Virchows Arch (2005) 446:1–9
DOI 10.1007/s00428-004-1157-3

REVIEW ARTICLE

Gerhard Faller · Thomas Kirchner

Immunological and morphogenic basis of gastric mucosa atrophy and metaplasia

Received: 28 July 2004 / Accepted: 30 September 2004 / Published online: 4 December 2004
© Springer-Verlag 2004

Abstract Chronic gastritis with gastric mucosa atrophy, intestinal metaplasia and endocrine cell hyperplasia are alterations with an increased risk for the development of gastric neoplasias. Immunological studies in autoimmune gastritis, in atrophic *Helicobacter pylori* gastritis and in studies with transgenic mice point to a central role of the parietal cell in the development of gastric mucosa atrophy. Destruction of gastric epithelial cells alone might not be sufficient for the loss of complete gastric glands. Gastric atrophy, endocrine cell hyperplasia and intestinal and pancreatic metaplasia can be regarded as the result of altered morphogenesis within the gastric mucosa. Impaired expression of the gastric morphogenic factor Sonic Hedgehog by parietal cells and increased expression of the transcriptional activators of intestinal and pancreatic differentiation, namely CDX2 and PDX1, seem to be crucial for the development of gastric atrophy and for intestinal, endocrine and pancreatic transdifferentiation processes. Altered expression of these morphogenic factors is partly caused by changes in the gastric milieu. Further studies concerning the normal and pathological morphogenesis of the gastric mucosa and related tissues might give new insight into the pathogenesis of gastric atrophy and metaplasia.

Keywords Gastric atrophy · Autoimmune gastritis · Metaplasia · Morphogenesis · Transdifferentiation

Introduction

Chronic gastritis is among the most prevalent chronic inflammatory conditions in man. However, most affected persons do not suffer from any clinically relevant complaints but usually remain asymptomatic for a long time. Chronic gastritis comprises two main entities, namely *Helicobacter pylori* (*H. pylori*) gastritis and autoimmune gastritis. In most cases, chronic *H. pylori* gastritis mainly affects the antrum mucosa, whereas the body mucosa shows only mild inflammatory changes. In contrast, autoimmune gastritis (AIG) predominantly affects the gastric body mucosa, which additionally shows severe mucosa atrophy, while the gastric antrum shows no more than a mild chronic inflammation. This reversal distribution and the different aetiologies have led to the classification of chronic gastritis into type A (autoimmune and corpus-predominant) and type B (*H. pylori*-induced and antrum predominant) [91]. However, it is well accepted that not only autoimmune gastritis but also a subset of chronic *H. pylori* gastritis show a corpus predominant phenotype with corpus mucosa atrophy, which means a depletion of the specific gastric glandular cells, namely acid-producing parietal cells and zymogenic chief cells [18]. Atrophic *H. pylori* gastritis and autoimmune gastritis almost always show extensive intestinal metaplasia. The particular clinical relevance of atrophic corpus gastritis with intestinal metaplasia lies in its association with the development of gastric adenocarcinoma [55, 83, 93]. Additionally, gastric neuroendocrine tumours are also linked to gastric atrophy in human autoimmune gastritis [56, 66, 93] and in an animal model of *H. pylori* gastritis [41]. Prevention or repression of gastric atrophy and metaplasia might protect from the development of gastric neoplasias. Therefore, more and detailed information on the pathogenesis of these early events in gastric tumorigenesis is needed. Here, we review the current and emerging concepts of the immunological and morphogenic pathomechanisms of gastric mucosa atrophy and metaplasia.

G. Faller (✉) · T. Kirchner
Institute of Pathology,
Krankenhausstrasse 8–10, 91054 Erlangen, Germany
e-mail: Gerhard.Faller@patho.imed.uni-erlangen.de
Tel.: +49-9131-8522524
Fax: +49-9131-8524745

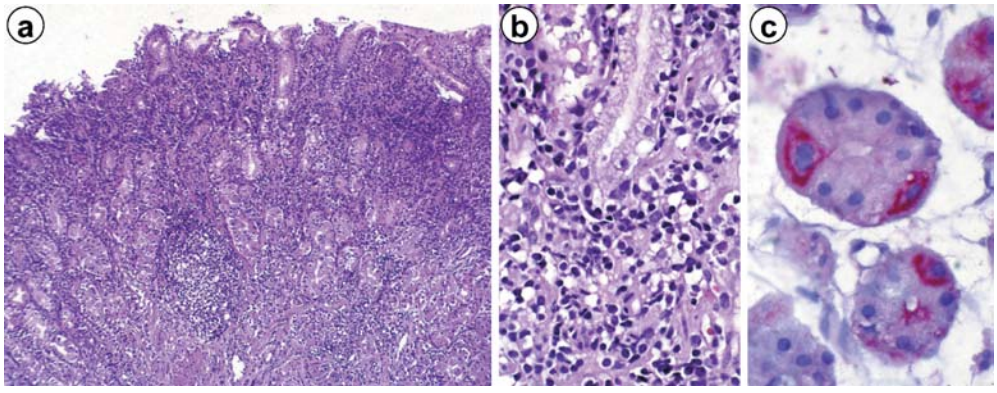

Fig. 1 Corpus predominant *Helicobacter pylori* gastritis (**a**) with focal gland destruction (**b**). Antigastric autoantibodies reactive against canaliculi within parietal cells (**c**) were detectable in the patient's serum

Immunopathology of atrophic gastritis

Classic autoimmune gastritis

AIG represents the prototype of corpus-predominant, chronic atrophic gastritis. It is closely associated with autoantibodies against gastric parietal cells and with the development of pernicious anaemia [80]. In the normal Western population and in patients with dyspepsia, the prevalence of AIG and autoantibodies against murine parietal cells adds up to 2–8% [10, 28, 63]. Anti-parietal cell autoantibodies react with the α and β subunits of the gastric H,K-ATPase, the so-called gastric proton pump, which is essential for gastric acidification [14]. In addition to humoral autoimmune responses, autoreactive T cells against the α and β subunits of the gastric 6H,K-ATPase were recently found in autoimmune gastritis patients [9, 21]. Clinically, AIG shows marked hypochlorhydria and hypoacidity. This could partly be caused by the inhibitory effect of anti-parietal cell autoantibodies on the gastric H,K-ATPase [13]. However, it seems more likely that low acid production in AIG is due to the autoimmune-mediated loss of the antigen-bearing and acid-secreting cells [21].

The immunopathogenesis of AIG has been extensively investigated in animal models of experimental autoimmune gastritis (EAIG). EAIG can be induced in lymphopenic mice with or without thymectomy, in non-lymphopenic mice immunised with the gastric H,K-ATPase or in transgenic mice if anti-H,K-ATPase reactivity is induced. The histological and functional parameters of EAIG correspond widely with the human disease, including inflammatory infiltrates in the gastric mucosa, loss of parietal and chief cells and detection of autoantibodies as well as of autoreactive T cells against the gastric H,K-ATPase [3]. The humoral autoimmune response in EAIG is also directed against the α and β subunits of the proton pump [16, 39]; but, transfer of autoantibodies does not induce gastritis in the acceptor mice [34]. In contrast, adoptive transfer of splenocytes from gastritic mice induces autoimmune gastritis in the recipient, which indicates a key role of T cells in the immunopathogenesis of autoimmune gastritis. Further analysis pointed to the Th1-subset of CD4+ T cells, which have also been implicated in the human disease [21, 22, 44, 54]. Pathogenic CD4+ T cells are CD25 negative, whereas CD4+CD25+ regulatory T cells can abrogate autoimmunity in transfer experiments. Therefore, it is concluded that a balance between pathogenic and suppressor/regulatory CD4+ T cells is required for the maintenance of tolerance to gastric autoantigens [71, 77]. Much effort has been made to find out whether the α or β chain of the gastric H,K-ATPase is the inciting autoantigen. Mice rendered tolerant to the β subunit but not to the α subunit of the gastric H,K-ATPase by transgenic expression of these subunits under the control of major histocompatibility complex class-II promoter in the thymus are protected from autoimmune gastritis, indicating that the β subunit acts as an inciting autoantigen [1, 2]. Yet, a pathogenic role for α-reactive T cells in EAIG cannot be ruled out [78]. However, from the data obtainable thus far, it was speculated that α-specific T cells could be of lower avidity and of minor pathogenic relevance than β-specific T cells, and it was suggested that anti-gastric immune reactions in EAIG and in AIG are initiated by reactivity to the β subunit but spread to other epitopes, leading to an autoimmune response against the α subunit [81].

H. pylori gastritis with antigastric autoreactivity

As in classic AIG, a subtype of chronic *H. pylori* gastritis histologically also shows corpus predominant gastritis (Fig. 1a), active gland destruction (Fig. 1b) and body mucosa atrophy and intestinal metaplasia [18]. Apart from these morphological parallels between AIG and corpus predominant atrophic *H. pylori* gastritis, systematic investigations have revealed striking autoimmune pathogenic similarities. When tested on human gastric tissue, sera from patients with atrophic *H. pylori* gastritis frequently contain autoantibodies against canalicular structures within the gastric parietal cells (Fig. 1c). Presence of these anticanalicular autoantibodies in H. pyori gastritis correlates with clinical and histological parameters of corpus mucosa atrophy, including reduced acid secretion [28, 30, 59]. At least 50% of these autoantibodies react with the α subunit or against both α and β subunits of the gastric H,K-ATPase but not against the

β subunit alone [17]. Anti-parietal cell antibodies have also been described in an animal model of Helicobacter infection, which substantiates the finding in human disease [20]. The pathogenesis of the humoral autoimmune response in Helicobacter infection has not been solved. Early reports on the potential role of molecular mimicry between *H. pylori* and the host could not be confirmed in humans or in ferrets [20, 29]. However, and most interestingly, in patients with antigastric autoimmune reactions and current *H. pylori* infection, T cells have been cloned that showed cross-reactivity between various *H. pylori* peptide epitopes and the gastric H,K-ATPase. Almost all cross-reacting clones reacted against the α subunit; whereas, for most autoreactive but non-cross-reactive clones, the β subunit was the main target [4]. These results correspond well with the findings of anti-H,K-ATPase reactivity of antigastric autoantibodies in *H. pylori* gastritis just mentioned [17] and support the idea that in genetically susceptible individuals *H. pylori* infection triggers or accelerates the development of gastric autoimmunity [6]. Thus, *H. pylori* gastritis could progress to autoimmune gastritis via an intermediate stage described as active autoimmune gastritis without complete loss of glands [76, 82]. This concept is strengthened by observations that this particular pre-atrophic phenotype of autoimmune gastritis improves after *H. pylori* therapy [58]. However, and in contrast to classic AIG, in *H. pylori*-induced antigastric autoimmunity, the α subunit of the H,K-ATPase could be of higher pathogenic relevance than the β subunit.

Atrophic *H. pylori* gastritis has also been found in patients without any evidence for antigastric autoimmune reactions [28]. It is far beyond the scope of this review to describe the possible pathomechanisms in detail. Briefly, the presence of certain *H. pylori* virulence factors, particularly the vacuolating toxin (VacA) or the cytotoxin-associated pathogenicity island (Cag-PAI) were shown to be associated with atrophic gastritis [11, 27]; but, thus far, antigastric autoantibodies could not be correlated with Cag-positive *H. pylori* strains [7]. Instead, it is very possible that bacterial factors directly interact with epithelial cells. For example, CagE, a protein of the Cag-PAI, has been found to induce apoptosis of parietal cells in vitro [60]. Additionally, host factors such as the predominant T-helper subtype and/or the host's genetic background could also influence the course of gastritis [32, 35, 51, 62].

Questionable role of increased apoptosis in the development of gastric atrophy

It has been suggested that the loss of glandular cells in the aforementioned subtypes of atrophic gastritis are the consequence of increased cell death in the glandular compartment. Indeed, in several cross-sectional studies, increased apoptosis was reported in both chronic atrophic *H. pylori* gastritis and AIG [75, 92, 94].

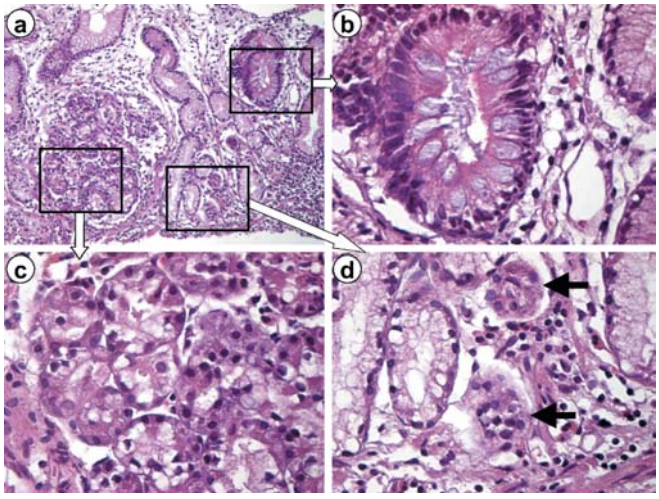

Fig. 2 End-stage autoimmune gastritis (**a**) showing extensive remodelling of the mucosa: intestinal metaplasia (**b**), pancreatic (acinar) metaplasia (**c**) and endocrine cell hyperplasia (*arrows* in **d**)

Increased apoptosis was also found in EAIG [40, 61]. Apoptosis in these gastric glands is mediated by Fas–Fas ligand interactions. In gastritic mice, Fas on parietal cells and Fas-ligand on H,K-ATPase-reactive T cells are upregulated, leading to destruction of antigen-bearing cells [61]. This was confirmed in a similar experimental approach in the human disease [21]. Additionally, thymectomised mice, deficient of Fas, are protected from gland destruction despite a significant inflammatory infiltrate in the glandular compartment. This provides convincing substantiation for an essential role of Fas-mediated parietal cell damage in the pathogenesis of gastric atrophy at least in experimental settings of autoimmune gastritis [53].

However, several arguments cast doubt on the exclusive role of increased apoptosis. First, in long-term follow-up studies, increased apoptosis was not correlated with the development of atrophy [88]. Second, increased loss of cells could be compensated by increased proliferation and gland regeneration [57]. Third, and most importantly, there is no convincing evidence for a significant autoimmune attack against gastric chief cells that are also lost in gastric atrophy [40]. Finally, increased apoptosis alone gives no explanation of the close association between gastric atrophy and the occurrence of intestinal metaplasia, endocrine cell hyperplasia and pancreatic metaplasia, as it can been seen in end stages of autoimmune gastritis (Fig. 2a, b, c, d).

Gastric atrophy—the result of altered gastric morphogenesis

From the data available, it cannot be ruled out that autoimmune-mediated apoptosis of parietal cells is a key event in the development of gastric atrophy. However, it must be assumed that additional and probably non-destructive pathomechanisms are also involved.

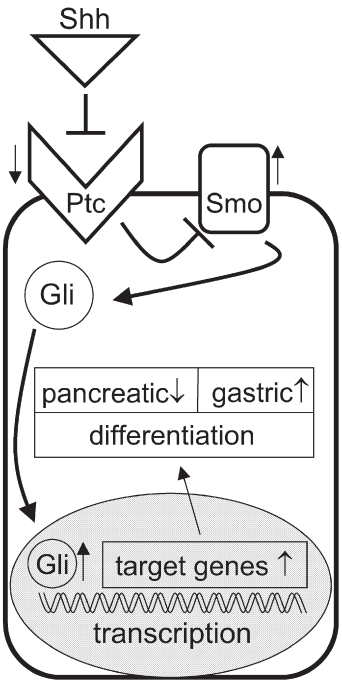

Fig. 3 Simplified overview of the Sonic Hedgehog signalling pathway and potential links to gastric and pancreatic differentiation

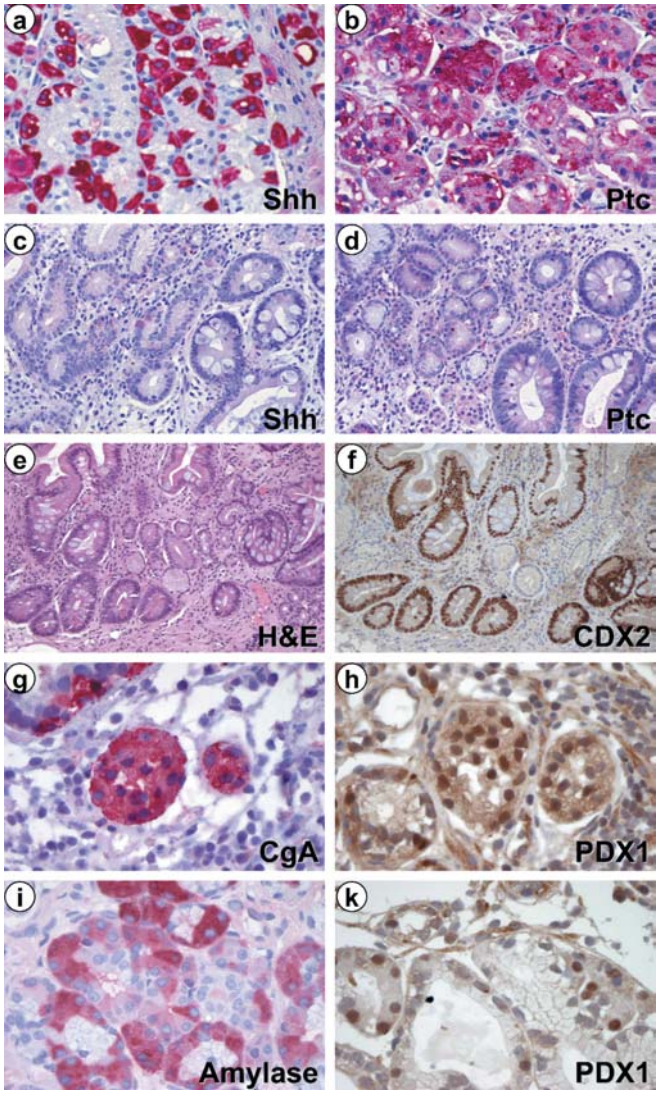

Fig. 4 Expression of the gastric morphogenic factor Sonic Hedgehog (Shh) and its receptor Patched (Ptc) in normal gastric mucosa (**a**, **b**) and in atrophic gastritis (**c**, **d**). In normal conditions, Shh is expressed exclusively in the parietal cells, whereas Ptc is additionally expressed in chief cells. In atrophic gastritis, both factors are not expressed. In intestinal metaplasia (**e**), the intestinal morphogenic factor CDX2 is expressed in the nuclei of metaplastic cells (**f**). Nodules of hyperplastic endocrine cells in atrophic gastritis co-express chromogranin A (**g**) and the pancreatic morphogenic factor PDX1 (**h**). Amylase-expressing foci of pancreatic (acinar) metaplasia (**i**) also show nuclear expression of PDX1 (**k**)

In EAIG, a significant increase of immature mucus-rich cells was observed, indicating that the normal development of chief cells is severely impaired [40]. The stop in chief cell differentiation could be caused by cytokines induced by the inflammatory infiltrate. However, thus far it is likely that parietal cells govern the differentiation program of other cell lines in the gastric gland and that this superior role of parietal cell is impaired in cases with anti-parietal cell autoimmunity [40]. This model is supported by experimental studies in transgenic mice showing that a selective loss of parietal cells not only leads to disturbances in the architecture of the gastric glands but additionally causes alterations or even a stop in the differentiation process of gastric chief cells [15, 50, 69, 74]. However, the factors by which this process is mediated were not identified in these studies.

Recent advances in developmental biology revealed a number of factors that are essential for the development of the gastrointestinal mucosa [67]. Embryonal differentiation processes are regulated through a number of signal cascades. One of these cascades starts with the morphogenic factor Sonic Hedgehog (Shh), which binds to its receptor Patched (Ptc), thus reducing the inhibitory effect of Ptc on another transmembrane protein, Smoothened (Smo). Shh signalling is finally carried out by members of the Gli-family of transcription factors (Fig. 3). Shh, an important nervous, craniofacial and limb morphogenic factor, is also involved in the development of the lung and gut [87]. Furthermore, and most interestingly, Shh knockout mice generated an intestinal- instead of gastric-type mucosa in the stomach, indicating that Shh plays a pivotal role in the morphogenesis of the gastric mucosa [65]. In human adults, we and others showed that Shh is almost exclusively expressed in gastric parietal cells (Fig. 4a), whereas the Shh-receptor Ptc is mainly expressed in gastric chief cells (Fig. 4b) [23, 85]. Thus, it might be possible that the parietal cell influences the differentiation process of other cell lines within the gastric gland via the Shh-Ptc signalling pathway. This is further strengthened by the fact that both Shh and Ptc are almost not detectable in conditions with reduced or abolished gastric morphogenesis, namely in gastric atrophy and intestinal metaplasia (Fig. 4c, d) [23, 86]. Loss of Shh might directly be

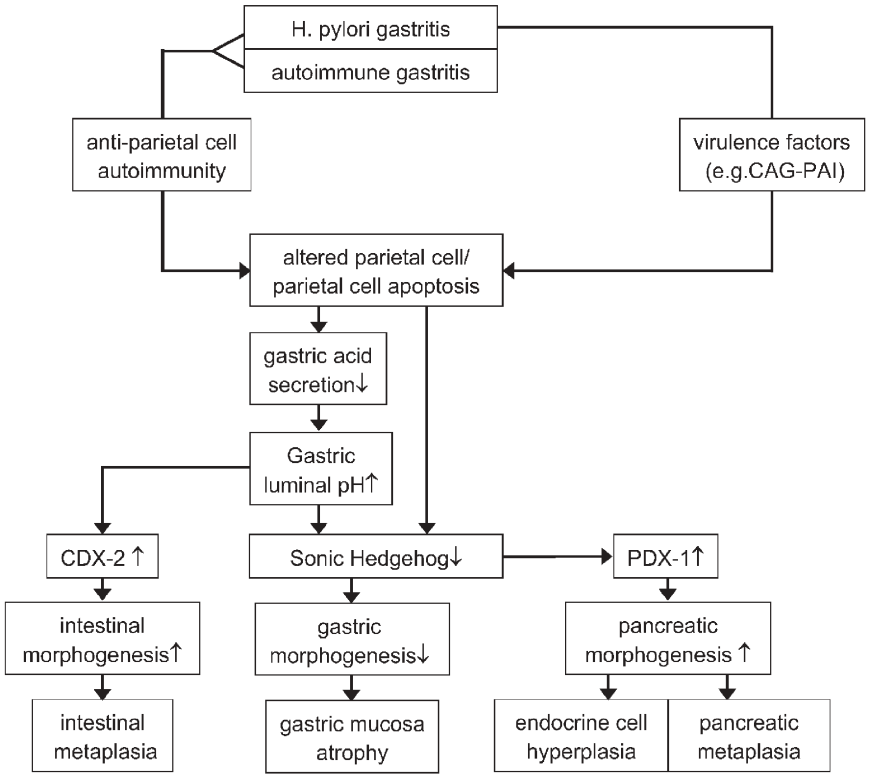

Fig. 5 Model for the immunological and morphogenic pathways in the development of gastric mucosa atrophy and metaplasia. The gastric parietal cell and the acidic milieu play a key role for autoimmune as well as for differentiation and transdifferentiation processes in the gastric corpus mucosa (see text for details)

caused by a loss of parietal cells, as seen in autoimmune gastritis. In addition, we were able to show that Shh is downregulated in hypoacidic conditions [23]. Hypoacidity might result from parietal cell apoptosis or from direct inhibition of the gastric H,K-ATPase by anti-H,K-ATPase autoantibodies [9]. Furthermore, hypoacidity-induced reduction of gastric morphogenesis via downregulation of gastric Shh signalling could explain a number of observations: first, the suppression of gastric epithelial cell differentiation in the developing and adult rat mucosa after omeprazole treatment [42, 43]; second, the depletion of differentiated glandular cells in mice overexpressing TGFα, a potent inhibitor of gastric acid secretion [70, 79]; and third, the potential development of gastric atrophy in *H. pylori*-infected patients taking proton-pump inhibitors [47, 48]. However, in clinical studies with non-infected patients treated by proton-pump inhibitors, no increase in corpus mucosa atrophy was observed [46]. Therefore, one might conclude that in addition to hypoacidity, other factors such as inflammatory cytokines or bacterial virulence factors are needed for the development of gastric atrophy. But thus far, any possible interference of such additional factors with Shh signalling remains speculative. Figure 5 briefly illustrates our current understanding of the autoimmunological and morphogenic pathomechanisms of gastric mucosa atrophy.

Remodelling of the gastric mucosa

Intestinal metaplasia

In contrast to other organ-specific autoimmune diseases, AIG shows extensive remodelling rather than significant scarring. As already mentioned, the remodelling of the mucosa comprises three alterations: intestinal metaplasia, pancreatic (acinar) metaplasia and endocrine cell hyperplasia (Fig. 2) [26, 38].

Advances in developmental biology have clearly shown that the caudal-type homeobox transcription factor 2 (CDX2) acts as master regulator for intestinal development and differentiation [33]. Loss of CDX2 expression leads to focal gastric differentiation in the colon [8]. However, aberrant expression of CDX2 in the upper gastrointestinal tract is a key event in the pathogenesis of Barrett's mucosa in the oesophagus and intestinal metaplasia (IM) in the stomach [64, 72]. Yet, the factors leading to aberrant CDX2 expression are only poorly understood.

Recent studies provided evidence that changes in the microenvironment within the upper gastrointestinal tract might influence CDX2 expression. Marchetti et al. found CDX2 upregulation in cultured oesophageal keratinocytes after exposure to acid. This corresponds to the close association of Barrett's mucosa with gastro-oesophageal reflux and consecutive lowered luminal pH in the oesophagus [52]. To study the role of the luminal milieu in transdifferentiation processes between intestinal- and gastric-type epithelium, gastric metaplasia of the duode-

num is a promising model because gastric metaplasia in the duodenum is closely associated with gastric hypersecretion and increased acid load in the duodenum [36, 84]. In our own studies, we were able to show that CDX2 expression in intestinal cells is lost in gastric metaplasia in the duodenum. Interestingly, in the intestinal cell line Caco2, CDX2 expression and expression of the CDX2 target gene sucrase-isomaltase are downregulated in acidic conditions, while the expression of gastric genes such as MUC5AC and MUC6 are upregulated [31]. The acid-induced loss of CDX2 expression in the development of gastric metaplasia in the duodenum might also reflect the pathomechanisms of IM in the stomach: gastric CDX2 expression and intestinal transdifferentiation in the gastric mucosa could be suppressed in the normal acidic situation in the corpus mucosa. Hypoacidity due to reduced acid secretion in gastric atrophy could allow upregulation of CDX2, resulting in IM (Fig. 4e, f). Although IM can also be found in cases without gastric atrophy, this concept could partly explain the strong association between gastric atrophy and IM. The possible pH-dependent morphogenic mechanism of IM in gastric atrophy is shown in Fig. 5.

Endocrine cell hyperplasia/endocrine pancreatic metaplasia?

Diffuse and nodular endocrine cell hyperplasia is a common finding in severe corpus mucosa atrophy (Fig. 4g) and a precursor lesion for gastric neuroendocrine tumours [93]. Phenotypically, hyperplastic endocrine cells mainly belong to gastric enterochromaffine-like cells [49]. Hypergastrinemia as consequence of hypoacidity is thought to play a pivotal role in the development of these lesions. However, additional relevant factors that are related to atrophic gastritis rather than hypergastinemia were postulated [19, 73]. Morphologically, endocrine nodules in atrophic gastric corpus mucosa resemble in some aspects islets of Langerhans in the pancreas. Since pancreatic hormones such as insulin or glucagon have not been found in these nodules, this view might be somewhat unconventional. But in the context of morphogenesis in the upper gastrointestinal tract, it is insofar intriguing, as Shh has been shown to inhibit pancreas development (Fig. 3) [5, 37]. In other words: loss of Hedgehog expression in the atrophic gastric mucosa might facilitate pancreatic differentiation [45].

Pancreatic organogenesis is regulated by a number of transcription factors. The pancreatic duodenal homeodomain transcription factor PDX1 plays an essential role in both early exocrine/endocrine pancreatic development and later in the regulation of insulin expression [25, 90]. We and others have recently shown that PDX1 is not expressed in the normal oxyntic mucosa but can be found in atrophic gastric body glands and in endocrine nodules (Fig. 4h) [12, 68]. In addition, so-called hyperplastic endocrine cells co-express the β subunit of the gastric H,K-ATPase and therefore obviously contain some characteristics of parietal cells. Hence, we speculated that endocrine nodules in atrophic gastritis could partly be regarded as the result of a transdifferentiation process in terms of endocrine pancreatic metaplasia rather than simple hyperplasia. Again, the parietal cell seems to play an important role in this transdifferentiation [12].

Pancreatic (acinar) metaplasia

Exocrine pancreatic (acinar) metaplasia (PM) of the stomach is mainly found in the gastro-oesophageal junction, and a congenital rather than an acquired origin of this lesion has been suggested [24, 89]. However, when present in the fundus mucosa, all cases with PM had histological changes consistent with AIG [24]. However, fundic PM was found in 50% of cases with AIG (Fig. 4i) [38]. As in endocrine nodules, the occurrence of exocrine PM could also be explained by decrease of Shh expression and subsequent increase of pancreatic development within the gastric mucosa. Indeed, our own studies revealed that the pancreatic morphogenic factor PDX1 is expressed in PM and in gastric glands surrounding PM, while PDX-1 is absent in normal glands of the gastric body mucosa (Fig. 4k) [12]. Interestingly, we found a cytoplasmic PDX1 reactivity in the parietal cells surrounding PM, which could indicate that, again, the gastric parietal cell plays a role in aberrant PDX1 expression. However, the meaning of this cytoplasmic PDX1 reactivity and the potential factors leading to PDX1 translocation from the cytoplasm to the nucleus in gastric epithelial cells are not understood. The potential morphogenic interrelation of gastric atrophy, endocrine cell hyperplasia and exocrine pancreatic metaplasia is outlined in Fig. 5.

Summary and future perspectives

Gastric mucosa atrophy and metaplasia are regarded as precursors of gastric epithelial neoplasias. Investigations of antigastric autoimmunity and of differentiation processes in the gastric mucosa have provided evidence that the gastric parietal cells are essential for the maintenance of gastric mucosa integrity. Transfer of the increasing knowledge of foregut development will increase the understanding of gastric mucosa alterations in the adult. Finally, the immunological and morphogenic analysis of gastric mucosa atrophy and metaplasia could show the way to new therapeutic approaches in the prevention of gastric neoplasias.

Acknowledgements Our studies were supported by grants from the Federal Ministry of Education and Research (BMBF) and the Interdisciplinary Centre of Clinical Research at the University of Erlangen-Nuremberg.

References

1. Alderuccio F, Toh BH, Tan SS, Gleeson PA, van Driel IR (1993) An autoimmune disease with multiple molecular targets abrogated by the transgenic expression of a single autoantigen in the thymus. J Exp Med 178:419–426
2. Alderuccio F, Gleeson PA, Berzins SP, Martin M, Van Driel IR, Toh BH (1997) Expression of the gastric H/K-ATPase alpha-subunit in the thymus may explain the dominant role of the beta-subunit in the pathogenesis of autoimmune gastritis. Autoimmunity 25:167–175
3. Alderuccio F, Sentry JW, Marshall AC, Biondo M, Toh BH (2002) Animal models of human disease: experimental autoimmune gastritis—a model for autoimmune gastritis and pernicious anemia. Clin Immunol 102:48–58
4. Amedei A, Bergman MP, Appelmelk BJ, Azzurri A, Benagiano M, Tamburini C, van der Zee R, Telford JL, Vandenbroucke-Grauls CM, D'Elios MM, Del Prete G (2003) Molecular mimicry between Helicobacter pylori antigens and H+, K+—adenosine triphosphatase in human gastric autoimmunity. J Exp Med 198:1147–1156
5. Apelqvist A, Ahlgren U, Edlund H (1997) Sonic hedgehog directs specialised mesoderm differentiation in the intestine and pancreas. Curr Biol 7:801–804
6. Appelmelk BJ, Faller G, Claeys D, Kirchner T, Vandenbroucke-Grauls CM (1998) Bugs on trial: the case of Helicobacter pylori and autoimmunity. Immunol Today 19:296–299
7. Asante MA, Mendall MA, Ballam L, Morris J, Northfield TC (1999) Relationship between Helicobacter pylori, gastric parietal cell antibodies and heat shock proteins. Eur J Gastroenterol Hepatol 11:1365–1370
8. Beck F, Chawengsaksophak K, Waring P, Playford RJ, Furness JB (1999) Reprogramming of intestinal differentiation and intercalary regeneration in Cdx2 mutant mice. Proc Natl Acad Sci U S A 96:7318–7323
9. Bergman MP, Amedei A, D'Elios MM, Azzurri A, Benagiano M, Tamburini C, van der Zee R, Vandenbroucke-Grauls CM, Appelmelk BJ, Del Prete G (2003) Characterization of H+, K+-ATPase T cell epitopes in human autoimmune gastritis. Eur J Immunol 33:539–545
10. Betterle C, Mazzi PA, Pedini B, Accordi F, Cecchetto A, Presotto F (1988) Complement-fixing gastric parietal cell autoantibodies. A good marker for the identification of type A chronic atrophic gastritis. Autoimmunity 1:267–274
11. Broutet N, Moran A, Hynes S, Sakarovitch C, Megraud F (2002) Lewis antigen expression and other pathogenic factors in the presence of atrophic chronic gastritis in a European population. J Infect Dis 185:503–512
12. Buettner M, Dimmler A, Magener A, Brabletz T, Stolte M, Kirchner T, Faller G (2004) Gastric PDX-1 expression in pancreatic metaplasia and endocrine cell hyperplasia in atrophic corpus gastritis. Mod Pathol 17:56–61
13. Burman P, Mardh S, Norberg L, Karlsson FA (1989) Parietal cell antibodies in pernicious anemia inhibit H+, K+-adenosine triphosphatase, the proton pump of the stomach. Gastroenterology 96:1434–1438
14. Callaghan JM, Khan MA, Alderuccio F, van Driel IR, Gleeson PA, Toh BH (1993) Alpha and beta subunits of the gastric H+/K(+)-ATPase are concordantly targeted by parietal cell autoantibodies associated with autoimmune gastritis. Autoimmunity 16:289–295
15. Canfield V, West AB, Goldenring JR, Levenson R (1996) Genetic ablation of parietal cells in transgenic mice: a new model for analyzing cell lineage relationships in the gastric mucosa. Proc Natl Acad Sci U S A 93:2431–2435
16. Claeys D, Saraga E, Rossier BC and Kraehenbuhl JP (1997) Neonatal injection of native proton pump antigens induces autoimmune gastritis in mice. Gastroenterology 113:1136–1145
17. Claeys D, Faller G, Appelmelk BJ, Negrini R, Kirchner T (1998) The gastric H+, K+-ATPase is a major autoantigen in chronic Helicobacter pylori gastritis with body mucosa atrophy. Gastroenterology 115:340–347
18. Correa P (1988) Chronic gastritis: a clinico-pathological classification. Am J Gastroenterol 83:504–509
19. Creutzfeldt W, Lamberts R (1992) Inter-relationship between serum gastrin levels, gastric mucosal histology and gastric endocrine cell growth. Digestion 51[Suppl 1]:76–81
20. Croinin TO, Clyne M, Appelmelk BJ, Drumm B (2001) Antigastric autoantibodies in ferrets naturally infected with Helicobacter mustelae. Infect Immun 69:2708–2713
21. D'Elios MM, Bergman MP, Azzurri A, Amedei A, Benagiano M, De Pont JJ, Cianchi F, Vandenbroucke-Grauls CM, Romagnani S, Appelmelk BJ, Del Prete G (2001) H(+),K(+)-atpase (proton pump) is the target autoantigen of Th1-type cytotoxic T cells in autoimmune gastritis. Gastroenterology 120:377–386
22. De Silva HD, Van Driel IR, La Gruta N, Toh BH, Gleeson PA (1998) CD4+ T cells, but not CD8+ T cells, are required for the development of experimental autoimmune gastritis. Immunology 93:405–408
23. Dimmler A, Brabletz T, Hlubek F, Hafner M, Rau T, Kirchner T, Faller G (2003) Transcription of sonic hedgehog, a potential factor for gastric morphogenesis and gastric mucosa maintenance, is up-regulated in acidic conditions. Lab Invest 83:1829–1837
24. Doglioni C, Laurino L, Dei Tos AP, De Boni M, Franzin G, Braidotti P, Viale G (1993) Pancreatic (acinar) metaplasia of the gastric mucosa. Histology, ultrastructure, immunocytochemistry, and clinicopathologic correlations of 101 cases. Am J Surg Pathol 17:1134–1143
25. Edlund H (2002) Pancreatic organogenesis—developmental mechanisms and implications for therapy. Nat Rev Genet 3:524–532
26. Eidt S, Oberhuber G, Schneider A, Stolte M (1996) The histopathological spectrum of type A gastritis. Pathol Res Pract 192:101–106
27. Eurohepygast Study Group (2002) Risk factors for atrophic chronic gastritis in a European population: results of the Eurohepygast study. Gut 50:779–785
28. Faller G, Steininger H, Kranzlein J, Maul H, Kerkau T, Hensen J, Hahn EG, Kirchner T (1997) Antigastric autoantibodies in Helicobacter pylori infection: implications of histological and clinical parameters of gastritis. Gut 41:619–623
29. Faller G, Steininger H, Appelmelk B, Kirchner T (1998) Evidence of novel pathogenic pathways for the formation of antigastric autoantibodies in Helicobacter pylori gastritis. J Clin Pathol 51:244–245
30. Faller G, Winter M, Steininger H, Konturek P, Konturek SJ, Kirchner T (1998) Antigastric autoantibodies and gastric secretory function in Helicobacter pylori-infected patients with duodenal ulcer and non-ulcer dyspepsia. Scand J Gastroenterol 33:276–282
31. Faller G, Dimmler A, Rau T, Spardena S, Hlubek F, Kirchner T, Brabletz T (2004) Evidence for an acid induced loss of Cdx2 expression in gastric metaplasia in the duodenum. J Pathol 203:904–908
32. Fox JG, Beck P, Dangler CA, Whary MT, Wang TC, Shi HN, Nagler-Anderson C (2000) Concurrent enteric helminth infection modulates inflammation and gastric immune responses and reduces helicobacter-induced gastric atrophy. Nat Med 6:536–542
33. Freund JN, Domon-Dell C, Kedinger M and Duluc I (1998) The Cdx-1 and Cdx-2 homeobox genes in the intestine. Biochem Cell Biol 76:957–969
34. Fukuma K, Sakaguchi S, Kuribayashi K, Chen WL, Morishita R, Sekita K, Uchino H, Masuda T (1988) Immunologic and clinical studies on murine experimental autoimmune gastritis induced by neonatal thymectomy. Gastroenterology 94:274–283
35. Furuta T, El-Omar EM, Xiao F, Shirai N, Takashima M, Sugimura H, Sugimurra H (2002) Interleukin 1beta polymorphisms increase risk of hypochlorhydria and atrophic gastritis and reduce risk of duodenal ulcer recurrence in Japan. Gastroenterology 123:92–105

36. Harris AW, Gummett PA, Walker MM, Misiewicz JJ, Baron JH (1996) Relation between gastric acid output, Helicobacter pylori, and gastric metaplasia in the duodenal bulb. Gut 39:513–520
37. Hebrok M (2003) Hedgehog signaling in pancreas development. Mech Dev 120:45–57
38. Jhala NC, Montemor M, Jhala D, Lu L, Talley L, Haber MM, Lechago J (2003) Pancreatic acinar cell metaplasia in autoimmune gastritis. Arch Pathol Lab Med 127:854–857
39. Jones CM, Callaghan JM, Gleeson PA, Mori Y, Masuda T, Toh BH (1991) The parietal cell autoantigens recognized in neonatal thymectomy-induced murine gastritis are the alpha and beta subunits of the gastric proton pump [corrected]. Gastroenterology 101:287–294
40. Judd LM, Gleeson PA, Toh BH, van Driel IR (1999) Autoimmune gastritis results in disruption of gastric epithelial cell development. Am J Physiol 277:G209–G218
41. Kagawa J, Honda S, Kodama M, Sato R, Murakami K, Fujioka T (2002) Enterocromaffin-like cell tumor induced by Helicobacter pylori infection in Mongolian gerbils. Helicobacter 7:390–397
42. Kakei N, Ichinose M, Tsukada S, Tatematsu M, Tezuka N, Furihata C, Yahagi N, Matsushima M, Miki K, Kurokawa K et al (1993) Effects of omeprazole on gastric mucosal growth and differentiation in developing rat. Biochem Biophys Res Commun 197:310–318
43. Kakei N, Ichinose M, Tatematsu M, Shimizu M, Oka M, Yahagi N, Matsushima M, Kurokawa K, Yonezawa S, Furihata C et al (1995) Effects of long-term omeprazole treatment on adult rat gastric mucosa—enhancement of the epithelial cell proliferation and suppression of its differentiation. Biochem Biophys Res Commun 214:861–868
44. Katakai T, Mori KJ, Masuda T and Shimizu A (1998) Differential localization of Th1 and Th2 cells in autoimmune gastritis. Int Immunol 10:1325–1334
45. Kim SK, Melton DA (1998) Pancreas development is promoted by cyclopamine, a hedgehog signaling inhibitor. Proc Natl Acad Sci U S A 95:13036–13041
46. Klinkenberg-Knol EC, Nelis F, Dent J, Snel P, Mitchell B, Prichard P, Lloyd D, Havu N, Frame MH, Roman J, Walan A, Group LT (2000) Long-term omeprazole treatment in resistant gastroesophageal reflux disease: efficacy, safety, and influence on gastric mucosa. Gastroenterology 118:661–669
47. Kuipers EJ, Lundell L, Klinkenberg-Knol EC, Havu N, Festen HP, Liedman B, Lamers CB, Jansen JB, Dalenback J, Snel P, Nelis GF, Meuwissen SG (1996) Atrophic gastritis and Helicobacter pylori infection in patients with reflux esophagitis treated with omeprazole or fundoplication. N Engl J Med 334:1018–1022
48. Lamberts R, Brunner G, Solcia E (2001) Effects of very long (up to 10 years) proton pump blockade on human gastric mucosa. Digestion 64:205–213
49. Lehy T, Roucayrol AM, Mignon M (2000) Histomorphological characteristics of gastric mucosa in patients with Zollinger–Ellison syndrome or autoimmune gastric atrophy: role of gastrin and atrophying gastritis. Microsc Res Tech 48:327–338
50. Li Q, Karam SM, Gordon JI (1996) Diphtheria toxin-mediated ablation of parietal cells in the stomach of transgenic mice. J Biol Chem 271:3671–3676
51. Macarthur M, Hold GL, El-Omar EM (2004) Inflammation and cancer. II. Role of chronic inflammation and cytokine gene polymorphisms in the pathogenesis of gastrointestinal malignancy. Am J Physiol Gastrointest Liver Physiol 286:G515–G20
52. Marchetti M, Caliot E, Pringault E (2003) Chronic acid exposure leads to activation of the cdx2 intestinal homeobox gene in a long-term culture of mouse esophageal keratinocytes. J Cell Sci 116:1429–1436
53. Marshall AC, Alderuccio F, Toh BH (2002) Fas/CD95 is required for gastric mucosal damage in autoimmune gastritis. Gastroenterology 123:780–789
54. Martinelli TM, van Driel IR, Alderuccio F, Gleeson PA, Toh BH (1996) Analysis of mononuclear cell infiltrate and cytokine production in murine autoimmune gastritis. Gastroenterology 110:1791–1802
55. Meining A, Bayerdorffer E, Muller P, Miehlke S, Lehn N, Holzel D, Hatz R, Stolte M (1998) Gastric carcinoma risk index in patients infected with Helicobacter pylori. Virchows Arch 432:311–314
56. Modlin IM, Lye KD, Kidd M (2003) Carcinoid tumors of the stomach. Surg Oncol 12:153–172
57. Moss SF, Valle J, Abdalla AM, Wang S, Siurala M, Sipponen P (1999) Gastric cellular turnover and the development of atrophy after 31 years of follow-up: a case-control study. Am J Gastroenterol 94:2109–114
58. Muller H, Rappel S, Wundisch T, Bayerdorffer E, Stolte M (2001) Healing of active, non-atrophic autoimmune gastritis by H. pylori eradication. Digestion 64:30–39
59. Negrini R, Savio A, Poiesi C, Appelmelk BJ, Buffoli F, Paterlini A, Cesari P, Graffeo M, Vaira D, Franzin G (1996) Antigenic mimicry between Helicobacter pylori and gastric mucosa in the pathogenesis of body atrophic gastritis. Gastroenterology 111:655–665
60. Neu B, Randlkofer P, Neuhofer M, Voland P, Mayerhofer A, Gerhard M, Schepp W, Prinz C (2002) Helicobacter pylori induces apoptosis of rat gastric parietal cells. Am J Physiol Gastrointest Liver Physiol 283:G309–G318
61. Nishio A, Katakai T, Oshima C, Kasakura S, Sakai M, Yonehara S, Suda T, Nagata S, Masuda T (1996) A possible involvement of Fas-Fas ligand signaling in the pathogenesis of murine autoimmune gastritis. Gastroenterology 111:959–967
62. Ohana M, Okazaki K, Oshima C, Kawasaki K, Fukui T, Tamaki H, Matsuura M, Asada M, Nishi T, Uchida K, Uose S, Nakase H, Iwano M, Matsushima Y, Hiai H, Chiba T (2003) Inhibitory effects of Helicobacter pylori infection on murine autoimmune gastritis. Gut 52:1102–1110
63. Oksanen A, Sipponen P, Miettinen A, Sarna S, Rautelin H (2000) Evaluation of blood tests to predict normal gastric mucosa. Scand J Gastroenterol 35:791–795
64. Phillips RW, Frierson HF Jr, Moskaluk CA (2003) Cdx2 as a marker of epithelial intestinal differentiation in the esophagus. Am J Surg Pathol 27:1442–1447
65. Ramalho-Santos M, Melton DA, McMahon AP (2000) Hedgehog signals regulate multiple aspects of gastrointestinal development. Development 127:2763–2772
66. Rindi G, Bordi C, Rappel S, La Rosa S, Stolte M, Solcia E (1996) Gastric carcinoids and neuroendocrine carcinomas: pathogenesis, pathology, and behavior. World J Surg 20:168–172
67. Roberts DJ (2000) Molecular mechanisms of development of the gastrointestinal tract. Dev Dyn 219:109–120
68. Sakai H, Eishi Y, Li XL, Akiyama Y, Miyake S, Takizawa T, Konishi N, Tatematsu M, Koike M, Yuasa Y (2004) PDX1 homeobox protein expression in pseudopyloric glands and gastric carcinomas. Gut 53:323–330
69. Scarff KL, Judd LM, Toh BH, Gleeson PA, Van Driel IR (1999) Gastric H(+),K(+)-adenosine triphosphatase beta subunit is required for normal function, development, and membrane structure of mouse parietal cells. Gastroenterology 117:605–618
70. Sharp R, Babyatsky MW, Takagi H, Tagerud S, Wang TC, Bockman DE, Brand SJ, Merlino G (1995) Transforming growth factor alpha disrupts the normal program of cellular differentiation in the gastric mucosa of transgenic mice. Development 121:149–161
71. Shevach EM (2000) Regulatory T cells in autoimmunity. Annu Rev Immunol 18:423–449
72. Silberg DG, Sullivan J, Kang E, Swain GP, Moffett J, Sund NJ, Sackett SD, Kaestner KH (2002) Cdx2 ectopic expression induces gastric intestinal metaplasia in transgenic mice. Gastroenterology 122:689–696
73. Solcia E, Rindi G, Larosa S, Capella C (2000) Morphological, molecular, and prognostic aspects of gastric endocrine tumors. Microsc Res Tech 48:339–348

74. Spicer Z, Miller ML, Andringa A, Riddle TM, Duffy JJ, Doetschman T, Shull GE (2000) Stomachs of mice lacking the gastric H,K-ATPase alpha-subunit have achlorhydria, abnormal parietal cells, and ciliated metaplasia. J Biol Chem 275:21555–21565
75. Steininger H, Faller G, Dewald E, Brabletz T, Jung A, Kirchner T (1998) Apoptosis in chronic gastritis and its correlation with antigastric autoantibodies. Virchows Arch 433:13–18
76. Stolte M, Baumann K, Bethke B, Ritter M, Lauer E, Eidt H (1992) Active autoimmune gastritis without total atrophy of the glands. Z Gastroenterol 30:729–735
77. Suri-Payer E, Amar AZ, Thornton AM, Shevach EM (1998) CD4+CD25+ T cells inhibit both the induction and effector function of autoreactive T cells and represent a unique lineage of immunoregulatory cells. J Immunol 160:1212–1218
78. Suri-Payer E, Amar AZ, McHugh R, Natarajan K, Margulies DH, Shevach EM (1999) Post-thymectomy autoimmune gastritis: fine specificity and pathogenicity of anti-H/K ATPase-reactive T cells. Eur J Immunol 29:669–677
79. Takagi H, Jhappan C, Sharp R, Merlino G (1992) Hypertrophic gastropathy resembling Menetrier's disease in transgenic mice overexpressing transforming growth factor alpha in the stomach. J Clin Invest 90:1161–1167
80. Toh BH, van Driel IR, Gleeson PA (1997) Pernicious anemia. N Engl J Med 337:1441–1448
81. Toh BH, Sentry JW, Alderuccio F (2000) The causative H+/K+ ATPase antigen in the pathogenesis of autoimmune gastritis. Immunol Today 21:348–354
82. Torbenson M, Abraham SC, Boitnott J, Yardley JH, Wu TT (2002) Autoimmune gastritis: distinct histological and immunohistochemical findings before complete loss of oxyntic glands. Mod Pathol 15:102–109
83. Uemura N, Okamoto S, Yamamoto S, Matsumura N, Yamaguchi S, Yamakido M, Taniyama K, Sasaki N, Schlemper RJ (2001) Helicobacter pylori infection and the development of gastric cancer. N Engl J Med 345:784–789
84. Van De Bovenkamp JH, Korteland-Van Male AM, Buller HA, Einerhand AW, Dekker J (2003) Metaplasia of the duodenum shows a Helicobacter pylori-correlated differentiation into gastric-type protein expression. Hum Pathol 34:156–165
85. van den Brink GR, Hardwick JC, Tytgat GN, Brink MA, Ten Kate FJ, Van Deventer SJ, Peppelenbosch MP (2001) Sonic hedgehog regulates gastric gland morphogenesis in man and mouse. Gastroenterology 121:317–328
86. van den Brink GR, Hardwick JC, Nielsen C, Xu C, ten Kate FJ, Glickman J, van Deventer SJ, Roberts DJ, Peppelenbosch MP (2002) Sonic hedgehog expression correlates with fundic gland differentiation in the adult gastrointestinal tract. Gut 51:628–633
87. Villavicencio EH, Walterhouse DO, Iannaccone PM (2000) The sonic hedgehog-patched-gli pathway in human development and disease. Am J Hum Genet 67:1047–1054
88. Vorobjova T, Maaroos HI, Sipponen P, Villako K, Uibo R (2001) Apoptosis in different compartments of antrum and corpus mucosa in chronic Helicobacter pylori gastritis. An 18-year follow-up study. Scand J Gastroenterol 36:136–143
89. Wang HH, Zeroogian JM, Spechler SJ, Goyal RK, Antonioli DA (1996) Prevalence and significance of pancreatic acinar metaplasia at the gastroesophageal junction. Am J Surg Pathol 20:1507–1510
90. Wilson ME, Scheel D, German MS (2003) Gene expression cascades in pancreatic development. Mech Dev 120:65–80
91. Wyatt JI, Dixon MF (1988) Chronic gastritis—a pathogenetic approach. J Pathol 154:113–124
92. Xia HH, Talley NJ (2001) Apoptosis in gastric epithelium induced by helicobacter pylori infection: implications in gastric carcinogenesis. Am J Gastroenterol 96:16–26
93. Ye W, Nyren O (2003) Risk of cancers of the oesophagus and stomach by histology or subsite in patients hospitalised for pernicious anaemia. Gut 52:938–941
94. Yoshimura T, Shimoyama T, Tanaka M, Sasaki Y, Fukuda S, Munakata A (2000) Gastric mucosal inflammation and epithelial cell turnover are associated with gastric cancer in patients with Helicobacter pylori infection. J Clin Pathol 53:532–536

Virchows Arch (2005) 446:10–14
DOI 10.1007/s00428-004-1143-9

ORIGINAL ARTICLE

Hajime Kuroda · Jun-ichi Tamaru · Goi Sakamoto · Kiyoshi Ohnisi · Shinji Itoyama

Immunophenotype of lymphocytic infiltration in medullary carcinoma of the breast

Received: 24 July 2004 / Accepted: 19 September 2004 / Published online: 30 November 2004
© Springer-Verlag 2004

Abstract Medullary carcinoma (MC) of the breast is characterized by large anaplastic cells and infiltration by benign lymphocytes. Patients with this pattern of breast carcinoma are considered to have a better prognosis than those with other histological subtypes. We reviewed cases of primary breast carcinoma that were surgically resected between 1990 and 2004. Of these, 13 cases of medullary carcinoma of the breast with lymphocyte infiltration were reported. Tests for CD3, CD4, CD8, CD20, CD56, TIA-1, and granzyme B were performed on paraffin sections. We found that the MC contained very few NK cells, as assessed by their reactivity with the CD56 antibodies. However, MC had a significantly greater percentage of CD3, CD8, TIA-1, and granzyme B lymphocytes infiltrating the stroma of the tumor. Furthermore, more CD8-positive than CD4-positive T-cell lymphocytes were present within the tumor cell nests in MC, as opposed to the proportion in usual ductal carcinoma. The infiltrating cytotoxic/suppressor T cells in MC represent host resistance against cancer, and the high grading of the T-cell infiltration could explain, in part, a key mechanism controlling the good prognosis for this type of tumor and solve the pathological paradox of MC.

H. Kuroda (✉) · J.-i. Tamaru · S. Itoyama
Department of Pathology,
Saitama Medical Center, Saitama Medical School 1981,
Tsujido, Kamoda, 350-8550 Kawagoe, Saitama, Japan
e-mail: hajime@saitama-med.ac.jp
Tel.: +81-49-2283522
Fax: +81-49-2283522

K. Ohnisi
Department of Surgery,
Saitama Medical Center,
Saitama, Japan

G. Sakamoto
Department of Breast Pathology,
Cancer Institute and Hospital,
Japanese Foundation for Cancer Research,
Japan

Keywords Medullary carcinoma · CD8 · CD56 · TIA-1 · Granzyme B

Introduction

In 1949, Moore and Foote described their experience with a well-circumscribed form of breast carcinoma with lymphoid stroma [10]. It was called medullary carcinoma (MC) and was recognized to have a favorable prognosis compared with other histological subtypes. However, it was not singled out as a distinct entity. In 1977, Ridolfi et al. redefined the histological criteria for typical and atypical MC [15]. In 1988, Wargotz and Silverberg found that cases having only one of the "atypical" features listed by Ridolfi et al.—intraductal carcinoma, sparse mononuclear infiltrate, or focal marginal infiltration—should not be excluded from the typical MC category [20]. There is also controversy over the prognosis in MC. Most authors state that MC has a more favorable prognosis when compared with invasive ductal carcinoma. However, numerous authors make the error of grading MC according to prognostic factors applicable to other breast carcinomas. In MC, neither the nuclear grading of the modified Bloom–Richardson scoring system nor mitotic activity applicable for other types of breast carcinoma is effective [12]. Some authors consider that this better prognosis is due, at least in part, to the presence of the lymphocytic infiltrate that is closely associated with the tumor [2, 5, 17, 18, 21, 22]. Questions persist concerning the specific characteristics of this histological subtype of breast carcinoma. One possible hypothesis for the improved prognosis in MC is that infiltrating lymphocytes in MC possess cytotoxic activity. The aims of this study were to characterize the immunophenotype of the lymphocytic infiltration and to define the association of these findings with the established prognosis of MC.

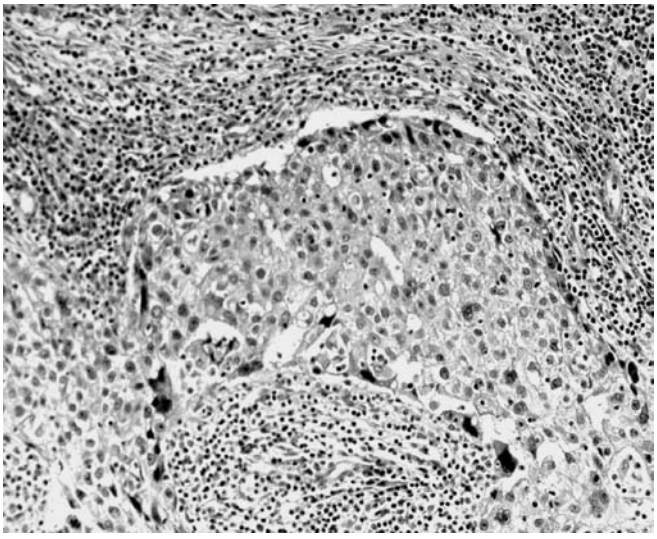

Fig. 1 Low-power microphotograph of medullary carcinoma. Carcinoma was distributed in sharply defined bands separated by stroma permeated predominantly by lymphoid cells

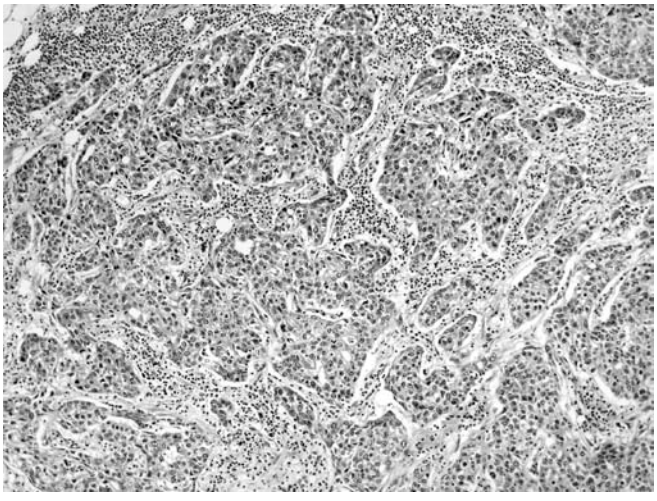

Fig. 2 Low-power microphotograph of medullary carcinoma showing the broad, interanastomosing sheets of the tumor cells with indistinct cell borders, as described by Ridolfi et al. [15]

Materials and methods

The subjects were cases of primary breast carcinoma that were surgically resected at Saitama Medical Center, Saitama Medical School between 1990 and 2004 and were reviewed for the histological presentation of MC. Of these, 13 cases were diagnosed as MC with abundant lymphocytic infiltration (Fig. 1, Fig. 2, Fig. 3). Paraffin-embedded slides stained with hematoxylin and eosin were used for the histological analysis. Histological typing was done using the criteria of Wargotz and Silverberg classification (Table 1) [20]. All of the histological slides were reviewed by two pathologists without knowledge of the clinical outcome. In addition, ten control specimens of infiltrating ductal carcinoma of the breast were selected from recent surgical samples that had been studied in our department and that contained abundant lymphocytic infiltration with nuclear grade 3.

Immunohistochemical staining was performed according to the following protocol. Consecutive sections from formalin-fixed, paraffin-embedded tissue blocks were cut at 5-μm intervals, deparaffinized, and dehydrated with xylene and graded alcohol. Pressure cooker pretreatment (1 cycle of 1 min) was performed at pH 6.0 for all antibodies. Endogenous peroxidase activity was quenched with 3% hydrogen peroxide at room temperature for 30 min. Sections were blocked with 10% goat serum for 60 min and then incubated with the primary antibody for 1 h at room temperature. Tests for CD3, CD4, CD8, CD20 (L26), CD56, TIA-1, and granzyme B were performed on paraffin sections. The primary antibodies and dilutions are summarized in Table 2.

For every case, the evaluation of the immunoreactions was done on slides, with lymphocytes infiltrating the MC as well as the control. The staining result for each antibody was scored by two authors, and a consensus score was obtained (Fig. 4, Fig. 5, Fig. 6). Grading of lymphocyte infiltration in cancer tissues was made according to the following standards, which are a modified method of the study by Ben-Ezra and Sheibani: 0=no positive cells; 1+=0–50%; 2+=50–75%; 3+=75–100% [2]. Multiple group comparisons were analyzed by Mann–Whitney U test. All statistical tests were considered significant at the $P<0.05$ level.

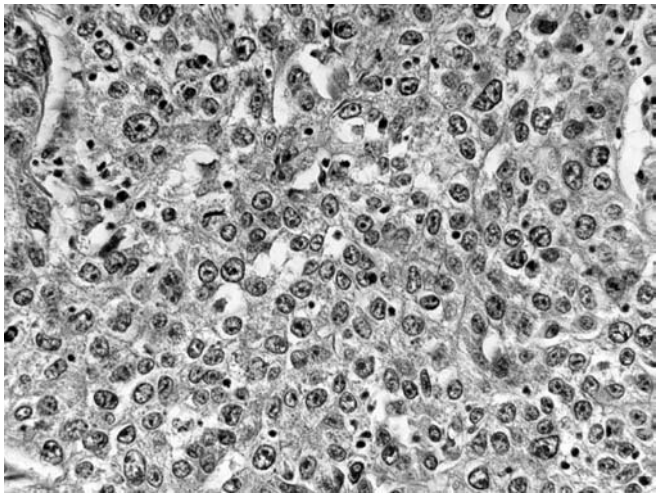

Fig. 3 High-power microphotograph of medullary carcinoma. This carcinoma had mitotic figures and pleomorphic nuclei

Table 1 Histological criteria for the diagnosis of medullary carcinoma. Modified from Wargotz and Silverberg [20]

Primary*
Predominantly circumscribed border
Syncytial growth>75%
Presence of admixed stromal mononuclear infiltrate
Grade 2 or 3 nuclei
Secondary**
Microscopically completely circumscribed
2+ to 3+ mononuclear infiltrate
Absence of in situ carcinoma

* Diagnosis of invasive ductal carcinoma is mandatory if any one of these criteria is not met

** Diagnosis of invasive ductal carcinoma is mandatory if two or more of these criteria are not met

Results

The results of the immunohistochemical analysis for immunophenotype are summarized in Table 3. The grading

Table 2 Monoclonal antibodies used in the study and the immunophenotypes of lymphocytes in breast cancer

Antibody	Clone	Source	Dilution	Main cellular expression
Anti-CD3	M7254	Dako-Japan	×100	T-cell lineage
Anti-CD4	1F6	Novocastra	×20	Helper T lymphocytes
Anti-CD8	C8/144B	Dako-Japan	×100	Cytotoxic/suppressor T lymphocytes
Anti-CD20	L26	Dako-Japan	×100	B-cell lineage
Anti-CD56	1B6	Novocastra	×50	NK cells, activated T cells
Anti-TIA-1	2G9	Immunotech	×50	Cytotoxic granule in cytotoxic T cells and NK cells
Granzyme B	GrB-7	Monosan	×20	Cytotoxic granule in cytotoxic T cells and NK cells

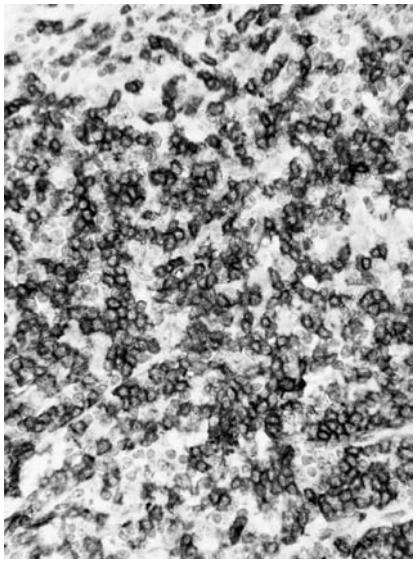

Fig. 4 Significant numbers of CD8-positive cells were seen within surrounding stroma in medullary carcinoma

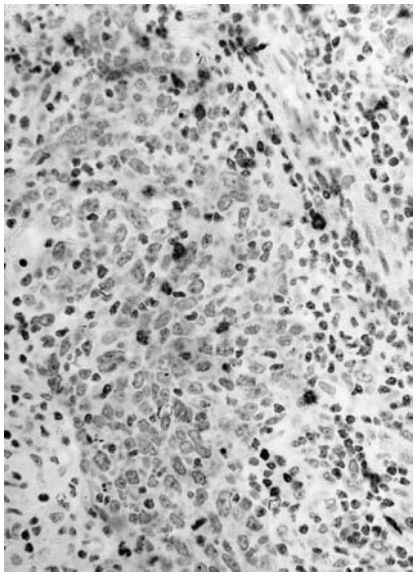

Fig. 5 Only a few CD56-positive cells were seen within the tumor cell nests and surrounding stroma in one of the medullary carcinoma cases

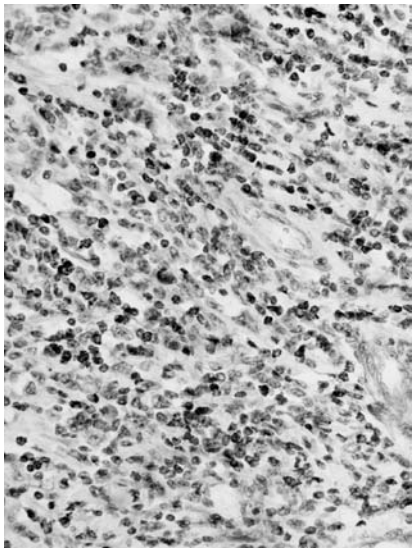

Fig. 6 Large numbers of granzyme-B-positive cells were seen infiltrating the stroma in medullary carcinoma

of CD3-positive T-lymphocytes infiltrating the stroma was significantly greater than that of CD20-positive T lymphocytes in the MC and control cases ($P<0.05$). In contrast, no significant difference was found between the grading of CD3-positive lymphocytes between these two groups in the surrounding stroma. The grading of CD8-positive lymphocytes in the surrounding stroma was significantly greater than that of the CD4-positive lymphocytes in the MC, as compared with those in the control cases ($P<0.05$). There were only two cases showing staining with CD56 antibodies, which detect NK cell-associated antigens. In these cases, the percentage of cells stained was usually less than the total percentage of T cells present.

The grading of TIA-1-positive cells was nearly equal to that of those stained with CD8. The grading of TIA-1-positive cells was not significantly greater than that of CD8-positive cells in the MC and control groups. The percentage of stromal TIA-1-positive cells was higher in the MC cases, although not significantly, than in the control cases.

The grading of granzyme-B-positive cells was consistently lower than that of TIA-1-and CD8-positive cells. However, the grading of granzyme-B-positive cells was

Table 3 The relationship between the histological classification and grading of lymphocyte infiltration with immunological markers of breast cancer

Cases	CD3	CD4	CD8	CD20	CD56	TIA-1	Granzyme B
MC cases							
1	3	1	2	1	0	2	2
2	3	0	3	1	0	3	1
3	3	1	3	1	0	3	2
4	2	1	2	1	0	2	3
5	3	0	3	1	0	2	2
6	3	1	3	1	0	3	2
7	3	0	3	1	1	3	2
8	3	1	2	1	0	2	2
9	3	1	3	1	0	3	1
10	1	1	2	1	0	2	1
11	3	2	3	1	0	3	2
12	3	1	3	1	1	2	2
13	3	1	2	1	0	2	1
Control cases							
1	3	3	1	1	0	2	1
2	3	3	2	1	0	1	1
3	3	2	1	1	0	2	1
4	3	3	2	1	0	2	1
5	3	3	3	0	0	2	1
6	3	3	2	1	0	3	1
7	3	3	2	1	0	3	0
8	3	3	2	1	0	3	1
9	3	3	2	1	0	2	1
10	3	3	2	2	0	3	1

* Significance was evaluated by Mann-Whitney's U test, and the p value indicates whether any significant difference existed between MC and general types of breast carcinoma

markedly higher in cases of MC, in contrast to that of the control cases ($P<0.05$).

Discussion

MC of the breast is a rare tumor that has a favorable prognosis [1, 4, 12, 13, 15, 20]. The characteristic histological features of this tumor are large anaplastic cells and infiltration by benign lymphocytes. Numerous authors make the error of grading MC according to prognostic factors applicable to other breast carcinomas. In MC, neither the nuclear grading of the modified Bloom–Richardson scoring system nor mitotic activity applicable for other types of breast carcinoma is effective. These problems are what we call the "paradox of MC." Some authors consider that this better prognosis is due, at least in part, to the presence of the lymphocytic infiltration, which is closely associated with the tumor. However, Ridolfi and Rapin classified MC using general diagnostic criteria and found that only about 30% of the cases fulfilled the strict criteria for that diagnosis [12, 15]. Even so, most authors, following Moore and Foote, retain this characteristic for the diagnosis [10].

As in previous studies of infiltrating ductal breast carcinomas, we found that the MCs contained very few NK cells, as assessed by their reactivity with CD56 antibodies. NK cells are a subpopulation of lymphocytes that have non-induced cell-mediated cytotoxicity against malignant tumor cells. They help protect the body against neoplasms and their metastatic dissemination by interacting with and destroying tumor cells. Therefore, it is not unreasonable to expect a higher percentage of CD56-positive cells with the NK phenotype to be present within MC. Bhan et al. reported that many NK cells, assessed by their reactivity with Leu-7 [3], were found in MC, which seems to differ from our results. However, similar to our findings, Ben-Ezra and Sheibani reported non-Leu-7-positive cases in 12 MC cases, in contrast to the study by Bhan et al. [3]. However, they did not describe the criteria required for a case to be considered MC. Furthermore, the result of the low percentage of CD56-positive cells might have been due to the small number of cases followed in our study. Thus, the NK-positive cell is scanty in the stroma of MC, and the mechanisms have still not been clarified.

Several authors have attempted to profile the lymphocyte subpopulations in breast carcinoma [2, 7, 8, 9, 16, 19]. These reports have shown a predominance of T cells and a paucity of B cells and NK cells. Attempts at further classification of these lymphocytes have led to disparate results, with some studies showing a predominance of T-helper cells and others showing a predominance of T-suppressor/cytotoxic cells. Furthermore, a survival advantage of marked lymphocytic infiltration has been demonstrated for several types of solid malignancies, including breast, renal, colon, malignant melanoma, and several others [6, 9, 11, 14].

Recently, antibodies that recognize antigens associated with the cytotoxic phenotype have become available by paraffin section. TIA-1 is a granule-associated RNA-binding protein that defines a subpopulation of CD8-positive T cells with cytotoxic activity. Granzyme B is a serine protease, expressed specifically by activated cytotoxic lymphocytes. Yakirevich et al. reported that MC is infiltrated by an increased percentage of lymphocytes

with cytotoxic potential and activity, TIA-1- and granzyme-B-positive cells [21]. For these reasons, TIA-1 and granzyme B are considered to be capable of suppressing MC progression.

In this study, MC had significantly higher percentages of CD3-, CD8-, TIA-1-, and granzyme-B-positive lymphocytes infiltrating the stroma of the tumor than those in the usual breast cancer. Thus, the increase in infiltrating cytotoxic lymphocytes in MC suggests that cytotoxically active lymphocytes may be an important mechanism governing the favorable prognosis.

In conclusion, our results indicate that cancer nests of MC are infiltrated by lymphocytes that express immunohistochemical markers of cytotoxic potential and activity. These results could explain, in part, a key mechanism controlling the good prognosis for this type of tumor and solve the pathological paradox of MC.

Acknowledgements We sincerely thank A. Adachi, M.D., I. Miura, M.D., Y. Toyosumi, M.D., S. Momose, M.D., T. Ougida, C.T., M. Abe, C.T., T. Saito, C.T., K. Kiuchi, C.T., K. Ohsawa, C.T., K. Matsuno, C.T., K. Hanami, C.T., Y. Ohno, C.T. and T. Masuda, C.T. for their technical assistance and advice.

References

1. Arlen M, Flores L, Elguezbal A, Levowitz BS (1976) Nodal response in medullary carcinoma of the breast. Am J Surg 131:263–266
2. Ben-Ezra J, Sheibani K (1987) Antigenic phenotype of the lymphocytic component of medullary carcinoma of the breast. Cancer 59:2037–2041
3. Bhan AK, DesMarais CL (1983) Immunohistologic characterization of major histocompatibility antigens and inflammatory cellular infiltrate in human breast cancer. J Natl Cancer Inst 71:507–516
4. Bloom HJG, Richardson WW, Filed JR (1970) Host resistance and survival in carcinoma of the breast a study of 104 cases of medullary carcinoma is a series of 1,411 cases of breast cancer followed for 20 years. BMJ 3:181–187
5. Gaffey MJ, Frierson HF, Mills SE, Boyd JC, Zarbo RI, Simpson JF, Gross LK, Weiss LM (1993) Medullary carcinoma of the breast. Identification of lymphocyte subpopulations and their significance. Mod Pathol 6:721–728
6. Gaudin C, Dietrich PY, Robache S, Guillard M, Escudier B, Lacombe MJ, Kumar A, Triebel F, Caignard A (1995) In vivo local expansion of clonal T cell subpopulations in renal cell carcinoma. Cancer Res 55:685–690
7. Georgiannos SN, Renaut A, Goode AW, Sheaff M (2003) The immunophenotype and activation status of the lymphocytic infiltrate in human breast cancers, the role of the major histocompatibility complex in cell-mediated immune mechanisms, and their association with prognostic indicators. Surgery 134:827–834
8. Hudson JM, Castilleja A, Murray JL, Honda T, Kudelka A, Singletary E, Wharton JT, Ioannides CG (1998) Growth and antigen recognition of tumor-infiltrating lymphocytes from human breast cancer. J Interferon Cytokine Res 18:529–536
9. Marrogi AJ, Munshi A, Merogi AJ, Ohadike Y, El-Habashi A, Marrogi OL, Freeman SM (1997) Study of tumor infiltrating lymphocytes and transforming growth factor-beta as prognostic factors in breast carcinoma. Int J Cancer 74:492–501
10. Moore OS, Foote FW (1949) The relatively favorable prognosis of medullary carcinomas of the breast. Cancer 2:635–642
11. O'Mahony AM, O'Sullivan GC, O'Connell J, Cotter TG, Collins JK (1993) An immune suppressive factor derived from esophageal squamous carcinoma induces apoptosis in normal and transformed cells of lymphoid lineage. J Immunol 151:4847–4856
12. Rapin V, Contesso G, Mouriesse H, Bertin F, Lacombe MJ, Piekarski JD, Travagli JP, Gadenne C, Friedman S (1988) Medullary breast carcinoma: a reevaluation of 95 cases of breast cancer with inflammatory stroma. Cancer 19:2503–2510
13. Reinfuss M, Stelmach A, Mitus J, Rys J, Duda K (1995) Typical medullary carcinoma of the breast: a clinical and pathological analysis of 52 cases. J Surg Oncol 60:89–94
14. Restifo NP, Marincola FM, Kawakami Y, Taubenberger J, Yannelli JR, Rosenberg SA (1996) Loss of functional beta 2-microglobulin in metastatic melanomas from five patients receiving immunotherapy. J Natl Cancer Inst 88:100–108
15. Ridolfi RL, Rosen PP, Port A, Kinne D, Mike V (1977) Medullary carcinoma of the breast: a clinicopathologic study with 10-year follow up. Cancer 40:1365–1385
16. Shimokawara I, Imamura M, Yamakawa N, Ishii Y, Kikuchi K (1982) Identification of lymphocyte subpopulations in human breast cancer tissue and its significance: an immunoperoxidase study with anti-human T-and B-cell sera. Cancer 49:1456–1464
17. Tanaka H, Hori M, Ohki T (1992) High endothelial venule and immunocomponent cells in typical medullary carcinoma of the breast. Virchows Arch 420:253–261
18. Tamiolakis D, Simopoulos C, Cheva A, Lambropoulou M, Kotini A, Jivannakis T, Papadopoulos N (2002) Immunophenotypic profile of tumor infiltrating lymphocytes in medullary carcinoma of the breast. Eur J Gynaec Oncol 23:433–436
19. Toso JF, Oei C, Oshidari F, Tartaglia J, Paoletti E, Lyerly HK, Talib S, Weinhold KJ (1996) MAGE-1-specific precursor cytotoxic T-lymphocytes present among tumor-infiltrating lymphocytes from a patient with breast cancer: characterization and antigen-specific activation. Cancer Res 56:16–20
20. Wargotz ES, Silverberg SG (1988) Medullary carcinoma of the breast: a clinicopathologic study with appraisal of current diagnostic criteria. Hum Pathol 19:1340–1346
21. Yakirevich E, Izhak OB, Rennert G, Kovacs ZG, Resnick MB (1999) Cytotoxic phenotype of tumor infiltrating lymphocytes in medullary carcinoma of the breast. Mod Pathol 12:1050–1056
22. Yazawa T, Kamma H, Ogata T (1993) Frequent expression of HLA-DR antigen in medullary carcinoma of the breast. A possible reason for its prominent lymphocytic infiltration and favorable prognosis. Appl Immunohistochem 1:289–296

Virchows Arch (2005) 446:15–20
DOI 10.1007/s00428-004-1114-1

ORIGINAL ARTICLE

Klaus Willenbrock · Christoph Renné · Philippe Gaulard · Martin-Leo Hansmann

In angioimmunoblastic T-cell lymphoma, neoplastic T cells may be a minor cell population. A molecular single-cell and immunohistochemical study

Received: 19 May 2004 / Accepted: 30 July 2004 / Published online: 5 October 2004
© Springer-Verlag 2004

Abstract The significance of T-cell proliferations in angioimmunoblastic lymphoma (AILD) is still enigmatic. Although classified as a malignant T-cell lymphoma in the World Health Organisation lymphoma classification, some cases of AILD lack dominant T-cell clones. In a previous study, based on single-cell polymerase chain reaction (PCR), we obtained similar results as studies of AILD using Southern blot or conventional PCR: some cases of AILD contained large T-cell clones, and, in other cases, T-cell clones were undetectable. As in single-cell studies, only a limited number of cells could be investigated; thus, we wanted to gain more insight into the amount and distribution of tumour cells. By applying triple immunofluorescent staining with antibodies directed against T-cell receptor Vβ-family-specific epitopes, we investigated T-cell populations in AILD and their localisation in the tissue in relation to B cells (CD20) and follicular dendritic cells (CD21). In two of five cases investigated, only a minority of the T-cells compartment belonged to the tumour clone. Neoplastic T cells were found throughout the tissue, including areas dominated by B cells.

Keywords AILD · T-cells · B-cells · Clonality · Single-cell PCR

K. Willenbrock (✉) · C. Renné · M.-L. Hansmann
Senckenbergisches Institut für Pathologie,
Klinikum der Johann Wolfgang Goethe Universität,
Theodor Stern Kai 7, 60590 Frankfurt am Main, Germany
e-mail: Willenbrock@em.uni-frankfurt.de
Tel.: +49-69-63015761
Fax: +49-69-63015241

P. Gaulard
Department of Pathology,
Hôpital Henri Mondor,
Créteil, France

Introduction

Angioimmunoblastic lymphadenopathy with dysproteinaemia (AILD) is a clinically and histopathologically defined malignant lymphoproliferative disorder [5, 14, 17]. In the World Health Organisation lymphoma classification, it is listed as a peripheral T-cell non-Hodgkin's lymphoma [6]. Patients affected with AILD present with non-specific symptoms, such as fatigue, fever, rash, generalised lymphadenopathy and hepatosplenomegaly. The lymph-node biopsy, however, displays a characteristic picture [9]. The lymph-node architecture is effaced and shows a polymorphous cellular infiltrate, prominent branching high endothelial venules and coarse irregular networks of follicular dendritic cells (FDC) [3, 5]. Using conventional molecular biologic techniques, clonal T-cell populations are detectable in approximately 70% of all cases [3, 13, 15, 20, 21]. In a previous investigation, we studied seven cases of AILD on the single-cell level [22]. T-cells and proliferating ($Ki67^+$) cells were microdissected from lymph nodes affected by AILD, and single-target gene amplification of T-cell receptor β (TCRβ) gene rearrangements was performed. Clonal T cells were detected in four out of seven cases, always among $CD4^+$ and $Ki67^+$ cells. Three cases lacked detectable T-cell clones on the single-cell level. Thus, we obtained similar results as studies carried out previously based on standard techniques such as Southern blot or conventional polymerase chain rection (PCR). To study tumour-cell dissemination on a large scale, single-cell PCR is not a suitable technique, as the procedure is time consuming and laborious, and, therefore, only a limited number of cells can be processed. To obtain a broader picture of the amount of T-cell tumour cells and their distribution in the tissue in relationship to B cells and FDC, we performed triple immunofluorescent staining, applying TCR Vβ-family-specific antibodies, CD20 and CD21. In one case, T cells were analysed at the single-cell level using amplification and sequence analysis of rearranged TCRβ genes from microdissected cells.

Materials and methods

Tissue samples

Lymph-node tissue diagnostic of AILD was collected from the files of the Departments of Pathology of the Henri Mondor Hospital, Créteil, France and the University of Kiel, Germany. Cases were reviewed using routine histology (haematoxylin and eosin, Giemsa) and immunohistochemistry. The diagnosis was based on the histological criteria detailed above. Four cases had been previously investigated for TCR gene rearrangements using single-cell PCR [22]. Frozen tissue of one further characteristic case was chosen for the single-cell study.

Whole tissue DNA analysis

Sections 10-μm thick of lymph-node tissue were cut and digested with proteinase K. DNA was extracted using the Qiagen DNA extraction kit as recommended by the manufacturer (Qiagen, Hilden, Germany). Analysis of IgH and TCRγ chain complementarity determining region-III length distributions was performed as described elsewhere [8, 12]. Briefly, DNA was extracted using a silica column system (QiaAmp, Qiagen). TCRγ and IgH gene rearrangements were amplified in separate reactions with consensus primers for V- and J-segments. PCR products were analysed on an automated sequencer (ABI377, Applied Biosystems, Darmstadt, Germany) using the GeneScan software. TCRβ gene rearrangements were amplified and sequenced using the same conditions and primers as described below for second-round single-cell PCR. For DNA amplification from paraffin-embedded tissue, an additional primer for the BJ2.4 segment was added to limit the length of PCR fragments to less than 450 base pairs (5′CCAGCTTACCCAGCACTGAGAGC 3′).

Triple immunofluorescent staining

Frozen tissue sections of five cases of AILD and one tonsil with reactive follicular hyperplasia were fixed in acetone for 10 min and dried. Slides were blocked with 3% bovine serum albumin in Tris-buffered saline for 30 min and a biotin-blocking kit as recommended by the manufacturer (DakoCytomation, Hamburg, Germany). Slides were incubated with an anti-CD21 antibody (1F8, DakoCytomation) for 45 min. After short washes with Tris-buffered saline, the slides were incubated with a biotinylated multilink (Bio Genex, San Ramon, California) for 30 min. The CD21 antibody was visualised using incubation with AMCA-Avidin D (Vector Laboratories, Burlington, California) for 30 min. Antibodies for TCR Vβ-segments [Vβ2 (MPB2D5), Vβ 13.1 (IMMU222), Vβ17 (E17.5F3) Beckman Coulter, Krefeld, Germany] were labelled with an Alexa Fluor 594-nm dye using the Zenon labelling kit as recommended by the manufacturer (Molecular probes, Leiden, Netherlands). For B-cell detection, a fluorescein isothiocyanate-conjugated antibody for CD20 was used (B-Ly1, DakoCytomation). After staining for CD21, slides were incubated with a mixture of the directly labelled antibodies (TCR Vβ and CD20) for 30 min, washed and fixed in 4% buffered formalin for 15 min.

Immunostaining and micromanipulation

Immunohistochemical staining of frozen tissue sections was performed as described [10], using monoclonal antibodies against CD20 (L26, DakoCytomation), TCRβ (βF1, T-Cell Diagnostics, Cambridge, UK), TCRVβ17 (E17.5F3, Beckman Coulter), dendritic cells (KiM4P, generously provided by R. Parwaresch, Kiel, Germany) and the proliferation marker Ki67 (MIB1, DakoCytomation). Single cells were mobilised and collected by a micropipette attached to a hydraulic micromanipulator from frozen sections and transferred into PCR tubes [10].

Single cell PCR

Amplification of rearranged TCRβ genes was performed according to an established protocol [18]. Briefly, micromanipulated cells were incubated with proteinase K. A first round of PCR was carried out in the same tube using a mix of 24 V-family- and 7 J-segment-specific primers. A second round of amplification was carried out in 96 well plates, adding 1 μl of the first-round reaction to eight separate reaction mixtures, each containing two to three V-primers and a mixture of internal J-primers. PCR products were gel purified and directly sequenced using the Big Dye cycle sequencing kit (Applied Biosystems) on an automated sequencer (ABI377, Applied Biosystems). Sequences were compared with germ-line genes in the Vbase database using the dnaplot software (http://www.dnaplot.de/index.html) and deposited in the European Molecular Biology Laboratory database (AJ 841706–AJ 841742).

Results

The cases reviewed for this study showed the typical morphology of AILD with effaced lymph-node architecture, a polymorphic cellular infiltrate and prominent high endothelial venules. Coarse irregular networks of FDC were seen using KiM4P immunostaining. Applying the CD20 antibody, distinct areas containing B cells were found in all cases (Fig. 1). Sheets of B cells were located either in subcapsular or in central nodules. In these areas, only scattered TCRβ^+ T cells could be detected. Between subcapsular and central lymph-node areas (intermediate area), TCRβ^+ T cells dominated, and only scattered CD20$^+$ cells were found. In the subcapsular region and central nodules, meshworks of FDC with diffuse borders to the intermediate area were detected.

Using triple immunofluorescent staining with monoclonal antibodies specific for the TCR Vβ family expressed by the tumour clones, the topology of the neoplastic cells in relation to B cells (CD20) and dendritic cells (CD21) was investigated in five cases of AILD. The monoclonal antibodies applied to detect T-cell clones are specific for Vβ-gene-segment families of the TCR (Vβ2, normally found in about 9.1%-; Vβ13.1, normally about 2.7%-; Vβ17, normally approximately 3.3% of TCRβ^+ T-cells, manufacturers specifications). They were selected to visualise the TCRVβ family of the T-cell clones detected in the PCR analysis reported here or carried out previously [22]. Tissue sections of tonsils with follicular hyperplasia were stained as controls. In accordance with the findings of the single-cell analysis carried out previously [22], varying numbers of tumour cells were found in the lymph-node tissue. Whereas, in three cases, the tumour clone clearly dominated in the tissue, in two cases, only a minority of the cells belonged to the clone (Fig. 2). In the AILD case, in which a single cell analysis was performed, approximately 10% of βF1$^+$ T cells were positive for Vβ17, indicating a low proportion of tumour cells. T cells belonging to the tumour clone were found throughout the tissue, sometimes in groups but present in all areas.

One of the cases, which showed good preservation of the areas defined in the CD20 immunostaining in frozen tissue was chosen for single-cell analysis. By whole-tissue

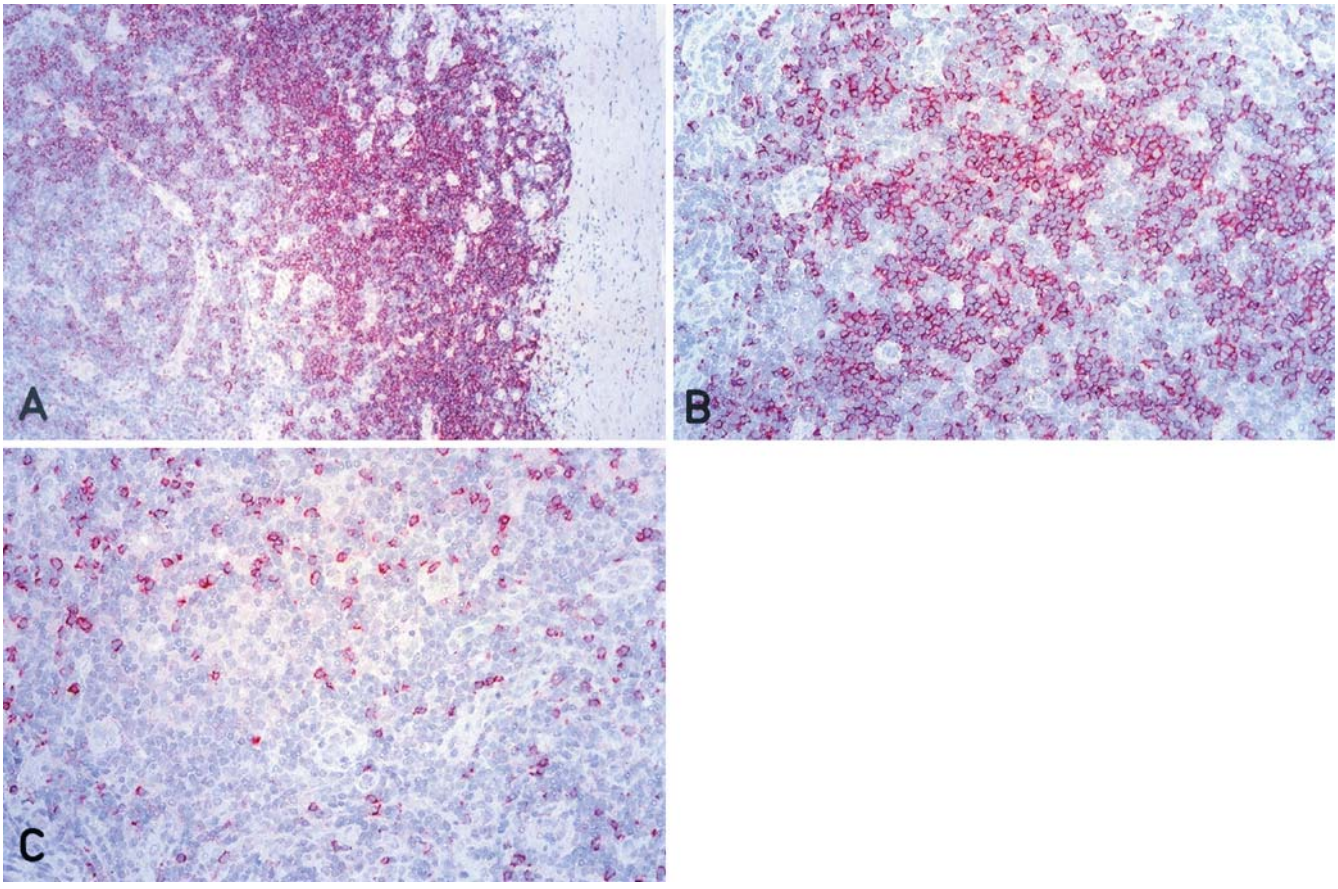

Fig. 1 Distribution of $CD20^+$ B-cells in angioimmunoblastic lymphoma. **A** Dense areas dominated by B cells subcapsular. **B** Scattered B cells in an intermediate area where mostly $\beta F1^+$ T cells are found. **C** Central B-cell nodule

Table 1 Single-cell analysis of T cells in different areas of a lymph node affected by angioimmunoblastic lymphoma

	Subcapsular area	Central nodule	Intermediate area
Sequence/cells	10/40	5/40	26/40
Clonal/sequence[a]	2/10	2/5	1/26
Controls (all areas)[b]	0/42		

[a] The sequence of the T-cell clone identified among the single T cells was identical to the out-of-frame T-cell receptor (TCR)β gene rearrangement obtained by whole-tissue DNA analysis. The in-frame rearrangement detected in the whole-tissue analysis was not amplified from single cells, for unknown reasons

[b] Buffer covering the slides and tubes containing polymerase chain reaction mixture but no cells were investigated in parallel with control for contamination artefacts in all cases

DNA PCR analysis for TCRγ and TCRβ gene rearrangements, a dominant T-cell clone was detected, whereas no dominant Ig gene rearrangement could be demonstrated.

T cells (n=120) micromanipulated from distinct areas were analysed for TCRβ gene rearrangements. Of rearranged TCRβ genes, 41 sequences were obtained, 14 of which were non-functional because they represented out-of-frame rearrangements or showed stop codons in the junctional region (Table 1). All TCRβ genes displayed complete sequence identity to the respective germ-line genes in line with the view that human T cells are generally not subject to somatic hypermutation [19]. Five non-functional sequences belonged to a dominant T-cell clone, which had also been identified by whole-tissue DNA analysis and, hence, likely represents the T-cell tumour clone in this case (Table 1). (A clonal in-frame TCRβ gene rearrangement detected in the whole tissue PCR was not obtained from the single cells, for unknown reasons). All other sequences were unrelated to each other. Sequences belonging to the T-cell clone were detected in two cells from the subcapsular area, one cell of the intermediate area and two cells from the central B-cell nodule. Thus, clonal T cells were found throughout the tissue and were also present in regions dominated by B cells.

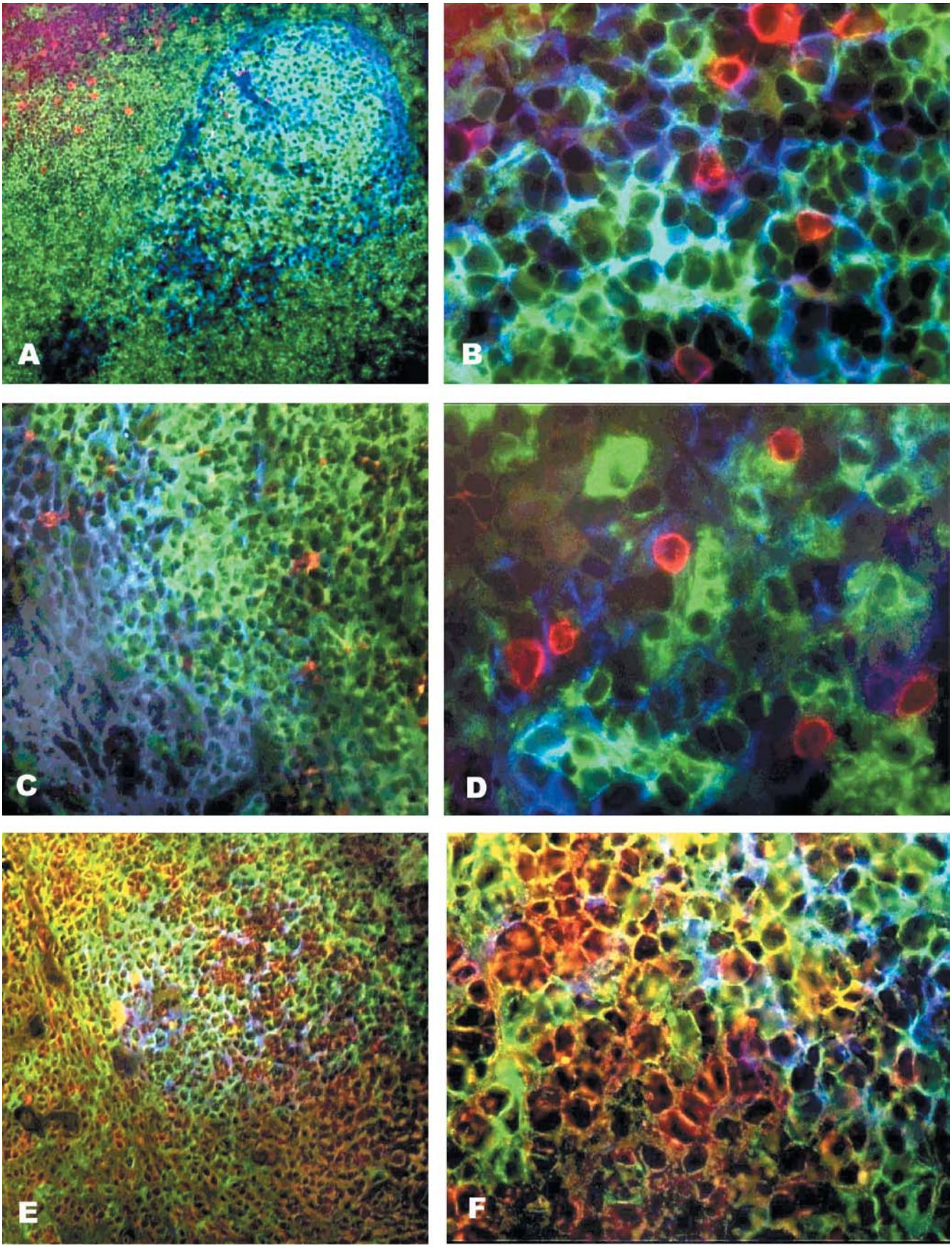
A
B
C
D
E
F

Discussion

Dominant clonal T cells are found in approximately 70% of all cases of AILD using Southern blot and conventional PCR and are thought to represent the neoplastic population [3, 13, 15, 20, 21]. In a previous study, we obtained similar results using a single-cell approach [22]. Based on micromanipulation of single cells from histological sections, single-cell PCR is a high-resolution technique. However, the number of cells that can be processed in one experiment is limited because of the lavishness of the procedure. For this reason, conclusions based on single-cell investigations concerning tumour-cell number and dissemination may be imprecise. To define the amount and distribution of tumour cells in different areas of the lymph node, we performed triple immunofluorescent staining. T cells were detected using antibodies directed against TCRVβ families. B cells and FDC were visualised applying anti-CD20 and anti-CD21 monoclonal antibodies, respectively.

In five of seven AILD cases, a disseminated distribution of the positively immunostained T cells could be found. In the AILD case investigated using single-cell PCR, T cells belonging to the tumour clone were not found to be preferentially represented in a defined lymph-node compartment.

In three of seven cases, the TCRVβ-family-positive T cells were aggregated in sheets and groups, whereas, in two of seven cases, only very few T cells were immunostained. The antibodies used to visualise T-cell clones are not thought to be clone specific but may also detect bystander T cells that use the same TCRVβ gene family. Considering this fact, the low number of positive T cells seems even more surprising. Although it might be possible, it seems unlikely that the T-cell clone lost the TCR on the cell surface. In three other cases, the positively stained cells were clearly dominating in concordance with the PCR results. The single-cell study in one of our cases in the investigation confirms the finding of minor clonal T-cell expansions in AILD. Surprisingly, some cases of AILD even lack detectable T-cell clones [20, 22].

Clonal T cells can be observed in different areas of AILD lymph nodes, including regions dominated by B cells. It is well known that, in lymphoproliferative disorders, the neoplastic clonal population must not be dominating in number. Good examples for this constellation are Hodgkin's lymphoma and T-cell-rich large B-cell lymphoma [1, 7, 11]. In addition, also part of the T-cell lymphomas of AILD type belong to this peculiar group of malignant lymphomas, in which tumour cells may attract reactive T-cell subsets. However, the aberrant setting in AILD lymph-node tissue, with unusual expression of a number of cytokines, which may contribute to the pathology of this disease [4, 16], must not necessarily be caused by a T-cell tumour clone. Apparently, T-cell clones as well as peculiar B-cell (oligo) clones develop in this setting [2, 20, 22], of which the causative agent has yet to be established.

Fig. 2 Triple immunofluorescent staining of T-cell receptor (TCR)Vβ2S1$^+$ T cells (*red*), CD20$^+$ B-cells (*green*) and CD21$^+$ follicular dendritic cells (*blue*). **A** Reactive tissue of a tonsil with follicular hyperplasia shows well-circumscribed networks of follicular dendritic cells. **B** B cells dominate in the follicles. Few TCRVβ2S1$^+$ T cells are present. **C**, **D** In this case of angioimmunoblastic lymphoma, the dendritic cells display typical irregular networks. In comparison with the normal tissue, the number of TCRVβ2S1$^+$ T-cells is not increased, although they are clonal, as could be shown by polymerase chain reaction. **E**, **F** In this case of AILD, sheets of neoplastic TCRVβ2S1$^+$ T-cells are present and clearly dominate by number

Acknowledgements We thank Prof. Dr. med. Reza Parwaresch and Prof. Dr. med. Hans-Heinrich Wacker for contributing tissue of AILD cases, Prof. Dr. rer. nat. Ralf Küppers for helpful discussion and Ekaterini Hadzoglou for excellent technical support. This work was supported by the Deutsche Krebshilfe, Dr. Mildred Scheel Stiftung.

References

1. Bräuninger A, Küppers R, Spieker T, Siebert R, Strickler JG, Schlegelberger B, Rajewsky K, Hansmann ML (1999) Molecular analysis of single B cells from T-cell-rich B-cell lymphoma shows the derivation of the tumor cells from mutating germinal center B cells and exemplifies means by which immunoglobulin genes are modified in germinal center B cells. Blood 8:2679–2687
2. Bräuninger A, Spieker T, Willenbrock K, Gaulard P, Wacker HH, Rajewsky K, Hansmann ML, Küppers R (2001) Survival and clonal expansion of mutating "forbidden" (immunoglobulin receptor-deficient) Epstein–Barr virus-infected B cells in angioimmunoblastic T cell lymphoma. J Exp Med 7:927–940
3. Feller AC, Griesser H, Schilling CV, Wacker HH, Dallenbach F, Bartels H, Kuse R, Mak TW, Lennert K (1988) Clonal gene rearrangement patterns correlate with immunophenotype and clinical parameters in patients with angioimmunoblastic lymphadenopathy. Am J Pathol 3:549–556
4. Foss HD, Anagnostopoulos I, Herbst H, Grebe M, Ziemann K, Hummel M, Stein H (1995) Patterns of cytokine gene expression in peripheral T-cell lymphoma of angioimmunoblastic lymphadenopathy type. Blood 10:2862–2869
5. Frizzera G, Moran EM, Rappaport H (1974) Angio-immunoblastic lymphadenopathy with dysproteinaemia. Lancet 866: 1070–1073
6. Jaffe ES, Ralfkiaer E (2001) Angioimmunoblastic T-cell lymphoma. In: Jaffe ES, Harris NL, Stein H, Vardiman JW (eds) Pathology and genetics of tumours of haematopoetic and lymphoid tissues. IARC Press, Lyon, France, pp 225–226
7. Kanzler H, Küppers R, Hansmann ML, Rajewsky K (1996) Hodgkin and Reed–Sternberg cells in Hodgkin's disease represent the outgrowth of a dominant tumor clone derived from (crippled) germinal center B cells. J Exp Med 4:1495–1505
8. Kneba M, Bolz I, Linke B, Bertram J, Rothaupt D, Hiddemann W (1994) Characterization of clone-specific rearrangement T-cell receptor gamma-chain genes in lymphomas and leukemias by the polymerase chain reaction and DNA sequencing. Blood 2:574–581
9. Knecht H, Schwarze EW, Lennert K (1985) Histological, immunohistological and autopsy findings in lymphogranulomatosis X (including angio-immunoblastic lymphadenopathy). Virchows Arch 1:105–124
10. Küppers R, Zhao M, Hansmann ML, Rajewsky K (1993) Tracing B cell development in human germinal centres by molecular analysis of single cells picked from histological sections. EMBO J 13:4955–4967

11. Küppers R, Rajewsky K, Zhao M, Simons G, Laumann R, Fischer R, Hansmann ML (1994) Hodgkin disease: Hodgkin and Reed–Sternberg cells picked from histological sections show clonal immunoglobulin gene rearrangements and appear to be derived from B cells at various stages of development. Proc Natl Acad Sci U S A 23:10962–10966
12. Linke B, Bolz I, Fayyazi A, von Hofen M, Pott C, Bertram J, Hiddemann W, Kneba M (1997) Automated high resolution PCR fragment analysis for identification of clonally rearranged immunoglobulin heavy chain genes. Leukemia 7:1055–1062
13. Lorenzen J, Li G, Zhao-Höhn M, Wintzer C, Fischer R, Hansmann ML (1994) Angioimmunoblastic lymphadenopathy type of T-cell lymphoma and angioimmunoblastic lymphadenopathy: a clinicopathological and molecular biological study of 13 Chinese patients using polymerase chain reaction and paraffin-embedded tissues. Virchows Arch 6:593–600
14. Lukes RJ, Tindle BH (1975) Immunoblastic lymphadenopathy. A hyperimmune entity resembling Hodgkin's disease. N Engl J Med 1:1–8
15. O'Connor NT, Crick JA, Wainscoat JS, Gatter KC, Stein H, Falini B, Mason DY (1986) Evidence for monoclonal T lymphocyte proliferation in angioimmunoblastic lymphadenopathy. J Clin Pathol 11:1229–1232
16. Ohshima KS, Suzumiya J, Kawasaki C, Kanda M, Kikuchi M (2000) Cytoplasmic cytokines in lymphoproliferative disorders: multiple cytokine production in angioimmunoblastic lymphadenopathy with dysproteinemia. Leuk Lymphoma 5–6: 541–545
17. Radaszkiewicz T, Lennert K (1975) Lymphogranulomatosis X (immunoblastic adenopathy): clinical features, treatment and prognosis. Dtsch Med Wochenschr 21:1157–1163
18. Roers A, Montesinos-Rongen M, Hansmann ML, Rajewsky K, Küppers R (1998) Amplification of TCRbeta gene rearrangements from micromanipulated single cells: T cells rosetting around Hodgkin and Reed-Sternberg cells in Hodgkin's disease are polyclonal. Eur J Immunol 8:2424–2431
19. Roers A, Hansmann ML, Rajewsky K, Küppers R (2000) Single-cell PCR analysis of T helper cells in human lymph node germinal centers. Am J Pathol 3:1067–1071
20. Smith JL, Hodges E, Quin CT, McCarthy KP, Wright DH (2000) Frequent T and B cell oligoclones in histologically and immunophenotypically characterized angioimmunoblastic lymphadenopathy. Am J Pathol 2:661–669
21. Weiss LM, Strickler JG, Dorfman RF, Horning SJ, Warnke RA, Sklar J (1986) Clonal T-cell populations in angioimmunoblastic lymphadenopathy and angioimmunoblastic lymphadenopathy-like lymphoma. Am J Pathol 3:392–397
22. Willenbrock K, Roers A, Seidl C, Wacker HH, Küppers R, Hansmann ML (2001) Analysis of T-cell Subpopulations in T-cell non-Hodgkin's lymphoma of angioimmunoblastic lymphadenopathy with dysproteinemia type by single target gene amplification of T cell receptor-beta gene rearrangements. Am J Pathol 5:1851–1857

Virchows Arch (2005) 446:21–27
DOI 10.1007/s00428-004-1120-3

ORIGINAL ARTICLE

Gustavo Valbuena · David H. Walker

Expression of CX3CL1 (fractalkine) in mice with endothelial-target rickettsial infection of the spotted-fever group

Received: 11 May 2004 / Accepted: 19 August 2004 / Published online: 5 October 2004
© Springer-Verlag 2004

Abstract Fractalkine (CX3CL1) is a chemokine expressed mainly by endothelial cells, which are the major cellular targets of rickettsiae. We used immunohistochemistry to investigate the normal expression of CX3CL1 in mice and the kinetics of expression of this chemokine throughout the course of lethal and sublethal rickettsial infections in a mouse model of spotted-fever group rickettsioses. The peak of expression of fractalkine on day 3 of infection coincided with the time of infiltration of macrophages into infected tissues and preceded the peak of rickettsial content in tissues.

Keywords Fractalkine · CX3CL1 · Rickettsia · Immunity · Spotted fever · Mouse

Introduction

Rickettsiae are obligately intracellular bacteria that primarily infect vascular endothelial cells and are transmitted by arthropods. They are separated into in two main groups: typhus and spotted fever. Rickettsiae belonging to the latter group polymerize host cellular actin to spread between cells [13, 14, 28], resulting in systemic multiorgan involvement. Rickettsiae of this spotted-fever group cause acute, potentially lethal diseases if not treated early with appropriate antibiotics [15]. They include Rocky Mountain spotted fever (caused by *Rickettsia rickettsii*) and boutonneuse fever (caused by *R. conorii*), among others [29, 30, 32].

Damage to endothelial cells in the lungs and brain produces the most significant clinical manifestations. Although the initial symptoms are not specific and resemble a flu-like syndrome, severe manifestations can develop, including delirium, seizures, coma, non-cardiogenic pulmonary edema/adult respiratory distress syndrome, interstitial pneumonia, hemorrhagic phenomena, peripheral edema and hypovolemic hypotension due to leakage of intravascular fluid into the extravascular space, which can result in acute renal failure [18, 32].

We have demonstrated in valid animal models [33, 34] that an effective anti-rickettsial immune response requires CD8+ T lymphocytes [6], capable of cytolysis and interferon (IFN)-γ production [5, 35]. We have also shown that natural killer (NK) cells are an important component of the early anti-rickettsial immune response [2]. Although it is known that the main target, endothelial cells, become activated upon rickettsial infection, as evidenced by the production of cytokines and expression of adhesion molecules [3, 17, 24, 25], the mechanism(s) whereby immune effector cells find rickettsia-infected endothelial cells and activate their effector functions is only now beginning to be explored. In this regard, we recently reported the possible role of the T-cell-targeting chemokines CXCL9 (Mig) and CXCL10 (IP-10) and found that they were expressed at very high levels early after experimental rickettsial infections [27]. Evidence from other systems, including in vitro flow studies [7], transplantation studies [12, 22] and studies of NK cell-mediated lysis [36], suggests that CX3CL1 might play an important role in the immune clearance of rickettsiae from the infected vasculature. We undertook the following morphological studies to investigate the expression and localization of this chemokine in a relevant animal model of the spotted-fever group rickettsioses.

Materials and methods

Rickettsia

Rickettsia conorii (Malish 7 strain) is a human isolate from South Africa with an unknown number of passages in the yolk sacs of embryonated chicken eggs. For all the experiments described in this study, a stock of *R. conorii* was produced by cultivation in specific pathogen-free embryonated chicken eggs. Yolk sacs from infected eggs with dead embryos were homogenized in a Waring blender,

G. Valbuena · D. H. Walker (✉)
Department of Pathology,
University of Texas Medical Branch,
301 University Boulevard, 77555-0609 Galveston, Texas
e-mail: dwalker@utmb.edu
Tel.: +1-409-7723989
Fax: +1-409-7722500

diluted to a 10% suspension in sucrose-phosphate-glutamate buffer (SPG; 0.218 M sucrose, 3.8 mM KH_2PO_4, 7.2 mM K_2HPO_4, 4.9 mM monosodium L-glutamic acid, pH 7.0) and aliquoted for storage at −80°C after discarding the pellet produced by low-speed centrifugation (200×*g*, 10 min). Rickettsial content of this stock was quantified by plaque assay (5.5×10^7 pfu/ml) [31], and the LD_{50} was determined experimentally in C3H/HeN mice (1 LD_{50}=1.65×10^4 pfu/ml) according to the method of Reed and Muench [21].

Animal model

The mouse model of endothelial-target spotted-fever group rickettsioses consists of *Rickettsia conorii* infection of C3H/HeN mice and has previously been described in detail [33]. All mice were housed in a biosafety level-3 facility and were infected intravenously (through the tail vein) with 0.25 LD_{50} of *R. conorii* for the sublethal dose study or 3 LD_{50} of *R. conorii* for the lethal dose study (in a volume of 300 μl in SPG buffer). Animals infected with the higher dose usually died 6–7 days later. In three separate experiments, eight mice received a sublethal dose of *R. conorii*, and three mice received a lethal dose. One mouse from each group was euthanized every other day by cervical dislocation, and all organs were harvested and divided for freezing at −20°C and for fixation in 10% buffered formalin or zinc fixative (BD Pharmingen, San Diego, CA). Tissues from uninfected mice were similarly processed and evaluated as negative controls. Organs fixed in formalin were transferred to 70% ethanol after 24 h to avoid overfixation. The experimental protocols comply with international standards and were reviewed and approved by the institutional review committee for animal use and care.

Quantitative real-time PCR

The rickettsial load was determined using real time polymerase chain reaction (PCR) (with Taqman probes) of the *Rickettsia*-specific gene *ompB* using the iCycler from BioRad (Hercules, CA) and the Brilliant quantitative PCR kit (Stratagene, La Jolla, CA). The cycling parameters and the primers and probes utilized have been reported previously [27]. The substrate for amplification was DNA purified from frozen samples using the Dneasy Tissue kit from Qiagen (Valencia, CA). The results were normalized to glyceraldehyde-3-phosphate dehydrogenase (GAPDH) in the same sample and expressed as copy number per 10^5 GAPDH copies (standard curves with more than 94% efficiency and linear amplification across 1 to 10^6–10^7 copies were used to obtain the copy number of the samples).

Immunohistochemistry

Sections (4–6 μm) from paraffin-embedded tissues fixed in 10% formalin in phosphate-buffered saline were antigen retrieved in citrate, pH 6.0, stained with affinity-purified goat anti-fractalkine (R&D Systems, Minneapolis, MN) and detected with biotinylated rabbit anti-goat, aviditin-biotin peroxidase complex and diaminobenzidine as a substrate (Vector Laboratories, Burlingame, CA). Zinc-fixed tissues from the same mice were used for the detection of the macrophage marker F4/80 with a rat anti-mouse F4/80 monoclonal antibody (Clone CI:A3–1; Serotec, Raleigh, NC) and biotinylated $F(ab')_2$ fragments of mouse-absorbed mouse anti-rat IgG (Jackson Immunoresearch, West Grove, PA) as a secondary reagent. In the absence of primary antibody or with non-immune goat or rat serum, no signal was detected.

Results

Expression of CX3CL1 (fractalkine) in mouse tissues with no inflammatory stimuli

We first investigated the normal basal expression of CX3CL1 in mouse tissues at the protein level using immunohistochemistry (Fig. 1a, b, c, d, e, g, and Fig. 2a). The immunohistochemical stain revealed that CX3CL1 was normally expressed in multiple areas of the vasculature of all organs examined, particularly in the endothelium of small arteries and arterioles. In the spleen, CX3CL1 was observed exclusively in the central arteries (Fig. 1d). In the lungs, there were multiple foci of expression that involved vessels of all sizes on what appeared to be mainly the arterial side (Fig. 2a); however, it was not possible to distinguish arteries from veins in the lungs with the hematoxylin stain used in immunohistochemistry. The liver expression of CX3CL1 was limited to the endothelium of vessels of the portal triads (Fig. 1b); while, in the kidney, it was detected in glomeruli, peritubular microvessels and in some tubular epithelial cells, most of which were adjacent to glomeruli and may be part of the proximal tubules (Fig. 1e). In the heart, fractalkine was detected in the endothelium of small arteries and some but not all microvessels (Fig. 1g). Finally, in the brain, CX3CL1 was detected on neurons, astrocytes and the endothelium of vessels of all sizes, including capillaries (Fig. 1a).

Expression of CX3CL1 (fractalkine) in mice infected with *Rickettsia conorii*

We next examined the expression of CX3CL1 in mice receiving either a lethal or sublethal inoculum of *R. conorii*. The immunohistochemical evaluation revealed that on day 3 of infection (both lethal and sublethal), the distribution of expression of CX3CL1 was increased, having become generalized throughout the vasculature of most organs examined (Fig. 1f, h and Fig. 2b, c). (Expression was identical in the lethal and sublethal models). In addition, the signal was more intense in infected mice than in the uninfected control animals. The only exception was the liver, where the expression of CX3CL1 remained confined to the vessels of the portal triads. Interestingly, between day 6 and day 10 of infection, in the sublethal model, the expression of CX3CL1 was downregulated in all organs and returned to the distribution observed under normal conditions in uninfected mice in all organs except the lung, where the signal was scarcely detectable (Fig. 2d).

Kinetics of rickettsial growth in C3H/HeN mice infected with *R. conorii*

We determined the rickettsial load in the lungs of the same mice used for fractalkine expression studies using

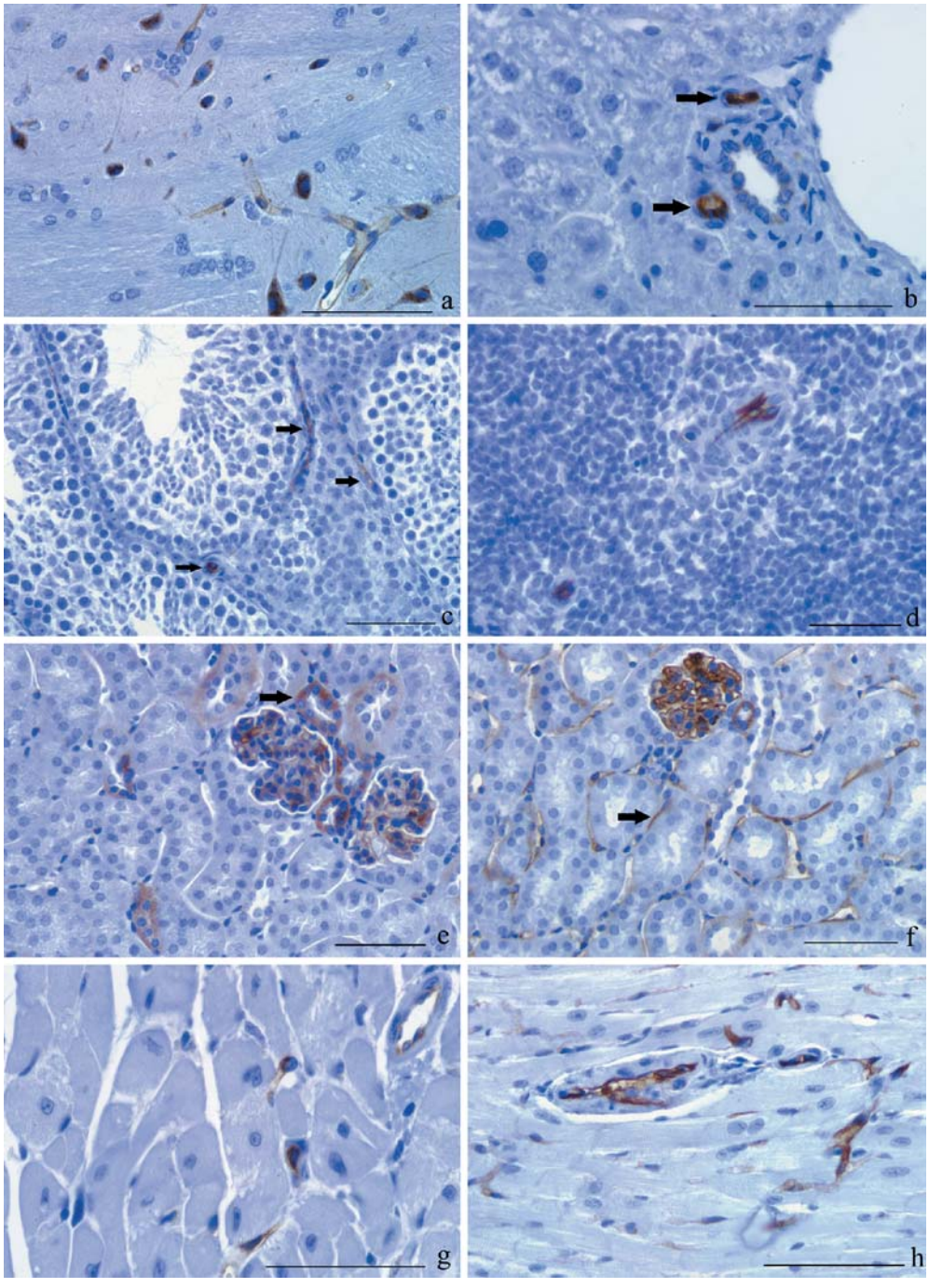

Fig. 1 Immunohistochemical analysis of the expression of CX3CL1 (fractalkine) (*brown*) in brain (**a** ×400), liver (**b** ×400), testis (**c** ×200), spleen (**d** ×200), kidney (**e** ×200 and **f** ×200) and heart (**g** ×400 and **h** ×400) of C3H/HeN mice with no inflammatory stimulus (**a**–**e**, **g**), or mice intravenously infected with a sublethal dose of *Rickettsia conorii* (**f** and **h**). Slight variations in magnifications are due to digital cropping (*scale bars*=100 μm). Fractalkine is expressed in the brain in neurons, astrocytes and vessels of all sizes (**a**). In the liver, its expression is limited to vessels of the portal triads (**b**, *arrows*) even during the course of rickettsial infections. In the testis and heart (**c** and **g**), fractalkine is observed in arteries and microvessels that seem to be on the arteriolar side of the microvasculature (*arrows*). In the spleen, fractalkine is observed normally in the central arteries (**d**). In the kidney, fractalkine is observed in glomeruli, some peritubular microvessels and some tubular epithelial cells (*arrow*). Around the third day of a rickettsial infection, fractalkine is expressed on almost all vessels as exemplified here in the kidney (**f**, *arrow* points to a capillary) and the heart (**h**)

real-time PCR of the rickettsial gene *ompB* (using Taqman probes). The PCR in these experiments was performed using DNA as a target, and the data were normalized against the eukaryotic gene encoding GAPDH. This was a valid approach, since rickettsiae are intracellular organisms. For these experiments, the results were expressed as number of *ompB* copies per 10^5 GAPDH copies. Mice inoculated with either a lethal or a sublethal dose of *R. conorii* had a progressive increase in rickettsial load, peaking on day 5 (Fig. 3). The animals receiving a lethal inoculum had approximately 30-fold higher rickettsial loads than mice receiving sublethal inocula. In the sublethal model, the rickettsial load progressively decreased after day 5, with a dramatic decline between day 5 and day 7.

Macrophage infiltration in mice infected with *Rickettsia conorii*

The early rise in expression of CX3CL1 coincides with the early activity of cells of the innate immune system. Since fractalkine targets macrophages in mice, we examined the kinetics of infiltration of these cells as as-

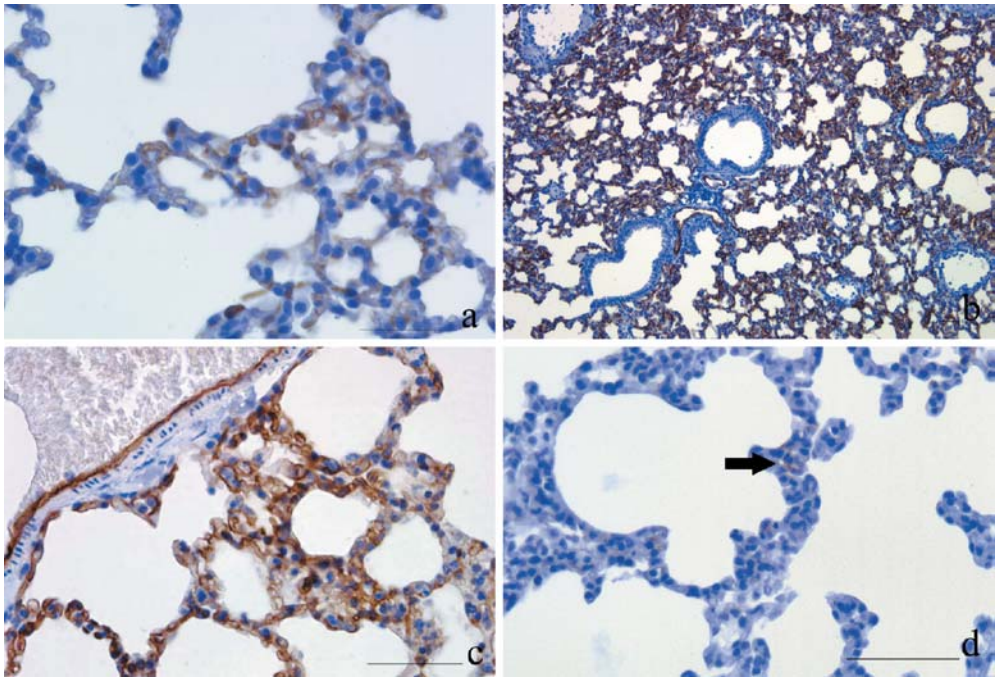

Fig. 2 Immunohistochemical analysis of the expression of CX3CL1 (fractalkine) (*brown*) in the lungs of normal uninfected C3H/HeN mice (**a** ×400) and C3H/HeN mice three days after intravenous infection with a sublethal dose of *Rickettsia conorii* (**b** ×100 and **c** ×400) and after 7 days of infection (**d** ×400). Slight variations in magnifications are due to digital cropping (*scale bars*=100 μm). Normally, fractalkine is expressed on multiple focal areas of the vasculature (**a**). Around the third day of a sublethal infection with *R. conorii*, fractalkine is expressed on all segments of the vasculature (**b** and **c**). Subsequently, between day 5 and day 7 of infection, the expression of fractalkine is downregulated to barely detectable levels (**d**, *arrow*)

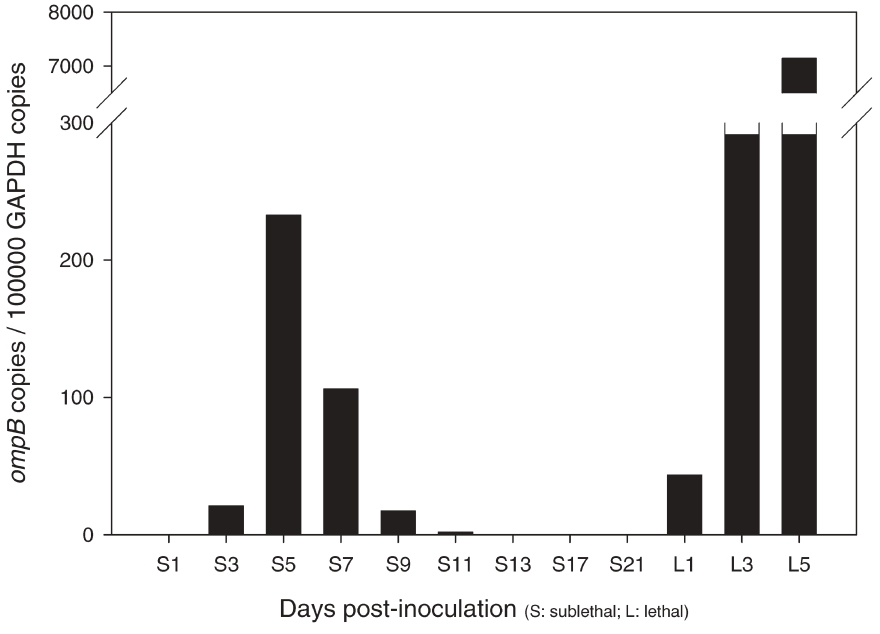

Fig. 3 Quantitative real-time polymerase chain reaction with Taqman probes of DNA from lungs of mice intravenously infected with either sublethal (S1–S21) or lethal doses (L1–L5) of *Rickettsia conorii* and sacrificed every other day. The number of copies of the rickettsial *ompB* gene was normalized by expressing this value relative to 10^5 copies of the eukaryotic gene GAPDH. All data points correspond to the means of three simultaneous amplifications with negligible standard deviations. The data presented are representative examples of two separate experiments

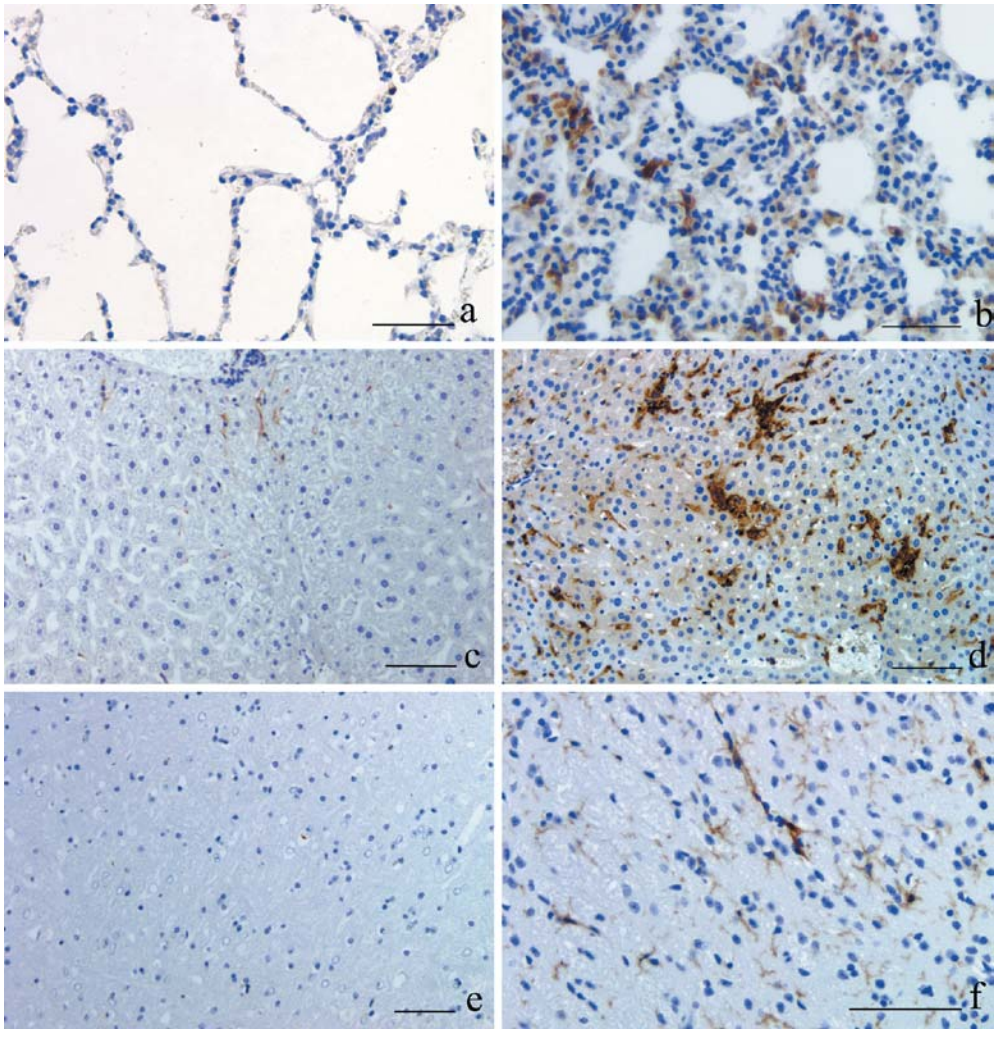

Fig. 4 Immunohistochemical analysis of the expression of the mouse macrophage antigen F4/80 (*brown*) in lungs (**a** ×200 and **b** ×400), livers (**c** ×200 and **d** ×200) and brains (**e** ×200 and **f** ×400) of normal uninfected C3H/HeN mice (**a**, **c**, and **e**) and C3H/HeN mice intravenously infected with a sublethal dose of *Rickettsia conorii* 4 days earlier (**b**, **d** and **f**). Slight variations in magnifications are due to digital cropping (*scale bars*=100 μm)

sessed by the immunohistochemical detection of the F4/80 antigen (Fig. 4). We found that macrophages are first detected infiltrating tissues starting 2–3 days after rickettsial infection. In the brain, it is likely that the F4/80 antigen detected is expressed by resident microglial cells (Fig. 4d, e).

Discussion

In this study, we describe the pattern of expression of the CX3C chemokine fractalkine (also known as CX3CL1) under normal non-inflammatory conditions and throughout the course of experimental endothelial-target bacterial infections caused by rickettsiae of the spotted-fever group in mice. We pursued this study because of our interest in understanding the mechanisms of localization and activation of effector leukocytes on rickettsia-infected endothelial cells. In this regard, we have recently shown that among several T-cell-targeting chemokines, the CXCR3 ligands, CXCL9 (Mig) and CXLC10 (IP-10), have the highest levels of expression [27] and, thus, might be important in the recruitment of CD8+ T cells, the most important effectors of anti-rickettsial immunity [6, 35] and also of NK cells, which are an important component of the early anti-rickettsial immune response [2].

Fractalkine (CX3CL1) differs from most other chemokines in that it has both adhesive and chemotactic functions [7, 11] and in that it is a transmembrane protein [1], although there is also a secreted form that results from proteolytic cleavage [9, 16]. In humans, CX3CL1 interacts with polarized Th1 cells but not Th2 cells [8] and preferentially attracts human leukocytes capable of inducing cytolysis, including CD8+ T cells, $\gamma\delta$ T cells and NK cells [20]. In mice, the receptor for CX3CL1 (CX3CR1) is not expressed by T cells, but it is found in microglial cells, monocytes, dendritic cells and subsets of NK cells [12]. Mouse fractalkine may, however, have an indirect action on T cells through the recruitment and activation of dendritic cells to sites of inflammation, as has been demonstrated in a mouse tumor model [10].

This is, to the best of our knowledge, the first study addressing the kinetics of expression and the localization of fractalkine (CX3CL1) throughout the natural history of an infectious disease that targets the main cellular source of this chemokine—endothelial cells. We found

that fractalkine was expressed normally, under non-inflammatory conditions, in vessels of different sizes (of most visceral organs) with an apparent preference for the arterial side of the vasculature (Fig. 1 and Fig. 2). In addition, although fractalkine is expressed in the ductal epithelial cells of human liver with inflammation and/or regenerative changes and in a human hepatocarcinoma cell line [4], our study revealed that, despite the severe inflammatory changes in the liver during rickettsial infection, fractalkine was only detected in the vessels of the portal triads, where it was normally detected under non-inflammatory conditions (Fig. 1b).

With the induction of inflammation caused by a systemic rickettsial infection, fractalkine expression changed on day 3 of infection, becoming detectable in vessels of all sizes, with the exception of the hepatic sinusoids (Fig. 1 and Fig. 2). After 5 days of infection (in both the lethal and sublethal model), fractalkine expression fell to levels below those observed under basal conditions (Fig. 2). Interestingly, macrophages infiltrated infected tissues around the time of the peak of expression of fractalkine (Fig. 4) and when rickettsial loads were still increasing (Fig. 3). This fact is relevant because fractalkine is an important mediator of monocyte recruitment [19].

We do not know the trigger for increased expression of fractalkine early after rickettsial infection of the endothelium. It is possible that rickettsiae could directly stimulate fractalkine expression through direct activation of NF-κB [23, 26], or it could be the consequence of the early rise in IFN-γ and tumor necrosis factor-α that has been observed during experimental rickettsial infections [2].

In conclusion, we demonstrated that mouse fractalkine (CX3CL1) was expressed normally, under non-inflammatory conditions, on endothelial cells of various segments of the vasculature, and its expression became generalized on the third day of a systemic endothelial-target rickettsial infection. The coincidental infiltration of macrophages at such a time justifies future studies with neutralizing antibodies and in mice with targeted disruption of the fractalkine gene or the gene for its receptor to determine the functional role of fractalkine in macrophage infiltration and the role of these cells in anti-rickettsial immunity.

Acknowledgements Sources of support: NIH grant RO1 AI21242 to D.H. Walker, College of American Pathologists Foundation Scholars Research Fellowship and James W. McLaughlin Predoctoral Fellowship awarded to G. Valbuena. We thank Susan Butler for her assistance with preparation of the manuscript.

References

1. Bazan JF, Bacon KB, Hardiman G, Wang W, Soo K, Rossi D, Greaves DR, Zlotnik A, Schall TJ (1997) A new class of membrane-bound chemokine with a CX3C motif. Nature 385:640–644
2. Billings AN, Feng HM, Olano JP, Walker DH (2001) Rickettsial infection in murine models activates an early anti-rickettsial effect mediated by NK cells and associated with production of gamma interferon. Am J Trop Med Hyg 65:52–56
3. Dignat-George F, Teysseire N, Mutin M, Bardin N, Lesaule G, Raoult D, Sampol J (1997) *Rickettsia conorii* infection enhances vascular cell adhesion molecule-1- and intercellular adhesion molecule-1-dependent mononuclear cell adherence to endothelial cells. J Infect Dis 175:1142–1152
4. Efsen E, Grappone C, DeFranco RM, Milani S, Romanelli RG, Bonacchi A, Caligiuri A, Failli P, Annunziato F, Pagliai G, Pinzani M, Laffi G, Gentilini P, Marra F (2002) Up-regulated expression of fractalkine and its receptor CX3CR1 during liver injury in humans. J Hepatol 37:39–47
5. Feng HM, Popov VL, Walker DH (1994) Depletion of gamma interferon and tumor necrosis factor alpha in mice with *Rickettsia conorii*-infected endothelium: impairment of rickettsicidal nitric oxide production resulting in fatal, overwhelming rickettsial disease. Infect Immun 62:1952–1960
6. Feng H, Popov VL, Yuoh G, Walker DH (1997) Role of T lymphocyte subsets in immunity to spotted fever group rickettsiae. J Immunol 158:5314–5320
7. Fong AM, Robinson LA, Steeber DA, Tedder TF, Yoshie O, Imai T, Patel DD (1998) Fractalkine and CX3CR1 mediate a novel mechanism of leukocyte capture, firm adhesion, and activation under physiologic flow. J Exp Med 188:1413–1419
8. Fraticelli P, Sironi M, Bianchi G, D'Ambrosio D, Albanesi C, Stoppacciaro A, Chieppa M, Allavena P, Ruco L, Girolomoni G, Sinigaglia F, Vecchi A, Mantovani A (2001) Fractalkine (CX3CL1) as an amplification circuit of polarized Th1 responses. J Clin Invest 107:1173–1181
9. Garton KJ, Gough PJ, Blobel CP, Murphy G, Greaves DR, Dempsey PJ, Raines EW (2001) Tumor necrosis factor-alpha-converting enzyme (ADAM17) mediates the cleavage and shedding of fractalkine (CX3CL1). J Biol Chem 276:37993–38001
10. Guo J, Zhang M, Wang B, Yuan Z, Guo Z, Chen T, Yu Y, Qin Z, Cao X (2003) Fractalkine transgene induces T-cell-dependent antitumor immunity through chemoattraction and activation of dendritic cells. Int J Cancer 103:212–220
11. Haskell CA, Cleary MD, Charo IF (1999) Molecular uncoupling of fractalkine-mediated cell adhesion and signal transduction. Rapid flow arrest of CX3CR1-expressing cells is independent of G-protein activation. J Biol Chem 274:10053–10058
12. Haskell CA, Hancock WW, Salant DJ, Gao W, Csizmadia V, Peters W, Faia K, Fituri O, Rottman JB, Charo IF (2001) Targeted deletion of CX(3)CR1 reveals a role for fractalkine in cardiac allograft rejection. J Clin Invest 108:679–688
13. Heinzen RA, Hayes SF, Peacock MG, Hackstadt T (1993) Directional actin polymerization associated with spotted fever group rickettsia infection of Vero cells. Infect Immun 61:1926–1935
14. Heinzen RA, Grieshaber SS, Van Kirk LS, Devin CJ (1999) Dynamics of actin-based movement by *Rickettsia rickettsii* in vero cells. Infect Immun 67:4201–4207
15. Holman RC, Paddock CD, Curns AT, Krebs JW, McQuiston JH, Childs JE (2001) Analysis of risk factors for fatal Rocky Mountain spotted fever: evidence for superiority of tetracyclines for therapy. J Infect Dis 184:1437–1444
16. Hundhausen C, Misztela D, Berkhout TA, Broadway N, Saftig P, Reiss K, Hartmann D, Fahrenholz F, Postina R, Matthews V, Kallen KJ, Rose-John S, Ludwig A (2003) The disintegrin-like metalloproteinase ADAM10 is involved in constitutive cleavage of CX3CL1 (fractalkine) and regulates CX3CL1-mediated cell-cell adhesion. Blood 102:1186–1195
17. Kaplanski G, Teysseire N, Farnarier C, Kaplanski S, Lissitzky JC, Durand JM, Soubeyrand J, Dinarello CA, Bongrand P (1995) IL-6 and IL-8 production from cultured human endothelial cells stimulated by infection with *Rickettsia conorii* via a cell-associated IL-1 alpha-dependent pathway. J Clin Invest 96:2839–2844
18. Kaplowitz LG, Fischer JJ, Sparling PF (1981) Rocky Mountain spotted fever: a clinical dilemma. 89–108

19. Lesnik P, Haskell CA, Charo IF (2003) Decreased atherosclerosis in CX3CR1−/− mice reveals a role for fractalkine in atherogenesis. J Clin Invest 111:333–340
20. Nishimura M, Umehara H, Nakayama T, Yoneda O, Hieshima K, Kakizaki M, Dohmae N, Yoshie O, Imai T (2002) Dual functions of fractalkine/CX3C ligand 1 in trafficking of perforin+/granzyme B+ cytotoxic effector lymphocytes that are defined by CX3CR1 expression. J Immunol 168:6173–6180
21. Reed LJ, Muench H (1938) A simple method of estimating fifty percent endpoints. Am J Hyg 27:493–497
22. Robinson LA, Nataraj C, Thomas DW, Howell DN, Griffiths R, Bautch V, Patel DD, Feng L, Coffman TM (2000) A role for fractalkine and its receptor (CX3CR1) in cardiac allograft rejection. J Immunol 165:6067–6072
23. Sahni SK, Van Antwerp DJ, Eremeeva ME, Silverman DJ, Marder VJ, Sporn LA (1998) Proteasome-independent activation of nuclear factor kappaB in cytoplasmic extracts from human endothelial cells by *Rickettsia rickettsii*. Infect Immun 66:1827–1833
24. Sporn LA, Lawrence SO, Silverman DJ, Marder VJ (1993) E-selectin-dependent neutrophil adhesion to *Rickettsia rickettsii*-infected endothelial cells. Blood 81:2406–2412
25. Sporn LA, Marder VJ (1996) Interleukin-1 alpha production during *Rickettsia rickettsii* infection of cultured endothelial cells: potential role in autocrine cell stimulation. Infect Immun 64:1609–1613
26. Sporn LA, Sahni SK, Lerner NB, Marder VJ, Silverman DJ, Turpin LC, Schwab AL (1997) *Rickettsia rickettsii* infection of cultured human endothelial cells induces NF-kappaB activation. Infect Immun 65:2786–2791
27. Valbuena G, Bradford W, Walker DH (2003) Expression analysis of the T-cell-targeting chemokines CXCL9 and CXCL10 in mice and humans with endothelial infections caused by rickettsiae of the spotted fever group. Am J Pathol 163:1357–1369
28. Van Kirk LS, Hayes SF, Heinzen RA (2000) Ultrastructure of *Rickettsia rickettsii* actin tails and localization of cytoskeletal proteins. Infect Immun 68:4706–4713
29. Walker DH (1982) Rickettsial diseases: an update. Monogr Pathol 188–204
30. Walker DH (1995) Rocky Mountain spotted fever: a seasonal alert. Clin Infect Dis 20:1111–1117
31. Walker DH, Cain BG (1980) The rickettsial plaque. Evidence for direct cytopathic effect of *Rickettsia rickettsii*. Lab Invest 43:388–396
32. Walker DH, TW Lane (1988) Rocky Mountain spotted fever: clinical signs, symptoms, and pathophysiology. In: Walker DH (ed) Biology of rickettsial diseases. CRC press, Boca Raton, pp 63–78
33. Walker DH, Popov VL, Wen J, Feng HM (1994) *Rickettsia conorii* infection of C3H/HeN mice. A model of endothelial-target rickettsiosis. Lab Invest 70:358–368
34. Walker DH, Popov VL, Feng HM (2000) Establishment of a novel endothelial target mouse model of a typhus group rickettsiosis: evidence for critical roles for gamma interferon and CD8 T lymphocytes. Lab Invest 80:1361–1372
35. Walker DH, Olano JP, Feng HM (2001) Critical role of cytotoxic T lymphocytes in immune clearance of rickettsial infection. Infect Immun 69:1841–1846
36. Yoneda O, Imai T, Goda S, Inoue H, Yamauchi A, Okazaki T, Imai H, Yoshie O, Bloom ET, Domae N, Umehara H (2000) Fractalkine-mediated endothelial cell injury by NK cells. J Immunol 164:4055–4062

Virchows Arch (2005) 446:28–33
DOI 10.1007/s00428-004-1126-x

ORIGINAL ARTICLE

Eugenio Maiorano · Gianfranco Favia · Saverio Capodiferro · Maria Teresa Montagna · Lorenzo Lo Muzio

Combined mucormycosis and aspergillosis of the oro-sinonasal region in a patient affected by Castleman disease

Received: 3 June 2004 / Accepted: 23 August 2004 / Published online: 5 October 2004
© Springer-Verlag 2004

Abstract One case of aspergillosis and mucormycosis occurring in a patient with stage-IV Castleman disease was investigated. The patient, who had undergone polychemotherapy and was in otherwise good general condition, without lymphadenopathies or imbalance of the immune system, presented with a palatal ulceration that progressively involved the palatal mucosa and bone, the paranasal sinuses and the orbit. Repeated cultural examinations were always negative. He had undergone multiple cytological smears of the inflammatory infiltration and biopsies of both the oral and nasal mucosa, which resulted in extensive necrotic debris and suppurative inflammation, and, on the very last biopsy, fungal hyphae, spores and conidia were also detected. These were large, branching, mostly non-septate hyphae, associated with conidiophores and conidia, the latter appearing dark brown to black in the histological preparations. Following the diagnosis of combined mucormycosis and aspergillosis, the patient underwent prolonged topic and systemic antibiotic treatment that resulted curative. Mucormycosis usually is a fatal complication of head and neck or systemic disorders, leading to severe immune suppression. Nevertheless, early diagnosis may be achieved using a combination of special stains and may lead to effective antibiotic treatment and cure of the patient, even if associated with other opportunistic infections, such as aspergillosis.

Keywords Mucormycosis · Aspergillosis · Castleman disease · Head and neck · Oral ulcer

E. Maiorano
Department of Pathological Anatomy and Genetics,
University of Bari,
Bari, Italy

G. Favia · S. Capodiferro
Department of Dental Sciences and Surgery,
University of Bari,
Bari, Italy

M. T. Montagna
Department of Internal Medicine and Public Medicine,
Section of Hygiene,
University of Bari,
Bari, Italy

L. Lo Muzio
Institute of Dental Sciences,
Università Politecnica delle Marche,
Ancona, Italy

E. Maiorano (✉)
Dipartimento di Anatomia Patologica e Genetica,
Piazza G. Cesare, 11–70124 Bari, Italy
e-mail: emaiorano@anatopat.uniba.it
Tel.: +39-080-5478292
Fax: +39-080-5478263

Introduction

Oro-facial lesions caused by systemic mycoses have been reported very rarely in Western countries [3, 7, 11, 13, 32]. Among some 100,000 different species of fungi, very few are pathogenic for man [8], and most of them show distinct geographical distribution. In recent years, the dramatic raise of immune-compromised patients, due to iatrogenic (mostly organ transplantation or immunosuppressive treatments) or infective causes (human immunodeficiency virus infection above all), resulted in increasing reports of systemic fungal infections in the Western world.

Isolated oro-facial mycotic lesions are occasionally encountered, with the exception of candidiasis; however, they are more commonly detected in association with respiratory tract or systemic fungal infection [26], most of the latter potentially being ominous or lethal for the patient.

Aspergillosis is the term used to identify the clinical syndromes resulting from infection with, colonisation by or allergic reactions due to *Aspergillus*. Of the almost 900 species of *Aspergillus*, the most often implicated in human diseases is *A. fumigatus* (50–70%). Aspergilli are ubiquitous and grow spontaneously in a variety of decaying organic materials. These organisms are routinely

isolated from tap water, soil, decaying vegetation, wet paint, food, dust and even sanitising agents used in hospitals. Aspergillus is not a person-to-person transmittable disease: spores may be liberated into the air and accidentally inhaled by human hosts. Inhalation of the conidiospores is extremely common but, unless there is massive inhalation or immune compromission, the occurrence of overt clinical diseases is a rare event.

Aspergilli appear as long filamentous fungi that reproduce by spores (conidia). In human tissues, these micro-organisms form septate hyphae that branch at 45-degree angles. Their morphological appearance in tissue specimens is indistinguishable from other moulds and, therefore, is not specific enough to make a definitive diagnosis of invasive aspergillosis, the latter usually being achieved by cultural methods.

Aspergillosis usually occurs in immune-suppressed or debilitated individuals [31], such as patients with neutropenia [17], leukaemia [10, 16, 18, 30], acquired immunodeficiency syndrome [23, 27], cancer [25], treated with corticosteroids or with otherwise imbalanced macrophagic functions [24]. In such instances, inhaled spores [22] invade blood vessels, causing thrombosis and infarction and can erode through the facial planes, cartilagine and bone [2].

Mucormycosis, or zygomycosis, is a rare and frequently lethal infection caused by opportunistic fungi, belonging to the family Mucoraceae, a class of the Zygomycetes [4]. These organisms have a world-wide distribution and grow spontaneously in a variety of decaying organic materials. Spores may be liberated into the air and accidentally inhaled by human hosts. Also, different species, such as Absidia, Apophysomyces, Mortierella, Saksenaae, Rhizomucor and Cunninghamella, may be responsible for mucormycosis in humans.

Mucormycetes are saprophytic aerobial fungi that grow in an acid layer and may colonise the oral mucosa, nose, maxillary sinuses and throat. More frequently, mucormycosis begins as a clinically subtle sinusitis or periorbital panniculitis, but, occasionally, patients with mucormycosis may be referred to dentists for dental pain or subperiostal swelling of the jaws [15]. Delayed diagnosis or inappropriate treatment may result in mucosal ulceration and bone destruction, leading to intra- and extra-oral mid-facial defects that require surgical intervention [15]. Nevertheless, mucormycosis frequently is lethal for the patients, due to extensive tissue destruction and brain involvement.

This study was aimed at describing the clinico-pathological features of a case of combined aspergillosis and mucormycosis, arising in a patient with generalised (stage IV) Castleman disease presenting with intra-oral ulcerations of the palatal and cheek mucosa and at illustrating the histopathological clues for accurate and prompt diagnosis.

Case report

A 66-year-old male patient, who had been suffering from generalised Castleman disease for several months, treated by poly-chemotherapy and in complete remission, reported an acute upper respiratory tract inflammation, with fever, hacking cough, left earache and an erythematous oro-pharyngeal eruption a few days prior to the appearance of palatal ulcers accompanied by loco-regional numbness. These signs were attributed to herpetic infection by both the patient and the general practitioner. Subsequently, the patient developed acute peri-orbital inflammation with oedema of the cheek and was referred to the Department of Dental Sciences and Surgery of the University of Bari.

At clinical examination, there was prominent tumefaction of the right hemi-face, involving the peri-orbital, zygomatic and maxillary areas, naso-sinusal congestion and diffuse ulcerative lesions of the palatal and cheek mucosa. Notwithstanding anti-inflammatory and antibiotic therapy, the palatal and cheek mucosa enlarged over the next few days, mimicking rapid neoplastic growth. Intra-oral examination disclosed a 3×3-cm painful palatal lump, with black central crusting and prominent oedematous–erythematous changes of the surrounding tissues. The entire area was indurated and markedly tender and evolved into a large tissue loss involving the palate and the alveolar bone in the following 24–48 h (Fig. 1). There were no signs of thrush, pharyngeal abnormalities or cervical lymphadenopathy, skin rash or systemic involvement by the disease. Computed axial and coronal tomographic scans were carried out and showed a soft tissue tumour-like expansion with central necrosis, involving the palatal mucosa and the paranasal sinuses (Fig. 2).

A peripheral blood test revealed mild neutropenia (WBC 4900/ml, with 65% neutrophils and 27% lymphocytes) but no other relevant abnormalities, including peripheral CD 4 T cells that were above 500/μl.

In consideration of the patient being affected by Castleman disease with possible intra-oral involvement, fine needle aspiration biopsy (FNAB) along with repeated sampling for microbiological tests were performed, which always resulted negative.

The FNAB samples were fixed in 50% ethyl alcohol and both smeared and stained with Papanicolau and Giemsa and embedded in paraffin, cut and stained with haematoxylin-eosin (H&E). The cyto-histological preparations showed non-specific suppurative inflammation in a background of macrophages and cellular debris admixed with acellular, weakly eosinophilic material.

Due to the persistence of the worrisome clinical suspicion of malignancy, an incisional biopsy was performed. Extensive purulence and necrosis of both the superficial and deep layers of the wound were noted. The surgical sample was formalin fixed, par-

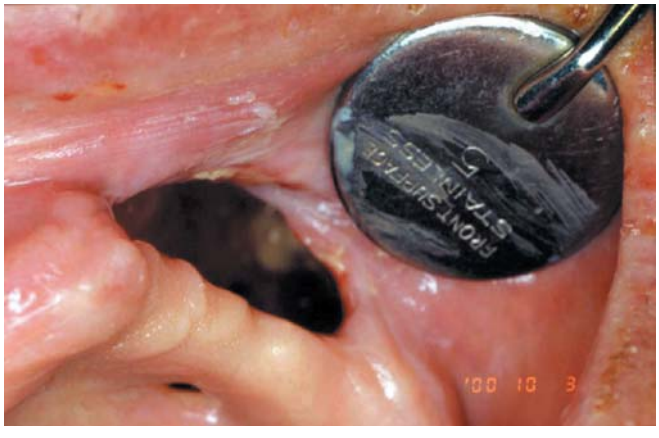

Fig. 1 Clinical features of combined mucormycosis and aspergillosis of the oral and sino-nasal tract. Evident tissue losses are evident in the hard palate and the alveolar maxillary bone

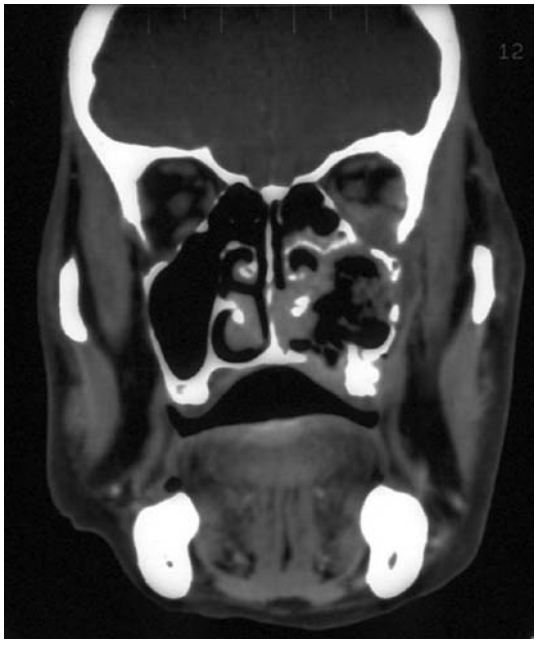

Fig. 2 Coronal view of computed tomography scan: multiple areas of bone rarefaction and resorption are evident in conjunction with diffuse thickening of the palatal, sino-nasal and orbital soft tissues

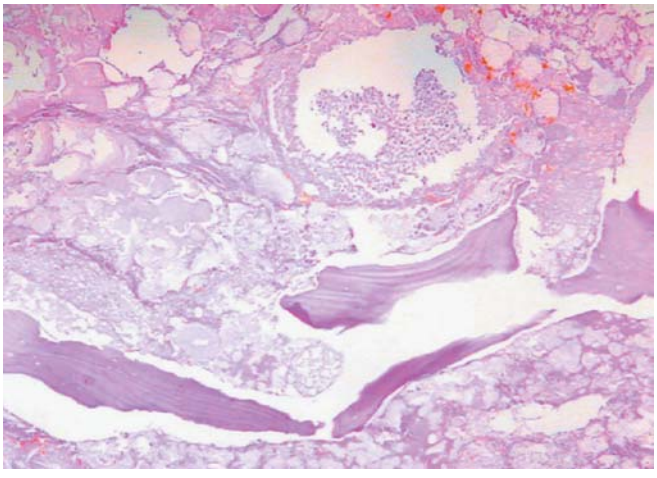

Fig. 3 The histopathological preparations showed unspecific neutrophilic infiltration, regressive and necrotic changes of residual structures and large collections of acellular and lightly stained material, which appeared flocculent or vaguely fibrillary with conventional stains. (Haematoxylin–eosin, ×20)

affin embedded, cut and stained with H&E, periodic acid Schiff (PAS), Giemsa, Grocott–Gomori silver methenamine method and Lugol's iodine solution.

Histologically, there was extensive mucosal and bone necrosis, suppurative neutrophilic infiltration, and most of the specimen consisted of acellular, weakly eosinophilic, non-structured filamentous material (Fig. 3). The latter, at higher magnification, was mainly composed of PAS-positive, elongated fungal hyphae that stained light blue with the Giemsa stain and dark brown to black with the Lugol's solution and the Grocott–Gomori silver methenamine method. These were mostly large, branching, non-septate fungal hyphae (Fig. 4) and were associated with umbrella-like conidiophores (sporangia) containing angulated and irregular

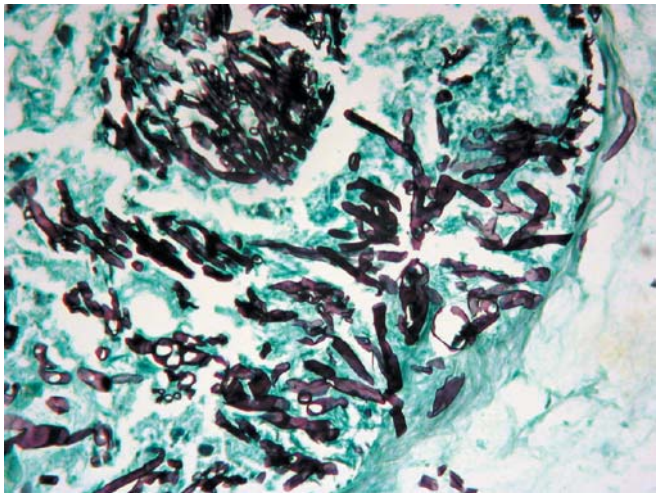

Fig. 4 Most mycotic hyphae were elongated and thick, branching and non-septate and stained dark brown to black with the Grocott–Gomori silver methenamine stain and Lugol's iodine solution. Their morphological features were most consistent with mucormycosis, although aspergillotic hyphae might look very much similar in histological preparations. (Grocott–Gomori silver methenamine stain, ×40)

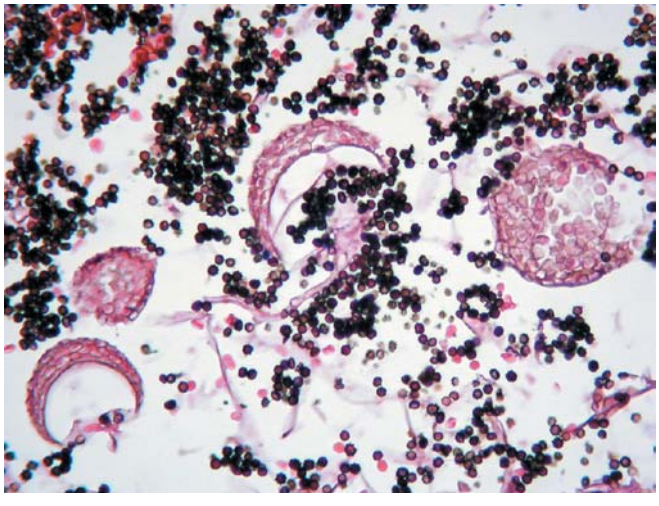

Fig. 5 Distinct areas of the histological preparations showed large umbrella-like or parachute-like structures containing pale-staining and larger spores (6–9 μm) of mucormycetes with a smooth surface and collections of smaller (3.5–4.5 μm) and darkly stained aspergillotic conidia demonstrating an echinulated profile at high magnification. (Lugol's iodine solution, ×40)

spores, 6–9 μm in diameter, which stained light pink or red with Lugol's solution and the Grocott–Gomori silver methenamine methods (Fig. 5). These morphological features were suggestive of infection by mucoraceae. Admixed with the latter, there were numerous smaller (3.5–4.5 μm) and darkly stained (with H&E, Lugol's solution and the Grocott–Gomori silver methenamine methods) conidia (Fig. 5) that demonstrated a roundish profile and an echinulated surface at higher magnification. In addition, these conidia were frequently associated with flower-like conidiophores (Fig. 6) that stained ocre to light brown with Lugol's solution and the Grocott–Gomori silver methenamine methods and were con-

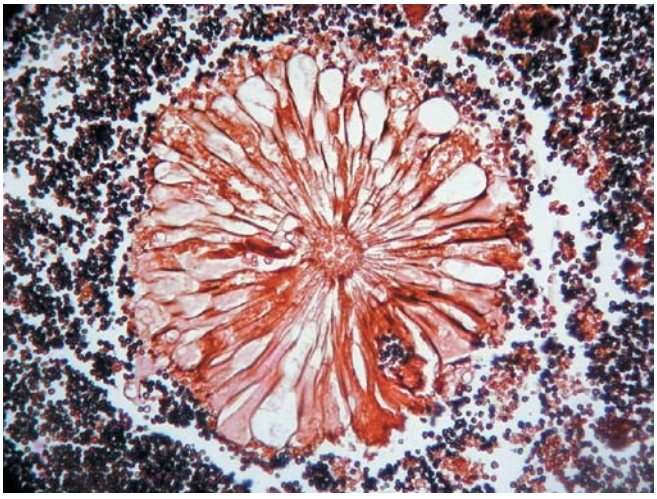

Fig. 6 Rare areas of the histological samples contained large conidiophores showing a flower-like appearance, staining ocre to light brown with Lugol's iodine solution or Grocott-Gomori's silver methenamine methods and surrounded by large collections of dark aspergillus conidia. (Lugol's iodine solution, ×20)

sistent with aspergillus infection, most probably *A. Flavus* or *A. Niger*.

Based on the clinical findings and the morphological features of the fungal organisms, the diagnosis of mucormycosis and concomitant aspergillosis was formulated. Nevertheless, cultural tests for fungi were repeatedly negative.

The patient underwent surgical debridement of the infected necrotic tissues, daily local nebulisation of amphotericin B and 2% potassium iodide for 6 months, along with systemic administration of high-dose (1 mg/kg/daily) amphotericin B intravenously for 2 months and oral itraconazole (100 mg twice a day) for 4 months. The patient is currently monitored every 6 months and is apparently completely cured of the fungal infections 3.5 years after the diagnosis.

Discussion

This study reports on the extremely unusual combined infection by mucormycosis and aspergillosis in an apparently healthy individual affected by systemic Castleman disease who was cured following accurate diagnosis and prompt local and systemic high-dose antifungal therapy.

Aspergillosis is a widely diffused disease [26] that may involve several distinct areas of human body, though the most typical clinical manifestations are: (1) allergic (extrinsic asthma, allergic bronchopulmonary aspergillosis) and extrinsic allergic alveolitis; (2) non-invasive colonisation of previously damaged tissue (aspergilloma) and (3) invasive disease (cutaneous, pulmonary, central nervous system, disseminated and naso-orbital aspergillosis) [29].

Aspergillosis of the head and neck, particularly the nose and paranasal sinuses, has been divided into four clinical types: allergic, non-invasive, invasive and fulminant. More recently, a semi-invasive form has been described, with bone destruction and erosion but without fungal tissue invasion, which may extend into the orbit and anterior cranial fossa [19, 21]. Invasive aspergillosis is rare and mainly affects immune-compromised hosts, causing destruction of the antral wall, antral pain, swelling, with or without sequelae from orbital invasion or intracranial extension. Following an initial sino-nasal localisation, oral lesions may develop, especially to the palate or the alveolar process, which appear as yellow to black necrotic ulcers of the palate or the posterior tongue [14, 23]. Delayed diagnosis or inappropriate treatment may result in massive tissue destruction and possible extension into the cranial base and/or vault and orbit, via the blood flow, and determine blindness, lethargy, seizure and eventually death [2]. Aspergillosis very rarely arises in healthy individuals and more commonly affects insulin-dependent diabetics with poorly controlled disease, immune-compromised patients [18, 28] or leukaemic patients [10, 16]. Non-invasive aspergillosis of the maxillary sinus may be associated with extrusion of root canal cements into the sinus, and it has been suggested that zinc oxide-based endodontic materials might promote the infection, as zinc may act as a growth factor for Aspergillus [20].

Most cases of mucormycosis or zygomycosis have been reported from the Caribbean, Latin America, Central and West Africa [4, 26], the disease possibly having wide distribution throughout the human body, the most typical clinical manifestations being: *rhino-cerebral m.*, *pulmonary m.*, *cutaneous m.*, *gastrointestinal m.* and *disseminated m.* [12].

The rhino-cerebral form usually is the most relevant for general and dental practitioners [26] and may involve the nose, the maxillary sinuses and different areas of the face. Patients experience nasal obstruction, bloody nasal discharge, facial pain, swelling or cellulitis, headache and visual disturbances with concurrent proptosis. Involvement of the cranial nerves with related symptoms is often present. The disease frequently extends to the cranial base and/or vault and the orbit, via the blood flow, and determines blindness, lethargy, seizure and eventually death. The involvement of maxillary sinuses may produce intraoral swelling of the maxillary alveolar process, the palate or both. Subsequently, the lesion may lead to palatal ulceration, the surface of the ulcers typically appearing black and necrotic.

As for aspergillosis, mucormycosis very rarely affects healthy individuals and more commonly arises in immune-compromised patients [5, 6, 13, 32]. Diabetic ketoacidosis was proven to abolish the normal serum inhibitory activity against zygomycetes [6]. Although in the current case, clinical and laboratory findings did not disclose immune depression at the time when the fungal infection became clinically evident, we cannot exclude that temporary immune depression might have occurred while the patient was undergoing systemic chemotherapy. At that time, the patient could have been infected by the two fungi, but it took several months to manifest the clinical signs depicted herein. This is quite a frequent event in patients affected by different haematological

malignancies, including Castleman disease, and undergoing chemo-radiotherapy.

The clinical diagnosis of aspergillosis or mucormycosis may be troublesome, especially for those cases exhibiting deep ulceration or destruction of the palate that simulate several different diseases, such as inflammatory lesions (tuberculosis and tertiary syphilis), malignancies of the palate, nose and maxillary sinuses (squamous cell carcinoma, salivary gland carcinomas, malignant odontogenic neoplasms) or local manifestations of systemic diseases (Wegener's granulomatosis, leukaemia and lymphoma) [26]. In such instances, radiological studies may help very little, showing non-specific bone resorption with cortical destruction, and mycological studies may result in absence of growth due to difficulties in effectively culturing mucormycetes and/or aspergilli obtained by superficial swabs of the lesions [26].

Consequently, most patients are subjected to different diagnostic procedures based on both cytological and histological studies. As in the present study, specimens obtained from the most superficial areas of the ulcerative/destructive lesions may result in necrotic debris and inflammatory cells only that do not allow an aetiological diagnosis and adequate treatment. In addition, routinely used staining techniques, such as Papanicolau or H&E stains, do not specifically highlight mycotic hyphae in general, and these could be easily overlooked among the inflammatory background of the cyto-histological preparations.

In such instances and if guided by the clinical suspicion of infection by unknown organisms, the use of ancillary stains, including PAS, the Grocott–Gomori silver methenamine method and Lugol's iodine solution, should be mandatory to highlight large, branching, non-septate hyphae (zygomycetes) or narrow (4 μm) regular width, branching, septate hyphae (Aspergillus). It should be noted that the mycotic hyphae detected in the current case did not allow proper identification of the infectious agent, as both Mucormycetes and Aspergilli may show similar morphology in histological preparations. A more accurate differential diagnosis between these two fungi derived from the detection of distinct umbrella-like sporangiophores suggestive of mucormycosis and flower-like conidiophores suggestive of aspergillosis. Also, mucor-mycotic sporangiophores are rarely evident in tissues exposed to air and have been seldom reported in the literature [4]. Additional histopathological features that may help for the diagnosis include the occurrence blood vessels necrosis in the absence of evident endo-perivascular inflammation and the presence of recently formed thrombi that frequently contain zygomycotic fungi.

Nevertheless, the latter were not prominent features of the current case, possibly due to former prolonged antibiotic therapy, which could have attenuated the virulence of both micro-organisms or to reciprocal partial inhibition by the concurrent infection by zygomycetes and aspergilli. Unfortunately, alternative diagnostic methods, such as the detection of circulating free antigens or immune complexes by enzyme-linked immunosorbent assay and radioimmunoassay techniques [1] do not allow satisfactory identification of these organisms, and, possibly, the wider use of immunohistochemistry or molecular approaches with polymerase chain reaction techniques will prove more effective for this purpose [2].

Both mucormycosis and aspergillosis usually are severe infections, with mortality rates ranging from 20% to 40% in immune-compromised patients [9] and approaching 80–90% in cases of disseminated infections or involvement of the brain structures [2]. Appropriate treatment must be instituted early, even before the results of cultural and/or histopathological studies have been obtained, and, currently, the administration of systemic amphotericin B (0.3–1.0 mg/kg/day in 5% dextrose intravenously) and surgical debridment of the lesions are considered the standard therapy [8, 12] and were proven effective in the current case.

References

1. Andriole VT (1993) Invasive aspergillosis: serologic diagnosis. Recent Results Cancer Res 132:117–125
2. Bodey GP (1999) Fungal infections in immunocompromised patients. II. Aspergillosis and cryptococcosis. Infect Dis Rev 1:87–92
3. Cangiano G, Longo F, Cangiano R (1998) Benign maxillofacial mucormycosis. Report of a case and review of the literature. Minerva Stomatol 47:613–616
4. Ciesla MC, Kammeyer PL, Yeldandi V, Petruzzelli GJ, Yong SL (2000) Identification of the asexual state of Rhizopus species on histologic tissue sections in a patient with rhinocerebral mucormycosis. Arch Pathol Lab Med 124:883–887
5. Cohen SG, Greenberg MS (1980) Rhinomaxillary mucormycosis in a kidney transplant patient. Oral Surg Oral Med Oral Pathol 50:33–38
6. Cox DT, Allen CM, Plouffe JF (1996) Locally invasive oral candidiasis mimicking zygomycosis in a patient with diabetic ketoacidosis. Oral Surg Oral Med Oral Pathol Oral Radiol Endod 81:70–73
7. Damante JH, Fleury RN (1998) Oral and rhinoorbital mucormycosis: case report. J Oral Maxillofac Surg 56:267–271
8. de Almeida OP, Scully C (1991) Oral lesions in the systemic mycoses. Curr Opin Dent 1:423–428
9. Denning DW (1998) Invasive aspergillosis. Clin Infect Dis 26:781–803
10. Dreizen S, Bodey GP, McCredie KB, Keating MJ (1985) Orofacial aspergillosis in acute leukemia. Oral Surg Oral Med Oral Pathol 59:499–504
11. Economopoulou P, Laskaris G, Ferekidis E, Kanelis N (1995) Rhinocerebral mucormycosis with severe oral lesions: a case report. J Oral Maxillofac Surg 53:215–217
12. Hauman CH, Raubenheimer EJ (1989) Orofacial mucormycosis. Oral Surg Oral Med Oral Pathol 68:624–627
13. Jones AC, Bentsen TY, Freedman PD (1993) Mucormycosis of the oral cavity. Oral Surg Oral Med Oral Pathol 75:455–460
14. Khatri ML, Stefanato CM, Benghazeil M, Shafi M, Kubba A, Bhawan J (2000) Cutaneous and paranasal aspergillosis in an immunocompetent patient. Int J Dermatol 39:853–856
15. Kurrasch M, Beumer J 3rd, Kagawa T (1982) Mucormycosis: oral and prosthodontic implications. A report of 14 patients. J Prosthet Dent 47:422–429
16. Myoken Y, Sugata T, Kyo TI, Fujihara M (1996) Pathological features of invasive oral aspergillosis in patients with hematologic malignancies. J Oral Maxillofac Surg 54:263–270
17. Myoken Y, Sugata T, Kyo T, Fujihara M, Mikami Y (1999) Antifungal susceptibility of Aspergillus species isolated from

invasive oral infection in neutropenic patients with hematologic malignancies. Oral Surg Oral Med Oral Pathol Oral Radiol Endod 87:174–179
18. Myoken Y, Sugata T, Kyo Ti T, Fujihara M, Kohara T, Katsu M, Tamura M, Mikami Y (2001) Invasive Aspergillus stomatitis in patients with acute leukemia: report of 12 cases. Clin Infect Dis 33:1975–1980
19. Notani K, Satoh C, Hashimoto I, Makino S, Kitada H, Fukuda H (2000) Intracranial Aspergillus infection from the paranasal sinus. Oral Surg Oral Med Oral Pathol Oral Radiol Endod 89:9–11
20. Odell E, Pertl C (1995) Zinc as a growth factor for Aspergillus sp. and the antifungal effects of root canal sealants. Oral Surg Oral Med Oral Pathol Oral Radiol Endod 79:82–87
21. Oyarzabal MF, Chevretton EB, Hay RJ (2000) Semi-invasive allergic aspergillosis of the paranasal sinuses. J Laryngol Otol 114:290–292
22. Perraud M, Piens MA, Nicoloyannis N, Girard P, Sepetjan M, Garin JP (1987) Invasive nosocomial pulmonary aspergillosis: risk factors and hospital building works. Epidemiol Infect 99:407–412
23. Rubin MM, Jui V, Sadoff RS (1990) Oral aspergillosis in a patient with acquired immunodeficiency syndrome. J Oral Maxillofac Surg 48:997–999
24. Schaffner A, Douglas H, Braude A (1982) Selective protection against conidia by mononuclear and against mycelia by polymorphonuclear phagocytes in resistance to Aspergillus. Observations on these two lines of defense in vivo and in vitro with human and mouse phagocytes. J Clin Invest 69:617–631
25. Schubert MM, Peterson DE, Meyers JD, Hackman R, Thomas ED (1986) Head and neck aspergillosis in patients undergoing bone marrow transplantation. Report of four cases and review of the literature. Cancer 57:1092–1096
26. Scully C, de Almeida OP (1992) Orofacial manifestations of the systemic mycoses. J Oral Pathol Med 21:289–294
27. Scully C, de Almeida OP, Sposto MR (1997) The deep mycoses in HIV infection. Oral Dis 3[Suppl 1]:S200–S207
28. Shibuya K, Coulson WF, Wollman JS, Wakayama M, Ando T, Oharaseki T, Takahashi K, Naoe S (2001) Histopathology of cryptococcosis and other fungal infections in patients with acquired immunodeficiency syndrome. Int J Infect Dis 5:78–85
29. Stevens DA, Kan VL, Judson MA, Morrison VA, Dummer S, Denning DW, Bennett JE, Walsh TJ, Patterson TF, Pankey GA (2000) Practice guidelines for diseases caused by Aspergillus. Infectious Diseases Society of America. Clin Infect Dis 30:696–709
30. Sugata T, Myoken Y, Kyo T, Fujihara M (1994) Invasive oral aspergillosis in immunocompromised patients with leukemia. J Oral Maxillofac Surg 52:382–386
31. Sugata T, Myoken Y, Kyo T, Fujihara M (1996) Oral aspergillosis in compromised patients. Oral Surg Oral Med Oral Pathol Oral Radiol Endod 81:632–633
32. Van der Westhuijzen AJ, Grotepass FW, Wyma G, Padayachee A (1989) A rapidly fatal palatal ulcer: rhinocerebral mucormycosis. Oral Surg Oral Med Oral Pathol 68:32–36

Virchows Arch (2005) 446:34–40
DOI 10.1007/s00428-004-1125-y

ORIGINAL ARTICLE

Kimihide Kusafuka · Keisuke Nakano · Yuji Hiraki · Chisa Shukunami · Hitoshi Nagatsuka · Noriyuki Nagai · Tamiko Takemura · Yutaku Sakaguchi · Kazuichi Okazaki · Michi Kusafuka · Hiroko Hisha · Susumu Ikehara

Expression and localization of cartilage-specific matrix protein chondromodulin-I mRNA in salivary pleomorphic adenomas

Received: 14 April 2004 / Accepted: 23 August 2004 / Published online: 11 November 2004
© Springer-Verlag 2004

K. Kusafuka (✉) · M. Kusafuka · H. Hisha · S. Ikehara
Department of Transplantation for Regeneration Therapy, sponsored by Otsuka Pharmaceutical Co. Ltd.,
Kansai Medical University,
10-15 Fumizono-cho, Moriguchi City, 570-8506 Osaka, Japan
e-mail: kusahukk@takii.kmu.ac.jp
Tel.: +81-06-69921001 x2472
Fax: +81-06-69948283

K. Kusafuka · T. Takemura
Department of Pathology,
Japanese Red Cross Medical Center,
4-1-22 Hiroo, Shibuya-ku, 150-8935 Tokyo, Japan

S. Ikehara
Regeneration Research Center for Intractable Disease,
Kansai Medical University,
10-15 Fumizono-cho, Moriguchi City, 570-8506 Osaka, Japan

S. Ikehara
Center for Cancer Therapy,
Kansai Medical University,
10-15 Fumizono-cho, Moriguchi City, 570-8506 Osaka, Japan

K. Nakano · H. Nagatsuka · N. Nagai
Patho-physiology Field,
Department of Oral Pathology and Medicine,
Graduate School of Medicine and Dentistry, Okayama University,
2-5-1 Shikata-cho, 700-8558 Okayama, Japan

Y. Hiraki · C. Shukunami
Department of Molecular Interaction and Tissue Engineering,
Institute for Frontier Sciences, Kyoto University,
53 Shogoinkawara-cho, Sakyo-ku, 606-8507 Kyoto, Japan

Y. Sakaguchi · H. Hisha · S. Ikehara
The First Department of Pathology,
Kansai Medical University,
10-15 Fumizono-cho, Moriguchi City, 570-8506 Osaka, Japan

Y. Sakaguchi · K. Okazaki
The Third Department of Internal Medicine,
Kansai Medical University,
10-15 Fumizono-cho, Moriguchi City, 570-8506 Osaka, Japan

S. Ikehara
Center for Transplantation,
Kansai Medical University,
10-15 Fumizono-cho, Moriguchi City, 570-8506 Osaka, Japan

Abstract Pleomorphic adenoma is the most common epithelial tumor in the salivary glands. This tumor frequently exhibits "mesenchyme"-like components, including myxoid or chondroid areas. Recently, using immunohistochemical techniques, we reported that cartilage-specific matrix protein, chondromodulin-I (ChM-I), was deposited on the inter-territorial matrix of the chondroid area in salivary pleomorphic adenomas and that ChM-I, which is also a strong angio-inhibitory factor, plays an important role in the avascular nature of the chondroid area and the chondroid formation in this type of tumor. To elucidate which cells express ChM-I mRNA in pleomorphic adenomas, we examined the expression and localization of ChM-I mRNA in this type of tumor using an in situ hybridization technique. Immunoreactivity for ChM-I was observed in the inter-territorial matrix of the chondroid area, especially around the lacunae, and in the cytoplasm of neoplastic myoepithelial cells of the myxoid element of pleomorphic adenomas. On in situ hybridization analysis, strong signals for ChM-I mRNA were detected in the cytoplasm of the lacuna cells of the chondroid element, and moderate to marked signals were observed in the cytoplasm of the neoplastic myoepithelial cells of the myxoid element. Signals for ChM-I mRNA were also seen in the cytoplasm of the spindle-shaped neoplastic myoepithelial cells in the transitional areas between the myxoid and chondroid elements of this tumor. Signals for ChM-I mRNA were not seen in the inner ductal cells or the fibrous element. These findings indicate that lacuna cells and neoplastic myoepithelial cells express ChM-I mRNA and that mature ChM-I, which lacuna cells and neoplastic myoepithelial cells translate, is deposited in the chondroid matrix of pleomorphic adenomas. In conclusion, lacuna cells and neoplastic myo-

epithelial cells express ChM-I mRNA ectopically in pleomorphic adenoma, and this plays an important role in chondroid formation and hypovascularity in this type of tumor.

Keywords Chondromodulin-I · Cartilaginous matrix · Pleomorphic adenoma · In situ hybridization · Immunohistochemistry

Introduction

Pleomorphic adenoma is the most common type of benign epithelial tumor in the salivary glands. Histologically, it shows "mesenchyme"-like components, including fibrous, hyaline, myxoid or chondroid areas. In particular, myxoid and chondroid elements have been considered to be derived from true mesenchymal cells, and pleomorphic adenoma has been considered to be a "true mixed tumor." Recent immunohistochemical and electron-microscopic examinations, however, have elucidated that this tumor is derived from epithelial cells and particularly from neoplastic myoepithelial cells [3, 4]. In the chondroid element, only lacuna cells were not distinguished from authentic chondrocytes, immunohistochemically and ultrastructurally [18]. We have reported that bone morphogenetic protein (BMP)-2 expressed in neoplastic myoepithelial cells may play a role in chondroid formation in a paracrine manner [13], whereas BMP-6 expressed in lacuna cells may play a role in maintenance of the cartilaginous phenotype of the chondroid element of pleomorphic adenoma in an autocrine manner [15]. Although BMPs are known to be strong inducers of bone and cartilage formation, ossification of the chondroid element is extremely rare. As binding between fibroblast growth factor (FGF) and FGF receptor-1 was reported to inhibit terminal differentiation of chondrocytes and calcification in vitro [12], we have reported that co-expression of FGF-2 and FGF receptor-1 in lacuna cells may play an essential role in the inhibition of ossification of the chondroid element in pleomorphic adenomas [14]. Although FGF-2 is also known to be a strong angiogenic factor [2, 5, 20], pleomorphic adenoma is a hypovascular tumor, due to the low density of CD34-positive endothelial cells [16]. Cartilage-specific matrix protein, bovine chondromodulin-I (ChM-I), has been shown to be a strong inhibitory factor against angiogenesis in vitro [8, 9], and human ChM-I has also been cloned [10]. Recently, using an immunohistochemical technique, we have shown that ChM-I is deposited in the inter-territorial matrix of the chondroid element of pleomorphic adenoma [16]. As ChM-I serves as a barrier against the angiogenic property of FGF-2, pleomorphic adenomas are hypovascular tumors. To confirm this immunohistochemical result, we examined which cells express ChM-I mRNA in pleomorphic adenomas, using an in situ hybridization method.

Materials and methods

Tissues

Cases of typical pleomorphic adenomas (n=25) were chosen from the pathology files of the Japanese Red Cross Medical Center, Tokyo, Japan, from the period 1986 to 2001. Eight specimens included normal salivary gland tissues. One bronchial cartilage tissue was used as positive control (Fig. 1A). These specimens were fixed in 10% buffered formalin at room temperature overnight, routinely processed and embedded in paraffin wax. Serial sections were then prepared. The "mesenchyme"-like stromas of pleomorphic adenomas are summarized in Table 1. Routinely processed paraffin sections were stained with hematoxylin and eosin.

Immunohistochemistry

Immunohistochemistry was carried out, as described previously [16]. Briefly, paraffin-embedded sections were deparaffinized in xylene and rehydrated. For ChM-I staining, deparaffinized sections were first pretreated with 0.1% hyaluronidase (H6254; Sigma Chemical Co., St. Louis MO) in acetate buffer, pH 5.0, for 45 min at 37°C, followed by two washes with phosphate-buffered saline (PBS), and they were then treated with 0.4% pepsin (P-6887; Sigma Chemical Co.) in 1.0 N HCl solution for 45 min at 37°C. All sections were washed in PBS and incubated for 30 min in 0.3% H_2O_2 in methanol. The polyclonal rabbit anti-ChM-I antibody, described previously [10, 16], was used and diluted 1:400. After incubation for 1 h at room temperature, sections were washed twice in PBS and incubated with biotinylated anti-rabbit or anti-mouse immunoglobulin antibodies (Dako Japan Co., Kyoto, Japan). After two additional washes, they were incubated in peroxidase-conjugated streptavidin (P397; Dako Japan Co.), followed by two washes in PBS. Bound peroxidase was developed with 0.02% 3,3′-diaminobenzidine in 0.1 mol/Tris buffer, pH 7.6, in 0.005% H_2O_2 for 5 min, and counterstaining was performed with 5% methyl green. As negative controls, the primary antibody was replaced with normal rabbit serum, PBS or was preadsorbed with recombinant mature human ChM-I protein.

For identification of neoplastic myoepithelial cells or lacuna cells, monoclonal mouse anti-α smooth muscle actin antibody (M0851: clone 1A4) and polyclonal rabbit anti-S-100 protein antibody (Z311) were purchased from Dako Japan Co. (Kyoto, Japan) and were diluted 1:50 and 1:400.

Probe preparation

Digoxigenin-11-UTP-labeled single strand RNA probes were prepared using a DIG Labeling Kit (Boehringer Mannheim Biochemical, Germany) according to the manufacturer's instructions. For generation of the ChM-I probe, a 1.0-kb fragment of human ChM-I cDNA was subcloned into pcDNA3 [10]. After transcription, 40 units of RNase-free DNase (Boehringer Mannheim) were added to the reaction mixture, and a further incubation was performed at 37°C for 10 min. Transcription products were recovered by ethanol precipitation with 25 μg of RNase-free glycogen (Boehringer Mannheim) as a carrier, and the precipitate was washed once with 70% ethanol, air dried and resuspended in 50 μl of diethyl pyrocarbonate-treated water.

In situ hybridization analysis

Serial 3-μm-thick sections were deparaffinized, dehydrated and incubated with 3 mg/ml of proteinase K (Boehringer Mannheim) in 10 mM Tris-HCl (pH 8.0) and 1 mM ethylenediaminetetraacetate (EDTA) for 10 min at 37°C. Following proteinase K treatment, the sections were fixed with 4% paraformaldehyde in 0.1 M sodium phosphate buffer and were washed once with 0.1 M phosphate buffer (PB) and equilibrated with 0.1 triethanolamine-HCl buffer

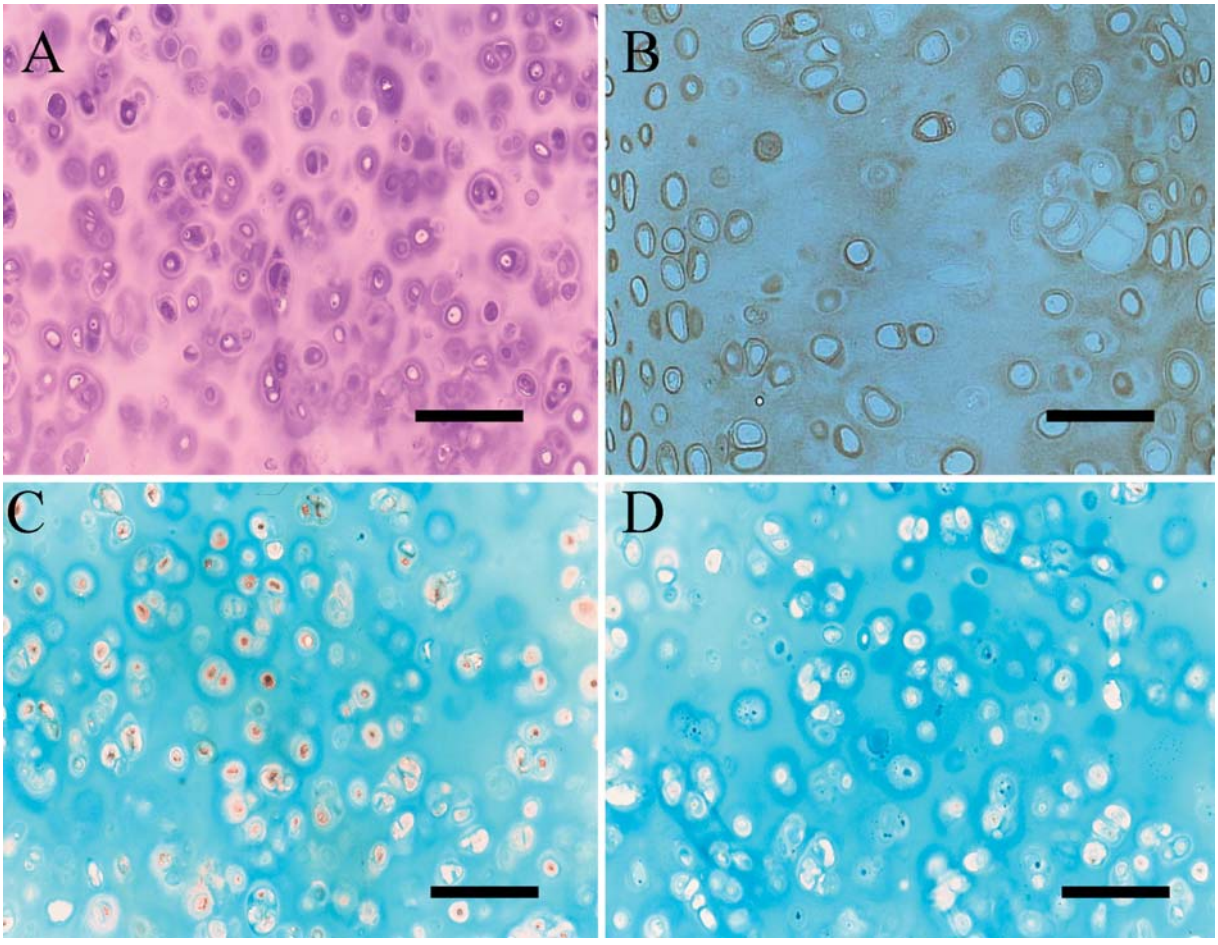

Fig. 1 **A** Typical histology of the normal bronchial cartilage. *Scale bar*=150 μm (hematoxylin and eosin staining ×150). **B** Moderate to strong immunoreactivity for chondromodulin-I (ChM-I) was observed in the inter-territorial regions around the lacunae of the bronchial cartilage. *Scale bar*=150 μm (immunostaining ×150). **C** Strong signals for ChM-I mRNA were observed in the cytoplasm of the chondrocytes of the bronchial cartilage. *Scale bar*=150 μm (in situ hybridization with anti-sense probe ×150). **D** No signals for ChM-I mRNA were seen in the chondrocytes using sense probe. *Scale bar*=150 μm (in situ hybridization with sense probe ×150)

Table 1 Cases of pleomorphic adenoma

Tubulo-glandular structures		Mesenchyme-like structures			
Inner cells	Outer cells*	Fibrous	Hyaline	Myxoid	Chondroid
21/25 (84.0%)	25/25 (100%)	13/25 (52.0%)	10/25 (40.0%)	22/25 (88.0%)	17/25 (68.0%)

* Outer cells included sheet-like structures and solid nests of neoplastic myoepithelial cells

(pH 8.0) for 2 min. Acetylation of the sections was performed by incubating with freshly prepared 0.25% acetic unhydride in 0.1 M triethanolamine-HCl buffer (pH 8.0) for 10 min at room temperature. After acetylation, sections were dehydrated by passage through 0.1 M PB and 70, 80, 90 and 100% ethanol twice for 15 s each, air dried. They were used for hybridization within 3 h. The hybridization solution contained 50% deionized formamide, 10% dextran sulfate, 1×Denhardt solution, 600 mM NaCl, 0.25% sodium dodecyl sulfate, 250 μl per μl of E. coli tRNA (proteinase treated), 10 mM DTT (dithiothreitol) and 0.1–2.0 mg/ml of digoxigenin-UTP-labeled RNA probe. The probe was diluted by hybridization solution and incubated at 85°C for 3 min. Hybridization solution was then placed on the sections, which were then covered by parafilm and incubated at 50°C for 16 h in a moisture chamber saturated with 50% formamide. After hybridization, the parafilm was dislodged with pre-incubated in 5×SSC (1×SSC=150 mM NaCl, 15 mM sodium citrate) at 50°C and then the slides were incubated with 50% formamide in 2×SSC for 30 min to remove the excess probe. The slides were incubated with 2×SSC and 0.2×SSC for 15 min twice at 50°C, respectively. For immunological detection, DIG nucleic acid detection kit (Roche) was used. The washed slides were incubated with DIG buffer 1 (100 mM Tris-HCl, pH 7.5, 150 mM NaCl) for 2 min and then with 1.5% blocking reagent in DIG buffer 1 for 60 min at room temperature. A diluted polyclonal sheep anti-digoxigenin Fab fragment (1:1000) in DIG buffer 1 was mounted on the sections and incubated for 30 min at room temperature. After immunoreaction, the slides were washed twice with DIG buffer 1 for 15 min and equilibrated with DIG buffer 3 (100 mM Tris-HCl, pH 9.5, 100 mM NaCl, 50 mM $MgCl_2$) for 3 min. Coloring solution containing 337.5 mg/ml of nitroblue

tetrazolium and 165.5 mg/ml of 5-bromo-4-chloro-3-indolylphosphate in DIG buffer 3 was mounted on the sections and incubated at room temperature until the signal–noise ratio was maximum. The reaction was stopped by rinsing the slides with 10 mM Tris-HCl, pH 8.0, 0.2 mM EDTA solution, and the slides were then mounted with counterstaining by methyl green. The controls included hybridization with sense probe. Neither anti-sense nor anti-digoxigenin antibody was used.

Results

Immunohistochemistry and in situ hybridization for ChM-I in the human bronchial cartilage

Moderate to strong immunoreactivity for ChM-I was observed in the inter-territorial regions around the lacunae of the cartilaginous tissues used as the positive control (Fig. 1B), whereas no immunoreactivity for ChM-I was seen in the negative controls: pre-absorption of the antibody with recombinant human ChM-I protein completely abolished immunoreactivity for ChM-I, and no staining was seen in the negative controls, in which the primary antibody was replaced with normal rabbit serum or PBS.

On in situ hybridization with anti-sense probe, strong signals for ChM-I mRNA were detected in the cytoplasm of the chondrocytes of the bronchial cartilages using this probe as the positive control, whereas no signals for ChM-I mRNA were seen in the bronchial cartilages using sense probe as the negative control or in the absence of anti-sense probe or the antibody (Fig. 1C, D). Therefore, this anti-sense probe is specific for ChM-I mRNA expression in our in situ hybridization system.

Immunohistochemistry for ChM-I and neoplastic myoepithelial cell markers in salivary pleomorphic adenomas

The results of immunohistochemical and in situ hybridization analysis in paraffin-embedded specimens are summarized in Table 2. Moderate immunoreactivity for ChM-I was observed in the cytoplasm of neoplastic myoepithelial cells in the myxoid elements (Fig. 2A) of pleomorphic adenomas (36.0%), while weak immunoreactivity was seen in the myxoid stroma (Fig. 2B). Almost all neoplastic myoepithelial cells, which exhibited the spindle-shaped appearance, in the myxoid elements of this type of tumor were positive for α-smooth muscle actin but negative for S-100 protein. Strong immunoreactivity for ChM-I was observed in the chondroid matrix (Fig. 2D), especially around the lacunae, in salivary pleomorphic adenomas (100%) (Fig. 2E). The lacuna cells of chondroid elements were positive for S-100 protein but negative for α-smooth muscle actin. Immunoreactivity for ChM-I was detected in neither fibrous nor hyaline stroma (0%, 0%) and, moreover, no immunoreactivity was seen in the normal salivary glands (data not shown).

In situ hybridization analysis for ChM-I in salivary pleomorphic adenomas

Ten typical cases of pleomorphic adenoma were chosen for in situ hybridization analysis. On in situ hybridization analysis with anti-sense probe, strong signals for ChM-I mRNA were detected in the cytoplasm of lacuna cells of chondroid elements of salivary pleomorphic adenomas, whereas moderate to strong signals for ChM-I mRNA were also observed in the cytoplasm of spindle-shaped neoplastic myoepithelial cells of myxoid elements (Fig. 2C, F) (Table 2). In a few cases, weak signals for ChM-I mRNA were seen in the neoplastic myoepithelial cells of hyaline elements of salivary pleomorphic adenomas and also in the periphery of the solid growth nests by outer cells. No signals for ChM-I mRNA were seen in the normal salivary glands, and no signals were seen in the negative controls using sense probe or in the absence of anti-sense probe or the antibody (data not shown).

Discussion

Pleomorphic adenoma of the salivary glands, the most frequent type of benign tumor, is considered as an epithelial tumor. We reported that, although FGF-2, a strong angiogenic factor [2, 5, 20], was expressed in pleomorphic adenoma, it was a hypovascular tumor due to the low

Table 2 Positivity and intensity for chondromodulin-I (ChM-I) immunohistochemistry and in situ hybridization analyses in salivary pleomorphic adenomas. *ASMA* α-smooth muscle actin, *IHC* immunohistochemistry, *ISH* in situ hybridization analysis,— no expression, + weak expression, ++ moderate expression, +++ strong expression

	Tubulo-glandular structures		Mesenchyme-like structures			
	Inner cells	Outer cells	Fibrous	Hyaline	Myxoid	Chondroid
ChM-I (IHC)	0/21(0%) —	0/25(0%) —	0/13(0%) —	0/10(0%) —	8/22(36%) ++	17/17(100%) +++
ASMA	0/21(0%) —	0/23(92%) —	10/13(77%) ++	17/22(77%) ++	7/10(70%) +++	0/17(0%) —
S-100 protein	13/21(62%) +	13/23(52%) ++	7/13(54%) ++	7/10(70%) +	3/22(14%) +	16/17(94%) +++
ChM-I (ISH)	0/10(0%) —	1/10(10%) ++	0/13(0%) —	1/10(10%) ++	10/10(100%) +++	10/10(100%) +++

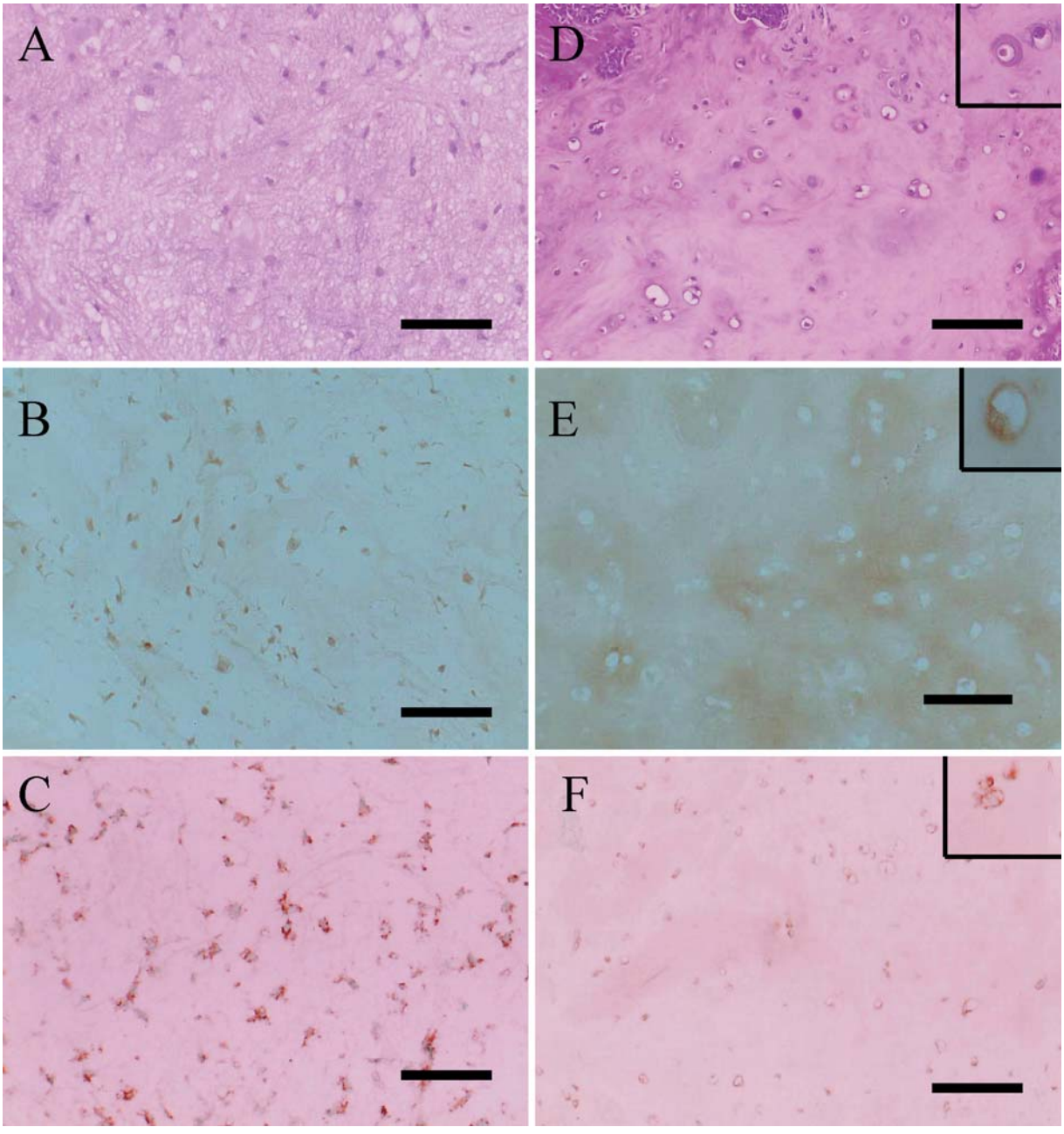

Fig. 2 **A** Typical histology of the myxoid regions of the pleomorphic adenomas. *Scale bar*=150 μm [hematoxylin and eosin (HE) staining ×150]. **B** Moderate immunoreactivity for chondromodulin-I (ChM-I) was seen in the cytoplasm of the spindle-shaped neoplastic myoepithelial cells in the myxoid regions of the pleomorphic adenomas. *Scale bar*=150 μm (immunostaining ×150). **C** Moderate to strong signals for ChM-I mRNA were observed in the cytoplasm of the spindle-shaped neoplastic myoepithelial cells of the myxoid regions of the pleomorphic adenomas. *Scale bar*=150 μm (in situ hybridization with anti-sense probe ×150). **D** Typical histology of the chondroid regions of pleomorphic adenomas. *Scale bar*=150 μm (HE staining ×150) *Inset* note the lacuna cell in the chondroid regions (HE staining ×400). **E** Strong immunoreactivity for ChM-I was observed in the chondroid matrix in the pleomorphic adenomas. *Scale bar*=150 μm (immunostaining ×150) *Inset* note the immunoreactivity for ChM-I was seen, especially, around the lacunae of the lacuna cells (immunostaining ×400). **F** Strong signals for ChM-I mRNA were detected in the cytoplasm of the lacuna cells of the chondroid regions of the pleomorphic adenomas. *Scale bar*=150 μm (in situ hybridization with anti-sense probe: ×150) *Inset* note the signals for ChM-I was seen in the lacuna cells (in situ hybridization with anti-sense probe ×400)

density of CD34-positive endothelial cells [14, 16]. Vascular endothelial cell growth factor (VEGF)-A was also expressed in the lacuna cells of the chondroid elements of pleomorphic adenomas (K. Kusafuka; unpublished data). We, therefore, thought that some strong angio-inhibitors should be present in pleomorphic adenomas, and a good candidate was ChM-I, a 25-kd glycoprotein purified from bovine epiphyseal cartilage [19], which has been identi-

fied as a novel endothelial cell growth inhibitor [8, 9]. ChM-I was reported to inhibit DNA synthesis and tube morphogenesis of cultured vascular endothelial cells in vitro, but this molecule stimulated DNA synthesis and proteoglycan synthesis in cultured growth plate chondrocytes in vitro [11, 19]. ChM-I is a glycoprotein of 121 amino acid residues and is encoded as the C-terminal portion of a large precursor (335 amino acids) [7]. Mature ChM-I is secreted from chondrocytes after proteolytic cleavage by a precursor-endopeptidase, furin [1, 6, 11]. In situ hybridization analysis indicated that ChM-I mRNA was expressed in the proliferating to upper hypertrophic chondrocytes in the growth plate of the long bones, but the expression of the gene was reduced in the lower hypertrophic and calcifying zones, allowing vascular invasion [21]. We demonstrated that angiogenic factors, FGF-2 and VEGF-A, were immunolocalized in the cytoplasm of lacuna cells of chondroid areas of salivary pleomorphic adenomas [14] (K. Kusafuka; unpublished data) but that ChM-I as an anti-angiogenic factor was immunolocalized in the inter-territorial spaces, especially around the lacunae, of the chondroid matrix in this type of tumor [16]. These findings suggest that mature ChM-I protein serves as a barrier against angiogenic property by FGF-2 or VEGF-A in salivary pleomorphic adenomas. In the present study, we have confirmed the immunolocalization pattern of ChM-I protein in salivary pleomorphic adenomas: ChM-I protein accumulated in the inter-territorial spaces around the lacunae of the cartilage matrix as well as the cartilage matrix itself, and this matrix molecule was also immunolocalized in the cytoplasm of the spindle-shaped neoplastic myoepithelial cells in the myxoid area. These results are similar to those of our previous immunohistochemical study [16]. In the present study, ChM-I mRNA was also expressed in the lacuna cells of the chondroid area and in the spindle-shaped neoplastic myoepithelial cells of the myxoid area of salivary pleomorphic adenomas. Therefore, the phenotype of lacuna cells was considered to be similar to that of the proliferating chondrocytes to the upper hypertrophic chondrocytes in the growth plate of the long bones. We also reported that BMP-6, which is considered to be a marker of the hypertrophic chondrocytes in the endochondral ossification process, is expressed in the lacuna cells of chondroid areas of salivary pleomorphic adenoma [15]. Taken together, the phenotype of lacuna cells was similar to that of the mature to upper hypertrophic chondrocytes of growth plate of the long bones. The spindle-shaped neoplastic myoepithelial cells of the myxoid area, which were positive for α-smooth muscle actin but negative for S-100 protein, expressed ChM-I mRNA. This finding suggests that some populations of neoplastic myoepithelial cells in the myxoid area are precursor cells with the chondrocyte-like phenotype. Recently, we reported that cartilage-derived morphogenetic protein-1/growth differentiation factor (GDF)-5, which is one of the BMP subfamily cloned from neonatal calf cartilage and which plays an important role in acceleration of the numbers of chondro-progenitor cells in the fetal long bones, was immunolocalized in the cytoplasm of cuboidal neoplastic myoepithelial cells around the chondroid area of a few cases of salivary pleomorphic adenomas [17]. We speculate that the cuboidal-shaped neoplastic myoepithelial cells are more similar to lacuna cells of the chondroid area than the spindle-shaped neoplastic myoepithelial cells. In the present study, however, we could not detect any expression of ChM-I mRNA in the cuboidal-shaped neoplastic myoepithelial cells near the chondroid areas.

In conclusion, pleomorphic adenoma expressed cartilage-specific matrix protein ChM-I protein and mRNA in the spindle-shaped neoplastic myoepithelial cells of the myxoid and in the lacuna cells of the chondroid areas. This molecule may play important roles in the chondroid formation and hypovascularity in salivary pleomorphic adenomas.

Acknowledgements We thank Mr. S. Sekiguchi, Mr. K. Wakamatsu, Mr. S. Hashimoto, Mr. A. Niizeki, Mr. E. Shimada and Ms. Y. Komatsuzaki from the Department of Pathology, Japanese Red Cross Medical Center, Tokyo, Japan, for their technical assistance. We are also grateful to Mr. T. Yoshizawa of Photo Studio, Tokyo Medical and Dental University, Tokyo, Japan, for his excellent microphotography. This work is supported by a grant from the "Science Frontier" program of the Ministry of Education, Culture, Sports, Science and Technology, a grant from Otsuka Pharmaceutical Co., Ltd. and a grant from Japan Immunoresearch Laboratories Co., Ltd. (JIMRO). The authors thank Mr. Hilary Eastwick-Field and Ms. K. Ando for their help in the preparation of this manuscript.

References

1. Azizan A, Holaday N, Naeme PJ (2001) Post-translational processing of bovine chondromodulin-I. J Biol Chem 276:23632–23638
2. Cordon-Cardo C, Vlodarsky I, Haimovitz-Friedman A, Hicklin D, Fuks Z (1990) Expression of basic fibroblast growth factor in normal human tissues. Lab Invest 63:832–884
3. Dardick I, Van Nostrand AWP, Jeans MTD, Rippstein P, Edward V (1983) Pleomoprhic adenoma. II: Ultrastructural organization of the "stromal regions." Hum Pathol 14:798–809
4. Erlandson RA, Cardon-Cardo D, Huggins PJ (1984) Histogenesis of benign pleomorphic adenoma (mixed tumor) of the major salivary glands. A ultrastructural and immunohistochemical study. Am J Surg Pathol 8:803–820
5. Folkman J, Klangsburn M (1969) Angiogenic factors. Science 235:442–447
6. Hatsuzawa K, Hosaka M, Nakagawa T, Nagase M, Shoda A, Murakami K, Nakayama K (1990) Structure and expression of mouse furin, a yeast Kex2-related protease. J Biol Chem 265:22075–22078
7. Hiraki Y, Tanaka H, Inoue H, Kondo J, Kamizono A, Suzuki F (1991) Molecular cloning of a new class of cartilage-specific matrix, chondromodulin-I which stimulates growth of cultured chondrocytes. Biochem Biophys Res Commun 175:971–977
8. Hiraki Y, Inoue H, Iyama K, Kamizono A, Ochiai M, Shukunami C, Iijima S, Suzuki F, Kondo J (1997) Identification of chondromodulin-I as a novel endothelial cell growth inhibitor; purification and its localization in the avascular zone of epiphyseal cartilage. J Biol Chem 272:32419–32426
9. Hiraki Y, Kono T, Sato M, Shukunami C, Kondo J (1997) Inhibition of DNA synthesis and tube morphogenesis of cultured vascular endothelial cells by chondromodulin-I. FEBS Lett 425:321–324

10. Hiraki Y, Mitsui K, Endo N, Takahashi K, Hayami T, Inoue H, Shukunami C, Tokunaga K, Kono T, Yamada M, Takahashi HE, Kondo J (1999) Molecular cloning of human chondromodulin-I, a cartilage-derived growth modulating factor, and its expression in Chinese hamster ovary cells. Eur J Biochem 260:869–878
11. Hosaka M, Nagahama M, Kim WS, Watanabe T, Hatsuzawa K, Ikemizu J, Mikami K, Nakayama K (1990) Arg-X-Lys/Arg-Arg motif as a signal for precursor cleavage catalyzed by furin within the constitutive secretory pathway. J Biol Chem 266:12127–12130
12. Kato Y, Iwamoto M (1990) Fibroblast growth factor is an inhibitor of chondrocyte terminal differentiation. J Biol Chem 265: 5903–5909
13. Kusafuka K, Yamaguchi A, Kayano T, Fujiwara M, Takemura T (1998) Expression of bone morphogenetic proteins in salivary pleomorphic adenomas. Virchows Arch 432:247–253
14. Kusafuka K, Yamaguchi A, Kayano T, Takemura T (1998) Immunohistochemical localization of fibroblast growth factors (FGFs) and FGF receptor-1 in human normal salivary glands and pleomorphic adenomas. J Oral Pathol Med 27:287–292
15. Kusafuka K, Yamaguchi A, Kayano T, Takemura T (1999) Immunohistochemical localization of bone morphogenetic protein-6 in salivary pleomorphic adenomas. Pathol Int 49:1023–1027
16. Kusafuka K, Hiraki Y, Shukunami C, Yamaguchi A, Kayano T, Takemura T (2001) Cartilage-specific matrix protein chondromodulin-I is associated with chondroid formation in salivary pleomorphic adenomas: immunohistochemical analysis. Am J Pathol 158:1465–1472
17. Kusafuka K, Luyten FP, De Bondt R, Hiraki Y, Shukunami C, Kayano T, Takemura T (2003) Immunohistochemical evaluation of cartilage-derived morphogenetic protein-1 and -2 in normal human salivary glands and pleomorphic adenomas. Virchows Arch 442:482–490
18. Mills SE, Cooper PH (1981) An ultrastructural study of cartilaginous zones and surrounding epithelium in mixed tumor of salivary glands and skin. Lab Invest 44:6–12
19. Mori Y, Hiraki Y, Shukunami C, Kakudo S, Shiokawa A, Kagoshima M, Man H, Hakeda Y, Kurokawa T, Suzuki F, Kumegawa M (1997) Stimulation of osteoblast proliferation by the cartilage-derived growth promoting factors chondromodulin-I and -II. FEBS Lett 406:310–314
20. Schultz-Osthoff K, Risau M, Vollmer E, Sorg C (1990) In situ detection of basic fibroblast growth factor by highly specific antibody. Am J Pathol 37:85–92
21. Shukunami C, Iyama K, Inoue H, Hiraki Y (1999) Spatiotemporal pattern of the mouse chondromodulin-I gene expression and its regulatory role in vascular invasion into cartilage during endochondral bone formation. Int J Dev Biol 43:39–49

Virchows Arch (2005) 446:41–45
DOI 10.1007/s00428-004-1142-x

ORIGINAL ARTICLE

R. Sedivy · K. Peters · G. Klöppel

Osteopontin expression in ductal adenocarcinomas and undifferentiated carcinomas of the pancreas

Received: 3 August 2004 / Accepted: 19 September 2004 / Published online: 26 November 2004
© Springer-Verlag 2004

Abstract Osteopontin (OPN) is a non-collagenous extracellular matrix protein with pleiotropic functions, including mediation of cell adhesion and migration. Recently, high OPN serum levels were found in pancreatic ductal adenocarcinomas (PDACs) in which OPN mRNA was identified in macrophages. We investigated OPN expression at the protein level in 15 PDACs and 10 undifferentiated pancreatic carcinomas (UCs), 4 of them with osteoclast-like giant cells (OCGCs), to find out whether the degree of OPN expression is related to tumor infiltration by macrophages and the adhesive capacity of tumor cells. With regard to its potential adhesive function, we compared OPN expression in PDACs and UCs with that of E-cadherin and β-catenin, two well-known adhesive molecules. OPN positivity was observed in two-thirds of PDACs (10/15) and in 7 UCs (7/10), including all 4 UCs with OCGCs. Apart from tumor cells, OPN was expressed in macrophages and OCGCs. When we assessed the relationship between the number of OPN-positive macrophages and tumor cells, we did not find any statistically significant correlation. There was also no correlation, either positive or negative, between OPN expression and E-cadherin and β-catenin expression. The results demonstrated that, in PDACs and UCs, OPN is expressed in both tumor-associated macrophages and tumor cells. The biological significance of this dual expression pattern is not yet known. It is, however, unlikely that OPN has an adhesive function, since its expression pattern differs distinctly from that of E-cadherin or β-catenin.

R. Sedivy (✉)
Department of Pathology,
Medical University Vienna,
Währinger Gürtel 18-20, 1090 Vienna, Austria
e-mail: roland.sedivy@meduniwien.ac.at
Tel.: +43-1-404003646

K. Peters · G. Klöppel
Department of Pathology,
University of Kiel,
Germany

Keywords Osteopontin · Pancreas · Carcinoma · E-cadherin · β-catenin

Introduction

Undifferentiated carcinomas (UCs) of the pancreas, which comprise 2–7% of all pancreatic exocrine tumors [10], are variants of pancreatic ductal adenocarcinoma (PDAC). They consist of bizarre, anaplastic cells and tumor giant cells lacking cohesion. Occasionally, UCs contain osteoclast-like giant cells (OCGCs), which represent a non-neoplastic cell population and stain for macrophage markers [21]. In a few instances, UCs with OCGCs may be found as a component of mucinous cystadenocarcinomas [18].

Osteopontin (OPN) is a non-collagenous phosphoprotein of the extracellular matrix with a molecular weight ranging from 36 kDa to 62 kDa [5]. OPN acts as a ligand of $\alpha_v\beta_3$ integrins and mediates cell adhesion and migration through its arginine-glycine-aspartate binding site [15]. It was originally isolated from bone and was found to be expressed in regular epithelium and macrophages [3, 4, 6, 8]. OPN expression has also been reported in various malignant tumors of epithelial and mesenchymal origin [1, 2, 7, 22], where it was detectable in both tumor cells and tumor-associated macrophages. OPN was found to be involved in adhesive interactions at the tumor/host interface. Acting as a ligand of $\alpha_v\beta_3$ integrins, OPN may contribute to tumor progression, thereby influencing the infiltrative and metastatic processes [2, 20].

In PDACs, oligonucleotide microarray studies revealed that OPN was overexpressed [9], and its serum levels were elevated in PDAC patients [11]. Although it has been shown that OPN mRNA is expressed in macrophages but not in PDAC tumor cells [11], it remains unclear where OPN is found at the protein level and how the protein expression pattern is related to the stromal infiltration by inflammatory cells, especially macrophages, and the differentiation of the tumor cells. We, therefore, recorded the immunohistochemical staining of

OPN in variously differentiated PDACs and also in UCs and attempted to correlate the OPN positivity in tumor cells with that of macrophages. Moreover, in view of OPN's potential function as a mediator of cell adhesion and migration, we investigated OPN expression in PDACs, which show cellular cohesiveness, and UCs, whose cells are dyscohesive [21]. We also compared the OPN expression pattern with those of E-cadherin and β-catenin, two important epithelial adhesion molecules, whose expression correlates with poor differentiation and prognosis [12].

Materials and methods

Surgical specimens

The study material comprised 25 cases, including 15 PDACs (7 well differentiated, 5 moderately, and 3 poorly), 6 UCs, and 4 UCs with OCGCs (2 associated with a mucinous cystadenocarcinoma). Paraffin-embedded tissue that had been collected during the period from 1985 to 2002 was retrieved from the files of the Departments of Pathology of the University of Kiel and the Medical University of Vienna. The age of the patients ranged from 39 years to 79 years. Of the patients, 17 were males, and 8 patients were females.

Immunohistochemistry

The tumor tissue was fixed in 10% formalin and embedded in paraffin. Serial sections (3-μm thick) were used for hematoxylin and eosin staining and immunohistochemistry. Slides were stained by the streptavidin-biotinylated peroxidase complex method utilizing primary antibodies raised against human osteopontin (1:30; clone 10A16, Immuno-Biological Laboratories Co., Ltd., Gunma, Japan), E-cadherin (1:5; clone SH 78–7, Zymed, Berlin, Germany), β-catenin (1:250; clone CAT-5H10, Zymed), Ki-67 (1:20; clone MM1, Novocastra Lab., Newcastle, UK), CD68 (1:100; clone PGM-1, DakoCytomation, Glostrup, Denmark), and the pan-cytokeratin Lu-5 (1:250; ascites, Biomedical AG, Augst, Switzerland). For OPN positivity, percentages lower than 30% of the tumor cells were scored as "+", 30–60% as "2+", and above 60% as "3+". The relationship between OPN-positive tumor cells and macrophages (identified by their CD68 positivity on a subsequent section) was assessed semi-quantitatively by determining the percentage of positively stained tumor/inflammatory cells in relation to negative tumor cells within three high power fields.

Statistics

All correlations were calculated using Spearman's correlation test. A two-tailed $P<5\%$ was considered significant. For statistical calculations, SPSS software, version 10.0.7, was used.

Results

OPN was occasionally expressed in the apical portion of centroacinar cells and the cells of intralobular ducts in tumor-free, non-inflamed portions of the resected pancreatic specimens. The cells of the main pancreatic duct and the islets were negative. Goblet cells in the duodenal epithelium showed strong reactivity, whereas other enterocytes were negative. In tumor-free areas showing chronic inflammatory changes, OPN expression was found in the apical part of all centroacinar cells and in the main pancreatic duct and the cells of the secondary ducts. Occasionally, cells of intrainsular ductular structures [19] in large islets also expressed OPN. Only rare endocrine cells of the islets were positive. E-cadherin and β-catenin were localized at the basolateral cell membrane of all exocrine cells. Their expression decreased in areas with inflammation.

Table 1 Osteopontin, E-cadherin, and β-catenin expression in pancreatic ductal adenocarcinomas. − negative, + ≤30% cells stained positively, *2+* 30–60% positive cells, *3+* >60% cells positive

Cases	Grade	E-cadherin	β-catenin	Osteopontin
01	1	+	2+	+
02	1	2+	3+	+
03	1	2+	3+	−
04	1	+	+	+
05	1	3+	3+	+
06	1	3+	3+	+
07	1	2+	2+	+
08	2	+	+	−
09	2	+	+	−
10	2	+	2+	+
11	2	+	+	−
12	2	+	2+	−
13	3	2+	+	2+
14	3	+	2+	3+
15	3	+	2+	3+

In the three poorly differentiated (G3) PDACs, moderate to strong OPN reactivity was found (Table 1). OPN was weakly expressed in six well-differentiated (G1) PDACs and in one moderately differentiated (G2) tumor (Fig. 1a). A predominantly apical, granular, and cytoplasmic staining pattern was seen. The remaining five cases (four G2 and one G1) were negative. In one case, perineurally infiltrating tumor cells showed a strong positive reaction, though most other tumor cells were negative for OPN. Tumor-associated macrophages were also strongly positive, regardless of whether they lay between the tumor glands or in the peritumoral area (Fig. 1b). A semi-quantitative assessment did not reveal any statistically significant correlation between the density of the tumor-associated OPN-positive macrophages and OPN-positive tumor cells. The extracellular matrix stained weakly to moderately in areas with high cellularity. Table 1 shows the E-cadherin and β-catenin expression. Both markers displayed membranous staining in most cases, while cytoplasmic staining was found only occasionally in poorly differentiated PDACs. The statistical calculations did not reveal any significant correlation between the grade of the PDAC and OPN expression.

Three UCs without OCGCs and all UCs with OCGCs showed cytoplasmic OPN expression (Table 2). One case revealed OPN positivity in tumor giant cells, in contrast to a negative reaction in all other tumor cells. The epithelial origin of these giant cells was confirmed by their negativity for the histiocytic marker CD68 and positivity for the pan-cytokeratin marker Lu-5. Tumor-associated macrophages were strongly positive for OPN in all cases.

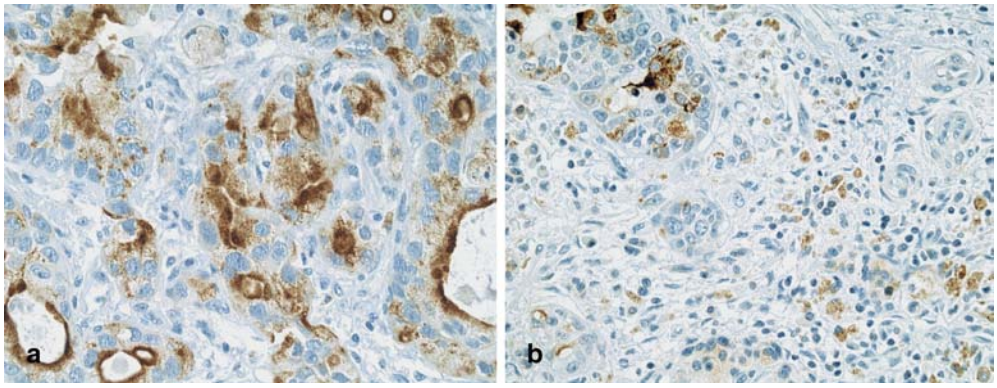

Fig. 1 Osteopontin expression in tumor cells (**A**) and tumor-associated macrophages (**B**) in pancreatic ductal adenocarcinomas

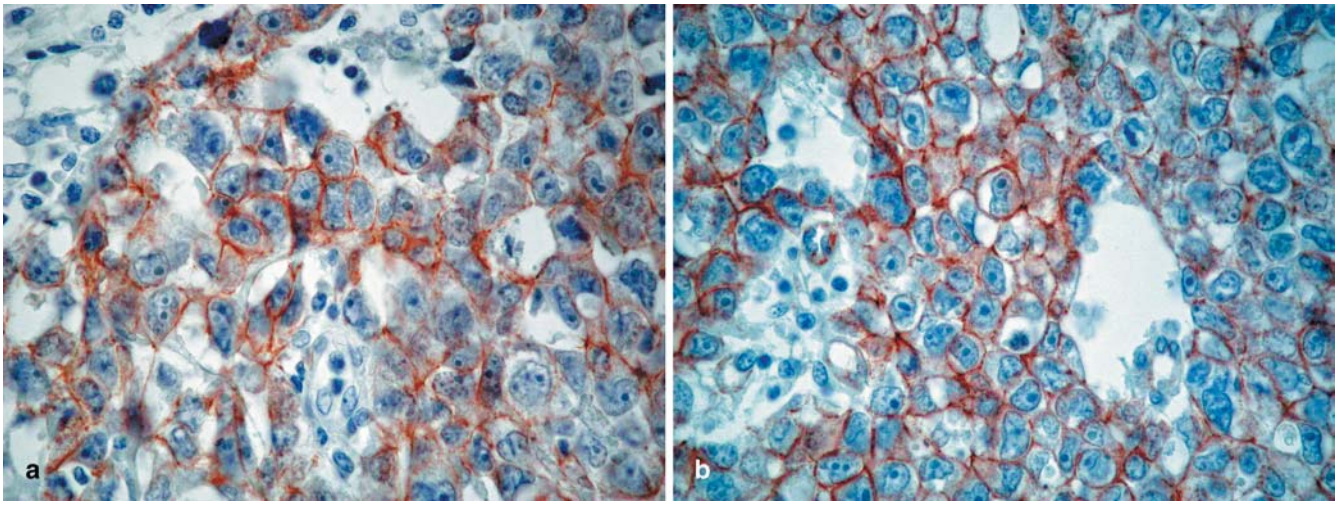

Fig. 2 E-cadherin (**A**), and β-catenin (**B**) expression in undifferentiated pancreatic carcinomas

Table 2 Immunohistochemical expression of osteopontin, E-cadherin, and β-catenin in undifferentiated carcinomas of the pancreas. – negative, + up to 30% cells stained positively, *2+* 30–60% positive cells, *3+* >60% cells stained positively. *UC* undifferentiated carcinoma, *OCGCs* osteoclast-like giant cells

Cases		E-cadherin	β-catenin	Osteopontin
Number	Diagnosis	Tumor cells		
01	UC	–	–	+
02	UC	–	–	–
03	UC	+	+	–
04	UC	3+	3+	–
05	UC	+	+	+#
06	UC	–	–	2+
07	UC (OCGCs)	– (–)	– (–)	+ (+)
08	UC (OCGCs)	– (–)	– (–)	3+ (3+)
09	UC (OCGCs)*	– (–)	+ (–)	2+ (2+)
10	UC (OCGCs)*	– (–)	+ (–)	3+ (+)

* UCs developed in mucinous cystadenocarcinoma components
\# Only in tumor giant cells

The extracellular tumor matrix expressed OPN only focally and weakly. The E-cadherin and β-catenin expression patterns were identical (Fig. 2). Two cases were aberrantly (non-membranous) positive for both markers; another case showed membranous expression. The remaining three UCs were negative. One case with weak E-cadherin and β-catenin expression also displayed a weak reaction with OPN (Table 2).

All UCs with OCGCs expressed OPN in the cytoplasm of most of the tumor cells. The OCGCs also expressed OPN (Fig. 3). The OPN-positive tumor cells co-expressed the pan-cytokeratin Lu-5. The mucinous epithelium of the two mucinous cystadenocarcinoma components did not react with OPN, whereas goblet-like cells stained strongly. E-cadherin was negative; whereas, β-catenin was weakly positive in two cases (Table 2).

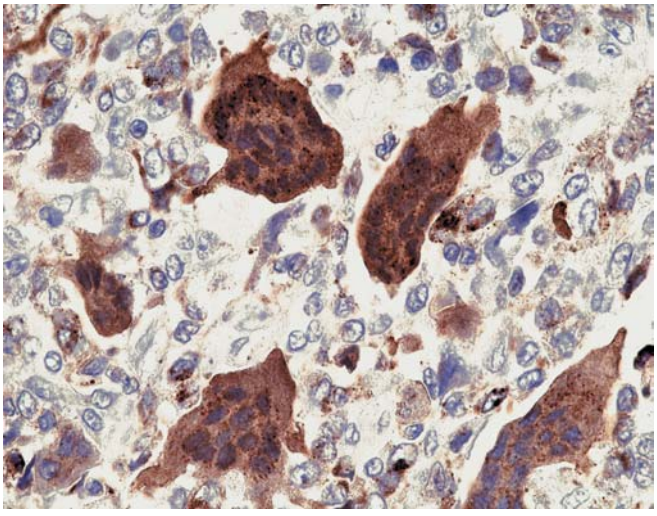

Fig. 3 Osteopontin expression in undifferentiated pancreatic carcinoma with osteoclast-like giant cells

Discussion

In this study of PDACs and UCs, we found OPN expression to be almost equal in the two malignancies (66% versus 70%). Apart from tumor cells, OPN was expressed in macrophages and OCGCs. Such a dual OPN expression has been reported in tumor cells and intermingled macrophages in cancers of the breast, lung, and gastrointestinal tract, including three pancreatic carcinomas [1, 2, 7]. Interestingly, OPN mRNA has not been detected thus far in tumor cells, including PDAC cells, though it has been to a remarkable degree in macrophages [11]. Only in cancers of the kidney and endometrium did both cell types reveal an elevated mRNA level. It was, therefore, suggested that macrophages are the main source of OPN, which is taken up secondarily by tumor cells [2]. In macrophages, the inflammatory cytokines interleukin-1 β and tumor necrosis factor-α appear to upregulate OPN expression [13]. Furthermore, OPN expression is elicited in response to pathological stimuli by various cell types, including endothelial cells, smooth-muscle cells [14], and T-lymphocytes [17], resulting in chemotaxis.

In our study, the assumption that the pancreatic carcinoma cells store OPN produced by the macrophages infiltrating the tumor seemed to be supported by the findings in the UCs with OCGCs, where both cell compartments were strongly positive for OPN. However, when we assessed the OPN expression in PDAC cells in relation to the density of associated OPN positive macrophages, there was no statistically significant correlation. This suggests that the conspicuous OPN expression pattern in UCs with OCGCs most likely does not reflect a general relationship between macrophages and tumor cells in pancreatic carcinomas, but is a special, so far unexplained, finding in UCs with OCGCs. Since OPN positivity has been described in multinucleated giant cells and epithelioid cells [16], the OCGCs' intense reactivity for OPN may be a feature of those macrophages that have been transformed into giant cells.

Recently, it was reported that serum OPN is useful as a diagnostic marker in patients with PDAC [11]. Provided that OPN is only produced and secreted by macrophages, this implies that PDAC might stimulate the secretion of OPN by tumor-associated macrophages. It would be interesting to know whether high OPN serum levels are observed, particularly in those PDACs in which the tumor cells also stain for OPN.

The OPN expression in the variously differentiated pancreatic carcinomas was heterogeneous. Well- and moderately differentiated PDACs expressed OPN only weakly, while poorly differentiated PDACs stained strongly for OPN. Among UCs, those without OCGCs showed weak OPN expression (except for one) and those with OCGCs revealed strong OPN expression. Because these findings do not reveal any clear relationship to the architectural differentiation in the carcinomas and, in particular, to the cohesiveness of the tumor cells, OPN most likely does not act as an adhesion molecule in these neoplasms.

To further evaluate the potential role of OPN as a tumor cell interface factor, we compared its expression with that of two known adhesion molecules, E-cadherin and β-catenin. We found that E-cadherin and β-catenin were rarely co-expressed with OPN in UCs. Only one case of UC and two cases of UC with OCGCs showed these markers simultaneously. As there was also no clear inverse correlation between aberrant or missing cadherin/catenin expression and positive OPN staining, the mechanisms leading to a loss of E-cadherin expression and to a change in β-catenin localization do not appear to be interrelated with those causing OPN expression.

In conclusion, OPN expression was found to varying degrees in PDACs and UCs, but its role in these tumors is poorly understood, because neither is there a clear correlation between OPN expression in macrophages and tumor cells nor is there an indication that it might act as an adhesion molecule.

References

1. Bellahcene A, Castronovo V (1995) Increased expression of osteonectin and osteopontin, two bone matrix proteins, in human breast cancer. Am J Pathol 146:95–100
2. Brown LF, Papadopoulos-Sergiou A, Berse B, Manseau EJ, Tognazzi K, Perruzzi CA, Dvorak HF, Senger DR (1994) Osteopontin expression and distribution in human carcinomas. Am J Pathol 145:610–623
3. Butler WT (1989) The nature and significance of osteopontin. Connect Tissue Res 23:123–126
4. Carlson I, Tognazzi K, Manseau EJ, Dvorak HF, Brown LF (1997) Osteopontin is strongly expressed by histiocytes in granulomas of diverse etiology. Lab Invest 77:103–108
5. Denhardt DT, Guo X (1993) Osteopontin: a protein with diverse functions. FASEB 7:1475–1482
6. Ellison JA, Barone FC, Feuerstein GZ (1999) Matrix remodeling after stroke. De novo expression of matrix proteins and integrin receptors. Ann N Y Acad Sci 890:204–222

7. Gaumann A, Petrow P, Mentzel T, Mayer E, Dahm M, Otto M, Kirkpatrick CJ, Kriegsmann J (2001) Osteopontin expression in primary sarcomas of the pulmonary artery. Virchows Arch 439:668–674
8. Giachelli CM, Lombardi D, Johnson RJ, Murry CE, Almeida M (1998) Evidence for a role of osteopontin in macrophage infiltration in response to pathological stimuli in vivo. Am J Pathol 152:353–358
9. Iacobuzio-Donahue CA, Ryu B, Hruban RH, Kern SE (2002) Exploring the host desmoplastic response to pancreatic carcinoma. Gene expression of stromal and neoplastic cells at the site of primary invasion. Am J Pathol 160:91–99
10. Klöppel G, Hruban RH, Longnecker D, Adler G, Kern S, Partanen T (2000) Ductal adenocarcinoma of the pancreas. Pathology and genetics of tumours of the digestive system. In: Hamilton S, Aaltonen L (eds) World Health Organisation Classification of Tumours. IARC Press, Lyon
11. Koopmann J, Fedarko NS, Jain A, Maitra A, Iacobuzio-Donahue C, Rahman A, Hruban RH, Yeo CJ, Goggins M (2004) Evaluation of osteopontin as biomarker for pancreatic adenocarcinoma. Cancer Epidemiol Biomarkers Prev 13:487–491
12. Li YJ, Ji XR (2003) Relationship between expression of E-cadherin-catenin complex and clinicopathologic characteristics of pancreatic cancer. World J Gastroenterol 9:368–372
13. Miyazaki Y, Tashiro T, Higuchi Y, Setoguchi M, Yamamoto S, Nagai H, Nasu M, Vassalli P (1995) Expression of osteopontin in a macrophage cell line and in transgenic mice with pulmonary fibrosis resulting from the lung expression of a tumor necrosis factor-alpha transgene. Ann N Y Acad Sci 760:334–341
14. O'Brien ER, Garvin MR, Stewart DK, Hinohara T, Simpson JB, Schwartz SM, Giachelli CM (1994) Osteopontin is synthesized by macrophage, smooth muscle, and endothelial cells in primary and restenotic human coronary atherosclerotic plaques. Arterioscler Thromb 14:1648–1656
15. Oldberg A, Franzen A, Heinegard D (1986) Cloning and sequence analysis of rat bone sialoprotein (osteopontin) cDNA reveals an Arg-Gly-Asp cell-binding sequence. Proc Natl Acad Sci U S A 83:8819–23
16. O'Regan A, Berman JS (2000) Osteopontin: a key cytokine in cell-mediated and granulomatous inflammation. Int J Exp Pathol 81:373–390
17. Patarca R, Saavedra RA, Cantor H (1993) Molecular and cellular basis of genetic resistance to bacterial infection: the role of the early T-lymphocyte activation-1/osteopontin gene. Crit Rev Immunol 13:225–246
18. Posen JA (1981) Giant cell tumor of the pancreas of the osteoclastic type associated with a mucous secreting cystadenocarcinoma. Hum Pathol 12:944–947
19. Pour PM, Pandey KK, Batra SK (2003) What is the origin of pancreatic adenocarcinoma? Mol Cancer 2:13–23
20. Rittling SR, Chambers AF (2004) Role of osteopontin in tumour progression. Br J Cancer 90:1877–1881
21. Solcia E, Capella C, Klöppel G (1997) Tumors of the pancreas. Atlas of Tumor Pathology. Armed Forces Institute of Pathology, Washington, DC
22. Sulzbacher I, Birner P, Trieb K, Lang S, Chott A (2002) Expression of osteopontin and vascular endothelial growth factor in benign and malignant bone tumors. Virchows Arch 441:345–349

Virchows Arch (2005) 446:46–51
DOI 10.1007/s00428-004-1123-0

ORIGINAL ARTICLE

Carmen Carda · Jaime Ferrer · Marien Vilanova · Amando Peydró · Antonio Llombart-Bosch

Anaplastic carcinoma of the thyroid with rhabdomyosarcomatous differentiation: a report of two cases

Received: 10 June 2004 / Accepted: 19 August 2004 / Published online: 29 October 2004
© Springer-Verlag 2004

Abstract Anaplastic carcinoma of the thyroid gland (ACT) is a highly malignant tumor that is almost invariably associated with a fatal outcome. It demonstrates a variety of peculiar histological features, with squamoid, giant cell and spindle cell growth patterns. The spindle cell variant of ACT is usually indistinguishable from a true sarcoma and it can simulate fibrosarcoma, malignant fibrous histiocytoma (MFH), hemangiopericytoma and angiosarcoma or rhabdomyosarcoma. Although a rhabdomyosarcomatous appearance has sometimes been mentioned in the literature, true skeletal muscle differentiation has never been consistently proved. We report two cases of ACT with rhabdomyosarcomatous differentiation, as demonstrated by means of immunohistochemistry and electron microscopy. Both cases disclosed a very similar histological appearance, with a main population of small, pleomorphic, round-to-oval cells arranged in a storiform pattern, admixed with scattered pleomorphic giant cells, an image similar to that of the usual type of MFH. Stains for epithelial markers showed only few, scattered, weakly positive cells. Thyroglobulin and calcitonin were negative in tumor cells in both cases. On the contrary, positivity to vimentin was strong and generalized. Immunomarkers of muscular differentiation showed a consistent positivity. At the ultrastructural level, the cells disclosed the same spindle and pleomorphic morphology, with large, bizarre nuclei and cytoplasm with abundant mitochondria, rough endoplasmic reticulum, secretory granules and lipid droplets. There were also cells with wide cytoplasm filled with filamentous material, either of actin or myosin, as well as Z-band material. In conclusion, the cases reported here show a clear-cut rhabdomyosarcomatous differentiation of ACT, confirmed both immunohistochemically and ultrastructurally, a feature not previously reported in the literature. These findings may contribute to the broadening of the differentiation spectrum of this unusual neoplasm.

Keywords Anaplastic carcinoma thyroid · Rhabdomyosarcomatous differentiation · Immunohistochemistry · Electron microscopy

C. Carda (✉) · J. Ferrer · M. Vilanova · A. Peydró · A. Llombart-Bosch
Department Pathology, Faculty of Medicine,
University of Valencia,
Av. Blasco Ibañez 17, 46010 Valencia, Spain
e-mail: carmen.carda@uv.es
Tel.: +96-386-8891
Fax: +96-386-4175

Introduction

Anaplastic (undifferentiated) carcinoma of the thyroid gland (ACT) is a highly malignant tumor that is almost invariably associated with a fatal outcome [3, 7, 16, 17, 26]. It demonstrates a variety of peculiar histological features, with squamoid, giant cell and spindle cell growth patterns [1, 3].

From the morphological point of view, the spindle cell variant of ACT is indistinguishable from a true sarcoma. Thus, ACT can simulate fibrosarcoma, malignant fibrous histiocytoma (MFH), hemangiopericytoma, angiosarcoma or rhabdomyosarcoma [8, 21, 22]. However, the presence of recognizable epithelial foci, immunohistochemical positivity for keratins and the ultrastructural presence of desmosomes and microvilli favor the diagnosis of an epithelial malignancy [1, 2, 10, 12, 14, 18, 19, 23].

Although a rhabdomyosarcomatous appearance has sometimes been mentioned in the literature [3, 17], true skeletal muscle differentiation has never been consistently proved. We report the first two cases of ACT with rhabdomyosarcomatous differentiation, as demonstrated by means of immunohistochemistry and electron microscopy.

Case reports

Case 1

A 59-year-old man with a personal history of heavy smoking and alcohol abuse was admitted to hospital because of a rapidly

growing neck mass, which had developed during the previous 3 months and was accompanied by dysphony and weight loss. Physical examination disclosed paralysis of the left recurrent nerve. A computerized axial tomography was performed, revealing the existence of a thyroid tumor invading the retrotracheal region. A right hemithyroidectomy was carried out, together with partial esophageal resection and pharingo-jejunostomy. Following surgery, the patient received radiation therapy (linear accelerator 18 Mv photons). A later computerized axial tomography demonstrated bilateral pulmonary metastases. The patient then received chemotherapy, but he developed a progressive respiratory distress and died 15 months after diagnosis and surgery. Autopsy was not allowed.

Case 2

A 62-year-old man with no interesting clinical history presented a rapidly enlarging mass in the left anterior cervical region. On physical examination, the tumor was nut-sized and apparently confined within the thyroid. A few days later, the patient suffered a sudden growth in the anterior region of his neck, together with severe hoarseness. A fine-needle aspiration biopsy was performed, followed by a total thyroidectomy and tracheostomy. The early postoperative period was satisfactory, with no remarkable event. After surgery, I^{131} gammagraphy was carried out, demonstrating cervical thyroid remnants. Chest radiography, hepatic ultrasonography and bone gammagraphy were negative. The patient was initially given radiotherapy, but after a few weeks he was lost for treatment and follow-up.

Materials and methods

After fixation of the surgical specimens in 10% formaldehyde solution, tissue samples were taken from different areas and embedded in paraffin. Multiple 3-μm sections were obtained by means of a standard microtome and then stained with haematoxylin and eosin. Immunohistochemistry was performed using paraffin-embedded material and the avidinbiotin-peroxidase technique. The antisera employed and their working dilution are shown in Table 1.

For electron microscopy examination, fresh specimens were fixed in 2.5% glutaraldehyde solution (buffered pH 7.4) and postfixed in 2% osmium tetroxide. After dehydration, the tissue blocks were embedded in Epon 812 (TAAB Lab, England). Ultrathin sections were stained with uranyl acetate and lead citrate, and examined under a Jeol-Jem 1010 electron microscope (Tokyo, Japan).

Results

Both cases disclosed a very similar histological appearance, with a large population of small, pleomorphic, round-to-oval cells arranged in a storiform pattern, admixed with scattered pleomorphic giant cells, an image similar to that of the usual type of MFH. In some areas, the small cells adopted a spindle cell configuration, with fascicles and bundles reminiscent of fibrosarcoma (Fig. 1a).

The small cells revealed a scant, pale cytoplasm, which was occasionally more prominent, giving the cell a rhabdomyoblast-like appearance. On the cell, however, no cross-striations were seen. The nuclei were irregular and showed prominent nucleoli. The pleomorphic giant cells were mono- and multinucleated, with bizarre, hyperchromatic nuclei and a wide, acidophilic, sometimes slightly granular cytoplasm. They were more abundant in case 2 (Fig. 1b). Atypical mitotic figures were frequent, reaching 18 mitoses per 10 high power fields (HPF) in case 1. Necrotic areas were prominent in both cases, often surrounded by a palisading of tumor cells. Both tumors showed a marked vascularization, the vessels sometimes adopting a branched pattern, similar to that of hemangiopericytoma. Pseudovascular channels, caused by artifactual retraction of tumor cells, were also seen in some areas. A diagnosis of anaplastic carcinoma was given in each case.

Both tumors grew in a markedly aggressive manner, substituting and entrapping the follicular parenchyma of the thyroid and invading the neighboring cervical structures, spreading into the skeletal muscles of the neck. Case 2 reached the esophageal wall, the tumor ulcerating the mucosa and forming an exophitically protruding mass.

Immunohistochemical results for epithelial markers (cytokeratin AE1/AE3 and CAM 5.2 cocktails, EMA) showed only few, scattered, weakly positive cells. The number of cells stained was not significantly different with any of these markers, which only showed strong reactivity in the entrapped thyroid follicles. Thyroglobulin and calcitonin were negative in tumor cells in both cases.

However, positivity to vimentin was strong and generalized. Immunomarkers of muscular differentiation showed a consistent positivity (Fig. 1c–h): muscle-specific actin (HHF35) was expressed by a large number of cells in case 1, in the form of islets of positive cells;

Table 1 List of primary antibodies used in immunohistochemistry

Antibody	Clone	Dilution	Source
CK	AE1 and AE3	1/50	DakoCytomation
CK 5.2	5D3	1/50	Novocastra
EMA	E29	1/200	DakoCytomation
Thyroglobulin	Polyclonal	1/500	DakoCytomation
Calcitonin	Polyclonal	1/500	DakoCytomation
Vimentin	V9	1/50	Novocastra
Muscle-specific actin	1A4	1/50	Biogenex
Desmin	DE-R-11	1/100	DakoCytomation
Smooth-muscle actin	1A4	1/50	DakoCytomation
Myoglobin	Polyclonal	1/200	DakoCytomation
MyoD1	5.8A	1/100	Novocastra
Myogenin	M-225	1/50	Santacruz biotechnology
CD 68	KP1	1/50	DakoCytomation

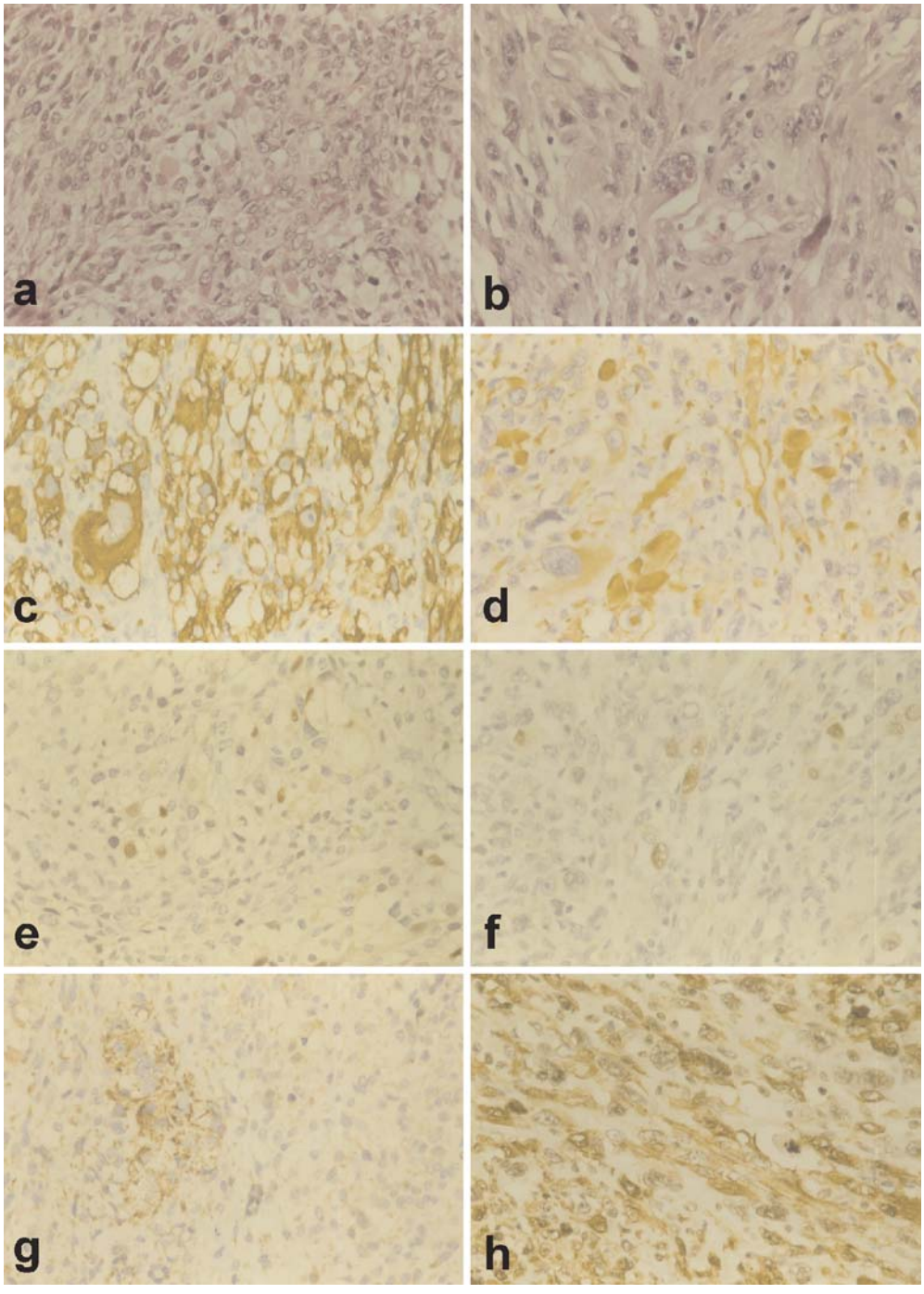

Fig. 1 Histological appearance and immunomarkers of muscular differentiation. **a** Round and oval cells in storiform pattern (case 1). **b** Pleomorphic cell population with small and giant cells (case 2). Muscle-specific actin (**c**; case 1), desmin (**d**; case 2), myogenin (**e**; case 1), myogenin (**f**; case 2), MyoD1 (**g**; case 1), smooth muscle actin (**h**; case 2)

whereas it reacted only focally in case 2. In contrast, desmin was more extensively expressed in case 2; myoglobin was widely positive in both cases; Myo-D1 showed clear nuclear positivity only in case 1 (staining less than 5% of tumor cells), with unspecific, scattered cytoplasmic reactivity in case 2; myogenin reacted against tumor cells in both cases, this reactivity being focal and more marked in case 1 (10–20% of tumor cells) than in case 2 (<5%); and, finally, smooth muscle actin was positive only in case 2, where it was expressed in a diffuse manner.

At the ultrastructural level, the cells disclosed the same spindle and pleomorphic morphology (Fig. 2c), with large, bizarre nuclei and cytoplasm with abundant mitochondria, rough endoplasmic reticulum and ribosomes, glycogen, lysosomes, secretory granules and lipid droplets (Fig. 2a). There were also cells with wide cytoplasm filled with filamentous material, either of actin (thin filaments) or myosin (thick filaments), as well as Z-band material (Fig. 2a, b). Rudimentary cell-to-cell junctions were found (Fig. 2c, inset).

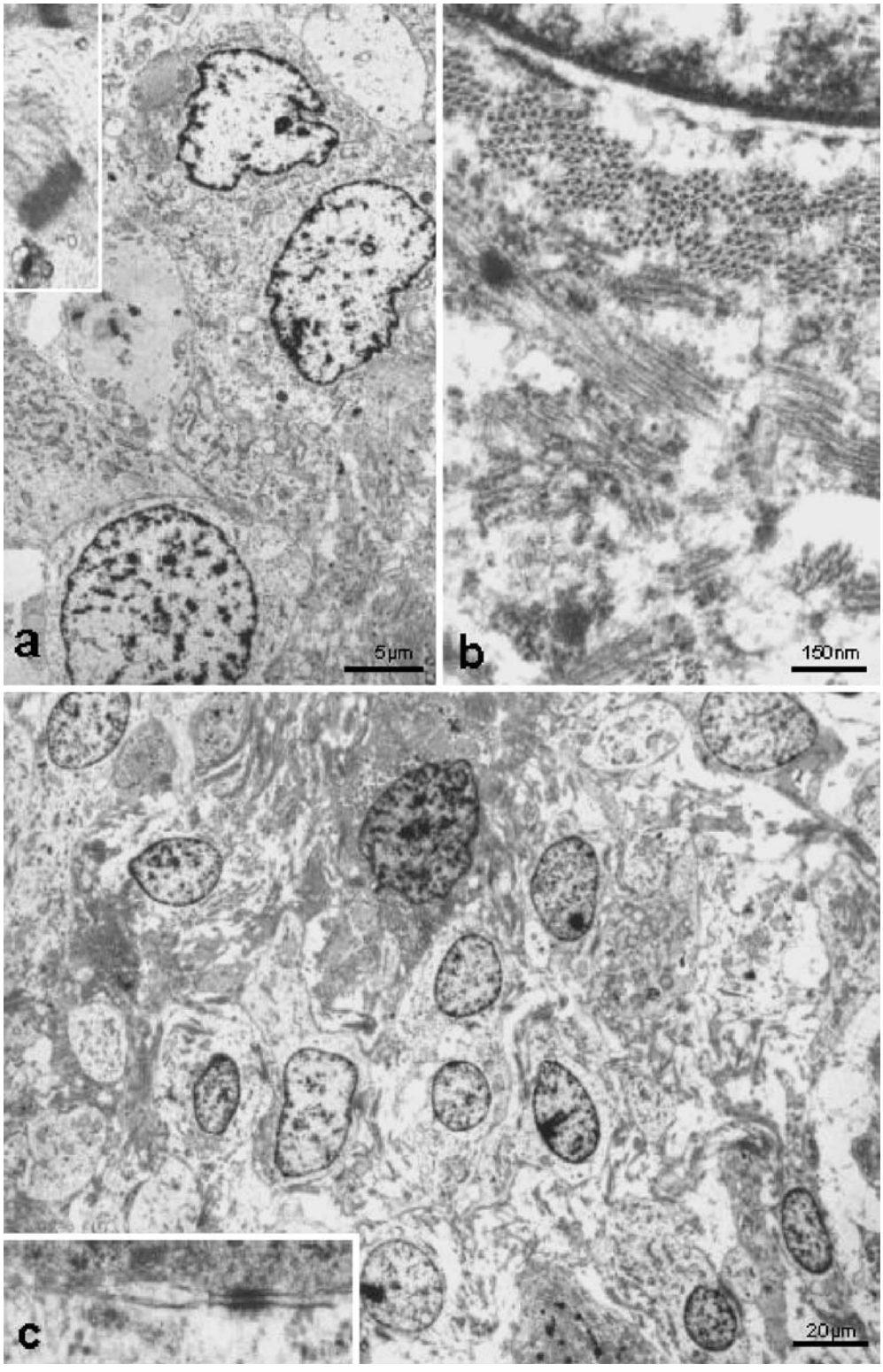

Fig. 2 Electron microscopic features. **a** Ultrastructural evidence of numerous organelles and myoblastic differentiation, thin filaments are placed randomly and with focal densities (*inset*; case 1). **b** Cross section showing thick and thin filaments, Z-band material and ribosomal complexes (case 2). **c** Tumor showing irregular cell size and nuclear shape with euchromatin, and isolated cell-to-cell junctions (*inset*; case 2)

Discussion

From the histological point of view, anaplastic thyroid tumors can resemble undifferentiated epithelial neoplasms or may be composed of spindle cells mimicking a sarcoma. The variety of peculiar histological features that characterize ACT has led to different morphological classifications, in which squamoid, giant cell and spindle cell growth patterns are the most accepted [3, 17, 26].

The spindle cell and pleomorphic variants of ACT are indistinguishable from a true sarcoma. In this sense, ACT has been repeatedly described as fibrosarcoma, malignant

fibrous histiocytoma, hemangiopericytoma, angiosarcoma or rhabdomyosarcoma [1, 3, 7, 8, 16, 17, 21, 22, 26]. However, the evidence of epithelial differentiation on an immunohistochemical and/or ultrastructural basis favors the diagnosis of an epithelial neoplasm [10, 11, 12, 13, 14, 15, 17, 18]. On the contrary, true sarcomas of the thyroid gland seem to be exceedingly unusual [3, 7, 16, 17, 26]. Altogether, this distinction appears rather academic, given the fact that both entities share a common clinical presentation and an almost invariably fatal outcome.

Despite the frequent notations of a rhabdomyosarcomatous appearance, no evidence of muscular differentiation has been consistently demonstrated. Some authors regard the pleomorphic variant of ACT as a mimicker of rhabdomyosarcoma, given the presence of spindle and pleomorphic cells arranged in a storiform pattern, often showing a wide, acidophilic cytoplasm [3, 17]. Nevertheless, neither immunoreactivity against muscular markers nor ultrastructural evidence of myogenic structures have been directly associated with this particular histological pattern of ACT. Isolated data of desmin expression [16] and ultrastructural presence of actin filaments [3] can be found in the literature, but they have not deserved any specific mention as indicative of skeletal or smooth muscle differentiation.

The cases reported here clearly showed skeletal muscle differentiation from the immunohistochemical point of view. First, the tumor cells of both cases reacted against muscle-specific actin and desmin, which are the most universally employed markers of myogenic commitment [20, 24, 25, 27, 28]. Desmin was more extensively expressed in case 2, but there was no doubt of its positivity in case 1, where well-defined islets of positive cells were seen. It has been shown, however, that actin and desmin can be expressed in different degrees by a variety of benign and malignant soft tissue tumors, thus making these two proteins not specific to muscle differentiation [24, 25]. Besides, muscle-specific actin can be seen (to a variable extent) in smooth muscle tumors—i.e., leyomiosarcoma, a malignancy also occurring in the thyroid gland [5, 13, 15, 29].

We also performed immunostaining against three specific skeletal muscle markers: myoglobin, Myo-D1 and myogenin. Care must be taken with the interpretation of the results using these antibodies, as has been frequently reported in the literature [4, 9]. This issue notwithstanding, we were able to demonstrate positivity to all three in the two cases studied. Myoglobin stained uniformly, clearly revealing the cytoplasms of tumor cells over a tea-colored background, a stain not attributable only to an edge-effect of the technique. Myo-D1 and myogenin are two myogenic transcriptional regulators, which appear to play a critical role in the commitment of mesenchymal progenitor cells to the myogenic cell line. These proteins are found in normal fetal muscle and are thought to be absent in adult muscle [6]. We found nuclear positivity against myogenin in both cases, although it was limited to a relatively small percentage of cells, which ranged from 5% to 20%. This variability has already been reported for the different subtypes of rhabdomyosarcoma, but it does not question the specificity of myogenin [4].

Ultrastructurally, there was a clear-cut skeletal muscle differentiation in both cases, defined by the presence of myofilaments and Z-bands in the cytoplasm of rhabdomyoblast-like tumor cells. Such definite structures have not been reported to date in ACT, despite an isolated mention to the existence of actin filaments [3]. Moreover, the cases reported here showed the mature form of myofilament disposition, i.e., thin filaments of actin surrounding a thick myosin filament. No ultrastructural features of smooth muscle differentiation were seen in any case, thus confirming the immunohistochemical expression of myogenic markers as corresponding to skeletal muscle.

The scarcely expressed epithelial phenotype finds correlation both immunohistochemically and ultrastructurally. The expression of cytokeratins was weak and focal, but mostly confined to rhabdomyoblast-like tumor cells. This feature has already been reported in ACT [19], and seems to correspond with the scarcity of epithelial differentiation as revealed by electron microscopy. In our cases, we could only find a few, rather rudimentary, desmosomes between some tumor cells, in the context of a loosely cohesive neoplastic population, most if not all undifferentiated carcinoma.

In conclusion, cases reported here show a clear-cut rhabdomyosarcomatous differentiation of ACT, confirmed both imunohistochemically and ultrastructurally, a feature not previously reported in the literature. These findings may contribute to the expansion of the spectrum of differentiation for this unusual neoplasm.

Acknowledgements This work was supported by FIS grant 01/0673.

References

1. Aldinger KA, Saaman NA, Ibáñez M (1978) Anaplastic carcinoma of the thyroid: a review of 84 cases of spindle and giant cell carcinoma. Cancer 41:2267–2275
2. Beltrami CA, Criante P, Di Loreto C (1989) Immunocytochemistry of anaplastic carcinoma of thyroid gland. Appl Pathol 7:122–133
3. Carcangiu ML, Steeper T, Zampi G, Rosai J (1984) Anaplastic thyroid carcinoma. A study of 70 cases. Am J Clin Pathol 83:135–158
4. Cessna MH, Zhou H, Perkins SL, Tripp SR, Layfield L, Daines C, Coffin CM (2001) Are myogenin and MyoD1 expression specific for rhabdomyosarcoma? A study of 150 cases, with emphasis on spindle cell mimics. Am J Surg Pathol 25:1150–1157
5. Chetty R, Clark SP, Dowling JP (1993) Leyomyosarcoma of the thyroid: immunohistochemical and ultrastructural study. Pathology 25:203–205
6. Dias P, Dilling M, Houghton P (1994) The molecular basis of skeletal muscle differentiation. Semin Diagn Pathol 11:3–14
7. Donnell CA, Pollock WJ, Sybers WA (1987) Thyroid carcinosarcoma. Arch Pathol Lab Med 11:1169–1172

8. Eusebi V, Carcangiu ML, Dina R (1990) Keratin-positive epithelioid angiosarcoma of the thyroid: a report of four cases. Am J Surg Pathol 14:737–747
9. Furlong MA, Mentzel T, Fanburg-Smith JC (2001) Pleomorphic rhabdomyosarcoma in adults: a clinicopathologic study of 38 cases with emphasis on morphologic variants and recent skeletal muscle-specific markers. Mod Pathol 14:595–603
10. Graham H, Daniel C (1974) Ultrastructure of an anaplastic carcinoma of the thyroid. Am J Clin Pathol 61:690–696
11. Hofstädter F (1980) Electron microscopic investigations about the differentiation of thyroid carcinoma. Pathol Res Pract 169:304–322
12. Hurlimann J, Gardiol D, Scazziga B (1987) Immunohistology of anaplastic thyroid carcinoma. A study of 43 cases. Histopathol 11:567–580
13. Iida Y, Katoh R, Yoshioka M, Oyama T, Kawaoi A (1993) Primary leyomyosarcoma of the thyroid gland. Acta Pathol Jpn 43:71–75
14. Jao W, Gould VE (1975) Ultrastructure of anaplastic (spindle and giant cell) carcinoma of the thyroid. Cancer 35:1280–1292
15. Kawahara E, Nakanishi I, Terahata S, Ikegaki S (1988) Leyomyosarcoma of the thyroid gland. A case report with comparative study of five cases of anaplastic carcinoma. Cancer 62:2558–2563
16. Lampertico P (1993) Anaplastic (sarcomatoid) carcinoma of the thyroid gland. Semin Diagn Pathol 10:159–168
17. LiVolsi VA (ed) (1990) Surgical pathology of the thyroid. In: Major problems in pathology, vol. 22. Saunders, Philadelphia, PA
18. LiVolsi VA, Brooks JJ, Arendash-Durand B (1987) Anaplastic thyroid tumors. Immunohistology. Am J Clin Pathol 87:434–442
19. Miettinen M, Franssila KO (2000) Variable expression of keratins and nearly uniform lack of thyroid transcription factor 1 in thyroid anaplastic carcinoma. Hum Pathol 31:1139–1145
20. Miettinen M, Lehto VP, Virtanen I (1984) Antibodies to intermediate filament proteins in the diagnosis and classification of human tumors. Ultrastruct Pathol 7:83–107
21. Mills SE, Stallings RG, Austin MB (1986) Angiomatoid carcinoma of the thyroid gland. Am J Clin Pathol 86:674–678
22. Ordóñez NG, Hickey RC, Samaan NA (1987) Anaplastic thyroid carcinoma. Cancer Bulletin 39:318–323
23. Ordóñez NG, El-Naggar AK, Hickey RC, Samaan NA (1991) Anaplastic thyroid carcinoma. Imunocytochemical study of 32 cases. Am J Clin Pathol 96:15–24
24. Rangdaeng S, Truong LD (1991) Comparative immunohistochemical staining for desmin and muscle-specific actin. A study of 576 cases. Am J Clin Pathol 96:32–45
25. Roholl PJ, Elbers HR, Prinsen R, Claessens JA, van Unnik JA (1990) Distribution of actin isoforms in sarcomas: an immunohistochemical study. Hum Pathol 21:1269–1274
26. Rosai J, Carcangiu ML, DeLellis RA (1992). Tumors of the thyroid gland (Atlas of tumor pathology). Armed Forces Institute of Pathology, Washington DC
27. Schürch W, Skalli O, Seemayer TA, Gabbiani G (1987) Intermediate filament proteins and acti isoforms as markers for soft tissue tumor differentiation and origin. I. Smooth muscle tumors. Am J Pathol 128:91–103
28. Skalli O, Gabbiani G, Babai F, Seemayer TA, Pizzolato G, Schürch W (1988) Intermediate filament proteins and acti isoforms as markers for soft tissue tumor differentiation and origin. II. Rhabdomyosarcomas. Am J Pathol 130:515–531
29. Thompson LDR, Wenig BM, Adair CF, Shmookler BM, Heffess CS (1997) Primary smooth muscle tumors of the thyroid gland. Cancer 79:579–587

Virchows Arch (2005) 446:52–55
DOI 10.1007/s00428-004-1147-5

ORIGINAL ARTICLE

Pao-Hsien Chu · Shih-Ming Jung · Ta-Sen Yeh · Hsin-Chiung Lin · Jaw-Ji Chu

MUC1, MUC2 and MUC5AC expressions in cardiac myxoma

Received: 27 June 2004 / Accepted: 19 September 2004 / Published online: 26 November 2004
© Springer-Verlag 2004

Abstract *Background.* Cardiac myxoma, the most common primary tumor of the heart, has a variable clinical presentation and immunohistochemical profile. An abundant mucopolysaccharidic matrix exists, including mucin, within cardiac myxoma. This investigation first reports the expressions of mucin genes in cardiac myxoma. *Methods.* A retrospective study was conducted between December 1976 and February 2003, comprising 101 consecutive patients with cardiac myxoma who were treated with surgical excision. Detailed clinical parameters also were reviewed. Mucin genes, namely MUC1, MUC2 and MUC5AC, were studied immunohistochemically in 47 randomly selected patients. *Results.* The study group contained 57 (57%) women and 44 (43%) men, with a mean age of 38±21 years. Their presentations included: asymptomatic (41%), dyspnea (35%), stroke (23%), chest pain (7%), fever (6%), syncope (5%) and tricuspid regurgitation (70%). The sample included 90 myxoma located in the left atrium, 3 (3%) recurrent myxoma and 8 (8%) myxoma not located in the left atrium. The myxoma did not differ with location or clinical event in terms of pathological scores, such as vascular proliferation, inflammation, cellularity, hyaline, calcification and thrombosis. Cardiac myxoma is characterized by excessive mucus secretion. Expression of membrane-associated MUC1 was considerably higher than that of the secreted mucins, MUC2 and MUC5AC ($P<0.05$). Furthermore, expression of MUC5AC is related to lesser embolism ($P<0.05$). *Conclusions.* This work first examined the immunohistochemical expression of mucin (MUC1, MUC2 and MUC5AC) in cardiac myxoma. This investigation then showed that the expression of representative membrane-associated mucin, MUC1, and/or secretory mucins, MUC2 and MUC5AC, in cardiac myxoma was associated with important tumor clinicopathological characteristics. Moreover, MUC5AC appears related to lesser embolism. This approach can help distinguish the potential roles of secretory mucins versus membrane-associated mucins in the development of cardiac myxoma.

Keywords Cardiac myxoma · Mucin genes · MUC1 · MUC2 · MUC5AC

P.-H. Chu (✉)
The First Cardiovascular Division,
Chang Gung Memorial Hospital, School of Medicine,
Chang Gung University,
199 Tun-Hwa North Road, 105 Taipei, Taiwan
e-mail: pchu@adm.cgmh.org.tw
Tel.: +886-3-328-1200
Fax: +886-3-327-1192

S.-M. Jung
Department of Pathology,
Chang Gung Memorial Hospital, Chang Gung University,
105 Taipei, Taiwan

T.-S. Yeh
Department of Surgery,
Chang Gung Memorial Hospital, Chang Gung University,
105 Taipei, Taiwan

H.-C. Lin
Department of Ophthalmology,
Chang Gung Memorial Hospital, Chang Gung University,
105 Taipei, Taiwan

J.-J. Chu
Division of Thoracic and Cardiovascular Surgery,
Chang Gung Memorial Hospital, Chang Gung University,
105 Taipei, Taiwan

Introduction

Myxoma is the most common benign neoplasm of the heart. Cardiac myxoma is also associated with many mucopolysaccharidic matrices, including mucin [1, 3, 4, 5]. Mucin gene expressions are both cell- and tissue specific. Furthermore, the mucin gene varies during cell differentiation and inflammation, and also evolves during carcinogenesis [6, 8]. The expression of mucin genes in cardiac myxoma has never been clarified [10]. Detailed immunohistochemical analysis of the cell surface-tethered mucin, MUC1, the mobile, gel-forming mucus layer,

MUC2, and MUC5AC, has been performed. Notably, the implications of mucins in cardiac myxoma require further consideration.

Mucins are high-molecular-weight glycoproteins containing oligosaccharides attached to serine or threonine residues of the protein apomucin backbone by *O*-glycosidic linkages. The glycosylated portion of the mucin backbone contains variable numbers of tandem repeats, flanked by unique domains with amino acid compositions different than the repeat domain. Mucins are responsible for the rheological properties of secreted mucus gels that lubricate and protect the producing mucous membranes. Moreover, mucins belong to a family containing 18 known gene products, including both large, secreted macromolecules (such as those encoded by MUC2, MUC5AC, MUC5B and MUC6 genes) and those with transmembrane domains (encoded by MUC1, MUC3, MUC4 and MUC12 genes) [8]. Mucin gene expression is relatively organ specific, and extensive loss of normal mucin gene regulation sometimes accompanies intestinal metaplasia or malignancy [9]. Mucins are receiving growing attention in the diagnosis and immunotherapeutic treatment of carcinomas.

This investigation first examined the delicated immunohistochemical expression of mucin (MUC1, MUC2 and MCU5AC) in cardiac myxoma, which has not been described elsewhere [3]. This investigation then attempted to determine whether the expression of representative membrane-associated and/or secretory mucins in cardiac myxoma linked with main clinicopathological tumor characteristics.

Materials and methods

This retrospective study conducted between December 1976 and February 2003 included 101 consecutive patients with cardiac myxoma who were treated by surgical excision. Detailed clinical parameters were also reviewed. The clinical charts displayed data on age, sex, presenting symptoms, echocardiographic characteristics and surgical procedures. Follow-up data were gathered from clinical records and standardized telephone interviews. Additionally, tumor size and morphological features were retrieved from the surgical pathology reports. All sections were stained with hematoxylin–eosin and examined for vascular proliferation, inflammation, cellularity, hyaline, calcification, thrombosis, fibrosis and Gamna–Gandy bodies. The clinical and pathological features of the cardiac myxomas were assessed statistically to identify morphological features related to embolism, atrial fibrillation and patient age on diagnosis. Echocardiographic features were also compared using the same pathological findings. All patients signed an informed consent document, and our institutional review board approved the study.

Immunohistochemical stainings for mucins: MUC1, MUC2 and MUC5AC

Mucin genes, including MUC1, MUC2 and MUC5AC, were studied immunohistochemically in 47 randomly selected patients. Formalin-fixed, paraffin-embedded tissues were cut into 4-μm sections and mounted on glue-coated slides. The slides then were treated by a modification of the avidin-biotin-peroxidase complex immunohistochemical method [3]. Slides were heated at 60°C for 60 min, then deparaffinized in xylene and rehydrated in graded alcohols. Endogenous peroxidase was blocked by incubation in 0.3% hydrogen peroxidase in methanol, and the slides were rehydrated and washed in phosphate-buffered saline (PBS), pH 7.4, for 15 min. Sections then were blocked using 10% normal goat serum in PBS with 1% bovine serum albumin for 15 min. The blocking serum was decanted and various primary antibodies (MUC1, 1:50, monoclonal, Novocastra, UK; MUC2, 1:100, monoclonal, Novocastra, UK; MUC5AC, 1:50, Novocastra, UK) were applied in PBS with 1% bovine serum albumin for 16 h at 4°C. Slides were washed in PBS with 1% Tween 20 for 10 min. Following three PBS rinses, biotinylated goat anti-rabbit immunoglobulin (Vector Labs, Burlingame, CA) at a dilution of 1:500 was applied for 30 min at room temperature. After another PBS rinse, avidin DH: biotinylated horseradish peroxidase complex (Vector Labs) was applied for 30 min. After a final PBS rinse, the tissue sections were reacted with 0.06% diaminobenzidine (Sigma Chemical Co.) for 5 min, rinsed, counter-stained with hematoxylin, dehydrated with graded alcohols, cleared with xylene and coverslipped with permount.

MUC1, MUC2 and MUC5AC first were interpreted using the following scale— – (negative), + (weakly positive), ++ (moderately positive) and +++ (strongly positive)—based on stained cell percentage and staining intensity. Stained cells with scale – or + were classified as immuno-negative, while those with scale ++ or +++ were considered immuno-positive. Statistical comparisons used the Fisher exact test, student *t*-test for unpaired data and Pearson correlation.

Results

Clinical findings

Patients comprised 57 (57%) women and 44 (43%) men with a mean age of 38±21 years (Table 1). All cases were sporadic myxomas rather than familial myxoma. The presentations included: asymptomatic (41%), dyspnea (35%), stroke (23%), chest pain (7%), fever (6%), syncope (5%) and mitral regurgitation (70%). Notably, the sample included 93 myxoma (92%) located in the left atrium and 8 (8%) myxoma located elsewhere, ranging in weight from 3 g to 64 g (mean 30.2 g).

Of 101 patients, 60 (59%) had abnormal electrocardiogram reports with non-specific ST-T changes. Sinus rhythm was observed in 41 patients (41%), atrial fibrillation in 4 patients (4%) and sinus arrhythmia in 1 patient (1%). All patients were diagnosed preoperatively using transthoracic echocardiography. The sample was free of false-positive diagnoses or perioperative mortality. These patients were followed for an average of 52±57 months (median, 32 months), and three (3%) recurrent myxomas were found.

Pathological findings

Microscopic examination revealed high levels of vascular proliferation (94%), hyaline formation (89%), congestive areas (79%) inflammation (57%) and multiple giant cells (47%) in the sample patients. Hemorrhagic foci (17%) and calcification (6%) were noted occasionally. However, there was no cardiac lithomyxoma in our study. No statistically significant differences appeared between the mucins staining pattern and pathological findings.

Table 1 Baseline characteristics of all cardiac myxomas (n=101) and mucin stains (n=47)

	Whole group	Mucins stains group	P value
Numbers	101	47	
Men	44 (43%)	22 (46%)	P>0.05
Women	57 (57%)	25 (53%)	P>0.05
Age (years)			
Mean±SD	38±21	40±17	
Range	13–71	24–65	
Location			
Left atrium	93 (92%)	45 (95.7%)	P>0.05
Left ventricle	2 (1.9%)	0 (0.0%)	P>0.05
Right atrium	4 (3.7%)	1 (2%)	P>0.05
Right ventricle	2 (1.9%)	1 (2%)	P>0.05
Recurrence	3 (3% and all in left atrium)	1 (2% and in left atrium)	P>0.05
Symptoms			
Asymptomatic	41 (41%)	22 (47%)	P>0.05
Dyspnea	35 (35%)	14 (30%)	P>0.05
Stroke	23 (23%)	10 (10%)	P>0.05
Syncope	5 (5%)	1 (2%)	P>0.05

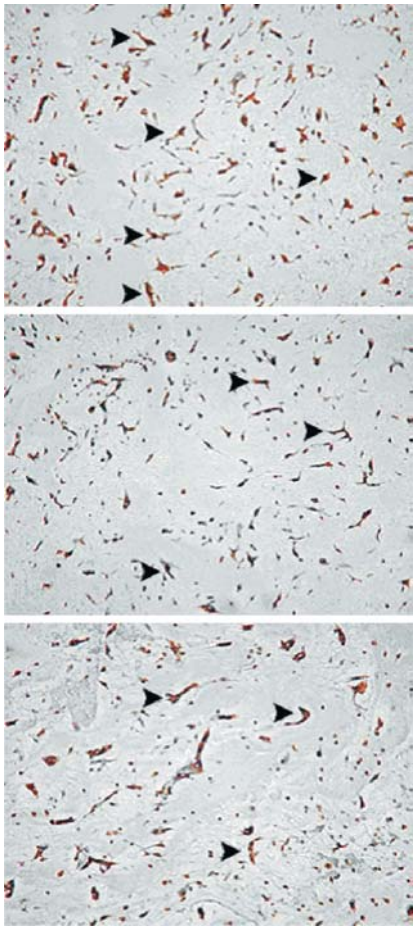

Fig. 1 The pictures display typical changes in a cardiac myxoma. The mucin genes, MUC1, MUC2 and MUC5AC, are clearly expressed (*arrows*; ×200)

Expression of MUC1, MUC2, and MUC5AC in cardiac myxoma and clinical parameters

Only some cardiac myxomas expressed immuno-negative mucin genes, including MUC1 and MUC5AC in 7 (15%) and MUC2 in 8 (17%) of 47 patients. Stained cell percentage and stain intensity scoring was MUC1 (1.69±0.97), MUC2 (1.24±0.77) and MUC5AC (1.26±0.83), respectively (Fig. 1). However, MUC1 had higher expression than MUC2 (P=0.018) and MUC5AC (P=0.024). MUC2 and MUC5AC did not differ significantly (P=0.949). Additionally, the expression MUC5AC (P=0.042) is correlated with less embolism but not the MUC1 (P=0.404) or MUC2 (P=0.9584).

Discussion

Myxoma is the most common benign neoplasm among cardiac tumors [1, 12]. The clinical presentation of cardiac myxomas is non-specific and determined by size, location and mobility. Patients typically present with one or more of intracardiac obstruction, embolism or constitutional symptoms.

Dyspnea is suspected to be caused by atrioventricular valve obstruction, and, in the present series, dyspnea affected 34% of patients (averaging 24–89%) [1]. Moreover, embolism is the classic typical symptom of cardiac myxomas, with an incidence ranging from 6% to 43% [1]. Embolism occurred in 23% of patients in the present series, consistent with other series. However, our relatively higher rate of asymptomatic cases (41%) was noted [1, 2]. Fibrotic, ossified, calcified myxomas mainly affect older patients, although the association was not statistically significant as in earlier studies. Moreover, our study did not have the uncommon lithomyxoma [2]. The recurrence rate in cardiac myxomas ranges between 3% and 12% for sporadic cases [8], such as those presented here, and 22% for cases involving Carney complex. Recurrence has been

linked to incomplete excision, multifocality and tumor fragmentation.

The morphological studies, such as vascular proliferation, hyaline formation, congestive areas, inflammation, hemorrhagic foci, calcification and multiple giant cells, were not statistically significant for clinical presentations as in previous reports [13].

Proliferating cardiac myxomas originate from subendocardial pluripotent primitive mesenchymal cells, which can differentiate within myxomas along various lineages (including epithelial, hematopoietic and muscular). Most microscopic examinations of myxomas reveal the myxomatous nature of the stroma, which contains abundant mucopolysaccharidic matrix [8]. We believe the characteristics of the mucins in cardiac myxoma require further investigation [3].

Mucins, the main component of mucus secretions, are high-molecular-weight and heavily glycosylated proteins synthesized by the mucosal epithelial cells that line the middle ear, trachea, digestive and reproductive tracts [1]. The upregulation of mucin genes is cell- and tissue specific but varies during cell differentiation [4] and microbe inflammation [9] and changes during tumorigenesis [5]. To date, 18 mucin genes have been identified [13].

The membrane-associated mucin MUC1 includes repeated cysteine-rich D-domains for polymerization. MUC1 is a widely used marker for squamous cell carcinomas and generally is produced by glandular epithelial cells related to ductal carcinoma invasion of the pancreas, cholangiocarcinomas of the liver [14] and breast tumors [11]. Levels of MUC1 expression in carcinomas correlate with tumor clinical stage and correlate inversely with patient survival prospects. MUC1 is scattered on chromosome 1q2, while MUC2 and MUC5AC map to 11p15.5 and encode secretory gel-forming mucins [4]. Secreted mucins include MUC2 (in cells with and without secretory granules) and MUC5AC (in surface and submucosal mucous cells). MUC2-unique sequences, mainly expressed in intestinal epithelial cells, appear to mediate polymerization. MUC2 is expressed in intraductal papillary tumors of the pancreas, bile duct cystadenocarcinomas, colonic cancer and defective polymerization of secreted mucin in ulcerative colitis [14]. Additionally, MUC5AC, primarily from airway and gastric epithelial cells, is related to mucus formation in adenocarcinomas [4]. Finally, MUC2 or MUC5AC production appears related to most non-invasive type tumors [5].

The cardiac myxoma, which may be related to chronic inflammation, expresses MUC1, MUC2 and MUC5AC in our study, thus indicating the possible mixed origins of the mucins that may be related to chronic inflammation and arise from multipotential mesenchymal cells. The cells of origin have been in dispute. A detailed immunohistochemical analysis of mucin genes was conducted, demonstrating that membrane-associated MUC1 may affect cardiac myxomas more than do secretory MUC2 and MUC5AC. Moreover, the upper regulation of MUC5AC is related to the lesser risk embolism in this study. The adaptation of mucin-based, histochemical classification to assess MUC gene expression has excellent potential and is likely to be more valuable still if reliably combined with mucin-linked glycosylation markers.

These findings reveal that mucin genes have novel pathological patterns related to clinical parameters. No previous investigations have explicated the expression of mucin genes in cardiac myxoma. Although the clinical implications of MUC1, MUC2 and MUC5AC in cardiac myxoma still need extended assessment, this result offers the potential for therapy based on monoclonal antibodies or vaccination approaches, as has already has been established for other tumor entities.

Acknowledgements Dr. Chu is supported by grants NHRI-EX91–9108SC, NHRI-EX92–9108SC and NHRI-EX93–9108SC from the National Health Research Institute of Taiwan. Dr. Jung is supported by CMRPG33044 from Chang Gung Memorial Hospital at Taiwan.

References

1. Acebo E, Val-Bernal JF, Gomez-Roman JJ, Revuelta JM (2003) Clinicopathologic study and DNA analysis of 37 cardiac myxomas: a 28-year experience. Chest 123:1379–1385
2. Basso C, Valente M, Casarotto D, Thiene G (1997) Cardiac lithomyxoma. Am J Cardiol 80:1249–1251
3. Chu PH, Jung SM, Yeh TS, Yeh CH, Wang CL (2004) Mucin genes expression in cardiac myxoma. Int J Clin Prac 58:306–309
4. Copin MC, Buisine MP, Devisme L, Leroy X, Escande F, Gosselin B, Aubert JP, Porchet N (2001) Normal respiratory mucosa, precursor lesions and lung carcinomas: differential expression of human mucin genes. Front Biosci 6:D1264–D1275
5. Corfield AP, Carroll D, Myerscough N, Probert CS (2001) Mucins in the gastrointestinal tract in health and disease. Front Biosci 6:D1321–D1357
6. Gum JR Jr (1995) Human mucin glycoproteins: varied structures predict diverse properties and specific functions. Biochem Soc Trans 23:795–799
7. Moniaux N, Escande F, Porchet N, Aubert JP and Batra SK (2001) Structural organization and classification of the human mucin genes. Front Biosci 6:D1192–D1206
8. Pinede L, Duhaut P, Loire R (2001) Clinical presentation of left atrial cardiac myxoma. A series of 112 consecutive cases. Medicine (Baltimore) 80:159–172
9. Porchet N, Buisine MP, Desseyn JL, Moniaux N, Nollet S, Degand P, Pigny P, Van Seuningen I, Laine A, Aubert JP (1999) MUC genes: a superfamily of genes? Towards a functional classification of human apomucins. J Soc Biol 193:85–99
10. Pucci A, Gagliardotto P, Zanini C, Pansini S, di Summa M, Mollo F (2000) Histopathologic and clinical characterization of cardiac myxoma: review of 53 cases from a single institution. Am Heart J 140:134–138
11. Rahn JJ, Dabbagh L, Pasdar M, Hugh JC (2001) The importance of MUC1 cellular localization in patients with breast carcinoma: an immunohistologic study of 71 patients and review of the literature. Cancer 91:1973–1982
12. Reynen K (1995) Cardiac myxomas. N Engl J Med 333:1610–1617
13. Rose MC, Nickola TJ, Voynow JA (2001) Airway mucus obstruction: mucin glycoproteins, MUC gene regulation and goblet cell hyperplasia. Am J Respir Cell Mol Biol 25:533–537
14. Yonezawa S, Sato E (1999) Expression of mucin antigens in human cancers and its relationship with malignancy potential. Pathol Int 47:813–830

Virchows Arch (2005) 446:56–63
DOI 10.1007/s00428-004-1145-7

ORIGINAL ARTICLE

Katharina Peters · Roswitha Panienka · Jinming Li · Günter Klöppel · Rennian Wang

Expression of stem cell markers and transcription factors during the remodeling of the rat pancreas after duct ligation

Received: 15 July 2004 / Accepted: 19 September 2004 / Published online: 30 November 2004
© Springer-Verlag 2004

Abstract Ligation of the pancreatic duct has been shown to induce islet cell neogenesis from duct cells in the adult rat pancreas. The transcription factors that regulate islet cell neogenesis and the phenotype of putative precursor cells involved in neogenesis are unknown. We, therefore, studied the expression of the transcription factors Pdx1, Pbx1, Meis2, Nkx2.2 and the putative stem cell markers c-Kit and nestin in rat pancreata 3, 5 and 7 days after duct ligation. Immunocytochemical staining revealed a subpopulation of cells in the ligated portion of the pancreas that was positive for the putative stem cell markers c-Kit and nestin. The c-Kit immunoreactivity was upregulated, reaching a peak at day 3, while nestin expression peaked at day 7. The c-Kit-positive cells were located among the duct and islet cells, while nestin-expressing cells were found scattered in the duct epithelium at day 3 and around the ducts at day 7. Both c-Kit- and nestin-positive cells showed high proliferative activity, as determined by BrdU labeling. Pdx1 and Nkx2.2 were found predominantly in the duct cells of the ligated pancreas. There were significant changes in the expression patterns of Pbx1 and Meis2 in the ductular complexes. The findings indicate that the stem cell markers c-Kit and nestin as well as the transcription factors Pdx1 and Nkx2.2 are upregulated in compartments of the pancreas that are involved in islet cell neogenesis after duct ligation.

K. Peters · R. Panienka · G. Klöppel
Department of Pathology,
University of Kiel,
Kiel, Germany

J. Li · R. Wang
Department of Physiology & Pharmacology,
Lawson Health Research Institute,
University of Western Ontario, Canada

K. Peters (✉)
Michaelisstrasse 11, 24105 Kiel, Germany
e-mail: k.peters@path.uni-kiel.de
Tel.: +49-431-5973485
Fax: +49-431-5973428

Keywords Islet cell neogenesis · Pancreatic duct ligation · Islet progenitor cell markers · Transcription factors

Introduction

The number of β-cells in an adult is established mainly during the fetal and perinatal period. It has been shown that during postnatal life, any further expansion of the pancreatic endocrine cell mass results either from the limited proliferation of the existing terminally differentiated islet cells or by a reiteration of ontogenic development, whereby new β-cells differentiate from the ductal epithelium, a process termed β-cell neogenesis [19]. In previous investigations, we were able to demonstrate in a pancreatic duct-ligation model in the rat that β-cell neogenesis was induced only in the duct-ligated portion of the pancreas [29]. Furthermore, the neogenetic regulation of new β-cell formation was assumed to be under the critical control of paracrine and autocrine factors [30]. It is, however, still unclear which transcription factors regulate β-cell neogenesis, and the precursor cells that give rise to new β-cells have not yet been clearly identified.

Our recent study examined the expression patterns of two putative stem cell markers, nestin and c-Kit, in the developing rat pancreas [32]. Nestin, a well-known neural stem cell marker, has been previously reported to be expressed within the adult ducts and islets, and nestin-positive cells have been shown to differentiate into pancreatic endocrine, exocrine and hepatic phenotypes in vitro [6, 33]. Similarly, c-Kit, a transmembrane protein whose ligand is stem cell factor, is of critical importance for early epithelial stem cell differentiation in hematopoiesis and gametogenesis. Recent studies showed that c-Kit mRNA is present in fetal and adult rat islets and is specifically transcribed in a subpopulation of β-cells, suggesting that mature β-cells may derive from c-Kit-positive cells during regeneration and neogenesis [16, 17, 32].

During pancreatic development, the morphological changes that occur as endocrine cells differentiate from

precursors are characterized by sequential changes in the expression of a group of transcription factors, such as Pdx1, Ngn3 and Pax4 [21]. These transcription factors, to which we limited our studies, include the pancreatic and duodenal homeobox gene 1 (Pdx1), Pbx1 and Nkx2.2. Pdx1 is crucial for embryonic pancreatic development and persists later in life within β-cells, where it has the important role of regulating insulin gene expression [15]. Pbx1 and Meis2 are known to form heteromeric complexes with each other and Pdx1 and have the capacity to alter the activity of Pdx1 [25]. Nkx2.2 is another transcription factor that is known to be expressed in the pancreatic islets [20]. It is required for the upregulation of Pdx1 expression in β-cells, and its expression is a critical step toward final β-cell differentiation [20]. Given the role of these transcription factors during β-cell development, it is important to investigate their expression profiles during the process of pancreatic remodeling and β-cell neogenesis in the duct-ligation model.

The aim of this study was, therefore, to monitor the expression patterns of the potential stem cell factors c-Kit and nestin and the transcription factors Pdx1, Pbx1, Meis2 and Nkx2.2 between day 3 and day 7 post-ligation, when the most pronounced neogenesis of islets occurs, using immunocytochemical and morphometric analysis. We detected two distinct undifferentiated cell types with high proliferative capacity that express the hematopoietic stem cell marker c-Kit or neural stem cell marker nestin within the ligated portion of the pancreas. Furthermore, we observed an increase in the expression of the transcription factors Pdx1 and Nkx2.2 in the ligated portion of the pancreas, suggesting that, in the duct-ligated model, islet neogenesis is accompanied by an increase in cells expressing putative progenitor markers and a dynamic change in transcription-factor patterning.

Materials and methods

Animals and tissue processing

Male Wistar rats weighing 280–300 g and kept in an environment of constant temperature, humidity and day–night cycle were used. The pancreatic duct ligation (PDL) was performed at the gastric and splenic segments, as described previously [29], according to a protocol approved by the ethics committee. Ligated animals were killed 3, 5 and 7 days after the operation. Pancreata from both the non-ligated head and the ligated tail portion were dissected, fixed in 4% paraformaldehyde and embedded in paraffin. To determine cell proliferation, 50 mg/kg body weight of bromodeoxyuridine (BrdU, Sigma, St. Louis, MO, USA) was injected intraperitoneally 1 h before the rats were sacrificed.

Immunohistochemistry and immunofluorescence

The tissue sections from both the non-ligated and ligated portions were immunostained with the primary antibodies against Pdx1 (gift of Christopher V.E. Wright, Vanderbilt University Medical Center, Nashville, TN, USA), antibodies against Pbx1 and Meis2, Nkx2.2 and c-Kit (Santa Cruz Biotechnology, Inc., Santa Cruz, CA, USA), rat nestin (PD PharMingen, Heidelberg, Germany), insulin (BioGenex, San Ramon, CA, USA) and BrdU (Roche, Mannheim, Germany), using either the avidin-biotin complex method (Vectastain ABC kit, ELITE, Vector Laboratories, Burlingame, CA, USA) or immunofluorescence, as described previously [28, 32].

Briefly, deparaffinized, rehydrated 4-µm sections were pretreated for 20 min with H_2O_2-blocking reagent (DakoCytomation, Hamburg, Germany) to block endogenous peroxidase. Nonspecific staining was blocked by incubation with normal goat serum for 15 min. For BrdU immunostaining, sections required pretreatment with 0.5% trypsin and 2 M HCl. All sections were incubated with a tested dilution of the primary antibody as listed above for 45 min and with the biotinylated secondary antibody for 30 min. Staining was visualized using diaminobenzidine (DAB; Substrate kit, Vector Laboratories) as chromogen.

To identify co-expression of phenotypes in both ligated and non-ligated pancreata and the percentage of c-Kit- or nestin-positive cells undergoing proliferation, double immunofluorescence staining was performed [32]. The fluorescent secondary antibodies (obtained from Jackson Immunoresearch Laboratories, West Grove, PA, USA) were fluorescein (fluorescein isothiocyanate) anti-mouse or anti-rabbit antibodies (1:100) or rhodamine (tetramethylrhodamine isothiocyanate) anti-rabbit or anti-mouse antibodies (1:100). Double-labeled images were recorded with a Leica DMIRE2 fluorescence microscope using Openlab image software (Improvision, Lexington, MA, USA). Controls were performed by omitting the primary antibody or secondary antibody. No staining was observed under the negative control conditions.

Morphometric analysis

Quantitative evaluation was performed using computer-assisted image analysis. A Zeiss Axioscope transmitted light microscope was connected via a camera to a PC computer, and, using the Northern Eclipse version 6.0 morphometric analysis software (Empix Imaging Co., Mississauga, ON, Canada), point counting of the immunopositive cells was conducted in each experimental group [28]. Point counting was performed in ten random fields per section, containing 12 islets and at least 500 ductal or acinar cells. This evaluation was repeated at least three to six times per time point. The BrdU labeling index of c-Kit- and nestin-immunopositive cells in the ligated pancreata was determined by double immunostaining and expressed as a percentage of the total number of c-Kit- or nestin-immunopositive cells counted.

Statistical analysis

Values are expressed as mean±SD. Statistical significance was determined by using a two-tailed unpaired student's *t*-test. Differences were considered to be statistically significant if $P<0.05$.

Results

Expression of c-Kit and nestin within the ligated portion of the pancreas

In our previous study, we demonstrated that the ligated pancreas undergoes pronounced changes in histology and cell growth. Most important was the transformation of acinar cells to cells with ductular features. These cells formed ductular complexes 3 days after PDL. Ductular complexes and original ducts formed the ductal compartment. No changes were observed in the non-ligated portion of the pancreas throughout the duration of the experiment [29]. In the present study, immunohistochemical staining revealed c-Kit-positive cells among the ductal and islet cells (Fig. 1A). c-Kit expression increased

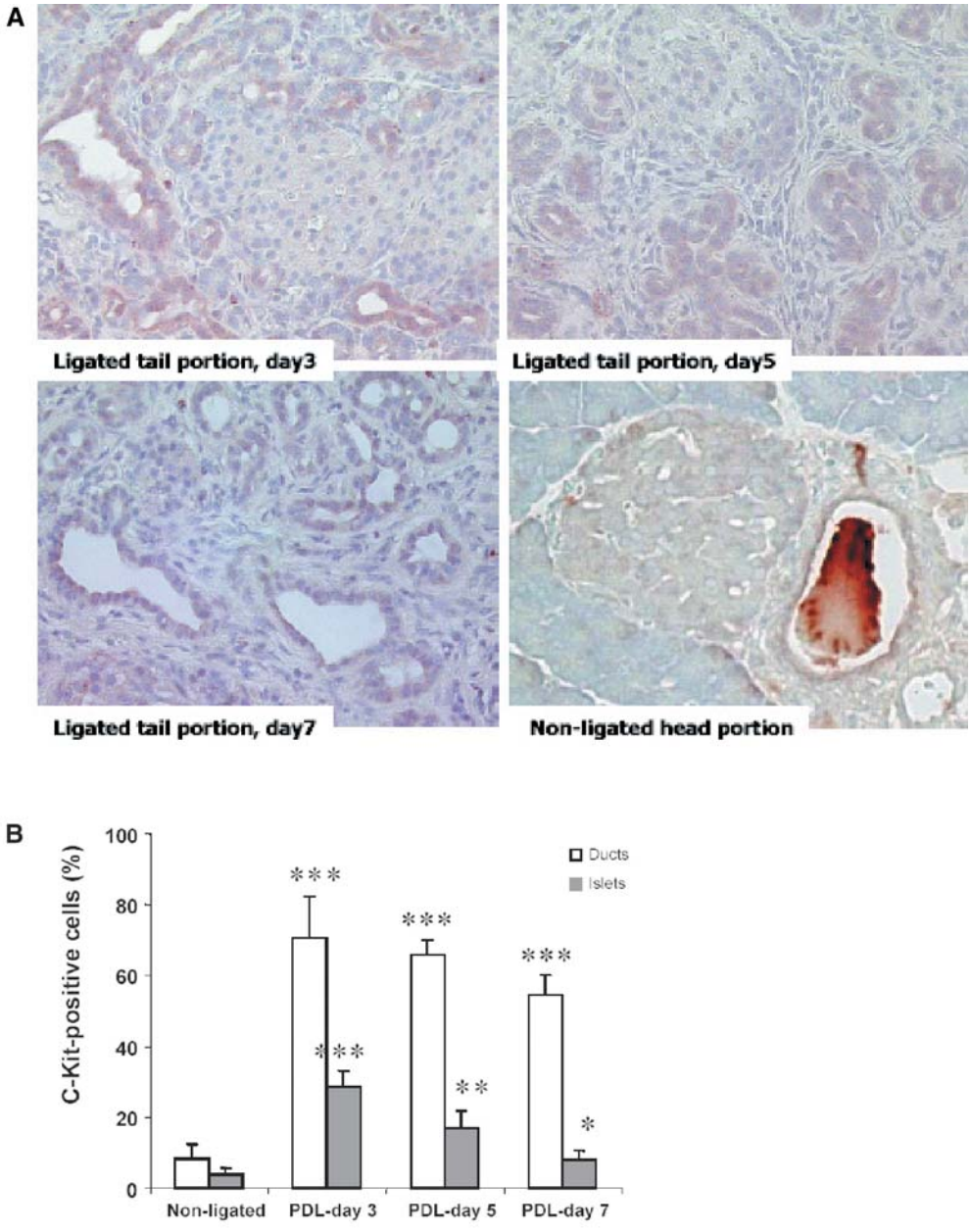

Fig. 1 Immunohistochemical staining demonstrating the presence of c-Kit expression in both the non-ligated and ligated rat pancreas (**A**) and quantitative analysis of the percentage of c-Kit located in the ductal and islet compartments (**B**). **P*<0.05, ***P*<0.01, ****P*<0.001 compared with the non-ligated portion of the pancreas. Original magnification ×400

significantly during ligation in both the ductal and islet cell compartments, reaching its peak on day 3 (70±11% versus 8±4% in the ductal cells and 29±5% versus 4±2% in the islet cells, *P*<0.005). Thereafter, there was a slight decrease (Fig. 1B). An increased number of nestin-expressing cells was found scattered within the ductal compartment on the first 3 days post-ligation. After that, the expression pattern shifted, so that nestin-positive cells were found encircling the ductular complexes (Fig. 2). At day 7, the number of nestin-expressing cells decreased. The nestin expression in the islet cells remained unchanged.

Expression of transcription factors within the ligated tail of the pancreas

Pdx1 expression increased significantly in the ductal compartment, reaching 71±9% on day 3 (*P*<0.006) and remaining at the same level on day 7 (Fig. 3A). Pdx1 expression in the islets did not increase (Fig. 3A). Nkx2.2 expression increased significantly by 6.5-fold in the ductal compartment on day 7, whereas, in the islets, there were no significant differences in expression (Fig. 3B, *P*<0.001). Interestingly, Pbx1 and Meis2 expression increased in the ductular complexes [Pbx1 62±7% on day 7 (*P*<0.04); Meis2 60±16% on day 7 (*P*<0.02)] (Fig. 4). The islet cells were Meis2 and Pbx1 positive in both the ligated and non-ligated portion of the pancreas.

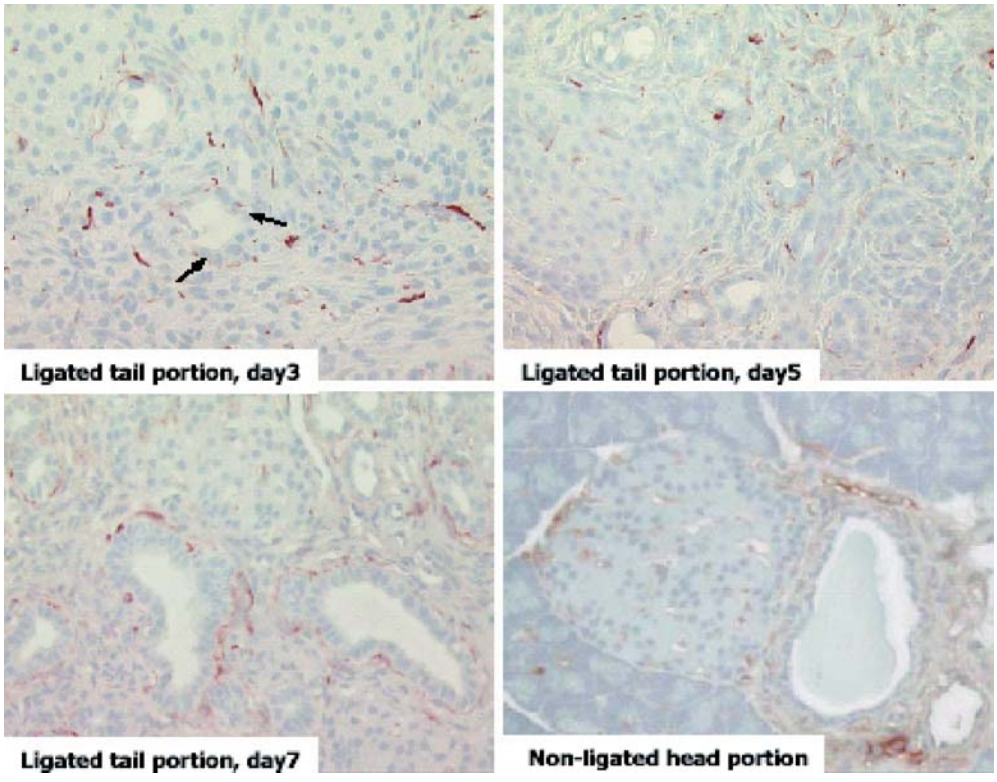

Fig. 2 Immunohistochemical staining demonstrating the presence of nestin expression in both the non-ligated and ligated rat pancreas. *Arrows* indicate nestin-positive cells within a duct. Original magnification ×400

Proliferation in the duct-ligated pancreas

The proliferation rate (BrdU labeling index) of both ductal and islet cells increased (ninefold and tenfold, respectively) on day 3 (Fig. 5). Interestingly, 15±3% of c-Kit-positive cells and 10±3% of nestin-positive cells were BrdU labeled (Fig. 5, inset).

Co-localization of c-Kit and nestin with ductal and endocrine cell markers in the ligated pancreas

Double-immunofluorescent staining revealed co-expression of CK20 with either c-Kit or nestin in both the ductal and islet cell compartments (Fig. 6A, C). There was no co-expression of insulin with either c-Kit or nestin (Fig. 6B, D). c-Kit was co-expressed with Pdx-1 in the duct and islet compartments (Fig. 7).

Discussion

Neogenesis of β-cells has been demonstrated to occur in the rat pancreas ligation model [29]. The putative progenitor cells, however, that differentiate into new islet cells, especially β-cells, have not been sufficiently identified, nor have the transcription factors associated with β-cell neogenesis been studied in detail. Our investigation demonstrates that the number of cells positive for the precursor cell markers c-Kit and nestin increases in the rat pancreas after duct ligation. Furthermore, immunohistochemical examination revealed that there is a dynamic expression of the individual components of transcription factor Pdx1 and Nkx2.2, increasing shortly after the occurrence of c-Kit- and nestin-positive cells in the ligated pancreas.

The fact that c-Kit-positive cells increased in the ductal and islet cell compartments after PDL and showed a high proliferative capacity stresses the role of c-Kit as a progenitor cell marker. This is further corroborated by the co-expression of cytokeratin 20, a ductal and progenitor cell marker [2]. Moreover, c-Kit was co-expressed with Pdx1 in ductal and islet cells. These findings are suggestive of a role of c-Kit as a progenitor cell marker, because, during pancreatic development, differentiated cells arise from ductal, Pdx1-positive progenitor cells. In adult animals, Pdx1 is expressed in proliferating ductal cells that are precursors of the cells of the endocrine and exocrine pancreas during regeneration [10, 23, 26]. Hence, the co-localization of c-Kit in Pdx1-immunopositive cells suggests that c-Kit expression may also mark precursors of the endocrine pancreas in the duct-ligation model. Whether these cells are finally able to differentiate into β-cells is unclear, since we failed to demonstrate co-localization of c-Kit with insulin. It may be speculated that this co-localization is time dependent and only occurs after the time period examined in this study or is transitory and escaped detection during our study. Another explanation could be that, during the development of the pancreas, c-Kit expression is probably only one of many steps, which might not necessarily be coupled with insulin expression. Finally, c-Kit may not be expressed in all endocrine precursor cells, as has been discussed in the literature [17].

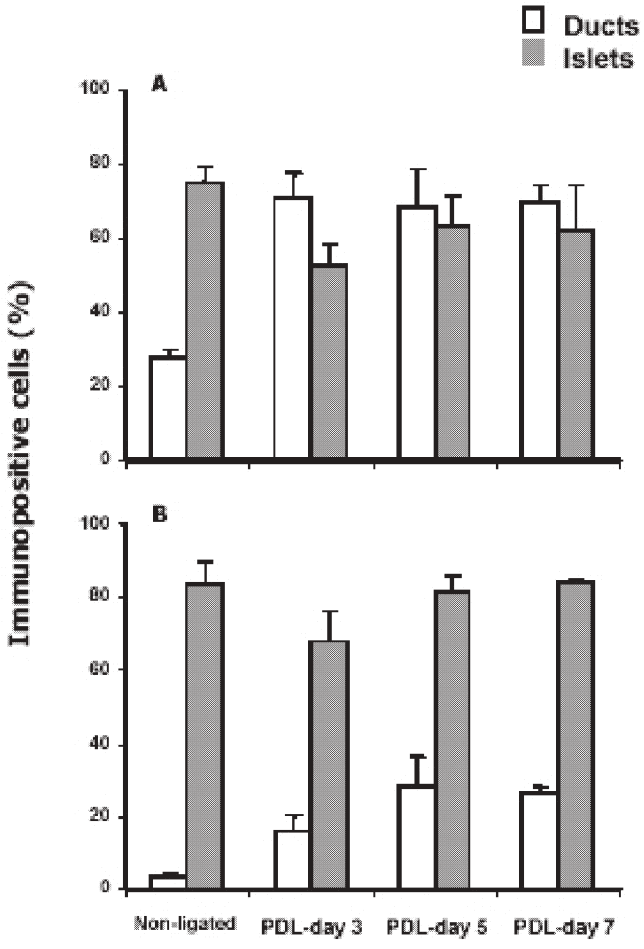

Fig. 3 Morphometric analysis of the transcription factors Pdx1- (**A**) and Nkx2.2- (**B**) expressing cells located amongst ductal and islet cells in the non-ligated and ligated pancreata. Statistical analysis showed significant differences in the expression of Pdx1 and NKx2.2 immunoreactivity within the ductal compartment between the non-ligated and ligated portions of the pancreas

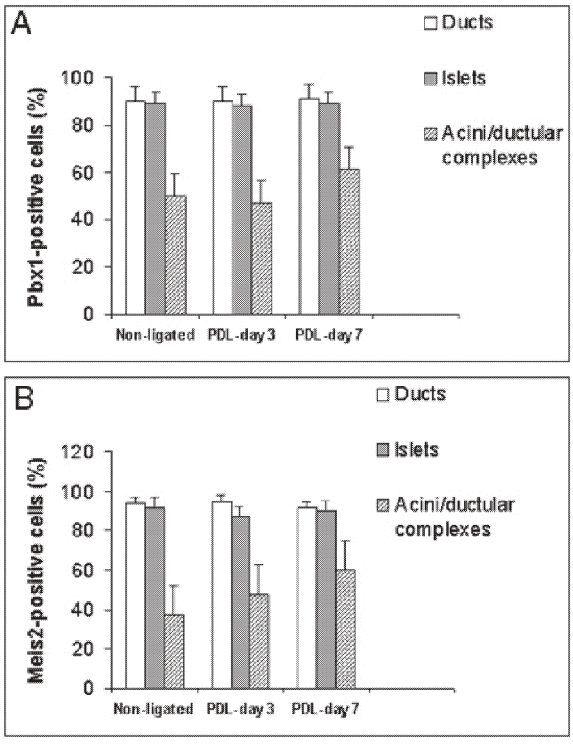

Fig. 4 Analysis of the transcription factors Pbx1 (**A**) and Meis2 (**B**) in different compartments in the non-ligated and ligated pancreas

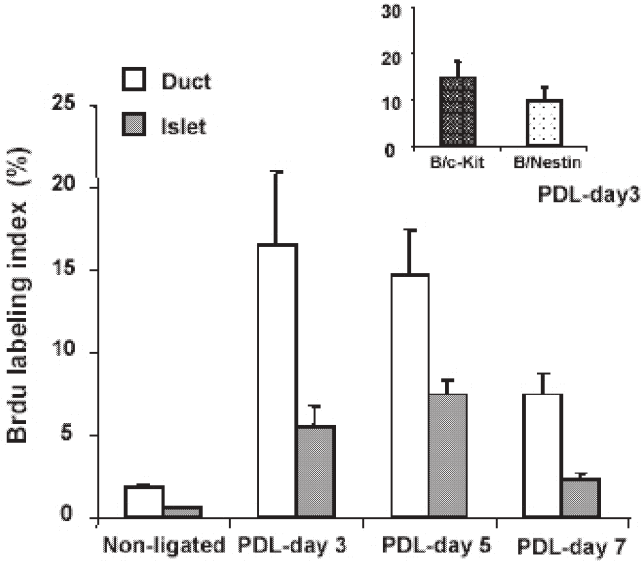

Fig. 5 BrdU labeling index of duct and islet cells in both the non-ligated and ligated rat pancreas and the proliferation rate of c-Kit- and nestin-positive cells at day 3 after ligation (*insert*)

Nestin has also been identified and used as a marker of islet cell precursors [4, 6, 14, 33], although it has not generally been accepted in this role [9, 11, 22]. It has also been postulated that nestin-expressing cells are merely reactive in nature [5, 11]. In our study, nestin expression, like that of c-Kit, was also increased after PDL. As nestin-positive cells also belong to the proliferating cell compartment and co-express CK20, they may have a function that is similar to that of c-Kit in this experimental setting. Similar to the c-Kit-expressing cells, we were unable to show co-expression with insulin, in contrast to other authors [4]. This might be due to the chosen investigation period. Our findings are further corroborated by a recent study by Kim et al. [8], who also failed to show co-expression of nestin and insulin in regenerating cells in a cell culture model after partial pancreatectomy. Therefore, it can be speculated that nestin-positive cells are either able to differentiate into different cell types or that their main objective is to maintain the morphology and control the growth of the islet, as has also been discussed by Treutelaar et al. [27].

PDL induced the neogenesis and/or upregulation of Pdx1 and Nkx2.2. The first transcription factor that was upregulated at day 3 after PDL was Pdx1. It was expressed mainly by the ductal cells and by the cells

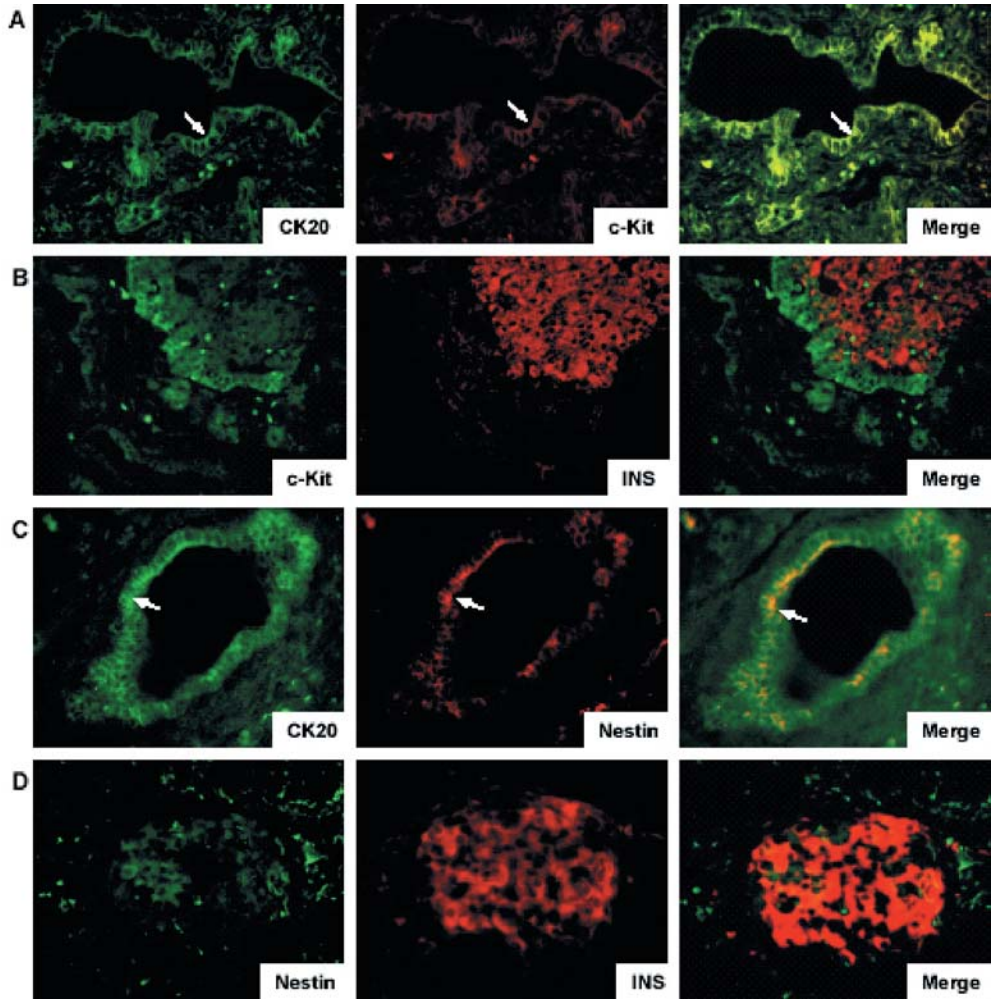

Fig. 6 Co-localization of CK20 [fluorescein isothiocyanate (FITC)] with c-Kit (**A**) or nestin (**C**) [tetramethylrhodamine isothiocyanate (TRITC)], insulin (TRITC) with c-Kit (**B**) or nestin (**D**) (FITC). *Arrows* indicate double-labeled cells. Original magnification ×400

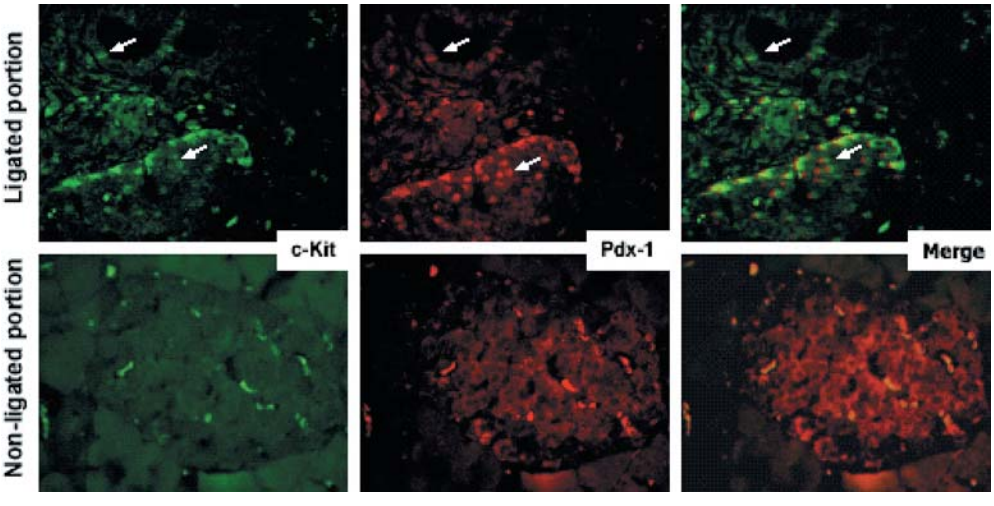

Fig. 7 Co-localization of c-Kit with Pdx1 in both the ligated (**A**) and non-ligated (**B**) rat pancreas. c-Kit is labeled by fluorescein isothiocyanate, while Pdx1 is labeled by tetramethylrhodamine isothiocyanate. *Arrows* indicate double labeled cells. Original magnification ×400

forming tubular complexes. This enhanced expression in ductal cells was accompanied by an increased expression of Nkx2.2 in ductal cells, a transcription factor on which differentiation of β-cells also depends [24]. Pbx1 expression was not enhanced until day 7. It was identified in the ductular complexes. Thus, expression of these transcription factors was dependent on time and compartment. These results suggest that the transcription factors play a role in regeneration and proliferation after duct ligation, especially in the duct cell compartment. Similar findings were reported in a duct-ligation model in the mouse [12]. The duct cell compartment is a well-known

source of potential migrating precursor cells [1, 23], and transformed acini might also serve as a harbor for regenerating cells. Our results suggest that the dimer of Pdx1:Pbx1 particularly promotes cellular proliferation and expansion of stem cells, resulting in islet cell regeneration from ductal and potentially acinar cells. This hypothesis is supported by findings in the literature reporting a complex of Pdx1:Pbx1 in acinar and ductal cell lines [13, 25]. It is further corroborated by the study by Dutta et al. [3], showing that Pdx:Pbx complexes are required for proliferation of cells of the ductal, endocrine or acinar lineages during development. Even the observation of Pdx1-positive cells in a subset of acinar cells and a few ductal cells [18, 31] and the close developmental relationship between embryonic acinar and islet cells [7] could speak in favor of this hypothesis.

The findings suggest that the remodeling and neoformation process that is initiated in the pancreas after PDL activates factors that are implicated in the differentiation of cells during the development of the pancreas. In connection with the findings on c-Kit and nestin, it can be deduced that PDL results in the occurrence of cells that display all the equipment necessary to give rise to new cells in the pancreas.

Acknowledgements This work was supported by grants from the Deutsche Forschungsgemeinschaft (PE 732/2–1) and SJHC Foundation Pearl Laird Fund Canada. Dr. Wang is supported by a University Faculty Award of Natural Science and Engineering Research Council of Canada (NSERC).

References

1. Bonner-Weir S, Sharma A (2002) Pancreatic stem cells. J Pathol 197:519–526
2. Bouwens L, Wang RN, De Blay E, Pipeleers DG, Klöppel G (1994) Cytokeratins as markers of ductal cell differentiation and islet neogenesis in the neonatal rat pancreas. Diabetes 43:1279–1283
3. Dutta S, Gannon M, Peers B, Wright C, Bonner-Weir S, Montminy M (2001) PDX:PBX complexes are required for normal proliferation of pancreatic cells during development. Proc Natl Acad Sci U S A 98:1065–1070
4. Huang H, Tang X (2003) Phenotypic determination and characterization of nestin-positive precursors derived from human fetal pancreas. Lab Invest 83:539–547
5. Humphrey RK, Bucay N, Beattie GM, Lopez A, Messam CA, Cirulli V, Hayek A (2003) Characterization and isolation of promoter-defined nestin-positive cells from the human fetal pancreas. Diabetes 52:2519–2525
6. Hunziker E, Stein M (2000) Nestin-expressing cells in the pancreatic islets of Langerhans. Biochem Biophys Res Commun 271:116–119
7. Kim SK, MacDonald RJ (2002) Signaling and transcriptional control of pancreatic organogenesis. Curr Opin Genet Dev 12:540–547
8. Kim SY, Lee SH, Kim BM, Kim EH, Min BH, Bendayan M, Park IS (2004) Activation of nestin-positive duct stem (NPDS) cells in pancreas upon neogenic motivation and possible cytodifferentiation into insulin-secreting cells from NPDS cells. Dev Dyn 230:1–11
9. Klein T, Ling Z, Heimberg H, Madsen OD, Heller RS, Serup P (2003) Nestin is expressed in vascular endothelial cells in the adult human pancreas. J Histochem Cytochem 51:697–706
10. Kritzik MR, Jones E, Chen Z, Krakowski M, Krahl T, Good A, Wright C, Fox H, Sarvetnick N (1999) PDX-1 and Msx-2 expression in the regenerating and developing pancreas. J Endocrinol 163:523–530
11. Lardon J, Rooman I, Bouwens L (2002) Nestin expression in pancreatic stellate cells and angiogenic endothelial cells. Histochem Cell Biol 117:535–540
12. Li M, Miyagawa J, Moriwaki M, Yuan M, Yang Q, Kozawa J, Yamamoto K, Imagawa A, Iwahashi H, Tochino Y, Yamagata K, Matsuzawa Y (2003) Analysis of expression profiles of islet-associated transcription and growth factors during beta-cell neogenesis from duct cells in partially duct-ligated mice. Pancreas 27:345–355
13. Liu Y, MacDonald RJ, Swift GH (2001) DNA binding and transcriptional activation by a PDX1.PBX1b.MEIS2b trimer and cooperation with a pancreas-specific basic helix-loop-helix complex. J Biol Chem 276:17985–17993
14. Lumelsky N, Blondel O, Laeng P, Velasco I, Ravin R, McKay R (2001) Differentiation of embryonic stem cells to insulin-secreting structures similar to pancreatic islets. Science 292:1389–1394
15. McKinnon CM, Docherty K (2001) Pancreatic duodenal homeobox-1, PDX-1, a major regulator of beta cell identity and function. Diabetologia 44:1203–1214
16. Oberg-Welsh C, Welsh M (1996) Effects of certain growth factors on in vitro maturation of rat fetal islet-like structures. Pancreas 12:334–339
17. Rachdi L, El Ghazi L, Bernex F, Panthier JJ, Czernichow P, Scharfmann R (2001) Expression of the receptor tyrosine kinase KIT in mature beta-cells and in the pancreas in development. Diabetes 50:2021–2028
18. Rooman I, Heremans Y, Heimberg H, Bouwens L (2000) Modulation of rat pancreatic acinoductal transdifferentiation and expression of PDX-1 in vitro. Diabetologia 43:907–914
19. Rosenberg L (1995) In vivo cell transformation: neogenesis of beta cells from pancreatic ductal cells. Cell Transplant 4:371–383
20. Rudnick A, Ling TY, Odagiri H, Rutter WJ, German MS (1994) Pancreatic beta cells express a diverse set of homeobox genes. Proc Natl Acad Sci U S A 91:12203–12207
21. Sander M, German MS (1997) The beta cell transcription factors and development of the pancreas. J Mol Med 75:327–340
22. Selander L, Edlund H (2002) Nestin is expressed in mesenchymal and not epithelial cells of the developing mouse pancreas. Mech Dev 113:189–192
23. Sharma A, Zangen DH, Reitz P, Taneja M, Lissauer ME, Miller CP, Weir GC, Habener JF, Bonner-Weir S (1999) The homeodomain protein IDX-1 increases after an early burst of proliferation during pancreatic regeneration. Diabetes 48:507–513
24. Sussel L, Kalamaras J, Hartigan-O'Connor DJ, Meneses JJ, Pedersen RA, Rubenstein JL, German MS (1998) Mice lacking the homeodomain transcription factor Nkx2.2 have diabetes due to arrested differentiation of pancreatic beta cells. Development 125:2213–2221
25. Swift GH, Liu Y, Rose SD, Bischof LJ, Steelman S, Buchberg AM, Wright CV, MacDonald RJ (1998) An endocrine-exocrine switch in the activity of the pancreatic homeodomain protein PDX1 through formation of a trimeric complex with PBX1b and MRG1 (MEIS2). Mol Cell Biol 18:5109–5120
26. Taguchi M, Yamaguchi T, Otsuki M (2002) Induction of PDX-1-positive cells in the main duct during regeneration after acute necrotizing pancreatitis in rats. J Pathol 197:638–646
27. Treutelaar MK, Skidmore JM, Dias-Leme CL, Hara M, Zhang L, Simeone D, Martin DM, Burant CF (2003) Nestin-lineage cells contribute to the microvasculature but not endocrine cells of the islet. Diabetes 52:2503–2512
28. Wang RN, Bouwens L, Klöppel G (1994) Beta-cell proliferation in normal and streptozotocin-treated newborn rats: site, dynamics and capacity. Diabetologia 37:1088–1096
29. Wang RN, Klöppel G, Bouwens L (1995) Duct-to islet-cell differentiation and islet growth in the pancreas of duct-ligated adult rats. Diabetologia 38:1405–1411

30. Wang RN, Rehfeld JF, Nielsen FC, Klöppel G (1997) Expression of gastrin and transforming growth factor-alpha during duct to islet cell differentiation in the pancreas of duct-ligated adult rats. Diabetologia 40:887–893
31. Wu KL, Gannon M, Peshavaria M, Offield MF, Henderson E, Ray M, Marks A, Gamer LW, Wright CV, Stein R (1997) Hepatocyte nuclear factor 3beta is involved in pancreatic beta-cell-specific transcription of the pdx-1 gene. Mol Cell Biol 17:6002–6013
32. Yashpal NK, Li J, Wang R (2004) Characterization of c-Kit and nestin expression during islet cell development in the prenatal and postnatal rat pancreas. Dev Dyn 229:813–825
33. Zulewski H, Abraham EJ, Gerlach MJ, Daniel PB, Moritz W, Muller B, Vallejo M, Thomas MK, Habener JF (2001) Multipotential nestin-positive stem cells isolated from adult pancreatic islets differentiate ex vivo into pancreatic endocrine, exocrine, and hepatic phenotypes. Diabetes 50:521–533

Virchows Arch (2005) 446:64–67
DOI 10.1007/s00428-004-1131-0

CASE REPORT

Romaric Croes · Maria Debiec-Rychter · Kristof Cokelaere · Rita De Vos · Anne Hagemeijer · Raf Sciot

Adult sclerosing rhabdomyosarcoma: cytogenetic link with embryonal rhabdomyosarcoma

Received: 7 June 2004 / Accepted: 25 August 2004 / Published online: 17 November 2004
© Springer-Verlag 2004

Abstract Rhabdomyosarcomas are classified into three well-defined categories: embryonal, alveolar and pleomorphic rhabdomyosarcoma. Recently, seven cases of an unusual adult type of rhabdomyosarcoma with a prominent hyaline sclerosis have been described. We report the hitherto unreported cytogenetic changes of an adult sclerosing rhabdomyosarcoma. A 79-year-old woman underwent an amputation for a rapidly growing soft tissue mass in the anterior compartment of the right lower leg. The tumor infiltrated the tibia. On histology, a fascicular spindle to round cell proliferation, embedded in a prominent hyaline matrix, was seen. Immunohistochemistry showed focal desmin, myogenin and MyOD1 expression, and electron microscopy revealed Z-band material. Cytogenetic analysis disclosed a 44–49,XX,+del(1)(p22)[2],+11,+16[5],+18[12],+21[3],-22 [cp13] karyotype. Using fluorescent in situ hybridization (FISH) analysis, the tumor cells were negative for *FOXO1A*-disrupting translocations specific for alveolar rhabdomyosarcoma. The chromosomal composition of malignant cells resembled the pattern of numerical changes frequently observed in embryonal rhabdomyosarcoma, suggesting a close relationship of an adult sclerosing rhabdomyosarcoma with this entity.

Keywords Sclerosing rhabdomyosarcoma · Embryonal rhabdomyosarcoma · Adults · Cytogenetic analysis · Immunohistochemistry

R. Croes · R. De Vos · R. Sciot
Department of Morphology and Molecular Pathology,
University Hospitals, K.U. Leuven,
Leuven, Belgium

M. Debiec-Rychter · A. Hagemeijer
Department of Human Genetics,
Catholic University of Leuven,
Leuven, Belgium

K. Cokelaere
Department of Pathology,
Jan Ypermanziekenhuis,
Ieper, Belgium

R. Sciot (✉)
Department of Pathology,
University Hospital St. Rafaël,
Minderbroedersstraat 12, 3000 Leuven, Belgium
e-mail: raf.sciot@uz.kuleuven.ac.be
Tel.: +32-16-336593
Fax: +32-16-336548

Introduction

Rhabdomyosarcomas are classified into embryonal (ERMS), alveolar (ARMS) and pleomorphic (PRMS) subtypes, which can be translated into significant clinical, morphological, molecular and prognostic differences. ERMS typically occurs in young children, ARMS usually in older children and adolescents and PRMS usually in older adults. ARMS usually shows a characteristic alveolar growth pattern, wreath-like tumor giant cells, a strong and uniform myogenin expression [6, 7] and the presence of specific PAX3/FOXO1A or PAX7/FOXO1A fusion proteins [1, 3, 10]. ERMS have many histological faces, ranging from a spindle-cell proliferation to a small blue round cell tumor with characteristic nuclear features and variable number of the characteristic differentiating cells with abundant eccentric eosinophilic, sometimes fibrillar cytoplasm (“tadpole”). There is a consistent immunoreactivity for muscle-specific actin and for desmin, MyOD1 or myogenin. EMRS do not show recurrent structural chromosomal rearrangements. The majority of reported tumors are hyperdiploid, showing gains of a variety of whole chromosomes, with trisomies/tetrasomies of chromosomes 2, 7, 8, 11, 12 and 13 being the most frequent (50–60% of the cases) [2, 5, 8, 9].

PRMS correspond to a very atypical and pleomorphic sarcoma with immunohistochemical or ultrastructural evidence of skeletal muscle differentiation. Recently, seven cases of an unusual adult type of rhabdomyosarcoma have been described [3, 5]. Due to the prominent hyaline sclerosis, these tumors do not clearly fit into the current classification of rhabdomyosarcoma. No cytogenetic description of adult sclerosing rhabdomyosarcoma

has been reported yet. Insight into the chromosomal changes might answer the question of whether these rare rhabdomyosarcomas represent a separate entity. This prompted us to report the cytogenetic changes in a case of adult sclerosing rhabdomyosarcoma.

Clinical history

A 79-year-old woman presented in August 2003 with a rapidly growing, sometimes painful soft tissue mass in the anterior compartment of the right lower leg infiltrating the tibia bone. She underwent an amputation of the distal femur and lower leg. On gross examination, the anterior compartment of the lower leg was completely occupied by a relatively well-delineated tumor from the surrounding soft tissues. On section, the tumor was gray to white in color, solid and rubbery in consistency and measured 6 cm in diameter (Fig. 1). The woman had no significant medical history to be retained. After surgery, no additional treatment was given. The woman presented 12 months after surgery with multiple skeletal and lung metastases and a solitary metastasis in the breast, the latter proven on biopsy.

Materials and methods

After sampling for frozen material, tumor samples were fixed in 6% buffered formalin, embedded in paraffin and stained with hematoxylin and eosin for routine histological examination. Indirect immunohistochemistry was performed on paraffin sections, using monoclonal alpha-smooth-muscle actin (dilution 1:40; Dako, Glostrup, Denmark), desmin (dilution 1:20; ICN-Cappel, Gent, Belgium), myogenin (dilution 1:30; Novocastra, Gent, Belgium), MyOD1 (dilution 1:10; Novocastra, Gent, Belgium), CD31 (dilution 1:50; Dako, Glostrup, Denmark), CD34 (dilution 1:10; Becton, Dickinson and Co, USA), CD99/Mic2 (dilution 1:200; Dako, Glostrup, Denmark), factor VIII (dilution 1:200; Dako, Glostrup, Denmark) and polyclonal S-100 protein (dilution 1:300; Dako, Glostrup, Denmark).

Small fragments of paraffin-embedded tissue were a second time fixed in 2.5% glutaraldehyde, 0.1 mol/l phosphate buffer. After postfixation in 1% osmiumtetroxide 0.1 mol/l phosphate buffer, the samples were dehydrated in graded series of alcohol and embedded in epoxy resin. Ultra-thin sections were cut stained with uranyl acetate and lead citrate and examined using a Zeiss EM10 electron microscope.

Chromosome metaphases were obtained after short-term culture of a primary tumor sample, using standard procedures. G-banded chromosomes were evaluated and classified according to the International System of Human Cytogenetic Nomenclature. Biotin-labeled BAC RP11–384O8 (containing *PAX3*/2q35), PAC RP3–394P21 (containing *PAX7*/1p36) and digoxigenin-labeled YAC 818B12 clone (from the CEPH mark 3 Mega YAC library, Paris, France) that contained sequences specific for *FOXO1A*/13q14 were used for dual-color FISH analysis.

Fig. 1 Gross examination of the tumor. The anterior compartment of the lower leg is completely occupied by a relatively well-delineated tumor, gray to white in color, solid and rubbery in consistency

Results

At low-power magnification, a moderate cellularity, a fascicular and pseudovascular growth pattern and a prominent hyaline sclerosis of the extracellular matrix characterized the tumor (Fig. 2). The tumor cells were either elongated spindle-shaped cells, plump primitive-appearing round cells with minute dense eosinophilic cytoplasm or medium sized with abundant eosinophilic cytoplasm with eccentrically placed nuclei resembling rhabdomyoblasts (Fig. 3). The enlarged nuclei were either hyperchromatic with irregular borders or vesicular with small nucleoli. Mitotic activity was increased up to 19 mitotic figures per 10 high power fields, and some atypical mitotic figures were found. Coagulative necrosis was only focally present.

The tumor cells stained positively for alpha-smooth-muscle actin and desmin (Fig. 4). A minority of tumor cells demonstrated expression of myogenin and MyOD1, and both stains were comparable. CD99 showed a focal expression, while no expression of S-100, CD31, CD34 or factor VIII was found.

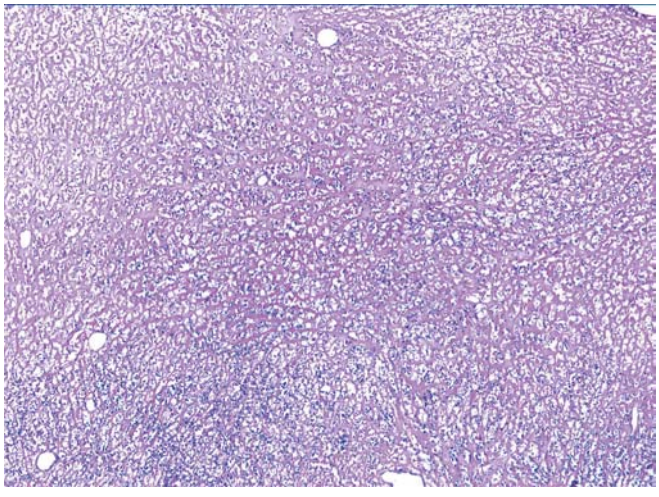

Fig. 2 The tumor is characterized by a moderate cellularity and a striking hyaline sclerosis of the intercellular matrix and a pseudovascular pattern (hematoxylin and eosin stain ×50)

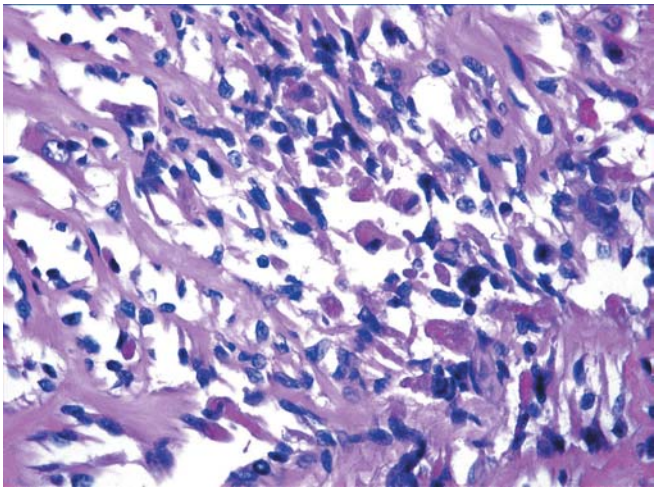

Fig. 3 Higher magnification shows either elongated spindle-shaped cells, plump primitive-appearing round cells with minute dense eosinophilic cytoplasm and medium-sized cells with abundant eosinophilic cytoplasm with eccentrically placed nucleus resembling rhabdomyoblasts (hematoxylin and eosin stain ×400)

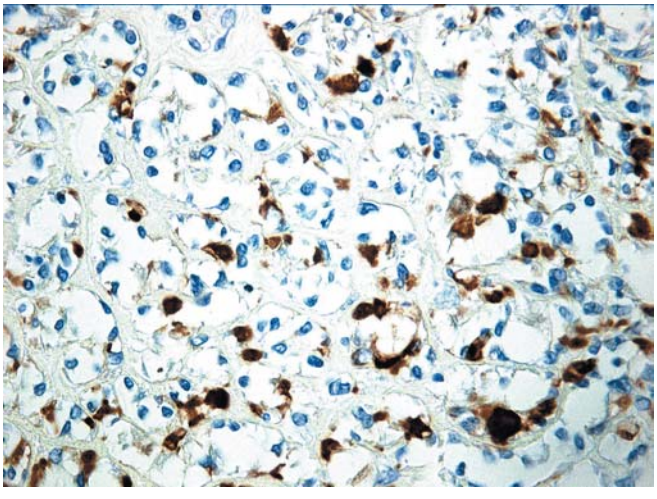

Fig. 4 The tumor cells show positivity for desmin (indirect immunoperoxidase stain ×200)

Electron microscopically, the tumor consisted of spindle-shaped cells lying in an abundant extracellular matrix rich in dense collagen fibers. The tumor cells had a cigar-shaped nuclei with peripheral chromatin. Their cytoplasms contained glycogen particles and haphazardly arranged myofilaments with prominent Z bands (Fig. 5).

Cytogenetic analysis disclosed a 44–49,XX,+del(1)(p22)[2],+11,+16[5],+18[12],+21[3],–22 [cp13] karyotype (Fig. 6). Sequential, dual-color FISH analysis using biotin-labeled BAC 384O8/*PAX3* or PAC 394P21/*PAX7* and digoxigenin-labeled YAC 818B12/*FOXO1A* probes revealed the presence of two green and two red signals over chromosomes 2 or normal 1p36 and 13q14, respectively, indicating the absence of a t(2;13)(q35;q14) or t(1;13)(p36;q14) translocation in the neoplastic cells and confirming the integrity of the *FOXO1A* gene.

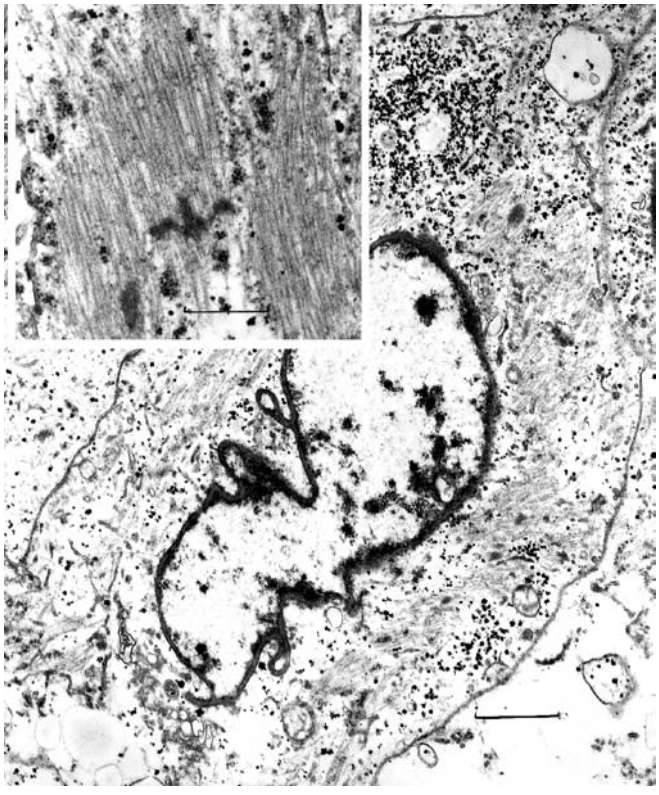

Fig. 5 Electron micrograph showing spindle-shaped tumor cells within their cytoplasm, glycogen particles and haphazardly arranged myofilaments with prominent Z bands (*inset*)

Discussion

The morphological features of the presented case correspond to a recently described unusual phenotype of rhabdomyosarcoma. Mentzel and Katenkamp reported a series of three cases of rhabdomyosarcoma in adults, all showing unusual sclerosing and pseudovascular features [7]. Subsequently, Folpe et al. published another four similar cases of adult rhabdomyosarcoma with the proposal to designate this very unusual hyalinizing, matrix-rich rhabdomyosarcoma occurring as "sclerosing rhabdomyosarcoma" [4]. This variant of adult rhabdomyosarcoma morphologically mimics sclerosing epithelioid fibrosarcoma, variants of osteosarcoma, chondrosarcoma or angiosarcoma. However, the combination of late adult age of onset, focal micro-alveolar architecture, the primitive round cell morphology with the presence of strap cells in one case, the predominance of MyOD1 expression rather than myogenin—a feature not present in the case we present—and the absence of ARMS-associated fusions genes made it unclear whether this variant of adult rhabdomyosarcoma represented a variant of ARMS or ERMS or, alternatively, represented a distinct type of rhabdomyosarcoma. In addition, the expression of alpha-smooth-muscle actin is of interest. Positivity for smooth-muscle actin was also present in half of the tested cases of Folpe et al. and in one of the three cases of Mentzel et al. Generally, alpha-smooth-muscle actin expression is seen in only about 4% of rhabdomyosarcomas. The fact that it

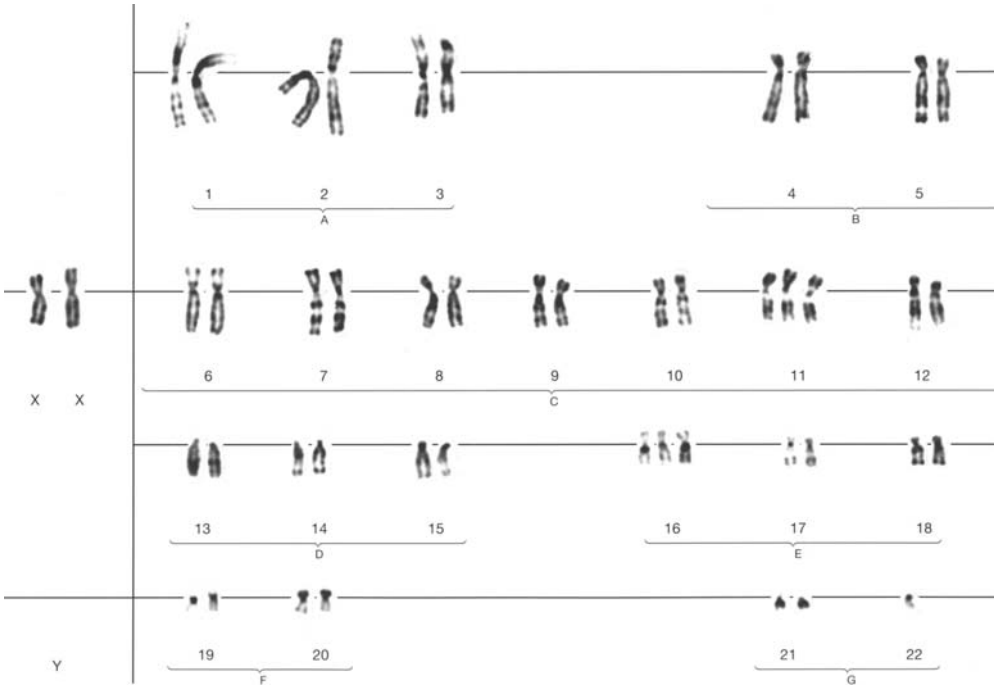

Fig. 6 Representative G-banded karyogram of a tumor cell, showing gain of chromosomes 11 and 16 and loss of chromosome 22

seems to be more frequently present in the adult sclerosing type of rhabdomyosarcoma might be of significance, but this needs more study.

The chromosomal changes of adult sclerosing rhabdomyosarcoma have hitherto not been reported. Since ARMS and ERMS have characteristic changes, it is of interest to know what chromosomal changes characterize the adult sclerosing type. In our case, all analyzed metaphases displayed gain of chromosome 11 and loss of chromosome 22, which was associated with the gain of the whole chromosomes 16, 18 and 21 and partial gain of chromosome 1 in a subset of cells. These numerical changes corresponded well with the range of chromosomal changes described in ERMS [8]. In particular, gains of chromosomes 11, 18 and 21 have been described as frequent numerical changes in ERMS. Importantly, translocations t(2;13)(q35;q14) and t(1;13)(p36;q14) were not found, excluding a relationship with ARMS. This cytogenetic profile supports the classification of adult sclerosing rhabdomyosarcoma as a clinical and morphological variant of ERMS.

Acknowledgements This text presents research results of the Belgian program on Interuniversity Poles of Attraction initiated by the Belgian Sate, Prime Minister's Office, Science Policy Programming. Its authors assume the scientific responsibility. The authors would like to acknowledge the COST support through the COST ACTION B19 "Molecular cytogenetics of solid tumors" in carrying out this work. Belinda Carleer and Lut Mekers are acknowledged for their excellent technical assistance. We thank Dr. C.D.M. Fletcher (Boston) for confirming the diagnosis.

References

1. Barr FG, Nauta LE, Davis RJ, Schafer BW, Nycum LM, Biegel JA (1996) In vivo amplification of the PAX3-FKHR and PAX7-FKHR fusion genes in alveolar rhabdomyosarcoma. Hum Mol Genet 5:15–21
2. Bridge J A, Liu J, Weibolt V, Baker KS, Perry D, Kruger R, Qualman S, Barr F, Sorensen P, Triche T, Suijkerbuijk R (2000) Novel genomic imbalances in embryonal rhabdomyosarcoma revealed by comparative genomic hybridization and fluorescence in situ hybridization: an intergroup rhabdomyosarcoma study. Genes Chromosomes Cancer 27:337–344
3. Davis RJ, D'Cruz CM, Lovell MA, Biegel JA, Barr FG (1994) Fusion of PAX7 to FKHR by the variant t(1;13)(p36;q14) translocation in alveolar rhabdomyosarcoma. Cancer Res 54:2869–2872
4. Folpe AL, McKenney JK, Bridge JA, Weiss SW (2002) Sclerosing rhabdomyosarcoma in adults: report of four cases of a hyalinizing, matrix-rich variant of rhabdomyosarcoma that may be confused with osteosarcoma, chondrosarcoma, or angiosarcoma. Am J Surg Pathol 26:1175–1183
5. Gordon T, McManus A, Anderson J, Min T, Swansbury J, Pritchard-Jones K, Shipley J (2001) Cytogenetic abnormalities in 42 rhabdomyosarcoma: a United Kingdom Cancer Cytogenetics Group Study. Med Pediatr Oncol 36:259–267
6. Kumar S, Perlman E, Harris CA, Raffeld M, Tsokos M (2000) Myogenin is a specific marker for rhabdomyosarcoma: an immunohistochemical study in paraffin-embedded tissues. Mod Pathol 13:988–993
7. Mentzel T, Katenkamp D (2000) Sclerosing, pseudovascular rhabdomyosarcoma in adults. Clinicopathological and immunohistochemical analysis of three cases. Virchows Arch 436:305–311
8. Mitelman F, Johansson B, Mertens F (eds) (2004) Mitelman database of chromosome aberrations in cancer. John Wiley & Sons, Inc., New York
9. Polito P, Dal Cin P, Sciot R, Brock P, Van Eyken P, Van den Berghe H (1999) Embryonal rhabdomyosarcoma with only numerical chromosome changes. Case report and review of the literature. Cancer Genet Cytogenet 109:161–165
10. Shapiro DN, Sublett JE, Li B, Downing JR, Naeve CW (1993) Fusion of PAX3 to a member of the forkhead family of transcription factors in human alveolar rhabdomyosarcoma. Cancer Res 53:5108–5112

Virchows Arch (2005) 446:68–72
DOI 10.1007/s00428-004-1132-z

CASE REPORT

Matthias Evert · Christiane Seiler · Frank Dombrowski

Aberrant acinar cell CA 19–9 expression and peri-insular acinar cell alterations in an adult human pancreas

Received: 3 July 2004 / Accepted: 26 August 2004 / Published online: 26 October 2004
© Springer-Verlag 2004

Abstract We herein report on a 23-year-old female patient who suffered from Crohn's disease and anorexia nervosa and died after long-term malnutrition and a perforated colitis. At autopsy, her pancreas displayed two peculiar findings. First, there was a constant and aberrant expression of CA 19–9 in the acinar cells. The expression of the carbohydrate antigen CA 19–9 is normally confined to duct-like epithelia, including centroacinar cells, while islet and acinar cells have repeatedly been reported to be immunohistochemically negative. Thus, to the best of our knowledge, our case is the first to show aberrant acinar CA 19–9 expression, and its potential meaning is discussed. Second, the pancreas showed a heterogeneity in acinar morphology, with peri-insular acini being considerably larger than tele-insular acini. The existence of enlarged peri-insular acini, mainly in animals, has occasionally been reported. Its origin, however, is still unclear. Some authors have proposed an influence of high insulin concentrations, exerted via the insulo-acinar capillary axis. We agree with the concept of an islet-derived mechanism. However, as we have observed a similar heterogeneity in streptozotocin- and autoimmune-diabetic rats, we presume that other islet hormones, in particular glucagon, might be more important for this phenomenon in the animals, as well as in the present case.

Keywords Pancreas · Anorexia · CA 19–9 · Peri-insular acini · Acino-ductal transformation

Introduction

In 1899, *Virchows Archiv* published a study of A.J. Jarotzky, which was the first to report on morphological differences between peri-insular (PA) and tele-insular (TA) acini in the murine pancreas [12]. Subsequently, several studies have provided additional clues as to a heterogeneity of acini in different species [4, 8, 10, 13, 18, 19]. PA have larger cells with larger nuclei, as well as a higher content of zymogen granula (the so-called "halos"), which do not get lost after injection of pilocarpine. The peri-insular location of these cells raised the suspicion that these differences derived from an influence of islet hormones, e.g., insulin [10, 13]. We observed similar differences in the morphology of PA and TA in streptozotocin- and autoimmune-diabetic rats but not in normoglycemic control animals. Recently, we encountered such an alteration for the first time in a human pancreas, which was investigated as part of an autopsy. A further peculiarity of this pancreas was the fact that CA 19–9, a marker that is typical for duct epithelia, was expressed in the vast majority of acinar cells, which, to the best of our knowledge, has not yet been described in the literature.

M. Evert (✉) · C. Seiler · F. Dombrowski
Institut für Pathologie,
Otto-von-Guericke-Universität, Magdeburg,
Leipziger Strasse 44, 39120 Magdeburg, Germany
e-mail: matthias.evert@medizin.uni-magdeburg.de
Tel.: +49-391-6713182
Fax: +49-391-6715818

Materials and methods

All tissue specimens were fixed in 10% buffered formalin and embedded in paraffin. Deparaffinized sections were stained with hematoxylin and eosin (H&E), periodic acid-Schiff, and acid fuchsin orange-G. Immunostaining (manufacturer and dilution in brackets) was done with antibodies directed against cytokeratin (CK) 7 (Novocastra, 1:50), CK 8 (Dako, 1:50), CK 19 (Novocastra, 1:100), CA 19–9 (Novocastra, 1:200), insulin (Biogenex, 1:100), glucagon (Dako, 1:1000), somatostatin (Quartett, undiluted), trypsin (Biotrend, 1:100), and alpha-amylase (Sigma, 1:1000), following antigen retrieval by microwave (CK 8, CA 19–9, alpha-amylase), papain (CK 19, trypsin) and/or protease pretreatment (CK 7, CK 19). No pretreatment was performed for the hormone immunohistochemistry. Diaminobenzidine served as a chromogen. Specimens were counterstained with hematoxylin. A positive control was used for monitoring the specificity of immunostaining. The rat pancreatic tissue was obtained after perfusion fixation of either streptozotocin- or autoimmune-diabetic animals as described previously [9].

Case history

The patient, a 23-year-old woman, was admitted to the hospital for severe weight loss and marked cachexia (body weight 32 kg; height 1.67 m; body-mass index 10.4 kg/m^2). She was suffering from severe malnutrition and was suspected to have developed anorexia nervosa. Furthermore, her clinical history included Crohn's disease, so that secondary anorexia in association with Crohn's disease was also considered in the differential diagnosis. Mucoviscidosis was excluded. A few days after her admission, she was affected by a heavy decrease in blood pressure and decreases in oxygen saturation, which could not be treated sufficiently despite intensive medical care and resuscitation measures. The patient died, and consent for autopsy was given.

Results

Autopsy confirmed the clinical diagnosis of Crohn's disease and revealed severe, segmental, ulcerous, and transmural enteritis and colitis, concentrating on the terminal ileum, descending colon, and sigmoid colon, respectively. The transmural colitis resulted in a perforation of the wall of the colon descendens, which was covered by the lateral abdominal wall, preventing diffuse peritonitis from developing.

The patient's constant refusal of food intake resulted in severe dystrophy of the inner organs (heart atrophy of 170 g); furthermore, we recognized hepatomegaly accompanied by hepatic steatosis (liver weight: 2330 g) and generalized edema with 600 ml ascites and bilateral pleural effusions (600 ml left, 150 ml right). The patient died of circulatory breakdown as a result of occult perforation of the colon and severe cachexia.

The pancreas was of moderate consistency. Histologically, we noted foci of moderate periductal and interlobular pancreatic fibrosis, as well as discrete intralobular pancreatic fibrosis without conspicuous inflammatory reaction (Fig. 1a). The acinar parenchyma was found to be atrophic focally. The following two additional findings were remarkable:

1. The exocrine cells of the pancreatic acini displayed a constant aberrant expression of CA 19–9 in more than 80% of the cells (Fig. 1b, c). In addition, however, they displayed the regular immunophenotype of acinar cells, i.e., expression of trypsin (Fig. 1d), amylase, and CK 8 and negativity for the ductal markers CK 7 (Fig. 1e) and CK 19. Only in areas of focal acinar atrophy and acino-ductal transformation, resulting in the formation of pseudo-ductular complexes, did the cells lose their acinar immunophenotype and expressed not only CA 19–9 but also the ductal types of cytokeratin. The ducts and centro-acinar cells generally showed the usual positive immunoreactions against CK 7, CK 19, and CA 19–9. The islet cells were positive only with antibodies against CK 8 and the corresponding hormones, the distribution of the different types of endocrine cells within the islets being normal.
2. The exocrine pancreas showed morphological heterogeneity. H&E staining revealed a concentric ring of enlarged acini around the major part of the islets when compared with the rest of the exocrine parenchyma (Fig. 2a, see also Fig. 1e). In addition to slightly enlarged nuclei, this enlargement was predominantly due to a higher amount in eosinophilic cytoplasm, i.e., to a higher content of zymogen granules. Due to autolysis, it cannot be determined whether the size of PA increased absolutely or whether it was a relative enlargement, thus, being a consequence of a stronger acinar atrophy in the TA. Regarding the aberrant immunoreaction against CA 19–9, there were no differences between PA and TA.

Discussion

CA 19–9 is a carbohydrate antigen that is located in the cell membrane and is related to the blood group antigens of the Lewis group (monosialosyl Le^a). It acquired significance as a tumor marker for different carcinomas of the digestive tract, including pancreatic carcinoma, and can be proven using immunohistochemistry. In normal pancreatic tissue, it is usually expressed in ductal and centroacinar cells [11, 20, 21]. Acinus cells and islet cells, however, have been described as negative. Therefore, the expression of acinus cells seen in our case should be considered a peculiarity. In our case, the distinct staining of pancreatic epithelia with negativity of stroma cells, the lacking expression in the islet cells, the successful control reactions, and identical results in several repetitions excluded a false-positive CA 19–9 immunoreaction. In addition, co-expression of trypsin and amylase proved the acinar origin of these cells and excluded the possibility of selective atrophy of merocrine acinar cells, so that only centroacinar and ductular cells were demonstrable. The pancreas showed foci of fibrosis without inflammatory reaction, possibly being the result of a past, clinically non-apparent pancreatitis or of the inanition per se [17]. A few segments displayed an almost complete acinar atrophy. In these segments, the ductally organized cells exclusively expressed ductal markers, including CA 19–9, with loss of acinar proteins. It has been postulated that the replacement of exocrine acini with pseudo-ductal complexes in pancreatitis is caused not only by an apoptotic elimination of part of the acinus cells but also by acino-ductal transdifferentiation of surviving acini [5, 6]. Therefore, one might hypothesize that in the CA 19–9-positive acinar cells in the present case, there exists a kind of intermediate stage to ductal differentiation and that CA 19–9 is expressed before the ductal cytokeratins. Intermediate stages of acino-ductal differentiation have indeed already been demonstrated in a transgenic mouse model [23] and just recently in a pancreatitis model in the rat [14]. However, we have not yet observed such an immunophenotypical expression pattern in chronic pancreatitis or pancreatic fibrosis in humans, nor has a positive reaction of CA 19–9 in acinar cells in chronic pancreatitis

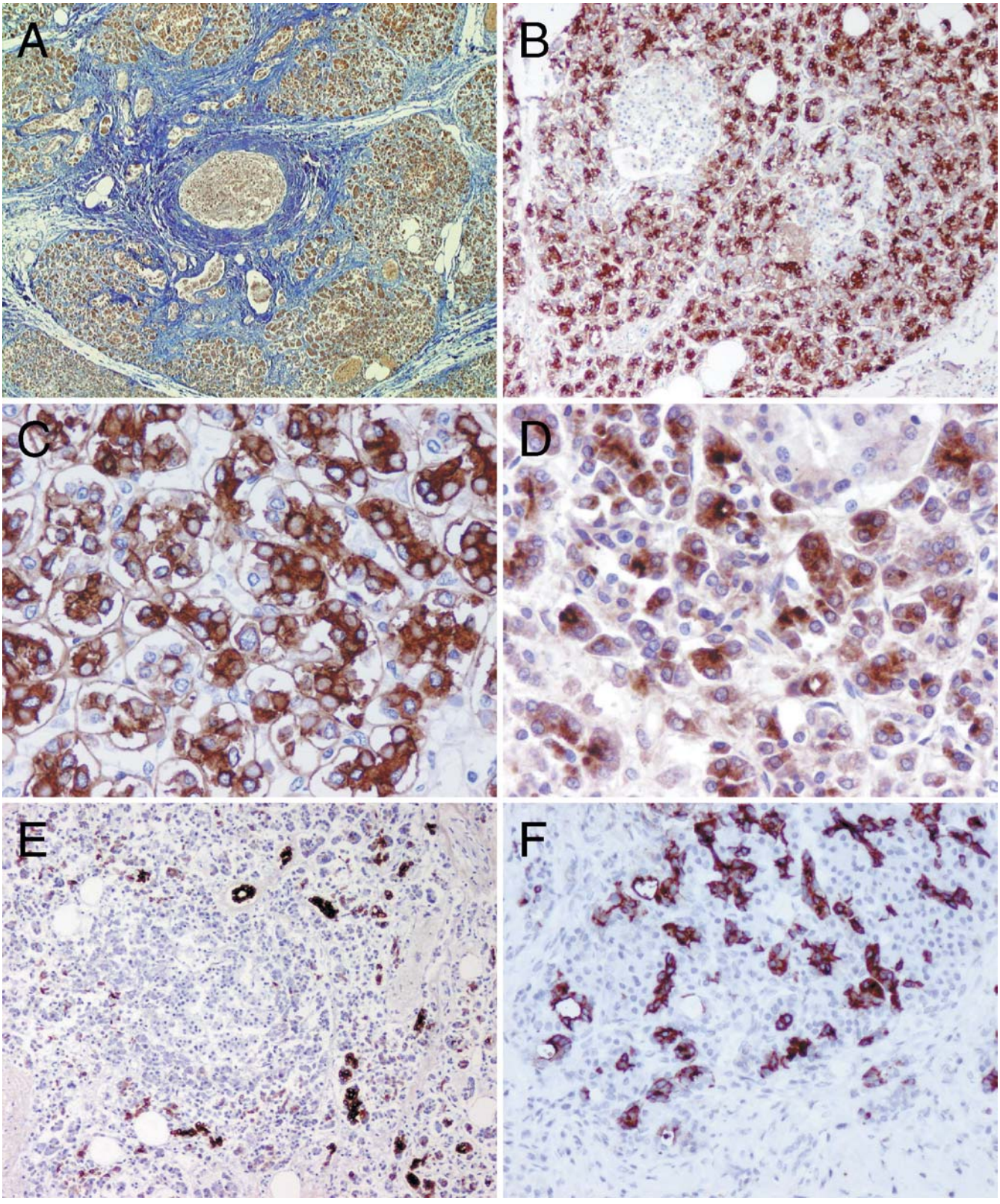

Fig. 1 A moderate periductal, interlobular, and discrete intralobular fibrosis was noted in the pancreas (**A**). The most striking immunohistochemical result was the expression of CA 19–9 in the majority of the acinar cells (**B**, **C**), which concurrently expressed typical acinar markers, such as trypsin (**D**) and amylase (not shown). The same acinar cells showed no expression for ductal cytokeratins, such as CK 7 (**E**) or CK 19 (not shown). Note also the ring of enlarged acini around the centrally located islet (**E**). **F** Typical CA 19–9 expression in an ordinary chronic pancreatitis. The immunoreactivity with the CA 19–9 antibody is, as usual, restricted to ductular and centroacinar cells. Acinar cells are negative. AFOG (Acid Fuchsin Orange-G) (**A**), CA 19–9 (**B**, **C**, **F**), trypsin, and CK 7 (**E**) immunostaining. *Original magnification*: ×21 (**A**), ×42 (**B**), ×429 (**C** and **D**), ×107 (**E**), ×214 (**F**)

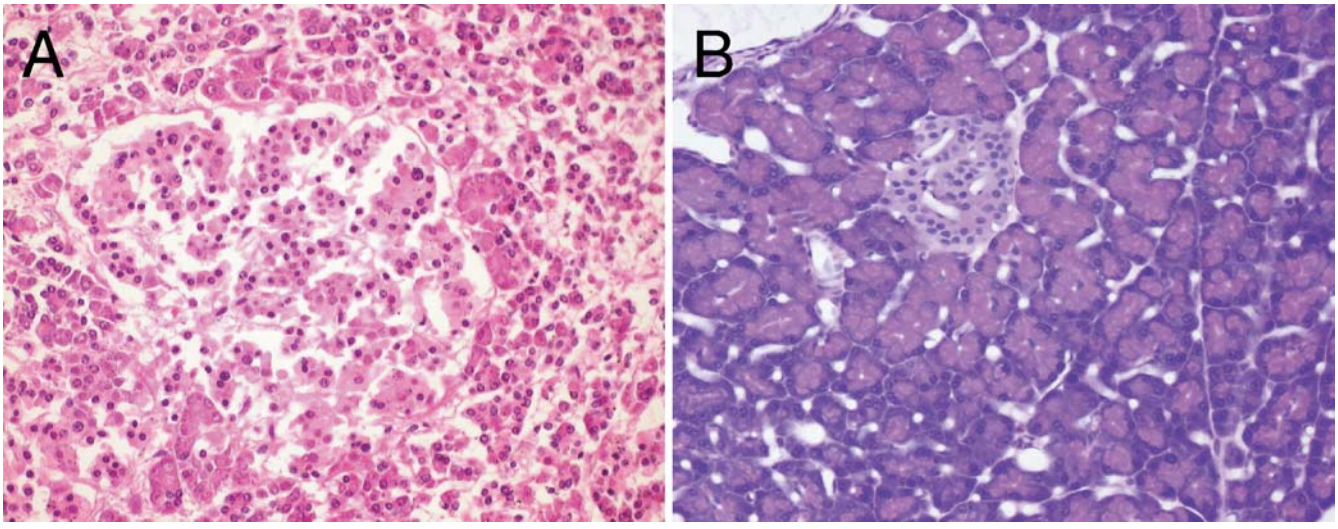

Fig. 2 The acini, located around the islet of Langerhans, are larger than in the periphery (**A**). This was a constant finding in the pancreas of the patient. **B** A similar enlargement of peri-insular acini in an autoimmune-diabetic BB rat. Due to the perfusion fixation, one can note here that this enlargement is mainly due to an increase in zymogen granules. Hematoxylin & eosin stain, *original magnification* ×214 (**A** and **B**)

been described in the literature [20, 21]. Therefore, one must assume that other factors, which may be associated with the complex metabolic situation, contribute to this unusual picture in our case.

The islet-like distribution of the pancreatic endocrine system and the insulo-acinar "portal" capillary system in mammals allow for the hypothesis that the islet hormones exert an influence on the exocrine parenchyma [7, 16]. Furthermore, it is known that differences exist between PA and TA in different species, such as rats, mice, and rabbits. It has been frequently observed in animals that PAs have larger cells with enlarged nuclei, a higher content of exocrine granula, a higher content of chymotrypsinogen, a lower content of amylase, and a different stainability with lectins [3, 4, 10, 13, 18, 19]. Burkl reported on larger PA in two human pancreata without giving detailed clinical data [9]. The major part of the morphological data were ascertained from morphometric analyses. Using the light microscope, however, no differences can usually be found in standardized staining procedures, as both the literature and our own experience have shown. The results of experiments performed in diabetic animals were controversial: some authors report that the peri-insular halos disappear in rats if diabetes was induced by alloxan or streptozotocin [2, 13]. However, only three and four diabetic animals were investigated, respectively. Our observation, based on investigations of more than 1000 animals, have revealed contradictory results and were in line with Malaisse-Lagae, who reported prominent halos in streptozotocin-diabetic rats but not in normoglycemic animals [15]. In our experiment, enlarged PA were a constant finding, and the stronger the diabetes was, the more recognizable the PAs were (Fig. 2b). It was also independent of the B-cell destroying mechanism and of the duration of the diabetes. We also presume that the influence of islet hormones leads to enlarged PAs. However, our results show that, in contrast to former assumptions [10, 13], insulin cannot be made responsible for this. We presume that other islet hormones, in particular glucagon, have to be taken into account. Although it is difficult to determine the exact influence of glucagon on acinar cells, as its effect on enzyme synthesis and on the degranulation behavior of acinar cells is dependent on dosage and time [1], the hyperglucagonemia, which prevailed in the animal experiment, might play an important role in the development of the enlarged PA.

Our patient was found to be affected by a strongly catabolic metabolism due to malnutrition. Therefore, one might expect that she had low systemic insulin and high glucagon levels. This would resemble in part the metabolic situation in the animal experiment and may, thus, have been important for the development of larger PA in her case also. This is supported by the study of Tamarin et al., who were able to induce these differences in food-deprived rats [22] and, most remarkably, by the very first study of A.J. Jarotzky in his inanition experiments in mice [12]. As early as 1899, he stated: "Bei totalem Hunger [...] erscheint jede Langerhans'sche Insel von einem Gürtel solcher Zellen umgeben, die in ihren Dimensionen beträchtlich vergrössert und mit eosinophilen Körnchen im wahren Sinne vollgestopft sind." (Author's translation: If completely food-deprived, each Langerhans islet seems to be surrounded by such cells, which are considerably enlarged and literally crammed with eosinophilic granules.)

Acknowledgement We are grateful to Mr. Bernd Wuesthoff for editing the manuscript.

References

1. Adler G (1977) Effect of glucagon on the secretory process in the rat exocrine pancreas. Cell Tissue Res 182:193–204
2. Augsteehn AA, Katsuoka K (1993) Morphometric studies on the juxta-insular and tele-insular acinar cells of the pancreas in the normal and streptozotocin-induced diabetic rats. J Electron Microsc 42:79–87
3. Bendayan M (1985) Morphometrical and immunocytochemical characterization of peri-insular and tele-insular acinar cells in the rat pancreas. Eur J Cell Biol 36:263–268
4. Bendayan M, Ito S (1979) Immunohistochemical localization of exocrine enzymes in normal rat pancreas. J Histochem Cytochem 27:1029–1034
5. Bockman DE (1995) Toward understanding pancreatic disease: from architecture to cell signaling. Pancreas 11:324–329
6. Bockman DE, Merlino G (1992) Cytological changes in the pancreas of transgenic mice overexpressing transforming growth factor alpha. Gastroenterology 103:1883–1892
7. Bonner-Weir S, Orci L (1982) New perspectives on the microvasculature of the islets of Langerhans in the rat. Diabetes 31:883–889
8. Burkl W (1949) Über Zymogenhöfe in der menschlichen Bauchspeicheldrüse. Wien Klin Wochenschr 61:264–267
9. Dombrowski F, Lehringer-Polzin M, Pfeifer U (1994) Hyperproliferative liver acini after intraportal islet transplantation in streptozotocin-induced diabetic rats. Lab Invest 71:688–699
10. Hellman B, Wallgren A, Petersson B (1962) Cytological characteristics of the exocrine pancreatic cells with regard to their position in relation to the islets of Langerhans. Acta Endocrinol 93:465–473
11. Itzkowitz SH, Yuan M, Fukushi Y, Lee H, Shi ZR, Zurawski V Jr, Hakomori S, Kim YS (1988) Immunohistochemical comparison of Le^a, monosialosyl Le^a (CA 19–9), and disialosyl Lea antigens in human colorectal and pancreatic tissues. Cancer Res 48:3834–3842
12. Jarotzky AJ (1899) Über die Veränderungen in der Größe und im Bau der Pankreaszellen bei einigen Arten der Inanition. Virchows Arch 155:409–450
13. Kramer MF, Tan HT (1968) The peri-insular acini of the pancreas of the rat. Z Zellforsch Mikrosk Anat 86:163–170
14. Lardon J, Huyens N, Rooman I, Bouwens L (2004) Exocrine cell transdifferentiation in dexamethasone-treated rat pancreas. Virchows Arch 444:61–65
15. Malaisse-Lagae F, Ravazzola M, Robberecht P, Vandermeers A, Malaisse WJ, Orci L (1975) Exocrine pancreas: evidence for topographic partition of secretory function. Science 190:795–797
16. Nakagawa A, Stagner JL, Samols E (1995) In situ binding of islet hormones in the isolated perfused rat pancreas: evidence for local high concentrations of islet hormones via the islet-acinar axis. Diabetologia 38:262–268
17. Overzier C (1949) Über chronische Inanition. Z Ges Inn Med 4:623–634
18. Posthuma G, Slow JW, Geuze HJ (1986) A quantitative immuno-electronmicroscopic study of amylase and chymotrypsinogen in peri- and tele-insular cells of the rat exocrine pancreas. J Histochem Cytochem 34:203–207
19. Putzke HP, Said F (1975) Different secretory responses of periinsular and other acini in the rat pancreas after pilocarpine injection. Cell Tissue Res 161:133–143
20. Schwenk J, Makovitzky (1989) Comparative study on the expression of the blood group antigens Le a, Le b, Le x, Le y and the carbohydrate antigens CA 19–9 and CA 50 in chronic pancreatitis and pancreatic carcinoma. Virchows Archiv 414:465–476
21. Takasaki H, Tempero MA, Uchida E, Buchler M, Ness MJ, Burnett DA, Metzgar RS, Colcher D, Schlom J, Pour PM (1988) Comparative studies on the expression of tumor-associated glycoprotein (TAG-72), CA 19–9 and DU-PAN-2 in normal, benign and malignant pancreatic tissue. Int J Cancer 42:681–686
22. Tamarin A, Wanamaker B, Sreebny LM (1963) The effect of inanition on the submandibular salivary glands and exocrine pancreas of the rat. Ann N Y Acad Sci 106:609–624
23. Wagner M, Lührs H, Klöppel G, Adler G, Schmid RM (1998) Malignant transformation of duct-like cells originating in transforming growth factor α transgenic mice. Gastroenterology 115:1254–1262

Virchows Arch (2005) 446:73–77
DOI 10.1007/s00428-004-1141-y

CASE REPORT

Akiteru Goto · Jun Nakajima · Kei Hara · Toshiro Niki · Masashi Fukayama

Lung adenocarcinoma associated with familial adenomatous polyposis. Clear cell carcinoma with beta-catenin accumulation accompanied by atypical adenomatous hyperplasia

Received: 20 August 2004 / Accepted: 19 September 2004 / Published online: 16 November 2004
© Springer-Verlag 2004

Abstract A 46-year-old man presented with a lung tumor 17 years after a subtotal colectomy and 13 years after a partial duodenectomy for familial adenomatous polyposis (FAP). There had been no malignant transformation in the specimens from his colectomy and duodenectomy, and a current gastrointestinal investigation revealed no evidence of malignancy. Pathological analysis of the lung tumor demonstrated adenocarcinoma with clear cells and a papillary structure, accompanied by tiny tumorous nodules in the background lung parenchyma. Many of the nodules were multifocal adenocarcinoma; however, some of the nodules demonstrated atypical adenomatous hyperplasia (AAH). This is the first case report of a lung adenocarcinoma accompanied by AAH in a FAP patient. Immunohistochemical and loss of heterozygosity studies revealed unique features of the lesions reflecting a disruption of the adenomatous poliposis coli–beta-catenin pathway.

Keywords Familial adenomatous polyposis · Lung adenocarcinoma · Beta-catenin · Adenomatous poliposis coli · Atypical adenomatous hyperplasia

A. Goto (✉) · T. Niki · M. Fukayama
Department of Human Pathology,
Graduate School of Medicine, University of Tokyo,
7-3-1, Hongo, Bunkyo-ku, 113-0033 Tokyo, Japan
e-mail: akiteru@m.u-tokyo.ac.jp
Tel.: +81-3-58413328
Fax: +81-3-38158379

J. Nakajima
Department of Cardiothoracic Surgery,
The University of Tokyo Hospital,
Tokyo, Japan

K. Hara
Department of Respiratory Medicine,
The University of Tokyo Hospital,
Tokyo, Japan

Introduction

Familial adenomatous polyposis (FAP) is an autosomal dominant condition caused by mutation of *APC* (*adenomatous poliposis coli*) gene and characterized by the development of multiple adenomas in the colon [2, 10]. FAP patients have also been reported to develop several types of extracolonic tumors, including desmoid tumors, gastric fundic gland polyps, and thyroid carcinomas [1, 6]. However, the pathological features of lung tumors in FAP have not yet been clarified. We report herein a lung adenocarcinoma in a patient with FAP with examination of beta-catenin immunoreactivity and a loss of heterozygosity (LOH) analysis of the *APC* gene.

Our study revealed that clear cell and papillary carcinoma with nuclear beta-catenin accumulation might have been specific to FAP-related lung cancer, and an accompanying condition of multiple atypical adenomatous hyperplasia (AAH) was also found.

Clinical history

A 46-year-old male presented with a cough and hemoptysis. He had a history of FAP and two previous operations: a subtotal colectomy at the age of 29 years for multiple colonic adenomas and a partial duodenectomy at the age of 33 years for duodenal adenomas. The colectomy specimen showed profuse polyps throughout the colon. Chest roentgenograms and computed tomography demonstrated a tumor in S9 of the left lower lobe of the lung surrounded by multiple nodules. Cytological examination of the bronchial washings indicated adenocarcinoma. Left lower lobectomy was performed. Recurrent tumors were identified in the left lung 16 months after lobectomy, and the patient died in 37 months after the lobectomy.

Materials and methods

Immunohistochemistry

Immunostaining of formalin-fixed paraffin-embedded sections of the case was preformed using the avidin-biotin technique via LSAB2 Kit (Dako Corp, CA, USA) with mouse monoclonal anti-

bodies against thyroid transcription factor-1 (TTF1) (8G7G3/1, Lab Vision Corp, CA, USA; 1:200), surfactant apoprotein (SP-A) (PE10, Dako Corp, CA, USA; 1:100), and beta-catenin (BD Biosciences Pharmingen, CA, USA; 1:1000). In the immunohistochemistries for TTF-1 and beta-catenin, antigen retrieval with autoclave treatment in 10 mM citrate buffer, pH 6.0, was performed.

LOH analysis of the *APC* gene

A series of 10-μm-thick sections from the lobectomy specimen were deparaffinized and stained with hematoxylin. Once the stained sections were dried, the tumor cells and normal bronchial cells were separately microdissected using a Leica Laser Capture Microdissection system (Leica Microsystems, Tokyo, Japan). Finally, 50–100 tumor cells and the same number of normal cells were microdissected from the specimens, and their genomic DNA was extracted as described elsewhere [3].

An LOH analysis of the chromosomal loci of *APC* was performed on the extracted DNA. For the *APC*-LOH analysis, polymerase chain reaction (PCR) was performed on extracted DNA with PCR primers flanking *Rsa*I restriction fragment length polymorphism within exon 11 [4]. Purified PCR products were digested with 30 U of *Rsa*I. The amplimer contained only one polymorphic restriction enzyme site, which yielded 85-bp and 48-bp fragments when present. The digested PCR products from tumor and normal tissues were electrophoresed on the same gels in parallel, stained with ethidium bromide, and photographed. A marked decrease in either the single uncut band or the two-cut bands in the tumor DNA (relative to normal tissue DNA) was taken as evidence for LOH.

Results

The resected specimen consisted of the left lower lobe of the lung with diaphragm. A yellowish solid tumor measuring 3.5×3.0×2.0 cm was identified in S9 of the left lung with numerous ill-defined white nodules of up to 5 mm in diameter in the background lung parenchyma (Fig. 1).

The main tumor was a papillary adenocarcinoma consisting mostly of columnar cells with clear cytoplasm (Fig. 2A, B). Many of the tiny nodules in the background lung parenchyma showed histological features indistinguishable from those of the main tumor; however, some showed significantly less structural and cytological atypia than the main tumor (Fig. 2C, D). These features met the diagnostic criteria for AAH.

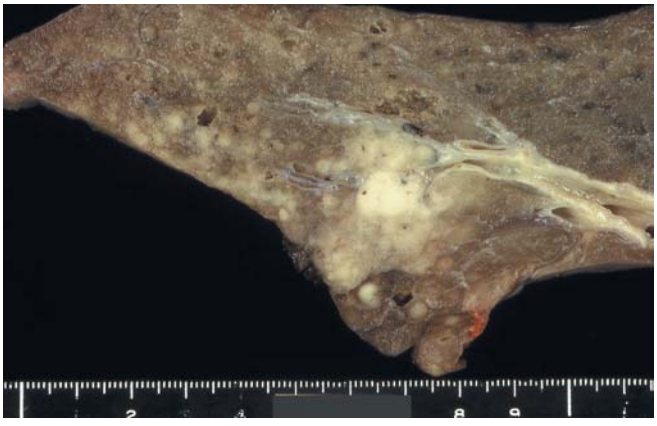

Fig. 1 Gross photograph of the specimen. An ill-defined yellowish solid tumor was identified in S9 of the left lung. Numerous tiny nodules were identified around the main tumor in the background lung parenchyma

Neoplastic cells of the main tumor and accompanying AAH shared a common phenotype with TTF1 (+), SP-A (+) (Fig. 3A, B). A combination of immunohistochemical examinations proved that the adenocarcinoma lacked biotin-rich optically clear nuclei.

Both the main tumor and accompanying AAH of the present case showed aberrant nuclear staining of beta-catenin with or without cytoplasmic or membranous staining (Fig. 3C, D), while immunoreactive beta-catenin was observed in the cellular membrane of the normal bronchiolar epithelium. LOH of the APC locus was observed in two different foci of the main tumor and two different accompanying AAHs, in contrast to background normal lung tissue of the present case (Fig. 4).

Discussion

The extracolonic tumors reported in FAP patients have included osteomas, desmoid tumors, gastric fundic gland polyps, duodenal polyps, and thyroid carcinomas. Rather than being incidental, all are basically caused by a germline mutation of the *APC* gene [1, 6]. Although no mutational analysis of the *APC* gene was performed in the present case, the pathological classification of the colectomy specimen as the profuse type of FAP suggests that the mutation might be present in codon 1250–1464 [8].

The lung carcinoma in the present case exhibited SP-A and TTF-1 immunoreactivity both specific and relatively specific to the carcinoma originating from the peripheral lung, thereby confirming its diagnosis as a primary lung carcinoma rather than a metastatic one [13]. An association with an abnormality of the *APC* gene was also observed. The carcinoma showed aberrant nuclear accumulation of beta-catenin, as well as LOH of the *APC* gene. APC protein is well known to degrade the unphosphorylated form of beta-catenin in the ubiquitin-mediated proteasome pathway to prevent its accumulation in the cytoplasm [11]. Bi-allelic inactivation of the *APC* gene induces a loss of functional APC protein, which in turn leads to an accumulation of beta-catenin in the nuclei and upregulation of the Wnt signaling pathway [11]. The lung adenocarcinoma in the present case was therefore confirmed to be a FAP-related lung carcinoma.

There has only been one previous case report of a lung cancer in an FAP patient, and the histology of the case was well-differentiated fetal adenocarcinoma (WDFA) or low-grade fetal-type adenocarcinoma (L-FLAC) [12]. Histology of the present lung adenocarcinoma was different from that of WDFA/FLAC, as it lacked characteristic findings of WDFA/FLAC, such as morules, complex tubular structure resembling tubular stage of the fetal lung, and biotin-rich optically clear nuclei [9]. Yet both the present case and previous case of L-FLAC/WDFA in FAP exhibited clear cytoplasm. In addition,

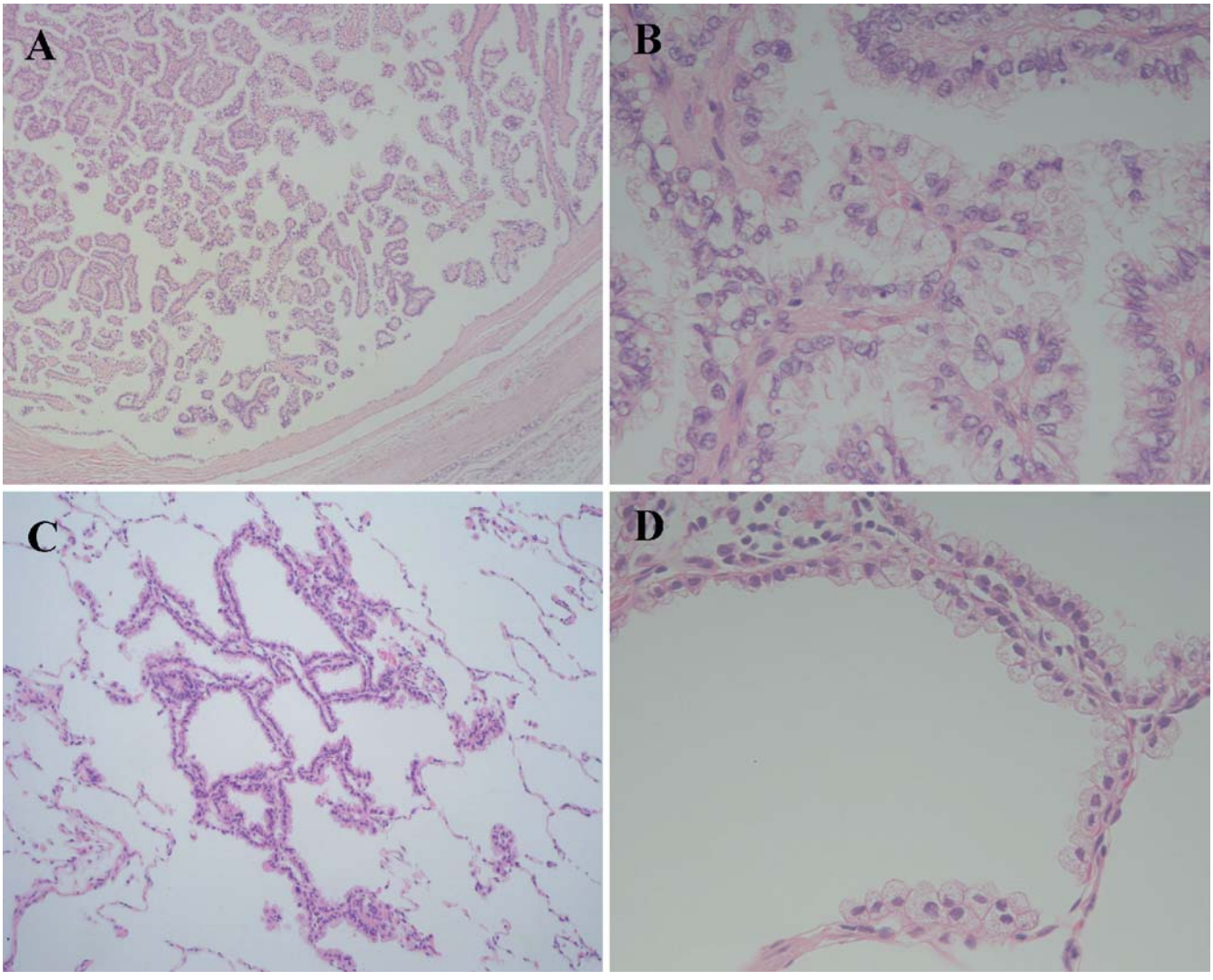

Fig. 2 Light photomicrographs of the lesions. **A** Main tumor was adenocarcinoma with papillary growth pattern throughout the tumor (×40). **B** Adenocarcinoma cells were columnar and showed clear cytoplasm (×400). **C** Atypical adenomatous hyperplasia (AAH) in the background lung parenchyma (×40). **D** AAH cells had less structural and cytological atypia than the main tumor (×400)

both showed characteristic nuclear accumulations of beta-catenin, while only 4% of conventional pulmonary adenocarcinoma showed its nuclear accumulation [9]. As the *beta-catenin* gene mutation was identified in sporadic cases of WDFA/L-FLAC, Nakatani's group speculated that the morphology of WDFA/L-FLAC might represent abnormality in APC/beta-catenin [9]. In the present FAP case, nuclear accumulation of beta-catenin in pulmonary adenocarcinoma might be caused by bi-allelic inactivation of *APC* gene through germ-line mutation and LOH, rather than mutation of the *beta-catenin* gene. On the basis of the histological finding in the present case, however, correlation between morphology and genetic abnormality was not as strict as Nakatani's group postulated. Carcinomas with abnormality in APC/beta-catenin might constitute one distinct group in clear cell carcinoma of the lung encompassing L-FLAC/WDFA and clear cell adenocarcinoma as observed in the present case.

In an examination of surgically resected lung adenocarcinomas, Kitagawa et al. found that extrapulmonary primary cancer was significantly more common in cases accompanied by AAH than in cases without AAH [5]. The finding suggested that a part of the patients with AAH might have a constitutional or genetic predisposition for the development of AAH together with extrapulmonary primary carcinoma. In fact, one case of AAH has been reported in a patient with Li-Fraumeni syndrome, a condition known to harbor germline mutation of *p53* [7]. The present case illustrates that FAP might be another genetic predisposition for the development of AAH in the lung, as AAHs of the present cases showed nuclear accumulation of beta-catenin and LOH of *APC* gene, which suggested causal relationship between FAP and development of pulmonary AAHs.

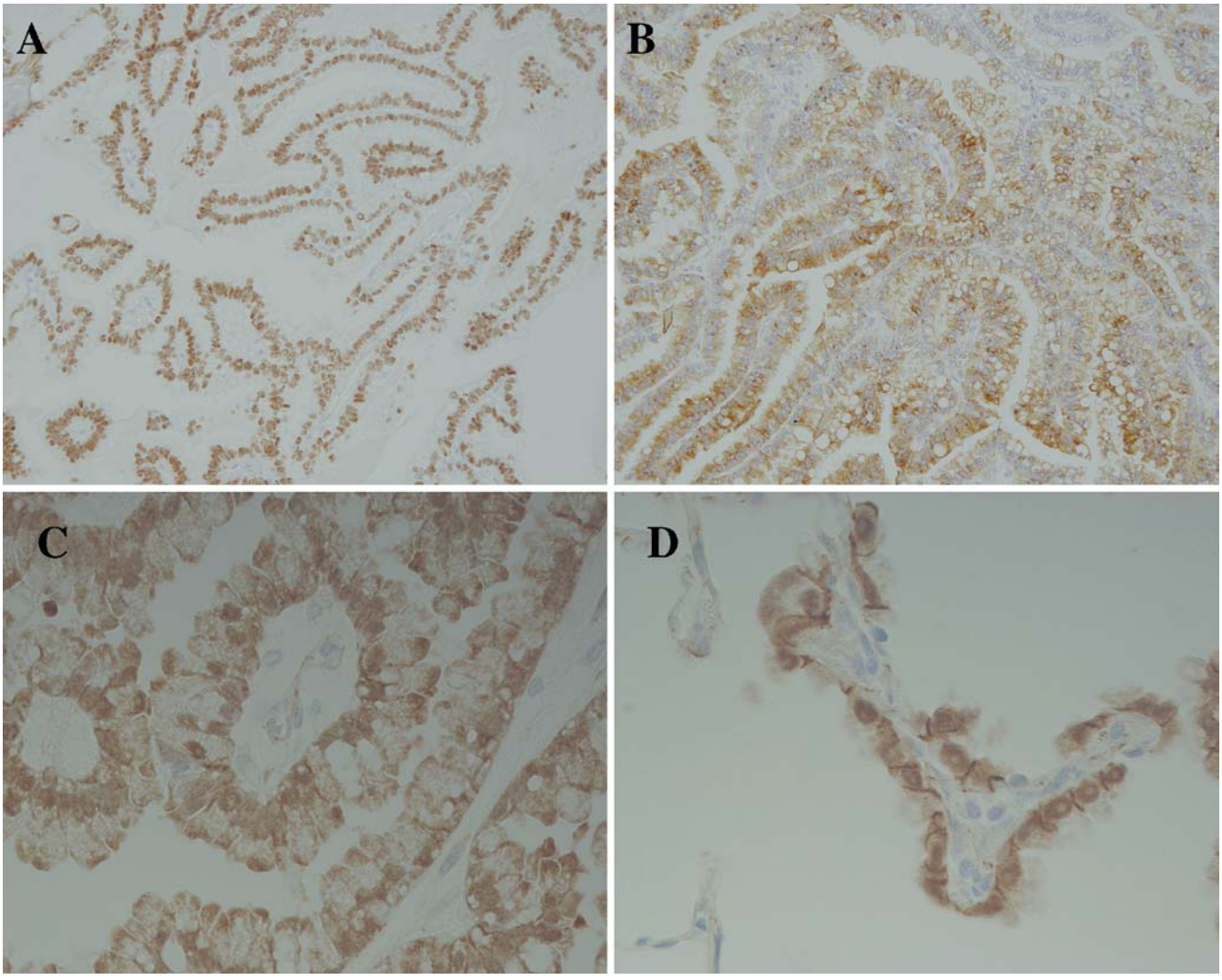

Fig. 3 Immunohistochemistry of the lesions. Adenocarcinoma was positive for immunohistochemistry of thyroid transcription factor-1 (**A**) and surfactant apoprotein (**B**) ×100. Adenocarcinoma (**C**) and atypical adenomatous hyperplasia (**D**) of the case showed nuclear accumulation of beta-catenin (×600)

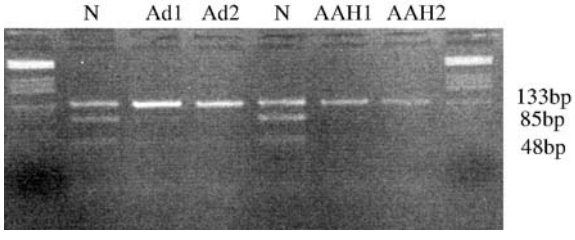

Fig. 4 Loss of heterozygosity of *APC* gene demonstrated by polymerase chain reaction. Lanes N, normal lung tissue of the case with bands of 133, 85, and 48 bp; lanes Ad1 and Ad2, adenocarcinoma tissues from the different sites of the main tumor, and lanes AAH1 (atypical adenomatous hyperplasia) and AAH2, AAH tissues from two AAHs of the background lung parenchyma, without the two-cut bands (85 bp and 48 bp)

References

1. Abraham SC, Nobukawa B, Giardiello FM, Hamilton SR, Wu TT (2000) Fundic gland polyps in familial adenomatous polyposis: neoplasms with frequent somatic adenomatous polyposis coli gene alterations. Am J Pathol 157:747–754
2. Campbell WJ, Spence RA, Parks TG (1994) Familial adenomatous polyposis. Br J Surg 81:1722–1733
3. Goto A, Kanda H, Ishikawa Y, Matsumoto S, Kawaguchi N, Machinami R, Kato Y, Kitagawa T (1998) Association of loss of heterozygosity at the p53 locus with chemoresistance in osteosarcomas. Jpn J Cancer Res 89:539–547
4. Ichihashi N, Kitajima Y (2000) Loss of heterozygosity of adenomatous polyposis coli gene in cutaneous tumors as determined by using polymerase chain reaction and paraffin section preparations. J Dermatol Sci 22:102–106
5. Kitagawa H, Goto A, Niki T, Hironaka M, Nakajima J, Fukayama M (2003) Lung adenocarcinoma associated with atypical adenomatous hyperplasia. A clinicopathological study with special reference to smoking and cancer multiplicity. Pathol Int 53:823–827

6. Kurihara K, Shimizu S, Chong J, Hishima T, Funata N, Kashiwagi H, Nagai H, Miyaki M, Fukayama M (2000) Nuclear localization of immunoreactive Beta-catenin is specific to familial adenomatous polyposis in papillary thyroid carcinoma. Jpn J Cancer Res 91:1100–1102
7. Nadav Y, Pastorino U, Nicholson AG (1998) Multiple synchronous lung cancers and atypical adenomatous hyperplasia in Li-Fraumeni syndrome. Histopathology 33:52–54
8. Nagase H, Miyoshi Y, Horii A, Aoki T, Ogawa M, Utsunomiya J, Baba S, Sasazuki T, Nakamura Y (1992) Correlation between the location of germ-line mutations in the APC gene and the number of colorectal polyps in familial adenomatous polyposis Cancer Res 52:4055–4057
9. Nakatani Y, Masudo K, Miyagi Y, Inayama Y, Kawano N, Tanaka Y, Kato K, Ito T, Kitamura H, Nagashima Y, Yamanaka S, Nakamura N, Sano J, Ogawa N, Ishiwa N, Notohara K, Resl M, Mark EJ (2002) Aberrant nuclear localization and gene mutation of Beta-catenin in low-grade adenocarcinoma of fetal lung type: up-regulation of the Wnt signaling pathway may be a common denominator for the development of tumors that form morules. Mod Pathol 15:617–624
10. Nishisho I, Nakamura Y, Miyoshi Y, Miki Y, Ando H, Horii A, Koyama K, Utsunomiya J, Baba S, Hedge P (1991) Mutations of chromosome 5q21 genes in FAP and colorectal cancer patients. Science 253:665–669
11. Peifer M, Polakis P (2000) Wnt signaling in oncogenesis and embryogenesis—a look outside the nucleus. Science 287:1606–1609
12. Wong RP, Hwang WS, Field SK (1995) Familial adenomatous polyposis and lung cancer. Surg Oncol 60:213–214
13. Yatabe Y, Mitsudomi T, Takahashi T (2002) TTF-1 expression in pulmonary adenocarcinomas. Am J Surg Pathol 26:767–773

Virchows Arch (2005) 446:78–81
DOI 10.1007/s00428-004-1148-4

CASE REPORT

Katsuhiko Mito · Kenji Kashima · Tsutomu Daa · Yoshiyuki Kondoh · Takashi Miura · Katsunobu Kawahara · Iwao Nakayama · Shigeo Yokoyama

Multiple calcifying fibrous tumors of the pleura

Received: 1 July 2004 / Accepted: 28 September 2004 / Published online: 30 November 2004
© Springer-Verlag 2004

Abstract Calcifying fibrous tumor (CFT) is a rare lesion characterized histologically by hypocellular hyalinized collagenous tissue with psammomatous and/or dystrophic calcifications and patchy lymphoplasmacytic infiltrates. CFT usually occurs in the somatic soft tissue of children and young adults but is rarely found in the pleura. We describe here an unusual case of multiple small CFTs in the right mediastinal pleura of a 54-year-old man who had a history of renal cell carcinoma. Suspecting pulmonary and pleural metastases, we performed wedge resection of the right middle lobe and local excision of two nodules in the right pleura. Light microscopy revealed metastatic lesions of renal cell carcinoma in the resected wedge. The pleural nodules were well circumscribed and composed of hypocellular, dense, hyalinized, collagenous tissue with scant lymphoplasmacytic infiltration and characteristic psammoma bodies. Immunohistochemical staining revealed that most spindle cells were positive for vimentin, CD34 and factor XIIIa, and negative for epithelial membrane antigen, keratin, smooth-muscle actin, desmin, S-100 protein and anaplastic lymphoma kinase. We made a histological diagnosis of CFT of the pleura, and the patient remains well 6 months after the wedge resection.

Keywords Calcifying fibrous tumor · Calcifying fibrous pseudotumor · Psammoma body · Pleura

K. Mito (✉) · K. Kashima · T. Daa · Y. Kondoh · I. Nakayama · S. Yokoyama
Department of Pathology,
Faculty of Medicine, Oita University,
Hasama-machi, 879-5593 Oita, Japan
e-mail: kmito@med.oita-u.ac.jp
Tel.: +81-97-5865683
Fax: +81-97-5865686

T. Miura · K. Kawahara
Second Department of Surgery,
Faculty of Medicine, Oita University,
Oita, Japan

Introduction

Calcifying fibrous tumor (CFT) is a rare fibrous lesion characterized histologically by hypocellular sclerotic tissue with psammomatous and/or dystrophic calcifications and patchy lymphoplasmacytic infiltrates [1, 2]. CFT was first described as a "childhood fibrous tumor with psammoma bodies" by Rosenthal and Abdul-Karim in 1988 [1]. In 1993, Fetsch et al. reported ten additional cases and renamed the entity "calcifying fibrous pseudotumor" for three reasons: the lesion is not limited to the pediatric population, the calcification is not limited to psammoma bodies and a neoplastic characterization seems inappropriate. In the newly published classification by the World Health Organization of tumors of soft tissue and bone, the designation "calcifying fibrous tumor (CFT)" is used for this entity [3]. Although CFT is known to occur at various sites, to our knowledge, only five cases have been reported in the pleura [4, 5, 6]. We describe here an unusual case of multiple small CFTs of the pleura.

Materials and methods

All surgically resected tissues were fixed in 10% formalin and embedded in paraffin. Sections 3-μm thick were stained with hematoxylin and eosin. Immunohistochemical analyses were performed by the avidin-biotin-peroxidase complex technique using a Histofine SAB-PO (MULTI) kit (Nichirei, Tokyo, Japan) and diaminobenzidine for visualization of binding of antibodies. We used antibodies against the following antigens: epithelial membrane antigen (prediluted; Dako, Carpinteria, CA, USA); keratin for wide spectrum screening; keratin subunits of 58, 56 and 52 kDa (prediluted; Dako); vimentin (prediluted; Dako); smooth-muscle actin (1:100; Dako); desmin (prediluted; Nichirei); S-100 protein (prediluted; Nichirei); CD34 (prediluted; Nichirei); factor XIIIa (1:20; Biogenesis, TOWN, UK) and anaplastic lymphoma kinase (1:100; Nichirei).

Clinical history

A 54-year-old Japanese man was diagnosed as having renal cell carcinoma and underwent a right nephrectomy. The histopatho-

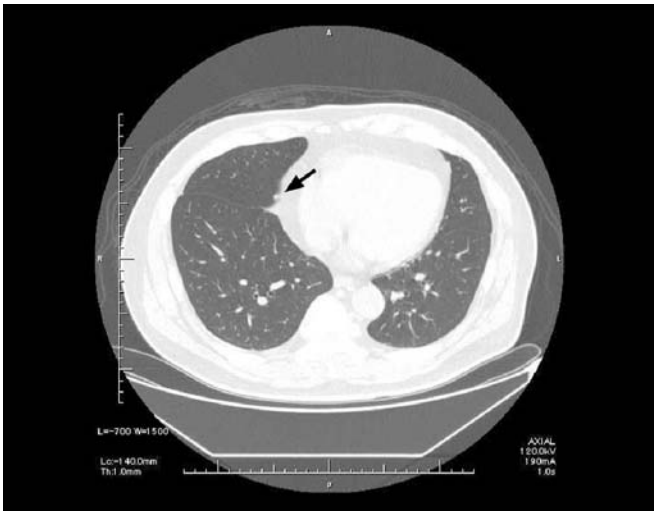

Fig. 1 A chest computed tomography scan reveals a small nodule (*arrow*) in the right mediastinal pleura

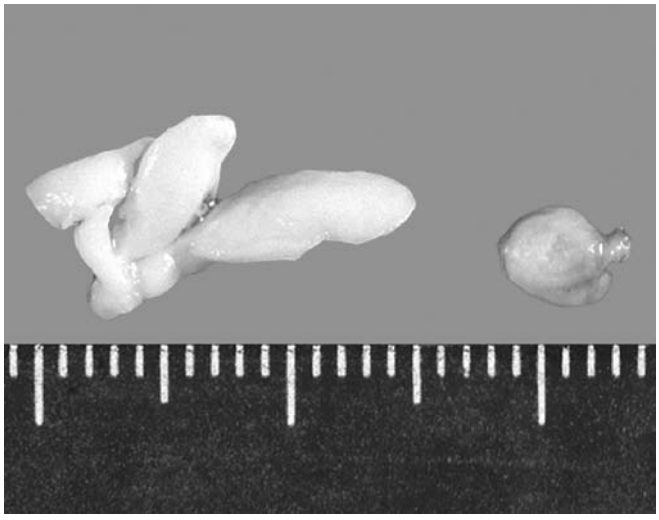

Fig. 2 The large arborized nodule (*left*) and the small dome-shaped nodule (*right*). (The scale is in cm)

logical diagnosis was clear cell carcinoma at stage III (T3aN0M0) according to the tumor node metastasis classification. The treatment for renal cell carcinoma was not received after operation. A computed tomography (CT) scan of the patient's chest 2 years later revealed several nodular lesions in both lungs and a nodule in the right mediastinal pleura (Fig. 1). No calcifications were detected. The patient had neither symptoms nor signs of respiratory disease and had no history of exposure to asbestos. The radiological images suggested a diagnosis of pulmonary and pleural metastases of renal cell carcinoma. To excise the lesions and to confirm the diagnosis, we performed wedge resection of the right middle lobe that contained intrapulmonary nodules and local excision of two protruding nodules located in the right parietal pleura, one of which had not been detected by CT. The patient's postoperative course was uneventful, and he was well 6 months after the resection.

Results

Pathological findings

The intrapulmonary nodules in the resected middle lobe were histologically identical to clear cell carcinoma of the kidney. Macroscopically, the two specimens of the pleura were firm and smooth surfaced. The large nodule measured 1.0×1.5×0.8 cm and was arborized in shape (Fig. 2, left), while the small nodule measured 0.5×0.5×0.5 cm and was dome shaped (Fig. 2, right). The cut surfaces revealed a solid, white, fibrous matrix without any hemorrhage or necrosis. A slightly gritty consistency was detected during sectioning. Under the light microscope, the two lesions resembled each other. Each was uniformly hypocellular and clearly circumscribed, without a fibrous capsule. Abundant hyalinized collagenous tissue was interspersed with bland spindle cells, scant lymphoplasmacytic infiltrate and small calcifications (Fig. 3). The calcifications had the laminated appearance that is typical of psammoma bodies (Fig. 4). These findings were consistent with a diagnosis of CFT.

Immunohistochemical staining revealed that most spindle cells were positive for vimentin, CD34 (Fig. 5, left) and factor XIIIa (Fig. 5, right) but negative for epithelial membrane antigen, keratin, smooth-muscle actin, desmin, S-100 protein and anaplastic lymphoma kinase (ALK).

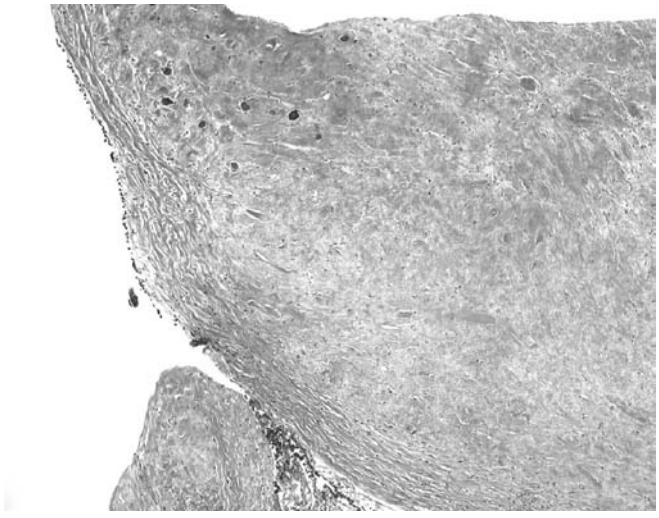

Fig. 3 Small calcifications (*upper left*) are visible in hypocellular, hyalinized collagenous tissue (hematoxylin and eosin, original magnification ×40)

Discussion

Although more than 60 cases have been reported, CFT is a rare lesion [7]. It occurs at various sites, including the subcutaneous and deep soft tissues of the extremities, trunk, neck and peritoneum and in the adrenal gland, lung and mediastinum, as well as in the pleura. In the thorax, specifically, 12 cases have been reported, including 5 in the pleura, 4 in the mediastinum, 2 in the lung and 1 in the chest wall [4, 5, 6, 8, 9, 10, 11, 12, 13]. The clinical features of the 5 previously reported cases in the pleura

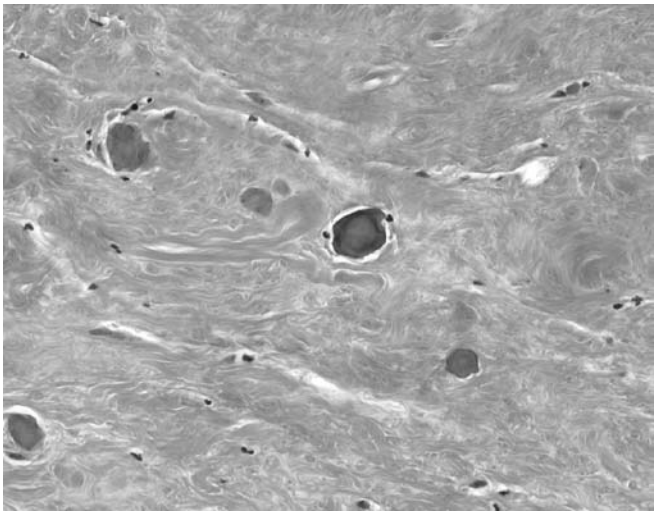

Fig. 4 Laminated psammomatous calcifications are evident (hematoxylin and eosin, original magnification ×400)

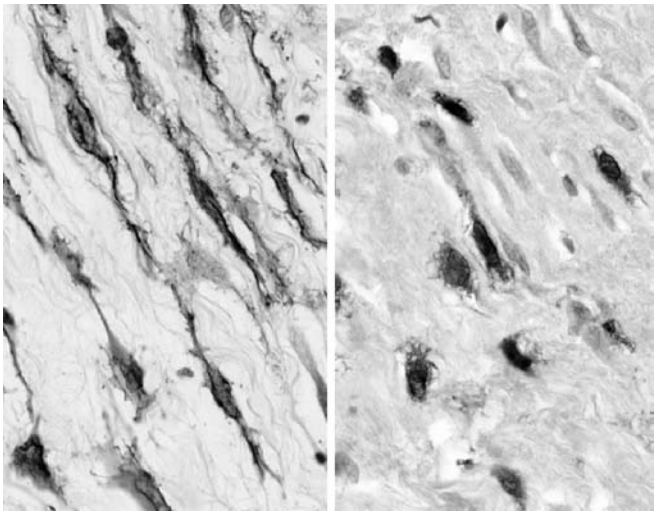

Fig. 5 Spindle cells were immunopositive for CD34 (*left*) and factor XIIIa (*right*) (original magnification ×400)

and the present case are summarized in Table 1 [4, 5, 6]. Of these lesions, 4 were in women and 2 in men. The ages of these 6 patients ranged from 23 years to 54 years, with mean age of 34 years. CFT of the pleura affects slightly older individuals than CFT of the somatic soft tissue, which is found mostly in children and young adults, with a mean age of 14.5 years [1, 2]. The excised lesions measured 1.5–12.5 cm in largest diameter. Of the 6 patients, 4 had multiple lesions. Of the patients, 3 presented with nonproductive cough and/or chest pain, while other the 3 were asymptomatic. Our patient had CFT simultaneously with pulmonary metastases of his renal call carcinoma. No history of prior respiratory illness was documented in the previous 5 cases. Our patient's metastatic carcinoma led us to discover lesions that were much smaller than those in the previously reported cases. There was no evidence of recurrence 6–12 months after resection in the previously reported cases. In the literature, most reported CFTs in the somatic soft tissue were solitary, and some cases were multiple [4, 5, 13, 14, 15]. The pleura might be a site that favors the simultaneous occurrence of multiple CFTs.

Careful examination of the criteria for CFT of the pleura allows it to be distinguished from other benign fibrous lesions, such as solitary fibrous tumor, old empyema or hemothorax, pleural plaque and inflammatory myofibroblastic tumor (IMT). Solitary fibrous tumor contains hyalinized collagen bundles similar to those in CFT, but it is usually associated with hypercellular areas and lacks psammomatous calcifications. Immunoreactivity for CD34, which characterizes solitary fibrous tumor [16], has been documented in a few cases of CFT [17, 18] and was also demonstrated in the present case. The expression of CD34 might reflect a common origin from submesothelial fibroblasts for both CFT and solitary fibrous tumor [17]. But most cases of CFT are negative for CD34 [14]; the original cell remains unknown. Although old empyema or hemothorax can result in a fibrous thickening of the pleura, the fibrosis is more diffuse than that in CFT, and there are no psammomatous calcifications. Pleural plaques usually occur in older patients with a history of exposure to asbestos. Discrimination between CFT and IMT can be difficult because both lesions are composed of spindle cells with lymphocytic infiltrates and, in addition, IMT is associated with occasional calcifications. However, IMT is usually hypercellular, with more frequent inflammatory infiltrates than those in CFT. In intrathoracic lesions, moreover, IMT is usually intraparenchymal compared with the pleura-based location of CFT. Some authors have suggested that CFT represents a sclerosing end-stage form of IMT [2, 10, 15]. Indeed, Van Dorpe et al. [15] reported a case of multiple peritoneal nodules in which CFT and IMT coexisted or were adjacent to each other, while

Table 1 Reported cases of calcifying fibrous tumor of the pleura. *NM* not mentioned, *RCC* renal cell carcinoma

Case	Age (years)/sex	Size* (cm)	Clinical presentation	Number of nodules	Recurrence (yes/no)/follow-up
1 [4]	23/Female	12.5	Chest pain	5	No/9 months
2 [4]	28/Female	6.5	No symptoms	2	No/12 months
3 [4]	34/Male	4.0	Chest pain Non-productive cough	1	NM
4 [5]	29/Female	4.5	No symptoms	Multiple	NM
5 [6]	38/Female	6.0	Chest pain	1	NM
Present case	54/Male	1.5	No symptoms (pulmonary metastases of RCC)	2	No/6 months

* Largest diameter

Pomplun et al. [10] reported a case of CFT that had arisen in a pulmonary inflammatory pseudotumor. However, recent studies suggest that CFT and IMT might be distinct from one another because of differences in immunodetectable expression of factor XIIIa, smooth-muscle actin, CD34 and ALK [13, 14, 19]. For example, CFT is immunopositive for factor XIIIa but immunonegative for ALK. Results for smooth-muscle actin and CD34 have been inconsistent. The present case was immunopositive for factor XIIIa and CD34, as was a previously reported CFT. A review of previous reports indicates that the etiology of CFT remains unclear, and it seems to be a heterogeneous entity. It seems likely that a variety of neoplastic and non-neoplastic fibrous lesions can be sclerotic and can even be associated with psammomatous and/or dystrophic calcifications at the end stage, which has also been called the "late sclerosing" or "burn-out" stage. It is probable that CFT includes various types of benign fibrous tumor or tumor-like lesions whose parent lesions have become so sclerotic that they are unrecognizable.

Some malignant tumors with desmoplasia and/or calcifications must also be included in differential diagnoses. Among pleural neoplasms, desmoplastic mesothelioma has a partially hypocellular collagenous appearance, but it is obviously invasive with bland necrosis or frankly sarcomatous areas. Moreover, immunoreactivity specific for cytokeratins is characteristic of desmoplastic mesothelioma [16]. Metastatic tumors with pleural calcifications have also been reported and include synovial sarcoma, giant cell tumor of the bone and carcinomas of the colon, ovary, breast and thyroid [20]. These metastatic tumors can be confused radiologically and, thus, a histological examination is necessary to confirm a definite diagnosis. The presence or absence of malignancy at other sites, associated pleural effusion or intrapulmonary masses might also be useful in distinguishing among possible diagnoses [21].

With respect to treatment, local excision appears to be adequate therapy for CFT of the pleura, as it is for CFT of somatic soft tissue [6]. However, local recurrence has been reported in a few cases [2, 13, 14].

The small CFTs in the present case were found incidentally during a search for pulmonary metastases of renal carcinoma by CT. It is possible that CFT of the pleura might be more frequent than is presently believed, since small CFTs might be readily overlooked in view of the absence of symptoms, the difficulties associated with radiological detection and the insignificant histological abnormalities.

Acknowledgements The authors thank Mr. S. Yano and Ms. T. Nakamatsu for their skilled technical assistance.

References

1. Rosenthal NS, Abdul-Karim FW (1988) Childhood fibrous tumor with psammoma bodies. Clinicopathologic features in two cases. Arch Pathol Lab Med 112:798–800
2. Fetsch JF, Montgomery EA, Meis JM (1993) Calcifying fibrous pseudotumor. Am J Surg Pathol 17:502–508
3. Montgomery E (2002) Calcifying fibrous tumour. In: Fletcher CDM, Unni KK, Mertens F (eds) Pathology and genetics of tumours of soft tissue and bone. IARC Press, Lyon, pp 77–78
4. Pinkard NB, Wilson RW, Lawless N, Dodd LG, McAdams HP, Koss MN, Travis WD (1996) Calcifying fibrous pseudotumor of pleura. A report of three cases of a newly described entity involving the pleura. Am J Clin Pathol 105:189–194
5. Hainaut P, Lesage V, Weynand B, Coche E, Noirhomme P (1999) Calcifying fibrous pseudotumor (CFPT): a patient presenting with multiple pleural lesions. Acta Clin Belg 54:162–164
6. Ammar A, El Hammami S, Horchani H, Sellami N, Kilani T (2003) Calcifying fibrous pseudotumor of the pleura: a rare location. Ann Thorac Surg 76:2081–2082
7. Lee HY, Chuah KL, Tan PH (2003) Test and teach. Diagnosis: calcifying fibrous pseudotumour. Pathology 35:166–169
8. Reed MK, Margraf LR, Nikaidoh H, Cleveland DC (1996) Calcifying fibrous pseudotumor of the chest wall. Ann Thorac Surg 62:873–874
9. Peachell M, Mayo J, Kalloger S, Flint J, English J (2003) Calcifying fibrous pseudotumour of the lung. Thorax 58:1018–1019
10. Pomplun S, Goldstraw P, Davies SE, Burke MM, Nicholson AG (2000) Calcifying fibrous pseudotumour arising within an inflammatory pseudotumour: evidence of progression from one lesion to the other? Histopathology 37:380–382
11. Dumont P, de Muret A, Skrobala D, Robin P, Toumieux B (1997) Calcifying fibrous pseudotumor of the mediastinum. Ann Thorac Surg 63:543–544
12. Jeong HS, Lee GK, Sung R, Ahn JH, Song HG (1997) Calcifying fibrous pseudotumor of mediastinum—a case report. J Korean Med Sci 12:58–62
13. Nascimento AF, Ruiz R, Hornick JL, Fletcher CD (2002) Calcifying fibrous "pseudotumor": clinicopathologic study of 15 cases and analysis of its relationship to inflammatory myofibroblastic tumor. Int J Surg Pathol 10:189–196
14. Hill KA, Gonzalez-Crussi F, Chou PM (2001) Calcifying fibrous pseudotumor versus inflammatory myofibroblastic tumor: a histological and immunohistochemical comparison. Mod Pathol 14:784–790
15. Van Dorpe J, Ectors N, Geboes K, D'Hoore A, Sciot R (1999) Is calcifying fibrous pseudotumor a late sclerosing stage of inflammatory myofibroblastic tumor? Am J Surg Pathol 23:329–335
16. Flint A, Weiss SW (1995) CD-34 and keratin expression distinguishes solitary fibrous tumor (fibrous mesothelioma) of pleura from desmoplastic mesothelioma. Hum Pathol 26:428–431
17. Weynand B, Draguet AP, Bernard P, Marbaix E, Galant C (1999) Calcifying fibrous pseudotumour: first case report in the peritoneum with immunostaining for CD34. Histopathology 34:86–87
18. Zamecnik M, Michal M, Boudova L, Sulc M (2000) CD34 expression in calcifying fibrous pseudotumours. Histopathology 36:183–184
19. Sigel JE, Smith TA, Reith JD, Goldblum JR (2001) Immunohistochemical analysis of anaplastic lymphoma kinase expression in deep soft tissue calcifying fibrous pseudotumor: evidence of a late sclerosing stage of inflammatory myofibroblastic tumor? Ann Diagn Pathol 5:10–14
20. Seo JB, Im JG, Goo JM, Chung MJ, Kim MY (2001) Atypical pulmonary metastases: spectrum of radiologic findings. Radiographics 21:403–417
21. Erasmus JJ, McAdams HP, Patz EF Jr, Murray JG, Pinkard NB (1996) Calcifying fibrous pseudotumor of pleura: radiologic features in three cases. J Comput Assist Tomogr 20:763–765

Virchows Arch (2005) 446:82–84
DOI 10.1007/s00428-004-1087-0

LETTER TO THE EDITOR

Hideo Hattori

Ciliated cyst of probable mullerian origin arising in the posterior mediastinum

Received: 2 February 2004 / Accepted: 7 July 2004 / Published online: 8 October 2004
© Springer-Verlag 2004

Sir, several types of cyst have been reported in the mediastinum. They include thymic cyst, bronchogenic cyst, esophageal cyst and celomic cyst [6]. Mullerian cyst arising in sites other than the female genital tract has been reported rarely in the literature. We report a mediastinal cyst that has a feature characteristic of a mullerian cyst.

An 18-year-old woman presented with an abnormal shadow on chest X-ray film during medical examination. She had otherwise neither anatomic abnormalities nor clinical symptoms. Computed tomographic scan and magnetic resonance imaging (MRI) revealed a lesion measuring 28×21×33 mm situated in the posterior mediastinum, in the right side of Th 5 level of vertebra, not in direct communication with tracheobronchial tree or esophagus. In T1-weighted scans of MRI, it was hypointense, while in T2-weighted scans, hyperintense signals were observed (Fig. 1). According to the radiological diagnosis of neurogenic tumor, surgical removal of the lesion was performed.

Immunohistochemical stainings were performed using a Ventana immunostainer (Ventana, Tacson, AZ). Primary antibodies used are commercially available AE1/AE3, CAM5.2, cytokeratin 7 (CK7), cytokeratin 19 (CK19), cytokeratin 20 (CK7), epithelial membrane antigen (EMA), desmin, 1A4, HHF35, CD10, estrogen receptor-α (ER), progesterone receptor (PR), cancer antigen 125 (CA125), calretinin, and carcinoembryonic antigen (CEA) (for details on the antibodies, see Table 1). Positive and negative controls were used in each assay. For ER and PR, deparaffinized sections were pretreated with microwave for 15 min in 95°C 10 mM citrate buffer at pH 6.0. For AE1/AE3, CAM5.2, CK7, CK19, calretinin and CK 20, deparaffinized sections were pretreated with trypsin in the automated staining procedure.

H. Hattori (✉)
Department of Pathology,
Kariya General Hospital,
Sumiyoshicho 5-15 Kariya, 448-0852 Aichi, Japan
e-mail: hattori.kariya-gh.pathol@kariya-gh.or.jp
Tel.: +81-566-212450
Fax: +81-566-258216

The lesion had ruptured during the removal procedure. It was a thin-walled but not translucent unilocular cyst, the inner surface of which was smooth and whitish in color.

The entire cyst was histologically examined. The cyst was lined by non-stratified cuboidal to columnar epithelium with no cytological atypia. Specifically, it was composed of ciliated cells, apocrine-like secretory cells and intercalated cells. Goblet cells were not found. Beneath the lining epithelium was an almost completely circumferential smooth-muscle layer, followed by loose connective tissue with abundant vascular channels. Cartilages and any types of glands were not observed (Fig. 2).

Lining epithelial cells of the cyst were positive for AE1/AE3, CAM 5.2, CK7 and CK19 in the cytoplasm. Apical surface of the lining cells stained occasionally positive with EMA and less conspicuously with CA125. Epithelial cells stained positive in the nucleus with ER and PR. They were negative for CK20, CEA, calretinin and CD10. Bundles of smooth-muscle cells stained diffusely positive with 1A4 and HHF-35 and less diffusely positive with desmin. Some of them were positive for ER and PR. They were negative for CD10 and calretinin (Table 1) (Fig. 3). We also examined ER and PR for a case of mediastinal bronchogenic cyst resected from an 18-year-old woman for a control, in which all of the cell types were entirely negative.

This is the first reported case of ciliated cyst of probable mullerian origin arising in the mediastinum. Ciliated cysts of probable mullerian origin in sites other than genitourinary organs or pelvis have been rarely reported. To my knowledge, only two categories have been known. Cutaneous ciliated cyst has a female preponderance, although a few male cases have been reported. This fact, together with morphological resemblance of lining cells to the epithelium of fallopian tube, has suggested their mullerian origin [2]. Retroperitoneal mullerian cyst represents another example of extra-genitourinary mullerian cyst. Only six cases of this entity have been reported, all the patients being adult women [4]. Pathological features presented in the recent case report of retroperitoneal

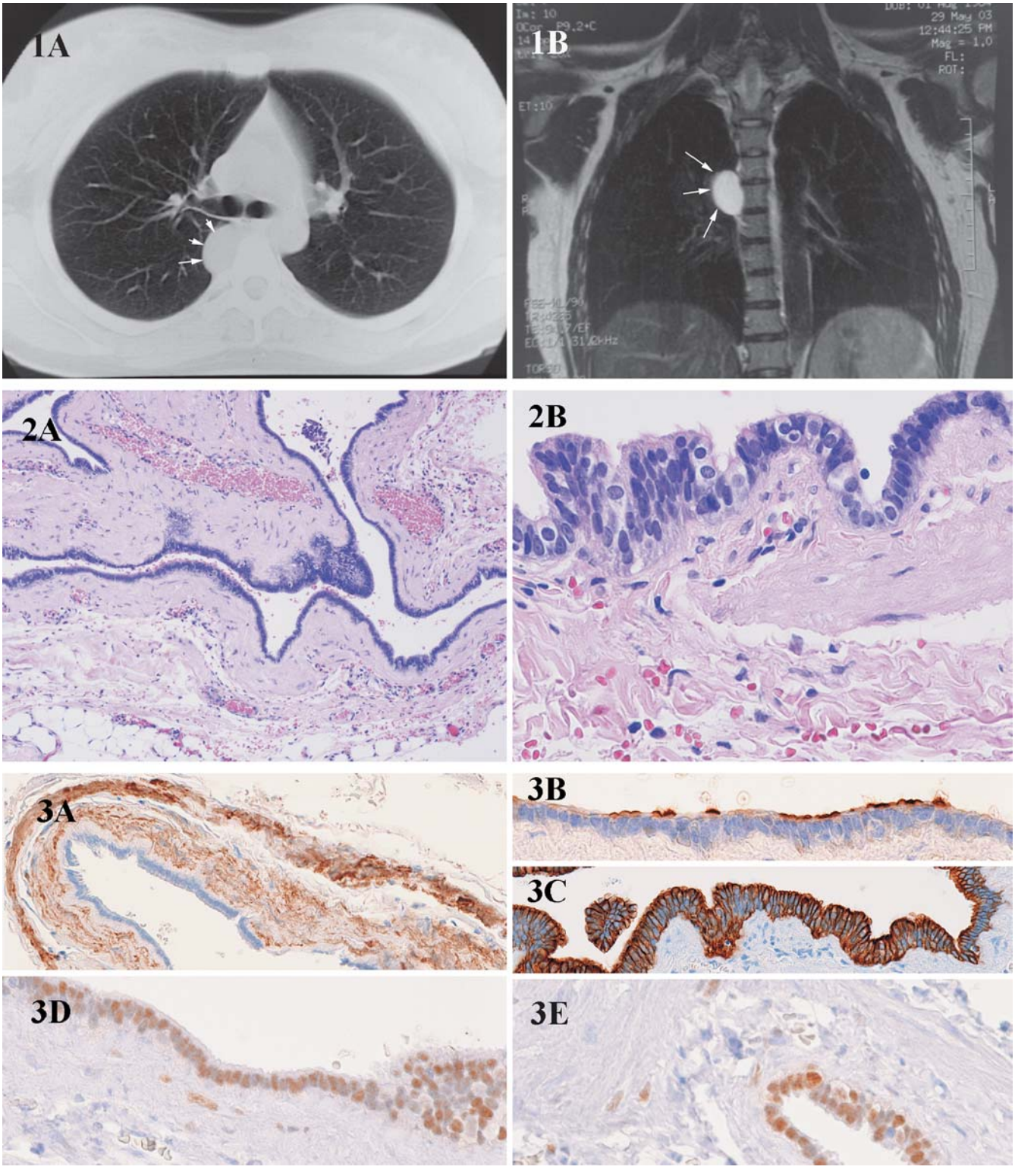

Fig. 1 Plain computed tomographic scan reveals a cystic lesion situated in the posterior mediastinum (*arrow*) (**A**). T2-weighted scans of MRI reveal hyperintense signals (*coronal view*) (**B**)

Fig. 2 The lesion is a thin-walled unilocular cyst with an almost completely circumferential smooth muscle layer (**A**), lined by non-stratified cuboidal to columnar epithelium composed of ciliated cells (some with clear cytoplasm), apocrine-like secretory cells and intercalated cells (**B**) (H&E; **A** ×100, **B** ×400)

Fig. 3 Bundles of smooth muscle cells stain diffusely positive with HHF-35 (**A**). Apical surface of the lining cells stained occasionally positive with epithelial membrane antigen (**B**). Lining epithelial cells of the cyst are positive for CK7 in the cytoplasm (**C**). The epithelial cells as well as some of the smooth muscle cells stain positive with ER (**D**) and PR (**E**) in the nucleus. (Diaminobenzidine; **A** ×100, **B** , **D** , **E** ×400, **C** ×200)

Table 1 Immunohistochemistry

Antibodies	Dilution and company	Result
Cytokeratin (AE1/AE3)	Prediluted; Dako, Carpenteria, CA	C+
Cytokeratin 7 (CK7) (OV-TL 12/30)	Prediluted; Dako	C+
Cytokeratin 19 (CK19) (RCK108)	1:50; Dako	C+
Cytokeratin (CAM 5.2)	Prediluted; Becton-Dickinson, Mountainview, CA	C+
Cytokeratin 20 (CK20) (Ks 20.8)	Prediluted; Dako	Negative
Epithelial membrane antigen (EMA) (E29)	Prediluted; Dako	A+
Cancer antigen 125 (CA125) (OC125)	Prediluted; Dako	A+
Carcinoembbryonic antigen (CEA) (polyclonal)	Prediluted, Dako	Negative
α-Smooth muscle actin (1A4)	1:200; Dako	M+
Muscle actin (HHF35)	Prediluted; Dako	M+
Desmin (D33)	Prediluted; Dako	M+
CD10 (56C6)	Prediluted; Novocastra, Newcastle, UK	Negative
Calretinin (DAK Calret1)	1:100; Dako	Negative
Estrogen receptor-α(ER) (6F11)	Prediluted; Ventana, Tacson, AZ	N+
Progesterone receptor (PR) (1A6)	Prediluted; Ventana	N+

C, cytoplasm of the epithelium; A, apical surface of the epithelium; M, smooth muscle cells; N, nucleus of the epithelial, and few smooth muscle, cells

mullerian cyst closely parallels the pathological features of our case, including histologic and immunohistochemical features of lining epithelia and the presence of a smooth muscle layer [4]. Ciliated cyst of probable mullerian origin in the mediastinum may have been misclassified as bronchogenic cysts. Most bronchogenic cysts arise in the middle mediastinum adjacent to trachea, bronchus or esophagus. Posterior mediastinum is not a typical site of occurrence of bronchogenic cyst. In one series of bronchogenic cysts, 2 of 69 cases were located lateroverteb rally, causing preoperative misdiagnoses for neurogenic tumors [5]. Alternatively, the two cases could have been examples of ciliated cyst of probable mullerian origin. Under light microscopic observations, a ciliated cyst of probable mullerian origin is not very different from a bronchogenic cyst. Distribution and configuration of ciliated cells could be similar to that in bronchogenic cysts. Moreover, apocrine-like secretary cells somehow resemble Clara cells. Absence of goblet cells, any types of glands, and cartilages would be helpful discriminating features. Immunohistochemical detection of ER could be helpful for the differential diagnosis concerned with such nonneoplastic lesions as mullerian or bronchogenic cysts because distribution of estrogen receptor-α in nonneoplastic cells is not high enough to be detected immunohistochemically in the organs other than those of mullerian derivation [1]. Differentials from other mediastinal cysts lined by non-ciliated epithelium will be straightforward. Pleural endometriosis may have similar features focally. In contrast with a mediastinal ciliated cyst, endometriosis presents with hemorrhage and pleural thickening [3]. The origin of a ciliated cyst in the mediastinum is as unclear as one arising in the skin or retroperitoneum. Although the site of occurrence is different, Konishi's postulate that their lesion is directly derived from the primary mullerian apparatus itself could also be applicable to our lesion [4]. Alternatively, it could have been derived from misplaced mesothelium and mesenchyme with characteristics of the secondary mullerian system. Although the histogenesis is not definitive, it would be necessary to differentiate a ciliated cyst of probable mullerian origin from a bronchogenic cyst of the mediastinum because of their different biological characteristics of the lining epithelia.

References

1. Brandenberger AW, Tee MK et al (1997) Tissue distribution of estrogen receptors alpha (ER-alpha) and beta (ER-beta) mRNA in the midgestational human fetus. J Clin Endocrinol Metab 82:3509–3512
2. Farmer ER, Herwig EB (1978) Cutaneous ciliated cysts. Arch Dermatol 114:70–73
3. Flieder DB, Moran CA, Travis WD et al (1998) Pleuropulmonary endometriosis and pulmonary ectopic deciduosis: a clinicopathologic and immunohistochemical study of 10 cases with emphasis on diagnostic pitfalls. Hum Pathol 29:1495–1503
4. Konishi E, Nakashima Y, Iwasaki T (2003) Immunohistochemical analysis of retroperitoneal Mullerian cyst. Hum Pathol 34:194–198
5. Ribet ME, Copin MC, Gosselin B (1995) Bronchogenic cysts of the mediastinum. J Thorac Cardiovasc Surg 109:1003–1010
6. Shimosato Y, Mukai K (1997) Mediastinal cysts. In: Tumors of the mediastinum. Atlas of tumor pathology, 3rd series. Armed Forces Institute of Pathology, Washington, DC, pp 263–267

Virchows Arch (2005) 446:85–87
DOI 10.1007/s00428-004-1092-3

LETTER TO THE EDITOR

Dimas Suárez-Vilela · Francisco Miguel Izquierdo-Garcia

Paraovarian hemangioma with immunoglobulin deposits in a patient with monoclonal gammopathy of uncertain significance and osteolytic lesions

Received: 6 April 2004 / Accepted: 8 July 2004 / Published online: 29 September 2004
© Springer-Verlag 2004

Sir, In 1990 Chan et al. [1] coined the descriptive term glomeruloid hemangioma (GH) for a distinctive vascular proliferation that occurs in patients with POEMS (polyneuropathy, organomegaly, endocrinopathy, M-protein, skin changes) syndrome or multicentric Castleman's disease. Microscopically, GH consists of multiple ectatic vascular structures containing aggregates of capillary loops closely resembling renal glomeruli. Typically these hemangiomas contain globular deposits of immunoglobulins in the endothelial cells.

We report a case of paraovarian hemangioma in a woman with monoclonal gammopathy of uncertain significance (MGUS) and osteolytic lesions in the skull. Microscopically this hemangioma was not glomeruloid, but as in the cases described by Chan et al. [1], it showed globular deposits of immunoglobulins in endothelial cells.

A 78-year-old woman with serum tests positive for hepatitis B virus was sent to our hospital after bicytopenia was discovered during a peripheral blood study (hemoglobin 10.8 g/dl, granulocytes 1800/mm^3). Immunoelectrophoresis showed a monoclonal band of IgG λ-immunoglobulin (2293 mg/l). Both the bone marrow aspiration and the trephine showed a hypoplasia, with a hematopoietic tissue-fatty tissue ratio of 30:70 and normal maturation gradient at the three series. The plasma cell count was 4%, all of them mature elements. On the immunohistochemical study, light chain restriction was not present. X-rays showed osteolytic lesions in frontal, parietal and occipital bones. The patient did not show polyneuropathy, cutaneous angiomatoid lesions or other features of POEMS syndrome. Eight months later she developed abdominal pain. During abdominal surgery, a left paraovarian nodule, attached to the ovarian surface and to a loop of the small bowel, was found. A left salpingoophorectomy was performed including the adhered loop of small bowel. The ovary measured 3×7 cm and contained a nodule in the meso of the ovary. This lesion measured 3.5×4.5 cm in diameter and was attached to the ovarian surface by a narrow pedicle. On cut section, the ovary had a unilocular cyst of 3.5 cm. The paraovarian nodule was red-brown, soft and friable, and it contained hemorrhagic areas. The fallopian tube was normal. The resected small bowel measured 18 cm in length and showed foci of transmural hemorrhagic infarction. Histologically the ovarian cyst was a simple serous one, surrounded by dense stroma. The paraovarian nodule corresponded to a vascular proliferation composed of a complex admixture of small anastomosing channels, as well as much larger vessels with dilated lumina and variably muscular walls (Fig. 1).There was multifocal thrombosis as well as large areas of infarction. Neither endothelial atypia nor multilayering was found. Fusiform cells with characteristics of pericytes were arranged

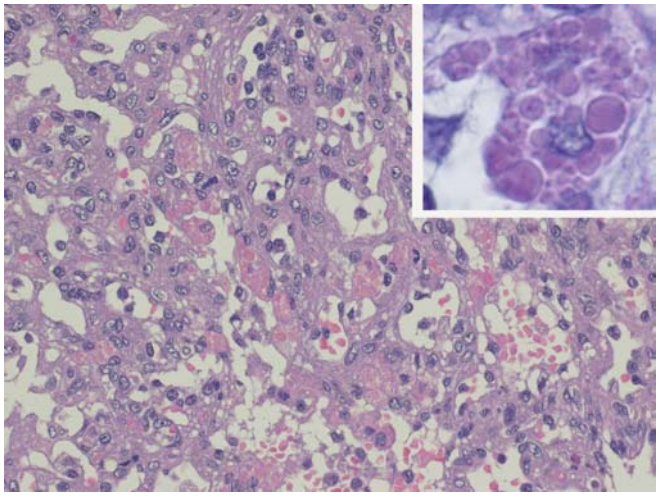

Fig. 1 Vascular channels lined by endothelial cells without nuclear atypia. Some showed homogeneous globules. *Inset* Vacuolized endothelial cells, filled with eosinophil globular structures (periodic acid–Schiff after diastase digestion)

D. Suárez-Vilela (✉) · F. M. Izquierdo-Garcia
Servicio de Anatomía Patológica,
Hospital de León,
Altos de la Nava s/n, 24008 León, Spain
e-mail: pacoizq20@hotmail.com
Tel.: +42-9-87237400
Fax: +42-9-87233322

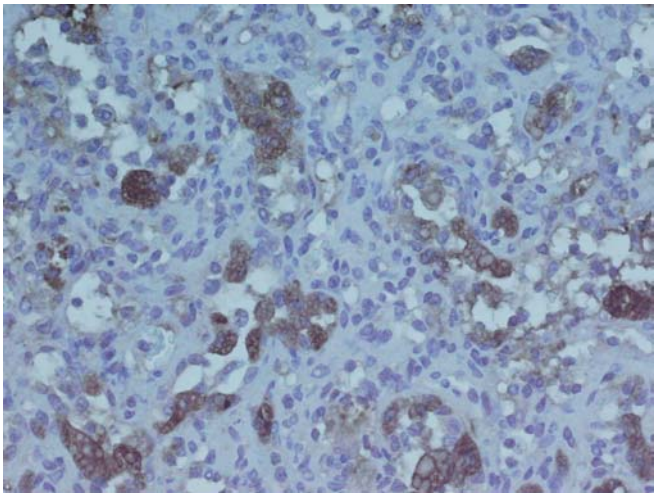

Fig. 2 Globules stained for IgG inside the cytoplasm of the endothelial cells

around the vessels. The cytoplasm of many of the endothelial cells was filled by eosinophilic globules of different sizes (Fig. 1 inset) that were stained by periodic acid–Schiff staining, being resistant to diastase digestion. These cells were positive for vimentin, CD34 (Novocastra), CD31 and factor VIII-associated antigen (Dako) and negative for KP1 (Dako) and AE1-AE3 (Signet) antibodies. Antibodies against IgG (Biogenex) and κ and λ light chains (Dako) strongly stained the cytoplasmic globules (Fig. 2). The fusiform cells of pericytic appearance were positive for smooth muscle actin (Novocastra). This vascular proliferation did not infiltrate the ovary, but it was very close to the vessels of the ovarian hilum and was delimited by a fibrous pseudocapsule.

The histological findings of this case corresponded to a hemangiomatoid tumor, not otherwise specified, with benign characteristics and globules of IgG and light chains in the cytoplasm of the endothelial cells. Similar immunoglobulin deposits are typically described in GHs [1, 4, 7, 8, 10, 11], which are cutaneous or visceral vascular lesions, so-called because they mimic the renal glomerules. This type of hemangioma occurs in patients with POEMS syndrome or is associated with multicentric Castleman's disease [1, 4, 7, 8, 10, 11]. Nowadays two major criteria (polyneuropathy and monoclonal plasma-proliferative disorder) and at least one minor criterion (bone lesions, organomegaly, endocrinopathy etc.) should be satisfied to strictly diagnose POEMS syndrome [2]. Our case does not accomplish all the criteria to be classified as POEMS syndrome inasmuch as the patient only presented MGUS as a major criterion and lytic bone lesions as a minor criterion. However, although polyneuropathy is present in all the cases of POEMS syndrome, some patients have a known plasma cell dyscrasia before the onset of neuropathy [2]. In this clinical context, the vascular paraovarian proliferation with immunoglobulin deposits in the endothelial cells may raise the possibility of an incomplete form of POEMS syndrome. However, in POEMS syndrome, different types of hemangiomas may appear, such as microvenular hemangioma, cherry hemangioma, multinucleated cell angiohistiocytoma and GH [7]. In some cases, the vascular lesions are indistinguishable from an ordinary cherry-type capillary hemangioma, and in other cases the lesions have features intermediate between a capillary hemangioma and the classic GH [1, 4, 7, 10, 11]. We think that the microscopic findings of our case correspond to a vascular lesion of difficult classification that present intermediate histological features between a "conventional hemangioma" and a GH. To our knowledge, a hemangioma with this appearance has not been described in an ovarian or paraovarian location, although in POEMS syndrome the vascular proliferation in the skin and lymph nodes is sometimes accompanied by similar visceral hemangiomatoid lesions, including involvement of serosa of the fallopian tube [1].

This case raises differential diagnosis with a heterogeneous group of vascular lesions included under the common denominator of reactive angioendotheliomatosis [5, 6]. This entity is characterized by cutaneous or visceral vascular proliferation that usually occurs in patients with diverse types of coexistent systemic disease. In those cases of reactive angoendotheliomatosis associated with abnormal circulating proteins, eosinophilic or hyaline globules can appear as intravascular microthrombi. Nevertheless, reactive angioendotheliomatosis do not contain immunoglobulin deposits inside the endothelial cells. So our case is more like GH.

It is still not clear whether the vascular lesions associated with POEMS syndrome are reactive or tumoral, but most of the authors think that they are reactive lesions [1, 4, 7, 8, 10, 11]. On this point, the immunoglobulin deposits in the endothelial cells could act as an angiogenic stimulus and so contribute to the development of the vessels [1]. In these cases, the entry of immunoglobulins and light chains from the plasma into the cytoplasm of the endothelial cells could be made through an internalization mechanism mediated by fibronectin and integrins [3, 9].

Acknowledgements We thank Dr. C.D.M. Fletcher of Brigham and Women's Hospital, Boston, MA, for the review of the case.

References

1. Chan JKC, Fletcher CDM, Hicklin GA, Rosai J (1990) Glomeruloid hemangioma: A distinctive cutaneous lesion of multicentric Castleman's disease associated with POEMS syndrome. Am J Surg Pathol 14:1036–1046
2. Dispenzieri A, Kyle RA, Lacy MQ, Rajkumar SV, Thereneau TM, Larson DR, Greipp PR, Witzig TE, Basu R, Suarez GA, Fonseca R, Lust JA, Gertz MA (2003) POEMS syndrome: definitions and long-term outcome. Blood 101:2496–2506
3. Fujii H, Nakatani K, Arita N, Ito MR, Terada M, Miyazaki T, Yoshida M, Ono M, Fujiwara T, Saiga K, Ota T, Ohtani H, Lockwood M, Sasaki T, Nose M (2003) Internalization of antibodies by endothelial cells via fibronectin implicating a novel mechanism in lupus nephritis. Kidney Int 64:1662–1670
4. Kishimoto S, Takenaka H, Shibagaki R, Noda Y, Yamamoto M, Yasuno H (2000) Glomeruloid hemangioma in POEMS

syndrome shows two different immunophenotypic endothelial cells. J Cutan Pathol 27:87–92
5. McMenamin ME, Fletcher CDM (2002) Reactive angioendotheliomatosis: a study of 15 cases demonstrating a wide clinicopathologic spectrum. Am J Surg Pathol 26:685–697
6. Ogawa K, Tada T, Takeuchi Y, Suenaga M, Suzuki S, Shirai T (2004) Reactive angioendotheliomatosis of the intestine. Am J Surg Pathol 28:257–261
7. Requena L, Sangueza OP (1997) Cutaneous vascular proliferations. 2. Hyperplasias and benign neoplasms. J Am Acad Dermatol 37:887–920
8. Rongioletti F, Gambini C, Lerza R (1994) Glomeruloid hemangioma: a cutaneous marker of POEMS syndrome. Am J Dermatopathol 16:175–178
9. Simionescu M, Simionescu N (1991) Endothelial transport of macromolecules: transcytosis and endocytosis. A look from cell biology. Cell Biol Rev 25:5–78
10. Tsai CY, Lai CH, Chan HL, Kuo TT (2001) Glomeruloid hemangioma—a specific cutaneous marker of POEMS syndrome. Int J Dermatol 40:403–406
11. Yang SG, Cho KH, Bang YJ, Kim CW (1998) A case of glomeruloid hemangioma associated with multicentric Castleman's disease. Am J Dermatol 20:266–270

Virchows Arch (2005) 446:88–90
DOI 10.1007/s00428-004-1122-1

LETTER TO THE EDITOR

Maria P. Foschini · Deborah Malvi · Christine M. Betts

Oncocytic carcinoma arising in Warthin tumour

Received: 20 July 2004 / Accepted: 19 August 2004 / Published online: 29 September 2004
© Springer-Verlag 2004

Sir, Warthin tumour (WT) of the parotid gland is by definition clinically benign, although on rare occasions it can give rise to malignant tumours, which originate from both the epithelial and lymphoid component. Among epithelial malignancies, mucoepidermoid carcinoma (MEC) [5] has been described in WT. This association is in keeping with the evidence that MEC is a "mitochondrion-rich" tumour, showing features of differentiation towards striated ducts [3].

Pure oncocytic cell carcinomas are a rarity in salivary glands and are thought to derive from the oncocytic epithelium of striated ducts. The purpose of the present paper is to report a case of oncocytic carcinoma (OC) arising in WT of parotid gland.

Clinical history

A 72-year-old woman presented with a nodule in the right parotid gland, which had slowly increased in size during the previous 12 months. On echography, the nodule had well-defined margins, was cystic and measured 2.7 cm in the greatest axis. A fine needle aspiration (FNA) was performed using a 25-g needle, which suggested the possibility of an unusual variant of WT. The nodule was surgically excised 2 months later. Following the histological diagnosis of carcinoma and as no residual tumour was detectable both on clinical and radiological grounds, a superficial parotidectomy with facial nerve sparing was performed. No residual tumour was found within the surgical specimen, and, therefore, no further treatment was administered. The patient presented 4 months later with enlarged right cervical lymph nodes, which showed metastatic deposits at histology. Skin metastases appeared 10 months later. The patient was then lost to follow-up soon after.

M. P. Foschini (✉) · D. Malvi
Section of Anatomic Pathology,
Department of Oncological Sciences,
University of Bologna at Ospedale Bellaria,
Via Altura 3, 40139 Bologna, Italy
e-mail: mariapia.foschini@ausl.bologna.it
Tel.: +39-051-6225523
Fax: +39-051-6225759

C. M. Betts
Department of Experimental Pathology,
University of Bologna,
Bologna, Italy

Cytology

Smears obtained on FNA were stained with Papanicolau and May Grunwald–Giemsa methods. Cytological smears were composed of proteinaceous material, containing cells with eosinophilic and granular cytoplasm, with atypical nuclei centrally located. Prominent nucleoli were seen. Clusters of spindle cells were noted. In addition, numerous mature lymphocytes were present.

Macroscopically, the tumour presented as a partially encapsulated nodule, which, on cut section, was partly cystic. On histology, at low power, the lesion showed typical architecture of WT, composed of prominent lymphoid stroma containing solid epithelial nests and glandular or cystic structures (Fig. 1A). The lesion appeared to be surrounded by a fibrous capsule. At higher magnification, the cystic spaces were lined by cuboidal cells, with eosinophilic and granular cytoplasm. The epithelium lining the cysts was focally pluristratified and showed prominent cytological atypia (Fig. 1B). In other areas of the nodule, there was a predominance of solid epithelial nests (Fig. 1C). The latter were composed of markedly atypical cells, oval to spindle in shape, with eosinophilic and granular cytoplasm and central nuclei with prominent nucleoli. Numerous atypical mitotic figures were also seen. Within these areas, the capsule appeared focally invaded by the neoplastic cells. No vascular invasion was seen.

At immunohistochemistry, the epithelial cells of the cystic and solid components were strongly positive for low-weight cytokeratin (monoclonal, clone MNF 166, diluted 1:200; Dako) and showed an intense and granular cytoplasmic positivity with the antibody recognising a mitochondrial antigen (monoclonal, clone 113–1, diluted 1:500; Biogenex) (Fig. 1D, E). Numerous neoplastic cells showed intense nuclear staining for Ki67 (monoclonal, clone MIB 1, diluted 1:200; Dako) and p53 (monoclonal,

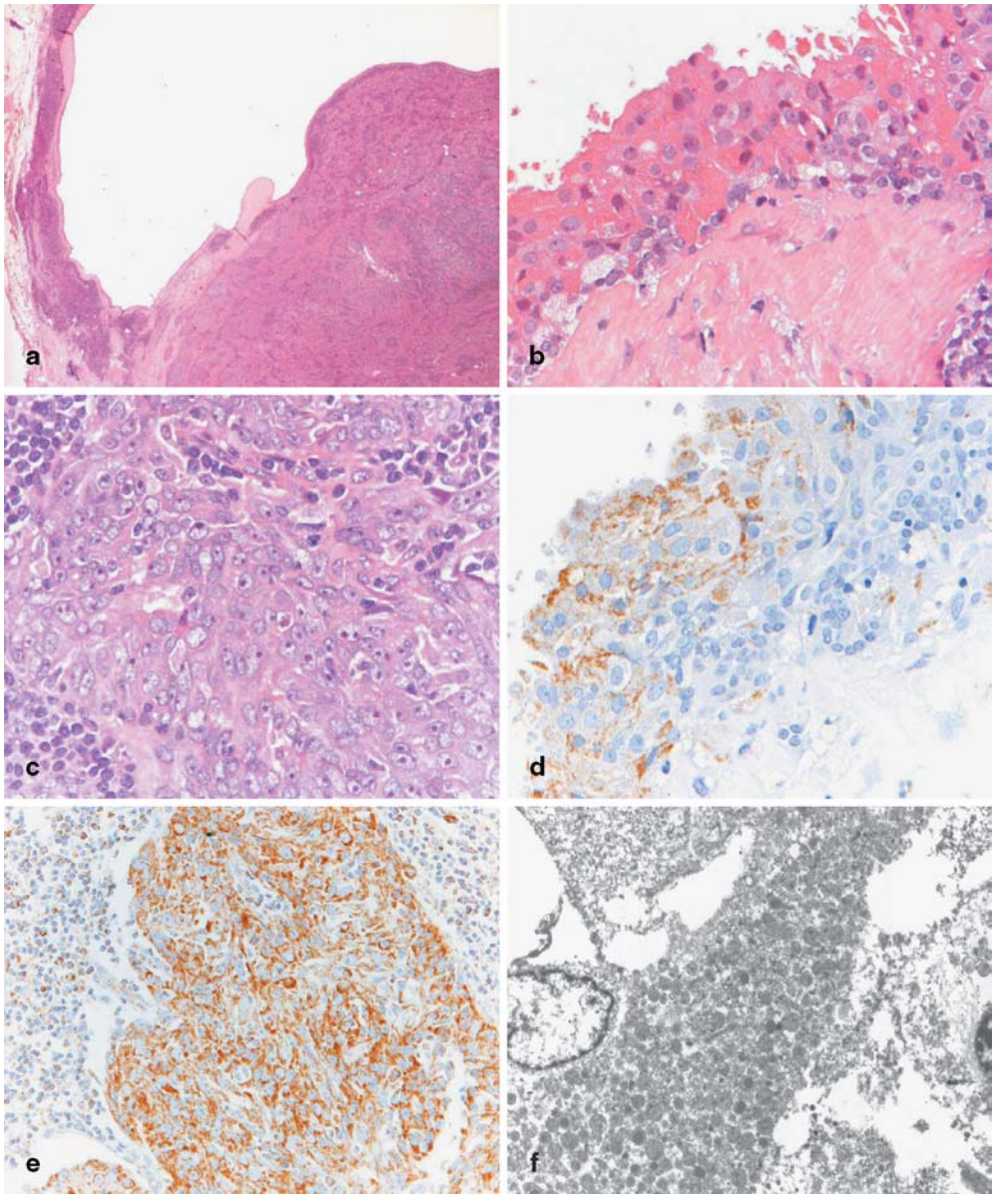

Fig. 1 **A** The nodule shows a cystic and a solid component. **B** The cystic component is lined by atypical eosinophilic cells. **C** The solid nests are composed of cells with eosinophilic cytoplasm, atypical nuclei showing prominent nucleolus. **D**, **E** The same cells are positive with the anti-mitochondrial antibody. **F** Electron microscopic examination reveals numerous mitochondria

clone DO-7, diluted 1:50l Dako). In addition, these latter two antibodies stained numerous cells of the cystic wall where the epithelium was pluristratified. Further immunohistochemical staining for smooth-muscle actin (Dako, monoclonal, clone 1A4, diluted 1:100) and calponin (Biogenex, monoclonal, clone CALP, diluted 1:60) did not reveal any myoepithelial cell component.

Small fragments obtained from paraffin blocks of the primitive and the metastatic lesions were used for ultrastructural investigation, which showed that the non-lymphoid neoplastic cells were engorged with numerous mitochondria (more than 80% of their cytoplasm) (Fig. 1F). The primary tumour, the lymph-node and skin metastases showed the same histological, immunohistochemical and ultrastructural features.

Oncocytes are cells with finely granular, eosinophilic cytoplasm, intensely positive with anti-mitochondrial antibody. These features correspond, on ultrastructural examination, to the presence of numerous mitochondria, occupying more than 60% of the cytoplasm [1]. The present case was composed of cells showing histological, immunohistochemical and ultrastructural features consistent with oncocytic differentiation.

Tumours mainly composed of oncocytes can arise in almost any organ. In salivary glands, oncocytic tumours are rare, and most of the reported cases are benign [2]. According to Dardick [2], WT and benign oncocytoma constitute the two extremes of a spectrum of lesions. Rare cases of OC in WT have been described to date [2, 5]. In the present case, a transition between benign and malignant epithelium lining the cystic component was observed, thus reinforcing the belief of a common origin of the two lesions.

Therefore, the present case has to be added to the list of cases previously reported of carcinomas arisen in WT, confirming the possibility of a malignant transformation

of the epithelium of WT. Prognosis of carcinomas arising in WT seems to be related to the type of carcinoma and to the extracapsular extension. In the case here described, despite only focal capsular involvement, OC gave rise to lymph-node and skin metastases. This behaviour confirms the highly aggressive nature of OC and the necessity for aggressive surgery [4].

In conclusion, the present case further confirms the possibility that, even if only rarely, neoplastic transformation can occur in WT. This possibility should be taken into consideration in preoperative diagnosis of WT.

References

1. Damiani S, Eusebi V, Losi L, D'Adda T, Rosai J (1998) Oncocytic carcinoma (malignant oncocytoma) of the breast. Am J Surg Pathol 22:221–230
2. Dardick I (1996) Color atlas/text of salivary gland tumor pathology. Igaku-Shoin Publishers, New York
3. Foschini MP, Marucci G, Eusebi V (2002) Low-grade mucoepidermoid carcinoma of salivary glands: characteristic immunohistochemical profile and evidence of striated duct differentiation. Virchows Arch 440:536–542
4. Goode K, Corio RL (1988) Oncocytic adenocarcinoma of salivary glands. Oral Surg Oral Med Oral Pathol 65:61–66
5. Nagao T, Sugano I, Ishida Y, Tajima Y, Furuya N, Kondo Y, Nagao K (1998) Mucoepidermoid carcinoma arising in Warthin tumor of the parotid gland. Report of two cases with histopathological, ultrastructural and immunohistochemical studies. Histopathology 33:379–386

Virchows Arch (2005) 446:91–92
DOI 10.1007/s00428-004-1128-8

LETTER TO THE EDITOR

Gaetano Magro · Antonina Torrisi · Antonietta Torrisi

Atypical/bizarre spindle-cell epithelial metaplasia in nodular goiter: a potential diagnostic pitfall

Received: 22 June 2004 / Accepted: 23 August 2004 / Published online: 23 October 2004
© Springer-Verlag 2004

Sir, Primitive spindle-cell tumor or tumor-like lesions of the thyroid are an uncommon finding. As far as thyroid tumors are concerned, apart from the well-known possibility that hyalinizing trabecular adenoma and anaplastic carcinomas may contain epithelial spindle cells, more rarely other tumors, such as follicular adenoma and papillary carcinoma, exhibit a metaplastic spindle-cell epithelial component [4]. In some primitive thyroid lesions, the spindle-cell component may be mesenchymal rather than epithelial in nature; this is the case of the solitary fibrous tumor and reactive lesions, such as the nodular fasciitis-like stroma of the papillary carcinoma and post-fine-needle aspiration spindle-cell nodules [1].

Spindle-cell epithelial metaplasia with nuclear pleomorphism may be occasionally seen in follicular adenoma (atypical adenoma) and focally even in nodular goiter. We report an unusual case of nodular goiter with an area of atypical spindle-cell epithelial metaplasia. A 54-year-old man underwent total thyroidectomy for bilateral nodular goiter. An unexpected finding was the presence of a 1.5-cm-sized, unencapsulated nodular area abruptly merging from an otherwise typical nodular goiter (Fig. 1A), composed mainly of spindle cells with bizarre hyperchromatic nuclei, similar to those observed in the so-called "atypical adenoma" (Fig. 1A, B, C). The cells, frequently arranged in whorls vaguely reminiscent of a nerve-sheath tumor (Fig. 1B), were set in a variably cellular fibrous to edematous stroma. Variable-sized thyroid follicles, some of which showed atypical nuclear pleomorphism, were frequently intermixed with the spindle-cell component, and transition morphological features from follicles to spindle cells were focally observed (Fig. 1B). Mitoses and necrosis were not observed. Immunohistochemical analysis showed a diffuse expression of thyroglobulin and vimentin in association with focal cytokeratin immunoreactivity in atypical spindle cells (Fig. 1D, E, F), while no reaction to calcitonin, S-100 protein, CD34, desmin and α-smooth-muscle actin was obtained. The immunohistochemical and morphological features supported the follicular-derived metaplastic epithelial nature of the atypical/bizarre spindle cells, similar to what is observed in spindle-cell component arising in association with papillary carcinoma and follicular adenoma of thyroid [4].

The spindle-cell metaplastic transformation of follicular epithelium is not at all surprising if we consider that both normal and neoplastic thyroid follicular cells in vitro may undergo an epithelial–mesenchymal transition with a fibroblastic-like appearance characterized by an acquisition of vimentin expression accompanied by a concurrent variable loss of cytokeratin [2, 3]. The present case contributes to widen the spectrum of the spindle-cell lesions, which can be encountered in diagnostic practice of thyroid pathology. Although atypical follicular cells may be expected in different thyroid diseases (follicular adenoma, nodular goiter, Basedow's disease) without adverse prognostic significance, their uncommon spindle-cell metaplastic transformation may alert pathologists, who should be aware of this possibility to avoid a diagnosis of malignancy.

G. Magro (✉) · A. Torrisi · A. Torrisi
Department G.F. Ingrassia,
Anatomia Patologica,
Via S. Sofia 87, 95123 Catania, Italy
e-mail: g.magro@unict.it

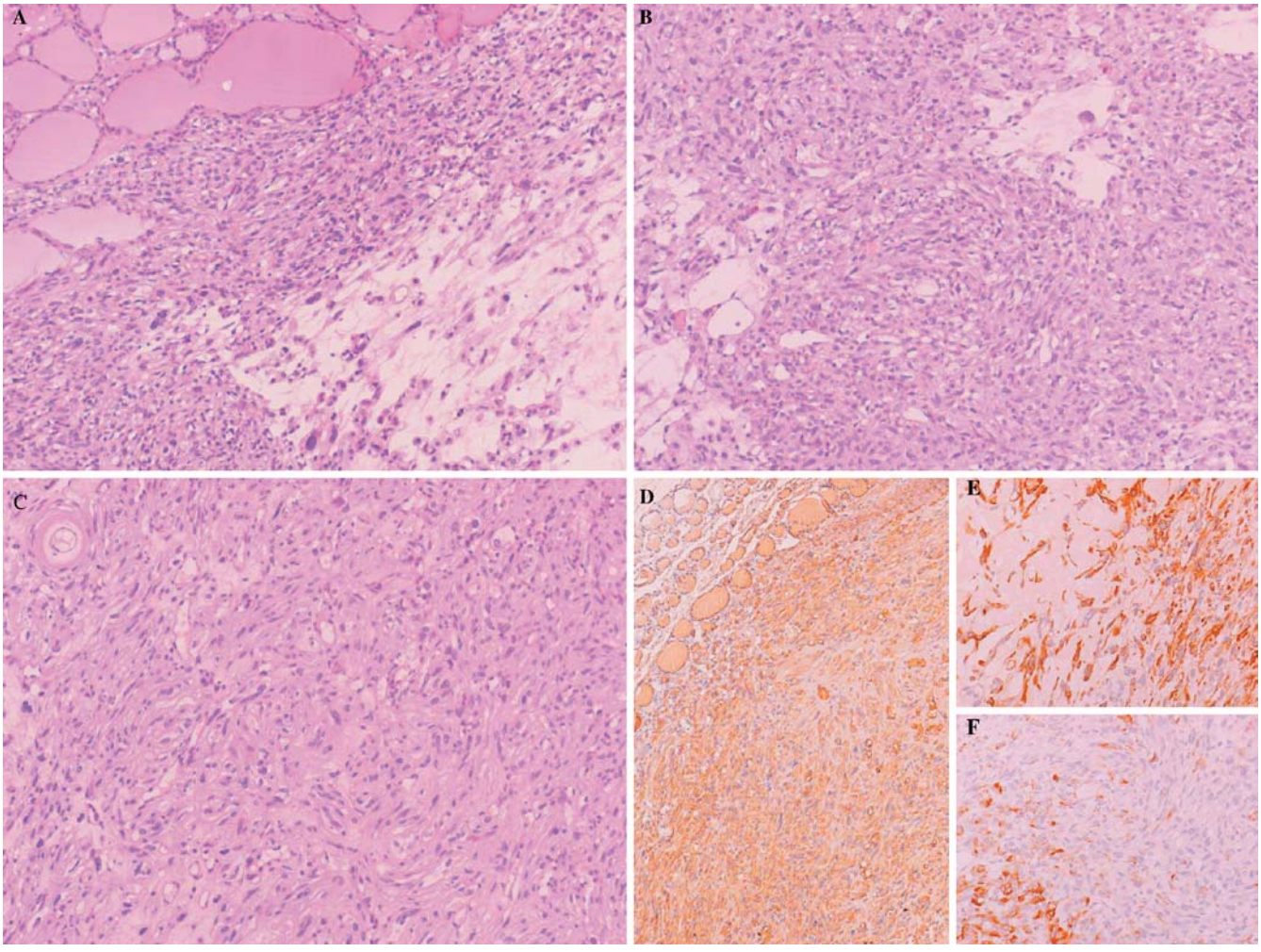

Fig. 1 Atypical/bizarre spindle cells closely intermingling with follicles (**A**) were frequently arranged in whorls (**C**). Transition from atypical follicular to spindle cells is evident (**B**). The spindle cells were diffusely immunoreactive to thyroglobulin (**D**) and vimentin (**E**) and focally to cytokeratin (**F**)

References

1. Baloch ZW, Wu H, LiVolsi V (1999) Post-fine-needle aspiration spindle cell nodules of the thyroid. Am J Clin Pathol 111:70–74
2. Greenburg G, Hay ED (1988) Cytoskeleton and thyroglobulin expression change during transformation of thyroid epithelium to mesenchyme-like cells. Development 102:605–622
3. Herrmann ME, Trevor KT (1993) Epithelial–mesenchymal transitions during cell culture of primary thyroid tumors? Genes Chromosomes Cancer 6:239–242
4. Vergilio J, Baloch ZW, LiVolsi V (2002) Spindle cell metaplasia of the thyroid arising in association with papillary carcinoma and follicular adenoma. Am J Clin Pathol 117:199–204

Virchows Arch (2005) 446:93–94
DOI 10.1007/s00428-004-1136-8

LETTER TO THE EDITOR

Shubhada Kane · Jay Mehta

Primary epithelioid hemangioendothelioma of the peritoneum—a diagnostic dilemma

Received: 16 August 2004 / Accepted: 2 September 2004 / Published online: 30 November 2004
© Springer-Verlag 2004

Dear Editors:
We report two cases of primary epithelioid hemangioendothelioma of the peritoneum presenting as omental masses. The first case was a 45-year-old male, and the second was a 12-year-old boy. Both the cases presented with an omental mass without ascites. Ultrasonographic examination showed normal abdominal organs, including liver. Chest X-ray was normal. A complete excision was performed in both the cases. Microscopy revealed lobules of epithelioid cells beneath a layer of mesothelium (Fig. 1). The tumor showed a bimorphic population consisting of large epithelioid cells with vesicular nuclei, prominent nucleoli and abundant pale eosinophilic cytoplasm. The second population of tumor cells exhibited clear, vacuolated cytoplasm (Fig. 2). Some of these cells showed eccentric nucleus and large intracytoplasmic lumina containing one or two erythrocytes (Fig. 3). Mucin stain was negative in the clear cells. Mitotic activity was not seen; there was no evidence of necrosis or spindled areas. Papillary growth pattern or glandular differentiation was not overtly evident. Immunohistochemically, the tumor cells expressed vimentin, factor VIII, CD 31 (Fig. 4) and CD 34 and were immunonegative for cytokeratin, epithelial membrane antigen, HBME-1, carcinoembryonic antigen, CD 15, Calretinin, c-kit (CD 117), smooth muscle actin (SMA) and S-100 protein. Considering the morphological appearance and the immunohistochemical profile, a diagnosis of primary epithelioid hemangioendothelioma of the peritoneum was rendered in both the cases.

Diffuse involvement of the peritoneum is usually associated with tumors of primary and secondary mullerian systems, mesothelioma or metastasis from gastric, colonic or pancreatic adenocarcinomas [1]. We have discussed these cases because of their rarity at this site, which leads to a diagnostic dilemma. The principle differential diagnosis of this tumor in adults is malignant mesothelioma, in view of the epithelioid nature of the tumor cells. However, intracytoplasmic lumina with red blood cells indicate abortive attempt at vascular differentiation and offers a diagnostic clue. The immunohistochemical profile of mesothelioma should further help to resolve this dilemma. The reason to differentiate these two histologically related entities is that epithelioid hemangioendothelioma is considered to be a low-grade malignant tumor with infrequent metastatic potential and a favorable prognosis in contrast with diffuse malignant mesothelioma, which has a very poor prognostic outlook. Secondly, it is necessary to differentiate the two entities because of insurance claims related to the occupational exposure to asbestos in case of mesothelioma.

The diagnostic dilemma becomes more acute in the pediatric age group when mesothelioma is ruled out on immunohistochemistry work-up, and a metastatic carcinoma is highly unlikely. In children, apart from mesothelioma, desmoplastic small round cell tumor (DSRCT)

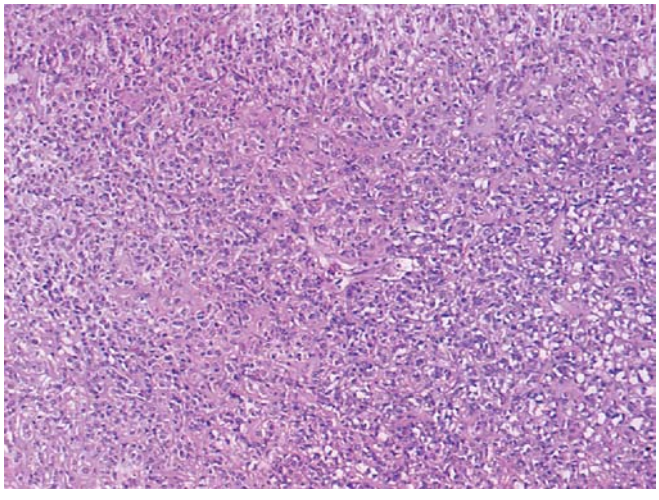

Fig. 1 Diffuse proliferation of a bimorphic population of tumor cells. Haematoxylin and eosin ×4

S. Kane (✉) · J. Mehta
Department of Pathology,
Tata Memorial Hospital,
Dr Ernest Borges Road, Parel, 400012 Mumbai, India
e-mail: drsvkane@rediffmail.com
Tel.: +91-22-24177272

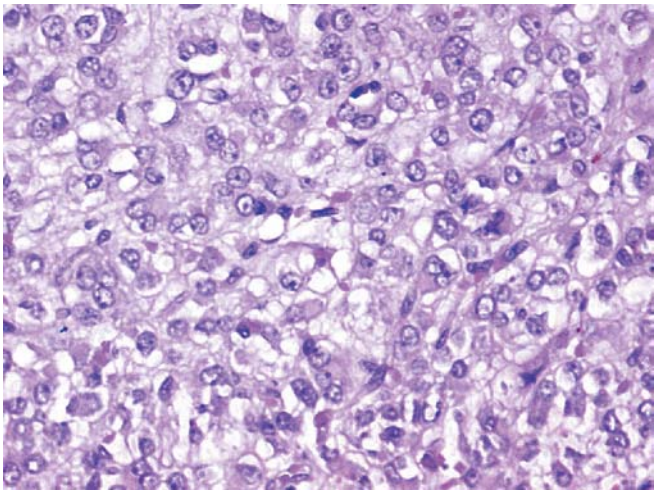

Fig. 2 Bimorphic population consisting of epithelioid cells with vesicular nuclei, prominent nucleoli and abundant pale eosinophilic cytoplasm and a second population of cells with clear, vacuolated cytoplasm and large intracytoplasmic lumina. Haematoxylin and eosin ×20

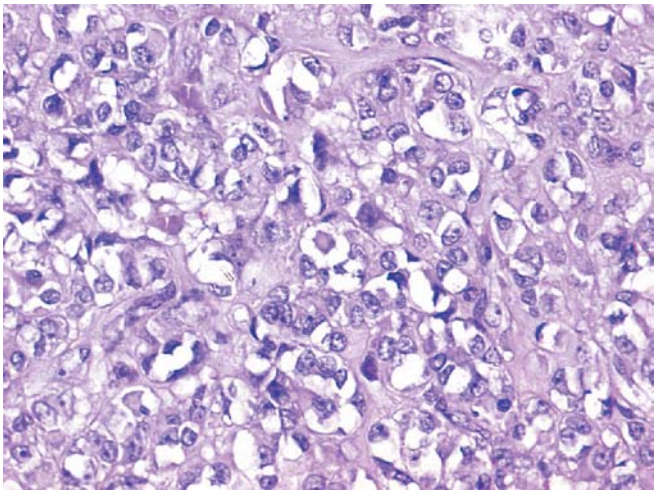

Fig. 3 Tumor cells showing eccentric nucleus and intracytoplasmic lumina containing erythrocytes (*arrow*). Haematoxylin and eosin ×40

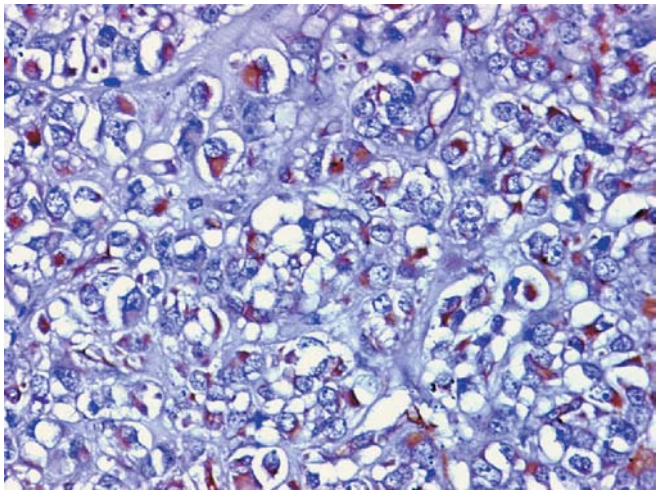

Fig. 4 Tumor cells immunostained with vascular marker CD 31

has to be considered in the differential diagnosis, which is also a primary peritoneal tumor and can exhibit epithelioid morphology. However, DSRCT is basically an aggressive round cell tumor, forming nests of irregular shapes separated by fibrous septae and showing brisk mitotic activity. In addition, its positivity with multiple immunohistochemistry markers (viz CK, Desmin, neuron-specific enolase) helps to separate this polyphenotypic tumor from epithelioid hemangioendothelioma. Besides, DSRCT is usually associated with ascites.

Thus, the rarity of these tumors, a low index of suspicion and their subsequent under-diagnosis precludes a correct histopathology report. A high index of suspicion followed by a battery of immunostains is necessary to reach a definite diagnosis. A wide excision and an accurate histological diagnosis is the key to the successful management of this rare low-grade vascular tumor of the peritoneum.

References

1. Attanoos RL, Dallimore NS, Gibbs AR (1997) Primary epithelioid hemangioendothelioma of the peritoneum—an unusual mimic of diffuse malignant mesothelioma. Histopathology 30:375–377

Virchows Arch (2005) 446:95–96
DOI 10.1007/s00428-004-1144-8

LETTER TO THE EDITOR

Gaetano Magro · Michele Bisceglia

Myofibroblastoma-like changes in fibro(stromo)-epithelial lesions of the breast: report of two cases

Received: 3 August 2004 / Accepted: 19 September 2004 / Published online: 30 November 2004
© Springer-Verlag 2004

Sir, Apart from the well-known epithelial/stromal tumors of the breast, such as fibroadenoma and phylloides tumors, another group of biphasic lesions, showing a wide morphological spectrum on a common basic theme, does exist. These lesions have been variably termed "fibroepithelial tumors," "hamartomas," "fibroadenoma variants," and "stromo-epithelial lesions" [1, 2, 3, 6]. The epithelial component usually features florid/sclerosing adenosis and ductal epithelial hyperplasia. The stromal component is usually composed of fibrous tissue in which mature lipomatous or cartilaginous or osseous components (hamartoma) may be occasionally encountered [6]. Although there is the possibility that stroma may also display a variable fibro/myofibroblastic and myoid differentiation [2, 3], to the best of our knowledge, myofibroblastoma-like changes have not been reported in mammary fibroepithelial (hamartomas) lesions.

Two women (25 years and 49 years) presented with two nodular breast masses, measuring 1.5 cm and 2 cm in greatest dimension, respectively, which were surgically excised with the pre-operative diagnosis of fibro-adenoma. Histologically, both surgical samples showed the typical features of the so-called "fibro-epithelial lesion," being composed of an admixture of glandular and stromal component proliferation. The epithelial component consisted of florid and sclerosing adenosis admixed with foci of typical ductal hyperplasia. In both cases, the stroma was completely replaced by bland-looking oval to spindle cells with pale to slightly eosinophilic cytoplasm, arranged in short irregularly intersecting fascicles, interrupted by thick bands of brightly eosinophilic collagen (Fig. 1A, B). Sometimes cells were nested grouped and similarly surrounded by thick collagen bands (Fig. 1C). Cells had round to spindle-shaped nuclei with one or two visible nucleoli (Fig. 1B). These stromal changes were closely reminiscent of myofibroblastoma, typical type, of the breast. Immunohistochemically, the cells of both cases had a similar profile: diffuse and strong immunoreactivity to vimentin and α-smooth-muscle actin (Fig. 1D) and focal staining to desmin, CD34, and bcl-2 protein. No staining was obtained for calponin, h-caldesmon, and S-100 protein. This immunophenotype, similar to what is observed in breast myofibroblastoma, is consistent with the fibro/myofibroblastic differentiation of stromal cells.

It is well known that mammary stroma has the capability of modulating its cellular phenotype as well as its extracellular matrix components upon several pathological conditions. As tumors of mammary stroma (fibroadenoma, myofibroblastoma, solitary fibrous tumor, leiomyoma), fibro(stromo)-epithelial lesions are examples in which presumptive fibroblast-like mammary stromal stem cells may undergo multidirectional mesenchymal differentiation [4, 5]. This event may well explain the occurrence of a stromal fibromatosis-like fibro/myofibroblastic and/or myoid (leiomyomatous) differentiation in these lesions [2, 3]. The present study provides evidence that mammary stromal cells in fibro-epithelial lesions may also acquire morphological and immunohistochemical features similar to those observed in myofibroblastoma, supporting the hypothesis that such cells (interlobular? and/or intralobular?) are the precursors of myofibroblastoma. Similar myofibroblastoma-like stromal changes have been reported in the more cellular areas of "pseudoangiomatous stromal hyperplasia," a lesion which is thought to be histogentically related to myofibroblastoma [7]. Although the characteristic slit-like spaces of this lesion are lacking in our cases, the possibility that we are dealing with a nodular, cellular variant of pseudoangiomatous stromal hyperplasia cannot be completely ruled out.

G. Magro (✉)
Dipartimento G.F. Ingrassia, Anatomia Patologica,
Università di Catania,
95123 Catania, Italia
e-mail: g.magro@unict.it
Tel.: +39-95-3782024
Fax: +39-95-3782023

M. Bisceglia
Servizio di Anatomia Patologica,
Ospedale Casa Sollievo della Sofferenza,
San Giovanni Rotondo, Foggia, Italia

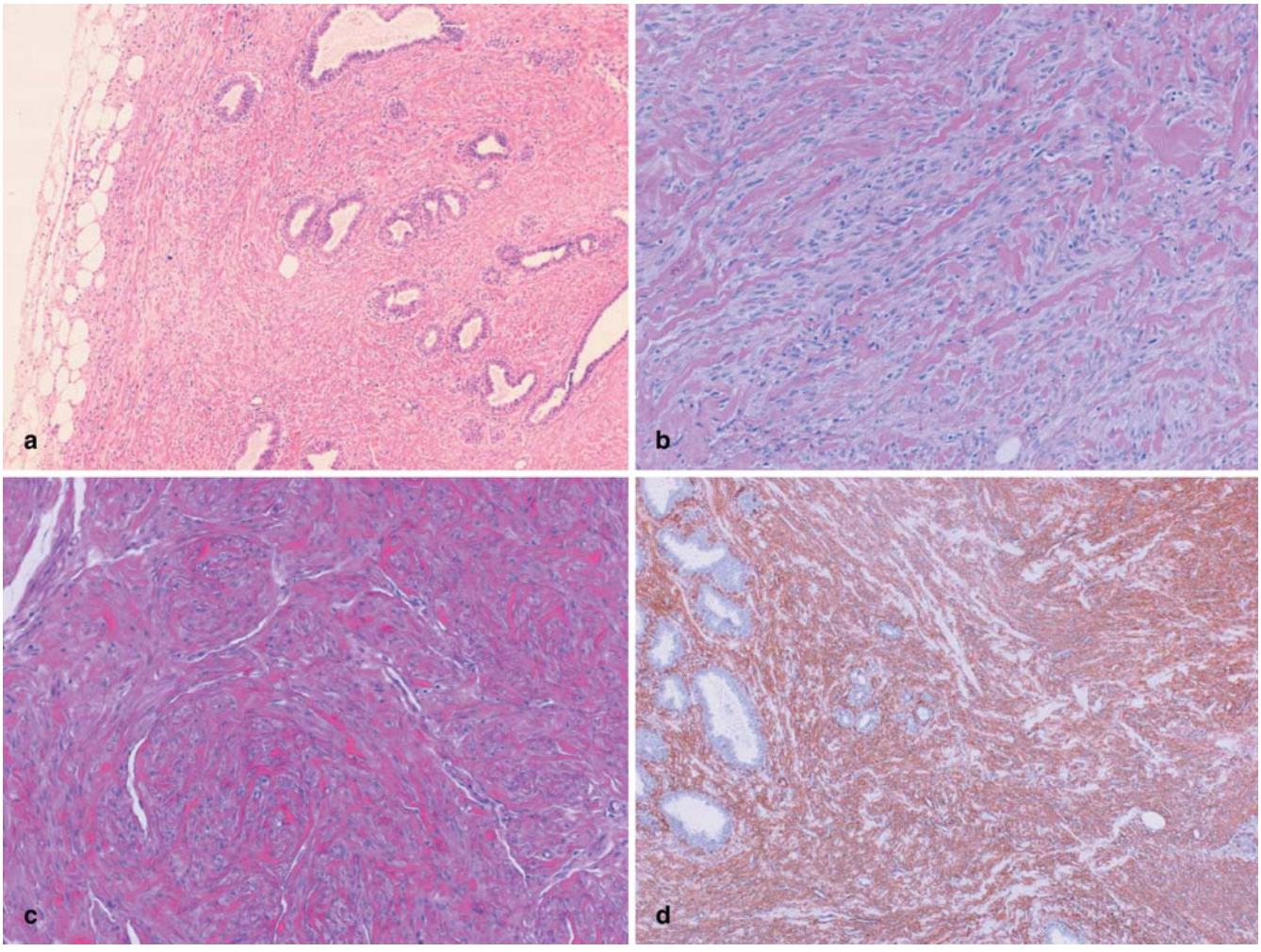

Fig. 1 Biphasic epithelial/stromal proliferation. **A** Nodular lesion with pushing borders, consisting of hyperplastic glandular and stromal components; stroma is occupied by spindle cells arranged in fascicles interrupted by eosinophilic thick collagen bands. **B** Area of stromal proliferation devoid of epithelial component, closely reminiscent of myofibroblastoma. **C** Stromal cells are arranged in small nests encircled by thick collagen bands. **D** All spindle stromal cells are immunoreactive with α-smooth-muscle actin

References

1. Azzopardi JG, Ahmed A, Millis RR (1979) Problems in breast pathology. Saunders, London
2. Bittesini LO, Dei Tos A, Doglioni C, Della Libera D, Laurino L, Fletcher CDM (1994) Fibroepithelial tumor of the breast with digital fibroma-like inclusions in the stromal component. Am J Surg Pathol 18:296–301
3. Di Tommaso L, Pasquinelli G, Damiani S (2003) Smooth muscle cell differentiation in mammary stromo-epithelial lesions with evidence of a dual origin: stromal myofibroblasts and myoepithelial cells. Histopathology 42:448–456
4. Magro G, Michal M, Bisceglia M (2001) Benign spindle cell tumors of the mammary stroma: diagnostic criteria, classification, and histogenesis. Pathol Res Pract 197:453–466
5. Magro G, Bisceglia M, Michal M, Eusebi V (2002) Spindle cell-lipoma like tumour, solitary fibrous tumour and myofibroblastoma of the breast: a clinico-pathological analysis of 13 cases in favour of a unifying histogenetic concept. Virchows Arch 440:249–260
6. Oberman HA (1989) Hamartomas and hamartoma variants of the breast. Semin Diagn Pathol 6:135–145
7. Powell CM, Cranor ML, Rosen PP (1995) Pseudoangiomatous stromal hyperplasia (PASH). A mammary stromal tumor with myofibroblastic differentiation. Am J Surg Pathol 19:270–277

Virchows Arch (2005) 446:97
DOI 10.1007/s00428-004-1149-3

LETTER TO THE EDITOR

Somma Pasquale · Diego Strianese · Gelsomina Mansueto · Fausto Tranfa

Epithelioid myoepithelioma of lacrimal gland

Received: 31 May 2004 / Accepted: 14 July 2004 / Published online: 26 November 2004
© Springer-Verlag 2004

Dear Editors:
Herein we describe a rare case of myoepithelioma of the lacrimal gland composed exclusively of epithelioid cells. A 57-year-old female had been complaining for 1 month of progressive swelling of the temporal region of the left orbit. Computed tomography scan revealed a lesion involving the left lacrimal gland. The lesion was entirely removed "en-bloc" along with the lacrimal gland. Grossly, the tumour was a well-circumscribed 3.5×25×1.5 cm mass. An extensive sampling was performed. The surgical specimen was routinely formalin fixed and paraffin embedded. Sections 5-μm thick were obtained and stained with haematoxylin-eosin. Immunostaining was performed on 5-μm serial sections. Histologically, the lesion showed a solid pattern of growth and was composed exclusively of cells with epithelioid (plasmacytoid) features. Atypical myoepithelial cells, abnormal mitotic figures, necrosis and invasive growth throughout the tumour were absent. Neoplastic cells were immunoreactive for vimentin (V9, Biogenex, 1:100), S-100 protein (15E2, Biogenex, 1:100), cytokeratin-7 (OV-TL 12/30, Biogenex, 1:100) and for smooth-muscle actin (1A4, Dako, 1:50). Because of these features, we regarded this tumour as benign. In the differential diagnosis, other benign and malignant lesions, such as fibrous histiocytoma, benign peripheral nerve sheath tumour, pleomorphic adenoma with abundant component of myoepithelial cells and malignant myoepithelioma [2] must be considered. Our case showed clear-cut morphological and immunohistochemical features of myoepithelioma that allowed us to easily distinguish it from the above-described benign and malignant proliferation of the lacrimal gland.

Myoepithelioma of the lacrimal gland is extremely rare, and thus far only seven cases have been reported [1, 4]. Of these cases, two were considered malignant [4] and one potentially malignant [6]. All but one showed spindle to cuboidal cells arranged in a solid or trabecular pattern [3].

Myoepithelial cells are generally immunoreactive for S-100, vimentin, cytokeratin, desmin, m-actin and sm-actin. There is a considerable variation in the immunoreactivity for these antigens in our case, as in the seven previously reported cases. These differences may be dependent on the degree of differentiation [5].

The size of the tumour prompted us to recommend a careful clinical follow-up. The patient had an uneventful post-operative course, and there has been no evidence of relapses over 24 months of follow-up.

S. Pasquale · G. Mansueto
Department of Biomorphological
and Functional Sciences Pathology Section,
"Federico II" University of Naples,
Italy

D. Strianese · F. Tranfa
Department of Ophthalmologic Sciences "Federico II" of Naples,
Italy

S. Pasquale (✉)
Via S. Renato 23, 80067 Sorrento (NA), Italy
e-mail: somma.pasquale@tiscalinet.it
Tel.: +39-81-7463433
Fax: +39-81-7463574

References

1. Bolzoni A, Pianta L, Farina D, Nicolai P (2004) Benign myoepithelioma of the lacrimal gland: report of a case. Eur Arch Otorhinolaryngol 2004 May 11 [Epub ahead of print]
2. Cheuk W, Chan JKC (2000) Salivary gland tumors. In: Fletcher diagnostic histopathology of tumors, Vol. I, 2nd edn. Churchill Livingstone, London, pp 231–311
3. Grossniklaus HE, Wojno TH, Wilson MW, Someren AO (1997) Myoepithelioma of the lacrimal gland. Arch Ophthalmol 115:1588–1590
4. Iida K, Sikishima K, Okido M, Sato S, Masuda Y (2001) A case of malignant myoepithelioma in the lacrimal gland. Nippon Ganka Gakkai Zasshi 105:42–46
5. Nakayama H, Miyazaki E, Hiroi M, Kikyoku H, Naruse K, Enzan H (1998) So-called neoplastic myoepithelial cells in chondroid syringoma/mixed tumors of the skin: their subtypes and immunohistochemical analysis. Pathol Int 48:245–253
6. Okudela K, Ito T, Iida MI, Kameda Y, Furuno K, Kitamura H (2000) Myoepithelioma of the lacrimal gland: report of a case with potentially malignant transformation. Pathol Int 50:238–243

Virchows Arch (2005) 446:98–99
DOI 10.1007/s00428-004-1188-9
© Springer-Verlag 2005

ACKNOWLEDGEMENT TO REFEREES

The Managing Editors are grateful to the following colleagues for generously giving their time in careful evaluation of the manuscripts submitted to *Virchows Archiv* in 2004:

Abdel Wahab N, London (GB)
Adsay N, Detroit (USA)
Alves V, San Paolo (BR)
Amann K, Erlangen (D)
Aubele M, Neuherberg (D)

Bachem M, Ulm (D)
Bamberger A-M, Hamburg (D)
Bannasch P, Heidelberg (D)
Barbareschi M, Trento (I)
Baretton G, Dresden (D)
Baud L, Paris (F)
Becker K-F, München (D)
Bertoni F, Bologna (I)
Bioulac Sage P, Bordeaux (F)
Bloemena E, Amsterdam (NL)
Boccon-Gibod L, Paris (F)
Bode-Lesniewska B, Zürich (CH)
Bordi C, Parma (I)
Boyde A, London (GB)
Brabletz T, Erlangen (D)
Bralet M-P, Paris (F)
Brambilla E, Grenoble (F)
Bras J, Amsterdam (NL)
Briner J, Aarau (CH)
Bruneval P, Paris (F)
Büttner R, Bonn (D)
Bussolati G, Torino (I)

Campo E, Barcelona (E)
Capella C, Varese (I)
Cardesa A, Barcelona (E)
Carneiro M, Porto (P)
Cathomas G, Liestal (CH)
Cazals Hatem D, Clichy (F)
Charpin C, Marseille (F)
Chott A, Wien (A)
Collan Y, Turku (FIN)
Collina G, Bologna (I)
Coupland SE, Berlin (D)
Cuvelier C, Ghent (B)

Damiani S, Bologna (I)
Damjanov I, Kansas City (USA)
De Pinieux G, Paris (F)
De Wolf-Peeters C, Leuven (B)
Deckert M, Köln (D)
Dei Tos A, Treviso (I)
DeLellis RA, Providence, RI (USA)
Denk H, Graz (A)
Denkert C, Berlin (D)
Desmouliere A, Bordeaux (F)
Diebold J, München (D)
Doglioni C, Milano (I)
Duarte MI, São Paulo (BR)
Duyckaerts C, Paris (F)

Ectors E, Leuven (B)

Facchetti F, Brescia (I)
Faller G, Erlangen (D)
Fend F, München (D)
Fisher C, London (GB)
Fléjou J-F, Paris (F)
Fletcher C, Boston (USA)
Folpe AL, Atlanta, GA (USA)
Foschini MP, Bologna (I)
Fouret P, Paris (F)
Fricke B, Bochum (D)
Füzesi L, Göttingen (D)

Gabbert H, Düsseldorf (D)
Gabbiani G, Genf (CH)
Galateau F, Caen (F)
Gale N, Ljubljana (SLO)
Gaulard P, Creteil (F)
Gerdes J, Borstel (D)
Giangaspero F, Rome (I)
Glasow A, London (GB)
Godfraind C, Bruxelles (B)
Goto A, Tokyo (J)
Gröne H, Heidelberg (D)
Guettier C, Villejuif (F)
Guski H, Berlin (D)

Hattori T, Shiga (J)
Hauptmann S, Halle a.d. Saale (D)
Hauschild A, Kiel (D)
Hayes M, Vancouver (CDN)
Helpap B, Singen (D)
Herbst H, Münster (D)
Höfler G, Graz (A)
Hofman P, Nice (F)
Hofstädter F, Regensburg (D)
Hogendoorn P, Leiden (NL)
Housset C, Paris (F)
Ichihara S, Nagoya (J)
Imura J, Shimotsuga (J)
In't Veld P, Brussels (B)
Junker K, Bochum (D)

Kanitakis J, Lyon (F)
Keller G, München (F)
Kerjaschki D, Wien (A)
Kern M, Köln (D)
Kim CJ, Seoul (ROK)
Kirchner T, Erlangen (D)
Klimstra D, New York (USA)
Knüchel-Clarke R, Aachen (D)
Koerner F, Boston (USA)
Komminoth P, Baden (CH)
Kreipe H, Hannover (D)
Krenn V, Berlin (D)
Kristiansen G, Berlin (D)
Kusafuka K, Moriguchi City (J)

La Rosa S, Varese (I)
Lacroix C, Le Kremlin-Bicêtre (F)
Lamovec J, Ljubljana (SLO)
Langner C, Graz (A)
Lavergne-Slove A, Paris (F)
Lax S, Graz (A)
Lazure T, Le Kremlin-Bicêtre (F)
Lebeau A, München (D)
Leithner A, Graz (A)
Lenzen S, Hannover (D)
Llombart-Bosch A, Valencia (E)
Löhr J-M, Mannheim (D)
Löning T, Hamburg (D)
Longnecker D, Lebanon (USA)
Lueftner D, Berlin (D)
Lüttges J, Kiel (D)

Machinami R, Tokyo (J)
Magro G, Catania (I)
Maiorano E, Bari (I)
Malecki M, Warsaw (PL)
Marx A, Würzburg (D)
Melamed J, New York (USA)
Mentzel T, Friedrichshafen (D)
Michal M, Pilsen (CZ)
Miettinen M, Washington (USA)
Mikuz G, Innsbruck (A)
Milde-Langosch K, Hamburg (D)

Miyazawa K, Yokohama (J)
Moch H, Zürich (CH)
Möller P, Ulm (D)
Molina T, Paris (F)
Molinie V, Paris (F)
Moll R, Marburg (D)
Montironi R, Torrette di Ancona (I)
Moran C, Houston, TX (USA)
Mori K, Shiga (J)
Müller K-M, Bochum (D)
Müller-Hermelink HK, Würzburg (D)
Mukai K, Tokyo (J)
Murphy N, Dublin (IRL)
Mutter G, Boston (USA)

Nabeshima K, Fukuoka (J)
Nesland J, Oslo (N)
Niedobitek G, Erlangen (D)
Nizze H, Rostock (D)
Nochy D, Paris (F)

Oberhuber G, Überlingen (D)
Offerhaus G, Amsterdam (NL)
Offner F, Feldkirch (A)
Ott G, Würzburg (D)

Papotti M, Orbassano (Torino) (I)
Paulus W, Münster (D)
Pession A, Bologna (I)
Petersen I, Berlin (D)
Peuchmaur M, Paris (F)
Popper H, Graz (A)

Ramos S, Ribeirão Preto (BR)
Raphael M, Le Kremlin-Bicêtre (F)
Reichart P, Berlin (D)
Remberger K, Homburg/Saar (D)
Ribalta Farres T, Barcelona (E)
Rindi G, Parma (I)
Riva C, Varese (I)
Röcken C, Magdeburg (D)
Rosai J, Milano (I)
Roskams T, Leuven (B)
Rossi M, Ribeirão Preto (BR)
Ruediger T, Würzburg (D)
Rüschoff J, Kassel (D)

Saeger W, Hamburg (D)
Santucci M, Florence (I)
Sapino A, Turin (I)
Sarbia M, München (D)
Schirmacher P, Heidelberg (D)
Schlegel J, München (D)
Schmidt D, Mannheim (D)
Schmitt M, München (D)
Schulz A, Giessen (D)
Scoazec J-Y, Lyon (F)
Seelentag W, Lausanne (CH)
Selves J, Toulouse (F)
Shia J, New York (USA)
Shipley J, London (GB)
Sibony M, Paris (F)
Sipos B, Kiel (D)
Sivridis E, Alexandroupolis (GR)
Skalova A, Plzen (CZ)
Slootweg P, Utrecht (NL)
Soares P, Porto (P)
Sobrinho-Simoes M, Porto (P)
Solcia E, Pavia (I)
Somma P, Naples (I)
Sophie F, Le Kremlin Bicêtre (F)
Specht K, München (D)
Stachura J, Krakow (PL)
Stallmach T, Zürich (CH)
Stawowy P, Berlin (D)
Stoerkel F, Wuppertal (D)
Stolte M, Bayreuth (D)

Tahara E, Hiroshima (J)
Tallini G, Bologna (I)
Tannapfel A, Leipzig (D)
Tavassoli F, New Haven, CT (USA)
Terracciano L, Basel (CH)
Thiele J, Köln (D)
Thiene G, Padua (I)
Thivolet-Bejui F, Lyon (F)
Tot T, Falun (S)
Tran van Nhieu J, Creteil (F)
Tsukamoto T, Nagoya (J)
Tuccari G, Messina (I)
Tyynella-Vesterinen J, Helsinki (FIN)

Van den Oord J, Leuven (B)
Van der Wal A, Amsterdam (NL)
Van Krieken J, Nijmegen (NL)
Van Marck E, Antwerpen (Wilrijk) (B)
Viale G, Milano (I)
Voit C, Berlin (D)
Von Herbay A, Harrow (GB)
Vortmeyer A, Bethesda MD (USA)

Wendum D, Paris (F)
Werner M, Freiburg (D)
Wittekind C, Leipzig (D)
Woenckhaus W, Greifswald (D)

Zamboni G, Negrar-Verona (I)
Zimmermann D, Zürich (CH)
Zimmermann U, Greifswald (D)
Ziol M, Bondy (F)

Virchows Arch (2005) 446:100
DOI 10.1007/s00428-004-1202-2
© Springer-Verlag 2005

ANNOUNCEMENTS

19–24 April 2005
10th International Congress on Oral Cancer
Crete, Greece

Creta Maris Conference Centre

- The 10th International Congress on Oral Cancer is supported by the World Health Organization, the International Union Against Cancer, the International Congress on Oral Cancer, the Hellenic Association for the Research and Treatment of Oral Cancer, and the Hellenic Cancer Society
- The Congress theme is *The Oral Cancer Patient: the anthropocentric approach to a multidisciplinary problem*
- A number of Keynote Lectures will be delivered by international leaders in their specialties
- Limited attendance Courses will be provided for interested participants
- Deadline for abstract submission: November 30th, 2004
- Accepted abstracts for oral and poster presentations will be published as a supplement to the journal Oral Oncology. Details at www.harcourt-international.com/journals/oron
- Social events include Presidents Reception, Cretan Night and Gala Dinner

Further details at www.icooc-2005.org or from the Congress President at rapidis@icooc-2005.org

9–13 May 2005
Diagnostic Histopathology of Breast Disease
Hammersmith Hospital (Imperial College Faculty of Medicine), London, UK

A week-long course designed for pathologists at Consultant and Senior Trainee level. The course provides a comprehensive coverage of the Histopathology of Breast Disease, with special emphasis on areas that pose diagnostic difficulties. The participants with be given ample time to study histological preparations, followed by illustrated discussion of the cases. There will be special sessions dealing with the interpretation of core biopsies and fine needle aspirations. There will also be several daily talks dealing with specific topics, given by eminent breast pathologists and followed by discussion. The topics will include reporting breast biopsies, immunohistochemistry, receptors and c-erbB-2 assessment, dealing with the gross specimen, prognostic factors, proliferative lesions/carcinoma in situ, problems in breast pathology and mucinous lesions of the breast. The faculty will include Ian Ellis, Christopher Elston, Andrew Hanby, Stephen Humphreys, Andrew Lee, Naomi Livni, Sarah Pinder and Sami Shousha

Further details from:
Wolfson Conference Centre,
Hammersmith Hospital,
Du Cane Road,
London W12 ONN, UK
Tel.: (44) 20 8383 31 17/3227/3245
Fax (44) 20 8383 2428
E-mail: wcc@imperial.ac.uk

3–4 June 2005
16th Ljudevit Jurak International Symposium on Comparative Pathology
Under the auspices of the European Society of Pathology and Academy of Medical Sciences of Croatia
Multimedial center Sestre milosrdnice University Hospital, Zagreb, Croatia

The main symposium topic is surgical pathology and frozen sections analysis. Symposium includes following sections: Pathological Morphology of the Human and Animal Diseases, Iatrogenic, Environmental and Experimental Pathology, Herman Jurak Round Table on Rheumatological Pathology, Clinical Forensic Pathology, Slide Seminars *in Histopathology and Cytopathology*, Quiz on Pathology.

Registration fee before April 1st – 100 EUR
Registration fee after April 1st – 150 EUR

Information: Davor Tomas, M.D.
Ljudevit Jurak University
Department of Pathology
Sestre milosrdnice University Hospital
Vinogradska 29
10000 Zagreb, Croatia
Tel.: +385 / 3787 909
Fax: +385 / 3787 244
E-mail: juraks@kbsm.hr
http://www.kbsm.hr/Jurak/symposium.htm

13–24 June 2005
International course on Laboratory Animal Science
Utrecht, The Netherlands

A two week intensive course on laboratory animal science will be organized at the Division of Laboratory Animal Science – Utrecht, The Netherlands in June 2005. This course is organized once a year since 1993.
The objective of this course is to present basic facts and principles that are essential for the humane use and care of animals and for the quality of research.
The contents of the course are in line with recommendations of the Federation of European Laboratory Animal Science Associations (FELASA) regarding the training of the young scientist whose research involves the use of vertebrate animals.
The course may also be of interest for those who intend to set up a similar course at their location. For this purpose, during the course the acquisition of teaching materials can be discussed with the course committee.

For information and application forms please contact:
Mr. Stephan van Meulebrouck, MA
Division of Laboratory Animal Science
Faculty of Veterinary Medicine
P.O. Box 80.166
3508 TD Utrecht
The Netherlands
Tel.: +31-30-2532033
Fax: +31-30-2537997
E-mail: pdk@las.vet.uu.nl
Internet: http://las.vet.uu.nl>Education and Training>International Course

Virchows Arch (2005) 446: 101–111
DOI 10.1007/s00428-004-1180-4

REVIEW ARTICLE

A. C. Langheinrich · R. M. Bohle

Atherosclerosis: humoral and cellular factors of inflammation

Received: 11 September 2004 / Accepted: 17 November 2004 / Published online: 2 February 2005
© Springer-Verlag 2005

Abstract In the past decade, atherosclerosis has come to be recognized as active and inflammatory rather than simply a passive process of lipid infiltration or a reparative process after endothelial injury. In general, atherosclerosis can be considered as an intramural chronic inflammation resulting from interactions between modified lipoproteins, monocyte-derived macrophages, lymphocytes, and the normal cellular elements of the arterial wall. The process of inflammation occurs in response to functional and structural injury through a variety of known and unknown stimuli and is active over years and decades. Here, we review recent experimental and human studies of inflammatory mechanisms underlying the pathogenesis of atherosclerosis.

Keywords Atherosclerosis · Inflammation · Pathogenesis · Review literature · History

Introduction

"I have therefore felt no hesitation in siding with the old view in this matter, and in admitting an inflammation of the arterial coat to be the starting point of the so-called atheromatous degeneration; and I have moreover endeavoured to show that this kind of inflammatory affection of the arterial coat, is in point of fact exactly the same as what is universally termed endocarditis, when it occurs in the parietes of the heart. Thus we have here an active process, which really produces new tissues, but then hurries on to destruction in consequence of its own development" (Virchow R. Cellular Pathology. A more precise account of fatty metamorphosis. 1858; Lecture XVI, 383–408; translated from the second edition of the original by Frank Chance, 1860). Although modern molecular techniques were not available in the middle of the 19th century, many topics of Virchow's observations on the inflammatory genesis of atherosclerosis have turned out to be true.

With the beginning of the last century, the pathophysiological aspects of plaque development were investigated by a number of researchers. In 1913, Anitschkow [60] first described the role of cholesterol accumulation in the vessel wall for the development of atherosclerosis. He also described the "Cholesterinesterphagozyten", which today is known as foam cells, derived from macrophages. In the last three decades, our knowledge has expanded by a large number of findings, based on morphological, immunohistochemical and molecular methods. In this context, one major contribution was the discovery by Brown and Goldstein of the low-density lipoprotein (LDL)-receptor and its importance for the development of atherosclerosis.

Experimental models of atherosclerosis

The modern theory of atherogenesis, championed by Russell Ross [55], is the "response to injury hypothesis", which states that atherosclerosis is an excessive fibroproliferative response to an insult upon the arterial wall. Although several theories or hypothesis about atherogenesis have been proposed during the past decades, up to now, none can prove entirely satisfactory.

At present, atherosclerosis has come to be recognized as active and inflammatory, rather than simply a passive process of lipid infiltration or reactive process after injury. The underlying molecular mechanisms responsible for inflammatory reactions in atherogenesis have been studied extensively.

It has been a longstanding goal of many investigators to create animal models for lipoprotein disorders and atherosclerosis to identify genes that may modify athero-

A. C. Langheinrich
Department of Diagnostic Radiology, Universitätsklinikum,
Klinikstr. 36,
35392 Giessen, Germany

R. M. Bohle (✉)
Department of Pathology, Universitätsklinikum,
Langhansstrasse 10,
35392 Giessen, Germany
e-mail: Rainer.Bohle@patho.med.uni-giessen.de
Tel.: +49-641-9941110
Fax: +49-641-9941169

genesis and lesion progression. Because atherosclerosis is a complex disease, it was difficult to establish animal models producing similar long-term lesions, as they are found in advanced human plaques. In 1908, Ignatowski et al. [31] described early vascular alterations under the influence of hypercholesterolemic food in rabbits. During the last century, first, hypercholesterolemic models, predominantly in rabbits and mice [4], then, injury models in rats and mice [1], and, later, genetic systems of transgenic and knockout mice [53] were used.

Over the last decade, the mouse has become the predominant species used to create models of atherosclerosis.

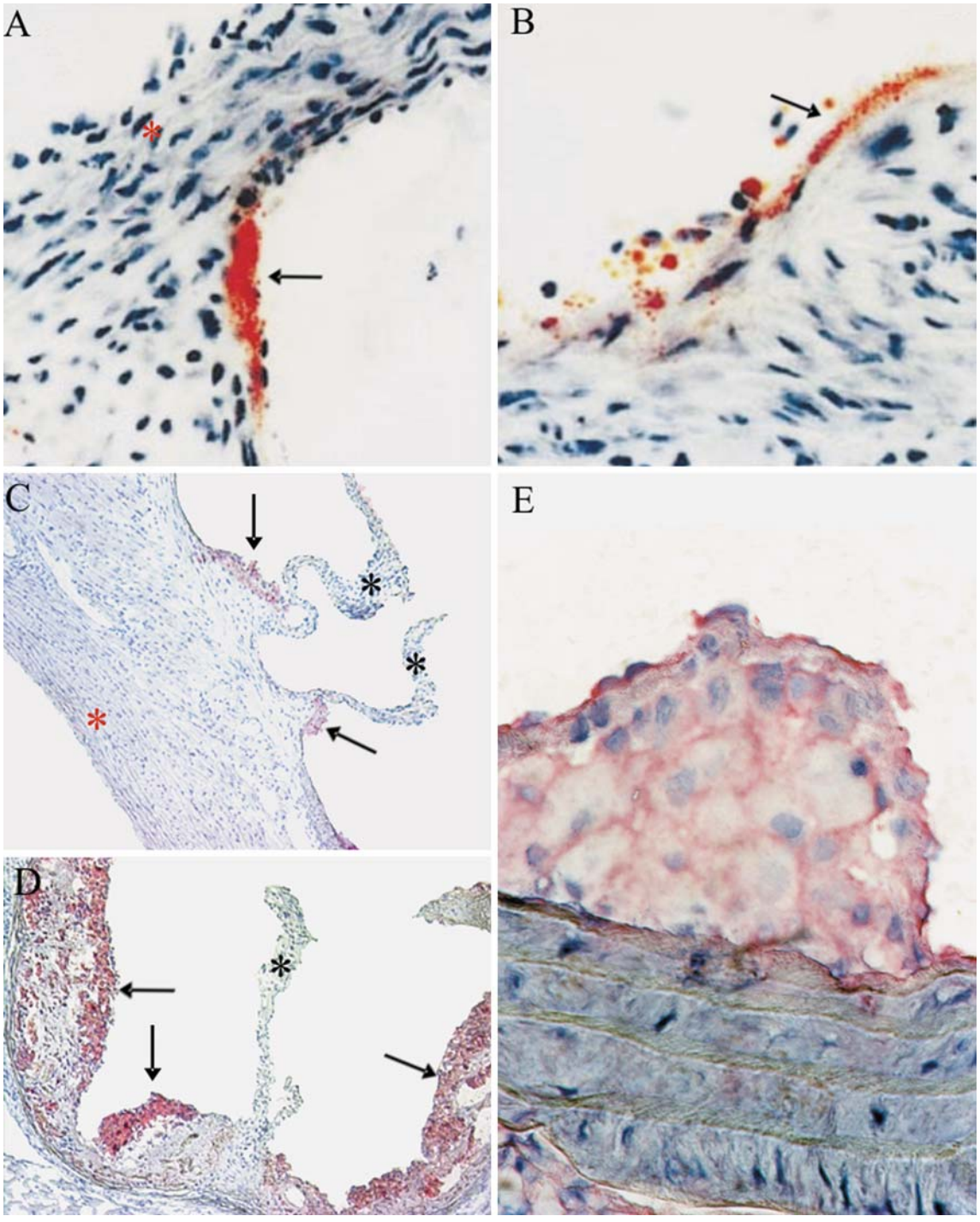

Fig. 1 Typical cross-section of the aortic root at the level of the aortic cusps after 24 weeks in C57/BL-mice with subendothelial tiny early lesions (**A**, **B**; *black arrow*). The aortic root was cryosectioned and stained for lipids with oil red O. Lesion development can be shown in apoE-deficient mice after 12 weeks (**C**) and 24 weeks (**D**) (original magnification ×10). An atherogenic diet induces development of fatty lesions with monocyte/macrophage adhesion to the intima in apoE-deficient mice after 8 weeks (**E**). (CD11b immunohistochemistry, alkaline phosphatase–antialkaline phosphatase, counterstained with hemalaun, original magnification ×100)

The earliest mouse model of atherosclerosis is the diet-induced model, which was first characterized during the 1960s in Robert Wissler's laboratory. In this model, animals received a diet containing 10% fat and 1.5% cholesterol, and mice developed early fatty lesions near the aortic cusps after 6 months. Shortly thereafter, they achieved further success in mouse studies using a diet containing 30% fat, 5% cholesterol, and 2% cholic acid. This led to tiny atherosclerotic lesions in certain strains of inbred mice, such as C57/BL. In 1987, Paigen et al. [47] demonstrated lesion development in C57/BL mice over more than 12 months. Lesions were very small at 4–5 months of age, and they usually did not develop beyond the early foam-cell, fatty-streak stage. These atherosclerotic lesions were comparable with early lesions of human atherosclerosis (Fig. 1A, B). Progressive and complicated plaques could not be induced by these models.

In 1992, Andrew Plump knocked out the mouse apolipoprotein E gene using the embryonic stem cells and homologous recombination (Fig. 1C, D, E). The apoE-deficient mouse was the first model in which atherosclerotic lesions progressed beyond the foam cell stage. The lesions grew so large that they could be observed macroscopically without any staining after 24 weeks.

Meanwhile, hundreds of inbred lines have been established. Both congenic strains and recombinant strains are available to facilitate genetic experimentation. The apoE- and LDL receptor-deficient mice have been most widely used.

Morphologically, lesions of these double knockout mice (i.e., apoE$^{-/-}$/LDL$^{-/-}$) bear considerable structural homology to human atherosclerosis. They develop from 8 weeks to 33 weeks from early fatty lesions up to fibroatheromas, as well as to fibroproliferative calcified and complicated lesions. Beyond this, inflammatory cells occur early and "post-inflammatory" lesions can be observed. As inflammation is characterized by cellular and humoral events, we will focus on these factors during the development of both human and experimental atherosclerosis.

Cellular components of inflammation

Endothelial cells

Endothelial cells regulate the traffic and functions of leukocytes by expressing receptors, adhesion molecules, and cytokines. It is evident that inflammatory responses and immunity involve close interactions between immunocompetent cells and vascular endothelial cells. The recruitment of leukocytes into sites of inflammation triggers a cascade of sequential events controlled by these cells. The endothelial cells are known to express several adhesion receptors belonging to different families, including integrins and selectins. The endothelium also produces vasoconstrictor substances, such as endothelin and angiotensin II (AT II). AT II not only acts as a vasoconstrictor but also acts as a pro-oxidant [59] and stimulates production of endothelin. Endothelin and AT II promote proliferation of smooth muscle cells and, thereby, contribute to plaque formation [15]. Dysfunction and/or damage of the endothelium initiates a number of events that promote atherosclerosis, including increased endothelial permeability, platelet aggregation, leukocyte adhesion, and generation of cytokines. Decreased production or activity of nitric oxide (NO), manifested as impaired vasodilatation, may be one of the earliest signs of endothelial dysfunction. Furthermore, lack of NO increases oxidative modification of LDL cholesterol, which is regarded as one of the major mechanisms of atherosclerosis [63]. Impaired activity or production of NO leads to events that promote atherosclerosis, such as vasoconstriction, platelet aggregation, smooth muscle cell proliferation and migration, leukocyte adhesion, and oxidative stress [16]. Recently, Wassmann et al. [67] demonstrated a marked reduction of atherosclerotic lesions if genetic disruption of the AT1A receptor inhibits vascular oxidative stress and endothelial dysfunction in apoE$^{-/-}$/AT1A$^{-/-}$ double knockout mice. This study supported the hypothesis that the reduction of oxidative stress, e.g., by antioxidants or by genetics, is associated with an improvement of endothelial function and decreased atherosclerotic lesion formation [3].

Monocytes

The ubiquitous monocyte, the precursor of macrophages in all tissues, is present in every stage of atherogenesis. Recruitment of monocytes from the peripheral blood to the intima of the vessel wall is a primordial event in atherogenesis, an event that appears to depend on the local presence of high amounts of LDL. Endothelial cells and smooth muscle cells are known to release substances causing oxidative modification of LDL, suggesting that oxidized LDL (oxLDL) may be an important atherogenic factor [62]. Monocyte recruitment is initiated by oxLDL, leading to enhanced transmigration of monocytes, upregulated exposure of adhesion molecules on a variety of cells, and chemoattractant production and release.

Activated monocyte-derived macrophages are scavenging and antigen-presenting cells. They secrete cytokines, chemokines, growth-regulating molecules, and metalloproteinases and other hydrolytic enzymes. The continuing entry, survival, and replication of mononuclear cells in lesions depend, in part, on factors such as macrophage colony-stimulating factor and granulocyte-macrophage colony-stimulating factor for monocytes and interleukin (IL)-2 for lymphocytes. Continued exposure to macrophage colony-stimulating factor permits macrophages to survive and possibly to multiply within the lesions [21].

A significant amount of data support the hypothesis that subendothelial modified LDLs provide the initiating ligands for the macrophage, and these are recognized by scavenger receptors. The class B scavenger receptor (CD36) is shown to be highly regulated in monocytes/macrophages during differentiation and to be present in lipid-laden macrophages in atherosclerotic lesions [25]. Febbraio et al. [17] demonstrated a marked reduction of

atherosclerotic lesions in CD36-apoE double null mice compared with controls. This study supported the hypothesis that monocytes/macrophages are key mediators of atherogenesis and that the scavenger receptor CD36 could play a profound impact on lesion development. Further, it is very likely that AT II synthesis occurs within foam cells, as they show a strong expression of CD143, angiotensin-converting enzyme [42].

T lymphocytes

There is an abundance of circumstantial evidence that T and B cells play a role in atherogenesis. T lymphocytes are found in human atherosclerotic plaques and, therefore, T cells have been implicated in the pathogenesis of atherosclerosis. Several studies also suggest that T lymphocytes in lesions are in the activated state and influence gene expression in neighboring cells. CD25, a marker of T-cell activation is co-localized with $CD4^+$ T cells in human and apoE-deficient mouse lesions [70]. Detection of interferon γ in atherosclerotic lesions [22] suggests that T cells release cytokines, which may influence gene expression in neighboring cells or the lesion. Therefore, T cells are not simply bystanders in atherosclerotic lesions. They actively participate in the lesion progression, possibly through the release of cytokines. Song et al. [58] demonstrated a 54% reduction in lesion development in $LDL^{-/-}$ and recombinase-activating gene-1 (RAG-1) double knockout mice. By 8 weeks, RAG1/low-density lipoprotein receptor (LDLR) double knockout mice lesions were significantly smaller than LDLR knockout lesions, pointing toward a significant delay in lesion development.

In contrast, Daugherty et al. [12] investigated the effects of total lymphocyte deficiency of atherosclerosis by crossing apoE-deficient mice with mice deficient in recombinase-activating gene-2, which is required for normal B and T lymphocyte development. In this study, it was shown that the absence of functional T lymphocytes did not influence the extent of aortic lesions in apoE-deficient mice.

B lymphocytes

The possibility of B-cell involvement in atherosclerosis has been based on the finding of immunoglobulins in atherosclerotic lesions and circulating autoantibodies to oxLDL in both humans and animals with atherosclerosis [68]. Zhou et al. [69] showed that immunization with homologous plaque homogenate as well as homologous malondialdehyde (MDA)-LDL inhibits plaque growth in apolipoprotein E-knockout mice. This effect was associated with high titers against MDA-LDL and oxidized cardiolipin, suggesting that B-cell responses mediated protection against atherosclerosis. Because the immunoglobulin isotype switch implied T-cell help, T-cell–B-cell cooperation during immune responses may play a role in protection against atherosclerosis. These data confirm findings from Laurat et al. [35], demonstrating in vivo that downregulation of T helper cell reduces atherogenesis in apolipoprotein E-knockout mice. Dimayuga et al. [14] present further evidence for a protective role of B cells in vascular disease. They have used a periadventitial cuff to induce intimal hyperplasia in the carotid artery of mice and assessed the role of adaptive immunity by comparing immunodeficient RAG-1 knockout mice with immunocompetent C57/BL controls. In this study, lesions were up to fivefold larger in the RAG-1 knockout mice, which lack T and B cells. The underlying mechanisms by which B cells exert their antiatherogenic effects remain unclear.

In contrast, Dansky et al. [11] determined whether an intact immune system is necessary for the formation of atherosclerotic lesions. In their study, immunodeficient mice with hypercholesterolemia and atherosclerosis by crossbreeding the apolipoprotein E-deficient mouse with the RAG-1 knockout mouse were investigated. No differences in lesion size and progression to fibrous lesions were observed. Therefore, they concluded that functional T and B lymphocytes are not necessary for the formation of fibroproliferative lesions in immunodeficient animals. A study in rabbits [49] has suggested that the humoral immune system protects against atherosclerotic plaque formation. Immunization of LDL receptor-deficient rabbits with oxLDL results in increases in the titer of antibodies against oxLDL and also reduced atherosclerosis by 30%. Despite some conflicting data regarding B and T lymphocyte involvement, the majority of studies imply that cellular immunity may actually play a protective role against atherosclerosis.

Granulocytes

As for the inflammatory cells, granulocytes are rarely detected during early and progressive human atherogenesis. Neutrophils in atherosclerotic lesions have not received much consideration, despite accumulating evidence suggesting a link between systemic inflammation and acute coronary syndromes.

Mehri et al. [41] assessed the interactions among neutrophils, platelets, and arterial responses to injury in porcine carotid arteries after balloon injury. In this study, neutropenia was achieved by treatment with cyclophosphamide (50 mg/kg, 4 days prior to the experiment), which decreased circulating leukocyte count by 92% and almost abolished neutrophil aggregation to N-formyl-methionyl-leucyl-phenylalanine without affecting blood platelet count, hematocrit, hemoglobin concentration, or whole blood platelet aggregation to adenosine diphosphate. Neutropenia produced a 50% reduction in whole blood platelet aggregation, resulting in a significant inhibition of platelet deposition to deeply injured arteries, and decreased vasoconstriction. They concluded that neutrophils can influence the vasoconstrictive response at the site of endothelial injury in vivo.

Previous clinical studies have demonstrated intense in vivo neutrophil activation in unstable angina pectoris and

acute myocardial infarction. Metha et al. [40] reported a 15-fold increase in plasma levels of peptide Bβ, a marker of elastase release, in patients with unstable angina pectoris compared with those in patients with stable angina pectoris.

Activated neutrophils are known to release a variety of proteolytic enzymes, all of which have the potential for tissue destruction. In particular, neutrophil elastase has been shown to mediate both degradation of basement membrane constituents and endothelial damage. Naruko et al. [45] proved neutrophil infiltration in humans in culprit lesions of acute coronary syndromes. Interestingly, patients who died of acute myocardial infarction had neutrophils within the plaque, although their number varied widely. In contrast, neutrophils were extremely rare in coronary lesions obtained from patients who died of non-cardiovascular diseases.

Infection and inflammation

Several microorganisms (i.e., *Chlamydia pneumonia*, *herpes simplex virus* and *cytomegalovirus*) have been implicated in the pathogenesis of atherosclerosis. This issue is under considerable discussion. At present, the role of microbial infection is controversial.

Chlamydia pneumonia (Cp), as with all Chlamydia, is an obligate intracellular prokaryotic pathogen. Cp can infect and modify the physiology of different cell types and may transit from the lung via circulating monocytes and lymphocytes [43]. Shor et al. [56] were the first to demonstrate that Cp is present in atheromatous lesions of the coronary artery obtained at necropsy from South African patients using electron microscopy. Seroepidemiological studies in several countries have shown the incidence of IgG antibodies to Cp to be in excess of 50% and to be higher in men than in women [18]. Furthermore, Cp has been isolated by culture from atheromatous arteries. In ApoE-deficient mice infected intranasally with Cp, atheromas were more pronounced, and organisms could be recovered from the lesions [24].

Dechend et al. [13] reported tissue factor, PAI-1, and IL-6 overexpression in human endothelial cells and vascular smooth muscle cells infected with Cp. These findings were accompanied with an activation of NFκB and degradation of IκBα. Infected cells subsequently upregulate adhesion molecules and produce inflammatory cytokines. Smooth muscle cells respond to endothelial infection by proliferating [9], and direct infection of smooth muscle cells induces secretion of cytokines such as IL-6 and basic fibroblast growth factor, which may alter atheroma biology. In addition, Cp induces monocytes to oxidize lipoproteins and make them atherogenic [28]. Recent studies suggest that Cp triggers specific cell-mediated immunity within plaques, as evidenced by the detection of Chlamydia-specific T lymphocytes in atherosclerotic lesions [44]. Therefore, it also appears that not only humoral responses against Cp but also cell-mediated immunity, by way of antigen-specific T cells, may play a role in atherosclerosis. The frequency of Cp-responsive T cells in the peripheral blood is increased in patients with coronary heart disease (CHD) [20].

However, Jantos et al. [27] examined coronary atherectomy specimens from 50 patients, demonstrating low prevalence of Cp DNA in coronary atheroma, only 4 of 50 samples (8%) showed molecular evidence of Cp in atheroma detected using polymerase chain reaction (PCR) and nested PCR. Supporting these data by means of a closed, highly sensitive and specific real-time PCR, Cp was not detected in cerebrovascular atherosclerosis [2]. Overall, unequivocal evidence is still lacking that Cp is involved in atherogenesis.

Humoral markers of inflammation adhesion molecules

During the 1990s, it was found that mononuclear cell adherence is triggered by a number of adhesion molecules on endothelial cells, such as vascular cell adhesion molecule-1 (VCAM-1) and intercellular cell adhesion molecule-1 (ICAM-1), P-selectin, and E-selectin [10]. Expression of adhesion molecules is considered to be responsible for the endothelial adherence of monocytes and T lymphocytes and for their preferential binding to the arterial surface.

Depending on which assays are used, ICAM-1 and VCAM-1 are minimally or moderately expressed on resting endothelial cells. They are clearly upregulated at sites of inflammation and immune responses by the release of cytokines, such as tumor necrosis factor (TNF)α, IL-1, or interferon γ (IFNγ). Zibara et al. [71], when investigating quantitatively the expression of adhesion molecules in the vasculature of apoE-deficient mice in aortic arch lesions over a period of time (0–20 weeks of diet), observed that ICAM-1, VCAM-1, and platelet endothelial cell adhesion molecule-1 (PECAM-1) are reduced in fibrofatty and complex lesions but not in fatty streaks or in areas without lesions, indicating that the expression of adhesion molecules varies with the evolution of plaque from a fatty to a fibrous stage.

Direct evidence for the critical role of adhesion molecules in the initiation of atherosclerotic lesions has been derived from ICAM-1-deficient and ICAM-1$^{-/-}$ mice [8].

Recently, Wang et al. [66] demonstrated a significant increase of VCAM-1 and E-selectin in the endothelium of hyperhomocysteinemic rats and an increase in monocyte adhesion to the aortic endothelium.

Cytokines

IFN-γ is one of the most notable cytokines derived from T lymphocytes, and has been shown to mediate foam cell formation, proliferation of smooth muscle cells, and regulation of the production of metalloproteinases [38]. Furthermore, IFN-γ enhances the recruitment of immunocompetent cells by upregulating adhesion molecule expression on endothelial cells and, thus, may be a factor

involved in the continuous inflammatory response. The most direct evidence for the critical role for Th1 cells, IFN-γ, and IFN-γ-driven molecules in atherosclerosis is provided by mice with combined deficiencies of apolipoprotein E and IFN-γ receptor, in which the development of atheromata is significantly reduced in comparison with mice with only apoE deficiency, whereas exogenous IFN-γ enhances atherosclerosis [19].

After monocytes and T lymphocytes bind to the endothelial surface, they migrate into the subendothelial space. This subendothelial migration is induced by the presence of bioreactive mediators called "chemoattractants" in the intima. During the last 20 years, a variety of chemoattractants have been shown to be capable of inducing monocyte chemotaxis: oxLDL, Lp (a), cytokines (monocyte chemoattractant protein-1), IL-1 and TNF-α. Monocyte chemoattractant protein-1 (MCP-1), a C-C chemokine, one of the best-characterized chemoattractants, controls chemotaxis of mononuclear cells. MCP-1 and its receptor (CCR2) pathway recently attracted much attention, because the MCP-1/CCR2 pathway seems to be involved in the inflammatory aspect of atherogenesis [51]. Atheroma-forming cells (endothelial cells, smooth muscle cells and macrophages) express MCP-1 and CCR2, and activity in this pathway is increased in atherosclerotic lesions. Furthermore, activation of the MCP-1/CCR2 pathway induces adhesion molecules, proinflammatory cytokines, chemokines, and matrix metalloproteinases (MMPs) and, thus, accelerates atherosclerosis in hypercholesterolemic animals. Mice, deficient in MCP-1 and apoE, show a significant reduction in atherosclerotic lesion formation compared with controls [57]. Confirming these data, Inoue et al. [26] demonstrated for the first time that blockade of the MCP-1/CCR2 pathway by transfecting an *N*-terminal deletion mutant of the MCP-1 gene transfer markedly limited progression and destabilization of established atherosclerotic lesions. The blockade of MCP-1 decreased immunohistochemically detectable CD40 and CD40L expression within the atheroma and normalized the increased chemokines and cytokine TNF α, IL-6, IL-1β, and transforming growth factor β_1. These findings suggest that MCP-1 is a central mediator in the progression and destabilization of established atheroma and contributes not only to vascular inflammation but also to plaque destabilization and thrombosis.

Serum parameters of inflammation

C-reactive protein

C-reactive protein (CRP) is an established marker of systemic inflammation, reflecting elevated levels of proinflammatory cytokines, such as IL-6. Other inflammatory markers include fibrinogen, ILs, and vascular adhesion molecules.

If human CRP is expressed in apoE$^{-/-}$ mice, accelerated atherosclerosis occurs [50]. CRP was detected in lesions, which were associated with increased expression of AT1-R, VCAM-1, collagen expression, and C3 deposition.

The association of CRP with human cardiovascular disease has been documented in several studies: one of the major results was that CRP is a better predictor of the risk of cardiovascular events than LDL cholesterol [54]. Proatherogenic properties of CRP can be derived from secretion of IL-6 and endothelin-1 and decrease the expression of endothelial NO synthase in human endothelial cells. Furthermore, CRP activates macrophages to express cytokines and tissue factor and enhances the uptake of LDL [65].

It has widely been appreciated that CRP is not only an excellent biomarker of inflammation, but it is also a direct participant in atherogenesis. Therefore, CRP will provide a readily accessible marker for monitoring inflammatory responses in atherogenesis.

NO synthesis

One of the major endothelium-derived vasoactive mediators is NO. Asymmetric dimethylarginine (ADMA) is an endogenous inhibitor of NO synthase. Stuhlinger et al. [64] demonstrated that homocysteine-induced accumulation of ADMA was associated with reduced NO synthesis by endothelial cells and segments of pig aorta. Furthermore, this effect was associated with the reduced activity of dimethylarginine dimethylaminohydrolase, the enzyme that degrades ADMA. Boger et al. [5] tested the hypothesis that hyperhomocysteinemia is associated with an elevated plasma concentration of ADMA in cynomolgus monkeys fed an atherogenic or hyperhomocysteinemia diet for 4 weeks. In this study, it was clearly demonstrated that plasma levels of ADMA are elevated in hyperhomocysteinemia. Supplementation of the atherogenic diet with B vitamins decreased the plasma levels of homocysteine but did not affect the plasma levels of ADMA or endothelial function.

ADMA inhibits vascular NO production at concentrations found in pathophysiological conditions. ADMA is increased in plasma of humans with familial hypercholesterolemia [48]. In several prospective and cross-sectional studies, ADMA evolved as a marker of cardiovascular risk in certain populations, such as hemodialysis, hypertensive, diabetic, or intensive-care patients.

Homocysteine

The link between homocysteine and vascular pathology of atherosclerosis was first described almost 30 years ago. The S-adenosylhomocysteine hydrolase catalyses the hydrolysis of adenosylhomocysteine (AdoHcy) to free homocysteine and adenosine. In eucaryotic cells, this is the only source of homocysteine. AdoHcy is the product of all adenosylmethionine-dependent biological transmethylations, including DNA methylation, phospholipid methylation, protein carboxylmethylation, nicotinamide methylation, and catecholamine metabolism. These reactions have a wide

range of products and are common in all facets of biometabolism. Laukkanen et al. [34] reported hypomethylation in atherosclerotic lesions and found that local hypomethylation is associated with the development of atherosclerosis. Although the precise molecular mechanism is unknown, homocysteine causes endothelial dysfunction at several levels. Homocysteine alters the normal antithrombotic phenotype or the endothelium by enhancing the activities of factor XII and factor V. Furthermore, homocysteine also inhibits the expression of thrombomodulin, induces the expression of tissue factor, and suppresses the expression of heparan sulfate by the endothelium [37, 52]. It induces the expression of monocyte chemoattractant protein-1 and IL-8 in human aortic endothelial cells. In addition to promoting atherosclerosis through endothelial injury or dysfunction, homocysteine is also a potent mitogen for vascular smooth muscle cells. Confirming homocysteine's atherogenicity, Langheinrich et al. [33] demonstrated that when blocking the final step in the synthesis of homocysteine, atherosclerosis was markedly reduced in apoE-deficient mice, which might explain, in part, the atherogenicity of homocysteine.

Since McCully [39] hypothesized that elevated serum homocysteine concentrations could cause atherosclerosis, abundant epidemiological evidence from more than 20 case controls and cross-sectional studies involving over 2000 patients have validated this relationship. Vitamins B6 and B12 as well as folic acid have been shown to decrease serum homocysteine in humans, but it is not known whether this relatively mild reduction of homocysteine concentrations will reduce cardiovascular disease risk.

Matrix metalloproteinases

MMPs constitute a tightly regulated family of zinc-dependent endopeptidases that degrade most components of the extracellular matrix and basement membrane. They can also function in many other proteolytic processes. The members of the MMP family (23 identified at present) are divided into five classes, based on their structure and substrate specificities. These are collagenases, gelatinases, stromeolysins, and other MMPs. MMPs are synthesized, and most are secreted as zymogens, which are activated extracellulary by several proteinases (including plasmin, trypsin, chymotrypsin, kallikrein, cathepsin, and other MMPs). Activated MMPs are inhibited by tissue inhibitors of metalloproteinases (TIMPs; TIMP-1, -2, -3, and -4). They form non-covalent complexes with the active forms of MMPs, as well as with some pro-matrix metalloproteinases (proMMPs).

Up to now, there were only limited data suggesting direct evidence of the contribution of MMPs to the development of atherosclerotic lesions and plaque rupture. Recent findings of Lemaitre et al. [36] are of particular interest, as they demonstrate that the in vivo expression of MMP-1 in the macrophages of apoE knockout mice significantly decreases formation of atherosclerotic lesions, suggesting that remodeling of the extracellular matrix of atherosclerotic lesions by MMP-1 may affect atherosclerosis by preventing or delaying the progression of these lesions. Increased expression and activity of MMPs have been identified in various pathological processes, such as general inflammation, tumor metastasis, respiratory diseases, myocardial injury, vascular aneurysms, and remodeling. MMPs have been identified in human atherosclerotic plaque shoulders and regions of foam cell accumulation and may, thus, contribute to plaque vulnerability as well as de novo atherosclerotic remodeling.

Statins

Statins [3-hydroxy-3-methylglutaryl coenzyme-A (HMG-CoA) reductase inhibitors] are now widely used for the treatment of hypercholesterolemia. They competitively inhibit HMG-CoA reductase, reduce LDL levels more than other cholesterol-lowering drugs, and lower triglyceride levels in hypertriglyceridemic patients. Both simvastatin and lovastatin induce transcriptional activation of the NO synthase gene in human endothelial cells in vitro. Endothelial function improves in primates receiving a dose of pravastatin, which does not reduce LDL. Furthermore, both simvastatin and lovastatin exert a dose-dependent protective effect in an experimental stroke model, mediated by increased production of endothelial NO synthase rather than cholesterol lowering. Simvastatin and pravastatin reduce the proliferation of macrophages induced by oxidized LDL. Additionally, both drugs lower the accumulation of cholesteryl esters in macrophages. It is well established that statins inhibit the growth of lymphocytes and other blood mononuclear cells via multiple pathways unrelated to cholesterol metabolism [23], an effect whose therapeutic relevance is currently being investigated in patients with leukemia.

Chronic inhibition of endothelial NO synthesis by oral administration of N (omega)-nitro-L-arginine methyl ester (L-NAME) to rats induces early vascular inflammation as well as subsequent arteriosclerosis. In this study, Ni et al. [46] found that treatment with statins did not affect serum lipid levels but markedly inhibited the L-NAME-induced vascular inflammation and arteriosclerosis.

The Scandinavian Simvastatin Survival Study (4S) demonstrated a convincing reduction in total mortality among the subjects in the simvastatin group [61]. The reduction in coronary events in 4S was observed in both men and women, in individuals younger and older than 60 years of age, and in subjects with other risk factors, including smoking, hypertension, and diabetes. In addition, 4S reported a 30% reduction in cerebrovascular events. The Cholesterol And Recurrent Events (CARE) study extended the findings of 4S to individuals with average cholesterol levels. Post-hoc analysis revealed no reduction in coronary events among patients in the treatment group with baseline LDL levels below 125 mg/dl, which led the authors to suggest that statin treatment of CHD patients with low LDL levels may not be warranted. Diabetic subjects treated with pravastatin had a 25%

reduction in major coronary events compared with diabetic subjects taking placebo [29].

Imaging of atherosclerotic inflammatory lesions

Developing imaging technologies capable of identifying early and vulnerable atheromatous plaques in vivo is a major issue of clinical cardiovascular research. In the past decade, rival techniques for clinical and experimental assessment of atherosclerotic lesions have been developed, e.g., magnetic resonance imaging (MRI), multi-slice computed tomography (MSCT), or micro-computed tomography (micro-CT).

Recently, Chaabane et al. [7] developed a specific mouse antenna to evaluate the potential of high-resolution MRI at 2 Tesla (T) for direct noninvasive imaging of the aortic wall in apoE-deficient mice. In this study, they could demonstrate the technical feasibility for non-invasive imaging at 2 T to analyze in vivo atherosclerotic lesions in mice.

Several means of assessing human atherosclerotic plaque composition have been used with MRI: carbon-13 and proton spectroscopy, proton imaging, chemical shift imaging, water diffusion imaging, and magnetization transfer [6]. Different studies demonstrated the ability to obtain in vivo coronary MR vessel wall and plaque images in humans. In some of these MRI studies, characterization of vulnerable plaques was performed.

The introduction of MSCT with retrospectively gated electrocardiogram reconstructions has substantially modified the coronary imaging scenario. In fact, the results have been promising, since various plaque components (i.e. lipid-rich, fibrous, calcified) can be detected ex vivo

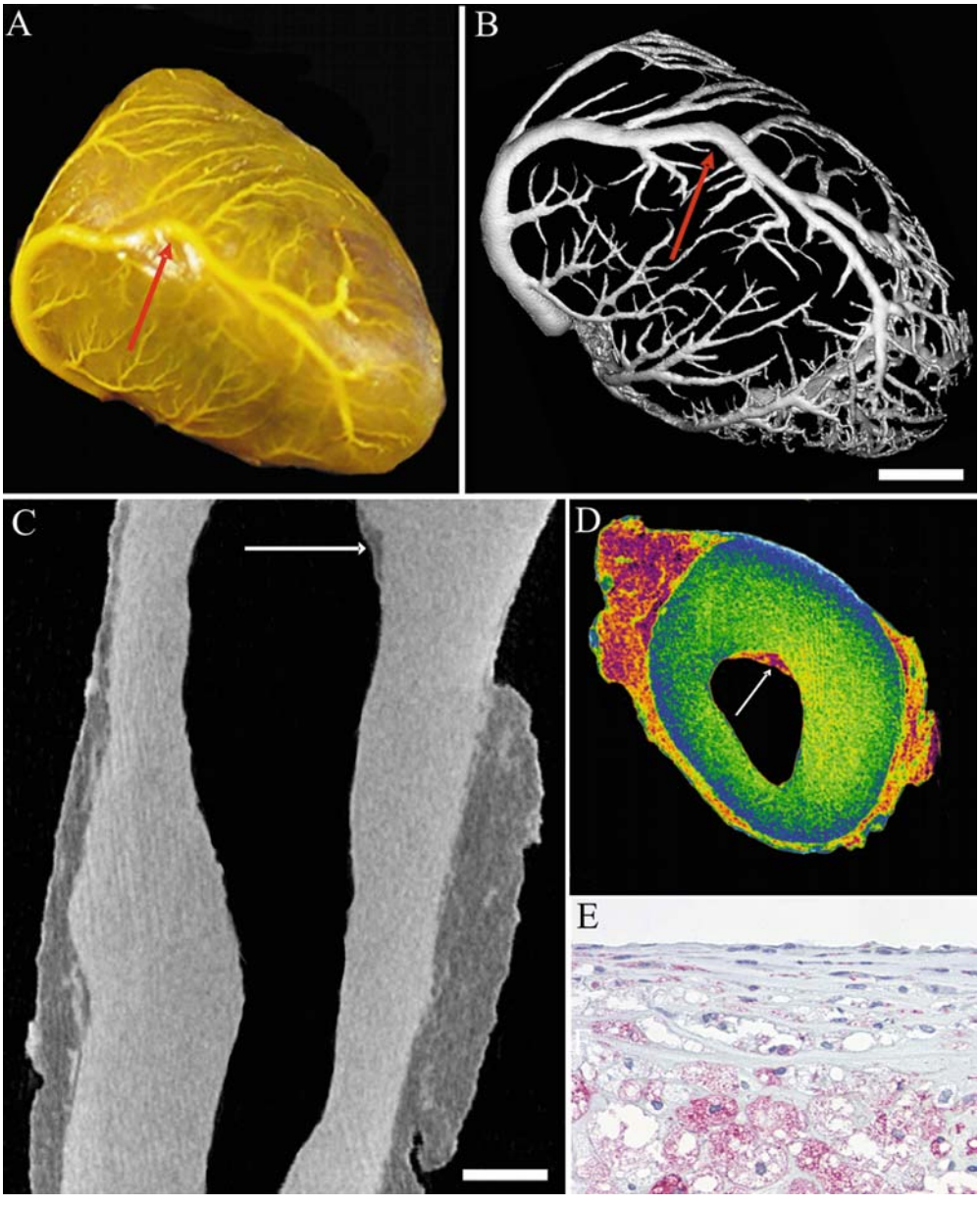

Fig. 2 Overview of a heart of an apoE$^{-/-}$/LDL$^{-/-}$ double knockout mouse (**A**) after ex-vivo perfusion of contrast agent (*red arrow*). The coronary tree can be extracted (**B**, *red arrow*) and quantitatively evaluated by three-dimensional micro-computed tomography (micro-CT) (*bar*=1 mm). Micro-CT reconstruction image of a human coronary artery segment shows a small atheromatous lesion (**C**, *white arrow*, *bar*=1.25 mm). Corresponding transverse micro-CT cross-section raw data image shows this lesion (**D**, *white arrow*, *bar*=1 mm). Photomicrograph of lesion classified as intimal lipid-rich plaque and stained for CD68 contains primarily macrophage-derived foam cells (**E**, original magnification ×40)

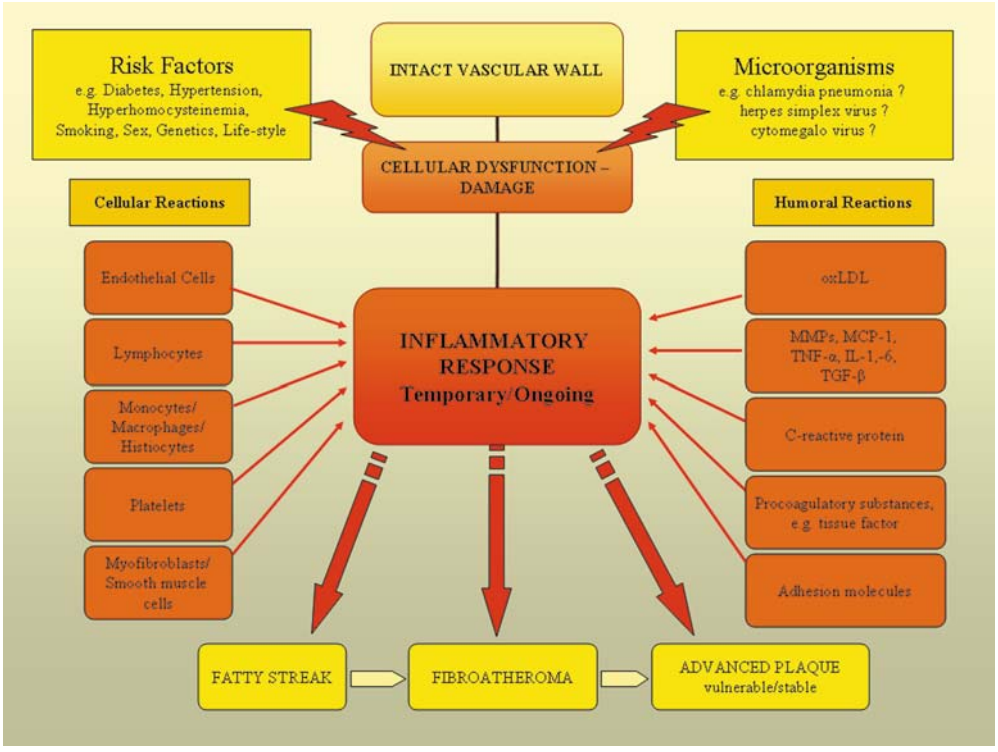

Fig. 3 Inflammatory factors of atherosclerosis. Schematic construction of the interrelationship between cellular and humoral factors involved in the inflammatory response of atherogenesis

in human hearts. In addition, Kopp et al. [30] were able to identify coronary vulnerable plaques by MSCT and intracoronary ultrasound.

In the past decade, micro-CT has become a powerful technique in laboratory investigation, as technical advances in computer speed and memory have enabled the generation of high-resolution images of small specimens. Using micro-CT, three-dimensional information of the coronary arteries can be obtained in apoE$^{-/-}$/LDL$^{-/-}$ mice at 19 weeks after birth (Fig. 2B). Additionally, in human coronary arteries [32], it was feasible to identify different plaque components and early foam cell plaques using gray-scale attenuation differences (Fig. 2C, D, E).

As quantitative information of the vasculature can be obtained in laboratory animals and human specimens (Fig. 2), imaging and monitoring of inflammatory lesions during the onset, during the course, and, e.g., after anti-inflammatory therapy of atherosclerosis can be qualitatively and quantitatively performed. Our current knowledge on inflammatory factors of atherosclerosis is summarized in Fig. 3.

Conclusion

Back to Virchow, regarding his initial understanding of inflammation, we are now able to "translate" his sight of atherogenesis. Although he described atherosclerosis as an "inflammation of the inner arterial coat to be the starting point of the so-called atheromatous degeneration", he misjudged in *res ipsa loquitur*. Degeneration, per se, might today be attributed to aging lesions of the arteries when pure intimal fibrosis occurs.

Concerning atherosclerosis, there is now much evidence that chronic inflammation and immune mechanisms are involved in genesis, especially during progression phase and during the onset of vulnerable plaques. Inflammation and immune mechanisms have many adverse effects in animal models. Study of the action of the inflammatory response in atherogenesis and its therapy is in its infancy, and much remains to be learned. As most of the work thus far has been done on experimental animals, mainly mice, the relevance of these observations to human disease remains to be determined. For instance, lesion formation in humans occurs with much less atherogenic pressure and, thus, proceeds at a more leisurely pace than in hypercholesterolemic mice. The inflammatory markers seem to be a powerful humoral predictor of cardiovascular disease in humans. Imaging techniques are on their way to detecting early and risky progressing lesions of atherosclerotic inflammation. Thus, within a short time, it is likely that therapy effects can be monitored in situ. Atherosclerotic inflammatory lesions will be accessible at the humoral and cellular levels to allow reasonable therapeutic strategies to suppress the key events of this disease.

References

1. Aliev G, Burnstock G (1998) Watanabe rabbits with heritable hypercholesterolaemia: a model of atherosclerosis. Histol Histopathol 13:797–817
2. Apfalter P, Barousch W, Nehr M et al (2004) No evidence of involvement of chlamydia pneumoniae in severe cerebrovascular atherosclerosis by means of quantitative real-time polymerase chain reaction. Stroke 35:2024–2028

3. Barry-Lane PA, Patterson C, van der Merwe M et al (2001) p47phox is required for atherosclerotic lesion progression in ApoE(−/−) mice. J Clin Invest 108:1513–1522
4. Belalcazar LM, Merched A, Carr B et al (2003) Long-term stable expression of human apolipoprotein A-I mediated by helper-dependent adenovirus gene transfer inhibits atherosclerosis progression and remodels atherosclerotic plaques in a mouse model of familial hypercholesterolemia. Circulation 107:2726–2732
5. Boger RH, Bode-Boger SM, Sydow K et al (2000) Plasma concentration of asymmetric dimethylarginine, an endogenous inhibitor of nitric oxide synthase, is elevated in monkeys with hyperhomocyst(e)inemia or hypercholesterolemia. Arterioscler Thromb Vasc Biol 20:1557–1564
6. Botnar RM, Stuber M, Kissinger KV et al (2000) Noninvasive coronary vessel wall and plaque imaging with magnetic resonance imaging. Circulation 102:2582–2587
7. Chaabane L, Soulas EC, Contard F et al (2003) High-resolution magnetic resonance imaging at 2 Tesla: potential for atherosclerotic lesions exploration in the apolipoprotein E knockout mouse. Invest Radiol 38:532–538
8. Collins RG, Velji R, Guevara NV et al (2000) P-selectin or intercellular adhesion molecule (ICAM)-1 deficiency substantially protects against atherosclerosis in apolipoprotein E-deficient mice. J Exp Med 191:189–194
9. Coombes BK, Mahony JB (1999) Chlamydia pneumoniae infection of human endothelial cells induces proliferation of smooth muscle cells via an endothelial cell-derived soluble factor(s). Infect Immun 67:2909–2915
10. Cybulsky MI, Iiyama K, Li H et al (2001) A major role for VCAM-1, but not ICAM-1, in early atherosclerosis. J Clin Invest 107:1255–1262
11. Dansky HM, Charlton SA, Harper MM et al (1997) T and B lymphocytes play a minor role in atherosclerotic plaque formation in the apolipoprotein E-deficient mouse. Proc Natl Acad Sci U S A 94:4642–4646
12. Daugherty A, Pure E, fel-Butteiger D et al (1997) The effects of total lymphocyte deficiency on the extent of atherosclerosis in apolipoprotein E−/− mice. J Clin Invest 100:1575–1580
13. Dechend R, Maass M, Gieffers J et al (1999) Chlamydia pneumoniae infection of vascular smooth muscle and endothelial cells activates NF-kappaB and induces tissue factor and PAI-1 expression: a potential link to accelerated arteriosclerosis. Circulation 100:1369–1373
14. Dimayuga P, Cercek B, Oguchi S et al (2002) Inhibitory effect on arterial injury-induced neointimal formation by adoptive B-cell transfer in Rag-1 knockout mice. Arterioscler Thromb Vasc Biol 22:644–649
15. Drexler H (1998) Factors involved in the maintenance of endothelial function. Am J Cardiol 82:3S–4S
16. Endres M, Laufs U, Huang Z et al (1998) Stroke protection by 3-hydroxy-3-methylglutaryl (HMG)-CoA reductase inhibitors mediated by endothelial nitric oxide synthase. Proc Natl Acad Sci U S A 95:8880–8885
17. Febbraio M, Hajjar DP, Silverstein RL (2001) CD36: a class B scavenger receptor involved in angiogenesis, atherosclerosis, inflammation, and lipid metabolism. J Clin Invest 108:785–791
18. Grayston JT (1992) Infections caused by Chlamydia pneumoniae strain. TWAR Clin Infect Dis 15:757–761
19. Gupta S, Pablo AM, Jiang X et al (1997) IFN-gamma potentiates atherosclerosis in ApoE knock-out mice. J Clin Invest 99:2752–2761
20. Halme S, Syrjala H, Bloigu A et al (1997) Lymphocyte responses to Chlamydia antigens in patients with coronary heart disease. Eur Heart J 18:1095–1101
21. Hamilton JA, Chan J, Byrne RJ et al (1998) MRL/lpr and MRL +/+ macrophage DNA synthesis in the absence and the presence of colony-stimulating factor-1 and granulocyte-macrophage colony-stimulating factor. J Immunol 161:6802–6811
22. Hansson GK, Holm J, Jonasson L (1989) Detection of activated T lymphocytes in the human atherosclerotic plaque. Am J Pathol 135:169–175
23. Hirai A, Nakamura S, Noguchi Y et al (1997) Geranylgeranylated rho small GTPase(s) are essential for the degradation of p27Kip1 and facilitate the progression from G1 to S phase in growth-stimulated rat FRTL-5 cells. J Biol Chem 272:13–16
24. Hu H, Pierce GN, Zhong G (1999) The atherogenic effects of chlamydia are dependent on serum cholesterol and specific to Chlamydia pneumoniae. J Clin Invest 103:747–753
25. Huh HY, Pearce SF, Yesner LM et al (1996) Regulated expression of CD36 during monocyte-to-macrophage differentiation: potential role of CD36 in foam cell formation. Blood 87:2020–2028
26. Inoue S, Egashira K, Ni W et al (2002) Anti-monocyte chemoattractant protein-1 gene therapy limits progression and destabilization of established atherosclerosis in apolipoprotein E-knockout mice. Circulation 106:2700–2706
27. Jantos CA, Nesseler A, Waas W et al (1999) Low prevalence of Chlamydia pneumoniae in atherectomy specimens from patients with coronary heart disease. Clin Infect Dis 28:988–992
28. Kalayoglu MV, Hoerneman B, La Verda D et al (1999) Cellular oxidation of low-density lipoprotein by Chlamydia pneumoniae. J Infect Dis 180:780–790
29. Keech A, Colquhoun D, Best J et al (2003) Secondary prevention of cardiovascular events with long-term pravastatin in patients with diabetes or impaired fasting glucose: results from the LIPID trial. Diabetes Care 26:2713–2721
30. Kopp AF, Schroeder S, Baumbach A et al (2001) Non-invasive characterisation of coronary lesion morphology and composition by multislice CT: first results in comparison with intracoronary ultrasound. Eur Radiol 11:1607–1611
31. Kritchevsky D (1995) Dietary protein, cholesterol and atherosclerosis: a review of the early history. J Nutr 125:589S–593S
32. Langheinrich AC, Braun-Dullaeus RC, Walker G et al (2003) Effects of 3–deazaadenosine on homocysteine and atherosclerosis in apolipoprotein E-deficient mice. Atherosclerosis 171:181–192
33. Langheinrich AC, Bohle RM, Greschus S et al (2004) Atherosclerotic lesions at micro CT: feasibility for analysis of coronary artery wall in autopsy specimens. Radiology 231:675–681
34. Laukkanen MO, Mannermaa S, Hiltunen MO et al (1999) Local hypomethylation in atherosclerosis found in rabbit ec-sod gene. Arterioscler Thromb Vasc Biol 19:2171–2178
35. Laurat E, Poirier B, Tupin E et al (2001) In vivo down-regulation of T helper cell 1 immune responses reduces atherogenesis in apolipoprotein E-knockout mice. Circulation 104:197–202
36. Lemaitre V, O'Byrne TK, Borczuk AC et al (2001) ApoE knockout mice expressing human matrix metalloproteinase-1 in macrophages have less advanced atherosclerosis. J Clin Invest 107:1227–1234
37. Lentz SR, Sadler JE (1991) Inhibition of thrombomodulin surface expression and protein C activation by the thrombogenic agent homocysteine. J Clin Invest 88:1906–1914
38. Matsumoto S, Kobayashi T, Katoh M et al (1998) Expression and localization of matrix metalloproteinase-12 in the aorta of cholesterol-fed rabbits: relationship to lesion development. Am J Pathol 153:109–119
39. McCully KS, Wilson RB (1975) Homocysteine theory of arteriosclerosis. Atherosclerosis 22:215–227
40. Mehta J, Dinerman J, Mehta P et al (1989) Neutrophil function in ischemic heart disease. Circulation 79:549–556
41. Merhi Y, Lacoste LL, Lam JY (1994) Neutrophil implications in platelet deposition and vasoconstriction after deep arterial injury by angioplasty in pigs. Circulation 90:997–1002
42. Metzger R, Bohle RM, Chumachenko P et al (2000) CD143 in the development of atherosclerosis. Atherosclerosis 150:21–31
43. Moazed TC, Kuo CC, Grayston JT et al (1998) Evidence of systemic dissemination of Chlamydia pneumoniae via macrophages in the mouse. J Infect Dis 177:1322–1325

44. Mosorin M, Surcel HM, Laurila A et al (2000) Detection of Chlamydia pneumoniae-reactive T lymphocytes in human atherosclerotic plaques of carotid artery. Arterioscler Thromb Vasc Biol 20:1061–1067
45. Naruko T, Ueda M, Haze K et al (2002) Neutrophil infiltration of culprit lesions in acute coronary syndromes. Circulation 106:2894–2900
46. Ni W, Egashira K, Kataoka C et al (2001) Antiinflammatory and antiarteriosclerotic actions of HMG-CoA reductase inhibitors in a rat model of chronic inhibition of nitric oxide synthesis. Circ Res 89:415–421
47. Paigen B, Morrow A, Holmes PA et al (1987) Quantitative assessment of atherosclerotic lesions in mice. Atherosclerosis 68:231–240
48. Paiva H, Laakso J, Laine H et al (2002) Plasma asymmetric dimethylarginine and hyperemic myocardial blood flow in young subjects with borderline hypertension or familial hypercholesterolemia. J Am Coll Cardiol 40:1241–1247
49. Palinski W, Miller E, Witztum JL (1995) Immunization of low density lipoprotein (LDL) receptor-deficient rabbits with homologous malondialdehyde-modified LDL reduces atherogenesis. Proc Natl Acad Sci U S A 92:821–825
50. Paul A, Ko KW, Li L et al (2004) C-reactive protein accelerates the progression of atherosclerosis in apolipoprotein E-deficient mice. Circulation 109:647–655
51. Peters W, Charo IF (2001) Involvement of chemokine receptor 2 and its ligand, monocyte chemoattractant protein-1, in the development of atherosclerosis: lessons from knockout mice. Curr Opin Lipidol 12:175–180
52. Poddar R, Sivasubramanian N, Di Bello PM et al (2001) Homocysteine induces expression and secretion of monocyte chemoattractant protein-1 and interleukin-8 in human aortic endothelial cells: implications for vascular disease. Circulation 103:2717–2723
53. Prescott MF, Sawyer WK, Von Linden-Reed J et al (1999) Effect of matrix metalloproteinase inhibition on progression of atherosclerosis and aneurysm in LDL receptor-deficient mice overexpressing MMP-3, MMP-12, and MMP-13 and on restenosis in rats after balloon injury. Ann N Y Acad Sci 878:179–190
54. Ridker PM, Rifai N, Rose L et al (2002) Comparison of C-reactive protein and low-density lipoprotein cholesterol levels in the prediction of first cardiovascular events. N Engl J Med 347:1557–1565
55. Ross R (1999) Atherosclerosis—an inflammatory disease. N Engl J Med 340:115–126
56. Shor A, Kuo CC, Patton DL (1992) Detection of Chlamydia pneumoniae in coronary arterial fatty streaks and atheromatous plaques. S Afr Med J 82:158–161
57. Smith JD, Trogan E, Ginsberg M et al (1995) Decreased atherosclerosis in mice deficient in both macrophage colony-stimulating factor (op) and apolipoprotein E. Proc Natl Acad Sci U S A 92:8264–8268
58. Song L, Leung C, Schindler C (2001) Lymphocytes are important in early atherosclerosis. J Clin Invest 108:251–259
59. Sowers JR (2002) Hypertension, angiotensin II, and oxidative stress. N Engl J Med 346:1999–2001
60. Stehbens WE (1999) Anitschkow and the cholesterol over-fed rabbit. Cardiovasc Pathol 8:177–178
61. Stein EA, Davidson MH, Dobs AS et al (1998) Efficacy and safety of simvastatin 80 mg/day in hypercholesterolemic patients. The Expanded Dose Simvastatin U.S. Study Group. Am J Cardiol 82:311–316
62. Steinberg D, Witztum JL (2002) Is the oxidative modification hypothesis relevant to human atherosclerosis? Do the antioxidant trials conducted to date refute the hypothesis? Circulation 105:2107–111
63. Steinberg D, Parthasarathy S, Carew TE et al (1989) Beyond cholesterol. Modifications of low-density lipoprotein that increase its atherogenicity. N Engl J Med 320:915–924
64. Stuhlinger MC, Tsao PS, Her JH et al (2001) Homocysteine impairs the nitric oxide synthase pathway: role of asymmetric dimethylarginine. Circulation 104:2569–2575
65. Verma S, Wang CH, Li SH et al (2002) A self-fulfilling prophecy: C-reactive protein attenuates nitric oxide production and inhibits angiogenesis. Circulation 106:913–919
66. Wang G, Woo CW, Sung FL et al (2002) Increased monocyte adhesion to aortic endothelium in rats with hyperhomocysteinemia: role of chemokine and adhesion molecules. Arterioscler Thromb Vasc Biol 22:1777–1783
67. Wassmann S, Czech T, Eickels M et al (2004) Inhibition of diet-induced atherosclerosis and endothelial dysfunction in apolipoprotein E/angiotension II type 1A receptor double-knockout mice. Circulation 110:27–32
68. Yla-Herttuala S, Palinski W, Butler SW et al (1994) Rabbit and human atherosclerotic lesions contain IgG that recognizes epitopes of oxidized LDL. Arterioscler Thromb 14:32–40
69. Zhou X, Stemme S, Hansson GK (1996) Evidence for a local immune response in atherosclerosis. CD4+ T cells infiltrate lesions of apolipoprotein-E-deficient mice. Am J Pathol 149:359–366
70. Zhou X, Caligiuri G, Hamsten A et al (2001) LDL immunization induces T-cell-dependent antibody formation and protection against atherosclerosis. Arterioscler Thromb Vasc Biol 21:108–114
71. Zibara K, Chignier E, Covacho C et al (2000) Modulation of expression of endothelial intercellular adhesion molecule-1, platelet-endothelial cell adhesion molecule-1, and vascular cell adhesion molecule-1 in aortic arch lesions of apolipoprotein E-deficient compared with wild-type mice. Arterioscler Thromb Vasc Biol 20:2288–2296

Virchows Arch (2005) 446:112–119
DOI 10.1007/s00428-004-1139-5

ORIGINAL ARTICLE

Pavlína Plevová · Eva Sedláková · Jana Zapletalová · Anna Křepelová · Petra Skýpalová · Zdeněk Kolář

Expression of the hMLH1 and hMSH2 proteins in normal tissues: relationship to cancer predisposition in hereditary non-polyposis colon cancer

Received: 22 January 2004 / Accepted: 30 August 2004 / Published online: 10 December 2004
© Springer-Verlag 2004

Abstract The majority of tumours in patients with hereditary non-polyposis colon cancer (HNPCC) occur in large intestine and endometrium; also, other tissues are at increased risk. We studied expression of hMLH1 and hMSH2 proteins in 148 normal samples of various tissues from non-HNPCC patients and in 14 normal colon tissues from HNPCC patients. Immunohistochemical technique was used. Intensity of nuclear staining, percentage of stained cells and H-scores were calculated. Tissues were divided into groups. Groups A, B and C included tissues with increased risk of cancer in HNPCC A) stomach, small and large bowel; (B) endometrium; (C) ovary, ureter, urinary bladder, kidney and liver. Group D tissues were without increased risk. Expression of the proteins was significantly higher in groups A, B and C compared with group D ($P<0.0001$, $P=0.0004$ for hMSH2 in C versus D). The expression was highest in testis. In colons of HNPCC patients, expression of the mutated gene product was significantly lower than in non-HNPCC patients. In conclusion, hMLH1/hMSH2 protein expression is constitutively higher in certain cell types of certain tissues, including the majority of tissues that are at increased risk of cancer in HNPCC. However, association of strong hMLH1/hMSH2 expression with cancer risk is not strictly valid.

Keywords Hereditary non-polyposis colon cancer · MLH1 protein expression · hMSH2 protein expression · Immunohistochemistry

P. Plevová (✉)
Předvrší 560, 725 26 Ostrava-Krásné Pole, Czech Republic
e-mail: pavlina.plevova@volny.cz
Tel.: +420-59-7372212
Fax: +420-59-7373293

P. Plevová · E. Sedláková · P. Skýpalová · Z. Kolář
Institute of Pathology and Laboratory of Molecular Pathology,
Medical Faculty of the Palacký University,
Hněvotínská 3, 775 15 Olomouc, Czech Republic

P. Plevová
Department of Medical Genetics,
University Hospital of Ostrava,
tř. 17.listopadu 1790, 708 52 Ostrava, Czech Republic

J. Zapletalová
Institute of Biophysics and Statistics,
Palacký University,
Hněvotínská 3, 775 15 Olomouc, Czech Republic

A. Křepelová
Institute of Genetics,
Faculty Hospital,
V úvalu 84, Prague-Motol, Czech Republic

Introduction

Germline mutations in *hMLH1* and *hMSH2* genes are linked to hereditary non-polyposis colon cancer (HNPCC), a cancer susceptibility syndrome with an autosomal dominant pattern of inheritance [1]. With respect to the *hMLH1* and *hMSH2* gene nature, their involvement in DNA mismatch repair (MMR) and their apparently ubiquitous expression patterns, at least as judged by assessment of mRNA, might lead one to expect that MMR deficiency would be associated with tumour development in tissues with a high rate of proliferation [15]. Nevertheless, the great majority of tumours in HNPCC patients occur in the large intestine and endometrium. Carcinomas of the stomach, small bowel, ovary, hepatobiliary and urinary tract have also increased incidence ratios, whereas the incidence of tumours of other rapidly proliferating tissues, such as the haematopoietic system, skin, mouth, mucosa or bronchoalveolar system, is not increased in these patients [3, 32]. The reasons why a higher incidence of cancers in *hMLH1*/*hMSH2* gene mutation carriers exists only in the specific organs and tissues mentioned above are not sufficiently explained. The aim of this study was to verify the hypothesis that a high incidence of cancers in specific types of tissues is related to the constitutive level of hMLH1/hMSH2 protein expression.

Table 1 Risk of cancer development in hMLH1/hMSH2 mutation carriers

Group	Cumulative cancer risk (%)	Times higher than general population risk	Reference
A			
Colon and rectum	78–82	10–40	[2, 3]
Stomach	13–19	4–13	[2, 3, 32]
Small bowel	1–4	25–100	[3, 32]
B			
Endometrium	43–62	14–60	[2, 3, 12, 33]
C			
Ovary	9–12	3.5–9	[2, 3, 32]
Urological tract	7–13		[2, 3]
Kidney	3–5	4	[2, 3]
Renal pelvis		17	[32]
Ureter	2–4	6–22	[2, 32]
Urinary bladder	2–4	6	[2, 3]
Hepatobiliary system	2–18	10	[2, 3, 32]
D			
Prostate		No increase	[3, 32]
Breast		No increase	[3, 32]
Lung/bronchus		No increase	[3, 32]
Thyroid gland		No increase	[3]
Melanoma		No increase	[3]
Pancreas		No increase	[3, 32]
Brain	3 [3]	No increase	[2, 19, 32]
Lymphatic/hematopoietic system		No increase	[3, 32]
Larynx		No increase	[32]
Uterine cervix		No increase	[3, 32]

Materials and methods

Materials

Expression of the hMLH1 and hMSH2 proteins was studied in formalin-fixed, paraffin-embedded archive tissue samples whose histological examination revealed normal morphology. We analysed 148 samples from 145 non-HNPCC patients. There were tissue samples of oral mucosa (3 samples), oesophagus (5), stomach (7), small bowel (7), colon and rectum (21), gallbladder (4), liver (5), pancreas (1), endometrium (16), uterine cervix (5), ovary (8), breast (9), kidney (3), ureter (9), urinary bladder (7), prostate (5), bronchi (3), lung (7), vocal cord (1), brain (3), peripheral nerve (2), bone marrow (5), thyroid gland (3), skin (6) and testis (3). We also analysed expression of the hMLH1 and hMSH2 proteins in normal colon tissue from ten *hMLH1* mutation carriers and four *hMSH2* mutation carriers.

Immunohistochemistry

Indirect immunohistochemical technique was used to detect the proteins [29]. Before immunostaining, heat-induced antigen retrieval was performed by treatment in a microwave oven (4×10 min at 900 W with a 1 min break between every 10 min), tissue sections being immersed in 10 mM citrate buffer, pH 6.0. Mouse monoclonal antibodies against hMLH1 protein (G168-15, PharMingen, San Diego, CA; prepared against full-length protein) and hMSH2 protein (G219-1129, PharMingen, San Diego, CA; prepared against full-length protein) and amplification system EnVision (DakoCytomation, Denmark) were used. The activity of peroxidase was visualised by diaminobenzidine. Positive control, a sample of colon tissue with a known immunoreactivity, was included in each set of samples analysed, as well as negative control, i.e. slides incubated with Tris buffer instead of the anti-hMLH1 or anti-hMSH2 antibodies. The intensity of nuclear staining was graded semi-quantitatively as "0" for no staining, "1" for weak staining, "2" for moderately strong staining and "3" for strong staining. With respect to the number of positive cells, the H-score was calculated, i.e. (% of cells with grade "1" staining×1)+(% of cells with grade "2" staining ×2)+(% of cells with grade "3" staining ×3). Nuclei of lymphocytes served as an internal control for grade "1" staining.

Statistical analysis

Expression of the hMLH1/hMSH2 proteins was compared among selected tissues, namely colon/rectum, small bowel, endometrium, ureter, ovary, kidney compared with breast, prostate, bronchi and testis. The tissues were also separated into four groups. Groups A, B and C included tissues with an increased risk of cancer in HNPCC patients; group D included tissues without an increased risk of cancer in HNPCC patients. The groups were selected according to the cumulative incidences reported in HNPCC patients compared with the general population (Table 1). The groups included: (A) high-risk tissues of the gastrointestinal tract—stomach, small bowel and large bowel glands; (B) endometrial glands; (C) other at-risk tissues: ovary–mesothelium, ureter–epithelium, urinary bladder–epithelium, kidney and liver tissues; (D) squamocellular epithelium of oral cavity, uterine cervix, oesophagus, skin and vocal cord, breast lobuli, prostatic glands, thyroid gland epithelium, haematopoietic cells of bone marrow, lung and bronchial epithelium, pancreatic and brain tissues, gallbladder epithelium, peripheral nerve and testis. H-scores were compared between these groups. The comparison of the H-scores between the groups was performed using analysis of variance and least significant difference tests. Differences in hMLH1 and hMSH2 H-scores for colon and rectum tissues between non-HNPCC and HNPCC patients were statistically analysed using a chi-square test.

Results

The hMLH1 and hMSH2 proteins were expressed in all the tested tissues. The tissues differed in the intensity of the protein expression (for H-scores in the particular tissues, see Table 2). The tissue with the most intensive protein expression was testis, with mean H-scores of 180 and 166.7 for hMLH1 and hMSH2, respectively. Sper-

Table 2 hMLH1 and hMSH2 expression in normal tissues of non-HNPCC patients

Group of tissues	No. of samples	H-scores: minimum/maximum/mean/median values	
		hMLH1	hMSH2
A			
Colon, rectum—epithelium	21	80/175/112.5/110	80/175/127.4/120
Small bowel—epithelium	7	85/130/111.7/112.5	105/140/124.3/130
Stomach—epithelium	7	100/130/112.5/110	100/180/144.3/160
Total in A	35	80/175/112.6/110	80/180/130.2/130
B			
Endometrium—glands			
Proliferation phase	8	100/180/136.4/130	135/195/160/155
Secretory phase	8	90/140/101.2/97.5	100/210/130/107.5
Total in B	16	90/180/117.7/100	100/210/145.3/142.5
C			
Ovary—mesothelium	8	100/135/117.5/120	110/175/133.8/127.5
Ureter—epithelium	9	100/135/112.8/115	110/130/119.4/117.5
Urinary bladder—epithelium	7	80/135/115/117.5	100/125/116.4/115
Kidney	3	70/80/76.7/80	70/80/76.7/80
Liver	5	75/100/91/100	80/120/106/100
Total in C	32	70/135/105.8/102.5	70/175/115.9/115
D			
Oral cavity—squamocellular epithelium	3	75/100/85/80	95/120/105/100
Uterine cervix—squamocellular epithelium	5	75/105/86/80	90/110/97/95
Oesophagus—squamocellular epithelium	5	70/100/88/90	90/115/100/95
Vocal cord—squamocellular epithelium	1	90	95
Breast—lobuli	9	50/100/75/70	70/105/88.3/90
Prostate—epithelium	5	70/100/88/90	70/120/89/90
Thyroid gland—epithelium	3	70/90/80/80	70/115/91.7/90
Bone marrow—haematopoietic cells	5	70/80/72.5/70	70/95/81/80
Lung	7	30/60/47.1/50	30/80/55.7/60
Bronchus	3	85/125/103.3/100	115/130/125/130
Pancreas	1	90	105
Skin—squamocellular epithelium	6	80/105/94.2/95	100/130/110.8/105
Brain	3	80/90/85/85	90/140/110/100
Gallbladder—epithelium	4	70/90/77.5/75	70/80/77.5/80
Total in D	60	30/125/75.8/80	30/140/90.1/90
Peripheral nerve	2	20/30/25/25	30/30/30/30
Testis	3	165/200/180/175	115/200/166.7/185

matogonia and spermatocytes expressed the proteins mostly at the "3" or "2" level, expression in Sertolli cells was weak and sperms and myoepithelial cells did not express the proteins. With regard to epithelial cells, the most intense staining was observed in endometrial epithelium. Staining at the "2" or "3" level was observed in about half of the cells in the proliferation phase (mean scores of 136.4 and 160, respectively) and at the "1" or "0" level in the secretory phase of the menstrual cycle (mean scores of 101.2 and 130, respectively). Strong expression was also observed in epithelial cells of all parts of the gastrointestinal tract. In small bowel and colon and rectum, mean H-scores were 111.7 and 112.5 for hMLH1 and 122.5 and 127.4 for hMSH2, respectively. The nuclei stained as "3" or "2" in the lower parts of the crypts; whereas, in the upper parts, the nuclei stained as "1" or "0". Expression in the cells of germline centres of lymphoid follicles was strong; whereas, lymphocytes outside germline centres stained as "1". In ovary, the most intensive expression was in oocytes, granulosa cells and mesothelial cells, whereas nuclei of theca externa cells and of corpus albicans cells did not express the protein. Mean H-scores for ovarian mesothelial cells were 117.5 and 133.8, respectively. The squamocellular epithelium of skin, oesophagus, mouth mucosa, uterine cervix and vocal cord expressed the proteins most intensively in the basal layers; whereas, in the upper layers, the expression was weak. Mean H-scores for these tissues ranged from 85.0 to 94.2 for hMLH1 and from 97.0 to 110.8 for hMSH2, the most intense staining being in squamocellular epithelium of the skin. In bone marrow, proerytroblasts and myeloblasts expressed the proteins most intensively, at the "3" or "2" level. Promyelocytes, myelocytes and metamyelocytes expressed the proteins at the "1" or "2" level, megakaryocytes at the "1" level. The expression in erythroblasts, bands, segments and lymphocytes was mostly negative or weakly positive. Mean H-scores for bone marrow were 72.5 and 81.0, respectively. In bronchi, the mean H-scores were 103.3 and 125.0, respectively, basal cells being mostly negative; whereas, cells at the surface of epithelium expressed the proteins strongly. Expression in bronchioli was weaker than in bronchi. For lung, mean H-scores were 47.1 and 55.7. Of alveolar epithelial type-I cells, 30–50% expressed the proteins at the "1" level, the others being negative; whereas, all type-II cells expressed the proteins mostly at the "1" level. Lung macrophages also expressed the proteins weakly. Relatively weak expression was seen in epithelia of

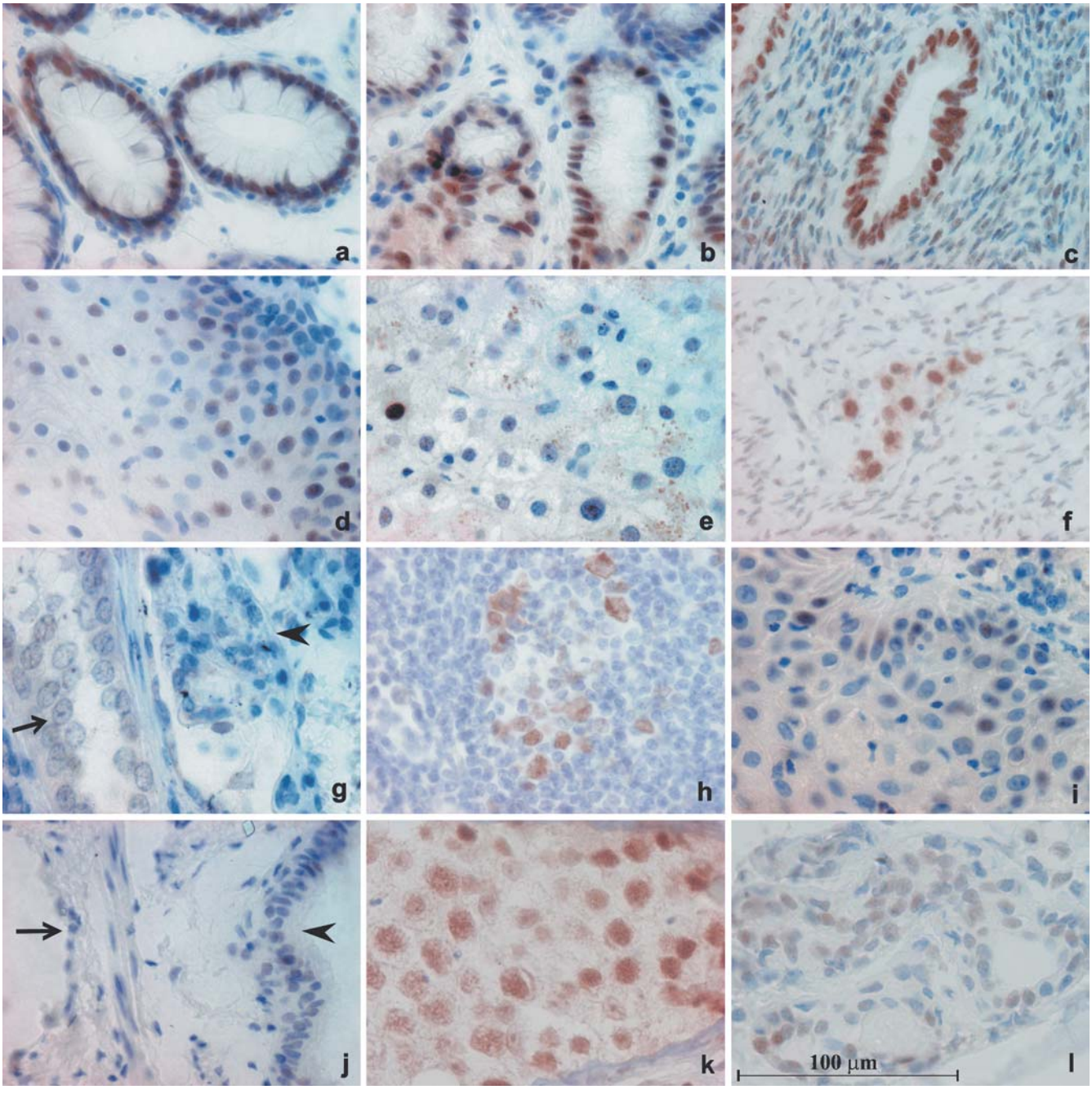

Fig. 1 Expression of hMSH2 protein in normal human tissues: colon—lower parts of crypts (**a**), stomach (**b**), endometrium (**c**), oesophagus—squamocellular epithelium (**d**), liver (**e**), ovary (**f**), kidney—tubules (*arrow*), glomerulus (*arrowhead*) (**g**), lymphoid follicle—germline centre (**h**), uterine cervix (**i**), lung—alveoli (*arrow*), bronchiolus (*arrowhead*) (**j**), testis (**k**), breast (**l**) (×1000). *Scale bar* 100 μm

breast, prostate and gall bladder, mean H-scores being 75.0, 88.0 and 77.5 for hMLH1 and 88.3, 89.0 and 77.5 for hMSH2, respectively. For kidney, both mean H-scores were 76.7. The majority of cells of tubules expressed the proteins at the "1" level, whereas in glomeruli, only half or less of podocytes and cells of the parietal layer of the Bowman capsule expressed the proteins weakly. Expression in the transitional epithelium of ureter and urinary bladder was moderately strong, mean H-scores being 112.8 and 115.0 for hMLH1 and 119.4 and 116.4 for hMSH2, respectively. In the brain, all neurons and astrocytes expressed the proteins at the "1" or "2" level. Expression in oligodendroglia was weak, and microglia did not express the proteins. Mean H-scores for brain tissue were 85 and 110, respectively. Stromal cells generally expressed the proteins mostly at grade "1" level. Expression of the hMSH2 protein in selected tissues is seen in Fig. 1.

Table 3 Comparison of hMLH1 and hMSH2 expression (H-scores) between epithelial cells of selected tissues, results of lowest significant difference tests

Tissue	Breast		Prostate		Bronchus		Testis	
	hMLH1	hMSH2	hMLH1	hMSH2	hMLH1	hMSH2	hMLH1	hMSH2
Colon, rectum	<0.0001	0.0001	0.015	0.002	NS	NS	<0.0001*	0.002*
Small bowel	0.001	0.003	0.052	0.013	NS	NS	<0.0001*	0.004*
Endometrium	<0.0001	<0.0001	0.005	<0.0001	NS	NS	<0.0001*	NS*
Ureter	0.0001	0.008	0.028	0.027	NS	NS	<0.0001*	0.001*
Ovary	<0.0001	0.0002	0.011	0.001	NS	NS	<0.0001*	0.016*
Kidney	NS*	NS*	NS*	NS*	NS*	0.014*	<0.0001*	<0.0001*

* Expression in the tissue in column is higher than in the tissue in line

Table 4 Statistical analysis of differences in H-scores for hMLH1/hMSH2 between selected groups of tissues, results of lowest significant difference tests

Group of tissues		D
	Protein	Significance
A	hMLH1	<0.0001
	hMSH2	<0.0001
B	hMLH1	<0.0001
	hMSH2	<0.0001
C	hMLH1	<0.0001
	hMSH2	0.0004

Comparison of H-scores between selected tissues is seen in Table 3. Expression of the proteins was significantly higher in epithelial cells of colon and rectum, small bowel, endometrium, ovary and ureter than in breast and prostate epithelia and significantly lower than in testis. There was no significant difference between expression in brochial epithelia compared with epithelia of colon and rectum, small bowel, endometrium, ovary and ureter. There was no statistical difference between H-scores for kidney tissue compared with breast, prostate and bronchi, except for hMSH2, which was significantly lower in kidney than in bronchi.

With regard to groups of tissues, mean H-score values for groups A, B, C and D were 112.6, 117.7, 105.8 and 75.8 for hMLH1 and 130.2, 145.3, 115.9 and 90.1 for hMSH2, respectively (Table 2). For statistical analysis, the tissues of peripheral nerve and testis were excluded from group D, because their H-scores highly differed from the other tissues, and this could influence the results. Results of the statistical analysis of H-score differences between particular groups of tissues are summarised in Table 4. Expression of the proteins was significantly higher in groups A, B and C than in group D ($P<0.0001$; hMSH2 for C compared with D, $P=0.0004$).

In colon and rectum of hMLH1/hMSH2 mutation carriers, expression of the mutated gene product was significantly lower than in non-HNPCC patients. With the exception of one sample from an *hMSH2* germline mutation carrier, we did not observe the typical intensive staining of hMLH1 protein in the lower parts of the crypts in hMLH1 mutation carriers and of hMSH2 protein in hMSH2 mutation carriers.

Discussion

To date, a comprehensive explanation of what defines the cancer spectrum in HNPCC has not been offered. Fearon suggests that the sites at risk must be exposed to an environmental injury that makes mutation or inactivation of the wild-type allele more likely at that location. This would appear to fit the gastric cancer story in HNPCC, given the fact that the earliest reported generations of HNPCC kindreds showed a gastric cancer excess that was even more common in certain families [8].

Using Western-blot analysis, the highest expression of the hMLH1, hMSH2 and hPMS2 proteins has been observed in the testis and ovary. Lower levels of expression were observed in brain, adrenal, heart, stomach, small intestine, skeletal muscle, liver, kidney, spleen and prostate [10, 20]. Western-blot analysis determines the content of the protein in the tissue in total and does not discriminate between particular cell types in the tissue. However, immunohistochemistry identifies the cells in the tissue that actually express the protein.

Tissues with high risk of cancer in HNPCC

Among the specific organ cancer risks, *hMLH1*/*hMSH2* heterozygous mutation carriers have the highest risk of colon and rectum cancer development—an 82% cumulative cancer incidence by the age of 70 years [3]. The cumulative cancer incidence of stomach cancer and small bowel cancer are also increased compared with that of the general population (Table 1) [2, 24]. The tissues of colon and rectum, small bowel and stomach express the hMLH1/hMSH2 proteins at a high level and a similar pattern; this strong expression is localised to the replicative compartment of lower part of the crypts, suggesting transcriptional or translational control analogous to other proteins involved in DNA replication and reflecting the requirement for protection of cells from DNA replication errors [15]. This pattern has been already described [6, 10, 32]. It seems logical that, in a rapidly replicating tissue with such a high need for MMR, inactivation of this function has unfavourable consequences, considering the direct exposure of the epithelium to cancerogens involved in the diet. In addition, mutations of MMR genes may lead to the accumulation of both environmental and en-

dogenous oxidative DNA lesions and should directly affect the ability of cells to induce apoptosis in response to DNA damage [4, 11, 23, 35]. Localisation of the highest cancer risk to colon corresponds to the general risk of cancer development in the digestive tract. Colon cancer is the most common one, six times more common than stomach cancer [21], which reflects the relatively long exposure of the epithelium to cancerogens in faeces.

Endometrial cancer is the second most common cancer in *hMLH1*/*hMSH2* heterozygous mutation carriers (Table 1) [12, 33]. The incidence of endometrial cancer exceeded that for colorectal cancer in women with HNPCC in one study [3]. Endometrial cancer is the most common cancer of the female reproductive organs [21]. Endometrial carcinoma of the endometroid type is common in HNPCC patients; this type shares some similar features with colorectal carcinoma—it often arises from benign precursors, endometrial hyperplasias [13]. The H-scores for endometrium were among the highest. This aside, a similarity in the epithelial morphology between colon and endometrium should be noted. The dependence of hMLH1/hMSH2 protein expression in endometrium on the phase of menstrual cycle has been described [13, 14]. The cyclic changes in endometrium with phases of high cell proliferation demanding effective protection from DNA replication errors might represent the factor that increases cancer risk in patients with hMLH1/hMSH2 inactivation.

Tissues with low risk of cancer in HNPCC

Female *hMLH1*/*hMSH2* heterozygous mutation carriers also have an increased risk of ovarian cancer (Table 1) [32]. The observed expression of the proteins in surface epithelium was relatively high in our study, which is in contrast to the findings by Fink and co-workers, who observed staining for hMLH1 and hPMS2 proteins in the nuclei of granulosa and stromal cells; whereas, surface epithelium and germ cells were non-reactive [10].

In regard to tumours of uroepithelial tract and kidney, HNPCC patients are at an increased risk of these tumours, although the spectrum of tumours differed in various studies [3]. In a study, 22 times the expected number of ureteral cancers and 17 times the expected number of carcinomas of the renal pelvis have been observed in HNPCC families, whereas the risks of renal cell and urinary bladder cancer were not raised [32]. In the general population, renal cell cancers represent more than 90% of kidney cancers; carcinomas of the renal pelvis represent 5% and ureteral cancers only 1% of these cancers [17]. In other studies, however, renal cell adenocarcinomas and carcinomas of the bladder and urethra were observed [2, 3]. The protein expression in transitional epithelia of ureter and urinary bladder was relatively high. However, this was not the case of kidney tissue.

The risk of hepatobiliary tumours is also increased in HNPCC patients [2, 3, 32]. However, the expression of the proteins in liver and gallbladder was moderate, comparable to the majority of non-risk tissues.

Non-risk tissues in HNPCC

No testicular tumours have been described in HNPCC patients [2, 3, 32]. This is in contrast to the strong expression of hMLH1 and hMSH2 proteins in germ cells of testis.

The expression of the proteins in the squamocellular epithelium of various organs was moderate. Deficiency of the MMR system does not effect cancer development in the squamocellular epithelium generally, neither in uterine cervix nor in oral cavity, oesophagus or elsewhere. This might be associated with a low probability of inactivation of the wild-type allele in this epithelium, corresponding to its localisation or with a preferential use of other protective systems with respect to specific cancerogens to which these tissues are in contact. The risk of cancer development in these epithelia increases with smoking. It is an interesting fact that the incidence of not only oesophageal or oral cavity cancer, but also of others in which an aetiology of smoking plays an important role, such as cancer of the lung, larynx or pancreas [21], is not raised in HNPCC patients.

Tissues with high risk of cancer in non-HNPCC patients

Bronchoalveolar cancer is one of the most common cancers. Its incidence is not increased in HNPCC patients [3, 32]. There was no significant difference between the protein expression in bronchial epithelium compared with high-risk tissues in HNPCC, including colon and rectum, small bowel, endometrium, ovary, ureter. The expression of hMSH2 was even significantly higher in bronchi than in kidney. This along with the above given facts about the incidence of other smoking-related cancer in HNPCC patients suggests that cancerogens involved in tobacco act through mechanisms that do not involve the DNA MMR system.

Breast and prostate cancers are two of the four most common cancers, along with colorectal and lung cancer [21]. The risks for breast and prostate cancer do not appear to be raised in HNPCC [3, 32], although there are cases of breast cancer in these patients [2]. Both tissues expressed the hMLH1/hMSH2 proteins at a moderate level. Breast tissue is the target tissue for cancer in another most common cancer predisposition syndrome, the hereditary breast/ovary cancer syndrome, resulting from germline mutations of the *BRCA1*/*BRCA2* genes [30, 31], and breast cancer occurrence in HNPCC patients might be associated with interactions between MMR and BRCA proteins [4]. When colon and breast tissues are compared, colonic crypts composed of large amounts of cells with a high need for functional MMR system are, in enormous numbers, exposed to cancerogens in faeces. In the breast tissue, there are relatively low numbers (compared with

colon) of lobuli composed by ductuli in non-lactating breast gland with relatively low hMLH1/hMSH2 protein expression. These conditions might suggest why inactivation of MMR system has more serious consequences for colon than for breast tissue. In the breast tissue, sex-hormone responsiveness is probably the main cancer-promoting factor [30, 31]. The 80% risk of cancer development in the breast in BRCA1/BRCA2 mutation carriers suggests that breast tissues preferentially use this system of DNA repair [30].

While quiet lymphocytes show weak expression of the proteins, activated lymphocytes in germline lymphoid follicles express the proteins strongly. Lymphomas are not involved in the common spectrum of extracolonic tumours in hMLH1/hMSH2 heterozygous mutation carriers [19]. However, lymphomas are involved in the spectrum of tumours developing in children with a constitutional homozygous inactivation of the hMLH1 gene, conceived from a consanguineous mating in HNPCC families [25, 26, 28]. This corresponds to the fact that mice homozygous for a mutation at the hMSH2 locus developed lymphomas [27], as has already been noticed [34]. The reason why preserved function of one allele of the gene is enough to protect lymphoid tissue from accumulation of mismatch errors might be that the exposure of the lymphoid tissue to cancerogens able to inactivate the wild-type allele is relatively low. The susceptibility to lymphoma development in homozygotes for hMLH1 or hMSH2 gene mutations might reflect accumulation of mismatches during rapid proliferation of lymphocytes in childhood. Leukaemias are also not involved in the spectrum of HNPCC-associated extracolonic tumours; again, leukaemias have been described in children with a constitutional homozygous inactivation of the hMLH1 and hMHS2 genes [25, 26, 28, 34].

We have observed a differential expression of hMLH1 and hMSH2 proteins in various tissues. Differences in p53 protein expression have also been observed in different tissues in response to various stimuli. P53-regulated gene expression patterns also differ not only in different cell types but also in response to different induction signals [5, 9]. Differences in p53 protein expression have been also found during human embryogenesis [16]. Although there was a statistically significant correlation between risk of cancer and hMLH1/hMSH2 expression in some tissues, this association is not stringent. There is no risk of cancer in the tissue with the highest expression of the proteins, testis. Expression of the proteins in bronchial epithelium, a non-risk tissue, is comparable with expression in the high-risk tissues. Despite a relatively low protein expression in the kidney, cancers arise there in HNPCC patients.

We have observed a significantly decreased expression of hMLH1 protein in colon tissue of hMLH1 mutation carriers and of hMSH2 protein in colon tissue of hMSH2 mutation carriers. The observed lack of increased expression of the proteins in low parts of the crypts, the replicative compartment, in most cases suggests that the tissue is not able to respond to increased demand on the protein in these patients. Experimental studies have shown that expression of the hMSH2 protein remains at a constant, high level throughout the cell cycle. hMLH1 protein levels are also high and expressed in all phases of the cell cycle, but a modest increase in late G_1 and in S phase has been observed [22, 23]. hMLH1 protein plays a regulatory role in the G_2–M arrest following treatment by ionising radiation and fluoropyrimidine [7, 23, 24]. hMLH1 and hMSH2 proteins are also involved in transcription-coupled repair of ultraviolet and oxidative damage, and their overexpression induces apoptosis of cells [4, 35]. Along with accumulation of DNA mismatches, mutations of these genes may lead to the accumulation of both environmental and endogenous oxidative DNA lesions, including those generated during normal metabolism, and should directly affect the ability of cells to induce apoptosis in response to endogenous DNA damage and some types of DNA damage, including ionising radiation, DNA-alkylating and other DNA-damaging agents [4, 11, 23, 35]. These mechanisms might contribute to the pathogenesis of cancer in HNPCC [4, 35].

In conclusion, the hMLH1 and hMSH2 proteins are widely expressed in various tissues of the human body. Their expression is constitutively higher in certain cell types of certain tissues, including the majority of those tissues that are at an increased risk of cancer development in patients with deficiency of hMLH1/hMSH2 function. However, the association of strong hMLH1/hMSH2 protein expression with cancer risk is not strictly valid. There are tissues with strong protein expression without an increased risk of cancer in HNPCC and at-risk tissues with a moderate level of protein expression. It is possible that, in some tissues, a constitutionally higher need of the protein along with other biological and environmental factors might be co-responsible for the increased risk of cancer development in these tissues under the conditions of *hMLH1*/*hMSH2* gene deficiency.

Acknowledgements This work was supported by Ministry of Health Care of the Czech Republic, grant no. NC/6741–3. I am indebted to reviewers for their helpful comments.

References

1. Aaltonen LA, Peltomäki P, Leach FS, Sistonen P, Pylkkanen L, Mecklin JP, Jarvinen H, Powell SM, Jen J, Hamilton SR et al (1993) Clues to the pathogenesis of familial colorectal cancer. Science 260:812–816
2. Aarnio M, Mecklin JP, Aaltonen LA, Nystrom-Lahti M, Jarvinen HJ (1995) Life-time risk of different cancers in hereditary non-polyposis colorectal cancer (HNPCC) syndrome. Int J Cancer 64:430–433
3. Aarnio M, Sankila R, Pukkala E, Salovaara R, Aaltonen LA, de la Chapelle A, Peltomaki P, Mecklin JP, Jarvinen HJ (1999) Cancer risk in mutation carriers of DNA-mismatch-repair genes. Int J Cancer 81:214–218
4. Bellacosa A (2001) Functional interactions and signaling properties of mammalian DNA mismatch repair proteins. Cell Death Differ 8:1076–1092

5. Benchimol S (2001) p53-dependent pathways of apoptosis. Cell Death Differ 8:1049–1051
6. Chiaravalli AM, Furlan D, Facco C, Tibiletti MG, Dionigi A, Casati B, Albarello L, Riva C, Capella C (2001) Immunohistochemical pattern of hMLH2/hMLH1 in familial and sporadic colorectal, gastric, endometrial and ovarian carcinomas with instability in microsatellite sequences. Virchows Arch 438:39–48
7. Davis TW, Vilson-Van Patten C, Meyers M, Kunugi KA, Cuthill S, Reznikoff C, Garces C, Boland CR, Kinsella TJ, Fishel T, Boothman DA (1998) Defective expression of the DNA mismatch repair protein, MLH1, alters G2-M cell cycle checkpoint arrest following ionizing radiation. Cancer Res 58:767–778
8. Fearon ER (1997) Human cancer syndromes: clues to the origin and nature of cancer. Science 278:1043–1050
9. Fei P, Bernhard EJ, El-Deiry WS (2002) Tissue-specific induction of p53 targets in vivo. Cancer Res 62:7316–7327
10. Fink D, Nebel S, Aebi S, Zheng H, Kim HK, Christen RD, Howell SB (1997) Expression of the DNA mismatch repair proteins hMLH1 and hPMS2 in normal human tissues. Br J Cancer 76:890–893
11. Fink D, Aebi S, Howell SB (1998) The role of DNA mismatch repair in drug resistance. Clin Cancer Res 4:1–6
12. Green SE, Bradburn DM, Varma JS, Burn J (1998) Hereditary nonpolyposis colorectal cancer. Int J Colorect Dis 13:3–12
13. Hamid AA, Mandai M, Konishi I, Nanbu K, Tsuruta Y, Kusakari T, Kariya M, Kita M, Shingo (2002) Cyclical change of hMSH2 protein expression in normal endometrium during the menstrual cycle and its overexpression in endometrial hyperplasia and sporadic endometrial carcinoma. Cancer 94:997–1005
14. Irving JA, Dupuis B, Wang L, Gilks CB (2002) Cyclical expression of the DNA mismatch repair enzyme hMLH1 in normal endometrium. Fertil Steril 78:195–196
15. Leach FS, Polyak K, Burrell M, Johnson K, Hill D, Dunlop MG, Wylie AH, Peltomaki P, de la Chapelle A, Hamilton SR, Kinzler KW, Vogelstein B (1996) Expression of the human mismatch repair gene hMSH2 in normal and neoplastic tissues. Cancer Res 56:235–240
16. Lichnovsky V, Kolar Z, Murray P, Hlobilkova A, Cernochova D, Pospisilova E, Vojtesek B, Nenutil R (1998) Differences in p53 and Bcl-2 expression in relation to cell proliferation during the development of human embryos. Mol Pathol 51:131–137
17. Lineham WM, Shipley WU, Longo DL (1989) Cancer of the kidney and ureter. In: DeVita VT, Hellman S, Rosenberg SA (eds) Cancer: principles and practice of oncology, 3rd edn. JB Lippicott, Philadelphia, pp 979–1007
18. Lynch HT, Watson P, Kriegler M, Lynch JF, Lanspa SJ, Marcus J, Smyrk T, Fitzgibbons RJ, Cristofaro G (1988) Differential diagnosis of hereditary nonpolyposis colorectal cancer (Lynch syndrome I and Lynch syndrome II). Dis Colon Rectum 31:372–377
19. Lynch HT, Smyrk TC, Watson P, Lanspa SJ, Lynch JF, Lynch PM, Cavalieri RJ, Boland CR (1993) Genetics, natural history, tumor spectrum, and pathology of hereditary nonpolyposis colorectal cancer. An updated review. Gastroenterology 104:1535–1549
20. Mello JA, Acharya S, Fishel R, Essigmann JM (1996) The mismatch-repair protein HMSH2 binds selectively to DNA adducts of the anticancer drug cisplatin. Chem Biol 3:579–589
21. Mendelsohn J (1991) Principles of neoplasia. In: Wilson JD, Braunwald E, Isselbacher KJ, Petersdorf RG, Martin JB, Fauci AS, Root RK (eds) Harrisons's principles of internal medicine, 12th edn. McGraw-Hill, Inc., New York, pp 1576–1586
22. Meyers M, Theodosiou M, Acharya S, Odegaard E, Wilson T, Lewis JE, Davis TW, Wilson-Van patten C, Rishel R, Boothman DA (1997) Cell cycle regulation of the human DNA mismatch repair genes hMSH2, hMLH1, and hPMS2. Cancer Res 57:206–208
23. Meyers M, Wagner MW, Hwang HS, Kinsella TJ, Boothman DA (2001) Role of the hMLH1 DNA mismatch repair protein in fluoropyrimidine-mediated cell death and cell cycle responses. Cancer Res 61:5193–5201
24. Paraf F, Gilquin M, Longy M, Gilbert B, Gorry P, Petit B, Labrousse F (2001) MLH1 and MSH2 protein immunohistochemistry is useful for detection of hereditary non-polyposis colorectal cancer in young patients. Histopathology 39:250–258
25. Pratt CB, Parham DM, Rao BN, Fleming ID, Dilawari R (1988) Multiple colorectal carcinomas, polyposis coli and neurofibromatosis. J Natl Cancer Inst 80:1170–1172
26. Pratt CB, Jane JA (1991) Multiple colorectal carcinomas, polyposis coli and neurofibromatosis, followed by multiple glioblastoma multiforme. J Natl Cancer Inst 83:880–881
27. Reitmair AH, Schmits R, Ewel A, Bapat B, Redston M, Mitri A, Waterhouse P, Mittrucker HW, Wakeham A, Liu B et al (1995) MSH2 deficient mice are viable and susceptible to lymphoid tumours. Nat Genet 11:64–71
28. Ricciardome MD, Özcelik T, Cevher B, Özdag H, Tuncer M, Gürgey A, Uzunalimoglu Ö, Cetinkaya H, Tanyeli A, Erken E, Özturk M (1999) Human MLH1 deficiency predisposes to hematological malignancy and neurofibromatosis type I. Cancer Res 59:290–293
29. Scartozzi M, Bianchi F, Rosati S, Galizia E, Antolini A, Loretelli C, Piga A, Bearzi I, Cellerino R, Porfiri E (2002) Mutations of hMLH1 and hMSH2 in patients with suspected hereditary nonpolyposis colorectal cancer: correlation with microsatellite instability and abnormalities of mismatch repair protein expression. J Clin Oncol 20:1203–1208
30. Thompson D, Easton DF, Breast Cancer Linkage Consortium (2002) Cancer incidence in BRCA1 mutation carriers. J Natl Cancer Inst 94:1358–1365
31. Venkitaraman AR (2002) Cancer susceptibility and the functions of BRCA1 and BRCA2. Cell 108:171–182
32. Watson P, Lynch PT (1993) Extracolonic cancer in hereditary nonpolyposis colorectal cancer. Cancer 71:677–685
33. Watson P, Vasen HF, Mecklin JP, Jarvinen H, Lynch HT (1994) The risk of endometrial cancer in hereditary non polyposis colorectal cancer. Am J Med 96:516–520
34. Whiteside D, McLeod R, Graham G, Steckley JL, Booth K, Somerville MJ, Andrew SE (2002) A homozygous germ-line mutation in the human MSH2 gene predisposes to hematological malignancy and multiple cafe-au-lait spots. Cancer Res 62:359–362
35. Zhang H, Richards B, Wilson T, Lloyd M, Cranston A, Thorburn A, Fishel R, Meuth M (1999) Apoptosis induced by overexpression of hMSH2 or hMLH1. Cancer Res 59:3021–3027

Virchows Arch (2005) 446:120–126
DOI 10.1007/s00428-004-1146-6

ORIGINAL ARTICLE

Naoyuki Homma · Gen Tamura · Teiichiro Honda · Zhe Jin · Kiyonari Ohmura · Sumio Kawata · Teiichi Motoyama

Hypermethylation of *Chfr* and *hMLH1* in gastric noninvasive and early invasive neoplasias

Received: 28 July 2004 / Accepted: 19 September 2004 / Published online: 10 December 2004
© Springer-Verlag 2004

Abstract Human tumors are genetically unstable, and the instability exists at two distinct levels—the chromosomal level and the nucleotide level. *Chfr* and *hMLH1* hypermethylation, which may lead to chromosomal instability (CIN) and microsatellite instability (MSI), respectively, was analyzed in gastric noninvasive neoplasias (NIN, Padova international classification) and submucosal invasive adenocarcinomas and in their corresponding non-neoplastic gastric epithelia. Results were compared with microsatellite status, p53 immunoreactivity, and cellular phenotype. Hypermethylation of *Chfr* and *hMLH1* was observed in: 10% (1/10) and 0% (0/10) of low-grade NIN (L-NIN); 63% (5/8) and 63% (5/8) of high-grade NIN, including suspicion for carcinoma without invasion (H-NIN); 36% (5/14) and 57% (8/14) of high-grade NIN, including carcinoma without invasion; and 35% (7/20) and 25% (5/20) of submucosal invasive adenocarcinomas, respectively. Hypermethylation was less frequent in L-NIN than H-NIN ($P<0.05$) for *Chfr* and was also less frequent in L-NIN than the others ($P<0.05$) for *hMLH1*. We failed to find a significant correlation between *Chfr* hypermethylation and chromosomal loss of heterozygosity, although hypermethylation of *hMLH1* was significantly associated with high-frequency MSI ($P<0.01$). Expression of p53 was not associated with *Chfr* or *hMLH1* methylation. As for cellular phenotype, hypermethylation of *Chfr* and *hMLH1* was frequent in tumors exhibiting the foveolar epithelial phenotype (50%, 2/4 and 75%, 3/4, respectively) and the ordinary phenotype (40%, 16/40 and 38%, 15/40, respectively), but never in those with the complete-type intestinal metaplastic phenotype (0%, 0/8 for both). In addition, hypermethylation of *Chfr* and *hMLH1* occurred concurrently ($P<0.01$); methylation was more frequent in patients over 70 years of age ($P<0.01$), and it was also present in some samples of non-neoplastic gastric epithelia from elderly patients. Thus, some gastric tumors with the foveolar or ordinary phenotype may develop as a result of age-related methylation of *Chfr* and *hMLH1*, although *Chfr* methylation was not associated with CIN.

Keywords *CHfr* · *hMLH1* · Hypermethylation · Gastric cancer

N. Homma · G. Tamura (✉) · T. Honda · Z. Jin · K. Ohmura · T. Motoyama
Department of Pathology,
Yamagata University School of Medicine,
990-9585 Yamagata, 2-2-2 Iida-nishi, Japan
e-mail: gtamura@med.id.yamagata-u.ac.jp

N. Homma · T. Honda · K. Ohmura · S. Kawata
Department of Gastroenterology,
Yamagata University School of Medicine,
Yamagata, Japan

Introduction

Human tumors are genetically unstable, and the instability exists at two distinct levels, the chromosomal level and the nucleotide level [22]. The subtle sequence instabilities represented by nucleotide-excision repair-associated instability and microsatellite instability (MSI) are rare. However, another form of instability, chromosomal instability (CIN), involving gains and losses of whole chromosomes, is likely to occur in most human malignancies [25]. Mutation of *p53* occurs in around 40%, and high-frequency MSI (MSI-H), which is induced by epigenetic inactivation of *hMLH1*, occurs in approximately 20% of gastric cancers [35]. Frequent gene abnormalities responsible for CIN have not yet been identified, although loss of heterozygosity (LOH), that is, loss of a maternal or paternal allele often accompanied by a gain of the opposite allele, is present in the majority of gastric cancers [27]. Genes that, when altered, can lead to CIN include those involved in chromosomal condensation, sister-chromatid cohesion, kinetochore structure and function, and centrosome/microtubule formation and dynamics, as well as "checkpoint" genes, which monitor the proper progression of the cell cycle [22]. Only a small fraction of CIN cancers is associated with dominant mutations in the human homologues of yeast spindle checkpoint genes *BUB1* [5, 13, 16] and *MAD2* [6, 23]. Although *p53* mu-

tation is frequently found in aneuploid cells of gastric cancer [37], it is unlikely that this mutation is generally responsible for CIN [22].

Recently, the *Chfr* [checkpoint with forkhead-associated (FHA) and ring finger (RF) gene], involved in the mitotic stress checkpoint, was cloned and localized to chromosome 12q24.33 [33]. Its product, CHFR, mediates the delayed entry into metaphase characterized microscopically by delayed chromosomal condensation [33]. In addition, CHFR promotes cell survival in response to mitotic stress [33]. CHFR possesses an N-terminal FHA domain, a central RF domain, and a C-terminal cysteine-rich (CR) region [33]. Based on functional analysis of *Chfr* deletion mutants, both the FHA and CR regions are required for its checkpoint function. CHFR also has ubiquitin ligase activity dependent on the RF domain [9]. Northern-blot analysis of *Chfr* using RNA from eight colon, osteosarcoma, and neuroblastoma cancer cell lines revealed that *Chfr* expression was absent in three cell lines [33]. Loss of *Chfr* expression due to hypermethylation of a CpG island in the promoter region has been observed in tumor cell lines and primary cancers of the lung, esophagus, and colon [10, 26, 34, 40]. Very recently, we have reported that two of ten gastric cancer cell lines (20%) showed *Chfr* promoter hypermethylation with resultant loss of expression, which could be restored by 5-aza-2′ deoxycytidine treatment; this was also found in 35% (25/71) of primary gastric cancers [15]. We speculated that *Chfr* promoter hypermethylation might lead to CIN based on the proposed function of CHFR mentioned above [33].

In the present study, we analyzed promoter methylation status of *Chfr*, a possible inducer of CIN, and *hMLH1*, an inducer of MSI, to confirm the association between methylation status of these genes and CIN, represented by LOH, or MSI. As methylation occurs at a very early stage of gastric carcinogenesis, we studied noninvasive neoplasias (NIN, classified according to the Padova international classification) [31] and in submucosal invasive adenocarcinomas. The results were also compared with p53 immunoreactivity and cellular phenotype [29].

Materials and methods

Samples

Samples of 52 gastric neoplasias (32 non-invasive and 20 submucosal invasive tumors) and their corresponding non-neoplastic gastric mucosa were studied. Of the specimens, 43 were obtained by surgical resection, and the others were obtained by endoscopic mucosal resection. All specimens were diagnosed histopathologically as either gastric adenoma or adenocarcinoma at the Department of Pathology, Yamagata University School of Medicine between 1998 and 2000. NINs were reclassified as 10 low-grade-NIN (L-NIN), 8 high-grade NIN (H-NIN), and 14 carcinoma without invasion (Ca-NIN) according to the Padova International Classification [31].

DNA extraction

Neoplastic and non-neoplastic portions were manually microdissected from different sets of ten serial, 10-μm-thick, formalin-fixed, paraffin-embedded tissue sections. DNA was extracted according to the method described previously [29].

Bisulfite modification and methylation-specific polymerase chain reaction

DNA samples were treated with bisulfite to convert all unmethylated cytosines to uracils, while leaving methylated cytosines unaffected. Briefly, 2 μg of genomic DNA was denatured by NaOH treatment and modified by sodium bisulfite. The samples were then purified using the Wizard DNA purification resin (Promega, Madison WI), treated with NaOH, recovered in ethanol, and resuspended in 30 μl of distilled water. Amplification was carried out in a 20-μl reaction volume containing 2 μl GeneAmp polymerase chain reaction (PCR) Gold Buffer (PE Applied Biosystems, Foster City, CA), 1.0 mM $MgCl_2$, 10 pM of each primer, 0.2 mM dNTPs, and 1U *Taq* polymerase (AmpliTaq Gold DNA polymerase, PE Applied Biosystems). After the mixture was heated at 95°C for 10 min, the PCR was performed in a thermal cycler (GeneAmp 2400, PE Applied Biosystems) for 35 cycles of denaturation at 95°C for 30 s, annealing at 55°C for 60 s, and extension at 72°C for 60 s, followed by a final 7-min extension at 72°C. A positive control (Sss I-treated DNA) and negative control (distilled water without DNA) were included for each amplification. The PCR products were separated on a 6% non-denaturing polyacrylamide gel. The following primer sets were used: 5′-GTA ATG TTT TTT GAT AGC GGC-3′ and 5′-AAT CCC CCT TCG CCG-3′ for methylated *Chfr* (106 bp); 5′-GGT TGT AAT GTT TTT TGA TAG TGG T-3′ and 5′-CAA ATC CCC CTT CAC CA-3′ for unmethylated *Chfr* (112 bp); and 5′-ACG TAG ACG TTT TAT TAG GGT CGC-3′ and 5′-CCT CAT CGT AAC TAC CCG CG-3′ for methylated *hMLH1* (115 bp).

Microsatellite analysis

PCR primers for microsatellite markers were obtained from Research Genetics (Huntsville, AL). Microsatellite markers were selected to cover chromosomal regions frequently deleted in gastric carcinomas [27, 38]. The following 12 primer pairs were used: D2S115 (2q), D4S404 (4p), D5S178 (5q), IL9 (5q), D6S265 (6p), D7S490 (7q), D11S900 (11q), MYH6 (14q), TP53 (17p), D17S1176 (17p), D18S46 (18q), and D21S1407 (21q). A marker for the mononucleotide repeat BAT-26 (2q) (Research Genetics), highly sensitive for MSI, was also used. PCR was performed as described previously [38]. PCR products were separated on 6% denaturing polyacrylamide gels. Assessment of LOH and MSI was also described previously [38]. Samples were defined as MSI-H if more than 30% of the loci observed were unstable, low-frequency MSI if less than 30% of loci were unstable, and microsatellite stable (MSS) if no unstable loci were observed [4].

Immunohistochemical staining for p53 protein

Immunostaining for p53 protein was performed using the monoclonal antibody Pab 1801 (Novocastra, New Castle, UK) (1:40 dilution) using a standard labeled streptavidin-biotin system (Nichirei, Tokyo, Japan).

Cellular phenotypic analysis

Sections from one or two representative paraffin blocks were stained with hematoxylin and eosin. In addition, the following histochemical and immunohistochemical staining was also performed: galactose oxidase-Schiff (GOS), paradoxical concanavalin

A (Con A), immunostaining with monoclonal antibody (mAb) 45M1 (Novocastra) [3], immunostaining with a MUC 2 mAb (Novocastra) [41], and immunostaining with a CD10 mAb (Novocastra) [11]. GOS and 45M1 were used to detect gastric foveolar mucin, Con A to detect pyloric gland cells and mucous neck cells, MUC 2 to detect intestinal goblet-cell mucin, and CD10 to detect brush borders in complete-type intestinal metaplasia. Immunohistochemical staining was performed on formalin-fixed, paraffin-embedded sections using standard labeled streptavidin-biotin methods (Nichirei). Cellular phenotypes for the 52 gastric neoplasias were defined as outlined previously [29].

Statistical analysis

Statistical analysis was performed using Fisher's exact probability test and Mann–Whitney's U test. *P* values of less than 0.05 were considered to be statistically significant.

Results

Hypermethylation of *Chfr* and *hMLH1*

Hypermethylation of *Chfr* and *hMLH1* was observed in 10% (1/10) and 0% (0/10) of L-NIN, 63% (5/8) and 63% (5/8) of H-NIN, 36% (5/14) and 57% (8/14) of Ca-NIN, and 35% (7/20) and 25% (5/20) of submucosal invasive adenocarcinomas, respectively (Fig. 1 and Table 1). Hypermethylation of *Chfr* and *hMLH1* occurred concordantly in 14 tumors ($P<0.01$) (Table 1). *Chfr* and *hMLH1* hypermethylation was also present in 8% (4/52) of the corresponding non-neoplastic gastric epithelia (Table 1). When hypermethylation was detected in non-neoplastic gastric epithelia, the corresponding tumors also exhibited hypermethylation, with the exception of a case of submucosal invasive carcinoma (no. 37) (Table 1).

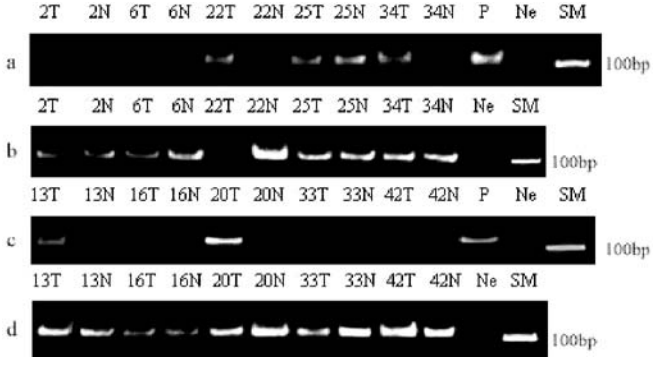

Fig. 1 An illustration of methylation-specific polymerase chain reaction (MSP). **a** Methylated-sequence-specific PCR for *Chfr*. **b** Unmethylated-sequence-specific PCR for *Chfr*. **c** Methylated-sequence-specific PCR for *hMLH1*. **d** Unmethylated-sequence-specific PCR for *Chfr*. *T* tumor, *N* non-neoplastic gastric mucosa, *P* positive control, *Ne* negative control, *SM* size marker. Methylated PCR products are present in 22T, 25T, 25N and 34T for *Chfr* (**a**) and in 13T and 20T for *hMLH1* (**c**). Unmethylated PCR products are present in all but 22T for *Chfr* (**b**) and all for *Chfr* (**d**)

Microsatellite alterations

MSI-H was observed in 10% (1/10) of L-NIN, none (0/8) of H-NIN, 36% (5/14) of Ca-NIN, and 15% (3/20) of submucosal invasive adenocarcinomas (Fig. 2 and Table 1). LOH in at least one chromosomal locus was observed in none of L-NIN (0/10) and H-NIN (0/8), 57% (8/14) of Ca-NIN, and 50% (10/20) of submucosal invasive adenocarcinomas (Fig. 2 and Table 1). No tumor exhibited both MSI-H and LOH, suggesting that these alterations are independent in the early stage of gastric carcinogenesis. The frequency of MSI-H + LOH was higher in Ca-NIN + invasive adenocarcinomas than L-NIN + H-NIN ($P<0.01$).

p53 Immunoreactivity

Nuclear accumulation of p53 protein was observed in 0% (0/10) of L-NIN, 13% (1/8) of H-NIN, 36% (5/14) of Ca-NIN, and 35% (7/20) of submucosal invasive adenocarcinomas (Table 1). The frequency of p53 expression was significantly higher in Ca-NIN + invasive adenocarcinomas than L-NIN + H-NIN ($P<0.05$).

Cellular phenotype

Neoplasias were classified as ordinary cellular phenotype (ordinary-type), complete-type intestinal metaplastic phenotype (CIM-type), or foveolar epithelial phenotype (foveolar-type) [29]. L-NIN is composed of 60% (6/10) ordinary-type, 30% (3/10) CIM-type, and 10% (1/10) foveolar-type; H-NIN of 100% (8/8) ordinary-type; Ca-NIN of 79% (11/14) ordinary-type, 7% (1/14) CIM-type, and 14% (2/14) foveolar-type; and submucosal invasive adenocarcinomas of 75% (15/20) ordinary-type, 20% (4/20) CIM-type, and 5% (1/20) foveolar-type (Table 1).

Correlation between *Chfr* and *hMLH1* methylation status and clinicopathological and molecular features

Although females exhibited more frequent hypermethylation of *Chfr* and *hMLH1* than males, this difference was not statistically significant. The mean age±SD of patients with and without hypermethylation of *Chfr* was 73.4±1.6 years and 67.7±1.5 years ($P<0.05$) and of *hMLH1* was 74.1±1.1 years and 67.4±1.6 years ($P<0.01$), respectively. Hypermethylation of *Chfr* was less frequent in L-NIN than H-NIN ($P<0.05$), and that of *hMLH1* was also less frequent in L-NIN than the others ($P<0.05$). As for cellular phenotype, hypermethylation of *Chfr* and *hMLH1* was frequently present in tumors exhibiting the foveolar-type (50%, 2/4 and 75%, 3/4, respectively) and the ordinary-type (40%, 16/40 and 38%, 15/40, respectively), but never in those with the CIM-type (0%, 0/8 for both). Expression of p53 protein was not associated with methylation status of *Chfr* or *hMLH1*. We failed to find a

Table 1 Clinicopathological and molecular features of gastric noninvasive and early invasive neoplasias. *L-NIN* low-grade noninvasive neoplasia, *H-NIN* high-grade noninvasive neoplasia including suspicion for carcinoma without invasion, *Ca-NIN* high-grade noninvasive neoplasia including carcinoma without invasion, *I* protruding-type, *IIa* superficial elevated-type, *IIc* depressed-type, *IIa+IIc* predominantly raised with central depression-type, *IIc+IIa* raised with predominance of central depression-type, *foveolar* gastric foveolar epithelial phenotype, *ordinary* ordinary phenotype, *CIM* complete intestinal metaplastic phenotype, *T* tumor, *N* non-neoplastic gastric mucosa, *MS* microsatellite, *MSS* microsatellite stable, *MSI-L* low frequency microsatellite instability, *MSI-H* high frequency microsatellite instability, *LOH* loss of heterozygosity present

Case no.	Age (years)	Sex	Size (mm)	Macroscopie type	Cellular phenotype	Methylation status[a]				p53 expression[b]	MS status
						Chfr (T)	Chfr (N)	hMLH1 (T)	hMLH1 (N)		
NIN											
1	68	Male	22	IIa	Ordinary	−	−	−	−	−	MSS
2	73	Male	16	IIa	Foveolar	−	−	−	−	−	MSI-H
3	55	Male	6	IIa	Ordinary	−	−	−	−	−	MSS
4	74	Male	12	IIa	Ordinary	−	−	−	−	−	MSS
5	71	Male	10	I	Ordinary	−	−	−	−	−	MSS
6	70	Male	13	IIa	CIM	−	−	−	−	−	MSS
7	80	Male	4	IIa	CIM	−	−	−	−	−	MSS
8	67	Male	25	IIa+IIc	Ordinary	−	−	−	−	−	MSS
9	67	Male	4	IIa	CIM	−	−	−	−	−	MSS
10	52	Male	37	IIa+IIc	Ordinary	+	−	−	−	−	MSS
H-NIN											
11	80	Male	33	IIa	Ordinary	+	+	+	−	−	MSS
12	71	Male	17	IIa	Ordinary	+	−	+	+	−	MSS
13	68	Female	16	IIc	Ordinary	−	−	+	−	−	MSS
14	73	Female	39	IIc+IIa	Ordinary	+	+	+	−	−	MSS
15	78	Male	30	IIc	Ordinary	+	−	−	−	−	MSS
16	64	Male	6	IIa	Ordinary	−	−	−	−	−	MSS
17	74	Male	7	IIa	Ordinary	+	−	+	−	+	MSS
18	55	Female	13	IIc	Ordinary	−	−	−	−	−	MSS
Ca-NIN											
19	73	Male	18	IIc	Ordinary	−	−	−	−	+	LOH
20	76	Male	14	IIa	Foveolar	+	−	+	−	−	MSI-H
21	59	Male	53	I	Ordinary	−	−	−	−	−	MSS
22	75	Male	25	IIa	Ordinary	+	−	+	−	−	MSI-L/LOH
23	66	Male	10,5	IIa	Ordinary	−	−	+	−	−	MSI-H
24	49	Male	16	IIc	Ordinary	−	−	−	−	+	LOH
25	80	Female	19	IIc	Ordinary	+	+	+	+	−	MSI-H
26	75	Male	28	IIc	Foveolar	−	−	+	−	−	MSI-H
27	66	Male	38	I+IIa	Ordinary	−	−	−	−	+	MSI-L/LOH
28	64	Female	28	IIc	CIM	−	−	−	−	−	LOH
29	73	Male	41	IIc+IIa	Ordinary	+	−	+	−	−	LOH
30	52	Male	19	IIc+IIa	Ordinary	−	−	−	−	+	LOH
31	70	Male	38	IIc+IIa	Ordinary	+	−	+	−	+	MSI-L/LOH
32	77	Female	38	IIc+IIa	Ordinary	−	−	+	+	−	MSI-H
Submucosal invasive carcinoma											
33	79	Male	12	IIc	CIM	−	−	−	−	+	MSS
34	79	Male	29	IIa	Foveolar	+	−	+	−	−	MSI-H
35	68	Male	18	IIa	Ordinary	+	+	+	−	−	MSI-H
36	80	Male	18	IIa	Ordinary	+	−	+	−	+	MSS
37	63	Male	53	IIc+IIa	CIM	−	−	−	+	+	LOH
38	67	Male	17	IIc+IIa	Ordinary	−	−	−	−	−	LOH
39	83	Male	19	IIc+IIa	Ordinary	−	−	−	−	+	MSS
40	51	Male	28	IIc+IIa	Ordinary	−	−	−	−	−	MSS
41	62	Male	25	IIc+IIa	Ordinary	−	−	−	−	−	MSI-L/LOH
42	72	Male	40	I	Ordinary	−	−	−	−	−	MSI-L/LOH
43	79	Male	59	I+IIa	Ordinary	−	−	−	−	−	MSS
44	75	Male	33	I	CIM	−	−	−	−	−	LOH
45	72	Male	23	IIc+IIa	Ordinary	+	−	−	−	−	MSS
46	59	Male	30	IIc+IIa	Ordinary	−	−	−	−	−	LOH
47	72	Female	27	IIc+IIa	Ordinary	+	−	−	−	+	LOH
48	82	Male	37	I	CIM	−	−	−	−	−	MSS
49	70	Male	32	IIc+IIa	Ordinary	+	−	+	−	+	LOH
50	79	Female	21	IIc+IIa	Ordinary	+	−	+	−	−	MSI-H
51	69	Male	18	IIc+IIa	Ordinary	−	−	−	−	+	LOH
52	69	Female	40	IIc+IIa	Ordinary	−	−	−	−	−	LOH

[a] −Unmethylated, + methylated
[b] −Negative, + positive

significant correlation between *Chfr* hypermethylation and chromosomal LOH, although hypermethylation of *hMLH1* was significantly associated with MSI-H ($P<0.01$). These results are summarized in Table 2.

Discussion

Many gastric cancers develop through defects in tumor suppressor genes (suppressor pathway) or DNA mismatch

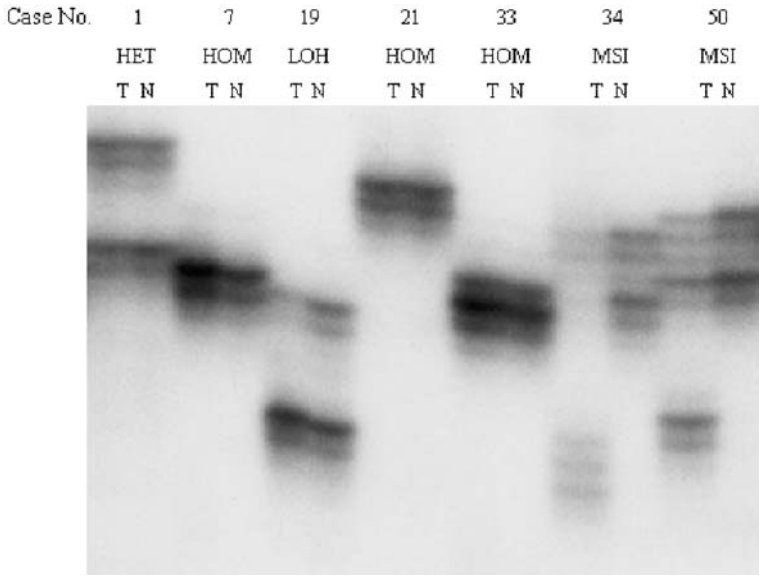

Fig. 2 An illustration of microsatellite analysis at TP53. Alterations are judged as microsatellite instability (MSI) when additional bands that are not seen in the corresponding normal DNA appear in the tumor DNA (cases 34 and 50), and loss of heterozygosity (LOH) when a band corresponding to one allele of the normal DNA is lost in the tumor DNA (case19). *T* tumor, *N* non-neoplastic gastric mucosa, *HET* heterozygosity, *HOM* homozygosity

Table 2 Correlation between methylation status of *Chfr* and *hMLH1* and clinicopathological features

Clinicopathological characteristics	*Chfr*			*hMLH1*		
	M (n=18)	U (n=34)		M (n=18)	U (n=34)	
Sex						
Male	14	29	NS	13	30	NS
Female	4	5		5	4	
Age						
< 70	2	20	*	3	19	*
≥ 70	16	14		15	15	
Padova classification						
L-NIN	1	9	**	0	10	* * **
H-NIN	5	3		5	3	
Ca-NIN	5	9		8	6	
Invasive carcinoma	7	13		5	15	
Cellular phenotype						
Foveolar phenotype	2	2	**	3	1	**
Ordinary phenotype	16	24		15	25	
CIM phenotype	0	8		0	8	
p53 immunoreactivity						
p53 positive	5	8	NS	4	9	NS
p53 negative	13	26		14	25	
MSI						
MSI-H	5	4	NS	8	1	*
MSS or MSI-L/LOH	13	30		10	33	

M, methylated; U, unmethylated; NS, not significant; *, p<0.01; **, p<0.05 by Fisher's exact test.

repair genes (mutator pathway) [36]. In suppressor pathway carcinogenesis, tumor suppressor genes were inactivated by any combination of mutations, LOH, and DNA methylation in both the paternal and maternal alleles [18]; whereas, tumors developed through the mutator pathway exhibited *hMLH1* promoter methylation and remained in the DNA diploid state [7]. Because the majority of gastric cancers exhibit LOH [27] and DNA aneuploidy [1], it is presumed that frequent genetic defects leading to CIN exist, although no such abnormalities directly associated with CIN have been identified. We postulated that *Chfr*, a possible inducer of CIN, might be associated with LOH; however, no such association was determined in the present study. Rather, *Chfr* methylation occurred concurrently with methylation of *hMLH1*, an inducer of MSI, and resultant mutator pathway carcinogenesis. There is an inverse relationship between CIN and MSI in early-stage gastric cancers of the differentiated type [17, 28], as well as in colorectal and endometrial cancers [22]. Actually, there were no tumors that exhibited both LOH and MSI-H in the present study. Therefore, there is no evidence that *Chfr* methylation leads to CIN in gastric cancer. Further studies are required to identify the important genes/mechanisms that lead to CIN in gastric cancer. The association between *Chfr* methylation and LOH in other tumors also should be analyzed.

The exact cause of concurrent hypermethylation of *Chfr* and *hMLH1* is unclear; however, it is known that tumors with the CpG island methylator phenotype show hypermethylation of multiple genes [30], and concerted hypermethylation has been reported in gastric cancer [20]. In addition, multiple tumor suppressor and tumor-related genes become methylated in non-neoplastic gastric epithelia during aging [42]. In the present study, hypermethylation of both *Chfr* and *hMLH1* was significantly associated with aging, and several corresponding non-neoplastic gastric epithelial samples also exhibited hypermethylation together with their tumors. We speculate that aging might induce concurrent hypermethylation of *Chfr* and *hMLH1*. *Chfr* delays entry into mitosis by negatively regulating the activation of the Cdc2 kinase at the G2–M transition [19]. *hMLH1* causes G2 arrest in the presence of DNA damage [2, 8, 14, 24]. Therefore, disruption of both *Chfr* and *hMLH1* may cooperatively accelerate entry into the mitotic phase.

The molecular pathway of gastric carcinogenesis depends on the histological background, and gastric cancers show distinct biological behaviors as a result of discernible cellular genetic and epigenetic alterations [36]. Methylation of *E-cadherin* in native gastric mucosa results in undifferentiated carcinomas [39], while methylation of *hMLH1* results in differentiated foveolar-type carcinomas [12]. Most differentiated gastric carcinomas (ordinary- and CIM-types), however, arise from intestinal metaplastic mucosa (incomplete and complete types, respectively) and exhibit structural alterations of tumor suppressor genes [36]. Approximately 20% of differentiated carcinomas of the ordinary-type have evidence of mutator pathway tumorigenesis [36]. In the present study, *hMLH1* hypermethylation was present in 75% (3/4) of foveolar-type and 38% (15/40) of ordinary-type but none (0%; 0/8) of CIM-type tumors. The results of *Chfr* hypermethylation were very similar to those of *hMLH1* hypermethylation, present in 50% (2/4) of foveolar-type and 40% (16/40) of ordinary-type but none (0%; 0/8) of CIM-type tumors. These results further support the tight linkage between cellular phenotype (histogenesis) and genetic/epigenetic alterations (molecular pathway).

The methylation status of *hMLH1* was significantly associated with microsatellite status in the present and previous studies [32]. However, this was not true for H-NIN. Although 53% (5/8) of H-NIN showed *hMLH1* hypermethylation, all of the H-NIN were MSS. It is possible that methylation of the *hMLH1* promoter CpGs, though detected by methylation-specific PCR, was not complete enough to shut down protein expression. When methylation reaches to involve the critical CpGs for protein expression, and the tumor suppressor function is lost, H-NIN may progress to Ca-NIN. The rarity of genetic alterations, including microsatellite alterations and *p53* mutations, in L-NIN and H-NIN has been noticed previously [17]. As for L-NIN, hypermethylation was very rare, and no such accumulations of genetic/epigenetic alterations have been observed between L-NIN and Ca-NIN, suggesting the absence of sequential progression of L-NIN to Ca-NIN, which may correspond to the results of *APC* mutation analyses in which mutations were frequent in gastric adenomas but exceptional in gastric cancers [21, 35].

In conclusion, our present observations suggest that some gastric tumors of the foveolar- or ordinary-type develop as a result of age-related methylation of *Chfr* and *hMLH1* in the native gastric mucosa or incomplete-type intestinal metaplastic mucosa.

References

1. Abad M, Ciudad J, Rincon MR, Silva I, Paz-Bouza JI, Lopez A, Alonso AG, Bullon A, Orfao A (1998) DNA aneuploidy by flow cytometry is an independent prognostic factor in gastric cancer. Anal Cell Pathol 16:223–231
2. Aquilina G, Crescenzi M, Bignami M (1999) Mismatch repair, G(2)/M cell cycle arrest and lethality after DNA damage. Carcinogenesis 20:2317–2326
3. Bara J, Gautier R, Mouradian P, Decaens C, Daher N (1991) Oncofetal mucin M1 epitope family: characterization and expression during colonic carcinogenesis. Int J Cancer 47:304–310
4. Boland CR, Thibodeau SN, Hamilton SR, Sidransky D, Eshleman JR, Burt RW, Meltzer SJ, Rodriguez-Bigas MA, Fodde R, Ranzani GN, Srivastava S (1998) A National Cancer Institute Workshop on microsatellite instability for cancer detection and familial predisposition: development of international criteria for the determination of microsatellite instability in colorectal cancer. Cancer Res 58:5248–5257
5. Cahill DP, Lengauer C, Yu J, Riggins GJ, Willson JK, Markowitz SD, Kinzler KW, Vogelstein B (1998) Mutations of mitotic checkpoint genes in human cancers. Nature 392:300–303
6. Cahill DP, da Costa LT, Carson-Walter EB, Kinzler KW, Vogelstein B, Lengauer C (1999) Characterization of MAD2B

and other mitotic spindle checkpoint genes. Genomics 58:181–187
7. Carvalho B, Pinto M, Cirnes L, Oliveira C, Machado JC, Suriano G, Hamelin R, Carneiro F, Seruca R (2003) Concurrent hypermethylation of gene promoters is associated with a MSI-H phenotype and diploidy in gastric carcinomas. Eur J Cancer 39:1222–1227
8. Cejka P, Stojic L, Mojas N, Russell AM, Heinimann K, Cannavo E, diPietro M, Marra G, Jiricny J (2003) Methylation-induced G(2)/M arrest requires a full complement of the mismatch repair protein hMLH1. EMBO J 22:2245–2254
9. Chaturvedi P, Sudakin V, Bobiak ML, Fisher PW, Mattern MR, Jablonsk SA, Hurle MR, Zhu Y, Yen TJ, Zhou BB (2002) Chfr regulates a mitotic stress pathway through its RING-finger domain with ubiquitin ligase activity. Cancer Res 62:1797–1801
10. Corn PG, Summers MK, Fogt F, Virmani AK, Gazdar AF, Halazonetis TD, El-Deiry WS (2003) Frequent hypermethylation of the 5′ CpG island of the mitotic stress checkpoint gene *Chfr* in colorectal and non-small cell lung cancer. Carcinogenesis 24:47–51
11. Danielsen EM, Vyas JP, Kenny AJ (1980) A neutral endopeptidase in the microvillar membrane of pig intestine: Partial purification and properties. Biochem J 191:645–648
12. Endoh Y, Tamura G, Ajioka Y, Watanabe H, Motoyama T (2000) Frequent hypermethylation of *hMLH1* gene promoter in differentiated-type tumors of the stomach with the gastric foveolar phenotype. Am J Pathol 157:717–722
13. Gemma A, Seike M, Seike Y, Uematsu K, Hibino S, Kurimoto F, Yoshimura A, Shibuya M, Harris CC, Kudoh S (2000) Somatic mutation of the *BUB1* mitotic checkpoint gene in primary lung cancer. Genes Chromosomes Cancer 29:213–218
14. Hawn MT, Umar A, Carethers JM, Marra G, Kunkel TA, Boland CR, Koi M (1995) Evidence for a connection between the mismatch repair system and the G2 cell cycle checkpoint. Cancer Res 55:3721–3725
15. Honda T, Tamura G, Waki T, Kawata S, Nishizuka S, Motoyama T (2004) Promoter hypermethylation of *Chfr* gene in neoplastic and non-neoplastic gastric epithelia. Br J Cancer 90:2013–2016
16. Imai Y, Shiratori Y, Kato N, Inoue T, Omata M (1999) Mutational inactivation of mitotic checkpoint genes, *hsMAD2* and *BUB1*, is rare in sporadic digestive tract cancers. Jpn J Cancer Res 90:837–840
17. Jin Z, Tamura G, Honda T, Motoyama T (2002) Molecular and cellular phenotypic profiles of gastric noninvasive neoplasia. Lab Invest 82:1637–1645
18. Jones PA, Laird PW (1999) Cancer epigenetics comes of age. Nat Genet 21:163–167
19. Kang D, Chen J, Wong J, Fang G (2002) The checkpoint protein Chfr is a ligase that ubiquitinates Plk1 and inhibits Cdc2 at the G2 to M transition. J Cell Biol 156:249–259
20. Kim H, Kim YH, Kim SE, Kim NG, Noh SH, Kim H (2003) Concerted promoter hypermethylation of *hMLH1*, *p16INK4A*, and *E-cadherin* in gastric carcinomas with microsatellite instability. J Pathol 200:23–31
21. Lee JH, Abraham SC, Kim HS, Nam JH, Choi C, Lee MC, Park CS, Juhng SW, Rashid A, Hamilton SR, Wu TT (2002) Inverse relationship between *APC* gene mutation in gastric adenomas and development of adenocarcinoma. Am J Pathol 161:611–618
22. Lengauer C, Kinzeler KW, Vogelstein B (1998) Genetic instabilities in human cancer. Nature 396:643–649
23. Li Y, Benezra R (1996) Identification of a human mitotic checkpoint gene: *hsMAD2*. Science 274:246–248
24. Meyers M, Wagner MW, Hwang HS, Kinsella TJ, Boothman DA (2001) Role of the hMLH1 DNA mismatch repair protein in fluoropyrimidine-mediated cell death and cell cycle responses. Cancer Res 61:5193–5201
25. Mitelman F (1994) Chromosomes, genes, and cancer. CA Cancer J Clin 44:133–135
26. Mizuno K, Osada H, Konishi H, Tatematsu Y, Yatabe Y, Mitsudomi T, Fujii Y, Takahashi T (2002) Aberrant hypermethylation of the *CHFR* prophase checkpoint gene in human lung cancers. Oncogene 21:2328–2333
27. Nishizuka S, Tamura G, Terashima M, Satodate R (1998) Loss of heterozygosity during the development and progression of differentiated adenocarcinoma of the stomach. J Pathol 185:38–43
28. Ogata S, Tamura G, Endoh Y, Sakata Y, Ohmura K, Motoyama T (2001) Microsatellite alterations and target gene mutations in the early stages of multiple gastric cancer. J Pathol 194:334–340
29. Ohmura K, Tamura G, Endoh Y, Sakata K, Takahashi T, Motoyama T (2000) Microsatellite alterations in differentiated-type adenocarcinomas and precancerous lesions of stomach with special reference to cellular phenotype. Hum Pathol 31:1031–1035
30. Paz MF, Avila S, Fraga MF, Pollan M, Capella G, Peinado MA, Sanchez-Cespedes M, Herman JG, Esteller M (2002) Germ-line variants in methyl-group metabolism genes and susceptibility to DNA methylation in normal tissues and human primary tumors. Cancer Res 62:4519–4524
31. Rugge M, Correa P, Dixon MF, Hattori T, Leandro G, Lewin K, Riddell RH, Sipponen P, Watanabe H (2000) Gastric dysplasia: The Padova international classification. Am J Surg Pathol 24:167–176
32. Sakata K, Tamura G, Endoh Y, Ohmura K, Ogata S, Motoyama T (2002) Hypermethylation of the *hMLH1* gene promoter in solitary and multiple gastric cancers with microsatellite instability. Br J Cancer 86:564–567
33. Scolnick DM, Halazonetis TD (2000) *Chfr* defines a mitotic stress checkpoint that delays entry into metaphase. Nature 406:430–435
34. Shibata Y, Haruki N, Kuwabara Y, Ishiguro H, Shinoda N, Sato A, Kimura M, Kayama H, Toyama T, Nishiwaki T, Kudo J, Terashita Y, Konishi S, Sugiura H, Fujii Y (2002) Chfr expression is downregulated by CpG island hypermethylation in esophageal cancer. Carcinogenesis 23:1695–1699
35. Tamura G (1996) Molecular pathogenesis of adenoma and differentiated adenocarcinoma of the stomach. Pathol Int 46:834–841
36. Tamura G (2002) Genetic and epigenetic alterations of tumor suppressor and tumor-related genes in gastric cancer. Histol Histopathol 17:323–329
37. Tamura G, Kihana T, Nomura K, Terada M, Sugimura T, Hirohashi S (1991) Detection of frequent *p53* gene mutations in primary gastric cancer by cell sorting and polymerase chain reaction single-strand conformation polymorphism analysis. Cancer Res 51:3056–3058
38. Tamura G, Sakata K, Nishizuka S, Maesawa C, Suzuki Y, Terashima M, Eda Y, Satodate R (1996) Allelotype of adenoma and differentiated adenocarcinoma of the stomach. J Pathol 180:371–377
39. Tamura G, Sato K, Akiyama S, Tsuchiya T, Endoh Y, Usuba O, Kimura W, Nishizuka S, Motoyama T (2001) Molecular characterization of undifferentiated -type gastric carcinoma. Lab Invest 81:593–598
40. Toyota M, Sasaki Y, Satoh A, Ogi K, Kikuchi T, Suzuki H, Mita H, Tanaka N, Itoh F, Issa JP, Jair KW, Schuebel KE, Imai K (2003) Epigenetic inactivation of *Chfr* in human tumors. Proc Natl Acad Sci U S A 100:7818–7823
41. Tytgat KM, Buller HA, Opdam FJ, Kim YS, Einerhand AW, Dekker J (1994) Biosynthesis of human colonic mucin: Muc2 is the prominent secretory mucin. Gastroenterology 107:1352–1363
42. Waki T, Tamura G, Tsuchiya T, Sato K, Nishizuka S, Motoyama T (2002) Promoter methylation status of *E-cadherin*, *hMLH1*, and *p16* genes in nonneoplastic gastric epithelia. Am J Pathol 161:399–403

Virchows Arch (2005) 446:127–135
DOI 10.1007/s00428-004-1160-8

ORIGINAL ARTICLE

I. D. Nagtegaal · C. G. S. Gaspar · L. T. C. Peltenburg · C. A. M. Marijnen · E. Kapiteijn · C. J. H. van de Velde · R. Fodde · J. H. J. M. van Krieken

Radiation induces different changes in expression profiles of normal rectal tissue compared with rectal carcinoma

Received: 27 November 2003 / Accepted: 20 August 2004 / Published online: 16 December 2004
© Springer-Verlag 2004

Abstract *Purpose:* Radiotherapy is a very effective adjuvant treatment for rectal cancer with little side effects. Its killing effect on tumor cells seems to be more profound than the effect on normal tissue. The molecular events caused by irradiation are mainly analyzed in in vitro and animal models; investigations on human material are rare. In the current study, we analyzed the effects of irradiation on gene expression in normal and tumor tissue of rectal cancer patients. *Methods and materials:* Normal and carcinoma tissue of patients from a randomized clinical trial of the benefits of preoperative radiotherapy were analyzed using the Affymetrix Human Cancer Gene Chip. Preoperative radiotherapy was given within 5 days prior to surgery. Results for normal tissue and tumor were compared to investigate the radiation-related differences between normal and tumor cells. We clustered the differentially expressed genes based on their functional annotation. Results were compared with immunohistochemical and literature data. *Results:* The majority of the investigated cancer-related genes remained unchanged by irradiation (92% in tumor tissue and 93% in normal tissue). The differentially expressed genes varied between tumor and normal tissue except for maspin and IL-8. Both in tumor and normal tissue, differentially expressed genes were present related to cell signaling and cycle control, apoptosis and cell survival and tissue response and repair. However, the spectrum of affected genes was totally different. *Conclusion:* Pre-existing differences in gene expression between normal tissue and tumor tissue might explain the differences in their responses to radiation. This change in response may explain the clinical beneficial effect of radiotherapy on tumor cells (low local recurrence rate) and the less severe effects on normal tissue (minor side effects).

Keywords Rectal cancer · Radiotherapy · Microarray · Apoptosis

I. D. Nagtegaal
Departments of Pathology,
Leiden University Medical Center,
Leiden, The Netherlands

I. D. Nagtegaal · E. Kapiteijn · C. J. H. van de Velde
Department of Surgery,
Leiden University Medical Center,
Leiden, The Netherlands

C. G. S. Gaspar · R. Fodde
Department of Human and Clinical Genetics,
Leiden University Medical Center,
Leiden, The Netherlands

L. T. C. Peltenburg · C. A. M. Marijnen
Department of Clinical Oncology,
Leiden University Medical Center,
Leiden, The Netherlands

I. D. Nagtegaal (✉) · J. H. J. M. van Krieken
Department of Pathology,
University Medical Center St. Radboud,
PO Box 9101, 6500 HB Nijmegen, The Netherlands
e-mail: I.Nagtegaal@pathol.umcn.nl
Tel.: +31-24-3615429
Fax: +31-24-3540520

Introduction

Radiotherapy is an effective form of treatment for many different cancer types. Recently, we showed, in the framework of the Dutch trial on preoperative radiotherapy in combination with total mesorectal excision (RT+TME trial), that in patients with rectal carcinoma, short-term preoperative radiotherapy decreases the local recurrence rate by more than 60% [11]. The risk of local recurrence, a major problem in rectal cancer treatment, has now been reduced to 2.4%. However, the beneficial effects of radiotherapy need to be weighed against the side effects on normal tissues. We recently described that the early side effects of short-term preoperative radiotherapy are acceptable [22]. Hence, this therapy has profound effects on tumor cells, with less damaging effects on normal tissue.

Since this approach turned out to be very effective in our trial, we set out to investigate in more detail the effects of radiotherapy on tumor tissues and the surrounding

microenvironment and analyze the differences between normal and tumor cells. Several molecular studies analyzed the effects of irradiation on tumor and normal cells by using in vitro and in vivo model systems. However, in vivo studies in humans are scarce, mainly due to technical limitations.

The general knowledge of the processes by which tissue responds to ionizing radiation has increased enormously, mainly as a result of in vitro and animal experiments [31]. Various cellular signaling systems recognize radiation damage in DNA, mitochondria and plasma membrane lipids and mediate the cytotoxic processes that lead to apoptosis but also to the cytoprotective response in favor of cell survival [32], not only in tumor cells but also in the surrounding stroma. Therefore, apart from the direct apoptotic response of tumor cells, effects on the tumor microenvironment may be important prognostic indicators. The inflammatory reaction to tissue injury (as caused by radiation) is mediated by different cell types: inflammatory cells, fibroblasts and endothelial cells (neoangiogenesis). We recently showed that quantitative changes in these cell types are observed after short-term preoperative radiotherapy for rectal cancer [25]. Intercellular signaling (through cytokines and chemokines) is associated with the response to tissue injury and repair [17].

The development of microarray techniques allows an extensive analysis of therapy-related reactions. In the current study, we have used both tumor and normal rectal tissue from patients participating in the Dutch RT+TME trial on the effect of preoperative radiotherapy on rectal cancer [11]. The effects of radiation on gene expression were studied in normal rectal tissue and carcinoma from both randomization arms of the trial (irradiated and non-irradiated). For a number of genes, we correlated our results on mRNA expression with protein expression using immunohistochemistry. In addition, we compared the literature data on radiation-induced expression with our results. We show that the combination of expression profiling with detailed morphological studies enlarges our insight in the complex processes underlying tissue response to radiation-induced cellular damage. The results indicate vast alterations in the control of both apoptosis and proliferation in rectal cancer and a differential response to radiation between normal and tumor tissue.

Materials and methods

Study population

Patients were selected from the RT+TME trial, a large Dutch multicenter trial in which 1530 patients were included from January 1996 until December 1999. This prospectively randomized trial evaluates TME surgery with or without preoperative radiotherapy (5×5 Gy) and showed that local recurrence risk decreased after radiation [11]. Patients with a resectable adenocarcinoma of the rectum were included in this study and were subsequently randomized for radiotherapy followed by TME surgery or for TME surgery alone. Radiotherapeutic, surgical and pathological procedures were standardized and quality controlled [23].

Patient selection for expression profiling by microarrays

From each randomization arm, ten patients with rectal adenocarcinoma were randomly selected based on the availability of fresh frozen tissue. From the same patients, ten normal rectal tissue samples were also selected. For patients in the radiotherapy arm, the total dose was 25 Gy (5×5 Gy), and the time between end of radiotherapy and surgery was less than or equal to 5 days. Patients from both treatment arms were matched for sex, tumor node metastasis (TNM) stage and disease-free survival. The male:female ratio was 1.5, the TNM distribution was 3/4/3 for TNM I, II and III, respectively. None of these patients developed a local or a distant recurrence after a median follow up of 42.9 months after surgery (range 29.5–53.9 months).

RNA preparation and analysis

Patient samples were derived from fresh frozen tissue, collected from the surgical specimen. All tumor and normal tissue samples were microscopically verified. Total RNA was extracted using the RNeasy Mini Kit (Qiagen GmbH, Hilden, Germany) according to the manufacturer's instructions, including a DNase treatment step (RNase-free DNase from Qiagen). RNA quantification was performed using a GeneQuant spectrophotometer (Pharmingen, San Diego, CA, USA). RNA integrity was tested by gel electrophoresis. The total RNA was pooled in four groups: irradiated and non-irradiated tumor, irradiated and non-irradiated normal tissue. For each pooled sample, 2 μg of total RNA was collected from ten individual samples.

Probe preparation

Double-stranded cDNA was synthesized using a high-performance liquid chromatography-purified oligo dT primer containing a T7 RNA promotor (5′-GGCCAGTGAATTGTAATACGACTCAC-TAT-AGGGAGGCGG-$(dT)_{24}$-3′) (GENSET Corporation, LaJolla, CA). After second-strand synthesis, reactions were extracted with phenol/chloroform PhaseLock gels (Eppendorf Inc., Westbury, NY). cDNA was precipitated with ethanol and resuspended in 12-μl diethyl pyrocarbonate-treated water. In vitro transcription was carried out using Bioarray High Yield RNA transcript Labeling Reagents (Enzo Diagnostics, Farmingdale, NY) following the manufacturer's instructions. Biotin-labeled cRNA was purified on a RNeasy column (Qiagen) and fragmented at 94°C for 35 min in fragmentation buffer (40 mM Tris-acetate, pH 8.1, 100 mM KOAc, 30 mM MgOAc). cRNA was added to the hybridization mixture containing four biotinylated hybridization controls (BioB, BioC, BioD, and Cre), as recommended by the manufacturer.

Array hybridization

Hybridization solution [100 mM 2-(N-morpholino) ethanesulfonic acid, 1 M NaCl, 20 mM ethylenediaminetetraacetate, 0.01% Tween 20] was used to prehybridize Affymetrix G110 Human Cancer microarray (Affymetrix UK Ltd., Abington, UK) for 10 min at 45°C. The prehybridization solution was removed and replaced with 130 μl of hybridization cocktail containing fragmented cRNA. The arrays were hybridized for 16 h at 45°C. After hybridization, arrays were washed on an Affymetrix fluidics station and stained with streptavidin-phycoerythrin [100 mM 2-(N-morpholino) ethanesulfonic acid, 1 M NaCl, 0.05% Tween 20, 0.005% Antifoam (0–30, Sigma chemicals, St. Louis, Missouri)], 2 mg/ml acetylated bovine serum albumin (BSA) and 5 μg/μl streptavidin R-phycoerythrin) (Molecular Probes Europe, Leiden, The Netherlands). Antibody amplification was performed for 10 min at 25°C (100 mM 2-(N-morpholino) ethanesulfonic acid, 1 M NaCl, 0.05% Tween 20, 0.005% Antifoam, 2 mg/ml acetylated BSA, 10 mg/ml normal goat IgG, 0.5 mg/ml biotinylated anti-streptavidin antibody) (Vector Laboratories, Burlingame, CA), followed by another

streptavidin-phycoerythrin staining. After staining, arrays were washed extensively in non-stringent wash buffer [6× SSPE (BioWhittaker, Walkersville, MD), 0.01% Tween 20, 0.005% Antifoam]. Arrays were scanned on a Hewlett-Packard GeneArray Scanner.

Data treatment

Affymetrix GENECHIP 4.0 software and the Gene Chip Expression Analysis Suite (Affymetrix) were used to determine which mRNAs were detected in non-irradiated and irradiated samples and which mRNAs were expressed at different levels between the samples. The images from the scanned chips were scaled such that the average intensity value for all arrays was adjusted to 500.

The expression level (average difference) for each gene was determined by calculating the average of differences in intensity (perfect match–mismatch) between its probe pairs. A gene was called differentially expressed when the difference call provided by the software was increased for upregulated genes, or decreased for downregulated genes, and the fold change was equal to or beyond three.

Patient selection for immunohistochemical analyses

Immunohistochemical analysis of normal rectal tissue was performed on the paraffin-embedded material from the same patients whose tumors were employed for the microarray analysis. For the immunohistochemical analysis of tumor tissue, we used a selection of 103 randomly selected patients from both randomization groups of the trial, as previously described [21]. The latter was preferred to the tumor material from the patients employed in the microarray analysis to improve the reliability of our data.

Antibodies and staining procedures for immunohistochemistry

Immunohistochemistry was performed on whole slides. To evaluate levels of apoptosis, the monoclonal antibody M30 (1:800) was used (Boehringer-Mannheim, Germany). This antibody is directed against a neo-epitope in the C-terminal domain of cytokeratin 18 that is exposed after cleavage by caspases during apoptosis. Proliferation was evaluated with the monoclonal antibody MIB-1 directed against Ki-67 (1:1600, Immunotech Coulter, Marseille, France). Other specific antibodies used for immunohistochemical analysis were directed against $p21^{waf1}$ (1:250, WAF1, Oncogene Research Products, Cambridge, MA), E-cadherin (1:100, Zymed laboratories, San Francisco, CA) and α-catenin (1:1000, Transduction Laboratories, Lexington, KY). Vascularization was studied using an anti-C31 antibody (JC70, 1:400, Dako, Glostrup, Denmark).

In brief, sections were de-paraffinized in xylene and re-hydrated. Endogenous peroxidase was blocked with 0.3% hydrogen peroxide in methanol for 20 min. Antigen retrieval was performed using 0.01 M citrate buffer. Subsequently, sections were pre-incubated with 1% bovine serum albumin. After overnight incubation with the primary antibody, the secondary biotin-conjugated antibody and a tertiary complex of streptavidin-avidin-biotin conjugated to 3-amino-9-ethyl-carbazole were applied. Finally, the sections were counterstained with Mayer's hematoxylin. Incubation with phosphate-buffered saline instead of the primary antibody served as a negative control.

Quantification methods

Apoptosis and proliferation were evaluated in all tumor slides by two independent investigators (IDN and CAMM). The tumor apoptotic index was defined as the number of positive tumor cells per mm^2 tumor tissue and was counted in ten high power (100×) fields for each tumor. The tumor proliferation index was defined as

Table 1 Radiation signaling. Differential mRNA expression between non-irradiated and irradiated rectal tissue. Fold changes are given between brackets and are calculated by relating the irradiated tissue to the non-irradiated tissue. The identifier represents the GenBank accession number

Function	Identifier	Gene	Normal tissue	Carcinoma
Damage recognition				
	U26455	Phosphatidylinositol 3-kinase homologue (ATM)		Up (3.0)
	U18300	Damage-specific DNA binding protein p48 subunit (DDB2)	Up (3.5)	
Cellular signaling				
	K00650	Fos proto-oncogene (c-fos)		Up (26.2)
	Z48541	Protein tyrosine phosphatase		Down (3.8)
	M93426	Protein tyrosine phosphatase zeta-polypeptide (PTPRZ)	Down (3.4)	
	U35234	Protein tyrosine phosphatase sigma	Down (4.3)	
	X68277	Protein tyrosine phosphatase (CL 100)		Up (3.4)
	U48807	MAP kinase phosphatase (MKP-2)	Up (4.9)	
	X06318	Protein kinase C (PKC) type beta I	Down (3.0)	
	X07109	Protein kinase C (PKC) type beta II	Down (3.4–4.3)	
	M35296	Tyrosine kinase arg	Down (8.8)	
	M59371	Protein tyrosine kinase (Eck)	Up (6.8)	
	X75208	HEK2 mRNA for protein tyrosine kinase receptor	Up (9.9)	
	X97630	Serine/threonine protein kinase EMK		Down (4.1)
	M19650	2,3–Cyclic nucleotide 3-phosphodiesterase		Up (3.0)
	U66619	SWI/SNF complex 60 KDa subunit (BAF60c)	Down (3.3)	
	D31815	Senescence marker protein-30 (SMP-30)	Down (4.5)	
	M14949	R-ras		Up (3.4)
	M12174	Ras-related rho		Up (12.7)
	M37190	Ras inhibitor		Up (3.8)
	L36463	Ras interactor	Up (9.2)	
Cell-cycle control				
	M92424	P53-associated mRNA	Up (3.5)	
	U14680	Breast and ovarian cancer susceptibility gene (BRCA1)	Up (5.9)	
	U03106	Wild-type p53 activated fragment-1 (p21 WAF1)		Up (4.2)

Table 2 Apoptosis. Differential mRNA expression between non-irradiated and irradiated rectal tissue. Fold changes are given between brackets and are calculated by relating the irradiated tissue to the non-irradiated tissue. The identifier represents the GenBank accession number

Identifier	Gene	Normal tissue	Carcinoma
X83492	Fas/Apo-1	Up (3.1)	
U28015	Caspase-3	Up (4.6)	
L22473	Bax alpha	Up (3.4)	
U19599	Bax delta	Up (4.4)	
X02612	Cytochrome P(1)-450		Down (3.2)
U04313	Maspin	Up (3.3–6.6)	Up (3.5–13.6)
M22489	Bone morphogenetic protein 2A (BMP-2A)	Up (3.2)	Up (3.0)

Table 3 Cell survival. Differential mRNA expression between non-irradiated and irradiated rectal tissue. Fold changes are given between brackets and are calculated by relating the irradiated tissue to the non-irradiated tissue. The identifier represents the GenBank accession number

Function	Identifier	Gene	Normal tissue	Carcinoma
Growth factors and receptors	S62539	Insulin receptor substrate-1	Down (4.5)	
	X57025	Insulin-like growth factor I (IGF-I)		Up (4.0)
		Insulin-like growth factor Ib		Up (4.1)
	M62402	Insulin-like growth factor binding protein 6 (IGFBP6)		Up (11.8)
	S37730	Insulin-like growth factor binding protein 2 (IGFBP2)	Up (17.6)	
	J00306	Somatostatin I	Up (7.8)	
	M10901	Glucocorticoid receptor alpha		Up (3.3)
	X51730	Progesterone receptor		Up (3.5)
	U07132	Steroid hormone receptor Ner-1		Up (7.9)
	M57399	Human nerve growth factor (HBNF-1)	Down (3.2)	
DNA repair				
	M60974	Growth arrest and DNA-damage-inducible protein (gadd45)	Up (3.1)	
	M63488	Human replication protein A 70-kDa subunit	Down (3.1)	
		Transcription factor Btf3 homologue	Down (3.1)	
	D50495	Transcription elongation factor S-II (hS-II-T1)	Down (10.1)	
	U86136	Telomerase-associated protein (TP-1)		Up (5.7)
	U43746	Breast cancer susceptibility gene (BRCA2)	Up (3.1)	
	M36067	DNA ligase I	Up (10.8)	
Proliferation				
	X65550	Antigen of monoclonal antibody Ki-67		Down (3.0)
	M11507	Transferrin receptor	Up (3.5–5.9)	

the number of tumor cells with nuclear Ki-67 staining per mm^2 tumor tissue and was counted in five high power (400×) fields per tumor. The number of high power fields to be counted was determined using the "running mean" method, as previously described [24]. In normal mucosa, five axially cut crypts were counted, as previously described [3]. Nuclei (Ki67) and cells (M30) were assessed as either positive or negative, and the percentages of positive cells were employed to determine the normal proliferation and apoptotic indexes, respectively.

Immunohistochemical staining of rectal tumors with the CD31 antibody was quantified using image analysis and expressed as the amount of vessel perimeter per mm^2 tumor. The E-cadherin and the α-catenin slides were evaluated by two independent observers (EK and JHJMvK). Membranous staining patterns of tumor cells were defined according to the following categories compared with the normal internal controls: loss (0–89% expression) and no or only focal loss of expression (90–100%).

p21 expression in tumor cells was evaluated in a semi-quantitative fashion by two independent investigators (CAMM and IDN or EK) and scored as absent (0% staining), intermediate (1–25% stained tumor cells) and high (>25% positive cells), as previously described [21].

Differences between the groups were analyzed using Chi-square testing. Differences between means were tested using the *t*-test method. P values ≤ 0.05 were considered significant.

Results

In this study, we evaluated the direct effects of irradiation on gene expression in rectal cancer and normal tissue using oligonucleotide microarrays. The material employed for the expression profiling experiments was derived from a prospective, randomized trial by the Dutch Colorectal Cancer Group to investigate the efficacy of short-term preoperative radiotherapy in combination with standardized total mesorectal excision [11]. To this aim, total RNA from irradiated and control tissues was employed to hybridize the GeneChip Human Cancer G110 Array by Affymetrix containing oligonucleotide probes for more than 1700 full-length genes previously linked to cancer (see also http://www.affymetrix.com/products/gc_g110_content.html).

In general, the expression level of the vast majority of the analyzed genes was not affected by irradiation of both tumor (n=1865, 91.7%) and normal rectal tissues (n=1886, 92.8%). When an arbitrary threefold threshold level was applied, a total of 47 genes, 39 and 8 of which up- and downregulated, respectively, were shown to be differentially expressed in tumor tissue. In normal tissue,

Table 4 Tissue response and repair. Differential mRNA expression between non-irradiated and irradiated rectal tissue. Fold changes are given between brackets and are calculated by relating the irradiated tissue to the non-irradiated tissue. The identifier represents the GenBank accession number

	Identifier	Gene	Normal tissue	Carcinoma
Cytokines and receptors	M27288	Oncostatin M		Up (3.8)
	J04765	Osteopontin		Up (4.9)
	M31165	Tumor necrosis factor-inducible protein (TSG-6)		Up (4.9)
	X54489	Melanoma growth stimulatory activity (MGSA)	Up (6.5)	
	AB000584	TGF-beta superfamily protein	Up (4.3)	
	M60556	Transforming growth factor beta-3		Up (5.6)
	U47011	Fibroblast growth factor 8 (FGF8)	Down (17.3)	
	M25897	Platelet factor 4 (PF4)	Up (4.2)	
	J05008	Endothelin-1 (EDN1)	Up (5.2)	
	K02215	Angiotensinogen		Up (5.9)
	U12471	Trombospondin-1	Up (14.4)	
	Z19585	Thrombospondin-4	Down (4.7)	
	M28130	Interleukin 8 (IL8)	Up (14.6)	Up (5.1)
	M11567	Angiogenin		Up (5.4)
		Vasoactive intestinal protein		Up (6.5)
	U11872	Interleukin-8 receptor type B (IL8RB)	Up (3.5)	
	U32324	Interleukin-11 receptor alpha chain		Down (3.2)
Adhesion molecules	D21254	OB-cadherin-1		Up (3.0)
	M94151	Alpha catenin		Down (3.4)
	D88799	Cadherin		Up (3.5)
Metalloproteases	X05232	Stromelysin		Up (4.9)
	L22524	Matrilysin		Up (9.1)
Other	M21389	Keratin type II		Up (13.6)
	J04430	Tartrate-resistant acid phosphatase type 5		Up (4.4)
		Immunoglobulin heavy chain, Vdjrc regions		Up (4.5)
	M95585	Hepatic leukemia factor		Down (3.5)
	D13666	Osteoblast specific factor (osf-2os)		Up (3.4)
	S76978	Prostate-specific membrane antigen		Up (3.4)
	U68019	Homo sapiens mad protein homologue (hMAD-3)		Up (10.2)
	U16307	Glioma pathogenesis-related protein (GliPR)	Up (3.5)	

Table 5 Miscellaneous. Differential mRNA expression between non-irradiated and irradiated rectal tissue. Fold changes are given between brackets and are calculated by relating the irradiated tissue to the non-irradiated tissue. The identifier represents the GenBank accession number

Identifier	Gene	Normal tissue	Carcinoma
U14383	Mucin 3 (MUC3)	Up (10.4)	
	Mucin 8 (MUC8)		Down (4.2)
	Adenylyl cyclase-associated protein 2	Down (3.8)	
S7754	NGFI-B/nur77 beta-type transcription factor homologue		Up (3.8)
M12529	Apolipoprotein E		Up (5.6)
D26561	Cellular DNA containing a fragment of HPV 5b	Up (3.0)	
J05036	Cathepsin E		Up (6.5)
M14758	P-glycoprotein (PGY1)		Up (15.3)

29 and 15 genes were up- and downregulated, respectively.

Next, we clustered the differentially expressed genes based on their functional annotation in relation to the biological processes involved in radiation response (Table 1, Table 2, Table 3, Table 4, Table 5). Among the genes involved in damage recognition, only ATM was up regulated in tumor, but not in normal tissue (Table 1). Of the genes involved in cellular signaling, 14 were differentially expressed, most of them protein phosphatases (n=4) and protein kinases (n=5). p21 was upregulated in tumor tissue, as confirmed by immunohistochemical (IHC) analysis (Fig. 1c).

A number of apoptosis-related genes were differentially expressed upon irradiation. IHC analysis showed that the level of apoptosis was increased upon irradiation in both normal and tumor tissues (Fig. 1a, b, Fig. 2). In both normal and tumor samples, maspin and BMP-2A were upregulated. In normal tissue, a number of genes involved in apoptosis were upregulated (Table 2), among which were caspase-3, Bax-genes and Fas/Apo-1. In contrast, ras-related genes were overexpressed in tumor after radiotherapy. Thus, the increase in apoptotic cells observed using IHC is differentially regulated between tumor and normal tissue.

In tumor tissue, proliferation was decreased, as indicated by the downregulation of Ki-67 at micro-array level (Table 3). IHC showed that proliferation was slightly decreased in tumor but not in normal tissues (Fig. 1b). Similar to apoptosis, proliferation appears to be differentially regulated between normal and tumor tissue, as shown by the spectrum of upregulated growth factors and

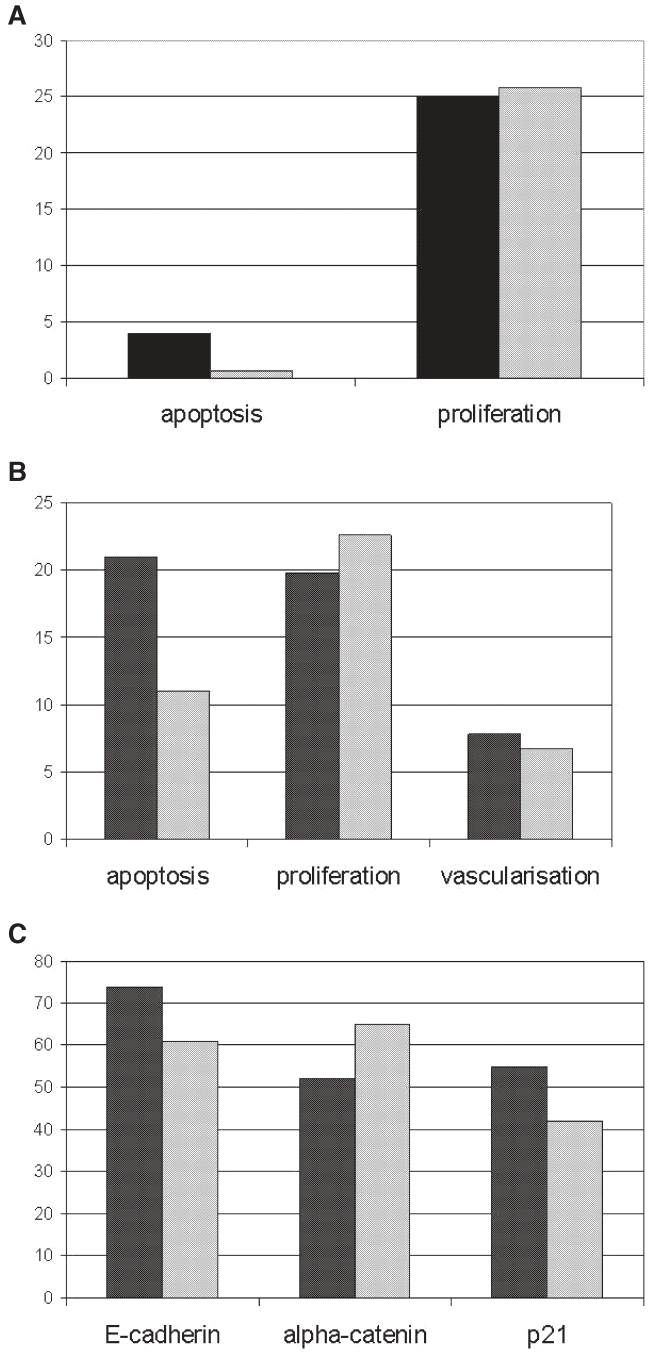

Fig. 1 Results of immunohistochemistry. **A** Changes in apoptosis and proliferation in normal tissue due to radiotherapy (P=0.06 and P=0.83, respectively). **B** Changes in apoptosis, proliferation and vascularization in tumor tissue due to radiotherapy (P=0.006, P=0.11 and P=0.03, respectively). **C** Changes in adhesion molecules (E-cadherin, α-catenin) and p21/waf in tumor tissue due to radiation (P=0.17, P=0.21 and P=0.16). Results are depicted as cells per square mm tumor (apoptosis and proliferation), as percentage of positive cells in normal tissue (apoptosis and proliferation) and as vessel perimeter per square mm tumor (vascularization). For E-cadherin, α-catenin and p21/waf1, percentages of tumors with positive staining are given. Irradiated samples are *black*; non-irradiated samples are *gray*

their receptors in normal tissue when compared with carcinoma.

Complex inflammatory responses were observed in tumor tissues, which were altered upon radiation [25]. Tissue repair characterized by inflammatory reaction, accompanied by vascular changes (Fig. 1b) and fibroblastic reaction (Table 4) was observed in both tumor and normal tissues. IHC showed a decrease in vascularization within the tumor microenvironment (Fig. 1b). In normal tissue, no change in vascularization was observed after irradiation.

Interleukin-8 was upregulated in both tumor and normal tissue, though the majority of cytokines were differentially expressed between the two tissue types. Effects of radiation on tumor–stroma interactions were also observed, as indicated by changes in metalloproteases and adhesion molecules (Table 4). E-cadherin was upregulated in irradiated tumor compared with non-irradiated tumor, while α-catenin showed a higher expression in non-irradiated tumor. This observation was confirmed by IHC (Fig. 1c).

Discussion

Radiation has severe effects on cells and tissues. Here, we show by expression profiling that radiotherapy differently affects normal and tumor tissues. Our results indicate that more than 90% of cancer-related genes remain unchanged upon radiation but that key genes in the control of proliferation, apoptosis and tissue repair are affected. Accordingly, the same processes are differentially affected in cancer and normal tissues as shown using IHC. Given the complexity of these processes, the use of expression profiling by microarray technology is necessary to obtain a more complete understanding of the molecular targets of radiotherapy in human cancer. Various studies by Northern blot analysis [35] and Taqman assays [10], as well as using immunohistochemistry [35] substantiate our microarray-based observations. For example, genes like P-glycoprotein (Table 5) and VIP (Table 4), known from the literature to be upregulated by radiation at the immunohistochemical level [8, 26], were confirmed to be upregulated in our expression profiles. In general, the majority of the genes found here to be differentially expressed have been described as being involved in the response and repair to tissue and DNA damage.

To minimize background levels and to obtain general information on gene expression before and after radiation, we chose to pool tumor as well as normal tissue samples. In this way, the individual differences between samples are smoothed, and the radiation-induced variations in gene expression patterns strengthened. Using this strategy, we pinpointed a number of genes known to be involved in the cellular reaction to radiotherapy, such as ATM (Table 1), cellular signaling molecules and genes involved in cell cycle control [2, 7, 13, 32]. Notably, p53, notwithstanding its role in cell cycle control after irradiation and its frequent mutation in colorectal carcinogen-

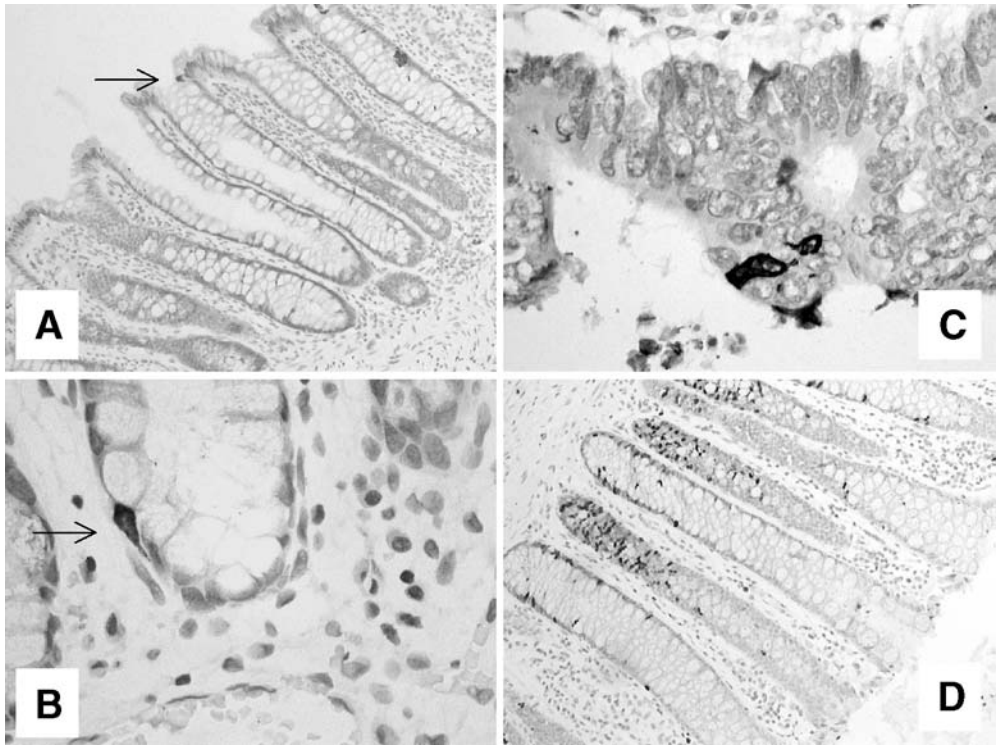

Fig. 2 Immunohistochemical conformation of changes in apoptosis and proliferation due to irradiation in normal and tumor tissue. **A** In normal rectal tissue, spontaneous apoptosis (*arrow*) is very infrequent, and apoptotic cells are never situated at the base of the crypts. The M30 antibody directed against the cleavage product of cytokeratin 18 is used to detect apoptotic cells. **B** Irradiation-induced apoptosis in normal tissue affects even the cells in the base of the crypts (*arrow*), as has been described in animal models [29]. **C** Apoptosis in tumor tissue; apoptosis is heterogeneously distributed. **D** Proliferation in normal tissue, demonstrated with the MIB1 antibody against Ki67

esis, was not differentially expressed. Although we showed recently that in normal tissue the p53 protein is clearly upregulated after radiotherapy and stays so for 7 days [21], the upregulation of p53 RNA is a very rapid and early event [19] and, therefore, not likely to be detected in the samples we used, with an interval between radiotherapy and surgery of 2–5 days. However, p53-regulated genes, such as gadd45 [37] (Table 3), p21 [18] (Table 1), TSG-6 [33] (Table 4) and maspin [39] (Table 2) are differentially expressed, suggesting the induction of a p53-mediated response.

The study of gene expression in whole tissue samples rather than in homogeneous cell types cultured in vitro provides additional information on the complex tissue responses to radiation. In Fig. 3, we provide a simplified representation of the sequence of molecular and cellular events induced by radiotherapy. First, a reorganization of the damaged tissues takes place. A delicate balance between tissue repair and scar formation is needed with the activation of cellular processes such as inflammation, (neo)angiogenesis and fibroblastic reactions. While absent immediately after irradiation [20], possibly due to the high sensitivity of lymphocytes, the presence of an inflammatory reaction in and around the tumor shifts back to non-irradiated levels within a week after termination of radiotherapy [25], suggesting the local production of chemotactic cytokines. Accordingly, our microarray analysis revealed the upregulation of chemoattractants such as IL-8 (Table 4), as well as other cytokines involved in the orchestration of the inflammatory reaction, such as osteopontin [1] (Table 4). Recently, it has been reported that both stromelysin and matrilysin (Table 4) might be involved in the regulation of osteopontin expression in vivo [1]. The genes coding for these proteases were found to be upregulated upon radiation in tumor tissue (Table 4). The upregulation in matrilysin mRNA in tumor tissue but not in normal tissue has been recently described [16].

Previous reports have shown a decrease of tumor vascularization after radiation [9, 15] using IHC. Furthermore, genes involved in the regulation of angiogenesis, such as trombospondin [5], interleukin-8 [14] and transforming growth factor (TGF) β[30] (Table 4) are differentially expressed in normal and tumor tissue. Recent literature suggests that the effects on the endothelial cell population in the intestine might be the most important factor in radiation damage in the gut [28].

Although tissue fibrosis is considered as one of the late effects of radiation, we have observed a fibroblastic reaction in and around the tumor as early as day 2 after irradiation [25]. The increased levels of TGFβ, Oncostatin M and the fibroblastic adhesion molecule OB-cadherin [34] provide molecular evidence for this finding. Reorganization of the tumor microenvironment includes changes in epithelial adhesion molecules. The upregulation of E-cadherin upon in vitro radiation has been previously reported [6] and confirmed in our study in rectal carcinoma using microarray and IHC. The expression of α-catenin was found to be decreased. The regulation of E-cadherin as well as of catenins is regulated by pathways involving TGFβ and protein kinase C [36], which are also differentially expressed due to irradiation.

Notably, gene expression profiles in normal and tumor tissue are affected by radiation in very distinct patterns. This may have been predicted from clinical data: the response of tumor tissue to short-term radiotherapy with regard to prognosis is generally good [11], and the effects

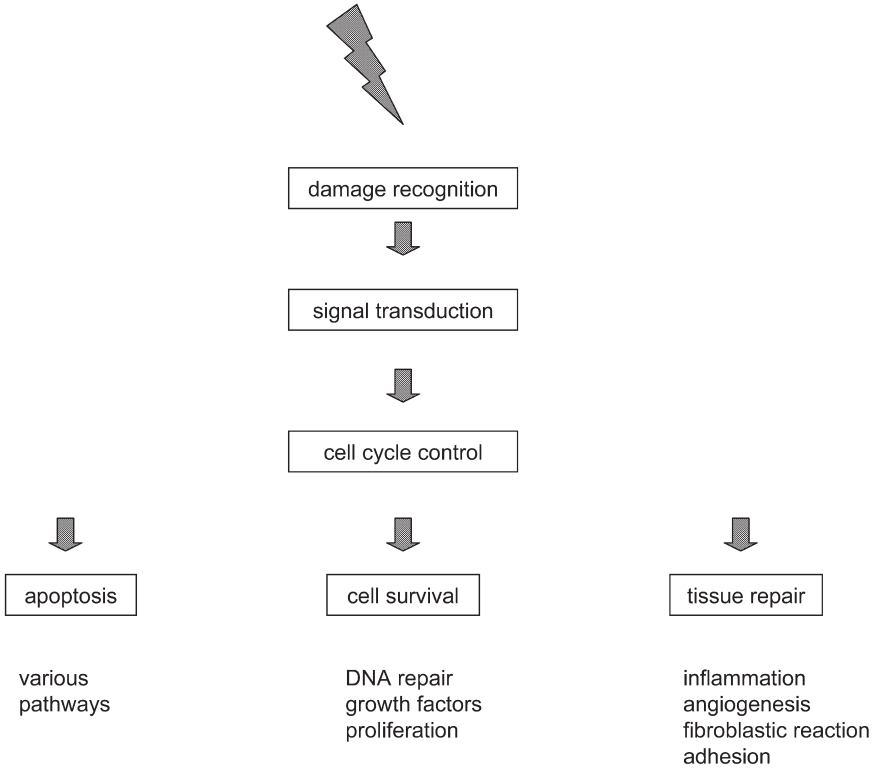

Fig. 3 Schematic representation of the events taking place after radiation on cellular and tissue level. On all levels, various interactions occur, and complex signaling mechanisms are involved. Damage recognition takes place in various locations throughout the cell (DNA, mitochondria, plasma membrane, etc.); as a consequence of damage recognition, various signaling pathways are engaged and give rise to both cellular and tissue reactions. The first line of control is executed by the induction of cell-cycle arrest, and, depending on the existing damage, cells go into apoptosis or survive. As a result of cell damage, reorganization of tissues takes place

on normal tissue are limited [22]. The differential expression patterns might be explained by the pre-existing differences in gene expression between normal tissue and tumor tissue. For example, MGSA (Table 4), strongly upregulated in tumor when compared with normal tissue [4, 27], is only upregulated in normal tissue upon radiation. The same holds true for the signaling molecule HEK2 [12] (Table 1). HBNF-1 (also known as pleiotrophin, Table 3) and protein tyrosine phosphatase zeta (Table 1), decreased in colorectal tumors compared with normal tissue [38], are downregulated by radiation only in normal tissue.

In conclusion, we showed that normal tissue and tumor tissue show different responses to radiation, which might be explained by the pre-existing differences in gene expression. The use of microarray technologies on patients' material provides data that give insight in the complex processes after the application of adjuvant therapy. The differences in clinical effects on normal and tumor cells are reflected by the outcome of the microarray experiments. Further research is needed to elucidate the exact mechanisms by which tumors, including stroma, and normal tissue react to irradiation.

Acknowledgement Grant support was provided by National Health Council (Ontwikkelingsgeneeskunde OWG 97/026).

References

1. Agnihotri R, Crawford HC, Haro H, Matrisian LM, Havrda MC, Liaw L (2001) Osteopontin, a novel substrate for matrix metalloproteinase-3 (stromelysin-1) and matrix metalloproteinase-7 (matrilysin). J Biol Chem 276:28261–28267
2. Artuso M, Esteve A, Bresil H, Vuillaume M, Hall J (1995) The role of the Ataxia telangiectasia gene in the p53, WAF1/CIP1(p21)- and GADD45-mediated response to DNA damage produced by ionising radiation. Oncogene 11:1427–1435
3. Bus PJ, Nagtegaal ID, Verspaget HW, Lamers CBHW, van Krieken JHJM, Griffioen G (1999) Mesazaline-induced apoptosis of colorectal cancer: on the verge of a new chemopreventive era? Aliment Pharmacol Ther 13:1397–1402
4. Cuenca RE, Azizkhan RG, Haskill S (1992) Characterization of GRO alpha, beta and gamma expression in human colonic tumours: potential significance of cytokine involvement. Surg Oncol 1:323–329
5. de Fraipont F, Nicholson AC, Feige JJ, VanMeir EG (2001) Thrombospondins and tumor angiogenesis. Trends Mol Med 7:401–407
6. Ebara T, Mitsuhashi N, Saito Y, Akimoto T, Niibe H (1998) Change in E-cadherin expression after X-ray irradiation of a human cancer cell line in vitro and in vivo. Int J Radiat Oncol Biol Phys 41:669–674
7. Fornace AJ Jr (1992) Mammalian genes induced by radiation; activation of genes associated with growth control. Annu Rev Genet 26:507–526
8. Hockerfelt U, Henriksson R, Franzen L, Norrgard O, Forsgren S (1999) Irradiation induces marked immunohistochemical expression of vasoactive intestinal peptide in colonic mucosa of man. Dig Dis Sci 44:393–401
9. Hopeweel JW, Young CMA (1978) Changes in the microcirculation of normal tissues after irradiation. Int J Radiat Oncol Biol Phys 4:53–58
10. Jin H, Yang R, Awad TA, Wang F, Li W, Williams SP, Ogasawara A, Shimada B, Williams PM, de Feo G, Paoni NF (2001) Effects of early angiotensin-converting enzyme inhibition on cardiac gene expression after acute myocardial infarction. Circulation 103:736–742
11. Kapiteijn E, Marijnen CAM, Nagtegaal ID, Putter H, Steup WH, Wiggers T, Rutten HJT, Pahlman L, Glimelius B, van Krieken JHJM, Leer JWH, van de Velde CJH (2001) Preop-

erative radiotherapy combined with total mesorectal excision for resectable rectal cancer. New Engl J Med 345:638–646
12. Kitahara O, Furukawa Y, Tanaka T, Kihara C, Ono K, Yanagawa R, Nita ME, Takagi T, Nakamura Y, Tsunoda T (2001) Alterations of gene expression during colorectal carcinogenesis revealed by cDNA microarrays after laser-capture microdissection of tumor tissues and normal epithelia. Cancer Res 61:3544–3549
13. Knebel A, Bohmer FD, Herrlich P (2000) Radiation-induced signal transduction. Methods Enzymol 319:255–272
14. Koch AE, Polverini PJ, Kunkel SL, Harlow LA, DiPietro LA, Elner VM, Elner SG, Strieter RM (1992) Interleukin-8 as a macrophage-derived mediator of angiogenesis. Science 258:1798–1801
15. Krishnan L, Krishnan EC, Jewell WR (1988) Immediate effect of irradiation on microvasculature. Int J Radiat Oncol Biol Phys 15:147–150
16. Kumar A, Collins H, van Tam J, Scholefield JH, Watson SA (2002) Effect of preoperative radiotherapy on matrilysin gene expression in rectal cancer. Eur J Cancer 38:505–510
17. Langberg CW, Hauer-Jensen M, Sung CC, Kane CJM (1994) Expression of fibrogenic cytokines in rat small intestine after fractionated irradiation. Radiother Oncol 32:29–36
18. Li Y, Jenkins CW, Nichols MA, Xiong Y (1994) Cell cycle expression and p53 regulation of the cyclin-dependent kinase inhibitor p21. Oncogene 9:2261–2268
19. Liu M, Dhanwada KR, Birt DF, Hecht S, Pelling JC (1994) Increase in p53 protein half-life in mouse keratinocytes following UV-B irradiation. Carcinogenesis 15:1089–1092
20. Marijnen CAM, Nagtegaal ID, Klein Kranenbarg E, Hermans J, van de Velde CJH, Leer JWH, van Krieken JHJM, Pathology Review Committee (2001) No downstaging after short-term preoperative radiotherapy in rectal cancer patients. J Clin Oncol 19:1976–1984
21. Marijnen CAM, Kapiteijn E, Nagtegaal ID, Mulder A, van de Velde CJH, Schrier PI, Peltenburg LTC, van Krieken JHJM (2002) p53 expression in rectal tissue after radiotherapy: remarkable long-term upregulation in normal mucosa versus extreme high frequency of functional loss in rectal carcinoma. Int J Radiation Oncology Biol Phys 52:720–728
22. Marijnen CAM, Kapiteijn E, van de Velde CJH, Martijn H, Steup WH, Wiggers T, Klein Kranenbarg E, Leer JWH (2002) Acute side effects and complications after short-term preoperative radiotherapy combined with total mesorectal excision in primary rectal cancer: report of a multicenter trial. J Clin Oncol 20:817–825
23. Nagtegaal ID, Klein Kranenbarg E, Hermans J, van de Velde CJH, van Krieken JHJM, Pathology Review Committee (2000) Pathology data in the central database of multicenter randomized trials need to be based on pathology reports and controlled by trained quality managers. J Clin Oncol 18:1771–1779
24. Nagtegaal ID, Marijnen CAM, Klein Kranenbarg E, Mulder A, Hermans J, van de Velde CJH, van Krieken JHJM (2001) Local and distant recurrences in rectal cancer patients are predicted by the nonspecific immune response; specific immune response has only systemic effect—a histopathological and immunohistochemical study. BMC Cancer 1:7
25. Nagtegaal ID, Marijnen CAM, Klein Kranenbarg E, Mulder A, Hermans J, van de Velde CJH, van Krieken JHJM (2002) Short-term preoperative radiotherapy interferes with the determination of pathological parameters in rectal cancer. J Pathol 197:20–27
26. Ng IO, Lam KY, Ng M, Kwong DL, Sham JS (1998) Expression of P-glycoprotein, a multidrug-resistance gene product, is induced by radiotherapy in patients with oral squamous cell carcinoma. Cancer 83:851–857
27. Notterman DA, Alon U, Sierk AJ, Levine AJ (2001) Transcriptional gene expression profiles of colorectal adenoma, adenocarcinoma, and normal tissue examined by oligonucleotide arrays. Cancer Res 61:3124–3130
28. Paris F, Fuks Z, Kang A, Capodieci P, Juan G, Ehleiter D, Haimovitz-Friedman A, Cordon-Cardo C, Kolesnick R (2001) Endothelial apoptosis as the primary lesion initiating intestinal radiation damage in mice. Science 293:293–297
29. Renehan AG, Bach SP, Potten CS (2001) The relevance of apoptosis for cellular homeostasis and tumorigenesis in the intestine. Can J Gastroenterol 15:166–176
30. Roberts AB, Sporn MB, Assoian RK, Smith JM, Roche NS, Wakefield LM, Heine UI, Liotta LA, Falanga V, Kehrl JH (1986) Transforming growth factor type beta: rapid induction of fibrosis and angiogenesis in vivo and stimulation of collagen formation in vitro. Proc Natl Acad Sci U S A 83:4167–4171
31. Rosen EM, Fan S, Rockwell S, Goldberg ID (1999) The molecular and cellular basis of radiosensitivity: implications for understanding how normal tissues and tumors respond to therapeutic radiation. Cancer Invest 17:56–72
32. Schmidt-Ullrich RK, Dent P, Mikkelsen RB, Valerie K (2000) Signal transduction and cellular radiation responses. Radiat Res 153:245–257
33. Seidita G, Polizzi D, Costanzo G, Costa S, Di Leonardo A (2000) Differential gene expression in p53-mediated G(1) arrest of human fibroblasts after gamma-irradiation or N-phosphoacetyl-L-aspartate treatment. Carcinogenesis 21:2203–2210
34. Thiagarajah JR, Gourmelon P, Griffiths NM, Lebrun F, Naftalin RJ, Pedley KC (2000) Radiation induced cytochrome c release causes loss of rat colonic fluid absorption by damage to crypts and pericryptal myofibroblasts. Gut 47:675–684
35. Thykjaer T, Workman C, Kruhoffer M, Demtroder K, Wolf H, Andersen LD, Frederiksen CM, Knudsen S, Orntoft TF (2001) Identification of gene expression patterns in superficial and invasive human bladder cancer. Cancer Res 61:2492–2499
36. Wang H, Chakrabarty S (2001) Requirement of protein kinase Calpha, extracellular matrix remodeling, and cell-matrix interaction for transforming growth factor beta-regulated expression of E-cadherin and catenins. J Cell Physiol 187:188–195
37. Xiao G, Chicas A, Olivier M, Taya Y, Tyagi S, Kramer FR, Bargonetti J (2000) A DNA damage signal is required for p53 to activate gadd45. Cancer Res 60:1711–1719
38. Yamakawa T, Kurosawa N, Kadomatsu K, Matsui T, Itoh K, Maeda N, Noda M, Muramatsu T (1999) Levels of expression of pleiotrophin and protein tyrosine phosphatase zeta are decreased in human colorectal cancers. Cancer Lett 135:91–96
39. Zou Z, Gao C, Nagaich AK, Connell T, Saito S, Moul JW, Seth P, Appella E, Srivastava S (2000) p53 regulates the expression of the tumor suppressor gene maspin. J Biol Chem 275:6051–6054

Virchows Arch (2005) 446:136–141
DOI 10.1007/s00428-004-1164-4

ORIGINAL ARTICLE

Zsuzsanna Varga · Rosmarie Caduff · Bernhard Pestalozzi

Stability of the HER2 gene after primary chemotherapy in advanced breast cancer

Received: 27 August 2004 / Accepted: 24 October 2004 / Published online: 14 January 2005
© Springer-Verlag 2005

Abstract We investigated whether alterations of the Her2 gene could be detected in breast cancer samples following primary chemotherapy in advanced breast cancer. The prospective study involved 23 patients with stage-II, -III or -IV breast cancer. All patients were treated with two to six cycles of fluorouracil-epirubicin and/or cyclophosphamid/epi-docetaxel. The Her2 protein and gene were assessed both on core needle biopsies prior to and on surgical specimens after completing chemotherapy using immunohistochemistry (IHC) and fluorescence in situ hybridization (FISH) methods. Estrogen and progesterone receptors (ER/PR) were also determined on both samples using IHC. Her2 status was modified in eight patients using IHC (35%) and in three patients using FISH (13%). Changes in ER/PR expression were detected in seven patients (30%). Our data suggest that alterations of the Her2 gene can occur, although not usually after primary or neoadjuvant chemotherapy. However, changes in ER/PR status seem to be a more common event; thus, both can lead to different therapeutic options. Intratumoral heterogeneity as well as sampling variations can contribute to modification of the Her2 status after primary chemotherapy.

Keywords Breast cancer · Chemotherapy · FISH · Her2 gene · Stability

Z. Varga (✉) · R. Caduff
Institute of Clinical Pathology,
University Hospital Zurich,
Schmelzbergstrasse 12, 8091 Zurich, Switzerland
e-mail: zsuzsanna.varga@usz.ch
Tel.: +41-1-2552449
Fax: +41-1-2554551

B. Pestalozzi
Department of Internal Medicine, Clinic of Oncology,
University Hospital Zurich,
Switzerland

Introduction

Overexpression and/or amplification of the Her2 gene and its protein product occur in approximately 25% of breast cancers [1, 12, 13, 20]. Clinical importance of Her2 positivity in breast cancer has been investigated in numerous previous studies, confirming shortened survival and worse clinical outcome in Her2-positive patients [6, 23, 25, 27]. Preferential and comparative detection methods of Her2 testing have been the subject of several investigations as well [2, 15, 17, 26]. Nevertheless, stability of the Her2 gene and protein after chemotherapy has not been thoroughly studied [7, 10, 22]. In routine practice, it is not common to determine Her2 status on breast cancer more than once during the disease course, postulating gene stability.

We addressed the question whether alterations of the Her2 gene and protein could be detected after primary chemotherapy using immunohistochemistry (IHC) and fluorescence in situ hybridization (FISH) methods on samples prior to and after chemotherapy.

Materials and methods

Sample collection

Initially, 26 patients with advanced breast cancer were enrolled in this prospective study, embracing a period from 2001 to 2004. Clinical charts were accessible through the files of the Clinic of Oncology of the University Hospital Zurich, Switzerland. Paraffin blocks were available from each patient in the Institute of Clinical Pathology of the University Hospital Zurich, Switzerland. Prior to primary chemotherapy, core needle biopsies and fine needle aspiration (FNA) were performed on all patients. In two patients (no. 6, no.12), no tumor tissue could be obtained on core biopsies; in one additional patient (no.19), there was no residual tumor confirmed on histology after chemotherapy. Therefore, these patients were excluded from the study later on. Mastectomy with axillary lymphonodectomy was the choice of surgery after completing chemotherapy in all patients.

Table 1 Summary of results. *P* values were analyzed using McNemar's test. *n.s.* not significant, *ER* estrogen receptors, *PR* progesterone receptors, *IHC* immunohistochemistry, *FISH* fluorescence in situ hybridization

	n	Pos→pos	Neg→neg	Neg→pos	Pos→neg	% Changed	*P* values
ER (absent versus + to ++++)	23	18	3	0	2	9	n.s.
PR (absent versus + to ++++)	23	9	9	2	3	22	n.s.
Her2 IHC (-/+ versus ++/+++)	23	5	10	2	6	35	n.s.
Her2 FISH $\geq$ 5 versus $\leq$5 copies	23	5	15	2	1	13	n.s.

Clinical features and histology

Of the patients, 22 presented with clinical stage-III or -IV breast cancer or with an inflammatory carcinoma. In 4 patients, clinical stage-II tumors were diagnosed. Positive axillary lymph nodes were detected clinically in 21 of 26 patients. Patients' ages ranged from 31 years to 72 years (mean age 50.3 years). All patients were administered neoadjuvant or primary chemotherapy consisting of several cycles (two to six) of fluorouracil-epirubicin and/or cyclophosphamid/epi-docetaxel.

All patients underwent core biopsy and FNA. In 2 patients, only FNA could be performed (these 2 patients were expelled from the cohort). The number of core biopsies per patient varied between two and four. All core biopsies were embedded in paraffin after fixation in 4% buffered formaldehyde. Slides 2-µm thick were prepared from each paraffin block and stained routinely with hematoxylin and eosin (H&E). The core biopsies confirmed invasive carcinoma in 24 patients, 17 corresponding to invasive ductal and 7 to invasive lobular subtypes (Fig. 1A, C). Of the tumors, one was well differentiated (G1), twelve were cases moderately differentiated (G2) and 10 carcinomas were graded as poorly differentiated (G3) on core biopsies according to the modified criteria of Bloom and Richardson.

Mastectomy specimens were processed similarly to the core biopsies. Paraffin blocks containing the best-preserved tumor area on H&E were selected for determining prognostic parameters. All immunohistochemical reactions and FISH analyses were performed on 2-µm thick slides. The mastectomy specimens revealed invasive carcinoma in 22 patients, representing all tumor stages as follows: pT1 (*n*=5), pT2 (*n*=9), pT3 (*n*=4) and pT4 (*n*=4). In one patient (no. 24), only lymphatic vessel invasion was detected without evidence of residual tumor mass. Another patient displayed extensive fibrosis without remaining invasive tumor cells or lymphatic invasion; for this reason, this patient was excluded from the study as well. Positive nodal status was confirmed in 13 of 23 cases. On histology, 4 cases diagnosed as lobular and ductal carcinoma, respectively, on core biopsy were identified as mixed carcinoma with ductal and lobular features—one case reported as ductal on the core biopsy showed predominantly lobular differentiation on the mastectomy specimen. Generally, there was abundant fibrosis in most mastectomy specimens (Fig. 1B). The invasive tumor cells exhibited typical histological changes after chemotherapy as hyperchromatic nuclei, pleomorphism and nuclear or cytoplasmic inclusions (Fig. 1D).

Immunohistochemistry

Her2

CB11 (anti-Her2 monoclonal antibody, Ventana, Tucson/AZ) was carried out with the Benchmark automated staining system (Ventana Medical Systems, Tucson/AZ). Cell membrane staining intensity was evaluated as follows: no or any detectable membrane signal in less then 10% of the tumor cells was considered as negative; weak incomplete membrane stain in more than 10% of the tumor cells was scored as 1+; moderate to strong complete membrane positivity in more than 10% of the tumor cells was considered as 2+ and 3+, respectively (Fig. 1E, F).

Estrogen and progesterone receptors

The detection of estrogen receptor (ER) (clone 6F11, Ventana, Tuscon/AZ) and progesterone receptor (PR) (clone 1A6, Ventana, Tucson/AZ) was carried out with the Benchmark automated staining system according to the manufacturers' prescriptions. For scoring of the reactions for ER and PR, the number of positively stained nuclei was assessed as follows: + $\leq$10%, ++ $\leq$50%, +++ $\leq$80%, ++++ 80–100%.

Her2/chromosome 17 FISH

FISH assay was carried out with two direct fluorescent-labeled DNA probes obtained from Pathvysion (Vysis, Abbot AG Diagnostic Division, Baar, Switzerland) according to the manufacturer's recommended protocol. The centromere region of chromosome 17 was visualized using a spectrum green-labeled probe, the Her2 gene with a spectrum orange-labeled probe. The probe mixture was hybridized on paraffin slides containing invasive tumor areas as controlled on an adjacent H&E-stained section. FISH was performed on all tumors irrespective of the result obtained using IHC.

With regard to scoring, a minimum of 60 non-overlapping nuclei were evaluated, and the ratio between Her2 gene and chromosome 17 was assessed. A tumor was considered amplified when the ratio (Her2/Chrom17) exceeded 2.0 (Fig. 1H). Among diploid tumor cells, a minimum of five Her2 copies was required for an amplified status; normal mean Her2 copy number was taken four signals or less (Fig. 1G).

Statistical analysis

Modifications after chemotherapy compared with results before treatment were analyzed using McNemar's test.

Results

Results are summarized in Table 1. Her2 status on IHC remained unchanged in 15 of 23 patients after chemotherapy (65%). Of the patients, 8 exhibited a different protein expression on mastectomy specimens (35%). The initial negative (+) IHC was found as positive (++ and +++, respectively) in 2 patients. Of the cases, 6 positive cases (++ and +++) on core biopsies were negative on the mastectomy specimens. Interestingly, 5 of 6 ++ positive cases on IHC were negative after chemotherapy. Among +++ positive tumors, there was one case with loss of protein expression after chemotherapy (case 8); however, this case showed gene amplification by FISH.

FISH stayed concordant in 20 of 23 patients (87%) on samples before and after chemotherapy. The initial negative FISH test in 2 patients showed clear gene amplification in both patients after therapy (same patients as on IHC). Another tumor with gene amplification on core biopsy was diagnosed as negative using FISH postoper-

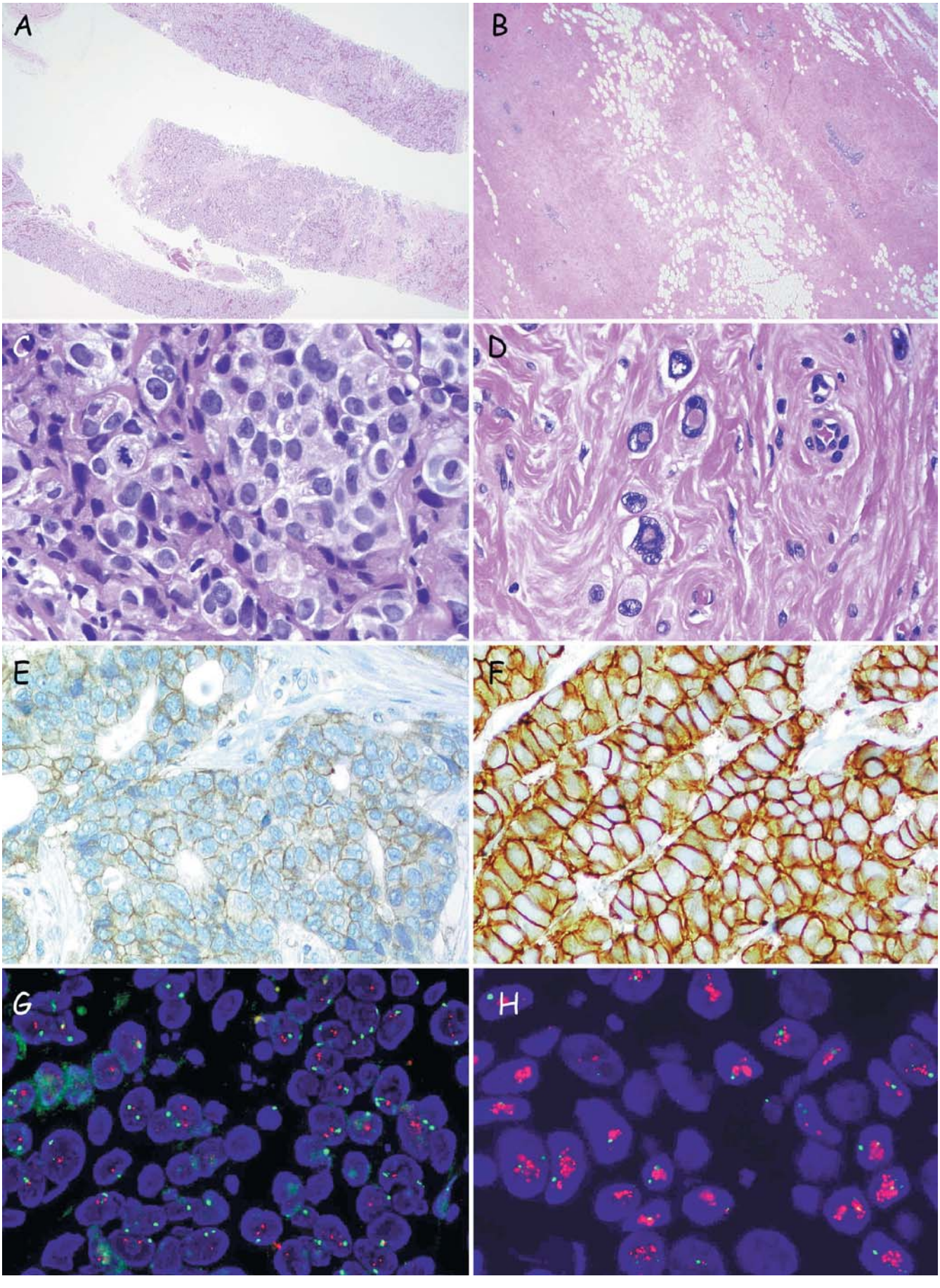
A
B
C
D
E
F
G
H

atively. All three cases with different Her2 gene status before and after chemotherapy corresponded to moderately differentiated invasive ductal carcinomas histologically. The chemotherapy protocol of these three patients included two to six cycles of fluorouracil–epirubicin. The six cases with loss of protein expression after chemotherapy kept a constant gene profile on the mastectomy specimens.

Difference in hormone receptor status was observed in 7 of 23 patients (30%). In 2 patients, the originally negative or weak positive tumor cells were found to express ER and/or PR strongly; in 5 other patients, the opposite constellation was seen. No statistically significant changes were found [*P*(ER)=0.5; *P*(PR)=1.0; *P*(Her2-IHC)=0.289; *P*(Her2-FISH)=1.0]. Results of the individual patients are presented in Table 2.

Discussion

Assessment of Her2 expression and correlation to response to primary or neoadjuvant chemotherapy or to prognosis at advanced breast cancer have been the subjects of several previous studies [5, 6, 14, 19, 23, 25, 27]. A few additional papers addressed the question recently whether the Her2 protein remains stable during induction chemotherapy using semi-quantitative and/or immunohistochemical methods [3, 4, 9, 16, 18, 21, 24].

Comparison of expression profile on both DNA and protein level before and after chemotherapy for breast cancer has not been investigated extensively [7, 11, 22]. We are aware of two previous papers determining Her2 gene characteristics on pre-treatment smears or cores and post-treatment sections by neoadjuvant treatment modality using a quantitative and an in situ hybridization (FISH) methodology, respectively [7, 22].

In our prospective cohort of 22 patients, we analyzed the Her2 gene and its protein product on core biopsies prior to induction chemotherapy and on the final mastectomy specimens on each patient using IHC and FISH methods. We were able to demonstrate in our series that modification of the Her2 gene after primary chemotherapy is a rare event, which occurs in a small percentage of the patients. Her2 gene status was modified in 3 of 23 patients, although this difference was not statistically significant (13%).

Our results are slightly higher than the observations of Dagrada et al.: in his series, gene alteration on previously negative Her2 status occurred only in 4% of the cases. However, in that study, pre-treatment smears and not core biopsies were used prior to induction therapy [7]. In a recent study of Taucher et al., a concordance of 100% was reached on core biopsies versus post-treatment specimens when results of IHC and FISH were analyzed combined [22].

In a similar study of Burstein et al., the preoperative Her2 status determined using IHC was reconfirmed using enzyme-linked immunosorbent assay postoperatively. In this patient selection, all initially negative cases remained negative; however, 17% of the originally strong positive cases were found to be negative [4].

Several previous studies addressed gene profile changing in Her2 status after neoadjuvant chemotherapy using IHC only; the results, however, represent a wide range from non-significant to relevant differences [3, 9, 16, 18, 21, 24].

Interestingly, discordance in Her2 status between primary versus metastatic, respectively, recurrent breast cancer disease seems to depend on chemotherapy performed in between, when using FISH methodology. Edgerton et al. found up to 25% discordant Her2 status in patients treated with chemotherapy; while in a study of Gansberg, where no chemotherapy was performed, the difference in Her2 status in primary and metastatic breast cancer was not significant [8, 11].

The mechanism and exact frequency in Her2 gene profile changing, loss or acquisition, after neoadjuvant chemotherapy is not fully understood. It has been suggested in several previous studies that both Her2 overexpression and gene amplification are early events in the tumor genesis, and both alterations remain stable during metastatic process and also for the duration of chemotherapy [7, 24].

As indicated by our results as well as in the papers of Dagrada et al. and Taucher et al., modification of the Her2 gene does not occur frequently, particularly when determining Her2 status on the genomic DNA level by means of FISH methodology [7, 22]. The same seems to be true for the hormone receptor stability after primary chemotherapy. The modification of estrogen and progesterone receptors could be observed in a small percentage of our patients after chemotherapy; however, these differences were not statistically significant. Our results appear to confirm similar previous observations in the literature. In the series of Faneyte et al., Bottini et al. and Penault-Llorca et al., slight changes in hormone receptor status could be detected, though none of the differences was statistically significant either [3, 9, 16].

In a subset of patients, however, the initial Her2 positive tumors, which are tested negative after induction therapy, may represent a downregulation of Her2 protein following antibody therapy; nevertheless, the clinical

Fig. 1 **A** Low-power view of core biopsies prior to chemotherapy, revealing large areas of invasive ductal carcinoma [hematoxylin and eosin (H&E stain)]. **B** Low-power view of a mastectomy specimen after chemotherapy, exhibiting abundant fibrosis containing scattered residual tumor cells (H&E stain). **C** High-power view of invasive tumor cells, showing uniform nuclei, finely dispersed chromatin and isolated mitoses (H&E stain). **D** High-power view of tumor cells, exhibiting large hyperchromatic nuclei, coarse chromatin and numerous nuclear inclusions (H&E stain). **E** Immunohistochemistry (2+) of Her2 protein, evidenced by moderate circumferential membranous reaction. **F** Immunohistochemistry (3+) of Her2 protein by strongly positive membranous staining. **G** Non-amplified Her2 gene. Fluorescence in situ hybridization (FISH) reaction reveals diploid tumor cells (*green signal*) with maximum two copies of the Her2 gene (*red signal*). **H** Amplified Her2 gene, FISH reaction demonstrates diploid cells (*green signal*) with large clusters and/or 10–12 copies of Her2 genes (*red signal*)

Table 2 Detailed results of individual patients. *ER* estrogen receptors, *PR* progesterone receptors, *IHC* immunohistochemistry, *FISH* fluorescence in situ hybridization

Patient no.	Before chemotherapy			After chemotherapy		
	ER/PR	Her2/IHC	Her2/FISH	ER/PR	Her2/IHC	Her2/FISH
1	++++ ++++	++	Diploid 2 copies	++++ +	+	Diploid 2 copies
2	+++ -	-	Diploid 2 copies	+++ -	-	Diploid 2 copies
3	+ -	++	Diploid 2 copies	- -	-	Diploid 2 copies
4	+++ +	-	Diploid 2 copies	++++ ++	+	Diploid 2 copies
5	+ -	++	Diploid 2 copies	++++ -	-	Diploid 2 copies
6	- -	+++	Not done Only cytology	++++ +++	-	Diploid 2 copies
7	+++ -	+	Diploid 2 copies	+++ -	+	Diploid 2 copies
8	- -	+++	Diploid 20 copies	- ++++	-	Diploid 20 copies
9	++++ +	+++	Diploid 12–15 copies	++++ -	+++	Diploid 12 copies
10	+ -	-	Diploid 2 copies	- -	-	Diploid 2 copies
11	++++ ++	+	Di/tetraploid 2–4 copies	++++ ++	+	Di/tetraploid 2–4 copies
12	Only cytology		Not done	++++ -	+++	Diploid 2 copies
13	+++ ++++	+	Diploid 2 copies	+++ +++	+	Diploid 2 copies
14	++++ -	+	Di/triploid 2–3 copies	++++ -	+++	Diploid 12 copies
15	++++ +++	+	Diploid 2 copies	++++ +++	++	Diploid 10 copies
16	+++ ++	-	Diploid 2 copies	++ +	-	Diploid 2 copies
17	- -	-	Diploid 2 copies	- +	-	Diploid 2 copies
18	+++ -	+++	Diploid 8 copies	++++ -	+++	Diploid 10–15 copies
19	- -	-	Diploid 2 copies	No residual tumor		
20	- -	+++	Diploid clusters	- -	+++	Diploid clusters
21	++++ ++	++	Diploid 2 copies	++++ ++	++	Diploid 2 copies
22	+++ +	+	Diploid 2 copies	++++ +++	+	Diploid 2 copies
23	++++ ++++	++	Diploid 2 copies	++++ -	+	Diploid 2 copies
24	+ -	+++	Diploid 6–8 copies	+++ -	+++	Diploid 10–12 copies
25	++++ ++	+	Diploid 8 copies	++++ +	+	Diploid 2 copies
26	++++ +	++	Diploid 2 copies	++++ -	+	Diploid 2 copies

significance of this phenomenon is not known at the moment [4]. Another possibility for discrepant findings after induction therapy is an intratumoral heterogeneity of Her2-expressing tumor cells along with tissue sampling error, both of which could eventually to some extent contribute to resistance or sensitivity to Herceptin or other chemotherapeutic agents [4].

In our series, modification of Her2 protein expression occurred more frequently among ++ positive cases, suggesting that +++ positive tumors using IHC are more stable during chemotherapeutic processes than ++ cases. Interestingly, Her2 ++ tumors using IHC in the absence of gene amplification were more common prior to than after chemotherapy in our study. Less favorable fixation of mastectomy specimens after chemotherapy with consecutive loss of epitopes and decreased sensitivity for IHC could be a possible explanation for this phenomenon.

Although predictive factors in a small percentage of cases can change after neoadjuvant or primary chemotherapy, it is advisable to measure these factors more than once during the disease course.

Acknowledgements The authors wish to thank Ms. Antje Nowotny for carrying out the fluorescence in situ hybridization reactions, Mr. Norbert Wey for his help in preparing the photographic illustrations and Prof. Dr. Burkhardt Seifert for performing the statistical analysis.

References

1. Allred DC, Harvey JM, Berardo M, Clark GM (1998) Prognostic and predictive factors in breast cancer by immunohistochemical analysis. Mod Pathol 11:155–168
2. Bartlett JMS, Going JJ, Mallon EA, Watters AD, Reeves JR, Stanton P, Richmond J, Donald B, Ferrier R, Cooke TG (2001) Evaluating Her2 amplification and overexpression in breast cancer. J Pathol 195:422–428
3. Bottini A, Berruti A, Bersiga A, Brunelli A. Brizzi MP, Di Marco B, Cirillo F, Bolsi G, Bertoli G, Alquati P, Dogliotti L (1996) Effect of neoadjuvant chemotherapy on Ki67 labeling index, c-erb-2 expression and steroid hormone receptor status in human breast tumors. Anticancer Res 16:3105–3110
4. Burstein HJ, Harris LN, Gelman R, Lester SC, Nunes RA, Kaelin CM, Parker LM, Ellisen LW, Kuter I, Gadd MA, Christian RL, Kennedy PR, Borges VF, Bunnell CA, Younger J, Smith BL, Winer EP (2003) Preoperative therapy with Trastuzumab and Paclitaxel followed by sequential adjuvant Doxorubicin/Cyclophosphamide for HER2 overexpressing stage II or III breast cancer: a pilot study. J Clin Oncol 21:46–53
5. Cleator S, Parton M, Dowsett M (2002) The biology of neoadjuvant chemotherapy for breast cancer. Endocr Relat Cancer 9:183–195
6. Cooke T, Reeves J, Lannigan A, Stanton P (2001) The value of the human epidermal growth factor receptor-2 (HER2) as a prognostic marker. Eur J Cancer 37:S3–S10
7. Dagrada GP, Mezzelani A, Alasio L, Ruggeri M, Romano R, Pierotti MA, Pilotti S (2003) HER-2/neu assessment in primary chemotherapy treated breast carcinoma: no evidence of gene profile changing. Breast Cancer Res Treat 80:207–214
8. Edgerton SM, Merkel DE, Moore DH, Thor AD (2000) HER-2/neu/ErbB2 status by immunohistochemistry and FISH: clonality and progression with recurrence and metastases (Abstract). Breast Cancer Res Treat 64:55
9. Faneyte IF, Schrama JG, Peterse JL, Reminjse PL, Rodenhuis S, van de Vijver MJ (2003) Breast cancer response to neoadjuvant chemotherapy: predictive markers and relation with outcome. Br J Cancer 88:406–412
10. Gansberg D, Lespagnard L, Rouas G, Paesmans M, Piccart M, Di Leo A, Nogaret JM, Hertens D, Verherst A, Larsimont D (2000) Sensitivity of HER-2/neu antibodies in archival tissue samples of invasive breast carcinomas. Am J Clin Pathol 113:675–682
11. Gansberg D, Di Leo A, Cardoso F, Rouas G, Pedrocchi M, Paesmans M, Verherst A, Bernard-Marty C, Piccart MJ, Larsimont D (2002) Comparison of HER-2 status between primary breast cancer and corresponding distant metastatic sites. Ann Oncol 13:1036–1043
12. Kaptain S, Tan LK, Chen B (2001) Her-2/neu and breast cancer. Diagn Mol Pathol 10:139–152
13. Kuter I (2001) Breast cancer. Oncologist 6:338–346
14. Mass RD, Press M, Anderson S, Murphy M, Slamon D (2001) Improved survival benefit from Herceptin (Trastuzumab) in patients selected by fluorescence in situ hybridization (FISH). Proc Am Soc Clin Oncol 20:22a
15. Pauletti G, Dandekar S, Rong HM, Ramos L, Peng H, Seshadri R, Slamon DJ (2000) Assessment of methods for tissue-based detection of the HER-2/neu alteration in human breast cancer: a direct comparison of fluorescence in situ hybridization and Immunohistochemistry. J Clin Oncol 18:3651–3664
16. Penault-Llorca F, Cayre A, Mishellany FB, Amat S, Feillel V, Bouedec G, Ferriere JP, De Latour M, Chollet P (2003) Induction Chemotherapy for breast carcinoma: predictive markers and relation with outcome. Int J Oncol 22:1319–1325
17. Press MF, Slamon DJ, Flom KJ, Park J, Zhou JY, Bernstein L (2002) Evaluation of Her2/neu gene amplification and overexpression: comparison of frequently used assay methods in a molecularly characterized cohort of breast cancer specimens. J Clin Oncol 20:3095–4005
18. Rasbridge SA, Gillett CE, Seymour AM, Patel K, Richards MA, Rubens RD, Millis RR (1994) The effects of chemotherapy on morphology, cellular proliferation, apoptosis and oncoprotein expression in primary breast carcinoma. Br J Cancer 70:335–341
19. Slamon DJ, Leyland-Jones B, Shak S, Fuchs H, Paton V, Bajamonde A, Fleming T, Eiermann W, Wolter J, Pegram M, Baselga J, Norton L (2001) Use of chemotherapy plus a monoclonal antibody against her2 for metastatic breast cancer that overexpresses Her2. N Engl J Med 344:783–792
20. Shackney SE, Silverman JF (2003) Molecular evolutionary patterns in breast cancer. Adv Anat Pathol 10:278–290
21. Stearns V, Singh B, Tsangaris T, Crawford JC, Novielli A, Ellis MJ, Isaacs C, Pennanen M, Tibery C, Farhad A, Slack R, Hayes DF (2003) A prospective randomized pilot study to evaluate predictors of response in serial core biopsies to single agent neoadjuvant Doxorubicin or Paclitaxel for patients with locally advanced breast cancer. Clin Cancer Res 9:124–133
22. Taucher S, Rudas M, Mader RM, Gnant M, Dubsky P, Roka S, Bachleitner T, Kandioler D, Steger G, Mittlbock M, Jakesz R (2003) Influence of neoadjuvant therapy with epirubicin and docetaxel on the expression of HER2/neu in patients with breast cancer. Breast Cancer Res Treat 82:207–213
23. Tulbah AM, Ibrahim EM, Ezzat AA, Ajarin DS, Rahad MM, El Weshi AM, Sorbris R (2002) HER-2/Neu overexpression does not predict response to neoadjuvant chemotherapy or prognosticate survival in patients with locally advanced breast cancer. Med Oncol 19:15–23
24. Vincent-Salomon A, Jouve M, Genin P, Frèneaux P, Sigal-Zafrani B, Caly M, Beuzeboc P, Pouillart P, Sastre-Garau X (2002) HER2 status in patients with breast carcinoma is not modified selectively by preoperative chemotherapy and is stable during the metastatic process. Cancer 94:2169–2173
25. Wang J, Buchholz TA, Middleton LP, Allred DC, Tucker SL, Kuerer HM, Esteva FJ, Hortobagyi GN, Sahin AA (2002) Assessment of histologic features and expression of biomarkers in predicting pathologic response to Anthracycline-based neoadjuvant chemotherapy in patients with breast carcinoma. Cancer 94:3107–3114
26. Wang S, Saboorian MH, Frenkel E, Hynan L, Gokaslan ST, Ashfaq R (2000) Laboratory assessment of the status of Her-2/neu protein and oncogene in breast cancer specimens: comparison of immunohistochemistry assay with fluorescence in situ hybridization assays. J Clin Pathol 53:374–381
27. Zhang F, Yang Y, Smith T, Kau SW, McConathy JM, Esteva FJ, Kuerer HM, Symmans WF, Buzdar AU, Hortobagyi GN, Pusztai L (2003) Correlation between HER-2 expression and response to neoadjuvant chemotherapy with 5-Fluorouracil, Doxorubicin, and Cyclophosphamide in patients with breast carcinoma. Cancer 97:1758–1765

Virchows Arch (2005) 446:142–149
DOI 10.1007/s00428-004-1137-7

ORIGINAL ARTICLE

Malcolm M. Hayes · David Lesack · Christophe Girardet · Marina Del Vecchio · Vincenzo Eusebi

Carcinoma ex-pleomorphic adenoma of the breast. Report of three cases suggesting a relationship to metaplastic carcinoma of matrix-producing type

Received: 23 July 2004 / Accepted: 8 September 2004 / Published online: 4 December 2004
© Springer-Verlag 2004

Abstract Three cases of carcinoma ex-pleomorphic adenoma of the breast are reported. Patients were 82, 60 and 56 years old and presented with a breast lump. All tumours showed areas of pleomorphic adenoma adjacent to typical areas of malignant transformation. These cases add to the spectrum of tumours shared by breast and salivary gland. The relationship between these neoplasms and metaplastic carcinoma of matrix-producing type is discussed.

Keywords Pleomorphic adenoma · Breast carcinoma · Metaplastic carcinoma

Introduction

Similarities in the embryogenesis of breast and salivary gland and the dual epithelial–myoepithelial cell differentiation in both anatomical sites account for the occurrence of salivary gland-type neoplasms in the breast [15]. Pleomorphic adenoma is one such benign neoplasm that occurs in both salivary gland and breast. In salivary gland, malignant transformation of pleomorphic adenoma is a well-recognised, albeit relatively, uncommon event. Malignant transformation can take the form of superimposed adenocarcinoma or development of a malignant mixed tumour with dual epithelial and mesenchymal elements [2, 16, 17, 18, 20, 21, 22, 28, 37, 38, 40, 43, 45]. Malignant pleomorphic adenoma has been reported to occur outside of the major salivary glands [11, 18]. To the best of our knowledge, malignant change arising in a pleomorphic adenoma of the breast has not been reported to date in the English language literature available to us for review. One previous record of ductal carcinoma co-existing with pleomorphic adenoma of the breast is noted, but the two tumours were separated from one another by normal intervening breast tissue [23].

M. M. Hayes (✉)
Department of Pathology,
British Columbia Cancer Agency,
Vancouver, BC, V5Z 4E6, Canada
e-mail: mhayes@bccancer.bc.ca
Tel.: +1-604-877-6098
Fax: +1-604-877-6178

D. Lesack
Department of Pathology,
Kelowna General Hospital,
Kelowna, Canada

C. Girardet
Histo et Cyto-pathologie Clinique,
Institut Central Des Hopitaux Valaisans,
France

M. Del Vecchio · V. Eusebi
Department of Pathology,
University of Bologna,
Italy

Clinical histories

Case 1

An 86-year-old woman presented with a suspicious palpable breast mass. Fine needle aspiration showed features of carcinoma. A left partial mastectomy was performed, which showed a 25-mm diameter circumscribed tumour, clear of the margin. There was no clinical evidence of metastatic disease to the axillary nodes or distant sites. Post-operative radiation was delivered to the breast and regional lymph nodes. Chemotherapy was not undertaken because of her advanced age and cardiomegaly. The patient remains free of disease 4 months after surgery.

Case 2

The patient was a 60-year-old woman who presented with an isolated nodule in the breast detected on a screening mammogram. A 14-mm circumscribed mass was present within 10 cm of excised breast fatty tissue. An axillary lymph-node dissection was performed, which showed 12 lymph nodes free of metastasis. Of these nodes, 2 contained nevus cells in their capsules. The patient remains free of disease 6 months after surgery.

Case 3

The patient was a 57-year-old woman who presented with a palpable mass in the left breast that she had noticed for about 3 months prior to diagnosis. A routine mammogram 7 months earlier was negative for abnormality. A diagnostic mammogram showed a 25-mm lobulated mass in the 12 o'clock position. Fine needle aspiration biopsy was positive for malignancy. A left modified radical mastectomy was performed, which revealed a 24-mm diameter tumour clear of the margins and ten axillary nodes negative for metastases. There was no clinical evidence of distant metastatic disease. She received a course of chemotherapy using adriamycin and cyclophosphamide. She remains free of disease 4.5 years later.

Materials and methods

All tissues were fixed in 10% buffered formalin, processed and embedded in paraffin wax as per standard histopathology protocols. Haematoxylin and eosin stain was performed on all blocks. Immunohistochemistry was performed on selected blocks using the Dako "EnVision+" biotin-free enhanced labelled polymer method [44] for all except the CD10 stain for which the Immunovision "Powervision" method [29] was employed. Sources and dilutions of the antibodies are reported in Table 1. The chromogenic in situ hybridisation for Her-2 neu was performed using the Zymed subtraction probe technology method [10, 41].

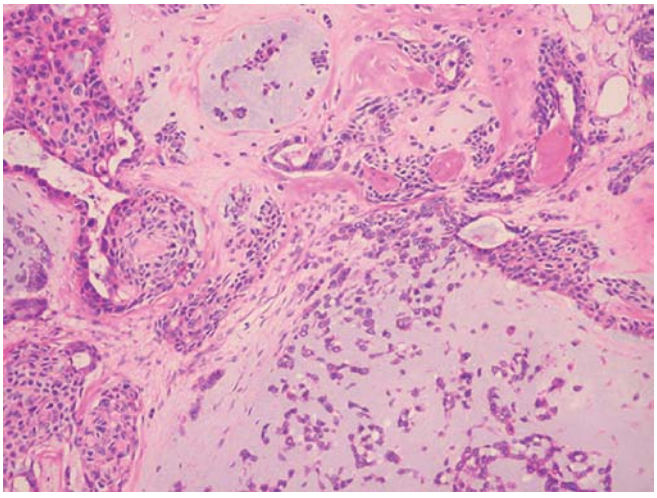

Fig. 1 Case 1. Photomicrograph to show areas of low-grade pleomorphic adenoma similar to that seen in salivary gland (haematoxylin and eosin ×150)

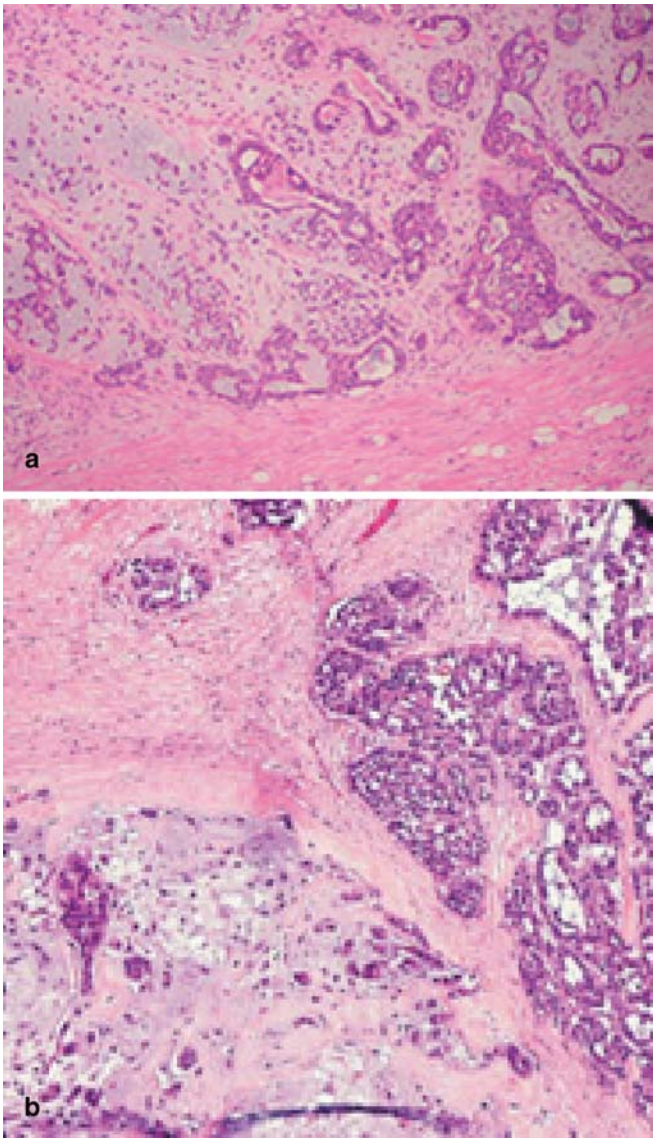

Fig. 2 a, b Cases 1 and 2. Circumscribed border of the benign component (haematoxylin and eosin ×100)

Table 1 Source and dilution of antibodies. *MSA* muscle specific actin, *HC myosin* heavy chain myosin, *K* keratin, *ER* oestrogen receptor

Antibody	Source	Clone	Dilution
P63	Dako	4A4	1:100
CD 10	Novocastra	56C6	1:50
MSA	Dako	HHF-35	1:50
HC myosin	Dako	SMMS-1	1:50
S 100 protein	University of Toronto	N/A	1:1500
Cam 5.2	BD Biosciences	CAM 5.2	Neat
K7	Dako	OV-TL 12/30	1:50
34βE12	Dako	34BE12	1:100
K 5/6	Dako	D5/16B4	1:50
MIB 1	Dako	MIB-1	1:100
P53	Dako	DO-7	1:100
ER	Novocastra	6F11	1:40
Her-2 neu	Dako	A485 polyclonal	1:500

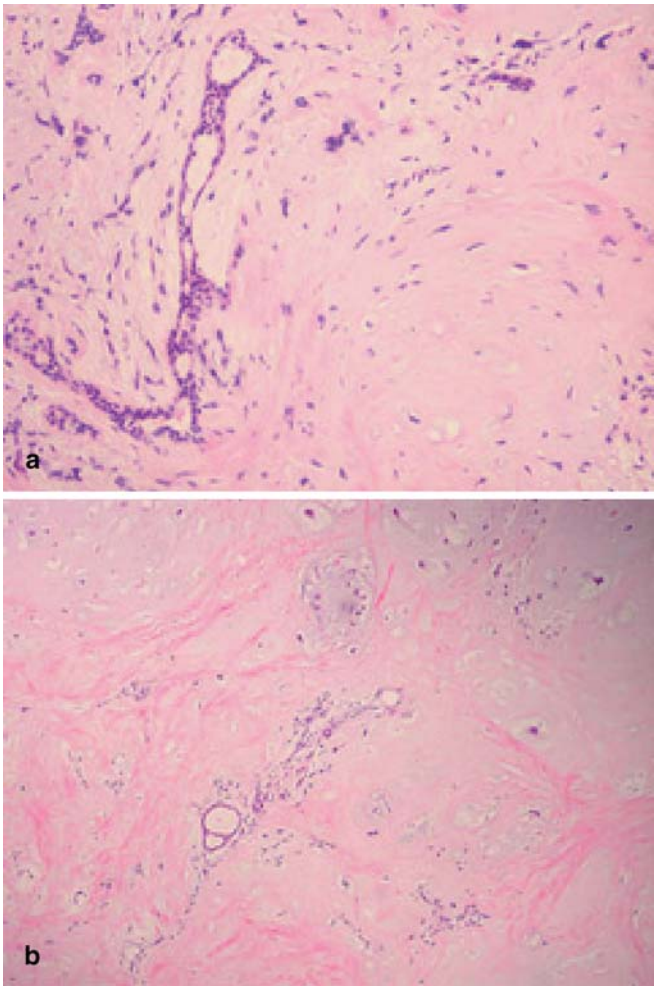

Fig. 3 a, b Case 3: Areas resembling pleomorphic adenoma. Benign-appearing ductal structures, bland periductal spindle cells and chords of epithelioid cells associated with nodules of cartilage (haematoxylin and eosin ×400 and ×200)

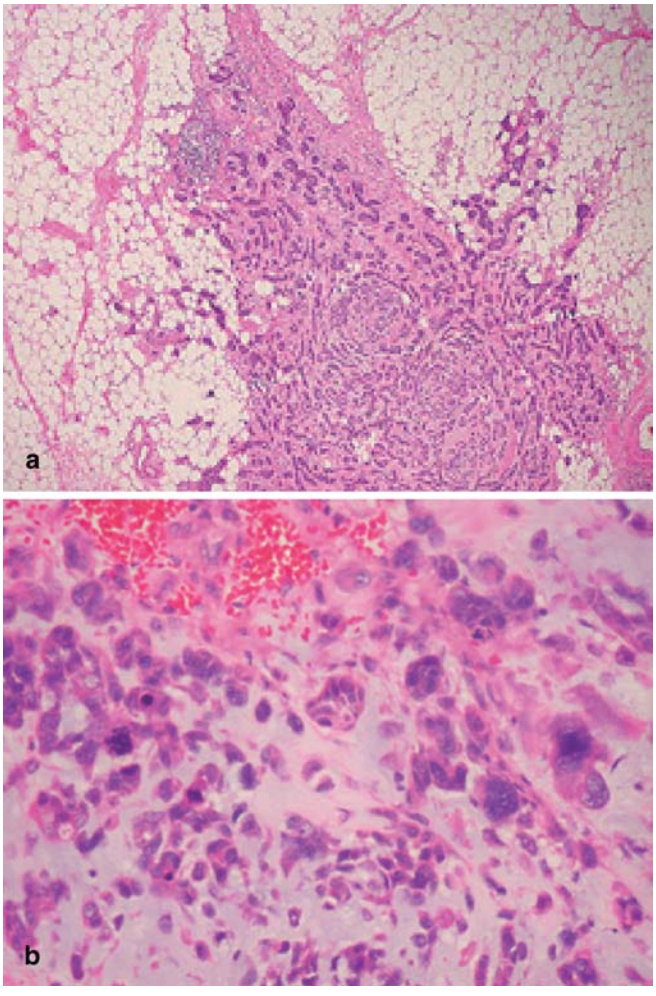

Fig. 4 Case 1. Component B. (**a**) Infiltrative growth pattern resembling invasive ductal carcinoma not otherwise specified (haematoxylin and eosin ×40). **b** Areas resembling high-grade metaplastic carcinoma (haematoxylin and eosin ×200)

Histological features

As all tumours were histologically similar, they will be described together. All three tumours were composed of two components. One component had the features of pleomorphic adenoma (component A), and the other showed features of overt malignancy (component B).

Component A

This component was histologically similar to typical pleomorphic adenoma of salivary gland (Fig. 1) and comprised approximately 60% of the tumour in case 1, a small area in case 2 and about 90% of the total neoplastic proliferation in case 3. This component had a circumscribed border in all cases and was composed of islands of chondroid tissue with interspersed small ductal structures (Fig. 2). Calcification of the chondroid stroma was seen in two of the three cases. Irregular sheets, nests and chords of epithelioid cells were also seen, and bland spindle cells were present between the ducts (Fig. 3). Uniform oval and spindle cells arranged in ill-defined chords and nests were present within the chondroid matrix (Fig. 1). The ductal structures had an internal layer of uniform columnar cells and an incomplete peripheral layer of myoepithelial cells as predominantly seen in cases 1 and 3. In these areas of the tumours, mitoses were very scanty, and necrosis was absent.

Component B

This was characterised by histologically malignant areas. In cases 1 and 3, there were areas that resembled grade-3 invasive ductal carcinoma not otherwise specified (NOS) and areas of high-grade metaplastic carcinoma with chondroid matrix. In case 2, the malignant component was pure high-grade matrix producing metaplastic carcinoma. In all cases, component B was seen at the periphery of neoplastic nodules invading the surrounding fat (Fig. 4 and Fig. 5). In case 1, extensive necrosis was present. At the periphery of the necrotic zones were garlands of markedly atypical epithelial cells showing remarkable nuclear pleomorphism and hyperchromasia. Mitotic figures were numerous, and some atypical mitoses were observed. Focally, an infiltrative border was noted with complex atypical glandular structures, sometimes associated with a desmoplastic stromal reaction, extending into the adjacent fat of the breast in a pattern seen in usual invasive ductal carcinoma NOS (Fig. 4 and Fig. 5). Some of the malignant areas also showed abundant chondroid matrix material resembling metaplastic carcinoma (Fig. 4 and Fig. 6). No malignant spindle-cell component was

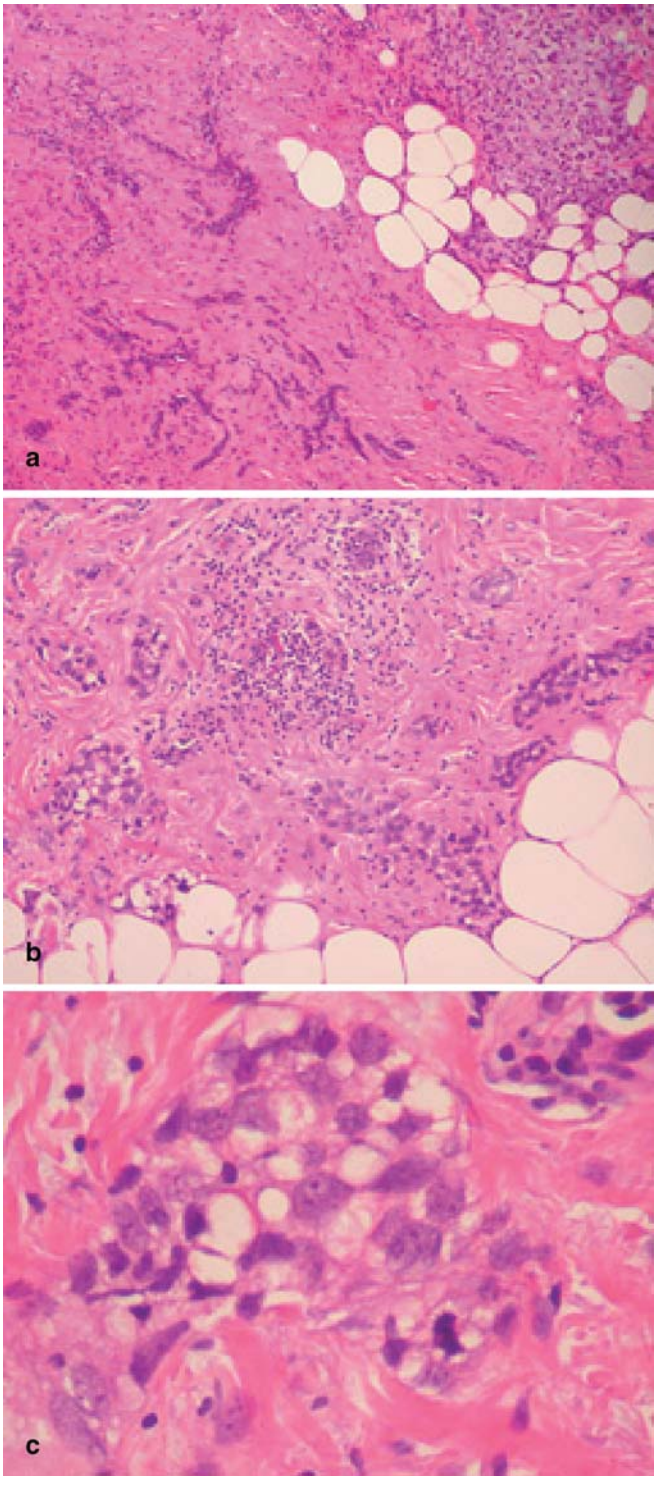

Fig. 5 a–c Case 3: Malignant areas showing infiltrative growth pattern, atypia and mitoses (haematoxylin and eosin ×100, ×200, ×400)

identified. A few ducts adjacent to the tumour contained high-grade solid in situ carcinoma.

In case 2, most of the tumour was composed of markedly pleomorphic cells floating in pools of myxochondroid matrix (Fig. 6). Numerous mitoses were seen in these areas, which resembled high-grade metaplastic carcinoma with matrix production.

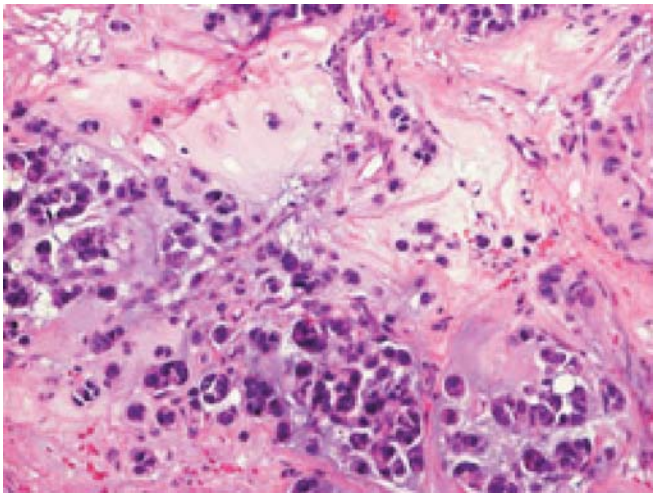

Fig. 6 Malignant areas of case 2 showing disorderly growth pattern and marked cytological atypia (×200)

Some of the malignant cells had an acinar arrangement and were associated with a desmoplastic fibrous stroma. High-grade ductal carcinoma in situ was seen in the adjacent breast tissue.

In case 3, a small peripheral area of the tumour showed features of grade-3 invasive ductal carcinoma NOS, and focal areas resembled high-grade metaplastic carcinoma with chondrosarcomatous differentiation. The chondroid lobules in the malignant component showed hypercellularity, marked cytological atypia, presence of mitoses and extensive necrosis. Between the lobules of atypical chondroid material were irregular groups and chords of pleomorphic epithelial cells exhibiting marked nuclear pleomorphism and hyperchromasia (Fig. 5). Mitoses and apoptotic cells were frequent in this component. No lymphatic or vascular invasion was seen. Within the tumour, a few ducts showed solid, grade-3 intraductal carcinoma.

Immunohistochemical features

Case 1 was studied for immunohistochemistry with all antibodies, and selected markers were employed in cases 2 and 3. Immunostains for p63, CD10, muscle-specific actin and smooth-muscle heavy-chain myosin highlighted myoepithelial cells in the benign component A of the tumours only (Fig. 7 and Fig. 8). Thus, some of the cells at the periphery of the ductal structures were positive for p63 as were many of the cells in the epithelioid nests. The epithelioid cells present in the chondroid matrix of component A were negative for p63. CD10 showed strong positive staining of the intertubular bland spindle cell component and the epithelioid and spindle cells present in the chondroid regions of the benign areas. The stains for muscle specific actin and smooth-muscle heavy-chain myosin showed surprisingly little staining in case 1 but good staining of periductal myoepithelial cells in case 3. Component B (malignant) areas failed to stain for myoepithelial markers except for focal positivity for p63 in the cells of the chondroid component. Both components (A and B) showed positive immunostaining for S-100 protein, but the staining was weak and patchy in the

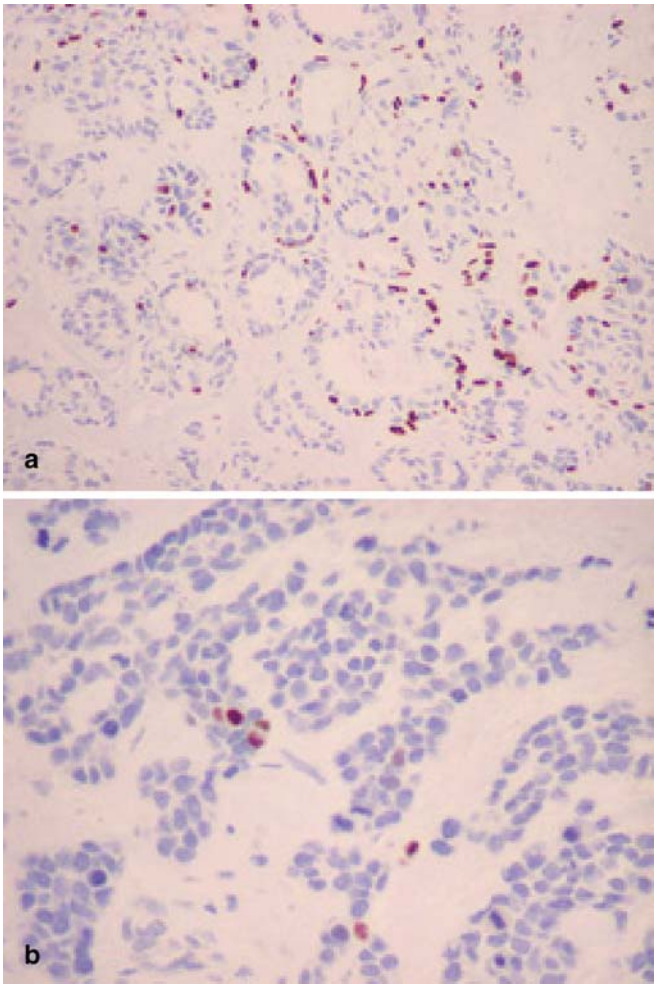

Fig. 7 Immunostain for p63 in case 1 showing a myoepithelial layer around many of the tubular structures in the benign areas (**a**; ×200) and scanty positive nuclei without an orderly arrangement in the malignant areas (**b**; ×400)

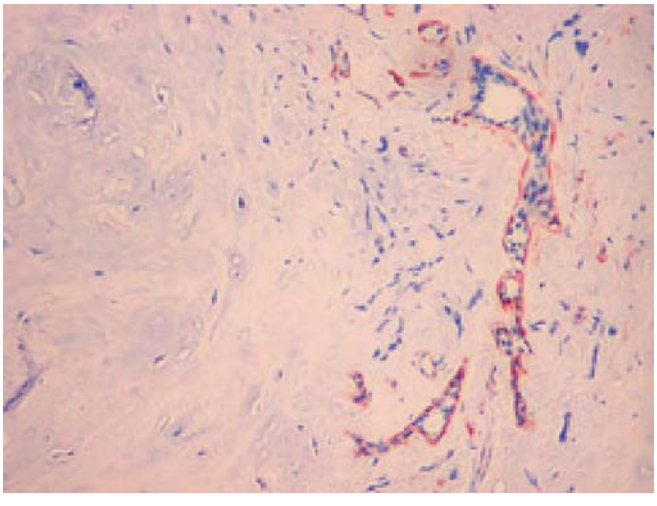

Fig. 8 Immunostain for muscle-specific actin demonstrating a periductal myoepithelial cell layer in the benign component (×200)

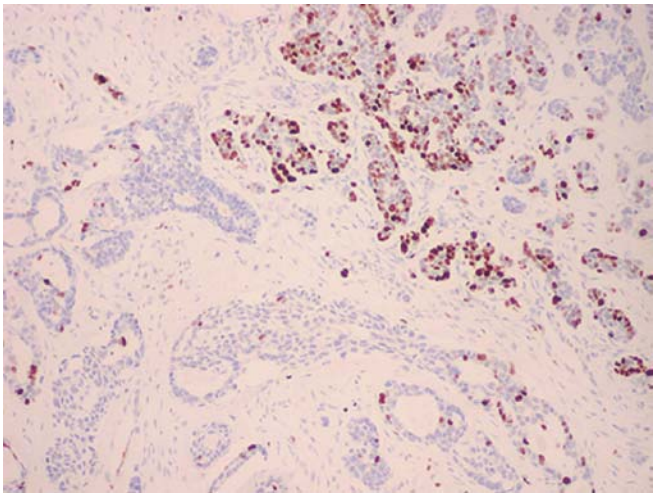

Fig. 9 Immunostain for Mib-1 in case 1. The scanty positive nuclei in the benign areas (*bottom left*) contrast with the numerous positive cells in the malignant areas (*top right*; ×200)

malignant areas of the tumours. In the benign areas, there was positive staining of almost all of the ductal epithelium, the surrounding myoepithelial cells, the epithelioid cell nests, the spindle cells and the chondroid cells. In case 1, staining for CK 5/6 was limited to the luminal cell layer of a few of the ductal structures in the benign areas of the tumour and to the majority of the cells in the malignant areas. The stain for Mib-1 showed scanty positive nuclei in the benign areas and numerous positive nuclei in the malignant areas (Fig. 9). The stain for p53 showed strong positive staining of more than 90% of nuclei in the malignant areas and patchy weak staining of the low-grade areas of the tumour in about 30% of nuclei. Immunostains for oestrogen receptors were negative in both components of the tumours, and Her-2 neu was not overexpressed or amplified in cases 1 and 3.

Discussion

The presence of salivary gland-type tumours in the breast has been known for a long time, but, in recent years, the spectrum of these lesions has been broadened to include oncocytic neoplasms [8], acinic cell carcinoma [9, 31] and mucoepidermoid carcinoma [6, 13, 42]. Although pleomorphic adenoma of the breast has been recognised for many years [1, 3, 4, 5, 7, 12, 19, 23, 25, 26, 30, 36, 46], as far as we are aware, its malignant counterpart has not been reported in the recent pathology literature. The recurrent pleomorphic adenoma of the breast reported by Soreide et al. did not show histological features of malignancy [36]. We believe that the three cases presented above meet the criteria for the diagnosis of carcinoma ex-pleomorphic adenoma, at least as defined in the salivary gland counterpart [17, 32, 33]. All three tumours showed benign or low-grade areas that were identical to pleomorphic adenoma of salivary gland. In addition, areas showing histological features of malignancy were seen

based on an infiltrative growth pattern, necrosis, marked cytological atypia, high mitotic rate, presence of atypical mitoses and high Mib-1 index.

Malignant transformation of pleomorphic adenoma of salivary glands has been shown to be associated with molecular changes, including expression of androgen receptor [27] and the amplification of Her-2 neu gene and overexpression of Her-2 neu protein [24, 35]. In two of the three cases presented above, there was no evidence of Her-2 neu amplification.

The differential diagnoses considered included matrix-producing metaplastic carcinoma, high-grade variant of adenoid cystic carcinoma and malignant adenomyoepithelioma. Part of the malignant areas of the tumours presented above resembled metaplastic carcinoma, but these neoplasms are typically uniformly high grade throughout and do not contain benign areas resembling pleomorphic adenoma. However, since there was no long history of a pre-existing stable nodule showing sudden onset of growth, one cannot entirely exclude the possibility of low-grade differentiated areas that resemble pleomorphic adenoma occurring within metaplastic carcinoma. Also, the usual abrupt transition between benign and malignant components seen in most cases of carcinoma ex-pleomorphic adenoma of salivary gland was less convincing in most of the cases described above, in which some areas of the tumour showed a transition from the benign-appearing areas to the high-grade malignant areas (Fig. 10). Furthermore, some cases of carcinoma ex-pleomorphic adenoma of salivary gland have been reported to show amplification of Her-2 neu gene, which was not apparent in our cases. Although a few tumour cells stained for p63, we were unable to demonstrate a definite myoepithelial component in the high-grade areas of the two cases available for immunohistochemistry. However, as elaborated elsewhere, the absence of a myoepithelial immunotype is not helpful in distinguishing between metaplastic carcinoma and carcinoma ex-pleomorphic adenoma because many metaplastic carcinomas exhibit myoepithelial markers [14], and the carcinoma component arising from malignant transformation of pleomorphic adenoma would not necessarily be expected to retain a myoepithelial immunotype. Similarly, the presence of a few ducts containing intraductal carcinoma adjacent to two of the three tumours is unhelpful in making this distinction. The presence of ductal carcinoma in situ is a useful diagnostic point to indicate the epithelial origin of a pure spindle cell metaplastic carcinoma [14] and to differentiate it from a sarcoma, but this feature is of no use to separate carcinoma ex-pleomorphic adenoma from metaplastic carcinoma. The exquisite organisation of myoepithelial cells at the periphery of ductal structures in the benign pleomorphic adenoma component of these lesions is the most compelling argument in favour of the diagnosis of carcinoma ex-pleomorphic adenoma rather than metaplastic carcinoma, since we believe this degree of organisation would be most unlikely in a metaplastic carcinoma with low-grade areas. Indeed, if such a differentiated change occurs in metaplastic matrix-producing carcinoma, it has not been illustrated in the literature we have reviewed. Furthermore, we believe that pleomorphic adenoma and metaplastic carcinoma of the breast likely represent two ends of a spectrum of neoplasia with potential for multiple lines of differentiation: epithelial,

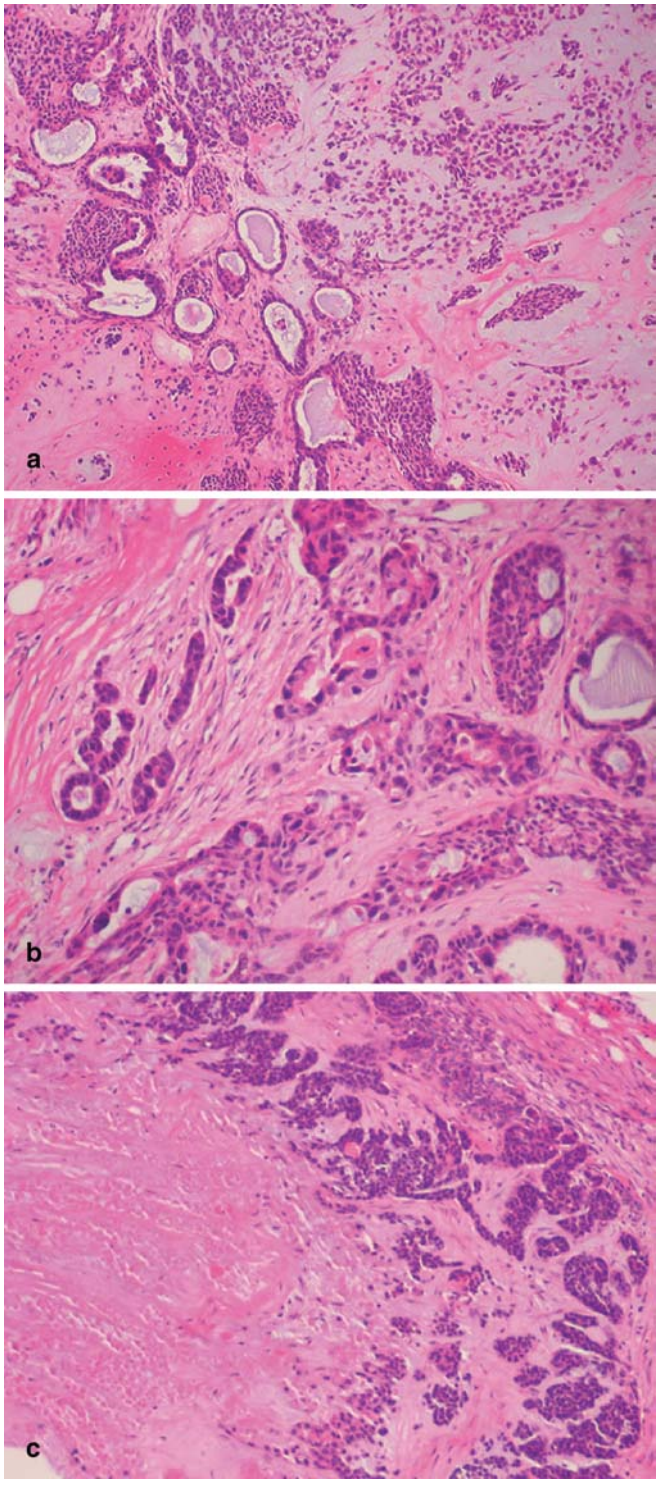

Fig. 10 a–c Panel to show transition from low-grade (**a**; ×100) through intermediate-grade (**b**; ×200) to high-grade (**c**; ×100) areas of the tumour in case 1

myoepithelial and mesenchymal. The transition from benign to malignant appearing areas illustrated in Fig. 10 supports this concept.

Although conceptually within the rubric of malignant epi-myoepithelial tumours (adenomyoepitheliomas), which can occasionally show matrix production [34, 39], the resemblance of the benign areas to pleomorphic adenoma warranted separation of this tumour as a distinct entity. Indeed, case 1 was referred with a suggested differential diagnosis of malignant adenomyoepithelioma or malignant pleomorphic adenoma. A diagnosis of adenoid cystic carcinoma was suggested by the referring pathologist for case 2, but the characteristic ductal structures and nodules of eosinophilic hyaline matrix of adenoid cystic carcinoma were not observed, and the presence of cartilage would be unusual for such a diagnosis.

The small number of cases reported and short clinical follow-up do not allow us to relate the histological features of malignancy to clinical outcome. Nevertheless, we think that the present tumours should be added to the list of neoplasms common to breast and salivary gland.

Acknowledgement Part of the work was financed with grants from MURST, Rome (40%), and the University of Bologna (ex 60%).

References

1. Agnantis NJ, Maounis N, Priovolou-Papaevangelou M, Baltatzis I (1992) Pleomorphic adenoma of the human female breast. Pathol Res Pract 188:235–241
2. Alvarez-Canas C, Rodilla IG (1996) True malignant mixed tumor (carcinosarcoma) of the parotid gland. Report of a case with immunohistochemical study. Oral Surg Oral Med Oral Pathol Oral Radiol Endod 81:454–458
3. Ballance WA, Ro JY, el-Naggar AK, Grignon DJ, Ayala AG, Romsdahl MG (1990) Pleomorphic adenoma (benign mixed tumor) of the breast. An immunohistochemical, flow cytometric, and ultrastructural study and review of the literature. Am J Clin Pathol 93:795–801
4. Betta PG, Spinoglio G (1992) Benign mixed salivary-type tumour of the breast. Eur J Surg Oncol 18:304–306
5. Bisceglia M, Nirchio V, Carosi I, Cappucci U, Decata A, Paragone T et al (1995) [Tumor and tumor-like benign mesenchymal lesions of the breast]. Pathologica 87:20–41
6. Chang LC, Lee N, Lee CT, Huang JS (1998) High-grade mucoepidermoid carcinoma of the breast: case report. Chang Keng I Hsueh Tsa Chih 21:352–357
7. Chen KT (1990) Pleomorphic adenoma of the breast. Am J Clin Pathol 93:792–794
8. Damiani S, Eusebi V, Losi L, D'Adda T, Rosai J (1998) Oncocytic carcinoma (malignant oncocytoma) of the breast. Am J Surg Pathol 22:221–230
9. Damiani S, Pasquinelli G, Lamovec J, Peterse JL, Eusebi V (2000) Acinic cell carcinoma of the breast: an immunohistochemical and ultrastructural study. Virchows Arch 437:74–81
10. Davison J, Morgan T, Hsi B, Xiao S, Fletcher J (1998) Subtracted, unique-sequence, in situ hybridization: experimental and diagnostic applications. Am J Pathol 153:1401–1409
11. Demirag F, Topcu S, Kurul C, Memis L, Altinok T (2003) Malignant pleomorphic adenoma (malignant mixed tumor) of the trachea: a case report and review of the literature. Eur Arch Otorhinolaryngol 260:96–99
12. Diaz NM, McDivitt RW, Wick MR (1991) Pleomorphic adenoma of the breast: a clinicopathologic and immunohistochemical study of 10 cases. Hum Pathol 22:1206–1214
13. Di Tommaso L, Foschini MP, Ragazzini T, Magrini E, Fornelli A, Ellis IO et al (2004) Mucoepidermoid carcinoma of the breast. Virchows Arch 444:13–19
14. Foschini MP, Dina RE, Eusebi V (1993) Sarcomatoid neoplasms of the breast: proposed definitions for biphasic and monophasic sarcomatoid mammary carcinomas. Semin Diagn Pathol 10:128–136
15. Foschini MP, Reis-Filho JS, Eusebi V, Lakhani SR (2003) Salivary gland-like tumours of the breast: surgical and molecular pathology. J Clin Pathol 56:497–506
16. Garner SL, Robinson RA, Maves MD, Barnes CH (1989) Salivary gland carcinosarcoma: true malignant mixed tumor. Ann Otol Rhinol Laryngol 98:611–614
17. Hellquist H, Michaels L (1986) Malignant mixed tumour. A salivary gland tumour showing both carcinomatous and sarcomatous features. Virchows Arch 409:93–103
18. Hemmi A, Hiraoka H, Mori Y, Wataya T, Sato H, Jinnai M et al (1988) Malignant pleomorphic adenoma (malignant mixed tumor) of the trachea. Report of a case. Acta Pathol Jpn 38:1215–1226
19. Kanter MH, Sedeghi M (1993) Pleomorphic adenoma of the breast: cytology of fine-needle aspiration and its differential diagnosis. Diagn Cytopathol 9:555–558
20. Kwon MY, Gu M (2001) True malignant mixed tumor (carcinosarcoma) of parotid gland with unusual mesenchymal component: a case report and review of the literature. Arch Pathol Lab Med 125:812–815
21. Lewis JE, Olsen KD, Sebo TJ (2001) Carcinoma ex pleomorphic adenoma: pathologic analysis of 73 cases. Hum Pathol 32:596–604
22. Manrique JJ, Albores-Saavedra J, Orantes A, Brandt H (1978) Malignant mixed tumor of the salivary-gland type, primary in the prostate. Am J Clin Pathol 70:932–937
23. Moran CA, Suster S, Carter D (1990) Benign mixed tumors (pleomorphic adenomas) of the breast. Am J Surg Pathol 14:913–921
24. Muller S, Vigneswaran N, Gansler T, Gramlich T, DeRose PB, Cohen C (1994) c-erbB-2 oncoprotein expression and amplification in pleomorphic adenoma and carcinoma ex pleomorphic adenoma: relationship to prognosis. Mod Pathol 7:628–632
25. Muthuphei MN (2000) Re: pleomorphic adenoma of the human breast. East African Med J 77:513
26. Narita T, Matsuda K (1995) Pleomorphic adenoma of the breast: case report and review of the literature. Pathol Int 45:441–447
27. Nasser SM, Faquin WC, Dayal Y (2003) Expression of androgen, estrogen, and progesterone receptors in salivary gland tumors. Frequent expression of androgen receptor in a subset of malignant salivary gland tumors. Am J Clin Pathol 119:801–806
28. Olsen KD, Lewis JE (2001) Carcinoma ex pleomorphic adenoma: a clinicopathologic review. Head Neck 23:705–712
29. Petrosyan K, Tamayo R, Joseph D (2002) Sensitivity of a novel Biotin-free detection reagent (Power Vision +). J Histotechnol 25:247–250
30. Reid-Nicholson M, Bleiweiss I, Pace B, Azueta V, Jaffer S (2003) Pleomorphic adenoma of the breast. A case report and distinction from mucinous carcinoma. Arch Pathol Lab Med 127:474–477
31. Schmitt FC, Ribeiro CA, Alvarenga S, Lopes JM (2000) Primary acinic cell-like carcinoma of the breast—a variant with good prognosis? (letter). Histopathology 36:286–289
32. Seifert G (1991) WHO International histological classification of tumours: histological typing of salivary gland tumours, 2nd edn. Springer, Berlin Heidelberg New York
33. Seifert G (1992) Histopathology of malignant salivary gland tumours. Eur J Cancer B Oral Oncol 28:49–56
34. Simpson RH, Cope N, Skalova A, Michal M (1998) Malignant adenomyoepithelioma of the breast with mixed osteogenic, spindle cell, and carcinomatous differentiation. Am J Surg Pathol 22:631–636

35. Skalova A, Starek I, Vanecek T, Kucerova V, Plank L, Szepe P et al (2003) Expression of HER-2/neu gene and protein in salivary duct carcinomas of parotid gland as revealed by fluorescence in-situ hybridization and immunohistochemistry. Histopathology 42:348–356
36. Soreide JA, Anda O, Eriksen L, Holter J, Kjellevold KH (1988) Pleomorphic adenoma of the human breast with local recurrence. Cancer 61:997–1001
37. Spiro RH, Huvos AG, Strong EW (1977) Malignant mixed tumor of salivary origin: a clinicopathologic study of 146 cases. Cancer 39:388–396
38. Stephen J, Batsakis JG, Luna MA, von der Heyden U, Byers RM (1986) True malignant mixed tumors (carcinosarcoma) of salivary glands. Oral Surg Oral Med Oral Pathol 61:597–602
39. Sugano I, Nagao T, Tajima Y, Ishida Y, Nagao K, Ooeda Y et al (2001) Malignant adenomyoepithelioma of the breast: a non-tubular and matrix-producing variant. Pathology International 51:193–199
40. Talmi YP, Halpren M, Finkelstein Y, Gal R, Zohar Y (1990) True malignant mixed tumour of the parotid gland. J Laryngol Otol 104:360–361
41. Tanner M (2000) Chromogenic in situ hybridization a practical alternative for fluorescence in situ hybridization to detect Her-2/neu oncogene amplification in archival breast cancer samples. Am J Pathol 157:1467–1472
42. Tjalma WA, Verslegers IO, De Loecker PA, Van Marck EA (2002) Low and high grade mucoepidermoid carcinomas of the breast. Eur J Gynaecol Oncol 23:423–425
43. Tortoledo ME, Luna MA, Batsakis JG (1984) Carcinomas ex pleomorphic adenoma and malignant mixed tumors. Histomorphologic indexes. Arch Otolaryngol 110:172–176
44. Vyberg M, Nielsen S (1998) Dextran polymer conjugate two-step visualization system for immunohistochemistry: a comparison of EnVision+ with two three-step avidin-biotin techniques. Appl Immunohistochem 6:3–10
45. Wahlberg P, Anderson H, Biorklund A, Moller T, Perfekt R (2002) Carcinoma of the parotid and submandibular glands—a study of survival in 2465 patients. Oral Oncol 38:706–713
46. Zafrani B, Bourquelot R, Chleq C, Mazabraud A (1985) [Mixed tumor of the breast (pleomorphic adenoma)]. Ann Pathol 5:213–215

Virchows Arch (2005) 446:150–156
DOI 10.1007/s00428-004-1151-9

ORIGINAL ARTICLE

Cora Pfisterer · Renaldo Faber · Lars-Christian Horn

Chorioamnionitis-induced changes of fetal extramedullar hematopoiesis in the second trimester of gestation. Is diagnosis from fetal autopsy possible?

Received: 23 August 2004 / Accepted: 15 September 2004 / Published online: 4 December 2004
© Springer-Verlag 2004

Abstract Chorioamnionitis, as the most frequent cause of second trimester abortions, is commonly diagnosed by histomorphological examination of placental tissue. We determined whether chorioamnionitis induces a fetal extramedullary hematopoietic response and estimated whether chorioamnionitis can be diagnosed from fetal liver alone. Clinical data and morphological and histological findings of 39 second trimester abortions, caused by chorioamnionitis, were compared with 32 age-matched control cases. Using hematoxylin and eosin staining, naphtol-ASD-chloracetate esterase and "Berliner Blau" reaction, total hematopoiesis, erythropoiesis, myelopoiesis and intracytoplasmatic iron of fetal liver were examined. In the study group, total hematopoiesis was increased compared with the controls (94.9% versus 84.4%). The same was seen in erythropoiesis (69.2% versus 56.2%, $P>0.05$). Chorioamnionitis resulted in a significant increase of fetal myelopoiesis with clustering of leukocytes in 56.4% ($P=0.001$). Neutrophiles were located predominantly intrasinusoidal and periportal (74.4%), while an isolated periportal location was often observed in controls (50.0%). Isolated perivenous iron storing was more often seen with chorioamnionitis (28.3% versus 3.1%) and correlated with the increasing severity of chorioamnionitis. It can be stated that infectious diseases, such as chorioamnionitis, increase fetal intrahepatic myelopoiesis as one defense mechanism. The morphology of fetal intrahepatic hematopoiesis and iron storing might also be helpful in the diagnosis of chorioamnionitis, especially when the placenta is not available for examination.

Keywords Chorioamnionitis · Fetal hematopoiesis · Second trimester of gestation · Inflammative abortion

C. Pfisterer (✉) · R. Faber
Department of Obstetrics and Gynecology,
University Hospital of Leipzig,
Philipp-Rosenthal-Strasse 55, 04103 Leipzig, Germany
e-mail: CoraPfisterer@gmx.net
Tel.: +49-341-9723595
Fax: +49-341-2252784

L.-C. Horn
Institute of Pathology,
University Hospital of Leipzig,
Liebigstrasse 26, 04103 Leipzig, Germany

Introduction

Chorioamnionitis is still one of the most frequent causes of fetal loss in the second trimester of gestation. Clinical signs of chorioamnionitis complicate about 2% of all gestations [27]. In several studies of necropsies of midtrimester miscarriages, a histological chorioamnionitis is responsible for 43–45.5% of the abortions [6, 22]. Some authors explain the high frequency of infection-induced abortions during the second trimester with the timing of initiation of the fetal immune response, meaning that only the fetus with a maturing immune system is able to generate the cytokine or hormonal response necessary to initiate labor [9]. In a study of 179 consecutive placentas from 14 weeks to 40 weeks of gestation, Sebire et al. [26] reported a peak prevalence (>90%) of chorioamnionitis-induced abortions at 20–24 weeks. In accordance, Lahra and Jeffery [11] proved the inverse relationship of the incidence of histological chorioamnionitis and gestational age in a large Australian pre-term cohort between 20 weeks and 34 weeks ($n=3928$). They observed a chorioamnionitis as a causative mechanism in 66% of abortions at the age of 20–24 weeks of gestation, while this part dropped to 16% at 34 weeks.

In general, the histological examination of placental tissue and umbilical cord is the main criterion for the diagnosis of a chorioamnionitis, the graduation of infection and the decision regarding a fetal systemic involvement in the inflammatory process.

During an infectious process, leukocytes in the placental tissue are derived from two different sources: the intervillous space (maternal origin) and the fetal surface blood vessels [1]. The emigration of leukocytes is always directional toward the amniotic cavity, presumably to-

ward an antigenic source. Pankuch et al. described this process as amniotropism [15].

Hematopoietic stem cells, deriving from the aortogonad-mesonephros region, colonize the fetal liver and later the bone marrow for developing the definitive fetal hematopoietic activity [8, 13]. During the mid-trimester period, the liver is the principal site of fetal hematopoiesis, where two functionally different compartments can be observed. Erythropoiesis takes place within the sinusoids of the parenchyma, while granulopoiesis is restricted to the mesenchymal tissue of the portal fields [28].

Our aim was to examine whether a chorioamnionitis causes a fetal hepatic cellular response in the second trimester of gestation. We determined whether there was a relationship between the severity of placental inflammation and diagnostic clinical features, on one hand, and the dimension of fetal response, on the other. Afterward, it was determined that a chorioamnionitis can be diagnosed by fetal autopsy alone, particularly if a placenta was not submitted for necropsy.

Materials and methods

The study examined 71 patients who had an abortion during the second trimester of gestation (63 single pregnancies, 8 twin pregnancies). Of those who had abortions, 39 resulted from a histological confirmed chorioamnionitis. Pre-term rupture of the membranes (PROM) occurred in 30 of these cases (76.9%). The fetal age ranged from 13 weeks to 25 weeks of gestation with a median age of 20 weeks. Of chorioamnionitis-induced abortions, 78.6% occurred between the 18th and the 23rd week of gestation with a maximum at the 23rd week (18.0%). The control group consisted of 32 fetuses with perinatal death deduced from non-infectious reasons, such as abruptio placentae with bleeding (n=7), placental dysmaturity (n=10), medical-induced abortion due to malformations (n=13) or abortion of unknown morphological origin (n=2). Matched-pair analysis was performed to select a study and control group with an appropriate gestational age (±1 week). The average maternal age in the study group was equal to the control cases at 28.8 years (±5.43) and ranged from 20 years to 40 years.

The diagnosis of an amnion infection syndrome (AIS) assumed a maternal axillar temperature raised over 37.5°C degrees together with a maternal leukocytosis above 16.0 Gpt/l and an elevated C-reactive protein (CRP) of more than 5.0 mg/l. Patients' symptoms of AIS could be determined from the clinical charts. But the duration of symptoms could not be stated in every case, as the majority of women were admitted with imminent abortions.

A histological chorioamnionitis was characterized by the presence of polymorphonuclear leukocyte infiltration of the amnion, chorionic plate and/or umbilical cord [1]. Depending on the extension of leukocytic infiltrates, a minimal, partial and complete infiltration was differentiated. An isolated amnionitis with inflammatory infiltrates in the amnion membranes was defined as a minimal leukocytic infiltration. In case of a partial infiltration, two of the below-mentioned compartments were affected, and leukocytes must have been present either in the amnion and/or chorionic plate and/or umbilical cord. A complete infiltration signified leukocytes in all three compartments [31]. Additionally, a semiquantitative analysis was performed, considering the amount of leukocyte infiltrations. In cases with a "moderate" infiltration, several leukocytes (>5) were seen in some neighboring microscopic fields. A "strong" infiltration was stated when many leukocytes were observed in many neighboring microscopic fields [31].

Clinical data were taken from the clinical files. The autopsies were performed by an experienced fetal pathologist according to the guidelines and recommendations of the Autopsy Committee of the College of American Pathologists and the Royal College of Pathologists of Great Britain [3, 30]. The description included body weight, head circumference, crown-rump and crown-heel lengths. The external description noted all major and minor malformations, color of the skin, hemorrhages and other abnormalities. A systemic examination of all major cranial, thoracic and abdominal organs was performed. Microscopic examination included histology of the heart, lungs, liver, kidneys, spleen, thymic gland and abdominal (mesenterial) lymph nodes in general. Depending on the clinical data, histological examination of additional organs was performed, including special staining procedures or immunohistochemistry. If the placenta was available, macroscopic description and histological examination were performed according to the recommendations of Benirschke and Kaufmann [1] and Vogel [31].

For examination of the fetal extramedullar hematopoietic activity, three clearly separated planes from tissue sections of the fetal liver were cut and stained after formalin fixation and paraffin embedding. Using the hematoxylin-eosin staining, total hematopoiesis and erythropoiesis were evaluated. Fetal myelopoiesis was examined with the naphtol-ASD-chloracetate esterase reaction. "Berliner Blau" reaction indicated location and quantity of intracytoplasmatic iron storing. Histological examination was blinded in that manner, in that the pathologist was unaware of clinical data during examination. For statistical analysis, proportions were compared using contingency tables or chi-square test. A two-tailed $P<0.05$ was considered significant. For calculations, we used the SPSS program (version 6.0.1.).

Results

The extension of leukocyte infiltration within the placental tissue was influenced by the gestational age at time of abortion (Table 1). A complete infiltration including all three compartments (chorioamnionitis and funisitis) was only seen between the 20th and 23rd week of gestation, concerning 11 study cases (28.2%).

A strong positive correlation between clinical symptoms of an AIS and a histopathological examination confirmed chorioamnionitis as a causative reason for the miscarriage. In 77.0% (n=30) of the study cases, clinicians diagnosed an AIS or had strong suspicion for placental inflammation. However, two study cases were clinically "silent", i.e., without any clinical symptoms of AIS (5.1%). The histological examination of these "silent" cases showed one minimal and one complete leukocytic infiltration of the placental tissue. In contrast, 52.0% of the cases in the control group represented no clinical symptoms for AIS. In one control case (4.0%), an elevated CRP, maternal leukocytosis and PROM were observed, and an infectious cause was suspected. Autopsy could not prove any inflammatory change.

Table 1 Placental leukocyte infiltration with reference to the gestational age

Infiltration	n	16–19 weeks (%)	≥20 weeks (%)
Minimal	8	50.0	50.0
Partial	20	50.0	50.0
Complete	11	0.0	100.0

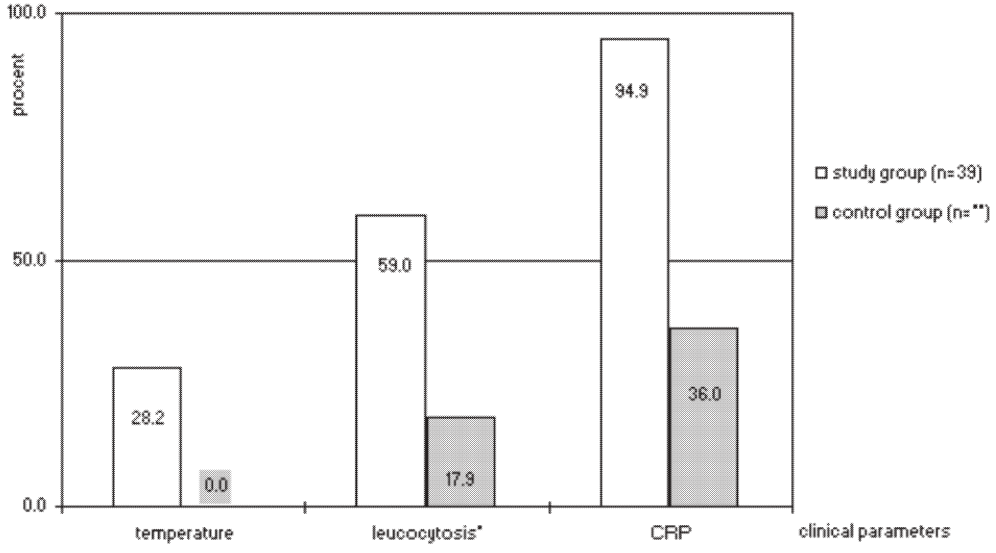

Fig. 1 Maternal axillary temperature (>37.5°C), leukocytosis (>16 Gpt/l) and C-reactive protein (CRP) (>5 mg/l) of study and control cases, *n*=number of fetuses, *statistically significant (*P*=0.0008), **number of control cases due to incomplete paraclinical data: temperature (*n*=32), leukocytosis (*n*=28), CRP (*n*=25)

Table 2 Fetal hepatic myelopoiesis, NASD staining

Characteristics	Classification	Study group (*n*=39)		Control group (*n*=32)	
		n	%	*n*	%
Intensity of leukocytes	Negative	0	0.0	6	18.8
	Isolated	17	43.6	20	62.4
	Grouped or confluated[b]	22	56.4	6	18.8
Location of leukocytes[a]	Intrasinusoidal	7	17.9	6	18.8
	Periportal	3	7.7	16	50.0
	Intrasinusoidal and periportal	29	74.4	4	12.4

[a] Excluding cases with a negative NASD result
[b] Statistically significant (*P*=0.001)

In assessing the clinical symptoms for AIS, a raised axillary temperature above 37.5°C degrees represented a very specific clinical marker. It was exclusively seen in connection with a chorioamnionitis (28.2%). The rate of maternal leukocytoses (>16.0 Gpt/l) among the study cases was significantly higher than at the control group (*P*=0.0008). The CRP, as shown in Fig. 1, tended to be a very sensitive, but less specific predictor for a placental infection (94.9% versus 36.0%).

The histocytological examination of the fetal hepatic tissue focused on the evaluation of the dimension and location of hematopoiesis, erythropoiesis, myelopoiesis and the detection as well as distribution of intracytoplasmatic iron.

As shown in Table 2, a chorioamnionitis caused strong alterations of fetal intrahepatic myelopoiesis. In each case of chorioamnionitis, fetal hepatic tissue represented leukocytes (100.0% versus 81.2%). Clustering and confluation of hepatic myelopoiesis was strongly associated with chorioamnionitis (56.4% versus 18.8%; *P*=0.001; Fig. 2). None of the control cases showed a confluation of leukocytes. The distribution of myelopoiesis was also altered. In cases with chorioamnionitis, leukocytes were predominantly seen both intrasinusoidal and in the portal fields (74.4% versus 12.4%). In the control cases, single leukocytes were observed in the connective tissue of the portal fields (50.0% versus 7.7%; Fig. 3). There was no correlation between the intensity or location of myelopoiesis in the fetal liver and the severity of chorioamnionitis (data not shown).

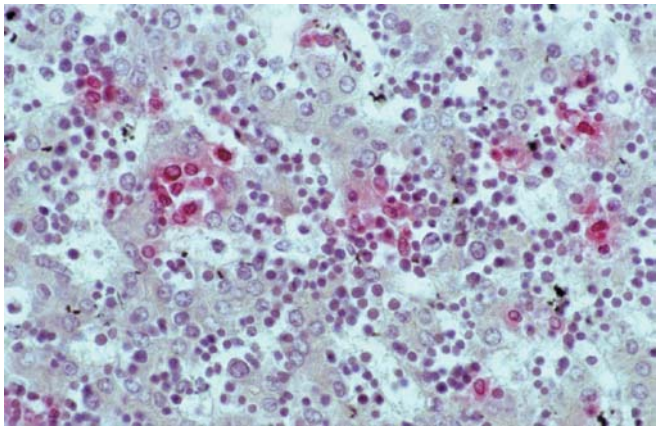

Fig. 2 Extramedullar myelopoiesis in a fetus of 18 weeks of gestation with chorioamnionitis. Positively stained cells represent a clustering and confluent pattern in the fetal liver (naphtol-ASD-chloracetate esterase reaction staining)

In cases with chorioamnionitis, colloidal iron, detected by Berliner Blau staining, was mainly seen ring-like

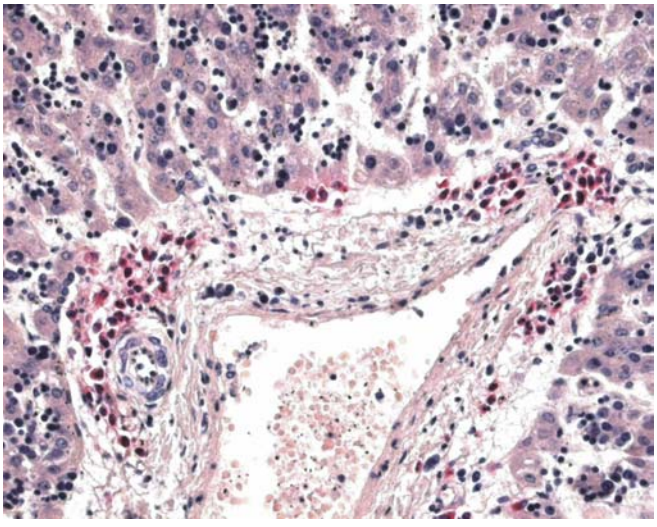

Fig. 3 Extramedullar myelopoiesis in a fetus of 20 weeks of gestation without chorioamnionitis. Positively stained leukocytes are restricted on the peripheral region of the portal area without a clustering between the hepatocytes (naphtol-ASD-chloracetate esterase reaction staining)

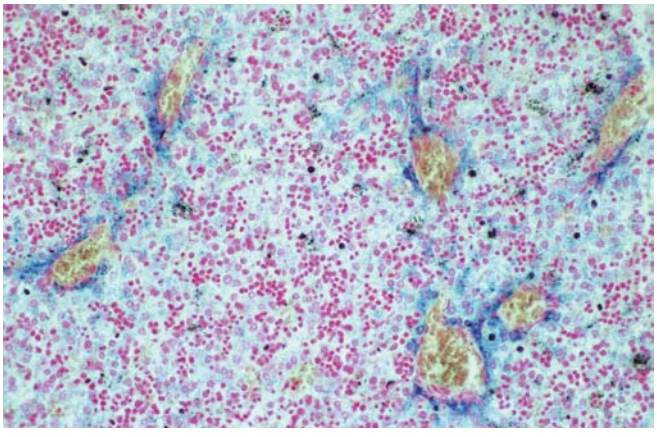

Fig. 4 Intrahepatic iron in a case with chorioamnionitis. Note the strong staining encircling the central veins in a fetus of the 23rd week of gestation (Berliner Blau staining)

around central veins (28.3% versus 3.1%; Fig. 4). As shown in Table 3, in the controls, iron was predominantly located in the portal fields (25.0% versus 5.1%; Fig. 5). There was a positive shift between the histologically confirmed severity of chorioamnionitis and iron-positive

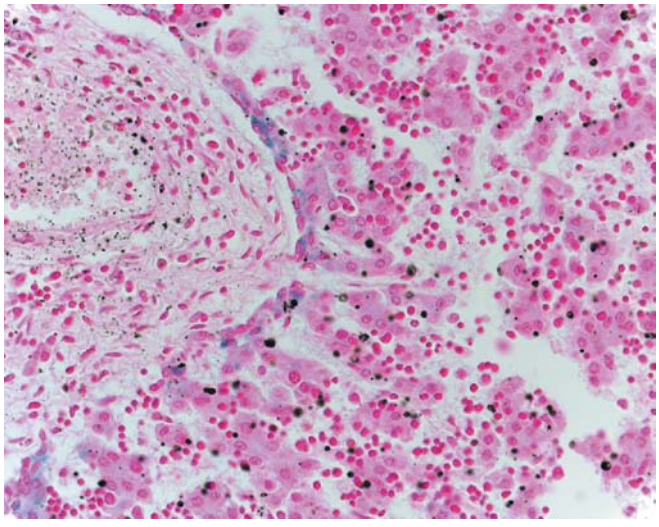

Fig. 5 Intrahepatic iron in a case without chorioamnionitis. Only moderate staining pattern around the periportal area in a fetus of 19 weeks of gestation is visible (Berliner Blau staining)

cases with isolated perivenous location (minimal placental leukocytic infiltration: 12.5% versus complete placental infiltration: 54.5%). The data indicate that there was a shift in iron staining from periportal to central perivenous location in fetal hepatic tissue in cases with chorioamnionitis.

Concerning the total hematopoiesis, there was a more diffuse distribution at the entire liver in cases complicated by chorioamnionitis (94.9% versus 84.4%, Table 4), but without statistical significance. However, focusing on portal fields, there were differences. Two-thirds or whole involvement was predominant in cases with chorioamnionitis (41.0% versus 9.1%), whereas involvement of the outer third was mainly detected in non-infectious-caused abortions (68.8% versus 43.6%, P=0.03). As observed in myelopoiesis, a clustering of erythropoietic cells is more often seen in cases caused by chorioamnionitis (69.2% versus 56.2%), which indicates an increased erythropoiesis.

Under special conditions, other fetal organs can be involved in hematopoietic processes. Of the fetuses, 61.5% aborted by chorioamnionitis represented hematopoietic foci in lung, pancreas and adrenal glands, whereas only 15.6% of the control cases showed extramedullar hematopoiesis in organs such as kidneys or adrenal glands

Table 3 Intensity and distribution of intracytoplasmatic iron; Berliner Blau staining

Characteristics	Classification	Study group (n=39)		Control group (n=32)	
		n	%	n	%
Intensity of iron	Negative	16	41.0	8	25.0
	Slight	13	33.3	14	43.8
	Increased	10	25.7	10	31.2
Location of iron[a]	Periportal	2	5.1	8	25.0
	Perivenous	11	28.3	1	3.1
	Perivenous and periportal	10	25.6	15	46.9

[a] Excluding cases with a negative result of the Berliner Blau staining

Table 4 Intensity and location of hematopoiesis and erythropoiesis; hematoxylin and eosin staining

Characteristics	Classification	Study group (n=39)		Control group (n=32)	
		n	%	n	%
Hematopoiesis	Isolated	2	5.1	5	15.6
	Diffuse	37	94.9	27	84.4
Erythron	Isolated	12	30.8	14	43.8
	In groups/confluated	27	69.2	18	56.2
Infiltration of portal fields	Negative	6	15.4	7	21.9
	1/3[a]	17	43.6	22	68.8
	2/3 to complete	16	41.0	3	9.3

[a] Statistically significant (P=0.03)

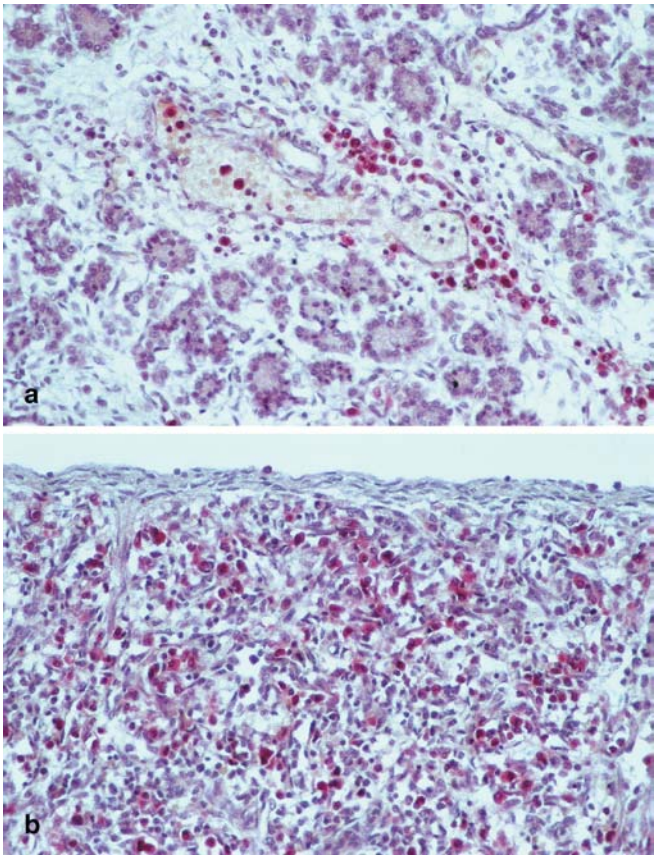

Fig. 6 Extramedullar myelopoiesis in a fetus of 21 weeks of gestation with chorioamnionitis. Detection of positively stained cells in the pancreas (**a**) and the spleen (**b**) with clustering (naphtol-ASD-chloracetate esterase reaction staining)

(P=0.0001). This represents a sixfold extension of fetal hematopoiesis in case of a chorioamnionitis (Fig. 6).

Discussion

Chorioamnionitis, as the leading cause for second trimester abortions, is responsible for 24%–44% of pregnancy failure [16, 19]. A standardized placental examination is common to verify the diagnosis of chorioamnionitis [21]. However, in some cases, the placenta is not submitted for histopathological examination, and it can be difficult or impossible to verify an inflammatory event as the possible causative agent for the abortion. Thus, the possibility of diagnosing a chorioamnionitis from fetal autopsy alone is important.

During the last years, many studies were focused on the fetal inflammatory response syndrome (FIRS) following a chorioamnionitis. This condition is characterized by an elevation of proinflammatory cytokines in fetal circulation with a multisystemic organ involvement [14, 23]. The inflammatory process that is responsible for the maternal syndrome during a chorioamnionitis frequently involves the fetus, proved by an elevated fetal plasma-interleukin-6 (IL-6) in those cases [4]. Pacora et al. [14] demonstrated that fetuses with a plasma-interleukin-6 (IL-6)>11 pg/ml had significantly higher rates of funisitis and/or chorionic vasculitis than fetuses with a plasma-IL-6<11 pg/ml, meaning that the histological manifestation of FIRS is a funisitis and/or chorionic vasculitis.

In the presented study, the majority of women with an inflammatory abortion showed clinical signs of an amnion infection syndrome (77.0%). Increased axillary temperature (>37.5°C) and a leukocytosis (>16.0 Gpt/l) were significant predictors for a chorioamnionitis-induced abortion (P>0.0008). Only 5.1% of the study cases had no clinical symptoms prior to abortion, independently of the extension of chorioamnionitis. Although Smulian et al. [27] took more clinical symptoms, such as uterine tenderness or fetal tachycardia, into account, they described 12.8% clinically silent cases of infectious second trimester abortions.

Concerning the histopathological examination of the placenta in the case of a chorioamnionitis, Vogel et al. [32] differed an isolated maternal reaction as minimal (amnionitis) and in part a partial granulocytic placental infiltration (amnionitis and chorionic vasculitis) from a fetomaternal reaction, meaning the other cases of partial and all complete infiltrations (amnion, chorion and umbilical cord). With respect to the gestational age, Benirschke and Kaufmann reported that neutrophils of placental inflammatory infiltrates prior to the 20th week of gestation are of maternal origin [1]. Interestingly, we saw leukocytic infiltrates in all three placental compartments (amnion, chorionic plate and umbilical cord) in accordance with a fetomaternal reaction exclusively in abortions between 20 weeks and 23 weeks of gestation (28.2%). However, 50% of the miscarriages caused by a chorioamnionitis with a partial or minimal inflammatory

placental involvement did not reach the 20th week of gestation.

In addition to the placental changes, it is common to find aspirated polymorphonuclear leukocytes in the lung, stomach or internal ear of the fetus in chorioamnionitis-induced abortions. However, in contrast to intrapulmonal leukocytes, only the intraalveolar inflammatory accumulation can be seen as a potent sign for the fetal involvement in the infection, which occurs mostly late in the process [1, 2].

During the mid-trimester of gestation, extramedullar hematopoietic activity is predominantly located in the hepatic tissue [20]. Without infection, liver shows a distinct distribution of the hematopoiesis with erythropoiesis mainly located within the sinusoids and granulopoiesis primarily occurring within the portal fields [24, 28]. While other maternal infections such as pyelonephritis or acute viral infection do not affect the fetal granulopoiesis, chorioamnionitis causes strong changes in fetal hematopoiesis [28, 29]. In the present study, clustering of leukocytes in the study group was significantly more frequent than among the cases without infection (P=0.001). In accordance with other papers [28], the majority of our study cases showed as an adaptive reaction to the chorioamnionitis granulocytes both in the sinusoids and portal fields (74.4% versus 12.4%). Confirming this hypothesis, the quantity of myelocytes of the controls was lower with a predominant location in the portal triads (50.0% versus 7.7%). The augmentation of extramedullary granulopoiesis further supports the assumption that granulocytes within the placental infiltrates are at least, in part, fetally derived [28].

In addition to the myelopoietic changes under infectious conditions, we observed a slight increase of the total hematopoiesis (94.9% versus 84.4%) and an adequate but not significant rise of the hepatical erythropoiesis (69.2% versus 56.2%). Unlike our observations, Stallmach and Karolyi [28] reported a reduced erythropoiesis by 20% and decreased hematopoiesis by 30% in all hepatic compartments in the case of a placental infection. However, Leikin et al. [12] described a significantly increased nucleated red blood cell count in 359 preterm infants in presence of a histological chorioamnionitis as a direct erythropoietic response in the fetus. Under normal conditions, erythropoiesis is restricted to the sinusoids of hepatic mesenchyme [28]. Confirming this distribution, erythropoiesis in most of our control cases was placed in the sinusoids and the outer third of portal fields (68.8% versus 43.6%, P=0.03). In case of a chorioamnionitis, erythropoietic activity was often expanded over the whole portal field and the sinusoids (41.0% versus 9.3%).

Moreover, the intracytoplasmatical storage of iron in the fetal liver was examined. Under normal conditions, the hepatic iron concentration and total iron storage shows no correlation with the gestational age [5]. We proved an intracytoplasmatical iron storing in fetuses aborted due to a chorioamnionitis less often as under normal conditions (59.0% versus 75.0%). A possible explanation could be an increased consumption of iron by erythropoiesis in the beginning of an infectious process. However, this observation could be a result of the limited sample size. Yet, in contrast to the quantity, a chorioamnionitis had major influence on the distribution of intracytoplasmatical iron. The isolated perivenous location of iron went nearly exclusively ahead with a placental infection. This phenomenon was more often observed with an increasing severity of a chorioamnionitis (28.3% versus 3.1%). In the majority of control cases, iron was placed both around the central veins and the portal fields (46.9% versus 25.6%) or isolated in the portal fields (25.0% versus 5.1%). According to our observations, Faa et al. [5] described an irregular acinar distribution of hepatic iron storing with a preferential periportal localization in stillborns without causative infectious events. Therefore, it can be suspected that isolated central perivenously placed iron can be used as a histomorphological criterion to diagnose a chorioamnionitis.

In addition to placental inflammations, other fetal or maternal conditions seem to have influence on the demand, transfer and storing of iron in the fetus. During a diabetic pregnancy, fetal hyperinsulinemia and hypoxia cause an increased fetal hemoglobin synthesis. This phenomenon is followed by a raised iron demand and mobilization, a reduced serum ferritin concentration and an increased expression of placental transferrin receptors to support the augmented erythropoiesis [17, 18]. Other authors observed a significant decreased total and highly sialylated transferrin as well as a reduced synthesis of placental transferrin receptors in cases of severe preeclampsia with negative impact on intrauterine growth [10, 33]. In malformed fetuses with bilateral renal agenesis (Potter's syndrome), the concentration of hepatic iron was only 26% of the control cases [7]. None of the study or control cases in our examination was affected by one of the discussed conditions.

Roge and Henriques [22] reported a fetal pneumonia as an additional diagnostic sign for detecting a chorioamnionitis in 32.0% (8/25) of cases. Schmidt et al. [25] observed an increased expression of interleukin-8-mRNA in addition to a leukocytic infiltration of the lung tissue as an intrauterine inflammatory fetal response. In our examination, more than half of the study cases represented an intrapulmonary aspiration of infected amnion fluid (53.9%). In addition to this finding, it should be considered that an intraalveolar fetal leukocytosis can be absent, even in cases with severe chorioamnionitis, if there was an long-standing anhydramnios.

Under physiological conditions, the fetal hematopoiesis is restricted to the liver and spleen during the second trimester of gestation [20]. We observed a significant extended hematopoiesis to the lung, pancreas and adrenal glands after a chorioamnionitis in 61.5% of study cases (P=0.0001). After the infection of amnion fluid, the inflammation reaches the fetus either directly from the placenta via umbilical vein or from the amnion fluid over the pulmonary tract or from the intestine by swallowing the amnion fluid via the portal vein [1, 28]. This could be a possible explanation for the selection of involved or-

gans. Just 15.6% of our control cases showed an expanded hematopoiesis, concerning kidneys or adrenal glands. The reasons for an extended hematopoiesis of fetuses without any inflammative conditions have not been elucidated yet.

We conclude that a chorioamnionitis causes significant changes of the fetal extramedullar hematopoiesis and intracytoplasmatic iron storing, indicating a fetal cellulary response to this inflammatory event. Morphological features of the fetal liver in cases with chorioamnionitis might be helpful in suspicion of infectious diseases, especially when placental tissue is not available for examination and in cases with long standing anhydramnios, in which pulmonary changes, indicating an AIS, are missed.

References

1. Benirschke K, Kaufmann P (2000) Infectious diseases. In: Benirschke K, Kaufmann P (eds) Pathology of the human placenta, 4th edn. Springer, New York, pp 591–685
2. Blanc WA (1961) Pathways of fetal and early neonatal infection: viral placentitis, bacterial and fungal chorioamnionitis. J Pediatr 59:473–496
3. Bove KE, The Autopsy Committee of the College of American Pathologists (1997) Practice guidelines for autopsy pathology. Arch Pathol Lab Med 121:368–376
4. Chaiworapongsa T, Romero R, Kim JC, Kim YM, Blackwell SC, Yoon BH, Gomez R (2002) Evidence for fetal involvement in the process of clinical chorioamnionitis. Am J Obstet Gynecol 186:1178–1182
5. Faa G, Sciot R, Farci AM, Callea F, Ambu R, Congui T, van Eyken P, Cappai G, Marras A, Costa V et al (1994) Iron concentration and distribution in the newborn liver. Liver 14:193–199
6. Gaillard DA, Paradis P, Lallemand AV, Vernet VM, Carquin JS, Chippaux CG, Visseaux-Coletto BJ (1993) Spontaneous abortions during the second trimester of gestation. Arch Pathol Lab Med 117:1022–1026
7. Georgieff MK, Petry CD, Wobken JD, Oyer CE (1996) Liver and brain iron deficiency in newborn infants with bilateral renal agenesis (Potter's syndrome). Pediatr Pathol Lab Med 16:509–519
8. Godin IE, Garcia-Porrero JA, Coutinho A, Dieterlen-Lievre LF, Marcos MA (1993) Para-aortic splanchnopleura from early mouse embryos contains Bla cell progenitors. Nature 364:67–70
9. Goldenberg RL, Hauth JC, Andrews WW (2000) Intrauterine infection and preterm delivery. NEJM 342:1500–1507
10. Khatun R, Wu Y, Kanenishi K, Ueno M, Tanaka S, Hata T, Sakamoto H (2003) Immunohistochemical study of transferrin receptor expression in the placenta of pre-eclamptic pregnancy. Placenta 24:870–876
11. Lahra MM, Jeffery HE (2004) A fetal response to chorioamnionitis is associated with early survival after preterm birth. Am J Obstet Gynecol 190:147–151
12. Leikin E, Garry D, Visintainer P, Verma U, Tejani N (1997) Correlation of neonatal nucleated red blood cell counts in preterm infants with histological chorioamnionitis. Am J Obstet Gynecol 177:27–30
13. Medvinsky AL, Dzierzak E (1996) Definitive hematopoiesis is autonomously initiated by the AGM region. Cell 86:897–906
14. Pacora P, Chaiworapongsa T, Maymon E, Kim YM, Gomez R, Yoon BH, Ghezzi F, Berry SM, Qureshi F, Jacques SM, Kim JC, Kadar N, Romero R (2002) Funisitis and chorionic vasculitis: the histological counterpart of the fetal inflammatory response syndrome. J Mat Fet Neonat Med 11:18–25
15. Pankuch GA, Cherouny PH, Botti JJ, Appelbaum PC (1989) Amniotic fluid leukotaxis assay as an early indicator of chorioamnionitis. Am J Obstet Gynecol 161:802–807
16. Petersson K, Bremme K, Bottinga R, Hofsjö A, Hulthen-Varli I, Kublickas M, Norman M, Papadogiannakis N, Wanggren K, Wolff K (2002) Diagnostic evaluation of intrauterine fetal deaths in Stockholm 1998–1999 Acta Obstet Gynecol Scand 81:284–292
17. Petry CD, Eaton MA, Wobken JD, Mills MM, Johnson DE, Georgieff MK (1992) Iron deficiency of liver, heart and brain in newborn infants of diabetic mothers. J Pediatr 121:109–114
18. Petry CD, Wobken JD, McKay H, Eaton MA, Seybold VS, Johnson DE, Georgieff MK (1994) Placental transferrin receptor in diabetic pregnancies with increased fetal iron demand. Am J Physiol 267:E507–E514
19. Pfisterer C, Horn LC, Faber R (2003) Aetiologie des Spontanabortes im 2. Trimenon—Ein Vergleich klinischer und pathologisch—anatomischer Befunde. Geburtsh Frauenheilk 63:248–254
20. Rahilly OR, Müller F (1999) Die Leber. In: Rahilly OR, Müller F (eds) Embryologie und Teratologie des Menschen. Verlag Hans Huber, Bern, pp 142–154
21. Redline RW, Faye-Petersen O, Heller D, Qureshi F, Savell V, Vogler C (2003) Amniotic infection syndrome: nosology and reproducibility of placental reaction patterns. Pediatr Dev Pathol 6:435–438
22. Roge HR, Henriques U (1992) Fetal and perinatal infections. A consecutive study. Path Res Pract 188:135–140
23. Romero R, Gomez R, Ghezzi F, Yoon BH, Mazor M, Edwin SS, Berry SM (1998) A fetal systemic inflammatory response is followed by the spontaneous onset of preterm parturition. Am J Obstet Gynecol 179:186–193
24. Rushton DI (1993) Liver and gall bladder. In: Keeling JW (ed) Fetal and neonatal pathology, 2nd edn. Springer, London, pp 373–401
25. Schmidt B, Cao L, Mackensen-Haen S, Kendziorra H, Klingel K, Speer CP (2001) Chorioamnionitis and inflammation of the fetal lung. Am J Obstet Gynecol 185:173–177
26. Sebire J, Goldin RD, Regan N (2001) Histological chorioamnionitis in relation to clinical presentation at 14–40 weeks of gestation. J Obstet Gynecol 21:242–245
27. Smulian JC, Shen-Schwarz S, Vintzileos AM, Lake MF, Anath CV (1999) Clinical chorioamnionitis and histologic placental inflammation. Obstet Gynecol 94:1000–1005
28. Stallmach T, Karolyi L (1994) Augmentation of fetal granulopoiesis with chorioamnionitis during the second trimester of gestation. Hum Pathol 25:244–247
29. Tamiolakis D, Kotini A, Jivannakis T, Papadopoulos N (2003) Induction of hepatic granulopoiesis due to chorioamnionitis during second trimester of development. Eur J Obstet Gynecol 110:164–168
30. The Royal College of Pathologists (1993) Guidelines for postmortem reports. The Royal College of Pathologists, London
31. Vogel M (1996) Atlas der morphologischen Plazentadiagnostik, 2nd edn. Springer, Berlin Heidelberg New York, pp 40–197
32. Vogel M, Lott E, Dudenhausen JW (1984) Korrelation von morphologischem Stadium und klinischem Symptom einer Amnionentzündung. In: Dudenhausen JW, Saling E (eds) Perinatale Medizin X. Thieme, Stuttgart, pp 266–267
33. Wu Y, Sakamoto H, Kanenishi K, Li K, Khatun R, Hata T (2003) Transferrin microheterogeneity in pregnancies with preeclampsia. Clin Chim Acta 332:103–110

Virchows Arch (2005) 446:157–163
DOI 10.1007/s00428-004-1135-9

ORIGINAL ARTICLE

J. F. Graadt van Roggen · J. A. M. van Unnik · I. H. Briaire-de Bruijn · P. C. W. Hogendoorn

Aggressive angiomyxoma: a clinicopathological and immunohistochemical study of 11 cases with long-term follow-up

Received: 23 June 2004 / Accepted: 7 September 2004 / Published online: 3 November 2004
© Springer-Verlag 2004

Abstract *Aims:* To report the clinicopathological and immunohistochemical features and longer term biological behaviour of aggressive angiomyxoma, an uncommon mesenchymal neoplasm occurring predominantly in the pelvi-perineal region of adults. Using immunohistochemistry, possible overexpression of CDK4 and MDM2 was analysed, which might point to (cyto)genetic alteration(s) in chromosome region 12q13–15, an area reported to be altered in this tumour entity. *Methods and results:* Cases (n=11) of aggressive angiomyxoma were retrieved from the consultation files of the Comprehensive Cancer Centre of the Middle Netherlands (IKMN) panel for soft tissue tumours. Clinical and follow-up information were obtained, and immunohistochemical analysis was performed using antibodies directed against vimentin, cytokeratin AE1/AE3, desmin, α-smooth-muscle actin, CD34, S-100 protein, oestrogen receptors, CDK4 and MDM2. Five patients were female (age range 24–47 years; median 39 years), and six patients were male (age range 36–69 years; median 44.5 years). Of 11 cases, 10 arose in the pelvi-perineal area and 1 arose in the abdominal cavity in close relation to the bladder. Morphology was consistent with previous reports of this entity. Immunohistochemically, 8 of 11 cases were desmin positive (5 of 5 positive in females; 3 of 6 positive in males), 6 of 11 cases were positive for α-smooth-muscle actin, 5 of 11 cases were CD34 positive, 11 of 11 cases, irrespective of gender, were positive for oestrogen receptors and 3 of 11 cases were positive for cytokeratin AE1/AE3. Strong, diffuse nuclear positivity for CDK4 expression was present in all 6 cases tested, while only 1 of 11 cases tested for MDM2 showed weak focal positivity. Clinical follow-up in all cases (range 1–216 months; median 72 months) showed one local recurrence (9%) after 36 months. No metastases or tumour-related deaths were noted. *Conclusions:* The sex distribution of cases reported in this study was roughly equal, in contrast to previous reports emphasising the predominance of this tumour in females. Our study confirms the local aggressive nature of aggressive angiomyxoma, although our local recurrence rate is lower than previous reports (9% versus 36–72%); no metastases and/or disease-related patient deaths were documented. All cases arising in females were positive for desmin, while three of the six cases arising in males were negative for desmin, supporting previous findings and indicating that the lesion may be somewhat different in males. The strong diffuse positivity for CDK4 in all six cases tested goes some way in implicating CDK4, either directly or indirectly, in tumourigenesis. The negative immunostaining for MDM2 would argue against functional amplification of this gene.

Keywords Soft tissue tumour · Sarcoma · Aggressive angiomyxoma · Myxoma · Cytogenetics

J. F. G. van Roggen · I. H. Briaire-de Bruijn · P. C. W. Hogendoorn (✉)
Department of Pathology,
Leiden University Medical Centre,
Building I, L1-Q, P.O. Box 9600, 2300RC Leiden, The Netherlands
e-mail: p.c.w.hogendoorn@lumc.nl
Tel.: +31-71-5266639
Fax: +31-71-5248158

J. F. G. van Roggen
Department of Pathology,
Diaconessenhuis, Leiden, The Netherlands

J. A. M. van Unnik
Comprehensive Cancer Centre of the Middle Netherlands,
Utrecht, The Netherlands

Introduction

Aggressive angiomyxoma is an uncommon, variably myxoid, mesenchymal neoplasm, occurring predominantly in the pelvi-perineal region of adults, with a reported female to male ratio of approximately 6:1 [1, 4, 7, 11, 17, 18]. The lesion appears to behave in a locally aggressive manner, with tumour recurrence often occurring years after the primary excision [1, 4, 7, 11, 17, 18]. Reported rates of local recurrence in larger series and follow-up reports vary from 36% to 72% [1, 4, 7, 11, 17, 18]. While aggressive angiomyxoma is generally regarded

as a benign lesion, two purported cases with metastases and associated tumour-related death have been documented to date [3, 16].

The histogenesis of this tumour remains enigmatic. Recent cytogenetic and molecular studies of aggressive angiomyxoma have identified a variety of genetic alterations, including chromosomal translocations, involving the long arm of chromosome 12, particularly in the chromosomal region 12q13–15 [2, 10, 12, 13, 14]. This genetic region appears to contain a number of genes implicated in the tumourigenesis of a number of mesenchymal tumours, including aggressive angiomyxoma [9]. *HMGIC*, a gene encoding a member of the high-mobility group of proteins, appears to be involved, possibly by amplification or translocation in most cases, although the molecular mechanisms by which the genetic heterogeneity in tumourigenesis might be explained remain elusive.

Using detailed long-term clinical follow-up information, we have described the clinicopathological features of 11 cases of aggressive angiomyxoma, particularly with respect to their biological behaviour. Additionally, using immunohistochemistry to assay protein expression—and thereby determining possible alteration in gene expression—of *MDM2* and *CDK4*, genes flanking the chromosomal region 12q13–15 and spanning the *HMGIC* locus, we have attempted to ascertain whether possible genetic alterations (e.g. gene amplification) might be present in this region.

Materials and methods

Cases (n=11) of aggressive angiomyxoma were retrieved from the consultation files of the Comprehensive Cancer Centre of the Middle Netherlands (IKMN) panel for soft tissue tumours, under the auspices of one of the authors (J.A.M.vU). Additional clinical and follow-up information was obtained from the original submitting pathologist following consultation with the treating physician (see Acknowledgements).

Representative formalin-fixed, paraffin-embedded material and/or unstained slides were available for routine haematoxylin and eosin (H&E) and alcian blue staining and immunohistochemical analysis in all cases. No frozen material or cell culture material was available for ancillary (cyto)genetic study.

H&E sections 4-μm thick were collectively re-examined in each case by the three pathologists involved in the paper (J.F.G.vR, J.A.M.vU, P.C.W.H). Staining for alcian blue was performed at pH 2.5. All immunohistochemical stains were performed using the avidin-biotin-peroxidase complex method. The antibodies, their sources, antigen retrieval method and dilutions used are documented in Table 1. All cases (n=11) were stained for cytokeratin AE1/AE3, desmin, α-smooth-muscle actin, S-100 protein, CD34, MDM2, vimentin and oestrogen receptor expression. Of 11 cases, 6 were screened for CDK4 expression. Appropriate positive and negative controls were used throughout.

In scoring the immunohistochemical stains, lesional positivity of more or less than 25% of the cells stained per mm^2 was em-

Table 1 Antibodies used for immunohistochemical analysis

Antibody	Clone	Dilution	Antigen retrieval	Source
Vimentin	–	1:2000	None	Eurodiagnostika
Cytokeratin AE1/AE3	–	1:4000	Citrate pretreatment	Chemicon International
Desmin	33	1:400	None	Sanbio
CD34	Qbend10	1:800	None	Neomarkers AL
Smooth-muscle actin	ASM-1	1:2000	None	Progen Immuno Diagnostika
S-100 protein	–	1:8000	None	Dako
MDM 2	–	1:400	Citrate pretreatment	Neomarkers AL
CDK4	–	1:10	Ethylenediaminetetraacetate pretreatment	Transduction lab AL
Oestrogen receptor	1D5	1:200	Citrate pretreatment	Dako

Table 2 Clinical details of 11 cases of aggressive angiomyxoma. *NED* no evidence of disease, *LR* local recurrence

Patient	Sex	Age, years	Site	Size, cm	Primary excision	Duration follow-up, months	Follow-up
AM 03	Male	57	Scrotum	5	Wide excision	72	NED
AM 04	Male	36	Left inguinal area	9.5	Intralesional	72	NED
AM 05	Male	44	Right epididymis	8	Intralesional	12	NED
AM 06	Female	39	Vulva	17	Intralesional	84	NED
AM 07	Female	31	Anterior abdominal wall/genital area	7	Intralesional	50	NED
AM 08	Female	39	Ligamentum latum	20	Intralesional	216	NED
AM 10	Male	38	Perineum	5	Intralesional	144	NED
AM 11	Female	24	Left vulva	5	Intralesional	48	LR (36 months), wide excision, NED 12 months later
AM 12	Female	47	Vagina	10	Intralesional	144	NED
AM 13	Male	69	Testis	6	Wide excision	1	Died, unrelated causes
AM 14	Male	45	Anterior to bladder: cavum retzii	15	Intralesional	72	NED

pirically used to distinguish between weak and stronger expression per case. The mitotic rate was expressed as the number of mitoses in 10 consecutive high-power fields (HPF; 1 HPF=0.159 mm^2 on the microscope used), counted in the most cellular areas.

Results

Clinical findings

The clinical features of the lesions are summarised in Table 2. The study group comprised 6 males (age range

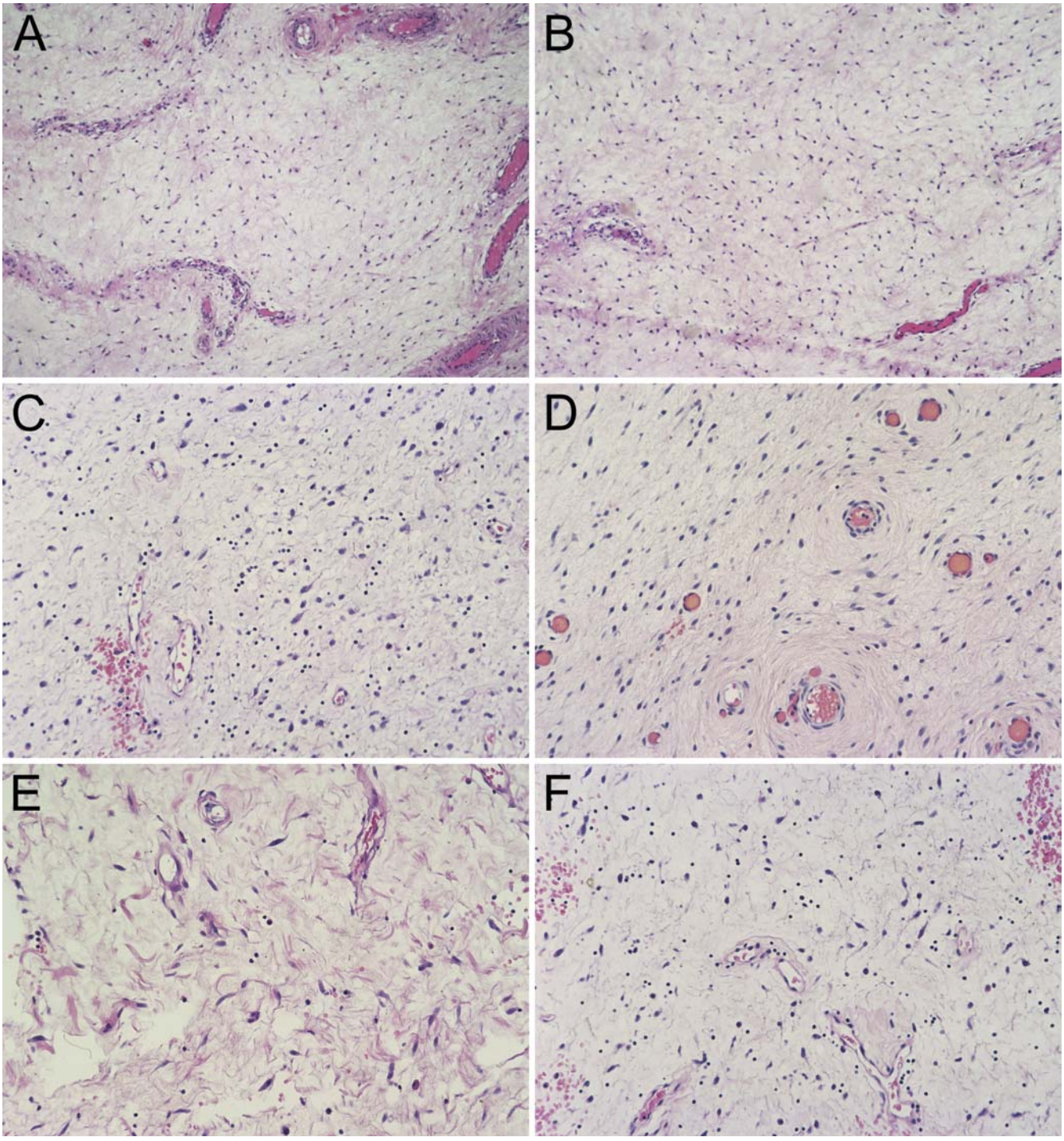

Fig. 1A–F The typical histological features of aggressive angiomyxoma. Lesions were composed of spindle-shaped cells with little or no nuclear polymorphism and variably elongated cytoplasm, set in a muco-myxoid stroma. Short bundles of spindle-shaped cells were occasionally present, often near, but not in continuity with vessels. Vascularity was variably composed of delicate to more hyalinised vessels (haematoxylin and eosin, **A** and **B** magnification ×100; **C**–**F** magnification ×200)

Table 3 Immunohistochemical data in 11 cases of aggressive angiomyxoma

Antigen/antibody	Number positive/number tested	Number positive/number tested	Total number cells positive/ number tested
	<25% cells positive/mm^2	>25% cells positive/mm^2	
Desmin	1/11	7/11	8/11
Smooth-muscle actin	3/11	3/11	6/11
CD34	2/11	3/11	5/11
Cytokeratin AE1/AE3	2/11	1/11	3/11
Vimentin	3/11	7/11	10/11
S-100 protein	0/11	0/11	0/11
Oestrogen receptor	2/11	9/11	11/11
MDM2	0/11	1/11	1/11
CDK4	0/6	6/6	6/6

36–69 years; median 44.5 years) and 5 females (age range 24–47 years; median 39 years); age range for the whole group was 24–69 years (median 39 years). All cases, except one (AM 14), were located in the soft tissues of pelvi-perineal area. Case AM 14 presented as a mass lesion within the pelvic cavity, in intimate association with the bladder. Specific details concerning clinical presentation were not available. Primary surgical excision was performed in all 11 cases. Due to the anatomic location, wide excision was only achieved in 2 cases (AM 03, AM 13). Surgical excision in the remaining 9 cases was intralesional (AM 04–08, AM 10–12, AM 14). It was not possible to quantitatively ascertain the residual tumour bulk following primary surgery in those cases with intralesional excision.

Follow-up information was available in all 11 cases (Table 2), with a median interval of 72 months (range 1–216 months). One of the two patients who underwent wide local excision had no evidence of disease 72 months after the initial surgery (AM 03); the other patient (AM 13) died 1 month after the surgical excision of causes unrelated to the tumour or the surgical procedure. The follow-up interval available for seven patients (AM 04, AM 06–08, AM 10, AM 12, AM 14) with primary intralesional tumour resection and who were free of disease at the last medical visit ranged from 50 months to 216 months (median 84 months). One patient with intralesional excision of the primary tumour (AM 11) developed a local recurrence 36 months after the initial surgery. The recurrence was excised with free margins, and the patient was disease free 12 months later (last medical visit). None of the patients developed metastases. There were no tumour-related deaths.

Pathological findings

Gross features

Tumours were unencapsulated and generally poorly circumscribed, varying in diametre from 5 cm to 20 cm (median size 8 cm) (Table 2); cut surfaces were variably mucoid.

Microscopic features

On microscopic examination, the tumours were generally composed of a uniform population of small spindle-shaped cells with ovaliform nuclei and poorly demarcated cytoplasm, set in a variably myxoid and collagenous stroma (Fig. 1A–F). Nuclear atypia was not present, and no mitoses were seen. Lesional cellularity was low to moderate; focally, more cellular foci were occasionally present. A single case had a more reticular architecture. The vascular architecture was variable, consisting of capillaries and larger vessels dispersed throughout the lesion focally, with perivascular hyalinisation. All tumours were poorly circumscribed and exhibited infiltration in the adjacent soft tissue. In the majority of cases, delicate bundles of smooth muscle could be identified. The smooth-muscle bundles were often near vascular structures but did not appear to arise from these vessels. Those lesions stained with alcian blue (pH 2.5) demonstrated variable stromal positivity.

Immunohistochemical features

The immunohistochemical data are summarised in Table 3. All 6 cases tested exhibited variably strong diffuse positivity for CDK4 (Fig. 2A), while only a single case out of 11 tested demonstrated focal weak expression for MDM2. Desmin was positive in the majority of cases (8 of 11). In 2 cases, 10–20% of lesional cells were positive, while, in the remaining cases, lesional positivity was more diffuse (Fig. 2B). Desmin was not expressed in 3 cases. All tumours demonstrated positivity for oestrogen receptors (Fig. 2C). Variable positivity was seen with the other markers used (Table 3); S-100 protein expression was absent in all cases.

Discussion

Myxoid tumours of soft tissue encompass a heterogeneous group of lesions characterised by a variable abundance of extracellular mucoid (myxoid) matrix. The predominant extracellular mucosubstances in soft tissue tumours are hyaluronic acid, keratan sulphate and chon-

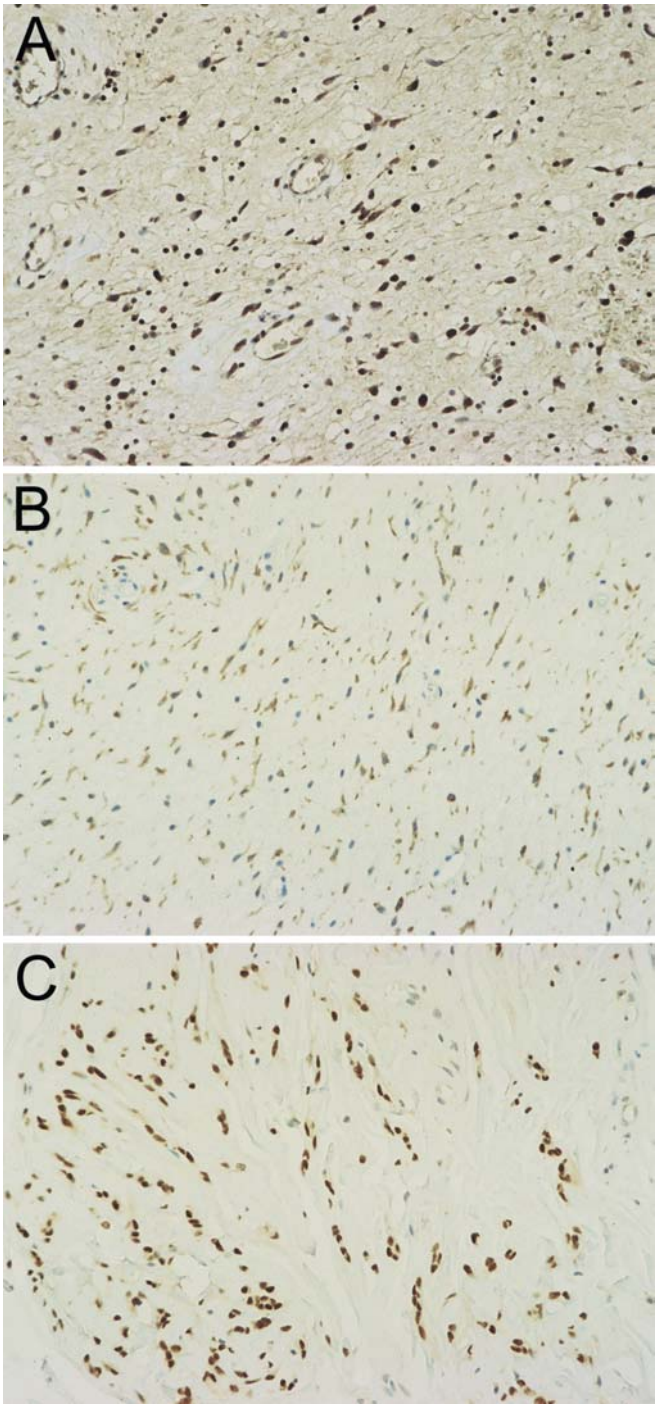

Fig. 2A–C Typical nuclear CDK4 (**A**), cytoplasmic desmin (**B**) and nuclear oestrogen (**C**) immunopositivity (magnification ×200)

droitin sulphate. An increase in the extracellular matrix, relative to the cellular component, accounts for the mucoid/myxoid lesional character and is clearly demonstrable using alcian blue staining. This group of tumours demonstrate significant variability in their biological behaviour and include benign lesions, tumours with a tendency to recur but not metastasise and frankly malignant neoplasms [6].

Steeper and Rosai first described nine cases of a distinctive, infiltrative, locally aggressive but non-metastasising fibro-myxoid soft tissue tumour arising in the pelvis and perineal area of young female patients, which they termed aggressive angiomyxoma [17]. In their series, local recurrences occurred as much as 14 years after the primary excision; no metastases were noted. Subsequent reports have validated their findings, confirmed the benign but local aggressiveness of this entity and documented the occurrence of aggressive angiomyxoma in males, albeit far less frequently [1, 4, 7, 11, 18]. The reported female to male ratio varies but is in the region of 6:1. Microscopically, the morphological spectrum has been well documented [1, 4, 7, 11, 17, 18]. Immunohistochemically, the vast majority of cases demonstrate positivity for desmin in the myoid bundles and/or stromal cells, while actins and CD34 may be variably positive. Oestrogen receptor expression is typically present [1, 4, 7, 11, 17, 18]. S-100 protein expression is absent.

Our series is interesting in that the sex distribution was roughly equal (six males, five females). This might represent consultation bias in that typical cases in young females are less likely to be submitted for second opinion, while cases occurring in males are more likely to be submitted for validation. Affected males (range 36–69 years, median age 44.5 years) tended to be somewhat older than females (range 24–47 years, median age 39 years), supporting previous observations [18]. Remarkably, despite the fact that the primary resection in the majority of our cases (9 of 11) was intralesional (with positive resection margins), our series was characterised by a very low rate of local recurrence (9%). None of the nine patients with positive margins following primary surgery received adjuvant radiotherapy, which might otherwise have accounted for this low recurrence rate. A single patient in our series (AM 11) developed a local recurrence 36 months after primary intralesional surgery. The remaining ten cases, with a median follow-up of 72 months (range 1–216 months), did not recur locally. This is in contrast to other series in which recurrence rates varied from 36% to 72% [4, 17]. We suspect that the true

Table 4 (Cytogenetic) alterations described in aggressive angiomyxoma

Author	Genetic alteration
Betz et al. [2]	46,XX,t(7;12)(q22–31;q13–14)
Horsman et al. [10]	45–50,XX,-12,-5,+der(5)t(5q15;?),-16,+der(16) t(5q;16q),-15,+der(15)t(15q13:?)(1–4),+/-frag.
Kazmierczak et al. [12]	46,XX,der(5)t(5;12)(q31;p11.2),der(12)t(5;12) (q31;p11)inv(12)(p11.2q15)
Kenny-Moynihan et al. [13]	45,X,-X
Nucci et al. [14]	46,XX,t(8;12)(p12;q15)

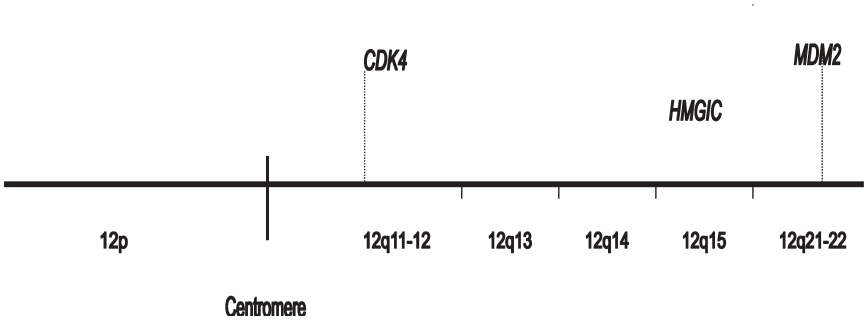

Fig. 3 Approximate cytogenetic location of *CDK4* and *MDM2* in the region 12q11–12q22, relative to *HMGIC* (not to scale)

recurrence rate for aggressive angiomyxoma probably lies somewhere between 9% and the previously reported recurrence rates for a number of reasons. Our cases were generally not routinely screened with radiological imaging studies at medical follow-up visits and relied on clinical symptomatology and physical examination to detect tumour recurrence. Due to the complex anatomic location of many of these lesions, physical examination alone is probably not sensitive enough to detect early recurrences. Additionally, it is clear from the literature that aggressive angiomyxoma is probably a slowly growing neoplasm with low mitotic activity and may, therefore, only present with local recurrence many years after the initial resection. Consequently, our follow-up period may still be too short to exclude the possibility of very late local recurrence.

Immunohistochemically, 8 of our 11 cases demonstrated significant desmin positivity in the myoid bundles and/or stromal cells. Interestingly, all the cases arising in females were positive for desmin, while 3 of the 6 cases arising in males were negative for desmin, supporting previous findings and indicating that the lesion may be somewhat different in males [18]. Cytokeratin positivity was present in 3 cases, a finding that has not been previously highlighted. This is nevertheless not surprising, since cytokeratin AE1/AE3 is a pankeratin, and numerous mesenchymal tumours are well known to express various cytokeratin subsets [8]. The remaining immunohistochemical findings were unremarkable with CD34 positivity present in 5 of 11 cases (45%) and smooth-muscle actin present in 6 of 11 cases (54%). Oestrogen receptor expression was present in all 11 cases, irrespective of gender, supporting previous reports [4].

Consequently, aggressive angiomyxoma is a mesenchymal neoplasm exhibiting infiltrative growth in the adjacent soft tissue and characterised by a potential for local recurrence, generally many years after the primary excision. Two cases with distant metastatic disease and associated patient death have been reported [3, 16]. While the morphological diagnostic accuracy in one case [16] is difficult to verify, the illustrative features provided in the other case [3] could well fit with metastatic aggressive angiomyxoma, underscoring the need for diligent clinical follow-up.

To date, the (cyto)genetic characteristics of five cases of aggressive angiomyxoma have been documented (Table 4) [2, 10, 12, 13, 14]. Three of these five cases demonstrate genetic aberrations involving, amongst others, the long arm of chromosome 12 and, in particular, the region 12q13–15, [2, 12, 14]; the fourth case exhibits monosomy of chromosome 12 [10]. 12q13–15 is a region that has been reported to be rearranged in numerous mesenchymal tumour entities, including, in addition to aggressive angiomyxoma, uterine leiomyomas and (atypical) lipomatous tumours [5, 9, 15]. This region contains a number of candidate genes, including *HMGI-C*, *CDK4*, *MDM2*, *SAS*, *GLI* and *GAD153* [5, 15]. *HMGI-C*, currently the candidate gene most favoured to be implicated in the pathobiology of aggressive angiomyxoma, encodes a DNA-binding protein belonging to the high mobility group family of proteins and is important for transcriptional regulation [9]. This gene appears to be intimately involved in the histogenesis of at least three cases of aggressive angiomyxoma (Table 4). *CDK4* (encoding a cyclin-dependent kinase) and *MDM2* ("murine double minute", encoding a zinc finger protein that contains a TP53 binding site) are two genes delineating the up- and downstream ends of 12q13–15 (Fig. 3) [5]. *CDK4* and *MDM2* are known to be amplified in a number of mesenchymal neoplasms. Type-D cyclins bind to and activate cyclin-dependent kinases such as *CDK4*. Consequently, amplification of *CDK4* could potentially promote cell-cycle progression. *MDM2* is known to inhibit wild-type TP53 activity, potentially promoting further amplification of *MDM2* and stimulating uncontrolled cellular proliferation [5]. All six cases in our series (AM 01–06) tested for immunohistochemical expression of CDK4 demonstrated strong diffuse nuclear positivity. This might support amplification (and consequently involvement) of *CDK4*. All cases in our series did not demonstrate immunohistochemical expression of MDM2, which would appear to make *MDM2* amplification in tumourigenesis of aggressive angiomyxoma unlikely. Unfortunately, fresh tumour tissue was not available for molecular genetic analysis, precluding a detailed analysis of this region (12q13–15) with regard to possible genetic alterations that might be present.

In this study, we have documented a morphological and immunohistochemical profile supporting previous reports. Interestingly, in contrast to previous studies, our series was characterised by a relatively low incidence of local recurrence (9%). Nevertheless, aggressive angiomyxoma has a definite potential for local, destructive recurrence, and follow-up of all cases is mandatory.

Strong immunohistochemical expression for CDK4 indicates its implication in tumourigenesis.

Acknowledgements The Comprehensive Cancer Centre of the Middle Netherlands, Utrecht, The Netherlands, under the auspices of one of the authors (J.A.M.vU) for the use of archival material. The following pathologists are thanked for their kind co-operation in providing the initial material and obtaining additional clinical follow-up information: J.R.J. Elbers, Saint Antonius Hospital, Nieuwegein; J.G. van den Tweel, University Medical Centre Utrecht, Utrecht; D.E. Israel, Lievensberg Hospital, Bergen op Zoom (two cases); C. van Heusden, Co-operative Hospitals East Groningen, Winschoten; U.G.J.M. van Haelst, Radboud Hospital/ Nijmegen Academic Medical Centre, Nijmegen; M.C.B.J.E. Tutein Nolthenius-Puylaert, Elkerliek Hospital, Helmond; R.J.M. Parren, Rijnstate Hospital, Arnhem; A.N. van Geel and M. Wijngaarden, Daniël den Hoed Kliniek, Rotterdam (four cases). All experiments performed for this paper comply with the laws as stipulated by the appropriate regularity authorities in the Netherlands.

References

1. Begin L, Clement P, Kirk M, Jothy S, McCaughey W, Ferenczy A (1985) Aggressive angiomyxoma of pelvic soft parts: a clinicopathologic study of nine cases. Hum Pathol 16:621–628
2. Betz J, Meloni A, U'ren L, Moore G, Sandberg A (1995) Cytogenetic findings in a case of angiomyxoma of the vaginal wall. Cancer Genet Cytogenet 84:157
3. Blandamura S, Cruz J, Vergara LF, Puerto IM, Ninfo V (2003) Aggressive angiomyxoma: a second case of metastasis with patient's death. Hum Pathol 34:1072–1074
4. Fetsch J, Laskin W, Lefkowitz M, Kindblom L, Meis-Kindblom J (1996) Aggressive angiomyxoma: a clinicopathologic study of 29 female patients. Cancer 78:79–90
5. Giesselson D, Hoglund M, Mertens F, Mitelman F, Mandahl N (1998) Chromosomal organization of amplified chromosome 12 sequences in mesenchymal tumors detected by fluorescence in situ hybridization. Genes Chromosomes Cancer 23:203–212
6. Graadt van Roggen JF, Hogendoorn PCW, Fletcher CDM (1999) Myxoid tumours of soft tissue. Histopathol 35:291–312
7. Granter S, Nucci M, Fletcher C (1997) Aggressive angiomyxoma: reappraisal of its relationship to angiomyofibroblastoma in a series of 16 cases. Histopathology 30:3–10
8. Hazelbag HM, Mooi WJ, Fleuren GJ, Hogendoorn PCW (1996) Chain-specific keratin profile of epithelioid soft-tissue sarcomas: an immunohistochemical study on synovial and epithelioid sarcoma. Appl Immunohistochem 4:176–183
9. Hes J (1998) Chromosomal translocations in benign tumors. The HMGI proteins. Am J Clin Pathol 109:251–261
10. Horsman D, Berean K, Salski C, Clement P (1991) Aggressive angiomyoma of the pelvis: cytogenetic findings in a single case. Cancer Genet Cytogenet 56:130–131
11. Iezzoni J, Fechner R, Wong L, Rosai J (1995) Aggressive angiomyxoma in males. A report of four cases. Am J Clin Pathol 104:391–396
12. Kazmierczak B, Dal Cin P, Wanschura S, Bartnitzke S, Van den Berghe H, Bullerdiek J (1998) Cloning and molecular characterization of part of a new gene fused to *HMGIC* in mesenchymal tumors. Am J Pathol 152:431–435
13. Kenny-Moynihan B, Hagen J, Richman B, McIntosh D, Bridge J (1996) Loss of an X chromosome in aggressive angiomyxoma of female soft parts: a case report. Cancer Genet Cytogenet 89:61–64
14. Nucci M, Weremowicz S, Neskey D, Sornberger K, Tallini G, Morton C et al (2001) Chromosomal translocation t(8; 12) induces aberrant *HMGIC* expression in aggressive angiomyoma of the vulva. Genes Chromosomes Cancer 32:172–176
15. Schoenmakers E, Wanschura S, Mols R, Bullerdiek J, Van den Berghe H, Van de Ven W (1995) Recurrent rearrangements in the high mobility group protein gene, HMGI-C, in benign mesenchymal tumours. Nat Genet 10:436–444
16. Siassi RM, Papadopoulos T, Matzel KE (1999) Metastasizing aggressive angiomyxoma. N Engl J Med 341:1772
17. Steeper TA, Rosai J (1987) Aggressive angiomyxoma of the female pelvis and perineum. Report of nine cases of a distinctive type of gynecologic soft-tissue neoplasm. Am J Surg Pathol 7:463–475
18. Tsang W, Chan J, Lee K, Fisher C, Fletcher C (1992) Aggressive angiomyxoma. A report of four cases occurring in men. Am J Surg Pathol 16:1059–1065

Virchows Arch (2005) 446:164–176
DOI 10.1007/s00428-004-1155-5

ORIGINAL ARTICLE

Yoshihide Fujigaki · Yoshinori Muranaka · Difei Sun · Tetsuo Goto · Hua Zhou · Masanori Sakakima · Hirotaka Fukasawa · Katsuhiko Yonemura · Tatsuo Yamamoto · Akira Hishida

Transient myofibroblast differentiation of interstitial fibroblastic cells relevant to tubular dilatation in uranyl acetate-induced acute renal failure in rats

Received: 1 July 2004 / Accepted: 6 October 2004 / Published online: 18 December 2004
© Springer-Verlag 2004

Abstract To investigate the mechanisms of myofibroblast differentiation of interstitial fibroblastic cells (FCs) in rats with uranyl acetate-induced acute renal failure (ARF), we examined the relationship between the expression of α-smooth muscle actin (α-SMA), myofibroblast phenotype and tubular dilatation as well as cell shape and adhesion of FCs. Peritubular α-SMA-positive myofibroblasts appeared after induction of ARF and extended along the damaged, dilated proximal tubules and then almost disappeared after proximal tubular recovery. The perimeter of proximal tubules correlated with fractional areas stained for α-SMA ($P<0.001$). Most α-SMA-positive cells did not incorporate [^{3}H]-thymidine, indicating a low proliferative activity. Transmission electron microscopy showed that FCs increasingly attached to the tubular basement membrane by elongated cytoplasm-containing microfilament bundles, which formed abundant adherens and gap junctions from day 4 to day 7. Scanning electron microscopy showed hypertrophic FCs covering large areas of tubules after induction of ARF. Administration of chlorpromazine, which can inhibit cytoskeletal movement, after induction of ARF partially inhibited myofibroblast differentiation of FCs immunohistochemically and morphologically and resulted in more dilated proximal tubules in concert with aggravation of renal dysfunction and inhibition of regenerative repair at day 4 than vehicle-administered rats. Our results indicate that mechanical tension, judged by tubular dilatation, may contribute to the induction of α-SMA phenotype with increased stress fiber formation and intercellular junctions in FCs to support damaged nephron structures by adjusting tensional homeostasis in rats with uranyl acetate-induced ARF.

Keywords Myofibroblast · α-Smooth muscle actin · Mechanical tension · Tubule · Acute renal failure

Y. Fujigaki (✉) · D. Sun · T. Goto · H. Zhou · M. Sakakima · H. Fukasawa · T. Yamamoto · A. Hishida
First Department of Medicine,
Hamamatsu University School of Medicine,
1-20-1 Handayama, 431-3192 Hamamatsu, Japan
e-mail: yf0516@hama-med.ac.jp
Tel.: +81-53-4352261
Fax: +81-53-4349447

Y. Muranaka
Research Equipment Center,
Hamamatsu University School of Medicine,
431-3192 Hamamatsu, Japan

K. Yonemura
Hemodialysis Unit,
Hamamatsu University School of Medicine,
431-3192 Hamamatsu, Japan

Introduction

Myofibroblasts are fibroblastic cells (FCs) that express α-smooth muscle actin (α-SMA), which is not expressed on fibroblasts in vivo [6, 27], and may well represent an intermediate state between fibroblasts and smooth muscle cells. Myofibroblasts display prominent cytoplasmic actin microfilaments (stress fiber), and they are connected to each other by adherens and gap junctions [6, 22, 23]. Stress fibers, which are thought to function as the contractile apparatus of non-muscle cells [4, 19, 26], consist of a highly organized array of thick contractile microfilament bundles that are formed by filamentous actin (F-actin) and actin-associated proteins [4]. Previous studies suggested that transforming growth factor-β, platelet-derived growth factor, and extracellular matrix, including cellular fibronectin, could transform fibroblasts to myofibroblasts [25]. It has been also reported that mechanical tension is crucial for differentiation and maintenance of the myofibroblast phenotype and that tissue contractility correlates with the expression of α-SMA both in vivo and in vitro [2, 11, 14, 29, 33].

We previously reported that after the induction of acute renal failure (ARF) by uranyl acetate in rats, interstitial α-SMA-positive myofibroblasts appeared around

the necrotic proximal tubules, developed along with the damaged proximal tubules, forming a network, and disappeared after the repair of proximal tubules [30]. We also demonstrated that the regeneration of tubules was inhibited by the suppression of the interstitial cellular response, including appearance of α-SMA-positive myofibroblasts by mycophenolate mofetil [31]. Thus, we assumed that myofibroblasts surrounding the denuded tubular basement membrane after the proximal tubular damage may originate from interstitial resident FCs [30] and act to protect the damaged nephron structures by providing contractility and resisting the stretching force, similar to the action of myofibroblasts in wound healing.

The present study was designed to determine the mechanisms and roles involved in the transient myofibroblast differentiation of the interstitial FCs in ARF. For this purpose, we examined the relationship between expression of α-SMA in FCs and dilatation of tubules (possible parameter of urinary flow-induced mechanical tension) in uranyl acetate-induced ARF in rats with or without chlorpromazine, which is known to inhibit cytoskeletal movement indirectly [18, 20, 24]. We also examined the morphological changes, mode of intercellular junctions, and cytoskeleton-associated proteins in FCs at light and electron microscopic levels.

Materials and methods

Induction of ARF

A total of 64 male Sprague-Dawley rats weighing 230–300 g (SLC Co. Shizuoka, Japan) were used in the present study. They received a single intravenous injection of 5 mg/kg of uranyl acetate, and 5 rats were sacrificed prior to and at 2, 4, 5, 7, 9, 15, and 21 days after uranyl acetate injection. Rats were anesthetized with intraperitoneal administration of pentobarbital sodium (30 mg/kg), then both kidneys were removed after a brief flush with phosphate-buffered saline (PBS). The right kidneys were bisected through the longitudinal axis, and one half of the kidney was fixed in 4% paraformaldehyde for histological examinations and another half was fixed in 2% glutaraldehyde for electron microscopy. Portions of the left kidney were snap frozen in N-hexan and stored at −70°C for immunofluorescence studies and α-SMA mRNA examination. For autoradiography, 6 rats received bolus intraperitoneal injections of [^{3}H]-thymidine [120 μCi/100 g body weight, Wako, Osaka, Japan] at 4 (n=2), 5 (n=2), and 7 (n=2) days after uranyl acetate injection, then were sacrificed 90 min later, and the kidneys were fixed in methacarn after a brief flush with PBS.

The effect of chlorpromazine on FCs

As reported by Takashima et al. [32], chlorpromazine-treated rats were too lethargic to drink water, so that no drinking water was given to the rats after chlorpromazine solution or its vehicle administration, and 3 ml of saline was injected intraperitoneally twice every day. In our preliminary study, all rats treated with the chlorpromazine solution (Sigma-Aldrich Co., St. Louis, MO) at a daily dose of 2.5 mg/100 g body weight intraperitoneally every 12 h from day 3 to day 5 or from day 5 to day 7 after induction of ARF died within 2 days. Thus, the experimental period was limited from day 2 to day 4 after ARF induction. The chlorpromazine solution (n=5) or its vehicle saline (n=4) at a daily dose of 2.5 mg/100 g body weight was injected intraperitoneally every 12 h from day 2 to day 4 after induction of ARF. Normal rats received the same dose of chlorpromazine solution (n=5) or its vehicle saline (n=4) as controls. Rats were sacrificed at day 4 for the measurement of serum creatinine by the enzymatic method (Mizuho Med, Saga, Japan) and for histological examinations.

Histochemistry and immunohistochemistry

For histological examination, 4% paraformaldehyde-fixed, 4-μm thick sections were stained with periodic acid-Schiff (PAS). For immunohistochemistry, sections were deparaffinized, and endogenous peroxidase was blocked by treatment with 3% H_2O_2 for 30 min. The sections were then incubated with mouse monoclonal anti-human α-SMA (Dako, Glostrup, Denmark), mouse monoclonal anti-Ki67 (Novocastra, Newcastle upon Tyne, UK) as a cell proliferation marker or polyclonal rabbit anti-vinculin (H-300, Santa Cruz, CA) and reacted with the biotinylated donkey polyclonal antibody against mouse IgG (Chemicon International Inc., Temecula, CA) or rabbit IgG (Chemicon), respectively, for 30 min at room temperature. Then, avidin-conjugated peroxidase (Nichirei, Tokyo, Japan) was added for 30 min. The reaction products were visualized using incubation with diaminobenzidine.

For control sections, the first antibodies were omitted or replaced by normal mouse or rabbit IgG. Signals in both control and experimental sections were negative or negligible.

Immunohistochemistry for α-SMA and autoradiography

After immunostaining the methacarn-fixed sections with α-SMA, slides were dehydrated, air-dried, dipped in NTB2 emulsion (Eastman Kodak Co., Rochester, NY), and placed in light tight boxes. Following a 4-week incubation at 4°C, slides were developed (D19; Eastman Kodak) and counterstained with hematoxylin and eosin. The numbers of α-SMA-positive cells containing nuclei labeled with [^{3}H]-thymidine (>5 nuclear grains) among nuclei-containing α-SMA-positive cells in the interstitium were counted in 20 randomly selected fields of the outer stripe of the outer medulla (OSOM) at days 4, 5, and 7 at ×400 magnification, and the mean percentage of α-SMA-positive cells containing nuclei labeled with [^{3}H]-thymidine was calculated.

Fluorescence studies

Fluorescence study was performed on 4-μm cryostat sections fixed in cold acetone. The specific fluorescence labeling of F-actin was performed with Alexa fluor phalloidin 568 (Cosmo Bio Co., Tokyo). Indirect immunofluorescence study was performed with mouse monoclonal anti-human α-SMA or rabbit polyclonal anti-connexin43 (gap junction protein, C6219, Sigma) followed by fluorescein isothiocyanate-conjugated donkey anti-mouse IgG (Chemicon) or fluorescein isothiocyanate-conjugated donkey anti-rabbit IgG (Chemicon), respectively. The staining intensity was determined semiquantitatively using a grading system of scales: −, ±, +, ++, and +++.

Transmission electron microscopy

Small portions of renal tissues were fixed in 2% glutaraldehyde in 0.1 M phosphate buffer (pH 7.4) at 4°C for 2 h, postfixed in 1% OsO_4 resolved in the same buffer for 1 h, and then embedded in Epon. Ultra-thin sections were counterstained with uranyl acetate and lead citrate and then examined under an electron microscope (JEM-1220, JEOL, Japan).

Scanning electron microscopy

For scanning electron microscopy, the glutaraldehyde-fixed kidneys were placed en bloc in 30% KOH aqueous solution for 10 min

at 60°C to remove extracellular matrices such as collagen fibrils and basal laminae [35]. After KOH treatment, the kidneys were washed several times in phosphate buffer and divided into small pieces with a fine needle and forceps under a dissecting microscope. The tissues were then dehydrated with t-butyl alcohol and dried by freeze-drying using t-butyl alcohol. The dried tissues were then attached to aluminum stubs; the deposition of the osmium-metal coating was carried out by plasma chemical vapor deposition method [1] and examined under a scanning electron microscope (S-800, Hitachi, Japan).

Measurement of proximal tubular perimeter

The proximal tubular perimeter was measured in 40 cross-sections of proximal tubule, which showed PAS-positive brush border, necrotic injury, or proliferative figures in the upper half of the OSOM at ×400 magnification in each animal. Each proximal tubule was considered necrotic when it included any tubular cell profiles, such as vacuolar degeneration, necrosis, and desquamation. The mean score in each rat represented the average score of the proximal tubular perimeter.

α-SMA-positive and vinculin-positive areas

For semi-quantification of α-SMA-positive or vinculin-positive interstitial areas in the upper half of the OSOM, point counting was performed using the method reported by Badid et al. [3]. A total of 20 high-power fields at ×400 magnification per section were counted in each animal. The percentage of fractional area (percentage of positive area relative to the total area counted in the section) was calculated using the following formula: percentage of fractional area=number of grid intersections with positive staining/total number of grid intersections ×100.

Ki67-positive regenerating proximal tubular cells

For semi-quantitative analysis, the number of Ki67-positive proximal tubular cells in the OSOM was counted at ×400 magnification. The number of immunoreactive cells in each rat represented the average number of 20 fields examined, and the mean number in each group was displayed in histograms.

α-SMA mRNA

The methods for total RNA extraction and polymerase chain reaction (PCR) were reported in detail previously [31]. To semi-quantitate PCR products and to confirm the integrity of RNAs, a housekeeping gene, glyceraldehyde-3-phosphate dehydrogenase (GAPDH), was co-amplified. We used the primers of α-SMA [5′-CGATAGAACACGGCATCATC (sense) and 5′-CATCAGGCA-GTTCGTAGCTC (antisense)] to yield a 525-bp product [10] and of GAPDH [5′-AATGCATCCTGCACCACCAA (sense) and 5′-GTAGCCATATTCATTGTCATA (antisense)] to yield a 515-bp product [17]. Amplification was performed at 32 cycles with both α-SMA and GAPDH primers in the ascending curve of amplification. PCR products were electrophoresed, the density of each

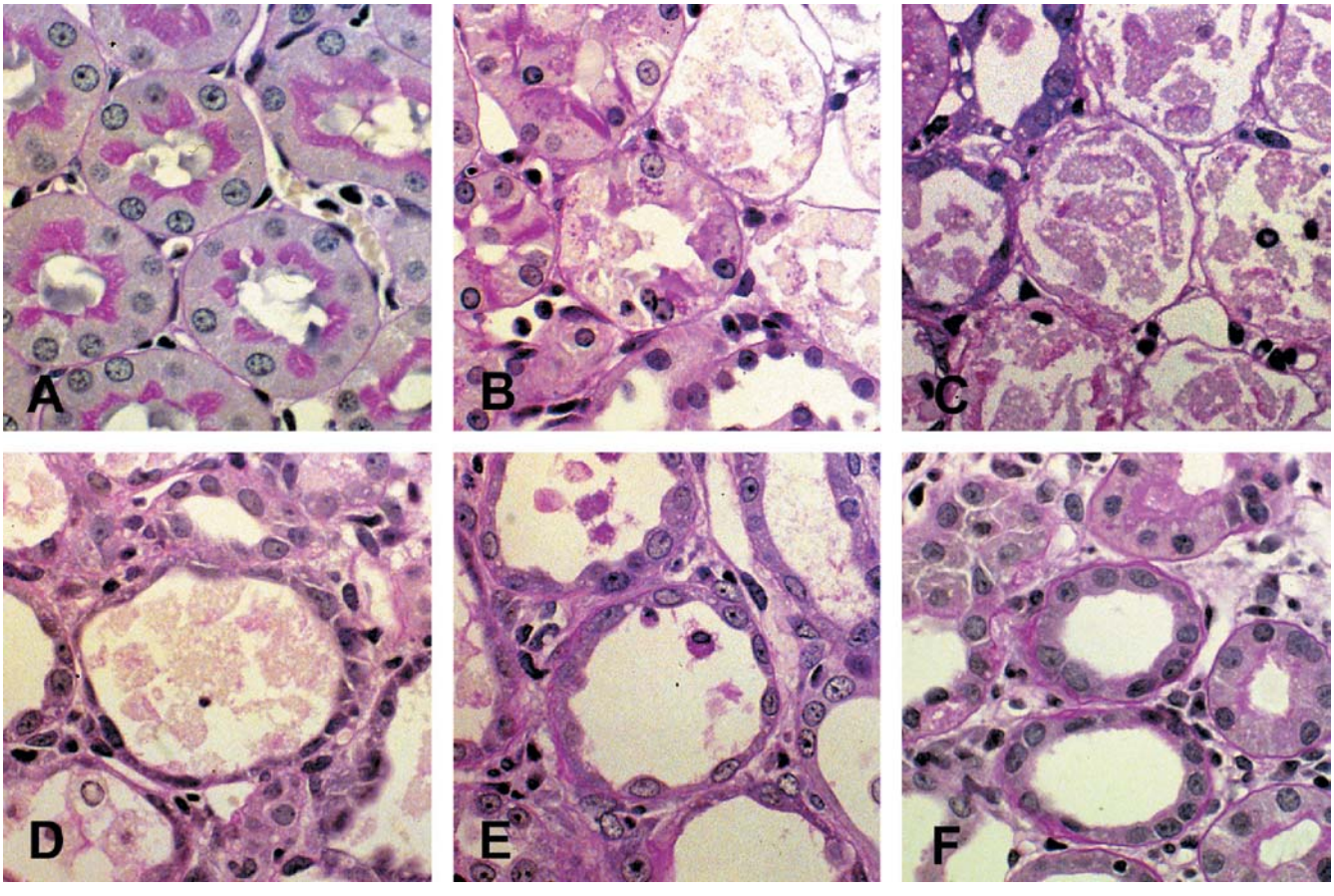

Fig. 1 Photomicrographs of periodic acid-Schiff-stained sections, showing proximal tubular injury (**B**, **C**) and repair (**D**–**F**) in the outer stripe of outer medulla after induction of acute renal failure (ARF). Prior to induction of ARF (**A**), day 2 (**B**), day 4 (**C**), day 7 (**D**), day 9 (**E**), day 15 (**F**)

DNA band was measured with NIH Image, and the mRNA levels for α-SMA were expressed as a ratio of the optical density units relative to GAPDH.

Statistical analysis

Data are expressed as mean±SD. Differences between data sets were examined for statistical significance using one-way analysis of variance followed by Fisher's *t*-test. Correlation coefficients were determined using Pearson's correlation coefficient. A P value of <0.05 was accepted as statistically significant.

Results

Perimeter of proximal tubules during tubular damage and recovery

Necrosis of proximal tubules was detected around corticomedullary junctions as early as day 2 after induction of ARF, developed throughout the OSOM from day 4 to day 5, and was almost substituted by epithelial relining by day 7 (Fig. 1 and Fig. 2). Measurement of perimeter of proximal tubules in the upper half of the OSOM revealed that tubular dilatation occurred significantly at day 4, peaked at day 7, then returned to almost normal level by day 15 (Fig. 3A).

Appearance of α-SMA-positive myofibroblasts

In normal rats, α-SMA staining was not detected in tubules or interstitial cells (Fig. 4A). α-SMA-positive cells, i.e., myofibroblasts, initially appeared exclusively around damaged proximal tubules with denuded tubular basement membrane as early as day 2 (Fig. 2 and Fig. 4B), extending along with the progression to severe tubular damage, forming a network around necrotic and/or regenerating tubules mainly throughout the OSOM between day 4 and day 7 (Fig. 2 and Fig. 4C, D, G). Most peritubular α-SMA expression began to decrease from day 9,

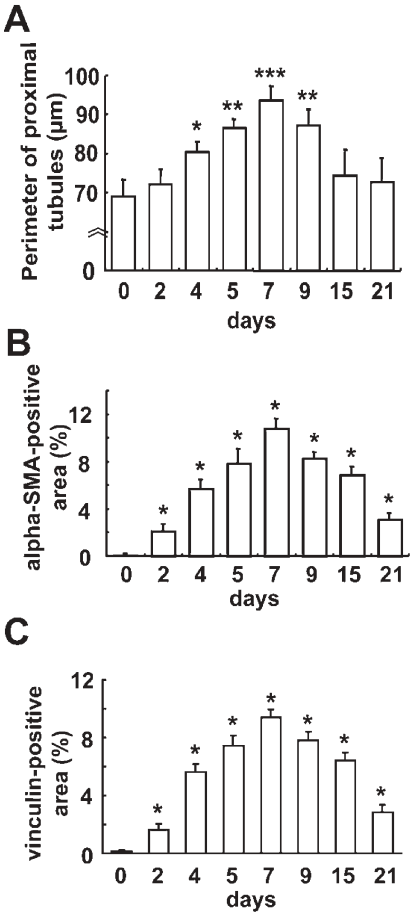

Fig. 3 A Morphometric analysis of proximal tubular perimeter in the upper half of the outer stripe of outer medulla (OSOM). Data are mean±SD of five rats. *P<0.05, **P<0.01, ***P<0.001 versus normal control. **B** Morphometric analysis of α-smooth muscle actin-positive area in the upper half of the OSOM. *P<0.001 versus normal control. Data are mean±SD of five rats. **C** Morphometric analysis of vinculin-positive interstitial area in the upper half of the OSOM. Data are mean±SD of five rats. *P<0.001 versus normal control

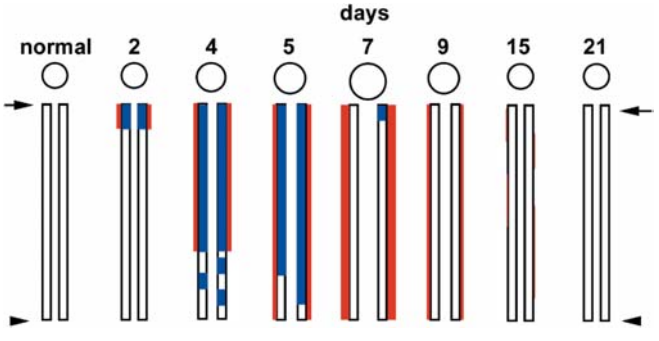

Fig. 2 Schematic drawing of the sequence of changes in proximal tubules in the outer stripe of outer medulla (OSOM) after the induction of acute renal failure. *Arrows* border between cortex and OSOM. *Arrowheads* border between OSOM and inner stripe of outer medulla. *Blue areas* indicate necrotic tubules and *red areas* indicate α-smooth muscle actin-positive myofibroblasts. *Circles* show changes in perimeter of proximal tubules

Fig. 4 Photomicrographs of immunohistochemical findings for α-smooth muscle actin (SMA)-positive interstitial cells (*brown color*). Prior to induction of acute renal failure (ARF) (**A**), day 2 (**B**), day 4 (**C**), day 5 (**H**), day 7 (**D** and **G**), day 15 (**E**), day 21 (**F**) after induction of ARF. **A**–**F** Serial changes in α-SMA-positive interstitial cells in outer stripe of outer medulla (OSOM). **E** At day 15, peritubular α-SMA staining became faint. **F** At day 21, α-SMA positive cells were seen only around the very dilated tubule. **G** Lower magnification of kidney section, on which nuclear staining was not performed. Note the formation of a network of α-SMA-positive interstitial cells in OSOM. **H** Autoradiograph with immunohistochemistry for α-SMA. Proliferating proximal tubular cells are identified by the presence of tritium (*black nuclear grains*, *arrowheads*), but most α-SMA-positive cells in the interstitium show lack of tritium at day 5. Note one proliferating α-SMA-positive cell (*large arrow*) and all non-proliferating α-SMA-positive cells (*small arrows*). *CO* cortex

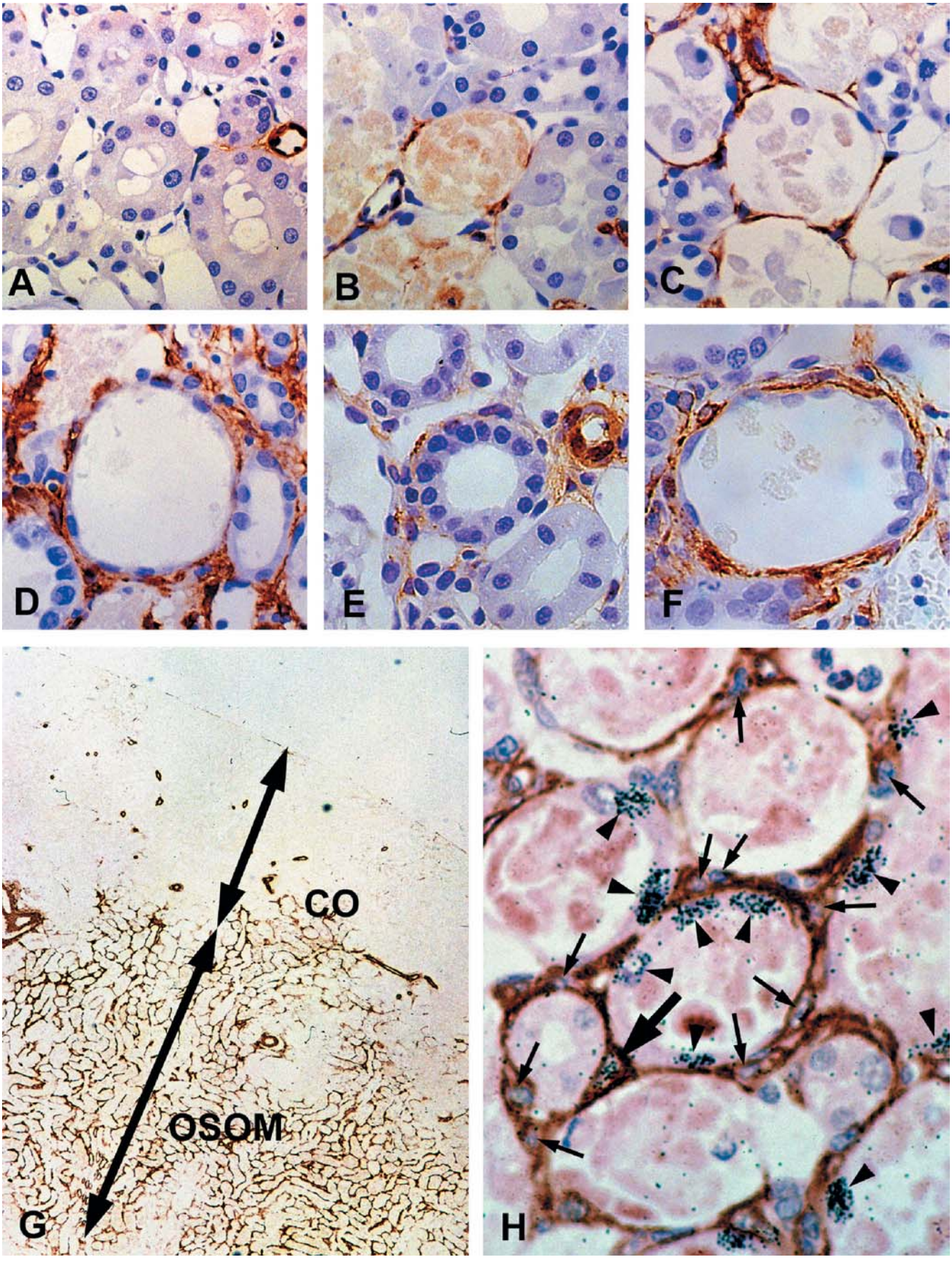
A
B
C
D
E
F
CO
OSOM
G
H

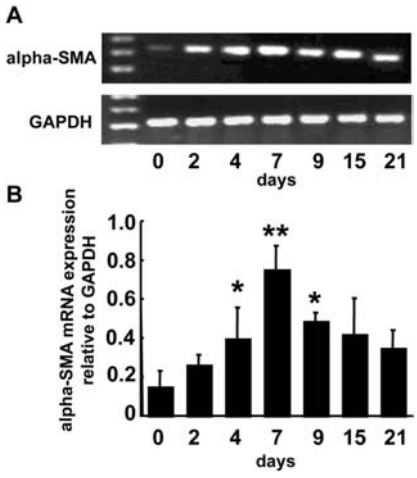

Fig. 5 Expression of α-smooth muscle actin (SMA) mRNA (**A**) and α-SMA mRNA expression relative to glyceraldehyde-3-phosphate dehydrogenase (GAPDH) mRNA (**B**). Data are mean±SD of five rats. **P*<0.05, ***P*<0.001

became faint by day 15, (Fig. 4E) and almost disappeared by day 21 (Fig. 2). By day 21, α-SMA-positive cells were present only around occasionally dilated tubules (Fig. 4F). Proportion of [^{3}H]-thymidine radiolabeled α-SMA-positive cells in the interstitium was 0.7% at day 4, 0.8% at day 5, and 0.5% at day 7 (Fig. 4H), indicating a low proliferative activity of α-SMA-positive cells.

Morphometric analysis of α-SMA-positive area revealed that α-SMA-positive interstitial areas in the upper half of the OSOM were significantly increased at day 2, peaked at day 7, and then gradually decreased (Fig. 3B). There was a positive correlation between the perimeter of proximal tubules and fractional area of α-SMA staining (n=40, r=0.826, P<0.001). At day 4, the expression of α-SMA mRNA was approximately threefold that of the normal control, and it gradually increased to reach a peak level at day 7, then decreased (Fig. 5).

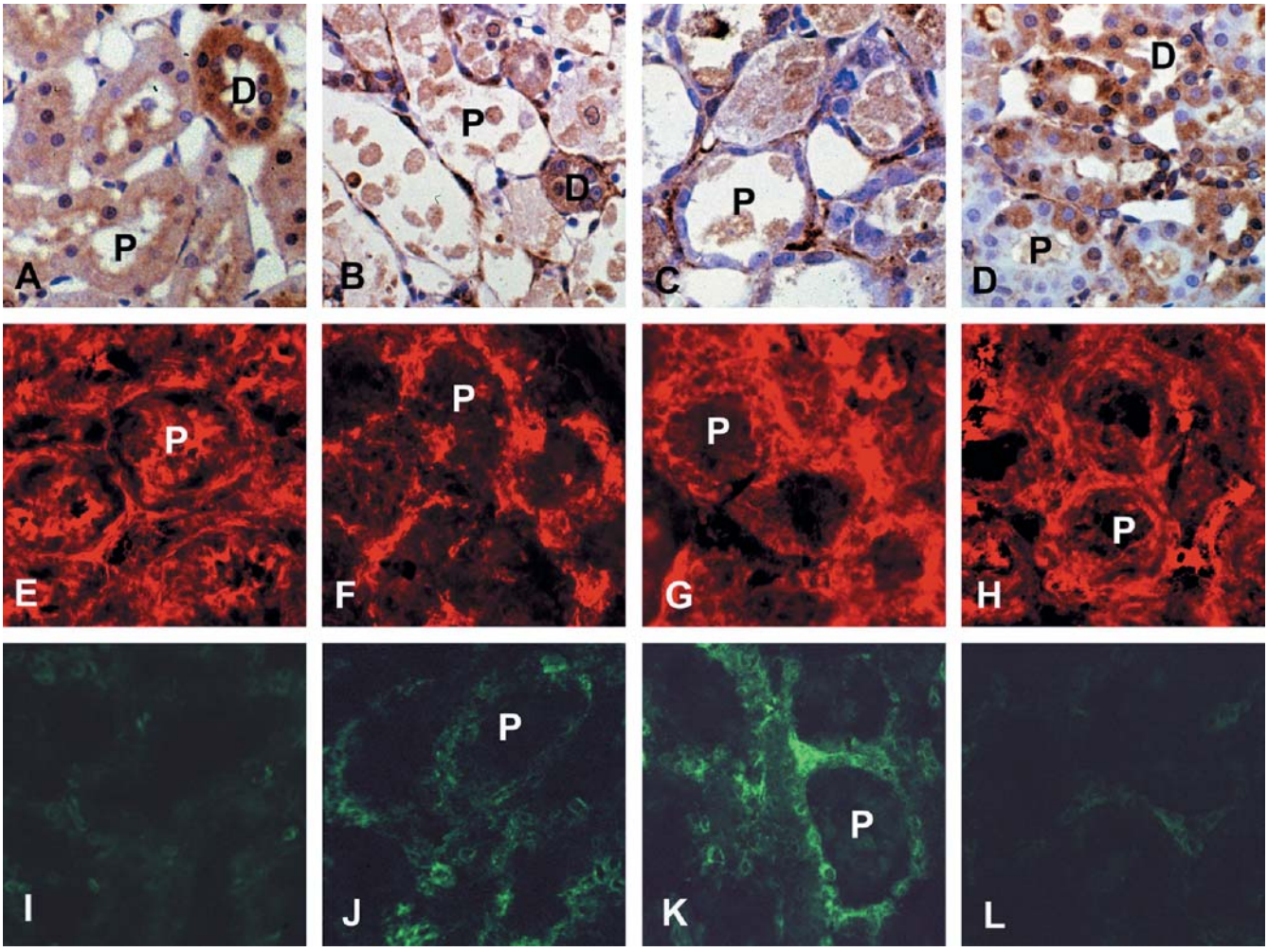

Fig. 6 Immunohistochemistry for vinculin (**A**–**D**), Alexa fluor phalloidin 568 for filamentous actin (**E**–**H**) and immunofluorescence for connexin43 (**I**–**L**) in the outer stripe of outer medulla prior to (**A**, **E** and **I**) and at days 4 (**B**, **F** and **J**), 7 (**C**, **G** and **K**), 15 (**H**, **L**), and 21 (**D**) after induction of acute renal failure. *P* proximal tubules, *D* distal tubules

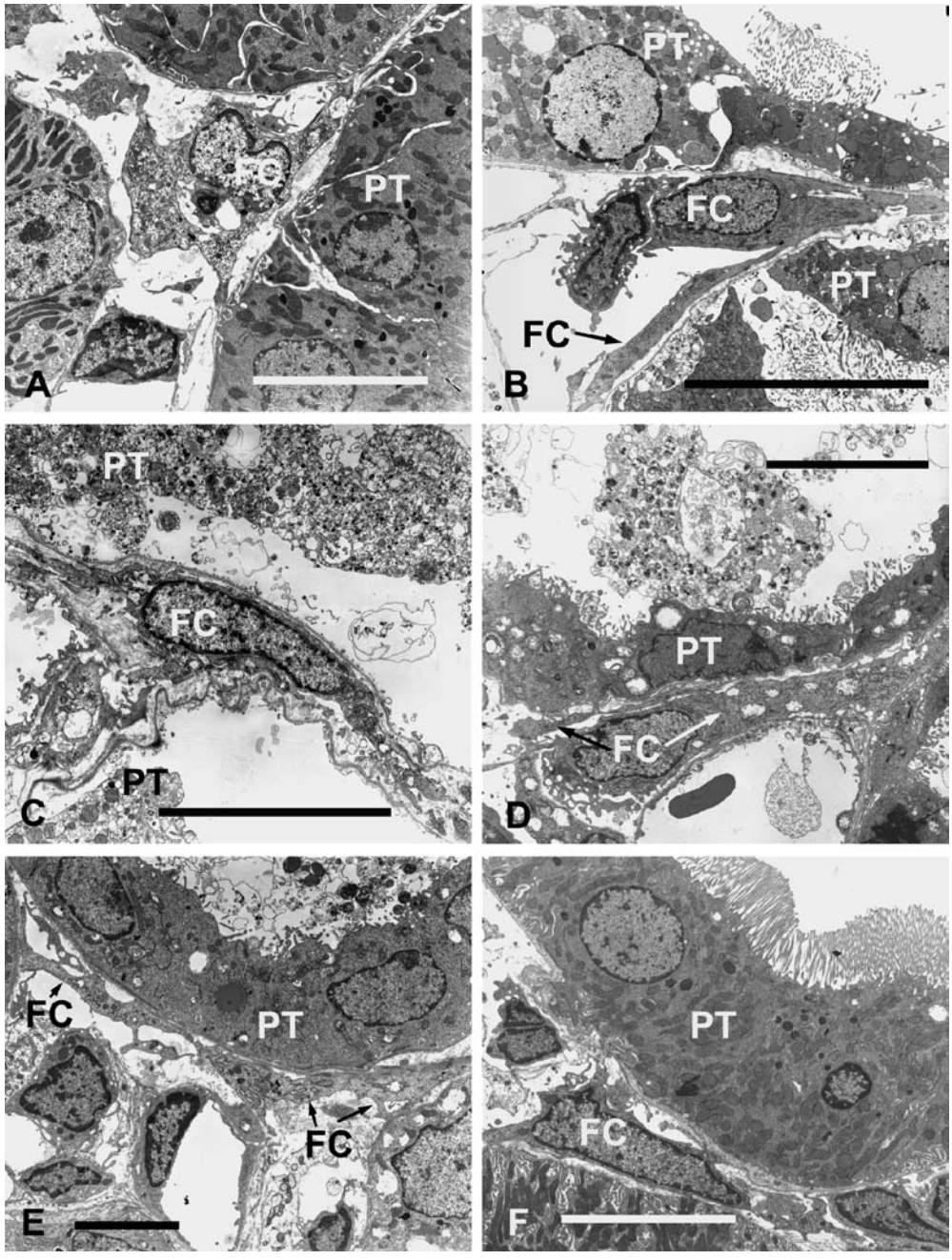

Fig. 7 Transmission electron micrographs of FCs in the outer stripe of outer medulla prior to (**A**) and at days 2 (**B**), 4 (**C**), 7 (**D**, **E**), and 15 (**F**) after induction of acute renal failure. In normal kidney, interstitial fibroblastic cells (FCs) located beneath the tubular basement membrane showed extended cellular processes, which attached to the tubular basement membrane through the narrow portion of the cellular processes, containing thin cortical microfilament bundles (**A**). At day 2 and day 4, FCs increasingly attached the tubular basement membrane, on which damaged proximal tubule could be seen, by extended cellular processes and/or elongated cell body containing thick microfilament bundles (**B**, **C**). FCs covered tubular basement membrane at large areas at day 7, when immature proximal tubular cell proliferated on tubular basement membrane (**D**) and formed a network (**E**). At day 15, FCs showed similar appearance of FCs in normal kidneys (**F**). *PT* proximal tubules. *Bars*=5.0 μm

Immunohistochemistry for vinculin and immunofluorescence study for F-actin, α-SMA, and connexin43

In normal rats, immunoreactive vinculin was detected in distal nephron and slightly in the cytoplasm and brush border of proximal tubules but not in the interstitium (Fig. 6A). Few vinculin-positive cells were found in the interstitium as early as day 2 and increased from day 4 to day 7 (Fig. 6B, C). Vinculin-positive interstitial cells decreased from day 9, but few were found in the interstitium and in the cytoplasm of some proximal tubules until day 21 (Fig. 6D). Morphometric analysis revealed that vinculin-positive interstitial areas in the upper half of the OSOM were significantly increased at day 2, peaked at day 7, and then gradually decreased (Fig. 3C).

In normal kidneys, staining for F-actin was found along the axis of the brush border of proximal tubules and at right angles to the tubular axis in the basal cytoplasm of tubules, but staining was very weak in the interstitium (Fig. 6E). The increased interstitial staining for F-actin was significant throughout the OSOM as early as day 2. At day 4, when denuded tubular basement membrane was abundant, the interstitial staining was clearly identified (Fig. 6F) and then peaked at day 7 (Fig. 6G). F-actin staining was also found in regenerating proximal tubular cells at day 7 (Fig. 7G) and almost returned to the basal level (i.e., normal kidneys) by day 15 (Fig. 6H, Table 1).

Table 1 Summary of staining for filamentous actin (F-actin), α-smooth muscle actin (SMA), and connexin43 in the interstitium. staining intensities: – negative, ± trace, + weak, ++ moderate, +++ strong

	Day 0	Day 2	Day 4	Day 5	Day 7	Day 9	Day 15	Day 21
F-actin	±	+[a]	++	++ to +++	+++	+	±	±
α-SMA	–	±[b]	++	++ to +++	+++	+ to ++	± to +	±
Connexin43	–	±[c]	+	+ to ++	++	±	–	–

[a] Throughout the outer stripe of outer medulla
[b] Around the corticomedullary junction
[c] Throughout the outer stripe of outer medulla

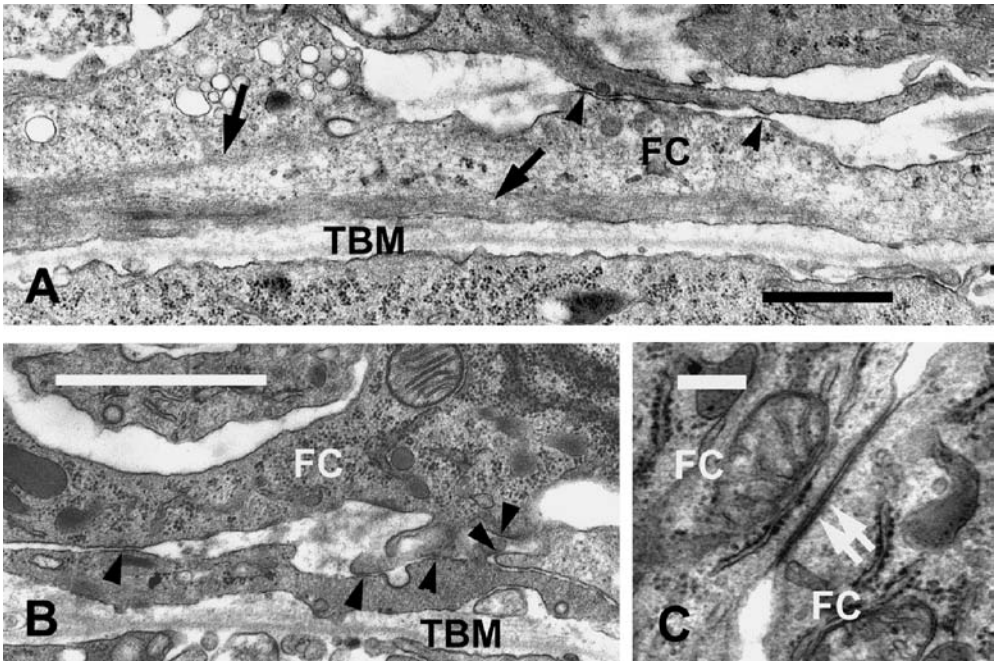

Fig. 8 Transmission electron micrographs of fibroblastic cells (FCs) at day 5. FCs tightly attached the tubular basement membrane, on which regenerating proximal tubular cells could be seen, by extended cellular processes containing thick microfilament bundles (*arrows*) (**A**). Numerous adherens junctions (**A**, **B**) and gap junctions (**C**) were found at sites of contact between neighboring processes of FCs. *PT* proximal tubules, *TBM* tubular basement membrane. *Bars*=1.0 μm (**A**, **B**), *bars*= 0.3 μm (**C**)

In contrast to the interstitial F-actin staining, α-SMA-positive cells initially appeared around the corticomedullary junction as described above. Since immunofluorescence study may be a more sensitive method than immunohistochemistry under some conditions, immunofluorescence study for α-SMA was also performed. The findings of immunofluorescence for α-SMA were similar to that of immunohistochemistry for α-SMA (Table 1).

In normal kidneys, very sparse immunofluorescent dots for connexin43 were observed in the interstitium (Fig. 6I). Connexin43 dots in the peritubular regions slightly increased as early as day 2, then numerous dots appeared, reaching peak intensity at day 7 (Fig. 6J, K). By day 15, the density of fluorescent dots decreased to the level of normal controls (Fig. 6L, Table 1).

Transmission electron microscopic findings of FCs

In OSOM of normal kidneys, the interstitial FCs exhibited extended cellular processes attached to the tubular basement membrane, with the narrow portion of the cellular processes containing thin microfilament bundles (Fig. 7A). After induction of ARF, FCs increasingly attached to the tubular basement membrane, on which damaged proximal tubules as well as regenerating, immature proximal tubules could be seen, by extended cellular processes and/or elongated cell bodies containing thick microfilament bundles (Fig. 9B, C, D, E). Bare tubular basement membrane was largely covered with FCs, as if FCs supported the tubular structures (Fig. 7C). Adherens junctions (Fig. 8A, B) and gap junctions (Fig. 8C) were increasingly found at the sites of contact between neighboring processes of FCs from day 4 to day 7, with FCs forming a network around the proximal tubules (Fig. 7C, D, E). By day 15, most FCs showed features similar to FCs in normal kidneys (Fig. 7F), and apparent apoptotic figures of FCs were not found.

Scanning electron microscopic findings of FCs

Scanning electron microscopy of KOH-digested normal tissues showed that FCs covered the tubules only partially with their extended, thin cellular processes and/or cell bodies (Fig. 9A). After induction of ARF, FCs became hypertrophic, anastomosed with the cellular processes, and covered large parts of tubules (Fig. 9B, C). However, by day 15, most FCs appeared similar to FCs of normal kidneys (Fig. 9D). During experimental periods, apparent

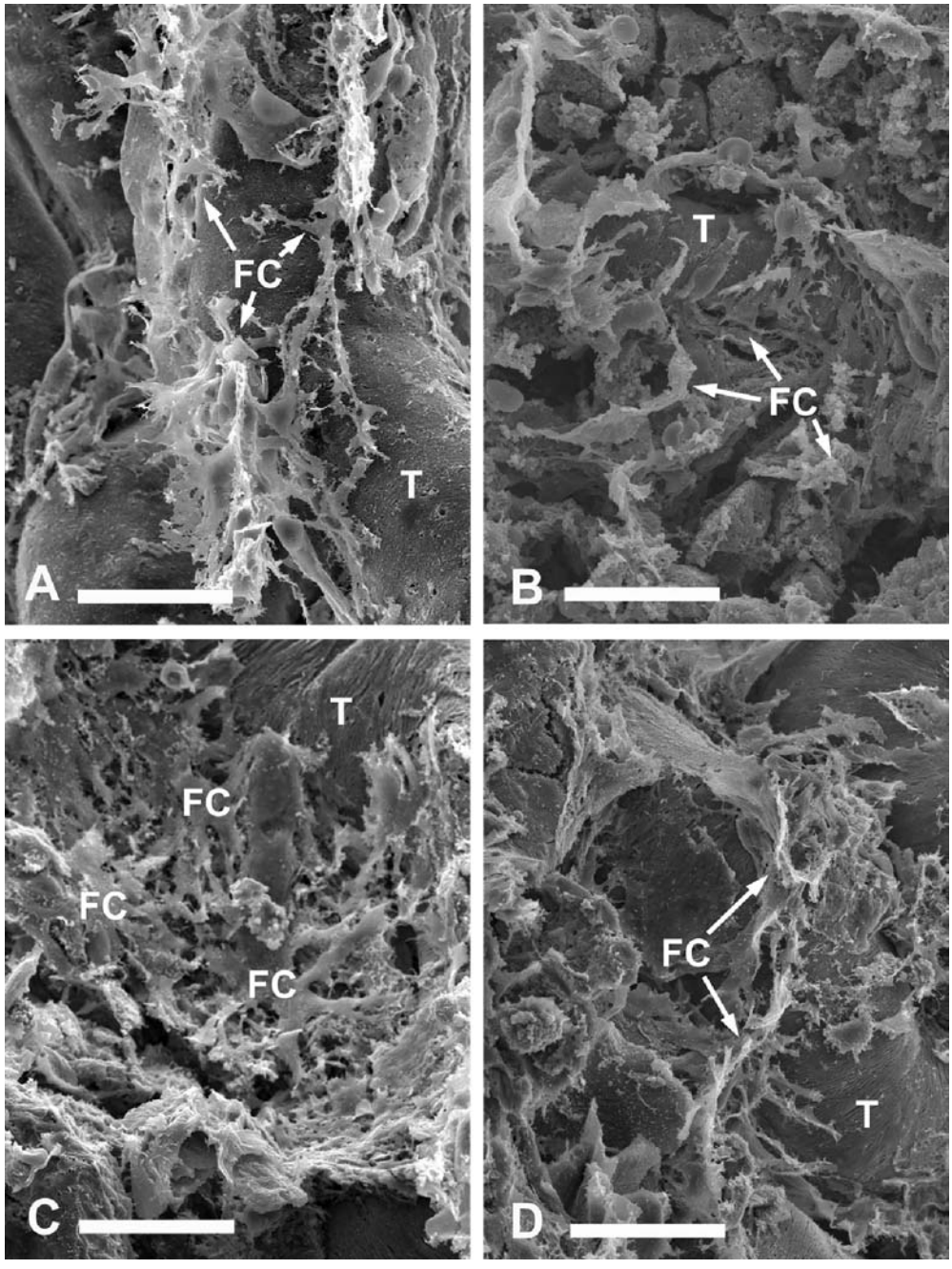

Fig. 9 Scanning electron micrographs of fibroblastic cells (FCs) in the outer stripe of outer medulla after KOH treatment prior to (**A**) and at days 4 (**B**), 7 (**C**), and 15 (**D**) after induction of acute renal failure. In normal kidney, FCs partially covered the tubules with their extended, thin cellular processes and/or cell bodies (**A**). At day 4, FCs became hypertrophic, anastomosed through cellular processes, and covered a large part of the tubules (**B**). These findings were more prominent at day 7 (**C**). At day 15, the appearance of FCs reverted to that of normal kidneys (**D**). *T* tubular cells. *Bars*=25.0 μm

migratory figures of tubular cells into the interstitium could not be found.

The effect of chlorpromazine on myofibroblast differentiation of FCs and the repair after ARF induction

In chlorpromazine-treated normal rats, α-SMA staining was not detected in the interstitium, and F-actin staining was very weak in the interstitium (not shown). These findings were similar to those in vehicle-treated normal rats. In chlorpromazine-treated ARF rats at day 4, stainings for α-SMA and F-actin in the interstitium were partially reduced when compared with those in vehicle-treated ARF rats at day 4 (Fig. 10A, B, C, D). Using transmission electron microscopy, chlorpromazine-treated

Fig. 10 Immunofluorescence for α-smooth muscle actin (**A**, **B**) and alexa fluor phalloidin 568 for filamentous actin (**C**, **D**) in the outer stripe of outer medulla in vehicle-treated acute renal failure (ARF) rats at day 4 (**A**, **C**) and in chlorpromazine-treated ARF rats at day 4 (**B**, **D**). *P* proximal tubules. Transmission electron micrographs of fibroblastic cells (FCs) in vehicle-treated (**E**) and chlorpromazine-treated ARF rats at day 4 (**F**). *P* proximal tubules. *Bars*=5.0 μm. Photomicrographs of immunostaining for Ki67-positive proximal tubular cells (*arrows*) (**G**, **H**) in vehicle-treated (**G**) and chlorpromazine-treated (**H**) ARF rats at day 4

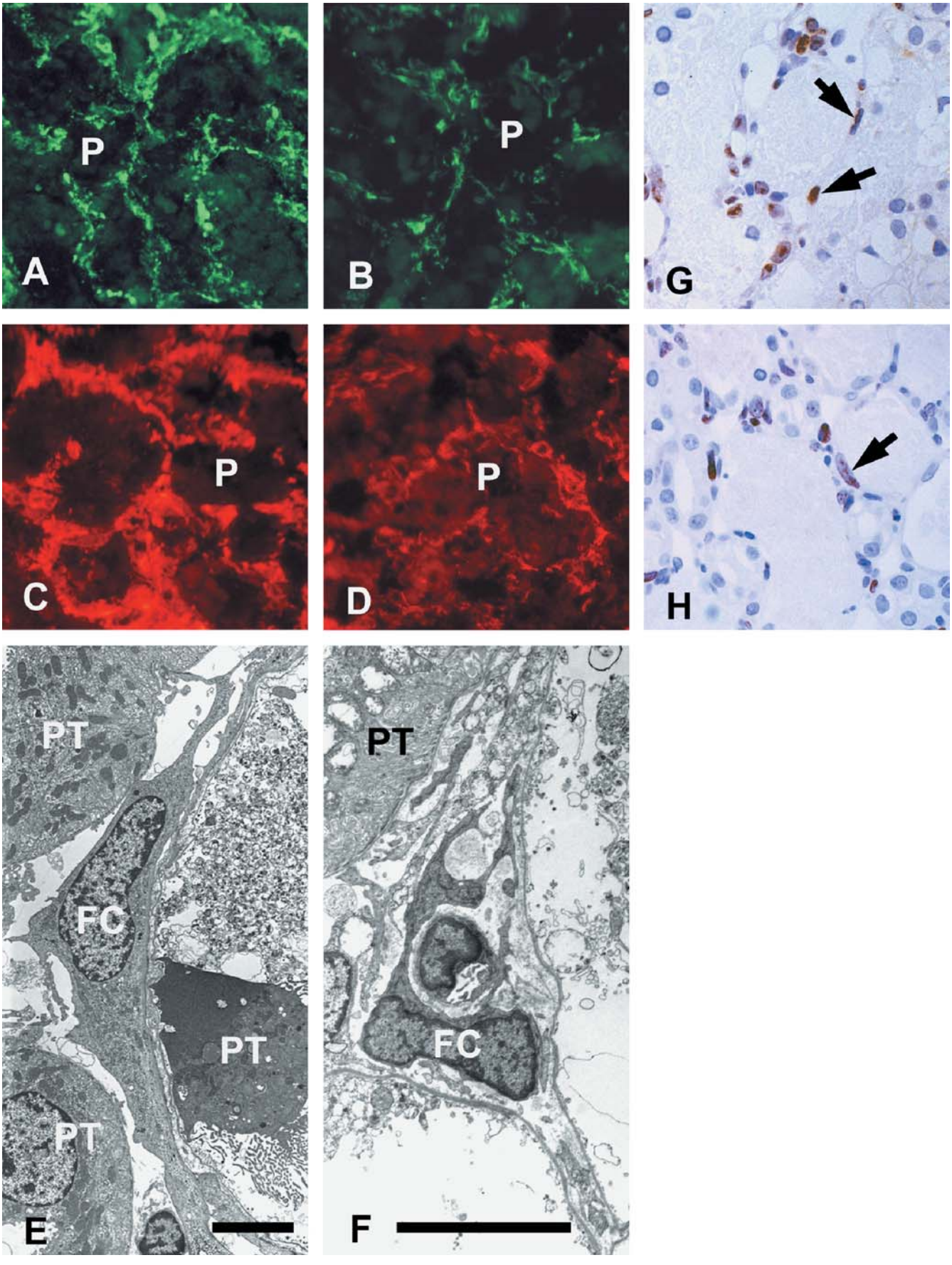
A
P
B
P
G
C
P
D
P
H
PT
FC
PT
PT
E
PT
FC
F

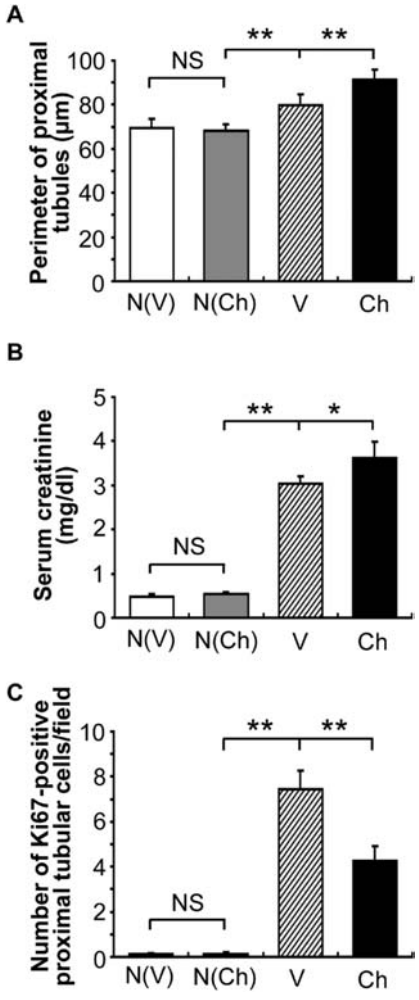

Fig. 11 Proximal tubular perimeter in the upper half of the outer stripe of outer medulla (**A**), serum creatinine levels (**B**) and the number of Ki67-positive proximal tubular cells per field in the upper half of the OSOM (**C**). *N(V)* vehicle-treated normal rats (n=4), *N(Ch)* chlorpromazine-treated normal rats (n=5), *V* vehicle-treated acute renal failure (ARF) rats (n=4), *Ch* chlorpromazine-treated ARF rats (n=5). Data are mean±SD of four or five rats. *P<0.05 versus normal control (con); *P<0.01; **P<0.001; *NS* no significant difference

normal rats showed comparable morphology of interstitial FCs with that in vehicle-treated normal rats. Chlorpromazine-treated ARF rats at day 4 (Fig. 10F) showed less attachment of FCs to the tubular basement membrane and fewer elongated cell bodies of FCs containing thick microfilament bundles than vehicle-treated ARF rats at day 4 (Fig. 10E). These findings indicated that chlorpromazine administration partially inhibited myofibroblast differentiation of FCs after induction of ARF. There was no difference of the perimeter of proximal tubules, serum creatinine level, and the number of Ki67-positive regenerating proximal tubular cells between chlorpromazine- and vehicle-treated normal rats (Fig. 11A, B, C). The perimeter of proximal tubules in chlorpromazine-treated ARF rats at day 4 was significantly longer than that in vehicle-treated ARF rats at day 4 (Fig. 11A). In chlorpromazine-treated ARF rats at day 4, the number of Ki67-positive regenerating proximal tubular cells was significantly reduced, and serum creatinine level was significantly increased compared with vehicle-treated ARF rats at day 4 (Fig. 10G, H and Fig. 11B, C). The data suggested that myofibroblast differentiation of FCs may play a contractile role on damaged nephron structures and a beneficial role on the recovery in uranyl acetate-induced ARF.

Discussion

Previously, we demonstrated transient expression of α-SMA in FCs in uranyl acetate-induced ARF in rats [30] and its beneficial role on tubular recovery [31]. In the present study, we investigated the possible mechanisms of myofibroblast differentiation of FCs and found transient proximal tubular dilatation after induction of ARF; there was a significant correlation between the perimeter of proximal tubules and fractional areas of α-SMA staining. We assumed the tubular dilatation to reflect the presence of high mechanical tension toward tubular basement membrane and matrix around FCs possibly by intratubular pressure due to obstruction of urinary flow by desquamated cellular components and cast formation [15]. However, it is also possible that the loss of stability due to toxic effects of uranyl acetate on tubular epithelial cells may cause the tubular dilatation.

It has been reported that mechanical tension is important for the development of fibroblast contractile features such as stress fiber formation [11, 29, 33] and acquisition of α-SMA phenotype [2, 14] both in vitro and in vivo. Therefore, this might apply to the present model. Mechanical tension is reported to induce actin polymerization (F-actin) and stress fiber formation [5, 12, 36]. Previous studies also reported the early formation of F-actin during wound healing and the rapid loss of actin stress fibers in fibroblasts after load release, suggesting that the physical integrity of stress fibers [16] provides an important prerequisite for α-SMA expression and myofibroblast contraction [14]. In agreement with these findings, our study showed that increased F-actin expression may precede α-SMA expression (Table 1).

Myofibroblasts are reported to display prominent cytoplasmic actin microfilaments [6, 23], and they are connected to each other by both adherens and gap junctions [22, 23]. Ultrastructural examination of FCs revealed that after induction of ARF, FCs became hypertrophic and showed increased number and length of cytoplasm-containing microfilament bundles that connected with other FCs and with the tubular basement membrane, through the formation of abundant adherens and gap junctions. In our study, F-actin and vinculin increased in FCs in parallel with myofibroblast differentiation. It is possible that F-actin and vinculin may play roles to form adherens junctions [9, 34] in myofibroblasts in this model. Abundant punctuate immunofluorescence for connexin43 was observed in the interstitium after induction of ARF,

indicating myofibroblast gap junction with connexin43 [28]. Since functional gap junctions have been identified between myofibroblasts in the wound healing process [8, 28], it is possible that there is functional gap junctional intercellular communication among myofibroblasts around damaged proximal tubules in uranyl acetate-induced ARF.

Administration of chlorpromazine, one of several calmodulin antagonists that inhibit cytoskeletal movement indirectly [18, 20, 24], after induction of ARF partially inhibited myofibroblast differentiation of FCs immunohistochemically and morphologically and resulted in more dilated proximal tubules at day 4 when compared with vehicle-administered rats. This supports the idea that tubular dilatation in this model should reflect an existence of mechanical tension. However, chlorpromazine treatment inhibited the regenerative repair of proximal tubule, as judged by Ki67-positive proximal tubular cells, and aggravated renal dysfunction, as judged by serum creatinine level. The findings suggested that an acquisition of myofibroblast phenotype in FCs and formation of a network of myofibroblasts around denuded tubular basement membrane may contribute to protecting damaged nephron structures by providing contractility and a cushion that resists any stretching force [13], resulting in promoting the recovery. ARF rats treated with chlorpromazine during the later phase of this model died with lethargy within 2 days. The exact cause of death is not clear, but the possible cause of death is uremia caused by lack of recovery from ARF.

It was reported that tubular epithelial-myofibroblast transdifferentiation and its migration may contribute to interstitial myofibroblast accumulation in progressive tubulointerstitial fibrosis in the rat remnant kidney [21]. However, since proximal tubules showed negative α-SMA staining during experimental periods, as well as no characteristic morphology of myofibroblast and no migratory figures into the peritubular interstitium through the tubular basement membrane using transmission and scanning electron microscopy, interstitial FCs should be the origin of myofibroblasts in this model. Fibroblast activation is a transitory process in wound healing, as myofibroblasts may disappear by apoptosis in the last steps of the repair process [7]. As there is no definitive marker for rat renal interstitial FCs, it is unclear what percentage of interstitial FCs expressed α-SMA and whether the number of interstitial FCs (including myofibloblasts) increased or remained stable in this model. However, α-SMA-positive myofibroblasts did not show active proliferation by [^{3}H]-thymidine incorporation study or apoptosis on an electron microscopic level, suggesting that the fate of myofibroblasts may mainly revert to the resident form of FCs.

In conclusion, increased mechanical tension by proximal tubular damage may contribute to the induction of α-SMA phenotype, together with increased stress fiber formation and intercellular junctions in interstitial FCs to support the structure of the damaged nephron by adjusting tensional homeostasis in uranyl acetate-induced ARF in rats.

Acknowledgements This work was partially supported by a Grant-In-Aid for scientific research (C; No.13671107) from the Ministry of Education, Science, Sports and Culture, Japan.

References

1. Akahori H, Handa M, Yoshida H, Kozuka Y (2000) Osmium-metal coating device using hollow-cathode plasma CVD method. J Electron Microsc 49:735–744
2. Arora PD, Narani N, McCulloch CA (1999) The compliance of collagen gels regulates transforming growth factor-beta induction of alpha-smooth muscle actin in fibroblasts. Am J Pathol 154:871–882
3. Badid C, Mounier N, Costa AM, Desmouliere A (2000) Role of myofibroblasts during normal tissue repair and excessive scarring: interest of their assessment in nephropathies. Histol Histopathol 15:269–280
4. Burridge K (1981) Are stress fibres contractile? Nature 294:691–692
5. Burridge K, Chrzanowska-Wodnicka M (1996) Focal adhesions, contractility, and signaling. Annu Rev Cell Dev Biol 12:463–518
6. Darby I, Skalli O, Gabbiani G (1990) α-smooth muscle actin is transiently expressed by myofibroblasts during experimental wound healing. Lab Invest 63:21–29
7. Desmouliere A, Redard M, Darby I, Gabbiani G (1995) Apoptosis mediates the decrease in cellularity during the transition between granulation tissue and scar. Am J Pathol 146:56–66
8. Gabbiani G, Chaponnier C, Huttner I (1978) Cytoplasmic filaments and gap junctions in epithelial cells and myofibroblasts during wound healing. J Cell Biol 76:561–568
9. Geiger B, Ginsberg D (1991) The cytoplasmic domain of adherents-type junction. Cell Motil Cytoskel 20:1–6
10. Ghassemifar MR, Tarnuzzer RW, Chegini N, Tarpila E, Schultz GS, Franzen LE (1997) Expression of alpha-smooth muscle actin, TGF-beta 1 and TGF-beta type II receptor during connective tissue contraction. In Vitro Cell Dev Biol Anim 33:622–627
11. Grinnell F, Zhu M, Carlson MA, Abrams JM (1999) Release of mechanical tension triggers apoptosis of human fibroblasts in a model of regressing granulation tissue. Exp Cell Res 248:608–619
12. Hall A (1998) Rho GTPases and the actin cytoskeleton. Science 279:509–514
13. Hinz B, Celetta G, Tomasek JJ, Gabbiani G, Chaponnier C (2001) Alpha-smooth muscle actin expression upregulates fibroblast contractile activity. Mol Biol Cell 12:2730–2741
14. Hinz B, Mastrangelo D, Iselin CE, Chaponnier C, Gabbiani G (2001) Mechanical tension controls granulation tissue contractile activity and myofibroblast differentiation. Am J Pathol 159:1009–1020
15. Hishida A, Yonemura K, Ohishi K, Yamada M, Honda N (1988) The effect of saline loading on uranium-induced acute renal failure in rats. Kidney Int 33:942–946
16. Ingber DE (1997) Tensegrity: the architectural basis of cellular mechanotransduction. Annu Rev Physiol 59:575–599
17. Ishidoya S, Morrissey J, McCracken R, Reyes A, Klahr S (1995) Angiotensin II receptor antagonist ameliorates renal tubulointerstitial fibrosis caused by unilateral ureteral obstruction. Kidney Int 47:1285–1294
18. Kakiuchi S, Sobue K (1983) Control of the cytoskeleton by calmodulin and calmodulin-binding proteins. Trends Biochem Sci 208:454–459
19. Kreis TE, Birchmeier W (1980) Stress fiber sarcomeres of fibroblasts are contractile. Cell 22:555–561
20. Levin RM, Weiss B (1979) Selective binding of antipsychotics and other psychoactive agents to the calcium-dependent acti-

vator of cyclic nucleotide phosphodiesterase. J Pharmacol Exp Ther 208:454–459
21. Ng YY, Huang TP, Yang WC, Chen ZP, Yang AH, Mu W, Nikolic-Patersion DJ, Atkins RC, Lan HY (1998) Tubular epithelial-myofibroblast transdifferentiation in progressive tubulointerstitial fibrosis in 5/6 nephrectomized rats. Kidney Int 54:864–876
22. Petridou S, Masur SK (1996) Immunodetection of connexins and cadherins in corneal fibroblasts and myofibroblasts. Invest Ophthalmol Vis Sci 37:1740–1748
23. Powell DW, Mifflin RC, Valentich JD, Crowe SE, Saada JI, West AB (1999) Myofibroblasts. I. Paracrine cells important in health and disease. Am J Physiol 277:C1–C9
24. Rahwan RG, Piascik MF, Witiak DT (1979) The role of calcium antagonism in the therapeutic action of drugs. Can J Physiol Pharmacol 57:443–460
25. Sappino AP, Schurch W, Gabbiani G (1990) Differentiation repertoire of fibroblastic cells: expression of cytoskeletal proteins as marker of phenotypic modulations. Lab Invest 63:144–161
26. Serini G, Gabbiani G (1999) Mechanisms of myofibroblast activity and phenotypic modulation. Exp Cell Res 250:273–283
27. Skalli O, Ropraz P, Trzeciak A, Benzonana G, Gillessen D, Gabbiani G (1986) A monoclonal antibody against alpha-smooth muscle actin: a new probe for smooth muscle differentiation. J Cell Biol 103:2787–2796
28. Spanakis SG, Petridou S, Masur SK (1998) Functional gap junctions in corneal fibroblasts and myofibroblasts. Invest Ophthalmol Vis Sci 39:1320–1328
29. Squier CA (1981) The effect of stretching on formation of myofibroblasts in mouse skin. Cell Tissue Res 220:325–335
30. Sun DF, Fujigaki Y, Fujimoto T, Yonemura K, Hishida A (2000) Possible involvement of myofibroblasts in cellular recovery of uranyl acetate-induced acute renal failure in rats. Am J Pathol 157:1321–1335
31. Sun DF, Fujigaki Y, Fujimoto T, Goto T, Yonemura K, Hishida A (2002) Mycophenolate mofetil inhibits regenerative repair in uranyl acetate-induced acute renal failure by reduced interstitial cellular response. Am J Pathol 161:217–227
32. Takashima N, Kawachi H, Oite T, Nishi S, Arakawa M, Shimizu F (1993) Effect of chlorpromazine on kinetics of injected monoclonal antibody in MoAb-induced glomerular injury. Clin Exp Immunol 91:135–140
33. Tomasek JJ, Haaksma CJ, Eddy RJ, Vaughan MB (1992) Fibroblast contraction occurs on release of tension in attached collagen lattices: dependency on an organized actin cytoskeleton and serum. Anat Rec 232:359–368
34. Tsukita SH, Tsukita SA, Nagafuchi A, Yonemura S (1992) Molecular linkage between cadherins and actin filaments in cell–cell adhesions junctions. Curr Opin Cell Biol 4:834–839
35. Ushiki T, Murakumo M (1991) Scanning electron microscopic studies of tissue elastin components exposed by a KOH-collagenase or simple KOH digestion method. Arch Histol Cytol 54:427–436
36. Wang N, Butler JP, Ingber DE (1993) Mechanotransduction across the cell surface and through the cytoskeleton. Science 260:1124–1127

Virchows Arch (2005) 446:177–180
DOI 10.1007/s00428-004-1154-6

ORIGINAL ARTICLE

Christian Andree · Roland Sedivy

Discovery of a letter from Rokitansky to Virchow about subependymal corpora amylacea

Received: 6 September 2004 / Accepted: 6 October 2004 / Published online: 4 December 2004
© Springer-Verlag 2004

Abstract Until recently, Rokitansky and Virchow were thought to have never exchanged letters. Recently, however, a letter from Rokitansky to Virchow dated 1853 was discovered. In this letter, Rokitansky commented on Virchow's discovery of subependymal corpora amylacea. This report comprises an English translation of this letter together with a historical appraisal and a short comment on the importance of corpora amylacea in the brain.

Keywords Rokitansky · Virchow · Corpora amylacea · Brain · Polyglucosan diseases · Ageing

Introduction

Until recently, no correspondence between the two doyens of pathology, Rokitansky (1804–1878) and Virchow (1821–1902) (Fig. 1), was known to exist. We are fortunate to be able to present a letter from Rokitansky to Virchow (Fig. 2), which was found by one of the authors (Christian Andree) at the Berlin-Brandenburg Academy of Sciences [15]. It is a three and a half page-long letter dated 10 November 1853, Vienna, which is published here for the first time in an English translation.

Letter

Dear Sir: Professor Kölliker will inform you about the matter that prompted me to contact him. I take the liberty of recommending the same to you.

Furthermore, I am influenced by my interest in your discovery of the specific nature of corp[ora] amyl[ac]ea in the ependyma of the brain ventricle. Yesterday evening I received the first issue of volume 6 of your Archives, and today I hastened to see what you write about them. It is exactly as you say; I just had the opportunity to examine the ependyma covering a large tubercle, loosened by a serous effusion in the vicinity of the ventricles, in which a great number of such bodies were embedded. Other objects are not immediately available with which to pursue this discovery further, but in the interest of the matter I cannot help adding the following observations: I have found these corp[ora] amyl[ac]ea, as they actually should be called, in the "atrophic" [N.] opticus, as you mentioned, but also in a dull gray translucent moisture in the medullary fascicles of the spinal cord and the brain leading to atrophy of the medulla and, repeatedly and of considerable size, in osteomalacic bones. They always attracted my attention because they differed in appearance from other lamellated bodies, and I distinguished them especially from these because they dissolved in the native moisture by gentle heating. For some time I was confused and inclined to consider them lamellated globules of fat, because the same dissolution occurred when ether was added. However, the manner in which they dissolved in aqueous liquid showed me otherwise; it was not like the melting of solid fat. The process of dissolution of these bodies differs somewhat from amylum bodies in that, although they first swell up, they do not develop cracks, as would be caused by pressure, but expand to a certain degree and then disappear all of a sudden. All of the substances in which I saw them were connective tissue bases.

Allow me to report this incidental information in the interest of your fine discovery and to assure you of my highest esteem.

Yours sincerely
Rokitansky
Vienna, the 10 November 1853
R. Virchow, Esq.

Dedicated to the 200th anniversary of Carl Rokitansky's birth

C. Andree
Institute for History of Medicine and Pharmacy,
University Kiel,
Germany

R. Sedivy (✉)
Department of Pathology,
Medical University Vienna,
Währinger Gürtel 18-20, 1090 Wien, Austria
e-mail: roland.sedivy@meduniwien.ac.at

Fig. 1 Carl Rokitansky (1804–1878) and Rudolf Virchow (1821–1902) facing each other—whether they ever met personally is unclear (pictures taken from "Galerie berühmter Kliniker, J. Hirschfeld 1877, Collectio Sedivy)

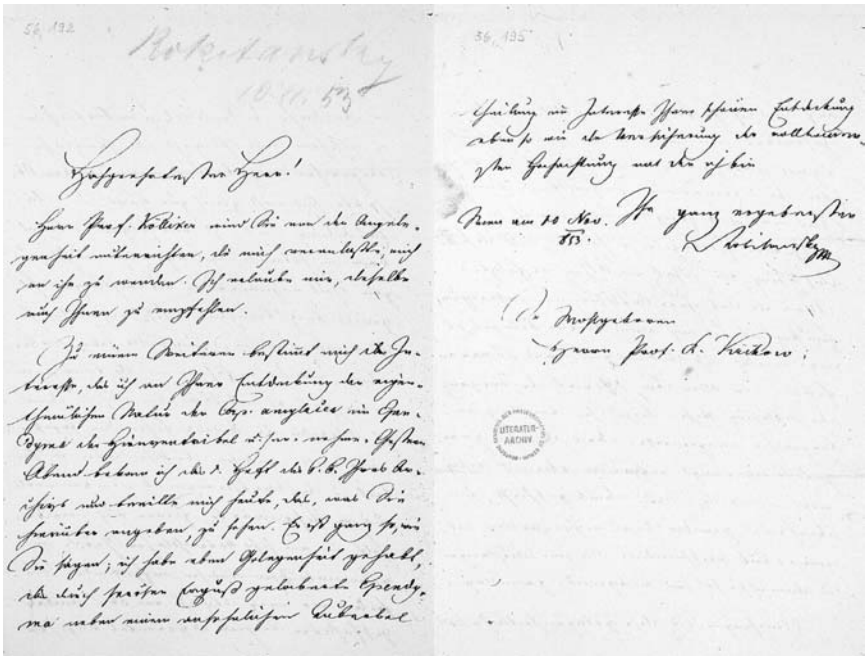

Fig. 2 Rokitansky's letter to Virchow dated 10 November 1853. The figure shows the first and the last pages (Berlin-Brandenburg Academy of Sciences [15])

Medicohistorical comment

This letter leads us directly into the scientific discussion of the mid-19th century. It was a time of epistemological change in medicine from a phenomenological orientation to a true scientific approach based on experimental methods. In contrast to Rokitansky, who represented humoropathological ideas, following the example of Andral (1797–1876), Virchow (1854) based his investigations strictly on experiments. Virchow's first years in Würzburg were exclusively devoted to his work in pathology and not, as in later times, to politics. In particular, he tried to solve morphological problems by applying chemical analysis and microscopy. On these aspects, Virchow had lively discussions with his colleagues Kölliker (1817–1905) and Scherer (1814–1869) [2]. Regarding corpora amylacea (CA), Virchow had already published on these enigmatic bodies in 1851, together with what he called "amyloid" deposits, which he had found in kidneys and ovaries [1]. Virchow was very interested in the chemical properties of such deposits [16]. Finally, in 1854, he discovered differences in the chemical properties that enabled amyloid bodies to be differentiated from CA [17].

CA were first noted by J.E. Purkinyê (Purkinje; 1787–1869) in 1837 [4, 9]. They were described in more detail, as mentioned above, by Virchow, who demonstrated their reactivity with iodine [17]. In the ensuing years, CA were considered to have no pathological significance. Their

origin was thought to be neuronal; others favoured astrocytes as the main source [4, 5]. It was believed that they were only post-mortem artefacts or hyaline degenerations of mesoglia or protein precipitates [7, 10]. All of these studies shared the observation that CA are more prominent in older age groups and in chronic neurological diseases. Investigations of their biological role involving histochemical, immunohistochemical and ultrastructural methods started within the last decades. In 1969, Sakai and co-workers [12] showed that CA are composed of polyglycosans. Using immunohistochemistry, Cisse et al. demonstrated that CA react with antibodies against ubiquitin and several heat shock proteins [6]. These findings indicated that the accumulation of proteins reflects sustained physiological stress. The latest overview was given by J.B. Cavanagh [5]. It is recommended to the reader interested in further details.

Pathohistological comment

CA are small (10–12 μm), basophilic, round-spherical, concentrically lamellated bodies found in the brain (Fig. 3), heart, skeletal muscle, liver, prostate, thyroid and lung in various species and in various conditions. In the brain, CA are glycoproteinaceous inclusions that accumulate in astroglia and other brain cells during ageing and in other neurodegenerative conditions. Topographically, in aged brains, CA are distributed mainly in perivascular and subependymal localisations and beneath the subpial border of the hippocampus. In adult polyglucosan body disease and type-IV glycogenosis, CA have been found throughout the nervous system. Although CA (amyloid or starch bodies) are similar to other neurological CA, such as Lafora (-like) bodies and Bielschowsky bodies, they appear in different situations. In particular, Lafora bodies, which are pathognomonic of myoclonic epilepsy, have a slightly different staining pattern because of variations in the esterification of the glucose polymer [12]. Cavanagh, therefore, suggested maintaining the separate nomenclature [5]. CA in other organs, such as the prostate, liver, thyroid and lung, do not share the histochemical features of brain CA and are therefore unrelated to polyglucosan bodies. The biogenesis of CA remains largely unclear. It has been shown that the sulfhydryl agent, cysteamine, promotes the accumulation of CA-like bodies in cultured rat astroglia. Human and rat CA stained positively with periodic acid-Schiff and react immunohistochemically with mitochondrial epitopes and ubiquitin [13]. Regarding their importance, it has been suggested that CA are indicators of neurodegeneration [5, 6, 14]. CA are now thought to be sequestrated glucose polymers of potentially hazardous products of cellular metabolism derived from the ageing process, but also from any disease with harmful products [8]. In normal health, the main role of CA is protection from these harmful products of metabolic activity [5]. The immunohistochemical finding that nestin filaments are part of CA supports the idea of an additional regulated disposal system in the brain [3].

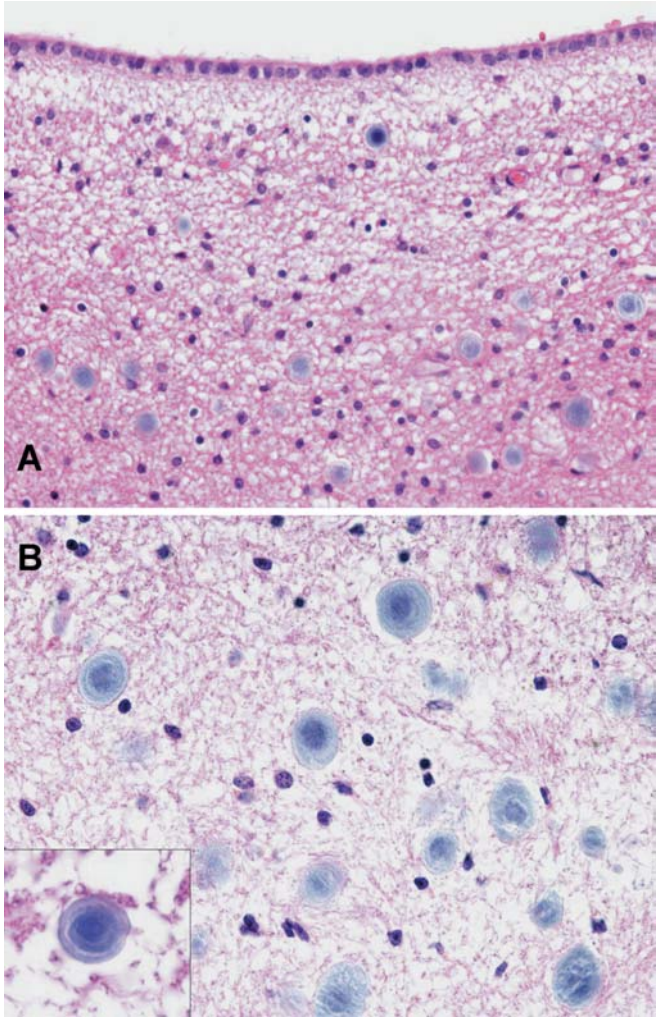

Fig. 3 Subependymal corpora amylacea (CA) in an elderly person. **A** Overview (original magnification ×100). **B** Detail (original magnification ×600). The inset shows CA with typical concentrically lamellated structure

Concluding remarks

Rokitansky's letter (dated 10 November 1853) cited the Archives of Pathological Anatomy and Physiology and Clinical Medicine, volume 6, 1854 [17]. This issue, however, appeared already in early November 1853. The particular article is dated 4 September 1853; an addendum displays the date 25 September 1853. This may explain why Rokitansky was able to read this article before the official time of publication. At the time, it was not unusual for issues of journals to appear much earlier than indicated by the printed year. Virchow mentioned in the addendum to his article that Rokitansky and Kölliker had seen CA in the N. opticus and retina, respectively. When mentioning Rokitansky, Virchow used the passive voice, indicating that he was not sure whether Rokitansky really had observed them. We speculate that this fact was the background behind his letter to Virchow.

On the first pages of the same volume (ref. [17] p. 3–33), Virchow unexpectedly praised Rokitansky's work and the Vienna School of Medicine. In the years before, he had criticised the humeropathological interpretation of blood diseases in Rokitansky's manual of pathological anatomy [11] strongly and in a very unfriendly manner [18]. Although the criticism of Rokitansky's theory of dyscrasis was justified, the harsh and derisive words used by Virchow would hardly have prompted Rokitansky to write an amicable letter. However, he approached Virchow without resentment and wrote approvingly of "your discovery of the specific nature of corpora amylacea" and closed his letter with "in the interest of your fine discovery and to assure you of my highest esteem".

Acknowledgements The authors are indebted to Dr. Christine Haberler (Department of Neuropathology, Medical University Vienna) for providing histological slides of corpora amylacea in the brain and to Mrs. Dege for editing the manuscript.

References

1. Ackerknecht EH (1957) Rudolf Virchow, Ferdinand Enke, Stuttgart, p 55f
2. Andree C (2001) Der Briefwechsel Rudolf Virchows mit den Eltern, 1839–1864. In: Andree C (ed) First complete edition: Rudolf Virchow—Sämtliche Werke, Blackwell Wissenschafts-Verlag, Berlin, p 969 (about Kölliker A), p 1003 (about Scherer JJ)
3. Buervenich S, Olson L, Galter D (2001) Nestin-like immunoreactivity of corpora amylacea in aged human brain. Mol Brain Res 94:204–208
4. Catola G, Achúcarro N (1906) Uber die Entstehung der Amyloidkörperchen im Zentranervensystem Virchows. Arch f Path Anat 184:454–469
5. Cavanagh JB (1999) Corpora-amylacea and the family of polyglucosan diseases. Brain Res Rev 29:265–295
6. Cisse S, Perry G, Lacoste-Royal G, Cabana T, Gauvreau D (1993) Immunohistochemical identification of ubiquitin and heat-shock proteins in corpora amylacea from normal aged and Alzheimer's disease brains. Acta Neuropathol (Berl) 85:233–240
7. Ferraro A, Damon LA (1931) The histiogenesis of amyloid bodies in the central nervous system. Arch Pathol 12:229–244
8. Mohanty SK, Radotra BD, Banerjee AK (2004) Ageing changes in the human brain: a histochemical and immunohistochemical study. Neuropathology 24:8–15
9. Purkinje JE (1837) Bericht über die Naturforscherversammlung zu Prag im Jahre 1837 (cit. ref. 4)
10. Robertson WF (1900) A textbook of pathology in relation to mental disease. WF Clay, Edinburgh
11. Rokitansky Carl (1846) Handbuch der allgemeinen pathologischen Anatomie, Wien, Braumüller & Seidel
12. Sakai M, Austin J, Witmer F, Trueb L (1970) Studies in myoclonus epilepsy (Lafora body form). II. Polyglucosans in systemic deposits in myoclonus epilepsy and corpora amylacea. Neurology 20:160–176
13. Schipper HM (1998) Experimental induction of corpora amylacea in adult rat brain. Microsc Res Tech 43:43–48
14. Singhrao SK, Neal JW, Newman GR (1993) Corpora amylacea could be an indicator of neurodegeneration. Neuropathol Appl Neurobiol 19:269–276
15. Virchow R (1807) estate fasc.
16. Virchow R (1852) Einige Bemerkungen über Bau und Zusammensetzung der Corpora amylacea des Menschen. Verhandlungen der physikalisch-medizinischen Gesellschaft zu Würzburg; II, pp 51–53
17. Virchow R (1854) Über eine im Gehirn und Rückenmark des Menschen aufgefundene Substanz mit der chemischen Reaction der Cellulose. Arch Path Anat u Physiol u Klin Med 6:135–138
18. Virchow Rudolf (1846), Rokitansky, Handbuch der allgemeinen pathologischen Anatomie, Literarische Beilage, Preußische Medicinal-Zeitung XV pp 237–238, pp 243–244

Virchows Arch (2005) 446:181–184
DOI 10.1007/s00428-004-1156-4

CASE REPORT

Carla Oliveira · Herculano Moreira · Raquel Seruca · Manuel Cardoso de Oliveira · Fátima Carneiro

Role of pathology in the identification of hereditary diffuse gastric cancer: report of a Portuguese family

Received: 27 August 2004 / Accepted: 30 September 2004 / Published online: 11 December 2004
© Springer-Verlag 2004

Abstract Mutations in E-cadherin gene are the underlying genetic defect in approximately one-third of the hereditary diffuse gastric cancer (HDGC) families described to date. Positive family history of diffuse gastric cancer and early age of onset of gastric tumours are the clinical criteria currently used to qualify for HDGC. In the present study, we describe a Portuguese family with HDGC that was selected for *CDH1* mutation screening after histological observation of the gastrectomy specimen of one member, who died at the age of 23 years from widely invasive diffuse gastric carcinoma. The detection in the surgical specimen of tiny foci of intramucosal diffuse carcinoma as well as in situ carcinoma lesions and pagetoid spread of signet ring cells raised the hypothesis of HDGC, which was confirmed by pedigree analysis of the family and detection of *CDH1* germline mutation. We conclude that there are morphological hints that may help in the identification of HDGC.

The authors wish it to be known that Carla Oliveira and Herculano Moreira should be regarded as joint first authors

C. Oliveira · R. Seruca · M. Cardoso de Oliveira · F. Carneiro (✉)
Institute of Molecular Pathology and Immunology,
University of Porto (IPATIMUP),
Rua Dr Roberto Frias s/n, 4200-465 Porto, Portugal
e-mail: fcarneiro@ipatimup.pt
Tel.: +351-2-25570700
Fax: +351-2-25570799

H. Moreira · M. Cardoso de Oliveira
Department of Surgery,
Hospital S. João,
Porto, Portugal

F. Carneiro
Department of Pathology,
Hospital S. João,
Porto, Portugal

R. Seruca · M. Cardoso de Oliveira · F. Carneiro
Medical Faculty,
University of Porto,
Porto, Portugal

Keywords E-cadherin · Hereditary diffuse gastric cancer · In situ carcinoma · Pagetoid spread

Introduction

Knowledge regarding pathology and genetic basis of familial gastric cancer has greatly increased in the last years, due to the definition of hereditary diffuse gastric cancer (HDGC) syndrome and the discovery of segregating germline mutations in the E-cadherin (*CDH1*) gene [2, 6]. Mutations in *CDH1* are the underlying genetic defect in one-third of the HDGC families [9]. Clinical criteria to qualify for HDGC were established by the International Gastric Cancer Linkage Consortium (IGCLC) [2]. The thorough study of prophylactic gastrectomies performed in asymptomatic carriers of germline *CDH1* mutations led to the identification of precursor lesions of HDGC, such as in situ signet ring cell carcinoma and pagetoid spread [3].

In the present study, we describe a Portuguese family with HDGC that was selected for *CDH1* mutation screening after morphological observation of the gastrectomy specimen of one member with early-onset diffuse gastric carcinoma. The detection of multiple foci of diffuse carcinoma and in situ carcinoma with pagetoid spread raised the hypothesis of HDGC, which was confirmed by pedigree analysis and detection of *CDH1* germline mutation.

Case report

A 23-year-old female reported in early 2001 for investigation of frequent epigastric pain, hematemesis and anaemia. Endoscopy revealed a large gastric ulcer. Multiple endoscopic biopsies showed the presence of chronic gastritis and signet ring cell carcinoma. The patient was submitted to total gastrectomy with oesophago-jejunostomy. A tumour (8×5×5 cm) was observed in the body of the stomach, with serosal invasion and metastases in 6 of 18 regional lymph nodes (pT3N1Mx). The patient died 9 months after surgery. Autopsy was not performed.

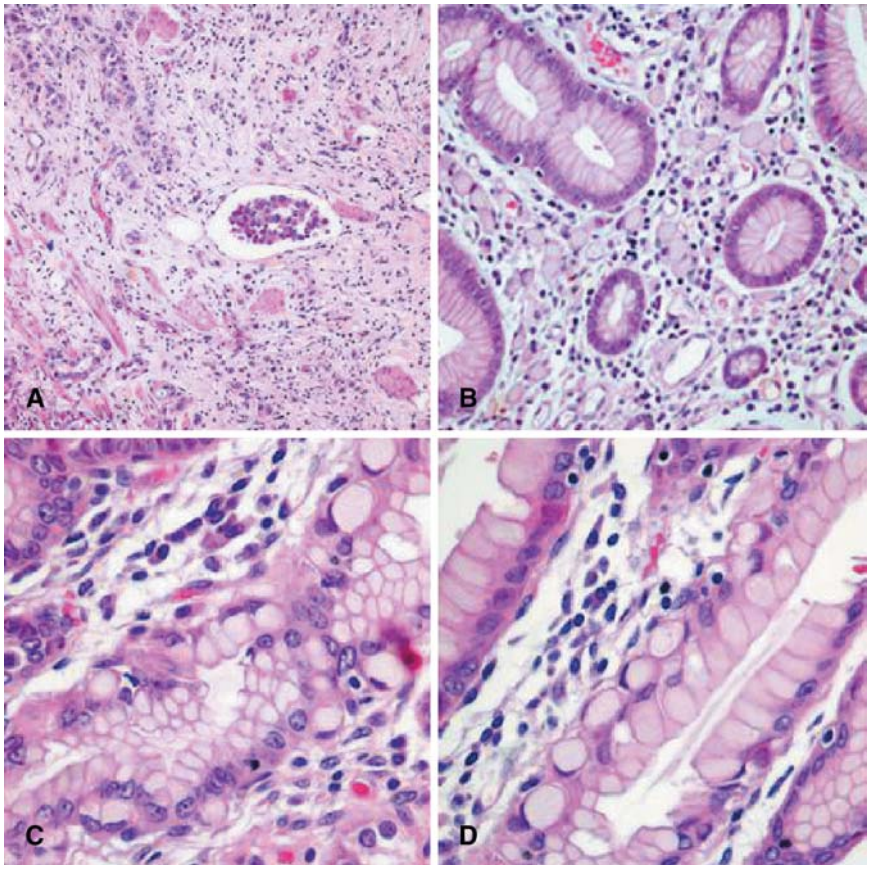

Fig. 1 Different lesions observed in the proband. **A** Widely invasive diffuse carcinoma [haematoxylin and eosin (H&E), ×10]. **B** Tiny focus of intramucosal diffuse carcinoma displaying signet ring cell phenotype (H&E, ×20). **C** In situ carcinoma (H&E, ×40). **D** Pagetoid spread of signet ring cells along an adjacent foveolae (H&E, ×40)

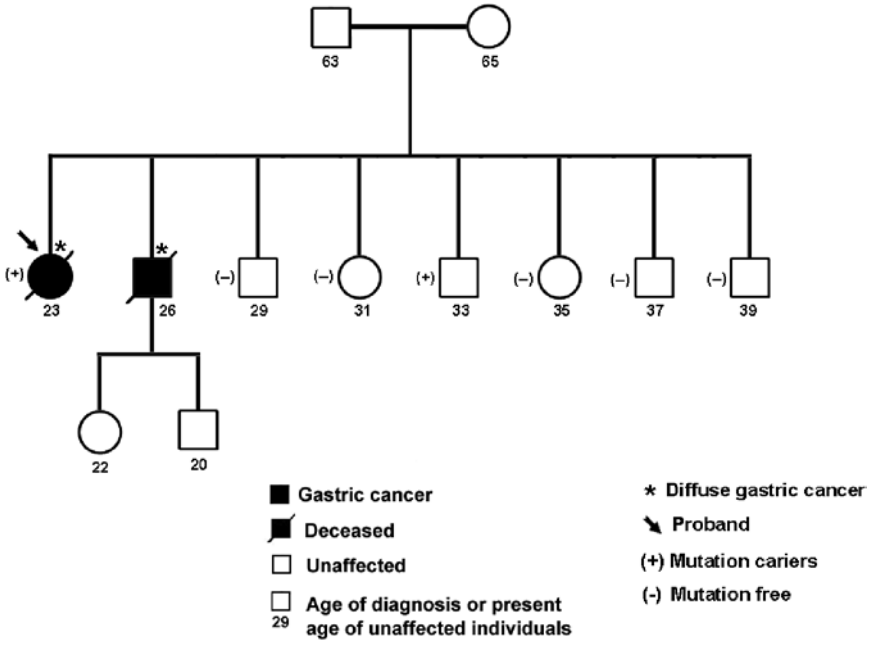

Fig. 2 Pedigree of the family. The age of onset of the tumours or the present age of unaffected individuals is shown underneath the symbols: + carriers of germline mutation, – subjects that did not carry the mutated alleles in the germline DNA, *arrow* proband, *asterisk* patients with histologically confirmed diffuse gastric cancer

Using histology, the tumour showed the features of diffuse/signet ring cell carcinoma (Fig. 1A). Several tiny foci of intramucosal signet ring cell carcinoma were identified away from the main tumour (Fig. 1B). Furthermore, foci of in situ carcinoma were observed, characterised by the presence of signet ring cells partially substituting the epithelial lining of glands (Fig. 1C). Pagetoid spread of signet ring cells was observed along adjacent foveolae (Fig. 1D). The similitude of these lesions with those described in prophylactic gastrectomies from germline *CDH1* mutation carriers [3, 7] raised the hypothesis of HDGC, which was further investigated.

Family history of gastric cancer was collected. The patient had an older brother who had died 14 years previously with diffuse gastric carcinoma, at the age of 26 years (Fig. 2). The diagnosis was

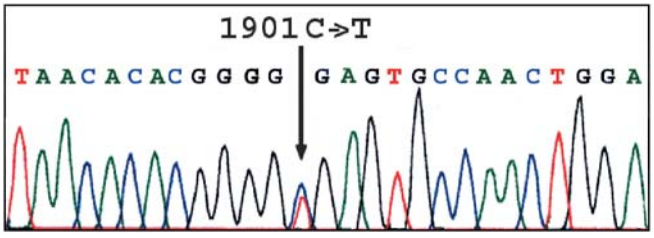

Fig. 3 Sequencing analysis showing the 1901 C>T transition in exon 12 leading to an amino acid substitution from alanine to valine in codon 634

confirmed by the histological evaluation of available haematoxylin and eosin-stained slides. Living members of this family were asked to provide informed consent to proceed for genetic testing for *CDH1* germline mutations. DNA was extracted from normal gastric tissue from the proband of this family, and *CDH1* mutation screening revealed the presence of a heterozygous missense mutation at position 1901 (C>T) in codon 634 (Fig. 3), leading to an amino acid substitution from Ala to Val [8]. Mutation screening was not performed in the 26-year-old brother who died from gastric cancer, due to unavailability of paraffin-embedded tissue. The remaining six asymptomatic siblings were also tested, after informed consent, and one (33-year old) was found to be a mutation carrier of the same *CDH1* mutation identified in the proband. The parents refused genetic testing.

Discussion

The collection of family history and the identification of several affected individuals in the same kindred are commonly the first steps towards the identification of familial/hereditary syndromes. Familial gastric cancer is an uncommon disease; HDGC is even less common and difficult to address on clinical and therapeutic grounds. Criteria for the identification of HDGC was first established by the IGCLC [2] and recently updated by Brooks-Wilson and colleagues [1].

In this report, we describe a family with HDGC in which a germline *CDH1* mutation was detected after morphological identification of multifocal diffuse/signet ring cell gastric carcinoma and in situ carcinoma lesions with pagetoid spread. The patient herein reported carried a missense mutation, which was first reported in a colon carcinoma cell line, as giving rise either to truncated proteins due to the activation of a cryptic splice-site created by the mutation, together with full length proteins carrying the amino acid substitution expected to occur after the missense mutation [12]. Soon after, this missense mutation was found in a Portuguese early-onset diffuse cancer patient who died at the age of 30 years [11]. By in vitro functional analysis, the A634V mutation proved to induce dramatic changes in cell adhesion, motility and invasion [11].

In addition to the patient who died from multifocal diffuse gastric cancer (the case herein reported), we have identified another mutation carrier, a brother who remains asymptomatic. Most probably, the brother who died from diffuse gastric cancer was also a mutation carrier, but we could not prove it due to lack of tissue for genetic analysis. One of the parents must be an obligate carrier, since two of their children carry the same germline *CDH1* mutation. Efforts to obtain informed consent for genetic testing in the parents were fruitless.

Huntsman and colleagues described foci of early diffuse gastric cancer in 100% of the prophylactic gastrectomy specimens from asymptomatic *CDH1* mutation carriers [7] and showed that gastric cancer developed in all of them, meaning that carriers of a germline *CDH1* mutation have a lifetime risk of developing early gastric cancer close to 100%. However, it is conceivable that not all pathological changes will develop into clinically significant cancer, leading to a decrease in the observed penetrance, as it seemed to occur in this family, regarding one of the parents and the asymptomatic son. Pharoah and colleagues [10] estimated the cumulative risk of clinically detected gastric cancer for men to be 67% and for women to be 83% at the age of 80 years.

The mutation identified in this family typed as a missense mutation and proved to be pathogenic in functional assays [11]. The program of surveillance of asymptomatic *CDH1* mutation carriers is being performed, in this family, according to the recommendations of Fitzgerald and Caldas [5]. The asymptomatic brother of the proband (aged 33 years) and both parents (one of which an obligate carrier) are currently under genetic counselling and intensive endoscopic surveillance, aiming to identify an early curable lesion.

According to Charlton and colleagues [4], chromoendoscopy using a pH-sensitive dye, congo red, following stimulation by pentagastrin, may be useful in performing multiple targeted biopsies in highlighted areas along the program of endoscopic surveillance.

In summary, the case we report was first considered as an early-onset diffuse gastric cancer, and histopathological features led to the collection of family history and genetic testing, which turned out to be positive for a germline *CDH1* mutation, proving the diagnosis of HDGC in this Portuguese family. For pathologists, the take-home lesson from this case is that there are morphological hints that may help in the identification of HDCG.

Acknowledgements This study was funded by grants from Fundação para a Ciência e a Tecnologia, Portugal (POCTI/35374/CBO/2000 and POCTI/MGI/35586/1999) and by Programa Operacional Ciência, Tecnologia e Inovação (POCTI), of QCA III.

References

1. Brooks-Wilson AR, Kaurah P, Suriano G, Leach S, Senz J, Grehan N, Butterfield YS, Jeyes J, Schinas J, Bacani J, Kelsey M, Ferreira P, MacGillivray B, MacLeod P, Micek M, Ford J, Foulkes W, Australie K, Greenberg C, LaPointe M, Gilpin C, Nikkel S, Gilchrist D, Hughes R, Jackson CE, Monaghan KG, Oliveira MJ, Seruca R, Gallinger S, Caldas C, Huntsman D (2004) Germline E-cadherin mutations in hereditary diffuse gastric cancer: assessment of 42 new families and review of genetic screening criteria. J Med Genet 41:508–517

2. Caldas C, Carneiro F, Lynch HT, Yokota J, Wiesner GL, Powell SM, Lewis FR, Huntsman DG, Pharoah PD, Jankowski JA, MacLeod P, Vogelsang H, Keller G, Park KG, Richards FM, Maher ER, Gayther SA, Oliveira C, Grehan N, Wight D, Seruca R, Roviello F, Ponder BA, Jackson CE (1999) Familial gastric cancer: overview and guidelines for management. J Med Genet 36:873–880
3. Carneiro F, Huntsman DG, Smyrk TC, Owen DA, Seruca R, Pharoah P, Caldas C, Sobrinho-Simões M (2004) Model of the early development of diffuse gastric cancer in E-cadherin mutation carriers and its implications for patient screening. J Pathol 203:681–687
4. Charlton A, Blair V, Shaw D, Parry S, Guilford P, Martin IG (2004) Hereditary diffuse gastric cancer: predominance of multiple foci of signet ring cell carcinoma in distal stomach and transitional zone. Gut 53:814–820
5. Fitzgerald RC, Caldas C (2004) Clinical implications of E-cadherin associated hereditary diffuse gastric cancer. Gut 53:775–778
6. Guilford P, Hopkins J, Harraway J, McLeod M, McLeod N, Harawira P, Taite H, Scoular R, Miller A, Reeve AE (1998) E-cadherin germline mutations in familial gastric cancer. Nature 392:402–405
7. Huntsman DG, Carneiro F, Lewis FR, MacLeod PM, Hayashi A, Monaghan KG, Maung R, Seruca R, Jackson CE, Caldas C (2001) Early gastric cancer in young, asymptomatic carriers of germ-line E-cadherin mutations. N Engl J Med 344:1904–1909
8. Oliveira C, Ferreira P, Nabais S, Campos L, Ferreira A, Cirnes L, Castro Alves C, Veiga I, Fragoso M, Regateiro F, Moreira Dias L, Moreira H, Suriano G, Carlos Machado J, Lopes C, Castedo S, Carneiro F, Seruca R (2004) E-cadherin (*CDH1*) and p53 rather than SMAD4 and caspase-10 germline mutations contribute to genetic predisposition in Portuguese gastric cancer patients. Eur J Cancer 40:1897–1903
9. Oliveira C, Suriano G, Ferreira P, Canedo P, Kaurah P, Mateus R, Ferreira A, Ferreira AC, Oliveira MJ, Figueiredo C, Carneiro F, Keller G, Huntsman D, Machado JC, Seruca R (2004) Genetic screening for familial gastric cancer. Hereditary Cancer Clin Pract 2:51–64
10. Pharoah PD, Guilford P, Caldas C, International Gastric Cancer Linkage Consortium (2001) Incidence of gastric cancer and breast cancer in *CDH1* (E-cadherin) mutation carriers from hereditary diffuse gastric cancer families. Gastroenterology 121:1348–1353
11. Suriano G, Oliveira C, Ferreira P, Machado JC, Bordin MC, De Wever O, Bruyneel EA, Moguilevsky N, Grehan N, Porter TR, Richards FM, Hruban RH, Roviello F, Huntsman D, Mareel M, Carneiro F, Caldas C, Seruca R (2003) Identification of *CDH1* germline missense mutations associated with functional inactivation of the E-cadherin protein in young gastric cancer probands. Hum Mol Genet 12:575–582
12. Vecsey-Semjen B, Becker KF, Sinski A, Blennow E, Vietor I, Zatloukal K, Beug H, Wagner E, Huber LA (2002) Novel colon cancer cell lines leading to better understanding of the diversity of respective primary cancers. Oncogene 21:4646–4662

Virchows Arch (2005) 446:185–188
DOI 10.1007/s00428-004-1093-2

CASE REPORT

Sandy Azoulay · Camilo Adem · Michel Gatineau · Jean-François Finet · Hayssam Bakdach · Jean-François Regnard · Frédérique Capron

Pericardial ectopic thymoma

Received: 1 April 2004 / Accepted: 2 July 2004 / Published online: 11 December 2004
© Springer-Verlag 2004

Abstract Primary intrapericardial thymoma is an unusual localization. We report a case of a patient with an isolated and primary pericardial thymoma. This 72-year-old woman presented with dyspnea, dysphony and myalgia. The radiological evaluation revealed an intrapericardial mass. Surgical exploration showed a hemorrhagic and infiltrative tumor in the pericardial sac, while the mediastinum was free of tumor. Surgical biopsies and, later, an ablation of pericardial mass were done. The tumor was a thymoma, composed of large epithelial cells and immature T lymphocytes and was classified B2 according to the World Health Organization classification (1999). Clinically, a myasthenia gravis was revealed. We discuss the few cases reported in the literature.

Keywords Thymoma · Pericardium · Ectopic thymoma · Myasthenia gravis

S. Azoulay · C. Adem · J.-F. Finet · F. Capron (✉)
Service d'Anatomie pathologique,
Groupe Hospitalier de la Pitié-salpêtrière,
47-83 Bd de l'Hôpital, 75013 Paris, France
e-mail: frederique.capron@psl.ap-hop-paris.fr
Tel.: +33-1-42177773
Fax: +33-1-42177777

M. Gatineau
Service de Pneumologie,
Groupe Hospitalier de la Pitié-salpêtrière,
47-83 Bd de l'Hôpital, 75013 Paris, France

H. Bakdach
Clinique Chirurgicale du Val d'Or,
16 rue Pasteur, 92211 Saint Cloud Cedex, France

J.-F. Regnard
Service de Chirurgie Thoracique,
Hôtel Dieu,
1 Place du parvis Notre Dame, 75001 Paris, France

Introduction

Thymomas, as tumors originating from the epithelial elements of the thymus, are more often located in the anterior mediastinum, sometimes extending to the superior compartment. However, some thymomas can occur in an unusual location, secondary to a probable failure in embryological thymic displacement. Among ectopic locations, authors have reported cases occurring in the neck, the inferior or posterior mediastinum, the bronchial tract and the diaphragm [3, 8, 12]. Rarely, isolated and solitary pericardial thymomas, without another tumor site, have been described [11]. We report a case of primary intrapericardial thymoma, revealing a myasthenia gravis. The clinicopathological and immunohistochemical features of this tumor are presented, along with a literature review of ectopic presentation.

Clinical history

A 72-year-old woman presented with dyspnea, dysphony and myalgia. She had a long personal history, with endometriosis, depression, polymyostis, nephrotic syndrome and Parkinson's disease. She had polymyositis with finger retraction and muscular weakness 20 years prior to presentation, treated by corticotherapy. On a recent chest-X-ray, there was a slight enlargement of the heart. The superior aerodigestive endoscopy found a left recurrent nerve deficit. A 5-cm solid mass, located in the pericardium, was observed on computed tomography scan, while the mediastinum was free of tumor. On surgical exploration, a solitary mass was identified, precisely in the aorta–pulmonary sinus, between the left superior pulmonary vein and the left pulmonary artery. It was large, infiltrative and extremely hemorrhagic, and its base of implantation could not be noted. Multiple biopsies were performed. Later, on surgical exploration, the mediastinum was free of tumor. The pericardial mass was completely excised, as well as a proximal bronchial enlarged lymph node.

Materials and methods

Tumor tissues from biopsies and surgical excision were routinely fixed in formalin (10%), embedded in paraffin and subsequently stained with hematoxylin–eosin–saffron. A panel of antibodies

(provider, dilution) was also applied to paraffin sections, using automated immunohistochemical technique (Dako), CD3 (Dako, 1/100), CD5 (Tebu Novocastra, 1/25), CD20 (Dako, 1/250), AE1/AE3 (Biogenex, 1/50), CD1A010 (Beckman-Coulter, prediluted) and TTF1 (Dako, 1/50).

Results

Macroscopically, the tumor was in the pericardium and measured approximately 6×4×3 cm. The cut surface revealed a white solid mass, with a 4-cm hemorrhagic and cystic area (Fig. 1). Its base of implantation was exactly in the pericardium and measured 2 cm. Microscopically, biopsies and tumor tissues had similar profiles. Low-power view of tumor sections showed lobulated architecture with two different cell types. At higher magnification, a medium-sized mesh of epithelial cells intermixed with abundant lymphocytes (Fig. 2). The epithelial cells were ovoid with eosinophilic cytoplasm and oval nuclei with fine chromatin, regular outline and prominent nucleoli. These cells were connected to each other by enlarged eosinophilic cytoplasmic processes. There was no atypia and no mitotic figure. The lymphocytes were small and round, with a scant cytoplasm. Another histopathological hallmark was the formation of perivascular clear spaces, bordered by palisading epithelial cells and sometimes containing serous fluid and lymphocytes. On the surgical mass, the tumor invades the pericardium, while the bronchial lymph node was metastatic with extracapsular extension.

Immunohistochemical studies showed that cells expressed cytokeratin (AE1/AE3), confirming their epithelial nature and highlighting their connected network (Fig. 3). The lymphocytes expressed CD3, CD5 and CD1a, and were recognized as immature T lymphocytes, i.e. thymocytes (Fig. 4). Very few lymphocytes were CD20 positive, while TTF1 did not mark any tumor cell. Putting together the clinical, the morphological and the immunohistochemical findings, this tumor was classified as a thymoma located in the pericardium. The tumor was malignant according to Levine and Rosai's classification [4] because it invaded the pericardium and because of the presence of metastatic lymph node. Pathologically, it was classified B2 according to the World Health Organization (WHO) classification (1999) or mixed lymphocytic and polygonal epithelial cell type, as known as cortical thymoma in Muller–Hermelink classification [6]. Morphological description of thymic tumors and concordances among classifications are summarized in Table 1 [9].

Fig. 1 Cut surface of the resected pericardial tumor showing the intrapericardial development of the lesion

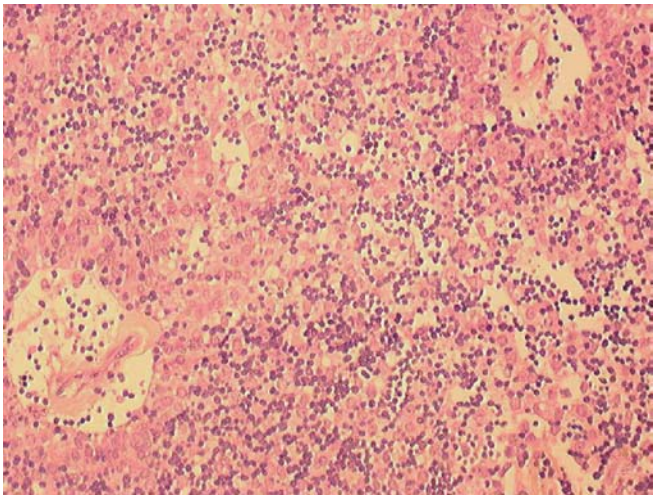

Fig. 2 Photomicrograph emphasizing the two cells populations, and the perivascular empty spaces (×400)

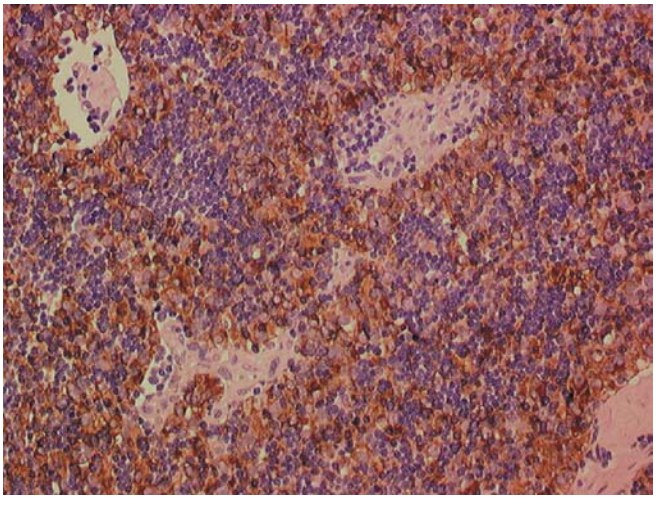

Fig. 3 Immunohistochemistry using AE1/AE3 antibody highlighting the large epithelial cells and their connected network (×400)

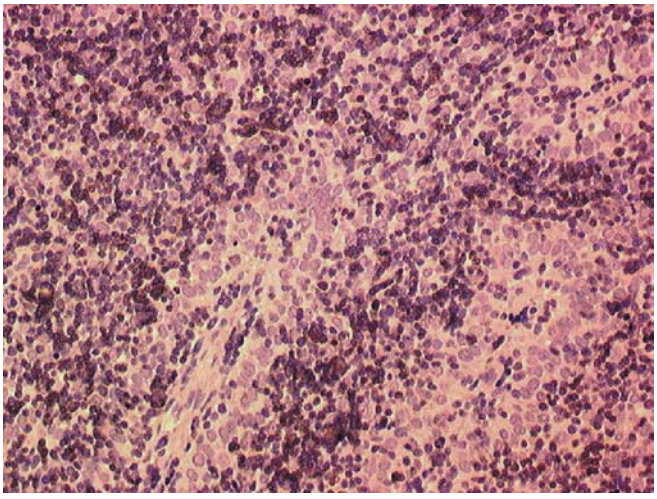

Fig. 4 Immunohistochemistry using the CD1a antibody highlighting the immature T-lymphocytes (×400)

Upon the discovery of a thymoma, complementary exams were done and revealed the existence of myasthenia gravis. Our hypothesis is that some of her symptoms, such as muscular weakness and dysphony, could be explained by the myasthenia gravis. The patient died of post-operative complications, and there was no autopsy performed.

Discussion

Primary intrapericardial thymomas are unusual neoplasms that have been rarely reported in the literature [1, 11]. To our knowledge, there are only three reported cases in this location, one surgical case and two autopsy cases, but with no associated myasthenia gravis (reviewed in Table 2). In 1996, Ben Hami et al. reported the case of a primary pericardial thymoma, revealed by pericardic effusion [1]. This report concerns a 54-year-old man, without history or sign of myasthenia gravis, who presented with thoracic pain and fever. On surgical explorations, hemorrhagic fluid in the pericardial sac was sampled, and a mass, infiltrating the heart, was biopsied. In this case, the mediastinum was also free of tumor. The tumor was composed of spindle cells, small lymphocytes and focally large polygonal cells. It was, therefore, classified as mixed thymoma (Muller–Hermelink) or AB (WHO) (Table 1). The patient was treated by chemotherapy and radiation therapy. In 1997, Maurizio Mirra et al. reported a retrospective evaluation of autopsy cases (between 1980 and 1995 in an Italian general hospital) [7]. Approximately 31,000 postmortem investigations were encoded, 57 thymomas were on record and only 2 cases of thymomas showing an exclusive intrapericardial growth were retrieved. The patients were 61 years and 82 years of age; both were women. They died of chronic diseases. There was no history or sign of myasthenia gravis. At autopsy, both tumors were in the pericardium, attached to the lateral or posterior wall of the parietal pericardium with a broad base and measuring 6–10 cm in largest dimension. There was no infiltration of myocar-

Table 1 Morphological description and concordances between classifications

Description	Muller–Hermelink	World Health Organization
Spindle cells accompanied by few lymphocytes (immature)	Medullary thymoma	A
Mixed spindle and round cells, with foci rich in lymphocytes (immature)	Mixed thymoma	AB
Round cells and abundant lymphocytes (immature)	Predominantly cortical thymoma	B1
	Cortical thymoma	B2
Round cells, with mild atypia and rare lymphocytes (immature)	Well-differentiated thymic carcinoma	B3
Atypic cells accompanied by few lymphocytes (mature)	Thymic carcinoma	C

Table 2 Literature review of pericardial thymomas

Authors, years	Sex, age (years)	Presentation	Myasthenia gravis	Pathology	Classification (World Health Organzation)	Treatment
Ben Hami, 1996 [1]	Male, 54	Thoracic pain, fever	Absent	Spindle and large polygonal cells, lymphocytes	AB	Chemotherapy Radiation therapy
Mirra, 1997 [7]	Female, 61	Autopsy	Absent	Spindle cells, lymphocytes	A	-
	Female, 82	Autopsy	Absent	Spindle cells, lymphocytes	A	-
Current case	Female, 72	Dyspnea, dysphony, myalgia	Present	Large polygonal cells, lymphocytes	B2	Surgery

dium in both tumors. Histologically, both were spindle cell thymomas or medullary type (Muller–Hermelink) or A (WHO) (Table 1). In all four cases, including our case, thymomas were only located in the pericardium, without any other tumor site. That eliminates pericardial invasion by mediastinal malignant thymoma. The alternative possibility of a solitary metastasis from a small undetected primary tumor in the thymus can not be totally eliminated, especially knowing that myasthenia gravis can reveal microscopic thymoma [10]. However, in our review, we did not find any such reported case. Thus, the diagnosis of ectopic pericardial primary thymoma was kept. The thymus is embryologically derived from the third pair of pharyngeal pouches, and during the development it descends into the anterior mediastinum. Ectopic locations of the thymus usually result from failure of the organ to descend or from an excessive descent. Classically, reported ectopic sites were cervical, middle or inferior mediastinum, as well as diaphragmatic sites [3, 12]. More rarely, other ectopic thymomas arose in the supraclavicular region, in the pleura and intrapulmonary regions [2, 8]. All these unusual sites of thymomas may pose a serious diagnostic challenge for pathologists. Differential diagnoses could be malignant lymphoma, particularly of the lymphoblastic type, and carcinoma (primary or metastatic), especially small cell lung carcinoma [5]. The large epithelial cells scattered in the background aid in distinguishing thymoma from lymphoblastic lymphoma. Immunohistochemical stains, particularly cytokeratin, may be very supportive in difficult cases, by highlighting the presence of an epithelial cell component drawing a connected network. The identification of an immature lymphoid cell component expressing CD1a should distinguish thymoma from carcinoma. Moreover, unlike thymoma, cells of small cell lung tumor have high mitotic count, and a specific marker can be useful in this context, such as TTF1, expressed in 80% of small cell lung carcinoma. Another histological sign that should alert the pathologist to the possibility of thymoma is the identification of perivascular clear spaces.

We have reported that thymoma may occur in the pericardium as a lesion independent from a mediastinal tumor. It can be, therefore, considered as an ectopic location of thymoma accompanied with clinical manifestation. The presence of myasthenia gravis in a patient with no mediastinal tumor should encourage the clinician to pursue investigations looking at ectopic sites for thymoma.

References

1. Ben Hami B, Caulet-Maugendre S, Valla J, Heresbach-Le Berre N, Kernec J, Laurent M, Ramee MP (1996) Primary pericardial thymoma: an unusual etiology of neoplastic pericarditis. Ann Pathol 16:445–448
2. Fushimi H, Tanio Y, Kotoh K (1998) Ectopic thymoma mimicking diffuse pleural mesothelioma: a case report. Hum Pathol 29:409–410
3. Jansen JD, Johnson FE (1990) Fatal ectopic thymoma. Ann Thorac Surg 50:469–470
4. Levine GD, Rosai J (1978) Thymic hyperplasia and neoplasia: a review of current concepts. Hum Pathol 9:495–515
5. Loire R, Hellal H (1993) Neoplastic pericarditis. Study by thoracotomy and biopsy in 80 cases. Presse Med 22:244–248
6. Marino M, Muller-Hermelink HK (1985) Thymoma and thymic carcinoma. Relation of thymoma epithelial cells to the cortical and medullary differentiation of thymus. Virchows Arch 407:119–149
7. Mirra M, Zanella M, Bussani R, Falconieri G (1997) Intrapericardial thymoma: report of two incidental autopsy cases and review of the literature. Arch Pathol Lab Med 121:59–63
8. Moran CA, Suster S, Fishback NF, Koss MN (1995) Primary intrapulmonary thymoma. A clinicopathologic and immunohistochemical study of eight cases. Am J Surg Pathol 19:304–312
9. Okumura M, Miyoshi S, Fujii Y, Takeuchi Y, Shiono H, Inoue M, Fukuhara K, Kadota Y, Tateyama H, Eimoto T, Matsuda H (2001) Clinical and functional significance of WHO classification on human thymic epithelial neoplasms: a study of 146 consecutive tumors. Am J Surg Pathol 25:103–110
10. Poulard G, Mosnier JF, Dumollard JM, Prades JM, Convers P, Boucheron S (1994) Microscopic thymoma and myasthenia gravis. Ann Pathol 14:203–204
11. Salih Deveci M, Ceyhan K, Deveci G, Finci R (2001) Pericardial rhabdomyomatous spindle cell thymoma with mucinous cystic degeneration. Histopathology 38:479–481
12. Salyer WR, Eggleston JC (1976) Thymoma: a clinical and pathological study of 65 cases. Cancer 37:229–249

Virchows Arch (2005) 446:189–193
DOI 10.1007/s00428-004-1168-0

CASE REPORT

Nicolas Ortonne · Christiane Copie-Bergman · Philippe Remy · Marie-Hélène Delfau-Larue · Miguel A. Alonso · Xavier Mariette · Judith Dierlamm · Karen Leroy · Philippe Gaulard

Mucosa-associated lymphoid tissue lymphoma of the thymus: a case report with no evidence of MALT1 rearrangement

Received: 25 August 2004 / Accepted: 27 October 2004 / Published online: 14 January 2005
© Springer-Verlag 2005

Abstract We report a case of thymic mucosa-associated lymphoid tissue (MALT) lymphoma (TML) that presented as an asymptomatic mediastinal mass in a 40-year-old woman with a past history of Sjögren syndrome. This case had the characteristic clinical and pathological features of TML, as found in most of the 24 previously reported cases, i.e., autoimmune context, especially Sjögren syndrome, IgA secretion, large epithelial cysts, lymphoepithelial lesions involving residual Hassal's corpuscles, epithelial cysts, and a marked plasmacytic differentiation with IgA expression. Reverse-transcription polymerase chain reaction for t(11;18)(q21;q21) was negative, in agreement with recently published data. In this case, investigation for t(14;18)(q32;q21) using fluorescent in situ hybridization was also performed and supplied negative results. Neoplastic cells were negative for MAL, a marker of primary mediastinal large B cell lymphoma (PMBL). Altogether, these findings further support that among MALT lymphomas, TML have peculiar clinical and morphological characteristics and appear not to involve MALT1 rearrangement. They also suggest the absence of a relationship between TML and PMBL.

Keywords Thymic MALT lymphoma · Sjögren syndrome · t(11;18)(q21; q21) - t(14 ;18)(q32;q21) - MAL

N. Ortonne (✉) · C. Copie-Bergman · K. Leroy · P. Gaulard
Département de Pathologie,
Hôpital Henri Mondor, AP-HP,
avenue du Maréchal de Lattre de Tassigny 51,
94010 Créteil, France
e-mail: nicolas.ortonne@hmn.ap-hop-paris.fr
Tel.: +33-1-49812732
Fax: +33-1-49812733

P. Remy
Service de Nephrologie,
Hôpital Henri Mondor,
94010 Créteil, France

M.-H. Delfau-Larue
Service d'Immunologie Biologique et INSERM U617,
Hôpital Henri Mondor,
94010 Créteil, France

M. A. Alonso
Centro de Biologia Molecular "Severo Ochoa",
Universidad Autonoma de Madrid and Consejo Superior de Investigaciones Cientificas,
Cantoblanco, Madrid, Spain

X. Mariette
Service de Rhumatologie,
CHU de Bicêtre,
94270 le Kremlin Bicêtre, France

J. Dierlamm
Genetic Laboratory,
University Hospital Hamburg-Eppendorf,
Hamburg, Germany

Introduction

Marginal zone B-cell lymphomas arising from mucosa-associated lymphoid tissue (MALT) represent an important proportion of extranodal lymphomas. They commonly present as a localized disease and are usually indolent. Since the initial description in the gastrointestinal tract by Isaacson and Wright in 1983, subsequent studies revealed that this type of lymphoma may occur in many organs, including lung, salivary gland, thyroid, conjunctiva, or skin. Lymphomas primarily developing in the thymus mainly comprise lymphoblastic T-cell lymphoma, Hodgkin lymphoma, and a subset of diffuse large B-cell lymphoma, also called primary mediastinal large B-cell lymphoma. Thymic MALT lymphoma (TML) was first recognized in 1990 by Isaacson et al., who described the first two cases [7]. Since then, to our knowledge, 24 cases have been reported [4, 6, 8, 9, 12, 13, 14, 15, 16, 17, 19, 21, 22]. We report an additional case of TML in which complete molecular studies for MALT1 rearrangement were performed and, MAL expression was investigated.

Clinical history

A 40-year-old Caucasian woman had an asymptomatic mediastinal anterior mass diagnosed on a routine chest radiograph. She had a 12-year past history of Sjögren syndrome (SS), associated with primitive biliary cirrhosis. She had renal deficiency due to acute interstitial nephritis related to her SS. She complained of mouth and ocular dryness. Physical examination was otherwise normal. Laboratory investigations revealed normocytic, normochromic anemia, proteinuria, and hypercreatininemia related to renal deficiency. A monoclonal IgA peak was found on immunological studies from both serum (11 g/l) and urine samples. Bone marrow smears and bone radiographs were normal. A large thymic mass was removed through a median sternotomy, and MALT lymphoma was diagnosed. Staging procedures revealed no other localization (gastric endoscopy with biopsies, bone marrow biopsy, and computed scan), resulting in an Ann Arbor stage-I disease. The patient received no other treatment. As renal dysfunction gradually deteriorated, 11 years after diagnosis, she underwent hemodialysis followed by kidney transplantation. At that time, an iliac lymph node was removed, which disclosed partial involvement by a lymphoma with morphological and phenotypic features of marginal zone MALT lymphoma.

Materials and methods

Histopathology and immunohistochemistry

Formalin-fixed surgical specimens were routinely processed, embedded in paraffin, and stained with hematoxylin–eosin. Immunohistochemical procedures were performed on paraffin sections with the Ventana automated immunostainer (Ventana Medical Systems, Tucson, AZ, USA) and antibodies for CD20/L26, CD79a, IgD, Bcl2, MUM1/IRF4 (Dako SA, Glostrup, Denmark), CD138 (Serotec, United Kingdom), CD5, CD10, CD23 (Novocastra, Newcastle, United Kingdom), Cytokeratin/KL1, Mib1/Ki67 (Immunotech, Marseille, France), and MAL protein (M. Alonso). Direct immunofluorescence tests were performed with fluorescein-conjugated antibodies directed against IgA, IgG, IgM (Dako SA) as well as kappa and lambda light chains (Becton-Dickinson, San Jose, USA).

Molecular studies

Samples of the surgical specimens were snap frozen in liquid nitrogen for molecular studies. For immunoglobulin heavy chain (IgH) gene rearrangement study, DNA was extracted from frozen sections, and the polymerase chain reaction (PCR) was used with standard procedures, as previously described [10]. Investigation for the API2-MALT1 fusion transcript was performed using reverse-transcription (RT)-PCR technique. Total RNA was also extracted from frozen tissue and reverse transcribed, and cDNA was then amplified with different API2-MALT1 primer couples, in parallel with known positive and negative controls [11]. Investigation for the t(14;18)(q32;q21) involving MALT1 and IgH genes was done using a specific two-color interphase fluorescent in situ hybridization (FISH) assay, as previously described [18].

Results

Histopathological analysis of the thymic mass revealed an effacement of the architecture by a dense diffuse lymphoid infiltrate (Fig. 1A) admixed with few residual lymphoid follicles. The infiltrate was composed of small lymphocytes, centrocyte-like cells, monocytoid-like cells, and numerous mature plasma cells. Large cells were rare, scattered within the infiltrate. Large cysts, lined by two or three layers of flattened epithelial cells and containing eosinophilic hyaline material, were observed within the infiltrate (Fig. 1B). Many residual Hassall corpuscles with central keratinization were present, most of them showing conspicuous lymphoepithelial lesions (Fig. 1C). The epithelial cysts also contained lymphoepithelial lesions.

Immunohistochemistry showed that neoplastic cells expressed CD79a and disclosed heterogeneous expression of CD20 and CD138 (Fig. 1D), in agreement with plasmacytic differentiation. Neoplastic cells were negative for CD5, CD10, CD23, IgD, and Bcl-6 but expressed Bcl-2. They were also positive for MUM-1/IRF4. Interestingly, neoplastic cells did not express MAL. Immunofluorescence studies revealed that the neoplastic cells disclosed cytoplasmic IgA (Fig. 1D, insert) with monotypic kappa light chain restriction. Lymphoepithelial lesions were highlighted by cytokeratin staining, which showed a branched network of epithelial elements (Fig. 1E).

Molecular studies showed a clonal rearrangement of the IgH gene. Investigation for API2-MALT1 by RT-PCR supplied negative results in contrast with positive control. No IgH-MALT1 fusion transcripts could be evidenced by FISH analyses (Fig. 1F). These findings thus indicated that MALT1 rearrangements involving the t(11;18)(q21; q21) and t(14 ;18)(q32;q21) were absent in this case.

Discussion

We report a case of TML that presented as an asymptomatic mediastinal mass in a 40-year-old woman with a past history of SS. To the best of our knowledge, 24 TML cases have been previously reported [4, 6, 8, 9, 12, 13, 14, 15, 16, 17, 19, 21, 22]. Among them, most occurred in middle-aged women, and 14 were of Asian origin. The female predominance in TML is in agreement with the development of TML in a context of autoimmune disease. With the present case, 16 (64%) of the 25 patients had autoimmune disease, including SS in 11 of them. It is now admitted that MALT lymphomas derive from inflammatory antigen-driven precursor lesions. The best example is given by the pathogenic link between gastric MALT lymphoma and *Helicobacter pylori* gastritis. An important issue is whether there could be an inflammatory precursor lesion of the thymus preceding the development of TML. Recently, Parrens et al. have shown that an acquired MALT tissue can develop in the thymus in a setting of *myasthena gravis* and/or other connective tissue diseases [17]. This finding strongly supports the hypothesis that TML primarily develops in the thymus on a precursor lesion. Whether SS can promote the development of an acquired thymic MALT tissue is questionable and is an interesting issue, which could give an explanation to the link between TML and SS.

Morphological features of TML are those of MALT lymphoma of other sites, except for the presence of a marked plasma cell component and of particular epithelium-lined cysts. As previously discussed [6], these cysts

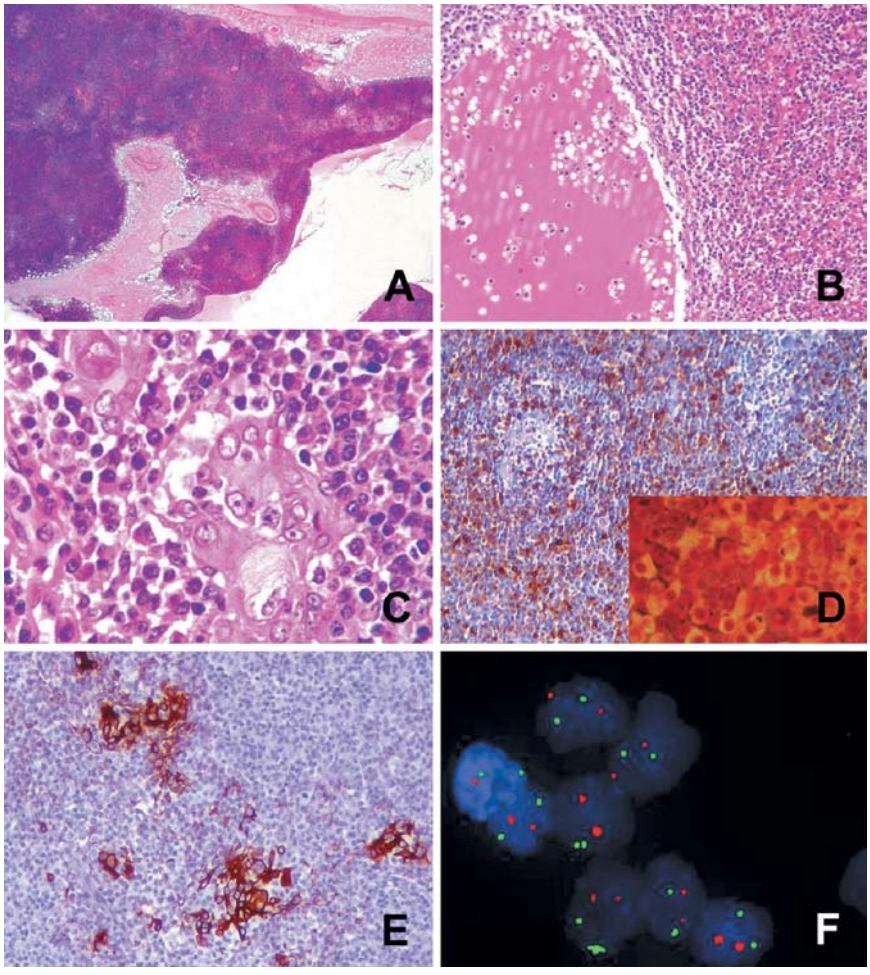

Fig. 1 The architecture of the thymus is effaced by a diffuse infiltrate of small lymphocytes (**A**, hematoxylin–eosin, ×50), with presence of epithelial cysts containing eosinophilic material and showing lymphopepithelial lesions (**B**, hematoxylin–eosin, ×200). At higher magnification, Hassall corpuscles containing lymphoepithelial lesions are seen (**C**, hematoxylin–eosin, ×400). The expression of CD138 by many lymphocytes highlights the marked plasmacytic differentiation (**D**, immunohistochemistry, ×200). Immunofluorescent study showing diffuse IgA expression by the neoplastic lymphocytes (**D**, *insert*, immunofluorescence, ×200). Cytokeratin immunostaining shows residual Hassall corpuscles dissociated by lymphoepithelial lesions, forming a branched network of epithelial cells (**E**, immunohistochemistry, ×200). The t(14;18)(q32;q21) fluorescent in situ hybridization assay on interphase cells, with staining of the immunoglobulin heavy chain gene on chromosome 14 (*green signal*) and the MALT1/MLT gene on chromosome 18 (*red signal*), shows a normal signal constellation (**F**)

may derive from the thymic medullary epithelial structures. Immunophenotype of TML is also similar to that of classical MALT lymphoma, namely CD20+, CD5−, CD10−, CD23−, IgD−. However, it is noteworthy that the majority of TML cases express a monoclonal IgA heavy chain. The reason why TML displays an IgA restriction is unclear.

MALT lymphomas are thought to derive from postgerminal cells. This is in agreement with the MUM1+ and Bcl-6− phenotype observed in our case. Recently, however, somatic hypermutations of the IgH V gene with intraclonal heterogeneity were reported in one case [8], a finding that has been hypothesized to reflect the reentry of neoplastic lymphocytes of TML into the germinal center environment of the reactive follicles.

Until now, no recurrent karyotypic abnormalities have been described in TML. Cytogenetic studies, however, have been conducted in only one case and revealed a normal karyotype [12]. Besides the t(1;14)(p22;q32), which is found in a minority of MALT lymphoma [20], and, to date, has never been investigated in TML, two recurrent translocations are associated with a proportion of MALT lymphomas. The translocation t(11;18)(q21;q21) represents the most frequent chromosomal abnormality in MALT lymphomas [5]. This translocation involves the API2 gene, an inhibitor of apoptosis, and the MALT1 gene. The resulting API2-MALT1 fusion protein is thought to have an increased anti-apoptotic activity, thereby conferring a survival advantage to MALT lymphomas and allowing antigen-independent proliferation. According to recent data, the frequency of this alteration depends upon the site of involvement, being observed in 30% and 50% of MALT lymphomas of the stomach and lung, respectively; whereas, it is rare or absent in thyroid

Table 1 Clinical and biological characteristics of reported cases of thymic mucosa-associated lymphoid tissue lymphoma, including the present case

Parameters	Number of cases (%)
Female	18/25 (72%)
Asian	14/16 (88%)
Asymptomatic thymic mass	25/25 (100%)
Autoimmune manifestations	18/25 (72%)
Sjögren syndrome	11/25 (44%)
Circulating monoclonal IgA	6/16 (38%)
Epithelial cysts	19/26 (73%)
IgA+ tumoral cells	14/20 (70%)
Plasmacytic differentiation	25/25 (100%)
Lymphoepithelial lesions in Hassal corpuscles	16/22 (73%)
T-cell clone	19/21 (90%)

and salivary glands [11]. In our case and in the 15 cases investigated by Inagaki et al., no API2-MALT1 fusion transcript could be detected, indicating that the t(11;18)(q21;q21) is not involved in the pathogenesis of TML. Recently, Streubel B et al. described the t(14;18)(q32;q21) involving the MALT1 and IgH genes as another recurrent abnormality in MALT lymphomas, being present in 18% of MALT lymphomas of the salivary glands and in a variable proportion of MALT lymphoma of the liver, skin, and ocular adnexae, but absent in the stomach, intestine, and lung [18]. It is unclear whether this translocation is present among TML cases. In our case, however, sensitive FISH studies did not detect this translocation, suggesting that it may not play a role in the pathogenesis of TML.

Among diffuse large B-cell lymphomas, primary mediastinal large B-cell lymphoma (PMBL) is a distinct clinicopathological entity that also occurs as an anterior mediastinal mass [1]. It has been hypothesized that PMBL could represent the high-grade counterpart of TML. However, as discussed by Inagaki et al., the younger age of onset, the lack of association with autoimmune disease, and the absence of Ig expression by tumoral cells in PMBL are arguments against a relationship between TML and PMBL. In addition, immunophenotype of PMBL appears to be distinct from TML, since PMBL commonly expresses CD23 and does not show IgA restriction. In a recent study, we showed that MAL, a proteolipid component of lipid rafts in T lymphocytes, is recurrently expressed in neoplastic cells of a majority (70%) of PMBLs, as well as in a subset of normal thymic B cells which are candidates to be the normal cell counterpart of PMBLs [2, 3]. Neoplastic cells in the present case were negative for MAL immunostaining, a finding that may further argue against a relationship between PMBL and TML.

In conclusion, primary MALT lymphoma of the thymus appears to be a rare condition, often characterized by its occurrence in a context of autoimmunity, especially SS, the presence of particular epithelial cysts, and a marked plasmacytic differentiation with monoclonal IgA expression and secretion (Table 1). Therefore, the association of thymic enlargement to a monoclonal circulating IgA in a context of autoimmune disease, especially SS, is suggestive of TML. Absence of MAL expression in this case further supports the absence of relationship between TML and PMBL. To date, the t(11;18)(q21;q21) was never reported in TML. Together with the absence of t(14;18)(q32;q21) seen in our case, this suggests that MALT1 rearrangement is not involved in the pathogenesis of TML, a finding to be confirmed by further studies.

References

1. Cazals-Hatem D, Lepage E, Brice P, Ferrant A, d'Agay MF, Baumelou E, Briere J, Blanc M, Gaulard P, Biron P, Schlaifer D, Diebold J, Audouin J (1996) Primary mediastinal large B-cell lymphoma. A clinicopathologic study of 141 cases compared with 916 nonmediastinal large B-cell lymphomas, a GELA ("Groupe d'Etude des Lymphomes de l'Adulte") study. Am J Surg Pathol 20:877–888
2. Copie-Bergman C, Gaulard P, Maouche-Chretien L, Briere J, Haioun C, Alonso MA, Romeo PH, Leroy K (1999) The MAL gene is expressed in primary mediastinal large B-cell lymphoma. Blood 94:3567–3575
3. Copie-Bergman C, Plonquet A, Alonso M, Boulland M, Marquet J, Divine M, Möller P, Leroy K, Gaulard P (2002) MAL expression in lymphoid cells: further evidence for MAL as a distinct marker of primary mediastinal large B-cell lymphomas. Mod Pathol 11:1172–1180
4. Di Loreto C, Mariuzzi L, De Grassi A, Beltrami CA (1996) B cell lymphoma of the thymus and salivary gland. J Clin Pathol 49:595–597
5. Dierlamm J, Wlodarska I, Michaux L, Stefanova M, Hinz K, Van Den Berghe H, Hagemeijer A, Hossfeld DK (2000) Genetic abnormalities in marginal zone B-cell lymphoma. Hematol Oncol 18:1–13
6. Inagaki H, Chan JK, Ng JW, Okabe M, Yoshino T, Okamoto M, Ogawa H, Matsushita H, Yokose T, Matsuno Y, Nakamura N, Nagasaka T, Ueda R, Eimoto T, Nakamura S (2002) Primary thymic extranodal marginal-zone B-cell lymphoma of mucosa-associated lymphoid tissue type exhibits distinctive clinicopathological and molecular features. Am J Pathol 160:1435–1443
7. Isaacson PG, Chan JK, Tang C, Addis BJ (1990) Low-grade B-cell lymphoma of mucosa-associated lymphoid tissue arising in the thymus. A thymic lymphoma mimicking myoepithelial sialadenitis. Am J Surg Pathol 14:342–351
8. Kamimura K, Nakamura N, Ishibashi T, Maruyama Y, Abe M (2002) Somatic hypermutation of immunoglobulin heavy chain variable region genes in thymic marginal zone B-cell lymphoma of MALT type of a patient with Sjogren's syndrome. Histopathology 40:294–296
9. Kim D, Nam E, Yi J, Shin H, Kim I (1998) Mucosa-associated lymphoid tissue (MALT) lymphoma of the thymus. Int J Surg Pathol 6:229–234
10. Lechapt-Zalcman E, Challine D, Delfau-Larue MH, Haioun C, Desvaux D, Gaulard P (2001) Association of primary pleural effusion lymphoma of T-cell origin and human herpesvirus 8 in a human immunodeficiency virus-seronegative man. Arch Pathol Lab Med 125:1246–1248
11. Liu H, Ye H, Dogan A, Ranaldi R, Hamoudi RA, Bearzi I, Isaacson PG, Du MQ (2001) T(11;18)(q21;q21) is associated with advanced mucosa-associated lymphoid tissue lymphoma that expresses nuclear BCL10. Blood 98:1182–1187
12. Lorsbach RB, Pinkus GS, Shahsafaei A, Dorfman DM (2000) Primary marginal zone lymphoma of the thymus. Am J Clin Pathol 113:784–791
13. McCluggage WG, McManus K, Qureshi R, McAleer S, Wotherspoon AC (2000) Low-grade B-cell lymphoma of mucosa-associated lymphoid tissue (MALT) of thymus. Hum Pathol 31:255–259

14. Moriyama E, Yokose T, Kodama T, Matsuno Y, Hojo F, Takahashi K, Nagai K, Nishiwaki Y, Ochiai A (2000) Low-grade B-cell lymphoma of mucosa-associated lymphoid tissue in the thymus of a patient with pulmonary amyloid nodules. Jpn J Clin Oncol 30:349–353
15. Nagasaka T, Lai R, Harada T, Chen YY, Chen WG, Arber DA, Weiss LM (2000) Coexisting thymic and gastric lymphomas of mucosa-associated lymphoid tissues in a patient with Sjogren syndrome. Arch Pathol Lab Med 124:770–773
16. Nakamura S, Koshikawa T, Kaba S, Tokoro Y, Suchi T, Kurita S (1993) Imprint cytology of low-grade B-cell lymphoma of mucosa-associated lymphoid tissue arising in the thymus: a case report. Diagn Cytopathol 9:665–667
17. Parrens M, Dubus P, Danjoux M, Jougon J, Brousset P, Velly JF, de MA, Merlio JP (2002) Mucosa-associated lymphoid tissue of the thymus hyperplasia vs lymphoma. Am J Clin Pathol 117:51–56
18. Streubel B, Lamprecht A, Dierlamm J, Cerroni L, Stolte M, Ott G, Raderer M, Chott A (2003) T(14;18)(q32;q21) involving IGH and MALT1 is a frequent chromosomal aberration in MALT lymphoma. Blood 101:2335–2339
19. Takagi N, Nakamura S, Yamamoto K, Kunishima K, Takagi I, Suyama M, Shinoda M, Sugiura T, Oyama A, Suzuki H et al (1992) Malignant lymphoma of mucosa-associated lymphoid tissue arising in the thymus of a patient with Sjogren's syndrome. A morphologic, phenotypic, and genotypic study. Cancer 69:1347–1355
20. Willis TG, Jadayel DM, Du MQ, Peng H, Perry AR, Abdul-Rauf M, Price H, Karran L, Majekodunmi O, Wlodarska I, Pan L, Crook T, Hamoudi R, Isaacson PG, Dyer MJ (1999) Bcl10 is involved in t(1;14)(p22;q32) of MALT B cell lymphoma and mutated in multiple tumor types. Cell 96:35–45
21. Yamasaki S, Matsushita H, Tanimura S, Nakatani T, Hara S, Endo Y, Hara M (1998) B-cell lymphoma of mucosa-associated lymphoid tissue of the thymus: a report of two cases with a background of Sjogren's syndrome and monoclonal gammopathy. Hum Pathol 29:1021–1024
22. Yokose T, Kodama T, Matsuno Y, Shimosato Y, Nishimura M, Mukai K (1998) Low-grade B cell lymphoma of mucosa-associated lymphoid tissue in the thymus of a patient with rheumatoid arthritis. Pathol Int 48:74–81

Virchows Arch (2005) 446:194–199
DOI 10.1007/s00428-004-1161-7

CASE REPORT

Yasuhiko Kimura · Kenji Kashima · Tsutomu Daa · Yoshiyuki Kondo · Kazuhiro Yada · Atsushi Sasaki · Toshifumi Matsumoto · Seigo Kitano · Nobuhiro Kubo · Shigeo Yokoyama

Biotin-rich intranuclear inclusions in morule-lacking adenocarcinoma of the gallbladder: a new category of "neoplastic/non-morular" lesions

Received: 3 August 2004 / Accepted: 8 October 2004 / Published online: 13 January 2005
© Springer-Verlag 2005

Abstract Biotin-rich intranuclear inclusions, also called "optically clear nuclei," are observed in various neoplastic and non-neoplastic lesions, including pregnancy-related endometrium and benign and malignant neoplasms with morular structures. A recent study reported that lesions with biotin-rich intranuclear inclusions can be classified as "(non-neoplastic) pregnancy-related endometrial" and as "(neoplastic) morular" category. In the present report, we describe two cases of well-differentiated adenocarcinoma of the gallbladder in which biotin-rich intranuclear inclusions were found without morular structures. Immunohistochemically, as reported previously, the intranuclear inclusions were positive for biotin and two biotin-binding enzymes (pyruvic acid carboxylase and propionyl CoA carboxylase). Intranuclear expression of β-catenin was also observed in neoplastic cells with and without intranuclear inclusion. We also detected a frame shift mutation of APC gene in one case but no mutation of β-catenin gene in both cases. Although intranuclear expression of β-catenin by mutation of APC gene might contribute to carcinogenesis in our cases, the relationships among intranuclear expressions of β-catenin, biotin, biotin-binding enzymes and intranuclear inclusions remain unclear. Our cases are the first neoplastic lesions with biotin-rich intranuclear inclusions that lacked morular structures. We propose a new "neoplastic/non-morular" category for lesions with biotin-rich intranuclear inclusions.

Keywords Biotin · Biotin-binding enzymes · β-Catenin · APC · Mutation · Intranuclear inclusion · Gallbladder

Y. Kimura (✉) · K. Kashima · T. Daa · Y. Kondo · K. Yada · S. Yokoyama
Department of Pathology, Faculty of Medicine,
Oita University,
Hasama-machi, 879–5593 Oita, Japan
e-mail: kimuray@med.oita-u.ac.jp

A. Sasaki · T. Matsumoto · S. Kitano
Department of Surgery, Faculty of Medicine,
Oita University,
Oita, Japan

N. Kubo
Kouseiren Tsurumi Hospital,
Beppu, Japan

Introduction

Biotin is a form of vitamin B that acts as a coenzyme in reactions catalyzed by biotin-binding enzymes, such as pyruvic acid carboxylase (PAC), propionyl CoA carboxylase (PCC), acetyl CoA carboxylase (ACC), and carbamoyl phosphate synthetase (CPS). A large amount of biotin is present in the liver, kidney, pancreas, mammary gland, skeletal muscle, salivary gland, and adipose tissue [5, 24]. Intranuclear expression of biotin was initially reported in ovarian endometrioid adenocarcinoma by Tsujimoto et al. [21]. Thereafter, Yokoyama et al. [23] found intranuclear expression of biotin in pregnancy-related endometrial glands. The biotin-rich part in the nuclei looks like an intranuclear inclusion, which is homogeneously pale to slightly eosinophilic with occasional marginated chromatin. Prior to the reports of Tsujimoto et al. [21] and Yokoyama et al. [23], these nuclear changes in pregnancy-related endometrial glands had been reported by Mazur et al. [9] in 1983, who called them "optically clear nuclei (OCN)".

Morules (or morulas) are mulberry-like structures composed of small, round to short-spindle epithelial cells. They have been identified in benign and malignant neoplasms of various organs in addition to their well-described presence in endometrioid hyperplasia and endometrioid adenocarcinoma [6]. Nakatani et al. [11] reported that the constituent cells of morules in well-differentiated fetal adenocarcinoma of the lung had biotin-rich intranuclear inclusions with morphologies similar to those seen in pregnancy-related endometrial glands. Since their report, such intranuclear inclusions have been found in a variety of benign and malignant neoplasms with morular structures, including cribriform-morular variant

of papillary carcinoma of the thyroid, uterine and ovarian endometrioid adenocarcinoma, colonic adenoma and adenocarcinoma, pyloric gland-type adenoma of the gallbladder and pancreatoblastoma [3, 9, 10, 13, 15, 17, 18, 21]. Moreover, the nuclear expression of β-catenin in morule-associated neoplasms is considered to correlate with the formation of morules [4, 7, 11, 14]. In Wnt signaling pathway, which is implicated in cellular proliferation, morphology, motility, axis formation and organ development and mutations of β-catenin, APC and Axin genes result in abnormal intranuclear accumulation of β-catenin [2].

Although the biotin-rich intranuclear inclusions seem to be observed in heterogeneous lesions, Gamachi et al. [6] demonstrated that they constantly co-existed with two biotin-binding enzymes (PAC and PCC) and classified the lesions with intranuclear inclusions as "(non-neoplastic) pregnancy-related endometrial" and "(neoplastic) morular" categories. We describe here two cases of adenocarcinoma of the gallbladder, representing previously undescribed neoplastic lesions with biotin-rich intranuclear inclusions, despite the absence of morular structures. We propose a new "neoplastic/non-morular" category for the present cases.

Case report

Two patients, each with a gallbladder tumor, a 78-year-old female (case 1) and a 76-year-old male (case 2), were admitted. The former patient had a history of 10 years of hypertension, 5 years of C-type chronic hepatitis and thyroidectomy for thyroid cancer. Case 2 had a 2-year history of chronic heart failure due to aortic stenosis, appendectomy and radical operation of inguinal hernia. Serum levels of tumor markers in both patients were within normal limits, including carbohydrate antigen 19–9, carcinoembryonic antigen and alpha-fetoprotein. They underwent cholecystectomy. Intraoperatively, the common bile duct was unremarkable, and regional lymph nodes were not enlarged.

Materials and methods

Tissue samples of each case were fixed in 10% formalin and embedded in paraffin. Sections were cut at 4 μm thickness and mounted on silane-coated glass slides. Sections of each sample were stained with hematoxylin and eosin for histopathological diagnosis.

Immunohistochemical staining

Immunostaining was performed on formalin-fixed paraffin-embedded tissue sections by the Envision+ technique (Dako, Carpinteria, CA). The primary antibodies used were monoclonal MUC5AC-specific antibody (1:100; Novocastra, Newcastle upon Tyne, UK), monoclonal MUC6-specific antibody (1:100; Novocastra), monoclonal HGM45 antibody (1:50; Novocastra), monoclonal biotin-specific antibody (1:100; Dako), monoclonal β-catenin-specific antibody (1:100; Novocastra), monoclonal estrogen receptor-α-specific antibody (1:50; Dako), monoclonal estrogen receptor-β-specific antibody (1:100; Dako), monoclonal progesterone receptor-specific antibody (1:800; Dako) and individual rabbit antisera against biotin-binding enzymes, namely, PAC, PCC, ACC and CPS. The latter four antisera were generated at Oita University by immunization of rabbits with chemically synthesized peptides that were based on amino acid sequences. The sequences of peptides and the results of characterizations using immunoblotting and immunoelectron microscopy can be found in our previous reports [6, 8, 16]. Prior to immunostaining of β-catenin, PCC and CPS, antigen retrieval was conducted by heating in an autoclave for 10 min. Final visualization was carried out by diaminobenzidine.

Additionally, 12 carcinomas of gallbladder, including 7 well- to moderately differentiated (tubular) adenocarcinomas, 3 papillary adenocarcinomas and 2 adenosquamous carcinomas were used as controls.

Mutational analysis of exon 15 of APC gene and exon 3 of CTNNBI gene

Mutational analyses of β-catenin and APC genes were performed in the two cases, using DNA extract from paraffin sections of a representative tissue block. Extraction of genomic DNA was performed by TaKaRa DEXPAT (TaKaRa Biomedicals, Otsu, Japan) according to the instructions provided by the manufacturer. Genomic DNA was amplified in nested polymerase chain reaction (PCR). PCR was performed with 40 cycles of denaturation at 95°C for 5 min, annealing at 58°C for 2 min and extension at 72°C for 1 min, with a predenaturing time of 5 min and a final extension time at 10 min. Three sets of primers were used for nested PCR with final amplification of the 156- to 178-bp fragment of exon 3 of the β-catenin gene encompassing the region of the GSK-3β phosphorylation site known to contain activating mutations. The primer sequences were 1U 5′-AAAGTAACATTTCCAATCTACTAATGC-3′ and 1D 5′-CTGTGGTAGTGGCACCAGAA-3′; 2U 5′-AAGCGGCTGTTAGTCACTGG-3′ and 2D 5′-AAAATCCCTGTTCCCACTCA-3′; 3U 5′-GCCACTACCACAGCTCCTTC-3' and 3D 5'-TCAAAACTGCATTCTGACTTTCA-3'.

Seven sets of primers were used for nested PCR with final amplification of the 126- to 176-bp fragment of exon 15 (codons 1274 to 1523) of the APC gene, which has been already reported to be a mutation cluster region in non-FAP colorectal tumors. The primer sequences are 1U 5′-ACTCCAATATGTTTTCAAGATG-3′ and 1D 5′-GGAACTTCGCTCACAGGAT-3′; 2U 5'-GCAGATTCTGCTCTAATACCCT-3′ and 2D 5′-AACAGCTTTGTGCCTGGCT-3′; 3U 5′-CTGCAGGGTTCTAGTTTATC-3′ and 3D 5′-ATCAAGTGAACTGACAGAAG-3′; 4U 5′-GACCCCACTCATGGCAT-3′; 4D 5′-TTACTTCTGCTTGGTGGCAT-3′; 5U 5′-GATCTTCCAGATAGCCCTGG-3′ and 5D 5′-TCTTTTCAGCAGTAGGTGCTTT-3′; 6U 5′-AAACAGCTCAAACCAAGCGA-3′ and 6U 5′-TCTGGAGTACTTTCCGG-3′; 7U 5′-CAGAGGGTCCAGGTTCTTCC-3′ and 7D 5′-TCCTGAACTGGAGGCATTATTC-3′.

PCR–single-strand conformation polymorphism (SSCP) was carried out as follows; PCR products were denatured 1:1 in denaturing solution at 95°C for 2.5 minutes and thereafter directly placed on ice to prevent reannealing of the single stranded product. Electrophoresis was performed using a GeneGel Excel 12.5/24 kit (Pharmacia Biotech AB, Sweden) using the instructions recommended by the manufacturer. The running conditions were 600 V for 1 h at 15°C. After electrophoresis, the gels were stained with DNA silver staining kit (Amersham Biosciences AB). When abnormal patterns were observed on SSCP analysis, the PCR products were electrophoresed on the 1% agarose gel. After staining with ethidium bromide, the bands of interest were excised carefully using a clean razor blade. PCR products were purified with the Quantum Prep Freeze 'N Squeeze DNA Gel Extraction Spin Column (Bio-Rad Lab., Hercules, CA) and were ligated into the TA cloning vector pCR2.1 (Invitrogen, Carlsbad, CA). Plasmid DNA from the recombinant clones was extracted using the QIAprep Miniprep Kit (Qiagen, Valencia, CA). Subsequent nucleotide sequence analyses were performed with an ABI 310 DNA sequencer (Applied Biosystems, Foster City, CA) using the ABI PRISM BigDye Terminators v3.0 Cycle Sequencing Kit (Applied Biosystems).

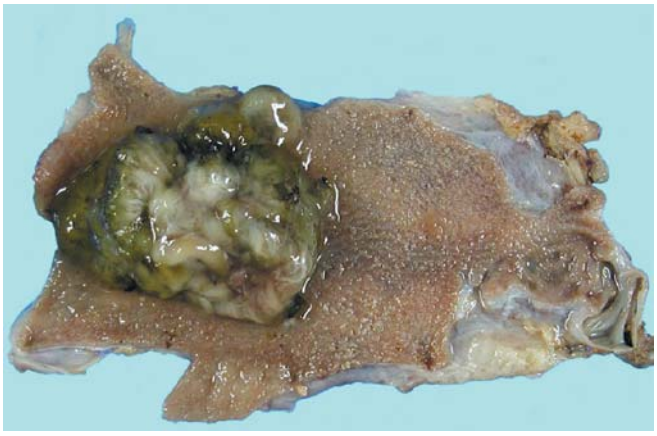

Fig. 1 Case 1. A gelatinous cauliflower-like tumor is located in the fundus of gallbladder

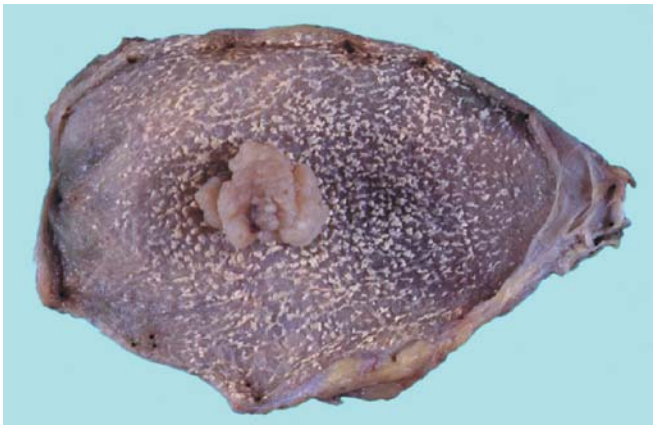

Fig. 3 Case 2. A lobulated polypoid tumor is located in the body of gallbladder in a background of strawberry appearance

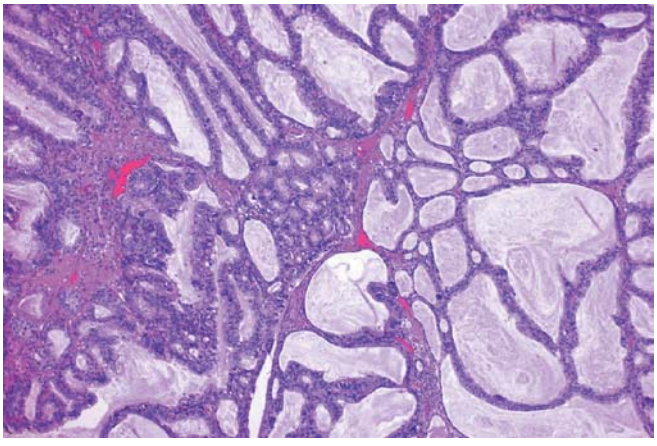

Fig. 2 Case 1. The tumor shows a papillotubular growth with abundant extracellular mucin

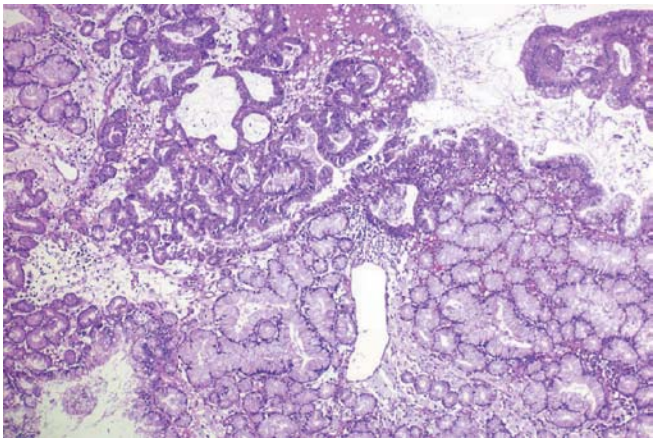

Fig. 4 Case 2. The tumor shows a papillotubular growth. Bland pale cells (*bottom*) and basophilic atypical cells (*top*) correspond to pyloric gland-type adenoma and well-differentiated adenocarcinoma, respectively

Results

In case 1, a tumor measuring 45 mm in diameter was located in the fundus of the gallbladder and was a sessile, soft, cauliflower-like mass with a gelatinous surface (Fig. 1). The wall showed focal thickening. Microscopically, proliferating tumor cells showed a papillotubular pattern with invasion of the muscular layer. Marked accumulation of mucin was noted extracellularly as well as intracellularly, resembling mucinous adenocarcinoma in some parts of the lesion. The final diagnosis was well-differentiated adenocarcinoma (Fig. 2).

In case 2, a pedunculated tumor measuring 25 mm in diameter was located in the body of gallbladder, and the mucosal surface in the non-tumorous areas showed a so-called strawberry appearance, which was consistent with cholesterosis (Fig. 3). Microscopically, the tumor was composed of papillotubular structures lined by cuboidal to columnar cells. Some neoplastic cells absolutely lacked nuclear atypia with pale cytoplasm, but others showed mild to moderate atypia consistent with well-differentiated adenocarcinoma. No invasion was seen. A diagnosis of pyloric gland-type adenoma with well-differentiated adenocarcinoma in situ was made (Fig. 4).

Interestingly, in all sections of both cases, intranuclear inclusions reminiscent of OCNs were occasionally found in neoplastic glands without any morular structures. In case 2, however, they were detected only in adenocarcinoma in situ, but not in the adenomatous portion. The intranuclear inclusions were homogeneously eosinophilic and covered by marginal condensed chromatin (Fig. 5a, b).

Immunohistochemical results were common to both cases. The neoplastic cells were positive for MUC5AC, HGM45 and MUC6, expressing gastric mucin. In addition, the intranuclear inclusions were positive for biotin and two biotin-binding enzymes (PAC and PCC) (Fig. 6a, b, c) but negative for the other two biotin-binding enzymes (ACC and CPS). Intranuclear expression of β-catenin was detected in the neoplastic cells with and without the intranuclear inclusions in both cases (Fig. 6d), including adenoma and adenocarcinoma in situ in case 2. No nuclear expression of ER-α, ER-β and PgR was observed.

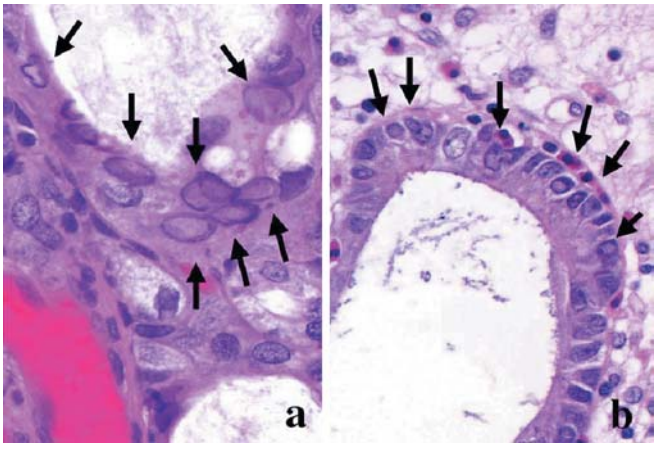

Fig. 5 Intranuclear inclusions (*arrows*) are evident without morular structures in cases 1 (**a**) and 2 (**b**)

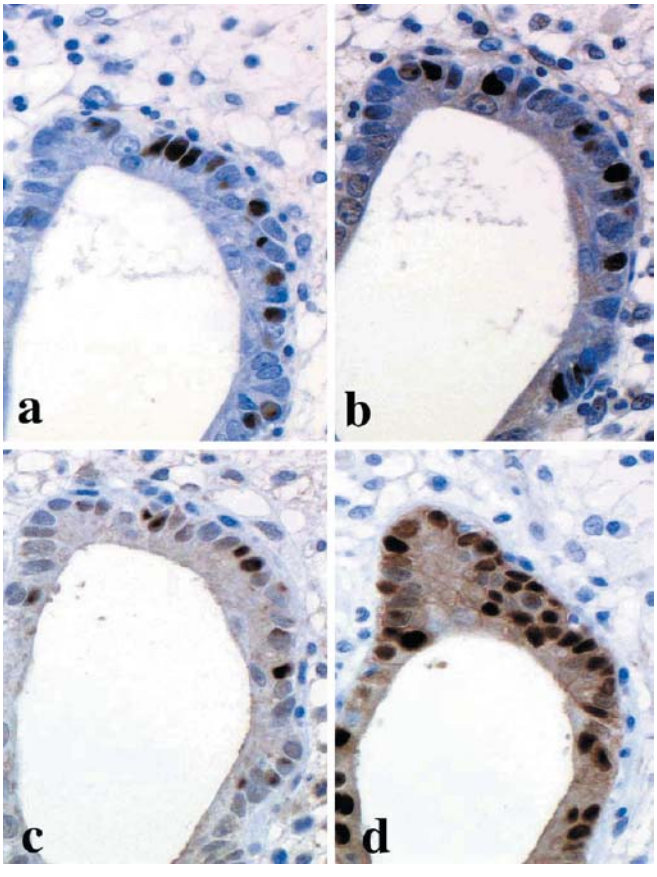

Fig. 6 Immunostaining for biotin, pyruvic acid carboxylase (PAC), propionyl CoA carboxylase (PCC), and β-catenin in serial sections of Fig. 5b (case 2). Biotin (**a**), PAC (**b**) and PCC (**c**) are positive in the intranuclear inclusions. Intranuclear expression of β-catenin (**d**) is observed in both neoplastic cells with and without intranuclear inclusions

Abnormal patterns were detected in the APC gene using SSCP analysis in case 1, and a frame shift mutation (AAGAGAGAGAGT to AAGAGAGAGT) of the APC gene was confirmed by DNA sequencing (Fig. 7). However, no mutation of β-catenin gene was detected in both cases. The 12 control samples demonstrated neither the morular structure nor the biotin-rich intranuclear inclusions, histologically and immunohistochemically.

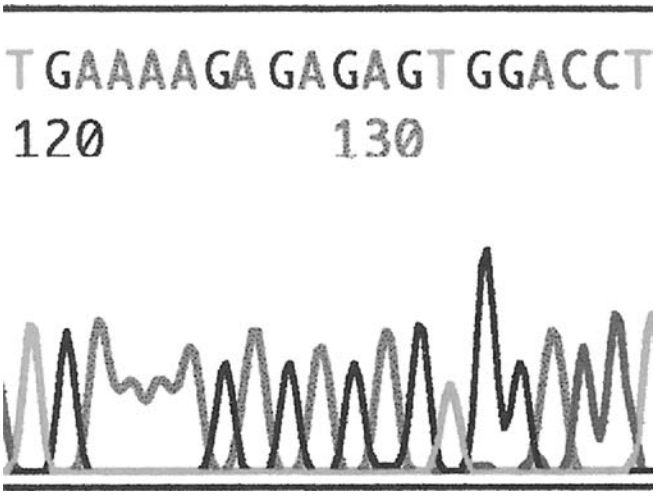

Fig. 7 The frame-shift mutation (AAGAGAGAGAGT to AAGAGAGAGT) of APC gene is detected by DNA sequencing (case 1)

Discussion

The biotin-rich intranuclear inclusions appear similar to viral inclusion bodies of herpes simplex virus-infected cells and cause a false positivity by immunohistochemical technique using biotinylated antibodies, such as the avidin-biotin complex (ABC) method. Practically, attention should be paid to such intranuclear inclusions when making a diagnosis of herpes simplex virus infection and evaluating intranuclear antigen using the ABC method. Fortunately, however, these intranuclear inclusions are observed in only a few lesions; pregnancy-related endometrial glands and neoplasms with morular structures. According to the report by Gamachi et al. [6], only one exceptional case was an ovarian endometrioid adenocarcinoma, which showed biotin-rich intranuclear inclusions without morular structures in a postmenopausal elderly woman. However, they considered that the pathogenesis of the case was the same as pregnancy-related endometrial category, resulting from hormonal influence of numerous stromal luteinized cells. Apart from the case of ovarian endometrioid adenocarcinoma, to our knowledge, there is no report of neoplasms with biotin-rich intranuclear inclusions and without morular structures or hormonal influences. As Gamachi et al. [6] emphasized, although morphologically similar intranuclear inclusions have occasionally been observed in various neoplastic and non-neoplastic lesions, they do not contain biotin. The 12 control samples in this study demonstrated no biotin-rich intranuclear inclusions either. We believe that the present two cases are extremely exceptional.

The biotin-rich intranuclear inclusions were considered to be induced by female sex hormones, since they

were initially detected in pregnancy-related endometrial glands and ovarian endometrioid adenocarcinoma with numerous stromal luteinized cells [9, 17, 21]. Although, Nakatani et al. [10] reported that morules with biotin-rich intranuclear inclusions in well-differentiated fetal adenocarcinoma of the lung lacked ER-α and PgR, they recently found ER-β expression in a series of morular lesions [12]. In our cases, although serum levels of sex hormones were not measured, ER-α, ER-β and PgR were immunohistochemically negative. Thus, we considered that our cases were unrelated to the effects of female sex hormones.

Gamachi et al. [6] classified various lesions with biotin-rich intranuclear inclusions into "(non-neoplastic) pregnancy-related endometrial" and "(neoplastic) morular" categories [6]. Moreover, they found that intranuclear biotin always coexisted with two mitochondrial biotin-binding enzymes (PAC and PCC) in all lesions. Despite the absence of morular structures in the present cases, intranuclear inclusions were observed in neoplastic cells, and their immunohistochemical results were the same as the previous report by Gamachi et al., that is, they were positive for biotin, PAC and PCC but negative for ACC and CPS. Both cases ware also positive for gastric mucin (HGM45, MUC5AC and MUC6). It is interesting that both neoplasms with biotin-rich intranuclear inclusions of the gallbladder, pyloric gland-type adenoma with morular structures and the present case, expressed gastric mucin. However, it is not clear whether the expression of gastric mucin is a common dominator or just incidental for the biotin-rich intranuclear inclusions in the neoplasms of the gallbladder.

Intranuclear expression of β-catenin and mutations of APC gene and/or β-catenin gene have been reported in the neoplasms of morular category, including thyroid carcinoma [4], ovarian carcinoma [7, 14] and well-differentiated fetal adenocarcinoma of the lung [11]. Nakatani et al. [11] surmised that the abnormality of Wnt signaling pathway or intranuclear accumulation of β-catenin was related to the formation of morules. In terms of neoplasms of the gallbladder, mutations of β-catenin gene were detected much more frequently in adenoma, especially in pyloric gland-type adenoma, than in adenocarcinoma [22]. In β-catenin-related tumorigenesis, it is considered that intranuclear accumulation of β-catenin is, in general, induced by alteration and/or mutation of APC and β-catenin genes, resulting in activation of oncogenic genes such as c-myc and cyclin D1 [1, 20]. However, the Ki-67 labeling index in morular structures was very low, despite overexpression of β-catenin and cyclin D1 [19]. These findings suggest that intranuclear accumulation of β-catenin in the neoplasms of morular category is related to morphogenesis of morular structures but not to cell proliferation. Our two cases also showed intranuclear β-catenin in both neoplastic cells with and without intranuclear inclusions. By DNA sequencing, APC gene mutation was detected in one case, while no mutation of β-catenin gene was found in both cases. Because our cases lacked morular structures, it is likely that intranuclear β-catenin plays a role in carcinogenesis or cell proliferation. However, the relationship among intranuclear expression of β-catenin, biotin and biotin-binding enzymes, as well as the mechanism of transportation of biotin and biotin-binding enzymes to the nucleus are still not clear.

To date, there is no report to our knowledge of neoplasms with biotin-rich intranuclear inclusions that lack both morular structures and participation of female sex hormones. We reported here two cases of adenocarcinoma of the gallbladder with biotin-rich intranuclear inclusions that lacked morular structures. We propose a "neoplastic/non-morular" category for lesions with biotin-rich intranuclear inclusions, along with "pregnancy-related endometrial" and "(neoplastic) morular" categories.

Acknowledgements The authors thank Ms. M. Hisaka, Ms. F. Kawamura, Mr. S. Yano, Ms. T. Nakamatsu and Ms. E. Katsuki for their skilled technical assistance.

References

1. Brabletz T, Herrmann K, Jung A, Faller G, Kirchner T (2000) Expression of nuclear β-catenin and c-myc is correlated with tumor size but not with proliferative activity of colorectal adenomas. Am J Pathol 156:865–870
2. Cadigan KM, Nusse R (1997) Wnt signaling: a common theme in animal development. Genes Dev 11:3286–3305
3. Cameselle-Teijeiro J, Chan JKC (1999) Cribriform-morular variant of papillary carcinoma: a distinctive variant representing the sporadic counterpart of familial adenomatous polyposis-associated thyroid carcinoma? Mod Pathol 12:400–411
4. Cameselle-Teijierio J, Ruiz-Ponte C, Loidi L, Suarez-Penaranda J, Baltar J, Sobrinho-Simoes M (2001) Somatic but not germline mutation of the APC gene in a case of cribriform-morular variant of papillary thyroid carcinoma. Am J Clin Pathol 115:486–493
5. Dakshinamurti K, Mistry SP (1963) Tissue and intracellular distribution of biotin-COOH in rats and chicks. J Biol Chem 238:294–296
6. Gamachi A, Kashima K, Daa T, Nakatani Y, Tsujimoto M, Yokoyama S (2003) Aberrant intranuclear localization of Biotin, Biotin-binding enzymes and β-Catenin in pregnancy-related endometrium and morule-associated neoplastic lesions. Mod Pathol 16:1124–1131
7. Gamallo C, Palacios J, Moreno G, Calvo de Mora J, Suarez A, Armas A (1999) β-Catenin expression pattern in stage I and II ovarian carcinomas. Relationship with β-catenin gene mutations, clinicopathological features, and clinical outcome. Am J Pathol 155:527–536
8. Lu CS, Kashima K, Daa T, Yokoyama S, Yanagisawa S, Nakayama I (2000) Immunohistochemical study of the distribution of endogenous biotin and biotin-binding enzymes in ductal structures of salivary gland tumors. J Oral Pathol Med 29:445–451
9. Mazur MT, Hendrickson MR, Kempson RL (1983) Optically clear nuclei: an alteration of endometrial endometrium in the presence of trophoblast. Am J Surg Pathol 7:415–423
10. Nakatani Y, Kitamura H, Inayama Y, Ogawa N (1994) Pulmonary endodermal tumor resembling fetal lung: the optically clear nucleus is rich in biotin. Am J Surg Pathol 18:637–642
11. Nakatani Y, Masudo K, Miyagi Y, Inayama Y, Kawano N, Tanaka Y, Kato K, Ito T, Kitamura H, Nagashima Y, Yamanaka S, Nakamura N, Sano J, Ogawa N, Ishiwa N, Notohara K, Resl M, Mark EJ (2002) Aberrant nuclear localization and gene mutation of β-catenin in low-grade adenocarcinoma of fetal lung type: up-regulation of the Wnt signaling

pathway may be a common dominator for the development of tumors that form morules. Mod Pathol 15:617–624
12. Nakatani Y, Masudo K, Nozawa A, Inayama Y, Yamanaka S, Ito T, Kitamura H, Notohara K, Kashima K, Yokoyama S, Tsujimoto M, Tamai S, Abe Y, Resl M, Mark EJ (2004) Biotin-rich, optically clear nuclei express estrogen receptor-β: tumors with morules may develop under the influence of estrogen and aberrant β-catenin expression. Hum Pathol 35:869–874
13. Okamoto Y, Kashima K, Daa T, Yokoyama S, Nakayama I, Noguchi S (1995) Morule with biotin-containing intranuclear inclusions in thyroid carcinoma. Pathol Int 45:573–579
14. Saegusa M, Okayasu I (2001) Frequent nuclear β-catenin accumulation and associated mutations in endometrioid-type endometrial and ovarian carcinomas with squamous differentiation. J Pathol 194:59–67
15. Sasaki A, Yokoyama S, Arita T, Inomata M, Kashima K, Nakayama I (1999) Morules with biotin-containing optically clear nuclei in colonic tubular adenoma. Am J Surg Pathol 23:336–341
16. Sato T, Kashima K, Gamachi A, Daa T, Nakayama I, Yokoyama S (2002) Immunohistochemical localization of pyruvate carboxylase and carbamyl-phosphate synthetase I in normal and neoplastic human pancreatic tissues. Pancreas 25:130–135
17. Sickel JZ, disant'Agenese PA (1994) Anomalous immunostaining of "optically clear" nuclei in gestational endometrium: a potential pitfall in the diagnosis of pregnancy-related herpes virus infection. Arch Pathol Lab Med 118:831–833
18. Tanaka Y, Ijiri R, Yamanaka S, Kato K, Nishihara H, Nishi T, Misugi K (1998) Pancreatoblastoma: optically clear nuclei in squamoid corpuscles are rich in biotin. Mod Pathol 11:945–949
19. Tanaka Y, Kato K, Notohara K, Nakatani Y, Miyake T, Ijiri R, Nishimata S, Ishida Y, Kigasawa H, Ohama Y, Tsukayama C, Kobayashi Y, Horie H (2003) Significance of aberrant (cytoplasmic/nuclear) expression of beta-catenin in pancreatoblastoma. J Pathol 199:185–190
20. Tetsu O, McCormick F (1999) β-Catenin regulates expression of cyclin D1 in colon carcinoma cells. Nature (London) 398:422–426
21. Tujimoto M, Noguchi M, Taki I (1991) Immunohistochemical and electron microscopic study of the intranuclear inclusion bodies containing biotin in the ovarian endometrioid carcinoma. J Clin Electron Microsc 24:5–6
22. Yanagisawa N, Mikami T, Saegusa M, Okayasu I (2001) More frequent β-catenin exon 3 mutations in gallbladder adenoma than in carcinomas indicate different lineages. Cancer Res 61:19–22
23. Yokoyama S, Kashima K, Inoue S, Daa T, Nakayama I, Moriuchi A (1993) Biotin-containing intranuclear inclusions in endometrial glands during gestation and puerperium. Am J Clin Pathol 99:13–17
24. Wood GS, Warnke R (1981) Suppression of endogenous avidin-binding activity in tissues and its relevance to biotin-avidin detection systems. J Histochem Cytochem 29:1196–1204

Virchows Arch (2005) 446:200–201
DOI 10.1007/s00428-004-1152-8

LETTER TO THE EDITOR

Triantafyllia Koletsa · Valentini Tzioufa · Antonios Michalopoulos · Stylianos Apostolidis · Basilios Papadopoulos · Prodromos Hytiroglou

Ciliated hepatic foregut cyst communicating with the gallbladder

Received: 14 July 2004 / Accepted: 1 October 2004 / Published online: 4 December 2004
© Springer-Verlag 2004

Dear Editors: Ciliated hepatic foregut cyst (CHFC) has previously been considered to be a rare lesion. However, in the last 15 years, the advent of radiological procedures has resulted in the publication of a number of case reports as well as three case series [1, 3, 4], suggesting that this entity has been underreported because it is usually asymptomatic. CHFC has a strong predilection for segment IV of the liver (medial segment of left lobe) and is lined by respiratory-type epithelium, similar to that seen in bronchogenic and esophageal cysts. Therefore, CHFC is believed to be of maldevelopmental origin, arising from remnants of the embryonic foregut, which, in addition to the liver, also forms the tracheobronchial tree, esophagus and other organs. Review of the literature has disclosed seven cases of CHFC located in the gallbladder wall [1, 2]. No communication between the cyst and the gallbladder lumen was found in any of these cases. To our knowledge, this is the first report of a CHFC connected to the gallbladder through a patent duct.

A 39-year-old woman presented with colicky pain in the right upper quadrant of the abdomen, which was accompanied by nausea. There was no fever or jaundice. Murphy's sign was positive. The patient's past medical history was remarkable for appendectomy at 18 years of age and lithiasis of the right kidney at 19 years. Laboratory findings on admission were unremarkable, including: white blood cell count 7320 per mm^3, hematocrit 44.9%, hemoglobin 14.9 g/dl, platelets 221×10^3 per mm^3, bilirubin 0.69 mg/dl, aspartate aminotransferase 19 U/l (nl: 0–37 U/l), alanine aminotransferase 16 U/l (nl: 0–41 U/l), alkaline phosphatase 58 U/l (nl: 40–129 U/l), gamma glutamyl transferase 23 U/l (nl: 8–61 U/l), albumin 3.99 g/dl and globulin 2.67 g/dl. Testing for hepatitis B surface antigen and hepatitis C antibody was negative. Serum levels of carcinoembryonic antigen, CA 19–9 antigen and CA 50 antigen were within normal ranges.

Abdominal ultrasonography showed a cystic structure in the liver measuring 64×31 mm. The gallbladder and large bile ducts appeared normal. No other pathology was noted. Abdominal computed tomography scan suggested that the cystic structure was multilocular and was closely associated with the gallbladder (Fig. 1A). On magnetic resonance imaging, the cyst was localized in segment V of the liver, in close relation to the gallbladder, and measured 51×50 mm. On surgery, it was found that the gallbladder and the cyst communicated through a short duct measuring approximately 2 cm, which was located at the junction of the body and neck. An additional duct, connecting the cyst with the cystic duct, was visualized on intraoperative cholangiography. The cyst contained bile and bile sludge. The gallbladder, its connection to the cyst and portions of the cyst wall were resected. The common bile duct was explored and was found to be free of stones or bile sludge; a Kehr T-tube was placed. A portion of omentum was then placed in the residual cavity. No stones were identified within the gallbladder.

On gross examination, the gallbladder measured 7.5×2.7 cm, had a wall thickness of 0.3 cm and was lined by velvet-like, green-tan mucosa with yellow specks. The connecting duct, measuring 0.1–0.2 cm in diameter, was identified. The portions of cyst wall that were received for examination were flat, gray-tan tissue fragments, measuring up to 3.1 cm in greatest dimension.

Histological examination showed a multilocular cyst with a fibrous wall, which was lined by ciliated, pseudostratified, columnar epithelium (Fig. 1B). Occasional goblet cells were present. The fibrous tissue contained

T. Koletsa · V. Tzioufa · P. Hytiroglou (✉)
Department of Pathology,
Aristotle University Medical School,
540 06 Thessaloniki, Greece
e-mail: phitir@med.auth.gr
Tel.: +30-231-0999218
Fax: +30-231-0999229

A. Michalopoulos · B. Papadopoulos
Department of Surgery,
Aristotle University Medical School,
Thessaloniki, Greece

S. Apostolidis
Department of Descriptive Anatomy,
Aristotle University Medical School,
Thessaloniki, Greece

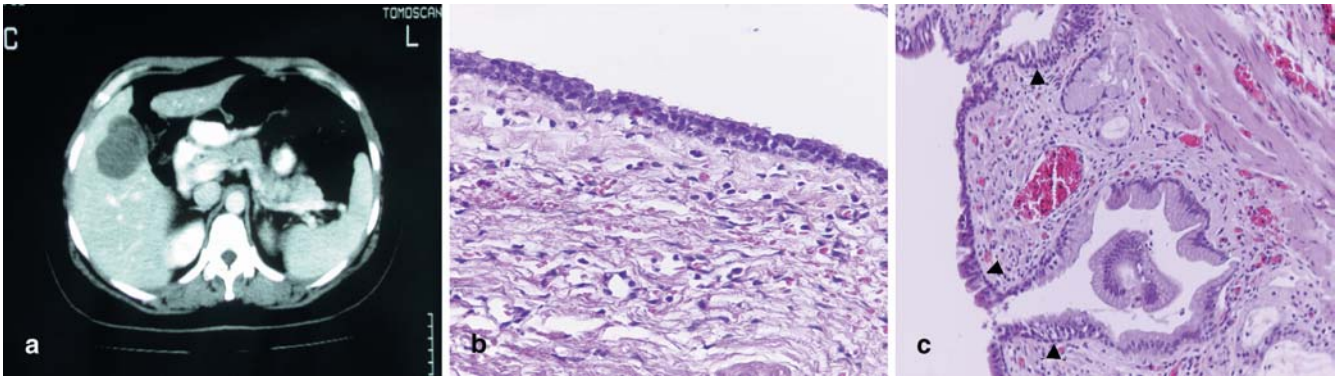

Fig. 1 **A** A multilocular cystic structure is seen on computed tomography scan. **B** The cyst is lined by respiratory type epithelium. **C** In the region of the connecting duct, there are alternating areas of respiratory type (*arrowheads*) and biliary epithelium [**B** Hematoxylin and eosin (H&E) ×400; **C** H&E ×200]

many myofibroblasts and rare strands of smooth muscle fibers, as confirmed by immunohistochemical stains for smooth-muscle actin and desmin. Within the outer portions of the wall, occasional small bile ducts were present. In some areas, a thin rim of compressed hepatic parenchyma was present adjacent to the fibrous wall. Sections of the gallbladder showed chronic cholecystitis and cholesterolosis. A smooth transition between the biliary and the respiratory-type epithelia was evident in the region of the connecting duct (Fig. 1C). The wall of the duct had a fibromuscular layer, which was in continuity with that of the gallbladder. Immunohistochemical stains for cytokeratins 7 and 19 showed areas of positivity in both biliary and respiratory type epithelia; whereas, stains for cytokeratin 20 were negative. In addition, the respiratory type epithelium of the cyst had a similar pattern of positive immunostaining for thyroid transcription factor-1 (TTF-1) as control sections of bronchial epithelium that were stained simultaneously. TTF-1 positivity was seen in many cells, especially basal ones.

The nature of the epithelial lining of the cyst in the present case indicated the diagnosis of CHFC. Nevertheless, what makes this case unique is the presence of a communication between the cyst and the gallbladder lumen, suggesting that the connecting duct was part of the malformation. This is supported by the presence of a fibromuscular layer in the duct wall, which was in continuity with the fibromuscular layer of the gallbladder, and by the presence of an additional aberrant duct connecting the cyst with the cystic duct. Knowledge of the existence of such malformations is useful information for physicians performing hepatobiliary surgery.

CHFC is usually asymptomatic [1, 4]. Abdominal pain is the most common complaint in symptomatic patients, including the one we report. However, review of the literature suggests that the symptoms of these patients, as well as the abnormal liver function tests that have sometimes been noted, cannot always be attributed with certainty to the presence of the cyst [4]. In one reported case, compression of the portal vein by a CHFC resulted in portal hypertension and splenomegaly; whereas, in another case, compression of the large extrahepatic bile ducts caused jaundice [2]. Although CHFC has traditionally been thought of as a lesion lacking any malignant potential, three recently published cases of squamous cell carcinoma arising in CHFC have changed this view [5]. Therefore, CHFC should be regarded as a lesion of which the clinical spectrum has not yet been fully defined.

References

1. Chatelain D, Chailley-Heu B, Terris B, Molas G, Le Caë A, Vilgrain V, Belghiti J, Degott C, Flejou JF (2000) The ciliated hepatic foregut cyst, an unusual bronchiolar foregut malformation: a histological, histochemical, and immunohistochemical study of 7 cases. Hum Pathol 31:241–246
2. Dardik H, Glotzer P, Silver C (1964) Congenital hepatic cyst causing jaundice: report of a case and analogies with respiratory malformations. Ann Surg 159:585–592
3. Terada T, Nakanuma Y, Kono N, Ueda K, Kadoya M, Matsui O (1990) Ciliated hepatic foregut cyst. A mucus histochemical, immunohistochemical, and ultrastructural study in three cases in comparison with normal bronchi and intrahepatic bile ducts. Am J Surg Pathol 14:356–363
4. Vick DJ, Goodman ZD, Deavers MT, Cain J, Ishak KG (1999) Ciliated hepatic foregut cyst: a study of six cases and review of the literature. Am J Surg Pathol 23:671–677
5. Vick DJ, Goodman ZD, Ishak KG (1999) Squamous cell carcinoma arising in a ciliated hepatic foregut cyst. Arch Pathol Lab Med 123:1115–1117

Virchows Arch (2005) 446:202–203
DOI 10.1007/s00428-004-1158-2

LETTER TO THE EDITOR

F. Alameda · L. Pijuan · L. Ferrer · M. L. Mariñoso · M. Muset · I. Soler · E. Gimferrer · S. Serrano

Human papilloma virus detection in liquid cytology, in situ hybridization and polymerase chain reaction

Received: 10 June 2004 / Accepted: 30 September 2004 / Published online: 13 January 2005
© Springer-Verlag 2005

Sir, Nowadays, the detection of high-risk human papilloma virus (HPV) is relevant to select those cases of cervical atypical squamous cells of undetermined significance (ASCUS) that probably will progress to cancer. In addition to morphology, we have several techniques, such as in situ hybridization (HIS) or polymerase chain reaction (PCR), to detect viral DNA in different samples. Liquid cytology is promoted in gynecological screening to have homogeneous material preserved for further study in suspicious cases, avoiding anxiety and the time spent taking a second sample. We decided to compare HPV detection in liquid cytology (ThinPrep Cytic) with HIS (Dako Genpoint) and PCR (HPVfast Pharma Gen S.A.), both wide-range HPV serotypes, using morphology as gold standard [1, 2, 3].

We selected 18 women with previous diagnoses of ASCUS or low-grade squamous intraepithelial lesions (LSIL) using conventional pap-smear and took a sample from each for liquid cytology. From this suspension, we prepared two slides—one stained with Papanicolau for morphology and one for HIS—the rest was used for PCR. We assessed the different nuclear alterations (enlargement, hypercromacy, irregular contours, binucleation, and perinuclear halos). In the HIS slide, we separated nuclear and cytoplasmic positivity. We registered in both slides the volume of pathological cells. PCR was considered positive when it showed a 450-pb band, which corresponded to HPV genoma, in addition to the 1200-pb band of control.

Results

From 18 cases, 14 were LSIL with clear morphology of HPV infection, and 4 were ASCUS with few or no HPV nuclear changes. Results of HIS and PCR are in Table 1.

From 13 HIS-positive cases, 11 were PCR-positive in the rest of the material. Of these, we found 4 cases with only cytoplasmic granular positivity—all 4 with very few affected cells. On a second screening of these 4 cases, we found one single nuclear-positive cell in 3 of these cases, and only 1 showed the positivity exclusively on the cytoplasm. This case was an LSIL. We performed PCR procedures using samples obtained from scraping the cytoplasmic positive of these 4 cases. The results were negative. We believe that in clinical practice, the cases with only cytoplasmic positivity should be confirmed with a PCR.

From 5 HPV-negative cases, 2 were PCR positive. In this short series, the sensibility and specificity were similar for both techniques: 84.6% and 60%, respectively.

Conclusions

– Though our series is short, both techniques have shown similar sensibility (84.6%) and specificity (60%) to detect HPV in liquid cytology. Discordances and false negatives may be justified because of the paucity of affected cellularity in all samples.

F. Alameda (✉) · L. Pijuan · L. Ferrer · M. L. Mariñoso · M. Muset · I. Soler · E. Gimferrer · S. Serrano
Hospital del Mar,
Department of Pathology,
Passeig Maritim 25-29, 08003 Barcelona, Spain
e-mail: 86780@imas.imim.es
Tel.: +34-932483031
Fax: +34-932483131

Table 1 Comparative results between polymerase chain reaction (PCR) and in situ hybridization (HIS) positive (+) and negative (–) cases. *LSIL* low-grade squamous intraepithelial lesions, *ASCUS* atypical squamous cells of undetermined significance

	HIS+	HIS–	Total
PCR +	11 (9 LSIL; 2 ASCUS)	2 (2 LSIL)	13
PCR–	2 (2 LSIL)	3 (1 LSIL; 2 ASCUS)	5
Total	13	5	18

– As pathologists, we prefer using HIS first, because we can appreciate morphology with positivity.
– When only cytoplasmic positivity is found, we suggest looking further for nuclear positivity or confirming it with PCR.

References

1. Iftner T, Villa LL (2003) Human papillomavirus technologies. J Nat Cancer Inst Monographs 2003:80–88
2. Yarkin F, Chauvin S (2003) Detection of HPV DNA in cervical specimens collected in cytologic solution by ligation-dependent PCR. Acta Cytol 47:450–456
3. Evans MF, Mount SL, Beatty BG, Cooper K, Phil D (2002) Biotinyl-tyramide-based in situ hybridization signal patterns distinguish human papillomavirus type and grade of cervical intraepithelial neoplasia. Mod Pathol 15:1339–1347

Virchows Arch (2005) 446:204–205
DOI 10.1007/s00428-004-1159-1

LETTER TO THE EDITOR

G. Marucci · C. M. Betts · M. Michal · M. P. Foschini

Peripheral ameloblastoma with Merkel cells

Received: 6 September 2004 / Accepted: 30 September 2004 / Published online: 10 December 2004
© Springer-Verlag 2004

Sir, Peripheral ameloblastoma (PA) is an exophytic tumour of the soft tissues overlying the tooth-bearing areas of maxilla and mandible, showing the same histological features as intraosseous ameloblastoma [4]. Merkel cells (MC) are clear cells localised in the basal layer of the epidermis, which are positive with anti-cytokeratin (CK) 7 and 20 antibodies and negative with S100 protein. In the oral mucosa, CK 20-positive cells, consistent with MC, are common. In samples from oral cavity mucosa [2], they have been observed in a variable percentage (up to 75%). MC in oral mucosa are polymorphic: among typical round to oval MC are admixed dendritic ones [5]. The exact function of MC, both in the skin and oral mucosa, is still unknown. In the present study, a case of PA with numerous MC within the neoplastic epithelium and in the perilesional mucosa is reported.

A 48-year-old-man presented with a gingival polypoid mass (measuring 2.5 cm in greatest axis) with an ulcerated surface on the left maxillary alveolar ridge. On radiography, there was no bone involvement. Following the histological diagnosis of PA, made on an incisional biopsy, radical surgical excision was performed.

G. Marucci · M. P. Foschini
Section of Pathology, Department of Oncological Sciences,
University of Bologna, Bellaria Hospital,
Bologna, Italy

C. M. Betts
Department of Experimental Pathology,
University of Bologna,
Bologna, Italy

M. Michal
Sikl's Department of Pathology,
Charles University, Medical Faculty Hospital,
Alej Svobody 80, 30460 Pilsen, Czech Republic

M. P. Foschini (✉)
Anatomia Patologica,
Ospedale Bellaria,
Via Altura 3, 40139 Bologna, Italy
e-mail: mariapia.foschini@ausl.bologna.it
Tel.: +39-051-6225523
Fax: +39-051-6225759

On haematoxylin and eosin-stained sections, the tumour consisted of nests and trabeculae showing a basaloid pattern with peripheral palisading. Neoplastic epithelium was in continuity with overlying surface epithelium (Fig. 1A, B).

CK 20 (DakoCytomation, dilution 1:40; clone KS 20.8) evidenced sparse MC within the neoplastic epithelium and numerous MC in the surrounding mucosa. MC were mainly dendritic and localised at the periphery of the neoplastic nests (Fig. 2A, B).

To establish whether MC are normally present in ameloblastoma, five cases of intraosseous ameloblastoma and two further cases of PA were studied with CK 20. Furthermore, to verify whether MC colonise tumours arising in contact with the oral mucosa, five cases of benign and malignant tumours (one pleomorphic adenoma, one myoepithelioma, one adenoid-cystic carcinoma and two mucoepidermoid carcinomas) with neoplastic epithelium in continuity with overlying oral surface epithelium have been studied with CK20. All the cases were retrieved from the files of the Department of Anatomic Pathology of the University of Bologna (Italy) at Bellaria Hospital.

None of these latter cases shows CK 20-positive cells, consistent with MC, while they were present in the perilesional mucosa. Thus, the PA, rich in MC, reported here seems to be an unique case. To the best of our knowledge, this phenomenon had not been previously described in oral cavity neoplasias. Furthermore, none of our control cases showed MC hyperplasia, while it is well known in the skin, where trichoblastomas rich in MC have been reported [3]. It is difficult to understand why MC are present in the neoplastic epithelium of PA.

One possible explanation could be a colonisation of the neoplastic epithelium by MC. A similar phenomenon is well known in the skin, where melanocytes colonise carcinoma [1] probably as a consequence of motility induced by cytokines. This possibility is suggested by the fact that MC showed dendritic processes. However, it seems to be a rare feature, since we could not detect it in the other cases studied.

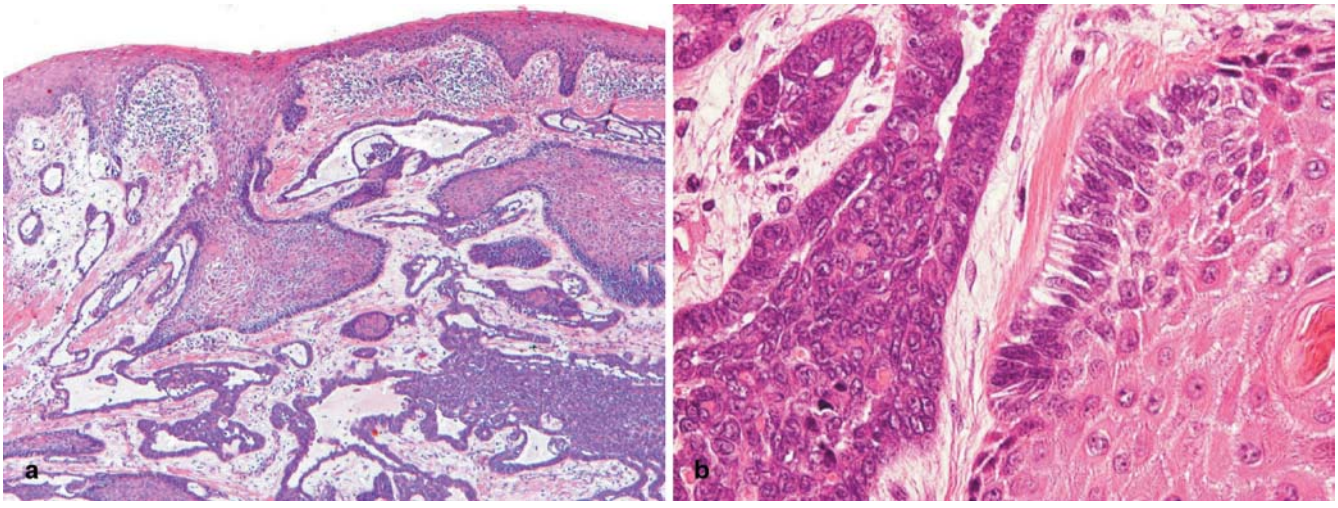

Fig. 1 A, B Peripheral ameloblastoma; neoplastic epithelium was in continuity with the overlying surface epithelium

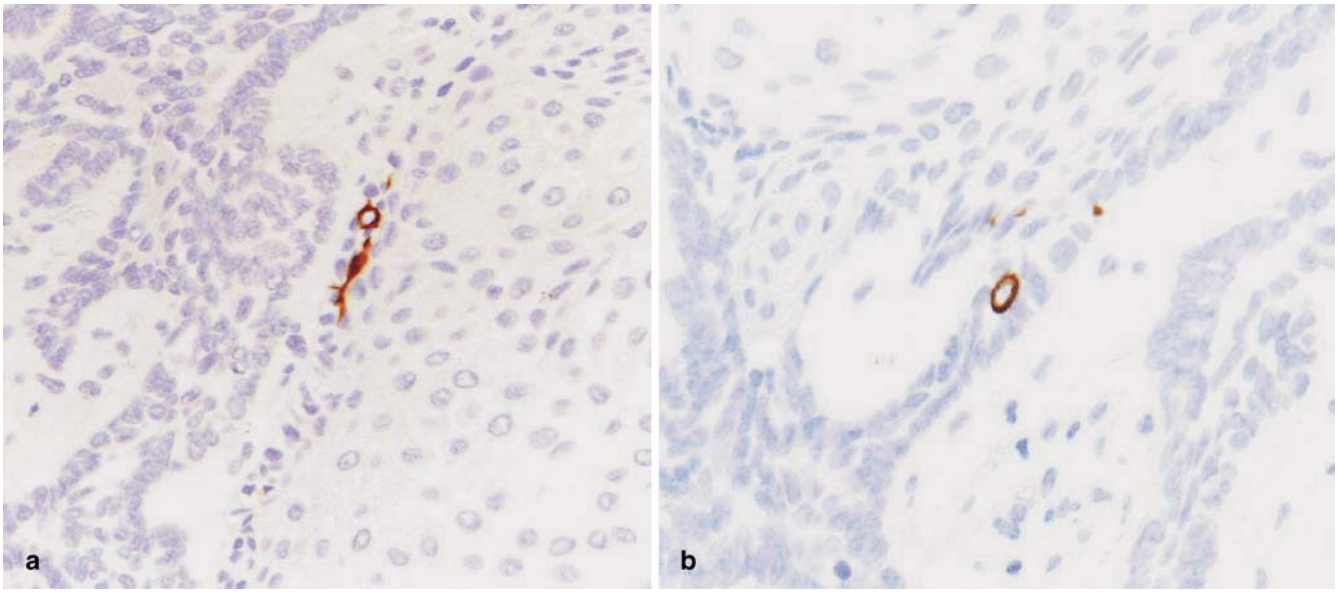

Fig. 2 A, B Immunostaining with CK 20 showed dendritic cells localised at the periphery of the neoplastic nests, consistent with Merkel cells

The histogenesis of PA has not been clearly elucidated. According to Philipsen et al. [4], some PA may arise from the basal cells of oral mucosa, producing a "basaloid" neoplasia, rich in MC, similar to the surrounding mucosa. The presence of MC in the PA described here appears to support this hypothesis.

References

1. Azzopardi JG, Eusebi V (1977) Melanocyte colonization and pigmentation of breast carcinoma. Histopathology 1:21–30
2. Barrett AW, Cort EM, Patel P, Berkovitz BK (2000) An immunohistochemical study of cytokeratin 20 in human and mammalian oral epithelium. Arch Oral Biol 45:879–887
3. Collina G, Eusebi V, Capella C, Rosai J (1998) Merkel cell differentiation in trichoblastoma. Virchows Arch 433:291–296
4. Philipsen HP, Reichart PA, Nikai H, Takata T, Kudo Y (2001) Peripheral ameloblastoma: biological profile based on 160 cases from the literature. Oral Oncology 37:17–27
5. Tachibana T, Kamegai T, Takahashi N, Nawa T (1998) Evidence for polymorphism of Merkel cells in the adult human oral mucosa. Arch Histol Cytol 61:115–124

Virchows Arch (2005) 446:206–207
DOI 10.1007/s00428-005-1221-7
© Springer-Verlag 2005

ANNOUNCEMENTS

19–24 April 2005
10th International Congress on Oral Cancer
Crete, Greece

Creta Maris Conference Centre

- The 10th International Congress on Oral Cancer is supported by the World Health Organization, the International Union Against Cancer, the International Congress on Oral Cancer, the Hellenic Association for the Research and Treatment of Oral Cancer, and the Hellenic Cancer Society
- The Congress theme is *The Oral Cancer Patient: the anthropocentric approach to a multidisciplinary problem*
- A number of Keynote Lectures will be delivered by international leaders in their specialties
- Limited attendance Courses will be provided for interested participants
- Deadline for abstract submission: November 30th, 2004
- Accepted abstracts for oral and poster presentations will be published as a supplement to the journal Oral Oncology. Details at www.harcourt-international.com/journals/oron
- Social events include Presidents Reception, Cretan Night and Gala Dinner

Further details at www.icooc-2005.org or from the Congress President at rapidis@icooc-2005.org

9–13 May 2005
Diagnostic Histopathology of Breast Disease
Hammersmith Hospital (Imperial College Faculty of Medicine), London, UK

A week-long course designed for pathologists at Consultant and Senior Trainee level. The course provides a comprehensive coverage of the Histopathology of Breast Disease, with special emphasis on areas that pose diagnostic difficulties. The participants with be given ample time to study histological preparations, followed by illustrated discussion of the cases. There will be special sessions dealing with the interpretation of core biopsies and fine needle aspirations. There will also be several daily talks dealing with specific topics, given by eminent breast pathologists and followed by discussion. The topics will include reporting breast biopsies, immunohistochemistry, receptors and c-erbB-2 assessment, dealing with the gross specimen, prognostic factors, proliferative lesions/carcinoma in situ, problems in breast pathology and mucinous lesions of the breast. The faculty will include Ian Ellis, Christopher Elston, Andrew Hanby, Stephen Humphreys, Andrew Lee, Naomi Livni, Sarah Pinder and Sami Shousha

Further details from:
Wolfson Conference Centre,
Hammersmith Hospital,
Du Cane Road,
London W12 ONN, UK
Tel.: (44) 20 8383 31 17/3227/3245
Fax (44) 20 8383 2428
E-mail: wcc@imperial.ac.uk

2–3 June 2005
Thyroid Pathology for the Practicing Pathologist
15 rue de l'Ecole de Médecine, Paris, France

A 2-day course will take place in Paris again under the auspices of the French Division of the I.A.P.
This course will be given in English by Prof.M.Sobrinho-Simoes (Porto) and Prof.R.Heimann (Brussels).
It will consist of lectures alternating with slide reviews and a slide seminar over a multihead microscope. The cases of this seminar will be sent (on CD) before the meeting.
The audience will be limited to 22 participants.
Course fees: 390 euros (320 euros for members of any I.A.P.division). The fees include registration,hand-out, CD of the slide seminar and coffee breaks.

For further information please contact:
Mrs.M. Fontanière
Administrative Secretary
French Division of the I.A.P.
32 Cours Albert Thomas
69008, Lyon, France
Fax: +33 4 78754311
E-mail: academie.pathologie@wanadoo.fr

3–4 June 2005
16th Ljudevit Jurak International Symposium on Comparative Pathology
Under the auspices of the European Society of Pathology and Academy of Medical Sciences of Croatia
Multimedial center Sestre milosrdnice University Hospital, Zagreb, Croatia

The main symposium topic is surgical pathology and frozen sections analysis. Symposium includes following sections: Pathological Morphology of the Human and Animal Diseases, Iatrogenic, Environmental and Experimental Pathology, Herman Jurak Round Table on Rheumatological Pathology, Clinical Forensic Pathology, Slide Seminars *in Histopathology and Cytopathology*, Quiz on Pathology.

Registration fee before April 1st – 100 EUR
Registration fee after April 1st – 150 EUR

Information: Davor Tomas, M.D.
Ljudevit Jurak University
Department of Pathology
Sestre milosrdnice University Hospital
Vinogradska 29
10000 Zagreb, Croatia
Tel.: +385 / 3787 909
Fax: +385 / 3787 244
E-mail: juraks@kbsm.hr
http://www.kbsm.hr/Jurak/symposium.htm

13–24 June 2005
International course on Laboratory Animal Science
Utrecht, The Netherlands

A two week intensive course on laboratory animal science will be organized at the Division of Laboratory Animal Science – Utrecht, The Netherlands in June 2005. This course is organized once a year since 1993.
The objective of this course is to present basic facts and principles that are essential for the humane use and care of animals and for the quality of research.
The contents of the course are in line with recommendations of the Federation of European Laboratory Animal Science Associations (FELASA) regarding the training of the young scientist whose research involves the use of vertebrate animals.
The course may also be of interest for those who intend to set up a similar course at their location. For this purpose, during the course the acquisition of teaching materials can be discussed with the course committee.

For information and application forms please contact:
Mr. Stephan van Meulebrouck, MA
Division of Laboratory Animal Science
Faculty of Veterinary Medicine
P.O. Box 80.166
3508 TD Utrecht
The Netherlands
Tel.: +31-30-2532033
Fax: +31-30-2537997
E-mail: pdk@las.vet.uu.nl
Internet: http://las.vet.uu.nl>Education and Training>International Course

26–29 July 2005
Practical Pulmonary Pathology
London, UK

This course is designed to provide histopathology and cytopathology trainees and consultants with an opportunity to study diagnostic lung pathology in a comprehensive manner. It comprises lectures and practical microscopy sessions, the latter making up roughly half the time and consisting of individual study of a unique collection of cases.

Further details and application forms are available from:
Professor B Corrin
Brompton Hospital
London SW3 6NP, UK
Fax: +44 20 7351 8293
E-mail: b.corrin@ic.ac.uk

Virchows Arch (2005) 446:208–215
DOI 10.1007/s00428-005-1203-9

EUROPATH NEWS 1/2005

European Society
of
Pathology

Editors
Dr. Grete Krag Jacobsen
University Department of Pathology,
Teilumbuilding Rigshospitalet
Blegdamsvej 9,
DK-2100 Copenhagen Ø, Denmark
Tel.: +45 3545 5450
Fax: +45 3545 5414
e-mail: grete.krag.jacobsen@rk.hosp.dk

Dr. Bjørn Risberg
Department of Pathology
The Norwegian Radium Hospital
0310 Oslo, Norway
Tel.: +47-22934174
Fax: +47-22508554
e-mail: brisberg@labmed.uio.no

The newsletter of the European Society of Pathology, EUROPATH NEWS, is sponsored by Leica Microsystems Nussloch GmbH

Newsletter of the European Society of Pathology

Presidential Address

Dear Members,

The year 2004 has been productive and enriching for the ESP. The principal scientific and educational activities have been the 2nd Intercontinental Congress of Pathology in Iguaçu, Brazil, the EuroCellPath meeting in Girona, Spain, and the European School of Pathology (ESCOP) courses in Turin, Italy, and in three other cities, mainly in eastern Europe. These are good indicators of the professional vitality and dynamism of our society. This is reflected in our official journal, *Virchows Archiv*, whose impact factor has jumped to 2.357 from 2.045. Furthermore, important administrative problems have been tackled at various business meetings during 2004: one Extraordinary General Assembly(GA), three Executive Committee (EC) meetings and one Advisory Council (AC).

On 6–7 February, both the EC and AC met in Paris with Pierre Bedossa and the French organizing committee, to help set up the final programme for the 20th ESP Congress to be held in September 2005. At the same time, an Extraordinary General Assembly was held in which the nomination of Niki Agnantis as President-Elect and of Roderick Simpson as Secretary (until the Paris congress) was approved. At the same time, the GA urged the EC to elaborate new rules for election of its officers, as well as to undertake the necessary steps for legal approval of the new statutes, which had had to be modified, in order to give the ESP a proper basis in law.

From 9 to 12 May, under the guidance of Fred Bosman, the EuroCellPath meeting was organized by Josep Lloreta in Girona, Spain, near the Catalan Costa Brava. This meeting was a success not only scientifically, but also socially. Genomic, transcriptomic and proteomic aspects were discussed in detail. A very stimulating round table discussion on the applications of array genomics and proteomics in pathology closed the activities. It became clear that there had to be closer interactions between EuroCellPath and ESCOP.

The 2nd Intercontinental Congress of Pathology was held in Iguaçu, Brazil, from 9 to 13 June, under the joint auspices of the ESP, the Latin American Society of Pathology and the Brazilian Society of Pathology. This was a most enjoyable and carefully prepared meeting, organized by Fernando Soares, Luiz Fernando Bleggi-Torres, José Vassallo and Brazilian colleagues. In particular, the ESP Working Groups were very active and well represented. The EC held a deliberating meeting in Iguaçu.

An Editorial Board meeting of*Virchows Archiv* was held on 24 September in Frankfurt, Germany. General satisfaction was expressed by all participants (Springer staff, the Editor-in-Chief and Managing Editors and the ESP Editorial Consultants), especially for the substantial rise in the journal's impact factor rate in 2003 as compared with 2002, which was mainly due to the efforts of the past Editor-in-Chief Günter Klöppel. His successor Heinz Höfler was quite optimistic with the opportunities for further improvement offered by the new online system, introduced in February 2003 by Springer for manuscript submission and editorial processing. It was widely felt that the joint venture in *Virchows Archiv* between Springer and ESP is bound to be beneficial for both sides. Negotiations for renewal of the contract are being scheduled for February–March 2005 and it is hoped that a satisfactory agreement will be reached before the congress in Paris.

The activities of the ESCOP, under the leadership of Gianni Bussolati, have increased this year despite financial limitations. The regular autumn course in Turin, Italy, was held on 23–29 September 2004 and covered "Pathology of the Uterus, Bladder and Prostate". In addition, other successful courses were held in Krakow, Poland, Ankara, Turkey, and Craiova, Romania.

On 19–20 November 2004, the Executive Committee met in Barcelona, where the following main items were considered:

Important Information

EuroPath News appears in *Virchows Archiv* four times a year, i.e. February, May, August and November. ESP members who want to publish information in *EuroPath News* should send the manuscript by e-mail to the editor (GKJ) *2 months ahead*of publication. Information only for the website should be sent to the editor of the website (BR).

e-mail: grete.krag.jacobsen@rh.hosp.dk
e-mail: brisberg@labmed.vio.no

For further information look at the ESP home page: http.//129.240.38.9/esp/

Contact person
Prof. Niki J. Agnantis
University Department of Pathoogy, Medical School of Joanina
GR-45110 Ioannina, Greece
e-mail: nagnanti@cc.uoi.gr

a. ESP Statutes: After very few, purely formal, amendments, the final version was accepted by the Belgian Ministry of Justice and was ready for publication in the appendices of the *Belgisch Staatsblad* on 26 November 2004. This important step was possible thanks to the persistent and enthusiastic work of several members, espe-cially Mia Marichal and Roderick Simpson.
b. Rules for the election of officers and members of the Executive Committee: The EC accepted the recommendations proposed by Michael Wells. Distinction was made between the procedure for election of officers and that for the election of other members of the committee. It was considered that for the time being no change of rules was needed for the elec-tion of the latter, since the existing procedure had been satisfactory, as, for example, factors of geography and sub-speciality have to be taken into account (see Attachment I).
c. Fred Bosman is the candidate proposed by the EC for President-Elect. Accordingly, in order to fulfil the requirements established by the rules for election of officers, this announcement is also a call for any further nominations from the membership. In the event of there being any other nomination, it must be submitted to the President within a period of 6 weeks, starting from the date of the first publication of this notice on the ESP website, http://www.europathology.org (see also Attachment I for details), or in the newsletter.
d. Roderick Simpson is the candidate proposed by the EC for Secretary. Accordingly, in order to fulfil the requirements established by the rules for election of officers, this announcement is also a call for further nominations from the membership. In the event of there being any other nomination, it must be submitted to the President within a period of 6 weeks, starting from the date of the first publication of this notice on the ESP website, http://www.europathology.org (see also Attachment I for details), or in the newsletter.
e. Several colleagues, well known members of our society, all of them in good financial standing, have been proposed as candidates for the four ordinary members of the EC to be replaced in Paris. Their election will follow the rules foreseen in Attachment I.
f. Grete Krag Jacobsen and Björn Risberg have finished the complex adaptation of the newsletter and the website for a quick flow of informative contents. In their increasingly demanding task they will have the assistance of Pieter Slootweg of Nijmegen, The Netherlands.
g. Barcelona, Spain, has been proposed by the EC as the site for the 3rd Intercontinental Congress of Pathology 2008. Josep Antoni Bombi is the proposed organizer. The GA, to be held in Paris on 7 September 2005, will have the opportunity to give its opinion.
h. Florence, Italy, has been proposed by the EC as the site of the 22nd European Congress of Pathology 2009, with Prof. Marco Santucci as proposed organizer. The GA, to be held in Paris on 7 September 2005, will have the opportunity to give its opinion.
i. Modifications of the by-laws are being prepared, to adapt them according to the current needs. They will be fully discussed at the next EC in Porto, Portugal, to be held on 16 April 2005, on occasion of the 14th Porto Cancer Meeting, organized by Manuel Sobrinho-Simoes.

The task ahead of us is formidable, as we accommodate the vitality and increased activity of our membership, with input coming from many parts of Europe. This constantly creates new scientific and educational challenges that need to be adequately promoted, coordinated and whenever possible sponsored. The congresses of Paris 2005, Ioannina 2006, Istanbul 2007, Barcelona 2008 and Florence 2009 are our main references for the future.

Last but not least, let me wish to all of you and to our Society all the best for the New Year. I very much hope to see you at the Paris Congress to celebrate its success together.

Sincerely yours,

Antonio Cardesa
President
Barcelona, January 2005

Attachment I

Elections of officers and other members of the Executive Committee:

1. *Election of officers*:
   a. The President will ask the advice of a Nominations Committee (composed of past presidents still active in the Society) to make proposals for candidates for each post, and these will be given to the Executive Committee.
   b. Following discussion and, if necessary, voting by simple majority, the Executive Committee will recommend this or another candidate to the membership at large. Approval by the individual of their own candidature must be given and an abbreviated CV of no more than one page provided.
   c. The recommendation of the Executive Committee to the membership at large will be published inthenewsletter and on the ESP website. This will be accompanied by a call for other nominations. Such nominations must be approved by the individuals themselves and each must be supported by at least 5% of members in good standing and accompanied by an abbreviated CV of no more than one page.
   d. After 6 weeks of publication on the ESP website or in the newsletter, and in the event of there being no other nominations for a particular post from the membership at large, the recommended candidate will be duly presented for formal approval at the General Assembly.
   e. In the event of other correctly proposed nominations for any particular post arising from the membership at large, a general ballot will be held; this could be either postal or by equivalent electronic means or by secret vote of members at the next appropriate congress. The successful candidate will be elected by simple majority, and will be duly presented for approval at the General Assembly. The method of conducting the ballot will be determined by the Executive Committee.

2. *Election of the eight additional Executive Committee members*:
   a. Nominations will be sought from a variety of sources, to include the President, members of the Executive Committee and the Advisory Council.
   b. Nominations should be sent to the Secretary, who will present them to the Executive Committee. After discussion, these should be sent to the Nominations Committee for comments and advice. Approval by the individual of his or her own candidature must be given and an abbreviated CV of no more than one page provided.
   c. Following discussion and, if necessary, voting by simple majority, the Executive Committee will approve the candidates, taking account of geographical and sub-speciality factors to ensure wide representation of the membership at large.
   d. The recommendation of the Executive Committee to the membership at large will be published in the newsletter and on the ESP website.
   e. The recommended candidates will be duly presented for formal approval at the General Assembly.

Past and Future Activities of the European School of Pathology (ESCOP)

In the past year, ESCOP courses have continued to focus on diagnostic histopathology. The now well-established general plan of the courses starts with two courses, each lasting 3 days, held in Turin in Villa Gualino at the end of September with 35–40 students participating. Villa Gualino is a modern 60–70-room building with teaching facilities and a restaurant.

Care is taken in selection of participants, favouring advanced residents and young pathologists from different European countries, and to date 15 countries have been represented.

The course leader, who is an internationally recognized expert in a specific field, is responsible for the programme and selection of cases and he or she is usually assisted by two or three collaborators.

The courses follow a scheme, which students have appreciated: a lecture on a given topic is followed by a slide seminar on selected pertinent cases. The participants have free time to run through the slides at the microscope, and after that the cases are discussed and commented on by the experts using video projection. No more than three to four topics are offered each day. At the end of the 3-day course, an anonymous evaluation is performed.

The aim of the courses is not only to update capabilities of diagnostic classification, but also to make students aware of the mental processes leading to diagnoses and to build up a network of friendship and mutual exchange among young European colleagues dedicated to our specia-lity.

It is now customary that the successful courses given in Turin are repeated in branches established in other seats.

In 2004 the ESCOP courses thus comprised:

a. Courses in Turin: one on "Pathology of the Uterus", 23–25 September, run by J. Prat with the assistance of X. Matias-Guiu and S. Carinelli, and one on "Pathology of the Urinary Tract and the Prostate", 27–29 September, run by F. Algaba with the assistance of A. Lòpez-Beltran. Forty students from 14 countries participated and it appeared from the evaluation that the participants appreciated the courses and the dedication of the teachers very much.
b. Courses in Krakow with local organizer J. Stachura: one on "Liver and Biliary Tumours" run by P. Bedossa and one on "The Pancreas" run by G. Klöppel, both courses previously held in Turin in 2003.
c. A course in Ankara with local organizer S.D. Sak: "Lung Pathology" run by H. Popper and previously held in Turin in 1999.

In 2005 the ESCOP activities will focus on three topics:

1. Financing: We have to face the fact that internal financing out of the budget of the supporting organizations, i.e. ESP and ISI, is not enough to sustain the expanding activities in Turin and in the other branches. Therefore financing will be sought from the EU (Marie Curie programmes), from European scientific programmes to be launched in 2005 and from a journal publisher.
2. Telepathology: The Turin headquarter will record cases presented in past courses, making consultation of such cases possible using the Internet and virtual microscope technology. We hope that this approach will boost the diagnostic impact of the courses, since past participants will be able to show and discuss cases with colleagues at their local laboratory. This approach will also favour the efficacy of the ESCOP courses in the various branches.
3. Implementation of courses in the ESCOP branches in Krakow (Poland), Ankara (Turkey) and Craiova (Romania) in collaboration with the local organizers, J. Stachura (Krakow), S.D. Sak (Ankara) and E. Plesea and D. Enache (Craiova). The programmes of these courses will soon be announced.

Gianni Bussolati

ESP Working Groups

Chairmen
Breast Pathology:
Ian Ellis
Nottingham City Hospital
NHS Trust, Hucknall Road
Nottingham NG5 1PB, UK
Tel.: +44-115-969
Fax: +44-115-9627769
e-mail: ian.ellis@nottingham.ac.uk

Cytopathology:
Fernando Schmitt
IPATIMUP
Rua Roberto Frias s/n
4200 Porto, Portugal
Tel.: +35-1-225570700
Fax: +35-1-225570799
e-mail: fschmitt@ipatimup.pt

Electron Microscopy:
Brian Eyden
Diagnostic Electron Microscopy
Christie Hospital NHS Trust 167
Manchester M20 4BX, UK
Tel.: +44-161-4463292
Fax: +44-161-4463300
e-mail: Brian.Eyden@christie-tr.nwest.nhs.uk

Endocrine Pathology:
Ronald de Krijger
Dept. of Pathology,
Josephine Nefkens Institute,
Erasmus MC University Medical Center
P.O. Box 1738
3000 DR Rotterdam
The Netherlands
Tel.: +31-10-4087901
Fax: +31-10-4089487
e-mail: r.dekrijger@erasmusmc.nl

Gastrointestinal Pathology:
Jan van Krieken
Department of Pathology
UMC St. Radboud
P.O. Box 9101
6500 HB Nijmegen
The Netherlands
Tel: +31 24 361 4352
Fax : +31 24 354 0520
e-mail: j.vankrieken@pathol.umcn.nl

Gynaecological Pathology:
Efthimios Sivridis
Democritus University of Thrace
Medical School
Dept. of Pathology
P.O. Box 128
68100 Alexandroupolis
Greece
Tel./Fax: +30-551-222212
e-mail: pathlab@users.duth.gr

Head and Neck Pathology:
Pieter J Slootweg
UMC St Radboud
Department of Pathology
Huispost 437, P.O. Box 9101
6500 HB Nijmegen
The Netherlands
Tel.: +31-243614314
Fax: +31-243540520
e-mail: .slootweg@pathol.umcn.nl

Molecular Pathology:
Heinz Höfler
Institut für Pathologie
der Technischen Universität
München
Ismaninger Str. 22
81675 München
Germany
Tel.: +49-89-41406123
Fax: +49-81-41406123
e-mail: Hoefler@lrz.tu-muenchen.de

Co-chairperson:
Generoso Bevilacqu
Divisione di Anatomia Pathologica
Via Roma 57
56126 Pisa
Italy
Tel.: +39-050/992889
Fax: +39-050/992706
e-mail: g.bevilacqua@med.unipi.it

Nephropathology:
Dušan Ferluga
Institute of Pathology
Faculty of Medicine University
of Ljubljana
Korytkova 2
1000 Ljubljana
Slovenia
Tel.: +386-1-5437137
Fax: +386-1-5437104
e-mail: dusan.ferluga@mf.uni-lj.si

Pulmonary Pathology:
Frédérique Capron
Serv. d' Anatomie
et Cytologi Patologiques
Hopital Antoine-Béclére
157, Rue de la Port de Trivaux
92141 Calamart Cedex
France
e-mail: frederique.capron
@psl.ap-hop-paris.fr

Skin Pathology:
Martin Gerald Cook
Department of Histopathology
Royal Surrey County Hospital
Egerton Road, Park Barn
GB-Guilford
Surrey GU2 5XX, UK
Fax: +44-148-3452718
e-mail: mgc@globalnet.uk

Soft-Tissue Tumours:
Angelo P. Dei Tos
Dept. of Pathology
Regional Hospital of Treviso
Piazza Ospedale 1
31110 Treviso
Italy
Tel.: +39-0422-322706
Fax: +39-0422-322663
e-mail: apdeitos@ulss.tv.it

Uropathology:
Gregor Mikuz
Dept. of Pathology
University of Innsbruck
Mullerstrasse 344
6020 Innsbruck
Austria
Fax: +43-512-58208815
e-mail: gregor.mikuz@uibk.ac.at

Report from the ESP Cytopathology Working Group

The Cytopathology Working Group of the ESP was established in 2000 during the intercongress meeting of the ESP on Madeira. Our main goal is to provide scientific knowledge in this field, to integrate cytopathology in the pathology practice and to link with cytology societies around the world.

Since our establishment, we have been responsible for the scientific activities in the following ESP congresses and intercongress meetings: Berlin 2001, Baveno 2002, Ljubljana 2003 and Foz do Iguassu 2004. We have contributed with slide seminars, symposiums, short courses and business meetings, with a significant participation of the ESP members from many different countries.

In 2004, the Cytopathology Working Group obtained international recognition from the International Academy of Cytology (IAC). For the first time, we organized a joined Satellite Symposium (IAC-ESP) entitled: "FNA: What's new in the 21st century", during the XV International Congress of Cytology, Santiago do Chile, April 2004. At the same time a Liaison Committee with the IAC was created with the following appointed members: F. Schmitt (Chairman), Portugal; I. Amendoeira, Portugal; U. Baandrup, Denmark; P. Firat, Turkey; C. La Cruz, Spain; A. Maria Puig, Spain; B. Risberg, Norway; L. Skoog, Sweden and P. Zeppa, Italy. The main objective of this committee is to organize joint activities during IAC and ESP meetings.

For 2005, we are involved in the scientific programme of the 20th European Congress of Pathology to be held in Paris. Besides a symposium and a business meeting, we are preparing a slide seminar with participation of young pathologists interested in cytology.

As chairman and co-chairpersons (L. Skoog and E. Tani, Sweden) of the Working Group on Cytopathology, we would like to invite you to participate actively in our group.

Professor Fernando Schmitt
Chairman, Cytopathology WG-ESP

Address for information:
IPATIMUP
Rua Roberto Frias s/n
4200 Porto, Portugal
e-mail: fernando.schmitt@ipatimup.pt
Tel.: +35-1-225570700
Fax: +35-1-225570799

Recent and Forthcoming Activities of the Electron Microscopy Working Group

The Electron Microscopy (EM) Working Group comprises pathologists and scientists working in diagnostic pathology and biomedical research with a special interest in electron microscopy. Members of the Working Group wish to promote EM by taking part in meetings at the ESP congresses and intercongresses as well as furthering EM by personal contacts. For this, a list of pathologists and scientists with an interest in ultrastructural pathology has been established and is constantly being updated as new individuals wish to participate. The latest update in September 2004 listed 97 members, and a website for the Working Group will shortly be established.

The EM Working Group participated in the Ljubljana Congress in September 2003, with two short courses and a slide seminar covering many aspects within the field.

Current objectives of the EM Working Group are to finalize details for a short course on tumours, and a precongress meeting on non-neoplastic disease, for the Paris Congress of September 2005.

Dr. Brian Eyden (PhD)
Department of Histopathology
Christie Hospital NHS Trust
Wilmslow Road
Manchester M20 4BX
UK
Tel.: +44-161-4463292
Fax: +44-161-4463300
e-mail: brian.eyden@christie-tr.nwest.nhs.uk

Information from the Working Group on Endocrine Pathology

The Working Group on Endocrine Pathology of the ESP is composed of 55 members throughout Europe. Apart from the chairman, there is a secretary and an advisory board, which are listed below. Anyone with an interest and experience in endocrine pathology is encouraged to become a member, by sending their address to the chairman or secretary. Membership is free of charge.

The working group organizes slide seminars, courses, and symposia, predominantly during ESP meetings, such as the European Congress of Pathology in September 2005 in Paris, France, and the interim meeting in May 2006 in Ioannina, Greece. Collaboration with other endocrine societies is promoted, especially with our North American counterpart, the Endocrine Pathology Society, which is reflected by a session on the new WHO Classification of Endocrine Tumours during the ESP congress in Paris, where some of the editors will present this classification.

Furthermore, the working group intends to create a platform for the exchange of research plans, as well as for setting up multicentre collaborations for relatively rare endocrine diseases and/or tumours. Initiatives in this field are also welcomed by the chairman and the secretary.

Ronald de Krijger
Rotterdam, December 2004

Chairman:
Ronald de Krijger, MD, PhD
Dept. of Pathology
Josphine Nefkens Institute
Erasmus MC – University Medical Center
P.O. Box 1738
3000 DR Rotterdam
The Netherlands
Tel.: +31-10-4087901
Fax: +31-10-4089487
e-mail: r.dekrijger@erasmusmc.nl

Secretary:
Marco Volante, MD, PhD
Dept. of Pathology
University of Torino
Via Santena 7
10126 Torino
Italy
Tel.: +39-011-6706539
Fax: +39-011-6635267
e-mail: marco.volante@unito.it

Advisory Board:
Prof. Paul Komminoth, MD, PhD
Institute of Pathology
Dept. of Medical Services
Kantonsspital Baden
5404 Baden
Switzerland
Tel.: +41-56-4863901
Fax: +41-56-4863919
e-mail: paul.komminoth@ksb.ch

Prof. Günter Klöppel, MD, PhD
Dept. of Pathology
University of Kiel
Michaelisstrasse 11
24105 Kiel
Germany
Tel.: +49-431-5973400
Fax: +49-431-5973460
e-mail: g.kloeppel@path.uni-kiel.de

Prof. Manuel Sobrinho-Simoes, MD, PhD
Dept. of Pathology & IPATIMUP
Medical Faculty of Porto
Rua Roberto Frias s/n
4200 Porto
Portugal
Tel.: +35-1-225090591
Fax: +35-1-225570799
e-mail: sobrinho.simoes@ipatimup.pt

Prof. Xavier Matias-Guiu, MD, PhD
Dept. of Pathology
Hospital Univ. Arnau de Vilanova
Avenida Alcalde Rovira Roure 80
25198 Lleid
Spain
Tel.: +34-973-248754
e-mail: xmatias@arnau.scs.es

Report from the ESP Head and Neck Pathology Working Group 2004

Meetings

Several ESP Working Group members attended the 2nd Intercontinental Congress of Pathology in Rio de Janeiro and Foz do Iguassu, 9–13 June 2004. In Rio de Janeiro, P.J. Slootweg gave a lecture on the impact of molecular biology for diagnostic and therapeutic management of patients with head and neck cancer.

At the meeting in Foz do Iguassu, Working Group members A. Cardesa, M.A. Luna, N. Gale, S. di Palma, R. Simpson, M. Santucci, Leivo, A. Skalova, M. Therkildsen, and P.J. Slootweg participated in various parts of the programme (slide seminar, short course, companion meeting and conference).

On behalf of the Working Group, M. Luna received an Honorary Diploma to acknowledge all his efforts in the promotion of head and neck pathology.

At the 12th Congress of the International Association of Oral Pathologists (IAOP), Madrid, 6–11 September 2004, P.J. Slootweg, A. Cardesa, M.A. Luna and R. Simpson spoke in the session "Update of Tumours of the Salivary Glands".

In addition, ESP Working Group members R. Simpson, A. Skálová, S. di Palma and P.J. Slootweg participated in various symposia and slide seminars at the IAP International Congress, Brisbane, Australia, 10–15 October 2004.

Scientific Collaboration

A multicentric study on papillary squamous carcinoma of the head and neck has been initiated by Prof. N. Gale and Prof. A. Cardesa and many members are contributing cases for this study.

At the WHO Classification of Head and Neck Tumours Consensus Conference, held in Lyon, France, 15–19 July 2003, several members of the Working Group participated: N. Gale, A. Cardesa, R. Simpson, A. Skálová, F. Bertoni, P.J. Slootweg, I. van der Waal, G. Jundt, J.W. Eveson, L. Michaels and A. Sandison.

Forthcoming Meetings

In association with the 20th European Congress of Pathology in Paris, 3–8 September 2005, a pre-meeting of the ESP Working Group and the North American Society of Head and Neck Pathology of the US and Canadian Academy of Pathology will be organized on 2 September 2005. At this 1-day meeting, an expert panel will discuss approximately 20 cases which in daily practice resulted in diagnostic difficulty or the differential diagnostic considerations resulted in severe prognostic implications.

At the congress a slide seminar, a symposium and a short course concerning head and neck pathology are scheduled to take place.

Other Activities

The ESCOP course on Head and Neck Pathology that was previously run twice in Turin will be given in Krakow, Poland, 6–9 June 2005, with the lecturers A. Cardesa, R. Simpson, and P.J. Slootweg.

Pieter J. Slootweg

Working Group on Nephropathology

Background

Until the 19th European Congress of Pathology in Ljubljana, nephropathology was included in the Working Group on Uropathology, which covers primarily surgical pathology, so that nephropathology as a non-neoplastic topic has been barely visible. Due to particular efforts of the organizers, at the Ljubljana Congress nephropathology was included on an equal basis to other fields and there was a great interest in these sessions. There has been unanimous opinion that the Working Group on Nephropathology should be established and a proposal for the foundation of an ESP Working Group on Nephropathology was prepared, presented by the ESP President at the General Assembly on 10 September 2003, after which the foundation of the Working Group on Nephropathology was approved.

Structure

Following the Ljubljana Foundation Meeting, the structure of the Working Group on Nephropathology is:

Chairman:	Prof. Dušan Ferluga (Ljubljana, Slovenia); e-mail: dusan.ferluga@mf.uni-lj.si
Secretary:	Dr. Alenka Vizjak (Ljubljana, Slovenia); e-mail: alenka.vizjak@mf.uni-lj.si
Executive members:	Prof. Jan A. Bruijn (Leiden, The Netherlands)
	Prof. Jean-Pierre Cosyns (Brussels, Belgium)
	Dr. Dominique Droz (France)
	Dr. Franco Ferrario (Milan, Italy)
	Prof. Peter Furness (Leicester, UK)
	Prof. Hermann-Josef Gröne (Heidelberg, Germany)
	Prof. Isin Kilicaslan (Istanbul, Turkey)
	Prof. Dontscho Kerjaschki (Vienna, Austria)
	Dr. Eugen Mandache (Bucharest, Romania)
	Prof. Niels Marcussen (Aarhus, Denmark)
	Prof. Michael. J. Mihatsch (Basel, Switzerland)
Advisers:	Prof. J. Charles Jennette (Chapel Hill, USA)
	Prof. Jan J. Weening (Amsterdam, The Netherlands)

Goals

- Establishment of a database of all pathologists and any holders of a MD, PhD, DVM or equivalent degree who have demonstrated interest and involvement in the field of renal pathology
- Collaboration with the existing international and national nephropathology and nephrology groups and societies in Europe, North America and other continents
- Scientific and educational programmes for the ESP congresses, other meetings and courses
- Training programme and certification in nephropathology (including kidney transplant pathology)
- International research projects
- Exchange of views and expertise

Communication

Proposals and suggestions for enhancing the activity of the working group are appreciated and an open forum for discussion between individuals engaged in nephropathology is enabled by e-mail.

Forthcoming Meetings

The working group, in collaboration with the organizers of the 20th European Congress of Pathology, to be held in Paris on 3–8 September 2005, has prepared a programme of four congress scientific sessions devoted to nephropathology and transplantation, as well as a 1-day Nephropathology Pre-congress Meeting – "Updates in Nephropathology and Transplantation" – to be held in Paris on 3 September 2005.

D. Ferluga

IUCP
Ioannina University
Courses in Pathology
First announcement

Prostate
Pathology – Oncology

Ioannina, May 25-27 2005

Preliminary list of speakers

Ass. Prof. Y. Alalmanos (GR)
Ass. Prof. E. Briasoulis (GR)
Dr. E. Eleftheriades (GR)
Ass. Prof. A. Kyroudi-Boulgari (GR)
Dr. P. Hamilton (UK)
Dr. D. McManus (UK)
Ass. Prof. R. Montironi (I)
Ass. Prof. K. Pavlaki (GR)
Dr. C. Petraki (GR)
Prof N. Sofikitis (GR)
Ass. Prof. N. Stavropoulos (GR)
Assoc. Prof. C. Tsampoulas (GR)

*Examination with multiple-choice questions.
*Credit hours: 13.30'

Topics

Epidemiology
Therapeutic management
Grading and staging
Histology and function
Specific techniques in prostate Pathology
Molecular pathology
Predictive factors in prostate cancer
S.S. Pitfalls in prostate lesions
Preneoplastic prostatic lesions
Surgical treatment
Screening for prostate cancer
Imaging

The European Society of Pathology

Dear Colleague,

It will surely not have escaped your attention that *Virchows Archiv* is now the Official Journal of the European Society of Pathology.

But did you realise what benefits membership in the society offer you?

- A subscription to the journal *Virchows Archiv* at no extra charge – this is automatically sent to every member every month.
- Access to the journal online (take a look at http://link.springer.de). If you are already a member of ESP but have not yet registered for your free electronic access, you will find the necessary form to complete online here too.
- A discount of 20% on most titles published by Springer. To take advantage of this, simply send your order directly to the publisher, with details of your membership.
- Attendance at the Society's conferences at a reduced fee.

If you have not yet joined the European Society of Pathology, why not do so now?
Simply complete and return the form enclosed. If you are already a member, please wait for our renewal letter for 2004.

We look forward to welcoming you as a member in 2005

Yours sincerely

A. Cardesa
President
European Society of Pathology

H. van Krieken
Treasurer
European Society of Pathology

H. Höfler
Managing Editor
Virchows Archiv

Application for Membership of the EUROPEAN SOCIETY OF PATHOLOGY

For formatting of old application, please follow old application (old Newsletter, p. 238)

This application can also be downloaded from our website:
http://www.Europathology.org

Please complete the following form (block capitals please) and return it to the Office of the Treasurer

FAMILY NAME: .....

First Name(s): .....

Male ❑ Female ❑

Place and date of birth: .....

Title/Present Position: Prof. ❑ Dr. ❑ Resident ❑

Other: .....

Please clearly indicate which one of the following addresses should be used for subsequent correspondence, mailings, and listing in the Members Handbook:

❑ PRIVATE ADDRESS:

Name: .....
Street: .....
Postcode .....
City: .....
Country: .....

❑ INSTITUTE / OFFICE ADDRESS:

Name Institute: .....
Department: .....
Street: .....
Postcode: .....
City: .....
Country: .....
Telephone: .....
Telefax: .....
E-mail: .....

FIELDS OF INTEREST: .....

Date: ..... Signature of Applicant: .....

Please mail or fax the completed application form to:

ESP – OFFICE OF THE TREASURER,
Prof. Dr. H. VAN KRIEKEN,
University Medical Center Nijmegen
Dept. of Pathology / 437 PA
P.O.Box 9101
6500 HB NIJMEGEN, The Netherlands

Tel.: +31-24-3614352
Fax: +31-24-3540520
e-mail: j.vankrieken@pathol.umcn.nl

Your acceptance as a member of E.S.P. will be confirmed in due course.

Virchows Arch (2005) 446: 219–224
DOI 10.1007/s00428-005-1217-3

REVIEW ARTICLE

Antoine de Mascarel · Agnès Ruskone-Fourmestraux · Anne Lavergne-Slove · Francis Megraud · Pierre Dubus · Jean-Philippe Merlio

Clinical, histological and molecular follow-up of 60 patients with gastric marginal zone lymphoma of mucosa-associated lymphoid tissue

Received: 12 October 2004 / Accepted: 11 January 2005 / Published online: 2 March 2005
© Springer-Verlag 2005

Abstract The persistence of gastric lymphoma after *Helicobacter pylori* eradication may be difficult to evidence on endoscopic and histological examination. The aims of the study were to evaluate the detection of monoclonal immunoglobulin H (IgH) gene rearrangement in endoscopically infiltrated and normal mucosa at diagnosis and during follow-up in order to determine its clinical and prognostic impact. We studied 60 gastric marginal zone lymphomas of mucosa-associated lymphoid tissue (MALT), and IgH monoclonality was detected at diagnosis in 52 patients (87%). The endoscopically normal mucosa contained clonal lymphomatous cells in 69% of cases before remission. A complete histological remission (HR) was observed in 28 patients (47%). Among them, 23 were followed for molecular remission (MR). The median delay was 10 months to achieve HR and 18 months to achieve MR. Interestingly, patients with HR but not MR had a longer delay to achieve HR (21 months) (P=0.0006) and a more frequent clonal normal mucosa at diagnosis (88%) than patients with both HR and MR (10 months and 39%, respectively). The presence of monoclonal B cells at both infiltrated and normal sites may therefore identify patients with a longer delay to achieve complete response, suggesting that molecular dissemination may require therapeutic intensification.

Keywords MALT · Lymphoma · *Helicobacter pylori* · *IgH* gene · Monoclonality

Introduction

Gastric marginal zone lymphoma of mucosa-associated lymphoid tissue (MALT) is strongly associated with colonisation of the gastric mucosa by *Helicobacter pylori* [7, 19], and high rates of complete remission can be obtained by *H. pylori* eradication therapy [2, 8, 10–14, 16, 17, 20]. The stability of the remissions remains difficult to understand. From a multicentre study by the "Groupe Français d'Etude des Lymphomes Digestifs" (GELD), for which clinical results of this study were previously reported [13], the sequential follow-up biopsies of this study were analysed for immunoglobulin heavy gene (IgH) rearrangement by means of polymerase chain reaction (PCR). The aims of the present study were: (1) to search for monoclonality in endoscopically infiltrated (I) mucosa and evaluate the molecular follow-up comparatively to clinical and histological follow-up; and (2) to search for monoclonality in endoscopically normal (N) mucosa and evaluate its predictive value for histological remission (HR) and relapse.

Patients, materials and methods

From 1995 to 2000, 60 consecutive patients with localised gastric marginal zone lymphoma of MALT (GL) were included in a multicenter study by GELD.

Patients suspected of having a histological diagnosis of low-grade GL on the basis of routine endoscopic biopsies were asked to participate in the study. A second gastroscopy prior to *H. pylori* treatment allowed the biopsy of multiple tissue specimens in the infiltrated (I) lesions and in the endoscopically normal (N) mucosa. Biopsies were fixed in

Part of this work was presented at the 2002 Annual Meeting of the United States and Canadian Academy of Pathology and published in abstract form (Mod Pathol 2002;15:126A).

A. de Mascarel (✉) · F. Megraud · P. Dubus · J.-P. Merlio
Department of Pathology, University Victor Segalen Bordeaux 2,
Hôpital Haut-Lévêque,
33604 Pessac cedex, France
e-mail: antoine.demascarel@chu-bordeaux.fr
Tel.: +33-5-57656467
Fax: +33-5-57656453

A. Ruskone-Fourmestraux
Department of Gastroenterology, Hôtel Dieu, AP-HP,
1 place du Parvis Notre Dame,
75181 Paris cedex 04, France

A. Lavergne-Slove
Department of Pathology, Hôpital Lariboisière,
2 avenue Ambroise Paré,
75475 Paris cedex 10, France

formalin and frozen. The endoscopic diagnosis of N mucosa was always confirmed histologically. The diagnosis of GL was confirmed by a review committee of four pathologists according to Isaacson's criteria [7] and Wotherspoon's scoring system [20]. Post-treatment biopsies were examined by the same panel of pathologists. Complete HR was diagnosed whenever the biopsies showed no sign of lymphoma, but small basal clusters of lymphocytes and scattered plasma cells were sometimes visible.

Extension of the disease was defined according to the Ann Arbor staging system modified by Musshoff [9] and included gastric endoscopic ultrasonography, ileocolonoscopy, abdominal CT scan and bone marrow biopsy.

Final inclusion criteria were a histologically proven low grade MALT GL (score 5) with a localised tumour at stage IE (parietal involvement) or IIE1 (contiguous nodal involvement) based on abdominal CT scan and gastric endoscopic ultrasonography.

All patients received the same anti-*H. pylori* treatment (lansoprazole, amoxicillin and clarithromycin), as described elsewhere [13].

During follow-up, endoscopic biopsies were performed as initially in the area of both suspected infiltrated mucosa (I) and normal mucosa (N). The first control was performed one month after the end of treatment, thereafter every 3 months until HR or every 6 months after HR during the first 2 years and then each year. For all patients, lymphoma HR was confirmed by at least three series of consecutive follow-up examinations. Patients with persistence of the initial macroscopic lesions or progression of the initial tumour pattern at control endoscopy, or patients whose HR was not complete 12 months after treatment were considered as showing no HR. These patients were referred for total gastrectomy.

The monoclonality of immunoglobulin heavy (IgH) chain FR3-JH gene rearrangement was studied as previously described [4]. DNA was extracted from a fresh-frozen part of endoscopic biopsy specimens of I mucosa and N mucosa by means of cell lysis with 160 μg proteinase K in a 200-μl Tris HCl 0.01 mol/l, NaCl 0.4 mol/l buffer for 12 h at 52°C. After heat inactivation at 100°C for 15 min, lysates were snap-frozen. A 10-μl aliquot containing approximately 500 ng DNA was used for each PCR. Two primer pairs (Ca1/Ca2 and Ca1/VLJH) were used in separate standard 35-cycle PCRs for each sample. A 20-μl aliquot was run on a 10% acrylamide-bisacrylamide 19/1 gel, then stained with ethidium bromide. PCR products were viewed under ultraviolet light illumination. At each endoscopic time point, a pair of DNA samples from infiltrated (I) and normal (N) mucosa was analysed and electrophoresed in comparison with the initial DNA of I mucosa.

Statistical analyses

The association between N mucosa monoclonality or polyclonality and the achievement of HR or no HR was evaluated using the Chi-square test. Similarly, the association between N mucosa monoclonality or polyclonality and the achievement of HR with MR or HR without MR was evaluated.

The impact of MR or no MR on HR delay was evaluated in 23 patients with HR using the Student *t*-test.

Results

Sixty patients with localised gastric marginal zone lymphomas of MALT and molecular study were enrolled in the study. The age of patients ranged from 25 years to 74 years (median 55.4 years) with a male-to-female ratio of 37:23. There were 45 patients (75%) in stage IE and 15 (25%) in stage IIE.

Clinical follow-up

Of the 60 patients, 28 (47%) achieved a complete endoscopic remission and HR, whereas 32 patients (53%) showed no response or endoscopic progression (Fig. 1).

Of the 32 non-responders, 4 patients who did not accept surgery presented a histological persistence of MALT lymphoma 12, 20, 24 and 39 months after *H. pylori* eradication. After a mean delay of 11.1 months (range, 3–36 months) after the initial histological diagnosis, the other 28 patients were referred for surgery. In these 28, the histological stomach examination showed a gastric marginal zone lymphoma of MALT without a diffuse large B cell component, and 21 of these patients have been followed (7 lost to follow-up) for a median of 25.9 months (range, 2–54 months), none of them presenting with relapse.

In the group of 28 patients with HR, the mean delay to achieve HR was 13 months (range, 2–35 months) and the mean follow-up after HR was 19.3 months (range, 0–61 months). Of these 28 patients, 3 presented with a relapse 11, 15 and 37 months after HR. Histological examination of the relapse showed a gastric marginal zone lymphoma of MALT in 2 and a diffuse large B cell lymphoma in 1.

Molecular follow-up

For the 60 patients, 368 N and I PCR-paired analyses were performed, with an average of 3 pairs per patient (range, 2–13) (Fig. 2).

In 8 patients (13.3%), all PCR analyses showed polyclonality with an average of 3.3 pairs of PCR per patient (range, 1–5). Of these, 3 patients underwent gastrectomy and 5 patients with HR were not operated on.

In 52 patients (86.7%), PCR analyses showed the presence of IgH monoclonality at diagnosis (Table 1):

- Of 52, 29 (55.8%) did not regress histologically. Four were endoscopically followed for a mean period of 23.8 months (range, 12–39 months) after the histological diagnosis and 25 were operated on after a mean delay of 11.1 months (range, 3–36 months) after the diagnosis. All showed the same clone found from the

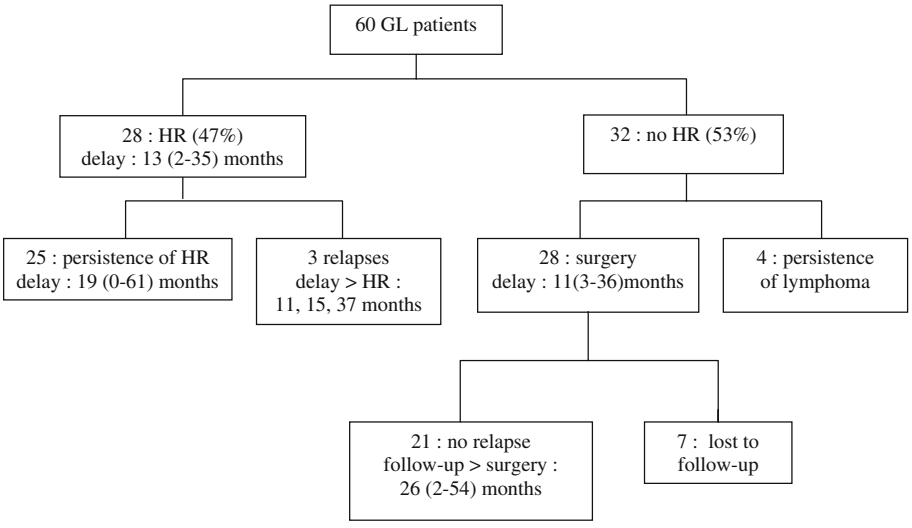

Fig. 1 Flowchart showing the clinical and histological follow-up of 60 patients with gastric MALT lymphomas (GL) after *H. pylori* eradication. *HR* histological remission

sequential biopsies at follow-up. For these 29 patients with neither HR nor molecular remission (MR), 68 paired-PCR analyses were positive: 27 of 68 only in I mucosa, 38 of 68 in both I and N mucosa, and 3 of 68 only in N mucosa (in I mucosa, DNA was not amplified in two and polyclonal in one). Therefore, I mucosa was positive in 65 of 68 samples (95.6%) and N mucosa was positive in 41 of 68 samples (60.3%).

– Of 52, 23 (44.2%) regressed histologically (HR). Among these, a first group of 13 (56.5%) also presented with MR. Their average delay to HR was 9.5 months (range, 4–18 months), their average delay to MR was 17.5 months (range, 5–36 months), and the average delay between HR and MR was 7.2 months (range, 0–29 months). The average follow-up period after MR was 14.5 months (range, 0–30 months). In this group, 23 pairs of PCR were positive: 14 of 23 only in I mucosa, 6 of 23 in both I and N mucosa, and 3 of 23 only in N mucosa (in I mucosa, DNA was not amplified in one and polyclonal in two). So I mucosa was monoclonal in 20 of 23 (87%) and N mucosa was monoclonal in 9 of 23 (39.1%). In this group with HR and MR, two patients relapsed with a gastric marginal zone lymphoma of MALT 11 months and 15 months after HR and 11 months and 9 months after MR, respectively. Unfortunately, the relapse could not be studied using PCR. A second group of 10 from 23 patients with HR (43.5%) did not present with MR with an average HR delay of 21.3 months (range, 2–35 months) and an average follow-up of 6.4 months (range, 0–35 months) after HR. In this group, 33 pairs of PCR were positive: 4 of 33 only in I mucosa, 28 of 33

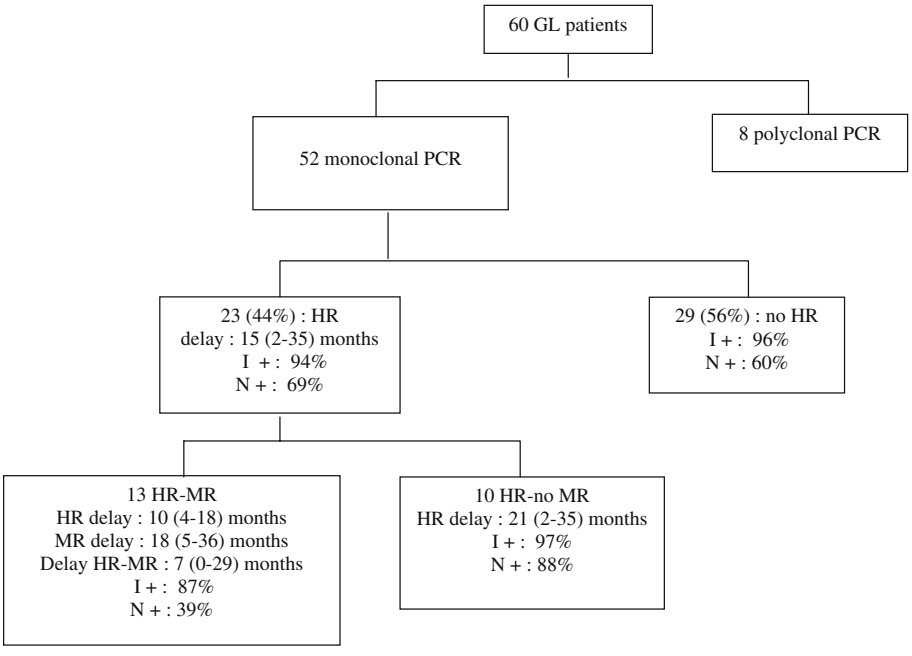

Fig. 2 Sixty MALT gastric lymphomas (GL). Flowchart showing the molecular follow-up of patients with monoclonal histological remission (HR) and the percentage of positive polymerase chain reactions (PCR) according to the infiltrated (I) and normal (N) biopsy mucosa during the histological lymphoma period. *MR* molecular remission

Table 1 Fifty-two clonal MALT lymphomas. *PCR* polymerase chain reaction, *HR* histological remission, *MR* molecular remission

Patients	Pairs of PCR+ (*)	I only (%)	N only (%)	I + N (%)	I (%)	N (%)
52	124	36	6	50	94	69
29 no HR	68	40	4	56	96	60
23 HR	55	33	7	62	95	69
13 HR–MR	23	61	13	26	87	39
10 HR, no MR	28	12	3	85	97	88

Percentage of positive PCRs according to the endoscopically infiltrated (I) or normal (N) biopsy mucosa during histological lymphoma period

(*) Every pair of PCR corresponds to 2 PCRs (I and N mucosa) which can be positive in I or N or both sites

in both I and N mucosa, and 1 of 33 only in N mucosa; so, I mucosa was positive in 32 of 33 (97%) and N mucosa was positive in 29 of 33 (87.9%). In this group, there was no clinical or histological relapse.

– We found no association between N mucosa monoclonality and the risk to achieve HR. However, in the 23 patients with HR, N mucosa polyclonality was statistically associated with MR achievement (χ^2=0.026). The 13 patients with MR also achieved HR after a shorter delay than the 10 patients without MR (Student *t*-test, *P*=0.0006).

Discussion

Histological follow-up

Since the first reports on gastric lymphoma regression after anti-*H. pylori* eradication [17, 20], various remission rates have been observed ranging from 50% [16] to, more frequently, 70% [2, 3, 6, 8, 10, 11, 14, 18] and even 100% [11]. With a remission rate of 46.7% (28 of 60 patients), our data are equivalent to those of Steinbach et al. [16]. In both series, the mixing of stage IE and IIE1 patients might explain such a low rate. Indeed, in our series, 45% of the non-responders had a stage IIE. Among the 32 non-operated patients, all but one presented stage IE without any nodal enlargement at endoscopic ultrasonography and 28 (87.5%) achieved a complete HR. This rate is similar to the proportion (range, 70–100%) of patients at stage IE in most series [2, 3, 6, 8, 10, 11, 14, 18]. HR of lymphoma was observed after a median period of 13 months, a finding similar to that in the series of 50 patients reported by Neubauer et al. (15 months) [10] but shorter than the series of 56 patients documented by Savio et al. (24 months) [15]. However, shorter delays to HR have been reported by others [2, 8, 11, 18].

There was a good correlation between the endoscopic and histological aspects of I and N mucosa in most, if not all, cases, especially at diagnosis of MALT on I samples, while N samples did not exhibit any lymphomatous infiltration. The same histological scores between fresh and paraffin-embedded samples were observed by Aiello et al. [1]. Moreover, they also found that 99% of samples showed an identical mono- and polyclonal pattern. Therefore, we analysed DNA extracted from freshly frozen fragments of I and N mucosa without histological examination, as several fragments taken at the same sites served as controls.

The presence of lymphomatous cells in N mucosa also underlines the interest of examining endoscopically N mucosa for monoclonality. Histologically, this N mucosa has been considered as normal or to contain small non-specific lymphoid aggregates and/or clustered plasma cells. Such an observation has already been reported by Du et al. [5] who demonstrated that monoclonal cells may be widely disseminated among non-lymphomatous lymphocytic infiltrates and in clustered plasma cells. For this reason, they studied five gastrectomy specimens of MALT lymphoma by microdissection and PCR. Cloning and sequencing of PCR products of different non-lymphomatous lymphoid or plasma cell infiltrates revealed monoclonal IgH rearrangement identical to that detected in lymphoma lesions. The data reported by Yamauchi et al. [21] also suggest that many gastric MALT lymphomas are multi-focal. They studied ten gastrectomy specimens which showed two or more lesions and found identical monoclonal IgH rearrangement between the different lesions in about 60% of cases. In our study, 47% of gastric marginal zone lymphomas of MALT achieved a complete HR after a median delay of 13 months after eradication of *H. pylori*.

In our series of 60 gastric marginal zone lymphomas of MALT, 52 of 60 patients (87%) had a monoclonal IgH gene rearrangement, a finding similar to the rates observed by Bertoni et al. [3]. Such a percentage is slightly higher than those reported by other groups (ranging from 61% to 73%) [8, 10, 15, 18]. The use of two separate sets of FR3-JH primers may account for such rates of monoclonal detection without the need of FR1-JH primers [4]. In our series, the rate of monoclonality was not different between

Table 2 Percentage of residual molecular disease in patients with histological remission (HR) with gastric MALT lymphoma

Series	HR patients with molecular follow-up	Residual molecular disease
Bayerdoffer et al. 1995 [2]	16	3 (19%)
Savio et al. 1996 [14]	9	3 (33%)
Neubauer et al. 1997 [10]	31	22 (71%)
Montalban et al. 2001 [8]	11	9 (82%)
Thiede et al. 2001 [18]	44	22 (50%)
Bertoni et al. 2002 [3]	34	19 (66%)
Present study, 2004	23	10 (44%)

patients without HR (29 of 32, 91%) and those with HR (23 of 28, 82%). In the 23 patients with HR, 13 achieved MR after a mean follow-up of 18 months and an average of 7 months after HR. This interval is in the range of that of 5 months reported by Nobre-Leitao et al. [11] but shorter than those observed by Thiede et al. (12 months) [18] or Savio et al. (13 months) [15]. After HR, Bertoni et al. [3] observed the achievement of MR in 16 of 19 patients at 1 year of follow-up and in 3 of 19 at 2 years. The percentage of residual molecular disease (44%) observed in our patients lies in the range reported in the literature (19% to 82%) (Table 2).

Interestingly, endoscopically and histologically, N mucosa often exhibited the same monoclonal profile as I mucosa. The pathological I mucosa was much more frequently monoclonal (94%) than the N mucosa (69%). The percentage of monoclonality in N mucosa was similar between the histologically responder and non-responder patients. In the cases in which a clone was found in the N mucosa but not in the I biopsy, there may be several explanations for such a discrepancy including DNA degradation, absence of histological control of the sample taken for DNA extraction and molecular study.

However, in the group of 23 patients with HR, the percentage of N mucosa positivity was lower for the 13 patients with MR (39%) than for the 10 without MR (88%), and a statistical link between N mucosa status and MR achievement was found. Moreover, the mean delay to achieve HR for MR patients was significantly shorter (9.5 months) than that for the non-MR patients (21.3 months). Therefore, a monoclonal infiltration at both I and N sites might be associated with a longer delay to achieve both MR and HR.

The dissemination of lymphomatous cells in N mucosa might also favour relapse. However, this was unlikely in our study since the two patients who relapsed after HR had a monoclonal I mucosa and a polyclonal N mucosa at diagnosis. The involvement of N mucosa by lymphomatous cells might therefore identify patients with more disseminated disease that would require a more efficient and/or a longer therapeutic scheme to achieve complete eradication.

Acknowledgement The authors thank Jean Christophe Garoste for technical work in clonality analyses.

References

1. Aiello A, Giardini R, Tondini C, Balzarotti M, Diss T, Peng H, Delia D, Pilotti S (1999) PCR-based clonality analysis: a reliable method for the diagnosis and follow-up monitoring of conservatively treated gastric B-cell MALT lymphomas? Histopathology 34:326–330
2. Bayerdorffer E, Neubauer A, Rudolph B, Thiede C, Lehn N, Eidt S, Stolte M (1995) Regression of primary gastric lymphoma of mucosa-associated lymphoid tissue type after cure of *Helicobacter pylori* infection. MALT lymphoma study group. Lancet 345:1591–1594
3. Bertoni F, Conconi A, Capella C, Motta T, Giardini R, Ponzoni M, Pedrinis E, Novero D, Rinaldi P, Cazzaniga G, Biondi A, Wotherspoon A, Hancock BW, Smith P, Souhami R, Cotter FE, Cavalli F, Zucca E, International Extranodal Lymphoma Study Group, United Kingdom Lymphoma Group (2002) Molecular follow-up in gastric mucosa-associated lymphoid tissue lymphomas: early analysis of the LY03 cooperative trial. Blood 99:2541–2544
4. de Mascarel A, Dubus P, Belleannee G, Megraud F, Merlio JP (1998) Low prevalence of monoclonal B cells in *Helicobacter pylori* gastritis patients with duodenal ulcer. Human Pathol 29:784–790
5. Du MQ, Diss TC, Dogan A, Ye HT, Aiello A, Wotherspoon AC, Pan LX, Isaacson PG (2000) Clone-specific PCR reveals wide dissemination of gastric MALT lymphoma to the gastric mucosa. J Pathol 192:488–493
6. Fischbach W, Dragosics B, Kolve-Goebeler ME, Ohmann C, Greiner A, Yang Q, Bohm S, Verreet P, Horstmann O, Busch M, Duhmke E, Muller-Hermelink HK, Wilms K, Allinger S, Bauer P, Bauer S, Bender A, Brandstatter G, Chott A, Dittrich C, Erhart K, Eysselt D, Ellersdorfer H, Ferlitsch A, Fridrik MA, Gartner A, Hausmaninger M, Hinterberger W, Hugel K, Ilsinger P, Jonaus K, Judmaier G, Karner J, Kerstan E, Knoflach P, Lenz K, Kandutsch A, Lobmeyer M, Michlmeier H, Mach H, Marosi C, Ohlinger W, Oprean H, Pointer H, Pont J, Salabon H, Samec HJ, Ulsperger A, Wimmer A, Wewalka F (2000) Primary gastric B-cell lymphoma: results of a prospective multicenter study. The German-Austrian gastrointestinal lymphoma study group. Gastroenterology 119:1191–1202
7. Isaacson PG (1994) Gastrointestinal lymphoma. Human Pathol 25:1020–1029
8. Montalban C, Santon A, Boixeda D, Redondo C, Alvarez I, Calleja JL, de Argila CM, Bellas C (2001) Treatment of low grade gastric mucosa-associated lymphoid tissue lymphoma in stage I with *Helicobacter pylori* eradication. Long-term results after sequential histologic and molecular follow-up. Haematologica 86:609–617
9. Musshoff K (1977) Clinical staging classification of non-Hodgkin's lymphomas. Strahlentherapie 153:218–221
10. Neubauer A, Thiede C, Morgner A, Alpen B, Ritter M, Neubauer B, Wundisch T, Ehninger G, Stolte M, Bayerdorffer E (1997) Cure of *Helicobacter pylori* infection and duration of remission of low-grade gastric mucosa-associated lymphoid tissue lymphoma. J Natl Cancer Inst 89:1350–1355
11. Nobre-Leitao C, Lage P, Cravo M, Cabecadas J, Chaves P, Alberto-Santos A, Correia J, Soares J, Costa-Mira F (1998) Treatment of gastric MALT lymphoma by *Helicobacter pylori* eradication: a study controlled by endoscopic ultrasonography. Am J Gastroenterol 93:732–736
12. Roggero E, Zucca E, Pinotti G, Pascarella A, Capella C, Savio A, Pedrinis E, Paterlini A, Venco A, Cavalli F (1995) Eradication of *Helicobacter pylori* infection in primary low-grade gastric lymphoma of mucosa-associated lymphoid tissue. Ann Intern Med 122:767–769
13. Ruskone-Fourmestraux A, Lavergne A, Aegerter PH, Megraud F, Palazzo L, de Mascarel A, Molina T, Rambaud JL (2001) Predictive factors for regression of gastric MALT lymphoma after anti-*Helicobacter pylori* treatment. Gut 48:297–303
14. Savio A, Franzin G, Wotherspoon AC, Zamboni G, Negrini R, Buffoli F, Diss TC, Pan L, Isaacson PG (1996) Diagnosis and posttreatment follow-up of *Helicobacter pylori*-positive gastric lymphoma of mucosa-associated lymphoid tissue: histology, polymerase chain reaction, or both? Blood 87:1255–1260
15. Savio A, Zamboni G, Capelli P, Negrini R, Santandrea G, Scarpa A, Fuini A, Pasini F, Ambrosetti A, Paterlini A, Buffoli F, Angelini GP, Cesari P, Rolfi F, Graffeo M, Pascarella A, Valli M, Mombello A, Ederle A, Franzin G (2000) Relapse of low-grade gastric MALT lymphoma after *Helicobacter pylori* eradication: true relapse or persistence? Long-term post-treatment follow-up of a multicenter trial in the north-east of Italy and evaluation of the diagnostic protocol's adequacy. Recent Results Cancer Res 156:116–124

16. Steinbach G, Ford R, Glober G, Sample D, Hagemeister FB, Lynch PM, McLaughlin PW, Rodriguez MA, Romaguera JE, Sarris AH, Younes A, Luthra R, Manning JT, Johnson CM, Lahoti S, Shen Y, Lee JE, Winn RJ, Genta RM, Graham DY, Cabanillas FF (1999) Antibiotic treatment of gastric lymphoma of mucosa-associated lymphoid tissue. An uncontrolled trial. Ann Intern Med 131:88–95
17. Stolte M, Eidt S (1993) Healing gastric MALT lymphomas by eradicating *H. pylori*? Lancet 342:568
18. Thiede C, Wundisch T, Alpen B, Neubauer B, Morgner A, Schmitz M, Ehninger G, Stolte M, Bayerdorffer E, Neubauer A, German MALT Lymphoma Study Group (2001) Long-term persistence of monoclonal B cells after cure of *Helicobacter pylori* infection and complete histologic remission in gastric mucosa-associated lymphoid tissue B-cell lymphoma. J Clin Oncol 19:1600–1609
19. Wotherspoon AC, Ortiz-Hidalgo C, Falzon MR, Isaacson PG (1991) *Helicobacter pylori*-associated gastritis and primary B-cell gastric lymphoma. Lancet 338:1175–1176
20. Wotherspoon AC, Doglioni C, Diss TC, Pan L, Moschini A, de Boni M, Isaacson PG (1993) Regression of primary low-grade B-cell gastric lymphoma of mucosa-associated lymphoid tissue type after eradication of *Helicobacter pylori*. Lancet 342:575–577
21. Yamauchi A, Tomita Y, Miwa H, Sakamoto H, Sugiyama H, Aozasa K (2001) Clonal evolution of gastric lymphoma of mucosa-associated lymphoid tissue type. Mod Pathol 14:957–962

Virchows Arch (2005) 446: 225–231
DOI 10.1007/s00428-004-1186-y

ORIGINAL ARTICLE

Ana Carolina Galtarossa Xavier · Sheila Aparecida Coelho Siqueira · Luciano José Megale Costa · Thais Mauad · Paulo Hilário Nascimento Saldiva

Missed diagnosis in hematological patients—an autopsy study

Received: 22 September 2004 / Accepted: 23 November 2004 / Published online: 15 February 2005
© Springer-Verlag 2005

Abstract Autopsy findings of missed diagnoses that would probably have changed management or prognosis occur in up to 29% of cases in general hospitals. Such proportions may be higher in subsets of patients with complex diseases. We reviewed 2908 consecutive autopsies performed over a period of 29 months in a large-volume hospital, analyzing 118 autopsies of patients with hematological malignancies or severe aplastic anemia. A review of macroscopic reports as well as microscopic examination of tissue samples was performed. Medical records were reviewed for clinical diagnoses. Discordances between clinical and autopsy diagnoses were classified using Goldman's criteria. Additionally, we searched for clinical parameters correlated with occurrence of class-I discrepancy using a multivariate method. Median age was 46.5 years, and 25.4% had received a hematopoietic stem-cell transplant. Overall, 11.9% (6.6–19.1%) of patients died before conclusion of the hematological diagnosis and 33% (24.6–42.3%) died with no active hematological disease. We found class-I discrepancy in 31.3% (23.1–40.5 %) of cases. The most common among these diagnoses were hematological disease, pneumonia and gastrointestinal bleeding. In a univariate analysis, being elderly (P=0.04) was positively correlated with the finding of class-I discrepancies; while, having received previous specific hematological treatment (P=0.0005) or hematopoietic stem-cell transplants (P=0.013), or being admitted to a specialized hematology unit (P=0.0006) were negatively correlated to the occurrence of such discrepancies. Multivariate analysis showed that care in a specialized hematology unit (OR 0.34, 0.12–0.93) was independently associated with lower occurrence of discrepancies. We concluded that critical diagnoses are often missed in highly complex hematological patients especially in the absence of admission to specialized hematology units.

Keywords Autopsy · Hematological neoplasms · Anemia · Aplastic · Medical errors

A. C. G. Xavier (✉)
Department of Pathology, Sao Paulo University Medical School, University of Colorado Health and Science Center,
Campus Box 8117,
PO Box 6511, 80045 Aurora, CO
e-mail: ana.xavier@uchsc.edu
Tel.: +303-724-3148
Fax: +303-724-3889

S. A. C. Siqueira
Department of Pathology
Sao Paulo University Medical School,
Av. Dr. Arnaldo 455,
01246–903 Sao Paulo, SP, Brazil

L. J. M. Costa
Department of Medical Oncology, University of Colorado Health and Science Center,
Sao Paulo University Medical School,
Campus Box 8117,
PO Box 6511, 80045 Aurora , CO

T. Mauad
Department of Pathology
Sao Paulo University Medical School,
Av. Dr. Arnaldo 455,
01246–903 Sao Paulo, SP, Brazil

P. H. Nascimento Saldiva
Department of Pathology
Sao Paulo University Medical School,
Av. Dr. Arnaldo 455,
01246–903 Sao Paulo, SP, Brazil

Introduction

For more than one century, autopsy studies have offered outstanding benefits to clinical medicine. Post-mortem macroscopic and microscopic evaluation of organs and tissues have not only helped pathologists to understand mechanisms of diseases but also verified clinical diagnoses and provided data for epidemiologists.

However, for the last few decades autopsy rates have decreased worldwide as can be exemplified by North American data showing autopsy rates of 50% in the 1950s and less than 10% in the 1990s [9, 29]. Different reasons have been offered for this fact, including reduced rates of consent from relatives, legal issues concerning exposition of phy-

sicians' errors, and non-reimbursement for such procedures [11, 20, 21, 23]. Factors known to influence autopsy rates are the type and size of hospital and the age of patients, with a higher rate of autopsy in large teaching hospitals and young adults [1, 7, 9].

Many authors have stated that autopsy is still fundamental for medicine despite a recent increase in the use of more complex diagnostic methods. In fact, they have published autopsy series in different areas of medicine showing between 0% and 29% of missed diagnoses that would have changed management if known pre-mortem [3, 5, 14, 15, 18, 19, 28, 29, 31, 32].

Frequency of missed important diagnoses, however, may be even higher in specific populations with particularly severe and rare diseases. For example, 38% of autopsies performed in patients with congenital heart disease revealed evidence of missed diagnoses that would have changed management [30]. In another series, at least one important missed diagnosis was found in 61% of immunocompromised surgical patients [22].

Hematological malignancies and aplastic anemia constitute a special group of diseases due to their low incidence, high mortality, complex diagnostic steps that are required for their care, and for the need of aggressive therapeutic methods. Clinical management often includes immunosuppression, intensive chemotherapy, and/or bone marrow or peripheral blood stem-cell transplantation (PBSCT). In this setting, an extremely wide sort of disorders may thrive including bacterial, viral and fungal infections, bleeding episodes, metabolic imbalances, or even direct infiltration of malignant cells into vital organs [2, 17]. As a result, it is possible that discrepancies between clinical and post-mortem diagnoses occur at higher rates in this population. Although several autopsy studies addressing discrepancies in oncological diseases have been performed [6, 26, 27], few have focused specifically on hematological neoplasms. Provencio et al. studied autopsies of Hodgkin's disease patients and found a 43% rate of discrepancy between the clinical and autopsy diagnoses [4]. In another study, Nigro et al. showed that 16% of pediatric leukemia patients who died at a single institution had at least one important diagnosis found during autopsy that had been missed clinically [24].

In this study, we compared autopsy findings and clinically suspected diagnoses in 118 patients who died with hematological malignancies or aplastic anemia at one institution. We intended to estimate the frequency of missed major diagnoses that affected outcomes and to search for factors related to occurrence of such discrepancies in the diagnosis of these diseases.

Methods

Inclusion of cases

This study was performed at the Department of Pathology, University of Sao Paulo that is linked to Hospital das Clinicas, a large-volume, high-complexity hospital in the city of Sao Paulo, Brazil that covers all main medical and surgical specialties with an average annual autopsy rate of 60%. The study protocol was approved by the Internal Review Board of the Hospital.

We included autopsy cases from January 2001 to May 2003 that received clinical or post-mortem diagnosis of a hematological malignancy or aplastic anemia. These conditions were analyzed together due to similarities in disease severity and management with complex and toxic therapies and frequent infectious, hemorrhagic and metabolic complications.

Medical records were fully reviewed with attention to patient age, sex, length of inpatient care, clinic and laboratorial diagnosis of hematological disease, treatments given, clinical intercurrences and their management. Patients whose medical records were unavailable, incomplete, or unreadable were excluded. We considered a diagnosis as clinically performed if the assistant physician registered it in medical records or prescribed for it a widely recognized specific therapy (e.g., ganciclovir for cytomegalovirus infection). For each patient, an unlimited number of diagnoses were extracted according to these criteria. Also based on medical records, we obtained the major suspected immediate cause of death (e.g., septic shock). All diagnoses were linked to an International Statistical Classification of Diseases and Related Health Problems, tenth revision (ICD-10) code [16].

Review of autopsies

For each case, a full description of macroscopic findings was available and used for further extraction of post-mortem diagnoses. At least one clinical hematologist and a pathologist reviewed the microscopic findings from each case, based on standard hematoxilin and eosin slides and special stains or immunohistochemical studies as needed. Similarly to clinical diagnosis, pathological findings were extracted and coded according to ICD-10. Cases in which autopsy studies were incomplete were excluded.

Study of discrepancies

Two clinical hematologists compared autopsy diagnoses with clinical hypotheses. Each diagnosis was classified by consensus between the two hematologists as being in accordance with clinical suspicion, being an incidental finding, or supporting a discrepancy with clinical hypothesis. Discrepancies were categorized according to Goldman's criteria [14], based on diagnostic relevance to the proximate cause of death and missed opportunities for management changes (Table 1).

The proportion of patients with at least one missed diagnosis that would affect management and/or prognosis (class I) was reported. Similarly, we estimated the proportion of patients with at least one missed major diagnosis (class I or II). For each Goldman's class, the most common autopsy diagnoses were ranked. Additionally, we estimated the proportion of patients who died after therapy with no evidence of the

Table 1 Goldman's classification for missed diagnoses (12)

Goldman's classification	Description
Class I	Major diagnoses for which detection before death, in all probability, would have led to a change in management that might have resulted in cure of prolonged survival
Class II	Major diagnoses for which detection before death would probably not have led to a change in management because no good therapy had been available at that time, because the patient presented with an acute cardiopulmonary arrest that was appropriately treated, because the patient had already received appropriate therapy although the diagnosis was not known, or because the patient had refused further evaluation or therapy
Class III	Minor diagnoses that were related to the terminal disease process but that were not directly related to death
Class IV	Minor diagnoses that were either important unrelated diagnoses that might eventually have affected prognosis or processes that contributed to death in a terminally ill patient

hematological disease, the proportion of patients with no cause of death identified even after autopsy, and the proportion of patients whose major suspected immediate cause of death disagreed with pathological findings.

Finally, we investigated clinical characteristics associated with occurrence of class-I and major (class-I or -II) discrepancies. For that, each case was categorized in accordance with age (<19 years, 19–64 years, >64 years), sex, presence of previous treatment for the hematological condition, presence of recent treatment for the hematological condition (<1 month), time since hematological diagnosis (<1 month or not), treatment with bone marrow or PBSC transplantation, place of inpatient care (specialized unit or not) and length of admission (<72 h, ≥72 h).

Table 2 Hematological diagnoses (n=118)

Diagnosis	ICD-10	n (%)
Non-Hodgkin's lymphoma	C83, C84, C85	22 (18.6)
Acute myelogenous leukemia	C92.0	19 (16.1)
Multiple myeloma	C90	18 (15.3)
Acute lymphoblastic leukemia	C91.0	17 (14.4)
Chronic myelogenous leukemia	C92.2	16 (13.6)
Aplastic anemia	D61	8 (6.8)
Myelodisplastic syndrome	D46	5 (4.2)
Myeloproliferative syndrome*	D47.1	4 (3.4)
Hodgkin's disease	C81	4 (3.4)
Chronic lymphoid leukemia	C91.1	4 (3.4)
Hairy cell leukemia	C91.4	1 (0.8)

*Except chronic myelogenous leukemia

Statistics

NCSS 2000 Stat System (NCSS, Kaysville, Utah, USA) and Microsoft Excel software were employed in the statistical processing of data. Simple proportions were reported with their 95% confidence intervals. Clinical characteristics were treated as categorical variables as presented above. Proportions of discrepancies (class I and major) were calculated for each category defined by the presence or absence of a clinical characteristic and compared using the chi-square test. Additionally, the independence of the association with the occurrence of class-I discrepancy was assessed with use of a stepwise forward-selection logistic-regression analysis. Results are reported as odds ratios with 95% confidence intervals. Two-sided P values of less than 0.05 were considered to indicate statistical significance.

Table 3 Most commonly missed diagnoses according to Goldman's class

Diagnose	ICD-10	n
Class I		
Hematological disease	C81, C83, C85, C90, C91.0, C91.4	15
Pneumonia	J18	5
Gastrointestinal hemorrhage, NOS*	K92.2	3
Congestive heart failure	I50.0	2
Acute pancreatitis	K85	2
Pulmonary embolism	I26	2
Invasive pulmonary aspergillosis	B44.0	2
Pulmonary edema	J81	2
Class II		
Pneumonia	J18	9
Hematological disease	C83, C91.0	5
Invasive pulmonary aspergillosis	B44.0	5
Pulmonary hemorrhage	R04.8	4
Other forms of aspergillosis	B44.8	2
Pulmonary candidiasis	B37.1	2
Class III		
Hemosiderosis	E83.1	17
Secondary malignant neoplasm of kidney and renal pelvis	C79.0	9
Pleural effusion in conditions classified elsewhere	J91	9
Secondary malignant neoplasm of other unspecified digestive organ	C78.8	5
Pulmonary hemorrhage	R04.8	4
Class IV		
Pulmonary hemorrhage NOS*	R04.8	14
Pulmonary edema	J81	8
Gastrointestinal hemorrhage, NOS*	K92.2	7
Nontraumatic intracerebral hemorrhage	I61	6
Pleural effusion in conditions classified elsewhere	J91	6
Secondary malignant lung neoplasm	C78.0	5
Chronic tubulo-interstitial nephritis	N11	5

*NOS—not otherwise specified

Results

During the period covered by the present study, 2908 autopsies were performed at our institution, including the 147 (5%) autopsies of patients with either a pre-mortem or post-mortem diagnosis of a hematological malignancy or aplastic anemia. Of these 147, 118 cases met the inclusion criteria for further analysis; 29 were excluded because of incomplete or unavailable medical records or incomplete autopsy.

Median age was 46.5 years (interquartile range 29.7), 61 patients were male (51.7%), 30 (25.4%) had received a bone marrow transplant (BMT) or PBSCT, and patients were hospitalized for a median of 11.5 days (interquartile range 18). Hematological diagnoses, with their respective International Statistical Classification of Diseases and Related Health Problems, tenth revision (ICD-10) codes, are displayed in Table 2.

Before conclusion of the hematological diagnosis (10 non-Hodgkin's lymphoma, 2 multiple myeloma, 1 hairy cell leukemia, and 1 chronic lymphoid leukemia) 14 patients (11.9%, 95% c.i. 6.6–19.1%) died, and for 5 patients (4.2%, 1.3–9.6%) the diagnosis of a definitive cause of death was not possible even after autopsy. Autopsy of 39 patients (33%, 24.6–42.3%) did not show any evidence of active hematological disease probably due to prior satisfactory response to treatment. In 7 patients (5.9%, 2.4–11.8%), the major suspected immediate cause of death was in disagreement with the autopsy finding.

Table 4 Patients with class-I discrepancy. *AA* aplastic anemia, *ALL* acute lymphocytic leukemia, *AML* acute myelogenous leukemia, *CLL* chronic lymphocytic leukemia, *CML* chronic myelogenous leukemia, *HCL* hairy cell leukemia, *HD* Hodgkin's disease, *MDS* myelodisplastic syndrome, *MM* multiple myeloma, *NHL* non-Hodgkin lymphoma, *ARDS* acute respiratory distress syndrome

Diagnosis	Age (years)	Clinical cause of death	Missed class-I diagnosis
ALL	5	Septic shock	Relapsed ALL
ALL	78	Coma, undefined cause	Pulmonary hemorrhage
HCL	46	Respiratory failure, pneumonia	HCL
NHL	40	Respiratory failure, pneumonia	NHL, congestive heart failure
NHL	62	ARDS, undefined cause	Pulmonary involvement from NHL
AA	14	Septic shock, enteritis	Fungal sepsis (*Candida sp*)
NHL	68	Undefined	Acute pancreatitis
MM	69	Shock, undefined cause	MM, bacterial pneumonia, pulmonary embolism
NHL	53	Pulmonary cryptococcosis	NHL
AML	64	Septic shock, pneumonia	CNS bleeding
MDS	79	Respiratory failure, shock, undefined cause	Congestive heart failure
MM	72	Undefined	Bacterial pneumonia
NHL	64	Arrhythmia	NHL
ALL	30	Respiratory failure, pulmonary hemorrhage	Gastrointestinal bleeding
ALL	23	Respiratory failure, undefined cause	Pulmonary invasive aspergillosis
NHL	27	Septic shock, undefined cause	NHL
NHL	61	Respiratory failure, shock, undefined cause	Intestinal perforation, NHL
HD	20	Undefined	Pneumonia
NHL	72	Undefined	NHL
AA	24	Respiratory failure, undefined cause.	Gastrointestinal bleeding
MPS	58	Undefined	Pulmonary edema
AA	13	Septic shock, undefined cause	Pulmonary invasive aspergillosis, pulmonary candidiasis
HD	76	Septic shock, pneumonia	HD
ALL	18	Septic shock	CMV pneumonitis
NHL	80	Septic shock, pneumonia	NHL
MM	42	Undefined	Aspiration pneumonia
NHL	64	Septic shock, pneumonia	NHL
MM	83	Septic shock, pneumonia	Acute pancreatitis
CML	27	Septic shock, pneumonia	Toxic hepatitis
NHL	43	Septic shock, pneumonia	NHL, pulmonary embolism
MM	73	Septic shock, undefined cause	MM
CLL	64	Shock, undefined cause.	Gastrointestinal bleeding, pulmonary edema,
CLL	53	Coma, undefined cause	Pneumonia
MM	67	Shock, tumor lysis	Gastrointestinal bleeding, pneumonia
ALL	28	Septic shock, pneumonia	Cerebral toxoplasmosis
NHL	61	Coma, undefined cause	Myocardial infarct, NHL
MM	61	Septic shock, pneumonia	Endocarditis

Overall 544 autopsy diagnoses were made. Of these, 171 (31.4%) were in full agreement with clinical hypothesis and management, 47 (8.6%) were considered class-I, 46 (8.4%) class-II, 102 (18.7%) class-III, and 110 (20.2%) class-IV missed diagnoses. Of the diagnoses, 68 (12.5%) were considered incidentals and did not fit in any of Goldman's class. Most frequent diagnoses for each of Goldman's classes are displayed in Table 3.

Of the patients, 37 (31.3%, 23.1–40.5%) had at least one class-I missed diagnosis and 66 (55.9%, 46.565%) had at least one major (class-I or -II) missed diagnosis. Table 4 displays clinical information and autopsy findings for the 37 cases that had class-I discrepancy.

Class-I discrepancies were more common in elderly patients (>64 years P=0.04) and in patients who had not received previous specific treatment (P=0.0005), had not been treated with marrow or PBSC transplantation (P= 0.013), or had not been treated in a specialized unit (P= 0.0006). Major discrepancies were more common in patients that had not received previous specific treatment (P=0.001), whose diagnosis of the hematological disease had been made in the prior month (P=0.04), had not been treated with marrow or PBSC transplantation (P=0.04) or had not been treated in a specialized unit (P=0.048) (Table 5).

Table 5 Occurrence of discrepancy per clinical characteristic

Characteristic	Class I		Major	
	(%)	*P* value	(%)	*P* value
Age (years)				
<19	28.6	0.87*	50	0.87*
18–64	25.6		51.8	
>64	52.4	0.04*	76.2	0.08*
Sex				
Female	38.6		57.9	
Male	24.6	0.10	54.1	0.67
Previous specific treatment				
Yes	23.7		48.4	
No	60	0.0005	84	0.001
Treatment <1 month				
Yes	23.8		52.3	
No	40	0.06	60	0.41
Diagnosis of the hematological disease <1 month				
Yes	41.0		68.2	
No	25.7	0.08	48.6	0.04
Marrow or PBSC transplantation				
Yes	14.4		40	
No	37.5	0.013	71.4	0.04
Care in a specialized unit				
Yes	16.1		46.5	
No	45.2	0.0006	64.6	0.048
Length of inpatient care				
<72 h	40.8		55.5	
≥72 h	28.6	0.23	56.1	0.96

* When compared with the intermediate age group

Table 6 Multivariate analysis of clinical characteristics related to occurrence of class-I discrepancy

	OR	*P* value
Age 19–64 years	0.62 (0.25–1.56)	0.31
Sex (male)	0.57 (0.24–1.39)	0.22
Previous specific treatment	0.40 (0.13–1.16)	0.09
Care in a specialized unit	0.34 (0.12–0.93)	0.04

Multivariate analysis involving age, sex, previous specific treatment and care in a specialized unit showed that only care in a specialized unit was independently and inversely related to occurrence of class-I discrepancy (Table 6).

Discussion

This study covers a large number of autopsy cases with complex hematological diseases addressing discrepancies between clinical hypotheses and autopsy findings. To the authors' best knowledge, this is the first study that not only reports discrepancy in this population but also searches for subsets of patients that are at increased risk to suffer from misdiagnosis and for clinical characteristics independently related to occurrence of class-I discrepancy.

All cases came from a large and highly specialized teaching hospital, so it is not expected that constraints in diagnostic technologies or therapeutic modalities would adversely affect patients' care and, consequently, increase the frequency of autopsy discrepancies. The authors did not influence attending physicians' attitudes toward request of autopsy during execution of this study. It is possible that autopsied cases were those with high likelihood of discrepancies, leading to overestimation of discrepancy rate. However, this is an inherent problem to all studies with similar design and, we believe, was minimized in this study by the high autopsy rate at our institution. Some medical records could not be checked due to unavailability. These cases were excluded from all analyses and are believed to distribute by chance in our sample, not under-representing any specific disease.

The post-mortem examination was effective in disclosing the cause of death in 95.8% of cases, reinforcing autopsy as an effective method to check accuracy of clinical diagnosis and to provide key epidemiological data regarding the cause of death in this specific setting. Another published series addressing cancer patients admitted in a specialized ICU also showed a high proportion (28 in 34) of deaths appropriately explained by autopsy [13]. The value of the post-mortem examination is also attested to by the observation that autopsy findings controverted or failed to corroborate the major immediate cause of death suspected clinically in 5.9% of cases in this series.

In 11.9% of cases, patients died without a conclusive premortem diagnosis of a hematological disease, often because they presented with severe clinical complications leading to premature deaths despite intensive supportive treatment. Such data is in accordance with a previous series published by Veress et al. that showed a 15% prevalence of missed malignancies in general population autopsies, half of which

were lethal [33]. Similarly, Burton et al. found 44% of malignant neoplasms during autopsies not clinically detected in a general population series [6].

We found a relatively high occurrence (33%) of patients dying with no macro- or microscopic evidence of the hematological disease. This data reinforces infections, hemorrhage, and metabolic imbalances as severe clinical complications in these patients making their management challenging and, not uncommonly, leading to fatal outcomes. As most of the hematological disorders included have difficult, risky treatments with low response rate, deaths with no post-mortem evidence of disease occurred in a selected subset of potentially curable patients for whom therapeutic toxicity was lethal. This proportion can be compared with 26% of patients with pediatric leukemia dying in remission, as reported in another published series [24]. Taken together, these data suggest that an even higher degree of awareness for toxic effects is needed, as well as a low threshold to order diagnostic tests and to start empirical complementary therapeutic interventions targeted at these possible frequent clinical complications.

Detection of missed diagnoses has been a major goal of autopsy for decades. With this purpose, Goldman et al., in 1983, introduced a structured classification of missed diagnoses considering not only the occurrence of discrepancies but also how previous detection would have changed management [14]. In that series of 300 autopsies, 10% showed at least one major diagnosis that, if performed before death, would have changed management. A similar proportion was found in a larger series, with 2537 retrospective cases from a teaching hospital, where in 244 cases the primary disease was found only during autopsy [12]. A recent retrospective review from a Brazilian teaching hospital [10] covered 252 cases with both autopsy and a medical-records review with systematic pairing, revealing an 8.3% frequency of Goldman's class-I discrepancies in an unselected population. In our institution, a recent analysis of 300 unselected autopsy cases found 7.0% of class-I discrepancy (unpublished data, Dr. Paulo H.N. Saldiva, personal communication).

In the present series, 31.3% of patients had autopsy findings that would have changed the management and potentially the prognosis if they had been detected before death (class-I discrepancy). This proportion was much higher than those found in previous series addressing unselected pathologies [10, 12, 14, 29], including prior reviews at our institution. As previously suggested by other series of uncommon and complex diseases [4, 22, 30], the focus on high complexity disorders may predispose to elevated rates of discrepancy.

While analyzing only class-I discrepancies, it is surprising that hematological disease was the most common discrepant diagnosis. This reflects the same previously discussed aspects of complexity of diagnosis performance and severity of the patient's illness. Unfortunately, a delay from the patient to see a doctor, long trips from referring services to a high-complexity center, or even prolonged stays in the emergency department may have postponed appropriate diagnosis and care, contributing to disease progression and acute complications.

Other main class-I discrepant diagnoses were infection and toxic effects. These etiologies were also dominant among class-II discrepancies, which is in accordance with expectations from previous reports. In fact an autopsy study reported by Nosari et al. [25] listed infection as the cause of death in 63% of hematological patients. Chandrasekar et al. [8] reported an autopsy result of 56 BMT or PBSC recipients and found that appropriate diagnoses were not performed before death in 9 of 14 patients with cytomegalovirus, 6 of 13 with yeast infection, and 4 of 6 with Aspergillus infection. Again, it reinforces the need for a more aggressive diagnostic and therapeutic approach to toxic complications in these patients.

A second major purpose of the present study was to describe the difference in discrepancy rates in accordance with clinical characteristics. We found that elderly patients (>64 years), those that had not been previously treated, and those who had been admitted to non-specialized hematology units encountered a higher risk of having an important missed diagnosis that would potentially change the management (class I), while patients who underwent BMT or PBSCT were at a lower risk. Additionally, using a multivariate method, we found that care in a specialized hematology unit was independently protective for class-I discrepancy. Similarly, patients with recent diagnosis prior to death (<1 month) and those not previously treated were at higher risk while those who had undergone a BMT or PBSCT were at a lower risk of having a missed major diagnosis (class I or class II).

Other studies addressing factors associated with discrepancies in hematological or cancer patients are underrepresented in the literature. A series published by Battle et al. [5] with 2067 autopsies collected from 32 university and community hospitals located throughout the United States recorded type and size of hospital (small community hospitals), age (old age) and sex (female) as factors associated with occurrence of important discrepancies. In another series, Mort et al. [22] showed an interesting relationship between length of stay in a surgical intensive care unit and occurrence of major discrepancies, largely nosocomial infections. Remarkably, none of these series used multivariate methods to try to clarify which factors where independently correlated with discrepancies. Our data points to factors that are certainly interconnected (e.g., BMT recipients are most likely young, etc.) so a multivariate analysis becomes crucial. Only care in a non-specialized unit such as an emergency department, internal medicine ward, ICU, etc. was independently associated with class-I discrepancy. It may reflect a greater severity of illness in these patients or may, instead, suggest a non-optimal diagnostic work-up when hematologists do not directly assist these patients. Finally, this study may not have been powerful enough to distinguish independent effects of other factors.

Taken together, these facts might be useful clinically in fostering a greater suspicion of a missed diagnosis leading to more intensive diagnostic evaluation in subsets of pa-

tients. Our data also suggest that admitting patients to specialized units might by itself avoid some discrepancies.

Overall, autopsy provides important information for general clinical practice and also in patients with complex hematological diseases. Our findings suggest that special efforts should be spent toward improving the diagnostic strategies used while caring for patients with hematological malignancies and aplastic anemia, with the goal of making diagnoses faster and more accurate. Involving hematologists early whenever these patients are treated in non-specialized units, and encouraging larger numbers of autopsies especially at academic centers where the structure of multidisciplinary meetings conveys the results of these postmortem examinations to the physicians in charge of these patients, may further decrease discrepancies in the future. We believe that current technology, with newer and more powerful diagnostic techniques being utilized while patients are still alive, does not obviate the need for autopsies, which continue to constitute a traditional, cheaper, and humbling way to learn with, and from, our errors.

Acknowledgements We are in debt to Dr. Robert L. Gottlieb for careful review of this manuscript. ACGX received financial support from FAPESP (Fundação de Amparo à Pesquisa do Estado de São Paulo). L.J.M.C. received financial support from CAPES (Coordenação de Aperfeiçoamento de Pessoal de Nível Superior).

References

1. Ahronheim JC, Bernholc AS, Clark WD (1983) Age trends in autopsy rate. JAMA 250:1182–1186
2. Albanell J, Baselga J (2000) Systemic therapy emergencies. Semin Oncol 27:347–361
3. Anderson RE (1984) The autopsy as an instrument of quality assessment. Classification of premortem and postmortem diagnostic discrepancies. Arch Pathol Lab Med 108:490–493
4. Avgerinos DV, Bjornsson J (2001) Malignant neoplasms: discordance between clinical diagnoses and autopsy findings in 3,118 cases. APMIS 109:774–780
5. Battle RM, Pathak D, Humble MS, et al (1987) Factors influencing discrepancies between premortem and postmortem diagnoses. JAMA 258:339–344
6. Burton EC, Troxclair DA, Newman III WP (1998) Autopsy diagnoses of malignant neoplasms. How often are clinical diagnoses incorrect? JAMA 280:1245–1248
7. Campion EW, Reder VA, Mulley AG, Thibault GE (1986) Age and the declining rate of autopsy. J Am Geriatr Soc 34:865–868
8. Chandrasekar PH, Weinmann A, Shearer C (1995) Autopsy-identified infections among bone marrow transplant recipients: a clinico-pathologic study of 56 patients. Bone Marrow Transplant 16:675–681
9. Council on Scientific Affairs (1987) Autopsy — a comprehensive review of current issues. JAMA 258:364–369
10. Coradazzi AL, Morganti ALC, Montenegro MRG (2003) Discrepancies between clinical diagnosis and autopsy findings. Braz J Med Biol Res 36:385–391
11. Friederici HHR (1988) Reflections on the *post mortem* audit. JAMA 260:3461–3465
12. Friederici HHR, Sebastian M (1984) Autopsies in a modern teaching hospital. A review of 2,537 cases. Arch Pathol Lab Med 108:518–521
13. Gerain J, Sculier JP, Malengreaux A, Rykaert C, Themelin L (1990) Causes of deaths in an oncologic intensive care unit: a clinical and pathological study of 34 autopsies. Eur J Cancer 26:377–381
14. Goldman L, Sayson R, Robbins S, Cohn LH, Bettmann M, Weisberg M (1983) The value of the autopsy in three medical eras. N Engl J Med 308:1000–1005
15. Gough J (1985) Correlation between clinical and autopsy diagnosis in a community hospital. CMAJ 133:420–422
16. International Statistical Classification of Diseases and Related Health Problems, 1989 Revision, Geneva, World Health Organization, 1992
17. Kelly KM, Lange B (1997) Oncologic emergencies. Ped Oncol 44:809–830
18. Landefeld CS, Goldman L (1989) The autopsy in clinical medicine. Mayo Clin Proc 64:1185–1189
19. Landefeld CS, Chren MM, Myers A, Geller R, Robbins S, Goldman L (1988) Diagnostic yield of the autopsy in a university hospital and a community hospital. N Engl J Med 318:1249–1254
20. Marwick C (1995) Pathologists request autopsy revival. JAMA 273:1889–1891
21. McPhee SJ, Bottles K (1985) Autopsy: moribund art or vital science? Am J Med 78:107–113
22. Mort TC, Yeston NS (1999) The relationship of pre mortem diagnoses and post mortem findings in a surgical intensive care unit. Crit Care Med 27:299–303
23. Nemetz PN, Beard M, Ballard DJ, et al (1989) Resurrecting the autopsy: benefits and recommendations. Mayo Clin Proc 64:1065–1076
24. Nigro JF, Gresik MV, Fernbach J (1990) Value of the post mortem examination in a pediatric population with leukemia. J Pediatr 116:350–354
25. Nosari A, Barberis M, Landonio G, et al (1991) Infections in haematologic neoplasms: autopsy findings. Haematologica 76:135–140
26. de Pangher Manzini V, Revignas MG, Brollo A (1995) Diagnosis of malignant tumor: comparison between clinical and autopsy diagnoses. Hum Pathol 26:280–283
27. Provencio M, Espana P, Salas C, Navarro F, Bonilla F (2000) Hodgkin's disease: correlation between causes of death at autopsy and clinical diagnosis. Ann Oncol 11:59–64
28. Pujol Farriols R, Bernet Vidal M, Castellsague J, Esquius Soriguera J, Raguer Sanz E, Yetano Laguna V (1994) Correlation between clinical and autopsy diagnosis at a general hospital. Ann Med Intern 11:372–376
29. Shojania KG, Burton EC, McDonald KM, Goldman L (2003) Changes in rates of autopsy-detected diagnostic errors over time. JAMA 298:2849–2856
30. Sun CC, Alonsonzana G, Love JC, Li L, Straumanis JP (2003) The value of autopsy in pediatric cardiology and cardiovascular surgery. Hum Pathol 34:491–496
31. Thurlbeck WM (1981) Accuracy of clinical diagnosis in a Canadian teaching hospital. CMAJ 125:443–447
32. Tse GM, Lee JC (2000) A 12 month review of autopsies performed at a university affiliated teaching hospital in Hong Kong. Hong Kong Med J 190–194
33. Veress B, Alafuzoff AI (1994) A retrospective analysis of clinical diagnoses and autopsy findings in 3,042 cases during two different time periods. Hum Pathol 25:140–145

Virchows Arch (2005) 446: 232–238
DOI 10.1007/s00428-004-1171-5

ORIGINAL ARTICLE

Cecilia M. Borromeo · Xavier Pottier · Peter A. In't Veld · Miriam A. Pipeleers-Marichal · Leonard Kaufman · Daniel G. Pipeleers · Christiaan F. Van Schravendijk

Heterogeneity in distribution of amyloid-positive islets in type-2 diabetic patients

Received: 24 September 2004 / Accepted: 4 November 2004 / Published online: 27 January 2005
© Springer-Verlag 2005

Abstract Amyloid-containing (A+) islets are characteristic for type-2 diabetes (T2D), but their abundance seems variable among patients. It is unclear whether the distribution of A+ islets follows a certain pattern or occurs randomly throughout the pancreatic organ. We investigated the topography of A+ islets in eight pancreata of T2D patients and eight sex- and age-matched non-diabetic subjects. Transversal sections of head, body and tail segments were stained with synaptophysin combined with Congo red to map/quantify islet tissue and amyloid. In the eight T2D pancreata, the overall percentage of A+ islets varied from 4% to 85%. Further analysis in body and tail indicated that peripheral regions exhibited higher percentages of A+ islets than central regions (averages of, respectively, 30% and 17%, $P<0.05$). Non-diabetic control pancreata also exhibited A+ islets, albeit at a 25-fold lower frequency; a tendency towards higher percentage of A+ islets in peripheral versus central regions was also observed. The higher percentage A+ islets in peripheral regions was associated with a higher density and relative islet over exocrine surface area. These observations on heterogeneity in abundance and distribution of A+ islets need consideration when sampling tissue for studies on human islet amyloidosis. The present methodology allows us to further investigate the susceptibility to amyloidosis of islets in peripheral regions of the pancreas.

C. M. Borromeo · X. Pottier · P. A. In't Veld · M. A. Pipeleers-Marichal · D. G. Pipeleers · C. F. Van Schravendijk (✉)
Diabetes Research Centre, Brussels Free University—VUB, Laarbeeklaan 103, 1090 Brussels, Belgium
e-mail: Chris.van.Schravendijk@vub.ac.be
Tel.: +32-2-4774558
Fax: +32-2-4774515

L. Kaufman
Department of Biostatistics and Medical Informatics, Brussels Free University—VUB, Belgium

Keywords Islet amyloid · Type-2 diabetes · Human pancreas · Morphometry · Islets of Langerhans

Introduction

Islet amyloid is considered as a characteristic lesion of type-2 diabetes (T2D) [4, 13, 25]. Its formation appears more pronounced in more severe and long-standing cases [11], but little is known about the underlying mechanisms. Amyloid-containing (A+) islets also seem not to be uniformly distributed within affected organs. They were reported to be markedly less abundant in the pancreatic polypeptide (PP)-rich lobe of the ventral head than in other segments, suggesting a role of islet composition in the formation of amyloid [2]. An unequal distribution of islet lesions was previously noticed in the pancreas of type-1 diabetic patients, where beta cell depletion varied greatly from one lobe to another [6, 15]. These observations suggest that pathological processes in man do not affect all islets, or at least not all simultaneously, raising the possibility that inter-islet variations in microanatomy and/or in beta cell functions influence susceptibility to disease [7, 14, 15, 20, 21]. This would be compatible with the view that pancreatic beta cells can participate in their disease process, at a degree that varies with their own intercellular heterogeneity [14, 16, 21]. It is not necessarily in conflict with the apparently homogeneous distribution of islet amyloidosis in transgenic mice [22], since induction of amyloid formation in this animal model may be much more synchronised than that in the pancreas of T2D patients. Thus, it remains unclear thus far whether the distribution of islet amyloidosis follows a certain pattern or whether it occurs randomly throughout the organ. This emphasises the need for topography studies in human tissue before a homogeneous or heterogeneous distribution model can be adopted. The present study investigated the occurrence and distribution of A+ islets in the pancreas of T2D patients and their matched non-diabetic controls. A mapping technique was developed to compare the distribution within or between whole organ sections of head, body and tail segments and

between PP-poor and PP-rich parts of the head segment. If a topographic heterogeneity is found, underlying reasons may become apparent and, thus, help in the understanding of amyloid development in human islet tissue. Such a finding would also have methodological implications in terms of tissue sampling for studies on islet amyloidosis in T2D.

Materials and methods

Human tissue

The 8 T2D pancreata analysed in this study were collected from a consecutive series of 14 pancreata from T2D patients. All organs were obtained within 6 h post-mortem according to procedures approved by the ethics committee of the hospital of the Dutch-speaking Free University of Brussels. Of 14 T2D pancreata, 10 were found to contain Congo red (CR)-positive islets, but 2 exhibited an excessive fat accumulation, with infiltrations around the islet tissue, which interfered with the present analysis. Pancreata of 8 age- and sex-matched non-diabetic subjects were also collected according to the same standards as the T2D organs. Each pancreas was divided into four segments: ventral and dorsal head, body and tail. Tissue slices were cut perpendicular to the longitudinal axis except for the ventral head, where they were made parallel to this axis. Tissue was fixed in 4% neutral buffered formalin and embedded in paraffin. Each slice was sectioned while maintaining the gland's outer contour in the section. Preliminary experiments indicated that single sections are representative of the distribution of islet amyloid in the segment. For each T2D pancreas, 4 segments were examined and, minimally, 77 islets per segment. Analysis in the control group was restricted to the body and tail segments, where A+ islets in central and peripheral organ regions could be compared (see also paragraph on whole-section mapping).

CR staining and immunohistochemistry

CR was used for staining amyloid [10, 17] and synaptophysin antibody for immunocytochemical staining of islet endocrine cells [26]. During the pilot phase of the study, it was found that the combination of these stains was optimal when performing CR staining first, followed by immunohistochemistry for synaptophysin. With this method, the initial stages of islet amyloid in structurally intact islets could be detected.

Paraffin sections 5-μm thick were first deparaffinised and then microwave-treated in 10 mM citrate buffer to unmask antigen epitopes. Endogenous peroxidase activity was blocked in 3% H_2O_2-methanol, followed by the CR staining as described previously [10, 17]. Sections were incubated with rabbit anti-human synaptophysin antibody (1:10; A10010, Dako, Denmark), which identifies both PP-rich and PP-poor islets. The PP-rich ventral head and PP-poor dorsal head regions were confirmed using immunocytochemical analysis with rabbit anti-human pancreatic polypeptide antibody (1:50,000; R. Chance, Lilly Res. Lab., Indianapolis, USA). After an overnight incubation at 4°C with the primary antibody, the binding was visualised using a biotinylated goat anti-rabbit antibody (1:300; RPN 1004, Amersham), (horseradish peroxidase)-labelled streptavidin-biotin complex (K377, Dako, Denmark) and DAB (3′-diaminobenzidine tetrahydrochloride). Islets were classified A+ when CR fluorescence was observed, with a lower measurable detection limit of 1.25 μm^2.

Islet image analysis

Images of A+ islets were captured using fluorescence microscopy (Axioplan 2 Image, Zeiss, Oberkochen, Germany) by a CCD camera (Sensys, Photometrics ltd., Tucson, Arizona), coupled to a Quips Pathvysion (VYSIS, Downers Grove, IL, USA) image analysis system. Multi-plane images were taken combining a brightfield image for synaptophysin immunoreactivity with a fluorescence image for CR obtained through filter set 00 (Zeiss, ex 530–585, em LP615). Islet surface areas were measured semi-automatically using IP-lab (Scanalytics, Fairfax, VA, USA) image analysis software at a screen magnification of ×20.

Whole-section mapping

To obtain an overview of all islets in a section, whole sections were scanned by an Epson Perfection 1200U flatbed scanner with transilluminating film adapter at 2500 dpi. In the scanned images, islets were detected with minimally 13 synaptophysin-positive nucleated cells in the section. In addition, x and y coordinates were assigned to each of the islets. This mapping technique allowed for the examination of whether the presence and size of amyloid deposits correlated with their topographic localisation in the tissue (Fig. 1). For each section, the geometric midpoint (gmp) was determined by coordinates:

$$X_{gmp} = \frac{x_{min} + x_{max}}{2} \text{ and } Y_{gmp} = \frac{y_{min} + y_{max}}{2}, \quad (1)$$

where minimum and maximum values for both X and Y are derived from the corresponding mapping database. These gmp coordinates were then used to calculate the distance (Di) of each individual islet (Xi/Yi) relative to the gmp:

$$Di = \sqrt{\left[\left(Xi - X_{gmp}\right)^2 + \left(Yi - Y_{gmp}\right)^2\right]} \quad (2)$$

In each section, the islet with the highest Di (max Di) represented the most peripherally located islet. A comparison was made between islets located in the periphery of the gland and those in the centre. Islets were, therefore,

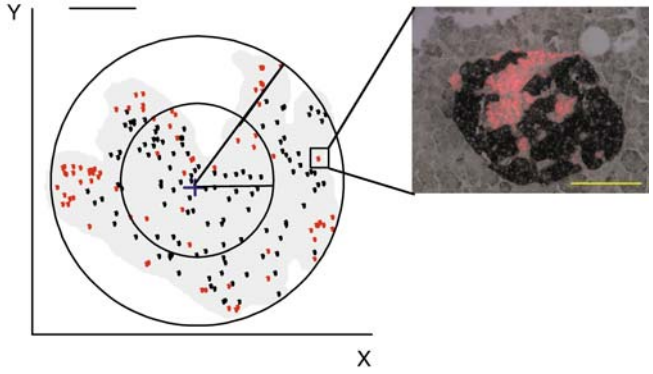

Fig. 1 Schematic representation of a whole tissue section, divided into a central region and a peripheral region (see Materials and methods). *Inset* shows a representative amyloid-containing islet immunostained for synaptophysin (in *brown*) and Congo-red stained for amyloid. *Black dots* amyloid-negative islets. *Red dots* amyloid-containing islets. *Blue cross* section geometric midpoint. *Grey area* shape of the section. *Scale bar for section*=5 mm; *Scale bar for inset*=100 µm. Please note that actual islet sizes are smaller than the dot size in this representation

ranked according to their distance from gmp (Di=0) and most peripherally located islets in the section (max Di). The peripheral region was defined as Di≥max Di/2 and central region as Di<max Di/2 (Fig. 1). The head region could not be used for this analysis, as the anatomy of this part of the gland, being composed of two ontogenetically different parts, precludes the same sort of cross-sectioning that was used for the body and tail parts. Only the body and tail sections of all 16 pancreata were, thus, used to determine the (A+) and amyloid-negative (A−) islets in the central and peripheral regions.

Islet density was defined as the number of islets per cm^2 exocrine tissue area and islet relative surface area as the synaptophysin surface area over the exocrine surface area. Exocrine surface area was measured semi-automatically using IP-lab image analysis software. The section was outlined and then auto-scanned so that the highlighted area corresponding to the exocrine surface area was taken into account.

Statistical analyses

Data processing and statistical analysis was performed using Statview software (Abacus Concepts, Berkeley, CA, USA) and SPSS 10 (SPSS Inc., Chicago, IL, USA). Repeated measures analysis of variance with two within-subject factors was used to assess the differences between values in central and peripheral zones. The paired *t*-test and Wilcoxon signed ranks test were used when two groups were compared. For all analyses, a *P* value of 0.05 or less (two-tailed) was considered to be statistically significant.

Results

Occurrence and segmental distribution of A+ islets in the pancreas

For each organ of the T2D group, sections from all segments were analysed for the presence of A+ islets. With the selected definition for A+ islets, 10 of 14 T2D cases were found to exhibit A+ islets. As described in methods, 2 of these organs were not further analysed due to excessive fat accumulation. Among the 8 others, 4 presented less than 10% of A+ islets, whereas the 4 others had 25–85% A+ islets (Table 1). In the non-diabetic group, 5 of 8 pancreata were found to exhibit A+ islets. Of these, 3 presented 2% and up to 3% A+ islets, while the two others had less than 1% of A+ islets (Table 1). There was no obvious correlation between the percentage of A+ islets and age, sex, body mass index and, for the T2D group, time since diagnosis (Table 1).

Table 1 Clinical data of type-2 diabetes (T2D) subjects (nos. 1–8) and sex- and age-matched non-diabetics (nos. 9–16): % amyloid positive (A+) corresponds to all islets that were analysed in the dorsal head, body and tail (T2D group) and in the body and tail (non-diabetic group). Most T2D patients were under some form of oral hypoglycaemic therapy. *BMI* body mass index

Subject no.	Sex	Age (years)	BMI	Major cause of death	% A+ islets	Years after diagnosis	Subject no.	Sex	Age (years)	BMI	Major cause of death	%A+ islets
1	Male	90	19	Myocarditis	85	10	9	Male	88	16	Sepsis	0.1
2	Female	85	23	Cardiac failure	30	5	10	Female	87	21	Respiratory failure	3
3	Male	74	27	Respiratory failure	29	3	11	Male	77	23	Cerebral haemorrhage	2
4	Male	74	23	Respiratory failure	25	12	12	Male	74	21	Respiratory failure	0
5	Male	79	24	Sepsis	8	45	13	Male	78	25	Septic shock	0
6	Male	66	30	Hypovolemic shock	6	5	14	Male	65	20	Respiratory failure	2
7	Male	71	18	Terminal kidney failure	5	34	15	Male	73	29	Cardiogenic shock	0
8	Male	69	37	Cardiogenic shock	4	>1	16	Male	65	23	Cardiac failure	0.3

Table 2 Comparison of amyloid-positive (A+) islets in different pancreatic segments in the type-2 diabetic group (T2D) versus the non-diabetic group (NonD). Results are expressed as the number of A+ islets over the total number of islets and as percentage. *N.S.* not significant. Wilcoxon signed ranks test was also used for the comparison of the respective groups and similar results were obtained

Patient no.	Head (A+/Total) (%)		Body	Tail	Patient no.	Body	Tail
T2D	Ventral	Dorsal	A+/Total (%)	A+/Total (%)	NonD	A+/Total (%)	A+/Total (%)
1	11/157 (7)	46/77 (60)	157/185 (85)	234/252 (93)	9	0/436 (0)	1/388 (0.26)
2	10/343 (3)	65/186 (35)	55/149 (37)	44/209 (21)	10	3/84 (4)	7/315 (2)
3	6/103 (6)	24/151 (16)	76/196 (39)	111/375 (30)	11	7/236 (3)	3/291 (1)
4	4/117 (3)	44/91 (48)	28/127 (22)	54/296 (18)	12	0/241 (0)	0/473 (0)
5	0/115 (0)	14/98 (14)	5/154 (3)	17/188 (9)	13	0/179 (0)	0/435 (0)
6	0/166 (0)	4/97 (4)	5/220 (2)	26/287 (9)	14	1/136 (0.74)	7/304 (2)
7	9/170 (5)	5/97 (5)	9/240 (4)	20/354 (6)	15	0/243 (0)	0/268 (0)
8	0/254 (0)	1/142 (1)	11/224 (5)	10/128 (8)	16	0/217 (0)	2/455 (0.44)
P value		0.03[a]	N.S.[b]	N.S.[c]			N.S.[d]

[a]Paired *t*-test derived *P* values calculated for the ventral versus the dorsal head segment (P=0.03)
[b]Paired *t*-test derived *P* values calculated for the dorsal head versus the body segment
[c]Paired *t*-test derived *P* values calculated for the body versus the tail segment of the T2D group (nos. 1–8)
[d]Paired *t*-test derived *P* values calculated for the body versus the tail segment of the matched non-diabetic group (nos. 9–16)

When the percentage of A+ islets was determined per segment in the T2D group, a marked difference was noticed between the ventral head segment identified by PP staining and the rest of the pancreas: for all A+ organs, the ventral head presented less than 10% of A+ islets, whereas higher percentages occurred in the other parts, including the dorsal head (Table 2). On average, 3% ventral head islets were A+ versus 22% of dorsal head islets (P=0.03, Table 2). This difference was noticed in both organs with the higher percentage of A+ islets (nos. 1–4, 4% ventral versus 35% dorsal) and those with the lower percentage (nos. 5–8, 1% ventral versus 6% dorsal). No statistically significant differences were found among the percentage of A+ islets in dorsal head, body and tail (Table 2).

In the control group, the percentage of A+ islets in the body and tail segments was considerably lower than in the T2D group, ranging from 0% to 0.44% at its lowest and up to 4% at its highest. Similar to the T2D group, however, no significant differences were found in the percentage of A+ islets between the body and tail segments (Table 2).

Distribution of A+ islets over central and peripheral regions of the pancreas

Upon visual inspection of tissue section maps from the T2D group, A+ islets appeared preferentially localised in the peripheral region (Fig. 1 and Fig. 2). This was confirmed by the topographical analysis of body and tail segments, which together represent the major part of the organ. Each tissue section was divided in a circular central and a circular peripheral region, with an outer diameter that was twice that of the inner circle (Fig. 1). The surface of the peripheral regions was, thus, consistently larger than that of the central regions, which may explain their larger number of sectioned islets (Table 3). The percentage of A+ islets was higher in peripheral regions than in central ones, both in body and tail segments (Table 4, averages of 30% A+ in peripheral and 17% in central regions). This was the case for both A+ rich and A+ poor organs (Table 4, analysis of variance repeated measures, P<0.01). When combining data collected in body and tail, A+ poor organs

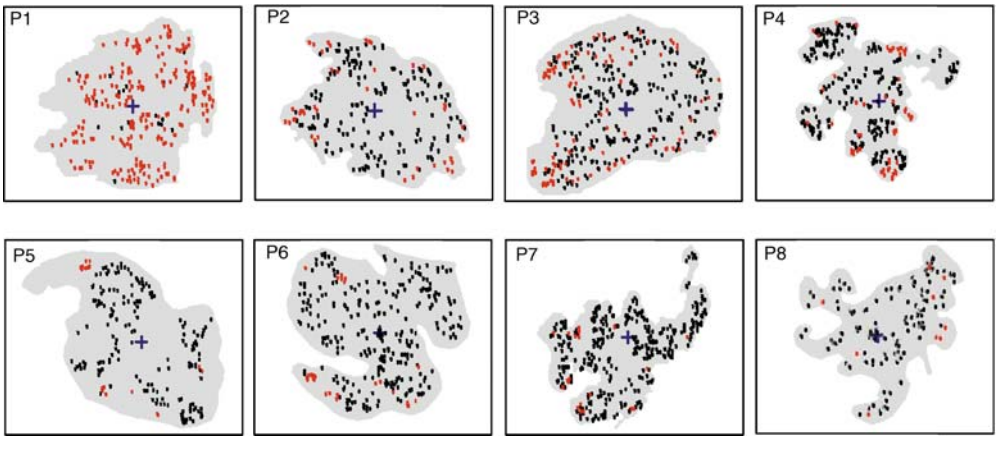

Fig. 2 Schematic representation of the distribution of amyloid-affected islets in the tail sections of all pancreatic organs from the type-2 diabetes group. The grey area represents the shape of the section. *Black dots* amyloid-negative islets. *Red dots* amyloid-containing islets. *Blue cross* section geometric midpoint

Table 3 Distribution of islet density per segment and per region in the type-2 diabetic group (T2D) versus the non-diabetic group (NonD). Data represent means±SEM. *%Exo SA* relative islet over exocrine surface area

Segment	Region	Islet number		Islet surface area	
		Per section	Per cm^2	10^3 μm^2	% Exo SA
T2D					
Body	Center	78±11[a]	105±22[b]	15.0±2.6	1.4±0.2[c]
	Periphery	109±10	131±15	15.0±2.0	2.0±0.3
Tail	Center	108±15[a]	158±29[b]	18.8±4.3	2.8±0.5[c]
	Periphery	153±18	184±29	19.5±3.8	3.5±0.7
Body	Center+periphery	187±14[d]	120±18[e]	14.9±2.2	1.7±0.2[f]
Tail	Center+periphery	261±30	178±27	19.3±3.9	3.1±0.5
NonD					
Body	Center	90±16	91±10	14.3±0.9	1.3±0.2
	Periphery	132±23	101±14	15.9±1.5	1.7±0.3
Tail	Center	176±17	227±36	17.2±1.4	4.2±0.8
	Periphery	191±19	293±41	16.2±1.2	5.3±1.2
Body	Center+periphery	222±37[g]	94±12[h]	15.3±1.2	1.5±0.2[i]
Tail	Center+periphery	366±29	256±37	16.7±1.3	4.7±1.0

Statistical significance of differences in: type-2 diabetic (T2D) group between center and periphery in same segment (upper panel) is calculated by repeated measures analysis of variance ([a]C versus P, P=0.006; B versus T, P=0.046; Int, P=0.535), ([b]C versus P, P=0.027; B versus T, P=0.021; Int, P=.993), ([c]C versus P, P=0.024; B versus T, P=0.028; Int, P=0.593). Statistical significance of differences between: body and tail (lower panel) by paired t-test [d]P=0.046, [e]P=0.011, [f]P=0.025. Wilcoxon signed ranks test generated similar results except for [d] where P=0.068. *C* center, *P* periphery, *B* body, *T* tail, *Int* interaction. Nondiabetic (NonD) group: between body and tail (lower panel) by paired t-test [g]P=0.01, [h]P=0.004, [i]P=0.014. Wilcoxon signed ranks test generated similar results

(nos. 5–8) presented 9% A+ islets in the peripheral region and only 1% in the central region (Table 4). These differences illustrate the risk for sampling errors when studying islet amyloidosis in T2D.

In the control group, a trend towards a higher percentage of A+ islets in the peripheral region was observed in both body and tail segments, albeit not statistically significant. Compared with the T2D group, the percentages of A+ islets in the peripheral region of the body and tail segments were lower by 21-fold and 26-fold, respectively (Table 4).

Table 4 Percentage A+ islets in central and peripheral regions of body and tail segments of type-2 diabetes group (T2D) and the non-diabetic group (NonD): data represent means±SEM of percentage amyloid-positive (A+) islets in T2D and NonD groups

Pancreatic segments	Central region	Peripheral region
T2D		
Body and tail in A+ rich group (P1–4)	33±11	50±11[a]
Body and tail in A+ poor group (P5–8)	1±0.45	9±1[b]
Body (P1–8)	17±9	30±11[c]
Tail (P1–8)	17±11	29±10[d]
NonD		
Body (P9–16)	0±0	1.4±0.8
Tail (P9–16)	0.4±0.3	1.1±0.5

Upper panel of T2D group: statistical differences between central and peripheral regions calculated by analysis of variance repeated measures [a]P=0.006, [b]P=0.002, or by paired t-test [c]P=0.03, [d]P=0.009 in the lower panel. Wilcoxon signed ranks test was used for the comparison of the respective groups and similar results were obtained

In view of the differences in percentage of A+ islets between peripheral and central regions of the T2D group, we examined whether these regions differed in islet surface area or islet number. No difference was measured in the mean islet surface area of both regions (Table 3). However, both the mean islet number per cm^2 and the relative islet surface areas were higher in peripheral than in central regions (P<0.03, Table 3, upper panel). This analysis also indicated a higher islet density in the whole tail segment, as reflected by a higher islet number per cm^2 and a higher islet over exocrine surface area (average of 3.1% in tail versus 1.7% in body, Table 3, lower panel). Similar differences were found when central or peripheral regions were compared between body and tail segments (Table 3).

In the control group, all parameters (islet number, islet density, islet surface area and relative islet density) displayed a trend towards higher values in the peripheral regions of both the body and tail segments without reaching significance. Similar to the T2D group, the tail segments of the control group had significantly higher islet density (per cm^2 and relative islet density) than the body segments (Table 3).

Discussion

A+ islets are considered to be a characteristic lesion of T2D, occurring, according to some authors, in 90% of patients versus less than 12% in non-diabetics [3, 4, 11].

Other studies report a wide variability, both in patients and age-matched controls, making the difference between average percentages smaller than in references 3, 4 and 11 [19, 24, 25]. When present, A+ islets do not always account for the majority of the islet population, their prevalence varying from 1% to 99% of the islets examined within the organ [2, 4, 11, 18, 19, 24, 25, 27]. This diversity might well be related to the heterogeneity in pathogenesis and clinical history of the studied cases; precautions to standardise studies in this respect have received little attention so far.

Variations in sampling of tissue may represent additional causes for the variation in data published thus far [2, 4, 11, 24, 27]. The segment from where tissue was recovered is not always stated, and only few studies specify the number of islets analysed per segment. Most studies indicate the number of islets analysed per organ, but these numbers vary from 20 to 500, raising the question as to whether all data carry the same degree of representation for the degree of amyloidosis in a particular organ.

In the present study, we have analysed a total of 555–887 islets per organ in the T2D group (composed of comparable numbers from ventral and dorsal head, body and tail segments), while in the non-diabetic group, a total of 399 to 824 islets per organ were analysed (all together, more than 10,500 islets in 16 organs were analysed). Although collected from a small series of organs, our data confirm the wide variability in prevalence of A+ islets in type-2 diabetic patients and indicate a new form of heterogeneity in their topography within the pancreatic organ.

As in other reports [4, 11, 25], A+ islets were not found in all organs (none detected in 4 of 14 organs) and, when detected, represented often less than 10% of the islet population (in 4 of the 8 analysed organs). We do not consider this a consequence of a lack of sensitivity of our amyloid staining method, since apparently the early stages of visible islet amyloid in structurally intact islets could also be detected. Previous studies have indicated or proposed a correlation between the degree of islet amyloidosis and duration of T2D [11], degree of insulin resistance and of islet failure [27]. Our study was not intended to search for clinical associations but to investigate whether A+ islets were homogeneously or heterogeneously distributed over the pancreatic organ of type-2 diabetic patients.

Quantitative morphometry on five organs has previously indicated that A+ islets occur throughout the dorsal head, body and tail segments, while being rare in the ventral head segment where the pancreatic polypeptide-rich islets are located [2]. Our data confirm this observation. In none of our eight T2D pancreata was the percentage of A+ islets in the ventral head higher than 7%, whereas the percentages in other segments were systematically higher, up to 93%. However, no statistically significant differences were found between the percentage of A+ islets in dorsal head, body and tail, while higher percentages A+ islets in tail versus body and head segments were suggested previously [24]. In our study, the organs with, respectively, low or high average A+ islets exhibited low or high values in these three segments.

Imaging of whole transverse tissue sections led us to distinguish a non-uniform distribution of A+ islets in the body and tail segments. Head segments could not be sectioned using the same method (which preserves the organ border) and were not, therefore, analysed. In both body and tail segments of the T2D group, peripheral regions exhibited a higher percentage of A+ islets than central regions. Interestingly, almost identical averages were counted in the central (17%) and in the peripheral (30%) regions of both segments. The higher percentage of A+ islets in the periphery could not be attributed to a larger average islet surface area, which could have facilitated detection, nor to the difference in the exocrine surface area of central versus peripheral regions. It was associated with a higher number of islets per surface area (islet density) as well as a higher relative islet surface area in peripheral versus central regions, in both body and tail. The non-diabetic group exhibited approximately 25-fold lower A+ islets in the body and tail segments than the T2D group. Again, most of these A+ islets were found in the peripheral regions of both segments, where islet densities were slightly higher than in the central regions. This finding further illustrates the heterogeneity in the microanatomy of the endocrine pancreas.

The present morphometric analysis reports a higher islet density in tail versus body segments (48% more islets per cm^2 and 82% higher relative islet surface area in the T2D group). While these findings are new for the T2D pancreas, they are consistent with an old notion for non-diabetic pancreata [8, 9], as well as with our own observations in the matched control group of pancreata from non-diabetic subjects.

We have previously demonstrated the existence of a heterogeneity in both the rat and human beta cell population, but the evidence comes largely from in vitro observations [21] and has not yet been extrapolated to pancreatic islets in situ. The present observations provide in situ signs of a heterogeneity in islet lesions in the pancreas of T2D patients and are thus consistent with the concept that heterogeneity in the pancreatic beta cell population can predispose to a heterogeneity in the pathogenic process. Such heterogeneity could, for example, be correlated to cellular ageing; not all islets in the pancreas have the same age, and it has been suggested that older islets will be positioned more distantly from the centrally located ducts [23]. This or any other functional heterogeneity may be correlated to factors that predispose islets to an increased deposition of amyloid under diabetic conditions. Among these are a higher cellular content and local production of islet amyloid polypeptide (IAPP) [1] and an increased lysosomal activity, such as has been observed in Alzheimer's disease [5, 12]. The present observations and methodology allow the identification of pathogenic markers that reveal this heterogeneity during the early stages of islet amyloidosis.

Acknowledgements The authors thank Dan Ardelean for performing the autopsies, as well as Geert Stangé and Nicole Buelens for technical assistance. This study was supported by the Flemish Research Foundation [Fonds voor Wetenschappelijk Onderzoek (FWO)] (grants G.0358.03 and G.0376.97), the Belgian Science Policy (Interuniversity Attraction Poles Grant P5/17) and by the Research Council of the Flemish Free University of Brussels, VUB.

References

1. Clark A (1992) Islet amyloid: an enigma of type 2 diabetes. Diabetes Metab Rev 8:117–132
2. Clark A, Holman RR, Matthews DR, Hockaday TDR, Turner RC (1984) Non-uniform distribution of islet amyloid in the pancreas of "maturity-onset" diabetic patients. Diabetologia 27:527–528
3. Clark A, Wells CA, Buley ID, Cruickshank JK, Vanhegan RI, Matthews DR, Cooper GJ, Holman RR, Turner RC (1988) Islet amyloid, increased A-cells, reduced B-cells and exocrine fibrosis: quantitative changes in the pancreas in type 2 diabetes. Diabetes Res 9:151–159
4. Clark A, Saad MF, Nezzer T, Uren C, Knowler WC, Bennett PH, Turner RC (1990) Islet amyloid polypeptide in diabetic and non-diabetic Pima Indians. Diabetologia 33:285–289
5. Furuta K, Yang XL, Chen JS, Hamilton SR, August JT (1991) Differential expression of the lysosome-associated membrane proteins in normal human tissues. Arch Biochem Biophys 365:75–82
6. Gepts W, De Mey J (1978) Islet cell survival determined by morphology. An immunocytochemical study of the islets of Langerhans in juvenile diabetes mellitus. Diabetes 27[Suppl 1]:251–261
7. Jorns A (1994) Immunocytochemical and ultrastructural heterogeneities of normal and glibenclamide stimulated pancreatic beta cells in the rat. Virchows Arch 425:305–313
8. Klöppel G, In't Veld PA (1997) Morphology of the pancreas in normal and diabetic states. In: KGMM Alberti, P Zimmet, RA DeFronzo (eds) International textbook of diabetes mellitus, 2nd edn. John Wiley & Sons, pp 287–313
9. Lazarus SS, Volk BW (1962) The pancreas in human and experimental diabetes. Grune & Stratton, New York
10. Linke RP (2000) Highly sensitive diagnosis of amyloid and various amyloid syndromes using Congo red fluorescence. Virchows Arch 436:439–448
11. Maloy AL, Longnecker DS, Greenberg ER (1981) The relation of islet amyloid to the clinical type of diabetes. Hum Pathol 12:917–922
12. Mathews PM, Guerra CB, Jiang Y, (2002) Alzheimer's disease-related overexpression of the cation-dependent mannose 6-phosphate receptor increases Abeta secretion: role for altered lysosomal hydrolase distribution in beta-amyloidogenesis. J Biol Chem 277:5299–5307
13. Opie E (1901) The relation of diabetes mellitus to lesions of the pancreas. Hyaline degeneration of the islands of Langerhans. J Exp Med 5:527–540
14. Pipeleers D (1987) The biosociology of pancreatic beta cells. Diabetologia 30:277–291
15. Pipeleers D, Ling Z (1992) Pancreatic beta cells in insulin-dependent diabetes. Diabetes Metab Rev 8:209–227
16. Pipeleers D, Hoorens A, Marichal-Pipeleers M, Van de Casteele M, Bouwens L, Ling Z (2001) Role of pancreatic beta-cells in the process of beta-cell death. Diabetes 50[Suppl 1]:S52–S57
17. Puchtler H, Sweat F (1965) Congo red as a stain for fluorescence microscopy of amyloid. J Histochem Cytochem 13:693–694
18. Sakuraba H, Mizukami H, Yagihashi N, Wada R, Hanyu C, Yagihashi S (2002) Reduced beta-cell mass and expression of oxidative stress-related DNA damage in the islet of Japanese type II diabetic patients. Diabetologia 45:85–96
19. Sempoux C, Guiot Y, Dubois D, Moulin P, Rahier J (2001) Human type 2 diabetes: morphological evidence for abnormal beta-cell function. Diabetes 50[Suppl 1]:S172–S177
20. Stefan Y, Meda P, Neufeld M, Orci L (1987) Stimulation of insulin secretion reveals heterogeneity of pancreatic B cells in vivo. J Clin Invest 80:175–183
21. Van Schravendijk CF, Kiekens R, Pipeleers DG (1992) Pancreatic beta cell heterogeneity in glucose-induced insulin secretion. J Biol Chem 267:21344–21348
22. Wang F, Hull RL, Vidal J, Cnop M, Kahn SE (2001) Islet amyloid develops diffusely throughout the pancreas before becoming severe and replacing endocrine cells. Diabetes 50:2514–2520
23. Watanabe T, Yaegashi H, Koizumi M, Toyota T, Takahashi T (1999) Changing distribution of islets in the developing human pancreas: a computer-assisted three-dimensional reconstruction study. Pancreas 18:349–354
24. Westermark P, Wilander E (1978) The influence of amyloid deposits on the islet volume in maturity onset diabetes mellitus. Diabetologia 15:417–421
25. Westermark P, Wilander E, Westermark GT, Johnson KH (1987) Islet amyloid polypeptide-like immunoreactivity in the islet B cells of type 2 (non-insulin-dependent) diabetic and non-diabetic individuals. Diabetologia 30:887–892
26. Wiedenmann B, Franke WW, Kuhn C, Moll R, Gould VE (1986) Synaptophysin: a marker protein for neuroendocrine cells and neoplasms. Proc Natl Acad Sci U S A 83:3500–3504
27. Zhao HL, Lai FM, Tong PC, Zhong DR, Yang D, Tomlinson B, Chan JC (2003) Prevalence and clinicopathological characteristics of islet amyloid in Chinese patients with type 2 diabetes. Diabetes 52:2759–2766

Virchows Arch (2005) 446: 239–245
DOI 10.1007/s00428-004-1167-1

ORIGINAL ARTICLE

Claudio Sorio · Paola Capelli · Daniele Lissandrini · Patrick S. Moore · Piera Balzarini · Massimo Falconi · Giuseppe Zamboni · Aldo Scarpa

Mucinous cystic carcinoma of the pancreas: a unique cell line and xenograft model of a preinvasive lesion

Received: 30 July 2004 / Accepted: 26 October 2004 / Published online: 2 February 2005
© Springer-Verlag 2005

Abstract Pancreatic mucinous cystic tumors (MCT) are proliferations of mucin-producing epithelia supported by an ovarian-like stroma. They are classified into adenomas (MCA), borderline (MCB) and noninvasive or invasive carcinomas (MCC). The molecular mechanisms underlying their clinical behavior are poorly understood, partly due to the lack of cellular models. We report the establishment of MCC1, the first cell line from a pancreatic MCT, deriving from the highly dysplastic cell component of a noninvasive MCC. MCC1 has mutations in codon 12 of K-*RAS* (GGT>GAT), codon 58 of *P16* (CGA>TGA) and codon 132 of *P53* (AAG>AGG). The *FHIT* and *DPC4* genes are unaltered. Immunohistochemistry shows abnormal expression of MUC1 and p53, loss of p16 and retention of Fhit and Dpc4 in both the cell line and the highly dysplastic cells of the primary lesion. The morphological and molecular features of MCC1 and its corresponding primary tumor are consistent with a model for non-invasive MCC, where K-*RAS*, *P16*, *P53* and MUC1 alterations are pre-invasive changes associated with progression of malignancy of MCT from adenoma to carcinoma. MCC1 is sensitive to 5-fluorouracil, representing the first assessment of drug sensitivity for MCC. Finally, MCC1 is a suitable model for preclinical studies, as it grows in immunodeficient mice.

C. Sorio · P. Capelli · D. Lissandrini · P. S. Moore · G. Zamboni · A. Scarpa (✉)
Dipartimento di Patologia, Università di Verona,
Strada Le Grazie 8,
37134 Verona, Italy
e-mail: aldo.scarpa@univr.it
Tel.: +39-045-8027617
Fax: +39-045-8027136

P. Balzarini
Istituto di Anatomia Patologica,
Università di Brescia,
Italy

M. Falconi
Dipartimento di Scienze Chirurgiche e Gastroenterologiche, Università di Verona,
Italy

Keywords Pancreas · Mucinous cystic tumor · Carcinoma · Cell line · Xenograft

Introduction

Mucinous cystic tumors (MCT) are among the most frequent cystic neoplasms arising in the pancreas [25]. They occur almost exclusively in women and are localized in the body-tail of the pancreas. MCTs are characterized by a cystic structure that is not connected to the native pancreatic duct system and contain a proliferation of mucinous lining epithelium surrounded by a dense, ovarian-like stroma. This latter feature also distinguishes them from other mucinous pancreatic tumors. Surgical removal is mandatory, given the potential malignant behavior of this lesion. In fact, the neoplastic epithelium shows variable degrees of dysplasia that are the basis for the recent World Health Organization (WHO) classification of these tumors into adenomas (MCA), borderline tumors (MCB) and noninvasive and invasive carcinomas (MCC) [25]. The prognosis of these cancers has been shown to depend on the extent of tumor invasion at the time of diagnosis [21, 22, 24]. A comparison of the clinical and pathological features of MCTs arising in the pancreas and those observed in the liver and retroperitoneum reveals a striking resemblance between these lesions, suggesting that they arise from similar cells. Interestingly, these MCTs show the same histopathological and cell lineage differentiation pattern in both the epithelium and the stroma as in MCTs of the ovary. This led to the hypothesis that these tumors might arise from ectopic ovarian tissue [24].

The molecular mechanisms underlying progression of malignancy in MCT are poorly understood, partly due to the absence of adequate cellular models. In fact, while numerous cell lines derived from the much more frequent and aggressive pancreatic ductal adenocarcinoma have been established and extensively characterized [16, 19], no cell line derived from pancreatic MCT has been reported to date. Particularly true for rare neoplasms, the availability of large amounts of viable neoplastic cells is limited,

and substantial progress may be achieved only by the exploitation of a cellular model.

In this report, we describe the isolation and characterization of MCC1, the first cell line derived from a mucinous cystic carcinoma of the pancreas. This model will be particularly useful in studies aimed at the elucidation of molecular aspects of pancreatic MCT and its relationship with other pancreatic neoplasms as well as with mucinous cystic neoplasms arising in different organs. MCC1 can also grow in immunodeficient mice, making it a suitable model for pre-clinical studies.

Materials and methods

Clinicopathological data

The primary mucinous cystic carcinoma was obtained from a 69-year-old female patient who underwent splenopancreasectomy in June 1997 with curative intent. Radiological examination including computerized tomography scan and nuclear magnetic resonance showed a sharp-edged ovoid neoformation of about 7 cm of largest diameter. The lesion was cystic with a liquid content and a central solid area. Informed consent for the utilization of samples from the resected specimen for research purposes was obtained. Macroscopic examination revealed that the pancreatic tail was almost completely substituted by a cystic lesion of 6×7 cm, lacking any communication with the duct system. It had a smooth outer surface and a fibrous pseudocapsule, contained mucin-like fluid and was rich in papillary vegetations. Histological diagnosis was of mucinous cystic carcinoma non-invasive, according to the WHO classification [25]. No lymph-node metastasis was detected in the nine lymph nodes isolated from the surgical specimen. The patient is well and alive to date and was not submitted to chemotherapy.

Culture procedure

Part of the lesion was removed under sterile conditions and transferred in Leibovitz medium (Leibovitz L-15, BioWhittaker, Bergamo, Italy) kept at 4°C until transfer to the cell culture facility. For culture, the tissue was finely minced and transferred into 6-well cell culture dishes (Beckton-Dickinson, Milano, Italy) after resuspension in RPMI 1640 containing 10% fetal bovine serum (Gibco-BRL), 2 mM glutamine, 80 μg/ml gentamicin sulphate and 2.5 μg/ml amphotericin B (Sigma-Aldrich, Milan, Italy). The cells were maintained at 37°C in a humidified atmosphere with 5% CO_2, and the medium was changed twice a week.

Duplication time

The duplication time for the cell line was determined by performing the readings with Alamar blue (Biosource International, Milan, Italy) at 24-h intervals as described below once a linear phase of growth was determined for a given cellular concentration.

Cyogenetic analysis

The cytogenetic study was performed in G-banded metaphases cells obtained from a 5-day-old culture and analysis of a total of 20 cells.

Table 1 MCC1 expression of epithelial/mesenchymal antigens. + Positive staining graded from one to three plus according to the intensity, − negative stain. *IHC* immunohistochemistry

Antigen	Source/clone	IHC staining Histological sample	IHC staining Cell line
CK7	Dako Corporation (clone OV-TL 12/30)	+	+
CK 8.18.19	CALTAG Laboratories (clone NCL5D3)	++	++
CK20	Dako	−	−
Carcinoembryonic antigen	Dako	Not done	−
Ber-EP4	Dako	+	+
CDX2	BioGenex (clone CDX2–88)	+	+
Vimentin	CALTAG Lab. (clone V9)	− (Stroma +)	−
Chromogranin A	Dako-A3	−	−
Neuron-specific enolase	Dako	ND	−
Estrogen receptor	Dako (clone 1D5)	− (Stromal cells +)	−
Progesterone receptor	DAKO (clone 1A6)	− (Stromal cells ++)	−
MUC-1	BD-Pharmingen (clone HMPV)	+ (High-grade dysplasia/carcinoma)/−	+
MUC-2	Biotrend Chemikalien (clone CCP58)	−	−
p53	BioSource International (clone DO-1)	++ (High-grade dysplasia/carcinoma)/−	++
p16	Dako (Clone E6H4)	− (High-grade displasia/carcinoma)/+	−
DPC4/Smad4	Santa Cruz	++	++
FHIT	Zymed	++	++

Molecular analysis

All samples were analyzed for mutations in exon 1 of the K-*RAS* gene, exons 1 and 2 of *P16*, exons 5–9 of *P53* and exons 8–11 of *DPC4* using direct sequencing of polymerase chain reaction (PCR)-amplified DNA fragments. Primers for amplification of the *P53* [17], *P16* [26], K-*RAS* [18] and *DPC4* genes [7] were as described. Methylation-specific PCR for the 5′ CpG island of the *P16* gene was carried out as described [9].

Immunocytochemical analysis

The phenotypic profile of MCC1 was analyzed using the antibodies detailed in Table 1. For immunocytochemistry, tissues were formalin fixed and paraffin embedded, while cells were cultured on glass slides, washed with PBS (phosphate buffered saline: 0.1 M NaCl, 2 mM KCl, 8 mM Na_2HPO_4, 1 mM KH_2PO_4, pH 7.4) and fixed in cold acetone. The slides were then rehydrated in PBS and pre-incubated with 10 mM phenylhydrazine in PBS to block endogenous peroxidase activity. Slides were rinsed four times in PBS and incubated with protein-blocking agent

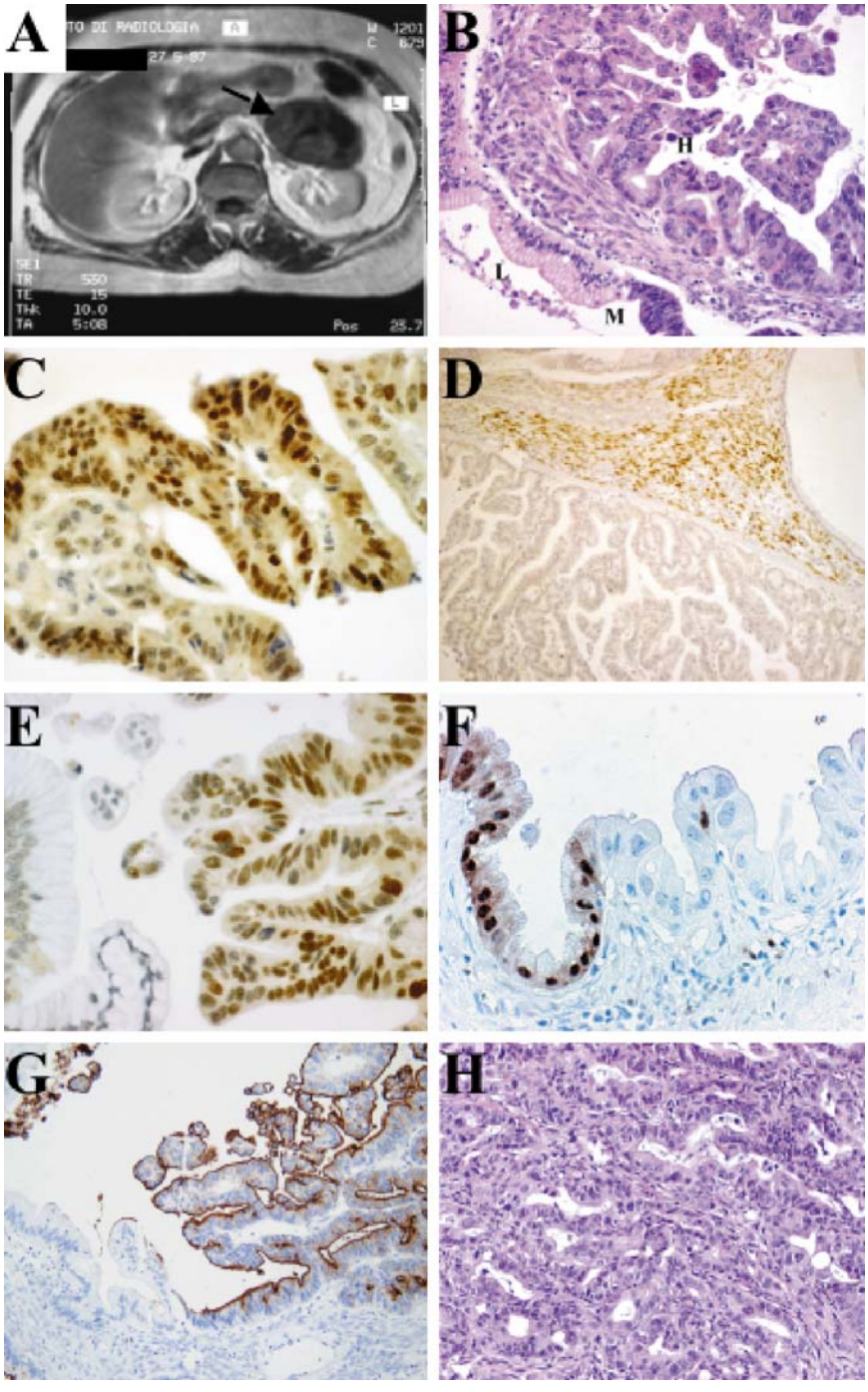

Fig. 1 Morphological and molecular features of primary mucinous cystic carcinoma and MCC1 xenograft. **A** Nuclear magnetic resonance image showing the cystic lesion (*black arrow*) containing vegetating solid protrusions. **B** Hematoxylin and eosin stain of the primary tumor showing papillary protrusions lined by low- (*L*), moderate- (*M*) and high-grade (*H*) dysplastic epithelium (×20). **C** Immunostaining for CDX2 shows nuclear positivity for this marker of intestinal epithelia (×40). **D** Immunostaining for progesterone receptor shows staining of the ovarian-like stroma (×10). **E** p53 immunostaining reveals positive nuclei in highly dysplastic cells (*right*) and no staining in low-grade cells (*left*) (×40). **F** Expression of p16 is lost in dysplastic cells (×40). **G** MUC1 immunostaining is positive in highly dysplastic cells (×20). **H** Morphology of MCC1 xenograft grown in nu/nu mice showing the close resemblance with the highly dysplastic area of the primary tumor shown in **B** (×20)

(UltraTech HRP Kit Immunotech) for 10 min at room temperature. To visualize the presence of specific antigens, the streptavidin-biotin-HRP staining method was used, and antibody localization was visualized with the diaminobenzidine reaction.

Tumorigenicity in nu/nu mice

Subconfluent MCC1 cells were trypsinized and, 1×10^6 cells in 0.2 ml of PBS were injected subcutaneously into the left flank of a total of 14 5-week-old *nu/nu* Swiss mice weighing 18–22 g (Charles River, Milan, Italy). The animal research complied with Italian national legislation and with the Verona University policy on the Care and Use of Animals and with related codes of practice.

Results

A cell line was established from a pancreatic mucinous cystic carcinoma excised from a patient undergoing resection for a cystic lesion of the pancreatic tail (Fig. 1). This cell line was designed as mucinous cystic carcinoma 1 (MCC1). When the original explant was kept in culture, the fibroblast contamination was minimal, and the epithelial component began to grow within few days, as judged by morphology and immunophenotyping. The cells were subcultured after they reached 80% confluence and were cryopreserved at early passages. The cryopreserved cells could be successfully re-cultured and xenografted in nu/nu mice.

Histopathology of the primary neoplasm

The tumor lacked any communication with the duct system and contained mucin-producing epithelium supported by an ovarian-like stroma (Fig. 1). This epithelium showed a variable degree of changes ranging from low- to high-grade dysplasia. The dysplastic changes were multifocal and mainly detected in tumor areas, which grossly showed papillations. Low-grade dysplastic areas were characterized by columnar cells with abundant cytoplasm, basally located nuclei with only slight enlargement and no mitotic figures. Moderately dysplastic epithelium showed pseudostratification with crowding of slightly irregular, hyperchromatic nuclei that had one or more nucleoli. In the areas of high-grade dysplasia, the epithelium was multilayered and formed irregular papillary projections and cribriform structures composed of cells with marked nuclear atypia and frequent mitotic figures. Extensive sampling of the margins revealed absence of capsule invasion and lymph-node metastasis. Therefore, the diagnosis was non-invasive mucinous cystic carcinoma.

Morphological and growth features of MCC1 cell line

The morphological characteristics of MCC1 are shown in Fig. 2, where, in accordance with its epithelial origin, an adherent growth pattern and a flattened polygonal morphology is evident. The cells often presented multiple nucleoli and grew with a trabecular pattern. Several polynucleated cells were observed. The doubling time in standard culture medium was 72±12 h (n=4).

Cytogenetic analysis

A complex karyotype was revealed with presence of both numerical and structural chromosome aberrations. A number of different chromosomes were involved in deletion, translocation and addition of material of unknown origin, and a marker chromosome was present. The cytogenetic analysis can be summarized as follows: 69, XX, -X, del(3)(p10)x2, +del(3)(p13), -6, -8, +del(9)(q21), +del(11)(q10), +del(11)(p10), -15, -17, der(18)t(?9;18)(?q22;q23), add(19)(q13), +add(19)(q13), +20, +21, der(22)t(?9;22)(q21;p13), -22, +mar.

Mutational analysis

Molecular analysis showed the presence of a mutation in codon 12 of the K-*RAS* gene (GGT>GAT), in codon 58 of the *P16* gene (CGA>TGA) and in codon 132 of the *P53* gene (AAG>AGG). Neither de novo methylation in *P16* nor mutations in *DPC4/SMAD4* were found.

Immunophenotyping

The immunophenotype of MCC1 included the analysis of a panel of epithelial and mesenchymal markers as well as evaluation of MUC1, MUC2, Fhit, p53, p16 and Dpc4/Smad4 expression. The results are detailed in Table 1 and representative results shown in Fig. 1. In summary, the epithelial nature of MCC1 was confirmed by the cytoplasmic expression of cytokeratins, membranous Ber-EP4 and nuclear CDX2 antigens, associated with the absence of

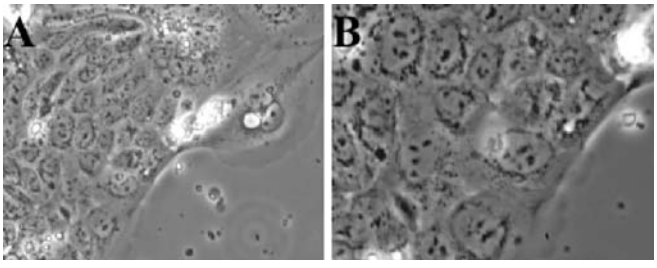

Fig. 2 Morphology of MCC1 cell line. **A** MCC1 cells display epithelial morphology, adhesion to the surface and a cohesive growth pattern (phase contrast ×20). **B** Higher magnification (×40) shows well-represented perinuclear secretory granules and multiple nucleoli

Table 2 ID_{50} for 5-fluorouracil

Cell line	5-fluorouracil (μM)
MCC1	40.6 (*n*=4)
CFPAC1	227 (*n*=4)
PACA44	<2.7 (*n*=3)
PANC1	193 (*n*=4)

immunoreactivity for vimentin, chromogranin A, S100 and neuron-specific enolase. MUC-1 was expressed in both the cell line and the high-grade dysplasia/carcinoma cells of the primary lesion. Anti-p53 antibody stained the same cell populations as anti-MUC1. Conversely, p16 expression was lost in highly dysplastic cells. Dpc4 was expressed in both the cell line and all the cell components of the primary tumor sample. The absence of CK20 immunostaining is not surprising, as this marker has been reported to be present in only 5–20% of the cells within human pancreatic ductal adenocarcinomas, while CK9–19 was expressed in all the cells [12]. MUC2 did not stain either the cell line or the primary tumor.

Sensitivity to 5-FU

We evaluated the effect of 5-FU on MCC1 compared with the ductal adenocarcinoma cell lines PANC-1, CF-PAC1 and PACA 44. The doses of 5-FU ranged from 2.7 μM to 700 μM. The results are detailed in Table 2.

MCC1 grows in nu/nu mice

MCC1 cell suspension was injected subcutaneously in 14 nu/nu mice. All implants were successful. The cytological appearance of the xenografted cancers closely resembled that of the highly dysplastic areas of the primary tumor (Fig. 1).

Discussion

We report the establishment of MCC1, the first cell line obtained from a MCT of the pancreas. This cell line also grows in nu/nu mice. MCC1 can be considered a model for non-invasive MCC and is characterized by the expression of MUC1, mutational activation of the K-*RAS* gene, inactivation of *P53* and *P16* genes, and a wild-type *DPC4/SMAD4* gene.

MCC1 derives from a non-invasive MCC. In fact: (i) histological examination of the specular part of the sample used to obtain the cell line showed a noninvasive epithelium with variable degrees of dysplasia; (ii) extensive sampling of both the tumor and its capsule did not show any invasion, and no lymph-node metastasis was detected; (iii) the patient is alive and well 7 years after surgery in the absence of chemotherapy.

The origin of the MCC1 cell line from highly dysplastic cells of the primary tumor is demonstrated by both morphological and molecular data: (i) all 14 xenografts obtained from MCC1 were tumors composed of highly dysplastic cells; (ii) overexpression of MUC1 and inactivation of the *P53* and *P16* genes detected in MCC1 cell line were restricted to the highly dysplastic cells of the primary tumor, whose low dysplastic cells did not show these anomalies.

The morphological and molecular analysis of MCC1 and its corresponding primary tumor are consistent with a model for pancreatic non-invasive MCC, where K-*RAS*, *P16*, *P53* and MUC1 alterations are pre-invasive changes associated with progression of malignancy of MCT from adenoma to carcinoma. This model is also supported by the information available on primary MCTs, as K-*RAS* mutations have been found in 20% of MCA, *P53* inactivation in 50% of MCC, and *DPC4* loss has been suggested as a marker of invasive capability of MCC [3, 11].

In more detail, the molecular data on primary MCT is summarized as follows. K-*RAS* mutations have been reported to occur with increasing frequency along the malignant progression of MCT, occurring in 20% of benign, 33% of borderline and 89% of malignant MCTs [3, 11]. Seven MCC have been analyzed for *P16*, *P53* and *DPC4* aberrations, and all cases had alterations in at least one of these tumor suppressor genes [6]. Furthermore, the analysis of a large series of these tumors, including 22 MCA, 12 MCB and 22 MCC (16 invasive and 6 non-invasive), showed that immunohistochemical staining for p53 was detected in 11 cases, all of which were MCC, while all MCAs and MCBs were p53 negative. It is worthwhile noting that 10 of the 11 p53-positive cases were invasive MCCs, and the last was a non-invasive MCC. Interestingly, in the invasive MCCs, p53 staining was already present in the severely dysplastic non-invasive epithelium [24]. As p53-positive immunostaining in tumors is due to the accumulation of a protein with prolonged half-life due to gene mutation, it is highly probable that positively staining MCCs also harbor *P53* mutations. This is well demonstrated by our cell line, which has a point mutation in the *P53* gene and nuclear accumulation of the mutated p53 protein that parallels the immunostaining of the highly dysplastic area of the primary non-invasive MCC from which it was derived. Finally, *DPC4* has been studied by immunohistochemistry in 36 MCTs, including 23 adenomas, 1 borderline, 5 non-invasive carcinomas and 7 invasive carcinomas. In six of the seven invasive MCC, Dpc4 expression was lost in invasive foci, while non-invasive areas retained normal Dpc4 expression [10]. Taken together, all the molecular features described in primary MCT further strengthen the conclusion that MCC1 represents a model for non-invasive MCC.

Of interest, the observed pattern of aberrations including the mutation of K-*RAS*, *P53* and *P16* is similar to that observed in mucinous cystic ovarian tumors, consistent with the hypothesis that pancreatic MCT might arise from residual ovarian ectopic tissue [24]. In fact, in ovarian tumors, alterations in *P53* have been associated with the malignant phenotype, while mutations in *K-RAS* and *P16* have been correlated with mucinous differentiation [4, 5, 15].

The MCC1 cell line showed MUC1 expression as the highly dysplastic areas of the corresponding primary tumor. Only one study has reported on the expression of MUC apomucins in pancreatic MCT [14]. Non-invasive MCTs were reported to be MUC5AC positive and MUC1 negative. MUC1 expression was observed only in cases with an invasive component. The expression of MUC1 has also been associated with another type of mucinous tumor of the pancreas, namely intraductal papillary mucinous tumor, and in particular with highly dysplastic/carcinoma in situ and invasive components [1, 13, 23]. Expression of MUC1 has been found in various adenocarcinomas of distinct origin and shown to exert inhibitory effects on the immune response [2]. Expression of MUC1 apomucin has been reported in both ducts and acini of normal pancreas and is constantly expressed during the process of ductal neoplastic transformation, while MUC2 expression is not observed [20]. MUC2 is ectopically expressed by mucinous carcinomas of the colon, pancreas, breast and ovary [8], but its expression is restricted to goblet cells scattered within the epithelium of mucinous cystic neoplasms [14].

Of clinical interest, while surgery is the treatment of choice for patients with MCC, chemotherapy is necessary when spreading from the original site occurs. No indication regarding the optimal chemotherapeutic regimen active against MCCs is available. This fact reflects the rarity of the disease and the absence of in vitro and in vivo models that might help to select the most promising drugs or drug combinations suitable for clinical trials. MCC1 showed moderate to high sensitivity to 5-FU in vitro, when compared with pancreatic ductal carcinoma cell lines. This experiment represents, to our knowledge, the first direct assessment of drug sensitivity for MCCs. The capability of this cell line to grow as a xenograft also makes it a suitable model for pre-clinical studies.

Acknowledgements This work was supported by: Associazione Italiana Ricerca Cancro, Milan, Italy; Fondazione Cassa di Risparmio (Bando 2001), Verona, Italy; CNR-diagnostica molecolare, Ministero Università and Ministero Sanita', Rome, Italy; and European Community Grant QLG1-CT-2002–01196.

References

1. Adsay NV, Merati K, Basturk O, Iacobuzio-Donahue C, Levi E, Cheng JD, Sarkar FH, Hruban RH, Klimstra DS (2004) Pathologically and biologically distinct types of epithelium in intraductal papillary mucinous neoplasms: delineation of an "intestinal" pathway of carcinogenesis in the pancreas. Am J Surg Pathol 28:839–848
2. Agrawal B, Krantz MJ, Reddish MA, Longenecker BM (1998) Cancer-associated MUC1 mucin inhibits human T-cell proliferation, which is reversible by IL-2. Nat Med 4:43–49
3. Bartsch D, Bastian D, Barth P, Schudy A, Nies C, Kisker O, Wagner HJ, Rothmund M (1998) K-ras oncogene mutations indicate malignancy in cystic tumors of the pancreas. Ann Surg 228:79–86
4. Caduff RF, Svoboda-Newman SM, Ferguson AW, Johnston CM, Frank TS (1999) Comparison of mutations of Ki-RAS and p53 immunoreactivity in borderline and malignant epithelial ovarian tumors. Am J Surg Pathol 23:323–328
5. Fujita M, Enomoto T, Murata Y (2003) Genetic alterations in ovarian carcinoma: with specific reference to histological subtypes. Mol Cell Endocrinol 202:97–99
6. Gerdes B, Wild A, Wittenberg J, Barth P, Ramaswamy A, Kersting M, Luttges J, Kloppel G, Bartsch DK (2003) Tumor-suppressing pathways in cystic pancreatic tumors. Pancreas 26:42–48
7. Hahn SA, Bartsch D, Schroers A, Galehdari H, Becker M, Ramaswamy A, Schwarte-Waldhoff I, Maschek H, Schmiegel W (1998) Mutations of the DPC4/Smad4 gene in biliary tract carcinoma. Cancer Res 58:1124–1126
8. Hanski C, Hofmeier M, Schmitt-Graff A, Riede E, Hanski ML, Borchard F, Sieber E, Niedobitek F, Foss HD, Stein H, Riecken EO (1997) Overexpression or ectopic expression of MUC2 is the common property of mucinous carcinomas of the colon, pancreas, breast, and ovary. J Pathol 182:385–391
9. Herman JG, Graff JR, Myohanen S, Nelkin BD, Baylin SB (1996) Methylation-specific PCR: a novel PCR assay for methylation status of CpG islands. Proc Natl Acad Sci U S A 93:9821–9826
10. Iacobuzio-Donahue CA, Wilentz RE, Argani P, Yeo CJ, Cameron JL, Kern SE, Hruban RH (2000) Dpc4 protein in mucinous cystic neoplasms of the pancreas: frequent loss of expression in invasive carcinomas suggests a role in genetic progression. Am J Surg Pathol 24:1544–1548
11. Jimenez RE, Warshaw AL, Z'Graggen K, Hartwig W, Taylor DZ, Compton CC, Fernandez-del Castillo C (1999) Sequential accumulation of K-ras mutations and p53 overexpression in the progression of pancreatic mucinous cystic neoplasms to malignancy. Ann Surg 230:501–511
12. Jimenez RE, Z'Graggen K, Hartwig W, Graeme-Cook F, Warshaw AL, Fernandez-del Castillo C (1999) Immunohistochemical characterization of pancreatic tumors induced by dimethylbenzanthracene in rats. Am J Pathol 154:1223–1229
13. Luttges J, Zamboni G, Longnecker D, Kloppel G (2001) The immunohistochemical mucin expression pattern distinguishes different types of intraductal papillary mucinous neoplasms of the pancreas and determines their relationship to mucinous noncystic carcinoma and ductal adenocarcinoma. Am J Surg Pathol 25:942–948
14. Luttges J, Feyerabend B, Buchelt T, Pacena M, Kloppel G (2002) The mucin profile of noninvasive and invasive mucinous cystic neoplasms of the pancreas. Am J Surg Pathol 26:466–471
15. Milde-Langosch K, Ocon E, Becker G, Loning T (1998) p16/MTS1 inactivation in ovarian carcinomas: high frequency of reduced protein expression associated with hyper-methylation or mutation in endometrioid and mucinous tumors. Int J Cancer 79:61–65
16. Moore P, Sipos B, Orlandini S, Sorio C, Real F, Lemoine N, Gress T, Bassi C, Klöppel G, Kalthoff H, Löhr M, Scarpa A (2001) Genetic profile of 22 pancreatic carcinoma cell lines: analysis of K-ras, p53, p16 and DPC4/Smad4. Virchows Arch 439:798–802
17. Scarpa A, Capelli P, Zamboni G, Oda T, Mukai K, Bonetti F, Martignoni G, Iacono C, Serio G, Hirohashi S (1993) Neoplasia of the ampulla of Vater. Ki-ras and p53 mutations. Am J Pathol 142:1163–1172
18. Scarpa A, Zamboni G, Achille A, Capelli P, Bogina G, Iacono C, Serio G, Accolla RS (1994) Ras-family gene mutations in neoplasia of the ampulla of Vater. Int J Cancer 59:39–42
19. Sipos B, Moser S, Kalthoff H, Torok V, Lohr M, Kloppel G (2003) A comprehensive characterization of pancreatic ductal carcinoma cell lines: towards the establishment of an in vitro research platform. Virchows Arch 442:444–452
20. Terada T, Ohta T, Sasaki M, Nakanuma Y, Kim YS (1996) Expression of MUC apomucins in normal pancreas and pancreatic tumours. J Pathol 180:160–165
21. Wilentz RE, Albores-Saavedra J, Zahurak M, Talamini MA, Yeo CJ, Cameron JL, Hruban RH (1999) Pathologic examination accurately predicts prognosis in mucinous cystic neoplasms of the pancreas. Am J Surg Pathol 23:1320–1327

22. Wilentz RE, Albores-Saavedra J, Hruban RH (2000) Mucinous cystic neoplasms of the pancreas. Semin Diagn Pathol 17:31–42
23. Yonezawa S, Taira M, Osako M, Kubo M, Tanaka S, Sakoda K, Takao S, Aiko T, Yamamoto M, Irimura T, Kim YS, Sato E (1998) MUC-1 mucin expression in invasive areas of intraductal papillary mucinous tumors of the pancreas. Pathol Int 48:319–322
24. Zamboni G, Scarpa A, Bogina G, Iacono C, Bassi C, Talamini G, Sessa F, Capella C, Solcia E, Rickaert F, Mariuzzi GM, Kloppel G (1999) Mucinous cystic tumors of the pancreas: clinicopathological features, prognosis, and relationship to other mucinous cystic tumors. Am J Surg Pathol 23:410–422
25. Zamboni G, Klöppel G, Hruban R, Longnecker D, Adler G (2000) Mucinous cystic neoplasms of the pancreas. In: Hamilton S, Aaltonen L (eds) Tumours of the digestive system, 2nd edn. Oxford University Press, Berlin
26. Zhang SY, Klein-Szanto AJ, Sauter ER, Shafarenko M, Mitsunaga S, Nobori T, Carson DA, Ridge JA, Goodrow TL (1994) Higher frequency of alterations in the p16/CDKN2 gene in squamous cell carcinoma cell lines than in primary tumors of the head and neck. Cancer Res 54:5050–5053

Virchows Arch (2005) 446: 246–250
DOI 10.1007/s00428-004-1197-8

ORIGINAL ARTICLE

Naoki Kanomata · Tomoyuki Yokose · Tomoyuki Kamijo · Hiroyuki Yonou · Takahiro Hasebe · Naoki Itano · Koji Kimata · Atsushi Ochiai

Hyaluronan synthase expression in pleural malignant mesotheliomas

Received: 28 June 2004 / Accepted: 6 December 2004 / Published online: 25 February 2005
© Springer-Verlag 2005

Abstract Hyaluronan (HA) is thought to play several important roles in tumor growth, tumorigenicity, and tumor dissemination and metastasis. Recently, three isoforms of hyaluronan synthase (HAS) have been cloned. Our objective was to determine which of the HAS isoforms were expressed in pleural malignant mesotheliomas, the most representative lesion of HA-producing tumors. We studied 10 cases of pleural malignant mesothelioma using novel antibodies of HAS. We compared HAS expression patterns of mesothelioma and pulmonary adenocarcinoma. Immunohistochemically, 9 of 10 (90%) cases of mesothelioma had extensive reaction to anti-HAS1 and anti-HAS2 antibodies, while HAS3 overexpression was present in 4 of 10 cases (40%). Of 20 cases of pulmonary adenocarcinoma, 5 overexpressed HAS1 (25%), 16 of 20 HAS2 (80%), and 4 of 20 HAS3 (20%). The expression level of HAS1 was significantly higher in mesotheliomas than in pulmonary adenocarcinoma (P=0.0036). Our data suggests that HAS1 might be a useful positive marker of malignant mesothelioma. However, a definitive conclusion should be based on further large-scale studies.

Keywords Hyaluronan synthase · Hyaluronan · Malignant mesothelioma · Adenocarcinoma · Immunohistochemistry

N. Kanomata · T. Yokose · T. Kamijo · H. Yonou · T. Hasebe · A. Ochiai (✉)
Pathology Division, National Cancer Center Research Institute East,
6-5-1 Kashiwanoha,
277-8577 Kashiwa, Chiba, Japan
e-mail: aochiai@east.ncc.go.jp
Tel.: +81-4-71346855
Fax: +81-4-71346865

N. Itano · K. Kimata
Institute for Molecular Science of Medicine
Aichi Medical University,
Japan

Introduction

Increasing evidence suggests that hyaluronan (hyaluronic acid, HA) plays several important roles in tumor growth, tumorigenicity, and tumor dissemination and metastasis in various tumors [14, 15, 22, 29, 33]. For example, the overexpression of hyaluronan synthases (HASs) makes tumor cells more aggressive [10, 12, 16, 18]. Furthermore, the administration of sodium HA enhances the metastatic potential of tumor cells [26]. In pleural malignant mesotheliomas, the concentration of HA is often elevated in the pleural fluid, and highly elevated HA has been considered a useful tumor marker [8, 19–21, 23, 24, 27]. HA has been reported to increase the malignant properties of mesothelioma cells [17]. Human hyaluronan synthases have been recently cloned [11, 25, 30]; however, the isoform expression of HAS in mesothelioma has not yet been studied in clinical specimens. We examined pleural mesotheliomas using newly developed anti-HAS antibodies and immunohistochemistry. The HAS expression pattern of mesotheliomas was compared with the pattern of pulmonary adenocarcinomas and discussed.

Materials and methods

We identified 10 cases of pleural malignant mesothelioma; from all, histological paraffin-block specimens were available. The cases came from the pathology files of Matsudo National Hospital and from the National Cancer Center Hospital East. The patients' hospital charts were reviewed to obtain clinical information. We reviewed gross photography, photocopies, hematoxylin and eosin slides, and special staining and immunostaining slides for each case and confirmed that all of the 10 cases met the criteria of malignant mesothelioma [4, 6, 9]. We also extracted paraffin blocks of 20 consecutive cases of pulmonary adenocarcinoma.

HA staining was performed according to a previously described method [33], with minor modifications. After deparaffinization and hydration, endogenous peroxidase activity was quenched by a 30-min incubation in 0.3%

Table 1 Clinicopathological findings of theten mesotheliomas. *N/A* not available, *HABP* biotinylated hyaluronate-binding probe, *HAS* hyaluronan synthase, *NED* no evidence of disease, *DOD* dead of disease, *AWD* alive with disease

Case no.	Age (years)	Hyaluronan in pleural fluid (mg/l)	Histology	Specimen	HABP	HAS1	HAS2	HAS3	Follow-up
1	63	N/A	Epithelioid	Pleuro-pneumonectomy	−	1+	4+	−	Lost
2	68	N/A	Epithelioid	Pleuro-pneumonectomy	−	4+	4+	−	NED 75 months
3	48	79	Epithelioid	Pleuro-pneumonectomy	−	3+	3+	2+	Lost
4	66	26	Sacomatoid	Pleuro-pneumonectomy	4+	4+	3+	2+	NED 51 months
5	52	240	Epithelioid	Pleuro-pneumonectomy	3+	4+	4+	1+	DOD 10 months
6	54	1170	Epithelioid	Pleuro-pneumonectomy	4+	4+	4+	3+	DOD 57 months
7	70	N/A	Epithelioid	Needle biopsy	4+	4+	4+	4+	DOD 1 month
8	61	54	Epithelioid	Needle biopsy	1+	3+	4+	4+	DOD 3 months
9	49	N/A	Epithelioid	Needle biopsy	–	4+	4+	–	AWD 4 months
10	54	247	Epithelioid	Needle biopsy	2+	4+	2+	3+	AWD 2 months

hydrogen peroxide in methanol. Following incubation in 10% bovine serum albumin for 10 min, the sections were incubated with a biotinylated hyaluronate-binding probe (1:500; SKK, Nagoya, Japan) for 1 h at room temperature. After the specimens were thoroughly washed in phosphate buffered saline, peroxidase-labeled streptavidin (Dako, Glostrup, Denmark) was applied for 30 min. The chromogen used was 3, 3′-diaminobenzidine tetrahydrochloride (DAB) (Dojindo, Kumamoto, Japan). The specificity of the biotinylated probe was studied using control sections treated with streptomyces hyaluronidase (Seikagaku Corp., Tokyo, Japan), 10 TRU/ml in 0.1 M phosphate buffer, pH 5.0, containing 0.15 M sodium chloride, 1 mM ethylene diamine tetraacetate, 1 mM iodoacetic acid, 1 mM phenylmethylsulfonyl fluoride, and 1 μg/ml pepstatin A at 37°C for 30 min prior to applying the probe. Sections without the probe also acted as negative controls.

The polyclonal antibodies to HAS1, HAS2, and HAS3 were raised in rabbits by subcutaneous injection of the synthetic peptides: VRRLCRRRSGGTRVGV, corresponding to amino acids 568–582 of HAS1; CGRRKKGQQY DMVLDV, corresponding to the amino acids 537–552 of HAS2; and CGKKPEQYSLAFAEV, corresponding to amino acids 541–555 of HAS3, which had been coupled to keyhole limpet hemacyanin. The specificity of the purified antibodies has been confirmed [28].

Immunostaining was performed using the LSAB2 peroxidase kit (Dako). To enhance the immunostaining, 10 min proteinase K (0.4 mg/ml, Dako) digestion was performed for the anti-HAS1 and anti-HAS3 antibodies. Microwave antigen retrieval in the Target Retrieval Solution (Dako) was employed for the anti-HAS2 (95°C, 20 min). The sections were incubated for 16 h at 4°C with the antibodies diluted to 25 μg/ml, respectively. The chromogen was DAB. Sections without primary antibodies were used as negative controls.

Results of HA staining and immunostaining were reported as follows: −, <1% reactivity; 1+, 1–25%; 2+, 26–50%; 3+, 51–75%; and 4+, 76–100%. For the immunostaining of HAS, 3+ and 4+ were defined as overexpression.

Statistical analysis was performed using StatView version 5.0 (SAS Institute Inc., Cary, NC, USA). Differences were analyzed using the Mann–Whitney U-test. A value of $P<0.05$ was considered statistically significant. All tests were two-tailed.

Results

The clinical characteristics, histological findings, HA staining, and immunohistochemistry results of the ten mesothelioma patients are summarized in Table 1. The patients consisted of nine men and one woman, with ages ranging from 48 years to 70 years (mean, 59 years). One patient (case 8) had an apparent history of occupational exposure to asbestos. The pleural hyaluronate concentration as measured using enzyme-linked immunosorbent assay (ELISA) was known in six patients, ranging from 26 mg/l to 1160 mg/l (mean, 303 mg/l).

HA staining was varyingly positive in fibroblasts, muscle, endothelium, and adipose tissue. Of ten mesothelioma cases, six (60%) showed membranous and/or cytoplasmic staining on application of the biotinylated HA-binding

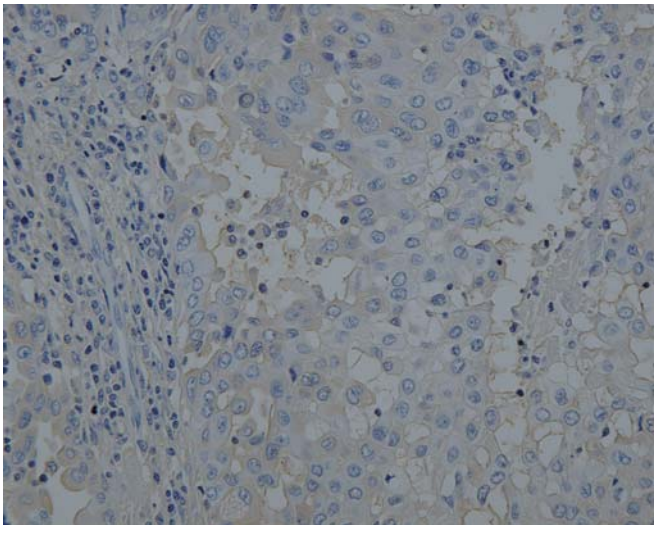

Fig. 1 Epithelioid mesothelioma (case 5) showing membranous and cytoplamic staining of the biotinylated hyaluronate-binding probe

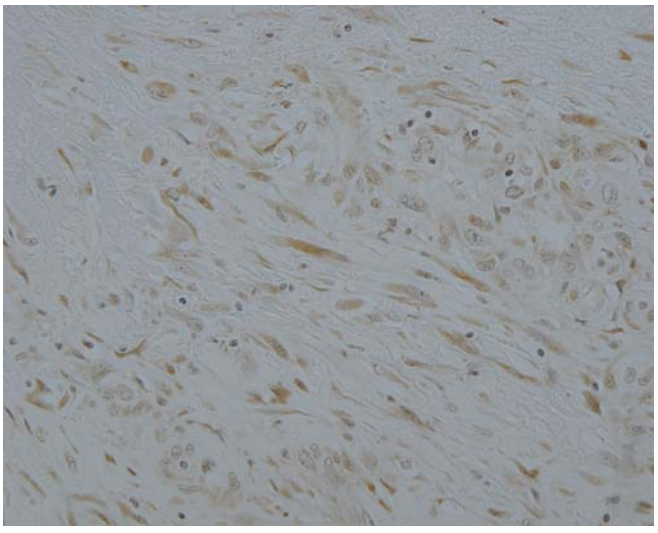

Fig. 2 Hyaluronan synthase 1 immunoreactivity in a sarcomatoid mesothelioma (case 4)

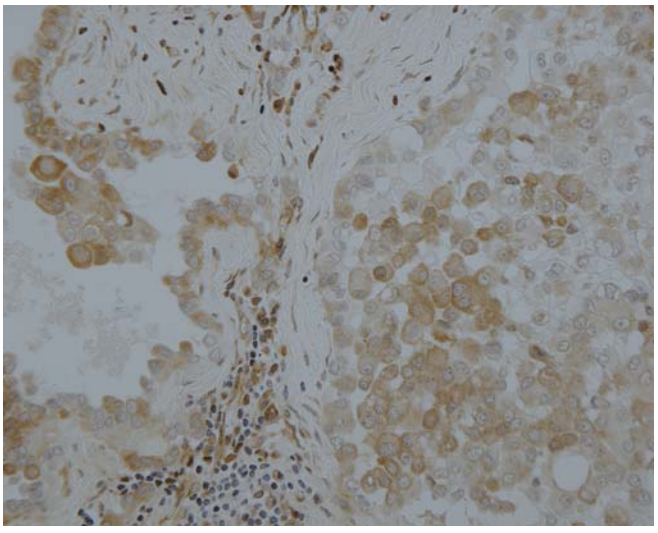

Fig. 4 Hyaluronan synthase 3 immunoreactivity in an epithelioid mesothelioma (case 6)

probe (Fig. 1), and the reaction disappeared with hyaluronidase digestion.

The immunohistochemical findings revealed that the bronchial epithelium and bronchial submucosal glands uniformly reacted to all anti-HAS antibodies, whereas the expression in other reactive/non-neoplastic tissues was variable. Nine of ten cases (90%) of mesothelioma had an extensive cytoplasmic reaction to anti-HAS1 and anti-HAS2 antibodies (Fig. 2, Fig. 3). HAS3 overexpression was present in four of ten mesotheliomas (40%) (Fig. 4). Other clinicopathological findings, including the HA concentration in the pleural fluid, did not correlate with the results for HA staining or HAS immunostaining.

Of the 20 cases of pulmonary adenocarcinoma, 5 overexpressed HAS1 (25%), 16 of 20 HAS2 (80%), and 4 of 20 HAS3 (20%) (Table 2). The expression level of HAS1 was significantly higher in mesotheliomas than in pulmonary adenocarcinomas (P=0.0036, Table 3), whereas HAS2 and

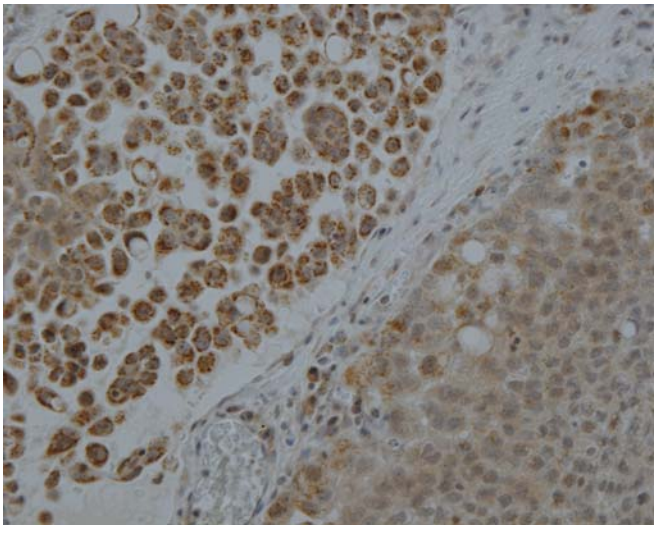

Fig. 3 Intense granular cytoplasmic expression of hyaluronan synthase 2 in an epithelioid mesothelioma (case 3)

Table 2 Hyaluronan synthase (HAS) expression in plumonary adenocarcinomas

Case no.	HAS1	HAS2	HAS3
1	1+	4+	1+
2	1+	4+	2+
3	2+	4+	1+
4	1+	3+	2+
5	3+	4+	4+
6	1+	4+	2+
7	−	2+	1+
8	4+	4+	3+
9	−	3+	−
10	4+	4+	2+
11	1+	4+	1+
12	−	2+	1+
13	−	2+	−
14	2+	3+	1+
15	4+	4+	4+
16	4+	4+	3+
17	−	4+	−
18	1+	2+	−
19	−	3+	−
20	1+	4+	1+

Table 3 Comparison of hyaluronan synthase (HAS) expression between mesotheliomas and adenocarcinomas

	HAS1	HAS2	HAS3
Mesothelioma	3.40±0.97	3.60±0.70	1.90±1.60
Adenocarcinoma	1.50±1.50	3.40±0.82	1.45±1.28
P value	0.0036*	0.5378	0.4703

*P<0.05

HAS3 expression level did not differ significantly between the mesotheliomas and the adenocarcinomas (P=0.5378 for HAS2, P=0.4703 for HAS3).

Discussion

Malignant mesotheliomas are known to produce HA [3–5, 8, 19–21, 23, 24, 27, 31]. Most previous HA studies on mesotheliomas have had only diagnostic objectives. As far as we know, no previous reports have examined the presence of HAS using clinical mesothelioma specimens, and only two articles using cell lines are available on this subject. Dobra et al. [7] reported that both epithelioid and fibroblast-like mesothelioma cell lines exhibited HAS1 mRNA expression, and Li and Heldin [17] reported that HAS2-transfected Mero-25 cells exhibited more anchorage independence and cell motility. Thus, the study of HAS expression in clinical material is meaningful.

In the present study, diffuse mesotheliomas, including a sarcomatoid case (case 4), had extensive HAS expression. Using semiquantitative reverse-transcriptase polymerase chain reaction methods, the fibroblast-like mesothelioma cell has been reported to have a smaller amount of HAS1 RNA than the epithelioid mesothelioma cell [7]. Our immunohistochemistry is likely to have good sensitivity for the detection of HAS, even in the sarcomatoid mesothelioma case.

Conventional histochemistry and HA-binding probe studies have shown that mesothelioma cells were most probably the main source of HA in mesothelioma patients [2, 5, 13]. However, Asplund et al. [1], in their in vitro study, claimed that mesothelioma cells produced only a minute amount of HA, whereas normal mesothelial cells and fibroblasts synthesized large quantities of HA. Our immunohistochemical study showed that the HAS expression in mesothelioma cells is striking and that it was greater or at least equal to the surrounding tissue. This suggests mesothelioma cells are the main source of HA in vivo in mesothelioma patients. HAS1 and HAS2 overexpression was present in 90% of the mesothelioma cases, while HAS3 expression was rather limited (four of ten, 40%). HAS1 and HAS2 are considered crucial for mesothelioma.

The pulmonary adenocarcinomas had lower expression of HAS1 than the mesotheliomas, whereas the adenocarcinomas expressed HAS2 and HAS3 at similar levels to the mesotheliomas. These findings suggest that HAS1 might be a useful marker in distinguishing mesothelioma from pulmonary adenocarcinoma. HAS1 might be the factor most responsible for massive pleural effusion in mesothelioma. However, the present study was limited in scale and lacked a variety of tumors, and a definitive conclusion on the usefulness of HAS1 as a marker should be based on further large-scale studies. The elevated mRNA for the HAS1 gene was reported to correlate with poor prognosis of colon cancer [32]. Immunohistochemical study of HAS expression, including in non-pulmonary carcinomas, would therefore be valuable.

We showed that HAS expression is evident in mesothelioma cells. Antibody therapy against HAS and/or antisense therapy using HAS genes could be used in the treatment of mesothelioma patients, and, even if they fail to produce a cure, at least they would work to control the troublesome pleural effusion produced by this fatal tumor.

This is just the beginning of the study of this fascinating enzyme and mesotheliomas. Further expansive studies of HAS using immunohistochemistry and quantitative methods such as ELISA in various tumors and benign/reactive disease will be valuable.

Acknowledgements This work was supported in part by a Grant-in-Aid for Cancer Research from the Ministry of Health, Labour and Welfare and by a Grant-in Aid for Second Term Comprehensive 10-Year Strategy for Cancer Control from the Ministry of Health, Labour and Welfare in Japan. N. K., T. K., and H. Y. are recipients of Research Resident Fellowships from the Foundation for Promotion of Cancer Research, Tokyo.

References

1. Asplund T, Versnel MA, Laurent TC, Heldin P (1993) Human mesothelioma cells produce factors that stimulate the production of hyaluronan by mesothelial cells and fibroblasts. Cancer Res 53:388–392
2. Azumi N, Underhill CB, Kagan E, Sheibani K (1992) A novel biotinylated probe specific for hyaluronate. Its diagnostic value in diffuse malignant mesothelioma. Am J Surg Pathol 16:116–121
3. Battifora H (1999) The pleura. In: Sternberg SS (ed) Diagnostic surgical pathology. Lippincott Williams and Wilkins, Philadelphia, pp 1117–1145
4. Battifora H, McCaughey WTE (1995) Tumors of the serosal membranes. Atlas of tumor pathology. Armed Forces Institute of Pathology, Washington, DC
5. Benjamin CJ, Ritchie AC (1982) Histological staining for the diagnosis of mesothelioma. Am J Med Technol 48:905–908
6. Churg A, Colby TV, Cagle P, Corson J, Gibbs AR, Gilks B, Grimes M, Hammar S, Roggli V, Travis WD (2000) The separation of benign and malignant mesothelial proliferations. Am J Surg Pathol 24:1183–1200
7. Dobra K, Andang M, Syrokou A, Karamanos NK, Hjerpe A (2000) Differentiation of mesothelioma cells is influenced by the expression of proteoglycans. Exp Cell Res 258:12–22
8. Harington JS, Wargner JC, Smith M (1963) The detection of hyaluronic acid in pleural fluids of cases with diffuse pleural mesotheliomas. Br J Exp Pathol 44:81–83
9. Henderson DW, Shilkin KB, Whitaker D (1998) Reactive mesothelial hyperplasia vs mesothelioma, including mesothelioma in situ: a brief review. Am J Clin Pathol 110:397–404
10. Ichikawa T, Itano N, Sawai T, Kimata K, Koganehira Y, Saida T, Taniguchi S (1999) Increased synthesis of hyaluronate enhances motility of human melanoma cells. J Invest Dermatol 113:935–939
11. Itano N, Kimata K (1996) Molecular cloning of human hyaluronan synthase. Biochem Biophys Res Commun 222:816–820
12. Itano N, Sawai T, Miyaishi O, Kimata K (1999) Relationship between hyaluronan production and metastatic potential of mouse mammary carcinoma cells. Cancer Res 59:2499–2504
13. Kannerstein M, Churg J, Magner D (1973) Histochemistry in the diagnosis of malignant mesothelioma. Ann Clin Lab Sci 3:207–211
14. Kimata K, Honma Y, Okayama M, Oguri K, Hozumi M, Suzuki S (1983) Increased synthesis of hyaluronic acid by mouse mammary carcinoma cell variants with high metastatic potential. Cancer Res 43:1347–1354

15. Knudson W (1996) Tumor-associated hyaluronan. Providing an extracellular matrix that facilitates invasion. Am J Pathol 148: 1721–1726
16. Kosaki R, Watanabe K, Yamaguchi Y (1999) Overproduction of hyaluronan by expression of the hyaluronan synthase Has2 enhances anchorage-independent growth and tumorigenicity. Cancer Res 59:1141–1145
17. Li Y, Heldin P (2001) Hyaluronan production increases the malignant properties of mesothelioma cells. Br J Cancer 85:600–607
18. Liu N, Gao F, Han Z, Xu X, Underhill CB, Zhang L (2001) Hyaluronan synthase 3 overexpression promotes the growth of TSU prostate cancer cells. Cancer Res 61:5207–5214
19. Martensson G, Thylen A, Lindquist U, Hjerpe A (1994) The sensitivity of hyaluronan analysis of pleural fluid from patients with malignant mesothelioma and a comparison of different methods. Cancer 73:1406–1410
20. Meyer K, Chaffee E (1939) Hyaluronic acid in pleural fluid associated with malignant tumor involving pleura and peritoneum. Proc Soc Exp Biol Med 42:797–800
21. Nurminen M, Dejmek A, Martensson G, Thylen A, Hjerpe A (1994) Clinical utility of liquid-chromatographic analysis of effusions for hyaluronate content. Clin Chem 40:777–780
22. Peterson RM, Yu Q, Stamenkovic I, Toole BP (2000) Perturbation of hyaluronan interactions by soluble CD44 inhibits growth of murine mammary carcinoma cells in ascites. Am J Pathol 156: 2159–2167
23. Pettersson T, Froseth B, Riska H, Klockars M (1988) Concentration of hyaluronic acid in pleural fluid as a diagnostic aid for malignant mesothelioma. Chest 94:1037–1039
24. Roboz J, Greaves J, Silides D, Chahinian AP, Holland JF (1985) Hyaluronic acid content of effusions as a diagnostic aid for malignant mesothelioma. Cancer Res 45:1850–1854
25. Shyjan AM, Heldin P, Butcher EC, Yoshino T, Briskin MJ (1996) Functional cloning of the cDNA for a human hyaluronan synthase. J Biol Chem 271:23395–23399
26. Tan B, Wang JH, Wu QD, Kirwan WO, Redmond HP (2001) Sodium hyaluronate enhances colorectal tumour cell metastatic potential in vitro and in vivo. Br J Surg 88:246–250
27. Thompson ME, Bromberg PA, Amenta JS (1969) Acid mucopolysaccharide determination. A useful adjunct for the diagnosis of malignant mesothelioma with effusion. Am J Clin Pathol 52: 335–339
28. Tominaga A, Tajima S, Ishibashi A, Kimata K (2001) Reticular erythematous mucinosis syndrome with an infiltration of factor XIIIa+ and hyaluronan synthase 2+ dermal dendrocytes. Br J Dermatol 145:141–145
29. Turley EA, Tretiak M (1985) Glycosaminoglycan production by murine melanoma variants in vivo and in vitro. Cancer Res 45:5098–5105
30. Watanabe K, Yamaguchi Y (1996) Molecular identification of a putative human hyaluronan synthase. J Biol Chem 271:22945–22948
31. Waxler B, Eisenstein R, Battifora H (1979) Electrophoresis of tissue glycosaminoglycans as an aid in the diagnosis of mesotheliomas. Cancer 44:221–227
32. Yamada Y, Itano N, Narimatsu H, Kudo T, Morozumi K, Hirohashi S, Ochiai A, Ueda M, Kimata K (2004) Elevated transcript level of hyaluronan synthase1 gene correlates with poor prognosis of human colon cancer. Clin Exp Metastasis 21:57–63
33. Zhang L, Underhill CB, Chen L (1995) Hyaluronan on the surface of tumor cells is correlated with metastatic behavior. Cancer Res 55:428–433

Virchows Arch (2005) 446: 251–258
DOI 10.1007/s00428-004-1190-2

ORIGINAL ARTICLE

Muna Sabah · Robert Cummins · Mary Leader · Elaine Kay

Leiomyosarcoma and malignant fibrous histiocytoma share similar allelic imbalance pattern at 9p

Received: 23 November 2004 / Accepted: 28 November 2004 / Published online: 25 February 2005
© Springer-Verlag 2005

Abstract Formalin-fixed, paraffin-embedded tissue from 45 soft tissue sarcomas was analysed for allelic imbalance/loss of heterozygosity (AI/LOH) of chromosome 9. The specimens consisted of 17 cases of soft tissue leiomyosarcoma (LMS), 4 cases of cutaneous LMS, 22 cases of conventional malignant fibrous histiocytoma (MFH) and 2 cases of angiomatoid fibrous histiocytoma. All cases were categorised morphologically and immunohistochemically. DNA was microdissected from normal and neoplastic tissues. AI/LOH was performed using six microsatellite markers on the 9p region. The frequency of allelic imbalance at different loci on chromosome 9p was analysed in LMS and MFH and then compared with values previously examined in synovial sarcoma and malignant peripheral nerve sheath tumour. Although AI/LOH and microsatellite instability (MSI) were more frequent in MFH, LMS and MFH groups showed similar patterns of allelic imbalance at the 9p region. Alterations of chromosome 9p have been reported in many cell lines and tumours including LMS and MFH. 9p21 region encodes $p16^{INK4A}$ and $p15^{INK4B}$. Allelic imbalance observed at 9p 21 in this study suggests that alterations of the negative cell cycle regulators may be an important step in the pathogenesis of MFH and LMS. However, the most frequent allelic imbalance was observed at 9p24 at D9S230. Alterations of this locus were very rare in synovial sarcoma and malignant peripheral nerve sheath tumours and were absent in cutaneous LMS and angiomatoid fibrous histiocytoma. This locus may point to the existence of a genetically altered tumour suppressor gene involved in the pathogenesis of LMS and MFH. Our results support the hypothesis that MFHs may represent a morphological pathway in tumour progression of LMSs.

Keywords Leiomyosarcoma · Malignant fibrous histiocytoma · Loss of heterozygosity · Chromosome 9 · Allelic imbalance · D9S230

M. Sabah · R. Cummins · M. Leader · E. Kay
Department of Histopathology, Beaumont Hospital and Royal College of Surgeons in Ireland, Dublin

M. Sabah (✉)
Department of Histopathology, Education and Research Centre, The Royal College of Surgeons in Ireland, Beaumont Hospital, Dublin 9
e-mail: munasabah@eircom.net
Tel.: +353-1-8092541
Fax: +353-1-8093720

Introduction

Leiomyosarcoma (LMS) is a relatively common neoplasm of adult life. It includes tumours of uterine, gastrointestinal, soft tissue and cutaneous origin. Cutaneous LMS has a better prognosis than LMS of soft tissue.

For many years, malignant fibrous histiocytoma (MFH) has been regarded as the most common type of soft tissue sarcoma of late adulthood. The latest World Health Organization classification of soft tissue tumours [10] regards MFH as a synonym for undifferentiated sarcomas and, therefore, the diagnosis of MFH has become a diagnosis of exclusion and is reserved for tumours showing no other line of differentiation. This study was carried out to determine and compare the frequency of allelic imbalance at different loci on chromosome 9p in LMS and MFH. This chromosomal region is frequently targeted during malignant transformation as it contains at least two known tumour suppressor genes $p16^{INK4A}$ [15, 24] and $p15^{INK4B}$[12, 21]. Both genes are located at 9p21 and encode nuclear proteins that have been shown to block cell cycle progression at the G1-S transition.

The aim of this study was to examine the frequency of allelic imbalance at 9p and to compare the pattern of allelic imbalance with that previously identified in synovial sarcomas and malignant peripheral nerve sheath tumours.

Materials and methods

Tissue samples and pathological analysis

Included in the study were 22 cases of formalin-fixed, paraffin-embedded MFH, 2 cases of angiomatoid fibrous histiocytoma and 21 cases of extra-uterine, extra-gastro-intestinal LMS including four cases of LMS of skin. The diagnosis in each case was based on standard histological and immunohistochemical features and was reviewed by the Dublin Soft Tissue Tumour Panel. The cases were graded according to the FNCLCC scoring system [26].

A summary of number of cases, histological type and tumour grade is outlined in Table 1 and Table 2 for LMS and MFH, respectively.

DNA microdissection

Two parallel, 8-μm thick sections were de-waxed in xylene, rehydrated through various alcohol grades, rinsed well in distilled water and finally stained with haematoxylin. Using the haematoxylin and eosin sections as a template, normal and tumour areas were microdissected under a stereomicroscope. Multiple areas of the tumour were sampled.

Genomic DNA extraction

Proteinase K solution [60 μl; 20 mg/ml proteinase K (Roche Diagnostics, Mannheim) in 50 mM Tris HCl pH 7.4, 0.1 mM ethylene diamine tetraacetic acid (EDTA), 1% Tween] was added to normal and tumour tissue pellets which were then digested at 55°C for 72 h.

Table 1. LMS cases, histological type and tumour grade

Case no.	Histological type	Grade
1	Conventional	Low grade
2	Conventional	Intermediate grade
3	Conventional	Intermediate grade
4	Conventional	Intermediate grade
5	Conventional	Intermediate grade
6	Conventional	High grade
7	Conventional	High grade
8	Conventional	High grade
9	Conventional	High grade
10	Conventional	High grade
11	Conventional	High grade
12	Conventional	High grade
13	Conventional	High grade
14	Pleomorphic	High grade
15	Pleomorphic	High grade
16	Pleomorphic	High grade
17	Pleomorphic	High grade
18	LMS of skin	Intermediate grade
19	LMS of skin	Intermediate grade
20	LMS of skin	Intermediate grade
21	LMS of skin	Intermediate grade

Table 2. MFH cases, histological type and tumour grade

Case no.	Histological type	Grade
1	Angiomatoid fibrous histiocytoma	Low grade
2	Angiomatoid fibrous histiocytoma	Low grade
3	Storiform	Intermediate grade
4	Storiform	Intermediate grade
5	Storiform	Intermediate grade
6	Storiform	Intermediate grade
7	Storiform	Intermediate grade
8	Storiform	Intermediate grade
9	Storiform	High grade
10	Storiform	High grade
11	Storiform	High grade
12	Storiform	High grade
13	Storiform	High grade
14	Storiform	Intermediate grade
15	Storiform	Intermediate grade
16	Storiform	Intermediate grade
17	Storiform	High grade
18	Storiform	High grade
19	Storiform	High grade
20	Storiform	High grade
21	Storiform	High grade
22	Inflammatory MFH	High grade
23	Inflammatory MFH	High grade
24	Giant cell MFH	High grade

Polymerase chain reaction amplification

Six fluorescent Cy5 end-labelled microsatellite markers that map to the 9p region were used. Four markers map to 9p21—D9S916, D9S1814, D9S974 and D9S942. The latter two are within the coding sequence of $p16^{INK4A}$. D9S916 is telomeric to $p16^{INK4A}$and $p15^{INK4B}$, whereas D9S1814 is centromeric to $p15^{INK4B}$. D9S171 is at 9p13 (proximal to $p16^{INK4A}$ and $p15^{INK4B}$). D9S230 is at 9p24.

Polymerase chain reaction (PCR) amplifications were performed in a final volume of 20 μl and consisted of 1×PCR reaction buffer, 200 μM dNTPs, 1 mM $MgCl_2$(Promega, Madison, WI), 2 pmol Cy5-labelled forward and reverse primers (TAGN, Newcastle) and 1 μl sample DNA digest. After denaturation at 95°C for 5 min, 2 μl *Taq* (1 U/μl) (Promega, Madison, WI) was added at 80°C. A touchdown PCR was then carried out consisting of two cycles at 95°C for 1 min, 1 min at an initial annealing temperature (Table 3), and 72°C for 1 min. Subsequent steps consisted of two cycles each with annealing temperatures reduced by 2°C until 30 cycles were carried out at the final annealing temperature. A final extension step at 72°C for 10 min completed the reactions. Following PCR, 5-μl PCR products mixed with agarose loading dye were electrophoresed through 12% polyacrylamide mini gels. The DNA fragments were

Table 3. Primer sequence, PCR product size and annealing temperatures used in touchdown PCR for each primer

Marker	Primer sequence	Initial annealing temperature (°C)	Final annealing temperature (°C)	PCR product size (bp)
D9S230	Forward 5′-acaggtcaccacccttcaac-3′ Reverse 5′-acaggagaagagctgaggca-3′	65	59	190–207
D9S916	Forward 5′-gatgtccagttgtcccttcataa-3′ Reverse 5′-atagactgccaaatttttggacc-3′	61	55	165–185
D9S974	Forward 5′-cctggtctggatcataaaatgaa-3′ Reverse 5′-tgtggaaattttctgtctggttc-3′	61	55	180–207
D9S942	Forward 5′-aagcaagattccaaacagtaaaca-3′ Reverse 5′-ttcgtttcacttttgagttttcc-3′	59	53	155–180
D9S1814	Forward 5′-tgtcagtggtatttacctttttgg-3′ Reverse 5′-cagaaggtcagtaggttcacagg-3′	61	55	160–180
D9S171	Forward 5′-agctaagtgaacctcatctctg-3′ Reverse 5′-tgattgttaataaagtagcccc-3′	59	53	112–131

visualised by means of ethidium bromide staining under ultraviolet light.

Allelic imbalance/loss of heterozygosity assay

The PCR products were diluted in distilled water, mixed with Cy5.5-labelled DNA size ladder and then analysed on an OpenGene analyser (Visible Genetics, Toronto, Ontario). Allelic ratios in both normal and tumour samples were calculated and compared. The area under each peak, representing each allele in the microsatellite pair, was obtained using the GeneObjects Fragment Analysis Tool, and an allele ratio was calculated by dividing the area under the larger peak by the area under the smaller peak in each of the normal and tumour DNA samples. A ratio of ratios between the normal and tumour PCR products was calculated to give an overall allele ratio. The cut-off value for allelic imbalance/loss of heterozygosity (AI/LOH) was 0.74, as was previously published from studies in our laboratory [1, 22, 24]. Microsatellite instability (MSI) was defined as the presence of novel alleles or extra peaks in the tumour DNA sample not seen in the normal DNA.

In questionable cases, the PCR amplification and AI/LOH analysis were repeated to ensure consistency in the results.

Results

Clinicopathological features

LMS of soft tissue (17 of 21) were morphologically classified into conventional (13 cases) (Fig. 1A) and pleomorphic type (4 cases). All cases of pleomorphic type were high-grade sarcomas. Conventional LMS cases consisted

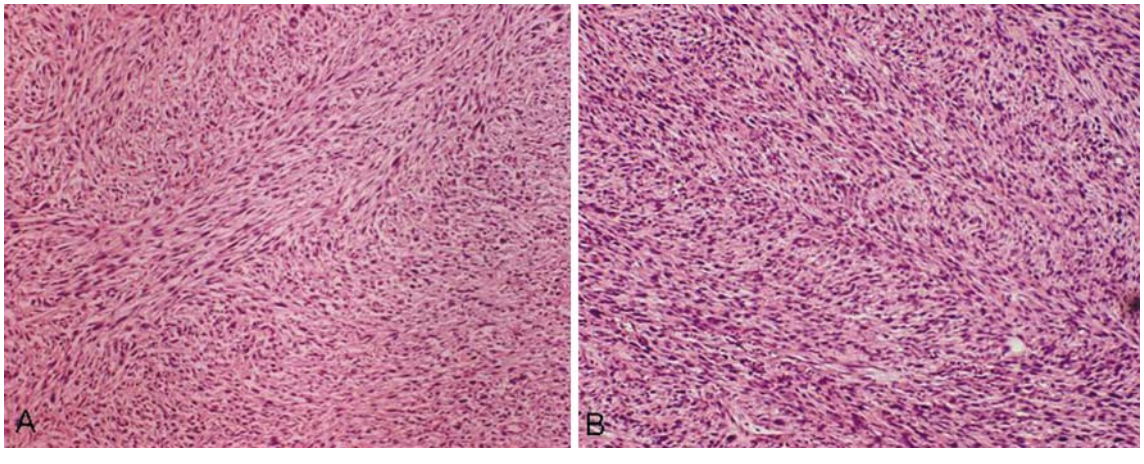

Fig. 1 Haematoxylin and eosin of conventional soft tissue leiomyosarcoma (LMS; **A**) and storiform malignant fibrous histiocytoma (MFH; **B**). Original magnification ×100

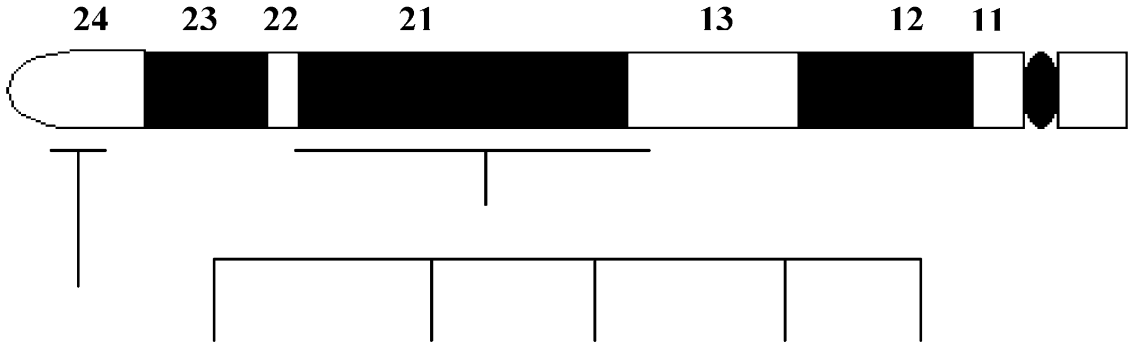

LMS	D9S230	D9S916	D9S974	D9S942	D9S1814	D9S171
Case 1	⊘	○	⊘	○	●	○
Case 2	●	●	●	●	⊘	●
Case 3	⊘	⊘	⊘	⊘	●	○
Case 4	⊘	●	⊘	○	○	○
Case 5	●	●	⊘	●	⊘	●
Case 6	●	●	●	●	⊘	○
Case 7	⊘MSI	⊘	●	○	○	●
Case 8	⊘	●	○	○	⊘	⊘
Case 9	●	○	⊘	●	○	⊘
Case 10	●	○	⊘	●	○	⊘
Case 11	⊘	●	○	⊘	●	○
Case 12	⊘	●	⊘	●	⊘	●
Case 13	●	●	⊘	●	⊘	○
Case 14	●	●	●	●	⊘	●
Case 15	●	○	○	⊘	○	○
Case 16	●	○	○	⊘	○	○
Case 17	●	●	○	⊘	●	●
Case 18	○	○	⊘	⊘	⊘	●
Case 19	⊘	○	●	●	⊘	○
Case 20	○	⊘	●	○	⊘	○
Case 21	⊘	⊘	⊘	●	⊘	⊘

Fig. 2 Microsatellite map of allelic imbalance/loss of heterozygosity (AI/LOH) of 9p for leiomyosarcoma (LMS), with tabulated results. *Filled circle* AI/LOH, *open circle* no AI/LOH, *strike-through circle* uninformative (homozygosity)

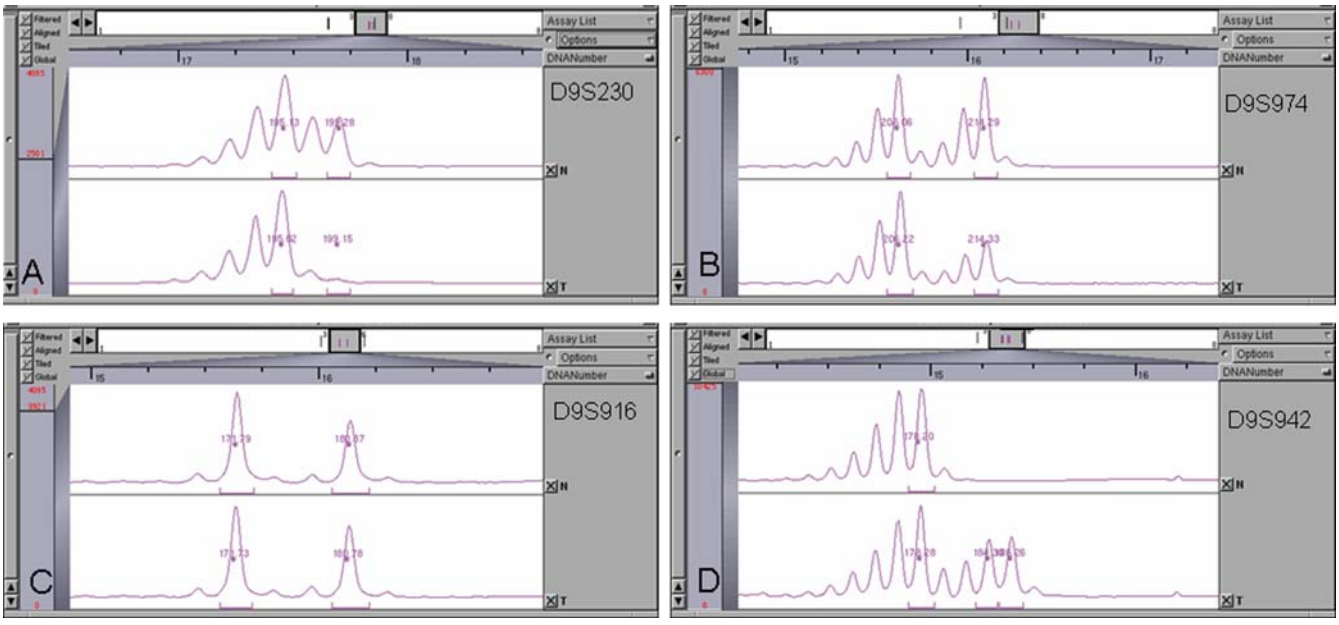

Fig. 3 Almost complete loss of the second allele at D9S230 in soft tissue leiomyosarcoma (LMS; **A**). Loss of heterozygosity (LOH) at D9S974 in cutaneous LMS (**B**). Retention of heterozygosity at D9S916 in angiomatoid fibrous histiocytoma (**C**). MSI at D9S942 in MFH (**D**)

of 1 low-grade, 4 intermediate-grade and 8 high-grade sarcomas. There were 4 cases of cutaneous dermal LMS. These were all intermediate grade sarcomas.

MFH specimens consisted of 19 cases of storiform MFH (Fig. 1B) (9 intermediate grade and 10 high grade), 2 cases of inflammatory MFH (high grade), 1 case of giant cell MFH (high grade) and 2 cases of angiomatoid fibrous histiocytoma. Angiomatoid fibrous histiocytoma was previously considered as a subtype of MFH and now is considered as a separate entity of low-grade malignancy [3, 7, 27].

AI/LOH results

The average informative rate per marker was 62% (range from 33% to 81%).

Leiomyosarcoma

The AI/LOH data are summarised in Fig. 2. For soft tissue LMS, the most frequent imbalance was at 9p24 at D9S230 locus (100%) (Fig. 3A). AI/LOH values at D9S916, D9S974, D9S942, D9S1814 and D9S171 were as follows: 67, 44, 67, 40 and 43%, respectively. Only one case (case 7) revealed MSI at D9S230. In cutaneous LMS, the most frequent allelic imbalance was identified within the coding sequence of $p16^{INK4A}$ at D9S974 (Fig. 3B) and D9S942 (100% and 67% of the informative cases, respectively). AI/LOH at D9S171 was 33%. Cutaneous LMS cases were uninformative for D9S1814. There was no evidence of AI/LOH at D9S916 and D9S230. Cutaneous LMS cases showed no evidence of MSI with any marker examined.

Malignant fibrous histiocytoma

The AI/LOH data are summarised in Fig. 4. Angiomatoid fibrous histiocytoma showed no evidence of allelic imbalance on 9p region at any of the six microsatellite markers examined (Fig. 3C).

The most frequent allelic imbalance in conventional MFH was at 9p24 at D9S230 locus. This was seen in13 of 14 informative cases (93%) of conventional MFH. AI/LOH values at D9S916, D9S974, D9S942, D9S1814 and D9S171 were 86, 83, 75, 71 and 61%, respectively. MSI was observed in 6 cases (Fig. 3D). There was no apparent correlation between the histological grade of the tumour and AI/LOH. Of 6 cases with MSI, 5 were high-grade sarcomas.

Discussion

AI/LOH analysis was performed in this study using six microsatellite markers at the 9p region. Four markers map to 9p21—D9S916, D9S1814, D9S974 and D9S942. The latter two are within the coding sequence of $p16^{INK4A}$. D9S171 is at 9p13 (proximal to $p16^{INK4A}$ and $p15^{INK4B}$). D9S230 is at 9p24.

A comparative analysis between the most frequent allelic imbalances in these two types of soft tissue sarcomas demonstrated that both types of tumours have similar recurrent patterns of allelic imbalance on 9p. AI/LOH was more frequent in MFH than LMS. MSI was rare in LMS but was detected in 6 cases of MFH.

Alterations of chromosome 9 have been previously reported using comparative genomic hybridization (CGH) in MFH [25] and in LMS of soft tissue [20]. Derre et al. compared chromosomal imbalances in these two groups of sarcomas using the CGH technique and found that loss of

MFH	D9S230	D9S916	D9S974	D9S942	D9S1814	D9S171
Case 1	○	○	○	○	○	○
Case 2	○	⊘	⊘	○	⊘	⊘
Case 3	⊘	●	●	⊘	⊘	⊘
Case 4	⊘	○	●	○	●	○
Case 5	●	⊘MSI	⊘	⊘	⊘	○
Case 6	●	●	●	○	●	○
Case 7	●	●	○	●	⊘	●
Case 8	●	⊘	⊘	●	○	⊘
Case 9	⊘	●	⊘	●	○	○
Case 10	⊘	⊘	⊘	⊘	⊘	●
Case 11	⊘	●	⊘	⊘	⊘	●
Case 12	○	●	○	●	⊘	●
Case 13	⊘	●	●	●	⊘	⊘
Case 14	●	●	⊘	●	⊘	●
Case 15	●	●	●	⊘MSI	⊘	●
Case 16	●	⊘MSI	⊘	⊘	●	●
Case 17	●MSI	●	⊘	●	●	●
Case 18	●	⊘MSI	⊘	●	⊘	●
Case 19	●	●	●	⊘	⊘	●
Case 20	●	⊘	●	⊘MSI	⊘	○
Case 21	●	⊘	●	●	⊘	⊘
Case 22	⊘	●	●	○	⊘	●
Case 23	⊘	○	⊘	⊘	●	○
Case 24	●	⊘	●	⊘	⊘	○

Fig. 4 Microsatellite map of allelic imbalance/loss of heterozygosity (AI/LOH) of 9p for malignant fibrous histiocytoma (MFH), with tabulated results. *Filled circle* AI/LOH, *open circle* no AI/LOH, *strike-through circle* Uninformative (homozygosity)

chromosome 9 was highly recurrent [5]. Studies based on LOH have the advantage over CGH studies of identifying small areas of allelic imbalance at different bands of the chromosome [6].

In this study, AI/LOH at 9p21 region was a common finding in LMS (soft tissue and skin) and MFH cases (excluding angiomatoid fibrous histiocytoma), suggesting that this chromosomal region may play a role in the pathogenesis of these tumours. However, the most frequent allelic imbalance was at 9p24 at D9S230. This was detected in 100% of soft tissue LMS and in 93% of conventional MFH cases. Interestingly this allelic imbalance was not detected in the LMS of skin.

Alterations of the chromosomal band 9p21 have been reported in different types of human tumours and cell lines [15, 21] including soft tissue sarcomas [25] and MFH of the bone [17]. This chromosomal region harbours $p15^{INK4B}$[12, 21] and $p16^{INK4A}$ [15, 24], which are likely candidates for tumour suppressor genes since they encode nuclear proteins that have been shown to block cell cycle progression at the G1-S transition by their ability to interfere with the catalytic activity of cyclin D/CDK4 complexes [24]. Allelic imbalance at D9S230 at the end of the chromosome may reflect imbalance of the entire short arm of chromosome 9 or it may suggest the possible existence of a putative tumour suppressor gene that may be important in the pathogenesis of these sarcomas at this locus. We found allelic imbalance at D9S230 in 100% of soft tissue LMS cases and in 93% of conventional MFH cases. This is in contrast to the level of allelic imbalance at this locus found in previous work in this department involving ten cases of synovial sarcoma (one of six informative cases) (unpublished data) and ten cases of malignant peripheral nerve sheath tumour (one of seven informative cases) [23].

Unlike LMS of soft tissue, cutaneous LMS is usually associated with good prognosis due to the small size and the superficial location of the tumour. The consistent finding of allelic imbalance at D9S230 in LMS of soft tissue and its absence in cutaneous LMS may suggest that this chromosomal region is essential for the development of the former and not so for the latter.

It is now widely accepted that the morphological pattern of pleomorphic MFH may be shared by a wide variety of poorly differentiated malignant mesenchymal neoplasms, and this tumour may represent a collection of sarcomas of diverse types, particularly LMSs [13] in which subtle differentiation has been overlooked, rather than a homogeneous entity [2, 4, 8, 9, 14, 18, 27]. Furthermore, it has been reported that the giant cell variant shares characteristics common to giant cell-rich osteosarcoma of soft tissue [11] and a number of inflammatory MFH may overlap with inflammatory LMS [19].

Therefore, the diagnosis of MFH is one of exclusion following thorough sampling and the use of ancillary techniques. The genetic profile of MFH is difficult to evaluate because of the lack of specific diagnostic features or immunohistochemistry used throughout the years. However, it has been reported that MFH and LMS tumours have similar comparative genomic hybridisation imbalances [5] and similar genome expression patterns [16].

Angiomatoid fibrous histiocytoma is a distinctive tumour of childhood, which was formerly classified within the conventional MFH subgroup but is now reclassified with the fibrohistiocytic tumours of low-grade malignancy because of its associated excellent rate of survival [3, 7, 27]. Our findings support this new classification and show that the angiomatoid fibrous histiocytoma is different from the conventional MFH. Although only two cases of angiomatoid fibrous histiocytoma were examined, neither showed allelic imbalance with any of the six microsatellite markers examined.

In conclusion, MFH and LMS share similar allelic imbalance at 9p, particularly at D9S230. While alterations at this locus may represent changes common to pleomorphic sarcomas, they were rare in synovial sarcomas and malignant peripheral nerve sheath tumours. This would suggest that this locus may harbour a tumour suppressor gene that is involved in the genesis of MFH and LMS. It further supports the hypothesis that MFH and LMS are related and that MFHs may represent a morphological pathway in tumour progression of LMSs.

Acknowledgement The authors wish to acknowledge the Dublin Soft Tissue Tumour Panel for reviewing the diagnosis of the cases in this study.

References

1. Butler D, Collins C, Mabruk M, Barry Walsh C, Leader MB, Kay EW (2000) Deletion of the FHIT gene in neoplastic and invasive cervical lesions is related to high-risk HPV infection but is independent of histopathological features. J Pathol 192: 502–510
2. Costa MJ (1994) Malignant fibrous histiocytoma phenotype in pleomorphic sarcoma differentiation in recurrent disease. Arch Pathol Lab Med 118:160–164
3. Costa MJ, Weiss SW (1990) Angiomatoid malignant fibrous histiocytoma. A follow-up study of 108 cases with evaluation of possible histologic predictors of outcome. Am J Surg Pathol 14:1126–1132
4. Dehner LP (1988) Malignant fibrous histiocytoma. Nonspecific morphologic pattern, specific pathologic entity, or both? Arch Pathol Lab Med 112:236–237
5. Derre J, Lagace R, Nicolas A, Mairal A, Chibon F, Coindre JM, Terrier P, Sastre X, Aurias A (2001) Leiomyosarcomas and most malignant fibrous histiocytomas share very similar comparative genomic hybridization imbalances: an analysis of a series of 27 leiomyosarcomas. Lab Invest 81:211–215
6. Dib C, Faure S, Fizames C, Samson D, Drouot N, Vignal A, Millasseau P, Marc S, Hazan J, Seboun E, Lathrop M, Gyapay G, Morissette J, Weissenbach J (1996) A comprehensive genetic map of the human genome based on 5,264 microsatellites. Nature 380:152–154
7. Fanburg-Smith JC, Miettinen M (1999) Angiomatoid "malignant" fibrous histiocytoma: a clinicopathologic study of 158 cases and further exploration of the myoid phenotype. Hum Pathol 30:1336–1343
8. Fletcher CD (1987) Malignant fibrous histiocytoma? Histopathology 11:433–437

9. Fletcher CD (1992) Pleomorphic malignant fibrous histiocytoma: fact or fiction? A critical reappraisal based on 159 tumors diagnosed as pleomorphic sarcoma. Am J Surg Pathol 16:213–228
10. Fletcher CD, van den Berg E, Molenaar WM (2002) Pleomorphic malignant fibrous histiocytoma/undifferentiated high grade pleomorphic sarcoma. In: Fletcher CD, Unni KK, Mertens F (eds) Pathology and genetics of tumours of soft tissue and bone. IARCPress, Lyon, France. pp 120–122
11. Guccion JG, Enzinger FM (1972) Malignant giant cell tumor of soft parts. An analysis of 32 cases. Cancer 29:1518–1529
12. Hannon GJ, Beach D (1994) p15INK4B is a potential effector of TGF-beta-induced cell cycle arrest. Nature 371:257–261
13. Hasegawa T, Hasegawa F, Hirose T, Sano T, Matsuno Y (2003) Expression of smooth muscle markers in so called malignant fibrous histiocytomas. J Clin Pathol 56:666–671
14. Hollowood K, Fletcher CD (1995) Malignant fibrous histiocytoma: morphologic pattern or pathologic entity? Semin Diagn Pathol 12:210–220
15. Kamb A, Gruis NA, Weaver-Feldhaus J, Liu Q, Harshman K, Tavtigian SV, Stockert E, Day RS, III, Johnson BE, Skolnick MH (1994) A cell cycle regulator potentially involved in genesis of many tumor types. Science 264:436–440
16. Lee YF, John M, Edwards S, Clark J, Flohr P, Maillard K, Edema M, Baker L, Mangham DC, Grimer R, Wooster R, Thomas JM, Fisher C, Judson I, Cooper CS (2003) Molecular classification of synovial sarcomas, leiomyosarcomas and malignant fibrous histiocytomas by gene expression profiling. Br J Cancer 88:510–515
17. Martignetti JA, Gelb BD, Pierce H, Picci P, Desnick RJ (2000) Malignant fibrous histiocytoma: inherited and sporadic forms have loss of heterozygosity at chromosome bands 9p21–22-evidence for a common genetic defect. Genes Chromosomes Cancer 27:191–195
18. Meister P (1996) Malignant fibrous histiocytoma: histomorphological pattern or tumor type. Pathol Res Pract 192:877–881
19. Merchant W, Calonje E, Fletcher CD (1995) Inflammatory leiomyosarcoma: a morphological subgroup within the heterogeneous family of so-called inflammatory malignant fibrous histiocytoma. Histopathology 27:525–532
20. Miyajima K, Oda Y, Tamiya S, Shimizu K, Hachitanda Y, Tsuneyoshi M (2003) Cytogenetic and clinicopathological analysis of soft-tissue leiomyosarcomas. Pathol Int 53:163–168
21. Nobori T, Miura K, Wu DJ, Lois A, Takabayashi K, Carson DA (1994) Deletions of the cyclin-dependent kinase-4 inhibitor gene in multiple human cancers. Nature 368:753–756
22. Sabah M, Cummins R, Leader M, Kay E (2004) Loss of heterozygosity of chromosome 9p and loss of $p16^{INK4A}$ expression are associated with malignant gastrointestinal stromal tumours. Mod Pathol 17:1364–1371
23. Sabah M, Cummins R, Leader M, Kay E (2005) Loss of heterozygosity of chromosome 9p and loss of $p16^{(INK4A)}$ expression in malignant peripheral nerve sheath tumours. Appl Immunohistochem Mol Morphol (in press)
24. Serrano M, Hannon GJ, Beach D (1993) A new regulatory motif in cell-cycle control causing specific inhibition of cyclin D/CDK4. Nature 366:704–707
25. Simons A, Schepens M, Jeuken J, Sprenger S, van de Zande G, Bjerkehagen B, Forus A, Weibolt V, Molenaar I, van den Berg E, Myklebost O, Bridge J, van Kessel AG, Suijkerbuijk R (2000) Frequent loss of 9p21 (p16(INK4A)) and other genomic imbalances in human malignant fibrous histiocytoma. Cancer Genet Cytogenet 118:89–98
26. Trojani M, Contesso G, Coindre JM, Rouesse J, Bui NB, De Mascarel A, Goussot JF, David M, Bonichon F, Lagarde C (1984) Soft-tissue sarcomas of adults; study of pathological prognostic variables and definition of a histopathological grading system. Int J Cancer 33:37–42
27. Weiss SW, Goldblum JR (2001) Enzinger and Weiss's Soft Tissue Tumors (4th edn) Mosby, USA

Virchows Arch (2005) 446: 259–264
DOI 10.1007/s00428-004-1173-3

ORIGINAL ARTICLE

Kuniyuki Oka · Koji Oohira · Yasushi Yatabe · Toshio Tanaka · Kozo Kurano · Rie Kosugi · Minoru Murata · Hando Hakozaki · Toshio Nishikawa · Yutaka Tsutsumi

Fulminant myocarditis demonstrating uncommon morphology—a report of two autopsy cases

Received: 31 August 2004 / Accepted: 3 November 2004 / Published online: 25 January 2005
© Springer-Verlag 2005

Abstract Two autopsy cases of fulminant myocarditis demonstrating uncommon morphology were studied. Subjects included two male patients: a 42-year-old (case 1) and a 39-year-old (case 2). Both cases had fever, chest or epigastric pain, electrocardiographic abnormalities, prominent elevation of serum glutamic oxaloacetic transaminase, glutamic pyruvic transaminase, lactic dehydrogenase and creatine phosphokinase. They were treated with intra-aortic balloon pumping and percutaneous cardiopulmonary support, and they died at 3 days and 4 days after admission (total course of 10 days and 9 days), respectively. Case 1 showed focal necrosis, severe myocardial dystrophic calcification positive for Kossa stain, inflammatory edema, lymphocyte and macrophage infiltration and extravasation of erythrocytes. Case 2 showed acute inflammation and severe myocardial necrosis with neutrophilic abscess, lymphocyte and macrophage infiltration, cell debris and purulent exudate. Calcified, degenerative and necrotic cardiac myocytes and macrophages were reacted with anti-Enterovirus antibody (clone 5-D8/1), which recognizes an epitope on the VP1 peptide of most Coxsackievirus, echovirus, poliovirus and enterovirus strains. Therefore, the present two cases may be compatible with fulminant enterovirus-associated myocarditis. Using reverse transcriptase-semi-nested polymerase chain reaction, picornaviral RNA was detected in the amplified products extracted from the paraffin-embedded myocardial sample of case 1 but not in case 2.

Keywords Fulminant myocarditis · Enteroviruses · VP1 · Picornaviral RNA · Dystrophic calcification

K. Oka (✉)
Pathology, Mito Saiseikai General Hospital,
3-3-10 Futabadai, Mito,
311-4198 Ibaraki , Japan
e-mail: oka-k@gb3.so-net.ne.jp
Tel.: +81-29-2549049
Fax: +81-29-2549099

K. Oohira · K. Kurano · R. Kosugi · M. Murata
Cardiology, Mito Saiseikai General Hospital,
Mito,
Ibaraki, Japan

Y. Yatabe
Department of Pathology and Molecular Diagnostics
Aichi Cancer Center Hospital,
Nagoya,
Aichi, Japan

T. Tanaka
Department of Infection and Immunology,
SRL Inc.,Hachioji,
Tokyo, Japan

H. Hakozaki
Pathology, Fukushima Rosai Hospital,
Iwaki,
Fukushima, Japan

T. Nishikawa
Department of Pathology, Tokyo Women Medical College,
Tokyo, Japan

Y. Tsutsumi
Department of Pathology
Fujita Health University School of Medicine,
Homei,
Aichi, Japan

Introduction

Viruses are the most common cause of myocarditis. Coxsackieviruses A and B and other enteroviruses probably account for most myocarditis cases [24]. It is often difficult to isolate the virus from the tissues after onset of clinical symptoms. Serological studies and viral DNA or RNA analyses in the myocardium using a gene amplification by polymerase chain reaction (PCR) or reverse transcriptase (RT)-PCR [21] and an in situ hybridization method may identify the agents. The positive rate of the genome is only 20–30%, and the clinical significance is questionable [15]. Whether the viruses are a direct cause of the myocardial injury or they initiate an immune response that cross-reacts with myocardial cells is undetermined in most cases [12]. T cells may damage virus-infected myocytes by reacting against viral antigens expressed on the cell membrane.

Fulminant myocarditis is a severe type of acute non-specific myocarditis and indicates fatal myocarditis [1]. The disease showed complete atrioventricular block, repeated unconscious attack, advanced cardiogenic shock, high increase of heart muscle-related enzymes, multiple organ failure syndrome and high fatality rate. Its typical electrocardiogram included abnormal Q wave, ST/T abnormality and electrical axis deviation.

Myocardial dystrophic calcification following acute myocarditis is uncommon in adult patients without renal failure, although the calcification has been observed in necrotic tissue following experimental viral myocarditis and acute myocarditis in human newborns and infants [19, 25].

Human enteroviruses of the picornavirus family include polioviruses, Coxsackieviruses A and B, echoviruses and enteroviruses. The viral particles are 25–30 nm in diameter and consist of a RNA and a viral capsid. The capsid contains four proteins, VP1 through VP4. Serotype-specific antigenic sites are located predominantly in VP1. A monoclonal antibody, 5-D8/1, developed by Yousef et al. [28], is specific for an epitope conserved on VP1. Using an immunohistochemical method, VP1 was detected in scattered myocytes in myocarditis and was localized often adjacent to necrosis [9, 16, 29].

PCR assays allow a rapid detection of viral genomes in paraffin-embedded tissue samples, are easy to use in a clinical laboratory and have revealed an association between enterovirus infection and myocarditis [2, 6, 11, 23]. Herein, we report two autopsy cases of fulminant myocarditis demonstrating uncommon morphology and VP1 positivity in the cytoplasms of the cardiac myocytes and macrophages. Picornaviral RNA was detected in one of them.

Clinical summary and pathological findings

Case 1

A 42-year-old male noticed common cold-like symptoms at the beginning of June 2002 and had pain in the chest on 6 June. His temperature was 38.3°C, and he was treated with intravenous infusion of antibiotics. On 9 June, he developed dyspnea and weak blood pressure and was admitted to the coronary care unit of our hospital for suspicion of myocarditis. Chest radiology showed mild cardiomegaly with prominent pulmonary congestion. Electrocardiogram showed complete atrioventricular block with a ventricular rate of 30 beats per minute, for which the QRS configuration was an incomplete right branch block with left axis deviation. Echocardiogram showed slight dilatation, hypertrophy and severe hypokinetic wall motion of left ventricle (LV) with LV ejection fraction of 24%. Coronary angiogram revealed no significant stenosis. Left ventriculogram was not performed because of hemodynamic deterioration. Laboratory findings on 9 June and 12 June revealed 21,670 IU/l and 1660 IU/l of glutamic oxaloacetic transaminase (GOT), 8822 IU/l and 1496 IU/l of glutamic pyruvic transaminase (GPT), 28,952 IU/l and 6142 IU/l of lactic dehydrogenase (LDH) and 5477 IU/l and 24,562 IU/l of creatine phosphokinase (CPK), respectively. Serum calcium and phosphate levels were 6.8 mg/dl (normal range of Ca; 8.4–10.8 mg/dl) and 11.5 mg/dl (normal range of P; 2.7–4.5 mg/dl) on 9 June and 6.2 mg/dl and 7.3 mg/dl on 12 June, respectively. On 10 June, assays of virus antibodies revealed anti-Coxsackie A9, B1, B2, B3, B4, B5, B6 ×4, anti-cytomegalovirus (CMV)-IgM, 0.26 (normal; under 0.80) and anti-CMV-IgG, 7.5 (normal under 2.0). Artificial respiration, pacing catheter intra-aortic balloon pumping (IABP), percutaneous cardiopulmonary support (PCPS), and hemodialysis were started. The patient's general condition worsened. At 3 days after admission (total course of 10 days, on 12 June), he showed falling blood pressure and respiratory failure and died. A pair serum analysis was not performed.

An autopsy was conducted 1.5 h after death. The heart measured 13×9×8.5 cm in size and weighed 438 g. Its macroscopical finding showed hypertrophic dilatation with degenerative foci. The microscopic finding contained: (1) prominent basophilic dense granular materials in the swollen cytoplasm of the heart muscle (Fig. 1a), collapse, myocytolysis, patchy foci of necrosis; (2) marked infiltration of lymphocytes, macrophages and hemophagocytic

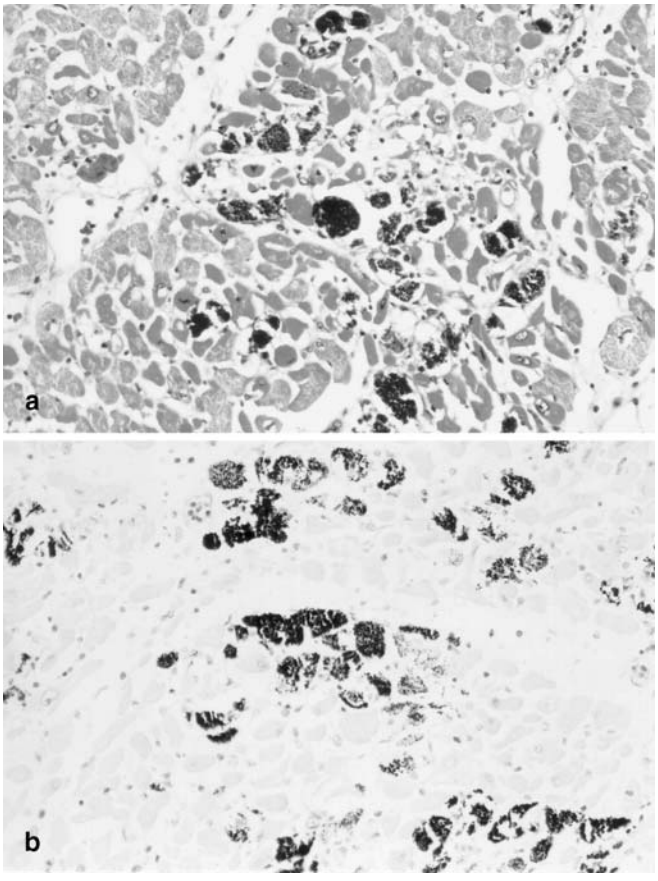

Fig. 1 Case 1. **a** Basophilic dense granules in their swollen cytoplasm of heart muscle cells and infiltration of lymphocytes and macrophages among myofibrils are seen. Hematoxylin and eosin stain ×200. **b** Basophilic materials are strongly positive for Kossa stain ×200

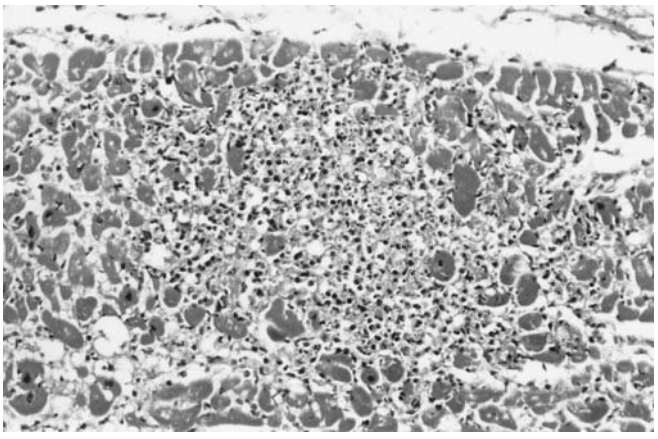

Fig. 2 Case 2. Massive myocytolysis, patchy necrotic foci, neutrophilic abscess and infiltration of lymphocytes and cell-debris-laden macrophages are observed. Hematoxylin and eosin stain ×200

cells; (3) interstitial inflammatory edema and hemorrhage and (4) separation and destruction of individual myofibers. Basophilic materials were strongly positive for Kossa stain (Fig. 1b). Some ulcers, approximately 1 cm in diameter, were observed in the lower esophagus, followed by accumulation of a large amount of coffee-ground-like materials in the stomach and tarry stools in the intestinal tract. Centrolobular necrosis caused by passive congestion was also seen. No inflammatory reaction was revealed in any other organs.

Case 2

A 39-year-old male presented with a high fever of 39.8°C on 16 April, 2002. He could not eat anything because of epigastric discomfort. Epigastralgia and short breath were reinforced, and he was admitted to our hospital for suspicion of hepatorenal dysfunction and acidosis: 954 IU/l of GPT, 1891 IU/l of LDH, 1148 IU/l of CPK, 57.9 mg/dl of blood urea nitrogen, 1.59 mg/dl of creatinine and −11.4 of base excess. Chest radiology showed mild cardiomegaly with prominent pulmonary congestion. Electrocardiogram showed atrial fibrillation with a ventricular rate of 110 beats per minute, for which the QRS configuration was left axis deviation, complete right branch block and ST elevation in leads II, III, aVF and V1 to V3. Echocardiogram showed slight hypertrophy and no dilatation of LV. The wall motion of LV was severe diffuse hypokinetic, especially of the inferior region, and LV ejection fraction was 30%. Coronary angiogram revealed no significant stenosis. Laboratory findings on 21 April and 23 April revealed 4427 and 26,696 IU/l of GOT, 1932 and 8266 IU/l of GPT, 7516 and 35,498 IU/l of LDH and 1139 and 4,817 IU/l of CPK, respectively. Serum calcium and phosphate levels were 7.8 mg/dl and 5.8 mg/dl on 21 April. On 23 April, assays of virus-neutralizing antibodies revealed anti-Coxsackie A9, B1, B2, B3, B4, B5, B6, influenza A, measles, rubella (under ×4), anti-adenovirus, influenza B, CMV (×8) and anti-herpes simplex virus (×4). Endomyocardial biopsy treated on 22 April showed myocarditis, showing severe neutrophilic leukocyte and lymphocyte infiltration in the myocardium, focal to diffuse. He developed ventricular tachycardia and shock condition and was treated with PCPS, IABP and continuous hemodialysis filtration. At 4 days after admission (total course of 9 days, on 24 April), he repeated ventricular fibrillation and showed falling blood pressure, respiratory failure and died. A pair serum analysis was not performed.

The autopsy was performed 2 h after death. The heart measured 13.5×9×8.5 cm in size and weighed 412 g. The macroscopic finding showed patchy and irregular-shaped necrotic foci in the heart. Microscopic findings included the following: (1) massive myocytolysis, collapse of heart muscles and patchy necrotic foci; (2) neutrophilic abscess formation with cell-debris-laden macrophages, infiltration of neutrophils, lymphocytes and macrophages (Fig. 2); (3) purulent exudate, interstitial edema and (4) separation and destruction of individual myofibers. Massive hemorrhage of both lungs (left 582 g, right 924 g), passive congestion of the liver (1595 g), accumulation of casts in the tubules of both kidneys and hypercellular bone marrow were observed. No inflammatory reaction was revealed in any other organs.

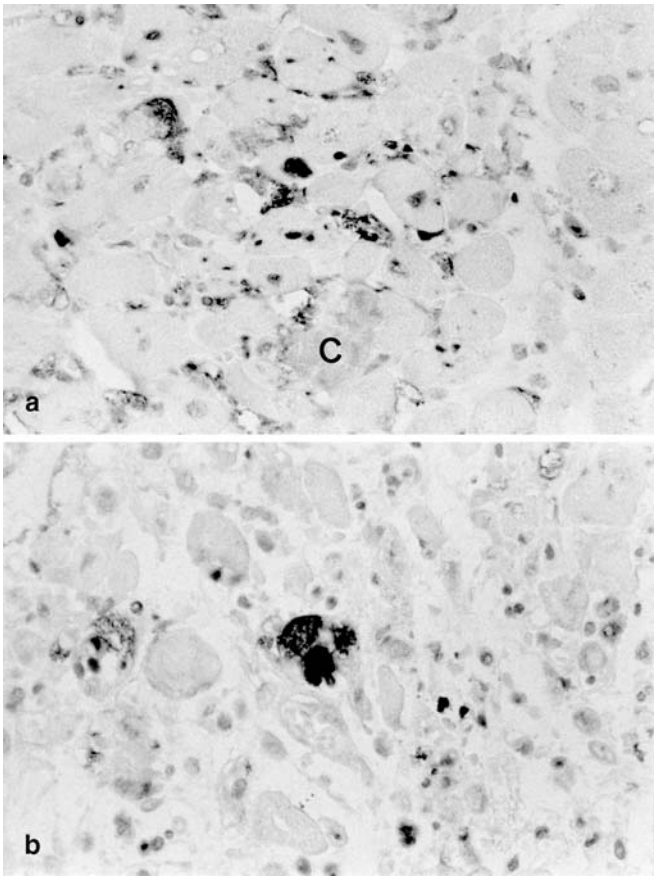

Fig. 3 Calcified, degenerative and necrotic heart muscle cells and macrophages are positive for VP1 in their cytoplasm (**a** case 1, **b** case 2). Dystrophic calcification (**c**) is seen (**a**). Immunostain ×200

Results

Immunohistochemical findings

Immunohistochemical staining using a monoclonal antibody, NCL-ENTERO (Clone 5-D8/1, Novocastra, UK), showed strong cytoplasmic staining of calcified, degenerative and necrotic myocytes in cases 1 and 2 (Fig. 3a, b). The antibody recognizes an epitope on the VP1 peptide, which is highly converted within the enterovirus group, except for hepatitis A virus. This reacts with most Coxsackievirus, echovirus, poliovirus and enterovirus strains. Macrophages were also positive for VP1.

Many lymphocytes infiltrated in the myocardium were positive for CD3 and CD8 (Fig. 4a) and negative for CD20 and CD56. Some lymphocytes were positive for CD4 in case 1, and only a few lymphocytes were positive for CD4 in case 2. Some lymphocytes were positive for granzyme B, showing a fine granular pattern (Fig. 4b). No perforin-positive lymphocyte was observed in either case 1 or case 2. Many macrophages positive for CD68 infiltrated in necrotic foci and among myofibrils. Langerhans' cells positive for S-100 protein were not observed.

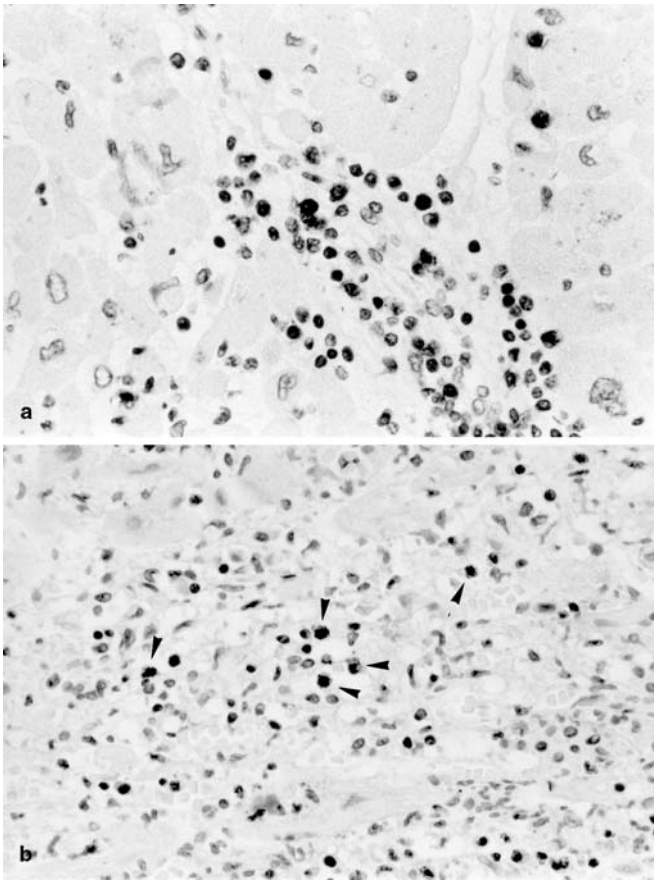

Fig. 4 Many lymphocytes infiltrated in the myocardium are positive for CD8 (**a**, case 1). Some lymphocytes are positive for granzyme B, showing a fine granular pattern (*arrowheads*, **b**, case 2). Immunostain ×200

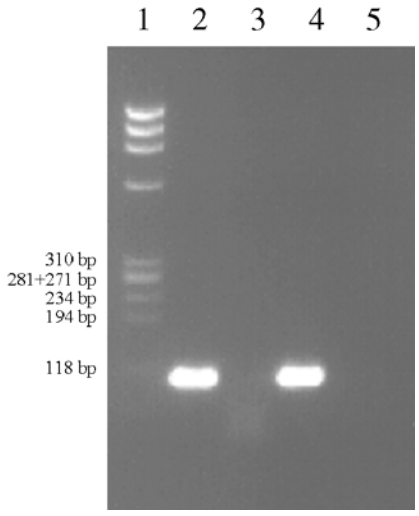

Fig. 5 Results of a reverse-transcripted-semi-nested polymerase chain reaction in myocardial samples from two patients for picornaviral RNA. A discrete band around 100 bp is detected with the amplification for picornaviral RNA in case 1 (lane 2) but not in case 2 (lane 3). Lane 1, molecular size marker (ϕχ174DNA digested with *Hae* III). Lane 2, case 1 sample. Lane 3, case 2 sample. Lane 4, positive control (poliovirus-1). Lane 5, negative control (Hela cell)

Picornaviral RNA detection

Total RNA was extracted from paraffin-embedded myocardial samples as described. Briefly, 10-μm-thick sections were dewaxed with xylene, washed with ethanol and incubated in the lysis buffer containing 1% sodium dodecyl sulfate, 10 mM Tris buffer (pH 8.0), 10 mM ethylenediaminetetraacetate, 150 mM NaCl and 200 μg/ml proteinase K at 56°C overnight, followed by extracting total RNA using an acid quanidium thiocyanate-phenol-choloroform method. Integrity of extracted RNA was confirmed by PCR of 120 bp fragment of β-actin. To detect picornavirus RNA, semi-nested RT-PCR for picornaviral RNA was performed using a forward primer, 5′-GGC CCC TGA ATG CGG CTA A-3′ and a reverse primer, 5′-GAA ACA CGG ACA CCC AAA GT-3′ for first PCR and a forward primer that was the same as first PCR and reverse primer 5′-ACC CAA AGT AGT CGG TTC CGC-3′ in second PCR. The amplified products were electrophoresed in 3% agarose gel, stained with ethidium bromide and photographed under ultraviolet light. A discrete band around 100 bp was detected with the amplification for picornaviral RNA in case 1 (lane 2 in Fig. 5) but not case 2 (lane 3 in Fig. 5).

Discussion

Of the reported five patients with dystrophic calcification following acute myocarditis or giant cell myocarditis, three showed normal calcium level, and one did not have the description [5, 13, 20, 22]. The remaining one [26] showed hypocalcemia (6.0 mg/dl), which was similar to our case. Hypocalcemia and myocardial calcification may imply abnormality of calcium metabolism and myocardial

calcium overload. Electron microscopy revealed calcium deposits bound to the sarcolemma and T-tubules and extensive calcium accumulation in swollen mitochondria of necrotic myocardial cells [20, 22]. The sarcoplasmic reticulum specifically regulates calcium flow, which is necessary for rapid contraction and relaxation. Cardiac muscle cells contain numerous mitochondria, reflecting the need for continuous aerobic metabolism in heart muscle. From these findings, cardiotropic viral infection occurred in myocardial cells, massive myocardial damage followed, abnormal calcium metabolism developed, calcium overload and accumulation appeared in degenerated and necrotic heart muscle cells and, finally, dystrophic calcification took place irreversibly. Therefore, case 1 was suggested to be the sixth adult case. The reported four patients and case 1 died 10–27 days after initial presentation. The remaining reported one patient is alive. It was clear that these consecutive phenomena occurred for a short time. Similarly, the mouse heart of 14 days after successive infection with Coxsackievirus B3 and encephalomyocarditis virus showed myocardial calcification and massive cellular infiltration with necrosis [19].

Generally, local deposits of calcium occur in caseous lesions of tuberculosis, old infarcts, atheromatous arteries and diseased heart valves, etc. [17]. That is, dystrophic calcification occurs in old lesions. Therefore, the myocardial calcification in case 1 was somewhat different from dystrophic calcification described in textbooks [17].

In general, the mechanism of dystrophic calcification may be as follows: necrosis or degeneration of the tissue induces release of enzymes and consequently, calcium accumulation in mitochondria in a process coupled with electron transport, uptake of equivalent amounts of phosphates, breakdown of organic phosphates, alteration of pH and, finally, deposition of $CaPO_4$ as granular matrix inclusions [4, 17]. There are multifunctional proteins that facilitate interaction with minerals, other matrix molecules and cells and may regulate dystrophic calcification [7]. They include osteopontin, osteonectin, osteocalcin and γ-carboxyglutamic acid-containing protein [7].

Case 2 showed massive myocardial necrosis and not only CD8-positive small lymphocyte infiltration but also neutrophilic abscess formation. In general, there is infiltration by lymphocytes, plasma cells and eosinophils in most acute myocarditis cases, and neutrophils may also be present if there is severe necrosis of muscle fibers [3]. GOT, GPT and LDH values showed the different tendency from on admission day to on death day between case 1 and case 2. GOT, GPT and LDH values increased about five times on death day in case 2 compared with those on admission day. Therefore, neutrophilic infiltration may be ascribed to more massive necrosis of heart muscle cells in case 2. Case 2 will catch a larger quantity of viruses and make a stronger immune response to the agent and tissue necrosis than case 1.

From the clinical course, morphology and VP1-positive immunohistochemical findings, we diagnosed two cases as fulminant enterovirus-associated myocarditis. Three studies have been reported using an immunohistochemical method with the same antibody against VP1. Dettmeyer et al. [9] detected VP1 in the heart muscle cells of postmortem myocardial samples of four children with suspected sudden infant death syndrome. Li et al. [16] also reported that VP1 was present in myocardial tissues from 11 patients with myocarditis. In addition, Zhang et al. [29] observed that VP1 was localized in cytoplasm of myofibrils of 13 patients with myocarditis. Furthermore, two studies about fulminant myocarditis and other virus infections from enterovirus have been described. Koga et al. [14] reported two child cases in which herpes simplex virus-1- or Epstein–Barr virus-positive signals were observed in the nuclei of myocardiac fibers. In addition, Miura et al. [18] observed the presence of influenza A in cardiac myocytes using an immunohistochemical analysis with patient's immunoglobulins.

Cytotoxic T lymphocytes (CTLs) kill antigen-bearing target cells. Two principal mechanisms of T-cell-mediated damage were discovered: (1) perforin-granzyme-dependent killing and (2) Fas–Fas ligand-dependent killing [8]. Perforins and granzymes are soluble mediators contained in the lysosome-like granules of CTLs. Perforins can perforate the plasma membranes of the target cells that are under attack by CD8+ lymphocytes. Granzymes are neural serine proteases that are stored in specialized lytic granules of CTLs and in neural killer cells and are delivered into the target cells via the perforin-induced pores. Exocytosis of granzyme-containing granules in the cytoplasm of the target cell leads to the induction of DNA fragmentation and apoptosis of the target cell. In the present two cases, many CD8-positive lymphocytes infiltrated in the myocardium; however, granzyme B-positive lymphocytes were few. Calcified, degenerative, necrotic foci of two cases were much larger compared with the numbers of granzyme B-positive lymphocytes infiltrated in the heart. Moreover, neither CD56-positive nor perforin-positive lymphocytes were observed. Therefore, the possibility of supporting the perforin-granzyme-killing mechanism was not produced from our findings. Koga et al. [14] reported that CD8-positive T-lymphocytes induced by virus infection might play an important role in the damage to heart muscle cells in fulminant myocarditis. Feeley et al. [10] reported that immunohistochemistry for T lymphocyte is a useful and reliable means of confirming a diagnosis of myocarditis. Young et al. [27] reported that myocardial damage may be due to the action of perforin-secreting lymphocytes in viral myocarditis.

Reports [2, 6, 11, 23] and a review article [21] about the demonstration of viral RNA in paraffin-embedded endocardial biopsy specimens were found. Satoh et al. [23] reported that enteroviral RNA was present in 21 of 44 patients with myocarditis by real-time RT-PCR method. Baasner et al. [2] reported that enteroviruses could be detected in 14 of 60 children with sudden infant death syndrome. Cioc and Nuovo [6] demonstrated Coxsackie virus B in five cases with sudden unexpected death by in situ viral detection method using PCR-amplified viral RNA. Hilton et al. [11] reported the demonstration of Coxsackie viral RNA in formalin-fixed tissue sections from

two of ten childhood myocarditis cases by a combined study using in situ hybridization and PCR. In the present study, case 1 was considered to be enterovirus-associated myocarditis because of VP1 expression in cardiac myocytes and macrophages and picornaviral RNA detection. Case 2 may be also considered to be enterovirus-associated myocarditis because of the presence of VP1, despite the absence of picornaviral RNA in the myocardial sample, because the detection site of the picornaviral RNA genome was located in 5′-NCR and not in the VP1-coding region.

Acknowledgements This study was supported by a grant-in aid from Mito Saiseikai General Hospital, MSGH, Mito, and TAKETOSHI Medical Research Fund, Oyama, Tochigi, Japan. The authors thank Drs. H. Hanawa, E. Itoh, and S. Abe (Department of Cardiology, Niigata University School of Medicine, Niigata, Japan) for thoughtful advice, and Mrs. T. Kawasaki, W. Tanno, H. Yonekawa, Mrs. S. Koyamatsu, Miss T. Tobita and Mrs. M. Koshihara (Pathology, MSGH) for skillful technical assistance and Mr. D. Mrozek (Medical English Service, Kyoto, Japan) for English revision.

References

1. Aoyama N, Izumi T, Hiramori K et al (2002) National survey of fulminant myocarditis in Japan: therapeutic guidelines and long-term prognosis of using percutaneous cardiopulmonary support for fulminant myocarditis (special report from a scientific committee). Circ J 66:133–144
2. Baasner A, Dettmeyer R, Graebe M, Rissland J, Madea B (2003) PCR-based diagnosis of enterovirus and parvovirus B19 in paraffin-embedded heart tissue of children with suspected sudden infant death syndrome. Lab Invest 83:1451–1455
3. Chandrasoma P, Taylor CR (1998) Myocarditis. In: Concise pathology, 3rd edn. Appleton & Lange, Stanford, pp 367–368
4. Cheville NF (1994) Consequences of acute cell injury: necrosis, recovery, and hypertrophy. In: Ultrastructural pathology. An introduction to interpretation. Iowa State University Press, Ames, pp 81–123
5. Chow LTC, Chow WH (1992) Intracellular calcification: an unusual histological feature of acute myocarditis. Histopathology 21:385–387
6. Cioc AM, Nuovo GJ (2002) Histologic and in situ viral findings in the myocardium in cases of sudden, unexpected death. Mod Pathol 15:914–922
7. Cotran RS, Kumar V, Collins T (1999) Dystrophic calcification. In: Robbins pathologic basis of disease, 6th edn. Saunders, Philadelphia, pp 43–45
8. Cotran RS, Kumar V, Collins T (1999) T cell-mediated cytotoxity. In: Robbins pathologic basis of disease, 6th edn. Saunders, Philadelphia, p 206
9. Dettmeyer R, Baasner A, Schlamann M, Haag C, Madea B (2002) Coxsackie B3 myocarditis in 4 cases of suspected sudden infant death syndrome: diagnosis by immunohistochemical and molecular-pathologic investigations. Pathol Res Pract 198:689–696
10. Feeley KM, Harris J, Suvarna SK (2000) Necropsy diagnosis of myocarditis: a retrospective study using CD45RO immunohistochemistry. J Clin Pathol 53:147–149
11. Hilton DA, Variend S, Pringle JH (1993) Demonstration of Coxsackie virus RNA in formalin-fixed tissue sections from childhood myocarditis cases by in situ hybridization and the polymerase chain reaction. J Pathol 170:45–51
12. Huber SA (1997) Autoimmunity in myocarditis: relevance of animal models. Clin Immunol Immunopathol 83:93–102
13. Itoh E, Saitoh H, Miida T et al (1997) An autopsied case of acute myocarditis with myocardial calcification. Jpn Circ J 61:798–802
14. Koga M, Fujiwara M, Ariga S et al (2001) $CD8^+$ T-lymphocytes infiltrate the myocardium in fulminant herpes virus myocarditis. Pediatr Pathol Mol Med 20:189–195
15. Koide H, Kitaura Y, Deguchi H et al (1992) Genomic detection of enteroviruses in the myocardium-studies on animal hearts with Coxsackievirus B3 myocarditis and endomyocardial biopsies from patients with myocarditis and dilated cardiomyopathy. Jpn Circ J 56:1081–1093
16. Li Y, Bourlet T, Andreoletti L et al (2000) Enteroviral capsid protein VP1 is present in myocardial tissues from some patients with myocarditis or dilated cardiomyopathy. Circulation 101:231–234
17. Macfarlane PS, Reid R, Callander R (2000) Calcification. In: Pathology illustrated, 5th edn. Churchill Livingstone, Edinburgh, p 25
18. Miura M, Asaumi Y, Wada Y et al (2001) A case of influenza subtype A virus-induced fulminant myocarditis: an experience of percutaneous cardio-pulmonary support (PCPS) treatment and immunohistochemical analysis. Tohoku J Exp Med 195:11–19
19. Okada I, Matsumori A, Tomioka N, Kawai C (1992) Successive infection of Coxsackievirus B3 and encephalomyocarditis virus: an animal model of chronic myocarditis. J Pathol 167:341–347
20. Olbrich HG, Herrmann G, Vandeplassche G et al (1990) Calcium overload in human giant cell myocarditis. J Clin Pathol 43:650–653
21. Romeo JR (1999) Reverse-transcription polymerase chain reaction detection of the enteroviruses. Arch Pathol Lab Med 123:1161–1169
22. Rossi MA, Santos CS (2003) Sepsis-related microvascular myocardial damage with giant cell inflammation and calcification. Virchows Arch 443:87–92
23. Satoh M, Nakamura M, Akatsu T et al (2003) Expression of Toll-like receptor 4 is associated with enteroviral replication in human myocarditis. Clin Sci (London) 104:577–584
24. Schoen FJ (1999) Myocarditis. In: Robbins pathologic basis of disease, 6th edn. Saunders, Philadelphia, pp 584–587
25. Stallion A, Rafferty JF, Warner BW, Ziegler MM, Ryckman FC (1994) Myocardial calcification: a predictor of poor outcome for myocarditis treated with extracorporeal life support. J Pediatr Surg 29:492–494
26. Wada A, Nakata T, Tsuchihashi K et al (1993) Massive myocardial calcification of right and left ventricles following acute myocarditis complicated with rhabdomyolysis-induced acute renal failure. Jpn Circ J 57:567–572
27. Young LH, Joag SV, Zheng LM, Lee YS, Young JD (1990) Perforin-mediated myocardial damage in acute myocarditis. Lancet 336:1019–1021
28. Yousef GE, Brown IN, Mowbray JF (1987) Derivation and biochemical characterization of an enterovirus group-specific monoclonal antibody. Intervirology 28:163–170
29. Zhang H, Li Y, Peng T et al (2000) Localization of enteroviral antigen in myocardium and other tissues from patients with heart muscle disease by an improved immunohistochemical technique. J Histochem Cytochem 48:579–584

Virchows Arch (2005) 446: 265–269
DOI 10.1007/s00428-004-1175-1

ORIGINAL ARTICLE

Li Wen Hu · Edson Aparecido Liberti · Maria Luiza Morais Barreto-Chaves

Myocardial ultrastructure in cardiac hypertrophy induced by thyroid hormone—an acute study in rats

Received: 20 July 2004 / Accepted: 8 November 2004 / Published online: 25 January 2005
© Springer-Verlag 2005

Abstract The early responses of the myocardium ultrastructure under thyroid dysfunction conditions, hemodynamic parameters, cardiac hypertrophy and ultrastructural evaluations were performed in hypothyroid and hyperthyroid rats submitted to different doses [T4–25 and T4–100; 0.025 mg and 0.1 mg kg^{-1} body weight (BW)·per day, respectively)]. All groups were treated for 7 days. The animals were sacrificed, the hearts were excised and weighed and the left ventricle tissue samples were processed for transmission election microscopy. Systolic blood pressure (SBP) was not altered by administration of T4. An increased heart rate and ratio of heart weight to body weight (HW/BW) were found in the hyperthyroid rats. However, the SBP and HW/BW decreased significantly in hypothyroid rats. No significant ultrastructural alterations were detected when the hypothyroid and T4–25 groups were compared with the control group. Alterations of cardiomyocytes nuclei of these groups were also not detected. Notably, disorganization of intercellular junctions was observed in many cardiomyocytes of T4–100 group. The present results indicate that in the early stages of hyperthyroidism, the cardiac hypertrophy development was mainly due to direct effects of thyroid hormone. Despite cardiac hypertrophy development, there is no ultrastructural evidence of myocardial degeneration.

Keywords Thyroid hormone · Cardiac hypertrophy · Cardiomyocytes · Transmission electron microscopy

L. W. Hu · E. A. Liberti · M. L. M. Barreto-Chaves (✉)
Laboratory of Cellular Biology and Functional Anatomy,
Department of Anatomy, Biomedical Sciences Institute,
University of São Paulo,
Av. Prof. Lineu Prestes 2415, Cidade Universitária,
05508–900 São Paulo, Brazil
e-mail: mchaves@usp.br
Tel.: +55-11-38159695
Fax: +55-11-30917366

Introduction

Over the past several decades, many neural and hormonal stimuli have been related to cardiac muscle growth, including, but not limited to, α- and β-adrenergic agonists, ANG II, glucocorticoids, insulin, growth hormone, glucagons and thyroxine (T4) [17]. In addition, several studies have demonstrated that the heart is an important target for thyroid hormone [15], which promotes an increase in myocyte transverse diameter with no changes in the collagen levels [13]. General features of thyroid hormone action include enhanced contraction strength/velocity and increased speed of diastolic relaxation in the hyperthyroid state [5, 21, 22]. In contrast, these mechanisms are decreased in hypothyroid animals [10]. Accordingly, Ferreira et al. [11] have observed the predominant appearance of myofibrillar disarray, associated with disorganization of cytoskeletal proteins in the deep myocardium. Disrupted/swollen mitochondria and myofibrolysis scattered in the myocardium of long-term thyrotoxic rats have also been reported [24]. However, reports describing cardiomyocyte ultrastructural alterations in hyperthyroid and hypothyroid myocardium are scarce. This study was initiated to examine some of the early responses of the myocardium ultrastructure in rats induced to hyper- and hypothyroidism conditions.

Materials and methods

Care and use of laboratory animals were performed according to National Institutes of Health guidelines. Male Wistar rats, weighing 200–260 g, were obtained from the Instituto de Ciências Biomédicas, University of Sao Paulo. The animals were maintained in individual cages with food and water ad libitum. Initially, rats were randomized into four groups: hypothyroid (Hypo), hyperthyroid (Hyper; T4–25 and T4–100) and control. In the Hypo group, the rats were surgically thyroidectomized and treated during a

period of 7 days with methimazole (0.05%) added to the drinking water. Hyperthyroidism was induced in T4–25 and T4–100 rats by daily intraperitoneal injections of T4 [0.025 mg kg^{-1} body weight (BW) per dayand 0.1 mg kg^{-1} BW per day, respectively)], for 7 days. In all groups, systolic blood pressure (SBP) and heart rate (HR) were measured daily at approximately the same time of day by tail-cuff plethysmograph, an indirect method for measuring blood pressure (Kent Scientific, USA). In addition, the BW was measured daily. The SBP and BW were last determined immediately preceding death. Rats were familiarized with the apparatus for a total of 7 days before measurements were taken. Afterward, the animals were anesthetized with pentobarbital sodium (45 mg/kg, intraperitoneally), and the heart was dissected and weighed. Fragments with approximately 2 mm of thickness were obtained from each left ventricle. These fragments were fixed in 2.5% glutaraldehyde in cacodilate buffer. The specimens were immersed in a 1% osmium-tetroxide phosphate buffer solution for 1 h post-fixation. Next, they were embedded in araldite using routine procedures for transmission electron microscopy [19] and examined with a Philips EM-301 electron microscope.

Statistical analysis

Statistical analysis was performed using one-way analysis of variance (ANOVA), and P values <0.05 were accepted as statistically significant. Tukey's post-hoc test was used to make individual comparisons between groups when a significant change was observed with ANOVA. The data are shown as mean±SD.

Results

The hemodynamic parameters of SBP and HR after T4 administration and thyroidectomy (Hypo group) are summarized in Table 1. Notably, neither dose of thyroid hormone affected SBP. However, SBP significantly decreased in hypothyroid rats. In addition, both doses of T4 treatment significantly increased HR. The BW at the beginning of the experiment was the same in all groups studied. In both T4-treated groups, a significant increase in heart weight to body weight ratio (HW/BW) was detected when compared with control group (19.5% and 21.3%, respectively).

Table 1 Hemodynamic parameters and heart weight-to-body weight ratio in all experimental groups. Values are expressed as mean±SD. T4–25, rats treated with 0.025 mg kg^{-1}·thyroxine per day; T4–100, 0.1 mg kg^{-1}·thyroxine per day^{-1}

Groups	n	Systolic blood pressure (mmHg)	Heart rate (beats/min)	Heart weight (mg)/body weight (g)
Control	8	142.8±7.08	378.7±20.4	2.69±0.09
T4–25	8	142.2±17.4	426.5±30.5[a]	3.22±0.14[c]
T4–100	8	142.8±7.97	444.3±37.3[b]	3.27±0.08[c]
Hypothyroid	7	104.6±14.0[c]	361.7±25.7	2.23±0.07[c]

[a] P<0.05 versus control
[b] P<0.01 versus control
[c] P<0.001 versus control

In the controls, myocardial tissue showed a typical structure. There were no ultrastructural changes either within cardiomyocytes (i.e., within sarcoplasma, contractile apparatus and organelles) or in intercellular spaces. No significant ultrastructural alterations were detected when the hypothyroid (Fig. 1B) or the T4–25 (Fig. 1A) groups were compared with the control group. The normal aspect of cardiomyocytes with typical myofibrillar arrangement exhibiting the preserved sarcomeric structure was maintained. Also, the mitochondria were preserved and intermingled with cardiomyocytes. In all groups, including the T4–100 group, the presence of disrupted mitochondria or mitochondria containing large vacuoles were not observed. However, although the number of these structures was not determined, apparently, they were more numerous in the T4–100 group (Fig. 1C). In addition, ultrastructural modification in the cardiomyocytes nuclei of hypothyroid and T4–25 groups were not observed when compared with the control group (Fig. 1F), where the nuclear chromatin was homogeneous, exhibiting small and widespread dense areas. Moreover, a thin layer of dense chromatin was verified, joining the inner surface of the nuclear membrane. A relevant aspect observed in the nuclei of T4–100 animals was the presence of large concentrations of chromatin constituting a thick layer in the inner boundary of the nuclear membrane (Fig. 1G). Probably, the main feature in T4–100 group was the alteration in the intercalated discs of cardiomyocytes (Fig. 1E). They showed clumps of adherens junctions in areas where two or three neighboring cells were joined. In the control (Fig. 1D), hypothyroid and T4–25 groups, these structures were not altered, being formed by regular arrays of junctions arranged in steps.

Discussion

Disorders of the thyroid gland are the most frequent endocrine diseases, but the alterations in adult conditions are reversible and can be corrected with adjustment of circulatory thyroid hormone levels. In the present report, we have investigated the ultrastructural changes in the myocardium induced by an acute alteration of T4 levels. Using the same experimental model, we have previously demonstrated that both the T4 doses, as those used in this study, were able to induce a significant increase on the cross-sectional myocyte width, which was not accompanied by marked cardiac fibrosis [13].

The effect of thyroxine-promoting cardiac hypertrophy has been well documented in chronic hyperthyroidism, which has typically been associated with simultaneous increases in blood pressure [4]. However, in this acute study, there was no difference in systolic blood pressure between T4-treated animals and control-group animals, indicating that the cardiac hypertrophy was not due to elevated

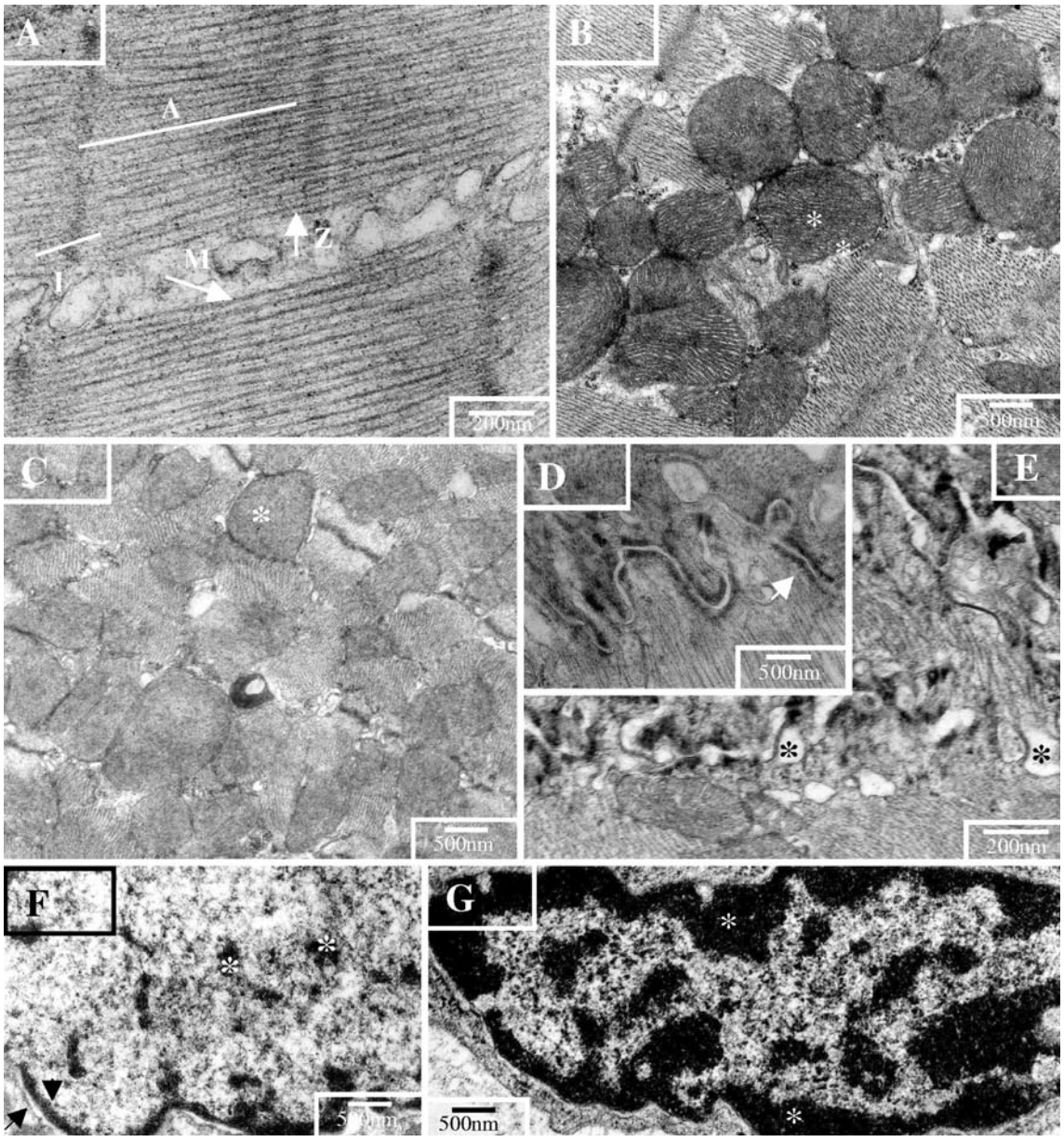

Fig. 1 Transmission electron micrographs of the myocardium. **A** Normal aspects of the A and I bands, M and Z discs in the myocardium of T4–25 group. **B**, **C** Non-altered mitochondria (*) and myofibrils (*arrow*) in the heart of hypothyroid (**B**) and T4–100 (**C**) groups. **D** An intercalated disc in control group with its characteristic sinuous aspect, where adherens junctions are evidenced (*arrow*). **E** A completely disorganized intercalated disk in the myocardium of T4–100 group; note the presence of wide spaces (*). **F** In the control group, the cardiomyocyte nucleus exhibits sparse (*) and a thin layer of dense chromatin (*arrow*) in the inner boundary of the nuclear membrane (*arrowhead*). **G** A large concentration of chromatin constituting a thick layer (*) in the inner boundary of the nuclear membrane in T4–100 group

hemodynamic parameters. Although dissociation between elevated arterial pressure and increased myocardial mass has been observed in this acute model of cardiac hypertrophy, hypothyroid rats presented decreased SBP and HW/BW ratio. This demonstrates that basal levels of thyroid hormone are very important for cardiac tissue metabolism and development and for maintenance of hemodynamic parameters. Furthermore, this dissociation suggests the existence of stimuli other than blood pressure that are responsible for the development and regression of cardiac hypertrophy [18]. Then, the indirect effects seem to be mediated mainly by up- or downregulation of alpha- and beta-adrenergic receptors [3], while the direct effects of thyroid hormone result from its binding to nuclear receptors, which function as transcription factors [6, 23]. Furthermore, a series of studies have recently shown important non-genomic effects of thyroid hormone, inducing different cytosolic signaling cascades, which can directly affect the gene expression [2, 9, 14].

Ultrastructural investigations of myocardial hypertrophy have demonstrated several characteristic changes in the various subcellular constituents of the myocytes [1, 12]. Additionally, the application of ultrastructural techniques has been useful in studies of cellular growth, allowing one to examine to what degree and in what sequence various subcellular components respond to growth stimuli.

As demonstrated in this study, in the myocardium of T4–25 and hypothyroid rats, no myofibrillar disarray or other significant ultrastructural alterations were detected. These results agree with Ferreira et al. [11] but differ from observations of the other authors [8, 24]. This discrepancy may be related to different dosages of T4 and/or to duration of treatment. Thyroid hormone presents profound effects on mitochondrial morphology and phenotype in cardiac muscle [20, 25]. Furthermore, Craft-Cormney and Hansen [8] demonstrated a significant increase in mitochondrial volume in the cardiac tissue, which characterized myocardial hypertrophy induced by thyroxine. In our study, we did not observe any alterations either morphology or phenotype of the mitochondria in all groups studied. However, although the number of these structures was not determined, apparently, they were more numerous in the T4–100 group. This apparent increase in the number of mitochondria is in accordance with other data previously obtained, since the literature on myocardial hypertrophy in hyperthyroidism indicates that, in such cases, myocytes are frequently characterized by multiple mitochondria [7, 16].

For effective cardiac contraction, strong adhesion between muscle cells and the transmission of the nervous stimulus from cell to cell are required [11]. Both these features depend on the existence of efficiently functioning intercalated discs. The intercalated discs of many cardiac muscle cells from T4–100 rats lost their staggered appearance and were seen as a disorganized group of adherens and gap junctions. This occurrence may be the consequence of a non-parallel arrangement of the muscle cells; probably, it will result in a loss of effective contraction force in the most affected areas.

In conclusion, the present study demonstrates that in the early stages of hyperthyroidism, the cardiac hypertrophy development was mainly due to direct effects of thyroid hormone. Despite cardiac hypertrophy development, there is no ultrastructural evidence of myocardial degeneration. However, it is still not clear how significant myocardial damage actually takes place in cardiac hypertrophy induced by thyroid hormone. We know, particularly from previous reports, that the mechanisms by which the animal model hyperthyroidism-induced cardiac hypertrophy occurs is multifactorial. Further studies are required to determine the intensity and severity of myocardial alterations promoted by low doses of T4 chronically.

References

1. Anversa P, Olivetti G, Melissar M, Loud A (1979) Morphometric study of myocardial hypertrophy induced by abdominal aortic stenosis. Lab Invest 38:341–349
2. Bassett JH, Harvey CB, Williams GR (2003) Mechanisms of thyroid hormone receptor-specific nuclear and extra nuclear actions. Mol Cell Endocrinol 31:1–11
3. Bilezikian JP, Loeb JN (1983) The influence of hyperthyroidism and hypothyroidism on α- and β-adrenergic receptor systems and adrenergic responsiveness. Endoc Rev 414:378–387
4. Bing RF, Briggs RSJ, Burden AC, Rusell GI, Swales JD, Thurston H (1980) Reversible hypertension and hypothyroidism: arterial pressure and hormone relationships. Clin Endocrinol 13:339–342
5. Biondi B, Palmieri EA, Fazio S, Cosco C, Nocera, M, SaccaL, Filetti S, Lombardi G, Perticone F (2000) Endogenous clinical hyperthyroidism affects quality of life and cardiac morphology and function of young and middle-aged patients. J Clin Endocrinol Metab 85:4701–4705
6. Brent GA, Moore DD, Larsen PR (1991) Thyroid hormone regulation of gene expression. Annu Rev Physiol 53:17–35
7. Callas G, Hayes IR (1974) Alteration in the fine structure of cardiac muscle mitochondria induced by hyperthyroidism. Anat Rec 178:539
8. Craft-Cormney C, Hansen JT (1980) Early ultrastructural changes in the myocardium following thyroxine-induced hypertrophy. Virchows Arch 33:267–273
9. Davis PJ, Davis FB (2002) Nongenomic actions of thyroid hormone on the heart. Thyroid 12:459–466
10. Di Meo S, de Martino Rosaroll P, Pito MC, De Leo T (1992) Modification of electrophysiological properties of rat heart with age. Arch Int Physiol Biochem Biophys 100:7–11
11. Ferreira PJ, L'Abbate C, Abrahamsohn A, Gouveia CA, Moriscot A (2003) Temporal and topographic ultrastructural alterations of rat heart myofibrils caused by thyroid hormone. Microsc Res Technique 62:451–459
12. Goldstein MA, Sordahl LA, Schwartz A (1974) Ultrastructural analysis of left ventricular hypertrophy in rabbits. J Mol Cell Cardiol 6:265–273
13. Hu LW, Benvenuti LA, Líberti EA, Carneiro-Ramos MS, Barreto-Chaves MLM (2003) Thyroxine-induced cardiac hypertrophy: influence of adrenergic nervous system versus renin-angiotensin system on myocyte remodeling. Am J Regul Comp Physiol 285:R1473–R1480
14. Kavok NS, Krasilnikova OA, Babenko NA (2001) Thyroxine signal transduction in liver cells involves phospholipase C and phospholipase D activation. Genomic independent action of thyroid hormone. BMC Cell Biol 2:5
15. Klein I, Ojamaa K (2001) Thyroid hormone targeting the heart. Endocrinology 142:11–12
16. Korenyi-Both A, Korenyi-Both I, Vages BC (1981) Thyrotoxic myopathy pathomorphological observation of human material and experimentally induced thyrotoxicosis in rats. Acta Neuropath 53:237–248
17. Marchant C, Brown L, Sernia C (1993) Renin-angiotensin system in thyroid dysfunction in rats. J Cardiovasc Pharmacol 22:449–455
18. Morgan HE, Kenneth M, Baker MD (1991) Cardiac Hypertrophy: mechanical, neural, and endocrine dependence. Circulation 83:13–24
19. Reynolds ES (1963) The use of lead citrate at high pH as an electron opaque stain in electron microscopy. J Cell Biol 17:208–212
20. Soboll S (1993) Thyroid hormone action on mitochondrial energy transfer. Biochem Biophys Acta 1144:1–16

21. Sun ZQ, Ojamaa K, Nakamura TY, Coetzee WA (2001) Thyroid hormone increases pacemaker activity in rat neonatal atrial myocytes. J Mol Cell Cardiol 33:811–824
22. Sussman MA (2001) When the thyroid speaks, the heart listens. Circ Res 89:557–559
23. Tsai MJ, O'Malley BW (1994) Molecular mechanisms of action of steroid/thyroid receptor superfamily members. Ann Rev Biochem 63:451–486
24. Wajdowicz A, Dabrós W, Zaczek M (1996) Myocardial damage in thyrotoxicosis ultrastructural studies. Pol J Pathol 47:127–133
25. Wrutniak-Cabello C, Casas F, Cabello G (2001) Thyroid hormone action in the mitochondria. J Mol Endocrinol 26:67–77

Virchows Arch (2005) 446: 270–277
DOI 10.1007/s00428-004-1184-0

ORIGINAL ARTICLE

Kazuto Yamazaki

CD10- and CD34-positive periglandular stromal cells in pulmonary benign metastasizing leiomyoma with metaplastic adenomyomatous glands: an ultrastructural and immunohistochemical study

Received: 20 July 2004 / Accepted: 22 November 2004 / Published online: 2 February 2005
© Springer-Verlag 2005

Abstract Two Japanese females, 36 years and 52 years old, with episodes of uterine leiomyoma, were operated on for pulmonary benign metastasizing leiomyomas (PBMLs) in their peripheral lung. Conventional light microscopic, ultrastructural, and immunohistochemical studies revealed that the PBMLs possessed an adenomyomatous histology, consisting of metaplastic glandular structures and stromal or smooth-muscle cell proliferation. In the tumorous nodules of the PBMLs, epithelial cells with the characteristics of lung epithelial cells of type-II pneumocytes were observed, together with ciliated and non-ciliated bronchiolar epithelial cells in the entrapped and metaplastic glands. The present study pointed out the unique periglandular stromal cells of fibroblastic cells, which were lacking the immunohistochemically conventional characteristics of normal lung smooth muscle cell but showed unique characteristics—ultrastructurally: fibroblastic lacking well-developed myofilaments with dense patches and well-developed external lamina; but immunohistochemically: CD10+, CD34+, alpha-smooth-muscle actin+, desmin−, estrogen receptor+, and progesterone receptor+. It was speculated that glandular metaplasia from entrapped respiratory epithelia cells might be introduced by the possible inductive interactions of periglandular mesenchymal stromal cells. Putative microenvironmental inductive roles were postulated for the periglandular stromal fibroblasts to induce a metaplastic change toward the glands from pre-existing lung epithelial cells revealing adenomyomatous features.

Keywords Type-II pneumocyte · Surfactant proteins · Mesenchymal stromal cells · Inductive microenvironment · Entrapped respiratory epithelial cells

K. Yamazaki (✉)
Department of Pathology, Saiseikai Central Hospital,
l-4-17 Mita, Minatoku,
108-0073 Tokyo , Japan
e-mail: KazutoYamazaki@aol.com
Tel.: +81-3-34518211
Fax: +81-3-34516102

Introduction

The pulmonary benign metastasizing leiomyoma (PBML) is a well-known but rather rare disease, usually encountered in women with a history of benign uterine leiomyoma and slowly growing multiple small nodules in the lung [1, 2, 4, 7, 9, 12–22]. These tumors usually demonstrate composite discrete small nodules in the peripheral lung, commonly showing the unique histology of adenomyomatous nodules, usually consisting of metaplastic glands possibly derived from entrapped lung epithelial cells and benign-looking smooth-muscle proliferations originating from the preexisting uterine leiomyoma [1, 2, 4, 7, 9, 12–22]. The epithelial inclusions are usually lined with cuboidal type-II pneumocytes without atypia or sometimes with bronchiolar epithelium [4, 7, 13]. The diagnostic descriptive of multiple fibroleiomyomatous hamartoma (MFLH) of the lung is morphologically identical to, and is now recognized as the same lesion as, the so-called PBML [4, 7]. A report has included three male cases with similar lesions where the tumors were believed to represent metastatic leiomyosarcomas with a hyper-well-differentiated histology [22]. Canzonieri et al. [2] proposed a unified histogenetic view of uterine leiomyoma with vascular invasion, intravenous leiomyomatosis, and PBML. They regarded the uterine leiomyoma with vascular invasion as the apparent precursor of intravenous leiomyomatosis and PBML. Others believe that PBML could be more satisfactorily explained by the concept of multifocality [3]. Takemura et al. [19] reported a case of benign metastasizing leiomyoma not only in the lung but also in the heart. Despite the interpretation of their hamartomatous nature [15], their common origin from uterine leiomyoma cells has been clearly demonstrated by the recent progress in molecular genetic techniques [20] (X-linked human androgen receptor gene: HUMARA). Furthermore, their sensitive nature to sex hormones has allowed attempts with hormonal therapy to achieve satisfactory success [14, 16–18, 21].

In the present report, interest is focused upon the histogenesis of the adenomyomatous histological pattern in the tumor tissue, possibly derived from entrapped lung epi-

thelial cells. Based on the results of ultrastructural and immunohistochemical studies, the author speculates that entrapped and morphologically changed metaplastic glands could be introduced by the possible inductive interactions of mesenchymal (smooth-muscle or fibroblastic) cells originating from the uterus and preexisting pulmonary epithelial cells. Putative inductive roles were assumed for the periglandular stromal fibroblasts for induction of a metaplastic change toward the arrays of cuboidal-shaped type-II pneumocytes, or sometimes bronchiolar epithelial cells from preexisting lung epithelial cells, revealing adenomyomatous features [13].

Clinical history

Case 1

A 36-year-old Japanese female was admitted to the hospital for evaluation and treatment of abnormal chest X-ray shadows with multiple small nodules in her peripheral lung. She had an episode of enucleation therapy for a 5.5× 7.5×4.8 cm and 140 g uterine leiomyoma with the histopathological diagnosis of conventional benign uterine leiomyoma. No vascular invasion was detected in the uterine leiomyoma. An abnormal shadow on chest X-ray with a single small nodule in the upper right peripheral lung had been noted in the patient approximately 4 years prior to the present admission. She had been followed up since with periodic chest X-ray and computed tomography (CT) scan checkups. The tumor size had gradually increased, and, 10 months prior to the admission, multiple small nodules appeared in her peripheral lung. CT scan findings showed a total number of more than ten nodules of less than 1.0 cm in diameter (Fig. 1A). Although a diagnosis of metastatic lung tumors was suspected, a thorough study was unable to identify the primary lesion. The patient underwent biopsy with video-assisted thoracic surgery (VATS) for the histopathological evaluation of the lesions in the upper S3a segment of her right lung. She was discharged after the pathological diagnosis of PBML, has been treated with hormonal therapy (hormonal manipulation of estrogen deprivation) after the operation, and followed up in the outpatient clinic without any serious changes.

Case 2

A 52-year-old Japanese female was admitted to the hospital for the excisional biopsy of a nodular lesion of approximately 1.5 cm in diameter in the S10 segment of her right lung. A nodular lesion had been noted approximately 4 months previously during examination of her gynecological problems related to a left ovarian clear cell adenocarcinoma. At that time, she had undergone extirpation of the uterus and bilateral uterine adnexa with an omentectomy for the clear cell adenocarcinoma in the left ovary. No vascular invasion was detected in the excised uterine leiomyoma. She had undergone a left ovarian cystectomy for a benign endometrial cyst 5 years prior to the last procedure. In her excised uterus, chronic cervicitis with squamous metaplasia, adenomyosis, and a benign leiomyoma of approximately 2 cm in diameter were revealed at that time, after the pathological examination of the excised uterus. After the most recent procedure, the patient had received anti-cancer chemotherapy and had been followed up to examine the growth of the nodule in her right lung with the periodic chest X-ray and CT scan checkups. The size of the lung tumor remained unchanged, and, to rule out the possibility of lung metastasis from the ovarian carcinoma, she underwent a VATS biopsy for the histopathological evaluation of the lesion in the S10 segment of her right lung. She was discharged after the pathological diagnosis of PBML and followed up without additional chemotherapy or hormone therapy in the outpatient clinic.

Materials and methods

The biopsied lung tissues, containing a total number of three tumors of PBML from the two cases, were examined with conventional light microscopy, light microscopic immunohistochemistry, and transmission electron microscopy.

Light microscopy and immunohistochemistry

The excised PBML tissue specimens were fixed in 15% formalin, embedded in paraffin wax, and processed using conventional histological techniques for sectioning and staining in hematoxylin and eosin, periodic acid-Schiff, and alcian blue. Immunohistochemical staining was performed using formalin-fixed, paraffin-embedded tissue sections and the Envision method (Dako, CA, USA) with or without appropriate pretreatment [23–25]. Primary antibodies for surfactant apoprotein A, surfactant apoprotein B (SP-B), prosurfactant apoprotein C (proSP-C), Clara cell 10 (CC 10), CA125, cytokeratin 7, cytokeratin 20, desmin, HHF-35 (muscle actin), alpha-smooth-muscle actin, estrogen receptor, progesterone receptor, Ki-67, p53, HMB45, CD10, leukocyte common antigen (LCA), CD34, c-kit, early membrane antigen (EMA), TTF-1, and secretory component were used.

Electron microscopy

The excised PBML tissue was fixed in 2.5% glutaraldehyde, postfixed in 1% osmium tetroxide, dehydrated using graded alcohol solutions, and embedded in epoxy resin. Ultrathin sections were stained using uranyl acetate and lead citrate and examined using a JEOL 1200 EXII transmission electron microscope [23–25].

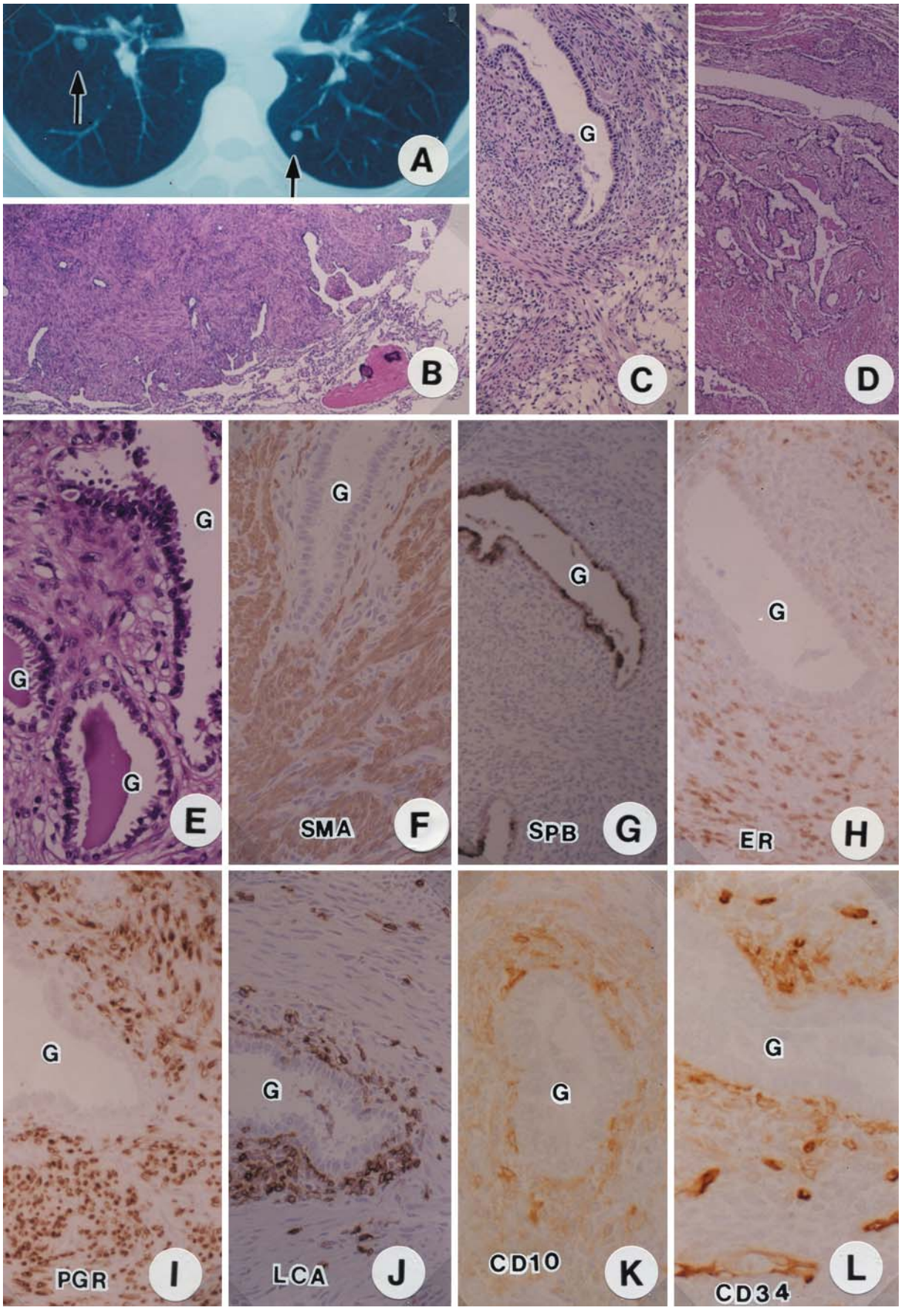
A
B
G
C
D
G
G
G
E
G
SMA
F
G
SPB
G
G
ER
H
G
PGR
I
G
LCA
J
G
CD10
K
G
CD34
L

◀ **Fig. 1** Lung computed tomography (CT) scanography, light micrograph of pulmonary benign metastasizing leiomyoma. *G* glandular structure of adenomyomatous area in the tumor tissue. **A** Lung CT scanography. Small nodular lesions distributed in the both lung (*arrows*) in case 1. **B** Low-power view of adenomyomatous tumor tissue associated with small ectopic ossicle. Hematoxylin and eosin stain in case 1, ×38. **C** Hematoxylin and eosin stain in case 1. Adenomyomatous histology, ×95. **D** Low-power view of adenomyomatous tumor tissue. Hematoxylin and eosin stain in case 2, ×38. **E** Hematoxylin and eosin stain in case 2. Adenomyomatous histology. Rather sparse distribution of spindle-shaped stromal cells in the periglandular area. Decapitating features in gland lining cells with eosinophilic amorphous luminal contents, ×190. **F** Immunostain for alpha-smooth-muscle actin (SMA) in case 1. Cytoplasm of proliferating smooth muscle cells stains positively. Periglandular stromal cells lacking the stains ×180. **G** Immunostain for surfactant protein B (SPB) in case 1. Many of the lining cells of the gland (G) stain positively in their cytoplasm, ×180. **H** Immunostain for estrogen receptor (ER) in case 1. Many of the nuclei of proliferating smooth-muscle cells stain positively, ×180. **I** Immunostain for progesterone receptor (PGR) in case 1. Many of the nuclei of proliferating smooth muscle cells stain positively ×180. **J** Immunostain for leukocyte common antigen (LCA, CD45RB) in case 1. Many leukocyte aggregated in the periglandular stroma stain positively in their membrane or cytoplasm, ×180. **K** Immunostain for CD10 in case 1. Periglandular stromal cells stain faintly positive in their membrane or cytoplasm, ×360. **L** Immunostain for CD34 in case 1. Not only definitive stain in the vascular endothelial cells but also periglandular stromal cells stain faintly positive in their membrane or cytoplasm ×360

Results

Gross findings

In the excised lung tissue from case 1, two small nodules of 6 mm and 3 mm in diameter were found. In the excised lung tissue from case 2, one small nodule of 15 mm in diameter was found.

Light microscopy and light microscopic immunohistochemistry

All three tumors showed similar adenomyomatous histology. With the background proliferation of stromal spindle-shaped smooth-muscle cells, tubular glandular structures with various shape and size were seen (Fig. 1B, C, D, E). Around the tubular glandular structures, periglandular loose stromal tissue demonstrated unique features, showing a mixture of a loose meshwork of sparsely distributed fibroblastic cells and associated lymphoid inflammatory cells (Fig. 1C, E). Small vascular structures and lymphoid inflammatory cells could be observed in the edematous periglandular stroma and contained the dendritic fibroblastic cells (Fig. 1C, E). The glandular epithelium was of a columnar shape with, or occasionally without, definitive apical cilia and mucin production. Some glands contained eosinophilic amorphous materials (Fig. 1E). Many of the small epithelial structures, including the gland-like structures, were usually lined with cuboidal type-II pneumocytes without atypia and no bronchiolar epithelia in both cases. In case 2, however, large gland-like spaces were sometimes lined with bronchiolar epithelial cells demonstrating occasional ciliation. Neither the stromal spindle-shaped smooth-muscle cells nor the glandular epithelium demonstrated significant nuclear atypism or abnormal mitotic figures (Fig. 1C, E).

The immunohistochemical findings revealed stromal spindle-shaped smooth-muscle cells with positive staining for desmin, HHF-35 (muscle actin), alpha-smooth-muscle actin (Fig. 1F), estrogen receptor, and progesterone receptor (Fig. 1H, I). Glandular epithelia were sometimes stained positively for surfactant apoprotein A, SP-B, proSP-C, CC 10, CA125, cytokeratin 7, cytokeratin 20, EMA, TTF-1, and secretory component (Fig. 1G). No positive staining was seen for estrogen or progesterone receptors (Fig. 1H, I). In the edematous periglandular stroma, fibroblastic spindle-shaped cells were not positive for definitive smooth-muscle cell markers of desmin, HHF-35 (muscle actin), and alpha-smooth-muscle actin (Fig. 1F). They stained positively for estrogen and progesterone receptors and CD10 (Fig. 1H, I, K). Some of them stained weakly for CD34 (Fig. 1H, I, K, L). Many of the lymphoid inflammatory cells in the edematous periglandular stroma stained for LCA (Fig. 1J). A few mast cells stained positively for c-kit. Ki-67 stained positively to various degrees in the tumor tissue, but HMB 45 and p53 did not stain positively. CD34 was distributed mainly in the endothelial cells of the vasculature (Fig. 1L).

Smooth-muscle cells in the non-tumorous lung tissue, that is, smooth-muscle cells in the vascular and bronchial wall, were positive for definitive smooth-muscle cell markers of desmin, HHF-35 (muscle actin), and alpha-smooth-muscle actin, but they did not reveal any of the staining characteristics of estrogen and progesterone receptors or CD10. Some of them occasionally stained positive for CD34.

Electron microscopy

Three ultrastructurally constitutional components could be discerned within the tumor nodule (Fig. 2A): an epithelial glandular component, the periglandular loose stromal layer, and definitive smooth-muscle bundles (Fig. 2A). The glandular epithelium showed a columnar shape with, or sometimes without, apical cilia and mucin production (Fig. 2A, B, C and Fig. 3A and Fig. 4A, B). In case 1, most of the epithelial cells revealed well-developed short microvillous cytoplasmic projections of the apical cell membrane, lamellar inclusions characterized in type-II pneumocytes, and apico-lateral cellular junctions facing the surface lumina (Fig. 3A); definitive type-II pneumocytes of cellular differentiation could be observed. In the apical region in particular, the observed characteristics included well-developed microvillous cytoplasmic folding and granules with high or medium electrodense finely granular contents (Fig. 3A). Vacuoles were characteristically included in the cytoplasm, known as multivesicular and multilamellar bodies (Fig. 3A). In the basal portion of the glandular epithelia, well-developed basal lamina could be seen, continuing to the loose fibro-cellular stroma meshwork (Fig. 2A, B, C, Fig. 3A, Fig. 4A). In case 2, many of

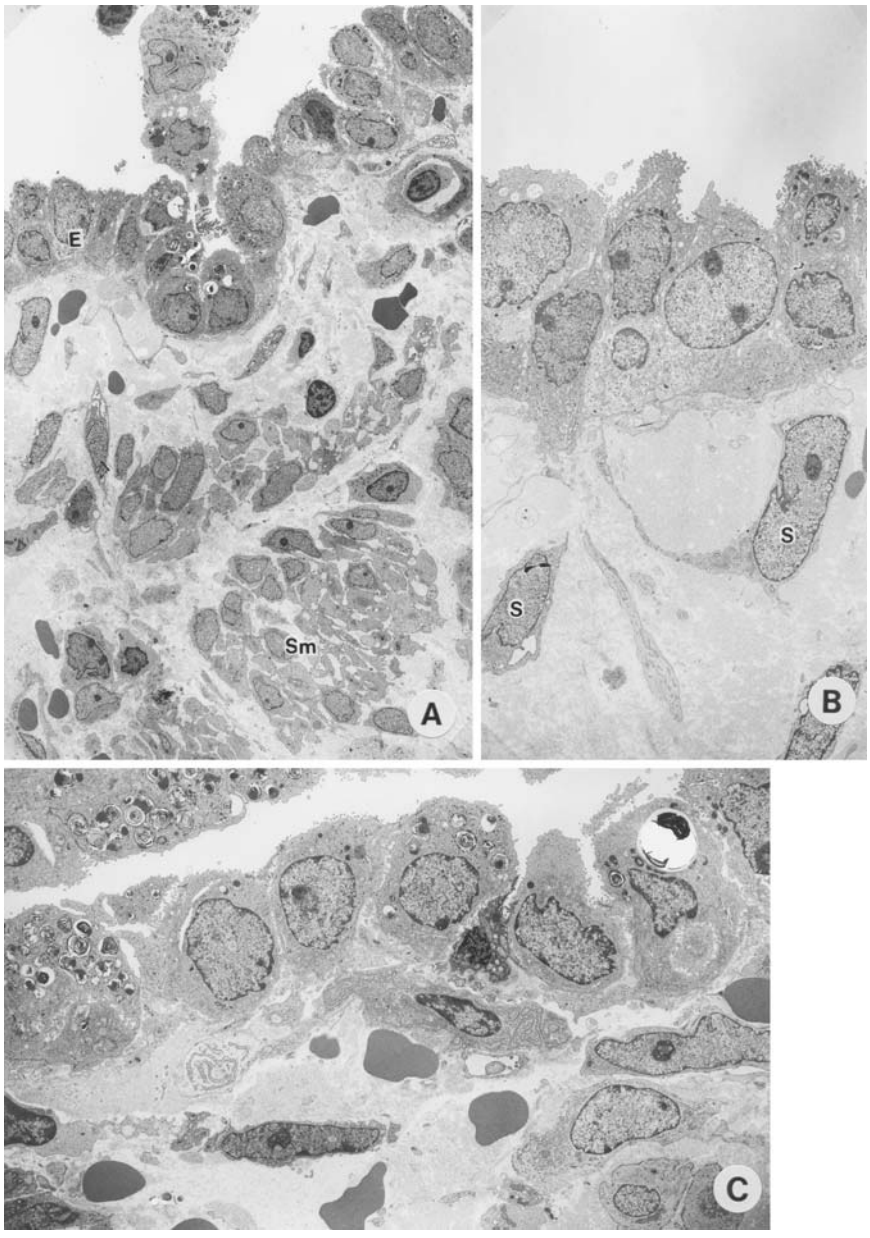

Fig. 2 Transmission electron micrographs of pulmonary benign metastasizing leiomyoma in case 1. **A** Low-power view of the periglandular area in the pulmonary benign metastasizing leiomyoma. Between the layers of epithelial gland lining type-II pneumocytes (E) and compact arrays of proliferating smooth muscle cells (Sm), spindle-shaped or stellate-shaped stromal cells distributed in the sparse fashion associated with some inflammatory lymphoid cells ×1800. **B** Fibroblastic primitive stromal cells in the periglandular area (S), ×3500. **C** Fibroblastic primitive stromal cells in the periglandular area. In the *lower right* corner, smooth-muscle is seen, ×3500

the epithelial cells revealed the feature of not only type-II pneumocytes but also ciliated columnar epithelial cells or Clara cells without cilia (Fig. 4A, B).

In the edematous periglandular stroma, fibroblastic spindle-shaped cells did not reveal definitive smooth-muscle cell features, but demonstrated spindle-shaped or satellite-shaped mesenchymal dendritic features with well-developed rough-surfaced endoplasmic reticulum (Fig. 2B, C, Fig. 3A, B, Fig. 4A). They had embedded, or were intimately associated with, fibrous collagen fibers. They lacked intermediate-type myofilaments, with a focal dense patch, incomplete external lamina, or frequent features of membrane-associated pinocytic vesicles (Fig. 2B, C, Fig. 3A, B, Fig. 4A, B). Among the loose cellular meshwork, small blood vessels, mast cells, lymphocytes, and granulocytes were distributed, associating the dendritic cell processes of the periglandular stromal fibroblasts (Fig. 2A, C, Fig. 3A, Fig. 4A).

Stromal spindle-shaped smooth-muscle cells, which were the main constituents of the tumor, showed ultrastructurally definitive smooth-muscle features of intermediate-type myofilaments with focal dense patches, incomplete external lamina, and frequent features of membrane-associated pinocytic vesicles (Fig. 2A, Fig. 3B). Occasionally, isolated cilia could be seen generated from the perikaryotic cytoplasm.

Discussion

In the present case, the differential histopathological diagnoses included hamartomas with a prominent smooth-mus-

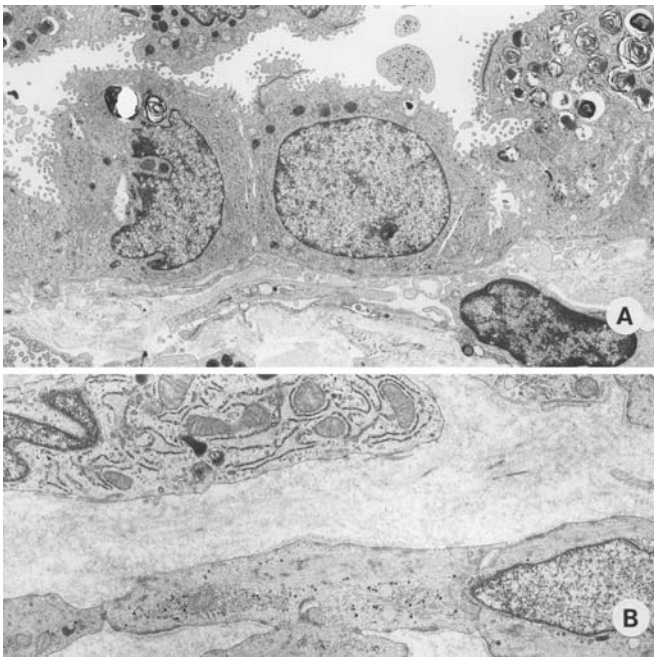

Fig. 3 A Metaplastic epithelial cells in the adenomyomatous area of the pulmonary benign metastasizing leiomyoma. Multilamellar bodies in the apical areas of type-II pneumocytes with well-developed apical microvilli and apico-lateral cellular junctions ×7000. **B** A fibroblastic primitive stromal cell with well-developed rough-surfaced endoplasmic reticulum (rER) (in the *upper left*) and smooth-muscle cells (in the *lower half*) with well-developed intracytoplasmic myofilaments with dense patches in the tumor tissue, ×18,000

cle component, low-grade leiomyosarcomas (primary or metastatic), primary leiomyoma, lymphangioleiomyomatosis, plasma cell granulomas, metaplastic smooth-muscle cell proliferation in focal scars and fibrotic lung disease, and other spindle cell tumors (especially spindle cell carcinoid and intrapulmonary solitary fibrous tumors) [4, 5, 7]. Pulmonary endometriosis has previously been reported in the literature [8]. Careful histopathological examination of the lesion can rule out the possibility of the others [4, 5, 7].

Although the other histopathological diagnostic name of MFLHs might exist, as well as arguments as to whether they are true metastasizing or primary tumors, the present case could be safely assumed to be PBML [1, 2, 4, 7, 9, 12–22] through the characteristic clinical history and histopathological studies. Compared with pre-existing smooth-muscle cells in the non-tumorous lung tissue, such as smooth-muscle cells in the vascular and bronchial walls, the PBML or stromal tumor cells in the present tumorous growth showed, immunohistochemically, some different characteristics in the positive staining for estrogen and progesterone receptors, CD34, and CD10 [1, 2, 4, 7, 9, 12–22]. The isolated cilia occasionally observed might be indicative of an active cell cycle in the present proliferating smooth-muscle cells and, taken together with the recent genetic study of the HUMARA gene, might be supportive of findings for the metastasizing theory of the tumor [20]. Huang et al. [15] reported focal immunoreactivity for the HMB-45 antibody in PBML tumor cells. In the present cases, no tumor cells stained positively for HMB 45.

The ultrastructural study of Herrera et al. [13] demonstrated that the gland-like spaces represent entrapped alveoli and terminal respiratory bronchioles. In the present study, both the immunohistochemistry and electron microscopy indicated the PBML epithelial glands consisted of epithelial cells of type-II pneumocytes or occasionally bronchiolar epithelial cells. However, their constitutional population and the shape of the gland-like spaces were different from the normal or physiological state of the alveoli or bronchioles. These conformational changes could be regarded as a kind of metaplasia, which is consistent with the notion of glandular metaplastic change [4, 7, 11].

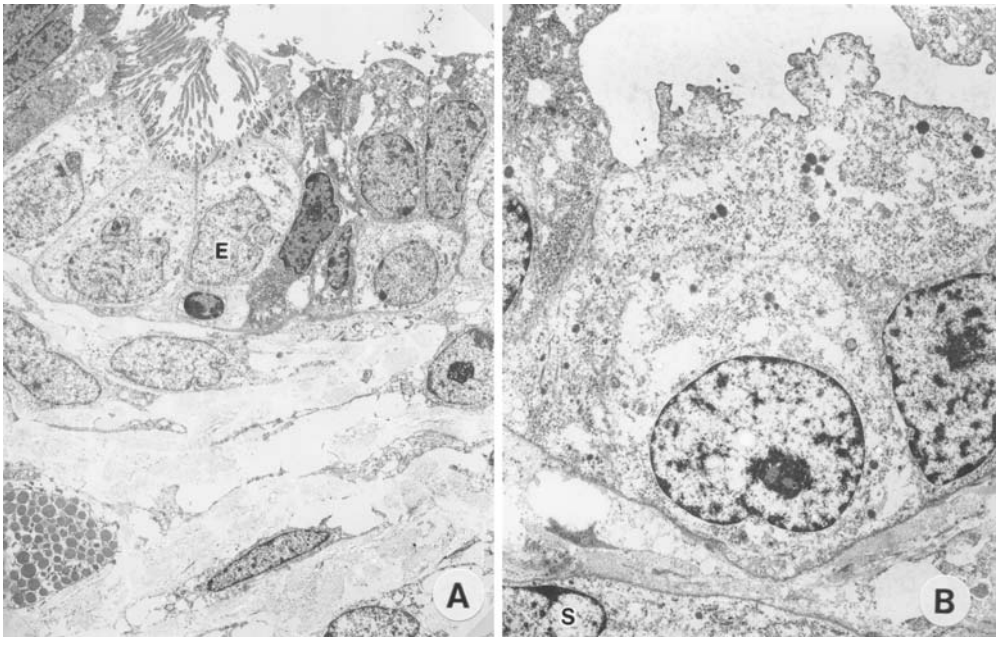

Fig. 4 Transmission electron micrographs of pulmonary benign metastasizing leiomyoma in case 2. **A** Ciliated and non-ciliated columnar epithelial cells (E) lining the adenomatous glands in the tumor nodule. Beneath the epithelial layer, spindle-shaped or stellate-shaped fibroblastic cells distributed in the rather loose stromal tissue. A mast cell in the peri-glandular loose stromal tissue (M) ×3,500. **B** Clara-like epithelial cells with apical decapitation and apical small electron dense secretory granules lining the adenomatous metaplastic gland. Basal lamina. A subepithelial fibroblastic stromal cell (S), ×7000

The phenomenon of metaplasia (or synonymous transdifferentiation) is defined as occurring when a certain differentiated type of cell is formed from other already differentiated cells [4, 7, 11]. In the present case, interest is focused upon the histogenesis of the adenomyomatous histological pattern in the tumor tissue. After a thorough ultrastructural and immunohistochemical study, the author speculates that metaplastic glands could be introduced by the possible inductive interactions of mesenchymal (stromal fibroblastic) cells, possibly originating from the uterus, and pre-existing pulmonary epithelial cells [11]. Putative inductive roles were assumed for the periglandular fibroblasts to induce the well-developed metaplastic change toward type-II pneumocytes or bronchiolar epithelial cells from pre-existing lung epithelial cells, revealing adenomyomatous features [11].

An interface or boundary between the metaplastic gland and proliferated smooth-muscle cells, well-developed basal lamina, and fibroblastic spindle cells was frequently seen. The cells had the appearance of primitive fibroblastic or mesenchymal cells, extending thin cytoplasmic processes and intimately associating with the basal lamina of the metaplastic gland [10, 11]. In the interfaces of the glandular-stromal area of the edematous periglandular stroma, unique primitive stromal fibroblastic cells with an immunohistochemical distribution of CD10 and CD34—but lacking other definitive smooth-muscle cell markers—were seen [6]. Interestingly, periglandular stromal fibroblasts showed, immunohistochemically, positive staining for some hematopoietic precursor cell markers of CD10 and CD34. CD10 (CALLA, neutral endopeptidase, mettaloendopeptidase) is a zinc-binding metalloprotease that cleaves peptides on the amino side of hydrophobic amino acids, thereby reducing the local concentrations of peptide hormones [6]. CD10 is usually distributed in some hematopoietic cells and their counterparts in neoplasms. CD10 is recognized to stain endometrial stroma but is focally positive in many female genital smooth-muscle neoplasms [6], while the stromal cell distribution of a CD34 antigen is now well known [6]. In this study, the author has demonstrated that PBMLs contain a population of CD10-positive fibroblastic cells arranged adjacent to the entrapped non-neoplastic pulmonary epithelial elements. Although these cells stain similarly to endometrial stromal cells, and endometrial stromal differentiation could be seen in uterine smooth muscle tumors, it might be possible to interpret these fibroblastic cells as the result of focal endometrial stromal differentiation. Although it is very hard to fully discuss the provenance and classification of this periglandular stromal cell-type, these cells might represent some kind of myofibroblast, fibroblast, abortive smooth-muscle cell, a cell with endometrial stromal differentiation, or a simple primitive mesenchymal stromal cell, etc. Detailed and possible mechanisms of the induction theory need to be explained in the future.

As for how mesenchymal–epithelial interaction is achieved, a part of the significant cell-to-cell, cell-to-matrix, and epithelial–mesenchymal interactions was revealed by this study [10, 11]. Metaplasia is thought to arise from genetic re-programming of stem cells. Chemicals, vitamins, or growth factors most likely play a role in such metaplasia, such as retinoic acid or bone morphogenetic factors [11]. Metaplasia is a unique pathological phenomenon introduced by active inductive cellular interactions of stromal microenvironment and the parenchimo-epithelial component [11]. Thus, in the specimens of this study, metaplastic glands had a lamina propria-like stroma tissue, which contained the unique periglandular stromal cells of immature or fibroblastic stroma cells. They showed unique characteristics, ultrastructurally lacking well-developed myofilaments with dense patches and well-developed external lamina and, immunohistochemically, CD10+, CD34+, alpha-smooth-muscle actin+, desmin−, estrogen receptor+, progesterone receptor+, and associated LCA-positive lymphoid inflammatory cells. These immunohistochemical reactions might be interpreted as having some functional significance. The ideas about how the stromal components might induce the particular morphology of the entrapped epithelial elements might be highly speculative and not supported directly by data from this study alone. However, it would be hard to believe something specific to the uterine stroma is responsible for this metaplasia, since a similar metaplastic change could be seen to be associated with a range of other pulmonary mesenchymal lesions (both primary and metastatic), such as solitary fibrous tumor, pulmonary hamartoma, and metastatic sarcomas from diverse sites [23, 24]. This study and discussion still do not quite clarify the exact intentions of the author concerning new viewpoints of the causal and formal pathogenesis of metastases of "low-grade malignant uterine leiomyosarcomas" (which is the correct term).

Acknowledgements The authors would like to acknowledge the technical assistance of T. Nagai and K. Fujita with the electron microscopy studies, M. Furihata, T. Kohno, K. Nagawatari, A. Furusawa, T. Ooyama, and S. Sasahara for the help with light microscopic and immunohistochemical studies, and the valuable discussions and help offered by Drs. K.Suemasu, H. Orikasa, H. Nomori, I Ootuka, H. Horio, T. Aoki, H. Kayano, J. Shiraishi, and Y. Mori.

References

1. Abramson S, Gilkeson RC, Goldstein JD, Woodard PK, Eisenberg R, Abramson N (2001) Benign metastasizing leiomyoma: clinical, imaging, and pathological correlation. AJR Am J Roentgenol 176:1766–1409
2. Canzonieri V, D'Amore ES, Bartoloni G, Piazza M, Blandamura S, Carbone A (1994) Leiomyomatosis with vascular invasion. A unified pathogenesis regarding leiomyoma with vascular microinvasion, benign metastasizing leiomyoma and intravenous leiomyomatosis. Virchows Arch 425:541–545
3. Cho K, Woodruff JD, Epstein JI (1989) Leiomyoma of the uterus with multiple extrauterine smooth muscle tumors: a case report suggesting multifocal origin. Hum Pathol 20:80–83
4. Colby T, Koss MN, Travis WD (1995) Atlas of tumor pathology. 21 Tumors of the lower respiratory tract. Armed Forces Institute of Pathology, Washington, D.C.
5. Colby T, Yousem SA (1997) Lungs. Histology for pathologists. Lippincot–Raven Publishers, Philadelphia
6. Dabbs D (2002) Diagnostic immunohistochemistry. Churchill Livingstone, New York

7. Dail D, Hammar SP (1993) Pulmonary pathology. Springer, Berlin Heidelberg New York
8. Duskova J, Vitkova I (2001) Pulmonary endometriosis. Cas Lek Cesk 140:214–216
9. Esteban J, Allen WM, Schaerf RH (1999) Benign metastasizing leiomyoma of the uterus. Arch Pathol Lab Med 123:960–962
10. Ghadially F (1997) Ultrastructural pathology of the cell and matrix. Butterworth–Heinemann, Boston
11. Gilbert S (2000) Developmental biology. Sinauer Associates Inc., Sunderland
12. Goyle K, Moore DF Jr, Garrett C, Goyle V (2003) Benign metastasizing leiomyomatosis: case report and review. Am J Clin Oncol 26:473–476
13. Herrera G, Mile PA, Greenberg H, Reimann BE, Weisman IM (1983) The origin of the pseudoglandular spaces in metastatic smooth muscle neoplasm of uterine origin. Report of a case with ultrastructure and review of previous cases studied by electron microscopy. Chest 83:270–274
14. Horstmann J, Pietra GG, Harman JA, Cole NG, Grinspan S (1977) Spontaneous regression of pulmonary leiomyomas during pregnancy. Cancer 39:314–321
15. Huang P, Chen JT, Chia-Man C, Kwan PC, Ho WL (2000) "Benign metastasizing leiomyoma of the lung: a case report." J Formos Med Assoc 99:948–951
16. Jacobson T, Rainey EJ, Sussex CW (1995) Pulmonary benign metastasising leiomyoma: response to treatment with goserelin. Thorax 50:1225–1226
17. Jautzke G, Muller-Ruchholtz E, Thalmann U (1996) Immunohistological detection of estrogen and progesterone receptors in multiple and well differentiated leiomyomatous lung tumors in women with uterine leiomyomas (so-called benign metastasizing leiomyomas). A report of 5 cases. Pathol Res Pract 192:215–223
18. Kardy M, Sievers C, Engelmann C (1999) Pulmonary leiomyomatosis in women after hysterectomy for uterine myoma. Benign metastasizing leiomyoma? Acta Chir Hung 38:57–61
19. Takemura G, Takatsu Y, Kaitani K, Ono M, Ando F, Tanada S, Niwa H, Tankawa H, Fujiwara T, Yamabe H (1996) Metastasizing uterine leiomyomas. A case with cardiac and pulmonary metastasis. Pathol Res Pract 192:622–629
20. Tietze L, Ginther K, Horbe A, Pawlik C, Klostherhalfen B, Handt S, Merkelbach-Bruse S (2000) Benign metastasizing leiomyoma: a cytologenetically balanced but clonal disease. Hum Pathol 31:126–128
21. Uchida T, Tokumaru T, Kojima H, Nakagawaji K, Imaizumi M, Abe T (1992) A case of multiple leiomyomatous lesions of the lung: an analysis of flow cytometry and hormone receptors. Surg Today 22:265–268
22. Wolff M, Silva F, Kaye G (1979) Pulmonary metastases (with admixed epithelial elements) from smooth muscle neoplasms. Report of nine, cases, including three males. Am J Surg Pathol 3:325–342
23. Yamazaki K (2003) An ultrastructural, immunohistochemical, and cytogenetical study of monophasic synovial sarcoma: Implications of the frequent ultrastructure of oligocilia and concentric membranous bodies with positive immunostaining for VS38c and MEF2. Ultrastruct Pathol 27:235–241
24. Yamazaki K (2004) Electron microscopy and immunohistochemistry studies of pulmonary carcinosarcomas expressing the transcription factor MEF-2 and showing significant cell-to-cell, cell-to-matrix, and epithelial-mesenchymal interactions. Virchows Arch 442:542–553
25. Yamazaki K (2003) Pulmonary well-differentiated fetal adenocarcinoma expressing lineage-specific transcription factors (TTF-1 and GATA-6) to respiratory epithelial differentiation: an immunohistochemical and ultrastructural study. Virchows Archiv 442:393–399

Virchows Arch (2005) 446: 278–286
DOI 10.1007/s00428-004-1176-0

ORIGINAL ARTICLE

Judit Nagy · Liliána Z. Fehér · István Sonkodi · József Lesznyák · Béla Iványi · László G. Puskás

A second field metachronous Merkel cell carcinoma of the lip and the palatine tonsil confirmed by microarray-based comparative genomic hybridisation

Received: 9 September 2004 / Accepted: 8 November 2004 / Published online: 25 February 2005
© Springer-Verlag 2005

Abstract Merkel cell carcinoma was diagnosed in a 79-year-old Caucasian woman. The tumour was localised to the upper lip and was in stage T2. After successful cryosurgery and a 7-year tumour-free period, a new tumour developed in her palatine tonsil. Histologically and immunohistochemically, this resembled the tumour in the lip. The regional lymph nodes were devoid of metastasis. The paraffin-embedded material of the two tumours and the unaffected lymphatic tissue were analysed with DNA microarrays for comparative genomic hybridisation to assess the genetic relationship of the tumours. In both tumours, regions on 2p and 10p were commonly over-represented, while 41 regions on chromosomes 1–4, 6, 8–9, 11 and 14–22 were commonly under-represented. Chromosomes 1, 3, 4, 16–18 and X were most frequently involved in the DNA losses. In gene copy numbers in the two tumours, 31 chromosome locations were found to be differently affected. The partly similar and partly different molecular patterns indicated a genetic relationship between the tumours and excluded the possibility that the tonsillar tumour was a metastasis. The findings suggest that a genetically altered field was the reason for the development of the tonsillar cancer; thus, it can be regarded pathogenetically as a second field tumour.

J. Nagy · I. Sonkodi
Department of Oral Medicine, Department of Dentistry and Oral Surgery, University of Szeged, Faculty of Medicine, Szeged, Hungary

L. Z. Fehér · L. G. Puskás (✉)
Laboratory of Functional Genomics, Biological Research Centre, Hungarian Academy of Sciences,
P.O. Box 521, 6701 Szeged , Hungary
e-mail: pusi@brc.hu
Tel.: +36-62-599782
Fax: +36-62-432576

J. Lesznyák
Department of Histopathology, Bács-Kiskun County Hospital, Kecskemét, Hungary

B. Iványi
Department of Pathology, University of Szeged, Szeged, Hungary

Keywords Merkel cell carcinoma · Second field tumour · Comparative genomic hybridisation · DNA microarray · Chromosome imbalances

Introduction

Merkel cells are found in the skin and in those parts of the mucosa derived from the ectoderm [11]. These cells are the origin of a rare, malignant neuroendocrine tumour that occurs predominantly in the sun-exposed areas of the skin called Merkel cell carcinoma (MCC) [1, 2, 4, 19, 20, 22, 28]. Local recurrence and regional or distant metastases generally develop within a short period of time. Oropharyngeal metastasis is very rare, and metastasis to the palatine tonsil has been described in only one case [27]. A perioral or intraoral localisation of the MCC is very infrequent: [13, 20] to date, 10 cases of MCC of the lip [35] and 14 cases of intraoral MCCs have been described [3, 16, 20]. During the past decade, we treated and followed up an elderly woman with MCC of the upper lip. After a long tumour-free period, an anaplastic carcinoma with neuroendocrine features developed in her palatine tonsil, raising the possibility of a late haematogenous metastasis, a second field tumour or a second primary tumour.

The term “secondary field tumour” was introduced in 1953 by Slaughter et al., who examined slides from patients with head and neck cancer [29]. It was observed that all of the epithelium beyond the margins of the tumours displayed histological alterations, and 11% of the patients were found to have more than one independent area of malignancy. The authors concluded that the mucosa of the head and neck had undergone a change, perhaps due to carcinogen exposure, and was, therefore, more susceptible to the development of foci of malignant transformation. Organs in which field cancerisation has been described since then are the oral cavity, oropharynx, larynx, lung, oesophagus, colon, skin, vulva, cervix, breast, renal pelvis, ureter and bladder [5–7, 10].

The determination of molecular patterns of first and second tumours has become a valuable tool to explore the

relationship between them: similar aberrations indicate a metastasis, partly different aberrations indicate a second field tumour and different aberrations denote a second primary tumour [5, 6, 10]. In the present study, we identified the molecular patterns with comparative genomic hybridisation (CGH) with microarray technology. Array-based CGH consists of a series of mapped artificial bacterial chromosomes or sequenced cDNA clones on glass slides, to which DNA from test and control samples is hybridised [8, 19–21, 30]. This approach allows the determination of copy number changes of chromosome regions without a need for tissue cultures and the preparation of metaphase spreads, as DNA extracted from a tumour specimen is used. Another major advantage of CGH is that archived specimens can be also studied. We applied human cDNA microarrays as a tool, DNA from paraffin-embedded tumour materials (from both the primary and secondary tumours) as test probes and DNA from normal lymph nodes as control probes.

Previous CGH studies of MCCs have identified divergent regions that are affected, with a small number of similarities between the samples analysed. Recurrent chromosomal imbalances detected using CGH analysis were loss of 3p, 4p15-pter, 10q, 13q and 17p and gains of 1q, 3q, 5p, 6, 8q, 18 and 20 [12, 24, 33, 34]. In the present study, we detected some of the previously found regions and also numerous novel regions with chromosomal imbalances. Copy number changes of nine chromosome regions detected by CGH were analyzed using real-time quantitative polymerase chain reaction (QPCR). Potential oncogenes, tumour suppressor and apoptotic genes mapped to regions detected as changed were also recorded. The results suggest that a genetically altered field was the reason for the development of the tonsillar cancer; thus, it can be regarded pathogenetically as a second field tumour.

Materials and methods

Case report

Between 1970 and 2003, 4418 patients with malignant orofacial tumours were treated in our clinic. One of these patients suffered from MCC. A 79-year-old Caucasian woman presented with a tumour in her upper lip. She was an outdoor worker and never smoked. She was disturbed only about the aesthetics. The physical examination revealed a 2–3-cm firm, compact mass in the skin of the upper lip on the left side. It was sharply separated from its surroundings and had a teleangiectatic surface (Fig. 1). The tumour was classified as stage T2. No regional lymph-node metastasis was detected. Surgical resection of the tumour and removal of the regional lymph nodes were suggested, but she refused it. As an alternate therapy, a biopsy was taken, and cryotherapy was applied according to the standard protocol. Light microscopy revealed that the tumour was confined to the dermis and was sharply separated from the epidermis (Fig. 2a). The tumour cells were arranged in nests and cords. Cytologically, the tumour cells were monomorphic, the nuclei were round and the chromatin pattern was finely granular and "dusty". The nucleoli were small; often two or even three were detected. The cytoplasm was scanty. The mitotic rate was high (six to ten figures/high-power field). The Grimelius staining was negative. The results of immunostainings are shown in Table 1 and Fig. 2. The histological and immunohistochemical features pointed to MCC of the lip. Following the histological diagnosis, distant metastases in the lungs and bones were searched for, with negative results.

Fig. 1 Tumourous mass sharply separated from the surroundings in the skin of the upper lip

In the 7-year follow-up, the patient was in a tumour-free condition. After 7 years, she was admitted to the County Hospital with a left palatine tonsillar tumour. This tumour was resected in part, and the regional lymph nodes were removed. Histologically, the tumour displayed features of anaplastic carcinoma (Fig. 3). The results of immunostainings are summarised in Table 1. The histological and immunohistochemical features pointed to MCC of the lip. Following the histological diagnosis, distant metastases in the lungs and bones were searched for, with negative results.

The morphological appearance of the tumour resembled that of the MCC of the lip. A further excision was performed 3 months later. The morphological and immunohistochemical features of the tonsillar tumour were essentially the same as observed 3 months earlier. The patient died at home on the 20th postoperative day. Autopsy was not performed.

Sample preparation, labelling

Paraffin-embedded tissues (200–500 mg) were deparaffinised in hexane and washed with ethanol. DNA was purified

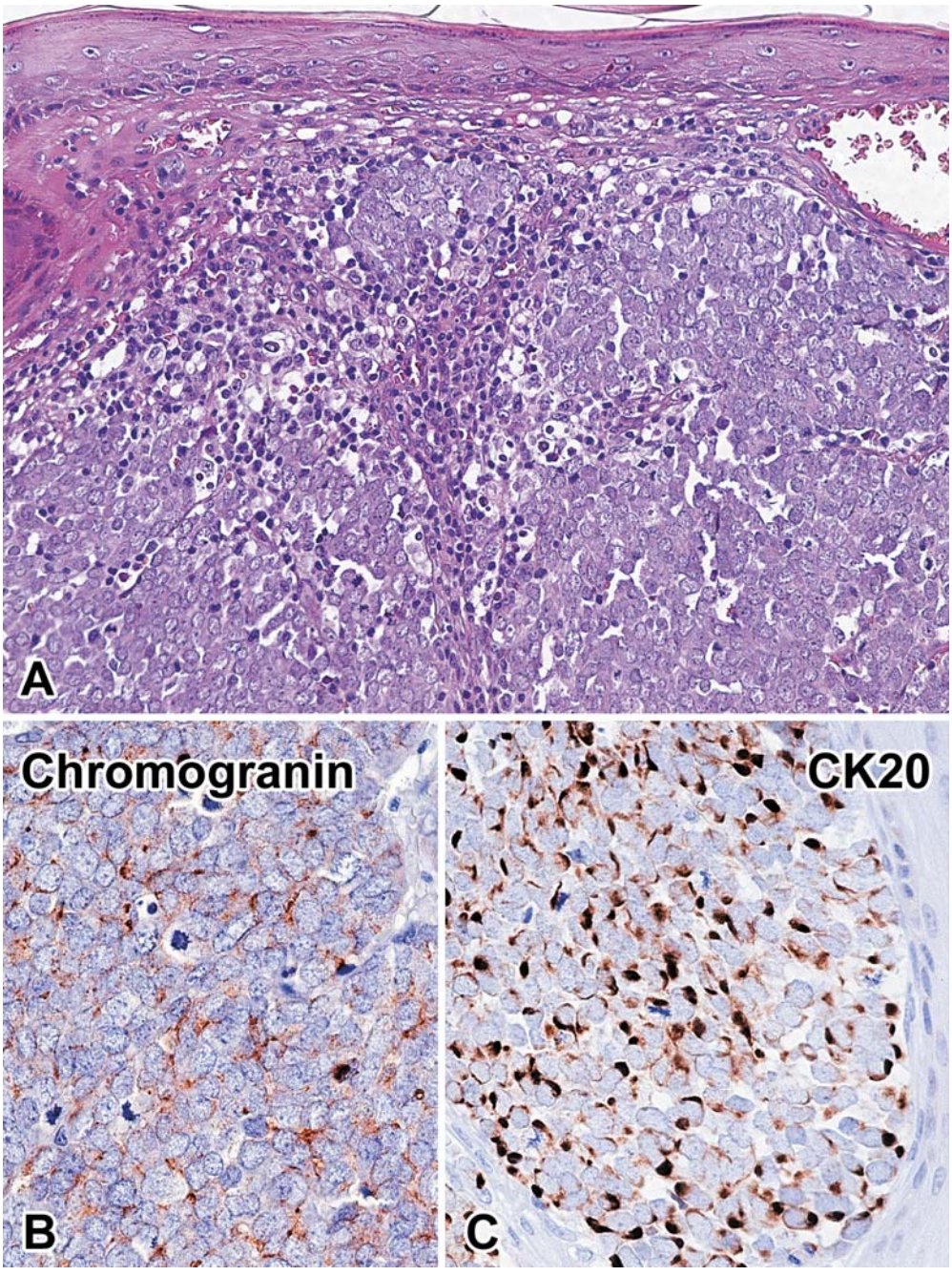

Fig. 2 Merkel cell carcinoma of the lip. **A** Small, monomorphic tumour cells fill the dermis arranged in nests and cords. The nuclei exhibit moulding. Haematoxylin-eosin ×200. **B** Chromogranin positivity of tumour cells ×400. **C** Paranuclear dots by cytokeratin-20 staining ×400

Table 1 Immunohistochemical findings

Immunohistochemical markers	Lip tumour	Tonsillar tumour
AE1/AE3	+++	+++
Cytokeratin	20	20
Paranuclear dots	+++	++
Chromogranin	++	+
Synaptophysin	–	–
TTF	–	–
HMB–45	–	–
CEA	–	–
Lymphoid markers	–	–

by using the DNA purification kit from Macherey-Nagel (Düren, Germany) according to the manufacturer's instructions. First, 100 ng genomic DNA from each sample was amplified with a modified version of the DOP (degenerate oligonucleotide primed) PCR protocol using a real-time PCR instrument to follow the amplification [9, 15]. Reactions were performed in a total volume of 100 µl. The cycling parameters were as follows: heat start at 95°C for 4 min, 8 cycles of 94°C denaturation for 50 s, 45°C annealing for 2 min to 72°C with 0.2°C/s and extension at 72°C for 90 s. After the 8 cycles, the reaction mix was separated into two 50-µl portions, and SybrGreen was added to the mix (1× final concentration, Molecular

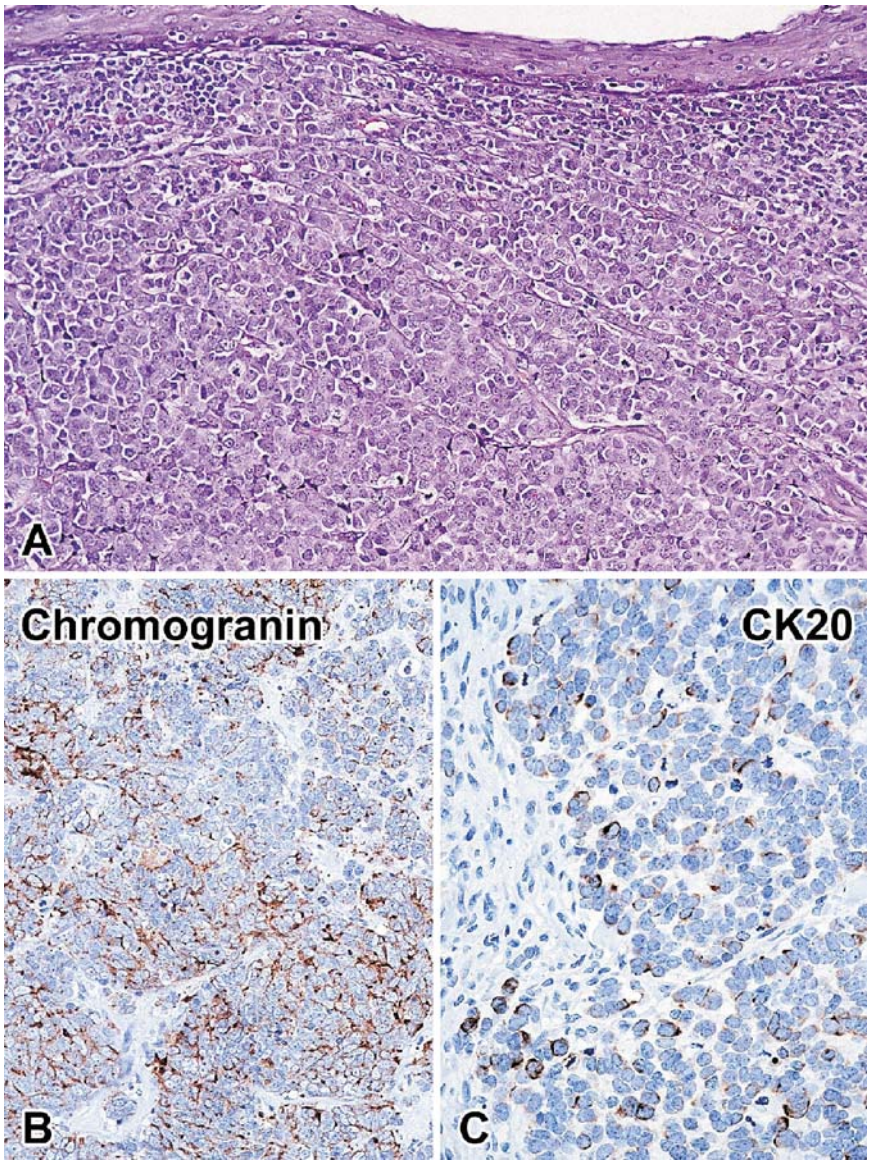

Fig. 3 A Anaplastic carcinoma of the tonsil. Hematoxylin-eosin ×200. **B** Chromogranin positivity in the tumour cells ×400. **C** Some tumour cells display paranuclear dots by cytokeratin-20 staining ×400

Probes, Eugene, USA). The following cycling protocol was performed in a real-time PCR instrument, RotorGene 2000 (RotorGene, Sydney, Australia): denaturation at 95°C for 40 s, annealing at 58°C for 1 min and extension at 72°C for 80 s. The cycling was performed just before the reaction reached the plateau to avoid over-amplification of the products (usually in 18–22 cycles). The PCR products were purified on PCR-purification columns (Bioneer, Daejeon, Korea). Next, 100 ng purified DNA was labelled with another round of PCR in the presence of Cy3-dUCTP (0.05 mM) in a total volume of 50 μl with the same parameters for 20 cycles as in the second PCR. In all these reactions, UN primer (5′-CCGACTCGAGNNNNNNATGTGG-3′) was used in a 1-μM concentration [31]. The reactions were performed with ExTaq DNA polymerase in 1× buffer (Takara, Tokyo, Japan). The labelled PCR products were purified with the PCR purification kit (Bioneer). The eluted DNA was dried in a Speed-Vacuum.

Hybridisation, scanning, data processing

The labelled DNA was reconstituted in ChipHyb hybridisation buffer (Ventana Discovery, Tuchon, USA) containing 20 μg human Cot DNA and 5 μg salmon sperm DNA (Invitrogen). Hybridisation was performed on human cDNA microarrays having 3200 gene-specific samples in duplicate in 200 μl using the Ventana hybridisation station (Ventana) at 42°C for 8 h [25, 26]. After hybridisation, the slides were washed twice in 0.2×sodium saline citrate at room temperature for 10 min and then dried. Scanning and data analysis were performed as described previously [21]. Briefly, data presented in this study were calculated from the results of four data points obtained from two separate labelling and hybridisation protocols. The background-corrected intensity data was filtered for flagged spots and weak signal. Technical replicates on the same array were averaged. Data were excluded in cases where technical replicates were significantly different. Normalisation was

performed using the print-tip LOWESS method [36]. Next, we used the one-sample *t*-test to determine the genes to be regarded as changed in copy number. Logarithm was taken from each ratio to fulfil the *t*-test's requirement for a normal distribution. Genes for which the mean of log-ratios across the biological replicates was equal to zero at a significance level α=0.05 were considered to have an unchanged copy number. However, genes with a *P* value smaller than α and where the average-fold change (over- or under-representation) of the four data points were at least twofold were considered as changes in DNA copy number.

Real-time QPCR

The confirmatory real-time QPCR was performed on a RotorGene 2000 instrument with gene-specific primers and the SybrGreen protocol on non-amplified genomic DNA. Reactions were performed in a total volume of 20 µl (50 ng genomic DNA from each sample, 5 pmol/each forward and reverse primer, 1× BioRad SYBRGreen buffer, BioRad, Hungary) with the following protocol: denaturation for 10 min at 95°C, and 45 cycles of 25 s denaturation at 95°C, 25 s annealing at 59°C and 25 s extension at 72°C. Fluorescent signals were collected after each extension step at 72°C. Curves were analysed with the RotorGene software, using dynamic tube and slope correction methods, ignoring data from cycles close to baseline. Primers were designed by using the ArrayExpress software (Applied Biosystems). Relative ratios were normalised to the Ct values obtained with the dihydrofolate reductase gene probe and calculated with the Pfaffl method [23]. The PCR primers used in this study are listed in Table 2. All the PCRs were performed four times in separate runs.

Results

CGH analysis

We analysed the primary MCC and the tumour of the tonsil, applying CGH with DNA from paraffin-embedded tumour material as the probes. Relative DNA losses and gains were determined for each tumour sample by normalising the intensities to the values obtained after hybridisation with labelled probes from normal lymphoid tissue.

Using microarray-based CGH, numerous changes in chromosome copy numbers were observed in both tumours investigated. Both tumours showed complex DNA copy number changes, with an abundance of DNA losses and a few DNA gains. Of the regions, 41 were detected with a DNA loss and 4 regions with a DNA gain (Table 3). CGH revealed regions on 2p and 10p to be commonly over-represented and regions on 1p, 1q, 2p, 2q, 3p, 3q, 4q, 5q, 6p, 6q, 7q, 8p, 9p, 9q, 11p, 11q, 12q, 14q, 15q, 16p, 16q, 17p, 17q, 18q, 19p, 20p, 21q, 22q and X to be commonly under-represented. Chromosomes 1, 2, 3, 17 and 18 were most frequently involved in the DNA losses. According to the intensity ratios, monosomy of the X chromosome is postulated. Besides the commonly affected regions, 31 additional chromosome locations were found to be differently affected in gene copy numbers in the two tumours. Common, primary MCC-specific and secondary tumour-specific changes are listed in Table 3. While 22 regions could be observed with the secondary tonsil cancer-specific DNA loss, only 6 regions were specifically under-represented in the case of the primary MCC. All other DNA losses were common in both tumours. Only 2 regions, 2p23 and 10p15, exhibited common gains, and 3 regions, 2p25, 12q12 and 15q14, showed over-representation in the case of MCC.

Potential oncogenes and tumour suppressor and apoptotic genes mapped to regions detected as changed were

Table 2 Sequences of the oligonucleotides (5′-3′) used in this study

Gene	Chromosome location	Forward primer	Reverse primer	Product size (bp)
Steroid 5-alpha-reductase 2	2p23	CAGAAGCCCCAAGCAACTTT	CCTTCTTGAACAGGTCCTGAGAA	69
Hepatocyte nuclear factor-3 alpha	14q12-q13	CTCAAGAGTTGCTTGACCGAAA	GGGCCATCTGTGGGTAGAGA	67
Zinc finger protein	19q13.43	GAAATTTCCCTGCCAGACCTT	CATGAAGCCCCACTCTGAGAGT	73
Androgen receptor (dihydro-testosterone receptor)	Xq12	CGGAAATGATGGCAGAGATCA	TGGGCTTGACTTTCCCAGAA	66
C8FW phosphoprotein	8q24.13	GGACGATACCCCTTCCATGA	GTCCACGCCGAATTTTGG	61
Cardiac myosin binding protein-C	11p11.2	GCCTAAATCCGAGCATCTGTTT	TGCACTCTCAGGGAATTTGAGA	70
EST	15q14	CCTGATTCCAGAAAAGCAAGTGT	CACTGAGATTACCGGGCATGA	76
Cytochrome P_{450}, subfamily XIA	15q22	CTGGTGCAAGTGGCCATCTA	AATTTTCCGGGTCGAAGAAGA	64
EST similar to phosphatidylcholin transfer protein	17q23	CACAAGGCTATGCACAAAGCA	GGAAACTGAGGCGTCAAGATG	68
Dihydrofolate reductase	5q14	CTGTCATGGTTGGTTCGCTAAA	TGCCGATGCCCATGTTC	60

Table 3 Common and individual gains and losses of Merkel cell carcinoma and the tonsillar tumour detected using comparative genomic hybridization

	Deletion	Amplification
Both tumours	1p36, 1p31, 1p13, 1q21–23, 1q32, 1q42.13, 2p13, 2p11.2, 2q35, 3p21, 3q13.2, 3q14.3, 3q26–28, 4p16, 4q21, 5q35, 6p21, 6q24, 7q21, 8p21, 8q24, 9p12, 9q34, 11p11.2, 11q13, 11q23.3, 12q24.1, 14q11.2, 15q23–24, 16p13–12, 16q24, 17p13, 17q12, 17q23, 18q12, 18q21, 19p13, 20p13, 21q22, 22q13.1, X monosomy	2p23, 10p15
Merkel cell carcinoma	11p11.2, 11q12.3, 12q13, 16p13.1, 17q21.1, 17q25	2p25, 12q12, 15q14
Mesopharynx	1p34.1–32.2, 1p21–22, 1q42, 2q37, 4p16.3, 4q28.3, 5q11.1, 5q22, 5q31–32, 7p14, 8p22–24.13, 10q21.1, 11pter-p15.5, 12q14.3, 14q11.2, 14q31–32, 15q11–13, 16q23–24, 17q21.3-q23, 20q13.1, 21q22.13, 22q11	–

also analysed. The genes mapped to regions that were changed in both tumour samples are listed in Table 4, while changes characteristic of only one tumour are presented in Table 5.

Confirmation of CGH data

The copy number changes of several chromosome regions detected using CGH were submitted for QPCR analysis. Specific primers were designed (Table 2) and used to amplify affected DNA regions of the genome using non-amplified genomic DNA as template. Relative ratios were normalised to the copy numbers of the dihydrofolate reductase gene, because this did not show any alteration in copy number in either tumour and gave reproducible results in all cases. Nine regions exhibiting DNA losses or gains in both tumours were selected for QPCR. In seven cases, the common alterations were confirmed, while in two cases, only MCC-specific changes could be detected (Table 6).

Discussion

MCCs are highly divergent when analysed for chromosome aberrations [12, 24, 34]. Reported recurrent chromosomal imbalances detected using CGH analysis were loss of 3p, 10q, 13q and 17p and gains of 1q, 3q, 5p and 8q [34]. In the present study, we could also detect the loss of 3p and 17p, but none of the above-mentioned amplified regions could be confirmed (Table 3, Fig. 4). In another study, only 3 of the 10 MCCs exhibited common gains and losses, and they shared a gain of 8q21-q22 and a loss of 4p15-pter [24]. In the present study, the 4p16 region was also found to be deleted in both the primary and secondary tumours. Unfortunately, to date, no known tumour suppressor gene has been mapped to this region (Table 4). Speleman's group detected losses involving the entire chromosome 10 or

Table 4 Apoptotic genes and tumour suppressors mapped to regions with common chromosomal aberrations. Apoptotic and tumour suppressor genes in bold character. Apoptotic and tumour suppressor-related genes in italics in brackets

Chromosome location In both tumours	Apoptotic genes	Tumour suppressors
1p36	**DFFB, TP73, CASP9** *(CDC42, MFN2)*	**UBE4B, TUSC3, PRDM 2, C1orf1, ALPL** *(E2F2, TP73)*
1p31	–	**CLCA2**
1p13	–	**ST7L**
1q21–23	**MCL1, DAP3, TNFSF6** *(MUC1, APCS, CRP, SELL)*	
2p13		**MAD**
3p21.3	*(CCR3)*	**RASSF1, BAP1** *(SEMA3B)*
3q26–28	*(ETV5, OPA1)*	**TSBF1**
4p16		*(GAK)*
4q21	*(SNCA)*	
5q35		*(PDLIM7)*
6p21	**BAK1, TNF** *(HSPA)*	*(CDKN1A)*
6q24		**SASH1** *(PLAGL1)*
8p21	**BNIP3** (*CLU*)	***PDGFRL*** *(CNOT7, PDLIM2)*
8q24		*(RNF139)*
9q34	**TRAF2** *(ABL1)*	
11p11.2	*(MADD)*	
11q13	**DPF2, BAD, FADD** (*RELA, CCND1, RAD9A*)	**DOC-1R, MEN1** *(ST3, CCND1, SHANK2)*
11q23.3		**THY1**
12q24.1	*(SCA2)*	
16p13–12	**ASC**	**TSC2**
16q24		**WFDC1, GAS8, MGC15419, CBFA2T3**
17p13		***TP53, HIC1, OVCA2, DPH2L1***
17q12	*(CCR7)*	*(MPP3)*
18q21	*(BCL2)*	**DCC, SERPINB5 (E2F5)**
19p13		**DIRAS1** *(TJP3, SMARCA4, GIPC3)*
21q22	*(MX1)*	
22q13.1	*(HMOX1)*	**ST13**
Xp22.1	*(SH3KBP1)*	
Xq12		**ING2**
Xq28		**RPL10**

Table 5 Apoptotic genes and tumour suppressors mapped to regions with chromosomal aberrations specific to Merkel cell carcinoma or tonsillar tumour. Apoptotic and tumour suppressor genes in bold character. Apoptotic and tumour suppressor related genes in italics in brackets

Chromosome location	Apoptotic genes	Tumour suppressors
In Merkel cell carcinoma		
11p11.2	*(MADD)*	
12q13	*(CDK2, KRT18, NR4A1, WNT1)*	
17q25	**BIRC5**	
In mesopharynx		
1p34.1–32.2		**FABP3**
3p22–21		**ADPRTL3**
5q11.1	*(LOC145908)*	
5q22		**MCC**
5q31–32		**C5orf7**
10q21.1	*(CDC2)*	
11pter-p15.5	*(CTSD, HRAS)*	**MRVI1**
14q31–32	**SIVA**	
16q23–24	*(LOC145908)*	**CBFA2T3**
21q22.13		**RUNX1**
22q11	**BID**	**MYO18B**

partial loss of the chromosome 10 long arm in one-third of the MCC cases they analysed with a possible loss of heterozygosity of 10q23, including the PTEN tumour-suppressor gene [33]. In our case, deletion of this region was not observed in either tumour sample.

In previous observations, series of MCCs showed no evidence of high-level amplification [34]. Recurrent gains of chromosomes 1, 6, 18q and 20 were detected in 2 cases [12]. In our case, only two regions, 2p and 10p were commonly over-represented. In a very recent study, 19 primary MCCs were analysed by CGH, and, in 13 samples, extensive gains and losses were detected [17]. It was shown that a majority of the alterations were gains, while only a few common losses were detected, mainly in regions 4q, 13q and 16q. Neither of our gains was found in any of the 19 cases they analysed. Most of the losses were detected in at least 1 case reported in the above-mentioned study, but the 13 MCCs exhibited a very heterogeneous pattern, with diverse regions with losses.

Our CGH results revealed several new and a few other previously known chromosomal regions that have been presumed to be involved in the pathogenesis of MCC. We found 2 common gains and 41 common losses in the two samples. However, in 31 chromosome locations, we observed differences in gene copy numbers between the two tumours. From the results obtained by CGH analysis, we believe that the mesopharynx cancer and the MCC of the lip derived from the same, genetically altered field; thus, the mesopharynx cancer can be regarded as a second field tumour. From the results obtained using CGH analysis, we hypothesise that Merkel cells in two adjacent anatomical sites, i.e. in the lip and mesopharynx, underwent same precancerous genetic alteration, and both tumours arose from a common cell clone. If our hypothesis is correct, the mesopharynx cancer can be regarded as a second field tumour.

Several oncogenes and tumour-suppressor and apoptotic genes were assumed to be changed in their copy number, as many of them were mapped to the regions having changes in their copy number in one or both of the tumours (Table 4 and Table 5). The limitation of this list is that, in these cases, the deletions of the genes themselves were not proved in this study; only those regions were determined that were located to certain regions or proximity to regions where DNA segments on the microarrays originated.

The microarray-based CGH techniques used in this study could result in distorted data, especially when paraffin-embedded tissue is the target. Another limitation of this study is that the deleted regions were determined using hybridisations based on complementary cDNA—genomic DNA annealing events, which could generate more biases. In consequence of the above problems, we determined the reliability of the results obtained by the CGH microarray using real-time QPCR. Ten genes were selected to follow

Table 6 Confirmation of comparative genomic hybridisation data using quantitative real-time polymerase chain reaction (QPCR). Only two common losses could not be confirmed. Gains are indicated as grey background

Microarray data confirmed using QPCR	Clone name	Accession no.	Chromosome location	Distance
Both tumours	Steroid 5-alpha-reductase 2 (SRD5A2)	M74047	2p23	31724
	Hepatocyte nuclear factor-3 alpha	U39840	14q12-q13	36052
	Zinc finger protein	AF020591	19q13.43	63450
	Androgen receptor (dihydrotestosterone receptor)	M23263	Xq12	63075
	C8FW phosphoprotein	AJ000480	8q24.13	126404
	ESTs, Highly similar to Phosohatidylcholine transfer protein	AA933627	17q23	54340
	Cytochrome P_{450}, subfamily XIA	M14565	15q23–24	70670
Merkel cell carcinoma	EST	N22765	15q14	no data
	Cardiac myosin binding protein-C	U91629	11p11.2	49310

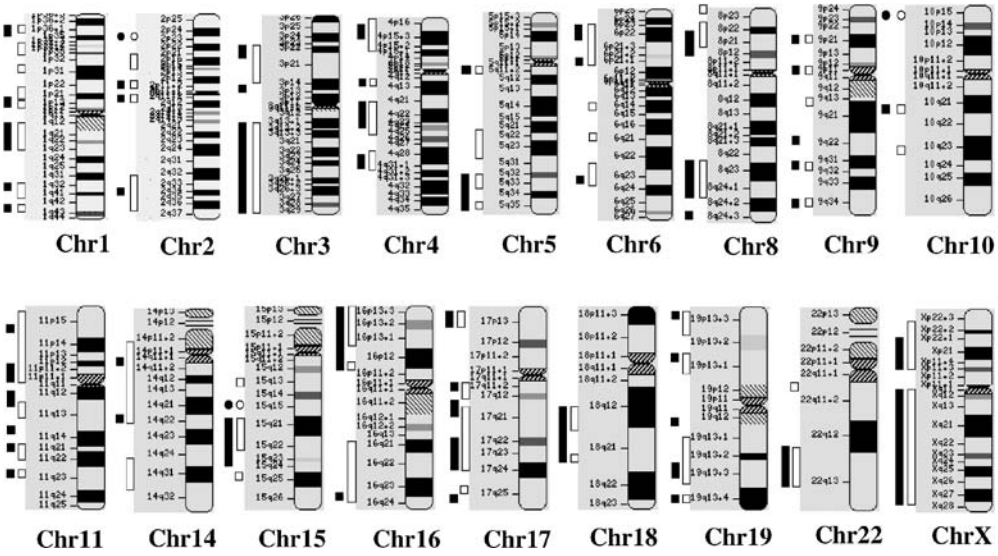

Fig. 4 Copy number aberrations found using microarray comparative genomic hybridisation analysis and real-time polymerase chain reaction of primary Merkel cell carcinoma (MCC) and the tonsillar cancer. *Boxes* on the left side of each chromosome ideogram show regions of reduced copy number (losses of DNA in the tumour genome). *Circles* on the left side of each chromosome ideogram show regions of increased copy number (gains of DNA in the tumour genome). *Filled boxes* denote MCC and *empty boxes* tonsillar tumour

the copy number changes by QPCR. Of the ten genes, one exhibited no changes in the copy number found using CGH microarray analysis in all cases: the dihydrofolate reductase gene. Therefore, it was used as an internal control. The copy numbers of all the other nine genes (sequences and chromosome locations are listed in Table 2, accession numbers are listed in Table 6) were related to this inner control. We used DNA purified from normal lymphoid tissue as control and determined copy number changes of the other two tumours (Table 3, Fig. 4). We confirmed the deletions in seven cases for both tumours, and two were confirmed for only MCC. Although the number of the confirmatory real-time QPCRs was limited and, therefore, does not allow determine the reliability of the CGH methods, the main purpose of the study was to determine the relation of the two tumours, not a precise determination of the deleted regions.

In summary, the partly different molecular patterns obtained using CGH, the similar histological features and the close proximity to the primary tumour indicate that the tonsillar cancer was a second field tumour. The common origin was further confirmed, because of three early markers (9p, 3p and 17p) two of them (9p and 17p) were common in both cancer samples, one (17p) bearing the tp53 tumour suppressor marker gene. The common copy number changes do not support the possibility that the tonsillar cancer was a second primary tumour. The tonsils are very rare and unusual sites of metastatic disease in MCC. There are three reports in the literature describing oropharyngeal metastasis of a MCC [18, 27, 31]. In all these reports, the metastasis occurred within 24 months after resection of the primary tumour. In our case, it was clinically very unlikely that the tonsillar tumour was a metastasis of the MCC of the lip, because no local recurrence, regional lymph-node metastasis or distant haematogenous metastases were observed in the 7-year follow-up. In harmony with the clinical situation, the molecular patterns of the two tumours were not similar, therefore, the possibility of a metastasis could be rejected. Although the concept of second primary tumours and field cancerisation has been formulated for oral and oropharyngeal squamous cell carcinomas [5], our results indicate that Merkel cells in adjacent anatomic sites may also be the targets of field cancerisation.

Acknowledgements This work was supported by a grant from the Hungarian Ministry of Health (ETT 400/2003). LGP is supported by the János Bolyai fellowship of the Hungarian Academy of Sciences.

References

1. Antoniades K, Giannouli TH, Kaisaridou D (1988) Merkel cell carcinoma in a patient with Recklinghausen neurofibromatosis. Int J Oral Maxillofac Surg 27:213–214
2. Bellome J, Bays DR (1998) Merkel cell carcinoma of the ear: report of case. J Oral Maxillofac Surg 56:984–988
3. Benning TL, Vollmer RT, Crain BJ, Shelburne JD (1990) Neuroendocrine carcinoma of the oral cavity. Mod Pathol 3:631
4. Bickle K, Glass LF, Messina JL, Fenske NA, Siegrist K (2004) Merkel cell carcinoma: a clinical, histopathologic, and immunohistochemical review. Semin Cutan Med Surg 23:46–53
5. Braakhuis BJ, Tabor MP, Leemans CR, van der Waal I, Snow GB, Brakenhoff RH (2002) Second primary tumors and field cancerization in oral and oropharyngeal cancer: molecular techniques provide new insights and definitions. Head Neck 24:198–206
6. Braakhuis BJ, Tabor MP, Kummer JA, Leemans CR, Brakenhoff RH (2004) A genetic explanation of Slughter's concept of field cancerization. Cancer Res 63:1727–1730
7. Califano J, van der Riet P, Westra W, Nawroz H, Clayman G, Piantadosi S, Corio R, Lee D, Greenberg B, Koch W, Sidransky D (1996) Genetic progression model for head and neck cancer: implications for field cancerization. Cancer Res 56:2488–2492
8. Cowell JK, Wang YD, Head K, Conroy J, McQuaid D, Nowak NJ (2004) Identification and characterisation of constitutional chromosome abnormalities using arrays of bacterial artificial chromosomes. Br J Cancer 90:860–865
9. Furák J, Troján I, Szőke T, Tiszlavicz L, Bodosi M, Kahán ZS, Micsik T, Puskás LG, Balogh Á (2002) Development of brain metastasis 5 years before the appearance of the primary lung cancer: messenger metachronous metastasis. Ann Thorac Surg 75:1016–1017

10. Ha PK, Califano JA (2003) The molecular biology of mucosal field cancerization of the head and neck. Crit Rev Oral Biol Med 14:363–369
11. Halata Z, Grim M, Baumann KI (2003) Friedrich Sigmund Merkel and his "Merkel cell", morphology, development, and physiology: review and new results. Anat Rec 271:225–239
12. Harle M, Arens N, Moll I, Back W, Schulz T, Scherthan H (1996) Comparative genomic hybridization (CGH) discloses chromosomal and subchromosomal copy number changes in Merkel cell carcinomas. J Cutan Pathol 23:391–397
13. Hashimoto K (1972) Fine structure of Merkel cell in human oral mucosa. J Invest Dermatol 58:381–387
14. Hodgson G, Hager JH, Volik S, Hariono S, Wernick M, Moore D, Nowak N, Albertson DG, Pinkel D, Collins C, Hanahan D, Gray JW (2001) Genome scanning with array CGH delineates regional alterations in mouse islet carcinomas. Nat Genet 29:459–464
15. Huang Q, Schantz SP, Rao PH, Mo J, McCormick SA, Chaganti RS (2000) Improving degenerate oligonucleotide primed PCR-comparative genomic hybridization for analysis of DNA copy number changes in tumours. Genes Chromosomes Cancer 28:395–403
16. Koss LG, Spiro RH, Hajdu S (1972) Small cell (oat cell) carcinoma of minor salivary gland origin. Cancer 30:737
17. Larramendy ML, Koljonen V, Bohling T, Tukiainen E, Knuutila S (2004) Recurrent DNA copy number changes revealed by comparative genomic hybridization in primary Merkel cell carcinomas. Mod Pathol 17:561–567
18. Lehnerdt KH, Broicher R, Tschubel K, Walther E (2001) Der interessante Fall Nr.49. Laryngorhinootologie 80:687–689
19. Longo F, Califano L, Mangone GM, Errico ME (1999) Neuroendocrine (Merkel cell) carcinoma of the oral mucosa: report of case with immunohistochemical study and review of the literature. J Oral Pathol Med 28:88–91
20. Mir R, Sciubba JJ, Bhuiya TA, Blomquist K, Zelig D, Friedman E (1988) Merkel cell carcinoma arising in the oral mucosa. Oral Surg Oral Med Oral Pathol 65:71–75
21. Ónody A, Zvara Á, Hackler Jr L, Vígh L, Ferdinandy P, Puskás LG (2003) Effect of classic preconditioning on the gene expression pattern of rat hearts: a DNA microarray study. FEBS Letters 536:35–40
22. Park GC, Shelton JB, Ow RA, Todd DH (1999) Merkel cell carcinoma of the lower lip. Arch Otolaryngol Head Neck Surg 125:907–911
23. Pfaffl MW (2001) A new mathematical model for relative quantification in real-time RT-PCR. Nucleic Acids Res 29:e45
24. Popp S, Waltering S, Herbst C, Moll I, Boukamp P (2002) UV-B-type mutations and chromosomal imbalances indicate common pathways for the development of Merkel and skin squamous cell carcinomas. Int J Cancer 99:352–360
25. Puskás LG, Hackler L Jr, Kovács G, Kupihár Z, Zvara Á, Micsik T, van Hummelen P (2002) Recovery of cyanine-dye nucleotide triphosphates. Anal Biochem 305:279–281
26. Puskás LG, Zvara Á, Hackler L Jr, Micsik T, van Hummelen P (2002) Production of bulk amounts of universal RNA for DNA microarrays. Biotechniques 33:898–904
27. Reichel OA, Mayr D, Issing WJ (2003) Oropharyngeal metastasis of a Merkel cell carcinoma of the skin. Eur Arch Otorhinolaryngol 260:258–60
28. Schmidt-Westhausen A, Reichert PA, Gross UM (1996) Gingival metastasis of Merkel cell carcinoma: a case report. J Oral Pathol Med 25:44–47
29. Slaughter DP, Southwick HW, Smejkal W (1953) "Field cancerization" in oral stratified squamous epithelium. Cancer 6:963–968
30. Snijders AM, Nowak N, Segraves R, Blackwood S, Brown N, Conroy J, Hamilton G, Hindle AK, Huey B, Kimura K, Law S, Myambo K, Palmer J, Ylstra B, Yue JP, Gray JW, Jain AN, Pinkel D, Albertson DG (2001) Assembly of microarrays for genome-wide measurement of DNA copy number. Nat Genet 29:263–264
31. Telenius H, Carter NP, Bebb CE, Nordenskjold M, Ponder BA, Tunnacliffe A (1992) Degenerate oligonucleotide-primed PCR: general amplification of target DNA by a single degenerate primer. Genomics 13:718–725
32. Tesei F, Farneti G, Cavicchi O, Antonelli P, Zanetti G, Leone O (1992) View from beneath: pathology in focus. A case of Merkel cell carcinoma metastatic to tonsil. J Laryngol Otol 106:1100–1102
33. Van Gele M, Leonard JH, Van Roy N, Cook AL, De Paepe A, Speleman F (2001) Frequent allelic loss at 10q23 but low incidence of PTEN mutations in Merkel cell carcinoma. Int J Cancer 92:409–413
34. Van Gele M, Leonard JH, Van Roy N, Van Limbergen H, Van Belle S, Cocquyt V, Salwen H, De Paepe A, Speleman F (2002) Combined karyotyping, CGH and M-FISH analysis allows detailed characterization of unidentified chromosomal rearrangements in Merkel cell carcinoma. Int J Cancer 101:137–145
35. Vigneswaren N, Müller S, Lense E, Stacey B, Hewan-Lowe K, Weathers DR (1992) Merkel cell carcinoma of the labial mucosa. Oral Surg Oral Med Oral Pathol 74:193–200
36. Yang YH, Dudoit S, Luu P, Lin DM, Peng V, Ngai J, Speed TP (2002) Normalization for cDNA microarray data: a robust composite method addressing single and multiple slide systematic variation. Nucleic Acids Res 30:e15

Virchows Arch (2005) 446: 287–299
DOI 10.1007/s00428-004-1194-y

ORIGINAL ARTICLE

Thomas Kalinski · Sabine Krueger · Antje-Friederike Pelz · Peter Wieacker · Roland Hartig · Martin Röpke · Regine Schneider-Stock · Frank Dombrowski · Albert Roessner

Establishment and characterization of the permanent human cell line C3842 derived from a secondary chondrosarcoma in Ollier's disease

Received: 29 August 2004 / Accepted: 6 December 2004 / Published online: 25 February 2005
© Springer-Verlag 2005

Abstract The permanent human cell line C3842 was established from a secondary chondrosarcoma in a typical case of Ollier's disease. In the present study, we analyzed the morphological, cytogenetic and molecular biological characteristics of the cultured cells in comparison with the original tumor and investigated the invasion properties of the tumor model using functional imaging of proteolysis, matrigel assay and chick chorioallantoic membrane assay. C3842 cells exhibit the typical features of malignant cartilage tumor cells in vitro, including the expression of collagen types II, IX, XI and aggrecan. The proteolytic ability of C3842 cells is attributed to the expression of several proteases, such as cathepsin B, urokinase plasminogen activator and matrix-metalloproteinase-2, which enable the cells to degrade collagen type I and to permeate matrigel matrix. In accordance with the biological features in vivo, C3842 cells are not able to invade through the epithelium of the chick chorioallantoic membrane. In conclusion, the cell line C3842 provides the first model of a secondary chondrosarcoma in Ollier's disease in vitro, which is characterized by distinct features of such malignant cartilage tumors.

T. Kalinski (✉) · S. Krueger · R. Schneider-Stock · F. Dombrowski · A. Roessner
Department of Pathology, Otto-von-Guericke-University, Leipziger Strasse 44, 39120 Magdeburg, Germany
e-mail: kalinski@medizin.uni-magdeburg.de
Tel.: +49-391-6717874
Fax: +49-391-67290724

A.-F. Pelz · P. Wieacker
Department of Human Genetics, Otto-von-Guericke-University, Magdeburg, Germany

R. Hartig
Department of Immunology, Otto-von-Guericke-University, Magdeburg, Germany

M. Röpke
Department of Orthopedics, Otto-von-Guericke-University, Magdeburg, Germany

Keywords Cell line · Secondary chondrosarcoma · Ollier's disease

Introduction

Chondrosarcoma is the second most frequent primary malignant tumor of bone and accounts for about one-quarter of all primary bone sarcomas [13]. In the majority of cases, conventional chondrosarcomas arise as primary lesions in the trunk bones, the femur or the humerus. The peak age incidence is in the fifth to seventh decades of life, with a slight preference for male patients [4]. As chondrosarcomas have little sensitivity to chemotherapy or radiation, a complete surgical excision of the tumor is essential. The prognosis of chondrosarcoma then correlates with the histological grade (from 1 to 3) of the tumor based on cytological criteria, such as cellularity, nuclear size and nuclear polymorphism [24, 41].

Secondary chondrosarcomas are histologically indistinguishable from their primary counterparts. If the predisposing condition is not included in the microscopic sections, the diagnosis depends on clinical or radiological findings. Among the predisposing conditions is Ollier's disease, which is a rare skeletal disorder that exhibits a multifocal intramedullary proliferation of hypercellular dysplastic cartilage and a high risk of developing malignant bone tumors, particularly chondrosarcomas [25]. Primarily, the lesions affect short and long tubular bones of the extremities, but trunk bones, such as the scapula and ribs, can also be involved. The histology appears to be similar to that of enchondromas, with minimal cellular atypia and increased cellularity.

In contrast to multiple osteochondromas, most cases of Ollier's disease occur sporadically [28]. No recurrent cytogenetic alterations have been reported in Ollier's disease and related secondary chondrosarcomas. In single cases of secondary chondrosarcomas, losses of heterozygosity at chromosomes 9p21 (*p15/p16* locus), 13q14 (*Rb1* locus) and 1p were identified [5, 30]. At the molecular genetic level, no specific point mutations in protooncogenes or

tumor suppressor genes have been described either for primary or secondary chondrosarcomas.

Permanent cell lines of human chondrosarcomas are rare. The few established cell lines correspond to grade-1, grade-2 and grade-3 tumors [9, 10, 18, 22, 38]. However, none of these cell lines correspond to a secondary chondrosarcoma. Here, we report on the establishment and characterization of the first permanent human cell line of a secondary chondrosarcoma grade 2 in Ollier's disease.

Materials and methods

Clinical data

A 38-year-old male patient with Ollier's disease developed a chondrosarcoma grade 2 in the right proximal tibia, which was treated by resection of the tumor 3 years ago. Benign cartilage tumors were detected in the right tibia, the right scapula and the right fourth finger. A recurrence occurred 3 years after the resection of the tumor, and a second chondrosarcoma was diagnosed in the distal tibia. The patient was treated by completely resecting the proximal tibia, followed by implantation of a prosthesis and resection of the tumor in the distal tibia. Metastases were not detected.

Tumor cell culture

Specimens of the recurrent chondrosarcoma were obtained immediately after the resection of the proximal tibia. The tumor tissue was minced aseptically using a pair of scissors and passed through a steel mesh. The cell suspension was subdivided into 35-mm dishes with RPMI-1640 medium (Sigma-Aldrich, Taufkirchen, Germany) supplemented with 10% fetal bovine serum (Biochrom, Berlin, Germany) and 1× penicillin/streptomycin (PAA, Pasching, Austria). The cell cultures were incubated at 37 C in a humidified atmosphere containing 5% CO_2. After a few days, the tumor cells became adherent and were further subcultured after detachment using 1:250 trypsin/ethylenediaminetetraacetate (EDTA) (PAA, Pasching, Austria). The medium was changed twice a week. One of the proliferating clones was further expanded and maintained for more than 30 passages until today. Cell counts were performed in duplicate after detachment using a Beckman Coulter Z2 counter. Cell proliferation was analyzed fourfold after 2, 4, 6, 8 and 10 days, starting from 2×10^5 cells in 25-cm^2 culture flasks.

Morphological examination

Light microscopy

Cells ($n=1\times10^5$) were seeded on 9.4-cm^2 Lab-Tek II Chamberslides (Nunc, Wiesbaden, Germany), fixed after 48 h using 4% paraformaldehyde and Giemsa stained. Paraffin sections of the tumor tissue 4 µm thick were deparaffinized, rehydrated and stained using hematoxylin and eosin.

Electron microscopy

Cells ($n=1\times10^5$) were seeded on 35-mm Petriperm dishes (Vivascience, Hannover, Germany) and fixed overnight after 48 h with 1% glutaraldehyde in phosphate-buffered saline (pH 7.4). Pieces of the plastic film base of the dishes (2×2 mm) with the fixed cells were postfixed with 2% osmium tetroxide, dehydrated and embedded in EPON 812. Thin sections were stained with lead citrate and uranyl acetate and examined with a Zeiss EM 900 (Leo, Oberkochem, Germany) at 80 kV.

Cytogenetic and molecular-cytogenetic studies

Conventional chromosome analyses

Conventional chromosome analyses were performed on cells of passage 1 of the cell line. Cell and chromosome preparations, as well as Giemsa-staining and GTG banding were performed following modified standard procedures [3]. We analyzed 5 Giemsa-stained and 17 GTG-banded metaphases of passage one. The International System for Human Cytogenetic Nomenclature was used for karyotyping [29].

Fluorescence in situ hybridization

Fluorescence in situ hybridization (FISH) was performed on cultured cells of passages 1, 20 and 25 of the cell line. The probe used was a spectrum orange-labeled alpha satellite probe for chromosome 7 (CEP 7, locus D7Z1; Abbott, Wiesbaden, Germany). FISH was achieved according to a modified supplier's protocol. The fluorescent signal was detected using a Zeiss Axioplan Imaging 2 microscope (Zeiss, Jena, Germany) and Applied Imaging software (Applied Imaging, Newcastle upon Tyne, UK). We analyzed 55 (passage 1), 132 (passage 20) and 238 (passage 25) interphase nuclei.

Molecular genetic studies

DNA from formalin-fixed, paraffin-embedded tissue (dysplastic cartilage and tumor) was prepared using the NucleoSpin Tissue kit (Macherey-Nagel, Düren, Germany) according to the manufacturer's instructions. DNA from cultured cells of passages 1 and 25 was isolated using a standard proteinase K-phenol-chloroform extraction protocol [33]. Exons 1 and 2 of the *p16* gene were analyzed using polymerase chain reaction (PCR)-single-stranded conformational polymorphism as described previously [36].

Exons 4 to 8 of the *p53* gene were also analyzed using PCR-single-stranded conformational polymorphism. Prim-

er sequences, annealing temperatures and product sizes are shown in Table 1. A 25-µl PCR mix contained 100 ng or 150 ng (exon 4) DNA, 12.5 pmol primers each (TibMolBiol, Berlin, Germany), 160 µM of each dNTP, 50 mM Tris-HCl, 1.5 mM $MgCl_2$, and 0.1 U HotGoldstar DNA polymerase (Eurogentec, Seraing, Belgium). The PCR conditions consisted of 35 cycles at 94 C for 60 s, annealing (56–58 C) for 60 s and extension at 72 C for 150 s. The PCR products were detected on ultrathin polyacrylamide gels (0.4 mm thick and 8–12%, depending on the fragment lengths to be separated) at 15 C for 2 h in horizontal electrophoresis (Multiphor; Pharamcia Biotech). DNA fragments were visualized using a modified silver-staining protocol [8]. For single-strand conformation polymorphism (SSCP) analysis, a 4.5-µl aliquot of the PCR sample was mixed with 4.5 µl of 100% formamide buffer (0.05% bromphenol and 0.05% xylencyanol) and denatured at 98 C for 5 min, subsequently chilled on ice and applied to a 0.5×MDE gel (Mutation Detection Enhancement, AT Biochem, Malvern, PA, for exons 7 and 8), to T6C1 gels (Amersham Biosciences, Uppsala, Sweden, exons 4 and 5) or to 8% polyacrylamide gels with 10% glycerol (for exon 6).

Exons 1 and 2 of *N*-, *K*-, and *H-ras* genes (35 cycles at 94 C for 60 s, annealing (55–60 C) for 60 s, extension at 72 C for 150 s) were amplified in a 25-µl mix with 100 ng DNA and 12.5 pmol of each primer, 140 µM of each dNTP, 50 mM Tris-HCl, 1.5 mM $MgCl_2$, and 0.1 U of HotGoldstar DNA polymerase. Primer sequences, annealing temperatures and product sizes are shown in Table 1. All PCR products were directly sequenced on an ABI310 sequencer (Perkin Elmer, Weiterstadt, Germany).

Immunohistochemical characterization

Cells (n=1×10^5; <10th passage) were seeded on 9.4 cm^2 Lab-Tek II Chamberslides (Nunc, Wiesbaden, Germany) and fixed after 48 h using 4% paraformaldehyde. Paraffin sections 4 µm thick of the tumor tissue were deparaffinized and rehydrated. The slides were exposed to the following antibodies: anti-collagen type I, anti-collagen type II (Acris Antibodies, Hiddenhausen, Germany); anti-cathepsin B, anti-urokinase plasminogen activator (uPA), anti-plasminogen-activator inhibitor (PAI-1), anti-matrix-metalloproteinase (MMP)-1, -2, -3, anti-tissue inhibitor of metalloprotease (TIMP)-1 (Calbiochem, Bad Soden, Germany); anti-TIMP-3 (Santa Cruz Biotechnology, Heidelberg, Germany). The antibodies were diluted 1:5 (anti-uPA), 1:20 (anti-collagen type II, anti-MMP-2), 1:30 (anti-MMP-3), 1:50 (anti-cathepsin B, anti-TIMP-1), 1:100 (anti-collagen type I, anti-MMP-1) and 1:200 (anti-PAI-1, anti-TIMP-3) in a buffer containing 50 ml RPMI-1640, 450 ml bidistilled water, 50 ml fetal bovine serum and 0.5 g sodium acid (pH between 7.4 and 7.6). Prior to incubation for 60 min at 37 C, an antigen retrieval was necessary for anti-collagen type II and anti-PAI-1 reactions (30 min in a microwave oven at 600 W in 10 mM citrate buffer, pH 6.0), as well as for anti-uPA and anti-MMP-2 reactions for 20 min at 450 W in 1 mM EDTA buffer, pH 8.0). Bound primary antibodies were detected using the Vectastain ABC alkaline phospha-

Table 1 Primers used for molecular genetic analyses

Target	Primer sequence	Annealing temperature (°C)	Fragment size (bp)
p53 exon 4	S: 5′-ATC TAC AGT CCC CCT TGC CG-3′ A: 5′-GCA ACT GAC CGT GCA AGT CA-3′	56	293
p53 exon 5	S: 5′-TTC ACT TGT GCC CTG ACT T-3′ A: 5′-ACC CTG GGC AAC CAG CCC TGT C-3′	58	270
p53 exon 6	S: 5′-ACC ATG AGC GCT GCT CAG AT-3′ A: 5′-AGT TGC AAA CCA GAC CTC AGG C-3′	58	236
p53 exon 7	S: 5′-CTT GCC ACA GGT CTC CCC AA-3′ A: 5′-GAG GCT GGG GCA CAG CAG GCC AGT G-3′	58	168
p53 exon 8	S: 5′-ACT GCC TCT TGC TTC TCT TT-3′ A: 5′-AAG TGA ATC TGA GGC ATA AC-3′	58	236
N-ras exon 1	S: 5’-ATG ACT GAG TAC AAA CTG GT-3’ A: 5’-CTC TAT GGT GGG ATC ATA TT-3’	57	111
N-ras exon 2	S: 5’-CAA GTG GTT ATA GAT GGT GA-3’ A: 5’-AGG AAG CCT TCG CCT GTC CT-3’	60	110
K-ras exon 1	S: 5’-ATG ACT GAA TAT AAA CTT GT-3’ A: 5’-CTC TAT TGT TGG ATC ATA TT-3’	57	111
K-ras exon 2	S: 5’-GCA AGT AGT AAT TGA TGG AG-3’ A: 5’-AGA AAG CCC TCC CCA GTC CT-3’	55	111
H-ras exon 1	S: 5’-TGA CGG AAT ATA AGC TGG TG-3’ A: 5’-TCG TCC ACA AAA TGG TTC TGG-3’	56	91
H-ras exon 2	S: 5’-AGG TGG TCA TTG ATG GGG AG-3’	58	109

tase kit (Vector Laboratories, Burlingame, CA) according to the manufacturer's recommendations. A substrate containing 44 ml of Tris buffer, 16 ml of propandiol, 0.025 g of levamisole, 0.125 g of new fuchsin, 0.3 ml of sodium nitrate (4%), 0.0315 g of naphthol as-bi phosphate and 0.4 ml of methylformamide (pH 8.5) was used for staining. The slides were counterstained with hematoxylin and mounted in gelatin. Paraffin-embedded tissue sections of a human fetal limb, a breast carcinoma and a giant cell tumor with known positivity for the particular antibodies were used as positive controls. Staining intensity was scored into four categories: negative, weakly positive, moderately positive and strongly positive. Staining extensity was scored as 0 when less than 5% of tumor cells were stained, 1 when 5–30% of tumor cells were positive, 2 when 31–70% of tumor cells were positive and 3 when greater than 71% of tumor cells were positive in ten high power fields.

Detection of specific mRNA using RT-PCR and real-time quantitative RT-PCR

Total RNA was extracted from 200 mg of fresh frozen tumor tissue and from 4×10^6 cultured cells (<10th passage) using guanidinium thiocyanate-acid phenol-chloroform [11]. In addition, RNA was extracted from 200 mg of fresh frozen adult joint cartilage. Prior to RNA extraction, cartilage and tumor tissues were pulverized using a mortar and a pestle exposed to liquid nitrogen. Reverse transcription (RT) was carried out using M-MLV RT and Oligo(dT) 15 Primer (Promega, Mannheim, Germany) according to the manufacturer's recommendations. The primer pairs used for the detection of beta-actin, beta-2-microglobulin, aggrecan, alpha-1 chain of collagen types I, II, IX and XI, cathepsin B, MMP-1, -2, and -3, and uPA are shown in Table 2. Next, 20 pmol of each primer were combined with 1 µl of 10 mM dNTP mixture, 5 µl of a 10× PCR reaction buffer (containing 500 mM KCl, 15 mM $MgCl_2$ and 130 mM Tris, pH 9.0) and 1.25 U of *Taq* DNA Polymerase (Promega, Mannheim, Germany). The PCR conditions consisted of 35 cycles at 94 C for 30 s, annealing (52–56 C) for 40 s and extension at 72 C for 1 min.

For the standardization of the copy number in real-time quantitative PCR, PCR products of beta-2-microglobulin and cathepsin B genes were cloned into the pCR2.1-TOPO vector (Invitrogen, Karlsruhe, Germany) and used in calculated quantifications in subsequent reactions. The quantitative PCRs were performed using a qPCR Mastermix kit (Qbiogene, Heidelberg, Germany) according to the manufacturer's recommendations. The standard temperature profile was as follows: 30 s at 95 C followed by 40 cycles of 0 s at 95 C, 5 s at 54 C, respectively, 58 C and 18 s at 72 C.

Table 2 Primers used for reverse-transcription polymerase chain reaction (RT-PCR) and real-time quantitative RT-PCR. *UPA* urokinase plasminogen activator, *MMP* matrix-metalloproteinase

Target	Primer sequence	Annealing temperature (°C)	Fragment size (bp)
Beta-actin	S: 5′-TGA CGG GGT CAC CCA CAC TGT GCC CAT CTA-3′ A: 5′-CTA GAA GCA TTT GCG GTG GAC GAT GGA GGG-3′	56	660
Beta-2-Microglobulin	S: 5′-CCA GCA GAG AAT GGA AAG TC-3′ A: 5′-GAT GCT GCT TAC ATG TCT CG-3′	54	269
Aggrecan	S: 5′-TGA GGA GGG CTG GAA CAA GT-3′ A: 5′-GGA GGT GGT AAT TGC AGG GA-3′	56	349
Alpha-1 chain of collagen I	S: 5′-AAG GAC AAG AGG CAT GTC TG-3′ A: 5′-GAG GGA GTT TAC AGG AAG CA-3′	56	449
Alpha-1 chain of collagen II	S: 5′-CTG GCT CCC AAC ACT GCC AA-3′ A: 5′-TCC TTT GGG TTT GCA ACG GA-3′	56	412
Alpha-1 chain of collagen IX	S: 5′-GGG CCC AGA ACA CAT AGT CC-3′ A: 5′-CTC CTC TCC ACG CCA ATC AT-3′	56	685
Alpha-1 chain of collagen XI	S: 5′-CGT AAC AAC CCT CGC AAT GA-3′ A: 5′-CTC CAC GCT GAT TGC TAC CC-3′	56	463
Cathepsin B	S: 5′-GAT CTA GGA TCC GGC TTC-3′ A: 5′-GTC AGA GAT GGC TTC CAC-3′	58	379
MMP-1	S: 5′-CTG AAG GTG ATG AAG CAG CC-3′ A: 5′-AGT CCA AGA GAA TGG CCG AG-3′	56	428
MMP-2	S: 5′-ACA ACT TTG AGA AGG ATG GC-3′ A: 5′-CTT GGT GTA GGT GTA AAT GG-3′	52	500
MMP-3	S: 5′-CTC ACA GAC CTG ACT CGG TT-3′ A: 5′-CAC GCC TGA AGG AAG AGA TG-3′	56	294
UPA	S: 5′-CTT GCT GAA GAT CCG TTC CA-3′	52	447

Functional imaging of proteolysis

Well chamber slides (n=8) were coated with 25 µg DQ-collagen type-I fluorescein conjugate (Molecular probes, Leiden, Netherlands) per 1 ml 2% gelatin/sucrose or 1:1 diluted Matrigel (BD Biosciences, Heidelberg, Germany). The tumor cells were seeded for 24–48 h onto the matrix. The chamber slides were fixed with 4% paraformaldehyde and counterstained with 4′-6′-diamidino-2-phenylindole (DAPI). A confocal laser scanning microscope TCS SP2 (Leica Microsystems, Bensheim, Germany) was used for the microscopic analysis. Confocal image data obtained with a 63×/1.4 N.A. oil immersion objective and CLSM software (Leica Microsystems) were processed with ImageJ software, optimizing images in brightness and contrast and pseudo-coloring them: green for fluorescein isothiocyanate and blue for DAPI. The fluorescing structures were visualized on serial confocal optical sections.

In vitro invasion assay

Invasion of chondrosarcoma cells was evaluated by Matrigel assay, as described previously, using polycarbonate Transwell filters of 8.0 µm pore size (Corning, Acton, MA) [21]. Cells (n=5×10^4) were seeded onto the filters, coated with 100 ng of Matrigel matrix (BD Biosciences, Heidelberg, Germany) and incubated at 37 C in a humidified atmosphere for 72 h. Cells migrating through the filters and attaching to the lower sites of the Transwell filters were harvested with 1:250 trypsin/EDTA (PAA, Pasching, Austria) and counted using a Beckman Coulter Z2 counter. The percentage of invasive cells was calculated from 100% controls grown under identical culture conditions for 72 h in 48 well plates. All invasion assays and quantifications were performed in triplicate.

Chick chorioallantoic membrane assay

The chick chorioallantoic membrane assay was performed as described previously [23]. Fertilized hen's eggs were incubated in a humidified chamber at 37 C. At day 4 of the incubation, a hole was drilled in the pointed pole of the shell, enlarged to a round window of about 2 cm and covered with a tape. On day 6 of the incubation, a silicone ring (1-mm thick with a 5-mm inner circle) was placed onto the chorioallantoic membrane. Next, 2.5–10×10^5 cells in a volume of 20 µl culture medium were seeded into the ring. Tumor growth was checked daily using stereomicroscopy. The incubation was stopped at day 12. The chorioallantoic membrane was fixed in 4% paraformaldehyde and embedded in paraffin. Sections 4 µm were prepared and stained using hematoxylin–eosin.

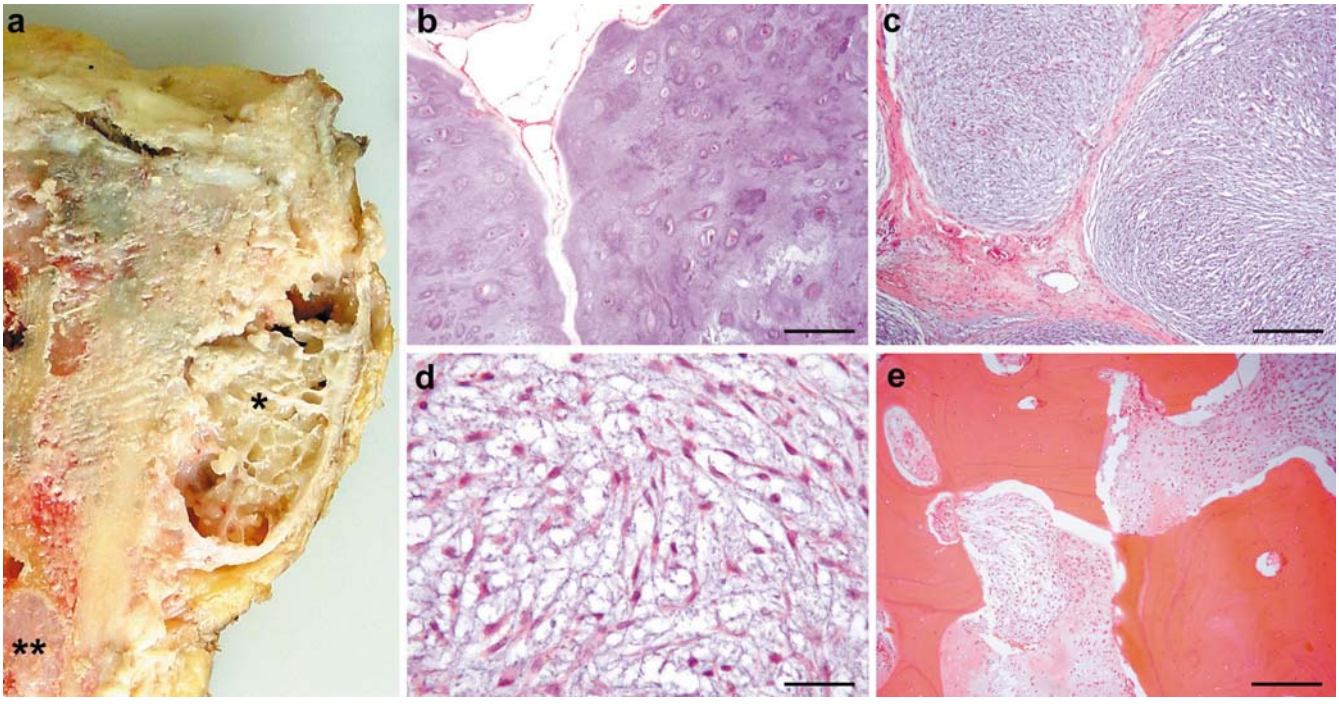

Fig. 1 Macroscopy of the secondary chondrosarcoma (*) and the dysplastic cartilage (**) (**a**). Histology of the dysplastic cartilage with hyaline matrix and moderate cellularity, Hematoxylin–eosin (HE), *scale bar*=100 µm (**b**). Histology of the secondary chondrosarcoma with myxoid matrix and increased cellularity, HE, *scale bar*=100 µm (**c**). Higher magnification showing spindle-shaped tumor cells with enlarged nuclei and increased atypia, HE, *scale bar*=50 µm (**d**). Infiltrative and destructive growth of the secondary chondrosarcoma in cortical bone, HE, *scale bar*=100 µm (**e**)

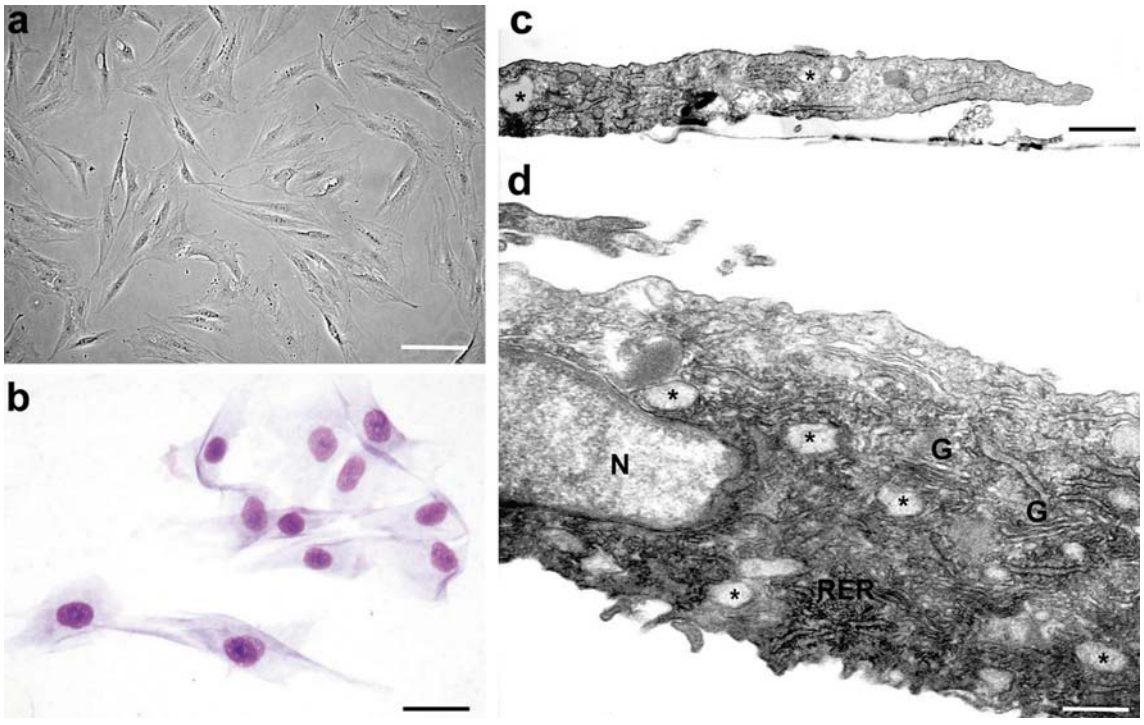

Fig. 2 Morphological appearance of C3842 cells in vitro, phase contrast, *scale bar*=50 µm (**a**). Fixed C3842 cells cultured on chamberslides, Giemsa, *scale bar*=20 µm (**b**). Ultrastructural appearance of C3842 cells with cytoplasmic vacuoles (*), *scale bar*=1.1 µm (**c**). Higher magnification with the nucleus (N), rough endoplasmatic reticulum (RER), Golgi fields (G) and cytoplasmic vacuoles (*), *scale bar*=0.4 µm (**d**)

Results

Morphological findings

Gross examination of the resected distal tibia revealed cartilage tumor masses in the medullary cavity, measuring 6.5 cm and 4.5 cm in largest dimension. The latter showed infiltration and disruption of the cortical bone with extraosseous extension and myxoid change (Fig. 1A). Appropriately, two distinct cartilage tumor components were distinguishable microscopically. One of them corresponded to dysplastic cartilage with moderate cellularity and slight cellular atypia (Fig. 1B). The other corresponded to a chondrosarcoma grade 2 and was composed of spindle-shaped cells with enlarged oval nuclei and increased atypia in a myxoid stroma (Fig. 1C, D). The cellularity of this component was markedly increased. The aggressive behavior was proved by the observation of infiltrative growth in the cortical bone (Fig. 1E). Both components exhibited a lobulated architecture with fibrous septa containing blood vessels. Additional intracartilage blood vessels were observed in the aggressive component.

The morphological appearance of the aggressive tumor component was preserved in vitro (Fig. 2A, B). The tumor cells grew in loose associations, without profuse evidence of cluster formation. Close monolayers were formed in confluent state. Ultrastructurally, the tumor cells were rich in Golgi fields and cytoplasmic vacuoles next to abundant endoplasmic reticulum and numerous mitochondria (Fig. 2C, D).

Growth properties

Proliferation counts revealed a moderate growth rate for the tumor cells (10th passage; Fig. 3). The growth rate maintained stable up to recent passages (>30th). The mean doubling time was approximately 10 days. Confluency was reached after 10–14 days, starting from 2×10^5 cells in 25-cm^2 culture flasks. The saturation density was calculated as about 1.8×10^4 cells/cm^2.

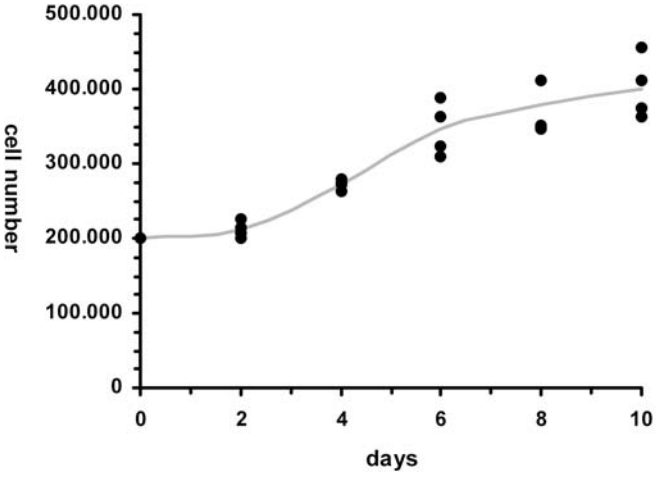

Fig. 3 Growth properties of C3842 cells in 25-cm^2 culture flasks starting from 2×10^5 cells

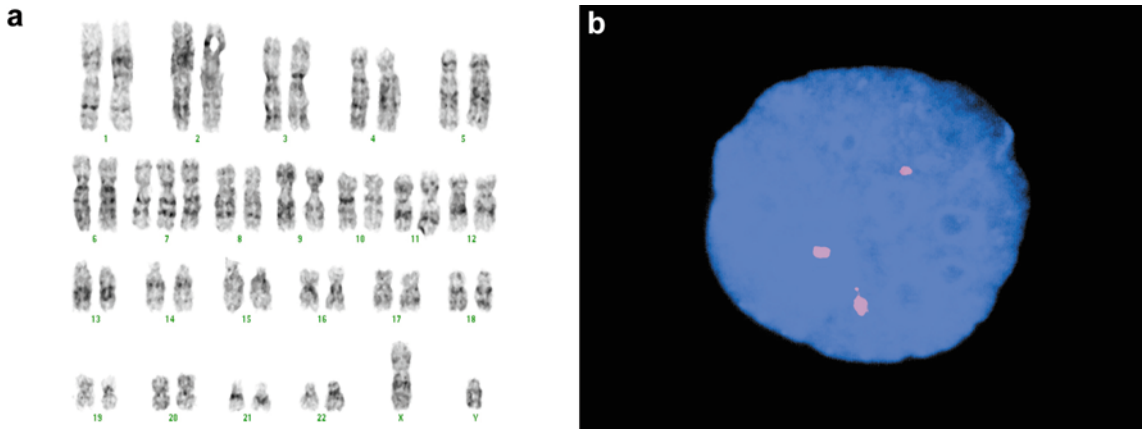

Fig. 4 Karyogram demonstrating trisomy 7 in C3842 cells of passage 1 (**a**). Fluorescent in situ hybridization analysis with labeled centromere-specific probe for chromosome 7 (CEP 7) showing three signals (**b**)

Cytogenetic and molecular-cytogenetic studies

Conventional chromosome analyses

Altogether, we analyzed 17 metaphases of passage 1. Eight metaphases showed a normal diploid karyotype; nine metaphases were aberrant. Four of these aberrant metaphases had a near-tetraploid chromosome number. Four other aberrant metaphases had 47 chromosomes with trisomy 7 (Fig. 4A). Another aberrant metaphase showed trisomy 8 and monosomy 22. The complete karyotype of passage one was 88~92, XXYY[4]/47,XY,+7[4]/46,XY [8].

FISH analyses

Of the interphase nuclei, 55 (passage 1), 132 (passage 20) and 238 (passage 25) could be analyzed. The centromere-

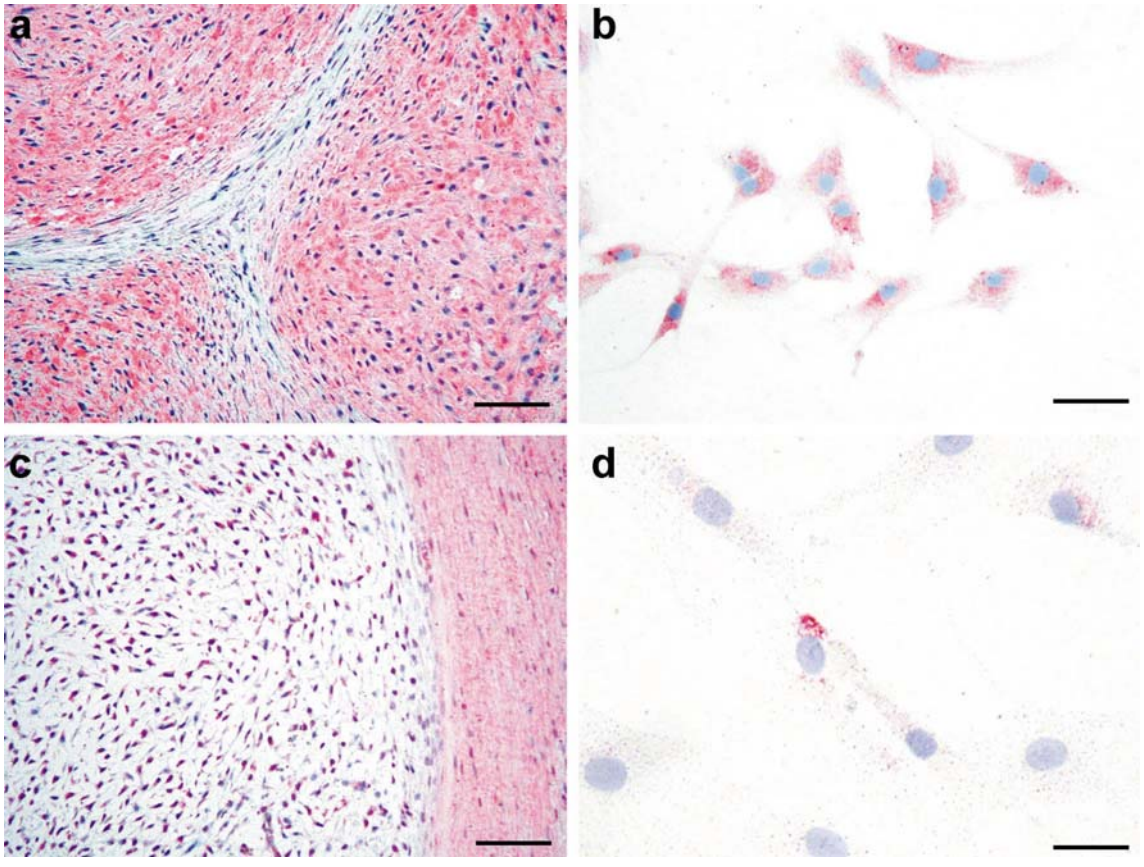

Fig. 5 Collagen type-II expression in the cytoplasm and the cartilage matrix of the secondary chondrosarcoma, *scale bar*=100 µm (**a**) and in C3842 cells, *scale bar*=25 µm (**b**). Focal expression of collagen type I in the secondary chondrosarcoma cells, in the adjacent fibrous tissue, *scale bar*=100 µm (**c**) and in the cytoplasm of individual C3842-cells, *scale bar*=20 µm (**d**)

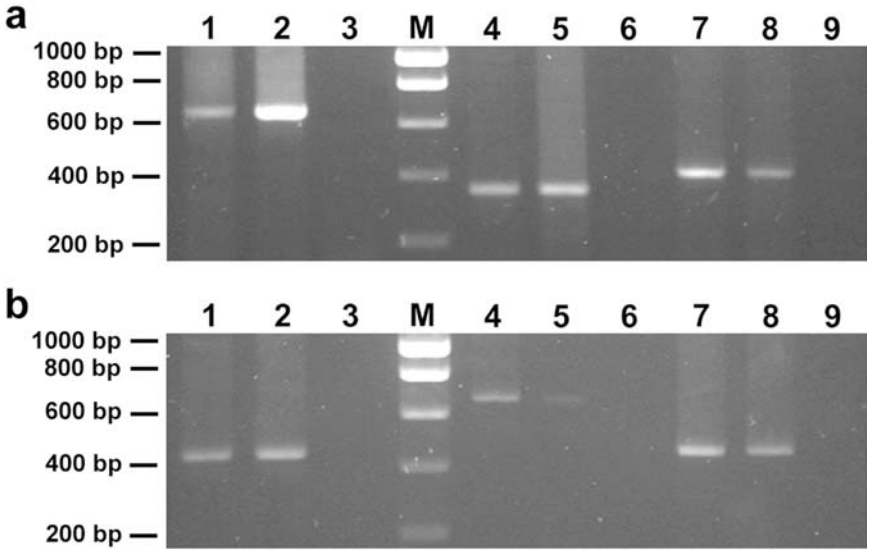

Fig. 6 Agarose gel electrophoresis of reverse-transcription polymerase chain reactions for beta-actin (*lane1–3*), aggrecan (*lane 4–6*), collagen type II (*lane 7–9*) (**a**) and collagen type I (*lane 1–3*), IX (*lane 4–6*), XI (*lane 7–9*) (**b**) for the tumor (*lanes 1, 4 and 7*) and the C3842-cells (*lanes 2, 5 and 8*). *Lanes 3, 6 and 9* negative controls. *M* marker

specific probe CEP 7 confirmed trisomy 7 (Fig. 4B) in 10 (18.2%) of the 55 interphase nuclei of passage 1, in 19 (14.4%) of the 132 interphase nuclei of passage 20 and in 25 (9.7%) of 258 interphase nuclei of passage 25. Interphase nuclei with four red signals for chromosome 7 were not detected in cells of passage 1 but in 15 (11.4%) of 132 interphase nuclei of passage 20 and in 20 (7.7%) of 258 interphase nuclei of passage 25.

Molecular genetic studies

PCR-SSCP analyses revealed no mutations for *p16* exons 1 and 2 or for *p53* exons 4–8 in the cultured cells and the tumor or the dysplastic cartilage. No mutations were detected using direct sequencing of *N*- and *H-ras* exons 1 and 2 and *K-ras* exon 1. In exon 2 of *K-ras*, a heterozygous point mutation from GAG to GAA, which does not lead to an amino acid substitution, was found in codon 62, affecting the tumor and the cultured cells but not the dysplastic cartilage.

Expression of cartilage matrix constituents

Immunohistochemical examination of the tumor tissue and the cultured cells revealed a positive reaction for collagen type II (Fig. 5A, B). In addition to the cytoplasm of the cells, it was mainly the myxoid matrix that was positively stained in the tumor tissue. The fibrous septa of the tumor tissue acted as an internal negative control. In the cell cultures, a strong cytoplasmic staining for collagen type II was observed in the majority of cells. For collagen type I, a positive immunohistochemical reaction of the matrix was noted in the vicinity of bone trabeculae and in the adjacent fibrous tissue. The cytoplasmic staining of the tumor cells was not continuous. In addition to a focal positivity, most tumor cells were only weakly positive or completely negative. Less than 5% of the cultured tumor cells showed cytoplasmic positivity (Fig. 5C, D).

The RT-PCR proved the expression of the alpha-I chain of collagen type I and type II in the tumor tissue and in the cultured cells. Aggrecan and the alpha-I chain of collagen types IX and XI were also detected in all samples (Fig. 6A, B).

Table 3 Immunohistochemical expression profile of proteases and protease inhibitors. Extensity scores: 0=<5%, 1=5–30%, 2=31–70%, 3=>71% positive tumor cells. Intensity scores: − negative, + weakly, ++ moderately, +++ strongly positive. *UPA* urokinase plasminogen activator, *PAI-1* anti-plasminogen-activator inhibitor, *MMP* matrix-metalloproteinase, *TIMP* tissue inhibitor of metalloprotease

	Tumor				Cultured cells	
	Invasion front		Internal tumor			
	Extensity	Intensity	Extensity	Intensity	Extensity	Intensity
Cathepsin B	2	++	2	++	3	+++
UPA	3	+++	3	++	3	+++
PAI-1	3	+++	3	+++	3	+++
MMP-1	3	+++	1	++	1	+
MMP-2	3	+++	1	++	2	++
MMP-3	3	+++	1	++	0	−
TIMP-1	1	++	0	−	0	−

Expression of proteases and protease inhibitors

The immunohistochemical expression profile of proteases and protease inhibitors are shown in Table 3. There were differences in the expression pattern between the bone invasion fronts and the internal parts of the tumor. At the invasion fronts, all proteases and protease inhibitors examined were detected. In other areas of the tumor, the expression of matrix metalloproteinases and their inhibitors was markedly reduced or (partially) absent. Besides TIMP-1 and TIMP-3, MMP-3 was virtually not detectable in cultured cells, whereas MMP-2 was clearly expressed (Fig. 7G, H, I). UPA and PAI-1 were almost constantly found in the tumor and in the cultured cells (Fig. 7D, E, F). Cathepsin B was demonstrated focally, particularly at the periphery of the tumor and at the invasion fronts (Fig. 7A, B, C). Typically, a granular cytoplasmic staining with varying intensities between individual tumor cells was observed. Associated macrophages in the fibrous septa of the tumor served as an additional internal positive control. In the cultured cells, cathepsin B was expressed more strongly.

The expression of all proteases examined was demonstrated by RT-PCR in the tumor and in the cultured cells (Fig. 8A, C). Quantitative RT-PCR of cathepsin B demonstrated an elevated expression level in the cultured cells (Fig. 8B).

Degradation of extracellular matrix

The degradation of the DQ-collagen type-I fluorescein conjugate mixed with gelatin/sucrose appeared as fine fluorescing structures on the cell surfaces and also in intracellular vesicles (Fig. 9A). When the DQ-collagen type-I fluorescein conjugate was mixed with Matrigel, the fluorescent

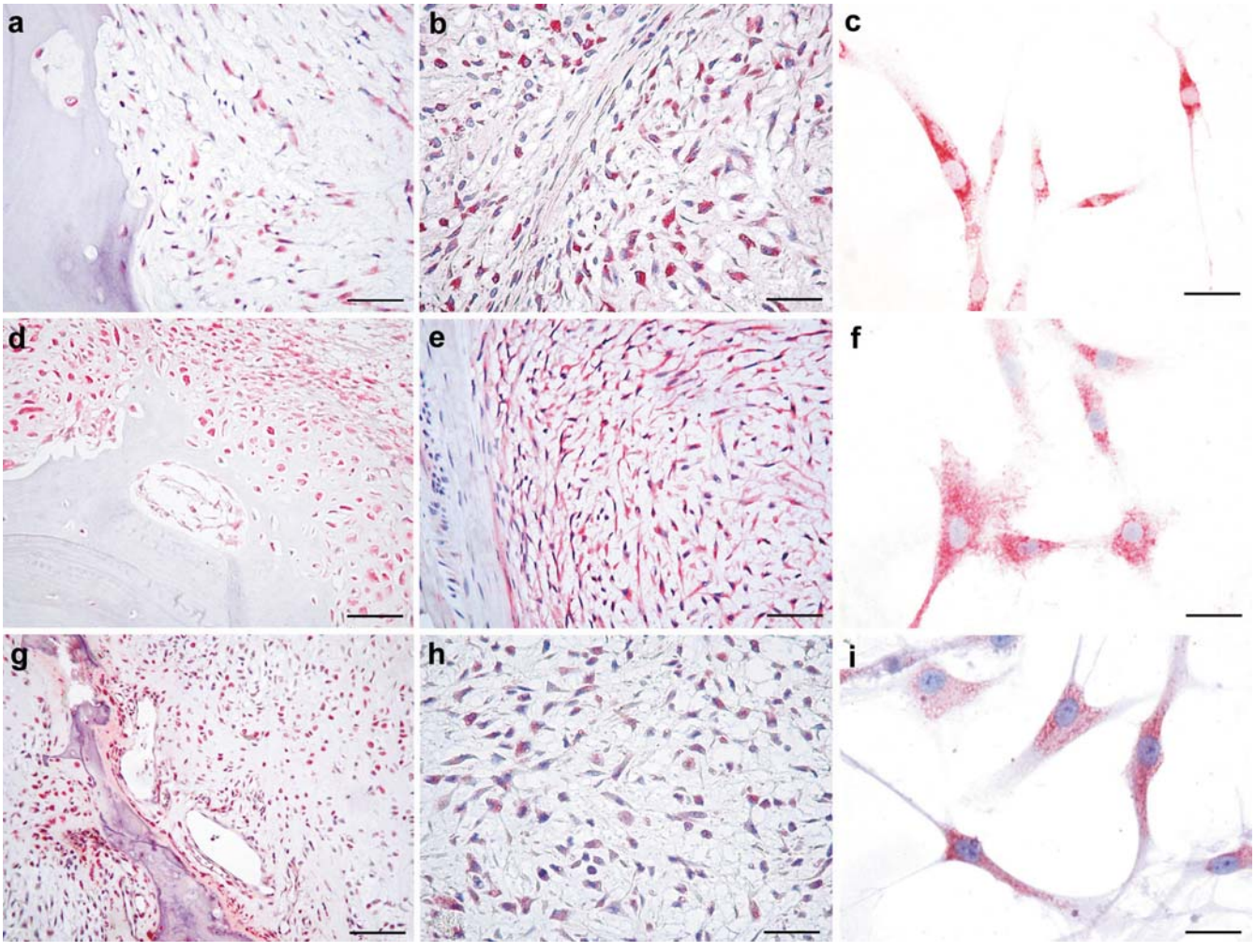

Fig. 7 Focal expression of cathepsin B in the secondary chondrosarcoma at the bone invasion front, *scale bar*=50 µm (**a**), in the internal tumor, *scale bar*=50 µm (**b**) and in C3842 cells, *scale bar*=20 µm (**c**). Marked expression of uPA at the bone invasion front, *scale bar*=50 µm (**d**), in the internal tumor, *scale bar*=50 µm (**e**) and in C3842 cells, *scale bar*=20 µm (**f**). Expression of MMP-2 at the bone invasion front, *scale bar*=100 µm (**g**), in the internal tumor, *scale bar*=50 µm (**h**) and in C3842 cells, *scale bar*=20 µm (**i**)

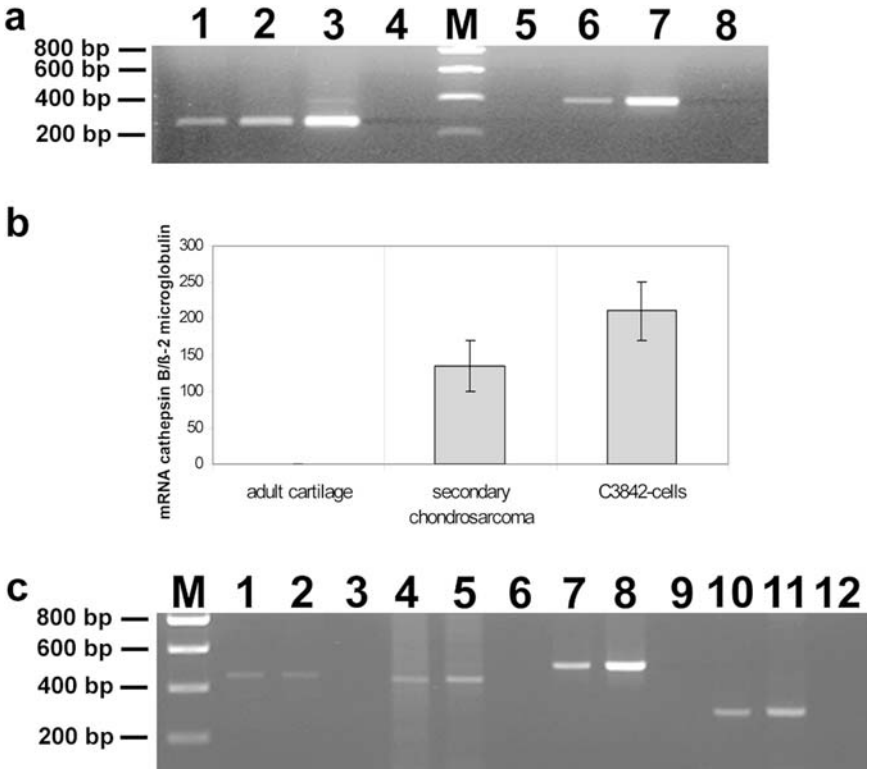

Fig. 8 Agarose gel electrophoresis of reverse-transcription polymerase chain reactions (RT-PCR) for beta-2-microglobulin (*lanes 1–4*) and cathepsin B (*lane 5–8*) for adult joint cartilage (*lanes 1 and 5*), the secondary chondrosarcoma (*lanes 2 and 6*) and the C3842 cells (*lanes 3 and 7*), *lanes 4 and 8* negative controls, *M* marker (**a**). Quantitative RT-PCR results for cathepsin B in adult cartilage, the secondary chondrosarcoma and C3842 cells in correlation to beta-2-microglobulin (**b**). Agarose gel electrophoresis of RT-PCRs for urokinase plasminogen activator (*lanes 1–3*), MMP-1 (*lanes 4–6*), MMP-2 (*lanes 7–9*) and MMP-3 (*lanes 10–12*) for the secondary chondrosarcoma (*lanes 1, 4, 7 and 10*) and the C3842 cells (*lanes 2, 5, 8 and 11*), *lanes 3, 6, 9 and 12* negative controls, *M* marker (**c**)

signal was also detected intracellularly but was mainly detected pericellularly in sector-like structures (Fig. 9B).

Invasive potential in vitro

Of 5×10^4 cultured cells seeded onto matrigel-coated Transwell filters, an average of 3840 cells permeating the filters in 72 h was detected in repeated Matrigel assays. This number corresponded to approximately 7.5% of the population in the control cell cultures grown under identical conditions.

Tumorigenicity in chick chorioallantoic membrane

The tumor cells formed three-dimensional aggregates on the surface of the chorioallantoic membrane, particularly at the inner circle of the silicone ring (Fig. 10A, B). The tumor cells did not invade the stroma of the chorioallan-

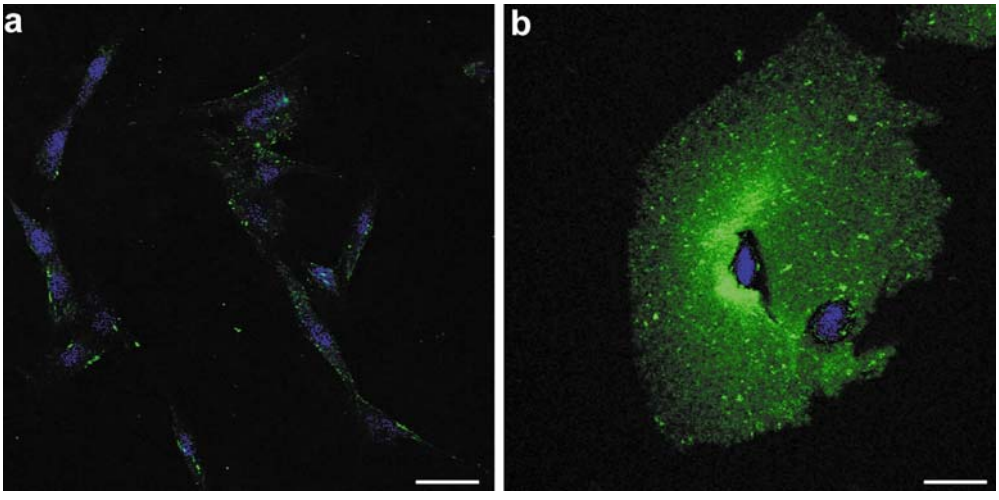

Fig. 9 Degradation of DQ-collagen type I fluorescein conjugate mixed with gelatin/sucrose (**a**) or Matrigel (**b**) by C3842-cells, *scale bars*=25 µm

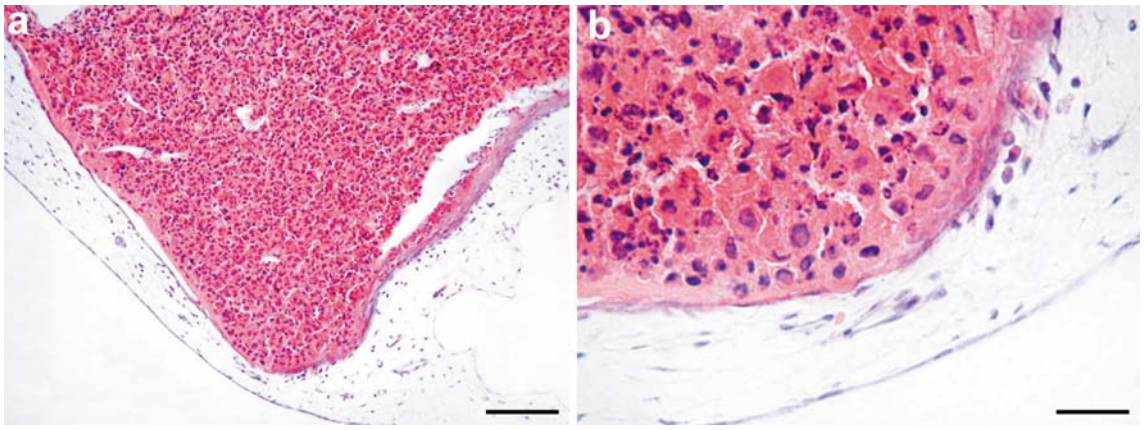

Fig. 10 Formation of three-dimensional tumor cell aggregates on the surface of the chorioallantoic membrane, Hematoxylin–eosin (HE), *scale bar*=100 µm (**a**) without stroma invasion, HE, *scale bar*=25 µm (**b**)

toic membrane. Necrotic changes were apparent in a great number of cells.

Discussion

Of all conditions predisposed to secondary chondrosarcoma, including Ollier's disease, Maffucci's syndrome, multiple hereditary exostoses, solitary osteochondroma, solitary enchondroma, Paget's disease or radiation injury, Ollier's disease has an exceptional position, owing to its long-term clinical course, starting in early childhood with slow-growing cartilage masses that may continue to grow even during adulthood. The latter represents the basic difference from solitary enchondromas, which exhibit a limited growth potential. In contrast to multiple hereditary exostoses, cases of Ollier's disease occur sporadically [28]. If secondary chondrosarcomas occur in Ollier's disease, the tumors are indistinguishable from primary chondrosarcomas, and the prognosis is exactly the same [13]. Therefore, secondary chondrosarcomas in Ollier's disease provide valuable models for further studies of the tumorigenesis of chondrosarcomas.

To our knowledge, C3842 is the first human cell line of a secondary chondrosarcoma in Ollier's disease. It exhibits typical features of the original tumor, which have been preserved in vitro. The morphological and ultrastructural characteristics of the C3842 cells were in accordance with the typical phenotypes in chondrosacomas grade 2 [17, 35].

The cytogenetic data on chondrosarcomas are heterogeneous and almost inappropriate for the differentiation of primary and secondary chondrosarcomas. Besides heavily rearranged karyotypes, peridiploidy with numerical or structural chromosomal aberrations is frequently found in chondrosarcomas [7, 27]. Secondary chondrosarcomas in osteochondroma are characterized by near haploidy and subsequent polyploidy in some cases [6]. Cytogenetic data on secondary chondrosarcomas in Ollier's disease are rare. Only two cytogenetically characterized cases have been documented in the literature: in one case, genetic analyses revealed losses of heterozygosity at the *Rb1* and the *p15/16* loci [5]. In another case, deletion of chromosome 1p was found [30]. In contrast to this, the majority of the C3842 cells were diploid, but trisomy 7 and near tetraploidy were detected using conventional chromosome analyses in passage 1. The number of diploid cells remained relatively stable during the cultivation up to the 25th passage, as demonstrated by FISH.

Mutations of protooncogenes and tumor suppressor genes are frequent findings in a variety of malignant tumors but are rare in chondrosarcomas [31]. In accordance with this, we did not detect any alterations in *p16*, *p53*, *N-ras* and *H-ras* genes in C3842-cells, the original tumor or the dysplastic cartilage. The heterozygous point mutation of the *K-ras* gene, which does not change the amino acid sequence, is attributed to the tumor and to the C3842-cells but not to the dysplastic cartilage.

Mature chondrocytes are characterized by the expression of typical cartilage matrix constituents, including aggrecan, collagen types II, IX and XI [1, 39, 40]. The matrix composition of cartilage tumors may be similar to normal cartilage in enchondromas or may be altered in chondrosarcomas [39]. The appearance of additional types of collagen, such as type I, has been attributed to a dedifferentiation in chondrosarcomas [2]. Together with the reduction of collagen type-II expression, this phenomenon has also been reported to occur in dedifferentiating chondrocytes in cell cultures [16]. However, chondrocytes with a phenotypic diversity may be found in the same tumor [1].

The expression of the typical cartilage matrix constituents, including collagen types II, IX, XI and aggrecan, was demonstrated in the tumor and in the C3842 cells. Collagen type I was also detected, but to a lesser extent than collagen type II. A preservation of the collagen type-II expression was also described for other chondrosarcoma cell lines [9, 18, 22, 38] except one [10]. However, a lack of collagen type-II expression was observed in some higher passages of C3842 cells (not shown), indicating an artificial change to a more dedifferentiated phenotype [16].

The degradation of the extracellular matrix is an essential step in the complex process of tumor cell invasion and metastasis [15]. The overexpression of matrix-degrading proteins, such as cathepsin B, uPA and MMPs, is of prognostic value in a variety of malignant tumors [14]. In chondrosarcomas, the overexpression of cathepsin B and

uPA is associated with a high rate of local recurrences and with an increased risk of distant metastasis [20]. The overexpression of MMP-2 is associated with tumor grade, suggesting a potential role in invasiveness [20, 32, 37].

The expression of cathepsin B, uPA, MMP-1, -2 and -3 was demonstrated in the tumor and in the C3842 cells. Varying expression levels of cathepsin B, MMP-1, -2 and -3 were detected at the bone invasion fronts and in the internal areas of the tumor, indicating a modulation of the invasive phenotype according to the microenvironmental conditions. In contrast to this, urokinase and its inhibitor PAI-1 were almost constantly detected, suggesting a rather constitutive expression. The coactivaton of PAI-1, which has been reported in several malignant tumors, can be interpreted as an overall upregulation of the plasminogen activation system and an attempt to prevent a complete stroma destruction [19]. A similar phenomenon was observed for TIMP-1 and -3 at the invasion fronts. The reduction of MMP-1 and -3 expression in C3842 cells may be attributed to the artificial conditions in vitro.

However, a wide spectrum of extracellular matrix components may be degraded by the C3842 cells, including collagen type I. The degradation products of the quenched collagen type I were detected both extracellularly and intracellularly, as described for DQ-collagen type IV in colon carcinoma cells [34]. Differences in the pericellular arrangement and the extension of the degradation products are attributed to the matrix composition with gelatin/sucrose or Matrigel, which may influence the expression, secretion and cell-surface localization of several proteases.

The degradation of the extracellular matrix was also demonstrated at a functional state by the Matrigel assay, which may be attributed to the expression of MMP-2 in particular [12]. However, this method does not necessarily correlate with the invasive behavior in vivo [26]. Accordingly, C3842 cells were not able to invade through the epithelium of the chorioallantoic membrane. However, this fits well with the biological behavior of the original tumor with its slow and bone destructive growth.

In conclusion, the cell line C3842 provides a unique model of a rare secondary chondrosarcoma in Ollier's disease that exhibits well-defined characteristics of malignant cartilage tumors in vitro and that will be subject to further functional investigations into secondary chondrosarcomas.

Acknowledgement This work was supported by a grant from the Bundesministerium für Bildung und Forschung (BMBF), NBL3-program.

References

1. Aigner T, Dertinger S, Vornehm SI, Dudhia J, von der Mark K, Kirchner T (1997) Phenotypic diversity of neoplastic chondrocytes and extracellular matrix gene expression in cartilaginous neoplasms. Am J Pathol 150:2133–2141
2. Aigner T, Muller S, Neureiter D, Illstrup DM, Kirchner T, Bjornsson J (2002) Prognostic relevance of cell biologic and biochemical features in conventional chondrosarcomas. Cancer 94:2273–2281
3. Barch MJ (ed) (1991) The ACT Cytogenetics laboratory manual, 2nd edn. Raven Press, New York
4. Bertoni F, Bacchini P, Hogendoorn PCW (2002) Chondrosarcoma. In: Fletcher CDM, Unni KK, Mertens F (eds) Pathology and genetics of tumours of soft tissue and bone. IARC Press, Lyon, pp 247–251
5. Bovee JV, van Roggen JF, Cleton-Jansen AM, Taminiau AH, van der Woude HJ, Hogendoorn PC (2000) Malignant progression in multiple enchondromatosis (Ollier's disease): an autopsy-based molecular genetic study. Hum Pathol 31:1299–1303
6. Bovee JV, van Royen M, Bardoel AF, Rosenberg C, Cornelisse CJ, Cleton-Jansen AM, Hogendoorn PC (2000) Near-haploidy and subsequent polyploidization characterize the progression of peripheral chondrosarcoma. Am J Pathol 157:1587–1595
7. Bridge JA, Bhatia PS, Anderson JR, Neff JR (1993) Biologic and clinical significance of cytogenetic and molecular cytogenetic abnormalities in benign and malignant cartilaginous lesions. Cancer Genet Cytogenet 69:79–90
8. Budowle B, Chakraborty R, Giusti AM, Eisenberg AJ, Allen RC (1991) Analysis of the VNTR locus D1S80 by the PCR followed by high-resolution PAGE. Am J Hum Genet 48:137–144
9. Chano T, Okabe H, Saeki Y, Ishizawa M, Matsumoto K, Hukuda S (1998) Characterization of a newly established human chondrosarcoma cell line, CS-OKB. Virchows Arch 32:529–534
10. Chansky H, Robbins JR, Cha S, Raskind WH, Conrad EU, Sandell LJ (1998) Expression of cartilage extracellular matrix and potential regulatory genes in a new human chondrosarcoma cell line. J Orthop Res 16:521–530
11. Chomczynski P, Sacchi N (1987) Single-step method of RNA isolation by acid guanidinium thiocyanate-phenol-chloroform extraction. Anal Biochem 162:156–159
12. Deryugina EI, Luo GX, Reisfeld RA, Bourdon MA, Strongin A (1997) Tumor cell invasion through matrigel is regulated by activated matrix metalloproteinase-2. Anticancer Res 17:3201–3210
13. Dorfman HD, Czerniak B (1998) Bone Tumors. Mosby Inc., St. Louis
14. Duffy MJ (1992) The role of proteolytic enzymes in cancer invasion and metastasis. Clin Exp Metastasis 10:145–155
15. Duffy MJ (1996) Proteases as prognostic markers in cancer. Clin Cancer Res 2:613–618
16. Elima K, Vuorio E (1989) Expression of mRNAs for collagens and other matrix components in dedifferentiating and redifferentiating human chondrocytes in culture. FEBS Lett 258:195–198
17. Erlandson RA, Huvos AG (1974) Chondrosarcoma: a light and electron microscopic study. Cancer 34:1642–1652
18. Gil-Benso R, Lopez-Gines C, Lopez-Guerrero JA, Carda C, Callaghan RC, Navarro S, Ferrer J, Pellin A, Llombart-Bosch A (2003) Establishment and characterization of a continuous human chondrosarcoma cell line, ch-2879: comparative histologic and genetic studies with its tumor of origin. Lab Invest 83:877–887
19. Hackel C, Czerniak B, Ayala AG, Radig K, Roessner A (1997) Expression of plasminogen activators and plasminogen activator inhibitor 1 in dedifferentiated chondrosarcoma. Cancer 79: 53–58
20. Hackel CG, Krueger S, Grote HJ, Oshiro Y, Hodges S, Johnston DA, Johnson ME, Roessner A, Ayala AG, Czerniak B (2000) Overexpression of cathepsin B and urokinase plasminogen activator is associated with increased risk of recurrence and metastasis in patients with chondrosarcoma. Cancer 89: 995–1003
21. Krueger S, Kellner U, Buehling F, Roessner A (2001) Cathepsin L antisense oligonucleotides in a human osteosarcoma cell line: effects on the invasive phenotype. Cancer Gene Ther 8:522–528

22. Kunisada T, Miyazaki M, Mihara K, Gao C, Kawai A, Inoue H, Namba M (1998) A new human chondrosarcoma cell line (OUMS-27) that maintains chondrocytic differentiation. Int J Cancer 77:854–859
23. Kunzi-Rapp K, Genze F, Kufer R, Reich E, Hautmann RE, Gschwend JE (2001) Chorioallantoic membrane assay: vascularized 3-dimensional cell culture system for human prostate cancer cells as an animal substitute model. J Urol 166:1502–1507
24. Lee FY, Mankin HJ, Fondren G, Gebhardt MC, Springfield DS, Rosenberg AE, Jennings LC (1999) Chondrosarcoma of bone: an assessment of outcome. J Bone Joint Surg Am 81:326–338
25. Liu J, Hudkins PG, Swee RG, Unni KK (1987) Bone sarcomas associated with Ollier's disease. Cancer 59:1376–1385
26. Mackinnon WB, Hancock R, Dyne M, Russell P, Mountford CE (1992) Evaluation of an in vitro invasion assay for use on solid tissue samples and cultured cells. Invasion Metastasis 12:241–252
27. Mandahl N, Gustafson P, Mertens F, Akerman M, Baldetorp B, Gisselsson D, Knuutila S, Bauer HC, Larsson O (2002) Cytogenetic aberrations and their prognostic impact in chondrosarcoma. Genes Chromosomes Cancer 33:188–200
28. Mertens-F, Unni-K (2002) Enchondromatosis: Ollier disease and Mafucci syndrome. In: Fletcher CDM, Unni KK, Mertens F (eds) Pathology and genetics of tumours of soft tissue and bone. IARC Press, Lyon, pp 356–357
29. Mitelman F (1995) An international system for human cytogenetic nomenclature. S. Karger, Basel
30. Ozisik YY, Meloni AM, Spanier SS, Bush CH, Kingsley KL, Sandberg AA (1998) Deletion 1p in a low-grade chondrosarcoma in a patient with Ollier disease. Cancer Genet Cytogenet 105:128–133
31. Pompetti F, Rizzo P, Simon RM, Freidlin B, Mew DJ, Pass HI, Picci P, Levine AS, Carbone M (1996) Oncogene alterations in primary, recurrent, and metastatic human bone tumors. J Cell Biochem 63:37–50
32. Sakamoto A, Oda Y, Iwamoto Y, Tsuneyoshi M (1999) Expression of membrane type 1 matrix metalloproteinase, matrix metalloproteinase 2 and tissue inhibitor of metalloproteinase 2 in human cartilaginous tumors with special emphasis on mesenchymal and dedifferentiated chondrosarcoma. J Cancer Res Clin Oncol 125:541–548
33. Sambrook J, Russell DW (2001) Molecular cloning. Cold Spring Harbor Laboratory Press, New York
34. Sameni M, Dosescu J, Moin K, Sloane BF (2003) Functional imaging of proteolysis: stromal and inflammatory cells increase tumor proteolysis. Mol Imaging 2:159–175
35. Schajowicz F, Cabrini RL, Simes RJ, Klein-Szanto AJ (1974) Ultrastructure of chondrosarcoma. Clin Orthop 100:378–386
36. Schneider-Stock R, Boltze C, Lasota J, Miettinen M, Peters B, Pross M, Roessner A, Gunther T (2003) High prognostic value of p16INK4 alterations in gastrointestinal stromal tumors. J Clin Oncol 21:1688–1697
37. Soderstrom M, Aro HT, Ahonen M, Johansson N, Aho A, Ekfors T, Bohling T, Kahari VM, Vuorio E (2001) Expression of matrix metalloproteinases and tissue inhibitors of metalloproteinases in human chondrosarcomas. APMIS 109:305–315
38. Takigawa M, Tajima K, Pan HO, Enomoto M, Kinoshita A, Suzuki F, Takano Y, Mori Y (1989) Establishment of a clonal human chondrosarcoma cell line with cartilage phenotypes. Cancer Res 49:3996–4002
39. Ueda Y, Oda Y, Tsuchiya H, Tomita K, Nakanishi I (1990) Immunohistological study on collagenous proteins of benign and malignant human cartilaginous tumours of bone. Virchows Arch 417:291–297
40. Vornehm SI, Dudhia J, Von der Mark K, Aigner T (1996) Expression of collagen types IX and XI and other major cartilage matrix components by human fetal chondrocytes in vivo. Matrix Biol 15:91–98
41. Welkerling H, Kratz S, Ewerbeck V, Delling G (2003) A reproducible and simple grading system for classical chondrosarcomas. Analysis of 35 chondrosarcomas and 16 enchondromas with emphasis on recurrence rate and radiological and clinical data. Virchows Arch 443:725–733

Virchows Arch (2005) 446: 300–304
DOI 10.1007/s00428-004-1138-6

CASE REPORT

T. Mentzel · J. Toennissen · A. Rütten · J. Schaller

Palmar atypical lipomatous tumour with spindle cell features (well-differentiated spindle cell liposarcoma): a rare neoplasm arising in an unusual anatomical location

Received: 10 August 2004 / Accepted: 8 September 2004 / Published online: 18 February 2005
© Springer-Verlag 2005

Abstract Lipomatous tumours, both benign and malignant, arising on the hands are uncommon. We present a rare atypical lipomatous tumour with spindle cell features (synonym: well-differentiated spindle cell liposarcoma) arising on the left palm of a 54-year-old male patient. The neoplasm presented as a long-standing, exophytic neoplasm measuring 9×9 cm. The well-circumscribed neoplasm was completely excised, and margins were tumour free. Histologically, the neoplasm showed features closely resembling spindle cell lipoma, being composed of mature adipocytic cells associated with bland, neuroid spindle cells staining positively for CD34. However, focally, atypia of adipocytic and stromal cells as well as scattered lipoblasts were noted, and immunohistochemical stainings showed focal overexpression of MDM 2 and CDK4. Aypical lipomatous tumour with spindle cell features may arise very rarely in palmar location and has to be distinguished from a number of benign and malignant mesenchymal neoplasms.

Keywords Atypical lipomatous tumour · Liposarcoma · Soft tissue tumours · Hand · Immunohistochemistry

T. Mentzel (✉) · A. Rütten
Dermatopathologische Gemeinschaftspraxis,
Siemensstrasse 6/1,
88048 Friedrichshafen, Germany
e-mail: tmentzel@w-4.de
Tel.: +49-7541-604431
Fax: +49-7541-604410

J. Toennissen
Department of Plastic and Hand Surgery,
Katholisches Klinikum Duisburg,
Germany

J. Schaller
Department of Dermatohistology,
Katholisches Klinikum Duisburg,
Germany

Introduction

Atypical and malignant lipomatous tumours represent the largest single group of atypical/malignant mesenchymal neoplasms in adults. The histological subtypes, including atypical lipomatous tumour (synonym: well-differentiated liposarcoma) and dedifferentiated liposarcoma, as well as myxoid and pleomorphic liposarcoma are separate diseases with distinct and different clinical, histological and genetic features [5]. Atypical lipomatous tumours (ALT) are intermediate, locally aggressive lipogenic neoplasms composed of atypical adipocytic cells showing significant variations in size and shape and nuclear atypia in stromal and adipocytic cells. Usually, scattered hyperchromatic stromal cells and mono- or multi-vacuolated lipoblasts are seen; however, the presence of lipoblasts is no longer regarded as a *conditio sine qua non* for the diagnosis of ALT [15]. Histologically, ALT can be subdivided into four main subtypes, including adipocytic (lipoma-like), sclerosing, inflammatory and spindle cell type; often more than one morphological pattern is seen in the same lesion. The spindle cell variant of ALT represents a recently characterised rare subtype of ALT [6] and is composed of slightly atypical spindle-shaped tumour cells associated with an atypical adipocytic component and set in a fibrous and/or myxoid matrix. Spindle cell ALT has been described in subcutaneous and deep soft tissues [6] as well as in unusual locations, such as the oral cavity [16] and the orbit [4]. We present a case of a spindle cell ALT (well-differentiated spindle cell liposarcoma) arising on the palm of a male patient and discuss the differential diagnosis.

Case report

In March 2003, a 54-year-old male patient presented with a long-standing (more than 5 years), slowly growing lesion on his left palm. Clinically, an exophytic neoplasm measuring 9×9 cm was seen (Fig. 1); however, the patient still refused excision. Magnetic resonance imaging showed

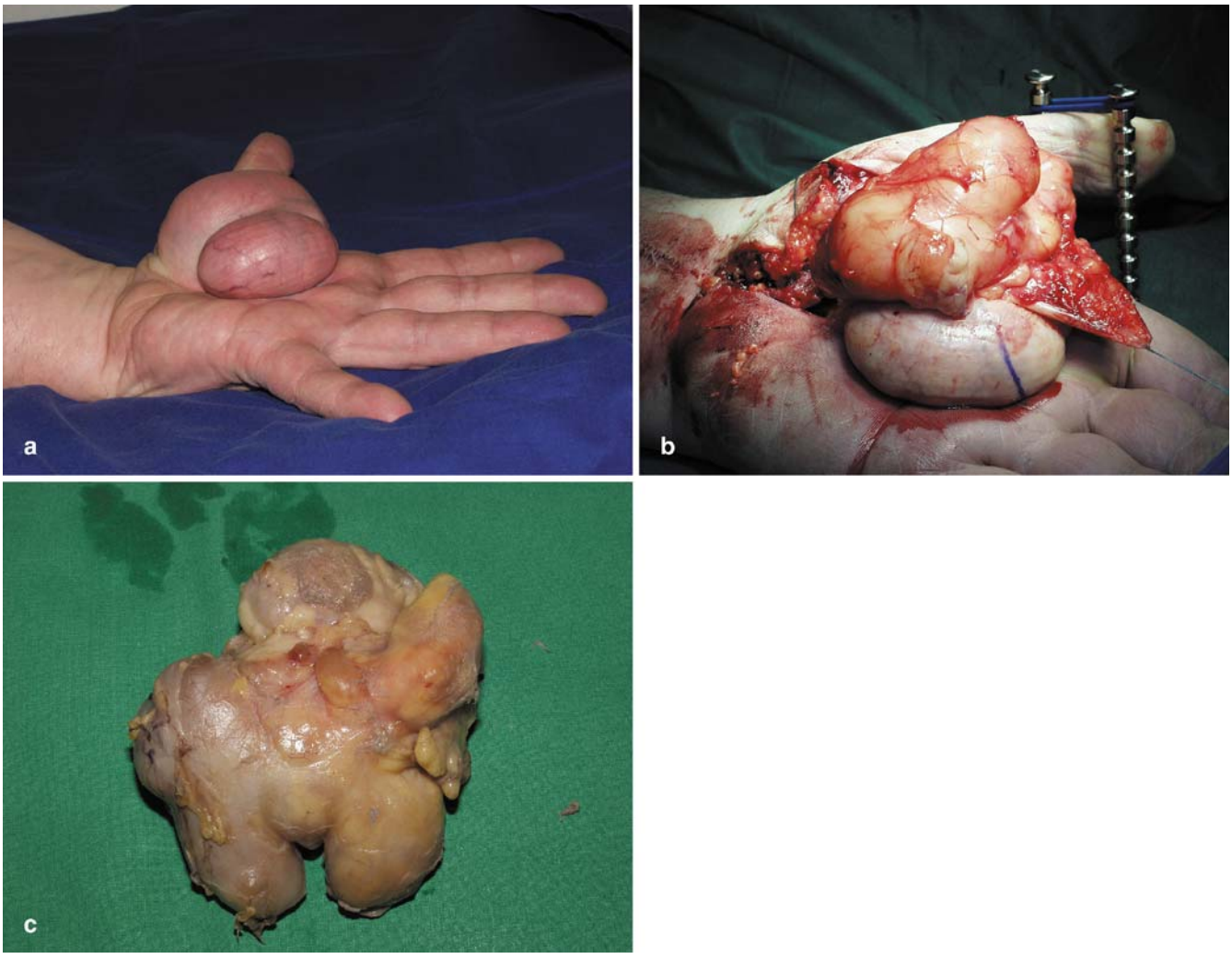

Fig. 1 **a** Clinically, a large, exophytic neoplasm with smooth surfaces arising on the palm is seen. **b** Intraoperatively, a well-circumscribed and partly encapsulated neoplasm is noted. **c** Grossly, the lobulated as well as nodular neoplasm is partly encapsulated and is grey-white as well as yellow, suggesting lipogenic differentiation

changes compatible with a lipomatous lesion. After a diagnostic biopsy in October 2003, the neoplasm was excised completely and with tumour-free margins. Intraoperatively, a nodular, well-circumscribed as well as encapsulated neoplasm was noted (Fig. 1). There is no sign of recurrence at 8 months.

Materials and methods

Material of the biopsy and the excision was fixed in 4% buffered formalin, routinely processed and embedded in paraffin; 4-µm-thick sections were stained with haematoxylin and eosin. In addition, representative sections were stained immunohistochemically by the labelled streptavidin biotin technique using commercially available antibodies; antigen retrieval was used for all antibodies. The antibodies used, their sources and dilutions are given in Table 1. Appropriate positive and negative controls were used in each case.

Table 1 Immunohistochemical reagents used. *ASMA* alpha-smooth-muscle actin

Antibody	Clone	Dilution	Source
Desmin	D33	1:200	Dako, Glostrup, Denmark
ASMA	1A4	1:300	Dako, Glostrup, Denmark
S-100 Protein	Polyclonal	1:4000	Dako, Glostrup, Denmark
CD34	Qbend10	1:50	Dako, Glostrup, Denmark
CD34	HPCA-1	1:100	Becton and Dickinson
CD68	PG-M1	1:200	Dako, Glostrup, Denmark
CD31	JC70A	1:100	Dako, Glostrup, Denmark
CDK4	DCS-31	1:400	Biosource
MDM 2	IF2	1:200	Zymed

Results

The biopsy showed an irregular admixture of mature adipocytic cells and cytologically uniform spindle-shaped cells containing bland, elongated, neuroid nuclei set in a slightly

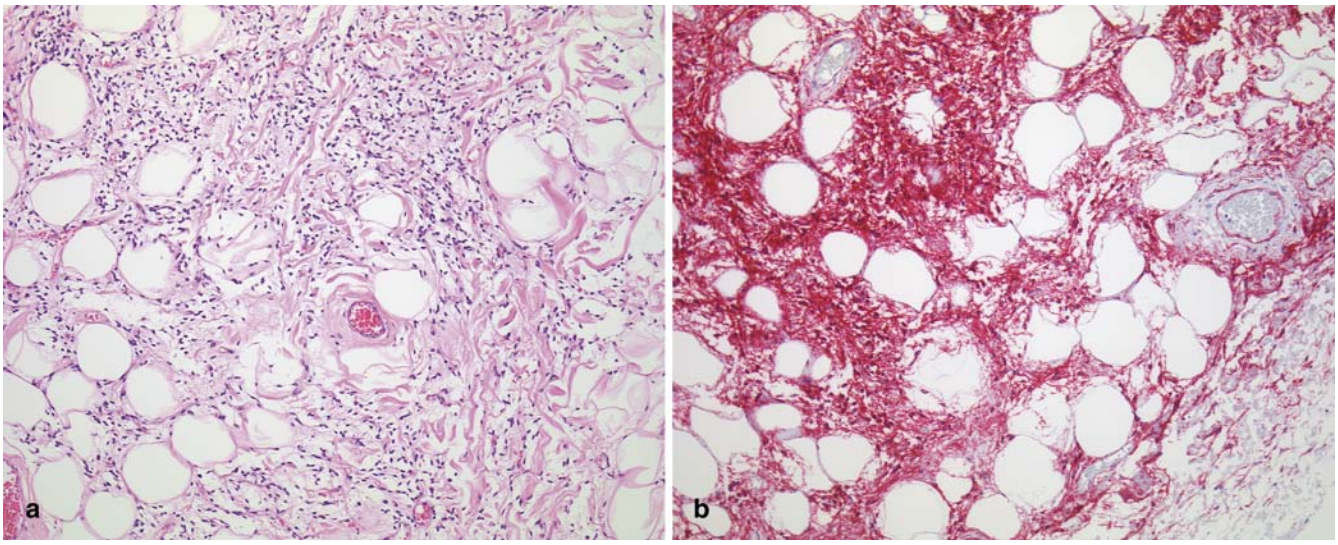

Fig. 2 **a** The material of the biopsy is composed of mature adipocytic cells closely associated with bland spindled cells set in a collagenous background with hyalinised collagen fibres. **b** Immunohistochemically, spindled cells stain positively for CD34

myxoid stroma with scattered inflammatory cells. Immunohistochemically, spindled cells stained homogenously positive for CD34 with two different antibodies (Fig. 2). The diagnosis of a lipogenic neoplasm with spindle cells resembling spindle cell lipoma was given tentatively. The completely excised neoplasm again showed features closely resembling spindle cell lipoma. However, in addition, tumour areas with marked nuclear atypia and scattered lipoblasts were present. In these areas, adipocytic cells showed striking variations in size and shape, and scattered enlarged stromal cells with enlarged and hyperchromatic nuclei were noted (Fig. 3). Spindled cells stained positively again for CD34 but were negative for S-100 protein. Some tumour cells showed nuclear staining for CDK4 and MDM 2. Focally, cellular areas composed mainly of spindle-shaped, CD34-positive cells set in a myxoid matrix with numerous small vessels were seen, and scattered inflammatory cells as well as necrobiotic changes were present. The final diagnosis was ALT with spindle cell features (well-differentiated spindle cell liposarcoma).

Discussion

Lipomatous neoplasms, both benign and malignant, arising on the hands are uncommon, and most cases have been reported in clinical journals [1–3, 7, 11, 12, 17, 18, 21]. Spindle cell lipoma and pleomorphic lipoma represent ends of a common histological spectrum. Most of these neoplasms occur as encapsulated subcutaneous lesions on the neck and back, usually of males, and are composed of a variable admixture of mature adipocytes and CD34-positive spindled, hyperchromatic round cells and multinucleated giant cells set in an often myxoid stroma with hyalinised collagen bundles [8, 22]. In contrast, purely dermal spindle cell/pleomorphic lipomas are rather ill-defined lesions, arising more frequently in female patients, and show a wider anatomic distribution [9]. To the best of our knowledge, only one case of a pleomorphic lipoma arising on the palm has been reported previously [10].

Although morphological features of the biopsy were almost indistinguishable from spindle cell lipoma, this diagnosis was suggested tentative only, knowing the clinical features of the presented case and the rarity of these neoplasms in palmar location. Given the presence of atypical stromal cells, scattered lipoblasts and variations of size and shape of adipocytic cells, the diagnosis of ALT with spindle cell features (well-differentiated spindle cell liposarcoma) was established. This diagnosis was further substantiated by the focal overexpression of MDM 2 and CDK4. Atypical lipomatous tumours are characterised by ring- or giant marker chromosomes derived from the q13–15 region of chromosome 12, and amplification of this region results in amplification of *MDM 2, CDK4* (and *SAS, GLI*) genes [19, 20].

ALT with spindle cell features (well-differentiated spindle cell liposarcoma) has to be distinguished from a number of benign and malignant mesenchymal lesions. Spindle cells in perineurioma and neurofibroma stain positively for perineurial (epithelial membrane antigen, claudin, Glut-1) and neural markers (S-100 protein), respectively. ALT with spindle cells may show a prominent expression of CD34 as in the presented case; however, the presence of atypical adipocytic and stromal cells as well as the overexpression of CDK4 and MDM 2 are of help in the distinction from spindle cell lipoma. Haemosiderotic fibrohistiocytic lipomatous lesions arise predominantly on the foot and ankle mostly in middle-aged women and are composed of mature adipocytic cells associated with plump spindled cells, scattered inflammatory cells and abundant iron pigment [14]. Fibrohistiocytic lipoma may also occur rarely on the hands; however, these neoplasms are composed of (myo)fibroblastic cells and mature adipocytes without prominent atypia [13]. Dermatofibrosarcoma protuberans is characterised by a diffusely infiltrative growth and a storiform pattern of bland spindle cells without an atypical lipogenic component.

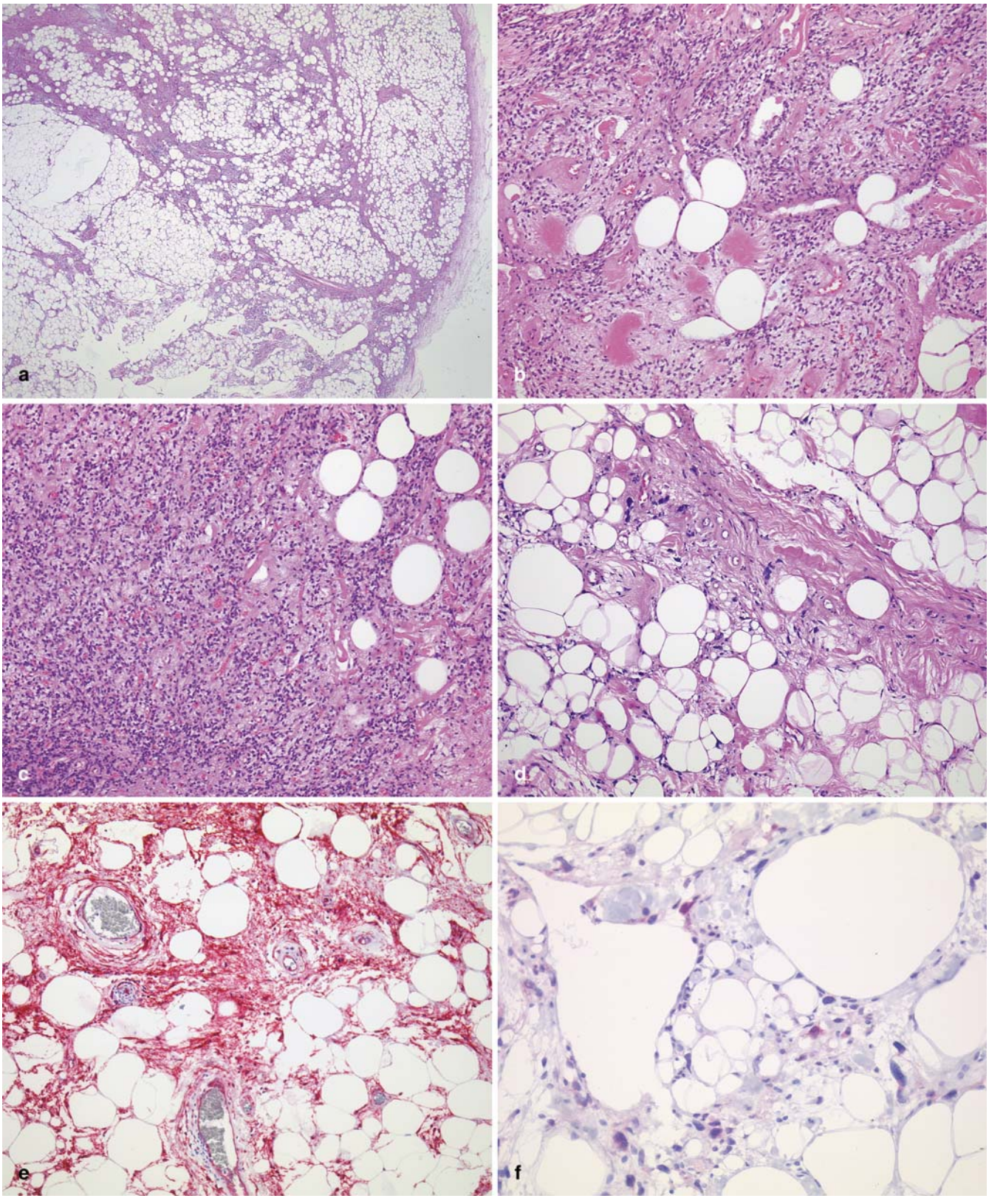

Fig. 3 **a** The excised neoplasm is well circumscribed and partly encapsulated. Even on low-power view, atypical adipocytic and stromal cells are evident. **b** In some areas, morphological features are indistinguishable from spindle cell lipoma, showing an admixture of mature adipocytes with bland spindled cells. **c** Focally, cellular areas composed of bland spindled and round cells set in a myxoid matrix with numerous capillaries were present. **d** In other tumour areas, striking atypia of lipogenic and stromal cells was seen. Note variations of size and shape of adipocytic cells as well as the presence of enlarged cells with enlarged and hyperchromatic nuclei. **e** Most spindled and pleomorphic cells stained positively for CD34. **f** Some tumour cells show weak nuclear expression of CDK4

The distinction of ALT with spindle cell features from low-grade dedifferentiated liposarcoma with a gradual dedifferentiation may be problematic. However, the spindle cell proliferation in low-grade dedifferentiated liposarcoma is usually nonlipogenic, and often a higher degree of cellularity and atypia is present somewhere.

In summary, the present report describes features of a rare ALT with spindle cell features (well-differentiated spindle cell liposarcoma) arising in an exceptionally rare location, and the differential diagnoses are discussed.

Acknowledgement The authors are very grateful to Professor Dr. C.D.M. Fletcher, Boston, MA, who kindly confirmed the diagnosis.

References

1. Babins DM, Lubahn JD (1994) Palmar lipomas associated with compression of the median nerve. J Bone Joint Surg Am 76: 1360–1362
2. Bailey SC, Bailey B, Smith NT, Van Tassel P, Thomas (2001) Brain metastasis from a primary liposarcoma of the digit. Case report. Am J Clin Oncol 24:81–84
3. Booher RJ (1965) Lipoblastic tumors of the hands and feet. Review of the literature and report of thirty-three cases. J Bone Joint Surg Am 47:727–740
4. Cai YC, McMenamin ME, Rose G, Sandy CJ, Cree IA, Fletcher CDM (2001) Primary liposarcoma of the orbit: a clinicopathological study of seven cases. Ann Diagn Pathol 5:255–266
5. Dei Tos AP, Pedeutour F (2002) Atypical lipomatous tumour/well-differentiated liposarcoma. In: Fletcher CDM, Unni KK, Mertens F (eds) WHO classification of tumours. Tumours of soft tissue and bone. IARS Press, Lyon, France
6. Dei Tos AP, Mentzel T, Newman PL, Fletcher CDM (1994) Spindle cell liposarcoma, a hitherto unrecognized variant of liposarcoma. Analysis of six cases. Am J Surg Pathol 18:913–921
7. De Smet L, Bande S, Fabry G (1994) Giant lipoma of the deep palmar space, mimicking persistent carpal tunnel syndrome. Acta Orthop Belg 60:334–335
8. Enzinger FM, Harvey DA (1975) Spindle cell lipoma. Cancer 36:1852–1859
9. French CA, Mentzel T, Kutzner H, Fletcher CDM (2000) Intradermal spindle cell/pleomorphic lipoma: a distinct subset. Am J Dermatopathol 22:496–502
10. Hayashi T, Tsuda N, Shimada O, Maeda H (1989) A pleomorphic lipoma of the palm-comparison to spindle cell lipoma. Gan No Rinsho 35:437–441
11. Hoehn JG, Farber HF (1983) Massive lipoma of the palm. Ann Plast Surg 11:431–433
12. Kaminsky CA, de Kaminsky AR, Chajchir A, Costantin (1987) Palmar subcutaneous lipoma. Cutis 40:29–32
13. Marshall-Taylor C, Fanburg-Smith JC (2000) Fibrohistiocytic lipoma: twelve cases of a previously undescribed benign fatty tumor. Ann Diagn Pathol 4:354–360
14. Marshall-Taylor C, Fanburg-Smith JC (2000) Hemosiderotic fibrohistiocytic lipomatous lesion. Ten cases of a previously undescribed fatty lesion of the foot/ankle. Mod Pathol 13:1192–1199
15. Mentzel T, Fletcher CDM (1995) Lipomatous tumours of soft tissues: an update. Virchows Arch 427:353–363
16. Nascimento AF, McMenamin ME, Fletcher CDM (2002) Liposarcomas/atypical lipomatous tumors of the oral cavity: a clinicopathological study of 23 cases. Ann Diagn Pathol 6:83–93
17. Ogose A, Kobayashi H, Morita T, Hasegawa K, Hirata (2000) Well-differentiated liposarcoma of the hand. Case report. Scand J Plast Reconstr Surg Hand Surg 34:185–187
18. Oster LH, Blair WF, Steyers CM (1989) Large lipomas in the deep palmar space. J Hand Surg (Am) 14:700–704
19. Pedeutour F, Forus A, Coindre JM, Berner JM, Nicolo G, Michiels JF (1999) Structure of the supernummerary ring and giant rod chromosomes in adipose tissue tumors. Genes Chromosomes Cancer 24:30–41
20. Rosai J, Akerman M, Dal Cin P, DeWever I, Fletcher CDM, Mandahl N, Mertens F, Mitelman F, Rydholm A, Sciot R, Tallini G, Van den Berghe H, Van de Van W, Vanni R, Willen H (1996) Combined morphologic and karyotypic study of 59 atypical lipomatous tumors: evaluation of their relationship and differential diagnosis with other adipose tissue tumors. Am J Surg Pathol 20:1182–1189
21. Sawhney KK, McDonald JM, Jaffe HW (1975) Liposarcoma of the hand. Am Surg 41:117–120
22. Shmookler BM, Enzinger FM (1981) Pleomorphic lipoma: a benign tumor simulating liposarcoma. A clinicopathologic analysis of 48 cases. Cancer 47:126–133

Virchows Arch (2005) 446: 305–309
DOI 10.1007/s00428-004-1163-5

CASE REPORT

Sebastian Aulmann · Philipp A. Schnabel · Birgit Helmchen · Hendrik Dienemann · Peter Drings · Herwart F. Otto · Hans Peter Sinn

Immunohistochemical and cytogenetic characterization of acantholytic squamous cell carcinoma of the breast

Received: 8 August 2004 / Accepted: 11 October 2004 / Published online: 25 January 2005
© Springer-Verlag 2005

Abstract Primary acantholytic squamous cell carcinoma (ASCC) of the breast is a rare and aggressive variant of invasive breast cancer. Here we report two new cases of ASCC and their immunohistochemical and cytogenetic characterization. One case was associated with systemic metastases and death and the other with local failure prior to loss of follow-up. Using comparative genomic hybridization (CGH), both tumors showed a high overall number of chromosomal imbalances with a similar pattern of gains and losses. Genetic aberrations common to both tumors included losses at 3p11-p25, 5q21-q31, 8p, 9, 13p13-q21, 16q12-q21, and 17p and gains at 1q31-qter, 7p, 18q12-qter, 19q, and 20. Immunohistochemically, the tumors were characterized by high proliferative activity, an uncommon cytokeratin expression profile, reduced E-cadherin staining, and overexpression of p53 and epithelial growth factor receptor (EGFR). The results of our analyses suggest that genetic alterations observed in ASCC of the breast include imbalances commonly observed in both mammary adenocarcinoma and squamous cell carcinoma of other locations. Furthermore, the overexpressed EGFR could be a possible therapeutic target for individual cases of this aggressive tumor type.

Keywords Acantholytic squamous cell carcinoma · Breast · Comparative genomic hybridization · Immunohistochemistry

S. Aulmann (✉) · P. A. Schnabel · B. Helmchen · H. F. Otto · H. P. Sinn
Department of Pathology, University of Heidelberg,
INF 220/221,
69120 Heidelberg, Germany
e-mail: sebastian_aulmann@med.uni-heidelberg.de
Tel.: +49-6221-562666
Fax: +49-6221-565251

H. Dienemann · P. Drings
Thoraxklinik Heidelberg,
Amalienstraße 6,
69126 Heidelberg, Germany

Introduction

Pure squamous cell carcinoma of the breast is a rare disease, accounting for approximately 0.05% of all breast neoplasms [5, 20]. The acantholytic variant was first described in 1989 by Eusebi et al. [6], who presented three cases that had been collected internationally. Another account of a well-documented acantholytic squamous cell carcinoma (ASCC) of the breast was published by Parramore et al. In 1999 [16], three further cases were included in a case series reported by Banerjee et al. in 1992 [2]. Histologically, these tumors are characterized by the formation of irregular spaces lined by atypical squamous epithelial cells leading to a pseudoglandular or pseudoangiosarcomatous appearance. In addition, solid and spindle cell areas are typically present to a varying extent [6]. The clinical course of the published cases suggests a highly aggressive behavior, most patients developing widespread metastases and dying within months from diagnosis.

Here, we report the clinicopathological and immunohistochemical features of two further cases of ASCC of the breast. In addition, both tumors were screened for chromosomal imbalances using comparative genomic hybridization (CGH).

Clinical history

Patient 1

A 48-year-old female presented to the Thoraxklinik Heidelberg, Germany, in January 2003 with a 3–4 cm tumorous mass in the upper lobe of the left lung with local infiltration of the posterior chest wall. The patient had suffered from tuberculosis 13 years previously, leading to extensive residual scarring in both lungs. A transbroncheal lung biopsy was performed and diagnosed as poorly differentiated non-small cell carcinoma, compatible with a scar carcinoma. Physical examination revealed a small, palpable tumor in the right breast approximately 1.5 cm in diameter. Initially, no further metastases were clinically de-

tected. Because of the extensive post-tuberculous changes in the left lung making operative treatment impossible, irradiation of the left upper lobe was initiated.

After 4 weeks, osteolytic bone metastases were diagnosed in the left pubic bone and the left radius, and the breast tumor had increased to almost 3 cm in diameter. It was excised for further diagnosis and sent to the Department of Pathology of the Heidelberg University Hospital. Gross examination showed a firm, grayish-white tumor with circumscribed margins and a maximum diameter of 2.8 cm (Fig. 1a). Histologically, there were areas with atypical spindle cells (Fig. 1d) and areas with prominent acantholysis, leading to the formation of irregular channels, lined by atypical tumor cells (Fig. 1c). Between both patterns, nests of focally keratinizing, atypical squamous epithelial cells were recognized (Fig. 1b). The tumor cells showed a high grade of nuclear atypia and many prominent mitoses. Within the tumor and in the surrounding breast tissue, a predominantly solid-growing, high-grade in situ ductal component without recognizable squamoid features was observed (Fig. 1b). On the basis of these findings, the diagnosis of a primarily metastasizing ASCC of the breast was established. Routinely performed immunohistochemistry for estrogen and progesterone receptors as well as for the Her2 proto-oncogene showed negative results.

The patient was treated palliatively with irradiation of symptomatic bone metastases and died 4 months after the first admission to hospital. No post-mortem examination was performed.

Patient 2

A 55-year-old female presented to the Heidelberg University Womens' Hospital in 1993 with a palpable breast mass approximately 2.5 cm in greatest diameter. The patient's clinical history had been unremarkable, and clinical investigation revealed no distant metastases. She was treated with breast-conserving surgery. Histologically, the tumor showed the same two growth patterns described above (Fig. 2). However, compared with case 1, the spindle cell areas were less prominent, and there were larger areas of necrosis. As in case 1, there was no detectable expression of the estrogen and progesterone receptors and no overexpression of the Her2 oncogene product. Surrounding the tumor, foci of a predominantly solid-growing, intermediate-grade ductal carcinoma in situ without squamoid features as well as a small, well-differentiated invasive ductal carcinoma with strong hormone receptor expression were observed. While the invasive tumor was excised in total, the in situ component focally reached into the surgical resection margin. The diagnosis of heterogeneously differentiated carcinoma was initially made, and the case was sent to a consultant pathologist (R. R. Millis, London, United Kingdom), who established the diagnosis of invasive carcinoma with features of acantholytic carcinoma of the breast. No axillary dissection was performed. The patient suffered from two local recurrences 15 months and 25 months after diagnosis, which were treated surgically, and was lost to follow-up shortly thereafter.

Materials and methods

Immunohistochemistry

Paraffin sections of representative tumor areas were immunostained on an automated staining system (Techmate 500+, DakoCytomation, Hamburg, Germany) with the avidin-biotin-complex peroxidase staining system. Primary antibodies and slide pre-treatment are summarized in Table 1.

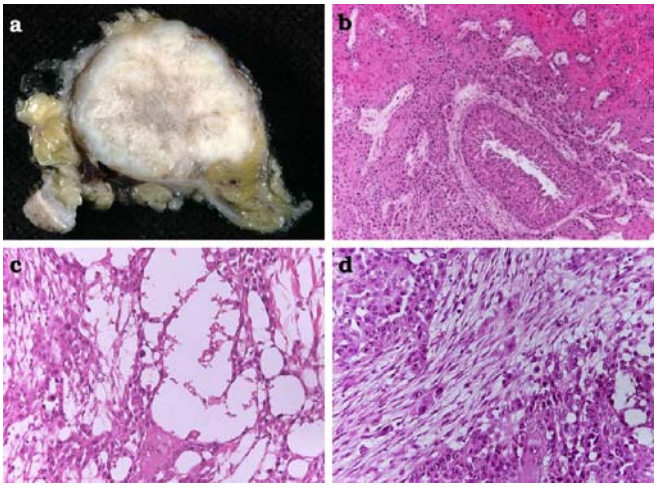

Fig. 1 Tumor 1. **a** Cut surface showing a firm, grayish-white tumor with circumscribed margins. **b** Low-power view (original magnification ×40) showing solid areas and the associated in situ carcinoma. **c** High-power view (original magnification: 1:200) of prominent acantholysis. **d** Merging of spindle cell and acantholytic areas (original magnification ×200)

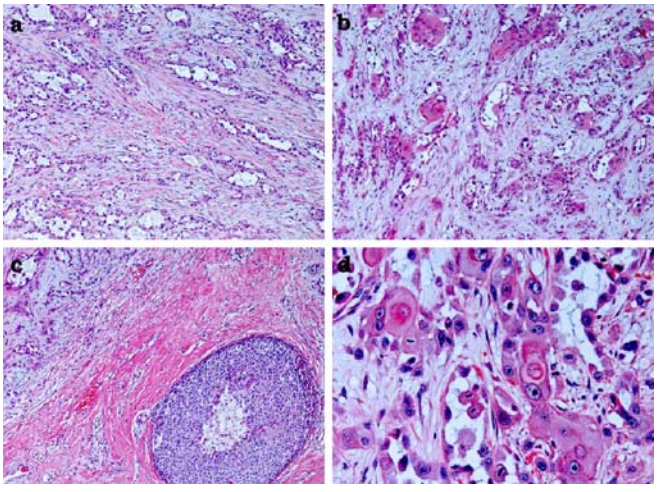

Fig. 2 Tumor 2. **a** Transition between acantholytic and spindle cell patterns. **b** Small nests of solidly growing cells with focal keratinization. **c** Associated in situ ductal component (original magnification **a**–**c** ×100). **d** High-power view (original magnification ×400)

Table 1 List of antibodies, dilution and pretreatment

Antigen	Clone	Manufacturer	Dilution	Pretreatment
Estrogen receptor	1D5	DakoCytomation, Glostrup, Denmark	1:80	Microwave/ citrate buffer
Progesterone receptor	PgR636	DakoCytomation	1:80	Microwave/ citrate buffer
Her2	(Polyclonal)	DakoCytomation	1:500	Microwave/ citrate buffer
Epithelial growth factor receptor	31G7	Zymed, San Francisco, CA, USA	1:50	Pronase E digestion
p53	DO7	DakoCytomation	1:100	Microwave/ citrate buffer
E-cadherin	HECD1	Takara Bio Inc, Shiga, Japan	1:500	Microwave/ citrate buffer
Syndecan-1	MI15	DakoCytomation	1:25	Microwave/ citrate buffer
Cytokeratin 5	XM26	Novocastra, Newcastle, UK	1:100	Microwave/ citrate buffer
Cytokeratin 13	DEK13	Novocastra	1:25	Pronase E digestion
Cytokeratin 8/18	5D3	Novocastra	1:100	Pronase E digestion

Comparative genomic hybridization

Tumor DNA was isolated from three to four representative 20-µm paraffin sections after microdissection of the complete area containing invasive carcinoma, including squamous, acantholytic, and spindle cell areas. The collected tissue was digested using Proteinase K and ethanol precipitated as described previously [1]. Control DNA was isolated from paraffin-embedded normal placenta tissue.

Tumor DNA was labeled using biotin-16-dUTP (Roche, Mannheim, Germany), and control DNA was labeled using digoxigenin-11-dUTP (Roche, Mannheim, Germany) using nick translation according to the manufacturer's instructions. Then, 1 µg of biotin-labeled tumor DNA, 1 µg of digoxigenin-labeled control DNA, and 50 µg Cot-1-DNA (Gibco/BRL, Gaithersburg, MD, USA) were co-denatured with normal metaphase spreads (Vysis, Downers Grove, IL, USA) on an in situ polymerase chain reaction thermocycler (Perkin Elmer, Monza, Italy) and hybridized at 37°C for 24–48 h in a humid chamber. Post-hybridization washes and detection of hybridized DNA using fluorescein and rhodamine were performed as described previously [18]. Image analysis was performed using an epifluorescence microscope (Zeiss, Wetzlar, Germany) and the ISIS CGH software package (Metasystems, Altlußheim, Germany).

Results

Immunohistochemistry

Ki-67 immunohistochemistry showed high proliferative activity of the tumor cells (80–90% positively stained nuclei in tumor 1 and 45–60% in tumor 2) with a slightly lower labeling index in the solid cell nests than in the spindle cell and acantholytic tumor component. Cytokeratin (CK) staining revealed a strong expression of CK5 in the acantholytic, spindle cell, and solid areas of both cases (Fig. 3a), while CK13 staining was limited to the solid and keratinizing cell nests. CK8/18 expression was weakly and focally detected with a slight predisposition for the spindle cell and acantholytic tumor components (Fig. 3b, c). There was no detectable hormone receptor expression. Both tumors showed an overexpression of the epithelial growth factor receptor (EGFR, Fig. 3d) and p53 (Fig. 3e); Her2 was not overexpressed. While there was no detectable loss of syndecan-1 staining, E-cadherin expression was completely lost in acantholytic and spindle cell areas; only in the keratinising squamous cell nests was weak membrane reactivity retained (Fig. 3f).

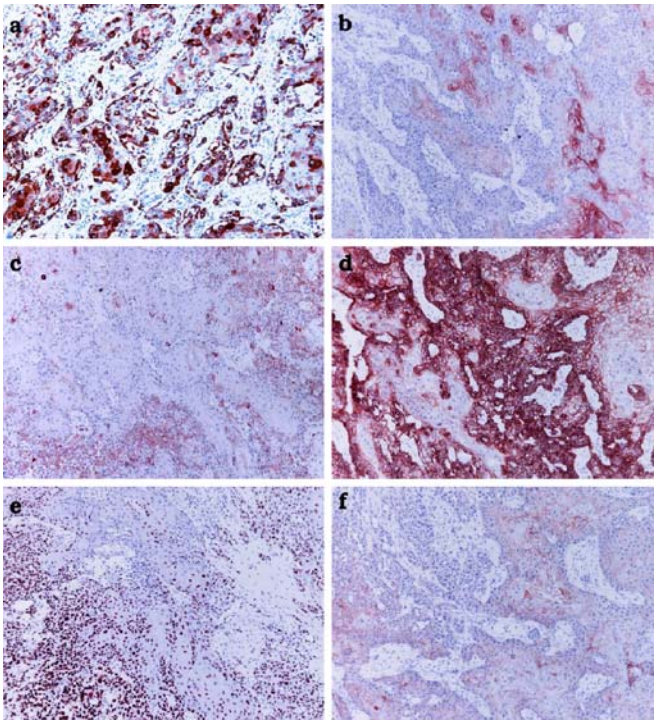

Fig. 3 Immunohistochemical staining reveals a strong expression of cytokeratin (CK) 5 (**a**, original magnification ×100), a weak expression of CK13 (**b**, original magnification ×40) and CK8/18 (**c**, ×40), an overexpression of epithelial growth factor receptor (**d**, ×40) and p53 (**e**, ×40), and a reduced E-cadherin expression (**f**, ×40)

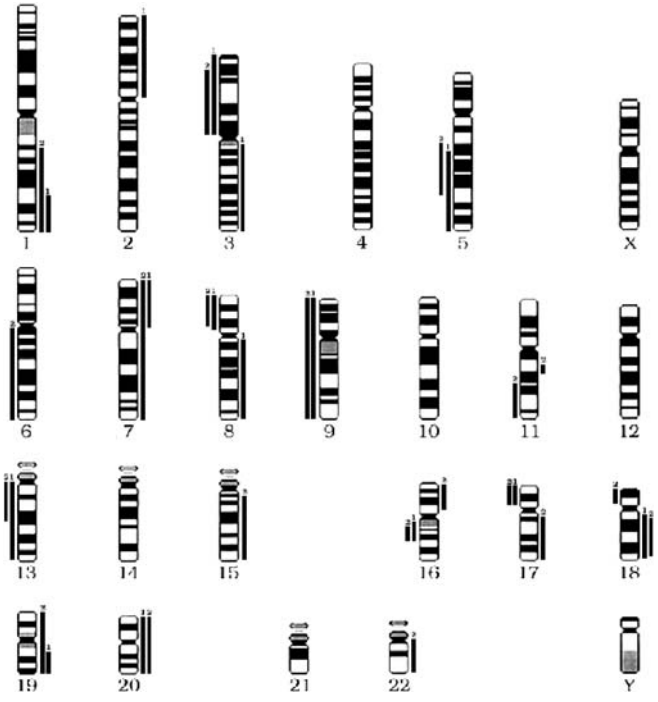

Fig. 4 Chromosomal imbalances detected by comparative genomic hybridization. *Bars* on the *left side* of chromosomes represent losses, bars on the *right side* gains of genetic material. *Small numbers* on top of each *bar* relate to tumor 1 or 2, respectively

Comparative genomic hybridization

Both tumors showed a high overall number of genomic alterations (n=14 and n=18, respectively). Specifically, tumor 1 had losses of chromosomal material at 3p, 5q14–5qter, 8p, 9, 13, 16qcen-16q22, 17p and gains of 1q31–1qter, 2p, 3q, 7p, 8q, 18q, 19q, and 20. Tumor 2 showed losses at 3pcen-3p25, 5q14–5q31, 6q, 8p, 9, 11q21-qter, 16q12-q22, 17p, 18p and gains at 1q22–1qter, 7, 15q, 16p, 17q, 18q12–18qter, 19, 20, and 22q as well as an amplicon at 11q13–11q14. The chromosomal imbalances are summarized in Fig. 4.

Discussion

ASCC is a distinct tumor entity that has been recognized as a variant of squamous cell carcinoma in the recently published World Health Organization classification of tumors of the breast and female genital organs [4]. Histologically, it is characterized by the formation of prominent, irregular spaces and clefts within the tumor leading to a pseudoglandular or pseudoangiosarcomatous appearance. The most common site of ASCC is the skin, where these tumors were first described by Lever in 1947 as adenoacanthoma of the sweat glands [12]. ASCCs of the skin account for up to 10% of all cutaneous squamous cell carcinomas [17] and have been associated with an increased malignant potential by some authors [15]. In the breast, pure squamous cell carcinoma is rare, although approximately 4% of invasive ductal carcinomas show foci of squamous cell metaplasia [7]. Over the last 20 years, only seven cases of primary ASCC of the breast have been reported [2, 6, 16]. However, Eusebi et al. [6] reviewed the older case series by Gersell and Katzenstein [8] and Toikkanen [20] and pointed out that, based on their histological description, probably several of their cases showed acantholytic features. In a large series of 100 breast carcinomas, in which spindle cell areas comprised more than half of the neoplasms, Wargotz et al. [22] identified partial or complete squamous differentiation in approximately one-third of the cases. Further, the authors observed areas of broad channels lined by plump endothelioid epithelial cells mimicking angiosarcoma in several cases as well as angioid areas as a frequent minor component. Apparently, there is a degree of overlap between ASCC and a subset of spindle cell carcinomas, indicating that these tumors may represent similar or possibly even identical biological entities.

Concordant with our findings in ASCC, previous studies have reported positive cytokeratin immunostaining and negative hormone-receptor status in typical squamous cell carcinomas [13, 24] and spindle cell carcinomas of the breast [14, 22]. Furthermore, Nakayama et al. [14] observed an overexpression of p53 and a high proliferative activity as detected by Ki67 immunostaining in a case of spindle cell carcinoma. In our cases, cytokeratin immunohistochemistry showed strong expression of CK5 and weak and only focal expression of CK13 and CK8/18. While the co-expression of CK5 and CK13 is commonly observed in squamous cell carcinoma [19], the cytokeratin 8/18 staining, which is typically seen in complex glandular epithelia, was an unexpected finding. In adenocarcinoma of the breast, a strong expression of CK5 combined with a reduced CK8/18 staining has been associated with the stem-cell phenotype, based on the hypothesis that tumors expressing CK5 arise from different precursor cells than CK8/18-positive tumors [11]. These tumors have been reported to carry high numbers of genetic alterations as detected using CGH and typically lack expression of hormone receptors or Her2. Interestingly, overexpression of EGFR and p53, which are frequently observed in squamous cell carcinomas arising in other organs, has also been associated with the stem cell phenotype of breast cancer [11], in contrast with more common types of breast cancer, which show a glandular cytokeratin expression pattern. Based on these findings, squamous cell carcinoma of the breast might arise from adult mammary gland stem cells, the CK13 expression possibly reflecting the metaplastic squamous cell differentiation.

Comparative genomic hybridization has previously been shown to be a reliable tool for the cytogenetic characterization of paraffin-embedded archival tissue samples [10]. Using CGH, both tumors showed a high overall number of numeric imbalances, reflecting a gross chromosomal instability. Therefore, the data have to be interpreted carefully. While the losses of chromosome 3p are a typical finding in squamous cell carcinomas of different locations [23], gains of 1q and losses on the long arm of chromosome 16 are frequently observed in adenocarcinomas of the breast [21].

Gains of chromosome 7p might reflect the EGFR overexpression, while the losses of 17p include the p53 gene locus, possibly leading to an overexpression of the functionally impaired protein.

The acantholytic variant of squamous cell carcinoma is characterized by a loss of cohesive growth and the formation of irregular spaces and clefts. In ASCC of the skin, different molecular alterations have been associated with this loss of cellular adhesion, including loss of E-cadherin or syndecan-1 [3]. While we found no loss of syndecan-1 staining, both tumors showed a complete absence of E-cadherin in acantholytic and spindle cell areas. Whether this loss of E-cadherin expression is a regulative phenomenon or based on a genetic inactivation of the HCD1 gene (both tumors had losses of chromosomal material at 16q22.1) remains speculative. However, loss of E-cadherin results in a lack of adherens junctions, a mechanism that has previously been shown to lead to an altered cellular motility associated with rapid metastasis [9].

In conclusion, the results of our analyses suggest that genetic alterations in ASCC of the breast include imbalances commonly seen in both mammary adenocarcinomas and squamous cell carcinomas of other locations. Additionally, we observed a co-expression of both glandular- and squamous-type cytokeratins. E-cadherin immunohistochemistry suggests an impaired cellular adhesion, which may explain the peculiar histological appearance of these tumors and contribute to the observed aggressive clinical behavior. Although primary ASCC of the breast is a rare neoplasm making randomized clinical trials almost impossible, the overexpressed EGFR might provide a therapeutic target in individual cases of metastasized tumors.

Acknowledgements We would like to thank Angelika Bönisch, Andrea Müller and Waltraud Schmitz for excellent technical assistance. We would also like to express particular appreciation to Dr. Rosemary R. Millis (Hedley Atkins/Cancer Research UK Breast Pathology Laboratory, Guy's Hospital, London, UK) who critically read the manuscript and provided many valuable comments.

References

1. Aulmann S, Bläker H, Penzel R, Rieker RJ, Otto HF, Sinn HP (2003) CTCF gene mutations in invasive ductal breast cancer. Breast Cancer Res Treat 80:347–352
2. Banerjee SS, Eyden BP, Wells S, McWilliam LJ, Harris M (1992) Pseudoangiosarcomatous carcinoma: a clinicopathological study of seven cases. Histopathol 21:13–23
3. Bayer-Garner IB, Smoller BR (2001) The expression of syndecan-1 is preferentially reduced compared with that of E-cadherin in acantholytic squamous cell carcinoma. J Cutan Pathol 28:83–89
4. Eggers JW, Chesney TM (1984) Squamous cell carcinoma of the breast. Hum Pathol 15:526–531
5. Ellis IO, Schnitt SJ, Sastre-Garau X et al (2003) Invasive breast carcinoma. In: Tavassoli FA, Devilee P (eds) Pathology and genetics of tumours of the breast and female genital organs (World Health Organization classification of tumours). IARC Press, Lyon, pp 13–59
6. Eusebi V, Lamovec J, Cattani MG, Fedeli F, Millis RR (1986) Acantholytic variant of squamous-cell carcinoma of the breast. Am J Surg Pathol 10:855–861
7. Fisher ER, Palekar AS, Gregorio RM, Paulson JD (1983) Mucoepidermoid and squamous cell carcinomas of breast with reference to squamous metaplasia and giant cell tumors. Am J Surg Pathol 7:15–27
8. Gersell DJ, Katzenstein AL (1981) Spindle cell carcinoma of the breast. Hum Pathol 12:550–561
9. Handschuh G, Candidus S, Luber B, Reich U, Schott C, Oswald S, Becke H, Hutzler P, Birchmeier W, Hofler H, Becker KF (1999) Tumor-associated E-cadherin mutations alter cellular morphology, decrease cellular adhesion and increase cellular motility. Oncogene 18:4301–4312
10. Isola J, DeVries S, Chu L, Ghazvini S, Waldman F (1994) Analysis of changes in DNA sequence copy number by comparative genomic hybridization in archival paraffin-embedded tumor samples. Am J Pathol 145:1301–1308
11. Korsching E, Packeisen J, Agelopoulos K, Eisenacher M, Voss R, Isola J, van Diest PJ, Brandt B, Boecker W, Buerger H (2002) Cytogenetic alterations and cytokeratin expression patterns in breast cancer: integrating a new model of breast differentiation into cytogenetic pathways of breast carcinogenesis. Lab Invest 82:1525–1533
12. Lever WF (1947) Adenoacanthoma of sweat glands: carcinoma of sweat glands with glandular and epidermal elements: report of four cases. Arch Dermatol Syphilol 56:157–171
13. Moisidis E, Ahmed S, Carmalt H, Gillett D (2002) Primary squamous cell carcinoma of the breast. ANZ J Surg 72:65–67
14. Nakayama Y, Iwasaki H, Iwanaga S, Nakamura H, Shiroshita T, Kikuchi M, Jozaki H, Hashimoto M, Ikeda S (1997) Spindle cell carcinoma of the breast: a case report and an immunohistochemical study including p53 and Ki-67 expression. Pathol Int 47:404–411
15. Nappi O, Pettinato G, Wick MR (1989) Adenoid (acantholytic) squamous cell carcinoma of the skin. J Cutan Pathol 16:114–121
16. Parramore B, Hanly M, Yeh KA, McNeely T (1999) Acantholytic variant of squamous cell carcinoma of the breast: a case report. Am Surg 65:467–469
17. Petter G, Haustein UW (2000) Histologic subtyping and malignancy assessment of cutaneous squamous cell carcinoma. Dermatol Surg 26:521–530
18. Rieker RJ, Joos S, Bartsch C, Willeke F, Schwarzbach M, Otano-Joos M, Ohl S, Hogel J, Lehnert T, Lichter P, Otto HF, Mechtersheimer G (2002) Distinct chromosomal imbalances in pleomorphic and in high-grade dedifferentiated liposarcomas. Int J Cancer 99:68–73
19. Scarpatetti M, Tsybrovskyy O, Popper HH (2002) Cytokeratin typing as an aid in the differential diagnosis of primary versus metastatic lung carcinomas, and comparison with normal lung. Virchows Arch 440:70–76
20. Toikkanen S (1981) Primary squamous cell carcinoma of the breast. Cancer 48:1629–1632
21. Vos CB, ter Haar NT, Rosenberg C, Peterse JL, Cleton-Jansen AM, Cornelisse CJ, van de Vijver MJ (1999) Genetic alterations on chromosome 16 and 17 are important features of ductal carcinoma in situ of the breast and are associated with histologic type. Br J Cancer 81:1410–1418
22. Wargotz ES, Deos PH, Norris HJ (1989) Metaplastic carcinomas of the breast. II. Spindle cell carcinoma. Hum Pathol 20:732–740
23. Yokoyama S, Yamakawa K, Tsuchiya E, Murata M, Sakiyama S, Nakamura Y (1992) Deletion mapping on the short arm of chromosome 3 in squamous cell carcinoma and adenocarcinoma of the lung. Cancer Res 52:873–877
24. Zoltan TB, Konick L, Coleman RJ (2001) Pure squamous cell carcinoma of the breast in a patient with previous adenocarcinoma of the breast: a case report and review of the literature. Am Surg 67:671–673

Virchows Arch (2005) 446: 310–315
DOI 10.1007/s00428-004-1174-2

CASE REPORT

B. Bode-Lesniewska · J. Hodler · A. von Hochstetter · L. Guillou · U. Exner · R. Caduff

Late solitary bone metastasis of a primary pulmonary synovial sarcoma with SYT-SSX1 translocation type: case report with a long follow-up

Received: 5 September 2004 / Accepted: 12 November 2004 / Published online: 25 January 2005
© Springer-Verlag 2005

Abstract Primary synovial sarcoma outside its classical presentation in para-articular soft tissue of young patients is rare but regularly reported. One of the rarest primary locations is the lung. We describe a 73-year-old female patient who presented with a solitary malignant bone tumor 8 years after the resection of a lung neoplasm. The bone tumor was classified as an osteosarcoma and the lung tumor as an atypical carcinoid tumor at their first respective diagnostic work-ups. The resection of the affected humerus with allograft and endoprosthesis implantation followed. Reevaluation of the tumor samples at the time of the local recurrence of the bone tumor 6 years following the initial symptoms of the bone tumor lead to the reclassification of both specimens as synovial sarcomas. Both neoplasms contained the SYT-SSX1 type of the diagnostic translocation t(X;18) as detected by the reverse-transcription polymerase chain reaction analysis. The patient died 14 years after the resection of the primary synovial sarcoma of the lung and 6 years following the occurrence of the bone metastasis. This prolonged clinical course is uncommon for the SYT-SSX1 translocation, which, in other locations, is usually associated with an unfavorable prognosis.

B. Bode-Lesniewska (✉) · A. von Hochstetter · R. Caduff
Department of Pathology, University Hospital Zurich,
8091 Zurich, Switzerland
e-mail: beata.bode@usz.ch
Tel.: +41-1-2554051
Fax: +41-1-2554551

J. Hodler
Department of Radiology, Balgrist Hospital,
University of Zurich,
Switzerland

L. Guillou
University Institute of Pathology,
Lausanne, Switzerland

U. Exner
Department of Orthopaedic Surgery, Balgrist Hospital,
University of Zurich,
Switzerland

Keywords Synovial sarcoma · Lung tumor · Bone metastasis · Gene translocation

Introduction

Synovial sarcomas, which account for approximately 10% of all malignant soft-tissue tumors, arise most commonly in the para-articular tissues in adolescents and young adults [13, 25]. It has become increasingly apparent, however, that synovial sarcomas may arise in a wide variety of other sites, including head and neck, mediastinum, heart, kidney, prostate, esophagus and vulva, and that they also occur in elderly patients [6]. There are four different morphological subtypes of synovial sarcoma: biphasic, monophasic spindle cell type, monophasic glandular type and poorly differentiated. While the histological diagnosis of a classical biphasic subtype is usually not difficult, the other types may be confounded with many other entities, especially when presenting in an unusual clinical context. The identification of the specific cytogenetic alteration in form of a balanced translocation t(X;18) with fusion product between SYT and SSX genes allows reliable diagnosis and/or confirmation of the diagnosis of a synovial sarcoma [13]. The correct diagnosis leads to the institution of the proper treatment and the estimation of prognostic factors. Although at present, surgery is still the mainstay of the treatment of synovial sarcomas and although there are no specific adjuvant methods (except for the notion of better response to some chemotherapy regimes), the situation may change in the future. The results of molecular studies on the oncogenic mechanism of the SYT-SSX fusion product [10, 11, 20] and on the expression profiles of synovial sarcomas [1, 21] may possibly allow the development of tumor-specific medications with the best candidate targeted at present being epidermal growth factor receptor.

Spindle cell tumors of the lung fall into several prognostically and pathogenetically different categories, such as sarcomatous carcinomas, malignant mesotheliomas and sarcomas. Primary sarcomas of the lung are exceedingly rare and constitute about 0.1% of malignant lung tumors.

Reports of primary synovial sarcomas of the lung and pleura began to appear with increasing frequency in recent years due to the potent diagnostic tools in the form of immunohistochemistry and molecular genetics [5, 12, 18].

We present an unusual case of a late solitary bone metastasis—at first erroneously diagnosed as an osteosarcoma—occurring 8 years after a resection of a primary pulmonary synovial sarcoma—at first erroneously diagnosed as an atypical carcinoid tumor—with confirmatory molecular analysis of the SYT-SSX translocation. Thanks to this examination, both tumors proved to represent manifestations of the same disease (monophasic synovial sarcoma), despite differing diagnoses in the preceding biopsies.

Case report

A 73-year-old female patient presented in September 1995 with slowly progressive pain in her right shoulder and weight loss. Within few weeks, the intensity of the pain increased and was also present at night. Standard radiographs obtained in December 1996 demonstrated an extensive aggressive, osteolytic lesion in the proximal humerus (Fig. 1A). Scintigraphically, no other bone lesions were found. An incisional biopsy of the tumor was performed in January 1996. The histological diagnosis was consistent with small cell osteosarcoma. The thorough staging procedure revealed no other tumor manifestations, specifically no pulmonary or bone metastases. The patient rejected an amputation, and the transarticular resection of the proximal humerus with implantation of an allograft and endoprosthesis was performed in January 1996 without direct complications. The postoperative follow-up was uneventful, with satisfying healing and no metastases radiologically.

In March 1998, 2 years later, standard radiographs and computed tomography of the chest demonstrated small pulmonary nodules compatible with metastatic spread. The patient declined further diagnostic and therapeutic procedures, and radiological follow-up showed slow progression of the pulmonary findings. Local recurrence of the tumor in the right humerus in August 2000, 4 years after the resection of the proximal humerus, proved unresponsive to radiation therapy. An accelerated growth as well as development of exulcerated tumor necrosis prompted palliative resection in December 2001. The patient died within 1 week of postoperative cardiac complications, 14 years following the resection of the pulmonary primary tumor. The patient was a housewife, and her medical history was otherwise uneventful, except for a remote history of a cholecystectomy, high blood pressure and slight aortic valve stenosis. No autopsy was performed.

At review, the tumor tissue resected in December 2001 as well as the previous histological specimens from this location were strongly suggestive of a monophasic spindle cell synovial sarcoma. The careful study of the patient file revealed the history of an operation of a lung tumor 8 years prior to the current onset of symptoms in the right shoulder (Fig. 1B) with the histological diagnosis of an atypical carcinoid tumor. At the time of the lung resection, no other tumor manifestations were found clinically and radiologically. The slides and paraffin blocks of this tumor could be recovered from another institution. The comparison of the morphology, immunohistochemical properties and the status of the t(X;18) proved identical tumor cell types morphologically and immunohistochemically with the same SYT-SSX1 translocation specific for synovial sarcoma.

Materials and methods

Clinical information was obtained from the files of the medical facilities where the patient had been treated. The study was performed in accordance with the guidelines of the local ethics commission. Histological material from the lung and bone tumors was fixed in buffered 4% formalin

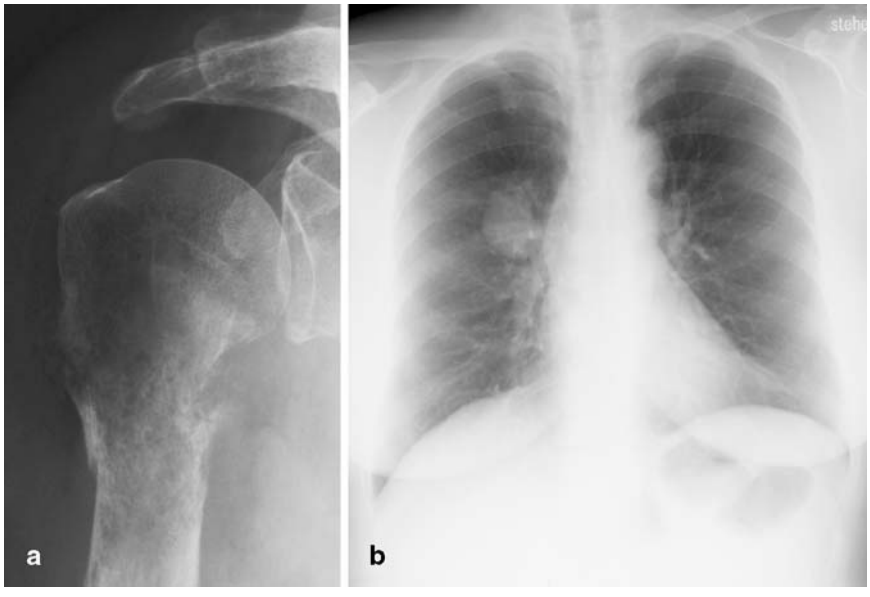

Fig. 1 **A** Extensive osteolytic tumor in the metaphysis of the proximal right humerus (standard radiograph). **B** Proximally located lung tumor resected 8 years prior to the presentation of the bone lesion (standard radiograph)

and embedded in paraffin according to standard procedures. Sections (1–2 μm) were cut for conventional histology and immunohistochemistry. The following antibodies were used: pan-cytokeratin (1:250; Biomedicals AG, Augst, Switzerland), early membrane antigen (EMA, 1:20; Dako, Glostrup, Denmark), S100 (1:3000; Dako), CD34 (1:50; Serotec Ltd., Oxford, UK), synaptophysin (1:30; Dako), chromogranin (1:50; Dako), alpha-smooth-muscle actin (SMA) (1:20,000; Sigma, St. Louis, USA), desmin (1:20; Dako). Immunohistochemistry was performed on deparaffinized sections using the Ventana NexES automated staining system with diaminobenzidine as substrate. For antigen retrieval, slides were either enzymatically predigested or heated in citrate buffer for 3 min using a pressure cooker. Slides were counterstained with hemalaum. The quality of the reactions was controlled on tissue slides with known reaction patterns stained in parallel with the examined probes.

Reverse-transcription polymerase chain reaction

RNA extraction and reverse-transcription polymerase chain reaction (RT-PCR) analysis were performed as previously described [14]. For subtyping SYT-SSX fusion transcripts, 3 μl of each PCR product was enzymatically hydrolyzed at 65°C for 1 h with 5 units of the restriction enzyme *Taq*I (Roche Diagnostics) in a final volume of 10 μl. The digestion patterns of the PCR products were analyzed on 2% agarose gels and visualized using ethidium bromide staining. The size of digested products were 65 bp and 32 bp for the SYT-SSX1 fusion gene transcripts, but remained at 97 bp for SYT-SSX2.

Subtyping was determined in parallel by single-strand conformation polymorphism (SSCP) analysis. Aliquots of 5 μl of PCR products were mixed with 5 μl of denaturing buffer (0.1 M NaOH and 2 mM ethylenediaminetetraacetate), heated at 50°C for 10 min. After addition of 1 μl of formamide dye, the samples were immediately loaded onto a 40% mutation detection enhancement (MDE) gel (FMC BioProducts, Rockland, Maine USA) and electrophoresed in 0.5×Tris–borate–EDTA (TBE) buffer at 20°C and 300 V (20 V/cm) for 5 h. The gels were stained with a SYBR Gold gel stain (Molecular Probes, Eugene, OR, USA) diluted 1:10,000 in 1×TBE buffer and visualized under ultraviolet light using a charge-coupled device camera.

Results

Pathological findings

Lung tumor (1987)

The resected right upper lobe contained a 3-cm whitish, well-circumscribed tumor mass in the vicinity of a proximal segmental bronchus without infiltration of the mucosa. Microscopically, the tumor consisted of plump, oval and spindle cells densely packed, partially infiltrating the outer bronchial wall (Fig. 2A). Focally, a trabecular pattern was found. The mitotic activity was 12 mitoses per 10 high power fields. No necrosis or lymph-node metastases were found.

Bone tumor (1996 and 2001)

The incisional biopsy contained hypercellular tumor tissue consisting of closely packed plump spindle and oval cells with scant cytoplasm, indistinct cell borders, arranged in irregularly intersecting fascicles or in a haphazard fashion. There were some variably ramifying and gaping, thin-walled vascular channels with a hemagiopericytoma-like appearance. Small foci of ossification (Fig. 3A) were present. Mitotic figures were easily found. The resected proximal humerus contained a large tumor mass with a longitudinal diameter of 8 cm, destroying the cortical bone

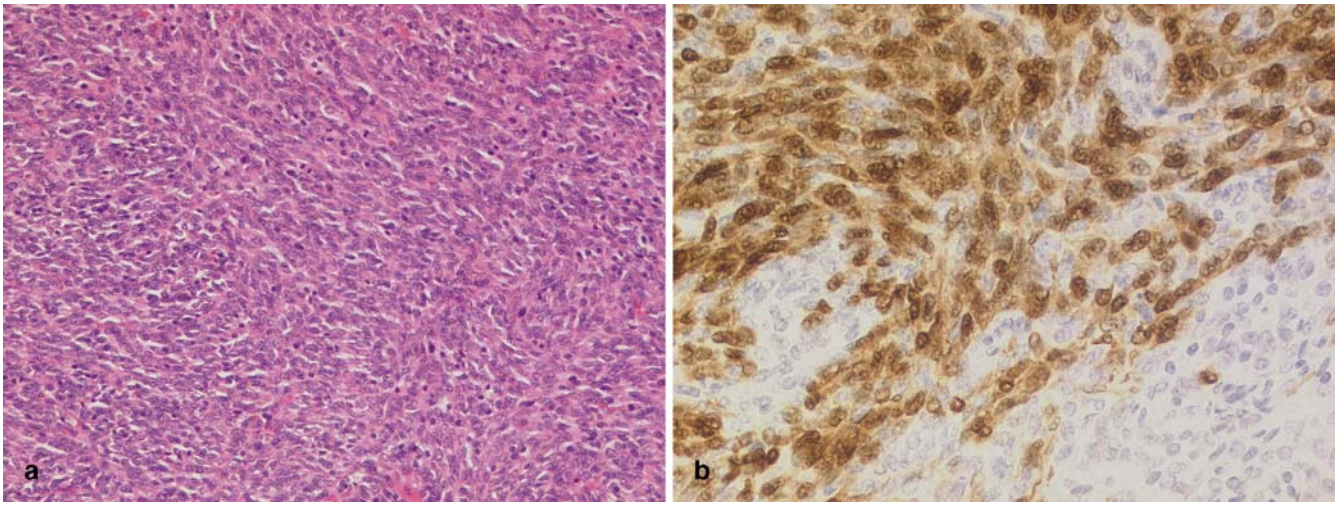

Fig. 2 Lung tumor. **A** Plump, relative monomorph spindle cells (hematoxylin and eosin ×10). **B** Intracytoplasmatic and nuclear expression of S100 protein (×20)

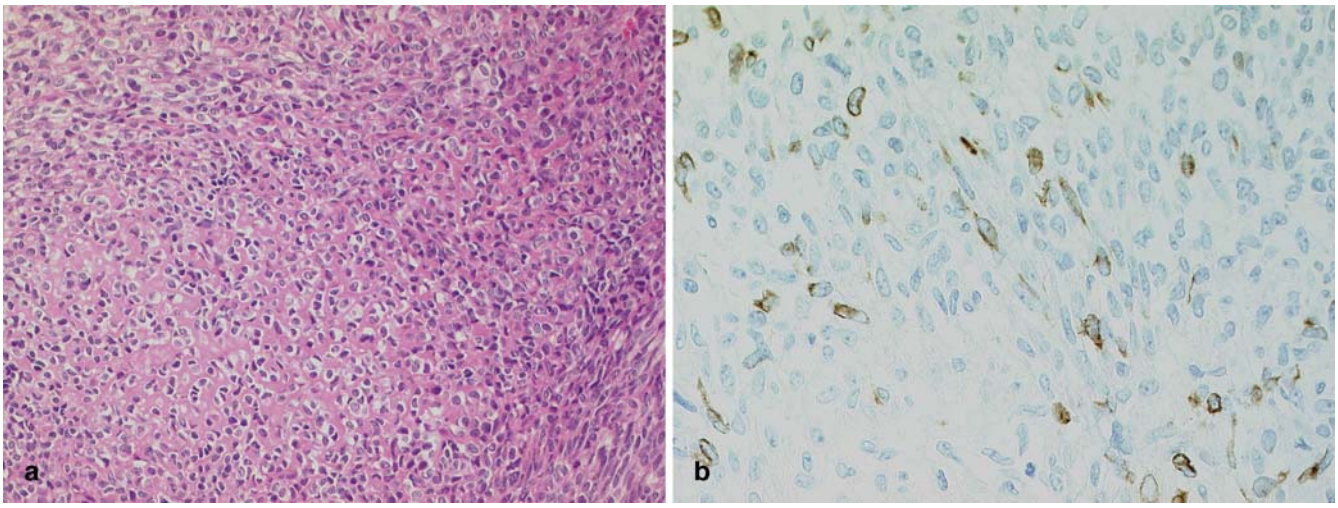

Fig. 3 Humerus tumor. **A** Spindle and oval tumor cells with focal osteoid production (hematoxylin and eosin ×200). **B** Expressin of cytokeratin by individual tumor cells (×400)

and minimally infiltrating the adjacent soft tissue. The tumor tissue was similar to the biopsy material, but areas with matrix hyalinization and slender spindle cells were more prominent. No tumor necrosis except for the biopsy site was noted. The recurrent tumor following radiotherapy was partially necrotic, showing high mitotic activity and somewhat stronger pleomorphism.

Immunohistochemistry

The lung tumor was negative for cytokeratin, EMA, synaptophysin, chromogranin and showed focal positivity for S100 (Fig. 2B). Contrary to the biopsy and resection material of the bone tumor, the recurrence showed focal positivity for cytokeratin and EMA. Focal positivity for S100 was present in all bone tumor specimen (Fig. 3B). Other markers remained negative.

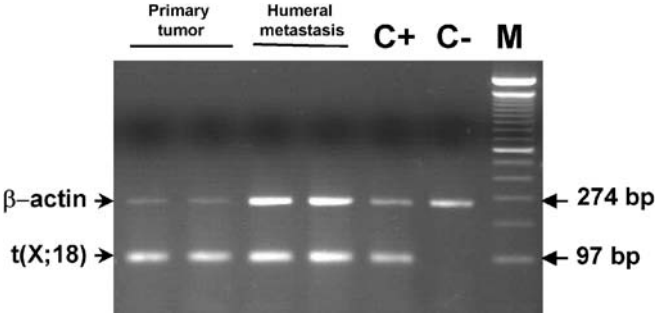

Fig. 4 Detection of the t(X;18) (SYT-SSX) translocation in the primary lung tumor (*lanes 1 and 2*), in the humeral metastasis (*lanes 3 and 4*), using reverse-transcription polymerase chain reaction (PCR). For each sample, two PCR amplifications were performed in parallel, both containing the primer set necessary for the amplification of SYT-SSX fusion gene transcripts and a set of primers for the ubiquitously expressed β-actin gene transcripts (positive control). A biphasic synovial sarcoma was used as a positive control (*lane 5*) for the t(X;18) detection. Negative control consisted of t (X;18)-negative desmoid tumor. *Lane 7* pGEM DNA size markers (Promega Madison, WI)

RT-PCR for SYT-SSX translocation

SYT-SSX fusion transcripts were detected in both primary lung tumor and humeral metastasis. Subtyping using SSCP showed that both were of SYT-SSX1 type (Fig. 4).

Discussion

The definition of synovial sarcoma has strikingly changed since its initial description in the beginning of the 20th century. Due to its commonly para-articular location, the tumor was initially falsely considered to originate from the synovial lining of joints. The most recent definition of synovial sarcoma includes the occurrence of a specific genetic abnormality [13]. After observation of the translocation between chromosome X and 18 in synovial sarcomas in 1986 [11], the fusion products of SYT-SSX with its variants -SSX1, -SSX2 and -SSX4 were described, depending on the SSX gene involved. The oncogenic potential of this gene is currently a subject of many studies [1, 10, 20, 21, 25]. The abnormalities mentioned above are specific to synovial sarcoma and are found in more than 95% of this tumor type with isolated reports on related cytogenetic abnormalities [23]. There are, at present, no convincing reports of its occurrence in other tumor types [4, 8, 14]. Thanks to the progress in molecular techniques, the detection of the fusion product is currently possible on standard pathological paraffin-embedded archive material [2, 4]. According to several reports, synovial sarcomas in unusual locations or in unusual clinical contexts have been previously diagnosed under various names, such as "classical" soft tissue fibrosarcoma for cases of monophasic fibrous synovial sarcoma [25] or embryonal sarcoma of the kidney for renal monophasic synovial sarcomas [3]. In our patient, the difficulty in classifying the lung neoplasia resulted in the diagnosis of an atypical carcinoid tumor.

We present a case where a synovial sarcoma was not considered as a diagnostic possibility either during the primary presentation in the lung or during the work-up of the solitary bone metastasis 8 years later. The examination of the local recurrence of the bone metastasis with review of all the slides and the molecular analysis of the SYT-SSX fusion product allowed the diagnosis of a primary lung synovial sarcoma. This tumor type is very rare, as the primary in the lung. Only about 50–60 cases (most of them monophasic spindle cell type and only two of the biphasic type) have been recorded in the English-language literature [5, 12, 16, 18, 22, 24]. This probably underestimates the prevalence of the disease, due to the diagnostic difficulties in differentiating among various spindle cell tumors of the lung. Many entities must be considered, namely sarcomatous carcinoma, malignant mesothelioma, spindle cell thymoma invading the lung, metastatic melanoma or—in women—metastatic malignant mixed Müllerian tumor and, of particular importance, metastatic sarcoma. Other primary sarcoma types also occurring in the lung must be taken into account, such as leiomyosarcoma, malignant peripheral nerve sheath tumor, solitary fibrous tumor, fibrosarcoma and mesenchymal chondrosarcoma. The eventual diagnosis of a spindle cell tumor of the lung depends in many cases on the results of the immunohistochemical reactions and—if the synovial sarcoma is a morphological consideration—on the molecular analysis.

Due to the small number of the described synovial sarcomas of the lung, the course of the disease is not yet fully known. There are only few reports with specific reference to the SYT-SSX translocation type [5, 16, 22, 24]. Patients with the SYT-SSX2 translocation, generally considered to have a relatively favorable outcome [17, 19], fared poorly and died within months. Most patients (including the patient described in the current study) with the SYT-SSX1 fusion product demonstrated a prolonged disease course with survival of up to 14 years, but a few died as early as at 12 months [16, 22, 24].

Synovial sarcoma in elderly patients is uncommon. Less than 10% of synovial sarcomas occur in patients over 60 years. Chan et al. [6] analyzed 32 patients older than 60 years with synovial sarcoma. They concluded that the tumors in this age group occur more often in unusual locations and have more often poorly differentiated morphology. Four of their cases were primaries of the lung, with none being metastatic at 36–48 months of follow-up.

The possibility of a primary bone synovial sarcoma presenting metachronously as lung tumor may theoretically be considered in our patient. However, the long time lag between both tumor presentations as well as the lacking clinical skeletal symptoms at the time of the lung resection make this possibility unlikely. Synovial sarcoma metastasizes predominantly hematogenously, most commonly to the lung (90–100% of the patients with metastases), followed by lymph nodes (<10%) and, in rare cases, by bone marrow [25]. At least two cases of a primary pulmonary sarcoma have been reported as metastatic to bone [16, 22]. A primary synovial sarcoma of bone is practically unknown. Hiraga [15] describes a radius tumor with morphological properties of a synovial sarcoma and the t(X;18) translocation, but there is no mention of the past medical history of the patient, and the possibility of a late metastasis (as in our case) is not excluded. The tendency of the synovial sarcoma for late metastases is well known and is mirrored in marked differences between short- and long-term survival [25]. The case of Cohen [7] probably represents a classical presentation of a synovial sarcoma in the para-articular soft tissue of the knee of a 22-year-old man with secondary infiltration of the tibia. Because no radiological or pathological documentation is included, the topography of the tumor cannot be definitively estimated.

The necessity of molecular testing in every case of a synovial sarcoma has been discussed in the recent paper of Coindre [9]. The authors conclude that this examination is not required in every case. Diagnosing synovial sarcoma in its classical biphasic form and/or classical clinical presentation does not cause any difficulty. It is, however, more problematic in its more common, monophasic spindle cell variant or poorly differentiated type. Because, in many cases, the immunohistochemistry is not sufficient, the option of molecular testing represents a helpful alternative.

In conclusion, the presented case demonstrates that for the proper understanding of the natural course of some of the rare mesenchymal tumors, very long follow-ups must be taken into account. The possibility of molecular testing for the presence and type of the t(X;18) translocation is valuable in the differential diagnosis of spindle cell malignant tumors and allows precise classification of some of them. Its role for the prognosis of the primary pulmonary synovial sarcoma remains to be established.

References

1. Allander SV, Illei PB, Chen Y, Antonescu CR, Bittner M, Ladanyi M, Meltzer PS (2002) Expression profiling of synovial sarcoma by cDNA microarrays: association of ERBB2, IGFBP2, and ELF3 with epithelial differentiation. Am J Pathol 161:1587–1595
2. Argani P, Zakowski MF, Klimstra DS, Rosai J, Ladanyi M (1998) Detection of the SYT-SSX chimeric RNA of synovial sarcoma in paraffin-embedded tissue and its application in problematic cases. Mod Pathol 11:65–71
3. Argani P, Faria PA, Epstein JI, Reuter VE, Perlman EJ, Beckwith JB, Ladanyi M (2000) Primary renal synovial sarcoma: molecular and morphologic delineation of an entity previously included among embryonal sarcomas of the kidney. Am J Surg Pathol 24:1087–1096
4. Bijwaard KE, Fetsch JF, Przygodzki R, Taubenberger JK, Lichy JH (2002) Detection of SYT-SSX fusion transcripts in archival synovial sarcomas by real-time reverse transcriptase-polymerase chain reaction. J Mol Diagn 4:59–64
5. Boroumand N, Raja V, Jones DV, Haque AK (2003) SYT-SSX2 variant of primary pulmonary synovial sarcoma with focal expression of CD117 (c-Kit) protein and a poor clinical outcome. Arch Pathol Lab Med 127:201–204
6. Chan JA, McMenamin ME, Fletcher CD (2003) Synovial sarcoma in older patients: clinicopathological analysis of 32 cases with emphasis on unusual histological features. Histopathology 43:72–83
7. Cohen IJ, Issakov J, Avigad S, Stark B, Meller I, Zaizov R, Bar-Am I (1997) Synovial sarcoma of bone delineated by spectral karyotyping. Lancet 350:1679–1680

8. Coindre JM, Hostein I, Benhattar J, Lussan C, Rivel J, Guillou L (2002) Malignant peripheral nerve sheath tumors are t(X;18)-negative sarcomas. Molecular analysis of 25 cases occurring in neurofibromatosis type 1 patients, using two different RT-PCR-based methods of detection. Mod Pathol 15:589–592
9. Coindre JM, Pelmus M, Hostein I, Lussan C, Bui BN, Guillou L (2003) Should molecular testing be required for diagnosing synovial sarcoma? A prospective study of 204 cases. Cancer 98:2700–2707
10. de Bruijn DR, dos Santos NR, Kater-Baats E, Thijssen J, van den Berk L, Stap J, Balemans M, Schepens M, Merkx G, van Kessel AG (2002) The cancer-related protein SSX2 interacts with the human homologue of a Ras-like GTPase interactor, RAB3IP, and a novel nuclear protein, SSX2IP. Genes Chromosomes Cancer 34:285–298
11. dos Santos NR, de Bruijn DR, van Kessel AG (2001) Molecular mechanisms underlying human synovial sarcoma development. Genes Chromosomes Cancer 30:1–14
12. Essary LR, Vargas SO, Fletcher CD (2002) Primary pleuro-pulmonary synovial sarcoma: reappraisal of a recently described anatomic subset. Cancer 94:459–469
13. Fisher C, de Bruijn DRH, Geurts van Kessel A (2002) Synovial sarcoma. In: Fletcher CDM, Unni KK, Mertens F (eds) WHO pathology and genetics. Tumours of soft tissue and bone. IARC Press, Lyon, pp 200–204
14. Guillou L, Coindre J, Gallagher G, Terrier P, Gebhard S, de Saint Aubain Somerhausen N, Michels J, Jundt G, Vince DR, Collin F, Trassard M, Le Doussal V, Benhattar J (2001) Detection of the synovial sarcoma translocation t(X;18) (SYT-SSX) in paraffin-embedded tissues using reverse transcriptase-polymerase chain reaction: a reliable and powerful diagnostic tool for pathologists. A molecular analysis of 221 mesenchymal tumors fixed in different fixatives. Hum Pathol 32:105–112
15. Hiraga H, Nojima T, Isu K, Yamashiro K, Yamawaki S, Nagashima K (1999) Histological and molecular evidence of synovial sarcoma of bone. A case report. J Bone Joint Surg Am 81:558–563
16. Hisaoka M, Hashimoto H, Iwamasa T, Ishikawa K, Aoki T (1999) Primary synovial sarcoma of the lung: report of two cases confirmed by molecular detection of SYT-SSX fusion gene transcripts. Histopathology 34:205–210
17. Kawai A, Woodruff J, Healey JH, Brennan MF, Antonescu CR, Ladanyi M (1998) SYT-SSX gene fusion as a determinant of morphology and prognosis in synovial sarcoma. N Engl J Med 338:153–160
18. Kuhnen C, Mentzel T, Haas V (1999) [Primary synovial sarcoma of the lung.] Pathologe 20:130–134
19. Ladanyi M, Antonescu CR, Leung DH, Woodruff JM, Kawai A, Healey JH, Brennan MF, Bridge JA, Neff JR, Barr FG, Goldsmith JD, Brooks JS, Goldblum JR, Ali SZ, Shipley J, Cooper CS, Fisher C, Skytting B, Larsson O (2002) Impact of SYT-SSX fusion type on the clinical behavior of synovial sarcoma: a multi-institutional retrospective study of 243 patients. Cancer Res 62:135–140
20. Morimoto Y, Ouchida M, Ozaki T, Kawai A, Ito T, Yoshida A, Inoue H, Shimizu K (2003) Splicing isoform of SYT-SSX fusion protein accelerates transcriptional activity and cell proliferation. Cancer Lett 199:35–43
21. Nielsen TO, Hsu FD, O'Connell JX, Gilks CB, Sorensen PH, Linn S, West RB, Liu CL, Botstein D, Brown PO, van de Rijn M (2003) Tissue microarray validation of epidermal growth factor receptor and SALL2 in synovial sarcoma with comparison to tumors of similar histology. Am J Pathol 163:1449–1456
22. Okamoto S, Hisaoka M, Daa T, Hatakeyama K, Iwamasa T, Hashimoto H (2004) Primary pulmonary synovial sarcoma: a clinicopathologic, immunohistochemical, and molecular study of 11 cases. Hum Pathol 35:850–856
23. Storlazzi CT, Mertens F, Mandahl N, Gisselsson D, Isaksson M, Gustafson P, Domanski HA, Panagopoulos I (2003) A novel fusion gene, SS18L1/SSX1, in synovial sarcoma. Genes Chromosomes Cancer 37:195–200
24. Terasaki H, Niki T, Hasegawa T, Yamada T, Suzuki K, Kusumoto M, Fujimoto K, Hayabuchi N, Matsuno Y, Shimoda T (2001) Primary synovial sarcoma of the lung: a case report confirmed by molecular detection of SYT-SSX fusion gene transcripts. Jpn J Clin Oncol 31:212–216
25. Weiss SW, Goldblum JR (2001) Malignant soft tissue tumors of uncertain type. In: Enzinger and Weiss's soft tissue tumors, 4th edn. Mosby, St. Louis, pp 1483–1571

Virchows Arch (2005) 446: 316–321
DOI 10.1007/s00428-004-1178-y

CASE REPORT

Aleodor A. Andea · David S. Klimstra

Adenocarcinoma arising in a tailgut cyst with prominent meningothelial proliferation and thyroid tissue: case report and review of the literature

Received: 20 August 2004 / Accepted: 10 November 2004 / Published online: 25 February 2005
© Springer-Verlag 2005

Abstract Tailgut cysts (retrorectal cystic hamartomas) are rare lesions occurring in the retrorectal/presacral space of young women, considered to be of developmental origin. In this study, we report the clinicopathological characteristics of an adenocarcinoma developing in an unusual tailgut cyst. A 47-year-old female presented with a 3-month history of an enlarging presacral mass, extending into the gluteal area. The patient underwent surgical resection. Microscopic examination revealed a mucinous adenocarcinoma with intestinal features arising in a tailgut cyst. In addition to the usual components previously described in this lesion (cuboidal, columnar, ciliated or squamous epithelial lining with scattered smooth muscle fibers in the wall), our case was unique in that it was associated with a meningothelial proliferation and benign thyroid tissue with oncocytic changes. These additional features bring into question the proposed hindgut origin of tailgut cysts.

Keywords Tailgut cyst · Adenocarcinoma · Retrorectal cystic hamartoma · Thyroid · Meningothelial

Introduction

Tailgut cysts (TGCs) are rare lesions of presumed developmental origin that occur in the presacral area of young adults, predominantly females [8]. They are composed of uni- or multilocular cysts lined by a variety of epithelia. Malignant transformation in TGCs has been only rarely documented. In this study, we report a case of an adenocarcinoma arising in a TGC that also exhibits unique features compared with previously described similar lesions.

A. A. Andea · D. S. Klimstra (✉)
Memorial Sloan-Kettering Cancer Center,
Department of Pathology,
1275 York Avenue,
New York, NY, 10021, USA
e-mail: klimstrd@mskcc.org
Tel.: +1-212-6395905

Clinical presentation

The patient was a 47-year-old female presenting with a 3-month history of an enlarging and painful mass in the gluteal area. On physical examination, a 4×4-cm, tender mass was identified in the intergluteal crease. On magnetic resonance imaging, the mass appeared to be located in the presacral space and to extend posteriorly over the tip of the coccyx. The differential diagnosis based on imaging studies included a benign soft tissue tumor or a chordoma. The patient serum carcinoembryonic antigen (CEA) levels were not elevated. Surgical resection with clear margins was carried out subsequently. The last follow-up, 6 years postoperatively, showed the patient to be healthy and free of disease.

Materials and methods

The specimen was grossed according to the standard protocol in place. Sections 5-μm thick stained with hematoxylin and eosin were obtained from paraffin-embedded tissue. Immunoperoxidase stains were performed on selected sections using an automated Ventana apparatus [for AE1/AE3, CK7, CK20, epithelial membrane antigen (EMA), monoclonal CEA, MIB1, p53 and thyroglobulin] as well as following a manual protocol (for MUC-1, MUC-2, p21, p27, p16, beta-catenin, DPC-4, hMLH1 and hMSH1).

Results

Pathological findings

The macroscopic specimen consisted of an 8-cm portion of fibrofatty tissue partially covered by skin. Upon sectioning, a 4-cm lobulated and multicystic mass with a gelatinous to solid cut surface was identified (Fig. 1).

Microscopic examination of the gelatinous mass revealed a mucinous adenocarcinoma composed of cystic mucin-filled spaces lined completely or partially by intestinal-type

Fig. 1 Gross picture of the specimen reveals a mucinous cystic mass

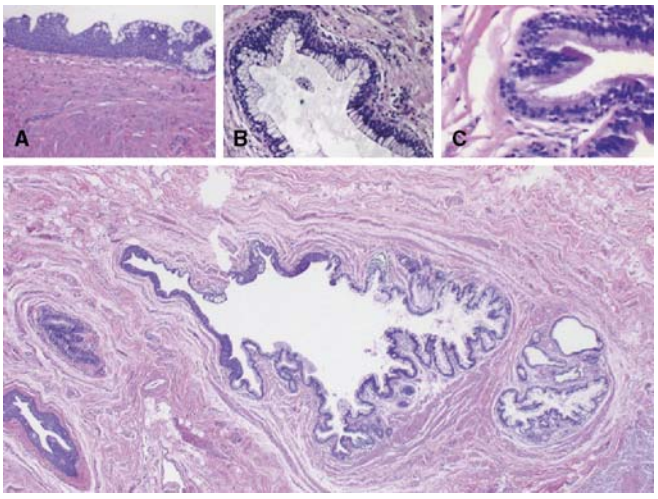

Fig. 3 Tailgut cyst composed of cystic spaces lined by a variety of benign epithelia and surrounded by discontinuous bundles of smooth muscle. *Inset* stratified squamous epithelium (**A**), mucinous lining (**B**), respiratory ciliated epithelium (**C**)

epithelium exhibiting variable cytological and architectural atypia ranging from a cytologically bland lining to one composed of cells with hyperchromatic nuclei and cribriforming architecture. Also identified were pools of mucin containing floating dysplastic epithelial cells (Fig. 2).

Adjacent to the aforementioned mass, several cystic structures were noted, lined by a benign epithelium with variable histology, including simple cuboidal, mucinous, ciliated respiratory, stratified squamous and transitional (Fig. 3). The walls of these cysts contained smooth muscle fibers; however, a well-formed muscular layer was not identified (Fig. 3). Some of the cystic structures surrounded by smooth muscle fibers were lined by dysplastic epithelium, suggesting that they represent dysplasia in a preexisting benign lesion (Fig. 4). Immunohistochemical stains showed the tumor cells to be positive for cytokeratin 20, CEA (membranous and cytoplasmic pattern), MUC-1 (focal apical staining) and MUC-2 (diffuse cytoplasmic staining) and negative for cytokeratin 7 (Table 1, Fig. 5). The proliferation marker Ki-67 exhibited a moderately increased labeling index in the carcinoma relative to the non-neoplastic epithelium, and there was no abnormal expression of p53. Other immunohistochemical stains showed normal expression patterns: beta-catenin (membranous staining), DPC-4 (retained nuclear and cytoplasmic staining), hMLH1, hMSH2 (retained nuclear staining).

Another distinctive feature encountered in this lesion was the presence of aggregates of cells with bland, round to ovoid nuclei and indistinct cytoplasmic membranes suggesting meningothelial differentiation. Focally, the cells formed meningothelial whorls (Fig. 6). Prominent psammomatous calcifications were also noted in these areas. The meningothelial cells were found to express EMA using immunohistochemistry and were negative for cytokeratin (Fig. 6).

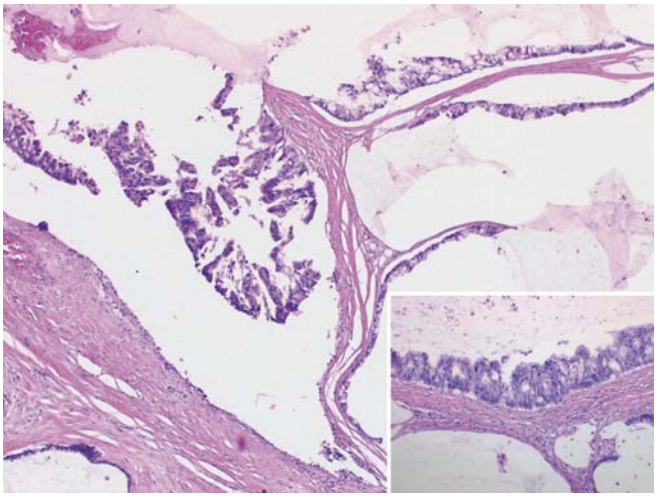

Fig. 2 Mucinous adenocarcinoma composed of cystic spaces filled with mucin and partially lined by a malignant appearing epithelium. *Inset* high power

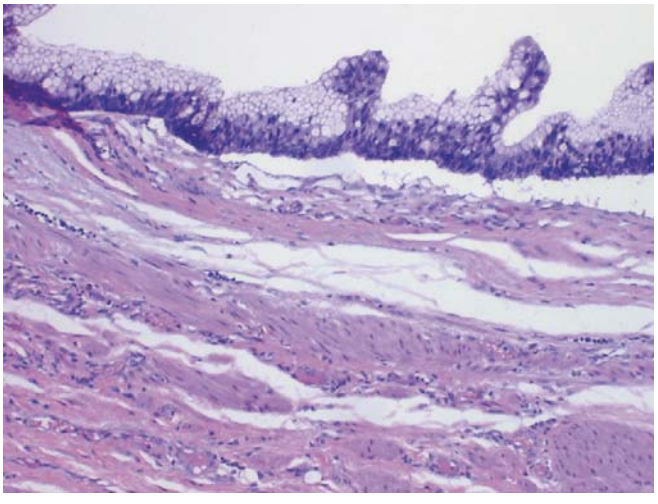

Fig. 4 Some of the cystic spaces were lined by dysplastic epithelium but were also surrounded by scattered smooth muscle bundles, consistent with a carcinoma developing in a pre-existing tailgut cyst

Table 1 Immunohistochemical profile of the mucinous adenocarcinoma arising in a retrorectal cystic hamartoma. *ADC* adenocarcinoma, *POS* positive, *N* negative

Antibody	Company/dilution	Result		
		ADC	Meningothelial cells	Thyroid tissue
Cytokeratin 7	Ventana prediluted	N		
Cytokeratin 20	Ventana prediluted	POS		
Monoclonal carcinoembryonic antigen	Ventana prediluted	POS (apical and cytoplasmic)		
MIB 1	Ventana prediluted	12%–34%		
MUC-1	Santa Cruz 1:500	POS (focally)		
MUC-2	Novocastra 1:200	POS (diffuse)		
P53[a]	Ventana prediluted	N		
P21	Oncogene Science 1:100	12%		
P27	Dako 1:1 k	70%		
P16[1]	Oncogene Science 1:100	N		
Beta-catenin	BD Transduction 1:200	POS (normal membranous staining)		
DPC-4	Santa Cruz 1:500	POS (normal staining)		
hMLH1	OBD Pharmingen 1:200	POS (normal staining)		
hMSH2	Oncogene Science 1:400	POS (normal staining)		
AE1/AE3	Ventana Prediluted	POS	N	POS
Epithelial membrane antigen	Ventana Prediluted		POS	
Thyroglobulin	Ventana Prediluted			POS

[a]Staining index <1% was regarded as negative

Adjacent to the cysts, there was another tissue type morphologically resembling thyroid tissue composed of epithelioid cells in a follicular arrangement containing luminal colloid-like material. The cells had abundant granular eosinophilic, cytoplasm and round nuclei with prominent nucleoli resembling thyroid Hurthle cells. Immunohisto-

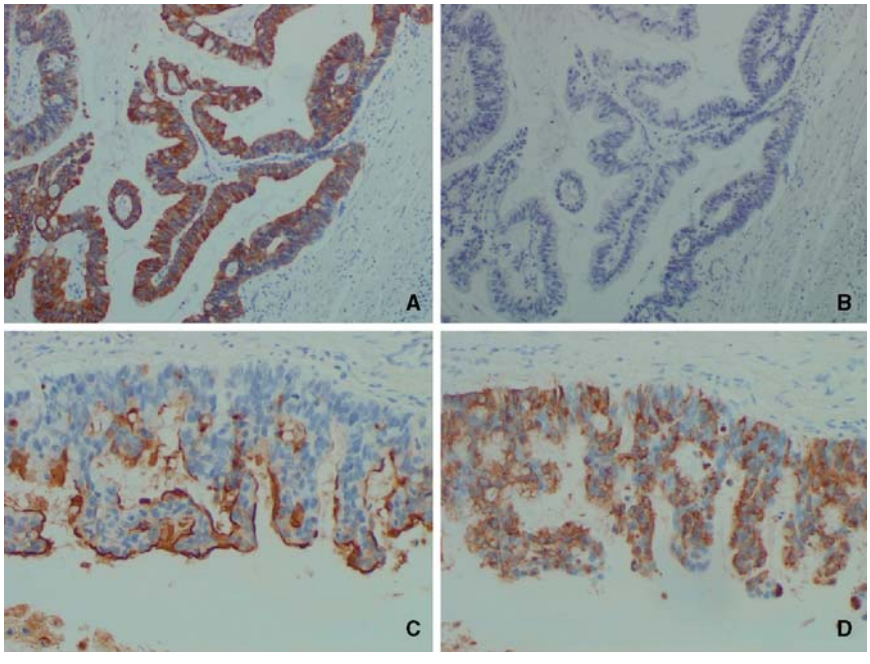

Fig. 5 Immunohistochemical profile of the mucinous carcinoma. **A** Cytokeratin 20. **B** Cytokeratin 7. **C** MUC-1. **D** MUC-2

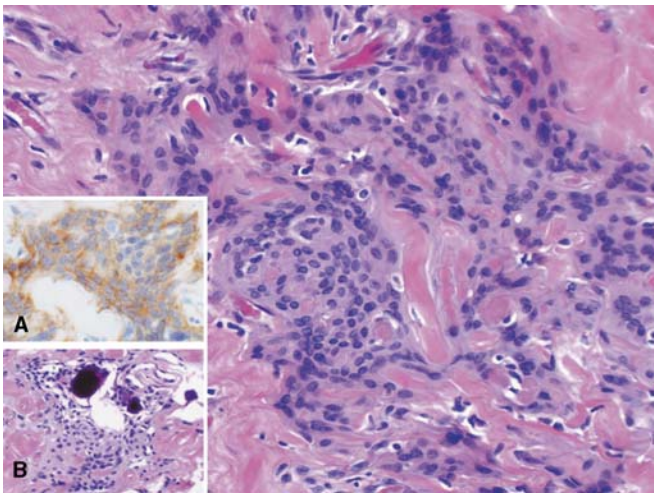

Fig. 6 Meningothelial proliferation was identified adjacent to the tailgut cyst. *Inset* epithelial membrane antigen stain (**A**), prominent psamomma-type calcifications (**B**)

chemical stains revealed intense expression of cytokeratin and thyroglobulin, confirming the thyroid differentiation (Fig. 7).

Discussion

TGCs are considered to be of developmental origin, arising from vestiges of the embryonic hindgut [4, 8]. In the course of normal development, the embryo forms a true tail at about 28–35 days of gestation. The embryonic hindgut (as well as the neural tube) extends into the tail, constituting the tailgut or postanal gut. The tail along with the tailgut undergoes regression by the eighth week of gestation. It is hypothesized that a failure to regress of the embryological tailgut results in formation of a TGC [4, 8, 29].

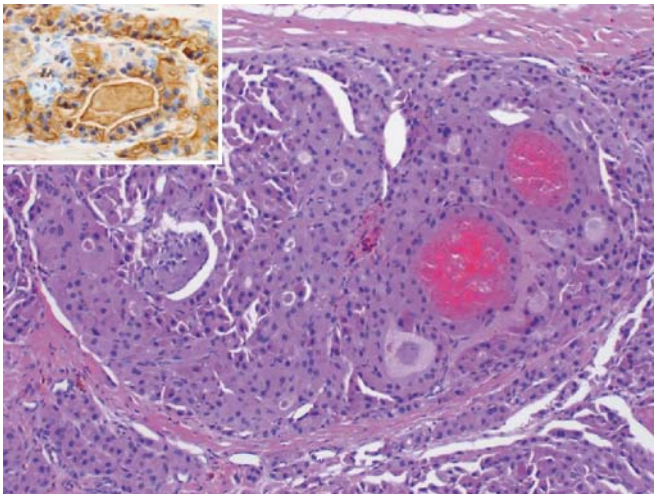

Fig. 7 Thyroid tissue identified adjacent to the tailgut cyst. *Inset* positive staining with antibodies against thyroglobulin confirms the thyroid differentiation

TGC, also known as retrorectal cystic hamartoma, cyst of postanal intestine, tail gut vestiges, or myoepithelial hamartoma of the rectum [3, 8, 10, 11, 34, 35], usually presents in adult life [8]. Only rare cases have been described in infants [8, 28, 36]. Between 75% and 90% of the reported cases occur in females [8, 11, 31], the reason for such a predilection being unclear. About 50% of the cases are discovered incidentally; the rest of the patients complain of symptoms related to the retrorectal location, such as rectal fullness, constipation, discomfort while sitting, rectal bleeding, or infections [7, 8, 14, 22, 30]. Digital rectal examination discloses a well-defined palpable presacral mass compressing the rectum [30]. Imaging studies reveal a multiloculated lesion in the retrorectal/presacral area limited anteriorly by the rectum, posteriorly by sacrum, superiorly by the peritoneal reflection, inferiorly by the levators ani and coccyges muscles, and laterally by ureters and iliac vessels [11].

Grossly, the lesion is usually composed of multilocular cysts ranging in size from 1 cm to 15 cm (average diameter 3.9 cm) and having a clear to thick mucoid or opaque greenish content [8]. The cysts are lined by a variety of epithelia, including stratified squamous, columnar, cuboidal, ciliated columnar, mucinous, gastric, and transitional [8, 30]. Scattered bundles of smooth muscle fibers are invariably present in the wall, separated from the lining by a thin layer of fibrous tissue; however, the cysts are not invested with a well-defined muscular layer (as opposed to rectal duplication cysts) [8, 22, 30]. Typically, skin adnexae, neural elements, and heterologous mesenchymal tissues are not identified [30], which helps in differentiating this entity from teratoma, another cystic lesion that may occur in this anatomic location.

Malignant transformation of a TGC is a rare occurrence. The first report of an adenocarcinoma arising in a TGC came from Ballantine in 1931 [2]. Since then, 17 cases have been reported (Table 2). Interestingly, the tumors reported included both adenocarcinomas (11 cases) and neuroendocrine tumors (5 cases). One case of sarcoma arising in a TGC was also reported [25]. Among the cases illustrated, one was a well-differentiated mucinous (colloid)-type adenocarcinoma [24]. In addition, 2 more cases of moderately to poorly differentiated mucinous adenocarcinomas were also described [7, 24]. In 2 cases of adenocarcinoma, an increase in serum CEA was demonstrated [19, 33].

The case reported here represents an example of a mucinous (colloid) intestinal-type adenocarcinoma developing in a TGC. Although the morphology and the immunohistological phenotype of our case (positive for cytokeratin 20, CEA, MUC-2, negative for cytokeratin 7) were similar to those of colo-rectal carcinomas, there are several features suggesting that this lesion developed within a preexisting TGC rather than extending from the intestinal tract. First, there was no connection of the tumor to the rectal wall. Second, some of the cysts lined by high-grade dysplastic epithelium contained smooth muscle fibers, similar to the benign TGCs, suggesting that they represent a non-invasive component of the tumor.

Table 2 Reported malignant transformation arising in a tailgut cyst

No.	Author, year	No. of cases	Malignancy
1	Graadt van Roggen et al. [7], 1999	1	Moderately to poorly-differentiated mucinous (colloid) adenocarcinoma
2	Ballantine [2], 1932	1	Adenocarcinoma
3	Marco et al. [18], 1982	1	Adenocarcinoma
4	Hjermstad et al. [8], 1988	1	Poorly differentiated adenocarcinoma
5	Schwartz et al. [33], 2000	1	Well- to moderately differentiated adenocarcinoma
6	Levert et al. [14], 1996	1	Adenocarcinoma
7	Lim et al. [15], 1998	1	Adenocarcinoma
8	Moreira et al. [24], 2001	2	Mucinous (colloid) adenocarcinoma
9	Maruyama et al. [19], 1998	1/1	Moderately differentiated adenocarcinoma
10	Prasad et al. [30], 2000	2/5	Well-differentiated intestinal type adenocarcinoma (1) and neuroendocrine carcinoma (1)
11	Mourra et al. [26], 2003	1/1	Well-differentiated neuroendocrine carcinoma
12	Horenstein et al. [9], 1998	1/1	Carcinoid
13	Lin et al. [16], 1992	1/1	Carcinoid
14	Schnee et al. [32], 1994	1/1	Carcinoid
15	Moulopoulos et al. [25], 1999	1/3	Sarcoma

A unique feature of our case compared with previously reported TGCs is the presence of thyroid tissue and of a meningothelial proliferation with prominent psammoma bodies. While elements such as pancreatic acini, islets of Langerhans [30], and even glomus bodies [21] have been anecdotally identified in association with TGCs, there are, to our knowledge, no reports of other tissues, including meningothelial or thyroid. This interesting feature raises a more fundamental issue regarding the differential diagnosis between TGCs and teratomas. If one follows a strict definition, TGCs could be considered under the teratoma category, since they contain cells originating from all three germ cell layers: ectoderm (squamous epithelium), endoderm (intestinal-type epithelium) and mesoderm (smooth muscle). Some authors maintain, however, that the diagnosis of teratoma should be employed only when the lesion contains dermal appendages, neural tissue, or heterologous mesenchymal elements such as bone or cartilage, which classically are not encountered in TGCs [8]. Supporting a non-teratomatous origin are the claims that the squamous epithelium is likely of endodermal rather than ectodermal origin and also that all the different epithelia (including ciliated type) can be found in the embryonic gastrointestinal tract. Moreover, the majority of sacrococcygeal teratomas occur in neonates and frequently demonstrate intralesional calcifications, fat, and bony destruction of coccyx or sacrum, features that are usually absent in TGCs that tend to occur in middle-aged women [8, 11]. A case like ours, where an otherwise classic TGC (albeit with malignant transformation) contains unusual elements, seems to question the proposed origin of TGCs from the caudal hindgut (which should not contain meningothelial or thyroid tissue), suggesting that the distinction from teratoma is not necessarily straightforward. Even though one can make the assumption that the meningothelial cells arose from remnants of the caudal neural tube (which also extends into the embryonic tail and undergoes regression), it is difficult to explain the origin of thyroid tissue in this region without invoking a teratomatous process. We decided to designate our case as a TGC because it demonstrates the stereotypic appearance, the characteristic organization, and the clinical presentation of a TGC and not of a classic teratoma but with the mention that our case supports the contention that maybe all TGCs represent teratomatous processes.

Among the few cases of sacrococcygeal teratomas arising in adults, there were only three cases (two females and one male) in which an associated adenocarcinoma was present (in two cases the tumor was associated with the teratoma [23, 27], while in one case the adenocarcinoma followed resection of a histologically mature teratoma [13]). One patient died 2 months after operation with leptomeningeal involvement by carcinomatosis, the second died 2 years after resection, and the third was free of disease at 2 years follow-up. By comparison, our patient with adenocarcinoma arising in a TGC was well and free of disease at 6 years follow-up; however, a relevant comparison cannot be made, due to the small number of cases. To further complicate the issue, some of the reported cases of adult sacrococcygeal teratomas may actually be examples of TGC, since the description does not mention the presence of dermal appendages, neural tissue, bone, or cartilage.

Other differential diagnoses of TGCs include epidermoid and dermoid cysts, rectal duplication cyst, and anal gland cyst. Epidermoid cysts are lined only by stratified squamous epithelium and lack smooth muscle fibers in the wall. Dermoid cysts contain, in addition, dermal appendages. Duplication cysts are usually unilocular and are lined by an intestinal or respiratory epithelium. Many of them are located prerectally, whereas TGCs are invariably retrorectal. As opposed to TGCs, they have a well-defined, double-layered muscular wall with occasional ganglion cells [1, 12, 17, 20]. Malignant transformation of an enteric duplication cyst has been also reported [5]. Anal gland cysts have a similar histology to TGCs, and anal gland carcinomas can be confused with adenocarcinomas involving a TGC. The distinguishing feature is the location of anal gland cysts in close proximity to the anal sphincter

and not in the retrorectal/presacral space. Finally, another differential diagnosis is with chordoma, which is the most common primary sacral lesion. In this case, imaging studies show evidence of sacral bone destruction with a heterogeneous mass that extends into soft tissue [6, 36].

In conclusion, TGCs (retrorectal cystic hamartomas) represent a distinct clinico-pathological entity that occurs in adult women and originates in the tailgut vestiges. Clinical diagnosis is, at times, difficult due to the non-specific symptoms or asymptomatic nature of the lesion. Malignant transformation in the form of adenocarcinoma or neuroendocrine tumors, although rare, does occur; therefore, complete resection of these lesions is recommended. Our case was unusual in that, besides a classic TGC with malignant transformation in the form of a mucinous adenocarcinoma, it also contained areas showing meningothelial proliferation and ectopic thyroid tissue, raising questions regarding the proposed origin of TGCs.

References

1. Alavanja G, Kaderabek DJ, Habegger ED (1995) Rectal duplication in an adult. Am Surg 61:997–1000
2. Ballantine BM (1931) Sacrococcygeal tumors. Adenocarcinoma of a cystic congenital embryonal remnant. Arch Pathol 14: 1–9
3. Campbell WL, Wolff M (1973) Retrorectal cysts of developmental origin. Am J Roentgenol Radium Ther Nucl Med 117:307–313
4. Caropreso PR, Wengert PA Jr, Milford HE (1975) Tailgut cyst —a rare retrorectal tumor: report of a case and review. Dis Colon Rectum 18:597–600
5. Crowley LV, Page HG (1960) Adenocarcinoma arising in presacral enterogenous cyst. Arch Pathol 69:64–66
6. Dahan H, Arrive L, Wendum D, Docou le Pointe H, Djouhri H, Tubiana JM (2001) Retrorectal developmental cysts in adults: clinical and radiologic–histopathologic review, differential diagnosis, and treatment. Radiographics 21:575–584
7. Graadt van Roggen JF, Welvaart K, de Roos A, Offerhaus GJ, Hogendoorn PC (1999) Adenocarcinoma arising within a tailgut cyst: clinicopathological description and follow up of an unusual case. J Clin Pathol 52:310–312
8. Hjermstad BM, Helwig EB (1988) Tailgut cysts. Report of 53 cases. Am J Clin Pathol 89:139–147
9. Horenstein MG, Erlandson RA, Gonzalez-Cueto DM, Rosai J. (1998) Presacral carcinoid tumors: report of three cases and review of the literature. Am J Surg Pathol 22:251–255
10. Jao SW, Beart RW Jr, Spencer RJ, Reiman HM, Ilstrup DM. (1985) Retrorectal tumors. Mayo Clinic experience, 1960–1979. Dis Colon Rectum 28:644–652
11. Johnson AR, Ros PR, Hjermstad BM (1986) Tailgut cyst: diagnosis with CT and sonography. AJR Am J Roentgenol 147: 1309–1311
12. La Quaglia MP, Feins N, Eraklis A, Hendren WH (1990) Rectal duplications. J Pediatr Surg 25:980–984
13. Lack EE, Glaun RS, Hefter LG, Seneca RP, Steigman C, Athari F (1993) Late occurrence of malignancy following resection of a histologically mature sacrococcygeal teratoma. Report of a case and literature review. Arch Pathol Lab Med 117:724–728
14. Levert LM, Van Rooyen W, Van Den Bergen HA (1996) Cysts of the tailgut. Eur J Surg 162:149–152
15. Lim KE, Hsu WC, Wang CR (1998) Tailgut cyst with malignancy: MR imaging findings. AJR Am J Roentgenol 170:1488–1490
16. Lin SL, Yang AH, Liu HC (1992) Tailgut cyst with carcinoid: a case report. Zhonghua Yi Xue Za Zhi (Taipei) 49:57–60
17. MacLeod JH, Purves JK (1970) Duplications of the rectum. Dis Colon Rectum 13:133–137
18. Marco V, Autonell J, Farre J, Fernandez-Layos M, Doncel F. (1982) Retrorectal cyst-hamartomas. Report of two cases with adenocarcinoma developing in one. Am J Surg Pathol 6:707–714
19. Maruyama A, Murabayashi K, Hayashi M, Nakano H, Isaji S, Uehara S, Kusuda T, Miyahara S, Kondo A, Yabana T (1998) Adenocarcinoma arising in a tailgut cyst: report of a case. Surg Today. 28:1319–1322
20. Mboyo A, Monek O, Massicot R, Martin L, Destuynder O, Lemouel A, Aubert D (1997) Cystic rectal duplication: a rare cause of neonatal intestinal obstruction. Pediatr Surg Int 12: 452–454
21. McDermott NC, Newman J (1991) Tailgut cyst (retrorectal cystic hamartoma) with prominent glomus bodies. Histopathology 18:265–266
22. Mills SE, Walker AN, Stallings RG, Allen MS Jr (1984) Retrorectal cystic hamartoma. Report of three cases, including one with a perirenal component. Arch Pathol Lab Med 108: 737–740
23. Monteiro M, Cunha TM, Catarino A, Tome V (2002) Case report: sacrococcygeal teratoma with malignant transformation in an adult female: CT and MRI findings. Br J Radiol 75:620–623
24. Moreira AL, Scholes JV, Boppana S, Melamed J (2001) p53 Mutation in adenocarcinoma arising in retrorectal cyst hamartoma (tailgut cyst): report of 2 cases—an immunohistochemistry/immunoperoxidase study. Arch Pathol Lab Med 125: 1361–1364
25. Moulopoulos LA, Karvouni E, Kehagias D, Dimopoulos MA, Gouliamos A, Vlahos L (1999) MR imaging of complex tailgut cysts. Clin Radiol 54:118–122
26. Mourra N, Caplin S, Parc R, Flejou JF (2003) Presacral neuroendocrine carcinoma developed in a tailgut cyst: report of a case. Dis Colon Rectum 46:411–413
27. Ng EW, Porcu P, Loehrer PJ Sr (1999) Sacrococcygeal teratoma in adults: case reports and a review of the literature. Cancer 86:1198–202
28. Oh JT, Son SW, Kim MJ, Kim L, Kim H, Hwang EH (2000) Tailgut cyst in a neonate. J Pediatr Surg 35:1833–1835
29. Peyron A (1928) Les vestiges embryonnaires de la region sacro-coccygienne et leur role dans la production des kystes ou tumeurs d'origine congenitale. Bull Assoc Fr Etude Cancer. 17:613–632
30. Prasad AR, Amin MB, Randolph TL, Lee CS, Ma CK (2000) Retrorectal cystic hamartoma: report of 5 cases with malignancy arising in 2. Arch Pathol Lab Med 124:725–729
31. Pyo DJ (1990) Tailgut cyst (retrorectal cyst hamartoma): case report and review. Mt Sinai J Med 57:249–252
32. Schnee CL, Hurst RW, Curtis MT, Friedman ED (1994) Carcinoid tumor of the sacrum: case report. Neurosurgery 35:1163–1167
33. Schwarz RE, Lyda M, Lew M, Paz IB (2000) A carcinoembryonic antigen-secreting adenocarcinoma arising within a retrorectal tailgut cyst: clinicopathological considerations. Am J Gastroenterol 95:1344–1347
34. Theuerkauf FJ Jr, Hill JR, ReMine WH (1970) Presacral developmental cysts in mother and daughter: report of cases. Dis Colon Rectum 13:127–132
35. Uhlig BE, Johnson RL (1975) Presacral tumors and cysts in adults. Dis Colon Rectum 18:581–589
36. Williams LS, Rojiani AM, Quisling RG, Mickle JP (1998) Retrorectal cyst-hamartomas and sacral dysplasia: MR appearance. Am J Neuroradiol 19:1043–1045

Virchows Arch (2005) 446: 322–324
DOI 10.1007/s00428-004-1181-3

CASE REPORT

Gianluca Marucci · Christine M. Betts · Luciano Liguori · Vincenzo Eusebi

Basaloid carcinoma of the pancreas

Received: 15 September 2004 / Accepted: 17 November 2004 / Published online: 22 February 2005
© Springer-Verlag 2005

Abstract A case of basaloid carcinoma of the pancreas in a 26-year-old woman is reported. The tumour was constituted by solid nests of relatively uniform neoplastic cells with hyperchromatic nuclei and scant cytoplasm, showing distinct peripheral palisading. There were necrotic areas and deposition of hyaline material, suggesting a basement membrane-like substance. Small foci of clear-cut squamous differentiation were present. Tumour cells were positive for cytokeratin 14 and P63 and negative for neuroendocrine and acinic cell markers. Ultrastructurally, the tumour was constituted by polygonal cells with round nuclei containing clumped chromatin. Occasional tight junctions and keratin filaments were present. Basaloid carcinomas may arise in several sites of the body, the most frequent being the anus and oesophagus, and have poor clinical outcome. The present case appears to be, to the best of our knowledge, the first documented example in the literature of basaloid carcinoma of the pancreas.

Keywords Pancreas · Basaloid carcinoma · Undifferentiated carcinoma

G. Marucci (✉) · V. Eusebi
Section of Pathology, Department of Oncology,
University of Bologna, Bellaria Hospital,
Via Altura 3,
40139 Bologna, Italy
e-mail: gianluca.marucci@ausl.bologna.it
Tel.: +39-51-6225523
Fax: +39-51-6225759

C. M. Betts
Department of Experimental Pathology,
University of Bologna,
Bologna, Italy

L. Liguori
Section of Surgery, Bellaria Hospital,
Bologna, Italy

Introduction

Basaloid carcinoma is a rare variant of poorly differentiated carcinoma observed in a variety of anatomic sites, including the anus [11], oesophagus [3], colon [6], lung [2], thymus [5], larynx [13], prostate [4], breast [8] and uterine cervix [10]. We report a case of basaloid carcinoma of the pancreas, a site not hitherto described.

Clinical history

A 26-year-old female patient presented with a rapidly worsening jaundice. She had a history of ankylosing spondylitis, but no signs of previous neoplasms were evident. Computed tomography scan revealed a tumour of the head of the pancreas together with a marked dilatation of gallbladder. Retroperitoneal lymph nodes appeared enlarged. All indices of cholestasis were altered. Two days before the operation, total amylase was 194 U/l (normal range: 0–220 U/l) and lipase was 244 U/l (normal range: 0–60 U/l).

A duodeno-cephalo-pancreasectomy was performed. Total amylase was 24 U/l and lipase was 16 U/l,3 days after the operation. The patient was treated with a chemotherapy protocol, including gemcitabine and oxaliplatin. The patient is alive with widespread metastases (lymph nodes, bone and muscle) 8 months after the operation.

Macroscopically, on the cut surface, a white, firm nodule measuring 3.5 cm was observed within the pancreas, involving the intrapancreatic portion of the common bile duct. Microscopically, the neoplasm was characterised by solid nests and sheets of relatively uniform tumour cells with hyperchromatic nuclei and scant cytoplasm. The neoplastic elements at the edge of the sheets and nests were forming distinctive palisades (Fig. 1 and Fig. 2). Mitoses were numerous (mean of three per high power field ×400). There were large foci of coagulation necrosis. In the centre of the tumour nests, eosinophilic hyaline material was observed. It was positive with periodic-acid Schiff after dia-

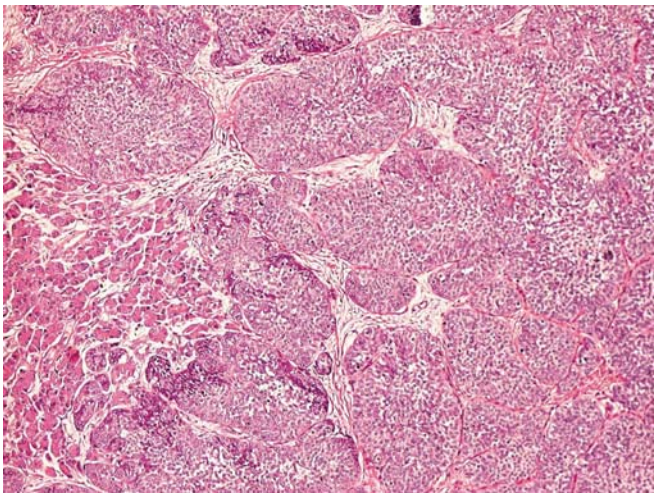

Fig. 1 The tumour architecturally forms sheets and nests of neoplastic cells

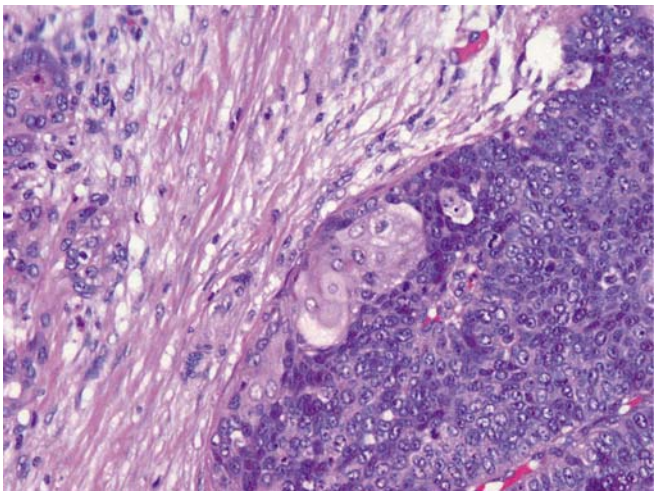

Fig. 3 A small whorly nest of squamoid elements

stase digestion, as well as for laminin and collagen IV. Small foci of squamous cells were observed (Fig. 3).

Tumour cells were diffusely immunoreactive for cytokeratin 14 (Dako; monoclonal: LL002; dilution: 1:100), P63 (Neomarkers; monoclonal: 4A4; dilution 1:200) (Fig. 4) and p53 (Dako; monoclonal: DO-7; dilution 1:50) and focally for carcinoembryonic antigen (Dako; dilution 1:1500); the same cells were negative for chromogranin (Biogenex; monoclonal: LK2H10; dilution 1:400), cytokeratin 7 (Dako; monoclonal: OV-TL 12/30; dilution 1:100), cytokeratin 8 (Dako; monoclonal: 35βH11; dilution 1:50), lysozyme (Dako; dilution 1:3000) and α1-antitrypsin (Dako; dilution 1:300). Of the neoplastic population, 20% resulted positive with antibody anti-Ki67 (Dako; monoclonal: MIB-1; dilution 1:200).

Ultrastructurally, the tumour was constituted by polygonal cells with round nuclei containing clumped chromatin. There were occasional tight junctions, and keratin filaments were seen dispersed in the cytoplasm (Fig. 5).

Discussion

Basaloid carcinomas are poorly differentiated and clinically aggressive tumours with features superficially reminiscent of basal cell carcinoma of the skin. These tumours share with basal cell carcinoma of the skin the "immature" looking cells, with hyperchromatic nuclei, scant cytoplasm, numerous mitoses and peripheral palisading cells. At a variance with the skin tumours, the deep-seated basaloid carcinomas show necrotic areas and are clinically aggressive with high incidence of metastases. Cases of basaloid carcinomas described at various levels all share similar features, which were also observed in the present tumour. Negativity for chromogranin and acinic cell markers ruled out poorly differentiated carcinoma of endocrine or acinic cell nature, while clinical history and instrumental investigation excluded a metastasis [1].

Basaloid pancreatic carcinoma is not included in the current World Health Organization classification. Hayashi et al. in 1956 published a study on "so-called basal cell carcinoma of undifferentiated type" [7].

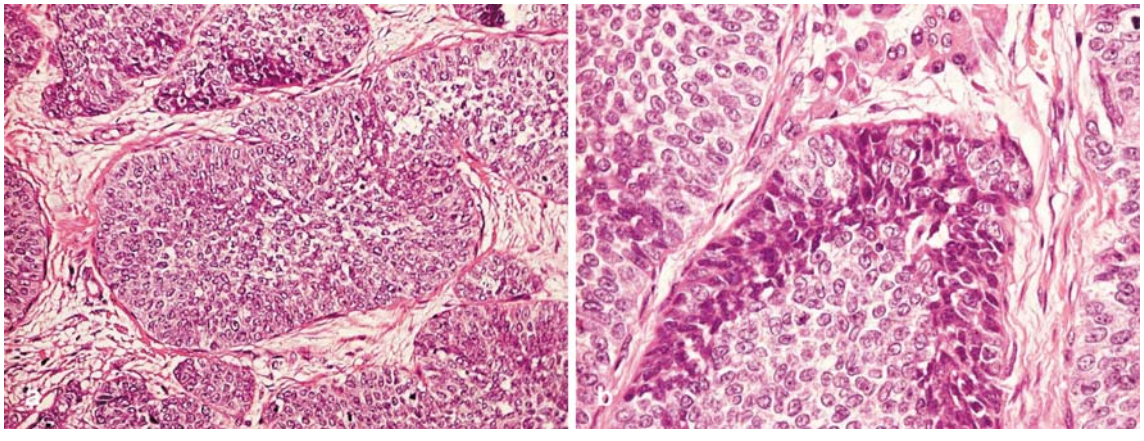

Fig. 2 A The edge of this nest evidences cells forming palisades. **B** The neoplastic elements display roundish nuclei with small nucleoli

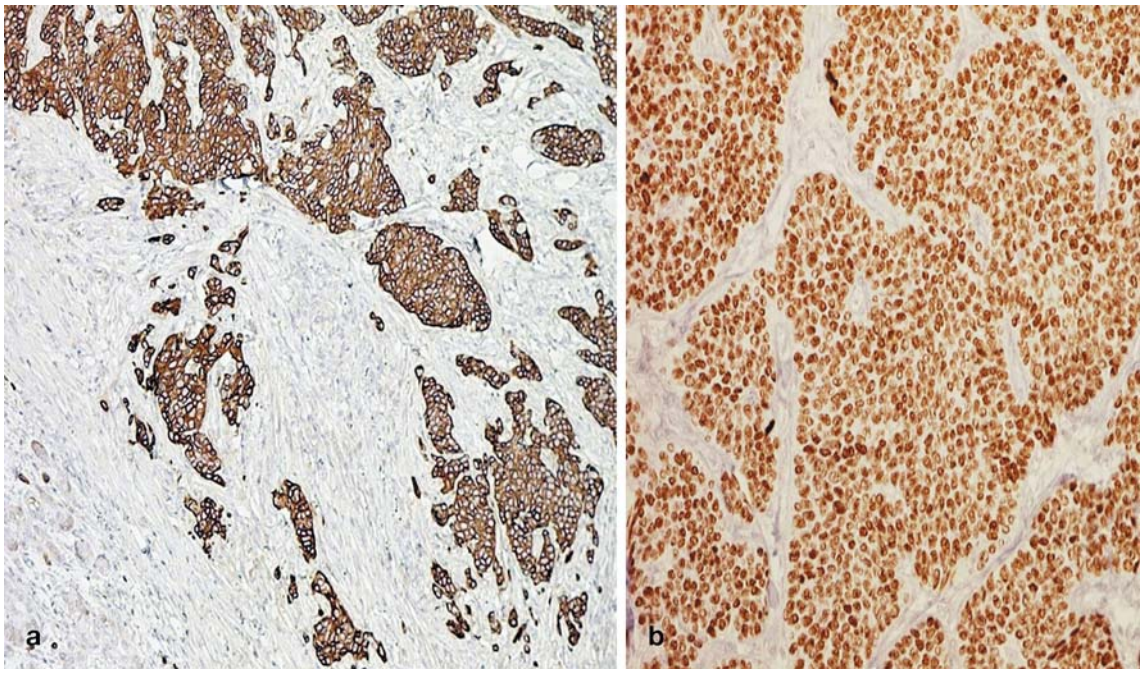

Fig. 4 A The neoplastic cells react for keratin 14. **B** Virtually all nuclei are positive for P63

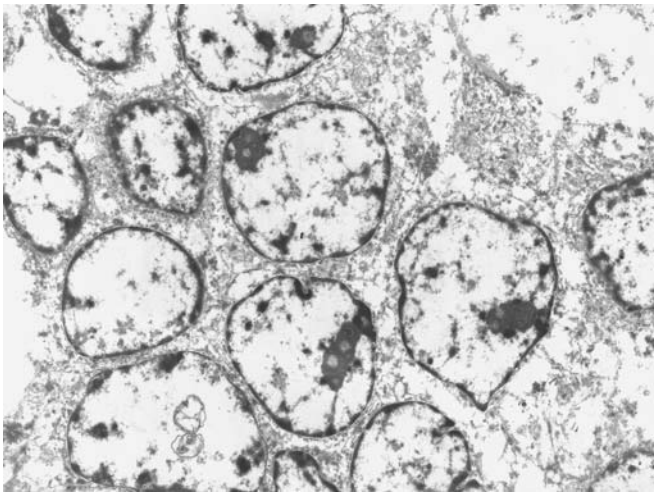

Fig. 5 The neoplastic cells show roundish nuclei. Their cytoplasm contains thin filaments

In the Armed Forces Institute of Pathology fascicle of the pancreas, 3 years later, the basal cell variant of carcinoma wasn't mentioned, but a case was reported with histological features similar to those of the present case, which was called "carcinoma simplex" or "medullary carcinoma" [9].

The present case was seen in a 26-year-old patient, an age at which more frequently unusual variants of pancreatic adenocarcinoma occur [12]. It is possible that the present basaloid carcinoma has originated from progenitor cells with pluripotent differentiation capacity. It displayed immunopositivity for cytokeratin 14 and P63, which stain basal/myoepithelial cells, a finding also shared by similar tumours of the breast [8].

In conclusion, the existence of a basaloid variant of pancreatic carcinoma, even though extremely rare, should be taken into consideration, especially in view of the ominous prognosis.

References

1. Adsay NV, Andea A, Basturk O et al (2004) Secondary tumors of the pancreas: an analysis of a surgical and autopsy database and review of the literature. Virchows Arch 444:527–535
2. Brambilla E, Moro D, Veale D et al (1992) Basal cell (basaloid) carcinoma of the lung: a new morphologic and phenotypic entity with separate prognostic significance. Hum Pathol 23:993–1003
3. Cho KJ, Jang JJ, Lee SS, Zo JI (2000) Basaloid squamous carcinoma of the oesophagus: a distinct neoplasm with multipotential differentiation. Histopathology 36:331–340
4. Denholm SW, Webb JN, Howard GC, Chisholm GD (1992) Basaloid carcinoma of the prostate gland: histogenesis and review of the literature. Histopathology 20:151–155
5. Iezzoni JC, Nass LB (1996) Thymic basaloid carcinoma: a case report and review of the literature. Mod Pathol 9:21–25
6. Hall-Craggs M (1982) Basaloid tumor of the sigmoid colon. Hum Pathol 13:497
7. Hayashi K, Matsuyama K, Suga T, Tauchi H (1956) On the varied histological picture of cancer of the pancreas; on the so-called basal cell carcinoma of undifferentiated type. Gan 47:793–794
8. Jones C, Nonni AV, Fulford L, Merrett S, Chaggar R, Eusebi V, Lakhani SR (2001) CGH analysis of ductal carcinoma of the breast with basaloid/myoepithelial cell differentiation. Br J Cancer 85:422–427
9. Kneeland FV (1959) Tumors of the pancreas. Atlas of tumor pathology, section VII, fascicles 27 and 28. Armed Forces Institute of Pathology, Washington DC, pp 64–65
10. Kurman RJ, Norris HJ, Wilkinson E (1992) Basaloid carcinoma. In: Kurman RJ, Norris HJ, Wilkinson E (eds) Tumors of the cervix, vagina and vulva. Atlas of tumor pathology, 3rd series, fascicle 4. Armed Forces Institute of Pathology, Washington DC, pp 198–199
11. Lone F, Berg JW, Stearns MW Jr (1960) Basaloid tumors of the anus. Cancer 13:907–913
12. Lüttges J, Stigge C, Pacena M, Klöppel G (2004) Rare ductal adenocarcinoma of the pancreas in patient younger than 40 years. Cancer 100:173–182
13. Wain SL, Kier R, Vollmer RT, Bossen EH (1986) Basaloid-squamous carcinoma of the tongue, hypopharynx and larynx: report of 10 cases. Hum Pathol 17:1158–1166

Virchows Arch (2005) 446: 325–332
DOI 10.1007/s00428-004-1182-2

CASE REPORT

Johannes Moeller · Manfred G. Krukemeyer · Lars Morawietz · Max Schmeding · Anja Dankof · Ulf Neumann · Veit Krenn · Claudia Berek

Molecular case report: IgVH analysis in acute humoral and cellular liver allograft rejection suggests a selected accumulation of effector B cells and plasma cells

Received: 10 September 2004 / Accepted: 17 November 2004 / Published online: 16 February 2005
© Springer-Verlag 2005

Abstract Acute cellular (CLR) and humoral liver allograft rejection (HLR) are the most important immunological obstacles to successful liver transplantation. In HLR, serum antibodies play the central pathogenetic role. In CLR, CD3+ T lymphocytes drive the destructive immune response. Although CLR and HLR show different clinical symptoms and can be kept apart in most cases, they share histomorphological similarities. In CLR, hepatic B lymphocytes and plasma cells as well as B-cell-activating cytokines have recently been described, indicating that, in addition to T cells, antibody-mediated mechanisms might be involved. To analyze the impact of hepatic B cells in CLR and HLR, the immunoglobulin (Ig) variable (V)-region gene repertoire was determined from tissue of one case of CLR and one case of HLR. Complement deposits and lymphocytic infiltrate were determined using immunohistochemistry. T cells, B lymphocytes and plasma cells could be detected in both cases, whereas C3c and C4d deposits could only be demonstrated in the HLR case. The molecular analysis of 63 V-region genes showed that B cells in both allografts expressed selected V-gene repertoires. All sequences differed from the putative germline sequences by multiple somatic mutations. This suggests a clonal expansion of selected effector B cells in the portal tracts of liver allografts. Locally accumulated B cells and their antibodies might be involved in IgG-mediated complement activation in CLR and HLR.

Keywords Liver transplantation · Humoral rejection · Cellular rejection · B lymphocytes · Immunoglobulins

J. Moeller · M. G. Krukemeyer · L. Morawietz · A. Dankof · V. Krenn
Institute for Pathology, University Hospital Charite, Schumannstrasse 20/21, 10117 Berlin, Germany

M. Schmeding · U. Neumann
Department for Surgery, University Hospital Charite, Augustenburger Platz 1, 13353 Berlin, Germany

C. Berek (✉)
Deutsches Rheumaforschungszentrum, Schumannstrasse 20/21, 10117 Berlin, Germany
e-mail: berek@drfz.de
Tel.: +49-30-28460711
Fax: +49-30-28460712

Introduction

Despite new potent immunosuppressants, acute cellular liver allograft rejection (CLR) is still a common and severe complication after orthotopic liver transplantation. Compared with CLR, humoral liver rejection (HLR) is a rather rare but severe complication, which is mainly based on autoantibodies directed against blood-group antigens. CLR and HLR show different clinical symptoms and can be kept apart in most cases. However, they share histopathological similarities with respect to infiltrating B and T lymphocytes [1, 3, 4, 7, 11, 13, 15, 17]. In a recently published study, B lymphocytes, plasma cells, chemokines and complement factor C4d were detected in tissue biopsies of CLR, suggesting that, in addition to the T-cell response, a local B-cell response may be involved in the pathogenesis of CLR [7]. In xenotransplants, highly mutated complementary-determining regions (CDRs) were found in infiltrating B cells, indicating a pathogenetic role of somatic mutations in maturation of immunoglobulin G (IgG) in xenotransplants. Only few molecular analyses on human liver allograft rejection have been carried out [14], and no data exist on the molecular B-cell response in human liver allograft rejection, in neither HLR nor CLR. To further evaluate the role of intrahepatic B cells in liver rejection, sequences of IgV_H- and V_L-region genes were determined in one case of HLR and one case of CLR.

Clinical history

Patient 1 (L53) with HLR was a 25-year-old woman undergoing liver transplantation due to acute liver failure of

unknown origin. Postoperative immunosuppression was based on tacrolimus and steroids. She developed fever and rising liver enzymes 8 days after surgery. Histological examination of a needle biopsy revealed the histological features of a humoral rejection with portal inflammatory infiltration, endothelitis and large hemorrhagic necroses [5]. After 3 days of steroid pulse therapy, liver function tests improved initially. However, in the further course, the liver function decreased, resulting in graft failure and consecutive liver re-transplantation.

Patient 2 (L55) with CLR was a 53-year-old man with liver re-transplantation for recurrent hepatitis C 3 years after initial orthotopic liver transplantation. Postoperative immunosuppression was based on tacrolimus and steroids. Initial graft function was excellent, yet 1 week after surgery, liver enzymes deteriorated. The liver biopsy then demonstrated a low portal inflammatory infiltration with lymphocytes attached to endothelia, confirming acute rejection grade 1.

In both cases, the blood serology revealed no IgM antibodies against Epstein–Barr virus, cytomegalovirus and hepatitis-C virus; however, the serum copy numbers of the viral genes have not been assessed.

Materials and methods

Tissue preparation

Immediately after puncture, parts of the biopsies were fixed in 4% buffered formalin. About one-fifth was cryopreserved and stored at −80°C. In addition to the above-mentioned serological examinations, there was no detection of hepatitis-C, cytomegalo or Epstein–Barr virus infection in either of the transplant biopsies using reverse-transcription polymerase chain reaction (RT-PCR). Using a DMRBE microscope (LEITZ, Germany), histopathological evaluation of the rejection was conducted by a pathologist specializing in transplant pathology (V.K.) according to the rejection activity index (RAI) score [2].

Immunohistochemistry

Tissue sections of 4–6 µm were deparaffinized and antigens demasked using a pressure cooker (citrate buffer, pH 6). Biotin-labeled primary antibodies specific for B cells (CD20, Dako, concentration 7 mg/l), for plasma cells (CD38, Novocastra; dilution 1:100), for T cells (CD3, Dako, concentration 10 mg/l) and for the complement factors C3c and C4d (Biomedica, concentration 20 mg/l) were used. Staining was performed using the streptavidin-biotin method according to the manufacturer's instructions (LSAB-Kit, Dako). Newfuchsin (Dako) was used as a chromogene, and sections were counterstained with hematoxylin. Tonsil tissue sections were used as positive control; negative controls were obtained by omitting the primary antibody. Biopsies from acute kidney transplant rejection served as positive controls for C4d.

Table 1 Variable (V)-region genes isolated from patient L55. Sequences derived from an independent reverse-transcription polymerase chain reaction reaction are distinguished by their first number, V(D)J and C-region genes are indicated, depending on the primer used for cDNA amplification it was possible to determine the IgG subclass. The ratio of replacement to silent (R/S) mutations in framework region (FR) is based on the number of somatic mutations in FRI to FRIII, for V_H- regions the ratio of R/S in the complementary-determining region (CDR) was calculated from the number of somatic mutations in CDRI and CDRII, for V_k- and V_λ-regions for CDRI, CDRII and CDRIII. *nd* not done, *n.a.* not applicable

Sequence	V-region gene			C-region	R/S	
	V	DH	J		CDR	FR
3.1	1–18	1–26	JH4b	IgG3	6/1	2/3
8.9	1–46	nd	JH3b	IgG1	5/4+del	9/4
14.1	1–46	nd	JH4b	IgA	4/0	1/2
8.2	1–69	4–17	JH4b	IgG1	6/1	8/3
8.10	1–69	3–03	JH4b	IgG1	15/1	7/7
3.2	3.15	nd	JH6	IgG1/2	5/2	5/5
10.1	3–23	5–05	JH4b	IgM	2/1	4/2
3.3	3–23	7–27	JH5b	IgG1/2	nd	nd
8.3	3–73	2–2	JH5b	IgG1	6/3	6/5
3.4[a]	4–04	3–10	JH5b	IgG1/2	3/0	0/1
2.1[a]	4–04	3–10	JH5b	IgG1/2	2/1	2/2
3.5	4–4	1–7	JH5b	IgG1/2	5/2	6/7
14.2	4–04	4–17	JH6b	IgA	8/2	5/4
8.12	4–30.1	3–09	JH4b	IgG1	7/0	7/3
3.6	4–39	nd	JH4b	IgG1/2	12/3	12/8
2.2	4–39	1–07	JH4b	IgG1/2	n.a.	n.a.
10.2	4–39	7–27	JH4b	IgM	1/0	1/0
3.7	4–59	2–21	JH4b	IgG1/2	5/1+del	5/4
3.8	4–59	6–13	JH4b	IgG3	0/0	5/1
8.6	4–59	5–24	JH4b	IgG1	6/4	9/8
10.3	4–59	nd	JH4b	IgM	10/0	2/2
13.1, 13.2[b]	4–61	3–22	JH4b	IgA	5/2	10/5
1.1 – 1.3[b]	4.61	3–22	JH4b	IgG	5/2*	10/5*
1.4[b]	4–61	3–22	JH4b	IgG	3/1	7/3
8.5[b], 8.11[b]	4–61	3–22	JH4b	IgG1	3/1*	7/3*
3.9[b]	4–61			IgG	6/1	6/2
10.4	4–61	3–22	JH2b	IgM	3/0	2/2
4.1	L6		Jk5	Kappa	5/2	3/3
4.2	L8		Jk3	Kappa	5/1	2/1
4.3	L12		Jk1	Kappa	7/0	1/4
4.4	012/02		Jk2	Kappa	4/2	5/9
4.5	012/02		Jk2	Kappa	1/1	2/0
4.6	012/02		Jk5	Kappa	9/3	3/3
11.1	1c		J2/3	Lambda	5/2	3/0
11.2	2e		JL2/3	Lambda	3/1	4/2
11.3	31		JL2/3	Lambda	4/0	4/4
11.4	3h		JL2/3	Lambda	2/0	0/0
11.5	8a		JL3b	Lambda	5/6	5/3

[a, b]Superscripts denote sequences with an identical rearrangement
*Indicates that sequences differ by 1 to 2 nucleotides from each other, the common number of somatic mutations is given

RNA extraction and V-gene amplification

Cryopreserved liver tissue (30 mg) from both patients as well as control tissue from a routine follow-up biopsy from one patient after liver transplantation without signs of HLR or CLR were homogenized under liquid nitrogen in guanidinium-isothiocyanate buffer, and the total RNA was extracted using the RNeasy Mini Kit (QIAGEN). The amount of RNA was determined using photometry. The quality of the RNA was assessed by comparing the 18-s and 28-s RNA on agarose gel. In addition, the quantity of mRNA was tested using PCR amplification of β actin.

V-region genes were amplified using RT-PCR (OneStep RT-PCR Kit, Qiagen) with 50 ng of RNA for each amplification. The constant regions of the H and the L chains were separately transcribed using primers specific for IgM: 5′-ACGGGGAATTCTCACAGGAGAC, IgG: 5′-CACGC TGCAGATGTAGGTCTGG, IgA: 5′-GAGGCTCAGCGG GAAGACCTTG, kappa L-chain: 5′-AAGATGAAGACA GATGGTGCAGCCAC and lambda L-chain: 5′-GGGCG GGAA CAGAGTGACCG. In addition, cDNA was transcribed using a primer specific for the membrane exon of IgG1: 5′-ATGAAGATGGTGTAGGTCGTCC.

V-region genes were amplified (94°C 1 min, 67°C 1 min, 72°C 1 min, 40 cycles, 72°C 10 min) after adding a mixture of V_H, Vκ and Vλ primers, respectively [6]. PCR products were ligated with Quick ligase kit into the TA vector (Invitrogen) and sequenced using the ABI prism sequencer (Applied Biosystems). The short sequence of the C-region gene does not allow one to distinguish between IgG1 and IgG2, but permits one to determine IgG3 and IgG4. V-region sequences isolated from the mRNA of membrane-bound IgG1 are distinguished by the prefixes 8 (patient L55, CLR) and 9 (patient L53, HLR) (Table 1). The presumptive germline gene was determined using V-base (Tomlinson, Cambridge, UK).

Results

Histological features

Histology of HLR revealed the characteristic appearance of an early humoral rejection: a portal inflammatory infiltration with lymphocytes, plasma cells and macrophages, the lymphocytes also being located in and near to endothelia

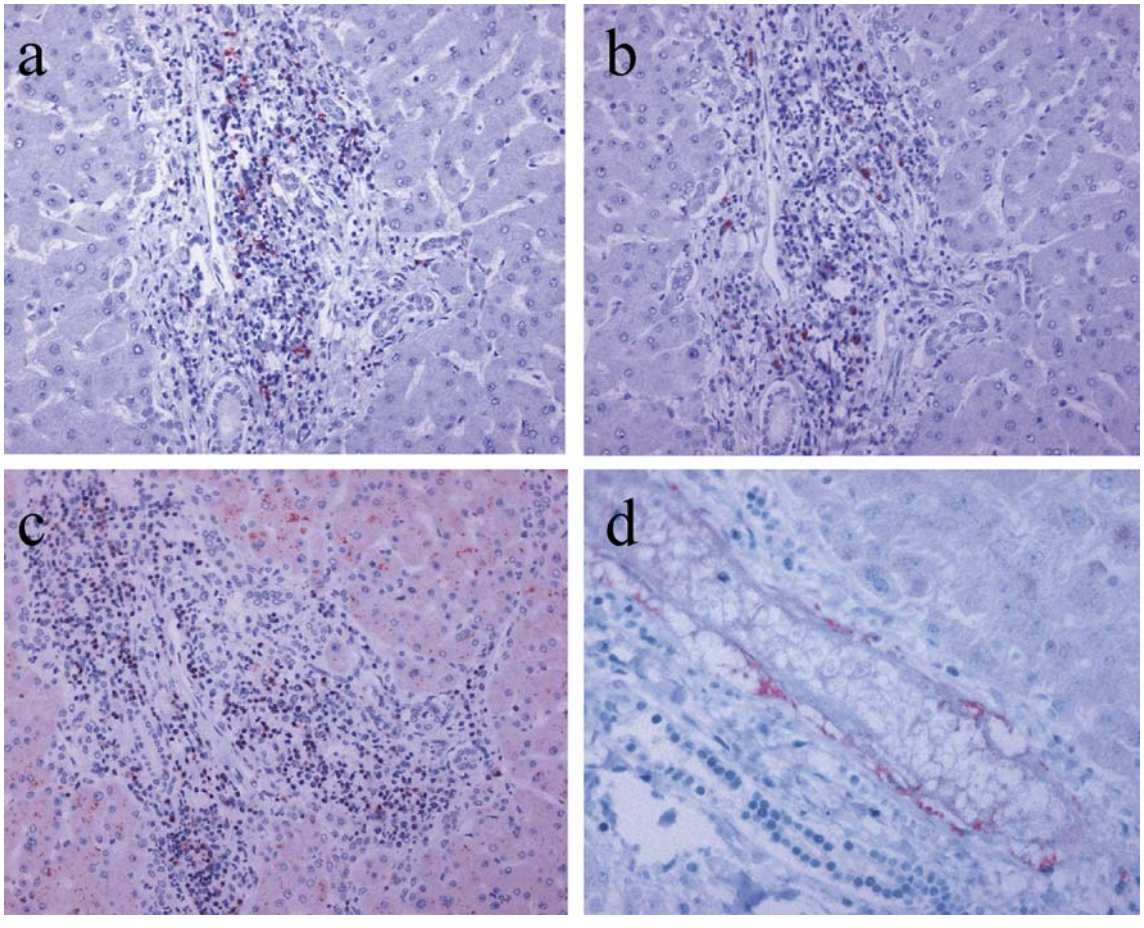

Fig. 1 Definition of cellular infiltrate and complement deposition in a humoral liver allograft rejection (HLR) biopsy (patient L53). The inflammatory infiltrate in the portal tracts with B lymphocytes (**a**) and plasma cells (**b**) is definite but lower in number when compared with T lymphocytes (**c**). Clearly visible C4d deposits can be found in the vicinity of small blood vessels (**d**). (**a** CD20, **b** CD38, **c** CD3 immunohistochemistry, original magnification ×200; **d** C4d immunohistochemistry, original magnification ×400)

Table 2 Variable (V)-region genes isolated from patient L53. Sequences derived from an independent reverse-transcription polymerase chain reaction are distinguished by their first number, V(D)J and C-region genes are indicated, depending on the primer used for cDNA amplification it was possible to determine the IgG subclass. The ratio of replacement to silent (R/S) mutations in framework region (FR) is based on the number of somatic mutations in FRI to FRIII, for V_H- regions the ratio of R/S in the complementary-determining region (CDR) was calculated from the number of somatic mutations in CDRI and CDRII, for V_k- and V_λ-regions for CDRI, CDRII and CDRIII. *nd* not done

Sequence	V-region gene			C-region	R/S	
	V	DH	J		CDR	FR
5.25	1–02	6–13	JH4b	IgG1/2	8/1	11/5
9.9	1–02	nd	nd	IgG1	11/0	6/3
5.23, 5.26	1–08	2–15	JH4b	IgG1/2	11/2	6/3
5.22	3–48	6–19	JH4b	IgG1/2	11/4	13/5
5.10, 5.12	3–66	nd	JH4b	IgG1/2	4/1	6/2
9.1, 9.3,9.4,9.11	3–74	nd	JH4	IgG1	6/3	4/2
5.17	4-b	3–16	JH3b	IgG1/2	9/4	15/10
5.1	4–30.1	1.01	JH4b	IgG1/2	2/2	2/2
5.5[c]	4–30.1	2–15	JH5b	IgG1/2	7/2	5/3
5.24[c]	4–30.1	2–15	JH5b	IgG1/2	8/3	8/6
5.27	4–30.1	4–17	JH4b	IgG1/2	6/1	8/5
5.4	4–30.4	2–15	JH6b	IgG1/2	6/1	13/4
5.28	4–30.4	2–21	JH4b	IgG4	8/2	3/2
9.10	4–30	4–17	JH4b	IgG1	4/0	5/0
5.29	4–34	2–15	JH4b	IgG1/2	5/1	7/8
5.21	4–39	nd	JH4b	IgG1/2	8/0	7/5
9.2, 9.6, 9.12	4–39	6–13	JH5b	IgG1	0/0	1/2*
9.7, 9.8	4–59	2–15	JH4b	IgG1	9/4	12/11*
5.7	4–59	4–23	JH4b	IgG1/2	7/1	6/6
5.2,5.3,5.15,5.19	4–59	6–19	JH4b	IgG1/2	2/1*	5/2*
5.13	4–59	nd	JH4b	IgG3	9/4	15/10
5.14[d]	6–01	nd	nd	IgG1/2	6/1	3/4
5.30[d]	6–01	nd	nd	IgG1/2	5/1	5/5
6.1	L8		Jk5	Kappa	3/2	3/5
12.1	4b		JL3/3	Lambda	2/1	1/2

[c, d]Superscripts denote sequences with an identical rearrangement
*Indicates that sequences differ by 1 to 2 nucleotides from each other, the common number of somatic mutations is given

(endothelitis) and periportal and centrilobular hemorrhagic necrosis. A high number of the venules exhibited severe endothelitis with fibrin thrombi.

CD20+ B lymphocytes and CD38+ plasma cells showed a predominantly portal distribution with a diffuse pattern. Rarely, small-sized aggregates were observed, while follicular structures were not detected. Isolated, single B lymphocytes were localized in the vicinity of venules and near to necrotic areas (Fig. 1a, b, c).

C3c and C4d deposits of variable size were seen in the inflammatory infiltrate of portal tracts and near to the border of necrotic areas. Capillaries of the portal tracts and liver sinus in the vicinity of portal tracts showed a partially focal and partially diffuse accumulation of C4d (Fig. 1d).

All of the portal tracts in the CLR biopsy exhibited a mixed infiltrate, containing lymphocytes, macrophages and few eosinophils. A minority of the bile ducts were cuffed and infiltrated by inflammatory cells; the bile duct nuclei showed mild reactive changes. A small number of CD20+ lymphocytes and CD38+ plasma cells were diffusely distributed in the portal tracts. No C3c and C4d deposits could be demonstrated in the case of CLR.

B cells in the transplanted liver tissue expressed a selected V-gene repertoire

To determine the V-gene repertoire, different PCR reactions were performed (sequence 1.n to 15.n), and a total of 31 VH, 6 Vk and 5 Vl sequences from the tissue of patient L55 and 35 VH, 1 Vk and 1 Vl from patient L53 were analyzed. For patient L55, in addition to IgG, IgM and IgA sequences were also determined (Table 1). Interestingly, for both patients, sequences of the IgG3 or IgG4 subclass were isolated, an Ig subclass which is rarely expressed in peripheral blood B-cells (4/24 IgG sequences). The analysis of the V_H-gene repertoire showed that 27 of 43 rearrangements used a gene of the VH4-, 8 of 43 of the VH1- and only 7 of 43 of the VH3-gene family. In addition, a single VH6 rearrangement was isolated. This strong bias toward rearrangements of the VH4-gene family was seen for both patients (Table 1 and Table 2) as well as for the control biopsy (data not shown).

```
                                  CDRI                  --------CDRII----------

VH1-02      QVQLVQSGAEVKKPGASVKVSCKASGYTFTGYYMHWVRQAPGQGLEWMGWINPNSGGTNYAQKFQG
VH1-08      ----------------------------S-DIN-----T---------M-----N-G-------
5.23        ........----------------------N-DI------A--------F-S--TDN-Y-T-N---
5.25        ........------------------N-GD--T--L-L---H------C----T-D-KF-R----


                                                    - CDRIII - J -
VH1-02      RVTMTRDTSISTAYMELSRLRSDDTAVYYCAR   YSAG    FDYW
VH1-08      ------N-----------S---E---------
5.23        ------S-P-K-------S-T-E--------IGWY----SLP--F-
5.25        G--L---A------------K---A-------DPM----KT.--S-
```

Fig. 2 Independent VDJ rearrangements with an identical amino acid motif in the CDRIII. Sequences 5.23 and 5.25 are compared with their closest germline genes VH1–02 and VH1–08. Amino acid sequences are given in single letter code. CDRs are indicated. Dashes indicate identity with the top line, dot shows different length of the CDRIII for sequence 5.25. Common amino acid motif in the CDRIII is high lighted

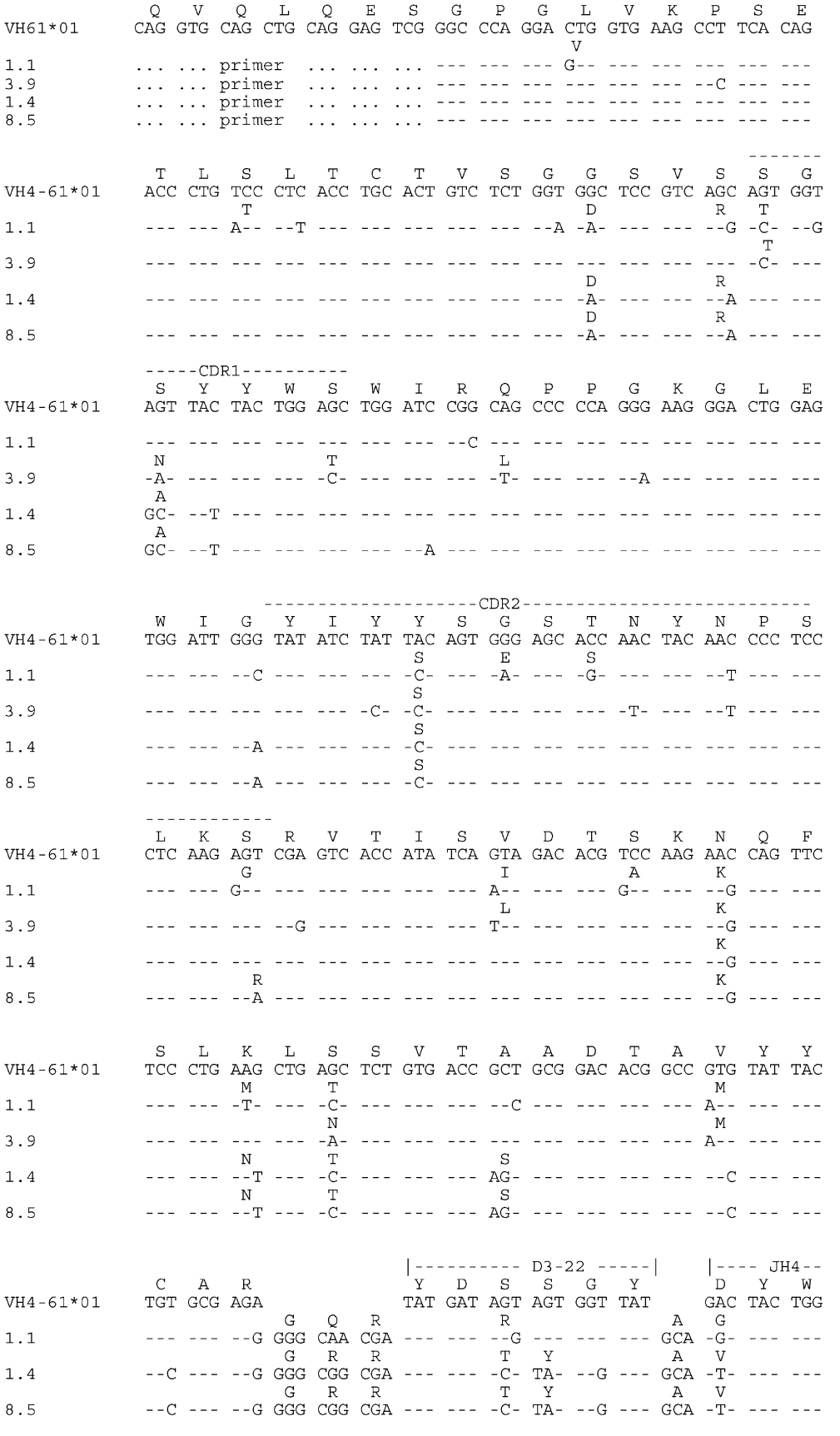

Fig. 3 Clonal expansion and V-gene diversification of B-cell clones isolated from rejected liver tissue. Sequences with an identical rearrangement but a different pattern of somatic mutations are shown. Clone b (**a**) is derived from patient L55 and clone d (**b**) from patient L53. Sequences are compared with the putative germline sequences. *Dashes* indicate identity with top line. Nucleotide differences and the predicted amino acid exchanges are given. The genealogical trees (**c**) show the stepwise accumulation of somatic mutations in the V-region genes expressed in B-cell clone b isolated from patient L55

Fig. 3 (continued)

```
                 Q   V   Q   L   Q   Q   S   G   P   G   L   V   K   P   S   Q
VH6-1        CAG GTA CAG CTG CAG CAG TCA GGT CCA GGA CTG GTG AAG CCC TCG CAG
5.30         ... ... primer  ... ... ... --- --- --- --- --- --- --- --- ---
5.14         ... ... primer  ... ... ... --- --- --- --- --- --- --- --- ---

                                                                     ---------
                 T   L   S   L   T   C   A   I   S   G   D   S   V   S   S   N
VH6-1        ACC CTC TCA CTC ACC TGT GCC ATC TCC GGG GAC AGT GTC TCT AGC AAC
5.30         --- --- --- --- --- --- --- --- --- --- --- --- --- --- --- ---
5.14         --- --- --- --- --- --- --- --- --- --- --- --- --- --- --- ---

                ---CDRI----------------
                 S   A   A   W   N   W   I   R   Q   S   P   S   R   G   L   E
VH6-1        AGT GCT GCT TGG AAC TGG ATC AGG CAG TCC CCA TCG AGA GGC CTT GAG
                             S                   R
5.30         --- --- --- --- -G- --- --- --- -G- --- --- --- --- --- --- ---
                             S
5.14         --- --- --- --- -G- --- --- --- --- --- --- --- --- --- --- ---

                                 ------------------------------------CDRII----------
                 W   L   G   R   T   Y   Y   R   S   K   W   Y   N   D   Y   A
VH6-1        TGG CTG GGA AGG ACA TAC TAC AGG TCC AAG TGG TAT AAT GAT TAT GCA
                             K                                   S   E
5.30         --- --- --- -A- --- --- --- --- --- --- --- --- -G- --A --- --C
                             K                       Q           S   E
5.14         --- --- --- -A- --- --- --- --- --- C-- --- --- -G- --A --- ---

                -------------------
                 V   S   V   K   S   R   I   T   I   N   P   D   T   S   K   N
VH6-1        GTA TCT GTG AAA AGT CGA ATA ACC ATC AAC CCA GAC ACA TCC AAG AAC
                             T                       S   S       A
5.30         --- --- --- --- -C- --- --- --- --- -GT T-C --- G-- --- --- ---
                             R           V           T   A
5.14         --C --- --- -G- --- --- G-C --- --- -C- G-- --- --- --- --- ---

VH6-1        CAG TTC TCC CTG CAG CTG AAC TCT GTG ACT CCC GAG GAC ACG GCT GTG
                             Q
5.30         --- --- --- -A- --A --T --- --- --- --- --- --- --- --- --- --A

5.14         --- --- --- --A --- --C --- --- --- --- --- --- --- --- --- --T

                                     ---------------CDRIII--------------
VH6-1        TAT TAC TGT GCA AGA GAG GGC CGG GGA AGT GGC TTC CCT ACC TGG
                                 Q   G
5.30         --- --- --- --C CA- -G- --- --- --- --- --- --- --- --- ---
                                 Q   G
5.14         --- --- --- --C CA- -G- --- --- --- --- --- --- --- -G- ---
```

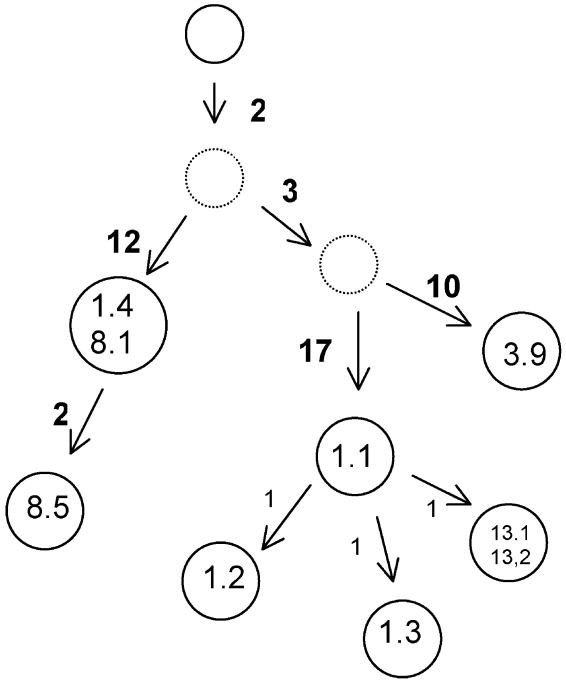

In comparison with germline V-genes, all isolated V-region sequences carried somatic mutations. On average, 14 nucleotide exchanges per VH region were seen in sequences from patient L55 and 19 in sequences from patient L53. Somatic mutations preferentially accumulated within the CDR of the V-region genes. The finding of a high ratio of replacement to silent mutations (R/S) in the CDRs (on average R/S=3.7) but not in the framework region (FR) (on average R/S=1.3), suggested that cells accumulating within the transplanted liver are selected for their affinity [16]. This interpretation is further supported by the finding of sequences with different VDJ rearrangements but identical amino acid motifs in the CDRIII. For example, sequences 5.23 and 5.25 used related VH1 genes, which were joined to D2–15 and D 6–19, respectively (patient L53, Table 2). Nevertheless, a motive of four identical amino acids was seen in the CDRIII (Fig. 2).

In the tissue sample from patient L55, a B-cell clone expressing a VH4–61/DH3–22/JH4b rearrangement seemed to be over represented (clone b, Table 1), as sequences were isolated when IgA, total IgG and membrane-bound IgG1 were amplified by RT-PCR. All VH sequences belonging to this clone shared two somatic mutations. During clonal expansion, further somatic mutations were introduced into the V-region gene. The genealogical tree shows the stepwise accumulation of up to 21 additional nucleotide exchanges (Fig. 3a). In addition, two IgG sequences with an identical VH4–04/DH3–10/JH5b rearrangement were isolated, which differed in their pattern of somatic mutations. These sequences had only one single nucleotide exchange in common (clone a, Table 1).

From the tissue sample of patient L53, sequences with an identical rearrangement but a different pattern of somatic mutations were again isolated. Sequences derived from the B-cell clone d (Table 2) had a VH4–30.1/DH2–15/JH4b rearrangement. These V_H regions had 16 somatic mutations in common. Whereas sequence 5.5 had a single additional somatic mutation, sequence 5.24 carried nine further nucleotide exchanges. Sequences with the VH6–01 rearrangement (clone d, Table 2) had only four somatic mutations in common; however, both sequences accumulated multiple additional nucleotide exchanges (11 or 12 substitutions, respectively). The control biopsy showed VH diversification, but no clonal expansion could be established among the VH gene sequences (data not shown).

Discussion

The involvement of antibodies in rejection of organ transplants is increasingly recognized as a relevant pathomechanism, other than in xenografts [17] and kidney and heart [9] transplants. Two recent studies demonstrated depositions of C3c and C4d in humoral [5] and cellular [7] liver rejection, suggesting an involvement of B lymphocytes and plasma cells in both acute humoral and cellular liver allograft rejection to a different extent.

The analysis of the IgV-gene repertoire had a great impact in the understanding of B-cell responses in various inflammatory and autoimmune diseases [6, 8, 12] but had never been applied to liver allograft rejection. It has been applied to other organ transplants; however, only xenotransplantations have been examined [17], and no data exist on the IgV-gene repertoires of B-cells in allografts.

HLR is mostly triggered by anti-donor blood group A/B antibodies and C3c deposits. The latter were demonstrated in the sinusoidal lumina, which indicates a complement-mediated destruction of liver parenchyma [5]. Immunohistochemical studies of CLR biopsies showed that B lymphocytes and plasma cells accumulate in the portal tracts, and C4d deposits are found along the capillaries in cases with high RAI scores, whereas transplant biopsies without rejection show hardly any infiltrating B cells or plasma cells [7]. Furthermore, B-cell-activating chemokines were detected using PCR in liver biopsies of CLR, both indicating that, in addition to T lymphocytes, intrahepatic B cells might be involved in acute CLR.

Our analysis of the V-gene repertoire in two patients after orthotopic liver transplantation provides, for the first time, evidence for the hypothesis that B cells and plasma cells might be specifically involved in the pathogenesis of CLR and HLR. This is supported by the accumulation of B-cell clones, expressing a restricted V-gene repertoire and having a selected pattern of somatic mutations. The finding of identical rearrangements, which differed from each other by up to 23 somatic mutations (clone d, Table 2), speaks for antigen activation of B cells and a clonal expansion within the liver tissue. Such clonal expansion was not found in control tissue from a liver transplant without signs of rejection. Since no lymphatic follicles could be detected in both CLR and HLR biopsies, it seems that an antigen-selected migration is responsible for B-cell and plasma cell colonization of portal fields in CLR and HLR.

This is the first experimental evidence that B cells might be specifically involved in human liver allograft rejection. In xenotransplants, a high number of replacement mutations in the CDRs have been found, providing evidence for the role of somatic mutations in the maturation of IgG xenoantibodies [17]. This is well in line with our findings, since the majority of the somatically highly mutated immunoglobulin genes belonged to the IgG isotype. Clonally expanded B cells in the portal fields may contribute to liver tissue rejection either by the ability of B cells to present antigens [10] or by immunoglobulin-mediated complement activation.

It is unknown, exactly, which antigens induce this B-cell response, although HLA antigens appear to be the most relevant antigens in HLR [5]. Since the antigens responsible for HLR and CLR are still enigmatic, the clarification of intrahepatic B-lymphocyte and plasma cell specificity by recombinant expression of IgV_H/V_L genes could help to identify rejection-specific antigens. Antigens responsible for liver allograft rejection may be defined in this way and, thus, may open new avenues for diagnostics and immunotherapy.

Acknowledgements The excellent technical assistance of Ms. Gabriele Fernahl and Ms. Janine Karle is gratefully acknowledged. This work was supported by the SFB 421. The Deutsches Rheumaforschungszentrum is supported by the Berlin Senate of Research and Education.

References

1. Demetris AJ, Jaffe R, Tzakis A, Ramsey G, Todo S, Belle S, Esquivel C, Shapiro R, Markus B, Mroczek E (1988) Antibody-mediated rejection of human orthotopic liver allografts. A study of liver transplantation across ABO blood group barriers. Am J Pathol 132:489–502
2. Demetris A, Adams D, Bellamy C, Blakolmer K, Clouston A, Dhillon AP, Fung J, Gouw A, Gustafsson B, Haga H, Harrison D, Hart J, Hubscher S, Jaffe R, Khettry U, Lassman C, Lewin K, Martinez O, Nakazawa Y, Neil D, Pappo O, Parizhskaya M, Randhawa P, Rasoul-Rockenschaub S, Reinholt F, Reynes M, Robert M, Tsamandas A, Wanless I, Wiesner R, Wernerson A, Wrba F, Wyatt J, Yamabe H (2000) Update of the International Banff Schema for Liver Allograft Rejection: working recommendations for the histopathologic staging and reporting of chronic rejection. An International Panel. Hepatology 31:792–799
3. Dollinger MM, Howie SE, Plevris JN, Graham AM, Hayes PC, Harrison DJ (1998) Intrahepatic proliferation of "naive" and "memory" T cells during liver allograft rejection: primary immune response within the allograft. FASEB J 12:939–947
4. Dubel L, Farges O, Johanet C, Sebagh M, Bismuth H (1998) High incidence of antitissue antibodies in patients experiencing chronic liver allograft rejection. Transplantation 65:1072–1075
5. Haga H, Egawa H, Shirase T, Miyagawa A, Sakurai T, Minamiguchi S, Yamabe H, Manabe T, Tanaka K (2004) Periportal edema and necrosis as diagnostic histological features of early humoral rejection in ABO-incompatible liver transplantation. Liver Transpl 10:16–27
6. Kim HJ, Krenn V, Steinhauser G, Berek C (1999) Plasma cell development in synovial germinal centers in patients with rheumatoid and reactive arthritis. J Immunol 162:3053–3062
7. Krukemeyer MG, Moeller J, Morawietz L, Rudolph B, Neumann U, Theruvath T, Neuhaus P, Krenn V (2004) Description of B-lymphocytes and plasma cells, complement and chemokines/receptors in acute liver allograft rejection. Transplantation 78:65–70
8. Magalhaes R, Stiehl P, Morawietz L, Berek C, Krenn V (2002) Morphological and molecular pathology of the B-cell response in synovitis of rheumatoid arthritis. Virchows Arch 441:415–427
9. Michaels PJ, Fishbein MC, Colvin RB (2003) Humoral rejection of human organ transplants. Springer Semin Immunopathol 25:119–140
10. Mitchison NA (2004) T-cell-B-cell cooperation. Nat Rev Immunol 4:308–312
11. Neumann UP, Guckelberger O, Langrehr JM, Lang M, Schmitz V, Theruvath T, Schonemann C, Menzel S, Klupp J, Neuhaus P (2003) Impact of human leukocyte antigen matching in liver transplantation. Transplantation 75:132–137
12. Stott DI, Hiepe F, Hummel M, Steinhauser G, Berek C (1998) Antigen-driven clonal proliferation of B cells within the target tissue of an autoimmune disease. The salivary glands of patients with Sjogren's syndrome. J Clin Invest 102:938–946
13. Takakura K, Kiuchi T, Kasahara M, Inomata Y, Tanaka K (1999) Humoral immunity in acute cellular rejection after living-donor liver transplantation. Transplant Proc 31:526–527
14. Tannapfel A, Geissler F, Witzigmann H, Hauss J, Wittekind C (2001) Analysis of liver allograft rejection related genes using cDNA-microarrays in liver allograft specimen. Transplant Proc 33:3283–3284
15. Vella JP, Magee C, Vos L, Womer K, Rennke H, Carpenter CB, Hancock W, Sayegh MH (1999) Cellular and humoral mechanisms of vascularized allograft rejection induced by indirect recognition of donor MHC allopeptides. Transplantation 1999 67:1523–1532
16. Weigert M (1986) The influence of somatic mutation on the immune response. Prog Immunol VI: 138–142
17. Wu GD, Gochi E, Jin YS, Swensson J, Starnes VA, Cramer DV (2001) Maturation of xenoantibody gene expression during the humoral immune response of rats to hamster xenografts. Xenotransplantation 8:291–302

Virchows Arch (2005) 446: 333–337
DOI 10.1007/s00428-004-1192-0

CASE REPORT

Corwyn Rowsell · Jane Sirbovan · Marc K. Rosenblum · Bayardo Perez-Ordoñez

Primary chordoid meningioma of lung

Received: 5 October 2004 / Accepted: 2 December 2004 / Published online: 16 February 2005
© Springer-Verlag 2005

Abstract Primary meningiomas of the lung are rare. Most pulmonary meningiomas are typical syncytial or transitional meningiomas with smaller numbers of fibrous-type tumors. Herein, we report an unusual pulmonary tumor with the microscopic, immunohistochemical, and ultrastructural characteristics of a chordoid meningioma. The tumor was composed of cords and fascicles of small- to medium-sized spindle and epithelioid cells with eosinophilic cytoplasm and round nuclei with finely dispersed chromatin. The tumor cells were surrounded by an abundant mucoid, vacuolated stroma. The periphery of the tumor was enveloped by a significant lymphoplasmacytic infiltrate. The neoplastic cells were positive for vimentin and epithelial membrane antigen only. The unusual morphology of the tumor caused significant diagnostic difficulties. The differential diagnosis included inflammatory myofibroblastic tumor, spindle cell myoepithelioma, and extraskeletal myxoid chondrosarcoma. To the best of our knowledge, this is possibly the first description of an extracranial or intrapulmonary chordoid meningioma.

Keywords Lung · Meningioma · Chordoid meningioma

C. Rowsell · B. Perez-Ordoñez (✉)
Department of Pathology, University Health Network,
Princess Margaret Hospital,
610 University Avenue,
Toronto, Ontario , M4N 3M5, Canada
e-mail: bayardo.perez-ordonez@uhn.on.ca
Tel.: +1-416-9462104
Fax: +1-416-9466579

C. Rowsell · B. Perez-Ordoñez
Department of Pathobiology and Laboratory Medicine,
University of Toronto,
Ontario, Canada

J. Sirbovan
Department of Pathology, The Scarborough Hospital,
Toronto, Ontario, Canada

M. K. Rosenblum
Department of Pathology, Memorial Sloan-Kettering
Cancer Center,
New York, New York, USA

Introduction

In this report, we describe an unusual pulmonary neoplasm with the morphological features of a chordoid meningioma. Primary pulmonary meningiomas are rare tumors. They were initially recognized by Erlandson [8], with approximately 20 or so cases subsequently described as single case reports or small series [2, 4, 6, 7, 9, 12, 14, 15, 17, 19, 21, 22]. Most cases of primary pulmonary meningioma have been typical syncytial or transitional meningiomas with smaller numbers of fibrous meningiomas [12, 14, 16].

Chordoid meningioma is an uncommon variant of meningothelial neoplasm first recognized by Kepes in 1988 [13]. Chordoid meningiomas constitute approximately 0.5% of all meningiomas [5]; microscopically, they resemble chordomas and are characterized by featuring spindle and epithelioid cells in clusters and cords with a mucoid or myxoid matrix. The tumor cells often show a vacuolated cytoplasm. Typically, the tumors are associated with a variable lymphoplasmacellular infiltrate [5]. Steilen-Gimbel et al. [20] described an unbalanced translocation *t*(1;3)(p12–13;q11) as a unique feature of chordoid meningiomas [20]. This is possibly the first report of an extracranial or primary pulmonary chordoid meningioma. A computer search of the National Library of Medicine/Pub Med database revealed no previous reports of extracranial or intrapulmonary chordoid meningiomas.

Case report

The patient is a previously healthy 51-year-old male with an asymptomatic right lower lung mass. The tumor was discovered on a routine chest X-ray performed as part of a general physical examination by his family doctor. Subsequent bronchoscopy and a chest computed tomography scan demonstrated a 4.0 cm mass, which was partially obstructing the right lower lobe. The patient underwent a lobectomy. Subsequent investigations revealed no evidence of extrapulmonary disease. He remains well and free of disease 8 months after surgery.

Fig. 1 Surgical specimen showing a multinodular mass with glistening surface adjacent to bronchus

Pathological findings

The surgical specimen showed a 4.0-cm, tan-white mass surrounding the proximal right lower lobe bronchus. The tumor grew along the bronchial tree into segmental bronchi. The tumor was well circumscribed and multilobulated and exhibited a glistening surface (Fig. 1).

The specimen was fixed in neutral, buffered formalin, routinely processed, with tissue sections embedded in paraffin. The sections were cut 4 μm thick and were stained with hematoxylin and eosin. Representative sections were also stained with Mayer's mucicarmine, periodic acid-Schiff (PAS), and PAS-D. Immunohistochemical stains were performed with the antibodies listed in Table 1. Tissue for electron microscopy was fixed in universal fixative, routinely processed, stained with uranyl acetate, and examined in a JEOL 1200 electron microscope.

The tumor was predominantly composed of cords and fascicles of small- to medium-sized spindle and epithelioid cells with pale eosinophilic cytoplasm and round nuclei with finely dispersed chromatin and inconspicuous nucleoli (Fig. 2). Numerous cytoplasmic vacuoles were present. The tumor cells were surrounded by an abundant pale eosinophilic mucoid stroma, often with large vacuoles. The periphery of the tumor was surrounded by sheets and nodules of plasma cells and small round lymphocytes with no cytological atypia (Fig. 3). Small areas of the tumor showed ill-defined nodules resembling whorls of a more typical transitional meningioma (Fig. 4A). Clusters of macrophages and histiocytes with foamy, reticular cytoplasm were frequently seen. A significant portion of the tumor was intrabronchial and demonstrated focal destruction of the bronchial cartilage. No cytological atypia, mitotic activity, or necrosis was present.

The tumor cells were diffusely positive for epithelial membrane (EMA) (Fig. 4B) and vimentin. They were negative for keratins (AE1/AE3, cam 5.2), keratin 14, keratin 19, 34βE12, S-100, smooth-muscle actin, muscle-specific actin, desmin, calponin, p63, CD34, chromogranin, synaptophysin, and glial fibrillary acid protein.

Ultrastructurally, the tumor cells demonstrated features consistent with a meningioma. The cells showed elongated interdigitating cytoplasmic processes joined by small ill-formed cell junctions (Fig. 5). The tumor cells were surrounded by amorphous material. No basement membrane was seen. Inflammatory cells were present.

Discussion

Primary pulmonary meningiomas are uncommon but well-recognized neoplasms [2, 4, 6, 9, 12, 14, 15, 17, 19, 21, 22]. Most reported cases have been typical syncytial or transitional-type meningiomas with smaller numbers of fibrous meningiomas [12, 14, 16]. Some exceedingly rare cases of primary malignant pulmonary meningiomas have also been described [8, 17]. In this report, we described a peculiar pulmonary neoplasm with the morphological and immunohistochemical features of chordoid meningioma [5, 13]. The tumor was composed of epithelioid and

Table 1 Antibodies used

Antibody	Clone	Source	Dilution
Vimentin	Vim 3β4	American Research Products	1/200
AE1/AE3		Dakocytomation	1/500
Cam 5.2		Becton Dickinson	1/50
Epithelial membrane antigen	MC5	Ventana	Prediluted
34βE12		Ventana	Prediluted
Keratin 14	LL002	Novocastra	1/100
Keratin 19	B170	Novocastra	1/250
Glial fibrillary acid protein		Ventana	Prediluted
S-100		Dakocytomation	1/2000
Smooth-muscle actin	1A4	Ventana	Prediluted
Muscle-specific actin	HHF35	Dakocytomation	1/100
Desmin	D33	Dakocytomation	1/200
Calponin		Dakocytomation	1/100
p63	7JUL	Novocastra	1/15000
CD34	QBEND10	Dakocytomation	1/1000
Chromogranin	LK2H/0	Biomeda	1/400
Synaptophysin		Ventana	Prediluted

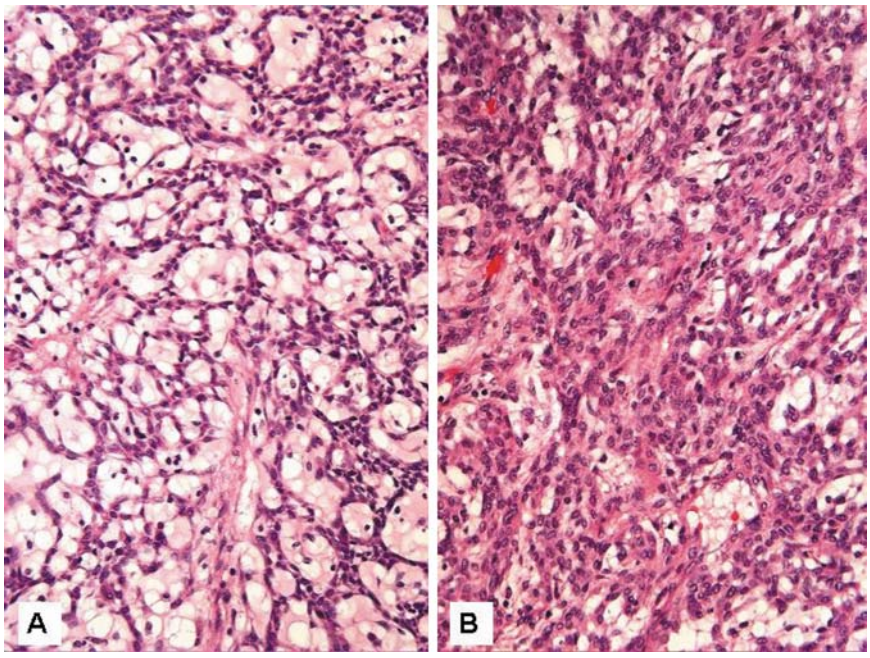

Fig. 2 Chordoid meningioma with spindle cells arranged in cords and surrounded by abundant mucoid material (**A**). Cellular areas of pulmonary chordoid meningioma with spindle cells with eosinophilic cytoplasm

spindle cells arranged in cords surrounded by abundant pale mucoid matrix. The periphery of the tumor was enveloped by an abundant infiltrate composed of small lymphocytes and plasma cells. Chordoid meningioma is an uncommon variant of meningioma first recognized by Kepes in 1988 [13]. This is possibly the first report of an extracranial or primary pulmonary chordoid meningioma.

The diagnosis of pulmonary chordoid meningioma presented considerable diagnostic difficulties. The main differential diagnoses considered in our case were: inflammatory myofibroblastic tumor (IMT), spindle cell myoepithelioma of the lung, and extraskeletal myxoid chondrosarcoma (EMC). IMT was the most difficult lesion to exclude from the differential diagnosis. However, IMT is a neoplasm composed of fibroblasts and myofibroblasts showing variable expression of actins and desmin [3]. In contrast, the tumor reported herein demonstrated a significantly different phenotype with absent expression for actins, desmin, and calponin and positive immunoreactivity for EMA. A pulmonary spindle cell myoepithelioma [23] was also a strong diagnostic consideration. However, spindle cell myoepitheliomas lack the distinct inflammatory component seen in this tumor. Furthermore, they typically demonstrate dual epithelial and muscle differentiation with expression of various keratins and muscle markers [18]; these markers were negative in this patient's tumor. EMC

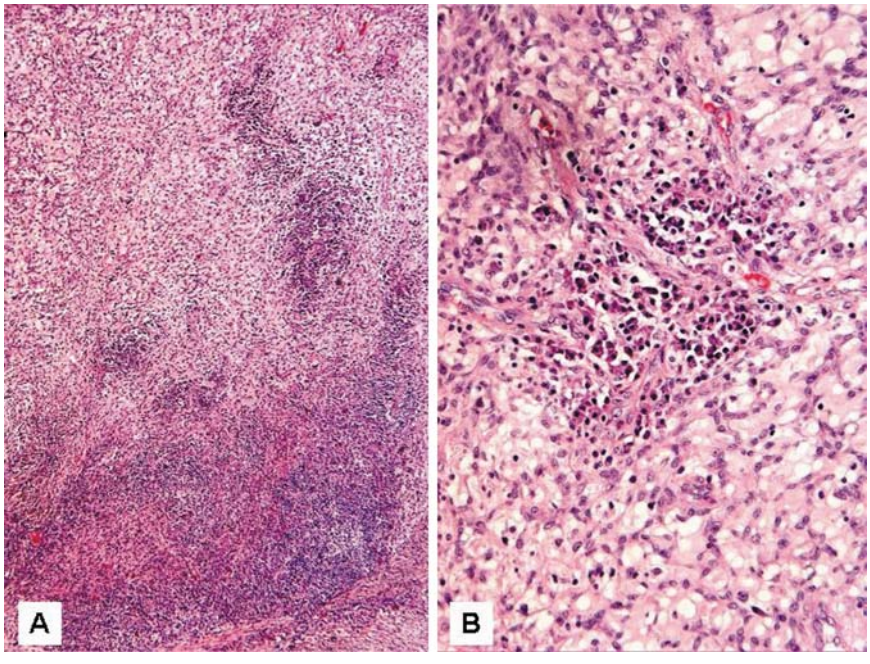

Fig. 3 The tumor was surrounded by lymphocytes and plasma cells (**A**). Clusters of plasma cells admixed with tumor cells (**B**)

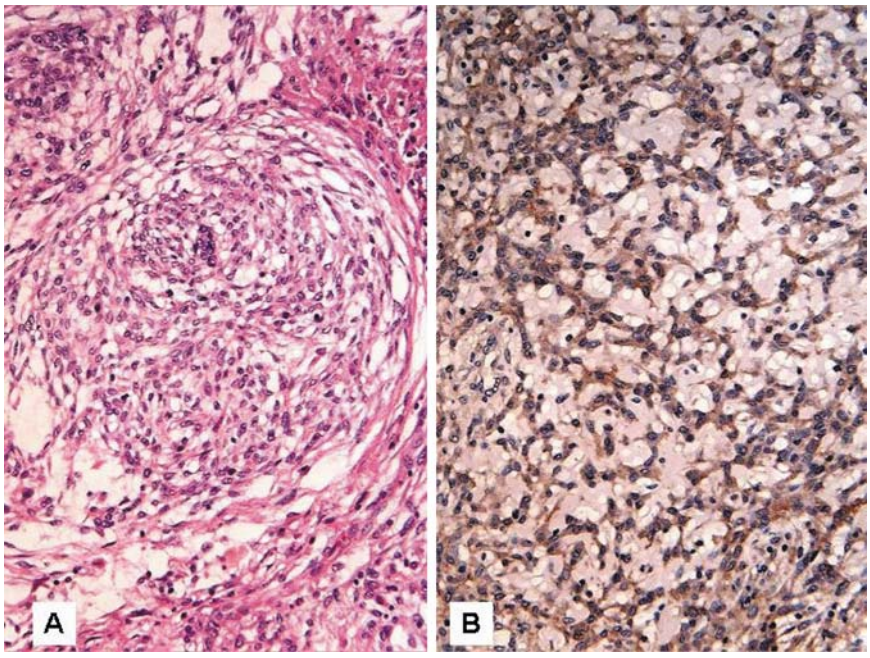

Fig. 4 Spindle cells arranged in a meningothelial nodule (**A**). This was a focal finding. Tumor cells with positive expression of epithelial membrane antigen (EMA) (**B**)

is a low-grade sarcoma occurring mainly in extremities and less commonly in head and neck [1]. These tumors often show neuroendocrine differentiation [10]. We excluded the possibility of EMC in our patient based on the absence of extrapulmonary disease, the inflammatory infiltrate present in the tumor, the spindle cell component—usually not present in most ECM—and the absence of neuroendocrine differentiation.

The origin of primary pulmonary meningiomas remains unknown. Ectopic embryonic rests of meningothelial, meningothelial differentiation of pluripotential stem cells, and the so-called minute pulmonary meningothelial-like nodule (MPMN) have been proposed as putative precursors of pulmonary meningiomas [16, 19]. It appears unlikely that MPMNs are related to pulmonary meningiomas, since the coexistence of pulmonary meningioma and MPMNs in the same patient has only rarely been reported [19]. Furthermore, a recent study comparing the mutational genotype of MPMNs and primary intracranial, spinal, and sinonasal meningiomas found that genetic abnormalities on chromosomes 22q, 14q, and 1p were common in meningiomas; whereas, they were absent in MPMNs [11]. In conclusion, it appears that despite morphological, immunohistochemical, and ultrastructural similarities, MPMNs are unlikely to represent precursors lesions of pulmonary meningiomas.

In summary, we report an unusual pulmonary neoplasm with the pathological features of a chordoid meningioma. Recognition of these neoplasms in extracranial locations

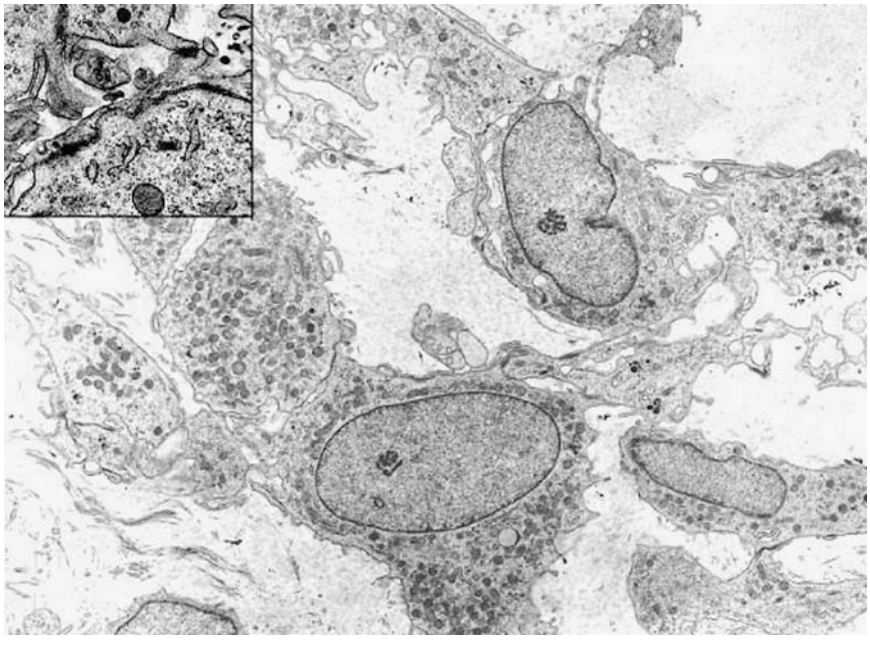

Fig. 5 Electron microscopy shows that the tumor was composed of spindle and stellate cells with elongated cell processes joined by poorly formed cell junctions (*inset*). The cytoplasm contains abundant mitochondria, rough endoplasmic reticulum, and occasional lipid vacuoles. The extracellular matrix consists of amorphous material with scanty collagen (×8000)

requires familiarity with their morphological features, a high index of suspicion, and the use of appropriate immunohistochemical and ultrastructural studies. The long-term prognosis of this tumor is unknown; although most primary pulmonary meningiomas have behaved in a benign manner with only isolated examples of malignant tumors. The long-term prognosis of intracranial chordoid meningiomas still remains controversial. Couce et al. [5] reported a recurrence rate of 39%; however, all but one of these tumors had undergone subtotal resection. The tumor in our patient appears completely resected.

References

1. Antonescu CR, Argani P, Erlandson RA, Healey JH, Ladanyi M, Huvos AG (1998) Skeletal and extraskeletal myxoid chondrosarcoma: a comparative clinicopathologic, ultrastructural, and molecular study. Cancer 83:1504–1521
2. Cesario A, Galetta D, Margaritora S, Granone P (2002) Unsuspected primary pulmonary meningioma. Eur J Cardiothorac Surg 21:553–555
3. Coffin CM, Humphrey PA, Dehner LP (1998) Extrapulmonary inflammatory myofibroblastic tumor: a clinical and pathological survey. Semin Diagn Pathol 15:85–101
4. Comin CE, Caldarella A, Novelli L, Janni A (2003) Primary pulmonary meningioma: report of a case and review of the literature. Tumori 89:102–105
5. Couce ME, Aker FV, Scheithauer BW (2000) Chordoid meningioma: a clinicopathologic study of 42 cases. Am J Surg Pathol 24:899–905
6. de Perrot M, Kurt AM, Robert J, Spiliopoulos A (1999) Primary pulmonary meningioma presenting as lung metastasis. Scand Cardiovasc J 33:121–123
7. Drlicek M, Grisold W, Lorber J, Hackl H, Wuketich S, Jellinger K (1991) Pulmonary meningioma. Immunohistochemical and ultrastructural features. Am J Surg Pathol 15:455–459
8. Erlandson RA (1981) Diagnostic transmission electron microscopy of human tumors. Masson Publishing, New York
9. Flynn SD, Yousem SA (1991) Pulmonary meningiomas: a report of two cases. Hum Pathol 22:469–474
10. Goh YW, Spagnolo DV, Platten M, Caterina P, Fisher C, Oliveira AM, Nascimento AG (2001) Extraskeletal myxoid chondrosarcoma: a light microscopic, immunohistochemical, ultrastructural and immuno-ultrastructural study indicating neuroendocrine differentiation. Histopathology 39:514–524
11. Ionescu DN, Sasatomi E, Aldeeb D, Omalu BI, Finkelstein SD, Swalsky PA, Yousem SA (2004) Pulmonary meningothelial-like nodules: a genotypic comparison with meningiomas. Am J Surg Pathol 28:207–214
12. Kaleem Z, Fitzpatrick MM, Ritter JH (1997) Primary pulmonary meningioma. Report of a case and review of the literature. Arch Pathol Lab Med 121:631–636
13. Kepes JJ, Chen WY, Connors MH, Vogel FS (1988) "Chordoid" meningeal tumors in young individuals with peritumoral lymphoplasmacellular infiltrates causing systemic manifestations of the Castleman syndrome. A report of seven cases. Cancer 62:391–406
14. Lockett L, Chiang V, Scully N (1997) Primary pulmonary meningioma: report of a case and review of the literature. Am J Surg Pathol 21:453–460
15. Maiorana A, Ficarra G, Fano RA, Spagna G (1996) Primary solitary meningioma of the lung. Pathologica 88:457–462
16. Moran CA, Hochholzer L, Rush W, Koss MN (1996) Primary intrapulmonary meningiomas. A clinicopathologic and immunohistochemical study of ten cases. Cancer 78:2328–2333
17. Prayson RA, Farver CF (1999) Primary pulmonary malignant meningioma. Am J Surg Pathol 23:722–726
18. Savera AT, Zarbo RJ (2004) Defining the role of myoepithelium in salivary gland neoplasia. Adv Anat Pathol 11:69–85
19. Spinelli M, Claren R, Colombi R, Sironi M (2000) Primary pulmonary meningioma may arise from meningothelial-like nodules. Adv Clin Pathol 4:35–39
20. Steilen-Gimbel H, Niedermayer I, Feiden W, Freiler A, Steudel WI, Zang KD, Henn W (1999) Unbalanced translocation t(1;3)(p12–13;q11) in meningiomas as the unique feature of chordoid differentiation. Genes Chromosomes Cancer 26:270–272
21. Strimlan CV, Golembiewski RS, Celko DA, Fino GJ (1988) Primary pulmonary meningioma. Surg Neurol 29:410–413
22. Ueno M, Fujiyama J, Yamazaki I, Uchiyama T, Ishikawa Y, Satoh Y (1998) Cytology of primary pulmonary meningioma. Report of the first multiple case. Acta Cytol 42:1424–1430
23. Veeramachaneni R, Gulick J, Halldorsson AO, Van TT, Zhang PL, Herrera GA (2001) Benign myoepithelioma of the lung: a case report and review of the literature. Arch Pathol Lab Med 125:1494–1496

Virchows Arch (2005) 446: 338–341
DOI 10.1007/s00428-004-1199-6

CASE REPORT

A. M. Luebke · T. Schlomm · B. Gunawan ·
H. Bonkhoff · L. Füzesi · A. Erbersdobler

Simultaneous tumour-like, atypical basal cell hyperplasia and acinar adenocarcinoma of the prostate: a comparative morphological and genetic approach

Received: 19 October 2004 / Accepted: 6 December 2004 / Published online: 22 February 2005
© Springer-Verlag 2005

Abstract Basal cell tumours of the prostatic gland are rare, and the classification is difficult. In the present case report, a large, tumour-like proliferation of atypical basaloid cells was found incidentally in a prostatectomy specimen that otherwise contained a conventional acinar adenocarcinoma. The basaloid cells displayed a solid or adenoid-cystic growth pattern and strongly expressed high-molecular-weight cytokeratins and bcl-2. A high Ki-67 index was recorded within the atypical basaloid cells, by far exceeding the one counted in the conventional adenocarcinoma. However, there were no definite criteria for a malignant behaviour of the basal cell tumour. Comparative genomic hybridisation from microdissected tumour cells yielded losses at the short arms of chromosomes 8 and 12 in the conventional adenocarcinoma and a normal karyotype in the basal cell tumour. The pathological findings favoured the diagnosis of an atypical basal cell hyperplasia.

Keywords Prostatic neoplasms · Basal cell tumour · Comparative genomic hybridisation

A. M. Luebke · T. Schlomm
Department of Urology, University of Hamburg, Germany

B. Gunawan · L. Füzesi
Institute of Pathology, University of Göttingen, Germany

H. Bonkhoff
Institute of Pathology, Berlin, Germany

A. Erbersdobler (✉)
Institute of Pathology
University Hospital Hamburg-Eppendorf,
Martinistrasse 52,
22081 Hamburg, Germany
e-mail: erbersdo@uke.uni-hamburg.de
Tel.: +49-40-428036513
Fax: +49-40-428035038

Introduction

Conventional acinar adenocarcinoma is the single most important entity among prostatic malignancies, comprising more than 90% of neoplasms in this gland. Nowadays, these tumours are thought to derive from basal reserve cells and differentiate towards secretory prostatic epithelial cells. However, rare carcinomas can also differentiate towards the other epithelial cell types existing in the prostate [5, 14]. Primary small cell carcinomas or prostatic carcinoids are histogenetically related to endocrine cells in the prostate, and transitional cell carcinomas resemble epithelium lining the large prostatic ducts. The spectrum of tumours and tumour-like lesions with primary basaloid features ranges from focal basal cell hyperplasia to basal cell carcinoma [3, 4, 8]. However, the terminology of basal cell proliferations is confusing, and criteria defining malignancy within this entity are ill-defined. In the present case report, a large, incidental, tumour-like basal cell hyperplasia was found in a prostatectomy specimen, together with a conventional acinar adenocarcinoma, thus allowing for comparative morphological and genetic investigations.

Clinical history

A 59-year-old patient underwent a radical prostatectomy due to a biopsy-confirmed, acinar prostatic carcinoma. The patient had no previous medical history, except for an umbilical hernia. He denied any significant lower urinary tract voiding symptoms. Urine analysis showed no evidence of hematuria or urinary tract infection. The total prostate-specific antigen (PSA) level was 4.03 ng/ml, with a free-PSA fraction of 0.84 ng/ml and a free/total-PSA percentage of 20.84%. The digital rectal and transrectal ultrasound examinations revealed a 70-g prostate with suspicion for a T2a-stage prostate carcinoma, affecting the right lobe. A ten-core ultrasound-guided prostate biopsy proved a moderately differentiated adenocarcinoma (Gleason score 3+3) in the basal and middle portion of the right lobe.

After risk stratification using preoperative nomograms [7], the patient opted for a bilateral nerve-sparing radical retropubic prostatectomy without pelvic lymph-node dissection.

Materials and methods

The prostatectomy specimen weighed 76 g and was completely embedded for histological investigations according to the Stanford protocol [13]. Briefly, after separation of apex, base and seminal vesicles, the trunk of the prostate gland was sectioned in 3- to 5-mm steps. Paraffin sections, 5 µm in thickness, were routinely stained with haematoxylin and eosin. Selected sections were stained with astra-blue and periodic acid-Schiff's reagent (PAS) or subjected to immunohistochemistry using the alkaline phosphatase anti-alkaline phosphatase method. The following primary antibodies were employed: PSA (clone ER-PR8; Linaris, Wertheim-Bettingen, Germany), high-molecular-weight cytokeratin (clone 34βE12; Enzo Diagnostics, Farmingdale, NY, USA), Ki-67 (clone Mib-1; Dianova, Hamburg, Germany), bcl-2 (clone 124; Dako, Glostrup, Denmark), oestrogen receptor (clone 1D5; Dako) and progesterone receptor (clone PR10A9; Immunotech, Marseille, France). The expression of PSA, high-molecular-weight cytokeratin, bcl-2, oestrogen receptor and progesterone receptor was assessed semiquantitatively (0, +, ++, +++). The percentage of tumour cells expressing the Ki-67 antigen was evaluated by counting at least 1000 cells in "hot-spot areas".

Tumour areas were marked on the histological sections by a water-resistant pen. Volumes of both distinct tumours were measured separately by computer-assisted planimetry multiplied with the thickness of tissue blocks and corrected for fixation shrinkage by a factor of 1.5 [13].

Microdissection of tumour cells was performed on membrane bound, haematoxylin and eosin-stained slides using the PALM MicroLaser system (P.A.L.M. Bernried, Germany). Microdissection yielded approximately 150–300 tumour cells, which has been shown in previous experiments to be sufficient material for the following investigations [15]. DNA extraction from microdissected material and whole genome amplification was also performed as previously described [15].

Comparative genomic hybridisation (CGH) was performed essentially as described [10]. For each analysis, the averaged chromosome-specific green-to-red fluorescence ratios from at least ten well-selected metaphases were plotted using the Quips CGH software (Applied Imaging, Newcastle, UK). Relative copy number changes were interpreted as gains when the average green-to-red ratio exceeded 1.2 (1.5 for amplifications) and as losses when the corresponding ratio was less than 0.8.

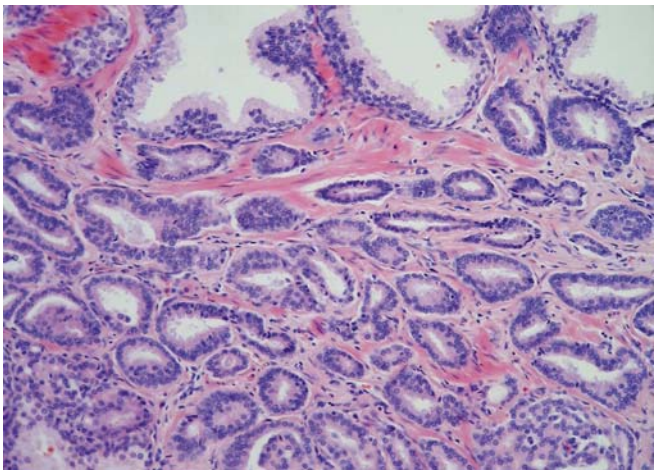

Fig. 1 Conventional acinar adenocarcinoma (Gleason 3+3) in the peripheral zone. Haematoxylin & eosin, original magnification ×250

Results

Pathological findings

Histological investigation of the prostatectomy specimen confirmed the conventional prostatic adenocarcinoma, consisting of small, tubular proliferations (Fig. 1). The tumour cells strongly expressed PSA but not high-molecular-weight cytokeratins or bcl-2. Immunohistochemistry with an antibody against the Ki-67 antigen disclosed a proliferation rate of 2.6%. Tumour foci were located in the peripheral zones on both sides. Total tumour volume of these foci was calculated as 1.518 cm^3.

However, in the medial areas of the gland, there were also atypical proliferations of basaloid cells in irregular nests with peripheral palisading. The cells showed nuclear crowding with frequent mitoses and discernible nucleoli (Fig. 2). Focal squamous metaplasia with discrete keratinisation was present (Fig. 3, left). Furthermore, some basaloid proliferations were made of cribriform glands with "punched-out"

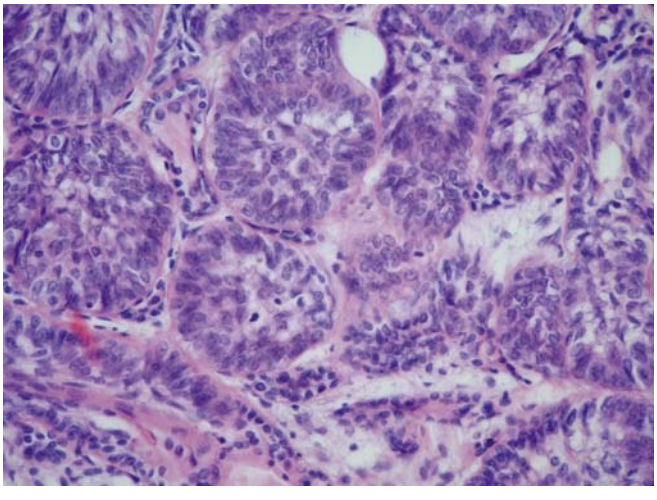

Fig. 2 Atypical basal cell hyperplasia with solid nests of basaloid cells. Haematoxylin & eosin, original magnification ×400

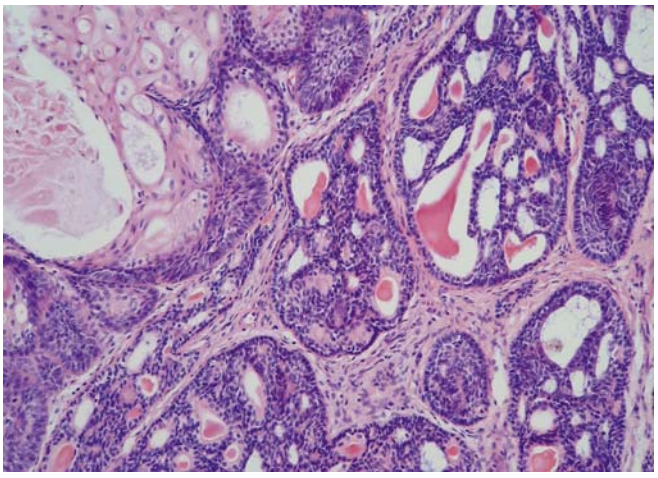

Fig. 3 Atypical basal cell hyperplasia with squamoid metaplasia (*left*) and adenoid-cystic growth pattern (*right*). Haematoxylin & eosin, original magnification ×250

spaces filled with PAS-positive material, thus giving an adenoid-cystic carcinoma-like appearance (Fig. 3, right). However, perineural invasion, necrosis or extraprostatic extension was not evident. A cellular, sometimes myxoid stroma surrounded the epithelial nests. The atypical basaloid cells strongly expressed high-molecular-weight cytokeratins (Fig. 4) and bcl-2. A high proliferation rate of 10.2% was recorded. Only a focal and weak expression of PSA was present at the interface between the atypical basaloid proliferations and normal prostate glands. This basal cell tumour measured 8.871 cm^3. There was no extraprostatic extension or seminal vesicle invasion. All margins of resection were free of tumour cells.

CGH profile obtained from microdissected tumour cells from the conventional, acinar adenocarcinoma displayed losses of genetic material at the short arms of chromosomes 8 and 12, respectively. However, amplified DNA from microdissected basaloid tumour cells generated a normal karyotype by means of CGH.

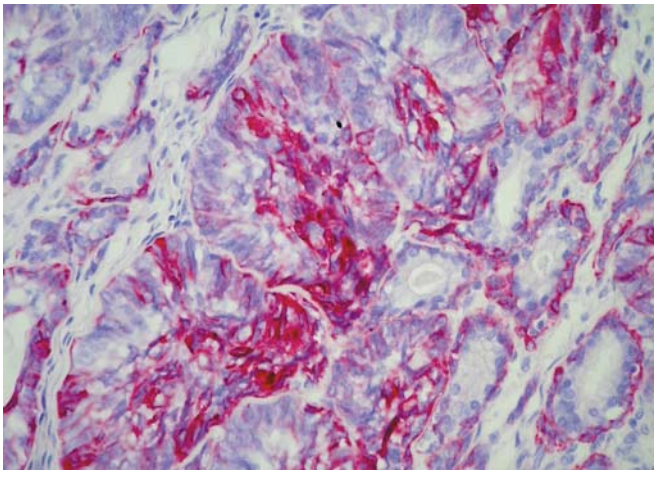

Fig. 4 Atypical basal cell hyperplasia with expression of high-molecular-weight cytokeratins. Immunohistochemistry with the antibody 34βE12; alkaline phosphatase anti-alkaline phosphatase method; original magnification ×400

Table 1 Results of morphological and genetic analyses. *0* no expression, + weak focal expression, ++ weak diffuse or intense focal expression, +++ intense diffuse expression

	Atypical basal cell tumour	Conventional acinar adenocarcinoma
Location	Transition zone	Peripheral zone
Tumour volume	8.871 cm^3	1.518 cm^3
Prostate-specific antigen	+	+++
High-molecular-weight CK	++	0
Bcl-2	++	0
Oestrogen receptor	0	0
Progesterone receptor	0	0
Ki-67 index	10.2%	2.6%
Comparative genomic hybridisation results	Normal karyotype	−8p; −12p

A diagnosis of conventional prostatic adenocarcinoma, Gleason 3+3, and a concomitant, tumour-like, atypical basal cell hyperplasia was made. Table 1 gives a comparison of the morphological and genetic findings in both lesions.

Discussion

Prostatic basal cell proliferations exhibit a morphological continuum ranging from focal basal cell hyperplasia to basal cell carcinoma [3, 4, 6, 8]. Whereas a focal hyperplasia of basal cells can frequently be observed in the setting of benign hyperplasia, tumour-like proliferations or real neoplasms consisting of basal cells are rare. Furthermore, there is a confusing variety of terms, such as “fetalisation of the prostate”, “embryonal hyperplasia”, “adenoid basal cell tumour”, “basal cell adenoma”, and more. Adenoid cystic carcinoma in the prostate is now regarded a morphological variant of basal cell carcinoma [2].

As basal cell proliferations of the prostate do not contribute to the overall PSA serum level of the patient, these tumours are often detected incidentally in tissue specimens removed for benign hyperplasia or carcinoma. Sometimes, however, the basal cell tumour itself may be the reason for obstructive symptoms.

Definite histological criteria for malignancy in basal cell tumours include necrosis, perineural invasion, extraprostatic extension and metastasis. Nuclear atypia, prominent nucleoli, an infiltrative- or adenoid-cystic growth pattern, a high Ki-67 index, and a strong bcl-2 expression are considered further evidence for an aggressive behaviour by some authors [17]. However, there are no clear histological definitions for grouping basaloid tumours in distinct categories.

Clinically, most basal cell tumours of the prostate are supposed to have indolent biological potential. However, there are several reports on aggressive basal cell carcino-

mas with distant metastases and adverse clinical outcome [9, 12].

In the present case, no certain criteria for a malignant behaviour were present. We do not share the opinion of Yang et al. [17], who claim that a high Ki-67 index and bcl-2 expression are helpful in distinguishing malignant from benign basal cell tumours. In our opinion, basal cell proliferations typically display bcl-2 expression and a high Ki-67 index, as this cell type is believed to harbour the prostatic stem cell in the normal prostate. Therefore, it is not surprising that the basal cell tumour in the present case displayed an even higher Ki-67 index than the concomitant prostatic carcinoma. However, the infiltrative and adenoid-cystic growth pattern as well as some nuclear atypia in the present case justify the term "atypical, tumour-like hyperplasia" [6]. Another appropriate term would be "adenoid basal cell tumour", as proposed by Grignon et al. [8].

To our best knowledge, no systematic genetic analyses have been performed on basal cell tumours of the prostate. We analysed both the basal cell tumour and the conventional acinar adenocarcinoma of the present case with CGH. By use of laser microdissection, we could guarantee a clear separation between tumour and stromal cells of both tumour types. The conventional acinar carcinoma displayed losses of the short arms of chromosomes 8 and 12. Losses at 8p are one of the most common cytogenetical aberrations in prostate cancer and are believed to be an early event in prostate carcinogenesis [16, 18]. However, losses at 12p have been rarely reported in prostate carcinomas [1, 18]. When present, they are supposed to play a role in the progression of that disease [11].

In contrast to the conventional acinar carcinoma, the CGH from the basal cell tumour yielded a normal karyotype. However, CGH is a method for evaluating genetic alterations at the microscopic level, serving mostly as a sort of whole genome screening for chromosomal imbalances. Balanced chromosomal translocations cannot be detected by CGH at all. Therefore, by using this method, we cannot definitely exclude the presence of submicroscopic deletions, amplifications or other genetic or epigenetic alterations in the present case. It is also impossible to differentiate between a hyperplastic and a neoplastic process by the finding of a normal karyotype. Nevertheless, a normal CGH profile would be unusual for an overtly malignant tumour and rather supports the diagnosis of a tumour-like hyperplastic process. Further cases have to be investigated by means of clinics, morphology and molecular biology to reach a reliable classification of basal cell tumours of the prostate.

References

1. Alers JC, Krijtenburg PJ, Vis AN, Hoedemaeker RF, Wildhagen MF, Hop WC, van Der Kwast TT, Schroder FH, Tanke HJ, van Dekken H (2001) Molecular cytogenetic analysis of prostatic adenocarcinomas from screening studies: early cancers may contain aggressive genetic features. Am J Pathol 158:399–406
2. Cohen RJ, Goldberg RD, Verhaart MJS, Cohen M (1993) Adenoid cyst-like carcinoma of the prostate gland. Arch Pathol Lab Med 117:799–801
3. Denholm SW, Webb JN, Howard GCW, Chisholm GD (1992) Basaloid carcinoma of the prostate gland: histogenesis and review of the literature. Histopathology 20:151–155
4. Devaraj LT, Bostwick DG (1993) Atypical basal cell hyperplasia of the prostate. Immunophenotypic profile and proposed classification of basal cell proliferations. Am J Surg Pathol 17:645–659
5. Dhom G (1990) Unusual prostatic carcinomas. Pathol Res Pract 186:28–36
6. Epstein JI, Armas OA (1992) Atypical basal cell hyperplasia of the prostate. Am J Surg Pathol 16:1205–1214
7. Graefen M, Noldus J, Pichlmeier U, Haese A, Hammerer P, Fernandez S, Conrad S, Henke R, Huland E, Huland H (1999) Early prostate-specific antigen relapse after radical retropubic prostatectomy: prediction on the basis of preoperative and postoperative tumor characteristics. Eur Urol 36:21–30
8. Grignon DJ, Ro JY, Ordonez NG, Ayala AG, Cleary KR (1988) Basal cell hyperplasia, adenoid basal cell tumor, and adenoid cystic carcinoma of the prostate gland: an immunohistochemical study. Hum Pathol 19:1425–1433
9. Iczkowski KA, Ferguson KL, Grier DD, Hossain D, Banerjee SS, McNeal JE, Bostwick DG (2003) Adenoid cystic/basal cell carcinoma of the prostate: clinicopathologic findings in 19 cases. Am J Surg Pathol 27:1523–1529
10. Kallioniemi OP, Kallioniemi A, Piper J, Isola J, Waldman FM, Gray JW, Pinkel D (1994) Optimizing comparative genomic hybridization for analysis of DNA sequence copy number changes in solid tumors. Genes Chromosomes Cancer 10:231–243
11. Kibel AS, Huagen J, Guo C, Isaacs WB, Yan Y, Pienta KJ, Goodfellow PJ (2004) Expression mapping at 12p12-13 in advanced prostate carcinoma. Int J Cancer 109:668–672
12. Mastropasqua MG, Pruneri G, Renne G, De-Cobelli O, Viale G (2003) Basaloid cell carcinoma of the prostate. Virchows Arch 443:787–791
13. McNeal JE, Villers AA, Redwine EA, Freiha FS, Stamey TA (1990) Histologic differentiation, cancer volume, and pelvic lymph node metastasis in adenocarcinoma of the prostate. Cancer 66:1225–1233
14. Randolph TL, Amin MB, Ro JY, Ayala AG (1997) Histologic variants of adenocarcinoma and other carcinomas of prostate: pathologic criteria and clinical significance. Mod Pathol 10:612–629
15. Stoecklein NH, Erbersdobler A, Schmidt-Kittler O, Diebold J, Schardt JA, Izbicki JR, Klein CA (2002) SCOMP is superior to degenerated oligonucleotide primed-polymerase chain reaction for global amplification of minute amounts of DNA from microdissected archival tissue samples. Am J Pathol 161:43–51
16. Visakorpi T, Kallioniemi AH, Syvanen AC, Hyytinen ER, Karhu R, Tammela T, Isola JJ, Kallioniemi OP (1995) Genetic changes in primary and recurrent prostate cancer by comparative genomic hybridization. Cancer Res 55:342–347
17. Yang XJ, McEntee M, Epstein JE (1998) Distinction of basaloid carcinoma of the prostate from benign basal cell lesions by using immunohistochemistry for bcl-2 and Ki-67. Hum Pathol 28:1447–1450
18. Zitzelsberger H, Engert D, Walch A, Kulka U, Aubele M, Hofler H, Bauchinger M, Werner M (2001) Chromosomal changes during development and progression of prostate adenocarcinomas. Br J Cancer 84:202–208

Virchows Arch (2005) 446: 342–343
DOI 10.1007/s00428-004-1162-6

LETTER TO THE EDITOR

Simonetta Piana · Silvia Asioli

Blue nevus of the nasal mucosa

Received: 3 September 2004 / Accepted: 11 October 2004 / Published online: 25 January 2005
© Springer-Verlag 2005

Dear Editor,

Blue nevi are uncommon pigmented proliferations of melanocytes [5]. They can be solitary or multiple; although they mainly present in the skin, they have been reported in many other sites, such as breast, lymph node, orbit, and genital tract. They also have been found in mucosas, mainly conjunctiva, genital [6], and oral mucosa [4, 7]. In maxillary sinuses [1], they probably arise from melanocytes usually located in the epithelium and stroma of the respiratory mucosa [8, 9]. We describe a case of blue nevus of the nasal mucosa; as far as we know, it has never been previously reported in this location.

A 40-year-old man with chronic otitis presented for a routine clinical examination at the ear, nose, and throat department. His past medical history was unremarkable. The patient showed no unusual skin pigmentations. After a physical examination, no lesions were found except a single, small, intensely pigmented spot, 2 mm in greatest axis, on the nasal mucosa.

S. Piana (✉) · S. Asioli
Department of Pathology, Room 1.030,
Arcispedale Santa Maria Nuova,
Viale Risorgimento 80,
42100 Reggio Emilia, Italy
e-mail: Simonetta.piana@asmn.re.it
Tel.: +39-0522-295919
Fax: +39-0522-296945

An excisional biopsy of the spot was taken. The specimen was fixed in formalin, completely embedded in paraffin, and some 5-mm sections were cut. Routine hematoxylin and eosin stainings were performed, and immunohistochemistry was carried on according to standard protocols, using two commercially available antibodies (S100 protein and MART-1), together with positive controls.

Histologically, the lesion consisted of a relatively ill-defined proliferation of heavily pigmented cells, intermingled within the respiratory glands (Fig. 1). At higher power, the cells were polygonal, had round nuclei, and an abundant, melanin-laden cytoplasm (Fig. 1, insert). No mitotic figures were noted. On immunohistochemistry, these cells strongly reacted with S-100 protein and MART-1 (Fig. 2), even after bleaching. Morphological findings were consistent with a blue nevus arising in the respiratory mucosa of the nasal cavity.

Among differential diagnoses, a melanoma arising in nasal mucosa was considered; the monomorphic and bland appearance of the proliferating cells and the absence either of mitotic activity or of an infiltrating growth pattern ruled out a melanocytic malignancy.

Blue nevus may also occur in the setting of syndromes, such as Carney complex [3] or familial multiple blue nevi [2]. In this case, the patients showed neither spotty pigmentation of the skin nor signs or symptoms indicating a multisystem disorder. These findings confirm that blue nevus can arise in mucosal sites and that its unusual location is possible, even outside the setting of a syndrome.

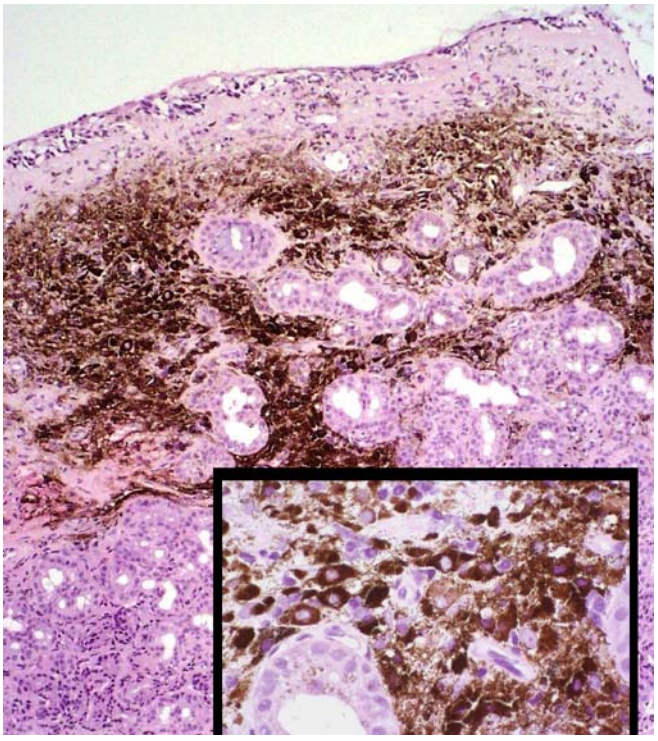

Fig. 1 The lesion consists of a proliferation of pigmented cells, intermingled within the respiratory glands. At higher power, the nuclei are round, and the cytoplasms are granular (*insert*)

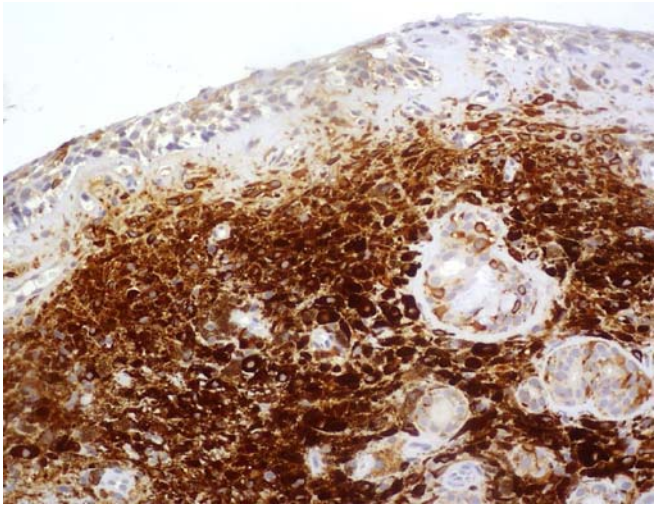

Fig. 2 MART-1 highlights the cytoplasm of the proliferating cells

References

1. Aneiros J, O'Valle F, Garcia del Moral R, Gomez Morales M, Alvaro T (1989) Blue nevus of the maxillary sinus. An immunohistochemical and electron microscopic study. Acta Otorhinolaryngol Belg 43:163–167
2. Blackford S, Roberts DL (1991) Familial multiple blue naevi. Clin Exp Dermatol 16:308–309
3. Carney JA (1995) Carney complex: the complex of myxomas, spotty pigmentation, endocrine overactivity, and schwannomas. Semin Dermatol 14:90–98
4. Flaitz CM, McCandless G (2001) Palatal blue nevus in a child. Pediatr Dent 23:354–355
5. Gonzales-Campora R, Galera-Davidson H, Vazquez-Ramirez FJ, Diaz Cano S (1994) Blue nevus: classical types and related entities. A differential diagnostic review. Pathol Res Pract 190:627–635
6. Izquierdo MJ, Pastor MA, Carrasco L, Moreno C, Kutzner H, Sangueza OP, Requena L (2001) Epithelioid blue nevus of the genital mucosa: report of four cases. Br J Dermatol 145:496–501
7. Pinto A, Raghavendra S, Lee R, Derossi S, Alawi F (2003) Epithelioid blue nevus of the oral mucosa: a rare histologic variant. Oral Surg Oral Med Oral Pathol Oral Radiol Endod 96:429–436
8. Thompson LD, Wieneke JA, Miettinen M (2003) Sinonasal tract and nasopharyngeal melanomas: a clinicopathologic study of 115 cases with a proposed staging system. Am J Surg Pathol 27:594–611
9. Uehara T, Matsubara O, Kasuga T (1987) Melanocytes in the nasal cavity and paranasal sinus. Incidence and distribution in Japan. Acta Pathol Jpn 37:1105–1114

Virchows Arch (2005) 446: 344–345
DOI 10.1007/s00428-004-1179-x

LETTER TO THE EDITOR

Bella Maly · Alexander Maly · Itzhak Pappo · Karen Meir · Orit Pappo

Pleomorphic variant of invasive lobular carcinoma of the male breast

Received: 28 September 2004 / Accepted: 15 November 2004 / Published online: 22 February 2005
© Springer-Verlag 2005

Dear Editors:
Lobular carcinoma of the male breast is extremely rare, with approximately 20 reported cases in the literature, all of the classic type [2, 4]. Herein, we describe a case of pleomorphic lobular carcinoma occurring in a male breast, with documentation of E-cadherin immunostaining.

A 44-year-old Ashkenazi (Eastern European) Jewish man, with three children, presented with a left breast mass of approximately 4 months duration. There was no history of trauma, gynecomastia, liver disease, estrogen administration, or drug use. The patient's family history was significant in that both of his grandmothers died of breast carcinoma. Physical examination revealed a firm mass localized beneath the nipple. There were no palpable axillary lymph nodes. Excisional biopsies of the breast mass were followed by mastectomy with axillary lymph node dissection.

The specimen consisted of a firm, gray-white mass with poorly circumscribed margins, measuring 2.5×2.0 cm. Microscopic sections showed an infiltrating tumor composed of discohesive pleomorphic tumor cells. Few ducts were seen, one of which showed ductal carcinoma in situ, solid type, intermediate grade (Fig. 1). The tumor cells infiltrated in a classic single linear pattern with a concentric targetoid pattern around neoplastic and non-neoplastic ducts. Individual tumor cells were large, with eccentric nuclei with irregular nuclear borders and some enlarged nucleoli (Fig. 2). The cell cytoplasm was frequently eosinophilic and vacuolated with intracytoplasmic lumina (signet-ring cell appearance). Occasional multinucleated cells were observed. Few mitoses were seen. Neither necrosis nor calcifications were found. There was no evidence of gynecomastia. The nipple was normal. There were 13 axillary lymph nodes without metastases.

Immunohistochemical studies demonstrated positive membrane staining for E-cadherin in the non-neoplastic ducts and in the intraductal carcinomatous component and complete loss of E-cadherin expression in the invasive component (Fig. 3). The Ki-67 proliferation index was positive in 5% of the tumor cells. Staining for gross cystic disease fluid protein (GCDFP-15)—the apocrine differentiation marker—was negative. The tumor cells were found to be positive for both estrogen and progesterone receptors and negative for Her-2/*neu* protein. Subsequent genetic screening for BRCA (tumor suppressor gene) mutations was negative in this patient. The diagnosis of pleomorphic invasive lobular carcinoma, grade 3, was made. The patient was treated with radiotherapy and chemotherapy and was alive and well, without evidence of recurrent or metastatic disease, 2 years after surgery.

Carcinomas of the male breast, grossly and microscopically, are remarkably similar to those seen in females. As such, they can be in situ or invasive [5]. The predominant histological type in males, in all large series, has been infiltrating duct carcinoma, with scattered reports of infiltrating lobular carcinoma, all of the classical type, characterized by small, round, regular cells, arranged in single lines, with a targetoid pattern of infiltration.

Pleomorphic lobular carcinoma, which was defined in 1992 in the female breast, has a poorer prognosis than its classic counterpart [1]. This subtype demonstrates an infiltrative pattern identical to that of classic lobular carcinoma; however, the nuclei show greater pleomorphism, increased chromatin clumping, increased mitotic activity, single or multiple prominent nucleoli, and, usually, abundant cytoplasm. The degree of nuclear atypia may approach that which is found in infiltrating duct carcinoma, but the invasive pattern characteristic of the classic lobular variant is always well maintained.

Immunohistochemical staining for E-cadherin may help in the differential diagnosis. E-cadherin is an epithelium-specific molecule involved in cell-to-cell adhesion. As such,

B. Maly (✉) · A. Maly · K. Meir · O. Pappo
Department of Pathology, Hadassah University Hospital,
Kiryat Hadassah,
p.o.b.12000, 91120 Jerusalem, Israel
e-mail: Maly_Bella@ yahoo.com
Fax: +972-2-6426268

I. Pappo
Department of Surgery, Assaf Harofeh Medical Center,
Zerifin, Israel

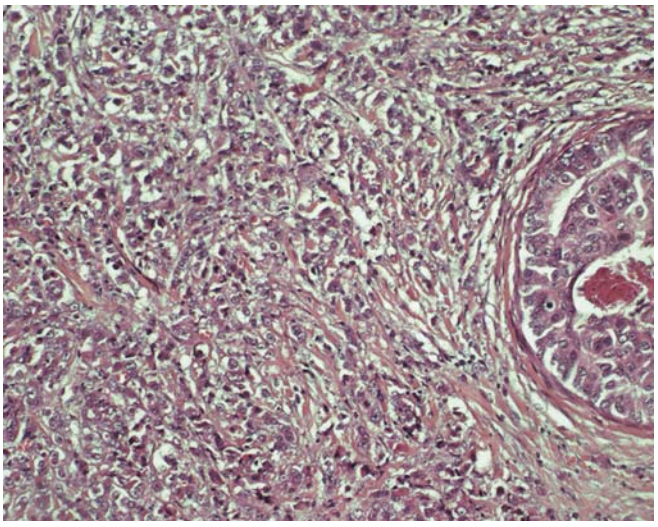

Fig. 1 Invasive lobular carcinoma and ductal carcinoma in situ. (Hematoxylin and eosin stain; original magnification ×50)

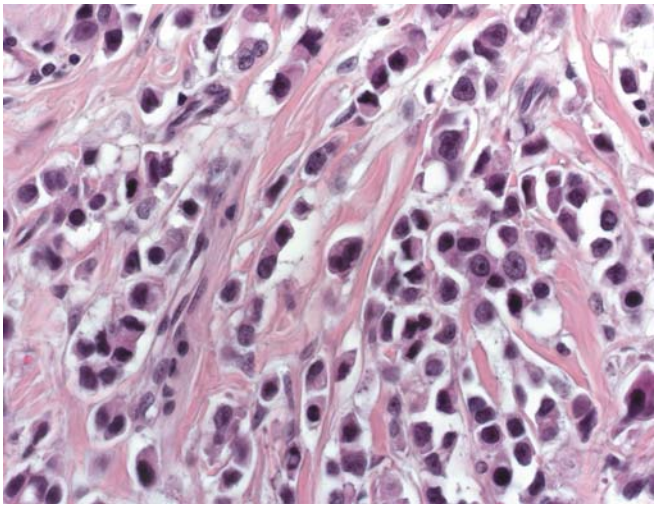

Fig. 2 Pleomorphic invasive lobular carcinoma. The tumor cells show abundant cytoplasm, eccentrically placed pleomorphic hyperchromatic nuclei. Note some cells with prominent nucleoli and multinucleated cells. (Hematoxylin and eosin stain; original magnification ×400)

it acts as a tumor invasion suppressor gene. While moderate to strong membrane expression of E-cadherin is seen in invasive and in situ ductal carcinoma (85% or more), most invasive lobular carcinomas show complete loss of expression. Lobular carcinoma in situ may display weak

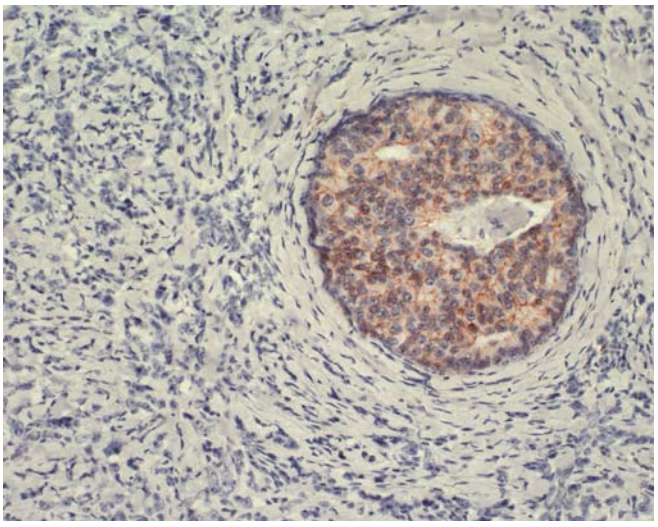

Fig. 3 Complete loss of E-cadherin expression in cells of invasive lobular carcinoma. Focus of ductal carcinoma in situ shows strong staining for E-cadherin. (E-cadherin immunostain with hematoxylin counterstain, original magnification ×100)

E-cadherin reactivity. In patients with invasive lobular carcinomas, intraductal carcinomatous components tend to display strong immunoreactivity for E-cadherin [3], as in our case. The prognosis of breast carcinoma in males, as in females, is dependent on clinical stage, histological type, and microscopic grade and correlates with proliferative activity.

In summary, to the best of our knowledge, the present case represents the first report of a pleomorphic lobular carcinoma in the male breast, with documented negative immunohistochemical staining for E-cadherin.

References

1. Eusebi V, Magalhaes F, Azzopardi JG (1992) Pleomorphic lobular carcinoma of the breast: an aggressive tumor showing apocrine differentiation. Hum Pathol 23:655–662
2. Michaels BM, Nunn CR, Roses DF (1994) Lobular carcinoma of the male breast. Surgery 115:402–405
3. Moll R, Mitze M, Frixen UH, Brichmeier W (1993) Differential loss of E-cadherin expression in infiltrating ductal and lobular breast carcinomas. Am J Pathol 143:1731–1732
4. Nance KVA, Reddick RL (1989) In situ and infiltrating lobular carcinoma of the male breast. Hum Pathol 20:1220–1222
5. Sasco AJ, Lowenfels AB, Pasker-De Jong P (1993) Epidemiology of male breast cancer: a meta-analysis of published case-control studies and discussion of selected aetiological factors. Int J Cancer 53:538–549

Virchows Arch (2005) 446: 346–347
DOI 10.1007/s00428-004-1196-9

LETTER TO THE EDITOR

Gaetano Magro · Aurelio Di Benedetto · Giuseppe Sanges · Filippo Scalisi · Rita Alaggio

Rhabdomyomatous mesenchymal hamartoma of oral cavity: an unusual location for such a rare lesion

Received: 21 August 2004 / Accepted: 6 December 2004 / Published online: 22 February 2005
© Springer-Verlag 2005

Sir, Rhabdomyomatous mesenchymal hamartoma (RMH) is a rare congenital lesion occurring in the skin, particularly of the face and neck [4]. The term hamartoma has been histologically proven as a lesion composed of a disordered mixture of mature adipose, skeletal muscle tissue, adnexal structures and sometimes blood vessels and nerves [4, 5]. Although RMH is usually a solitary lesion, it can be multiple and associated with uncommon congenital abnormalities [5]. The etiology of RMH is still unclear, but it is likely that an aberrant embryological development or migration of mesodermally derived tissues due to micro-environmental modifications and/or genetic factors may play a pathogenetic role.

We first report two cases of RMH arising as polypoid masses of oral cavity. This is an unusual site for such a lesion, as all cases of RMH reported in the English literature (approximately 25 cases) have typically been located in the skin, with only one case occurring in the nares [2, 4]. Patient 1 is a 15-day-old female infant who presented with multiple polypoid masses of tongue, the largest one measuring 1 cm in diameter (Fig. 1A). Patient 2 is a 1-month-old male infant presenting with a single polypoid mass of the left palatine tonsil, measuring 1.5 cm in greatest dimension. In both cases, the lesions were surgically excised with free margins. After a 6-month (case 1) and 2-year (case 2) clinical follow-up, no recurrence was observed.

Histological examination in both cases showed the typical features of RMH: a polypoid mass covered by squamous epithelium (case 1) or alternating squamous and respiratory type epithelium (case 2) with an underlying disordered admixture of mature skeletal muscle fibers, islands of mature adipose tissue and salivary glands (case 1) (Fig. 1B) or submucosal seromucinous glands (case 2) (Fig. 2). Characteristically, the skeletal muscle fibers haphazardly surrounded both salivary glands (case 1) or seromucinous glands (case 2). Blood vessels of venular type were found admixed among the adipose tissue. No cytological atypia, necrosis or mitosis was observed.

The present case widens the anatomic location of RMH, indicating the oral cavity as a possible involved site. This is not only of academic interest, as both fetal rhabdomyoma and embryonal rhabdomyosarocma (botryoid subtype) may present as polypoid masses in the same sites [1, 3]. Unlike RMH, they lack any additional mature tissue component as integral part of the lesion. Although these tumors may contain a variable amount of differentiated skeletal muscle cells, there is a morphological spectrum of skeletal muscle differentiation, ranging from undifferentiated round to spindle-shaped to well-differentiated mature cells with cross-striations, which is not seen in RMH.

G. Magro (✉)
Dipartimento G.F. Ingrassia, Anatomia Patologica,
Università di Catania,
Catania, Italia
e-mail: g.magro@unict.it
Tel.: +39-95-3782024
Fax: +39-953-782023

A. Di Benedetto · G. Sanges · F. Scalisi
Dipartimento Assistenziale Chirurgia Generale, Specialistica,
Anestesia e Rianimazione Chirurgia Pediatrica,
Università di Catania,
Catania, Italia

R. Alaggio
Dipartimento Scienze Oncologiche e Chirurgiche,
Università di Padova,
Italy

Fig. 1 A Case 1: rhabdomyomatous mesenchymal hamartoma presenting with multiple polypoid masses of the tongue. **B** Case 1: mature striated muscle fibers are seen in the dermis, closely admixed with salivary glands

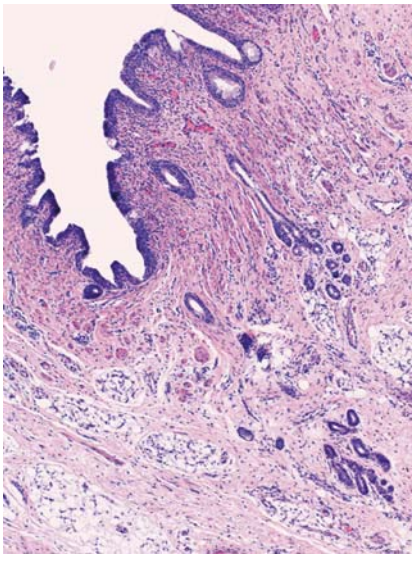

Fig. 2 Case 2: polypoid mass covered by respiratory type epithelium; bundles of mature striated muscle, islands of adipose tissue and glandular structures are seen in sub-epithelial connective tissue

References

1. Corio RL, Lewis DM (1979) Intraoral rhabdomyomas. Oral Surg Oral Med Oral Pathol 48:525–531
2. Farris PE, Mannin S, Vuitch F (1992) Rhabdomyomatous mesenchymal hamartoma. Am J Dematopathol 14:64
3. Peters E, Cohen M, Altini M, Murray J (1989) Rhabdomyosarcoma of the oral and paraoral region. Cancer 63:963–966
4. Rosenberg AS, Kirk J, Morgan MB (2002) Rhabdomyomatous mesenchymal hamartoma: an unusual dermal entity with a report of two cases and a review of the literature. J Cutan Pathol 29:238–243
5. Sahn EE, Garen PD, Pai GS, Levkoff AH, Hagerty RC, Maize JC (1990) Multiple rhabdomyomatous mesenchymal hamartomas of skin. Am J Dermatopathol 12:485–491

Virchows Arch (2005) 446:348–349
DOI 10.1007/s00428-005-1231-5
© Springer-Verlag 2005

ANNOUNCEMENTS

19–24 April 2005
10th International Congress on Oral Cancer
Crete, Greece

Creta Maris Conference Centre

- The 10th International Congress on Oral Cancer is supported by the World Health Organization, the International Union Against Cancer, the International Congress on Oral Cancer, the Hellenic Association for the Research and Treatment of Oral Cancer, and the Hellenic Cancer Society
- The Congress theme is *The Oral Cancer Patient: the anthropocentric approach to a multidisciplinary problem*
- A number of Keynote Lectures will be delivered by international leaders in their specialties
- Limited attendance Courses will be provided for interested participants
- Deadline for abstract submission: November 30th, 2004
- Accepted abstracts for oral and poster presentations will be published as a supplement to the journal Oral Oncology. Details at www.harcourt-international.com/journals/oron
- Social events include Presidents Reception, Cretan Night and Gala Dinner

Further details at www.icooc-2005.org or from the Congress President at rapidis@icooc-2005.org

9–13 May 2005
Diagnostic Histopathology of Breast Disease
Hammersmith Hospital (Imperial College Faculty of Medicine),
London, UK

A week-long course designed for pathologists at Consultant and Senior Trainee level. The course provides a comprehensive coverage of the Histopathology of Breast Disease, with special emphasis on areas that pose diagnostic difficulties. The participants with be given ample time to study histological preparations, followed by illustrated discussion of the cases. There will be special sessions dealing with the interpretation of core biopsies and fine needle aspirations. There will also be several daily talks dealing with specific topics, given by eminent breast pathologists and followed by discussion. The topics will include reporting breast biopsies, immunohistochemistry, receptors and c-erbB-2 assessment, dealing with the gross specimen, prognostic factors, proliferative lesions/carcinoma in situ, problems in breast pathology and mucinous lesions of the breast. The faculty will include Ian Ellis, Christopher Elston, Andrew Hanby, Stephen Humphreys, Andrew Lee, Naomi Livni, Sarah Pinder and Sami Shousha

Further details from:
Wolfson Conference Centre,
Hammersmith Hospital,
Du Cane Road,
London W12 ONN, UK
Tel.: (44) 20 8383 31 17/3227/3245
Fax (44) 20 8383 2428
E-mail: wcc@imperial.ac.uk

2–3 June 2005
Thyroid Pathology for the Practicing Pathologist
15 rue de l'Ecole de Médecine, Paris, France

A 2-day course will take place in Paris again under the auspices of the French Division of the I.A.P.
This course will be given in English by Prof.M.Sobrinho-Simoes (Porto) and Prof.R.Heimann (Brussels).
It will consist of lectures alternating with slide reviews and a slide seminar over a multihead microscope. The cases of this seminar will be sent (on CD) before the meeting.
The audience will be limited to 22 participants.
Course fees: 390 euros (320 euros for members of any I.A.P.division). The fees include registration,hand-out, CD of the slide seminar and coffee breaks.

For further information please contact:
Mrs.M. Fontanière
Administrative Secretary
French Division of the I.A.P.
32 Cours Albert Thomas
69008, Lyon, France
Fax: +33 4 78754311
E-mail: academie.pathologie@wanadoo.fr

3–4 June 2005
16th Ljudevit Jurak International Symposium on Comparative Pathology
Under the auspices of the European Society of Pathology
and Academy of Medical Sciences of Croatia
Multimedial center Sestre milosrdnice University Hospital,
Zagreb, Croatia

The main symposium topic is surgical pathology and frozen sections analysis. Symposium includes following sections: Pathological Morphology of the Human and Animal Diseases, Iatrogenic, Environmental and Experimental Pathology, Herman Jurak Round Table on Rheumatological Pathology, Clinical Forensic Pathology, Slide Seminars *in Histopathology and Cytopathology*, Quiz on Pathology.

Registration fee before April 1st – 100 EUR
Registration fee after April 1st – 150 EUR

Information: Davor Tomas, M.D.
Ljudevit Jurak University
Department of Pathology
Sestre milosrdnice University Hospital
Vinogradska 29
10000 Zagreb, Croatia
Tel.: +385 / 3787 909
Fax: +385 / 3787 244
E-mail: juraks@kbsm.hr
http://www.kbsm.hr/Jurak/symposium.htm

13–24 June 2005
International course on Laboratory Animal Science
Utrecht, The Netherlands

A two week intensive course on laboratory animal science will be organized at the Division of Laboratory Animal Science – Utrecht, The Netherlands in June 2005. This course is organized once a year since 1993.
The objective of this course is to present basic facts and principles that are essential for the humane use and care of animals and for the quality of research.
The contents of the course are in line with recommendations of the Federation of European Laboratory Animal Science Associations (FELASA) regarding the training of the young scientist whose research involves the use of vertebrate animals.
The course may also be of interest for those who intend to set up a similar course at their location. For this purpose, during the course the acquisition of teaching materials can be discussed with the course committee.

For information and application forms please contact:
Mr. Stephan van Meulebrouck, MA
Division of Laboratory Animal Science
Faculty of Veterinary Medicine
P.O. Box 80.166
3508 TD Utrecht
The Netherlands
Tel.: +31-30-2532033
Fax: +31-30-2537997
E-mail: pdk@las.vet.uu.nl
Internet: http://las.vet.uu.nl>Education and Training>International Course

26–29 July 2005
Practical Pulmonary Pathology
London, UK

This course is designed to provide histopathology and cytopathology trainees and consultants with an opportunity to study diagnostic lung pathology in a comprehensive manner. It comprises lectures and practical microscopy sessions, the latter making up roughly half the time and consisting of individual study of a unique collection of cases.

Further details and application forms are available from:
Professor B Corrin
Brompton Hospital
London SW3 6NP, UK
Fax: +44 20 7351 8293
E-mail: b.corrin@ic.ac.uk

Virchows Arch (2005) 446: 351–359
DOI 10.1007/s00428-004-1198-7

ORIGINAL ARTICLE

Philipp Stawowy · Heike Kallisch · Núbia Borges Pereira Stawowy · Dietger Stibenz · John P. Veinot · Michael Gräfe · Nabil G. Seidah · Michel Chrétien · Eckart Fleck · Kristof Graf

Immunohistochemical localization of subtilisin/kexin-like proprotein convertases in human atherosclerosis

Received: 9 August 2004 / Accepted: 6 December 2004 / Published online: 9 March 2005
© Springer-Verlag 2005

Abstract Integrins are heterodimeric α/β receptors that link the cytoskeleton with the extracellular matrix, thereby regulating several cell functions important in atherosclerosis. In vitro, the subtilisin/kexin-like proprotein convertases (PCs), namely PC5 and furin, have been shown to be responsible for the endoproteolytic activation of the αv integrin subunit. Based on their cleavage activity, these PCs are potential targets in atherosclerosis. In the present study, we investigated the localization of furin and PC5 in different stages of human atherosclerosis. Immunohistochemical analysis of furin and PC5 revealed their presence in vascular smooth-muscle cells and endothelial cells in atherosclerotic and non-atherosclerotic lesions. However, in the more advanced lesions, furin and PC5 staining was significantly expressed in macrophages/foam cells. In vitro, THP-1 derived macrophages contained furin and PC5, and maturation of monocytes to macrophages was accompanied by enhanced αvβ3 cell-surface expression. Inhibition of furin/PC5 with the specific pharmacological furin-like PC-inhibitor dec-CMK inhibited αv endoproteolytic activation but did not abolish αvβ3 cell-surface expression. This indicates that furin/PC5 is required for αv endoproteolytic activation but not for αv routing and sorting to the cell surface. In conclusion, our study demonstrates that furin and PC5 are significantly expressed in mononuclear cells in advanced human atherosclerotic lesions, where they regulate αv endoproteolytic activation.

Keywords Atherosclerosis · Proprotein convertases · Furin · Integrins · Endoproteolytic cleavage · Macrophages

P. Stawowy (✉) · H. Kallisch · N. Borges Pereira Stawowy · D. Stibenz · M. Gräfe · E. Fleck · K. Graf
Department of Medicine/Cardiology,
Deutsches Herzzentrum Berlin,
Augustenburger Platz 1,
13353 Berlin, Germany
e-mail: stawowy@dhzb.de
Tel.: +49-30-45932413
Fax: +49-30-45932415

J. P. Veinot · M. Chrétien
Diseases of Aging and Regional Protein Chemistry Centers,
Ottawa Health Research Institute,
University of Ottawa,
Ontario, Canada

N. G. Seidah
Laboratory of Biochemical Neuroendocrinology,
Clinical Research Institute,
Montréal, Quebec, Canada

Introduction

Atherosclerosis is a progressive inflammatory disease, characterized by the accumulation of lipids, vascular smooth-muscle cells (VSMCs) and mononuclear cells (MNCs) within the arterial wall [16]. Cellular processes involved are directed by growth factors, chemokines and adhesion molecules [23], most of which are synthesized as larger precursor proteins. Maturation of precursor proteins involves limited endoproteolytic cleavage as well as post-translational modifications, leading to the generation of biologically active molecules. Endoproteolytic activation of proproteins typically requires the presence of suitable subtilisin/kexin-like proprotein convertases (PCs) [25]. This family of calcium-dependent serine proteinases includes seven mammalian PCs, characterized by activating precursors at basic amino acid residues with the general cleavage motif: (K/R)-(X*n*)-(K/R)↓ [25]. Members in this group include PC1 (also named PC3), PC2, PC4, PACE4, furin, PC5A&B (also known as PC6) and PC7/LPC [25]. In addition, the more recently discovered pyrolysin-like subtilase, SKI-1/S1P [24, 26], has been shown to cleave proproteins at non-basic amino acid residues with the consensus motif (R/K)-X-(hydrophobic)-Z↓ (where Z is variable), whereas the novel neural apoptosis-regulated convertase 1 (NARC-1)/PC8 cleaves its own pro-segment at $VFAQ^{153}$↓ [27].

Except for PC4, which is confined to germinal cells [19], PCs exhibit widespread cell and tissue distribution [25]. Furin is the prototype convertase found within the constitutive secretory pathway [37] and has been shown to cycle between the trans-Golgi network (TGN) and cell surface

through the endocytic pathway [36]. Both furin and its closely related isozyme, PC5 [25], are present in VSMCs [31] and macrophages [18]. Based on their cleavage activity, these PCs are potential intermediates in the development and progression of atherosclerosis through the activation of growth factors and adhesion molecules.

Such a potential target are the α-integrin subunits. Integrins are α/β heterodimeric cell-surface receptors, which link the cytoskeleton with the extracellular matrix, mediating mechanotransduction and bi-directional signaling [15]. Integrin αvβ3 and its major receptor, vitronectin, are upregulated in human atherosclerotic lesions [10, 14, 39], and inhibition of αv-integrins attenuates neointima formation in animal models [7], underlining their importance. Several of the α-subunits (e.g., α3, α5, α6, α7, αIIb and αv) consist of disulfide-bound light and heavy chains, generated by endoproteolytic cleavage. In vitro studies demonstrated that PC5 and, to a lesser extent, furin are the major integrin convertases [17]. We recently reported that αv endoproteolytic activation is required for αv-dependent outside-in signaling and subsequent activation of tyrosine kinases in VSMCs [33] and that PC5 co-localizes in the neointima with αv following balloon injury in rodent arteries [32]. Thus, the present study investigated the cellular expression of furin and PC5, as well as their putative substrate, αv, in different stages of human atherosclerosis.

Materials and methods

The furin-like proprotein convertase inhibitor decanoyl-RVKR-chloromethylketone (dec-CMK) [12] was purchased from Bachem. All other chemicals were from Sigma. Cell culture media and materials were from GIBCO. The following primary antibodies were used: anti-actin and anti-α-smooth-muscle actin (α-SMA; clone 1A4) were both from Sigma; anti CD68, anti vimentin and anti CD31 were from Dako and antibodies to the αv NH_2-terminal sequence (VNR139) or αv C-terminal sequence (AB1930) were from Calbiochem and Chemicon, respectively. Rabbit antibodies to furin [18] and PC5 [8] were from the Clinical Research Institute.

Tissue samples and immunohistochemistry

Human femoral arteries (n=15) of various atherosclerotic plaque stages (Stary I/II n=3, Stary III n=4; Stary IV/V n=5; Stary VI n=3) were investigated. Atherosclerotic lesion classification was carried out independently by two experienced investigators according to American Heart Association criteria [29, 30]. Paraffin sections 3 μm thick were cut on poly-lysine-precoated slides (10%; Sigma FRG). Deparaffinization and rehydration were done using three charges of xylene and a graded series of ethanol (100–50%), followed by several washings in phosphate-buffered saline (PBS, containing 0.01% Triton-X100). Immunohistochemistry was done using the DAB Zymed Histostain-Plus kit (Zymed Laboratories, # 85–9843). For co-localization studies, double-label immunocytochemical stainings were performed by combining alkaline phosphatase (Alkaline Phosphatase Substrate Kit, cat. # SK-5300 Vector Red or cat. # SK-5100 Vector Blue) and horseradish peroxidase activity (diaminobenzidine), as described previously [32]. Incubation with primary antibodies was done overnight at 4°C. Antibodies used were diluted as follows: α-SMA 1:50; CD68 1:50, CD31 1:50, αv-integrin (targeting the C-terminus; AB1930) 1:250, PC5 1:250 and furin 1:500. Specificity controls were done by omission of the first antibody and/or incubation with non-immune IgGs. Arteries were routinely stained with Accustin Elastic stain (Sigma) and Masson Trichrome (Bio-Optica). Microscopy was carried out on an Olympus BX61, using analySIS imagine software.

Cell culture

The human monocytic leukemia THP-1 cell line was obtained from DSMZ (Deutsche Sammlung von Mikroorganismen und Zellkulturen GmbH, Germany). Cells were routinely propagated in RPMI 1640 supplemented with 10% fetal calf serum, 2 mM L-glutamine, 100 U/ml penicillin and 100 μg/ml streptomycin and incubated at 95% relative humidity and 5% CO_2 at 37°C. Differentiation of THP-1 monocytes to macrophages occurred in the presence of 100 nM phorbol 12-myristate 13-acetate (PMA) for 48 h [38]. Following macrophage differentiation, medium was changed, cells washed and PMA removed. In inhibition experiments, cells were treated with the furin-like PC-inhibitor dec-CMK (50 μM; 48 h) [12]. Cell viability was monitored by propidium iodide fluorescence-activated cell sorter (FACS) analysis. Experiments were done (at least) in triplicate.

Immunofluorescence

THP-1 macrophages (THP-1/Mφ) were let to adhere on gelatin-coated (0.2%) plastic chamber slides (Nunc) and then fixed with 4% buffered methanol (20 min) at room temperature. Non-specific binding was blocked with 10% normal-goat serum, followed by washing with PBS/0.01% Triton-X100 several times. Primary antibodies (all diluted 1:50) were incubated overnight at 4°C. After washing with PBS/0.01% Triton-X100 several times, fluorescein isothiocyanate (FITC)- or Avidin D-Texas Red (TXR)-conjugated secondary antibodies were used (Vector). Specificity con-

Fig. 1 Immunohistochemical staining of proprotein convertase 5 (PC5) in the intact human artery (serial sections; type-I lesion): Van Gieson (**A**), α-smooth-muscle actin (SMA) (**B**), PC5 (**C**), control (**D**). **E** PC5 co-localized with α-SMA (*small arrow* PC5, *brown*; *triangle* α-SMA, *red*). **F** Some PC5 immunoreactivity was found in endothelial cells. PC5 expression in Stary type-III lesion (serial sections): Van Gieson (**G**), CD68 (**H**), α-SMA (**I**), co-localization of PC5 (*brown*) with CD68 (*blue*) (**J**). *Arrows* in **B**, **C**, **H** and **I** lamina elastica interna. *Bar* in **F** for **E** lamina elastica interna, *Bar* in **G** for **A**, **B**, **C**, **D**, lamina elastica interna. *Bar* in **I** for **H** lamina elastica interna

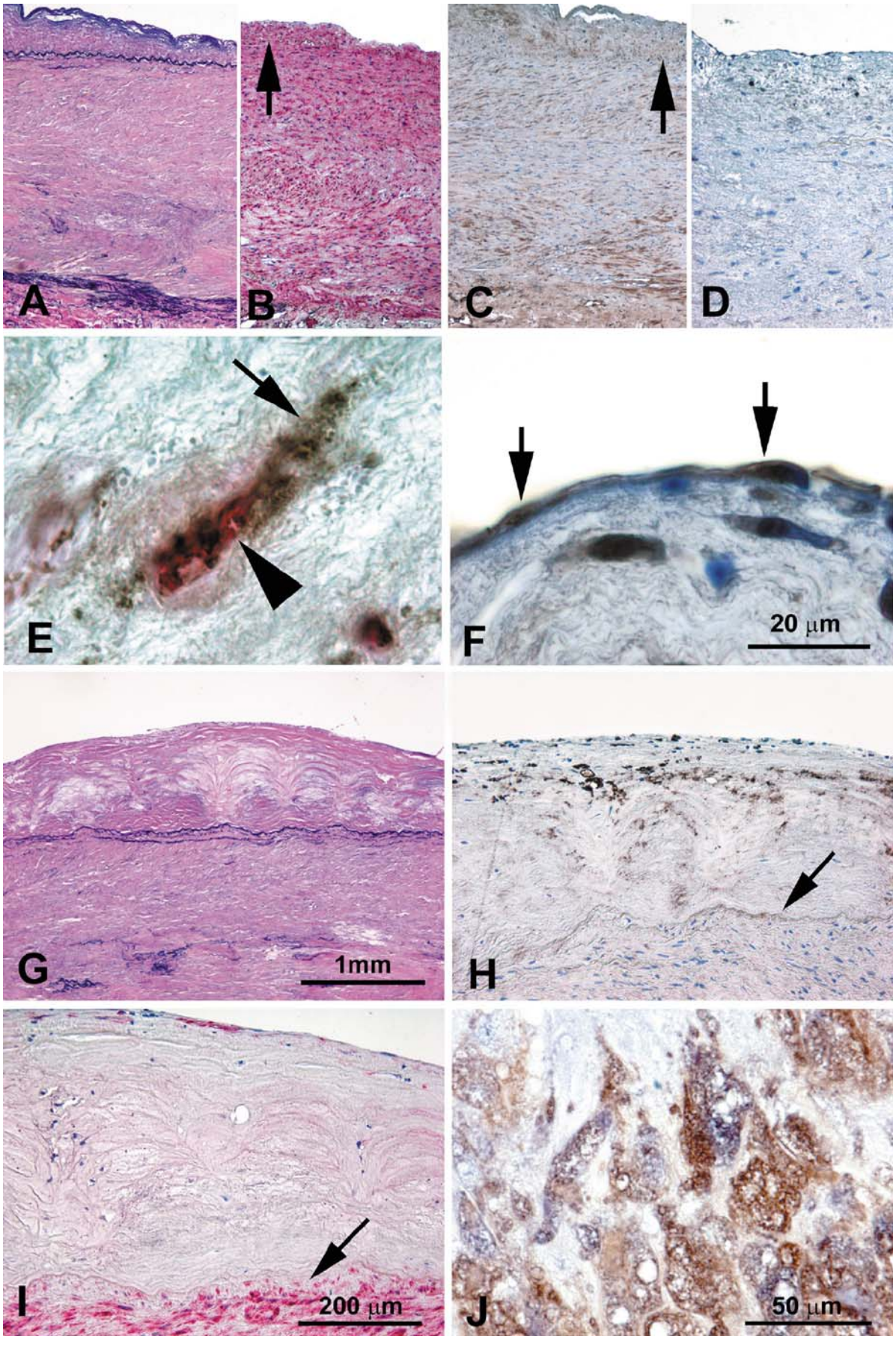
A
B
C
D
E
F
20 μm
G
1mm
H
I
200 μm
J
50 μm

trols were done by omission of the first antibody and/or incubation with non-immune IgGs.

Western-blot analysis

Immunoblotting was done as described [31] with modifications. Proteins were extracted in a buffer (20 mM Tris, pH 7.5; 150 mM NaCl; 1 mM ethylene diamine tetraacetate; 1 mM ethylene glycol tetraacetic acid; 1% Triton X-100; 2.5 mM Na-pyrophosphate; 1 mM Na_3VO_4) containing freshly dissolved protease inhibitors (Complete EDTA-free, Bohringer). Up to 25 μg of proteins were mixed with sample buffer and applied on 10% sodium dodecyl sulfate polyacrylamide gel electrophoresis (SDS-PAGE) with or without reduction with β-mercaptoethanol. Following migration, proteins were transferred onto nitrocellulose membranes (BioRad). The membranes were first incubated overnight at 4°C with the primary anti-αv-antibody (targeting either the NH_2-terminus [VNR139, diluted 1:5000] or C-terminus [AB1930, diluted 1:500]), followed by incubation with donkey anti-rabbit or donkey anti-mouse IgG-peroxidase (Dianova). Peroxidase activity product was revealed with the ECL-method (Amersham). Blots were reblotted with an anti-actin antibody (Sigma, diluted 1:5000) to assess equal protein loadings.

FACS analysis

Monocytic THP-1 or THP-1/Mφ (200,000 cells/sample), with or without dec-CMK treatment, was washed once with PBS–0.2% NaN_3–0.15% bovine serum albumin (BSA)–1 mg/ml hIgG (500×g, 5 min, 5°C), giving a final volume of 300 μl. After addition of 2.5 μg isotypic (mIgG1: CYMBUS, CBL600) or specific antibody (mouse-anti αvβ3: Chemicon, mIgG1, MAB1976), samples were incubated for 30 min at 5°C and washed again as described above. Then, mouse primary antibodies 5.6 μg goat F(ab')2-anti-mouse IgG(H+L)-FITC (Jackson Immunotech; # 115–096–062) were added and incubated for 30 min at 5°C in the dark. Finally, samples were washed once with PBS–0.2% NaN_3–0.15% BSA–1 mg/ml hIgG (500×g, 5 min, 5°C). The fluorescence of the cells was measured with the

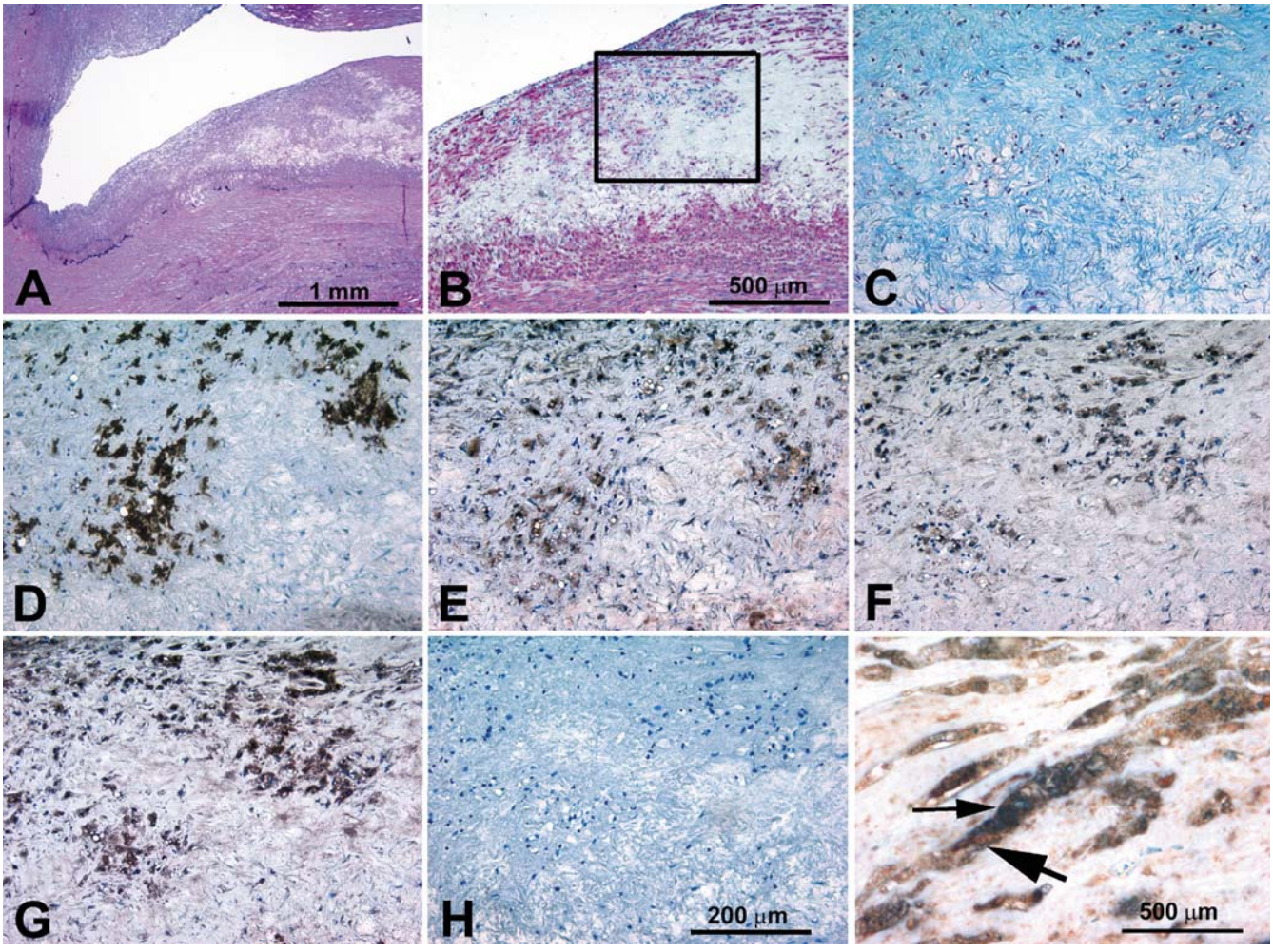

Fig. 2 Expression of proprotein convertases (PC) furin and PC5 in Stary type-V lesion (serial sections): Van Gieson (**A**), α-smooth-muscle actin (**B**), trichrome staining (**C**), CD68 (**D**), PC5 (**E**), furin (**F**), αv integrin (**G**) and control (**H**). **I** Furin (*brown, larger arrow*) co-localized with CD68 (*blue, smaller arrow*). *Bar* in **H** for **C**, **D**, **E**, **F**, **G**

FACScan (BD Biosciences, USA) in the fluorescence-1-channel (20000 events/sample). Generation of the fluorescence histograms and calculation of the median and mean fluorescence values of the different populations were done using the WinMDI 2.8 software after gating.

Results

Expression of furin and PC5 in human atherosclerotic lesions

In the intact human artery (Stary type-I atherosclerotic lesion, characterized by accumulation of VSMCs in the intima in the absence of lipids or macrophage/foam cells), PC5 staining revealed a low, diffuse expression pattern throughout media and intima, which correlated with the localization of α-SMA on serial sections (Fig. 1A, B, C, D). Furin staining revealed a comparable localization in intact arteries (data not shown). Expression of PC5 in VSMCs was confirmed by co-localization studies of PC5 with α-SMA (Fig. 1E). PC5 was also noticed in endothelial cells (Fig. 1F), both in non-atherosclerotic and atherosclerotic arteries.

The more progressive atherosclerotic lesion (preatheroma/atheroma, Stary type-III/IV lesion) is characterized by the presence of CD68-positive macrophages/foam cells within the neointima as well as accumulation of extracellular lipid pools but contains few VSMCs in the neointima (Fig. 1G, H, I). Co-localization studies of PC5 and CD68 revealed the presence of PC5 in macrophages/foam cells (Fig. 1J).

In the advanced atherosclerotic lesion (fibroatheroma; Stary type-V lesion), a lipid-rich core is contained by a VSMC-rich fibrous cap (Fig. 2A, B). Within the neointima, lipid-laden macrophages are found (Fig. 2B, C). Staining of serial section revealed a comparable expression of CD68-positive macrophages/foam cells (Fig. 2D), PC5 (Fig. 2E)

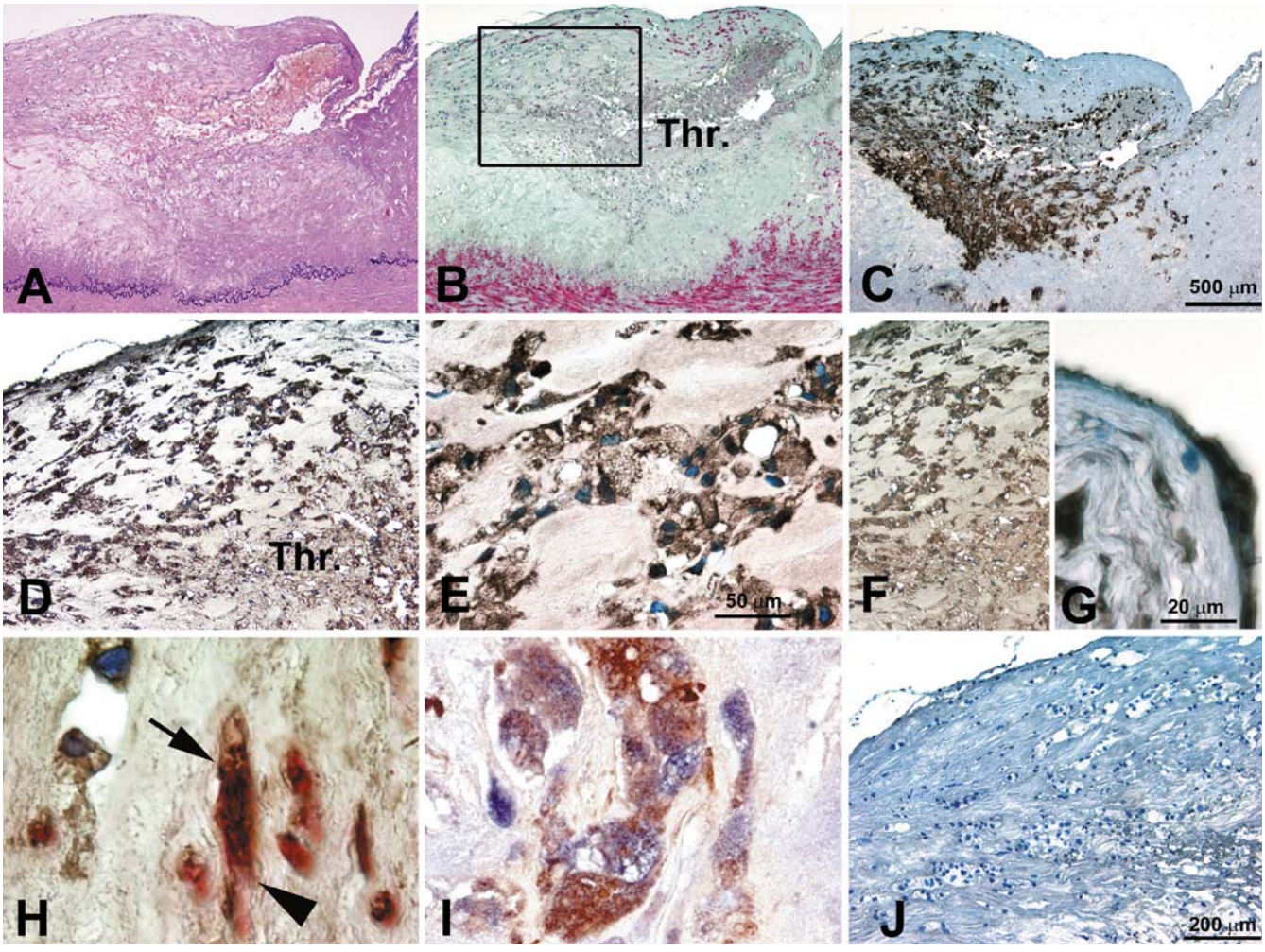

Fig. 3 Immunohistochemical analysis of furin and proprotein convertase 5 (PC5) in a complicated Stary type-VI lesion (serial sections). **A** Van Gieson, a large lipid core is contained by a thin fibrous cap, which is ruptured with thrombus (Thr.). **B** α-Smooth-muscle actin (SMA). **C** CD68. **D**, **E** PC5. **F** Furin on serial sections. **G** Some furin was also found in endothelial cells. **H** Furin (*brown, smaller arrow*) co-localized with α-SMA (*red, triangle*). **I** αv (*brown*) co-localized with CD68 (*blue*) as well. **J** Control. *Bar* in **C** for **B** and **C**; in **J** for **D** and **F**; in **G** for **H** and **I**

and furin (Fig. 2F) as well as their putative substrate αv integrin (Fig. 2G, H). As PC5, furin also co-localized with CD68 (Fig. 2I).

The complicated plaque (Stary type-VI lesion) demonstrates a large necrotic core, with a thin plaque cap (containing few VSMCs), but contains a high number of CD68-positive macrophages/foam cells at the rupture site/in the thrombus (Fig. 3A, B, C). Macrophages at the rupture site expressed PC5 (Fig. 3D, E) and furin (Fig. 3F). As PC5, furin staining was found in endothelial cells (Fig. 3G) and VSMCs (Fig. 3H). Integrin αv was localized in macrophages as well (Fig. 3I). A control staining is depicted in Fig. 3J.

Expression of furin, PC5 and αv integrin in THP-1/macrophages

For in vitro studies, the human monocytic cell line THP-1 was differentiated to THP-1/macrophages (THP-1/Mφ) by 100 nM PMA treatment (48 h) [38] and PMA then removed. THP-1 cells were chosen to reduce the variability in experiments with human monocyte-derived macrophages. THP-1/Mφ have been shown to behave more like native monocyte-derived macrophages than those from other monocytic cell lines [1]. Upon macrophage differentiation by PMA, cells adhere, and display a Golgi apparatus and rough endoplasmic reticulum as well as free ribosomes and microvilli [38]. Figure 4A shows the phase contrast image of the typical "pancake-like" morphology of PMA-differentiated THP-1/Mφ. The THP-1/Mφ express CD68 (Fig. 4B) and vimentin (Fig. 4C), as marker proteins of macrophage differentiation [6]. A prominent TGN is found (Fig. 4D) and both furin (Fig. 4E) and PC5 (Fig. 4F) display a perinuclear "TGN-like" staining.

Furin-like PCs are required for αv-activation in THP-1/macrophages

Non-differentiated, monocytic THP-1 cells do not express αv integrin [13]. Whereas no αv was found in monocytic THP-1 cells using immunoblotting, THP-1/Mφ expressed increased αv levels (Fig. 5A). This was accompanied by an enhanced cell-surface expression of the αvβ3 heterodimer on THP-1/Mφ (Fig. 5B, C). To further investigate the function of furin/PC5 for αv endoproteolytic activation in THP-1/Mφ, cells were incubated with the specific pharmacological furin-like PC-inhibitor dec-CMK (50 μM; 48 h) [12]. Endoproteolytic cleavage of αv was then investigated on reducing and non-reducing SDS-PAGE, using the αv-antibody targeting the NH_2-terminus (VNR139), and cell surface expression of cleaved and uncleaved αv was investigated by FACS analysis. On reducing SDS-PAGE, when disulphide-bound heavy (125 kDa) and light αv chains (25 kDa) [35] are separated, only the 125-kDa mature αv is found in THP-1/Mφ (Fig. 5D). In contrast, furin/PC5 inhibition with dec-CMK completely inhibited

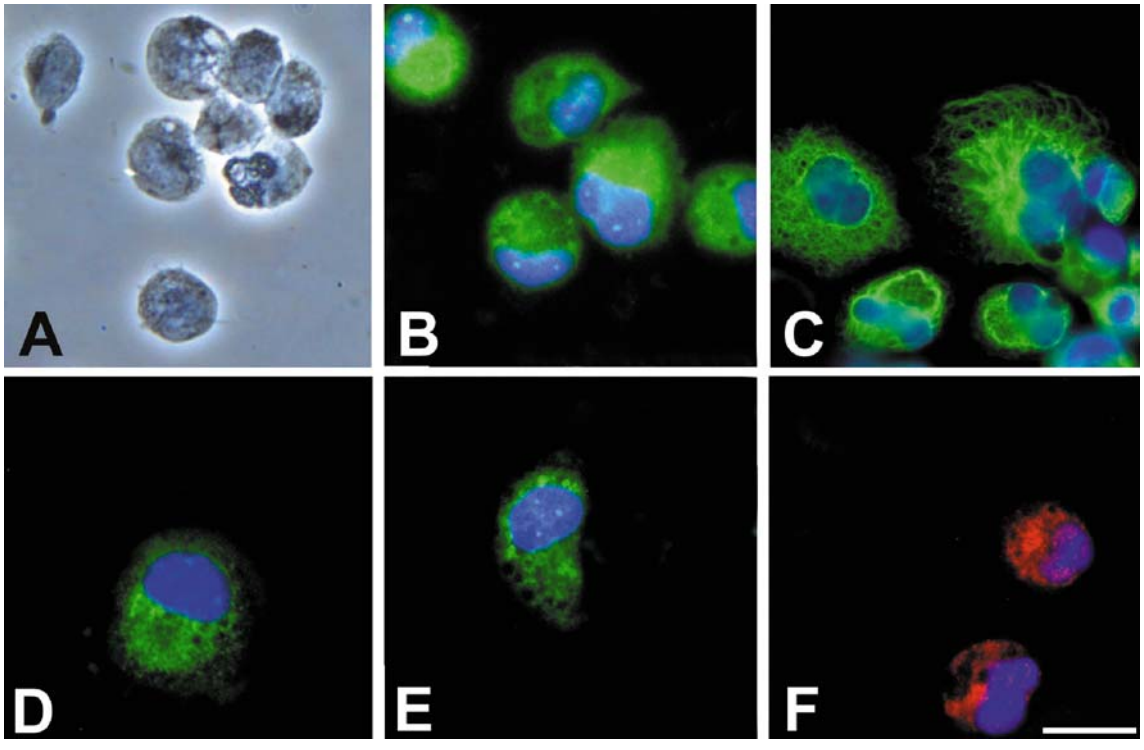

Fig. 4 THP-1 monocytes were differentiated to THP-1/Mφ by phorbol 12-myristate 13-acetate (PMA) (100 nM; 48 h), cells were then washed, and PMA was removed. THP-1/Mφ were than platted for immunofluorescence analysis. **A** The typical phase contrast image of THP-1/Mφ. These cells expressed CD68 (**B**) and vimentin (**C**) as markers of macrophage maturation. A prominent *trans*-Golgi network (TGN) is found (**D** TGN38 staining) and cells express furin (**E**) and proprotein convertase 5 (PC5) (**F**). *Bar* 25 μM

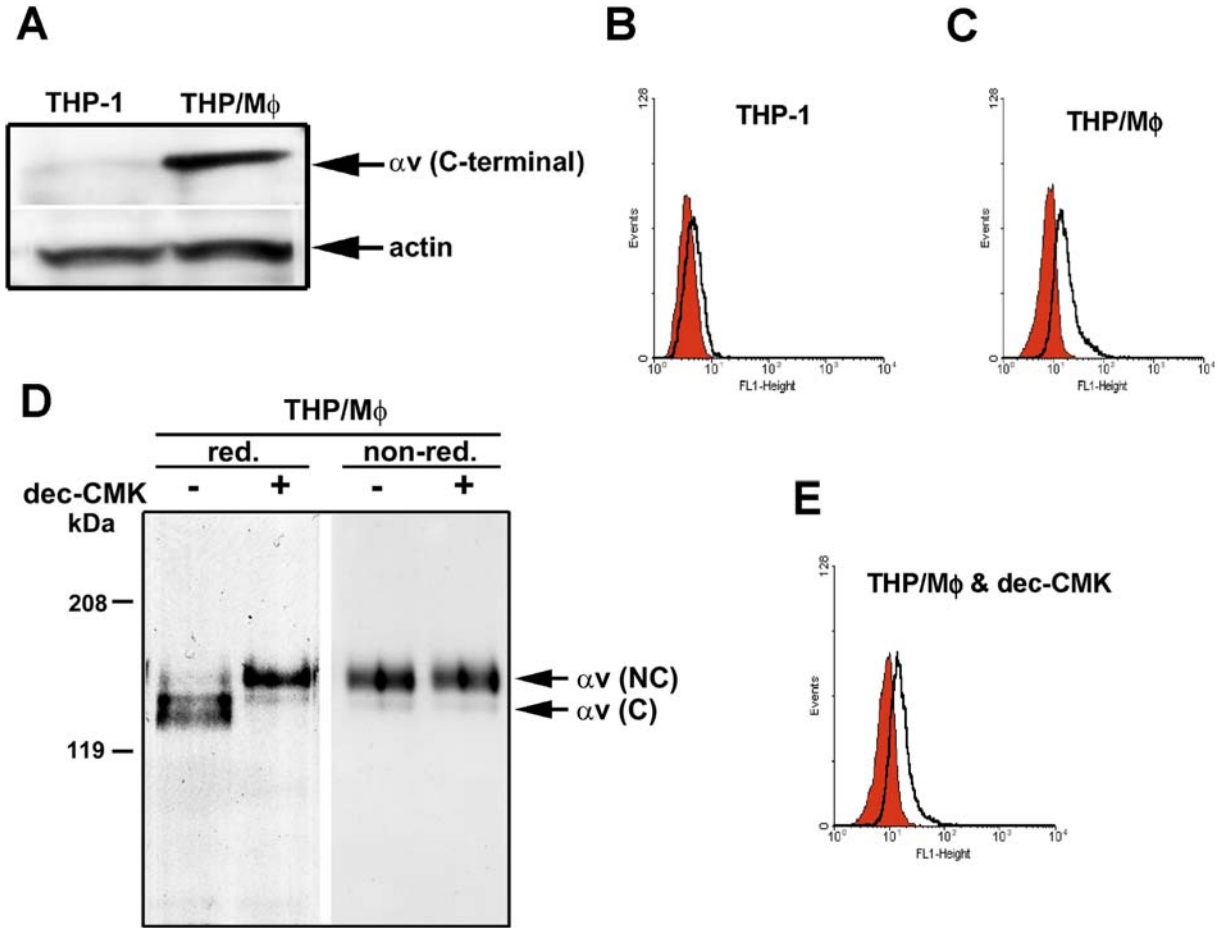

Fig. 5 Maturation of THP-1 cells to THP-1/Mφ increased αv protein levels (**A**). Immunoblotting is done with an antibody targeting the C-terminus (25 kDa) on reducing sodium dodecyl sulfate polyacrylamide gel electrophoresis (SDS-PAGE). Reblotting with actin was done to demonstrate equal protein loadings. On THP-1/Mφ enhanced αvβ3 cell surface expression is found (**B** THP-1; **C** THP-1/Mφ). The furin-like PC-inhibitor dec-CMK (50 μM) inhibited endoproteolytic activation of the 150 kDa non-cleaved (*NC*) αv to the 125 kDa cleaved (*C*) integrin subunit, as investigated on reducing (red.) and non-reducing (non-red.) SDS-PAGE (**D**; antibody VNR139, targeting the NH_2-terminus). However, dec-CMK did not abolish αvβ3 cell surface expression on THP-1/Mφ (**E**)

αv-activation in THP-1/Mφ, evident by the 150-kDa αv precursor on reducing SDS-PAGE (Fig. 5D). Blotting of control THP-1/Mφ and dec-CMK-treated THP-1/Mφ demonstrated no changes in αv levels upon inhibition of furin/PC5 on non-reducing gels (Fig. 5D). However, FACS analysis revealed that dec-CMK treatment and, thus, consequent inhibition of αv activation did not abolish αvβ3 expression on the cell surface of THP-1/Mφ (Fig. 5E).

Discussion

The present study investigated the expression of furin and PC5 in different stages of human atherosclerotic lesions. Both proprotein convertases were detectable in endothelial cells (ECs), VSMCs and MNCs, namely macrophages/foam cells. Although the number of specimens investigated in the present study is relatively small, our study indicates that the expression pattern of furin and PC5 changes with the progression of the atherosclerotic lesion. Whereas little furin and PC5 was found in the initial lesion, in which staining was mostly identified in VSMCs, a significant number of macrophages/foam cells expressed furin and PC5 in the advanced and complicated atherosclerotic plaque. Both furin and PC5 co-localized with their putative substrate αv in MNCs, the principal inflammatory cell type involved in the initiation, progression and complication of atherosclerosis [16].

Mononuclear cells play a major role in inflammation, immunity and tissue repair. Entry of the vessel wall by MNCs is a highly coordinated process, initiated by tethering and rolling, followed by adhesion and finally transmigration of the endothelial cell barrier [28]. Recruitment and diapedesis of MNCs requires the expression of adhesion molecules on MNCs and ECs, including VCAM-1 and α-integrins [28], and is directed by growth factors, such as MCP-1 expressed in ECs and MNCs [41]. Expression of adhesion molecules is essential for MNC antigen presentation, cytotoxicity, phagocytosis, tissue recruitment and chemotaxis, as well as release of inflammatory mediators [28]. The integrin superfamily is pivotal for MNC signaling [3] and activation of αvβ3 has been shown to modulate

αLβ2-dependent MNC adhesion/migration, essential for transmigration of an endothelial cell monolayer [40].

Concomitant to transmigration, the process of monocyte to macrophage maturation occurs, rendering the cells ready for their participation in the tissue inflammatory process [20]. Following macrophage maturation, growth factors, such as M-CSF, enhance scavenger receptor A and CD36 expression, enabling macrophages to endocytose modified lipoproteins, leading to foam cell formation [16]. Progression of the atherosclerotic lesion occurs by further accumulation of lipids and VSMC proliferation/migration as well as extracellular matrix protein synthesis/deposition, involving growth factors, such as transforming growth factor-β derived from macrophages [23]. Vulnerable plaque lesions are characterized by a large lipid core, contained by a thin fibrous cap and the accumulation of MNCs [5], which contribute to fibrous cap weakening through the expression and release of matrix metalloproteinases (MMPs) [11]. MMP activities are partly controlled by integrins in MNCs [34].

Experimental studies demonstrated that the inhibition of αvβ3 [4] or α4 [21] integrin attenuates macrophages homing/content as well as restenosis following balloon injury in atherosclerotic rabbits. Taken together, these studies clearly demonstrate α-integrins as potential targets in atherosclerosis and restenosis. However, there has been little focus on the maturation of α-integrins by PCs, which may potentially lead to novel strategies.

The mature αv-subunit consists of disulfide-bound heavy (125 kDa) and light (25 kDa) chains, derived from endoproteolytic cleavage of a 150-kDa αv precursor protein [35]. Activation of α-integrins occurs most likely in the TGN [22, 32], where furin/PC5 is localized. In VSMCs, PC5 is required for αv activation [33], and both PC5 and, to a lesser extent, furin have been identified as major integrin convertases among several PCs investigated [17].

Using the αvβ3(−/−) monocytic THP-1 human cell line [13] as a model for macrophage maturation, the present study demonstrates that monocyte differentiation is accompanied by enhanced cell-surface expression of αvβ3. Generally macrophages, which express furin and PC5, are believed to exhibit a significantly higher reactivity than monocytes [20]. Our study demonstrates that furin/PC5 is required for αv activation in THP-1/Mφ. However, even though inhibition of furin/PC5 with the furin-like PC-inhibitor dec-CMK [12] completely inhibited αv endoproteolytic activation, it did not abolish αvβ3 cell-surface expression. Thus, endoproteolytic cleavage of αv by furin/PC5 seems not to be a prerequisite for its sorting and routing to the cell surface, and cleavage does not control heterodimerization with the β-subunit. Indeed, uncleaved α-subunits are expressed on the cell surface and maintain their RGD-binding capacities, but cleavage likely controls integrin-dependent signaling pathways [2, 9, 33]. Thus, endoproteolytic cleavage of α-subunits by furin/PC5 does not represent solely precursor maturation but may be a novel strategy to modulate integrin-dependent signaling events important for atherosclerosis and vascular remodeling.

Acknowledgements This work was supported by grants from the Bundesministerium für Bildung und Forschung (BMBF) (CAN02/005) to PS and EF and Canadian Institutes of Health Research (CIHR) (MGP-44363) to NGS. JPV and MC were supported from the Heart and Stroke Foundation of Ontario (NA4337 and T4891) and the Canadian Stroke Network.

References

1. Auwerx J (1991) The human leukemia cell line, THP-1: a multifaceted model for the study of moncyte-macrophage differentiation. Experientia 47:22–31
2. Berthet V, Rigot V, Champion S, Secchi J, Fouchier F, Marvaldi J, Luis J (2000) Role of endoproteolytic processing in the adhesive and signaling functions of alphavbeta5 integrin. J Biol Chem 275:33308–33313
3. Berton G, Lowell CA (1999) Integrin signaling in neutrophils and macrophages. Cell Signal 9:612–635
4. Bishop GG, McPherson JA, Sanders JM, Hesselbacher SE, Feldman MJ, McNamara CA, Gimple LW, Powers ER, Mousa SA, Sarembock IJ (2001) Selective alpha(v)beta(3)-receptor blockade reduces macrophage infiltration and restenosis after balloon angioplasty in the atherosclerotic rabbit. Circulation 103:1906–1911
5. Buja LM, Willerson JT (1994) Role of inflammation in coronary plaque disruption. Circulation 89:503–505
6. Cabanas C, Sanchez-Madrid F, Aller P, Yague E, Bernabeu C (1990) Phorbol esters induce differentiation of U-937 human promonocytic cells in the absence of LFA-1/ICAM-1-mediated intercellular adhesion. Eur J Biochem 191:599–604
7. Coleman KR, Braden GA, Willingham MC, Sane DC (1999) Vitaxin, a humanized monoclonal antibody to the vitronectin receptor (alpha v beta 3), reduced neointima hyperplasia and total vessel area after balloon injury in hypercholesteremic rabbits. Circ Res 84:1268–1276
8. de Bie I, Marcinkiewicz M, Malide D, Lazure C, Nakayama K, Bendayan M, Seidah NG (1996) The isoforms of the proprotein convertase PC5 are sorted to different subcellular compartments. J Cell Biol 35:1261–1275
9. Delwel GO, Kuikman I, van der Schors RC, de Melker AA, Sonnenberg A (1997) Identification of the cleavage sites in the alpha6A integrin subunit: structural requirements for cleavage and functional analysis of the uncleaved alpha6Abeta1 integrin. Biochem J 324:263–272
10. Dufourcq P, Louis H, Moreau C, Daret D, Boisseau MR, Lamaziere JM, Bonnet J (1998) Vitronectin expression and interaction with receptors in smooth muscle cells from human atheromatous plaque. Arterioscler Thromb Vasc Biol 18:168–176
11. Galis ZS, Sukhova GK, Lark MW, Libby P (1994) Increased expression of matrix metalloproteinases and matrix degradating activity in vulnerable regions of human atherosclerotic plaques. J Clin Invest 94:2493–2503
12. Hallenberger S, Bosch V, Angliker H, Shaw E, Klenk HD, Garten W (1992) Inhibition of furin-mediated cleavage activation of HIV-1 glycoprotein gp160. Nature 360:358–361
13. Hermann P, Armant M, Brown E, Rubio M, Ishihara H, Caspary RG, Lindberg FP, Armitage R, Maliszewski C, Delespesse G, Sarfati M (1999) The vitronectin receptor and its associated CD47 molecule mediate proinflammatory cytokine synthesis in human monocytes by interaction with soluble CD23. J Cell Biol 144:767–775
14. Hoshiga M, Alpers CE, Smith LL, Giachelli CM, Schwartz SM (1995) Alpha-v beta-3 integrin expression in normal and atherosclerotic artery. Circ Res 77:1129–1135
15. Hynes RO (1992) Integrins: versatility, modulation, and signaling in cell adhesion. Cell 69:11–25
16. Libby P (2002) Inflammation in atherosclerosis. Nature 420:868–874

17. Lissitzky JC, Luis J, Munzer JS, Benjannet S, Parat F, Chretien M, Marvaldi J, Seidah NG (2000) Endoproteolytic processing of integrin pro-alpha subunits involves the redundant function of furin and proprotein convertase (PC) 5A, but not paired basic amino acid converting enzyme (PACE) 4, PC5B or PC7. Biochem J 346:133–138
18. Marcinkiewicz M, Marcinkiewicz J, Chen A, Leclaire F, Chrétien M, Richardson P (1999) Nerve growth factor and proprotein convertases furin and PC7 in transected sciatic nerves and in nerve segments cultured in conditioned media: their presence in Schwann cells, macrophages, and smooth muscle cells. J Comp Neurol 403:471–485
19. Mbikay M, Tadros H, Ishida N, Lerner CP, De Lamirande E, Chen A, El-Alfy M, Clermont Y, Seidah NG, Chretien M, Gagnon C, Simpson EM (1997) Impaired fertility in mice deficient for the testicular germ-cell protease PC4. Proc Natl Acad Sci U S A 94:6842–6846
20. Osterud B, Bjorklid E (2003) Role of monocytes in atherogenesis. Physiol Rev 83:1069–1112
21. Patel SS, Thiagarajan R, Willerson JT, Yeh ET (1998) Inhibition of alpha4 integrin and ICAM-1 markedly attenuate macrophage homing to atherosclerotic plaques in ApoE-deficient mice. Circulation 97:75–81
22. Rigot V, Andre F, Lehmann M, Lissitzky JC, Marvaldi J, Luis J (1999) Biogenesis of alpha6beta4 integrin in a human colonic adenocarcinoma cell line. Involvement of calnexin. Eur J Biochem 261:659–666
23. Ross R (1993) The pathogenesis of atherosclerosis: a perspectives for the 1990s. Nature 362:801–809
24. Sakai J, Rawson RB, Espenshade PJ, Cheng D, Seegniller AC, Goldstein JL, Brown MS (1998) Molecular identification of the sterol-regulated luminal protease that cleaves SREBPs and controls lipid composition of animal cells. Mol Cell 2:505–514
25. Seidah NG, Mbikay M, Marcinkiewicz M, Chrétien M (1998) The mammalian precursor convertases: paralogs of the subtilisin/kexin family of calcium-dependent serine proteinases. In: Hook VYH (ed) Proteolytic and cellular mechanisms in prohormone and proprotein processing. R.G. Landes Company, Georgetown, TX, pp 49–76
26. Seidah NG, Mowla SJ, Hamelin J, Mamarbachi AM, Benjannet S, Touré BB, Basak A, Munzer JS, Marcinkiewicz J, Zhong M, Barale JC, Lazure C, Murphy RA, Chrétien M, Marcinkiewicz M (1999) Mammalian subtilisin/kexin isozyme SKI-1: a widely expressed proprotein convertase with a unique cleavage specificity and cellular localization. Proc Natl Acad Sci U S A 96: 1321–1326
27. Seidah NG, Benjannet S, Wickham L, Marcinkiewicz J, Jasmin SB, Stifani S, Basak A, Prat A, Chrétien M (2003) The secretory proprotein convertase neural apoptosis-regulated convertase 1 (NARC-1): liver regeneration and neuronal differentiation. Proc Natl Acad Sci U S A 100:928–933
28. Springer TA (1994) Traffic signals for lymphocyte recirculation and leukocyte emigration: the multistep paradigm. Cell 76:301–314
29. Stary HC, Chandler AB, Glagov S, Guyton JR, Insull W Jr, Rosenfeld ME, Schaffer SA, Schwartz CJ, Wagner WD, Wissler RW (1994) A definition of initial, fatty streak, and intermediate lesions of atherosclerosis. A report from the Committee on Vascular Lesions of the Council on Arteriosclerosis, American Heart Association. Arterioscler Thromb 14:840–856
30. Stary HC, Chandler AB, Dinsmore RE, Fuster V, Glagov S, Insull W Jr, Rosenfeld ME, Schwartz CJ, Wagner WD, Wissler RW (1995) A definition of advanced types of atherosclerotic lesions and a histological classification of atherosclerosis. A report from the Committee on Vascular Lesions of the Council on Arteriosclerosis, American Heart Association. Arterioscler Thromb Vasc Biol 15:1512–1531
31. Stawowy P, Blaschke F, Kilimnik A, Goetze S, Kallisch H, Chrétien M, Marcinkiewicz M, Fleck E, Graf K (2002) Proprotein convertase PC5 regulation by PDGF-BB involves PI3-kinase/p70(s6)-kinase activation in vascular smooth muscle cells. Hypertension 39:399–404
32. Stawowy P, Graf K, Goetze S, Roser M, Chrétien M, Seidah NG, Fleck E, Marcinkiewicz M (2003) Coordinated regulation and colocalization of alpha v integrin and its activating enzyme proprotein convertase PC5 in vivo. Histochem Cell Biol 119: 239–245
33. Stawowy P, Kallisch H, Veinot JP, Kilimnik A, Prichett W, Goetze S, Seidah NG, Chrétien M, Fleck E, Graf K (2004) Endoproteolytic activation of alpha (v) integrin by proprotein convertase PC5 is required for vascular smooth muscle cell adhesion to vitronectin and integrin-dependent signaling. Circulation 109:770–776
34. Stefanidakis M, Ruohtula T, Borregaard N, Gahmberg CG, Koivunen E (2004) Intracellular and cell surface localization of a complex between alphaMbeta2 integrin and promatrix metalloproteinase-9 progelatinase in neutrophils. J Immunol 172:7060–7068
35. Suzuki S, Argraves WS, Pytela R, Arai H, Krusius T, Pierschbacher MD, Ruoslahti E (1986) cDNA and amino acid sequences of the cell adhesion protein receptor recognizing vitronectin reveal a transmembrane domain and homologies with other adhesion protein receptors. Proc Natl Acad Sci U S A 83:8614–8618
36. Takahashi S, Nakagawa T, Banno T, Watanabe T, Murakami K, Nakayama K (1995) Localization of furin to the trans-Golgi network and recycling from the cell surface involves Ser and Tyr residues within the cytoplasmic domain. J Biol Chem 270: 28397–28401
37. Thomas G (2002) Furin at the cutting edge: from protein traffic to embryogenesis and disease. Nat Rev Mol Cell Biol 3:753–766
38. Tsuchiya S, Kobayashi Y, Goto Y, Okumura H, Nakae S, Konno T, Tada K (1982) Induction of maturation in cultured human monocytic leukemia cells by a phorbol diester. Cancer Res 42:1530–1536
39. Veinot JP, Srivasta S, Carlson P (1999) Beta 3 integrin—a promiscuous integrin involved in vascular pathology. Can J Cardiol 15:762–770
40. Weerasinghe D, McHugh KP, Ross FP, Brown EJ, Gisler RH, Imhof BA (1998) A role for the alphavbeta3 integrin in the transmigration of monocytes. J Cell Biol 142:595–607
41. Wilcox JN, Nelken NA, Coughlin SR, Gordon D, Schall TJ (1994) Local expression of inflammatory cytokines in human atherosclerotic plaques. J Atheroscler Thromb 1:S10–S13

Virchows Arch (2005) 446: 360–368
DOI 10.1007/s00428-004-1201-3

ORIGINAL ARTICLE

U. Jeschke · C. Kunert-Keil · I. Mylonas · A. Hammer · B. Schiessl · I. Lomba · C. Kuhn · S. Schulze · K. Friese

Expression of glycodelin A in decidual tissue of preeclamptic, HELLP and intrauterine growth-restricted pregnancies

Received: 22 November 2004 / Accepted: 13 December 2004 / Published online: 9 March 2005
© Springer-Verlag 2005

Abstract During pregnancy, the placenta produces a variety of proteins that are responsible for the establishment of the foeto–maternal tolerance and circulation. The aim of this study was to investigate the expression of glycodelin A (formerly named PP14) in decidual tissue of placentas with intrauterine growth restriction (IUGR), preeclamptic patients, hemolysis, elevated liver, low-platelet (HELLP) patients and normal decidual tissue. Slides of paraffin-embedded decidual tissue of patients with IUGR, preeclamptic patients, HELLP patients and normal-term placentas were incubated with either polyclonal or monoclonal antibodies against glycodelin A. Staining reaction was performed with the ABC reagent. Intensity of immunohistochemical reaction on the slides was analysed using a semi-quantitative score. In addition, expression of glycodelin mRNA was analysed by in situ hybridisation. Expression of glycodelin A was significantly reduced in decidual cells of placentas with IUGR and HELLP, as investigated with both monoclonal and polyclonal antibodies and in situ hybridisation. However, preeclamptic decidual tissue showed no significantly different expression of intensity of glycodelin mRNA compared with normal placental tissue controls. A reduced expression of glycodelin A by decidual cells seems to be related to IUGR and HELLP. Therefore, glycodelin A might play an important role in the pathogeneses of these diseases.

Keywords Glycodelin · Intrauterine growth restriction · Preeclampsia · HELLP · Decidua

U. Jeschke, C. Kunert-Keil and I. Mylonas contributed equally to this article.

U. Jeschke (✉) · I. Mylonas · B. Schiessl · I. Lomba · C. Kuhn · S. Schulze · K. Friese
Ludwig-Maximilians-University Munich,
1st Department of Obstetrics and Gynaecology,
Maistrasse 11,
80337 Munich, Germany
e-mail: udo.jeschke@med.uni-muenchen.de

C. Kunert-Keil
Ernst Moritz Arndt University of Greifswald,
Institute of Pathophysiology,
Karlsburg, Germany

I. Mylonas
University of Rostock,
Faculty of Science,
Universitätsplatz 1,
18051 Rostock, Germany

A. Hammer
Medical-University Graz,
Institute of Histology and Embryology,
Graz, Austria

B. Schiessl
School of Surgical and Reproductive Sciences
(Obstetrics and Gynaecology),
University of Newcastle upon Tyne,
Framlington Place,
Newcastle upon Tyne, NE2 4HH,
United Kingdom

Introduction

The glycoprotein glycodelin has been predominantly localised to organs of the genital tract in humans [23], baboons [13] and rats [17]. Glycodelin in humans, previously known as placental protein 14 (PP14) [3], is expressed in glandular epithelium of the endometrium [15] and decidua [14]. It is known that glycodelin suppresses the cytolytic capacity of natural killer (NK) cells in vitro [27]. A relationship between serum levels of glycodelin and enhanced probability of abortion has been suggested in former investigations [35]. Glycodelin was shown to have a molecular weight of 28,000 with two identical subunits held together by noncovalent bonds and a carbohydrate content of 17.5%. Glycodelin has a unique carbohydrate configuration, consisting of sialylated LacdiNAc structures, which are very unusual in mammals [7]. Julkunen and co-workers confirmed the findings of homology between glycodelin and β-lactoglobulins by deducing the complete amino acid sequence of glycodelin [16]. Two isoforms of glycodelin

have been described: glycodelin A, isolated from amniotic fluid, and a similar glycoprotein, glycodelin S, which is found in seminal plasma but is differentially glycosylated from glycodelin A [19].

We have recently shown that the immunosuppressive glycoprotein glycodelin is an efficient inhibitor of the E-selectin-mediated cell adhesion. Due to its high concentration in the decidua and its potential ability to block selectin-mediated cell adhesion, glycodelin may play an important role in foetal maternal defence mechanisms and in maintaining pregnancy [12]. In another study, we showed that glycodelin A significantly stimulated the hCG protein and mRNA release of term placental trophoblast cells [11, 30] and inhibited the hPL release of these cells. Our results indicated further that glycodelin A has paracrine effects in reproductive tissues and the maternal–trophoblast interface. These data support the concept that glycodelin A is a modulator of trophoblast function.

It is already known that glycodelin promotes the angiogenic response in human umbilical cord vein endothelial cells (HUVECs). Increased migration and tube formation of HUVECs were found in the presence of a glycodelin peptide (Gp), and this increase was blocked by an antibody to Gp and by an anti-vascular endothelial growth factor (VEGF) antibody, suggesting that the angiogenic effects of glycodelin might be mediated by VEGF [34]. Because glycodelin is a major secretory decidual product during pregnancy and plays a role in angiogenesis, this protein may provide an important marker of decidual development in normal, preeclamptic, and HELLP (hemolysis, elevated liver, low-platelet) pregnancies and those with intrauterine growth restriction (IUGR).

Therefore the aims of this study were: (1) to assess glycodelin A expression in IUGR, preeclamptic, HELLP and in normal control decidual tissues with the use of specific monoclonal and polyclonal antibodies and (2) to investigate glycodelin mRNA expression using in situ hybridisation methods in the same decidual tissue panel used for immunohistochemistry.

Materials and methods

Tissue samples

Decidual tissues were obtained from 27 placentas of women giving birth in the 1st Department of Obstetrics and Gynaecology of the LMU Munich. Six placentas with IUGR (mean date of delivery±SD: 33±3 weeks of gestation), eight placentas with preeclampsia (PE) (mean date of delivery: 33±3.2 weeks of gestation), five placentas with HELLP (mean date of delivery: 33.8±2.9 weeks of gestation) and eight normal placentas (mean date of delivery: 38.2±3 weeks of gestation) were used for the study. The study was approved by the ethics committee of the LMU Munich, Germany, and informed consent was obtained from the patient.

Table 1 Antibodies used for immunohistochemical characterisation of decidual tissue samples using immunohistochemistry and immunofluorescence

Antibody	Clone	Isotype	Concentration (μg/ml)	Source
Glycodelin	UCI-2	Rabbit IgG	2.0	Bioscience AG
Glycodelin A	A87-B/D2	Mouse IgG	2.0	Glycotope GmbH
Prolactin	N1549	Rabbit IgG	2.0	DakoCytomation
CD 45	T29/33	Mouse IgG	2.0	DakoCytomation
Cytokeratin-Cy-3 labeled	A45-B/B3	Mouse IgG	2.0	Micromet

Immunohistochemistry

Immunohistochemistry on paraffin sections (7 μm) of the different decidual tissue specimens was done by incubating the slides in methanol/H_2O_2 (30 min) to inhibit endogenous peroxidase activity, followed by washing in phosphate-buffered saline (PBS) (5 min) and treating with goat serum (20 min, 22°C) to reduce non-specific background staining. Incubation with the primary antibody (Table 1) was done overnight at 4°C. Specific binding of the antibodies used to glycodelin A was analysed using Western-blot analysis [2, 12]. Sections were thoroughly incubated with the biotinylated secondary antibody (1 h, 22°C) and avidin-biotinylated peroxidase (45 min, room temperature). Between each step, sections were washed with PBS (pH 7.4). Peroxidase staining reaction was done with diaminobenzidine/H_2O_2 (1 mg/ml; 5 min) and stopped in tap water (10 min).

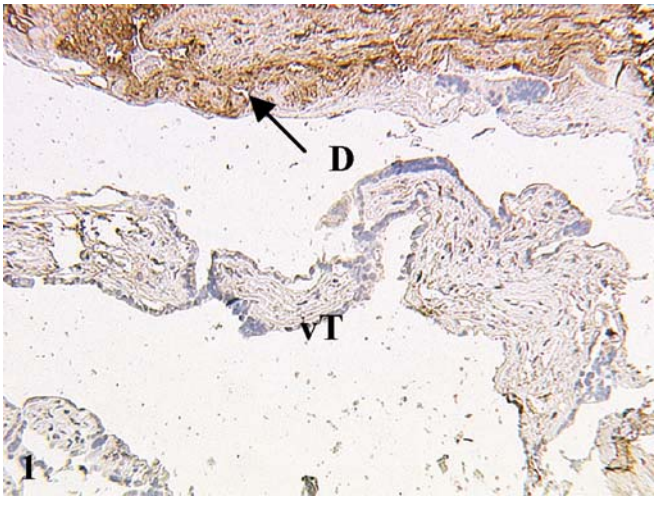

Fig. 1 Expression of glycodelin in normal term decidua (D) marked with an *arrow* at the implantation side. Placental villi (vT) do not express glycodelin, whereas a strong staining for this molecule can be observed in the decidua ×10 lens

Sections were counterstained in hemalaun (1 min) and then cover-slipped. In controls, the primary antibody was replaced with pre-immune mouse serum with positive and negative controls being included. All specimens were evaluated by a pathologist. The intensity and distribution patterns of the staining reaction were evaluated by two blinded, independent observers, including a gynaecological pathologist, using the semi-quantitative immunoreactive score (IRS), as previously described [31], and used to asses steroid receptors [25] and cathepsin D [26] expression in human endometrial tissue. The IRS was calculated by multiplication of optical staining intensity (graded as 0=no, 1=weak, 2=moderate and 3=strong staining) and the percentage of positive stained cells (0=no staining, 1=<10% of the cells, 2=11–50% of the cells, 3=51–80% of the cells and 4=>81% of the cells) and without knowing the pathological evaluation, the diagnosis or the standard performed hematoxylin reaction of each specimen.

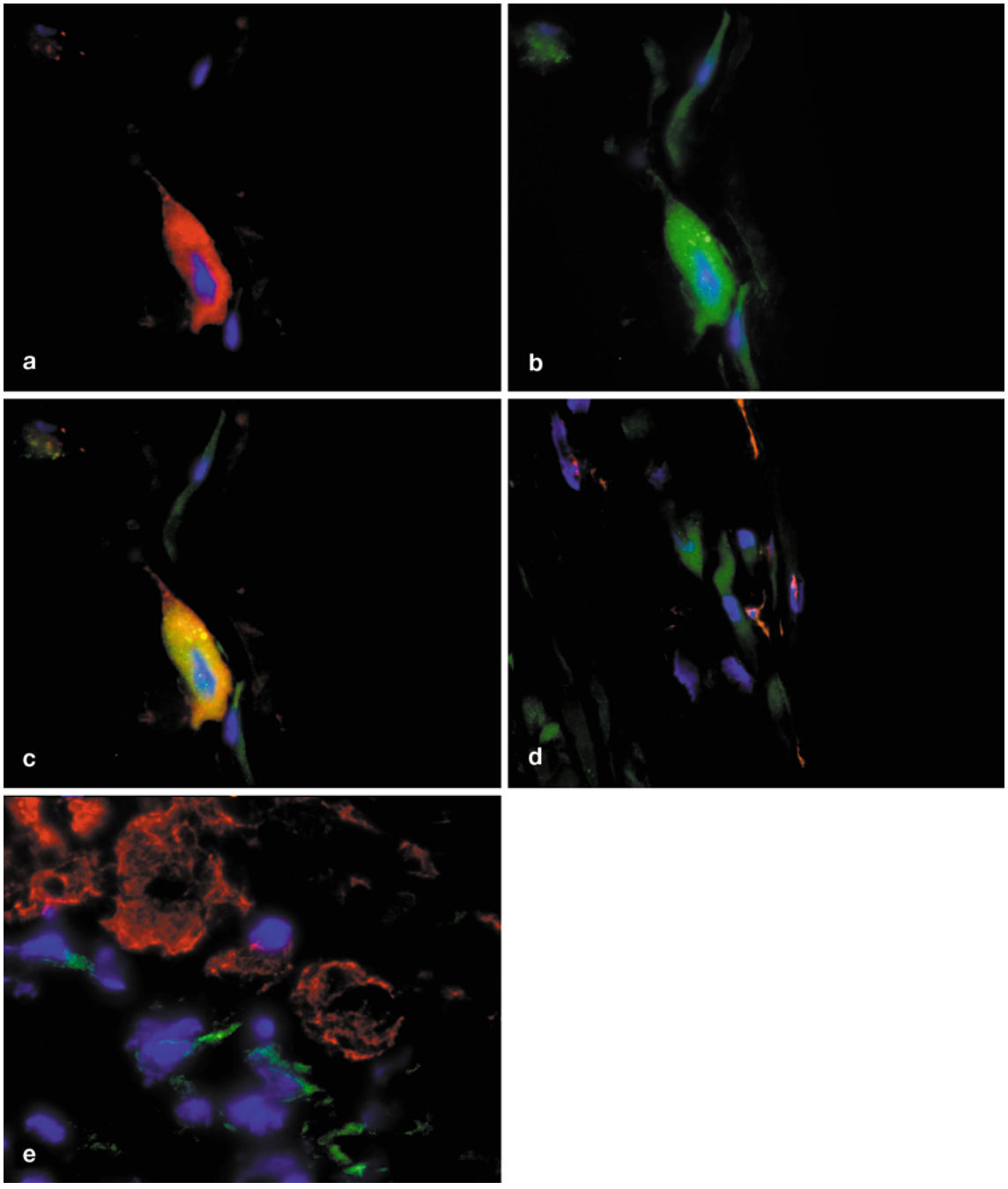

Fig. 2 Double staining for glycodelin (A87-B/D2) (**a**) and prolactin (**b**) in normal decidual tissue, counterstaining with 4′-6′-diamidino-2-phenylindole. Triple-filter excitation (**c**) ×63 lens. Glycodelin-positive cells in the decidua (polyclonal antibody UCI-2) do not express CD45 (×40 lens) (**d**) nor cytokeratin (monoclonal antibody A87-B/D2) ×63 lens (**e**). Cy2 staining is coloured in green, whereas Cy3 staining is coloured in red

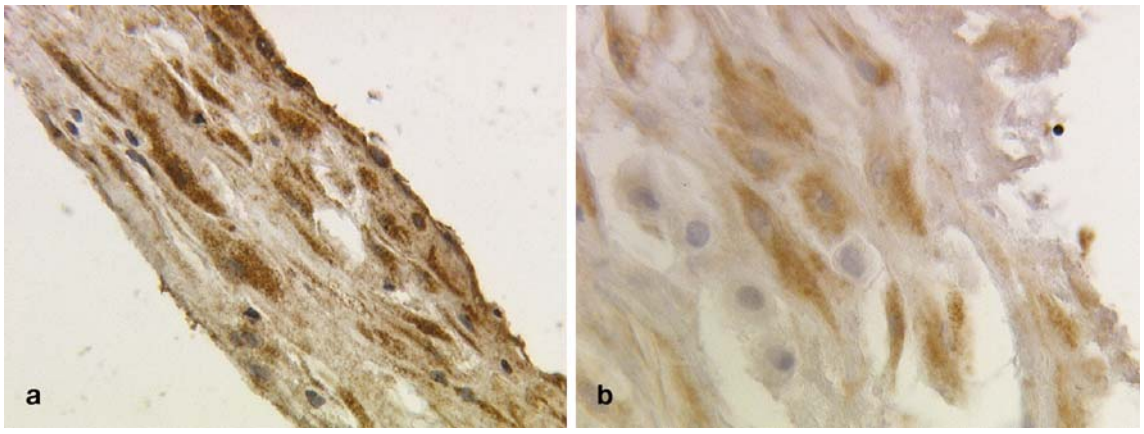

Fig. 3 Expression of glycodelin A in normal-term decidual tissue visualised with the polyclonal antibody UCI-2, ×25 lens (**a**) and with the monoclonal antibody A87-B/D2 ×40 lens (**b**)

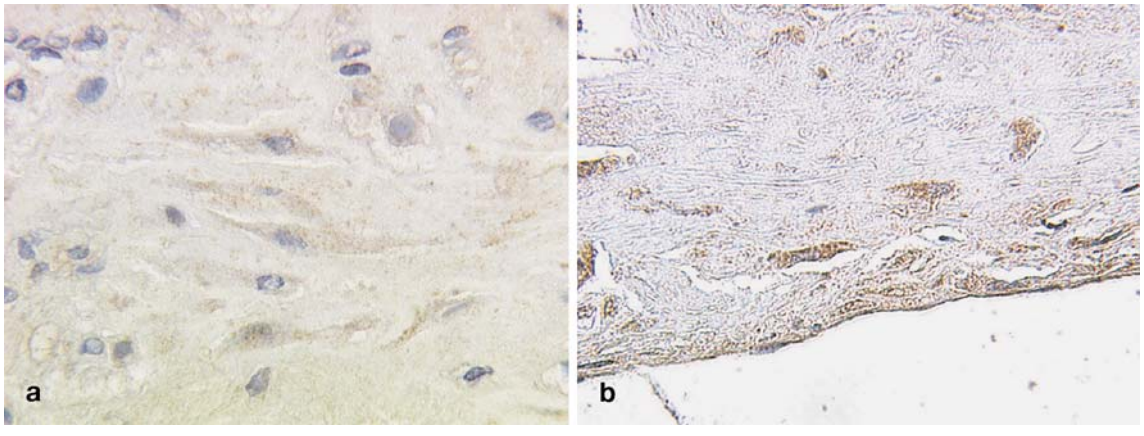

Fig. 4 Expression of glycodelin A in intrauterine growth-retarded decidual tissue visualised with the polyclonal glycodelin antibody UCI-2 ×40 lens (**a**) and with the monoclonal antibody A87-B/D2, ×25 lens (**b**)

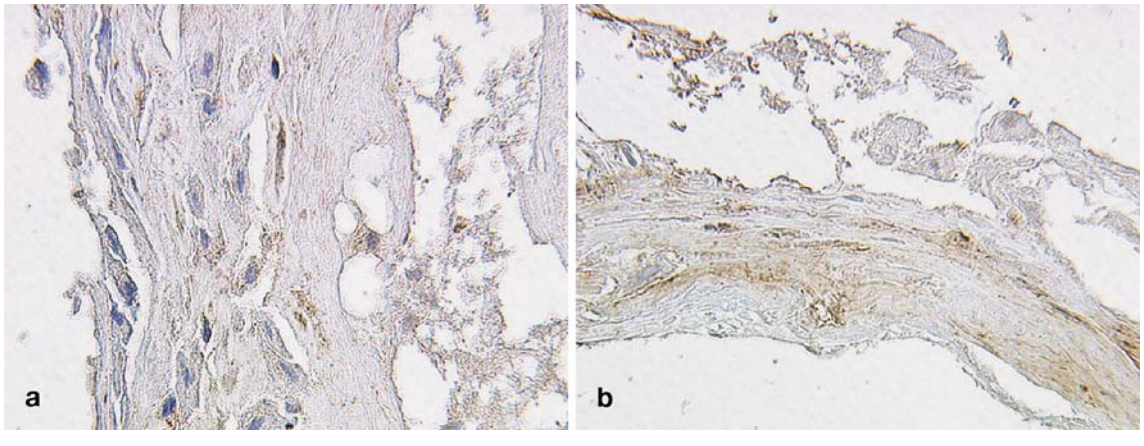

Fig. 5 Expression of glycodelin A in preeclamptic decidual tissue visualised with the polyclonal antibody UCI-2 ×25 lens (**a**) and with the monoclonal antibody A87-B/D2, ×25 lens (**b**)

Immunofluorescence double staining

For the characterisation of glycodelin-expressing cells in decidual tissue, cryosections were examined. All samples were fixed in 5% buffered formalin. Antibodies used for the experiments are listed in Table 1. They were diluted to 2 µg/ml with PBS, and incubated with the slides overnight at 4°C. After washing, Cy2-labeled goat anti-mouse IgG or Cy3-labeled goat anti-rabbit IgG (both Dianova), diluted 1:200, served as second antibody. Alternatively, Cy2-labeled goat anti-rabbit IgG and Cy3-labeled goat anti-mouse IgG (Dianova), diluted 1:200, were used as second antibody in some cases. The slides were finally embedded in mounting buffer containing 4′,6-diamino-2-phenylindole, resulting in staining of the nucleus. Slides were examined with a Zeiss (Jena, Germany) Axiophot photomicroscope. Digital images were obtained with a digital-camera system (CF20DXC, KAPPA Messtechnik, Gleichen, Germany) and saved on computer.

Preparation of riboprobes

A 227-bp fragment of the glycodelin cDNA (position +41 to +268) was cloned into the EcoR1 restriction site of pBluescript SK (Stratagene, Germany) and labelled with DIG (digoxigenin) by in vitro transcription using the DIG RNA labelling Kit (SP6/T7) (Roche Biochemicals, Germany) as previously described [17]. The antisense cRNA was used for the detection of glycodelin mRNA, whereas the sense cRNA probe served as a negative control.

In situ hybridisation analysis of glycodelin on paraffin sections

Non-radioactive in situ hybridisation was performed on paraffin sections (4 µm) that had been fixed in 4% paraformaldehyde. Sections were rehydrated and permeabilised by pepsin digestion (750 µg/ml pepsin in 0.2 M HCl, 37°C, 30 min). Post-fixation (paraformaldehyde 4%, 20 min, 4°C) was followed by acetylation using 0.25% acetic anhydride in triethanolamine (0.1 M, pH 8.0, 15 min). After dehydration in ethanol (70%, 95%, 100%), the sections were hybridised for 16 h (56°C) in a solution containing 25% formamide, 0.3 M NaCl, 10% dextran sulfate, 20 mM Tris-HCl pH 7.5, 1 mM ethylene diamine tetraacetate, 1× Denhardt's (Ficoll, polyvinylpyrrolidone, bovine serum albumin), 0.1 ng/ml herring sperm DNA, 0.5 mg/ml t-RNA, 0.1 mg/ml polyuridylic acid and 125 ng DIG-labelled cRNA probe. After washing with 50% formamide in 1×sodium saline citrate, sections were incubated with RNase A followed by additional washing steps and incubation with blocking reagent (Roche Biochemicals, Germany). Bound riboprobe was visualised using incubation with alkaline phosphatase-conjugated anti-DIG antibody (Roche Biochemicals, Germany) and subsequent substrate reaction using 5-bromo-4-chloro-3-indolyl phosphate/nitroblue-tetrazolium chloride.

Computerised analysis of glycodelin mRNA expression

The level of glycodelin mRNA expression was determined in a blinded fashion in one run with identical staff, equipment and chemicals. From each section, five digital pictures were taken at random of different places of the decidual tissue (200-fold magnification; 3CCD colour camera; Hitachi HV-C20 M; Hitachi Denshi Ltd, Japan, and Axiolab, Carl Zeiss, Germany). For standardisation of the measurement in each picture, the optical density of white background colour was attuned to 250. For all sections, we assessed the mean optical density and the quantity of pixels that had a positive reaction for Gd using the KSRun software (imaging system KS400, release 3.0; Zeiss, Vision GmbH, Germany).

Statistical analysis

The SPSS/PC software package, version 10.01 (SPSS, Munich, Germany), was used for collection, processing and statistical analysis of all data. Statistical analysis was performed using the non-parametrical Mann Whitney U test for comparison of the means. $P<0.05$ values were considered statistically significant.

Results

Characterisation of glycodelin-expressing cells in decidual tissue

First experiments showed that decidual tissue from normal human pregnancy gave a positive staining for glycodelin. For these, glycodelin expression was exclusively found in the decidua, whereas no staining could be detected in placental villi, neither in the trophoblast layer, nor in the villous stroma (Fig. 1). To determine which cells present in the decidua basalis express glycodelin, a fluorescence double labelling with cell markers (prolactin for decidual stromal cells, cytokeratin for trophoblast cells and CD45 for maternal leukocytes) and glycodelin antibodies was performed. The staining with the monoclonal anti-glycodelin antibody A87-B/D2 in combination with the polyclonal anti-prolactin antibody showed that the decidual stromal cells expressed glycodelin (Fig. 2a, b, c). Decidual leukocytes did not express glycodelin as could be verified by the combination of an anti-CD45 antibody with the polyclonal anti-glycodelin antibody UCI-2 (Fig. 2d). A third set of slides incubated with the anti-glycodelin antibody A87-B/D2 and afterwards with the anti-cytokeratin (CK) antibody A45-B/B3 showed that glycodelin A-positive cells in the decidua were CK negative (Fig. 2e) and, therefore, could neither be trophoblast cells nor epithelial cells of the uterine glands.

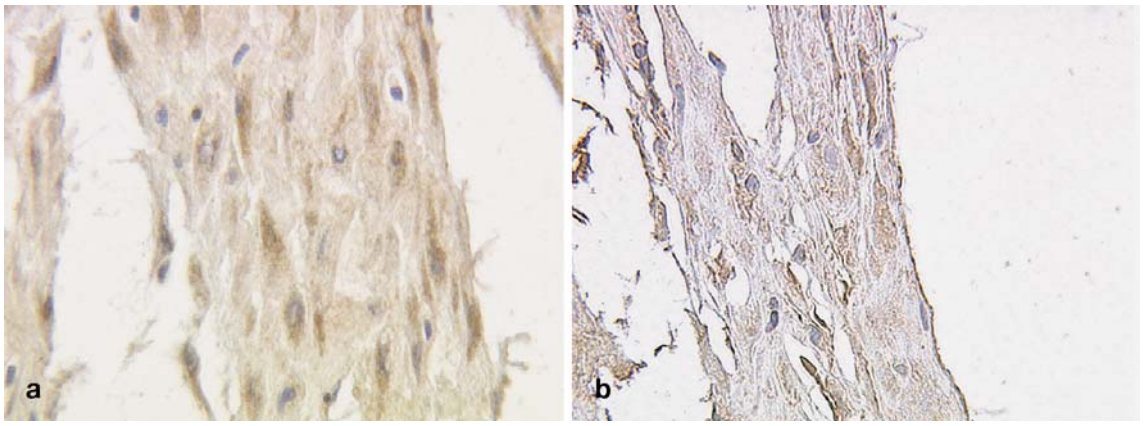

Fig. 6 Expression of glycodelin A in hemolysis, elevated liver, low platelet decidual tissue visualised with polyclonal antibody ×25 lens (**a**) and with the monoclonal antibody A87-B/D2, ×25 lens (**b**)

Immunohistochemistry for the comparison of normal and pathological pregnancies

We found a strong expression of glycodelin A in the decidua of normal control placentas with the polyclonal glycodelin antibody UCI-2 (Fig. 3a) as well as with the monoclonal antibody A87-B/D2 (Fig. 3b). The expression of glycodelin A was significantly reduced in the decidual cells of all three types of pathological pregnancies investigated: IUGR placentas (Fig. 4a, polyclonal glycodelin antibody, Fig. 4b, A87-B/D2, $P<0.001$), preeclamptic placentas (Fig. 5a, polyclonal glycodelin antibody, Fig. 5b, A87-B/D2, $P<0.001$) and HELLP placentas (Fig. 6a, polyclonal glycodelin antibody, Fig. 6b, A87-B/D2, $P<0.002$). A summary of decidual glycodelin expression intensity in the placentas investigated is summarised in Fig. 7.

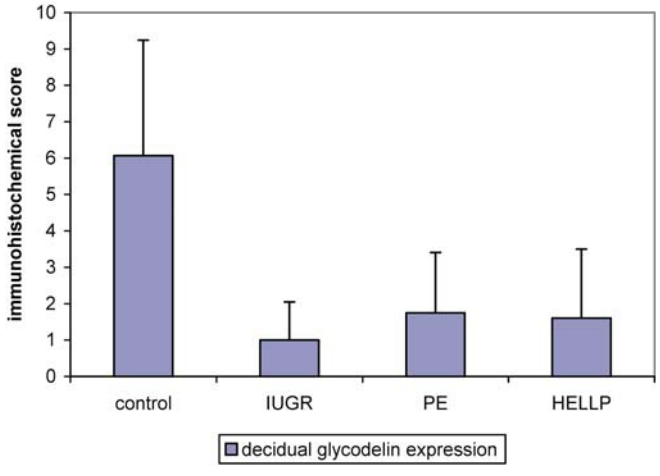

Fig. 7 Staining intensity of glycodelin in normal, preeclamptic and intrauterine growth-restricted (IUGR) decidual tissue determined by the semi-quantitative immunohistochemical immunoreactive score on the different tissue slides. Data shown represent mean±SEM. Differences in glycodelin expression in normal and IUGR decidual tissue, preeclamptic and hemolysis, elevated liver, low platelet decidual tissue are statistically significant ($P=0.000$, $P=0.000$ and $P=0.001$)

In situ hybridisation

As was to be expected because of the results obtained using immunohistochemistry, the expression of glycodelin mRNA was most intense in the decidua of normal control placentas (Fig. 8a). In decidual cells of IUGR placentas, the expression of glycodelin mRNA was significantly reduced compared with normal pregnancies (Fig. 8c, $P<0.012$). Preeclamptic placentas did also show a reduced expression of glycodelin A in decidual cells. This reduction, however, was not significant (Fig. 8e). HELLP tissue showed the same trend of significantly reduced mRNA for glycodelin in decidual cells (Fig. 8g, $P<0.007$) as IUGR placentas. All control sections that were incubated with the sense cRNA probe were devoid of any reaction (Fig. 8b, d, f, h).

The densitometric quantification of the glycodelin mRNA staining intensity showed the strongest mRNA expression in normal decidual cells. Comparable relative intensities in expression of glycodelin mRNA in preeclamptic placentas and significantly reduced expression of glycodelin mRNA were estimated in IUGR and HELLP placentas from mRNA levels (Fig. 9).

Discussion

As all cells present in placental villi were devoid of staining for glycodelin, our investigation focused on the decidua. For identification of glycodelin-expressing cells in this tissue, double-immunofluorescence methods were employed. Decidua cells are described to express prolactin [4]; therefore, we used this protein as a marker for the definition of the uterine stromal cells that change under the influence of pregnancy-associated hormones to decidua cells. These decidua cells were found to express glycodelin A; a result that verifies data obtained by Tseng et al. [36]. Glycodelin could not be found on CD 45-positive cells nor on cells reacting with the antibody for cytokeratin. Therefore, glycodelin is not expressed by trophoblast nor by maternal immune cells but only by decidua cells.

Normal foetal growth depends on several factors modulated by the foetus, the placenta and the mother. Small

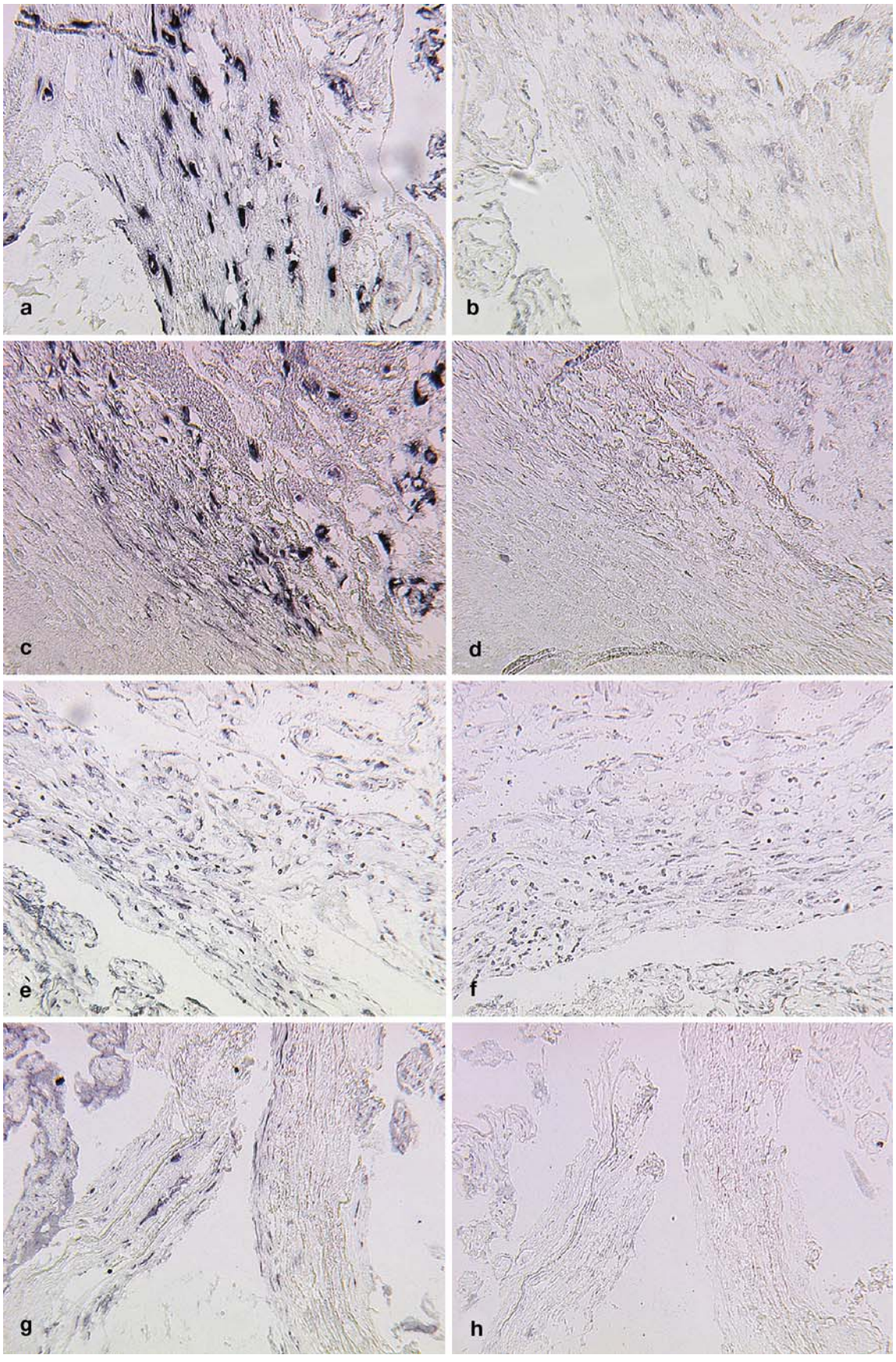

Fig. 8 Expression of glycodelin mRNA in normal decidual tissue (**a**: antisense, **b**: sense), intrauterine growth-restricted decidual tissue (**c**: antisense, **d**: sense), preeclamptic decidual tissue (**e**: antisense, **f**: sense) and hemolysis, elevated liver, low platelet decidual tissue (g: antisense, h: sense) detected by in situ hybridisation (×10 lens)

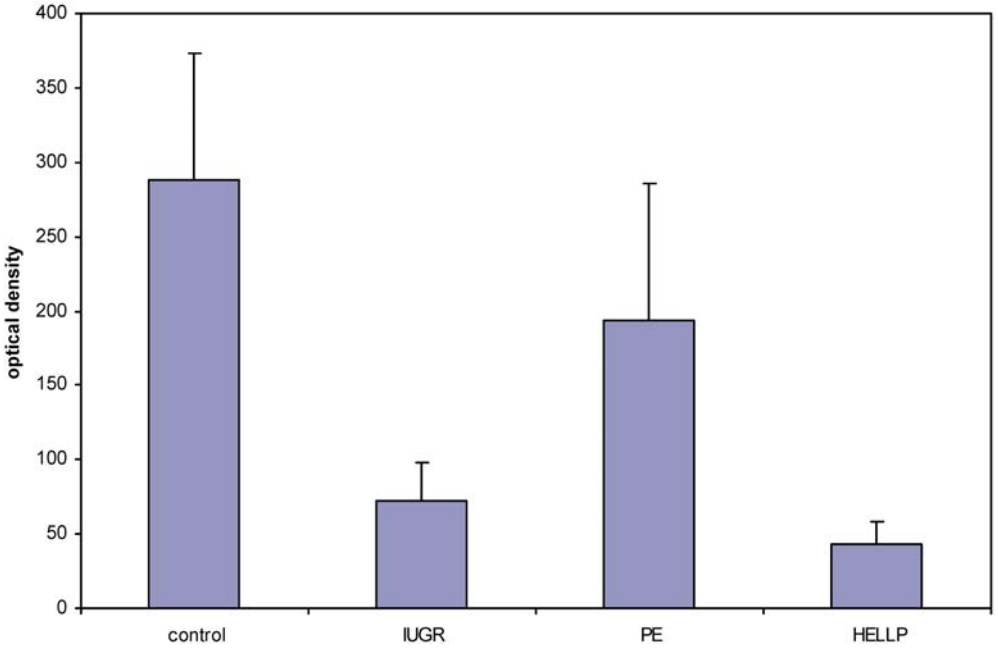

Fig. 9 Staining intensity of glycodelin mRNA by in situ hybridisation reaction in normal, intrauterine growth-restricted, preeclamptic and hemolysis, elevated liver, low platelet decidual tissue determined by a computerised analysis. Data shown represent mean±SEM

foetuses due to IUGR are at higher risk for poor perinatal and long-term outcome [1]. PE is characterised by hypertension, oedema and proteinuria and affects about 3% of all pregnancies [32]. PE is associated with IUGR and impairment in blood flow to the uterine circulation. IUGR, however, is not associated with hypertension, oedema and proteinuria. HELLP is a syndrome of haemolysis, elevated liver enzymes and low-platelet count [33]. Our investigations on glycodelin mRNA and protein expression on decidual tissue showed that this protein as well as its mRNA is significantly reduced in IUGR and HELLP decidual cells compared with those in normal pregnancies. In preeclamptic deciduas, only the expression of glycodelin protein is significantly reduced, whereas the mRNA level is not.

There exists only little information on glycodelin expression and gestational hypertension or growth retardation. Iino et al. [10] investigated serum concentration of placental protein 14 (PP14), which is the former name for glycodelin, in 129 healthy pregnant women and 40 women with gestational hypertension either with or without proteinuria at similar weeks. In normal pregnancy, maternal serum PP14 levels decreased towards term. In gestational hypertension, the values were higher than normal. The presence or absence of proteinuria did not affect these results [10]. In contrast, Howell et al. [8] demonstrated a slight reduction in the median values of PP14 in pregnancies complicated by hypertension. In addition to these early results, Howell et al. found that levels of PP12 were significantly elevated in patients with severe PE, whereas PP14 levels were unaffected [9]. Recent investigations showed that cord serum glycodelin concentrations were unaltered in diabetic pregnancies with hypertensive disorders (chronic hypertension, pregnancy-induced hypertension or PE) or foetal macrosomia compared with normal controls [22].

To our knowledge, this is the first report on glycodelin expression in decidual cells of IUGR and HELLP placentas. Glycodelin has immunosuppressive properties. This is important because the human conceptus is a semiallograft that is not subject to the laws of classical transplantation immunity. In contrast to other mucosal sites, where B cells, plasma cells, mast cells and eosinophils play an important role, the number of these cells in the decidua is negligible. In first trimester decidua, the main populations are $CD56^{+}$ NK-like cells (large granular lymphocytes, 70%), macrophages (20%) and T cells (10%) [6, 18]. NK cells have the ability to kill foreign cells without any prior exposure. Both glycodelin and the NK cells are abundant at the foeto–maternal interface. Glycodelin inhibits NK cell activity [27], and it stimulates the Th2-type cytokine production in monocytes [24], shown by an increased production of IL-6 and IL-10 following glycodelin exposure [20, 21]. Glycodelin directly inhibits T-cell activity [28] on an early phase of activation by diminishing T-cell responses in the contact site at the time of T-cell receptor triggering and inducing T-cell apoptosis [29]. In pregnancies complicated by PE or HELLP syndrome, an increase of foetal DNA in the maternal serum indicates an increased lysis of foetal cells by maternal immune cells [5].

In summary, glycodelin protein expression is significantly reduced in PE, IUGR or HELLP decidual cells. Glycodelin mRNA expression is significantly reduced in IUGR and HELLP decidual cells. Because glycodelin is known to be a major immunosuppressive protein of the implantation side, reduced suppression of the maternal immune response can be discussed for PE, IUGR or HELLP syndrome. Further investigations are necessary to show if reduced glycodelin expression is accompanied with increased activation of maternal immune response.

References

1. Baschat AA, Hecher K (2004) Fetal growth restriction due to placental disease. Semin Perinatol 28:67–80
2. Bergemann C, Reimer T, Muller H, Hosel A, Briese V, Friese K, Jeschke U (2003) Stimulation of hCG protein and mRNA levels in trophoblast tumour cells Jeg3 and BeWo by glycodelin A. Anticancer Res 23:1107–1113
3. Bohn H, Kraus W, Winckler W (1982) New soluble placental tissue proteins: their isolation, characterization, localization and quantification. Placenta 4[Suppl]:67–81
4. Bonney RC, Franks S (1990) The endocrinology of implantation and early pregnancy. Baillieres Clin Endocrinol Metab 4: 207–231
5. Brune T, Hornung T, Koch HG, F GR, Louwen F (2004) The increased lysis of fetal cells in the mother after pregnancies complicated by pre-eclampsia or HELLP syndrome is not the result of a specific anti-fetal cytotoxicity of the mother. Am J Reprod Immunol 51:174–179
6. Bulmer JN, Morrison L, Longfellow M, Ritson A, Pace D (1991) Granulated lymphocytes in human endometrium: histochemical and immunohistochemical studies. Hum Reprod 6: 791–798
7. Dell A, Morris HR, Easton RL, Panico M, Patankar M, Oehniger S, Koistinen R, Koistinen H, Seppala M, Clark GF (1995) Structural analysis of the oligosaccharides derived from glycodelin, a human glycoprotein with potent immunosuppressive and contraceptive activities. J Biol Chem 270:24116–24126
8. Howell RJ, Bolton AE, Chard T (1986) Placental protein 14 (PP14) in late pregnancy. Arch Gynecol 239:27–29
9. Howell RJ, Economides D, Teisner B, Farkas AG, Chard T (1989) Placental proteins 12 and 14 in pre-eclampsia. Acta Obstet Gynecol Scand 68:237–240
10. Iino K, Julkunen M, Sjoberg J, Seppala M (1986) Is decidua affected in gestational hypertension? Indication by elevated PP14 levels. Acta Obstet Gynecol Scand 65:367–370
11. Jeschke U, Richter DU, Walzel H, Bergemann C, Mylonas I, Sharma S, Keil C, Briese V, Friese K (2003) Stimulation of hCG and inhibition of hPL in isolated human trophoblast cells in vitro by glycodelin A. Arch Gynecol Obstet 268:162–167
12. Jeschke U, Wang X, Briese V, Friese K, Stahn R (2003) Glycodelin and amniotic fluid transferrin as inhibitors of E-selectin-mediated cell adhesion. Histochem Cell Biol 119:345–354
13. Joshi SG, Szarowski DH, Bank JF (1981) Decidua-associated antigens in the baboon. Biol Reprod 25:591–598
14. Julkunen M, Rutanen EM, Koskimies A, Ranta T, Bohn H, Seppala M (1985) Distribution of placental protein 14 in tissues and body fluids during pregnancy. Br J Obstet Gynaecol 92: 1145–1151
15. Julkunen M, Koistinen R, Sjoberg J, Rutanen EM, Wahlstrom T, Seppala M (1986) Secretory endometrium synthesizes placental protein 14. Endocrinology 118:1782–1786
16. Julkunen M, Seppala M, Janne OA (1988) Complete amino acid sequence of human placental protein 14: a progesterone-regulated uterine protein homologous to beta-lactoglobulins. Proc Natl Acad Sci U S A 85:8845–8849
17. Keil C, Husen B, Giebel J, Rune G, Walther R (1999) Glycodelin mRNA is expressed in the genital tract of male and female rats (Rattus norvegicus). J Mol Endocrinol 23:57–66
18. King A, Birkby C, Loke YW (1989) Early human decidual cells exhibit NK activity against the K562 cell line but not against first trimester trophoblast. Cell Immunol 118:337–344
19. Koistinen H, Koistinen R, Dell A, Morris HR, Easton RL, Patankar MS, Oehninger S, Clark GF, Seppala M (1996) Glycodelin from seminal plasma is a differentially glycosylated form of contraceptive glycodelin-A. Mol Hum Reprod 2:759–765
20. Laird SM, Li TC, Bolton AE (1993) The production of placental protein 14 and interleukin 6 by human endometrial cells in culture. Hum Reprod 8:793–798
21. Laird SM, Tuckerman E, Li TC, Bolton AE (1994) Stimulation of human endometrial epithelial cell interleukin 6 production by interleukin 1 and placental protein 14. Hum Reprod 9:1339–1343
22. Loukovaara M, Leinonen P, Teramo K, Koistinen R (2004) Cord serum glycodelin concentrations in normal pregnancies and pregnancies complicated by diabetes. Arch Gynecol Obstet 270:161–164
23. Mazurkiewicz JE, Bank JF, Joshi SG (1981) Immunocytochemical localization of a progestagen-associated endometrial protein in the human decidua. J Clin Endocrinol Metab 52: 1006–1008
24. Miller RE, Fayen JD, Chakraborty S, Weber MC, Tykocinski ML (1998) A receptor for the lipocalin placental protein 14 on human monocytes. FEBS Lett 436:455–460
25. Mylonas I, Speer R, Makovitzky J, Richter DU, Briese V, Jeschke U, Friese K (2000) Immunohistochemical analysis of steroid receptors and glycodelin A (PP14) in isolated glandular epithelial cells of normal human endometrium. Histochem Cell Biol 114:405–411
26. Mylonas I, Makovitzky J, Richter DU, Jeschke U, Briese V, Friese K (2003) Cathepsin D expression in normal, hyperplastic and malignant endometrial tissue: an immunohistochemical analysis. Acta Histochem 105:245–252
27. Okamoto N, Uchida A, Takakura K, Kariya Y, Kanzaki H, Riittinen L, Koistinen R, Seppala M, Mori T (1991) Suppression by human placental protein 14 of natural killer cell activity. Am J Reprod Immunol 26:137–142
28. Rachmilewitz J, Riely GJ, Tykocinski ML (1999) Placental protein 14 functions as a direct T-cell inhibitor. Cell Immunol 191:26–33
29. Rachmilewitz J, Riely GJ, Huang JH, Chen A, Tykocinski ML (2001) A rheostatic mechanism for T-cell inhibition based on elevation of activation thresholds. Blood 98:3727–3732
30. Reimer T, Koczan D, Briese V, Friese K, Richter D, Thiesen HJ, Jeschke U (2000) Absolute quantification of human chorionic gonadotropin-beta mRNA with TaqMan detection. 4. Mol Biotechnol 14:47–57
31. Remmele W, Hildebrand U, Hienz HA, Klein PJ, Vierbuchen M, Behnken LJ, Heicke B, Scheidt E (1986) Comparative histological, histochemical, immunohistochemical and biochemical studies on oestrogen receptors, lectin receptors, and Barr bodies in human breast cancer. Virchows Arch 409:127–147
32. Schlembach D (2003) Pre-eclampsia—still a disease of theories. Fukushima J Med Sci 49:69–115
33. Sibai BM (2004) Diagnosis, controversies, and management of the syndrome of hemolysis, elevated liver enzymes, and low platelet count. Obstet Gynecol 103:981–991
34. Song M, Ramaswamy S, Ramachandran S, Flowers LC, Horowitz IR, Rock JA, Parthasarathy S (2001) Angiogenic role for glycodelin in tumorigenesis. Proc Natl Acad Sci U S A 98:9265–9270
35. Tomczak S, Briese V, Kunkel S, Muller H (1996) Serum placental protein 14 (PP14) levels in patients with threatened abortion. Arch Gynecol Obstet 258:165–169
36. Tseng L, Mazella J (2002) Endometrial cell specific gene activation during implantation and early pregnancy. Front Biosci 7:1566–1574

Virchows Arch (2005) 446: 369–378
DOI 10.1007/s00428-004-1177-z

ORIGINAL ARTICLE

E. Herpel · S. Singer · C. Flechtenmacher · M. Pritsch · F.-U.Sack · S. Hagl · H. A. Katus · M. Haass · H. F. Otto · P. A. Schnabel

Extracellular matrix proteins and matrix metalloproteinases differ between various right and left ventricular sites in end-stage cardiomyopathies

Received: 5 August 2004 / Accepted: 10 November 2004 / Published online: 2 April 2005
© Springer-Verlag 2005

Abstract This study was undertaken to investigate whether there might be differences in the distribution of extracellular matrix (ECM) proteins and matrix metalloproteinases (MMPs), depending on their specific sites within the heart. We investigated 33 explanted human hearts, 15 with dilated cardiomyopathy (DCM) and 18 with ischemic cardiomyopathy (ICM). Transmural samples from the right ventricle, the interventricular septum and the left ventricle, either from near the apex or from near the base were taken from every heart. Frozen sections were processed for connective tissue staining and immunohistochemistry for collagens type I, III, IV, laminin and fibronectin, as well as MMP-1, -2 and -9. Volume densities of laminin in ICM as well as of fibronectin and collagen types I and IV in DCM showed significant differences between right and left ventricular sites. The volume densities of matrix proteins usually did not reveal significant differences among the three left ventricular sites tested in both DCM and ICM. MMPs partly showed differences between the right and the left ventricular myocardium. These results suggest that the distributions of ECM proteins and MMPs differ between the two ventricles in both end-stage DCM and ICM. This gives rise to the hypothesis that a specific pattern of ECM degradation exists in the right and left ventricular myocardium.

Keywords Extracellular matrix · Remodeling · Cardiomyopathies · Left ventricle · Right ventricle

E. Herpel · S. Singer · C. Flechtenmacher · H. F. Otto · P. A. Schnabel
Department of Pathology, University of Heidelberg, INF 220/1, 69120 Heidelberg, Germany
e-mail: philipp_schnabel@med.uni-heidelberg.de
Tel.: +49-6221-396496
Fax: +49-6221-565251

M. Pritsch
Department of Medical Biometry, University of Heidelberg, Germany

F.-U. Sack · S. Hagl
Department of Cardiac Surgery, University of Heidelberg, Germany

Introduction

The extracellular matrix (ECM) surrounds myocytes and myofibroblasts and is responsible for the three-dimensional spatial arrangement necessary for the integrity and metabolic function in the tissue of the intercellular space [14, 20, 33]. The ECM is not a static structure but is remodeled constantly [5, 31].

Some of the important components of the ECM are collagen types I and III and fibronectin, which ensure the structural integrity of adjoining myocytes and the connecting of the myocytes to the surrounding vasculature. Other components are laminin and collagen type IV, which are predominantly located in basement membranes [21, 32].

The ECM builds a continuum among different cell types within the myocardium and provides a structural supporting network to maintain myocardial geometry during the cardiac cycle [27]. Disruption or discontinuities within the fibrillar ECM network result in a loss of normal structural support, resulting in myocyte fascicles being subjected to abnormal stress and strain patterns during the cardiac cycle, which, in turn, result in changes in myocardial geometry and function [26].

The enzyme system that is responsible for ECM degradation within the myocardium is particularly relevant for the development of dilated cardiomyopathy (DCM) and ischemic cardiomyopathy (ICM). Therefore, it is necessary to understand the way in which enzyme system works [7, 22, 23].

Matrix metalloproteinases (MMPs) are members of a family of more than 20 zinc-dependent enzymes. Much evidence indicates that they play an important role in tissue remodeling. They can be subdivided into four groups, based upon their substrate specificity and primary structure [6, 15, 30]. The first group, the collagenases, including MMP-1 (interstitial collagenase), can all cleave fibrillar collagen types I and III. A second group consists of MMP-2 and MMP-9, also called gelatinases. They have the ability to degrade gelatin and collagen type IV, which are components of basement membranes [9]. Another group of MMPs are called stromelysins [9]. Group 4 contains the membrane-

type MMPs, which degrade several ECM components, such as collagen types I and III, laminin and fibronectin. They are also able to activate other MMPs [9].

It is crucial to keep the activity of these enzymes under tight control, because they are capable of degrading the complete ECM. The regulation of MMP activity in normal myocardium can be controlled at the transcriptional level as well as at the activation level (e.g., by the plasminogen/plasmin system). Activated MMPs can also be inhibited by their endogenous inhibitors, the tissue inhibitors of matrix metalloproteinases (TIMPs), which are able to bind MMPs in a ratio of 1:1 [10, 14].

Previous studies on DCM or ICM have shown a dysregulation and upregulation of collagenolytic activity, which leads to interruption and disorganization of the ECM and to cardiac dysfunction [10, 18, 25].

As of yet, there have not been many studies systematically comparing different sites in the heart or investigating the pattern of distribution of ECM proteins and MMPs [2, 3]. Further, most studies preparing ventricular myocardium have not described exactly from which site within the left or right ventricle the samples were taken from. Besides that, many authors have only prepared one site per ventricle [20, 21, 25, 26, 35].

Thus, the purpose of the present study was to compare the patterns of distribution of total connective tissue, of matrix proteins, of MMPs and TIMP-1 in four defined regions in the myocardium of explanted hearts. First, we wanted to examine whether there are differences between right and left ventricular myocardium and, second, whether there are differences among the three sites of the left ventricle. Therefore, for each heart, we investigated transmural samples from the right ventricle, the septal region and the left ventricle, taking a sample from near the apex and another from near the base. Patients had been suffering from DCM or ICM.

Materials and methods

Patients

The material consisted of 33 explanted human hearts. Of the patients, 15 had been suffering from DCM, 18 from ICM. Four different sites were investigated for each heart. Transmural samples ware taken from the right ventricle, from the interventricular septum and from the left ventricle—in each case, one from near the apex and another from near the base. The tissue samples were taken immediately after explantation and were embedded in Tissue Tek (Sakura, Netherlands, Batch # 4583000) and stored at −70°C.

Cryosections 4-μm thick were cut at −20°C with a Frigocut E (Reichert-Jung Model 2800, Nussloch, Germany) and then fixed in acetone. Until use they were stored at −70°C.

The mean age of the patients at the time of heart transplantation (HTX) was 53.2 years (SD: 12.0 years); 6 were female, 27 male. The mean age at the time of HTX in the cohort of DCM, including 2 female and 13 male patients, was 47.1 years (SD: 14.4 years). The mean age of the 4 female and 14 male patients suffering from ICM was 58.3 years (SD: 6.3 years).

Immunohistochemistry

Sections were washed in phosphate buffered saline (PBS) twice for 5 min and processed for 20 min with a mixture of CAS-block, albumin and γ-venin to saturate non-specific immunoglobulin binding sites and then incubated for 1 h at room temperature in a humidified chamber with specific antibodies:

Collagen type I	(Cat. no. 2150-0020 Bio Trend, Köln, Germany), polyclonal rabbit, 1:100
Collagen type III	(Cat. no. MU 167-UC BioGenex, San Ramon, CA, USA), monoclonal mouse, 1:200
Collagen type IV	(Cat. no. MU-379-UC BioGenex), monoclonal mouse, 1:200
Fibronectin	(Code no. A0 245 Dako, Denmark), polyclonal rabbit, 1:800
Laminin	(Cat. no. PU078-UP BioGenex), polyclonal rabbit, 1:50
MMP-1 (IHC)	(Cat. no. 551000 BD Biosciences PharMingen, San Diego, CA, USA), monoclonal mouse, 1:100
MMP-2 (Ab-4)	(Cat. no. IM 51 Oncogene Research Products, Boston, MA, USA), monoclonal mouse, 1:25
MMP-9 (Ab-7)	(Cat. no. IM 61 Oncogene), monoclonal mouse, 1:100
TIMP-1 (Ab-4)	(Cat. no. IM 63 Oncogene), monoclonal mouse, 1:20

All antibodies were diluted with common-antibody diluent from BioGenex.

For rabbit antibodies, as negative control, rabbit isotype control from Zytomed, San Francisco, CA, USA (Cat. no. 0861 99) was used. As negative control for mouse antibodies, mouse IgG from Dako (Code no. XO 931) was used. Afterward, sections were washed twice in PBS. In the following step, the second block, consisting of antibody-diluent and goat serum, was applied and incubated for 20 min. Thereafter, goat-anti-mouse from the "supersensitive-detection-kit" (BioGenex, Cat. no. ZA 000-UM) diluted 1:20 for mouse antibodies and IgG-Biotin-anti-Rabbit (Zymed Cat. no. 62-6140) diluted 1:400 for rabbit antibodies were applied for 30 min. After being washed twice in PBS, they were incubated with streptavidin-alkaline-phosphatase from the "supersensitive-detection-kit" (BioGenex). Before staining was performed with Fast-Red, the sections were washed twice in PBS. Contrast staining was carried out using haemalum (Cat. no. S2020 Dako, Denmark). Lastly, sections were coverslipped with Glycergel (Cat. no. C0 563, Dako).

The morphometric analysis was carried out by "random system sampling" on a grid through a light microscope

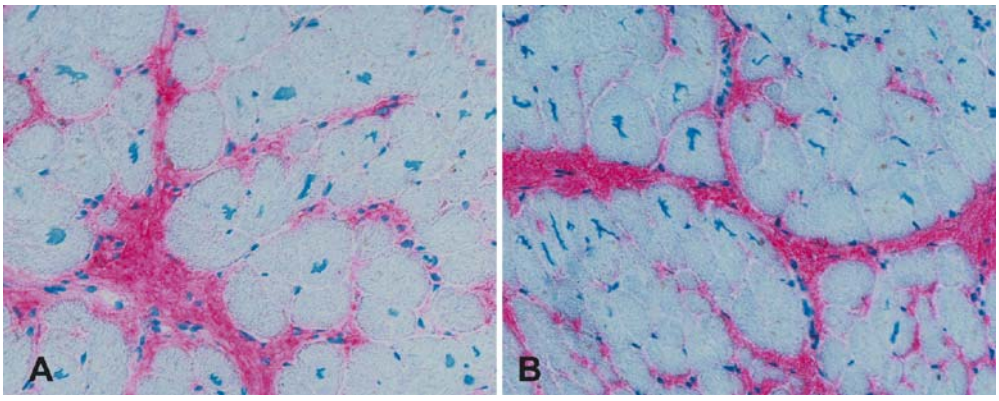

Fig. 1 A Perimysial expression of collagen type I in dilated cardiomyopathy, immunohistological staining. **B** Perimysial expression of collagen type I in ischemic cardiomyopathy, immunohistological staining

using the point-counting method [8, 36]. The parameters within the perimysium (collagen types I and III, fibronectin) were investigated at a final magnification of ×200, and the parameters in the endomysial space (collagen IV, laminin) were investigated at a final magnification of ×1000 with a Zeiss Axioscope (Jena, Germany). Per tissue block, 20 fields in ×200 magnification and 35 fields in ×1000 magnification were measured.

The cells with positive reactions for MMPs and TIMP-1 were counted under the Zeiss microscope at a final magnification of ×400. The areas of the cryotome sections were measured with Optimas 5.2, Leiden, Netherlands, and the Hi Resolution CCD-IRIS camera (Sony, Tokyo, Japan).

Statistics

The distribution of the various ECM parameters at the different sites was visualized using boxplots. The distributions of MMPs and TIMPs were described by mean and SD. The Wilcoxon-signed-rank-test was applied to test for differences in the distributions of the matrix proteins, MMPs and TIMP-1 among the various sites. Test results with P values$\leq$0.05 were regarded as statistically significant.

Due to the multiple testing, however, the P values cannot be interpreted in a confirmatory sense. Adjustment of the local significance levels in the various tests was not feasible due to the large number of comparisons and the explorative nature of the investigation.

Results

Qualitative morphology of myocardial interstitium

In DCM and ICM hearts, collagen type I was primarily expressed in the perimysium (Fig. 1). Collagen type III was mainly expressed in the perimysium and also, to some extent, in the endomysium. In contrast, collagen type IV was expressed in the endomysium and framed the cardiomyocytes (Fig. 2), as did the glycoprotein, laminin. Fibronectin was primarily expressed in the perimysium. MMP-1, MMP-2, MMP-9 and TIMP-1 were located in interstitial cells and (myo)fibroblasts. No positive signals were found within cardiomyocytes.

Immunohistochemistry and morphometry of matrix proteins, MMPs and TIMP-1

In DCM, there were greater volume densities of ECM components than in ICM. In both groups, collagen type III made up the greatest fraction, followed by fibronectin and collagen type I. Laminin and collagen type IV were less strongly expressed.

Comparing the four sites, in most cases we found no statistically significant differences between the volume densities, although the right ventricle, the two sites of the left ventricle and the interventricular septum descriptively showed different volume densities (Fig. 3 and Fig. 4).

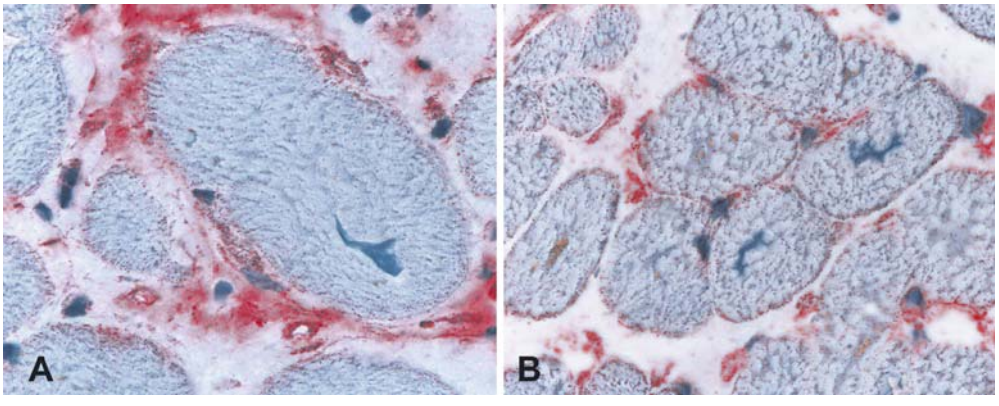

Fig. 2 A In dilated cardiomyopathy, diffuse extracellular immunohistological staining for collagen type IV can be seen in the endomysium. **B** Immunohistochemical staining for collagen type IV in dilated cardiomyopathy. Positively stained vascular basement membranes of endothelial cells and smooth muscle cells were also found in the myocardium

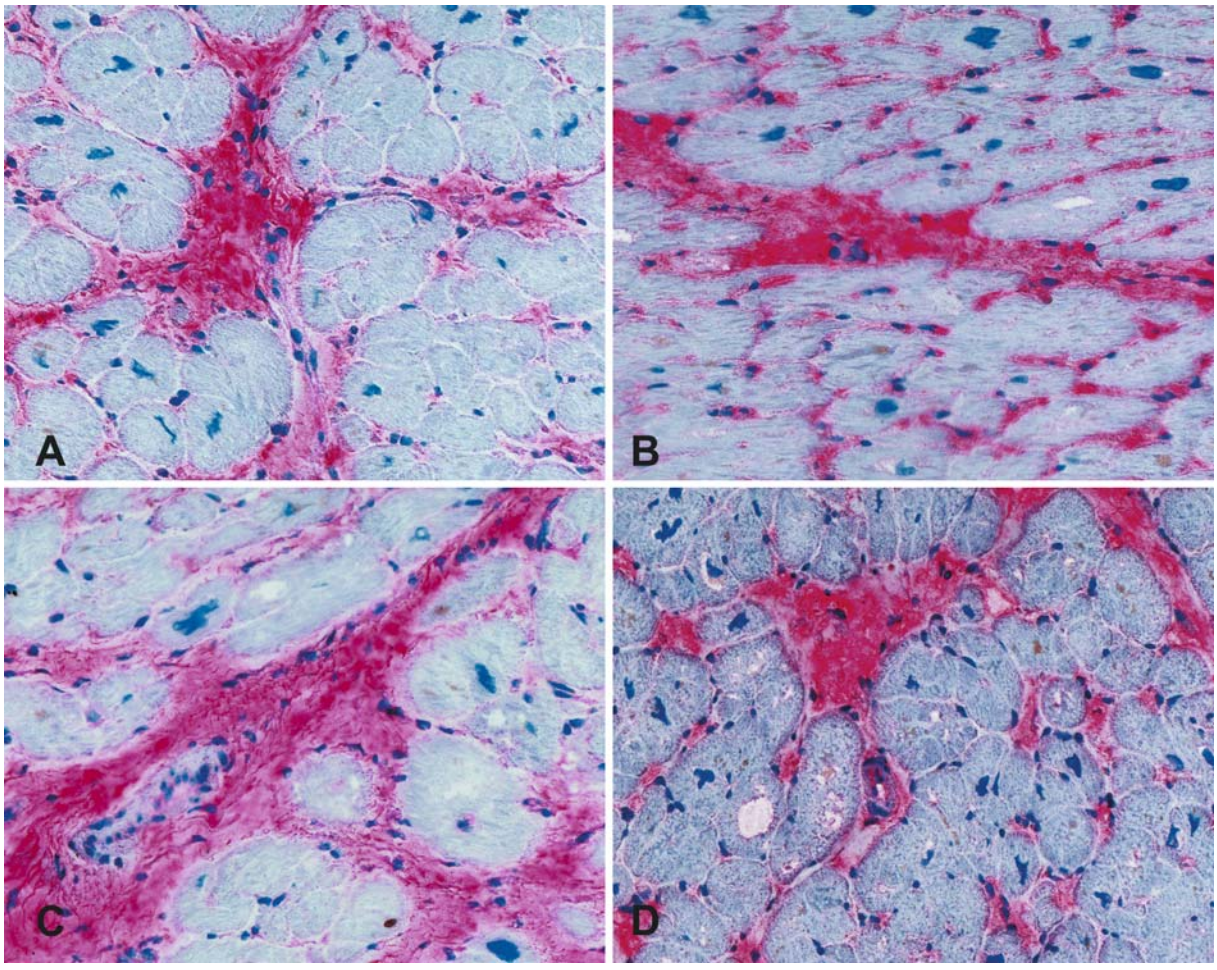

Fig. 3 Immunohistochemical staining for fibronectin in dilated cardiomyopathy showed significant differences between the right ventricle and (**A**) the left ventricle (**C**) near the apex. No differences were found in comparison with the left ventricle near the base (**B**) or the interventricular septum (**D**)

Results of the immunohistochemistry of the matrix proteins related to the different sites are indicated as volume densities in Fig. 5. Only a few comparisons revealed significant differences. In ICM, the content of laminin in the right ventricle was decreased in comparison with all other sites. Volume densities of collagen type III were different between the interventricular septum and the left ventricle near the apex (Table 1). In DCM, the volume densities of fibronectin and collagen type I were significantly higher in the left ventricle near the apex than in the right ventricle. Collagen type IV in DCM was decreased in the right ventricle relative to the interventricular septum or the left ventricle near the base.

Using the histochemical connective tissue stain, no significant differences between the sites were found in DCM. In ICM, significantly decreased values in the left ventricle near the base in comparison with the interventricular septum or the left ventricle near the apex were detected (Table 1). The standard deviations of the matrix proteins were mostly greater in DCM than in ICM (Fig. 5).

The results for matrix metalloproteinases and their inhibitors are listed in Table 1 and Table 2. The MMPs and TIMP-1 showed only a few significant differences between the sites tested. In ICM, the right ventricle showed more cells per mm^2 than the interventricular septum or the left ventricle near the base.

MMP-9 values in the right ventricle were increased in comparison with the interventricular septum. In dilated cardiomyopathy, significant differences were only found for three comparisons. The right ventricle in MMP-1 showed more cells per mm^2 than the interventricular septum and fewer cells than the left ventricle near the apex. The left ventricle near the base showed an increased number of MMP-2-positive cells in comparison with the interventricular septum.

TIMP-1 did not show any significant difference within number of positive cells between the sites in DCM or in ICM. However, TIMP-1 and the MMPs showed a great range in all the sites tested (Table 1).

Discussion

This study was designed to test the hypothesis that there are differences in the pattern of distribution of the matrix proteins, MMPs and TIMP-1 involved in the remodeling

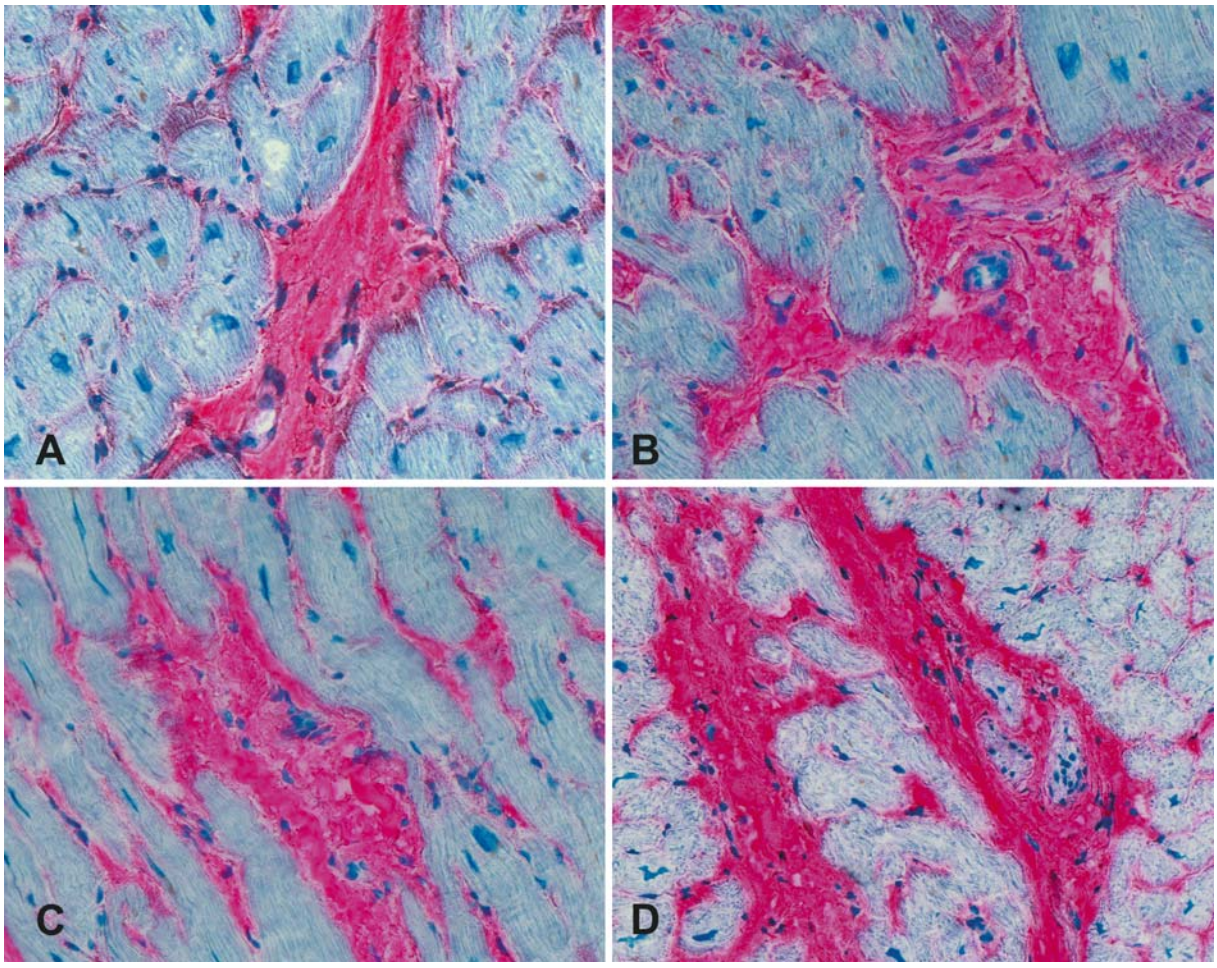

Fig. 4 Immunohistochemical staining for collagen type III in ischemic cardiomyopathy showed a significant difference between the left ventricle near the apex (**C**) and the interventricular septum (**D**). Right ventricle (**A**) and left ventricle (**B**) near the base

processes according to whether they occur at left or at right ventricular sites. To our knowledge, there have not been many studies systematically comparing left and right ventricular myocardium or even different sites in the heart. In addition, many groups have only prepared one site per ventricle [20, 21, 25, 26, 35], and most of these groups have not described exactly from which site within the left or right ventricle their samples were taken. Also, most studies only investigated the total amount of fibrosis using connective tissue staining [2, 3]. They did not focus on the different proteins existing in the ECM.

Therefore, the purpose of the present study was to determine and to compare the patterns of distribution of total connective tissue as well as of above-noted ECM components in four defined regions in the myocardium of explanted hearts. We wanted to examine first, whether there are differences between right and left ventricular myocardium and, second, whether there are differences among the three sites of the left ventricle.

As mentioned above, we wanted to know if there are differences in total connective tissue staining between right and left ventricular myocardium. This could be expected because of different stress-strain patterns existing in the two ventricles. Beltrami et al. [2] investigated the amount of fibrosis in left and right ventricular myocardium in ICM. Although, in their study, the right and left ventricle were sliced into seven sections, only two sections (out of the middle of each ventricle) were used to perform connective tissue staining. In these sections, they described larger amounts of fibrosis within the left ventricle than in the right ventricle. Another study that focused on DCM showed an increased amount of fibrosis on the left side of the interventricular septum in comparison with the right side [35]. Therefore, and because of above-noted aspects, we also expected differences of total connective tissue staining. However, we also found different values for total connective tissue staining between the right and the left ventricular sites, which have unfortunately not been significant.

In addition to our investigations on total connective tissue staining, we also wanted to examine whether the pattern of distribution of matrix proteins differed between right and left ventricular myocardium. Using immunohistochemistry, we were able to detect the matrix proteins either in peri- and/or endomysium of right and left ventricular myocardium. These qualitative results were similar to those from other studies dealing with DCM and ICM, which found the same matrix proteins in peri- and endomysium [16, 21, 29]. When comparing volume densities of collagen types I, III,

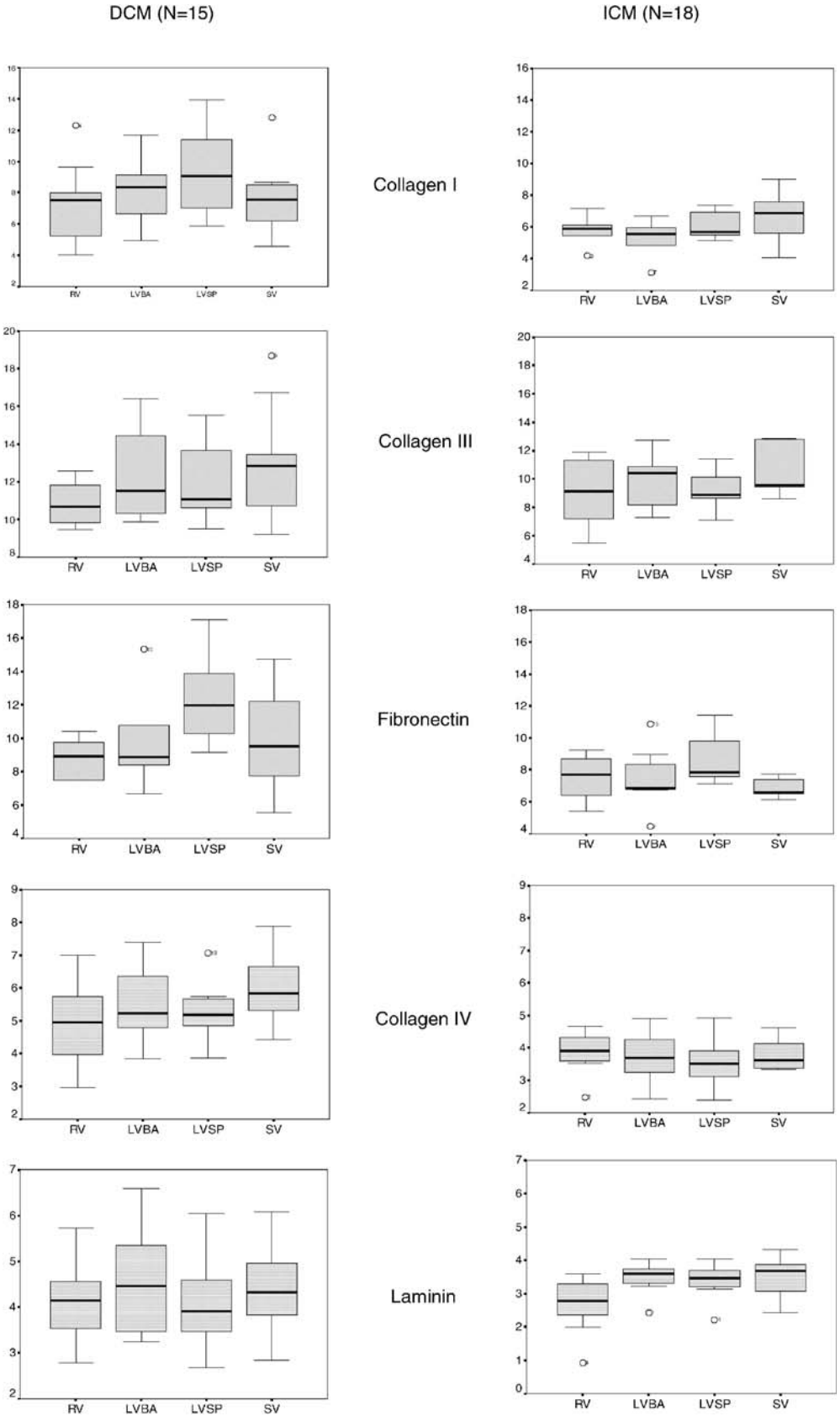

Fig. 5 Volume densities of collagen types I, III and fibronectin in the perimysium and of collagen type IV and laminin in the endomysium in dilated cardiomyopathy (DCM) and ischemic (ICM) cardiomyopathy. Mean±SD. *RV* right ventricle. *LVBA* left ventricle near the base. *LVSP* left ventricle near the apex. *SV* interventricular septum

Table 1 Comparison of *P* values from matrix proteins, matrix metalloproteinases (MMPs) and tissue inhibitors of matrix metalloproteinases (TIMP)-1 in dilated cardiomyopathy (DCM) and ischemic (ICM) cardiomyopathy. *RV* right ventricle, *LVba* left ventricle near the base, *LVap* left ventricle near the apex, *SV* interventricular septum, $V_{V\,peri}$ volume density in perimysium, $V_{V\,endo}$ volume density in endomysium

	P values					
	RV compared with LVba	RV compared with LVap	RV compared with SV	LVba compared with LVap	LVba compared with SV	Lvap compared with SV
DCM						
$V_{V\ peri}$collagen I	0.657	0.05*	0.534	0.209	0.722	0.034*
$V_{V\ peri}$collagen III	0.131	0.272	0.11	0.722	0.767	0.594
$V_{V\ peri}$fibronectin	0.237	0.005*	0.11	0.123	0.612	0.11
$V_{V\ endo}$collagen IV	0.046*	0.173	0.019*	0.754	0.422	0.064
$V_{V\ endo}$ laminin	0.345	0.875	0.249	0.075	0.552	0.158
$V_V$connective tissue	0.878	0.203	0.79	0.374	0.721	1.169
MMP-1	0.363	0.036*	0.027*	0.363	0.363	0.427
MMP-2	0.753	0.272	0.060	0.600	0.013*	0.158
MMP-9	0.069	0.46	0.245	0.394	0.865	0.460
TIMP-1	0.388	0.209	0.173	0.925	0.650	0.778
ICM						
$V_{V\ peri}$collagen I	0.721	0.499	0.182	0.515	0.221	0.139
$V_{V\ peri}$collagen III	0.203	1.000	0.086	0.051	0.790	0.012*
$V_{V\ peri}$fibronectin	0.859	0.091	0.937	0.086	0.285	0.059
$V_{V\ endo}$collagen IV	0.152	0.26	0.203	0.114	0.814	0.484
$V_{V\ endo}$ laminin	0.021*	0.017*	0.016*	0.515	0.477	0.508
$V_V$connective tissue	0.484	0.214	0.310	0.037*	0.036*	0.285
MMP-1	0.007*	0.133	0.022*	0.306	0.420	0.711
MMP-2	0.26	0.638	0.929	0.093	0.959	1.000
MMP-9	0.062	0.811	0.035*	0.177	0.877	0.068
TIMP-1	0.272	0.069	0.356	0.438	0.557	0.777

*$P \leq 0.05$ is significant

IV, laminin and fibronectin, we found statistically significant differences for perimysial as well as for endomysial laminin and collagen type IV (Table 1). The other matrix proteins also showed differences within their volume densities, which were not statistically significant. As in our study, an examination of acute ischemia in human myocardium also found an increase in the relative content of collagens in the left ventricle compared with that of the right [1]. Unfortunately, we have not found any other studies focusing on quantitative comparisons of matrix proteins in left and right ventricular myocardium. Thus, our findings have to be interpreted carefully, because they cannot be compared with other studies. Despite this, however, our observations in patients with different cardiomyopathies suggest that specific patterns of ECM degradation exist in the failing right and left ventricular myocardium, which lead to different patterns of distribution of matrix proteins in the two ventricles.

Table 2 Expression of matrix metalloproteinases (MMP)-1, MMP-2, MMP-9 and tissue inhibitors of matrix metalloproteinases (TIMP)-1 (mean ± SD) in dilated (DCM) and ischemic (ICM) cardiomyopathy at various sites. *RV* right ventricle, *LVba* left ventricle near the base, *LVap* left ventricle near the apex, *SV* interventricular septum

	Numbers of cases	RV (cells/mm^2)	LVba (cells/mm^2)	LVap (cells/mm^2)	SV (cells/mm^2)
DCM					
MMP-1	15	2.06±1.00	1.95±2.07	1.46±0.81	1.34±0.84
MMP-2	15	5.51±3.36	5.89±3.63	4.34±2.51	3.32±1.20
MMP-9	15	1.18±1.20	0.78±1.09	0.84±0.70	0.78±1.22
TIMP-1	15	0.15±0.27	0.25±0.28	0.51±1.16	0.26±0.29
ICM					
MMP-1	18	2.27±1.10	1.55±1.34	1.72±1.09	1.71±1.17
MMP-2	18	5.15±3.74	4.41±1.70	4.22±2.28	4.24±2.58
MMP-9	18	1.25±0.98	0.78±0.84	1.21±1.15	0.67±0.86
TIMP-1	18	0.11±0.13	0.16±0.18	0.22±0.39	0.22±0.31

We also wanted to know whether different sites of the left ventricle show differences in the pattern of distribution of total connective tissue staining and matrix proteins. Thus, we investigated the septal region, the left ventricle near the apex and the base. Comparisons between these different parts of the left ventricle (Fig. 5) showed differences in volume densities. Although these differences were somewhat similar to the differences found upon comparison of the left and right ventricular myocardium, they were not statistically significant. Again, we are aware of only a few other studies referring to different left ventricular sites. For example, one study on total connective tissue staining described comparisons within the interventricular septum as

mentioned above [35]. Although we found a few differences in the expression of ECM components between the left ventricular sites, no definite statement on the distribution of matrix proteins is possible, because there are no data available that could support our findings. Therefore, further studies in combination with biochemical analysis should be performed.

Studies on dilated or ischemic cardiomyopathy have shown a dysregulation and upregulation of collagenolytic activity [11, 37]. Therefore, we wanted to know whether there were differences in the pattern of distribution of MMPs and TIMP-1 even within left ventricular sites or between right and left ventricular myocardium.

Wang et al. [37] described an intracellular action of MMP-2 during acute myocardial ischemia and reperfusion injury. Florholmen et al. were able to show an upregulation of TIMP-2 expression in cardiomyocytes [11]. However, we found no positive signals for MMPs and TIMPs within cardiomyocytes. We only detected positive signals in fibroblasts.

Due to remodeling, one working hypothesis was that there could be an increase in MMPs within areas that contain larger amounts of their substrates [34]. However, there was usually no evident relationship between MMP expression and the amount of fibrosis. On the one hand, a few MMPs were expressed to a larger extent at right or left ventricular sites, although their substrates were not found to be increased in the same areas. For example, in DCM, collagen type IV was expressed in larger amounts in the left ventricle near the base than in the right ventricle. Although collagen type IV is a substrate of MMP-9 [4], this MMP was not increased in the left ventricle near the base when compared with the right ventricle (Table 1). In ICM, laminin was found to a larger extent within the left ventricle than in the right ventricle, but MMP-2, which can cleave laminin [12], was not expressed more strongly in the left ventricle than in the right ventricle. However, in DCM and ICM, several MMPs were quantitatively increased in the right ventricle compared with left ventricular regions. As for the matrix proteins, these differential MMP expression levels confirm a difference between left and right ventricular myocardium. Differences have been described in other studies [34].

In the three left ventricular sites, only MMP-2 and -9 showed one significant comparison each, although the other comparisons showed differences within the number of positive cells (Table 1). Again, we found no data in literature focusing on different sites of the left ventricle.

The amount of TIMP-1-positive cells was very low in general. The same situation was observed in other studies [17, 19]. As the natural inhibitor of MMP-1, TIMP-1 builds a complex in a stoichometric molar ratio of 1:1. However, a comparison of the number of cells measured in this study showed fewer cells for TIMP-1 than for MMP-1 (Table 2). Further, we found no significant differences between the left and right ventricular regions, which first could be due to the aspect that our method was not able to distinguish between activated and inactivated cells. Second, we also found a great range for TIMP-1-data (Table 1).

Unfortunately, we are not able to compare most of our results to other studies, because there have not been many studies comparing different sites in the heart. However, our results suggest that the remodeling process in the left and right ventricular myocardium is different in end-stage DCM and ICM, which leads to different patterns of distribution for matrix proteins, MMPs and TIMPs. This is reflected by our findings on tested ECM components, which showed a tendency toward differences between the two ventricles.

Although we found a few differences in the expression of ECM components between the interventricular septum and the left ventricular myocardium near the apex and the base, no definite statement on the pattern of distribution of matrix proteins and MMPs is possible because of the above-noted limitations. However, altogether, our data give rise to the hypothesis that there might be differences in remodeling within the left ventricular sites.

End note

In all, some limitations to this study must be recognized. Due to the problem of multiple testing, it is not possible to safely distinguish significant results achieved by chance from those reflecting a true difference. However, the number of hearts tested was relatively small, and interindividual variability in pathological characteristics also has to be considered. So, possible differences might have been missed statistically due to lack of power. However, in this study the hearts were carefully selected. DCM hearts with an additional coronary heart disease (even one-vessel disease) or valvular disease were not included in the study. Also, no hearts with additional valvular disease were included in the ICM group. From both groups, hearts with additional surgical procedures (e.g., implantation of a defibrillator or an assist device) were excluded. Therefore, the number of hearts in the DCM group (n=15) and the ICM group (n=18) was relatively small. The number of samples (n=4 per heart) and the number of test fields per sample (20 test fields in ×200 magnification and 35 in ×1000 magnification per sample) and the number of test points (100 test points per test field) was high enough when regarding sampling efficiency [13]. Altogether, in this study, 1,980,000 test points were counted for all tested matrix proteins.

The purpose of this study was to investigate whether differences in the pattern of distribution of matrix proteins exist in different sites of the heart. To our knowledge, we are the first group to compare the pattern of distribution in four different sites within one heart. It was not our intention to deal with total amount of matrix proteins, and, therefore, our study was limited on volume densities. In morphometry, volume densities usually describe the relationship of defined structures or tissues to a reference volume [36]. Hence, it would be interesting to see if there is a relationship between volume densities and the total amount of matrix proteins. So, further studies on total protein present should be performed using northern blot to determine the total amount of protein present or reverse-transcription polymerase chain reaction to determine the m-RNA.

Furthermore, we did not investigate the remodeling process in patients with milder forms of DCM or ICM. Our study only included patients suffering from end-stage cardiomyopathies (New York Heart Association stages III and IV); therefore, a heterogeneous pattern of fibrosis could already be expected within the different sites of the heart. Further, all these patients with end-stage cardiomyopathies were treated with specific pharmacological interventions, which may have influenced matrix proteins and MMP abundance and activity [24, 28]. Last, all MMP values showed a great variability.

Acknowledgements This work was supported by the Forschungsfoerderungs-Programm of the University of Heidelberg, project-no. 150 /2001. The authors thank Ms. G. Gorsberg and Ms. B. Hofmann for their excellent technical assistance and Ms. U. Horr and Mr. J Moyers for their help with preparation of the photographs.

References

1. Adler CP, Neuburger M, Herget GW, Mühlbach D (1997) Regeneration processes in human myocardium after acute ischaemia-quantitative determination of DNA, cell number and collagen content. Virchows Arch 430:149–153
2. Beltrami CA, Finato N, Rocco M, Feruglio GA, Puricelli C, Cigola E, Quaini F, Sonnenblick EH, Olivetti G, Anversa P (1994) Myocardial function/valvular heart disease/hypertensive heart disease: structural basis of end-stage failure in ischemic cardiomyopathy in humans. Circulation 89:151–163
3. Beltrami CA, Finato N, Rocco M, Feruglio GA, Puricelli C, Cigola E, Sonnenblick EH, Olivetti G, Anversa P (1995) The cellular basis of dilated cardiomyopathy in humans. J Mol Cell Cardiol 27:291–305
4. Birkdal-Hansen H (1995) Proteolytic remodeling of extracellular matrix. Curr Opin Cell Biol 7:728–735
5. Bosman FT, Stamenkovic I (2003) Functional structure and composition of the extracellular matrix. J Pathol 200:423–428
6. Coker ML, Doscher MA, Thomas ChV, Galis ZS, Spinale FG (1999) Matrix metalloproteinase synthesis and expression in isolated myocyte preparations. Am J Physiol Heart Circ Physiol 277:777–787
7. Coker ML, Zellner JL, Crumbley AJ, Spinale FG (1999) Defects in matrix metalloproteinase inhibitory stoichiometry and selective MMP induction in patients with nonischemic or ischemic dilated cardiomyopathy. Ann N Y Acad Sci 878:559–562
8. Corradi D, Callegari S, Benussi S, Nascimbene S, Pastori P, Calvi S, Maestri R, Astorri E, Pappone C, Alfieri O (2004) Regional left atrial interstitial remodeling in patients with chronic atrial fibrillation undergoing mitral-valve surgery. Virchows Archiv 445:498–505
9. Diez J (2002) Emerging role of matrix metalloproteinases in the pathophysiology of cardiac diseases. Eur J Clin Invest 32:291–294
10. Feldman AM, Li YY, McTiernan CF (2001) Matrix metalloproteinases in pathophysiology and treatment of heart failure. Lancet 357:654–655
11. Florholmen G, Andersson KB, Yndestad A, Austbø B, Henriksen UL, Christensen G (2004) Leukaemia inhibitory factor alters expression of genes involved in rat cardiomyocyte energy metabolism. Acta Physiol Scan 180:133–142
12. Giannelli G, Falk-Marzillier J, Schiraldi O, Stetler-Stevenson WG, Quaranta V (1997) Induction of cell migration by matrix metalloproteinase-2 cleavage of laminin. Science 277:225–228
13. Gunderson HJG, Osterby R (1981) Optimizing sampling efficiency of stereological studies in biology or "Do more less well!" J Microscopy 121:65–73
14. Heeneman S, Cleutjens JP, Faber BC, Creemers EE, van Suylen RJ, Lutgens E, Cleutjens KB, Daemen MJ (2003) The dynamic extracellular matrix: intervention strategies during heart failure and atherosclerosis. J Pathol 200:516–525
15. Ishikawa Y, Asuwa N, Ishii T, Ito K, Akasaka Y, Masuda T, Zhang L, Kiguchi H (2000) Collagen alteration in vascular remodeling by hemodynamic factors. Virchows Arch 437:138–148
16. Klappacher G, Franzen P, Haab D, Mehrabi M, Binder M, Plesch K, Pacher R, Grimm M, Pribill I, Eichler HG, Glogar HD (1995) Measuring extracellular matrix turnover in the serum of patients with idiopathic or ischemic dilated cardiomyopathy and impact on diagnosis and prognosis. Am J Cardiol 75:913–918
17. Li YY, Feldman AM, Sun Y, McTiernan CF (1998) Differential expression of tissue inhibitors of metalloproteinases in the failing human heart. Circulation 98:1728–1734
18. Li YY, McTiernan CF, Feldman AM (2000) Interplay of matrix metalloproteinases, tissue inhibitors of metalloproteinases and their regulators in cardiac matrix remodeling. Cardiovasc Res 46:214–224
19. Lu L, Gunja-Smith Z, Woessner JF, Ursell PC, Nissen T, Galardy RE, Xu Y, Zhu P, Schwartz GG (2000) Matrix metalloproteinases and collagen ultrastructure in moderate myocardial ischemia and reperfusion in vivo. Am J Physiol Heart Circ Physiol 279:601–609
20. Mundhenke M, Schwartzkopff B, Strauer B (1997) Structural analysis of arteriolar and myocardial remodelling in the subendocardial region of patients with hypertensive disease and hypertrophic cardiomyopathy. Virchows Arch 431:265–273
21. Nogami K, Kusachi S, Nunoyama H, Kondo J, Endo C, Yamamoto K, Murakami T, Tsuji T (1996) Extracellular matrix components in dilated cardiomyopathy. Jpn Heart J 37:483–494
22. Pauschinger M, Knopf D, Petschauer S, Doerner A, Poller W, Schwimmbeck PL, Kuhl U, Schultheiss HP (1999) Dilated cardiomyopathy is associated with significant changes in collagen type I/III ratio. Circulation 99:2750–2756
23. Pauschinger M, Chandrasekharan K, Li J, Schwimmbeck PL, Noutsias M, Schultheiss HP (2002) Remodeling der extrazellulären Matrix bei dilatativer Kardiomyopathie. Herz 27:677–682
24. Reinhardt D, Sigusch HH, Hensse J, Tyagi SC, Korfer R, Figulla HR (2002) Cardiac remodelling in end stage heart failure: upregulation of matrix metalloproteinase (MMP) irrespective of the underlying disease, and evidence for a direct inhibitory effect of ACE inhibitors on MMP. Heart 88:525–530
25. Rossi MA (1991) Patterns of myocardial fibrosis in idiopathic cardiomyopathies and chronic Chagasic cardiopathy. Can J Cardiol 7:287–294
26. Rossi MA (1998) Pathologic fibrosis and connective tissue matrix in left ventricular hypertrophy due to chronic arterial hypertension in humans. J Hypertension 16:1031–1041
27. Rossi MA, Abreu MA, Santoro LS (1998) Connective tissue skeleton of the human heart. A deminstration by cell-maceration scanning electron microscope methode. Circulation 97:934–935
28. Sandmann S, Bohle RM, Dreyer T, Unger T (2000) The T-type calcium channel blocker mibefradil reduced interstitial and perivascular fibrosis and improved hemodynamic parameters in myocardial infarction-induced cardiac failure in rats. Virchows Arch 436:147–157
29. Schaper J, Speiser B (1992) The extracellular matrix in the failing human heart. Basic Res Cardiol 87[Suppl]:303–309
30. Soini Y, Satta J, Määttä M, Autio-Harmainen H (2001) Expression of MMP-2, MMP-9, MT1-MMP, TIMP-1and TIMP-2 mRNA in valvular lesions of the heart. J Pathol 194:225–231
31. Spinale FG (2002) Matrix metalloproteinases. Regulation and dysregulation in the failing heart. Circ Res 90:520–530
32. Stamenkovic I (2003) Extracellular matrix remodelling: the role of matrix metalloproteinases. J Pathol 200:448–464
33. Tyagi SC (1997) Proteinases and myocardial extracellular mat rix turnover. Moll Cell Biochem 168:1–12

34. Tyagi SC, Campbell SE, Reddy HK, Tjahja E, Voelker DJ (1996) Matrix metalloproteinase activity expression in infarcted, noninfarcted and dilated cardiomyopathic human hearts. Mol Cell Biochem 155:13–21
35. Unverferth DV, Baker PB, Swift SE, Chaffee R, Fetters JK, Uretsky BV, Thompson ME, Leier CV (1986) Extent of myocardial fibrosis and cellular hypertrophy in dilated cardiomyopathy. Am J Cardiol 57:816–820
36. Wang W, Schulze CJ, Suarez-Pinzon WL, Dyck JRB, Sawicki G, Schulz R (2002) Intracellular action of matrix metalloproteinase-2 accounts for acute myocardial ischemia and reperfusion in injury. Circulation 106:1543–1549
37. Weibel ER (ed) (1979) Stereological methods, vol.1. Practical methods for biological morphometry, 1st edn. Academic Press, London, pp 101–161

Virchows Arch (2005) 446: 379–382
DOI 10.1007/s00428-004-1165-3

ORIGINAL ARTICLE

Gustavo Valbuena · David H. Walker

Changes in the adherens junctions of human endothelial cells infected with spotted fever group rickettsiae

Received: 17 June 2004 / Accepted: 25 October 2004 / Published online: 19 March 2005
© Springer-Verlag 2005

Abstract Rickettsiae of the spotted fever group are obligately intracellular bacteria that primarily infect the vascular endothelium, invade adjacent cells propelled by actin polymerization, and cause severe systemic diseases. Endothelial dysfunction and vascular leakage develop as a consequence; this effect is the pathophysiological mechanism that explains most clinical manifestations. Here we report that rickettsial infection of cultured primary human endothelial cells is associated with the formation of gaps in the interendothelial adherens junctions, occurring late during the course of in vitro infections but not early, even when rickettsial loads are significant.

Keywords Rickettsia · Rocky Mountain spotted fever · Mediterranean spotted fever · Vascular leakage · Endothelial cells · Adherens junction

Introduction

Rocky Mountain spotted fever (caused by *Rickettsia rickettsii*) and Mediterranean spotted fever (caused by *R. conorii*) are severe systemic infectious diseases [16, 17, 19] caused by the obligately intracellular bacteria, *Rickettsia* of the spotted fever group [20]. The main target cells of rickettsiae are endothelial cells lining the vasculature, and rickettsiae spread among them through stimulation of directional host cell actin polymerization [6, 7] using a mechanism that resembles the formation of cellular filopodia [5, 8]. Increased microvascular permeability as a consequence of endothelial changes triggered by rickettsial infection is hypothesized to play a predominant role in the pathogenesis of these infections; however, the mechanistic aspects of spotted fever group rickettsioses are still poorly understood. Proposed mechanisms include endothelial denudation, oxidative stress, and response to autocrine and paracrine inflammatory mediators. We hypothesize that, in addition to those mechanisms, spotted fever group rickettsiae, through their actin polymerizing activity, may disrupt the function of one of the elements of the endothelial barrier, the adherens junctions, whose stability depends on the integrity of the actin cytoskeleton.

G. Valbuena
School of Medicine, Universidad de Los Andes,
Bogota, D.C., Colombia

G. Valbuena · D. H. Walker (✉)
Department of Pathology, University of Texas Medical Branch,
301 University Boulevard,
Galveston, Texas , 77555-0609, USA
e-mail: dwalker@utmb.edu
Tel.: +1-409-772-3989
Fax: +1-409-772-2500

Materials and methods

Rickettsia

Rickettsia conorii (Malish 7 strain) is a human isolate from South Africa with an unknown number of passages in the yolk sacs of embryonated chicken eggs. For all the experiments described in this study, a stock of *R. conorii* was produced by cultivation in specific pathogen-free embryonated chicken eggs. Yolk sacs from infected eggs with dead embryos were homogenized in a Waring blender, diluted to a 10% suspension in sucrose-phosphate-glutamate buffer (0.218 M sucrose, 3.8 mM KH_2PO_4, 7.2 mM K_2HPO_4, 4.9 mM monosodium L-glutamic acid, pH 7.0) and aliquotted for storage at −80°C after discarding the pellet produced by low-speed centrifugation (200×*g*, 10 min). Rickettsial content of this stock was quantified by plaque assay (5.5×10^7 pfu per ml) [18], and the LD_{50} was determined experimentally in C3H/HeN mice (1 $LD_{50}=1.65\times10^4$ pfu/ml) according to the method of Reed and Muench [11].

Endothelial cells

Human umbilical vein endothelial cells were isolated from fresh umbilical cords according to standard protocols [4] and used at passages 1 to 3 for all experiments. They were grown using endothelial growth medium (EGM) with the EGM bullet kit (Cambrex, East Rutherford, NJ). Confluent

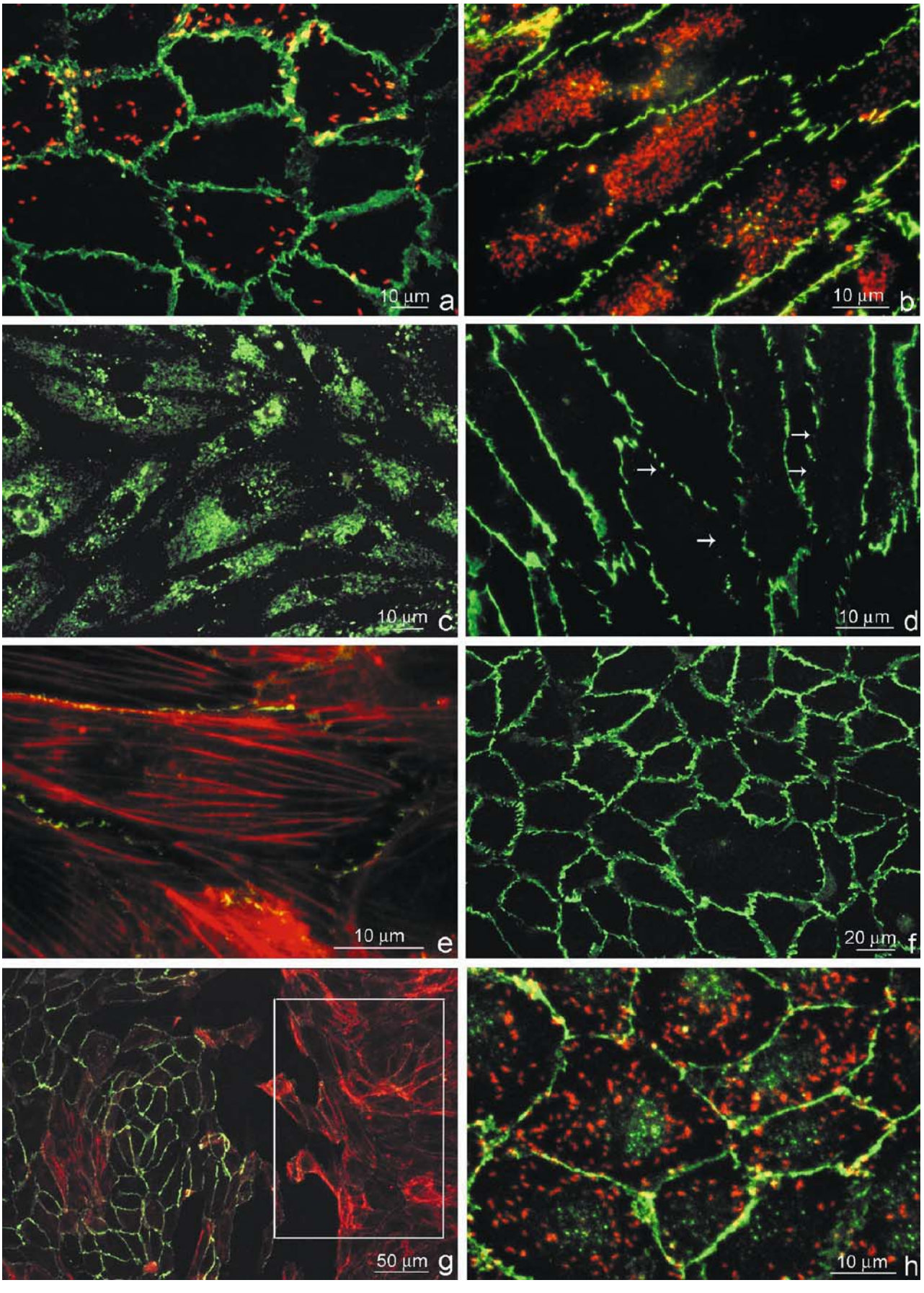
10 µm
a
10 µm
b
10 µm
c
10 µm
d
10 µm
e
20 µm
f
50 µm
g
10 µm
h

endothelial monolayers were grown in 8-chamber slides coated with 0.1% gelatin (Sigma, St. Louis, MO) and infected with 4×10^4 (high dose), 4×10^3 (medium dose), or 4×10^2 (low dose) pfu of *R. conorii*. Uninfected cells were used as negative controls.

Immunofluorescence

Cells were washed with phosphate-buffered saline (PBS) containing calcium (Sigma, St. Louis, MO) and fixed with cold methanol or 0.4% paraformaldehyde in PBS at 6, 12, 24, 36, 48, 72 or 96 h after infection. Each experiment was repeated three times. The adherens junction proteins examined and the antibodies used were the following: β-catenin (Clone 14, Transduction Laboratories, Lexington Kentucky), α-catenin (clone 5, Transduction Laboratories, Lexington Kentucky), pp120 (clone 98, Transduction Laboratories, Lexington Kentucky), plakoglobin (Clone Pg5.1, Biodesign International, Kennebunk, Maine), α-catenin (rabbit polyclonal, Zymed Laboratories, San Francisco, CA), cadherin-5 or VE-cadherin (Clone TEA1/31, Biodesign International, Kennebunk, Maine). Rickettsiae were detected with a rabbit polyclonal IgG antibody against *R. conorii*. Secondary anti-mouse IgG biotinylated antibodies and fluorescein isothiocyanate-streptavidin were obtained from Vector Laboratories (Burlingame, CA). Rabbit primary polyclonal antibodies were detected with goat anti-rabbit IgG labeled with rhodamine (Sigma, St. Louis, MO). Rhodamine-phalloidin (Molecular Probes, Eugene, OR) was used in some experiments to localize actin filaments.

Results

Morphological changes in rickettsia-infected endothelial cells

Rickettsiae were detected using immunofluorescence starting at 6 h of infection, even with the lowest inoculum used (4×10^2 pfu). At this point, endothelial cells were polygonal and uniform in size (Fig. 1a). As the infection progressed, particularly after 36 h (48 h for the low-dose inoculum), detached endothelial cells were seen floating in the supernatant, while the remaining attached endothelial cells became larger and acquired a spindle shape (Fig. 1b, c, d, e). It is likely that cellular self-renewal through mitosis, in addition to increased cellular size, played a role in maintaining the growth surface covered with cells, since many detached cells were evident when the medium was changed every 48 h. In fact, some rickettsia-infected cultures were kept for up to 30 days, and endothelial cells always covered the growth surface despite their cytoplasm being filled with rickettsiae (Fig. 1c).

Intercellular gaps in rickettsia-infected endothelial cells

The development of interendothelial gaps is an indication of discontinuities in the adherens junctions. We observed these changes with all anti-adherens junction protein antibodies used after 36 h with medium-dose and high-dose inocula and after 48 h with low dose inocula (Fig. 1d). The formation of such gaps coincided with a change in endothelial cellular shape from small polygonal (Fig. 1a, f, h) to large spindle (Fig. 1b, d), which was also associated with stress fibers (Fig. 1e). Also, rickettsiae were not consistently observed adjacent to the gaps. The only adherens junction protein that behaved differently was plakoglobin, because the intensity of staining of it decreased (or was undetectable) at the time that gaps became evident as assessed using the immunofluorescent staining of the other adherens junction proteins (Fig. 1f, g). Such reduced staining was similar to that observed in repairing monolayers of endothelial cells wounded physically (Fig. 1g). Despite the presence of significant numbers of intracellular rickettsiae, no changes in the continuity and linearity of the adherens junctions were detected at time points of rickettsial infection earlier than 36 h, for medium- and high-dose inocula, or 48 h for the low-dose rickettsial inoculum (Fig. 1a, h).

◀ **Fig. 1** Fluorescent detection of adherens junction proteins, rickettsiae, and actin in human endothelial cells infected with spotted fever group rickettsiae. **a** β-Catenin (*green*) is linear in a mature endothelial monolayer after 24 h of rickettsial (*red*) infection (similar findings were observed with all other antibodies; not shown). **b** VE-cadherin (*green*) linearity is lost and delineates larger spindle endothelial cells after 72 h of rickettsial (*red*) infection. **c** Endothelial cells with the cytoplasm distended by spotted fever group rickettsiae (*green*) after 1 month of infection. **d** Interendothelial gaps (*arrows*) revealed by β-catenin staining (*green*) after 72 h of rickettsial infection. **e** Actin stress fibers (*red*) and loss of intercellular pp120 (*green*) in spindled endothelial cells after 72 h of rickettsial infection. **f** Linear continuous staining of plakoglobin (*green*) in uninfected endothelial cells. **g** Loss of plakoglobin signal (*green*) in an area of repair (*white rectangle*) in an endothelial monolayer wounded physically with a stick (filamentous actin is stained *red*). **h** Interendothelial adherens junctions are uninterrupted (plakoglobin, *green*) in monolayers infected for less than 36 h with a medium-dose inoculum of *R. conorii* (*red*)

Discussion

The vascular barrier function of the endothelium is regulated by a balance between contractile forces of the cytoskeleton and cellular adhesive forces, which include cell–matrix adhesions (focal adhesions) and cell–cell adhesions (tight junctions and adherens junctions) [1, 3]. Adherens junctions are formed by the homophilic binding of the transmembrane protein VE-cadherin (or cadherin 5) and the cytoplasmic proteins p120, α and β catenins, and plakoglobin (or γ-catenin), which mediate binding to the actin cytoskeleton [10]. In view of the fact that spotted fever group rickettsiae stimulate polymerization of host actin, an activity that may disrupt the host cell cytoskeleton and thus the stability of the adherens junctions, we sought to investigate the localization of the adherens junction proteins VE-cadherin, plakoglobin, pp120, α-catenin, and β-catenin at various time points in endothelial cells infected with different doses of *R. conorii*, a member of the spotted fever group rickettsiae.

We observed that rickettsial infection of endothelial cells was associated with the development of discontinuities in the localization of adherens junction proteins (i.e., intercellular gaps) at late time points during the course of in vitro infections (more than 36 h) (Fig. 1b, d, e) but not at early time points (Fig. 1a, h). These observations, together with the coincidental change in cellular shape from polygonal to spindle (Fig. 1b, c, d, e), the inconsistent localization of rickettsiae adjacent to the interendothelial gaps, and the simultaneous formation of prominent actin stress fibers (Fig. 1e), suggest that changes in the localization and staining characteristics of the adherens junction proteins during rickettsial infections are not a direct consequence of disruption of the actin cytoskeleton by rickettsiae. Therefore, we now hypothesize that the development of interendothelial gaps during rickettsial infections results from two phenomena: (1) endothelial denudation followed by an endothelial physiological reparative response and (2) an inflammatory response as a consequence of the activation of receptors through paracrine signals [9, 14] or possibly as a result of rickettsia-mediated activation of the transcription factor NF-κB [12, 13, 15]. The latter could direct the activation of various inflammatory pathways, thus, leading to the development of contractile forces that involve the actin and microtubule cytoskeleton [3]. Interestingly, this effect occurs not only as a consequence of binding of inflammatory mediators to their endothelial receptors but also as a result of leukocyte adhesion to the endothelium [2]. Thus, future studies should analyze possible changes in the interendothelial junctional complexes when other physiological elements, such as leukocytes and platelets, are introduced into the system.

Acknowledgements We thank Susan Butler for her assistance with preparation of the manuscript. Sources of support: NIH grant RO1 AI21242 to David H. Walker.

References

1. Aurrand-Lions M, Johnson-Leger C, Imhof BA (2002) Role of interendothelial adhesion molecules in the control of vascular functions. Vasc Pharmacol 39:239–246
2. Del Maschio A, Zanetti A, Corada M, Rival Y, Ruco L, Lampugnani MG, Dejana E (1996) Polymorphonuclear leukocyte adhesion triggers the disorganization of endothelial cell-to-cell adherens junctions. J Cell Biol 135:497–510
3. Dudek SM, Garcia JG (2001) Cytoskeletal regulation of pulmonary vascular permeability. J Appl Physiol 91:1487–1500
4. Gimbrone MA Jr, Cotran RS, Folkman J (1974) Human vascular endothelial cells in culture. Growth and DNA synthesis. J Cell Biol 60:673–684
5. Gouin E, Egile C, Dehoux P, Villiers V, Adams J, Gertler F, Li R, Cossart P (2004) The RickA protein of *Rickettsia conorii* activates the Arp2/3 complex. Nature 427:457–461
6. Heinzen RA (2003) Rickettsial actin-based motility: behavior and involvement of cytoskeletal regulators. Ann N Y Acad Sci 990:535–547
7. Heinzen RA, Hayes SF, Peacock MG, Hackstadt T (1993) Directional actin polymerization associated with spotted fever group Rickettsia infection of Vero cells. Infect Immun 61:1926–1935
8. Jeng RL, Goley ED, D'Alessio JA, Chaga OY, Svitkina TM, Borisy GG, Heinzen RA, Welch MD (2004) A *Rickettsia* WASP-like protein activates the Arp2/3 complex and mediates actin-based motility. Cell Microbiol 6:761–769
9. Kaplanski G, Teysseire N, Farnarier C, Kaplanski S, Lissitzky JC, Durand JM, Soubeyrand J, Dinarello CA, Bongrand P (1995) IL-6 and IL-8 production from cultured human endothelial cells stimulated by infection with *Rickettsia conorii* via a cell-associated IL-1 alpha-dependent pathway. J Clin Invest 96:2839–2844
10. Lampugnani MG, Ejana E (1997) Interendothelial junctions: structure, signalling and functional roles. Curr Opin Cell Biol 9:674–682
11. Reed LJ, Muench H (1938) A simple method of estimating fifty percent endpoints. Am J Hyg 27:493–497
12. Sahni SK, Van Antwerp DJ, Eremeeva ME, Silverman DJ, Marder VJ, Sporn LA (1998) Proteasome-independent activation of nuclear factor kappaB in cytoplasmic extracts from human endothelial cells by *Rickettsia rickettsii*. Infect Immun 66:1827–1833
13. Sahni SK, Rydkina E, Joshi SG, Sporn LA, Silverman DJ (2003) Interactions of *Rickettsia rickettsii* with endothelial nuclear factor-kappaB in a "cell-free" system. Ann N Y Acad Sci 990:635–641
14. Sporn LA, arder VJ (1996) Interleukin-1 alpha production during *Rickettsia rickettsii* infection of cultured endothelial cells: potential role in autocrine cell stimulation. Infect Immun 64:1609–1613
15. Sporn LA, Sahni SK, Lerner NB, Marder VJ, Silverman DJ, Turpin LC, Schwab AL (1997) *Rickettsia rickettsii* infection of cultured human endothelial cells induces NF-kappaB activation. Infect Immun 65:2786–2791
16. Walker DH (1995) Rocky Mountain spotted fever: a seasonal alert. Clin Infect Dis 20:1111–1117
17. Walker DH (2002) *Rickettsia rickettsii*: as virulent as ever. Am J Trop Med Hyg 66:448–449
18. Walker DH, Cain BG (1980) The rickettsial plaque. Evidence for direct cytopathic effect of *Rickettsia rickettsii*. Lab Invest 43:388–396
19. Walker DH, Raoult D (2000) *Rickettsia rickettsii* and other spotted fever group rickettsiae (rocky mountain spotted fever and other spotted fevers). In: Mandell GL, Bennett JE, Dolin R (eds) Principles and practice of infectious diseases. Churchill Livingstone, New York, pp 2035–2042
20. Walker DH, Bouyer DH (2003) Rickettsia. In: Murray PL, Baron EJ, Jorgensen JH, Pfaller MA, Yolken RH (eds) Manual of clinical microbiology. ASM Press, Washington, pp 1005–1014

Virchows Arch (2005) 446: 383–393
DOI 10.1007/s00428-004-1187-x

ORIGINAL ARTICLE

O. Hes · T. Vanecek · D. M. Perez-Montiel · I. Alvarado Cabrero · M. Hora · S. Suster · J. Lamovec · R. Curik · V. Mandys · M. Michal

Chromophobe renal cell carcinoma with microcystic and adenomatous arrangement and pigmentation—a diagnostic pitfall. Morphological, immunohistochemical, ultrastructural and molecular genetic report of 20 cases

Received: 3 October 2004 / Accepted: 30 November 2004 / Published online: 9 March 2005
© Springer-Verlag 2005

Abstract We present clinical, morphological, immunohistochemical, ultrastructural and molecular genetic features of 20 cases of a peculiar form of chromophobe renal cell carcinoma (CRCC) with morphology differing from that of conventional CRCC. Microscopically, the typical features of the tumors were microcystic arrangement and formation of adenomatous structures. Microcystic areas were composed of smaller eosinophilic and bigger pale cells having cytological appearance typical of conventional CRCC. Cytological features of the adenomatous structures were mostly different from those of conventional CRCC. They had a typical columnar arrangement with nuclei positioned at the base of the glandular structures and a small amount of a deeply eosinophilic cytoplasm often endowed with brush border facing the lumen of the glands. In addition, all the tumors showed a brown pigmentation. The pigmentation was located mostly extracellularly, where it formed pools of heavy deposits. Microscopic calcifications present in all cases formed psammoma bodies or else the calcifications were more extensive and amorphous in shape. Ultrastructurally, the cells showed features characteristic of CRCC: typical cytoplasmic vesicles were 100–700 nm in size and mitochondria had tubulovesicular, lamellar or circular cristae. Some tumor cells contained dark, variously sized electron-dense pigment granules. Neither melanosomes nor membrane-bound neurosecretory granules were seen. Using fluorescence in-situ hybridization probes for chromosomes 1, 2, 6, 10, 13, 17 and 21, the tumors revealed massive loss of tested chromosomes typical for conventional CRCC. Monosomy of chromosomes 1, 2, 6, 10, 13 and 21 was found in 100, 36, 91, 82, 82, 82 and 64% of cases, respectively. None of the cases showed mutation of exons 9, 11, 13 and 17 of the c-kit gene. The important feature of pigmented microcystic chromophobe renal cell carcinoma is a relatively benign biological behavior and the absence of distant metastases and sarcomatoid transformation.

Keywords Pigmented chromophobe renal cell carcinoma · Microcystic · Adenomatous · Columnar change · Calcifications · C-kit gene

O. Hes · T. Vanecek · M. Michal (✉)
Department of Pathology,
University Hospital, Charles University,
Plzen, Czech Republic
e-mail: michal@medima.cz
Tel.: +420-377104630
Fax: +420-377104650

D. M. Perez-Montiel
Department of Pathology, INCAN,
Mexico City, United States of Mexico

I. Alvarado Cabrero
Department of Pathology, Centro Medico,
Mexico City, United States of Mexico

M. Hora
Department of Urology, University Hospital,
Charles University,
Plzen, Czech Republic

S. Suster
Department of Pathology, OSU,
Columbus, OH, USA

J. Lamovec
Department of Pathology,
Institute of Oncology,
Ljubljana, Slovenia

R. Curik
Department of Pathology,
University Hospital Ostrava,
Czech Republic

V. Mandys
Department of Pathology, 3rd Faculty of Medicine,
Charles University,
Prague, Czech Republic

Introduction

In 1998, we described five cases of so-called pigmented microcystic chromophobe renal cell carcinoma (PMCRC). The pigment was visible at the gross, light microscopic and ultrastructural levels. Histochemical and ultrastructural characteristics of the pigment had features of lipochrome pigment. The most striking feature was a very peculiar morphological architecture of all tumors. Tumors were arranged in a tubular pattern forming microcystic structures in some areas [31]. The study was not, however, accompanied by any molecular genetic findings to support the hypothesis that these tumors with a highly misleading morphology belong to the family of chromophobe renal cell carcinomas (CRCCs). Since this publication, we have collected, in total, 20 cases of this peculiar type of CRCC. We report clinical, morphological, immunohistochemical, ultrastructural, and molecular genetic features of these peculiar renal tumors.

Materials and methods

From 191 CRCCs, 20 tumors that corresponded to the original description of PMCRC [31] were selected. These tumors were retrieved from more than 9,000 renal neoplasms from the files of Tumor Registry of Charles University Hospital, Plzen, from the files of Departments of Pathology of Institute Nacional de Cancerologia and Centro Medico, Mexico City, and from the files of Department of Pathology of the Ohio State University. Most of the 20 selected tumors were accessed via consultation. The most frequent diagnosis of the referring pathologists was "renal cell carcinoma NOS (not otherwise specified)".

Morphological analysis

Tissues for light microscopy were fixed in 4% formaldehyde and embedded in paraffin using routine procedures. Sections 5 μm thick were cut from the tissue blocks and stained with hematoxylin and eosin, periodic acid Schiff (PAS) with and without diastase digestion, Schmorl method, Ziehl-Nielsen method, Masson method with and without bleaching (4 h and 24 h), iron stain and Hale's colloidal iron stain [17, 33].

Immunohistochemical analysis

Immunohistochemical staining was performed using the following primary antibodies: epithelial membrane antigen (monoclonal, DakoCytomation, Glostrup, Denmark), cytokeratins-AE_1-AE_3 (monoclonal, NeoMarkers, Fremont, CA), CAM 5, 2 (monoclonal, Becton Dickinson, San Jose, CA), parvalbumin (monoclonal, Sigma, Steinheim, Germany), vimentin (monoclonal, NeoMarkers) synaptophysin (polyclonal, DakoCytomation), chromogranin (monoclonal, DakoCytomation), S100 protein (monoclonal, Novocastra, Newcastle), HMB45 (monoclonal, DakoCytomation, Newcastle), Carpenteria, CA), c-kit (CD 117, polyclonal, DakoCytomation), and Ki 67 (polyclonal, DakoCytomation). The primary antibodies were visualized using the supersensitive streptavidin-biotin-peroxidase complex (Biogenex, San Ramon, CA). Appropriate positive control tissues used with the primary antibodies were employed.

Ultrastructure

Small pieces of the formaldehyde-fixed wet tissue of four cases were postfixed in glutaraldehyde and routinely processed for electron microscopy. Small pieces of paraffin-embedded tissues were retrieved from an additional eight cases. Tissues were deparaffinized according to protocol of Widehn and Kindblom and reprocessed for ultrastructure examination [48]. Ultrathin sections were stained with uranyl acetate and lead citrate and viewed in a Philips EM 208S electron microscope.

Molecular genetic analysis

DNA extraction

DNA was extracted from formalin-fixed, paraffin-embedded tissues. Several 10-μm thick sections were cut from each block. DNA was isolated using the DNeasy Tissue Kit (QIAgen, Hilden, Germany) according to manufacturer's protocol. In several cases, where quality or amount of extracted DNA were low, microconcentration with Microcon 100 (Millipore, Billerica, MA, USA) according to manufacturer's protocol was carried out.

Mutation status of the exons 9, 11, 13 and 17 of the c-kit gene (accession number U63834)

Polymerase chain reaction (PCR) was carried out using primers shown in Table 1. These primers were modified with the help of Poland java script (http://www.biophys.uni-duesseldorf.de/local/POLAND/poland.html) [41] by GC-clamp addition (Table 1) to create a thermostabile domain suitable for temperature gradient gel electrophoresis (TGGE) analysis. The reaction conditions were as follows: 12, 5 μl HotStart *Taq* PCR Master Mix (QIAgen, Hilden, Germany), 10 pmol each primer, 100 ng template DNA and distilled water up to 25 μl. The amplification program consisted of denaturation at 95°C for 15 min and then 40 cycles of denaturation at 95°C for 1 min, annealing at 54°C for 1 min and extension at 72°C for 1.5 min for all amplicons. The program was finished by 72°C incubation for 7 min. Screening of mutations was performed by heteroduplex analysis on TGGE (Biometra, Goettingen, Germany) on 8% denaturing acrylamide gel (AA:bis-AA [37.5:1], 7 M Urea, 1× MOPS, 2% glycerol) with temperature gradients shown in Table 1 and, in several cases, by direct sequencing.

Table 1 Polymerase chain reaction primers and TGGE condition. *GC-clamp 1* CGCCCGCCGCGCCCCGCGCCCGGCCCGCCGCCCCCGCCCG; *GC-clamp 2* CGGC; *GC-clamp 3* CGGGCGGGGGC GGCGGGCCGGGCGCGGGGCGCGGCGGGCG; *GC-clamp 4* GCGGGCGGCGCGGGGCGCGGGCCGGGCGGCGGGGGCGGGC; *GC-clamp 5* GGGCG

Exons	Name	Primers	Modification	TGGE condition
Exon 9a[1]	c-kit e9aNF	GAGTAAGCCAGGGCTTTTGTT		48–55°C
	c-kit e9aNR-GC	CGTGCCATTGTGCTTGAAT	GC-clamp 1	1 h 30 min
Exon 9b[2]	c-kit e9bNF	CCGTTTGGAAAGCTAGTGGT		48–52°C
	c-kit e9bNR-GC	CAGAGCCTAAACATCCCCTTA	GC-clamp 1	1 h 45 min
Exon 11*	c-kit e11 F-GC	CTATTTTTCCCTTTCTCCCC	GC-clamp 2	45.5–49.5°C
	c-kit e11 R-GC	TACCCAAAAAGGTGACATGG	GC-clamp 3	1 h 30 min
Exon 13	c-kit E13F-GC	CATGCGCTTGACATCAGTTT	GC-clamp 4	49–55°C
	c-kit E13R-GC	CAATAAAAGGCAGCTTGGACA	GC-clamp 5	1 h 30 min
Exon 17	c-kit E17F-GC	GGTTTTCTTTTCTCCTCCAACC	GC-clamp 4	47–53°C
	c-kit E17R	TGCAGGACTGTCAAGCAGAG		1 h 30 min

[1]5′ end of exon 9
[2]3′ end of exon 9
*Primers published elsewhere [47]

Molecular cytogenetic analysis

Isolation of nuclei

Paraffin-embedded tissue with no or minimal infiltration with non-neoplastic tissue was chosen for analysis. Several 40-μm sections were cut from paraffin blocks and deparaffinized in xylene twice for 30 min. After that, the tissue was rehydrated in 100, 96, 70 and 50% ethanol series and twice in distilled water, each for 30 min. Then, tissue was digested with proteinase K in 50 mM Tris, 10 mM ethylene diamine tetraacetic acid (EDTA) and 10 mM NaCl (pH 7.0) buffer at 37°C for 1 h. After digestion, proteinase K solution was carefully removed, and isolated nuclei were washed once with phosphate buffered saline (PBS). Nuclei were then fixed with two changes of freshly prepared methanol/acetic acid (3:1) fixative solution, resuspended by vortexing and vigorous pipetting in 100 μl fixative and frozen at −70°C until ready for fluorescence in-situ hybridization (FISH).

Pretreatment

The pretreatment was done according to the protocol of Paternoster et al. [36] with several modifications. Briefly, 10 μl of isolated nuclei were placed on a positively charged slide and dried at 65°C for 15 min. The slide was then gradually incubated at 37°C in 10 mM citric acid (pH 6.0) for 15 min, in 2×sodium saline citrate (SSC; pH 7.0) for 15 min and in 0.5% pepsin in 0.9% NaCl (pH 1.5) for 12–16 min. After that, the slide was immersed into 2×SSC at room temperature for 5 min and dehydrated in 70, 85 and 100% ethanol series, each for 3 min. The dried slide was then denatured in 70% formamide/2×SSC (pH 7.0) for 8 min at 77°C and dehydrated in ice-cold 70, 85 and 100 ethanol series.

FISH

An aliquot of 2 μl of one of the chromosome satellite probe numbers 1, 2, 6, 7 (as a control, see below), 10, 17 and unique sequence probes 13 and 21, directly labeled with Rhodamine (Q-BIOgene, Illkirch Cedex, France), and 8 μl of hybridization buffer were mixed, denatured at 96°C for 10 min and placed on the ice. The whole volume of probe mix was applied on dried denatured specimen, covered with the coverslip, sealed and hybridized at 37°C overnight. Then, the coverslip was carefully removed and the specimen was incubated in 0.5×SSC/0.1% sodium dodecyl sulfate (SDS) for 5 min at 37°C. After that, the slide was placed in the dark until completely dry, counterstained with DAPI II (Vysis, Downers Grove, IL, USA), and viewed under a fluorescence microscope Olympus BX 60.

Counting and scoring

Numbers of signals from at least 100 non-overlapping cell nuclei were counted for each case and every chromosome. The cut-off value for monosomy and for polysomy was determined on several normal kidney tissues from studied cases and on several normal kidney tissues from different samples using probes for chromosomes 1, 2, 6, 10, 13, 17 and 21. Additionally, a probe for chromosome 7, which was not included in the study and an aberration of which in CRCC is relatively rare, was used as another control on several normal and tumor tissues. In all cases, the number of a single signal never exceeded 25% and the number of more than two signals never exceeded 20%. The specimen was then considered as monosomic when at least 25% of nuclei with only one signal were found and polysomic when at least 20% of nuclei bore three and more signals.

Results

Clinical features of the cases are presented in Table 2. Patients presented with gross hematuria, microcytic anemia, loin pain and abdominal discomfort, or the tumors were detected incidentally. The age of the patients ranged from 32 years to 83 years (mean 59.65 years). Of the patients, 12 were males and 8 were females. Case no. 5 was a particularly interesting case. The patient was a 73-year-old Caucasian female with PMCRC combined with angiomyolipoma which collided with the PMCRC component. The size of the renal tumor was 4×3.7×4 cm. Moreover, in the same surgical session, an inflammatory fibroid polyp (Vanek's tumor) of 2×1.1×1 cm was excised from the stomach mucosa. The same patient had a history of surgery for moderately differentiated follicular carcinoma of the thyroid gland 8 years prior to the nephrectomy. No signs of metastatic spreading or of a further progression of the thyroidal tumor were documented. One of the patients (case 11) was treated for seminoma of the right testis by orchiectomy and chemotherapy 22 years before the diagnosis of PMCRC. In one patient (case 18), lentigo maligna was diagnosed independently on the left arm at the time of nephrectomy.

Follow-up data is known for 19 of 20 patients in the time period 0.2–8 years (mean 2.82 years). All but one of the patients are well, without signs of further dissemination of the disease. One patient died 2 months after nephrectomy of an unrelated cause.

Grossly, the tumors were unencapsulated but well demarcated from kidney parenchyma. In one patient (case 19), a grossly visible invasion to the renal pelvis was noted. The size of the tumors ranged from 1.9 cm to 20 cm in the largest dimension (mean 8.41 cm). Tumors had a tan, brown or gray color. Some parts of the tumors looked as though sprayed with soot particles. The dark gray coloration was unevenly distributed through the tumorous mass. Some tumors had grossly visible cysts, focal hemorrhages, and calcifications. The extensive grossly visible necrotic areas were noted in 3 of 20 tumors. Some tumors had a spongy appearance on the cut surface.

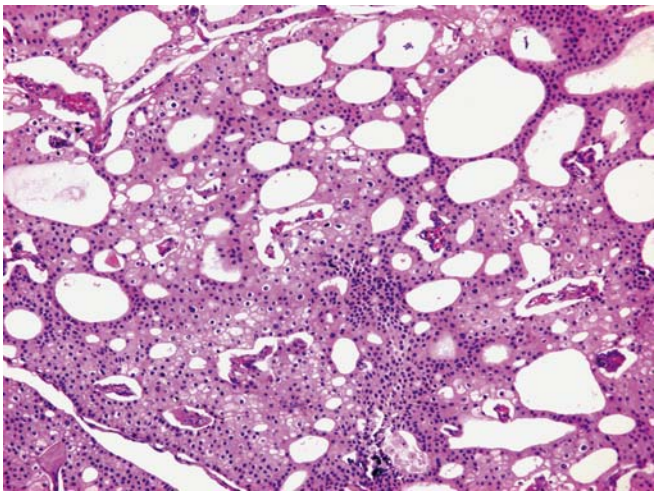

Fig. 1 The typical feature of the tumors was a microcystic arrangement and formation of adenomatous structures

Microscopically, the typical feature of the tumors was a microcystic arrangement and formation of adenomatous structures (Fig. 1). Microcystic areas were composed of smaller eosinophilic and bigger pale cells with a cytological appearance typical of conventional CRCC. They were composed of cells with copious eosinophilic to granular or clear cell cytoplasm and one or two nuclei of 10–15 μm with raisinoid quality and perinuclear clearing. The cytological features of the adenomatous structures were quite

Table 2 Clinical features of pigmented microcystic chromophobe cell carcinoma. *AW* alive and well, *LE* lost of evidence, *DUKR* death of unknown reasons, *Diam.* largest diameter

Case no.	Sex	Age (years)	Lateralization	Size (cm)	Follow-up
1	Male	73	Left	5×5×5	8 years AW
2	Male	70	Left	Diam. 5.5	2 years AW
3	Female	83	Right	Diam. 10	3 years AW, than LE
4	Male	34	Right	Diam. 13	6 years AW
5*	Female	73	Left	12×8×6	1.5 years AW
6	Female	48	Right	6.5×4×4	LE
7	Female	37	Left	4×3.5×3	1 year AW
8	Male	62	Right	Diam. 5	8 years AW
9	Male	75	Right	Diam. 12	3 years AW
10	Female	60	Right	2.8×2.5×2.5	2 years AW
11	Male	32	Left	Diam. 7	2 years AW
12	Male	67	Right	Diam. 14	DUKR 2 months later
13	Male	51	Right	9.5×6.5×7.5	2 years AW
14	Male	50	Right	Diam. 20	3 years AW
15	Female	71	Right	6.5×4×4.5	2 years AW
16	Male	76	Right	14×10×13	2 years AW
17	Female	51	Right	5×4×4	2 years AW
18	Female	71	Right	Diam. 6.5	3 years AW
19	Male	56	Right	8×7×6.5	2 years AW
20	Male	53	Left	Diam. 1.9	1 year AW

*Data referred to patient no 5 are concerning pigmented chromophobe renal cell carcinoma only

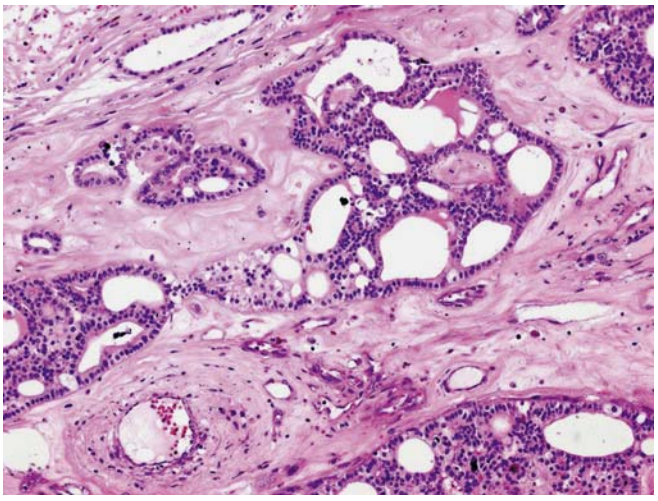

Fig. 2 The adenomatous pattern showed columnar arrangement of the cells with nuclei positioned at the base of the glandular structures often endowed with a brush border facing the lumen of the glands

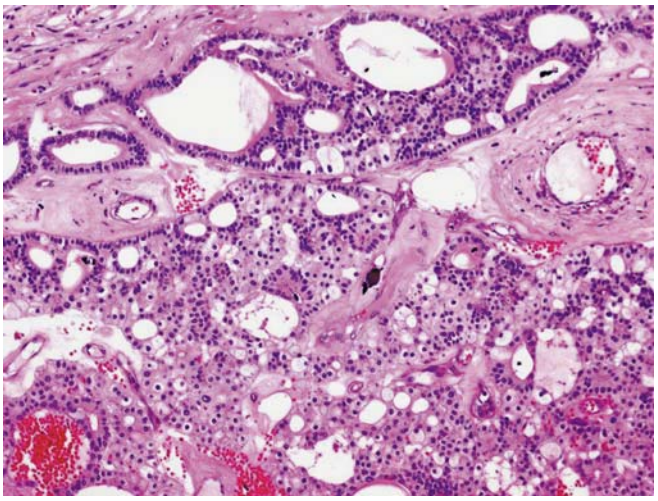

Fig. 4 There are seen transitions between the microcystic and adenomatous components

different from the conventional CRCC. It was this pattern which, when predominated, made the diagnosis of CRCC most difficult. The adenomatous pattern showed columnar arrangement of the cells with nuclei positioned at the base of the glandular structures and a small amount of a deeply eosinophilic cytoplasm often endowed with a brush border facing the lumen of the glands (Fig. 2). These glands were frequently set in a fibrous background, and they were formed either of single tubules or they were arranged in more complicated adenomatous cribriform formations with "Roman bridges". These cribriform structures were not much different from those seen in mammary pathology (Fig. 3). Sometimes the incipient columnar change was observed even in the microcystically arranged areas of the tumors. Wide transitions between the microcystic and adenomatous components were frequent (Fig. 4). An interesting cellular arrangement consisting of small cells with dark nuclei and a small amount of an eosinophilic cytoplasm was found focally in areas with the adenomatous pattern (Fig. 5). These areas bore a similarity with small cell variant of renal oncocytoma [18] (Fig. 6). Besides these two main patterns, bigger multicystic spaces separated by one or two rows of neoplastic cells were noted and rarely formed even a majority of the tumorous mass (Fig. 7). In four cases, the cystic areas were combined with a solid-alveolar pattern typical of conventional CRCC. No sarcomatoid transformation was noted in any of the cases. Light to dark brown pigmentation was present in all cases, but the intensity varied from very prominent to focal and inconspicuous. When the pigmentation was located extracellularly, it often formed pools of heavy deposits of the pigmentation (Fig. 8). Rarely the pigment was seen intracellularly. Microscopic calcifications

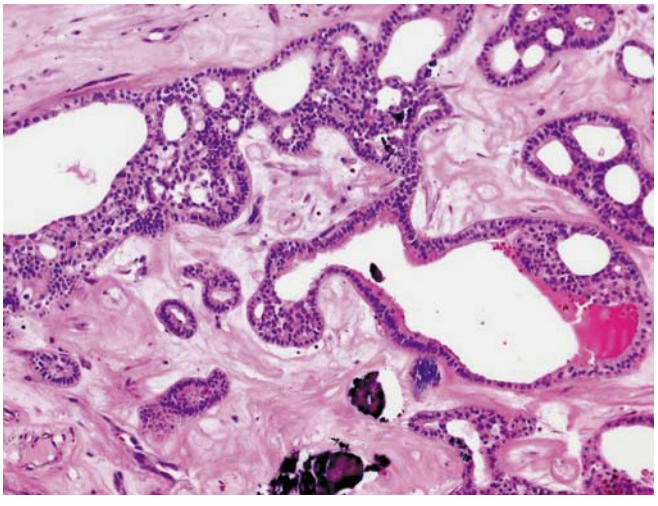

Fig. 3 The glands were frequently set in a fibrous background and they were formed either of single tubules or they were arranged in a more complicated adenomatous cribriform formations with "Roman bridges"

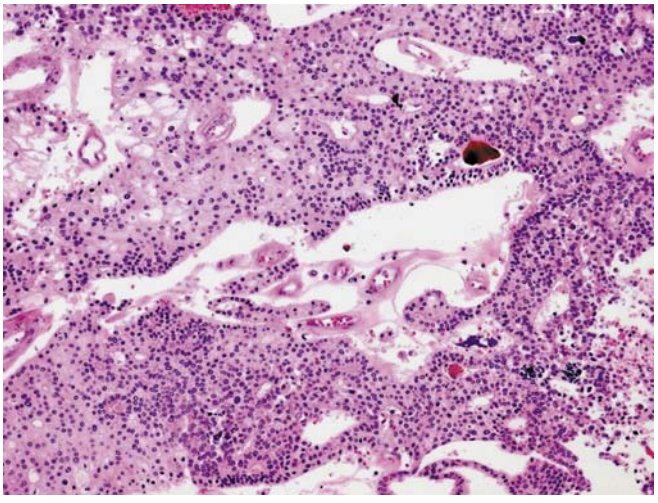

Fig. 5 An interesting cellular arrangement consisting of small cells with dark nuclei and a small amount of an eosinophilic cytoplasm was found focally in areas with the adenomatous pattern

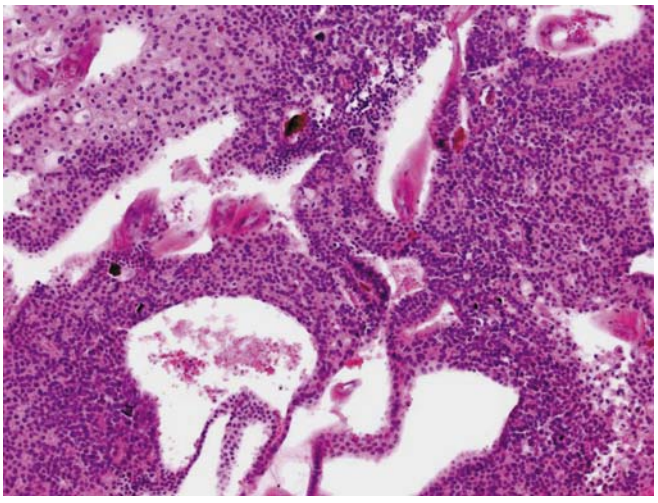

Fig. 6 Areas of the tumor with small cells had the appearance of small cell variant of renal oncocytoma

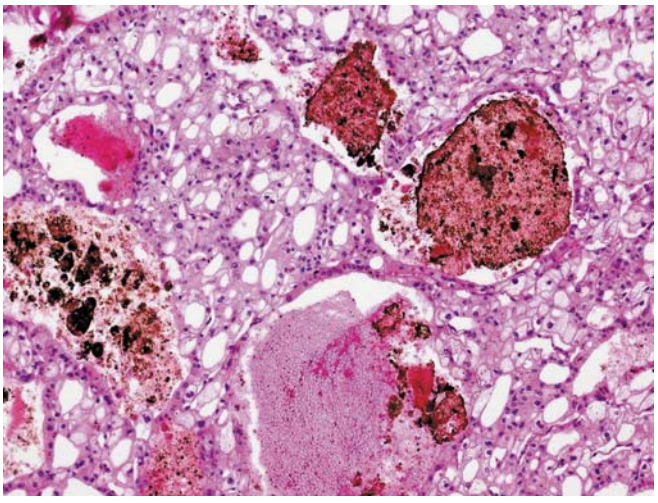

Fig. 8 Extracellular pigmentation often formed pools of heavy deposits

were found in all cases. They formed psammoma bodies or the calcifications were more extensive, amorphous and irregular in shape (Fig. 9). Von Kossa and Alizarin red stains reacted positively with these calcifications. Almost all tumors contained at least small microscopic necrotic areas. In three cases, the tumors contained extensive regressive changes, i.e., necroses and hyalinization with extensive calcifications.

The tumor cells were PAS negative and stained with Hale's colloidal iron (Fig. 10) with a variable intensity depending on fixation artifacts. The pigment stained positively with Masson Fontana stain, PAS with and without prior diastase pretreatment, Ziehl-Nielsen stain and it was blue-green in Schmorl reaction. The iron stain was focally positive in extracellular pigment deposits.

The results of immunohistochemical examinations are summarized in Table 3. All cases were positive for epithelial membrane antigen (EMA) and variably positive for cytokeratins. The majority of the cases reacted with parval-

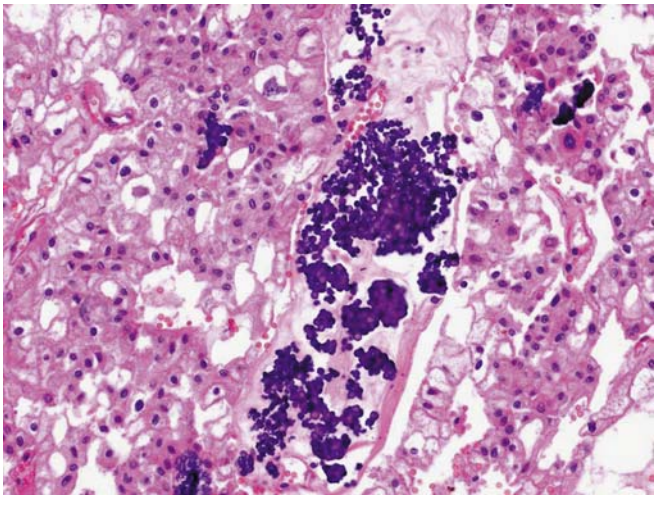

Fig. 9 When the calcifications were more extensive, they were amorphous and irregular in shape

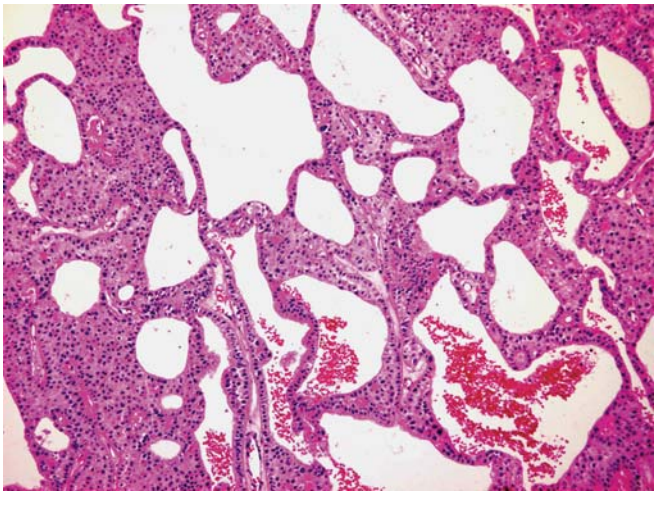

Fig. 7 The bigger multicystic spaces divided by one or two rows of cells sometimes formed a majority of the tumorous mass

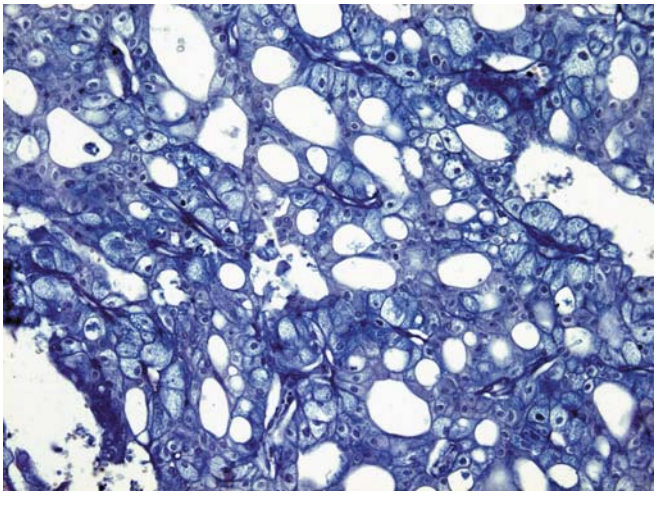

Fig. 10 Positivity with Hale's colloidal iron stain

Table 3 Results of immunohistochemical examination. *EMA* epithelial membrane antigen, *AE1-AE3* cytokeratin, *CAM 5.2* cytokeratin, *Parv.* parvalbumin, *Vim.* vimentin, *Syn.* synaptophysin, *Chrom.* chromogranin, *hpf* high power field, *Foc* focal

Case no.	EMA	AE1-AE3	CAM 5.2	Parv.	Vim.	Syn.	Chrom.	HMB45	S100	CD 117	Ki 67
1	+++	−	++	+	−	−	−	−	−	Foc +	0–1/hpf
2	++	+	++	+	+	−	−	−	−	−	3–4/hpf
3	++	−+	+	−+	−	−	−	−	−	−	2–3/hpf
4	++	++	++	−	−	−	−	−	−	−	3–4/hpf
5	+++	++	+	−+	+	−	−	−	−	−	1–2/hpf
6	+++	++	++	+−	+	−	−	−	−	−	0–1/hpf
7	+++	++	−	+	−	−	−	−	−	−	1–3/hpf
8	+++	+	+	+	−	−	−	−	−	−	5–7/hpf
9	++	++	+	−	−	−	−	−	−	−	3–5/hpf
10	+++	−+	−	+	−	−	−	−	−	−	0–1/hpf
11	+++	++	+	+	−	−	−	−	−	Foc +	2–3/hpf
12	++	++	+	+	+	−	−	−	−	−	0–3/hpf
13	+++	−+	+++	+	−	−	−	−	−	−	1–5/hpf
14	++	+	++	+	−	−	−	−	−	−	2–4/hpf
15	++	+	+	−	−	−	−	−	−	−	1–2/hpf
16	+++	+	+	+−	−	−	−	−	−	−	1–2/hpf
17	++	+	++	−	−	−	−	−	−	−	1–2/hpf
18	++	+++	−	+	+	−	−	−	−	−	1–3/hpf
19	+++	+	+	−	+	−	−	−	−	−	5–8/hpf
20	++	+	++	+	−	−	−	−	−	−	4–7/hpf

bumin. A weak and focal positivity with vimentin was noted in 6 of 20 tumors. Small groups of cells reacted with c-kit antibody in 2 of 20 tumors. The tumor cells were negative for the antibodies to HMB45, S-100 protein, synaptophysin and chromogranin.

The ultrastructural examination revealed cells with poorly formed junctions and external lamina. There were two major intracellular components—typical cytoplasmic vesicles as usually seen in CRCC [6], 100–700 nm in size (Fig. 11); and mitochondria with tubulovesicular, lamellar or circular cristae. Besides normal looking mitochondria there were degenerating mitochondrias with alternating inner cristae in orientation. Some tumor cells contained dark, variously sized electron-dense pigment granules. The pigment granules were round to polygonal or amorphous in shape (Fig. 12). We found places in the tumors where the vesicles seemed to contain tiny grains of the same dark, electron-dense material as in the granules. Neither melanosomes nor membrane-bound neurosecretory granules could be detected in any of the cases.

In Table 4, there are results of mutation analysis of exons 9, 11, 13 and 17 of c-kit gene. In three cases, heterozygotic C to T alteration at position 81,349 of the c-kit gene was found. This mutation has no effect on amino-acid sequence. No additional mutation was found in all successfully analyzed samples (16 of 20).

Table 5 presents the FISH results for all the patients. Of the 19 studied cases (case no. 20 was not analyzed), FISH

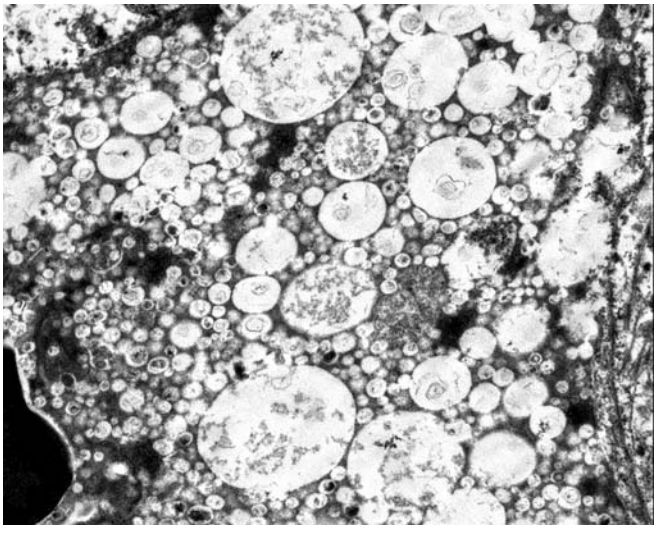

Fig. 11 The tumors contained cytoplasmic microvesicles typical for CRCC having 100–700 nm in size

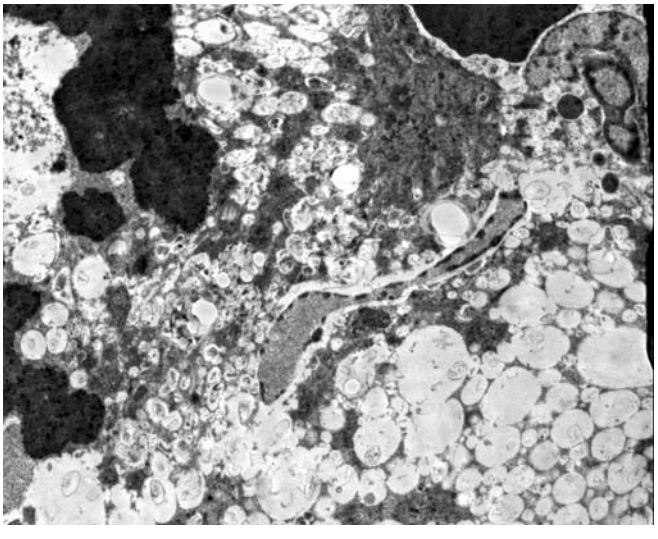

Fig. 12 The pigment granules were amorphous in shape (left side of the figure)

Table 4 Results of c-kit mutation analysis screening. *F* amplification failed

Case no.	Exon 9a[1]	Exon 9b[2]	Exon 11	Exon 13	Exon 17
1	F	F	F	F	F
2	–	–	–	–	+[3]
3	–	–	–	–	–
4	–	–	–	–	–
5	–	–	–	–	–
6	–	–	–	–	–
7	F	F	F	F	F
8	F	F	F	F	F
9	–	–	–	–	–
10	–	–	–	–	+[3]
11	–	–	–	–	–
12	–	–	–	–	–
13	–	–	–	–	–
14	–	–	–	–	–
15	–	–	–	–	+[3]
16	–	–	–	–	–
17	F	F	F	F	F
18	–	–	–	–	–
19	–	–	–	–	–
20	–	–	–	–	–

[1] 5′ end of exon 9
[2] 3′ end of exon 9
[3] In cases no. 2, 10 and 15, C to T alteration at the position 81,349 with no impact to amino-acid chain was found (for details see text)

Table 5 Results of fluorescence in situ hybridization analysis. *M* monosomy, *D* disomy, *F* failed, *ND* not done

Case no.	Chromosomes						
	1	2	6	10	13	17	21
1	F	F	F	F	F	F	F
2	M	M	M	M	M	M	D
3	M	D	M	M	M	M	M
4	F	F	F	F	F	F	F
5	F	F	F	F	F	F	F
6	M	M	M	M	M	M	D
7	F	F	F	F	F	F	F
8	F	F	F	F	F	F	F
9	M	D	M	M	M	M	M
10	M	D	M	M	D	M	D
11	M	M	M	M	M	M	D
12	M	M	M	M	M	M	M
13	F	F	F	F	F	F	F
14	M	D	M	M	M	M	M
15	F	F	F	F	F	F	F
16	M	D	M	M	M	M	M
17	F	F	F	F	F	F	F
18	M	D	M	D	D	D	M
19	M	D	D	D	M	D	M
20	ND	ND	ND	ND	ND	ND	ND

using probes for chromosomes 1, 2, 6, 10, 13, 17 and 21 was successful in 11 cases. These analyses reveal a massive loss of tested chromosomes. Monosomy of chromosomes 1, 2, 6, 10, 13 and 21 was found in 100, 36, 91, 82, 82, 82 and 64% of cases, respectively.

Discussion

CRCC was first described by Thoenes and colleagues in 1985 [43]. CRCC represents approximately 5% of the carcinomas of the kidney. It is important to distinguish it from other malignancies, because it has a better prognosis than most other types of renal cell carcinomas. According to the proportion of cells with an abundant pale cytoplasm and eosinophilic cells, CRCC has traditionally been separated into the classic type composed of both cell types and the chromophil eosinophilic cell type [25, 32, 44]. In 1998, we published a type of CRCC that contains pigmented cells and large extracellular deposits of lipochrome in addition to eosinophilic cells and cells with abundant pale cytoplasm. The most striking features of this variant of CRCC are a peculiar microtubullar or microcystic pattern, pigmentation and the constant presence of calcifications [31].

Clinical features of all PMCRC were similar to that of renal carcinomas. The patients presented with gross hematuria, loin pain and abdominal discomfort, or the tumors were detected incidentally. The age of the patients was in accordance with the data of the literature [1, 30]. The size of PMCRC corresponded with published series of CRCC; however, the size was slightly bigger [1, 30, 32]. Interestingly, the biological behavior of PMCRC, despite the stage, was generally favorable. Metastases were absent at the time of the diagnosis and no further spread or recurrence of the disease was documented at follow-up in 19 of 20 cases.

The microcystic and tubulo-cystic pattern is not unique for the PMCRC variant of CRCC. However, the architectural features resembling “Roman bridging” of intraductal and invasive breast cancer in some areas are highly unusual for CRCC. Martignoni et al. described a tubulocystic pattern in 30% of CRCC in their series [30]. However, the connection of an unusual histological pattern, extensive pigmentation and microcalcifications altogether forms a misleading histological appearance, which caused most of the cases sent to us in consultation to be diagnosed as renal cell carcinoma NOS by referring pathologists.

Only a few reports dealing with pigmented renal cell carcinomas have been published in the English written literature. The occurrence of the lipochrome in CRCC at the ultrastructural level has been described by Bonsib et al. However, no pigment was observed at the light microscopic level in his report [7]. Kamishina et al. published a case of renal cell carcinoma that contained pigment at both the light and ultrastructural level in 1995 [22]. The same group of authors published altogether five cases of pigmented renal cell carcinomas 2 years later [15]. The macroscopic appearance of one case is very similar to our grossly documented cases [15, 22]. Histochemically and ultrastructurally, the

pigment resembled neuromelanin. There were, however, no described light microscopic or ultrastructural features corresponding to CRCC. Another case report of melanin-pigmented clear (conventional) renal cell carcinoma was published in 2001 by Lei et al. [26].

The occurrence of a lipochrome pigment is not unique to the PMCRC. It was described in primary pigmented nodular adrenocortical disease [39, 46] and adenomas of the adrenal glands [5, 9, 12, 24, 29] in thyroids of patients with a history of minocycline ingestion [3, 20] and in various organs and conditions of the gastrointestinal tract [16].

In 3 of 20 tumors, prominent regressive changes were noted, which are very unusual for typical CRCCs [10]. Calcifications are mentioned in the minority of published cases of typical CRCC in the literature [1, 11]. However, irregular calcifications were present in almost 50% of cases in a large series of 100 CRCCs [30]. Extensive calcification and ossification was noted in one of our cases, similar to a case described previously in 2002 [50]. We hypothesize that all these calcifications, pigmentation and adenomatous to (micro)cystic changes in our cases are probably consequences of microhemorrhages and necroses.

Our results of an immunohistochemical examination corresponded approximately with other immunohistochemical analyses of CRCC [10, 13, 42]. All cases were positive for EMA and variably positive for cytokeratins. The majority of the cases reacted with parvalbumin. No reactivity with "melanotic" markers was noted. An interesting study was published recently. In 88% of CRCCs and 71% of oncocytomas, c-kit expression was detected by immunohistochemistry suggesting that c-kit expression could be used for distinguishing CRCC from other renal cell carcinomas [38]. In contrast, only focal and weak immunohistochemical positivity was revealed in 2 of 20 PMCRCs in our study. These results were also supported by mutation screening of exons 9, 11, 13 and 17 of the c-kit gene, which are the most commonly altered in several types of neoplasia [28, 47]. Although we found alteration of exon 17 at nucleotide position 81,349 in three cases, this nucleotide is the third in the codon 798 (Ile), its alteration has no effect on amino acid sequence and it is probably a rare polymorphism. No additional mutation of the c-kit gene was found in successfully analyzed samples. We had obtained similar results when we had analyzed 10 cases of conventional CRCC for the mutation of c-kit, not included in this series. No case of conventional CRCC revealed mutation of exons 9, 11, 13 and 17 of the c-kit gene (unpublished observation).

Many molecular genetic and cytogenetic studies revealed that specific chromosomal aberrations are a common feature of renal cell carcinoma. Heidelberg classification is based on such findings. According to this classification, loss of chromosomes 1, 2, 6, 10, 13, 17 and 21 is one of the characteristics for CRCCs [23]. Speicher et al. revealed under-representation of chromosome 1 in 17 of 19 CRCCs, loss of entire chromosomes 2, 10 and 13 in 16 of 19 CRCCs, loss of chromosomes 6 and 21 in 15 of 19 CRCCs and loss of chromosome 17 in 13 of 19 cases using comparative genomic hybridization [40]. Comparative genomic hybridization was used in a recently published study of Junker et al. Combined loss of chromosomes 1, 2, 6, 10, 13, 17 and 21 represented a typical alteration of CRCC [21].

In our molecular cytogenetic analysis, monosomy of the majority or all of chromosomes 1, 2, 6, 10, 13, 17 and 21 was found in all successfully analyzed cases (Table 5). These results are in a good concordance with molecular genetic and cytogenetic data for CRCC published by other authors [8, 19, 21, 23, 35, 40, 49] and support our hypothesis that PMCRC is only an unusual morphologic variant of CRCC, without major differences in immunohistochemical and cytogenetic profile.

PMCRC seems to have an excellent prognosis. In none of the 19 patients in our series with a follow-up (0.2–8 years) did local recurrence or metastatic disease occur. As CRCC is well known to be the most frequent type of renal cell carcinoma to give rise to sarcomatoid carcinomas of the kidney [2], we reviewed all 14 cases of CRCC in which a component of this highly aggressive type of carcinoma was found in our files. In none of the 14 cases of sarcomatoid CRCC have we found features of PMCRC. In this respect, the excellent prognosis of PMCRC can be compared with a similar behavior of multilocular cystic type of clear renal cell carcinoma [34].

In terms of differential diagnosis, PMCRC is a challenging tumor: in light of its much more indolent behavior in comparison with other renal cell carcinomas, it is important to distinguish it from latter types. It can be very difficult to distinguish from renal oncocytoma (RO). In general, RO may show a broad spectrum of appearances, the most common being the alveolar, tubular, trabecular and tubulocystic patterns with focal papillary prominences or cystic arrangement, which are similar to PMCRC. The polygonal tumor cells of RO are typically uniform with usually abundant granular eosinophilic cytoplasm packed with mitochondria [4, 37]. Psammoma bodies and calcification are quite frequently present both in ROs and PMCRC. The dark brown pigmentation and architectural characteristics of tumors we present are therefore helpful morphological diagnostic features of PMCRC. PMCRC also differs from RO by the presence of typical raisinoid nuclei, which are virtually absent in RO [45]. We documented typical numerous intracytoplasmic vesicles within the cytoplasm of PMCRC. The karyotypes of RO fall into three categories: (1) normal, (2) loss of chromosome 1 or the short arm of chromosome 1 and (3) loss of the Y chromosome and occasionally monosomy 14, structural rearrangements involving chromosome 11 band q13 [27].

The granular variant of clear renal cell carcinoma (CIRCC) is another entity, which should be concerned in the differential diagnosis. Although a variety of histological patterns has been described for CIRCC, a complicated organoid structure of PMCRC has not been reported [14]. Moreover, the typical cytological appearance of CRCC cells, such as raisinoid nuclei, perinuclear clearing, etc., is present in all cases in our series [45].

The presence of large pools of dark pigmentation raises the possibility of metastatic melanoma. This condition should be considered especially when it coincides with skin melanoma as in one case (no. 18) in our series. The patient

underwent nephrectomy for renal tumor and, subsequently, the diagnosis of lentigo maligna of the skin was established. Any type of metastatic melanoma should express "melanocytic" markers, such as S-100 protein or HMB45. Both reactions were entirely negative in all cases. Moreover, clearly epithelial morphological and immunohistochemical nature and organoid pattern of PMCRC speaks strongly against the diagnosis of melanoma.

In summary, we enlarged our previously published study of unusual PMCRC and added cytogenetic analysis. Our results indicate that PMCRC is an unusual morphologic variant of CRCC with a cytogenetic and immunohistochemical profile corresponding to usual forms of CRCC. The gradual transitions between the adenomatous component and classic CRCC component are indirect evidence that the adenomatous component is an integral part of the tumor rather than a collision tumor. The important feature of PMCRC is its relatively benign biological behavior and the absence of distant metastases and sarcomatoid transformation.

References

1. Akhtar M, Kardar H, Linjawi T, McClintock J, Ali MA (1995) Chromophobe cell carcinoma of the kidney. A clinicopathologic study of 21 cases. Am J Surg Pathol 19:1245–1256
2. Akhtar M, Tulbach A, Kardar H, Ali MA (1997) Sarcomatoid renal cell carcinoma: the chromophobe connection. Am J Surg Pathol 21:1188–1195
3. Alexander CB, Herrera GA, Jaffe K, Yu H (1985) Black thyroid. Clinical manifestations, ultrastructural findings, and possible mechanisms. Hum Pathol 16:72–78
4. Amin MB, Crotty TB, Tickoo SK, Farrow G (1997) Renal oncocytoma, a reappraisal of morphologic features with clinicopathologic findings in 80 cases. Am J Surg Pathol 21:1–12
5. Baker MR (1938) A pigmented adenoma of the adrenal. Arch Pathol 26:845–852
6. Bonsib SM (1996) Renal chromophobe cell carcinoma. The relationship between cytoplasmic vesicles and colloidal iron stain. J Urol Pathol 4:9–14
7. Bonsib SM, Lager DJ (1990) Chromophobe cell carcinoma. Am J Surg Pathol 14:260–267
8. Bugert P, Kovacs G (1996) Molecular differential diagnosis of renal cell carcinomas by microsatellite analysis. Am J Pathol 149:2081–2088
9. Caplan RH, Virata RL (1974) Functional black adenoma of the adrenal cortex. A rare cause of primary aldosteronism. Am J Clin Pathol 62:97–103
10. Cochand-Priollet B, Molinié V, Bougaran J, Bouvier R, Dauge-Geffroy, Desligniéres S, Fournet JC, Gross P, Lesourd A, Saint-André JP, Toublanc M, Vieillefond A, Wassef M, Fontaine A, Groleau L (1997) Renal chromophobe cell carcinoma and oncocytoma. A comparative morphologic, histochemical, and immunohistochemical study of 124 cases. Arch Pathol Lab Med 121:1081–1086
11. Crotty TB, Farrow GM, Lieber MM (1995) Chromophobe cell renal carcinoma: clinicopathological features of 50 cases. J Urol 154:964–967
12. Damron TA, Schelper RL, Sorensen L (1987) Cytochemical demonstration of neuromelanin in black pigmented adrenal nodules. Am J Clin Pathol 87:334–341
13. DeLong WH, Sakr W, Grignon DJ (1996) Chromophobe renal cell carcinoma. A comparative histochemical and immunohistochemical study. J Urol Pathol 4:1–8
14. Eble JN, Sauter G, Epstein JI, Sesterhenn IA (eds) (2004) Tumours of the urinary system and male genital organs. IARC Press, Lyon
15. Fukuda T, Kamishima T, Emura I, Takastuka H, Suzuki T (1997) Pigmented renal cell carcinoma: accumulation of abnormal lysozomal granules. Histopathology 31:38–46
16. Ghadially FN, Walley VM (1994) Melanoses of the gastrointestinal tract. Histopathology 25:197–207
17. Hale CW (1946) Histochemical demonstration of acid mucopolysaccharides in animal tissues. Nature 204:745–747
18. Hes O, Michal M (2001) Small cell variant of renal oncocytoma —a rare and misleading type of benign renal tumor. Int J Surg Pathol 9:215–222
19. Iqbal MA, Akhtar M, Ulmer C, Al-Dayel F, Paterson MC (2000) FISH analysis in chromophobe renal-cell carcinoma. Diagn Cytopathol 22:3–6
20. Jennings TA, Sheehan ChE, Chodos RB, Figge J (1996) Follicular carcinoma associated with minocycline-induced black thyroid. Endocrin Pathol 7:345–348
21. Junker K, Weirich G, Amin MB, Moravek P, Hindermann W, Schubert J (2003) Genetic subtyping of renal cell carcinoma by comparative genomic hybridization. Recent Results Cancer Res 162:169–175
22. Kamishima T, Fukuda T, Emura I, Tanigawa T, Naito M (1995) Pigmented renal cell carcinoma. Am J Surg Pathol 19:350–356
23. Kovacs G, Akhtar M, Beckwith BJ, Bugert P, Cooper CS, Delahunt B, Eble JN, Fleming S, Ljungberg B, Medeiros LJ, Moch H, Reuter VE, Ritz E, Roos G, Schmidt D, Srigley JR, Storkel S, van den Berg E, Zbar B (1997) The Heidelberg classification of renal cell tumours. J Pathol 183:131–133
24. Lam KY, Wat MS (1996) Adrenal cortical black adenoma. Report of two cases and review of the literature. J Urol Pathol 4:183–190
25. Latham B, Dickersin R, Oliva E (1999) Subtypes of chromophobe renal cell carcinoma. An ultrastructural and histochemical study of 13 cases. Am J Surg Pathol 23:530–535
26. Lei JY, Middleton LP, Guo XD, Duray PH, McWilliams G, Linehan WM, Merino MJ (2001) Pigmented renal clear cell carcinoma with melanotic differentiation. Hum Pathol 32:233–236
27. Lindgren V, Paner GP, Omeroglu A, Campbell SC, Waters WB, Flanigan RC, Picken MM (2004) Cytogenetic analysis of a series of 13 renal oncocytomas. J Urol 171:602–604
28. Longley BJ, Reguera MJ, Ma Y (2001) Classes of c-KIT activating mutations: proposed mechanisms of action and implications for disease classification and therapy. Leuk Res 25: 571–576
29. Macadam RF (1971) Black adenoma of the human adrenal cortex. Cancer 27:116–119
30. Martignoni G, Eble JN, Brunelli M, Cheng L, Pea M, Delahunt B (2003) Chromophobe renal cell carcinoma: a clicopathologic study of 100 cases. Mod Pathol 16:161A
31. Michal M, Hes O, Švec A, Ludvíková M (1998) Pigmented microcystic chromophobe cell carcinoma: a unique variant of renal cell carcinoma. Ann Diagn Pathol 2:149–153
32. Morell-Quadreny L, Gregori-Romero M, Llombart-Bosch A (1996) Chromophobe renal cell carcinoma. Pathologic, ultrastructural, immunohistochemical, cytofluorometric and cytogenetic findings. Pathol Res Pract 192:1275–1281
33. Muller G (1955) Uber eine Vereinfachung der Reaktion nach Hale (1946). Acta Histochem 2:68–70
34. Murad T, Komaiko W, Oyasu R, Bauer K (1991) Multilocular cystic renal cell carcinoma. Am J Clin Pathol 95:633–637
35. Nagy A, Buzogany I, Kovacz G (2004) Microsatellite allelotyping differentiates chromophobe renal cell carcinomas from oncocytomas and identifies new genetic changes. Histopathology 44:542–546
36. Paternoster SF, Brockman SR, McClure RF, Remstein ED, Kurtin PJ, Dewald GW (2002) A new method to extract nuclei from paraffin-embedded tissue to study lymphomas using interphase fluorescence in situ hybridization. Am J Pathol 160:1967–1972

37. Perez-Ordonez B, Hamed G, Campbell S, Erlandson RA, Russo P, Gaudin PB, Reuter VE (1997) Renal oncocytoma: A clinicopathologic study of 70 cases. Am J Surg Pathol 21:871–883
38. Petit A, Castillo M, Santos M, Mellado B, Alcover JB, Mallofré C (2004) KIT expression in chromophobe renal cell carcinoma. Comparative immunohistochemical analysis of KIT expression in different renal cell neoplasms. Am J Surg Pathol 28:676–678
39. Shenoy BV, Carpenter PC, Carney JA (1984) Bilateral primary pigmented nodular adrenocortical disease. Rare cause of the Cushing syndrome. Am J Surg Pathol 8:335–344
40. Speicher MR, Schoell B, du Manoir S, Schrock E, Ried T, Cremer T, Storkel S, Kovacs A, Kovacs G (1994) Specific loss of chromosomes 1, 2, 6, 10, 13, 17, and 21 in chromophobe renal cell carcinomas revealed by comparative genomic hybridization. Am J Pathol 145:356–364
41. Steger G (1994) Thermal denaturation of double-stranded nucleic acids: prediction of temperatures critical for gradient gel electrophoresis and polymerase chain reaction. Nucleic Acids Res 25:2760–2768
42. Taki A, Nakatani Y, Misugi K, Yao M, Nagashima Y (1999) Chromophobe renal cell carcinoma: an immunohistochemical study of 21 Japanese cases. Mod Pathol 12:310–317
43. Thoenes W, Storkel S, Rumpelt HJ (1985) Human chromophobe cell renal carcinoma. Virch Arch B 48:207–217
44. Thoenes W, Storkel S, Rumpelt HJ, Moll R, Baum HP, Werner S (1988) Chromophobe cell renal carcinoma and its variants-A report on 32 cases. J Pathol 155:277–287
45. Tickoo SK, Amin MB (1998) Discriminant nuclear features of renal oncocytoma and chromophobe renal cell carcinoma. Analysis of their potential utility in the differential diagnosis. Am J Surg Pathol 110:782–787
46. Travis WD, Tsokos M, Doppman JL, Nieman L, Chrousos GP, Cutler Jr GB, Lynn Loriaux D, Norton JA (1989) Primary pigmented nodular adrenocortical disease. Am J Surg Pathol 13:921–930
47. Wardelmann E, Neidt I, Bierhoff E, Speidel N, Manegold C, Fischer HP, Pfeifer U, Pietsch T (2002) C-kit mutations in gastrointestinal stromal tumors occur preferentially in the spindle rather than in the epithelioid cell variant. Mod Pathol 15: 125–136
48. Widehn S, Kindblom LG (1988) A rapid and simple method for electron microscopy of paraffin embedded tissue. Ultrastr Pathol 12:131–136
49. Wilhelm M, Veltman JA, Olshen AB, Jain AN, Moore DH, Presti JC Jr, Kovacs G, Waldman FM (2002) Array-based comparative genomic hybridization for the differential diagnosis of renal cell cancer. Cancer Res 62:957–960
50. Wu SL, Fishman IJ, Shannon RL (2002) Chromophobe renal cell carcinoma with extensive calcification and ossification. Ann Diagn Pathol 6:244–247

Virchows Arch (2005) 446: 394–401
DOI 10.1007/s00428-004-1166-2

ORIGINAL ARTICLE

Jukka Tienari · Sanna Lehtonen · Eero Lehtonen

CD2-associated protein in human urogenital system and in adult kidney tumours

Received: 3 September 2004 / Accepted: 26 October 2004 / Published online: 23 March 2005
© Springer-Verlag 2005

Abstract We studied expression of CD2-associated protein (CD2AP) in human urogenital system and in adult kidney tumours. In the cortex of normal kidney, CD2AP was expressed in all types of tubules and in the glomeruli. Labelling was more intense in cytokeratin 7- and in Tamm–Horsfall-positive tubules than in proximal tubules. In the medulla, expression was observed in the collecting ducts. Urothelium and the epithelium of prostatic acini, seminal vesicles, seminiferous tubules, epididymal ducts, Fallopian tube, endometrium and endocervix as well as granulosa cells showed moderate to strong CD2AP positivity. In syncytiotrophoblast, the expression was weaker than in cytotrophoblast. Endometrial stroma was negative, but decidualised stroma was weakly positive. Clear cell renal cell carcinoma (RCC) (n=63) showed a weak expression. Type-I papillary RCCs (n=4) and papillary adenomas (n=3) were negative. The epithelium lining the cysts in multilocular cystic RCCs (n=3) and in cystic nephroma (n=1) was strongly positive. Chromophobe RCCs (n=2), oncocytomas (n=3) and urothelial carcinomas (n=2) were moderately positive. The results show that CD2AP displays a specific expression pattern in human urogenital organs and that distinct expression is shown in several types of kidney tumours but not in type-I papillary RCCs or in papillary adenomas.

Keywords CD2AP · Renal cell carcinoma · Oncocytoma · Papillary adenoma of the kidney · Histological subtype

J. Tienari (✉)
Department of Pathology, Helsinki University Central Hospital/
Peijas Hospital and HUSLAB,
Sairaalakatu 1,
01400, Vantaa, Finland
e-mail: jukka.tienari@hus.fi
Tel.: +358-9-47167695
Fax: +358-9-47167577

S. Lehtonen · E. Lehtonen
Department of Pathology, Haartman Institute and Helsinki
University Central Hospital, University of Helsinki,
P.O. BOX 21, 00014 Helsinki, Finland

Introduction

Renal cell carcinoma (RCC) is a group of malignancies arising from the epithelium of the renal tubules [8]. The different histological subtypes of RCC are believed to originate from specific segments of kidney tubules. The histological subtype of RCC is known to influence the outcome of the patients [1, 24, 32]. The majority of the cases, however, represent the conventional clear cell RCC.

One of the recently identified scaffolding proteins is CD2-associated protein (CD2AP), an 80-kDa protein that contains multiple domains implicated in protein–protein interactions [7, 20, 21]. CD2AP was identified from T cells as a CD2-adhesion molecule-associating protein [7] and the human counterpart of CD2AP, CMS, was cloned as a protein binding to the focal-adhesion molecule $p130^{CAS}$ [20]. We identified the protein in differential screening for developmentally regulated genes from embryonic mouse kidney cDNA library as a gene that was strongly upregulated upon mesenchyme-to-epithelium transition during kidney development [17, 21].

In the glomeruli, CD2AP localises to the slit diaphragm and links nephrin and podocin to phosphoinositide 3-OH kinase (14, 33). CD2AP knockout (−/−) mice develop a congenital nephrotic syndrome with podocyte foot-process effacements and die at 6 weeks of age from renal failure [34]. The CD2AP +/− heterozygous mice develop glomerular changes at 9 months of age with a histological pattern similar to that in human focal segmental glomerulosclerosis [19].

CD2AP is also connected to another kidney disease characterised by loss of cell morphology and polarity, namely autosomal dominant polycystic kidney disease (ADPKD), which can be caused by mutations in PKD1 or PKD2 genes, which encode proteins polycystin-1 and polycystin-2, respectively [15, 16, 26]. CD2AP interacts with polycystin-2 [21]. ADPKD manifests as cystic dilatations of kidney tubules and glomerular capsules, which are believed to develop as a consequence of increased proliferation and dedifferentiation of renal tubule epithelial cells [28]. The disease is usually associated with epithelial hy-

perplasia and polypoid foci and, in about 20% of the cases, also with adenomas [11].

In the developing mouse kidney, CD2AP is upregulated in the aggregating metanephric mesenchyme cells. Upon maturation of the nephrons, the signal becomes weak in proximal tubules, whereas immunoreactivity in the glomeruli and distal tubules remains until adulthood. Both during embryonic development and in the adult mouse kidney, CD2AP can be detected abundantly in the collecting ducts [21, 23]. Here, we have studied the expression of CD2AP in human kidney tubules and other components of the urogenital system and compared it with the CD2AP expression in adult kidney tumours.

Materials and methods

Tissue selection

Samples of kidney tumours from patients operated in Peijas hospital during 1994–2002 were retrieved from the archives of Peijas hospital. All the patients had been treated with surgical radical nephrectomy. Three samples of normal kidney were from kidneys that had contained tumours in the opposite poles. Almost all tumour samples also contained adjacent normal kidney as internal controls. Tumours were classified according to the World Health Organization classification of tumours [8]. Nuclear grading was determined following the Fuhrman system [9].

Immunohistochemistry

Immunohistochemical analysis was performed with antibodies listed in Table 1. Tissue samples were fixed in 10% formalin and embedded in paraffin. In stainings for CD2AP, CD10 and cytokeratin 7, the sections were microwaved in 10 mM citrate buffer, pH 6.0 (30 min 160 W) to retrieve antigens. The primary and secondary antibodies were diluted in phosphate-buffered saline containing 1% bovine serum albumin, and the incubations were at room temperature for 1 h. Detection was carried out using StreptABComplex/HRP Duet, Mouse/Rabbit kit (Dako) and diaminobenzidine tetrahydrochloride. Light microscopy was performed with an Olympus BH 2 microscope. The slides were examined by two pathologists (J.T. and E.L.). Negative controls included slides incubated in buffer without the primary antibody and tissues known to be negative for CD2AP, such as skeletal muscle and fibrous tissue. Endothelium of blood vessels served as a positive control for CD2AP. Normal kidney tissue adjacent to tumour tissue was used as an internal positive control for CK7 and CD10.

Table 1 Antibodies used in the study. (*MW* microwave oven treatment)

Antibody	Source	Dilution, antigen retrieval
CD2AP (H290)	Santa Cruz, Santa Cruz, CA	1:100, MW
CD10 (NCL-CD10–270)	Novocastra, Newcastle upon Tyne, UK	1:100, MW
Cytokeratin 7 (Clone OV-TL 12/30)	Dako, Clostrup, Denmark	1:100, MW
Tamm–Horsfall (TH)	Cedarlane laboratories, Hornby, Ontario	1:500, no antigen retrieval

In almost all cases, the tumour tissues showed a rather homogeneous staining pattern for CD2AP. Therefore, in the case of CD2AP, the expression in the tumour tissues was graded by comparing it with the adjacent normal kidney: a strong reaction (+++) was similar to that seen in urothelium and medullary collecting ducts, a moderate reaction (++) was similar to that observed in cortical collecting ducts and a weak reaction (+) corresponded to that observed in proximal tubules. Staining weaker than that seen in proximal tubules was interpreted as negative. In the cases of CD10 and CK 7, many tumours showed considerable intratumoural variation in staining intensities with strongly positive components intermingled with entirely negative components. Therefore, a different scoring system was used for CD10 and CK7. The scoring of the tumour tissue was graded according to the proportion of tumour cells showing positive staining: −, no staining; +, positive staining in less than 33% of the cells; ++, positive staining in 33 to 66% of the cells; +++, positive staining in more than 66% of the cells.

Results

Normal kidney

We studied immunohistochemically the expression of CD2AP in normal human kidney. CD10 was used as a marker for proximal tubules, Tamm–Horsfall as a marker for thick ascending limbs of the loops of Henle and for the distal convoluted tubules and cytokeratin 7 as a marker for distal tubules and collecting ducts [13, 22, 25, 35].

In the cortex of human kidney, CD2AP appeared to be expressed widely in different types of tubules as well as in the glomeruli (Fig. 1A, B, C, D). The expression was weak in CD10-positive proximal tubules and moderate in cytokeratin 7-positive and in Tamm–Horsfall-positive tubules. In the medulla, CD2AP expression was more restricted. A strong expression was observed only in cytokeratin 7-positive tubules that could morphologically be identified as collecting ducts (Fig. 1E, F, G). Urothelium was also strongly positive.

Reproductive organs

Prostatic acinar secretory epithelial cells were moderately positive for CD2AP, whereas the basal cells of the acinar epithelium were strongly positive (Fig. 2A). The epithelium of seminal vesicles was moderately positive (not shown). In testis, spermatocytes and spermatogonia were moderately

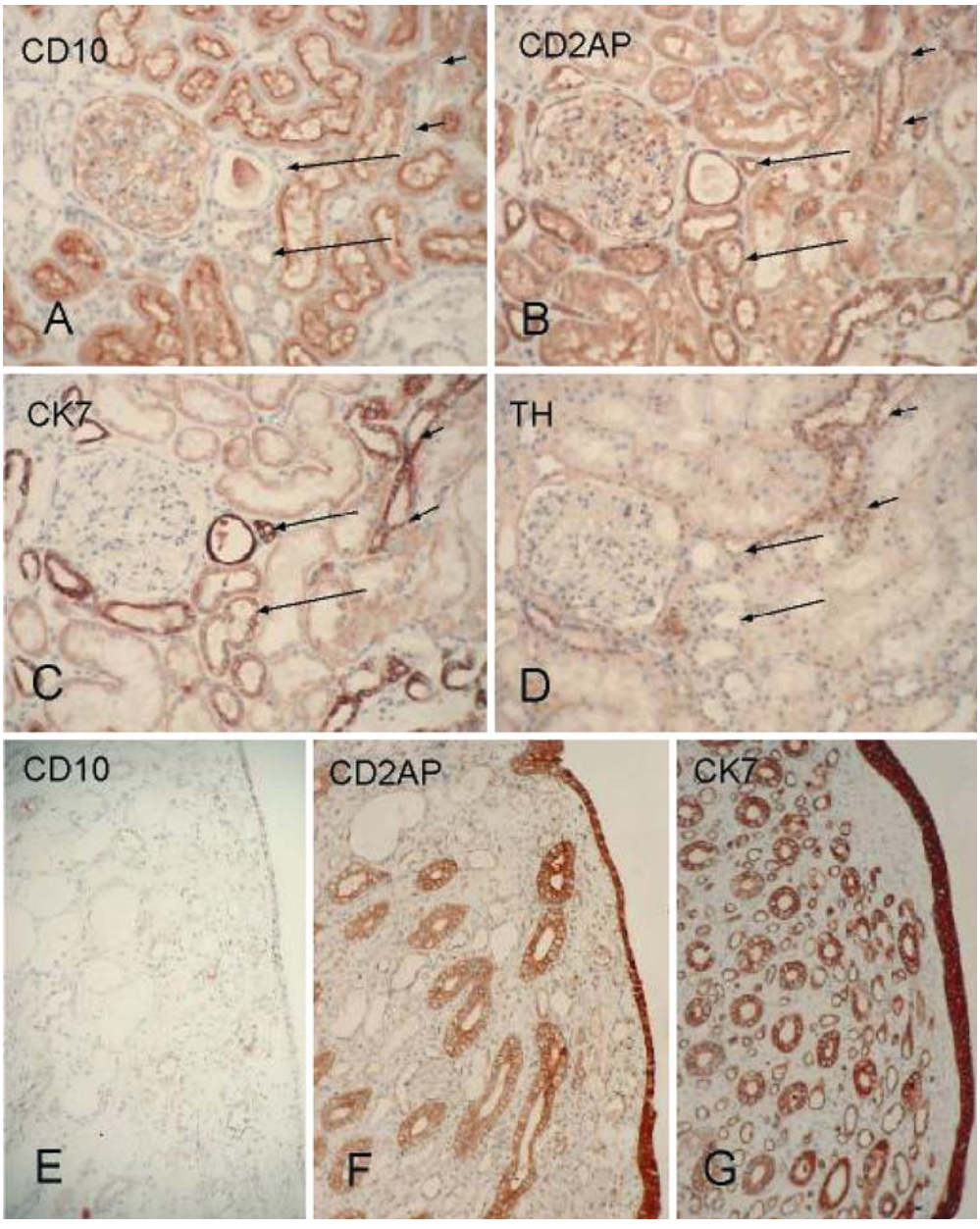

Fig. 1 Serial sections of human kidney immunostained for CD10 (**A**, **E**), CD2-associated protein (CD2AP) (**B**, **F**), cytokeratin 7 (**C**, **G**) and Tamm–Horsfall protein (**D**). In the cortex (**A**–**D**), both the glomeruli and the tubules are positive for CD2AP. Some of the cytokeratin 7-positive tubules (*long arrows*) and Tamm–Horsfall-positive tubules (*short arrows*) show a stronger staining for CD2AP than the CD10-positive proximal tubules. In the medulla (**E**–**G**), only collecting ducts and urothelium are distinctly CD2AP positive (original magnification ×200)

positive, while Leydig cells were weakly positive (Fig. 2B). The tall columnar cells of the ductal epithelium of epididymis were moderately positive, whereas the basal cells were strongly positive (Fig. 2C). The surface epithelium of ovaries was strongly positive (not shown). Granulosa cells were moderately positive, while ovarial stroma was negative (Fig. 2D). The epithelium of Fallopian tube was moderately positive (Fig. 2E). Endometrial epithelium was moderately positive, while endometrial stroma was negative (Fig. 2F). Decidualised endometrial stroma was weakly positive (Fig. 2G). In placenta, the cytotrophoblast was strongly positive, while the syncytiotrophoblast was moderately positive (Fig. 2H). The glandular epithelium of uterine cervix was moderately positive, while squamous epithelium was weakly positive (not shown).

Kidney tumours

Surgical specimens containing kidney tumours were studied (Table 2). Of the cases, 63 represented conventional clear cell RCC, most of which express CD10 [3]. Seven tumours showed papillary structures and small cells with scant pale cytoplasms and expressed cytokeratin 7 but were negative or only focally positive for CD10. Four of these tumours were more than 5 mm in diameter and were classified as type-I papillary RCC, and three were less than 5 mm and were classified as papillary adenomas [6, 8]. One papillary tumour consisted of larger cells than the other papillary tumours and expressed widely CD10 but only focally cytokeratin 7. It was classified as type-II papillary RCC. Three tumours consisted almost entirely of cysts lined by a single layer of cells with only occasional small groups

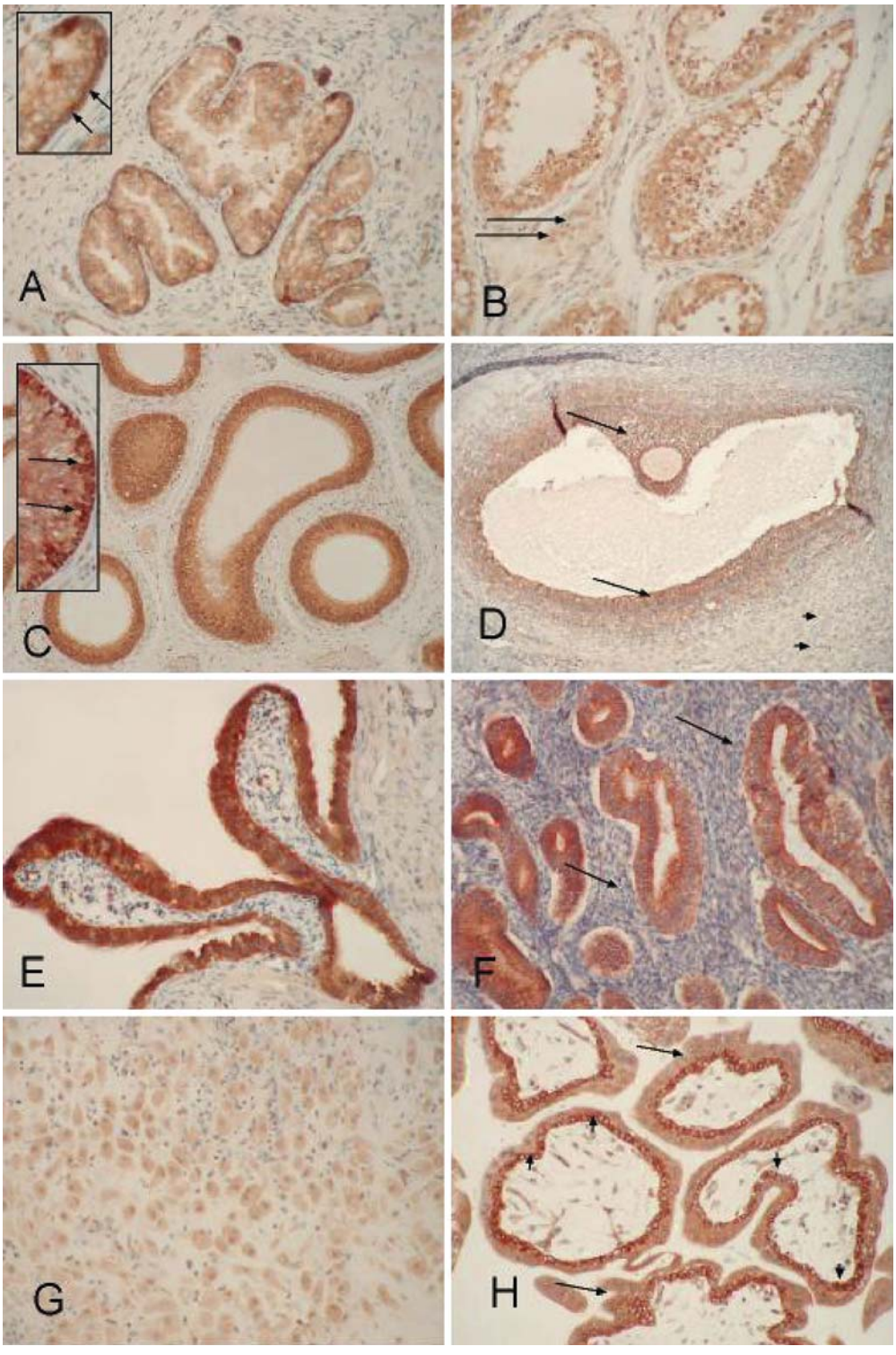

Fig. 2 Human reproductive tissues immunostained for CD2-associated protein (CD2AP). Moderate positivity is seen in prostatic acinar epithelium (**A**) while basal cells are strongly positive (*insert*, *arrows*). Spermatocytes and spermatids of seminiferous tubules of testis (**B**) are moderately positive, while Leydig cells are weakly positive (*arrows*). Ductal epithelium of epididymis (**C**) is moderately positive, while basal cells are strongly positive (*insert*, *arrows*). Granulosa cells of ovarian follicles (**D**, *arrows*) are moderately positive while ovarian stroma (*arrowheads*) is negative. Epithelium of Fallopian duct (**E**) is moderately positive. Endometrial epithelium (**F**) is moderately positive, while stroma (*arrows*) is negative. Decidualised stromal cells in uterus (**G**) are weakly positive. Cytotrophoblast (*arrowheads*) of placenta (**H**) is strongly positive, while syncytiotrophoblast (*arrows*) is weakly positive for CD2AP [original magnification ×200 (**A**, **B**, **E**–**H**; ×100 (**C**, **D**); ×400 (*inserts*)]

of clear cells in the septa and were positive with varying intensity for CD10 and for cytokeratin 7. They were classified as multilocular cystic RCCs. One tumour consisted entirely of cysts lined by a single layer of cells positive for cytokeratin 7 but negative for CD10 and was classified as a cystic nephroma. Two tumours showed abundant granular cytoplasms and were negative for CD10 but strongly positive for cytokeratin 7 and were classified as chromophobe RCCs; whereas, three tumours with abundant granular cytoplasms were negative for both CD10 and cytokeratin 7 and were classified as oncocytomas. Two tumours were urothelial carcinomas.

The conventional clear cell RCCs showed a rather similar staining pattern for CD2AP, which indicated a uniform low-level expression (Fig. 3A, B, C). The type-I papillary RCCs and papillary adenomas were almost entirely negative for

Table 2 Expression of CD2-associated protein (CD2AP), CD10 and CK7 in adult human kidney tumors. Semi-quantitative analysis of expression of CD2AP, CD10 and CK7 was performed on immunoperoxidase-stained sections of kidney tumours. In the case of CD2AP, the expression in the tumour cells was relatively homogeneous, and the scoring was based on comparisons with the normal kidney in the same section. In the case of CD10 and CK7, the scoring was based on the proportion of tumour cells showing positive staining to the marker. For details, see Materials and methods. *RCC* renal cell carcinoma

	n	CD2AP	CD10	CK7
Clear cell RCC	63	+	++ [1]	+/– [1]
Type-I papillary RCC	4	–	+/– [2]	+++
Type-II papillary RCC	1	++	++	+
Papillary adenoma	3	–	–	+++
Multilocular cystic RCC	3	+++	++	+
Cystic nephroma	1	+++	–	+++
Chromophobe RCC	2	++	–	+++
Oncocytoma	3	++	–	–
Urothelial carcinoma	2	++	na	na

[1]Ten cases of clear cell RCCs were immunostained for CD10 and CK7. All of them were positive for CD10, but only three were distinctively positive for CK7 although three others showed weak focal positivity

[2]Of the four cases of type-I papillary RCC, two showed focal positivity for CD10

CD2AP (Fig. 3D, E, F). However, type-II papillary RCC was moderately positive (not shown). The neoplastic epithelium lining the cysts in multilocular cystic RCC was strongly positive for CD2AP (Fig. 4A, B, C). The epithelium in cystic nephroma was also strongly positive for CD2AP (Fig. 4D, E, F). A moderate staining for CD2AP was observed in chromophobe RCCs and in oncocytomas (Fig. 5). Urothelial carcinomas were also moderately positive for CD2AP (not shown).

Discussion

CD2AP is a scaffolding protein that is induced during kidney differentiation. It shows a distinct expression pattern in normal developing and adult mouse kidney and associates with proteins involved in kidney diseases, including nephrin and polycystin-2 [7, 21, 23, 33]. Previous studies on CD2AP expression in human kidney have focused on the glomeruli [10, 12, 23]. This is the first study investigating the expression of CD2AP in human kidney tubules as well as in urinary and reproductive organs and in different adult kidney tumours.

In the cortex of normal human kidney, CD2AP was rather ubiquitous, as the protein was observed in the glomeruli as well as in all the tubules. The glomerular staining was a result of a strong CD2AP expression in podocytes [10, 12, 23]. Extraglomerularly, the staining was more intense in

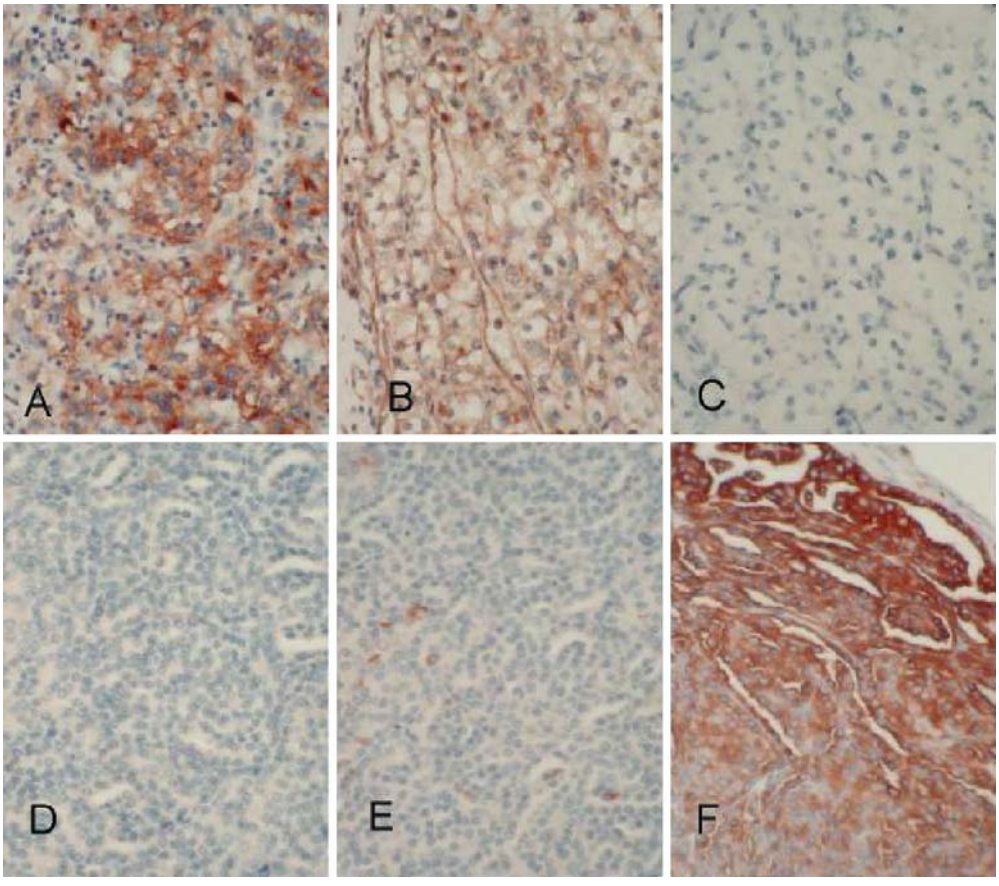

Fig. 3 Kidney tumours immunostained for CD10 (**A**, **D**), CD2-associated protein (CD2AP) (**B**, **E**) and cytokeratin 7 (**C**, **F**). A clear cell renal cell carcinoma (RCC) is positive for CD10 (**A**) but expresses only low levels of CD2AP (**B**) and is negative for cytokeratin 7 (**C**). A papillary adenoma is negative for CD10 (**D**) and CD2AP (**E**) but positive for cytokeratin 7 (**F**) (original magnification ×400)

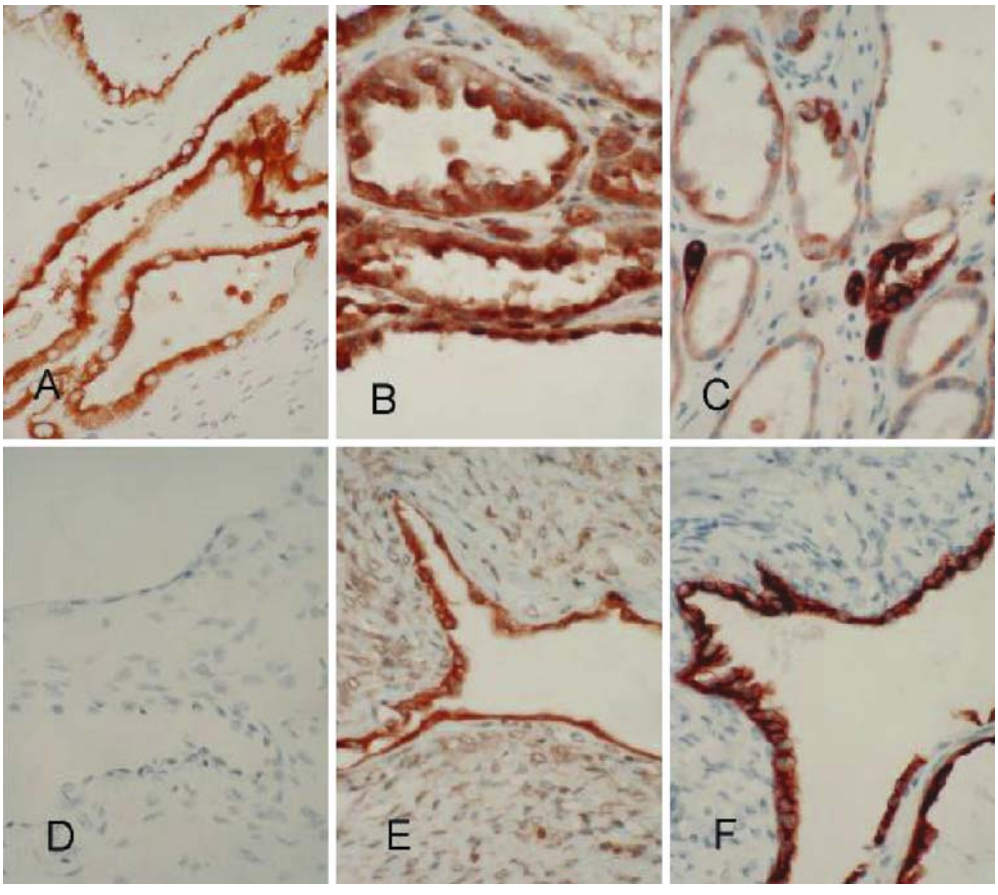

Fig. 4 Cystic kidney tumours immunostained for CD10 (**A**, **D**), CD2-associated protein (CD2AP) (**B**, **E**) and cytokeratin 7 (**C**, **F**). A multilocular cystic renal cell carcinoma is strongly positive for CD10 (**A**) and CD2AP (**B**) and focally positive for cytokeratin 7 (**C**). A benign cystic nephroma is negative for CD10 (**D**) but positive for CD2AP (**E**) and cytokeratin 7 (**F**) (original magnification ×400)

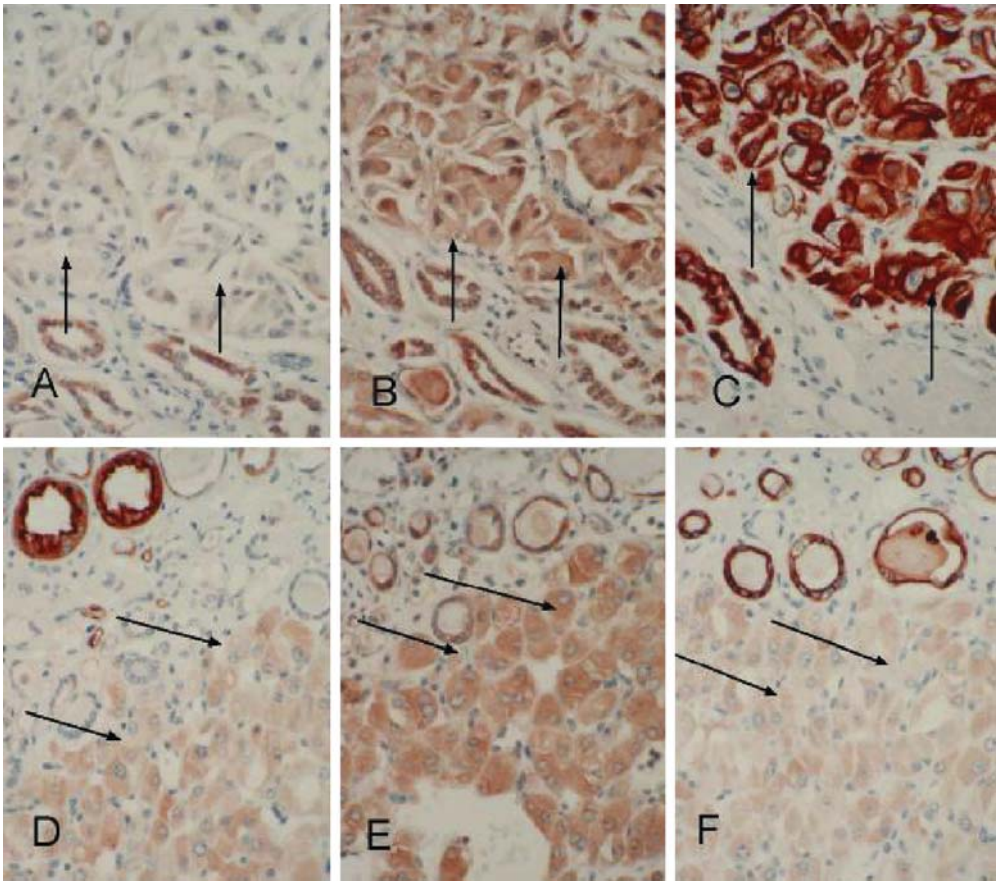

Fig. 5 Kidney tumours with granular cytoplasms immunostained for CD10 (**A**, **D**), CD2-associated protein (CD2AP) (**B**, **E**) and cytokeratin 7 (**C**, **F**). A chromophobe renal cell carcinoma (*arrows*) is negative for CD10 (**A**), positive for CD2AP (**B**) and strongly positive for cytokeratin 7 (**C**). A benign oncocytoma (*arrows*) is negative for both CD10 (**D**) and cytokeratin 7 (**F**) but positive for CD2AP (**E**) (original magnification ×400)

cytokeratin 7- and in Tamm–Horsfall-positive tubules than in proximal tubules, indicating that CD2AP is moderately expressed in the thick ascending limbs of the loops of Henle and/or in the distal convoluted tubules as well as in the collecting ducts [25, 35]. In the medullary areas, the expression of the protein was more restricted, as it was seen only in collecting ducts and in urothelium. These results are in accordance with reports on the localisation of CD2AP in mouse kidney [21, 23]. The CD2AP expression observed here also resembles the expression of polycystin-2 and polcystin-1 in normal human kidney. These proteins are prominently expressed by maturing proximal and distal tubules during development but show a more pronounced distal expression pattern in adult life [30]. ADPKD is, in 15% of the cases, caused by mutations in the PKD2 gene that encodes polycystin-2 [26]. There is, however, variation in the disease progression among patients. Changes in interacting proteins have been proposed as putative factors that could contribute to such variations by reducing or increasing the amount and stability of assembled protein complexes, thus affecting signalling pathways necessary for proper maintenance of the renal epithelial architecture in kidney tubules [31]. Since CD2AP interacts with polycystin-2 and colocalises to the same nephron segments in human kidney, it could be involved in the changes of kidney tubule epithelial cell morphology and tissue architecture of ADPKD-2 patients. Further studies are warranted to assess the role of CD2AP in ADPKD-2.

Distribution of CD2AP in mouse extrarenal tissues has been reported notably in epithelia and in endothelium [23]. This study did not, however, cover reproductive organs. Our results show that CD2AP is widely expressed in the epithelial cells in male and female reproductive organs. In some cases, such as the basal cells of prostatic acini and epididymal ducts as well as cytotrophoblast, a proliferating cell type shows a stronger staining than a mature cell type, such as the secretory epithelial cells of prostatic acini, the tall columnar epithelium of epididymal ducts or the syncytiotrophoblast, respectively. CD2AP expression was found in some cell types that otherwise do not typically show epithelial features, such as granulosa cells and Leydig cells. Decidualisation of endometrial stroma also appears to result in a weak induction of CD2AP expression. Our results suggest that CD2AP may have varying roles in the formation and maintenance of cellular architecture and/or in specialised cell functions of diverse cell types.

In hope of finding morphologically undetectable subtypes among the conventional clear cell RCCs, we immunostained 63 samples of such tumours from different patients with CD2AP antibodies. The morphologically typical clear cell RCCs showed, however, irrespective of their nuclear grades, a rather uniform staining pattern with CD2AP antibodies, which indicated a low level of expression of this protein.

Interestingly, the type-I papillary RCCs and the papillary adenomas consisting of similar small cells with scant pale cytoplasms appeared to lack CD2AP almost entirely. Besides the cytological and immunohistochemical resemblance, these tumours showed karyotypic similarities [5, 8, 18]. The lack of CD2AP in these tumours could reflect an origin from the CD2AP-negative medullary tubules. However, the loss of CD2AP expression in the papillary adenoma and carcinoma cells could also be connected to their neoplastic transformation. Mutations in PKD2 cause autosomal dominant polycystic kidney disease with kidney cysts and epithelial hyperplasia in mice [38]. The predisposition to develop adenomas by ADPKD patients with mutation in the PKD2 gene coding for polycystin-2, an interaction partner of CD2AP, and the lack of CD2AP in sporadic papillary adenomas and carcinomas raise the possibility that the CD2AP-polycystin-2 complex could be involved in the growth control of these tumour cells or their precursors. Thus, CD2AP could be implicated in the processes that lead to an increased cell proliferation of tubular epithelium and/or papillary neoplasias in ADPKD patients as well as in sporadic cases. However, papillary RCC is known to be a heterogeneous entity. In our material, one tumour showed features of type-II papillary RCCs and expressed CD2AP moderately.

The classification of cystic RCCs has been controversial, since some authors consider multilocular cystic RCC as a clinicopathological entity, whereas others suggest that it is a variant of conventional clear cell RCC [4, 27, 29]. In this respect, it is significant that the neoplastic epithelium lining the cysts in multilocular cystic RCCs was distinctively more strongly CD2AP positive than the solid-type clear cell RCCs. Cystic nephroma has been shown to have ultrastructural features similar to collecting ducts [37]. Kidney tumours composed of cells with granular cytoplasms, such as chromophobe RCC and oncocytoma, have been suggested to be histogenetically related to the intercalated cells of the collecting duct system [2, 36]. The distinct CD2AP expression observed in these tumours is in line with a direction of differentiation towards collecting duct-type cells, since this protein in the normal kidney is strongly expressed in collecting ducts. Similarly, normal urothelium is CD2AP positive, and, in line with this, urothelial carcinomas were also positive for CD2AP.

The results show that with the exception of papillary adenomas and type-I papillary carcinomas, CD2AP is expressed in several types of adult kidney tumours. CD2AP does not reveal any distinct subtypes among the prevalent clear cell RCCs, but it might offer a marker that could, in some cases, be used for differentiating non-papillary RCC from papillary RCC or for identifying different subtypes of papillary RCCs.

Acknowledgements We thank Mrs. Tuulikki Leinonen for excellent technical assistance. The work was supported by the Clinical Research Fund of Helsinki University Central Hospital, Finland and Academy of Finland, Finnish Cultural Foundation, and Wihuri Foundation, Finland. The study was approved by the Helsinki University Central Hospital Ethics Committee.

References

1. Amin MB, Amin MB, Tamboli P, Javidan J, Stricker H, de-Peralta Venturina M, Deshpande A, Menon M (2002) Prognostic impact of histologic subtyping of adult renal epithelial neoplasms: an experience of 405 cases. Am J Surg Pathol 26:281–291
2. Amin MB, Crotty TB, Tickoo SK, Farrow GM (1997) Renal oncocytoma: a reappraisal of morphologic features with clinicopathologic findings in 80 cases. Am J Surg Pathol 21:1–12
3. Avery AK, Beckstead J, Renshaw AA, Corless CL (2000) Use of antibodies to RCC and CD10 in the differential diagnosis of renal neoplasms. Am J Surg Pathol 24:203–210
4. Bielsa O, Lloreta J, Gelabert-Mas A (1998) Cystic renal cell carcinoma: pathological features, survival and implications for treatment. Br J Urol 82:16–20
5. Brown JA, Anderl KL, Borell TJ, Qian J, Bostwick DG, Jenkins RB (1997) Simultaneous chromosome 7 and 17 gain and sex chromosome loss provide evidence that renal metanephric adenoma is related to papillary renal cell carcinoma. Urology 158:370–374
6. Delahunt B, Eble JN (1997) Papillary renal cell carcinoma: a clinicopathologic and immunohistochemical study of 105 tumors. Mod Pathol 10:537–544
7. Dustin, ML, Olszowy MW, Holdorf AD, Li J, Bromley S, Desai N, Widder P, Rosenberger F, van der Merwe PA, Allen PM, Shaw AS (1998) A novel adaptor protein orchestrates receptor patterning and cytoskeletal polarity in T-cell contacts. Cell 94:667–677
8. Eble JN, Sauter G, Epstein JI, Sesterhen IA (eds) (2004) Pathology and genetics of tumours of the urinary system and male genital organs. WHO Classification of tumors. IARC Press, Lyon
9. Fuhrman SA, Lasky LC, Limas C (1982) Prognostic significance of morphologic parameters in renal cell carcinoma. Am J Surg Pathol 6:655–663
10. Gagliardini E, Benigni A, Tomasoni S, Abbate M, Kalluri R, Remuzzi G (2003) Targeted downregulation of extracellular nephrin in human IgA nephropathy. Am J Nephrol 23:277–286
11. Gregoire JR, Torres VE, Holley KE, Farrow GM (1987) Renal epithelial hyperplastic and neoplastic proliferation in autosomal dominant polycystic kidney disease. Am J Kidney Dis 9:27–38
12. Heidet L, Bongers EM, Sich M, Zhang SY, Loirat C, Meyrier A, Broyer M, Landthaler G, Faller B, Sado Y, Knoers NV, Gubler MC (2003) In vivo expression of putative LMX1B targets in nail-patella syndrome kidneys. Am J Pathol 163:145–155
13. Holm-Nielsen P, Pallesen G (1988) Expression of segment-specific antigens in the human nephron and in renal epithelial tumors. APMIS 4[Suppl]:48–55
14. Huber TB, Hartleben B, Kim J, Schmidts M, Schermer B, Keil A, Egger L, Lecha RL, Borner C, Pavenstadt H, Shaw AS, Walz G, Benzing T (2003) Nephrin and CD2AP associate with phosphoinositide 3-OH kinase and stimulate AKT-dependent signaling. Mol Cell Biol 23:4917–4928
15. Igarashi P, Somlo S (2002) Genetics and pathogenesis of polycystic kidney disease. J Am Soc Nephrol 13:2384–2398
16. International Polycystic Kidney Disease Consortium (1995) Polycystic kidney disease: the complete structure of the PKD1 gene and its protein. Cell 81:289–298
17. Jansson, S, Olkkonen V, Martin-Parras L, Chavrier P, Stapleton M, Zerial M, Lehtonen E (1997) Mouse metanephric kidney as a model system for identifying developmentally regulated genes. J Cell Physiol 173:147–151
18. Jiang F, Richter J, Schraml P, Bubendorf L, Gasser T, Sauter G, Mihatsch MJ, Moch H (1998) Chromosomal imbalances in papillary renal cell carcinoma: genetic differences between histological subtypes. Am J Pathol 153:1467–1473
19. Kim JM, Wu H, Green G, Winkler CA, Kopp JB, Miner JH, Unanue ER, Shaw AS (2003) CD2-associated protein haploinsufficiency is linked to glomerular disease susceptibility. Science 300:1298–1300
20. Kirsch KH, Georgescu MM, Ishimaru S, Hanafusa H (1999) CMS: an adapter molecule involved in cytoskeletal rearrangements. Proc Natl Acad Sci U S A 96:6211–6216
21. Lehtonen S, Ora A, Olkkonen VM, Geng L, Zerial M, Somlo S, Lehtonen E (2000) In vivo interaction of the adapter protein CD2-associated protein with the type 2 polycystic kidney disease protein, polycystin-2. J Biol Chem 275:32888–32893
22. Leroy X, Moukassa D, Copin MC, Saint F, Mazeman E, Gosselin B (2000) Utility of cytokeratin 7 for distinguishing chromophobe renal cell carcinoma from renal oncocytoma. Eur Urol 37:484–487
23. Li G, Ruotsalainen V, Tryggvason K, Shaw AS, Miner JH (2000) CD2AP is expressed with nephrin in developing podocytes and is found widely in mature kidney and elsewhere. Am J Physiol Renal Physiol 279:F785–F792
24. Ljungberg B, Alamdari FI, Stenling R, Roos G (1999) Prognostic significance of the Heidelberg classification of renal cell carcinoma. Eur Urol 36:565–569
25. Mathers ME, Pollock AM, Marsh C, O'Donnell M (2002) Cytokeratin 7: a useful adjunct in the diagnosis of chromophobe renal cell carcinoma. Histopathology 40:563–567
26. Mochizuki T, Wu G, Hayashi T, Xenophontos SL, Veldhuisen B, Saris JJ, Reynolds DM, Cai Y, Gabow PA, Pierides A, Kimberling WJ, Breuning MH, Deltas CC, Peters DJM, Somlo S (1996) PKD2, a gene for polycystic kidney disease that encodes an integral membrane protein. Science 272:1339–1342
27. Murad T, Komaiko W, Oyasu R, Bauer K (1991) Multilocular cystic renal cell carcinoma. Am J Clin Pathol 95:633–637
28. Nadasdy T, Laszik Z, Lajoie G, Blick KE, Wheeler DE, Silva FG (1995) Proliferative activity of cyst epithelium in human renal cystic diseases. J Am Soc Nephrol 5:1462–1468
29. Nassir A, Jollimore J, Gupta R, Bell D, Norman R (2002) Multilocular cystic renal cell carcinoma: a series of 12 cases and review of the literature. Urology 60:421–427
30. Ong AC, Ward CJ, Butler RJ, Biddolph S, Bowker C, Torra R, Pei Y, Harris PC (1999) Coordinate expression of the autosomal dominant polycystic kidney disease proteins, polycystin-2 and polycystin-1, in normal and cystic tissue. Am J Pathol 154:1721–1729
31. Peters DJ, Breuning MH (2001) Autosomal dominant polycystic kidney disease: modification of disease progression. Lancet 358:1439–1444
32. Renshaw AA, Richie JP (1999) Subtypes of renal cell carcinoma. Different onset and sites of metastatic disease. Am J Clin Pathol 111:539–543
33. Shih NY, Li J, Cotran R, Mundel P, Miner JH, Shaw AS (2001) CD2AP localizes to the slit diaphragm and binds to nephrin via a novel C-terminal domain. Am J Pathol 159:2303–2308
34. Shih NY, Li J, Karpitskii V, Nguyen A, Dustin ML, Kanagawa O, Miner JH, Shaw AS (1999) Congenital nephrotic syndrome in mice lacking CD2-associated protein. Science 286:312–315
35. Sikri KL, Foster CL, MacHugh N, Marshall RD (1981) Localization of Tamm–Horsfall glycoprotein in the human kidney using immuno-fluorescence and immuno-electron microscopical techniques. J Anat 132:597–605
36. Storkel S, Steart PV, Drenckhahn D, Thoenes W (1989) The human chromophobe cell renal carcinoma: its probable relation to intercalated cells of the collecting duct. Virchows Arch 56: 237–245
37. Tang TT, Harb JM, Oechler HW, Camitta BM (1984) Multilocular renal cyst: electron microscopic evidence of pathogenesis. Am J Pediatr Hematol Oncol 6:27–32
38. Wu G, D'Agati V, Cai Y, Markowitz G, Park JH, Reynolds DM, Maeda Y, Le TC, Hou H Jr, Kucherlapati R, Edelmann W, Somlo S (1998) Somatic inactivation of Pkd2 results in polycystic kidney disease. Cell 93:177–188

Virchows Arch (2005) 446: 402–410
DOI 10.1007/s00428-005-1205-7

ORIGINAL ARTICLE

Ilona Kovács · Krisztina Pocsai · Gabriella Czifra · László Sarkadi · Géza Szucs · Zoltán Nemes · Zoltán Rusznák

TASK-3 immunoreactivity shows differential distribution in the human gastrointestinal tract

Received: 29 October 2004 / Accepted: 15 December 2004 / Published online: 24 March 2005
© Springer-Verlag 2005

Abstract The presence and distribution of TASK-3 immunopositivity (a channel with potential oncogenic significance) was investigated in the human gastrointestinal system. The immunohistochemical reactions were performed with two commercially available polyclonal antibodies, targeting different epitopes of the channel protein. Experiments conducted on frozen and formalin-fixed samples indicated that the application of a suitable antigen retrieval (AR) technique was essential to produce consistent, strong and reproducible TASK-3-specific immunolabelling of the formalin-fixed tissue. The lack of or inappropriate selection of the AR resulted in false-negative reactions. As for the distribution of the TASK-3 channels, strong immunolabelling was observed in the gastric and large intestinal mucosa, with particularly prominent immunoreactivity of the epithelial cells. In contrast, the smooth-muscle layers demonstrated weak TASK-3 positivity. Intense TASK-3 expression was noted in both the exocrine and endocrine pancreas, but the islets of Langerhans exhibited more powerful reactions. The ductal apparatus of the submandibular gland and lymphocytes situated in pericolonic lymph nodes were also TASK-3 positive. Strong TASK-3 positivity could also be observed in malignant gastrointestinal tumours, with intense nuclear-perinuclear labelling of some of the tumour cells. The present findings suggest that TASK-3 channels may have roles in the gastrointestinal functions, including insular hormone secretion.

Keywords TASK-3 channels · Human tissue · Immunohistochemistry · Antigen retrieval · Gastrointestinal tract

I. Kovács · L. Sarkadi
Department of Pathology,
HBM Kenézy Gyula County Infirmary,
Bartók Béla u. 2-26,
Debrecen, 4043, Hungary

K. Pocsai · G. Czifra · G. Szucs · Z. Rusznák (✉)
Department of Physiology, Medical and Health Science Centre,
University of Debrecen,
Debrecen, P.O. Box 22, 4012, Hungary
e-mail: rz@phys.dote.hu
Tel.: +36-52-416634
Fax: +36-52-432289

Z. Nemes
Department of Pathology, Medical and Health Science Centre,
University of Debrecen,
Debrecen, P.O. Box 24, 4012, Hungary

Introduction

TASK (or *T*WIK-related *a*cid *s*ensitive K^+) channels are important representatives of the twin-pore-domain K^+ channel superfamily [1, 4, 8, 9, 15, 18, 20, 21, 25, 35, 36]. It has been suggested that TASK channels are responsible for the high K^+ permeability of the cells at rest, playing very important roles in determining their resting membrane potential, input resistance and excitability [9]. Besides acting as the most important background conductance, TASK channels also detect changes of the extracellular pH [9, 21, 25, 26, 36] as they close on extracellular acidification.

TASK channels seem to have a variety of physiological functions. They are involved in the regulation of aldosterone secretion [5, 6] and may also participate in the control of breathing [3, 16]. Furthermore, TASK channels seem to be the targets of certain volatile anaesthetics [27, 33], and they are also involved in the regulation of cell apoptosis [24]. Most interestingly, TASK-3 channels may also be of importance in certain pathological conditions, as suggested by Mu et al. [31], reporting on the genomic amplification of the *KCNK9* gene (encoding the TASK-3 channel protein) in a significant percentage of patients suffering from breast cancer. The direct oncogenic potential of the gene and its functional protein product has also been demonstrated [34].

To investigate and fully understand the physiological significance as well as the oncogenic role of the TASK channels, it would be imperative to have a proper understanding of their tissue distribution, including their cellular and possible subcellular localisations. Although the presence of TASK-specific mRNA sequences has been noted in a number of tissues and cells (brain, lung, testis, pancreas,

kidney, astrocytes, etc.) [28, 36, 37], only limited information is available about the distribution of TASK channels within a certain tissue or organ, especially in tissue samples with human origin. In situ hybridisation might provide information about the cellular localisation of TASK-specific mRNA, but it does not indicate whether the protein product is also available. Considering these points, the immunohistochemical detection of the TASK-channel proteins seems to be an important technique in exploring and understanding the significance of TASK channels. In fact, the recently reported oncogenic potential of the TASK-3 channels [31, 34] even further necessitates a reliable technique for the detection of TASK-3-specific proteins in formalin-fixed, paraffin-embedded histopathological tissue specimens with the commercially available anti-TASK-3 antibodies to be able to perform retrospective studies concerning the expression of these channels in a variety of malignant tumours. One must note, however, that in formalin-fixed tissue samples, the antigen protein is not only immobilized but is often hidden after the formation of methylene bridges [14, 29], hence the application of the most effective antigen retrieval (AR) technique may be essential to get reliable and reproducible results.

In the present study, the tissue distribution of the TASK-3 channel protein was investigated in the human gastrointestinal tract. Specific emphasis was laid upon the confirmation of the specificity of the reactions and on finding the most consistent AR technique. Our results show that false-negative reactions may occur in the absence of AR or when an inappropriate AR is utilised. As for the distribution of the TASK-3 specific immunolabelling, strong immunoreactivity was observed in the gastrointestinal mucosa, particularly in the epithelial cells of the stomach and large intestines. TASK-3 positivity could be seen in the exocrine as well as in the endocrine pancreas, the latter providing stronger immunoreaction. TASK-3 positivity was also found in carcinomas affecting the gastrointestinal tract.

Materials and methods

Immunohistochemistry

The experiments on human tissues were conducted with the approval and authorisation of the ethics committee of the University of Debrecen as well as with the written consent of the patients or their relatives. The tissue samples (with the exception of the cerebellum) were excised during surgical interventions for intra- or postoperative histopathological diagnosis. Immediately after surgical removal, the tissue samples were frozen or fixed in 4% buffered formalin (24 h) and embedded in paraffin wax.

Sections 4 μm thick were cut from both the frozen and the formalin-fixed, paraffin-embedded tissue samples. When the immunolabelling was performed on formalin-fixed tissues, either no AR was applied or one of the following AR techniques was employed (Table 1).

The AR (if applicable) was followed by blocking the endogenous peroxidase activity with a 3% H_2O_2 solution (10 min, room temperature). Non-specific binding was prevented by incubating the sections with Protein Block Serum Free Reagent (5 min, room temperature; Dako, Glostrup, Denmark). The tissue sections were then incubated overnight with one of the primary antibodies (Table 2).

Next, the sections were rinsed with phosphate-buffered saline (PBS) (3×5 min). If the primary antibody was raised in goat, then the sections were incubated with biotinylated anti-goat secondary antibodies [30 min; 1:100 (Dako)], rinsed with PBS again then exposed to horseradish–peroxidase–conjugated streptavidin (30 min; 1:500; room temperature). The immunoreaction was visualised using a diamino-benzidine (DAB) kit (Vector Laboratories, CA, USA). When the primary antibody was raised in rabbit, the EnVision detection system (Dako) was employed (with DAB visualisation).

In most of the cases, counterstaining (haematoxylin) was also performed. All immunoreactions were investigated sing a Nikon Eclipse 600-W microscope (Nikon, Tokyo, Japan), equipped with an RT Color CCD camera. The images were acquired using the Spot RT v3.5 software.

Table 1 Summary of the antigen retrieval methods

Type of antigen retrieval	Protocol	Duration (min)
Proteolytic treatment	Pronase (0.1%)	3
Microwave oven (750 W)	8 mM Tris-buffer (pH=8.4)	15
	1 mM ethylenediaminetetraacetate buffer (pH=8.0)	15
High temperature at high pressure (pressure cooker)	0.1 M citrate buffer (pH=6.0)	2

Table 2 Comparison of the primary antibodies

Source company	Santa Cruz Biotechnology Inc.[a]	Alomone Labs Ltd.[b]
Antibody code	Sc-11320	APC-044
Specificity	Anti-TASK-3, human specific	Anti-TASK-3, human and rat specific
Raised in	Goat	Rabbit
Type of antibody	Polyclonal	Polyclonal
Epitope	Near to the carboxy terminus of the channel protein	Extracellular, near to the P1 loop (corresponding to amino acid residues 57–73)
Incubation period	Overnight	Overnight
Antibody dilution	1:100	1:800
Final antibody concentration	2 μg/ml	1 μg/ml

[a]Santa Cruz, CA, USA
[b]Jerusalem, Israel

Control experiments were regularly performed where the primary antibodies were co-incubated with the antibody-specific blocking peptides (supplied by the manufacturer of the primary antibody) according to the instructions provided. When formalin-fixed sections were used, these preadsorption control experiments were conducted after the application of the most effective AR technique (Tris incubation, see below).

Western blotting

The tissue samples were deep frozen in liquid nitrogen and fragmented thereafter. The small tissue pieces were placed into homogenization buffer (20 mM Tris–HCl, 5 mM ethyleneglycoltetraacetic acid, 1 mM 4-(2-aminoethyl)benzenesulfonyl fluoride, 20 μM leupeptin, pH 7.4; all from Sigma) and disrupted by sonication on ice. Protein content of samples was measured by a modified bicinchoninic acid protein assay (Pierce, Rockford, IL, USA). Total cell lysates were mixed with sodium dodecyl sulfate-polyacrylamide gel electrophoresis (SDS-PAGE) sample buffer and boiled for 10 min at 100°C. The samples were subjected to SDS-PAGE (7.5% gels were loaded with 80–160 μg protein per lane) and transferred to nitrocellulose membranes (BioRad Laboratories, CA, USA). Membranes were then blocked with 5% dry milk in PBS and probed with TASK-3-specific primary antibodies (Santa Cruz 1:50; Alomone 1:800). The secondary antibody was either a biotin-conjugated goat anti-rabbit IgG antibody (BioRad 1:1,000) or biotin-conjugated rabbit anti-goat IgG antibody (Vector Laboratories, CA, USA 1:1,000). In control experiments, specificity of staining was assessed by incubating the membrane with antibodies preincubated with the corresponding synthetic blocking peptides, a procedure that completely prevented the immunosignal in all cases. The immunoreactive bands were visualised using an enhanced chemiluminescence Western-blotting detection kit (Amersham, Little Chalfont, England) on light-sensitive films (AGFA, Brussels, Belgium) or by using a Fujifilm Labs-3000 dark box (Tokyo, Japan).

Results

In the first step of the experiments, the optimal antibody dilution and the most effective AR technique had to be found for the antibody obtained from the Alomone Labs Ltd., as no prior experience existed with this particular type of primary antibody. Human cerebellar sections were used as positive controls for these immunoreactions, as it has been already demonstrated that the TASK-3-specific mRNA had the highest level in this tissue [28], with very intense anti-TASK-3 immunolabelling of the Purkinje cells and strong positivity of the granular and molecular layers [37].

Figure 1 demonstrates the results of immunolabelling with the Alomone anti-TASK-3 antibody in the absence (Fig. 1a) and in the presence of various AR methods (Fig. 1b–e). All the immunoreactions demonstrated in Fig. 1 were performed simultaneously after applying the relevant type of AR. As can be clearly seen, the immunolabelling was very weak in the absence of AR (Fig. 1a) or after the pronase treatment of the tissue sections (Fig. 1b). However, after applying citrate (Fig. 1c), Tris (Fig. 1d) or ethylenediaminetetraacetate (EDTA) incubation (Fig. 1e), the positive immunoreaction of the cerebellum was obvious. Although all three methods resulted in clear and distinct immunopositivities, the Tris application gave the most powerful labelling of the expected structures (Purkinje cells—see insets; granule and molecular layers). On the bases of this and similar labellings of the cerebellum, Tris, citrate and EDTA incubations were employed when other, formalin-fixed tissue samples were investigated. There were no major differences between the immunopositivity patterns of the various samples after applying these AR techniques, but the intensity of the labelling was always stronger after Tris incubation, hence these images are demonstrated in the rest of the present work. Figure 1f shows the result of a control experiment.

Various dilutions of the primary antibody were tested in this stage of the present work, ranging from 1:200 to 1:4,000, and the 1:800 dilution (corresponding to 1 μg/ml final antibody concentration) proved to be the most suitable.

Figure 2 gives an overview of the distribution of the TASK-3-specific immunopositivity in the human large intestine. The top row of panels (a1–a3) demonstrates the result when the primary antibody, purchased from Santa Cruz Biotechnology Inc., was employed (Fig. 2a1–a3 shows the results in a frozen section, after formalin fixation and after preadsorption of the primary antibody, respectively). The brown labelling, indicating the TASK-3-specific staining, is obvious in the large intestinal mucosa, and the strong reactivity of the epithelial cells is particularly noteworthy. It could also be concluded that after the formalin fixation, the application of the Tris-AR resulted in a similar immunopositivity pattern (targeting the large intestinal epithelium) than the one observed in frozen tissue sections, although the intensity of the reaction was somewhat weaker. The absence of AR did not result in appreciable immunopositivity (not shown).

The results demonstrated in Fig. 2a clearly suggest that the large intestinal epithelium had strong TASK-3 expression. This suggestion is strongly corroborated by the findings yielded after the application of the other type of primary antibody (Alomone Labs Ltd.). Results in all panels demonstrated in Fig. 2b, c were obtained from the same patient. The immunoreactions shown in panels b1–b3 and c1–c3 were conducted on frozen and formalin-fixed, paraffin-embedded sections, respectively. In the cases of the frozen sections, strong TASK-3 expression of the large intestinal epithelium (Fig. 2b1, b2) and the neural structures belonging to the myenteric plexus could be observed (Fig. 2b3). Western-blot experiments were also performed with both types of primary antibodies; in the inset of Fig. 2b1, the result of such a trial is demonstrated. In addition to the fact that the Western-blot experiments gave a single immunopositive band, it is important to point out that a much thicker band could be observed in the case of the colonic mucosa

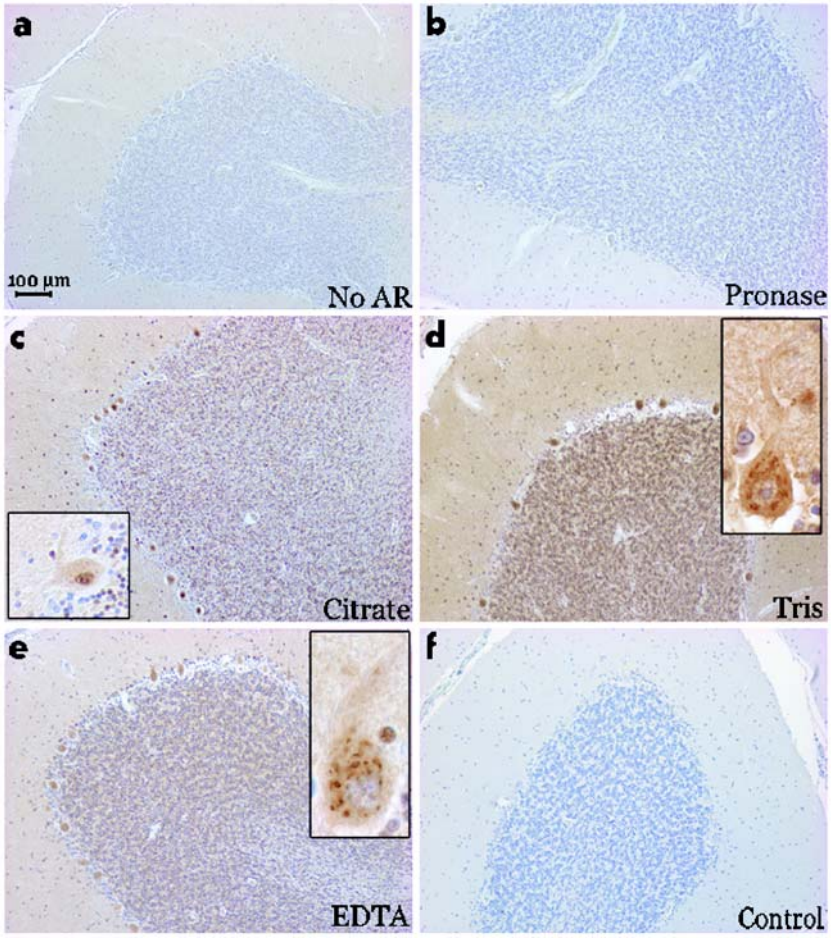

Fig. 1 The effect of various antigen retrieval (*AR*) methods on the TASK-3-specific immunolabelling of formalin-fixed, paraffin-embedded human cerebellar sections. **a** Result of the immunolabelling in the absence of AR. **b**–**e** Immunopositivity in the presence of various AR techniques (for details, see Materials and methods). *Insets* in **c**, **d** and **e** demonstrate the immunolabelling of Purkinje cells. **f** Result of the immunolabelling in the presence of the specific blocking peptide. The preadsorption control was performed after applying Tris-AR. The dilution of the primary antibody (Alomone Labs) was 1:800 in every case. The *scale bar* in **a** is applicable for all other panels

than in the case of the colonic smooth muscle, indicating that the TASK-3-specific protein content of the mucosa was more significant than that of the muscular layer of the large intestine. This observation was in perfect agreement with the immunohistochemistry data (for comparison, see Fig. 2b1 and the inset of Fig. 2b3).

Figure 2c1–c3 demonstrates the TASK-3-specific labelling of the tissue block presented in Fig. 2b1–b3 after the application of a routine histological preparation (formalin fixation, paraffin embedding) and Tris-AR. As shown in Fig. 2c1, the tissue retained its TASK-3-specific reaction, without inducing false-positive reactivity; although the intensity of the labelling was somewhat reduced. This finding was even more obvious when images were taken at higher magnification (Fig. 2c2). The evaluation of the immunolabelling was easier when an oil immersion objective was used (see the inset of Fig. 2c2). The neural elements belonging to the myenteric plexus gave strong and distinct TASK-3 positivity, even after formalin fixation when Tris-AR was used (Fig. 2c3, inset shows a low-power view of the same area). Preadsorption control experiments were conducted on frozen tissue samples as well as on formalin-fixed sections, and neither experiment resulted in appreciable immunopositivity (data not shown). Large intestinal tissue samples excised from five more patients were also investigated, resulting in identical findings.

Figure 3 demonstrates the TASK-3-specific immunolabelling of some other gastrointestinal structures. The gastric epithelium showed strong anti-TASK-3 labelling (Fig. 3a and b); the immunoreaction appeared to be strong in the cytoplasm as well as in or around the nuclei of the individual cells. As opposed to the reaction seen in the gastric mucosa, the smooth-muscle layer of the stomach (Fig. 3c) did not show prominent TASK-3 positivity, as only the nuclear–perinuclear region of some of the smooth-muscle cells demonstrated TASK-3 labelling. The result of a control experiment is also shown (Fig. 3e).

The presence of TASK-3-specific immunopositivity could also be seen in malignant tumours. As Fig. 3d illustrates, tumour cells showed definite TASK-3 positivity on the surface and in the cytoplasm, and the particularly strong labelling of the nuclear–perinuclear region is also noteworthy.

Western-blot experiments were also performed. As the optical density values of the individual bands indicate, there was no difference between the TASK-3 expressions of the corpus and cardia (Fig. 3f). In Fig. 3g, three samples were used, excised from the smooth-muscle layer and mucosa of the healthy part of a stomach as well as from the malignant gastric tumour of the same patient, respectively. The Western-blot data were in good agreement with the immunohistochemistry observations presented in Fig. 3a–e, indicating

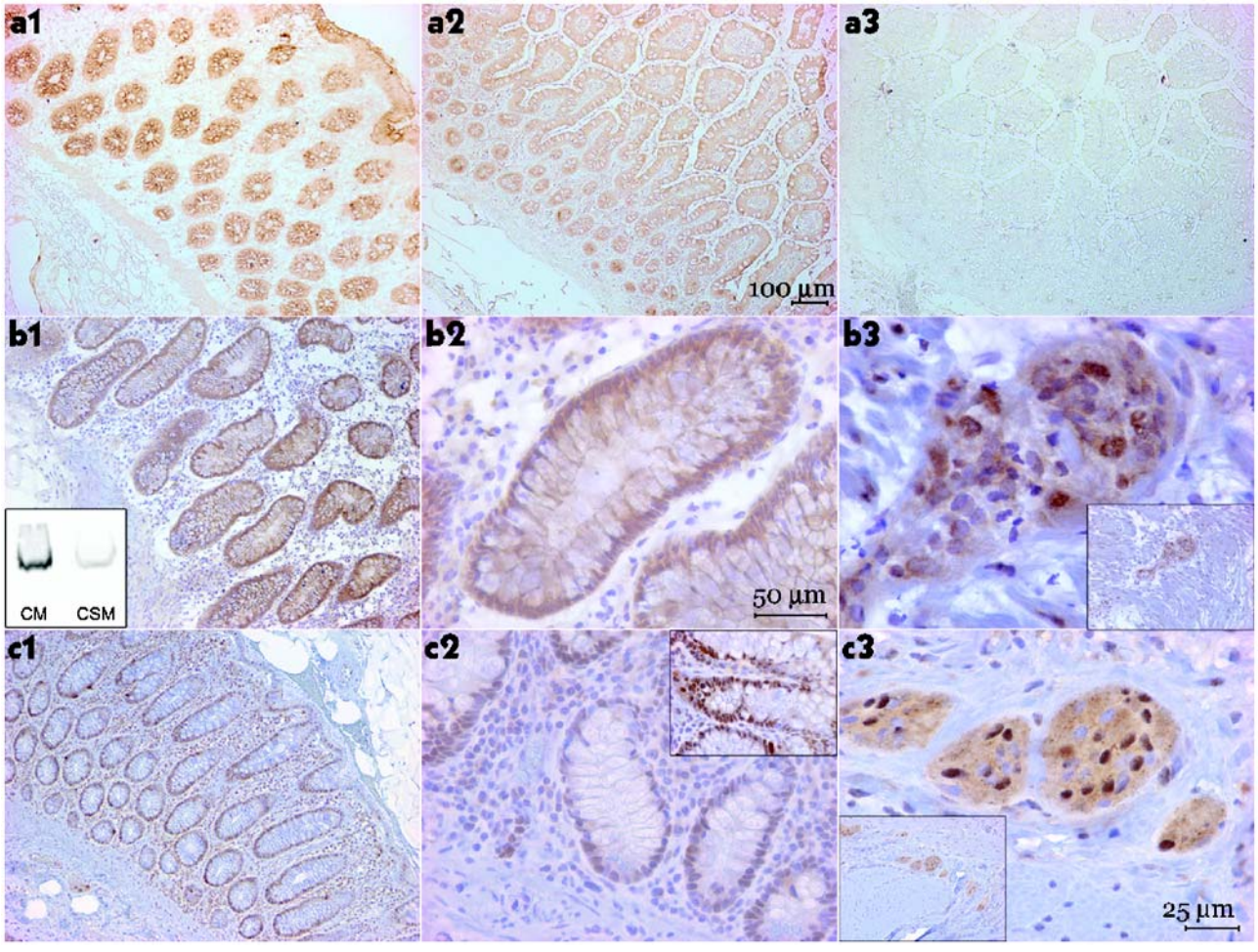

Fig. 2 TASK-3 immunolabelling of the large intestine. **a1**–**a3** Results of the immunolabellings achieved when the primary antibody obtained from Santa Cruz Biotechnology was employed; whereas in the rest of the panels the primary antibody obtained from Alomone Labs was used. **a1** TASK-3 specific reaction of a frozen large intestinal section. **a2** was conducted on a tissue section prepared from the same tissue block, after formalin fixation, paraffin embedding and Tris-AR. The result of the preadsorption control experiment is shown in **a3** (formalin-fixed tissue section, subjected to Tris-AR). No counterstaining was applied in these cases. **b1**–**b3** Immunopositivity seen in the case of a frozen tissue sample excised from a different patient. **b1** A low-power and a **b2** high-power view of the large intestinal epithelium. The *inset* of **b1** shows the result of a Western-blot experiment when the tissue samples were obtained from the large intestinal mucosa (*CM*) and smooth-muscle layer of the colon (*CSM*). The same amount of protein was loaded in both lanes. The immunopositive bands appeared at 84 kDa. **b3** Immersion objective view of a neural structure identified as part of the myenteric plexus. The lower-magnification view of the same area is demonstrated in the *inset*, providing an overview of the weak TASK-3 positivity of the smooth-muscle layer. **c1**–**c3** TASK-3 immunolabelling of the same tissue sample shown in **b1**–**b3** after completing the formalin fixation, paraffin embedding and Tris-AR. The organisation of the individual images is similar to **b1**–**b3**. The *inset* of **c2** shows an oil immersion view of TASK-3 reactivity of the intestinal epithelium. The *scale bar* of **a2** is applicable for **a1**, **a3**, **b1** and **c1**. The *scale bar* of **b2** is applicable for **c2**. The *scale bar* of **c3** is applicable for **b3**

that the TASK-3 channels are more abundantly expressed in the gastric mucosa than in the smooth-muscle layer. The Western-blot experiments also confirmed that the gastric cancer shown in Fig. 3d expressed TASK-3 channels as well. Altogether, gastric tissue samples isolated from six different patients were employed, resulting in identical findings.

Figure 3h illustrates the TASK-3 expression pattern of the submandibular gland, where the ductal epithelium showed the strongest immunoreaction. In Fig. 3I, a pericolonic lymph node is demonstrated, illustrating the general observation that lymphocytes showed definite TASK-3 positivity.

Figure 4 shows the TASK-3-specific labelling of the pancreas. The images demonstrated in panels a, b and c, d were taken from two different tissue samples excised from two different patients and incubated with anti-TASK-3 antibodies obtained from Santa Cruz and Alomone, respectively. Preadsorption controls were conducted in each case (insets). Although both the exocrine and endocrine pancreas showed definite TASK-3-specific immunolabelling, the immunopositivity of the islets of Langerhans proved to be more intense than that of the exocrine portion. No anti-TASK-3 labelling was observed in the connective tissue, which was in sharp contrast to the strong labelling of the adjacent exocrine and endocrine structures. Pancreatic tis-

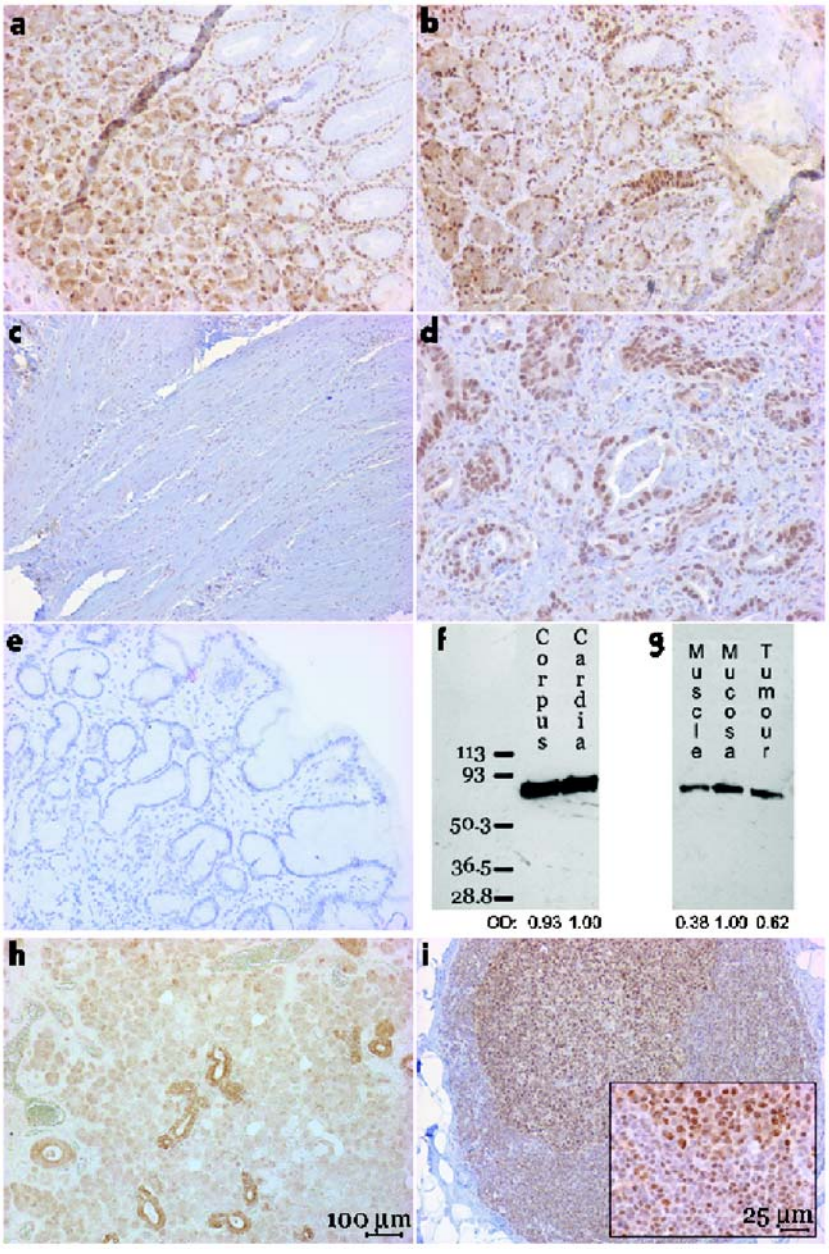

Fig. 3 TASK-3 immunolabelling of the stomach, submandibular gland and gastrointestinal lymph nodes. All immunohistochemical reactions were conducted on formalin-fixed and paraffin-embedded tissue sections, after Tris-AR. When the immunolabelling shown in **h** was performed, the primary antibody obtained from Santa Cruz Biotechnology, was employed; all other panels were produced using the primary antibody obtained from Alomone Labs. The tissue sections shown in **a**–**e** were prepared from the tissue blocks excised from the stomach of the same patient. **a**–**d** TASK-3 immunolabelling of the mucosa of the corpus, mucosa of the antrum, smooth-muscle layer and a moderately differentiated gastric cancer, respectively. **e** Result of the preadsorption control experiment. The Western blot shown in **f** was performed by using frozen, homogenised samples excised from two different parts of the stomach of a different patient. **g** Result of another Western-blot experiment (with a tissue sample obtained from the patient whose immunohistochemistry results are demonstrated in **a**–**e**), where the samples were excised from the smooth-muscle layer, mucosa and cancer of the same stomach, respectively. The same amount of protein was loaded in all simultaneously performed Western-blot experiments; the optical density of the individual bands are provided, relative to the most intense band. **h** TASK-3-specific labelling of the submandibular gland. **I** TASK-3 labelling of a pericolonic lymph node. In the *inset*, an oil immersion view of the lymph node is demonstrated. The *scale bar* of **h** is applicable for all panels

sue samples obtained from five different patients (none of them showed any symptoms of diabetes mellitus) were investigated with identical results.

As this was the first report on the distribution pattern of the TASK-3 immunoreactivity in the human gastrointestinal tract, during the experiments, specific emphasis was laid upon the confirmation of the specificity of the immu-

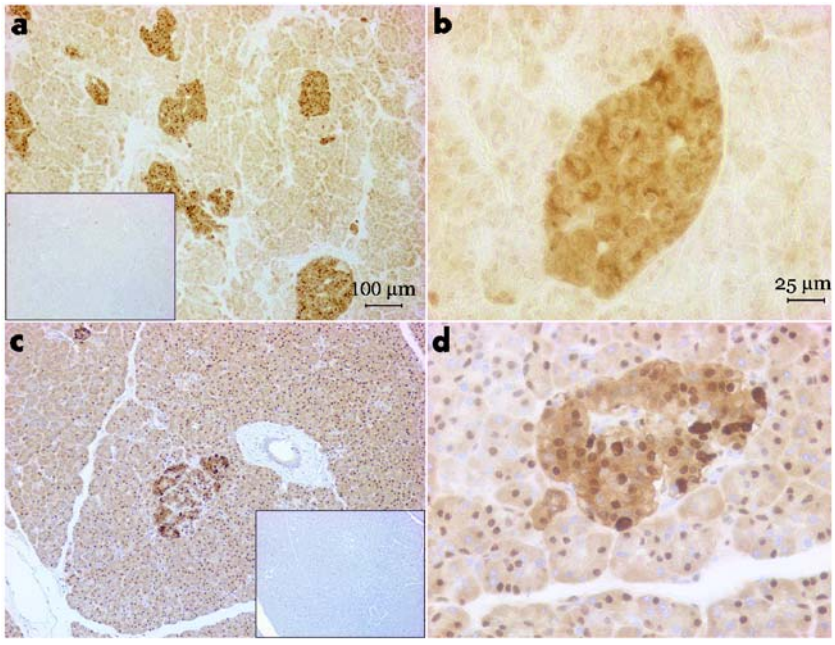

Fig. 4 TASK-3 immunoreactivity of the pancreas. **a**, **b** Results were obtained after using the primary antibody obtained from Santa Cruz Biotechnology; **c**, **d** Results were produced after employing the primary antibody obtained from Alomone Labs. In all cases formalin-fixed, paraffin-embedded tissue samples were used, which subsequently underwent Tris-AR. **a**, **c** A low-magnification view of the TASK-3 labelling of the pancreas. **b**, **d** High-magnification images. The lack of immunoreactivity of the connective tissue is worth noting, along with the intense reaction of the islets of Langerhans. The *insets* demonstrate the results of the immunolabelling when the primary antibodies were preincubated with their specific blocking peptides. The *scale bars* shown in **a** and **b** are applicable for **c** and **d**, respectively

nolabelling. The following findings indicate the specificity of the immunoreactions demonstrated in this work:

1. Two different primary antibodies, targeting different epitopes of the channel protein (one close to the C-terminus, the other one close to the N-terminus) were employed, resulting in the same immunopositivity pattern.
2. Preadsorption controls were regularly performed on both frozen tissue samples and on formalin-fixed specimens. In the latter case, the control experiments were always conducted after the application of the most effective AR technique. None of the control experiments gave recognisable TASK-3-specific immunopositivity. As an additional test of specificity, isotype controls were also conducted, where the sections were preincubated with non-immunised rabbit serum (1:10,000–1:30,000). These reactions gave either no appreciable reaction (large intestine and stomach), or just a diffuse, very weak staining (pancreas) could be observed.
3. The applicability of the AR technique was confirmed by comparing the immunopositivity pattern achieved after AR to the already established TASK-3 expression pattern (cerebellum) as well as to the reaction obtained on frozen sections, where the epitopes are well preserved. Although slight differences could be seen in terms of the intensity of the reactions, the distribution of immunopositivity was always the same in both cases (i.e. in frozen or formalin-fixed tissue samples).
4. Western blotting was performed in all frozen tissue samples (stomach and large intestine). The results of the Western-blot experiments confirmed the specificity of the antibodies, and the semi-quantitative Western-blot analysis (densitometry) was in prefect agreement with the immunohistochemistry data.

Discussion

In this paper, it is demonstrated that the application of an appropriate AR technique is essential to investigate the distribution of the TASK-3-specific immunoreactivity in formalin-fixed tissue sections. This finding is in good agreement with the general opinion that the application of polyclonal antibodies on formalin-fixed tissue samples requires the search and utilisation of the most suitable AR technique to achieve optimal immunolabelling (see a recent review by Montero [30]). The present work also showed that the expression of the TASK-3 channels is more widespread than it could be thought on the bases of the data concerning the concentration of TASK-3 specific mRNA in various tissues [28].

The physiological and pathological roles of the TASK-3 channels could be more thoroughly understood if their tissue, cellular and subcellular localisations were described; thus, the investigation of the TASK-3 immunopositivity in various human tissues seems to be imperative. As TASK-specific antibodies are commercially available now, such projects are relatively straightforward to commence. Although it is possible to conduct these studies on frozen tissue samples, the application of the universal fixative,

formaldehyde, is usually more convenient. However, formaldehyde (or more specifically methylene glycol, in which form the original molecule exists in phosphate buffer, where it is dissolved) produces methylene bridges between various groups of proteins. It has been established a long time ago that amino, imino, amido, peptide, guanydil, carboxyl and SH groups or aromatic rings may all participate in the genesis of such links [10–13, 32]. However, the production of these cross-bridges alters the structure of the original protein to such an extent that its ability to react with the specific antibodies may be very severely compromised or even prevented, resulting in weak or sometimes false-negative immunoreactions. To alleviate this problem, various AR techniques are employed, which usually try to take advantage of the fact that the altered (either increased or reduced) pH, heat or the application of proteolytic enzymes may improve the ability of the antibodies to bind to the appropriate epitopes [2].

The AR techniques applied in the present study are relatively standard techniques in the everyday histopathodiagnostic arsenal [38, 39]. The results showed that the Tris incubation proved to be the most effective AR method, giving consistent and reliable results in all tissues investigated.

When the possible functions of the TASK channels are considered in the gastrointestinal system, it must be noted that the secretum of the large intestinal mucosa is rich in K^+. It is not fully understood yet, however, what types of K^+ channels are responsible for the K^+ traffic through the apical and basolateral membranes (for a recent review, see [23]). The roles of certain maxi K^+ channels and ROMK-type K^+ channels have been proposed, but our understanding of the other possible K^+ channel types participating in this process is fairly limited. In the basolateral membrane of the large intestinal epithelium, the function of certain cAMP-activated and Ca^{2+}-activated K^+ channels seems to be the most significant, but the roles of other types of K^+ channels cannot be excluded either. Our observation that TASK-3 channels are present in the colonic epithelium suggests that these channels may contribute to the K^+ secretion of these cells.

In the pancreas, several functions may be attributed to the TASK channels. It has been indicated that in Cl^- secretory epithelia (including the pancreas) the presence and activity of K^+ channels and the subsequent K^+ movement provides the driving force for the Cl^- movement. The significance of certain Ca^{2+}-activated K^+ channels has already been noted in this process [19, 22], and the present findings suggest that TASK-3 channels might also be involved in the K^+ traffic through the cell membrane of the pancreatic acinar cells.

A very important and potentially useful observation of the present work is the significant TASK-3 expression of the insular cells. Obviously, more experimental work is required to assess the functional consequences, but it is possible that TASK-3 channels might oppose the depolarisation force induced by the closure of the ATP-sensitive K^+ channels; hence, they may be involved in the regulation of the hormone secretion. Furthermore, the presence and function of TASK-3 channels in the β cells may provide an additional explanation for the known effects of the altered extracellular pH on the insulin secretion [17].

Obviously, TASK-3 channels might be involved in the secretory functions of the gastric mucosa as well. However, the fact that malignant tumours of the stomach, large and small intestines and breast cancers (unpublished observations) also express TASK-3 channels is clearly worth attention, especially in the light of the observation that a rather prominent TASK-3 positivity could be noticed in and around the nuclei of the tumour cells. Intense nuclear–perinuclear staining was also observed in lymphocytes and in certain cells of the gastrointestinal mucosa. However, at this moment it is not clear whether the TASK-3 expression is associated with the endoplasmic reticulum only (similar to the situation described in the case of cultured astrocytes [37]) or whether the TASK-3 channels are also present in the nuclear membrane.

Finally, it is also worth considering that, based on the oncogenic potential of the functional TASK-3 channels [31, 34], it has been suggested that TASK-3-specific blockers (such as ruthenium red [7]) might serve as potential anti-cancer drugs. In the light of the data presented in the present work, particular attention should be given to the unwanted side effects of such TASK-3 inhibiting substances, as they might severely interfere with various gastrointestinal functions and with the pancreatic insulin and glucagon production.

Acknowledgements This work was supported by a grant from the Hungarian Science Foundation (OTKA-046067). The authors are indebted to Mrs. E. Károlyi and Mrs. T. Kálmánczy for their professional work on the tissue sections and to Dr. T. Bíró for his valuable suggestions about the Western-blot experiment. The experiments presented here complied with the current laws of Hungary. The tissue samples were investigated with the approval and authorisation of the ethics committee of the University of Debrecen as well as with the written consent of the patients or their relatives.

References

1. Ashmole I, Goodwin PA, Stanfield PR (2001) TASK-5, a novel member of the tandem pore K^+ channel family. Pflugers Arch 442:828–833
2. Bell PB Jr, Rundquist I, Svensson I, Collins VP (1987) Formaldehyde sensitivity of a GFAP epitope, removed by extraction of the cytoskeleton with high salt. J Histochem Cytochem 35: 1375–1380
3. Buckler KJ, Williams BA, Honore E (2000) An oxygen-, acid- and anaesthetic-sensitive TASK-like background potassium channel in rat arterial chemoreceptor cells. J Physiol 525:135–142
4. Chapman CG, Meadows HJ, Godden RJ, Campbell DA, Duckworth M, Kelsell RE, Murdock PR, Randall AD, Rennie GI, Gloger IS (2000) Cloning, localisation and functional expression of a novel human, cerebellum specific, two pore domain potassium channel. Brain Res Mol Brain Res 82:74–83
5. Czirják G, Fischer T, Spät A, Lesage F, Enyedi P (2000) TASK (TWIK-related acid-sensitive K^+ channel) is expressed in glomerulosa cells of rat adrenal cortex and inhibited by angiotensin II. Mol Endocrinol 14:863–874

6. Czirják G, Enyedi P (2003a) TASK-3 dominates the background potassium conductance in rat adrenal glomerulosa cells. Mol Endocrinol 16:621–629
7. Czirják G, Enyedi P (2003b) Ruthenium red inhibits TASK-3 potassium channel by interconnecting glutamate 70 of the two subunits. Mol Pharmacol 63:646–652
8. Decher N, Maier M, Dittrich W, Gassenhuber J, Bruggemann A, Busch AE, Steinmeyer K (2001) Characterization of TASK-4, a novel member of the pH-sensitive, two-pore domain potassium channel family. FEBS Lett 492:84–89
9. Duprat F, Lesage F, Fink M, Reyes R, Heurteaux C, Lazdunski M (1997) TASK, a human background K^+ channel to sense external pH variations near physiological pH. EMBO J 16:5464–5471
10. Fraenkel-Conrat H, Brandon BA, Olcott HS (1947) The reaction of formaldehyde with proteins. IV. Participation of indole groups. Gramicidine. J Biol Chem 168:99–118
11. Fraenkel-Conrat H, Olcott HS (1948a) The reaction of formaldehyde with proteins. V. Cross-linking between amino and primary amide or guanidyl groups. J Am Chem Soc 70:2673–2684
12. Fraenkel-Conrat H, Olcott HS (1948b) The reaction of formaldehyde with proteins. VI. Cross-linking of amino groups with phenol, imidazole and indole groups. J Biol Chem 174: 827–843
13. Fraenkel-Conrat H, Mecham DK (1949) The reaction of formaldehyde with proteins. VII. Demonstration of intermolecular cross-linking by means of osmotic pressure measurements. J Biol Chem 177:477–486
14. French D, Edsall JT (1945) Reactions of formaldehyde with amino acids and proteins. Adv Protein Chem II:277–335
15. Girard C, Duprat F, Terrenoire C, Tinel N, Fosset M, Romey G, Lazdunski M, Lesage F (2001) Genomic and functional characteristics of novel human pancreatic 2P domain K^+ channels. Biochem Biophys Res Commun 282:249–256
16. Hartness ME, Lewis A, Searle GJ, O'Kelly I, Peers C, Kemp PJ (2001) Combined antisense and pharmacological approaches implicate hTASK as an airway O_2 sensing K^+ channel. J Biol Chem 276:26499–26508
17. Hutton JC, Sener A, Herchuelz A, Valverde I, Boschero AC, Malaisse WJ (1980) The stimulus-secretion coupling of glucose-induced insulin release. XLII. Effects of extracellular pH on insulin release: their dependency on nutrient concentration. Horm Metab Res 12:294–299
18. Kim D, Gnatenco C (2001) TASK-5, a new member of the tandem-pore K^+ channel family. Biochem Biophys Res Commun 284:923–930
19. Kim SJ, Greger R (1999) Voltage-dependent, slowly activating K^+ current (I_{Ks}) and its augmentation by carbachol in rat pancreatic acini. Pflugers Arch 438:604–611
20. Kim Y, Bang H, Kim D (1999) TBAK-1 and TASK-1, two-pore K^+ channel subunits: kinetic properties and expression in rat heart. Am J Physiol 277:H1669–H1678
21. Kim Y, Bang H, Kim D (2000) TASK-3, a new member of the tandem pore K^+ channel family. J Biol Chem 275:9340–9347
22. Köttgen M, Hoefer A, Kim SJ, Beschorner U, Schreiber R, Hug MJ, Greger R (1999) Carbachol activates a K^+ channel of very small conductance in the basolateral membrane of rat pancreatic acinar cells. Pflugers Arch 438:597–603
23. Kunzelmann K, Mall M (2002) Electrolyte transport in the mammalian colon: mechanisms and implications for disease. Physiol Rev 82:245–289
24. Lauritzen I, Zanzouri M, Honoré E, Duprat F, Ehrengruber MU, Lazdunski M, Patel AJ (2003) K^+-dependent cerebellar granule neuron apoptosis. J Biol Chem 278:32068–32076
25. Leonoudakis D, Gray AT, Winegar BD, Kindler CH, Harada M, Taylor DM, Chavez RA, Forsayeth JR, Yost CS (1998) An open rectifier potassium channel with two pore domains in tandem cloned from rat cerebellum. J Neurosci 18:868–877
26. Lopes CM, Zilberberg N, Goldstein SA (2001) Block of Kcnk3 by protons. Evidence that 2-P-domain potassium channel subunits function as homodimers. J Biol Chem 276:24449–24452
27. Meadows HJ, Randall AD (2001) Functional characterisation of human TASK-3, an acid-sensitive two-pore domain potassium channel. Neuropharmacology 40:551–559
28. Medhurst AD, Rennie G, Chapman CG, Meadows H, Duckworth MD, Kelsell RE, Gloger II, Pangalos MN (2001) Distribution analysis of human two pore domain potassium channels in tissues of the central nervous system and periphery. Brain Res Mol Brain Res 86:101–114
29. Meyer KH (1929) Die Chemie der Micelle und ihrer Anwendung auf biochemische und biologische Probleme. Biochem Z 208:1–31
30. Montero C (2003) The antigen–antibody reaction in immunohistochemistry. J Histochem Cytochem 51:1–4
31. Mu D, Chen L, Zhang X, See L-H, Koch CM, Yen C, Tong JJ, Spiegel L, Nguyen KCQ, Servoss A, Peng Y, Pei L, Marks JR, Lowe S, Hoey T, Jan LY, McCombie WR, Wigler MH, Powers S (2003) Genomic amplification and oncogenic properties of the KCNK9 potassium channel gene. Cancer Cell 3:297–302
32. Nitschmann von HS, Hadorn H (1944) Die Umsetzung des Caseins mit Formaldehyd. V. Über des Verhalten der e-Aminogruppen des Lysins und der Peptidogruppen. Helv Chim Acta 27:299–312
33. Patel AJ, Honore E, Lesage F, Fink M, Romey G, Lazdunski M (1999) Inhalational anesthetics activate two-pore-domain background K^+ channels. Nat Neurosci 2:422–426
34. Pei L, Wiser O, Slavin A, Mu D, Powers S, Jan LY, Hoey T (2003) Oncogenic potential of TASK3 (Kcnk9) depends on K^+ channel function. Proc Natl Acad Sci U S A 100:7803–7807
35. Rajan S, Wischmeyer E, Xin Liu G, Preisig-Müller R, Daut J, Karschin A, Derst C (2000) TASK-3, a novel tandem pore domain acid-sensitive K^+ channel. An extracellular histidine as pH sensor. J Biol Chem 275:16650–16657
36. Reyes R, Duprat F, Lesage F, Fink M, Salinas M, Farman N, Lazdunski M (1998) Cloning and expression of a novel pH-sensitive two pore domain K^+ channel from human kidney. J Biol Chem 273:30863–30869
37. Rusznák Z, Pocsai K, Kovács I, Pór Á, Pál B, Bíró T, Szucs G (2004) Differential distribution of TASK-1, TASK-2 and TASK-3 immunoreactivities in the rat and human cerebellum. Cell Mol Life Sci 61:1532–1542
38. Shi S-R, Key ME, Kalra KL (1991) Antigen retrieval in formalin-fixed, paraffin-embedded tissues: an enhancement method for immunohistochemical staining based on microwave oven heating of tissue sections. J Histochem Cytochem 39:741–748
39. Shi S-R, Cote RJ, Young I, Imam SA, Taylor CR (1996) Use of pH 9.5 Tris HCl buffer containing 5% urea for antigen retrieval immunohistochemistry. Biotech Histochem 71:190–196

Virchows Arch (2005) 446: 411–415
DOI 10.1007/s00428-005-1210-x

ORIGINAL ARTICLE

Tomonori Sasahira · Yoshihiko Akama · Kiyomu Fujii · Hiroki Kuniyasu

Expression of receptor for advanced glycation end products and HMGB1/amphoterin in colorectal adenomas

Received: 29 November 2004 / Accepted: 5 January 2005 / Published online: 24 March 2005
© Springer-Verlag 2005

Abstract Receptor for advanced glycation end products (RAGE) is associated with invasion, metastasis, and poor prognosis in colorectal cancer. We studied the expression of RAGE in colorectal adenomas to elucidate the role of RAGE in cancer development. Expressions of RAGE and high-mobility group box-1 (HMGB1)/amphoterin RAGE ligand were examined in 96 colorectal adenomas using immunohistochemistry and in situ hybridization, respectively. Positivity and expression pattern of RAGE were compared with atypia, histological types, size, and HMGB1/amphoterin expression. Of 96 adenomas, 34 (35%) showed RAGE expression. RAGE positivity was significantly higher in adenomas with severe atypia (18/20, $P<0.0001$) and large-sized adenomas (−15 mm) (18/22, $P<0.0001$). RAGE expression showed three patterns: cytosolic ($n=10$), luminal ($n=14$), and membranous ($n=10$). Cytosolic pattern was associated with mild atypia and small size (−5 mm). Membranous pattern was associated with severe atypia, villous histological type, and co-expression with overexpressed HMGB1/amphoterin. These results suggest that RAGE expression, especially with membranous pattern, is associated with malignant potential of colorectal adenomas.

Keywords RAGE · HMGB1/amphoterin · Colorectal adenoma · Atypia

Introduction

Receptor for advanced glycation end products (RAGE), isolated as a 35-kDa multiligand receptor belonging to the immunoglobulin superfamily, is implicated in homeostasis, development of embryonic neuron, inflammation, and tissue damage in diabetes mellitus and Alzheimer's disease [11]. Major ligands of RAGE are amphoterin, which is an extracellular form of chromosomal high-mobility group box-1 (HMGB1) protein, advanced glycation end products, S100/calgulanin, and amyloid-beta [5, 10, 12, 14]. Recently, RAGE has been regarded as a tumor invasion- and metastasis-related gene [1, 6–9, 12]. Taguchi et al. reported that RAGE accelerates tumor cell migration, invasion, and metastasis in rat C6 glioma cells [12]. Abe et al. reported that RAGE regulates growth and metastasis of human melanoma [1]. We also reported that RAGE is strongly associated with invasive and metastatic ability of gastric, colon, and prostate cancer [6–9]. In particular, expression of RAGE was significantly correlated with tumor progression and metastasis, and coexpression of RAGE and the ligand, HMGB1/amphoterin, is correlated closely with poor prognosis of colon cancer [8]. Biologically, RAGE and HMGB1/amphoterin accelerates cell growth, migration, invasion, and vascular endothelial growth factor (VEGF) production in colon cancer cells [6]. Thus, RAGE and the ligand, HMGB1/amphoterin, are vital factors in the progression of colon cancer.

Colorectal adenomas are generally considered to be precancerous lesions of colon cancer in biological and genetic situations [13]. Malignant potential of colorectal adenomas is evaluated histopathologically [2, 4]. In genetic events, p53 mutation is the most striking marker for suggesting malignant potential in adenoma [15]. In the present study, we studied the expression of RAGE in colorectal adenomas to elucidate the role of RAGE for acquisition of malignant potential in colorectal adenomas.

T. Sasahira · Y. Akama · K. Fujii · H. Kuniyasu (✉)
Department of Molecular Pathology,
Nara Medical University,
840 Shijo-cho,
Kashihara, Nara, 634-8521, Japan
e-mail: cooninh@zb4.so-net.ne.jp
Tel.: +81-744-223051
Fax: +81-744-257308

Materials and methods

Tumor specimens

Formalin-fixed, paraffin-embedded tumor specimens of human colorectal adenomas ($n=96$) were selected at random from Nara Medical University Hospital, Kashihara,

Japan. Mean age was 62 years (32–78 years). Sex ratio was 66:30 (male/female). Histological types, degree of atypism, and size of adenomas are summarized in Table 1. No significant difference was found in numbers of atypism among four histological types (P=0.9782). As for size of adenoma, serrated adenomas showed many small-sized adenomas; in contrast, villous adenomas showed large-sized lesions (P<0.0001).

Immunohistochemistry

Consecutive 4-μm sections were cut from each block, and immunostaining was performed using the immunoperoxidase technique following antigen retrieval with pepsin (Dako, Carpinteria, CA, USA) treatment for 20 min. After endogenous peroxidase block by 3% H_2O_2–methanol for 15 min, specimens were rinsed with phosphate-buffered saline (PBS). Anti-RAGE antibody (clone-20, Santa Cruz Biotechnology Inc., Santa Cruz, CA) was used at 1 μg/ml for primary antibody and incubated at room temperature for 2 h. The specimens were rinsed with PBS and incubated at room temperature for 1 h with secondary antibody conjugated to peroxidase diluted at 0.5 μg/ml (anti-goat IgG, Medical & Biotechnological Laboratories Co., Ltd., Nagoya, Japan). All specimens were then rinsed with PBS and color-developed using diaminobenzidine (DAB) solution (Dako). After being washed with water, specimens were counter-stained with Meyer's hematoxylin (Sigma, St. Louis, MO, USA). Immunostaining of all specimens was performed to ensure the same condition of antibody reaction and DAB exposure.

Table 1 Cases of colorectal adenomas

Histological type	Degree of atypism[a]	Size[b]		
		−5 mm	−10 mm	−15 mm
Tubular	Mild (n=18)	10	8	0
	Moderate (n=18)	10	4	4
	Severe (n=8)	4	2	2
	Total (n=44)	24	14	6
Tubulovillous	Mild (n=12)	4	6	2
	Moderate (n=12)	6	2	4
	Severe (n=8)	0	6	2
	Total (n=32)	10	14	8
Villous	Mild (n=2)	0	0	2
	Moderate (n=6)	0	2	4
	Severe (n=2)	0	0	2
	Total (n=10)	0	2	8
Serrated	Mild (n=4)	2	2	0
	Moderate (n=4)	2	2	0
	Severe (n=2)	0	2	0
	Total (n=10)	4	6	0

[a] P=0.9782 by two-tailed chi-square test
[b] P<0.0001 by two-tailed chi-square test

Evaluation of immunoreactivity

The immunoreactivity was classified into four grades according to the number of RAGE-positive cells and the intensity of the reaction in individual cells in contrast to the vascular endothelial cells in the same specimen. Grades were classified into four grades: grade I, almost all cells showing no immunoreactivity; grade II, 5–25% of tumor cells showing weak to moderate immunoreactivity compared with the endothelial cells [8, 9]; grade III, 25–50% of tumor cells showing moderate to intense immunoreactivity compared with the endothelial cells; grade IV, over 50% of tumor cells showing moderate to intense immunoreactivity compared with the endothelial cells. Cases with grade III–IV staining were defined as RAGE expression positive.

In situ hybridization

In situ hybridization (ISH) was performed as described previously [8, 9]. The sequence of the microprobe for HMGB1/amphoterin was 5′-CCC AGT TTC TTC GCA ACA TCA C-3′ (referred to as GenBank accession No. X12597). The probe was conjugated to fluorescein isothiocyanate (FITC) on the 5′-end (Sigma Genosys, Ishikari, Japan). Non-counterstained ISH slides were examined using densitometric scanning with computer-capturing image analysis (NIH image software, National Institutes of Health, Bethesda, MD). Levels of HMGB1/amphoterin expression were graded as follows: normal, expression equal to those in normal mucosal epithelium adjacent to adenoma; moderate, expression less than two times that of normal mucosal epithelium; marked, expression more than two times that of normal mucosal epithelium.

Statistical analyses

Statistical differences in RAGE expression were calculated with the two-tailed chi-square test by Stat View Version 4.5 (SAS Institute, Inc., Cary, NC), and a P value of <0.05 was considered as statistically significant.

Results

Expression of RAGE in colorectal adenomas

As shown in Fig. 1, we classified the RAGE immunoreactivity to three patterns: cytosolic, luminal, and membranous pattern. In the cytosolic pattern, RAGE was mainly found in the cytoplasm of epithelial cells (Fig. 1a). In the luminal pattern, RAGE was detected in the cell surface of the luminal side of epithelial cells but was not linked with intracellular mucin (Fig. 1b). In the membranous pattern, RAGE was located on the cell–cell boundary and submembranous cytoplasm (Fig. 1c). RAGE expression was strong in all cases with membranous pattern. In the non-

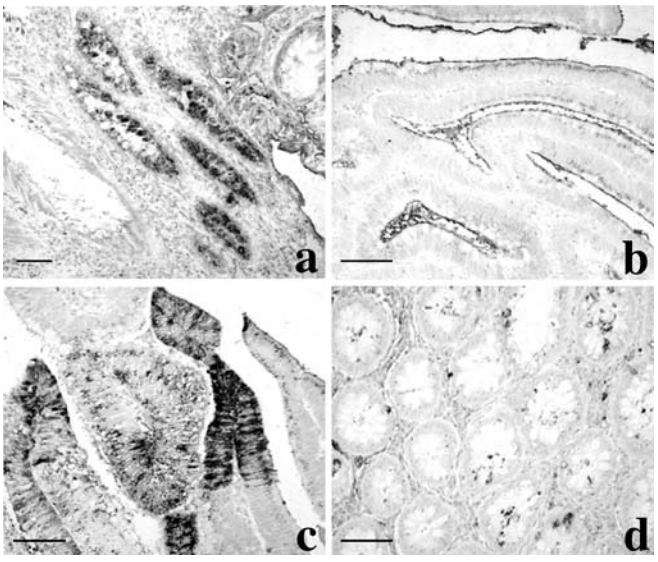

Fig. 1 Receptor for advanced glycation end products (RAGE) expression in colorectal adenomas and colorectal mucosa. RAGE expression was examined using immunohistochemistry. **a** Cytosolic pattern in a tubular adenoma with moderate atypia. **b** Luminal pattern in a tubulovillous adenoma with moderate atypia. **c** Membranous pattern in a villou adenoma with severe atypia. **d** Nonneoplastic mucosa. *Bar* 100 μm

neoplastic mucosa, RAGE expression was not detected (Fig. 1d).

Relationship of RAGE expression to atypia of colorectal adenomas

Of 96 colorectal adenomas, adenomas with mild, moderate, and severe atypia were 36, 40, and 20, respectively (Table 2). RAGE positivities in adenomas with mild, moderate, and severe atypia were 6% (2/36), 35% (14/40), and 90% (18/20), respectively ($P<0.0001$). In two RAGE-positive adenomas with mild atypia, only a cytosolic pattern was found. In 14 RAGE-positive adenoma with moderate atypia, four cytosolic patterns (29%), eight luminal patterns (57%), and two membranous patterns (14%) were found. In 18 RAGE-positive adenomas with severe atypia, four cytosolic patterns (22%), six luminal patterns (33%), and eight membranous patterns (44%) were found. Membranous pattern in adenomas with severe atypia was significantly associated ($P=0.0323$).

Table 2 Relationship of receptor for advanced glycation end products (RAGE) expression to atypism of adenomas

RAGE pattern	Degree of atypia		
	Mild (n=36)	Moderate (n=40)	Severe (n=20)
Positive[a]	2 (6%)	14 (35%)	18 (90%)
Pattern[b]			
Cytosolic	2	4	4
Luminal	0	8	6
Membranous	0	2	8

[a] $P<0.0001$ by two-tailed chi-square test
[b] $P=0.0323$ by two-tailed chi-square test

Table 3 Relationship of receptor for advanced glycation end products (RAGE) expression to histological type of adenomas

RAGE pattern	Histological pattern			
	Tubular (n=44)	Tubulovillous (n=32)	Villous (n=10)	Serrated (n=10)
Positive[a]	8 (18%)	14 (44%)	8 (80%)	4 (40%)
Pattern[b]				
Cytosolic	2	6	0	2
Luminal	4	4	4	2
Membranous	2	4	4	0

[a] $P=0.0015$ by two-tailed chi-square test
[b] $P=0.3075$ by two-tailed chi-square test

Relationship of expression RAGE to histological types of adenomas

Histological types of colorectal adenomas were classified as tubular (n=44), tubulovillous (n=32), villous (n=10), and serrated (n=10) (Table 3). RAGE positivities in adenomas with tubular, tubulovillous, villous, and serrated adenomas were 18% (8/44), 44% (14/32), 80% (8/10), and 40% (4/10), respectively ($P=0.0015$). In the tubular and tubulovillous adenomas, three RAGE expression patterns were found. In eight RAGE-positive villous adenomas, four luminal patterns (50%), four membranous patterns (50%), and no cytosolic patterns were found. In contrast, two cytosolic patterns (50%), two luminal patterns (50%), and no membranous patterns were found in serrated adenomas. No significant difference was detected in RAGE expression patterns among four histological types.

Relationship of RAGE expression and size of colorectal adenomas

Sizes of colorectal adenomas were classified into three groups: −5 mm in diameter (n=36), −10 mm (n=40), and −15 mm (n=20) (Table 4). RAGE positivities in adenomas sized −5, −10, and −15 were 11% (4/38), 33% (12/36), and

Table 4 Relationship of receptor for advanced glycation end products (RAGE) expression to size of adenomas

RAGE pattern	Size of adenomas		
	−5 mm (n=38)	−10 mm (n=36)	−15 mm (n=22)
Positive[a]	4 (11%)	12 (33%)	18 (82%)
Pattern[b]			
Cytosolic	4	2	4
Luminal	0	6	8
Membranous	0	4	6

[a] $P<0.0001$ by two-tailed chi-square test
[b] $P=0.0265$ by two-tailed chi-square test

Table 5 Relationship of receptor for advanced glycation end products (RAGE) expression to high-mobility group box-1 (HMGB1)/amphoterin expression

HMGB1/amphoterin expression[a]	RAGE expression pattern		
	Cytosolic (n=10)	Luminal (n=14)	Membranous (n=10)
Normal	6	3	0
Moderate	4	4	0
Marked	0	7	10
Coexpression of RAGE and overexpressed HMGB1/amphoterin[b]	4 (40%)	11 (79%)	10 (100%)

[a] P<0.0001 by two-tailed chi-square test
[b] P=0.0084 by two-tailed chi-square test

82% (18/22), respectively (P<0.0001). In four RAGE-positive adenomas sized −5 mm, only a cytosolic pattern was found. In RAGE-positive adenomas sized −10 mm or −15 mm, three RAGE expression patterns were found. Cytosolic pattern in adenomas sized −5 mm was significantly associated (P=0.0265).

Co-expression of RAGE and HMGB1/amphoterin in adenomas

Finally, we examined the co-expression of RAGE and the tumor-associated ligand, HMGB1/amphoterin (Table 5) [6]. HMGB1/amphoterin is a housekeeping gene with constitutive expression; in contrast, cancer cells overexpress and secrete HMGB1/amphoterin [3, 8]. In RAGE-negative adenomas, HMGB1/amphoterin expression levels were graded as normal, which meant that the expression is equal to that in non-neoplastic colorectal mucosa. In 10 RAGE-positive adenomas with cytosolic pattern, 4 (40%) showed overexpression of HMGB1/amphoterin (P=0.0004). In contrast, all 21 RAGE-positive adenomas with luminal and membranous patterns overexpressed HMGB1/amphoterin. In particular, all RAGE-positive adenomas with membranous pattern showed HMGB1/amphoterin overexpression at high levels (more than two times higher than that in non-neoplastic mucosa) (P<0.0001). Co-expression of RAGE and overexpressed HMGB1/amphoterin was most frequently found in adenomas with membranous RAGE pattern (10/10, P=0.0084) (Fig. 2).

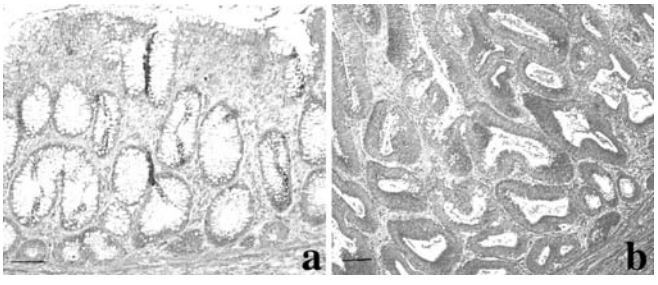

Fig. 2 High-mobility group box-1 (HMGB1)/amphoterin expression in colorectal adenomas. HMGB1/amphoterin expression was examined by in situ hybridization. **a** Moderate expression in a tubular adenoma with mild atypia. **b** Marked expression in a tubular adenoma with severe atypia. *Bar* 100 μm

Discussion

RAGE is one of the key factors of tumor progression and metastasis due to biological effects associated with cell growth, motility, invasion, and production of angiogenic factors [1, 6–9, 12]. In the present study, RAGE expression was strongly associated with atypia and size of colorectal adenomas. RAGE positivity was significantly higher in adenomas with severe atypia (P<0.0001) and large-sized adenomas (−15 mm) (P<0.0001). Expression pattern of RAGE was different in each group of atypia: cytosolic pattern in mild atypia (2/2, 100%); luminal pattern in moderate atypia (8/14, 57%); membranous pattern in severe atypia (8/18, 44%). In particular, frequency of membranous pattern was significantly different among atypia: 0 in mild atypia, 14% in moderate atypia, and 44% in severe atypia. In small adenomas (−5 mm), all RAGE-positive adenomas showed cytosolic pattern, whereas adenomas with moderate (−10 mm) and large (−15 mm) sizes showed mainly luminal or membranous patterns. With regard to RAGE expression and histological types, comparison without regard to atypia showed no significant difference among histological types. Villous adenomas showed luminal or membranous patterns. Three of four tubulovillous adenomas with severe atypia showed luminal or membranous pattern, which was found in villous components but not in tubular components in these adenomas.

RAGE is a membrane-bound protein [11], and we previously found membranous expression pattern of RAGE in cancer cells [7–9]. Colorectal adenomas with severe atypia and villous type are thought to possess malignant potentials [2, 4]. In this study, membranous and luminal patterns were associated with severe atypia and villous adenomas.

Importantly, adenomas with membranous pattern RAGE expression expressed HMGB1/amphoterin at significantly higher levels than those adenomas with cytosolic or luminal pattern. HMGB1/amphoterin is a RAGE ligand, which accelerates cancer cell growth, migration, invasion, and VEGF production in colorectal cancer cells [6]. Our data suggest that RAGE is activated with HMGB1/amphoterin in an autocrine manner [6]. Co-expression of RAGE and HMGB1/amphoterin is significantly associated with metastases to lymph nodes and distal organs and poor prognosis in any stage of colorectal cancer [8]. We also found RAGE and HMGB1 are increased successively not only cancer tissues but precancerous colon mucosa in azoxymethane-induced rat colon cancer model (data not shown). These results suggest that RAGE expression, especially with membranous pattern, is associated with malignant potential of colorectal adenomas.

Acknowledgements This work was supported in part by Grant-in-Aid for Scientific Research from The Ministry of Education, Culture, Sports, Science and Technology, Japan.

References

1. Abe R, Shimizu T, Sugawara H, Watanabe H, Nakamura H, Choei H, Sasaki N, Yamagishi S, Takeuchi M, Shimizu H (2004) Regulation of human melanoma growth and metastasis by AGE–AGE receptor interactions. J Invest Dermatol 122: 461–467
2. Coutsoftides T, Lavery I, Benjamin SP, Sivak MVJ (1979) Malignant polyps of the colon and rectum: a clinicopathologic study. Dis Colon Rectum 22:82–86
3. Fages C, Nolo R, Huttunen HJ, Eskelinen E, Rauvala H (2000) Regulation of cell migration by amphoterin. J Cell Sci 113: 611–620
4. Fenoglio-Preiser CM, Hutter RV (1985) Colorectal polyps: pathologic diagnosis and clinical significance. CA Cancer J Clin 35:322–344
5. Hsieh HL, Schafer BW, Weigle B, Heizmann CW (2004) S100 protein translocation in response to extracellular S100 is mediated by receptor for advanced glycation endproducts in human endothelial cells. Biochem Biophys Res Commun 316:949–959
6. Kuniyasu H, Chihara Y, Kondo H (2003) Differential effects between amphoterin and advanced glycation end products on colon cancer cells. Int J Cancer 104:722–727
7. Kuniyasu H, Chihara Y, Kondo H, Ohmori H, Ukai R (2003) Amphoterin induction in prostatic stromal cells by androgen deprivation is associated with metastatic prostate cancer. Oncol Rep 10:1863–1868
8. Kuniyasu H, Chihara Y, Takahashi T (2003) Co-expression of receptor for advanced glycation end products and the ligand amphoterin associates closely with metastasis of colorectal cancer. Oncol Rep 10:445–448
9. Kuniyasu H, Oue N, Wakikawa A, Shigeishi H, Matsutani N, Kuraoka K, Ito R, Yokozaki H, Yasui W (2002) Expression of receptors for advanced glycation end-products (RAGE) is closely associated with the invasive and metastatic activity of gastric cancer. J Pathol 196:163–170
10. Schmidt AM, Hofmann M, Taguchi A, Yan SD, Stern DM (2000) RAGE: a multiligand receptor contributing to the cellular response in diabetic vasculopathy and inflammation. Semin Thromb Hemost 26:485–493
11. Schmidt AM, Yan SD, Yan SF, Stern DM (2001) The multiligand receptor RAGE as a progression factor amplifying immune and inflammatory responses. J Clin Invest 108:949–955
12. Taguchi A, Blood DC, del Toro G, Canet A, Lee DC, Qu W, Tanji N, Lu Y, Lalla E, Fu C, Hofmann MA, Kislinger T, Ingram M, Lu A, Tanaka H, Hori O, Ogawa S, Stern DM, Schmidt AM (2000) Blockade of RAGE-amphoterin signalling suppresses tumour growth and metastases. Nature 405:354–360
13. Vogelstein B, Fearon ER, Hamilton SR, Kern SE, Preisinger AC, Leppert M, Nakamura Y, White R, Smits AM, Bos JL (1988) Genetic alterations during colorectal-tumor development. N Engl J Med 319:525–532
14. Yan SD, Chen X, Fu J, Chen M, Zhu H, Roher A, Slattery T, Zhao L, Nagashima M, Morser J, Migheli A, Nawroth P, Stern D, Schmidt AM (1996) RAGE and amyloid-beta peptide neurotoxicity in Alzheimer's disease. Nature 382:685–691
15. Yasui W, Akama Y, Yokozaki H, Semba S, Kudo Y, Shimamoto F, Tahara E (1997) Expression of p21WAF1/CIP1 in colorectal adenomas and adenocarcinomas and its correlation with p53 protein expression. Pathol Int 47:470–477

Virchows Arch (2005) 446: 416–420
DOI 10.1007/s00428-005-1214-6

ORIGINAL ARTICLE

Pavlina Cejkova · Andreas Zettl · Anne K. Baumgärtner · Andreas Chott · German Ott · Hans Konrad Müller-Hermelink · Petr Starostik

Amplification of *NOTCH1* and *ABL1* gene loci is a frequent aberration in enteropathy-type T-cell lymphoma

Received: 21 October 2004 / Accepted: 12 January 2005 / Published online: 9 March 2005
© Springer-Verlag 2005

Abstract We have shown previously that amplification of chromosomal region 9q34 is the most frequent aberration in enteropathy-type T-cell lymphoma (ETL). To determine the minimum amplified 9q34 region and identify possible candidate gene(s), we performed a detailed microsatellite screening and quantitative real-time PCR (QPCR) on 26 ETL cases. Microsatellite analysis revealed allelic imbalance in both *ABL1* and *NOTCH1* gene loci (microsatellites D9S290–D9S1847 and D9S158 flanking the former and latter genes, respectively) localized in the band 9q34. The results were confirmed by TaqMan-based QPCR showing amplification of *ABL1* and *NOTCH1* exons in 50% and 65% of cases, respectively. Amplifications of the *NOTCH1* gene were more frequent than of the *ABL1* gene; moreover, the analyzed *NOTCH1* exon consistently displayed higher levels of amplification than *ABL1* coding sequences. From 9q34 known genes, *NOTCH1* could thus be the primary target of genomic DNA amplification in ETL.

Keywords T-cell lymphoma · Genetic analysis · Lymphomagenesis · Coeliac disease · Chromosome 9 · Amplification

P. Cejkova · P. Starostik (✉)
Department of Pathology and Laboratory Medicine,
Roswell Park Cancer Institute,
Elm & Carlton Streets,
Buffalo, NY, 14263, USA
e-mail: petr.starostik@roswellpark.org
Tel.: +1-716-8458136
Fax: +1-716-8457638

A. Zettl · A. K. Baumgärtner · G. Ott · H. K. Müller-Hermelink
Institute of Pathology,
Würzburg University,
Würzburg, Germany

A. Chott
Clinical Institute of Pathology,
Vienna General Hospital,
Vienna, Austria

Introduction

Enteropathy-type T-cell lymphoma (ETL) is a malignant intestinal lymphoma associated with late presentation, rapid progression, severe side effects (bowel perforation), and absence of specific therapy. Intriguingly, this disease displays the same genetic background as celiac disease [10], namely the HLA genotype DQA1*0501, DQB1*0201 [13], and occurs solely as a sequel of either refractory celiac disease or ulcerative colitis. Little is known about specific aberrations in this disease. Unlike the majority of lymphomas presenting with a typical primary translocation, e.g., t(14;18) in follicular lymphoma, no translocations have yet been found in ETL [4, 24, 30]. In previous studies, we identified the amplification of 9q34 to be the most frequent aberration occurring in ETL. Besides several putative gene-encoding sequences, the 9q34 region also encompasses gene loci of two important hematopoietic regulatory genes: *ABL1* and *NOTCH1*. In the presented work, we further delineated and narrowed the region in 9q34 implicated in the amplifications and show that both *ABL1* and *NOTCH1* genes are affected by genomic DNA amplification in 9q34.

Materials and methods

Patients and samples

For the study, 26 ETL cases from cancer registries at the Institute of Pathology of the Würzburg University in Würzburg, Germany, and the Clinical Institute of Pathology, Vienna General Hospital, Vienna, Austria, on which sufficient both tumor and normal (mostly muscle) tissue was available, were selected. The samples were exclusively paraffin-embedded/formalin-fixed blocks. The diagnosis was established according to the criteria of the World Health Organization (WHO) Classification of Lymphoid Tumors [15] by means of morphological and immunophenotypic analyses of tissue sections using standard staining methods.

Microscopic dissection and DNA extraction

In each case, 16 serial 10-μm-thick tissue sections were cut. The first and last cuts were stained with hematoxylin and eosin to assure high tumor content and as guidance for the following microdissection. Remaining tissue sections were stained with Nuclear-Fast Red to precisely delineate tumor-containing areas. Under microscope, areas showing ETL were scraped to be used for microsatellite analysis. The collected tissue was deparaffinized with xylene before digestion. DNA extraction was performed using proteinase K and phenol-chloroform according to routine molecular biology protocols. A polymerase chain reaction (PCR)-based clonality analysis assay for TCR-γ gene rearrangement [29] was performed on all DNA samples to assure the control normal DNA did not contain the lymphoma clone.

Microsatellite analysis

Microsatellite analysis was performed using a panel of six repeats: D9S1821, D9S290, D9S1847, D9S1818, D9S1826, and D9S158 (Ensembl, Sanger Institute; http://www.sanger.ac.uk). Primer sequences for the amplification of microsatellites were retrieved from Genome Database (http://www.gdb.org). PCR primers were synthesized at MWG Biotech (High Point, NC), and one oligonucleotide of each primer pair was labeled with fluorescent dye phosphoramidites FAM or HEX. Thirty cycles were carried out in a PE-9600 thermal cycler (ABI, Foster City, CA) in a total volume of 20 μL. Aliquots of the PCR reactions were then mixed with size standard and formamide, denatured, and subjected to electrophoresis on an ABI 3100 DNA Sequencer (ABI, Foster City, CA). The automatically collected data were analyzed using GeneScan and Genotyper software as described in the manufacturer's manual. Only genotypes heterozygous for a given locus were regarded as informative; homozygosity and microsatellite instability (MSI) rendered the particular locus unevaluable for loss of heterozygosity (LOH) or amplification. In heterozygous genotypes, ratios of both alleles in normal and tumor tissues were calculated. If these ratios showed a difference of more than 40%, the genotype was determined to display allelic imbalance. All aberrations were confirmed by repeating the experiments. For further determination of LOH or amplification in a locus, first the unchanged allele was identified (by comparison with other microsatellites showing no change in the same multiplex PCR) and then the ratios of the allele showing decreased or increased signal to the unchanged allele were calculated; first for control DNA and then for the tumor. Increase of the ratio by 40% in the tumor (compared with the control) was considered amplification; a decrease by 40% was considered LOH.

Quantitative PCR

Quantitative PCRs were performed in triplicate on the ABI 7700 Sequence Detection System instrument (ABI, Foster City, CA) under standard conditions using the TaqMan Universal PCR Master Mix (ABI, Foster City, CA). DNA quantities were normalized using two reference loci located on chromosomes usually unaltered in ETL: D6S310 and D14S79. Primers for target loci (*ABL1*, *NOTCH1*) were designed to amplify regions spanning across exon–intron boundaries. TaqMan probes labeled on the 5′ end with 6′ carboxy fluorescein (FAM) and on the 3′ end with TAMRA and primers were synthesized by MWG Biotech (High Point, NC). Primer sequences: *ABL1* (intron 6–7/exon 7) forward primer 5′AGGAGCTCTCATGGGTGAACA 3′, reverse primer 5′ GTTCTCCCCTACCAGGCAGTT 3′, probe (FAM)-5′ CCTTTCTTAGAGATCTTGCTGCCC 3′-(TAMRA); *NOTCH1* (intron 22–23/exon 23) forward primer 5′ GCTTGGGCCACTGACGAA 3′, reverse primer 5′ AGTCGTCCACGTTGATCTCACA 3′, probe (FAM)-5′ TGCACACCTGCGGGGCCA 3′-(TAMRA); D6S310 forward primer 5′ CCAGGGCTACACTTTCAGGTTT 3′, reverse primer 5′ GGAAGGGCTAGGAAGTGCTATG 3′, probe (FAM)-5′ TGCCTTCTGCAATCTGGATCCCAAA 3′-(TAMRA); D14S79 forward primer 5′ TGAGACGG AGTCTCGCTCTGT 3′, reverse primer 5′ TCCAAAAGT CAGAGGTTTCAGTGA 3′, probe (FAM)-5′ CACGCC ATTGCACTCCAGCCTG 3′-(TAMRA).

Sample DNAs were compared with standard DNA (calibrator) pooled from 23 unrelated normal individuals using the relative quantification ΔΔCt technique [19]. DNA copy numbers greater than 2.8 were considered to be gains and those less than 1.2 losses.

Results

We previously performed comparative genomic hybridization (CGH) and microsatellite studies on a group of 26 ETL specimens and detected several consistent abnormalities. The most frequent aberration identified in this lymphoma was the amplification of chromosomal region 9q34. This amplification was detected by CGH in 58% of the examined lymphomas [32] and in 40% by microsatellite analysis [2]. To analyze this amplification further we carried out a detailed analysis of the 9q34 region using six microsatellite markers: D9S1821, D9S290, D9S1847, D9S1818, D9S1826, and D9S158. These repeats cover approximately 10 Mbp of the amplified region (Ensembl, Sanger Institute; http://www.sanger.ac.uk) and are on average about 2 Mbp apart. Microsatellite results revealed allelic imbalance in 16 of 26 studied cases (62%) (Fig. 1). To reliably distinguish LOH from genomic amplification, multiplex PCR reactions with the marker showing allelic imbalance and minimally one other marker used as an internal control were performed. Additionally, the microsatellite analysis results were compared with CGH data, which were available on 58% of these tumors. None of the amplifications as determined by microsatellite analysis appeared as loss of signal by CGH. Genotypes displaying allelic imbalance in the 9q34 region centered around the *ABL1* gene locus (D9S290–D9S1847) in a subgroup of ETL. However, in

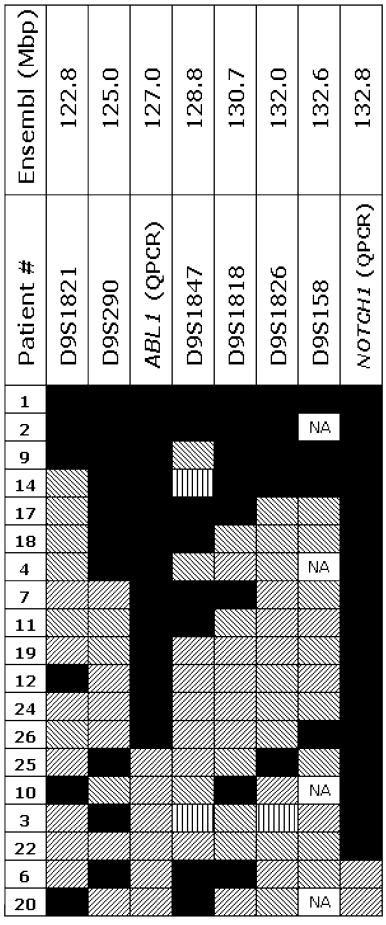

Fig. 1 Genetic aberrations in 9q34 by microsatellite analysis and quantitative real-time polymerase chain reaction (QPCR). *Rows* individual cases, *columns* microsatellites or QPCR assay targets analyzed (with their position on chromosome 9 depicted according to the Ensembl database). *Black* genomic DNA amplification; *falling stripes* homozygote; *ascending stripes* heterozygote; *vertical stripes* microsatellite instability; *NA* no PCR amplificate. Only cases displaying allelic imbalances or those positive for genomic DNA amplification by QPCR are shown

other cases, multiple discontinuous allelic imbalances involving both the *ABL1* and *NOTCH1* loci could be seen.

There are several genes or putative gene-coding sequences localized in the 9q34 chromosomal band. Two of them, *ABL1* and *NOTCH1*, are genes very well known for their key roles in hematopoietic malignancies and would be thus primary candidates for gene(s) dysregulated in ETL. To further ascertain which of the known genes located between or in close vicinity to repeats showing the most aberrations would be a good candidate for genomic DNA amplification and to confirm the microsatellite analysis results we performed a TaqMan-based QPCR. Using primers spanning exon–intron boundaries, we analyzed *ABL1* exon 7 and *NOTCH1* exon 23 for copy number amplifications. The results revealed that *NOTCH1* genomic DNA was more frequently amplified then the *ABL1* gene locus (65% and 50%, respectively, Fig. 1). *NOTCH1* also consistently showed higher levels of amplification than *ABL1* (median 4.1 and 2.82 DNA copies, respectively, Fig. 2). It thus seems that the *NOTCH1* gene locus could be the primary target of genomic DNA amplification in the region 9q34 in ETL.

Discussion

Previously, we reported amplification of 9q34 to be the most frequent aberration found in ETL. In this study, we further narrowed down the minimum amplified region in the chromosomal band 9q34. The results of microsatellite analysis performed on the lymphomas actually favored the *ABL1* as primary target of the amplifications. However, in multiple cases, the allelic imbalances were discontinuous, not showing any consistent pattern. We therefore analyzed *ABL1* exon 7 and *NOTCH1* exon 23 for copy number amplifications by means of QPCR using TaqMan probes. Interestingly, the number of amplification-positive cases went up as the QPCR detected the *ABL1* or *NOTCH1* gene amplifications in cases negative by microsatellite analysis. The percentage of cases positive for the *ABL1* amplification in-

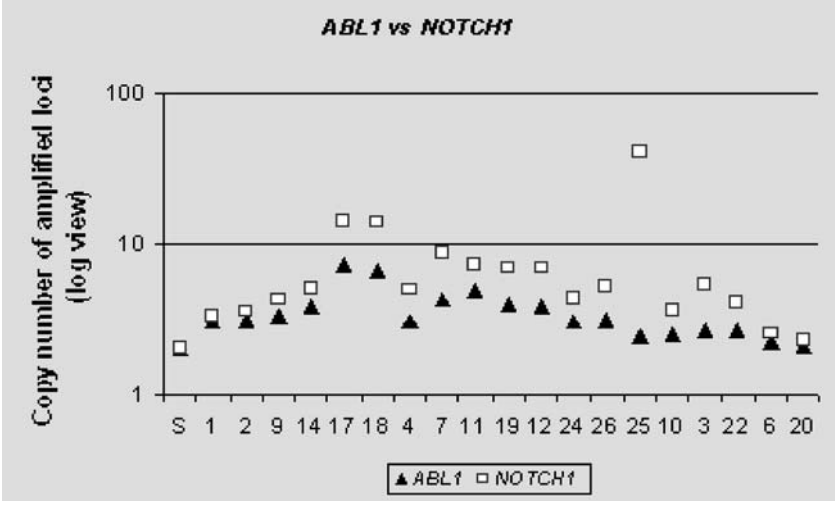

Fig. 2 Amplification of *ABL1* and *NOTCH1* gene loci by quantitative real-time polymerase chain reaction (QPCR). *X* axis represents each case; *Y* axis shows genomic DNA copy number of *NOTCH1* (exon 23) and *ABL1* (exon7) gene loci (*empty boxes* and *black triangles*, respectively; log scale). *S*=standard pooled DNA showing two DNA copies for both analyzed loci

creased from 38.5% (D9S290) or 30.8% (D9S1847) to 50%; the *NOTCH1* amplification-positive cases went up from 15.4% (D9S158) to 65.4%. Both these hematopoietically significant genes thus seem to be targeted by the amplifications. Such amplifications of genomic DNA could be one mechanism of how to induce their permanent overexpression, resulting in constitutive signaling that could predispose to ETL.

ABL1 is a ubiquitously expressed tyrosine kinase that is fused to *BCR* in CML and precursor B-ALL cases with the t(9;22)(q34;q11) translocation [6, 7], to *ETV6* in leukemias with the t(9;12)(q34;p13) translocation [11] and to *NUP214* in episomes consisting of *ABL1* and *NUP214* amplicons in T-cell acute lymphoblastic leukemia (T-ALL) [12]. Exclusive amplification of *ABL1* was described in the CML-derived cell line K562 [5], in a patient with CML in lymphoid blast crisis [18], and in three cases of secondary AML [28]. Recently, amplification involving the *ABL1* gene was described in several cases of T-ALL. The fusion gene products of the above-mentioned translocations deregulate pathways controlling cell growth and cell cycling. In normal cells, the *ABL1* oncogene has been implicated in processes of cell differentiation, cell division, cell adhesion, and stress response. Activity of the ABL1 protein is negatively regulated by its SH3 domain, and deletion of the SH3 domain turns ABL1 into an oncogene. Its DNA-binding activity is regulated by CDC2-mediated phosphorylation, suggesting a cell cycle function for *ABL1*. So far, it is not completely clear how *ABL1* contributes to oncogenesis. Several possible ways of signaling through downstream targets involving PI3-kinase, RAS, RAF and the proapoptotic protein BAD [27], JAK2 tyrosine kinase [31], MYC and anti-apoptotic BCL2 [16] were outlined. Up to this day, it has not been fully elucidated whether only a quantitative change in expression (overexpression) of wild-type *ABL1* is sufficient to render the same or similar phenotype as fused *BCR-ABL1* or other mutants of the *ABL1* gene itself.

Unlike *ABL1*, the *NOTCH1* gene encodes a transmembrane receptor, a critical regulator of multiple developmental pathways. It has the capacity to induce apoptosis in B cells [20], whereas it promotes survival in T cells [8]. Its role in leukemogenesis was identified as early as in 1991 by Ellisen et al. [9] who described a t(7;9)(q34;q34.3) in T-ALL, causing overexpression of truncated *NOTCH1* mRNA missing the anchoring amino terminus under the influence of the T-cell receptor promoter. Such *NOTCH1* activation leads to leukemia induction as shown previously [1, 25]. Activated *NOTCH1* signaling mediated by the wild-type protein has been shown to play a role in pathogenesis of anaplastic large cell lymphoma (ALCL) [17], where *NOTCH1* is highly expressed and its interaction with *Jagged1* through homotypic or heterotypic cell–cell interactions was shown to directly contribute to lymphomagenesis. Signaling through nuclear transcriptional repressor *CSL*, known also as *RBP-Jκ*, stimulates the transcription of downstream target genes such as *HES1* and *HES5* hairy enhancer of split and *HRT/HERP* [14, 22]. However, genetic evidence points also to the existence of a so-far poorly characterized *CSL*-independent signaling pathway [3, 23]. Recently, it was shown that activated *NOTCH1* inhibits p53-induced apoptosis through a PI3K-PKB/Akt-dependent pathway [21, 26]. PI3-kinase thus could represent a common pathway involved in both *ABL1* and *NOTCH1* downstream signaling. Synergistic activation of this pathway by both *ABL1* and *NOTCH1* could potentiate their impact on inhibition of apoptosis and facilitate cell cycle deregulation by *ABL1*. However, such hypotheses require further investigations. The answer will surely yield further insights into molecular mechanisms underlying the development of ETL.

Nevertheless, there is still the possibility remaining that a different unknown oncogene is the target of amplifications in the 9q34 chromosomal region. The amplifications in the 9q34 are concentrated around the *ABL1* gene between the D9S290 and D9S1847 microsatellites (3.8 Mbp apart). This interval contains numerous genes and ETSs. However, we found multiple discontinuous amplifications in the 9q34 chromosomal band in 27% of analyzed ETLs. These randomly appearing amplifications do not pinpoint any particular specific interval in 9q34 as a locus of the amplified oncogene.

We have shown previously that amplification of 9q34 is the most frequent allelic imbalance in ETL. In the present work, we identified two genes affected by the 9q34 amplification, *ABL1* and *NOTCH1,* with the latter the most frequently amplified (two-thirds of cases). This finding is of interest, as it would point future investigations toward exploration of the role of *NOTCH1* in the pathogenesis of this disease. Additional RNA/protein-based studies are required to confirm the primary target status of *ABL1* and *NOTCH1* and possibly identify new, so-far unknown gene (s) located in 9q34 being involved in the tumorigenesis of ETL.

References

1. Aster JC, Xu L, Karnell FG et al (2000) Essential roles for ankyrin repeat and transactivation domains in induction of T-cell leukemia by *notch1*. Mol Cell Biol 20:7505–7515
2. Baumgartner AK, Zettl A, Chott A et al (2003) High frequency of genetic aberrations in enteropathy-type T-cell lymphoma. Lab Invest 83:1509–1516
3. Bush G, diSibio G, Miyamoto A et al (2001) Ligand-induced signaling in the absence of furin processing of *Notch1*. Dev Biol 229:494–502
4. Carbonnel F, Lavergne A, Messing B et al (1994) Extensive small enteropathy-type T-cell lymphoma of low-grade malignancy associated with a new chromosomal translocation. Cancer 73:1286–1291
5. Collins SJ, Groudine MT (1983) Rearrangement and amplification of *c-abl* sequences in the human chronic myelogenous leukemia cell line K-562. Proc Natl Acad Sci U S A 80:4813–4817
6. De Klein A, van Kessel AG, Grosveld G et al (1982) A cellular oncogene is translocated to the Philadelphia chromosome in chronic myelocytic leukaemia. Nature 300:765–767
7. De Klein A, Hagemeijer A, Bartram CR et al (1986) *bcr* rearrangement and translocation of the *c-abl* oncogene in Philadelphia positive acute lymphoblastic leukemia. Blood 68: 1369–1375

8. Deftos ML, Bevan MJ (2000) *Notch* signaling in T cell development. Curr Opin Immunol 12:166–172
9. Ellisen LW, Bird J, West DC et al (1991) *TAN-1*, the human homolog of the *Drosophila notch* gene, is broken by chromosomal translocations in T lymphoblastic neoplasms. Cell 66: 649–661
10. Ferguson A, Kingstone K (1996) Coeliac disease and malignancies. Acta Paediatr Suppl 412:78–81
11. Golub TR, Goga A, Barker GF et al (1996) Oligomerization of the *ABL* tyrosine kinase by the Ets protein TEL in human leukemia. Mol Cell Biol 16:4107–4116
12. Graux C, Cools J, Melotte C et al (2004) Fusion of *NUP214* to *ABL1* on amplified episomes in T-cell acute lymphoblastic leukemia. Nat Genet 36:1084–1089
13. Howell WM, Leung ST, Jones DB et al (1995) HLA-DRB, -DQA, and -DQB polymorphism in celiac disease and enteropathy-associated T-cell lymphoma. Common features and additional risk factors for malignancy. Hum Immunol 43:29–37
14. Iso T (2001) HERP, a novel heterodimer partner of HES/E(spl) in *Notch* signaling. Mol Cell Biol 21:6080–6089
15. Jaffe ES, Harris NL, Stein H et al (2001) Pathology and genetics of tumours of haematopoietic and lymphoid tissues. World Health Organization classification of tumours. IARC Press, Lyon, pp 157–160
16. Jaiswal S, Traver D, Miyamoto T et al (2003) Expression of *BCR*/*ABL* and *BCL-2* in myeloid progenitors leads to myeloid leukemias. Proc Natl Acad Sci U S A 100:10002–10007
17. Jundt F, Anagnostopoulos I, Forster R et al (2002) Activated *Notch1* signaling promotes tumor cell proliferation and survival in Hodgkin and anaplastic large cell lymphoma. Blood 99: 3398–3403
18. Kenner L, Beham-Schmid C, Kerbl R et al (1999) *ABL* amplification in a patient with lymphoid blast crisis of chronic myelogenous leukaemia. Virchows Arch 434:255–257
19. Livak KJ, Schmittgen TD (2001) Analysis of relative gene expression data using real-time quantitative PCR and the 2 (-Delta Delta C(T)) method. Methods 25:402–408
20. Morimura T, Goitsuka R, Zhang Y et al (2000) Cell cycle arrest and apoptosis induced by *Notch1* in B cells. J Biol Chem 275:36523–36531
21. Nair P, Somasundaram K, Krishna S (2003) Activated *Notch1* inhibits p53-induced apoptosis and sustains transformation by human papillomavirus type 16 E6 and E7 oncogenes through a PI3K-PKB/Akt-dependent pathway. J Virol 77:7106–7112
22. Nakagawa O (2000) Members of the HRT family of basic helix–loop–helix proteins act as transcriptional repressors downstream of *Notch* signaling. Proc Natl Acad Sci U S A 97: 13655–13660
23. Ordentlich P, Lin A, Shen CP et al (1998) *Notch* inhibition of E47 supports the existence of a novel signaling pathway. Mol Cell Biol 18:2230–2239
24. Ott G, Katzenberger T, Siebert R et al (1998) Chromosomal abnormalities in nodal and extranodal CD30+ anaplastic large cell lymphomas: infrequent detection of the t(2;5) in extranodal lymphomas. Genes Chromosomes Cancer 22:114–121
25. Pear WS, Aster JC, Scott ML et al (1996) Exclusive development of T cell neoplasms in mice transplanted with bone marrow expressing activated *Notch* alleles. J Exp Med 183:2283–2291
26. Sade H, Krishna S, Sarin A (2004) The anti-apoptotic effect of *Notch-1* requires p56lck-dependent, Akt/PKB-mediated signaling in T cells. J Biol Chem 279:2937–2944
27. Skorski T, Bellacosa A, Nieborowska-Skorska M et al (1997) Transformation of hematopoietic cells by *BCR*/*ABL* requires activation of a PI-3k/Akt-dependent pathway. EMBO J 16: 6151–6161
28. Tanaka K, Arif M, Eguchi M et al (1997) Frequent jumping translocations of chromosomal segments involving the *ABL* oncogene alone or in combination with *CD3-MLL* genes in secondary leukemias. Blood 89:596–600
29. Trainor KJ, Brisco MJ, Wan JH et al (1991) Gene rearrangement in B- and T-lymphoproliferative disease detected by the polymerase chain reaction. Blood 78:192–196
30. Wright DH, Jones DB, Clark H et al (1991) Is adult-onset coeliac disease due to a low-grade lymphoma of intraepithelial T lymphocytes? Lancet 337:1373–1374
31. Xie S, Wang Y, Liu J et al (2001) Involvement of Jak2 tyrosine phosphorylation in *Bcr–Abl* transformation. Oncogene 20:6188–6195
32. Zettl A, Ott G, Makulik A et al (2002) Chromosomal gains at 9q characterize enteropathy-type T-cell lymphoma. Am J Pathol 161:1635–1645

Virchows Arch (2005) 446: 421–429
DOI 10.1007/s00428-004-1193-z

ORIGINAL ARTICLE

A. Schütz · W. Härtig · M. Wobus · J. Grosche · Ch. Wittekind · G. Aust

Expression of ADAM15 in lung carcinomas

Received: 10 September 2004 / Accepted: 6 December 2004 / Published online: 9 March 2005
© Springer-Verlag 2005

Abstract ADAM15, a member of the ADAM (a disintegrin and metalloprotease) family, is a membrane protein containing both protease and adhesion domains and may, thus, be involved in tumor invasion and metastasis. The aim of this study was to analyze the expression of ADAM15 and its potential ligand, integrin αvβ3 (CD51/CD61), in lung carcinoma cell lines and tissues. Most small cell lung carcinomas (SCLCs) and non-SCLC cell lines were ADAM15, αv and β3 integrin mRNA positive. Half of the cell lines expressed ADAM15, and three expressed the αvβ3 heterodimer at the cell surface as shown using flow cytometry. Paraffin sections of pulmonary epithelial tumors, including SCLCs (n=26), squamous cell cancer (SCCs, n=27) and adenocarcinomas (ACs, n=17) were stained with antibodies to the ectosolic and cytosolic domain of ADAM15 and αvβ3 integrin complex. The results were scored (0–12, according to Remmele's score). Normal epithelial cells of the lung were negative or slightly positive for ADAM15 (score<2). The score was always significantly higher for tumor cells. ACs showed the strongest staining (tumor center; ADAM15ecto; mean±SEM; 5.47±1.04), whereas SCLCs only showed weak ADAM15 expression (2.67±0.42; SCCs: 3.62±0.62). Frequently, significantly stronger ADAM15 expression has been shown in tumor cells located at the front of invasion compared with those within solid formations. Overall analysis of all tumor specimens and each tumor type revealed no significant correlation between tumor stage or degree of differentiation and ADAM15 ectosolic or cytosolic domain expression in tumor cells. Both molecules are often co-localized in the same tumor cells in ADAM15- and αvβ3 integrin-positive carcinomas. In summary, lung carcinoma cell lines and tissues were frequently ADAM15 positive.

Keywords ADAM 15 · Integrin · Lung carcinoma

A. Schütz (✉) · C. Wittekind
Institute of Pathology,
University of Leipzig,
Liebigstrasse 26,
04103 Leipzig
e-mail: schuetza@medizin.uni-leipzig.de
Tel.: +49-341-9715074
Fax: +49-341-9715009

W. Härtig · J. Grosche
Paul Flechsig Institute for Brain Research,
University of Leipzig,
Germany

M. Wobus · G. Aust
Institute of Anatomy,
University of Leipzig,
Germany

Introduction

ADAMs—a disintegrin and metalloprotease family also referred to as metalloprotease disintegrins or metalloprotease/disintegrin/cysteine-rich (MDC) proteins—consist of 34 putative membrane-linked proteins with a unique multidomain structure that, in many cases, comprises an amino-terminal metalloproteinase domain followed by a disintegrin domain (a potential integrin binding domain), a cysteine-rich sequence, and a membrane-proximal epithelial growth factor-like sequence [13, 38, 46, 47]. They frequently have large cytoplasmic domains with potential signaling properties. ADAMs have been implicated in a wide variety of functions, including basement membrane degradation and cell–cell and cell–matrix interactions [31, 46]. They play an important role in ectodomain shedding, the process by which biologically active, soluble forms of cytokines, growth factors and their receptors are released from membrane-bound precursors [44]. The separate domains in ADAMs would enable the cell both to interfere with integrin binding to the extracellular matrix and to degrade that matrix, suggesting a role in cell migration.

Human ADAM15 (MDC15, or metargidin) is the only ADAM with the arginine-glycine-aspartic acid (RGD) cell adhesion motif in the integrin-binding loop of the disintegrin domain [31]. ADAM15 interacts in an RGD-dependent manner, with the integrins αvβ3 and α5β1, via its disintegrin domain [15, 34, 50]. Non-RGD-dependent

interactions between ADAM15 and α9β1 integrin have also been identified [3]. ADAM15 is present in normal smooth-muscle and endothelial cells, mesangial cells and specific areas of the hippocampus and cerebellum [19, 22, 32]. Despite the pronounced expression of ADAM15 in these tissues, no major developmental defects or pathological phenotypes were evident in adam15$^{-/-}$ mice [22].

One of the interaction partners of ADAM15, αvβ3 integrin, has relatively restricted cellular and tissue distribution. This integrin can bind to a variety of extracellular matrix proteins, including vitronectin, fibronectin, fibrinogen, thrombospondin, Von Willebrand factor, and denatured collagen [28], and it is able to recruit cytoskeletal and signaling proteins to focal adhesion sites [29]. Its expression and activity is tightly regulated during a variety of biological processes, including cell proliferation and survival as well as tumor progression and metastasis [10, 25, 37, 39]. In contrast, studies on the presence of ADAM15 in tumors are rare [16], although its biochemical structure and potential activities suggest an involvement in tumor–cell interactions and migration. Here, we investigated the expression and co-localization of ADAM15 and the αvβ3 integrin heterodimer in lung tumor cell lines and tissues by flow cytometry and immunohistology.

Materials and methods

Cell lines and cells

The human small cell lung cancer (SCLC) cell lines NCI-H82, NCI-H69 and non-SCLC cell lines A549 (adenocarcinoma) [30], Colo-699 (adenocarcinoma), LCLC-103H (large cell) [3], Oka-C-1 (squamous cell carcinoma) [2], EPLC-272H (squamous cell carcinoma) [18], KNS-62 (squamous cell carcinoma) [40], BEN (squamous cell carcinoma) and MR65 (squamous cell carcinoma) were obtained from American Type Culture Collection, European Collection of Cell Cultures, and German Collection of Microorganisms and Cell Cultures.

Reverse-transcription polymerase chain reaction

Total cellular RNA was isolated using the QIAGEN total RNA isolation kit (QIAGEN GmbH, Hilden, Germany). cDNA was synthesized from 1 μg RNA in a 20-μl standard reaction mixture containing 200 U Superscript II RNaseH reverse transcriptase (Invitrogen GmbH, Karlsruhe, Germany). The following intron-overspanning primer pairs were designed: ADAM15 s (5′- ggc tgg cag tgt cgt cct acc aga ggg -3′)/r (5′- ggt gca ccc agc tgc agt tca gct cag tcc -3′), αv integrin s (5′- gat ggc aaa gga gta ctt ccc -3′)/r (5′- cgc tat caa ttc ctc aca ctg c -3′) and β3 integrin s (5′- gcc ttg gcg ccc tgc tca tct -3′)/r (5′- ccc caa atc cct ccc cac aaa tac -3′), resulting in 420 bp, 270 bp, and 291 bp polymerase chain reaction (PCR) products.

Flow cytometry

Antibodies were supplied by R&D Systems GmbH (Wiesbaden, Germany; anti-ADAM15 cytosolic domain rabbit polyclonal, anti-ADAM15 ectodomain goat polyclonal), Chemicon (Temecula, US; anti-integrin αvβ3 heterodimer monoclonal) and BD Biosciences (Heidelberg, Germany; CD51=αv single chain monoclonal; CD61=β3 single chain monoclonal). Cells (3×10^5) were incubated with the first antibody at the desired concentration for 25 min at 4 C. The cells were washed and stained with the appropriate one of the following secondary antibodies: goat anti-rabbit-fluorescein isothiocyanate (FITC), rabbit anti-goat-Cy2, or goat anti-mouse-FITC (all Dianova, Hamburg, Germany) (30 min, 4 C). After washing, the cells were analyzed by means of flow cytometry (FACSscan, Becton Dickinson, Mountain View, CA).

Biochemical characterization of ADAM15

Surface labeling of A549 cells was performed using D-Biotin-N-hydroxysuccinimide ester (Roche Diagnostics GmbH, Mannheim, Germany) [11]. Lysates of 1×10^7 cells were prepared in 50 mM Tris-HCl, 0.15 M NaCl, pH 8.0, 1 mM phenylmethylsulfonyl fluoride and used for immunoprecipitation with 10 μg of anti-human ADAM15 ectosolic or cytosolic domain antibody as well as 40 μl protein G plus/protein A agarose (Calbiochem-Novabiochem GmbH, Schwalbach, Germany) for 2 h with rotation at 4 C [41]. Samples were electrophoresed through 7.5% sodium dodecyl sulfate polyacrylamide gel and transferred to nitrocellulose, which was probed with streptavidin/horseradish peroxidase (DakoCytomation GmbH, Hamburg, Germany), and processed by enhanced chemiluminescence (ECL) on Hyper-ECL X-Ray films (Amersham Biosciences, Freiburg, Germany).

Patients

The study covered a series of 70 primary carcinomas of the lung, including SCLCs (n=26), squamous-cell carcinomas (SCCs, n=27) and adenocarcinomas (ACs, n=17), that were obtained from patients undergoing biopsy (SCLCs) or surgery at the University of Leipzig. The study was approved by the local committees of medical ethics; all patients gave written consent. None of the patients had received chemotherapy or radiotherapy before surgery. Histological diagnosis and staging were established following the tumor, lymph node and metastasis classification proposed by the International Union Against Cancer. Each tumor was further examined for differentiation according to the most dedifferentiated part of the tumor (grade 1: well-differentiated; grade 2: moderately differentiated; grade 3: poorly differentiated; grade 4: undifferentiated). SCLCs were graded as G4 tumors according to the definition [42]. The characteristics of the patients are summarized in Table 1.

Table 1 Characteristics of the patients. *TNM* tumor, lymph node and metastasis classification, *UICC* International Union Against Cancer, *ACC* adenocarcinoma, *SCC* squamous cell cancer, *SCLC* small-cell lung carcinoma

Tumor type	Age (mean±SEM)	Sex (male/female)	*n*	Grading				TNM, T-category				TNM, N-category				TNM, M-category		UICC stage			
				G1	G2	G3	G4	T1	T2	T3	T4	N0	N1	N2	N3	M0	M1	I	II	III	IV
SCC	66.4±5.7	17/10	27	0	15	12	0	9	13	3	2	17	9	1	0	27	0	14	8	5	0
AC	59.9±11.4	9/6	17	0	11	6	0	9	5	1	2	13	2	1	1	15	2	8	1	4	2
SCLC	66.6±9.8	18/7	26	-	-	-	26	Biopsy specimen only													

Tissue samples were embedded in paraffin or snap-frozen in liquid nitrogen.

Immunostaining of tissues

Serial paraffin sections were cut at 4 μm and deparaffinized. The sections were treated with 3.0% H_2O_2 for 20 min to reduce endogenous peroxidase activity. Unspecific binding sites were blocked by 5% goat normal serum (Dianova) for 30 min. For immunoperoxidase staining, the sections were incubated with primary antibodies against ADAM15 ectosolic and cytosolic domain and αvβ3 integrin for 2 h at 37 C. Detection was performed using the BioGenex Super Sensitive Detection System (San Ramon, CA, USA). Negative control was performed by omitting the specific primary antibody. Endothelial cells of small vessels within the tumor were used for internal positive control. Immunoreactivity was scored semi-quantitatively using a light microscope (Axioskop, Carl Zeiss, Jena, Germany) by two independent investigators who were unaware of the histological results. The final positive-cell count was performed after examination of the entire slide to avoid overestimation due to focal heterogeneity. At least 200 tumor cells and bronchioalveolar cells in representative areas without necrosis or regression were examined on each section and scored according to Remmele [36], a method originally introduced for receptor analysis in breast carcinomas. The percentage of positive cells was judged ranging from 1 to 4 (1: <10%, 2:10–50%, 3: 51–80%; 4: >80% positive tumor cells), and the level of staining intensity was estimated to grades between 0 and 3 (0: negative, 1: weak, 2: moderate,

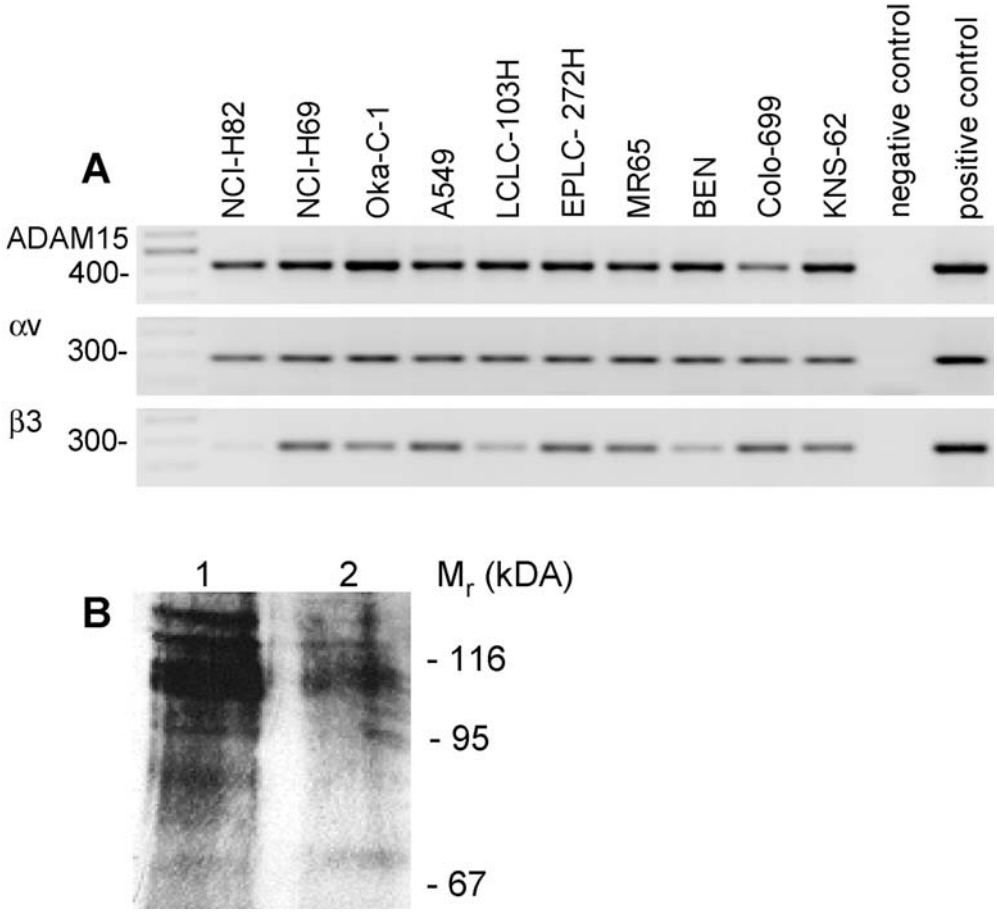

Fig. 1 Expression of ADAM15 and αvβ3 integrin in lung carcinoma cell lines. **A** Reverse-transcription polymerase chain reaction for ADAM15, αv and β3 integrin mRNA. **B** Detection of ADAM15 with antibodies against the cytosolic domain (*lane 1*) and the ectodomain (*lane 2*) on A549 cells after immunoprecipitation

3: strong staining). Multiplying positive-cell numbers by staining intensity yielded the score (0–12). We considered samples as positive where the score was higher than 2. A score of 3–6 was regarded as moderate and >6 as strong.

We selected two cases of each tumor type for double-immunofluorescence staining [17]. Sections were blocked with 5% normal goat serum and 0.3% Triton X-100 in phosphate-buffered saline for 1 h and incubated in a cocktail of ADAM15 cytosolic domain and biotin-conjugated mouse anti-αvβ3 integrin primary antibodies (15 h, all steps at room temperature) for ADAM15 cytosolic domain and αvβ3 integrin labeling. After that, sections were incubated with a mixture of Cy3-conjugated goat anti-rabbit IgG and Cy2-tagged streptavidin (Jackson) for 2 h. The sections were blocked with 5% normal donkey serum (Dianova) and incubated with a cocktail of Cy3-conjugated donkey anti-goat IgG and Cy2-tagged streptavidin (Dianova) for ADAM15 ectodomain and αvβ3 integrin detection. Finally, sections were inspected using a confocal laser-scanning microscope (LSM 510, Carl Zeiss). Projection images were assembled using Zeiss LSM Viewer shareware software (version 3.0).

Results

Expression of ADAM15 and αvβ3 integrin in lung carcinoma cell lines

All lung carcinoma cell lines were positive for ADAM15 and αv integrin mRNA (Fig. 1a). β3 integrin mRNA was not detected in NCI-H82 cells and was only slightly present in LCL-103H and BEN cells. Half of the cell lines expressed ADAM15 at the cell surface as shown using flow cytometry.

This result was confirmed by immunoprecipitation of surface-biotinylated A549 cells. A major immunoreactive band at 97 kDa corresponding to the predicted size of the mature, prodomain prototypically processed ADAM15 form was detected under reducing conditions with the ADAM15 cytosolic domain antibody (Fig. 1b, lane 1). This band was also observed with the ADAM15 antibody raised against the ectodomain (lane 2). However, the apparent signal was much weaker. One explanation for this discrepancy could be that this antibody has lower affinity or binds to an epitope, which was cleaved from most molecules. The observed 112-kDa and 116-kDa bands could represent ADAM15 proforms [27]. Some slightly lower molecular weight bands of 85, 83 and 67 kDa were detected, perhaps resulting from proteolytic processing.

Three different antibodies have been used for the detection of the αvβ3 integrin in flow cytometry. Two antibodies detect the single molecules, whereas the third only detects the expressed heterodimer. Although most cell lines were αv (CD51) positive, seven of them did not express β3 (CD61), and only three of the cell lines were, therefore, positive for the αvβ3 heterodimer. Two of the cell lines, A549 and LCLC-103H, expressed ADAM15 and the αvβ3 heterodimer simultaneously at the cell surface. SCLC cell lines were negative for ADAM15 as well as αvβ3 integrin at the surface.

Expression of ADAM15 in lung tissues

Tumor cells at the tumor margin or in front of invasion, tumor cells within the tumor center and normal epithelial cells in adjacent small bronchioli were scored. The highest scores were determined in ACs, whereas SCLCs showed only a very weak ADAM15 staining regardless of which ADAM15 antibody was used (Fig. 2). ADAM15 ectodomain-positive tumors were always positive for ADAM15 cytosolic domain.

Among the tumor cells, we frequently observed a heterogeneous staining pattern for ADAM15 dependent on the location of the tumor cell in the same tissue sample. We frequently found stronger expression of ADAM15 in cells that were located at the front of invasion, whereas tumor cells located within solid formations, such as glandular or trabecular structures, showed weaker staining, irrespective of which ADAM 15 antibody had been used or which histological type of lung carcinoma had been analyzed (Fig. 2). The score was always significantly lower in normal epithelium than in either tumor area examined.

SCLCs showed a significantly higher ADAM15 ectodomain staining score for tumor cells at the invasion front than that of tumor cells located within solid tumor structures. Similar results were obvious for staining with the ADAM15 cytosolic domain antibody in ACs. We found nearly identical staining patterns with ADAM15 ectosolic and cytosolic domain antibodies. There was no difference between the score for tumor cells at the front of invasion and in the tumor center. No significant difference between the tumor cells at the invasion front and in the tumor center was seen using the ADAM15 ectodomain antibody in SSCs. Analysis of the ADAM15 cytosolic domain revealed a score at the front of invasion that was significantly higher than those obtained in the tumor center.

Interestingly, one case showed strong expression of the ADAM15 cytosolic and ectodomain (score 9 versus 6) in squamous cell metaplasia of bronchus epithelium adjacent to infiltrates of small cell lung carcinoma (Fig. 3g, h).

Overall analysis of all tumor specimens did not reveal any significant correlation between tumor stage, lymph node involvement, distant metastasis or degree of differentiation and ADAM15 ectosolic or cytosolic domain expression in tumor cells. Further, we did not find any statistically significant correlation to lymph or blood vessel infiltration.

αvβ3 Integrin expression in lung normal tissue and carcinoma

Tissue samples were stained only with the antibody recognizing the αvβ3 heterodimer. The epithelium from normal lung was mostly αvβ3 integrin negative. Only normal bronchioli showed weak staining for αvβ3 integrin. Fur-

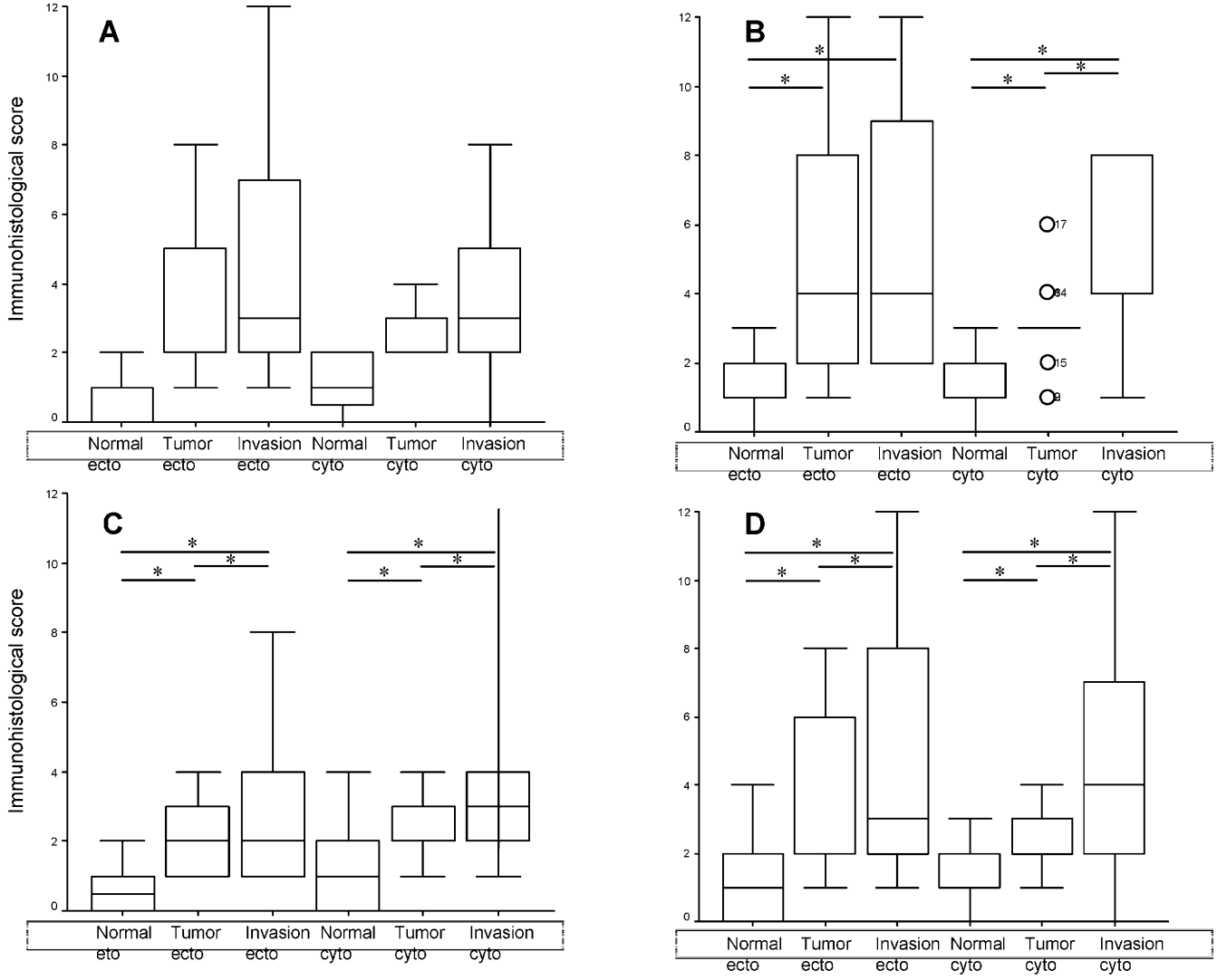

Fig. 2 Statistical analysis of ADAM15 cytosolic and ectodomain expression scores in all carcinomas from the present study (**A**), only adenocarcinomas (ACs) (**B**), squamous cell cancers SCCs (**C**) and small-cell lung carcinomas (SCLCs) (**D**). Note the significant differences between ADAM15 cytosolic and ectodomain expression in normal lung tissue (normal), at the front of invasion (invasion) and in the tumor center (tumor), marked with *asterisks*. Raw data (**B**) are marked with *circles*

thermore, the endothelium of small vessels in the interstitium showed αvβ3 integrin staining.

In contrast, the lung carcinomas expressed αvβ3 in about half of the cases (51.7%, score 3.17±0.76); αvβ3 integrin staining was nearly homogeneous in all types of carcinomas. We did not observe either predominance within scattered tumor cells or stronger expression at the front of invasion. The portion of αvβ3 integrin-positive cell was different, depending on tumor type. Of SCCs, 64.3% were weakly or moderately stained for αvβ3 integrin. Only a few tumors were strongly positive (7.4%). A higher proportion was strongly positive for the integrin heterodimer (23.1%) in the SCLC group. Of the tumors, 30.7% revealed weak or moderate staining. Of ACs, 52.9% were stained weakly or moderately for αvβ3 integrin, whereas 27.4% of the tumors were strongly positive. As described for ADAM15, moderate staining for αvβ3 integrin was found in squamous cell metaplasia of the bronchus (Fig. 3).

Co-localization of ADAM15 and αvβ3 integrin

Double immunostaining and confocal laser scanning microscopy were used to demonstrate co-localization of αvβ3 integrin and ADAM15. Two αvβ3 integrin- and ADAM15-positive tumors of each tumor type were analyzed. The distribution of the molecules was comparable with that found by single immunolabeling. A different portion of double- and single-stained cells was found, depending on tumor type and ADAM15 epitope detected. The number of double-stained tumor cells varied from 5.7% in SCCs up to 22.7% in ACs. Due to the more homogeneous distribution of the αvβ3 integrin, most of the cells (up to 90.0%) were only positive for this molecule. A direct spatial relationship of the two molecules could be demonstrated in some tumors (Fig. 4). Microscopy revealed predominantly perinuclear and membrane-associated localization of the ADAM 15 cytosolic and ectodomain as well as αvβ3 integrin.

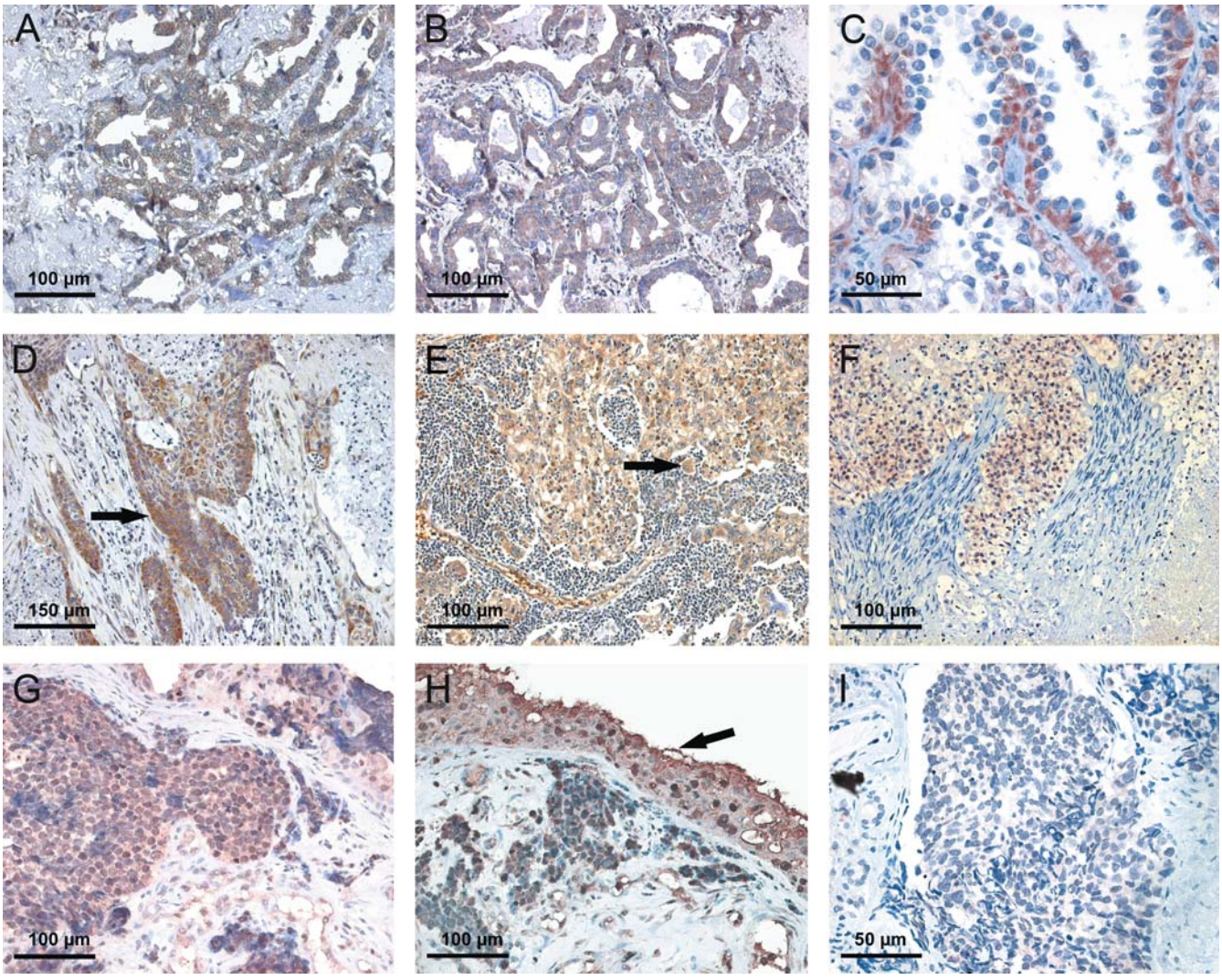

Fig. 3 Immunolocalization of ADAM15 ectosolic and cytosolic domain as well as αvβ3 integrin in lung carcinomas. Strong expression of ADAM15 ectodomain and cytosolic domain in adenocarcinomas (ACs) (**A**, **B**). Typical weak and moderate expression of the ADAM15 ectodomain and cytosolic domain in squamous cell cancers (SCCs); note the remarkably stronger expression in tumor cells at the front of invasion (**D**, **E**; *arrow*). Small-cell lung carcinomas (SCLCs) and squamous cell metaplasias (*arrow*) in the bronchus were positive for ADAM15 ectosolic and cytosolic domain (**G**, **H**). AC tumor cells were strongly positive for αvβ3 integrin (**C**). Weak to moderate expression of αvβ3 integrin in typical SCCs and SCLCs is shown in **F** and **I**

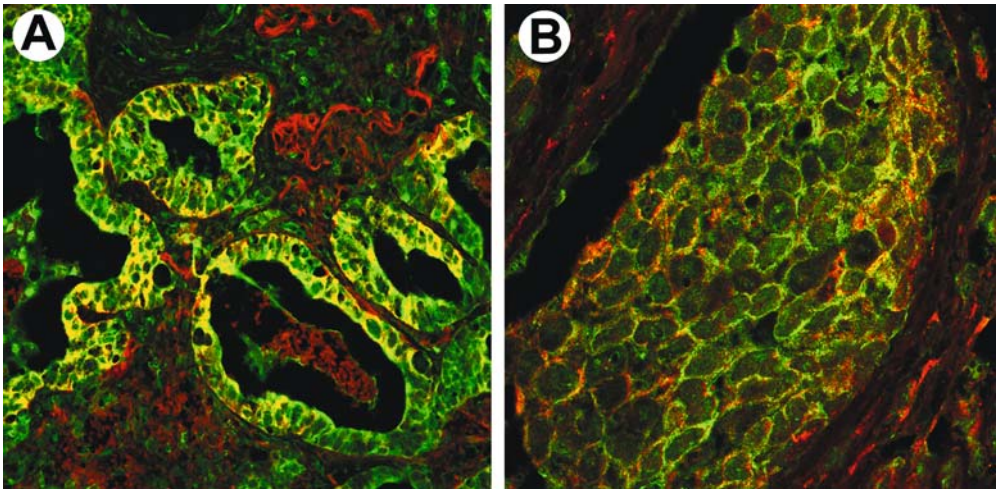

Fig. 4 ADAM15 immunoreactivity (*red*) in spatial relationship to αvβ3 integrin (*green*) expression in lung carcinomas. A high number of ADAM15 cytosolic domain and αvβ3 integrin double stained cells was present in adenocarcinoma (AC) (**A**). Note the double stained cells characterized by a yellow fluorescence signal. Compared with this example, fewer cells were double-stained in a typical small-cell lung carcinoma (SCLC) case (ADAM15 ectodomain and αvβ3 integrin staining) (**B**)

Discussion

Lung carcinomas of various tumor types showed higher ADAM15 expression than normal lung epithelium. Although the labeling score for ADAM did not correlate to tumor grade or stage, the result raises the question as to the function of this molecule within tumors.

ADAM15 is a multifunctional molecule as suggested by its structure. It possesses a metalloprotease domain, which is active, as shown by degrading the extracellular matrix proteins collagen IV and denaturated collagen I [32]. The natural substrate of ADAM15 has not yet been identified. However, proteolytic activity in carcinomas would not only facilitate cell migration by allowing the degradation of the matrix and cell detachment but could also promote cell movement trough its surrounding extracellular matrix barrier.

The disintegrin domain of ADAM15 binds to several integrins on the cell surface [14, 34, 50], thus associating proteolytic activity with tumor cell migration. This has been convincingly shown in mesangial cell migration [32]. However, ADAM15 activity must be tightly regulated, since non-physiological overexpression of ADAM15 enhances cell–cell interaction, as suggested by decreased migration and monolayer permeability [20]. The disintegrin domain of ADAM15, expressed as soluble recombinant protein, has potential therapeutic efficacy not only in tumor angiogenesis by preventing the interaction of ADAM15 with αvβ3 on endothelial cells during tumor angiogenesis but also in tumor growth and metastasis [43]. A 78% reduction tumor growth has been observed in human MDA-MB-231 tumors engrafted into nude mice bearing the transferred disintegrin domain. Moreover, 74% fewer B16F10 melanoma lung metastases were found in C57BL/6 mice [43] in the presence of the disintegrin domain. Perhaps the isolated disintegrin domain competes with the action of membrane-bound ADAM15 during its multiple inhibitory actions by preventing ADAM15 association with binding proteins. Further investigations will support the potential clinical use of the isolated disintegrin domain as a potent and promising cancer agent.

ADAMs contain a N-terminally located prodomain. The ADAM15 pro-protein with a molecular weight of nearly 110 kDa [27, 31] includes a pro-protein convertase cleavage site between its proprotease and metalloprotease domains. As shown here on A549 cells, the majority of the detectable protein lacks the prodomain, resulting in a mature 97-kDa molecule. This suggests that ADAM15 is active in lung carcinomas, although neither ADAM15 antibody used could distinguish between the proform and mature form of the molecule. Moreover, if present, soluble extracellular protein domains of ADAM15 could not be detected. Certain ADAMs have been shown to exist as secreted proteins as a result of alternative splicing, or at least in one case, self-shedding [46].

Half of the lung carcinoma cell lines express the ADAM15 ectodomain at the cell surface. Whether the ectodomain is cleaved from the surface in ADAM15 ecftodomain-negative cell lines or whether the molecule is located within the cells is unclear. Mouse ADAM15 expressed in Cos-7 cells has a predominantly perinuclear localization, which raises the possibility that ADAM15 may also have intracellular functions, such as a role in intracellular protein maturation [31].

Up to now, there has not been much in the way of data published on the expression of ADAM15 in tumors. ADAM15 cDNA was cloned from a human breast cancer cell line [27]. Malignant hematological and tissue-derived cell lines express ADAM15 mRNA and known splice variants [48, 49]. There is a markedly strong upregulation of ADAM15 in chondrosarcomas compared with adult normal articular cartilage [4]. Increased ADAM15 mRNA and proteins have been detected in tissues undergoing remodeling [4]. High levels of ADAM15 expression in macrophage-like and fibroblast-like synoviocytes and plasma cells are a histological feature most prominent in rheumatoid arthritis synovial tissue [5]. ADAM15 is upregulated in developing atherosclerotic lesions where smooth-muscle cells migrate into the intimal space to form lesions but is not expressed in normal vessels [19]. A potential role for ADAM15 in pathological neovascularization has recently been shown [22].

We not only found ADAM15 upregulation in the tumors but also demonstrated higher ADAM15 expression at the invasion front compared with the tumor center. Carcinoma cells located at the invasion front and, thus, interacting with the stromal microenvironment are thought to display a characteristic phenotype involved in invasive, migrating, and proliferating activities, which could also be the case for ADAM15-overexpressing cells in several lung carcinomas. Frequent co-localization of Cox-2 and laminin-5 γ2 at the invasion front in early-stage lung adenocarcinomas has been described [35]. A lack of homogeneous staining for β-catenin and β-catenin target genes has been frequently observed at the invasion front in colorectal adenocarcinomas [1, 6, 7, 21, 23]. Cells in the tumor center often retained a membranous expression of β-catenin where the molecule maintains adherens junctions. In contrast, a strong nuclear expression of β-catenin, now working as a transcription facor, was predominantly localized at the invasion front. Thus, the invasion front highly expresses β-catenin target genes, which are important contributors to the hallmarks of cancer, proliferation (c-myc and cyclin D1), invasion and metastasis (CD44, laminin-5γ2, MMP-7, MT1-MMP), angiogenesis (vascular endothelial growth factor) and others [6, 7, 21, 23]. Additionally, we demonstrated an increase in ADAM15 in squamous cell metaplasia. Thus, ADAM15 upregulation may be an early event in cancerogenesis.

ADAM15 is able to interact with αvβ3 integrin via its disintegrin domain. αvβ3 integrin expression is very restricted in normal epithelium [33]. In malignant tissues, tumor-associated blood vessels frequently express elevated levels of αvβ3 integrin. Additionally, αvβ3 integrin expression may occur in malignant cells. In part, αvβ3 integrin facilitates prostate cancer metastasis into bone by mediating prostate cancer cell adhesion and migration [12]. Expressed on melanoma cells, this integrin can bind and localize active MMP-2 on the cell surface, facilitating cell-mediated collagen degradation and directed cellular invasion [9]. β3

Expression is associated with tumor invasiveness in gastric carcinoma [24]. In multiple myelomas, αvβ3 integrin engagement enhances cell invasiveness [37]. Tumor αvβ3 cell integrin makes an important contribution to arrest in the lung and early metastasis formation [45]. Moreover, the molecules promote extravasation of αvβ3 integrin-expressing tumor cells in the liver [25]. In contrast to the study by Koukoulis et al. [26], who described a variable intense reaction for αv in SCCs and ACs similar to that of the bronchial epithelium [26] and no staining for β3 in immunohistology, we could demonstrate that variable expression in αvβ3 using reverse-transcription PCR and fluorescence-activated cell sorter analysis in lung tumor cell lines and using immunohistology in lung carcinomas. Additionally, Bredin et al. [8] revealed that two of five lung cancer cell lines express the β3 chain. Furthermore, we demonstrated that both molecules were sometimes co-localized in the same tumor cell in ADAM15 as well as in αvβ3 integrin-positive lung tumors. In tissue cultures, ADAM disintegrin domains can interact with integrins on neighboring cells, but whether they can interact with integrins on the same cell is not yet known.

Taken together, ADAM15 expression appears as a typical sign of lung carcinoma cell lines and tissues. The multifunctionality of ADAM15 suggests a role for the molecule in tumor-cell migration and invasion.

Acknowledgements We would like to thank M. Steinert (currently at the Städtisches Krankenhaus Martha-Maria Halle-Dölau) for providing tissues, and D. Sittig for her contribution in performing experiments. This study was supported by the Interdisciplinary Center for Clinical Research (IZKF) Leipzig at the Faculty of Medicine, University of Leipzig (project D6 and Z10, 01KS9504).

References

1. Akbari O, Panjwani N, Garcia S, Tascon R, Lowrie D, Stockinger B (1999) DNA vaccination: transfection and activation of dendritic cells as key events for immunity. J Exp Med 189:169–178
2. Asahi Y, Kubonishi I, Imamura J, Kamioka M, Matsushita H, Furihata M, Ohtsuki Y, Miyoshi I (1996) Establishment of a clonal cell line producing granulocyte colony-stimulating factor and parathyroid hormone-related protein from a lung cancer patient with leukocytosis and hypercalcemia. Jpn J Cancer Res 87:451–458
3. Bepler G, Koehler A, Kiefer P, Havemann K, Beisenherz K, Jaques G, Gropp C, Haeder M (1988) Characterization of the state of differentiation of six newly established human non-small-cell lung cancer cell lines. Differentiation 37:158–171
4. Bohm BB, Aigner T, Gehrsitz A, Blobel CP, Kalden JR, Burkhardt H (1999) Up-regulation of MDC15 (metargidin) messenger RNA in human osteoarthritic cartilage. Arthritis Rheum 42:1946–1950
5. Bohm BB, Aigner T, Blobel CP, Kalden JR, Burkhardt H (2001) Highly enhanced expression of the disintegrin metalloproteinase MDC15 (metargidin) in rheumatoid synovial tissue. Arthritis Rheum 44:2046–2054
6. Brabletz T, Jung A, Hermann K, Gunther K, Hohenberger W, Kirchner T (1998) Nuclear overexpression of the oncoprotein beta-catenin in colorectal cancer is localized predominantly at the invasion front. Pathol Res Pract 194:701–704
7. Brabletz T, Jung A, Dag S, Hlubek F, Kirchner T (1999) beta-catenin regulates the expression of the matrix metalloproteinase-7 in human colorectal cancer. Am J Pathol 155:1033–1038
8. Bredin CG, Sundqvist KG, Hauzenberger D, Klominek J (1998) Integrin dependent migration of lung cancer cells to extracellular matrix components. Eur Respir J 11:400–407
9. Brooks PC, Stromblad S, Sanders LC, von Schalscha TL, Aimes RT, Stetler-Stevenson WG, Quigley JP, Cheresh DA (1996) Localization of matrix metalloproteinase MMP-2 to the surface of invasive cells by interaction with integrin alpha v beta 3. Cell 85:683–693
10. Carreiras F, Denoux Y, Staedel C, Lehmann M, Sichel F, Gauduchon P (1996) Expression and localization of alpha v integrins and their ligand vitronectin in normal ovarian epithelium and in ovarian carcinoma. Gynecol Oncol 62:260–267
11. Cole SR, Ashman LK, Ey PL (1987) Biotinylation: an alternative to radioiodination for the identification of cell surface antigens in immunoprecipitates. Mol Immunol 24:699–705
12. Cooper CR, Chay CH, Pienta KJ (2002) The role of alpha(v) beta(3) in prostate cancer progression. Neoplasia 4:191–194
13. Duffy MJ, Lynn DJ, Lloyd AT, O'Shea CM (2003) The ADAMs family of proteins: from basic studies to potential clinical applications. Thromb Haemost 89:622–631
14. Eto K, Puzon-McLaughlin W, Sheppard D, Sehara-Fujisawa A, Zhang XP, Takada Y (2000) RGD-independent binding of integrin alpha9beta1 to the ADAM-12 and -15 disintegrin domains mediates cell–cell interaction. J Biol Chem 275:34922–34930
15. Eto K, Huet C, Tarui T, Kupriyanov S, Liu HZ, Puzon-McLaughlin W, Zhang XP, Sheppard D, Engvall E, Takada Y (2002) Functional classification of ADAMs based on a conserved motif for binding to integrin alpha 9beta 1: implications for sperm-egg binding and other cell interactions. J Biol Chem 277:17804–17810
16. Gutwein P, Oleszewski M, Mechtersheimer S, Agmon-Levin N, Krauss K, Altevogt P (2000) Role of Src kinases in the ADAM-mediated release of L1 adhesion molecule from human tumor cells. J Biol Chem 275:15490–15497
17. Hartig W, Riedel A, Grosche J, Edwards RH, Fremeau RT Jr, Harkany T, Brauer K, Arendt T (2003) Complementary distribution of vesicular glutamate transporters 1 and 2 in the nucleus accumbens of rat: relationship to calretinin-containing extrinsic innervation and calbindin-immunoreactive neurons. J Comp Neurol 465:1–10
18. Heidtmann HH, Salge U, Havemann K, Kirschke H, Wiederanders B (1993) Secretion of a latent, acid activatable cathepsin L precursor by human non-small cell lung cancer cell lines. Oncol Res 5:441–451
19. Herren B, Raines EW, Ross R (1997) Expression of a disintegrin-like protein in cultured human vascular cells and in vivo. FASEB J 11:173–180
20. Herren B, Garton KJ, Coats S, Bowen-Pope DF, Ross R, Raines EW (2001) ADAM15 overexpression in NIH3T3 cells enhances cell–cell interactions. Exp Cell Res 271:152–160
21. Hiendlmeyer E, Regus S, Wassermann S, Hlubek F, Haynl A, Dimmler A, Koch C, Knoll C, van Beest M, Reuning U, Brabletz T, Kirchner T, Jung A (2004) Beta-catenin up-regulates the expression of the urokinase plasminogen activator in human colorectal tumors. Cancer Res 64:1209–1214
22. Horiuchi K, Weskamp G, Lum L, Hammes HP, Cai H, Brodie TA, Ludwig T, Chiusaroli R, Baron R, Preissner KT, Manova K, Blobel CP (2003) Potential role for ADAM15 in pathological neovascularization in mice. Mol Cell Biol 23:5614–5624
23. Jung A, Schrauder M, Oswald U, Knoll C, Sellberg P, Palmqvist R, Niedobitek G, Brabletz T, Kirchner T (2001) The invasion front of human colorectal adenocarcinomas shows co-localization of nuclear beta-catenin, cyclin D1, and p16INK4A and is a region of low proliferation. Am J Pathol 159:1613–1617
24. Kawahara E, Ooi A, Nakanishi I (1995) Integrin distribution in gastric carcinoma: association of beta 3 and beta 5 integrins with tumor invasiveness. Pathol Int 45:493–500

25. Kikkawa H, Kaihou M, Horaguchi N, Uchida T, Imafuku H, Takiguchi A, Yamazaki Y, Koike C, Kuruto R, Kakiuchi T, Tsukada H, Takada Y, Matsuura N, Oku N (2002) Role of integrin alpha(v)beta3 in the early phase of liver metastasis: PET and IVM analyses. Clin Exp Metastasis 19:717–725
26. Koukoulis GK, Warren WH, Virtanen I, Gould VE (1997) Immunolocalization of integrins in the normal lung and in pulmonary carcinomas. Hum Pathol 28:1018–1025
27. Kratzschmar J, Lum L, Blobel CP (1996) Metargidin, a membrane-anchored metalloprotease-disintegrin protein with an RGD integrin binding sequence. J Biol Chem 271:4593–4596
28. Kuhn K, Eble J (1994) The structural bases of integrin-ligand interactions. Trends Cell Biol 4:256–261
29. Lewis JM, Cheresh DA, Schwartz MA (1996) Protein kinase C regulates alpha v beta 5-dependent cytoskeletal associations and focal adhesion kinase phosphorylation. J Cell Biol 134:1323–1332
30. Lieber M, Smith B, Szakal A, Nelson-Rees W, Todaro G (1976) A continuous tumor-cell line from a human lung carcinoma with properties of type II alveolar epithelial cells. Int J Cancer 17:62–70
31. Lum L, Reid MS, Blobel CP (1998) Intracellular maturation of the mouse metalloprotease disintegrin MDC15. J Biol Chem 273:26236–26247
32. Martin J, Eynstone LV, Davies M, Williams JD, Steadman R (2002) The role of ADAM 15 in glomerular mesangial cell migration. J Biol Chem 277:33683–33689
33. Natali PG, Hamby CV, Felding-Habermann B, Liang B, Nicotra MR, Di Filippo F, Giannarelli D, Temponi M, Ferrone S (1997) Clinical significance of alpha(v)beta3 integrin and intercellular adhesion molecule-1 expression in cutaneous malignant melanoma lesions. Cancer Res 57:1554–1560
34. Nath D, Slocombe PM, Stephens PE, Warn A, Hutchinson GR, Yamada KM, Docherty AJ, Murphy G (1999) Interaction of metargidin (ADAM-15) with alphavbeta3 and alpha5beta1 integrins on different haemopoietic cells. J Cell Sci 112:579–587
35. Niki T, Kohno T, Iba S, Moriya Y, Takahashi Y, Saito M, Maeshima A, Yamada T, Matsuno Y, Fukayama M, Yokota J, Hirohashi S (2002) Frequent co-localization of Cox-2 and laminin-5 gamma2 chain at the invasive front of early-stage lung adenocarcinomas. Am J Pathol 160:1129–1141
36. Remmele W, Hildebrand U, Hienz HA, Klein PJ, Vierbuchen M, Behnken LJ, Heicke B, Scheidt E (1986) Comparative histological, histochemical, immunohistochemical and biochemical studies on oestrogen receptors, lectin receptors, and Barr bodies in human breast cancer. Virchows Arch 409:127–147
37. Ria R, Vacca A, Ribatti D, Di Raimondo F, Merchionne F, Dammacco F (2002) Alpha(v)beta(3) integrin engagement enhances cell invasiveness in human multiple myeloma. Haematologica 87:836–845
38. Seals DF, Courtneidge SA (2003) The ADAMs family of metalloproteases: multidomain proteins with multiple functions. Genes Dev 17:7–30
39. Seftor RE (1998) Role of the beta3 integrin subunit in human primary melanoma progression: multifunctional activities associated with alpha(v)beta3 integrin expression. Am J Pathol 153:1347–1351
40. Takaki T (1980) An epithelial cell line (KNS-62) derived from a brain metastasis of bronchial squamous cell carcinoma. J Cancer Res Clin Oncol 96:27–33
41. Tamura GS, Dailey MO, Gallatin WM, McGrath MS, Weissman IL, Pillemer EA (1984) Isolation of molecules recognized by monoclonal antibodies and antisera: the solid phase immunoisolation technique. Anal Biochem 136:458–464
42. Travis WD, Bramila E, Müller-Hermelink HK, Curtis CH (2004) WHO classification of tumours: tumours of the lung, pleura, thymus and heart. IARC Press, Lyon
43. Trochon-Joseph V, Martel-Renoir D, Mir LM, Thomaidis A, Opolon P, Connault E, Li H, Grenet C, Fauvel-Lafeve F, Soria J, Legrand C, Soria C, Perricaudet M, Lu H (2004) Evidence of antiangiogenic and antimetastatic activities of the recombinant disintegrin domain of metargidin. Cancer Res 64:2062–2069
44. Turner AJ, Hooper NM (1999) Role for ADAM-family proteinases as membrane protein secretases. Biochem Soc Trans 27:255–259
45. Wang H, Fu W, Im JH, Zhou Z, Santoro SA, Iyer V, DiPersio CM, Yu QC, Quaranta V, Al Mehdi A, Muschel RJ (2004) Tumor cell alpha3 beta1 integrin and vascular laminin-5 mediate pulmonary arrest and metastasis. J Cell Biol 164:935–941
46. White JM (2003) ADAMs: modulators of cell-cell and cell-matrix interactions. Curr Opin Cell Biol 15:598–606
47. Wolfsberg TG, Primakoff P, Myles DG, White JM (1995) ADAM, a novel family of membrane proteins containing a disintegrin and metalloprotease domain: multipotential functions in cell–cell and cell–matrix interactions. J Cell Biol 131:275–278
48. Wu E, Croucher PI, McKie N (1997) Expression of members of the novel membrane linked metalloproteinase family ADAM in cells derived from a range of haematological malignancies. Biochem Biophys Res Commun 235:437–442
49. Yasui A, Matsuura K, Shimizu E, Hijiya N, Higuchi Y, Yamamoto S (2004) Expression of splice variants of the human ADAM15 gene and strong interaction between the cytoplasmic domain of one variant and Src family proteins Lck and Hck. Pathobiology 71:185–192
50. Zhang XP, Kamata T, Yokoyama K, Puzon-McLaughlin W, Takada Y (1998) Specific interaction of the recombinant disintegrin-like domain of MDC-15 (metargidin, ADAM-15) with integrin alphavbeta3. J Biol Chem 273:7345–7350

Virchows Arch (2005) 446: 430–437
DOI 10.1007/s00428-005-1208-4

ORIGINAL ARTICLE

Liesbeth Hameetman · Petra Kok · Paul H. C. Eilers · Anne-Marie Cleton-Jansen · Pancras C. W. Hogendoorn · Judith V. M. G. Bovée

The use of Bcl-2 and PTHLH immunohistochemistry in the diagnosis of peripheral chondrosarcoma in a clinicopathological setting

Received: 22 September 2004 / Accepted: 30 December 2004 / Published online: 3 March 2005
© Springer-Verlag 2005

Abstract Distinguishing osteochondroma from low-grade secondary peripheral chondrosarcoma can be difficult. In osteochondroma, growth-signalling pathways are thought to be downregulated through exostosin (EXT) inactivation. A previous pilot study focusing on expression of putative EXT downstream effectors indicated that progression of osteochondroma towards grade I chondrosarcoma was characterised by upregulation of Bcl-2 and parathyroid hormone-like hormone (PTHLH). We investigated their use as diagnostic markers in a large nationwide series of 71 osteochondromas and 34 chondrosarcomas. Bcl-2 immunohistochemistry proved to be a valuable diagnostic tool: scoring negative in 95% (specificity) of the osteochondromas and positive in 57% (sensitivity) of the chondrosarcomas, reaching a positive predictive value of 84% and negative predictive value of 82%. Positivity was not related to age, hereditary status, gender or thickness of the cartilage cap. Presence of internal controls and verification using mRNA in situ hybridisation strengthened the reliability of the immunohistochemical staining. PTHLH showed more variable staining, being positive in osteochondromas from females or adolescent males, suggesting age- and gender-dependent expression. Thus, in cases where the distinction between osteochondroma and chondrosarcoma is difficult, Bcl-2 is a valuable diagnostic marker for malignancy, regardless of tumour size, patient gender or age, and this can be extended with PTHLH for non-adolescent male patients.

Keywords Bone neoplasm · Bcl-2 · PTHLH · Osteochondroma · Exostosis

L. Hameetman · P. Kok · A.-M. Cleton-Jansen · P. C. W. Hogendoorn · J. V. M. G. Bovée (✉)
Department of Pathology, Leiden University Medical Centre, L1-Q, PO Box 9600,
2300 RC Leiden, The Netherlands
e-mail: j.v.m.g.bovee@lumc.nl

P. H. C. Eilers
Department of Medical Statistics,
Leiden University Medical Centre,
Leiden, The Netherlands

Introduction

Chondrosarcoma is a slowly growing, malignant, cartilaginous tumour. It is the second most frequent bone sarcoma, after osteosarcoma [25]. Fifteen percent of the chondrosarcomas—so-called secondary peripheral chondrosarcomas—develop within the cartilage cap of a pre-existent osteochondroma [25]. Osteochondroma can occur as a solitary lesion or in the context of multiple osteochondromas (MOs), a familial skeletal disorder with autosomal dominant inheritance [8]. Malignant transformation is reported to be low: <1% [8] in solitary osteochondromas and 0.5–3% in MO cases.

Mutations in the *Exostosin-1 (EXT1)* or *Exostosin-2 (EXT2)* genes located at 8q24 and 11p11–12, respectively, are responsible for MO [1, 29, 33]. These genes have been identified to act as tumour suppressor genes [7]. The EXT proteins are involved in the biosynthesis of heparan sulphate (HS) [28]. In the growth plate, HS proteoglycans (HSPGs) are involved in Indian Hedgehog (IHh) signalling, a pathway that regulates proliferation, organisation and differentiation of chondrocytes (Fig. 1) [2]. In the post-natal growth plate, IHh binds to Patched (Ptc) in the hypertrophic zone, inducing expression of parathyroid hormone-like hormone (PTHLH), which binds to its receptor in the transition zone [32]. Subsequent upregulation of B-cell lymphoma-2 (Bcl-2) in the proliferative zone [2] inhibits chondrocyte differentiation, which downregulates IHh secretion in the pre-hypertrophic zone. Altered expression of *EXT* genes will probably affect HSPG synthesis and, consequently, the IHh feedback loop.

In daily practice, it is sometimes difficult to distinguish both radiologically [15] and histologically [24] osteochondromas from low-grade chondrosarcomas. The diagnosis is usually based on a combination of clinicoradiological and histological findings. A correct diagnosis is required for optimal treatment of the patient, since for osteochondromas there can be a wait-and-see policy or marginal excision, whereas for chondrosarcomas possible mutilating en bloc resection is required. Immunohistochemical or molecular markers can be useful to improve the reliability

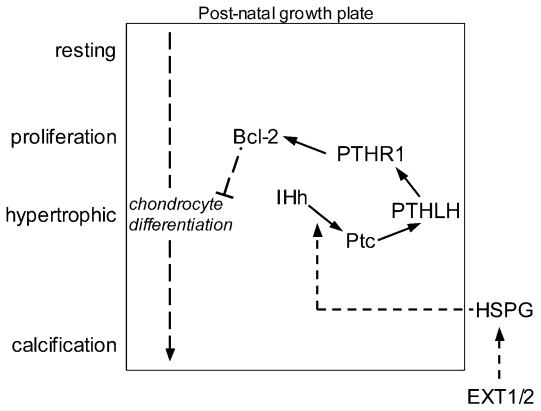

Fig. 1 Indian Hedgehog (IHh)/parathyroid hormone-like hormone (PTHLH) growth-restraining feedback loop in the post-natal growth plate. In the growth plate, resting chondrocytes differentiate to proliferative, pre-hypertrophic, hypertrophic and finally calcifying chondrocytes. In the post-natal growth plate, *IHh* binds to Patched in the hypertrophic zone, inducing expression of PTHLH, which binds to its receptor in the transition zone [32]. Upregulation of Bcl-2 in the proliferative zone [2] inhibits chondrocyte differentiation, which downregulates IHh secretion in the pre-hypertrophic zone. Diffusion of IHh is facilitated by heparan sulphate proteoglycans (HSPG). These proteins depend on EXT proteins for HS polymerisation

of the diagnosis. So far, these have not been found. A previous pilot study, focusing on the protein expression of several putative downstream effectors of EXT in cartilaginous tumours [9], suggested that upregulation of PTHLH and Bcl-2 characterises progression of osteochondroma towards grade I secondary peripheral chondrosarcoma. To investigate whether Bcl-2 and PTHLH can be used in a diagnostic setting irrespective of age, gender or MO status, data and specimens from a large nation-wide series of cases of osteochondromas and grade I peripheral chondrosarcomas were collected; the specimens were screened for PTHLH and Bcl-2 protein expression by means of immunohistochemistry. In a subset of tumours, transcription of the Bcl-2 gene was verified by means of mRNA in situ hybridisation.

Materials and methods

Patient material of the present series

A list of all patients between 1975 and August 2001 diagnosed with osteochondroma or chondrosarcoma secondary to osteochondroma was obtained through the Pathological Anatomical District Automised Archives (Foundation PALGA). This anonymised database contains full conclusions of pathology reports for every patient in the Netherlands. From 20 different medical centres, 400 tumour specimens with a diagnosis of osteochondroma or secondary peripheral chondrosarcoma were able to be retrieved. For all cases, the histology was revised by two expert bone tumour pathologists (P.C.W.H. and J.V.M.G.B.) according to the 2002 World Health Organisation (WHO) classification [4, 19]. Thickness of the cartilage cap was obtained from gross pathology or, if available, radiology reports. A cartilage cap thicker than 20 mm in adult patients, increased cellularity combined with hyperchromatic plump nuclei of uniform size and the more than occasional presence of binucleated cells were applied as criteria for malignancy, according to the most recent WHO classification [4]. For diagnosis of secondary peripheral chondrosarcoma, the presence of a pre-existent osteochondroma had to be described in the pathology report. The selection retrieved from PALGA contained, after revision, 68 peripheral chondrosarcomas of which 40 were diagnosed grade I according to Evans et al. [14]. Tumours that were used in the pilot series (n=11) [9] and recurrences (n=14), with the exception of 2 because there was no tissue available of the primary lesions, were excluded, rendering 17 new grade I peripheral chondrosarcomas from 16 patients for our study, including 1 MO patient with 2 grade I peripheral chondrosarcomas secondary to 2 different osteochondromas. An additional 6 grade I secondary peripheral chondrosarcoma cases originated from the 2001–2002 files of the Netherlands Committee of Bone Tumours, resulting in a total number of 23 grade I secondary peripheral chondrosarcomas from 22 patients. Osteochondromas of the pilot series (n=22) [9] were excluded from the osteochondromas of the PALGA selection, after which 49 osteochondromas were randomly selected. These lesions originated from 38 patients.

Since an unequivocal family history was not always available, multiplicity of osteochondromas was considered as criterion for MO, as was done previously [6, 9]. The diagnosis of multiple osteochondromas can be made when at least two separate lesions are observed [8]. Although theoretically patients with only one osteochondroma documented could have MO, for this study we considered an osteochondroma to be solitary when other lesions were absent according to the PALGA results and/or the pathology reports. From the PALGA selection, patient data could only be obtained by review of pathology reports. Further clinical or radiological data could not be retrieved due to anonymisation.

Immunohistochemistry

Immunohistochemical reactions were performed according to standard laboratory methods [10]. Antigen retrieval consisted of pre-treatment in trypsin or citrate buffer for PTHLH or Bcl-2, respectively. The monoclonal Bcl-2 antibody (clone 124, DAKO, Glostrup, Denmark) was used in a 1:100 dilution. Tonsil was used as a positive control. Lymphocytes and osteoclasts served as internal positive controls for Bcl-2. The polyclonal PTHLH antibody (Oncogene, San Diego, CA, USA) was diluted 1:25. Normal skin was used as external positive control. Occasionally, positive osteoclasts were found. The immunolabelling was detected by an avidin–biotin complex and 3,3′-diaminobenzidine as a chromogen (DAKO). Sections were counterstained with hematoxylin.

To include tumours from the previous study [9] in the statistical analysis, four grade I peripheral chondrosarcomas from that series were stained simultaneously with those from the present series to ensure similar staining scores for intensity and percentage of positive cells.

Evaluation and scoring

Four observers evaluated the staining in pairs independently, and discrepancies among the observers were re-evaluated by all four in concert. Scoring was performed as described previously [6, 13]. Both staining intensity (0=no staining, 1=weak, 2=moderate and 3=strong intensity, relative to the internal positive control) and percentage of positive tumour cells (0=0%, 1=1–24%, 2=25–49%, 3=50–74% and 4=75–100% positive tumour cells) were evaluated. The staining score was calculated as the sum of staining intensity and percentage of positive tumour cells. A staining score of more than 3 was considered positive to prevent the possibility of single positive cells reducing the diagnostic value of Bcl-2 or PTHLH [9, 13]. A tumour was only scored negative when a positive internal control was present. The scoring was performed blinded towards clinicopathological data.

Statistical analysis

For statistical analysis, the 22 osteochondromas and 11 grade I secondary chondrosarcomas from the previous series [9] were included, rendering a combined total series of 71 osteochondromas and 34 grade I secondary peripheral chondrosarcomas from 93 patients (Table 1). Fisher's exact test was used to compare different groups. Specificity (chance that an osteochondroma is negative), sensitivity (chance that a chondrosarcoma is positive), positive predictive value (chance that a positive tumour is a chondrosarcoma) and negative predictive value (chance that a negative tumour is an osteochondroma) were calculated for PTHLH and Bcl-2. The median thickness of the cartilage cap of osteochondromas and chondrosarcomas was compared using the Student's *t*-test. The same was done for the median thickness of the cartilage cap of Bcl-2-positive and Bcl-2-negative chondrosarcomas. The PTHLH expression in osteochondromas was evaluated using the Fisher's exact test. For visualisation of PTHLH expression in osteochondromas of male patients, the curve and the approximate 95% confidence intervals were estimated using P-splines [12], to model the logit of the probability. The optimal weight of the penalty was determined by Akaike Information Criterion [22]. A P value <0.05 was considered significant.

RNA in situ hybridisation

For Bcl-2 mRNA in situ hybridisation, a probe was constructed from a reverse-transcription polymerase chain reaction product. Primers (forward 5′TCCACCTGACCCTCCGC3′ and reverse 5′AACAGAGGCCGCATGCTG3′) were designed for Bcl-2 cDNA to obtain a 351-bp product encompassing exons 1 and 2 that was ligated into a pGEM3 vector (Promega, Madison, WI, USA). The DNA construct was sequenced to verify the correct insert. Sense and antisense digoxigenin (DIG)-labelled riboprobes were made by means of transcription using SP6 and T7 RNA polymerase (Roche, Basel, Switzerland), respectively, following the instructions provided by the manufacturer. The in situ hybridisation was performed as described previously [11], with minor modifications. The sections were hybridised at 62°C for 16 h with 100 ng/ml riboprobe, and the wash steps in 2×SSC with 50% formamide and 0.1×SSC with 20 mM β–mercaptoethanol were performed at 62°C. The DIG-labelled hybrids were visualised with mouse anti-DIG (Sigma, St. Louis, MO, USA), rabbit anti-mouse, APAAP (both DAKO) and BCIP/NBT (Roche, Basel, Switzerland).

Results

Patient data of the present series

In the present series, formalin-fixed, paraffin-embedded material was used from 72 tumour specimens (49 osteochondromas and 23 grade I peripheral chondrosarcomas) from 60 patients. The clinical and tumour-related data of these patients together with that of the patients from the previous series [9] are summarized in Table 1. The cartilage caps of secondary peripheral chondrosarcomas were significantly thicker than the caps of osteochondromas (P>0.0001). One osteochondroma of a 25-year-old male patient had a cap of 25 mm. However, the lesion did not show any cytonuclear features of malignancy [4] and was

Table 1 Clinical and tumour-related data of the combined total series (present and previous study taken together)

	Osteochondroma	Peripheral chondrosarcoma
Present study	38 patients (49 tumours)	22 patients (23 tumours)
Previous study [9]	22 patients (22 tumours)	11 patients (11 tumours)
Total	60 patients (71 tumours)	33 patients (34 tumours)
Male versus female	36 versus 18[a]	20 versus 13
Median age at diagnosis (years)	17[a] (range 2–49)	36 (range 16–82)
Multiple osteochondromas (MO)	33/46[b]	6/19[b]
Median thickness of cartilage cap (mm)	5[b] (range 1–25)	40[b] (range 6–220)

[a]For six patients, data on age and gender were not available
[b]Only patients with unequivocal measurements of thickness of cartilaginous cap (n=46) and MO status (n=65) were included

Table 2 Results of Bcl-2 and parathyroid hormone-like hormone (PTHLH) immunohistochemistry

		Diagnosis	
		Osteochondroma present (combined total) series	Peripheral chondrosarcoma present (combined total) series
Bcl-2	Negative	37 (56)	9 (12)
	Positive	3 (3)	9 (16)
PTHLH	Negative	11 (28)	2 (4)
	Positive	36 (37)	21 (30)
Bcl-2 negative	PTHLH negative	6 (21)	1 (3)
	PTHLH positive	30 (31)	8 (9)
Bcl-2 positive	PTHLH negative	0 (0)	0 (0)
	PTHLH positive	3 (3)	9 (16)

therefore diagnosed as benign. There were three grade I secondary peripheral chondrosarcomas with cartilage caps thinner than 20 mm but with overt cytonuclear atypia. There were no recurrences or, as expected, no metastases of osteochondromas reported in the study cohort retrieved by PALGA. Of the 22 patients with grade I secondary peripheral chondrosarcomas, seven had one or more recurrences. There were no metastases of the grade I secondary peripheral chondrosarcomas reported.

Immunohistochemistry (present series)

Of the 49 osteochondromas included in the present series, 40 osteochondromas could be evaluated, of which only three (7%) were positive for Bcl-2. In contrast, of the 23 chondrosarcomas of the present series, 18 could be evaluated of which half were positive (Table 2). Thus, 9 osteochondromas and 5 chondrosarcomas in the present series could not be analysed for Bcl-2 protein expression, primarily due to loss of sections, as a result of antigen retrieval, or because the internal control was negative. Of the seven chondrosarcomas that recurred, two were positive for Bcl-2. Of 49 osteochondromas, 47 could be evaluated for PTHLH; of these, 36 tumours (77%) were positive for PTHLH while 21 of 23 (91%) of the chondrosarcomas were positive (Table 2). Two osteochondromas were excluded from the PTHLH analysis because of loss of the sections. Representative examples of the immunohistochemical staining of Bcl-2 and PTHLH are shown in Fig. 2.

RNA in situ hybridisation

On a subset of tumours, the specificity of the immunohistochemical staining of Bcl-2 was validated by means of RNA in situ hybridisation. The mRNA expression showed a 100% correlation with the Bcl-2 protein expression. Four Bcl-2-positive tumours (two osteochondromas and two grade I secondary peripheral chondrosarcomas) had high mRNA expression of Bcl-2 in the tumour cells (Fig. 2d). At the same time, in two Bcl-2 negative osteochondromas

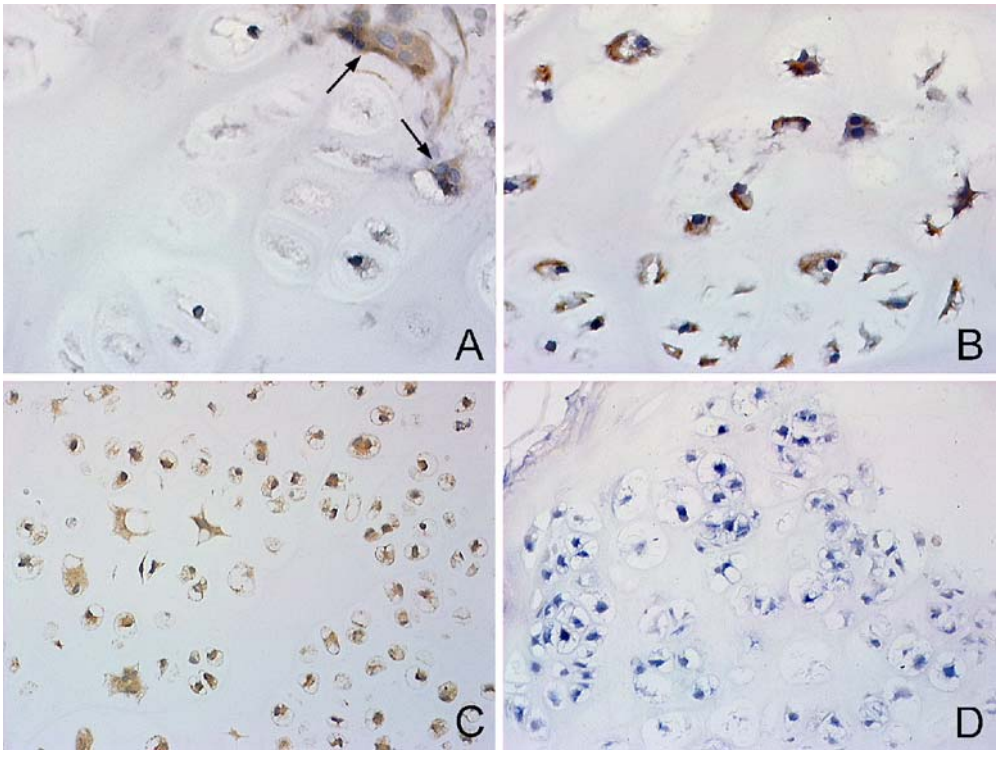

Fig. 2 Bcl-2 and parathyroid hormone-like hormone (PTHLH) protein expression in osteochondromas and peripheral chondrosarcomas. Light-micrograph showing immunohistochemical staining of hereditary osteochondroma without Bcl-2 expression, scored as negative (**a**). Positive osteoclasts indicated by *arrows* were used as a positive internal control; **b** grade I chondrosarcoma secondary to a sporadic osteochondroma, scored as positive. The tumour clearly demonstrates moderate Bcl-2 expression in 50–75% of the cells; **c** grade I chondrosarcoma demonstrating moderate PTHLH expression in almost all tumour cells, scored positive. **d** Light micrograph of Bcl-2 mRNA in situ hybridisation of a low-grade chondrosarcoma with a positive staining score for Bcl-2 protein. All tumour cells demonstrate Bcl-2 mRNA expression

Table 3 Parathyroid hormone-like hormone (PTHLH) in osteochondroma (combined total series)

Age range (years)	Male		Female	
	Positive[a]	Percentage	Positive[a]	Percentage
0–9	2/4	50%	3/3	100%
10–19	13/19	68%	7/10	70%
20–29	1/8	13%	1/4	25%
30–39	1/3	33%	3/3	100%
40–49	0/3	0%	1/1	100%
Total[b]	17/37	45%	15/21	71%

[a]The number of positive osteochondromas/total number of osteochondromas that could be evaluated
[b]Seven cases were omitted because information on gender was unavailable

and two Bcl-2 negative grade I secondary peripheral chondrosarcomas, no Bcl-2 mRNA expression was found in the tumour cells, even though a positive internal control was present.

Statistical analysis

Given the matching staining results of 4 grade I peripheral chondrosarcomas from the previous study that were re-stained in the present study, results from 22 osteochondromas and 11 grade I secondary peripheral chondrosarcomas [9] (summarised in Tables 1 and 2) were included in the statistical analysis to increase statistical power. The difference in Bcl-2 expression between osteochondromas and grade I chondrosarcomas was highly significant ($P<0.001$). The high specificity (95%) and the high positive predictive value of 84% indicated that Bcl-2 positivity supports the diagnosis of grade I peripheral chondrosarcoma. However, progression towards chondrosarcoma cannot be excluded when a tumour is Bcl-2 negative due to its low sensitivity of 57% and negative predictive value of 82%. Within the group of grade I peripheral chondrosarcomas, there was no relationship between the size of the lesion and Bcl-2 staining ($P=0.70$).

PTHLH expression was less supportive in the differential diagnosis (specificity 43%, sensitivity 88%, positive predictive value 45% and negative predictive value 88%).

For 83 cases from the combined total series, both Bcl-2 and PTHLH expression could be evaluated (Table 2). Combining the results of the two tests did not strengthen the diagnostic value. All cases with absent PTHLH expression were also negative for Bcl-2 expression.

There was no difference in PTHLH or Bcl-2 expression between MO- and non-MO-related tumours ($P=0.16$).

Within the osteochondroma group, most male patients between 10 years and 19 years (68%) and most female patients (71%) were positive for PTHLH (Table 3). This increase in PTHLH-positive osteochondromas in adolescent male patients was significant when compared with the other male age groups ($P=0.008$). The probability that an osteochondroma of a male patient is positive for PTHLH depending on the patient's age is visualised in Fig. 3. For grade I peripheral chondrosarcomas, no difference in PTHLH expression was seen between male and female patients, nor was there any age- or gender-specific expression pattern found for Bcl-2.

Discussion

The differential diagnosis between osteochondroma and low-grade secondary peripheral chondrosarcoma is usually based on a combination of clinical, histological and radiological findings [4]. Treatment can differ substantially from local marginal surgery or wait-and-see policy for osteochondromas to sometimes mutilating en bloc resection for chondrosarcomas. A valid diagnosis is therefore needed to determine which treatment and follow-up strategy is required. As of yet, there are no markers available to discriminate between benign and low-grade malignant cartilaginous tumours. Immunohistochemistry would be an ideal additional diagnostic tool to help stratify the treatment strategy.

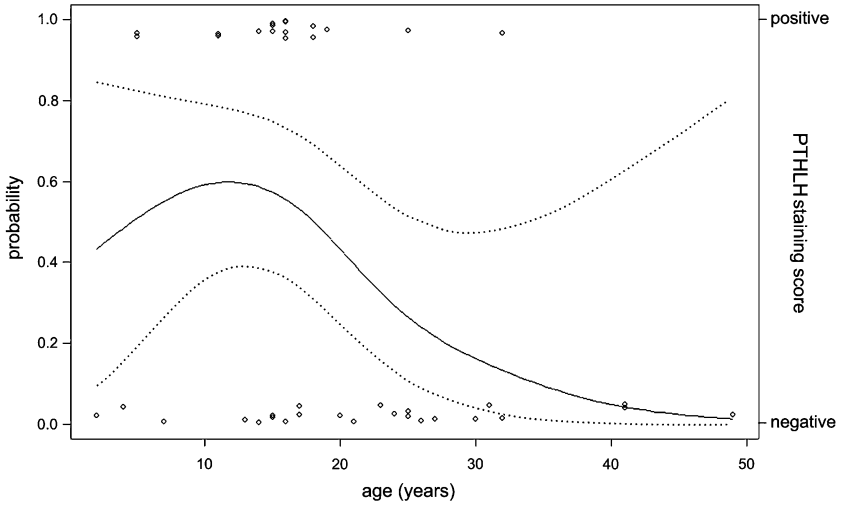

Fig. 3 Parathyroid hormone-like hormone (PTHLH) expression in osteochondromas of male patients. PTHLH staining scores of osteochondromas of male patients (*right y*-axis) are plotted against the patients' ages. The *curve* represents the probability (*left y*-axis) that an osteochondroma of a male patient is PTHLH positive [12]. The *dotted lines* represent the approximate 95% confidence intervals. The possibility of a male patient with a positive osteochondroma decreases after the age of 20 years

In a previous smaller pilot study focusing on the expression of several putative downstream effectors of EXT in cartilaginous tumours [9], we demonstrated that molecules from IHH/PTHLH- and FGF/FGFR signalling are mostly absent in osteochondromas. In chondrosarcomas, re-expression of FGF2, FGFR1, PTHLH, Bcl-2 and p21 was found, and expression levels increased with increasing histological grade. Expression of PTHLH and Bcl-2 was significantly higher in grade I chondrosarcoma than in osteochondroma [9], suggesting that these molecules play a role in malignant transformation. To further investigate whether Bcl-2 and/or PTHLH immunohistochemistry could be used in a diagnostic setting, we collected a large multi-institute series of osteochondromas and grade I secondary peripheral chondrosarcomas using our national pathology database.

The staining for Bcl-2 was significantly higher in grade I peripheral chondrosarcomas than in osteochondromas. Only 3 of the 59 osteochondromas that could be evaluated for Bcl-2 in the previous and present series combined were positive, leading to a high specificity of 95%. These 3 tumours had a staining score of four, just above the selected threshold. Histologically, these 3 tumours did not meet the WHO criteria for malignancy [4]. From the literature, it is known that less than 1% of the solitary and 0.5–3% of the hereditary osteochondromas can progress towards chondrosarcoma [9]. It may be that these three cases are osteochondromas prone to malignant transformation.

In the literature Bcl-2 expression has been described as a tumour progression marker but also as a marker for good prognosis [18]. This can be attributed to the different functions of Bcl-2 in both apoptosis and cell cycle regulation. However, it can also be ascribed to the use of different staining techniques, different Bcl-2 antibodies and a bias in selecting cut-off points [23]. In our study, tumours were only included in the analysis if there was an internal positive control (lymphocytes/osteoclasts), thereby preventing misinterpretation due to technical problems and allowing a correlation between staining intensity of the tumour cells and the internal positive control. Bcl-2 is not a specific marker for grade I peripheral chondrosarcoma, since a subset of these tumours was Bcl-2 negative (12 of 28). Probably, these tumours have an alternative as yet unknown mechanism independent of Bcl-2 for malignant transformation. There was no relationship between Bcl-2 expression and thickness of the cartilage cap in grade I secondary peripheral chondrosarcoma. Thus, expression of Bcl-2 gives additional information about the lesion, independent of the size of the cartilage cap.

PTHLH showed more variable staining in this present large series of osteochondromas than in small pilot series. Interestingly, the PTHLH-positive osteochondromas consisted mostly of tumours from female or adolescent male patients, suggesting that other signalling pathways influence PTHLH expression, such as the involvement of steroids (e.g. oestrogen). It has been shown that in the rat uterus PTHLH expression is regulated by steroids [26]. In addition, oestrogen initiates the pubertal growth spurt and causes growth plate fusion at the end of puberty [31]. Oestrogen also affects differentiation and proliferation of chondrocytes and is involved in extracellular matrix production [5]. In the growth plate the oestrogen receptors are co-expressed in late proliferating and hypertrophic chondrocytes, the same area where components of the IHh/PTHLH growth-restraining feedback loop are expressed (Fig. 1) [21, 30, 32]. This suggests that oestrogen could directly influence the feedback loop. Since osteochondroma histologically resembles the organisation of an epiphyseal growth plate, one could speculate that, in osteochondroma, oestrogen also affects PTHLH expression.

There is little additional diagnostic value when Bcl-2 and PTHLH immunohistochemistry data are combined. Not all tumours that are PTHLH positive are Bcl-2 positive (19 of 59, 32%). This suggests that in cartilaginous tumours PTHLH does not necessarily inhibit chondrocyte differentiation by upregulating Bcl-2. PTHLH can also stop differentiation by downregulating BMP6, an autocrine stimulator of chondrocyte differentiation [17]. Interestingly, all cases without PTHLH expression also demonstrated absence of Bcl-2 expression. In the IHh/PTHLH growth-restraining feedback loop, Bcl-2 is downstream of PTHLH (Fig. 1) and it therefore seems plausible that in at least a subset of cartilaginous tumours PTHLH regulates Bcl-2. However, PTHLH expression does not necessarily upregulate Bcl-2.

mRNA in situ hybridisation, which was performed to validate our immunohistochemical results, showed that the Bcl-2 protein expression is most probably regulated at the transcription level because mRNA was absent in Bcl-2 immunohistochemistry-negative tumours and present in tumours positive for Bcl-2 protein expression. In the literature, it has been described that IL-2 can regulate Bcl-2 expression

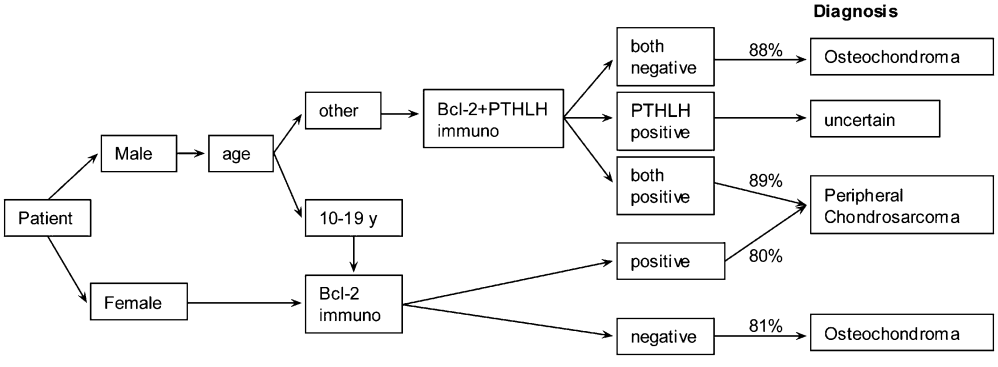

Fig. 4 Proposed flow chart for diagnosis. Patients are stratified for gender and age, and immunohistochemistry experiments are performed. Via the results of the immunohistochemistry, the flow chart ends in a recommended diagnosis. The reliability of the diagnosis is indicated in percentages

at the transcription level [16] and therefore one can speculate that PTHLH could act in a similar fashion.

The expression of Bcl-2 and PTHLH in cartilaginous tumours has also been studied previously by others [3, 20, 27]. However, no distinction has been made between central and peripheral chondrosarcomas. Amling et al. [3] found that Bcl-2 was upregulated in high-grade chondrosarcomas, which is in concordance with the results of central chondrosarcomas in our pilot series [9]. This is unlike peripheral chondrosarcomas where Bcl-2 is already expressed in grade I lesions. Similar to our results, these studies found that practically all chondrosarcomas and most benign lesions had expression of PTHLH, which increased with increasing histological grade. The present study is the first that focuses specifically on osteochondromas and grade I secondary peripheral chondrosarcomas.

Based on our immunohistochemical findings, we propose a flow chart for the use of Bcl-2 and PTHLH immunohistochemistry (Fig. 4) to assist in those cases where, despite the combination of clinical, radiological and histological data, the differential diagnosis between osteochondroma and grade I secondary peripheral chondrosarcoma is difficult. For female and adolescent male patients, only the Bcl-2 expression is informative and positive staining favours malignancy. For non-adolescent male patients, immunohistochemistry for both Bcl-2 and PTHLH can be performed, although PTHLH has limited additional value. When Bcl-2 and PTHLH are both positive, a diagnosis of chondrosarcoma is supported. When both stainings are negative, a diagnosis of osteochondroma is favoured.

Acknowledgements The contribution of the Dutch national pathology database 'Stichting PALGA' and the Netherlands Committee of Bone Tumours to this study is thankfully acknowledged. The authors gratefully acknowledge Hans J. Baelde and Ayse Yavas for expert technical assistance, Dr. M. Karperien for fruitful discussions, Klaas G. van der Ham for graphical assistance and the different medical centres that shared their cases with us. This work was financially supported by the Dutch Cancer Society (grant-no. RUL 2002–2738) and was presented in part at the 91st annual meeting of the United States and Canadian Academy of Pathology (USCAP, 2002) and the 15th annual meeting of the European Musculoskeletal Oncology Society (EMSOS, 2002). All investigations were performed according to the national ethics guidelines for the use of patient material.

References

1. Ahn J, Ludecke H-J, Lindow S, Horton WA, Lee B, Wagner MJ, Horsthemke B, Wells DE (1995) Cloning of the putative tumour suppressor gene for hereditary multiple exostoses (EXT1). Nat Genet 11:137–143
2. Amling M, Neff L, Tanaka S, Inoue D, Kuida K, Weir E, Philbrick WM, Broadus AE, Baron R (1997) Bcl-2 lies downstream of parathyroid hormone related peptide in a signalling pathway that regulates chondrocyte maturation during skeletal development. J Cell Biol 136:205–213
3. Amling M, Posl M, Hentz MW, Priemel M, Delling G (1998) PTHrP and Bcl-2: essential regulatory molecules in chondrocyte differentiation and chondrogenic tumors. Verh Dtsch Ges Pathol 82:160–169
4. Bertoni F, Bacchini P, Hogendoorn PCW (2002) Chondrosarcoma. In: Fletcher CDM, Unni KK, Mertens F (eds) World Health Organisation classification of tumours. Pathology and genetics of tumours of soft tissue and bone. IARC Press, Lyon
5. Bland R (2000) Steroid hormone receptor expression and action in bone. Clin Sci (Lond) 98:217–240
6. Bovée JVMG, Cleton-Jansen AM, Kuipers-Dijkshoorn N, Van den Broek LJCM, Taminiau AHM, Cornelisse CJ, Hogendoorn PCW (1999) Loss of heterozygosity and DNA ploidy point to a diverging genetic mechanism in the origin of peripheral and central chondrosarcoma. Genes Chromosomes Cancer 26:237–246
7. Bovée JVMG, Cleton-Jansen AM, Wuyts W, Caethoven G, Taminiau AHM, Bakker E, Van Hul W, Cornelisse CJ, Hogendoorn PCW (1999) EXT-mutation analysis and loss of heterozygosity in sporadic and hereditary osteochondromas and secondary chondrosarcomas. Am J Hum Genet 65:689–698
8. Bovée JVMG, Hogendoorn PCW (2002) Multiple osteochondromas. In: Fletcher CDM, Unni KK, Mertens F (eds) World Health Organization classification of tumours. Pathology and genetics. Tumours of soft tissue and bone. IARC Press, Lyon
9. Bovée JVMG, Van den Broek LJCM, Cleton-Jansen AM, Hogendoorn PCW (2000) Up-regulation of PTHrP and Bcl-2 expression characterizes the progression of osteochondroma towards peripheral chondrosarcoma and is a late event in central chondrosarcoma. Lab Invest 80:1925–1933
10. Bovée JVMG, Van den Broek LJCM, De Boer WI, Hogendoorn PCW (1998) Expression of growth factors and their receptors in adamantinoma of long bones and the implications for its histogenesis. J Pathol 184:24–30
11. De Boer WI, van Schadewijk A, Sont JK, Sharma HS, Stolk J, Hiemstra PS, van Krieken JH (1998) Transforming growth factor beta1 and recruitment of macrophages and mast cells in airways in chronic obstructive pulmonary disease. Am J Respir Crit Care Med 158:1951–1957
12. Eilers PHC, Marx BD (1996) Flexible smoothing with *B*-splines and penalties. Stat Sci 11:89–102
13. Elkhuizen PHM, Voogd AC, Van den Broek LJCM, Tan ITC, Van Houwelingen HC, Leer J-WH, Van de Vijver MJ (1999) Risk factors for local recurrence after breast-conserving therapy for invasive carcinomas: a case-control study of histological factors and alterations in oncogene expression. Int J Radiat Oncol Biol Phys 45:73–83
14. Evans HL, Ayala AG, Romsdahl MM (1977) Prognostic factors in chondrosarcoma of bone. A clinicopathologic analysis with emphasis on histologic grading. Cancer 40:818–831
15. Geirnaerdt MJ, Hogendoorn PCW, Bloem JL, Taminiau AHM, Van der Woude HJ (2000) Cartilaginous tumors: fast contrast-enhanced MR imaging. Radiology 214:539–546
16. Gomez J, Martinez A, Gonzalez A, Garcia A, Rebollo A (1998) The Bcl-2 gene is differentially regulated by IL-2 and IL-4: role of the transcription factor NF-AT. Oncogene 17:1235–1243
17. Grimsrud CD, Romano PR, D'Souza M, Puzas JE, Reynolds PR, Rosier RN, O'Keefe RJ (1999) BMP-6 is an autocrine stimulator of chondrocyte differentiation. J Bone Miner Res 14:475–482
18. Gurova KV, Gudkov AV (2003) Paradoxical role of apoptosis in tumor progression. J Cell Biochem 88:128–137
19. Khurana J, Abdul-Karim F, Bovée JVMG (2002) Osteochondroma. In: Fletcher CDM, Unni KK, Mertens F (eds) World Health Organization classification of tumours. Pathology and genetics. Tumours of soft tissue and bone. IARC Press, Lyon
20. Kunisada T, Moseley JM, Slavin JL, Martin TJ, Choong PF (2002) Co-expression of parathyroid hormone-related protein (PTHrP) and PTH/PTHrP receptor in cartilaginous tumours: a marker for malignancy? Pathology 34:133–137
21. Lanske B, Karaplis AC, Lee K, Luz A, Vortkamp A, Pirro A, Karperien M, Defize LHK, Ho C, Mulligan RC, Abou-Samra A-B, Juppner H, Segre GV, Kronenberg HM (1996) PTH/PTHrP receptor in early development and Indian hedgehog-regulated bone growth. Science 273:663–666

22. Lindsey JK, Jones B (1998) Choosing among generalized linear models applied to medical data. Stat Med 17:59–68
23. Martin B, Paesmans M, Berghmans T, Branle F, Ghisdal L, Mascaux C, Meert AP, Steels E, Vallot F, Verdebout JM, Lafitte JJ, Sculier JP (2003) Role of Bcl-2 as a prognostic factor for survival in lung cancer: a systematic review of the literature with meta-analysis. Br J Cancer 89:55–64
24. Mirra JM, Gold R, Downs J, Eckardt JJ (1985) A new histologic approach to the differentiation of enchondroma and chondrosarcoma of the bones. A clinicopathologic analysis of 51 cases. Clin Orthop 201:214–237
25. Mulder JD (ed) (1993) Radiologic atlas of bone tumors. Elsevier, Amsterdam
26. Paspaliaris V, Petersen DN, Thiede MA (1995) Steroid regulation of parathyroid hormone-related protein expression and action in the rat uterus. J Steroid Biochem Mol Biol 53:259–265
27. Pateder DB, Gish MW, O'Keefe RJ, Hicks DG, Teot LA, Rosier RN (2002) Parathyroid hormone-related Peptide expression in cartilaginous tumors. Clin Orthop 198–204
28. Simmons AD, Musy MM, Lopes CS, Hwang L-Y, Yang Y-P, Lovett M (1999) A direct interaction between EXT proteins and glycosyltransferases is defective in hereditary multiple exostoses. Hum Mol Genet 8:2155–2164
29. Stickens D, Clines G, Burbee D, Ramos P, Thomas S, Hogue D, Hecht JT, Lovett M, Evans GA (1996) The EXT2 multiple exostoses gene defines a family of putative tumour suppressor genes. Nat Genet 14:25–32
30. Van der Eerden BCJ, Gevers EF, Lowik CW, Karperien M, Wit JM (2002) Expression of estrogen receptor alpha and beta in the epiphyseal plate of the rat. Bone 30:478–485
31. Van der Eerden BCJ, Karperien M, Wit JM (2001) The estrogen receptor in the growth plate: implications for pubertal growth. J Pediatr Endocrinol Metab 14(Suppl 6):1527–1533
32. Van der Eerden BCJ, Karperien M, Gevers EF, Lowik CWGM, Wit JM (2000) Expression of Indian Hedgehog, PTHrP and their receptors in the postnatal growth plate of the rat: evidence for a locally acting growth restraining feedback loop after birth. J Bone Miner Res 15:1045–1055
33. Wuyts W, Van Hul W, Wauters J, Nemtsova M, Reyniers E, Van Hul E, De Boulle K, De Vries BBA, Hendrickx J, Herrygers I, Bossuyt P, Balemans W, Fransen E, Vits L, Coucke P, Nowak NJ, Shows TB, Mallet L, Van den Ouweland AMW, McGaughran J, Halley DJJ, Willems P (1996) Positional cloning of a gene involved in hereditary multiple exostoses. Hum Mol Genet 5:1547–1557

Virchows Arch (2005) 446: 438–441
DOI 10.1007/s00428-004-1169-z

ORIGINAL ARTICLE

Andreas Leithner · Andreas Weinhaeusel · Petra Zeitlhofer · Horst Koch · Roman Radl · Reinhard Windhager · Alfred Beham · Oskar A. Haas

Evidence of a polyclonal nature of myositis ossificans

Received: 11 August 2004 / Accepted: 31 October 2004 / Published online: 11 March 2005
© Springer-Verlag 2005

Abstract Myositis ossificans is a localized, self-limiting, reparative lesion that is composed of reactive hypercellular fibrous tissue and bone. Although it is clearly a benign lesion, its clinical, radiological, and histological appearance may sometimes mimic a malignant tumor. Whether myositis ossificans represents a monoconal or polyclonal hyperplastic proliferation is not yet known. To address this question, we therefore extracted DNA from the respective paraffin-embedded tumor tissues of nine women with a median age of 50 years at diagnosis (range: 20–84 years) and studied the X inactivation pattern by means of methylation-sensitive polymerase chain reaction and primers that target the polymorphic CGG trinucleotide repeat of the FMR1 gene. The fact that we did not detect any skewing of the X inactivation pattern in the five successfully analyzed cases corroborates the notion that myositis ossificans results from a polyclonal proliferation and confirms that it is a reactive, reparative process. Analysis of the X inactivation pattern may, thus, supplement the differential diagnostic work-up of cases with an uncertain histology, at least in the informative proportion of female patients.

Andreas Leithner and Andreas Weinhaeusel contributed equally to this work.

A. Leithner · R. Radl · R. Windhager
Department of Orthopedic Surgery, Medical University Graz,
Graz, Austria

A. Weinhaeusel · P. Zeitlhofer · O. A. Haas (✉)
Children's Cancer Research Institute (CCRI),
St. Anna Children's Hospital,
Kinderspitalgasse 6,
1090 Vienna, Austria
e-mail: oskar.haas@ccri.at
Tel.: +43-1-40170480
Fax: +43-1-40170437

H. Koch
Department of Surgery, Division of Plastic Surgery,
Medical University Graz,
Graz, Austria

A. Beham
Institute of Pathology, Medical University Graz,
Graz, Austria

Keywords Myositis ossificans · DNA methylation · X inactivation · Polymerase chain reaction · FMR1

Introduction

According to the World Health Organization classification of tumors, published in 2002, myositis ossificans (also known as myositis ossificans circumscripta or traumatica) is a localized, self-limiting, reparative lesion that is composed of reactive hypercellular fibrous tissue and bone [7]. A preceding trauma is believed to be the initiating event in most instances and is noted in 40–70% of the published cases [4, 5, 7]. Although there is no doubt regarding the benign nature of this lesion, its clinical, radiological, and histological appearance may sometimes mimic a malignant tumor [4]. In particular, a biopsy of cellular inner and middle layers alone may result in an erroneous diagnosis of a sarcoma [6]. Furthermore, such lesions can occasionally resemble many of the radiological characteristics that are frequently associated with malignancy [1]. Particularly, in such instances, a distinguishing laboratory marker would be helpful, one of which could be the determination of the clonality pattern of the respective tissue. Whereas malignant as well as benign neoplastic proliferations evolve in the overwhelming majority from a single cell clone, reactive hyper-proliferations are polyclonal. Despite the benign nature of myositis ossificans, it is still not yet known whether it results from a polyclonal or monoclonal proliferation. We, therefore, set out to investigate this issue by determining the X inactivation pattern, in the respective lesions, in affective female patients.

Materials and methods

Patients, tissue processing, and DNA extraction

For our analysis, we selected nine female patients with histologically verified myositis ossificans utilizing the documentation system AURA (Institute of Medical Informatics, Graz, Austria). The median age at diagnosis was 50 years

(range: 20–84 years). Patient characteristics, including location and type of procedure, are summarized in Table 1. Previous trauma was noted in two cases. At presentation, the radiological features of three patients were suspicious for a sarcoma. An intralesional excision was performed in five, a marginal resection in one, and a biopsy only in three patients. Two patients were lost to follow-up after 1 month. The mean follow-up of the other seven patients was 34±26 months (mean±standard deviation) with a minimum follow-up period of 4 months. In one patient, the tumor recurred once after 8 months from the primary operation.

Tissue samples that were obtained from the nine patients at surgery were fixed in 4.5% formaldehyde and were paraffin embedded according to standard procedure and analyzed histologically (Fig. 1). For the analysis of the X inactivation patterns, these formalin-fixed, paraffin-embedded tissue blocks were retrieved from the archival files of the Department of Pathology. Prior to the inclusion in the study, a senior pathologist reviewed the slides for the accuracy of the initial diagnosis. From four patients, peripheral blood was also available for comparative analysis.

Analysis of the X chromosome inactivation pattern

The clonality pattern of the respective tissue samples was assessed with the help of a previously published methylation-sensitive polymerase chain reaction (MS-PCR) test system that enables the concurrent semi-quantitative comparison of the methylated and unmethylated alleles of a polymorphic GCC trinucleotide repeat within the FMR1 gene [8]. For this purpose, we extracted DNA from paraffin-embedded tissue sections and peripheral blood of the patients using NucleoSpin columns (Macherey-Nagel, Düren, Germany). DNA extracted from peripheral blood of four healthy women and eight patients with acute leukemia and an acquired trisomy X served as negative and positive controls, respectively (Fig. 2A). DNA derived from tissue sections was added to 0.5 µg salmon sperm DNA (SSP) to protect the DNA from further degradation and loss during deamination and subsequent recovering

Table 1 Patient characteristics of nine females with myositis ossificans. *NED* no evidence of disease, *REC* recurrence, *CR* complete remission

No.	Age (years)	Location	Operation	Follow-up (months)	Status
1	36	Elbow	Intralesional excision		Lost
2	84	Thigh	Intralesional excision		Lost
3	50	Thigh	Intralesional excision	70	NED
4	33	Thigh	Intralesional excision	66	NED
5	60	Hand	Intralesional excision	39	NED
6	20	Thigh	Intralesional excision	29	REC
7	58	Arm	Biopsy	14	CR
8	58	Thigh	Biopsy	4	CR
9	39	Thigh	Marginal resection	12	NED

Fig. 1 Macroscopic and histological presentation of myositis ossificans. **A** Gross appearance of myositis ossificans in a young adult female (patient no. 6) presenting as a tumorous lesion with a grayish-white cut surface. **B** Low-power view showing the typical zonation with fasciitis like features (fl), immature osteoid (io), peripheral bone formation (bf), and residual skeletal muscle (sm). Original magnification ×50

procedures. Tissue DNA (in SSP) and peripheral blood (PB) DNA (0.5 µg) was deaminated in sodium bisulfite at 55°C for 2 h as previously described [8]. Following DNA recovery with QiaSpin-Columns (Quiagen, Hilden, Germany), 4 µl of deaminated DNA was used to amplify the FMR1 repeat with MS-PCR (25 µl final volume) [8]. SSP does not result in any unspecific amplification (data not shown). Of the respective PCR products, 4 µl was separated on Spreadex 500 EL analytical gels (Elchrom Scientific AG, Cham, Switzerland) in an Elchrom Submerged electrophoresis system for 3 h, 120 V at 35°C constant temperature and stained with SYBR Green according to the manufacturer's recommendations.

Results

Owing to the generally poor quality of the degraded DNA that was extracted from the paraffin-embedded tissues, we were only successful in amplifying six of the nine DNA

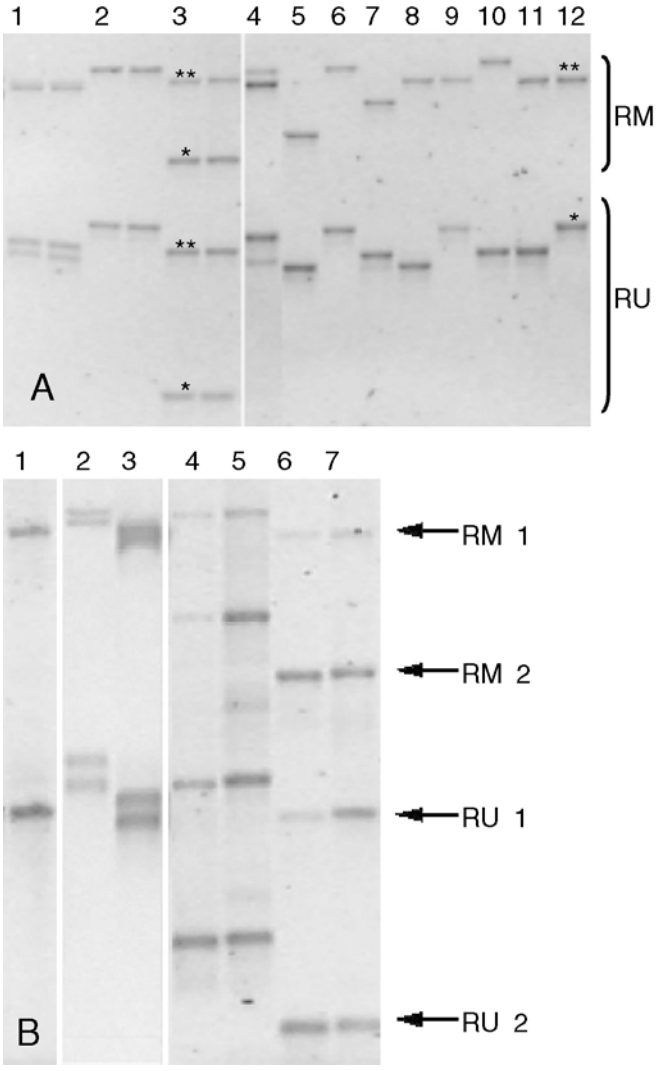

Fig. 2 Representative examples of the electrophoretic band patterns from various control samples (**A**) and patients (**B**). *RM*, *RM 1 & RM 2* methylated alleles, *RU*, *RU 1 & RU 2* unmethylated alleles. **A** *Lanes1–3* show duplicate amplifications. In normal heterozygote females with a random X inactivation pattern (1, 3), four distinct bands of equal intensity can be distinguished that represent the two unmethylated (RU) and methylated (RM) alleles (designated with * and ** for ease of orientation in sample 3). In homozygous individuals with a random X inactivation (sample 2), only one allele is seen in the methylated and unmethylated forms. *Lane 4* shows the pattern of a normal heterozygous female with skewed X inactivation, which leads to the intensification of one allele in the methylated and the other in the unmethylated form. *Lanes 5–12* derive from heterozygous female patients with an acquired duplicated X chromosome in 69–85% of their leukemic cell population. The methylated copy of the one and the unmethylated copy of the other allele are seen (two instead of four bands), which clearly designates the presence of a monoclonal cell population. **B** Myossitis ossificans is not derived from clonal expansion. Polymerase chain reaction (PCR) products corresponding to either the methylated (RM) or unmethylated (RU) FMR1 repeat and different alleles (1, 2) are present in all informative tissue samples (*arrows* indicate PCR products of lanes 7 and 8). PCR products 1–7: 1 homozygous (uninformative) and 2, 3 heterozygous (informative) tissue samples from different individuals; 4, 5 and 6, 7 (tissue and blood, respectively) of two heterozygous individuals. Product size of methylation-sensitive PCR products: RM=120 bp+repeat size; RU=64 bp+repeat size according to Weinhaeusel et al. [4]

samples. Of these, five samples were heterozygous and, thus, informative. In such cases, a random X inactivation pattern generated four electrophoretic bands of similar intensity. A skewed X inactivation pattern, however, would indicate the presence of a monoclonal cell population and lead to the intensification of one methylated and the opposite unmethylated allele and, accordingly, to a diminution of the alternate methylated and unmethylated allelic bands, respectively. We found that in all five informative cases all four bands were always of approximately equal intensity, both in the tissue as well as in the corresponding PB control samples (Fig. 2A, B).

Discussion

These results, therefore, imply that, as expected, myositis ossificans is a non-neoplastic, polyclonal regenerative process. Given the commonly reported post-traumatic origin and the generally benign clinical course with occasional total regressions, these confirmatory results are not surprising. However, as pointed out earlier and as experienced in three of the eight patients reported herein, the clinical, radiological and magnetic resonance tomography appearance of rapidly growing and markedly inhomogeneous soft tissue masses may be difficult to distinguish from a progressive neoplasm [1]. The most important clinico-pathological differential diagnoses of myositis ossificans are, therefore, osteosarcoma and other types of soft tissue sarcoma as well as malignant fibrous histiocytoma [4]. Furthermore, the presence of a rapidly proliferating mesenchyme with numerous mitoses in biopsy material may occasionally add to the confusion and lead to the misinterpretation of this benign process with a malignant sarcomatous process [4]. Particularly in such an instance, the determination of the clonality pattern may certainly aid to the differential diagnostic clarification, which is of course of utmost importance, because the self-limiting reparative myositis ossificans requires no further treatment after biopsy.

X chromosome inactivation-based clonality assays, such as the one presented herein, have already previously been successfully applied to examine other benign soft tissue lesions, for example the aggressive fibromatosis [2]. One of the pitfalls that may impede the correct interpretation of the outcome of such clonality assays results from the potential contamination of the targeted tissue with infiltrating or surrounding “non-tumorous” tissue. To avoid these problems, we have, therefore, only used tissue sections for our analyses that were carefully selected by an expert pathologist. Moreover, based on previous dilution experiments, we also know that we are able to identify a clonal cell population even in the presence of 20–30% contaminating background with the applied MS-PCR test system. Another advantage of using the FMR1 trinucleotide repeat polymorphism for such clonality studies is that, except for the repeat expansion-associated FRAXA syndrome, we have thus far never observed any aberrant de novo methylation of this region in normal or diseased subjects [4]. This issue is of importance, because it has become more and

more evident that the most frequently used clonality marker, the HUMARA gene polymorphism, is also subjected to de novo methylation in many instances. Particularly, when HUMARA is used as the sole clonality marker, such a de novo methylation will not become evident and, therefore, lead to a wrong interpretation of the test result [3]. The variations in the tissue- and PB-derived inactivation patterns are, rather, due to technical than physiological differences, with the dissimilar DNA quality most likely being the main contributor (Fig. 2B). For instance, the amount of DNA obtained from single 10-µm paraffin tissue sections was almost not measurable after staining with Hoechst 33258. Nevertheless, supplementation with SSP significantly improved the DNA deamination and MS-PCR amplification procedures without falsifying the results, at least in the majority of cases.

In conclusion, the present study: (1) provides evidence for the polyclonal nature of myositis ossificans and (2) demonstrates that for female patients the analysis of the X-chromosomal inactivation could serve as a further diagnostic tool in cases of an uncertain histology after a biopsy with only a limited amount of tissue available.

Acknowledgements Supported by a grant of the Austrian Society of Orthopedic Surgeons (1/03) and by a grant of the Austrian Science Fund (FWF, project P15150).

References

1. Kransdorf MJ, Meis JM, Jelinek JS (1991) Myositis ossificans: MR appearance with radiologic–pathologic correlation. Am J Roentgenol 157:1243–1248
2. Li M, Cordon CC, Gerald WL, Rosai J (1996) Desmoid fibromatosis is a clonal process. Hum Pathol 27:939–943
3. McDonald HL, Gascoyne RD, Horsman D, Brown CJ (2000) Involvement of the X chromosome in non-Hodgkin lymphoma. Genes Chromosomes Cancer 28:246–257
4. Mirra JM (1989) Myositis ossificans. In: Mirra JM (ed) Bone tumors. Clinical, radiological, and pathologic correlations. Lea & Febiger, Philadelphia, pp 1550–1586
5. Nuovo MA, Norman A, Chumas J, Ackerman LV (1992) Myositis ossificans with atypical clinical, radiographic, or pathologic findings: a review of 23 cases. Skeletal Radiol 21:87–101
6. Resnick D, Niwayama G (1981) Myositis ossificans traumatica. In: Resnick D, Niwayama G (eds) Diagnosis of bone and joint disorders. With emphasis on articular abnormalities. Saunders, Philadelphia, pp 3152–3159
7. Rosenberg AE (2002) Myositis ossificans and fibroosseous pseudotumors of digits. In: Fletcher CDM, Unni KK, Mertens F (eds) World Health Organization classification of tumours. Pathology and genetics of tumours of soft tissue and bone. International Agency for Research on Cancer, Lyon, pp 52–53
8. Weinhausel A, Haas OA (2001) Evaluation of the fragile X (FRAXA) syndrome with methylation-sensitive PCR. Hum Genet 108:450–458

Virchows Arch (2005) 446: 442–450
DOI 10.1007/s00428-005-1212-8

ORIGINAL ARTICLE

Wilko Weichert · Glen Kristiansen · Klaus-JürgenWinzer · Mathias Schmidt · Volker Gekeler · Aurelia Noske · Berit-Maria Müller · Silvia Niesporek · Manfred Dietel · Carsten Denkert

Polo-like kinase isoforms in breast cancer: expression patterns and prognostic implications

Received: 16 September 2004 / Accepted: 10 January 2005 / Published online: 23 March 2005
© Springer-Verlag 2005

Abstract Polo-like kinase (PLK) family members are known to be functionally involved in mitotic signaling and in cytoskeletal reorganization in both normal and malignant cells. In this study, expression of PLK1 and PLK3 was determined immunohistochemically in tissue specimens of 135 breast carcinomas, and expression was correlated with clinicopathological parameters and patient prognosis. Strong PLK isoform overexpression was observed in 42.2% (PLK1) and 47.4% (PLK3) of breast carcinomas when compared with non-transformed breast tissue. A positive correlation of PLK isoform expression with tumor grade, vascular invasion, erbB2/HER-2 expression and markers of proliferative activity was evident. Additionally, an inverse correlation of PLK isoform expression and estrogen receptor status was observed. Overexpression of PLK3 but not of PLK1 was significantly linked to reduced median overall (P<0.001) and relapse-free (P=0.021) survival time. PLK3 expression remained an independent prognostic factor for overall (RR=3.2, P=0.002) and relapse-free (RR=2.9, P=0.049) survival in multivariate survival analysis. These results suggest PLK3 as a novel independent prognostic marker in breast cancer and hint toward a role for PLK isoform overexpression in disease progression. Therefore, in vivo inhibition of PLK family members might represent a rewarding approach in the development of new anticancer drugs for this tumor entity.

W. Weichert (✉) · G. Kristiansen · A. Noske · B.-M. Müller · S. Niesporek · M. Dietel · C. Denkert
Institute of Pathology, Charité University Hospital,
Schumannstraße 20/21,
10117 Berlin, Germany
e-mail: wilko.weichert@charite.de
Tel.: +49-30-450536006
Fax: +49-30-450536922

K.-J. Winzer
Breast Center, Charité University Hospital,
Berlin, Germany

M. Schmidt · V. Gekeler
Altana Pharma AG,
Konstanz, Germany

Keywords Breast carcinoma · Immunohistochemistry · Polo like kinase · Mitosis · Survival

Introduction

Breast cancer is the most common malignant tumor in women in the western world with 215,990 estimated new cases in the United States in 2004. With approximately 40,110 cases of cancer death in 2004, in women it ranks second only to lung cancer as the most common cause of death from malignancies in the US [14]. In Germany, 47,517 estimated new cases of breast cancer and 17,814 cancer-related deaths were reported in 2000 [3]. Although advances in detection and treatment of breast cancer have been made, only a moderate decline of disease-specific mortality has been achieved in the last 10 years. Even in cases with a low risk of disease progression and a presumably favorable outcome, the diagnosis of breast cancer imposes a substantial burden on the patients and their families. Surgical treatment, hormonal therapy, radiotherapy and chemotherapy are the cornerstones in the treatment of breast carcinoma [11], but despite all efforts, this tumor entity still remains a major cause of malignancy-related death in women, which indicates that the biology of this tumor entity is still poorly understood.

One of the oldest but still promising ideas for the development of new chemotherapeutics is to inhibit uncontrolled cell proliferation in order to diminish tumor growth and/or to induce tumor cell apoptosis. Most recently, this goal regained attractiveness through the rapid progress of molecular biology, which leads to the definition of proteins potentially suitable for new targeted chemotherapeutic approaches.

Polo-like kinase (PLK) isoforms are known to play a crucial role in cell proliferation. They regulate the entry into, the progression through and the exit out of mitosis [2, 7, 23] in almost all cell types and species investigated so far. Expression of members of this kinase family in malignancies is of special interest, because it is known that inhibitory strategies targeting PLK isoforms hinder tumor

cells to progress through mitosis and subsequently induce tumor cell death and, therefore, reduce tumor growth [8, 20, 25].

Since the first description of the Drosophila gene *polo* 15 years ago [28], homologues of this serine/threonine kinase have been identified in a broad variety of different species including yeast, bacteria, mice and humans. To date, the family of human PLKs comprises four isoenzymes named PLK1 to PLK4, formerly designated as PLK, SNK, FNK and SAK, respectively [21].

The expression patterns of PLK1 are quite well defined in a variety of human tumors [6, 13, 17, 18, 29, 31, 35–39] and have revealed a potential prognostic role in some of these entities. Yet, information on the expression of the three other PLK isoforms is sparse and the results are conflicting.

Therefore, we aimed to investigate the expression patterns of PLK1 and PLK3 in breast carcinomas and to correlate our findings with clinicopathological parameters including hormone receptor status, markers of proliferative activity, and patient survival. The goal of our study was to clarify whether alterations in PLK isoform expression might play a role in disease progression. Furthermore, we wanted to know whether expression of PLK isoforms might be a new prognostic marker in breast cancer.

Materials and methods

Patients

Tissue samples from 135 patients (median age 61.8 years, range 28.0–88.3 years) who underwent surgery for primary breast cancer in the Breast Center of the Charité University Hospital between 1991 and 1996 were used in this study. Patients with known distant metastasis at the time of diagnosis and patients with bilateral carcinomas were not included in the study. Of the patients, 98 (72.6%) underwent surgery by the same surgeon (K.J.W.). Follow-up data on overall survival were available for all patients. Within the follow-up time, 39 patients (28.9%) died. Median follow-up time of patients still alive at the endpoint of analysis was 88.6 months. Data on relapse-free survival was available for 101 patients. Of those patients, 19 (18.8%) relapsed, defined as first clinical or pathological evidence of locoregional or distant recurrent disease.

Clinicopathological characteristics

Data on histology, tumor size, nodal status, vascular invasion and tumor grade were extracted from the pathological report at primary diagnosis. The group of malignant tissue comprises all major tumor types of breast cancer. In detail, 108 (80%) invasive ductal carcinomas, 16 (11.9%) invasive lobular carcinomas and 11 (8.1%) carcinomas of other histology were investigated. Nodal status was reclassified according to the 6th edition of the TNM classification. Cases were graded according to the Bloom–Richardson Grading modified by Elston and Ellis with defining the respective scores for tumor architecture, nuclear polymorphism and mitotic figure count [9]. Expression status for estrogen receptor, progesterone receptor and erbB2/Her-2 was, if available, also extracted from the primary pathological report. For a subset of cases, the exact number of mitotic figures per ten high power fields was recounted on standard H&E sections. Additionally, in a subset of cases, the exact fraction of tumor cells with immunohistochemically detectable expression of Ki-67 (clone MIB-1) was evaluated by defining the fraction of Ki-67-positive nuclei in 100 tumor cells.

Antibody specificity

For immunohistochemical detection of PLK isoenzymes on tissue samples, monoclonal mouse antibodies against PLK1 (BD Transduction Laboratories, San Diego, CA, USA) and PLK3 (FNK) (BD Transduction Laboratories) were used on 5-μm-thick paraffin sections. For both antibodies, specificity had been tested in preceding functional or expression studies [1, 6, 8, 34]. To further ascertain antibody specificity, a His-tagged human PLK1 peptide (amino acids 1 to 623 of the protein) was expressed in a baclovirus system and purified by means of nickel chromatography. Preincubation experiments showed that immunostaining for PLK1 but not for PLK3 could be blocked by the PLK1 protein. In addition, Western-blot experiments revealed that the PLK1 but not PLK3 antibody reacted with the PLK1 protein (data not shown).

Immunohistochemistry

For antigen retrieval, deparaffinized slides were boiled for 5 min in 0.01 M sodium citrate buffer, pH 6.0, in a pressure cooker. Subsequently, slides were allowed to cool down for another 5 min in the same buffer. After several rinses in Tris-buffered saline (TBS) and pre-treatment with blocking medium (Dako, Glostrup, Denmark) for 5 min, slides were incubated with primary antibody diluted 1:500 (PLK1/PLK3) in antibody diluent solution (Zymed, San Francisco, CA, USA) for 20 min at room temperature and then at 4°C overnight. After washing slides in TBS, a streptavidin–biotin system was used according to the manufacturer's instructions (BioGenex, San Ramon, CA, USA). For color development, a fast red system (Sigma, Deisenhofen, Germany) was used. The slides were counterstained and cover slipped using Aquatex (Merck, Gernsheim, Germany).

Double-immunostaining of tissue slides

For immunolabelling of PLK isoforms, slides were processed as described above. After color developed, slides were washed in PBS and subsequently incubated with a 1:50 dilution of primary polyclonal rabbit antibody directed against human Ki-67 (Dako) for 20 min at room temperature and subsequently at 4°C overnight. After washing slides in TBS, bound antibody was detected using the

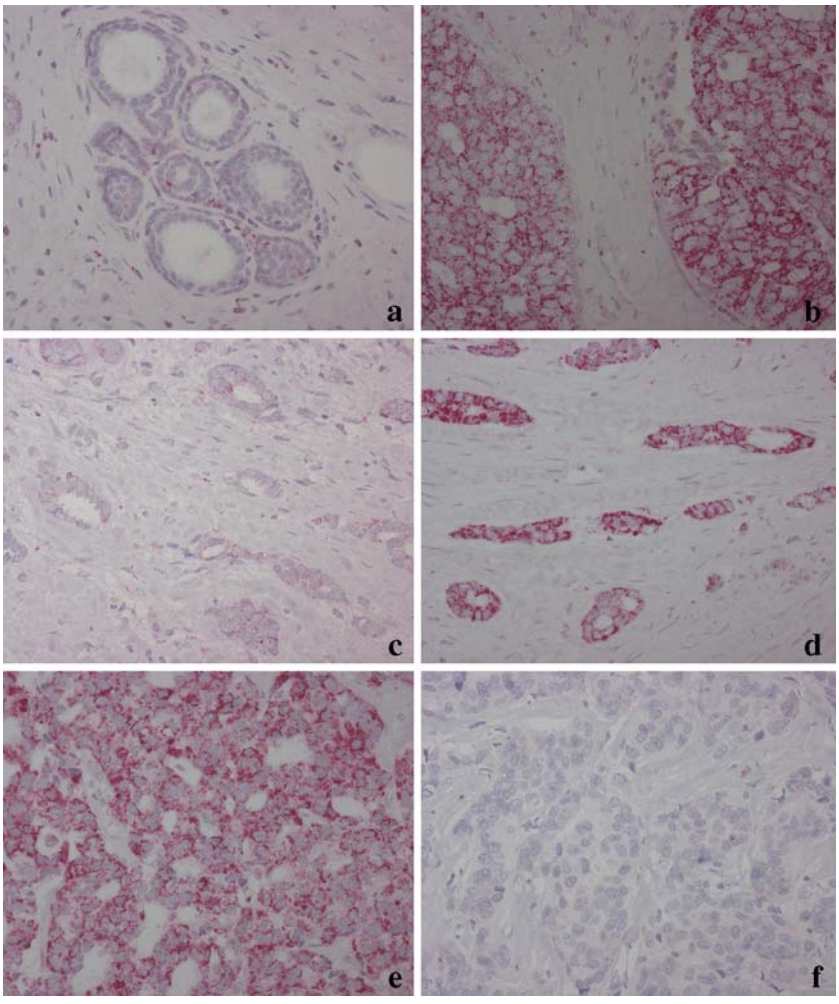

Fig. 1 Expression of polo-like kinase (PLK) isoforms in breast tissue. **a** Normal breast tissue with patchy weak expression of PLK1. **b** Ductal carcinoma in situ (*DCIS*) showing strong homogeneous expression of PLK3. **c**, **d** Invasive ductal carcinoma being scored as negative for PLK1 (**c**) and positive for PLK3 (**d**). **e**, **f** Invasive ductal carcinoma with strong expression of PLK1 (**e**) but without significant PLK3 positivity (**f**)

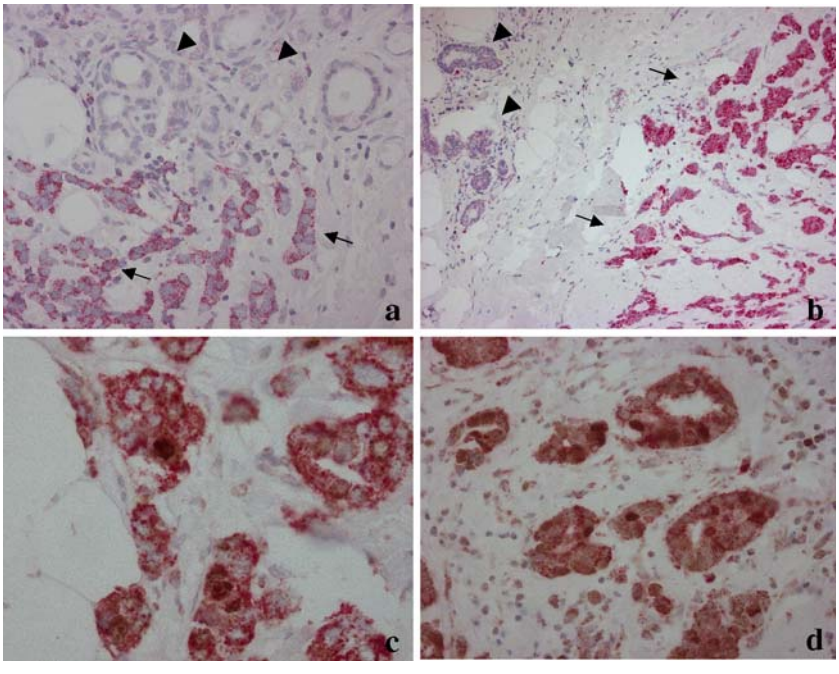

Fig. 2 Differential expression of polo-like kinase (PLK) isoforms in breast tissue and colocalization of PLK isoform expression and Ki-67 expression. **a** Invasive lobular carcinoma (*arrows*) infiltrating non-transformed breast parenchyma (*arrowheads*). Note strong overexpression of PLK1 in the tumor tissue. **b** Invasive ductal carcinoma (*arrows*) showing strong overexpression of PLK3 in comparison with the adjacent normal breast tissue (*arrowheads*). Coexpression of PLK1 (**c**) and PLK3 (**d**) (red staining of the cytoplasm), and of Ki-67 (brown staining of the nucleus) in breast carcinomas. Part of the tumor cells showed coexpression of both proteins, while a considerable number of tumor cells were PLK isoform positive but remained Ki-67 negative

Table 1 Distribution of clinicopathological parameters and polo-like kinase (PLK) isoform expression in the study population and correlation analysis of selected factors with PLK isoform expression

Characteristic	All cases	PLK1 negative	PLK1 positive	*P*-value	PLK3 negative	PLK3 positive	*P*-value
All cases							
	135 (100%)	78 (57.8%)	57 (42.2%)	–	71 (52.6%)	64 (47.4%)	–
Age							
≤60 years	59 (43.7%)	37 (62.7.%)	22 (37.3%)	0.380[a]	32 (54.2%)	27 (45.8%)	0.862[a]
>60 years	76 (56.3%)	41 (53.9%)	35 (46.1%)		39 (51.3%)	37 (48.7%)	
Histology							
Invasive ductal	108 (80%)	58 (53.7%)	50 (46.3%)	0.087[b]	55 (50.9%)	53 (49.1%)	0.364[b]
Invasive lobular	16 (11.9%)	13 (81.3%)	3 (18.7%)		11 (68.8%)	5 (31.2%)	
Other	11 (8.1%)	7 (63.6%)	4 (36.4%)		5 (45.5%)	6 (54.5%)	
Tumor size							
≤20 mm	102 (75.6%)	59 (57.8%)	43 (42.2%)	1.000[a]	56 (54.9%)	46 (45.1%)	0.423[a]
>20 mm	33 (24.4%)	19 (57.6%)	14 (42.4%)		15 (45.5%)	18 (54.5%)	
Lymph-node status							
N0/N1mic	90 (66.7%)	55 (61.1%)	35 (38.9%)	0.436[c]	52 (57.8%)	38 (42.2%)	0.116[c]
N1	11 (8.1%)	5 (45.5%)	6 (54.5%)		4 (36.4%)	7 (63.6%)	
N2	18 (13.3%)	9 (50%)	9 (50%)		9 (50%)	9 (50%)	
N3	16 (11.9%)	9 (56.3%)	7 (43.7%)		6 (37.5%)	10 (62.5%)	
Grade[d]							
G1	42 (32.0%)	29 (69%)	13 (31%)	0.029[c]	29 (69%)	13 (31%)	0.001[c]
G2	61 (46.6%)	34 (55.7%)	27 (44.3%)		33 (54.1%)	28 (45.9%)	
G3	28 (21.4%)	12 (42.9%)	16 (57.1%)		8 (28.6%)	20 (71.4%)	
Blood vessel invasion							
VX	116 (85.9%)	72 (62.1%)	44 (37.9%)	0.022[a]	65 (56%)	51 (44%)	0.081[a]
V1	19 (14.1%)	6 (31.6%)	13 (68.4%)		6 (31.6%)	13 (68.4%)	
Estrogen receptor[e]							
Negative	32 (34%)	11 (34.4%)	21 (65.6%)	0.001[a]	14 (43.7%)	18 (56.3%)	0.048[a]
Positive	62 (66%)	44 (71%)	18 (29%)		41 (66.1%)	21 (33.9%)	
Progesterone receptor[e]							
Negative	36 (76.6%)	24 (66.7%)	12 (33.3%)	1.000[a]	25 (69.4%)	11 (30.6%)	0.702[a]
Positive	11 (23.4%)	8 (72.7%)	3 (27.3%)		9 (81.8%)	2 (18.2%)	
erbB2/Her-2[e]							
Negative	75 (87.2%)	43 (57.3%)	32 (42.7%)	0.214[a]	41 (54.7%)	34 (45.3%)	0.049[a]
Positive	11 (12.8%)	4 (36.4%)	7 (63.6%)		2 (18.2%)	9 (81.8%)	
PLK3 expression							
Negative	71 (52.6%)	62 (87.3%)	9 (12.7%)	<0.001[a]	–	–	–
Positive	64 (47.4%)	16 (25%)	48 (75%)		–	–	

[a]Fisher's exact test
[b]Chi-square test
[c]Chi-square test for trends
[d]Four cases had to be left out in determination of tumor grade (not definable)
[e]Data were available only in a subset of carcinomas

peroxidase/anti-peroxidase method due to standard protocol with standard antibody dilutions as supplied by the manufacturers (Dako). Color development was performed using a DAB+ system (Dako). Finally, slides were mounted using Aquatex.

Evaluation of immunohistochemical tissue staining

Immunohistochemical tissue staining was evaluated by two pathologists (W.W. and C.D.) who were blinded toward patients' characteristics. To achieve a more exact quantification of the immunostaining, an immunoreactivity scoring system (IRS) was applied. For this purpose, the mean number of cells stained (0 = no cells stained, 1 = less then 10% of cells stained, 2 = 10–50% of cells stained, 3 = 51–80% of cells stained, 4 = more than 80% of cells stained) and staining intensity (0 = negative, 1 = weak, 2 = moderate, 3 = strong) were evaluated. Subsequently, the respective IRS for each case was calculated by multiplication of these two parameters. Distribution of IRS scores for both proteins comprised the whole range of possible IRS scores with a slight accumulation toward the high IRS score end of the scale. For statistical analysis, cases were grouped as either

Table 2 Correlation analysis of mitotic index parameters with ungrouped polo-like kinase (PLK) isoform expression scores

Characteristic	Tested cases	PLK-1 score correlation	*P*-value[a]	PLK-3 score correlation	*P*-value[a]
Mitotic figure count	64	0.440	<0.001	0.471	<0.001
Proliferation index (Ki-67)	81	0.270	0.015	0.281	0.011

[a]Spearman's rank order correlation

PLK isoform negative (IRS 0–6) or PLK isoform positive (IRS 7–12). Cases with discordant IRS scores were discussed at a multiheaded microscope until consensus was achieved.

Statistical analysis

Statistical correlation between several clinicopathological factors and expression of PLK was assessed using either chi-square test, chi-square test for trends, Fisher's exact test or Spearman's test for rank order correlation. The probability of differences in overall and relapse-free survival as a function of time was determined using the Kaplan–Meier method, with a log-rank test to probe for significance. Multivariate survival analysis was performed using the Cox model of proportional hazards. *P* values smaller than 0.05 were considered significant. For all statistical procedures SPSS v10.0 software was used.

Results

Expression of PLK isoforms in breast tissue

Morphologically normal breast epithelium of terminal ductal-lobular units was negative for both, PLK1 and PLK3. Only occasionally was a weak expression of both proteins in both the luminal epithelial and myoepithelial cells noted (Figs. 1, 2).

In contrast, expression of PLK1 and PLK3 was increased in breast carcinomas. A strong expression of PLK1 protein in the cytoplasm of the tumor cells was shown in 57 (42.2%) invasive breast carcinomas. For PLK3, 64 (47.4%) carcinomas showed a strong cytoplasmic staining (Figs. 1, 2). However, a weak scattered expression of both proteins was also observed in almost all cases scored as PLK isoform negative. Nuclear PLK1/3 expression was detectable in neither tumor epithelium nor tumor stroma. Ductal carcinoma in situ, if present on the tissue samples examined, usually expressed PLK isoforms in the same intensity range as the respective invasive tumor (Fig. 1).

Statistical analysis revealed a significant positive correlation of the expression of PLK1 with the expression of PLK3 ($P<0.001$) in the study cohort. However, 16 (20.5%) of 78 PLK1-negative tumors were scored as PLK3 positive, whereas only 9 (12.7%) of 71 PLK3-negative tumors were PLK1 positive (Table 1).

Correlation of PLK isoform expression with clinicopathological factors

A significant positive correlation ($P=0.022$) of PLK1 expression with vascular invasion status could be established. No significant correlation for PLK1 and PLK3 expression with histological type, tumor stage or nodal status was observed (Table 1).

Additionally, expression of both proteins showed a significant positive correlation with histopathological tumor grade (PLK1: $P=0.029$, PLK3: $P=0.001$). Since the Bloom–Richardson grading system is a three-tiered scoring system incorporating mitotic rate, nuclear polymorphism and architecture, additional correlation analyses of the expression of PLK isoforms with each element of the grading system were performed. A significant positive correlation—as determined using the chi-square test for trends—of the expression of both PLK1 and PLK3 with the scores for both nuclear poly-

Table 3 Univariate overall and relapse-free survival analysis for several clinicopathological factors and for polo-like kinase (PLK) isoform expression

	Overall survival (months)	Standard error	*P*-value[a]	Relapse-free survival (months)	Standard error	*P*-value[a]
Age						
≤60 years	108.38	5.34	0.3275	85.95	6.87	0.1538
>60 years	98.84	5.24		104.02	5.19	
Tumor size						
≤20 mm	105.51	4.22	0.1832	105.51	4.47	0.0203
>20 mm	95.73	8.36		81.69	7.97	
Lymph-node status						
N0/ N1mic	106.90	4.30	0.0001	109.27	4.15	0.0202
N1	110.78	11.72		77.89	7.42	
N2	109.76	9.62		65.64	9.39	
N3	64.59	13.56		75.75	14.35	
Grade						
G1	110.57	5.80	0.0900	107.60	4.26	0.0202
G2	104.97	5.59		96.87	6.17	
G3	84.65	10.39		77.47	10.75	
PLK1						
Negative	109.12	4.64	0.1126	103.12	5.17	0.0952
Positive	95.18	6.27		88.08	7.20	
PLK3						
Negative	116.98	4.06	0.0001	106.64	5.06	0.0213
Positive	86.71	6.09		74.95	4.73	

[a]Log-rank test

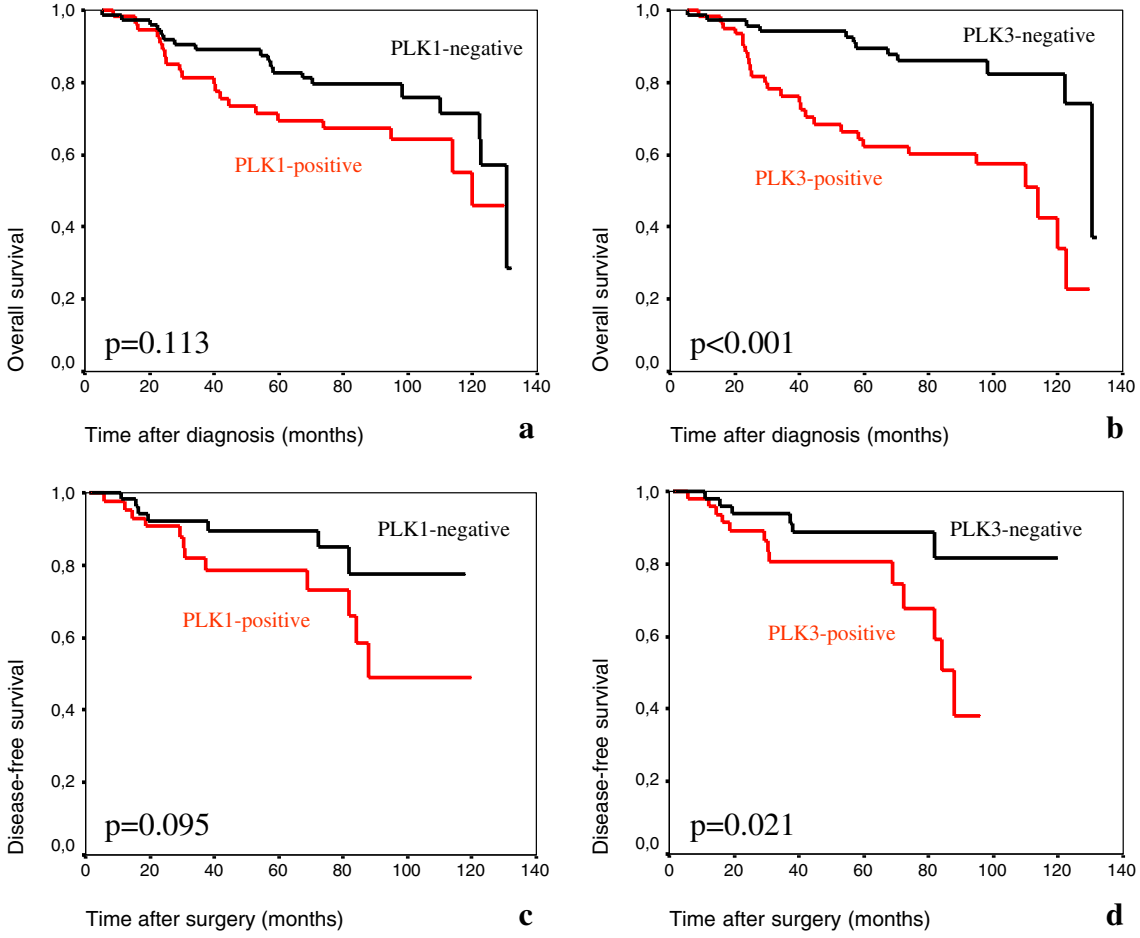

Fig. 3 Overall survival (**a**, **b**) and relapse-free survival (**c**, **d**) in dependence of polo-like kinase (PLK)1 (**a**, **c**) and PLK3 (**b**, **d**) expression (for details, see text)

morphism (PLK1: P=0.01, PLK3: P=0.003) and mitotic figure count (PLK1: P=0.004, PLK3: P<0.001) was evident. No correlation of the expression of both proteins with the score for tumor architecture could be observed (data not shown).

Correlation of PLK isoform expression with mitotic index

Since PLK isoforms have been reported to play a crucial role in the regulation of the cell cycle, correlation analysis of PLK isoform expression and indicators of proliferative activity was performed. Expression of both PLK1 and PLK3 showed a significant positive correlation with mitotic figure count (per ten HPF) and proliferation index (Ki-67), as determined by Spearman's test for rank order correlations. The correlation coefficient for PLK1 with mitotic figure count and with proliferation index was 0.44 (P<0.001) and 0.27 (P=0.015), respectively. For PLK3, correlation with mitotic figure count and proliferation index reached a coefficient of 0.47 (P<0.001) and 0.28 (P=0.011), respectively (Table 2). However, as reflected by the r values, the correlation between expression of both proteins with indicators of tumor proliferation reached only a moderate (mitotic figures) to weak (proliferation index) strength. This observation is supported by the fact that no strict colocalization of both proteins with Ki-67 expression was evident (Fig. 2).

Correlation of PLK isoform expression with the expression of hormonal receptors and erbB2/Her-2

Both, PLK1 and PLK3 expression were negatively correlated with estrogen receptor status (PLK1: P=0.001, PLK3: P=0.048). Additionally, a significant positive correlation between PLK3 expression and erbB2/Her-2 expression was found (P=0.049). No correlation for the expression of both proteins with progesterone receptor status was evident (Table 1).

Correlation of PLK isoform expression and clinicopathological factors with survival

As expected, nodal status had a significant impact on patient prognosis for both overall survival (P<0.001) as well as relapse-free survival (P=0.020). Additionally, tumor size (P=0.020) and tumor grade (P=0.020) were significant pre-

Table 4 Multivariate survival analysis for overall survival under consideration of polo-like kinase (PLK)3 expression status

	Overall survival		
	RR	95%CI	*P*-value
Age			
Per year	1.029	0.998–1.062	0.067
Tumor size			
Per mm	0.955	0.954–1.039	0.831
Lymph-node status			
Per positive node	1.069	1.020–1.122	0.006
Grade			
G1	1.000		
G2	0.851	0.345–2.102	0.727
G3	1.398	0.522–3.742	0.505
PLK3			
Negative	1.000		
Positive	3.193	1.523–6.693	0.002

dictors for relapse-free survival (Table 3). PLK3 expression, but not PLK1 expression also showed significant impact on both overall survival ($P<0.001$) and relapse-free survival ($P=0.021$) in univariate Kaplan–Meier analysis (Table 3, Fig. 3). Mean overall survival was reduced from 117.0 months in the PLK3-negative group to 86.7 months in the PLK3-positive group. The estimated overall 5-year survival rate of patients with PLK3-negative tumors was 90% and was diminished in patients with PLK3-positive tumors to 63%. Mean relapse-free survival reached 106.6 months for PLK3-negative patients and 75.0 months for PLK3-positive patients. The estimated 5-year relapse-free survival rates for PLK3-negative and PLK3-positive patients were 89% and 81%, respectively.

Multivariate survival analysis for overall and relapse-free survival was performed under consideration of all parameters that reached significance in univariate survival analysis for overall or disease-free survival. Additionally, patient age was included. Besides the nodal status, PLK3 expression remained the only independent prognostic factor for overall survival ($P=0.002$) and relapse-free survival ($P=0.049$). Patients, whose tumors were PLK3 positive, suffered a 3.2-fold increased risk of dying and a 2.9-fold risk of developing recurrent disease within the given time interval when compared with patients with PLK3-negative tumors (Tables 4, 5).

Table 5 Multivariate survival analysis for relapse-free survival under consideration of polo-like kinase (PLK)3-expression status

	Relapse-free survival		
	RR	95%CI	*P*-value
Age			
Per year	0.983	0.942–1.026	0.435
Tumor size			
Per mm	0.981	0.923–1.042	0.525
Lymph-node status			
Per positive node	1.084	1.014–1.158	0.018
Grade			
G1	1.000		
G2	2.803	0.333–23.582	0.343
G3	6.638	0.748–58.896	0.089
PLK3			
Negative	1.000		
Positive	2.899	1.006–8.358	0.049

Discussion

Since the discovery of *polo* in Drosophila 15 years ago by Sunkel and Glover [28], a wealth of information on the function of members of this protein family has been obtained. Most studies have concentrated on the pivotal role of polo homologues in the control of the mitotic machinery of both normal and malignant cells of different species. It is known that PLK1 is highly overexpressed in the G2/M transition of the cell cycle [2] and that regular isoenzyme function is essential for the entry into, progression through and exit out of mitosis by activation of several mitotic key enzymes such as cdc25c [32], cyclin B1 [40] and the anaphase-promoting complex [10] by phosphorylation. Furthermore, PLK1 activity triggers the dissociation of cohesins from their chromosomal binding sites [27]. Additional functions of PLK1 in the regulation of centrosome function might contribute substantially to its central role in the execution of mitosis [5]. For PLK isoforms, other than PLK1, data on function is sparse and contradictory. For PLK3, some authors reported an increased expression and activation in G2/M as well [4, 24], while others found no change in enzyme activity or expression levels throughout the cell cycle [1]. In *Saccharomyces cerevisiae* both PLK3 and PLK1 are capable of rescuing cdc5 (the polo homologue in this species) temperature-sensitive mutants at restrictive temperatures [24], which hints at a functional overlap of both enzymes. These results are in line with our observation in breast cancer, that expression of both proteins PLK1 and PLK3 correlates with each other and with indicators of proliferative activity, although other authors failed to show a correlation of PLK1 expression with markers of proliferation in a much smaller study on breast cancer [38]. However, correlation of indicators of mitosis and PLK isoform expression has been observed in other tumor entities such as colon cancer [29] and ovarian cancer [35]. Nevertheless, our data indicate that not all of the variation in PLK isoform expression levels in breast cancer can be explained by the variations in the mitotic activity of tumors. Therefore, it is intriguing to speculate that other functions of PLK overexpression in breast carcinomas might exist. Support for this hypothesis came from functional studies that reported a role for PLK3 in the control of synaptic plasticity of irreversibly postmitotic neuronal cells [16] and in the control of golgi reassembly and protein transport [5], both functions being intimately related to the control of microtubule dynamics. Another study reported an overexpression of PLK3 in adherent versus non-adherent macrophages and identified CIB, a small protein involved in integrin signaling, as an interaction partner for PLK3 [12]. Our observation of a positive correlation of PLK isoform

expression with vascular invasion, an event which is centrally interconnected with a change of adhesiveness and invasiveness of tumor cells, might give some support to this hypothesis, which, however, needs further studies for substantiation.

But what might be the reason for the strong and homogeneous overexpression of PLK isoforms we observed in a subset of carcinomas? An apparent explanation for this phenomenon might be, that PLK isoform overexpression is the consequence of an enhanced mitotic activity in tumors. In fact, a correlation of PLK isoform expression with markers of mitotic activity could be established in our study. However, there are several arguments against this hypothesis. First, in former studies and in our present study, discordances between PLK isoform expression and mitotic activity of tumors became apparent, which could not be sufficiently explained. Furthermore, in our study, we observed cases with strong PLK isoform expression in almost 100% of tumor cells, a number that by far exceeds the rate of cells that can be expected to be in G2/M phase and certainly exceeds the proliferation rate of these cases. An alternative explanation for PLK isoform deregulation in tumors might be that either enhanced transcription by altered intracellular signal transduction or chromosomal overrepresentation of the respective gene locus leads to high cellular protein levels, which in turn may enhance mitotic activity. In fact, chromosomal amplifications of 16p12, the gene locus of PLK1 have been described in 38% of primary breast carcinomas [30] a rate which is very near to the rate of 42.2% of cases overexpressing PLK1 protein in our study.

Most recently, Lee et al. [19] reported that PLK1 phosphorylates BRCA2 in breast cancer cells. They concluded that this specific phosphorylation might alter BRCA2 function, which subsequently could lead to genetic instability, which represents another possible functional explanation of the adverse effect that PLK isoform overexpression had on patient prognosis in breast cancer.

Our finding of a significant negative correlation of PLK isoform expression with estrogen receptor status in breast cancer is in direct contrast to the results of other authors [38], who reported a positive correlation of both parameters in a markedly smaller study on breast carcinomas. However, it is well known that estrogen receptor-negative breast cancers tend to show a higher proliferative capacity [15, 26], although the mechanisms responsible for this phenomenon are complex and incompletely understood [22]. Our results may indicate that aberrant overexpression of PLK isoforms could contribute to the ability of estrogen receptor-negative cancers to circumvent steroid hormone dependency for the control of their proliferative capacity.

In recent studies, no correlation between the proliferative activity of a tumor and erbB2/HER-2 expression was observed [33], although there is evidence that erbB2/HER-2 downstream signaling also affects the function of several cell cycle regulators [41]. To our knowledge little is known on possible signaling between erbB2/HER-2 and PLK isoforms. Whether a functional link between PLK3 and erbB2/Her-2 exists remains to be demonstrated.

The concept of defining PLK isoforms as potential targets for new anticancer drugs recently obtained strong support by several studies that showed that inhibition of PLK1 either by RNA interference [20, 25] or antisense strategies [8] in several carcinoma cell lines including breast cancer cell lines dramatically interferes with tumor growth and induces apoptosis in vitro and in vivo. The consistently reported overexpression of PLK isoforms in various human tumor entities in vivo [6, 13, 17, 18, 29, 31, 35–39], which we could confirm for breast cancer, might provide an important link of such functional data into the clinic.

In summary, we demonstrated that two PLK isoforms, PLK1 and PLK3, are strongly overexpressed in a high proportion of breast carcinomas. Importantly, overexpression of PLK3 is significantly and independently linked to a poor patient prognosis. These results point to a potential role of PLK isoforms in the progression of breast cancer and define them as attractive targets for new chemotherapeutic approaches in this tumor entity. Despite the wealth of information about deregulated PLK expression in tumor cells, the exact mechanisms by which deregulated PLKs contribute to breast cancer development and progression remains subject to further studies.

Acknowledgements We are grateful to Lisa Glanz for excellent technical assistance and Martina Eickmann for critical reading and help in the preparation of the manuscript.

References

1. Bahassi el M, Conn CW, Myer DL, Hennigan RF, McGowan CH, Sanchez Y, Stambrook PJ (2002) Mammalian Polo-like kinase 3 (Plk3) is a multifunctional protein involved in stress response pathways. Oncogene 21:6633–6640
2. Barr FA, Sillje HH, Nigg EA (2004) Polo-like kinases and the orchestration of cell division. Nat Rev Mol Cell Biol 5:429–440
3. Bertz J, Hentschel S, Hundsdörfer G, Kaatsch P, Katalinic A, Lehnert M Schön D, Stegmaier C, Ziegler H (2004) Krebs in Deutschland. 4. überarbeitete, aktualisierte Ausgabe. Arbeitsgemeinschaft Bevölkerungsbezogener Krebsregister in Deutschland, Saarbrücken
4. Chase D, Feng Y, Hanshew B, Winkles JA, Longo DL, Ferris DK (1998) Expression and phosphorylation of fibroblast-growth-factor-inducible kinase (Fnk) during cell-cycle progression. Biochem J 333:655–660
5. Dai W, Wang Q, Traganos F (2002) Polo-like kinases and centrosome regulation. Oncogene 21:6195–6200
6. Dietzmann K, Kirches E, von Bossanyi P, Jachau K, Mawrin C (2001) Increased human polo-like kinase-1 expression in gliomas. J Neuro-Oncol 53:1–11
7. Donaldson MM, Tavares AA, Hagan IM, Nigg EA, Glover DM (2001) The mitotic roles of Polo-like kinase. J Cell Sci 114:2357–2358
8. Elez R, Piiper A, Kronenberger B, Kock M, Brendel M, Hermann E, Pliquett U, Neumann E, Zeuzem S (2003) Tumor regression by combination antisense therapy against Plk1 and Bcl-2. Oncogene 22:69–80
9. Elston CW, Ellis IO (1991) Pathological prognostic factors in breast cancer. I. The value of histological grade in breast cancer: experience from a large study with long-term follow-up. Histopathology 5:403–410

10. Golan A, Yudkovsky Y, Hershko A (2002) The cyclin–ubiquitin ligase activity of cyclosome/APC is jointly activated by protein kinases Cdk1-cyclin B and Plk. J Biol Chem 277: 15552–15557
11. Goldhirsch A, Wood WC, Gelber RD, Coates AS, Thurlimann B, Senn HJ (2003) Meeting highlights: updated international expert consensus on the primary therapy of early breast cancer. J Clin Oncol 21:3357–3365
12. Holtrich U, Wolf G, Yuan J, Bereiter-Hahn J, Karn T, Weiler M, Kauselmann G, Rehli M, Andreesen R, Kaufmann M, Kuhl D, Strebhardt K (2000) Adhesion induced expression of the serine/threonine kinase Fnk in human macrophages. Oncogene 19:4832–4839
13. Ito Y, Miyoshi E, Sasaki N, Kakudo K, Yoshida H, Tomoda C, Uruno T, Takamura Y, Miya A, Kobayashi K, Matsuzuka F, Matsuura N, Kuma K, Miyauchi A (2004) Polo-like kinase 1 overexpression is an early event in the progression of papillary carcinoma. Br J Cancer 90:414–418
14. Jemal A, Tiwari RC, Murray T, Ghafoor A, Samuels A, Ward E, Feuer EJ, Thun MJ; American Cancer Society (2004) Cancer statistics, 2004. CA Cancer J Clin 54:8–29
15. Jensen EV, Cheng G, Palmieri C, Saji S, Makela S, Van Noorden S, Wahlstrom T, Warner M, Coombes RC, Gustafsson JA (2001) Estrogen receptors and proliferation markers in primary and recurrent breast cancer. Proc Natl Acad Sci U S A 98:15197–15202
16. Kauselmann G, Weiler M, Wulff P, Jessberger S, Konietzko U, Scafidi J, Staubli U, Bereiter-Hahn J, Strebhardt K, Kuhl D (1999) The polo-like protein kinases Fnk and Snk associate with a Ca(2+)- and integrin-binding protein and are regulated dynamically with synaptic plasticity. EMBO J 18:5528–5539
17. Knecht R, Elez R, Oechler M, Solbach C, von Ilberg C, Strebhardt K (1999) Prognostic significance of polo-like kinase (PLK) expression in squamous cell carcinomas of the head and neck. Cancer Res 59:2794–2797
18. Kneisel L, Strebhardt K, Bernd A, Wolter M, Binder A, Kaufmann R (2002) Expression of polo-like kinase (PLK1) in thin melanomas: a novel marker of metastatic disease. J Cutan Pathol 29:354–358
19. Lee M, Daniels MJ, Venkitaraman AR (2004) Phosphorylation of BRCA2 by the Polo-like kinase Plk1 is regulated by DNA damage and mitotic progression. Oncogene 23:865–872
20. Liu X, Erikson RL (2003) Polo-like kinase (Plk)1 depletion induces apoptosis in cancer cells. Proc Natl Acad Sci U S A 100:5789–5794
21. Manning G, Whyte DB, Martinez R, Hunter T, Sudarsanam S (2002) The protein kinase complement of the human genome. Science 298:1912–1934
22. Nicholson RI, McClelland RA, Robertson JF, Gee JM (1999) Involvement of steroid hormone and growth factor cross-talk in endocrine response in breast cancer. Endocr Relat Cancer 6:373–387
23. Nigg EA (1998) Polo-like kinases: positive regulators of cell division from start to finish. Curr Opin Cell Biol 10:776–783
24. Ouyang B, Pan H, Lu L, Li J, Stambrook P, Li B, Dai W (1997) Human Prk is a conserved protein serine/threonine kinase involved in regulating M phase functions. J Biol Chem 272:28646–28651
25. Spänkuch-Schmitt B, Bereiter-Hahn J, Kaufmann M, Strebhardt K (2002) Effect of RNA silencing of polo-like kinase-1 (PLK1) on apoptosis and spindle formation in human cancer cells. J Natl Cancer Inst 94:1863–1877
26. Spyratos F, Ferrero-Pous M, Trassard M, Hacene K, Phillips E, Tubiana-Hulin M, Le Doussal V (2002) Correlation between MIB-1 and other proliferation markers: clinical implications of the MIB-1 cutoff value. Cancer 94:2151–2159
27. Sumara I, Vorlaufer E, Stukenberg PT, Kelm O, Redemann N, Nigg EA, Peters JM (2002) The dissociation of cohesin from chromosomes in prophase is regulated by Polo-like kinase. Mol Cell 9:515–525
28. Sunkel CE, Glover DM (1988) Polo, a mitotic mutant of Drosophila displaying abnormal spindle poles. J Cell Sci 89:25–38
29. Takahashi T, Sano B, Nagata T, Kato H, Sugiyama Y, Kunieda K, Kimura M, Okano Y, Saji S (2003) Polo-like kinase 1 (PLK1) is overexpressed in primary colorectal cancers. Cancer Sci 94:148–152
30. Tirkkonen M, Tanner M, Karhu R, Kallioniemi A, Isola J, Kallioniemi OP (1998) Molecular cytogenetics of primary breast cancer by CGH. Genes Chromosomes Cancer 21:177–184
31. Tokumitsu Y, Mori M, Tanaka S, Akazawa K, Nakano S, Niho Y (1999) Prognostic significance of polo-like kinase expression in esophageal carcinoma. Int J Oncol 15:687–692
32. Toyoshima-Morimoto F, Taniguchi E, Nishida E (2002) Plk1 promotes nuclear translocation of human Cdc25C during prophase. EMBO Rep 3:341–348
33. Volpi A, Nanni O, De Paola F, Granato AM, Mangia A, Monti F, Schittulli F, De Lena M, Scarpi E, Rosetti P, Monti M, Gianni L, Amadori D, Paradiso A (2003) HER-2 expression and cell proliferation: prognostic markers in patients with node-negative breast cancer. J Clin Oncol 21:2708–2712
34. Wang Q, Xie S, Chen J, Fukasawa K, Naik U, Traganos F, Darzynkiewicz Z, Jhanwar-Uniyal M, Dai W (2002) Cell cycle arrest and apoptosis induced by human Polo-like kinase 3 is mediated through perturbation of microtubule integrity. Mol Cell Biol 22:3450–3459
35. Weichert W, Denkert C, Schmidt M, Gekeler V, Wolf G, Köbel M, Dietel M, Hauptmann S (2004) Polo like kinase isoform expression is a prognostic factor in ovarian carcinoma. Br J Cancer 90:815–821
36. Weichert W, Schmidt M, Gekeler V, Bellach J, Denkert C, Stephan C, Jung K, Loening S, Dietel M, Kristiansen G (2004) Polo like kinase 1 is overexpressed in prostate cancer and linked to higher tumor grades. Prostate 60:240–245
37. Wolf G, Elez R, Doermer A, Holtrich U, Ackermann H, Stutte HJ, Altmannsberger HM, Rubsamen-Waigmann H, Strebhardt K (1997) Prognostic significance of polo-like kinase (PLK) expression in non-small cell lung cancer. Oncogene 14:543–549
38. Wolf G, Hildenbrand R, Schwar C, Grobholz R, Kaufmann M, Stutte HJ, Strebhardt K, Bleyl U (2000) Polo-like kinase: a novel marker of proliferation: correlation with estrogen-receptor expression in human breast cancer. Pathol Res Pract 196:753–759
39. Yamada S, Ohira M, Horie H, Ando K, Takayasu H, Suzuki Y, Sugano S, Hirata T, Goto T, Matsunaga T, Hiyama E, Hayashi Y, Ando H, Suita S, Kaneko M, Sasaki F, Hashizume K, Ohnuma N, Nakagawara A (2004) Expression profiling and differential screening between hepatoblastomas and the corresponding normal livers: identification of high expression of the PLK1 oncogene as a poor-prognostic indicator of hepatoblastomas. Oncogene 23:5901–5911
40. Yuan J, Eckerdt F, Bereiter-Hahn J, Kurunci-Csacsko E, Kaufmann M, Strebhardt K (2002) Cooperative phosphorylation including the activity of polo-like kinase 1 regulates the subcellular localization of cyclin B1. Oncogene 21:8282–8292
41. Zhou BP, Hung MC (2003) Dysregulation of cellular signaling by HER2/neu in breast cancer. Semin Oncol 30:38–48

Virchows Arch (2005) 446: 451–455
DOI 10.1007/s00428-004-1170-6

CASE REPORT

Yoshifumi Makimoto · Kazuki Nabeshima · Hiroshi Iwasaki · Akiko Ishiguro · Tatsu Miyoshi · Takeshi Shiraishi · Akinori Iwasaki · Takayuki Shirakusa

Inflammatory myofibroblastic tumor of the posterior mediastinum: an older adult case with anaplastic lymphoma kinase abnormalities determined using immunohistochemistry and fluorescence in situ hybridization

Received: 23 August 2004 / Accepted: 30 October 2004 / Published online: 19 March 2005
© Springer-Verlag 2005

Abstract Inflammatory myofibroblastic tumor (IMT) is a rare neoplasm that usually occurs in children and young adults. Anaplastic lymphoma kinase (ALK) abnormalities in IMT, determined using immunohistochemistry and/or molecular genetic studies, including fluorescence in situ hybridization (FISH), have almost been limited to children and young adults. In elderly cases of IMT, these ALK abnormalities are very rare. We report on a case of IMT arising in the posterior mediastinum of a 59-year-old Japanese man that showed ALK abnormalities determined using immunohistochemistry and FISH, suggesting the neoplastic nature of a subset of IMTs in older patients similar to those in younger ones and the presence of an additional mechanism(s) that allows them to start to grow late.

Keywords Inflammatory myofibroblastic tumor · ALK · Immunohistochemistry · FISH

Introduction

Inflammatory myofibroblastic tumor (IMT) is characterized by a proliferation of fibroblasts and myofibroblasts associated with inflammatory cells, predominantly occurring in the abdominal cavity of children and young adults [4, 5]. Recently, the pathogenesis of IMT has been highlighted by studies on molecular genetics: various gene fusions involving anaplastic lymphoma kinase (ALK) at chromosome 2p23 have been described in approximately 50% of cases of IMTs, suggesting the neoplastic nature of a subset [3, 6, 7, 12, 15]. These ALK abnormalities, which are associated with a high incidence of recurrence, are more frequent in children and young adults and are extremely rare in older adults [6, 7, 12]. We report here a case of mediastinal IMT in an older adult patient, which showed ALK abnormalities detected using immunohistochemistry and FISH.

Y. Makimoto · K. Nabeshima (✉) · H. Iwasaki · A. Ishiguro
Department of Pathology,
Fukuoka University School of Medicine,
7-45-1 Nanakuma, Jonan-ku,
814-0180 Fukuoka , Japan
e-mail: kaznabes@fukuoka-u.ac.jp
Tel.: +81-92-8011011
Fax: +81-92-8617300

Y. Makimoto · T. Miyoshi · T. Shiraishi · A. Iwasaki · T. Shirakusa
Second Department of Surgery,
Fukuoka University School of Medicine,
Fukuoka, Japan

Clinical history

A 59-year-old Japanese man with no subjective symptoms was admitted to our hospital due to a mediastinal tumor found on an annual routine chest radiograph (Fig. 1A). Chest computed tomography scan (Fig. 1B) and magnetic resonance imaging showed a well-circumscribed mass (5×5 cm in diameter) with an extrapleural sign in the posterior mediastinum. The differential diagnosis on the imaging studies included a solitary fibrous tumor and neurogenic tumors. The patient underwent tumor excision. The surgery revealed a tumor protruding into the right pleural cavity, completely covered by the parietal pleura. It was located within the posterior mediastinum, with no connection to great vessels, trachea and the heart. The postoperative course was uneventful, with no complications.

Materials and methods

Immunohistochemistry

Immunoperoxidase staining of formalin-fixed, paraffin-embedded sections was performed using Envision labeled polymer reagent (Dako, Glostrup, Denmark). The primary

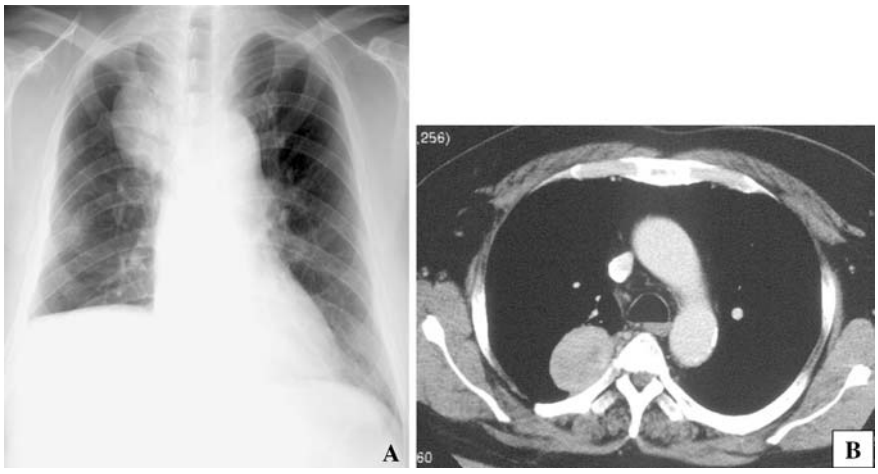

Fig. 1 A Chest radiograph showing a well-circumscribed mass at the mediastinal side of the right upper lung field. **B** A chest computed tomography scan revealing a well-circumscribed mass in the right posterior mediastinum with an extrapleural sign

antibodies used include monoclonal antibodies against ALK (ALK1, dilution 1:25; Dako), alpha-smooth muscle actin (1A4, dilution 1:50; Dako), vimentin (V9, dilution 1:50; Dako), calponin (CALP, dilution 1:500; Dako), CD34 (QBEnd 10, dilution 1:100; IMMUNO TEC, Marseille, France), desmin (D33, dilution 1:25; Dako), h-caldesmon (h-CD, dilution 1:500; Dako) and p53 (DO-7, dilution 1:50; NOVO CASTRA, Newcastle, UK) and a polyclonal antibody against cytokeratin (dilution 1:1000; Dako).

FISH protocol

Paraffin-embedded tissue sections were processed using the Vysis Paraffin Pretreatment Kit protocol (Vysis, Inc., Downers Grove, IL), substituting xylene in place of the Hemo-De clearing agent. Protease digestion was done for 30–100 min. Slides were denatured in 70% formamide/2×sodium saline citrate at 75°C for 6 min followed by dehydration in an ethanol series. Fluorescence in situ hybridization (FISH) was performed with the Vysis LSI ALK probe according to the

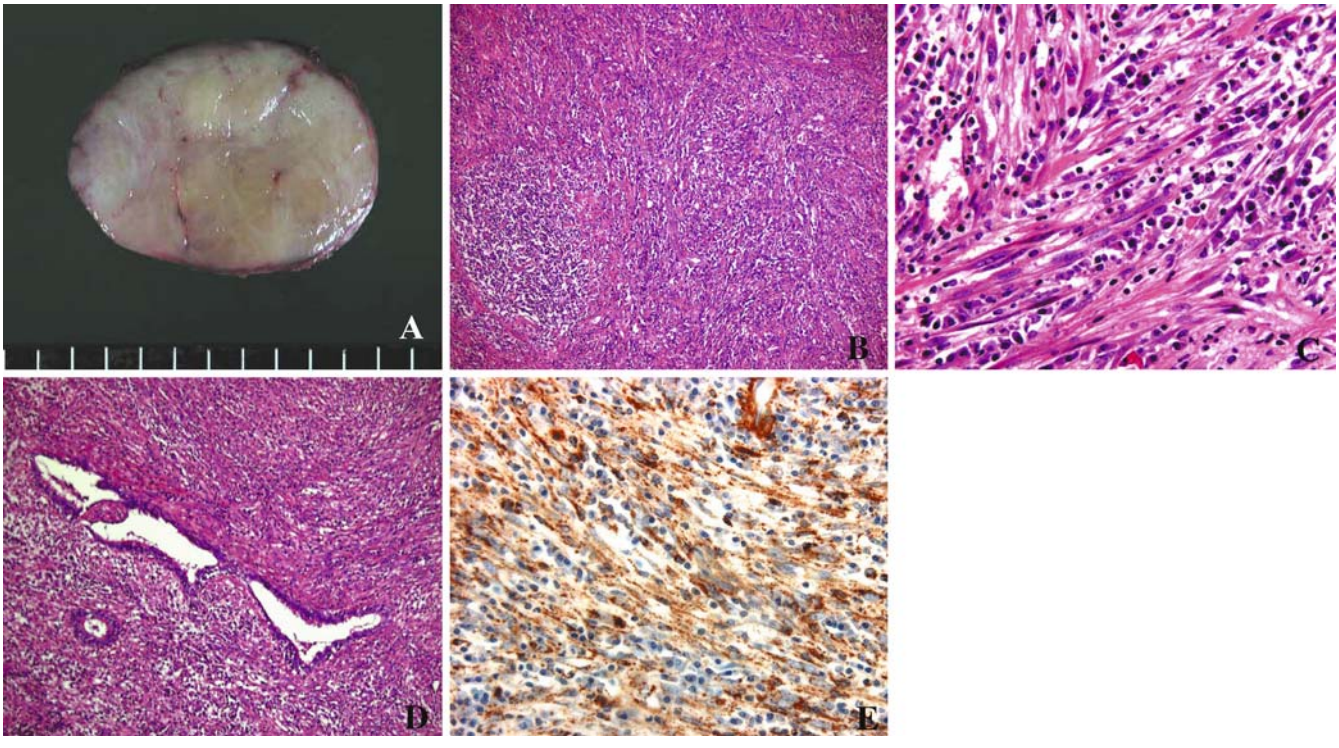

Fig. 2 A Gross appearance. **B** Myofibroblastic cells showing compact fascicles with dense lymphoplasmacytic infiltration. **C** Myofibroblastic cells having elongated or plump nuclei and nucleoli. **D** Duct-like spaces lined by bronchial epithelium at the periphery of the lesion. **E** Immunohistochemical positive reactivity for ALK in the cytoplasm of myofibroblastic cells. Original magnification ×100 (**D**); ×200 (**B**); ×400 (**C, E**)

manufacturer's instructions (Vysis). The slides were counterstained with DAPI (4′-6′-diamino-2-phenyl-indole; Sigma Chemical Co., St. Louis, MO) and visualized using an in situ imaging system (Isis, Carl Zeiss Vison, Oberkochen, Germany). More than 200 nuclei were examined for ALK gene rearrangements.

Results

Pathological findings

The lesion was well defined, firm and gray in color, measuring 5.0×4.3×3.5 cm (Fig. 2A). Neither necrosis nor hemorrhage was found. Microscopically, the tumor showed a proliferation of spindle-shaped myofibroblastic cells with elongated or plump nuclei, forming compact fascicles or storiform patterns, accompanied by prominent lymphoplasmacytic infiltration (Fig. 2B, C), indicative of a compact spindle cell type of IMT. Mitotic figures were rarely seen (less than 1/50 hpf). No cellular atypia was observed. Some duct-like spaces lined by bronchial epithelium were seen at the periphery of the lesion (Fig. 2D).

Immunohistochemical findings

Immunohistochemical examination showed a strong cytoplasmic positivity for ALK (Fig. 2E). Tumor cells were also positive for alpha-smooth muscle actin, vimentin, calponin, p53 (approximately 10%) and negative for desmin, CD34, h-caldesmon and cytokeratins. Duct-like spaces lined by bronchial epithelium were positive for cytokeratins.

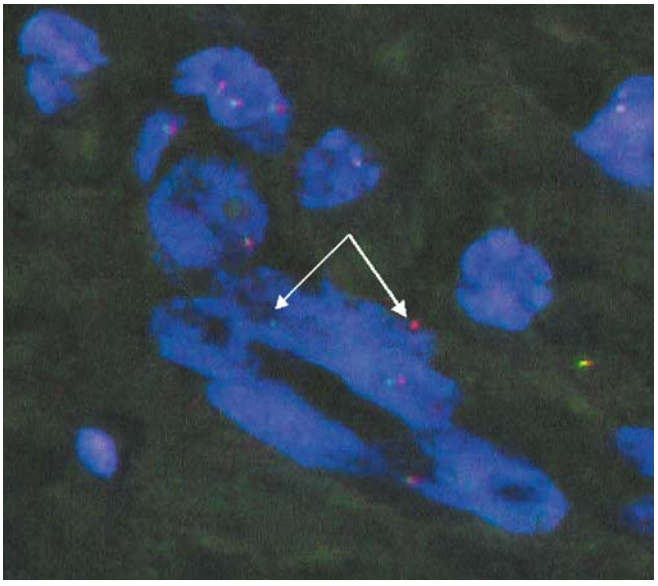

Fig. 3 Fluorescence in situ hybridization with the LSI ALK Dual Color, Break Apart Rearrangement probe (Vysis) showing a split of telomeric (*red signal*) and centromeric (*green signal*) probes in tumor cell nuclei (*arrow*)

FISH findings

The FISH results showed ALK gene rearrangements, as characterized by separation of the centromeric and telomeric probes on either side of the common ALK breakpoint onto different chromosomes (Fig. 3).

Discussion

IMT is a relatively rare spindle cell neoplasm that typically occurs in central soft tissues and viscera of children and young adults [4, 5]. It is characterized by a proliferation of fibroblasts and myofibroblasts associated with inflammatory cells. IMT was originally viewed as a reactive tumor-like lesion because of the favorable outcome of most of these lesions after complete surgical resection. However, the local recurrence rate of IMT is approximately 25%, and the metastatic rate ranges from 5% to 11% in various studies [4–6]. Moreover, chromosomal translocation involving the ALK gene has recently been discovered in approximately 50% of IMTs in children and young adults [3, 6, 12, 15]. Several ALK fusion partner genes, including TPM3 and TPM4 [15], clathrin heavy chain [2] and cysteinyl-tRNA synthetase [8] have also been identified. These aggressive behavior and ALK abnormalities support the neoplastic nature of a subset of IMTs.

The above genomic rearrangements and overexpression of the ALK gene are uncommon in adults over 40 years old [6, 15], and only several reports, including our case, have shown the ALK abnormalities detected using immunohistochemistry and clonal cytogenetic rearrangements in such older adults [7, 10, 18]. These suggest the neoplastic nature of IMTs in older patients similar to those in younger ones. Moreover, an additional mechanism may be present for IMT in older patients to grow very slowly with a late onset in spite the same ALK abnormalities.

The prognostic factors of IMT have not been established [5]. Coffin et al. demonstrated the influence of ALK status on the clinical outcome of IMT: ALK-positive IMTs had a higher recurrence rate, but the difference between the groups with or without ALK abnormalities was not statistically significant [6]. Recent studies suggested that a combination of atypia, ganglion-like cells, aneuploidy and p53 expression was associated with more aggressive clinical behavior [1, 13]. Our case showed p53 expression and ALK abnormalities, suggesting the necessity for a careful follow-up.

IMT can occur throughout the body, and the most common sites of extrapulmonary IMT are the mesentery and omentum [4]. The mediastinum is an uncommon site, with the occurrence rate of 1.1–5.5% in several large studies [3, 4, 17]. As far as we know, seven cases of mediastinal IMT have been reported in the English literature [3, 4, 9, 14, 17, 19–21]. Only one of the seven patients was an adult over 40 years old [17]. Thus, our case was the second mediastinal IMT in an adult over 40 years old.

The differential diagnosis in mediastinum includes several neoplastic and non-neoplastic conditions, such as solitary fibrous tumor (SFT), inflammatory fibrosarcoma,

Hodgkin's disease, neurogenic tumors and sclerosing/fibrosing mediastinitis. As for SFT, the lack of a prominent inflammatory cell infiltrate and a myofibroblastic phenotype on immunohistochemical study and the presence of CD34 reactivity in proliferating fibroblastic cells serve to distinguish SFT from IMT [16]. Moreover, SFT cells are intimately admixed with extracellular collagen fibers. Histological distinction from inflammatory fibrosarcoma is sometimes very difficult, although it favors the retroperitoneum and mesentery in children. The major discriminatory features are reported to be those of nuclear atypia and the presence of very cellular fascicular areas in inflammatory fibrosarcoma [17]. ALK abnormalities determined using immunohistochemistry and FISH also helped the distinction in our case. In view of the florid inflammatory component and stromal collagenization, Hodgkin's disease (nodular sclerosis and mixed cellularity) is also considered in the differential diagnosis [17]. Successful demonstration of classical Reed–Sternberg cells and Hodgkin cells substantiates this diagnosis. Neurogenic tumors make up a high proportion of the posterior mediastinal neoplasms and include tumors of the sympathetic nervous systems and those of peripheral nerve sheath. For the sympathetic nervous system tumors, such as ganglioneuroblastoma and ganlioneuroma, their histopathological appearances tend to be sufficiently distinctive to allow their differentiation. The peripheral nerve sheath tumors include schwannoma, neurofibroma and malignant peripheral nerve sheath tumor (MPNST). The lack of a myofibroblastic phenotype and their characteristic histological features help in distinction of schwannoma and neurofibroma from IMT. For MPNST, a combination of high cellularity, higher mitotic activity and nuclear atypia together with the lack of a myofibroblastic phenotype serve to differentiate it from IMT. From a morphological point of view, IMT and a non-neoplastic condition, sclerosing/fibrosing mediastinitis [also proposed as idiopathic fibroinflammatory lesion (IFL) of the mediastinum] might show similar histological features. Although the early stage of IFL highlights large numbers of vimentin- and actin-positive spindle cells in edematous fibromyxoid tissue, only fewer numbers of vimentin-positive, actin-negative spindle cells are demonstrated in collagenous, sclerosing stroma in the advanced stages [11]. Thus, distinction from IMT is easier in the advanced stage. ALK abnormalities also help the distinction. Moreover, IFL predominantly involves the anterior mediastinum and has a more aggressive behavior, which might lead to an acute presentation, such as superior vena cava syndrome [11].

Here, we report a case of IMT in 59-year-old man with ALK abnormalities, suggesting the neoplastic nature of IMTs in older patients and necessity for careful follow-up. Further studies on the clinical, pathological and genetic background in more IMT cases occurring in older patients are required to elucidate their characteristics.

References

1. Biselli R, Ferlini C, Fattorossi A, Boldrini R, Bosman C (1996) Inflammatory myofibroblastic tumor (inflammatory pseudotumor): DNA flow cytometric analysis of nine pediatric cases. Cancer 77:778–784
2. Bridge JA, Kanamori M, Ma Z, Pickering D, Hill DA, Lydiatt W, Lui MY, Colleoni GW, Antonescu CR, Ladanyi M, Morris SW (2001) Fusion of the ALK gene to the clathrin heavy chain gene, CLTC, in inflammatory myofibroblastic tumor. Am J Pathol 159:411–415
3. Chan JK, Cheuk W, Shimizu M (2001) Anaplastic lymphoma kinase expression in inflammatory pseudotumors. Am J Surg Pathol 25:761–768
4. Coffin CM, Watterson J, Priest JR, Dehner LP (1995) Extrapulmonary inflammatory myofibroblastic tumor (inflammatory pseudotumor). A clinicopathologic and immunohistochemical study of 84 cases. Am J Surg Pathol 19:859–872
5. Coffin CM, Humphrey PA, Dehner LP (1998) Extrapulmonary inflammatory myofibroblastic tumor: a clinical and pathological survey. Semin Diagn Pathol 15:85–101
6. Coffin CM, Patel A, Perkins S, Elenitoba-Johnson KS, Perlman E, Griffin CA (2001) ALK1 and p80 expression and chromosomal rearrangements involving 2p23 in inflammatory myofibroblastic tumor. Mod Pathol 14:569–576
7. Cook JR, Dehner LP, Collins MH, Ma Z, Morris SW, Coffin CM, Hill DA (2001) Anaplastic lymphoma kinase (ALK) expression in the inflammatory myofibroblastic tumor: a comparative immunohistochemical study. Am J Surg Pathol 25:1364–1371
8. Cools J, Wlodarska I, Somers R, Mentens N, Pedeutour F, Maes B, De Wolf-Peeters C, Pauwels P, Hagemeijer A, Marynen P (2002) Identification of novel fusion partners of ALK, the anaplastic lymphoma kinase, in anaplastic large-cell lymphoma and inflammatory myofibroblastic tumor. Genes Chromosomes Cancer 34:354–362
9. Crespo C, Navarro M, Gonzalez I, Lorente MF, Gonzalez R, Mayol MJ (2001) Intracranial and mediastinal inflammatory myofibroblastic tumour. Pediatr Radiol 31:600–602
10. Debiec-Rychter M, Marynen P, Hagemeijer A, Pauwels P (2003) ALK-ATIC fusion in urinary bladder inflammatory myofibroblastic tumor. Genes Chromosomes Cancer 38:187–190
11. Flieder DB, Suster S, Moran CA (1999) Idiopathic fibroinflammatory (fibrosing/sclerosing) lesions of the mediastinum: a study of 30 cases with emphasis on morphologic heterogeneity. Mod Pathol 12:257–264
12. Griffin CA, Hawkins AL, Dvorak C, Henkle C, Ellingham T, Perlman EJ (1999) Recurrent involvement of 2p23 in inflammatory myofibroblastic tumors. Cancer Res 59:2776–2780
13. Hussong JW, Brown M, Perkins SL, Dehner LP, Coffin CM (1999) Comparison of DNA ploidy, histologic, and immunohistochemical findings with clinical outcome in inflammatory myofibroblastic tumors. Mod Pathol 12:279–286
14. Karnak I, Senocak ME, Ciftci AO, Caglar M, Bingol-Kologlu M, Tanyel FC, Buyukpamukcu N (2001) Inflammatory myofibroblastic tumor in children: diagnosis and treatment. J Pediatr Surg 36:908–912
15. Lawrence B, Perez-Atayde A, Hibbard MK, Rubin BP, Dal Cin P, Pinkus JL, Pinkus GS, Xiao S, Yi ES, Fletcher CD, Fletcher JA (2000) TPM3-ALK and TPM4-ALK oncogenes in inflammatory myofibroblastic tumors. Am J Pathol 157:377–384
16. Nielsen GP, O'Connell JX, Dickersin GR, Rosenberg AE (1997) Solitary fibrous tumor of soft tissue: a report of 15 cases, including 5 malignant examples with light microscopic, immunohistochemical, and ultrastructural data. Mod Pathol 10:1028–1037
17. Ramachandra S, Hollowood K, Bisceglia M, Fletcher CD (1995) Inflammatory pseudotumour of soft tissues: a clinicopathological and immunohistochemical analysis of 18 cases. Histopathology 27:313–323

18. Sastre-Garau X, Couturier J, Derre J, Aurias A, Klijanienko J, Lagace R (2002) Inflammatory myofibroblastic tumour (inflammatory pseudotumour) of the breast. Clinicopathological and genetic analysis of a case with evidence for clonality. J Pathol 196:97–102
19. Souid AK, Ziemba MC, Dubansky AS, Mazur M, Oliphant M, Thomas FD, Ratner M, Sadowitz PD (1993) Inflammatory myofibroblastic tumor in children. Cancer 72:2042–2048
20. Yamaguchi M, Yoshino I, Osoegawa A, Kameyama T, Tagawa T, Fukuyama S, Oda Y, Tsuneyoshi M, Maehara Y (2003) Inflammatory myofibroblastic tumor of the mediastinum presenting as superior vena cava syndrome. J Thorac Cardiovasc Surg 126:870–872
21. Yamamoto H, Oda Y, Saito T, Sakamoto A, Miyajima K, Tamiya S, Tsuneyoshi M (2003) p53 Mutation and MDM 2 amplification in inflammatory myofibroblastic tumours. Histopathology 42:431–439

Virchows Arch (2005) 446: 456–459
DOI 10.1007/s00428-005-1207-5

CASE REPORT

Isabela Werneck da Cunha · Luiz Paulo Kowalski · Fernando Augusto Soares

Dedifferentiated liposarcoma of the oral cavity with angiosarcomatous dedifferentiation

Received: 7 December 2004 / Accepted: 22 December 2004 / Published online: 2 April 2005
© Springer-Verlag 2005

Abstract We report a unique case of a 42-year-old woman with a dedifferentiated liposarcoma of the soft tissue of the oral cavity with angiosarcomatous dedifferentiation. Liposarcomas compromising the head and neck region are very unusual, and most of the cases in oral cavity show a well-differentiated pattern. Dedifferentiation in liposarcomas occurs in about 10% of the cases and, when it occurs, the dedifferentiated areas usually resemble high-grade fibrosarcoma or pleomorphic sarcoma. Divergent differentiation might also occur. To the best of our knowledge, there are only nine cases of dedifferentiated liposarcoma of the oral cavity, none of which show an angiosarcomatous dedifferentiation.

Keywords Sarcomas · Soft tissue · Oral · Head and neck

Introduction

Adipocytic tumors are common mesenchymal tumors. The great majority of adipose tissue tumors are benign tumors, although liposarcomas represent the most common histological type of sarcomas. Most liposarcomas arise in the extremities and retroperitoneum. Liposarcomas compromising the head and neck region are very unusual and even less common in sites of the oral and maxillofacial region, accounting for approximately 0.3% of all liposarcomas [7].

I. W. da Cunha (✉) · F. A. Soares
Department of Pathology, Centro de Tratamento e Pesquisa,
Hospital do Câncer, A. C. Camargo,
R. Prof Antônio Prudente 211, Liberdade,
01509-900 São Paulo, Brazil
e-mail: iwcunha@hcancer.org.br
Tel.: +55-11-32725103
Fax: +55-11-32725185

L. P. Kowalski
Department of Head and Neck Surgery,
Centro de Tratamento e Pesquisa,
Hospital do Câncer, A. C. Camargo,
São Paulo, Brazil

There are very few series of oral liposarcomas (OLSs), with less than 100 cases reported so far. Most of the cases in oral cavity show a well-differentiated pattern [7, 17]. Nascimento et al. [17] studied 23 cases of atypical lipomatous tumors/OLS, in which 21 cases were classified as atypical lipomatous tumor, 1 as myxoid liposarcoma, and only 1 case as dedifferentiated OLS. Fanburg-Smith et al. [7] reported 18 cases of OLS, 10 of which were cases of atypical lipomatous tumor, 5 cases of myxoid liposarcoma and 3 cases of dedifferentiated OLS.

Dedifferentiation in liposarcomas occurs in about 10% of the cases, and it can be defined as a non-lipogenic sarcoma of variable histological grade juxtaposed of atypical lipomatous tumors/well-differentiated liposarcoma [1]. Most of the dedifferentiated liposarcomas display extenive areas of high-grade dedifferentiation resembling high-grade fibrosarcoma or pleomorphic sarcoma [15]. Divergent dedifferentiation, such as myosarcomatous or osteosarcomatous, can also occur [6, 15, 16, 25].

Clinical history

A 42-year-old woman sought medical attention at the outpatient clinic of the Medical and Research Center Hospital for Cancer, São Paulo, Brazil, with complaints of swelling and a rapid-growth tumoral mass of the right cheek region (Fig. 1). In 1997, she had reported a small enlargement in the same region, and a magnetic resonance image examination demonstrated a small mass with density comparable with mature adipose tissue. There were no alterations in the characteristics of the mass until 2001, when an ultrasound showed a 1-cm nodular lesion in the gingival sulcus. A fine-needle aspiration was performed, with no evidence of malignant cells. The patient reported a sudden and rapid growth of the lesion in 2003. The patient underwent resection of the lesion.

The histological examination of the surgical specimen demonstrated a dedifferentiated liposarcoma with angiosarcomatous dedifferentiation with tumor extension to the surgical margins. After the diagnosis, the patient under-

Fig. 1 X-ray showing a tumoral mass in the right cheek region

went a second surgery for a complete excision of the tumor and adjuvant radiotherapy. She had no signs of recurrence or metastasis in her 1-year follow-up.

Materials and methods

Pathological examination of the first surgery revealed a 6.0×3.5×2.4-cm lobulated and yellow mass similar to a lipoma. A firm white nodular area measuring approximately 1.2 cm in its greatest diameter was observed. The two areas had different histological findings (Fig. 2a). The first one was characterized by well-differentiated liposarcoma showing adipocytes with variation in size, focal nuclear atypia and hypercromasia. Some lipoblasts could also be observed (Fig. 2b). The nodular white area was composed of spindle cells with severe nuclear atypias arranged in sheets or forming rudimentary vascular channels (Fig. 2c). The immunohistochemistry demonstrated strong expression of CD31 and CD34 (Fig. 3) and negative stains for muscle markers and S100 protein.

The material of the second surgery corresponded to two nodules separated by adipose tissue, a parotid gland and one lymph node. The histological aspect was the same as the first specimen. The parotid gland and the lymph node were not infiltrated by the neoplasm.

Discussion

Liposarcomas are the most common among the adult soft tissue sarcomas and account for approximately 20% of all mesenchymal tumors. They occur almost exclusively in adults and are most often found in the thigh or retroperitoneum. Diagnostic criteria for liposarcoma have been well established for a long time, and very few changes in liposarcomas nomenclature have been observed [11]. Liposarcomas are separated into histological subtypes with different microscopic appearances and slightly different behavior characteristics. They are histologically classified as atypical lipomatous tumor/well-differentiated liposarcoma, myxoid liposarcoma, pleomorphic liposarcoma, dedifferentiated liposarcoma and mixed-type liposarcoma [11]. Although the only major modifications in the histological classification of liposarcomas was the inclusion of dedifferentiated liposarcoma, new variants and new concepts secondary to best knowledge of genetics and molecular pathology of these tumors were introduced [2].

Sarcomas of the head and neck region are unusual neoplasm, with their major series having no equal approaches, making it very difficult to evaluate their real incidence. Some of them are found in children [8, 24], and differences between the primary sites included are also observed. For instance, some series in these children include tumors occurring in the scalp as head and neck sarcomas, but others include angiosarcomas of the scalp as primary skin sarcomas. The incidence of head and neck sarcomas has been estimated in frequencies between 0% and 9% of

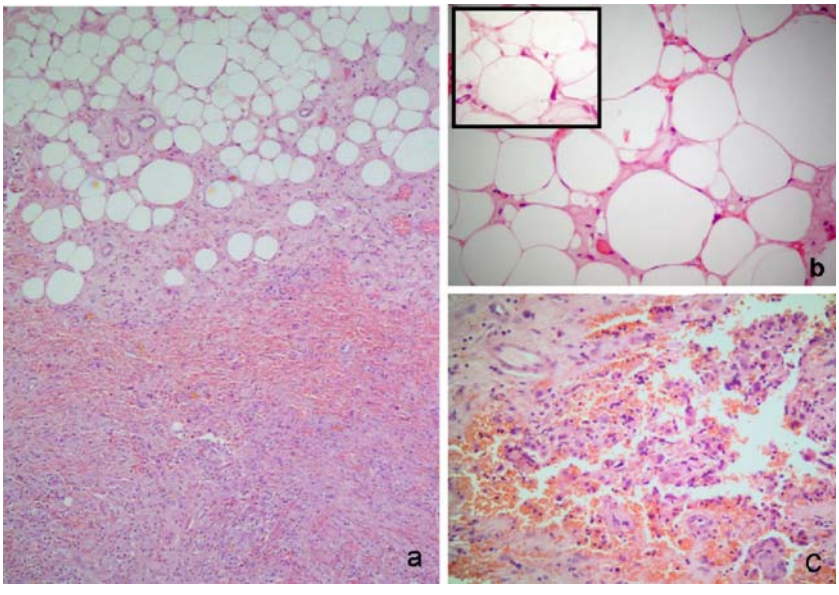

Fig. 2 The tumor has two distinct areas represented by a well-differentiated liposarcoma (*upper*) and a dedifferentiated area (*bottom*) [**a** hematoxylin and eosin (HE), ×40]; a well-differentiated liposarcoma area is demonstrated in **b** that shows lipocytes with wide range of size and shape and in detail (*insert*) the presence of nuclear atypia (**b** HE, ×200, insert ×400); dedifferentiated area shows atypical spindle cells forming rudimentary vascular channels (**c** HE, ×100)

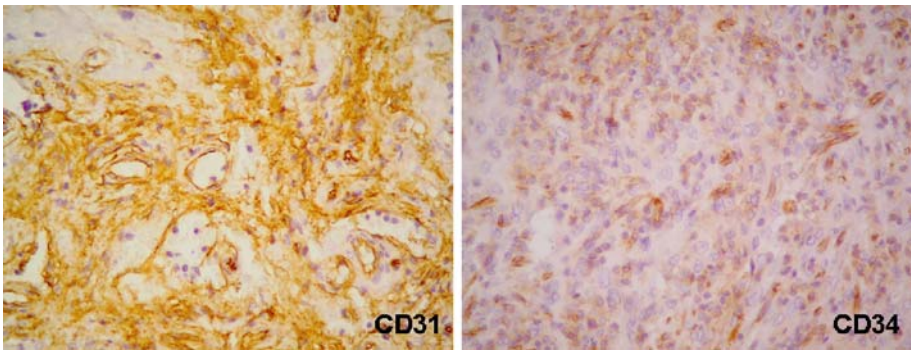

Fig. 3 The dedifferentiated areas show strong positives for CD31 and CD34

all sarcomas [4, 5, 14, 20, 21]. In an evaluation of the distribution of sarcomas in head and neck primary sites, it is found that the head and neck sarcoma registry have noted 214 cases and, among them, the most common sites were parotid and neck region (20% of the cases), face and forehead (18%), maxilla and palate (13%), scalp (12%) and mandible (11%) [24]. There have been few occurrences of head and neck sarcomas found in the oral cavity, and the majority of those reported have a common fibrosarcomatous background [8]. Oral cavity liposarcomas corresponded to only 5–8% of all cases of head and neck liposarcomas [12, 24] and, according to Fanburg-Smith et al. [7], OLSs correspond to 0.3% of the liposarcomas.

Knowledge of adipocytic tumors of the oral cavity is restricted primarily to case reports [3, 7, 10]. There are very few documented series of oral adipocytic tumors available in the literature, and the most common histological type is the lipoma. Among the malignant, it is difficult to evaluate because the concept of atypical lipomatous tumors are quite recent. Nascimento et al. [17] reported that 21 of 23 oral adipocytic tumors were atypical lipomatous tumors. Prior to this series, myxoid liposarcoma was the most common histological type. Golledge et al. [12] reviewed the literature and found a very similar number of well-differentiated, myxoid and pleomorphic OLS. The tongue is the most common primary site according to Nascimento et al. [17].

Dedifferentiation in well-differentiated liposarcomas is defined by the coexistence of a non-lipogenic sarcoma of variable histological grade and atypical lipomatous tumors/well-differentiated liposarcoma [1]. The concept of dedifferentiated liposarcoma (DDLS) was introduced by Evans in 1979, and it is similar to what occurs in other

Table 1 Clinicopathological characteristics and follow-up of five cases of dedifferentiated liposarcoma of the oral cavity reported in the literature and the present case

Case reported by (reference)	Age (years)/sex	Anatomic location (size in cm)	Duration and clinical history	Type of dedifferentiation	Follow-up information (outcome)
Diamond et al. [3]	57/male	Cheek (8)	7-year mass, with rapidly increased in size in few weeks	Spindle cell pattern with areas showing multinucleated giant cells	12 months (without recurrence)
Fanburg-Smith et al. [7]	39/male	Tongue (6)	2 years, nodule	Bland spindle proliferation and scattered floret cells	6 years follow-up (without recurrence)
Fanburg-Smith et al. [7]	56/male	Left buccal mucosa (5)	Two recurrences following wide excision at 18 months and 28 months	Spindled pleomorphic liposarcoma-like areas	26-year follow-up, six recurrences
Nascimento et al. [17]	72/male	Tongue (0.7)	N/A	Heterologous cartilage	2 years (without recurrence)
Nascimento et al. [17]	83/female	Tongue (2.5)	Nodule	Nonlipogenic rounded tumors cells	N/A
Present report	42/female	Cheek (6)	7-year mass, with rapidly increasing size in few weeks	Spindle cells with nuclear atypias arranged in sheets or forming rudimentary vascular channels	12 months (without recurrence)

N/A: not available

sarcomas. It has been reported that it can occur in approximately 10% of the cases, and various histological types of sarcomas have been documented, including high- or low-grade sarcomas [15, 19]. The most frequent sarcomas recognized in the dedifferentiated areas are fibrosarcomas and pleomorphic sarcomas [15]. There is limited data available on the prognosis of DDLS, but McCormick et al. [16] suggested that they have a better prognosis than other pleomorphic sarcomas. DDLS occurs mainly in the retroperitoneum, and there are very few findings reported in cases of the head and neck region. We were able to find nine reported cases of DDLS in the head and neck region [3, 7, 13, 15–17], and five on them are primarily in the oral cavity [3, 7, 17] (Table 1).

DDLS may exhibit heterologous differentiation in approximately 5–10% of cases. The heterologous differentiation apparently does not affect clinical outcome. Most often the line of heterologous differentiation is neural/meningeal-like [18], myogenic [6] or osteo/chondrosarcomatous dedifferentiation [25]. To the best of our knowledge, there is only one reported case of an angiosarcomatous dedifferentiation in a liposarcoma of the mediastinum in a 45-year-old man [6]. This tumor measured 10×8×6 cm and had an appearance of a lipoma with areas of hemorrhage. Microscopically, it was found to be a dedifferentiated liposarcoma with areas of vasoformation within the dedifferentiated component. No immunohistochemistry was performed. The patient was alive without recurrence after 1-year follow-up.

There is no report in literature of an angiosarcomatous dedifferentiation in a liposarcoma in the head and neck region. Also, there are very few cases of primary angiosarcomas in the oral cavity [9, 22, 23].

In conclusion, oral liposarcomas are rare tumors, and most of them are well-differentiated tumors. Dedifferentiation in oral liposarcomas is very unusual, and we report the first case of oral liposarcoma with angiosarcomatous dedifferentiation.

Acknowledgements We thank Juliana and Andrew Jernigan for the english review.

References

1. Dei Tos AP, Pedeutour F (2002) Dedifferentiated liposarcoma. In: Fletcher CDM, Unni KK, Mertens F (eds) Pathology and genetics. Tumors of soft tissue and bone. IARC Press, Lyon, pp 38–39
2. Dei Tos AP (2000) Liposarcoma: new entities and evolving concepts. Ann Diagn Pathol 4:252–266
3. Diamond C, Prince ME, Covert AA, Morris SF (2002) Dedifferentiated liposarcoma of the cheek: case report and literature review. J Otolaryngol 31:125–128
4. Enterline HT, Culberson JD, Rochlin DB, Brady LW (1960) Liposarcoma: a clinical and pathological study of 53 cases. Cancer 13:932–950
5. Enzinger FM, Winslow DJ (1962) Liposarcoma: a study of 103 cases. Virchows Arch 335:367–388
6. Evans HL, Khurana KK, Kemp BL, Ayaka AG (1994) Heterologous elements in dedifferentiated component of dedifferentiated liposarcoma. Am J Surg Pathol 18:1150–1157
7. Fanburg-Smith JC, Furlong MA, Childers EL (2002) Liposarcoma of the oral and salivary gland region: a clinicopathologic study of 18 cases with emphasis on specific sites, morphologic subtypes, and clinical outcome. Mod Pathol 15:1020–1031
8. Farr HW (1981) Soft tissue sarcomas of the head and neck. Semin Oncol 8:185–189
9. Favia G, Lo ML, Serpico R et al (2002) Angiosarcoma of the head and neck with intraoral presentation. A clinicopathological study of four cases. Oral Oncol 38:757–762
10. Favia G, Maiorano E, Orsini G, Piatelli A (2001) Myxoid liposarcoma of the oral cavity with involvement of the periodontal tissues. J Clin Periodontol 28:109–112
11. Fletcher CDM, Unni KK, Mertens F (eds) (2002) Pathology and genetics. Tumors of soft tissue and bone. IARC Press, Lyon
12. Golledge J, Fisher C, Rhys-Evans PH (1995) Head and neck liposarcoma. Cancer 76:1051–1058
13. González-Louis C, Ibarrola C, Ballestin C, Martanez-Tello FJ (2002) Dedifferentiated liposarcoma of the pyriform sinus: report of a case and review of the literature. Int J Surg Pathol 10: 75–79
14. Hashimoto H, Enjoji M (1982) Liposarcoma: a clinicopathologic sub-typing of 52 cases. Acta Pathol Jpn 32:933–948
15. Henricks WH, Chu YC, Goldblum JR, Weiss SW (1997) Dedifferentiated liposarcoma. A clinicopathological analysis of 155 cases with a proposal for an expanded definition of dedifferentiation. Am J Surg Pathol 21:271–281
16. McCormick D, Mentzel T, Behem A, Fletcher CD (1994) Dedifferentiated liposarcoma. Clinicopathologic analysis of 32 cases suggesting a better prognostic subgroup among pleomorphic sarcomas. Am J Surg Pathol 18:1213–1223
17. Nascimento AF, McMenamin ME, Fletcher CDM (2000) Liposarcomas/atypical lipomatous tumors of the oral cavity: a clinicopathologic study of 23 cases. Ann Diagn Pathol 6:83–93
18. Nascimento AG, Kurtin PJ, Guillou L, Fletcher CDM (1998) Dedifferentiated liposarcoma. A report of nine cases with a peculiar neural-like whirling pattern associated with metaplastic bone formation. Am J Surg Pathol 22:945–955
19. Nascimento AG (2001) Dedifferentiated liposarcoma. Semin Diagn Pathol 18:263–266
20. Spittle MF, Newton A, MacKenzie DH (1970) Liposarcoma: a review of 60 cases. Br J Cancer 24:696–704
21. Stout AP (1994) Liposarcoma: malignant tumor of lipoblasts. Ann Surg 119:86–107
22. Tabata M, Sugihara K, Matsui R et al (1999) Angiosarcoma of the tongue: report of a case with immunohistochemical findings. J Oral Pathol Med 28:92–95
23. Triantafillidou K, Lazaridis N, Zaramboukas T (2002) Epithelioid angiosarcoma of the maxillary sinus and maxilla: a case report and review of the literature. Oral Surg Oral Med Oral Pathol Oral Radiol Endo 94:333–337
24. Wanebo HJ, Koness J, MacFarlane JK, Eilber FR, Byers RM, Elias G, Spiro RH (1942) Head and neck sarcoma: report of the head and neck sarcoma registry. Head Neck 14:1–7
25. Yamamoto T, Matsushita T, Manui T, Mizuno K, Minami R, Hayashi Y, Hanioka K (2000) Dedifferentiated liposarcoma with chondroblastic osteosarcomatous dedifferentiation. Pathol Int 50:558–561

Virchows Arch (2005) 446: 460–462
DOI 10.1007/s00428-005-1213-7

CASE REPORT

Joji Sekine · Masanobu Anami · Shuichi Fujita · Michael Vieth · Tsugio Inokuchi

A case of mucoepidermoid carcinoma with melanin pigmentation manifested in the palate

Received: 31 October 2004 / Accepted: 12 January 2005 / Published online: 9 March 2005
© Springer-Verlag 2005

Abstract This paper describes the first documented case of mucoepidermoid carcinoma (MEC) with melanin pigmentation manifested in the palate. Histopathological sections showed a neoplasm composed of epidermoid, mucous-producing and intermediate cells. Numerous large cells contained dark pigmented materials. Fontana Masson staining revealed dendritic melanocytes and melanin granules. HMB-45, Melan A and S-100 protein were all positive for melanocytes. Histopathological examination was not typical for malignant melanoma; the lesion was diagnosed as a low-grade MEC with melanin pigmentation.

Keywords Mucoepidermoid carcinoma · Melanin · Minor salivary gland · Palate · Immunohistochemistry

M. Vieth received a research grant from the Japanese Society of Pathology at the Institute of Pathology, Shiga University of Medical Science, Ohtsu, Japan

J. Sekine (✉) · T. Inokuchi
Division of Oral and Maxillofacial Surgical Reconstruction and Functional Restoration,
Department of Developmental and Reconstructive Medicine,
Graduate School of Biomedical Sciences,
Nagasaki University,
1-7-1 Sakamoto,
Nagasaki, 852-8588, Japan
e-mail: georges@net.nagasaki-u.ac.jp
Tel.: +81-95-8497704
Fax: +81-95-8497705

M. Anami
Division of Pathology, Nagasaki University Hospital,
Nagasaki, Japan

S. Fujita
Division of Oral Pathology and Bone Metabolism,
Department of Developmental and Reconstructive Medicine,
Graduate School of Biomedical Sciences,
Nagasaki University,
Nagasaki, Japan

M. Vieth
Institute of Pathology, Otto-von-Guericke Universität,
Magdeburg, Germany

Introduction

Mucoepidermoid carcinoma (MEC) is a common malignant tumor which occurs in the salivary glands and constitutes 23% of all malignant tumors of the salivary glands [3]. To the best of our knowledge, MEC with melanin pigmentation is extremely rare in the oral cavity and only two cases, one in the lip [8] and the other in the buccal mucosa [1], have been reported. The present paper describes the first documented case of MEC with melanin pigmentation manifested in the hard palate. Both immunohistochemical features and histopathological findings are presented. The histogenesis of the melanin is also discussed.

Case report

A 26-year-old Japanese female with a chief complaint of a small dark spot measuring 7 mm in diameter in the hard palate was referred to our hospital. The patient's past medical history was unremarkable.

Excisional biopsy with a 4-mm surgical margin was performed. Histopathological sections revealed a noncapsulated neoplasm composed of epidermoid cells, mucous-producing cells and intermediate cells. These three types of cells formed small proportions of solid tumor nests, which were involved with the minor salivary glands. The major part of the tumor consisted of many cystic structures lined by mucous-producing cells on the luminal surface. The tumor lesion was attached to the lobes of the normal minor salivary gland by connective tissue but was not in direct contact with the normal squamous epithelium of the oral mucosa. In the epidermoid as well as intermediate cells of the tumor, many dark pigmented intracytoplasmic inclusions were present (Fig. 1). These pigmentations were also seen in the basal cell layer of the mucosal epithelium and in the subepithelial layer but not in the adjacent minor salivary glands. Fontana Masson staining revealed melanin granules in the melanocytes with dendritic cytoplasmic elongations (Fig. 2). Some of the slides bleached by peroxidase and potassium permanganate solution showed the absence of any positive staining

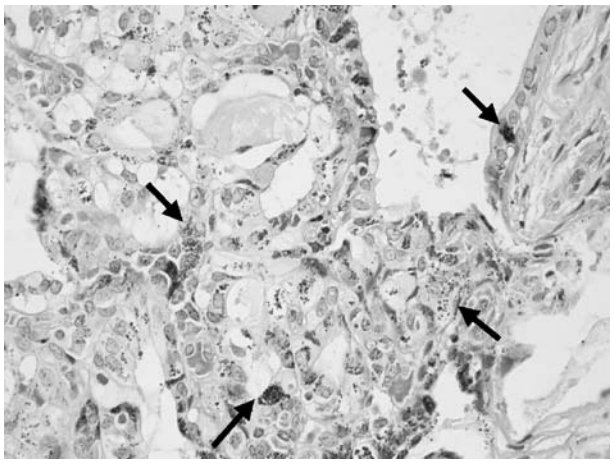

Fig. 1 Photograph showing tumor composed of epidermoid, mucous-producing and intermediate cells. *Arrows* black pigmented materials. Hematoxylin and eosin (HE) staining, original magnification ×400

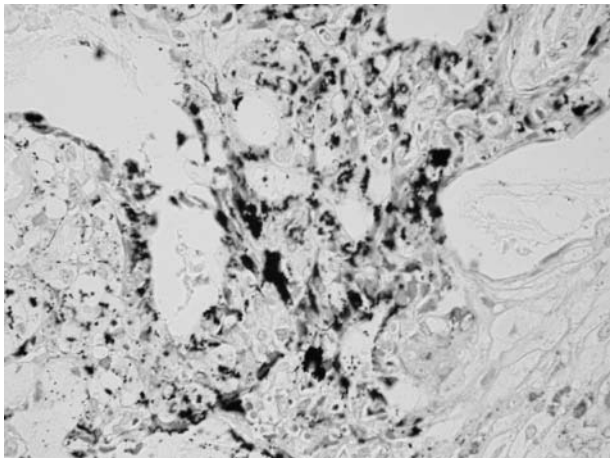

Fig. 2 Fontana Masson staining showing pigmented dendritic melanocytes and melanin granules. Original magnification ×400

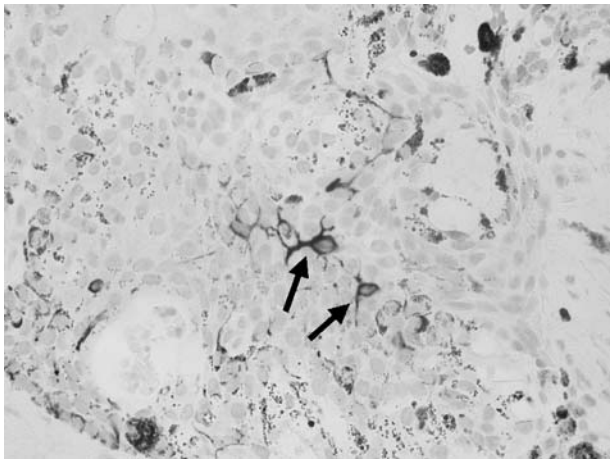

Fig. 3 HMB-45 immunostaining showing dendritic melanocytes (*arrows*). Original magnification ×400

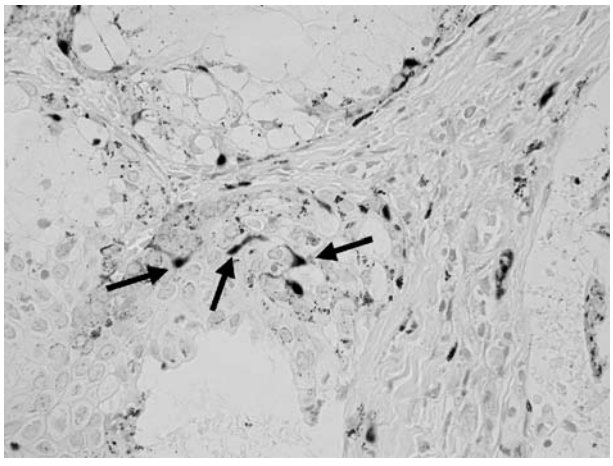

Fig. 4 Melan A immunostaining showing dendritic melanocytes (*arrows*). Original magnification ×400

for melanin. Immunostaining for HMB-45 (Fig. 3), and Melan A and S-100 protein (Fig. 4) showed a positive reaction in some of the melanocytes. However, pigmented neoplastic cells were negative. The lesion was diagnosed as a low-grade MEC derived from the minor salivary glands of the hard palate with melanin pigmentation.

Discussion

Melanocytes are derived embryologically from neural crest tissue and are not a constituent of normal salivary tissue [5], although melanocytes and melanin granules are reported to exist in the human minor salivary gland system [6]. Melanocytes are sometimes scattered in the periductal and periacinar regions around the duct system [6], and a case of benign salivary gland tumor with melanin pigmentation was recently reported [7]. In the present case, pigmented inclusions within dendritic melanocytes and melanin granules were detected histopathologically as well as histochemically; these were not present in the normal minor salivary gland but were found in the tumor and in the normal epithelium around the components of the MEC. Azzopardi et al. investigated melanocyte colonization and pigmentation of breast carcinomas, which occur frequently in the dermal–epidermal interface [2]. Hirakawa et al. described nasopharyngeal oncocytic metaplasia with melanin pigmentation [4]. Both reports mentioned the existence of a migration factor from cancer cells or oncocytic cells to the melanocyte thus acting as a stimulating factor for melanin production. Although the mechanism through which cells are associated with the melanin pigmentation is unclear, these melanin pigmentations were assumed to have been transferred from the adjacent dendritic melanocytes [4] and it might just be a secondary melanocyte colonization. Further research is necessary to clarify this issue.

References

1. Aufdemorte TB, van Sickels JE, Glass BJ (1985) Melanin pigmentation in a mucoepidermoid tumor of a minor salivary gland. J Oral Maxillofac Surg 43:876–879
2. Azzopardi JG, Eusebi V (1977) Melanocyte colonization and pigmentation of breast carcinoma. Histopathology 1:21–30
3. Eneroth CM (1971) Salivary gland tumors in the parotid gland, submandibular gland, and the palate region. Cancer 27:1415–1418
4. Hirakawa E, Miki H, Ohmori M, Kobayashi S, Haba R, Nagai Y (1999) Melanin pigmented oncocytic metaplasia of the nasopharynx. Virchows Arch 434:455–457
5. Renaut AJ (1996) Melanoma arising within the parotid salivary gland—a case report and review of management. Eur J Surg Oncol 22:201–202
6. Takeda Y (2000) Existence and distribution of melanocytes and HMB-45-positive cells in the human minor salivary glands. Pathol Int 50:15–19
7. Takeda Y, Satoh M, Nakamura S (2004) Pigmented pleomorphic adenoma, a novel melanin-pigmented benign salivary gland tumor. Virchows Arch 445:199–202
8. Thomas KM, Hutt MSR, Borgstein J (1980) Salivary gland tumors in Malawi. Cancer 46:2328–2334

Virchows Arch (2005) 446: 463–466
DOI 10.1007/s00428-005-1215-5

CASE REPORT

Arzu Ensari · Berna Savas · Aylin Okcu Heper · Isinsu Kuzu · Ramazan Idilman

An unusual presentation of *helicobacter pylori* infection: so-called "Russell body gastritis"

Received: 6 December 2004 / Accepted: 12 January 2005 / Published online: 3 March 2005
© Springer-Verlag 2005

Abstract *Helicobacter pylori* (*H. pylori*) is a "slow" bacterial pathogen, which induces several gastroduodenal diseases. Varying degrees of inflammation can be present in the gastric mucosa of patients infected with *H. pylori*. The case presented here is a male patient suffering from dyspepsia and nausea. His upper gastrointestinal endoscopy revealed pan gastritis. Histological examination of multiple gastric biopsies taken from the body and antrum showed a rare morphological expression of *H. pylori* gastritis characterized by diffuse plasma cell infiltration with extensive Russell body formation. Diffuse infiltration of plasma cells with Russell bodies in gastric mucosa can cause difficulties in differentiation from neoplastic processes. However, immunohistochemically, the infiltrating cells in the gastric mucosa stained negatively with cytokeratins while they expressed both kappa and lambda light chains showing their polyclonal nature. The presence of diffuse plasma cells with Russell bodies in the gastric mucosa may represent a different presentation of *H. pylori* gastritis. There are only two case reports of similar presentation and both have been called "Russell body gastritis".

Keywords *Helicobacter pylori* · Russell body gastritis

Introduction

Helicobacter pylori (*H. pylori*) is a major etiological agent in a variety of gastroduodenal diseases including chronic gastritis, peptic ulcer, gastric cancer, and lymphoma [1, 2, 8, 9]. Varying degrees of mucosal inflammation and atrophy can be present in gastric biopsies infected with this microorganism. *H. Pylori* infection causes damage to both superficial and glandular epithelial cells. Cellular injury may be inflicted directly by the bacteria or by mechanisms mediated by inflammation or apoptosis [6]. Bacterial attachment and superficial cell activation results in the rapid recruitment of neutrophils in the gastric mucosa, followed by lymphocytes, and later by plasma cells [4, 6]. Plasmacytic infiltrate is the hallmark of chronic inflammation of gastric mucosa. However, plasma cells containing Russell bodies, which are thought be accumulations of condensed intercisternal immunoglobulin (Ig) in the cytoplasm of plasma cells [7], are extremely rare in *H. pylori* gastritis. There are only two case reports of plasma cells with Russell bodies infiltrating the gastric mucosa in the English literature [3, 11].

The case presented here has characteristic features of so-called "Russell body gastritis" associated with *H. pylori* infection.

A. Ensari (✉) · B. Savas · A. Okcu Heper · I. Kuzu
Department of Pathology, Medical School, Ankara University, Ankara, Turkey
e-mail: aensari@ato.org.tr
Tel.: +90-312-3103010
Fax: +90-312-3106370

R. Idilman
Department of Gastroenterology, Medical School, Ankara University , Ankara, Turkey

Clinical history

A 70-year-old male patient suffering from dyspepsia and nausea for the last 6 months was admitted to the Department of Gastroenterology, Ankara University Medical Faculty. He had a history of essential hypertension and benign prostatic hyperplasia. His physical examination was normal except for slight tenderness in the epigastric area. Routine blood tests revealed hypochromic microcytic anemia, consistent with iron deficiency. Upper gastrointestinal endoscopy revealed flattened gastric folds and edema, which were suggestive of pan gastritis. Multiple gastric biopsies from the body and antrum were taken for histopathological examination.

Materials and methods

Biopsy samples were fixed in 10% formalin, processed routinely, and embedded in paraffin. Sections (4 μm thick)

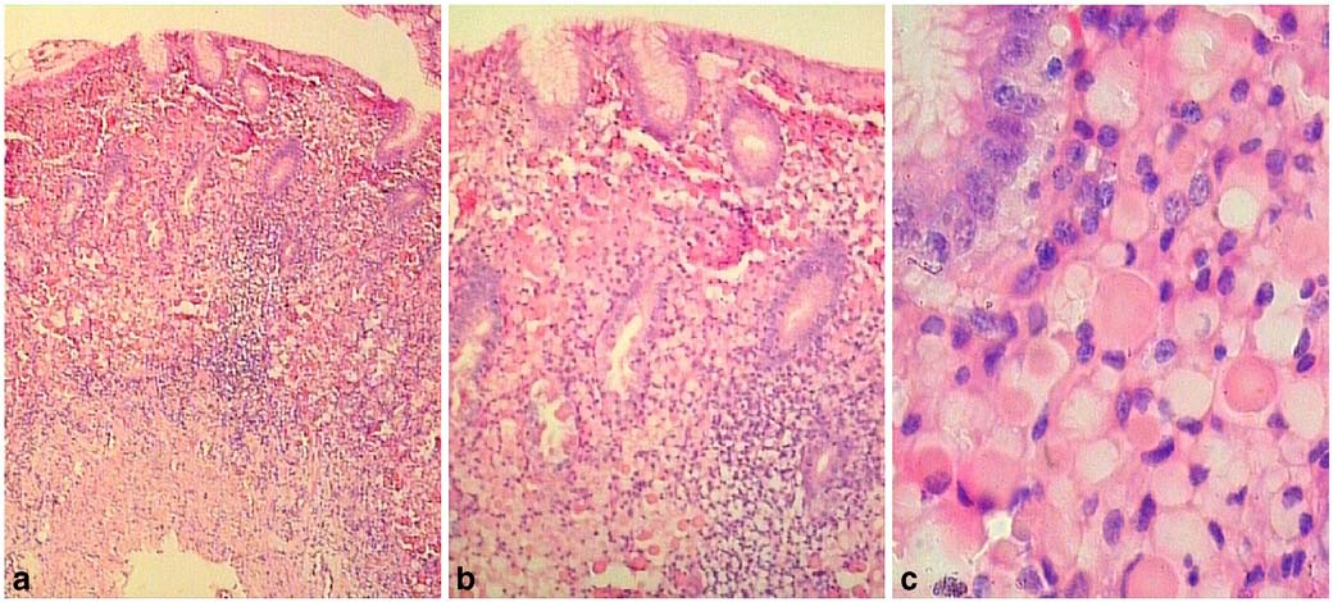

Fig. 1 **a**, **b** Gastric biopsy showing diffuse infiltration of lamina propria by monomorphous cells with large eosinophilic cytoplasms and eccentric nuclei (hematoxylin and eosin; ×100 and ×200, respectively). **c** High-power view of expanded lamina propria by the infiltrating plasma cells and numerous round eosinophilic intracytoplasmic inclusions, so-called Russell bodies (hematoxylin and eosin; oil immersion)

were taken from the paraffin blocks and stained with hematoxylin and eosin (H&E) for light microscopic examination. Immunohistochemical examination was performed using a streptavidin-biotin peroxidase technique (Zymed, US) and AEC as chromogen. Monoclonal antibodies used included pan-cytokeratin (pan CK; clone 5D3+LP34, Neomarkers, California), CD20 (clone L26, Novocastra, UK), CD79a (clone JCB117, Dako, California), CD68 (clone PG-M1, Dako, California), plasma cell antigen (PCA; clone VS38c, Dako, California), kappa (clone HP-6054, Novocastra, UK) and lambda (clone kp-53, Novocastra, UK) light chains.

Results

Histopathological findings

Histopathological examination of the gastric biopsies revealed atrophy with moderate mononuclear cellular in-

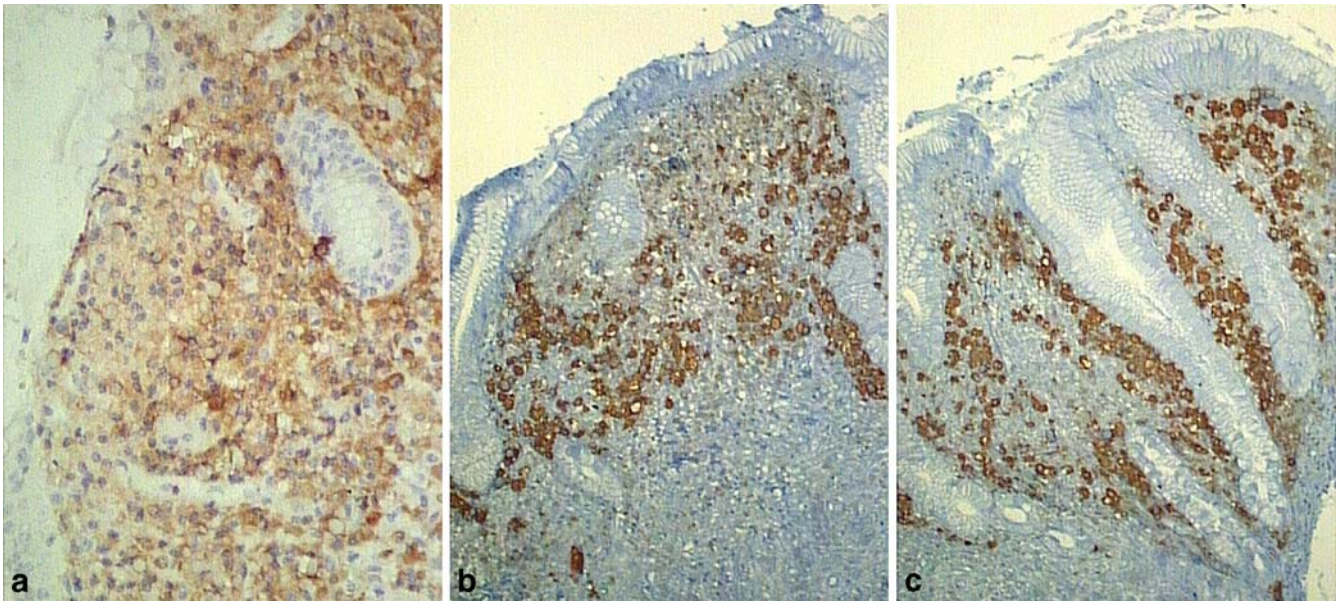

Fig. 2 **a**–**c** Infiltrating cells showing diffuse cytoplasmic positivity with anti-CD79a, anti-κ immunoglobulin light chain, and anti-λ immunoglobulin light chain, respectively (streptavidin-biotin peroxidase; ×200)

filtration in the lamina propria and polymorphonuclear leukocyte infiltration of glandular epithelium in the gastric antrum. In the lamina propria of the corpus mucosa, in addition to the findings found in antral mucosa, a diffuse infiltration of cells—with large eosinophilic cytoplasm and eccentric nuclei somewhat resembling plasma cells—was observed (Fig. 1a, b). On higher magnification, these cells had numerous round eosinophilic intracytoplasmic inclusions, so-called Russell bodies (Fig. 1c). Colonization by *H. pylori* was observed on the surface of foveolar cells in H&E and modified Giemsa stains.

Immunohistochemical findings

Immunohistochemically, the infiltrating cells were positive with CD79a (Fig. 2a) and PCA, while no staining was observed with CD20, CD68 or pan CK. The cells expressed both kappa (Fig. 2b) and lambda (Fig. 2c) light chains showing their polyclonal nature. The case was diagnosed as *H. pylori* gastritis with extensive Russell body formation.

Following this diagnosis, immune and protein electrophoreses together with a bone marrow trephine biopsy were performed in order to exclude a plasma cell neoplasia. No abnormalities were found in either test while bone marrow biopsy showed a normal plasma cell ratio. Follow-up of the patient since the diagnosis has shown him to be well; however, he refused to be re-examined endoscopically after *H. pylori* treatment.

Discussion

Russell bodies, first described by Russell in 1890 [10], are considered to represent aggregates of Igs resulting from secretory disturbance of plasma cells [7]. Plasma cells with Russell bodies can be seen in a variety of mucosal surfaces, including gastrointestinal tract in association with chronic inflammation such as *H. pylori* gastritis.

Recently, two case reports of chronic gastritis showing plasma cell infiltration with extensive Russell body formation have been published. In the first report, Tazawa and Tsutsumi presented a 53-year-old male showing localized accumulation of plasma cells containing Russell bodies in association with infection of *H. pylori* and defined this pathology as "Russell body gastritis" [11]. The most recent case presented by Erbersdobler et al., was an 80-year-old female with non-*H. pylori*-associated gastritis, characterized by a diffuse plasma cell infiltration with Russell bodies [3]. Both cases had a focal nature of plasma cell accumulation detected either endoscopically or histologically [3, 11], while the current case is characterized by diffuse and extensive accumulation of Russell bodies presenting as a diffuse pan gastritis on endoscopy.

H. pylori stimulates cytokine production by epithelial cells that recruit and activate immune and inflammatory cells in the underlying lamina propria, causing chronic active gastritis. Although epidemiological evidence shows that infection generally occurs in children, the inflammatory changes progress throughout life [5, 9]. *H. pylori* has also been associated with gastroduodenal ulcers and gastric cancer [5]. These more severe manifestations of the infection usually occur later in life and only in a minority of infected subjects [1, 2]. In addition, the stimulation of cytokine production by epithelial cells and activation of the immune system lead to the formation of lymphoid aggregates, which may show progression to MALTomas [8].

The presence of diffuse plasma cell infiltration with extensive Russell body formation is suggestive of an interaction between *H. pylori* and gastric immune system. It could be speculated that the formation of Russell bodies may result from over-stimulation of plasma cells by mucosal pathogens such as *H. pylori*, leading to accumulation of excess amounts of Igs in the cytoplasm. In support of this view, *H. pylori* has been detected both in the present case and in the case reported by Tazawa and Tsutsumi [11]. However, the presence of Russell bodies in *H. pylori* gastritis seems to be a very rare finding, thus a direct role of this pathogen in Russell body formation is highly unlikely.

Though the clinical significance (if any) of Russell bodies in *H. pylori* gastritis is not known, histopathologically extensive infiltration of plasma cells with Russell bodies in gastric mucosa can cause confusion with neoplastic processes such as signet ring cell carcinoma, malignant lymphoma and solitary plasmacytoma. Interestingly, the low-power view of our case strongly suggested diffuse infiltration of signet ring cells; whereas, eosinophilic round intracytoplasmic inclusions within the infiltrating cells were easily detected on higher magnification. The benign nature of infiltrating plasma cells demonstrated by immunohistochemistry and the lack of lymphoepithelial lesion-like features excluded a malignant lymphoma or plasmacytoma, while negative staining with cytokeratins helped to differentiate the lesion from a carcinoma.

The present case is a good example of an unusual presentation of ordinary *H. pylori* gastritis, which can either easily be missed or misinterpreted during daily microscopy routine. However, we believe that such histopathological pictures need to be recognized and even deserve to be called by distinct names.

References

1. Bolin TD, Hunt TR, Korman MG, Lambert JR, Lee A, Talley NJ (1995) *Helicobacter pylori* a gastric neoplasia: evolving concepts. Med J Aust 163:235–255
2. Chan AO, Chu KM, Yuen ST, Leung SY, Lam SK, Wong J (2001) Synchronous gastric adenocarcinoma and mucosa-associated lymphoid tissue lymphoma in *Helicobacter pylori* infection; comparing reported cases between the east and west. Am J Gastroenterol 96:1922–1924
3. Erbersdobler A, Petri S, Lock G (2004) Russell body gastritis. An usual, tumor-like lesion of the gastric mucosa. Arch Pathol Lab Med 128:915–917
4. Ernst PB, Crowe SE, Reyes VE (1997) How does *Helicobacter pylori* cause mucosal damage? The inflammatory response. Gastroenterology 113:S35–S42
5. Ernst PB, Gold BD (2000) The disease spectrum of *Helicobacter pylori*: the immunopathogenesis of gastroduodenal ulcer and gastric cancer. Annu Rev Microbiol 54:615–640

6. Genta RM (1997) Role of *Helicobacter pylori* infection in cancer. *Helicobacter pylori*, inflammation, mucosal damage, and apoptosis: pathogenesis and definition of gastric atrophy. Gastroenterology 113:S51–S55
7. Hsu SM, Hsu PL, McMillan PN, Fanger H (1982) Russell bodies: a light and electron microscopic immunoperoxidase study. Am J Clin Pathol 77:26–31
8. Isaacson PG (1990) Lymphomas of mucosa-associated lymphoid tissue (MALT). Histopathology 16:617–619
9. Kokoska ER, Kauffman GL Jr (2001) *Helicobacter pylori* and the gastroduodenal mucosa. Surgery 130:13–16
10. Russell W (1890) An address on a characteristic organism of cancer. BMJ 2:1356–1360
11. Tazawa K, Tsutsumi Y (1998) Localized accumulation of Russell body-containing plasma cells in gastric mucosa with *helicobacter pylori* infection: "Russell body gastritis". Pathol Int 48:242–244

Virchows Arch (2005) 446: 467–469
DOI 10.1007/s00428-004-1153-7

LETTER TO THE EDITOR

Simonetta Piana · Silvia Asioli · Alberto Cavazza

Benign Müllerian inclusions coexisting with breast metastatic carcinoma in an axillary lymph node

Received: 6 September 2004 / Accepted: 1 October 2004 / Published online: 23 March 2005
© Springer-Verlag 2005

Sir, Within lymph nodes, benign inclusions can occur and are typically found incidentally during regional dissection. Their importance relies on the differential diagnosis with metastatic carcinoma. Many types of inclusions have been reported, including salivary gland and breast tissue, squamous epithelium, thyroid follicles, mesothelial and melanocytic cells [5, 8], and Müllerian-type epithelium [8]. So called Müllerian inclusions are found almost exclusively in women and mainly in pelvic lymph nodes; their appearance is very similar to peritoneal endosalpingiosis and, like endosalpingiosis, they can mimic metastasis from ovarian carcinoma. Only one case of Müllerian inclusion has been described in sovradiaphragmatic lymph nodes thus far [1]. As they are usually found during lymph-node dissection, they can present alone or in association with several types of malignancies [6, 7]; recently, two cases have been reported associated with lymphangioleyomiomatosis in retroperitoneal lymph nodes [4]. We describe an additional case of Müllerian-type inclusion in an axillary lymph node, coexisting with a metastasis, in a woman with breast cancer.

A 44-year-old woman underwent a right superolateral quadrantectomy for breast cancer, with axillary lymph-node dissection. Grossly, the breast showed a 1.4-cm grayish lump; in the axillary dissection, 28 lymph nodes were found. The resected specimens were fixed in 10% buffered formalin, embedded in paraffin, sectioned, and stained with hematoxylin and eosin. Histologically, in the breast, a ductal infiltrating carcinoma was present; it was made up of solid nests and ribbons of epithelial cells, with round nuclei and abundant cytoplasm, with no evidence of tubular differentiation (Fig. 1a). Two lymph nodes showed some micrometastases (less than 2 mm) in the subcapsular sinuses,

S. Piana (✉) · S. Asioli · A. Cavazza
Arcispedale Santa Maria Nuova, Department of Pathology,
Viale Risorgimento 80,
42100 Reggio Emilia, Italy
e-mail: Simonetta Piana@asmn.re.it
Tel.: +39-0522-295919
Fax: +39-0522-296945

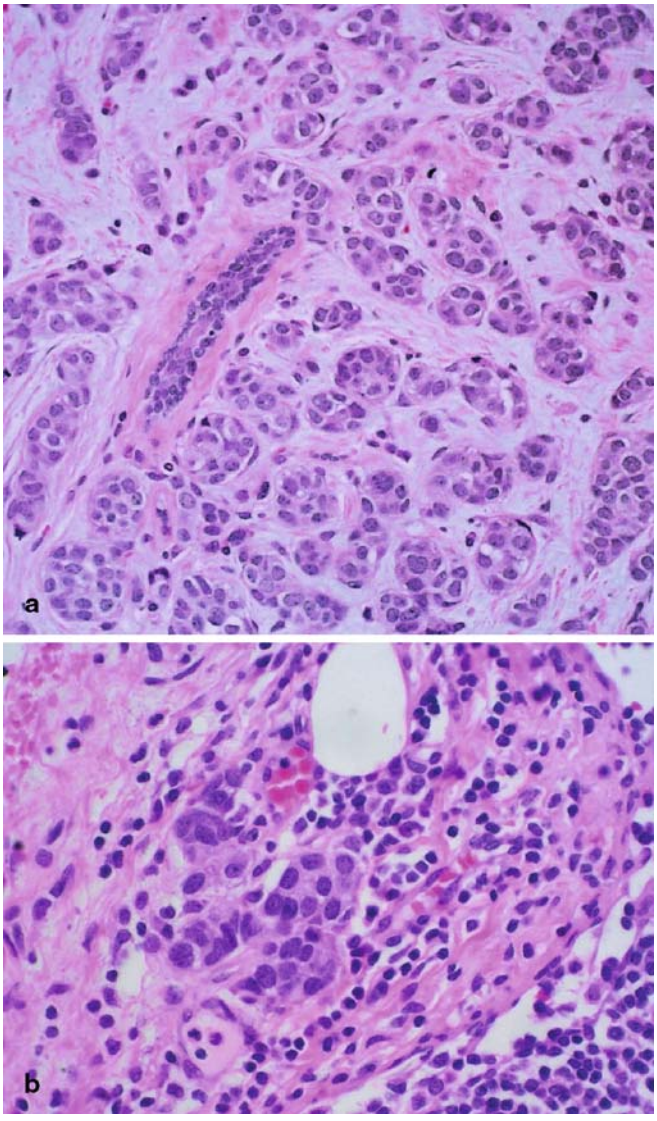

Fig. 1 The primitive breast carcinoma is constituted by solid nests and trabeculae of epithelial cells, without tubular differentiation (**a**). A high-power view of the solid, metastatic nests in the lymph node (**b**)

which were constituted by solid epithelial nests; their appearance reflects the morphological features of the primitive breast carcinoma (Fig. 1b).

In one of these lymph nodes, few glandular structures were noted within the capsule, clearly distinct from the micrometastasis, without an accompanying endometrial-like stroma (Fig. 2a). These glands were lined by a monolayer of low-cuboidal to columnar, bland ciliated cells, resembling Fallopian tube epithelium. In multiple sections, a little psammoma body was seen just below the epithelial lining (Fig. 2b). Immunohistochemically, the lining cells had a staining profile typical of the Müllerian system [2, 3], since they were strongly positive with cytokeratins AE1/AE3 and cytokeratin 7 (Fig. 3a), estrogen (Fig. 3b) and progesterone receptors (Fig. 3c); they resulted negative with cytokeratin 20 and CD10. Metastatic deposits were immunoreactive with cytokeratins AE1/AE3, cytokeratin 7 (Fig. 4a), and estrogen receptors (Fig. 4b); they resulted negative with progesterone, cytokeratin 20, and CD10.

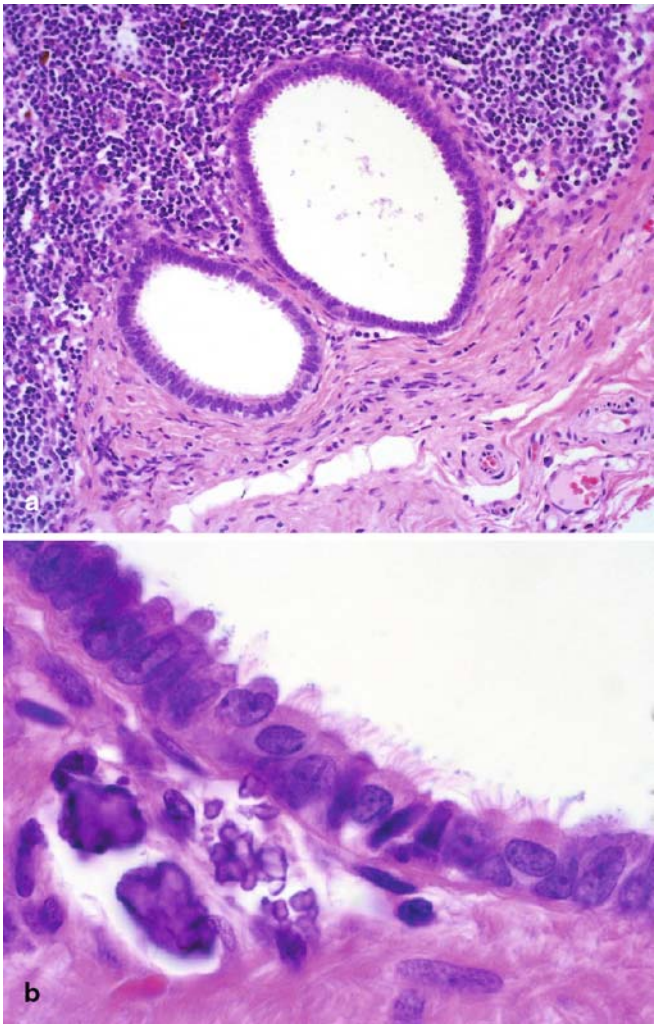

Fig. 2 Few glandular structures are present within the lymph-node capsule, without an accompanying endometrial-like stroma (**a**). The glands are lined by a monolayer of low-cuboidal to columnar, bland ciliated cells, with a little psammoma body just below the epithelial lining (**b**)

This lesion fulfils the morphological criteria for endosalpingiosis of the lymph node, that is, a Müllerian-type inclusion, quite common in pelvic lymph nodes but exceedingly rare in extraabdominal ones. Microscopic features favor the benign nature of the lesion, as it lacks mitoses, cellular atypia, and desmoplastic stromal reaction.

The present case is peculiar because of the previously unreported association between lymph-node endosalpingiosis and metastatic breast carcinoma; it is worth noting

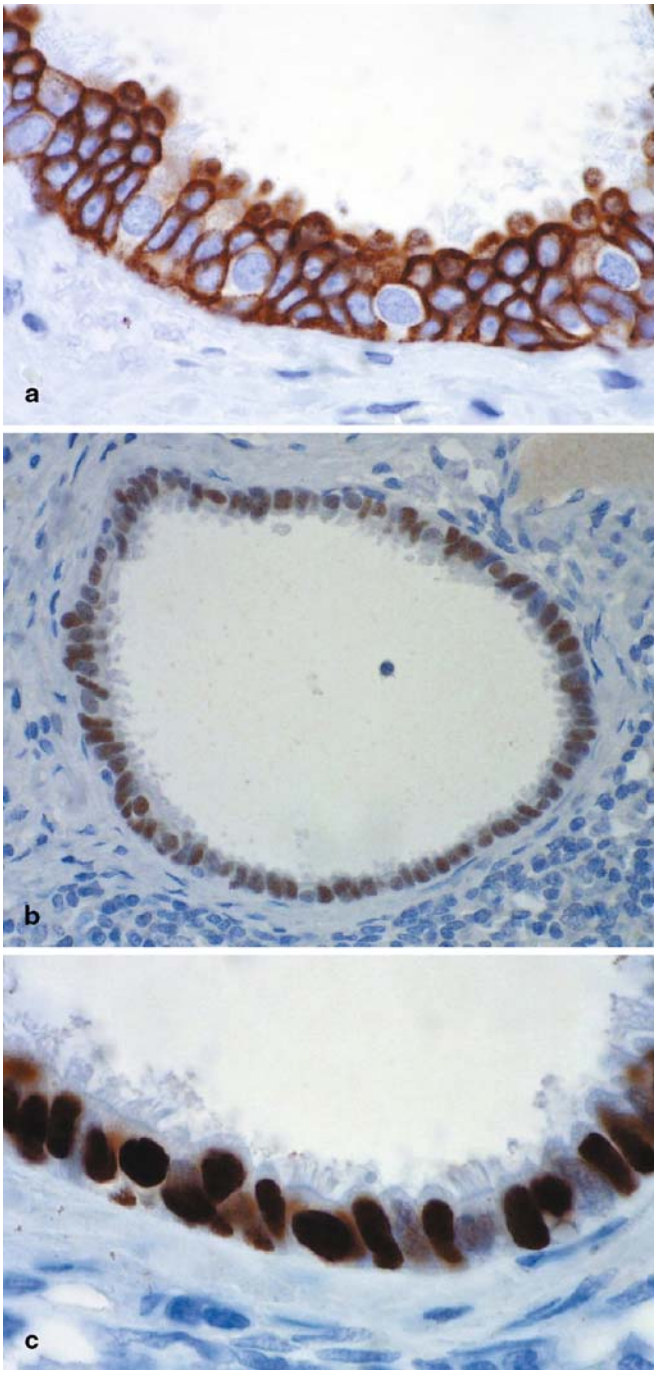

Fig. 3 The lining cells are immunoreactive with cytokeratin 7 (**a**), estrogen receptors (**b**), and progesterone receptor (**c**)

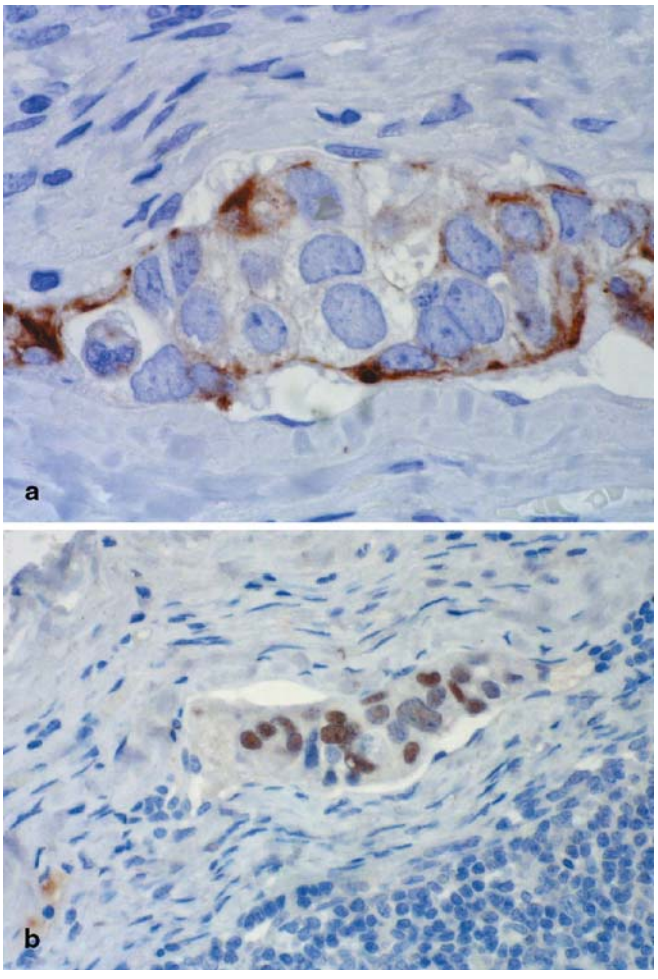

Fig. 4 Micrometastases are positive with cytokeratin 7 (**a**) and estrogen receptors (**b**)

that the immunohistochemical profile in Müllerian inclusions and in breast carcinoma is superimposable, and only morphological features allow the differential diagnosis.

References

1. Henley JD, Michael HB, English GW, Roth LM (1995) Benign Müllerian lymph node inclusions. An unusual case with implications for pathogenesis and review of the literature. Arch Pathol Lab Med 119:841–844
2. Horn LC, Bilek K (1995) Frequency and histogenesis of pelvic retroperitoneal lymph node inclusions of the female genital tract. An immunohistochemical study of 34 cases. Pathol Res Pract 191:991–996
3. Konishi E, Nakashima Y, Iwasaki T (2003) Immunohistochemical analysis of retroperitoneal Müllerian cyst. Hum Pathol 34:194–198
4. Matsui K, Travis WD, Gonzales R, Terzian JA, Rosai J, Moss J, Ferrans VJ (2001) Association of lymphangioleiomyomatosis (LAM) with endosalpingiosis in the retroperitoneal lymph nodes: report of two cases. Int J Surg Pathol 9:155–162
5. Parkash V, Vidwans M, Carter D (1999) Benign mesothelial cells in mediastinal lymph nodes. Am J Surg Pathol 23:1264–1269
6. Shen SC, Bansal M, Purrazzella R, Malviya V, Strauss L (1983) Benign glandular inclusions in lymph nodes, endosalpingiosis and salpingitis isthmica nodosa in a young girl with clear cell adenocarcinoma of the cervix. Am J Surg Pathol 7:293–300
7. Tsuchiya A, Kikuchi Y, Matsuoka T, Yashima R, Abe R, Suzuki T (1999) Endosalpingiosis of non metastatic lymph nodes along the stomach in a patient with early gastric cancer: report of a case. Surg Today 29:264–265
8. Warnke RA, Weiss LM, Chan JKC, Clery ML, Dorfman RF (1995) Glandular inclusions in lymph node. In: Tumors of the lymph nodes and spleen, Atlas of tumor pathology, 3rd series, AFIP, Washington

Virchows Arch (2005) 446: 470–472
DOI 10.1007/s00428-004-1200-4

LETTER TO THE EDITOR

Ondrej Daum · Jiri Klecka · Jiri Ferda · Vladimir Treska · Tomas Vanecek · Radek Sima · Petr Mukensnabl · Michal Michal

Gastrointestinal stromal tumor of the pancreas: case report with documentation of KIT gene mutation

Received: 17 August 2004 / Accepted: 12 December 2004 / Published online: 9 March 2005
© Springer-Verlag 2005

Sir, mesenchymal tumors of the pancreas are exceedingly rare, accounting for less than 1% of all pancreatic tumors, and most of them have been reported in small series or as single case reports. This group of pancreatic tumors includes leiomyosarcoma, malignant peripheral nerve sheath tumor, malignant fibrous histiocytoma, liposarcoma, rhabdomyosarcoma, hemangiopericytoma, schwannoma and solitary fibrous tumor. In the gut, mesenchymal tumors are more common, and the majority of these are formed by gastrointestinal stromal tumors (GISTs). GISTs are defined as KIT-positive mesenchymal spindle cell or epithelioid neoplasms showing differentiation toward the interstitial cell of Cajal. GISTs occur most commonly in the stomach (60–70%), small intestine (20–25%), colorectum (5%) and esophagus (<5%). They were also occasionally reported in extragastrointestinal sites, such as urinary bladder, gallbladder, omentum and mesentery [1]. We report a case of a GIST of the pancreatic head in a 70-year-old woman exhibiting all diagnostic histopathological, immunohistochemical and molecular genetic features, which has not yet been properly documented in this location. Although Neto et al. published a case of pancreatic GIST recently, evaluation of c-kit mutations as well as computed tomography (CT) scan or microphotograph documenting pancreatic location of the tumor is missing in their report [7].

Our case concerns a 70-year-old Caucasian woman who was incidentally found to have an epigastric mass during physical examination performed for a uroinfection in November 2003. Otherwise, there were no clinical signs of biliary obstruction, and tumor markers were negative. CT scans showed a tumorous cystic-like lesion with low-density values in the central part of the tumor, with a 5- to 8-mm-thick rim enhanced very strongly in the arterial phase. The solid part of the tumor contained grain-like calcifications. The tumor was localized in the pancreatic head, and the surrounding parenchyma showed signs of involution. There were no signs of dilatation of the biliary or pancreatic ducts. Duodenum was displaced by expansion of the tumor peripherally. The size of the tumor was 5×4×5 cm (Fig. 1).

Whipple's hemipancreatoduodenectomy with pancreatojejunoanastomosis, choledochojejunoanastomosis and gastrojejunoanastomosis (Heidelberg modification) was performed in December 2003. Dilatation of biliary and pancreatic ducts was absent. The diameter of the choledochus was 0.9 cm, the diameter of the pancreatic duct distal to the tumor was only 1 mm, thus causing the pancreatojejunoanastomosis to be difficult to perform.

On macroscopic examination, a 10×8×6 cm tumor was found in the head of the pancreas. The distance from the resection margin was 2 mm. It was unencapsulated and well demarcated but shown to infiltrate the duodenal wall. The cut surface was rubbery and white, with zones of necrosis, hemorrhage and a central 4×2×2 cm irregular cavity filled with serous-hemorrhagic fluid and debris.

Histologically, the tumor was adjacent to pancreatic glandular tissue (Fig. 2); it consisted predominantly of spindle cells with acidophilic cytoplasm and plump nuclei

O. Daum · P. Mukensnabl
Sikl's Department of Pathology,
Medical Faculty Hospital,
E. Benese 13,
305 99 Plzen (Pilsen), Czech Republic

J. Klecka · V. Treska
Surgical Clinic,
Medical Faculty Hospital,
Alej Svobody 80,
323 18 Plzen (Pilsen), Czech Republic

J. Ferda
Radiological Clinic,
Medical Faculty Hospital,
Alej Svobody 80,
323 18 Plzen (Pilsen), Czech Republic

T. Vanecek · R. Sima · M. Michal (✉)
Sikl's Department of Pathology,
Laborator Spec. Diagnostiky,
Medical Faculty Hospital,
Alej Svobody 80,
323 18 Plzen (Pilsen), Czech Republic
e-mail: michal@medima.cz
Tel.: +420-19-603886633
Fax: +420-19-377104650

Fig. 1 Abdominal computed tomography scan: axial image showing the cystic-like lesion of the pancreatic head

with prominent nucleoli. However, some parts of the mass primarily contained epithelioid cells. Perinuclear vacuolization in neoplastic cells was quite common. Peripheral parts of the tumor were cellular with fascicular arrangement, focally reminiscent of a schwannoma-like nuclear palisading pattern. Skeinoid fibers were readily discernible in the extracellular matrix. Central parts were hypocellular, showing perivascular hyalinization, myxoid changes of the stroma, foci of hemorrhagic necrosis and cystic degeneration. The hyalinized areas showed small foci of calcifications as well. We observed 2 mitoses per 50 high-power fields (HFP). The tumor infiltrated into the muscularis propria of the adjacent duodenal wall; however, nearly the whole bulk of the tumor mass was located in the pancreatic head, whereas only peripheral layers of the duodenal muscular wall were infiltrated. Immunohistochemically, neoplastic cells were positive for antibodies against vimentin, CD117 (Fig. 3), smooth-muscle actin and muscle-specific actin; whereas, reactions with antibodies against cytokeratins, S-100, CD34 and desmin were negative. Proliferative index counted as a proportion of MIB-1-positive cells was 2%. On molecular genetic examination, deletion of six base pairs in exon 11 of c-kit, causing loss of Gln at position 556 and Trp at position 557 of the KIT protein, were found.

The postoperative course was complicated, with moderate bronchopneumonia and formation of an external pancreatocutaneous fistula treated by drainage. The fistula disappeared in May 2004. Since then, the patient has been doing well, with no evidence of tumor recurrence or metastases on an abdominal CT scan performed at the end of May 2004. The patient is currently treated according to the STI-571 protocol.

To the best of our knowledge, this is the first proper description of a pancreatic GIST, since the above-mentioned case of Neto et al. lacks evaluation of c-kit mutations as well as CT scan or microphotograph documenting pancreatic location of the tumor. We think that the localization of such a dominant bulk within the pancreas together with the fact that the tumor caused displacement of adjacent duodenum on CT scans are sufficient to consider the pancreas as the primary site of the tumor. We cannot fully exclude that some cases of pancreatic GISTs are hidden behind the diagnoses of leiomyosarcomas that are occasionally described in small series or as single cases [4, 6, 8]. However, differential diagnosis between smooth-muscle tumors and GISTs is of crucial importance. Neither leiomyoma nor leiomyosarcoma can be successfully treated by the recently developed efficient therapy by the inhibitor of the tyrosine kinase activity of c-kit, known as STI-571 (imatinib mesylate, Gleevec) used for treating GISTs. Although there may be some morphological overlap between smooth-muscle tumors and GIST, the overwhelming majority of cases can be diagnosed by immunohistochemistry, in regard to the fact that smooth-muscle tumors tend to be desmin positive and KIT negative, in contrast to GISTs—most of which are KIT positive and desmin negative [5]. As for the biological behavior of GISTs, a few reports stated several markers predicting potential for aggressive growth or metastasizing of the tumor, varying from one author to

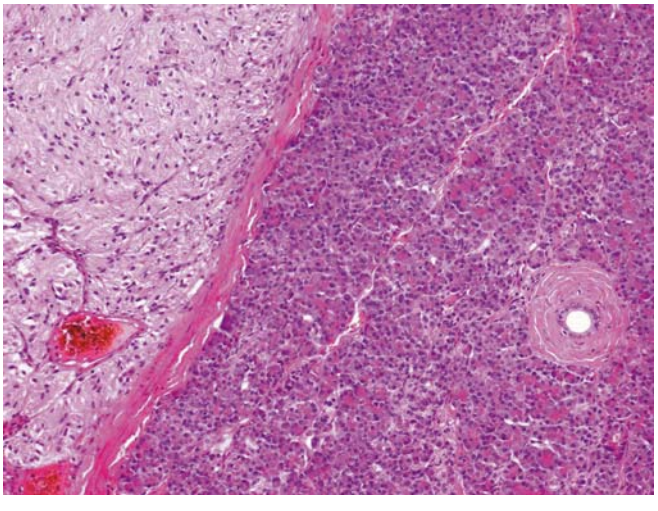

Fig. 2 Gastrointestinal stromal tumor adjacent to the pancreatic acini. Hematoxylin and eosin, ×100

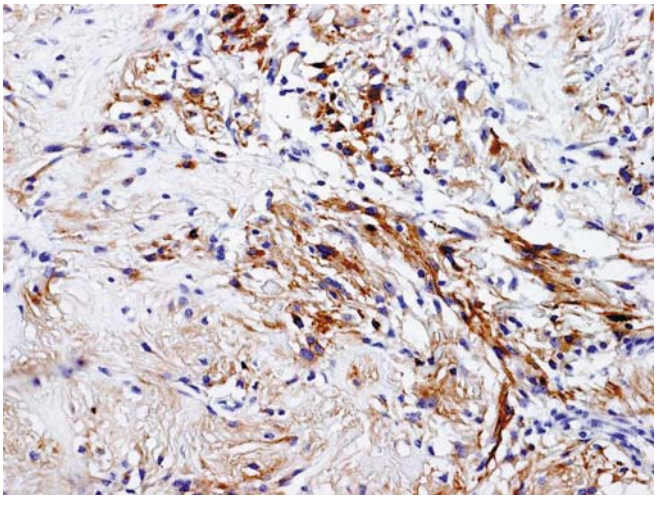

Fig. 3 CD117 immunohistochemical positivity of the spindle cells. CD117, ×200

another. Currently, according to the National Institutes of Health Consensus Conference, tumor size and mitotic count are accepted as the most important predictors of aggressive behavior [2].

The case of pancreatic GIST reported by Neto et al. was considered to belong to the "high-risk" category because of its large size. Unfortunately, mutational status of KIT gene of the tumor was not mentioned in their article.

Our case was a 10-cm large predominantly spindle cell tumor with foci of necrosis, and its mitotic count was 2/50 HPFs. Therefore, it belongs to the "intermediate risk of aggressive behavior" category of the classification provided by the Consensus Conference. Results of molecular genetic investigation, which revealed deletion of six base pairs in exon 11 of c-kit, causing loss of Gln at position 556 and Trp at position 557 of the KIT protein, further support the prediction of aggressive behavior according to some authors. Heinrich even claims that systematic sequencing of exon 11 of c-kit, which encodes the juxtamembrane domain of KIT protein, coupled with evaluation of the entire c-kit coding sequence in GISTs that lack juxtamembrane region mutations, reveals oncogenic c-kit mutations in most GISTs, irrespective of histological grades [3].

In conclusion, we report the first case of primary pancreatic GIST with not only radiological and immunohistochemical but with molecular genetic documentation of mutation of KIT gene.

References

1. Dei Tos AP (2003) The reappraisal of gastrointestinal stromal tumors: from Stout to the KIT revolution. Virchows Arch 442: 421–428
2. Fletcher CDM, Berman JJ, Corless C, Gorstein F, Lasota J, Longley BJ, Miettinen M, O'Leary TJ, Remotti H, Rubin BP, Shmookler B, Sobin LH, Weiss SW (2002) Diagnosis of gastrointestinal stromal tumors: a consensus approach. Hum Pathol 33:459–465
3. Heinrich MC, Rubin BP, Longley BJ, Fletcher JA (2002) Biology and genetic aspects of gastrointestinal stromal tumors: KIT activation and cytogenetic alterations. Hum Pathol 33:484–495
4. Komoda H, Nishida T, Yumiba T, Nishikawa K, Kitagawa T, Hirota S, Ito T, Matsuda H (2002) Primary leiomysarcoma of the pancreas—a case report and case review. Virchows Arch 440:334–347
5. Miettinen M, Lasota J (2001) Gastrointestinal stromal tumors—definition, clinical, histological, immunohistochemical, and molecular genetic features and differential diagnosis. Virchows Arch 438:1–12
6. Nesi G, Pantalone D (2001) Primary leiomyosarcoma of the pancreas. A case report and review of the literature. Arch Pathol Lab Med 125:152–155
7. Neto MRM, Machuca TN, Pinho RV, Yuasa LD, Bleggi-Torres LF (2004) Gastrointestinal stromal tumor: report of two unusual cases. Virchows Arch 444:594–596
8. Zalatnai A, Kovács M, Flautner L, Sipos B, Sarkady E, Bocsi J (1998) Pancreatic leiomyosarcoma. Case report with immunohistochemical and flow cytometric studies. Virchows Arch 432:469–472

Virchows Arch (2005) 446: 473–474
DOI 10.1007/s00428-005-1270-y
© Springer-Verlag 2005

ANNOUNCEMENTS

9–13 May 2005
Diagnostic Histopathology of Breast Disease
Hammersmith Hospital (Imperial College Faculty of Medicine), London, UK

A week-long course designed for pathologists at Consultant and Senior Trainee level. The course provides a comprehensive coverage of the Histopathology of Breast Disease, with special emphasis on areas that pose diagnostic difficulties. The participants with be given ample time to study histological preparations, followed by illustrated discussion of the cases. There will be special sessions dealing with the interpretation of core biopsies and fine needle aspirations. There will also be several daily talks dealing with specific topics, given by eminent breast pathologists and followed by discussion. The topics will include reporting breast biopsies, immunohistochemistry, receptors and c-erbB-2 assessment, dealing with the gross specimen, prognostic factors, proliferative lesions/carcinoma in situ, problems in breast pathology and mucinous lesions of the breast. The faculty will include Ian Ellis, Christopher Elston, Andrew Hanby, Stephen Humphreys, Andrew Lee, Naomi Livni, Sarah Pinder and Sami Shousha

Further details from:
Wolfson Conference Centre,
Hammersmith Hospital,
Du Cane Road,
London W12 ONN, UK
Tel.: (44) 20 8383 31 17/3227/3245
Fax (44) 20 8383 2428
E-mail: wcc@imperial.ac.uk

2–3 June 2005
Thyroid Pathology for the Practicing Pathologist
15 rue de lEcole de Mdecine, Paris, France

A 2-day course will take place in Paris again under the auspices of the French Division of the I.A.P.
This course will be given in English by Prof.M.Sobrinho-Simoes (Porto) and Prof.R.Heimann (Brussels).
It will consist of lectures alternating with slide reviews and a slide seminar over a multihead microscope. The cases of this seminar will be sent (on CD) before the meeting.
The audience will be limited to 22 participants.
Course fees: 390 euros (320 euros for members of any I.A.P. division). The fees include registration,hand-out, CD of the slide seminar and coffee breaks.

For further information please contact:
Mrs.M. Fontanire
Administrative Secretary
French Division of the I.A.P.
32 Cours Albert Thomas
69008, Lyon, France
Fax: +33 4 78754311
E-mail: academie.pathologie@wanadoo.fr

3–4 June 2005
16th Ljudevit Jurak International Symposium on Comparative Pathology
Under the auspices of the European Society of Pathology and Academy of Medical Sciences of Croatia
Multimedial center Sestre milosrdnice University Hospital, Zagreb, Croatia

The main symposium topic is surgical pathology and frozen sections analysis. Symposium includes following sections: Pathological Morphology of the Human and Animal Diseases, Iatrogenic, Environmental and Experimental Pathology, Herman Jurak Round Table on Rheumatological Pathology, Clinical Forensic Pathology, Slide Seminars *in Histopathology and Cytopathology*, Quiz on Pathology.

Registration fee before April 1st – 100 EUR
Registration fee after April 1st – 150 EUR

Information: Davor Tomas, M.D.
Ljudevit Jurak University
Department of Pathology
Sestre milosrdnice University Hospital
Vinogradska 29
10000 Zagreb, Croatia
Tel.: +385 / 3787 909
Fax: +385 / 3787 244
E-mail: juraks@kbsm.hr
http://www.kbsm.hr/Jurak/symposium.htm

13–24 June 2005
International course on Laboratory Animal Science
Utrecht, The Netherlands

A two week intensive course on laboratory animal science will be organized at the Division of Laboratory Animal Science – Utrecht, The Netherlands in June 2005. This course is organized once a year since 1993.
The objective of this course is to present basic facts and principles that are essential for the humane use and care of animals and for the quality of research.
The contents of the course are in line with recommendations of the Federation of European Laboratory Animal Science Associations (FELASA) regarding the training of the young scientist whose research involves the use of vertebrate animals.
The course may also be of interest for those who intend to set up a similar course at their location. For this purpose, during the course the acquisition of teaching materials can be discussed with the course committee.

For information and application forms please contact:
Mr. Stephan van Meulebrouck, MA
Division of Laboratory Animal Science
Faculty of Veterinary Medicine
P.O. Box 80.166
3508 TD Utrecht
The Netherlands
Tel.: +31-30-2532033
Fax: +31-30-2537997
E-mail: pdk@las.vet.uu.nl
Internet: http://las.vet.uu.nl>Education and Training>International Course

26–29 July 2005
Practical Pulmonary Pathology
London, UK

This course is designed to provide histopathology and cytopathology trainees and consultants with an opportunity to study diagnostic lung pathology in a comprehensive manner. It comprises lectures and practical microscopy sessions, the latter making up roughly half the time and consisting of individual study of a unique collection of cases.

Further details and application forms are available from:
Professor B Corrin
Brompton Hospital
London SW3 6NP, UK
Fax: +44 20 7351 8293
E-mail: b.corrin@ic.ac.uk

22–23 September 2005
Breast Diagnostic Histopathology Update
Hammersmith Hospital (Imperial College), London, UK

A 2-day course designed for pathologists at Consultant and Senior Trainee level. The course is a shorter version of the week long course and is also suitable for those who have previously attended that course and wish to participate in discussing new developments in the field. The course will be based on 30, mostly new, cases derived from the arcives of Hammersmith, Charing Cross, Nottingham City and Cambridge Addenbrook's Hospitals and is slanted to practical diagnostic pathology with special emphasis on areas that pose diagnostic difficulties. The participants will be given ample time to study histological preparations, followed by illustrated discussion of the cases. In addition there will be several talks on specific topics, given by breast pathology specialists followed by discussions. The topics will include issues in the interpretation of breast biopsies, examination of breast biopsies after neo-adjuvant chemotherapy, breast immunohistochemistry, dealing with the gross specimen, fibro-epithelial and spindle cell lesions; papillary, lobular, apocrine and metaplastic lesions, proliferative lesions/ carcinoma in situ and sentinel lymph node biopsy. The faculty will include Ian Ellis, Mary Falzon, Andrew Lee, Sarah Pinder and Sami Shousha.

Further details from:
Wolfson Conference Centre,
Hammersmith Hospital,
Du Cane Road,
London W12 ONN, UK
Tel.: (44) 20 8383 3117/3227/3245
Fax: (44) 20 8383 2428
E-mail: wcc@imperial.ac.uk

1–2 December 2005
International Symposium on "Salivary Gland Tumours; Present Concepts of Diagnosis and Management"
Amsterdam, The Netherlands

For further information please contact congress secretariat
Mrs. D. Chavalking
Vrije Universiteit Medical Center (Vumc)
Department of Oral and Maxillofacial Surgery/Oral Pathology
PO Box 7057
1007 MB Amsterdam
The Netherlands
Tel.: +31-20-444-4039
Fax: +31-20-444-4046
E-mail: d.chevalking@vumc.nl
Internet: www.vumc.nl

Virchows Arch (2005) 446: 475–482
DOI 10.1007/s00428-005-1264-9

REVIEW ARTICLE

Xavier Dolcet · David Llobet · Judit Pallares · Xavier Matias-Guiu

NF-kB in development and progression of human cancer

Received: 21 January 2005 / Accepted: 30 March 2005 / Published online: 27 April 2005
© Springer-Verlag 2005

Abstract The nuclear factor kB (NF-kB) comprises a family of transcription factors involved in the regulation of a wide variety of biological responses. NF-kB plays a well-known function in the regulation of immune responses and inflammation, but growing evidences support a major role in oncogenesis. NF-kB regulates the expression of genes involved in many processes that play a key role in the development and progression of cancer such as proliferation, migration and apoptosis. Aberrant or constitutive NF-kB activation has been detected in many human malignancies. In recent years, numerous studies have focused on elucidating the functional consequences of NF-kB activation as well as its signaling mechanisms. NF-kB has turned out to be an interesting therapeutic target for treatment of cancer.

Keywords NF-kB · Cancer · Apoptosis

The NF-κB signaling pathway

NF-κB is not a single gene but a family of closely related transcription factors that includes five genes NF-κB1 (p50/p105), NF-κB2 (p52/p100), RelA (p65), c-Rel and RelB. These five genes give raise to seven proteins that share a Rel Homology Domain (RHD) in their sequence. The RHD mediates their dimerization, interaction with their specific inhibitors, and DNA binding. There are two types of NF-κB proteins [32]: 1) RelA, c-Rel and RelB are synthesized in their mature forms and contain a transactivation domain which interacts with the transcriptional apparatus; and 2) NF-κB1-p105/p50 and NF-κB2-p100/p52 that are synthesized in a precursor form. The precursor forms (p100 and p105) contain C-terminal ankyrin repeats that are proteolysed by the proteasome resulting in the production of the mature (p50 and p52) proteins. Both p50 and p52 contain the DNA binding domain but lack a transactivation domain.

In most types of cells, NF-κB dimers are predominantly cytoplasmic due to their interaction with the inhibitors of NF-kB (IkBs) and therefore remain transcriptionally inactive. The IkBs (IkBα, IkBβ, IkBε and Bcl-3) encompass a family of proteins that contain ankyrin repeats, which interact with the RDH domains of NF-κB proteins. IkBα, IkBβ and IkBε interact with NF-κB dimers, being responsible for their retention in the cytoplasm. Bcl-3 is a peculiar member of the family, because it contains a transactivation domain and may interact with p50 or p52 homodimers, acting as a transcriptional coactivator. IkBα, IkBβ, and IkBε contain two conserved serines that become phosphorylated by the IkB kinases (IKKs). Upon phosphorylation, IkBs undergo proteasome-dependent degradation [32]. The IKK is a complex formed by the catalytic IKKα and IKKβ subunits and the regulatory subunit IKKγ.

Activation of NF-κB may result from different signaling pathways triggered by a variety of cytokines, growth factors and tyrosine kinases. Enhanced expression of members of the epidermal growth factor receptor, insulin growth factor receptor, and tumor necrosis factor receptor families may be responsible for NF-κB activation. Moreover, activation of other signaling pathways, such as Ras/MAPK and PI3K/Akt, are also involved in activation of NF-kB.

Different molecular mechanisms of NF-κB activation have been proposed (Fig. 1) [2, 20]. In the so-called *canonical* or *classical* NF-κB pathway, dimers contain either RelA or c-Rel, together with p50. The dimers are held inactive in the cytoplasm by their interaction with IkB proteins (Ghosh and Karin, 2002; 17, 20]. This pathway is typically triggered by pro-inflammatory cytokines and viral infections. Upon activation, the IKKβ subunit is the major responsible for IkB phosphorylation in serine residues. After phosphorylation, IkB proteins undergo ubiquitin-dependent degradation by the proteasome, and NF-κB is translocated to the nucleus, where it acts as nuclear transcription factor. Figure 2 shows nuclear translocation of RelA sub-

X. Dolcet · D. Llobet · J. Pallares · X. Matias-Guiu (✉)
Department of Pathology and Molecular Genetics,
Hospital Universitari Arnau de Vilanova,
University of Lleida,
Av Alcalde Rovira Roure 80,
25198 Lleida, Spain
e-mail: xmatias@arnau.scs.es

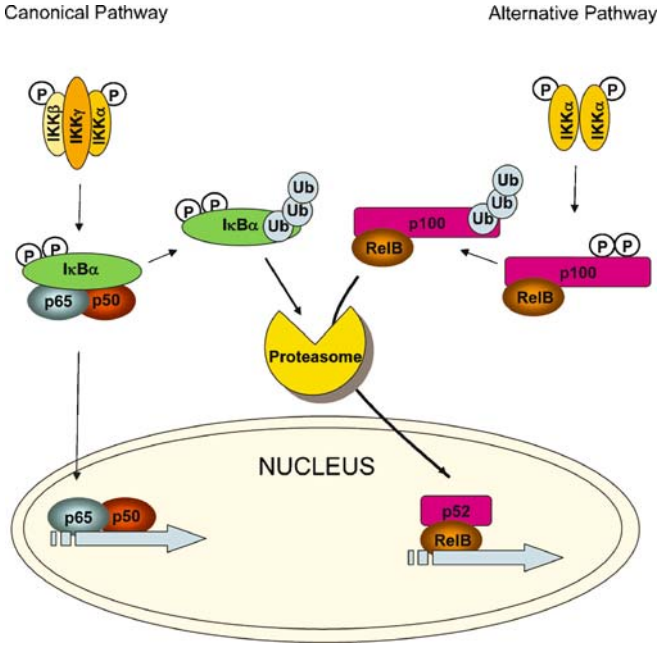

Fig. 1 Canonical and alternative pathways of NF-kB activation

unit in endometrial stromal cells as a result of stimulation with TNF-α, by the canonical pathway.

The *alternative pathway* is activated by members of the tumor necrosis factor (TNF) family, such as lymphotoxin B and BAFF. The dimers contain RelB and p100 subunits [60]. This pathway mainly activates IKKα, which phosphorylates p100 that is subsequently proteolysed to generate the p52 mature form [17, 59]. Then, the dimers translocate to the nucleus, where they can activate transcription of specific target genes.

Although the dimers that result from the canonical and alternative pathways are the most commonly produced (RelA-p50, c-Rel-p50, RelB-p52), other types of heterodimers (c-Rel-RelA, c-Rel-c-Rel) or homodimers (p50–p50 and p52–p52) may also be generated. Each NF-κB dimer is likely to have distinct regulatory functions.

As mentioned before, unlike the other members of the IKB family, Bcl-3 associates with p50 or p52 homodimers in the nucleus to act as a transcriptional co-activator.

Activation of NF-κB must be a tightly regulated event. In normal cells, NF-κB becomes activated only after the appropriate stimuli, and up-regulates the transcription of its target genes. Afterwards, regulatory mechanisms return NF-κB to its inactive state. NF-κB activation is therefore an inducible and transient process. In tumoral cells, different types of molecular alterations may result in impaired regulation of NF-κB activation. In such case, NF-kB loses its inducibility and becomes constitutively activated. This leads to deregulated expression of genes under NF-κB control. Among them, there are genes involved in regulation of apoptosis, cell cycle control, adhesion or migration. Since alterations in all these processes participate in development and progression of cancer, there is a clear link between NF-κB and carcinogenesis.

Regulation of apoptosis

NF-κB may activate the transcription of several genes involved in the suppression of cell death by both mitochondrial (intrinsic) and death receptor (extrinsic) pathways. NF-κB may up-regulate the expression of proteins that interfere the death receptor apoptotic pathway. One of these target proteins is the FLICE-like inhibitory protein (FLIP)

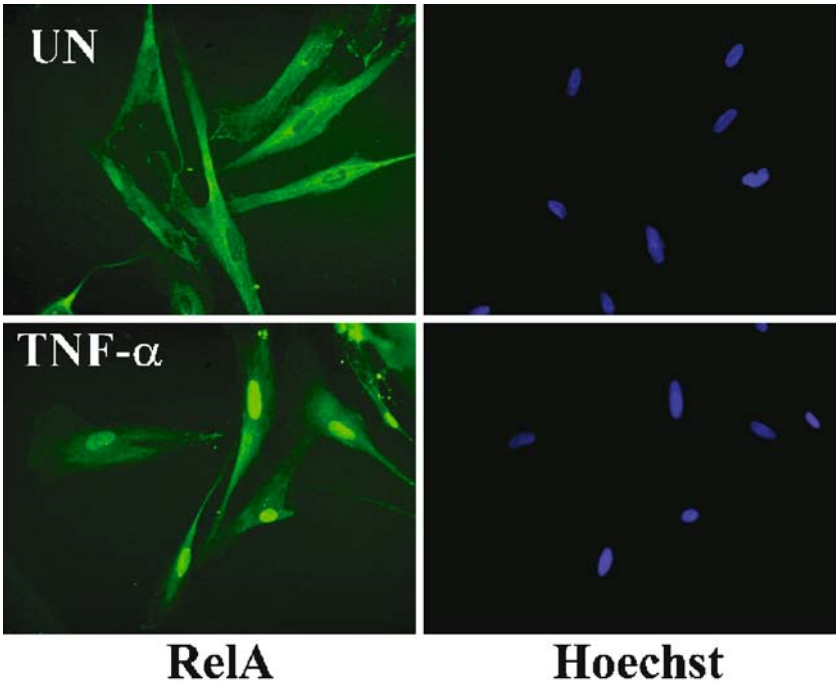

Fig. 2 Nuclear translocation of p65/RelA in endometrial stromal cells as a result of stimulation with TNFα

[35, 41]. FLIP shares a high degree of homology with caspase-8 but lacks protease activity and competes with caspase-8 for the binding to the Death-Inducing Signaling Complex (DISC). Thus, high levels of FLIP prevent caspase-8 recruitment to the DISC. Up-regulation of FLIP has been reported in many tumors. It is believed that FLIP expression may explain the resistance to death receptor apoptosis in some types of tumor [3, 18, 28, 29, 50, 52, 63]. Other proteins of the TNF-α signaling cascade such as TRAF2 and TRAF6 may also be targets of NF-κB. These proteins may lead to activation of pro-survival signaling by TNF [67].

NF-κB also induces the expression of the Inhibitors of Apoptosis (IAPs) [13, 62, 67] and some members of the anti-apoptotic Bcl-2 family [10, 37]. The IAPs (c-IAP1, c-IAP2, and XIAP) suppress apoptosis induced by both extrinsic and intrinsic pathways through direct inhibition of effector caspases (caspases-3, -6, -7, and 9), whereas the anti-apoptotic members of the bcl-2 family antagonize the function of the proapoptotic members A1/BFL1 and Bcl-XL.

We have mentioned before that the PI3K/Akt signaling pathway may be responsible for activation of NF-κB. The PTEN tumor suppressor gene is a negative regulator of the pro-survival PI3K/Akt signaling pathway. Thus, abnormalities in PTEN may aberrantly activate the PI3K/Akt pathway, and subsequently NF-κB. However, two recent reports have shown that NF-kB may also down-regulate the expression of PTEN [34, 66]. Thus, a decrease in PTEN expression may cause increased Akt activity and suppression of apoptosis [12]. Genetic alteration of both alleles of PTEN occurs in a wide variety of human cancers, with the highest frequency of inactivation in glioblastoma and endometrial carcinoma [38, 39]. In many tumors, the frequency of reduced PTEN expression exceeds that of genetic alteration. Although epigenetic inactivation of PTEN by promoter methylation may account for decreased PTEN expression in a percentage of cases, it seems obvious that the constitutive activation of NFkB could be responsible for down-regulation of PTEN in an additional subset of tumors.

It is generally accepted that NF-κB activation is responsible for apoptosis resistance. However, recent evidences support a pro-apoptotic role of certain dimers of NF-κB. It has been speculated that NF-kB may exert a dual function, either as an inhibitor or an activator of apoptotic cell death, depending on the levels of RelA and c-Rel [9].

Furthermore, NF-κB may interfere with the transcriptional activity of p53, since it inhibits p53-induced apoptosis, by up-regulating anti-apoptotic genes, and down-regulating p53 levels.

Regulation of proliferation and invasiveness

NF-κB promotes cell cycle progression, by regulating the expression of several genes involved in the cell cycle machinery such as cyclins D1, D2, D3 and cyclin E [19, 22, 23, 27], c-myc and c-mycb [8, 14, 36, 64]. NF-kB-induced cyclin D1 expression appears to be a key element in mammary gland development and breast carcinogenesis [73]. As happens in apoptosis, in some scenarios NF-kB may have growth inhibitory effects. For example, NF-kB activation can suppress the proliferation of keratinocytes [21] and c-Rel overexpression induces cell cycle arrest in HeLa cells [1].

On the other hand, NF-κB induces the expression of cell adhesion molecules (ICAM-1, E-selectin), and proteins involved in invasion (matrix metalloproteinases). Several angiogenic factors, including vascular endothelial growth factor (VEGF), are also promoted by NF-κB. Moreover, NF-κB induces the expression of cycloxygenase-2 (COX-2), which is important in many tumors, for example, colonic carcinoma.

NF-κB alterations in human cancer

Several animal models have provided evidences for a role of NF-κB in cancer. For example, v-Rel, a viral homologue of c-Rel, was identified as the transforming gene of an avian retrovirus, which is highly oncogenic, and causes aggressive lymphomas and leukemias in chickens [16]. v-REL is the oncoprotein of the reticuloendotheliosis (REV-T) retrovirus.

Moreover, some viral oncoproteins may interact with the IKK complex, and cause NF-kB activation. The Tax oncoprotein from the human T-cell leukemia virus I (HTLV-I) induces NF-κB activity, and activation of NF-κB was shown to be required for transformation of rat fibroblasts by HTLV-I tax protein [69]. Moreover, the Epstein–Barr virus, implicated in Burkitt's lymphoma and Hodgkin lymphoma, is also capable of inducing persistent NF-κB activation; the EBV nuclear antigen-2 (EBNA-2) and latent membrane protein-1 (LMP-1) increase NF-κB transcriptional functions [43].

A wide variety of haematopoietic proliferations may show alterations in the expression or activity of members of the NF-κB signaling pathway. For example, amplification of c-Rel, on chromosome 2p14-15, resulting in an increased gene expression, occurs in 23% cases of extranodal diffuse large cell lymphoma and non-Hodgkin B-cell nodal lymphomas [25, 30, 54]. However, recent evidences suggest that the amplification on 2p14-15, may not necessarily cause abnormal c-REL activation, suggesting that other genes at the vicinity of c-REL may be the real functional target of the amplification event [26].

Chromosomal rearrangements or deletions affecting the NF-κB2 locus, on chromosome 10q24, resulting in the loss of ankyrin repeats of p100 and generation of constitutively active p52 protein, have been associated with B-cell and T-cell lymphomas and multiple myelomas [42, 46, 47].

Some B-cell lymphocytic leukemias may present a t(14;19)(q32;q13) translocation. Bcl-3 is located on human chromosome 19q13 and it is located near to the chromosomal breakpoint [49]. This translocation results in increased expression of Bcl-3. Since Bcl-3 acts as a transcriptional co-activator of p50 or p52 homodimers, Bcl-3 overexpression leads to an increased NF-kB activity [4] and up-regulation

of its transcriptional targets such as cyclin D1 [68]. Recently, the expression of Bcl-3 has been analyzed in a large series of lymphomas [6].

The infrequent detection of genetic alterations of the genes coding for NF-κB subunits in human cancer has lead to the evaluation of other genes involved in the activation of NF-kB. One of the key regulators of NF-kB activation is the IkB family of proteins. Alterations in these genes may affect the ability of the IkBs to inhibit NF-kB, which would lead to constitutive NF-κB activity. Loss-of-function mutations in IkBα, resulting in high constitutive nuclear activity of NF-kB, are characteristic of Reed–Sternberg cells in Hodgkin lymphoma [5, 31]. This implies a tumor suppression function for IkBs.

It has also been shown that the oncogenic fusion protein BCR-ABL, which corresponds to the Philadelphia chromosome of chronic myeloid leukemia, may activate NF-κB [56]. Moreover, tumorigenesis driven by ABL-BCR-expressing cells may be blocked if NF-κB is inhibited.

In solid tumors, high levels of c-Rel have been found in non-small cell lung carcinoma [44] and breast cancer [61]. A recent report has provided direct evidence of the function of c-Rel in breast carcinogenesis. The authors generated a transgenic mouse that overexpressed c-Rel in the mammary gland; a 31.6% of mice developed one or more mammary tumours and had increased expression of NF-kB target genes, such as cyclin D1, c-myc and Bcl-XL [57]. Moreover, the classic forms of NF-κB (p50–p65) have been shown to be activated in some breast cancers, although other authors have found nuclear accumulation of p52 and Bcl-3 along with c-Rel, rather than p65. Finally, selective activation of Bcl-3, p50 and p52 is present in breast carcinoma compared with non-tumoral breast tissue, and correlates with increased expression of cyclin D1 [11].

NF-κB activation has been also identified in squamous cell carcinomas of the head and neck. Inhibition of NF-κB activity in these tumors inhibits cell survival and tumor growth. Active Bcl-3/p50 complexes have also been found in nasopharyngeal carcinoma [64].

Although RelA, RelB and NF-kB1 alterations are rare in human cancer, these subunits are constitutively activated in a wide variety of human tumors. Increased RelA nuclear localization or activity is present in many tumors and is associated with tumor progression. Nair et al. [45] demonstrated an increased NF-κB nuclear immunostaining and p65–p50 activity associated with progression in cervical squamous cell carcinomas. Gastric carcinoma shows increased nuclear translocation of RelA in comparison with adjacent normal epithelial cells. In gastric cancer, Rel A correlated with tumor invasion-related clinicopathological features such as lymphatic invasion of tumor cells, depth of invasion, peritoneal metastases and tumor size [58].

Moreover, defective IkBα were found in several solid tumors such as breast, colon, ovarian, pancreatic, bladder, prostate carcinomas and melanoma [55].

The upstream IkB kinases are also constitutively active in some types of cancer. The expression of IKKα has been correlated with increased expression of NF-kB and COX-2 in colorectal carcinomas. In contrast, absent or minimal expression of COX-2, NF-κB, and IKKa has been found in non-neoplastic colon epithelial cells [8].

Genetic alterations in signaling pathways that regulate NF-κB activation may also result in increased or constitutive NF-κB activity. Two proteins frequently mutated in human cancers are the tumor suppressor PTEN and Ras proto-oncogene. The possible role of PTEN has been previously discussed. NF-kB is an important downstream effector of oncogenic Ras transformation [15, 40, 48].

NF-κB and chemo/radio-resistance

Tumors with constitutive NF-kB activation usually show increased resistance to chemotherapy. NF-kB may be responsible for blocking the efficacy of chemotherapy and radiation in some types of tumor cells. It has been suggested that NF-kB may induce the expression of the multidrug resistance P-glycoprotein. In some tumors, cells exposed to radiation or certain chemotherapeutic drugs show enhanced activation of NF-kB. On the other hand, inhibition of NF-kB improves the apoptotic response to radiation therapy.

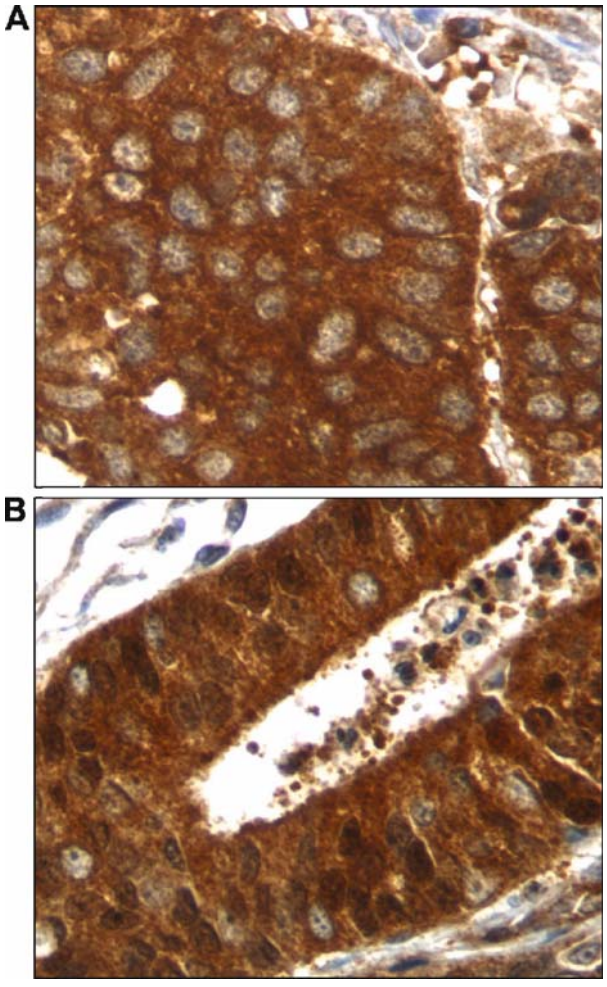

Fig. 3 Cytoplasmic (**a**) and nuclear (**b**) immunoreactivity for p65 in sections of an endometrioid carcinoma of the endometrium

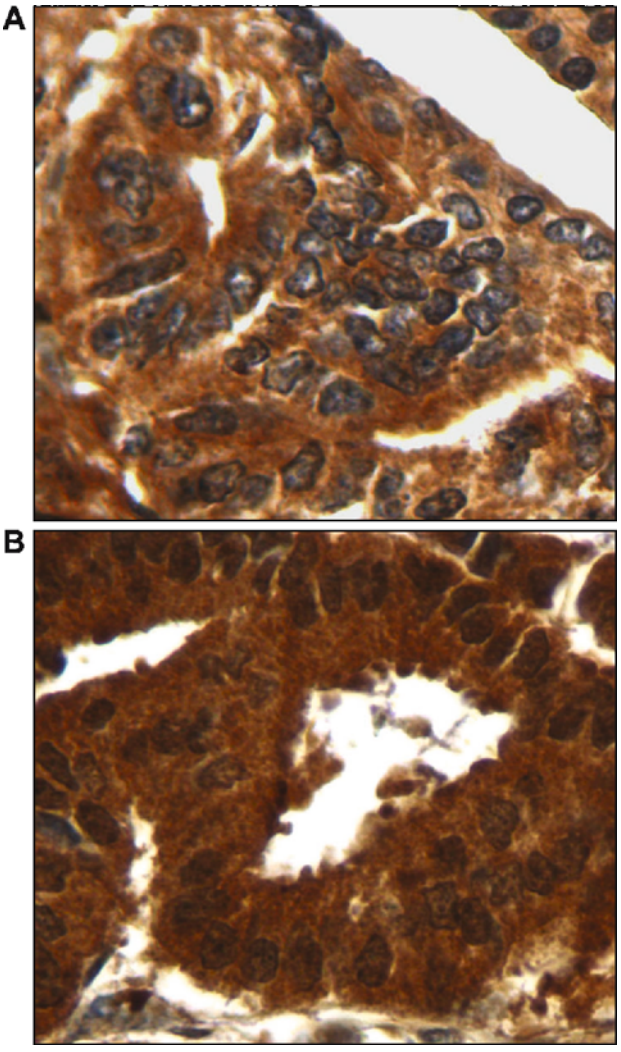

Fig. 4 Cytoplasmic (**a**) and nuclear (**b**) immunoreactivity for c-Rel in sections of an endometrioid carcinoma of the endometrium

NF-kB has also been suggested to be required for taxol-induced cell death.

NF-κB and cancer therapy

Several studies have addressed the identification of putative NF-kB inhibitors as therapeutic agents for cancer. Since NF-kB activation is the result of a multi-step signaling pathway, these compounds may target different points of the signaling process. For example, some anti-inflammatory drugs may inhibit NF-kB by interfering with IKK activity [70–72]. Other substances such as curcumin, trans-resveratrol or parthenolide are natural compounds that have been demonstrated to inhibit IKK activity [24, 33, 53, 70]. Another way to approach NF-kB inhibition is to target the process of proteasome degradation. Proteasome inhibitors prevent NF-kB activation by blocking the degradation of IkBs, NF-kB1/p105 or NF-kB2/p100.

Immunostaining for NF-κB

As shown in this review, there is much evidence pointing to a role for NF-κB activation, in tumor development and progression, but also in chemo- and radioresistance, and even in cancer therapy. Thus, it seems likely that pathologists will be asked to evaluate the status of NF-κB in tumors for investigational or practical purposes.

We have mentioned that activation of NF-κB signaling pathway results in translocation of NF-κB subunits to the nucleus. Therefore, NF-κB activation can be identified by the presence of positive nuclear immunostaining with antibodies specific for the different subunits of NF-κB. Figures 3 and 4 show the cytoplasmic and nuclear immunostaining that can be observed for the subunits RelA and c-Rel. Double staining procedures, or immunostaining of serial sections can be useful to identify the dimers involved in a specific type of cell, as well as the putative targets of

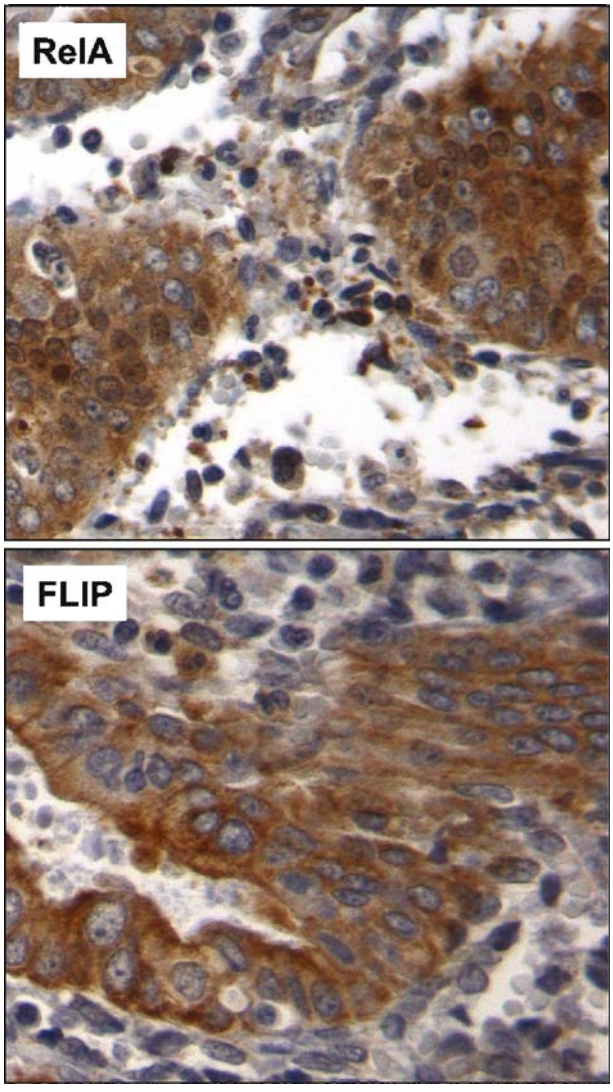

Fig. 5 Nuclear immunostaining for RelA in an endometrioid carcinoma of the endometrium associated with an increase in Flip immunoexpression

NF-κB activation. Figure 5 shows coexpression of RelA subunit with its putative target FLIP [51].

Acknowledgements Supported by grants FISS 01/1656, FISS PI020227, SAF 2004-05250 and 2002XT00115. X.D. holds a postdoctoral fellowship supported by Department d'Universitats, Recerca i Societat de la Informació, Generalitat de Catalunya (2003RED0018). J.P. holds a research fellowship from the Fondo de Investigaciones Sanitarias, Ministerio de Sanidad y Consumo (BEFI-02/9007). DLL holds a research fellowship from AECC-Catalunya contra el Cancer-Lleida.

References

1. Bash J, Zong WX, Gelinas C (1997) c-Rel arrests the proliferation of HeLa cells and affects critical regulators of the G1/S-phase transition. Mol Cell Biol 17:6526–6536
2. Bonizzi G, Karin M (2004) The two NF-kappaB activation pathways and their role in innate and adaptive immunity. Trends Immunol 25:280–288
3. Bullani RR, Huard B, Viard-Leveugle I, Byers HR, Irmler M, Saurat JH, Tschopp J, French LE (2001) Selective expression of FLIP in malignant melanocytic skin lesions. J Invest Dermatol 117:360–364
4. Caamano JH, Perez P, Lira SA, Bravo R (1996) Constitutive expression of Bc1-3 in thymocytes increases the DNA binding of NF-kappaB1 (p50) homodimers in vivo. Mol Cell Biol 16: 1342–1348
5. Cabannes E, Khan G, Aillet F, Jarrett RF, Hay RT (1999) Mutations in the IkBa gene in Hodgkin's disease suggest a tumour suppressor role for IkappaBalpha. Oncogene 18:3063–3070
6. Canoz O, Rassidakis GZ, Admirand JH, Medeiros LJ (2004) Immunohistochemical detection of BCL-3 in lymphoid neoplasms: a survey of 353 cases. Mod Pathol 17:911–917
7. Charalambous MP, Maihofner C, Bhambra U, Lightfoot T, Gooderham NJ (2003) Upregulation of cyclooxygenase-2 is accompanied by increased expression of nuclear factor-kappa B and I kappa B kinase-alpha in human colorectal cancer epithelial cells. Br J Cancer 88:1598–1604
8. Chen F, Castranova V, Shi X (2001) New insights into the role of nuclear factor-kappaB in cell growth regulation. Am J Pathol 59:387–397
9. Chen F, Wang M, O'Connor JP, He M, Tripathi T, Harrison LE (2003) Phosphorylation of PPARgamma via active ERK1/2 leads to its physical association with p65 and inhibition of NF-kappa beta. J Cell Biochem 90:732–744
10. Chen QM, Tu VC (2002) Apoptosis and heart failure: mechanisms and therapeutic implications. Am J Cardiovasc Drugs 2:43–57
11. Cogswell PC, Guttridge DC, Funkhouser WK, Baldwin AS Jr (2000) Selective activation of NF-kappa B subunits in human breast cancer: potential roles for NF-kappa B2/p52 and for Bcl-3. Oncogene 19:1123–1131
12. Datta SR, Brunet A, Greenberg ME (1999) Cellular survival: a play in three Akts. Genes Dev 13:2905–2927
13. Deveraux QL, Roy N, Stennicke HR, Van Arsdale T, Zhou Q, Srinivasula SM, Alnemri ES, Salvesen GS, Reed JC (1998) IAPs block apoptotic events induced by caspase-8 and cytochrome c by direct inhibition of distinct caspases. EMBO J 17: 2215–2223
14. Duyao MP, Kessler DJ, Spicer DB, Bartholomew C, Cleveland JL, Siekevitz M, Sonenshein GE (1992) Transactivation of the c-myc promoter by human T cell leukemia virus type 1 tax is mediated by NF kappa B. J Biol Chem 267:16288–16291
15. Finco TS, Westwick JK, Norris JL, Beg AA, Der CJ, Baldwin AS Jr (1997) Oncogenic Ha-Ras-induced signaling activates NF-kappaB transcriptional activity, which is required for cellu lar transformation. J Biol Chem 272:24113–24116
16. Gilmore TD (1999) Multiple mutations contribute to the oncogenicity of the retroviral oncoprotein v-Rel. Oncogene 18: 6925–6937
17. Greten FR, Karin M (2004) The IKK/NF-kappaB activation pathway—a target for prevention and treatment of cancer. Cancer Lett 206:193–199
18. Griffith TS, Chin WA, Jackson GC, Lynch DH, Kubin MZ (1998) Intracellular regulation of TRAIL-induced apoptosis in human melanoma cells. J Immunol 161:2833–2840
19. Guttridge DC, Albanese C, Reuther JY, Pestell RG, Baldwin AS Jr (1999) NF-kappaB controls cell growth and differentiation through transcriptional regulation of cyclin D1. Mol Cell Biol 19:5785–5799
20. Hayden MS, Ghosh S (2004) Signaling to NF-kappaB. Genes Dev 18:2195–2224
21. Hinata K, Gervin AM, Jennifer Zhang Y, Khavari PA (2003) Divergent gene regulation and growth effects by NF-kappa B in epithelial and mesenchymal cells of human skin.Oncogene 22:1955–1964
22. Hinz M, Krappmann D, Eichten A, Heder A, Scheidereit C, Strauss M (1999) NF-kappaB function in growth control: regulation of cyclin D1 expression and G0/G1-to-S-phase transition. Mol Cell Biol 19:2690–2698
23. Hinz M, Loser P, Mathas S, Krappmann D, Dorken B, Scheidereit C (2001) Constitutive NF-kappaB maintains high expression of a characteristic gene network, including CD40, CD86, and a set of antiapoptotic genes in Hodgkin/Reed–Sternberg cells. Blood 97:2798–2807
24. Holmes-McNary M, Baldwin AS Jr (2000) Chemopreventive properties of trans-resveratrol are associated with inhibition of activation of the IkappaB kinase. Cancer Res 60:3477–3483
25. Houldsworth J, Mathew S, Rao PH, Dyomina K, Louie DC, Parsa N, Offit K, Chaganti RS (1996) REL proto-oncogene is frequently amplified in extranodal diffuse large cell lymphoma. Blood 87:25–29
26. Houldsworth J, Olshen AB, Cattoretti G, Donnelly GB, Teruya-Feldstein J, Qin J, Palanisamy N, Shen Y, Dyomina K, Petlakh M, Pan Q, Zelenetz AD, Dalla-Favera R, Chaganti RS (2004) Relationship between REL amplification, REL function, and clinical and biologic features in diffuse large B-cell lymphomas. Blood 103:1862–1868
27. Hsia CY, Cheng S, Owyang AM, Dowdy SF, Liou HC (2002) c-Rel regulation of the cell cycle in primary mouse B lymphocytes. Int Immunol 14:905–916
28. Irisarri M, Plumas J, Bonnefoix T, Jacob MC, Roucard C, Pasquier MA, Sotto JJ, Lajmanovich A (2000) Resistance to CD95-mediated apoptosis through constitutive c-FLIP expression in a non-Hodgkin's lymphoma B cell line. Leukemia 14: 2149–2158
29. Irmler M, Thome M, Hahne M, Schneider P, Hofmann K, Steiner V, Bodmer JL, Schroter M, Burns K, Mattmann C, Rimoldi D, French LE, Tschopp J (1997) Inhibition of death receptor signals by cellular FLIP. Nature 388:190–195
30. Joos S, Otano-Joos MI, Ziegler S, Bruderlein S, du Manoir S, Bentz M, Moller P, Lichter P (1996) Primary mediastinal (thymic) B-cell lymphoma is characterized by gains of chromosomal material including 9p and amplification of the REL gene. Blood 87:1571–1578
31. Jungnickel B, Staratschek-Jox A, Brauninger A, Spieker T, Wolf J, Diehl V, Hansmann ML, Rajewsky K, Kuppers R (2000) Clonal deleterious mutations in the IkappaBalpha gene in the malignant cells in Hodgkin's lymphoma. J Exp Med 191:395–402
32. Karin M, Ben-Neriah Y (2000) Phosphorylation meets ubiquitination: the control of NF-[kappa]B activity. Annu Rev Immunol 18:621–663
33. Keifer JA, Guttridge DC, Ashburner BP, Baldwin AS Jr (2001) Inhibition of NF-kappa B activity by thalidomide through suppression of IkappaB kinase activity. J Biol Chem 276:22382–22387

34. Kim KM, Lee YJ (2004) Amiloride augments TRAIL-induced apoptotic death by inhibiting phosphorylation of kinases and phosphatases associated with the P13K-Akt pathway. Oncogene (in press)
35. Kreuz S, Siegmund D, Scheurich P, Wajant H (2001) NF-kappaB inducers upregulate cFLIP, a cycloheximide-sensitive inhibitor of death receptor signaling. Mol Cell Biol 21:3964–3973
36. La Rosa FA, Pierce JW, Sonenshein GE (1994) Differential regulation of the c-myc oncogene promoter by the NF-kappa B rel family of transcription factors. Mol Cell Biol 14:1039–1044
37. Lee JU, Hosotani R, Wada M, Doi R, Kosiba T, Fujimoto K, Miyamoto Y, Tsuji S, Nakajima S, Nishimura Y, Imamura M (1999) Role of Bcl-2 family proteins (Bax, Bcl-2 and Bcl-X) on cellular susceptibility to radiation in pancreatic cancer cells. Eur J Cancer 35:1374–1380
38. Li J, Yen C, Liaw D, Podsypanina K, Bose S, Wang SI, Puc J, Miliaresis C, Rodgers L, McCombie R, Bigner SH, Giovanella BC, Ittmann M, Tycko B, Hibshoosh H, Wigler MH, Parsons R (1997) PTEN, a putative protein tyrosine phosphatase gene mutated in human brain, breast, and prostate cancer. Science 275:1943–1947
39. Matias-Guiu X, Catasus L, Bussaglia E, Lagarda H, Garcia A, Pons C, Munoz J,Arguelles R, Machin P, Prat J (2001) Molecular pathology of endometrial hyperplasia and carcinoma. Hum Pathol 32:569–577
40. Mayo MW, Wang CY, Cogswell PC, Rogers-Graham KS, Lowe SW, Der CJ, Baldwin AS Jr (1997) Requirement of NF-kappaB activation to suppress p53-independent apoptosis induced by oncogenic Ras. Science 278:1812–1815
41. Micheau O, Lens S, Gaide O, Alevizopoulos K, Tschopp J (2001) NF-kappaB signals induce the expression of c-FLIP. Mol Cell Biol 21:5299–5305
42. Migliazza A, Lombardi L, Rocchi M, Trecca D, Chang CC, Antonacci R, Fracchiolla NS, Ciana P, Maiolo AT, Neri A (1994) Heterogeneous chromosomal aberrations generate 3′ truncations of the NFKB2/lyt-10 gene in lymphoid malignancies. Blood 84:3850–3860
43. Mosialos G (1997) The role of Rel/NF-kappa B proteins in viral oncogenesis and the regulation of viral transcription. Semin Cancer Biol 8:121–129
44. Mukhopadhyay T, Roth JA, Maxwell SA (1995) Altered expression of the p50 subunit of the NF-kappa B transcription factor complex in non-small cell lung carcinoma. Oncogene 11:999–1003
45. Nair A, Venkatraman M, Maliekal TT, Nair B, Karunagaran D (2003) NF-kappaB is constitutively activated in high-grade squamous intraepithelial lesions and squamous cell carcinomas of the human uterine cervix. Oncogene 22:50–58
46. Neri A, Chang CC, Lombardi L, Salina M, Corradini P, Maiolo AT, Chaganti RS, Dalla-Favera R (1991) B cell lymphoma-associated chromosomal translocation involves candidate oncogene lyt-10, homologous to NF-kappa B p50. Cell 67:1075–1087
47. Neri A, Fracchiolla NS, Roscetti E, Garatti S, Trecca D, Boletini A, Perletti L, Baldini L, Maiolo AT, Berti E (1995) Molecular analysis of cutaneous B-and T-cell lymphomas. Blood 86:3160–3172
48. Norris JL, Baldwin AS Jr (1999) Oncogenic Ras enhances NF-kappaB transcriptional activity through Raf-dependent and Raf-independent mitogen-activated protein kinase signaling pathways. J Biol Chem 274:13841–13846
49. Ohno H, Takimoto G, McKeithan TW (1990) The candidate proto-oncogene bcl-3 is related to genes implicated in cell lineage determination and cell cycle control. Cell 60:991–997
50. Olsson A, Diaz T, Aguilar-Santelises M, Osterborg A, Celsing F, Jondal M, Osorio LM (2001) Sensitization to TRAIL-induced apoptosis and modulation of FLICE-inhibitory protein in B chronic lymphocytic leukemia by actinomycin D. Leukemia 15:1868–1877
51. Pallares J, Martinez-Guitarte JL, Dolcet X, Llobet D, Rue M, Palacios J, Prat J, Matias-Guiu X (2004) Abnormalities in the NF-kappaB family and related proteins in endometrial carcinoma. J Pathol 204:569–577
52. Panka DJ, Mano T, Suhara T, Walsh K, Mier JW (2001) Phosphatidylinositol 3-kinase/Akt activity regulates c-FLIP expression in tumor cells. J Biol Chem 276:6893–6896
53. Plummer SM, Holloway KA, Manson MM, Munks RJ, Kaptein A, Farrow S, Howells L (1999) Inhibition of cyclo-oxygenase 2 expression in colon cells by the chemopreventive agent curcumin involves inhibition of NF-kappaB activation via the NIK/IKK signalling complex. Oncogene 18:6013–6020
54. Rao PH, Houldsworth J, Dyomina K, Parsa NZ, Cigudosa JC, Louie DC, Popplewell L, Offit K, Jhanwar SC, Chaganti RS (1998) Chromosomal and gene amplification in diffuse large B-cell lymphoma. Blood 92:234–240
55. Rayet B, Gelinas C (1999) Aberrant rel/nfkb genes and activity in human cancer. Oncogene 18:6938–6947
56. Reuther JY, Reuther GW, Cortez D, Pendergast AM, Baldwin AS Jr (1998) A requirement for NF-kappaB activation in Bcr-Abl-mediated transformation. Genes Dev 12:968–981
57. Romieu-Mourez R, Kim DW, Shin SM, Demicco EG, Landesman-Bollag E, Seldin DC, Cardiff RD, Sonenshein GE (2003) Mouse mammary tumor virus c-rel transgenic mice develop mammary tumors. Mol Cell Biol 23:5738–5754
58. Sasaki N, Morisaki T, Hashizume K, Yao T, Tsuneyoshi M, Noshiro H, Nakamura K, Yamanaka T, Uchiyama A, Tanaka M, Katano M (2001) Nuclear factor-kappaB p65 (RelA) transcription factor is constitutively activated in human gastric carcinoma tissue. Clin Cancer Res 7:4136–4142
59. Senftleben U, Cao Y, Xiao G, Greten FR, Krahn G, Bonizzi G, Chen Y, Hu Y, Fong A, Sun SC, Karin M (2001) Activation by IKKalpha of a second, evolutionary conserved, NF-kappa B signaling pathway. Science 293:1495–1499
60. Solan NJ, Miyoshi H, Carmona EM, Bren GD, Paya CV (2002) RelB cellular regulation and transcriptional activity are regulated by p100. J Biol Chem 277:1405–1418
61. Sovak MA, Bellas RE, Kim DW, Zanieski GJ, Rogers AE, Traish AM, Sonenshein GE (1997) Aberrant nuclear factor-kappaB/Rel expression and the pathogenesis of breast cancer. J Clin Invest 100:2952–2960
62. Takahashi R, Deveraux Q, Tamm I, Welsh K, Assa-Munt N, Salvesen GS, Reed JC (1998) A single BIR domain of XIAP sufficient for inhibiting caspases. J Biol Chem 273:7787–7790
63. Thomas RP, Farrow BJ, Kim S, May MJ, Hellmich MR, Evers BM (2002) Selective targeting of the nuclear factor-kappaB pathway enhances tumor necrosis factor-related apoptosis-inducing ligand-mediated pancreatic cancer cell death. Surgery 132:127–134
64. Thornburg NJ, Pathmanathan R, Raab-Traub N (2003) Activation of nuclear factor-kappaB p50 homodimer/Bcl-3 complexes in nasopharyngeal carcinoma. Cancer Res 63:8293–8301
65. Toth CR, Hostutler RF, Baldwin AS Jr, Bender TP (1995) Members of the nuclear factor kappa B family transactivate the murine c-myb gene. J Biol Chem 270:7661–7671
66. Vasudevan KM, Gurumurthy S, Rangnekar VM (2004) Suppression of PTEN expression by NF-kappa B prevents apoptosis. Mol Cell Biol 24:1007–1021
67. Wang CY, Mayo MW, Korneluk RG, Goeddel DV, Baldwin AS Jr (1998) NF-kappaB antiapoptosis: induction of TRAF1 and TRAF2 and c-IAP1 and c-IAP2 to suppress caspase-8 activation. Science 281:1680–1683
68. Westerheide SD, Mayo MW, Anest V, Hanson JL, Baldwin AS Jr (2001) The putative oncoprotein Bcl-3 induces cyclin D1 to stimulate G(1) transition. Mol Cell Biol 21:8428–8436
69. Xiao G, Cvijic ME, Fong A, Harhaj EW, Uhlik MT, Waterfield M, Sun SC (2001) Retroviral oncoprotein Tax induces processing of NF-kappaB2/p100 in T cells: evidence for the involvement of IKKalpha. EMBO J 20:6805–6815

70. Yamamoto Y, Gaynor RB (2001) Role of the NF-kappaB pathway in the pathogenesis of human disease states. Curr Mol Med 1:287–296
71. Yamamoto Y, Yin MJ, Lin KM, Gaynor RB (1999) Sulindac inhibits activation of the NF-kappaB pathway. J Biol Chem 274:27307–27314
72. Yin MJ, Yamamoto Y, Gaynor RB (1998) The anti-inflammatory agents aspirin and salicylate inhibit the activity of I(kappa) B kinase-beta. Nature 396:77–80
73. Yu Q, Geng Y, Sicinski P (2001) Specific protection against breast cancers by cyclin D1 ablation. Nature 411:1017–1021

Virchows Arch (2005) 446: 483–488
DOI 10.1007/s00428-005-1254-y

ORIGINAL ARTICLE

Young Hwa Soung · Jong Woo Lee · Su Young Kim · Si Hyung Seo · Won Sang Park · Suk Woo Nam · Sang Yong Song · Joung Ho Han · Cheol Keun Park · Jung Young Lee · Nam Jin Yoo · Sug Hyung Lee

Mutational analysis of EGFR and K-RAS genes in lung adenocarcinomas

Received: 10 December 2004 / Accepted: 7 March 2005 / Published online: 7 April 2005
© Springer-Verlag 2005

Abstract Both *epidermal growth factor receptor* (*EGFR*) and *RAS* gene mutations contribute to the development of non-small cell lung cancer (NSCLC). Because RAS is one of the downstream molecules in the EGFR signal transduction, the association between the somatic mutations of *EGFR* and *RAS* may be important in the pathogenesis of NSCLC . However, to date, such data are lacking. In this study, we analyzed the hotspot regions of *K-RAS* gene (codons 12, 13, 59 and 61) and *EGFR* gene (exons 18, 19 and 21) in 153 NSCLC tissue samples including 69 adenocarcinomas. Overall, we detected 30 *EGFR* mutations (19.6%) and 6 *K-RAS* mutations (3.9%) in the 153 NSCLCs. In the 69 adenocarcinomas, 26 *EGFR* mutations (37.7%) and six *K-RAS* mutations (8.7%) were detected. Of note, the 26 tumors with *EGFR* mutations did not harbor any *K-RAS* mutations, and the six tumors with *K-RAS* mutations did not harbor any *EGFR* mutations. Inverse relationship between *K-RAS* and *EGFR* mutations in the lung adenocarcinoma was statistically significant (P=0.046, χ^2 test). As regards smoking history, *EGFR* mutation was significantly associated with never-smoking history, whereas *K-RAS* mutation was significantly associated with smoking history. Our data suggest that mutations of *EGFR* and *K-RAS* genes might separately, but not cooperatively, contribute to lung adenocarcinoma pathogenesis, and that EGFR and K-RAS mutants could separately be anti-neoplastic targets in lung adenocarcinomas.

Y. H. Soung · J. W. Lee · S. Y. Kim · S. H. Seo · W. S. Park · S. W. Nam · J. Y. Lee · N. J. Yoo · S. H. Lee (✉)
Department of Pathology, College of Medicine,
The Catholic University of Korea,
505 Banpo-dong, Socho-gu,
Seoul, 137-701, South Korea
e-mail: suhulee@catholic.ac.kr
Tel.: +82-2-5901188
Fax: +82-2-5376586

S. Y. Song · J. H. Han · C. K. Park
Department of Pathology, Samsung Medical Center,
Sungkyunkwan University School of Medicine,
Seoul, South Korea

Keywords EGFR · K-RAS · Mutation · Lung cancer · Oncogene

Abbreviations PCR: polymerase chain reaction · SSCP: single strand conformation polymorphism · EGFR: epidermal growth factor receptor · NSCLC: non-small cell lung cancer · BAC: bronchioloalveolar carcinoma

Introduction

Lung cancer is the most common cause of cancer deaths in both men and women worldwide, with non-small cell lung cancer (NSCLC) accounting for approximately 80% of these cases [8]. Despite advances in surgical and chemotherapeutic intervention, survival has improved very little over the past few decades, with an overall cure rate of <15% [19].

The epidermal growth factor receptor (EGFR), a receptor protein tyrosine kinase, contributes to a number of processes in tumor survival and growth activity, thus making it a promising molecular target for cancer therapy [9]. One of the agents that target the EGFR is the orally active EGFR tyrosine kinase inhibitor gefitinib (Iressa), which has given significant clinical benefit to NSCLC patients [6, 11, 21]. However, since not all NSCLC patients exhibit the same response, there is considerable interest in prognostic indicators that might predict the response to gefitinib. Recently, three research groups discovered that somatic mutations of *EGFR* gene in the NSCLC could predict significant clinical responses to gefitinib [13–15]. Most of the *EGFR* somatic mutations were exclusively detected in the adenocarcinomas (including bronchioloalveolar carcinomas). The mutations were detected in the exons 18, 19 and 21 that encode the intracellular kinase domain. The mutations detected in the exon 18 would substitute the amino acid G719 in the P-loop, while those detected in the exon 21 would substitute amino acids in the activation domain (L858 and L861). The mutations in the exon 19 were in-frame deletions that may alter the structure of αC helix. All of the *EGFR* mutations affect amino acids near the ATP-binding pocket that is targeted by gefitinib. Functional assays revealed that the

hotspot mutants of EGFR had a higher EGF-dependent activation than the wild-type EGFR had [13–15, 18].

Activation of the RAS pathway also plays a critical role in cell proliferation, and is frequently activated in cancer cells by the somatic mutation [4]. In NSCLC, the *K-RAS* mutations are more common in adenocarcinoma than those in the other histologic types and have been detected in approximately 7–40% of lung adenocarcinomas [7]. Of note, RAS pathway is one of the major signaling pathways that mediate the downstream effects of EGFR activation. Although genetic alterations of both *EGFR* and *K-RAS* genes are important in the pathogenesis of NSCLC, to date the data that analyzed the relationship between the incidences of *EGFR* and *K-RAS* mutations in NSCLC is lacking. In this study, we analyzed 153 NSCLCs, including 69 adenocarcinomas, for the detection of both *EGFR* and *K-RAS* gene mutations, and found the inverse relationship between *EGFR* and *K-RAS* mutations in lung adenocarcinomas.

Materials and methods

Methacarn-fixed tissues of 153 human NSCLC tissue samples were randomly obtained from surgically treated patients. These samples consisted of 69 adenocarcinomas (including 20 adenocarcinomas with bronchioloalveolar carcinoma features and three pure bronchioloalveolar carcinomas), 70 squamous cell carcinomas, three adenosquamous carcinomas and 11 large cell carcinomas. We analyzed the primary tumors, but not the metastatic lesions of the NSCLC. The male to female ratio was 111:42. Ages of the patients ranged from 36 to 79 years, with an average of 59.6 years. The patients consisted of 91 current smokers, eight former smokers and 54 non-smokers (Tables 1 and 2). Approval was obtained from the Catholic University of Korea, College of Medicine's institutional review board for this study. Informed consent was provided according to the Declaration of Helsinki.

Table 2 Patient characteristics and association with the mutation status of *EGFR* gene. *SQ* squamous cell carcinoma; *AD* adenocarcinoma including bronchioloalveolar carcinoma; *LC* large cell carcinoma; *ASQ* adenosquamous cell carcinoma

Characteristics	Total	*EGFR* mutation-positive (% of the total *EGFR* mutation-positive cases)	*EGFR* mutation-negative (% of the total *EGFR*-mutation negative cases)
	n=153	*n*=30	*n*=123
Sex			
Male	111	13 (43.3)	98 (79.7)
Female	42	17 (56.7)	25 (20.3)
Histology			
SQ	70	2 (6.7)	68 (55.3)
AD	69	26 (86.6)	43 (35.0)
LC	11	0 (0)	11 (8.9)
ASQ	3	2 (6.7)	1 (0.8)
Smoking history			
No	54	25 (83.4)	29 (23.6)
Former	8	1 (3.3)	7 (5.7)
Current	91	4 (13.3)	87 (70.7)

Through the microdissection, tumor cells and normal cells were selectively procured from hematoxylin and eosin-stained slides of the same patients using a 30G1/2 hypodermic needle (Becton Dickinson, Franklin Lakes, N.J., USA) affixed to a micromanipulator, as described previously [12]. DNA extraction was performed by a modified single-step DNA extraction method [12]. Because all of the *EGFR* mutations in the NSCLC have been detected within exons 18, 19 and 21 in the previous studies [13–15], we analyzed the mutations in these three exons by polymerase chain reaction (PCR)-single strand conformation polymorphism (SSCP) analysis. Radioisotope ([^{32}P] dCTP) was incorporated into the PCR products for detection by

Table 1 Summary of *EGFR* and *K-RAS* mutations in the lung cancers. *AD* adenocarcinoma including bronchioloalveolar carcinoma; *SQ* squamous cell carcinoma, *ASQ* adenosquamous carcinoma; *LC* large cell carcinoma

Gene (exon)	Mutations	Histology				
	Nucleotide change (predicted amino acid change)	AD	SQ	ASQ	LC	Total
EGFR (exon 19)	2236_2250delGAATTAAGAGAAGCA (E746_A750del)	1	0	0	0	1
EGFR (exon 19)	2235_2249delGGAATTAAGAGAAGC (E746_A750del)	6	1	1	0	8
EGFR (exon 19)	2240_2257delTAAGAGAAGCAACATCTC (L747_753del insS)	1	0	0	0	1
EGFR (exon 19)	2245_2253delGAAGCAACA (E749_T751del)	1	0	0	0	1
EGFR (exon 19)	2254_2276delTCTCCGAAAGCCAACAAGGAAAT, 2252delC (T751_I559del insN)	1	0	0	0	1
EGFR (exon 21)	2573T>G (L858R)	16	1	1	0	18
	No. of mutations (% of cancers with mutations in each histology)	26 (37.7)	2 (2.9)	2 (66.7)	0 (0)	30 (19.6)
	No. samples screened	69	70	3	11	153
K-RAS (exon 1)	34G>T (G12C)	3	0	0	0	3
K-RAS (exon 1)	35G>T (G12V)	2	0	0	0	2
K-RAS (exon 1)	35G>A (G12D)	1	0	0	0	1
	No. of mutations (% of cancers with mutations in each histology)	6 (8.7)	0 (0)	0 (0)	0 (0)	6 (3.9)
	No. samples screened	69	70	3	11	153

autoradiogram. After SSCP, bands showing mobility shifts were cut out from the dried gel, re-amplified for 30 cycles, and sequenced using the cyclic sequencing kit (Perkin-Elmer, Foster City, Calif., USA). The procedures of PCR and SSCP analysis were performed as described previously [12]. We analyzed *K-RAS* mutations at codons 12, 13, 59 and 61 by both PCR-SSCP and direct DNA sequencing.

Results

PCR and subsequent SSCP analysis of the *EGFR* gene identified aberrantly migrating bands compared with the wild-type bands (Fig. 1). None of the corresponding normal samples from the same patients showed evidence of mutations by SSCP (Fig. 1), indicating that the mutations had risen somatically. Enrichment and DNA sequence analysis of the aberrantly migrating bands led us to identify that 30 out of the 153 samples harbored *EGFR* mutations (19.6%) (Table 1). The *EGFR* mutations were detected in the exon 19 (12 mutations) and exon 21 (18 mutations), but not detected in the exon 18. Of the *EGFR* mutations detected in the exon 21, all of the mutations were the known hotspot mutation at the nucleotide 2573 (2573T→G) that would result in an amino acid change (L858R). In exon 19, we found five types of in-frame *EGFR* mutations and the most common one was 2235_2249delGGAATTAAGAGAAGC,

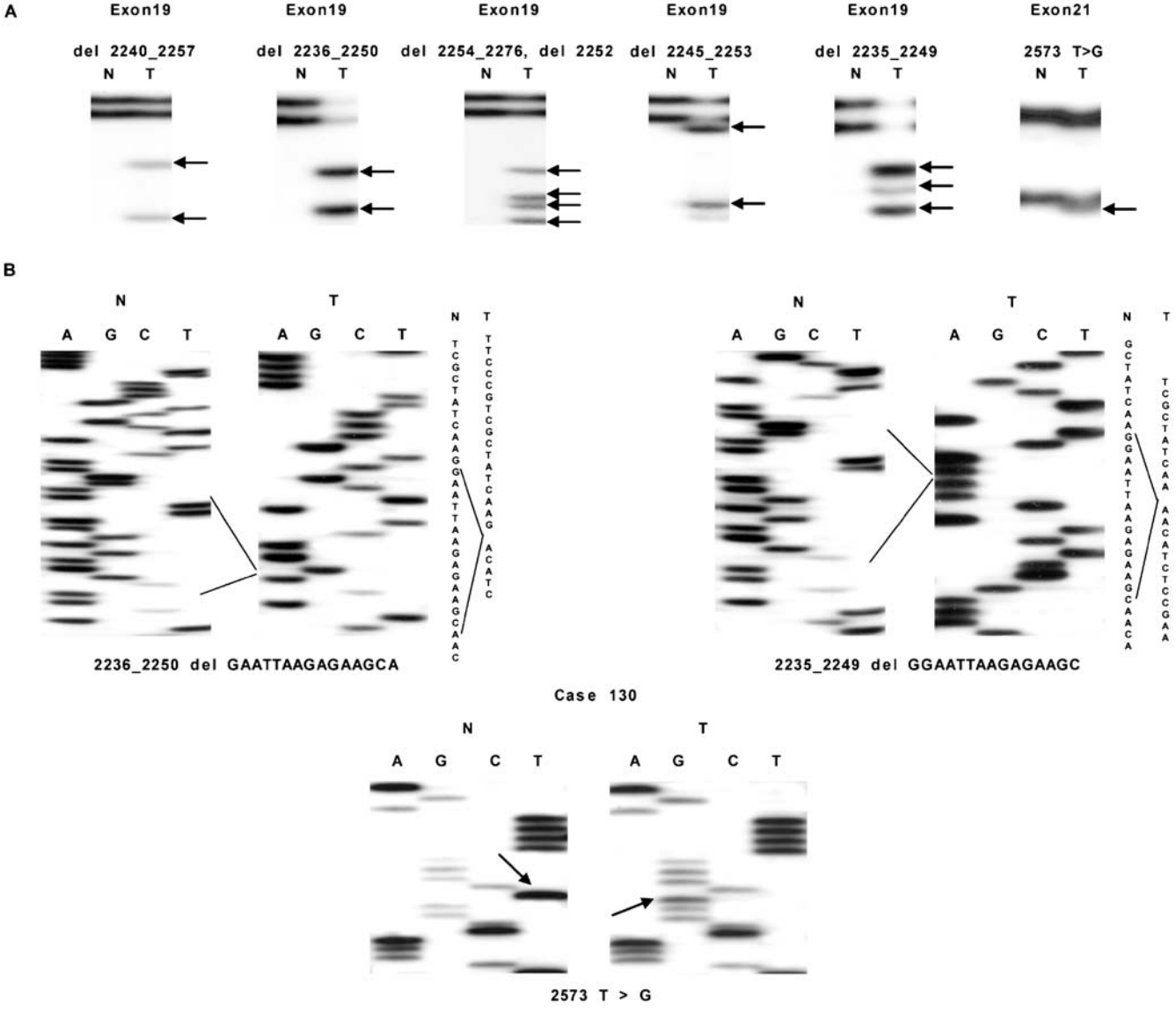

Fig. 1 PCR-SSCP of *EGFR* gene in the NSCLC. Representative data of SSCP (**A**) and DNA sequencing analysis (**B**) of *EGFR* DNA from tumors (lane T) and normal tissues (lane N). **a**: SSCPs of DNA in exons 19 and 21 from the tumors (*T*) show wild type bands and additional aberrant bands (*arrows*) as compared with SSCP from corresponding normal cells of the same patients (*N*). **B**: Sequencing analysis from the aberrant bands in (**A**). Numbering of cDNA of *EGFR* was carried out with respect to the ATG start codon (GenBank)

which would result in in-frame deletion of five amino acids (E746_A750del).

According to the histologic types, the *EGFR* mutations were identified in 26 of the 69 adenocarcinomas (38%), two of the 70 squamous cell carcinomas (3%), two of the three adenosquamous carcinomas (67%) and none of 11 large cell carcinomas (0%). The incidence of the *EGFR* mutation in the adenocarcinomas was significantly higher than that of the squamous cell carcinomas (Fisher's exact test, $P<0.01$). Furthermore, the incidence of the *EGFR* mutations was significantly associated with being female (Fisher's exact test, $P<0.01$) and never-smoking history (Fisher's exact test, $P<0.01$) (Table 2).

We also analyzed *K-RAS* mutations in the same 153 NSCLC tissue samples. In agreement with the previous reports that *K-RAS* mutations have been detected mainly in adenocarcinoma type of NSCLC [7, 17], we detected six *K-RAS* mutations (8.7%) of the 69 adenocarcinomas, but not in other types of NSCLC (Fig. 2, Table 1). The mutations consist of three 34G→T (G12C), two 35 G→T (G12V) and one 35G→A (G12D). Interestingly, the 26 tumors with *EGFR* mutations did not harbor any *K-RAS* mutations, and the six tumors with *K-RAS* mutations did not harbor any *EGFR* mutations. The inverse relationship between K-RAS and *EGFR* mutations was statistically significant (Table 3; $P=0.046$, χ^2 test). The incidence of *K-RAS* mutation was significantly associated with smoking history (Fisher's exact test, $P<0.05$). There was no association of either *EGFR* and *K-RAS* mutations with patient's age, size of the tumor and number of lymph nodes with tumor metastasis.

Table 3 Relationship of *EGFR* and *K-RAS* mutations in lung adenocarcinomas

	EGFR mutation (+)	EGFR mutation (−)	Total
K-RAS mutation (+)	0	6	6
K-RAS mutation (−)	26	37	63
Total	26	43	69

Discussion

The previous observations that signaling pathways of EGFR and K-RAS are overlapped [4] led us to analyze the relationship between the incidences of mutations of these two genes in NSCLC. We observed that most of the *EGFR* mutations (26 of the total 30 mutations) and all of the *K-RAS* mutations were detected in the adenocarcinoma type. Furthermore, there was an inverse relationship between the occurrences of *EGFR* and *K-RAS* mutations in the adenocarcinomas. As regards the inverse relationship between *EGFR* and *K-RAS* mutations, there have been

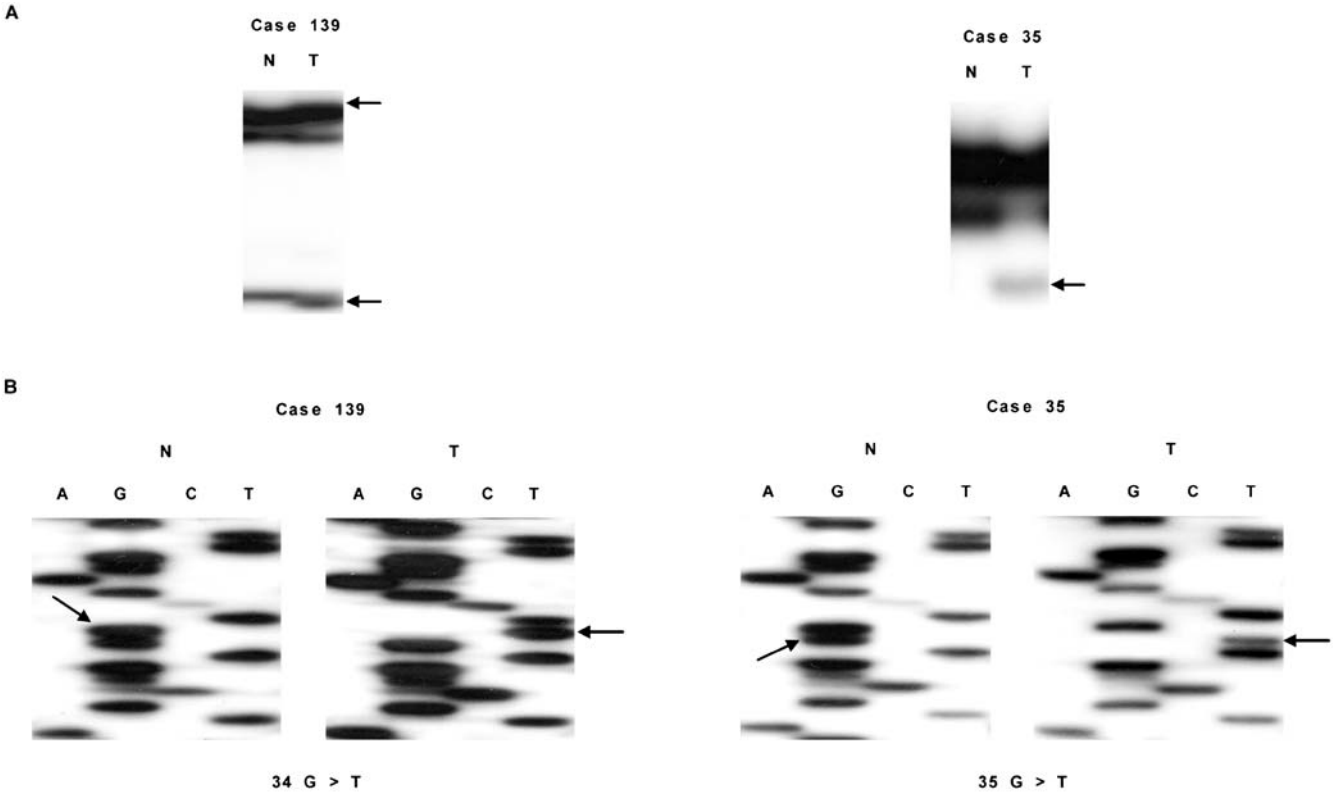

Fig. 2 PCR-SSCP of *K-RAS* gene in the NSCLC. Representative data of SSCP (**A**) and DNA sequencing analysis (**B**) of *K-RAS* DNA from tumors (lane T) and normal tissues (lane N). **A**: SSCPs of DNA in the exon 1 from the tumors (T) show wild type bands and additional aberrant bands (*arrows*) as compared to SSCP from corresponding normal cells of the same patients (N). **B**: Sequencing analysis from the aberrant bands in (**A**). Numbering of cDNA of *K-RAS* was done in respect to the ATG start codon (GenBank)

genetic epidemiology data that support that. For the smoking history, *K-RAS* mutation was strongly associated with cigarette smoking in lung adenocarcinomas [2], whereas *EGFR* mutation was commonly found in NSCLCs from never smokers as apposed to former or current smokers [13–15]. In the current study, we also observed that *K-RAS* mutation was associated with cigarette smoking and that *EGFR* mutation was associated with non-smoking status (Table 2). These data suggested the possibility that *EGFR* and *K-RAS* mutations target different subsets of lung adenocarcinomas.

So far, more than ten types of *EGFR* mutations in the exon 19 have been reported [13–15]. Of the five types of the exon 19 mutations detected in the present study, three (2236_2250delGAATTAAGAGAAGCA, 2235_2249delGGAATTAAGAGAAGC and 2240_2257- delTAAGAGAAGCAACATCTC) were the previously reported mutations, while the remaining two (2245_2253 delGAAGCAACA, and 2254_2276delTCTCCGAAAGCCAACAAGGAAAT with 2252delC) were novel mutations that would also result in the in-frame deletion of the amino acids near the ATP-binding pocket. The *EGFR* mutations in the kinase domain were reported in 3–32% of the adenocarcinomas, and the mutations were more frequent in patients from Japan than in those from the United States [13–15]. The incidence of the *EGFR* mutation in our study (37.7% of the Korean patients with lung adenocarcinoma) is similar to that of the Japanese patients [14], confirming the racial difference of the *EGFR* mutation in lung cancers. Regarding *K-RAS* gene, the incidence of the mutation in the lung adenocarcinomas in this study was 8.7%, which was at the low part of the 7–40% reported in the previous studies [2, 7, 17]. The lower incidence of *K-RAS* mutation is unlikely to be a result of low sensitivity of the detection methods, because we used both direct sequencing and SSCP, which have been used to detect *K-RAS* mutations in the previous studies [2, 7, 17].

What would be the difference in the oncogenic effects between the EGFR-mutated and the K-RAS-mutated lung adenocarcinomas? The major downstream pathways mediating oncogenic effects of EGFR are activation of ERKs via RAS, and AKT via PI3K [10]. Given the observation that EGFR mutants in the kinase domain selectively activated AKT pathway with no effects on the ERK pathway via RAS [18], the EGFR mutation would result in the increased survival of the affected cancer cells by AKT. Although RAS mutants mainly activate the ERK pathway [20], they also activate AKT via PI3K [16]. Therefore, the K-RAS mutants would result in both increased survival and proliferation of the affected cancer cells. However, the exact consequences of the *K-RAS* and *EGFR* mutations in the complicated cellular contexts should be further analyzed in future studies.

Findings of *EGFR* mutations in NSCLC raised several critical questions. One of them was as to whether other components of the EGFR signaling could be drug targets. In the current study, our data suggested that the lung adenocarcinomas with the *EGFR* mutations might comprise an adenocarcinoma group that is distinct from those with *K-RAS* mutations. Therefore, the EGFR mutants as well as the RAS mutants could separately be anti-neoplastic targets in the different sets of lung adenocarcinomas. The most impressive examples of recent cancer therapies used the small-molecule inhibitors for tyrosine kinases such as imanitib, trastzumab and gefitinib [3, 5, 21]. In addition, several inhibitors of the RAS mutants and downstream molecules of RAS are now in clinical trials for cancer therapy [1]. In this respect, the present study may provide the basic information of lung adenocarcinomas for future therapies targeting *EGFR* and *RAS* mutations.

Acknowledgements This work was supported by the Korea Science & Engineering Foundation (KOSEF) through the Cell Death Disease Research Center at The Catholic University of Korea (R13-2002-005-01004-0).

References

1. Adjei AA (2001) Blocking oncogenic Ras signaling for cancer therapy. J Natl Cancer Inst 93:1062–1074
2. Ahrendt SA, Decker PA, Alawi EA, Zhu YYR, Sanchez-Cespedes M, Yang SC, Haasler GB, Kajdacsy-Balla A, Demeure MJ, Sidransky D (2001) Cigarette smoking is strongly associated with mutation of the K-ras gene in patients with primary adenocarcinoma of the lung. Cancer 92:1525–1530
3. Arteaga CL, Moulder SL, Yakes FM (2002) HER (erbB) tyrosine kinase inhibitors in the treatment of breast cancer. Semin Oncol 29:4–10
4. Downward J (2003) Targeting RAS signalling pathways in cancer therapy. Nat Rev Cancer 3:11–22
5. Druker BJ, Sawyers CL, Kantarjian H, Resta DJ, Reese SF, Ford JM, Capdeville R, Talpaz M (2001) Activity of a specific inhibitor of the BCR-ABL tyrosine kinase in the blast crisis of chronic myeloid leukemia and acute lymphoblastic leukemia with the Philadelphia chromosome. N Engl J Med 344:1038–1042
6. Fukuoka M, Yano S, Giaccone G, Tamura T, Nakagawa K, Douillard JY, Nishiwaki Y, Vansteenkiste J, Kudoh S, Rischin D, Eek R, Horai T, Noda K, Takata I, Smit E, Averbuch S, Macleod A, Feyereislova A, Dong RP, Baselga J (2003) Multi-institutional randomized phase II trial of gefitinib for previously treated patients with advanced non-small-cell lung cancer. J Clin Oncol 21:2237–2246
7. Graziano SL, Gamble GP, Newman NB, Abbott LZ, Rooney M, Mookherjee S, Lamb ML, Kohman LJ, Poiesz BJ (1999) Prognostic significance of K-ras codon 12 mutations in patients with resected stage I and II non-small-cell lung cancer. J Clin Oncol 17:668–675
8. Jemal A, Tiwari RC, Murray T, Ghafoor A, Samuels A, Ward E, Feuer EJ, Thun MJ, American Cancer Society (2004) Cancer statistics, 2004. Cancer J Clin 54:8–29
9. Jorissen RN, Walker F, Pouliot N, Garrett TP, Ward CW, Burgess AW (2003) Epidermal growth factor receptor: mechanisms of activation and signalling. Exp Cell Res 284:31–53
10. Kamata T, Feramisco JR (1984) Epidermal growth factor stimulates guanine nucleotide binding activity and phosphorylation of ras oncogene proteins. Nature 310:147–150
11. Kris MG, Natale RB, Herbst RS, Lynch TJ Jr, Prager D, Belani CP, Schiller JH, Kelly K, Spiridonidis H, Sandler A, Albain KS, Cella D, Wolf MK, Averbuch SD, Ochs JJ, Kay AC (2003) Efficacy of gefitinib, an inhibitor of the epidermal growth factor receptor tyrosine kinase, in symptomatic patients with non-small cell lung cancer: a randomized trial. JAMA 290:2149–2158
12. Lee JY, Dong SM, Kim SY, Yoo NJ, Lee SH, Park WS (1998) A simple, precise and economical microdissection technique for analysis of genomic DNA from archival tissue sections. Virchows Arch 433:305–309

13. Lynch TJ, Bell DW, Sordella R, Gurubhagavatula S, Okimoto RA, Brannigan BW, Harris PL, Haserlat SM, Supko JG, Haluska FG, Louis DN, Christiani DC, Settleman J, Haber DA (2004) Activating mutations in the epidermal growth factor receptor underlying responsiveness of non-small-cell lung cancer to gefitinib. N Engl J Med 350:2129–2139
14. Paez JG, Janne PA, Lee JC, Tracy S, Greulich H, Gabriel S, Herman P, Kaye FJ, Lindeman N, Boggon TJ, Naoki K, Sasaki H, Fujii Y, Eck MJ, Sellers WR, Johnson BE, Meyerson M (2004) EGFR mutations in lung cancer: correlation with clinical response to gefitinib therapy. Science 304:1497–1500
15. Pao W, Miller V, Zakowski M, Doherty J, Politi K, Sarkaria I, Singh B, Heelan R, Rusch V, Fulton L, Mardis E, Kupfer D, Wilson R, Kris M, Varmus H (2004) EGF receptor gene mutations are common in lung cancers from "never smokers" and are associated with sensitivity of tumors to gefitinib and erlotinib. Proc Natl Acad Sci USA 101:13306–13311
16. Rodriguez-Viciana P, Warne PH, Dhand R, Vanhaesebroeck B, Gout I, Fry MJ, Waterfield MD, Downward J (1994) Phosphatidylinositol-3-OH kinase as a direct target of Ras. Nature 370:527–532
17. Slebos RJ, Hruban RH, Dalesio O, Mooi WJ, Offerhaus GJ, Rodenhuis S (1991) Relationship between K-ras oncogene activation and smoking in adenocarcinoma of the human lung. J Natl Cancer Inst 83:1024–1027
18. Sordella R, Bell DW, Haber DA, Settleman J (2004) Gefitinib-sensitizing EGFR mutations in lung cancer activate anti-apoptotic pathways. Science 305:1163–1167
19. Sridhar SS, Seymour L, Shepherd FA (2003) Inhibitors of epidermal-growth-factor receptors: a review of clinical research with a focus on non-small-cell lung cancer. Lancet Oncol 4: 397–406
20. Vojtek AB, Hollenberg SM, Cooper JA (1993) Mammalian Ras interacts directly with the serine/threonine kinase Raf. Cell 74:205–214
21. Wakeling AE, Guy SP, Woodburn JR, Ashton SE, Curry BJ, Barker AJ, Gibson KH (2002) ZD1839 (Iressa): an orally active inhibitor of epidermal growth factor signaling with potential for cancer therapy. Cancer Res 62:5749–5754

Virchows Arch (2005) 446: 489–496
DOI 10.1007/s00428-005-1244-0

ORIGINAL ARTICLE

Norbert Arens · Uwe Bleyl · Ralf Hildenbrand

HER2/*neu*, p53, Ki67, and hormone receptors do not change during neoadjuvant chemotherapy in breast cancer

Received: 25 November 2004 / Accepted: 26 February 2005 / Published online: 19 April 2005
© Springer-Verlag 2005

Abstract The selection of a systemic breast cancer therapy is based on the expression pattern of immunohistochemical prognostic markers. In our study we sought to determine whether neoadjuvant chemotherapy may alter these expression patterns within the tumors. Our hypothesis was that the expression of the immunohistochemical prognostic markers does not differ between tissue specimens before and after neoadjuvant chemotherapy. We determined the protein expression levels of estrogen receptor, progesterone receptor, Ki67, p53 and HER2/*neu* in the core biopsy and the resected tumor sample from 25 patients receiving neoadjuvant chemotherapy. As a control group, we analyzed sample pairs from 30 patients who did not receive neoadjuvant chemotherapy. Additionally, we determined the relative HER2/*neu* gene copy number by FISH and/or real-time PCR. There were no significant differences in the changes in expression patterns from the core biopsy to the treated resected tumor between those who had received neoadjuvant chemotherapy and the control group. We suggest that it is sufficient to analyze the prognostic factors from either the core biopsy prior to chemotherapy or the treated tumor sample instead of investigating both samples. This would markedly reduce the costs.

Keywords Chemotherapy · HER2/*neu* · Prognostic factors · Immunohistochemistry · Real-time PCR

Introduction

The reliable estimation of prognostic factors in breast cancer samples is a prerequisite for selection of the optimal therapeutic strategy. Besides the classical prognostic factors such as axillary lymph node status, tumor size, and tumor grading and typing, there are many tumor biological prognostic factors such as estrogen receptor (ER), progesterone receptor (PgR), proliferation-associated antigen Ki67, tumor suppressor gene p53, and proto-oncogene HER2/*neu* (epidermal growth factor receptor homolog).

Although predictive factors are more valuable clinically, the only clearly validated predictive factors are ER and PgR expression levels, which predict response to hormonal therapy. Determination of ER and PgR in biopsies of infiltrating carcinomas prior to therapeutic manipulation has become standard practice in the management of patients with breast cancer. Considerable attention has been directed at identification of additional prognostic and particularly predictive factors that might guide more appropriate individualization of therapy. In this regard, HER2/*neu* has been the focus of intensive study over the past decade. In a pivotal study in 1987, Slamon et al. [21] carried out a multivariate analysis in node-positive patients and showed that HER2/*neu* gene amplification independently predicts overall survival and disease-free survival. Since then, most large studies have confirmed HER2/*neu* status—generally measured by gene amplification or receptor protein overexpression—as a significant independent predictor of prognosis in multivariate analysis in node-positive patients.

Recently, the timing of adjuvant chemotherapy in relation to surgery has been extensively investigated. The early use of chemotherapy seems to reduce the number of chemoresistant cell clones [23]. The effect of preoperative chemotherapy on survival was investigated in a recently published study by the National Surgical Adjuvant Breast and Bowel Project [8]. This randomized trial did not find a difference in time to recurrence or time to death when preoperative and postoperative chemotherapy were compared. However, preoperative chemotherapy can be regarded as an "in vivo" chemosensitivity test and this seems to be advantageous for postoperative therapy, where evaluation of the tumor response is very difficult. There are two major indications for neoadjuvant chemotherapy in breast cancer: (1) disproportion of breast and tumor size; (2) preoperative chemotherapy is indicated in primary inflammatory breast carcinomas.

N. Arens (✉) · U. Bleyl · R. Hildenbrand
Pathologisches Institut,
Universitätsklinikum Mannheim gGmbH,
Theodor-Kutzer-Ufer 1–3,
68167 Mannheim, Germany
e-mail: Norbert.Arens@path.ma.uni-heidelberg.de
Tel.: +49-621-3833772
Fax: +49-621-3832005

Prior to neoadjuvant chemotherapy large-core needle biopsies are performed to obtain tumor tissue for histopathological examination. After breast cancer is diagnosed by the pathologist, the neoadjuvant chemotherapy is performed and followed by surgical removing of the tumor. Both the needle core biopsy (CB) and the excised tumor after chemotherapy allow the determination of prognostic and predictive factors.

We questioned whether the expression of routinely determined prognostic and predictive factors change during chemotherapy.

The determination of prognostic and predictive factors, e.g. ER and HER2/*neu*, in breast cancer is an important issue to address since knowledge of the expression patterns of these factors is necessary in selecting the best option for further therapy. If the cytotoxic drugs of a chemotherapy change prognostic and predictive factors their reliability might be reduced and their predictive value might be lost, and one has to raise the question whether these factors should be determined in the CB (prior to chemotherapy) or in the excised tumor (after chemotherapy). Are prognostic and predictive factors reliable after chemotherapy? In the present study we examined established prognostic and predictive factors in matching pairs of CB and chemotherapy-treated tumor samples. We compared the expression of hormone receptors, HER2/*neu*, p53 and Ki67 in sample pairs (CB and resected tumor samples) of chemotherapy-treated patients and patients who had not received neoadjuvant chemotherapy.

Material and methods

Patients

Matched tumor samples were obtained from 25 patients before and after neoadjuvant chemotherapy. The primary sample of each pair was obtained by ultrasound-guided CB prior to chemotherapy. CB samples were 1.2 mm in diameter and between 10 and 18 mm in size. The diameter of the untreated tumors (25.8±13.95 mm) was determined by mammography and ultrasound.

As a control group, matched CB and whole tumor samples were obtained from 30 patients who did not receive neoadjuvant chemotherapy (staging pT1–pT4b, pN0–pN1biii, pMx; grading G1–G3). The median tumor size in this group was 21.1±20.49 mm. Molecular markers were determined in the CB samples and in the untreated resected tumor samples 1 to 11 days following CB.

The characteristics of the patients and their tumors are shown in Tables 1 and 2, respectively.

Preoperative chemotherapy was performed as follows. Of the 25 patients, 12 received Adriamycin at a dose of 50 mg/m^2 and docetaxel at a dose of 75 mg/m^2 every 14 days for four cycles. Adriamycin was administered as a short i.v. infusion over 15 min, followed immediately by a 1-h infusion of docetaxel diluted in 250 ml NaCl. The other 13 patients received Adriamycin at a dose of 60 mg/m^2 and cyclophosphamide at a dose of 600 mg/m^2 every 21 days for four cycles. Thereafter, docetaxel at a dose of 100 mg/m^2 was given every 21 days for four cycles. The 23 patients with ER-positive tumors (Table 2) received tamoxifen (20 mg) once daily starting on the first day of chemotherapy. Surgery was performed 14–28 days following chemotherapy. In 21 patients modified radical mastectomy and in 4 patients breast-conserving surgery was performed. In all patients axillary lymph nodes were dissected.

Table 1 Patient characteristics

		Chemotherapy group (n=25)	Control group (n=30)
Age (years)	Mean	53.5	63.4
	Range	29–69	41–83
pT stage	1	6	20
	2	6	6
	3	1	0
	4	12	4
Lymph node stage	pN0	5	16
	pN1/2	20	14

Tissue samples were processed according to routine procedures and embedded in paraffin. Sections were cut and stained with H&E for histopathological diagnosis. Tumors were classified according to the TNM system (pT1–pT4b, N0–N1biii, pMx), and graded according to the Elston and Ellis system [7] (G1–G3).

Nine patients in the chemotherapy group exhibited lymphangiosis carcinomatosa of the dermis (inflammatory carcinoma, stage pT4). Inflammatory carcinoma is a classic indication for treatment with neoadjuvant chemotherapy. There were more pT4 stage tumors in the chemotherapy group than in the control group even though the mean tumor sizes did not differ significantly. Furthermore, there were more patients with lymph node involvement in the chemotherapy group than in the control group. This is based on the fact that the clinical appearance of an inflammatory carcinoma is histopathologically characterized as lymphangiosis carcinomatosa of the dermis.

Table 2 Characteristics of tumors in the chemotherapy and control groups

		Chemotherapy group (n=25)		Control group (n=30)	
		Core biopsy	Whole tumor	Core biopsy	Whole tumor
Grade	1	3	0	6	6
	2	21	9	21	22
	3	1	16	3	2
HER2/*neu* expression	Negative	17	17	24	23
	Positive	8	8	6	7
ER expression	Negative	2	2	1	1
	Positive	23	23	29	29
PgR expression	Negative	6	4	2	2
	Positive	19	21	28	28

Methods

Immunohistochemistry

Immunostaining procedure Each tissue sample was fixed in 4% formaldehyde and then routinely processed in paraffin wax. The anti-ER (clone 1D5), anti-PgR (clone PgR636), and anti-Ki67 (clone MIB-1) antibodies (all mouse monoclonal) as well as the HercepTest system for the detection of the HER2/*neu* expression came from DAKO (Hamburg, Germany). Expression of p53 was detected with a mouse monoclonal antibody (clone DO-7; Jackson ImmunoResearch, West Grove, Pa.). Immunohistochemistry was performed using a standard biotin-streptavidin method with the appropriate antigen retrieval method for each antibody. With exception of the HercepTest, we used Fast Red (Roche, Mannheim, Germany) as chromogen. Nuclei were counterstained with hematoxylin, with exception of the hormone receptors.

The HercepTest was applied strictly according to the manufacturer's instructions. HER2/*neu* overexpression was indicated by an intense brown staining (using diaminobenzidine as chromogen) of the cell membrane.

Assessment of staining results ER and PgR staining was evaluated according to the immunoreactive score (IRS) as described by Remmele and Stegner [20]. Two observers assessed the steroid receptors semiquantitatively using a scoring system for the staining intensity of nuclei (0=no staining, 1=weak staining, 2=moderate staining, 3=strong staining) and also a scoring system for the number of stained carcinoma cells given as percent of all carcinoma cells (0=staining of no cells, 1=staining of <10%, 2=staining of 10–50%, 3=51–80%, 4=staining of >80%). The IRS was calculated in each case as the product of the two scores.

For the determination of HER2/*neu* protein overexpression, only the membrane staining pattern and intensity of invasive tumor cells were scored. The proportion of positively stained invasive cells was estimated. Interpretation was independently performed by two observers (R.H. and N.A.) each blinded to the other and to the results of the other assays. Immunostaining was scored according to the criteria specified by DAKO for the interpretation of the HercepTest, which have also been used in trials of Herceptin [2, 3, 15, 22, 28]. The score ranged from 0 (negative) to 3+ (strong membrane signal).

Cancer cell proliferation was assessed by identification of Ki67-positive cells within the tissue section. The rate of proliferation is given as percent Ki67-positive cells of 1000 carcinoma cells per section. The rate of p53-positive cells is also given as percent of 1000 carcinoma cells.

Tumor regression was assessed using the tumor regression grading (TRG) system of Mandard et al. [13] as follows: TRG1, absence of residual cancer and extensive fibrosis; TRG2, rare residual cancer cells scattered through the fibrosis; TRG3, increased residual cancer cells but fibrosis still predominating; TRG4, residual cancer outgrowing fibrosis; TRG5, absence of regressive changes.

Fluorescence in situ hybridization

We performed fluorescence in situ hybridization (FISH) analysis in samples from 17 patients in the chemotherapy group (17 CB samples, 15 whole tumor samples) and from 10 patients in the control group (10 CB samples, 9 whole tumor samples) to determine the HER2/*neu* gene copy number using a PathVysion kit (Vysis, Downers Grove, Ill.). The procedure was performed according to the instructions of the kit supplier with slight modifications. In brief, 4 μm thick tissue sections were cut from the same paraffin block that was used for the immunohistochemical staining, and mounted on charged slides (Superfrost Plus, Menzel, Braunschweig, Germany). Following deparaffinization in xylol (3×5 min) and rehydration in 100% ethanol, the slides were incubated for 20 min in 0.2 N HCl. After several washes in 2xSSC, the tissue sections were incubated in 1 M NaSCN at 80°C for 30 min. Cytoplasm was removed from the nuclei by pepsin digestion (3 mg/ml pepsin; Sigma, Deisenhofen, Germany) in 0.9% NaCl (pH 2.0) at 37°C for 10 min. A postfixation step was added involving 10 min in 4% formaldehyde/phosphate-buffered saline. The hybridization mixture (including a centromere 17-specific, SpectrumGreen-labeled DNA probe and a HER2/*neu*-specific, Spectrum Orange-labeled DNA probe) was applied to the pretreated slides, a coverslip was added and the edges of the hybridization area were sealed with rubber cement. To allow hybridization the slides were incubated for 16–24 h in a humidified chamber at 37°C.

After hybridization the slides were washed twice for 5 min each time in 0.05×SSC at 42°C. The slides were then minced in 2×SSC/0.3% NP-40 and embedded in mounting medium (Vectashield, Burlingame, Calif.) containing DAPI (0.5 μg/ml, Sigma) for nuclear counterstaining.

The ratio of the HER2/*neu*-specific signal number to the centromere-17-specific signal number was estimated in 60 nuclei per sample. The threshold for amplification was set at 2.0. Nuclei without any HER2/*neu*- or centromere-specific signal were excluded from analysis. Up to 15 signals per nucleus were counted. When signal swarms were found indicating a high level of gene amplification, the signal number was arbitrarily set to a value of 16.

Quantification of the HER2/neu gene copy number by real-time PCR

DNA isolation In 29 of the 51 samples analyzed by FISH (see above), the HER2/*neu* gene level was additionally determined by real-time PCR.

From 5 to 15 consecutive 10-μm thick tissue sections were mounted on slides and stained with H&E. At the end of a dehydration procedure the slides were placed into 100% ethanol. Tissue areas with a high density of tumor cells were manually dissected from the wet sections using a sterile syringe needle and placed into the tissue lysis buffer of a DNA isolation kit (Macherey & Nagel, Düren, Germany). After isolation of the DNA according to the supplier's protocol, DNA was recovered in water. To increase

the concentration in the eluate, the DNA was dried in a SpeedVac and resolved in Tris, pH 8.0. An aliquot of 1–5 μl was used in each PCR experiment.

Hot-start PCR PCR was performed using a LightCycler-HER2/*neu* DNA quantification kit (Roche, Mannheim, Germany). A 112-bp fragment of the HER2/*neu* gene (17q11.2-21) and a 133-bp fragment of the reference gene located on chromosome 17 were amplified by PCR with specific primers. As two sets of hybridization probes were used, one labeled with LightCycler-fluorescein and LightCycler-Red 640 and the other with LightCycler-fluorescein and LightCycler-Red 705, both amplicons could be quantified simultaneously in one capillary. Tumor DNA samples as well as a calibrator DNA were analyzed in a PCR reaction under the following conditions. After an initial 6-min preincubation step at 95°C, 45 amplification cycles were performed each consisting of 95°C for 10 s, 58°C for 10 s and 72°C at 10 s. The fluorescence signals were measured after each primer annealing step.

Calculation of the relative amounts of HER2/neu DNA The relative amounts of HER2/*neu* DNA compared to the reference gene DNA were estimated using the LightCycler Relative Quantification software (Roche, Mannheim, Germany). At the end of the quantification procedure the results were expressed as the ratio of HER2/*neu* to reference gene copies in the sample, normalized to the ratio of the two genes in the calibrator DNA, that was set to one. A ratio of <2.0 was assumed to be negative for HER2/*neu* amplification and a ratio of ≥2.0 was assumed to be positive for HER2/*neu* amplification.

Statistics

Fisher's exact test was used to determine the association between the assay results and the assignment to one of the patient groups (neoadjuvant chemotherapy/control).

The following paired sample tests were used to determine the significance of the differences between the expression levels in the biopsies and the resected tumor samples within each group: the Wilcoxon test (HER2/*neu*, ER, and PgR), the McNemar test (p53), and the *t*-test for paired samples (Ki67).

Results

The histological effects of chemotherapy were evaluated by comparing samples taken before and after chemotherapy. In our study most patients showed a moderate to high response to chemotherapy. The residual degenerated and infarcted necrotic infiltrating carcinoma was characterized by a loss of normal staining properties and decreased architectural detail. Many macrophages and inflammatory cells were present. Healed sites showed fibrosis, stromal edema and increased vascularity compared to thin-walled vessels. Intraductal and intralymphatic residual carcinoma was often observed. In most samples tumor cells exhibited cytological changes that were possibly treatment-related effects. Carcinoma cells were enlarged due to an increased cytoplasmic volume. The cytoplasm of these cells often contained vacuoles or eosinophilic granules. Cellular borders were typically well defined, or the cells tended to shrink away from the stroma. Some carcinoma cells featured enlargement, pleomorphism, and hyperchromasia of their nuclei.

Estimation of the tumor regression grade in the chemotherapy-treated tumors revealed a broad range of response intensity. Two tumors that did not show any reduction in size after chemotherapy showed no regressive changes in the tissue sections, indicating that these tumors had not responded to chemotherapy at all. A moderate response was seen in 16 tumors (TRG3 or TRG4), and 7 showed a high degree of reduction as well as strong regressive changes within the tissue section and thus were assigned to TRG2. TRG1 tumors were excluded from our study due to the absence of tumor cells in the treated tissue sample.

Immunohistochemical staining results revealed no significant differences between CB and the resected tumor samples (ER, P=0.85; PgR, P=0.42; p53, P=0.32; Ki67, P=0.24; HER-2/*neu*, P=1.00), and no significant group-specific changes in immunohistochemical reactivity between CB and resected tumor samples could be identified (Table 3). Although evaluation of the staining results revealed rare slight differences, these changes did not reach significance. Both the chemotherapy group and the control group showed a high degree of concordance in the measurements of molecular markers between the CB samples and the resected tumor samples (Fig. 2a–d).

Table 3 Expression of prognostic factors in core biopsies and excised tissue specimens

Prognostic factor	Change[a]	Chemotherapy group (n=25)	Control group (n=30)
HER2/*neu*	↑	3	3
	→	20	24
	↓	2	3
ER	↑	3	4
	→	20	19
	↓	2	7
PgR	↑	2	5
	→	20	20
	↓	3	5
Ki67	↑	1	3
	→	19	27
	↓	5	0
p53	↑	1	2
	→	24	28
	↓	0	0

[a]Changes in immunohistochemically detected expression of prognostic factors in samples from the chemotherapy and control groups: ↑ IHC $score_{CB}$<IHC $score_{resected\ tumor}$; → IHC $score_{CB}$=IHC $score_{resected\ tumor}$; ↓ IHC $score_{CB}$>IHC $score_{resected\ tumor}$

No significant changes in HER2/*neu* levels following chemotherapy were detected in samples from the chemotherapy group compared to samples from the control group. Indeed, 80% of samples from both groups (20 of 25 from the chemotherapy group and 24 of 30 from the control group) revealed no change at all in expression between CB and resected tumor samples. Samples from two patients in the chemotherapy group showed a slight reduction in expression (HercepTest score 1+ → 0) but the final interpretation did not change and thus stayed "negative". Samples from three patients showed a slight increase in expression (score 0 → 1+ in two and 1+ → 2+ in one). The latter change could not be verified by FISH due to a HER2/*neu* to reference gene copy number ratio of 1.12 in the resected tumor sample (score 2+).

High correlations were found between immunohistochemistry data (HercepTest) and DNA analysis on the one hand, and between the results of the DNA analysis methods on the other. FISH was performed in 51 of 110 tumor samples, and evaluable hybridization signals were obtained in each sample investigated. Real-time PCR analysis was performed in 29 samples. Here, applicability was limited due to the low number of dissectible tumor cells in tumor samples after successful chemotherapy leading to a low DNA yield.

Of 38 samples negative by immunohistochemistry (HercepTest score 0/1+), 36 showed FISH ratios <2 (Fig. 1). Real-time PCR showed a high degree of correlation between relative gene copy number and protein expression level. In two samples a discrepancy between FISH and real-time PCR results was found. In both cases, evaluation of the FISH results revealed a slight overrepresentation of HER2/*neu* gene copies as compared to centromere copies, whereas real-time PCR values did not reach the amplification threshold. The tests were repeated with similar results. One of the samples was immunohistochemically allocated a score of 0, the other a score of 2+.

The HER/*neu* gene to reference gene ratio was generally increased in samples with a HercepTest score of ≥2. As a consequence, all samples with HER/*neu* overexpression or amplification (n=14) were also positive by PCR (range 2.29–15.74) as far as analyzed.

As already indicated by the immunohistochemistry results that HER2/*neu* expression did not change during chemotherapy, DNA analysis also revealed no significant difference between the CB samples and the treated tumor samples (Fig. 2e–f).

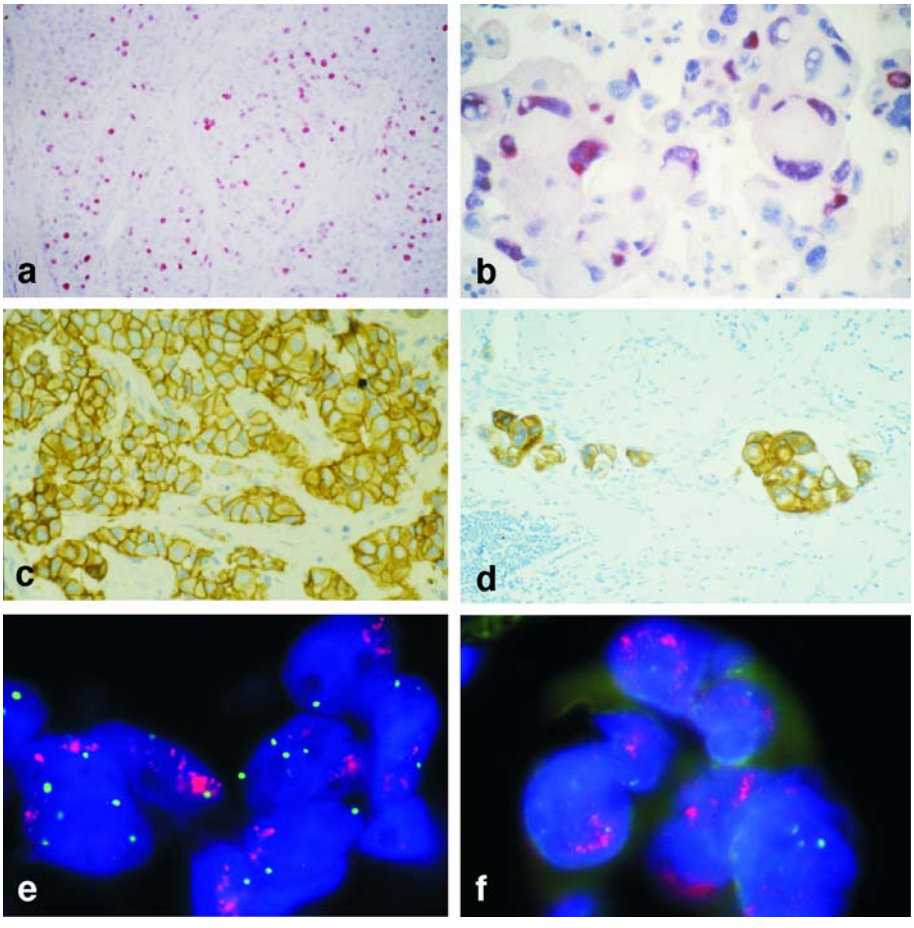

Fig. 1 Ki67 and HER2/*neu* staining in chemotherapy-treated and untreated tissue samples. **a**–**d** Ki67 and HER2/*neu* immunohistochemical staining with antibodies against Ki67 (**a**, **b**) and HER2/*neu* (HercepTest score 3+) (**c**, **d**) in a tumor before (**a**, **c**) and after (**b**, **d**) chemotherapy. Although the number of tumor cells is diminished in the post-treatment sample due to a high degree of tumor regression, expression of immunohistochemical markers is retained. **e**, **f** FISH results from the same sample as shown in **c** and **d** reveal strong HER2/*neu* overexpression. Nuclei in both samples before (**e**) and after chemotherapy (**f**) reveal a high level of amplification of the HER2/*neu* gene (*red signal*) as compared to the reference DNA (chromosome 17 centromer, *green signal*). **a** ×100; **c**, **d** ×200; **b** ×400; **e**, **f** ×1000

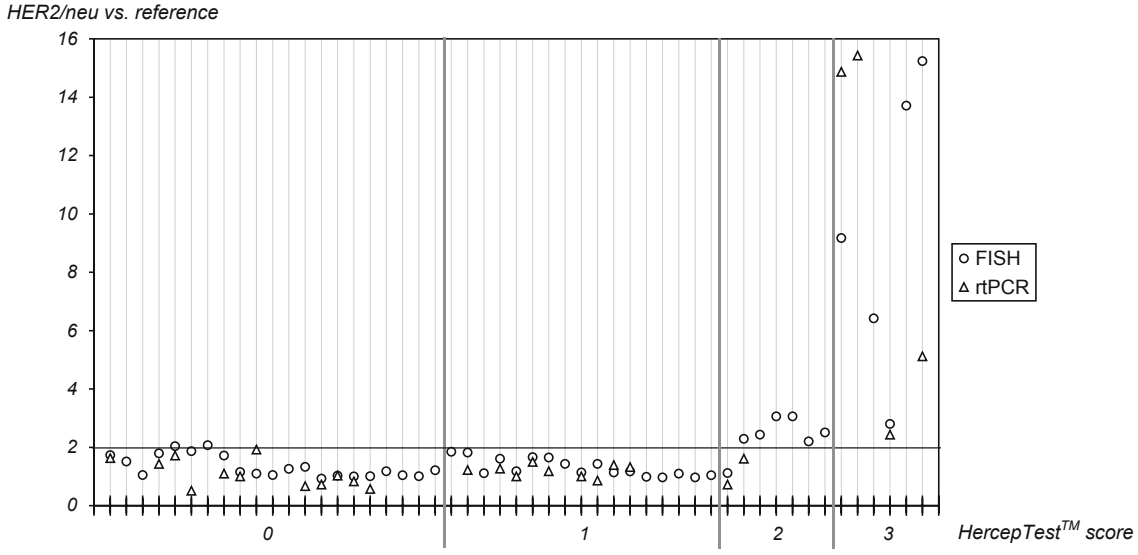

Fig. 2 Synopsis of the results from the HER2/*neu* analysis of 51 tumor samples on a genomic level (FISH, real-time PCR) and protein expression level (immunohistochemistry, HercepTest). Note the strong association between the relative gene copy number and the degree of protein expression

Discussion

HER2/*neu* oncoprotein is overexpressed due to gene amplification in numerous solid tumors [1, 5, 19, 21, 26]. Slamon et al. [21] first described the importance of HER2/*neu* in breast cancer in 1987 and many studies have confirmed its prognostic significance. Early studies used Southern blotting to define HER2/*neu* status, but currently, especially since the introduction of a therapeutic monoclonal anti-HER2/*neu* antibody (trastuzumab, Herceptin), the two most common methods used are immunohistochemistry and FISH. Both methods allow a reliable determination of HER2/*neu* at the protein level and the genomic level, respectively, even in formalin-fixed paraffin-embedded tissue samples.

An important topic in the context of neoadjuvant chemotherapy is the question as to whether prognostic factors including HER2/*neu* should be assessed in the CB or the resected tumor sample. Chemotherapy-treated tissue samples provide a pleomorphic appearance of the residual cells and exhibit regressive changes. Thus the question arises as to whether the expression of prognostic and predictive markers could be changed during neoadjuvant chemotherapy. Further evidence of the need for a direct comparison of HER2/*neu* expression in the primary sample and the chemotherapy-treated sample is given by the fact that Herceptin is synergistic with a variety of chemotherapies [14, 16]. Even if the mechanisms of the synergy observed with other chemotherapy agents in vitro is unknown, one could speculate that these synergistic effects arise from an increase in HER2/*neu* expression during chemotherapeutic treatment.

The results of our study disprove this hypothesis, since no significant changes in HER2/*neu* expression were seen. HER2/*neu* expression levels did not differ significantly between CB and resected tumor samples, either in the chemotherapy group or in the control group. This is in agreement with the results of two recent studies [25, 27]: non-overexpressed tumors did not become overexpressed and overexpressed tumors stayed overexpressed. This is also highly relevant to the use of Herceptin as second-line therapy: according to our data, neoadjuvant chemotherapy does not lead to a decrease in the HER2/*neu* expression level, thus the option of Herceptin therapy of the HER2/*neu*-overexpressing tumors is retained.

We confirmed our HER2/*neu* immunohistochemistry results by two different DNA analysis methods aimed at the coding gene. Comparison of the results from immunohistochemistry and gene copy revealed that overexpression remained strongly correlated with the amplification of the coding gene. The results of both FISH and real-time PCR analysis showed a correlation of nearly 100% with the immunohistochemistry results. This is in agreement with the results of previous studies (for review see reference 29). However, a major disadvantage of the real-time PCR method was the need for microdissection of tumor cells out of the regressively changed tissue of the chemotherapy-treated samples for DNA extraction. Even though the data from real-time PCR were reproducible and in concordance with the FISH data, FISH seems to be the method of choice for routine applications.

In a pilot study concerning immunohistochemical changes in a cohort of patients who received chemotherapy, Makris et al. [12] found a significant reduction in Ki67 expression associated with a diminished S-phase fraction in their treatment group. Our results concerning Ki67 revealed a similar tendency, as we found a decrease in Ki67 expression in 5 of 25 (20%) of the treated patients, although the difference did not reach significance in our study (P=0.239). In most previously reported studies a decrease in Ki67-associated pro-

liferation was observed. This was explained by disturbed signal transduction pathways due to the influence of the chemotherapeutic agent [4, 6, 10].

The immunohistochemical detection of the hormone receptors also did not reveal significant changes in either groups. For both ER and PgR the differences between the sample pairs were larger in the control group than in the chemotherapy group, indicating that the differences observed here might have originated rather from tumor cell heterogeneity than from chemotherapy. The positive–negative border (IRS 2) was never passed during chemotherapy. Previous studies in which hormone receptor changes following neoadjuvant chemotherapy have been analyzed have been more concerned with their predictive value. One study found a significant decrease in ER expression that was limited to the group of chemotherapy responders [9]. Considering all patients in the study, no significant change was observed. Similar to the results of our study, Taucher et al. [24] found a strong correlation of hormone receptor expression between CB and resected tumor samples in the control group, but also found significant changes in the chemotherapy group: increases in ER-negative samples and PgR-negative samples. The apparent contradiction between these findings and those of our study might be a result of the use of different scoring systems and group sizes.

Although data from the literature reveal that the expression of the cell cycle regulator p53 increases during chemotherapy [11, 17, 18], our study did not find any significant change in p53 expression, either in the chemotherapy group or in the control group.

Against the background of similar immunohistochemical staining results in CB and treated tumor samples in our study, we suggest that chemotherapy does not influence the HER2/*neu* level, the steroid receptor status, or Ki67 proliferation index in a statistically significant manner. This is an important issue to address since limitation of the diagnostic determination of the immunohistochemical markers to one of the two samples would markedly reduce the expense. However, the reliable determination of immunohistochemical prognostic and predictive factors requires the presence of residual tumor cells within the chemotherapy-treated tumor.

Conclusions

We conclude that neoadjuvant chemotherapy does not change the expression of HER2/*neu*, p53, Ki67, ER or PgR. Therefore it is sufficient to analyze expression of these proteins in either the pretreatment biopsy or the postchemotherapy resection specimen, provided that the degree of regression allows the evaluation of an appropriate number of tumor cells.

Acknowledgements The authors are grateful to Dr. Christel Weiß, Department for Medical Statistics, University Hospital Mannheim, for statistical advice.

References

1. Albino AP, Jaehne J, Altorki N, Blundell M, Urmacher C, Lauwers G, Niedzwiecki D, Kelsen DP (1995) Amplification of HER-2/neu gene in gastric adenocarcinomas: correlation with primary site. Eur J Surg Oncol 21:56–60
2. Baselga J, Norton L, Albanell J, Kim YM, Mendelsohn J (1998) Recombinant humanized anti-HER2 antibody (Herceptin) enhances the antitumor activity of paclitaxel and doxorubicin against HER2/neu overexpressing human breast cancer xenografts. Cancer Res 58:2825–2831
3. Baselga J (2001) Phase I and II clinical trials of trastuzumab. Ann Oncol 12 [Suppl 1]:S49–S55
4. Chang J, Powles TJ, Allred DC, Ashley SE, Clark GM, Makris A, Assersohn L, Gregory RK, Osborne CK, Dowsett M (1999) Biologic markers as predictors of clinical outcome from systemic therapy for primary operable breast cancer. J Clin Oncol 17:3058–3063
5. Coombs LM, Pigott DA, Sweeney E, Proctor AJ, Eydmann ME, Parkinson C, Knowles MA (1991) Amplification and overexpression of c-erbB-2 in transitional cell carcinoma of the urinary bladder. Br J Cancer 63:601–608
6. Dowsett M, Archer C, Assersohn L, Gregory RK, Ellis OPA, Salter J, Chang J, Mainwaring P, Boeddinghaus I, Johnston SR, Powles TJ, Smith IE (1999) Clinical studies of apoptosis and proliferation in breast cancer. Endocr Relat Cancer 6:25–28
7. Elston CW, Ellis IO (1991) Pathological prognostic factors in breast cancer. The value of histological grade in breast cancer: experience from a large study with long-term follow up. Histopathology 19:403–410
8. Fisher B, Brown A, Mamounas E, Wieand S, Robidoux A, Margolese RG, Cruz AB Jr, Fisher ER, Wickerham DL, Wolmark N, DeCillis A, Hoehn JL, Lees AW, Dimitrov NV (1997) Effect of preoperative chemotherapy on local regional disease in women with operable breast cancer: findings from National Surgical Adjuvant Breast and Bowel Project B-18. J Clin Oncol 15:2483–2493
9. Frassoldati A, Adami F, Banzi C, Criscuolo M, Piccinini L, Silingardi V (1997) Changes of biological features in breast cancer cells determined by primary chemotherapy. Breast Cancer Res Treat 44:185–192
10. Kuerer HM, Newman LA, Smith TL, Ames FC, Hunt KK, Dhingra K, Theriault RL, Singh G, Binkley SM, Sneige N, Buchholz TA, Ross MI, McNeese MD, Buzdar AU, Hortobagyi GN, Singetary SE (1999) Clinical course of breast cancer patients with complete pathologic primary tumor and axillary lymph node response to doxorubicin-based neoadjuvant chemotherapy. J Clin Oncol 17:460–469
11. MacGrogan G, Mauriac L, Durand M, Bonichon F, Trojani M, De Mascarel I, Coindre JM (1996) Primary chemotherapy in breast invasive carcinoma: predictive value of the immunohistochemical detection of hormonal receptors, p53, c-erbB-2, Mib-1, pS2 and GST pi. Br J Cancer 74:1458–1465
12. Makris A, Powles TJ, Allred DC, Ashley SE, Trott PA, Ormerod MG, Titley JC, Dowsett M (1999) Quantitative changes in cytological markers during primary medical treatment of breast cancer: a pilot study. Breast Cancer Res Treat 53:51–59
13. Mandard AM, Dalibard F, Mandard JC, Marnay J, Henry-Amar M, Petiot JF, Roussel A, Jacob JH, Segol P, Samama G, Ollivier J-M, Bonvalot S, Gignoux M (1994) Pathologic assessment of tumor regression after preoperative chemotherapy of esophageal carcinoma. Clinicopathologic correlations. Cancer 73:2680–2686
14. Nahta R, Esteva FJ (2003) HER-2-targeted therapy: lessons learned and future directions. Clin Cancer Res 9:5078–5084
15. Pegram MD, Lipton A, Hayes DF, Weber BL, Baselga JM, Tripathy D, Baly D, Baughman SA, Twaddell T, Glaspy JA, Slamon DJ (1998) Phase II study of receptor-enhanced chemosensitivity using recombinant humanized anti-p185HER2/neu monoclonal antibody plus cisplatin in patients with HER2/neu-overexpressing metastatic breast cancer refractory to chemotherapy treatment. J Clin Oncol 16:2659–2671

16. Pegram M, Hsu S, Lewis G, Pietras R, Beryt M, Sliwkowski M, Coombs D, Baly D, Kabbinavar F, Slamon D (1999) Inhibitory effects of combinations of HER-2/neu antibody and chemotherapeutic agents used for treatment of human breast cancers. Oncogene 18:2241–2251
17. Penault-Llorca F, Cayre A, Bouchet Mishellany F, Amat S, Feillel V, Le Bouedec G, Ferriere JP, De Latour M, Chollet P (2003) Induction chemotherapy for breast carcinoma: predictive markers and relation with outcome. Int J Oncol 22:1319–1325
18. Pohl G, Rudas M, Taucher S, Stranzl T, Steger GG, Jakesz R, Pirker R, Filipits M (2003) Expression of cell cycle regulatory proteins in breast carcinomas before and after preoperative chemotherapy. Breast Cancer Res Treat 78:97–103
19. Reles A, Marx D, Meden H (1991) C-erbB2 oncogene expression in ovarian cancers. Arch Gynaecol Obstet 250:183–184
20. Remmele W, Stegner HE (1987) Vorschlag zur einheitlichen Definierung eines immunreaktiven Score (IRS) für den immunhistochemischen Östrogenrezeptornachweis (ER-ICA) im Mammakarzinomgewebe. Pathologe 8:138–140
21. Slamon DJ, Clark GM, Wong SG, Levin WJ, Ullrich A, McGuire WL (1987) Human breast cancer: correlation of relapse and survival with amplification of HER2/neu oncogene. Science 235:177–182
22. Slamon DJ, Leyland-Jones B, Shak S, Fuchs H, Paton V, Bajamonde A, Fleming T, Eiermann W, Wolter J, Pegram M, Baselga J, Norton L (2001) Use of chemotherapy plus a monoclonal antibody against HER2 for metastatic breast cancer that overexpresses HER2. N Engl J Med 344:783–792
23. Surbone A, Norton L (1993) Kinetic concepts in the treatment of breast cancer. Ann N Y Acad Sci 698:48–62
24. Taucher S, Rudas M, Gnant M, Thomanek K, Dubsky P, Roka S, Bachleitner T, Kandioler D, Wenzel C, Steger G, Mittlböck M, Jakesz R (2003) Sequential steroid hormone receptor measurements in primary breast cancer with and without intervening primary chemotherapy. Endocr Relat Cancer 10:91–98
25. Taucher S, Rudas M, Mader RM, Gnant M, Sporn E, Dubsky P, Roka S, Bachleitner T, Fitzal F, Kandioler D, Wenzel C, Steger GG, Mittlböck M, Jakesz R (2003) Influence of neoadjuvant chemotherapy with epirubicin and docetaxel on the expression of HER2/neu in patients with breast cancer. Breast Cancer Res Treat 82:207–213
26. Tyson FL, Boyer CM, Kaufman R, O'Briant K, Cram G, Crews JR, Soper JT, Daly L, Fowler WC Jr, Haskill JS (1991) Expression and amplification of the HER-2/neu (c-erbB-2) protooncogene in epithelial ovarian tumors and cell lines. Am J Obstet Gynecol 165:640–646
27. Vincent-Salomon A, Jouve M, Genin P, Freneaux P, Sigal-Zafrani B, Caly M, Beuzeboc P, Pouillart P, Sastre-Garau X (2002) HER2 in patients with breast carcinoma is not modified selectively by preoperative chemotherapy and is stable during the metastatic process. Cancer 94:2169–2173
28. Vogel CL, Cobleigh MA, Tripathy D, Gutheil JC, Harris LN, Fehrenbacher L, Slamon DJ, Murphy M, Novotny WF, Burchmore M, Shak S, Stewart SJ, Press M (2002) Efficacy and safety of trastuzumab as a single agent in first-line treatment of HER2-overexpressing metastatic breast cancer. J Clin Oncol 20:719–726
29. Winston JS, Ramanaryanan J, Levine E (2004) HER-2/neu evaluation in breast cancer: are we there yet? Am J Clin Pathol 121 [Suppl 1]:S33–S49

Virchows Arch (2005) 446: 497–504
DOI 10.1007/s00428-005-1243-1

ORIGINAL ARTICLE

Marinke Westerterp · Linetta B. Koppert · Christianne J. Buskens · Hugo W. Tilanus · Fiebo J. W. ten Kate · Jacques J. H. G. M. Bergman · Peter D. Siersema · Herman van Dekken · Jan J. B. van Lanschot

Outcome of surgical treatment for early adenocarcinoma of the esophagus or gastro-esophageal junction

Received: 16 December 2004 / Accepted: 26 February 2005 / Published online: 19 April 2005
© Springer-Verlag 2005

Abstract Adenocarcinoma of the esophagus, or GEJ, has a poor prognosis. Early lesions [i.e. high grade dysplasia (HGD) or T1-carcinoma] are potentially curable. Local endoscopic therapies are promising treatment options for superficial lesions; however, for deeper lesions, surgical resection is considered to be the treatment of choice. To contribute to therapeutic decision-making, we retrospectively analysed the outcome of transhiatal esophagectomy in 120 patients with pathologically proven HGD (n=13) or T1-adenocarcinoma (n=107) of the distal esophagus or gastro-esophageal junction (GEJ). Tumors were subdivided into six different depths of invasion ('T1-mucosal' m1-m3, 'T1-submucosal' sm1-sm3), and the frequency of lymphatic dissemination and time to locoregional and/or distant recurrence were analysed. Only one of the 79 T1m1-3/sm1 tumors (1%) showed lymph node metastases as compared with 18 out of 41 T1sm2-3 tumors (44%). There was a significant difference in recurrence-free period between T1m1-m3/sm1 versus T1sm2-sm3 tumor patients (P log rank <0.0001), with 5-year recurrence-free percentages of 97% and 57%, respectively. In multivariate analysis including age, gender, tumor differentiation grade, N-stage and depth of invasion, only N-stage was an independent prognostic factor for recurrence-free period (hazard rate= 5.9, 95% CI 1.7–20.7). However, if N-stage was excluded from analysis, only depth of invasion (T1sm2-3 versus T1m1-m3/sm1) was an independent prognostic factor for recurrence-free period (hazard rate=7.5, 95% CI 2.0–27.7). These data indicate that T1m1-m3/sm1 adenocarcinomas of esophagus or GEJ show a very low risk of lymphatic dissemination and are therefore eligible for local endoscopic therapy. After transhiatal surgical resection, almost half of the patients with T1sm2-sm3 lesions develop recurrent disease within 5 years, and therefore need additional therapy to improve survival.

Keywords Barrett's esophagus · GEJ · Early cancer · Substage · Survival

M. Westerterp · C. J. Buskens · J. J. B. van Lanschot
Department of Surgery,
Academic Medical Center at the
University of Amsterdam,
Amsterdam, The Netherlands

L. B. Koppert · H. W. Tilanus
Department of Surgery,
Erasmus University Medical Center,
Rotterdam, The Netherlands

F. J. W. ten Kate
Department of Pathology,
Academic Medical Center at the University of Amsterdam,
Amsterdam, The Netherlands

J. J. H. G. M. Bergman
Department of Gastroenterology,
Academic Medical Center at the University of Amsterdam,
Amsterdam, The Netherlands

P. D. Siersema
Department of Gastroenterology and Hepatology,
Erasmus University Medical Center,
Rotterdam, The Netherlands

H. van Dekken (✉)
Department of Pathology, Josephine Nefkens Institute,
Erasmus University Medical Center,
PO Box 1738, 3000 DR Rotterdam, The Netherlands
e-mail: h.vandekken@erasmusmc.nl
Tel.: +31-10-4087499
Fax: +31-10-4089487

Introduction

The incidence of adenocarcinomas of the esophagus or gastro-esophageal junction is rising [7, 24, 33]. Due to increased awareness of the clinical importance of Barrett's esophagus, and the advent of better detection techniques [3, 30]), high grade dysplasia (HGD) and early esophageal adenocarcinoma are being diagnosed with increasing frequency in the Western world [5, 8, 32]. Early carcinoma is defined as a tumor limited to the mucosa or submucosa, irrespective of the presence of lymph node metastases [26]. These early carcinomas are potentially curable diseases,

but at present the extent of resection necessary to achieve cure is not clear.

Many institutions favor radical esophagectomy with lymphadenectomy as standard therapy for esophageal carcinoma. As this procedure is associated with substantial morbidity and mortality [31], the question rises if this extensive resection is also necessary in patients with early malignancies of the esophagus [22, 34]. To date, various techniques have been applied for the treatment of early esophageal carcinoma, i.e. local endoscopic, organ-preserving treatment modalities (e.g. endoscopic mucosal resection (EMR) or photodynamic therapy (PDT) [6, 9, 10]), limited surgical resection (e.g. Merendino operation or vagal-sparing esophagectomy [2, 27]) and radical esophagectomy with or without systematic lymphadenectomy (transthoracic or transhiatal).

In this study, we analyzed the outcome of transhiatal esophagectomy in 120 patients with early adenocarcinoma of the esophagus or gastro-esophageal junction. We subdivided this series of early cancers of the mucosa and submucosa into six successive layers (m1, m2, m3, sm1, sm2, sm3) in order to facilitate clinical decision making. Subsequently, we analysed whether a possible correlation between the depth of tumor infiltration on the one hand, and lymphatic dissemination and recurrence-free period on the other hand, was present.

Materials and methods

Patient materials

Data from all patients operated for carcinoma of the esophagus or gastro-esophageal junction (GEJ) in the Erasmus University Medical Center in Rotterdam and the Academic Medical Center at the University of Amsterdam, The Netherlands, were continuously collected in prospective databases between 1980 and 1993, respectively. A cancer was termed esophageal adenocarcinoma if the centre was clearly situated in the distal esophagus with or without specialised Barrett's epithelium. In addition, cancers at the GEJ in the presence of Barrett's epithelium were considered esophageal adenocarcinoma. A tumor was designated GEJ adenocarcinoma, if the centre was located at the junction in the absence of Barrett's mucosa, or if the centre of the tumor was seen in the gastric cardia. According to the Siewert classification, an esophageal adenocarcinoma would refer to type I, whereas a GEJ adenocarcinoma would be type II [25]. Between January 1980 and July 2002, 702 patients underwent subtotal esophageal resection with proximal gastrectomy for HGD or adenocarcinoma in Rotterdam; between January 1993 and July 2002, 398 patients underwent this same procedure in Amsterdam. All patients with a pathologically proven HGD (n=13) or pT1 invasive adenocarcinoma (n=107), who underwent a transhiatal resection, were included in the present study. All 13 HGD lesions were situated in Barrett's mucosa. The 107 pT1 carcinomas included 94 early cancers of the distal esophagus, of which 13 were classified as GEJ adenocarcinomas. None of the patients received (neo-)adjuvant chemo- and/or radiotherapy.

Histopathologic assessment

The resection specimens of all included patients were reviewed by two experienced pathologists (FJWtK, HvD) to determine size and location of the primary tumor, the number of resected and involved lymph nodes, and the radicality of resection. All tumors were graded, and staging was performed according to the 2002 UICC TNM classification [26]. The depth of tumor invasion was measured and subclassified based on the criteria proposed by the Japanese Society for Esophageal Diseases [13]. High-grade dysplasia (carcinoma in situ) arising in a Barrett segment was defined by the lack of obvious invasion through the basement membrane (HGD, m1). Intramucosal carcinoma was defined as tumor cells extending beyond the basement membrane into the lamina propria (m2), or as carcinomas with deepest invasion into the muscularis mucosae (m3). In the presence of a double muscularis mucosae (i.e. a superficial and a deep one in Barrett's mucosa), we considered the deep one as the pre-existing muscularis mucosae and the superficial one as newly formed [29]. Consequently, a carcinoma invading into the superficial, i.e. newly formed, muscularis mucosae was defined as m2 and invasion into the deeper (pre-existing) muscularis mucosae was defined as m3. Carcinomas infiltrating into the submucosa without invasion of the muscularis propria were further subclassified as invasion limited to the upper third (sm1), intermediate third (sm2), or lower third part of the submucosal layer (sm3).

Follow-up

Patients were followed until death or until April 2003 with a median follow-up time of 44 months (range, 1 day to 13.6 years). They were seen on a regular basis for 5 years in the outpatient clinic (at 3- to 4-month intervals for the first 2 years and at 6-month intervals thereafter). For the present study, patients and/or their family practitioners were contacted by telephone to assess their current status when the patient had been discharged after 5 years. No patients were lost to follow-up.

Statistical analysis

All statistical analyses were performed using the Statistical Software Package version 11.5 (SPSS INC., Chicago, IL, USA). Recurrence-free periods were calculated according to the Kaplan–Meier method and differences in recurrence-free period were assessed using the log-rank test. P-values <0.05 were considered statistically significant. The Cox regression model was used to analyse the independent prognostic value of different variables.

Results

Pathological findings in the esophagectomy specimens

Of the 1100 patients operated upon for HGD or adenocarcinoma in both institutions, 120 patients were found to have an early lesion and underwent a transhiatal resection. There were 103 men (85%) and 17 women (15%), with a median age of 65.4 years (range 31–83 years). One hundred and seven patients had an early lesion of the distal esophagus (94 adenocarcinomas, 13 HGDs), in all but two cases associated with specialised intestinal metaplasia (Barrett's epithelium). Thirteen patients had a GEJ carcinoma, i.e. four junction tumors without Barrett's metaplasia and nine gastric cardia adenocarcinomas. All the 13 HGD cases were associated with Barrett's mucosa. Of the 107 invasive adenocarcinomas, 26 were classified as well differentiated, 58 as moderately differentiated, and the remaining 23 tumors showed a poor differentiation grade.

Thirteen patients (11%) had a T1m1 tumor without clear invasion into the deeper layers (HGD, carcinoma in situ, Table 1). In 18 patients invasion was limited to the lamina propria (T1m2, 15%), 23 patients had the deepest tumor infiltration into the (deeper, pre-existent) muscularis mucosae (T1m3, 19%). In 25 patients, the tumor extended into the upper third of the submucosal layer (T1sm1, 21%), 23 of the patients had a cancer infiltrating into the intermediate one-third (T1sm2, 19%), and in 18 patients the carcinoma infiltrated into the lower third of the submucosal layer (T1sm3, 15%). Examples of each T1 substage are depicted in Fig. 1. Of the 79 patients with T1m1-m3 or sm1 cancers, only one patient (T1m3) showed lymph node metastasis (1%), whereas 18 out of 41 patients with T1sm2-sm3 tumors (44%) had lymph node metastases (Table 1). The 19 cases with lymph node involvement included 18 distal esophageal adenocarcinomas and one GEJ cancer. The mean number of resected lymph nodes was 8.6 (range 1–40). The ratio of infiltrated to removed lymph nodes in these 19 pN+ cases was 0.21, and the mean number of resected nodes was 10.0 (range 3–20). In 16 patients only regional lymph node metastases were present (paraesophageal, paracardial and/or along the lesser curvature), in three patients lymph nodes at the origin of the left gastric artery contained metastatic tumor (M1a).

Outcome after surgical resection

In all patients, microscopically complete resection (R0) of the tumor was achieved. Five patients died in the hospital (mortality=4%). Overall, the 120 patients with early lesions had a 5-year disease free survival of 68%. During follow-up 37 patients died. The proportions of patients without recurrence, per subgroup of depth of tumor invasion, are shown in Fig. 2. Recurrence-free period of patients with T1sm1 tumors did not differ from that of patients with T1m1, patients with T1m2, or patients with T1m3 tumors. However, recurrence-free period did significantly differ from that of patients with T1sm2 and T1sm3 tumors (Fig. 2). We therefore redefined depth of invasion into two subclasses, i.e. group I (T1m1, T1m2, T1m3 and T1sm1) and group II (T1sm2 and T1sm3), and subsequently compared recurrence-free periods in both groups. A significant difference in recurrence-free period was found between group I and group II (P logrank <0.0001, Fig. 3), with 5-year recurrence-free percentages of 97% (95% CI 93–100%) and 57% (95% CI 40–74%), respectively. Importantly, when patients with HGD were left out of analysis, the difference in recurrence-free period remained significant between T1m2, T1m3, T1sm1 (group I minus T1m1) and T1sm2, T1sm3 (group II) patients (P logrank <0.0001), with 5-year recurrence-free percentages of 96% (95% CI 92–100%) and 57% (95% CI 40–74%), respectively. Univariate Cox regression analysis to identify prognostic variables in the total group showed tumor differentiation grade, depth of tumor invasion and N-stage to be prognostic factors for recurrence-free period (P=0.001, P<0.0001 and P<0.0001, respectively; Table 2). In multivariate analysis including N-stage, only N-stage was an independent prognostic factor for recurrence-free period (HR 5.9, 95% CI 1.7–20.7, P=0.005). However, this concerns a retrospective analysis after surgery. If N-stage was excluded from analysis, i.e.

Table 1 Pathological features in 120 transhiatal esophagectomy specimens with high grade dysplasia (m1) or early invasive adenocarcinoma of the esophagus or gastro-esophageal junction

	T1m1	T1m2	T1m3	T1sm1	T1sm2	T1sm3	Total
Tumor characteristics	(n=13)	(n=18)	(n=23)	(n=25)	(n=23)	(n=18)	(n=120)
Lymph node involvement							
Negative	13	18	22	25	17	6	101
Positive	0	0	1	0	6	12	19
Locoregional recurrence							
Absent	13	17	23	25	19	14	111
Present	0	1	0	0	4	4	9
Distant recurrence							
Absent	13	18	22	24	19	13	109
Present	0	0	1	1	4	5	11
Mortality							
No	13	12	18	21	12	7	83
Yes	0	6	5	4	11	11	37

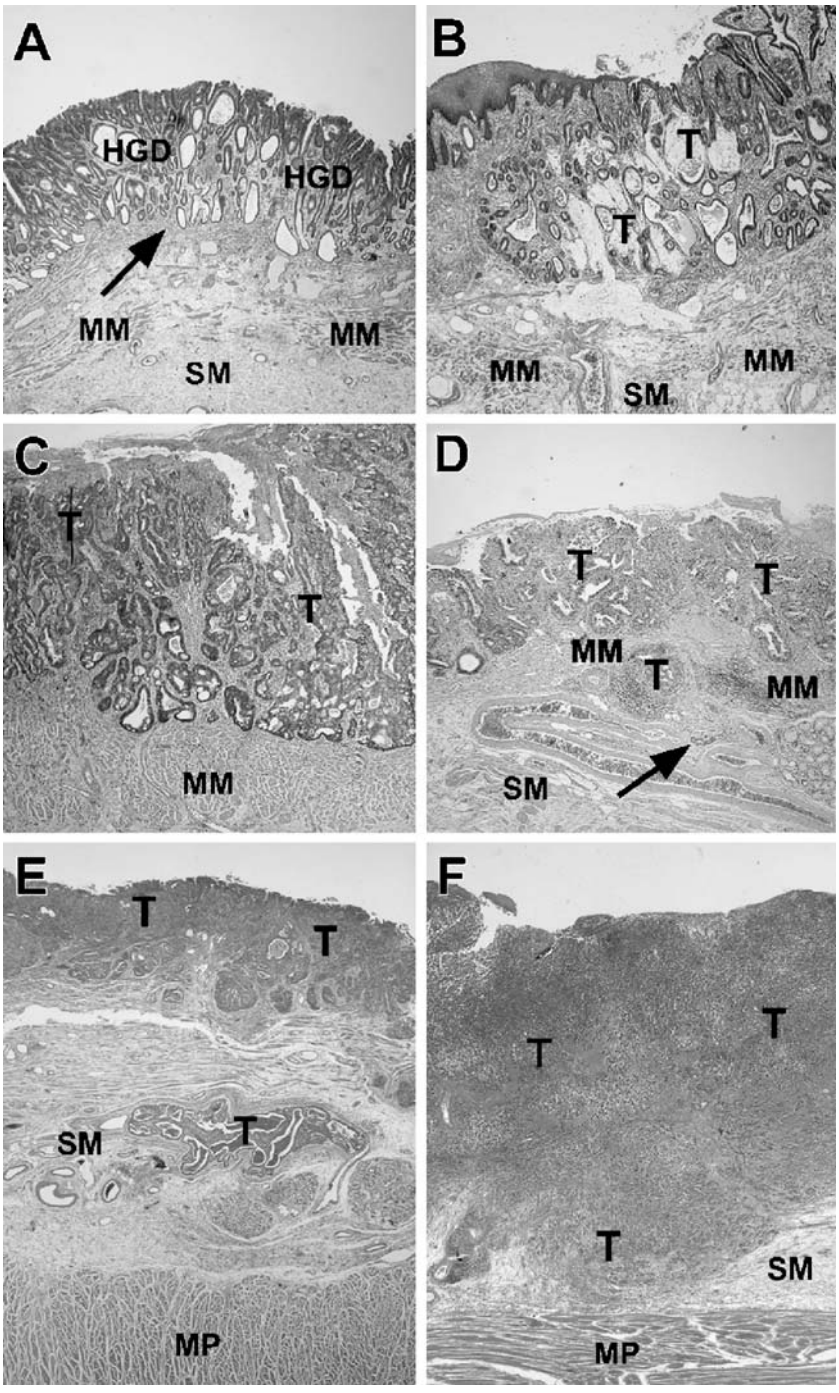

Fig. 1 Hematoxylin-eosin stained histological sections of examples of the six different subgroups for depth of tumor invasion. **a** T1m1, HGD; note the newly formed Barrett-associated muscularis mucosae (arrow) in relation to the pre-existent muscularis mucosae. **b** T1m2, a mucinous, well differentiated, intra-mucosal adenocarcinoma. **c** T1m3, adenocarcinoma reaches into the (pre-existent) muscularis mucosae. **d** T1sm1, a small group of tumor cells is present in the superficial submucosa (arrow). **e** T1sm2, carcinoma can be seen in the middle part of the submucosa, surrounded by vessels and esophageal salivary glands. **f** T1sm3, a poorly differentiated adenocarcinoma infiltrates the deep submucosa. **a**–**c** 4× objective, **d**–**f**, 2× objective. *HGD* high grade dysplasia; *MP* muscularis propria; *MM* muscularis mucosae; *SM* submucosa; *T* tumor

the prospective situation after histological examination of an EMR, only depth of invasion (T1sm2-3 versus T1m1-m3/sm1) was an independent prognostic factor for recurrence-free period (HR 7.5, 95% CI 2.0–27.7, P=0.002).

Alternatively, when recurrence-free survival instead of recurrence-free period was analysed, the significant difference between group I (T1m1, T1m2, T1m3, T1sm1) and group II (T1sm2, T1sm3) remained intact (P logrank= 0.0001) with 5-year recurrence-free survival percentages of 83% (95% CI 65–92%) and 42% (95% CI 25–59%), respectively. Again, when patients with HGD were left out of this analysis, a significant difference in recurrence-free survival remained (P logrank=0.0008) with 5-year recurrence-free survival percentages of 80% (95% CI 68–91%) and 42% (95% CI 25–59%), respectively.

During the follow-up period 18 patients developed tumor recurrence (Table 3). The mean interval between operation and recurrence was 16 months (range 4–85 months). Seven patients died because of locoregional tumor recurrence without evidence of distant disease, eight patients developed only distant recurrence (of whom one patient was still alive at the end of follow-up), and three patients died because of both locoregional and distant recurrence. One patient died because of a second primary carcinoma in the

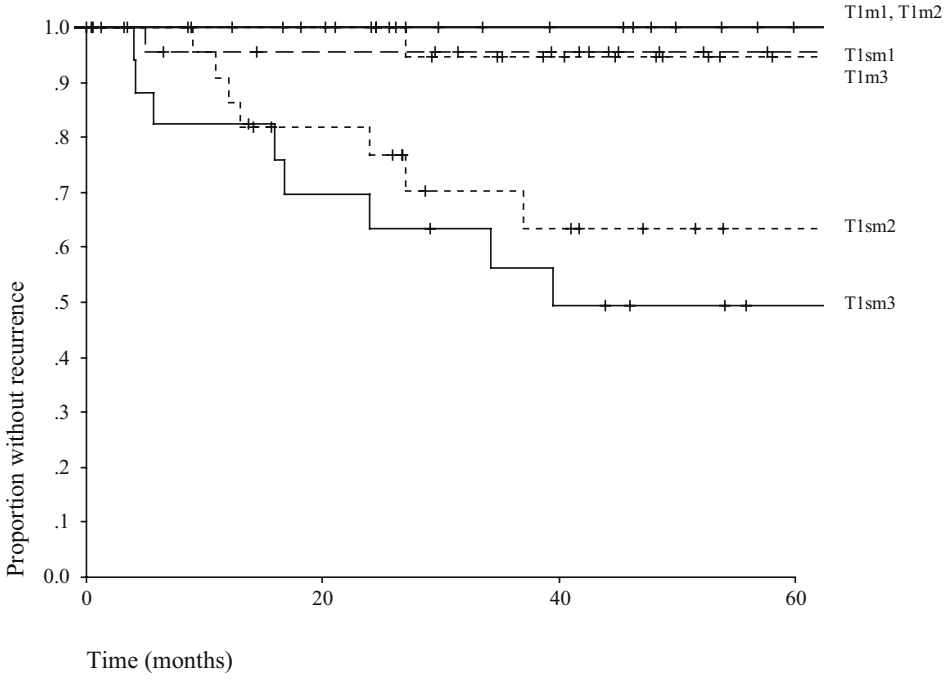

Fig. 2 Proportion of patients without recurrence for depth of tumor invasion subgroups T1m1, T1m2, T1m3, T1sm1, T1sm2 and T1sm3. Patients with T1sm1 did not differ from patients with T1m1, T1m2 or T1m3 (*P* logrank=0.5, 0.6 and 0.9, respectively), but differed from patients with T1sm2 or T1sm3 (*P* logrank=0.02 and 0.002, respectively). Tick marks represent censored patients, i.e. end of follow-up

No at risk

Total	120	94	64	34
T1m1	13	11	9	4
T1m2	18	15	8	6
T1m3	23	21	14	7
T1sm1	25	20	17	10
T1sm2	23	16	9	4
T1sm3	18	11	7	3

lung (Table 4). Twelve out of 18 patients who died following locoregional recurrence and/or distant metastases already had lymph node metastases at the time of resection. Recurrence-free period differed significantly between patients with N0 (n=101) and N+ (n=19) tumors (P logrank <0.0001, Fig. 4) with 5-year recurrence-free percentages of 94% (95% CI 89–99%) and 33% (95% CI 12–55%), respectively.

Discussion

We have created a detailed map of T1-substages of early Barrett's and GEJ cancers in relation to lymphatic dissemination and tumor recurrence. A favorable outcome was characterised by vertical tumor growth into, but not deeper than the upper layer of the submucosa. In contrast, cancers proliferating into the middle and deeper layers of the submucosa showed an unfavorable outcome with a high rate of recurrence after surgical resection. In our study the overall 5-year disease free survival was 68%, which is comparable to the sparse literature on this subject [11, 15, 19, 23, 28]. In the literature 5-year overall survival rates of 100% have been reported for T1 tumors limited to the mucosa, and rates declining to 63–100% for T1 tumors invading into the submucosa.

The group of T1m1-m3/sm1 tumors had lymph node metastases in only 1% as compared with 44% in the group of T1sm2-sm3 carcinomas. The very low frequency of lymphatic dissemination in the first group could not be attributed to the inclusion of 13 HGDs, as the recurrence-free period did not alter by excluding them from analysis. In another study from our group, the correlation between vertical cancer growth, angio-lymphatic permeation and the presence of lymph node metastasis has been investigated. However, this concerned only a subset of the present cohort that was operated on with various procedures [4].

The histopathological examination of endoscopically removed T1 adenocarcinomas in Barrett's esophagus can be difficult due to the presence of a double muscularis mucosae [29]. In Barrett's esophagus the mucosa consists of columnar epithelium, a superficial lamina propria, a superficial

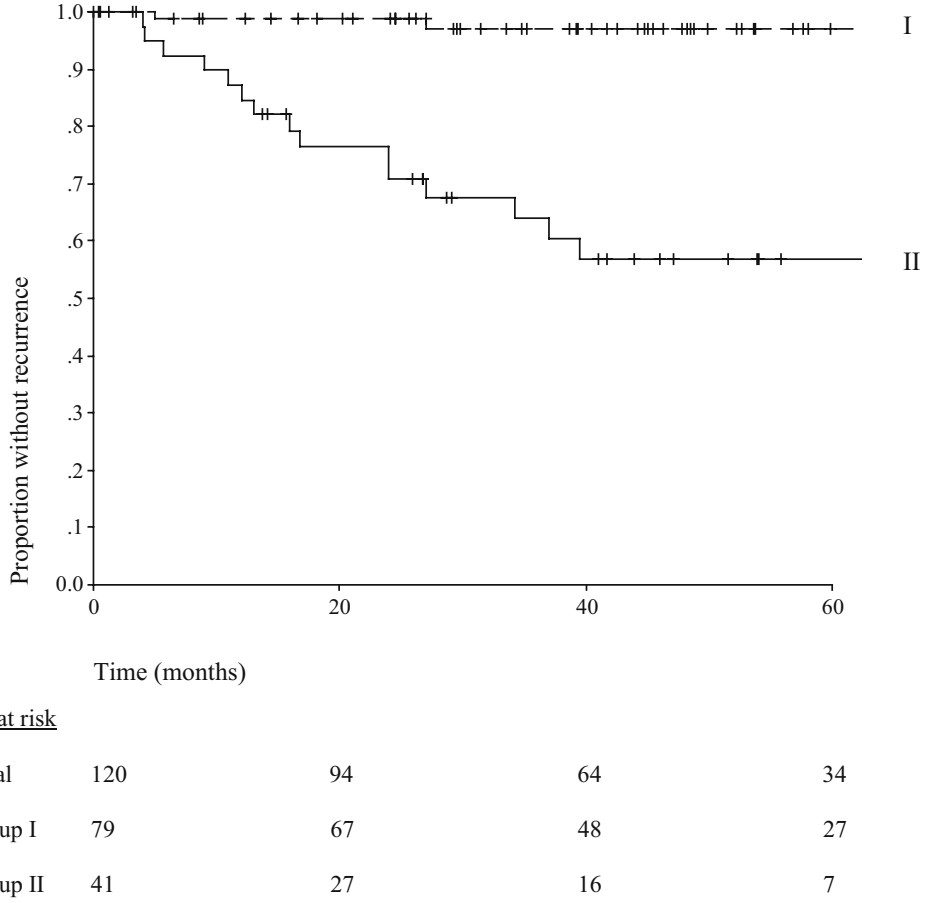

Fig. 3 Proportion of patients without recurrence, T1m1, T1m2, T1m3, T1sm1 (group I, broken line, *n*=79) versus T1sm2 or T1sm3 (group II, uninterrupted line, *n*=41). A clear difference can be seen between the two groups (*P* log-rank <0.0001). Five-year recurrence-free percentages for group I and group II were 97% (95% CI 93–100%) and 57% (95% CI 40–74%), respectively. Tick marks represent censored patients, i.e. end of follow-up

Table 2 Results of the Cox regression analysis, concerning recurrence-free period, in the total group of 120 early carcinomas

Prognostic factors	Univariate 5 years recurrence-free survival %	*P*-value	Multivariate[a] HR[b] (CI)[c]	*P*-value
Age[d]			1.0 (1.0–1.1)	0.8
Gender				
M[e]	81		1.0	
F	100	0.3	1.1 (0.1–9.9)	0.9
Tumor grade				
Well/Moderate[e]	87		1.0	
Poor	59	0.001	1.6 (0.6–4.4)	0.3
Depth of tumor invasion				
T1m1, T1m2, T1m3, T1sm1[e]	97		1.0	
T1sm2, T1sm3	57	<0.0001	3.1 (0.7–14.6)	0.2
N-stage				
N0[e]	94		1.0	
N1	33	<0.0001	5.9 (1.7–20.7)	0.005

[a]In multivariable analysis correction was carried out for the prognostic variables age, gender, tumour differentiation grade, depth of tumour invasion and N-stage; variables are mentioned in the column "Prognostic factors"
[b]Hazard Rate
[c]CI: 95% confidence interval
[d]In the multivariable analysis, age is included as a continuous variable
[e]Reference category

(newly formed) muscularis mucosae, a deep (pre-existent) lamina propria and a deep (pre-existent) muscularis mucosae. Precise classification of T1m2, T1m3 or T1sm1 cancer can be hampered, if there is doubt concerning the presence of the deep muscularis mucosae in the endomucosal resection specimen. Another, likely more important issue, is the correct classification of superficial tumor invasion of the submucosa in EMR specimens, because the deep (pre-existent) muscularis mucosae is not always a continuous structure [21]. However, our data indicate that this probably has no therapeutic consequences, since there is no

Table 3 Tumor recurrence: of the 18 patients, some patients had recurrence at more than one site

Recurrence	Number of patients
Locoregional	7
Distant	8
Bone	2
Pleural	3
Peritoneal	1
Liver	3
Truncal region	1
Both locoregional and distant	3
Truncal region	1
Bone	1
Supraclav lymph node	1

Table 4 Distribution of patients at the end of follow-up

Distribution	Number of patients
In-hospital mortality	5
Intercurrent death without disease	14
Death with locoregional recurrence only	7
Death with locoregional and distant recurrence	3
Death with distant recurrence only	7
Death due to second primary cancer	1
Alive with distant recurrence	1
Alive without evidence of disease	82
Total	120

difference in prognosis between T1m3 and T1sm1. Further, in our experience EMR substaging improves the selection procedure for surgical treatment of T1 cancers (Kerkhof et al., manuscript in preparation), whereas this cannot be achieved with sufficient accuracy by endoscopic ultrasound [14, 18].

The 5-year recurrence-free percentage of the patients with early tumors with lymph node invasion after transhiatal resection is disappointing (33%) and comparable with the prognosis of tumors with a more advanced T-stage and lymph node invasion [20]. The potential, particularly of the T1sm2-sm3 tumors, for both lymphatic and hematogenous dissemination already in an early stage is an indication of their aggressiveness. This might justify more radical treatment, i.e. transthoracic esophagectomy with extended lymphadenectomy of the posterior mediastinum, upper abdomen and perhaps even the neck [16]. Moreover, the unordered pattern of lymphatic dissemination in esophageal cancer, resulting in the frequent presence of tumor cells at a relatively large distance from the primary lesion [1], is once more a reason for extensive procedures. Extended resection is believed to reduce the rate of locoregional recurrence, thereby increasing the quality of life and prolonging the recurrence-free period and perhaps even survival. However, a more extensive resection for patients with early carcinomas could only be legitimated if it leads to a higher chance for cure. The possible advantages should be weighed against the increased risk of postoperative morbidity and mortality, since these patients are exposed to the higher risk of surgical complications [12].

To improve long term outcome, many institutes apply neoadjuvant chemoradiotherapy for advanced esophageal carcinoma, especially after the recent publication of favorable long term results of a randomized MRC trial comparing neoadjuvant chemotherapy followed by surgery versus surgery alone [17]. However, the poor prognosis of submucosal T1 tumors, and the high frequency of lymphatic dissemination indicate that these patients could also benefit from neoadjuvant chemoradiotherapy.

In conclusion, based on these results, we suggest that the combined group of mucosal (T1m1-m3) and superficial

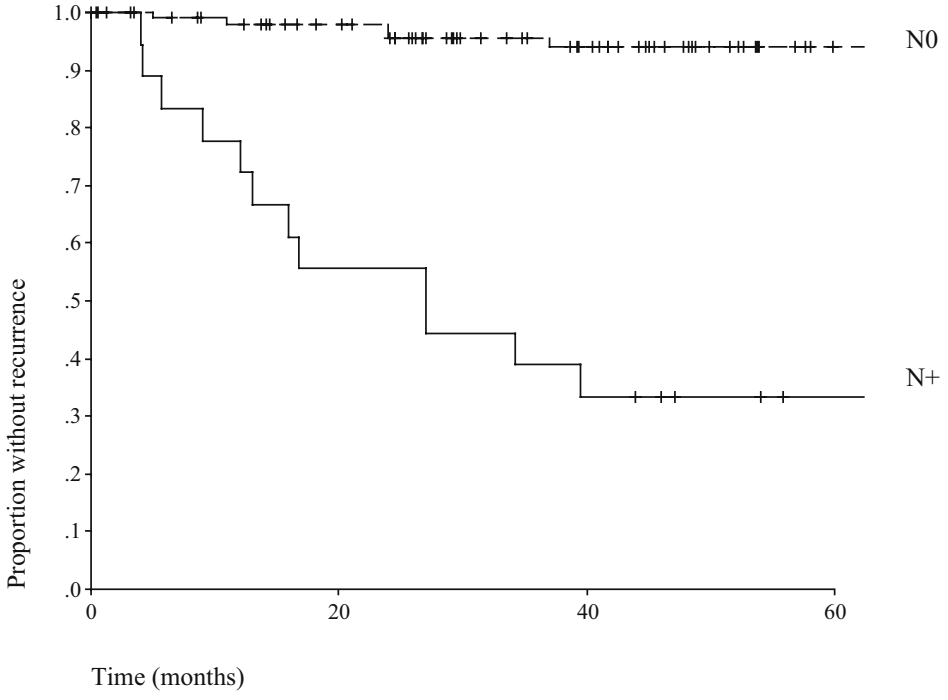

No at risk

Total	120	94	64	34
N0	101	84	58	33
N+	19	10	6	1

Fig. 4 Proportion of patients without recurrence, N0 (broken line, n=101) versus N+ (uninterrupted line, n=19). Patients with positive lymph nodes display a strikingly higher frequency of recurrence (P logrank <0.0001). Five-year recurrence-free percentages for N0 and N+ patients were 94% (95% CI 89–99%) and 33% (95% CI 12–55%), respectively. Tick marks represent censored patients, i.e. end of follow-up

submucosal (T1sm1) adenocarcinomas are eligible for local endoscopic treatment, since they carry only a 1% risk of lymphatic dissemination in combination with a 5-year recurrence-free period of 97%. For the T1sm2-sm3 adenocarcinoma group, which showed lymph node metastases in 44% and a recurrence-free period of 57%, surgical resection should be the treatment of choice. The substantial locoregional recurrence with or without distant dissemination after limited transhiatal resection is an argument in favor of more extensive surgery, and/or neo-adjuvant chemoradiation.

Acknowledgements The authors are grateful to W.C.J. Hop, PhD (Department of Epidemiology and Biostatistics, Erasmus University Medical Center, Rotterdam) for statistical advice.

References

1. Akiyama H, Tsurumaru M, Kawamura T, Ono Y (1981) Principles of surgical treatment for carcinoma of the esophagus: analysis of lymph node involvement. Ann Surg 194:438–446
2. Akiyama H, Tsurumaru M, Ono Y, Udagawa H, Kajiyama Y (1994) Esophagectomy without thoracotomy with vagal preservation. J Am Coll Surg 178:83–85
3. Bruno MJ (2003) Magnification endoscopy, high resolution endoscopy, and chromoscopy; towards a better optical diagnosis. Gut 52(Suppl 4):iv7–iv11
4. Buskens CJ, Westerterp M, Lagarde SM, Bergman JJ, ten Kate FJ, van Lanschot JJ (2004) Prediction of appropriateness of local endoscopic treatment for high-grade dysplasia and early adenocarcinoma by EUS and histopathologic features. Gastrointest Endosc 60:703–710
5. Bytzer P, Christensen PB, Damkier P, Vinding K, Seersholm N (1999) Adenocarcinoma of the esophagus and Barrett's esophagus: a population-based study. Am J Gastroenterol 94:86–91
6. Ell C, May A, Gossner L, Pech O, Gunter E, Mayer G, Henrich R, Vieth M, Muller H, Seitz G, Stolte M (2000) Endoscopic mucosal resection of early cancer and high-grade dysplasia in Barrett's esophagus. Gastroenterology 118:670–677
7. Falk GW (2002) Barrett's esophagus. Gastroenterology 122: 1569–1591
8. Froelicher P, Miller G (1986) The European experience with esophageal cancer limited to the mucosa and submucosa. Gastrointest Endosc 32:88–90
9. Gossner L, Stolte M, Sroka R, Rick K, May A, Hahn EG, Ell C (1998) Photodynamic ablation of high-grade dysplasia and early cancer in Barrett's esophagus by means of 5-aminolevulinic acid. Gastroenterology 114:448–455
10. Hage M, Siersema PD, van Dekken H, Steyerberg EW, Haringsma J, van de Vrie W, Grool TE, van Veen RLP, Sterenborg HCJM, Kuipers EJ (2004) 5-Aminolevulinic acid photodynamic therapy versus argon plasma coagulation for ablation of Barrett's oesophagus: a randomized trial. Gut 53:785–790
11. Holscher AH, Bollschweiler E, Schneider PM, Siewert JR (1995) Prognosis of early esophageal cancer. Comparison between adeno- and squamous cell carcinoma. Cancer 76:178–186
12. Hulscher JB, van Sandick JW, de Boer AG, Wijnhoven BP, Tijssen JG, Fockens P, Stalmeier PF, ten Kate FJ, van Dekken H, Obertop H, Tilanus HW, van Lanschot JJ (2002) Extended transthoracic resection compared with limited transhiatal resection for adenocarcinoma of the esophagus. N Engl J Med 347: 1662–1669
13. Japanese Society of Esophageal Diseases (1999) Guidelines for the clinical and pathologic studies on carcinoma of the esophagus, 9th edn. Kanehara, Tokyo
14. Kelly S, Harris KM, Berry E, Hutton J, Roderick P, Cullingworth J, Gathercole L, Smith MA (2001) A systematic review of the staging performance of endoscopic ultrasound in gastro-oesophageal carcinoma. Gut 49:534–539
15. Lerut T, Coosemans W, van Raemdonck D, Dillemans B, De Leyn P, Marnette JM, Geboes K (1994) Surgical treatment of Barrett's carcinoma:correlation between morphologic findings and prognosis. J Thorac Cardiovasc Surg 107:1059–1065
16. Lerut T, De Leyn P, Coosemans W, Van Raemdonck D, Scheys I, LeSaffre E (1992) Surgical strategies in esophageal carcinoma with emphasis on radical lymphadenectomy. Ann Surg 216:583–590
17. Medical Research Counsil Esophageal Cancer Working Group (2002) Surgical resection with or without preoperative chemotherapy in oesophageal cancer: a randomised controlled trial. Lancet 359:1727–1733
18. Meining A, Dittler HJ, Wolf A, Lorenz R, Schusdziarra V, Siewert JR, Classen M, Höfler H, Rösch T (2002) You get what you expect? A critical appraisal of imaging methodology in endosonographic cancer staging. Gut 50:599–603
19. Menke-Pluymers MB, Schoute NW, Mulder AH, Hop WC, van Blankenstein M, Tilanus HW (1992) Outcome of surgical treatment of adenocarcinoma in Barrett's oesophagus. Gut 33:1454–1458
20. Millikan KW, Silverstein J, Hart V, Blair K, Bines S, Roberts J, Doolas A (1995) A 15-year review of esophagectomy for carcinoma of the esophagus and cardia. Arch Surg 130:617–624
21. Offerhaus GJ, Correa P, van Eeden S, Geboes K, Drillenburg P, Vieth M, van Velthuysen ML, Watanabe H, Sipponen P, ten Kate FJ, Bosman FT, Bosma A, Ristimaki A, van Dekken H, Riddell R, Tytgat GN (2003) Report of an Amsterdam working group on Barrett esophagus. Virchows Arch 443:602–608
22. Pera M, Trastek VF, Carpenter HA, Allen MS, Deschamps C, Pairolero PC (1992) Barrett's esophagus with high-grade dysplasia: an indication for esophagectomy? Ann Thorac Surg 54: 199–204
23. Rice TW, Blackstone EH, Goldblum JR, DeCamp MM, Murthy SC, Falk GW, Ormsby AH, Rybicki LA, Richter JE, Adelstein DJ (2001) Superficial adenocarcinoma of the esophagus. J Thorac Cardiovasc Surg 122:1077–1090
24. Riegman PHJ, Vissers KJ, Alers JC, Geelen E, Hop WCJ, Tilanus HW, van Dekken H (2001) Genomic alterations in malignant transformation of Barrett's esophagus. Cancer Res 61: 3164–3170
25. Siewert JR, Stein HJ (1998) Classification of adenocarcinoma of the oesophagogastric junction. Br J Surg 85:1457–1459
26. Sobin LH, Wittekind C (2002) TNM classification of malignant tumours: International Union Against Cancer (UICC), 6th edn. Wiley-Liss, New York, pp 60–68
27. Stein HJ, Feith M, Mueller J, Werner M, Siewert JR (2000) Limited resection for early adenocarcinoma in Barrett's esophagus. Ann Surg 232:733–742
28. Streitz JM Jr, Ellis FH Jr, Gibb SP, Balogh K, Watkins E Jr (1991) Adenocarcinoma in Barrett's esophagus. A clinicopathologic study of 65 cases. Ann Surg 213:122–125
29. Takubo K, Sasajima K, Yamashita K, Tanaka Y, Fujita K (1991) Double muscularis mucosae in Barrett's esophagus. Hum Pathol 22:1158–1161
30. Van Dam J (2003) Novel methods of enhanced endoscopic imaging. Gut 52(Suppl 4):iv12–iv16
31. Van Lanschot JJ, Hulscher JB, Buskens CJ, Tilanus HW, ten Kate FJ, Obertop H (2001) Hospital volume and hospital mortality for esophagectomy. Cancer 91:1574–1578
32. Van Sandick JW, van Lanschot JJ, Kuiken BW, Tytgat GN, Offerhaus GJ, Obertop H (1998) Impact of endoscopic biopsy surveillance of Barrett's oesophagus on pathological stage and clinical outcome of Barrett's carcinoma. Gut 43:216–222
33. Wijnhoven BP, Tilanus HW, Dinjens WN (2001) Molecular biology of Barrett's adenocarcinoma. Ann Surg 233:322–337
34. Zaninotto G, Parenti AR, Ruol A, Costantini M, Merigliano S, Ancona E (2000) Oesophageal resection for high-grade dysplasia in Barrett's oesophagus. Br J Surg 87:1102–1105

Virchows Arch (2005) 446: 505–510
DOI 10.1007/s00428-005-1240-4

ORIGINAL ARTICLE

Peter Kornprat · Peter Rehak · Martina Lemmerer · Margit Gogg-Kamerer · Cord Langner

Analysis of trefoil factor family protein 1 (TFF1, pS2) expression in chronic cholecystitis and gallbladder carcinoma

Received: 5 December 2004 / Accepted: 22 February 2005 / Published online: 9 April 2005
© Springer-Verlag 2005

Abstract Trefoil factor family protein 1 (TFF1, pS2) interacts with mucins to protect gastrointestinal epithelium against injury and contributes to mucosal repair by promoting epithelial cell migration and restitution. Moreover, TFF1 has antiproliferative and anti-apoptotic effects and promotes cell scattering and invasion. We investigated TFF1 expression in healthy and inflamed non-neoplastic gallbladder mucosa as well as in gallbladder carcinomas (n=57) and corresponding metastases (n=18), using a tissue microarray technique. TFF1 immunoreactivity was absent in healthy mucosa, focally observed in epithelium with inflammatory changes and present in 35% of primary and 24% of metastatic cancer tissues. Immunoreactivity significantly decreased with increasing tumour stage (P=0.009) and increasing tumour grade (P=0.001). Patients with TFF1 positive tumours showed a more favourable outcome compared to patients with TFF1 negative tumours in univariate analysis (P=0.006). However, multivariate analysis proved resection status and tumour grade as the only independent prognostic factors. In conclusion, TFF1 is expressed in inflamed non-neoplastic gallbladder epithelium and in low stage and low grade gallbladder carcinomas. Thus, TFF1 may be the missing link between gallstones, chronic cholecystitis and gallbladder cancer. Further studies are needed to evaluate whether TFF1 immunostaining can be used as a diagnostic tool to identify patients with a more favourable outcome.

Keywords TFF1 · pS2 · Gallbladder carcinoma · Pathogenesis · Prognosis

P. Kornprat · M. Lemmerer
Department of Surgery,
Medical University of Graz,
Auenbruggerplatz 29,
8036 Graz, Austria

P. Rehak
Division of Biomedical Engineering & Computing,
Medical University of Graz,
Auenbruggerplatz 29,
8036 Graz, Austria

M. Gogg-Kamerer · C. Langner (✉)
Institute of Pathology,
Medical University of Graz,
Auenbruggerplatz 25,
8036 Graz, Austria
e-mail: cord.langner@meduni-graz.at
Tel.: +43-316-38583665
Fax: +43-316-384329

Introduction

Carcinoma of the gallbladder represents the most common malignant tumour of the biliary tract and the sixth most common cancer of the gastrointestinal tract [4]. Overall, this tumour entity shows a strong female predominance, with incidence rates up to 3 times higher among women than men. Prognosis is generally poor with a 32% 5-year survival rate for lesions confined to the gallbladder mucosa and a 10% 1-year survival rate for more advanced stages [13]. The main prognostic factors for gallbladder cancer are resection status and TNM stage [8, 23], and there is a correlation between the level of tumour invasion and the presence of lymph node metastases [13]. However, since gallbladder cancer is difficult to cure by surgery alone, identification of new prognostic biomarkers may help to identify patients who might benefit from additional therapy.

The trefoil factor family protein 1 (TFF1), originally called pS2, was first identified in the estrogen receptor positive MCF-7 human breast cancer cell line [20]. It belongs to a family of small protease-resistant proteins known as trefoil ("three leaves") peptides because of their distinctive three-loop structure formed by intrachain disulfide bonds. Three members of this family have been identified in humans: TFF1 (pS2), TFF2 or human spasmolytic polypeptide (SP) and TFF3 or intestinal trefoil factor (ITF) [35]. Depending on the methylation status of their proximal promoter regions, the TFF peptides are expressed in a site-specific pattern along the gastrointestinal tract [25]. Thus, TFF1 is expressed primarily in the stomach (superficial and foveolar epithelium) and TFF2 in the stomach (mucous neck

cells) and in the duodenum (Brunner's glands), whereas TFF3 predominates in the small and large intestine (goblet cells) [35].

Physiologically, TFFs are abundantly secreted peptides that interact directly with mucins to stabilize the mucous layer lining the gastrointestinal tract, thus protecting the epithelium against injury and maintaining the integrity of the mucosal barrier [37]. Moreover, TFFs contribute to mucosal repair promoting epithelial cell migration and mucosal restitution, and increased TFF expression has been demonstrated in response to epithelial damage and inflammation [35]. According to recent in vitro data, TFF1 is able to inhibit both proliferation (by delaying G1-S phase transition) and apoptosis (via the decrease of caspase-3, -6, -8, and -9 activities) in gastrointestinal epithelial cells [3]. Thus, TFF1 has an important role in regulating the balance between gastrointestinal cell proliferation, death and differentiation.

However, TFFs may also play a role in tumour biology. Support for this function has come mainly from observations that TFF levels in malignant tissues differ from that of corresponding normal tissues. Thus, TFFs are variably expressed by many types of human cancer, including breast, prostatic, gastric, colorectal and pulmonary adenocarcinomas [18].

In the biliary tract, TFF1 expression is increased in biliary diseases in response to injury, as is seen in epithelial damage elsewhere in the gastrointestinal tract [30, 33]. With respect to gallbladder cancer, only two studies investigating TFF1 expression exist which have yielded conflicting results and have not correlated pathologic data with clinical follow-up [26, 31]. Therefore, the current study was designed to investigate the expression of TFF1 in a large series of gallbladder cancers with respect to associations with tumour stage, tumour grade and histological subtype as well as impact on carcinogenesis and patient outcome.

Materials and methods

Case selection

Formalin-fixed and paraffin-embedded specimens of 57 primary gallbladder carcinomas from consecutive patients (40 women and 17 men; male/female ratio 2.4:1) operated between 4/1984 and 12/2002 were chosen for analysis. The mean and median age of patients at surgery were 71 and 72 years (range 35–91 years), respectively. Resection categories of primary tumours were R0 in 28 (49%), R1 in 16 (28%) and R2 in 13 (23%) cases, respectively. Corresponding syn-/metachronous lymph node (n=11) and hepatic (n=7) metastases were included in the study. PT categories were adjusted according to the UICC 2002 issue of the TNM-system [32]: stage pT1a was present in one (2%), pT1b in four (7%), pT2 in 23 (40%), pT3 in 27 (47%) and pT4 in two (4%) cases, respectively. For the conventional histopathologic examination of tumour specimens H&E-stained sections were used. Tumour grades and histological subtypes (variants) were evaluated according to WHO guidelines [1]. Ten cases of non-neoplastic, healthy and inflamed gallbladder tissue were analyzed for comparison. Ethical committee approval and informed consent are not required for retrospective studies dealing with archival material at our institution.

Immunohistochemistry

For immunohistochemical analysis, a tissue microarray technique was used which allows staining of a large number of specimens on one slide. One might argue that the analysis of only small tumour samples could yield unreliable data. However, this objection has been disproved by former studies [22]. Tissue microarrays (TMAs) were prepared using a manual tissue arraying instrument (Beecher, Silver Spring, Md., USA). The details of this technique have been described previously [11]. With respect to the well known heterogeneity of cancer tissues, between three and five cylindrical core biopsies, 0.6 mm in diameter, were taken from different sites of each tumour which had been selected on the original tumour slides to include all patterns of differentiation. Sections of 4 μm were mounted on Superfrost slides for immunohistochemical analysis using an automated immunostainer (DAKO-Autostainer, Universal Staining System; DAKO, Glostrup, Denmark). TMA sections were deparaffinized, rehydrated in graded alcohols and treated for 5 min with 1% H_2O_2. Sections were submitted to microwave antigen retrieval (30 min 160 W in 0.01 M sodium citrate buffer pH 6.0) and subsequently incubated for 30 min with a monoclonal mouse antibody anti-human TFF1 (pS2) antibody (Clone BC04, 1:50, DAKO). Binding of the primary antibody was assessed by the DAKO LSAB2 System HRP (AEC) Detection kit.

Immunohistochemical evaluation and controls

Immunohistochemical staining was evaluated in a semiquantitative fashion independently by two investigators (P. K. and C.L.) who were blinded regarding the clinicopathologic data, especially pT-stage and patients' outcome. Discrepancies were resolved by simultaneous reexamination of the slides by both investigators using a double-headed microscope. A distinct cytoplasmic staining was considered positive, and immunoreactivity was categorized as "focal" (+; <10% of tumour cells positive), "moderate" (++; 10–50%), or "extensive" (+++; >50%). Sections of breast cancer tissue served as positive controls. Negative controls included omission of the primary antibody and incubation with DAKO ChemMate Antibody Diluent.

Statistical analysis

Subgroups according to pT-stage, tumour grade and histological subtype were compared with respect to possible differences in immunoreactivity using the Chi-square test or Fisher's exact test, respectively. Patient outcome was investigated using the Kaplan–Meier method and compared by

the log-rank test. For multivariate testing a Cox's proportional hazards regression model for pT-stage, tumour grade, R-status of surgery and TFF1 expression was performed.

Results

Histopathology

Conventional histopathological evaluation showed tubular adenocarcinoma in 43/57 (75%) cases, whereas the remaining 14 tumours displayed either a papillary (n=5; 9%), mucinous (n=2; 4%), clear cell (*n*=2; 4%), signet-ring cell (*n*=1; 2%) or adenosquamous (*n*=4; 7%) morphology. WHO grading revealed 16 (28%) well differentiated (G1), 19 (33%) moderately differentiated (G2), 21 (37%) poorly differentiated (G3) carcinomas and one (2%) undifferentiated (G4) carcinoma. Lymphatic and venous invasion were detected in 41/57 (72%) and 16/57 (28%) primary tumours, respectively. In general, the histology of metastases was identical to that of corresponding primary tumours.

Immunohistochemistry

Cancer tissue allowing a reliable evaluation of TFF1 immunostaining was present in 52/57 (91%) primary tumours and 17/18 (94%) metastases, respectively. Overall, TFF1 immunoreactivity was seen in 18/52 (35%) primary cancer tissues (Fig. 1a) with only four tumours showing extensive immunostaining (Table 1). TFF1 expression was independent of gender, since immunoreactivity was seen in 14/38 (37%) female and 4/14 (29%) male patients. Regarding metastases, TFF1 immunoreactivity was seen in 4/17 (24%) cases, with three metastases showing only focal and one moderate immunostaining. Comparison of primary and syn-/metachronous metastatic cancer tissues yielded identical staining results in ten cases. In four cases, the primary tumours showed focal TFF1 immunoreactivity, whereas the corresponding metastases lacked immunostaining. In the remaining three cases focal TFF1 immunoreactivity of metastatic tissues was seen, whereas the corresponding primary tumours lacked immunostaining. Non-neoplastic gallbladder mucosa showed focal epithelial TFF1 expression in areas of inflammation (Fig. 1b), whereas healthy mucosa lacked TFF1 immunoreactivity.

TFF1 immunoreactivity of primary tumours decreased with increasing stage (13/24 (54%) pT1/pT2 versus 5/28 (18%) pT3/pT4; *P*=0.009) and increasing grade (16/30 (53%) G1/G2 versus 2/22 (9%) G3/G4; *P*=0.001), but was not found to be significantly associated with angioinvasion (7/14 (50%) L0/V0 versus 11/38 (29%) L1 and/or V1; *P*=0.2). Due to sample size, no significant association between TFF1 immunoreactivity and histological subtypes were found. However, it appears worth mentioning that 4/5 (80%) papillary adenocarcinomas showed at least moderate immunoreactivity.

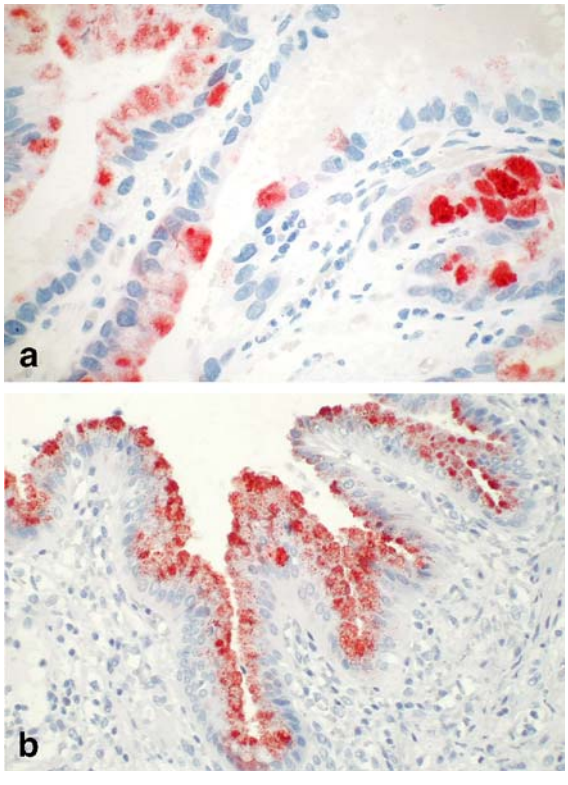

Fig. 1 Distinct cytoplasmic TFF1 immunoreactivity in a moderately differentiated tubular adenocarcinoma of the gallbladder (A, original ×400) and in non-neoplastic gallbladder epithelium with inflammatory alterations (B, original ×150)

Survival analysis

Follow-up data were available for all patients. The overall median survival time of all patients was 45 weeks (range 0.4–604) with a 1-year survival rate of 34% and 5-year sur-

Table 1 TFF1 immunoreactivity (+,<10% of cells positive; ++, 10–50% of cells positive; +++, >50% of cells positive) of primary gallbladder carcinomas related to tumour stage and tumour grade

Stage/grade	Gallbladder carcinomas (*n*=52)	
	N	%
Negative	34/52	65
+	5/52	10
++	9/52	17
+++	4/52	8
Overall positive	18/52	35
pT1a	1/1	100
pT1b	2/4	50
pT2	10/19	53
pT3	4/26	15
pT4	1/2	50
G1	8/13	62
G2	8/17	47
G3	2/21	10
G4	0/1	0

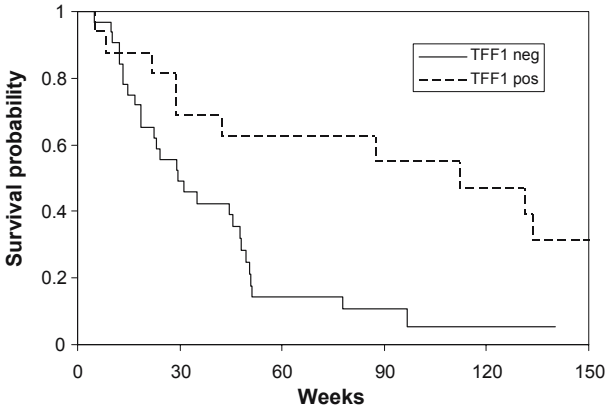

Fig. 2 Overall survival (weeks) of patients with gallbladder carcinoma related to TFF1 immunoreactivity (P=0.006; log-rank test)

vival rate of 6%, respectively. There were four (7%) procedure related deaths (within 28 days): two patients with pulmonary embolism, one patient with pneumonia and one patient with cholangitis and consecutive sepsis. Forty-four (77%) patients died (range 10–175 weeks, median=31 weeks) because of tumour progression, eight (14%) patients died (range 12–604 weeks, median=44 weeks) from causes unrelated to gallbladder cancer without evidence of residual tumour, and one (2%) patient currently is alive, but suffering from metastatic disease (90 weeks after surgery). Patients who underwent complete resection (R0) had a more favourable overall median survival (78 weeks, range 14–604) compared with patients with R1 resection (21 weeks, rage 5–90) and R2 resection (18 weeks, range 0.4–42), respectively (P<0.001, log-rank test). The 1-year survival rate was 63% for patients with R0 resection, 7% for R1 resection and 0% for R2 resection status, respectively. The 5-year survival rate of patients with R0 status was 11% (n= 6), whereas no patients with R1- or R2-resection were alive 5 years after surgery.

Regarding TFF1 expression, patients with TFF1 positive tumours showed a significantly longer median survival time (113 weeks, range 2–604) compared with patients with TFF1 negative tumours (30 weeks, range 0.4–140). Moreover, 57% of patients who died from causes unrelated to cancer had TFF1-positive tumours compared with 30% of patients who died due to tumour progression (P=0.006; log-rank test; Fig. 2). However, multivariate analysis proved only resection category >0 (RR 12.2, CI=4.5–33.6; P<0.001) and tumour grade >2 (RR 3.1, CI=1.4–7.0; P=0.005) as independent prognostic factors regarding survival, whereas both tumour stage and TFF1 lacked independent influence on patient outcome.

Discussion

TFF1 is variably expressed by many types of human cancer, including breast, prostatic, gastric, colorectal and pulmonary adenocarcinomas [18]. Two general patterns have emerged: TFFs either are overexpressed in tumours, whereas normal counterpart tissues express no or low levels of TFFs (e.g. breast, colon, prostate), or they are absent or reduced in tumours in contrast to high levels in the respective non-neoplastic tissue (e.g. stomach). It has been proposed by Lefebvre et al. [14] that TFF1 is a tumour suppressor gene. In support of this idea, TFF1 "knock-out" mice (*TFF1*−/−) constantly develop gastric adenomas and 30% develop invasive adenocarcinomas [14]. Accordingly, TFF1 gene inactivation by deletion, missense mutation and promoter methylation has been documented in human gastric cancer in several studies [9]. Interestingly, TFF1 protein expression is frequently down-regulated in intestinal-type gastric cancer, whereas the TFF1 protein is commonly expressed in diffuse-type gastric cancer cells [10, 15, 19]. This finding is supported by some recent in vitro data showing TFF1-mediated cell scattering and activation of invasion by kidney and colonic cancer cells as well as TFF1-induced angiogenesis implicating cyclooxygenase-2 and EGF receptor signalling, thus linking auto-/paracrine TFF1 expression to cancer progression [5, 27, 28].

Only two studies investigating TFF1 expression in gallbladder cancer exist [26, 31]. Seitz et al. [31] reported TFF1 immunostaining in up to 86% of cancer cases and in non-neoplastic mucosa with inflammatory alterations, whereas healthy gallbladder epithelium constantly lacked TFF1 expression. Roa et al. [26], however, found TFF1 expression in only 32% of cancer cases and in 60% of non-tumoural gallbladders. No associations with either stage or grade were reported and no correlation with clinical follow-up was performed.

According to our data, TFF1 immunostaining is absent in healthy gallbladder mucosa, but present in non-neoplastic mucosa with inflammatory changes and expressed in about one-third of primary gallbladder cancers as well as in about a quarter of cancer metastases. The similar expression in primary and metastatic tumour tissues has already been noted in colorectal carcinomas and corresponding metastases [6], indicating that pS2 may not contribute to the metastatic process. In our study, TFF1 expression by primary tumors decreased with increasing tumour stage and grade. Moreover, patients with TFF1-positive tumours showed a more favourable outcome compared to patients with TFF1-negative tumours in univariate analysis. Further studies including more patients are needed to decide whether TFF1 expression in gallbladder cancer might independently influence patient outcome.

However, our findings can be related to a recent study by Sasaki et al. [30], who examined the participation of TFF1 in the development and progression of intrahepatic cholangiocarcinoma associated with hepatolithiasis. According to their data, TFF1 expression was found to be increased in hepatolithiasis compared with control livers. In biliary epithelial dysplasia and in non-invasive cholangiocarcinoma, TFF1 was extensively expressed, whereas its expression was significantly decreased in invasive cancers, possibly related to methylation of the TFF1 promoter region [30]. A similar correlation between loss of TFF1 expression and tumour dedifferentiation and/or progression has been reported for breast [2], pancreatic [29] and endo-

metrial [12] adenocarcinomas, whereas positive TFF1 immunostaining has been correlated with poor prognosis in pulmonary adenocarcinomas [7] and transitional cell bladder tumours [17]. With respect to gastric cancer, Suarez et al. [34] reported a significant association between high intratumour TFF1 levels and unfavourable outcome, whereas two other groups failed to detect any impact on survival [19, 21].

The pathogenesis of gallbladder cancer has been related to cholelithiasis and chronic infection. Gallstones are found in almost all cases of gallbladder cancer [13] and chronic inflammation may contribute to the progression from epithelial dysplasia (intraepithelial neoplasia) to invasive carcinoma [36]. On the molecular level, loss of p16 and reduced p21(WAF1/CIP1) expression, as well as p53 overexpression are frequent events in gallbladder carcinogenesis [16, 24]. However, the pathogenetic mechanisms concerning the relationship between gallstones (and chronic inflammation) and gallbladder cancer are poorly understood.

Our results and recent data in the literature strongly suggest that TFF1 expression may play a role in the relationship between gallstones, chronic cholecystitis and gallbladder cancer. Gallstones and other agents causing chronic cholecystitis lead to alterations of gallbladder epithelium which are associated with TFF1 overexpression. TFF1 has a motogenic potential and can be regarded as an auto-/paracrine scatter factor promoting invasion (and angiogenesis). Moreover, inhibition of apoptosis by TFF1 may interrupt the death signal that is usually encountered by motile cells when they detach from the matrix. Once the first steps of cancer development are established, the antiproliferative effect of TFF1 may impede tumour growth. Thus, decreased TFF1 expression, possibly due to epigenetic effects, such as methylation of the TFF1 promoter region, may lead to increased tumour cell proliferation, promoting cancer progression.

In conclusion, TFF1 protein is absent in healthy gallbladder mucosa, but present and up-regulated in inflamed gallbladder epithelium and expressed in increased amounts in both primary and metastatic gallbladder cancers. TFF1 expression of primary tumours decreases with increasing tumor stage and grade. Moreover, patients with TFF1-positive tumours show a more favourable outcome compared to those with TFF1-negative tumours in univariate analysis. Finally, TFF1 may play a role in the relationship between gallstones, chronic cholecystitis and gallbladder cancer.

References

1. Albores-Saavedra J, Scoazec JC, Wittekind C, Sripa B, Menck HR, Soehendra N, Sriram PVJ (2000) Tumours of the gallbladder and extrahepatic bile ducts. In: Hamilton SR, Aaltonen LA (eds) WHO classification of tumours. Pathology and genetics. Tumours of the digestive system. IARC Press, Lyon, pp 203–218
2. Balleine RL, Clarke CL (1999) Expression of the oestrogen responsive protein pS2 in human breast cancer. Histol Histopathol 14:571–578
3. Bossenmeyer-Pourié C, Kannan R, Ribieras S, Wendling C, Stoll I, Thim L, Tomasetto C, Rio MC (2002) The trefoil factor 1 participates in gastrointestinal cell differentiation by delaying G1-S phase transition and reducing apoptosis. J Cell Biol 157:761–770
4. Donohue JH, Stewart AK, Menck HR (1998) The national cancer data base report on carcinoma of the gallbladder, 1989–1995. Cancer 83:2618–2628
5. Emami S, Le Floch N, Bruyneel E, Thim L, May F, Westley B, Rio MC, Mareel M, Gespach C (2001) Induction of scattering and cellular invasion by trefoil peptides in src- and RhoA-transformed kidney and colonic epithelial cells. FASEB J 15: 351–361
6. Hackel C, Falkenberg B, Gunther T, Lippert H, Roessner A (1998) The pS2 protein in colorectal carcinomas and metastases. Pathol Res Pract 94:171–176
7. Higashiyama M, Doi O, Kodama K, Yokouchi H, Inaji H, Nakamori S, Tateishi R (1994) Prognostic significance of pS2 protein expression in pulmonary adenocarcinoma. Eur J Cancer 30A:792–797
8. Ito H, Matros E, Brooks DC, Osteen RT, Zinner MJ, Swanson RS, Ashley SW, Whang EE (2004) Treatment outcomes associated with surgery for gallbladder cancer: a 20-year experience. J Gastrointest Surg 8:183–190
9. Katoh M (2003) Trefoil factors and human gastric cancer. Int J Mol Med 12:3–9
10. Kirikoshi H, Katoh M (2002) Expression of TFF1, TFF2 and TFF3 in gastric cancer. Int J Oncol 21:655–659
11. Kononen J, Bubendorf L, Kallioniemi A, Barlund M, Schraml P, Leighton S, Torhorst J, Mihatsch MJ, Sauter G, Kallioniemi OP (1998) Tissue microarrays for high-throughput molecular profiling of tumor specimens. Nat Med 4:844–847
12. Koshiyama M, Yoshida M, Konishi M, Takemura M, Yura Y, Matsushita K, Hayashi M, Tauchi K (1997) Expression of pS2 protein in endometrial carcinomas: correlation with clinicopathologic features and sex steroid receptor status. Int J Cancer 74:237–244
13. Lazcano-Ponce EC, Miquel JF, Munoz N, Herrero R, Ferrecio C, Wistuba II, Alonso de Ruiz P, Aristi Urista G, Nervi F (2001) Epidemiology and molecular pathology of gallbladder cancer. CA Cancer J Clin 51:349–364
14. Lefebvre O, Chenard MP, Masson R, Linares J, Dierich A, LeMeur M, Wendling C, Tomasetto P, Chambon P, Rio MC (1996) Gastric mucosa abnormalities and tumorigenesis in mice lacking the pS2 trefoil protein. Science 274:259–262
15. Leung WK, Yu J, Chan FK, To KF, Chan MW, Ebert MP, Ng EK, Chung SC, Malfertheiner P, Sung JJ (2002) Expression of trefoil peptides (TFF1, TFF2, and TFF3) in gastric carcinomas, intestinal metaplasia, and non-neoplastic gastric tissues. J Pathol 197:582–588
16. Li X, Hui AM, Shi YZ, Takayama T, Makuuchi M (2001) Reduced p21(WAF1/CIP1) expression is an early event in gallbladder carcinogenesis and is of prognostic significance for patients with carcinomas of the gallbladder. Hum Pathol 32:771–777
17. Lipponen PK, Eskelinen MJ (1994) Expression of pS2 protein transitional cell bladder tumours. J Pathol 173:327–332
18. Longman RJ, Thomas MG, Poulsom R (1999) Trefoil peptides and surgical disease. Br J Surg 86:740–748
19. Machado JC, Carneiro F, Ribeiro P, Blin P, Sobrinho-Simoes M (1996) pS2 protein expression in gastric carcinoma. An immunohistochemical and immunoradiometric study. Eur J Cancer 32A:1585–1590
20. Masiakowski P, Breathnach R, Bloch J, Gannon F, Krust A, Chambon P (1982) Cloning of cDNA sequences of hormone-regulated genes from the MCF-7 human breast-cancer cell line. Nucleic Acids Res 10:7895–7903
21. Müller W, Borchard F (1993) pS2 protein in gastric carcinoma and normal gastric mucosa: association with clinicopathological parameters and patient survival. J Pathol 171:263–269

22. Nocito A, Bubendorf L, Tinner ME, Suess K, Wagner U, Forster T, Kononen J, Fijan A, Bruderer J, Schmid U, Ackermann D, Maurer R, Alund G, Knonagel H, Rist M, Anabitarte M, Hering F, Hardmeier T, Schoenenberger AJ, Flury R, Jager P, Fehr LJ, Schraml P, Moch H, Mihatsch MJ, Gasser T, Sauter G (2001) Microarrays of bladder cancer tissue are highly representative of proliferation index and histological grade. J Pathol 194:349–357
23. North JH Jr, Pack MS, Hong C, Rivera DE (1998) Prognostic factors for adenocarcinoma of the gallbladder: an analysis of 162 cases. Am Surg 64:437–440
24. Parwani AV, Geradts J, Caspers E, Offerhaus GJ, Yeo CJ, Cameron JL, Klimstra DS, Maitra A, Hruban RH, Argani P (2003) Immunohistochemical and genetic analysis of non-small cell and small cell gallbladder carcinoma and their precursor lesions. Mod Pathol 16:299–308
25. Ribieras S, Lefebvre O, Tomasetto C, Rio MC (2001) Mouse Trefoil factor genes: genomic organization, sequences and methylation analyses. Gene 266:67–75
26. Roa I, Araya JC, Villaseca M, de Artxabala X, Ferreira A, Roa JC (1995) Gallbladder cancer: immunohistochemical expression of the protein related to estrogen receptor (p29) and of the protein induced by estrogen (pS2). Rev Med Chile 123:1333–1340
27. Rodrigues S, van Aken E, van Bocxlaer S, Attoub S, Nguyen QD, Bruyneel E, Westley BR, May FEB, Thim L, Mareel M, Gespach C, Enami S (2003) Trefoil peptides as proangiogenic factors in vivo and in vitro: implication of cyclooxygenase-2 and EGF receptor signaling. FASEB J 17:7–16
28. Rodrigues S, Attoub S, Nguyen QD, Bruyneel E, Rodrigue CM, Westley BR, May FEB, Thim L, Mareel M, Emami S, Gespach C (2003) Selective abrogation of the proinvasive activity of the trefoil peptides pS2 and spasmolytic polypeptide by disruption of the EGF receptor signaling pathways in kidney and colonic cancer cells. Oncogene 22:4488–4497
29. Sagol O, Tuna B, Coker A, Karademir S, Obuz F, Astarcioglu H, Kupelioglu A, Astracioglu I, Topalak O (2002) Immunohistochemical detection of pS2 protein and heat shock protein-70 in pancreatic adenocarcinomas. Relationship with disease extent and patient survival. Pathol Res Pract 198:77–84
30. Sasaki M, Tsuneyama K, Nakanuma Y (2003) Aberrant expression of trefoil factor family 1 in biliary epithelium in hepatolithiasis and cholangiocarcinoma. Lab Invest 83:1403–1413
31. Seitz G, Thelsinger B, Tomasetto G, Rio MC, Chambon P, Blin N, Welter G (1991) Breast cancer—associated protein pS2 expression in tumors of the biliary tract. Am J Gastroenterol 86: 1491–1494
32. Sobin LH, Wittekind C (eds) (2002) TNM classification of malignant tumors, 6th edn. Wiley-Liss, New York
33. Srivatsa G, Giraud AS, Ulaganathan M, Yeomans ND, Dow C, Nicoll AJ (2002) Biliary epithelial trefoil peptide expression is increased in biliary diseases. Histopathology 40:262–268
34. Suarez C, Vizoso F, Rodriguez JC, Garcia I, Raigoso P, Allende MT, Garcia-Muniz JL, Garcia-Moran M (2001) Prognostic significance of cytosolic pS2 protein content in gastric cancer. Int J Biol Markers 16:37–44
35. Taupin D, Podolsky DK (2003) Trefoil factors: initiators of mucosal healing. Nat Rev Mol Cell Biol 4:721–732
36. Tazuma S, Kajiyama G (2001) Carcinogenesis of malignant lesions of the gallbladder. The impact of chronic inflammation and gallstones. Langenbeck's Arch Surg 386:224–229
37. Tomasetto C, Masson R, Linares JL, Wendling C, Lefevre O, Chenard MP, Rio MC (2000) pS2/TFF1 interacts directly with the VWFC cysteine-rich domains of mucins. Gastroenterology 118:70–80

Virchows Arch (2005) 446: 511–516
DOI 10.1007/s00428-005-1239-x

ORIGINAL ARTICLE

Noelia Perez · Mireia Castillo · Yolanda Santos · David Truan · Rafael Gutierrez · Agustin Franco · Antonio Palacin · Josep Antoni Bombi · Elias Campo · Pedro L. Fernandez

Carcinosarcoma of the prostate: two cases with distinctive morphologic and immunohistochemical findings

Received: 12 December 2004 / Accepted: 21 February 2005 / Published online: 9 April 2005
© Springer-Verlag 2005

Abstract Carcinosarcomas (CS) of the prostate are very uncommon neoplasms defined by the admixture of malignant epithelial and mesenchymal components. We describe here two new examples of CS in two patients aged 66 and 77 years, the first without previous history of prostate adenocarcinoma and the second with a 5-year history of acinar type prostate adenocarcinoma. The diagnosis of CS was made on the cystoprostatectomy specimen in the first case and transurethral resection in the second case. Both biphasic tumours exhibited papillary areas of ductal differentiation and conventional adenocarcinoma in the epithelial component, as well as malignant fibrous histiocytoma and angiosarcomatous areas in the first case and solid, poorly differentiated epithelial areas with neuroendocrine features in the second case. Immunohistochemistry revealed over-expression of c-erb B2 in the papillary epithelial component of both cases, whereas the solid undifferentiated epithelial areas in the second patient expressed c-kit, CD10 and synaptophysin, thus conforming a very undifferentiated cell population. The angiosarcomatous component of the first case expressed CD31 and CD10. The clinical course of the cases was divergent; the first patient is free of disease after radical surgery and adjuvant therapy and the other died 5 months after the diagnosis of CS, having already developed liver metastases.

Keywords Prostate · Carcinosarcoma · Immunohistochemistry · Ductal

N. Perez · M. Castillo · A. Palacin · J. A. Bombi · E. Campo · P. L. Fernandez (✉)
Department of Pathology, Hospital Clinic,
C/Villarroel 170,
08036 Barcelona, Spain
e-mail: plfernan@clinic.ub.es
Tel.: +34-93-2275450
Fax: +34-93-2275717

Y. Santos · D. Truan · R. Gutierrez · A. Franco
Department of Urology, Hospital Clinic,
Barcelona, Spain

Introduction

Carcinosarcoma (CS) of the prostate is a very rare neoplasm, with fewer than 50 previous reports of well-documented cases to our knowledge [1, 3, 5, 8–15, 17–20, 22, 23, 26, 32, 34]. The World Health Organization (WHO) [6], despite classifying CS and sarcomatoid carcinoma together in the chapter of epithelial tumours, reflects the controversy regarding their histogenesis and nomenclature. The Armed Forces Institute of Pathology [33], on the other hand, classifies these entities separately, and defines CS as a haphazard admixture of obvious malignant epithelial and spindle cell foci, with the latter being truly sarcomatous, often with heterologous tissues such as cartilage or skeletal muscle. Therefore, the origin and proper designation of this type of neoplasm are still a matter of debate. From a practical point of view, CS should probably not be considered synonymous of sarcomatoid carcinoma of the prostate, as some authors have suggested [24, 28], which might lead to improved diagnostic accuracy and therefore to possible treatment or prognostic differences. Nevertheless, it seems to be currently accepted that the diagnosis of CS needs a morphologically suggestive appearance and a dual immunophenotype or ultrastructural demonstration of mesodermal differentiation.

We herein report two new cases fulfilling the criteria for this entity, each with distinctive and unusual clinical, morphological and immunohistochemical characteristics.

Clinical history

Case no. 1

A 66-year-old man presented with prostatism and was found to have an enlarged prostate on physical examination. The serum prostate-specific antigen (PSA) was 6.74 ng/ml at that time. Transrectal ultrasonography revealed a heterogeneous retroprostatic mass involving the right prostatic lobe with extrinsic infiltration of the rectal wall, measuring 78×77×61 mm altogether. Fine-needle biopsies were obtained, and the histological diagnosis was high-grade fuso-

cellular sarcoma involving the right prostatic lobe, whereas the left lobe biopsies only contained fibrous tissue. Clinical evaluation for metastases was negative. Cystoprostatectomy as well as rectum-sigmoidectomy and urinary diversion to colostomy were needed to ensure total resection of the tumour. Bilateral obturator lymphadenectomy was also performed. In addition, adjuvant chemotherapy (one cycle of adriamycin and ifosfamide) and radiotherapy (60 Gy) were administered. Serum PSA fell to non-detectable values after surgery, and the patient remains free of disease with a follow-up of 30 months.

Case no. 2

The patient was a 77-year-old man with a previous history of adenocarcinoma Gleason 8 (5+3) of acinar type diagnosed 5 years before the current episode, who did not receive further treatment because of his age and high surgical risk. Thirty-four months after the initial episode, transrectal ultrasonography demonstrated an enlargement of the prostatic gland, measuring 56×54×30 mm, and elevated PSA of 15.5 ng/ml. Androgen deprivation therapy (flutamide and leuprorelin) was indicated and followed for 9 months, and during that period PSA levels decreased to a nadir of 0.3 ng/ml. A palliative transurethral resection (TURP) was performed because of obstructive symptoms and the final diagnosis was made from this specimen. Clinical evaluation was negative for metastases at that time. Nevertheless, the patient died 5 months later due to septic shock of respiratory origin, having already developed massive liver metastases.

Material and methods

Histological sections (3–4 μm thick) were obtained from formalin-fixed, paraffin-embedded tissue and stained with hematoxylin and eosin for routine examination. Selected blocks in each case were processed for immunohistochemistry with the Envision method (Dako, Denmark) and stained with the Dako Techmate automatic stainer. The panel of antibodies is summarized in Table 1.

In the first case, fresh tissue was obtained for electron microscopy study, immediately fixed in 4% buffered glutaraldehyde and postfixed in osmium tetroxide. In the second case, formalin-fixed tissue was retrieved from the paraffin block but the quality of the material was inadequate for electron microscope analysis. The sample was examined with a JEOL 1200 EX II electron microscope.

Results

In the first patient, the cystoprostatectomy specimen measured 145×100×65 mm. Macroscopic examination of the prostate after formalin fixation revealed a whitrish cut surface with hemorrhagic and necrotic areas. The tumour involved the seminal vesicles and extended to extraprostatic tissues, with extrinsic infiltration of the rectum and the urinary bladder walls. Microscopically, a mixture of epithelial and mesenchymal elements was observed. The epithelial component consisted of conventional adenocarcinoma Gleason 8 (5+3) with ductal differentiation areas and multifocal involvement of both prostatic lobes. Ductal adenocarcinoma presented as large ductal structures with papillary or cribiform pattern and prominent cytologic atypia (Fig. 1a), in some of which comedonecrosis was present.

The mesenchymal component was predominantly peripheral in the prostate specimen and spindle cell and angiosarcomatous differentiation were observed. The spindle-cell proliferation focally displayed a storiform pattern and areas of prominent pleomorphism and nuclear atypia, with abundant eosinophilic cytoplasms and high mitotic activity (Fig. 1b), whereas angiosarcomatous areas were composed of interanastomosing vascular channels lined by plump polygonal cells with apically displaced, hyperchromatic nuclei (Fig. 1a). Large zones of necrosis and hemorrhage were also observed within the tumour. The epithelial and mesenchymal components were intimately associated and admixed in some areas with foci of apparently morphological transition. Obturator lymph nodes were bilaterally involved by pure adenocarcinoma.

The immunohistochemical study revealed positivity for CAM 5.2, AE1–AE3 cytokeratins and EMA in the epithelial component and focal staining for CAM5.2 in the areas of morphological transition, as well as a few isolated cells in the stroma (Fig. 1c). Conversely, vimentin diffusely stained the sarcomatous component as well as some epithelial cells. The epithelial component of the tumour was positive for PSA, and only the papillary areas of ductal adenocarcinoma

Table 1 Panel of antibodies, sources and working dilutions. *PSA* prostate specific antigen, *NSE* neuron specific enolase, *UEIA* ulex europaeus I agglutinin, *BL** biotinated lectin

Antibody	Source	Clone	Dilution
CAM5.2 cytokeratin	Becton–Dickinson	CM 5.2	1:100
EMA cytokeratin	Novocastra	GP1.4	1:600
AE1–AE3 cytokeratin	BioGenex	AE1/AE3	1:100
PSA	DAKO	A562	1:4000
Vimentin antibody	DAKO-0725	V9	1:100
Desmin antibody	DAKO-M0760	D33	1:400
NSE	Novocastra	5E2	1:400
Muscle specific actin	DAKO	1A4	1:12,000
S-100 protein	DAKO	Polyclonal	1:10,000
Synaptophysin	DAKO	SY 38	1:100
Chromogranin A	DAKO	DAK-A3	1:2000
CD34	Novocastra	QBEnd10	1:200
CD31	DAKO	JC/70A	1:40
α_1-antitrypsin	DAKO	Polyclonal	1:2000
UEIA	Vector	BL*	1:3000
CD10	Novocastra	56C6	1:25
c-Kit	DAKO	Polyclonal	1:25
c-erb B2	DAKO	Polyclonal	1:800
p53	Novocastra	BP53-12	1:50
MIB-1 antibody	Immunotech	MIB-1	1:400
Myoglobin	DAKO	Polyclonal	1:2000

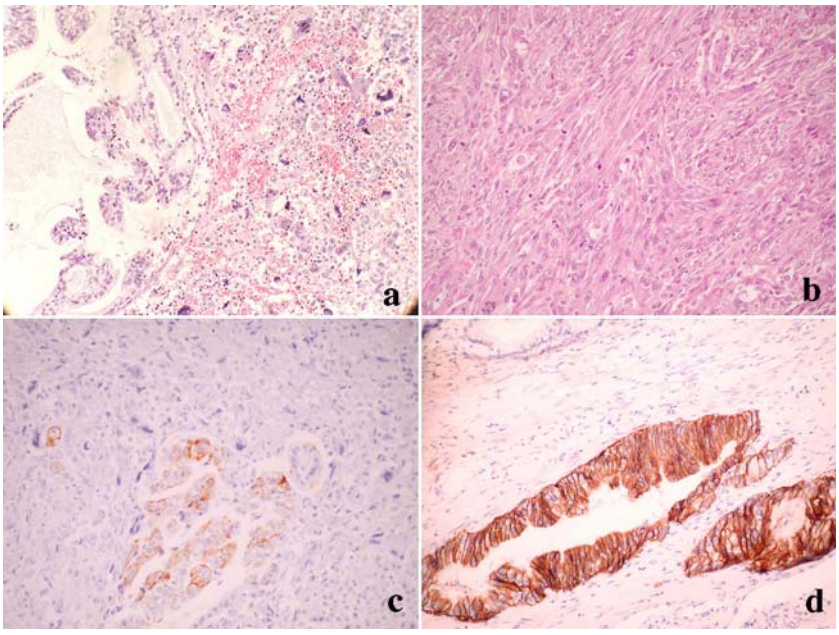

Fig. 1 **a** Ductal structures with papillary pattern (left) admixed with angiosarcoma in case 1 (original magnification ×100); **b** Detail of storiform pattern with numerous mitotic figures (original magnification ×100); **c** CAM 5.2 cytokeratin in a transition area. Positive staining of the glandular structure as well as in some isolated cells of the mesenchymal component (original magnification ×200); **d** Strong staining with membranous pattern for c-erb B2 in ductal adenocarcinoma areas (original magnification ×100)

showed c-erb B2 membranous stain (Fig. 1d). p53 was diffusely positive both in the epithelial and mesenchymal components, and MIB-1 antibody showed increased positivity in the mesenchymal areas. The angiosarcomatous areas expressed CD31 and CD10, whereas the storiform areas immunoreacted for α_1-antitrypsin.

The ultrastructural study performed in the storiform areas revealed fusiform cells showing well-developed and dilated rough endoplasmic reticulum and mitochondriae (Fig. 2a). In some cells, the rough endoplasmic reticulum was filled with intracisternal globules with lucent areas, suggestive of α_1-antitrypsin secretion (Fig. 2b). Some tight junctions and cytoplasmic filaments similar to vimentin were also observed. These findings were consistent with areas of malignant fibrous histiocytoma.

The TURP specimen of the second patient consisted of 3 g of prostatic fragments massively infiltrated by the tumour. Small areas of acinar adenocarcinoma were noticed, as well as papillary glands consistent with ductal adenocarcinoma (Fig. 3a), although solid epithelial neoplasm predominated in the sample. These solid epithelial areas exhibited high mitotic activity, and were composed of relatively uniform medium-sized cells with round to oval hyperchromatic nuclei and scant cytoplasm organized in nests and solid cords, some of them with central necrosis and some others with a peripheral palisade (Fig. 3b). The papillary ductal adenocarcinoma areas diffusely stained for c-erb B2 (Fig. 3c) and for CD10. The solid, poorly differentiated epithelial nests were positive for synaptophysin, c-kit (Fig. 3d), c-erb B2 with membranous pattern and

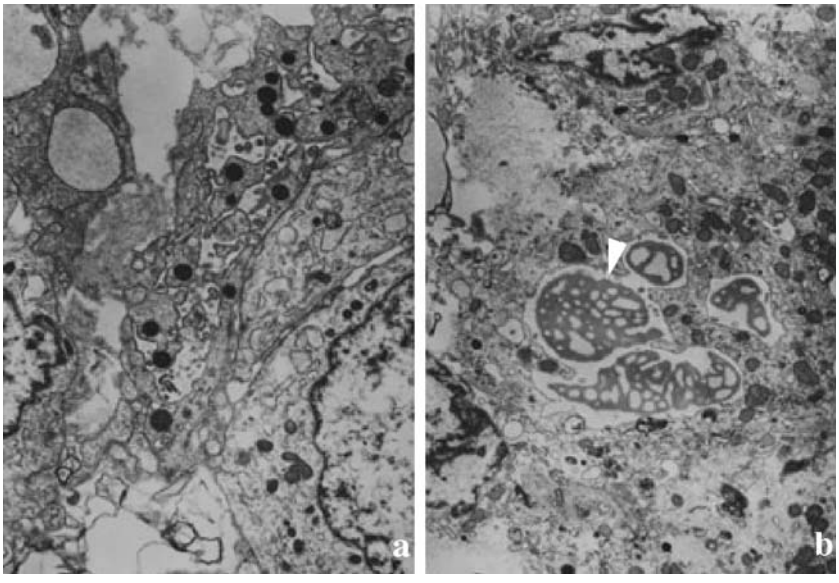

Fig. 2 **a** Electron microscope images showing mesenchymal cells with well-developed and dilated rough endoplasmic reticulum and mitochondriae (**b**) In some areas, the rough endoplasmic reticulum was filled with intracisternal globules exhibiting lucent areas (arrowhead), suggestive of α_1-antitrypsin secretion. (original magnification ×5000)

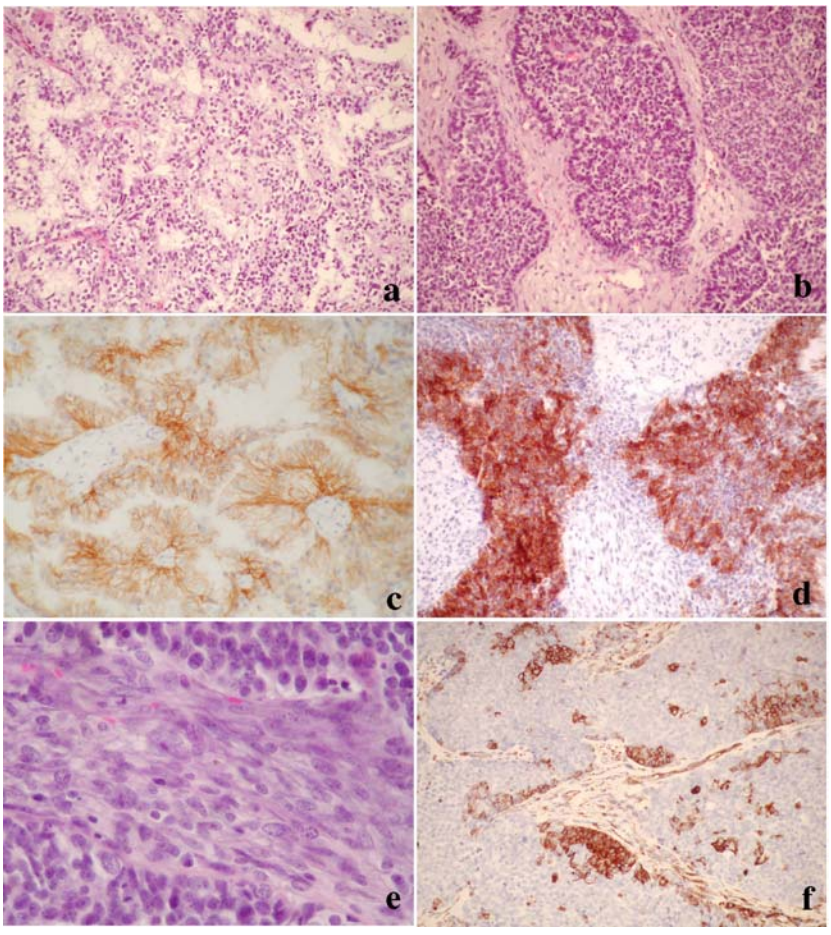

Fig. 3 **a** Ductal adenocarcinoma showing papillary pattern; **b** solid poorly differentiated epithelial nests with peripheral palisade; **c** c-erb B2 membranous staining in papillary ductal adenocarcinoma areas; **d** strong staining of the epithelial poorly differentiated epithelial nests with c-Kit antibody; **e** mesenchymal component showing spindle cells with pleomorphism and atypia between two epithelial nests; **f** vimentin antibody showing positive staining of the mesenchyme as well as of some epithelial cells of the vicinity (original magnifications ×100 except for (**e**) ×400)

Table 2 Results of the immunohistochemical panel for the two cases. *EMA* epithelial membrane antigen, *PSA* prostate specific antigen, *NSE* neuron specific enolase, *UEIA* ulex europaeus I agglutinin, + positive result, − negative result, *foc +transit* focal positivity in transitional mesenchyme-epithelial areas, *+solid* positive result in the solid, poorly differentiated areas, *+angio* positive in the angiosarcoma, *+storiform* positive in the storiform solid areas, *ND* not done, *+ductal* positive result in ductal adenocarcinoma areas

	Case 1		Case 2	
	Epithelial	Mesenchymal	Epithelial	Mesenchymal
CAM 5.2 cytokeratin	+	foc+transit	+	foc+transit
EMA	+	−	+	foc+transit
AE1–AE3 cytokeratin	+	−	+	foc+transit
PSA	+	−	+	−
Vimentin	−	+	foc+transit	+
Desmin	−	−	−	−
NSE	−	−	−	−
Muscle specific actin	−	−	−	−
S-100 protein	−	−	−	−
Synaptophysin	−	−	+solid	−
Chromogranin	−	−	−	−
CD34	−	−	−	−
CD31	−	+angio	−	−
α_1-antitrypsin	−	+storiform	ND	ND
UEIA	−	−	−	−
CD10	−	+angio	+	+
c-Kit	−	−	+	−
c-erb B2	+ductal	−	+ductal	−
p53	+30–40%	+90%	+90%	+40%
MIB-1	5%	60%	40%	80%
Myoglobin	−	−	−	−

CD10. PSA was only positive in the epithelial component. The stroma was also remarkable for the presence of spindle cells with prominent nuclear atypia and pleomorphism, some of them multinucleated, and plenty of atypical mitoses (Fig. 3e). A few areas of morphologic transition between the solid epithelial nests and the mesenchymal component of the tumour could be identified. The epithelial component of the tumour was positive for CAM 5.2, AE1-AE3 cytokeratin and EMA, and morphologically transitional areas and some mesenchymal cells were also positive for these antibodies. Conversely, vimentin diffusely stained the sarcomatous component and few epithelial cells (Fig. 3f). p53 was also tested and diffusely stained both the mesenchymal and the epithelial components. MIB-1 antibody demonstrated mitotic activity in the two components.

The search for other mesodermal differentiation in the two cases included a panel of several antibodies, which are summarized in Table 2, with negative results.

Discussion

Adenocarcinoma of the prostate is a frequent malignancy in elderly men, whereas pure sarcomas of the prostate (rhabdomyosarcomas in childhood and leiomyosarcomas in adult patients) account for less than 0.1% of prostatic tumours [33]. CS of the prostate is an exceedingly rare tumor, in which the demonstration of divergent but intimately admixed malignant epithelial and mesenchymal cell populations is required for appropriate diagnosis.

The malignant epithelial component of the two cases herein presented exhibited adenocarcinoma of acinar type, as well as papillary and cribiform areas of ductal differentiation, the latter finding previously reported in only one case of CS [22]. We observed intense and selective overexpression of c-erb B2 in these areas, this being the first report of such pattern in CS. This is an immunohistochemical feature seldom reported in conventional prostatic adenocarcinoma [27], but interestingly present in our two patients.

The solid poorly differentiated epithelial areas in the second case exhibited unusual immunohistochemical findings. These cells were positive for c-kit, CD10 and also synaptophysin. The pattern of c-kit in normal prostate has not been elucidated completely. To some authors, positivity of c-kit in the prostate detects mast cells [29]. Contrarily, others described the presence of interstitial cells, first in the guinea-pig [7] and more recently, in the human prostate [31]. The common embryologic origin of the prostate and the gut, and the existence of slow-wave potentials in the prostatic gland, could indicate a role of these cells as pacemakers. However, the undifferentiated epithelial cell population of our second case was also positive for CD10. This marker was described by Chu and Arber [4] in the apical surface of the prostatic large ductal epithelial cells in normal prostate, and in the surface and cytoplasm of cells in poorly differentiated adenocarcinoma with large ducts and cribiform and papillary pattern, whereas adenocarcinomas with small glands tended to be CD10 negative. On the other hand, Tawfic et al. [30] studied this marker in pathologic entities of the prostatic gland and observed increased expression of CD10 in areas of higher Gleason score. In our case, the co-expression of c-kit, CD10 and synaptophysin in the poorly differentiated epithelial population suggests a cell population with neuroendocrine features. The neuroendocrine differentiation in prostatic adenocarcinomas has been associated with poor prognosis due to the development of hormone-independency in vitro [25, 35]. It has been suggested that the androgen-independent disease progression in patients with prostate cancer after androgen ablation may often be due to the outgrowth of the stem cell population [2, 21], because such cells survive androgen deprivation in experimental models. The undifferentiated epithelial population of the second patient, who had followed hormonal deprivation therapy, could correspond to an example of such outgrowth.

Regarding the mesenchymal component, the first of our cases is the second prostatic CS with angiosarcomatous differentiation in the literature [32], this finding being very uncommon among the possible mesodermal differentiations described in CS of any location. The histological features and the expression of CD31 in these areas confirmed the vascular lineage of the tumoural component. The same case also exhibited areas of malignant fibrous histiocytoma, with three previous cases reported in the literature [5, 14, 18]. These spindle-cell areas expressed α_1-antitrypsin and the ultrastructural study was consistent with this diagnosis. In the second case, the mesenchymal component consisted of a poorly differentiated spindle-cell population in which no mesodermal differentiation could be documented, although it strongly immunoreacted with vimentin. In the two cases, it was possible to observe areas in which the epithelial and the mesenchymal components merged, supporting the existence of a sole biphasic tumour and not colliding neoplasms.

The evolution of the two patients was divergent. In the first patient, radical surgery was performed, and adjuvant therapy also administered and, surprisingly, he remains alive and free of disease 30 months later. Bilateral epithelial metastases had been documented in obturator lymph nodes in this patient. There are six reports of metastases to the lymph nodes involving both the mesenchymal and epithelial components [10, 13, 14, 19, 20, 34] or only the mesenchymal component [15], and only a few descriptions of metastatic pure adenocarcinoma [5]. Contrarily, the second patient died a few months after the discovery of CS and had already developed massive liver metastasis. The prognosis of this entity was classically considered dismal, but recent studies have postulated an improvement of prognosis after radical surgery in locally advanced cases that lack distant metastases [8, 14], thus suggesting that such initial treatment should be elected in these cases whenever it is possible.

In conclusion, this report offers insight into these very rare neoplasms, being these two CS unique cases because of their uncommon histopathological and immunohistochemical findings, among which c-erb B2 and c-kit expression could prove useful from a diagnostic and therapeutic point of view, if consistently expressed in larger series.

Acknowledgements The authors would like to thank Margarita Mainar, Elena Gonzalvo, Elena Rull and Cristina Durana for their technical assistance, and DAKO for contributing in the immunohistochemical studies. This work was supported by grants Red Temática del Cáncer, Instituto de Salud Carlos III, no. C03/10, FIS 01/1519 from Ministerio de Sanidad y Consumo and AECC de Barcelona.

References

1. Algaba F, Sole-Balcells FJ (1992) Carcinosarcoma of the prostate. Immunophenotype, morphologic course and clinicopathologic differential diagnosis. Arch Esp Urol 45:779–782
2. Bruchovsky N, Rennie PS, Coldman AJ, Goldenberg SL, To M, Lawson D (1990) Effects of androgen withdrawal on the stem-cell composition of the Shionogi carcinoma. Cancer Res 50:2275–2282
3. Canfield SE, Gans TH, Unger P, Hall SJ (2001) Postradiation prostatic sarcoma: de novo carcinogenesis or dedifferentiation of prostatic adenocarcinoma? Tech Urol 7:294–295
4. Chu P, Arber DA (2000) Paraffin-section detection of CD10 in 505 nonhematopoietic meoplasms. Am J Clin Pathol 113:374–382
5. Dundore PA, Cheville JC, Nascimento AG, Farrow GM, Bostwick DG (1995) Carcinosarcoma of the prostate. Report of 21 cases. Cancer 76:1035–1042
6. Eble JN, Sauter G, Epstein JI, Sesterhenn IA (eds) (2004) Tumours of the urinary system and the male genital organs. International Agency for Research on Cancer, Lyon
7. Exintaris B, Klemm MF, Lang RJ (2002) Spontaneous slow wave and contractile activity of the guinea pig prostate. J Urol 168:315–322
8. Fukawa T, Numata K, Yamanaka M, Miyamoto T, Kurokawa Y, Kanayama HO, Kagawa S, Utsunomiya M, Hirokawa M (2003) Prostatic carcinosarcoma: a case report and review of literature. Int J Urol 10:108–113
9. Ginesin Y, Bolkier M, Moskovitz B, Lichtig C, Levin DR (1986) Carcinosarcoma of the prostate. Eur Urol 12:441–442
10. Haddad JR, Reyes EC (1970) Carcinosarcoma of the prostate with metastasis of both elements: case report. J Urol 103:80–83
11. Hamlin WB, Lund PK (1967) Carcinosarcoma of the prostate: a case report. J Urol 97:518–522
12. Hokamura K, Kurozumi T, Tanaka K, Yamaguchi A (1985) Carcinosarcoma of the prostate. Acta Pathol Jpn 35:481–487
13. Kaneko Y, Yoshiki T, Fukumoto M, Oishi K, Yoshida O (1992) Carcinosarcoma of the prostate. Urol Int 48:105–107
14. Koleski FC, Turk TM, Wojcik EM, Albala DM (1999) Carcinosarcoma of the prostate. World J Urol 17:316–318
15. Krastanova LJ, Addonizio JC (1981) Carcinosarcoma of prostate. Urology 18:85–88
16. Kubosawa H, Matsuzaki O, Kondo Y, Takao M, Sato N (1993) Carcinosarcoma of the prostate. Acta Pathol Jpn 43:209–214
17. Lauwers GY, Schevchuk M, Armenakas N, Reuter VE (1993) Carcinosarcoma of the prostate. Am J Surg Pathol 17:342–349
18. Lindboe CF, Mjones J (1992) Carcinosarcoma of prostate. Immunohistochemical and ultrastructural observations. Urology 45:376–380
19. Martin SA, Fowler M, Catalona WJ, Boyarsky S (1979) Carcinosarcoma of the prostate: report of a case with ultrastructural observations. J Urol 122:709–711
20. Nazeer T, Barada JH, Fisher HA, Ross JS (1991) Prostatic carcinosarcoma: case report and review of literature. J Urol 146: 1370–1373
21. Pisters LL, Wang XH, Chung L, Hsieh JT (2001) Differential expression of c-erb B2/neu, epidermal growth factor receptor, cytokeratin 8, and the prostatic steroid-binding protein gene in rat ventral prostate during postnatal development. Prostate 47:164–171
22. Poblet E, Gomez-Tierno A, Alfaro L (2000) Prostatic carcinosarcoma: a case originating in a previous ductal adenocarcinoma of the prostate. Pathol Res Pract 196:569–572
23. Quay SC, Proppe KH (1981) Carcinosarcoma of the prostate: case report and review of the literature. J Urol 125:436–438
24. Randolph TL, Amin MB, Ro JY, Ayala AG (1997) Histologic variants of adenocarcinoma and other carcinomas of prostate: pathologic criteria and clinical significance. Mod Path 10:612–629
25. Rumpold H, Heinrich E, Untergasser G, Hermann M, Pfister G, Plas E, Berger P (2002) Neuroendocrine differentiation of human prostatic primary epithelial cells in vitro. Prostate 53: 101–108
26. Sak SD, Orhan D, Yaman O, Tulunay O, Ozdiler E (1997) Carcinosarcoma of the prostate. A case report and a possible evidence on the role of hormonal therapy. Urol Int 59:50–52
27. Sanchez KM, Mass R, Koch MO, Eckert GJ, Geary WA, Balbridge LA, Zhang S, Eble JN, Gheng L (2002) Evaluation of HER-2/neu expression in prostatic adenocarcinoma. Cancer 95:1650–1655
28. Shannon RL, Ro JY, Grignon DJ, Ordoñez NG, Johnson DE, Mackay B, Tetu B, Ayala AG (1992) Sarcomatoid carcinoma of the prostate. A clinicopathological study of 12 patients. Cancer 69:2676–2682
29. Simak R, Capodieci P, Cohen DW, Fair WR, Scher H, Melamed J, Drobnjak M, Heston WD, Stix U, Steiner G, Cordon-Cardo C (2000) Expression of c-kit and kit-ligand in benign and malignant prostatic tissues. Histol Histopathol 15: 365–374
30. Tawfic S, Niehans GA, Manivel JC (2003) The pattern of CD10 expression in selected pathologic entities of the prostate gland. Human Pathol 34:450–456
31. Van der Aa F, Roskams T, Blyweert W, Ridder D (2003) Interstitial cells in the human prostate: a new therapeutic target? Prostate 56:250–255
32. Wick MR, Young RH, Malvesta R, Beebe DS, Hansen JJ, Dehner LP (1989) Prostatic carcinosarcomas. Clinical, histologic, and immunohistochemical data on two cases, with a review of the literature. Am J Clin Pathol 92:131–139
33. Young RH, Srigley JR, Amin MB, Ulbright TM, Cubilla AL (eds) (2000) Tumors of the prostate gland, seminal vesicles, male urethra, and penis. Armed Forces Institute of Pathology, Washington
34. Zenklusen HR, Weymuth G, Rist M, Mihatsch MJ (1990) Carcinosarcoma of the prostate in combination with adenocarcinoma of the prostate and adenocarcinoma of the seminal vesicles: a case report with immunocytochemical analysis and review of the literature. Cancer 66:998–1001
35. Zhau HY, Chang SM, Chen BQ et al (1996) Androgen-repressed phenotype in human prostate cancer. Proc Natl Acad Sci USA 93:15152–15157

Virchows Arch (2005) 446: 517–524
DOI 10.1007/s00428-005-1204-8

ORIGINAL ARTICLE

Zsombor Melegh · Erzsébet Csernák · Erika Tóth · Zsuzsa Veleczki · Edina Magyarosy · Kálmán Nagy · Zoltán Szentirmay

DNA content heterogeneity in neuroblastoma analyzed by means of image cytometry and its potential significance

Received: 29 August 2004 / Accepted: 15 December 2004 / Published online: 13 April 2005
© Springer-Verlag 2005

Abstract The aim of this study was to determine the frequency and significance of the tumor DNA content heterogeneity in 33 previously untreated human neuroblastomas. We used image cytometry to selectively analyze neuroblasts by excluding karyorrhectic or stromal cells from cytometric measurements. DNA content heterogeneity with more than one clonal subpopulation on DNA histogram was found in 8 of 33 cases. Of these 8 cases, 4 showed MYCN amplification. Double labeling fluorescent in situ hybridization with probes for the centromeric region of chromosome 2 and MYCN gene was used to confirm the DNA content heterogeneity. DNA content heterogeneity was associated with poorer prognosis in this study ($P<0.05$). There was a significant correlation between euploidy (di- and tetraploidy) and worse prognosis, but only when heterogeneous neuroblastomas with euploid cell population were assigned to euploid tumors ($P=0.006$). Our results may explain the conflicting data in the literature regarding ploidy and suggest that DNA content heterogeneity and the presence of a euploid population may predict worse prognosis in neuroblastoma patients.

Keywords Neuroblastoma · Heterogeneity · Ploidy · Survival

Z. Melegh (✉) · E. Csernák · E. Tóth · Z. Veleczki · Z. Szentirmay
Department of Molecular Pathology,
National Institute of Oncology,
Budapest, Hungary
e-mail: eghbor@excite.com
Tel.: +36-1-2248600
Fax: +36-1-2248620

K. Nagy
Department of Haematology,
Child Welfare Center,
Borsod County Teaching Hospital,
Miskolc, Hungary

E. Magyarosy
Department of Haematology,
Heim Pal Children's Hospital,
Budapest, Hungary

Introduction

The risk grouping (biological staging) for neuroblastoma combines clinical characteristics (patient's age and stage), histopathology, and biological characteristics (MYCN oncogene amplification and tumor ploidy) for the assignment of treatment protocols, as defined by the Children's Cancer Study Group and Pediatric Oncology Study Group [21]. Amplification of the MYCN gene was one of the first markers found to be associated with worse outcome of the disease [18, 19]. Although investigated in several studies, the prognostic significance of euploidy (di- or tetraploidy) in neuroblastoma has been less firmly established. Specifically, conflicting results have been published in patients of young age [17]. However, in the majority of these studies, the authors either presumed that the tumors were homogeneous regarding ploidy or excluded heterogeneous tumors from statistical analysis. Flow cytometry (FCM) is not the best tool to determine DNA content heterogeneity either, as it does not permit morphological cell confirmation [11]. It has also been shown that additional cell populations may be masked on the DNA histogram [16]. However, it would be important to pick up heterogeneous tumors, as intratumor DNA content heterogeneity has been found to have prognostic value in several tumor types. In epithelial ovarian cancer, the incidence of tumor DNA heterogeneity has significantly correlated with lymph-node involvement and FIGO staging [24]. In pediatric tumors, a significant association between DNA ploidy heterogeneity and unfavorable histology or death due to disease was found specifically in Wilms' tumor [28]. It is presumable that DNA content heterogeneity in neuroblastoma, if it is present, may deeply influence the ploidy analysis and, similar to other tumors, might have prognostic relevance. To our knowledge the frequency and significance of intratumor DNA content heterogeneity in untreated human neuroblastomas has not been examined; therefore, its impact on statistical analysis and its prognostic significance is still unclear. Image cytometry (ICM) is an alternative approach for analyzing tumor ploidy as it is able to exclude normal diploid cells, cell debris, and multinucleated giant

cells from cytometric analysis and provides valuable correlation with morphology. ICM also appears more useful in determining whether a given sample with a high second peak twice the first peak is diploid with large G_2M phase or is genuinely tetraploid [11]. In this study, we used ICM and a recently published mathematical algorithm, which was developed at the Central Research Institute for Mathematics in cooperation with the National Institute of Oncology, Hungary [25]. As this algorithm allowed us to distinguish and separately analyze up to four cell populations per DNA histogram, it is a particularly useful tool to obtain reliable information about the DNA ploidy pattern of the cell subpopulations within the tumor. Thus, in this study, we have tried to describe the incidence of intratumoral DNA content heterogeneity in neuroblastoma and investigate specifically the aspect of its biological significance and the potential prognostic value of ploidy.

Patients, materials and methods

Patients and cell line

We studied frozen (−70°C) and/or fresh samples of neuroblastoma from 33 infants and children. The study group comprised 18 female and 15 male patients with an age range of 1 month to 137 months. Mean and median follow-up times were 34 months and 27 months, respectively. International Neuroblastoma Pathology Classification (modified Shimada classification) was used to determine the histopathological subtype of the tumors on the basis of mitosis-karyorrhexis index, histological type, and age [21].

Isolation of cell nuclei

Cell nuclei were obtained by touch-print smears from tumor tissue samples and stained with standard Feulgen reaction. We used Pararosalin (color index: 4250) for the preparation of the Schiff reagent. The optimum hydrolysis condition (1 M hydrochloric acid at 60°C for 8 min) was determined on the basis of the hydrolysis curves (time versus integrated optical density).

Image analysis

Cytometric measurements were performed using DNA TV image analyzer (Central Research Institute for Mathematics, National Institute of Oncology, Hungary) and a specific mathematical algorithm analysis. ICM was performed on touch preparations taking the guidelines of the SIOP Europe Neuroblastoma Pathology and Biology and Bone Marrow Group [2] into account. Those areas of the specimens that were used for touch print smears were fixed in 4% formalin and processed using a standard technique to paraffin wax. Sections were stained with hematoxylin and eosin. Only those smears were used for image analysis, at which more than 80% of the area comprised tumor tissue. Immunohistochemical studies with monoclonal S100 antibodies (Dako, Denmark) were done using the fixed, paraffin-embedded sections of the samples. By morphological and immunohistochemical valuation of the samples we could exclude cell debris, karyorrhetic and stromal cells from the analysis. The technical details and the mathematical analysis of the cumulative DNA histograms were the same as those described by Tamás et al. [25]. All corrections (shading, general and local background compensation, and glare) were executed by software procedures. An average of 15 variables—including morphometric, density, and nuclear texture parameters—were determined per nucleus. These parameters were used by an interactive learning algorithm, only to differentiate between cells of interest and reference cells. The digital pictures of all measured nuclei were stored in an image gallery for post-processing control. There were at least 1,000 neuroblasts included in each analysis. Lymphocytes and granulocytes were used as an internal diploid reference standard. The maximum likelihood method utilizing para-

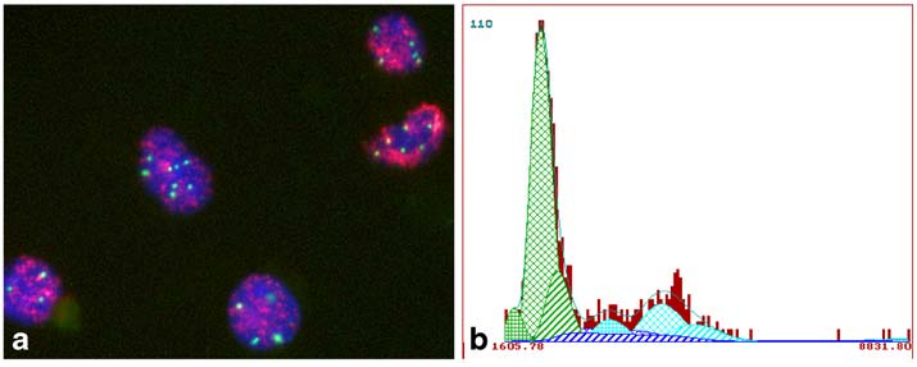

Fig. 1 **a** A single field from the dual-color fluorescent in situ hybridization (FISH) analysis of case 6. *Red dot* MYCN, *green dot* chromosome 2. Three cells can be seen with three, four and five green dots for chromosome two and two cells in mitosis with six and eight green dots for chromosome 2. Each cell shows MYCN amplification, indicating their tumoral origin. **b** Histogram from the same tumor sample (case 6). There is a dominant tetraploid population, which masks the G_1G_0 phase of a triploid and a pentaploid population, although the presence of three G_2 is quite obvious on the histogram. This is in keeping with the FISH result (**a**). The CV=3%, although, when this histogram is deconvoluted assuming only a single G_1G_0 phase, the CV is well over 10%

Table 1 Patient characteristics of 8 patients with heterogeneous and 25 patients with homogeneous tumors

Heterogeneous tumors								
Number	Sex[1]	Age (months)	Stage	Localization[2]	Histogram type	INPC[3] and histological type	N-myc status	Status[4]
1	2	12	II	Thorax	Diploid (1.04) Aneuploid (1.52) Pentaploid (2.48)	Unfavorable P differentiated	Amplified	AND
2	2	73	IV	Abdomen	Aneuploid (1.60) Tetraploid (2.04)	Unfavorable P differentiated	Amplified	DOD
3	2	22	IV	Retroperitoneum	Diploid (1.03) Aneuploid (1.24)	Unfavorable P differentiated	Non-amplified	DOD
4	1	9	I	–	Aneuploid(1.78) Pentaploid (2.52)	Favorable P differentiated	Amplified	AND
5	2	8	I	Retroperitoneum	Aneuploid (1.31) Aneuploid (1.84)	Unfavorable P differentiated	Non-amplified	AND
6	1	22	IV	–	Aneuploid (1.69) Tetraploid (2.04) Pentaploid (2.48)	Unfavorable P differentiated	Amplified	DOD
7	2	26	IV	Abdomen	Hypodiploid(0.83) Diploid (1.03)	Unfavorable P differentiated	Amplified	DOD
8	1	20	IV	Abdomen/retro	Peridiploid(1.16) Aneuploid (1.65) Tetraploid (2.03)	Unfavorable Undiff	Amplified	DOD
Homogeneous tumors								
Number	Sex[1]	Age (months)	Stage	Localization[2]	Histogram type	INPC[3] and histological type	N-myc status	Status[3]
1	2	5	II	Thorax	Aneuploid (1.28)	Favorable P differentiated	Non-amplified	AND
2	1	1	I	Adrenal gland	Aneuploid (1.42)	Favorable Differentiating	Non-amplified	AND
3	1	13	I	Thorax	Aneuploid (1.42)	Favorable P differentiated	Non-amplified	AND
4	1	27	III	Abdomen	Diploid (1.02)	Unfavorable P differentiated	Non-amplified	DOD
5	1	2	I	Adrenal gland	Aneuploid(1.42)	Favorable Differentiating	Non-amplified	AND
6	2	137	I	Thorax	Diploid (1.04)	Favorable GNB	Non-amplified	AND
7	2	5	III	Abdomen	Diploid (1.09)	Favorable P differentiated	Non-amplified	DOD
8	2	8	III	–	Diploid (1.06)	Unfavorable P differentiated	Amplified	DOD
9	1	75	III	Adrenal gland	Diploid (1.05)	Unfavorable Differentiating	Non-amplified	DOD
10	1	17	I	Thorax	Aneuploid (1.49)	Favorable Differentiating	Non-amplified	AND
11	2	42	III	Thorax	Peridiploid (1.12)	Unfavorable Differentiating	Non-amplified	AND
12	2	31	IV	Abdomen	Tetraploid (2.03)	Unfavorable P differentiated	Amplified	AND
13	1	15	I	Thorax	Aneuploid (1.77)	Favorable GN	Non-amplified	AND
14	1	31	IV	Adrenal gland	Peridiploid(1.14)	Unfavorable Differentiating	Non-amplified	DOD
15	2	72	III	Adrenal gland	Peridiploid(1.11)	Unfavorable P differentiated	Non-amplified	AND
16	1	26	IV	Adrenal gland	Peridiploid(1.16)	Unfavorable Undifferentiated	Amplified	AND
17	2	8	III	Adrenal gland	Aneuploid (1.26)	Favorable Differentiating	Non-amplified	AND
18	1	3	I	–	Aneuploid (1.35)	Favorable P differentiated	Amplified	AND
19	2	2	I	Adrenal gland	Aneuploid (1.73)	Favorable Differentiating	Non-amplified	AND
20	2	86	III	Bowel	Aneuploid (1.38)	Favorable GN	Non-amplified	AND
21	2	1	I	Adrenal gland	Aneuploid (1.62)	Favorable P differentiated	Non-amplified	AND

Table 1 (continued)

Heterogeneous tumors								
Number	Sex[1]	Age (months)	Stage	Localization[2]	Histogram type	INPC[3] and histological type	N-myc status	Status[4]
22	1	14	I	–	Aneuploid (1.66)	Unfavorable P differentiated	Non-amplified	AND
23	2	30	IV	Abdomen	Aneuploid (1.34)	Unfavorable Differentiating	Non-amplified	DOD
24	2	8	III	Retroperitoneum	Diploid (1.02)	Favorable P differentiated	Non-amplified	ARD
25	1	27	II	Retroperitoneum	Aneuploid (1.65)	Unfavorable Differentiating	Non-amplified	AND

[1] *1* Male, *2* female
[2] – No data
[3] International Neuroblastoma Pathology Classification: *undiff* stroma-poor, undifferentiated; *p differentiated* stroma-poor, poorly differentiated; *differentiating* stroma-poor, differentiating; *GNB* stroma-rich, ganglioneuroblastoma; *GN* stroma-dominant, ganglioneuroma
[4] *AND* alive with no evidence of disease, *DOD* dead of disease, *ARD* alive with residual disease

bolic optimization was used for decomposition of DNA histogram. The mathematical algorithm allowed separate analysis of up to four cell populations per given DNA histogram. The probability of the theoretical curve fitting the measured data (PROFI parameter) was also calculated. The exactness of the histogram decomposition was validated on the basis of the PROFI parameter. This feature is very important, as it let us decide whether a sample contains several subpopulations or a single cell population only, and is particularly useful when a dominant cell population masks additional subpopulations (Fig. 1). In these cases, where the presence of several G_0/G_1 peaks is not so obvious, only the mathematical algorithm helped us to recognize the additional subpopulations. Thus, tumor samples were accepted as heterogeneous only if the PROFI parameter (i.e., the exactness of the histogram decomposition) was better when the histogram was deconvoluted assuming more then one G_0/G_1 peak rather than a single G_0/G_1 peak. Using this mathematical algorithm, the coefficient of variants (CV) was always below 5%. DNA aneuploidy was defined on the basis of modified criteria used by Sergi et al. [19]: a discrete G_0/G_1 peak with a DNA index (DI) less than 0.85 or greater than 1.15 or less than 1.85 or greater than 2.15. A tumor was classified as tetraploid only if a large peak in the range of DI 1.85–2.15 was present with a visually detectable G_2/M phase.

Fluorescent in situ hybridization

Fluorescent in situ hybridization (FISH) was performed using commercially available MYCN/Alphasat 2 dual color probes for the centromeric alphoid DNA of chromosome 2 and for MYCN gene (QBiogene RFONC0224) according

Table 2 Characteristics of the eight heterogeneous tumors. *FISH* fluorescent in situ hybridization

No	Stage	Histogram type	Proportion of the population	No of Chr2 (FISH)	Proportion of Schwann cells
1	II	Diplod (1.04)	19.2%	2,3,4	0
		Aneuploid (1.52)	43.9%		
		Pentaploid (2.48)	36.9%		
2	IV	Aneuploid (1.60)	20.5%	3,4	0
		Tetraploid (2.04)	79.5%		
3	IV	Diploid (1.03)	28.8%	2	5%
		Aneuploid (1.24)	71.2%		
4	I	Aneuploid(1.78)	45.8%	3,5	1% (sparse)
		Pentaploid (2.52)	54.2%		
5	I	Aneuploid (1.31)	81.8%	2,3	1% (sparse)
		Aneuploid (1.84)	20.2%		
6	IV	Aneuploid (1.69)	4.6%	3,4,5	0
		Tetraploid (2.04)	81.6%		
		Pentaploid (2.48)	13.6%		
7	IV	Hypodiploid(0.83)	30.8%	2	0
		Diploid (1.03)	69.2%		
8	IV	Peridiploid (1.16)	57.2%	2,3,4	0
		Aneuploid (1.65)	11.5%		
		Tetraploid (2.03)	21.3%		

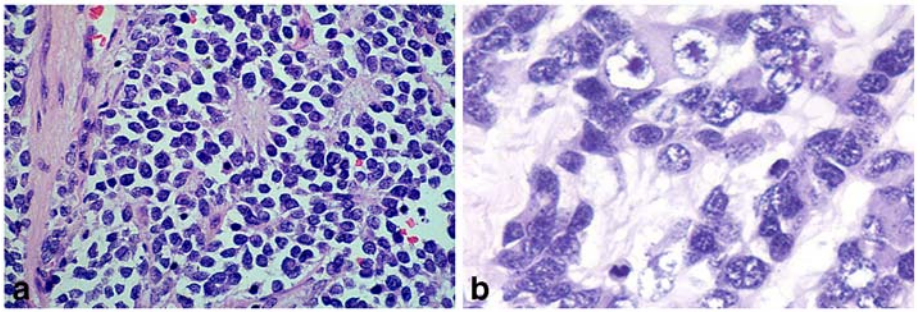

Fig. 2 **a** Representative picture of a poorly differentiated neuroblastoma with homogeneous ploidy pattern. The tumor comprises monomorphic neuroblasts with occasional Homer–Wright rosettes. **b** Large cells with clear nuclei and prominent nucleoli in a heterogeneous tumor with pentaploid clonal population on histogram (case 6)

to the guidelines of the SIOP Europe Neuroblastoma Pathology and Biology and Bone Marrow Group [2]. Stringency washing was in 1×sodium saline citrate (SSC) at 65°C for 5 min, and probe detection was according to standard procedures. Dual color probes were chosen for analysis, as it is particularly useful to differentiate between normal diploid cells and tumor cells on the basis of MYCN amplification, if it is present.

Statistical analysis

Survival rates at 36-month follow-up times and their 95% confidence intervals were estimated using the Kaplan-Meier and Greenwood methods, respectively. Survivals of subgroups were compared using a two-sided log-rank test. Potentially predictive factors were entered into a multivariate analysis using Cox proportional hazards regression model. For all statistical calculations, we used commercially available BMDP Statistical Software.

Results

ICM was performed on all 33 cases and the results are shown in Table 1. The DI of the tumors ranged from 0.8 to 2.5. In 8 of 33 cases (24.2%), more than one cell population was present. In 5 of these 8 cases, there were two cell populations present while 3 of 8 showed three cell populations (Fig. 1). Of these 5 cases, 1 contained aneuploid cell populations only, while 3 showed both aneuploid and euploid G_0G_1 peaks. The 3 tumors with three cell populations had both aneuploid and euploid populations. From all the cases 14 (42%) had only a single aneuploid peak and 11 (33%) contained only one euploid (peridi- or tetraploid) peak.

Having examined the number of cells in each subpopulation, in four of the five stage-IV tumors with both euploid and aneuploid subpopulations, the dominant population (i.e., that contained the most cells) was euploid (Table 2).

The FISH results showed good correlation with the ICM data (Table 2), although in those two cases (cases 3 and 7), in which a diploid and a peridiploid subpopulation were detected by ICM, only two chromosomes 2 were seen by means of FISH analysis. Presence of a diploid clone on ICM in heterogeneous tumors was also detected in cases 8 and 1. Ambros et al. [1] found that Schwann cells can appear on the histogram as an additional diploid peak, but according to their results these cells are reactive of origin and do not show any genetic abnormalities. In light of this, the fact that FISH analysis of cases 1 and 8 showed excess copies of MYCN gene in the diploid clonal population indicated that these cells are part of the tumor and are not stromal Schwann cells. Despite the presence of MYCN gain in case 1, this tumor is considered as non-amplified in the statistical analysis according to the criteria of MYCN amplification in neuroblastoma (at least ten copies), as it contained only eight copies of MYCN gene.

To further analyze the risk of Schwann cell contamination, we examined the same tissue samples, which were used for touch print smears, on haematoxilin-and-eosin-stained sections and S100 immunohistochemistry. The histological type of the heterogeneous tumors were either undifferentiated or poorly differentiated stroma poor neuroblastoma (Table 1), and contained few or no Schwann cells (Table 2). Therefore, it is highly unlikely that contamination by Schwann cells had had significant influence on the ICM results.

The histological appearance of stroma-poor neuroblastoma is usually a monomorphic pattern consisting of small blue round cells (Fig. 2a), or occasionally of larger cells with prominent nucleoli [20]. However, in heterogeneous tumors with higher nuclear DNA content, a slight heterogeneity of the histological pattern was seen, characterized by cells with large clear nuclei and prominent nucleoli (Fig. 2b) set in a dominant population of small round blue

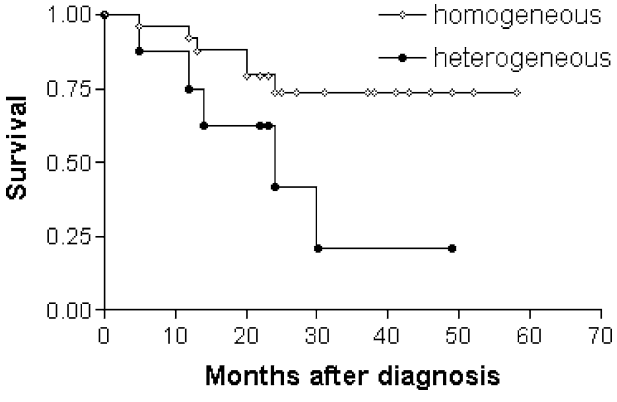

Fig. 3 Kaplan–Meier survival according to heterogeneity ($P<0.05$). Survival rates at 36-month follow-up times and their 95% confidence intervals (Kaplan Meier, Greenwood): homogeneous tumors 73.5% (57.0–94.8%); heterogeneous tumors 20.8% (3.85–100%)

Table 3 Correlation between prognostic factors and survival

Total	Aspect	Risk factor	Number	*P* value
33	Heterogeneity	Heterogeneous	8	0.0408
		Homogeneous	25	
33	MYCN	Amplified	8	0.0412
		Not amplified	25	
33	Stage	Stage 3,4	13	0.0004
		Stage 1,2	19	
33	Histology	Unfavorable	15	0.0039
		Favorable	18	
25	Ploidy	Euploid	11	0.0515
		Aneuploid	14	
33	Ploidy	Euploid present	17	0.0066
		Euploid not present	16	

cells. Nevertheless, it is not obvious whether these cells represent neuroblasts with high nuclear DNA content. The fact that the homogeneous tetraploid tumor(case 12) showed a monomorphic pattern of small blue round cells and that scattered larger cells with clear nuclei could also be seen in poorly differentiated neuroblastomas with homogeneous DNA content makes any further consideration that DNA content may correlate with cell morphology dubious. Survival was significantly better for those 25 children with tumors containing only one cell population on DNA histogram than for the eight children who had heterogeneous tumor ($P<0.05$), notwithstanding the relatively small sample size (Fig. 3, Table 3). There was no statistically significant correlation between DNA ploidy and survival when tumors with one cell population only were analyzed (Fig. 4, Table 3). When the heterogeneous tumors were also included in the statistical analysis, and the six tumors with both aneuploid and euploid cell populations were assigned to the euploid tumor group, we found significant correlation of euploidy and decreased survival (Fig. 5, Table 3).

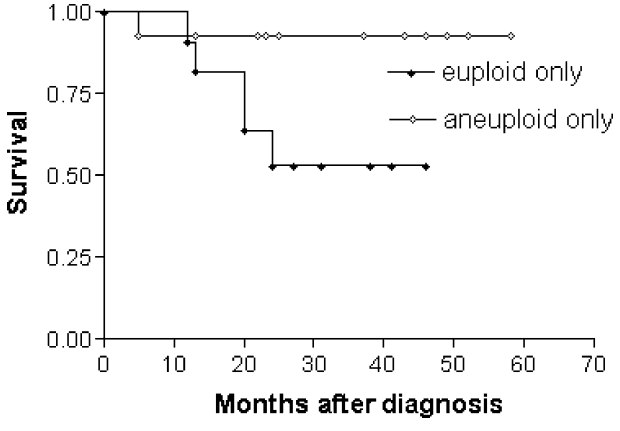

Fig. 4 Kaplan–Meier survival according to ploidy, if heterogeneous tumors are not included in the statistical analysis ($P=0.051$). Survival rates at 36-month follow-up times and their 95% confidence intervals: (Kaplan–Meier, Greenwood) euploid only 53% (29.9–94.0%); aneuploid only 92.86% (80.3–100%)

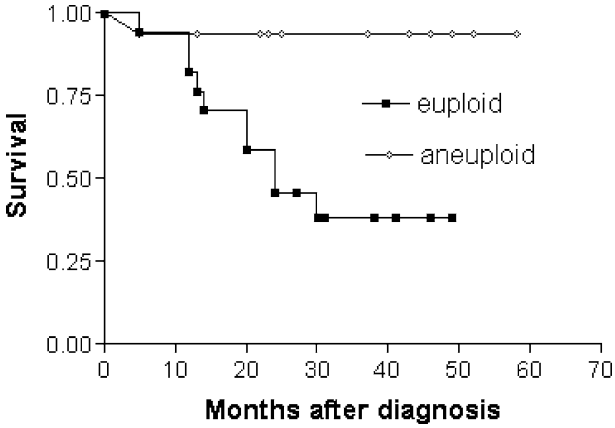

Fig. 5 Kaplan–Meier survival according to ploidy, if heterogeneous tumors with a euploid cell population are assigned to euploid tumors in the statistical analysis ($P<0.001$). Survival rates at 36-month follow-up times and their 95% confidence intervals (Kaplan Meier, Greenwood): euploid 38.1% (20.1–72.2%); aneuploid: 93.75% (82.61–100%)

By multivariate analysis we found stage as the only significant independent factor associated with overall survival.

Discussion

Although there are a few studies that have reported DNA content heterogeneity in neuroblastoma [4, 12], the frequency and significance of intratumoral DNA content heterogeneity in neuroblastoma has not yet been examined in detail. To the best of our knowledge, the only study that used ICM technology was the investigation carried out by Taylor and colleagues [26]. They described two cases with the presence of two G_0G_1 populations and two S phases. However, similar to the above studies, they did not distinguish them and considered these two tumors as aneuploid. A case with focal heterogeneity of ploidy has been reported also using FISH studies [8].

Our study suggests that, comprising of about one-quarter of the cases, DNA content heterogeneity is an important feature of neuroblastoma. According to the FISH results from these heterogeneous tumors, the tumor cells, exhibiting a different number of chromosomes 2, were arranged in a mixed haphazard pattern rather than in separate, well-circumscribed foci (Fig. 1). On histological examination, no convincing morphological signs of heterogeneity could be identified. In our view, occasional presence of larger cells, either in heterogeneous or in homogeneous tumors, is rather to be considered anaplastic features [15].

The eight heterogeneous tumors had significantly worse prognosis on Kaplan-Meier analysis than the homogeneous tumors, although heterogeneity did not prove to be an independent prognostic factor on multivariate analysis (Fig. 3). On the basis of this, it is conceivable that the worse survival of these patients may originate from other factors, such as associated genetic abnormalities, and that the DNA content heterogeneity is a result of the genetic in-

stability of the tumor. The presence of several subpopulations has been recently found to be associated with higher frequency of karyotypic abnormalities, supporting this argument [6]. Thus, it is possible that the DNA content heterogeneity is a sign rather than the cause of the worse prognosis. It is also notable that those patients with heterogeneous tumors who died of the disease had tumors that contained at least one euploid subpopulation (Table 1). This raises the possibility that euploidy has an adverse effect on the survival.

It is still debated in the literature whether the euploid (di- or tetraploid) tumors have a better outcome in neuroblastoma [17]. Although most authors have reported significant correlation between ploidy and survival rates or the prognostic variables [3, 5, 7, 9, 10, 23, 26], others [4, 17, 22, 27] did not find such an association. In our opinion, the conflicting results in the literature regarding the prognostic utility of ploidy may be explained, in part, by the presence of intratumor DNA content heterogeneity that is difficult to determine, mainly for two reasons. The first is the different grouping of the tumors by the authors. Since a relatively high proportion of tumors contain both aneuploid and euploid cell populations, the grouping of these cases can significantly influence the results. In this study, six of the eight tumors with DNA content heterogeneity contained both aneuploid and euploid fractions, and significant correlation of euploidy and worse survival was found only when the six heterogeneous tumors, containing both euploid and aneuploid cell populations, were assigned to the euploid tumor group (Fig. 5, Table 3). On the basis of these findings, it is conceivable that the presence of a euploid clone may predict worse prognosis in neuroblastoma patients. The fact that, in four of the five late-stage (stage IV) neuroblastomas with both euploid and aneuploid cell populations, the dominant population (i.e., that of the highest number of cells) on the DNA histogram was euploid suggests that these populations might have overgrown the aneuploid ones during the tumor evolution (Table 3). These findings are in keeping with those of Mora et al., who presumed that diploid may have a proliferative advantage over aneuploid populations [14].

The second reason for the different results in ploidy studies, in our view, is related to insufficient mathematical analysis of the histograms. Most of the authors reported only one or two G_0G_1 peaks in each histogram [3, 7, 9, 10, 27]. However, Kusufaka, Yalcin, and Huddart mentioned that samples with a high coefficient of variation (CV>10%) were excluded, considered as having excessive cellular debris. In fact, high values of CV (>10%) may indicate the presence of an additional cell population and should not be considered as a sign of cell degradation in each case [11, 13]. As we demonstrated, it is particularly true when a dominant cell population is present, which can mask additional subpopulations (Fig. 1). In these cases, with further decomposition of the histogram, assuming the presence of additional cell populations and using a mathematical algorithm, we could decrease the CV to under 5%. It has also been reported that thorough sample processing may improve the ability of FCM to detect additional cell populations on a histogram [18].

In conclusion, our results may explain the conflicting data in the literature regarding ploidy and emphasize the importance of the inclusion and proper assessment of heterogeneous tumors in the statistical analyses. We also found that DNA content heterogeneity and/or the presence of a euploid population may predict a worse prognosis in neuroblastoma. Further studies with more cases are necessary to determine the prognostic significance of DNA content heterogeneity in neuroblastoma.

Acknowledgements We are indebted to Jenőné Budai, Béláné Schád, and Józsefné Takács for their technical support, to Judit Müller, Péter Hauser, and Imre Rényi for collecting patient data, Gábor Borgulya for his help in the statistical analysis, and to Miklós Kónya for preparing the illustrations. This work was supported by NFKP 1/048, Széchenyi Project, Hungarian Ministry of Education and OTKA T30805 research fund. The experiments comply with the current laws of the country in which they were performed.

References

1. Ambros IM, Zellner A, Roald B, Amann G, Ladenstein R, Printz D, Gadner H, Ambros PF (1996) Role of ploidy, chromosome 1p, and Schwann cells in the maturation of neuroblastoma. N Engl J Med 334:1505–1511
2. Ambros PF, Ambros IM (2001) Pathology and biology guidelines for resectable and unresectable neuroblastic tumors and bone marrow examination guidelines. Med Pediatr Oncol 37: 492–504
3. Bourhis J, DeVathaire F, Wilson GD, Hartman O, Terrier-Lacombe MJ, Boccon-Gibod L, McNally NJ, Lemerle J, Riou G, Bénard J (1991) Combined analysis of DNA ploidy index and n-myc genomic content in neuroblastoma. Cancer Res 51:33–36
4. Carlsen NLT, Ørnvold K, Christensen IJ, Laursen H, Larsen JK (1992) Prognostic importance of DNA flow cytometrical, histopathological and immunohistochemical parameters in neuroblatomas. Virchows Arch A Pathol Anat Histopathol 420:411–418
5. Eckschlager T, Pilát D, Kodet R, Dahbiová R, Staňková J, Jašinská J, Hrušák O (1996) DNA ploidy in neuroblastoma. Neoplasma 43:23–26
6. Gisselsson D, Gorunova L, Höglund M, Mandahl N, Elfving P (2004) Telomere shortening and mitotic dysfunction generate cytogenetic heterogeneity in a subgroup of renal cell carcinoma. Br J Cancer 91:327–332
7. Huddart SN, Muir KR, Parkes SE, Mann JR, Stevens MCG, Raafat F, Smith K (1993) Retrospective study of prognostic value of DNA ploidy and proliferative activity in neuroblastoma. J Clin Pathol 46:1101–1104
8. Kerbl R, Ambros IM, Ambros PF, Lackner H, Dornbusch HJ, Urban CE (2002) Neuroblastoma with focal MYCN amplification and bone marrow infiltration: a staging and treatment dilemma. Med Pediatr Oncol 38:109–111
9. Kusafuka T, Fukuzawa M, Oue T, Yoneda A, Okada A, Satani M (1994) DNA flow cytometric analysis of neuroblastoma: distinction of tetraploidy subset. J Pediatr Surg 29:543–547
10. Ladenstein R, Ambros IM, Pötschger U, Amann G, Urban C, Fink FM, Schmitt K, Jones R, Slociak M, Schilling F, Ritter J, Berthold F, Gadner H, Ambros PF (2001) Prognostic significance of DNA di-tetraploidy in neuroblastoma. Med Pediatr Oncol 36:83–92
11. Lanigan D, McLean PA, Curan B, Leadre M (1993) Comparison of flow and static image cytometry in the determination of ploidy. J Clin Pathol 46:135–139

12. Look AT, Hayes FA, Nitschke R, McWilliams NB, Green AA (1984) Cellular DNA content as a predictor of response to chemotherapy in infants with unresectable neuroblastoma. N Engl J Med 311:231–235
13. McFadden PW, Clowry LJ, Daehnert K, Hause LL, Koethe SM (1990) Image analysis confirmation of DNA aneuploidy in flow cytometric DNA distributions having a wide coefficient of variation of the G_0/G_1 peak. Am J Clin Pathol 93:637–642
14. Mora J, Cheung N-KV, Gerald WL (2001) Genetic heterogeneity and clonal evolution in neuroblastoma. Br J Cancer 85: 182–189
15. Navarro S, Noguera R, Pellin A, Mejia C, Ruiz A, Llombart-Bosch A (2000) Pleomorphic anaplastic neuroblastoma. Med Pediatr Oncol 35:498–502
16. Rosenberg P, Wingren S, Guerrieri C (1997) Flow cytometric DNA-heterogeneity in paraffin-embedded endometrial cancer. Acta Oncol 36:23–26
17. Sawada T, Matsumara T (2000) DNA ploidy and prognosis of neuroblastoma. Pediatr Hemat Oncol 17:1–3
18. Schwab M (2004) MYCN in neuronal tumours. Cancer Lett 204:179–187
19. Seeger RC, Brodeur GM, Sather H, Dalton A, Siegel SE, Wong KY, Hammond D (1985) Association of multiple copies of the n-myc oncogene with rapid progression of neuroblastomas. N Engl J Med 313:1111–1116
20. Sergi C, Ehemann V, Beedgen B, Linderkamp O, Otto HF (1999) Huge fetal sacrococygeal teratoma with a completely formed eye and intratumoral DNA ploidy heterogeneity. Pediatr Dev Pathol 2:50–57
21. Shimada H, Nakagawa A (1999) Tumors of the neuroblastoma group. Int J Clin Oncol 4:123–132
22. Slavc I, Ellenborgen R, Jung WH, Vawter GF, Kretschmar C, Grier H, Korf BR (1990) Myc gene amplification and expression in primary human neuroblastoma. Cancer Res 50: 1459–1463
23. Tajiri T, Shono K, Tanaka S, Suita S (2002) Evaluation of genetic heterogeneity in neuroblastoma. Surgery 131:S283–S287
24. Takahashi Y, Takenaka A, Ishiguro T, Noda Y (1994) Intratumoral DNA heterogeneity correlated with lymph node involvement and surgical staging in epithelial ovarian cancer by flow cytometry. Cancer 73:3011–3104
25. Tamas L, Kraxner H, Mechtler L, Repassy G, Ribari O, Hirschberg A, Szentkuti G, Jaray B, Szentirmay Z (2000) Prognostic significance of P53 histochemistry and DNA histogram parameters in head and neck malignancies. Anticancer Res 20:4031–4037
26. Taylor SR, Locker JL (1990) A comparative analysis of nuclear DNA content and n-myc gene amplification in neuroblastoma. Cancer 65:1360–1366
27. Yalçin B, Kutlik T, Kansu E, Göğüş S, Canpinar H, Akyüz C, Büyükpamukçu M (2000) DNA content and proliferative activity in children with neuroblastoma. Pediatr Hemat Oncol 17:45–54
28. Yildiz I, Jaffe N, Aksoy F, al-Naggar AK (1994) Regional DNA content heterogeneity in Wilms' tumor: incidence and potential clinical relevance. Anticancer Res 14:1365–1370

Virchows Arch (2005) 446: 525–531
DOI 10.1007/s00428-005-1247-x

ORIGINAL ARTICLE

Takamitsu Sasaki · Kazuhiro Yoshida · Hideaki Kondo · Hitoshi Ohmori · Hiroki Kuniyasu

Heme oxygenase-1 accelerates protumoral effects of nitric oxide in cancer cells

Received: 23 November 2004 / Accepted: 1 March 2005 / Published online: 15 April 2005
© Springer-Verlag 2005

Abstract We examined the biological effects of nitric oxide (NO) and its mediator, heme oxygenase-1 (HO-1), in cancer. Urogenital cancer cell lines, SKRC, T24 and DU145, were treated with various concentrations of sodium nitroprusside (SNP), a NO donor. The medium nitrite concentration was exponentially increased according to the concentration of SNP. Cell growth inhibition by NO was observed only at high nitrite concentrations (>20 μ*M*) in DU145 and T24 cells. Nitrite did not inhibit the growth of SKRC cells at any of the concentrations used. Doxorubicin (DXR) inhibited cell growth in the three cell lines, whereas growth inhibition recovered in the presence of <10 μ*M* nitrite. The recovery of DXR-induced growth inhibition was closely associated with an increase in Bcl-2 in the presence of <10 μ*M* nitrite. Vascular endothelial growth factor (VEGF) secretion was also increased in the presence of <10 and <20 μ*M* nitrite, respectively, in DU145 and SKRC or T24 cells. The expression of HO-1 was associated with sensitivity to NO-induced growth inhibition at constitutive levels, and was induced by SNP treatment. HO-1 inhibition by HO-1 antisense S-oligodeoxynucleotide treatment increased NO-induced growth inhibition, and decreased Bcl-2 expression or VEGF secretion in the three cell lines. These findings suggest that the NO/HO-1 system has protumoral effects.

Keywords Nitric oxide · Hemeoxigenase-1 · Apoptosis · VEGF · Bcl-2

Abbreviations DXR: Doxorubicin · ELISA: Enzyme-linked immunosorbent assay · HO: Heme oxygenase · NO: Nitric oxide · S-ODN: 18-Mer S-oligodeoxynucleotide · SNP: Sodium nitroprusside · TAMs: Tumor-associated macrophages · VEGF: Vascular endothelial growth factor

Introduction

Recent studies have focused on the biologic effects of nitric oxide (NO). NO is a multifunctional biologic effector. Firstly, NO is a donor of oxidative stress, which works as a strong defense tool against pathologic microorganism. In addition, NO-associated oxidative stress plays a role in tissue damage in atherosclerosis, in diabetes mellitus, and in antitumoral activity by macrophages [10, 12, 14, 22, 28]. Secondly, NO affects vascular endothelial cells, causing them to dilate vessels and to proliferate to make new vasculature [1, 23]. Thirdly, NO provides antiapoptotic signals [21].

In cancer, NO has opposite effects on tumor cells. Antitumoral effects are provided by the NO-associated cytotoxic effect of tumor-associated macrophages (TAMs) [12]. Protumoral effects are provided by angiogenesis and the antiapoptotic effect of NO, which are associated with tumor growth, metastasis, and anticancer drug resistance [1, 16, 29]. The total direction of the effects of NO depends on the summation of this multimodal function of NO.

Relevant parameters affecting the summation of the effects of NO are NO concentration produced by TAMs and NO resistance of tumor cells. TAMs produce NO by the action of inducible NO synthase following activation by various factors, such as interferon-gamma and lipopolysaccharide [7, 24]. The concentration of NO produced

This work was supported by a Grant-in-Aid for Scientific Research (B) from the Japan Society for the Promotion of Science (KAKENHI: 15390130).

T. Sasaki · H. Kondo · H. Ohmori · H. Kuniyasu (✉)
Department of Molecular Pathology,
Nara Medical University,
840 Shijo-cho, Kashihara,
Nara, 734-8521, Japan
e-mail: cooninh@zb4.so-net.ne.jp
Tel.: +81-722-223015
Fax: +81-722-257308

K. Yoshida
Surgical Oncology,
Research Institute for
Radiation Biology and Medicine,
Hiroshima University,
Hiroshima, Japan

by TAMs varies widely, and its role is still a subject of controversy.

One of the mediators of the effects of NO is heme oxygenase (HO) which is a pivotal enzyme in the degradation of the heme group. HO contains isoforms including HO-1, an inducible isoform, and HO-2, a constitutively expressed isoform [25]. HO-1 is a ubiquitous stress-inducible enzyme which is induced by NO and reactive oxygen species, and is thought to provide cell resistance to NO cytotoxicity [8].

In this study, we examined the effects of NO on cell growth, cell survival against anticancer drugs and angiogenesis at various concentrations in three urogenital cancer cell lines to determine the summation of the effects of NO. We also examined the role of HO-1 in the effects of NO.

Materials and methods

Cell culture

The human renal cell carcinoma cell line, SKRC, was kindly provided by Dr. Y. Hirao (Nara Medical University, Nara, Japan). T-24 (a human bladder cancer cell line) and DU145 (a human prostate cancer cell line) were provided by the American Type Culture Collection. The cells were routinely maintained in RPMI-1640 (Sigma Chemical Co., St. Louis, Mo.) containing 10% FBS (Sigma) under an atmosphere of air containing 5% CO_2 at 37°C. All these cell lines carry a mutated p53 gene [4, 13]. To evaluate cell survival, the cells were treated with doxorubicin (DXR) (Sigma) at 0.25 μg/ml.

Preparation of conditioned medium

For enzyme-linked immunosorbent assay (ELISA), the cells were cultured in RPMI-1640 containing 10% FBS for 2 days. Then the conditioned medium was filtered through a 0.2-μm filter (Becton-Dickinson Labware, Bedford, Mass.). A VEGF human ELISA kit (Calbiochem, Darmstadt, Germany) was used for detection of VEGF in the conditioned medium according to the supplier's instructions. VEGF contents are presented in relation to the production by untreated cells (set to 100).

Nitric oxide (NO)

For NO treatment of cells, sodium nitroprusside (SNP) was used as a NO donor at the concentrations mentioned in the Results. NO concentrations were determined as a nitrite concentrations, which were measured by the Griess method. The culture medium was mixed with the same amount of Griess solution (1% sulfanilamide, 0.1% naphthylethylenediamine dihydrochloride, 2.5% phosphoric acid) and the optical density was measured at a wavelength of 540 nm after 10 min incubation. Nitrite concentrations were determined from a standard curve made with various concentrations of sodium nitrite.

Cell growth

Cultured cells were harvested from 80% confluent monolayer cultures by a brief trypsinization with 0.1% trypsin and 0.1% EDTA. The cells were seeded at the density of 2000 cells per well of 96-well tissue culture plates, and cultured for 12 h in regular medium. The cells were washed with phosphate-buffered saline (PBS) twice and treated under the conditions mentioned in the Results. Cell growth was evaluated after 48 h using the 3-(4,5-dimethylthiazol-2-yl)-2,5-diphenyltetrazolium bromide (MTT) assay.

Antisense phosphorothioate (S)-oligodeoxynucleotide assay

The 18-mer S-oligodeoxynucleotide (S-ODN) for the antisense sequence from the 1st to the 18th nucleotide of human heme oxygenase-1 (HO-1) cDNA (GenBank NM00 2133) were synthesized and purified by reverse-phase high-performance liquid chromatography (Sigma Genosys, Ishikari, Japan). The sequence of HO-1 antisense was 5′-AGG GGA GGC AGG CGT TGA-3′. The sense sequence 18-mers was for the negative control. Cells of each cell line were pretreated with 3 μ*M* of antisense or sense S-ODN for 6 days with medium exchange and addition of antisense or sense S-ODN every 2 days. After that, the cells were used for further experiments.

Immunoblot analysis

Whole cell lysates were prepared as described previously [20]. Lysates (50 μg) were subjected to immunoblot analysis using 12.5% SDS-polyacrylamide gel followed by electrotransferring onto nitrocellulose filters. The filters were incubated with primary antibodies and then with peroxidase-conjugated anti-goat IgG antibody (Medical and Biological Laboratories, Nagoya, Japan) in a secondary reaction. For internal control of the amount of protein loaded, tubulin was detected by the specific antibody (Zymed Laboratories, South San Francisco, Calif.). The immune complex was visualized using an ECL Western blot detection system (Amersham, Little Chalfont, UK). The antibodies used were anti-Bcl-2 antibody (DAKO Corporation, Carpinteria, Calif.) and anti-HO-1 antibody (Santa Cruz Biotechnology, Santa Cruz, Calif.). For semiquantification, the specific signals on immunoblotted membrane detected by each antibody were computer-captured and quantified by NIH image computer software (National Institutes for Health, Bethesda, Md.). The signal intensities were compensated by tubulin intensities as internal controls and are represented in relation to the standard production by untreated cells (set to 100).

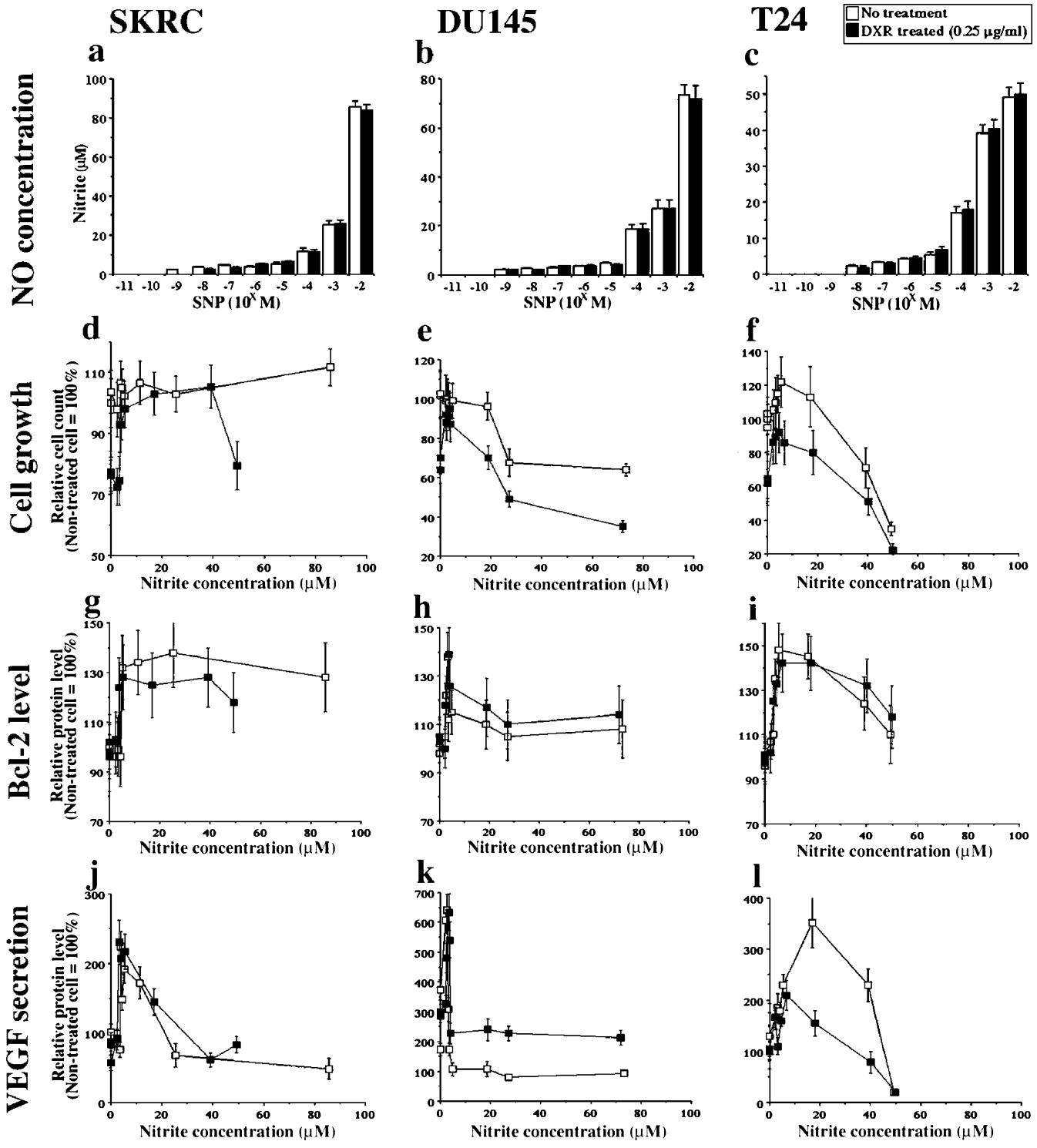

Fig. 1 Effect of SNP on NO production, cell growth, Bcl-2 expression, and VEGF secretion in cultures of three urogenital cancer cell lines. **a–c** Nitrite concentrations (measured by the Griess method) in the medium of cells treated with SNP at 10^{-11} to 10^{-2} *M*. **d–f** Growth of cells treated with SNP was compared with nitrite concentration in the medium. The cells were also treated with DXR to evaluate the effects of NO on cell survival. **g–i** Bcl-2 expression in SNP-treated cells detected by immunoblot analysis was compared with nitrite concentration in the medium. **j–l** VEGF secretion in SNP-treated cells detected by ELISA was compared with nitrite concentration in the medium. Protein levels (**g–l**) were standardized in relation to the constitutive level in each cell line, which was set to 100 (*error bars* ±SD)

Results

NO concentration provided by SNP

We first confirmed the effect of SNP, a NO donor, on NO concentrations in the culture medium. NO was detected in medium containing cells treated with SNP at 10^{-11} to 10^{-2} *M* (Fig. 1a–c). The NO concentration exponentially increased with increasing SNP concentration. The maximum NO concentrations detected in culture medium exposed to 10^{-2} *M* SNP were 84±4, 72±7, and 49±4 μ*M* in cultures of SKRC, DU145, and T24 cells, respectively.

Cell growth of SNP-treated cells

Cell growth in SNP-treated cells was determined using the MTT assay (Fig. 1d–f). Growth of DU145 and T24 cells was inhibited by exposure to >20 μ*M* nitrite. However, exposure to <10 μ*M* nitrite did not inhibit the growth of SKRC and DU145 cells, and increased the growth of T24 cells. In contrast, SKRC cells did not show any growth inhibition with any nitrite concentration.

To evaluate the effects of NO on cell survival, the cells were treated with DXR (Fig. 1d–f). DXR inhibited growth of SKRC, DU145, and T24 cells without SNP treatment by 24%, 37%, and 42%, respectively. To compare with cells untreated with DXR, DXR-induced growth inhibition recovered on exposure to <10 μ*M* nitrite in DU145 and T24 cells. DXR-treated SKRC cells showed recovery of growth inhibition on exposure to a wide range of nitrite concentrations (<40 μ*M*).

Bcl-2 production by SNP-treated cells

We next investigated Bcl-2 production in SNP-treated cells (Fig. 1g–i). In the three cell lines, Bcl-2 production was dose-dependently upregulated by exposure to <10 μ*M* nitrite regardless of DXR treatment. In SKRC cells, Bcl-2 production was increased by exposure to <40 μ*M* nitrite regardless of DXR treatment. In DU145 and T24 cells, Bcl-2 production was increased by exposure to <20 μ*M* nitrite regardless of DXR treatment. In the three cell lines, the levels of Bcl-2 production were correlated with the levels of cell growth.

VEGF secretion by SNP-treated cells

We next detected VEGF secretion in SNP-treated cells (Fig. 1i–l). In the three cell lines, VEGF secretion was dose-dependently upregulated by exposure to <10 μ*M* nitrite regardless of DXR treatment. In SKRC cells, VEGF secretion was also increased by exposure to <20 μ*M* nitrite of regardless of DXR treatment. In T24 cells with and without DXR treatment, VEGF secretion was also increased by exposure to <40 μ*M* and <20 μ*M* nitrite, respectively.

Fig. 2 Effect of HO-1 antisense S-ODN on cell growth, Bcl-2 expression, and VEGF secretion in cultures of three urogenital cancer cell lines. **a** HO-1 expression was detected by immunoblotting (*Sense HO-1* HO-1 sense S-ODN treatment,*Antisense HO-1* HO-1 antisense S-ODN treatment). Tubulin served as protein loading control. **b** HO-1 expression in SNP-treated cells. HO-1 protein levels were standardized to the constitutive level in T24 cells, which was set to 100. **c**–**e** Effect of HO-1 antisense S-ODN on growth of cells treated with various concentrations of SNP. **f** Bcl-2 expression was detected by immunoblotting in cells treated with HO-1 antisense or sense S-ODN. **g** VEGF in culture medium of cells treated with HO-1 antisense or sense S-ODN (**f**, **g** *SNP conc.* concentration of SNP used for cell treatment; **b**–**g** *S* HO-1 sense S-ODN treatment, *AS* HO-1 antisense S-ODN treatment;*error bars* ±SD) ▶

Effect of HO-1 antisense S-ODN

In the three cancer cell lines, HO-1 was expressed at various levels (Fig. 5a). HO-1 expression was higher in SKRC cells, which were resistant to NO-induced growth inhibition, than in T24 and DU145 cells, which were sensitive to NO-induced growth inhibition. HO-1 expression was increased by SNP treatment in the three cell lines in a dose-dependent manner (Fig. 2b–e). The increase in HO-1 in SKRC cells was the most prominent among the three cell lines. We then suppressed HO-1 expression by HO-1 antisense S-ODN to examine the role of HO-1 in NO-induced growth inhibition (Fig. 2a). In all cell lines, exposure to HO-1 antisense S-ODN inhibited growth in a NO concentration-dependent manner (Fig. 2c–e). NO-induced growth inhibitions of T24 and DU145 cells treated with HO-1 antisense S-ODN were respectively 21- and 104-times higher than those of untreated cells. In SKRC cells NO-induced growth inhibition also responded to treatment with HO-1 antisense S-ODN.

Bcl-2 expression in cells treated with SNP at the concentration yielding maximum Bcl-2 level in each cell line was decreased by exposure to HO-1 antisense S-ODN (Fig. 2f). SKRC cells treated with 10^{-5} *M* SNP showed 81% Bcl-2 expression on exposure to HO-1 antisense S-ODN compared to cells exposed to sense S-ODN. DU145 and T24 cells treated with 10^{-6} *M* and 10^{-5} *M* SNP, respectively, showed 68% and 74% Bcl-2 expression on exposure to HO-1 antisense S-ODN compared to cells exposed to sense S-ODN.

VEGF secretion in cells treated with SNP at the concentration yielding maximum VEGF secretion in each cell line was decreased by exposure to HO-1 antisense S-ODN (Fig. 2f). SKRC cells treated with 10^{-5} *M* SNP showed 78% Bcl-2 expression on exposure to HO-1 antisense S-ODN compared to cells exposed to sense S-ODN. DU145 and T24 cells treated with 10^{-7} *M* SNP showed, respectively, 82% and 85% Bcl-2 expression on exposure to HO-1 antisense S-ODN compared to cells exposed to sense S-ODN.

Discussion

In the present study, we studied the effects of NO on cell growth, survival, VEGF secretion, and HO-1 expression,

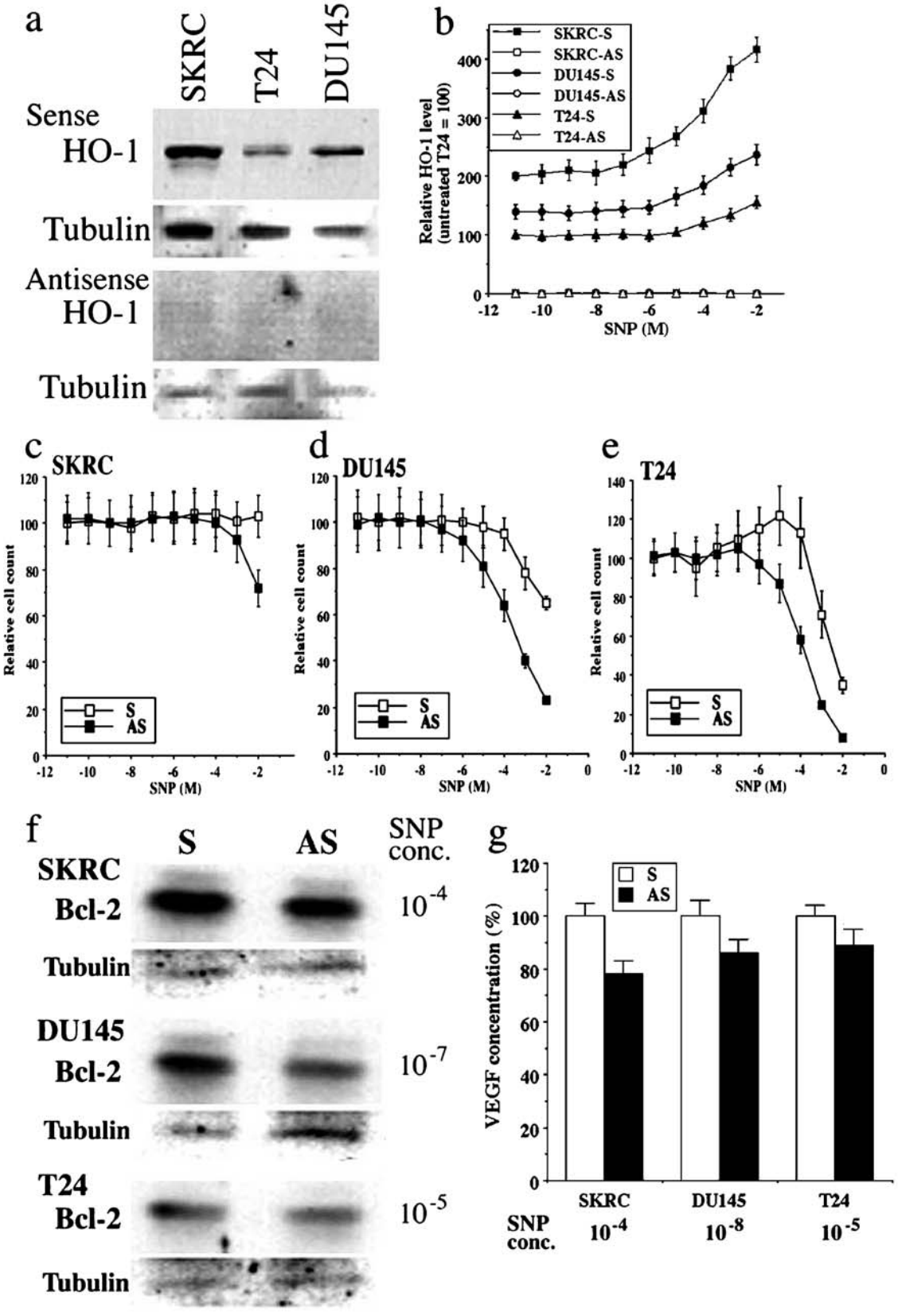
a
SKRC
T24
DU145
Sense
HO-1
Tubulin
Antisense
HO-1
Tubulin
b
SKRC-S
SKRC-AS
DU145-S
DU145-AS
T24-S
T24-AS
Relative HO-1 level
(untreated T24 = 100)
SNP (M)
c
SKRC
d
DU145
e
T24
Relative cell count
S
AS
SNP (M)
f
S
AS
SNP
conc.
SKRC
Bcl-2
Tubulin
DU145
Bcl-2
Tubulin
T24
Bcl-2
Tubulin
10-4
10-7
10-5
g
VEGF concentration (%)
S
AS
SKRC
DU145
T24
SNP
conc.
10-4
10-8
10-5

which are associated with resistance to NO-induced cell growth inhibition. The growth-inhibitory effect of NO was observed only at high nitrite concentrations (>20 μ*M*) in DU145 and T24 cells. Growth inhibition in those cell lines was not detected at nitrite concentrations <20 μ*M*. Moreover, SKRC cells did not show any growth inhibition on treatment with SNP at the concentrations used in the experiments.

Cell growth inhibition induced by DXR was decreased in the presence of various concentration of nitrite in the three cell lines. At undetectable nitrite concentrations, DXR inhibited cell growth to 60% to 70% in non-treated cells of the three cell lines. In contrast, at nitrite concentrations <10 μ*M*, growth inhibition induced by DXR recovered. Although the most effective concentration depended on the cell line, the concentration of nitrite reducing DXR-induced growth inhibition was similar to that increasing Bcl-2. At nitrite concentrations <10 μ*M*, Bcl-2 production was increased in a nitrite concentration-dependent manner. Kim et al. have reported that caspase-3 inhibition by NO is associated with suppression of Bcl-2 cleavage [18]. The increase in Bcl-2 protein in our experiments was also possibly associated with inhibition of Bcl-2 cleavage by NO. Thus, NO might act as a survival factor for cancer cells by inhibiting apoptotic processes and subsequently providing resistance to anticancer agents.

VEGF in the culture medium was increased by SNP treatment in the three cell lines in the present experiments. NO has been reported to upregulate the VEGF gene by enhancing the activity of hypoxia-induced factor (HIF)-1, and to dilate vascular vessels to increase blood flow [19, 30]. Although little is known about different effects of different concentrations of NO and the optimum NO concentrations for VEGF secretion, apoptosis inhibition might be associated with differences in intracellular signaling of NO.

We examined HO-1 as a factor susceptible to resistance to NO cytotoxicity in cancer cells. HO-1 expression is induced by NO by stabilization of HO-1 mRNA [6, 26]. Our data showed that HO-1 was increased by SNP treatment in a dose-dependent manner in the three cell lines. Inhibition of HO-1 expression by antisense S-ODN resulted in marked enhancement of NO-induced growth inhibition in NO-sensitive DU145 and T24 cells, and also NO-resistant SKRC cells. Constitutive levels of HO-1 expressions in the three cell lines were parallel to sensitivities to NO-induced growth inhibition. Therefore, overexpression of HO-1 might mediate cell protection to NO-induced cytotoxicity in cancer cells.

HO-1 antisense treatment decreased Bcl-2 expression and VEGF secretion in the three cancer cell lines. Carbon monoxide (CO), a by-product of the HO-1 enzymatic reaction, is a strong inducer of VEGF under hypoxic and normoxic conditions [9]. Reciprocally, VEGF prolongs HO-1 expression and activity [3]. HO-1 induction or HO-1 gene transfer reduces apoptosis with an increase in Bcl-2 in rat ischemic hearts [17] and liver grafts [5]. The mechanism by which HO-1 overexpression induces Bcl-2 expression is still unclear. However, CO produced by HO-1 inhibits apoptosis via p38 mitogen-activated proliferation kinase (MAPK) activation [2].

In our experiments, HO-1 overexpression was found in renal cell carcinomas, bladder cancer, and prostate cancer cells, and was especially associated with advanced disease of these cases. HO-1 overexpression and induction by NO has been reported in brain tumors [11, 26]. HO-1 enhances VEGF expression, vascular capillary formation, and blood flow in ischemic tissues and tumors [8, 27]. Inhibition of HO-1 suppresses colon cancer metastasis in mice [15]. HO-1 is, therefore, an important target of cancer treatment. HO-1 is induced by not only NO but also various growth factors and cytokines [25] which are produced by tumor cells. Understanding of the mechanism by which HO-1 is induced in tumors is needed to elucidate these processes.

Our results overall suggest that NO has protumoral effects through decreasing cell growth inhibition, an anti-apoptotic effect, and VEGF secretion. Overexpression of HO-1 in cancer cells provides resistance to the cytotoxicity of NO at high concentrations.

Acknowledgements We thank Miss Kaori Obara for excellent assistance in preparing the manuscript.

References

1. Ambs S, Merriam WG, Ogunfusika MO, Bennett WP, Ishibe N, Hussain SP, Tzeng EE, Geller DA, Billiar TR, Harris CC (1998) p53 and vascular endothelial growth factor regulate tumor growth of NOS2-expressing human carcinoma cells. Nat Med 4:1371–1376
2. Brouard S, Otterbein LE, Anrather J, Tobiasch E, Bach FH, Choi AM, Soares MP (2000) Carbon monoxide generated by heme oxygenase 1 suppresses endothelial cell apoptosis. J Exp Med 192:1015–1026
3. Bussolati B, Ahmed A, Pemberton H, Landis RC, Di Carlo F, Haskard DO, Mason JC (2004) Bifunctional role for VEGF-induced heme oxygenase-1 in vivo: induction of angiogenesis and inhibition of leukocytic infiltration. Blood 103:761–766
4. Cemazar M, Grosel A, Glavac D, Kotnik V, Skobrne M, Kranjc S, Mir LM, Andre F, Opolon P, Sersa G (2003) Effects of electrogenetherapy with p53wt combined with cisplatin on survival of human tumor cell lines with different p53 status. DNA Cell Biol 22:765–775
5. Coito AJ, Buelow R, Shen XD, Amersi F, Moore C, Volk HD, Busuttil RW, Kupiec-Weglinski JW (2002) Heme oxygenase-1 gene transfer inhibits inducible nitric oxide synthase expression and protects genetically fat Zucker rat livers from ischemia-reperfusion injury. Transplantation 74:96–102
6. Demple B (2004) Protection from the dark side of NO: signaling and cellular defenses against nitric oxide toxicity. IUBMB Life 56:59–64
7. Dinapoli MR, Calderon CL, Lopez DM (1996) The altered tumoricidal capacity of macrophages isolated from tumor-bearing mice is related to reduce expression of the inducible nitric oxide synthase gene. J Exp Med 183:1323–1329
8. Dulak J, Loboda A, Zagorska A, Jozkowicz A (2004) Complex role of heme oxygenase-1 in angiogenesis. Antioxid Redox Signal 6:858–866
9. Dulak J, Jozkowicz A, Foresti R, Kasza A, Frick M, Huk I, Green CJ, Pachinger O, Weidinger F, Motterlini R (2002) Heme oxygenase activity modulates vascular endothelial growth factor synthesis in vascular smooth muscle cells. Antioxid Redox Signal 4:229–240

10. Forstermann U, Mugge A, Alheid U, Haverich A, Frolich JC (1988) Selective attenuation of endothelium-mediated vasodilation in atherosclerotic human coronary arteries. Circ Res 62: 185–190
11. Hara E, Takahashi K, Tominaga T, Kumabe T, Kayama T, Suzuki H, Fujita H, Yoshimoto T, Shirato K, Shibahara S (1996) Expression of heme oxygenase and inducible nitric oxide synthase mRNA in human brain tumors. Biochem Biophys Res Commun 224:153–158
12. Hibbs JBJ, Vavrin Z, Taintor RR (1987) L-arginine is required for expression of the activated macrophage effector mechanism causing selective metabolic inhibition in target cells. J Immunol 138:550–565
13. Hinata N, Shirakawa T, Zhang Z, Matsumoto A, Fujisawa M, Okada H, Kamidono S, Gotoh A (2003) Radiation induces p53-dependent cell apoptosis in bladder cancer cells with wild-type-p53 but not in p53-mutated bladder cancer cells. Urol Res 31:387–396
14. Honing ML, Morrison PJ, Banga JD, Stroes ES, Rabelink TJ (1998) Nitric oxide availability in diabetes mellitus. Diabetes Metab Rev 14:241–249
15. Ishikawa T, Yoshida N, Higashihara H, Inoue M, Uchiyama K, Takagi T, Handa O, Kokura S, Naito Y, Okanoue T, Yoshikawa T (2003) Different effects of constitutive nitric oxide synthase and heme oxygenase on pulmonary or liver metastasis of colon cancer in mice. Clin Exp Metastasis 20:445–450
16. Jenkins DC, Charles IG, Thomsen LL, Moss DW, Holmes LS, Baylis SA, Rhodes P, Westmore K, Emson PC, Moncada S (1995) Roles of nitric oxide in tumor growth. Proc Natl Acad Sci U S A 92:4392–4396
17. Katori M, Buelow R, Ke B, Ma J, Coito AJ, Iyer S, Southard D, Busuttil RW, Kupiec-Weglinski JW (2002) Heme oxygenase-1 overexpression protects rat hearts from cold ischemia/reperfusion injury via an antiapoptotic pathway. Transplantation 73: 287–292
18. Kim YM, Kim TH, Seol DW, Talanian RV, Billiar TR (1998) Nitric oxide suppression of apoptosis occurs in association with an inhibition of Bcl-2 cleavage and cytochrome c release. J Biol Chem 273:31437–31441
19. Kimura H, Esumi H (2003) Reciprocal regulation between nitric oxide and vascular endothelial growth factor in angiogenesis. Acta Biochim Pol 50:49–59
20. Kuniyasu H, Yasui W, Kitahara K, Naka K, Yokozaki H, Akama Y, Hamamoto T, Tahara H, Tahara E (1997) Growth inhibitory effect of interferon-beta is associated with the induction of cyclin-dependent kinase inhibitor p27Kip1 in a human gastric carcinoma cell line. Cell Growth Differ 8:47–52
21. McGowan AJ, Fernandes RS, Samali A, Cotter TG (1996) Antioxidants and apoptosis. Biochem Soc Trans 24:229–233
22. Minor RLJ, Myers PR, Guerra RJ, Bates JN, Harrison DG (1990) Diet-induced atherosclerosis increases the release of nitrogen oxides from rabbit aorta. J Clin Invest 86:2109–2116
23. Palmer RM, Ferrige AG, Moncada S (1987) Nitric oxide release accounts for the biological activity of endothelium-derived relaxing factor. Nature 327:524–526
24. Shrivastava P, Singh SM, Singh N (2003) Effect of thymosin-alpha1 on the production of nitric oxide by tumor-associated macrophages. Neoplasma 50:47–53
25. Sikorski EM, Hock T, Hill-Kapturczak N, Agarwal A (2004) The story so far: molecular regulation of the heme oxygenase-1 gene in renal injury. Am J Physiol Renal Physiol 286:F425–F441
26. Takahashi K, Hara E, Suzuki H, Sasano H, Shibahara S (1996) Expression of heme oxygenase isozyme mRNAs in the human brain and induction of heme oxygenase-1 by nitric oxide donors. J Neurochem 67:482–489
27. Tozer GM, Prise VE, Motterlini R, Poole BA, Wilson J, Chaplin DJ (1998) The comparative effects of the NOS inhibitor, Nw-nitro-L-arginine, and the haemoxygenase inhibitor, zinc protoporphyrin IX, on tumour blood flow. Int J Radiat Oncol Biol Phys 42:849–853
28. Williams SB, Cusco JA, Roddy MA, Johnstone MT, Creager MA (1996) Impaired nitric oxide-mediated vasodilation in pasynthesistients with non-insulin-dependent diabetes mellitus. J Am Coll Cardiol 27:567–574
29. Xu W, Liu L, Smith GC, Charles G (2000) Nitric oxide upregulates expression of DNA-PKcs to protect cells from DNA-damaging anti-tumour agents. Nat Cell Biol 2:339–345
30. Xu W, Liu LZ, Loizidou M, Ahmed M, Charles IG (2002) The role of nitric oxide in cancer. Cell Res 12:311–320

Virchows Arch (2005) 446: 532–536
DOI 10.1007/s00428-005-1256-9

ORIGINAL ARTICLE

Peter J. Barth · Roland Moll · Annette Ramaswamy

Stromal remodeling and SPARC (secreted protein acid rich in cysteine) expression in invasive ductal carcinomas of the breast

Received: 20 December 2004 / Accepted: 7 March 2005 / Published online: 19 April 2005
© Springer-Verlag 2005

Abstract In the present study, we analyzed tumor associated stromal remodeling with special respect to SPARC (secreted protein acid rich in cysteine) expression. 25 invasive ductal carcinomas of the breast and corresponding tumor-free breast tissue were studied immunohistochemically (CD34, α-SMA, SPARC and TGFβ-R1). Tumor associated stroma was characterized by a loss of CD34 expression, paralleled by a gain in α-SMA. While SPARC expression was virtually absent from normal stromal cells in the tumor stroma, strong cytoplasmic SPARC reactivity was found in the majority of stromal cells. The TGFβ-R1 also showed stronger expression in the tumor stroma compared to that of the normal breast. Stromal response to antecedent core needle biopsy was similar to that observed in the tumor stroma. We conclude that SPARC overexpression is a constant and functionally important feature of invasive ductal carcinomas, since SPARC mediates stromal de-adhesion crucial for local tumor invasion and systemic spread, respectively. When considering changes of the stromal phenotype (normal: $CD34^+\alpha\text{-SMA}^-SPARC^-$ vs. carcinoma: $CD34^-\alpha\text{-SMA}^+SPARC^+$) as a tool in distinguishing benign from malignant breast lesion one has to keep in mind that the phenotype of granulation tissue in areas of antecedent biopsy resembles that of tumor stroma.

Keywords Stroma · Breast · Invasive ductal carcinoma · SPARC · CD34

Introduction

Stromal remodeling precipitated by invasive carcinomas is independent of the histologic type and primary tumor site, and shows uniform histological features as CD34 expression is lost in stromal cells, paralleled by a gain of α-SMA expression [3–6, 22]. CD34 is mainly found on hemopoetic precursor cells and endothelial cells [16]. In the microvasculature CD34 serves as an L-selectin ligand regulating leukocyte rolling and emigration into tissue [16]. On the other side, the function and significance of CD34 on stromal cells referred to as $CD34^+$ fibrocytes [8, 11] has up to now rarely been addressed and therefore remains enigmatic. However, $CD34^+$ fibrocytes constitute an important element of the connective tissue of various organs [3–6, 18, 19, 22, 27]. Although it remains to be clarified whether all $CD34^+$ fibrocytes histologically detected in the connective tissue derive from circulating cells, it appears reasonable to assume that stromal $CD34^+$ fibrocytes are at least closely related to circulating $CD34^+$ fibrocytes originally described by Bucala and coworkers in 1995 [8]. $CD34^+$ fibrocytes are capable of tissue matrix synthesis [11, 14] and have been shown to be potent antigen-presenting cells [10]. A loss of $CD34^+$ fibrocytes as described in most carcinomas might therefore favor local tumor invasion and subsequent systemic spread.

Stromal remodeling in invasive carcinomas is certainly an important prerequisite of local tumor invasion and distant spread. TGFβ has been reported to induce α-SMA upregulation in fibrocytes, and might therefore play a role in tumor associated stromal remodeling [1]. SPARC (secreted protein acid rich in cysteine) also devised as osteonectin or BM-40 belongs to the group of matricellular proteins and has been claimed as a member of the invasion associated cluster [15, 24]. We therefore undertook the present study to relate TGFβ-R and SPARC expression in stromal cells to the phenotypic alterations in malignancy induced stromal remodeling.

P. J. Barth (✉) · R. Moll · A. Ramaswamy
Institute of Pathology, Philipps-University Marburg,
Baldingerstraße,
35033 Marburg, Germany
e-mail: barthp@med.uni-marburg.de
Tel.: +49-6421-2862465
Fax: +49-6421-2865640

Materials and methods

The present study comprises a total of 25 breast biopsies obtained exclusively from women with proven invasive ductal carcinoma. The epidemiological data of the patients

Table 1 Tumor characteristics and epidemiologic data of patients investigated

Number: 25
Median age: 52 years (range: 29–80)
Grading: G1: 3, G2: 21, G3: 1
UICC: pT1b: 6, pT1c: 14, pT2: 5; pN0: 20, pN1a: 4, pN1mi:1

are summarized in Table 1, together with the major tumor characteristics.

After resection, tissues were fixed in a 10% formalin solution, embedded in paraffin, cut and stained H&E and PAS for routine purposes. In all cases tumor free tissue from resection margins was available for comparison. The site of previous core needle biopsy was included in the specimens in 14 cases.

Immunohistochemistry

CD34, α-SMA, SPARC and the TGFβ-R1 were detected immunohistochemically by means of the standard avidin biotin complex (ABC)-peroxidase method (ABC Elite Kit; Vector, Burlingame, Calif., USA) using 3,3′-diaminobenzidine (DAB) as chromogen. The primary antibodies and type of tissue pre-treatment are listed in Table 2. Microwave pretreatment was performed by heating the deparaffinized and rehydrated sections, immersed in 10 mM sodium citrate buffer (pH 6.0), in a microwave oven at 600 W for 3 or 4 times 5 min (see Table 2).

Double labeling of CD34 and TGFβ-R

For double labeling of CD34 and TGFβ-R1 sections were pre-treated by micro-wave heating for 4 times 5 min as described above. Thereafter TGFβ-R1 was detected by means of the ABC-alkaline phosphatase method (ABC-AP Kit; Vector, Burlingame, CA). As primary antibody, a monoclonal antibody against TGFβ-R1 (IgM, Novocastra, dilution 1:10 in PBS containing 1% horse serum) was used. Thereafter, sections were incubated with a biotinylated horse anti mouse IgM antibody (1:100 in PBS) followed by incubation with the avidin-biotin alkaline phosphatase complex. Histo Red (Linaris, Wertheim-Bettingen, Germany) was used as chromogen according to the instructions of the manufacturer. After rinsing in PBS for 5 min, CD34 was detected according to the ABC-peroxidase method using the Qbend10 (IgG1a) antibody at a dilution of 1:40 as primary antibody. Thereafter a biotinylated horse anti mouse IgG1 (1:100 in PBS) was applied and finally sections were incubated with the ABC peroxidase complex (VECTASTAIN Elite ABC Kit, Vector). Histo Green (Linaris) was used as chromogen according to the instructions of the manufacturer and resulted in a green color reaction, whereas the TGFβ-R1 stained red.

Semi-quantitative assessment of immunohistochemistry

Immunoreactivity of CD34, α-SMA and SPARC was assessed semi-quantitatively in the tumor free tissue, in the center and periphery of the tumor. The percentage of stromal cells expressing the respective antigen was graded as "0", "+", "++" and "+++" when up to 5%, more than 5% and up to 25%, more than 25% and up to 50% or more than 50% of stromal cells, respectively, disclosed immunoreactivity. Percentages were assessed by two independent observers, assuming that a microscopic high power field (objective 40x, microscopic magnification: ×400) harbors 100 stromal cells (range: 75–150). Immunohistochemical expression of TGFβ-R1 was assessed qualitatively as positive or negative.

Statistical analyses

Comparison of groups (tumor-free versus tumor periphery; tumor periphery versus tumor border) was performed using the χ^2-test defining $P<0.01$ to be statistically significant.

Results

Tumor free breast tissue

In the tumor free breast tissue $CD34^+$ fibrocytes were predominantly found in the lobular stroma, forming a dense network that surrounded ducts and acini (Fig. 1a). Most $CD34^+$ fibrocytes showed bipolar slender cytoplasmic processes which appeared to communicate with neighbouring $CD34^+$ fibrocytes. In the extralobular stroma, $CD34^+$ fibrocytes were found in the adventitia of small arteries and arterioles and few $CD34^+$ fibrocytes were detected in the collagen rich stroma remotely located from vessels. The tumor free stroma was devoid of α-SMA positive myofibroblasts. Immunohistochemically SPARC expression was found in myoepithelial cells and in endothelial cells of

Table 2 Antibodies applied for immunohistochmenistry and type of tissue pre-treatment. *dl* double labeling, *s* single staining

Antibody (Clone)	Source	Dilution	Tissue pre-treatment
CD34 (Qbend 10)	Dako, Hamburg, Germany	1:40 (dl)	
		1:50 (s)	Microwave 3×5 min, 600 W
SPARC	Novocastra, UK	1:40	Microwave 3×5 min, 600 W
TGFβ-R1 (8A11)	Novocastra, UK	1:10 (dl)	Microwave 4×5 min, 600 W
		1:25 (s)	Microwave 4×5 min, 600 W
α−SMA (ASM−1)	Progen, Heidelberg, Germany	1:200	0,1% Trypsin Tris/HCl 15 min 37°C

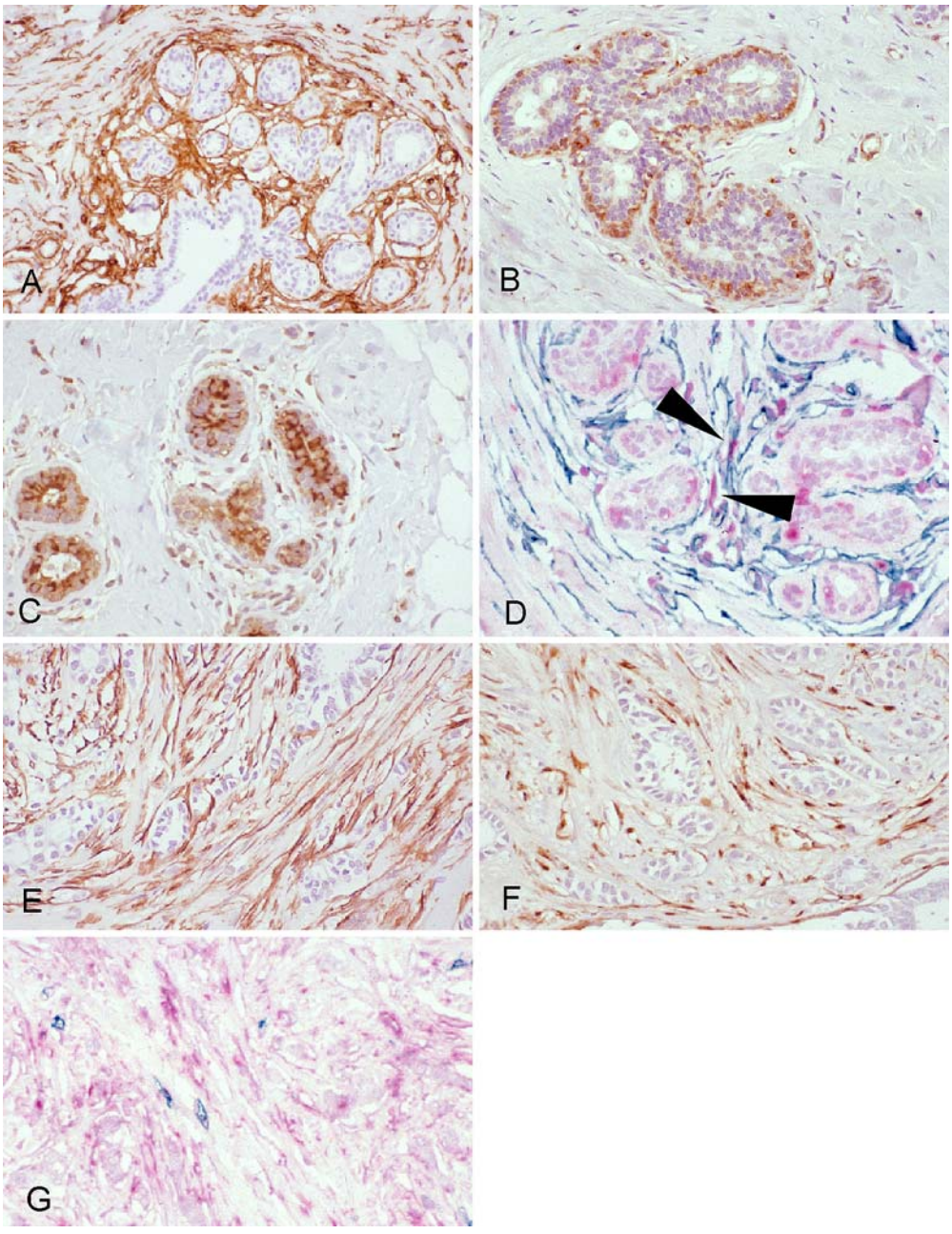

Fig. 1 The tumor-free lobular stroma consists of densely packed $CD34^+$ fibrocytes, the extralobular stroma discloses scattered $CD34^+$ fibrocytes (**a**). SPARC is immunohistochemically expressed in myoepithelial cells, few stromal cells and endothelial cells (**b**). TGFβ−R1 immunohistochemistry shows membrane staining of acinar epithelia and intra- and extralobular stromal cells (**c**). Double labeling shows co-expression of CD34 (green) and TGFβ−R1 (red, see arrows) in intralobular fibrocytes (**d**). The tumor associated stroma contains α-SMA positive myofibroblasts (**e**) that also show cytoplasmic SPARC immunoreactivity (**f**). Double labeling of the tumor tissue shows CD34 positivity (green) of endothelial cells, a loss of $CD34^+$ fibrocytes and strong TGFβ−R1 immunoreactivity (red) (**g**)

arterioles and capillaries (Fig. 1b, Table 3). In nine cases, a small population of stromal cells making up less then 5% of stromal cells were weakly positive for SPARC, in the remaining cases, stromal cells showed no SPARC immunoreactivity. TGFβ-R1 immunoreactivity was strong in lymphocytes, myoepithelial cells, a subpopulation of ductal and acinar epithelia and few intralobular fibrocytes (Fig. 1c). Double labeling of the TGFβ-R1 and CD34 showed the bipolar processes of CD34+ fibrocytes to be reactive with CD34, whereas the body of the cells exhibited positivity for TGFβ-R1 (Fig. 1d).

Invasive ductal carcinomas

The tumor associated stroma was virtually free of $CD34^+$ fibrocytes and the interface between tumor-free and tumor associated stroma showed an abrupt loss of $CD34^+$ fibrocytes. $CD34^+$ fibrocytes at the tumor border were morphologically identical to those located remotely from the tumor. In four cases, few residual $CD34^+$ fibrocytes were found in the tumor periphery, making up less than 5% of the stromal cells. The tumor associated stroma consisted of plump myofibroblasts showing intense cytoplasmic α-SMA immunoreactivity mostly displaying a tram track pattern (Fig. 1e). In all cases, stromal cells also showed strong cytoplasmic staining for SPARC (Fig. 1f). Comparison of the

Table 3 Semi-quantitative assessment of CD34, α-SMA and SPARC expression in tumor-free breast tissue, tumor center and tumor periphery, respectively

	CD34*,#				α-SMA*,#				SPARC*,#			
	0	+	++	+++	0	+	++	+++	0	+	++	+++
Tumor free	0	0	16	9	25	0	0	0	25	0	0	0
Tumor periphery	25	0	0	0	0	6	14	5	1	9	10	5
Tumor center	25	0	0	0	1	9	9	6	0	10	12	3

0: <5%, + >5% and <25%, ++ >25% and <50%, +++: >50% positive stromal cells, *P<0.01 for tumor free vs tumor periphery; #P>0.01 for tumor periphery vs tumor center

tumor center and periphery disclosed no statistically significant differences in α-SMA- and SPARC expression, respectively (Table 3). TGFβ-R1 immunoreactivity of tumor associated myofibroblasts was more intense compared to that observed in $CD34^+$ fibrocytes of the tumor free stroma (Fig. 1g).

In areas of antecedent biopsy, the granulation tissue showed a phenotype similar to that of the tumor stroma as the stromal cells showed strong expression of α-SMA and SPARC accompanied by a negative reaction of CD34.

Discussion

Porter and coworkers were the first to report SPARC expression in tumor associated stromal cells and assumed that SPARC expression "might contribute to some aspects of tumor progression" [21]. In the present study, stromal remodeling associated with invasive breast cancer, characterized by a loss of CD34 expression paralleled by a gain of α-SMA, is strongly related to an increased expression of SPARC (secreted protein acid rich in cysteine). The regulation of SPARC synthesis and secretion is elusive, but recent investigations have shown that TGFβ1 increases the synthesis of SPARC in stromal cells [2, 23] while SPARC vice versa interferes with the TGFβ1 signaling system [25]. These findings suggest a close functional relation of SPARC and TGFβ1 which may in part be reflected by a similar cellular distribution pattern observed in the present study in that, SPARC and the TGFβ-R1 are predominantly found in myoepithelial cells and few lobular stromal fibrocytes of the normal breast.

SPARC exerts three major functions: anti-proliferation, de-adhesion and regulation of ECM synthesis [7]. De-adhesion of the tumor associated stroma is defined as an intermediate state of adhesion caused by restructuring of focal adhesions and stress fibers mediated by matricellular proteins such as SPARC [17] and constitutes a prerequisite for tumor cell migration and tissue invasion [13]. Moreover, de-adhesion leads to alterations of the cytoskeleton in part characterized by synthesis of stress fibers, which histologically is reflected by the abundance of α-SMA positive myofibroblasts. In addition, TGFβ1 has also been reported to directly increase α-SMA expression in fibrocytes [1]. On the other side, the loss of CD34 expression in stromal cells can less easily be explained. In primary cultures of fibrocytes, a progressive time dependent loss of CD34 expression was observed [12, 20, 26]. Moreover, in vitro differentiation of $CD34^+$ fibrocytes from $CD14^+$ monocytes requires direct T-cell interaction, indicating that cell-cell contacts are crucial for the development and maintenance of CD34 expression in fibrocytes [1]. Therefore it appears to be reasonable that the loss of CD34 expression in stromal cells is at least in part due to a reduction and modification of cell-cell contacts mediated by SPARC. This assumption might additionally explain the phenotypic similarity of tumor stroma and granulation tissue. Chauhan and coworkers were the first to point out that stromal remodeling in carcinomas closely resembles granulation tissue and woung healing observed at sites of antecedent biopsy [9]. This is in keeping with the findings of the present study. Moreover, benign complex lesions of the breast such as radial scars are characterized by a focal loss of $CD34^+$ fibrocytes [22]. Thus, when considering the detection of $CD34^+$ fibrocytes as a tool in distinguishing benign from malignant breast lesions, it has to be kept in mind that a loss of this cell population does not automatically indicate malignancy. On the other side, the presence of $CD34^+$ fibrocytes excludes malignancy with a high degree of certainty [3, 9, 22].

References

1. Abe R, Donnelly SC, Peng T, Bucala R, Metz CN (2001) Peripheral blood fibrocytes: differentiation pathway and migration to wound sites. J Immunol 166:7556–7562
2. Abe K, Hibino T, Mishima H, Shimomura Y (2004) The cytokine regulation of SPARC production by rabbit corneal epithelial cells and fibroblasts in vitro. Cornea 23:172–179
3. Barth PJ, Ebrahimsade S, Ramaswamy A, Moll R (2002) $CD34^+$ fibrocytes in invasive ductal carcinoma, ductal carcinoma in situ, and benign breast lesions. Virchows Arch 440:298–303
4. Barth PJ, Ebrahimsade S, Hellinger A, Moll R, Ramaswamy A (2002) $CD34^+$ fibrocytes in neoplastic and inflammatory pancreatic lesions. Virchows Arch 440:128–133
5. Barth PJ, Ramaswamy A, Moll R (2002) $CD34^+$ fibrocytes in normal cervical stroma, cervical intraepithelial neoplasia III, and invasive squamous cell carcinoma of the cervix uteri. Virchows Arch 441:564–568
6. Barth PJ, Schenck zu Schweinsberg T, Ramaswamy A, Moll R (2004) CD34+ fibrocytes, α–smooth muscle antigen-positive myofibroblasts, and CD117 expression in the stroma of invasive squamous cell carcinomas of the oral cavity, pharynx, and larynx. Virchows Arch 444:231–234
7. Bradshaw AD, Sage EH (2001) SPARC, a matricellular protein that functions in cellular differentiation and tissue response to injury. J Clin Invest 107:1049–1054
8. Bucala R, Spiegel LA, Chesney J, Hogan M, Cerami A (1994) Circulating fibrocytes define a new leukocyte subpopulation that mediates tissue repair. Mol Med 1:71–81
9. Chauhan H, Abraham A, Phillips JR, Pringle JH, Walker RA, Jones JL (2003) There is more than one kind of myofibroblast: analysis of CD34 expression in benign, in situ, and invasive breast lesions. J Clin Pathol 56:271–276
10. Chesney J, Bacher M, Bender A, Bucala R (1997) The peripheral blood fibrocyte is a potent antigen-presenting cell capable of priming naive T cells in situ. Proc Natl Acad Sci USA 94:6307–6312

11. Chesney J, Metz C, Stavitsky AB, Bacher M, Bucala R (1998) Regulated production of type I collagen and inflammatory cytokines by peripheral blood fibrocytes. J Immunol 160:419–425
12. Espana EM, Kawakita T, Liu CY, Tseng SC (2004) CD-34 expression by cultured human keratocytes is downregulated during myofibroblast differentiation induced by TGF-beta1. Invest Ophthalmol Vis Sci 45:2985–2991
13. Framson PE, Sage EH (2004) SPARC and tumor growth: where the seed meets the soil? J Cell Biochem 92:679–690
14. Hartlapp I, Abe R, Saeed RW, Peng T, Voelter W, Bucala R, Metz CN (2001) Fibrocytes induce an angiogenic phenotype in cultured endothelial cells and promote angiogenesis in vivo. FASEB J 15:2215–2224
15. Iacobuzio-Donahue CA, Argani P, Hempen PM, Jones J, Kern SE (2002) The desmoplastic response to infiltrating breast carcinoma: gene expression at the site of primary invasion and implications for comparisons between tumor types. Cancer Res 62:5351–5357
16. Khan AI, Landis RC, Malhotra R (2003) L-Selectin ligands in lymphoid tissues and models of inflammation. Inflammation 27: 265–280
17. Murphy-Ullrich JE (2001) The de-adhesive activity of matricellular proteins: is intermediate cell adhesion an adaptive state? J Clin Invest 107:785–790
18. Nakayama H, Enzan H, Miyazaki E, Kuroda N, Naruse K, Hiroi M (2000) Differential expression of CD34 in normal colorectal tissue, peritumoral inflammatory tissue, and tumour stroma. J Clin Pathol 53:626–629
19. Nakayama H, Enzan H, Miyazaki E, Kuroda N, Naruse K, Kiyoku H, Toi M, Hiroi M (2001) CD34 positive stromal cells in gastric adenocarcinomas. J Clin Pathol 54:846–848
20. Phillips RJ, Burdick MD, Hong K, Lutz MA, Murray LA, Xue YY, Belperio JA, Keane MP, Strieter RM (2004) Circulating fibrocytes traffic to the lungs in response to CXCL12 and mediate fibrosis. J Clin Invest 114:438–446
21. Porter PL, Sage EH, Lane TF, Funk SE, Gown AM (1995) Distribution of SPARC in normal and neoplastic human tissue. J Histochem Cytochem 43:791–800
22. Ramaswamy A, Moll R, Barth PJ (2003) $CD34^{+}$ fibrocytes in tubular carcinomas and radial scars of the breast. Virchows Arch 443:536–540
23. Reed MJ, Vernon RB, Abrass IB, Sage EH (1994) TGF-beta 1 induces the expression of type I collagen and SPARC, and enhances contraction of collagen gels, by fibroblasts from young and aged donors. J Cell Physiol 158:169–179
24. Ryu B, Jones J, Hollingsworth MA, Hruban RH, Kern SE (2001) Invasion-specific genes in malignancy: serial analysis of gene expression comparisons of primary and passaged cancers. Cancer Res 61:1833–1838
25. Schiemann BJ, Neil JR, Schiemann WP (2003) SPARC inhibits epithelial cell proliferation in part through stimulation of the transforming growth factor-β-signaling system. Mol Biol Cell 14:3977–3988
26. Schmidt M, Sun G, Stacey MA, Mori L, Mattoli S (2003) Identification of circulating fibrocytes as precursors of bronchial myofibroblasts in asthma. J Immunol 171:380–389
27. Soma L, LiVolsi VA, Baloch ZW (2001) Dendritic interstitial and myofibroblastic cells at the border of salivary gland tumors. Arch Pathol Lab Med 125:232–236

Virchows Arch (2005) 446: 537–541
DOI 10.1007/s00428-004-1185-z

CASE REPORT

Ryoji Kushima · Michael Vieth · Ken-ichi Mukaisho · Rie Sakai · Hidetoshi Okabe · Takanori Hattori · Horst Neuhaus · Franz Borchard · Manfred Stolte

Pyloric gland adenoma arising in Barrett's esophagus with mucin immunohistochemical and molecular cytogenetic evaluation

Received: 3 October 2004 / Accepted: 22 November 2004 / Published online: 19 April 2005
© Springer-Verlag 2005

Abstract Pyloric gland adenoma is a recently described and very rare entity. The occurrence of adenoma is very unusual in Barrett's epithelium of the esophagus. We report a case of esophageal polyp showing the features of pyloric gland adenoma, which was surrounded by so-called specialized columnar epithelium. Immunohistochemically, most tumor glands were strongly positive for MUC6, except in the superficial layer. MUC5AC was positive in almost all tumor cells, but MUC2 and CD10 were negative in the tumor. MIB-1-positive proliferating cells were distributed throughout the tumor. Microdissection and comparative genomic hybridization analyses revealed losses on 2p24–25.2, 2q14.1-ter, 5q31.3–32, 6q23–24, 8q23–24.2, 11q22.3–24 and 18q21.1–22. This is the first case of pyloric gland adenoma found to arise in Barrett's epithelium of the esophagus, showing its unstable and precancerous nature.

R. Kushima (✉) · R. Sakai · H. Okabe
Division of Diagnostic Pathology,
Shiga University of Medical Science,
Seta, Otsu,
520-2192 Shiga, Japan
e-mail: kushima@belle.shiga-med.ac.jp
Tel.: +81-77-548-2621
Fax: +81-77-548-2407

M. Vieth · M. Stolte
Institute of Pathology, Klinikum Bayreuth,
95445 Bayreuth, Germany

K.-i. Mukaisho · T. Hattori
Department of Pathology,
Shiga University of Medical Science,
Otsu,
520-2192 Shiga, Japan

H. Neuhaus
Department of General Internal Medicine,
Evangelisches Krankenhaus Düsseldorf,
40217 Düsseldorf, Germany

F. Borchard
Institute of Pathology, Klinikum Aschaffenburg,
63739 Aschaffenburg, Germany

Keywords Pyloric gland adenoma · Barrett's epithelium · Esophagus · Mucin · CGH

Introduction

In Barrett's epithelium (BE), a rising incidence of adenocarcinoma has been described in the literature over recent decades. These adenocarcinomas are believed to develop through a metaplasia-dysplasia-carcinoma sequence [5, 6]. Intraepithelial neoplasia (dysplasia) may be broadly categorized as flat or associated with visible or raised lesions similar to those occurring in inflammatory bowel disease [20]. However, the occurrence of adenoma, a polypoid lesion composed of densely packed neoplastic glands similar to a colonic adenoma, is very unusual, and some authors have recently proposed a descriptive diagnostic term, such as BE-associated polypoid dysplasia [18].

Pyloric gland adenoma was first characterized by Borchard et al. [2], and Watanabe [26] described a similar lesion in the World Health Organization classification of gastric tumors in 1990. Borchard presented two cases of pyloric gland adenoma with transition to adenocarcinoma during two slide seminars in 1986 and 1987 (F. Borchard, personal communication). Similar adenomas of the gastric type were subsequently described in gastric heterotopia in the duodenum [14], in the pancreatic duct [1] and, in particular, in the gallbladder [7, 11, 17]. We recently reported a clinico-pathological analysis of 90 cases of pyloric gland adenoma [24].

The present study documents the first case of pyloric gland adenoma arising in BE. The cellular differentiation and molecular cytogenetic changes in this peculiar tumor are evaluated by means of mucin immunohistochemistry and comparative genomic hybridization (CGH).

Clinical summary

A 62-year-old Caucasian man had been followed up because of long-segment BE. In 2002, an upper gastrointes-

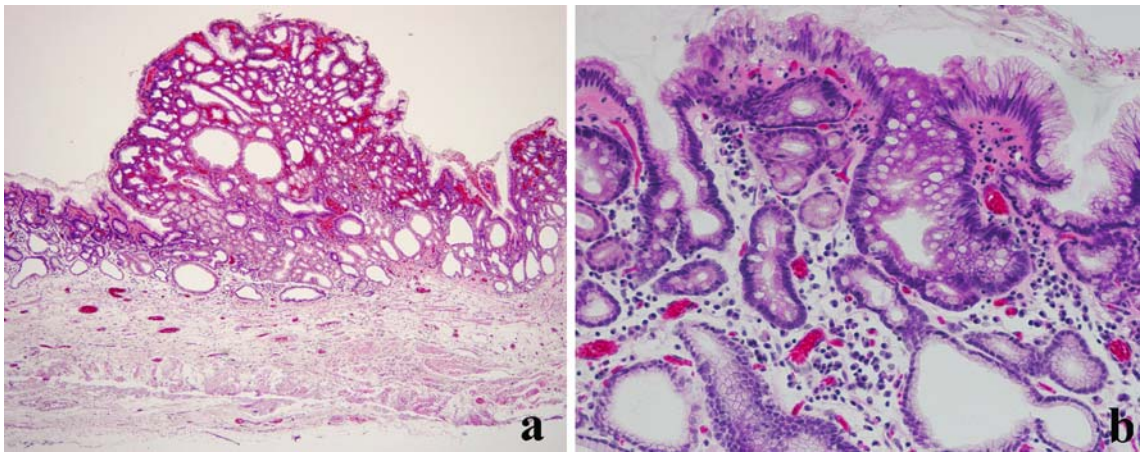

Fig. 1 a "Pyloric gland adenoma" surrounded by specialized columnar epithelium (SCE). Two-layered muscularis mucosae are seen. **b** Higher magnification of the SCE

tinal endoscopy disclosed a small nodular and polypoid lesion in BE, 25 cm distant from the incisors. Because of the suspicion that the tumor might be an early BE adenocarcinoma, the patient underwent an endoscopic resection of the questionable lesion. The lesion was completely removed with clear vertical and lateral margins. The patient is well after 3 years follow-up and developed no further neoplasia within his Barrett's segment.

Materials and methods

The tumor measured 3×2 mm with surrounding esophageal mucosa, was fixed in 10% formalin, sliced into two sections and embedded in paraffin. Paraffin blocks were available for routine histology and immunohistochemical studies. Immunohistochemical staining was carried out with the following monoclonal antibodies (mAbs): (1) MUC2 (Ccp58, 1:100; Novocastra, UK); (2) MUC5AC (CLH2, 1:100; Novocastra, UK); (3) MUC6 (CLH5, 1:100; Novocastra, UK) and (4) CD10 (56C6, 1:50; Novocastra, UK). A series of MUC2, MUC5AC, MUC6 and CD10 stains has been reported to be very useful in detecting the phenotypic expression of epithelial lesions of the gastrointestinal tract [16, 21]. MUC5AC, MUC6 and MUC2 specifically express, in gastric surface, mucous cells, pyloric gland cells and intestinal goblet cells of the mature gastrointestinal tract, respectively. MAb CD10 was used to detect the brush border of small intestinal absorptive cells and mAb MIB-1 to estimate the cell proliferation. The streptavidin-biotin method of detection was used. Peroxidase binding sites were visualized using the diaminobenzidine method, and the sections were lightly counterstained with hematoxylin.

We carried out microdissection of tumor cells from one 5-μm tissue section as described previously elsewhere [19]. Subsequently, these microdissected tissues were incubated in the proteinase K digestion. From the sample DNAs, whole genome was amplified using the method of degenerate oligonucleotide-primed polymerase chain reaction (DOP-PCR) [9]. We used 1 μl of DOP-PCR product as tumor DNA and gender-matched reference DNA and labeled with Cy 3-dCTP and Cy 5-dCTP (Perkin Elmer,

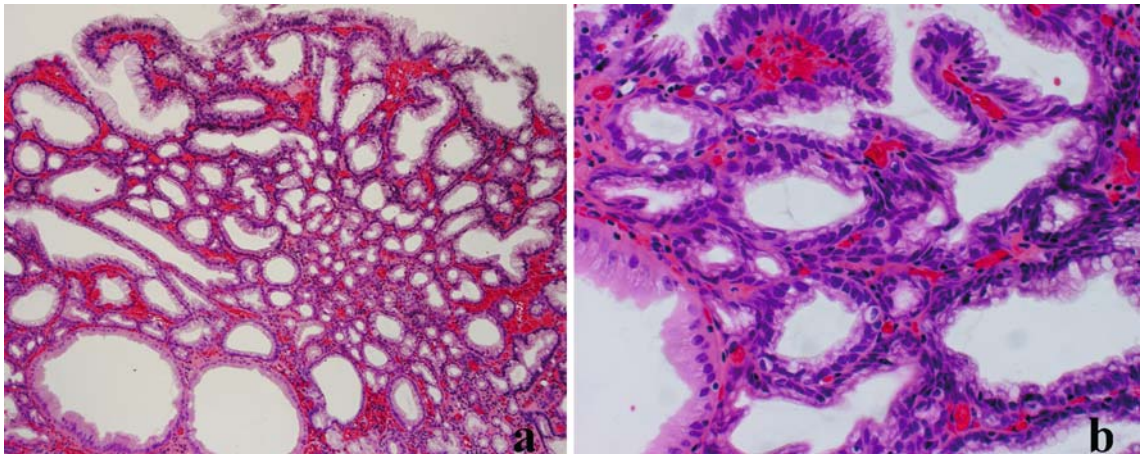

Fig. 2 Histological demonstration of the tumor. **a** The tumor consists of narrow to dilated tubules. They are lined by cuboidal to prismatic columnar epithelial cells that contain clear or pale eosinophilic cytoplasm. Superficial tumor cells were slightly higher in size than deeper ones. **b** Higher magnification of **a**. The tumor cell nuclei are small and oval or round in shape and contain small but conspicuous nucleoli

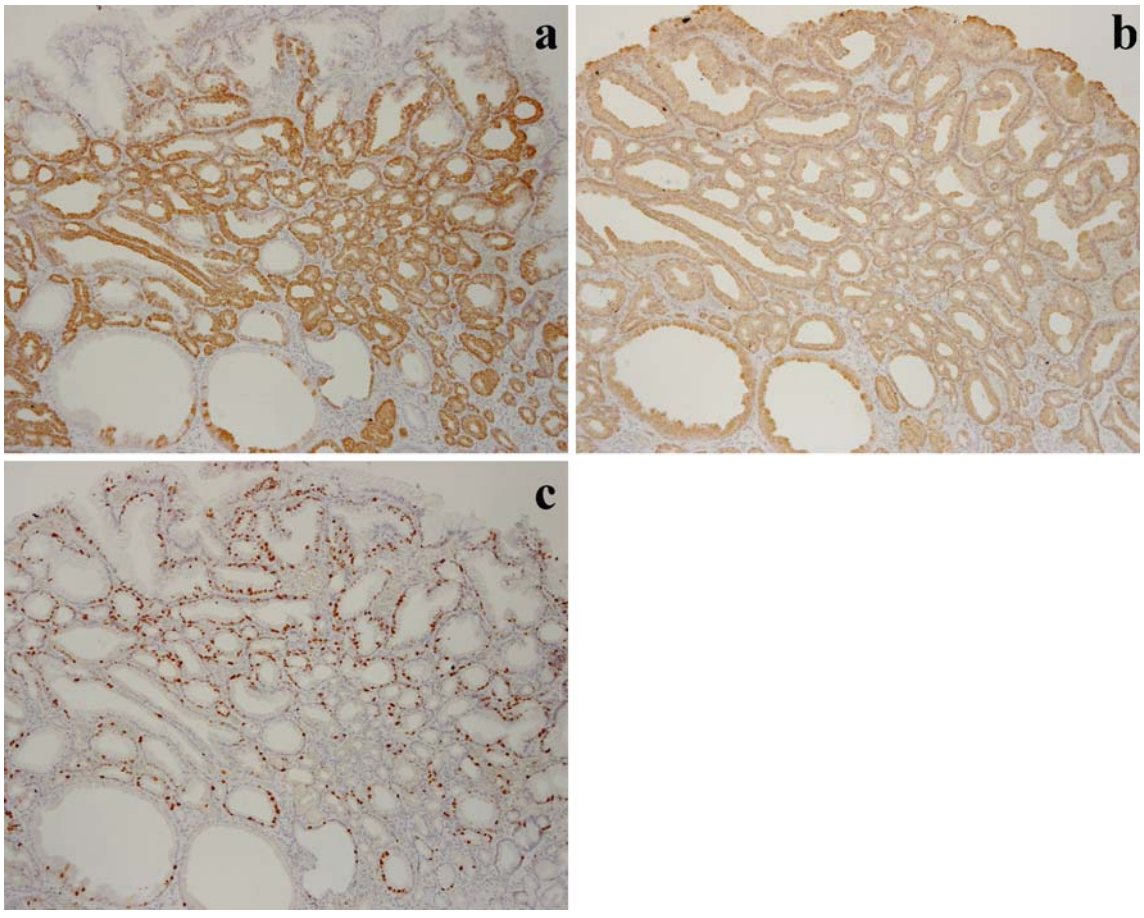

Fig. 3 Immunohistochemical demonstration of the tumor (serial sections of Fig. 2). **a** Most tumor glands are strongly positive for MUC6, except in the superficial layer. **b** MUC5AC is positive in almost all tumor cells. **c** MIB-1-positive proliferating cells are distributed throughout the tumor

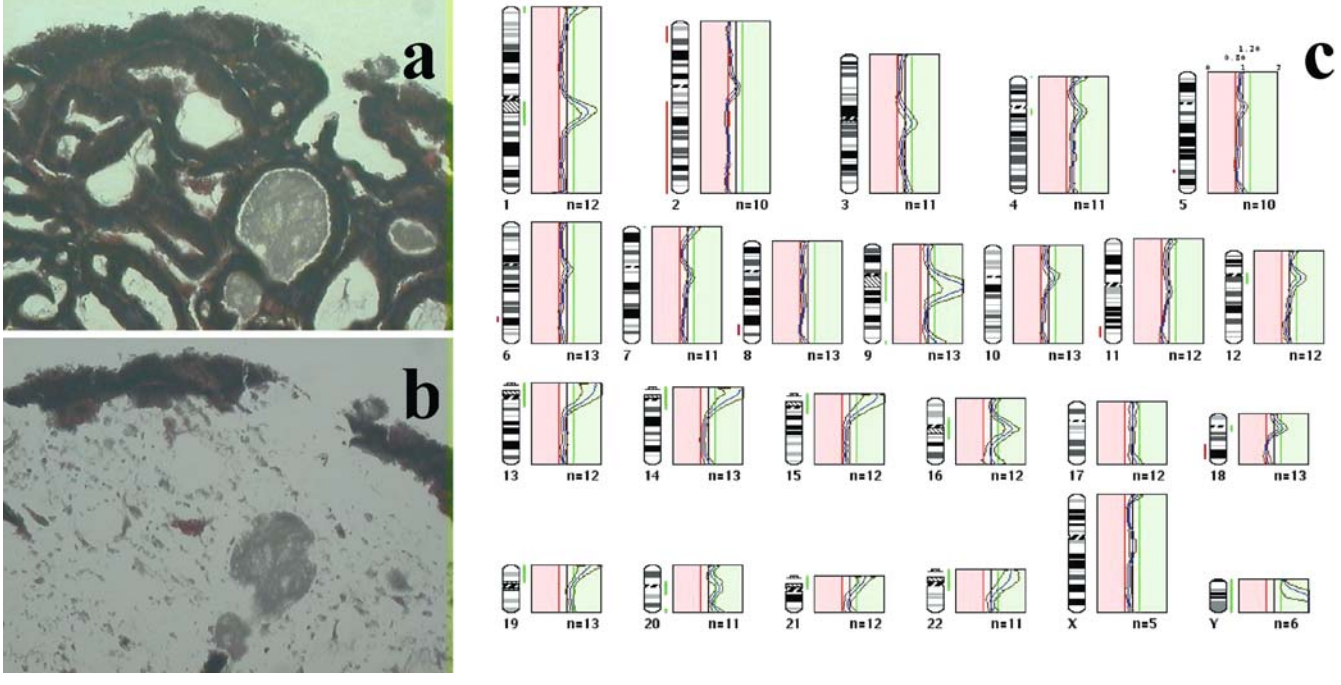

Fig. 4 Microdissection and comparative genomic hybridization (CGH) analyses of the tumor. **a** Pre-microdissection. **b** Post-microdissection. **c** CGH analysis shows losses on 2p24–25.2, 2q14.1-ter, 5q31.3–32, 6q23–24, 8q23–24.2, 11q22.3–24 and 18q21.1–22

USA), respectively, using random priming reaction. Gains and losses in DNA copy number were defined by green to red ratios (G/R) greater than 1.2 and less than 0.8, respectively. High-level gains (amplifications) were defined by a G/R greater than 1.5. Chromosomes 1p32-pter, 16p, 19, 22 and Y were excluded in the analyses [8].

Results

Pathological findings

A polypoid tumor, 2 mm in the longest diameter, was found to be surrounded by so-called specialized columnar epithelium (SCE), and two-layered muscularis mucosae was observed (Fig. 1). The tumor consisted of narrow or cystically dilated tubules. They were lined by cuboidal to prismatic columnar epithelial cells that contained clear cytoplasm or pale eosinophilic cytoplasm. Superficial tumor cells were slightly higher in size than deeper ones (Fig. 2a). The tumor cell nuclei were small and oval or round in shape and contained small but conspicuous nucleoli (Fig. 2b). These findings were identical to those described for pyloric gland adenoma of the stomach [24, 26] and some other digestive organs [10, 11, 14, 17].

Most tumor glands were strongly positive for MUC6, except in the superficial layer (Fig. 3a). MUC5AC was positive in almost all tumor cells (Fig. 3b), but MUC2 and CD10 were negative in the tumor. MIB-1-positive proliferating cells were distributed throughout the tumor (Fig. 3c). In the area of SCE surrounding the tumor, MUC5AC- and MUC6-positive cells tended to be located in the upper and lower portions of the glands, respectively. In the upper glands of SCE, there were scattered MUC2-positve goblet cells, most of which also expressed MUC5AC. CD10 positivity was focally found in the SCE area. Microdissection and CGH analyses revealed losses on 2p24–25.2, 2q14.1-ter, 5q31.3–32, 6q23–24, 8q23–24.2, 11q22.3–24 and 18q21.1–22 (Fig. 4).

Discussion

In our most recent clinico-pathological analysis of 90 cases of the pyloric gland adenoma, 15 cases (13%) were extragastric, but no esophageal case was encountered. Immediately after our publication, Michal et al. [15] described a case of pyloric gland adenoma underneath the normal squamous epithelium of the esophagus without BE. SCE of BE is identical to subtype of incomplete-type intestinal metaplasia of the stomach. Both metaplastic changes have widely been believed to be precancerous conditions, from which neoplasia of the gastric, gastrointestinal or intestinal phenotype may occur. Mucin histochemical analysis using mAbs against MUC2, MUC5AC and MUC6 recently revealed the mixed differentiation to intestinal and gastric phenotypes in SCE of BE and incomplete-type intestinal metaplasia of the stomach. Glickman demonstrated a higher frequency of MUC6 expression in SCE than in intestinal metaplasia of the stomach [4]. Therefore, it is very likely that the present tumor may have developed under induction of differentiation to pyloric gland-type cells in SCE of BE.

In the normal gastric mucosa or gastric metaplasia of extragastric mucosa, bi-directional differentiation of MUC5AC (apical part of the mucosa) and MUC6 (lower part of the mucosa) is displayed [12, 13]. However, the present tumor cells express both MUC6 and MUC5AC, except in the superficial layer, and MIB-1-positive cells were not localized as in intestinal-type adenomas [21]. Chromosomal aberrations found in the present tumor were partly common to those of Barrett's dysplasias, adenocarcinomas and gastric cardia adenocarcinomas [22, 23, 25]. These immunohistochemical and cytogenetic findings demonstrate that the tumor is immature, unstable and precancerous in nature. We recently demonstrated relatively high incidence of malignant transformation in pyloric gland adenomas [24]. Takei et al. [17] also showed a close association between pyloric gland adenomas and adenocarcinomas in the gallbladder. Pyloric gland adenoma of the gastric mucosa was first described by Elster [3] in 1976 but misinterpreted as adenoma-like hyperplasia of mucoid glands. In our experience, pyloric gland adenomas have been regarded as hyperplasia or hamartoma, and this entity has not been accepted, particularly in the Anglo-American literature, in the past. Endoscopists and pathologists must avoid misinterpretation and should be on the lookout for this type of tumor during routine examination.

In summary, we have presented the first case of pyloric gland adenoma arising in BE, showing its unstable and precancerous nature by mucin histochemical and cytogenetic methods.

References

1. Bakotic BW, Robinson MJ, Sturm PD, Hruban RH, Offerhaus GJ, Albores-Saavedra J (1999) Pyloric gland adenoma of the main pancreatic duct. Am J Surg Pathol 23:227–231
2. Borchard F, Ghanei A, Koldovsky U, Hengels KJ, Bückmann FW (1990) Gastrale Differenzierung in Adenomen der Magenschleimhaut. Immunohistochemische und elektronenmikroskopische Untersuchungen. Verh Dtsch Ges Pathol 74:528
3. Elster K (1976) Histologic classification of gastric polyps. In: Morson BC (ed) Pathology of the gastro-intestinal tract. Springer, Berlin Heidelberg New York, pp 78–92
4. Glickman JN, Shahsafaei A, Odze RD (2003) Mucin core peptide expression can help differentiate Barrett's esophagus from intestinal metaplasia of the stomach. Am J Surg Pathol 27:1357–1365
5. Haggitt RC, Tryzelaar J, Ellis FH, Colcher H (1978) Adenocarcinoma complicating columnar epithelium-lined (Barrett's) esophagus. Am J Clin Pathol 70:1–5
6. Hameeteman W, Tytgat GN, Houthoff HJ, van den Tweel JG (1989) Barrett's esophagus: development of dysplasia and adenocarcinoma. Gastroenterology 96:1249–1256
7. Itoi T, Takei K, Shinohara Y, Takeda K, Nakamura K, Horibe T, Sanada A, Ohno H, Matsubayashi H, Saito T, Watanabe H (1999) K-ras codon 12 and p53 mutations in biopsy specimens and bile from biliary tract cancers. Pathol Int 49:30–37

8. Kallioniemi OP, Kallioniemi A, Piper J, Isola J, Waldman FM, Gray JW, Pinkel D (1994) Optimizing comparative genomic hybridization for analysis of DNA sequence copy number changes in solid tumors. Genes Chromosomes Cancer 10:231–243
9. Kamitani S, Sugihara H, Shiomi H, Tani T, Hattori T (2000) Intratumoral regional variations in copy number of the chromosomal part revealed by microdissection and combined ploidy and comparative genomic hybridization analyses in esophageal squamous cell carcinoma. Cancer Genet Cytogenet 132:30–35
10. Kato N, Akiyama S, Motoyama T (2002) Pyloric gland-type tubular adenoma superimposed on intraductal papillary mucinous tumor of the pancreas. Pyloric gland adenoma of the pancreas. Virchows Arch 440:205–208
11. Kushima R, Remmele W, Stolte M, Borchard F (1996) Pyloric gland type adenoma of the gallbladder with squamoid spindle cell metaplasia. Pathol Res Pract 192:963–969
12. Kushima R, Borchard F, Hattori T (1997) A new aspect of gastric metaplasia in Crohn's disease: bidirectional (foveolar and pyloric) differentiation in so-called "pyloric metaplasia" in the ileum. Pathol Int 47:416–419
13. Kushima R, Manabe R, Hattori T, Borchard F (1999) Histogenesis of gastric foveolar metaplasia following duodenal ulcer: a definite reparative lineage of Brunner's gland. Histopathology 35:38–43
14. Kushima R, Rüthlein HJ, Stolte M, Bamba M, Hattori T, Borchard F (1999) "Pyloric gland-type adenoma" arising in heterotopic gastric mucosa of the duodenum, with dysplastic progression of the gastric type. Virchows Arch 435:452–457
15. Michal M, Curik R, Matler K, Benes Z (2003) Regarding the paper by Vieth et al. Virchows Archiv 442/4:317–321. Virchows Arch 443:589–590
16. Shiroshita H, Watanabe H, Ajioka Y, Watanabe G, Nishikura K, Kitano S (2004) Re-evaluation of mucin phenotypes of gastric minute well-differentiated-type adenocarcinomas using a series of HGM, MUC5AC, MUC6, M-GGMC, MUC2 and CD10 stains. Pathol Int 54:311–321
17. Takei K, Watanabe H, Itoi T, Saito T (1996) p53 and Ki-67 immunoreactivity and nuclear morphometry of "carcinoma-in-adenoma" and adenoma of the gall-bladder. Pathol Int 46:908–917
18. Thurberg BL, Duray PH, Odze RD (1999) Polypoid dysplasia in Barrett's esophagus: a clinicopathologic, immunohistochemical, and molecular study of five cases. Hum Pathol 30:745–752
19. Tokugawa T, Sugihara H, Tani T, Hattori T (2002) Modes of silencing of p16 in development of esophageal squamous cell carcinoma. Cancer Res 62:4938–4944
20. Torres C, Antonioli D, Odze RD (1998) Polypoid dysplasia and adenomas in inflammatory bowel disease: a clinical, pathologic, and follow-up study of 89 polyps from 59 patients. Am J Surg Pathol 22:275–284
21. Tsukashita S, Kushima R, Bamba M, Sugihara H, Hattori T (2001) MUC gene expression and histogenesis of adenocarcinoma of the stomach. Int J Cancer 94:166–170
22. van Dekken H, Alers JC, Riegman PH, Rosenberg C, Tilanus HW, Vissers K (2001) Molecular cytogenetic evaluation of gastric cardia adenocarcinoma and precursor lesions. Am J Pathol 158:1961–1967
23. Varis A, Puolakkainen P, Savolainen H, Kokkola A, Salo J, Nieminen O, Nordling S, Knuutila S (2001) DNA copy number profiling in esophageal Barrett adenocarcinoma: comparison with gastric adenocarcinoma and esophageal squamous cell carcinoma. Cancer Genet Cytogenet 127:53–58
24. Vieth M, Kushima R, Borchard F, Stolte M (2003) Pyloric gland adenoma: a clinico-pathological analysis of 90 cases. Virchows Arch 442:317–321
25. Walch AK, Zitzelsberger HF, Bruch J, Keller G, Angermeier D, Aubele MM, Mueller J, Stein H, Braselmann H, Siewert JR, Hofler H, Werner M (2000) Chromosomal imbalances in Barrett's adenocarcinoma and the metaplasia-dysplasia-carcinoma sequence. Am J Pathol 156:555–566
26. Watanabe H, Jass JR, Sobin LH (1990) Histological typing of oesophageal and gastric tumours. Springer, Berlin Heidelberg New York

Virchows Arch (2005) 446: 542–545
DOI 10.1007/s00428-005-1242-2

CASE REPORT

M. Vieth · R. Kushima · J. P. A. de Jonge ·
F. Borchard · F. Oellig · M. Stolte

Adenoma with gastric differentiation (so-called pyloric gland adenoma) in a heterotopic gastric corpus mucosa in the rectum

Received: 8 January 2005 / Accepted: 26 February 2005 / Published online: 19 April 2005
© Springer-Verlag 2005

Abstract In a 46-year-old man, a pedunculated rectal polyp measuring 3.0×3.0×2.0 cm was diagnosed histologically as a pyloric gland-type adenoma arising in heterotopic gastric corpus mucosa. The luminal site was covered by glands of the gastric foveolar type, displaying focal marked proliferation interpreted as low-grade intraepithelial neoplasia. A bidirectional gastric differentiation was found: most lower glandular structures showed positivity for the deep gastric mucin core protein Muc 6 and superficial positivity for gastric foveolar epithelium mucin core protein Muc 5AC. Pyloric gland adenoma has so far been described in one larger series only and a few case reports of the stomach, gallbladder, pancreatic duct and within heterotopic gastric corpus mucosa of the duodenal bulb. The present case report is the first case of a pyloric gland-type adenoma within a gastric corpus heterotopia of the rectal mucosa.

Keywords Pyloric-gland adenoma · Rectum polyp · Heterotopic gastric mucosa

M. Vieth (✉) · F. Oellig · M. Stolte
Institute of Pathology, Klinikum Bayreuth,
Preuschwitzer Straße 101,
95445 Bayreuth, Germany
e-mail: vieth.lkpathol@uni-bayreuth.de
Tel.: +49-921-4005602
Fax: +49-921-4005609

R. Kushima
Department of Clinical Science and Laboratory Medicine,
Division of Diagnostic Pathology,
Shiga University of Medical Science,
Ohtsu, Shiga, 520-2192, Japan

J. P. A. de Jonge
Institute of Pathology,
Nordhorn,
Hagenstraße 14,
48529 Nordhorn, Germany

F. Borchard
Institute of Pathology, Klinikum Aschaffenburg,
63703 Aschaffenburg, Germany

Introduction

Colorectal tumours are for the most part benign adenomas [9, 19]. Rarely does the histological work-up of a colorectal polypectomy specimen reveal heterotopic gastric mucosa. Tumours arising in such heterotopias should, however, always reveal a differentiation of the "tissue of origin". To date, the international literature contains reports on only 40 gastric heterotopias in rectal mucosa [2, 7, 14, 18, 22, 23, 28].

The majority of polyps of the stomach are non-neoplastic tumor-like lesions [24]. Only about 10% of all gastric polyps are adenomas [25].

Among the various types of gastric adenoma is an adenoma with gastric differentiation-a so-called pyloric gland adenoma (PGA), which is a rare variant [5, 25, 27] (approximately 2.7% of all gastric polyps [26]).

The present case is the first report of an adenoma with gastric differentiation (PGA) arising within heterotopic gastric mucosa within the rectum.

Case history

In a 46-year-old man undergoing screening colonoscopy, a rectal polyp was found incidentally. This was removed by snare biopsy and fixed in 4% formalin. Gross inspection of the pedunculated polyp measuring 3.0×3.0×2.0 cm, revealed a smooth surface and a spongiform cut surface showing multiple tiny cysts (see Fig. 1).

Histological findings

The polyp was worked up in its entirety in parallel slices. At the cut edge of the polyp, in addition to normal rectal mucosa, a transition to heterotopic gastric corpus mucosa was found (Fig. 2a). In the center the polyp was found histologically to comprise superficial gastric differentiated cells similar to foveolar epithelium. Here, proliferation of tall columnar cells arranged in two to three rows was found, together with somewhat enlarged nuclei and tiny apical

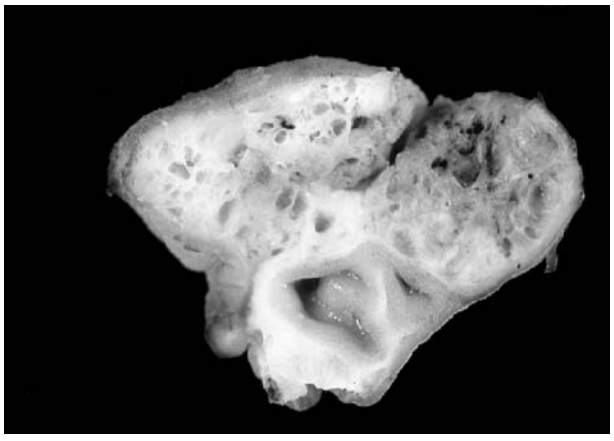

Fig. 1 Gross appearance of pyloric gland adenoma of the rectum within a gastric corpus heterotopia. On the cut surface with numerous small cystic dilatations within the deeper parts of the polyp

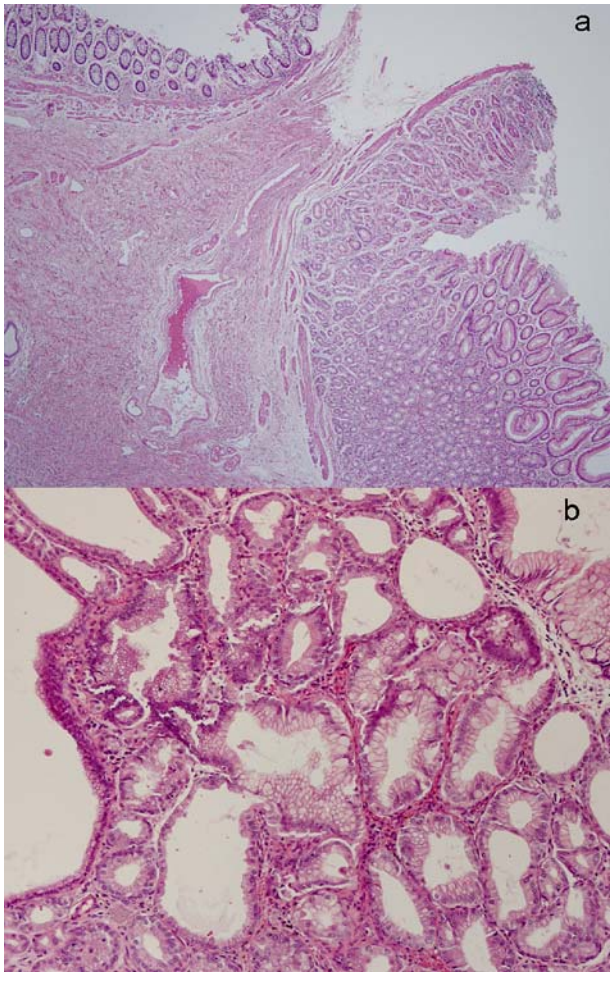

Fig. 2 **a** Cut edge of the pyloric gland adenoma with pre-existing parts of the corpus mucosal heterotopia and adjacent rectal mucosa (HE ×100); **b** Histological section of pyloric gland adenoma with superficial gastric-like foveolar cells. Deep glandular formations are lined by a single layer of cubic to columnar cells with clear cytoplasm and nuclei located at the base. (HE 200×)

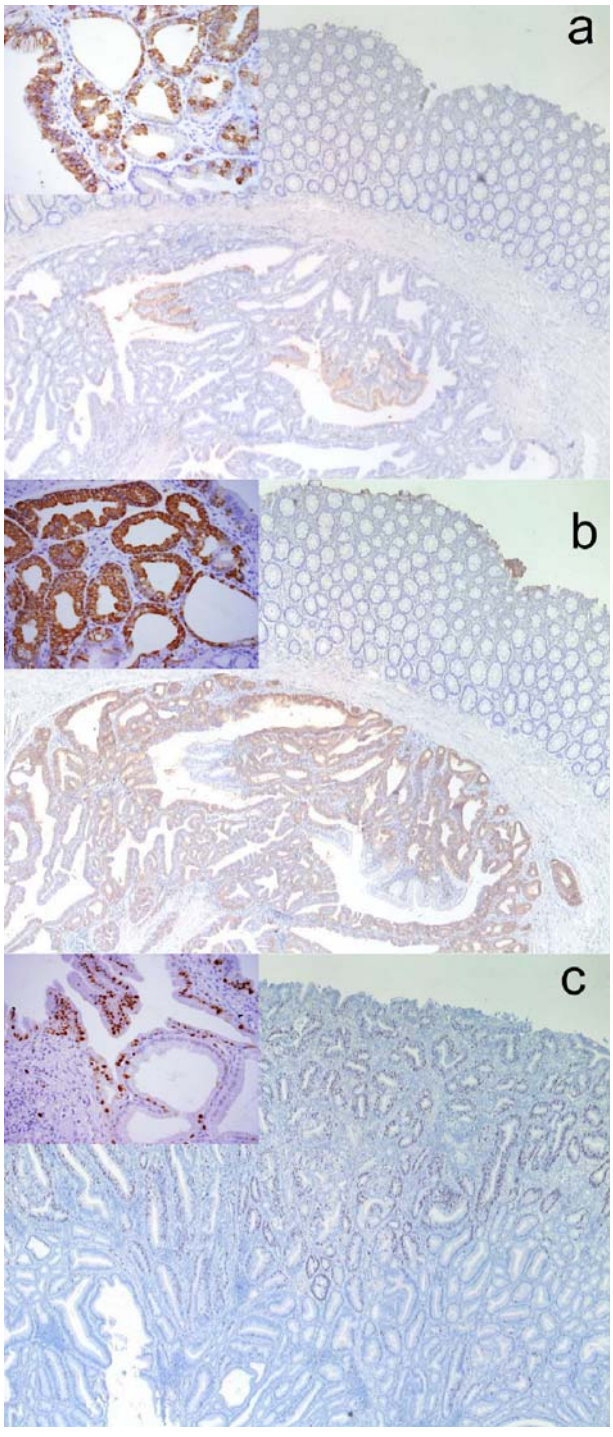

Fig. 3 **a** Immunhistochemistry of pyloric gland adenoma with mAb against foveolar mucin core protein apomucin 5AC, staining apical fovelar gastric glands, inset: ×400; **b** Incubation with mAB against deep gastric mucin apomucin 6 staining deep gastric glands (×100), inset: ×400; **c** Immunhistochemistry against Ki67 showing marked proliferation in circumscribed apical parts of the pyloric gland adenoma thus leading to the diagnosis of low-grade intraepithelial neoplasia (×200), inset: ×400

drops of mucin. In deeper sections there was a predominance of small tubular formations lying close together. These glandular formations were lined by a single layer of

cubic to columnar cells with a clear cytoplasm and nuclei located at the base (see Fig. 2b). The polypous tubular glands located up to the luminal side prompted the diagnosis of pyloric gland adenoma (PGA) within a gastric corpus mucosal heterotopia of the rectum.

In the adenoma portions of the polyp, typical zonal differentiation of PGA was detectable with deep pyloric like glands in the depth of the adenoma and only a small superficial layer of apical gastric foveolar epithelium. Also present in deeper sections were dilated, in part cystic, glandular tubules extending deep into the adjacent submucosa (see Fig. 3a, b). Neoplastic glands of the adenoma were found deep within the submucosa, of which some were cystically dilated. The apical portions revealed a positivity for the core protein of foveolar mucin Muc 5 AC [6] (CLH2; Novocastra Laboratories Ltd, Newcastle upon Tyne, UK) (see Fig. 3a). The basal portions of the PGA reacted positively for the core protein of deep gastric mucin Muc 6 (CLH5; Novocastra Laboratories) (see Fig. 3b). Incubation with the proliferation marker Ki67 (AB MIB 1; Dianova, Hamburg, Germany) revealed focally marked proliferation of cells in the superficial portions of the adenoma (Fig. 3c). The nuclei of the PGA cells were not polymorphic nor hyperchromatic. Despite the higher proliferation activity of focal apical parts of the adenoma, step sections revealed no pathological mitoses or transition to high-grade intraepithelial neoplasia or a carcinoma. Presumably, the displacement of neoplastic tubules into the submucosal layer might be a sequela of recurrent local lesions with pseudoinvasion of the glands of the pyloric gland adenoma. Since the lesion had been removed with a margin of clearance, only follow-up endoscopy was carried out. The patient has been free of tumor for 3 years.

Discussion

To our knowledge, a PGA arising within a heterotopic gastric corpus mucosa of the rectum has never before been described.

Heterotopic gastric mucosa in the colon or rectum has been described as a rarity in several reports, and may present as small sessile polyps [28]. As a result of repeated mechanical or peptic lesions, heterotopic gastric glands can, as in our case, be "displaced" into the submucosa in a pseudoinvasive mannor in analogy to similar changes in the stomach [13]. In any event, the clinical history of our patient is unremarkable concering prior rectal injury (e.g. rectal prolapse syndrome [18]).

The finding of parts of a pyloric gland adenoma within the submucosal layer of rectum within a heterotopic corpus mucosa includes the differential diagnosis of well differentiated adenocarcinoma but no mitoses, cytological abnormalities nor immunhistochemical evidence for abnormal proliferation within these displaced tubules were found. In conclusion, these tubules are therefore much more likely to represent pseudoinvasion than a well differentiated adenocarcinoma.

Epithelial differentiation in the gastrointestinal tract is triggered by homeobox gene activation and/or deactivation and the relation of activity between responsible genes [21]. This can be due to inflammatory reactions. Theoretically, it might be possible that gastric differentiation (including gastric "heterotopia") in the lower GI tract might be due to deregulation/reactivation of these genes [4]. This means that gastric heterotopia(-like) lesions can occur due to prior inflammatory reactions, too and must not merely be a result of epithelial displacement within the foetal period (e.g hypothesis of gut regenerative cell lineage by Mukaisho et al. [11]).

Gastric PGA was first described but misinterpreted by Elster [8]. To our knowledge, PGA was first described in the stomach simultaneously by Borchard et al. (1990) [5] and Watanabe et al. (1990) [27] and independently identified as an adenoma. Further case reports showed PGA in gastric metaplasia of the gallbladder mucosa [15, 17], pancreatic duct [1, 3, 12], and within a corpus mucosa heterotopia of the duodenal bulb [16], indicating that PGA can arise not only in gastric metaplasia but also in heterotopic gastric mucosa.

The rectal polyp described here confirms that such PGAs can arise in heterotopic gastric mucosa elsewhere in the gastrointestinal tract.

Since 1988, we have found 163 cases of pyloric gland adenoma among our gastric polyps. The follow-up study of our cases revealed that a relatively high percentage of these adenomas might progress to gastric [10] differentiated carcinomas [20]. Therefore, special care should be taken if a pyloric gland adenoma is identified [26].

Acknowledgement MV is supported by a grant of the Japanese Society of Pathology at Shiga University of Medical Science.

References

1. Amaris J (2002) Intraductal mucinous papillary tumor and pyloric gland adenoma of the pancreas. Gastrointest Endosc 56:441–444
2. Antonietta Pistoia M, Guadagni S, Ventura T, Pistoia F, Carboni M (1986) Gastric heterotopia of the rectum. Endoscopy 18:34
3. Bakotic BW, Robinson MJ, Sturm PD, Hruban RH, Offerhaus GJ, Albores–Saavedra J (1999) Pyloric gland adenoma of the main pancreatic duct. Am J Surg Pathol 23:227–231
4. Beck F, Chawengsaksophak K, Waring P, Playford RJ, Furness JB (1999) Reprogramming of intestinal differentiation and intercalary regeneration in Cdx2 mutant mice. Proc Natl Acad Sci U S A 96:7318–7323
5. Borchard F, Ghanei A, Koldovsky U, Hengels KJ, Bückmann FW (1990) Gastrale Differenzierung in Adenomen der Magenschleimhaut. Immunhistochemische und elektronenmikroskopische Untersuchungen. Verh Dtsch Ges Pathol 74:523
6. Borchard F, Bodensieck U, Koldovsky U (1993) Entwicklung des monoklonalen Antikörpers R3C4 gegen das foveoläre Muzin M1. Verh Dtsch Ges Pathol 74:523
7. Devereaux CE, Devereaux RG (1994) Heterotopic gastric mucosa of the rectum with a review of the literature. J Clin Gastroenterol 19:41–45
8. Elster K (1976) In: Morson BC (ed) Current topics in pathology 63. Springer, Berlin Heidelberg New York, p 86

9. Fenoglio–Preisser CM (1999) Gastrointestinal pathology. Lippincott–Raven, Philadelphia
10. Hanisch FG, Koldovsky U, Borchard F (1993) Monoclonal antibody 2B5 defines a truncated O-glycan, GlcNAc beta 1–3Gal beta 1–4GlcNAc beta 1–6 (GalNAc), on mucins from deep gastric and duodenal glands as well as metaplasia and neoplasia of gastric differentiation. Cancer Res 53:4791–4796
11. Mukaisho K, Miwa K, Kumagai H, Bamba M, Sugihara H, Hattori T (2003) Gastric carcinogenesis by duodenal reflux through gut regenerative cell lineage. Dig Dis Sci 48:2153–2158
12. Kato N, Akiyama S, Motoyama T (2002) Pyloric gland-type tubular adenoma superimposed on intraductal papillary mucinous tumor of the pancreas. Pyloric gland adenoma of the pancreas. Virchows Arch 440:205–208
13. Kato Y, Sugano H, Rubio CA (1983) Classification of intramucosal cysts of the stomach. Histopathology 7:931–938
14. Kestemberg A, Marino G, de Lima E, Garcia FT, Carrascal E, Arredondo JL (1993) Gastric heterotopic mucosa in the rectum with Helicobacter pylori-like organisms: a rare cause of rectal bleeding. Int J Colorectal Dis 8:9–12
15. Kushima R, Remmele W, Stolte M, Borchard F (1996) Pyloric gland type adenoma of the gallbladder with squamoid spindle cell metaplasia. Pathol Res Pract 192:963–969
16. Kushima R, Ruthlein HJ, Stolte M, Bamba M, Hattori T, Borchard F (1999) "Pyloric gland-type adenoma" arising in heterotopic gastric mucosa of the duodenum, with dysplastic progression of the gastric type. Virchows Arch 435:452–457
17. Laitio M (1975) Goblet cells, enterochromaffin cells, superficial gastric-type epithelium and antral-type glands in the gallbladder. Beitr Pathol 156:343–358
18. Levine DS (1987) "Solitary" rectal ulcer syndrome. Are "solitary" rectal ulcer syndrome and "localized" colitis cystica profunda analogous syndromes caused by rectal prolapse? Gastroenterology 92:243–253
19. Lewin KJ, Riddell RH, Weinstein WM (1992) Gastrointestinal pathology and its clinical implications. Igaku–Shoin, New York
20. Lohe B, Ghanei A, Koldovsky U, Borchard F (1990) Gastrale Differenzierung in Neoplasien der Gallenblase–Untersuchungen mit dem monoklonalen Antikörper 2B5. Verh Dtsch Ges Pathol 74:529
21. Mizoshita T, Inada K, Tsukamoto T, Kodera Y, Yamamura Y, Hirai T, Kato T, Joh T, Itoh M, Tatematsu M (2001) Expression of Cdx1 and Cdx2 mRNAs and relevance of this expression to differentiation in human gastrointestinal mucosa-with special emphasis on participation in intestinal metaplasia of the human stomach. Gastric Cancer 4:185–191
22. Murray FE, Lombard M, Dervan P, Fitzgerald RJ, Crowe J (1988) Bleeding from multifocal heterotopic gastric mucosa in the colon controlled by an H_2 antagonist. Gut 29:848–851
23. Seitz G, Schuder G (1987) Heterotopic gastric mucosa of the rectum. Pathologe 8:52–55
24. Stolte M, Sticht T, Eidt S, Ebert D, Finkenzeller G (1994) Frequency, location, and age and sex distribution of various types of gastric polyp. Endoscopy 26:659–665
25. Stolte M (1995) Clinical consequences of the endoscopic diagnosis of gastric polyps. Endoscopy 27:32–37
26. Vieth M, Kushima R, Borchard F, Stolte M (2003) Pyloric gland adenoma: a clinico-pathological analysis of 90 cases. Virchows Arch 442:317–321
27. Watanabe H, Jass JR, Sobin LH (eds) (1990) Histological typing of oesophageal and gastric tumours. Springer, Berlin Heidelberg New York
28. Wolff M (1971) Heterotopic gastric epithelium in the rectum: a report of three new cases with a review of 87 cases of gastric heterotopia in the alimentary canal. Am J Clin Pathol 55:604–616

Virchows Arch (2005) 446: 546–554
DOI 10.1007/s00428-005-1209-3

CASE REPORT

Ömer Uluoğlu · Nalan Akyürek · Aytuğ Üner ·
Uğur Coşkun · Ayşegul Özdemir · Nahide Gökçora

Interdigitating dendritic cell tumor with breast and cervical lymph-node involvement: a case report and review of the literature

Received: 12 November 2004 / Accepted: 30 December 2004 / Published online: 2 April 2005
© Springer-Verlag 2005

Abstract Interdigitating dendritic cell tumor (IDCT) is an extremely rare malignancy. It occurs primarily in lymph nodes, but extranodal involvement has also been reported. A 38-year-old woman with IDCT with breast and cervical lymph-node involvement is reported in this paper. To our knowledge, this is the first case of IDCT originating from the breast. In the breast and lymph node, the tumor displayed diffuse sheets, fascicles and storiform growth pattern. It was composed of oval to spindle cells with pale to eosinophilic cytoplasm, ill-defined cell outlines, oval nuclei with vesicular chromatin and prominent eosinophilic nucleoli. Mitotic activity was three per ten high-power fields. The neoplastic cells were intermingled with small mature lymphocytes and plasma cells. Immunohistochemical studies showed that the tumor cells were strongly and diffusely positive for vimentin, CD68, S-100 protein, CD45/leukocyte common antigen and fascin and focally positive for lysozyme, alpha-1 antitrypsin and CD4. Ki-67 labeling index was 10%. The patient was treated with combined therapeutic approaches, including surgery, radiotherapy and chemotherapy. IDCT has the potential for an aggressive clinical course. However, 32 months after the initial diagnosis, the patient is still alive and being followed with a stable tumor burden.

Keywords Interdigitating dendritic cell tumor · Breast · Prognosis · Immunohistochemistry

Ö. Uluoğlu · N. Akyürek
Department of Pathology,
Gazi University Medical School,
Ankara, Turkey

A. Üner · U. Coşkun
Department of Medical Oncology,
Gazi University Medical School,
Ankara, Turkey

A. Özdemir
Department of Radiology,
Gazi University Medical School,
Ankara, Turkey

N. Gökçora
Department of Nuclear Medicine,
Gazi University Medical School,
Ankara, Turkey

N. Akyürek (✉)
S. Ozdemir Mah. Percem Sok. No: 44/20,
06460 Dikmen-Ankara, Turkey
e-mail: akyurek@gazi.edu.tr

Introduction

Dendritic cells are nonlymphoid, nonphagocytic elements grouped under the immune accessory cells. Their primary role is the capture and presentation of the antigens and immune complexes. They share a common CD34+ stem cell with monocyte–macrophages [9, 13, 36, 37]. Dendritic cells include the follicular dendritic cells, Langerhans cells, interstitial dendritic cells, veiled cells (indeterminate) and interdigitating dendritic cells. While the origin of follicular dendritic cells is still controversial, the other dendritic cell types are thought to derive from the bone marrow. Different dendritic cell types can be distinguished by a combination of morphological and immunophenotypic features. Follicular dendritic cells are CD21+, CD23+, CD35+, CD1a− and S-100 protein±, and they show desmosomes on ultrastructural examination. Langerhans cells and interstitial dendritic cells are CD1a+, S-100 protein+, CD4+, CD21−, CD35−, CD68−, and they show characteristic Birbeck granules ultrastructurally. Veiled cells (indeterminate) display phenotypes similar to Langerhans cells but have no Birbeck granules and complex interdigitating cellular junctions [25, 37].

Interdigitating dendritic cells (IDCs) are located in the thymus and in the T-cell areas of peripheral lymphoid organs, including the paracortex and deep cortex of lymph nodes, the splenic periarterial lymphoid sheets and interfollicular areas of mucosa-associated lymphoid tissue [1, 8, 10, 11]. They are thought to derive from bone marrow precursors of monocytic lineage, and they function as potent antigen-presenting cells to T lymphocytes for initiating cellular immunity [10, 37]. IDCs are CD68+, S-100 protein+,

CD1a−, CD21− and CD35− and reveal complex interdigitating cellular junctions [25].

Interdigitating dendritic cell tumor (IDCT) is an uncommon neoplasm that usually occurs within the lymph nodes but also occasionally arises in extranodal sites such as the nasopharynx [32], testis [20], spleen [17], salivary gland [3], small intestine and mesentery [5, 21], tonsil [11], bladder [26] and skin [15, 25]. Up to now, including our case, 51 cases have been reported in the literature. To our knowledge, this is the first case of IDCT involving the parenchyma of the breast. We report the clinicopathological and immunohistochemical features of an IDCT of the breast with cervical lymph-node involvement and a review of the literature on IDCT.

Clinical history

A 38-year-old woman was admitted to the hospital in November 2001 with a 2-year history of painless, slow-growing bilateral masses in the neck, measuring 5 cm and 4 cm in diameters in the right and left cervical regions, respectively. No systemic symptoms were referred, and peripheral blood counts were normal. Physical examination revealed a firm and painless 3×2-cm mass in the upper outer quadrant of the right breast. An excisional biopsy was taken from the right cervical lymph node, and the diagnosis of angioimmunoblastic T-cell lymphoma was established. A trucut biopsy of the lesion in the breast was performed, which revealed nonspecific mastitis. The computerized tomography (CT) of the chest, abdomen and pelvis showed no other organ and lymph-node involvement. The bone

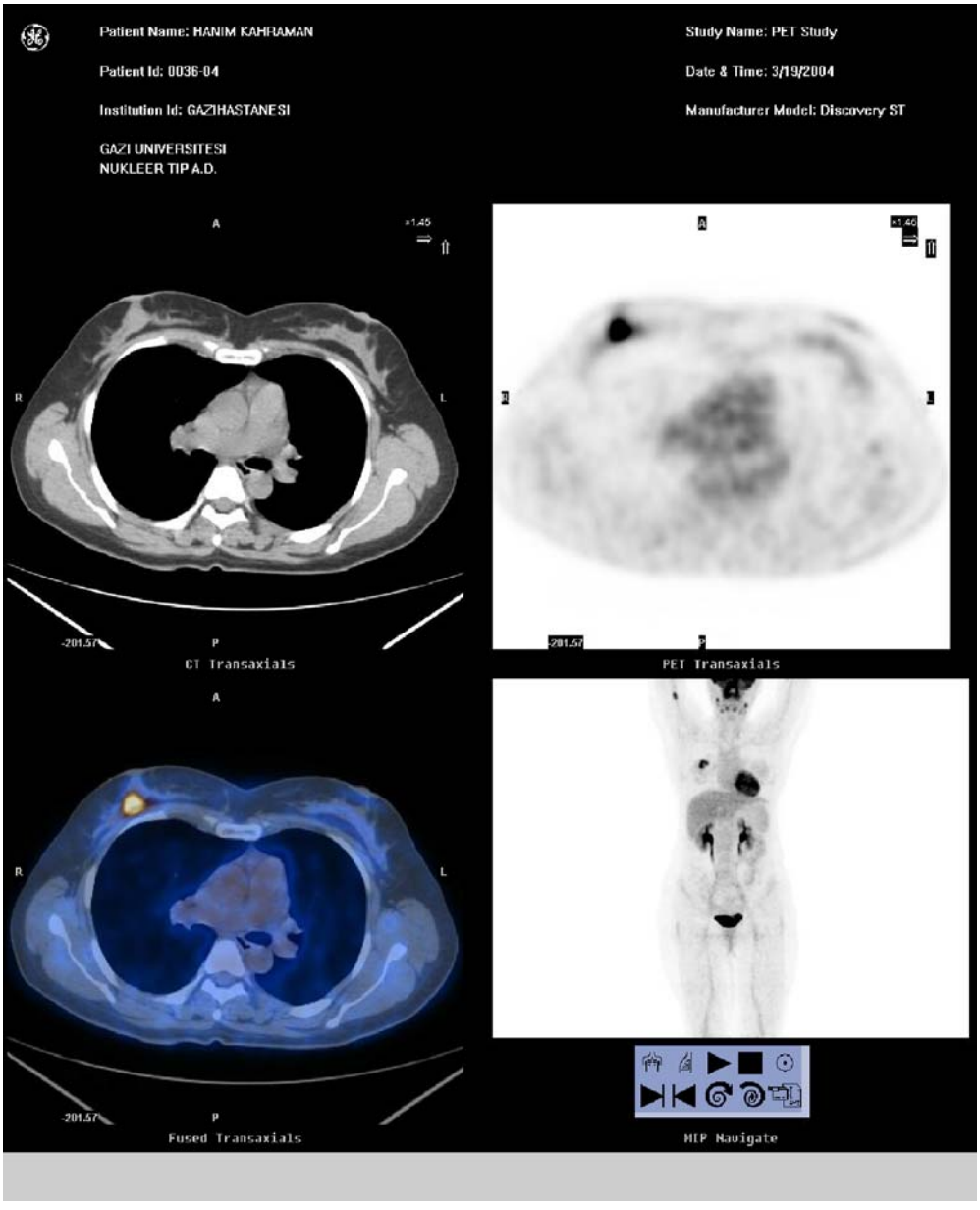

Fig. 1 Transaxial slices of positron emission tomography/computed tomography. There is increased accumulation of 18F-fluorodeoxyglucose in the right breast tissue [standard uptake value (SUV)=10.7]. The whole-body images also display the abnormal focal activity observed in the cervical lymph nodes (SUV=11.3)

marrow morphology and histology were normal. The patient was treated with 6 cycles of CHOP chemotherapy (cyclophosphamide, doxorubicin, vincristine and prednisone), and a partial response was obtained. Radiation therapy of 40 Gy to the involved field in the neck followed this treatment. After the treatment, the patient was periodically followed-up with physical examinations and CT scans of the head and neck, which revealed stability of the disease. No progression was observed in the clinical size of the breast lesion. The cervical lymph nodes were regressed to 1–2 cm in diameter.

Three years later, the patient had still no evidence of progression in her routine controls. In April 2004, breast ultrasonography revealed a solid mass of 26×11 mm size with multilobulated shape, central hyperechogenity and well-delineated margins. However, a control ultrasonography in June 2004 showed enlargement of the lesion, measured as 32×14 mm. At that time, positron emission tomography (PET) with [F-18] fluorodeoxyglucose was performed to evaluate the systemic involvement of the primary disease and its activity. PET scan revealed increased activities in bilateral cervical lymph nodes and the upper outer quadrant of the right breast (SUV=10.7) (Fig. 1). A few cervical lymph nodes in a maximum diameter of 1.4 cm were present.

The patient underwent lumpectomy for diagnostic purposes. In addition to the pathological examination of the breast lesion, the previous pathological specimens from the cervical lymph node were reevaluated. After the lumpectomy, the patient was free of disease and received no further therapy.

Materials and methods

Tissue specimens were fixed in formalin and embedded in paraffin, sectioned and stained with hematoxylin and eosin, Masson trichrome and reticulin silver. Immunohistochemical studies were performed on formalin-fixed tissue sections using the streptavidin–biotin–peroxidase method and employing a panel of antibodies including: cytokeratin (AE1+ AE3), vimentin, CD68, lysozyme, alpha-1 antitrypsin, S-100 protein, fascin, human leukocyte antigen (HLA)-DR, CD45 [leukocyte common antigen (LCA)], CD21, CD35, CD79a, CD15, CD30 (Ki-1), CD31, CD34, myeloperoxidase, epithelial membrane antigen (EMA), desmin, smooth-muscle actin, p53 (DO7), Ki-67 (MIB-1), HMB-45 (prediluted, NeoMarkers), CD4, CD8, CD3, CD20 (L26), CD23 and CD1a (prediluted, Novocastra). Appropriate pre-

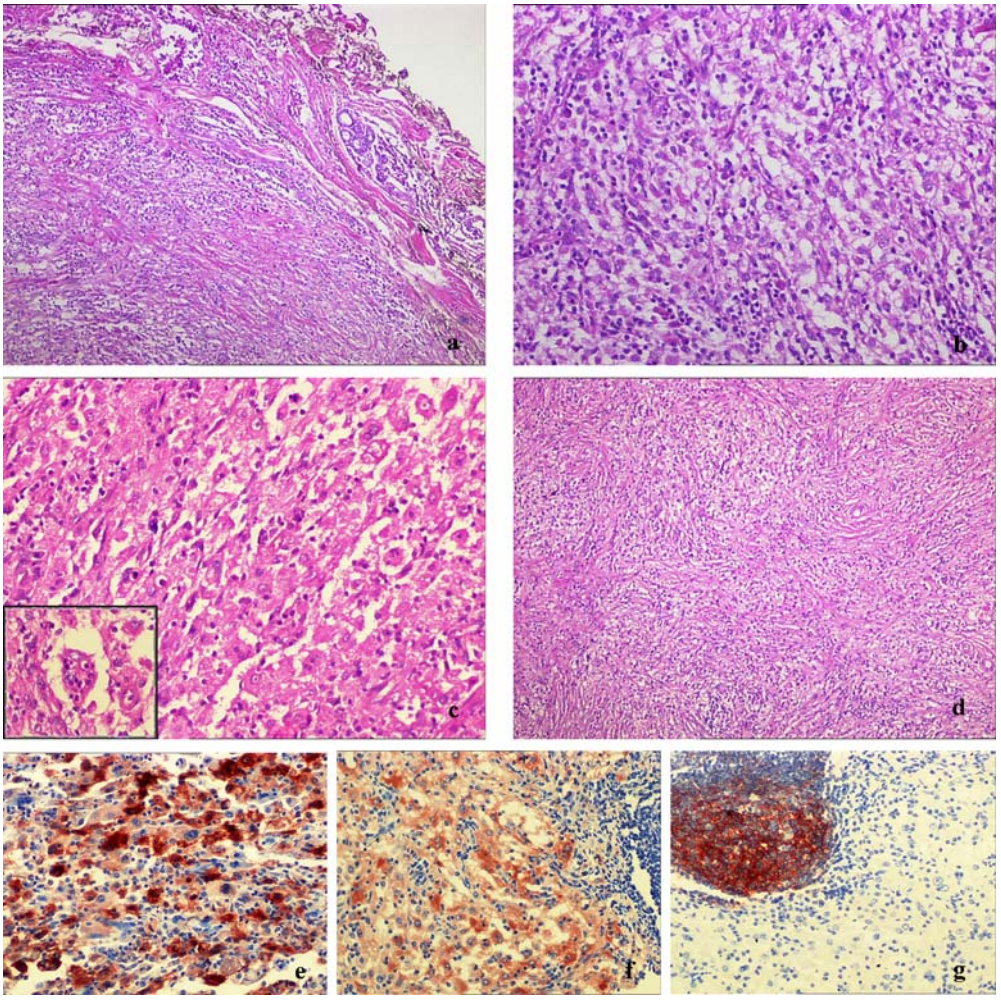

Fig. 2 **a** The tumor is well circumscribed by the adjacent breast parenchyma; hematoxylin and eosin (HE), ×40. **b** Interdigitating dendritic cell tumor composed of oval and polygonal cells arranged in sheets and an intermixed population of small lymphocytes; HE, ×100. **c** The tumor cells with vesicular nuclei and prominent nucleoli; HE, ×200. *Inset* multinucleate cells showing lymphophagocytosis; HE, ×200. **d** The tumor cells are arranged in a fascicular pattern; HE, ×40. **e** The tumor cells showed strong cytoplasmic and nuclear immunoreactivity for S-100 protein; streptavidin–biotin peroxidase (*SBP*)/3-amino-9-ethylcarbazole substrate (AEC) method, ×200. **f** The tumor cells are positive for fascin; SBP/AEC method, ×200. **g** The CD21 stain negative on the tumor cells but positive on the follicular dendritic cells in the lymphoid follicles; SBP/AEC method, ×100

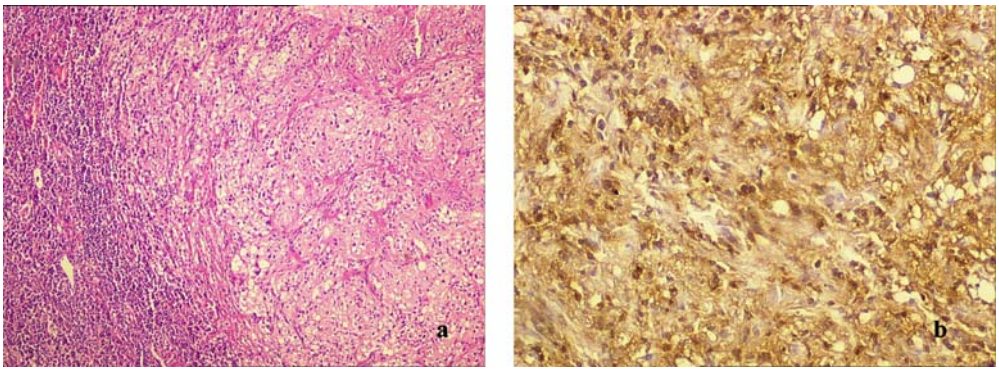

Fig. 3 **a** Cervical lymph node involved by oval–polygonal tumor cells with abundant eosinophilic cytoplasm and vesicular nuclei. There is background of small lymphocytes scattered throughout the tumor; hematoxylin and eosin, ×100. **b** The tumor cells are positive for S-100 protein streptavidin–biotin peroxidase/3,3′-diaminobenzidine tetrahydrochloride technique, ×200

treatment was performed for each antibody as required, and antigen–antibody reaction was visualized using either 3-amino-9-ethylcarbazole substrate (LabVision, NeoMarkers) or 3,3′-diaminobenzidine tetrahydrochloride (LabVision, NeoMarkers) as chromogen. To evaluate the specificity of the antibody, tissues known to have positive and negative reactions were used as controls.

Results

Upon gross examination, the tumor was a firm, well-circumscribed, white to tan nodule measuring 30 mm in diameter, surrounded by normal breast tissue. No evidence of necrosis or hemorrhage was detected grossly.

Histologically, the tumor was relatively well circumscribed from the adjacent breast tissue (Fig. 2a). The tumor displayed several growth patterns: cohesive sheets, fascicles and storiform. The major part of the tumor consisted of diffuse proliferation of cohesive large, polygonal or ovoid cells with abundant eosinophilic cytoplasm (Fig. 2b). The nuclei had round to oval, deeply grooved, vesicular chromatin pattern and irregular nuclear membranes and typically had a single, distinct, centrally located eosinophilic nucleolus (Fig. 2c). In some areas, the tumor was composed of spindle cells arranged in short intersecting fascicles, and focally there was a whorled pattern (Fig. 2d). The spindled tumor cells had slightly eosinophilic cytoplasms and indistinct cell borders. The minor part of the tumor showed deposition of collagen in between fascicles and was admixed with moderate numbers of small lymphocytes. Mitotic activity was three per ten high power fields. There were occasional multinucleated cells and large pleomorphic cells. Tumor cells showing phagocytosis of lymphocytes were commonly observed. Necrosis was not identified. The neoplastic cells were intermingled with small mature lymphocytes and plasma cells. Some of the ductal glands were entrapped within the tumor, and some of the lobules were also infiltrated by small lymphocytes. In the nonneoplastic breast parenchyma, there was a lymphoplasmacytic infiltrate and lymphoid follicles.

In the breast tumor, tumor cells were diffusely positive for vimentin, CD68, S-100 protein, CD45/LCA and focally positive for lysozyme and alpha-1 antitrypsin (Fig. 2e). Additionally, cytoplasmic staining was diffusely positive for fascin in the tumor cells (Fig. 2f). There was cytoplasmic CD4 staining in approximately 60% of tumor cells. The background small lymphocytes were predominantly T-cell lineage cells with very few B cells. No nuclear staining was observed for p53. However, Ki-67 labeling index was 10%. The tumor cells were negative for CD3, CD20, CD21, CD35, *CD1a*, CD30, CD15, cytokeratin, smooth-muscle actin, desmin and HMB-45 (Fig. 2g).

In the lymph node at reexamination, diffuse effacement of architecture was observed with absence of germinal centers. There were islands of large, plump, histiocytoid-appearing cells with ill-defined cell borders, abundant pale cytoplasms and large grooved nuclei with deep convolutions and prominent nucleoli. A mixed infiltrate, including small lymphocytes, plasma cells and histiocytes, was present (Fig. 3a). In addition, there was a marked proliferation of high endothelial venules. Mitosis was two per ten high-power fields. Necrosis was not observed.

Comparison with the patient's breast tumor, pleomorphic cells and fibrosis was absent. Immunohistochemical staining with a wide panel of antibodies was also performed in the lymph-node biopsy. The large neoplastic cells were positive for vimentin, LCA, CD68 and S-100 (Fig. 3b). Based upon these findings, the present case was diagnosed as IDCT of the breast with cervical lymph-node involvement.

Discussion

IDCT is an extremely rare neoplasm of presumed hematopoetic origin showing phenotypic features similar to those of IDCs [16]. IDCs are present not only in lymph nodes but also extranodally either as acquired lymphoid tissue or as part of the organized constitutive lymphoid tissue [20]. The presented tumor is the first case of IDCT of the breast involvement with concurrent nodal disease.

Including the present case, there have been 51 reported cases of IDCT in the literature. The clinical and pathological features of the reported cases are summarized in Table 1. IDCT generally occurs in adults. The median age at presentation is 58 years (range 2–88 years). The sex distribution is almost equal (male/female, 27:24). The patient usually presents with painless lymphadenopathy, but in approximately one-third of patients extranodal involvement develops at the time of presentation. Extranodal sites include nasopharynx [32], small intestine and mesentery [5, 21],

Table 1 Reported cases of interdigitating dendritic cell tumor. *AWD* alive with disease, *DOD* dead of disease, *FOD* free of disease, *D, NED* dead with no evidence of disease

Authors	Sex/Age (years)	Sites of involvement	Treatment	Follow-up
Lennert and Mohri [18]	Female/69	Lymph nodes	Not reported	Not reported
Feltkamp et al. 1981 [6]	Male/37	Mediastinum, cervical and axillary lymph nodes, skin	Chemotherapy, radiotherapy	DOD, 4 months
Turner et al. [32]	Male/17	Lymph nodes, spleen, liver, bone marrow	Chemotherapy	DOD, 4 months
	Male/30	Nasopharynx	Radiotherapy	AWD, 20 months
Daum et al. [5]	Male/43	Jejunum, mesenteric mass	Chemotherapy	D, NED, 5 months
Salisbury et al. [30]	Female/41	Lymph nodes	Chemotherapy, bone morrow transplantation	AWD, 6 months
Chan et al. [4]	Male/67	Lymph nodes, spleen, liver, lung, bone marrow	Chemotherapy	DOD, 1 week
van der Oord et al. [33]	Female/74	Axillary lymph node, mediastinum	Radiotherapy	FOD, not reported
Hui et al. [15]	Male/67	Skin, axillary lymph nodes	Not reported	AWD, 6 years
Nakamura et al. [22]	Male/58	Cervical, mesenteric lymph nodes, jejunum	Chemotherapy, radiotherapy, surgery	D, NED, 101 months
Rabkin et al. [28]	Male/17	Lymph nodes, spleen, bone marrow	Chemotherapy, radiotherapy	DOD, 9 months
	Female/13	Lymph nodes, spleen, mediastinum, ovaries, lung	Chemotherapy, surgery	DOD 3 months
Weiss et al. [35]	Male/60	Supraclavicular lymph node	Radiotherapy, surgery	FOD, 1 year, 5 year
	Male/34	Inguinal, thoracic lymph nodes, bone marrow, skin, liver, lung, heart, kidney, spleen	Chemotherapy, surgery, bone morrow transplantation	DOD, 10 months
Hammar et al. [13]	Male/67	Cervical lymph node	Surgery	FOD, 4 years
Yamakawa et al. [38]	Male/54	Lymph nodes, pleural effusion	Chemotherapy	AWD, 1 year
Horschowski et al. [14]	Male/8	Lymph nodes, colomesenteric mass	Chemotherapy	DOD, 8 months
Miettinien et al. [21]	Female/52	Lymph nodes, small intestine, abdominal masses	Chemotherapy, surgery	DOD, 16 months
	Male/58	Ileum, mesentery, liver	Chemotherapy, surgery	FOD, 12 months
Nakamura et al. [23]	Male/70	Submandibular lymph node	Untreated	FOD, 57 months
	Female/55	Cervical lymph node	Radiotherapy	FOD, 18 months
Rousselet et al. [29]	Female/20	Cervical, supraclavicular and mediastinal lymph nodes	Chemotherapy, radiotherapy	AWD, 24 months
Vasef et al. [34]	Female/56	Cervical and axillary lymph nodes	Predenisone	Not reported
Banner et al. [2]	Female/68	Caecum, lymph nodes	Chemotherapy	Not reported
Liu et al. [19]	Male/41	Lymph nodes, bone	Chemotherapy	AWD, 17 months
Andriko et al. [1]	Male/23	Cervical lymph node	Surgery, radiotherapy	Not reported
	Female/32	Cervical lymph node	Surgery	FOD, 8 years
Luk et al. [20]	Male/74	Testis	Surgery	FOD, 9 months
Gaertner et al. [11]	Male/61	Lymph nodes, chest wall, lung, spleen	Chemotherapy	AWD, 1, 5 years
	Male/70	Axillary lymph nodes	Surgery	FOD, 9 months
	Female/73	Inguinal lymph node, wide spread disease	Untreated	DOD, 2 months
	Female/77	Tonsil	Surgery, radiotherapy	FOD, 5 months
Kawachi et al. [17]	Female/86	Spleen, liver, bone marrow, abdominal lymph nodes	Surgery	DOD, 6 months
Olnes et al. [24]	Female/44	Lymph nodes, abdominal mass	Chemotherapy	FOD, 24 months
Pileri et al. [25]	Male/60	Multiple skin lesions	Chemotherapy	FOD
	Female/78	Inguinal lymph nodes	Surgery, radiotherapy	FOD
	Female/83	Axillary lymph nodes	Not reported	Relapse, not reported
	Male/67	Cervical lymph nodes	Not reported	Not reported

Table 1 (continued)

Authors	Sex/Age (years)	Sites of involvement	Treatment	Follow-up
Pillay et al. [26]	Female/10	Chest wall mass	Surgery	FOD, 10 years
	Female/12	Paravertebral mass	Chemotherapy, radiotherapy, surgery	FOD, 9 years
	Male/2	Lymph nodes	Chemotherapy	DOD, 29 months
	Female/6	Bladder	Chemotherapy, surgery	DOD, 5 months
Ylagan et al. [39]	Male/66	Intraparotid lymph nodes, cervical lymph node, lung, liver	Radiotherapy, surgery	DOD, 20 months
Barwell et al. [3]	Female/51	Salivary gland, lymph nodes	Surgery	FOD, 24 months
Grogg et al. [12]	Male/88	Intraparotid lymph node	Radiotherapy	D, NED, 24 months
	Male/15	Cervical lymph node	Surgery	FOD, 19 months
	Female/67	Lung, liver, abdominal lymph nodes	No treatment	DOD, 21 days
	Male/61	Axillary lymph nodes, inguinal lymph nodes, spleen, bone marrow	Chemotherapy	DOD, 5 months
	Female/72	Intraparotid lymph node	Radiotherapy	FOD, 7 months
	Female/68	Axillary lymph node	Not reported	Not reported
Present case	Female/38	Cervical lymph nodes, breast	Chemotherapy, radiotherapy, surgery	AWD, 32 months

testis [20], skin [15, 25], tonsil [11], spleen [17], chest wall [26], paraspinal area [26], bladder [26], salivary gland [3] and breast (present case). Nine cases without documented nodal involvement were reported in the literature [11, 20, 25, 26, 32]. Liver and/or spleen involvement have been described in approximately 20% of the cases [4, 12, 17, 21, 28, 32, 35, 39]. Six patients had bone marrow involvement [4, 12, 17, 28, 32, 35], and superior vena cava syndrome developed in two patients [6, 29]. Among patients with IDCT, eight patients were reported to have a previous or concurrent history of malignant neoplasms, including colon cancer [11], mycosis fungoides [18], follicular center cell lymphoma [13], T-lymphoblastic lymphoma [14], adenocarcinoma of the stomach [23], ductal carcinoma of the breast [23] and small lymphocytic lymphoma [11, 34]. Systemic symptoms, such as fatigue, fever and night sweats, have been reported [8]. Etiology is unknown [16]. Grossly, IDCTs are generally described as well-circumscribed nodular and lobulated masses that are yellow or white to tan and of solid consistency. Sometimes they may have focal areas of necrosis or hemorrhage [16].

In general, the tumor is composed of oval to spindle cells with pale to eosinophilic cytoplasm, ill-defined cell outlines, oval nuclei with vesicular chromatin and prominent eosinophilic nucleoli [11, 32, 33]. Characteristically, the tumor cells grow in diffuse sheets, fascicles and sometimes in a storiform pattern [25, 33]. Scattered multinucleated cells are common. Necrosis (either focal or as a microabscess) is rarely reported [21, 28, 29, 35]. The mitotic rate is variable but generally few in number (less then five per ten high power fields [16]. Phagocytosis has occasionally been seen as in the present case [4, 21, 32, 38]. Characteristic and a diagnostically valuable feature is the presence of small mature lymphocytes and plasma cells closely intermingled with the neoplastic cells [1, 35]. In addition, some of the cases showed histological features suggestive of aggressive clinical behavior, including foci of necrosis, marked nuclear pleomorphism, abnormal mitoses and high mitotic activity or high proliferative index (Ki-67 labeling), sometimes in combination [8, 17, 21]. Although the number of reported cases is limited, there was no association between these histological features or extranodal location and survival. However, our patient had none of these histological features and had a relatively long clinical course.

The diagnosis of IDCT can be confirmed with the use of immunohistochemistry and/or electron microscopy. Immunohistochemical studies showed that the tumor cells were positive for vimentin, LCA, S-100 protein, HLA-DR and CD68, but negative for B-cell and T-cell markers, CD1a, CD30 and follicular dendritic cell markers (CD21 and CD35) [8, 25]. Normal interdigitating reticulum cells present adenosine triphosphate activity, which was also demonstrated in most of the IDCT cases [4, 6, 8, 30, 31, 38]. Immunoreactivity for fascin, an actin-bundling protein expressed by follicular and IDC, has been recently proposed as an additional marker of IDCT [11, 17, 27]. The Ki-67 labeling index usually ranges between 10% and 20% [6]. Variable degrees of staining have been reported for CD1a, CD11c, CD4, CD14 and EMA [8, 25]. These immunohistochemical findings are compatible with our findings as for the others. Ultrastructurally, the tumor cells showed complex interdigitating cytoplasmic processes; however, well-formed desmosomes and Birbeck granules were absent [1, 13, 28, 38].

Because of its morphological heterogeneity, the differential diagnosis of IDCT is broad and includes both non-neoplastic and neoplastic entities. IDCTs can be round or polygonal, resembling histiocytes and epithelioid cells; they can also be spindle, mimicking mesenchymal cells. Inflammatory pseudotumor is characterized by prolifera-

tion of spindle cells, which are admixed with inflammatory cells. In contrast to IDCT, there is no morphological atypia or aggressive growth pattern, while the cellular population is polymorphic [8].

A number of spindle and epithelioid cell tumors, primary or metastatic to the breast, should be considered in the differential diagnosis. The spindle cell or metaplastic carcinoma may be excluded by considering the cytological characteristics of the tumor cells, the lack of any intraductal carcinoma or heterologue components and by the use of immunohistochemical studies. Unlike IDCT, the cells of carcinoma react with cytokeratin [27].

In the presence of spindle cell component, IDCT is confused with fibrosarcoma, leiomyosarcoma, rhabdomyosarcoma and malignant fibrous histiocytoma. Morphology, immunohistochemistry and ultrastructural features are helpful in differential diagnosis [11].

Metastatic carcinoma is ruled out by the absence of the other possible primary sites. Metastatic malignant melanoma closely resembles IDCT, since both neoplasms can have a similar immunohistochemical profile (S-100 positive, CD68±). Confirming the hematolymphoid nature of IDCT by staining for CD45 (LCA) is critical. In malignant melanoma, HMB-45 should also be positive, and melanosomes will be seen ultrastructurally [11].

Hematopoietic entities, such as those of histiocytic or dendritic origin, must be considered for the differential diagnosis. There are two reported cases of follicular dendritic cell tumor (FDCT) in the breast [7, 27]. The distinction of FDCTs from IDCT is of clinical importance given the reported aggressive behavior of subsets of IDCTs. Although IDCT tends to have plumpy, histiocyte-like cells with grooved nuclei, the compact fascicular pattern and storiform growth pattern with oval and spindle cells are observed in IDCT and FDCT. They share immunohistochemical positivity for fascin and CD68, but IDC tumors express S-100 protein, CD45 (LCA), HLA-DR, CD68, CD4 and, unlike FDCTs, lack staining with CD21 and CD35 [25]. In addition, Grogg et al. demonstrated that strong diffuse clusterin staining distinguishes FDCT from IDCT and Langerhanscell histiocytosis [12]. Ultrastructurally, they exhibit broad interdigitating cytoplasmic processes but no desmosome-type cellular junctions [25].

Histiocytic sarcomas are extremely rare neoplasms and show variable staining with the histiocytic markers and lysozyme in the absence of myeloid differentiation. There is no positivity for specific B- and T-cell-associated antigens, including antigen receptor gene rearrangements and S-100 protein [8, 21]. IDCTs have been reported to show varying degrees of histiocytic differentiation, and some cases of histiocytic sarcomas may express weak and focal S-100 protein staining as well; therefore, they display a hybrid immunophenotype of ordinary histiocytes and interdigitating dendritic cells. Because the precursors of histiocytes and IDCs have originated from similar bone marrow stem cell, the presence of hybrid phenotypes may be observed. Also, as observed in our case, IDCT cells show phagocytic activity, which is considered to be an important functional feature of histiocytes. Thus, the neoplasms of histiocytes and IDCs are considered to be closely related entities [17].

Sinus histiocytosis with massive lymphadenopathy (Rosai Dorfman disease) is a rare disorder, characterized as a nonmalignant proliferation of distinctive histiocytic/phagocytic cells within lymph-node sinuses and lymphatics in extranodal sites. The microscopic hallmark of the disease is represented by histiocytes with abundant pale eosinophilic cytoplasm, round vesicular nuclei with a single prominent nucleoli and demonstrating lymphophagocytosis or emperipolesis. Cellular morphology is more monotonous and less hyperchromatic, with rare atypical nuclei. Mitoses are infrequent. Immunohistochemically, the histiocytes are typically positive for S-100 protein and CD68 but are negative for CD1a.

Exclusion of the Langerhans cell histiocytosis was simplified by the lack of CD1a positivity and Birbeck granules ultrastructurally [25]. However, some authors have reported cases of IDCT expressing CD1a with the absence of Birbeck granules. Some investigators think that the origin of these tumors is the indeterminate cells [36].

Cases of IDCT involving the lymph nodes may be misdiagnosed as pleomorphic T-cell lymphoma, diffuse large B-cell lymphoma, anaplastic large cell lymphoma and Hodgkin lymphoma-lymphocyte depletion type. Absence of B-cell and T-cell lineage markers helped in excluding the large B-cell lymphoma and T-cell lymphoma. In Hodgkin lymphoma, diagnostic Reed–Sternberg cells were positive for CD15 and negative for S-100. Immunostaining for CD30 and EMA should be performed to exclude anaplastic large cell lymphoma, which often lacks CD3 expression [25].

In the current case, an initial diagnosis of angioimmunoblastic T-cell lymphoma within the cervical lymph node was yielded because of the effaced nodal architecture, presence of predominant populations of T cells characterized by a larger, more vesicular nucleus and more prominent nucleoli than small mature lymphocytes and marked proliferation of high endothelial venules. In the reexamination, however, islands of plump, large atypical cells with histiocytoid-like appearance, pale cytoplasm, vesicular nucleus and prominent nucleoli were seen. A revised diagnosis of IDCT was made when these neoplastic cells stained positively for S-100, LCA, vimentin and CD68. Miettinen et al. [21] reported two cases of IDCT of the small intestine that were initially diagnosed as true histiocytic lymphoma. So, once the dendritic cell tumor is suspected histologically, appropriate immunostaining must be performed to avoid the potential for misdiagnosis.

The World Health Organization used the term sarcoma/tumor due to variable cytological grade and the unknown/indolent biological behavior of this neoplasm [16].

Follow-up data are available for 45 of the 51 patients in the literature. The mean follow-up time is 25 months (range 1–120 months). Although some patients have died, with wide-spread disease in the spleen, liver, lung and bone marrow, others survived their illness over long periods of time. Compared with follicular dendritic neoplasms, IDCT

seems to behave more aggressively, with an overall median survival of 30 months. Approximately, one-third of these patients (15 of 45 patients) died in 1 week to 29 months [4, 6, 11, 12, 14, 17, 21, 26, 28, 32, 35, 39]. Of these cases, 3 died of other causes [5, 12, 22]. At the time of the last follow-up, 27 cases were still alive, 9 patients of which were alive with disease [11, 15, 19, 25, 29, 30, 32, 38] and 18 patients remained disease free [1, 3, 11–13, 20–22, 24–26, 32, 35]. These findings suggest that IDCTs display a variable behavior, ranging from a benign localized disease to a rapidly fatal disease [6, 25]. Treatment generally consists of surgical resection and chemotherapy regimens used for non-Hodgkin's lymphomas. Radiotherapy was reported to be used in several patients, alone or in combination with chemotherapy or surgery (Table 1). The response to therapy has been generally poor, but complete responses have been reported in one-third of cases [1, 3, 11, 12, 21, 23–26, 33, 35]. In the present case, although the initial diagnosis was not correct, the chemotherapy regimen given to the patient seems to be consistent with the therapies used in similar cases previously reported.

In conclusion, our case expands the possible sites of occurrence of IDCT. Its pathological diagnosis is often challenging because it mimics other primary and metastatic neoplasms of the lymph nodes. Based on the review of the present and previous cases, the minimal diagnostic criteria for the diagnosis of IDCT are the histological features as described above and the positive staining for CD45 (LCA), S-100 and CD68. An additional ultrastructural feature is essential to confirm the diagnosis of IDCT. In contrast to the reported aggressive behavior of IDCT, a partial remission was obtained in the present case. The patient showed a relatively indolent course with 32 months of survival after the diagnosis.

References

1. Andriko JW, Kaldiian EP, Tsokos M, Abbondanzo SL, Jaffe ES (1998) Reticulum cell neoplasms of lymph nodes: a clinicopathologic study of 11 cases with recognition of a new subtype derived from fibroblastic reticular cells. Am J Surg Pathol 22:1048–1058
2. Banner B, Beauchamp ML, Liepman M, Woda BA (1997) Interdigitating reticulum-cell sarcoma of the intestine: a case report and review of the literature. Diagn Cytopathol 17:216–222
3. Barwell N, Howatson R, Jackson R, Johnson A, Jarrett RF, Cook G (2004) Interdigitating dendritic cell sarcoma of salivary gland associated lymphoid tissue not associated with HHV-8 or EBV infection. J Clin Pathol 57:87–89
4. Chan WC, Zaatari G (1986) Lymph node interdigitating reticulum cell sarcoma. Am J Clin Pathol 85:739–744
5. Daum GS, Liepman M, Woda BA (1985) Dendritic cell phenotype in localized malignant histiocytosis of the small intestine. Arch Pathol Lab Med 109:647–650
6. Feltkamp CA, van Heerde P, Feltkamp-Vroom TM, Koudstaal J (1981) A malignant tumour arising from interdigitating cells: light microscopical, ultrastructural, immuno- and enzyme-histochemical characteristics. Virchows Arch 393:183–192
7. Fisher C, Magnusson B, Hardarson S, Smith ME (1999) Myxoid variant of follicular cell sarcoma arising in the breast. Ann Diagn Pathol 3:92–98
8. Fonseca R, Yamakawa M, Nakamura S, van Heerde P, Miettinen M, Shek TWK, Jensen OM, Rousselet MC, Tefferi A (1998) Follicular dendritic cell sarcoma and interdigitating reticulum cell sarcoma: a review. Am J Hematol 59:161–167
9. Foucar K, Foucar E (1990) The mononuclear phagocyte and immunoregulatory effector (M-PIRE) system: evolving concepts. Semin Diagn Pathol 7:4–18
10. Friess A (1976) Interdigitating reticulum cells in the popliteal lymph node of the rat: an ultrastructural and cytochemical study. Cell Tissue Res 170:43–60
11. Gaertner EM, Tsokos M, Derringer GA, Neuhauser TS, Arciero C, Andriko JW (2001) Interdigitating dendritic cell sarcoma: a report of four cases and review of the literature. Am J Clin Pathol 115:589–597
12. Grogg KL, Lae ME, Kurtin PJ, Macon WR (2004) Clusterin expression distinguishes follicular dendritic cell tumors from other dendritic cell neoplasms. Am J Surg Pathol 28:988–998
13. Hammar SP, Rudolph RH, Bockus DE, Remington FL (1991) Interdigitating reticulum cell sarcoma with unusual features. Ultrastruct Pathol 15:631–645
14. Horschowski N, Guitard AM, Arnoux I, Michel G, Thuret I, George F, Perrimond H (1993) Interdigitating cell sarcoma: occurrence during incomplete remission of a lymphoblastic lymphoma. Pathol Biol (Paris) 41:255–259
15. Hui PK, Feller AC, Kaiserling H et al (1987) Skin tumour of T accessory cells (interdigitating reticulum cells) with high content of T lymphocytes. Am J Dermatopathol 9:129–137
16. Jaffe ES (2001) Histiocytic and dendritic cell neoplasms. In: Jaffe ES, Harris NL, Stein H, Vardiman JW (eds) Tumours of haematopoietic and lymphoid tissues. IARC Press, Lyon pp 284–285
17. Kawachi K, Nakatani Y, Inayama Y, Kawano N, Toda N, Misugi K (2002) Interdigitating dendritic cell sarcoma of the spleen: report of a case with a review of the literature. Am J Surg Pathol 26:530–537
18. Lennert K, Mohri N (1978) Histopathology and diagnosis of non-Hodgkin's lymphomas. In: Vehrlinger E (ed) Malignant lymphomas other than Hodgkin's disease. Springer, Berlin Heidelberg New York, pp 448
19. Liu SM, Huang P-H, Liu JM (1998) Interdigitating reticulum cell tumor of lymph node: a case report and literature review. Pathol Int 48:974–980
20. Luk ISC, Shek TWH, Tang VWL, Ng WF (1999) Interdigitating dendritic cell tumor of the testis: a novel testicular spindle cell neoplasm. Am J Surg Pathol 23:1141–1148
21. Miettenen M, Fletcher CDM, Lasota J (1993) True histiocytic lymphoma of the small intestine: analysis of two S-100 protein-positive cases with features of interdigitating reticulum cell sarcoma. Am J Clin Pathol 118:285–292
22. Nakamura S, Hara K, Suchi T, Ito M, Ikeda H, Nagahama M, Nakayama A, Nakagawa A, Kaneshima H, Asai J (1988) Interdigitating cell sarcoma. A morphologic, immunohistologic and enzyme-histochemical study. Cancer 61:562–568
23. Nakamura S, Koshikawa T, Kitoh K, Nakayama A, Yamakawa M, Imai Y, Ishii K, Fujita M, Suchi T (1994) Interdigitating cell sarcoma: a morphologic and immunologic study of lymph node lesions in four cases. Pathol Int 44:374–386
24. Olnes MJ, Nicol T, Duncan M, Bohlman M, Erlich R (2002) Interdigitating dendritic cell sarcoma: a rare malignancy responsive to ABVD chemotherapy. Leuk Lymphoma 43:817–821
25. Pileri SA, Grogan TM, Harris NL, Banks P, Campo E, Chan JKC, Favera RD, Delsol G, De Wolf-Peeters C, Falini B, Gascoyne RD, Gaulard P, Gatter KC, Isaacson PG, Jaffe ES, Kluin P, Knowles DM, Mason DY, Mori S, Müller-Hermelink H-K, Piris MA, Ralfkiaer E, Stein H, Su I-J, Warnke RA, Weis LM (2002) Tumours of histiocyte and accessory dendritic cells: an immunohistochemical approach to classification from the International Lymphoma Study Group based on 61 cases. Histopathology 41:1–29
26. Pillay K, Solomon R, Daubenton JD, Sinclair-Smith CC (2004) Interdigitating dendritic cell sarcoma: a report of four pediatric cases and review of the literature. Histopathology 44:283–291

27. Pruneri G, Masullo M, Renne G, Taccagni G, Manzotti M, Luini A, Viale G (2002) Follicular dendritic cell sarcoma of the breast. Virchows Arch 441:194–199
28. Rabkin MS, Kjeldsberg CR, Hammond ME, Wittwer CT, Nathwani B (1988) Clinical, ultrastructural, immunohistochemical and DNA content analysis of lymphomas having features of interdigitating reticulum cells. Cancer 61:1594–1601
29. Rousselet M-C, François S, Croue A, Maigre M, Saint-Andre J-P, Ifrah N (1994) A lymph node interdigitating reticulum cell sarcoma. Arch Pathol Lab Med 118:183–188
30. Salisbury JR, Ramsay AD, Isaacson PG (1985) Histiocytic lymphoma: a report of a case with unusual phenotype. J Pathol 146:99–106
31. Stenman R, Pack M, Inaba K (1997) Dendritic cells in the T-cell areas of lymphoid organs. Immunol Rev 156:25–37
32. Turner RR, Wood GS, BekColby TV, Horning SJ, Warnke RA (1984) Histiocytic malignancies: morphologic, immunologic and enzymatic heterogeneity. Am J Surg Pathol 8:485–500
33. van den Oord JJ, de Wolf-Peeters C, de Vos R, Thomas J, Desmet VJ (1986) Sarcoma arising from interdigitating reticulum cells: report of a case, studied with light and electron microscopy, and enzyme- and immunohistochemistry. Histopathology 10:509–523
34. Vasef MA, Zaatari GS, Chan WC, Sun NCJ, Weiss LM, Brynes RK (1995) Dendritic cell tumours associated with low grade B-cell malignancies: report of three cases. Am J Clin Pathol 104:696–701
35. Weiss LM, Berry GJ, Dorfman RF, Banks P, Kaiserling E, Curtis J, Rosai J, Warnke RA (1990) Spindle cell neoplasm of lymph nodes of probable reticulum cell lineage: true reticulum cell sarcoma? Am J Surg Pathol 14:405–414
36. Weiss LM (2001) Histiocytic and dendritic cell proliferations. In: Knowles DM (ed) Neoplastic hematopathology. Lippincott, Williams and Wilkins, Philadelphia, pp 1815–1846
37. Wright-Brown V, McClain KL, Talpaz M, Ordonez N, Estrov Z (1997) Physiology and pathophysiology of dendritic cells. Hum Pathol 28:563–579
38. Yamakawa M, Matsuda M, Imai Y, Arai S, Harada K, Sato T (1992) Lymph node interdigitating cell sarcoma: a case report. Am J Clin Pathol 97:139–146
39. Ylagan LR, Bartlett NL, Kraus M (2003) Interdigitating dendritic reticulum cell tumor of lymph nodes: case report with differential diagnostic considerations. Diagn Cytopathol 28:278–281

Virchows Arch (2005) 446: 555–559
DOI 10.1007/s00428-005-1216-4

CASE REPORT

Olivier Ramuz · Bernard Lelong · Marc Giovannini · Jean-Robert Delpero · Philippe Rochaix · Luc Xerri · Jacques Hassoun · Jean-François Flejou · Geneviève Monges

"Sugar" tumor of the pancreas: a rare entity that is diagnosable on preoperative fine-needle biopsies

Received: 9 November 2004 / Accepted: 11 January 2005 / Published online: 9 April 2005
© Springer-Verlag 2005

Abstract This study is the second to report a pancreatic "sugar" tumor (ST) case. This ST was incidentally discovered in a 31-year-old woman using computed tomography scan (CT scan) for work-up of a hepatic focal nodular hyperplasia. Both CT scan and endoluminal ultrasonography (EUS) features evoked a 15-mm large benign endocrine tumor. Pathological examination of EUS-guided fine-needle aspiration biopsies could not confirm this diagnosis. Laparoscopic corporeo-caudal pancreatectomy was performed. The tumor was intrapancreatic, well circumscribed, and organized in sheets of epithelioid cells. The tumor cells expressed HMB-45 but did not express epithelial or endocrine immunohistochemical markers. These histophenotypic features are those of an extra pulmonary ST, which belong to the PEComa family of tumors. Retrospective examination of preoperative biopsies evidenced the same histophenotypic features. This observation highlights that STs should be considered in preoperative differential diagnosis of pancreas tumors, since they may be treated by limited surgical resection.

Keywords "Sugar" tumor · PEComa · Pancreas · Immunohistochemistry · Melanoma markers · Fine-needle aspiration · Endoluminal ultrasonography

O. Ramuz (✉) · L. Xerri · J. Hassoun · G. Monges
Department of Pathology, Institut Paoli-Calmettes,
Marseille, France
e-mail: ramuzo@marseille.fnclcc.fr
Tel.: +33-491-223457
Fax: +33-491-223573

B. Lelong · J.-R. Delpero
Department of Surgical Oncology,
Institut Paoli-Calmettes,
Marseille, France

M. Giovannini
Department of Medical Oncology,
Institut Paoli-Calmettes,
Marseille, France

P. Rochaix
Department of Pathology,
Institut Claudius Regaud,
Toulouse, France

J.-F. Flejou
Department of Pathology,
Hôpital Saint-Antoine,
Paris, France

Introduction

"Sugar" tumors (STs) have been described as "monophasic" angiomyolipomas (AMLs) that usually occur in lung. STs belong to a family of tumors called PEComas [2, 4]. PEComas are mesenchymal tumors composed of histologically and immunohistochemically distinctive perivascular epithelioid cells [2, 4].

The case of pancreatic (extra-pulmonary) ST that we report highlights that STs may be diagnosed by pathological examination of perendoscopic, ultrasonography-guided, fine-needle aspiration (FNA) biopsies and that ST should, therefore, be considered during the preoperative diagnosis of pancreatic tumors.

Clinical history

In October 2003, a 31-year-old woman complained of pain in the right hypochondriac region. She was otherwise well, and physical examination was unrevealing. She had no significant medical history. Abdominal ultrasonography evidenced a large nodular lesion in the right hepatic lobe. On computed tomography (CT) and resonance magnetic imaging abdominal scan, this hepatic lesion was 9 cm large, was located in the hepatic segments VII and VIII, and showed features of focal nodular hyperplasia (FNH).

In addition to the FNH, CT scan revealed a round, 15-mm-diameter, homogeneous, solid lesion in the pancreas

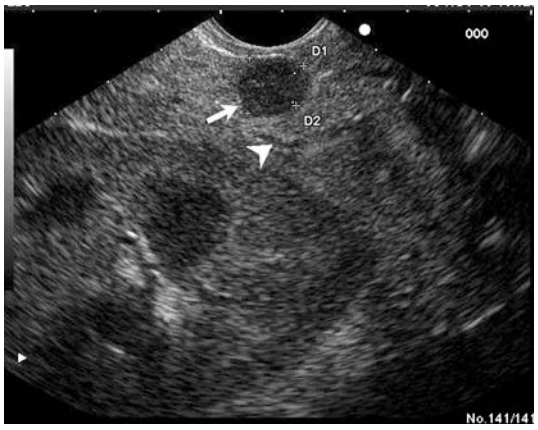

Fig. 1 Endoluminal ultrasonography examination of the pancreas. The Wirsung duct (*arrowhead*) was pushed away by a round, 15-mm diameter, homogeneous, hypoechogenic nodule (*arrow*) of the pancreas body. These features were reminiscent of a benign endocrine tumor

body. Endoluminal ultrasonography (EUS) showed an hypoechogenic nodule that was pushing the Wirsung duct away (Fig. 1). No loco-regional adenomegaly was found. These features were reminiscent of a benign endocrine tumor. Pathological examination of EUS-guided FNA cytological preparations and biopsies could neither confirm an endocrine tumor nor lead to any obvious diagnosis.

No additional lesion was found on chest, abdominal, and pelvic CT scans. At laparoscopy, a subcapsular tumor of the pancreas body was found. This tumor was located in the upper margin of the pancreas body, near the splenic vein. Laparoscopic ultrasonography showed the same features as EUS. Since no preoperative pathological diagnosis was available, the tumor was completely removed by laparoscopic corporeo-caudal pancreatectomy with spleen preservation. Neither metastases nor nodal enlargements were evidenced.

The patient is doing well 9 months after surgery, with neither evidence of tumor recurrence nor FNH alteration. Our patient did not display any signs of tuberous sclerosis complex after extensive clinicoradiological investigation.

Materials and methods

Tissue samples were fixed in 10% formalin and were entirely paraffin embedded. Paraffin sections 5 μm thick were cut and processed for hematoxylin and eosin or immunohistochemical staining.

Commercially available ready-to-use primary antibodies (Table 1) were used according to manufacturers' instructions. Detection was done using horseradish peroxidase-labeled secondary antibodies, diaminobenzidine or 3-amino, 9-ethyl-carbazole chromogens, and a Dako Autostainer device (DakoCytomation, Trappes, France). Staining controls were either internal or external, according to the antibody used.

Pathological findings

A firm, well-circumscribed, nodular, 15-mm-diameter lesion was found in the pancreas body. The cut surface was homogeneous, white tan, without any hemorrhagic areas.

Microscopic examination evidenced a cellular tumor that was sharply demarcated from the pancreas parenchyma, without any peripheral nodule (Fig. 2). At low magnification, tumor cells were organized in sheets, without lobulation. Loose, edematous areas but no necrotic foci were observed. Tumor cells were epithelioid and showed abundant clear to eosinophilic, granular cytoplasm (Fig. 3a). The nuclei were polymorphous, often eccentric, and sometimes with a prominent nucleolus or cytoplasmic inclusions. No mitoses were observed. An abundant, granular, periodic-acid Schiff-positive, diastase-sensitive material was evidenced in the cytoplasm of the tumor cells. Collections of foamy histiocytes and sparse lymphocytes were found throughout the tumor. No entrapped pancreatic structures were found within the tumor. The surrounding pancreatic parenchyma did not show any histological peculiarity.

The tumor cells expressed neither epithelial (KL1, CK7, CK20), endocrine (chromogranin A, synaptophysin) nor S-100 protein but showed a strong, diffuse, granular cytoplasmic HMB-45 immunostaining pattern (Table 1, Fig. 3b). Strong PNL2 and Melan-A immunohistochemistry (IHC) expression was found in 90–100% and 40–50% tumor cells,

Table 1 Immunohistochemical procedures and findings

Antibody	Source	Dilution	Result
KL1 (pan-cytokeratin)	Beckman-Coulter Immunotech, Marseille, France	1:150	−
Cytokeratin 7	Dakocytomation, Glosturp, Denmark	1:50	−
Cytokeratin 20	Dakocytomation	1:50	−
HMB-45	Immunotech	Undiluted (rtu)	++
Melan-A	Dakocytomation	1:20	+
PNL2	Culture Supernatant[a]	1:2	++
KBA.62	Beckman-Coulter Immunotech	Undiluted (rtu)	−
S-100 protein	Beckman-Coulter Immunotech	Undiluted (rtu)	−/+
Chromogranin A	Beckman-Coulter Immunotech	Undiluted (rtu)	−
Synaptophysin	Dakocytomation	Undiluted (rtu)	−
Smooth-muscle actin	Dakocytomation	1:200	+
Mib1 (Ki-67)	Dakocytomation	1:50	<1%

rtu ready-to-use primary antibody solution, − negative, −/+ scarce positive cells, + ≤50% positive cells, ++ >50% positive cells

[a]PNL2 monoclonal antibody was provided to us by PR [14]; PNL2 is also distributed by Dakocytomation

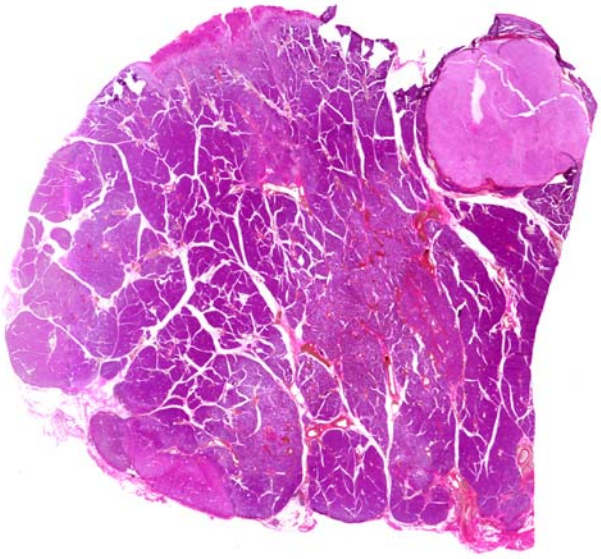

Fig. 2 Corporeo-caudal pancreatectomy with spleen preservation. Whole-mount section showing an intra-pancreatic, well-circumscribed, homogeneous, and nodular lesion. The tumor was sharply demarcated from the pancreatic parenchyma by a thin fibrous capsule

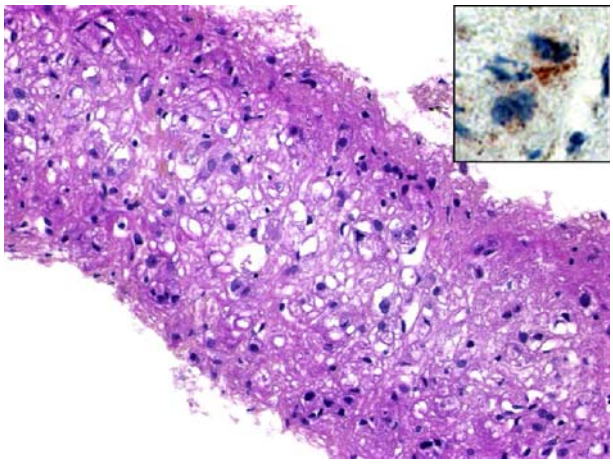

Fig. 4 Fine-needle aspiration biopsy. Retrospective examination evidenced the same epithelioid cells as in the surgical resection specimen. These cells showed cytoplasmic HMB-45 expression (*inlay*)

respectively, whereas no KBA.62 IHC expression was observed. Smooth-muscle actin but not desmin was expressed by some neoplastic cells. Nuclear stain for Mib1 (Ki-67) was found in rare cells (<1%). These morphological and phenotypical features led us to the diagnosis of "sugar" tumor of the pancreas.

Retrospective examination evidenced the same microscopic features on FNA biopsies, with HMB-45 immunoexpression by epithelioid tumor cells (Fig. 4).

Discussion

STs usually arise in the lung [2] and have been scarcely reported in extrapulmonary sites [6, 8, 17–19]. To our knowledge, only one typical case of pancreatic ST has been reported previously [19]. Moreover, Heywood et al. [7] have recently described a case of pancreatic AML with prominent epithelioid features reminiscent of ST. These morphological similarities between STs and AMLs highlight the fact that both tumors belong to the PEComas family [4]. STs are usually benign tumors; however, rare epithelioid PEComas have shown malignant behavior [1, 3, 11, 15, 18]. Increased mitotic rates have been reported in malignant PEComas, but no clear malignancy criteria have been developed yet. The ST case, which we report here, appeared histologically benign and remained without recurrence 9 months after surgical resection.

STs are epithelioid cell tumors that must be differentiated from carcinomas, especially from clear cell carcinomas, which may be either primary or metastatic [19]. Endocrine carcinoma may also be considered [19]. Moreover, clear cell features have been reported in pancreatic endocrine tumors that were associated with von Hippel–Lindau dis-

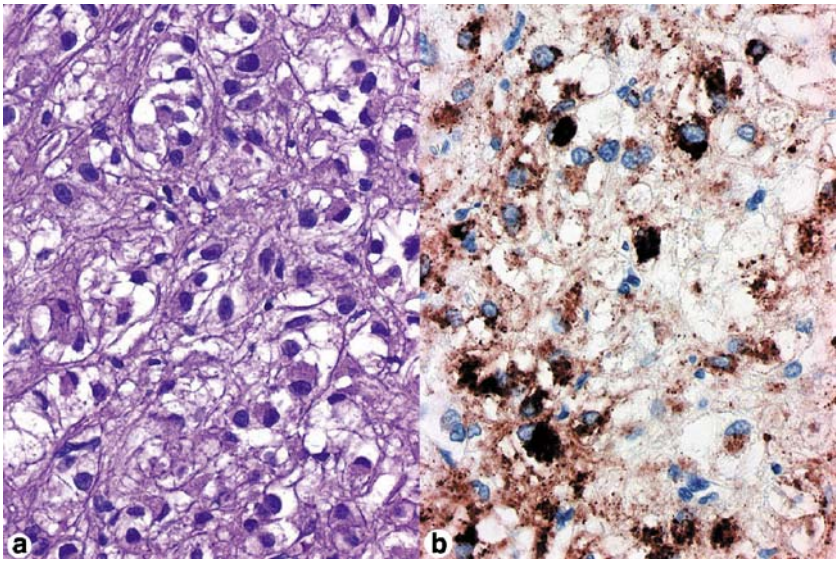

Fig. 3 Surgical resection. **a** The epithelioid cells were arranged in sheets, without any conspicuous pattern. The tumor cells were characterized by abundant, clear or eosinophilic cytoplasm and slightly atypical nucleus. A small, central nucleolus was sometimes observed. **b** The tumor cells expressed HMB-45

ease [10]. Some typical features of ST—lack of glandular pattern, necrosis, mitotic activity, epithelial (cytokeratins) and endocrine (chromogranin A, synaptophysin) markers IHC expression—will argue against carcinoma and endocrine tumor, while diffuse HMB-45 IHC expression will point to the correct diagnosis [2, 19]. All these typical features were met by our patient's tumor.

Clear cell sarcoma or melanoma usually show more atypical features than STs and express S-100 protein, whereas STs only show low, focal S-100 protein IHC expression. To be noticed, PEComas have been reported to express other melanogenesis markers: melan-A, tyrosinase, microphtalmia transcription factor, NKI/C3, and PNL2 [14, 16, 20]. Cytoplasmic, melanosoma-like granules have been evidenced in pancreatic STs [19]. Expression of muscle markers—α smooth actin, desmin, HHF-35—has also been reported [7, 19], and a muscle tumor will be ruled out by HMB-45 IHC expression. Our patient's tumor expressed α smooth actin but not desmin. The lack of c-kit (CD117) IHC expression argued against an epithelioid gastro-intestinal stromal tumor.

Pancreatic STs, like AMLs, are devoid of any specific symptoms [7, 19]. However, characteristic features of AML cannot be observed on CT scan, nor on magnetic resonance imaging, nor on preoperative frozen sections, because STs include no fat. Therefore, preoperative diagnosis of pancreatic ST relies on pathological examination.

Liquid-phase cytological preparations and/or biopsies can now be obtained by EUS-guided FNA. These kinds of samples are suitable for IHC, whereas usual cytological smears allow only morphological examination. IHC is crucial for preoperative differential diagnosis, because morphological features may be incomplete and/or impaired on FNA samples. Though STs are rare, pathologists must keep them in mind, since preoperative diagnosis of ST may allow limited surgical resection. On retrospective examination of our FNA biopsies, the epithelioid cells showed an IHC pattern typical for perivascular epithelioid cells and were HMB-45 positive.

STs are not associated with tuberous sclerosis, unlike angiomyolipomas [4]. In agreement with the observations of Zamboni et al. [19], our patient did not display any signs of tuberous sclerosis complex.

To our knowledge, we report here the first observation of simultaneous hepatic FNH and pancreatic ST. The simultaneous occurrence of FNH and a PEComa (an hepatic angiomyolipoma) has only been reported once [9]. FNH is a reactive, polyclonal process [13], whereas, PEComas have been described as neoplastic, monoclonal lesions [5, 12]. Therefore, the simultaneous occurrence of pancreatic ST and hepatic FNH, which we report, is probably incidental.

Conclusion

To our knowledge, this study is the second to report a case of pancreatic ST. STs are benign and display characteristic IHC features that can be evidenced on FNA samples. Therefore, STs should be considered in preoperative differential diagnosis of pancreas tumors, since they may be treated by limited surgical resection.

Acknowledgements We thank Dr. Lucile Andrac-Meyer, Christiane Bailly, Laurence Lamant, and Talal al-Saati for their kind help.

References

1. Bonetti F, Martignoni G, Colato C, Manfrin E, Gambacorta M, Faleri M, Bacchi C, Sin VC, Wong NL, Coady M, Chan JK (2001) Abdominopelvic sarcoma of perivascular epithelioid cells. Report of four cases in young women, one with tuberous sclerosis. Mod Pathol 14:563–568
2. Bonetti F, Pea M, Martignoni G, Doglioni C, Zamboni G, Capelli P, Rimondi P, Andrion A (1994) Clear cell ("sugar") tumor of the lung is a lesion strictly related to angiomyolipoma—the concept of a family of lesions characterized by the presence of the perivascular epithelioid cells (PEC). Pathology 26:230–236
3. Cibas ES, Goss GA, Kulke MH, Demetri GD, Fletcher CD (2001) Malignant epithelioid angiomyolipoma ('sarcoma ex angiomyolipoma') of the kidney: a case report and review of the literature. Am J Surg Pathol 25:121–126
4. Folpe AL (2002) Neoplasms with perivascular epithelioid cell differentiation (PEComas). In: Fletcher CDM, Unni KK, Mertens F (eds) Pathology and genetics of tumours of soft tissue and bone. IARC Press, Lyon, pp 221–222
5. Folpe AL, Goodman ZD, Ishak KG, Paulino AF, Taboada EM, Meehan SA, Weiss SW (2000) Clear cell myomelanocytic tumor of the falciform ligament/ligamentum teres: a novel member of the perivascular epithelioid clear cell family of tumors with a predilection for children and young adults. Am J Surg Pathol 24:1239–1246
6. Govender D, Sabaratnam RM, Essa AS (2002) Clear cell 'sugar' tumor of the breast: another extrapulmonary site and review of the literature. Am J Surg Pathol 26:670–675
7. Heywood G, Smyrk TC, Donohue JH (2004) Primary angiomyolipoma of the pancreas. Pancreas 28:443–445
8. Kung M, Landa JF, Lubin J (1984) Benign clear cell tumor ("sugar tumor") of the trachea. Cancer 54:517–519
9. Langner C, Homayounfar K, Ruten B, Fass J, Ruschoff J (2001) Concomitant occurrence of angiomyolipoma, focal nodular hyperplasia, bile duct adenoma, and cavernous hemangioma in the liver. Pathologe 22:417–423
10. Lubensky IA, Pack S, Ault D, Vortmeyer AO, Libutti SK, Choyke PL, Walther MM, Linehan WM, Zhuang Z (1998) Multiple neuroendocrine tumors of the pancreas in von Hippel–Lindau disease patients: histopathological and molecular genetic analysis. Am J Pathol 153:223–231
11. Martignoni G, Pea M, Rigaud G, Manfrin E, Colato C, Zamboni G, Scarpa A, Tardanico R, Roncalli M, Bonetti F (2000) Renal angiomyolipoma with epithelioid sarcomatous transformation and metastases: demonstration of the same genetic defects in the primary and metastatic lesions. Am J Surg Pathol 24:889–894
12. Paradis V, Laurendeau I, Vieillefond A, Blanchet P, Eschwege P, Benoit G, Vidaud M, Jardin A, Bedossa P (1998) Clonal analysis of renal sporadic angiomyolipomas. Hum Pathol 29:1063–1067
13. Paradis V, Laurent A, Flejou JF, Vidaud M, Bedossa P (1997) Evidence for the polyclonal nature of focal nodular hyperplasia of the liver by the study of X-chromosome inactivation. Hepatology 26:891–895
14. Rochaix P, Lacroix-Triki M, Lamant L, Pichereaux C, Valmary S, Puente E, Al Saati T, Monsarrat B, Susini C, Buscail L, Delsol G, Voigt JJ (2003) PNL2, a new monoclonal antibody directed against a fixative-resistant melanocyte antigen. Mod Pathol 16:481–490
15. Sale GE, Kulander BG (1988) 'Benign' clear-cell tumor (sugar tumor) of the lung with hepatic metastases ten years after resection of pulmonary primary tumor. Arch Pathol Lab Med 112:1177–1178

16. Stone CH, Lee MW, Amin MB, Yaziji H, Gown AM, Ro JY, Tetu B, Paraf F, Zarbo RJ (2001) Renal angiomyolipoma: further immunophenotypic characterization of an expanding morphologic spectrum. Arch Pathol Lab Med 125:751–758
17. Tanaka Y, Ijiri R, Kato K, Kato Y, Misugi K, Nakatani Y, Hara M (2000) HMB-45/melan-A and smooth muscle actin-positive clear-cell epithelioid tumor arising in the ligamentum teres hepatis: additional example of clear cell 'sugar' tumors. Am J Surg Pathol 24:1295–1299
18. Tazelaar HD, Batts KP, Srigley JR (2001) Primary extrapulmonary sugar tumor (PEST): a report of four cases. Mod Pathol 14:615–622
19. Zamboni G, Pea M, Martignoni G, Zancanaro C, Faccioli G, Gilioli E, Pederzoli P, Bonetti F (1996) Clear cell "sugar" tumor of the pancreas. A novel member of the family of lesions characterized by the presence of perivascular epithelioid cells. Am J Surg Pathol 20:722–730
20. Zavala-Pompa A, Folpe AL, Jimenez RE, Lim SD, Cohen C, Eble JN, Amin MB (2001) Immunohistochemical study of microphthalmia transcription factor and tyrosinase in angiomyolipoma of the kidney, renal cell carcinoma, and renal and retroperitoneal sarcomas: comparative evaluation with traditional diagnostic markers. Am J Surg Pathol 25:65–70

Virchows Arch (2005) 446: 560–565
DOI 10.1007/s00428-005-1241-3

CASE REPORT

Eleni Vrettou · Prodromos Hytiroglou · Nikolaos Sikas · Ioannis Soultoyannis · Zachary D. Goodman

Hepatic adenocarcinoma expressing inhibin in a young patient on oral contraceptives

Received: 12 January 2005 / Accepted: 24 February 2005 / Published online: 7 April 2005
© Springer-Verlag 2005

Abstract A case of primary hepatic carcinoma is reported, which occurred in a 24-year-old woman with a 10-year history of oral contraceptive use, and demonstrated unique morphologic and immunohistochemical features. The tumor was located in the left hepatic lobe, measured 14 cm at its widest, and showed histologic heterogeneity. The neoplastic cells were mostly arranged in trabecular and pseudoglandular growth patterns simulating hepatocellular carcinoma; however, in focal areas, small cystic, organoid and tubular patterns predominated. Immunohistochemical stains showed a phenotype consistent with biliary differentiation (positive staining for cytokeratin 7, cytokeratin 19, carcinoembryonic antigen and CA 19-9 antigen). The tumor cells were negative for markers that would be suggestive of hepatocytic or neuroendocrine differentiation. Interestingly, they were positive for inhibin, a protein that is known to be expressed in sex cord–stromal tumors of the ovary, trophoblastic neoplasms and adrenal cortical tumors, but not in hepatic tumors. However, no definite evidence of gonadal stromal, trophoblastic, or adrenocortical differentiation was identified on extensive immunohistochemical work-up. In conclusion, this unique case may represent a rare variant of cholangiocarcinoma expressing inhibin.

Keywords Adenocarcinoma · Cholangiocarcinoma · Inhibin · Liver

E. Vrettou · P. Hytiroglou (✉) · I. Soultoyannis
Department of Pathology, Aristotle University Medical School,
540 06 Thessaloniki, Greece
e-mail: phitir@med.auth.gr
Tel.: +30-2310-999218
Fax: +30-2310-999229

N. Sikas
The Interbalkan Medical Center,
Thessaloniki, Greece

Z. D. Goodman
The Armed Forces Institute of Pathology,
Washington, DC, USA

Introduction

Adenocarcinomas of the liver (intrahepatic cholangiocarcinomas) represent approximately 10% of primary carcinomas of this organ, and are thought to be derived from biliary epithelial cells. These tumors are known to be etiologically associated with parasitosis of the bile ducts, hepatolithiasis, congenital anomalies of the biliary tree, primary sclerosing cholangitis and Thorotrast exposure [2, 4]. Oral contraceptive steroids have also been suggested as possible etiologic agents of both intrahepatic and extrahepatic cholangiocarcinoma [1, 8]. In western countries, the majority of cholangiocarcinomas occur in patients without obvious predisposing factors.

While the commonest histologic appearance of cholangiocarcinoma is that of a tubular adenocarcinoma with abundant fibrous stroma, other architectural patterns may also be observed, including trabecular and papillary structures [2, 4]. Immunohistochemical stains typically show positivity for "biliary-type" cytokeratins (cytokeratins 7 and 19), carcinoembryonic antigen, epithelial membrane antigen, and antigen CA 19-9. Expression of inhibin is not a feature of either cholangiocarcinoma or any other primary hepatic tumor. This protein is commonly detected in gonadal stromal tumors and, occasionally, in other ovarian, trophoblastic and adrenal cortical neoplasms [3, 5–7, 9].

We report a unique case of hepatic adenocarcinoma with unusual histologic features, which expressed inhibin and occurred in a young patient on oral contraceptives.

Clinical history

A 24-year-old white woman presented with a 15-day history of nausea, vomiting and abdominal discomfort. Physical examination was remarkable for a palpable mass in the mid-upper abdomen. There were no other findings on complete systemic examination. The patient's past medical history was unremarkable. She was a non-smoker and occasionally consumed very small amounts of alcohol. She had

been on oral contraceptives (combination of 0.02 mg ethinylestradiol and 0.15 mg desogestrel) for 10 years.

Computed tomography (CT) scan of the abdomen showed a well-circumscribed mass, located in the left hepatic lobe and occupying the inferior and lateral borders. On administration of intravenous contrast, the lesion showed inhomogeneous enhancement, which was more intense on late images (Fig. 1a). On magnetic resonance images, the mass appeared well defined and measured 16.7×16.2 cm. It was multilobulated and inhomogeneous, with cystic changes, and showed enhancement after intravenous administration of paramagnetic contrast material (Fig. 1b). Biochemistry and hematology results were within normal limits. The serum levels of tumor markers, including carcinoembryonic antigen, CA 19-9 antigen and CA 125 antigen, were also within normal limits. A full hormonal screen, including follicle stimulating hormone, luteinizing hormone, prolactin, estradiol, progesterone, testosterone, dehydroepiandrosterone-S and thyroid-stimulating hormone, did not reveal any abnormality.

At laparotomy, the tumor mass was found to involve hepatic segments II and III and appeared to have a "pushing" rather than infiltrating border. A left lobectomy was performed. The lesion was excised intact, together with a 3-cm rim of hepatic parenchyma. The patient had an uneventful postoperative course and was discharged home 7 days following surgery. Since then (almost 3 years ago), she has been on follow-up with physical examination and tumor markers every 3 months, abdominal ultrasound scan every 6 months, and CT scan of thorax and abdomen every year. She has remained free of recurrence. No further treatment has been given.

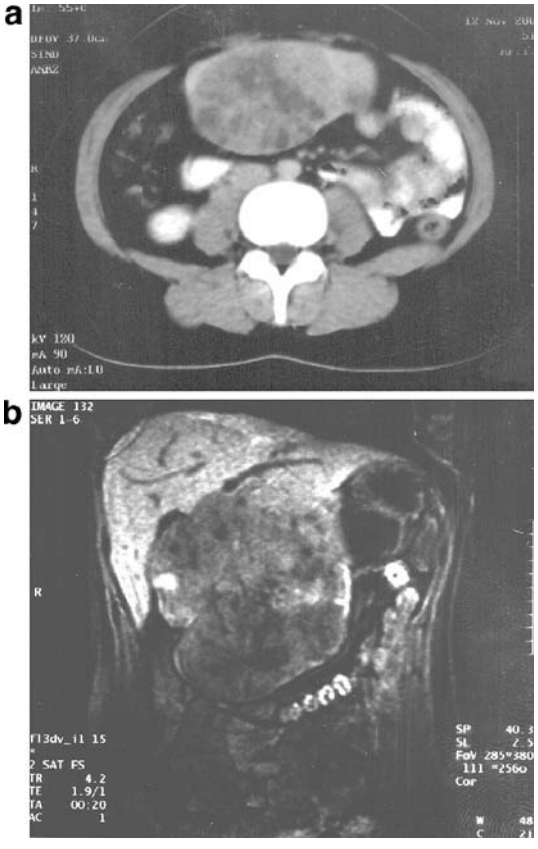

Fig. 1 Radiographic findings: **a** Abdominal CT scan showing a well-circumscribed tumor mass in the left hepatic lobe. **b** MRI of the abdomen: on fat saturation images, the tumor appears multilobulated and inhomogeneous, with focal cystic changes

Table 1 Summary of immunohistochemical stains. *HepPar-1* hepatocyte specific antigen; *CEA* carcinoembryonic antigen; *hCG* human chorionic gonadotropin; *NSE* neuron-specific enolase; *ER* estrogen receptor; *PR* progesterone receptor; *PAP* prostatic acid phosphatase

Antigen	Source of antibody	Clone	Result
Pancytokeratin	DAKO	AE1/AE3	Moderately positive
Cytokeratin 8/18	Becton Dickinson	cam5.2	Moderately positive
Cytokeratin 7	DAKO	OV TL 12/30	Strongly positive
Cytokeratin 19	DAKO	RCK108	Strongly positive
Cytokeratin 20	DAKO	Ks 20.8	Negative
HepPar-1	DAKO	OCH1E5	Negative
pCEA	DAKO	Polyclonal	Positive (cytoplasmic and membranous)
mCEA	DAKO	11-7	Negative
EMA	DAKO	E29	Negative
CA 19-9	DAKO	116-NS-19-9	Focally positive
CA 125	Novocastra	NCL-CA125	Negative
α-Fetoprotein	Signet	Polyclonal	Negative
hCG	Biocare	Polyclonal	Negative
NSE	Biocare	DT01-BC10	Negative
Chromogranin	Sanbio	Polyclonal	Negative
Synaptophysin	Ventana	Polyclonal	Negative
Somatostatin	Chemicon	Polyclonal	Negative
Insulin	DAKO	Polyclonal	Negative
Thyroglobulin	DAKO	DAK-Tg6	Negative
Calcitonin	Biogenex	Polyclonal	Negative
Vimentin	Biocare	V-9	Negative
Inhibin	DAKO	R1	Strongly positive
ER protein	DAKO	1D5	Negative
PR protein	Novocastra	1A6	Negative
PAP	DAKO	PASE/4LJ	Negative
S-100 protein	DAKO	Polyclonal	Rare positive cells
HMB-45	DAKO	HMB-45	Negative
CD10	Novocastra	56C6	Negative
CD34	Biogenex	Qbend/10	Negative
CD56	Novocastra	ERIC-1	Moderately positive
CD117 (c-kit)	Biotechnology	C-19	Negative
Ki-67	Immunotech	MIB1	5–10% of nuclei positive
p53	DAKO	D0-7	Negative

Materials and methods

Multiple sections of tumor and non-tumorous hepatic parenchyma were routinely processed for paraffin sections. Sections 4 μm thick were stained with hematoxylin–eosin and mucicarmine. Additional paraffin sections were used for immunohistochemical stains with a standard streptavidin–biotin staining protocol. The primary antibodies utilized and their sources are shown in Table 1.

Results

The surgical specimen weighted 940 g and measured 15× 14×7.5 cm. On sectioning, the specimen was almost com-

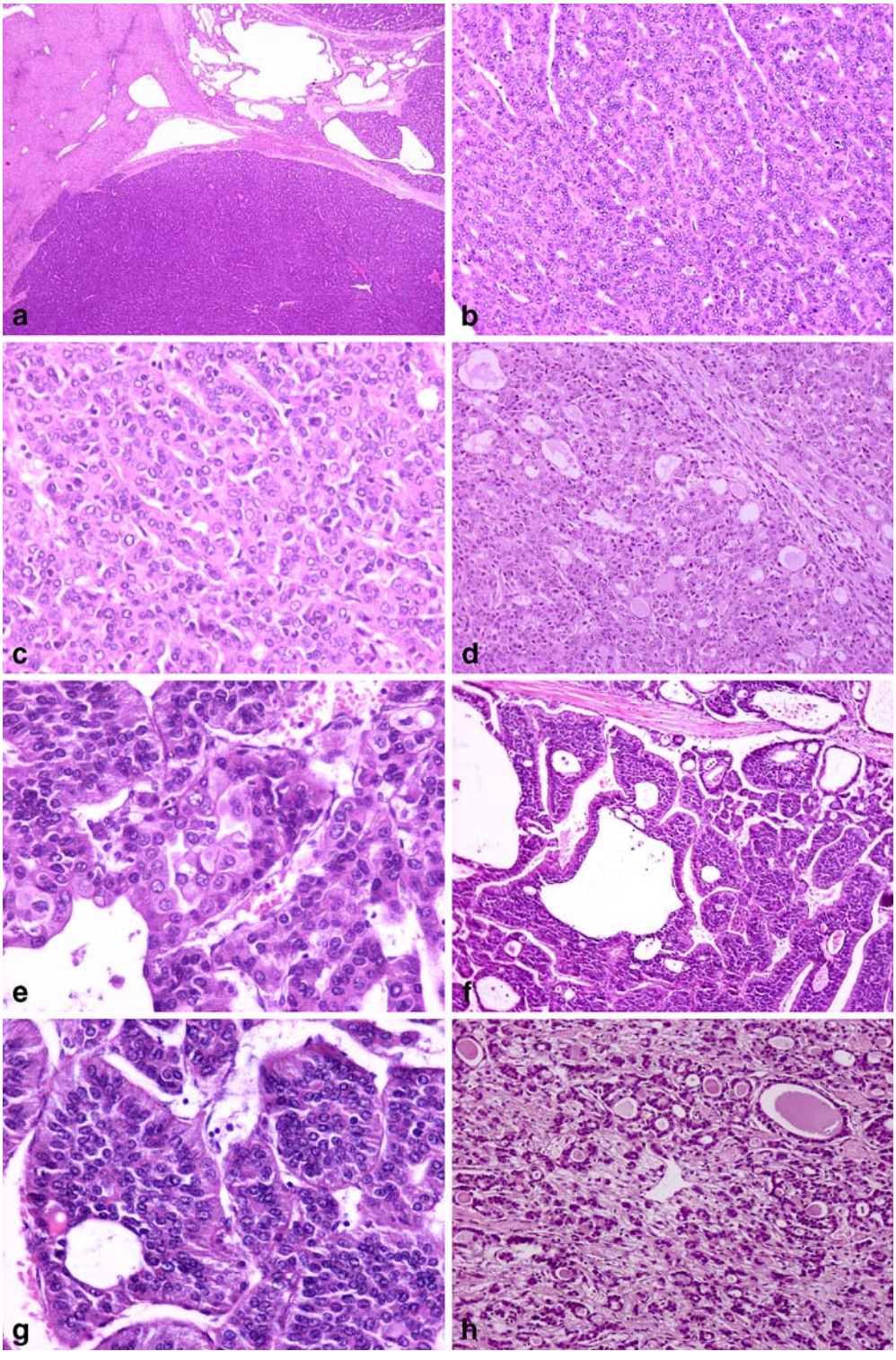

Fig. 2 Microscopic features. **a** Low-power view of the tumor shows areas of trabecular (bottom) and microcystic (top) architecture. **b** The trabeculae vary in thickness and are lined by endothelial cells. **c** High-power view shows cuboidal or columnar neoplastic cells with moderate nuclear pleomorphism. **d** In some areas, the cells form prominent pseudoglandular structures. **e** Occasional clusters of tumor cells with hepatocytoid features are present. **f**, **g** Focally, the tumor cells are arranged in organoid structures. **h** In a different area, the tumor cells form tubular structures within a loose fibrous stroma. (Original magnifications: **a**: ×20; **b**, **d**, **h**: ×100; **c**: ×200; **e**, **g**: ×400; **f**: ×40)

pletely occupied by a well-demarcated tumor, measuring 14 cm at its widest. The cut surface was tan, solid, with focal areas of microcystic change and extensive areas of hemorrhage.

Microscopic examination showed a carcinoma with predominantly trabecular architecture (Fig. 2a, b). The tumor cells were columnar or cuboidal, with roundish, hyperchromatic nuclei and moderate amounts of eosinophilic or amphophilic cytoplasm (Fig. 2c). Mitotic activity was mild. The trabeculae were several cells thick, and were lined by endothelial cells. The neoplastic cells within the trabeculae were often arranged in pseudoglandular structures, some-

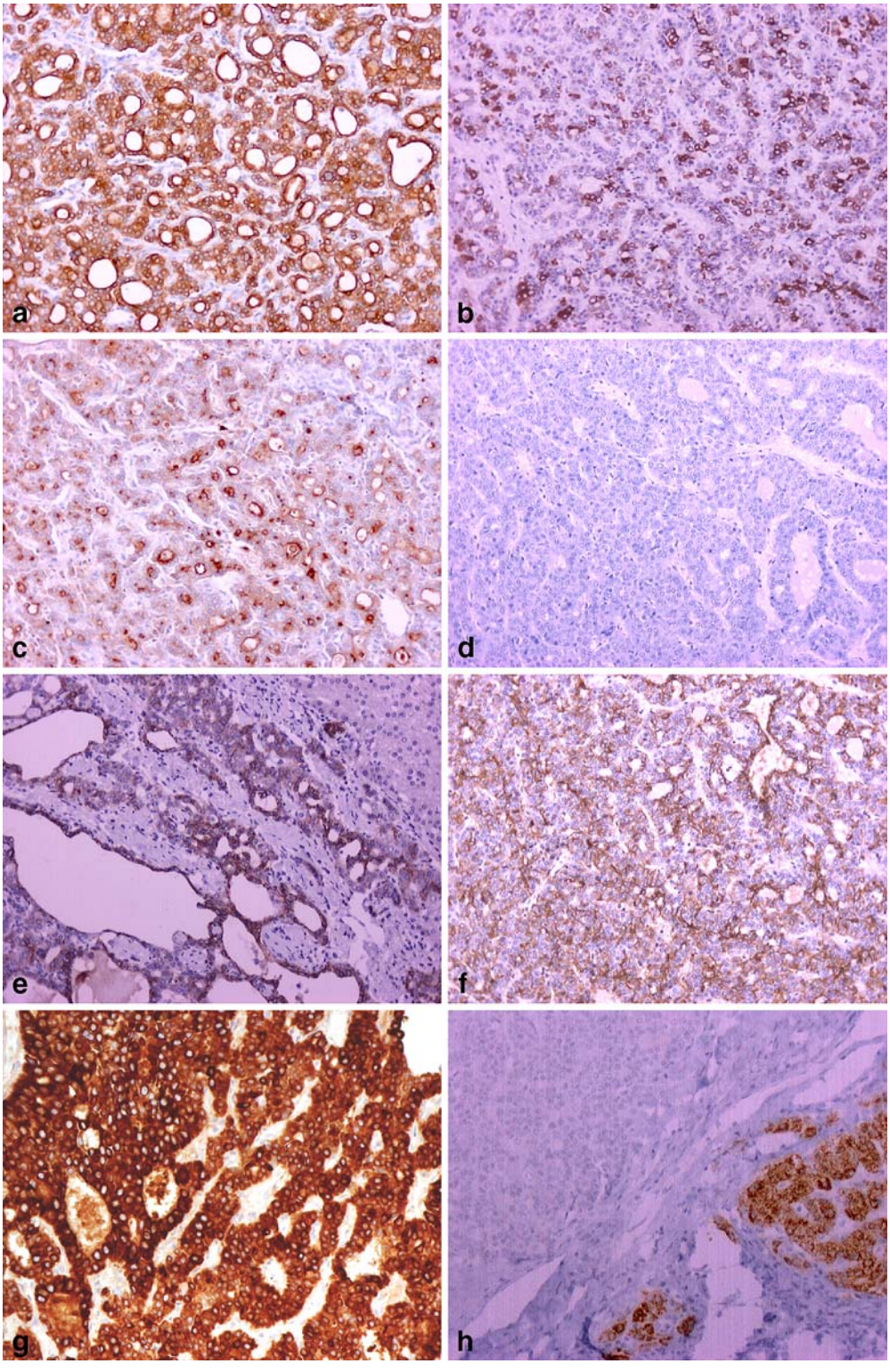

Fig. 3 Immunohistochemical findings: the tumor cells are positive for cytokeratin 7 (**a**) and cytokeratin 19 (**b**). Stains for carcinoembryonic antigen demonstrate cytoplasmic and membranous positivity with polyclonal (**c**), but not with monoclonal antibodies (**d**). The tumor cells are also positive for CA 19–9 (**e**), CD56 antigen (**f**) and inhibin (**g**). No positivity for HepPar-1 is seen in the neoplasm, as contrasted to nearby hepatocytes (**h**). (Original magnifications: **a**–**f**: ×100; **g**, **h**: ×200)

times containing amorphous eosinophilic material in the lumina (Fig. 2d). No bile production was seen. Mucicarmin stain was negative for mucin. In the central portion of some trabeculae, the tumor cells contained increased amounts of eosinophilic cytoplasm, resembling hepatocytes (Fig. 2e). In some areas, the neoplastic cells lined small cystic spaces (Fig. 2a, f) or formed organoid structures (Fig. 2f, g). In a small area close to the tumor edge, the tumor cells formed tubular structures, surrounded by a loose fibroconnective tissue stroma (Fig. 2h). The tumor contained foci of hemosiderin deposition, small foci of necrosis and occasional microcalcifications. The surrounding hepatic parenchyma appeared compressed, without evidence of pre-existing disease. The surgical margins of resection were free of tumor.

Due to the unusual histologic features of the tumor, extensive immunohistochemical stains were performed (Table 1). The neoplastic cells were positive for "biliary-type" cytokeratins (cytokeratins 7 and 19), carcinoembryonic antigen (cytoplasmic and membranous staining with polyclonal, but not with monoclonal antibodies), CA 19-9 antigen and CD56 antigen (Fig. 3a–f). They were also positive for inhibin (Fig. 3g). The tumor cells were negative for a variety of other markers, including those which would be suggestive of hepatocytic or endocrine differentiation (Table 1, Fig. 3h).

Discussion

Several aspects of the case reported herein are unusual. In the absence of chronic liver disease, hepatic carcinomas are rare in the 3rd decade of life, and, as a rule, represent hepatocellular carcinomas of the fibrolamellar variant. Our case did not demonstrate histologic features characteristic of fibrolamellar carcinoma. Since our patient did not have any other predisposing factor for tumor development, attention must be focused on the 10-year-long history of oral contraceptive use. In an analysis of possible etiologic factors in a series of 42 patients with intrahepatic cholangiocarcinoma, Altaee et al. found that 35% of the women had used oral contraceptives [1]. In a different study, a statistically significant association between the use of contraceptives and extrahepatic bile duct cancer was observed among women under 60 years of age [8].

The histologic features of our case are also unusual. In most areas, the predominant growth patterns were trabecular and pseudoglandular, simulating hepatocellular carcinoma. In several trabeculae, a neoplastic cell subpopulation with features suggestive of hepatocellular differentiation was also found. However, the tumor cell immunophenotype (cytokeratin 7 and 19 positive, carcinoembryonic antigen positive, CA 19-9 positive, hepatocyte specific antigen negative, α-fetoprotein negative) was consistent with a biliary tumor. Immunopositivity for CD56 antigen may also be supportive of biliary differentiation [10]. Because of the tendency of the neoplastic cells to form organoid structures, a variety of markers of endocrine differentiation were assessed, but were found to be negative.

The most unusual feature of this case was the strongly positive immunostaining for inhibin. This glycoprotein is known to be synthesized by granulosa cells, luteinized thecal cells, and hilus cells of the normal ovary, and to regulate reproductive functions in conjunction with activin [3]. Inhibin is widely accepted as a marker for sex cord tumors, especially for granulosa cell tumors, and appears to be helpful in the differential diagnosis of such tumors from other neoplasms affecting the ovary [5]. In addition, inhibin is expressed by syncytial trophoblastic cells and in neoplasms of trophoblastic origin, such as hydatidiform moles, placental site nodule, placental trophoblastic tumors, and choriocarcinoma [3, 7]. This protein is also expressed by the majority of adrenocortical adenomas and carcinomas [6, 9].

Inhibin expression is not considered a feature of primary hepatic neoplasms. On immunohistochemical studies, both hepatocellular carcinoma and cholangiocarcinoma have been found to be negative for this protein, with the exception of a single case of high-grade pleomorphic hepatocellular carcinoma [11–13]. In the absence of histologic and immunohistochemical evidence of gonadal stromal, trophoblastic or adrenocortical differentiation in the tumor we are reporting, we must conclude that this neoplasm represents a unique case of cholangiocarcinoma expressing inhibin. A possible association with oral contraceptive use may be suggested, but cannot be proven at the present time.

References

1. Altaee MY, Johnson PJ, Farrant JM, Williams R (1991) Etiologic and clinical characteristics of peripheral and hilar cholangiocarcinoma. Cancer 68:2051–2055
2. Anthony PP (2002) Tumours and tumour-like lesions of the liver and biliary tract: aetiology, epidemiology and pathology. In: MacSween RNM, Burt AD, Portmann BC, Ishak KG, Scheuer PJ, Anthony PP (eds) Pathology of the liver, 4th edn. Churchill Livingstone, London, pp 711–775
3. Azumi N, Czernobilsky B (2002) Immunohistochemistry. In: Kurman RJ (ed) Blaustein's pathology of the female genital tract, 5th edn. Springer, Berlin Heidelberg New York, pp 1251–1276
4. Ishak KG, Goodman ZD, Stocker JT (2001) Tumors of the liver and intrahepatic bile ducts. In: Atlas of tumor pathology, 3rd series, Fascicle 31. Armed Forces Institute of Pathology, Washington, pp 185–198
5. Kommoss F, Oliva E, Bhan AK, Young RH, Scully RE (1998) Inhibin expression in ovarian tumors and tumor-like lesions: an immunohistochemical study. Mod Path 11:656–664
6. Pelkey TJ, Frierson HF Jr, Mills SE, Stoler MH (1998) The alpha subunit of inhibin in adrenal cortical neoplasia. Mod Path 11:516–524
7. Shih IM, Kurman RJ (1999) Immunohistochemical localization of inhibin-alpha in the placenta and gestational trophoblastic lesions. Int J Gynecol Pathol 18:144–150
8. Yen S, Hsieh CC, MacMahon B (1987) Extrahepatic bile duct cancer and smoking, beverage consumption, past medical history, and oral contraceptive use. Cancer 59:2112–2116
9. Zhang PJ, Genega EM, Tomaszewski JE, Pasha TL, LiVolsi VA (2003) The role of calretinin, inhibin, melan-A, BCL-2, and C-kit in differentiating adrenal cortical and medullary tumors: an immunohistochemical study. Mod Path 16:591–597

10. Van Den Heuvel MC, Sloof MJH, Visser L, Muller M, De Jong KP, Poppema S, Gouw ASH (2001) Expression of anti-OV6 antibody and anti-N-CAM antibody along the biliary line of normal and diseased human livers. Hepatology 33:1387–1393
11. Renshaw AA, Granter SR (1998) A comparison of A103 and inhibin reactivity in adrenal cortical tumors: distinction from hepatocellular carcinoma and renal tumors. Mod Path 11:1160–1164
12. Iezzoni JC, Mills SE, Pelkey TJ, Stoler MH (1999) Inhibin is not an immunohistochemical marker for hepatocellular carcinoma. An example of the potential pitfall in diagnostic immunohistochemistry caused by endogenous biotin. Am J Clin Pathol 111:229–234
13. Lau SK, Prakash S, Geller SA, Alsabeh A (2002) Comparative immunohistochemical profile of hepatocellular carcinoma, cholangiocarcinoma, and metastatic adenocarcinoma. Hum Pathol 33:1175–1181

Virchows Arch (2005) 446: 566–568
DOI 10.1007/s00428-005-1253-z

CASE REPORT

Noelyn Anne Hung

Congenital "clear cell sarcoma of the kidney"

Received: 27 November 2004 / Accepted: 7 March 2005 / Published online: 19 April 2005
© Springer-Verlag 2005

Abstract At 31 weeks gestation, a hydropic male fetus died in utero with metastatic disease from a renal clear cell sarcoma. The tumor had metastasized to para–aortic and mediastinal lymph nodes, lung, pleura, and liver, leading to superior vena cava obstruction and pulmonary hypoplasia. The pathologic findings and cytogenetic analysis of the fetus and tumor are presented. In addition, review of the literature reveals six other cases aged <6 months of age, including two extrarenal cases.

Keywords Clear cell sarcoma kidney · Congenital · Metastatic · Cytogenetics

Introduction

Clear cell sarcoma of the kidney is a rare aggressive neoplasm of the pediatric population, which is even more rarely reported as a congenital tumor or in the first 6 months of life. The usual age of diagnosis is about 3 years old with a male predominance. Also called "bone metastasizing renal sarcoma", it has a propensity to metastasize to bone, lung, liver and lymph nodes. Extrarenal tumors with identical morphology and phenotype are also included in this report.

In this remarkable case, a hydropic male fetus died in utero with metastatic disease at 31 weeks gestation. The tumor was locally invasive, and had metastasized to para–aortic and mediastinal lymph nodes, leading to superior vena cava obstruction and pulmonary hypoplasia. Metastases were found in the lung, liver, and pleura. The pathologic findings, and cytogenetic analysis of the fetus and tumor are presented. In addition, review of the literature reveals six other cases aged <6 months of age, including two extrarenal cases.

N. A. Hung (✉)
Pathology Department,
University of Otago Medical School,
PO Box 913 Dunedin,
New Zealand
e-mail: Noelyn.hung@stonebow.otago.ac.nz
Tel.: +64-3-4740999
Fax: +64-3-4747813

Clinical history

A 36-year-old woman in her third pregnancy, with no significant past medical history or family history of pediatric or renal tumors, presented with decreased fetal movements. A 20 week gestation ultrasound scan by an experienced ultrasonographer assessed fetal anatomy as normal. A further scan performed at the time of presentation at 31 weeks for lack of fetal movements identified intrauterine demise of the fetus, and, labor was therefore induced. (The mother has since delivered a healthy term infant with no evidence of renal anomaly.)

The fetus was a grossly hydropic male fetus weighing 2665 g, crown–rump length 32 cm, crown–heel length 42 cm and foot length of 6.8 cm. The head circumference was 32.5 cm and abdominal circumference 32 cm. Within the chest cavity, the heart and both lungs were displaced to the left and the right pleural cavity contained 175 ml of serous fluid.

The pleural surface of the diaphragm and posterior part of the parietal pleura had multiple small tumor deposits. The heart was normal in weight and anatomy, weighing 11 g, but both the bilobed left lung and trilobed right lung were hypoplastic, weighing 12 g combined. A tumor nodule was present within the hilum of the left lung. The mediastinal nodes were grossly enlarged by metastatic tumor, and these extended around the superior vena cava and great vessels.

The right kidney weighed 24 g and tumor comprised at least 15 g, measuring 30 mm in diameter. The upper pole of the right kidney was replaced by tumor that invaded posteriorly into the retroperitoneal soft tissues close to the vertebrae and replaced para–aortic lymph nodes. The left kidney was normal, weighing 9 g. Both ureters and urinary bladder were normal. The left and right adrenals were normal, although the right adrenal gland was engulfed by tumor. Microscopically cytologic detail was evident in all organs despite intrauterine demise.

Materials and methods

Immunohistochemical studies were performed according to the manufacturer's protocol for the following antibody clones and dilutions: Vimentin Dako clone v9, 1:500 dilution, CD10 Novocastra clone 56C6 1:100, pan–cytokeratin MNF 116 Dako 1:100, S100 Dako 1:500, HMB–45 Dako 1:50, LCA Dako clone PD7/26, 1:100), CD30 Dako clone Ber H2 1:40, CD34 Dako clone QBEnd10, 1:50, CD99, EMA Dako clones E29, 1:100 and BerEP4, 1:200, and desmin Dako clone D33, 1:100, and BCL2 Dako clone 124, 1:50.

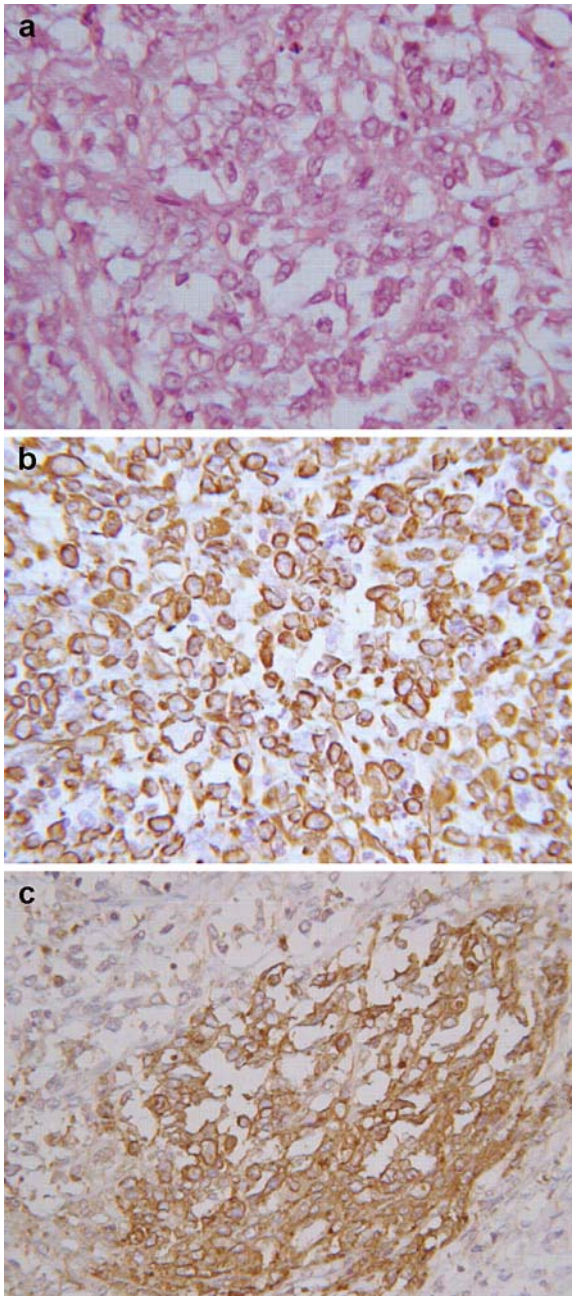

Fig. 1 **a** Hematoxylin stained section of non-necrotic areas of tumor, ×400 (**b** and **c**): vimentin and CD10 immunoperoxidase staining, respectively, ×400

G–banding cytogenetic analysis from primary culture was performed on fresh tissue from the normal kidney and tumor.

Results

Sections of the tumor showed a clear cell sarcoma of the kidney (Fig. 1a), consisting of an evenly dispersed network of fine arborizing vessels accompanied by a small amount of spindle–cell stroma occasionally defining nests and fascicles of tumor cells, consistent with the classical variant of clear cell sarcoma of the kidney. The tumor cells were of regular size with stellate cytoplasm. Finely dispersed chromatin was present in the nuclei, with inconspicuous nucleoli. Mitotic activity was moderate. Scattered pre–existent tubules or glomeruli were dispersed in the peripheral regions of the tumor, but the tumor invaded the surrounding soft tissues with metastatic deposits to the lungs, pleura, mediastinal lymph nodes, liver and para–aortic lymph nodes. Large areas of tumor necrosis were present in addition to scattered apoptotic figures. No areas of blastema or tubule formation were present. No evidence of nephrogenic rest formation was found in either kidney, as might be found in Wilms tumor. Osteoid–like non-birefringent matrix was not identified, as may be found in other variants of clear cell sarcoma of the kidney.

Immunohistochemistry was strongly and diffusely positive for vimentin (Fig. 1b), and focally strongly positive for CD10 (Fig. 1c). All other antibodies studied were negative.

Cytogenetics produced a 46XY karyotype from the normal tissue of the kidney, whereas the tumor produced a balanced translocation between chromosomes 13 and 14 (46,XY, t(13;14)(q12;q32) in the two metaphases that were suitable for analysis.

Discussion

The most commonly encountered congenital renal tumor is the low–grade malignant congenital mesoblastic nephroma that rarely occurs beyond the 4th month of life, and has an excellent prognosis provided resection is complete. Review of the literature reveals only a handful of cases of clear cell sarcoma of the kidney less than 6 months old, and no record of an intrauterine case [1–5, 8]. Two cases were reportedly included in the National Wilms Studies at age less than 6 months [5]. Three congenital cases reported separately in the literature [3, 4, 8] were diagnosed in the newborn period. Even though this represents a small number of cases, the usual predominance of male cases reported for older patients appears to hold true also for these younger cases, as presented in Table 1. Interestingly, two extrarenal cases were both female patients. A further female extrarenal case is also reported by Finn and Patterson [9], although this case is a month older than the group discussed herein.

The inability of an experienced ultrsonographer to diagnose the tumor in this case at 20 weeks gestation, even if

Table 1 Cases of clear cell sarcoma of the kidney reported in the literature. *A&W* alive and well, *DwD* dead with disease, *PR* perirenal, *NC* non-classical, *NS* not specified, *m* months, *NB* newborn

Author	Age	Sex	Site	Variant	Metastases	Follow-up	Outcome
Present case	Fetal	Male	Kidney	Classical	Multiple	–	DwD
Suzuki et al. 1983	NB	Male	Kidney	Classical	Negative/No PR invasion	12 m	A&W
Mazzoleni et al. 2003	NB	Male	Kidney	NC	Negative/No PR invasion	25 m	A&W
Kataoka et al. 1993	NB	Female	Ileal wall	NS	Multiple/local	1 m	DwD
Newbould and Kelsey 1993	4 m	Male	Kidney	Classical	PR invasion	NS	NS
Argani et al. 2000	5 m	Female	Ovary	Classical	NS	NS	NS
El Kababri et al 2004	5 m	NS	NS	NS	NS	NS	NS

present at that time, confirms the possibility for clear cell sarcoma of the kidney to grow and metastasize rapidly. The National Wilms Study report identified a favorable prognosis group of low stage [1], and indeed, the stage 1 congenital tumors in this group were reported to be alive and well without recurrence at 12 and 25 months.

However, the case reported herein, and, the case reported by Kataoka et al. [3], were stage 4 at presentation and pursued an aggressive course (despite surgery and chemotherapy including vincristine, cyclophosphamide, pirarubicin and cisplatin). The rapid demise in these cases suggests that both an aggressive and a more indolent form may exist, reflected in stage at presentation. It would seem premature, however, to propose that the prognosis of renal neoplasia of the sarcomatous type in the newborn should carry a favorable prognosis, and that aggressive therapy is not required [8].

Clear cell sarcoma of the kidney appears to arise from a primitive cell of the kidney and extrarenal cases may arise from mesonephric remnants, as all cases identified so far, even in older patients, have been associated with the pelvis or retroperitoneum [1]. This case has the typical immunoperoxidase profile with positive vimentin and CD10, and negative staining for keratins, CD99, EMA and desmin, which in addition to the morphological features, differentiates Wilms tumor, peripheral neuroectodermal tumor, and congenital mesoblastic nephroma. CD10 positivity has been reported in the developing kidney and clear cell sarcoma of the kidney [7].

Punnett et al. [6] found a 10;17 translocation in their case of clear cell sarcoma in an 11-month-old boy. In our case, a 13;14 translocation was found, but the significance of this finding is unclear, and no report of this translocation in other tumors exists to the best of the author's knowledge. Further reports of the cytogenetic findings in the clear cell sarcoma of the kidney in the English literature, were not identified.

Although rare, these cases illustrate that the so–called clear cell sarcoma of the kidney must be considered in the differential of congenital tumors, both intrarenal and extrarenal in location.

Acknowledgements The author wishes to thank Spencer Walker for his expert technical assistance.

References

1. Argani P, Perlman EJ, Breslow NE, Browning NG, Green DM, D'Angio GJ, Beckwith JB (2000) Clear cell sarcoma of the kidney: a review of 351 cases from the National Wilms Tumor Study Group Pathology Center. Am Surg Pathol 24(1):4–18
2. El Kababri M, Khattab M, El Khorassani M, Hessissen L, Kili A, Nachef MN, Cherradi N, Malihy A, Alhamany Z, Msefer-Alaoui F (2004) Clear cell sarcoma of the kidney. A study of 13 cases. Arch Pediatr 11(7):794–799
3. Kataoka Y, Shimada H, Sugimoto T, Mine H, Hachitanda Y, Doi Y, Sawada T, Weeks DA (1993) Congenital sarcoma in the terminal ileum histologically resembling clear cell sarcoma of the kidney: a case report with an immunohistochemical study. Hum Pathol 24(9):1026–1030
4. Mazzoleni S, Vecchiato L, Alaggio R, Cecchetto G, Zorzi C, Carli M (2003) Clear cell sarcoma of the kidney in a newborn. Med Pediatr Oncol 41(2):153–155
5. Newbould MJ, Kelsey AM (1993) Clear cell sarcoma of the kidney in a 4-month-old infant: a case report. Med Pediatr Oncol 21(7):525–528
6. Punnett HH, Halligan GE, Zaeri N, Karmazin N (1989) Translocation 10;17 in clear cell sarcoma of the kidney, a first report. Cancer Genet Cytogenet 41:123–128
7. Satoh F, Tsutsumi Y, Yokoyama S, Osamura RY (2000) Comparative immunohistochemical analysis of developing kidneys, nephroblastomas and related tumors: considerations on their histogenesis. Pathol Int 50(6):458–471
8. Suzuki H, Honzumi M, Itoh Y, Umehara N, Moriyama S, Funada M (1983) Clear cell sarcoma of the kidney seen in a 3-day-old newborn. Z Kinderchir 38(6):422–424
9. Finn LS, Patterson K (2000) Ovarian sarcoma with pathologic features of clear cell sarcoma of the kidney. Pediatr Dev Pathol 3:487–491

Virchows Arch (2005) 446: 569–576
DOI 10.1007/s00428-004-1189-8

MEETING REPORT

B. J. Lü · M. D. Lai · M. Dietel

An overview of the Sino–German symposium on new developments in surgical and basic pathology

Received: 8 December 2004 / Accepted: 8 December 2004 / Published online: 12 April 2005
© Springer-Verlag 2005

Introduction

For more than 100 years, a longstanding intense relationship based on many mutual activities has become part of Chinese and German medical history. For example, in 1907, Dr. Erich Paulun, a German doctor working in Shanghai around the turn of the 19th century, founded the first "Deutsche Medizinschule für Chinesen" (German Medical School for Chinese), later the Medical Faculty of the Tongji University (Shanghai and Wuhan). There, the tradition of a German-based medicine has been upheld until today, leading to student education with lectures in the German language. In Germany, many Chinese doctors have been and still are working while influencing the medical development of many fields. Traditional Chinese Medicine, for example, is very popular in Germany and adds a lot of stimulating ideas to so-called Western medicine. Due to the political situation, there was a period of silence beginning with World War II up to the 1980s, and, only after the policy of openness, could the co-operation be re-established step by step by strong activities from both sides. In the field of anatomical and surgical pathology, the recent years were dominated by the intention to share knowledge and skills as well as to exchange young colleagues. For example, a telepathology project was initiated between Shanghai, Chongching and Berlin, supported by the National Science Foundation of China and the Deutsche Forschungsgemeinschaft. To give these activities a framework, the authorities of the German and the Chinese Society of Pathology agreed to establish continuous interactions, e.g. with the presence of representatives at the annual meetings of each society. Among other reasons, this was to reflect the dramatically increasing importance of the People's Republic of China in the scientific community.

As a first step, a Sino–German Symposium on New Development in Surgical and Basic Pathology was held in Hangzhou, China, between 22 April 2004 and 24 April 2004. Attending this symposium were 23 leading pathologists from both countries, supported by the Sino–Germany Science Center and chaired by Professor Maode Lai (Zhejiang University, China) and Professor Manfred Dietel (Humboldt University, Germany). This meeting not only covered a comprehensive update of recent developments in surgical and basic pathology but also provided a general aspect of these fields in both countries. It intended to establish a forum to foster the communication and collaboration for pathologists of China and Germany. This report summarises the essential information from the meeting.

B. J. Lü · M. D. Lai
Department of Pathology, School of Medicine,
Zhejiang University,
Hangshou, PR China

M. Dietel (✉)
Institute of Pathology, Charité,
Berlin, Germany
e-mail: manfred.dietel@charite.de

Basic pathology

Professor Heinz Höfler (Technische Universität München, Germany) introduced overall aspects of molecular pathology in Germany. Professor Dietel gave an overview of DNA array technology in diagnostic pathology. This technology may provide molecular signatures for individual tumours as potential powerful indicators for diagnosis, therapy response and prognosis, etc. It will become possible to determine the biological behaviour of a given tumour much more precisely, for example, to predict the potential to metastasise, the resistance to cytostatic drugs or the individual prognosis. The diagnostic of genomic signatures may lead to a new approach of functional surgical pathology. Professor Lai reviewed the state of the art with regard to proteomics in cancer research and briefly mentioned one novel protein that overexpressed in colonic cancers in comparison with corresponding normal colonic mucosa and adjacent mucosa to cancers, detected by 2-D electrophoresis in the up-to-date study of his group on proteomics of colorectal cancer.

Professor Jie Zheng (Peking University, China) showed his group's extensive and intensive studies on a novel gene-

tumour metastasis-related gene (TMSG-1, Genebank accession: NP_037516; gi:7019445), which his group first discovered. This gene was first surrogated by mRNA differential display polymerase chain reaction (PCR) separately on four prostate cancer cell lines or subclones (*BE1*/*LH7* and*1E8*/*2B4*), as overexpressions in two subclones (*LH7* and *2B4*) with low invasive and metastatic capacity that had previously been verified by tumourigenesis and spontaneous metastasis in nude mice; then, its full-length cDNA sequence was obtained via sequencing and ESTs assembly, and its chromosomal location (1p) was also disclosed. Eventually, this gene was reconfirmed by Northern-blot technique on the four cell lines or subclones and prime in situ labelling on *2B4* subclone. Monoclonal antibody of TMSG-1 was produced using a standard hybridoma technique. Semi-quantitative reverse-transcription (RT)-PCR on six common human cancers revealed that the expression level was highest in prostate adenocarcinoma (grade IV) and recurrent poorly differentiated breast cancer while lowest in lung cancer. Nevertheless, a higher expression level was documented in poorly differentiated colonic adenocarcinoma than in well-differentiated cancers. Strong positive signals or cytoplasmic stains were found in *2B4* and *LH7* subclones by either Western-blot or immunocytochemical staining in contrast with negative results in the remaining *1E8* and *BE1*. For both breast and colorectal cancers, positive staining (++–+++) was more common in cancers with metastasis than without metastasis (36% versus 7.4% in breast and 52% versus 35% in colorectal). Biological effects of TMSG-1 gene transfection on two prostate cancer cell lines (*2B4* and *1E8*) were also studied. Both transfectants with TMSG-1 sense displayed considerably suppressed cell growth in the curve, obviously lower outside diameter (OD) ratio in mean transit time and reduced clone formation in soft agar clone formation assay, compared with those with vain vector or non-transfectants, while transfectants with anti-sense exhibited more active cell growth, a higher OD ratio and increased clone formation. However, cell apoptotic rate increased only in the sense transfectants and was relatively invariable in anti-sense or vain vector transfectants and non-transfectants.

Professor Weigang Fang (Peking University, China) presented his group's findings, showing the effects of agonists [adenosine triphosphate (ATP) and adenosine monophosphate-purine nucleoside phosphorylase] or antagonists (suramin, PD and SB) of P2 purinoreceptor Y (P2Y), a G protein coupled receptor, on mitogen-activated extracellular signal-regulated kinase-activating kinase (MEK)-mitogen-activated protein kinase (MAPK) or p38 signal transduction pathways in two prostate cancer cell lines, metastatic *1E8* and non-metastatic *2B4*, using Western-blot method. The activities of ERK1/2 and p38 were significantly enhanced by ATP in a time- and dose-dependent manner in both cell lines. However, these effects were dramatically suppressed by surman, PD and SB, indicating that P2Y activation could incur MEK-MAPK and p38 signal transduction pathways. Furthermore, P2Y receptor-induced ERK1/2 and p38 activation as well as NFB activity were found higher in metastatic *1E8* cells than in non-metastatic *2B4* cells, implying a potential signalling mechanism in regulating metastatic phenotype. In in vitro invasion assay, the invasion of both cell lines was stimulated by ATP in parallel with ERK1/2 and p38 activation, and this effect by ATP was blocked by pretreament with SB. While *1E8* and *2B4* both were transfected with dominant-negative MAPK kinase 1 (KA-MEK1), both KA-MEK1 transfectants showed an obvious decrease in passing through matrigel-coated membranes as well as ERK1/2 activities, as compared with pcDNA3 transfectants. MAP kinase phosphatase 5 (MKP5), a novel MKP that inactivates p38 and SAPK/JNK but not MAPK/ERK, was also found to incite cancer invasion by inhibiting ATP-induced p38 activation. As a corollary, activation of both downstream transduction pathways of P2Y receptor, ERK1/2 and p38, might be of great importance in promoting prostate cancer invasion, implying the significance of being potential therapeutic targets for this cancer. Further study revealed that both matrix metalloproteinases (MMPs) 2/9 and tissue inhibitor of metalloproteases 1/2 might not participate in ATP-induced cancer invasion, as their expressions were not influenced by ATP in *1E8* and *2B4* cells.

Severe acute respiratory syndrome

Severe acute respiratory syndrome (SARS) was a catastrophe in Spring 2003 worldwide, particularly in China, Singapore and Canada. Professor Mingpeng She (Chinese Academy of Medical Sciences & the Peking Union Medical College, China) reported a SARS model in *Macaca Mulata* (*Rhesus* monkeys), which was generated by giving SARS co-virus or lung tissue lysate from a patient who died from SARS via nasal cavity and bronchus or intravenously, then assessed by clinical symptoms (anal temperature and blood white counts) and virology assays (virus antibody detection, RT-PCR and coronavirus cultivation). The systematic pathological changes were observed up to 60 days after virus inoculation. Definite acute haemorrhagic interstitial pneumonia was seen in the monkey 5 days after virus inoculation, followed by lesions of acute interstitial and bronchial pneumonia in those monkeys 7, 10, 15, 20 and 30 days after virus infection. Even 60 days after virus inoculation, pathological changes, including the destruction of elastic fibres of septa with communication between neighbouring air sacs, expansion of alveoli and chronic pleuritis still appeared in monkeys, but the number of CD4+ or CD8+ infiltrating cells decreased 30 days and 60 days after virus infection. Hyaline membrane and desquamation of lining cells were seen in damaged alveoli but not so remarkable as that described in human autopsy findings. In addition to lung and pleural lesions, congestion of red pulp in spleen, proliferation of epithelial and endothelial cells in renal glomeruli and focal liver necrosis were also discovered during the SARS development. Professor Bingquan Wu (Peking University, China) introduced a method for gene detection of SARS coronavirus that had broad application for clinical diagnosis and surveillance investigation. They devised a pair of primers and a probe (molecular beacon), which were specific for the recognition of a highly conserva-

tive region between 15301 and 15480 of the SARS-related coronavirus polymerase gene sequences obtained from Genebank. In the real-time RT-PCR assay, the extent of SARS-related coronavirus amplification was measured in terms of the increase in fluorescence during the amplification process. The 145-bp fragment of PCR product was further confirmed using conventional PCR assay and proved using DNA sequencing to be identical to the target sequence to which the probe was hybridised. In 25 of 85 clinical specimens from patients with suspected SARS and all 6 SARS post-mortem cases during the epidemic in Beijing, SARS-related coronavirus was identified using this method.

Colorectal cancer

Professor Thomas Kirchner (University of Erlangen-Nuremberg, Germany) showed his group's recent studies on colorectal cancers. The progression of colorectal cancer is non-linear, which is driven by morphogenetic programs that derived from normal development (gastrulation). β-Catenin, an important molecule in the Wnt signalling pathway, had more prominent nuclear staining at the invasive front (usually with epithelial mesenchymal transition) than in the centre of the tumour, implicating a critical role in the morphogenesis by up-regulating its downstream target genes, including p16, MMP7, UPA and Lam-5γ2, etc. A study of invasion-associated gene expression profiles on 11 colorectal cancers (Affymetrix U133A chip containing 22283 genes) disclosed an intratumourous heterogeneity in colorectal carcinomas as 127 genes up and 49 down were found at the invasive fronts. The up genes could be separated into three subgroups, including the aforementioned known β-catenin target genes, lymphocyte genes and factors of angiogenesis. The gene expression profiles can be defined to identify targets for an interference of morphogenesis and colorectal cancer progression. Microsatellite instability accounts for 10–15% colorectal carcinogenesis. In comparison with microsatellite stability and microsatellite instability (MSI)-L cancers, MSI-H colorectal cancers are more frequently associated with right hemicolon location, mucinous, signet ring cell, cribriform or medullary subtypes, prominent intraepithelial lymphocytes and a Crohn's-like reaction, frameshift mutations in transforming growth factor (TGF)β-RII, insulin-like growth factor (IGF)-IIR and BAX, and relatively better prognosis despite poor differentiation. MSI-H colorectal cancers could occur in familial [hereditary nonpolyposis colonic cancer (HNPCC)] and sporadic settings. Different clinicopathological and molecular features were discovered in the two parallel pathways. HNPCC cancers, displaying germline mutations in mismatch genes (mainly hMLH1 and hMSH2), were associated with the traditional adenoma–carcinoma sequence and less concurrent serrated adenomas (2%) and mucinous adenocarcinomas (14%), whereas sporadic MSI-H cancers, characterised by hypermethylation in the promoter region of hMLH1 (methylator phenotype), were associated with serrated pathways and more concurrent serrated adenomas (17%) and mucinous adenocarcinomas (44%). Professor Kirchner also introduced three new routes for colorectal carcinogenesis, serrated route, juvenile polyp route and colitis-dysplasia-carcinoma route, which were inferred in the new World Health Organization (WHO) classification of tumours of the digestive system, in addition to traditional adenoma–carcinoma route. A multi-gene and multi-step process as the accumulation of mutations/loss of heterozygosity (LOH) at 5q, 12p, 18q and 17p, etc. has been widely accepted in the traditional adenoma–carcinoma sequence. Nevertheless, the combined mutations could only interpret 7% of colorectal cancers, implying the presence of other molecular models. Accumulating evidence suggested that MSI might be critical in the serrated pathway. In addition to an increased frequency of serrated polyps and adenomas adjacent to sporadic MSI-H colorectal cancers, molecular alterations, including hMLH1 inactivation and shift mutations in TGFβRII, BAX and IGFIIR were also uncovered. About 5–10% or 15–20% ulcerative colitis patients can develop colonic cancers in 20 years or 30 years, respectively. As invasion could occur in intraepithelial neoplasia in ulcerative colitis exhibiting relatively mild morphological changes, the criteria for high-grade intraepithelial neoplasia complicating colitis should be less severe than in adenomas. Both dysplasia-associated lesion or mass (DALM) and high-grade flat dysplasia are commonly associated with concurrent invasive cancers, frequently leading to total colonectomy. Hence, the discrimination between sporadic adenomas and DALM is pivotal. Despite frequent villous structure, high nuclear p53 and low nuclear β-catenin in DALM, the discrimination remains difficult.

Identification of new molecular markers associated with colorectal adenoma and cancer may uncover critical events involved in the initiation and progression of colorectal cancer and may be of great significance in the prevention, diagnosis and treatment of this cancer. Professor Lai and his group have done some intriguing work in this field. They generated three differentially expressed cDNA libraries from the same patient, A-N (colonic adenoma-normal mucosa), T-N (colonic adenocarcinoma-normal mucosa) and T-A (colonic adenocarcinoma-adenoma) using the suppression subtractive hybridisation method in 1999. Then, 109 clones were obtained in the A-N library, 95 in T-N and 98 in T-A. The insert sequences of all clones were amplified and verified by means of a reverse Northern-blot technique using digoxigenin (DIG)-labelled probes. A great number of genes, separated into known genes, hypothetical proteins and novel genes or unknown expressed sequence tag (EST), were obtained by traditional methods, such as sequencing, ESTs assembly and BLASTNing with a public database in combination with bioinformatics analysis based on a self-devised Linux-based platform, analysing nucleic sequences automatically. Unknown (n=25) EST sequences were submitted to GeneBank. The known genes were found to be associated with important biological functions, fundamentally associated with cytoskeleton, cell cycle and proliferation, immunity, metabolism and signal transduction pathways. Two candidate genes, IGFBP-rp1/B2 and RegIV, were further investigated. The known sequence of B2 gene

was separated from T-N library, and, by combining with the sequence from 5′RACE (rapid amplification of cDNA end) product, a sequence of 1125 bp was obtained which shared 1122/1125 identities with IGFBP-rP1, indicating that both genes were the same. Semi-quantitative RT-PCR and immunohistochemistry were used to detect the expression of B2 in colorectal cancer tissues and cell lines (*SW480*, *SW1116*, *SW620*, *HCT8*, *CoLo205* and *LoVo*). At the level of mRNA, the expression of B2/IGFBP-rP1 was high in colorectal carcinomas, moderate in adenomas and tissues adjacent to tumours and low in normal tissues. No expression of B2/IGFBP-rP1 was found in the five cell lines except *SW480*. Immunostaining of B2/IGFBP-rP1 was stronger in cancer tissues than in paired normal tissues. A stronger staining of B2/IGFBP-rP1 was seen at the invasive front of cancer than in the centre in 28.9% (22/76) of cancers, which were also associated with an increased frequency of lymph-node involvement, deeper invasion and stronger staining of B2/IGFBP-rP1 than the remaining cancers. Further exploration uncovered that the fasting glucose level was significantly correlated with IGFBP-rP1 expression in cancer tissues. In conclusion, B2/IGFBP-rP1 overexpression might play an important role in the initiation and progression of colorectal cancer and may be linked with an increased potential of invasion. Its expression may also be associated with fasting glucose level and the presence of diabetes mellitus. RegIV, a novel gene first isolated from a large inflammatory bowel disease library in 2001, was obtained in A-N library in a manner of contigs assembly using electronic cloning (in silico cloning) with the EST database. Semi-quantitative RT-PCR in 12 colorectal adenomas and 10 concurrent carcinomas indicated that Reg IV mRNA level was higher in all adenomas and in 9 of 10 concurrent colorectal carcinomas when compared with paired normal colorectal mucosa. Northern-blot analysis further supported these findings. Subsequent study of in situ hybridisation with DIG-labelled cRNA in 32 colorectal adenomas with varying degrees of dysplasia disclosed that Reg IV was overexpressed in 74% (14/19) of adenomas with mild or moderate dysplasia and 100% (13/13) in cases of adenoma with severe dysplasia, compared with paired normal tissues. In addition, higher levels of Reg IV mRNA were consistently scored in regions with more severe dysplasia within the same adenoma sample displaying varying degree of dysplasia. The strongest staining was seen within carcinomatous areas of the 12 adenoma cases. All these results support that overexpression of Reg IV may be an early event in colorectal carcinogenesis. Detection of Reg IV overexpression may be useful in the early assessment of carcinomatous transformation of adenoma.

Professor Lirong Chen (Zhejiang University, China) explored the histogenesis and neural differentiation in 20 gastrointestinal stromal tumours (GIST, all c-kit+) using electron microscopy and immunocytochemistry. The ultrastructural features for neural differentiation were observed in 7 GISTs, myogenic differentiation in 1 GIST and neither in 12 GISTs. Among 7 GISTs with ultrastructural features for neural differentiation, all were positive for both neuron-specific enolase (NSE) and CD99, and 5 or 4 cases were positive for S-100 and CD56, respectively. Hence, gastrointestinal autonomic nerve tumour should be regarded as a subtype of GIST, due to their overlapping morphological features, with GIST accompanying neural differentiation.

Lymphoid tumours

Professor Harald Stein (Berlin—Free University, Germany) introduced the development history and general features of the present WHO classification of lymphoid tumours and discussed recent molecular issues on non-Hodgkin's lymphoma. To achieve an international standard and to assess the diagnostic value of IgH rearrangement, a collaborative study of 48 European institutes (including 30 PCR laboratories) in seven national networks was carried out on 110 gastric biopsies. The histological diagnoses were reassessed by seven pathologists, without knowledge of the PCR results. Meanwhile, IgH PCR analysis was done without knowledge of the histological diagnoses using three Biomed-2 IgH primers, FR1, FR2 and FR3. Monoclonal IgH was identified in 2% (1/53) of gastritis cases, 22% (4/18) of borderline cases and 92% (24/26) of mucosa-associated lymphoid tissue (MALT) lymphomas, respectively. Thus, Professor Stein concluded that the distinction between true clonality from pseudoclonality was essential for a correct interpretation and possible when the PCR assay was repeated at least two times using primers of high quality. Mantle cell lymphoma (MCL), the unique small cell lymphoma with poor prognosis, was characterised by cyclin D1 overexpression as a result of t(11;14) leading to IgH-cyclin D1-fusion protein. However, an MCL gene expression signature defined a large subset of MCLs that expressed cyclin D1 and a novel subset that lacked cyclin-D1 expression. The more than 5 years in median survival was better in cyclin D1+ MCLs than in cyclin D1− MCLs. Furthermore, the gene expression profiles of leukaemic MCL cells was otherwise identical to the cyclin-D1-positive MCLs in a comparative study among MCL cell lines, leukaemic MCL cells and nodal MCL cells. Three chromosomal aberrations, trisomy 3, t(1;14) and t(11;18), were found in only a fraction of gastric MALT lymphomas as demonstrated by a study on molecular-cytogenetic comparison of MALT lymphoma and large B-cell lymphoma, which proposed that MALT lymphomas can be separated into different genetic subgroups. Furthermore, a clonal lymphoma progression occurred from the small to the large cell component was identified with accumulation of gains and losses of chromosomal material in the large cell component in MALT lymphoma plus large B-cell lymphoma. Aberrations overlapping with MALT lymphoma and MALT lymphoma plus large B-cell lymphoma included losses on chromosome 13, amplifications of the REL proto-oncogene or gains on chromosome 12. In addition, the large-cell component revealed gains on 8q24, including amplifications of the MYC proto-oncogene and losses on 2q. The large B-cell lymphoma had frequent gains on chromosomes 12 and 9, as well as on 11q, and losses on 6q. Diffuse large-cell B-cell lymphoma (DCBCL) is one of the most complicated lymphoid tumour

entities and has many WHO morphological variants and types. Recently, three gene-expression subgroups—germinal-centre B-cell-like (GCB type), activated B-cell-like (ABC type) and type-3 DCLBCL—were identified in a DNA microarray analysis on 240 DLBCLs, among which patients in GCB subgroup had the highest 5-year survival rate.

Another microarray study focused on centroblastic lymphoma (CBL) and Burkitt lymphoma confirmed that DLBCL of centroblastic morphology can be separated into a GCB type and ABC type. However, more than 50% of CBL was of the ABC type and all Burkitt lymphomas were the GCB type in contrast to the study above. The latter difference is probably due to a highly variable percentage of the tumour cells in biopsies. Reliable distinction between primary mediastinal (thymic) large B-cell lymphoma (PMLBCL) and common types of DLBCLs is only obtained via clinical information. However, this distinction can be reliably made by gene expression profiling without clinical information. Intriguingly, PMLBCL shared several features for downregulating Stat1, AK2, TRAF1 and IL13R, resembling classical Hodgkin's lymphoma. Another rare entity of DLBCL, plasmablastic lymphoma, can also be distinguished from DLBCL of ABC type and GCB type by gene expression profiling. Thus, at the close of his report, Professor Stein concluded that new scientific data should be integrated into the WHO classification concept, which would lead to the identification of new lymphoma diseases and sharpening of existing definitions.

Professor Gandi Li (Sichuan University, China) investigated 42 intestinal T-cell lymphomas (ITCL) in Chinese, including a broad pattern of clinicopathological features and molecular alterations. Neither immunosuppression nor clinical evidence of celiac disease at the time of diagnosis was implicated in all 42 patients. The prognosis was generally poor, as indicated by a short relapse period (4 patients relapsed within 24.3 months) and survival time (23 patients died with a median survival of 3.0 months), despite the fact that 6 patients with one site involvement had survived for 156 months. In comparison with enteropathy-type intestinal T-cell lymphomas (ETCLs), ITCLs had unusual clinical features, such as male predilection (33/42), young age (mean 30.4 years) and predominantly ileocecum and colon location (33/42). Histological patterns were similar in ITCLs and ETCLs, except that massive zonal necrosis and the absence of enteropathy were seen in ITCLs. Both immunophenotyping and Epstein–Barr virus (EBV) detection showed similar patterns as found in nasal NK/T cell lymphoma, including invariably CD56+ (12/42), TIA-1+ (39/42) and EBER+ 41/42 (97.62%). Owing to a peculiar EBV-associated entity with distinct clinicopathological features, ITCL in Chinese should be put into a catalogue separate from ETCL.

Professor Weiping Liu (Sichuan University, China) studied 185 cases of nasal NK/T-cell lymphoma. A routine diagnostic protocol for nasal NK/T-cell lymphomas was put forward, including morphological features for massive coagulative necrosis, mostly medium-sized atypical cells and increased vessels, immunophenotype displaying CD3ε+, CD20−, CD56+, TIA-1+ and granzyme B+, and EBER+ using in situ hybridisation. It was addressed that EBER in situ hybridisation was a more sensitive method for EBV detection (58/64) in this lymphoma on paraffin tissues than both PCR (19/28) and LMP-1 immunostaining (2/20). A follow-up study of 120 cases revealed that the general 1-year, 3-year and 5-year survival rates of NK/T-cell lymphoma were 71.80%, 55.40% and 54.10%, respectively. Lower tumour stage (I–II), free of recurrence and combined therapies were the most favourable prognosticators. In stage-I to -II tumours, the 1-year, 3-year and 5-year survival rates were 76.40%, 65.50% and 62.70%, respectively, in comparison with 38.20%, 23.60% and 0 in stage-III to -IV tumours. A nude mouse model and the cell line of NK/T-cell lymphoma were successfully generated from a secondary lymphoma in stomach, both of which might be of great significance for further study on this tumour. Afterwards, a cDNA microarray analysis on the lymphoma was carried out. A total of 265 differential expressed genes were identified, of which 178 were upregulated and 87 downregulated. Preliminary assessment suggested that 25 downregulated or 21 upregulated genes might be closely correlated with nasal NK/T-cell lymphoma.

Gynaecological tumours

Professor Manfred Dietel (Charité, Berlin, Germany) gave an overall aspect of considerable improvements of 2003 WHO Classification of Gynaegologic Tumours in comparison with the 1999 version. He explained changes of the diagnostic terminology in new the WHO classification. As an important example, the former category of "epithelial tumours of borderline malignancy (low malignant potential)" is condensed to the term "borderline tumour", and the term "low malignant potential" is avoided due to the considerable misunderstandings among pathologists and clinicians, resulting in distinct overtherapy. The serous borderline tumour of the ovary was particularly addressed. Immunohistochemistry, as well as new diagnostic procedures such as DNA cytophotometry, was recommended in the assessment of invasive foci (≤ 10 mm^2) for the diagnosis of serous borderline tumours with microinvasion, although no prognostic relevance can be attributed to microinvasion. As a new type, micropapillary serous borderline tumour was mentioned but not fully accepted by WHO 2003. Surface proliferations and peritoneal implants were common in serous borderline umours, however, only invasive or destructive implants are associated with unfavourable outcomes, whereas surface proliferations per se and non-invasive peritoneal implants are not strikingly correlated to poor prognosis. Therefore, it should be addressed that peritoneal implants be distinguished into an invasive and a non-invasive type according to the criteria recommended by WHO 2003.

With regard to endometrial carcinoma, a type I and II have to be separated, due to different clinicopathological features. Type-I cancer was low-grade prototypical endometrioid adenocarcinoma, which is associated with exogenous or endogenous hyperoestronism, endometrial hyperplasia, in particular, atypical hyperplasia, relatively good clinical

prognosis and higher oestrogen receptor or progesterone receptor overexpression, whereas type-II carcinoma exhibits a more aggressive behaviour, primarily in elderly patients, and higher p53 overexpression. A three-tiered grading system is adopted for type-I endometrial carcinoma, based on the component of solid growth pattern (without glandular formation). But WHO also supplemented that solid nests of cells showing squamous or morular differentiation do not increase the tumour grade, and bizarre nuclear atypia should raise the grade by one type, e.g. from 1 to 2 or 2 to 3. The new WHO classification defined the endometrial intraepithelial neoplasia in the uterine corpus, however, there is limited experience in clinical implementation at the present time.

In addition, the cervical squamous cell carcinoma with microinvasion has to be distinguished from high-grade cervical intraepithelial neoplasia (CIN 3) in the uterine cervix. Early invasion is indicated by more mature squamous cells extending from a focus of in situ carcinoma, luminal necrosis and intraepithelial squamous maturation as well as stromal oedema and a stromal desmoplastic and lymphocytic response, features that aid in its distinction from crypt involvement by CIN.

With regard to the CIN system, there is an increasing tendency to use a two-tiered classification of low- and high-grade CIN that equates to CIN 1 versus CIN 2 and 3, respectively (WHO Classification of Tumors, 2003, p 11). Further, the International Federation of Gynecology and Obstetrics definition of stage-1A carcinoma of the cervix was outlined in that the depth of invasion may not be greater than 5 mm, and the horizontal spread should measure 7 mm or less.

Professor Joachim Diebold (Ludwig-Maximilians-University München, Germany) focused on selected issues concerning the WHO Classification of Ovarian Tumours' classification of mucinous tumours, classification of extraovarian lesions associated with serous tumours and classification of primary extraovarian (peritoneal) serous tumours. A three-tiered grading system of ovarian carcinomas scored on growth pattern, nuclear pleomorphism and mitotic activity was recommended by the new WHO classification, as proposed by Silverberg in 2000. A prominent prognostic significance of the Silverberg grading was disclosed by multivariate Cox analysis. However, as listed in the WHO, clear cell carcinomas and mucinous carcinomas are not graded, due to absence of prognostic and/or therapeutic relevance, and endometrioid carcinoma or transitional carcinomas can be graded by use of the criteria for endometrial carcinomas or transitional carcinomas of the urinary tract. Mucinous adenocarcinomas of the ovary are rare, despite the presence of many subtypes. It was emphasised that mucinous metastases in the ovary from colorectal, appendiceal, gastric, pancreaticobiliary, and endocervical carcinomas are more common than primary ovarian mucinous carcinomas, and the differential diagnosis may be extremely difficult due to shared gross and microscopic features and overlapping immunophenotype. The two subtypes of mucinous borderline tumours of the ovary, the endocervical type and the intestinal type, have different clinical and morphological features. Intraepithelial carcinoma is defined as the presence of areas with severe atypia or more than three cell layers in the intestinal type of mucinous borderline tumours. Extraovarian lesions associated with serous tumours are not uncommon. They have clinicopathological features similar to their ovarian counterparts. Particular attention should be paid to Mullerian inclusion cysts as potential diagnostic pitfalls, due to their presence in 25–30% of pelvic and paraaortic lymph nodes. According to a recent report, primary peritoneal serous carcinomas are not rare (31 of 220, 14.1%). These carcinomas are defined using histology that is indistinguishable from primary ovarian carcinoma but normal-sized ovaries. In his review on molecular approaches to gynaecological tumours, Professor Diebold concluded that a molecular basis for the multi-step process of neoplastic transformation is only established for some gynaecological carcinomas, and the genetic changes identified so far only partially explain the phenotypic variability of gynaecological tumours. Type-I endometrial carcinoma is a good example for the paradigm of multi-step carcinogenesis. During the process of transformation from normal endometrium, simple hyperplasia, complex hyperplasia to low-grade and high-grade carcinoma under the estrogenic stimulation, underlying genetic alterations, including microsatellite instability and mutations involving PTEN, k-ras, β-catenin and p53, etc., are accumulating. Specifically, MSI-H endometrial carcinomas are associated with mucinous differentiation, favourable prognosis and PTEN mutation. Using comparative genomic hybridization (CGH), array accumulation of genetic aberrations was also found in the transformation of serous borderline tumours into invasive serous carcinoma, which is a rare event (≤1%). Most genetic aberrations in endometrial and ovarian tumours affect members of signalling pathways, growth factors and their receptors and regulatory molecules for cell cycle, differentiation and apoptosis. The activation of members of RAS and Wnt pathway is frequent in type-I endometrial carcinoma. For example, k-ras and β-catenin mutations were found in 16% or 31% type-I endometrial carcinomas, respectively. Several genes in the signalling pathways of receptor tyrosine kinases are frequently activated in epithelial ovarian tumours, including Her2/neu, Dab-2, Ras, Raf and PTEN, etc. Moreover, serous borderline tumours are characterised by activation of the RAS-BRAF pathway, suggesting a different molecular developmental pathway in contrast to invasive serous carcinomas. Professor Diebold also discussed the role of chromosome 20q for ovarian carcinogenesis, which harbours a high density of putatively relevant genes, such as CSE1L/CAS, EEF1A2, ZNF217, etc. Some studies proved that gains of transcription factor ZNF217 on 20q13.2 using fluorescent in situ hybridisation (FISH) and reduced overexpression of CAS/CSE1 on 20q13 were unfavourable prognostic factors in ovarian carcinomas.

Urothelial tumours

Professor Ferdinand Hofstädter (University Regensburg, Germany) compared the 2004 WHO Classification of Tu-

mours of the urinary system with the 1999 version and focused on several topics regarding urothelial tumours. Based on molecular and clinical data, urothelial tumours were separated into infiltrating tumours, which are defined as urothelial tumours that invade beyond the basement membrane, and non-invasive tumours, in which papilloma, papillary urothelial neoplasm of low-malignancy potential (PUNLMP) and non-invasive cancer are included. PUNLMP is not supposed to carry the label of cancer. A two-tiered grading system for urothelial epithelial cancer (low/high grade) substituted for the former three-tiered (G1–3) system to avoid G1–2 or G2–3 diagnosis, as was the case previously. In the 2004 WHO classification, flat lesion is not an independent type but a comprehensive entity exhibiting hyperplasia, reactive atypia, atypia of unknown significance, dysplasia (low-grade intraurothelial neoplasia) and carcinoma in situ. Hyperplasia and dysplasia, both as precursor lesions of urotheilial tumours, might be representative of two different pathways in carcinogenesis, the papillary or invasive pathway. The papillary pathway is genetically stable in most cases and associated with chromosome-1 (frequently the whole chromosome) loss and other rare genetic alterations, wheareas the invasive pathway is genetically unstable and frequently shows p53 mutations. Both lesions in cancer patients may be clonally related to the respective tumours as indicated by identical patterns of LOH analysis and chromosome-9 deletions in FISH as well as duplicate p53 mutation sequence in hyperplasia-papilloma-recurrent papilloma or dysplasia carcinoma in situ in the same patient. Oligoclonality or monoclonality of multifocal carcinoma was also discovered using similar methods in support of an intraluminal dissemination of multifocal cancers. Professor Hofstädter also reported the role of MSI and chromosome 8p deletions with several candidate genes (e.g. sfrp1 and TRAIL-R2). Loss of sfrp1 expression was found in 30% of urothelial carcinomas and associated with papillary growth pattern and lower survival rate of patients with invasive papillary tumours despite the fact that no mutation in the coding sequence and promoter region was identified in 20 urothelial carcinomas with 8p loss and five cell lines as well as rare promoter methylation (<10%). cDNA-array expression analysis might be beneficial for sharper tumour classification of urothelial tumours in a manner of hierarchical clusters. A gene expression analysis was found to contribute to discrimination of non-invasive from invasive papillary tumours via 40 differentially expressed genes.

Central nervous system tumours

Professor Otmar D. Wiestler (German Cancer Research Center, Heidelberg, Germany) addressed major changes in the new WHO Classification of Brain Tumours, including new tumour entities and variants, detailed criteria for diagnosis and tumour grading and molecular and genetic alterations. As listed in astrocytic neoplasms, pilocytic astrocytoma, diffuse low-grade astrocytoma, anaplastic astrocytoma and glioblastoma multiforme (GBM) are regarded as grades I, II, III and IV, respectively. Tanycytic ependymoma, pineal parenchymal tumour of intermediate differentiation, large cell medulloblastoma, rhabdoid meningioma and teratoma with malignant transformation were novel tumour variants in the new WHO fascicle; whereas, polar spongioblastoma, cysts and tumour-like lesions (Rathke cyst, nasal glioma) and locally invading cancers are not mentioned, while pituitary adenomas are put into another WHO fascicle. He also reviewed recent molecular advances in brain tumours. There are two different genetic pathways leading to GBM, type I (primary) *de novo* from precursor cells and type II (secondary) as progression from low-grade astrocytoma, with the exception of pilocytic astrocytoma, which is associated with indolent biological behaviour and rare progression. Amplification of EGFR and chromosome 10 LOH were most common in the tumorigenesis of type-1 GBM, while p53 or 17p LOH as well as 19q LOH were most common in type-II GBM. DNA aberrant methylation might also play an important role in the initiation and development of gliomas. In a study on GBM, oligodendroglioma and pilocytic astrocytoma using DMH CpG chips, tumour methylation-specific patterns were obtained, which not only helped the histopathological diagnosis but also guided the identification of multiple novel candidate genes. 1p and 19q LOH is frequently involved in oligodendroglial tumours. The LOH incidence at both loci was found higher in the oligodendroglioma (WHO II) than in the anaplastic oligodendroglioma (WHO III), implicating prognostic significance.

Classical and desmoplastic medulloblastoma had differences in tumourigenesis, as the classical was associated with 17p LOH and Myc amplification, while the desmoid was associated with 9p22 LOH and PTCH inactivation. Overexpression of c-Myc may be related to unfavourable prognosis in medulloblastoma patients. A recent study on 34 tumours also demonstrated that expression profilings via cDNA array chip can make desmoplastic and classic medulloblastoma distinguishable.

Lung tumours

Professor Iver Petersen (Charité, Berlin, Germany) reported on changes in the new WHO lung cancer classification, which will incorporate more clinical data (epidemiology, signs and symptoms, imaging, prognosis) and particular genetic characteristics on the still morphologically defined subtypes. Predictive factors being subdivided into clinical, histopathological and genetic parameters, however, opened the window for new subentities. Generally speaking, the morphological subtypes have remained essentially unchanged. The issue of morphological heterogeneity and phenotypical transitions is still contentious; on practical grounds, a minimal component of 10% is generally required to diagnose mixed tumour entities such as adenosquamous carcinoma, pleomorphic carcinoma or combined small carcinoma with a large cell component. A few variants of squamous cell carcinoma (SCC) are additionally mentioned, i.e. SCC resembling transitional cell carcinoma

and alveoloar space-filling type of peripheral SCC, which is growing without destruction of alveolar framework and represents about 5% of peripheral SCC. The latter is contrasting with the conventional expanding type of SCC, showing infiltration and destruction of the normal lung architecture. Spindle cell SCC has been grouped with sarcomatoid carcinoma. For adenocarcinoma, the Noguchi subtypes being defined by a mixture of gross and histological features were mentioned. These include type A (localised bronchioloalveolar carcinoma), type B (localised bronchioloalveolar carcinoma with central alveolar collapse), type C (localised bronchioloalveolar carcinoma with fibroblastic proliferation), type D (poorly differentiated adenocarcinoma), type E (tubular adenocarcinoma) and type F (papillary adenocarcinoma with a compressive growth pattern). This typing is of great significance in the assessment of clinical treatment and prognosis. Of the six types, types A and B, thought to be in situ peripheral adenocarcinoma, showed no lymph-node metastasis and the most favourable prognosis (100% 5-year survival). Thus, both cancers may be potentially cured by limited resection (e.g. wedge resection); however, the diagnosis needs a good computed tomography correlation and require entire sectioning for histology. Conversely, type C appeared to be an advanced stage of types A and B; whereas, types D, E and F are small but advanced adenocarcinomas with less favourable prognoses.

Professor Petersen also documented that molecular pattern analysis on the DNA, RNA or protein level using CGH, array-CGH, cDNA/oligo-microarray and mass spectrometry expression analysis may be able to refine the morphological tumour classification. In a cDNA array study on lung cancers and normal lungs, gene expression patterns not only segregated the four major morphological subtypes of lung tumours but also provided gene clusters characteristic of adenocarcinoma subgroups with morphological and survival difference. Furthermore, expression profile of large cell lung cancer was suggestive of epithelial–mesenchymal transition. Protein analysis using matrix-assisted laser desorption/ionisation time-of-flight revealed that the proteomic pattern of lung cancers could not only classify correctly 34 primary non-small cell lung cancers (NSCLC) and 8 normal lung samples according to 91 MS peaks but also discriminated 34 primary NSCLCs from 7 metastases or recurrent lung tumours as indicated by 23 distinct MS peaks. Six groups of lung cancers with prognostic differences were generated by analysing the proteomic patterns of 15 MS peaks.

UICC TNM staging

Professor Christian Wittekind (Leipzig University, Germany) summarised the improvements in the 6th edition of the International Union Against Cancer (UICC) tumour node metastasis (TNM) Classification of malignant tumours. He gave an overview on the changes of the different tumour entities as listed in the classification and made comments on the importance and clinical usefulness of them. R classification was introduced to describe the absence or presence of residual tumour after treatment. Three descriptors were designated R0 (no residual tumour), R1 (microscopic residual tumour), and R2 (macroscopic residual tumour). In the example of gastrectomy specimen, circumferential resection margin (CRM) has to be considered as margins in minor ligament, gastrocolic and mesocolic ligament, hepatoduodenal ligament and subserosal soft tissue in non-peritonealised regions. According to data of residual tumour in gastric carcinoma resection specimen from Erlangen Cancer Center, in R1-tumour patients, CRM was most frequently involved (67%, 79 of 118). As the sentinel lymph node is the first lymph node to receive lymphatic drainage from a primary tumour, it is a good indicator for lymph-node metastasis. Occasionally, there is more than one sentinel lymph node. The following designations are applicable when sentinel lymph node assessment is attempted: pNX(sn) (sentinel lymph node could node be assessed), pN0(sn) (no sentinel lymph node metastasis) and pN1(sn) (sentinel lymph node metastasis). Isolated tumour cells (ITCs) are single tumour cells or small clusters of cells not more than 0.2 mm in greatest dimension (micrometastasis $\leq$0.2 cm), which are usually detected using immunohistochemistry or molecular methods. However, ITCs do not typically show evidence of metastatic activity (e.g. proliferation or stromal reaction) or penetration of vascular or lymphatic sinus walls. In explaining further developments of the TNM system, the example colorectal carcinoma was mentioned: stage III is separated into stages IIIA, IIIB and IIIC. The 5-year survival rate was 59.8%, 42.0% and 27.3%, respectively. Finally, he addressed that the TNM system and its variables were essential important prognostic factors. In addition to these well-established factors, the UICC also considered the spectrum of prognostic factors in a new publication, including new promising molecular markers.

Acknowledgements The authors thank the contributors Lirong Chen, Joachim Diebold, Weigang Fang, Heinz Höfler, Ferdinand Hofstädter, Thomas Kirchner, Gandi Li, Weiping Liu, Iver Petersen, Mingpeng She, Harald Stein, Otmar D. Wiestler, Christian Wittekind, Bingquan Wu, Jie Zheng and all participants for the excellent lectures and interesting discussions. In particular, the great hospitality of the Chinese colleagues is very much acknowledged.

Virchows Arch (2005) 446: 577–578
DOI 10.1007/s00428-005-1278-3
© Springer-Verlag 2005

ANNOUNCEMENTS

2–3 June 2005
Thyroid Pathology for the Practicing Pathologist
15 rue de lEcole de Mdecine, Paris, France

A 2-day course will take place in Paris again under the auspices of the French Division of the I.A.P.
This course will be given in English by Prof. M. Sobrinho-Simoes (Porto) and Prof. R. Heimann (Brussels).
It will consist of lectures alternating with slide reviews and a slide seminar over a multihead microscope. The cases of this seminar will be sent (on CD) before the meeting.
The audience will be limited to 22 participants.
Course fees: 390 euros (320 euros for members of any I.A.P. division). The fees include registration,hand-out, CD of the slide seminar and coffee breaks.

For further information please contact:
Mrs. M. Fontanire
Administrative Secretary
French Division of the I.A.P.
32 Cours Albert Thomas
69008, Lyon, France
Fax: +33 4 78754311
E-mail: academie.pathologie@wanadoo.fr

3–4 June 2005
16th Ljudevit Jurak International Symposium on Comparative Pathology
Under the auspices of the European Society of Pathology and Academy of Medical Sciences of Croatia
Multimedial center Sestre milosrdnice University Hospital, Zagreb, Croatia

The main symposium topic is surgical pathology and frozen sections analysis. Symposium includes following sections: Pathological Morphology of the Human and Animal Diseases, Iatrogenic, Environmental and Experimental Pathology, Herman Jurak Round Table on Rheumatological Pathology, Clinical Forensic Pathology, Slide Seminars *in Histopathology and Cytopathology*, Quiz on Pathology.

Registration fee before April 1st – 100 EUR
Registration fee after April 1st – 150 EUR

Information: Davor Tomas, M.D.
Ljudevit Jurak University
Department of Pathology
Sestre milosrdnice University Hospital
Vinogradska 29
10000 Zagreb, Croatia
Tel.: +385 / 3787 909
Fax: +385 / 3787 244
E-mail: juraks@kbsm.hr
http://www.kbsm.hr/Jurak/symposium.htm

13–24 June 2005
International course on Laboratory Animal Science
Utrecht, The Netherlands

A two week intensive course on laboratory animal science will be organized at the Division of Laboratory Animal Science–Utrecht, The Netherlands in June 2005. This course is organized once a year since 1993.
The objective of this course is to present basic facts and principles that are essential for the humane use and care of animals and for the quality of research.
The contents of the course are in line with recommendations of the Federation of European Laboratory Animal Science Associations (FELASA) regarding the training of the young scientist whose research involves the use of vertebrate animals.
The course may also be of interest for those who intend to set up a similar course at their location. For this purpose, during the course the acquisition of teaching materials can be discussed with the course committee.

For information and application forms please contact:
Mr. Stephan van Meulebrouck, MA
Division of Laboratory Animal Science
Faculty of Veterinary Medicine
P.O. Box 80.166
3508 TD Utrecht
The Netherlands
Tel.: +31-30-2532033
Fax: +31-30-2537997
E-mail: pdk@las.vet.uu.nl
Internet: http://las.vet.uu.nl>Education and Training>International Course

26–29 July 2005
Practical Pulmonary Pathology
London, UK

This course is designed to provide histopathology and cytopathology trainees and consultants with an opportunity to study diagnostic lung pathology in a comprehensive manner. It comprises lectures and practical microscopy sessions, the latter making up roughly half the time and consisting of individual study of a unique collection of cases.

Further details and application forms are available from:
Professor B Corrin
Brompton Hospital
London SW3 6NP, UK
Fax: +44 20 7351 8293
E-mail: b.corrin@ic.ac.uk

22–23 September 2005
Breast Diagnostic Histopathology Update
Hammersmith Hospital (Imperial College), London, UK

A 2-day course designed for pathologists at Consultant and Senior Trainee level. The course is a shorter version of the week long course and is also suitable for those who have previously attended that course and wish to participate in discussing new developments in the field. The course will be based on 30, mostly new, cases derived from the arcives of Hammersmith, Charing Cross, Nottingham City and Cambridge Addenbrook's Hospitals and is slanted to practical diagnostic pathology with special emphasis on areas that pose diagnostic difficulties. The participants will be given ample time to study histological preparations, followed by illustrated discussion of the cases. In addition there will be several talks on specific topics, given by breast pathology specialists followed by discussions. The topics will include issues in the interpretation of breast biopsies, examination of breast biopsies after neo-adjuvant chemotherapy, breast immunohistochemistry, dealing with the gross specimen, fibro-epithelial and spindle cell lesions; papillary, lobular, apocrine and metaplastic lesions, proliferative lesions/ carcinoma in situ and sentinel lymph node biopsy. The faculty will include Ian Ellis, Mary Falzon, Andrew Lee, Sarah Pinder and Sami Shousha.

Further details from:
Wolfson Conference Centre,
Hammersmith Hospital,
Du Cane Road,
London W12 ONN, UK
Tel.: (44) 20 8383 3117/3227/3245
Fax: (44) 20 8383 2428
E-mail: wcc@imperial.ac.uk

1–2 December 2005
International Symposium on "Salivary Gland Tumours; Present Concepts of Diagnosis and Management"
Amsterdam, The Netherlands

For further information please contact congress secretariat
Mrs. D. Chavalking
Vrije Universiteit Medical Center (Vumc)
Department of Oral and Maxillofacial Surgery/Oral Pathology
PO Box 7057
1007 MB Amsterdam
The Netherlands
Tel.: +31-20-444-4039
Fax: +31-20-444-4046
E-mail: d.chevalking@vumc.nl
Internet: www.vumc.nl

Virchows Arch (2005) 446:579–584
DOI 10.1007/s00428-005-1271-x

EUROPATH NEWS 2/2005

European Society
of
Pathology

Editors
Dr. Grete Krag Jacobsen
University Department of Pathology,
Teilumbuilding Rigshospitalet
Blegdamsvej 9,
DK-2100 Copenhagen Ø, Denmark
Tel.: +45 3545 5450
Fax: +45 3545 5414
e-mail: grete.krag.jacobsen@rk.hosp.dk

Dr. Bjørn Risberg
Department of Pathology
The Norwegian Radium Hospital
0310 Oslo, Norway
Tel.: +47-22934174
Fax: +47-22508554
e-mail: brisberg@labmed.uio.no

Newsletter of the European Society of Pathology

Dear Members,

In this newsletter you can find the new statutes of the Society and the rules for election of officers and members of the Executive Committee, the latter in short form as the procedures were published in full length in the previous newsletter. Please read it carefully. New members are to be elected at the forthcoming congress in Paris in September 2005.

The Society hopes that many of you will accept the invitation from Pierre Bedossa, President of the Congress, and take the opportunity to come to the European Congress of Pathology in Paris and also join the General Assembly of the Society.

The application form for membership of the Society can be found at the end of the newsletter. Please give it to a colleague who has not yet applied.

Sincerely yours,
Grete Krag Jacobsen

Statues of the European Society of Patholgoy published in the appendices of the "Belgisch Staatsblad", on November 26, 2004

International Society with Humanitarian, Religious, Scientific or Pedagogic Aims

Article 1: Name

The international non-profit society "Société Européenne de Pathologie" has been established according to the Belgian law of 25 October 1919 and recognized by royal decree on 9 February 1970. From now on this Society shall be called "European Society of Pathology" (ESP). This Society is now subject to title III of the Belgian law of 27 June 1921 concerning non-profit societies, international non-profit societies and foundations.

Article 2: Seat

The seat of the Society is at Borchtlombeek, Benedenstraat 5, 1761, Belgium, with a working address at Anatomo-Pathologie, AZ-VUB, Jette, Laarbeeklaan 101, 1090, Belgium. The seat can be moved to any place in Belgium upon decision of the Executive Committee. All changes shall be submitted for publication to the appendices of the *Belgisch Staatsblad* ("Bijlagen tot het *Belgisch Staatsblad*") and communicated to the Justice Department of the Belgian Federal Government within 1 month following the decision.

Article 3: Social Aims

The Society is a non-profit society. The aims of the Society are to advance pathology in Europe and to facilitate communication between European pathologists. The term "pathology" includes all aspects of pathology. In order to achieve this aim, the Society will organize courses and congresses on a regular basis.

Article 4: Members

The Society will accept Belgians and persons of other nationalities.

The Society will consist of ordinary, retired and honorary members. The number of members is unrestricted, but is at least 30.

Ordinary members are pathologists and trainees in pathology and any other person, normally a medical, dental, veterinary or science graduate, who is or has been engaged in research and/or in teaching in connection with pathology.

Honorary members are persons with meritorious achievement in medicine, biology or any field directly related to pathology or the ESP.

Retired members are ordinary members who have obtained the retired member status upon request by letter, fax, e-mail or any other way of communication to the Executive Committee.

Article 5: Membership, Termination of Membership and Exclusion from the Society

5.1: Membership

Ordinary members are elected by the General Assembly upon submission of an application form to the Treasurer and fol-

Important Information

EuroPath News appears in *Virchows Archiv* four times a year, i.e. February, May, August and November. ESP members who want to publish information in *EuroPath News* should send the manuscript by e-mail to the editor (GKJ) *2 months ahead* of publication. Information only for the website should be sent to the editor of the website (BR).

e-mail: grete.krag.jacobsen@rh.hosp.dk
e-mail: brisberg@labmed.vio.no

For further information look at the ESP home page: http://129.240.38.9/espl

lowing nomination by the Executive Committee. Each member pays a yearly membership fee. Ordinary members may vote at the General Assembly and serve on committees, commissions and working groups.

Honorary members are elected by the General Assembly following nomination by the Executive Committee. The honorary members shall be exempted from paying a membership fee. Honorary members can participate in the General Assembly, but hold no votes. Honorary members may be appointed to commissions or working groups.

Retired members shall be exempted from paying a membership fee. Retired members can participate in the General Assembly, but hold no votes.

5.2: Termination of Membership

Membership can be terminated by letter, fax, e-mail or any other way of communication to the Executive Committee at least 6 months prior to a General Assembly.

5.3: Exclusion from the Society

Membership is cancelled automatically after 2 years of unpaid membership dues.

Any other exclusion of a member can only be decided by the General Assembly, after a proposal by the Executive Committee, through a resolution adopted by a majority of two-thirds of the members present or represented, provided the item is on the agenda of a regularly scheduled General Assembly. The member in question has the right to be heard by the Executive Committee.

Article 6: Membership fee

The annual membership fee is fixed by the General Assembly, after a proposal by the Executive Committee.

Article 7: General Assembly

The General Assembly is the supreme body of the Society. It supervises the activities of the Executive Committee.

7.1: Competence

1. At the General Assembly, the report of the President, as well as recommendations of the Executive Committee and Advisory Council, shall be presented and discussed for approval by the General Assembly.
2. The Treasurer will present the budget and accounts and the Finance Committee will present its report, all for final approval by the General Assembly.
3. The editors of the official publications of the ESP may be requested to provide information.
4. The activities of the working groups, commissions and committees of the ESP shall be briefly reported.
5. The General Assembly has the sole authority to change the statutes.
6. The General Assembly has the sole authority to approve and dismiss the Executive Committee members.
7. The General Assembly has the sole authority to liquidate the Society voluntarily and decides on the way the Society will be dissolved and how the assets will be settled.
8. The General Assembly has the sole authority to nominate and expel members.
9. The General Assembly has the sole authority to approve and to change the bye-laws.
10. The General Assembly has the sole authority to designate the venues of the forthcoming congresses.
11. The General Assembly has the sole authority to approve the contracts with the affiliated journals.
12. The General Assembly has the sole authority to recognize the working groups formally.

7.2: Composition

The General Assembly is composed of all the ordinary members; each ordinary member holds one vote. Retired ordinary members and honorary members can participate in the General Assembly, but hold no vote.

7.3: Meeting and Convocation

The General Assembly meets under the guidance of the Chairman of the Executive Committee at each biennial congress of the ESP, at a site specified in the notice of meeting.

The General Assembly may also be called upon request of one-third of the members of the ESP.

A notice of meeting including the agenda is sent out by the Secretary of the Executive Committee by letter, fax, e-mail or any other way of communication at least 3 months prior to the meeting.

The working language is English.

7.4: Decisions

A meeting of the General Assembly should be attended by at least 10% of the members.

All issues not provided for in these statutes shall be decided by a simple majority of the members present or represented at the General Assembly, the President having the casting vote in the event of a tie.

Another member who holds a special procuration may represent each ordinary member at the General Assembly. One ordinary member cannot represent more than three other members.

No valid decisions can be made on items not mentioned in the agenda.

If the meeting of the General Assembly is not attended by at least 10% of the or--dinary members of the Society, a new meeting of the General Assembly will be scheduled under the same conditions as the above-mentioned, and this assembly can take a final and valid decision on the proposal after approval by a simple majority of the members present and represented, the President having the casting vote in the event of a tie.

The resolutions of the General Assembly are entered in a register, signed by both the President and the Secretary, and recorded by the latter, who will deposit the register at the working address of the society on behalf of the members.

The decisions shall be communicated to all society members.

Article 8: Changes in the Statutes and Liquidation of the Society

Irrespective of articles 50§3, 55 and 56 of the law on non-profit societies, international non-profit societies and foundations, any proposal to amend the statutes or to liquidate the Society shall emanate from the General Assembly or at least 5% of all ordinary members.

Any proposal to change or amend the statutes or liquidate the Society shall first be submitted to the Secretary in writing for consideration by the Executive Committee. If the Executive Committee agrees with such a proposal, it must be put to the General Assembly.

The Executive Committee must give to all members of the Society at least 3 months' notice of the meeting of the General Assembly which will make a final decision on the proposal.

No decision shall be taken without an affirmative vote by a two-thirds majority of the members present and represented at the meeting of the General Assembly of the Society.

At least 25% of the ordinary members must be present or represented at this General Assembly.

Changes in the statutes or liquidation of the society is valid only after approval by the authorities, according to article 50§3 of the law, and after the formalities for publication in the "Bijlagen tot het *Belgisch Staatsblad*" are fulfilled, according to article 51§3 of the law.

The General Assembly decides on the way in which the Society will be dissolved and how its assets will be settled.

After liquidation, the net assets of the Society shall be transferred to a non-profit organization with a similar aim as the ESP or to a charity.

Article 9: Management

9.1: Powers

Between General Assemblies, an Executive Committee shall direct the Society.

The Executive Committee possesses full powers of management and administration, except for the functions assigned to the General Assembly. The Committee may delegate the management of day-to-day affairs and well-specified functions to its President, to another member of the Executive Committee or to a third person.

The Advisory Council assists the Executive Committee. The Council has a purely advisory role.

9.2: Composition

The Executive Committee is composed of at least 12 members, namely, four officers and eight Society members.

The officers shall be the President, the President-Elect, the Secretary and the Treasurer.

The Society will try to include at least one Belgian in the Executive Committee.

Nominations will be sought from the membership by advertisement in the newsletter.

The Executive Committee will make nominations for members of the Executive Committee.

This Committee is elected by the General Assembly for a period of 4 years.

The Secretary and the Treasurer can be re-elected immediately. The president is elected for a period of 2 years as a president-elect, followed by a 2-year presidency.

The officers and the members of the Executive Committee can be removed by the General Assembly, by a resolution accepted by a two-thirds majority of members present and represented.

Their function will also be terminated by death, resignation, civil incompetence and severe incapacity of health, discharge or end of term.

If an Executive Committee member prematurely terminates his function, the Executive Committee can elect a replacement.

The Executive Committee is assisted by an Advisory Council composed of members, each representing his or her national society. The Executive Committee upon approval by the General Assembly shall nominate the Chairman of the Council.

9.3: Meeting and Convocation

The Executive Committee meets as necessary and at least twice a year. Notice of the meeting will be circulated by the Secretary by mail, fax, e-mail or any other means of communication, at least 1 month prior to the meeting.

9.4: Resolutions

At least two-thirds of the Executive Committee members need to be present or represented to form a quorum.

Another member can represent a member of the Executive Committee, but each member can only represent one other member.

Resolutions are adopted by a majority of the members present or represented, the President having the casting vote in the event of a tie.

If the meeting of the Executive Committee is not attended by two-thirds of the members, a new meeting of the Executive Committee will be scheduled under the same conditions as the above-mentioned, and this meeting can take a final and valid decision with a simple majority of the members present or represented, irrespective of their number.

9.5: Registration of the Resolutions Taken by the Executive Committee

The resolutions of the Executive Committee are entered in a register, signed by both the President and the Secretary and recorded by the latter, who will maintain the register on behalf of the members, at the working address of the Society.

Article 10: Representation of the Society Towards Third Persons and Towards the Law

Except for special powers of attorney, all acts binding on the ESP are signed by the Secretary and the President of the Executive Committee, who need not give proof of their powers to a third person.

All legal proceedings, including the entering into and the prosecution of a lawsuit, are conducted, both as a plaintiff and as a defendant, by the Executive Committee represented by its President or a member of the Executive Committee designated by it for the purpose.

Article 11: Budgets and Accounts

The financial year begins 1 August and ends on 31 July. The budget and accounts of the ESP shall be submitted annually for provisional approval to the Executive Committee in accordance with article 53. Prior to the meeting of the General Assembly, the Treasurer will submit the accounts of the past two financial years to the Finance Committee composed of three Society members. Members of the Executive Committee cannot be members of the Finance Committee. The report of this Committee will be presented to the General Assembly together with the Treasurer's report and the respective accounts for final approval. In addition, the budget for the two forthcoming financial years will be discussed and approved by the General Assembly.

The yearly accounts have to be transferred to the Belgian Federal Government of Justice, in accordance with article 51 of the law.

Article 12: General Considerations

The Dutch version of the statutes is the only official version.

All cases not provided for by the present regulations and particularly the announcements to be made in the *Belgisch Staatsblad* shall be regulated in conformity with the provisions of the Belgian law of 27 June 1921, title III, concerning non-profit societies, international non-profit societies and foundations.

Attention please:

New procedures for the election of officers of the Society and members of the Executive Committee

A. *Election of officers*:
1. The President asks for the advice of the Nominations Committee (active past presidents) to make proposals for candidates for each post.
2. Proposals and the opinion of the Nominations Committee are presented to the Executive Committee.
3. The Executive Committee discusses and votes (by simple majority) on any proposals.
4. The Executive Committee recommends a candidate for each post to the membership at large. (Individuals must approve their own candidature and provide an abbreviated CV). The recommendation will be published in the newsletter and on the ESP website.
5. The published recommendation will be accompanied by a call for other nominations. Such nominations must be approved by the individuals themselves and each must be supported by a substantial number of members in good standing (initially this will be 5%) and accompanied by an abbreviated CV of no more than one page.
6. Six weeks later:
   Option A:
   No further nominations.
   Option B:
   i. One or more correctly proposed nominations.
   ii. A general ballot will be held (either postal or electronic or by secret vote of members at the next appropriate congress). The method of conducting the ballot will be determined by the Executive Committee.
   iii. The successful candidate will be elected by simple majority.
7. The successful nomination will be presented for approval at the General Assembly.
8. The General Assembly must approve that the procedure for choosing the new officer was carried out correctly. Further candidates cannot be proposed at the General Assembly.

B. *Election of the eight additional Executive Committee Members*:
1. Nominations to be sought from a variety of sources, to include the President, members of the Executive Committee and the Advisory Committee.
2. Nominations (with a short CV) should be sent to the Secretary.
3. The Secretary will present them to the Executive Committee.
4. The Executive Committee will discuss the candidates.

5. Nominations will be sent the Nominations Committee for comments and advice. (Individuals must approve their own candidature and provide an abbreviated CV).
6. The Executive Committee discusses the nominations, taking into account geographical and sub-speciality factors to ensure wide representation of the membership at large.
7. The Executive Committee decides, and if necessary votes (by simple majority), on the proposals.
8. The recommendations of the Executive Committee will be published in the newsletter and on the ESP website.
9. The recommended candidates will be presented for formal approval at the General Assembly. The General Assembly must approve that the procedure for choosing the new members of the Executive Committee was carried out correctly. Further candidates cannot be proposed at the General Assembly.

From the Meeting of the Executive Committee in Barcelona, November 2004

Front row, *left to right*: President-Elect Niki J. Agnantis, President Antonio Cardesa, Past President Gianni Bussolati. *Second row*, *left to right*: Veli-Pekka Letho, Grete Krag Jacobsen, Dilek Yilmazbayhan, Fatima Carneiro, President of the Advisory Council Günther Klöppel. *Back row*, *left to right*: Michael Wells, Roderick HW Simpson, Rastko Goluoh and Treasurer Jan van Kriecken. (Absent: Frederique Capron and Christine de Wolf-Peeters.)

Report on the Gastrointestinal Workshop, Ankara, 11–12 September 2004

On behalf of the ESP Working Group on Gastrointestinal Pathology, a Gastrointestinal Pathology Workshop was organized by Prof. Arzu Ensari on 11–12 September 2004, at the Department of Pathology, Ankara University Medical School, Turkey. Five distinguished speakers from various European countries gave excellent lectures and workshops: J. Offerhaus (The Netherlands), J.F. Flejou (France), M. Walker (UK), M.N. Marsh (UK) and A. Ristimaki (Finland); 80 pathologists attended the workshop. The topics of the lectures and slide discussions included Barrett's oesophagus, gastric intra-epithelial neoplasia and the Vienna Classification, gastric cancer and Cox-2, inflammatory gastroduodenal diseases and small intestine and intraepithelial lymphocytes. There were also endoscopy–microscopic interactive sessions presented by endoscopists and pathologists. Each workshop ended with a session on difficult cases presented by the participants and discussed with the speakers. Overall, the workshop had a lively and interactive atmosphere and each session scored 4.5 points out of 5 in the evaluation. Both the lecturers and the participants found the meeting to be successful and stated that they would hope to meet again in future workshops.

Arzu Ensari

Invitation to the 20th European Congress of Pathology

On behalf of the European Society of Pathology, the French Society of Pathology and the Organizing Committees, we warmly invite you to the 20th European Congress of Pathology to be held in Paris, 3–8 September 2005.

Over the years, progress in pathology has led to an improved understanding of the physiopathology of diseases and has provided strong help for assessing or designing new treatments. There is no doubt that in the near future pathology, with its multidisciplinary approaches, will continue to play a key role in everyday clinical practice while contributing to push back the frontiers of basic understanding. A congress like the Biannual Congress of the European Society of Pathology is the place of choice to gain information and to share recent advances on the many different aspects of our speciality.

This year, the 20th European Congress of Pathology will coincide with the 40th anniversary of the European Society of Pathology. The Congress Organizing Committee has put a lot of effort in creating an attractive scientific programme, addressing many of the key issues in pathology and focusing on the cutting edge of basic and clinical pathology. The congress will consist of several symposia and seminars, advanced teaching courses, free communications and poster sessions. Distinguished speakers will give keynote presentations. Sessions of submitted papers will be strongly evaluated. Our goal is to provide a forum for all pathologists and a bridge between education and research. As always, the Congress will offer the opportunity for old friends to meet again, and for colleagues from all over Europe and beyond to make new contacts, discuss their science and develop new ideas while enjoying the friendly atmosphere of Paris.

France is a major European crossroad. It is an ideal place to gather pathologists from countries of the north and the south of Europe and pathologists from the west and the east. Paris, on the banks of the River Seine, is one of the most scenic capitals in the world. Although resolutely looking

towards tomorrow, Paris has always been associated with history. Paris, the "city of light", has a tremendous historical, cultural, architectural and artistic heritage – nowhere else will you find finer monuments, museums, and of course fashion, food and wine. The "social" programme will try to incorporate all these different facets and will contribute towards making the 20th European Congress of Pathology in Paris an unforgettable "souvenir".

The Organizing Committee will do its utmost to ensure that you enjoy a happy and productive congress and looks forward to your active participation. We are convinced that your stay in Paris will be academically, educationally and socially rewarding.

We look forward to welcoming you to the 20th European Congress of Pathology.

Pierre Bedossa

President of the 20th European Congress of Pathology

All information available at: www.pathology-congress.com

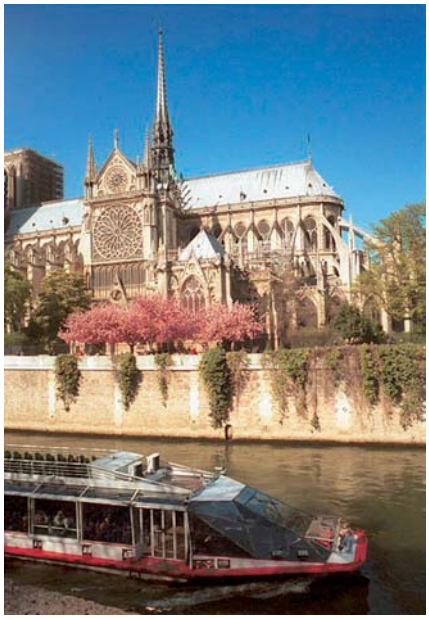

The European Society of Pathology

Dear Colleague,

It will surely not have escaped your attention that *Virchows Archiv* is now the Official Journal of the European Society of Pathology.

But did you realise what benefits membership in the society offer you?

- A subscription to the journal *Virchows Archiv* at no extra charge – this is automatically sent to every member every month.
- Access to the journal online (take a look at http://link.springer.de). If you are already a member of ESP but have not yet registered for your free electronic access, you will find the necessary form to complete online here too.
- A discount of 20% on most titles published by Springer. To take advantage of this, simply send your order directly to the publisher, with details of your membership.
- Attendance at the Society's conferences at a reduced fee.

If you have not yet joined the European Society of Pathology, why not do so now?
Simply complete and return the form enclosed.

We look forward to welcoming you as a member in 2005

Yours sincerely

A. Cardesa
President
European Society of Pathology

H. van Krieken
Treasurer
European Society of Pathology

H. Höfler
Managing Editor
Virchows Archiv

Application for Membership of the EUROPEAN SOCIETY OF PATHOLOGY

For formatting of old application, please follow old application (old Newsletter, p. 238)

This application can also be downloaded from our website:
http://www.Europathology.org

Please complete the following form (block capitals please) and return it to the Office of the Treasurer

FAMILY NAME: .....

First Name(s): .....

Male ❑ Female ❑

Place and date of birth: .....

Title/Present Position: Prof. ❑ Dr. ❑ Resident ❑

Other: .....

Please clearly indicate which one of the following addresses should be used for subsequent correspondence, mailings, and listing in the Members Handbook:

❑ PRIVATE ADDRESS:

Name: .....
Street: .....
Postcode .....
City: .....
Country: .....

❑ INSTITUTE / OFFICE ADDRESS:

Name Institute: .....
Department: .....
Street: .....
Postcode: .....
City: .....
Country: .....
Telephone: .....
Telefax: .....
E-mail: .....

FIELDS OF INTEREST: .....

Date: ..... Signature of Applicant: .....

Please mail or fax the completed application form to:

ESP – OFFICE OF THE TREASURER,
Prof. Dr. H. VAN KRIEKEN,
University Medical Center Nijmegen
Dept. of Pathology / 437 PA
P.O.Box 9101
6500 HB NIJMEGEN, The Netherlands

Tel.: +31-24-3614352
Fax: +31-24-3540520
e-mail: j.vankrieken@pathol.umcn.nl

Your acceptance as a member of E.S.P. will be confirmed in due course.

Virchows Arch (2005) 446: 585–588
DOI 10.1007/s00428-005-1276-5

REVIEW ARTICLE

A. Teymoortash · J. A. Werner

Tissue that has lost its track: Warthin's tumour

Received: 8 February 2005 / Accepted: 20 April 2005 / Published online: 24 May 2005
© Springer-Verlag 2005

Abstract The origin of cystadenolymphoma (Warthin's tumour) of the parotid gland is unknown. According to the most favoured hypothesis, Warthin's tumour results from the proliferation of salivary gland ductal cells that were entrapped in parotid lymph nodes during embryonal life. If this is correct, and the almost total lack of recurrence and malignant transformation of this lesion lends credence to this view, Warthin's tumour is correctly classified in the group of tumour-like lesions and should not be considered to be a monomorphic adenoma.

Keywords Warthin's tumour · Pathogenesis · Classification

Introduction

The average incidence rate of all salivary gland tumours is 5 per 100,000 [17]. According to the Hamburg Salivary Gland Registry, about 65% of those tumours are benign. Warthin's tumour of the parotid gland accounts for about 15% of all epithelial tumours of the parotid gland [22]. This tumour entity has always fascinated head and neck surgeons and pathologists, as its pathogenesis is still unknown. Not even the nomenclature of this disease is standardised. Currently more than 20 different terms are in use to describe this disease. The initial description of the tumour goes back to Hildebrand in 1895, who considered this disease a variant of lateral cyst of the neck [9]. In 1910, Albrecht and Arzt reported two tumours of the upper neck region which they interpreted as "confused tissue" in the entodermal pharyngeal anlage, particularly that of salivary glands, in the lymph nodes [2]. They called them papillary cystadenomas in lymph nodes. In the WHO classification, the disease was named Warthin's tumour after the pathologist who published the first two case reports in the American literature in 1929 [28]. He gave the tumour the name papillary cystadenoma lymphomatosum and regarded it as heterotopia of the mucous membrane of the accessory eustachian tube anlage. The term Warthin's tumour was chosen later, in order to avoid confusion with malignant lymphomas.

Warthin's tumours are well encapsulated lesions with cystic and solid areas. They usually occur at the caudal pole of the parotid gland. These tumours consist of an oncocytic epithelial cell component arranged in double layers, which develops cysts and papillary projections, and a variable stroma component with lymphoid tissue. A few Warthin's tumours (about 8%) show areas of squamous cell metaplasia and regressive changes.

Warthin's tumours most commonly present as an asymptomatic, slowly growing mass usually affecting men in the 5th and 6th decade. They occur extremely rarely in patients of Black African origin. In about 4–10% of cases, there is bilateral tumour development, which is commonly metachronous. In about 4% of cases, multiple Warthin's tumours may be observed in one parotid gland. They may occur simultaneously with pleomorphic adenomas, various types of carcinoma and malignant lymphomas [22]. These observations are important because the latter features are not shared by the other tumour entities of the salivary glands and they may therefore be helpful for the understanding of the pathogenesis of the disease.

Where does Warthin's tumour come from?

Although various theories have been put forward to explain the development of Warthin's tumour [6, 18], only two have ultimately remained. The first is the already mentioned hypothesis of heterotopia; the second is the theory

A. Teymoortash (✉) · J. A. Werner
Department of Otolaryngology, Head and Neck Surgery,
Philipps University,
Deutschhausstr. 3,
35037 Marburg, Germany
e-mail: teymoort@med.uni-marburg.de
Tel.: +49-6421-2866478
Fax: +49-6421-2866367
URL: www.ent-marburg.de

that this tumour is an adenoma with concomitant lymphocytic infiltration. According to the latter theory, when they are small and have a short history, Warthin's tumours consist mainly of epithelial components, while when they are large they show, in addition to their epithelial component, a lymphoid stroma. Since they are observed first, the epithelial components are therefore thought to be the fundamental neoplastic elements [1]. This theory was disproved by a recent study performed by Honda et al. [10], who showed that the epithelial tumour components, like the lymphocytic infiltrations [25], are polyclonal. If, however, neoplasia is defined as a monoclonal process, this kind of tumour cannot be considered to be a true neoplasm.

After Albrecht and Arzt [2] a large number of studies drew the conclusion that this tumour develops due to salivary gland heterotopia in peri- and intraparotideal lymph nodes [18, 27]. The main support for this theory is the detection of salivary duct inclusions in lymphoid tissue in foetuses and infants. During the embryogenesis of the parotid gland, epithelial cells from the oral mucosa happen to penetrate into lymphocyte-rich tissue. The late encapsulation of the parotid gland explains the occurrence of intraparotideal lymph nodes and heterotopic salivary gland remnants entrapped in the parotideal lymph nodes. According to this theory, Warthin's tumours have their origin in these epithelial inclusions. Luminal cells in the tumour in particular show a similar construction to the striated ducts of the normal glandular tissue and contain numerous mitochondria. The basally located cells are characterised by different degrees of differentiation and can be classified according to their cytokine expression as regenerative cells [20]. Besides the epithelial component with cysts of different sizes, these tumours are characterised by a stromal component with lymphocytic infiltrates and lymph follicles that correspond to the distribution of the lymphocytic infiltrations of a lymph node. However, the lymph node architecture is extensively displaced by the epithelial components. This hypothesis is further supported by the occurrence of tuberculosis, metastases and malignant lymphomas in the lymphoid stroma of those tumours [23].

In large registries, Warthin's tumours located outside of the parotid gland account for about 8% of the cases. Case reports concern particularly cervical lymph nodes, the submandibular gland, and the larynx [16]. We assume that more attention is paid to these rather rare locations than to the numerous Warthin's tumours located in the parotid gland which are extirpated worldwide. The extraparotid location and multicentric nature of these tumours can be explained by the last-mentioned hypothesis.

The hypothesis of heterotopia would at least partly confirm the theory established by Hildebrand, who considered this disease to be a variation of a lateral cervical cyst [9]. While it was previously thought that lateral cervical cysts develop from the 2nd to 4th pharyngeal cleft, the current opinion is that they are more likely to be heterotopic epithelial inclusions of tonsillar tissue in jugulodigastric lymph nodes [24, 29]. Thus, Hildebrand was not totally wrong with the hypothesis he published already in 1895, and his theory corresponds to the hypothesis of heterotopia.

Other studies discussed the importance of immunological reactions during the formation of Warthin's tumour. Due to the morphological similarities between Warthin's tumour and Hashimoto thyroiditis, Allegra [3] first established the hypothesis that Warthin's tumour originates on the basis of an immune reaction of delayed hypersensitivity type. From his point of view, metaplasia of the ductal epithelium of the parotid gland may lead to proliferation of the epithelium with cyst formation. Reabsorption and phagocytosis of the cystic contents may result in an immunological reaction with emigration of the immunocompetent cells, corresponding to a cell-mediated immune reaction. A number of immunohistochemical findings indicate that there is an immunological interaction between epithelium and lymphoid stroma. These results support the assumption that oncocytic cells represent the true tumour component and cause reactive hyperplasia of the lymphoid stroma.

In this context, further similarities between the lymphoid components of the tumour and the lymphoid tissue of the intestinal mucosa were found [15]. The subepithelial infiltrates consist mainly of B-cells containing a large number of IgA producing subpopulations. The epithelial cells of the tumour are able to transport IgA to the lumen. The numerous germinal centres in the lymphoid tissue also support the hypothesis of an active immune reaction. The hypothesis has been discussed that epithelial cells of Warthin's tumour may serve as antigen-presenting cells, similar to the cells of the intestinal mucosa, inducing and regulating immune reactions. Major histocompatibility complex class II antigens and also IL-1 have been detected in the luminal oncocytic cells. These results indicate a possible role of the luminal tumour cells as antigen-presenting cells, which may present luminal antigens to lymphoid stromal cells. The expression of MHC-II antigens and IL-1, however, did not depend on the density of the T-cells.

Figure 1 depicts the various steps in the development of Warthin's tumour according to the hypothesis of heterotopia and the possible immunological reactions involved.

What triggers the tumourous changes and promotes their development? The detection of EBV-DNA in tumour cells in some studies led to the hypothesis that EBV may play a pathogenetic role in the development of the tumours [19]. However, these results could not be confirmed by further studies [11].

Some studies also showed that a significant number of patients suffering from this disease are smokers, in contrast to patients with other salivary gland tumours [8, 30]. Smoking was discussed as an important aetiological factor. Warthin's tumour consists of oncocytic cells containing numerous mitochondria frequently showing structural abnormalities and reduced metabolic function. The oncocytic transformation of single striated epithelial cells represents a process within the salivary glands that is frequently observed in advanced age. This fact seems to correlate with age-related metabolic deficiencies. Smoking can lead to

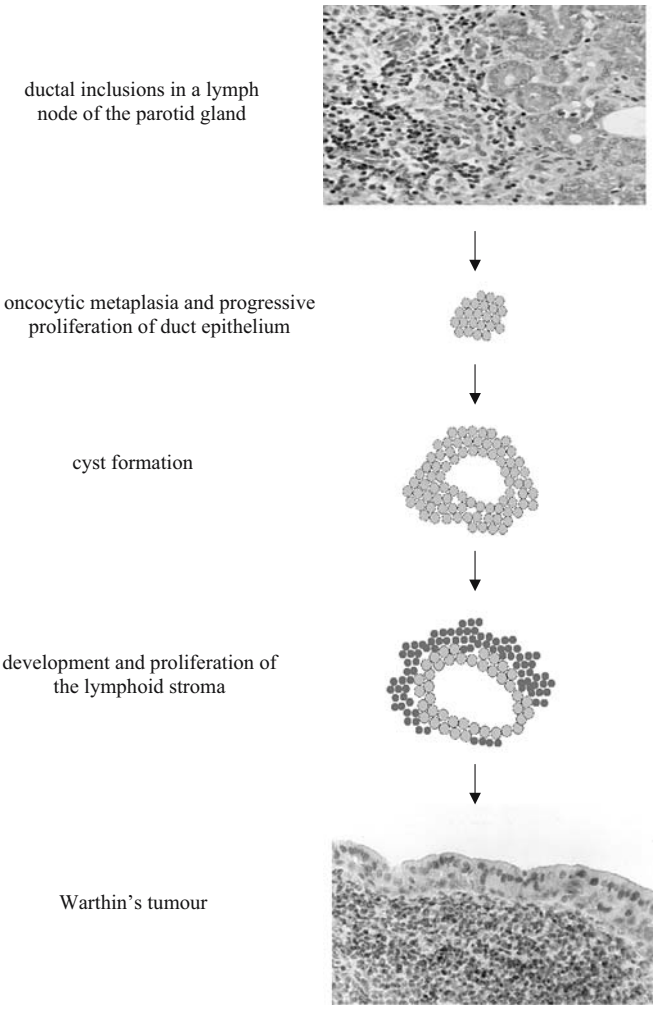

Fig. 1 Schematic representation of the changes in the salivary ducts during the development of Warthin's tumour

damage to mitochondrial DNA due to the development of numerous reactive oxygen species [4]. In this context, a high rate of deleted mitochondrial DNA has been detected in the oncocytic cells of Warthin's tumour [13].

The role of hormones in the aetiology of this disease has also been discussed. The salivary glands are not considered the classical target organs of steroid hormones and their possible contribution to salivary gland diseases is unclear. Only very few studies have dealt with this question. In some malignant salivary gland diseases and even in Warthin's tumour progesterone receptors have been found [26]. A correlation with hormones could possibly play an important role in the development of those tumours and provide an explanation for the dominance of the male gender. However, it must be considered that more males than females used to smoke so that the role of the individual factors remains unclear and the intrinsic factor stimulating the development of Warthin's tumour is still unknown (Fig. 2).

The cytogenetic data available on this tumour are rather scare. However, analysis of cytogenetic findings revealed,

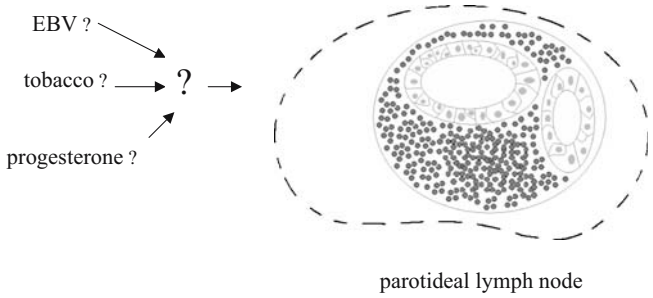

Fig. 2 Aetiological factors in the pathogenesis of Warthin's tumour

beside normal karyotypes, also structural alterations and numerical deviations in some cases [14]. Identification of cytogenetic subgroups in Warthin's tumour may suggest that it might be a pathogenetically heterogeneous group of lesions.

Another interesting aspect to be considered in the discussion of the aetiology of Warthin's tumour is manifest AIDS. In 3–6% of all HIV positive patients, cystic lymphoid hyperplasia occurs in the form of a cystic tumour of the parotid gland. In the context of this disease, a pathogenetic development from the epithelial salivary gland inclusions in the lymph nodes has also been discussed.

Conclusions

The details of the pathogenesis of Warthin's tumour are, as discussed above, still unclear. However, because of the arguments against a true neoplastic origin of this tumour, we favour a hypothesis combining immunological interactions between tumour cells and lymphocytic infiltrations with heterotopia.

In the WHO classification of salivary gland tumours, certain diseases of the salivary glands are considered tumour-like lesions [21]. Warthin's tumour may therefore also be classified in the group of tumour-like lesions, since both the epithelial and lymphoid tumour components are polyclonal in origin. The almost total lack of recurrence and malignant transformation of this tumour, similar to the situation in lateral cervical cysts, further supports this view. Multicentricity at first excision and growth from a new focus seem to be responsible for the cases of recurrence reported in the literature. Malignant transformation of this tumour, if it ever occurs, is extremely rare [7]. Most cases of reported malignancy can be attributed to a second tumour in association with Warthin's tumour [5]. On the basis of these clinical characteristics, a limited partial parotidectomy is recommended as an effective treatment of Warthin's tumour of the parotid gland [12].

Acknowledgements The authors would like to thank Professor Günter Klöppel and Kay Dege for critically reading the manuscript.

References

1. Aguirre JM, Echebarria MA, Martinez-Conde R, Rodriguez C, Burgos JJ, Rivera JM (1998) Warthin tumor. A new hypothesis concerning its development. Oral Surg Oral Med Oral Pathol Oral Radiol Endo 85:60–63
2. Albrecht H, Arzt L (1910) Beiträge zur Frage der Gewebsverirrung. I. Papilläre Cystadenome in Lymphdrüsen. Frankfurt Z Pathol 4:47–69
3. Allegra SR (1971) Warthin's tumor: a hypersensitivity disease? Ultrastructural, light, and immunofluorescent study. Hum Pathol 2:403–420
4. Allen JA, Coombs MM (1980) Covalent binding of polycyclic aromatic compounds to mitochondrial and nuclear DNA. Nature 287:244–245
5. Batsakis JG, Regezi JA (1987) The pathology of head and neck tumors: salivary glands, part 1. Head Neck Surg 1:59–68
6. Chapnik JS (1983) The controversy of Warthin's tumor. Laryngoscope 93:695–716
7. Foschini MP, Malvi D, Betts CM (2005) Oncocytic carcinoma arising in Warthin tumour. Virchows Arch 446:88–90
8. Gallo O, Bocciolini C (1997) Warthin's tumour associated with autoimmune diseases and tobacco use. Acta Otolaryngol 117:623–627
9. Hildebrand O (1895) Über angeborene epitheliale Cysten und Fisteln des Halses. Arch Klin Chir 49:167–206
10. Honda K, Kashima K, Daa T, Yokoyama S, Nakayama I (2000) Clonal analysis of the epithelial component of Warthin's tumor. Hum Pathol 31:1377–1380
11. Laane CJ, Murr AH, Mhatre AN, Jones KD, Lalwani AK (2002) Role of Epstein-Barr virus and cytomegalovirus in the etiology of benign parotid tumors. Head Neck 24:443–450
12. Leverstein H, van der Wal JE, Tiwari RM, van der Waal I, Snow GB (1997) Results of the surgical management and histopathological evaluataion of 88 parotid gland Warthin's tumours. Clin Otolaryngol 22:500–503
13. Lewis PD, Baxter P, Paul Griffiths A, Parry JM, Skibinski DO (2000) Detection of damage to the mitochondrial genome in the oncocytic cells of Warthin's tumour. J Pathol 191:274–281
14. Martins C, Fonseca I, Roque L, Soares J (1997) Cytogentic characterisation of Warthin's tumour. Oral Oncol 33:344–347
15. Ogawa Y, Hong SS, Toyosawa S, Chang CC, Yagi T (1990) Expression of major histocompatibility complex class II antigens and interleukin-1 by epithelial cells of Warthin's tumor. Cancer 66:2111–2117
16. Patterson JW, Wright ED, Camden S (1999) Extraparotid Warthin's tumor. J Am Acad Dermatol 40:468–470
17. Pinkston JA, Cole P (1999) Incidence rates of salivary gland tumors: results from a population-based study. Otolaryngol Head Neck Surg 120:834–840
18. Rauch S (ed) (1959) Papilläre Zystadenolymphome. (Die Speicheldrüsen des Menschen) Thieme, Stuttgart, pp 368–373
19. Santucci M, Gallo O, Calzolari A, Bondi R (1993) Detection of Epstein-Barr viral genome in tumor cells of Warthin's tumor of parotid gland. Am J Clin Pathol 100:662–665
20. Schwerer MJ, Kraft K, Baczako K, Maier H (2001) Cytokeratin expression and epithelial differentiation in Warthin's tumour and its metaplastic (infarcted) variant. Histopathology 39:347–352
21. Seifert G (1992) Tumour-like lesions of the salivary glands. The new WHO classification. Pathol Res Pract 188:836–846
22. Seifert G (1996) Warthin tumoren (Adenolymphome). In: Doerr W, Seifert G, Uehlinger E (eds) Oralpathologie I, Pathologie der Speicheldrüsen. Springer, Berlin Heidelberg New York, pp 440–463
23. Seifert G, Bull HG, Donath K (1980) Histologic subclassification of the cystadenolymphoma of the parotid gland. Analysis of 275 cases. Virchows Arch A Pathol Anat 388:13–38
24. Stoll W, Huttenbrink KB (1982) Die laterale halszyste: eine lymphknotenerkrankung. Laryngol Rhinol Otol 61:272–275
25. Takezawa K, Jackson C, Gnepp DR, King TC (1998) Molecular characterization of Warthin tumor. Oral Surg Oral Med Oral Pathol Oral Radiol Endo 85:569–575
26. Teymoortash A, Lippert BM, Werner JA (2001) Steroid hormone receptors in parotid gland cystadenolymphoma (Warthin's tumour). Clin Otolaryngol 26:411–416
27. Thompson AS, Bryant HC (1950) Histogenesis of papillary cystadenoma lymphomatosum (Warthin's tumor) of the parotid salivary gland. Am J Pathol 26:807–829
28. Warthin AS (1929) Papillary cystadenoma lymphomatosum. A rare teratoid of the parotid region. J Cancer Res 13:116–125
29. Wild G, Mischke D, Lobeck H, Kastenbauer E (1987) The lateral cyst of the neck: congenital or acquired? Acta Otolaryngol 103:546–550
30. Yu GY, Liu XB, Li ZL, Peng X (1998) Smoking and the development of Warthin's tumour of the parotid gland. Br J Oral Maxillofac Surg 36:183–185

Virchows Arch (2005) 446: 589–595
DOI 10.1007/s00428-005-1236-0

ORIGINAL ARTICLE

Vítor Trovisco · Paula Soares · Ana Preto · Inês Vieira de Castro · Jorge Lima · Patrícia Castro · Valdemar Máximo · Tiago Botelho · Severina Moreira · Ana Margarida Meireles · João Magalhães · Alexander Abrosimov · José Cameselle-Teijeiro · Manuel Sobrinho-Simões

Type and prevalence of *BRAF* mutations are closely associated with papillary thyroid carcinoma histotype and patients' age but not with tumour aggressiveness

Received: 13 January 2005 / Accepted: 17 February 2005 / Published online: 19 May 2005
© Springer-Verlag 2005

Abstract A high prevalence of the $BRAF^{V600E}$ somatic mutation was recently reported in several series of papillary thyroid carcinomas (PTC). This mutation appears to be particularly prevalent in PTC with a predominantly papillary architecture. Another *BRAF* mutation (K601E) was detected in a follicular adenoma and in some cases of the follicular variant of PTC. The few studies on record provided controversial data on the relationship between the occurrence of *BRAF* mutations and clinicopathologic parameters such as gender, age and tumour staging. In an attempt to clarify such controversies we decided to enlarge our previous series to 315 tumours or tumour-like lesions diagnosed in 280 patients, including a thorough analysis of several clinicopathologic features. The $BRAF^{V600E}$ mutation was exclusively detected in PTC with a papillary or mixed follicular/papillary architecture both of the conventional type (46%) and of other histotypes, such as microcarcinoma (43%), Warthin-like PTC (75%) and oncocytic variant of PTC (55%). The $BRAF^{K601E}$ mutation was detected in four of the 54 cases of the follicular variant of PTC (7%). The mean age of patients with conventional PTC harbouring $BRAF^{V600E}$ (46.7 years) was significantly higher ($P<0.0001$) than that of patients with conventional PTC without $BRAF^{V600E}$ (29.5 years). The *BRAF* ($BRAF^{V600E}$) mutated PTC did not exhibit signs of higher aggressiveness (size, vascular invasion, extra-thyroid extension and nodal metastasis) and were in fact less often multicentric than PTC without the mutation.

Keywords Thyroid · Papillary carcinoma · Follicular variant of PTC · Oncocytic variant · BRAF · Oncogene

V. Trovisco and P. Soares contributed equally to this work

Fundação para a Ciência e Tecnologia POCTI/FEDER (POCTI/NSE/48171/2002)

V. Trovisco · P. Soares · A. Preto · J. Lima · P. Castro · V. Máximo · T. Botelho · S. Moreira · A. M. Meireles · M. Sobrinho-Simões (✉)
IPATIMUP (Institute of Molecular Pathology and Immunology of the University of Porto),
R. Roberto Frias s/n,
4200 Porto, Portugal
e-mail: ssimoes@ipatimup.pt
Tel.: +351-22-5570700
Fax: +351-22-5570799

P. Soares · M. Sobrinho-Simões
Department of Pathology,
Medical Faculty of the University of Porto,
Porto, Portugal

I. V. de Castro
Department of Pathology,
Medical Faculty of the University of São Paulo,
São Paulo, Brazil

J. Magalhães · M. Sobrinho-Simões
Department of Pathology, Hospital São João,
Porto, Portugal

A. Abrosimov
Pathology Department,
Medical Radiology Research Centre,
Russian Academy of Medical Sciences,
Obninsk, Russia

J. Cameselle-Teijeiro
Department of Pathology,
Hospital Clínico Universitario,
University of Santiago de Compostela,
Santiago de Compostela, Spain

Introduction

Raf proteins are serine/threonine kinases that play an initial role in the enzymatic cascade of the MAPK signalling pathway Raf-MEK-ERK [16]. Mutations from valine to glutamic acid at the residue 600 (formerly referred as residue 599 [10]) of the *BRAF* gene, first described with a high frequency in melanoma [3, 7], were found to be highly prevalent in PTC in several series [6, 9, 13, 22, 26].

We have recently shown that the large variation of the mutation prevalence in different studies (29–69% of PTC) [6, 9, 13, 22, 26] probably reflects the different histotype

composition of the reported series. The mutation is almost exclusively detected in PTC with a papillary or mixed follicular/papillary architecture (conventional PTC; Warthin-like PTC; oncocytic variant of PTC with a predominantly papillary growth pattern), being extremely rare in other variants of PTC [24].

The follicular variant of PTC was characterized by the presence of another *BRAF* mutation (K601E) in three out of 32 cases (9%) [24]. This genetic alteration corresponds, like the V600E, to the activation segment of the *BRAF* gene (exon 15). It had been previously detected in rare cases of melanoma and colorectal carcinoma [3, 18] and, by our group, in two follicular adenomas of the thyroid [11, 22].

Xu and colleagues [26] reported that the $BRAF^{V600E}$ mutation was significantly more prevalent in PTC of males than those occurring in females and more prevalent, although without reaching statistical significance, in PTC of older individuals. Nikiforova and colleagues [15] found that the $BRAF^{V600E}$ mutation is significantly associated with older age of the patients but not with their gender. Finally, Namba and colleagues [13], Puxeddu and colleagues [17] and Kim and colleagues [8] did not find any significant association between the presence of the $BRAF^{V600E}$ mutation and the gender and age of patients.

Namba and colleagues [13] and Nikiforova and colleagues [15] reported that the $BRAF^{V600E}$ mutation was associated with tumour stages III and IV, and Xu and colleagues [26], Namba and colleagues [13] and Kim and colleagues [8] reported an association between $BRAF^{V600E}$ and metastatic tumours. In contrast to this, Puxeddu and colleagues [17] did not find any association between the presence of $BRAF^{V600E}$ in PTC and tumour staging, local invasiveness or lymph node metastasis.

In an attempt to clarify the aforementioned discrepancies and to reinforce (or refute) our previous data on the association between the occurrence of *BRAF* mutations and some PTC histotypes, we decided to enlarge our series of differentiated tumours of the thyroid and tumour-like lesions. We have specifically studied additional cases of conventional PTC and some PTC variants (follicular variant, oncocytic variant and microcarcinoma), as well as cases with more than one type of tumour. We also tried to elucidate any possible relationship between the occurrence of *BRAF* mutations and some clinicopathologic features (multicentricity, vascular invasion, extra-thyroid extension and lymph node metastasis).

Materials and methods

Materials Material from 280 patients with 315 tumours and tumour-like lesions of the thyroid was collected from seven institutions in four countries: Hospital de S. João/Medical Faculty of Porto, Porto, Portugal; IPATIMUP, Porto, Portugal; IPO, Lisboa, Portugal; Hospital de San Pau Y San Creu, Barcelona, Spain; Hospital Clínico Universitario, Santiago de Compostela, Spain; Hospital das Clínicas, Medical Faculty of the University of São Paulo, Brasil; Medical Radiological Research Centre of Russian Academy of Medical Sciences, Russian Federation. Two or three independent lesions (including six cases in which there were foci of nodular lymphocytic thyroiditis adjacent to PTC) were studied in 30 patients.

The histological classification was made according to the criteria of LiVolsi [12] and Rosai and colleagues [19] by three pathologists (I.V.C., A.A., M.S.S.) without information on *BRAF* data. Whenever there was a discrepancy, the case was discussed together under a multiple head microscope and a consensus diagnosis was reached.

Data on gender and age were available in 278 patients. The size of the tumours diagnosed as follicular adenoma, follicular carcinoma or PTC was available in 197 cases. In Table 1 we have summarized the histological classification of the lesions, the age and gender of patients and the size of the tumours.

Data on multicentricity, vascular invasion, extra-thyroid extension and lymph node metastasis were available in 93 of the 156 clinically evident PTC (all but 20 microcarcinomas).

One hundred lesions were added to the 215 tumours and tumour-like lesions that had been previously assessed for *BRAF* mutations in two previous studies [22, 24]. In 20 lesions, two (n=18) or three (n=2) different samples were screened for *BRAF* mutations. The DNA material was retrieved from paraffin blocks after careful microdissection performed by an experienced pathologist. DNA extraction was performed using the Puregene DNA Isolation Kit (GENTRA Systems, Minneapolis, Minn., USA) following the manufacturer's instructions. Cases in which there were doubts on the quality of the DNA preservation have not been included in the study.

BRAF mutation analysis To screen for *BRAF* mutations, we analysed DNA from tumour tissue. We studied the regions of *BRAF* where mutations were previously identified—AKT binding sites/G-rich loop region and activation segment—which are encoded by exon 11 and 15, respectively. Both exons were amplified by PCR using conditions described elsewhere [22]. The amplicons were then subjected to single stranded conformation polymorphism (SSCP) analysis: PCR reaction products of *BRAF* exons 11 and 15 were diluted 1:1 with loading buffer (95% formamide, 0.05% bromophenol blue and 0.05% xylene cyanol), denatured at 96°C for 10 min and cooled on ice for 5 min; electrophoresis of the denatured PCR products was carried out in non-denaturing 0.8X mutation detection enhancement (MDE) gels (BMA, Rockland, Maine, USA) at 180 V and 8°C for 15 h; PCR/SSCP products were visualized by standard DNA silver staining of the gels.

BRAF sequencing analysis Whenever a case presented aberrant bands in the SSCP analysis, the remaining PCR sample was subjected to a purifying treatment using Exonuclease I (New England Biolabs Inc., Beverly, USA) and shrimp alkaline phosphatase (Amersham Biosciences, Piscataway, N.J., USA) and subjected to automatic sequencing, using ABI Prism dGTP BigDye Terminator Ready Reaction Kit (Perkin-Elmer, Foster City, California)

Table 1 Gender ratio and mean age of the 280 patients with 315 thyroid tumours and tumour-like lesions according to the histological classification, as well as the size of the tumours, and the prevalence of $BRAF^{V600E}$ mutation[a]

Histotypes	No. of cases	Gender ratio (♀:♂)	Mean age (years±SE)	Tumour size (cm±SE)[b]	$BRAF^{V600E}$ mutation
Nodular lymphocytic thyroiditis	6	6:0	48.7±4.8	NA[c]	0/6 (0%)
Nodular goiter	39	6.8:1	49.4±2.3	NA[c]	0/39 (0%)
Follicular thyroid adenoma	58	4.8:1	44.1±2.1	3.6±0.3 (47)	1/58 (1.7%)[d]
Conventional	50	5.3:1	42.2±2.0	3.7±0.7(43)	1/50 (2%)[d]
Oncocytic variant	8	3:1	64.0±5.6	2.6±0.8(4)	0/8 (0%)
Follicular thyroid carcinoma[e]	24	6.7:1	44.7±4.0	3.5±0.4(21)	0/24 (0%)
Conventional[e]	15	13:1	40.6±3.5	3.7±0.6(14)	0/15 (0%)
Oncocytic variant	9	3.5:1	56.4±10.6	3.2±0.5(7)	0/9 (0%)
Mucoepidermoid carcinoma	12	3:1	31.4±7.0	Not available	0/12 (0%)
Papillary thyroid carcinoma[e]	176	7.3:1	40.5±1.4	2.7±0.2 (129)	55/176 (31.3%)
Conventional PTC	72	5.3:1	37.2±2.1	3.2±0.3(49)	33/72(45.8%)
Follicular variant of PTC	54	12.5:1	41.5±2.6	2.7±0.2(46)	4/54(7.4%)[d]
Oncocytic variant of PTC	22	9:1	45.7±2.9	3.5±0.7(12)	6/22 (27.3%)
Conventional pattern	11	8:1	46.6±3.5	2.6±0.5 (8)	6/11(54.5%)
Follicular pattern	11	10:1	44.9±4.5	5.2±1.4(4)	0/11(0%)
Warthin-like PTC[e]	8	7:0	50.1±4.5	1.7±0.3(7)	6/8(75%)
Microcarcinoma (PTC)	20	8:1	49.8±3.2	0.5±0.1(15)	6/20(30%)
Conventional pattern	14	13:1	45.7±3.1	0.5±0.1(13)	6/14(42.9%)
Follicular pattern	6	5:1	53.2±7.8	0.4±0.2 (2)	0/6(0%)

[a]There were 25 patients with two independent lesions and five with three independent lesions
[b]Number of cases analysed in each category within brackets
[c]*NA* not aplicable
[d]The $BRAF^{K601E}$ mutation was detected in one follicular adenoma and in four cases of follicular variant of PTC
[e]In a follicular carcinoma and a Warthin-like PTC the data on patients' gender and age were not available

and an ABI prism 3100 Genetic Analyser (Perkin-Elmer). Sequencing was performed on both strands using the aforementioned primers.

Statistical analysis The results are expressed as a percentage or mean±SE. Statistical analysis was performed both on the whole series and considering the different groups of lesions. For the analysis of the relationship between patients' age and *BRAF* status of the tumours, we used the unpaired *t*-test and ANOVA. Fisher's exact test was used in the statistical analysis of the other parameters. Results were considered statistically significant whenever $P<0.05$, and suggestively different whenever $P<0.1$.

Ethics statement Local ethical guidelines appropriate to each country were followed in this study.

Results

The age of the patients and, less obviously, their gender, differed according to the histotypes of the tumours (Table 1). Regarding age, patients with tumours exhibiting oncocytic (Hürthle cell) features were consistently older than patients presenting their non-oncocytic tumour counterparts (follicular adenoma: 64.0 years versus 42.2 years $P=0.001$; follicular carcinoma: 56.4 years versus 40.6 years $P=0.16$; conventional PTC: 46.6 years versus 37.2 years $P=0.11$; and follicular variant of PTC: 44.9 years versus 41.5 years $P=0.56$, respectively). Patients with Warthin-like PTC (50.1 years) were suggestively older ($P=0.06$) than those with conventional PTC (37.2 years). Finally, patients with conventional PTC were younger (37.2 years), though not significantly ($P=0.13$), than those with follicular variant of PTC (42.1 years).

With regard to gender, the most impressive difference concerned the higher predominance of women in patients with follicular variant of PTC (12.5:1) than in patients with conventional PTC (5.3:1), although this difference did not reach the threshold of statistical significance ($P=0.18$) (Table 1).

No significant differences were observed in the prevalence of *BRAF* mutations in the comparison of the cases from the seven institutions (data not shown).

The $BRAF^{V600E}$ mutation was detected in conventional PTC (46%), Warthin-like PTC (75%), and in oncocytic variant of PTC and microcarcinoma with papillary or mixed follicular/papillary architecture (55% and 43%, respectively) (Table 1).

The $BRAF^{K601E}$ mutation was only detected in the follicular adenoma previously reported [22] and in four out of 54 cases of the follicular variant of PTC (7%) (Table 1).

No *BRAF* mutations (V600E, K601E) were detected in any nodular goiter, any of the additional cases of follicular adenoma, nor in any follicular carcinoma (Table 1).

No mutations in exon 11 were detected in any case.

In Table 2, we have summarized the data concerning the 14 cases having more than one independent lesion in which

Table 2 Histological classification of the lesions in 14 patients presenting two or three independent lesions with and without *BRAF* mutations

Case	Carcinoma	BRAF
1	Papillary microcarcinoma (conventional)	V600E
	Oncocytic variant of PTC (conventional)	Wild-type
	Mucoepidermoid carcinoma	Wild-type
2	Nodular goiter	Wild-type
	Oncocytic variant of PTC (conventional)	V600E
3	Nodular lymphocytic thyroiditis	Wild-type
	Conventional PTC	V600E
4	Papillary microcarcinoma (conventional)	Wild-type
	Papillary microcarcinoma (conventional)	V600E
5	Nodular goiter	Wild-type
	Conventional PTC	Wild-type
	Conventional PTC	V600E
6	Nodular goiter	Wild-type
	Conventional PTC	V600E
7	Nodular goiter	Wild-type
	Oncocytic variant of PTC (conventional)	V600E
8	Nodular lymphocytic thyroiditis	Wild-type
	Nodular goiter	Wild-type
	Conventional PTC	V600E
9	Follicular variant of PTC	Wild-type
	Papillary microcarcinoma (conventional)	V600E
	Warthin-like PTC	V600E
10	Nodular lymphocytic thyroiditis	Wild-type
	Papillary microcarcinoma (conventional)	Wild-type
	Conventional PTC	V600E
11	Follicular carcinoma	Wild-type
	Warthin-like PTC	V600E
12	Nodular goiter	Wild-type
	Warthin-like PTC	V600E
13	Nodular lymphocytic thyroiditis	Wild-type
	Conventional PTC	V600E
14	Mucoepidermoid carcinoma	Wild-type
	Conventional PTC	V600E

at least one of them had a $BRAF^{V600E}$ mutation. No $BRAF^{V600E}$ mutations were detected in the "normal" thyroid parenchyma adjacent to PTC, regardless of the presence or absence of $BRAF^{V600E}$ mutation in the tumours (data not shown). We also did not detect any $BRAF^{V600E}$ mutation in any of the six cases of nodular lymphocytic thyroiditis adjacent to PTC, despite the existence of this mutation in four of the latter (Table 2). The same holds true regarding seven nodular goiters adjacent to $BRAF^{V600E}$ positive PTC, as well as two mucoepidermoid carcinomas and one follicular carcinoma that coexisted with $BRAF^{V600E}$ mutated PTC (Table 2). In the 20 cases in which more than one sample of the same lesion was screened, the same *BRAF* status was found in all the samples.

In Table 3 we have summarized the gender ratio and mean age±SE of the patients with conventional or follicular variant of PTC, as well as the mean size±SE of the tumours, and the percentage of multicentricity, vascular invasion, extra-thyroid extension and lymph node metastasis of the cases according to the presence or absence of *BRAF* mutation.

The mean age of the patients with conventional PTC with $BRAF^{V600E}$ (46.7 years) was significantly higher ($P<0.0001$) than that of patients with conventional PTC without *BRAF* mutation (29.5 years) (Table 3). In Fig. 1 we have summarized the distribution of cases of conventional PTC according to the age of patients and presence or absence of $BRAF^{V600E}$ mutation.

The cases of conventional PTC with $BRAF^{V600E}$ were less often multicentric (44%) than cases without *BRAF* mutation (82%) ($P=0.04$). The size of the tumours and the percentage of vascular invasion, extra-thyroid extension and lymph node metastasis were similar in conventional PTC with and without the $BRAF^{V600E}$ mutation (Table 3).

No significant differences in the gender ratio, mean age, multicentricity, vascular invasion, extra-thyroid extension and lymph node metastasis were found in the follicular variant of PTC (Table 3) nor in the groups with oncocytic variant of PTC and Warthin-like PTC (data not shown).

Discussion

The study of this large series confirms that the $BRAF^{V600E}$ mutation is not detected in any type of benign lesion or well differentiated carcinoma of the thyroid but PTC [6, 9, 13, 22, 26]. However, our series of PTC associated to lymphocytic thyroiditis is too small (six cases) to rule out definitively the occurrence of *BRAF* mutations in this particular setting.

The $BRAF^{V600E}$ mutation was not detected in any case of the oncocytic variants of follicular adenoma or follicular carcinoma, in contrast to its frequent occurrence in cases of the oncocytic variant of PTC. This finding supports the classification of the oncocytic carcinomas of the thyroid as variants of the corresponding histological types, instead of their grouping under the general term of "oncocytic carcinoma" [24]. This is in agreement with the results of Cheung and colleagues [5] and Belchetz and colleagues [2], who detected RET/PTC rearrangements in cases of the oncocytic variant of PTC, but not in the oncocytic variant of follicular carcinoma.

The present study confirms the close relationship between the occurrence of $BRAF^{V600E}$ and the architecture of the PTC [24]. The mutation appears to be mostly or exclusively detected in PTC exhibiting a papillary or mixed follicular/papillary growth pattern, regardless of being a conventional PTC or any of the PTC variants (Warthin-like, oncocytic variant and microcarcinoma).

Despite the substantial increase in the number of cases of the follicular variant of PTC and of the oncocytic variant of PTC with a follicular pattern of growth, we did not detect any $BRAF^{V600E}$ mutation in these histotypes: 0/54 (0%) in the follicular variant of PTC and 0/11 (0%) in cases of the oncocytic counterpart, in contrast to 33/72 (45.8%) in conventional PTC and 6/11 (54.5%) in the oncocytic variant of PTC with a conventional pattern of growth.

Table 3 Distribution of gender, age, size, multicentricity, vascular invasion, extra-thyroid extension and lymph node metastasis of the patients with conventional PTC and follicular variant of PTC according to tumour histotype and *BRAF* status

Histotype	Clinicopathologic feature	$BRAF^{WT\dagger}$	$BRAF^{mut\dagger}$	*P*-value
Conventional PTC (72 tumours in 69 patients)	Gender(♀:♂)	8.5:1 (38)	3.4:1 (31)	0.20
	Age (mean years±SE)	29.5±2.4 (38)	46.7±2.8 (31)	<0.0001
	Size (mean cm±SE)	3.1±0.4 (29)	3.2±0.4 (20)	0.82
	Multicentricity (positive/total)	0.82 (17)	0.44 (18)	0.04
	Vascular involvement (positive/total)	0.56 (17)	0.32 (18)	0.19
	Extra-thyroid extent (positive/total)	0.42 (17)	0.37 (18)	>0.9999
	Lymph node metastases (positive/total)	0.69 (17)	0.62 (18)	>0.9999
Follicular variant of PTC (54 tumours in 54 patients)	Gender (♀:♂)	15.7:1 (50)	3:1 (4)	0.27
	Age (mean years±SE)	42.7±2.6 (50)	34.8±6.7 (4)	0.40
	Size (mean cm±SE)	2.8±0.3 (42)	2.0±0.3 (4)	0.33
	Multicentricity (positive/total)	0.36 (36)	0.00 (3)	0.54
	Vascular involvement (positive/total)	0.19 (36)	0.00 (3)	>0.9999
	Extra-thyroid extent (positive/total)	0.08 (36)	0.00 (3)	>0.9999
	Lymph node metastases (positive/total)	0.17 (36)	0.00 (3)	>0.9999

†Number of cases analysed in each category within brackets

We found an additional case of the follicular variant of PTC with the $BRAF^{K601E}$ mutation, thus leading to an overall percentage of 7.4% of follicular variant of PTC with this genetic alteration. With the exception of its detection in two follicular adenomas, one included in the present series and another from a different study in post-Chernobyl tumours [11], the $BRAF^{K601E}$ mutation was not detected in any of the remaining 57 follicular adenomas, 39 nodular goiters and 24 follicular carcinomas. It was not also detected in any case of mucoepidermoid carcinoma or in any PTC histotype other than the follicular variant of PTC.

Altogether, our findings show that there is an association between two morphological types of a single entity (PTC with papillary or mixed follicular/papillary architecture and PTC with a follicular growth pattern) and two missense mutations of the *BRAF* gene (V600E and K601E).

Our data demonstrate, furthermore, the molecular singularity of the follicular variant of PTC, as Zhu and colleagues [27] had already shown with regard to the high prevalence of *Ras* mutations. These two findings support the existence of a molecular counterpart for the so-called hybrid follicular/papillary carcinoma [1, 4]. It seems also challenging to search for *BRAF* mutations in PTC apparently arising on pre-existing follicular adenomas [25].

The absence of $BRAF^{V600E}$ mutations in cases of the follicular variant of PTC and of the oncocytic variant of PTC with a follicular pattern of growth, which are much more frequent in women than in men (12.5:1 and 10:1 ♀:♂, respectively), explains why the different histotype composition of the different series may obscure the association between male gender and occurrence of the *BRAF* mutation (Table 3) [8, 13, 15, 17, 26].

The same holds true (influence of the histotype composition of the series) regarding the association between age of the patients and *BRAF* mutated tumours. Like Xu and colleagues [26] and Nikiforova and colleagues [15], we observed that patients with PTC lesions harbouring the $BRAF^{V600E}$ mutation are older than those presenting PTC lesions with wild-type *BRAF* (P=0.004). This age unbalance is substantially increased (more 17.2 years in average) when the comparison is restricted to patients with conventional PTC (P<0.0001).

The significantly older age of patients with conventional PTC displaying $BRAF^{V600E}$ (P<0.0001) indicates that

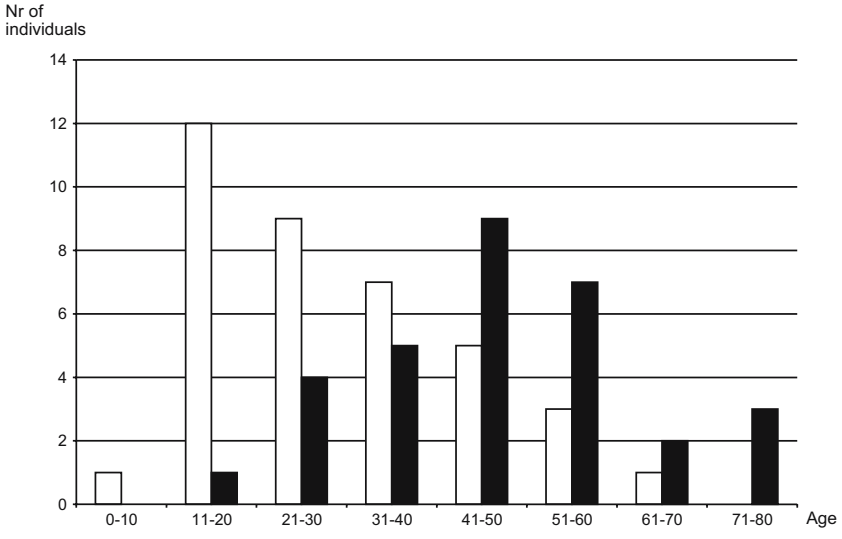

Fig. 1 Distribution of the age of 69 patients with conventional PTC with wild-type *BRAF* (□) and with the $BRAF^{V600E}$ mutation (■)*. *Patients with more than one tumour were considered only once: if any of the tumours was *BRAF* positive ($BRAF^{V600E}$) the patient was included in the "mutated" group

either the tumours with the mutation start their neoplastic development (initiation and/or early phase of promotion) in older individuals or, having started in a similar age period, progress slower than PTC without the mutation. The latter hypothesis fits with the possibility that the $BRAF^{V600E}$ mutation provides a less efficient tumourigenic stimulus to the thyrocytes than other genetic alterations, such as RET/PTC rearrangements. This possibility (i.e. weak tumourigenic stimulus of *BRAF* mutation) is supported by the findings of rare *BRAF* mutations in childhood PTC [11, 14], at variance with the younger age of patients with PTC associated to RET/PTC rearrangement [20, 23].

The *BRAF* mutated PTC of our series did not exhibit signs of clinical aggressiveness (size, vascular invasion, extra-thyroid extension and lymph node metastasis). The only difference between cases with and without *BRAF* mutation concerned the frequency of multicentric lesions, which was actually higher in conventional PTC without the mutation. Our data contrast with those of other groups [8, 13, 15, 26], who reported a positive association between *BRAF* mutations and tumour staging. As with age and gender, we think the different types and prevalence of *BRAF* mutations in the different PTC histotypes may contribute to explain this discrepancy.

Taken together, our results fit with the concept that *BRAF* mutations do not appear to confer per se a strong stimulus for neoplastic development in the thyroid. This does not mean, however, that PTC with *BRAF* mutation cannot progress towards less differentiated carcinomas, since our group, and others [13, 15, 21] have detected the $BRAF^{V600E}$ mutation in 10–35% of undifferentiated carcinomas of the thyroid.

Acknowledgements We thank Drs. Valeriano Leite and Xavier Matias-Guiu for having provided material from their hospitals. We are also grateful to Fundação para a Ciência e Tecnologia for grant support to Vítor Trovisco, Ana Preto, Jorge Lima, Patrícia Castro, Valdemar Máximo, Tiago Botelho, Severina Moreira and Ana Margarida Meireles.

References

1. Baloch ZW, LiVolsi VA (2002) Etiology and significance of the optically clear nucleus. Endocr Pathol 13:289–299
2. Belchetz G, Cheung CC, Freeman J, Rosen IB, Witterick IJ, Asa SL (2002) Hurthle cell tumors: using molecular techniques to define a novel classification system. Arch Otolaryngol Head Neck Surg 128:237–240
3. Brose MS, Volpe P, Feldman M, Kumar M, Rishi I, Gerrero R, Einhorn E, Herlyn M, Minna J, Nicholson A, Roth JA, Albelda SM, Davies H, Cox C, Brignell G, Stephens P, Futreal PA, Wooster R, Stratton MR, Weber BL (2002) BRAF and RAS mutations in human lung cancer and melanoma. Cancer Res 62:6997–7000
4. Castro P, Fonseca E, Magalhaes J, Sobrinho-Simoes M (2002) Follicular, papillary, and "hybrid" carcinomas of the thyroid. Endocr Pathol 13:313–320
5. Cheung CC, Ezzat S, Ramyar L, Freeman JL, Asa SL (2000) Molecular basis off hurthle cell papillary thyroid carcinoma. J Clin Endocrinol Metab 85:878–882
6. Cohen Y, Xing M, Mambo E, Guo Z, Wu G, Trink B, Beller U, Westra WH, Ladenson PW, Sidransky D (2003) BRAF mutation in papillary thyroid carcinoma. J Natl Cancer Inst 95:625–627
7. Davies H, Bignell GR, Cox C, Stephens P, Edkins S, Clegg S, Teague J, Woffendin H, Garnett MJ, Bottomley W, Davis N, Dicks E, Ewing R, Floyd Y, Gray K, Hall S, Hawes R, Hughes J, Kosmidou V, Menzies A, Mould C, Parker A, Stevens C, Watt S, Hooper S, Wilson R, Jayatilake H, Gusterson BA, Cooper C, Shipley J, Hargrave D, Pritchard-Jones K, Maitland N, Chenevix-Trench G, Riggins GJ, Bigner DD, Palmieri G, Cossu A, Flanagan A, Nicholson A, Ho JW, Leung SY, Yuen ST, Weber BL, Seigler HF, Darrow TL, Paterson H, Marais R, Marshall CJ, Wooster R, Stratton MR, Futreal PA (2002) Mutations of the *BRAF* gene in human cancer. Nature 417:949–954
8. Kim KH, Kang DW, Kim SH, Seong IO, Kang DY (2004) Mutations of the *BRAF* gene in papillary thyroid carcinoma in a Korean population. Yonsei Med J 45:818–821
9. Kimura ET, Nikiforova MN, Zhu Z, Knauf JA, Nikiforov YE, Fagin JA (2003) High prevalence of BRAF mutations in thyroid cancer: genetic evidence for constitutive activation of the RET/PTC-RAS-BRAF signaling pathway in papillary thyroid carcinoma. Cancer Res 63:1454–1457
10. Kumar R, Angelini S, Snellman E, Hemminki K (2004) BRAF mutations are common somatic events in melanocytic nevi. J Invest Dermatol 122:342–348
11. Lima J, Trovisco V, Soares P, Maximo V, Magalhaes J, Salvatore G, Santoro M, Bogdanova T, Tronko M, Abrosimov A, Jeremiah S, Thomas G, Williams D, Sobrinho-Simoes M (2004) BRAF mutations are not a major event in post-chernobyl childhood thyroid carcinomas. J Clin Endocrinol Metab 89:4267–4271
12. LiVolsi V (1990) Surgical pathology of the thyroid. Saunders, Philadelphia
13. Namba H, Nakashima M, Hayashi T, Hayashida N, Maeda S, Rogounovitch TI, Ohtsuru A, Saenko VA, Kanematsu T, Yamashita S (2003) Clinical implication of hot spot BRAF mutation, V599E, in papillary thyroid cancers. J Clin Endocrinol Metab 88:4393–4397
14. Nikiforova MN, Ciampi R, Salvatore G, Santoro M, Gandhi M, Knauf JA, Thomas GA, Jeremiah S, Bogdanova TI, Tronko MD (2004) Low prevalence of BRAF mutations in radiation-induced thyroid tumors in contrast to sporadic papillary carcinomas. Cancer Lett 209:1–6
15. Nikiforova MN, Kimura ET, Gandhi M, Biddinger PW, Knauf JA, Basolo F, Zhu Z, Giannini R, Salvatore G, Fusco A, Santoro M, Fagin JA, Nikiforov YE (2003) BRAF mutations in thyroid tumors are restricted to papillary carcinomas and anaplastic or poorly differentiated carcinomas arising from papillary carcinomas. J Clin Endocrinol Metab 88:5399–5404
16. Peyssonnaux C, Eychene A (2001) The Raf/MEK/ERK pathway: new concepts of activation. Biol Cell 93:53–62
17. Puxeddu E, Moretti S, Elisei R, Romei C, Pascucci R, Martinelli M, Marino C, Avenia N, Rossi ED, Fadda G, Cavaliere A, Ribacchi R, Falorni A, Pontecorvi A, Pacini F, Pinchera A, Santeusanio F (2004) BRAFV599E mutation is the leading genetic event in adult sporadic papillary thyroid carcinomas. J Clin Endocrinol Metab 89:2414–2420
18. Rajagopalan H, Bardelli A, Lengauer C, Kinzler KW, Vogelstein B, Velculescu VE (2002) Tumorigenesis: RAF/RAS oncogenes and mismatch-repair status. Nature 418:934
19. Rosai J, Carcangiu ML, DeLellis RA (1992) Tumours of the thyroid gland. Armed Forces Institute of Pathology, Washington
20. Soares P, Fonseca E, Wynford-Thomas D, Sobrinho-Simoes M (1998) Sporadic ret-rearranged papillary carcinoma of the thyroid: a subset of slow growing, less aggressive thyroid neoplasms? J Pathol 185:71–78

21. Soares P, Trovisco V, Rocha AS, Feijao T, Rebocho AP, Fonseca E, Vieira de Castro, I, Cameselle-Teijeiro J, Cardoso-Oliveira M, Sobrinho-Simoes M (2004) BRAF mutations typical of papillary thyroid carcinoma are more frequently detected in undifferentiated than in insular and insular-like poorly differentiated carcinomas. Virchows Arch 444:572–576
22. Soares P, Trovisco V, Rocha AS, Lima J, Castro P, Preto A, Maximo V, Botelho T, Seruca R, Sobrinho-Simoes M (2003) BRAF mutations and RET/PTC rearrangements are alternative events in the etiopathogenesis of PTC. Oncogene 22:4578–4580
23. Tallini G, Santoro M, Helie M, Carlomagno F, Salvatore G, Chiappetta G, Carcangiu ML, Fusco A (1998) RET/PTC oncogene activation defines a subset of papillary thyroid carcinomas lacking evidence of progression to poorly differentiated or undifferentiated tumor phenotypes. Clin Cancer Res 4:287–294
24. Trovisco V, Vieira de Castro I, Soares P, Maximo V, Silva P, Magalhaes J, Abrosimov A, Guiu XM, Sobrinho-Simoes M (2004) BRAF mutations are associated with some histological types of papillary thyroid carcinoma. J Pathol 202:247–251
25. Vickery AL Jr, Carcangiu ML, Johannessen JV, Sobrinho-Simoes M (1985) Papillary carcinoma. Semin Diagn Pathol 2: 90–100
26. Xu X, Quiros RM, Gattuso P, Ain KB, Prinz RA (2003) High prevalence of BRAF gene mutation in papillary thyroid carcinomas and thyroid tumor cell lines. Cancer Res 63:4561–4567
27. Zhu Z, Gandhi M, Nikiforova MN, Fischer AH, Nikiforov YE (2003) Molecular profile and clinical-pathologic features of the follicular variant of papillary thyroid carcinoma. An unusually high prevalence of ras mutations. Am J Clin Pathol 120:71–77

Virchows Arch (2005) 446: 596–603
DOI 10.1007/s00428-005-1258-7

ORIGINAL ARTICLE

Chun-Mei Cheng · Koichi Tsuneyama · Kazuhiro Matsui · Hiroyuki Takahashi · Shin Ishizawa · Yasuo Takano

Cytoplasmic expression of c-erbB2 in non-small cell lung cancers

Received: 9 January 2005 / Accepted: 7 March 2005 / Published online: 19 May 2005
© Springer-Verlag 2005

Abstract The aim of this study was to investigate the expression of c-erbB2 in non-small cell lung cancers (NSCLCs) with attention both to membranous and cytoplasmic reaction, and to try to elucidate the meaning of cytoplasmic expression of c-erbB2 in NSCLCs. Immunohistochemical c-erbB2 expression and related clinico-pathological features were examined in 312 surgically resected patient tissues of NSCLCs, including 175 cases of adenocarcinoma and 137 cases of squamous cell carcinoma. Immunostaining of inner- and ecto-domain of c-erbB2, mRNA expression and the quantitation of soluble c-erbB2 in cultured media were performed in five NSCLC cell lines. Cytoplasmic expression of c-erbB2 was observed more frequently than membranous, both in patient tissues and cell lines. Neither membranous nor cytoplasmic expression of c-erbB2 was significantly correlated with short outcome in NSCLCs. Membranous c-erbB2 was expressed by both inner and ecto-domain, while cytoplasmic c-erbB2 was expressed by either or both inner and ecto-domain. c-erbB2 mRNA was produced in most cell lines; however, the soluble form was only detectable in a cell line that only presented a membranous c-erbB2. In conclusion, cytoplasmic c-erbB2 of NSCLCs was not a full-length protein only expressed in cellular membrane, but reflected degenerated c-erbB2 fragments with less functional ability.

Keywords c-erbB2 · Cytoplasmic expression · Non-small cell lung cancers

C.-M. Cheng · K. Tsuneyama (✉) · H. Takahashi · S. Ishizawa · Y. Takano
Department of Pathology,
Toyama Medical and Pharmaceutical University,
2630 Sugitani,
Toyama, 930-0194, Japan
e-mail: ktsune@ms.toyama-mpu.ac.jp
Tel.: +81-764347237
Fax: +81-764345016

C.-M. Cheng · K. Tsuneyama
21st Century COE Program,
Toyama Medical and Pharmaceutical University,
2630 Sugitani,
Toyama, 930-0194, Japan

K. Matsui
Forensic Pathology,
Toyama Medical and Pharmaceutical University,
2630 Sugitani,
Toyama, 930-0194, Japan

Introduction

Non-small cell lung cancers (NSCLCs) are associated with high mortality world-wide and are responsible for the highest number of cancer-related deaths in Japan. c-erbB2 (HER-2), which is a transmembrane receptor with tyrosine kinase activity containing intracellular (inner), transmembrane and extracellular (ecto-) domain, heterodimerizes with other ErbB familial members to promote the transduction of proliferative and survival signals [21, 23]. Overexpression of c-erbB2 was found in a substantial group of human malignancies, and signified a poor clinical prognosis [23]. Using the Hercep Test (DAKO, Glostrup, Denmark), membranous immunohistochemical expression of c-erbB2 was well established as a rational evaluation and an essential index for Herceptin therapy in breast cancers [1, 5, 9, 11]. The correlation between c-erbB2 expression and outcome in NSCLCs has been reported in several studies with controversial discussion [7]. On the other hand, cytoplasmic expression of c-erbB2 was noted frequently in some cancer series, including NSCLCs [3, 4, 8, 11, 16], but its reasonable mechanism still remained unclear.

In this study, to elucidate whether cytoplasmic expression of c-erbB2 harboring a specific meaning in NSCLCs, both membranous and cytoplasmic immunohistochemical expression were investigated using a series of patient tissues and five cancer cell lines of NSCLCs.

Materials and methods

Study groups

Patient tissues

Three hundred and twelve surgically resected NSCLCs, including 175 cases of adenocarcinoma (ADC) and 137 cases of squamous cell carcinoma (SCC), registered in the Toyama Medical and Pharmaceutical University hospital during 1983-2002, were used to investigate expression of c-erbB2 by immunohistochemistry. According to the guidelines defined by the World Health Organization [20], the histological subtype of each case was re-evaluated by two of us (C.M.C. and K.T.) with available representative tissue sections. The pathologic tumor stage of each case was also determined according to the TNM classification defined by the International Union Against Cancer [19]. In each case, tumor samples fixed with buffered 10% formalin and embedded in paraffin were available. The 4 μm-thick tissue sections were cut and stained with hematoxylin-eosin (HE), Elastica-van Gieson, alcian blue and periodic acid-Schiff methods.

The clinical data were obtained from the patient files, including follow-up information. The end point for clinical follow-up was December 31, 2002. Neither chemotherapy nor radiotherapy was carried out for any patient prior to surgery.

Five lung cancer cell lines

Five NSCLC cell lines, including two ADC (KJ and PC-14) and three SCC (AOI, LC-1/sq and LC/1F) derived from Japanese patients, were obtained commercially from Riken Gene Bank (Tokyo, JAPAN). The media of RPMI160 for KJ and PC-14, Minimum Essential Medium Eagle for AOI and RPMI-1640:Nutrient Mixture F-12 (HamF12)+25 mM HEPES containing 10% FBS and 1% penicillin-streptomycin (Gibco, Invitrogen, Tokyo, Japan) for LC/1F and LC-1/sq were maintained, respectively, at 37 and 5% CO_2 moist condition. FBS and all kinds of media were obtained from Sigma Chemical Corporation (Sigma, N.Y., USA).

Evaluative criteria of immunohistochemical staining

In accordance with the scoring system of the Hercep Test recommended by DAKO, membranous activity was evaluated from grade 0 to 3, and each sample was placed in one of the four categories. In brief, grade 0=complete absence of membranous staining; grade 1=weak and incomplete membranous staining; grade 2=weak and complete or strong but incomplete membranous staining with greater than 10% of the cancer cells; grade 3=strong and complete membranous staining with more than 10% of cancer cells. A sample with grade 2 or 3 membranous activity would be defined as a tumor with positive membranous overexpression of c-erbB2. A sample showing prominent cytoplasmic staining in grade 0 or 1 membranous staining would be defined as a tumor with cytoplasmic expression of c-erbB2. The samples with complete absence of both membranous and cytoplasmic staining and with only weak/incomplete staining would be classified to a tumor with negative expression of c-erbB2.

Two of us (C.M.C., K.T.) assigned an immunostaining score to each sample independently. When the scores determined by the two investigators differed significantly from each other, a consensus score would be derived by a joint examination.

Immunohistochemistry

The 4 μm-thick tissue sections cut from the representative formalin-fixed-paraffin-embedded tissue blocks were immunostained by the peroxidase method (Envision System, DAKO, Carpinteria, Calif., US) as described previously [12] to firstly evaluate the localization and degree of expression of c-erbB2 using a rabbit polyclonal antibody against the inner domain of c-erbB-2 (Ab1-21N; Neomarkers, Fremont, Calif., USA). Human breast carcinoma was used as a positive control for c-erbB2 expression. Normal bronchial epithelium seldom showed a valuable positive expression for c-erbB2 and thus served as internal negative control. Immunohistochemical procedures of negative control included omission of the primary antibody and replacement of the primary antibody by normal mouse IgG in appropriate concentration. The membranous and cytoplasmic reactivity for c-erbB2 in cancer cells were evaluated separately in five randomly selected areas of 200-fold magnification.

The tumors with grade 3 membranous staining were classified as panel A, containing 18 cases, and tumors with strongly cytoplasmic staining without positive membranous overexpression were classified as panel B, containing 20 cases. They were selected to examine the distribution of intra-/extra-parts of c-erbB2 expressed in the cancer cells using two mouse monoclonal antibodies against inner (Novocastra, Claremont Place, UK; dilution, 1:40) and ectodomain (Nichirei, SV2-61γ, Tokyo, Japan; dilution,1:20) of c-erbB2.

Statistical analysis

All statistical analysis was performed using the Statistical Package for the Social Sciences (SPSS) 10.0 for WIN 98 (SPSS, Inc., Chicago, Ill., US). Chi-square test, Fisher's exact test, or log-rank test, were applied to examine the association of variables, depending on the nature of the variables and matching with the group size. For the survival analysis, the Kaplan-Meier method was performed with the log-rank test. Differences were considered significant when a P-value was <0.05.

RT-PCR

mRNA of five lung cancer cell lines were extracted by ISOGEN method (Nippon Gene Co. Ltd, Japan). The upper primer ACGGTGCAGCTGGTGACACAGCTTATG and the lower primer CAACTCCCGGAATCTTGGCCGACA TTCAGA coding the region of c-erbB2 were synthesized by Espec Oligo Service Corp. (Tsukuba, Ibaraki, Japan) to perform RT-PCR with RT-PCR-kit (TaKaRa Biomedicals, Otsu, Shiga, Japan) as described earlier [18]. The primers of housekeeping geneβ-actin (RIKEN Gene Bank, Tokyo, Japan) were also applied as a negative control.

Immunocytostaining

Autosmear

First, immunocytostaining for c-erbB2 by Autosmear method were performed in five cell lines. In brief, four adhesive cell lines (KJ, PC-14, AOI and LC-1/sq) were stuffed by trypsin (Sigma), and all five cell lines were made floating status. The floating cells of each kind were set on the two slides after centrifugation at 1500 rpm for 5 min, and then fixed by 90% alcohol for 10 min. The slides were incubated with primary antibodies against ecto-domain (mouse monoclonal, SV2-61γ, Nichirei; dilution,1:20) and inner domain of c-erbB2 (mouse monoclonal, CB11; Novocastra, Claremont Place, UK; dilution, 1:40) in a moist chamber under intermittent microwave (I-MW) (MI-77; Azumaya, Tokyo, Japan) for 15 min, respectively. After gentle rinsing with TBS, the peroxidase-labeled polymer for monoclonal antibody (EnVision System, DAKO, Carpineria, Calif., USA) was applied for 15 min in a wet chamber under I-MW. The later steps of developing color and counterstaining were performed similarly to immunohistochemistry as described above.

Lab-tek chamber

Next, immunocytostaining for c-erbB2 by Lab-Tek chamber method was performed in three adhesive cell lines (KJ, PC-14 and AOI) with their natural state of cell growth. In brief, the cell lines were cultured in Lab-Tek chamber (Nalge Nunc International, Naperville, Ill., US) for 24 h, the media was discarded, while attached cell lines were fixed on the slides with 70% alcohol for 10 min. Consequently, the slides were made with cytostaining that was similar to the autosmear method described above.

Enzyme immunoassay (EIA)

Using cultured media of each kind of lung cancer cell line at 24 and 48 h, respectively, the quantity of soluble c-erbB2 secreted from cells was determined by ErbB-2 EIA kit (Nichirei), which contained two mouse monoclonal antibodies against ectodomain of c-erbB2, SV2-61γ and 6G10. The protocol followed came from the information of kit provided by the Nichirei Corp.

Results

Patient characteristics

Clinicopathologic features of the patients with AD or SCC were summarized in Table 1. The mean age of patients with AD was quite similar to that of patients with SCC. SCC predominantly occurred in males when compared with AD ($P<0.001$), whereas a gender difference was not observed in patients with AD. The overall survival of patients with AD and SCC was 45 months (95% CI, 41–49) and 55 months (95% CI, 48–62), respectively. The significance between AD and SCC was not shown (survival curves are not shown). Multivariate analyses revealed that the tumor stage was an independent prognostic factor in not only the AD group but also the SCC group. This result confirmed our study group being an appropriate subject to conduct the following statistical analyses.

Table 1 Clinicopathologic features of 312 patients with non-small cell lung cancers. *ADC* adenocarcinoma; *SCC* squamous cell carcinoma

Variables	ADC *n*=175	SCC *n*=137	*P*-values
Age (years)			
Mean (range)	62.6 (29-84)	65.0 (37-88)	
Gender (male/female)	94/81	126/11	<0.01
Histological grade			<0.01
1	90 (51.4%)	23 (16.8%)	
2	45 (25.7%)	90 (65.7%)	
3	42 (22.9%)	24 (17.5%)	
T-factor			0.032
T1	109 (62.3%)	47 (34.3%)	
T2	56 (32%)	71 (51.8%)	
T3	8 (4.6%)	17 (12.4%)	
T4	2 (1.1%)	2 (1.5%)	
N-factor			0.252
N0	92 (52.5%)	82 (59.9%)	
N1	47 (26.9%)	47 (34.3%)	
N2	35 (20%)	8 (5.8%)	
N3	1 (0.6%)	0 (0%)	
Stage			<0.01
I	93 (53.1%)	76 (55.5%)	
II	38 (21.7%)	44 (32.1%)	
III	40 (22.9%)	16 (11.7%)	
IV	4 (2.3%)	1 (0.7%)	
Follow-up period (months)			
Mean (range)	33.0±1.8 (1–70)	34.8±2.0 (1–90)	
Outcome			0.535
Alive	88 (50.2%)	67 (48.9%)	
Died of disease	72 (41.1%)	46 (33.6%)	
Died of other disease	4 (2.3%)	6 (4.4%)	
Missing	11 (6.3%)	18 (13.1%)	

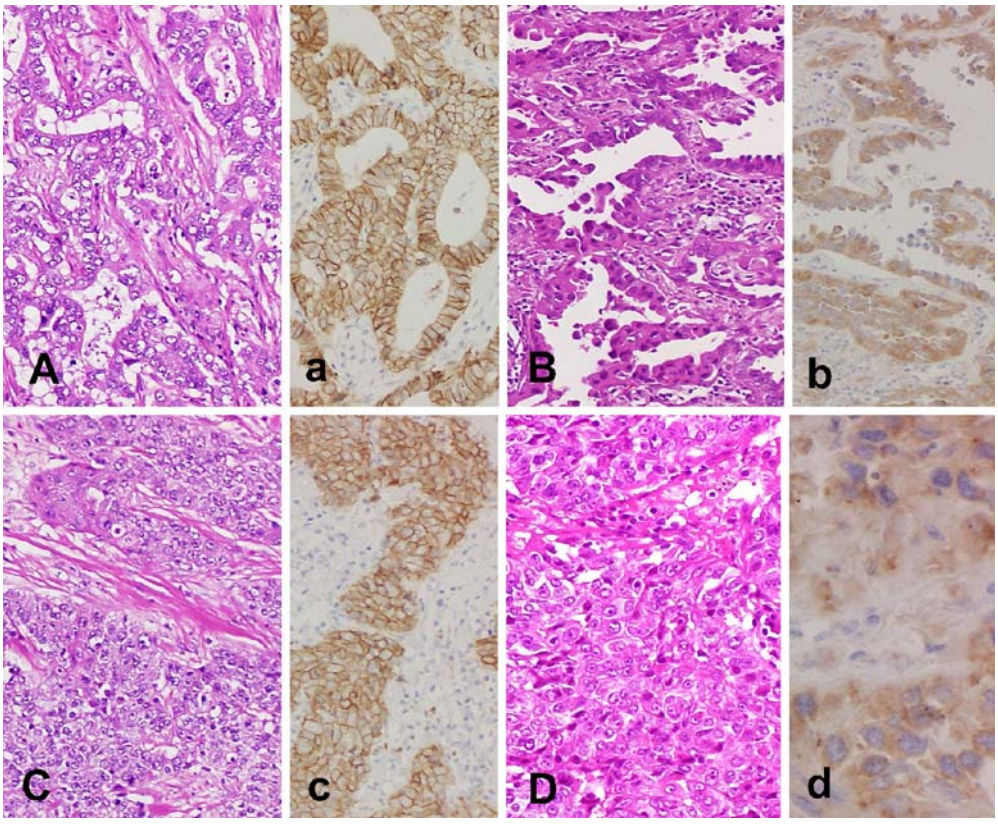

Fig. 1 H&E stain is shown in **A**, **B**, **C** and **D** and immunostaining of c-erbB2 was shown in **a**, **b**, **c**, **d**. Membranous expression of c-erbB2 (**a**) in the case of adenocarcinoma (**A**); cytoplasmic expression of c-erbB2 (**b**) in the case of adenocarcinoma (**B**); membranous expression of c-erbB2 (**c**) in the case of squamous cell carcinoma (**C**); cytoplasmic expression of c-erbB2 (**d**) in the case of squamous cell carcinoma (**D**) were observed. Neither stromal nor inflammatory cell showed any expression of c-erbB2 in each case (Original magnification, ×300 each)

Expression of c-erbB2 in patient tissues

Immunohistochemical reactivity for rabbit polyclonal antibody against inner domain of c-erbB2 was membranous or cytoplasmic in cancer cells, whereas stromal cells, including inflammatory cells, never showed immunoreactivity for c-erbB2 (Fig. 1). Based on the criteria listed above, the frequency of immunohistochemical c-erbB2 overexpression in 312 NSCLCs was compiled in Table 2. Membranous overexpression of c-erbB2 was not associated with overall survival of the patients. Two- and 5-year survivals of the group with membranous c-erbB2 overexpression were 75.9% and 33.3%, respectively, but those without it were 78.7% and 45.2%, respectively (P=0.281) (Fig. 2a). Cytoplasmic overexpression of c-erbB2 was not related to the patient's prognosis either (P=0.144) (Fig. 2b). This trend remained unchanged even if analyses under the condition of AD and SCC were divided (Fig. 2c and d).

Shown as Fig. 3 and Table 3, the cases both of panel-A and panel-B showed similar immunohistochemical reactivity and grade for a mouse monoclonal antibody against inner domain of c-erbB2 to them for a rabbit polyclonal antibody against inner domain of c-erbB2 shown in Fig. 1. For a mouse monoclonal antibody against ecto-domain of c-erbB2, the membranous reactivity was observed in 15 (82.2%) of 18 panel-A cases but not did in any panel-B case, whereas the cytoplasmic activity was noted in 6 (33.3%) of 20 panel-B cases but not did in any panel-A case.

Table 2 Frequency of c-erbB-2 overexpression in 312 non-small cell lung cancers

	c-erbB-2 overexpression	
	Membranous (%)	Cytoplasmic (%)
Adenocarcinoma (n=175)	19 (10.9)	134 (76.6)
Squamous cell carcinoma (n=137)	16 (11.7)	41 (29.9)

mRNA expression of c-erbB2 in five lung cancer cell lines

mRNA expression of β-actin located in 412 bp was found in 5 kinds of cell lines except dH_2O, and mRNA expression of c-erbB2 located in 555 bp was noted in KJ, PC-14, AOI and LC/1F cell lines except LC-1/sq cell line as well as dH_2O (Fig. 4).

Immunocytostaining of five lung cancer cell lines

The results of immunocytostaining from Autosmear (Fig. 5a) and Lab-Tak chamber methods (Fig. 5b) showed coordinated conformity, in which the KJ cell line presented stronger membranous and weaker cytoplasmic reactivity for either antibody against ecto-domain or inner domain of c-erbB2, but PC-14 and AOI showed only cytoplasmic expression. By the Autosmear method, LC/1F cell line

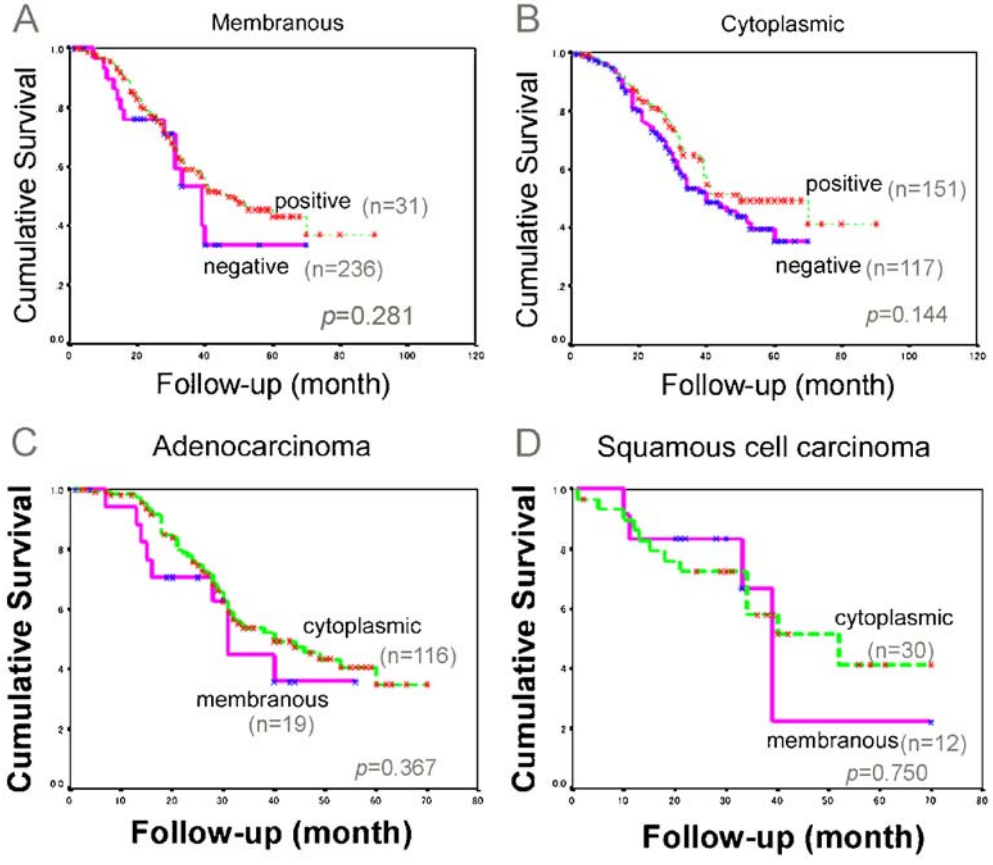

Fig. 2 **a** Survival curves of patients with and without membranous expression of c-erbB2. There was no significance between the overall survival of patients with or without membranous expression of c-erbB2. **b** Survival curves of patients with and without cytoplasmic expression of c-erbB2. There was no significance between the overall survival of patients with or without cytoplasmic expression of c-erbB2. **c** Survival curves of patients with adenocarcinoma (*ADC*) expressed membranous and cytoplasmic expression of c-erbB2. There was no significance between the overall survival of ADC patients expressed membranous and cytoplasmic expression of c-erbB2. **d** Survival curves of patients with squamous cell carcinoma (*SCC*) expressed membranous and cytoplasmic expression of c-erbB2. There was no significance between the overall survival of SCC patients that expressed membranous and cytoplasmic expression of c-erbB2

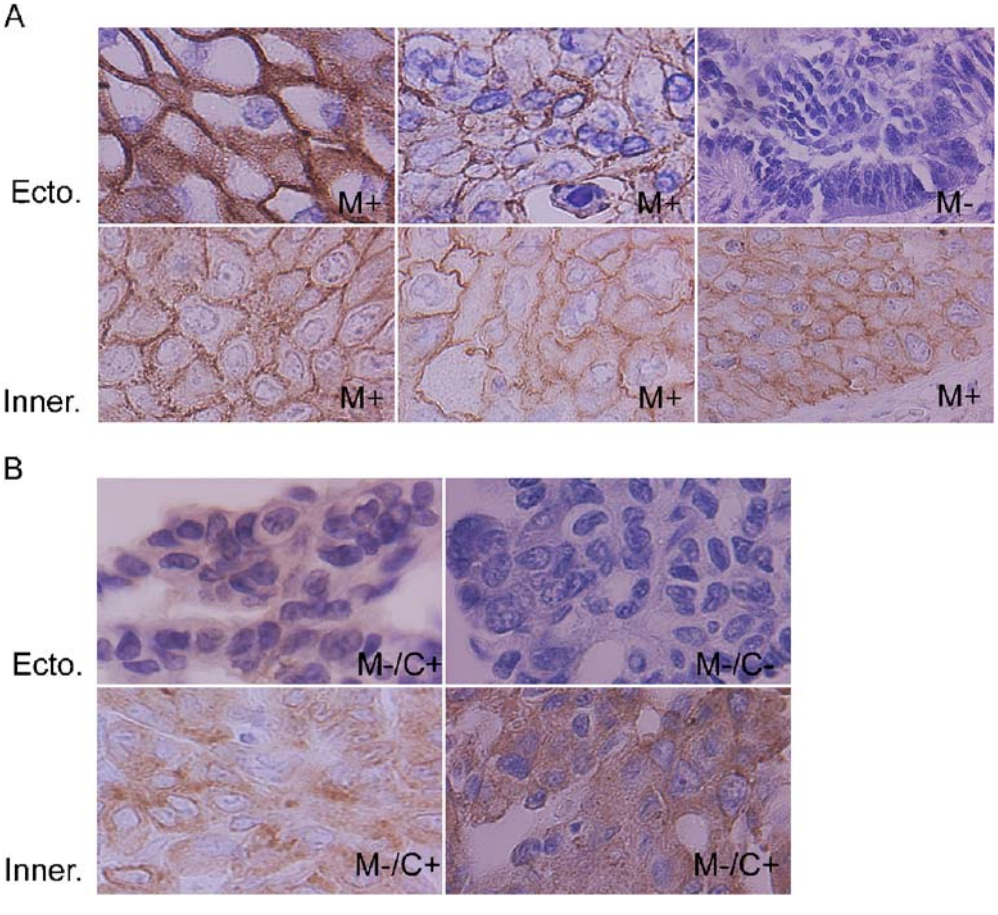

Fig. 3 Cases shown in **A**) and **B**) showed immunohistochemical reactivity and grade for monoclonal antibody against the inner domain of c-erbB2 (inferior, Inner.) to almost the same for polyclonal one, and more sensitivity compared to monoclonal antibody against the ecoto-domain (upper, Ecto.) (Original magnification, ×400 each)

Table 3 Patterns of c-erbB2 expression in patient tissues with NSCLCs

Anti-inner-domain**	Anti-ecto-domain*		
	M	C	N
Panel A (18 cases)	15	0	3
Panel B (20 cases)	0	6	14

M membranous expression; *C* cytoplasmic expression; *N* negative expression

*Anti-ecto-domain of c-erbB2 antibody: mouse monoclonal, SV2-61γ, NICHIREI

**Anti-inner-domain of c-erbB2 antibody: mouse monoclonal, CB11, Novocastra

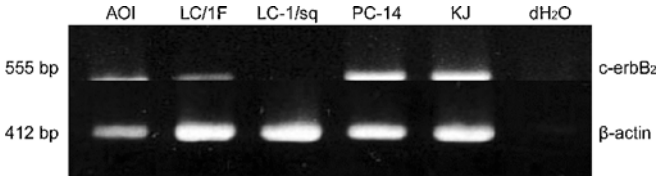

Fig. 4 mRNA expression of β-actin located in 412 bp was found in five cell lines except dH_2O, and mRNA expression of c-erbB2 located in 555 bp was noted in KJ, PC-14, AOI and LC/1F cell lines except LC-1/sq cell line and dH_2O

showed cytoplasmic reactivity only for an antibody against the inner domain of c-erbB2. Neither membranous nor cytoplasmic immunocytostaining of c-erbB2 was noted in the LC-1/sq cell line for any antibody against ecto- or inner domain. The results are shown in Table 4.

Quantitative analysis of soluble c-erbB2 of lung cancer cell lines by EIA

The soluble c-erbB2, equal to the detectable ectodomain of c-erbB2 in cultured media was only detectable and increased quantitatively from 24 h to 48 h in the KJ cell line, but was undetectable in any other cell line (Table 5).

Discussion

In the present study, we first investigated the immunohistochemical expression of c-erbB2 in 312 surgically resected NSCLCs with rabbit polyclonal antibody against inner domain of c-erbB2. According to the criteria of the Hercept test (DAKO), positive membranous expression of c-erbB2 with grade 2 and 3 was observed in almost 10% of either ADC or SCC, respectively. In contrast, cytoplasmic expression was more frequently found in 76.6% of ADC and 29.9% of SCC. Although patients with overexpression of either membranous or cytoplasmic in cancer cells showed a tendency for shorter survival, neither cases with membranous expression nor those with cytoplasmic expression showed a significant correlation with outcome, regardless of combining and dividing the ADC and SCC. These results were very similar to most previous reports on c-erbB2 research in NSCLCs, although other studies stated the difference in survival based on membranous c-erbB2 overexpression [14]. In our study, the index of membranous expression of c-erbB2 was cautiously evaluated using the principle described above, and approximately 10% of ADC limited in positive event. This result was fewer than the mean values reported previously [6, 7]. Meert et al. reviewed 30 eligible NSCLC studies, and stated that there was a potential bias in favor of the significant studies with an overestimation risk of the magnitude of the true effect of c-erbB2 overexpression [14]. The difference between positive evaluation and different immunohistochemical systems was not statistically significant.

On the other hand, the high frequency of cytoplasmic expression in our NSCLC series resembled other studies concerning and evaluating cytoplasmic expression of c-erbB2 as a positive action in their NSCLC studies [4, 16]. Absence of detectable membranous expression of c-erbB2 by immunohistochemistry could be interpreted as the probability of internalized receptors on membrane degrading rapidly in most cell culture systems [2] and newly synthesizing or synthesized molecules within the Golgi apparatus had not been transported and inserted into the membrane [16]. Although c-erbB2 has been broadly researched in breast, ovarian and other cancers, some potential signaling pathway of c-erbB2 in carcinogenesis still remained unclear [15]. Studies on cytoplasmic expression of c-erbB2 and its meaning in cancer cells are lacking. If cytoplasmic staining is specific, what does it mean? Does it indicate a mid-term phase of synthesizing and/or transporting of proteins, despite degradation of proteins?

In theory, the polyclonal antibody has higher sensitivity than monoclonal one, whereas the monoclonal antibody has higher specificity than polyclonal one. In the cases of panel A and panel B, immunoreactivity for a monoclonal antibody against the inner domain of cerbB2 showed a significant similarity to that for a polyclonal antibody against the inner domain, but a monoclonal antibody against the ecto-domain of c-erbB2 showed lower sensitivity both of membrane and cytoplasm. In addition, using the above two types of monoclonal antibodies against the ecto-domain and inner domain of c-erbB2, the immunostaining patterns of five lung cell lines was in agreement with that of tissue samples. The KJ cell line showed stronger membranous stain with weaker cytoplasmic stain, PC-14, AOI, LC/1F cell lines showed only cytoplasmic stain, and the LC-1/sq cell line had completely negative expression. By RT-PCR, except for the LC-1/sq cell, c-erbB2 mRNA expression was confirmed in four other cell lines. All of these results supported the reliability and specificity of immunohistochemistry conducted in this study. It was therefore confirmed that information from lung cancer cell lines was in accordance with that of tissue samples from patients with NSCLCs.

By EIA, soluble c-erbB2 corresponding to the ecto-domain portion was only detectable in the media of KJ cell line, but not in PC-14, AOI and LC/1F or LC-1/sq. This indicated a significant correlation between the soluble

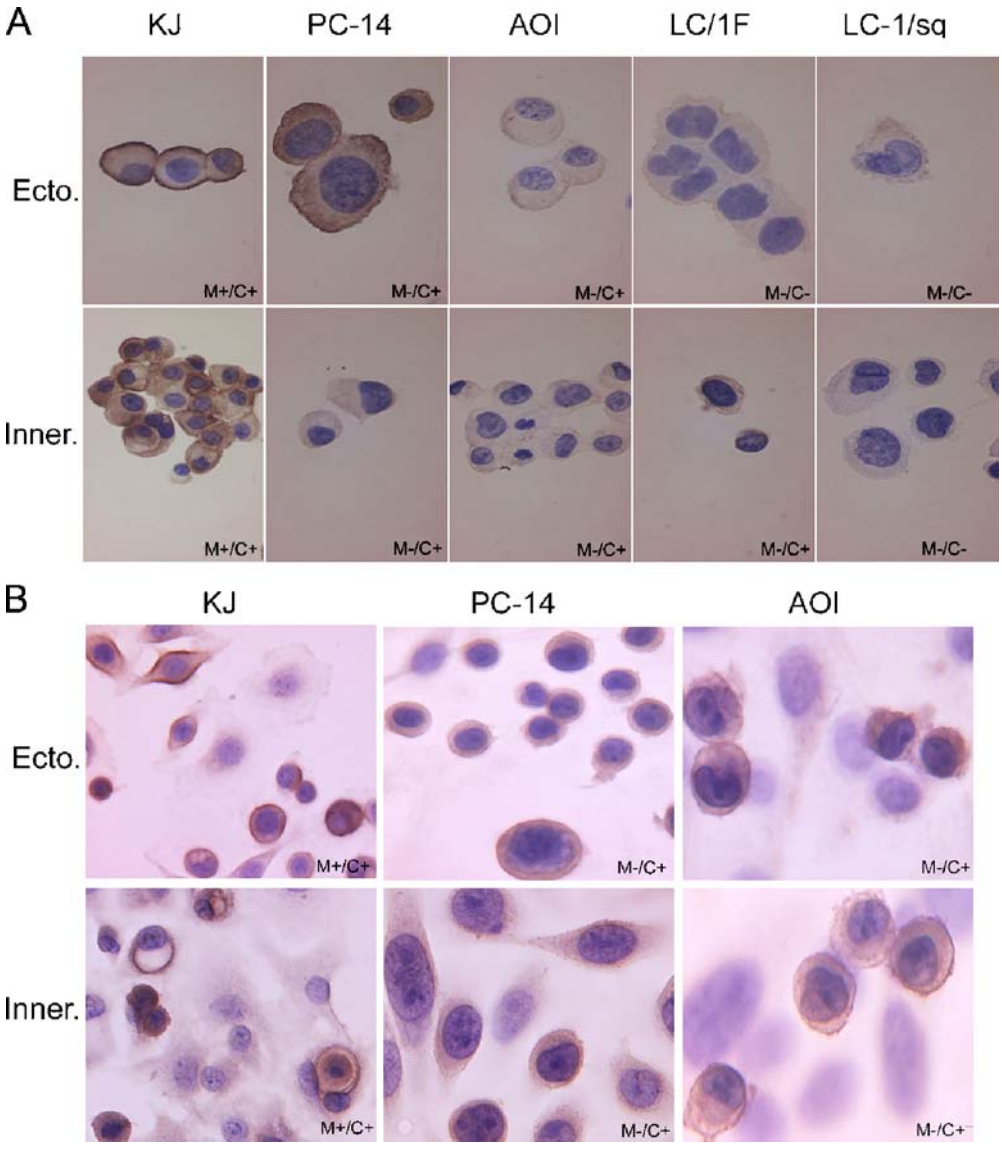

Fig. 5 **A** The results of immunocytostaining in five lung cancer lines with antibodies against ectodomain (*Ecto.*) and inner domain (*Inner.*) of c-erbB2 by the Autosmear method. KJ cell line showed stronger membranous and weaker cytoplasmic expression of c-erbB2 (M+/C+), but PC-14 and AOI showed only cytoplasmic expression (M-/C+) both with two antibodies against Ecto. and Inner. of c-erbB2. Whereas, LC/1F cell line just showed cytoplasmic expression (M-/C+) for anti-inner domain antibody (Inner.). Neither membranous nor cytoplamic expression of c-erbB2 was demonstrated in LC-1/sq with any antibody (Ecto. and Inner. M-/C-) (original magnification, ×400 each). **B** The results of immunocytostaining in three types of lung cancer lines (KJ, PC-14 and AOI) with antibodies against Ecto. and Inner. of c-erbB2 by the Lab-Tak chamber method showed same expression to that with Autosmear method (original magnification, ×400 each)

c-erbB2 and full-length c-erbB2, which showed membranous expression. However, no affinity was found between cytoplasmic expression and soluble c-erbB2 shed in cultured media of lung cancer cell lines. From the above results, it was clear that the membranous expression reflected a localization of full-length c-erbB2 consisting of both ecto- and inner domain in the membrane, where it played a role in some signaling pathways. This result was in agreement with studies that reported an excellent correlation between the ecto-domain released from the cytosols and the amount of full-length c-erbB2 extracted from the cell membrane in breast tumor specimens [22]. Elevated ectodomain molecule could be found in sera from patients with various carcinomas, 35% in breast carcinoma, approximately 21% in prostate cancer and 9% in ovarian carcinoma and in hepatoma, head and neck, cervical, gastric, colorectal and pancreatic carcinoma [21, 22].

Table 4 Characterization of lung cancer cell lines based on c-erbB2 expression by cytostaining

	Membrane		Cytoplasm	
Cell lines	Inner domain	Ecto-domain	Inner domain	Ecto-domain
KJ	+	+	+	+
PC-14	−	−	+	+
AOI	−	−	+	+
LC/IF	−	−	+	−
LC-1/sq	−	−	−	−

Table 5 Quantity of the soluble c-erbB2 secreted from 5 kinds of lung cancer cell lines into culture medium at 24 and 48 h

Cell lines	Quantity (ng/ml)	
	24 h	48 h
KJ	2.8	8.2
PC-14	0	0
AOI	0	0
LC/1F	0	0
LC-1/sq	0	0

Previous research reported that almost all antigen receptors were prominent targets of negative regulation for degeneration by signaling pathway such as Cbl family members, to provide a critical mechanism to ensure an appropriate immune response and homeostasis [15, 17]. A crucial physiological mechanism of attenuation of the ErbB family involving down-regulation of receptors from cell surface mediated by ubiquitin ligase Cbl, underwent ubiquitinization and delivered to lysosome for eventual degradation [24]. In addition, it was reported that the therapeutic anti-human ErbB2 antibody Trastuzumab (Herceptin) induced an ErbB2-Cbl interaction, which resulted in ErbB2 ubiquitinization and degeneration in breast cancer [10, 13].

In conclusion, we report herein that the cytoplasmic expression of c-erbB2 in NSCLCs might show aggregation of degraded c-erbB2 fragments of the ecto-domain, or/and inner domain portions in cytoplasm. To clarify the degraded mechanism probably contributing to a new prospective therapy of NSCLCs, the detailed researches would be carried out by further study.

Acknowledgements We particularly thank Mr. Tokimasa Kumada and Hideki Hatta for their excellent technical support. This work was supported in part by a grant from the 21st century COE program in Japan, R&D, for the practical use of university-based technology by matching government funds and private funds from the Ministry of Economy, Trade and Industry of Japan (No. 0320003), Grants-in-Aid for scientific research from the Japan Society for the Promotion of Science (No. 16790183), and from Honjin and Japan Diabetes Foundations. Support was also obtained from the Japanese Ministry of Education, Science, Sports and Culture, Grant-in-Aid for Scientific Research 14770072 and 15922084.

References

1. Baselga J, Norton L, Albanell J, Kim YM, Mendelsohn J (1998) Recombinant humanized anti-HER2 antibody (Herceptin) enhances the antitumor activity of paclitaxel and doxorubicin against HER2/neu overexpressing human breast cancer xenografts. Cancer Res 58:2825–2831
2. Beguinot L, Lyall RM, Willingham MC, Pastan I (1984) Down-regulation of the epidermal growth factor receptor in KB cells is due to receptor internalization and subsequent degradation in lysosomes. Proc Natl Acad Sci USA 81:2384–2388
3. Giatromanolaki A, Gorgoulis V, Chetty R, Koukourakis MI, Whitehouse R, Kittas C, Veslemes M, Gatter KC, Iordanoglou I (1996) C-erbB-2 oncoprotein expression in operable non-small cell lung cancer. Anticancer Res 16:987–993
4. Giatromanolaki A, Koukourakis MI, O'Byrne K, Kaklamanis L, Dicoglou C, Trichia E, Whitehouse R, Harris AL, Gatter KC (1996) Non-small cell lung cancer: c-erbB-2 overexpression correlates with low angiogenesis and poor prognosis. Anticancer Res 16:3819–3825
5. Hatanaka Y, Hashizume K, Kamihara Y, Itoh H, Tsuda H, Osamura RY, Tani Y (2001) Quantitative immunohistochemical evaluation of HER2/neu expression with HercepTestTM in breast carcinoma by image analysis. Pathol Int 51:33–36
6. Hirsch FR, Franklin WA, Veve R, Varella-Garcia M, Bunn PA Jr (2002) HER2/neu expression in malignant lung tumors. Semin Oncol 29:51–58
7. Hirsch FR, Varella-Garcia M, Franklin WA, Veve R, Chen L, Helfrich B, Zeng C, Baron A, Bunn PA Jr (2002) Evaluation of HER-2/neu gene amplification and protein expression in non-small cell lung carcinomas. Br J Cancer 86:1449–1456
8. Ibrahim SO, Lillehaug JR, Johannessen AC, Liavaag PG, Nilsen R, Vasstrand EN (1999) Expression of biomarkers (p53, transforming growth factor alpha, epidermal growth factor receptor, c-erbB-2/neu and the proliferative cell nuclear antigen) in oropharyngeal squamous cell carcinomas. Oral Oncol 35:302–313
9. Jacobs TW, Gown AM, Yaziji H, Barnes MJ, Schnitt SJ (2001) Specificity of HercepTest in determining HER-2/neu status of breast cancers using the United States Food and Drug Administration-approved scoring system. J Clin Oncol 17:1983–1987
10. Klapper LN, Waterman H, Sela M, Yarden Y (2000) Tumor-inhibitory antibodies to HER-2/ErbB-2 may act by recruiting c-Cbl and enhancing ubiquitination of HER-2. Cancer Res 60: 3384–3388
11. Kristiansen G, Yu Y, Petersen S, Kaufmann O, Schluns K, Dietel M, Petersen I (2001) Overexpression of c-erbB2 protein correlates with disease-stage and chromosomal gain at the c-erbB2 locus in non-small cell lung cancer. Eur J Cancer 37:1089–1095
12. Kumada T, Tsuneyama K, Hatta H, Ishizawa S, Takano Y (2004) Improved one-hour rapid immunostaining method using intermittent microwave irradiation: practicability based on five years application in Toyama Medical and Pharmaceutical University Hospital. Mod Pathol 17:1141–1149
13. Levkowitz G, Oved S, Klapper LN, Harari D, Lavi S, Sela M, Yarden Y (2000) c-Cbl is a suppressor of the neu oncogene. J Biol Chem 275:35532–35539
14. Meert AP, Martin B, Paesmans M, Berghmans T, Mascaux C, Verdebout JM, Delmotte P, Lafitte JJ, Sculier JP (2003) The role of HER-2/neu expression on the survival of patients with lung cancer: a systematic review of the literature. Br J Cancer 89:959–965
15. Murata S, Chiba T, Tanaka K (2003) CHIP: a quality-control E3 ligase collaborating with molecular chaperones. Int J Biochem Cell Biol 35:572–578
16. Piyathilake CJ, Frost AR, Manne U, Weiss H, Bell WC, Heimburger DC, Grizzle WE (2002) Differential expression of growth factors in squamous cell carcinoma and precancerous lesions of the lung. Clin Cancer Res 8:734–744
17. Rao N, Dodge I, Band H (2002) The Cbl family of ubiquitin ligases: critical negative regulators of tyrosine kinase signaling in the immune system. J Leukoc Biol 71:753–763
18. Semba K, Kamata N, Toyoshima K, Yamamoto T (1985) A v-erbB-related protooncogene, c-erbB-2, is distinct from the c-erbB-1/epidermal growth factor-receptor gene and is amplified in a human salivary gland adenocarcinoma. Proc Natl Acad Sci USA 82:6497–6501
19. Sobin LH, Wittekind C (eds.) (2002) Lung and pleural tumors. In: The TNM Classification of malignant tumours. UICC, International union against cancer. Wiley-Liss, Canada, pp 97–107
20. Travis WD, Brambilla E, Konrad Müller-Hermelink H, Harris CC (eds.) (2004) Malignant epithelial tumours, In: Pathology and genetics tumours of the lung, pleura, thymus and heart. World Health Organization Classification of Tumours, Springer, Berlin, pp 26–67
21. Wu JT (2002) C-erbB2 oncoprotein and its soluble ectodomain: a new potential tumor marker for prognosis early detection and monitoring patients undergoing Herceptin treatment. Clin Chim Acta 322:11–19
22. Wu JT, Astill ME, Gagon SD, Bryson L (1995) Measurement of c-erbB-2 proteins in sera from patients with carcinomas and in breast tumor tissue cytosols: correlation with serum tumor markers and membrane-bound oncoprotein. J Clin Lab Anal 9:151–165
23. Xu W, Marcu M, Yuan X, Mimnaugh E, Patterson C, Neckers L (2002) Chaperone-dependent E3 ubiquitin ligase CHIP mediates a degradative pathway for c-ErbB2/Neu. Proc Natl Acad Sci USA 99:12847–12852
24. Zhou P, Fernandes N, Dodge IL, Reddi AL, Rao N, Safran H, DiPetrillo TA, Wazer DE, Band V, Band H (2003) ErbB2 degradation mediated by the co-chaperone protein CHIP. J Biol Chem 278:13829–13837

Virchows Arch (2005) 446: 604–612
DOI 10.1007/s00428-005-1222-6

ORIGINAL ARTICLE

Guida Maria Portela-Gomes · Lars Grimelius · Mats Stridsberg · Enrica Bresaola · Giuseppe Viale · Giuseppe Pelosi

Expression of amino acid sequences of the chromogranin A molecule and synaptic vesicle protein 2 in neuroendocrine tumors of the lung

Received: 22 December 2004 / Accepted: 7 February 2005 / Published online: 20 May 2005
© Springer-Verlag 2005

Abstract Chromogranin A (CgA) and its valuable complement synaptic vesicle protein 2 (SV2) are neuroendocrine (NE) markers. Post-translational processing of CgA has been reported to vary in different NE cell types and tumors, but little is known regarding the expression of various CgA epitopes and SV2 in NE pulmonary tumors. We studied the immunoreactivity to six CgA epitopes and SV2 in ten typical (TC) and ten atypical (ACT) carcinoids, five large-cell NE carcinomas (LCNEC) and five small-cell carcinomas (SCLC), also comparing the results with clinicopathological characteristics of tumors. The sequences CgA 17–38 (vasostatin), 176–195 (chromacin), 375–384 (parastatin) and 411–424 (C-terminal parastatin) and SV2 were relevant markers for the CT/ATC group, whereas the antibody to CgA 176–195 was a better marker for the LCNEC/SCLC group. An inverse correlation was found between proliferative activity and granule-related markers in the CT/ACT group, and a direct correlation in poorly differentiated tumors. The expression of granule-related markers did not correlate with hormone content or clinical characteristics of NE tumors. The expression of CgA epitopes and SV2 occurs in all NE tumors, differing between better differentiated and poorly differentiated tumors but not within the respective groups.

Keywords Chromogranin A · SV2 · Neuroendocrine · Lung · Tumor · Fragment · Immunohistochemistry

G. M. Portela-Gomes · L. Grimelius
Unit of Pathology,
Department of Genetics and Pathology,
University Hospital,
751 85 Uppsala, Sweden

G. M. Portela-Gomes
Centre of Nutrition and Metabolism,
Lisbon University,
Lisbon, Portugal

M. Stridsberg
Department of Medical Sciences,
Clinical Chemistry,
University Hospital,
75185 Uppsala, Sweden

E. Bresaola · G. Viale · G. Pelosi
Division of Pathology and Laboratory Medicine,
European Institute of Oncology and
University of Milan School of Medicine,
Milan, Italy

G. Pelosi (✉)
Divisione di Anatomia Patologica e Medicina di Laboratorio,
Istituto Europeo di Oncologia,
Via G. Ripamonti 435,
20141 Milan, Italy
e-mail: giuseppe.pelosi@ieo.it
Tel.: +39-2-57489414
Fax: +39-2-57489417

Introduction

Neuroendocrine (NE) tumors of the lung are currently classified as typical carcinoid (TC), atypical carcinoid (ATC), large-cell NE carcinoma (LCNEC) and small-cell lung carcinoma (SCLC) [27]. Typical carcinoids are low-grade malignant tumors, ATC intermediate grade, and the two latter tumor types are highly malignant. The carcinoids account for 2% or less of all lung tumors, while LCNEC and SCLC represent together about 20% [7]. Different hormonal products have been immunohistochemically demonstrated in pulmonary NE tumors, some of which have given rise to endocrine-related syndromes, such as inappropriate secretion of antidiuretic hormone, Cushing syndrome, acromegaly or carcinoid syndrome [2]. Pulmonary carcinoids but not the high-grade NE tumors may also be associated with neoplastic or hyperplastic lesions of the pituitary and parathyroid glands and of endocrine pancreas, mainly as a part of MEN-1 syndrome [7].

Several studies have been carried out in order to identify histopathological characteristics useful in assisting the differential diagnosis of these tumor types and/or in predicting their biological behaviour [3, 13, 14, 27, 28]. The most specific and suitable markers so far for highlighting NE differentiation in lung tumors are chromogranin A (CgA) and synaptophysin (Syn), but more recently synaptic ve-

sicle protein 2 (SV2) has also been proposed as a useful marker for NE differentiation [22].

CgA is a glycoprotein localized in the secretory granules [29], whereas Syn is an integral membrane glycoprotein detectable in small vesicles [17]. SV2 has been demonstrated in vesicular structures of the mammalian nervous system [4] and in various NE cell types [22]. Recently, interest has been focused on the expression of various epitopes of the CgA molecule in different NE cell types of the gastroenteropancreatic system and derived tumors [23–25]. CgA has ten potential cleavage sites, which can give rise to post-translational processing of the CgA molecule. However, data on the prevalence and clinicopathological implications of the immunoreactivity to both different CgA epitopes and SV2 in NE tumors of the lung are lacking.

An essential factor for tumor growth is neoangiogenesis [9], which can be inferred by microvessel density (MVD) in tumor sections after selective immunostaining of endothelial cells [31]. In carcinoids of the gastroenteropancreatic system and in NE-differentiated adenocarcinomas of the prostate, the hypervascular status of the neoplasm has been linked to the presence of CgA-immunoreactive NE tumor cells, which produce a vascular endothelial growth factor [6, 16, 26]. Moreover, it has been shown that CgA is able to prevent the endothelial cell cytoskeleton rearrangement and vascular leakage mediated by cytokines [10], and that vasostatins may inhibit vascular contractions [1].

The aim of the present study was to analyse the expression of epitopes of the CgA molecule and SV2 in various types of NE lung tumors and to evaluate if these results can give additional information to other tumor characteristics, such as histological typing, tumor cell proliferation, neoangiogenesis and peptide hormone pattern.

Materials and methods

Patients and tumors

Tissue specimens from surgically resected pulmonary NE tumors from 30 patients (10 CT, 10 ACT, 5 LCNEC and 5 SCLC) were included in the study. The tissue specimens were fixed in buffered formalin and routinely processed to paraffin. These tumors were selected among 117 consecutive NE lung tumors of various histologic types, diagnosed at the Division of Pathology and Laboratory Medicine of the European Institute of Oncology, Milan, Italy, surgically removed between 1996 and 2002. To ensure an accurate staging, all tumors were removed by radical surgery, with extensive mediastinal lymph node dissection. All ten CT were arbitrarily chosen with no regional lymph node metastases at the time of diagnosis, whereas all the other tumours were metastatically spread to regional lymoh nodes. Lymph node metastases were at the pN1 (8 ACT, 4 LCNEC and 1 SCLC) or pN2 (5 ACT, 1 LCNEC, and 4 SCLC) level according to the last international tumor-node-metastasis (TNM) staging system (6th edn, 2003) [30], involving the hilar/peribronchial nodes or mediastinal nodes, respectively. One LCNEC and four SCLC patients underwent neo-adjuvant combination chemotherapy by using CAVE protocol (cyclophosphamide, doxorubicin, vincristine and etoposide).

For each case, all paraffin blocks were retrieved and archival hematoxylin-eosin sections reviewed. Tumor recurrences were seen in 12 (40%) patients (1 CT, 2 ACT, 4 LCNEC and 5 SCLC), with localization in ipsilateral lung (1 CT, 1 ACT, 4 LCNEC and 1 SCLC), liver (3 LCNEC and 2 SCLC), ovary (1 ACT), bone (3 SCLC), or brain (2

Table 1 Antibodies used in the current study

Antibodies	m/P	Clone	Specificity	Dilution	Source
CgA	m	LK2H10	CgA 250–301 N-terminal pancreastatin	1:1000	Boehringer-Mannheim, Mannheim, Germany
Synthetic human CgA (CgA2)	p	–	CgA 17–38 vasostatin	1:800	M. Stridsberg, Dept. Clin.Chem., Uppsala, Sweden
Synthetic human CgA (CgA4)	p	–	CgA 116–130 chromostatin	1:800	M. Stridsberg
Synthetic human CgA (CgA10)	p	–	CgA 176–195 chromacin	1:1600	M. Stridsberg
Synthetic human CgA (CgA11)	p	–	CgA 238–247	1:1600	M. Stridsberg
Synthetic human CgA (CgA8)	p	–	CgA 375–384 GE25 (mid-parastatin)	1:400	M. Stridsberg
Synthetic human CgA (CgA9)	p	–	CgA 411–424 C-terminal parastatin	1:800	M. Stridsberg
Synaptic vesicle protein 2	m	SV2	Synaptic vesicle protein 2	1:50	RB Kelly, Dept. Biochem. Biophys., UCSF, CA
Synaptophysin	m	SY 38	Synaptophysin	1:20	DakoCytomation, Glostrup, Denmark
ACTH	m	02A3	Human ACTH 24–39	1:100	DakoCytomation, Glostrup, Denmark
Calcitonin	p	–	Human calcitonin 1–32	1:20	DakoCytomation, Glostrup, Denmark
CD34	m	QBEnd/10	110 kD glycoprotein	1:400	DakoCytomation, Glostrup, Denmark
GRP/Bombesin	p	–	Human GRP 14–27	1:400	DakoCytomation, Glostrup, Denmark
Serotonin	m	5HT-H209	5-HT	1:10	DakoCytomation, Glostrup, Denmark
alpha-HCG	p	–	Alpha-chain	1:200	Signet Laboratories, Dedham, MA
Ki-67	m	MIB-1	Ki-67 antigen	1:400	Immunotech, Marseille, France

CgA chromogranin A; *m* monoclonal; *p* polyclonal

SCLC). The mean age of the patients at the time of surgery was 54±15 years (median: 59, range 26–75) for CT and ACT group, and 60±11 years (median: 59, range 45–74) for LCNEC and SCLC (NS). The gender distribution was 12 males (7 CT/ACT and 5 LCNEC/SCLC) and 18 females (13 CT/ACT and 5 LCNEC/SCLC). Complete clinical follow-up was available for all patients with a mean duration of 29±19 months (median 24; range 9–85); during this period eight (26.7%) died of disease (2 ACT, 3 LCNEC and 3 SCLC). No patients presented with MEN-1 or any other endocrine-related syndromes.

The diagnosis of NE tumor was based on previously refined morphological and immunohistochemical criteria, including immunoreactivity for pan-endocrine markers CgA, Syn, and for a variety of respiratory tract-related hormones, including GRP, calcitonin, ACTH, serotonin and alpha-HCG) [20, 21]. Tumor size ranged from 0.7 to 4.0 cm in CT (mean±SD: 2.4±0.9; median 2.45), from 1.2 to 6.2 cm in ATC (mean±SD: 2.7±1.5; median 2.25), from 3.1 to 8.0 cm in LCNEC (mean±SD: 4.9±1.8; median 4.5) and from 2.5 to 9.0 cm in SCLC (mean±SD: 4.5±2.8; median 3.0) (CT versus ACT, NS; LCNEC versus SCLC, P=0.060; CT/ACT versus LCNEC/SCLC, P=0.037).

Immunohistochemistry

Sections 5 μm thick were cut from representative tissue blocks and immunostained with polyclonal antibodies raised to six specific regions of the CgA molecule [amino acid sequences CgA 17–38 (vasostatin), 116–130 (chromostatin), 176–195 (chromacin), 238–247, 375–384 9 (mid-portion of parastatin) and 411–424 (C-terminal parastatin)], all previously characterized by Portela-Gomes and Stridsberg

Table 2 Distribution of chromogranin A fragments nd SV2 immunoreactivity according to tumor typing

Tumor type	17–38 vasostatin	116–130 chromostatin	176–195 chromacins	238–247	375–384 mid-parastatin (GE-25)	411–424 C-terminal parastatin	mCgA 250–301 N-terminal pancreastatin	SV-2
CT #11	2/*(**)	1/*(*)	3(4)/**	1/*	3/*	4/**	3(4)/*(*)	4/**
CT #12	4/**(*)	4/***	4/***	3/*	4/**(*)	3/*	4/***	4/***
CT #13	3/*(**)	2/*	4/**	1/*	3/*(**)	4/*	4/***	4/**(*)
CT #14	4/***	2/*(*)	4/***	4/**	3/**	4/*(*)	4/***	4/**
CT #15	3/***	2/*	4/***	3/**	3/**	3/*(*)	4/***	3/*
CT #16	4/***	2/*(*)	4/***	4/*(*)	4/***	4/*	4/***	2/*
CT #17	3/**	3/*	4/***	3/*(*)	4/***	3/**(*)	4/***	3/**
CT #18	4/***	3/*(*)	4/***	4/**	4/**	3/*	4/***	4/*(*)
CT #19	4/**(*)	1/*	4/***	1/*	4/*(*)	–	4/***	4/*(*)
CT #20	4/***	4/**	4/***	4/**	4/**(*)	4/*(*)	4/***	4/*(*)
ACT #1	4/***	3/*	4/***	4/**	4/***	4/***	4/***	4/**(*)
ACT #2	4/***	3/*	4/***	3/*(*)	4/***	3/*(**)	4/***	4/**(*)
ACT #3	3/*(**)	3/**	4/***	4/*(*)	4/***	4/*	4/***	4/**
ACT #4	4/***	2/*	3(4)/***	2(3)/*	3/**	3/*	3(4)/***	3/*(*)
ACT #5	4/***	3/*(*)	4/***	4/**	4/***	4/**(*)	4/*(*)	4/**(*)
ACT #6	4/***	1/**	4/***	4/*(*)	4/***	4/**	4/***	4/**
ACT #7	4/***	4/**(*)	4/***	4/*	4/**(*)	4/**	4/***	4/**(*)
ACT #8	4/***	4/**(*)	4/***	3/*	3/**(*)	3/**	4/**(*)	4/**(*)
ACT #9	4/*(**)	4/*(**)	4/***	3/*	3/**(*)	4/**(*)	4/***	3/*(*)
ACT #10	4/***	3/*(*)	4/***	3/(*)	4/*(*)	4/**	4/***	4/**
LCNEC #21	2(3)/**(*)	2/**(*)	4/**(*)	3/**	2/**	3/**	3/**(*)	1/*
LCNEC #22	2/*(*)	2/*	3/**(*)	2/*	3/*(**)	4/**	3/**(*)	–
LCNEC #23	3/*	3/*	4/**(*)	3/*	3/*	3(4)/*	3/**(*)	3/*
LCNEC #24	2/*(**)	3/*(**)	3/*(**)	3/(*)	2/*(**)	3/*	3/*(**)	2/(*)
LCNEC #25	1/**	1/**	4/**	–	3/*	3/*	1/***	–
SCLC #26	4/***	–	4/***	2/*	2/*	3/*	4/***	4/***
SCLC #27	2/*	2/*	2/**(*)	2/*	2/*	2/*	1/**	–
SCLC #28	–	4/*	4/**	4/*	3/*	4/*(*)	–	1/*
SCLC #29	3/*(**)	3/*(*)	4/*(**)	2/*	3/*	3/*(*)	4/*(**)	3/*
SCLC #30	3/*(**)	3/*	4/***	2/*	2/*	3/*(*)	4/***	4/**

mCgA monoclonal antibody to chromogranin A; *CT* typical carcinoid; *ACT* atypical carcinoid; *LCNEC* large-cell neuroendocrine carcinoma; *SCLC* small-cell lung carcinoma

Percentages of tumor cells displaying immunoreactivity: −, negative; 1, <10% positive; 2, 11–50% positive; 3, 51–90% positive; 4, >90% positive

Intensity of immunoreaction: ***, strong; **, moderate; *, weak; (*), very weak

[23, 25]. The SV2 antibody was instead monoclonal, and was previously characterized by Buckley and Kelly [4].

Dewaxed sections were initially treated with 5% hydrogen peroxide for 12 min for blocking endogenous peroxidase activity and reacted with the panel of reagents listed in Table 1 using either a Ventana NEXES automatic immunostainer (Ventana, Tucson, Ariz., USA) for commercial CgA (clone LK2H10), SV2 and CgA region-specific antibodies, or a Dako Autostainer (DakoCytomation, Glostrup, Denmark) for all the other reagents under investigation, both of which were used according to the manufacturers' suggestions. Whenever appropriate, before immunostaining the sections were pretreated in a microwave oven with either citrate buffer at pH 6.0 or EDTA buffer at pH8 as retrieval solution. Peroxidase activity was then developed with 3-3′-diaminobenzidine-copper sulphate (Sigma Chemical Co., St Louis, Mo., USA) to obtain a bright brownish-black end product. The control stainings for all reactions entailed (i) omission of the primary antibodies or (ii) replacement of the first layer of antibody by nonimmune serum diluted 1:10, (iii) replacement of the CgA region-specific antibodies by the diluent alone and preincubation (24 h) of primary antibodies with the relevant antigen (10 nmol per ml diluted antibody solution, respectively) before application to the sections. Appropriate internal positive controls represented by the scattered NE cells of the normal bronchial mucosa were checked in every staining run. n

The density of immunoreactive cells was semiquantitatively calculated on a five-tier scale, as being either negative or positive in <10%, 11–50%, 51–90% and >90% tumor cells, respectively. For CgA and SV2, the immunostaining intensity was also evaluated subjectively by using a three-tier scale (strong, moderate, weak/very weak). Tumor cell proliferation was evaluated by Ki-67 index and tumor neoangiogenesis was inferred by MVD after CD34 immunostaining of endothelial cells as previously detailed [19].

Statistical analysis

Qualitative data were compared using the Fisher exact *t*-test or chi-square test. Differences in continuous data (i.e. CgA fragments, SV2, MVD, Ki-67 index, tumour size) were contrasted employing the Mann–Witney test or the Kruskal–Wallis test if medians were compared between two or more groups, respectively. All correlation tests were calculated using Spearman's rank test (*r*). All *P*-values were based on two-sided testing.

Results

Immunostaining of scattered normal NE cells of adjacent bronchi and bronchioli with the various CgA region-specific antibodies and SV2 showed that immunoreactive cells to CgA 176–195, the monoclonal CgA antibody and SV2 were the most commonly observed, whereas only occasional or no immunoreactive cells were observed to CgA 116–130, 238–247 and 411–424.

The findings of immunostaining for both NE markers (commercial CgA and SV2) and region-specific epitopes of the CgA molecule are presented in Tables 2 and 3. Representative features of CgA molecule fragment and SV2 immunoreactivity are depicted in Figs. 1 and 2, respectively.

For the commercial CgA antibody and SV2, the frequency of immunoreactive cells was significantly higher in

Table 3 Chromogranin (*Cg*) A and SV2 immunoreactive cells in 30 pulmonary neuroendocrine tumours

Antibody	Tumour category	No. of tumors with different percentage intervals of immunoreactive cells (%)					
		neg	<10%	10–50%	50–90%	90–100%	*P*-value
CgA 17–38 (CgA2)	CT/ACT	0 (0)	0 (0)	1 (5)	4 (20)	15 (75)	
	LCNEC/SCLC	1 (10)	1 (10)	4 (40)	3 (30)	1 (10)	0.0059
CgA 116–130 (CgA4)	CT/ACT	0 (0)	3 (15)	5 (25)	7 (35)	5 (25)	
	LCNEC/SCLC	1 (10)	1 (10)	3 (30)	4 (40)	1 (10)	NS
CgA 176–195 (CgA10)	CT/ACT	–	–	0 (0)	2 (10)	18 (90)	
	LCNEC/SCLC	–	–	1 (10)	2 (20)	7 (70)	NS
CgA 238–247 (CgA11)	CT/ACT	0 (0)	3 (15)	1 (5)	7 (35)	9 (45)	
	LCNEC/SCLC	1 (10)	0 (0)	5 (50)	3 (30)	1 (10)	0.0126
CgA 375–384 (CgA8)	CT/ACT	–	–	0 (0)	7 (35)	13 (65)	
	LCNEC/SCLC	–	–	0 (0)	5 (50)	5 (50)	0.0002
CgA411–424 (CgA9)	CT/ACT	1 (5)	–	0 (0)	7 (35)	12 (60)	
	LCNEC/SCLC	0 (0)	–	1 (10)	7 (70)	2 (20)	NS
mabCgA	CT/ACT	0 (0)	0 (0)	–	2 (10)	18 (90)	
	LCNEC/SCLC	1 (10)	2 (20)	–	4 (40)	3 (30)	0.0061
SV2	CT/ACT	0 (0)	0 (0)	1 (5)	3 (15)	16 (80)	
	LCNEC/SCLC	3 (30)	2 (20)	1(10)	2 (20)	2 (20)	0.0063

CT carcinoid tumor; *ACT* atypical carcinoid tumor; *LCNEC* large-cell neuroendocrine carcinoma; *SCLC* small-cell lung carcinoma; *NS* not significant; *mabCgA* monoclonal antibody to chromogranin A

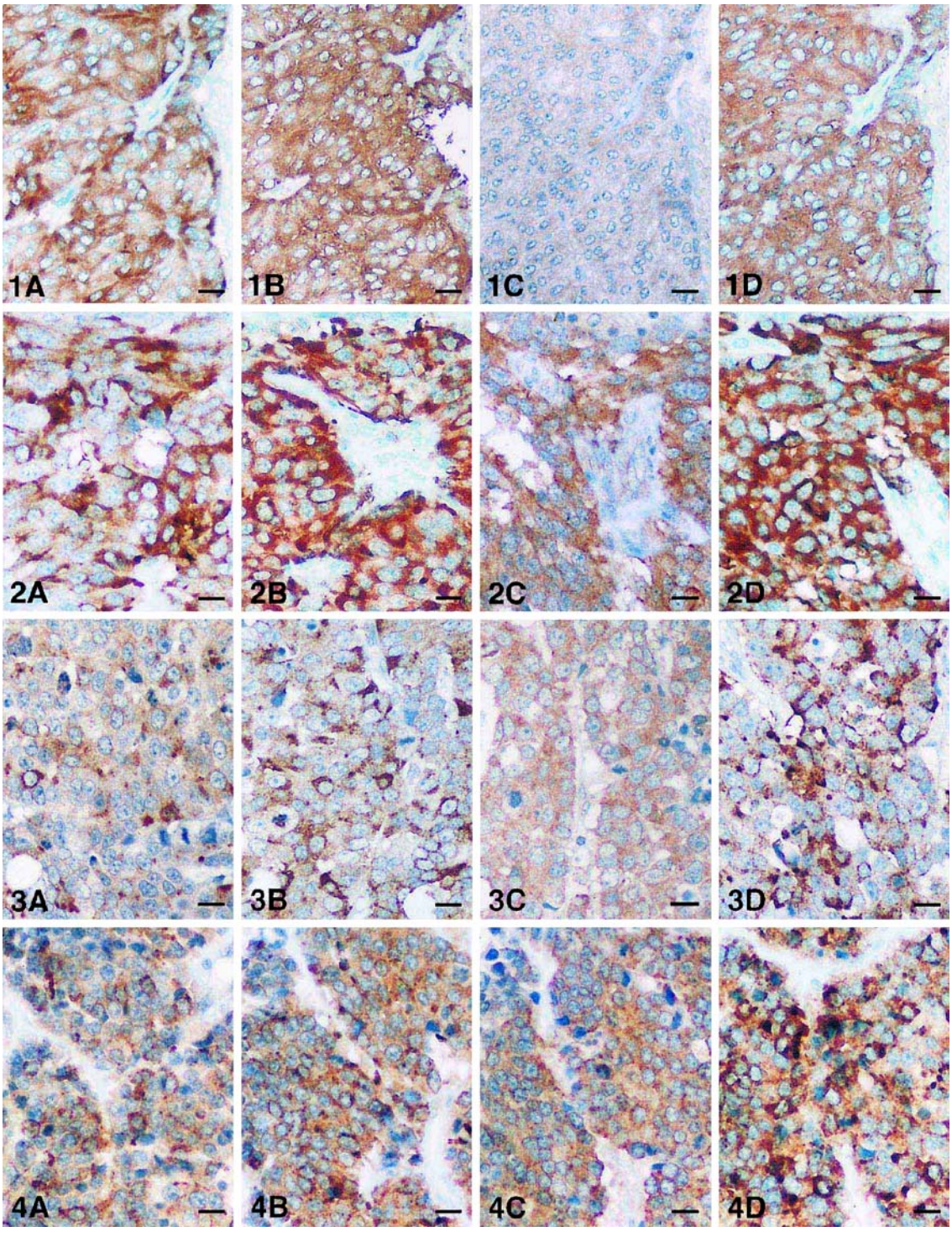

Fig. 1 Pulmonary neuroendocrine tumours immunostained with antibodies to three chromogranin A (*CgA*) amino acid sequences, namely CgA 17–38 (vasostatin) (**a**), CgA 176–195 (chromacin) (**b**), CgA 411–424 (C-terminal parastatin) (**c**), and with a commercial monoclonal CgA antibody (LK2H10) recognizing an epitope lying in the region CgA 250–284 (i.e. N-terminal pancreastatin) (**d**) (*bars* indicate 10 ηm). In the first line a typical carcinoid (CT #13) is shown. Most neoplastic cells display vasostatin immunoreactivity (**a**); virtually all show chromacin immunostaining (**b**); almost all are very faintly immunostained with the antibodies to parastatin (C-terminal region) (**c**); and the commercial antibodies reveal immunoreactivity in virtually all tumour cells (**d**). In the second line, an atypical carcinoid (ACT #9) is shown. Most cells are vasostatin-immunoreactive, but the staining intensity varies (**a**); virtually all tumour cells demonstrate strong chromacin immunoreactivity (**b**); most cells show weak immunoreactivity to parastatin (**c**) and strong immunoreactivity to the commercial antibody (**d**). In the third line, a large-cell neuroendocrine carcinoma (LCNEC #22) is shown. Almost half of the neoplastic cells show mainly weak immunoreactivity to vasostatin (**a**); most cells display immunoreactivity to the chromacin antibody, with varying intensities (**b**); almost all tumour cells show weak parastatin immunoreactivity (**c**); and the commercial antibody demonstrates immunoreactivity in most neoplastic cells (**d**). In the fourth line, a small-cell lung carcinoma (SCLC #29) is shown. Most cells display immunoreactivity with the four antibodies (**a**–**d**). With the parastatin antibody the immunostaining varies from weak to moderate (**c**), the other three immunostainings vary from weak to strong

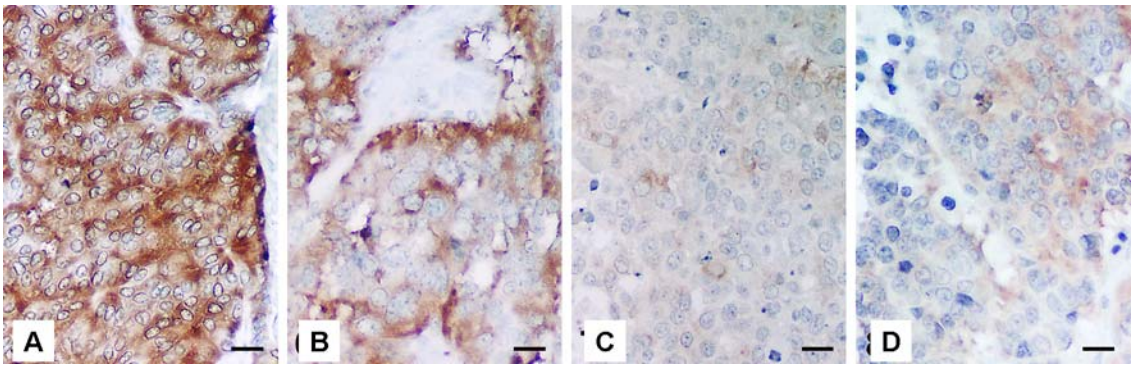

Fig. 2 Synaptic vesicle protein 2 (*SV2*) immunostaining of sections from the same four cases as reported in lines 1–4 of Fig. 1. More tumour cells are immunostained in the typical carcinoid (**a**) and atypical carcinoid (**b**) compared with the large-cell neuroendocrine carcinoma (**c**) and small-cell lung carcinoma (**d**). (Bars indicate 10 ηm)

the two differentiated tumor types compared with the two poorly differentiated (P=0.0061 and P=0.0063, respectively), but no quantitative differences were observed in between the two differentiated tumor types, nor in between the two poorly differentiated. No significant difference were seen between these two groups regarding Syn or serotonin immunoreactive cells or the immunoreactive cells to the other antibodies to the respiratory tract-related peptide hormones.

The intensity of several CgA fragments and SV2 immunostaining was stronger in the differntiated groups compared with the undifferentiated ones (Table 4). For both the differentiated NE tumors and the poorly differentiated considered as a whole, the frequency of cells stained for the SV2 antibody correlated rather well with those stained when using the commercial monoclonal CgA (r=0.786), Syn (r=0.869) and the CgA 17–38 (r=0.765), 176–195 (r=0.497) and 375–384 (r=0.448) antibodies (P<0.05). Such a relationship was, however, not found regarding the peptide immunoreactive cells.

The expression of CgA epitopes in the differentiated tumors agreed rather well, with the exception of the antibodies to CgA116–130 and 238–247. However, the prevalence of CgA immunoreactive cells to CgA region-specific antibodies did not differ significantly between CT and ACT. In the LCNEC/SCLC group, the most conserved CgA sequence was 176–195.

Statistically significant differences in the prevalence of either immunoreactive cells to all markers (Table 3) or immunostaining intensity (Table 4) were found between CT/ATC on one hand and LCNEC and SCLC on the other. In general, there was a close correlation between the staining intensity and the number of immunoreactive cells, i.e. the tumors that had a higher frequency of immunoreactive cells also showed a stronger immunoreactivity (Table 5). In the CT/ACT group, the expression of CgA 17–38 (r=0.675, P=0.001) and 375–384 (r=0.557, P=0.010), and in the LCNEC/SCLC group the expression for CgA 17–38 (r=0.876, P<0.001) correlated with the immunoreactivity for the commercial monoclonal antibody to CgA. In both tumor types, instead, no relationship was found between the expression of CgA epitopes and hormone products, apart from a weak correlation between CgA 116–130 (chromostatin) and GRP expression in CT/ACT tumors (r=0.474, P=0.034).

Proliferative activity as assessed by Ki-67 labelling index ranged from 0.5 to 9% (mean±SD: 3.7±2.8, median 3) in CT, from 5.8 to 16% (mean±SD: 9.8±3.8, median 9) in ACT, from 41 to 57% in LCNEC (mean±SD: 50.6±6.9, median 53) and from 51 to 84% (mean±SD: 66.4±15.1,

Table 4 Immunostaining intensity cells in 30 neuroendocrine tumours of the lung by histology

Antibody	Category	Levels of immunoreactivity (%)				
		neg	weak	moderate	strong	*P*-value
CgA 17–38 (CgA2)	CT/ACT	0 (0)	4 (20)	3 (15)	13 (65)	
	LCNEC/SCLC	1 (10)	6 (60)	2 (20)	1 (10)	0.0221
CgA 176–195 (CgA10)	CT/ACT	–	0 (0)	2 (10)	18 (90)	
	LCNEC/SCLC	–	2 (20)	6 (60)	2 (20)	0.0005
CgA 375–384 (CgA8)	CT/ACT	–	4 (20)	9 (45)	7 (35)	
	LCNEC/SCLC	–	9 (90)	1 (10)	0 (0)	0.0012
mabCgA	CT/ACT	0 (0)	2 (10)	1 (5)	17 (85)	
	LCNEC/SCLC	1 (10)	2 (20)	4 (40)	3 (30)	0.0153
SV2	CT/ACT	0 (0)	7 (35)	12 (60)	1 (5)	
	LCNEC/SCLC	3 (30)	5 (50)	1 (10)	1 (10)	0.0190

Differences in the distribution of 116–130 (chromostatin), 238–247 and 411–424 (C-terminal parastatin) CgA sequences were not statistically significant. Immunostaining intensity for synaptophysin, serotonin and all peptide hormones was not assessed in the study

Table 5 Correlations between number of immunoreactive cells and immunostaining intensity

Monoclonal antibody	Correlation coefficient	*P*-value
CgA 17–38 (CgA2)	0.754	<0.001
CgA 116–130 (CgA4)	0.428	0.018
CgA 176–195 (CgA10)	0.412	0.023
CgA 238–247 (CgA11)	0.536	0.002
CgA 375–384 (CgA8)	0.614	<0.001
CgA411–424 (CgA9)	0.670	<0.001
mabCgA	0.577	<0.001
SV2	0.830	<0.001

median 60) in SCLC. These differences were statistically significant between CT and ACT (P=0.003) but not between LCNEC and SCLC. In the former group, Ki-67 labelling index was inversely correlated (r=−0.506) with the expression of either CgA 176–195 or the commercial antibody to CgA (P=0.022), but not with SV2 expression, in the latter tumor group Ki-67 was directly correlated with CgA 17–38 (r=0.679), the commercial CgA antibody (r=0.601), and with SV2 expression (r=0.699) (P<0.05).

MVD was higher in more differentiated NE tumors than in LCNEC and SCLC, according to both Weidner's (P=0.037) and Chalkley's (P=0.050) methods, and in the former it was higher in CT than in ACT (P=0.011 and P=0.014, respectively). However, no relationship was observed between MVD and the immunoreactivity to SV2, the commercial CgA antibody or the various CgA epitopes.

Likewise, no relationship was found between the expression of CgA epitopes or SV2 immunoreactivity on one hand, and age, gender and tumor size on the other. Survival analysis according to the expression of CgA epitopes or SV2 immunoreactivity was not performed owing to the low number of events in the CT/ACT group and the small number of patients under evaluation in the LCNEC/SCLC group.

Discussion

The present study is the first investigation concerning the expression of various regions of CgA molecule and SV2 in a series of the four NE pulmonary tumor types. A broad spectrum of immunohistochemical markers have been proposed in the past to highlight NE differentiation in these tumor types, but CgA and/or Syn still remain the most exploited ones, owing to their close correlation with the ultrastructural evidence of neurosecretory granules [2, 5, 7, 15, 20, 21, 27, 28]. Knowledge about the expression of various CgA fragments and SV2 in these tumor types is limited, and our investigation was mainly aimed to map their expression pattern and evaluate if they can be helpful in the diagnostic approach to NE tumors of the lung.

The main findings of our study were that (i) several epitopes of the CgA molecule and SV2 were consistently expressed in the four NE tumor types of the lung, but to various extent, the two better differentiated tumors (carcinoids) expressing more CgA epitopes and SV2 than the poor differentiated tumors; (ii) CgA 17–38 (vasostatin), 176–195 (chromacin), 375–384 (mid-parastatin) and 411–424 (C-terminal parastatin) appear to be the most relevant CgA epitopes for the two differentiated tumor types, whereas CgA 176–195 (chromacin) was mostly expressed in the lower differentiated tumors; the commercial monoclonal CgA antibody and the SV2 antibody gave rise to a similar expression pattern; the expression pattern between the two differentiated tumor types did not differ significantly, nor did it differ between the two poor differentiated tumor types; (iii) a significant correlation was found between the expression of the three main NE markers (monoclonal CgA, SV2 and Syn); CgA 116–130 (chromostatin) showed a correlation with GRP; (iv) the expression of Syn and the peptide hormones analysed were not related to the tumor differentiation grade; (v) there seems to be a complex relationship between tumor cell growth and expression of granule-related markers in NE tumors of the lung; (vi) no relationship was noted between the expression of these NE granule-related markers and the hypervascular status or the clinical behaviour of the tumors.

Recently, Portela-Gomes et al. have reported a strong immunoreactivity for SV2 in three bronchial carcinoids, with a labelling intensity apparently more intense than that to Syn [22]. However, in the current study dealing with a larger amount of tumors, this finding was not confirmed, indicating that both markers seem to be equally useful in histopathological typing of pulmonary NE tumors.

The differential diagnosis between CT and ACT is sometimes difficult or impossible and the occurrence of mitosis (2–10 mitosis/10 high-power fields) and/or punctate necrosis are signs indicating ACT [27, 28]. The commercially CgA antibody showed a similar staining pattern as the three region-specific antibodies mentioned above; the former antibody is directed to the N-terminal part of pancreastatin, i.e. the midportion of the CgA molecule [23]. Our study shows that the CgA epitopes and SV2 are expressed mainly in the two differentiated tumor groups, but their patterns did not differ significantly, i.e. they are not helpful in histopathological differential diagnosis between CT and ACT.

In the two poorly differentiated tumor groups, the expression of CgA epitopes were limited; the most conserved CgA sequence was 176–195, confirming the previous report that chromacin is a useful general NE marker [23]. However, the CgA patterns and SV2 did not differ between these two poorly differentiated tumor types, i.e. these markers are not useful in differential diagnosis between LCNEC and SCLC.

The CgA epitope patterns and SV2, however, differed significantly between the differentiated NE tumors and the poorly differentiated ones. Accordingly, they could also assist in difficult differential diagnosis between carcinoids, either typical or atypical, and poorly differentiated tumors, especially in small crushed biopsy tissue fragments avoiding inappropriate treatments of the patients [12, 18].

The expression of CgA epitopes varied to some extent within the differentiated tumor group and a variation also occured within one and the same tumor. The CT and ACT tumors, with only one exception, demonstrated all the fragments, indicating that the whole CgA molecule was intact. In most of the tumors these fragments occurred in the majority of tumor cells. In all the poorly differentiated tumor cases one or more fragments were lacking, which means that only parts of the molecule were translated, or that the molecule was spliced, or that parts of the molecule were hidden in such a way the antibodies were unable to react with the corresponding epitopes.

Cunningham et al. [8] reported that only one of 24 bronchial carcinoids expressed vasostatin, which is in contrast with our findings where the majority of the differentiated tumors expressed that epitope. In both studies polyclonal rabbit antibodies were used, but the two antibodies were directed against different parts of the molecule: Cunningham et al. used antibodies against the CgA sequence 68–76 (vasostatin II), we used 17–38 (vasostatin I). Recently, Portela-Gomes and Stridsberg [23–25] demonstrated these two sequences of vasostatin (17–38 and 68–76) in enterochromaffin and enteroglucagon cells of the human gastrointestinal tract, as well as in insulin and glucagon cells of the human endocrine pancreas. Thus, these vasostatin epitopes occur in peptide and monoamine producing cells, but vasostatin is cleaved in a different way in NE lung tumors.

Other NE markers, such as Syn, serotonin and respiratory tract-related peptide hormones, did not differ significantly quantitatively in their expression between the differentiated tumors or between the poorly differentiated. The commercial CgA antibody, and antibodies to some CgA region-specific antibodies and SV2 are useful markers in differentiation between NE and non-endocrine lung tumors.

The tumor cell proliferation was inversely correlated to the tumor cell expression of the CgA commercial antibody and CgA sequences 176–195, but not with SV2, in the differentiated tumor groups. In the poorly differentiated groups there was a direct correlation between the proliferation index and the expression of SV2, CgA (commercial antibody) and vasostatin (CgA 17–38). Thus, it does not seem that CgA or its epitopes have any direct influence on the tumor cell proliferation. There was neither an apparent correlation between MVD on one hand and SV2 and CgA fragments on the other, nor between the expression of these proteins and clinical chracteristics of tumors. Altough neuroendocrine cells may contribute to tumor angiogenesis by expressing VEGF [26], the latter, however, may be functionally inhibited by CgA N-terminal fragments [11].

The demonstration of CgA fragments only indicates their existence but not if they are separate protein fragments or a part of a larger molecule. The existence of the whole CgA molecule seems, as mentioned above, to be rare and, if so, only occuring in differentiated tumors. Some of the CgA epitopes are known to have endocrine functions, such as vasostatins (CgA 1–113), chromostatin (124–147), chromacin (173–194), pancreastatin (250–301), catestatin (344–364) and parastatin (347–419). It is not clear if any of the fragments are released from the lung NE tumors into the vascular system, although elevated levels of circulating CgA are common in the blood of neuroendocrine tumor-bearing patients where could regulate the endothelial barrier function [11].

References

1. Angeletti RH, Aardal S, Serck-Hanssen G, Gee P, Helle KB (1994) Vasoinhibitory activity of synthetic peptides from the amino terminus of chromogranin A. Acta Physiol Scand 152: 11–19
2. Axiotis CA (2002) The neuroendocrine lung. In: Li Volsi V, Asa SL (eds) Endocrine pathology. Churchill Livingstone, New York, pp 261–296
3. Bohm J, Koch S, Gais P, Jutting U, Prauer HW, Hofler H (1996) Prognostic value of MIB-1 in neuroendocrine tumours of the lung. J Pathol 178:402–409
4. Buckley K, Kelly RB (1985) Identification of a transmembrane glycoprotein specific for secretory vesicles of neural and endocrine cells. J Cell Biol 100:1284–1294
5. Capella C, Heitz PU, Hofler H, Solcia E, Kloppel G (1995) Revised classification of neuroendocrine tumours of the lung, pancreas and gut. Virchows Arch 425:547–560
6. Chevalier S, Defoy I, Lacoste J, Hamel L, Guy L, Begin LR, Aprikian AG (2002) Vascular endothelial growth factor and signaling in the prostate: more than angiogenesis. Mol Cell Endocrinol 189:169–179
7. Corrin B (2000) Pathology of the lungs. Churchill Livingstone, London
8. Cunningham RT, Pogue KM, Curry WJ, Johnston CF, Sloan JM, Buchanan KD (1999) Immunostaining for vasostatin I distinguishes between ileal and lung carcinoids. J Pathol 187: 321–325
9. Ferrara N, Gerber HP, LeCouter J (2003) The biology of VEGF and its receptors. Nat Med 9:669–676
10. Ferrero E, Magni E, Curnis F, Villa A, Ferrero ME, Corti A (2002) Regulation of endothelial cell shape and barrier function by chromogranin A. Ann N Y Acad Sci 971:355–358
11. Ferrero E, Scabini S, Magni E, Foglieni C, Belloni D, Colombo B, Curnis F, Villa A, Ferrero ME, Corti A (2004) Chromogranin A protects vessels against tumor necrosis factor alpha-induced vascular leakage. FASEB J 18:554–556
12. Flieder DB (2002) Neuroendocrine tumors of the lung: recent developments in histopathology. Curr Opin Pulm Med 8:275–280
13. Granberg D, Wilander E, Oberg K, Skogseid B (2000) Prognostic markers in patients with typical bronchial carcinoid tumors. J Clin Endocrinol Metab 85:3425–3430
14. Granberg D, Wilander E, Oberg K, Skogseid B (1999) Decreased survival in patients with CD44-negative typical bronchial carcinoid tumors. Int J Cancer 84:484–488
15. Lloyd RV, Douglas BR, Young WF (2002) Endocrine diseases. American Registry of Pathology and the Armed Forces Institute of Pathology, Washington D.C.
16. Mazzucchelli R, Montironi R, Santinelli A, Lucarini G, Pugnaloni A, Biagini G (2000) Vascular endothelial growth factor expression and capillary architecture in high-grade PIN and prostate cancer in untreated and androgen-ablated patients. Prostate 45:72–79
17. Navone F, Jahn R, Di Gioia G, Stukenbrok H, Greengard P, De Camilli P (1986) Protein p38: an integral membrane protein specific for small vesicles of neurons and neuroendocrine cells. J Cell Biol 103:2511–2527
18. Nicholson SA, Beasley MB, Brambilla E, Hasleton PS, Colby TV, Sheppard MN, Falk R, Travis WD (2002) Small cell lung carcinoma (SCLC): a clinicopathologic study of 100 cases with surgical specimens. Am J Surg Pathol 26:1184–1197

19. Pelosi G, Fraggetta F, Pasini F, Maisonneuve P, Sonzogni A, Iannucci A, Terzi A, Bresaola E, Valduga F, Lupo C, Viale G (2001) Immunoreactivity for thyroid transcription factor-1 in stage I non-small cell lung carcinomas of the lung. Am J Surg Pathol 25:363–372
20. Pelosi G, Fraggetta F, Sonzogni A, Fazio N, Cavallon A, Viale G (2000) CD99 immunoreactivity in gastrointestinal and pulmonary neuroendocrine tumours. Virchows Arch 437:270–274
21. Pelosi G, Pasini F, Fraggetta F, Pastorino U, Iannucci A, Maisonneuve P, Arrigoni G, De Manzoni G, Bresaola E, Viale G (2003) Independent value of fascin immunoreactivity for predicting lymph node metastases in typical and atypical pulmonary carcinoids. Lung Cancer–J IASLC 42:203–213
22. Portela-Gomes GM, Lukinius A, Grimelius L (2000) Synaptic vesicle protein 2, a new neuroendocrine cell marker. Am J Pathol 157:1299–1309
23. Portela-Gomes GM, Stridsberg M (2001) Selective processing of chromogranin A in the different islet cells in human pancreas. J Histochem Cytochem 49:483–490
24. Portela-Gomes GM, Stridsberg M (2002) Chromogranin A in the human gastrointestinal tract: an immunohistochemical study with region-specific antibodies. J Histochem Cytochem 50: 1487–1492
25. Portela-Gomes GM, Stridsberg M, Johansson H, Wilander E, Grimelius L (2001) Chromogranin A in human neuroendocrine tumors: an immunohistochemical study with region-specific antibodies. Am J Surg Pathol 25:1261–1267
26. Terris B, Scoazec JY, Rubbia L, Bregeaud L, Pepper MS, Ruszniewski P, Belghiti J, Flejou J, Degott C (1998) Expression of vascular endothelial growth factor in digestive neuroendocrine tumours. Histopathology 32:133–138
27. Travis WD, Brambilla E, Muller-Hermelink HK, Harris CC (2004) Pathology and genetics of tumours of the lung, pleura, thymus and heart. IARC Press, Lyon
28. Travis WD, Rush W, Flieder DB, Falk R, Fleming MV, Gal AA, Koss MN (1998) Survival analysis of 200 pulmonary neuroendocrine tumors with clarification of criteria for atypical carcinoid and its separation from typical carcinoid. Am J Surg Pathol 22:934–944
29. Varndell IM, Lloyd RV, Wilson BS, Polak JM (1985) Ultrastructural evidence of chromogranin: a potential marker for the electron microscopic recognition of endocrine secretory granules. Histochem J 17:981–992
30. Watanabe Y (2003) TNM classification for lung cancer. Ann Thorac Cardiovasc Surg 9:343–350
31. Weidner N, Folkman J, Pozza F, Bevilacqua P, Allred EN, Moore DH, Meli S, Gasparini G (1992) Tumor angiogenesis: a new significant and independent prognostic indicator in early-stage breast carcinoma. J Natl Cancer Inst 84:1875–1887

Virchows Arch (2005) 446: 613–618
DOI 10.1007/s00428-005-1237-z

ORIGINAL ARTICLE

Wahiba Sakly · Badreddine Sriha · Ibtissem Ghedira · Françoise Bienvenu · Abdelkarim Ayadi · Mohamed Tahar Sfar · Alain Lachaux · Sadok Korbi · Jacques Bienvenu · Nicole Fabien

Localization of tissue transglutaminase and N (epsilon)-(gamma) -glutamyl lysine in duodenal cucosa during the development of mucosal atrophy in coeliac disease

Received: 17 November 2004 / Accepted: 17 February 2005 / Published online: 13 May 2005
© Springer-Verlag 2005

Abstract Expression and transamidation activity of tissue transglutaminase (tTG) may be involved in the morphological modifications leading to the mucosal atrophy observed in coeliac disease (CD). We aimed to investigate the localization of tTG within the duodenal mucosa during the development of villous atrophy. The localization and level of expression of Nε-(γ-glutamyl) lysine isopeptides which could reflect the transamidation activity of tTG were also analyzed. tTG and Nε-(γ-glutamyl) lysine were localized using an immunohistochemical technique on duodenal biopsies obtained from 75 patients with CD and 51 subjects with normal mucosa (control group). The number of cases displaying tTG-expressing cells in the basement membrane and lamina propria was significantly higher in CD patients than in the control group. Moreover, the intensity of tTG staining in these areas was higher in CD. In contrast, the number of biopsies with tTG-expressing enterocytes was significantly lower in CD than in the control group. There was no difference in Nε-(γ-glutamyl) lysine between the two populations. Tissue transglutaminase was differently expressed in the various areas of the mucosa according to the stage of atrophy, whereas the localization and the intensity of the labelling of Nε-(γ-glutamyl) lysine isopeptides did not show any modification. The preferential localization in the basement membrane and lamina propria may reflect the involvement of tTG in the development of mucosal atrophy in CD.

Keywords Tissue transglutaminase · Nε-(γ-glutamyl) lysine isopeptide · Duodenal mucosal atrophy · Coeliac disease

W. Sakly · J. Bienvenu · N. Fabien
Department of Immunology,
Lyon-Sud Hospital,
Lyon, France

W. Sakly · I. Ghedira
Department of Immunology,
University of Pharmacy,
Monastir, Tunisia

B. Sriha · S. Korbi
Department of Anatomopathology,
CHU Farhat Hached,
Sousse, Tunisia

F. Bienvenu
Department of Immunology,
Debrousse Hospital,
Lyon, France

A. Ayadi · M. Tahar Sfar
Department of Pediatrics,
Tahar Sfar Hospital,
Mahdia, Tunisia

A. Lachaux
Department of Pediatrics,
Edouard Herriot Hospital,
Lyon, France

N. Fabien (✉)
UF d'Auto-Immunité,
Centre Hospitalier Lyon-Sud,
69495 Pierre-Benite Cedex, France
e-mail: nicole.fabien@chu-lyon.fr
Tel.: +33-47-8866681
Fax: +33-47-8569060

Introduction

Tissue transglutaminase (type II) (tTG) has been identified as the major target of autoantibodies described and used as specific biological markers of coeliac disease (CD) [6]. The biological and physiological roles of tTG have been clarified, demonstrating that this enzyme is involved in major biological processes such as programmed cell death or apoptosis, wound repair, tissue stabilization, extracellular matrix organization and tissue homeostasis [1, 8, 11, 14, 16, 21]. Tissue transglutaminase catalyzes the formation of a covalent bond between the γ carboxamide groups of protein-bound glutamine and the ε amino groups of lysine residues on the same or different protein chains [2]. This Nε-(γ-glutamyl) lysine isopeptide bond leads to the production of cross-linked insoluble polymeric cellular pro-

teins [13]. Among the different proteins, gliadin has been shown to be a good substrate for tTG-catalyzed cross-linking. In addition, tTG mediates gliadin deamidation, thus promoting better presentation of this protein by the antigen presenting cells to T lymphocytes [18, 20]. The immune response following this presentation causes, at the least, the mucosal atrophy characteristic of CD. At the present time, little is known of tTG expression and transamidation activity, which could play a role in the morphological modifications observed during the development of mucosal atrophy.

The aim of our study was to investigate the localization of tTG within the different areas of duodenal mucosa at different stages of the atrophy observed in CD. In addition, the localization and level of expression of Nε-(γ-glutamyl) lysine isopeptides which could reflect the transamidation activity of tTG [7] were also analyzed. This study was performed in a large cohort of patients with CD compared with a control population suffering mostly from persistent gastrointestinal symptoms but without CD.

Materials and methods

Patients

The study was carried out on 126 patients including 75 patients with CD and 51 control subjects with no mucosal atrophy. Biopsies of duodenal mucosa (two to three specimens from each patient) were collected from the Department of Anatomopathology (CHU Farhat Hached, Sousse, Tunisia) after the patients and the children's parents had given their informed consent. The study was approved by the Research and Ethics Committee of the CHU Farhat Hached. The diagnosis was based on clinical symptoms characteristic of CD and was confirmed by histology of duodenal biopsy. The group of 75 patients with untreated CD included 47 children (15 boys and 32 girls, mean age 6 years 7 months, age range 11 months to 16 years) and 28 adults (six men and 22 women, mean age 25 years 7 months, age range 17–54 years). The severity of mucosal atrophy was defined according to the histological classification of Marsh [22] slightly modified as grade 1 or isolated increase of intraepithelial lymphocytes (up to more than 60 intraepithelial lymphocytes per 100 epithelial cells) with normal appearing villi and crypts, grade 2 or partial atrophy (PVA), grade 3 or subtotal atrophy (STVA), and grade 4 or total atrophy (TVA). Histopathological examination of the duodenal mucosa of CD patients showed PVA in 16 cases and STVA to TVA (S/TVA) in 59 cases. CD patients displayed typical clinical symptoms in 30 cases, isolated digestive symptoms such as chronic diarrhoea and abdominal pain in 24 cases, growth deficiency in 13 cases and anaemia in eight cases. Forty-eight out of 50 patients with PVA or S/TVA tested for the presence of IgA anti-endomysium antibodies were found to be positive for these antibodies.

A control group was chosen among patients who underwent duodenal biopsies because they suffered from significant gastrointestinal symptoms or other clinical signs suggestive of CD. Fifty-one subjects were selected as non-CD controls. This control group included 16 children (ten boys and six girls, mean age 8 years 7 months, age range 1–16 years) and 35 adults (13 men and 22 women, mean age 41 years, age range 17–82 years). These patients suffered from isolated digestive signs (chronic diarrhoea, abdominal pain and malabsorption signs) in 37 cases, anaemia in 11 cases and growth deficiency in three cases. In this control group, 43 patients had a normal mucosa with no atrophy and no increase of intraepithelial lymphocytes. The final diagnosis was not clearly established for these patients but celiac disease was totally excluded because of the strictly normal duodenal mucosa and negative serology for the classical markers, e.g IgA anti-endomysium, antitransglutaminase and antigliadin antibodies. In eight patients, a measurable but slight increase of intraepithelial lymphocytes was classified by the anatomopathologists as Marsh 0 because the lymphocyte count was less than 60 per 100 epithelial cells. One patient had Crohn's disease, three had giardiasis and four had infectious duodenitis, but as none of these eight patients had CD, they were included in the control group.

Immunohistochemistry

Duodenal biopsy samples were fixed in formalin and embedded in paraffin. Sections of 3–4 μm were prepared on glass slides coated with poly-L-lysine (Dako, Carpenteria, USA) and were incubated with citric solution pH 6 for 6 min in a microwave. Endogenous peroxidase was blocked by 3% H_2O_2 for 5 min. After two washes with Tris buffer saline (TBS) pH 7.4, the sections were incubated with 100 μl of either a mouse monoclonal IgG antibody to tTG (Clone CUB 7402) (Dako) diluted 1/50 in TBS, or mouse monoclonal IgM antibody to N-ε(γ-glutamyl) lysine (81D4) (CovaLab, Lyon, France) diluted 1/200 [7] for 30 min in a humid chamber at room temperature. Slides were washed twice with TBS and then incubated with peroxidase-conjugated rabbit anti-mouse IgG diluted at 1/1000 or peroxidase-conjugated goat anti-mouse IgM diluted at 1/1000 (Biorad, Marnes La Coquette, France). The reaction was developed by incubation with the substrate solution consisting of liquid diaminobenzidine chromogen and buffered substrate (imidazole-HCl buffer pH 7.5; Dako). The slides were counterstained with haematoxylin and eosin solution and mounted with glycerin (Dako). As negative controls, isotypic control mouse IgG (Becton Dickinson, San Jose, Calif., USA) and mouse IgM (Dako) were used instead of the primary antibody. The specificity of the antibody to N-ε(γ-glutamyl) lysine (81D4) for the N-ε(γ-glutamyl) lysine isopeptide was assessed in a previous work [23]. The presence or absence of tTG and N-ε(γ-glutamyl) lysine were analysed in the different areas of the mucosa, e.g enterocytes (cytoplasm and brush border), basement membrane, lamina propria and muscularis mucosa. A semiquantitative approach was used for the enterocytes with two ranges zero and positive when up to 10%

of these epithelial cells were positive. The number of positive cases for each area within the two groups of patients was thus determined. In parallel, the intensity of the staining in each area was evaluated by the investigator and classified as weak, moderate, or strong. To confirm the specificity of CUB 7402, following the manufacturer's instructions cryostat sections of breast carcinoma were used as positive controls; CUB 7402 stained the cytoplasm of the endothelial cells and the membrane of the tumoral cells that expressed a high level of tTG (data not shown).

Statistical analysis

Fisher's test was used to analyze the statistical significance of the number of duodenal biopsies displaying tTG-expressing areas in CD patients compared with the control group. A P-value <0.05 was considered as statistically significant.

Results

Localization of tTG within the mucosal duodenal sections

The expression of tTG was analyzed within the different histological areas of the duodenum, e.g enterocytes (cytoplasm and brush border), basement membrane, lamina propria and muscularis mucosa. The percentages of the different areas expressing the enzyme are summarized in Table 1 and representative immunohistochemical staining patterns is shown in Fig. 1.

The enzyme was localized with a moderate intensity within the cytoplasm of enterocytes in 54 out of 75 CD patients and in 47 out of 51 control patients (P=0.006) (Table 1, Fig. 1). Within the brush border, seven out of 75 CD and six out of 51 control patients expressed tTG with a weaker intensity in the control group.

The number of cases displaying tTG within the basement membrane was significantly higher in CD patients than in the control group (44/75 versus 20/51; P=0.045) (Table 1). In addition, tTG labelling was stronger in this area in CD mucosa than in control mucosa (Fig. 1). Isolated staining of the basement membrane was observed in ten cases whereas 34 cases showed staining both in the basement membrane and in the lamina propria.

In the lamina propria, tTG was expressed in 47 out of 75 CD and in four out of 51 control patients (P<0.0001) (Table 1). The precise localization was within some mononuclear cells expressing CD68 characteristic of the macrophage phenotype (data not shown). tTG-staining in this area was also stronger in the CD population than in the control population (Fig. 1).

Strong tTG staining was observed within the muscularis mucosa in all CD and all control patients.

In the control group, the number of cases expressing the enzyme in the different areas of the mucosa and the intensity of staining did not differ between patients who did and those who did not have increased intraepithelial lymphocytes.

Each of the biopsy specimens taken from a single patient showed the same pattern of staining in the different histological areas.

Relationship between the localization of tTG, the degree of atrophy and clinical symptoms

The results are summarized in Table 1. The number of cases with tTG-expressing enterocytes was significantly higher in the control group than in CD patients with either PVA (P=0.009) or S/TVA mucosa (P=0.022). Within the CD group, there was no statistically significant difference in the number of cases displaying weak staining between PVA (6/10) and S/TVA (26/44). Regarding the clinical data, the patients with S/TVA displayed typical clinical symptoms in 15 cases, chronic diarrhoea in eight cases, growth deficiency in one case and anaemia in two cases, whereas patients with PVA displayed typical clinical symptoms in two cases, growth deficiency in three cases and anaemia in one case.

The number of cases expressing tTG within the basement membrane was significantly higher in patients with S/TVA mucosa (37/59) in comparison with patients with normal mucosa (20/51) (P=0.021), whereas there was no statistically significant difference between patients with PVA (7/16) and normal controls (20/51). Concerning clin-

Table 1 Association of the histological area expressing tTG with the degree of atrophy of the duodenal mucosa. Grade of atrophy was determined according to Marsh's histological criteria (1990). *PVA* partial villous atrophy; *S/TVA* subtotal to total villous atrophy

	CD patients			Control group
	Villous atrophy	Stage of villous atrophy		Normal mucosa
	PVA+S/TVA n=75	PVA n=16	S/TVA n=59	n=51
Enterocytes				
Cytoplasm	54 (72%)	10 (63%)	44 (75%)	47*[(a)]**[(b)](92%)
Brush border	7 (9%)	4 (25%)	3 (5%)	6 (12%)
Basement membrane	44 (59%)	7 (44%)	37* (63%)	20 (39%)
Lamina propria	47*** (63%)	10*** (63%)	37*** (63%)	4 (8%)

P-values were shown; P-values less than 0.05 were regarded as statistically significant. *P<0.05; **P<0.01; ***P<0.0001; (a, b) Comparison between the stage of villous atrophy (a: PVA, b: S/TVA) and the normal mucosa

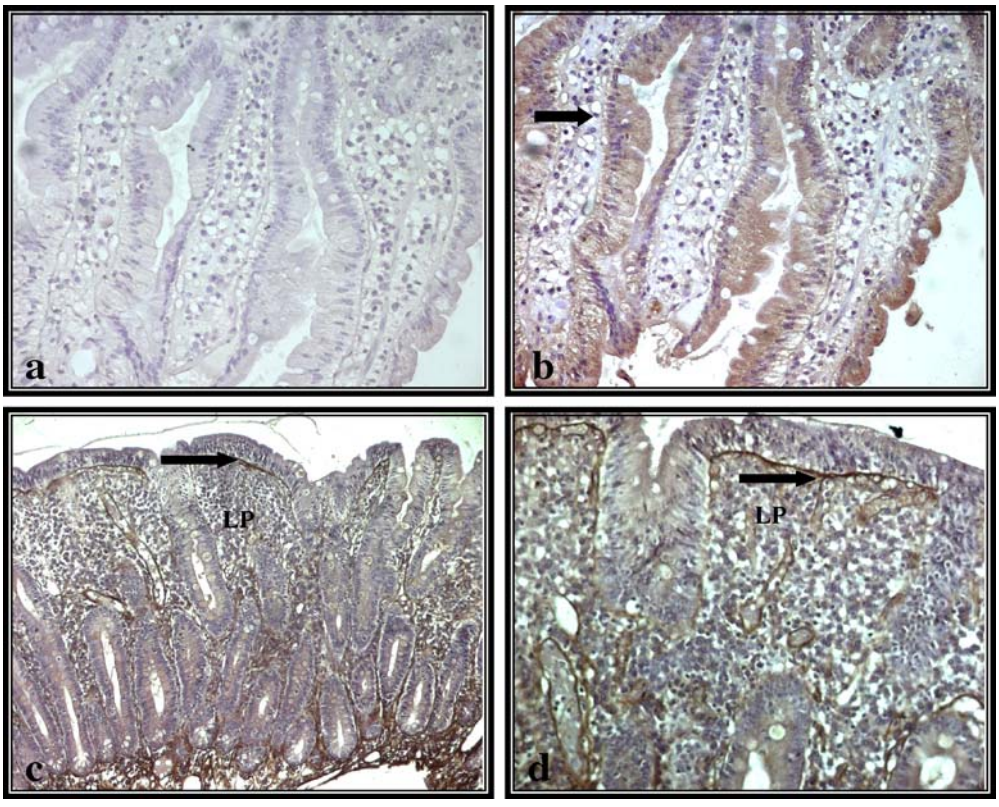

Fig. 1 Immunohistochemical analysis of tTG protein expression. **a**, **b** Normal duodenal biopsy specimen from a control subject. **a** negative control using an isotypic control mouse IgG. **b** tTG was detected using mouse monoclonal IgG antibody to tTG (clone CUB 7402) and was expressed in the enterocytes (*arrow*). **c**, **d** Subtotal villous atrophy of a duodenal biopsy specimen from a patient with untreated coeliac disease: tTG was localized within the basement membrane (*arrow*) and the lamina propria (*LP*) (magnification **a**, **b** ×20, **c** ×10 and **d** ×40)

ical data, patients with S/TVA had typical clinical symptoms in 14 cases, chronic diarrhoea in 16 cases, growth deficiency in five cases and anaemia in two cases, while patients with PVA had typical clinical symptoms in three cases, chronic diarrhoea in one case, growth deficiency in two cases and anaemia in one case. In the group with

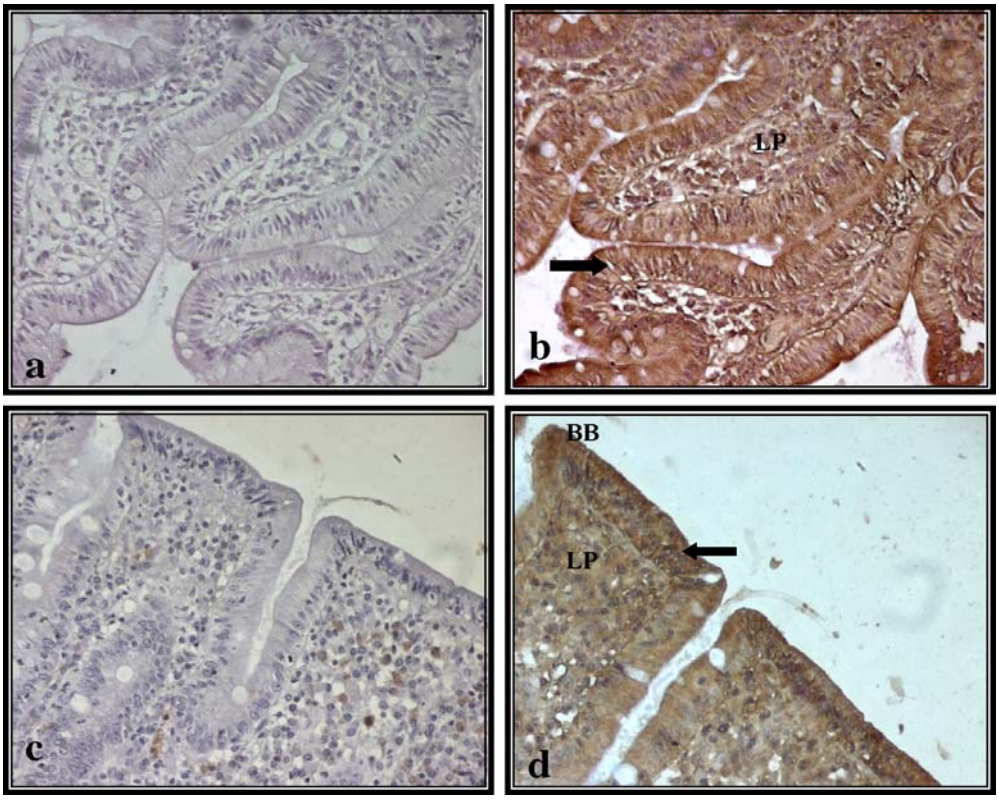

Fig. 2 Immunohistochemical analysis of Nε -(γ-glutamyl) lysine expression. **a**, **b** Normal duodenal biopsy specimen from a control subject. **a** negative control using an isotypic control mouse IgM. **b** the Nε-(γ-glutamyl) lysine detected using mouse monoclonal IgM antibody to N-ε(γ-glutamyl) lysine was localized in the brush border and cytoplasm of enterocytes (arrow), within the basement membrane and in the lamina propria (*LP*). **c**, **d** Subtotal villous atrophy of duodenal biopsy specimen from a patient with untreated coeliac disease. **c** Negative control using an isotypic control mouse IgM. **d** Nε-(γ-glutamyl) lysine was observed in the brush border and cytoplasm of enterocytes (arrow), within the basement membrane and in the LP Nε-(γ-glutamyl) lysine staining was more intense at the brush border (*BB*). Magnification: **a**, **b**, **c** and **d**: ×40

normal mucosa, the cases displaying tTG expression in the basement membrane were obtained from patients with digestive signs (nine patients with chronic diarrhoea and six patients with abdominal pain), isolated anaemia (four patients) or growth deficiency (one patient).

The number of cases displaying tTG expression in the lamina propria did not significantly differ between patients with S/TVA and patients with PVA. In normal mucosa, tTG was expressed in the lamina propria in only four cases, of whom three had digestive signs (one patient with chronic diarrhoea, two patients with abdominal pain) and one patient had growth deficiency.

There was no difference in the expression of tTG between adults and children.

Localization of Nε-(γ-glutamyl)lysine isopeptides within the mucosal duodenal sections

In all the duodenal biopsies, the Nε-(γ-glutamyl) lysine isopeptides were localized within the enterocytes (cytoplasm and brush border), lamina propria, and muscularis mucosa. Staining was stronger at the brush border than in the other areas but was similar between the CD and the control non-CD group (Fig. 2).

Discussion

Tissue transglutaminase, which is the major target antigen of specific autoantibodies in CD [6], may play a role in the pathogenesis of this intestinal disease. In the present study, we examined the localization and expression of this enzyme and of its substrate, the Nε-(γ-glutamyl) lysine isopeptides produced by the action of transglutaminase activity or transamidation activity [7]. This analysis was performed in the duodenal mucosa of a large cohort of CD patients with various stages of atrophy, as well as in non-CD patients with normal mucosa. In addition, we compared the localization of the enzyme with clinical parameters observed in CD and non-CD patients.

We found that the localization of tTG was modified during the development of duodenal mucosa atrophy. The enzyme was preferentially localized within the basement membrane and within the lamina propria in CD patients, compared with the non-CD control patients displaying normal mucosa. The expression of tTG within specific areas suggests that the enzyme could be translocated from the intracellular to the pericellular environment or could be synthesized by cells in the lamina propria such as macrophages. The externalization of tTG in the extracellular matrix has already been demonstrated [14]. The enzyme may be released as a result of increased intestinal gliadin permeability and tTG may be concentrated in the lamina propria and within the basement membrane to reinforce the deamidation of the toxic fraction of gliadin. Furthermore, it has been demonstrated that there is a significant increase of tTG mRNA and of its enzymatic activity, particularly in the subepithelial region of the lamina propria; tTG activity correlates well with the pattern of tTG protein expression [10]. In CD, it has been shown that tTG forms complexes with gliadin peptides within the duodenal mucosa in the extracellular matrix of the lamina propria and in the basement membrane [17]. The formation of these complexes may explain induction of tTG synthesis in such areas. In addition, redistribution of tTG to the extracellular matrix has also been demonstrated, a mechanism which may be involved in tissue stabilization following insult or inflammation [19]. The tTG expression within some specific areas could serve as an early indicator of the severity of mucosal atrophy. Expression of tTG staining within the basement membrane was in fact significantly associated with S/TVA mucosa, whereas there was no difference between PVA and normal mucosa. We then analyzed the relationship between clinical parameters and tTG expression within specific areas, and we showed that expression of the enzyme in these areas was not associated with a specific clinical sign such as digestive signs, anaemia or growth deficiency.

Our findings correlate with previous studies, especially concerning the localization of tTG in the basement membrane and lamina propria [4, 5, 9, 10, 15, 17]. We also found that the localization of tTG was more marked in the lamina propria than in the epithelium [4, 24]. However, other authors found an increased expression of tTG in enterocytes in CD mucosa compared with healthy mucosa [5, 10, 15]. Results were also discrepant for brush border localization, as we found similarity between the two groups, unlike previous studies which showed that tTG staining was more intense within the brush border in CD patients than in normal controls [5, 10]. These discrepancies are probably due to high heterogeneity in extracellular tTG expression within the duodenal biopsies. Localization in the muscularis mucosa was identical in the two groups, demonstrating that the enzyme is not modified in this area during the development of mucosal atrophy.

Our data indicate that increase and/or changes in localization and intensity of expression are a specific phenomenon which distinguishes the control group from the coeliac group. In addition, there was no difference within the control group between patients with and those without an increase of intraepithelial lymphocytes. A previous study comparing various intestinal inflammatory diseases displaying the same duodenal atrophy, such as some cases of Crohn's disease, suggested that these changes may be non-specific [10]. However, this previous study included only one patient with this disease; a larger population should be analyzed to strengthen this hypothesis.

The different localizations of tTG may occur in parallel with a modification of its enzymatic activity. tTG mediated gluten deamidation is more important than cross-linking of extracellular matrix proteins with respect to tissue injury [12]; an increase of tTG activity in gliadin deamidation has been reported in CD mucosa [3, 5, 17]. As a consequence this increased deamidation could inhibit transamidation. Transamidation is fundamental for protein cross-linking and maintenance of the integrity of the basement membrane [1] and its decrease could explain a defect in extra-

cellular matrix organization of the basement membrane that may be implicated in the mechanism of mucosal atrophy. However, in our study the localization and level of expression of Nε-(γ-glutamyl) lysine isopeptides were similar in the two populations of CD and non-CD patients. Thus, the cross-linking activity or transamidation function of tTG seems not to be modified during the development of CD.

In conclusion, our data demonstrate that the localization of tTG is modified, with preferential expression in the basement membrane and in the lamina propria of the mucosa during the development of duodenal atrophy whereas the localization and intensity of staining of the Nε-(γ-glutamyl) lysine isopeptide are not modified. These results may be important in clarifying the role(s) of tTG in CD.

Acknowledgements The authors thank Mr. El Alaoui (CovaLab, Lyon, France) for the gift of the mouse monoclonal IgM antibody to N-ε(γ-glutamyl) lysine and Mrs. Paola Damaso for secretarial assistance. This study was supported in part by the Hospices Civils de Lyon and the CMCU (Comité Mixte Franco-Tunisien pour la Coopération Universitaire). The experiments comply with the current laws of our countries.

References

1. Aeschlimann D, Thomazy V (2000) Protein crosslinking in assembly and remodelling of extracellular matrices: the role of transglutaminases. Connect Tissue Res 41:1–27
2. Birckbichler PJ, Dowben RM, Matacic S, Loewy AG (1973) Isopeptide bonds in membrane proteins from eukaryotic cells. Biochim Biophys Acta 291:149–155
3. Bruce SE, Bjarnason I, Peters TJ (1985) Human jejunal transglutaminase: demonstration of activity enzyme kinetics and substrate specificity with special relation to gliadin and celiac disease. Clin Sci 68:573–579
4. Brusco G, Muzi P, Ciccocioppo R, Biagi F, Cifone MG, Corazza GR (1999) Transglutaminase and coeliac disease: endomysial reactivity and small bowel expression. Clin Exp Immunol 118:371–375
5. Ciccocioppo R, Di Sabatino A, Ara C, Biagi F, Perilli M, Amicosante G, Cifone MG, Corazza GR (2003) Gliadin and tissue transglutaminase complexes in normal and coeliac duodenal mucosa. Clin Exp Immunol 134:516–524
6. Dieterich W, Ehnis T, Bauer M, Donner P, Volta I (1997) Identification of tissue transglutaminase as the auto-antigen of celiac disease. Nat Med 3:797–803
7. El Alaoui S, Legastelois S, Roch AM, Chantepie J, Quash G (1991) Transglutaminase activity and N epsilon (gamma glutamyl) lysine isopeptide levels during cell growth: an enzymatic and immunological study. Int J Cancer 48:221–226
8. El Alaoui S, Mian S, Lawry J, Quash G, Griffin M (1992) Cell cycle kinetics, tissue transglutaminase and programmed cell death (apoptosis). FEBS Lett 311:174–178
9. Ehrmann J, Kolek A, Kod'ousek R, Zapletalova J, Lisova S, Murray PG, Drabek J, Kolar Z (2003) Immunohistochemical study of the apoptotic mechanisms in the intestinal mucosa during children's coeliac disease. Virchows Arch 442:453–461
10. Esposito C, Paparo F, Caputo I, Porta R, Salvati VM, Mazzarella G, Auricchio S, Troncone R (2003) Expression and enzymatic activity of small intestinal tissue transglutaminase in celiac disease. Am J Gastroenterol 98:1813–1820
11. Fesus L, Thomazy V, Falus A (1987) Induction and activation of tissue transglutaminase during programmed cell death. FEBS Lett 224:104–108
12. Fleckenstein B, Molberg O, Qiao SW, Schmid DG, Von der Mulbe F, Elgstoen K, Jung G, Sollid LM (2002) Gliadin T cell epitope selection by tissue transglutaminase in celiac disease. Role of enzyme specificity and pH influence on the transamidation versus deamidation process. J Biol Chem 277:34109–34116
13. Folk JE, Finlayson JS (1977) The ε-(γ-glutamyl) lysine crosslink and the catalytic role of transglutaminases. Adv Protein Chem 31:1–133
14. Gaudry CA, Verderio E, Jones RA, Smith C, Griffin M (1999) Tissue transglutaminase is an important player at the surface of human endothelial cells: evidence for its externalization and its colocalization with the beta (1) integrin. Exp Cell Res 252:104–113
15. Hansson T, Ulfgren AK, Lindroos E, DannAEus A, Dahlbom I, Klareskog L (2002) Transforming growth factor-;β (TGF-β) and tissue transglutaminase expression in the small intestine in children with coeliac disease. Scand J Immunol 56:530–537
16. Melino G, Piacentini M (1998) Tissue transglutaminase in cell death: a downstream or a multifunctional upstream effector? FEBS Lett 430:59–63
17. Molberg O, McAdam S, Körner R, Quarsten H, Kristiansen C, Madsen L, Fugger L, Scott H, Noren O, Roepstorff P, Lundin KE, Sjöström H, Sollid LM (1998) Tissue transglutaminase selectively modifies gliadin peptides that are recognized by gut-derived T cells in celiac disease. Nat Med 4:713–717
18. Molberg O, McAdam, S, Lundin KE, Kristiansen C, Arentz-Hansen H, Kett K, Sollid LM (2001) T cells from coeliac disease lesions recognise gliadin epitopes deamidated in situ by endogenous tissue transglutaminase. Eur J Immunol 31:1317–1323
19. Nicholas B, Smethurst P, Verderio E, Jones R, Griffin M (2003) Cross-linking of cellular proteins by tissue transglutaminase during necrotic cell death: a mechanism for maintaining tissue integrity. Biochem J 371:413–422
20. Novak P, Man P, Tuckova L, Tlaskalova-Hogenova H, Bezouska K, Havlicek V (2002) Monitoring of in vitro deamidation of gliadin peptic fragment by mass spectrometry may reflect one of the molecular mechanisms taking place in coeliac disease development. J Mass Spectrom 37:507–511
21. Oliverio S, Amendela A, Rodolfo C, Spinedi A, Pacentini M (1999) Inhibition of tissue transglutaminase increases cell survival by preventing apoptosis. J Biol Chem 274:34123–34128
22. Revised criteria for diagnosis of coeliac disease (1990) Report of Working Group of European Society of Pediatric Gastroenterology and Nutrition. Arch Dis Child 65:909–911
23. Thomas V, Fournet G, Simonet F, Roch AM, Ceylan I, El Alaouia S, Quash G (2004) Definition of the fine specificity of the monoclonal antibody 81D4: its reactivity with lysine and polyamine isopeptide cross-links. J Immunol Methods 292:83–95
24. Thomazy V, Fesus L (1989) Differential expression of tissue transglutaminase in human cells. An immunohistochemical study. Cell Tissue Res 255:215–224

Virchows Arch (2005) 446: 619–625
DOI 10.1007/s00428-005-1238-y

ORIGINAL ARTICLE

Klaus Kapelari · Martin Fruehwirth · Andreas Heitger · Alfred Königsrainer · Raimund Margreiter · Burkhard Simma · Felix Albert Offner

Loss of intrahepatic bile ducts: an important feature of familial hemophagocytic lymphohistiocytosis

Received: 28 October 2004 / Accepted: 18 February 2005 / Published online: 20 May 2005
© Springer-Verlag 2005

Abstract Familial hemophagocytic lymphohistiocytosis (FHL) is a rare, fatal disorder of early infancy. We report two siblings with FHL whose symptoms were dominated by hepatic failure. Both presented with sudden-onset fever and hepatosplenomegaly with progressive abnormalities of clinical biochemistry indices of liver function. One died of hepatorenal failure. The other underwent liver transplantation. Autopsy and explant liver displayed portal and periportal infiltrates of T lymphocytes and histiocytes; an activation of the hepatic mononuclear phagocytic system with focal hemophagocytosis; and almost complete loss of interlobular bile ducts. Paucity of bile ducts dominated in a pre-transplant liver biopsy specimen (and transiently obscured the diagnosis of FHL). Disease recurred in the allograft, again with lymphohistiocytic infiltration and destruction of interlobular bile ducts. Consequently the patient underwent haploidentical peripheral stem cell transplantation. This patient is alive 5 years later. Loss of bile ducts may be an important feature of hepatic involvement by FHL.

Keywords FHL · Hepatic failure · Loss of bile ducts

K. Kapelari · M. Fruehwirth
Department of Pediatrics,
Medical University Innsbruck,
Innsbruck, Austria

A. Heitger
St. Anna Children's Hospital,
Vienna, Austria

A. Königsrainer · R. Margreiter
Department of Transplant Surgery,
Medical University Innsbruck,
Innsbruck, Austria

B. Simma
Department of Pediatrics,
Academic Teaching Hospital,
Feldkirch, Austria

F. A. Offner (✉)
Department of Pathology,
LKH Feldkirch-Academic Teaching Hospital
of the Medical University Innsbruck,
Carinagasse 47,
6800 Feldkirch, Austria
e-mail: felix.offner@lkhf.at
Tel.: +43-5522-3033400
Fax: +43-5522-3037521

Introduction

Hemophagocytic lymphohistiocytosis (HLH), a rare life-threatening hematological disorder characterized by an excessive infiltration of vital organs by T lymphocytes and histiocytes [4, 5], has two variants. One is primary and is genetically determined. The other is a secondary, or acquired, hemophagocytic syndrome, occurring in association with infections, malignancies, or immune disorders. Familial hemophagocytic lymphohistiocytosis (FHL), an inherited autosomal-recessive form of HLH, is invariably fatal without early diagnosis and bone marrow transplantation [8, 13]. It may occur in consanguineous families or be sporadic [4]. FHL is genetically heterogenous and may result from mutations in *PRF1*, the gene encoding perforin, mutations in *UnC13D*, the gene encoding the lytic granule priming factor hMunc13-4 or other yet unidentified genetic alterations [1, 3, 7, 15, 21]. Failure to find mutations does not exclude FHL. Various studies suggest that impaired cytotoxicity and defective triggering of apoptosis underlie FHL and that its symptoms are mediated by a proinflammatory hypercytokinemia [2, 6, 9, 10, 17]. As FHL is frequently triggered by infections, distinction between genetically determined and environmental types of HLH may be exceedingly difficult and sometimes impossible [22]. This may result in delayed or even inappropriate bone marrow transplantation. Children with FHL are usually profoundly ill at presentation. Characteristic symptoms include fever, hepatosplenomegaly, pancytopenia, and abnormalities of neurological function and coagulation. In severe cases, hepatic dysfunction may so dominate that liver biopsy is undertaken, frequently without considering

FHL. Correct interpretation of the microscopic liver abnormalities then may be essential to diagnosis [5, 18]. Loss of intrahepatic bile ducts is not a reported feature of FHL [5, 11, 12, 19]. We describe two siblings with FHL who presented with acute liver failure and in whom bile duct injury was prominent.

Case reports

Sibling 1

A 5-week-old girl was first seen in a peripheral hospital because of slow weight gain and persistent diarrhea. The brother of the patient had died as a neonate in a peripheral hospital (see below). There was metabolic acidosis, but values for ammonia, lactate, pyruvate, amino acids, and organic acids were within normal ranges. Lactose intolerance was diagnosed and a lactose-free diet was prescribed. She was discharged from the hospital despite persistent metabolic acidosis. Two months later she was again hospitalized for fever, recurrent abdominal pain, massive abdominal distension, bloody diarrhea, and marked weight loss. Clinical investigation revealed severe hepatosplenomegaly and features compatible with septicemia. Clinical biochemistry values suggested liver dysfunction. Coagulation studies were abnormal and the CRP (3.0 mg/dl) was elevated.

The girl was referred to the Intensive Care Unit of the Department of Pediatrics at the University Hospital of Innsbruck with severe hepatic dysfunction and suspected metabolic disease. Initial laboratory investigations showed severe neutropenia, lymphocytosis, thrombocytopenia, and various abnormalities suggestive of hepatic dysfunction, with hyperferritinemia (2982 μg/l) and hyperlipidemia (Table 1). Two days later the hemoglobin concentration and platelet count dropped (11.8 to 9.7 g/dl and 97 to 55×10^9/l, respectively). Repeated serologic screening found no evidence of viral hepatitis (hepatitis viruses A, B, C, D, and E; CMV; EBV; HSV; VZV; adenovirus; coxsackieviruses), no seroconversion or rise of antibodies suggestive for early acute phase infection, and no autoantibodies. Values for IgG, IgA and IgM were normal and there was no eosinophilia. Usual inborn errors of metabolism were excluded by extensive laboratory studies. The girl developed hepatorenal syndrome requiring peritoneal dialysis. Examination of a bone marrow aspirate, performed to evaluate severe cytopenia, showed hypocellularity with rare phagocytosing histiocytes, interpreted as consistent with parenteral nutrition and sepsis. Liver biopsy (Fig. 1; age 14 weeks) found severe cholestasis and a marked reduction of interlobular bile ducts, without hemophagocytosis. Fourteen days later, the patient developed acute hepatic failure (Table 1). Emergency liver transplantation was performed on day 25, using the mother's left lateral liver segments. Immunosuppression was started with methylprednisolone, azathioprine, and FK 506 (peak concentration 10.9 μg/l) immediately and was reduced to methylprednisolone and low-dose FK 506 on post-transplant day 8 due to severe leucopenia. Microscopy of the explanted liver and portal lymph nodes (Figs. 2 and 3) led to the diagnosis of FHL (see below). Chemotherapy with etoposide and dexamethasone (HLH 94 protocol) was started immediately [8]. However, despite chemotherapy, immunosuppression, and partial clinical remission, recurrence of the disease in the donor organ was diagnosed 16 days after transplantation (Fig. 4). This diagnosis was also supported by the laboratory findings of adequate immunosuppression (FK506 peak concentration of 6.9 μg/l) as well as hyperlipidemia (261 mg/dL), hyperferritinemia (3080 μg/l), and cytopenia

Table 1 Laboratory test results of proposita

	Admission	Day 25 (1 day before liver transplantation)	Day 41 (16 days after liver transplantation)	Normal range
Leucocytes	5.1×10^9/l	1.5×10^9/l	2.8×10^9/l	5.5–18.0
Segmented neutrophiles	8.5%	3.0%	61.5%	10–52
Lymphocytes	85%	89.5%	25.5%	39–72
Platelets	97×10^9/l	30×10^9/l	49×10^9/l	140–400
Aspartate aminotransferase (AST)	168 IU/l	240 IU/l	24 IU/l	9–26
Alanine aminotransferase (ALT)	692 IU/l	58 IU/l	25 IU/l	2–28
Alkaline phosphatase	298 IU/l	64 U/l	405 IU/l	170–460
Bilirubin, total	85.8 μmol/l	199.4 μmol/l	213.2 μmol/l	3.4–17
Bilirtubin, conjugated	84.1 μmol/l	192.7 μmol/l	200.9 μmol/l	0–3.4
Gamma-glutamyltranspeptidase (γGT)	285 IU/l	43 IU/l	94 IU/l	8–90
Cholinesterase (CHE)	2.39 kIU/l	2.14 kIU/l	2.83 kIU/l	3.5–8.5
Ammonia	53 μmol/l	48 μmol/l	n.d.	<48
Lactate dehydrogenase (LDH)	2,124 IU/l	671 IU/l	204 IU/l	200–495
Fibrinogen	93 mg/dl	<20 mg/dl	72 mg/dl	190–380
Ferritin	2982 μg/l	n.d.	3080 μg/l	6–340
Triglycerides	149 mg/dl	227 mg/dl	261 mg/dl	27–125

n.d.: not determined

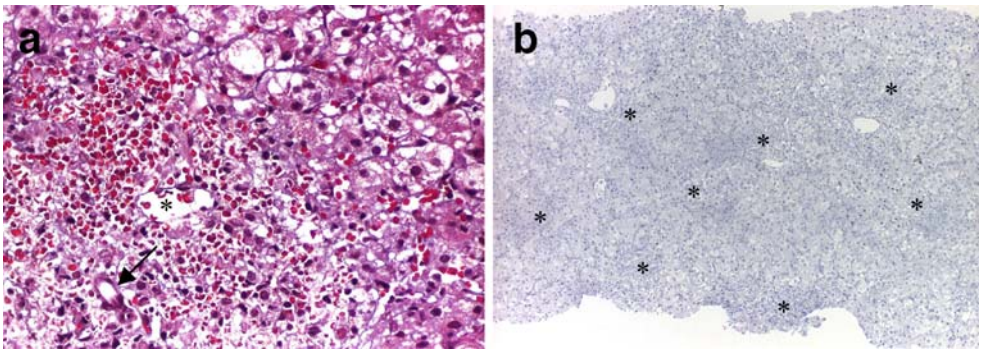

Fig. 1 Liver biopsy, proposita, 14 days before liver transplantation (**a**) Marked swelling of hepatocytes; cholestasis; and a mild to moderate infiltration of portal tracts by mononuclear cells. Note portal extravasation of erythrocytes. Hepatic arteriole (*arrow*), portal venule (*asterisk*) (Masson's trichrome, ×400). (**b**) Striking and complete loss of bile ducts, without even remnants of bile duct epithelium demonstrable in any of 16 portal tracts (*asterisks*) (anti-cytokeratin 7/hematoxylin, ×100)

at the time of allograft biopsy. In an attempt to cure the underlying disease, haploidentical peripheral stem cell transplantation from the patient's mother was performed 74 days after liver transplantation. The conditioning regimen consisted of busulfan, thiotepa, cyclophosphamide, and rabbit anti-thymocyte globulin. The second rationale of this approach was to induce allograft tolerance. Forty-three days after peripheral stem cell transplantation, microscopy of an allograft liver biopsy specimen showed no evidence of hemophagocytosis or rejection (data not shown). As reported elsewhere, 6 months after liver transplantation immunosuppressive therapyC could be stopped [13]. The patient is alive and well (August, 2004) 5 years after stem cell transplantation. Molecular analyses excluded a mutation of the *PRF1* gene, but have so far not revealed any other gene mutation (Dr. Janka, Department of Hematology and Oncology, Children's Hospital, University of Hamburg; personal communication).

Sibling 2

The older brother of the proposita had died as a neonate in a peripheral hospital. He was born vaginally one year before the proposita at a gestational age of 39 weeks and 5 days. His birth weight was 3300 *g*. The amniotic fluid was green; the genitourinary tract of the mother was colonized by group B streptococcus. On the 5th postnatal day the newborn exhibited features of sepsis, with disseminated intravascular coagulation and paralytic ileus. Laboratory investigation revealed thrombocytopenia ($50\times10^3/\mu l$), mild anemia (Hb 13.8 g/dl), and leucopenia. Clinical-biochemistry studies suggested slight hepatic dysfunction. Necrotizing enterocolitis was suspected, and laparotomy with enterocutaneous diversion was performed. After surgery, the patient developed acute hepatorenal failure. Death aged 9 days was ascribed to septic shock. Autopsy diagnoses included pneumonia, treatment-refractory septic shock,

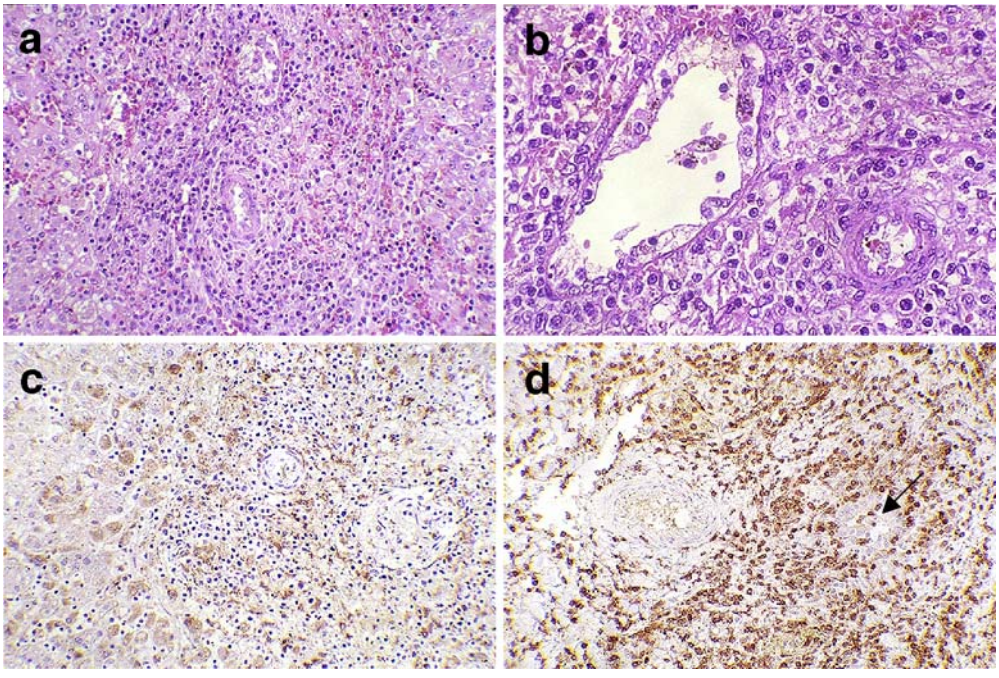

Fig. 2 Explanted liver, proposita. (**a**) Heavy portal and periportal infiltration by mononuclear inflammatory cells (HE, ×200). (**b**) Marked swelling of the endothelial cells, with lymphocytic endotheliitis (HE, ×400). (**c**) Activated von Kupffer cells and histiocytic infiltration of portal tracts (anti-CD68/hematoxylin, ×200). (**d**) The infiltrate was dominated by T lymphocytes. Residual bile ducts of intermediate size were severely damaged (*arrow*) by T cells (anti-CD3/hematoxylin, ×200)

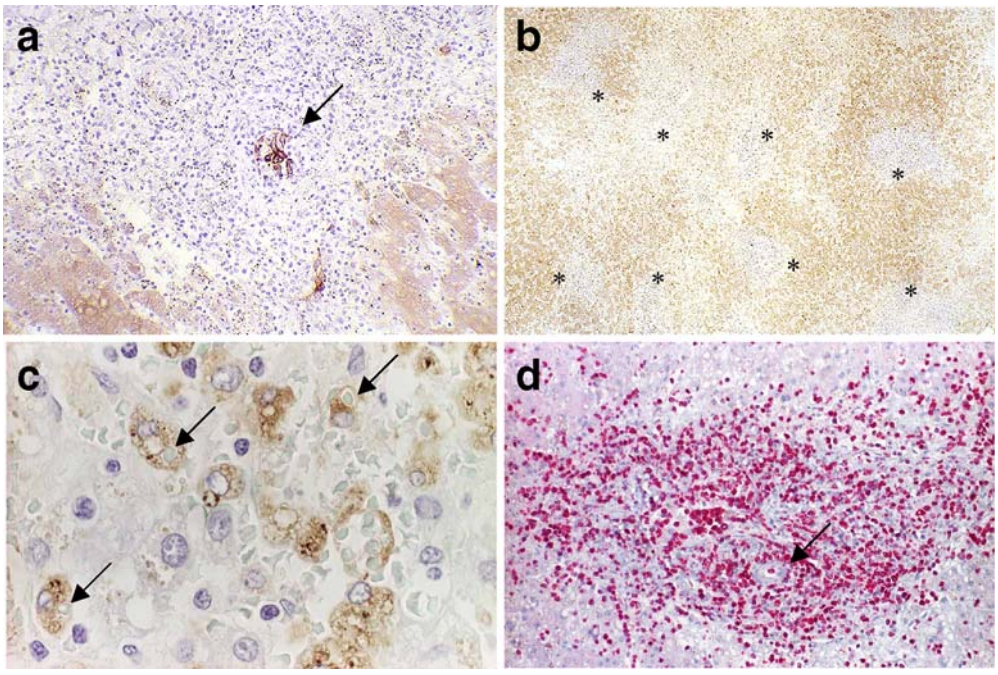

Fig. 3 Explanted liver, proposita. (**a**) One of the few remaining larger bile ducts (arrow) overrun by T lymphocytes (anti-cytokeratin 7/hematoxylin, ×100). (**b**) Overview demonstrating the widespread loss of interlobular bile ducts. Asterisks mark portal tracts. Immunohistochemical marking with anti-cytokeratin 7 highlights disappearance of bile ducts and lack of ductular proliferation (anti-cytokeratin 7/hematoxylin, ×40). (**c**) Hemophagocytosis was focally detected in von Kupffer cells and portal histiocytes; note CD68-expressing von Kupffer cells with ingested pale erythrocytes (*arrows*). (anti-CD68/hematoxylin, ×1000). (**d**) Strong expression of perforin by T cells infiltrating the portal tracts. Portal arteriole (*arrow*) (anti-perforin/hematoxylin, ×200)

and hepatitis of unknown cause. Review found hepatic abnormalities identical to those in the proposita, (Fig. 5).

Materials and methods

All specimens were fixed in 10% formalin, dehydrated through graded alcohols to xylene, and embedded in paraffin. Sections were stained with hematoxylin and eosin, Masson's trichrome, Gömöri, diastase-PAS, Perl's iron stain, orcein, and rhodanine. Antibodies used for immunological analyses are listed in Table 2.

Results

Proposita—native liver

The pre-transplant liver biopsy (Fig. 1a and b) showed a moderate ballooning of liver cells, focal necrosis of centrilobular hepatocytes, and pronounced intracanalicular cholestasis. Von Kupffer cells appeared hyperplastic and activated. Hemophagocytosis could not be demonstrated. The portal tracts revealed only mild mononuclear-cell infiltration by CD3-expressing T lymphocytes and a few CD68-expressing histiocytes. Substantial extravasation of

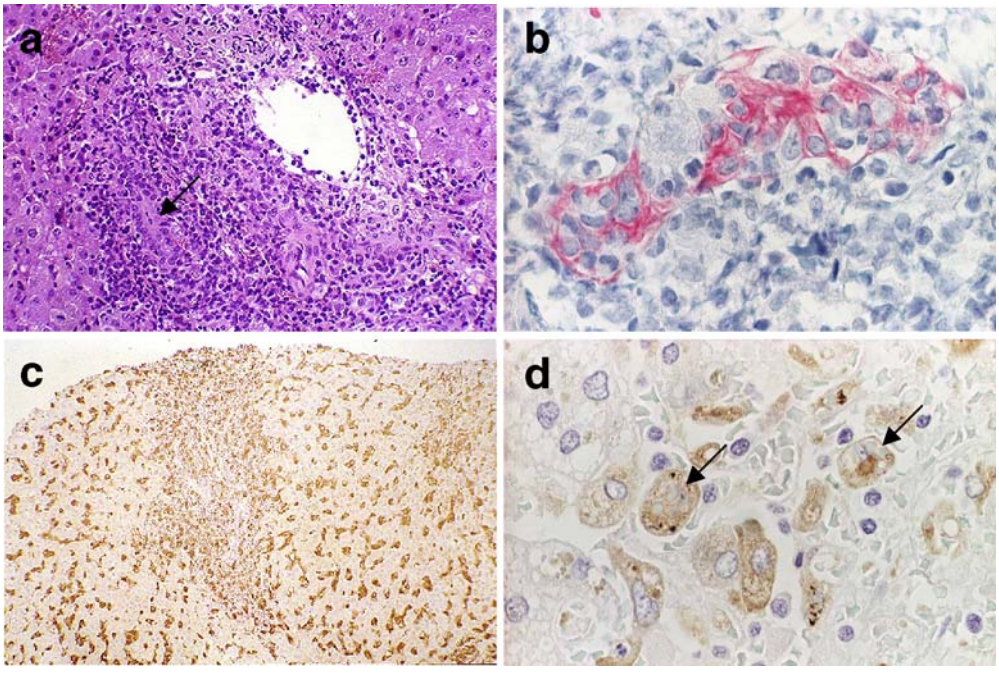

Fig. 4 Recurrent FHL in allograft liver, proposita. (**a**) Pronounced infiltration of portal tracts by T lymphocytes and histiocytes and swelling of the venous endothelium with undermining by T cells. Bile ducts were reduced in number and focally damaged severely by T lymphocytes (arrow) (HE, ×200). (**b**) Interlobular bile duct remnant marked with anti-cytokeratin 7 (anti-cytokeratin 7/hematoxylin, ×1000). (**c**) Marked activation of von Kupffer cells and infiltration of portal tracts by histiocytes (anti-CD68/hematoxylin, ×100). (**d**) Immunostaining for CD68 assisted in detecting focal hemophagocytosis and diagnosing recurrent FHL. Note ingested erythrocytes within von-Kupffer cells (anti-CD68/hematoxylin, ×1000)

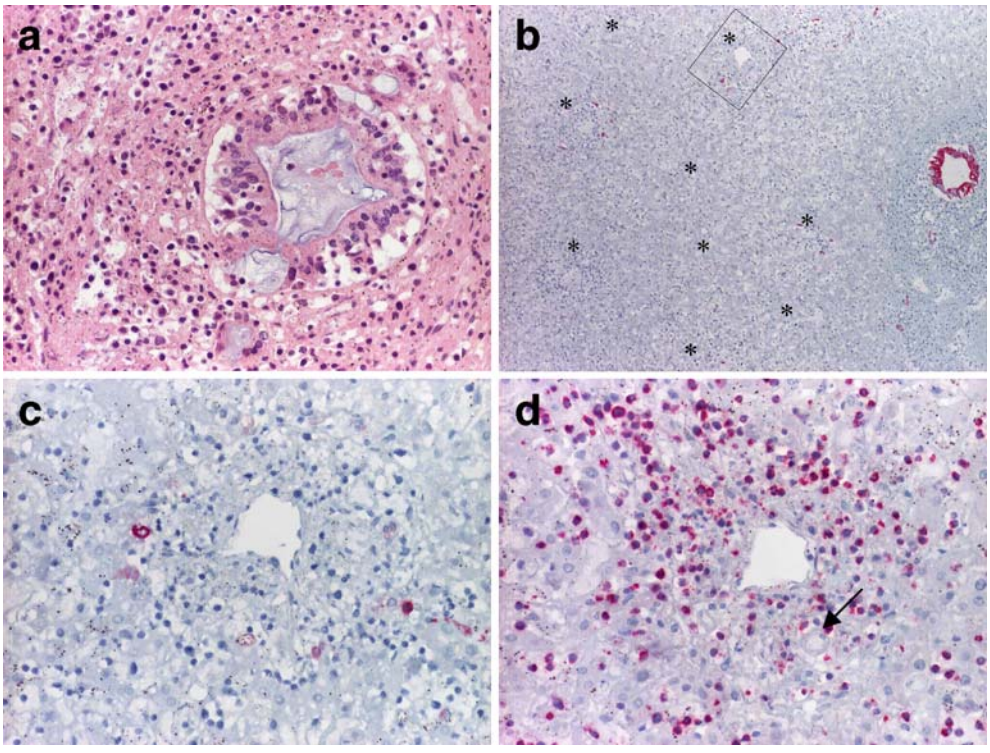

Fig. 5 Autopsy liver, brother. (**a**) Damage of remaining larger bile duct by infiltrating T cells (HE, ×400). (**b**) The bile duct shown in **a** was marked with anti-cytokeratin. The smaller interlobular bile ducts were completely lost. Portal tracts devoid of bile ducts are marked by asterisks. Rectangle corresponds to region shown in C and D (anti-cytokeratin 7/hematoxylin, ×100). (**c**) Portal tract devoid of interlobular bile duct (anti-cytokeratin 7/hematoxylin, ×400). (**d**) T lymphocytes infiltrating the portal tracts revealed strong expression of perforin. Arteriole (arrow) (anti-perforin/hematoxylin ×400)

erythrocytes was interpreted as indicating a leakiness of portal blood vessels. The most striking abnormality of the portal tracts, however, was complete loss of interlobular bile ducts. Neither bile ducts nor remnants of biliary epithelium could be detected in any of the 16 available portal tracts. Furthermore, there was no ductular proliferation or ductular metaplasia of periportal hepatocytes. This was confirmed by immunohistochemical evaluation with anti-cytokeratin 7 antibodies. No evidence of storage disorder was found; copper, copper-binding protein, and stainable iron were not demonstrable.

The explanted liver (Fig. 2), removed 14 days after liver biopsy, on macroscopy showed marked green discoloration, a normal attached gallbladder, and no evidence of necrosis. Microscopy disclosed portal tracts markedly expanded by dense mononuclear infiltrates resembling chronic hepatitis. Spill-over of the infiltrate into periportal regions was significant (Fig. 2a). Of note was a severe lymphocytic infiltration of both portal and central veins with undermining of the endothelium and endothelial-cell swelling that constituted endotheliitis (Fig. 2b). The infiltrate was dominated by T lymphocytes, with substantially fewer CD68-expressing histiocytes (Fig. 2c and d). Almost complete loss of interlobular bile ducts was confirmed. Immunohistochemical studies using a monoclonal antibody against cytokeratin 7 demonstrated that only a few larger portal tracts contained remnants of larger bile duct structures, with obvious patchy damage by T lymphocytes (Fig. 3a and b). The remaining biliary epithelial cells showed cytoplasmic swelling and reactive

Table 2 Antibodies used for immunohistochemistry

Antigen	Clone	Isotype	Dilution	Source
CD3	F7.2.38	IgG1 (mouse)	1:40	Dako
CD20	L26	IgG2a (mouse)	1:500	Dako
CD68	PG-M1	IgG3 (mouse)	1:100	Dako
CD68	KP1	IgG1 (mouse)	1:700	Dako
CD1a	O10	IgG1 (mouse)	–	Serotec
HLA-DR	DK22	IgG2a	1:100	Dako
S-100	Polyclonal	–	–	Dako
Cytokeratin 7	OV-TL 12/30	IgG1 (mouse)	1:200	Dako
HBc-AG	–	IgG2b (mouse)	–	ID Labs
HBSAG	–	IgG1 (mouse)	1:6	Linaris
CMV	CCH 2	IgG1 (mouse)	1:10	Dako
EBNA-2	F10-44-2	IgG2a (mouse)	1:30	Serotec
LMP	CS 1-4	IgG1 (mouse)	1:100	Dako
Perforin	5B10	IgG1 (mouse)	1:20	Novocastra

nuclear atypia. There was no ductular proliferation. Centrilobular hepatocytes showed single-cell necrosis with focal confluence. The remaining hepatocytes exhibited fatty change and ballooning with severe intracytoplasmic cholestasis. Hemophagocytosis could be demonstrated focally in CD68-expressing von Kupffer cells (Fig. 3c) and in the sinuses of adherent portal lymph nodes. In some portal vein branches we observed adherent thrombi of activated histiocytes. Microscopy of the gallbladder revealed focal infiltration by lymphocytes with damage to cholangiocytes. Mild siderosis of von Kupffer cells was demonstrated histochemically. Copper and copper-binding protein were not demonstrable. Hepatitis B virus surface and core antigens, cytomegalovirus antigens, EBV determined nuclear antigens-2, and EBV latent membrane protein-1 were not immunohistochemically demonstrable. Analysis of perforin expression revealed strong positivity within the portal and periportal inflammatory infiltrate (Fig. 3d). FHL was diagnosed.

Proposita—allograft liver

Microscopy of a core biopsy specimen of the allograft liver 16 days after transplantation showed parenchymal alterations identical to those in the explanted liver. The portal tracts were markedly infiltrated by lymphocytes and histiocytes. Bile ducts were very few. Some remaining interlobular bile ducts were infiltrated by T lymphocytes (Fig. 4a), others were overrun by mononuclear inflammatory cells (Fig. 4b). Destruction of bile ducts together with endotheliitis of portal veins prompted the differential diagnosis of acute allograft rejection. However, immunostains again confirmed an abundance of CD68-expressing histiocytes, marked activation of von Kupffer cells and focal hemophagocytosis (Fig. 4c and d). In line with the results of immunological analyses, the findings were interpreted as allograft involvement by FHL.

Brother's liver

Review of autopsy materials from the brother of the proposita showed liver lesions identical to those observed in the explant specimen. Again remarkable near-total loss of interlobular bile ducts (Fig. 5) was combined with pronounced hepatic infiltration by T-lymphocytes and histiocytes, and focal hemophagocytosis.

Discussion

Familial hemophagocytic lymphohistiocytosis is a rare disorder of infancy and childhood that is invariably fatal without early diagnosis and treatment. In many patients the diagnosis of FHL is difficult due to variability of clinical presentation, absence of proof of hemophagocytosis during the diagnostic work-up, and absence of a specific marker of the disease. Only 30% of the patients suffering from FHL are diagnosed when still alive [16].

We report two siblings who presented with symptoms of hemophagocytic lymphohistiocytosis (HLH) and liver failure. Acute hepatic failure in early infancy is primarily caused by inborn errors of metabolism, ischemic damage, viral infections, and neonatal hemochromatosis.

HLH is usually not supposed to present primarily with liver failure. However, four infants with FHL are described whose clinical picture on presentation strongly resembled that of our patients [14, 18, 20]. All these cases were initially misinterpreted as neonatal hemochromatosis, a differential diagnosis that may be particularly difficult and even lead to inappropriate liver transplantation [18].

Since molecular analysis of gene mutations may take too long to permit timely treatment, diagnosis of FHL must be based upon clinical, laboratory, and histopathologic findings. However, hemophagocytosis may be difficult to detect, particularly in the tissues most likely obtained to confirm the disorder, i.e. bone marrow and liver [19]. Particularly in bone marrow, hemophagocytosis may be assumed to be a consistent finding in FHL. At autopsy in 27 patients with FHL, however, active hemophagocytosis was seen in only 39% and 11% of bone marrow and liver specimens, respectively [16, 18]. Failure to document evidence of hemophagocytosis therefore does not exclude FHL. On the other hand, hemophagocytosis, particularly in bone marrow, may also be present in patients with metabolic disorders or acute sepsis, and is, therefore, not pathognomonic.

An important diagnostic pointer in liver specimens may be portal tract infiltration by T lymphocytes and histiocytes, resembling chronic hepatitis. These changes are found in approximately 85% of FHL specimens [5, 16]. Since chronic hepatitis is very rare in the neonatal period this may point to FHL. Both our patients had this hepatitis-like picture.

However, one of the most striking features in our cases was near-total loss and destruction of interlobular bile ducts. The lack of bile ducts was in fact interpreted as the most prominent finding in the initial liver biopsy specimen taken from the proposita 14 days before liver transplantation. Only mild portal tract involvement by mononuclear cells was noted; the diagnosis assigned thus was "loss of interlobular bile ducts, cause uncertain".

Loss of intrahepatic bile ducts in infants and children has been reported in many conditions. These include inborn errors of metabolism, chromosomal defects, prune belly syndrome, and a number of syndromatic or non-syndromatic idiopathic disorders as well as primary sclerosing cholangitis and Langerhans' cell histiocytosis [11]. FHL has not generally been appreciated as a potential cause of acquired paucity of interlobular bile ducts [5, 11, 12, 19]. How frequently destruction of intrahepatic bile ducts may occur and whether it may be restricted to certain genetically determined variants of FHL is unclear; such injury has also been described in other cases with severe hepatic involvement [18].

The pathogenesis of bile duct injury is unknown. It may be linked to aberrations in the activation of T lymphocytes and the regulation of cytokines [17]. Some bile ducts are obviously overrun and damaged by abnormally activated T lymphocytes. Direct cytokine-mediated injury to biliary epithelium may, however, be an alternative pathomechanism. The loss of bile ducts (pre-transplant biopsy specimen) appeared to antedate heavy infiltration of the portal tracts by lymphohistiocytic cells (explant specimen). This suggests that destruction of bile ducts may be an early event.

The combination of bile duct damage and endotheliitis seen in the allograft prompted the differential diagnosis of acute allograft rejection. Based on the extensive activation of the von Kupffer cells with focal hemophagocytosis and in conjunction with the clinical-biochemistry analyses, we interpreted the abnormalities seen in the allograft as recurrence of FHL. Recurrence of FHL after liver transplantion has recently also been described by Parizhskaya and colleagues [18].

Our observations indicate that loss of interlobular bile ducts may be an important feature of hepatic involvement by FHL. Molecular analyses did so far not reveal a causative mutation in our cases. However, they may help to clarify the association of hepatic bile duct damage with the various genetically determined variants of FHL.

Acknowledgements The support of Dr. Janka and Dr. zur Stadt (Department of Hematology and Oncology, Children's Hospital, University of Hamburg) is gratefully acknowledged. For their help the authors are grateful to Dr. Tauber, to Dr. Mikuz (Department of Pathology, Medical University Innsbruck) and Dr. Fichtel (Department of Pathology, General Regional Hospital Bozen, Italy).

References

1. Arico M, Imashuku S, Clementi R, Hibi S, Teramura T, Danesino C, Haber DA, Nichols KE (2001) Hemophagocytic lymphohistiocytosis due to germline mutations in SH2D1A, the X-linked lymphoproliferative disease gene. Blood 97:1131–1133
2. Arico M, Danesino C, Pende D, Moretta L (2001) Pathogenesis of haemophagocytic lymphohistiocytosis. Br J Haematol 114: 761–769
3. Clementi R, zur Stadt U, Savoldi G, Varoitto S, Conter V, De Fusco C, Notarangelo LD, Schneider M, Klersy C, Janka G, Danesino C, Arico M (2001) Six novel mutations in the PRF1 gene in children with haemophagocytic lymphohistiocytosis. J Med Genet 38:643–646
4. Farquhar JW, Claireaux AF (1952) Familial hemophagocytic histiocytosis. Arch Dis Child 27:519–525
5. Favara BE (1996) Histopathology of the liver in histiocytosis syndromes. Pediatr Pathol Lab Med 16:413–433
6. Feldmann J, Le Deist F, Ouachee-Chardin M, Certain S, Alexander S, Quartier P, Haddad E, Wulffraat N, Casanova JL, Blanche S, Fischer A, de Saint Basile G (2002) Functional consequences of perforin gene mutations in 22 patients with familial haemophagocytic lymphohistiocytosis. Br J Haematol 117:965–972
7. Goransdotter Ericson K, Fadeel B, Nilsson-Ardnor S, Soderhall C, Samuelsson A, Janka G, Schneider M, Gurgey A, Yalman N, Revesz T, Egeler R, Jahnukainen K, Storm-Mathiesen I, Haraldssson A, Poole J, de Saint Basile G, Nordenskjold M, Henter J (2001) Spectrum of perforin gene mutations in familial hemophagocytic lymphohistiocytosis. Am J Hum Genet 68: 590–597
8. Henter JI, Samuelsson-Horne A, Arico M, Egeler RM, Elinder G, Filipovich AH, Gadner H, Imashuku S, Komp D, Ladisch S, Webb D, Janka G, Histiocyte Society (2002) Treatment of hemophagocytic lymphohistiocytosis with HLH-94 immunochemotherapy and bone marrow transplantation. Blood 100: 2367–2373
9. Henter JI (2002) Biology and treatment of familial hemophagocytic lymphohistiocytosis: importance of perforin in lymphocyte-mediated cytotoxicity and triggering of apoptosis. Med Pediatr Oncol 38:305–309
10. Imashuku S, Hibi S, Sako M, Ishii T, Kohdera U, Kitazawa K, Ooe M, Naya M, Sawada H, Kawakami T (1998) Heterogeneity of immune markers in hemophagocytic lymphohistiocytosis: comparative study of 9 familial and 14 familial inheritance-unproved cases. J Pediatr Hematol Oncol 20:207–214
11. Ishak KG, Sharp HL (2000) Developmental abnormalities and liver disease in childhood. In: MacSween RNM, Burt AD, Portmann BC, Ishak KG, Scheuer PJ, Anthony PP (eds) Pathology of the liver. Churchill Livingstone, London, pp 107–154
12. Ludwig J, Batts K (eds) (1998) Practical liver biopsy interpretation. Diagnostic algorithms. ASCP Press, Chicago
13. Matthes-Martin S, Peters C, Königsrainer A, Fritsch G, Lion T, Heitger A, Kapelari K, Kronberger M, Offner F, Wrba F, Margreiter R, Gadner H (2000) Successful stem cell transplantation following orthotopic liver transplantation from the same haploidentical family donor in a girl with hemophagocytic lymphohistiocytosis. Blood 96:3997–3999
14. Menasche G, Feldmann J, Fischer A, de Saint Basile G (2005) Primary hemophagocytic syndromes point to a direct link between lymphocyte cytotoxicity and homeostasis. Immun Rev 203:165–179
15. Ohadi M, Lalloz MRA, Sham P, Zhao J, Dearlove AM, Shiach C, Kinsey S, Rhodes M, Layton DM (1999) Localization of a gene for familial hemophagocytic lymphohistiocytosis at chromosome 9q21.3-22 by homozygosity mapping. Am J Hum Genet 64:165–171
16. Öst A, Nilsson-Ardnor S, Henter JI (1998) Autopsy findings in 27 children with haemophagocytic lymphohistiocytosis. Histopathology 32:310–316
17. Osugi Y, Hara J, Tagawa S, Takai K, Hosoi G, Matsuda Y, Ohta H, Fujisaki H, Kobayashi M, Sakata N, Kawa-Ha K, Okada S, Tawa A (1997) Cytokine production regulating Th1 and Th2 cytokines in hemophagocytic lymphohistiocytosis. Blood 89:4100–4103
18. Parizhskaya M, Reyes J, Jaffe R (1999) Hemophagocytic syndrome presenting as acute hepatic failure in two infants: clinical overlap with neonatal hemochromatosis. Pediatr Dev Pathol 2:360–366
19. Scheuer PJ, Lefkowitch JH (eds) (2000) Liver biopsy interpretation. Saunders, New York
20. Senger C, Gonzalez-Crussi F (1999) Histiocytic-phagocytic infiltrates in the liver of an infant: a case clinically simulating perinatal hemochromatosis. J Pediatr Gastroenterol Nutr 29: 215–220
21. Stepp SE, Dufourcq-Lagelouse R, Le Deist F, Bhawan S, Certain S, Mathew PA, Henter JI, Bennett M, Fischer A, de Saint Basile G, Kumar V (1999) Perforin gene defects in familial hemophagocytic lymphohistiocytosis. Science 286: 1957–1959
22. Sung L, Weitzman SS, Petric M, King SM (2001) The role of infections in primary hemophagocytic lymphohistiocytosis: a case series and review of the literature. Clin Infect Dis 33: 1644–1648

Virchows Arch (2005) 446: 626–633
DOI 10.1007/s00428-005-1252-0

ORIGINAL ARTICLE

Shigeki Shiohara · Tanri Shiozawa · Tsutomu Miyamoto · Yu-Zhen Feng · Hiroyasu Kashima · Miyuki Kurai · Akihisa Suzuki · Ikuo Konishi

Expression of cyclins, p53, and Ki-67 in cervical squamous cell carcinomas: overexpression of cyclin A is a poor prognostic factor in stage Ib and II disease

Received: 26 January 2005 / Accepted: 4 March 2005 / Published online: 13 May 2005
© Springer-Verlag 2005

Abstract We previously reported the overexpression of cyclins in uterine cervical carcinoma; however, their clinicopathological significance remained undetermined. In the present study, we examined the immunohistochemical expression of cyclins (D1, E, A, B1), p53 and Ki-67 in squamous cell carcinoma (stage Ib+II; 80 cases, stage III+IV; 23 cases). Correlations between the expression of cyclins and clinicopathological parameters and patient survival were statistically evaluated. The results indicated that in the normal squamous epithelium, the expression of cyclins and Ki-67 was sporadically observed in the parabasal layer. Of the 103 cervical carcinomas, overexpression of cyclins D1, E, A, B1 and p53 was observed in 13 (13%), 23 (22%), 25 (24%), 18 (18%) and 23 (22%) cases, respectively, with a slight predominance in advanced stage tumors. The expression of cyclin D1, E, A and p53 significantly correlated with that of Ki-67 (Spearman's rank correlation). Univariate and multivariate analyses revealed that lymph node metastasis and cyclin A overexpression were independent prognostic factors for unfavorable outcomes in stage Ib+II patients. These findings suggest that the overexpression of various cyclins is involved in the acquisition of the vigorous growth potential of cervical carcinoma cells, and that cyclin A is an independent prognosticator of cervical carcinoma in early stages.

Keywords Cyclin · Ki-67 · p53 · Cervical cancer · Immunohistochemistry

S. Shiohara · T. Shiozawa (✉) · T. Miyamoto · Y.-Z. Feng · H. Kashima · M. Kurai · A. Suzuki · I. Konishi
Department of Obstetrics and Gynecology,
Shinshu University School of Medicine,
3-1-1 Asahi, Matsumoto, 390-8621, Japan
e-mail: tanri@hsp.md.shinshu-u.ac.jp
Tel.: +81-263-372718
Fax: +81-263-340944

Introduction

Uterine cervical cancer is the second most common malignancy among women worldwide. Although the prevalence of effective screening systems has reduced the number of cervical carcinoma patients in developed countries, more than 4000 deaths were still reported in the United States in 2002 [23]. It is well known that human papillomavirus (HPV) is the main etiologic factor of cervical carcinoma, and that more than 95% of cervical carcinomas have high-risk HPV types [4]. Two major viral proteins, E6 and E7, are known to bind p53 and retinoblastoma gene products (pRB), abrogating their functions as tumor suppressors, leading to an abnormal cell cycle machinery [5]. Although the loss of the cell "brake" system can be attributed to viral proteins, molecular mechanisms which actually promote cell proliferation are not fully elucidated.

Recent studies have revealed that cell growth is exquisitely controlled by interactions of cell cycle-related molecules such as cyclins, cyclin-dependent kinases (cdks) and tumor suppressor gene products [31, 32]. Cyclins D1, E, A and B1 are expressed in a cell cycle-specific manner, and they form complexes with their respective cdks. These complexes phosphorylate substrates such as pRB, leading to cell growth. On the other hand, tumor suppressor gene products, such as p53 and cdk inhibitors (cdkIs), suppress cell growth by counteracting cyclin/cdk functions [32]. In various malignancies, abnormalities of these cell cycle-related molecules, i.e. overexpression of cyclins/cdks and loss of tumor suppressor functions, have been reported [12]. Some of these abnormalities were shown to have prognostic value [12].

In cervical carcinoma, possible prognostic factors reported to date are overexpression of growth factors and receptors [11], angiogenetic factors [10], and type of HPV [7], in addition to clinicopathological parameters such as age, clinical stage, lymph node and parametrial involvement, and lymph vascular permeation [41]. We previously reported the overexpression of various classes of cell cycle-

related molecules associated with loss of steroid receptor expression in cervical intraepithelial neoplasias and invasive carcinomas [22]. However, the correlation of these factors with clinicopathological parameters and with patient survival remained undetermined. Therefore, we examined the immunohistochemical expression of cyclins (D1, E, A, B1), p53 and the proliferation marker Ki-67 in cervical squamous cell carcinoma to evaluate the relationship between the expression of cell cycle regulators and clinicopathological indicators. In addition, the prognostic significance of the expression of these cell cycle regulators was also analyzed.

Materials and methods

Histological materials

One hundred and three squamous cell carcinoma tissues of the uterine cervix were obtained from women (28–90 years of age) who underwent hysterectomy or biopsy at Shinshu University Hospital during 1990–1997. Each specimen was immediately fixed in 10% phosphate-buffered formalin for 24 h and embedded in paraffin. Each tissue sample was used with the approval of the Ethics Committee of Shinshu University, after obtaining written consent from the patients. Serial sections 3 μm thick were prepared for hematoxylin and eosin (H.E.) staining and immunostaining. The histological diagnosis was performed using an H.E.-stained slide. Of the 103 cervical carcinomas, 56 were stage Ib, eight were stage IIa, 16 were IIb, 18 were stage III and five were stage IV, according to the classification of the International Federation of Gynecology and Obstetrics (FIGO).

With regard to the treatment modality, 80 patients with stage Ib and II carcinoma primarily underwent radical hysterectomy with pelvic lymphadenectomy. Patients with high-risk factors such as parametrial invasion and lymph node metastasis received adjuvant postoperative treatment withwhole pelvic irradiation of 40–50 Gy (13 cases), cisplatin-based chemotherapy (11 cases), or both (22 cases). Clinicopathological factors including tumor size, lymph vascular permeation, parametrial involvement, and lymph node metastasis were evaluated in resected tissue specimens. The tumor size was determined from the longest axis of the tumor. The remaining 23 patients with stage III and IV tumors underwent whole pelvic irradiation (40–50 Gy) and intracavital brachytherapy.

Immunohistochemistry

Staining procedures

Immunostaining was performed using specific antibodies against cyclin D1 (DCS-6; Progen, Heidelberg, Germany). Antibodies against cyclin E (HE1), cyclin A (BF683), and cyclin B1 (GNS-1) were purchased from Santa Cruz Biotechnology (Santa Cruz, Calif., USA). Antibodies against p53 (Do-1) and Ki-67 were purchased from Immunotech (Marseille, France). Indirect immunohistochemical staining was performed by the avidin–biotin–peroxidase complex method using a Histofine SAB–PO detector kit (Nichirei, Tokyo, Japan) with microwave pretreatment as described previously [22].

Interpretation of immunohistochemical staining and statistical analysis

The specific staining of each antibody was identified in the nucleus with or without in the cytoplasm. In the present study, we evaluated only nuclear staining, since most of the cyclins are known to work in the nucleus [31, 32]. Cyclin B1 was reportedly expressed in the cytoplasm, and in this study, the positive staining for cyclin B1 was observed in both the nucleus and cytoplasm. Although the significance of subcellular distribution of cyclin B1 has not fully been elucidated, we have previously reported that the nuclear staining of cyclin B1 topologically correlated well with Ki-67 [34], thus suggesting an importance of nuclear staining. Immunoreactivity was evaluated as the percentage of positive cells among 500 tumor cells in more than three high power fields, and described as the positivity index (PI). In cervical carcinoma, cut-off PI values for the overexpression of cyclin D1, E, A, B1, p53 and Ki-67 were determined in reference to the mean PI values of each staining and previous studies [6, 13, 19, 28, 37], and were 5, 25, 25, 20, 10 and 50, respectively. The significance of the differences in PI between stages IB+II and stages III+IV was examined by Mann–Whitney *U*-test. A tied *P*-value of <0.05 was considered significant. Correlations between the expression of cyclins and Ki-67, and between cyclins and clinicopathological factors were examined using Spearman's rank correlation test. A tied *P*-value of <0.05 was considered significant. A correlation coefficient (ρ) greater than 0.4 or less than -0.4 was considered to represent a "strongly" positive or negative correlation. These analyses were made using the StatView system (Abacus, Berkeley, Calif., USA).

Survival analysis

Of the 103 patients examined in the present study, 29 (13 in the stage Ib+II group, 16 in the stage III+IV group) had died from the disease and the remaining 74 were alive with no evidence of disease at the last follow-up. The mean post-treatment follow-up period was 65.1±45.9 months. The prognostic factors used in the survival analysis were as follows: tumor size ($\geq$30 mm versus $<$30 mm), lymph vascular permeation (positive versus negative), stromal invasion ($\geq$1/2 versus $<$1/2), parametrial involvement (positive versus negative), pelvic lymph node metastasis (positive versus negative), overexpression of cyclins (D1, E, A, B1), p53, and Ki-67 (positive versus negative). The prognostic value of these parameters was evaluated first with a univariate analysis using Cox's proportional hazard model,

and then with a multivariate analysis. A *P*-value of <0.05 was considered significant.

Results

Expression of cyclins and p53

Positive staining for cyclin D1, E, A and B1 in the normal ectocervical epithelia was sporadically observed in parabasal cells (Fig. 1), with a PI of less than 5 for cyclin D1, E and A, and 10 for cyclin B1. The expression of p53 in the normal ectocervical epithelia was negative. In cervical carcinoma, the expression of cyclins (Fig. 2) and p53 was increased compared to that in the normal squamous epithelium. Of the 80 stage Ib+II cervical carcinomas, the number of cases with cyclin D1, E, A, B1, and p53 overexpression was 10 (13%), 14 (18%), 12 (15%), 8 (10%), and 17 (21%), respectively. Of the 23 stage III+IV carcinomas, the numbers of cases with cyclin D1, E, A, B1, and p53 overexpression were 3 (13%), 9 (39%), 13 (57%), 10 (44%), and 6 (26%), respectively. The PIs of each staining are summarized in Table 1. The mean PI for cyclin A in total cases was 16.0. The PI for cyclin A was higher in stage III+IV (25.1) than stage Ib+II (13.3) (P=0.0128). The mean PI of cyclin D1, E, B1, and p53 in total cases was 2.0, 12.3, 12.2, and 8.3, respectively. There was no significant difference in these factors between those with stage Ib+II and stage III+IV tumors. The mean PI of Ki-67 for all cases was 46.2, and there was no significant difference between stage I+II (46.1) and stage III+IV (46.9).

Correlation of cyclin expression and Ki-67

Correlations between the immunohistochemical expression of cyclins and Ki-67 are summarized in Table 2. In stage Ib+II tumors, the expression of cyclin D1, E, A, and p53 positively correlated with the expression of Ki-67 (*P*=0.0379 for cyclin D1, *P*=0.0053 for cyclin E, *P*=0.0065 for cyclin A, and *P*=0.0284 for p53). In stage III+IV tumors, the expression of cyclin D1, E, A, B1, and p53 strongly and positively correlated with the Ki-67 expression. The *P*-value for cyclin E, A, B1 and p53 was 0.0102, 0.0002, 0.0002 and 0.0423, respectively.

Correlation between the expression of cyclins and clinicopathological parameters

Correlations between the expression of cell cycle regulators and clinicopathological factors in stage Ib+II tumors are summarized in Table 3. Lymph vascular permeation was correlated positively with the expression of cyclin D1 and negatively with Ki-67 (*P*=0.0424 for cyclin D1, *P*=0.0140 for Ki-67). Stromal invasion was correlated negatively with the expression of p53 (*P*=0.0058). Lymph node metastasis was correlated negatively with the expres-

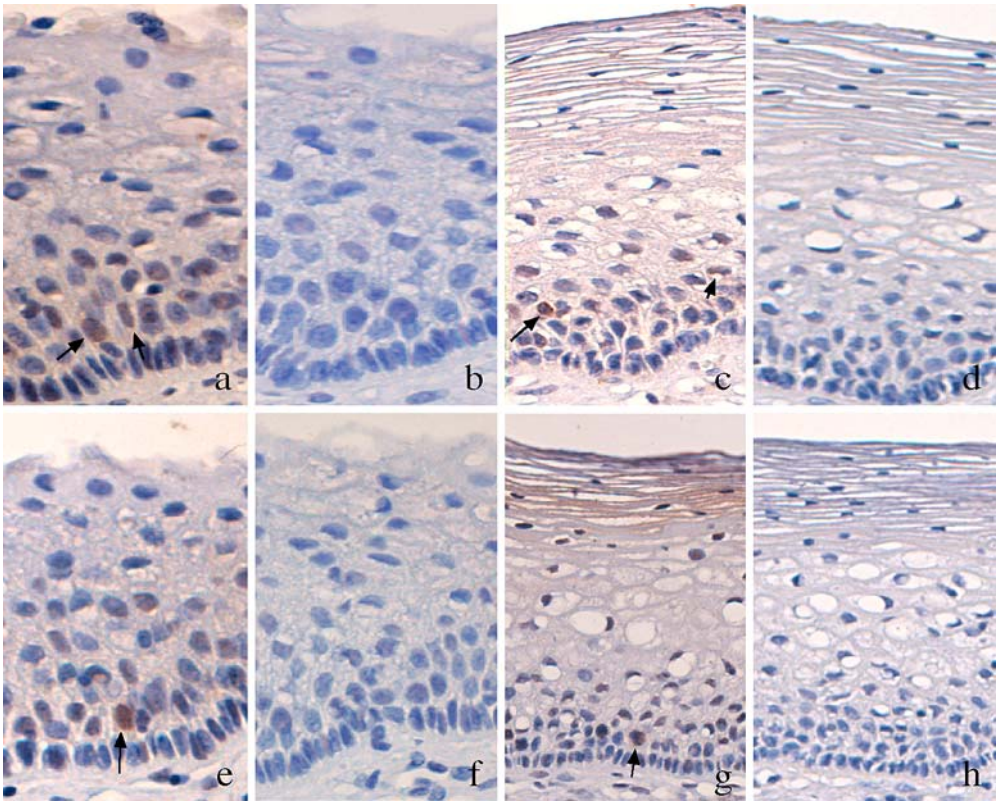

Fig. 1 Immunostaining of cyclin D1 (**a**, **b**), cyclin E (**c**, **d**), cyclin A (**e**, **f**) and cyclin B1 (**g**, **h**) in the normal squamous epithelium. b, d, f and h show negative control of the same sites. Positive cells (arrows) are sporadically observed in the parabasal layer. (**a**, **b**, **e**, **f**; ×200, **c**, **d**, **g**, **h**; ×175)

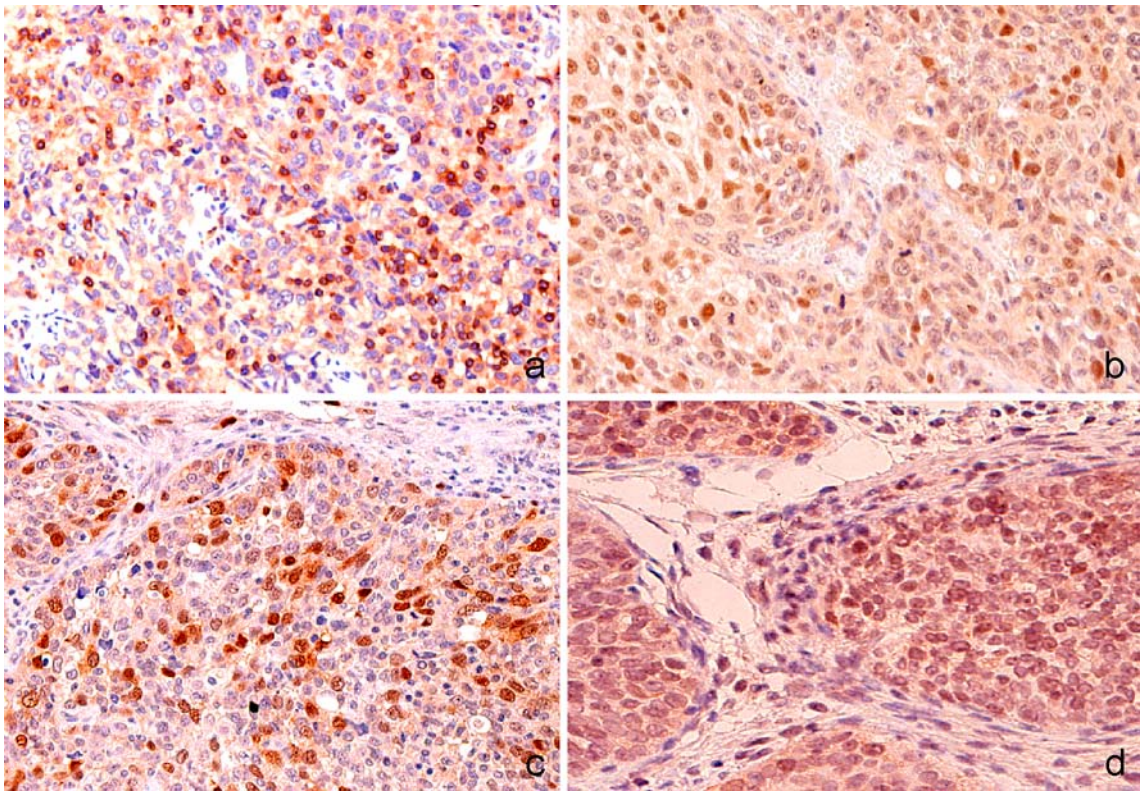

Fig. 2 Immunostaining of cyclin D1 (**a**), cyclin E (**b**), cyclin A (**c**) and cyclin B1 (**d**) in squamous cell carcinoma. **a**– **c**: nuclear-positive tumor cells are observed with a considerable heterogeneity among weak, cytoplasmic-positive cells (**a**; stage Ib, **b**; stage IIa, **c**; stage IIa, ×225). **d**: nuclear-positive cells with weak cytoplasmic staining are diffusely observed (stage Ib, ×250)

sion of Ki-67 (P=0.0170). Tumor size greater than 30 mm was negatively correlated with the expression of p53 (P= 0.0044). There were no significant correlations between cell cycle-related molecules and parametrial involvement.

Prognostic significance of the expression of cyclins, and clinicopathological factors in cervical carcinoma patients

Correlations between the expression of cell cycle regulators, Ki-67, clinicopathological parameters and survival in patients with stage Ib+II cervical carcinoma were analyzed by univariate and multivariate analyses (Table 4). The univariate analysis demonstrated that the overall survival was significantly shorter in patients with lymph node metastasis (P=0.0261, RR; 3.46) and those with cyclin A overexpression (P=0.0109, RR; 4.33) (Fig. 3). Of the 58 patients without lymph node metastasis, six (10.3%) died of the disease during the follow-up, whereas seven (31.8%) of 22 patients with lymph node metastasis died. Of the 68 patients without cyclin A overexpression, eight (11.8%) died of the disease, whereas five (41.7%) of 12 patients with cyclin A overexpression died. Other parameters did not show significant differences. We then examined whether there are strong correlations among each clinopathological and immunohistochemical parameter or not using a Spearman's rank correlation analysis. Since no "strong" correlations (i.e. ρ-value of more than 0.4 or less than −0.4)

Table 1 Result of immunostaining for cyclins and Ki-67

Factor	Stage Ib+II (80 cases)	Stage III+IV (23 cases)	Total	P value
Cyclin D1	2.0±5.9	1.9±5.4	2.0±5.8	0.5951
Cyclin E	9.8±17.7	20.9±27.8	12.3±20.7	0.1395
Cyclin A	13.3±12.5	25.1±19.9	16.0±5.2	0.0128
Cyclin B1	8.4±18.5	25.2±30.9	12.2±22.8	0.3264
p53	6.6±12.1	14.3±23.0	8.3±15.4	0.5903
Ki-67	46.1±19.8	46.9±25.8	46.2±21.0	0.4376

Each figure indicates the mean positivity index (PI)±SD
P-value of less than 0.05 is considered significant

Table 2 Correlation between the expression of cell cycle regulators and Ki-67 (Spearman's rank correlation)

Factors	Stage Ib+II		Stage III+IV		Total	
	P	ρ	P	ρ	P	ρ
Cyclin D1	0.0379	0.234	0.0526	0.423	0.0069	0.269
Cyclin E	0.0053	0.313	0.0102	0.548	0.0003	0.356
Cyclin A	0.0065	0.306	0.0002	0.806	0.0001	0.415
Cyclin B1	0.1609	0.158	0.0002	0.807	0.0010	0.326
p53	0.0284	0.247	0.0423	0.432	0.0011	0.322

A P-value of <0.05 was considered significant. A ρ-value (correlation coefficient) greater than 0.4 or less than −0.4 was considered to represent a "strongly" positive or negative correlation

Table 3 Correlation between the expression of cell cycle regulators and clinicopathological factors in stage Ib and II cervical carcinoma (Spearman's rank correlation)

	lymph vascular permeation	Stromal invasion (≧1/2)	Parametrial involvement	lymph node metastasis	Tumor size (≧30mm)
Cyclin D1					
P-value	0.0424	0.1763	0.8838	0.9087	0.7460
ρ-value	0.228	NE	NE	NE	NE
Cyclin E					
P-value	0.6147	0.5424	0.9683	0.6699	0.7323
ρ-value	NE	NE	NE	NE	NE
Cyclin A					
P-value	0.3290	0.1492	0.6999	0.9785	0.1784
ρ-value	NE	NE	NE	NE	NE
Cyclin B1					
P-value	0.9451	0.1822	0.4451	0.7708	0.8712
ρ-value	NE	NE	NE	NE	NE
p53					
P-value	0.0610	0.0058	0.0594	0.0881	0.0044
ρ-value	NE	−0.310	NE	NE	−0.321
Ki-67					
P-value	0.0140	0.2058	0.9688	0.0170	0.0564
ρ-value	−0.276	NE	NE	−0.269	NE

A *P*-value of less than 0.05 was considered significant. A ρ-value (correlation coefficient) greater than 0.4 or less than −0.4 was considered to represent a "strongly" positive or negative correlation. When the *P*-value was greater then 0.05, the respective ρ value was not examined (NE)

among the parameters were noted as shown in Table 3, we then performed a multivariate analysis using the same variables as used in the univariate analysis. The results again indicated that lymph node metastasis (*P*=0.0174, RR; 13.36) and cyclin A overexpression (*P*=0.0355, RR; 5.29) showed significant correlations. These findings indicated that the lymph node metastasis and cyclin A overexpression are independent prognostic factors for shorter survival in patients with surgically treated stage Ib+II cervical carcinoma. With regard to survival analysis in 23 patients with stage III+ IV carcinoma, the *P*-values determined by the univariate analysis for the overexpression of cyclin D1, E, A, B1, p53, and Ki-67 were 0.7608, 0.3878, 0.8236, 0.3650, 0.0997, and 0.7571, respectively. These results indicated that the overexpression of cell cycle-related molecules did not have prognostic significance in stage III+IV cervical carcinoma patients.

Discussion

The present study demonstrated that various cell cycle-related molecules were overexpressed in squamous cell carcinomas. Among the cyclins examined, the expression of cyclin A showed a significant positive correlation with that of Ki-67. Since cyclin A accelerates the cell cycle progression by binding to cdk2 in late G1 phase and to cdc2 in the G2-M phases [31, 32], the correlation between cyclin A and Ki-67 seems reasonable. Although cyclin A overexpression is reportedly caused by an increase in transcription [42], the molecular mechanisms involved in cyclin A transcription are not fully elucidated. One of the candidates of such an enhancer is p53 protein, because we previously showed a close topological correlation between the expression levels of cyclin A and p53 in endometrial

Table 4 Prognostic value of the clinicopathological parameters, and expression of cell cycle regulators and Ki-67 in patients with stage Ib and II cervical cancer

Cox's proportional hazard model				
Factors (No. of cases)	Univariate		Multivariate	
	P-value	RR (95%C I)	*P*-value	RR (95% CI)
LVP: positive (38)	0.2474	1.87 (0.61–5.71)	0.1875	0.28 (0.04–1.85)
StI: ≧1/2 (57)	0.6350	1.37 (0.38–4.97)	0.5416	0.58 (0.10–3.32)
PMI: positive (13)	0.4387	1.67 (0.46–6.07)	0.4875	2.17 (0.24–19.26)
LNM: positive (22)	0.0261	3.46 (1.16–10.35)	0.0174	13.36 (1.56–113.07)
TS: ≧30mm (38)	0.1104	2.61 (0.80–8.50)	0.3328	3.09 (0.32 –30.26)
Cyc D1: PI≧5 (10)	0.1301	2.74 (0.74–8.19)	0.1708	3.77 (0.57–25.11)
Cyc E: PI≧25 (14)	0.6019	1.41 (0.39–5.15)	0.8234	1.28 (0.14–11.53)
Cyc A: PI≧25 (12)	0.0109	4.33 (1.40–13.37)	0.0355	5.29 (1.12–25.02)
Cyc B1: PI≧20 (8)	0.4965	1.69 (0.37–7.67)	0.8854	0.84 (0.08–8.75)
p53: PI≧10 (17)	0.3465	1.76 (0.54–5.72)	0.7440	1.27 (0.30–5.45)
Ki-67: PI≧50 (35)	0.4193	1.57 (0.53–4.66)	0.6352	1.44 (0.32–6.39)

LVP lymph vascular permeation, *StI* stromal invasion, *PMI* parametrial involvement *LNM* lymph node metastasis, *TS* tumor size, *Cyc* cyclin, *RR* relative risk, *CI* confidence interval
P<0.05 was regarded as significant

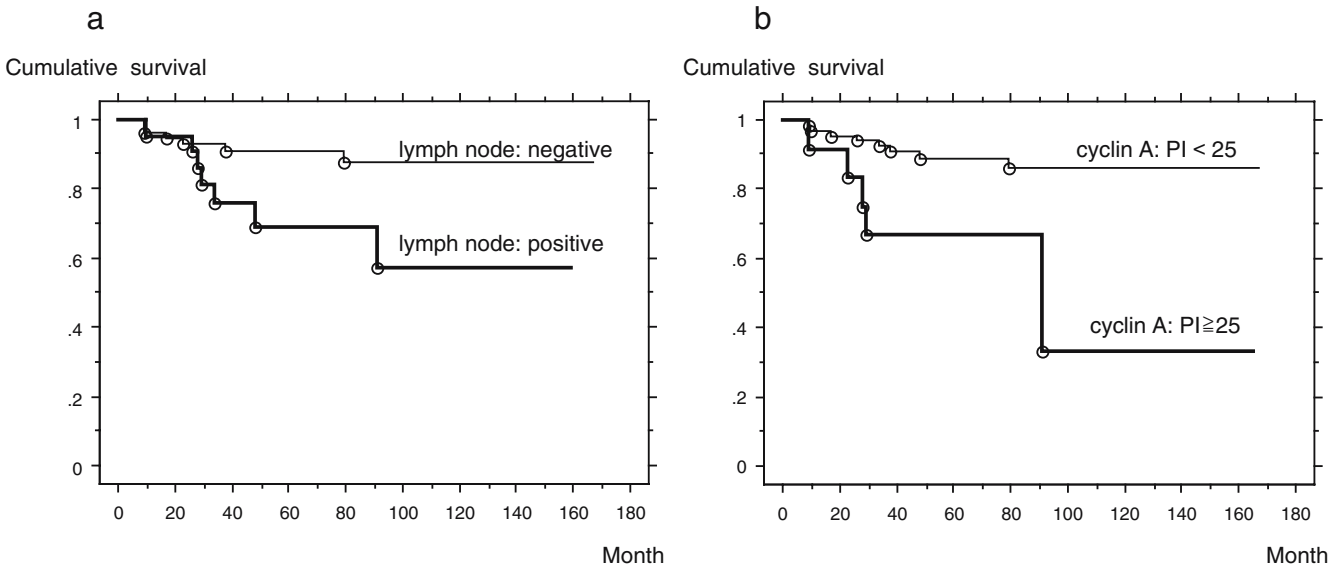

Fig. 3 Kaplan–Meier analysis of patients survival, with respect to lymph node metastasis (**a**) and cyclin A overexpression (**b**). The patients with positive lymph node metastasis and with cyclin A overexpression showed significantly poorer outcomes. The *P*-values are described in the text

carcinoma [33] and leiomyosarcoma [44]. However, no such spatial correlation between p53 and cyclin A was observed in the present study. Therefore, other mechanisms boosting cyclin A expression can be expected in cervical carcinoma. In this regard, HPV-E7 protein is reported to increase the expression of a transcription factor, E2F, which can activate the E2F-dependent promoter of the cyclin A gene [43].

In the present study, stage Ib+II patients with cyclin A overexpression exhibited a significantly shorter overall survival than those without cyclin A overexpression by multivariate analysis, and therefore cyclin A is an independent prognostic factor in early stage cervical carcinoma. In carcinomas of the breast and lung, overexpression of cyclin A has been reported as a prognostic factor for poor outcome [27, 40]. We have also reported that cyclin A is a prognosticator of uterine endometrial carcinoma [33] and uterine leiomyosarcoma [44]. The present result is in line with these reports. In contrast, a study by Van de Putte et al. reported that there was no prognostic significance of cyclin A overexpression in stage Ib cervical squamous cell carcinoma [39]. This difference may be due to the different selection of disease stages and different cut off values. To our knowledge, this is the first report of prognostic significance of cyclin A in stage Ib+II cervical carcinoma. The poor prognosis of patients with cyclin A-positive carcinoma may be attributed to the higher proliferative activity of the tumor, since the expression of cyclin A significantly correlated with Ki-67 expression. However, other cell cycle markers, such as cyclin D1, cyclin E and p53, did not show prognostic significance, although they also correlated with Ki-67. It is known that forced expression of cyclin A confers on non-neoplastic cells the anchorage-independency, that is an important hallmark of malignant transformation [16]. A recent study demonstrated that overexpression of cyclin A can suppress ultraviolet-induced, p53-mediated apoptosis [18]. Our preliminary experiments have shown that the forced expression of cyclin A in endometrial carcinoma cell lines resulted in the induction of cisplatin-resistance (unpublished observation). Accordingly, the tumor cells may acquire the specific biological characteristics via cyclin A overexpression, which may be related with the poor prognosis. On the other hand, we could not detect prognostic significance of cyclin A overexpression in stage III and IV tumors. Although the reason for this is unknown, it may be related to the limited number of cases examined.

In our series of cervical carcinoma, the clinicopathological parameters such as lymph node metastasis and lymph vascular permeation were not statistically correlated with the expression of cyclin A, but were correlated negatively with Ki-67. The results suggest that tumors with invasive or metastatic potentials have less growth activities. Recent research has indicated that tumor cells during invasion or metastasis are usually in the quiescent status of cell cycle [24, 25], such as G0 or early G1 phases in which Ki-67 is negative [14]. Therefore, negative correlations of Ki-67 with lymph node metastasis and lymph vascular permeation may represent that the presence of many quiescent tumor cells involved in the invasion or metastasis. However, further researches are needed to clarify the cell cycle status of cervical carcinoma cells in lymph node metastasis or vascular space invasion.

Cyclin D1 is expressed in the G1 phase of the cell cycle, forms a complex with cdk4 and 6 which phosphorylate pRB, resulting in cell cycle progression [31]. Therefore, cyclin D1 is regarded as an important G1 phase regulator. In the carcinoma tissues examined in the present study, although cyclin D1 expression increased compared to that in the normal epithelium, the mean PI (2.0) was relatively low. This result was consistent with a report by Skomedal et al. [35]. Cyclin D1 overexpression is reported in various

human malignancies. In breast carcinomas, overexpression of cyclin D1 has been reported to be a prognostic maker for favorable outcomes [3]. Conversely, in squamous cell carcinoma of the head and neck [26] and esophagus [38], overexpression of cyclin D1 has been reported to be a prognostic factor for poor outcomes. In addition, Bae et al. reported that the overexpression of cyclin D1 has prognostic significance in squamous cell carcinoma of the uterine cervix [2]. However, contrary to these reports, no prognostic value was detected in the present study, being similar with that of a previous report [35]. With regard to the expression mechanism of cyclin D1, Cattani et al. reported that the cyclin D1 gene amplification was associated with HPV infection, as oncoproteins E6 and E7 induce gene instability in laryngeal squamous cell carcinoma [8]. However, Southern et al. reported that cyclin D1 was frequently expressed in low risk HPV-infected low grade intra-epithelial lesions but not in high risk HPV-infected lesions [36].

The present study indicated that the p53, one of the most important transcription factors to control cell cycle progress and apoptosis, was nearly absent in the normal squamous epithelium, but was overexpressed in cervical squamous cell carcinoma. This result was consistent with the previous report [22]. It has been shown that the p53 is bound and inactivated by E6 oncoproteins in HPV-positive squamous cell carcinoma of the uterine cervix [5]. However, genetic analyses of p53 have demonstrated that p53 mutation is rare in cervical carcinoma [1]. In addition, Akasofu et al. reported that more than 50% of the tumor cells showed strong p53 staining in cases with p53 mutation [1]. In the present study, the mean PI of the p53 was 8.3 and the PI of most of p53-positive cases was less than 50. Therefore, though we have not performed the sequencing of p53 gene, the expression of p53 in the present study may represent an accumulation of wild-type p53 protein. Although, the significance of p53 protein accumulation in cervical tissues needs further investigation, a study reported that disease progression in ectocervical epithelia is associated with an increased incidence of apoptosis [21]. In this regard, the immunoreactive p53 could be involved in p53-mediated apoptosis. The prognostic significance of p53 protein accumulation is controversial. Chen and others claimed that p53 overexpression has prognostic value [9], while other reports stated it did not [20]. In the present study, we could not detect any prognostic significance of p53 in surgically treated stage Ib+II patients (P=0.3396) or in stage III+IV patients (P=0.0997), being consistent with the latter group of studies.

Overexpression of cyclin B1 and cyclin E was also observed in cervical carcinoma in the present study. Overexpression of cyclin E is an important prognostic factor of breast carcinoma [30], and cyclin B1 has been reported to have a prognostic impact in squamous cell carcinoma of the esophagus [37]. However, we did not find prognostic implications of cyclin E and B1 in the present study. Although this reason is not understood, a previous study has reported "unscheduled" expression of cyclin E and B1 in solid tumors, i.e. these cyclins were overexpressed irrespective of cell cycles [15].

Ki-67 staining has been evaluated extensively as a prognostic parameter in squamous cell carcinoma. Ho et al. [17] reported that those with increased Ki-67 labeling had shorter survival in stage I cervical carcinoma patients. In contrast, the increased labeling of Ki-67 was not associated with poor outcomes in cervical carcinoma patients with stage I [39] and stage III+IV [29] tumors. Although the exact reason for this discrepancy is unknown, our results are similar to those in the latter group.

In summary, the present study demonstrated various cyclins are overexpressed in squamous cell carcinomas, and considered to be involved in the gaining of the active growth potential of squamous cell carcinoma. In addition, cyclin A overexpression, as well as lymph node metastasis, was an independent prognosticator for unfavorable outcomes in patients with surgically treated stage Ib and II cervical cancer. Further studies are needed to clarify the biological roles of cyclin A overexpression other than growth stimulation.

Acknowledgements This work was supported in part by a Grant-in-aid for Scientific Research from the Ministry of Education, Science, Sports and Culture (No. 12671583 and No.14370527), Japan.

References

1. Akasofu M, Oda Y (1995) Immunohistochemical detection of p53 in cervical epithelial lesions with or without infection of human papillomavirus types 16 and 18. Virchows Arch 425: 593–602
2. Bae DS, Cho SB, Kim YJ, Whang JD, Song SY, Park CS, Kim DS, Lee JH (2001) Aberrant expression of cyclin D1 is associated with poor prognosis in early stage cervical cancer of the uterus. Gynecol Oncol 81:341–347
3. Barnes DM (1997) Cyclin D1 in mammary carcinoma. J Pathol 181:267–269
4. Bosch FX, Manos MM, Munoz N, Sherman M, Jansen AM, Peto J, Schiffman MH, Moreno V, Kurman R, Shah KV (1995) Prevalence of human papillomavirus in cervical cancer: a worldwide perspective. International Biological Study on Cervical Cancer (IBSCC) Study Group. J Natl Cancer Inst 87:796–802
5. Bosch FX, Lorincz A, Munoz N, Meijer CJ, Shah KV (2002) The causal relation between human papillomavirus and cervical cancer. J Clin Pathol 55:244–265
6. Brown DC, Cole D, Gatter KC, Mason DY (1988) Carcinoma of the cervix uteri: an assessment of tumour proliferation using the monoclonal antibody Ki67. Br J Cancer 57:178–181
7. Burger RA, Monk BJ, Kurosaki T, Anton-Culver H, Vasilev SA, Berman ML, Wilczynski SP (1996) Human papillomavirus type 18: association with poor prognosis in early stage cervical cancer. J Natl Cancer Inst 88:1361–1368
8. Cattani P, Hohaus S, Bellacosa A, Genuardi M, Cavallo S, Rovella V, Almadori G, Cadoni G, Galli J, Maurizi M, Fadda G, Neri G (1998) Association between cyclin D1 (CCND1) gene amplification and human papillomavirus infection in human laryngeal squamous cell carcinoma. Clin Cancer Res 4:2585–2589
9. Chen HY, Hsu CT, Lin WC, Tsai HD, Chang WC (2000) Prognostic value of p53 expression in stage IB1 cervical carcinoma. Gynecol Obstet Invest 49:266–271

10. Cheng WF, Chen CA, Lee CN, Wei LH, Hsieh FJ, Hsieh CY (2000) Vascular endothelial growth factor and prognosis of cervical carcinoma. Obstet Gynecol 6:721–726
11. Cho NH, Kim YB, Park TK, Kim GE, Park K, Song KJ (2003) P63 and EGFR as prognostic predictors in stage IIB radiation-treated cervical squamous cell carcinoma. Gynecol Oncol 91:346–353
12. Dictor M, Ehinger M, Mertens F, Akervall J, Wennerberg J (1999) Abnormal cell cycle regulation in malignancy. Am J Clin Pathol 112:S40–S52
13. Dong Y, Sui L, Tai Y, Sugimoto K, Hirao T, Tokuda M (2000) Prognostic significance of cyclin E overexpression in laryngeal squamous cell carcinomas. Clin Cancer Res 6:4253–4258
14. Gerdes J, Lemke H, Baisch H, Wacker HH, Schwab U, Stein H (1984) Cell cycle analysis of a cell proliferation-associated human nuclear antigen defined by the monoclonal antibody Ki67. J Immunol 133:1710–1715
15. Gong J, Ardelt B, Traganos F, Darzynkiewicz Z (1994) Unscheduled expression of cyclin B1 and cyclin E in several leukemic and solid tumor cell lines. Cancer Res 54:4285–4288
16. Guadagno TM, Ohtsubo M, Roberts JM, Assoian RK (1993) A link between cyclin A expression and adhesion-dependent cell cycle progression. Science 262:1572–1575
17. Ho DM, Hsu CY, Chiang H (2000) MIB-1 labeling index as a prognostic indicator for survival in patients with FIGO stage IB squamous cell carcinoma of the cervix. Gynecol Oncol 76: 97–102
18. Hsieh JK, Yap D, O'Connor DJ, Fogal V, Fallis L, Chan F, Zhong S, Lu X (2002) Novel function of the cyclin A binding site of E2F in regulating p53-induced apoptosis in response to DNA damage. Mol Cell Biol 22:78–93
19. Hui AM, Li X, Shi YZ, Takayama T, Torzilli G, Makuuchi M (2000) Cyclin D1 overexpression is a critical event in gallbladder carcinogenesis and independently predicts decreased survival for patients with gallbladder carcinoma. Clin Cancer Res 6:4272–4277
20. Hunt CR, Hale RJ, Buckley CH, Hunt J (1996) p53 expression in carcinoma of the cervix. J Clin Pathol 49:971–974
21. Isacson C, Kessis TD, Hedrick L, Cho KR (1996) Both cell proliferation and apoptosis increase with lesion grade in cervical neoplasia but do not correlate with human papillomavirus type. Cancer Res 56:669–674
22. Kanai M, Shiozawa T, Xin L, Nikaido T, Fujii S (1998) Immunohistochemical detection of sex steroid receptors, cyclins, and cyclin-dependent kinases in the normal and neoplastic squamous epithelia of the uterine cervix. Cancer 82: 1709–1719
23. Krivak TC, McBroom JW, Elkas JC (2002) Cervical and vaginal cancer. In: Berek JS (ed) Novak's gynecology, 13th edn. Lippincott Williams & Wilkins, Philadelphia, pp 1199–1211
24. Krtolica A, Ludlow JW (1996) Hypoxia arrests ovarian carcinoma cell cycle progression, but invasion is unaffected. Cancer Res 56:1168–1173
25. Krtolica A, Krucher NA, Ludlow JW (1999) Molecular analysis of selected cell cycle regulatory proteins during aerobic and hypoxic maintenance of human ovarian carcinoma cells. Br J Cancer 80:1875–1883
26. Michalides R, van Veelen N, Hart A, Loftus B, Wientjens E, Balm A (1995) Overexpression of cyclin D1 correlates with recurrence in a group of forty-seven operable squamous cell carcinomas of the head and neck. Cancer Res 55:975–978
27. Michalides R, van Tinteren H, Balkenende A, Vermorken JB, Benraadt J, Huldij J, van Diest P (2002) Cyclin A is a prognostic indicator in early stage breast cancer with and without tamoxifen treatment. Br J Cancer 86:402–408
28. Nozoe T, Korenaga D, Futatsugi M, Saeki H, Ohga T, Sugimachi K (2002) Cyclin A expression in superficial squamous cell carcinoma of the esophagus and coexisting infiltrated lymphocyte follicle. Cancer Lett 188:221–229
29. Oka K, Arai T (1996) MIB1 growth fraction is not related to prognosis in cervical squamous cell carcinoma treated with radiotherapy. Int J Gynecol Pathol 15:23–27
30. Porter PL, Malone KE, Heagerty PJ, Alexander GM, Gatti LA, Firpo EJ, Daling JR, Roberts JM (1997) Expression of cell-cycle regulators p27Kip1 and cyclin E, alone and in combination, correlate with survival in young breast cancer patients. Nat Med 3:222–225
31. Sherr CJ (1993) Mammalian G1 cyclins. Cell 73:1059–1065
32. Sherr CJ (1994) G1 phase progression: cyclin on cue. Cell 79:551–555
33. Shih HC, Shiozawa T, Kato K, Imai T, Miyamoto T, Uchikawa J, Nikaido T, Konishi I (2003) Immunohistochemical expression of cyclins, cyclin-dependent kinases, tumor-suppressor gene products, Ki-67, and sex steroid receptors in endometrial carcinoma: positive staining for cyclin A as a poor prognostic indicator. Hum Pathol 34:471–478
34. Shioazawa T, Li SF, Nakayama K, Nikaido T, Fujii S (1996) Relationship between the expression of cyclins/cyclin-dependent kinases and sex steroid receptors/Ki67 in normal human endometrial glands and stroma during the menstrual cycle. Mol Hum Reprod 2:745–752
35. Skomedal H, Kristensen GB, Lie AK, Holm R (1999) Aberrant expression of the cell cycle associated proteins TP53, MDM2, p21, p27, cdk4, cyclin D1, RB, and EGFR in cervical carcinomas. Gynecol Oncol 73:223–228
36. Southern SA, Herrington CS (1998) Differential cell cycle regulation by low- and high-risk human papillomaviruses in low-grade squamous intraepithelial lesions of the cervix. Cancer Res 58:2941–2945
37. Takeno S, Noguchi T, Kikuchi R, Uchida Y, Yokoyama S, Muller W (2002) Prognostic value of cyclin B1 in patients with esophageal squamous cell carcinoma. Cancer 94:2874–881
38. Takeuchi H, Ozawa S, Ando N, Shih CH, Koyanagi K, Ueda M, Kitajima M (1997) Altered p16/MTS1/CDKN2 and cyclin D1/PRAD-1 gene expression is associated with the prognosis of squamous cell carcinoma of the esophagus. Clin Cancer Res 3:2229–2236
39. Van de Putte G, Kristensen GB, Lie AK, Baekelandt M, Holm R (2004) Cyclins and proliferation markers in early squamous cervical carcinoma. Gynecol Oncol 92:40–46
40. Volm M, Koomagi R, Mattern J, Stammler G (1997) Cyclin A is associated with an unfavourable outcome in patients with non-small-cell lung carcinomas. Br J Cancer 75:1774–1778
41. Wright TC, Ferenczy A, Kurman RJ (2002) Carcinoma and other tumors of the cervix. In: Kurman RJ (ed) Blaustein's pathology of the female genital tract, 5th edn. Springer, Berlin Heidelberg New York, pp 325–346
42. Yasmeen A, Berdel WE, Serve H, Muller-Tidow C (2003) E- and A-type cyclins as markers for cancer diagnosis and prognosis. Expert Rev Mol Diagn 3:617–633
43. Zerfass K, Schulze A, Spitkovsky D, Friedman V, Henglein B, Jansen-Durr P (1995) Sequential activation of cyclin E and cyclin A gene expression by human papillomavirus type 16 E7 through sequences necessary for transformation. J Virol 69: 6389–6399
44. Zhai YL, Nikaido T, Shiozawa T, Orii A, Fujii S (1999) Ex pression of cyclins and cyclin-dependent kinases in smooth muscle tumors of the uterus. Int J Cancer 84:244–250

Virchows Arch (2005) 446: 634–639
DOI 10.1007/s00428-005-1249-8

ORIGINAL ARTICLE

Maciej Lopucki · Ivo Schmerold · Agnes Dadak · Henryk Wiktor · Hans Niedermüller · Marta Kankofer

Low dose magnetic fields do not cause oxidative DNA damage in human placental cotyledons in vitro

Received: 20 October 2004 / Accepted: 4 March 2005 / Published online: 19 April 2005
© Springer-Verlag 2005

Abstract The biological impact of low dose magnetic fields generated by electric appliances present in the human environment is still uncertain. In this study, human placentas served as a model tissue for the evaluation of the potential effect of oscillating low intensity magnetic fields on the concentration of 8-hydroxy-2′-deoxyguanosine (8-OH-dG) in cellular DNA. Cotyledons were dissected from placentas obtained immediately after physiological labours and exposed to magnetic fields (groups MF A, 2 mT, 50 Hz and MF B, 5 mT, 50 Hz) or sham exposed (group C) during an in vitro perfusion of 3 h. Cellular DNA was isolated, hydrolyzed and analyzed by HPLC. Native nucleosides were monitored at 254 nm and 8-OH-dG by electrochemical detection. Results were expressed as μmol 8-OH-dG/mol deoxyguanosine (dG). The concentrations of 8-OH-dG in group C, MF A and MF B were 28.45±15.27 μmol/mol dG, 62.80±31.91 μmol/mol dG, and 27.49±14.23 μmol/mol dG, respectively, demonstrating no significant difference between the groups. The results suggest that placental tissues possess a capacity to protect DNA against oxidative alterations by magnetic field of intensities previously shown to produce radical mediated DNA damage in rat brain cells in vivo and imbalances in electrolyte release of cotyledons under in vitro conditions.

Keywords Human placenta · Magnetic field · Oxidative DNA damage · 8-Hydroxy-2′-deoxyguanosine

M. Lopucki · H. Wiktor
I. Chair and Department of Obstetrics and Gynaecology,
Faculty of Medicine, Medical University School,
Staszica 16,
20-081 Lublin, Poland

I. Schmerold · A. Dadak
Institute of Pharmacology and Toxicology,
Department of Natural Sciences,
Veterinary University of Vienna,
Veterinärplatz 1,
1210 Vienna, Austria

H. Niedermüller
Institute of Physiology and Ludwig Boltzmann Institute
for Aging Research, Department of Natural Sciences,
Veterinary University of Vienna,
Veterinärplatz 1,
1210 Vienna, Austria

M. Kankofer (✉)
Department of Biochemistry,
Faculty of Veterinary Medicine,
Agricultural University,
Lubartowska 58 a,
20-123 Lublin, Poland
e-mail: kankofer@agros.ar.lublin.pl
Tel.: +48-81-7474023
Fax: +48-81-4456006

Introduction

Various appliances and electric tools induce magnetic fields with flux densities in the milliTesla (mT) range at a frequency of 50 Hz (Europe) or 60 Hz (USA). Such devices comprise vacuum cleaners, electric can openers, micro waves, portable heaters, fluorescent light fixtures, electric shavers, and television sets [2].

There are various publications on adverse biological effects and risks to human health associated with low dose exposures to magnetic fields occurring in the environment. The available information on the biological impact of magnetic fields of low energy is, however, contradictory due to variations of the biological systems studied and the biological endpoints analyzed [see review 24].

Some epidemiological studies suggest that exposure of humans to extremely low frequency magnetic fields leads to an increased incidence of cancer [8]. Other studies have shown no health risks following occupational extremely low frequency magnetic field exposure, indicating that the data on the biological effects of magnetic fields are ambiguous [14, 29], and therefore pointing to the need for further elucidation.

Nevertheless, published experimental data show that low frequency magnetic fields can exert various effects in living organisms. Among the effects observed are increases in enzyme reaction rates and transcript levels for specific genes

[7], genomic instability [33] and co-promoting effects in tumor development [5].

Chung et al. [3] reported that continuous exposure of rats between gestational days 6 and 20 to doses ranging between 0.005 mT and 0.5 mT (60 Hz) did not produce any biological effects in either dams or fetuses. Similar negative results were described by Negishi et al. [28] in rats following exposure to dose levels between 0.007 mT to 0.35 mT during days 8–15 of gestation. On the contrary, the exposure of rats of both sexes to 0.25 mT (50 Hz) for 90 days before mating showed some adverse effects on fertility, comprising an increased number of resorptions as well as a significantly decreased number of implantations and living fetuses per litter. Male rats exerted a partly reversible infertility [1].

McCann et al. [24] reviewed published studies on the effect on DNA both of magnetic and electric fields in a variety of experimental models including bacteria, *Drosophila melanogaster*, cultured human and animal derived cells and rats. Their overall conclusion was that electric and magnetic fields may exert genotoxic effects directly via damage to chromosomes or indirectly by alterations of DNA repair mechanisms. Indirect effects are presently understood to be induced by oxygen radical generation or impairment of antioxidative defence mechanisms.

An increase in DNA single- and double-strand breaks was found in brain cells of rats after acute exposure for 2 h to a 60-Hz magnetic field of 0.1–0.5 mT [15]. Ivancsits et al. [10] observed that intermittent exposure to a 50 Hz magnetic field causes a reproducible increase in DNA strand breaks in human diploid fibroblast cultures. Furthermore, it was shown that treatment with antioxidants such as melatonin and also spin-trap compounds blocks magnetic field induced single- and double-strand breaks in brain cell DNA [16]. Melatonin was documented to directly trap hydroxyl and peroxyl radicals [12]. These data suggest free radicals such as hydroxyl and peroxyl radicals to play a key role in magnetic field-induced DNA damage.

8-Hydroxy-2′-deoxyguanosine (8-OH-dG) is one of the most abundant cellular DNA lesions generated by reactive oxygen species (ROS). This guanine modification is often taken as a marker analyte of oxidative DNA damage in tissue and in urine following renal excretion [6, 18]. It was recently shown that increased levels of 8-OH-dG in placental cellular DNA can be associated with pathological conditions linked to oxidative stress [13, 34].

In order to gain a first insight into potential effects of oscillating low intensity magnetic fields in human placental tissue we have determined under defined in vitro conditions the levels of 8-OH-dG following acute exposures of cotyledons to magnetic fields with flux densities of 2 mT and 5 mT (50 Hz). This tissue was chosen for two reasons: (i) because it is a non-invasively obtainable human model matrix and (ii) to study whether magnetic fields with densities and a frequency ubiquitously occurring in the human environment acutely lead to oxidative DNA lesions in terms of concentrations of 8-OH-dG.

Material and methods

Human placentas collected in the I. Department of Obstetrics and Gynaecology, Faculty of Medicine, Medical University of Lublin (Poland) from physiological labours through natural births between weeks 38 and 41 of pregnancy were used in this study. Placentas were taken only from women (age ranging between 17 and 38 years, mean 26.3 years) with an uncomplicated pregnancy and a delivery without drug treatment. Exclusion criteria comprised hypertensive disorders, haemorrhage, intrauterine infection, fetal distress, abnormal placentation, oligo- and polyhydramnios, diabetes mellitus, collagen vascular disease, abuse of tobacco or alcohol, and neonatal weight below 2500 g and above 4500 g.

Only placentas with undamaged surfaces and fetal membranes preserved in at least one-third of the placenta circumference were used. Tissue with pathological arterial and venous systems (e.g. with additional cotyledons or marginal vessels) or with ruptures of the basal decidua was excluded. In order to ensure homologous specimen cotyledons were consistently dissected from the edge of the placenta.

The competent ethical commission of the Medical University in Lublin granted permission for this study.

Cotyledons were transferred into a chamber and perfused using an adapted dual closed perfusion system [19, 20, 25] as described by Schneider et al. [32]. Cotyledons were divided into three groups: a sham exposed control group (C, n=12) and two experimental groups exposed for 3 h to a magnetic field with a flux density of 2 mT (MF A, n=10) or 5 mT (MF B, n=9), each with a frequency of 50 Hz.

One cotyledon from each of the 31 placentas was perfused. The time passing from the delivery of the placenta to the beginning of the perfusion did not exceed 8 min. The mean weight of the placentas was 486.2±115.4 g and that of the cotyledon 32.2±12.3 g with a maximum diameter of less than 3.90 cm and a surface of less than 15.20 cm^2.

Tissue culture M 199 medium (Sigma, Poznan, Poland, pH 7.45) served as perfusion fluid; it contained glucose (2 g/l, Gliwa, Gliwice, Poland), Bactrim (1 ml/l, corresponding to 80 mg sulfamethoxazol/l and 16 mg trimethoprim/l, Polfa, Kutno, Poland), heparin (25,000 IU/l, Polfa), and dextran 40,000 (Sigma) at a concentration of 30 g/l in the fetal (F) and 7.5 g/l in the maternal circulation (M). In each experiment, 300 ml of the M solution and 120 ml of the F solution were used.

After preparation of the amniotic sac, two umbilical catheters (5.0 Fr; Balton, Warszawa, Poland) were inserted into the 3rd order fetal artery and vein, which run together. Following fixation of the catheters with Mersilk 3.0 sutures (Ethicon, Warszawa, Poland), perfusion of the fetal side was initiated. The flow in the fetal vessels was 3.0±0.1 ml/min and the pressure did not exceed 6.67 kPa. The maternal circulation was artificially maintained by insertion of 3 5.0 Fr catheters into the intervillous space through the chorionic

surface of each cotyledon. A flow rate of 14.0±0.2 ml/min was established.

Following washout of the blood from the fetal circulation with 20 ml perfusion fluid and from the maternal circulation with 50 ml, both circulations were closed. The perfusion fluid on the maternal side was oxygenated with a mixture of 95% O_2 and 5% CO_2, while the fetal fluid was saturated with a mixture of 95% N_2 and 5% CO_2.

The proper function of the human cotyledon in the perfusion system was confirmed by the lack of a maternal-fetal leakage greater than 1 ml/30 min. The difference of oxygen pressure in the fetal vein and artery was at least 60 mmHg throughout the experiment. Other parameters such as pH, pO_2 and pCO_2 of the perfusion fluids in the artery and vein of the maternal and fetal circulation were measured every 30 minutes using a blood gas analyser (Ciba Corning 248, Halstead, United Kingdom).

After 30 min of cotyledon adaptation in the perfusion chamber, the magnetic field was applied for experimental group MF A or MF B. The electromagnet consisted of 50,000 turns of copper wire (0.05 mm diameter) placed on a ferromagnetic core of 20 mm diameter. The magnetic field was generated by transformation of the power line current (220 V, 50 Hz). Teslometer (Aspan, Warszawa, Poland) measurements confirmed a uniform distribution of the magnetic field over a surface of 17.6 cm^2, ensuring exposure of the whole cotyledon. With the frequency of 50 Hz used in our experiment, the generation of an electric field was minimal and could be excluded as an influencing factor. Control placentas were perfused without application of the magnetic field.

At the end of the perfusion the cotyledon samples were taken from the central area and immediately frozen at -80°C.

Isolation and analysis of DNA

Cellular DNA was extracted from placentas (sample weight approximately 100 mg) by use of a Qiagen genomic DNA purification kit following the standard protocol as given by the manufacturer (Qiagen Blood and Cell Culture DNA Midi Kit; Qiagen GmbH, Hilden, Germany). Isolated DNA pellets were dried under a stream of N_2, dissolved overnight in 200 µl of 20 mmol/l sodium acetate buffer, pH 4.8, and digested with 20 µg nuclease P1 (Sigma; 30 min, 37°C); then 20 µl of Tris buffer (1 mol/l, pH 7.4) containing 1.3 IU of alkaline phosphatase (Roche Diagnostics GmbH, Vienna, Austria) was added, followed by a further incubation for 60 min at 37°C [6]. The DNA hydrolysate was directly applied onto an HPLC column.

The HPLC system comprised a Waters station with a 600 S controller, a 626 pump, a 717 plus autosampler, a 996 photodiode array detector and a serially connected 464 pulsed electrochemical detector equipped with a glassy carbon working electrode set at 0.6 V and an $Ag/AgCl_2$ reference electrode. Samples were injected into a Merck Superspher HPLC column (100 RP18e, 4 µm, 4.6×250 mm) and isocratically eluted (50 mmol/l KH_2PO_4, 5% acetonitrile, pH 4.1; flow 0.5 ml/min; oven temp 44°C). Ultrapure water produced by a MILLI-Q 185 plus system was used in this study [30].

Native nucleosides were monitored at 254 nm and 8-OH-dG by electrochemical detection. Authentic marker substances purchased from Sigma and Merck were used as standards. Peak areas served as integration parameters. Concentrations of 8-OH-dG were expressed as µmol/mol 2′-deoxyguanosine (dG). Concentrations of DNA were determined by comparison of the dG-peak areas of tissue samples with the dG-peak areas of known amounts of calf thymus DNA. The calibration curves for all native nucleosides and 8-OH-dG were linear within the relevant concentration ranges measured in placental DNA samples.

Table 1 Concentrations of 8-hydroxy-2′-deoxyguanosine (µmol/mol deoxyguanosine) in cellular DNA from perfused cotyledons sham exposed (group C) or exposed to 50 Hz magnetic fields of 2 mT (group MF A) or 5 mT (group MF B) for 3 h. *M* arithmetic mean, *SEM* standard error of the mean, *n* number of cotyledons

Group	*n*	M	SEM
C	12	28.45	15.27
MF A	10	62.80	31.91
MF B	9	27.49	14.23

Statistics

Comparative analysis of the results was performed using the Mann-Whitney *U*-test. A non-parametric test was used because the values did not show a normal distribution. A P-value<0.05 was considered as significant.

Results

Samples collected from group C showed 8-OH-dG levels ranging from 3.39 to 194.07 µmol/mol dG with a mean value of 28.45 µmol/mol dG; this group was statistically not different from groups MF A and MF B with mean levels of 62.80 µmol/mol dG (minimum 4.52 µmol/mol dG, maximum 264.63 µmol/mol dG) and 27.49 µmol/mol dG (minimum 2.60 µmol/mol dG, maximum 113.83 µmol/mol dG), respectively (Table 1).

Typical chromatograms of a placental hydrolysate are shown in Fig. 1. The ultraviolet absorbance peaks of the native nucleosides deoxycytosine (dC), deoxyguanosine (dG), deoxythymidine (dT), and deoxyadenosine (dA) are depicted in Fig. 1A. Minor peaks detected most probably represent hydrolysis products from residual RNA within the DNA preparations since their retention times resemble those of RNA nucleoside standards. In Fig. 1B the corresponding electrochemical 8-OH-dG chromatogram is shown. Included is a chromatogram of an 8-OH-dG standard run with 8-OH-dG eluted at approximately 9.85 min as a clearly separated peak.

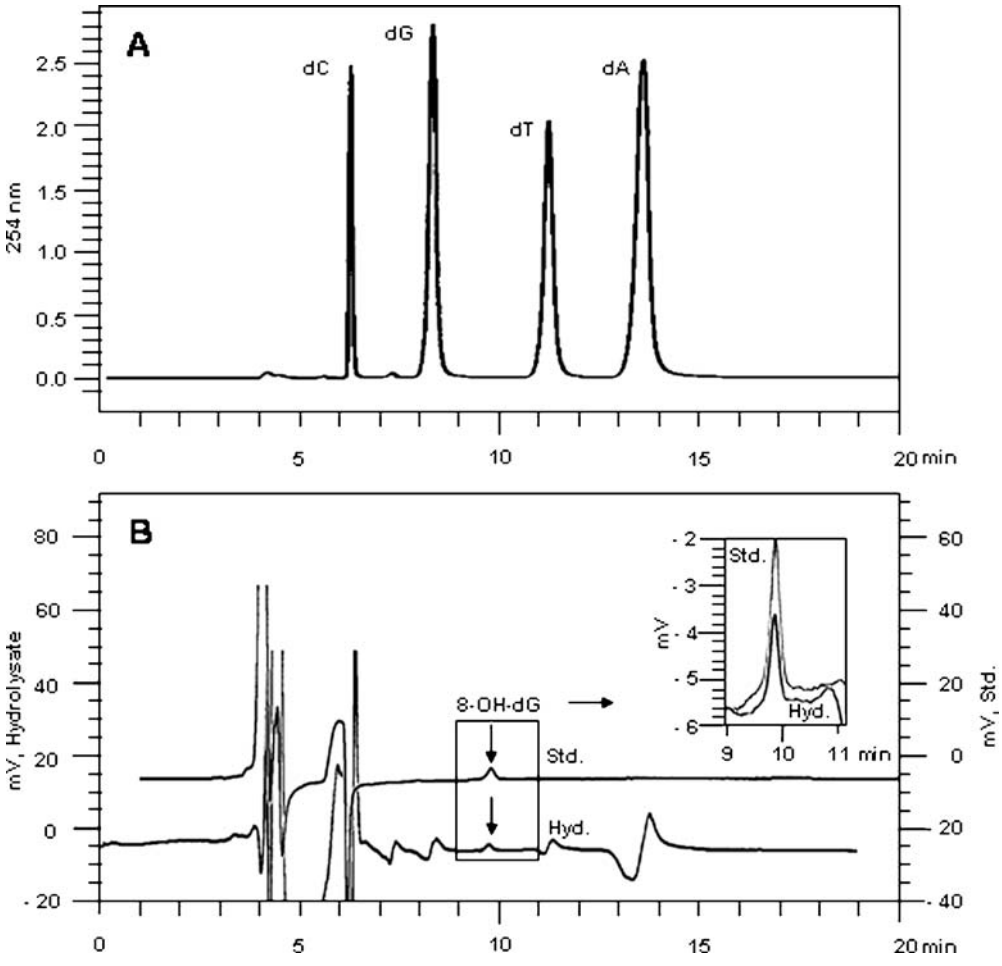

Fig. 1 UV and EC chromatograms of a DNA hydrolysate (*Hyd.*, 50 µl). DNA was isolated from 100 mg placental tissue using a commercial Quiagen DNA extraction kit, digested with nuclease P1 and alkaline phosphatase and subjected to reversed phase HPLC. The nucleosides dC (6.24 min), dG (8.31 min), dT (11.23 min), and dA (13.61 min) were monitored at 254 nm (**A**), 8-OH-dG (9.82 min) by electrochemical detection (**B**). Included is a chromatogram with 0.6 pmol 8-OH-dG standard (*Std.*; 9.85 min) dissolved in 60 µl distilled water

Discussion

The biological impact of the exposure to magnetic fields present in the human environment is difficult to assess due to the increasing number of sources emitting various field densities and frequencies. Practically all living organisms are continuously exposed in one way or another to magnetic fields of different types. The International Commission of Non-Ionising Radiation Protection proposed 0.5 mT per working day for occupational exposure and 0.1 mT per 24 h for the general population [9].

It is a matter of concern that pregnant women are also habitually exposed to low frequency magnetic fields. Their influence on placental function is not well studied. It is, however, known that 5 mT 50 Hz oscillating magnetic fields intensify the release of sodium ions from in vitro perfused cotyledons both to the fetal and maternal circulation [22]. Lopucki et al. [21] also observed that low-induction magnetic fields (2 mT, 50 Hz) activate apoptosis in the human placenta under in vitro conditions. Placental tissue is of particular interest because of its specific function and importance for the maintenance of pregnancy and fetal development. From an investigational viewpoint, it can be taken as a human model tissue available by non-invasive techniques; in vitro perfusion methods allow for the study of biochemical parameters under maintenance of its function.

The present study focused on the generation of 8-OH-dG in cellular DNA from perfused human placental tissue acutely exposed for 3 h to 2 mT or 5 mT magnetic fields with a frequency of 50 Hz. This flux density, although higher than 0.5 mT as proposed as occupational exposure limit by the ICNIRP per working day, was chosen because of its environmental relevance and its known detrimental effects in different biological systems including the placenta [10, 11, 21, 22, 31]. In order to ensure the maintenance of proper function of placenta during in vitro perfusion the duration of exposure was limited to 3 h. In combination with the chosen flux densities, this period is not far from actual exposure conditions of a normal day in the industrial world.

8-OH-dG was taken as an indicator of oxidative stress because this base lesion is widely accepted to reflect the status of oxidative DNA damage in tissues including the placenta of humans and other species [6, 18].

Under the conditions of this study both exposure levels did not yield any significant change of the 8-OH-dG concentrations in placental cellular DNA when compared to sham exposed controls. Mean concentrations of 8-OH-dG found in control samples were approximately 28 µmol/mol

dG and resembled those found by Daube et al. [4] in non-perfused placental tissues (8.7±1.6 per 10^6 dG).

The concentration of 8-OH-dG is subject to various parameters, including the individual and the site of the placenta where the specimen for analysis are taken from. This argument is reflected by recently published data generated with tissue samples taken from the mid-disc region of the chorionic plate from normal placentas (the middle between the edge of the placenta and the origin of the umbilical cord). In these investigations, the mean concentrations of 8-OH-dG of approximately 179±80 μmol/mol dG were found. This relatively high level was attributed to a single elevated concentration of approximately 1413 μmol 8-OH-dG/mol dG found in one out of 18 samples [34].

It must be remembered that the extent of oxidative DNA damage induced by exogenous sources depends on various factors including the oxidative status of the cells, the capability of antioxidative enzymatic and non-enzymatic processes to counteract free radical build-up, the availability of exogenous antioxidants, the iron homeostasis, processes of DNA repair and the kind of ROS generated. Most of these factors can be considered to be affected by the parameters of the intensity, dose, and frequency of magnetic fields.

Intermittent exposure was demonstrated to exert more impact on biological structures than continuous. Ivancsits et al. [10] observed a reproducible increase in DNA strand breaks in cultured human diploid fibroblasts following a discontinuous exposure (5 min on/10 min off for 24 h) to a 50 Hz magnetic field of 1 mT. In a different study, the same author [11] described an increase in DNA strand breaks in human diploid fibroblasts after up to 15 h of intermittent exposure to electromagnetic fields which declined to base levels after termination of exposure. The authors distinguished between single and double strand breaks and suggested, on the basis of their comet assay results, that single-strand DNA breaks are repaired within 30 min while double-strand breaks need 7–9 h for restoration.

The damage to DNA thus appears to be a complex function of the duration of exposure, magnetic flux density and the time of recovery.

Lai and Singh [17] showed that acute exposure of rats for 3 h to 60 Hz magnetic fields with intensities between 0.1 and 0.5 mT produced increases in DNA single and double strand breaks in brain cells. The authors supported the so-called free radical hypothesis, which postulates that extremely low frequency electromagnetic fields intensify free radical activity in cells thereby causing DNA damage and disturbance of other cellular processes and functions. ROS are believed to be involved in the complex process eventually leading to damage of DNA and other macromolecules [17, 23].

Our findings demonstrate that acute exposure of placental tissue to low dose magnetic fields (2 mT, 5 mT, 50 Hz) for 3 h does not cause oxidative damage in cellular DNA in terms of 8-OH-dG concentration. The lack of any significant effect on DNA oxidation under the conditions chosen is notable because magnetic fields of similar flux densities produced acute effects in other systems such as intermittently exposed cultured human fibroblasts [10].

Incubation of cotyledons for extended periods runs the risk for the tissue to drift away from a physiological status and to function in an artefactual manner not reflecting normal conditions. A potentially non-physiological status resulting from prolonged incubation periods was not systematically investigated in this study but both, decreased or increased 8-OH-dG levels, may occur due to malfunctions of pro- and antioxidative mechanisms.

Whether chronic exposure to low-dose magnetic fields can induce oxidative DNA damage in human placental tissue remains to be studied. For this purpose, a different experimental approach must be considered taking into account all ethical aspects in cases of studies including in vivo exposures.

Schmitz et al. [31] observed in mice exposed to a 50 Hz magnetic field with a mean flux densitiy of 1.5 mT for 8 weeks a significant increase in both unscheduled DNA synthesis and in situ nick translation in epithelial cells of the choroid plexus, but not in other types of brain cells in the cortex, hippocampus and cerebellum. In renal epithelial cells of the distal convoluted tubules and collecting ducts an increased synthesis of mitochondrial DNA was found. Presently, these cell specific vulnerabilities towards low dose magnetic fields are far from being understood.

The present study suggests placental tissue to possess a capacity to protect its DNA against oxidative damage by magnetic fields under conditions which were shown to produce imbalances in sodium, calcium, and magnesium concentrations both in the maternal and/or fetal circulation [22]. Whether the mature human placenta develops a specific resistance to low dose oscillating magnetic fields potentially based on rapidly responding adaptive mechanisms to preserve its physiological function remains to further studies. It is worth mentioning that pregnancy per se is described as a condition of oxidative stress maintained by placental mitochondrial activity [see review 27]. All major antioxidant systems are physiologically present in this tissue. Several DNA enzyme systems specific for 8-OH-dG repair are known; however, their activity and interaction in human placenta have not yet been studied. In addition, estriol, which rises with progession of gestation to levels 1000-fold higher than that of estradiol, was recently reported to act as an antioxidant and possibly to be involved as one component of the self-protection system against oxidative damage of human placental tissue [26].

Acknowledgements The authors express their gratitude to the Department of Physics, Agricultural University, Lublin, Poland, for theoretical calculations and for providing the electromagnetic device used in this study. The authors are also grateful to Harald Kühnel and Michael Balka (both Veterinary University of Vienna) and Wanda Rogowska (Medical University Lublin) for excellent technical assistance.

This study was supported by the Polish State Committee for Scientific Research (KBN 6 PO5E 04420).

References

1. Al-Akhras MA, Elbetieha A, Hasan MK, Al-Omari I, Darmani H, Albiss B (2001) Effects of extremely low frequency magnetic field on fertility of adult male and female rats. Bioelectromagnetics 22:340–344
2. Blank M (1995) Electromagnetic fields. Biological interactions and mechanisms. American Chemical Society, Washington, thesis, Columbia University, 223 pp
3. Chung MK, Kim JC, Myung SH, Lee DI (2003) Developmental toxicity evaluation of ELF magnetic fields in Sprague-Dawley rats. Bioelectromagnetics 24:231–240
4. Daube H, Scherer G, Riedel K, Ruppert T, Tricker AR, Rosenbaum P (1997) DNA adducts in human placenta in relation to tobacco smoke exposure and plasma antioxidant status. J Cancer Res Clin Oncol 123:141–151
5. Fedrowitz M, Kamino K, Loscher W (2004) Significant differences in the effects of magnetic field exposure on 7,12-dimethylbenz(a) anthracene-induced mammary carcinogenesis in two substrains of Sprague-Dawley rats. Cancer Res 64:245–251
6. Fraga CG, Shigenaga MK, Park JW, Degan P, Ames BN (1990) Oxidative damage to DNA during aging: 8-hydroxy-2′-deoxyguanosine in rat organ DNA and urine. Proc Natl Acad Sci USA 87:4533–4537
7. Goodman R, Blank M (2002) Insights into electromagnetic interaction mechanisms. J Cell Physiol 192:16–22
8. Hakansson N, Floderus B, Gustavsson P, Johansen C, Olsen JH (2002) Cancer incidence and magnetic field exposure in industries using resistance welding in Sweden. Occup Environ Med 59:481–486
9. International Commission on Non-Ionizing Radiation Protection (1998) Guidelines for limiting exposure to time-varying magnetic and electromagnetic fields up to 300 GHz. Health Phys 74: 494–522
10. Ivancsits S, Diem E, Pilger A, Rudiger H, Jahn O (2002) Induction of DNA strand breaks by intermittent exposure to extremely-low-frequency electromagnetic fields in human diploid fibroblasts. Mutat Res 519:1–13
11. Ivancsits S, Diem E, Jahn O, Rüdiger H (2003) Intermittent extremely low frequency electromagnetic fields cause DNA damage in a dose dependent way. Int Arch Occup Environ Health 76:431–436
12. Jajte J, Zmyslony M (2000) The role of melatonin in the molecular mechanism of weak, static and extremely low frequency (50 Hz) magnetic fields (ELF). Medycyna Pracy 51:51–57
13. Kankofer M, Schmerold I (2002) Spontaneous oxidative DNA damage in bovine retained and nonretained placental membranes. Theriogenology 57:1929–1938
14. Knave B (2001) Electromagnetic fields and health outcomes. Annal Acad Med, Singapore 30:489–493
15. Lai H, Singh NP (1997) Acute exposure to a 60-Hz magnetic field increases DNA strand breaks in rat brain cells. Bioelectromagnetics 18:156–165
16. Lai H, Singh NP (1997) Melatonin and N-tert-butyl-alpha-phenylnitrone block 60 Hz magnetic field-induced DNA single and double strand breaks in rat brain cells. J Pineal Res 22:152–162
17. Lai H, Singh NP (2004) Magnetic-field-induced DNA strand breaks in brain cells of the rat. Environ Health Perspect 112:687–694
18. Loft S, Fischer-Nielsen A, Jeding IB, Vistisen K, Poulsen HE (1993) 8-Hydroxydeoxyguanosine as a urinary biomarker of oxidative DNA damage. J Toxicol Environ Health 40:391–404
19. Lopucki M, Szymczyk G, Rogowska W, Morawska D, Kotarski J (2002) Studies on the methodical values of in vitro dual perfusion of the human cotyledon performed according to the Schneider method modified by Miller. I. Evaluation of pH values of the perfusion fluid in the arterial and venous circulations of the fetal and maternal systems. Gin Pol 73:653–657
20. Lopucki M, Szymczyk G, Polak G, Rogowska W, Wiktor H, Kotarski J (2002) Studies on the methodical values of in vitro dual perfusion of the human cotyledon performed according to the Schneider method modified by Miller. II. Evaluation of arterial pressure values in the fetal circulation. Gin Pol 73:658–661
21. Lopucki M, Tarkowski R, Wojcierowski J, Rogowska W, Pietruszewski S, Kornarzynski K, Kowalski P, Czekierdowski A, Kotarski J (2003) Effect of low-frequency magnetic field on placental apoptosis in the perfused human placental cotyledon. Arch Perinatal Med 9:47–51
22. Lopucki M, Czekierdowski A, Rogowska W, Kotarski J (2004) The effect of oscillating low intensity magnetic field on the Na^{+}, K^{+}, Ca^{++}, and Mg^{++} concentrations in the maternal and fetal circulation of the dually perfused human placental cotyledon. Bioelectromagnetics 25:329–337
23. Marnett LJ (2002) Oxy radicals, lipid peroxidation and DNA damage. Toxicology 181–182:219–222
24. McCann J, Dietrich F, Rafferty C (1998) The genotoxic potential of electric and magnetic fields: an update. Mutat Res 411:45–86
25. Miller RK, Wier PJ, Maulik D (1985) Human placenta in vitro: characterisation during 12 hours dual perfusion. Contrib Gynecol Obstet, Krager Basel 13:77–84
26. Mueller A, Koebnick C, Binder H, Hoffmann I, Schild RL, Beckmann MW, Dittrich R (2005) Placental defence is considered to control lipid peroxidation in pregnancy. Med Hypoth 64 (3):553–557
27. Myatt L, Cui X (2004) Oxidative stress in the placenta. Histochem Cell Biol 122:369–382
28. Negishi T, Imai S, Itabashi M, Nishimura I, Sasano T (2002) Studies of 50 Hz circularly polarized magnetic fields of up to 350 microT on reproduction and embryo-fetal development in rats: exposure during organogenesis or during preimplantation. Bioelectromagnetics 23:369–389
29. Reynolds P, Cone J, Layefsky M, Goldberg DE, Hurley S (2002) Cancer incidence in California flight attendants (United States). Cancer Causes Control 13:317–324
30. Schmerold I, Niedermüller H (2001) Levels of 8-hydroxy-2′-deoxyguanosine in cellular DNA from 12 tissues of young and old Sprague-Dawley rats. Exp Gerontol 36:1375–1386
31. Schmitz C, Keller E, Freuding T, Silny J, Korr H (2004) 50-Hz magnetic field exposure influences DNA repair and mitochondrial DNA synthesis of distinct cell types in brain and kidney of adult mice. Acta Neuropathol 107:257–264
32. Schneider H, Panigel M, Danicis J (1972) Transfer across the perfused human placenta of antipyrine, sodium and leucine. Am J Obstet Gynecol 114:822–828
33. Simko M, Richard D, Kriehuber R, Weiss DG (2001) Micronucleus induction in Syrian hamster embryo cells following exposure to 50 Hz magnetic fields, benzo(a)pyrene, and TPA in vitro. Mutat Res 495:43–50
34. Wiktor H, Kankofer M, Schmerold I, Dadak A, Lopucki M, Niedermüller H (2004) Oxidative DNA damage in placentas from normal and preeclamptic pregnancies. Virchows Arch 445: 74–78

Virchows Arch (2005) 446: 640–645
DOI 10.1007/s00428-005-1251-1

ORIGINAL ARTICLE

Christopher Burke · Glenda Gobe

Pontosubicular apoptosis ("necrosis") in human neonates with intrauterine growth retardation and placental infarction

Received: 7 January 2005 / Accepted: 4 March 2005 / Published online: 19 April 2005
© Springer-Verlag 2005

Abstract In a previous study of 37 autopsied stillbirths with non-dysmorphic intrauterine growth retardation (IUGR), 26 cases were associated with placental infarction, a morphologic marker of uteroplacental insufficiency. Nine of the 26 cases with both IUGR and placental infarction, where archival tissue was available, had grey matter ischaemic lesions that were subsequently identified as "pontosubicular necrosis". This lesion is now regarded as a localized form of apoptosis. A further eight third trimester stillbirth cases with both IUGR and placental infarction were ascertained prospectively. Sixteen of these 17 cases showed pontosubicular apoptosis, identified morphologically and verified using activated caspase-3 and TUNEL. Five of the 17 cases showed apoptosis in the frontal or temporal cortex as well. In this current study, pontosubicular apoptosis was strongly associated with IUGR and placental infarction in third trimester stillborns, suggesting that uteroplacental insufficiency leading to chronic fetal hypoxaemia may cause cerebral apoptosis.

Keywords Neonate · Pediatrics · Intrauterine growth retardation · Apoptosis · Necrosis

C. Burke
Department of Pathology,
Mater Hospitals,
Brisbane, Australia

C. Burke · G. Gobe
Discipline of Molecular and Cellular Pathology,
University of Queensland School of Medicine,
Herston Road,
Herston, Australia

C. Burke (✉)
Department of Pathology,
University of Sydney (DO6),
2006 Sydney, Australia
e-mail: christeph@bigpond.com
Fax: +61-2-93513429

Introduction

"Pontosubicular necrosis" was originally described by Friede [10] as a specific form of hypoxic prenatal or perinatal brain injury that led to karyorrhectic neuronal death in the basal pons and hippocampal subiculum. He noted that the vulnerable period for the development of pontosubicular necrosis is from the 30th week of gestation to the 2nd month post-term. Pontosubicular necrosis has been attributed to ischaemia, hyperoxia, hypoglycaemia and hypocapnia as well as hypoxia [20]. A close association with intraventricular haemorrhage has also been reported [25]. Karyorrhectic neurons have also been noted in lesser numbers in several other areas of the brain in pontosubicular necrosis [22]. Recent studies using electron microscopy, in situ detection of apoptotic DNA fragmentation and anti-activated caspase-3 immunohistochemistry have shown that neuronal death in pontosubicular necrosis is apoptotic [6, 24] and associated with expression of Fas, a tumour necrosis factor cell surface receptor [26].

In a previous study by us [7], a consecutive series of 37 autopsied stillbirths greater than 20 weeks gestation with non-dysmorphic IUGR was reported. Approximately one-third of the cases were related to pre-eclampsia, one-third to multiple gestation and one-third were idiopathic. Thirty-one of the 37 cases showed histologic evidence of ischaemic cerebral injury mainly in the cerebral white matter, and placental infarction was seen in 26 of 36 placentas. Following this study, it was noted that pontosubicular apoptosis was present in nine of the cases with both IUGR and placental infarction. This had not been detected initially because archival tissue blocks of both the pons and subiculum were available in only a small number of cases. The stillborn fetuses were all macerated to some degree and, as noted by Keeling [13], this limited the extent of the neuropathological assessment and the number of tissue blocks available for histological assessment in each case. Eight further cases of third trimester fetuses with both IUGR and placental infarction were ascertained prospectively. The aim of the study was to quantitate the extent of pontosubicular apoptosis in the 17 cases and document any

Table 1 Gestational age in post-conceptional weeks (GA) and percentage of apoptosis in pons, subiculum and frontal (*F*) or temporal (*T*) cortex of sections the study cases. *NA* not available from archival tissue bank; *H&E* haematoxylin and eosin tissue stain; *TUNEL* terminal dideoxyuridine transferase-mediated nick end labelling

	GA	Pons			Subiculum			Cerebral Cortex			
		H&E	TUNEL	Caspase	H+E	TUNEL	Caspase	Lobe	H&E	TUNEL	Caspase
1	35	4.1	0.1	3.1	NA	NA	NA	F	0	0	0.1
2	34	NA	NA	NA	0.8	0.4	0.6	NA	NA	NA	NA
3	34	10	3	10	15	2	16	F	0.5	0.1	.5
4	31	15	6	15	NA	NA	NA	F	0.5	0.1	0.5
5	37	0.5	0.2	5	2.7	0.2	5	F	0.6	0.1	0.5
6	30	NA	NA	NA	4	0.2	4	F	2.2	0.1	0.1
7	40	NA	NA	NA	8.5	6	10	T	1.4	0.1	2
8	38	7.8	8	10	12	6	8	F	7.5	0.6	12
9	40	4.3	NA	NA	NA	NA	NA	F	0.2	6	0.5
10	32	2.4	0.5	4	5.3	0.2	7	F	0.2	0	0.1
11	37	10	8	14	NA	NA	NA	F	0.5	0	0.5
12	37	9.3	6	8	16	10	12	T	0.1	0	0.1
13	37	20	9	20	NA			F	0.5	0	0.4
14	38	0	0	0	0	0	0	F	0	0	0
15	32	12	6	13	14	5	11	F	1.9	2	3
16	34	14	7	12	18.6	6	16	F	1.6	0	2
17	39	14	6	11	NA	NA	NA	F	0.1	0	0.2

apoptosis in the cerebral cortex as well, using both standard histology and stains specific for apoptosis. Placental infarction is a morphological marker of uteroplacental insufficiency in pregnancies complicated by IUGR [17]. IUGR associated with abnormal blood flow in the umbilical artery is associated with chronic fetal hypoxaemia [23]. If pontosubicular apoptosis were strongly associated with IUGR and placental infarction, it would suggest that uteroplacental insufficiency leading to chronic fetal hypoxaemia might cause cerebral apoptosis.

Materials and methods

Ethical approval for this study was granted by the Mater Hospitals Human Ethics Committee (Reference number 524c), Brisbane, Australia.

Cases and histological preparation

Seventeen autopsied cases of stillborn fetuses with IUGR and placental infarction and tissue blocks of the pons, the subiculum or both comprise the basis of this report. Nine cases were included in a previous study [7] involving 225 perinatal autopsies that extended over 4 years. In two of these nine cases, blocks from both the pons and subiculum were available. Another eight cases were identified prospectively over a further 5-year period from 305 perinatal autopsies performed in that time. In three of these cases, blocks from both the pons and subiculum were obtained. The growth retarded fetuses had growth parameters below the third centile for gestational age. Cases with congenital abnormalities and evidence of fetal infection were excluded. Placental infarcts were considered significant when they occupied 5% or more of the placental villous surface. At the time of autopsy, the brains and placentas were processed using standard methods. Brains were fixed in 20% buffered formalin with added glacial acetic acid and placentas were fixed in 10% buffered formalin before processing to paraffin blocks and sectioning onto Superfrost plus histological slides.

In addition to the study cases, five stillborn fetuses with normal growth, normal placentas and no pathological abnormality detected at autopsy were selected to determine whether cerebral apoptosis was present in fetuses presumed to be normal morphologically. There were no cases of placental abnormalities and no signs of acute hypoxia prior to fetal death death. Tables 1 and 2 list the gestational ages of the study and comparison cases, respectively.

Histology, TUNEL and immunohistochemistry

Sections from all the available brain tissue blocks were stained with haematoxylin and eosin (H&E) as well as TUNEL (terminal dideoxyuridine transferase-mediated nick end labelling) and anti-activated caspase-3 antibody. The TUNEL assay identifies strand breaks in DNA that are typical of apoptosis and, for this assay, the ApopTag Peroxidase In Situ Apoptosis Detection Kit was used according to the manufacturer's protocol for paraffin embedded sections

Table 2 Gestational age (*GA*) and percentage of apoptosis in pons, subiculum and cortex of sections of the comparison cases. *NA* not available from archival tissue bank; *BG* basal ganglia

	GA	Pons	Subiculum	Cortex	BG
1	38	0	0	0	
2	38	0	0	0	
3	44	0	0	0	
4	33	NA	0	0	0
5	41	0	NA	0	

(Serologicals Corporation, Chemicon, Boronia, Australia). Caspase-3 is considered the executioner caspase for induction of apoptosis and the structural disassembly of apoptosis is subsequent to its cleavage to an activated form [4]. Hence, activated caspase-3 antibody (Santa Cruz Biotechnology Inc., Calif., USA) was used for immunohistochemistry and further biochemical verification of apoptosis. Sections were pre-treated with proteinase K, and endogenous peroxidase activity was blocked by incubating sections in 1.0% hydrogen peroxide (H_2O_2), 0.1% sodium azide in Tris-buffered saline (TBS) for 10 min and washing 3×5 min in TBS. Normal goat serum (10% in TBS) was applied for 20 min to stop non-specific binding and the primary antibody (rabbit anti-activated caspase-3, diluted 1:100) was applied for 1 h at room temperature, followed by washing 3×5 min in TBS. The Dako Envision anti-(mouse, rabbit, goat) antibody was applied for 30 min, followed by washing 3×5 min in TBS. Colour was developed in diaminobenzidine tetrahydrochloride (DAB) with H_2O_2 for 5 min, sections were washed in running water for 5 min and lightly counterstained with Mayer's haematoxylin prior to dehydration in ethanols, clearing in xylene and mounting with glass coverslips in Depex. Positive and negative controls were performed for TUNEL and activated caspase-3.

Quantification of apoptosis

Apoptotic neurons on available sections from the pons, subiculum, and the frontal or temporal cortex were counted by two observers independently, using H&E, TUNEL and anti-activated caspase-3 stained sections. Using an eyepiece grid at ×400 magnification, a minimum of 1000 cells was counted in each brain region and the percentage of apoptotic cells was calculated. The morphological features of apoptosis used in the H&E slides were those described previously [8, 14]. For example, apoptosis was assessed as shrunken darkly staining cells with condensed, marginated nuclear chromatin and intact cell membranes or discrete apoptotic bodies comprising large dense, pyknotic, nuclear fragments usually surrounded by a narrow cytoplasmic rim. Any doubtful cells, such as apoptotic cells within vessels, were disregarded. Counts were made in affected areas of the pons, subiculum and cerebral cortex. The means of the cell counts for the two observers are presented for each of the three stains.

Results

Quantification of apoptosis

The results of the apoptotic cell counts on the H&E, TUNEL and anti-activated caspase-3 stained sections from the 17 study cases are given in Table 1 and apoptotic counts using H&E for the comparison cases in Table 2. Although we detected no apoptosis in sections of the comparison cases, we cannot exclude the occurrence of a minor degree of apoptosis that would be likely to occur normally in all fetal brains. Sixteen of the 17 study cases had apoptotic neurons in the pons, subiculum or both, whereas no apoptotic neurons were seen in the same regions in the comparison cases. In each of the 16 cases, the number of apoptotic neurons seen on the H&E stain was >1% in the affected areas. Apoptotic neurons were also seen in the frontal or temporal cortex in 14/17 study cases and none of the comparison cases. In five of these 14 cases, the counts were greater >1%. The lack of detectable apoptosis by any

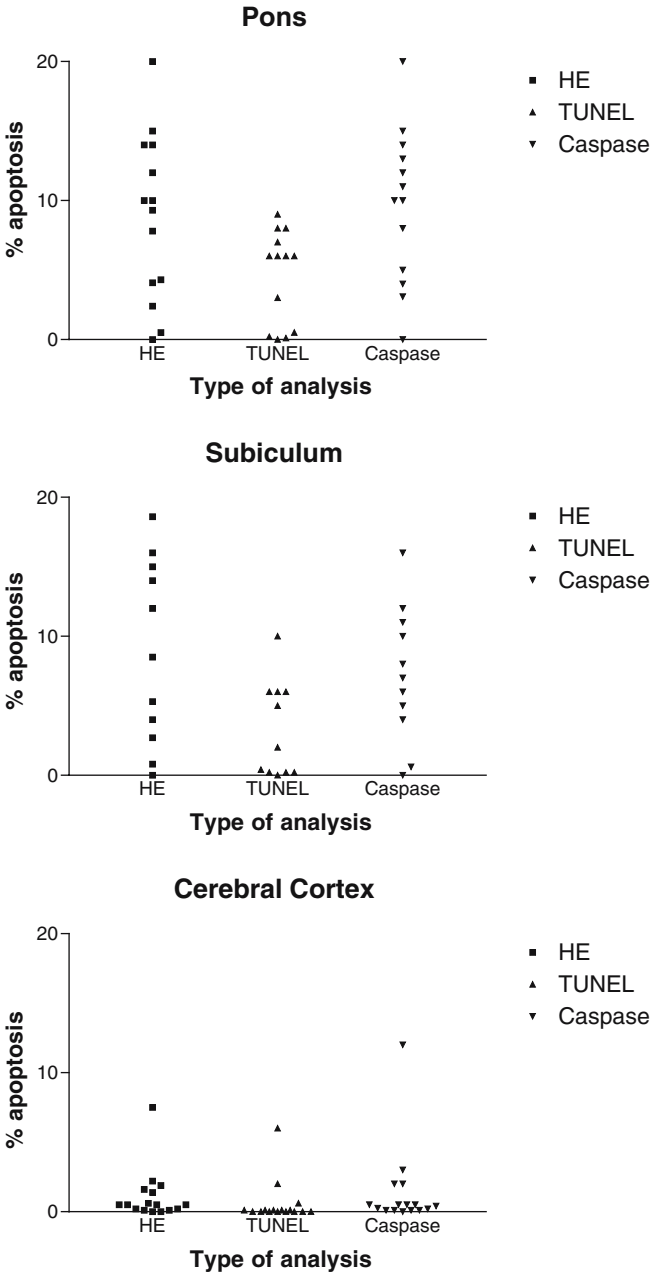

Fig. 1 Comparison of apoptotic counts for pons, subiculum and cerebral cortex using H&E, TUNEL and activated caspase-3 stains. Significance of correlations between H&E with TUNEL or caspase-3 is listed in Table 2. With one exception (H&E and TUNEL in subiculum, $P<0.1$), there was a significant correlation between these methods of assessing apoptosis in each case

Table 3 Regression analysis comparing apoptosis identified in haematoxylin and eosin (H&E)-stained sections with TUNEL (terminal dideoxyuridine transferase-mediated nick end labeling) or activated caspase-3 (*casp3*) for pons, subiculum and cerebral cortex (*cortex*)

	Slope	Intercept	R^c	Significance
Pons H&E vs TUNEL	0.843	0.416	0.462	$P<0.05$
H&E vs casp3	0.933	1.834	0.850	$P<0.001$
Subiculum H&E vs TUNEL	0.788	−0/354	0.411	NS
H&E vs casp3	0.943	1.254	0.783	$P<0.001$
Cortex H&E vs TUNEL	0.929	−0.319	0.779	$P<0.001$
H&E vs casp3	0.943	−0.178	1.520	$P<0.001$

method in case 14 is likely an example of biological variation, or mis-diagnosed IUGR. Figure 1 demonstrates the comparisons of counts for pons, subiculum and cerebral cortex for H&E, TUNEL and activated caspase-3 stains. Table 3 lists the results of the linear regression analysis for H&E with TUNEL or H&E with activated caspase-3 for each tissue type. With one exception (H&E and TUNEL in subiculum, $P<0.1$), there was a significant correlation between these methods of assessing apoptosis in each case (Table 3 for significance). In particular, these data indicate that detection of active caspase-3 is a reliable marker for apoptosis in formalin-fixed human tissue, and that neuronal apoptosis in pontosubicular necrosis/apoptosis is accompanied by a pronounced activation of caspase-3.

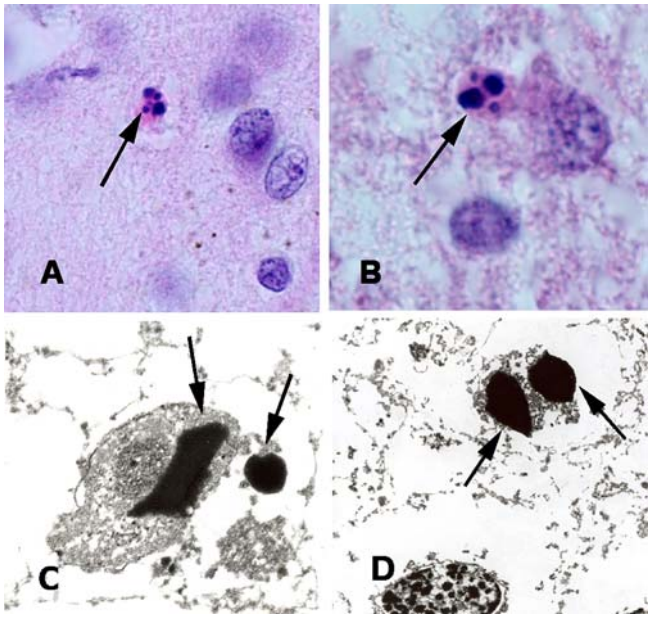

Fig. 2 Photomicroscopic examples of apoptosis as assessed using H&E stained sections are illustrated in **a** and **b** (arrows). The distinct condensation of the nuclear chromatin is visible in the arrowed cells. **c** and **d** demonstrate electron microscopy of apoptotic cells (*arrows*). Despite the loss of clear cell structure from the autopsy specimens, there is evidence of cell shrinkage and also the typical nuclear changes of apoptosis: condensed nuclear chromatin within a shrunken cytoplasm plus another nuclear bleb in **c**, and condensed and fragmented nuclear chromatin in crescentic forms in **d**

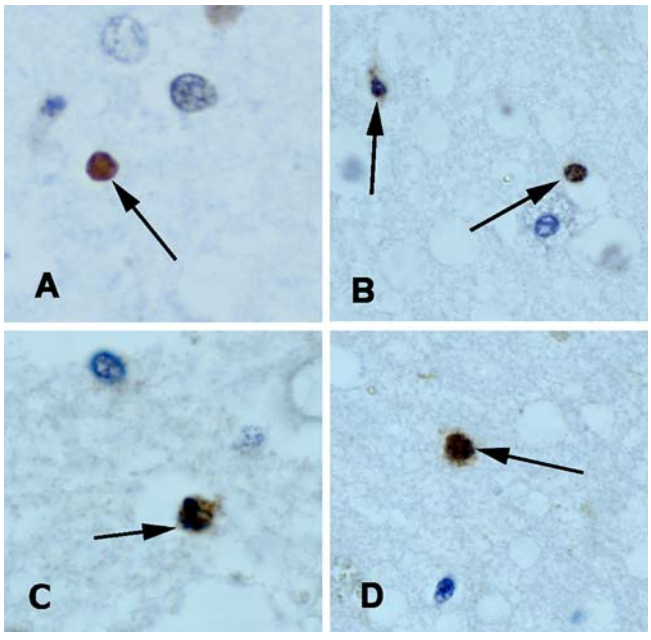

Fig. 3 TUNEL and activated caspase-3 stains are demonstrated in **a** and **b** (TUNEL) or **c** and **d** (activated caspase-3). Some morphological features of apoptotic cells (nuclear condensation and blebbing) are also visible in the *arrowed* cells

Microscopy of apoptosis

Photomicroscopic examples of apoptosis as assessed in H&E stained sections are illustrated in Fig. 2a and b. The distinct condensation of the nuclear chromatin is visible in the arrowed cells. Electron microscopic verification of apoptosis is demonstrated in Fig. 2c and d. Despite the loss of clear cell structure from the autopsy specimens, there is evidence of cell shrinkage and also the typical nuclear changes of apoptosis: condensed nuclear chromatin within a shrunken cytoplasm plus another nuclear bleb in Fig. 2c, and condensed and fragmented nuclear chromatin in crescentic forms in Fig. 2d. Further verification was provided with TUNEL and activated caspase-3 stains which are demonstrated in Fig. 3a-d. Figure 3a and b indicate TUNEL positive cells beside other non-stained nuclei and Fig. 3c and d demonstrate activated caspase-3 positive cells.

Discussion

The notable feature of the data presented above is that 16/17 consecutive third trimester stillborn fetuses with both IUGR and placental infarction coming to autopsy had typical neuronal apoptotic changes in the pons, subiculum or both. A comparison group of presumed normal stillborn fetuses with normal placentas did not show any histologic brain abnormality. Neuronal apoptosis was also present in the frontal or temporal cortex in 14/17 of the study cases, in five of these cases involving 1% of neurons counted.

These findings suggest that the unfavourable intrauterine environment in IUGR fetuses exposed to reduced uteroplacental blood flow can cause cerebral apoptosis. Several

studies [3, 9, 21] have shown increased apoptosis in placentas from pregnancies complicated by IUGR. The cause of this increase has not been elucidated in the quoted studies, but the current finding suggests that uteroplacental insufficiency may contribute to both placental and cerebral apoptosis in IUGR.

The results of the present study confirm the earlier work of Bruck and colleagues [6] and Stadelmann and colleagues [24] showing that neuronal death in pontosubicular "necrosis" is apoptotic. They somewhat contradict the view of Auer and Sutherland [2] that apoptotic cell death is controversial in human cerebral ischaemia. However, the latter authors were referring to acute cerebral infarction in adults, whereas the present study involves fetuses exposed to chronic intrauterine hypoxaemia.

In 15 of the 17 study cases, the number of apoptotic neurons seen on the H&E stain was >1% in the affected tissues. The neuronal counts mainly provide a comparison between cases rather than an accurate measure of the degree of apoptosis. However, there have been many studies, including one of ours [11], in which the significance of low counts of apoptosis, in terms of organ dysfunction, is discussed. For example, each histological section is a 4 μm tissue slice glimpsed at only a brief window of time. Apoptosis is a very rapid process and quickly cleared from tissues. The total effect over a long period of time in the current tissue would probably be a significant deletion of neuronal mass.

The results of the present study are also of interest in the light of recent experimental work by Lane and colleagues [16]. These authors showed that uteroplacental insufficiency in growth retarded fetal rats reduces the threshold for subsequent hypoxia-induced cerebral apoptotic injury. This may explain the increased susceptibility of IUGR human fetuses to intrapartum asphyxia [18].

The documented increase in apoptosis in the pons and subiculum in the stillborn fetuses examined in this study is of further interest in suggesting a possible basis for the neurodevelopment difficulties seen in children born with IUGR associated with uteroplacental insufficiency [12, 18]. The subiculum is linked to the entorhinal cortex, which in turn is the origin of the perforant path, one of the two main afferent pathways to the hippocampus. The pontine nuclei are part of the cortico-cerebellar pathway [1, 5]. A recent study in mice showed that a lesion in the entorhinal cortex may induce trans-synaptic death of perforant path neurons [15]. It seems plausible to suggest that damage to the subiculum and pons in IUGR human fetuses may lead to subsequent problems with memory and co-ordination.

In summary, the results of this study confirm that pontosubicular "necrosis" is more accurately described as pontosubicular apoptosis. This was verified using light and electron microscopy and special stains such as TUNEL and activated caspase-3. Pontosubicular apoptosis was strongly associated with IUGR and placental infarction, suggesting that the uteroplacental insufficiency leading to chronic fetal hypoxaemia may lead to cerebral apoptosis, which may contribute to subsequent functional neuro-developmental problems.

Acknowledgements Mr. Clay Winterford, Histology Services Unit, Discipline of Molecular and Cellular Pathology, The University of Queensland provided the expertise for the electron microscopy of the archival tissue samples.

References

1. Amaral DG, Insausti R (1990) Hippocampal formation In: Paxinos G (ed) The human nervous system. Academic, New York, pp 721–755
2. Auer RN, Sutherland GR (2002) Hypoxia and related conditions. In: Graham DI, Lantos PL (eds) Greenfield's neuropathology, 7th edn. Arnold, London, p 257
3. Barrio E, Calvo MT, Romo A, Alvarez R, Gutierrez JI, Naval J, Ferandez Longas A (2004) J Pediatr Endocrinol Metab 17 (Suppl 3):451–456
4. Boatright KM, Salvesen GS (2003) Mechanisms of caspase activation. Curr Opin Cell Biol 15:725–731
5. Brodal P, Bjaalie JG (1997) Salient anatomic features of the cortico–ponto-cereballar pathway. Prog Brain Res 114:227–249
6. Bruck Y, Bruck W, Kretzschmar HA, Lassmann H (1996) Evidence for neuronal apoptosis in pontosubicular neuron necrosis. Neuropathol Appl Neurobiol 22:23–29
7. Burke CJ, Tannenberg AE, Payton DJ (1997) Ischaemic cerebral injury, intrauterine growth retardation, and placental infarction. Dev Med Child Neurol 39:726–730
8. Edwards AD, Yue X, Cox P, Hope PL, Azzopardi DV, Squier MV, Mehmet H (1997) Apoptosis in the brains of infants suffering intrauterine cerebral injury. Pediatr Res 42:684–689
9. Erel CT, Dane B, Calay Z, Kaleli S, Aydinli K (2001) Apoptosis in the placenta of pregnancies complicated with IUGR. Int J Gynaecol Obstet 73:229–235
10. Friede RL (1972) Ponto-subicular lesions in perinatal anoxia. Arch Pathol 94:343–354
11. Gobe GC, Axelsen RA (1987) Genesis of renal tubular atrophy in experimental hydronephrosis in the rat. Role of apoptosis. Lab Invest 56:273–281
12. Hill RM, Verniaud WM, Deter RL, Tennyson LM, Rettig GM, Zion TE, Vorderman AL, Helms PG, McCulley LB, Hill LL (1984) The effect of intrauterine malnutrition on the term infant. Acta Paediatr Scand 73:482–487
13. Keeling JW (1993) Macerated stillbirth. In: Keeling JW (ed) Fetal and neonatal pathology. Springer-Verlag, London, pp 167–177
14. Kerr JF, Gobe GC, Winterford CM, Harmon BV (1995) Anatomical methods in cell death. Methods Cell Biol 46:1–27
15. Kovac AD, Kwidzinski E, Heimrich B, Bittigau P, Deller T, Nitsch R, Bechmann I (2004) Entorhinal cortex lesion in the mouse induces transsynaptic death of perforant path target neurons. Brain Pathol 14:249–257
16. Lane RH, Ramirez RJ, Tsirka AE, Kloesz JL, Mclaughlin MK, Gruetzmacher EN, Devaskar SU (2001) Uteroplacental insufficiency lowers the threshold towards hypoxia-induced cerebral apoptosis in growth-retarded rats. Brain Res 895:186–193
17. Laurini R, Laurin J, Marsal K (1994) Placental histology and fetal blood flow in intrauterine growth retardation. Acta Obstet Gynecol Scand 73:529–534
18. Low JA, Boston RW, Pancham SR (1972) Fetal asphyxia during the intrapartum period in intrauterine growth retarded infants. Am J Obstet Gynecol 113:351–357
19. Low JA, Handley-Derry MH, Burke SO, Peters RD, Pater EA, Killen Hl, Derrick BA (1992) Association of intrauterine fetal growth retardation and learning deficits at age 9 to 11 years. Am J Obstet Gynecol 167:1499–1505
20. Mito T, Kamei A, Takashima S, Becker LE (1993) Clinicopathological study of pontosubicular necrosis. Neuropediatrics 24:204–207
21. Smith SC, Baker PN, Symonds EM (1997) Increased placental apoptosis in intrauterine growth restriction. Am J Obstet Gynecol 177:1395–1401

22. Sohma O, Mito T, Mizuguchi M, Takashima S (1995) The prenatal age critical for the development of pontosubicular necrosis. Acta Neuropathol (Berl) 90:7–10
23. Soothill PW, Nicolaides KH, Cambell S (1987) Prenatal asphyxia, hyperlactic acidemia, hypoglycaemia and erythroblastosis in growth retarded fetuses. BMJ 294:1051–1053
24. Stadelmann C, Mews I, Srinivasan, A, Deckwerth TL, Lassman H, Bruck W (2001) Expression of cell death-associated proteins in neuronal apoptosis associated with pontosubicular neuron necrosis. Brain Pathol 11:273–281
25. Takashima S, Mito T, Houdou S, Ando Y (1989) Relationship between periventricular hemorrhage, leukomalacia and brainstem lesions in prematurely born infants. Brain Dev 11:121–124
26. Van Landeghem FKH, Felderhoff-Mueser U, Moysich A, Stadelmann C, Obladen M, Bruck W, Buhrer C (2002) Fas (CD95/Apo-1)/Fas ligand expression in neonates with pontosubicular neuron necrosis. Pediatr Res 51:129–135

Virchows Arch (2005) 446: 646–652
DOI 10.1007/s00428-005-1261-z

ORIGINAL ARTICLE

Fumio Ide · Kumi Obara · Kenji Mishima · Ichiro Saito · Kaoru Kusama

Ultrastructural spectrum of solitary fibrous tumor: a unique perivascular tumor with alternative lines of differentiation

Received: 9 December 2004 / Accepted: 10 March 2005 / Published online: 21 May 2005
© Springer-Verlag 2005

Abstract Eight tumors diagnosed as solitary fibrous tumor (SFT) of the oral cavity were studied. Histologic spectrum was entirely comparable with the extrapleural SFT of other sites. One tumor had glomus tumor-like foci. Immunohistochemical results confirmed most of the previous observations, indicating characteristic expression of vimentin, CD34, bcl-2, and CD99. Factor XIIIa and α-smooth muscle actin were less commonly reactive and a very few cells were faintly positive for factor VIII-related antigen and *Ulex europaeus* agglutinin 1. All were essentially negative for S-100 protein, desmin, CD31, and CD68. In stark contrast to the conclusive immunoprofile, ultrastructural investigation of six tumors demonstrated considerable cellular heterogeneity. Other than fibroblasts, perivascular undifferentiated cells and pericytes predominated, but endothelial cells were regularly present. There was a distinctive proliferation of pericytic cells in four tumors, one of which had glomoid foci of myopericytes. The extreme increase in number of Weibel-Palade bodies occurred in voluminous capillary endothelium. Occasional single and clustered cells with consistent features of endothelium showed intracytoplasmic lumen formation. Such composite cells constituted an integral segment of richly vascularized SFT. Myofibroblastic form smooth muscle differentiation was present in only a minority of cells. From phenotypic analysis by electron microscopy, SFT may originate from a unique, perivascular multipotent mesenchyme sharing with its lineage with pericytes, fibroblasts, and infrequently, endothelium. Consequently, morphological features of SFT may become diversely varied by whether predominantly constituent cells are undifferentiated, pericytic or fibroblastic in nature.

Keywords Endothelium · Myofibroblast · Oral mucosa · Pericyte · Perivascular undifferentiated cell · Solitary fibrous tumor

F. Ide (✉) · K. Obara · K. Mishima · I. Saito
Department of Pathology,
Tsurumi University School of Dental Medicine,
2-1-3 Tsurumi, Tsurumi-ku,
Yokohama, 230-8501, Japan
e-mail: ide-f@tsurumi-u.ac.jp
Tel.: +81-45-5808361
Fax: +81-45-5808361

F. Ide · K. Kusama
Department of Oral Pathology,
Meikai University School of Dentistry,
Saitama, Japan

Introduction

Solitary fibrous tumor (SFT) is a ubiquitous soft tissue tumor that has now been recognized in virtually all anatomic sites [11, 20, 29]. Histologic and immunohistochemical features have been extensively studied during the past 10 years and are well summarized in a seminal article [4]. To date, the origin and nature of SFT remain a conundrum. Since the immunoprofiling data are not specific, light microscopy alone is unable to clarify the phenotypic modulation capacity of tumor cells. There are many electron microscopic descriptions of extrapleural SFT [1–3, 7, 12–14, 16–18, 21–23, 27, 30]; however, most studies dealt very briefly with summations and specific mention was made only of the presence of fibro/myofibroblastic cells. Considering the premise that a variegation of histological patterns is the hallmark of SFT, it is curious that ultrastructural appearances were rather uniform in the literature [2, 7, 12, 16–18, 21].

In an attempt to elaborate the lineage of differentiation pursued by SFT, histologic, immunohistochemical and ultrastructural analyses were performed on eight cases arising in the oral cavity. The evidence that main cells comprising SFT are differentiating as true myofibroblasts was less than compelling. Rather, the principal line of origin was a perivascular undifferentiated mesenchyme inseparably tied to abnormally proliferating vascular supporting cells.

Materials and methods

Cases

As shown in Table 1, eight cases of oral SFT were retrieved from the surgical pathology files of our two institutions and from the personal consultation files of three of the authors (K.K.; case 1, F.I.; case 4, and K.M.; case 7).

Light microscopy and immunohistochemistry

Formalin-fixed and paraffin-embedded sections were stained with hematoxylin and eosin and examined immunohistochemically by the avidin-biotin peroxidase complex method, using the following antibodies: vimentin (clone 3B4, Dako, Glostrup, Denmark, 1:50), CD34 (clone QBEND10, Serotec; Washington D.C., USA; 1:80), bcl-2 (clone bcl-2/100/D5; Novocastra, Newcastle upon Tyne, UK; 1:50), CD99 (clone O13; Signet, Dedham, Mass., USA; 1:30), factor XIIIa (FXIIIa, polyclonal; Calbiochem, La Jolla, Calif., USA; 1:400), α-smooth muscle actin (SMA, clone 1A4; Sigma, St Louis, Mo., USA; 1:500), factor VIII-related antigen (FVIII, polyclonal; Dako; 1:500), *Ulex europaeus* agglutinin 1 (UEA 1; Dako; 1:3600), CD31 (clone JC/70A; Dako; 1;10), S-100 protein (polyclonal; Dako; 1:300), desmin (clone D33; Dako; 1;40), and CD68 (clone KP1; Dako; 1:200). Appropriate controls were tested simultaneously.

Electron microscopy

Fresh tissues from three tumors (cases 5, 6 and 8) were fixed in 2% glutaraldehyde, post-fixed in 1% osmium tetraoxide, and embedded in Epon. Ultrathin sections were stained with uranyl acetate-lead citrate and examined with an electron microscopy (JEM 100B). The remaining three tumors (cases 2, 3 and 4) were retrieved from wet tissues fixed in 10% buffered formalin and processed identically. In two consultation cases (cases 1 and 7), suboptimal material was not available for examination. To resolve problems of sampling error, various portions sampled included tumor cells in hypercellular, hypocellular fibrous, densely collagenized, hyalinized, myxoid, and glomoid areas as confirmed on light microscopy of toluidine blue sections.

Table 1 Clinical characteristics

Case	Age (yrs)	Sex	Location	Size (cm)
1	27	Female	L-PBS	1.5
2	52	Female	L-ALG	2
3	46	Male	L-RP	2
4	35	Female	Hard palate	0.7
5	67	Female	Soft palate	3
6	53	Male	L-ALG	1
7	48	Female	Tongue	1
8	35	Female	BM	1.5

L-PBS lower posterior buccal sulcus, *L-ALG* lower anterior lingual gingiva, *L-RP* lower retromolar pad, *BM* buccal mucosa

Results

Clinical features

All lesions were treated by simple local excision. Follow-up information was available in five patients, with duration ranging from 3 to 15 years, and to date, none have recurred. Three remaining cases (cases 5, 6 and 8) were recent.

Microscopic findings

At low magnification, all tumors were submucosal in localization. Their histological spectrum was diversely varied from case to case and area to area within a given tumor. Lesions were fairly well demarcated and at least partially encapsulated by a thin fibrous tissue. Despite circumscription, entrapment of salivary glands (cases 3 and 6), muscular tissues (cases 1, 7 and 8) and nerve bundles (case 8) could be found at the edges. Commonly, tumors were highly vascularized with branching, thin-walled, hemangiopericytoma-like vessels (Fig. 1a) and numerous capillaries showing prominent perivascular hyalinization (Fig. 1b). A diagnostic feature was so-called patternless architecture, characterized by a combination of altering hypercellular and hypocellullar foci. The former area was composed of haphazard, storiform, fascicular and/or wavy neuroid arrangement of bland-looking short spindled cells (Fig. 1c). In focal areas of one palatal tumor (case 6), uniform cuboidal cells with central round nuclei, discrete cell borders, and clear cytoplasm exhibited a concentric perivascular growth reminiscent of glomus tumor (Fig. 1d). The hypocellular area was richly collagenized (Fig. 1e), ranging from sclerosis (Fig. 1f) to hyalinized (Fig. 1g). There were a few amianthoid fibers in two lesions (cases 5 and 6). In two tumors (cases 6 and 8), focal myxoid stromal change was visible (Fig. 1h). One buccal tumor (case 8) contained mature fatty tissue. Inflammatory infiltrate was not a feature but mast cells were dispersed almost throughout. There was no mitotically active case and necrosis, and cytologic atypia were absent.

Immunohistochemical findings

In individual cases, there was no significant relationship between the histologic appearances and immunoprofile (Table 2). All tumors showed consistent positivity for vimentin, CD34, bcl-2, CD99, and FXIIIa. In most cases, staining for vimentin and CD34 was diffuse, with moderate to strong intensity (Fig. 1i), whereas that for bcl-2 and CD99 was more focal (Fig. 1j). On closer inspection, however, FXIIIa staining could be detected in interstitial dendrocytes but not in spindled tumor cells (Fig. 1k). Interestingly, most XIIIa-positive dendrocytic cells were non-

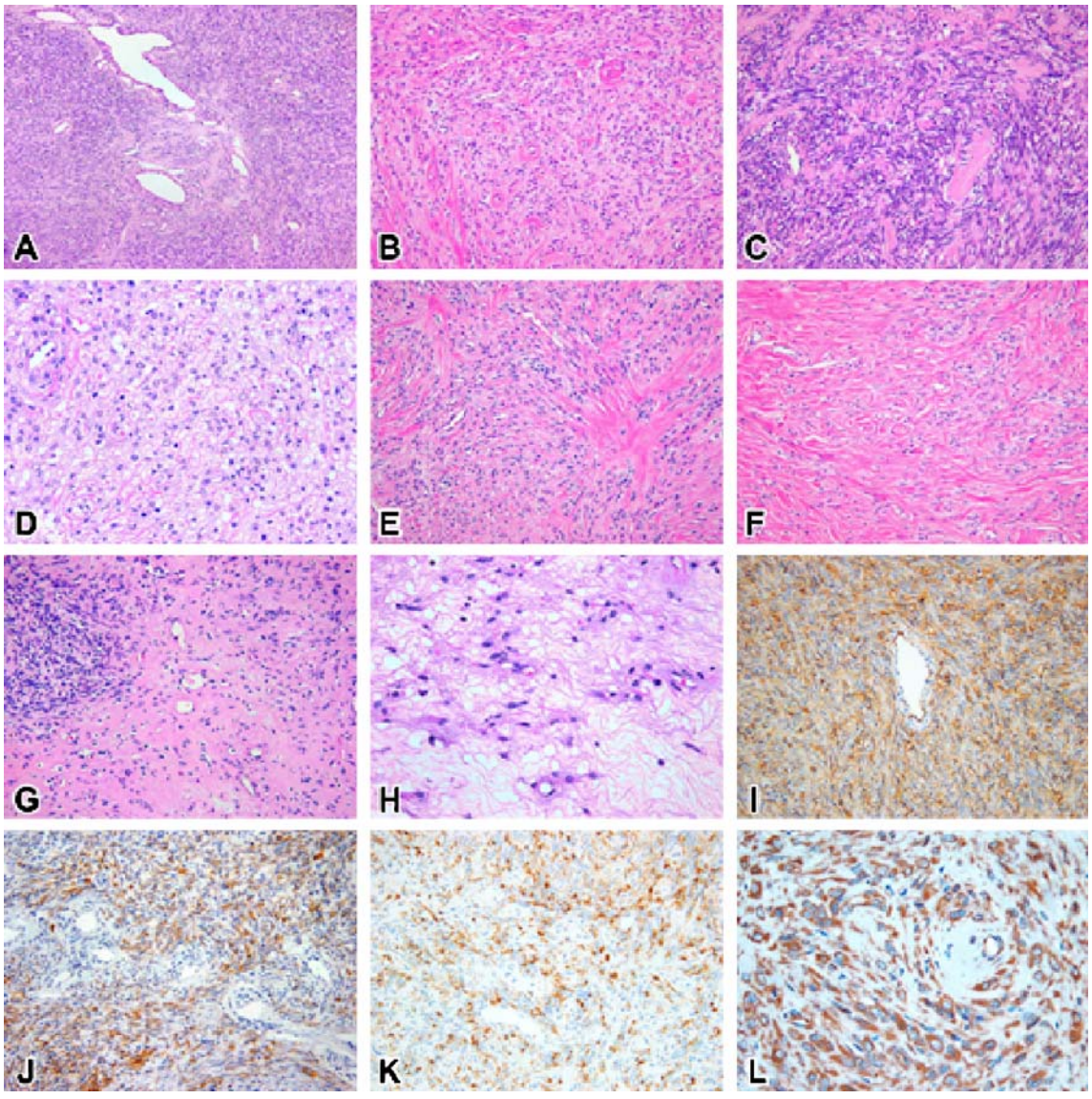

Fig. 1 **a** Hemangiopericytoma-like vasculature (case 1). **b** Numerous capillaries with perivascular hyalinization (case 5). **c** Bland spindly tumor cells (case 3). **d** Glomus-type proliferation (case 6). **e** Focal keroid-like sclerosis (case 6). **f** Densely collagenized stroma (case 4). **g** Hyalinized area (case 8). **h** Myxoid stroma (case 6). **i** Diffuse CD34 positivity (case 3). **j** Spindle tumor cells are mostly positive for bcl-2 (case 5). **k** Factor XIIIa reactivity in dendrocytes (case 2). **l** Strong positivity for α-smooth muscle actin in glomoid tumor cells (case 6)

reactive for CD34 [19]. Focal and limited staining for SMA was evident in four of eight tumors. In contrast, glomoid nests exhibited intense cytoplasmic positivity for SMA (Fig. 1l). All cases tested had faint staining of rare lesional cells for FVIII and four of them also showed UEA1 affinity. Essentially no immunoreactivity was present for CD31, S-100, desmin, and CD68.

Ultrastructural findings

Because of the limited experience, a comparison of the ultrastructural characteristics with immunohistochemical results failed to reveal any meaningful correlation in individual cases. Common to six tumors were vascular prominences with intercapillary stroma containing various mesenchymal cells in varying proportions. The following types were exclusively identified in each tumor: (1) a predominant line of tumor cells, herein described as undifferentiated cells, (2) pericytes, (3) fibroblasts, (4) transitional forms between pericytes and fibroblasts, (5) endothelium, (6) undetermined population that appeared to be intermediate between pericytic and endothelial cells, (7) dendritic macrophages, and (8) mast cells. Since the fine structure of fibroblastic lineage has been described in previous publications [2, 3, 12–14, 16–18, 22, 23, 30], we will focus on other features that are pertinent to the morphogenesis of SFT.

In all areas examined, a close topographic relationship between undifferentiated tumor cells, pericytes and endo-

Table 2 Immunohistochemical profile

Antibody	Positive cases	Grading[a]			
		1+	2+	3+	4+
Vimentin	8/8	0	0	2	6
CD34	8/8	1	1	1	5
Bcl-2	6/6	1	3	2	0
CD99	6/6	1	3	1	1
Factor XIIIa	6/6	0	3	2	1
SMA	4/8	4	0	0	0
Factor VIII	6/6[b]				
UEA 1	4/6[b]				
CD31	1/6[b]				
S-100 protein	1/8[b]				
Desmin	0/7				
CD68	0/7				

*SMA*α-smooth muscle actin, *UEA 1* Ulex europaeus agglutinin 1
[a]*1+* <25%, *2+* 25%–50%, *3+* 50%–75%, *4+* >75%
[b]Rare (<5%) and faintly positive cells

thelium could be readily visible (Fig. 2). Oval-to polygonal-or spindle-shaped tumor cells showed a high nucleocytoplasmic ratio and had simplified outlines. No distinguishing organelle suggestive of a specialized line of differentiation was evident (Fig. 3a). Even in the fibrous (Fig. 3b) and densely collagenized (Fig. 3c) areas, they contained only sparse rough endoplasmic reticulum and were not intimately associated with collagen fibrils. As one moved away from the vessels, there were certain differentiating cells with small bunches of thin filaments, and fragmented basal lamina. Tumor cells embedded in the hyalinized stroma had vacuoles and short segments of duplicated basal lamina (Fig. 3d, e).

Pericytes were also an outstanding cell type in all cases. They were present singly or in small groups, in close proximity to capillaries and usually entrapped within the same basement membrane surrounding endothelium (Fig. 2). Pericytic derivation was confirmed for recognition of microfilaments, pinocytotic vesicles and basal lamina (Fig. 4a) [5, 8]. As shown in Fig. 2d, in the absence of discrete basal lamina, numerous dense plaques were seen along the thin friable cell membrane. Four tumors (cases 3, 5, 6 and 8) had more differentiated pericytes characterized by prominent microfilaments with dense bodies, numerous pinocytotic vesicles, and thickened continuous basal lamina (Fig. 4b). Glomoid nests were composed of myopericytes which contained abundant microfilaments with attachment bodies in the plasmalemma as well as dense body formation (Fig. 4c).

Swollen endothelium lining the patent capillary lumen was rich in Weibel-Palade bodies (WPB, Fig. 5a) and often formed broad intercellular connections with tight junctions (Fig. 2a). There were many isolated endothelial cells with large cytoplasmic vacuole reminiscent of early vascular lumen (Fig. 5b). They were also characterized by skeins of microfilaments, discrete basal lamina, and occasional rudimentary cell junctions (Fig. 5c, inset); however, such structures varied considerably in amount and distribution from cell to cell. Throughout the lesion, cells showing multiple cytoplasmic processes, microfilaments, lysosomes, and focal duplicated basal lamina circumscription were conspicuous. They were compatible with XIIIa-positive dendrocytes (Fig. 5c).

Discussion

Since 1995 [15, 26], SFT has been rediscovered in a variety of extrapleural sites and now gained wide acceptance as a unique soft tissue tumor [4, 11, 20, 29]. However, the specific direction of differentiation for SFT is a lingering doubt.

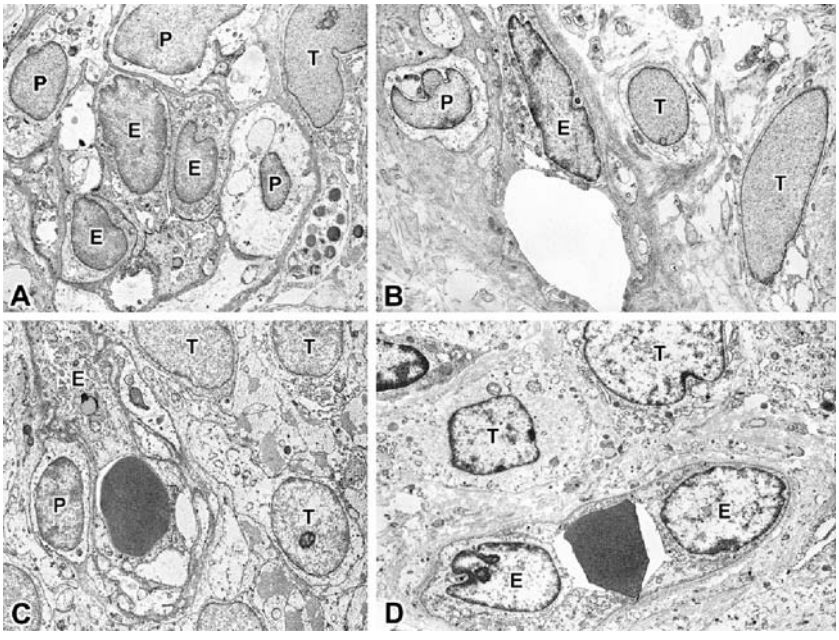

Fig. 2 Intimate relationship between undifferentiated tumor cells (*T*), pericytes (*P*) and endothelium (*E*). **a** Pericyte and tumor cell abut one another directly. Part of a granule-containing mast cell appears on the lower right corner (case 2, ×3500). **b** Partial investment of tumor cell by periendothelial basement membrane (case 5, ×3500). **c** Tumor cells arranged concentrically about capillary (case 3, ×3500). **d** Numerous dense plaques along thin plasmalemma of tumor cells (case 6, ×3500)

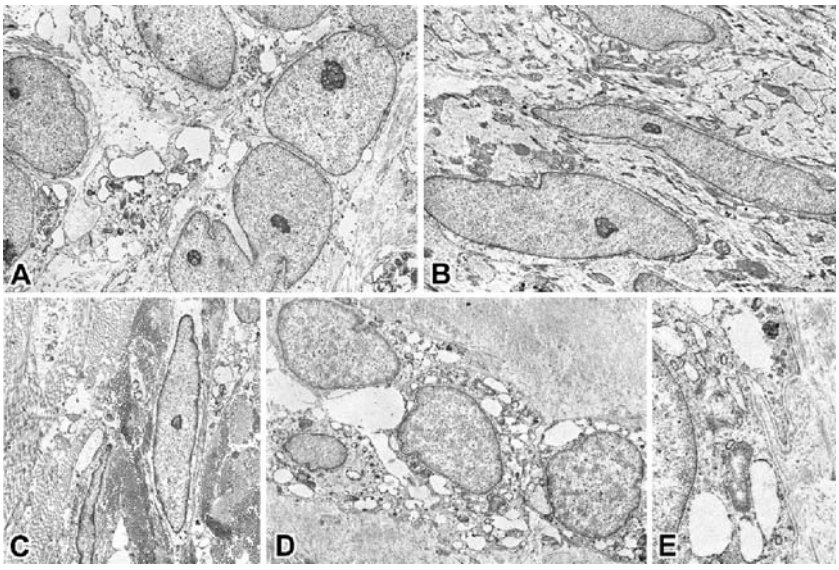

Fig. 3 Undifferentiated tumor cells from light microscopic areas corresponding to (**a**) hypercellular (case 3, ×5000), (**b**) fibrous (case 5, ×5000), (**c**) densely collagenized (case 8, ×3500), and (**d**) hyalinized foci (case 2, ×5000). **e** Discontinuous basal lamina, ×10,500

There is an organizational relationship of tumor cells and prominent vascular components in SFT. It would thus appear that tumor tissue may be responsible for an active angiogenesis in a certain stage of development. Our ultrastructural observations point to several valuable findings indicating angiogenic nature of SFT; there were hyperplastic vasoformative mesenchyme with clear-cut features of endothelium and pericytes. Endothelial cells and their equivalent were often dispersed singly in the stroma. Recent immunohistochemical studies also confirmed the phenotypic differentiation of SFT to vascular endothelial cells [24]. WPB in such cells were very few and smaller than in the putative normal counterpart and sometimes difficult to find; therefore, they have been either overlooked or ignored in previous evaluations [1–3, 7, 12–14, 16–18, 21–23, 27, 30].

Unlike endothelium, pericytes are cells of great versatility in soft tissue tumor pathology [11, 20, 29]. Because of the lack of established immunohistochemical marker, ultrastructural analysis is the only recommended way to confirm the pericytic population. Although contribution of a pericytic line to the morphogenesis of SFT has been theoretically proposed [11, 29], the specific relationship reported herein has not been adequately demonstrated. In our examination, lesional cells characterized by the total investment of basal lamina, numerous pinocytotic vesicles, and abundant microfilaments were commonly encountered. These attributes pertain to the population of pericytic cells [5, 8], but reflecting the relative non-specificity, none of these traits provides sufficient basis for identification of true pericytes without topographic relationship to vessels or association with periendothelial basement membrane [5, 8, 11, 20, 29]. In addition to the enigmatic type, one SFT demonstrated specialized smooth muscle phenotype to the extent that myopericytic origin is plausible. In selected fields, its fine structure was identical to those of glomus tumor [11, 29]. A full range of pericytic differentiation in our SFT series strongly argue against the complaint that these cells were the entrapped normal vascular smooth muscle. This example is particularly appealing in consideration with the plausibility of kinship between SFT and perivascular tumors. Recently, Thompson et al. [28] described an opposite case of sinonasal-type hemangiopericytoma with intermixed foci of SFT. This is significant, since the former is a tumor truly derived from, or putatively differentiating toward, myopericytes [11, 20, 29]. Such

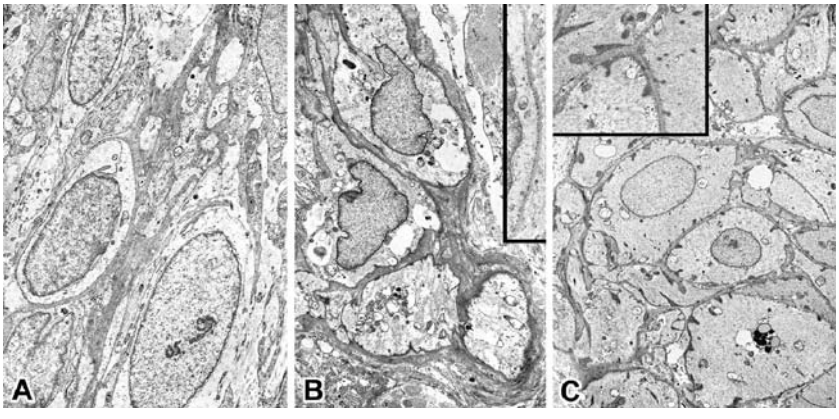

Fig. 4 Morphologic spectrum of pericytes. **a** Basal lamina formation around spindled tumor cells (case 3, ×3500). **b** Thickened basal lamina encasing pericytes (case 5, ×3500). Inset: Pinocytotic vesicles, ×14,000. **c** Myopericytes containing abundant myofilaments (case 6, ×3500). *Inset*: Dense and attachment bodies, ×14,000

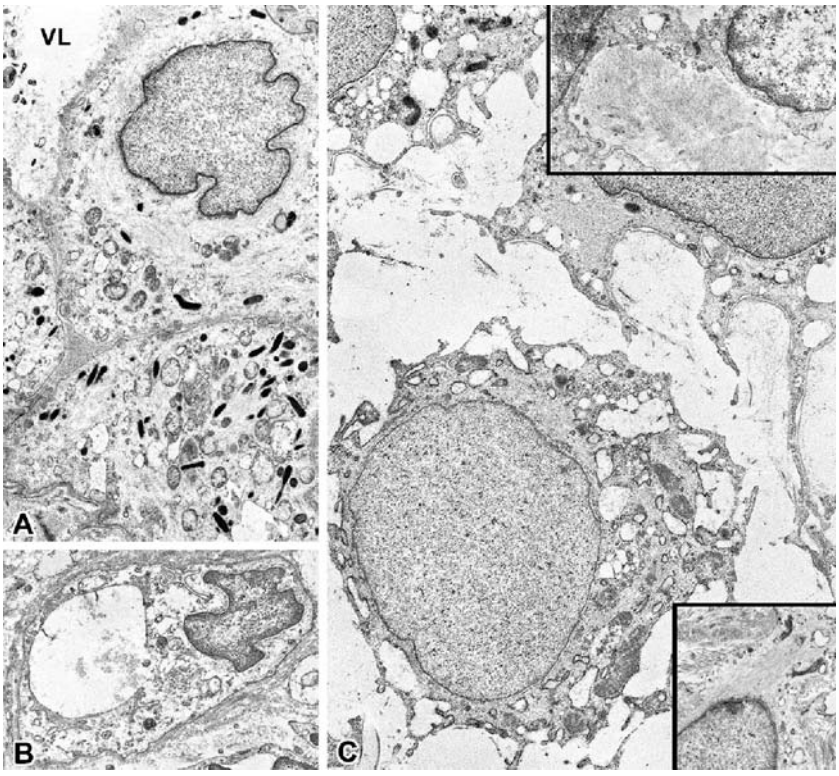

Fig. 5 Endothelial cells and macrophages. **a** Weibel-Palade bodies and microfilaments in capillary endothelium lining vascular lumen (*VL*) (case 5, ×8700). **b** Intracytoplasmic lumen formation (case 3, ×10,500). **c** Dendrocytic cells within myxoid area showing microfilaments, lysosomes, and interrupted duplicated basal lamina (case 6, ×12,500). Inset: rudimentary cell junction (upper right corner, ×10,500) and single endothelial cell embedded in fibrous stroma (lower right corner, ×4500)

conjoint microscopic features further advance the view that a subset of SFT is undoubtedly very close to a spectrum of tumors showing pericytic differentiation [11].

Myofibroblastic differentiation is an enigmatic term which has been used loosely to encompass a variety of fascicular spindle cell tumors [10]. Because of its principally reactive nature, a precise definition of myofibroblastic derivation is sometimes difficult in the neoplastic states [10, 25]. Although the concept of SFT composed predominantly of myofibroblasts has been accepted [11, 20], it is questioned whether such evidence has been unequivocally demonstrated. In truth, Nielsen et al. [22] found only one tumor showing ultrastructural features to support myofibroblastic differentiation in their large SFT series. In our own material, myofibroblasts were a small fraction of the cell population. These observations are in keeping with the reported lack or low frequency of staining for smooth muscle markers in SFT [1–3, 7, 12–18, 21, 23, 26, 27, 30]. The term myofibroblast probably encompasses a heterogeneous population of cells, i.e. myoid fibroblasts, myopericytes, vascular smooth muscle, and other myoid stromal cells [6, 10, 25]. Since they form part of a morphologic and histogenetic continuum, it is not always possible with certainty to define a cell type, even at the ultrastructual level. Accordingly, the possibility that spindle cells dominated by actin filaments with subplasmalemmal densities and enveloped by basal lamina may be pericytes rather than true myofibroblasts is undeniable [9].

In the present and some previous studies [1, 7, 12, 13, 22, 27], there were primitive mesenchymal cells in varying numbers, often dominating the picture. Taccagni et al. [27] concluded that such uncommitted cells may undergo differentiation towards one or more mature lines. Although favoring fibroblastic derivation, Nielsen et al. [22] stressed much less differentiated phenotype of SFT. Conceivably, undifferentiated cells grown in a circumferential perivascular fashion are a candidate responsible for tumor development, despite the apparent branching of the evolving lines, consisting in the formation of vascular element and perivascular collagen. Up to date, it has not been clear whether the reputed XIIIa-positive and CD34-negative dendrocyte proliferation is reactive in nature or an integral part of the tumor cell component. Although both dendrocytes and mast cells may play an interactive role in the propagation of SFT [19], there is no evidence that perivascular multipotent cells serve as precursors to dendrocytic lineage.

In summary, we analyzed the ultrastructural spectrum of SFT, specifically trying to suggest its possible link to pericytic tumors. Although the number of cases is limited and the individual cases represent significant heterogeneity, SFT may originate from a perivascular stem able to give rise to differentiate along 3 evolutional lines such as endothelial, pericytic, and fibroblastic, following a pathway that occurs in normal angiogenesis. In this context, it would be premature to simply classify SFT as a form of intrinsically fibro/myofibroblastic tumor [11, 20]. We find instead rather some justification that SFT fall into an umbrella concept of perivascular tumor category [29]. However, the possibility that SFT might have different ultrastructural characteristics in different sites should also be considered.

References

1. Alston SR, Francel PC, Jane JA (1997) Solitary fibrous tumor of the spinal cord. Am J Surg Pathol 21:477–483
2. Brunnemann RB, Ro JY, Ordonez NG, Mooney J, El-Naggar AK, Ayala AG (1999) Extrapleural solitary fibrous tumor: a clinicopathologic study of 24 cases. Mod Pathol 12:1034–1042
3. Carneiro SS, Scheithauer BW, Nascimento AG, Hirose T, Davis DH (1996) Solitary fibrous tumor of the meninges: a lesion distinct from fibrous meningioma. Am J Clin Pathol 106:217–224
4. Chan JKC (1997) Solitary fibrous tumour-everywhere, and a diagnosis in vogue. Histopathology 31:568–576
5. Dardick I, Hammar SP, Scheithauer BW (1989) Ultrastructural spectrum of hemangiopericytoma: a comparative study of fetal, adult, and neoplastic pericytes. Ultrastruct Pathol 13:111–154
6. Dictor M, Elner A, Andersson T, Ferno M (1992) Myofibromatosis-like hemangiopericytoma metastasizing as differentiated vascular smooth-muscle and myosarcoma. Myopericytes as a subset of "myofibroblasts". Am J Surg Pathol 16:1239–1247
7. Dorfman DM, To K, Dickersin GR, Rosenberg AE, Pilch BZ (1994) Solitary fibrous tumor of the orbit. Am J Surg Pathol 18:281–287
8. Erlandson RA, Woodruff JM (1998) Role of electron microscopy in the evaluation of soft tissue neoplasms, with emphasis on spindle cell and pleomorphic tumors. Hum Pathol 29:1372–1381
9. Eyden B (2001) Reactive pericytes vs myofibroblastic tumor cells. Arch Ophthalmol 119:459
10. Eyden B (2003) Electron microscopy in the study of myofibroblastic lesions. Semin Diagn Pathol 20:13–24
11. Fletcher CDM, Unni KK, Mertens F (2002) World health organization classification of tumours. Pathology and genetics of tumours of soft tissue and bone. International Agency for Research on Cancer, Lyon
12. Fukunaga M, Naganuma H, Nikaido T, Harada T, Ushigome S (1997) Extrapleural solitary fibrous tumor: a report of seven cases. Mod Pathol 10:443–450
13. Fukunaga M, Ushigome S, Nomura K, Ishikawa E (1995) Solitary fibrous tumor of the nasal cavity and orbit. Pathol Int 45:952–957
14. Gelb AB, Simmons ML, Weidner N (1996) Solitary fibrous tumor involving the renal capsule. Am J Surg Pathol 20:1288–1295
15. Hanau CA, Miettinen M (1995) Solitary fibrous tumor: histological and immunohistochemical spectrum of benign and malignant variants presenting at different sites. Hum Pathol 26: 440–449
16. Hasegawa T, Hirose T, Seki K, Yang P, Sano T (1996) Solitary fibrous tumor of the soft tissue. An immunohistochemical and ultrastructural study. Am J Clin Pathol 106:325–331
17. Hasegawa T, Matsuno Y, Shimoda T, Hasegawa F, Sano T, Hirohashi S (1999) Extrathoracic solitary fibrous tumors: their histological variability and potentially aggressive behavior. Hum Pathol 30:1464–1473
18. Huang H-Y, Sung M-T, Eng H-L et al (2002) Solitary fibrous tumor of the abdominal wall: a report of two cases with immunohistochemical, flow cytometric, and ultrastructural studies and literature review. APMIS 110:253–262
19. Ide F, Kusama K (2002) Solitary fibrous tumor is rich in factor $XIIIa^{+}$ dendrocytes. Am J Dermatopathol 24:449–450
20. Kempson RL, Fletcher CDM, Evans HL, Hendrickson MR, Sibley RK (2001) Atlas of tumor pathology. 30 Tumors of the soft tissues. Armed Forces Institute of Pathology, Washington, DC
21. Mentzel T, Bainbridge TC, Katenkamp D (1997) Solitary fibrous tumour: clinicopathological, immunohistochemical, and ultrastructural analysis of 12 cases arising in soft tissues, nasal cavity and nasopharynx, urinary bladder and prostate. Virchows Arch 430:445–453
22. Nielsen GP, O'Connell JX, Dickersin GR, Rosenberg AE (1997) Solitary fibrous tumor of soft tissue: a report of 15 cases, including 5 malignant examples with light microscopic, immunohistochemical, and ultrastructural data. Mod Pathol 10:1028–1037
23. O'Connell JX, Logan PM, Beauchamp CP (1995) Solitary fibrous tumor of the periosteum. Hum Pathol 26:460–462
24. Sawada N, Ishiwata T, Naito Z, Maeda S, Sugisaki Y, Asano G (2002) Immunohistochemical localization of endothelial cell markers in solitary fibrous tumor. Pathol Int 52:769–776
25. Schurch W, Seemayer TA, Gabbiani G (1998) The myofibroblast. A quarter century after its discovery. Am J Surg Pathol 22:141–147
26. Suster S, Nascimento AG, Miettinen M, Sickel JZ, Moran CA (1995) Solitary fibrous tumors of soft tissue. A clinicopathologic and immunohistochemical study of 12 cases. Am J Surg Pathol 19:1257–1266
27. Taccagni G, Sambade C, Nesland J, Rosa Terreni M, Sobrinho-Simoes M (1993) Solitary fibrous tumour of the thyroid: clinicopathological, immunohistochemical and ultrastructural study of three cases. Virchows Arch A Pathol Anat 422:491–497
28. Thompson LDR, Miettinen M, Wenig BM (2003) Sinonasal-type hemangiopericytoma. A clinicopathologic and immunophenotypic analysis of 104 cases showing perivascular myoid differentiation. Am J Surg Pathol 27:737–749
29. Weiss SW, Goldblum JR (2001) Enzinger and Weiss's soft tissue tumors, 4th edn. Mosby, St Louis
30. Wu SL, Vang R, Clubb FJ, Connelly JH (2002) Solitary fibrous tumor of the tongue: report of a case with immunohistochemical and ultrastructural studies. Ann Diagn Pathol 6:168–171

Virchows Arch (2005) 446: 653–662
DOI 10.1007/s00428-005-1219-1

ORIGINAL ARTICLE

Wael Swelam · Hiroko Ida-Yonemochi · Satoshi Maruyama · Kazufumi Ohshiro · Jun Cheng · Takashi Saku

Vascular endothelial growth factor in salivary pleomorphic adenomas: one of the reasons for their poorly vascularized stroma

Received: 11 November 2004 / Accepted: 24 January 2005 / Published online: 23 April 2005
© Springer-Verlag 2005

Abstract To better understand the poorly vascularized background of the stroma of pleomorphic adenomas, we attempted to determine the expression of molecules related to blood vessels and hypoxic conditions in pleomorphic adenoma. Surgical specimens and tumor cells in primary culture of salivary pleomorphic adenomas were used for immunohistochemistry for CD31, vascular endothelial growth factor (VEGF) and its receptors Flk-1 and Flt-1, as well as for hypoxia markers, such as hypoxia-inducible factor-1α (HIF-1α) and lactate dehydrogenase-1 (LDH). At the same time, alternative splicing modes of the VEGF gene and expression levels of the HIF-1α gene were analyzed in surgical specimens by means of reverse-transcription polymerase chain reaction (RT-PCR) and direct sequencing of the PCR products. In addition to co-immunolocalization with CD31+ vascular endothelial cells, VEGF and its receptors were demonstrated in normal duct epithelial and myoepithelial cells as well as in tumor cells in ductal structures and in myxochondroid stromata. Immunolocalizations for HIF-1α and LDH were confirmed in the VEGF-positive area. Immunofluorescence signals for VEGF and others were confirmed in pleomorphic adenoma cells in culture. RT-PCR results showed that there were at least four splicing modes of the VEGF gene, among which $VEGF_{121}$ was most enhanced, and higher HIF-1α levels in pleomorphic adenomas. The results suggest that pleomorphic adenoma cells produce VEGF in several functional forms for their own proliferation or differentiation, and that the VEGF expression is controlled by hypoxic circumstances of poorly vascularized pleomorphic adenomas.

W. Swelam · H. Ida-Yonemochi · S. Maruyama · K. Ohshiro · J. Cheng · T. Saku (✉)
Department of Tissue Regeneration and Reconstruction,
Division of Oral Pathology,
Niigata University Graduate School of Medical and Dental Sciences,
2-5274 Gakkocho-dori,
Niigata, 951-8514, Japan
e-mail: tsaku@dent.niigata-u.ac.jp
Tel.: +81-25-2272832
Fax: +81-25-2270805

Keywords Hypoxia · HIF-1α · Pleomorphic adenoma · Poorly vascular stroma · VEGF

Introduction

The colorful histology of pleomorphic adenoma is mainly due to its variety of stromal phenotypes from fibrous, hyaline, myxoid, and cartilaginous phenotypes. These varieties of stromal phenotypes depend on the proportion of local contents of extracellular matrix molecules including basement membrane-associated molecules, such as perlecan, type-IV collagen, laminin, entactin, and fibronectin, which have been thought to be produced by tumor cells themselves [29]. Despite such a colorful histology, the stroma of pleomorphic adenoma is always poor in vascularity [12, 37]. This is totally against the general idea of the highly vascular architectures of the neoplasm, on which anti-tumor therapeutic strategies have been devised [5].

Pleomorphic adenoma cells mimic to some extent salivary glandular structures in which inner duct epithelial cells and outer myoepithelial cells are arranged. However, in the stroma with myxoid or chondroid appearances, tumor cells show no such obvious glandular differentiation. Instead, they have several myoepithelial characteristics because they are immunohistochemically positive for myosin [28] or S-100 protein [3]. These tumor cells scattered in the myxochondroid area have been considered to have more potential to survive, because recurrences of pleomorphic adenomas are related to their myxochondroid phenotypes [11]. However, no explanation has been given as to why these tumor cells can potently survive in a poorly vascularized myxochondroid environment.

Vascular endothelial growth factor (VEGF) was first characterized as a modulator that induces endothelial differentiation [7]. Recently, however, it has been demonstrated that its distribution is not only limited in endothelial cells or endothelial progenitors but also in normal [34] or in neoplastic epithelial cells [34, 35], both of which are not in direct contact with blood circulation. In addition, its ex-

pression has been revealed to be regulated by hypoxia-responsive elements of the promoter region of the gene [4]. Thus, it is highly suspected that the expression of VEGF should be enhanced in pleomorphic adenomas in which hypoxic conditions are highly speculated, because tumor tissues are poorly vascularized.

In this study, our intent was to determine how VEGF is expressed in pleomorphic adenoma tissues and cells, and whether or not the background for their VEGF expression is related to hypoxic conditions. To this end, we performed (1) immunohistochemical analyses of VEGF, its receptors Flt-1 and Flk-1, and hypoxia-related molecules, such as hypoxia-inducible factor 1α (HIF-1α); and (2) reverse-transcription polymerase chain reaction (RT-PCR) analyses for alternative splicing modes of the VEGF gene and HIF-1α. We examined their modes of expression/localization to determine the possible mechanism for hypoxia-dependent VEGF regulation that enables pleomorphic adenoma cell proliferation or differentiation even in such a poorly vascularized environment.

Materials and methods

Materials

A total of 100 surgical samples of pleomorphic adenoma diagnosed in the Division of Oral Pathology, Niigata University Graduate School of Medical and Dental Sciences during the period 1995–2004 were reviewed histopathologically, and 20 typical samples (four parotid, three submandibular, two labial, and 11 palatal) with different compositions of epithelial–mesenchymal components were selected, in addition to seven cases of tumor-free normal submandibular gland. Surgical materials were fixed in 10% formalin, routinely processed and embedded in paraffin. Serial sections were cut at a thickness of 5 μm. One set of the sections was stained with hematoxylin and eosin (HE), and other sets were used for immunohistochemical staining of (1) VEGF and its two main receptors Flt-1 and Flk-1; (2) myoepithelial markers, such as cytokeratin14 (CK14) and S-100 protein; and (3) hypoxia-related molecules, such as hypoxia-inducible factor-1α (HIF-1α) and lactate dehydrogenase-1 (LDH).

Six fresh surgical samples of pleomorphic adenoma (three parotid, two submandibular, and one palatal) and two of normal submandibular gland were also used for RNA extraction and primary cell culture as described in the following sections.

Antibodies

Rabbit polyclonal antibodies against S-100 protein were purchased from Dako Ltd. (Glostrup, Denmark; diluted at 1:200). A mouse monoclonal antibody against CK14 was purchased from Sigma Chemicals Co. (St. Louis, MO, USA; 1:200). Mouse monoclonal antibodies against both VEGF (C-1) and Flk-1 (A-3) were purchased from Santa Cruz Biotech Inc. (Santa Cruz, CA, USA; 1:50). Rabbit polyclonal antibodies against Flt-1 were purchased from Oncogene Research Products (Darmstadt, Germany; 1:1, 000). A mouse monoclonal antibody against human CD31 (JC-70A) was purchased from Dako (1:50). A mouse monoclonal antibody against HIF-1α was purchased from Chemicon International Inc. (Temecula, CA, USA; 1:100). Rabbit polyclonal antibodies against LDH were purchased from Nordic Immunological Laboratories (Tilburg, Netherlands; 1:200). The primary antibodies used in this study are summarized in Table 1.

Immunohistochemistry

Immunohistochemical experiments were performed using the Envision peroxidase system for rabbit and mouse antibodies (Dako). After deparaffinization, sections were treated in 0.3% H_2O_2 in methanol for 30 min at room temperature to block endogenous peroxidase activities. The sections were then rinsed in 0.01 M phosphate buffered saline (PBS) and pretreated to restore antigenicity as follows: for S-100 protein, CK14, and CD31, the sections were treated with 0.1% (w/v) trypsin (type II, Sigma) in 0.05 M Tris–HCl (pH 7.6) containing 1% $CaCl_2$ for 30 min at 37°C. For VEGF, the sections were digested with proteinase K (5 μg/ml) for 30 min at 37°C. For Flk-1, Flt-1, and HIF-1 α immunostainings, sections were autoclaved in citrate buffer (pH 6.0) at 121°C for 10 min. After antigen retrieval treatments, the sections were incubated in 5% skim milk in PBS containing 0.05% Triton X-100 (PBST) for 30 min at 37°C to block non-specific protein bindings, and then the sections were incubated at 4°C overnight with the primary

Table 1 List of primary antibodies used in immunohistochemistry for pleomorphic adenoma

Antibody against	Immunogen		Clone	Dilution	Distributors
	Species	Origin			
Keratin 14	Human	Callus keratin	CKB1	1:200	Sigma
CD31	Human	Spleen	JC/70A	1:50	Dako
VEGF	Human	1–140 amino acids of human VEGF	C-1	1:50	Santa Cruz
Flk-1	Mouse	1158–1345 amino acids of mouse Flk-1	1–3	1:50	Santa Cruz
HIF-1α	Human	432–528 amino acids of human HIF-1α	*	1:100	Chemicon
Flt-1	Human	1164–1174 amino acids of human VEGFR-1	–	1:1,000	Oncogene
S-100	Bovine	Brain	–	1:200	Dako
LDH	Human	Erythrocytes	–	1:200	Nordic

*Mouse monoclonal antibody, clone name not available

antibodies. After rinsing in PBST, the sections were incubated with goat antibodies against rabbit or mouse IgGs conjugated with peroxidase-labeled dextgran polymers (EnVision+ peroxidase, rabbit/mouse; Dako) for 30 min at room temperature. The peroxidase reaction products were visualized by incubation with 0.02% 3,3′-diaminobenzidine (Dohjin Laboratories, Kumamoto, Japan) in 0.05 M Tris–HCl solution (pH 7.4) containing 0.005% H_2O_2. The sections were then counterstained with hematoxylin.

Cell culture

Six cases of pleomorphic adenomas were used for cell culture. Briefly, tissues were minced into small pieces, and 0.1 g of the tissues was incubated with 1 ml of Dulbecco's modified Eagle medium (DMEM; Gibco BRL, Grand Island, NY) containing 0.1% collagenase A (Boehringer Mannheim Biochemica, Darmstadt, Germany) in a plastic tube with a screw cap for 17 h at 37°C. Collagenase-digested tissues were filtrated on a sheet of nylon mesh, and the pass-through fractions were washed two times with DMEM. Recovered cells were plated into 35-mm plastic Petri dishes at a concentration of 5×10^4 cells in 2 ml of DMEM containing 10% fetal calf serum (FCS; ICN Pharmaceuticals, Costa Mesa, CA, USA), 1% glutamine, 50 μg/ml streptomycin and 50 IU/ml penicillin, and incubated at 37°C under humidified 5% CO_2/95% air atmosphere. When they reached confluency, they were served for immunofluorescence studies as described below.

Immunofluorescence

For immunofluorescent staining, cells were plated onto 4-well Lab-Tek II chamber slides purchased from Nalge Nunc International (Naperville, CA, USA), and 0.4×10^4 cells were used for each well. The chamber slides were fixed and stained 7 days after plating with an indirect immunofluorescent technique using the specific monoclonal or polyclonal antibodies against VEGF, Flk-1, Flt-1, and HIF-1α as mentioned above and rhodamine-conjugated goat anti-mouse or anti-rabbit IgG (Cappel Laboratories, Cochranville, PA, USA, 1:50) as described elsewhere [2].

Total RNA isolation and RT-PCR

Total RNA was extracted from fresh tissue specimens by the ISOGEN total RNA isolation reagent (Nippongene, Tokyo, Japan) according to the manufacturer's instructions. cDNAs were synthesized from RNA with the SuperScript Preamplification System (Gibco-BRL, Grand Island, NY, USA). Following RT, PCR was carried out in an Astec thermal cycler PC-800 (Astec Co. Ltd., Fukuoka, Japan) as follows: the reaction products of the RT were diluted with 1×PCR buffer [50 mM KCl, 10 mM Tris–HCl (pH 8.5), 1.5 mM, and 0.01% Triton X-100] to a final volume of 50 μl, which contained 100 ng each of a forward oligonucleotide primer and a reverse primer, additional dNTPs (final concentration of 0.2 mM), and 2.5 U of *Taq* DNA polymerase (Takara Shuzo Co. Ltd., Kyoto, Japan). The oligonucleotide primers flanking the VEGF gene (nucleotide numbers 1020–1666, No. BC058855, GeneBank) were synthesized as follows: 5′-TCGG GCCTC CGAAA CCATG A-3′ (forward) and 5′-CCTGG TGAGA GATCT GGTTC-3′ (reverse) to generate 721-, 673-, 580-, and 517-bp products corresponding to VEGF splicing variants 189, 165, 145, and 121, respectively. The thermocycling protocol during 30 amplification cycles was as follows: denaturation at 94°C for 2 min, annealing at 58°C for 2 min, and extension at 72°C for 2 min. The reaction was terminated with a final cycle of annealing (58°C for 1 min) and extension (72°C for 10 min). Exponential amplification was confirmed in the 30 cycles. As an internal standard, the glyceraldehyde-3-phosphate dehydrogenase (GAPDH) gene was also amplified (983 bp). The resultant spliced isoforms were confirmed by direct sequencing on an ABI PRISM 310 Genetic Analyzer (Applied Biosystems, Foster, CA, USA).

The oligonucleotide primers for the HIF-1α gene (nucleotide numbers 1806–1943, No. BT009776, GeneBank) were synthesized as follows: 5′-CCAGC AGACT CAAAT ACAAG AACC-3′ (forward) and 5′-TGTAT GTGGG TAGGA GATGG AGAT-3′ (reverse) to generate a 138-bp product. As an internal standard, a 367-bp fragment of the GAPDH gene was also amplified. The thermocycling protocol during 35 amplification cycles was as follows: denaturation at 94°C for 1 min, annealing at 60°C for 1 min, and extension at 72°C for 2 min. The reaction was terminated with a final cycle of annealing (60°C for 1 min) and extension (72°C for 7 min). The PCR products were analyzed by means of electrophoresis on 2% or 3% agarose gels.

Quantitative analysis

The image of electrophoresis was analyzed to determine relative amounts of each VEGF splicing variant to GAPDH with NIH Image, an image-processing and analyzing program. The relative values were analyzed using the student's *t*-test. A *P*-value of less than 0.001 was considered statistically significant.

Results

Immunohistochemistry

In normal salivary gland tissues, VEGF was strongly immunolocalized in epithelial cells of both striated and intercalated ducts, in addition to endothelial cells of blood capillaries or venules (Fig. 1a). The duct epithelial cells showed more intensive stainings for Flk-1 (Fig. 1b) and Flt-1 (Fig. 1c), receptors for VEGF. They were not always localized on the cell membrane but also diffusely in the cytoplasm. These three molecules were also immunolocalized in a granular fashion in serous acinar cells or in the

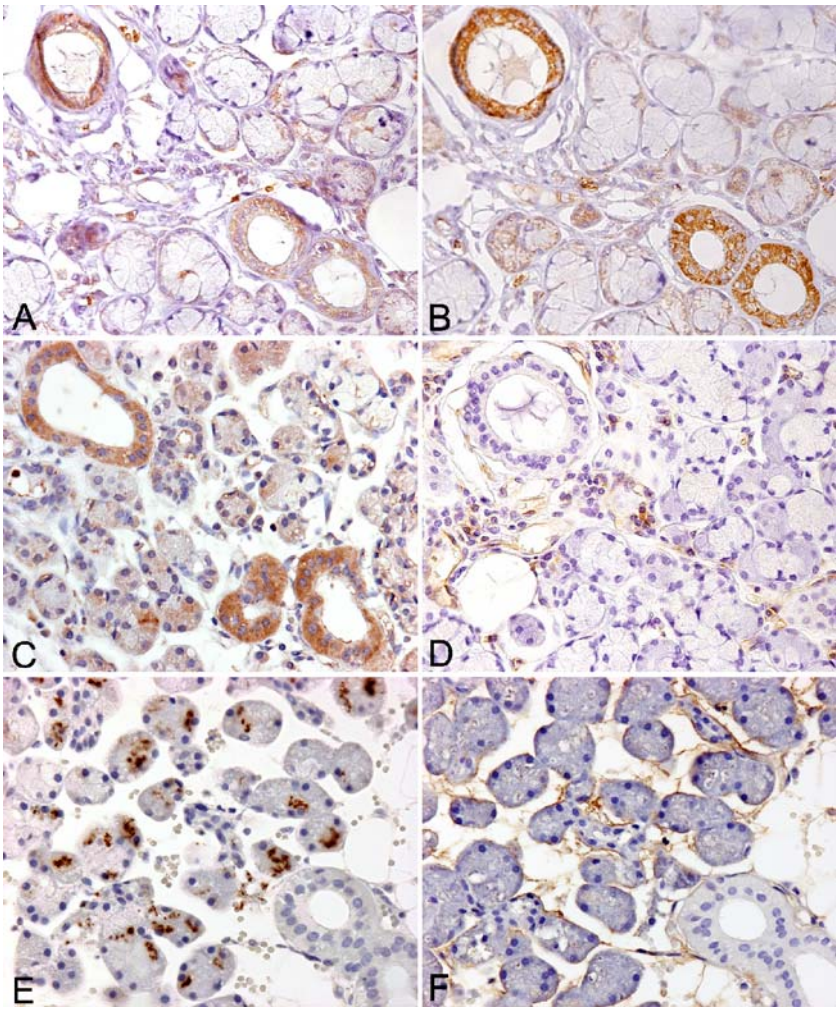

Fig. 1 Immunohistochemistry for vascular endothelial growth factor (VEGF; **a**), Flk-1 (**b**), Flt-1 (**c**), CD31 (**d**), HIF-1α (**e**), and lactate dehydrogenase (LDH; **f**) in the normal submandibular gland. Immunoperoxidase stain, hematoxylin counterstain, ×250. **a** VEGF, **b** Flk-1, and **c** Flt-1 were strongly immunolocalized in duct epithelial cells and serous acinar cells. Myoepithelial cells were occasionally immunopositive for these antigens. **d** CD31 was only localized in blood vascular endothelial cells in the interstitium. HIF-1α was localized in acinar cells in granular fashions (**e**), while LDH was mainly localized in interstitial connective tissues (**f**)

periphery of the acini, suggesting their expression in myoepithelial cells. Among them, VEGF was most evidently localized in myoepithelial cells (Fig. 1a). Since CD31 as an endothelial marker was only immunolocalized in blood channels (Fig. 1d), the localizations of VEGF and its receptors in salivary components were contrastively demonstrated. HIF-1α was immunolocalized in both acinar cells and intercalated duct epithelial cells (Fig. 1e), while LDH was mainly expressed in the extracellular space (Fig. 1f).

Next, we will describe the immunohistochemical results of pleomorphic adenoma tissues comparatively between solid areas and myxoid areas. S-100 protein and CK14 were expressed in tumor cells arranged in solid sheaths, while stellate-shaped cells in myxoid areas showed diffused and stronger signals mainly for S-100 protein (data not shown). VEGF was widely distributed in tumor cells forming sheet-like or ductal structures in the solid area. Those forming ductal structures were stronger than those arranged in sheets (Fig. 2a). In the myxoid area, stellate cells were strongly immunopositive for VEGF (Fig. 2b). Flk-1 was also intensively positive in tumor cells, especially those forming ductal structures (Fig. 2c). Flt-1 was mildly immunopositive in tumor cells with slightly more predominance in ductal cells (Fig. 2e). Stellate cells in the myxoid stroma were also immunopositive for Flk-1 (Fig. 2d) as well as for Flt-1 (Fig. 2f). Their positivities in the cytoplasm of stellate tumor cells were basically similar to those for VEGF. There were no immunopositive stainings for CD31 in either solid or myxoid areas, indicating that pleomorphic adenoma tissues were very poor in vascularity.

HIF-1α was immunolocalized in tumor cells forming small ductal structures within the solid area (Fig. 3a), while it was more widely and definitely localized in stellate cells in the myxochondroid area (Fig. 3b). LDH was immunolocalized along the basement membrane of ductal structures as well as within hyaline stroma within the solid area (Fig. 3c), while it was strongly labeled in the stellate cells and in some spider web-like fibrillar extracellular matrices (Fig. 3d). There was no definite difference in the staining patterns for these molecules among the samples from the parotid, submandibular, and minor salivary glands.

Immunofluorescence for pleomorphic adenoma cells in culture

Pleomorphic adenoma cells in culture at their subconfluency showed definite immunofluorescent signals for VEGF

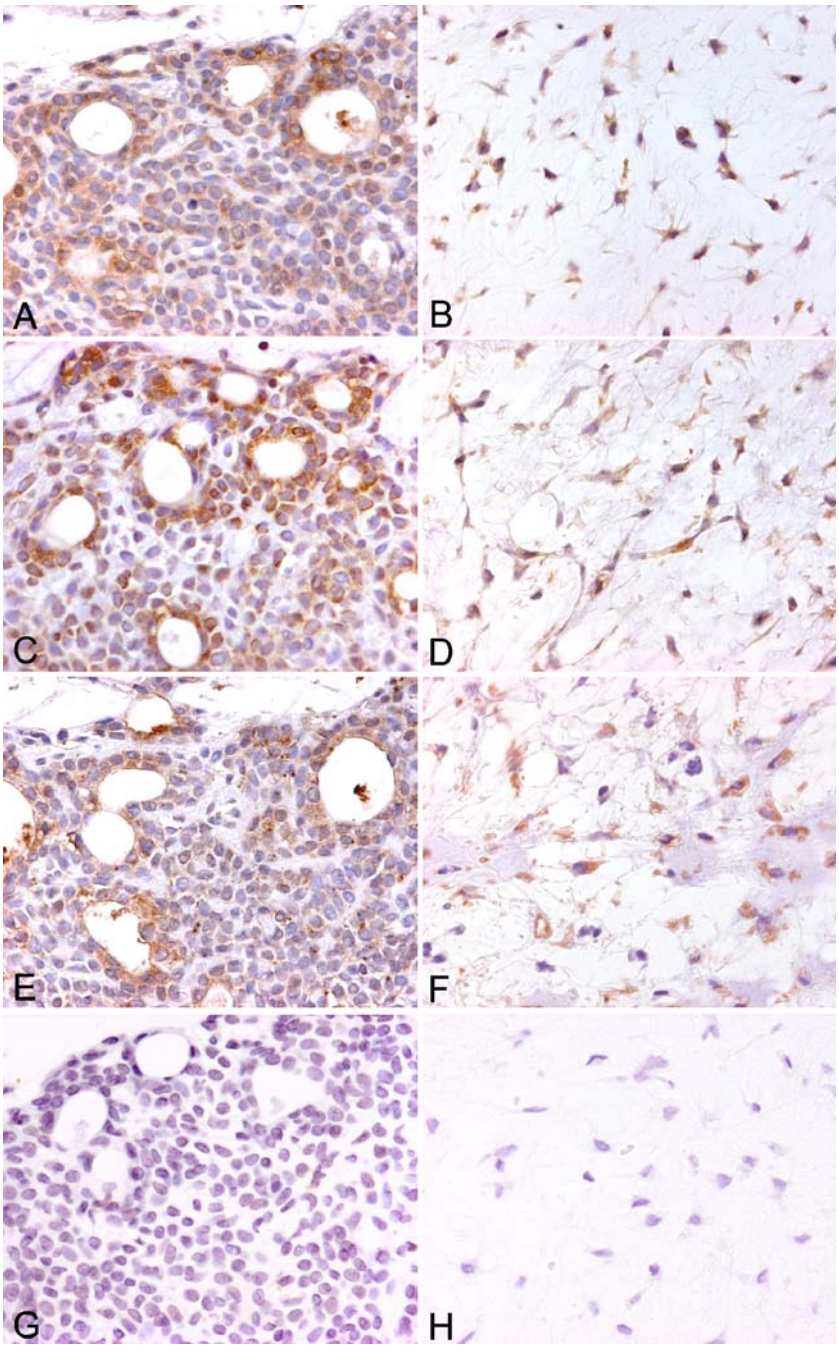

Fig. 2 Immunohistochemistry for vascular endothelial growth factor (VEGF; **a, b**), Flk-1 (**c, d**), Flt-1 (**e, f**), and CD31 (**g, h**) in solid (**a, c, e, g**) and myxoid (**b, d, f, h**) areas of pleomorphic adenoma. Immunoperoxidase stain, hematoxylin counterstain, ×250. In solid areas of pleomorphic adenomas, tumor cells forming duct-like structures were strongly positive for VEGF (**a**) and Flk-1 (**c**) and faintly positive for Flt-1 (**e**). In myxoid areas, most stellate-shaped tumor cells were immunopositive for VEGF (**b**) and Flk-1 (**d**), but only sporadic Flt-1 immunopositivities were found among them (**f**). Tumor cells were not immunopositive for CD31 either in solid (**g**) or myxoid areas (**h**)

(Fig. 4a), Flk-1 (Fig. 4b), Flt-1 (Fig. 4c), and HIF-1α (Fig. 4d). VEGF was strongly immunolocalized in the perinuclear area in punctuated patterns, while Flk-1 and Flt-1 were more diffusely localized around the nuclei. These findings suggested their localization in the Golgi apparatus for secretion. In contrast, HIF-1α was shown primarily within the nuclei and, at the same time, in the cytoplasm with faintly diffused as well as sharply punctuated patterns. The results suggest that pleomorphic adenoma cells produce VEGF and its receptors and that VEGF functions in an autocrine manner. Since HIF-1α signals were synchronized VEGF genes, it can be assumed that hypoxic stimulation might favor the VEGF expression. There was no difference in the staining pattern among the six samples.

Reverse-transcription polymerase chain reaction

Both in pleomorphic adenoma and normal submandibular gland tissues, PCR products for VEGF contained at least four bands with molecular masses of 721, 673, 580, and 517 bp, which corresponded to VEGF splicing variants 189, 165, 145 and 121, respectively (Fig. 5). The resultant products for VEGF were directly sequenced and shown to be

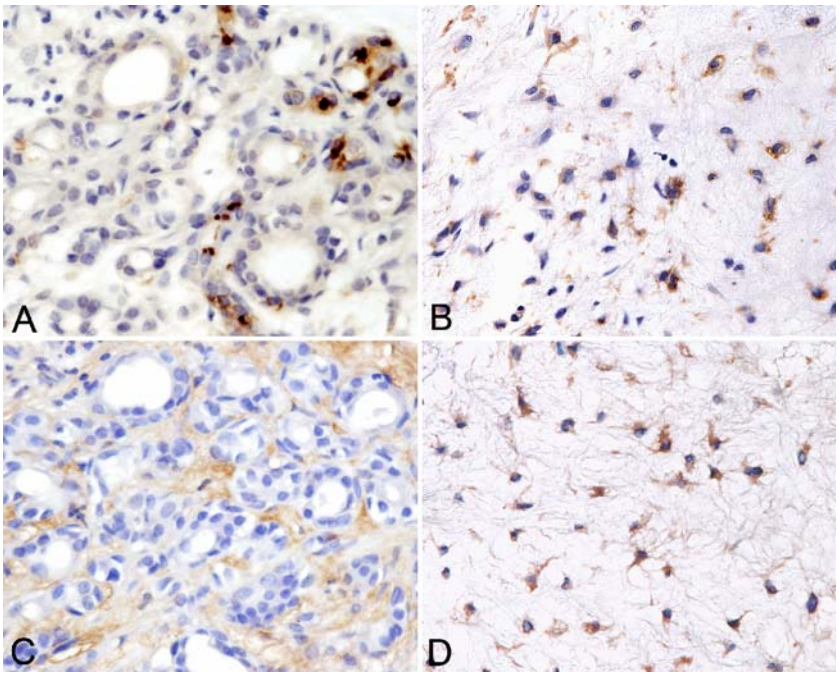

Fig. 3 Immunohistochemistry for hypoxia-related molecules HIF-1α (**a, b**) and lactate dehydrogenase (LDH; **c, d**) in solid (**a, c**) and myxoid (**b, d**) areas of pleomorphic adenoma. Immunoperoxidase stain, hematoxylin counterstain, ×250. In solid areas of pleomorphic adenoma, tumor cells forming minimal glandular structures or in the periphery of ductal structures were immunopositive for HIF-1α (**a**) and the stromal space was positive for LDH (**c**). In contrast, in myxoid area, most of the stellate-shaped cells were positive for both HIF-1α (**b**) and LDH (**d**), suggesting that tumor cells in myxoid areas are in more hypoxic conditions

consistent with their sequence registered in the NCBI GeneBank. Relative amounts of RT-PCR products for VEGF spliced variants were obtained by competitive PCR against GAPDH (983 bp). The bands electrophoresed in agarose gels were photographed and analyzed by NIH Image. The densitometric analyses showed that, among the VEGF splicing variants, $VEGF_{121}$ was always higher than any other variants in pleomorphic adenoma—irrespective of location—and in normal submandibular gland tissues, although the ratios of $VEGF_{121}$ against other variants were higher in tumor tissues. $VEGF_{189}$ and $VEGF_{165}$ were also evidently higher in pleomorphic adenomas than in normal salivary gland tissues.

Figure 6 shows RT-PCR results for HIF-1α in the same samples as shown in Fig. 5. There were statistically significant ($P<0.001$) higher levels of HIF-1α mRNA in pleomorphic adenomas than in normal salivary gland tissues. There were some relationships between the $VEGF_{121}$ and HIF-1α levels, indicating that pleomorphic adenoma tissues are involved in more hypoxic conditions than normal tissues are, which may have resulted in higher VEGF levels in pleomorphic adenomas. There was no definite

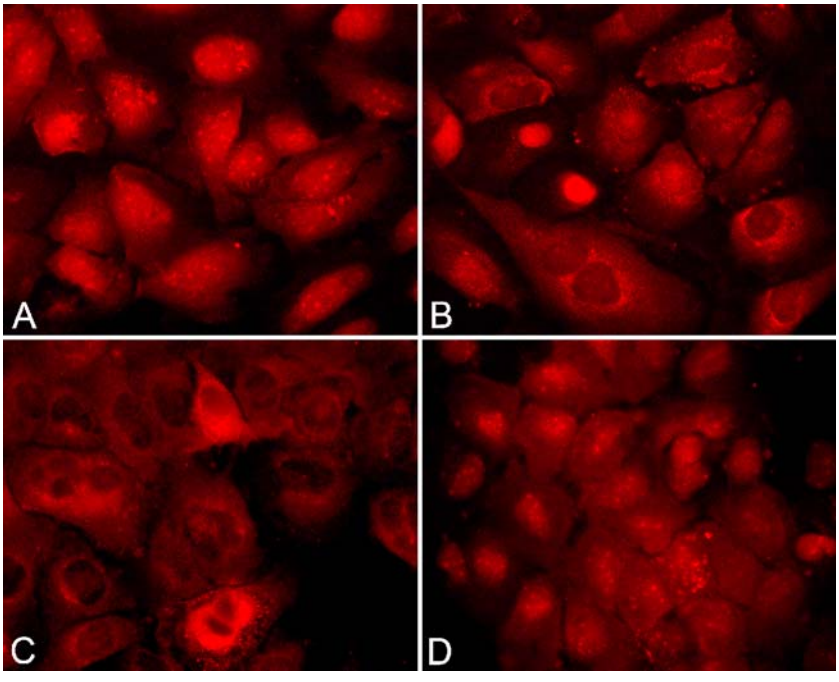

Fig. 4 Immunofluorescence for vascular endothelial growth factor (VEGF; **a**), Flk-1 (**b**), Flt-1 (**c**), and HIF-1α (**d**) in pleomorphic adenoma cells in culture. Indirect immunofluorescence, ×400. VEGF and its receptors Flk-1 and Flt-1 were biosynthesized and immunolocalized in pleomorphic adenoma cells in culture. There were punctuated VEGF signals in the perinuclear area, suggesting their localization in Golgi apparatus. HIF-1α was faintly and diffusely positive in the cytoplasm and more strongly in the nuclei. There were also characteristic punctuated signals for HIF-1α, which were scattered over the cytoplasm

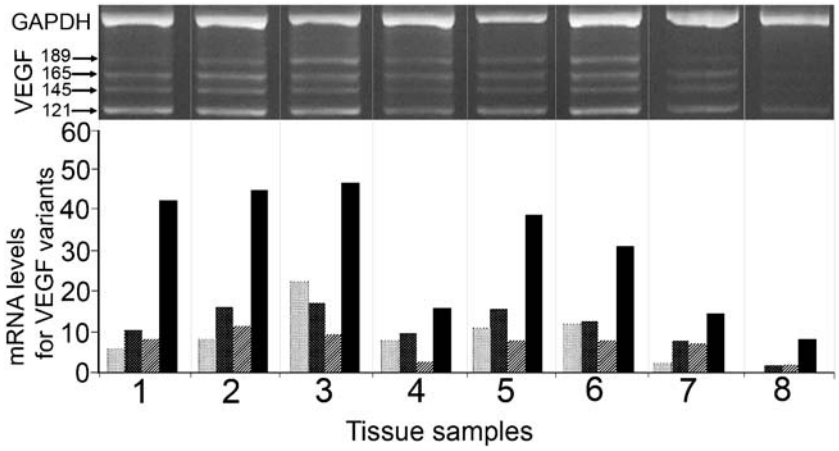

Fig. 5 Differential mRNA expression levels of vascular endothelial growth factor (VEGF) splicing variants in pleomorphic adenoma and normal submandibular gland tissues. Competitive reverse-transcription polymerase chain reaction (RT-PCR) products electrophoresed on 2% agarose gel and analyzed by densitometry. *Lane 1* 62-year-old female, submandibular gland; *lane 2* 41-year-old male, parotid; *lane 3* 26-year-old male, palate; *lane 4* 42-year-old female, parotid; *lane 5* 51-year-old female, parotid; *lane 6* 55-year-old female, submandibular; *lane 7* 56-year male, normal submandibular; *lane 8* 48-year-old female, normal submandibular. Higher mRNA expression levels of $VEGF_{121}$, $VEGF_{165}$, and $VEGF_{189}$ were obtained more often in pleomorphic adenomas (*lanes 1–6*) than in normal submandibular gland (*lanes 7 and 8*)

correlation between immunohistochemical and RT-PCR results for VEGF and HIF-1α, although higher levels for $VEGF_{121}$ and HIF-1α tended to occur in cases with predominant myxoid areas. There was no significant difference in terms of expression levels of both VEGF and HIF-1α between the parotid and the submandibular or the palatal salivary glands.

Discussion

The present results indicated that VEGF was produced by pleomorphic adenoma cells, and its signals were received by pleomorphic adenoma cells through Flt-1 or Flk-1. Since VEGF has been regarded as an important blood vascular endothelial modulator [6], its expression and function in pleomorphic adenoma cells were not expected. In addition to the immunolocalization of VEGF in pleomorphic adenoma, we were successful in the demonstration of VEGF splicing variants in the tumor tissue by means of RT-PCR, with no definite difference among the salivary gland types. Based on the immunohistochemical data in both normal salivary glands and pleomorphic adenomas, it was found that several particular VEGF signaling pathways may function not only in tumor cell proliferation but also in tumor cell arrangement. Our starting point of this study was the fact that pleomorphic adenoma is characterized by its poor vascularity in its stromal space whether it is hyaline, myxoid, or chondroid [12, 17, 19, 29, 37]. The poor vascularity in this particular tumor may be contrary to the general idea found in the textbook teaching which asserts that neoplastic tissues must be more vascularized than normal tissues [1]. In such a poor blood circulatory environment, how can tumor cells proliferate or even survive? This question was

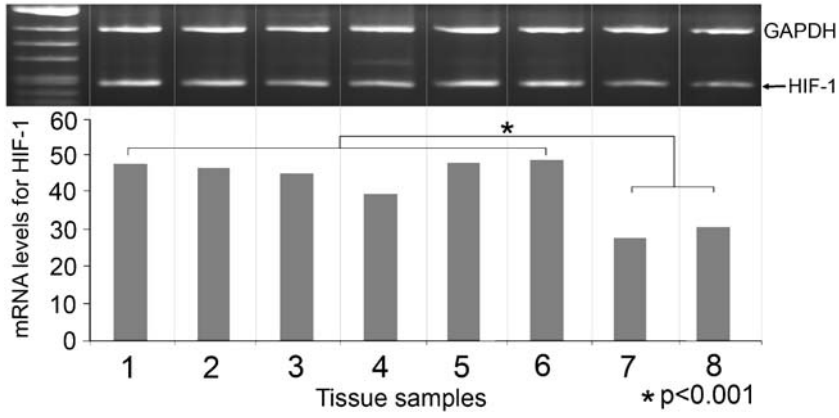

Fig. 6 Differential mRNA expression levels of HIF-1α in pleomorphic adenoma (*lanes 1–6*, samples in the same order as shown in Fig. 5) and normal submandibular gland (*lanes 7 and 8*) tissues. Competitive reverse-transcription polymerase chain reaction (RT-PCR) products electrophoresed on 3% agarose gel and analyzed by densitometry. Higher mRNA expression levels of HIF-1α were obtained more often in pleomorphic adenomas (*lanes 1–6*) than in normal submandibular gland (*lanes 7 and 8*). The difference was statistically significant ($P<0.001$) between pleomorphic adenomas and normal salivary glands

raised in the first step of our present investigation. In the beginning, we wanted to confirm the blood vessel population within the tumor tissue of pleomorphic adenoma, and we were able to reconfirm its poor vascularity by means of immunohistochemistry for endothelial markers such as CD31 or VEGF. However, to our surprise, the immunolocalization for VEGF involved more than just blood vessels, which we had not expected.

Immunohistochemically, we found that VEGF was localized in duct epithelial cells and some myoepithelial cells in normal salivary glands. The immunolocalization for Flk-1 and Flt-1, two of the VEGF receptors, was almost similar to that of VEGF. This result was also the same as previous data in normal salivary [22, 32] or mammary glands [20]. The present results and lines of previous evidence show that salivary gland cells are capable of producing and secreting VEGF under normal conditions. In pleomorphic adenoma tissues, however, VEGF expression was more characteristic. It was found in tubular structures as well as in stellate cells in the myxoid stroma. While Flk-1 and Flt-1 were immunolocalized in stellate cells, tumor cells forming tubular structures were more intensively positive for Flk-1. The tendency of Flk-1 predominance in tubular structures was consistent with the results in normal salivary glands, which obviously indicates that VEGF functions in formation and maintenance of ductal structures when it is recognized by Flk-1. A similar tendency in terms of tubule formation has already been reported in prostatic [8] and mammary [27] cancers. Since stellate cells that were diffusely scattered in the myxoid stroma were simultaneously immunopositive for VEGF, Flk-1, and Flt-1, these tumor cells seem to survive by an autocrine manner through both Flk-1 and Flt-1 signaling pathways, which has already been suggested in pancreatic [35] or prostatic [15] cancers.

Alternative splicing for the eight exons forming the VEGF gene has been shown to result in six spliced isoforms, which range in length from 121 to 206 amino acid residues ($VEGF_{121\text{-}206}$) [6, 26]. Most of the VEGF-producing tumor cells, such as those of germ cell tumors and breast and pulmonary tumors, appear preferentially to express $VEGF_{121}$, $VEGF_{165}$, and $VEGF_{189}$ more than normal cells do, indicating that these variants may function in tumor cell growth [8]. These splicing variants have been differentially immunolocalized in human kidney CEN4 cells: $VEGF_{165}$ with punctuated patterns in the perinuclear area and $VEGF_{189}$ with more diffused patterns in the cell surface and in the extracellular space [23]. Since both of the immunofluorescence patterns were found in pleomorphic adenoma cells in the present study, the presence of the two splicing forms seems to be also indicated morphologically. As to their receptors, some peculiar affinity of Flk-1 has been reported toward bindings with $VEGF_{145}$, $VEGF_{121}$, and $VEGF_{165}$, resulting in cell survival and proliferation in normal endothelial cells [31] or in intraepithelial carcinoma cells of the uterine cervix [18]. However, Flt-1 has been shown to have more affinities to $VEGF_{121}$ and $VEGF_{165}$, resulting in cellular proliferation and migration of the vascular endothelium [21, 33]. It is obvious that smaller VEGF variants can be recognized by both Flk-1 and Flt-1. However, at least in pleomorphic adenomas, most upregulated variants were shown to be $VEGF_{121}$, $VEGF_{165}$, and $VEGF_{189}$. $VEGF_{189}$ can be recognized by Flk-1 as a mitogenic signal when it is cleaved by urokinase-type plasminogen activator, although its intact form can be recognized only by Flt-1 [25]. In either way, the simultaneous signaling from the two receptors may play an important role in proliferation and maintenance of pleomorphic adenoma cells in the myxochondroid stroma where blood supplies are basically poor.

VEGF splicing variants lacking totally or partially the area encoded by exon 7, which were represented as $VEGF_{121}$ or $VEGF_{165}$, have been shown to be soluble and have lower binding affinity for heparin [10, 38]. In normal salivary glands, VEGF soluble isoforms have been thought to function mainly in increasing vascular permeability during the salivary secretory process [22, 32]. However, this does not seem to be the case in pleomorphic adenomas, because there is no sufficient blood circulation within the stromal space of pleomorphic adenomas. Instead, these free or soluble isoforms seem to be free from heparin binding and easily stimulate tumor cell proliferation in the myxochondroid stroma of pleomorphic adenoma, where heparan sulfate proteoglycan is rich [29]. At the same time, this particular heparan sulfate-rich setting may be related to the pronounced expression level for $VEGF_{189}$, which has higher binding affinity for heparan sulfates. In addition to heparan sulfate proteoglycans, the myxochondroid stroma has been shown to be rich in connective tissue growth factor (CTGF) [13, 30] and chondromodulin-I [17], which are also regarded as angiogenic inhibitors.

Moreover, the VEGF gene contains a hypoxia response element (HRE) that acts as an enhancer of VEGF gene expression [4, 9]. This HRE contains a consensus binding site for HIF-1α, which is expressed when cells are exposed to low oxygen tension [36]. The increase of HIF-1α levels has been shown to increase subsequently VEGF mRNA levels in human solid tumors, such as salivary adenoid cystic carcinomas [14] and colorectal adenomas/adenocarcinomas [16]. This molecular sequence caused by hypoxia can be reasonably applied to the present results in pleomorphic adenomas. In the present study, we were successful for the first time in demonstrating HIF-1α and LDH at both protein and gene levels in pleomorphic adenoma cells and tissues. The strong and characteristic immunofluorescence signals for HIF-1α may indicate that it functions within the nuclei and is then metabolized in the cytoplasm and that the protein levels for HIF-1α are already elevated in pleomorphic adenoma cells in their normal culture condition. Sharply punctuated and various-sized granular immunofluorescence signals for HIF-1α in the cytoplasm may imply that ubiquitination and proteasomal degradation of HIF-1α occurred after it activated its target genes [24], because VEGF was immunolocalized in the Golgi area at the same time, which indicated that it was ready for secretion by that time. The results may explain why pleomorphic adenoma cells can survive in poorly vascularized stromal spaces. The upregulation of VEGF, especially $VEGF_{121}$, due to tumor cells' own expression of hypoxia-related modulators, such as HIF-1α and LDH, may compensate for the poor vascular

milieu of the stroma of pleomorphic adenomas for proliferation of tumor cells.

In conclusion, the present study gave an answer to the question why pleomorphic adenoma cells can survive or even proliferate in their poorly vascularized stroma. The result indicated clearly that pleomorphic adenoma cells expressed VEGF in several spliced forms, which should have been induced by their hypoxic conditions due to avascularity, and that they seemed to receive particular splicing variant signals from Flt-1 and Flk-1, which might function in proliferation and tubular differentiation, respectively.

Acknowledgements This work was supported by Grants-in-Aid for Scientific Research from the Japan Society for the Promotion of Science and from the Ministry of Education, Culture, Sports, Science and Technology, Japan.

References

1. Bronchud MH, Foote MA, Giaccone G, Olopade O, Workman P (2004) Principles of molecular oncology. 2nd edn. Humana, New Jersey, pp 411–442
2. Cheng J, Irié T, Munakata R, Kimura S, Nakamura H, He RG, Lui AR, Saku T (1995) Biosynthesis of basement membrane molecules by salivary adenoid cystic carcinoma cells: an immunofluorescence and confocal microscopic study. Virchows Arch 426:577–586
3. Dardick I, van Nostrand AW (1985) Myoepithelial cells in salivary gland tumors—revisited. Head Neck Surg 7:395–408
4. Dibbens JA, Miller DL, Damert A, Risau W, Vadas MA, Goodall GJ (1999) Hypoxic regulation of vascular endothelial growth factor mRNA stability requires the cooperation of multiple RNA elements. Mol Biol Cell 10:907–919
5. Eatock MM, Schatzlein A, Kaye SB (2000) Tumour vasculature as a target for anticancer therapy. Cancer Treat Rev 26:191–204
6. Ferrara N, Gerber HP, LeCouter J (2003) The biology of VEGF and its receptors. Nat Med 9:669–676
7. Ferrara N, Henzel WJ (1989) Pituitary follicular cells secrete a novel heparin-binding growth factor specific for vascular endothelial cells. Biochem Biophys Res Commun 161:851–858
8. Ferrer FA, Miller LJ, Lindquist R, Kowalczyk P, Laudone VP, Albertsen PC, Kreutzer DL (1999) Expression of vascular endothelial growth factor receptors in human prostate cancer. Urology 54:567–572
9. Forsythe JA, Jiang BH, Iyer NV, Agani F, Leung SW, Koos RD, Semenza GL (1996) Activation of vascular endothelial growth factor gene transcription by hypoxia-inducible factor 1. Mol Cell Biol 16:4604–4613
10. Goerges AL, Nugent MA (2003) Regulation of vascular endothelial growth factor binding and activity by extracellular pH. J Biol Chem 278:19518–19525
11. Hamada T, Matsukita S, Goto M, Kitajima S, Batra SK, Irimura T, Sueyoshi K, Sugihara K, Yonezawa S (2004) Mucin expression in pleomorphic adenoma of salivary gland: a potential role for MUC1 as a marker to predict recurrence. J Clin Pathol 57:813–821
12. Hirokawa M, Tamura M, Horiguchi H, Wakatsuki S, Sano T (2001) Abnormal venous structures in salivary gland tumors: vasculature characteristics of pleomorphic adenoma. APMIS 109: 625–630
13. Inoki I, Shiomi T, Hashimoto G, Enomoto H, Nakamura H, Makino K, Ikeda E, Takata S, Kobayashi K, Okada Y (2002) Connective tissue growth factor binds vascular endothelial growth factor (VEGF) and inhibits VEGF-induced angiogenesis. FASEB J 16:219–221
14. Ishibashi H, Shiratuchi T, Nakagawa K, Onimaru M, Sugiura T, Sueishi K, Shirasuna K (2001) Hypoxia-induced angiogenesis of cultured human salivary gland carcinoma cells enhances vascular endothelial growth factor production and basic fibroblast growth factor release. Oral Oncol 37:77–83
15. Jackson MW, Roberts JS, Heckford SE, Ricciardelli C, Stahl J, Choong C, Horsfall DJ, Tilley WD (2002) A potential autocrine role for vascular endothelial growth factor in prostate cancer. Cancer Res 62:854–859
16. Jiang YA, Fan LF, Jiang CQ, Zhang YY, Luo HS, Tang ZJ, Xia D, Wang M (2003) Expression and significance of PTEN, hypoxia-inducible factor-1 alpha in colorectal adenoma and adenocarcinoma. World J Gastroenterol 9:491–494
17. Kusafuka K, Hiraki Y, Shukunami C, Yamaguchi A, Kayano T, Takemura T (2001) Cartilage-specific matrix protein chondromodulin-I is associated with chondroid formation in salivary pleomorphic adenomas: immunohistochemical analysis. Am J Pathol 158:1465–1472
18. Michalski B, Zielinski T, Fila A, Mazurek U, Poreba R, Wilczok T (2003) Correlation between transcriptional activity of vascular endothelial growth factor (VEFG) and transcriptional activity of its receptors (FLT-1 and FLK-1) in low-grade squamous intraepithelial lesions (LSIL) of uterine cervix. Ginekol Pol 74: 805–810
19. Neureiter D, Bohmer J, Kirchner T, Aigner T (1999) Pleomorphic adenomas of the parotid express different mesenchymal phenotypes: demonstration of matrix gene expression products characteristic of the fibroblastic and chondrocytic cell lineages. Histopathology 35:373–379
20. Nishimura S, Maeno N, Matsuo K, Nakajima T, Kitajima I, Saito H, Maruyama I (2002) Human lactiferous mammary gland cells produce vascular endothelial growth factor (VEGF) and express the VEGF receptors, Flt-1 and KDR/Flk-1. Cytokine 18:191–198
21. Orecchia A, Lacal PM, Schietroma C, Morea V, Zambruno G, Failla CM (2003) Vascular endothelial growth factor receptor-1 is deposited in the extracellular matrix by endothelial cells and is a ligand for the alpha 5 beta 1 integrin. J Cell Sci 116:3479–3489
22. Pammer J, Weninger W, Mildner M, Burian M, Wojta J, Tschachler E (1998) Vascular endothelial growth factor is constitutively expressed in normal human salivary glands and is secreted in the saliva of healthy individuals. J Pathol 186:186–191
23. Park JE, Keller GA, Ferrara N (1993) The vascular endothelial growth factor (VEGF) isoforms: differential deposition into the subepithelial extracellular matrix and bioactivity of extracellular matrix-bound VEGF. Mol Biol Cell 4:1317–1326
24. Paul SA, Simons JW, Mabjeesh NJ (2004) HIF at the crossroads between ischemia and carcinogenesis. J Cell Physiol 200:20–30
25. Plouet J, Moro F, Bertagnolli S, Coldeboeuf N, Mazarguil H, Clamens S, Bayard F (1997) Extracellular cleavage of the vascular endothelial growth factor 189-amino acid form by urokinase is required for its mitogenic effect. J Biol Chem 272: 13390–13396
26. Poltorak Z, Cohen T, Neufeld G (2000) The VEGF splice variants: properties, receptors, and usage for the treatment of ischemic diseases. Herz 25:126–129
27. Restucci B, Borzacchiello G, Maiolino P, Martano M, Paciello O, Papparella S (2004) Expression of vascular endothelial growth factor receptor Flk-1 in canine mammary tumours. J Comp Pathol 130:99–104
28. Saku T, Okabe H, Yagi Y, Sato E, Tsuda N (1984) A comparative study on the immunolocalization of keratin and myosin in salivary gland tumors. Acta Pathol Jpn 34:1031–1040
29. Saku T, Cheng J, Okabe H, Koyama Z (1990) Immunolocalization of basement membrane molecules in the stroma of salivary gland pleomorphic adenoma. J Oral Pathol Med 19:208–214
30. Shakunaga T, Ozaki T, Ohara N, Asaumi K, Doi T, Nishida K, Kawai A, Nakanishi T, Takigawa M, Inoue H (2000) Expression of connective tissue growth factor in cartilaginous tumors. Cancer 89:1466–1473

31. Soker S, Gollamudi-Payne S, Fidder H, Charmahelli H, Klagsbrun M (1997) Inhibition of vascular endothelial growth factor (VEGF)-induced endothelial cell proliferation by a peptide corresponding to the exon 7-encoded domain of VEGF165. J Biol Chem 272:31582–31588
32. Taichman NS, Cruchley AT, Fletcher LM, Hagi-Pavli EP, Paleolog EM, Abrams WR, Booth V, Edwards RM, Malamud D (1998) Vascular endothelial growth factor in normal human salivary glands and saliva: a possible role in the maintenance of mucosal homeostasis. Lab Invest 78:869–875
33. Usui T, Ishida S, Yamashiro K, Kaji Y, Poulaki V, Moore J, Moore T, Amano S, Horikawa Y, Dartt D, Golding M, Shima DT, Adamis AP (2004) VEGF164(165) as the pathological isoform: differential leukocyte and endothelial responses through VEGFR1 and VEGFR2. Invest Ophthalmol Vis Sci 45:368–374
34. Viac J, Palacio S, Schmitt D, Claudy A (1997) Expression of vascular endothelial growth factor in normal epidermis, epithelial tumors and cultured keratinocytes. Arch Dermatol Res 289: 158–163
35. von Marschall Z, Cramer T, Hocker M, Burde R, Plath T, Schirner M, Heidenreich R, Breier G, Riecken EO, Wiedenmann B, Rosewicz S (2000) De novo expression of vascular endothelial growth factor in human pancreatic cancer: evidence for an autocrine mitogenic loop. Gastroenterology 119:1358–1372
36. Waltenberger J, Mayr U, Pentz S, Hombach V (1996) Functional upregulation of the vascular endothelial growth factor receptor KDR by hypoxia. Circulation 94:1647–1654
37. Xu H, Shimizu Y, Niki T, Nagasaka H, Kawamura H, Ooya K (2003) Pleomorphic adenoma of the submandibular salivary glands with marked ossification. J Oral Pathol Med 32:499–501
38. Zhang HT, Scott PA, Morbidelli L, Peak S, Moore J, Turley H, Harris AL, Ziche M, Bicknell R (2000) The 121 amino acid isoform of vascular endothelial growth factor is more strongly tumorigenic than other splice variants in vivo. Br J Cancer 83:63–68

Virchows Arch (2005) 446: 663–673
DOI 10.1007/s00428-005-1265-8

ORIGINAL ARTICLE

Hideki Fujii · Shuichi Seki · Sawako Kobayashi · Takuya Kitada · Nobuyoshi Kawakita · Keishi Adachi · Hiroko Tsutsui · Kenji Nakanishi · Hiromi Fujiwara · Yoshinori Ikarashi · Masaru Taniguchi · Kronenberg Mitchell · Masaru Ikemoto · Yuji Nakajima · Tetsuo Arakawa · Kenji Kaneda

A murine model of NKT cell-mediated liver injury induced by alpha-galactosylceramide/D-galactosamine

Received: 8 November 2004 / Accepted: 25 March 2005 / Published online: 20 May 2005
© Springer-Verlag 2005

Abstract Natural killer-T (NKT) cells are rich in the liver. However, their involvement in liver injury is not fully understood. We developed here a new murine model of NKT-cell-activation-associated liver injury, and investigated a role of tumor necrosis factor alpha (TNF-α) and Fas in pathogenesis. We injected intraperitoneally alpha-galactosylceramide (α-GalCer), an NKT-cell stimulant, into D-galactosamine (GalN)-sensitized mice. Survival rate, pathological changes of the liver, and plasma concentrations of cytokines were studied. Alpha-GalCer/GalN administration gave a lethal effect within 7 h, making pathological changes such as massive parenchymal hemorrhage, hepatocyte apoptosis, sinusoidal endothelial cell injury, and close apposition of lymphocytes to apoptotic hepatocytes. Anti-NK1.1 mAb-pretreated mice and Vα14NKT knock out (KO) mice did not develop liver injury. Tumor necrosis factor-alpha (TNF-α) and interferon-gamma (IFN-γ) were elevated at 4 h in the plasma. These cytokines were produced by hepatic lymphocytes as demonstrated by in vitro stimulation with α-GalCer. The lethal effect was suppressed in TNF-α KO mice, TNF receptor-1 KO mice, and *lpr/lpr* (Fas deficient) mice, whereas it was not in IFN-γ KO mice. These results indicate that the present liver injury is characterized by parenchymal hemorrhage and hepatocyte apoptosis, and mediated by TNF-α secretion and direct cytotoxicity of α-GalCer-activated NKT cells.

Keywords Parenchyma hemorrhage · Apoptosis · TNF-α · IFN-γ · Fas

H. Fujii (✉) · S. Seki · S. Kobayashi · T. Kitada · N. Kawakita
Department of Hepatology,
Osaka City University Graduate
School of Medicine,
1-4-3 Asahimachi, Abeno-ku,
Osaka, 545-8585, Japan
e-mail: rolahideki@med.osaka-cu.ac.jp
Tel.: +81-6-66453811
Fax: +81-6-66463603

H. Fujii · M. Ikemoto · Y. Nakajima · K. Kaneda
Department of Anatomy,
Osaka City University Graduate
School of Medicine,
Osaka, Japan

K. Adachi · H. Tsutsui · K. Nakanishi
Core Research for Evolutional
Science and Technology,
Japan Science and Technology Agency,
Kawaguchi, Japan

H. Tsutsui · K. Nakanishi
Department of Immunology and
Medical Zoology,
Hyogo College of Medicine,
Nishinomiya, Japan

H. Fujiwara
Biomedical Research Center,
Osaka University Graduate School of Medicine,
Suita, Japan

Y. Ikarashi
Pharmacology Division,
National Cancer Center Research Institute,
Tokyo, Japan

M. Taniguchi
Institute of Physical and Chemical Research,
Research Center for Allergy and Immunology,
Tokyo, Japan

M. Taniguchi
Chiba University Graduate School of Medicine,
Chiba, Japan

K. Mitchell
La Jolla Institute for Allergy and Immunology,
San Diego, CA, USA

T. Arakawa
Department of Gastroenterology,
Osaka City University Graduate School of Medicine,
Osaka, Japan

Abbreviations NK: natural killer · NKT: natural killer-T · α-GalCer: alpha-galactosylceramide · GalN: D-galactosamine · SEB: staphylococcal enterotoxin B · TNF-α: tumor necrosis factor alpha · IFN-γ: interferon gamma · TNFR1: TNF receptor-1 · FasL: Fas ligand · LPS: lipopolysaccharide · iNKT: invariant NKT · KO: knock out · mAb: monoclonal antibody · ALT: alanine transaminase · IL: interleukin · TUNEL: terminal deoxynucleotidyl transferase-mediated nick end labeling · WT: wild type · SECs: sinusoidal endothelial cells · RT-PCR: reverse transcription- polemerase chain reaction

Introduction

There are large populations of macrophages (or Kupffer cells), natural killer (NK) cells, and natural killer-T (NKT) cells in the liver even in the steady state. In pathological conditions, they are activated, and play roles in the defense against microbes and tumor cells [6, 12, 38]. Inflammation thus induced often causes liver injury. Several murine models of liver injury have been developed by stimulating these cell populations. Many of the models are related to macrophage activation with lipopolysaccharide (LPS). Hepatotoxicity of LPS is augmented by priming animals with *Propionibacterium acnes*, which stimulates macrophages, NK cells and T cells to produce cytokines [44, 50] or sensitizing animals with D-galactosamine (GalN), a transcriptional inhibitor [13]. Hepatitis is also induced by activation of T cells with concanavalin A (Con A), a T-cell mitogen [24, 26, 32, 54], staphylococcal enterotoxin B (SEB), a superantigen, or anti-CD3 monoclonal antibody (mAb) [14, 56]. It was recently reported that NKT-cell activation is induced by treatment with alpha-galactosylceramide (α-GalCer) [40]. Administration of this agent induces liver injury, but the extent of damage is limited [40].

NKT cells are a T-cell subset defined as $NK1.1^+$ αβT-cell $receptor^+$ cells [2, 15]. They regulate Th1 and Th2 immune responses by producing various immunoregulatory cytokines such as interleukin-4, interferon gamma (IFN-γ) and tumor necrosis factor alpha (TNF-α) [2], and exert direct cytotoxicity against target cells by either perforin- or Fas-dependent mechanism [21]. NKT cells are specifically stimulated with α-GalCer presented by CD1d molecule on dendritic cells [22]. They are deeply involved in the development of several human diseases such as type I diabetes [53], systemic sclerosis [45], multiple sclerosis [18], systemic lupus erythematosis [46], primary biliary cirrhosis [23], and alcoholic hepatitis [31].

In this study, in order to make a murine model of NKT-cell activation-associated liver injury, we activated hepatic NKT cells with α-GalCer in GalN-sensitized mice, and analysed pathological changes. We also revealed that TNF-α/TNF receptor-1 (TNFR1) pathway is mainly involved in the pathogenesis.

Materials and methods

Animals

Specific pathogen-free, female C57BL/6 (B6) wild-type (WT) mice aged 6–7 weeks old, and female B6-*lpr/lpr* mice of the same age were purchased from Nippon SLC (Shizuoka, Japan). Female TNF-α-knock out (KO) mice and TNFR1 KO mice on a B6 background were purchased from Jackson Laboratories (Bar Harbor, ME, USA). Female IFN-γ-KO mice were kindly provided by Dr. Yoichiro Iwakura at Tokyo University, Japan [47]. Vα 14NKT KO on a B6 background mice lacking invariant NKT (*i*NKT) cells were described elsewhere [7]. Animals were fed of standard chow pellet and water ad libitum. The experimental protocol was approved by the Animal Research Committee of Osaka City University (Guide for Animal Eeperiments, Osaka City University).

Induction of liver injury

A single dose of 0.5 μg α-GalCer (kindly provided by Dr. Kazuhiro Motoki, Research Center, Kirin Beer Co., Tokyo, Japan) and that of 10 mg GalN (Wako Pure Chemicals, Tokyo, Japan) were intraperitoneally injected into the mice at the same time. Lethality was scored up to 12 h after the challenge.

Pretreatments of mice

Mice were pretreated with several agents before α-GalCer/GalN administration. Some mice were subjected to intraperitoneal injections of z-VAD-fmk (Wako Pure Chemicals) in the doses of 0.25 mg at −15 min and 0.1 mg at 1 h [5]. Some mice were subjected to intraperitoneal injections of 50 μl rabbit anti-asialo GM1 antibody (Wako Pure Chemical Industries) once daily at −4, −3, −2 and −1 day or 400 μg anti-NK1.1. mAb (BD Biosciences, Rockeysville, Md., USA) once daily at −3 days in order to deplete NK cells and NK/NKT cells, respectively [43].

Assay of plasma alanine transaminase (ALT) levels

Blood was collected at various time intervals after α-GalCer/GalN administration, and plasma ALT levels were determined using a HITACHI 7250 auto-analyzer.

Organ index

The liver, spleen, kidney, lung, and heart were taken and weighed. Organ index was calculated as follows. Organ index (%)=organ weight/body weight×100.

Histology

The liver was fixed in 10% formalin, and embedded in paraffin. Sections were stained with hematoxylin and eosin (H-E). For electron microscopy, the liver was perfusion-fixed with 1.5% glutaraldehyde in 0.062 M cacodylate buffer, pH 7.4, plus 1% sucrose for 3 min via the portal vein, and post-fixed in 1% OsO_4 in 0.1 M phosphate buffer, pH 7.4, for 2 h. They were embedded in Polybed (Polyscience Inc., Warrington, Pa., USA). Thin sections were stained with uranyl acetate and lead citrate, and observed under a JEM-1200EX electron microscope (JEOL, Tokyo, Japan) at 80 kV.

TUNEL method

For detection of apoptosis, paraffin sections were stained by terminal deoxynucleotidyl transferase (TdT)-mediated dUTP nick end labeling (TUNEL) technique using an In Situ Apoptosis Detection Kit (Takara Shuzo Co., Ltd, Shiga, Japan). Three mice were used for each group. Three sections were made per liver, and five microscopic fields (×400) were examined to obtain a minimum count of 2000 hepatocytes.

Measurement of TNF-α and IFN-γ

Plasma levels of TNF-α and IFN-γ were quantitated by enzyme-linked immunosorbent assay (ELISA) kits FACTOR-TEST-X (Genzyme, Cambridge, Mass., USA) and INTERTEST-γ (Genzyme), respectively. TNF-α levels in the whole liver were determined as previously described [33]. Assays were performed as indicated by the manufacturer. Each sample was determined in duplicate.

RNA preparation and reverse transcription-polymerase chain reaction (RT-PCR)

Total liver RNA was extracted by using ISOGEN (Nippon Gene, Tokyo, Japan) according to the manufacturer's instructions, and 0.3 μg of the sample was reverse-transcribed into cDNA using the One Step RT-PCR Kit (QIAGEN, Valencia, California). The sequences of oligonucleotide primers are: 5′ TNF-α, CAT GAT CCG CGA CGT; 3′ TNF-α, GTG GTT TGC TAC GAC G; 5′ TNFR1, CTG CTG TCA CTG GTG CTC CTG; 3′ TNFR1, CAC ACA CCG TGT CCT TGT CAG; 5′ GAPDH, GAG GCC GGT GCT GAG TAT GT; 3′ GAPDH, TCA TTG AGA GCA ATG CCA GC. We quantified gene expression as previously described [54]. Briefly, The thermal cycle program was set to anneal at 58° for a total of 32 cycles. The expected fragment length was 283 bp for TNF-α, 349 bp for TNFR1 and 650 bp for GAPDH.

Preparation and culture of hepatic lymphocytes

Hepatic lymphocytes were prepared from WT and TNF-α KO mice by gradient centrifugation of Percoll (Amersham, Uppsala, Sweden) as previously described [16]. This fraction included dendritic cells and monocytes in addition to lymphocytes. Cells from three mice were pooled. They were prepared at the concentration of 2.0×10^5 cells/200 ml/well, and cultured with 0, 1, 10, and 100 ng/ml α-GalCer for 72 h at 37°. TNF-α and IFN-γ in the culture medium were measured by ELISA. Three mice were used for one experiment.

Flow cytometric analysis

Hepatic lymphocytes isolated from the liver were stained with FITC-conjugated anti-CD3 mAb (PharMingen, San Diego, Calif., USA) and PE-conjugated α-GalCer/CD1d tetramer [30]. Stained cells were analyzed on a FACS Calibur (Becton Dickinson, San Jose, Calif., USA) using Cell Quest software (Becton Dickinson). Liver lymphocytes were gaited according to their forward and side scatter profiles.

Statistics

The data was expressed as the mean±standard deviation (SD). Significant difference was evaluated by an unpaired Student's *t*-test.

Results

Lethal effect of α-GalCer on GalN-sensitized mice

Neither sensitization with GalN (10 mg per mouse) nor NKT cell activation with α-GalCer (0.5, 1.0 and 2.0 μg per mouse) was lethal to WT mice. On the other hand, com-

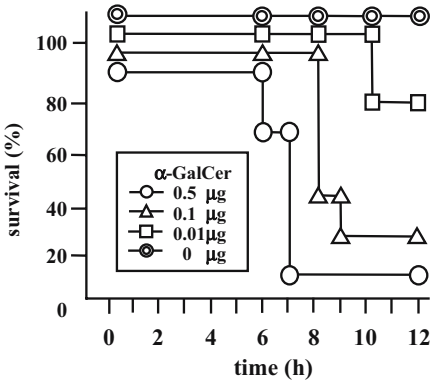

Fig. 1 A dose-dependent lethal effect of α-GalCer on GalN-sensitized WT mice. Five animals were used for each group

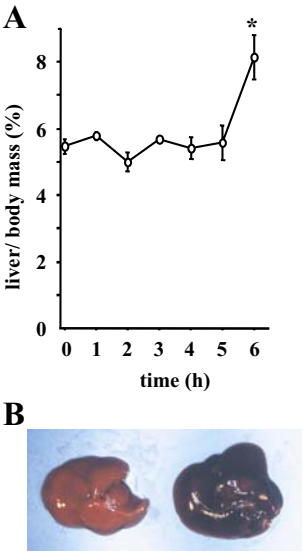

Fig. 2 **a** Time course of the liver index in WT mice after treatment with α-GalCer/GalN. The data represent the mean±SD (n=3 mice for each time period). *P<0.01 versus 0 h. **b** A macroscopic view of the livers from untreated WT mice (left side) and α-GalCer/GalN-treated WT mice at 6 h (right side). The latter liver is swollen and congested

bination of sensitization with GalN and NKT-cell activation with α-GalCer (0.01-0.5 μg per mouse) induced very high mortality in WT mice within 7 h in a dose-dependent manner (Fig. 1). All mice died at 0.5 μg α-GalCer, so we used this dose in the following experiments.

Induction of liver injury by α-GalCer/GalN administration

By α-GalCer/GalN administration, the liver index was unchanged until 5 h. It then abruptly went up at 6 h (Fig. 2a). Macroscopically, the liver was swollen, and congested (Fig. 2b). The spleen, lung, and heart, on the other hand, showed no significant increase in organ index (Table 1).

In H-E stained sections, the livers from untreated mice (Fig. 3a) and those from GalN (10 mg)-treated mice (Fig. 3c) showed no pathological changes. In α-GalCer (0.5 μg)-treated mice, a moderate infiltration of lymphocytes was seen in the sinusoids (Fig. 3b). When treated with α-GalCer (0.5 μg)/GalN (10 mg), the liver showed massive parenchyma hemorrhage at 5 h (Fig. 3d). Many hepatocytes underwent apoptosis as demonstrated by TUNEL (Fig. 3e) and H-E staining (Fig. 3f). The space among apoptotic hepatocytes was filled with many erythrocytes (Fig. 3f). Despite such prominent pathological changes, plasma ALT activity did not increase (=33.0±16.4 IU/l; n=5) at 5 h. In the spleen, lung, kidney and heart, neither hemorrhage nor apoptosis was observed (data not shown). Quantitative analysis demonstrated that hepatocyte apoptosis appeared at 3 h, and progressively increased in number until 6 h. Approximately 30 apoptotic cells were counted per 200 hepatocytes at 6 h (Fig. 4).

Pathological changes were further investigated by electron microscopy. At 4 h, hepatocytes showed "pre-apoptotic alterations [1]", i.e. swelling of mitochondria and disappearance of microvilli (Fig. 5a). Apoptotic hepatocytes shrinked, and as the result the space of Disse was extended. At 5 h, SECs showed a significant decrease in the number fenestrated (Fig. 5b). Some of them were disrupted in places, allowing extravasation of erythrocytes (Fig. 5c). Lymphocytes migrated into the space of Disse, and made a direct contact with hepatocytes (Fig. 5d, e), or entered the cytoplasm of the latter cells, representing "emperipolesis [10]" (Fig. 5c). Large granular lymphocytes (LGLs), the morphological relevance to NK and NKT cells [38, 52], were also found in the extrasinusoidal space (Fig. 5f). Several hepatocytes showed nuclear chromatin condensation, being conjugated with lymphocytes, and produced apoptotic bodies (Fig. 5d). Apoptotic bodies were phagocytozed by adjacent hepatocytes as previously reported [3, 11]. A wide extrasinusoidal space produced by elimination of apoptotic hepatocytes was filled with many erythrocytes.

It is reported that, when SECs are functionally impared, hyaluronic acid is selectively taken up by SECs, and increases in serum concentration [8]. Hyaluronic acid increased in plasma level at 4 h, and further went up at 5 h after α-GalCer/GalN treatment (Fig. 6).

Involvement of NKT cells in the liver injury

Pretreatment with anti-asialo GM1 neither decreased the lethality nor suppressed the liver injury after α-GalCer/GalN treatment (Fig. 7). Pretreatment with anti-NK1.1 mAb, on the other hand, increased the survival. Vα14NKT KO mice all survived up to 12 h, and did not develop liver injury (Fig. 7). These data indicate that NKT cells, but not NK cells, are involved in the lethal effect of α-GalCer/GalN.

Involvement of TNF-α and TNFR1 in the liver injury

We measured plasma concentrations of TNF-α and IFN-γ at various time intervals after administration of GalN alone, α-GalCer alone and α-GalCer/GalN (Fig. 8). No appreciable elevation of both cytokines was detected in GalN-treated mice. Alpha-GalCer administration increased plasma TNF-α and IFN-γ in both GalN-non-sensitized and sensitized mice to similar levels, although the peak of TNF-α in the latter mice somewhat delayed (4 h) compared

Table 1 Organ indices in control (vehicle alone-treated) and α-GalCer/GalN-treated WT mice at 6 h after administration

Organs	Control	α-GalCer/GalN
Liver	4.94±0.53	8.40±0.53*
Spleen	0.35±0.03	0.48±0.09
Kidney	1.25±0.07	1.36±0.07
Lung	0.88±0.09	0.91±0.06
Heart	0.51±0.04	0.50±0.03

Organ index (%)=organ weight/body weight ×100. The data is represented by the mean±SD. n=3 mice
*P<0.01 versus control

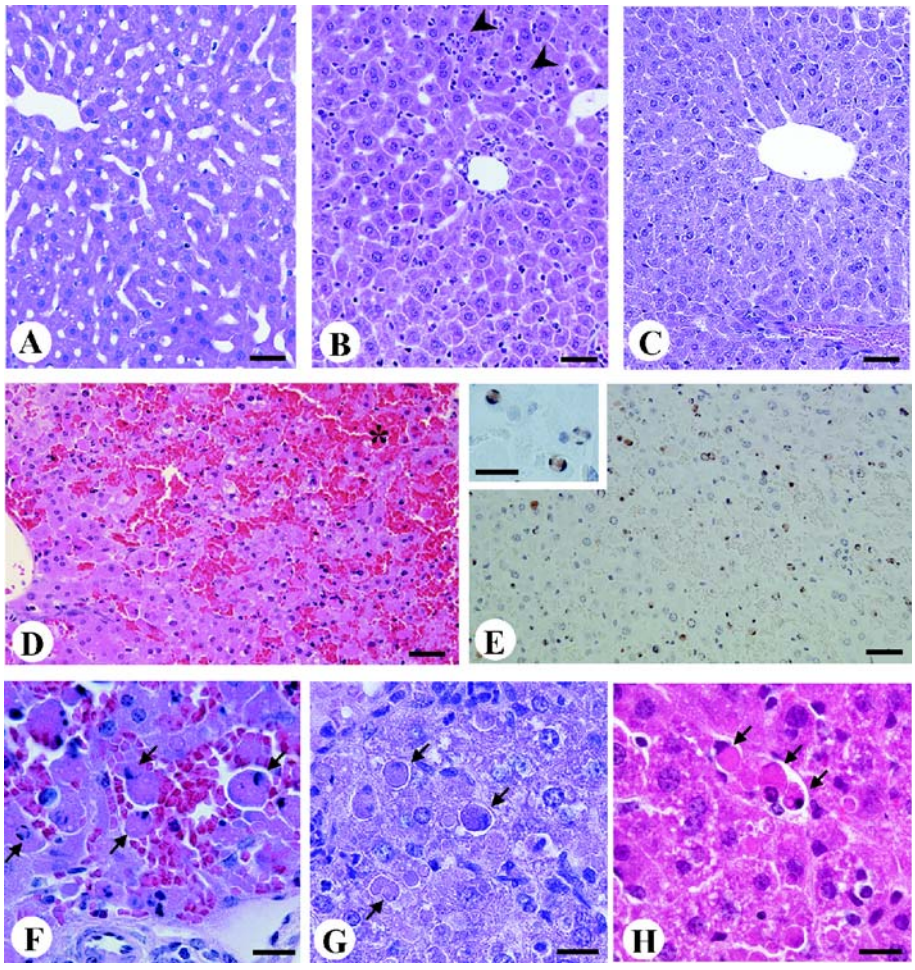

Fig. 3 Light microscopy of the liver. **a** Untreated WT mice. Bar=60 μm. **b** WT mice at 5 h after administration of 0.5 μg α-GalCer alone. Lymphocyte infiltration (*arrowheads*) is seen in the parenchyma. However, the hepatic injury is negligible. Bar=60 μm. **c** WT mice at 5 h after administration of 10 mg GalN alone. No appreciable changes are seen. Bar=60 μm. **d-f** WT mice at 6 h after administration of α-GalCer (0.5 μg)/GalN (10 mg). **D**. Hemorrhage (*asterisks*) in the liver parenchyma. Bar=60 μm. **e** A TUNEL-stained serial section of **d**. Many hepatocytes in the lesion are positively stained. Bar=60 μm. *Inset*. Higher magnification of TUNEL-positive hepatocytes. Bar=30 μm. **f** A higher magnification of H-E stained sections. Apoptotic hepatocytes (*arrows*) have eosinophilic cytoplasm and chromatin-condensed nuclei. The space around them is filled with many erythrocytes. Bar=30 μm. **g** TNF-α KO mouse at 12 h after α-GalCer/GalN administration. There are a small number of apoptotic hepatocytes (*arrows*), but no appreciable hemorrhage is seen. Bar=30 μm. **h** TNFR1 KO mouse at 12 h. There are several apoptotic hepatocytes (*arrows*). Bar=30 μm

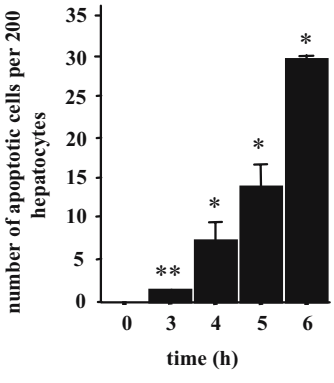

Fig. 4 Timecourse of the number of apoptotic hepatocytes per 200 hepatocytes after α-GalCer/GalN administration. Apoptotic hepatocytes were identified in H-E stained sections. The data represent the mean±SD (n=3 mice for each time period). *P<0.01, **P<0.05 versus 0 h

to the former mice (2 h) (Fig. 8). We next measured TNF-α levels in the liver tissue. No appreciable amount of TNF-α was detected in the liver from untreated mice. By treatment with α-GalCer/GalN, liver TNF-α significantly increased to 29.75±6.15 pg/ml (n=3) at 4 h.

In order to investigate the role of cytokines in the lethal effect and liver injury, we used KO mice. While IFN-γ KO mice gave a survival curve similar to WT mice, TNF-α KO mice all survived up to 12 h (Fig. 9). In IFN-γ KO mice, the liver became swollen and dark, and the liver index significantly increased as seen in WT mice (Fig. 10). Under a light microscope, parenchyma hemorrhage and hepatocyte apoptosis were observed in IFN-γ KO mice (data not shown). In TNF-α KO mice, on the other hand, the liver was macroscopically normal (data not shown), and the liver index did not increase (Fig. 10). Apparent hemorrhage was not induced, but there was a small number of apoptotic

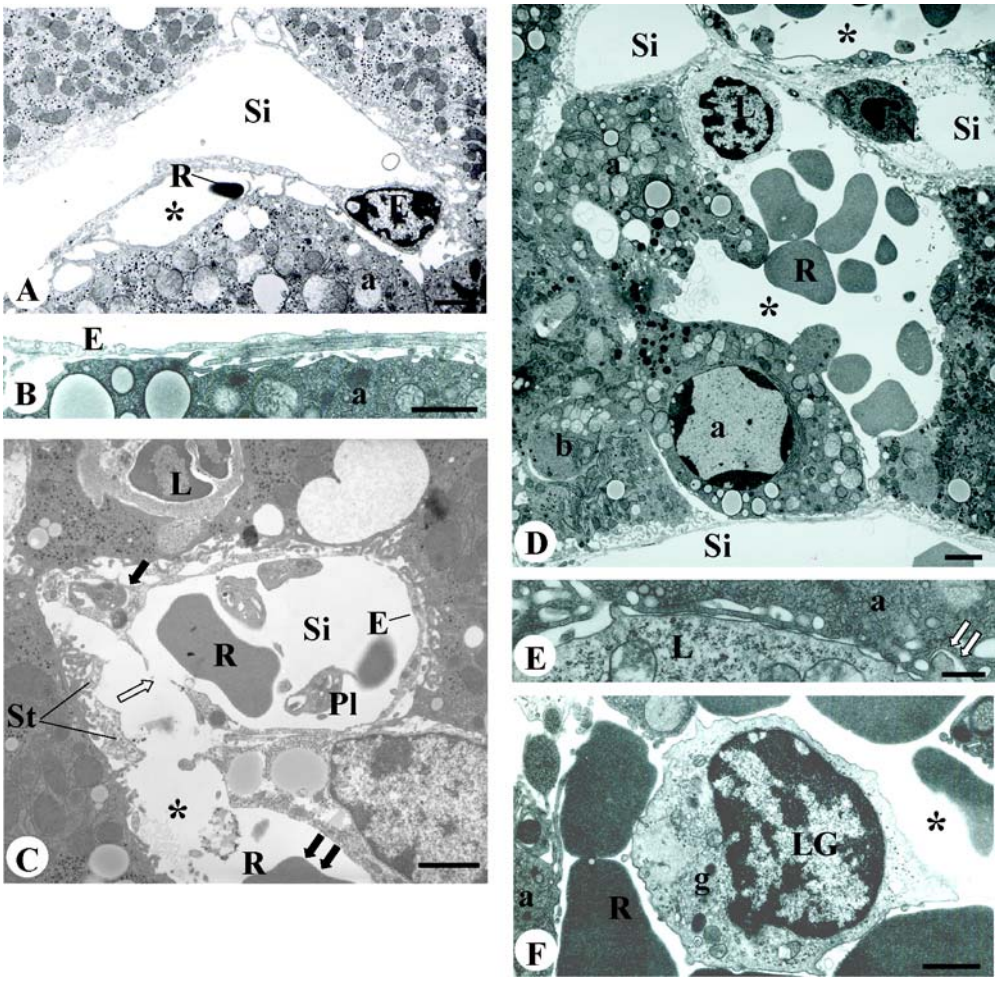

Fig. 5 Electron microscopy of the liver at 4 h (**a**) and 5 h (**b**–**f**). **a** Hepatocytes show the feature of early-phase apoptosis (*a*), i.e. decrease of microvilli and swelling of mitochondria. Erythrocytes (*R*) are seen in the extended space of Disse (*asterisks*). The sinusoidal lining is well preserved. *E*, SECs. *Si*, sinusoids. Bar=2 μm. **b** High magnification of SECs. Although the sinusoidal lining is mostly preserved, the fenestrae of SECs (*E*) decrease in number. *a*, apoptotic hepatocytes. Bar=1 μm. **C**. SECs (*E*) show disruption (*open arrow*). In the sinusoid (*Si*), red blood cells (*R*) and platelets (*Pl*) are seen. The space of Disse (*asterisks*) is extended, and contains red blood cells (*R with double arrows*) and platelets (*arrow*). Lymphocytes (*L*) enter the cytoplasm of hepatocytes, representig the feature of empelipolesis. Bar=2 μm. **d** Apoptotic hepatocytes (*a*) with chromatin-condensed nuclei and swollen mitochondria are disrupted, forming apoptotic bodies (*b*), which are phagocytosed by a neighboring hepatocyte. A lymphocyte (*L*) is closely apposed to apoptotic hepatocytes. The wide extrasinusoidal space (*asterisks*) is formed after elimination of apoptotic hepatocytes, being filled with erythrocytes (*R*). *Si,* sinusoids. *N*, neutrophils. Bar=2 μm. **e** A higher magnification of lymphocyte-apoptotic hepatocyte contact shown in Fig. 5d. A lymphocyte (*L*) extend a small projection (*large arrow*) into the apoptotic hepatocyte (*a*). *Double open arrows*, a cytoplasmic projection of the lymphocyte. Bar=0.5 μm. **f** A large granular lymphocyte (*LG*) containing dense granules (*g*) is seen in the extrasinusoidal space (*asterisks*). *R*, erythrocytes. *a*, apoptotic hepatocytes. *b*, apoptotic bodies. Bar=1 μm

hepatocytes and lymphocyte infiltration in and outside the sinusoid were seen (Fig. 3g).

We next examined if this TNF-α-associated liver injury developed through TNFR1. RT-PCR analysis demonstrated that TNFR1 was constitutively expressed in the normal liver and was similarly expressed at 2 and 4 h after α-GalCer/GalN treatment (Fig. 11). TNFR1 KO mice all survived after treatment (Fig. 9) in spite of a significant elevation of liver TNF-α [101.01±36.06 pg/ml (n=3) at 4 h] which was comparable to that in WT mice. Pathological changes were very similar to those seen in TNF-α KO mice, i.e. there were a small number of apoptotic hepatocytes and no hemorrhage in the parenchyma (Fig. 3h).

Flow cytometric analysis demonstrated that hepatic lymphocytes from WT mice contained *i*NKT cells, which were identified as $CD3^+CD1d^+$ cells, in the proportion of 12% (Fig. 12). TNF-α KO mice had a similar number of *i*NKT cells in the liver. In vitro stimulation with α-GalCer induced both TNF-α and IFN-γ production by WT hepatic lymphocytes (Fig. 13). Hepatic lymphocytes from TNF-α KO mice did not produce TNF-α by stimulation with α-GalCer, but did appreciable amounts of IFN-γ.

Since it is reported that there are caspase-dependent [17] and independent [27] pathways for apoptosis, we next examined the involvement of caspase in the present model. Pretreatment of mice with z-VAD-fmk, a broad inhibitor

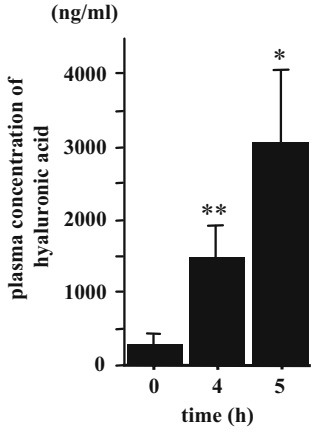

Fig. 6 Timecourse of the plasma concentration of hyaluronic acid after α-GalCer/GalN administration. The data represent the mean±SD (n=3 mice for each time period). *P<0.01, **P<0.05 versus 0 h

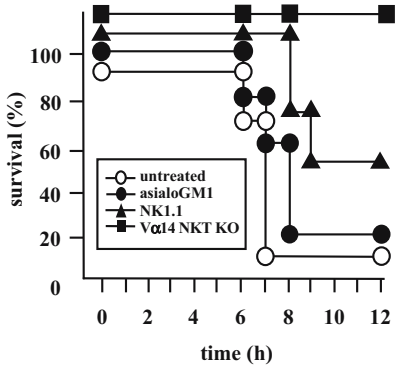

Fig. 7 Involvement of NKT cells but not NK cells in the lethal liver injury with α-GalCer/GalN. Four to eight mice were used for each group. Animals received 50 μl/mouse anti-asialo GM1 at 3, 2 and 1 day before α-GalCer/GalN administration or 400 μg/mouse anti-NK1.1 mAb at 3 days before administration. Vα14NKT KO mice all survived, and pretreatment with anti-NK1.1 mAb improved the survival

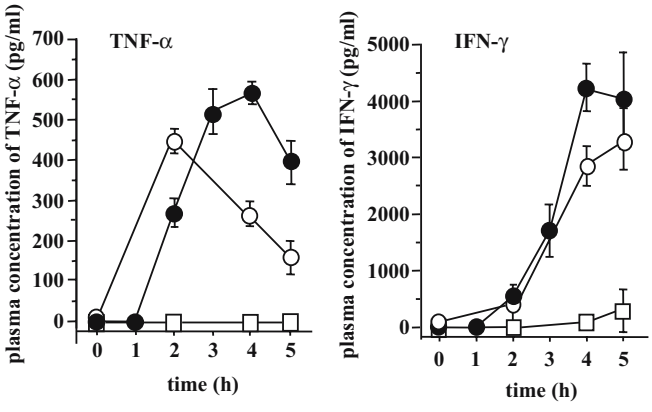

Fig. 8 Involvement of TNF-α but not IFN-γ in the α-GalCer/GalN-induced lethal liver injury. Timecourse of plasma TNF-α (left) and IFN-γ (right) concentrations in WT mice after treatment with α-GalCer alone (○), GalN alone (□), or α-GalCer/GalN (•). The data represent the mean±SD (n=3 mice per group)

for caspase, increased the survival after α-GalCer/GalN-induced liver injury (Fig. 14).

The histological findings of hepatocyte apoptosis in TNF-α KO mice and hepatocyte apoptosis in close proximity to lymphocytes raised the possibility that direct cytotoxicity of lymphocytes might be also involved in the liver injury. The *lpr/lpr* (Fas-deficient) mice showed an improved survival (Fig. 15). The mice that survived showed neither hepatocyte apoptosis nor hemorrhage in the liver (data not shown). Plasma TNF-α was elevated at 4 h to 330±150 pg/ml (n=3), comparable with that in WT mice (350±50 pg/ml, n=3).

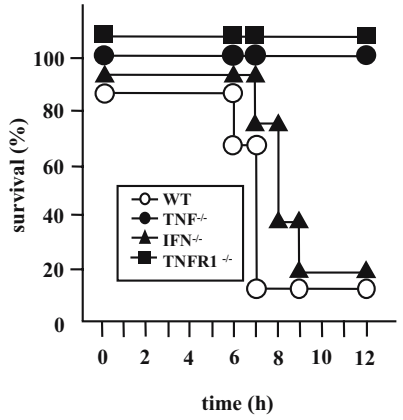

Fig. 9 TNF-α KO mice and TNFR1 KO mice all survived, whereas IFN-γ KO mice all died as well as WT mice within 9 h after α-GalCer/GalN administration. Five to ten animals were used for each group

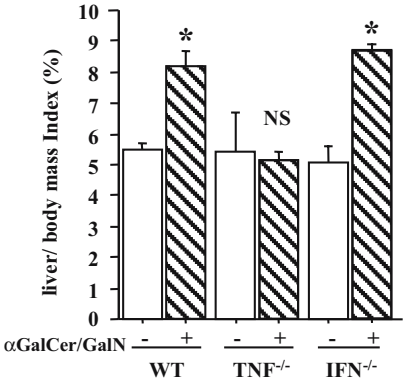

Fig. 10 The liver index significantly increased in WT and IFN-γ KO mice, while not in TNF-α KO mice, at 6 h after α-GalCer/GalN administration. The data represent the mean±SD (n=3 mice). *P<0.01 versus without treatment. NS, not significant

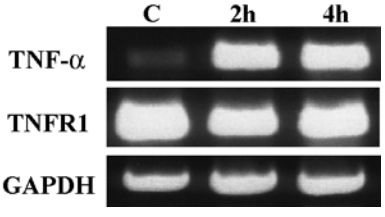

Fig. 11 RT-PCR analysis of untreated and α-GalCer/GalN treated WT mice. The levels of TNF-α mRNA increased after treatment of α-GalCer/GalN. The levels of TNFR1 mRNA did not change before or after treatment. The levels of GAPDH mRNA were used as positive control

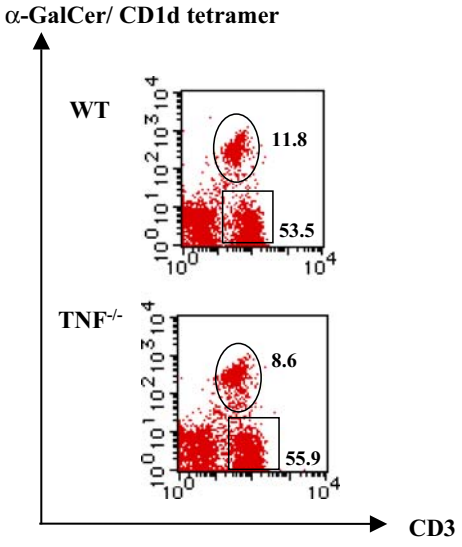

Fig. 12 In vitro production of TNF-α and IFN-γ by hepatic lymphocytes stimulated with α-GalCer. Flow cytometric analysis of hepatic lymphocytes from untreated WT and TNF-α KO mice. A representative data from three experiments is shown. The liver from TNF-α KO mice contained NKT cells in a proportion similar to that from WT mice

Discussion

The present study demonstrated that specific activation of NKT cells with α-GalCer gave a lethal effect on GalN-sensitized mice. Among the organs, pathological changes were only found in the liver. The liver injury was pathologically characterized by massive liver parenchyma hemorrhage and hepatocyte apoptosis. A direct cause of death seems to be hypovolemic shock after intrahepatic bleeding as indicated by the fact that the amount of bleeding reached 0.45–0.6 g, which corresponds over 30% of circulating blood (=1.8 ml) [9].

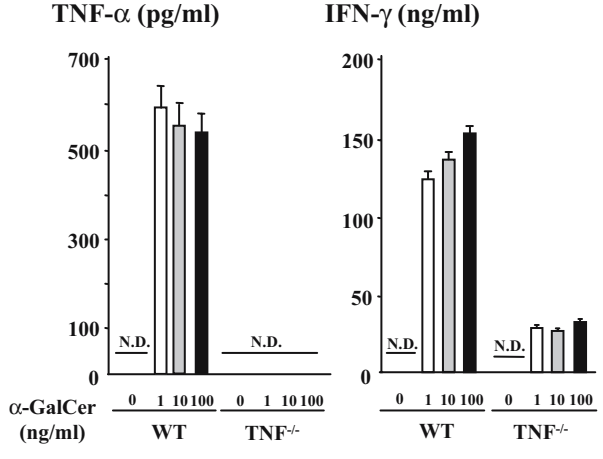

Fig. 13 In vitro production of TNF-α and IFN-γ by hepatic lymphocytes from WT and TNF-α KO after 72-h culture with 0, 1, 10 and 100 ng/ml α-GalCer. ND, not detected. Hepatic lymphocytes from WT mice produce both cytokines with α-GalCer at a dose of larger than 1 ng/ml

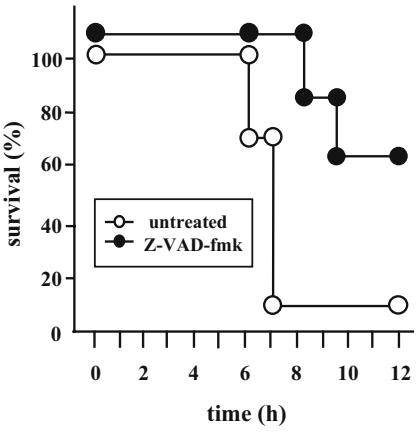

Fig. 14 Involvement of caspase in the α–GalCer/GalN-induced lethal liver injury. The survival rate of WT mice pretreated without and with z-VAD-fmk after α-GalCer/GalN administration. Five to ten mice were used for each group. Pretreatment of mice with z-VAD-fmk considerably improved the survival

Parenchyma hemorrhage developed in association with SEC injury and hepatocellular damage. Morphological and functional alterations to SECs were shown by defenestration/disruption and elevation of plasma hyaluronic acid [8], respectively. SEC disruption follows defenestration and elevation of hyaluronic acid [55]. Although it is not known whether these morphological changes are the events related to apoptosis, apoptotic changes of SECs have been well documented, e.g. SECs are susceptibile to Fas-mediated apoptosis [35], and killing of SECs precedes the parenchyma hemorrhage and hepatocyte death [51]. Furthermore, TNF-α increases the susceptibility of liver endothelial cells to Fas-mediated apoptosis [4]. We observed here that red blood cells passed through injured endothelial barrier, and filled the space generated after hepatocyte destruction. Such communication between the sinusoidal lumen and perisinusoidal space is characteristic of human peliosis hepatis [57]. The present murine model therefore provides a clue for elucidating the pathogenesis of this disease as well.

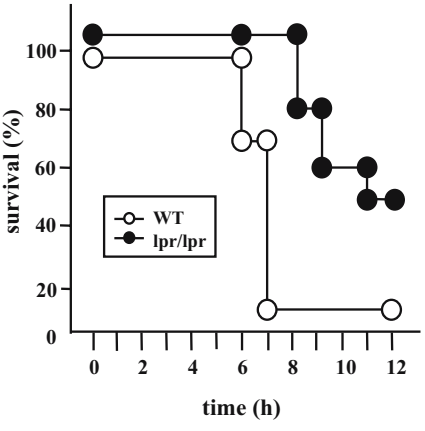

Fig. 15 The survival rate of WT mice and *lpr/lpr* mice after α-GalCer/GalN administration. Ten mice were used for each group. The survival rate increased in *lpr/lpr* mice

In this study, apoptotic change was predominant, while necrosis was negligible. Consistent with this finding, ALT did not increase in the plasma. In human acute and fulminant hepatitis, apoptotic changes of hepatocyte are frequent, but massive necrosis and elevation of transaminase also occur [20, 41, 48] different from the present model. It is reported that hepatocyte apoptosis induces transmigration of neutrophils which mediate hepatocyte necrosis [19]. If animals could have survived longer than 6 h in this model, hepatocyte necrosis should have occurred following apoptosis, and showed elevation of transaminase.

In order to reveal the mechanism of liver injury, we first investigated the implication of NKT cell activation. It is reported that hepatic NKT cells are activated by α-GalCer, and exert cytotoxicity against target cells [40]. In this study, pretreatment of mice with anti-NK1.1 mAb increased the survival, whereas that with anti-asialo GM1 did not. Furthermore, Vα14NKT KO mice neither showed parenchyma hemorrhage nor hepatocyte apoptosis, and survived long. These results indicate that NKT cells rather than NK cells are essential for induction of liver injury. It has been demonstrated that α-GalCer-activated NKT cells produce IFN-γ and TNF-α [2, 15]. In this study, we detected elevation of plasma TNF-α and IFN-γ levels in α-GalCer/GalN-treated mice. In vitro experiment confirmed that α-GalCer-activated hepatic NKT cells are capable of producing these cytokines, suggesting that hepatic NKT cells seem to induce liver injury through TNF-α and IFN-γ production.

We next examined the involvement of TNF-α in liver injury. TNF-α KO mice survived without showing massive parenchyma hemorrhage. The number of apoptotic hepatocytes were small. FACS analysis demonstrated that TNF-α KO mice possessed a substantial number of hepatic *i*NKT cells, although they were somewhat less responsive to α-GalCer compared to *i*NKT cells from WT mice, indicating that resistance to liver injury in TNF-α KO mice is not due to the absence of *i*NKT cells. Vα14NKT KO mice were also resistant to liver injury. These mice did not produce TNF-α after α-GalCer/GalN treatment (data not shown). Furthermore, GalN has a sensitizing effect on hepatocytes for TNF-α-induced apoptosis [28]. These data indicate that endogenous TNF-α is responsible for parenchyma hemorrhage and lethality, and is involved in hepatocyte apoptosis. It is reported that z-VAD-fmk, a broad caspase inhibitor which inhibits both TNF-α/TNFR1-mediated apoptosis and Fas/FasL-mediated one [25], prevents TNF-α-mediated hepatotoxicity and hepatocyte apoptosis in the LPS/GalN model [19]. In this study, pretreatment with z-VAD-fmk increased the survival to 60% at 12 h, indicating that the present liver injury is related to the caspase-dependent pathway for apoptosis. In contrast to TNF-α, IFN-γ was not required for inducing the pathological changes in the present model.

TNF-α functions through two distinct surface receptors, a 55 kD receptor (TNFR1) and a 75 kD receptor (TNFR2). TNFR1 predominantly signals soluble TNF, whereas TNFR2 recognizes membrane-associated TNF. It is intriguing to note that each signal pathway plays a different role in the development of TNF-dependent liver injuries. The TNFR1-mediated pathway, but not TNFR2-mediated one, is essential for the development of LPS/GalN-induced liver injuries [39], while Con A-induced hepatitis primarily depends on the activation of TNFR2-mediated signalings [24, 26, 54]. The experiments using TNFR1 KO mice demonstrated that α-GalCer/GalN-induced liver injury depends on TNFR1 as well as other models in GalN-sensitized mice.

Apoptotic hepatocytes appeared in TNF-α KO mice after α-GalCer/GalN treatment, although the number was much less compared to WT mice, suggesting that mechanisms other than TNF-α may be also involved in induction of hepatocyte apoptosis. Nakagawa et al. [37] described that α-GalCer-activated hepatic NKT cells directly damage the hepatocytes via Fas/FasL signaling. In this study, Fas-deficient *lpr/lpr* mice survived in a higher percentage. Furthermore, conjugation of extrasinusoidally migrating lymphocytes to apoptotic hepatocytes was often encountered. These data suggest the involvement of a direct cytotoxicity of NKT cells through Fas/FasL interaction in liver injury.

Several murine models of liver injury are reported (Table 2). The LPS/GalN model shows the lethality, pathological features (hemorrhage and apoptotic death of

Table 2 Murine models for hepatitis in previous and present studies

Treatments	Lethality (%)	ALT (U/l)	TNF-α (pg/ml)	IFN-γ (pg/ml)	Reference
1) Macrophage activation-mediated					
LPS (10 mg/kg)	0	nt	800	1000	42
LPS (5–20 μg/kg)/GalN	100	6000 (6 h)	500–1500	1000	42, 56
LPS (50–800 μg/kg)/*P.acnes*	90	3500 (12 h)	50,000–300,000	150,000	44, 50
2) T-cell activation-mediated					
Con A (20 mg/kg)	0	8000 (24 h)	200	3000	32
SEB (200 μg/mouse)/GalN	100	nt	100	5000	56
3) NKT-cell activation-mediated					
GalCer (25–100 μg/kg)	0	300 (24 h)	400	3300	40, this study
GalCer (25 μg/kg)/GalN	100	30 (6 h)	600	4300	this study
4) Others					
TNF-α/GalN	100	10,000 (8 h)	nt	nt	36

GalN was used in a dose of 600–700 mg/kg. *P. acnes* was used in a dose of 20–50 mg/kg

hepatocytes) [19, 29] and cytokine profiles (relatively small amounts of TNF-α and IFN-γ) similar to the present model. Liver-specific injury [58] and TNF-dependency [39] are also similar. There are, however, several differences between them. For example, in this model, TNF-α KO mice showed mild liver injury as represented by a small number of apoptotic hepatocytes and moderate elevation of ALT (=556.7±367.0 IU/l; *n*=3) at 12 h, whereas, in the LPS/GalN model, they showed neither histological changes nor elevation of ALT [39]. Furthermore, *lpr/lpr* mice survived α-GalCer/GalN-induced liver injury, whereas they were sensitive to LPS/GalN-induced one [34].

In summary, NKT-cell activation induces severe hepatitis as well as macrophage activation does. The present NKT-cell-mediated liver injury is pathologically characterized by parenchyma hemorrhage and hepatocyte apoptosis, both of which develop mainly by the action of TNF-α secreted by α-GalCer-stimulated NKT cells and in part by a direct cytotoxicity of possible NKT cells. It has been recently reported that activation of NKT cell with α-GalCer induces prominent liver injury in HBs-tg B6 mice which express a transgene-encoded hepatitis B surface antigen [49], suggesting the involvement of NKT-cell activation in the development of type B hepatitis in the human. The present model may be also useful for investigating human vascular disease of the liver like peliosis.

Acknowledgements The authors thank Dr. Yoichiro Iwakura for providing us with IFN-γ-deficient mice. We are grateful to Ms. Miki Yamauchi and Mr. Masahide Sakabe, Department of Anatomy, Osaka City University, Graduate School of Medicine, for their technical supports.

References

1. Angermuller S, Kunstle G, Tiegs G (1998) Pre-apoptotic alterations in hepatocytes of TNFα-treated galactosamine-sensitized mice. J Histochem Cytochem 46:1175–1183
2. Bendelac A, Rivera MN, Park SH, Roark JH (1997) Mouse CD1-specific NK1 T cells: development, specificity, and function. Annu Rev Immunol 15:535–562
3. Bursch W, Taper HS, Lauer B, Schulte-Hermann R (1985) Quantitative histological and histochemical studies on the occurrence and stages of controlled cell death (apoptosis) during regression of rat liver hyperplasia. Virchows Arch B Cell Pathol Incl Mol Pathol 50:153–166
4. Cardier JE, Schulte T, Kammer H, Kwak J, Cardier M (1999) Fas (CD95, APO-1) antigen expression and function in murine liver endothelial cells: implications for the regulation of apoptosis in liver endothelial cells. FASEB J 13:1950–1960
5. Cauwels A, Janssen B, Waeytens A, Cuvelier C, Brouckaert P (2003) Caspase inhibition causes hyperacute tumor necrosis factor-induced shock via oxidative stress and phospholipase A2. Nat Immunol 4:387–393
6. Crispe IN (2003) Hepatic T cells and liver tolerance. Nat Rev Immunol 3:51–62
7. Cui J, Shin T, Kawano T, Sato H, Kondo E, Toura I, Kaneko Y, Koseki H, Kannno M, Taniguchi M (1997) Requirement for Vα14 NKT cells in IL-12-mediated rejection of tumors. Science 278:1623–1626
8. Deaciuc IV, Bagby GJ, Lang CH, Spitzer JJ (1993) Hyaluronic acid uptake by the isolated, perfused rat liver: an index of hepatic sinusoidal endothelial cell function. Hepatology 17:266–272
9. Diehl KH, Hull R, Morton D, Pfister R, Rabemampianina Y, Smith D, Vidal JM, van de Vorstenbosch C; European Federation of Pharmaceutical Industries Association and European Centre for the Validation of Alternative Methods (2001) A good practice guide to the administration of substances and removal of blood, including routes and volumes. J Appl Toxicol 21:15–23
10. Dienes HP (1989) Viral and autoimmune hepatitis. Morphologic and pathogenetic aspects of cell damage in hepatitis with potential chronicity. Verroff Pathol 132:1–107
11. Dini L, Pagliara P, Carla EC (2002) Phagocytosis of apoptotic cells by liver: a morphological study. Microsc Res Tech 57:530–540
12. Emoto M, Kaufmann SH (2003) Liver NKT cells: an account of heterogeneity. Trends Immunol 24:364–369
13. Galanos C, Freundenberg MA, Reutter W (1979) Galactosamine-induced sensitization to the lethal effects of endotoxin. Proc Natl Acad Sci USA 76:5939–5943
14. Gantner F, Leist M, Jilg S, Germann PG, Freudenberg MA, Tiegs G (1995) Tumor necrosis factor-induced hepatic DNA fragmentation as an early marker of T cell-dependent liver injury in mice. Gastroenterology 109:166–176
15. Godfrey DI, Hammond KJ, Poulton LD, Smyth MJ, Baxter AG (2000) NKT cells: facts, functions and fallacies. Immunol Today 21:573–583
16. Hashimoto W, Takeda K, Anzai R, Ogasawara K, Sakihara H, Sugiura K, Seki S, Kumagai K (1995) Cytotoxic NK1.1 Ag+ αβ T cells with intermediate TCR induced in the liver of mice by IL-12. J Immunol 154:4333–4340
17. Hengartner MO (2000) The biochemistry of apoptosis. Nature 407:770–776
18. Illes Z, Kondo T, Newcombe J, Oka N, Tabira T, Yamamura T (2000) Differential expression of NK T cell V alpha24Jalpha Q invariant TCR chain in the lesionsof multiple sclerosis and chronic inflammatory demyelinating polyneuropathy. J Immunol 164:4375–4381
19. Jaeschke H, Fisher MA, Lawson JA, Simmons CA, Farhood A, Jones DA (1998) Activation of caspase 3 (CPP32)-like proteases is essential for TNF-α-induced hepatic parenchymal cell apoptosis and neutrophil-mediated necrosis in a murine endotoxin shock model. J Immunol 160:3480–3486
20. Kasahara I, Saitoh K, Nakamura K (2000) Apoptosis in acute hepatic failure: histopathological study of human liver tissue using the tunel method and immunohistochemistry. J Med Dent Sci 47:167–175
21. Kawano T, Cui J, Koezuka Y, Toura I, Kaneko Y, Sato H, Kondo E, Harada M, Koseki H, Nakayama T et al (1998) Natural killer- like nonspecific tumor cell lysis mediated by specific ligand-activated Vα14 NKT cells. Proc Natl Acad Sci USA 95:5690–5693
22. Kawano T, Cui J, Koezuka Y, Toura I, Kaneko Y, Motoki K, Ueno H, Nakagawa R, Sato H, Kondo E et al (1997) CD1d-restricted and TCR-mediated activation of Vα14 NKT cells by glycosylceramides. Science 278:1626–1629
23. Kita H, Naidenko OV, Kronenberg M, Ansari AA, Rogers P, He XS, Koning F, Mikayama T et al. (2002) Quantitation and phenotypic analysis of natural killer T cells in primary biliary cirrhosis using a human CD1d tetramer. Gastroenterology 123:1031–1043
24. Künsters S, Tiegs L, Alexopoulou M, Pasparakis E, Douni G, Künstle H, Bluchmann A, Wendel K, Pfitzenmaier G, Kollias G, Grell M (1997) In vivo evidence for a functional role of both tumor necrosis factor (TNF) receptors and transmembrane TNF in experimental hepatitis. Eur J Immunol 27:2870–2875
25. Künstle G, Leist M, Uhlig S, Revesz L, Feifel R, MacKenzie A, Wendel A (1997) ICE- protease inhibitors block murine liver injury and apoptosis caused by CD95 or by TNF-α. Immunol Lett 55:5–10

26. Künstle G, Hentze H, Germann P-G, Tiegs G, Meergans T, Wendel A (1999) Concanavalin A hepatotoxicity in mice: tumor necrosis factor-mediated organ failure independent of caspase-3-like protease activation. Hepatology 30:1241–1251
27. Leist M, Jäattelä M (2001) Four deaths and a funeral: from caspases to alternative mechanisms. Nat Rev Mol Cell Biol 2:589–598
28. Leist M, Gantner F, Bohlinger I, Germann PG, Tiegs G, Wendel A (1994) Murine hepatocyte apoptosis induced in vitro and in vivo by TNF-α requires transcriptional arrest. J Immunol 153:1778–1788
29. Leist M, Gantner F, Bohlinger I, Tiegs G, Germann PG, Wendel A (1995) Tumor necrosis factor-induced hepatocyte apoptosis precedes liver failure in experimental murine shock models. Am J Pathol 146:1220–1234
30. Matsuda JL, Naidenko OV, Gapin L, Nakayama T, Taniguchi M, Wang CR, Koezuka Y, Kronenberg M (2000) Tracking the response of natural killer T cells to a glycolipid antigen using CD1d tetramers. J Exp Med 192:741–754
31. Minagawa M, Deng Q, Liu ZX, Tsukamoto H, Dennert G (2004) Activated natural killer T cells induce liver injury by Fas and tumor necrosis factor-alpha during alcoholic consumption. Gastroenterology 126:1387–1399
32. Miyazawa Y, Tsutsui H, Mizuhara H, Fujiwara H, Kaneda K (1998) Involvement of intrasinusoidal hemostasis in the development of concanavalin A-induced hepatic injury in mice. Hepatology 27:497–506
33. Mohammed FF, Smookler DS, Taylot SE, Fingleton B, Kassiri Z, Sanchez OH, English JL, Matrisian LM, Au B, Yeh WC et al. (2004) Abnormal TNF activity in Timp3-/- mice leads to chronic hepatic inflammation and failure of liver generation. Nat Genet 36:969–977
34. Morikawa A, Sugiyama T, Kato Y, Koide N, Jiang GZ, Takahashi K, Tamada Y, Yokochi T (1996) Apoptotic cell death in the response of D-galactosamine-sensitized mice to lipopolysaccharide as an experimental endotoxic shock model. Infect Immun 64:734–738
35. Muschen M, Warskulat U, Douillard P, Gilbert E, Haussinger D (1998) Regulation of CD95(APO-1/Fas) receptor and ligand expression by lipopolysaccharide and dexamethasone in parenchymal and nonparenchymal rat liver cells. Hepatology 27:200–208
36. Nagaki M, Naiki T, Brenner DA, Osawa Y, Imose M, Hayashi H, Banno Y, Nakashima S, Moriwaki H (2000) Tumor necrosis factor α prevents tumor necrosis factor receptor-mediated mouse hepatocyte apoptosis, but not Fas-mediated apoptosis: role of nuclear factor-κB. Hepatology 32:1272–1279
37. Nakagawa R, Nagafune I, Tazunoki Y, Ehara H, Tomura H, Iijima R, Motoki K, Kamishohara M, Seki S (2001) Mechanism of the antimetastatic effect in the liver and of the hepatocyte injury induced by α-galactosylceramide in mice. J Immunol 166:6578–6584
38. Nakatani K, Kaneda K, Seki S, Nakajima Y (2004) Pit cells as liver-associated natural killer cells: morphology and function. Med Electron Microsc 37:29–36
39. Nowak M, Gaines GC, Rosenberg J, Minter R, Bahjat FR, Rectenwald J, Mackay SL, Edwards CK III, Moldawer LL (2000) LPS-induced liver injury in D-galactosamine- sensitized mice requires secreted TNF-α and the TNF-p55 receptor. Am J Physiol Regul Integr Comp Physiol 278:R1202–R1209
40. Osman Y, Kawamura T, Naito T, Takeda K, Van Kaer L, Okumura K, Abo T (2000) Activation of hepatic NKT cells and subsequent liver injury following administration of α-galactosylceramide. Eur J Immunol 30:1919–1928
41. Pretet JL, Pelletier L, Bernard B, Coumes-Marquet S, Kantelip B, Mougin C (2000) Apoptosis participates to liver damage in HSV-induced fulminant hepatitis. Apoptosis 8:655–663
42. Sass G, Heinlein S, Agli A, Bang R, Schümann J, Tiegs G (2002) Cytokine expression in three mouse models of experimental hepatitis. Cytokine 19:115–120
43. Seki S, Hashimoto W, Ogasawara K, Satoh M, Watanabe H, Habu Y, Hiraide H, Takeda K (1997) Antimetastatic effect of NK1+ T cells on experimental haematogenous tumor metastases in the liver and lungs of mice. Immunology 92:561–566
44. Shimizu Y, Margenthaler JA, Landeros K, Otomo N, Doherty G, Flye MW (2002) The resistance of P. acnes-primed interferon γ-deficient mice to low-dose lipopolysaccharide-induced acute liver injury. Hepatology 35:805–814
45. Sumida T, Sakamoto A, Murata H, Makino Y, Takahashi H, Yoshida S, Nishioka K, Iwamoto I, Taniguchi M (1995) Selective reduction of T cells bearing invariant Vα24 JαQ antigen receptor in patients with systemic sclerosis. J Exp Med 182:1163–1168
46. Sumida T, Maeda T, Taniguchi M, Nishioka K, Stohl W (1998) TCRαV24 gene expression in double negative T cells in systemic lupus erythematosus. Lupus 7:565–568
47. Tagawa Y, Sekikawa K, Iwakura Y (1997) Suppression of concanavalin A-induced hepatitis in IFN-γ-/- mice, but not in TNF-α-/- mice: role for IFN-γ in activating apoptosis of hepatocytes. J Immunol 159:1418–1428
48. Tokushige K, Yamaguchi N, Ikeda I, Hashimoto E, Yamauchi K, Hayashi N (2000) Significance of soluble TNF receptor-I in acute-type fulminant hepatitis. Am J Gastroenterol 95:2040–2046
49. Trobonjaca Z, Leithäuser F, Möller P, Schirmbeck, Reimann J (2001) Activating immunity in the liver. I. Liver dendritic cells (but not hepatocytes) are potent activators of IFN-γ release by liver NKT cells. J Immunol 167:1413–1422
50. Tsuji H, Mukaida N, Harada A, Kaneko S, Matsushita E, Nakanuma Y, Tsutsui H, Okamura H, Nakanishi K, Tagawa Y et al. (1999) Alleviation of lipopolysaccharide-induced acute liver injury in Propionibacterium acnes-primed IFN-γ-deficient mice by a concomitant reduction of TNF-α, IL-12, and IL-18 production. J Immunol 162:1049–1055
51. Wanner GA, Mica L, Wanner-Schmid E, Kolb SA, Hentze H, Trentz O, Ertel W (1999) Inhibition of caspase activity prevents CD95-mediated hepatic microvascular perfusion failure and restores Kupffer cell clearance capacity. FASEB J 13:1239–1248
52. Watanabe H, Miyaji C, Kawachi Y, Iiai T, Ohtsuka K, Iwanaga T, Takahashi-Iwanaga H, Abo T (1995) Relationships between intermediate TCR cells and NK1.1+T cells in various immune organs. NK1.1+T cells are present within a populations of intermediate TCR cells. J Immunol 155:2972–2983
53. Wilson SB, Kent SC, Patton KT, Orban T, Jackson RA, Exley M, Porcelli S, Schatz DA, Atkinson MA, Balk SP (1998) Extreme Th1 bias of invaiant Valpha24 JalphaQ T cells in type 1 diabetes. Nature 391:177–181
54. Wolf D, Hallmann R, Sass G, Sixt M, Kusters S, Fregien B, Trauwein C, Tiegs G (2001) TNF- alpha-induced expression of adhesion molecules in the liver is under the control of TNFR1 — relevance for concanavalin A-induced hepatitis. J Immunol 166:1300–1307
55. Yachida S, Kokudo Y, Wakabayashi H, Maeba T, Kaneda K, Maeta H (1998) Morphological and functional alterations to sinusoidal endothelial cells in the early phase of endotoxin-induced liver failure after partial hepatectomy in rats. Virchows Arch 433:173–181
56. Yasuda S, Nagaki M, Moriwaki H (2002) Staphylococcal enterotoxin B induces hepatic injury and lethal shock in endotoxin-resistant C3H/HeJ mice despite a deficient macrophage response. J Endotoxin Res 8:253–261
57. Zafrani ES, Cazier A, Baudelot AM, Feldmann G (1984) Ultrastructural lesions of the liver in human peliosis. A report of 12 cases. Am J Pathol 114:349–359
58. Zhou BR, Gumenscheimer M, Freudenberg M, Galanos C (2003) A striking correlation between lethal activity and apoptotic DNA fragmentation of liver in response of D-galactosamine-sensitized mice to a non-lethal amount of lipopolysaccharide. Acta Pharmacol Sin 24:193–198

Virchows Arch (2005) 446: 674–676
DOI 10.1007/s00428-005-1255-x

LETTER TO THE EDITOR

Najat Mourra · Maité Lewin · Alain Sautet · Rolland Parc · Jean-Francois Flejou

Epithelioid solitary fibrous tumor in the ischioanal fossa

Received: 14 December 2004 / Accepted: 7 March 2005 / Published online: 13 May 2005
© Springer-Verlag 2005

Dear Editor:
Solitary fibrous tumor (SFT) is a rare mesenchymal tumour initially described in the pleural cavity, but later reports have documented its occurrence in various extrapleural sites, including the abdomen [3, 5, 6]. The diagnosis of these tumors has generally been fraught with difficulties, because of their histologic variability. They can display storiform, hemangiopericytic, herring-bone, neural-type palisading, and diffuse sclerosing areas [4].

We describe the second case of SFT in the ischioanal fossa, characterized by epithelioid areas. To our knowledge, this feature has not been documented in this location before.

A 67-year-old male, with unremarkable medical history, presented with urinary problems. Rectal examination revealed a fullness in the right side of the rectum. MRI study showed the presence of a 14×8 cm moderately circumscribed, heterogeneous solid mass, with high vascularity, and central necrosis, occurring in the right ischioanal fossa (Fig. 1). This mass was extra-peritoneal in location, with resultant superio-left displacement of the levator musculature and the rectum. The tumor was totally excised. No further therapy was given, and the patient recovered well, without evidence of recurrence as yet (6 months of follow-up).

N. Mourra (✉) · J.-F. Flejou
Department of Pathology, Hôpital St-Antoine,
184, rue du faubourg St-Antoine,
75012 Paris, France
e-mail: najat.mourra@sat.ap-hop-paris.fr
Tel.: +33-1-49282178
Fax: +33-1-49282878

M. Lewin
Department of Radiology, Hopital St-Antoine, AP-HP,
Paris, France

A. Sautet · R. Parc
Department of Surgery, Hopital St-Antoine, AP-HP,
Paris, France

Grossly, the excised lesion was a well circumscribed, partially encapsulated, rounded mass, measuring 13×12×8 cm. On section, the mass had multinodular, gray-whitish and firm appearance, with myxoid and hemorrhagic changes at the center (Fig. 2).

Microscopically, the tumor was characterized by prominent vascularity, with numerous small and mid-sized caliber vessels, with hyalinized wall "hemangiopericytoma-like" and significant variation in cellularity (Fig. 3). Hypercellular areas were predominant at the periphery, they displayed compact clusters of epithelioid neoplastic cells, with abundant eosinophilic cytoplasm, and distinct cell borders (Fig. 4). The nuclei were round with finely dispersed chromatin and small nucleoli. There was no nuclear atypia and mitoses were difficult to find (<1/10 HPF). Necrosis was prominent at the center, as well as myxoid degeneration. There was no storiform pattern, neuroid appearance, or diffuse sclerosing areas, even after multiple sampling of the tumor. The surgical margins were found to be clear.

Immunohistochemically, tumor cells were strongly positive for vimentin, CD34 (Fig. 3, inset), BCL2 (Fig. 4, inset), and moderately for CD99 (MIC 2). Scattered cells reacted with KL1. Immunostains for EMA, actin, desmin, CD117 (c-Kit), and S100 protein, were negative.

The diagnosis of epithelioid SFT, with unpredictable prognosis was made. SFT is an uncommon spindle cell neoplasm that was first described as a distinctive pleural lesion in 1931. In subsequent decades, extra-thoracic SFTs have increasingly been recognized. In this paper, we report the second case of SFT arising in the ischioanal fossa; the first was described by Dudkiewicz et al. in 2004 [2]. What makes the present lesion apparently unique, is the presence of epithelioid features. This morphologic variability may contribute to more difficulties in diagnosing these tumours, especially on percutaneous biopsy.

Histologically, these tumours are characterized by a variety of growth patterns, with admixture in a various proportion of bland spindle cell cytology, alternating hyper- and hypocellular areas, keloid-like hyalinisation, and a frequently prominent branching vasculature often described as

Fig. 1 RMI : 14 cm moderately circumscribed, heteregeneous solid mass, with high vascularity, and central necrosis

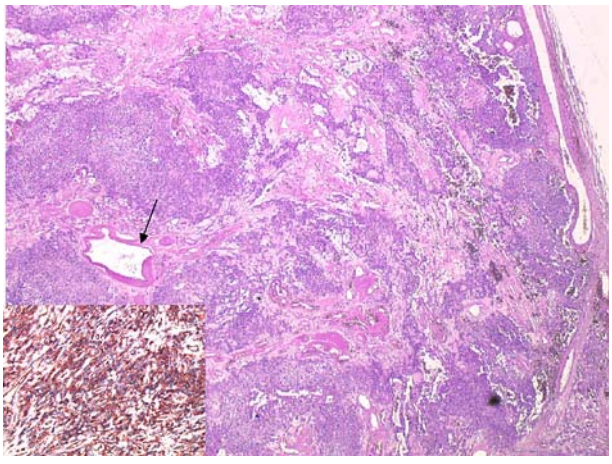

Fig. 3 Well circumscribed tumor, with numerous small and mid-sized vessels, with hyalinized wall (arrow) "hemangiopericytoma-like" and variation in cellularity. Strong immunostaining positivity of the tumor cells with CD34 (inset)

"hemangiopericytoma-like". Areas showing an angiofibroma-like appearence, neural-type fascicle areas, with wavy nuclei, and occasional herring-bone patterns are also reported [5]. Other less frequently observed cytological features are nuclear palisading, compact clusters of polygonal cells, and small cells [4].

All these patterns were absent in our observation, which was composed entirely of epithelioid cells. The term "epithelioid SFT" was proposed for the first time in 2003 by Alberto et al., when they reported a mediastinal SFT, with predominantly epithelioid cells, exhibiting histopathological and immunohistochemical features intermediate between those of SFT and those of cellular adenomatoid tumor [1]. Unlike this observation, SFT was entirely composed of epithelioid cells in our case, and only scattered tumor cells were positive for cytokeratin.

This epithelioid growth pattern contributes to further difficulties in differential diagnosis of these tumors with other soft tissue neoplasms, with epithelioid features, such as epithelioid sarcoma, schwannoma, leiomyosarcoma, and malignant gastrointestinal stromal tumor. Immunohistochemical stains will be of great value by demonstrating positivity of epithelioid cells with vimentin, CD34, BCL2, and CD99, and their negativity with CD117 (c-Kit), epithelial, neural, and muscular markers.

The behaviour of extrathoracic SFTs is unpredictable, comparable to their pleural counterparts, although they have an increased risk of local recurrence. Positive surgical margins, tumor size greater than 10 cm, and the presence of malignant component (necrosis, marked cellularity, nuclear atypia, and more than four mitoses/10 HPF) predict worse-metastasis-free survival [3]. Whether this epithelioid pattern represents another atypical histological features SFT awaits further studies with larger numbers of cases.

In summary, we report a case of epithelioid SFT arising in the ischioanal fossa, which highlights the difficulties encountered in the diagnosis of SFTs because of their histologic variability. One should bear in mind that epithelioid features may exist, and could be prominent in some

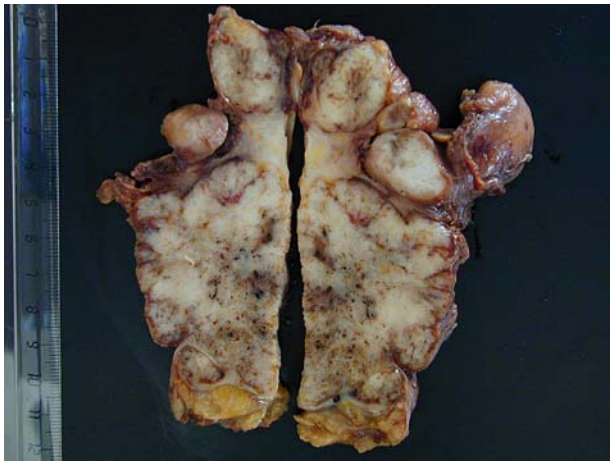

Fig. 2 Gross section : multinodular, gray-whitish mass, with myxoid and hemorrhagic changes at the center

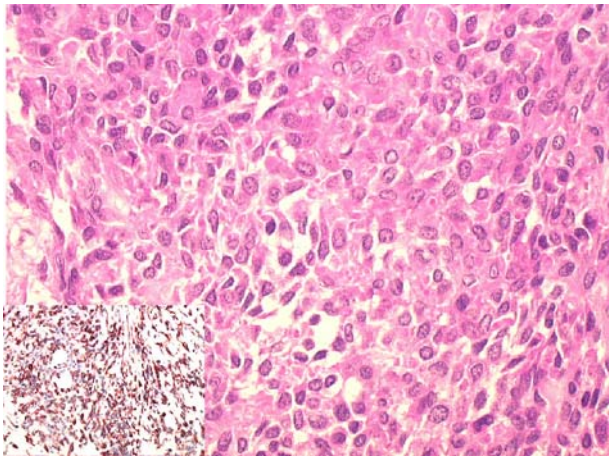

Fig. 4 High power view of epithelioid tumor cells, with abundant eosinophilic cytoplasm, distinct cell borders, and round nuclei, without atypia and mitosis. Diffuse immunostaining positivity of tumor cells with BCL2 (inset)

cases. Our observation emphasizes the importance of an appropriate immunohistochemical panel in the differential diagnosis of epithelioid cell neoplasms in the pelvis. Identification of this pattern of SFT is of importance, to avoid misdiagnosis with other more aggressive conditions in the soft tissue location.

References

1. Alberto MM, Varshney D, Fullet C (2003) Mediastinal epithelioid solitary fibrous tumor. Arch Pathol Lab Med 127: e212–e215
2. Dudkiewicz M, Deschenes JL, Bloom C, Gordon PH (2004) Solitary fibrous tumor of the ischioanal fossa: report of a case and review of the literature. Dis Colon Rectum 47:535–537
3. Gold JS, Antonescu CR, Hadju C, Ferrone CR, Hussain M, Lewis JL (2002) Clinicopathologic correlates of solitary fibrous tumors. Cancer 94:1057–1068
4. Hasegawa T, Matsuno Y, Shimoda T, Hasegawa F, Sano T, Hirohashi S (1999) Extrathoracic solitary fibrous tumors: their histological variability and potentially aggressive behavior. Hum Pathol 30:1464–1473
5. Suster P, Nascimento AG, Miettinen M, Sickel JZ, Moran CA (1995) Solitary fibrous tumors of soft tissue: a clinicopathologic and immunohisochemical study of 12 cases. Am J Surg Pathol 19:1257–1266
6. Vallat-Decouvelaere AV, Dry SM, Fletcher CDM (1998) Atypical and malignant solitary fibrous tumors in extrathoracic locations. Evidence of their comparability to intra-thoracic tumors. Am J Surg Pathol 22:1501–1511

Virchows Arch (2005) 446: 677–679
DOI 10.1007/s00428-005-1259-6

LETTER TO THE EDITOR

Gaetano Magro · Kamila Benkova · Michal Michal

Meningioma-like tumor of the thyroid. A previously undescribed variant of follicular adenoma

Received: 25 February 2005 / Accepted: 7 March 2005 / Published online: 13 May 2005
© Springer-Verlag 2005

Dear Editor:
Recently one of us (G.M.) reported in *Virchows Archiv* [4] the possibility that nodular goiter may contain follicular-derived atypical/bizarre spindle cells that may represent a potential diagnostic pitfall. In this regard, we have encountered a unique spindle cell thyroid tumor bearing a striking morphological resemblance to a meningioma. To the best of our knowledge, such a lesion has not been previously reported in English literature.

A 69-year-old woman underwent resection of the right lobe of the thyroid. One year after the excision, the patient is without signs of the disease. Grossly, a nodule measuring 2×2×5 cm^3, and whitish in color was detected at the lower pole of the lobe. Histological examination revealed a capsulated tumor showing an overall morphological appearance closely reminiscent of a transitional type meningioma (Fig. 1a-c). The tumor was composed of an intimate admixture of small/medium-sized thick-walled vessels with intervening proliferation of bland-looking ovoid to spindle-shaped cells. The hallmark feature was the arrangement of cells in whorls, most of which appeared to be centered around the above mentioned blood vessels (Fig. 1a, b). In some areas, the cells had a more compact, syncytial-like configuration, or lined numerous varying-sized empty spaces or more rarely follicular-like structures containing esosinophilic material (Fig. 1c). The neoplastic cells had a pale to slightly eosinophilic cytoplasm, with a round to ovoid nucleus, sometimes with one or two small nucleoli. Only rarely were intranuclear pseudoinclusions seen. Psammoma bodies, nuclear pleomorphism, mitoses, necrosis, and inflammatory cells were absent. Deeply eosiniophilic colloid with peripheral scalloping typical of papillary carcinoma of the thyroid was absent. The tumor was highly vascularized. The blood vessels were characteristically small to medium-sized, round-shaped, and had distinctive thick walls due to collagen and/or fibrin deposition. Foamy histiocytes were observed in the walls and/or within the lumen of vessels, and less frequently they were scattered throughout the tumor. No capsular or vascular invasion was found. Immunohistochemical analysis revealed that neoplastic cells were stained with both thyroglobulin (Fig. 1d) and TTF-1 (Fig. e). Only a minority of cystic spaces, easily identified on H and E, contained thyroglobulin-positive material (Fig. 1d). Both cytokeratins and EMA were strongly expressed in the cells lying cystic spaces, and only weakly in spindled cells forming whorls. Vimentin stained variably tumor areas, being generally more expressed in spindle-shaped cells. No immunoreactivity to calcitonin, S-100 protein, parathormone, CD34, CD31, desmin and α-smooth muscle actin was obtained. The expression of thyroglobulin and TTF-1 by neoplastic cells supported the follicular origin of the lesion; antibodies anti-pancytokeratins and EMA were helpful in better highlighting a follicular configuration in some tumor areas, that was under-recognized on H and E examination. On the basis of the morphological and immunohistochemical features, we believe that the lesion described herein is to be interpreted as a histological variant of a follicular adenoma. Although follicular adenoma may occasionally exhibit a varying amount of spindle cells [3, 5, 7] and/or numerous blood vessels with marked degenerative changes (i.e. thrombosis and/or collagenization of walls) [5], it is the peculiar arrangement of cells in whorls around collagenized vessels to impart the present tumor a peculiar meningioma-like appearance. A similar growth pattern has only been rarely and focally detected in follicular thyroid adenoma (personal unpublished observations).

Differential diagnosis mainly includes meningioma and, given the prominent angiocentricity of tumor, the wide group of pericytic (vascular) tumors (hemangiopericytoma,

G. Magro (✉)
Dipartimento G.F. Ingrassia, Anatomia Patologica,
Università di Catania,
Catania, Italy
e-mail: g.magro@unict.it

K. Benkova
Faculty Hospital Bulovka,
Prague, Czech Republic

M. Michal
Sikl's Department of Pathology, Charles University Hospital,
Pilsen, Czech Republic

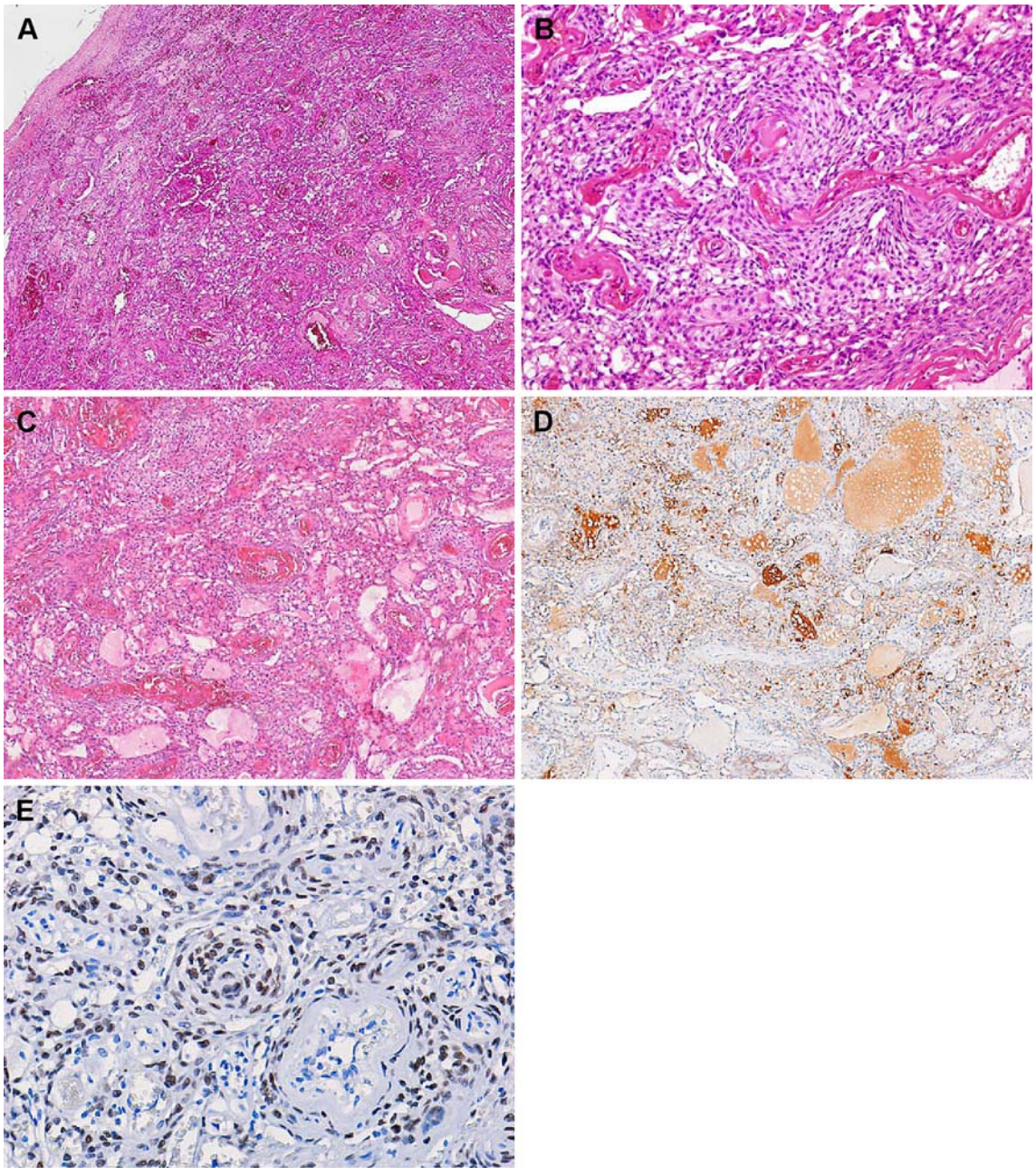

Fig. 1 (**a**) Low magnification of tumor showing a transitional-type meningioma-like appearance. (**b**) Cells are arranged in whorls around blood vessels with hyalinized walls. (**c**) Tumor area in which follicular-like structures are seen. (**c**) Thyroglobulin stains colloidal material within follicles. Less intense staining is also observed in cellular component. (**d**) Neoplastic cells are immunoreactive to TTF-1

glomus tumor, glomangioma/myoma, myopericytoma). Primary ectopic meningiomas are exceedingly rare neoplasms usually occurring in the head and neck region or to the paravertebral soft tissues. Although the occurrence of a meningioma in lung is accepted [6], the detection of such a tumor at a visceral site, including thyroid, is probably a metastasis from a malignant cranial tumor [2]. Pericytic tumors are composed of α-smooth muscle actin-positive cells showing a continuous morphological spectrum, ranging from primitive-appearing round cells to spindled cells with overt features of smooth muscle differentiation [1]. Immunohistochemistry, revealing a follicular-derived epithelial phenotype of neoplastic cells, was helpful in ruling out both meningioma and pericytic tumors.

The present case widens the histological spectrum of follicular thyroid adenoma. The meningioma-like features should be interpreted as a variant on the theme of the follicular-derived spindle cell metaplasia, a phenomenon which is known to occur occasionally in both benign and malignant thyroid lesions [3–5, 7]. The importance of recognizing this variant for pathologist is to avoid confusion with other benign and malignant spindle cell lesions.

Acknowledgements The authors thank Dr. Juan Rosai for confirming the diagnosis.

References

1. Folpe AL, McMenamin ME (2002) Pericytic (perivascular) Tumours. In: Fletcher CDM, Unni KK, Mertens F (ed) Pathology and genetics of tumors of soft tissue and bone. WHO, Lyon, pp 135–139
2. Hasan R, Marshall MC Jr, Medhi M, Arshad A, Braun A, Panageas E (2001) Meningioma metastatic to thyroid gland. Endocr Pract 7:370–374
3. Hazard JB, Kenyon R (1954) Atypical adenoma of the thyroid. Arch Pathol 58:554–563
4. Magro G, Torrisi A, Torrisi A (2005) Atypical/bizarre spindle-cell epithelial metaplasia in nodular goiter: a potential diagnostic pitfall. Virchows Arch 446:91–92
5. Rosai J, Carcangiu ML, DeLellis RA (1992) Tumors of the thyroid gland. In: Atlas of tumor pathology, Third Series, Washington
6. Spinelli M, Claren R, Colombi R, Sironi M (2000) Primary pulmonary meningioma may arise from meningothelial-like nodules. Adv Clin Pathol 4:35–39
7. Vergilio J, Baloch ZW, LiVolsi V (2002) Spindle cell metaplasia of the thyroid arising in association with papillary carcinoma and follicular adenoma. Am J Clin Pathol 117:199–204

Virchows Arch (2005) 446: 680–681
DOI 10.1007/s00428-005-1267-6

LETTER TO THE EDITOR

Thomas Longerich · Knut Ketterer · Burkhard M. Helmke · Helmut Friess · Peter Schirmacher

Tumor induced local fibrogenic effect by hepatic metastasis of insulinoma

Received: 17 January 2005 / Accepted: 30 March 2005 / Published online: 19 May 2005
© Springer-Verlag 2005

To the Editor:

Here we report an interesting phenomenon of peritumoral fibrotic architectural alteration of the non-tumorous liver, most likely induced by a diffusible, tumor-derived factor. A 47-year-old male Caucasian patient developed a metachronous hepatic metastasis of an insulinoma, which had been resected by partial pancreas tail-resection 13 years ago. Seven years later, recurrent hypoglycaemic episodes emerged and the patient received total pancreas left-resection, splenectomy and lymph node dissection. Several lymph node metastases were diagnosed in the peripancreatic fat tissue and the splenic hilus demonstrating malignancy. The patient now became symptomatic again with recurrent, spontaneous hypoglycemic episodes (serum glucose values lowered to 30 mg/dl). Neither abdominal ultrasound nor contrast-enhanced MRI detected a focal liver lesion, but liver metastasis was proven by a rise in serum insulin levels in the *vena hepatica propria* (3.2-fold increase of c-peptide and 9-fold increase of insulin values after selective intra-arterial calcium stimulation). Intraoperative ultrasound disclosed a single lesion in liver segment 6, which was resected. The gross specimen contained a relatively sharp demarcated, yellowish nodule, measuring 0.5 cm in diameter surrounded by liver tissue of micronodular texture. Immunohistologically, the tumor cells stained strongly for insulin (Fig. 1A). The immediately surrounding liver tissue showed severe fibrotic change, which was clearly demonstrable in connective tissue stains. The type of fibrosis was clearly discernible and different from tumor desmoplasia or capsule formation (Fig. 1B). Peritumorous focal nodular hyperplasia was ruled out by the lack of typical occluded or atypical vascular structures, well demarcated nodular hepatocellular proliferation, and by the fact that the fibrotic change faded out into the surrounding liver tissue, thus showing some kind of gradient formation [1]. The fibrogenic effect was not detectable in more than 1 cm distance from the metastasis and was also absent in a synchronous liver biopsy taken far away from the tumor (insert 1C). The restriction of the phenomenon to the immediate surrounding of the tumor with some kind of gradient formation strongly suggested activity of a tumor derived, diffusible factor. A likely candidate was insulin, which was highly expressed and secreted by the tumor cells. The growth-promoting effect of insulin appears to be mediated through activation of insulin-like growth factor I receptor (IGF-IR) and insulin receptor substrate-1 (IRS-1) [2]. In particular, it has been demonstrated that insulin stimulates proliferation and collagen type I expression of human hepatic stellate cells (HSC), which express insulin receptor, IGF-I-R, and IRS-1 [4]. Recently, Novosyadlyy et al. suggested that stimulation of the IGF axis by IGF-I and insulin is relevant in vivo for the process of fibrogenesis during acute and chronic liver injury [3]. Underlying stimulation and myofibroblastic transformation of HSC and/or portal fibroblasts in our case was suggested by smooth-muscle actin positive cells within the cirrhotic septa (Fig. 1D). Since the phenomenon was only detectable in the immediate surrounding, excessive insulin concentrations appear to be required to solely excert the fibrogenic effect in vivo. However, it remains an open question whether increased systemic insulin concentrations have confounding fibrogenic activity. Interestingly, patients with non-alcoholic fatty liver disease (NAFLD) associated with type 2 diabetes mellitus develop liver cirrhosis more frequently than non-diabetic patients [5]. In contrast to patients with

T. Longerich · B. M. Helmke · P. Schirmacher
Institute of Pathology,
University of Heidelberg,
Heidelberg, Germany

K. Ketterer · H. Friess
Department of General Pathology and
Department of General Surgery,
University of Heidelberg,
Heidelberg, Germany

T. Longerich (✉)
Institute of Pathology,
Im Neuenheimer Feld 220,
69120 Heidelberg, Germany
e-mail: thomas.longerich@med.uni-heidelberg.de
Tel.: +49-6221-562609
Fax: +49-6221-565251

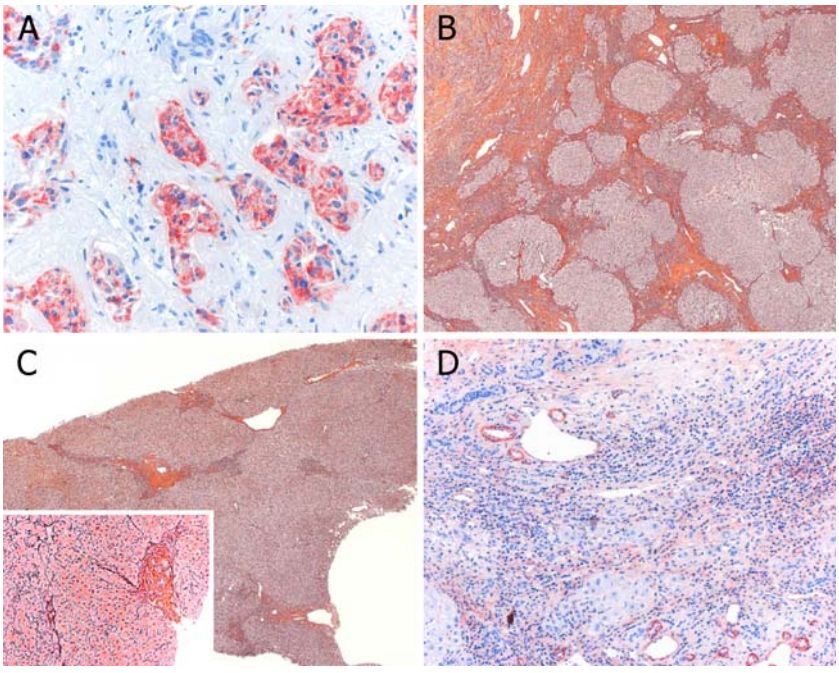

Fig. 1 Tumor cells stain strongly positive for insulin (**a**, original magnification 200×). The fibrotic architectural change of the nontumorous liver in the immediate surrounding of the insulinoma metastasis shows some gradient formation (**b**, 25×, modified Gomori's stain). Liver tissue distant to the metastasis (**c**, 25×, modified Gomori's stain) as well as an additional biopsy taken far away from the tumor (insert C, 50×) show only mild portal fibrosis. The fibrous septa as well as the vessels stain positive for alpha_smooth muscle actin (**d**, 25×)

NAFLD, we detected only mild steatosis in the parenchyma surrounding the metastasis, which was probably due to the absence of insulin resistance in these hepatocytes.

References

1. Iordanidis F, Hytiroglou P, Drevelegas A, Kodonas F, Ioannidis I, Nenopoulou H, Papadimitriou CS (2002) A 25-year-old man with a large hepatic tumor and multiple nodular lesions. Semin Liver Dis 22:97–102
2. Kahn CR (1985) The molecular mechanism of insulin action. Annu Rev Med 36:429–451
3. Novosyadlyy R, Tron K, Dudas J, Ramadori G, Scharf JG (2004) Expression and regulation of the insulin-like growth factor axis components in rat liver myofibroblasts. J Cell Physiol 199:388–398
4. Svegliati-Baroni G, Ridolfi F, Di Sario A, Casini A, Marucci L, Gaggiotti G, Orlandoni P, Macarri G, Perego L, Benedetti A, Folli F (1999) Insulin and insulin-like growth factor-1 stimulate proliferation and type I collagen accumulation by human hepatic stellate cells: differential effects on signal transduction pathways. Hepatology 29:1743–1751
5. Younossi ZM, Gramlich T, Matteoni CA, Boparai N, McCullough AJ (2004) Nonalcoholic fatty liver disease in patients with type 2 diabetes. Clin Gastroenterol Hepatol 2:262–265

Virchows Arch (2005) 446: 682
DOI 10.1007/s00428-005-1284-5
© Springer-Verlag 2005

ANNOUNCEMENTS

26–29 July 2005
Practical Pulmonary Pathology
London, UK

This course is designed to provide histopathology and cytopathology trainees and consultants with an opportunity to study diagnostic lung pathology in a comprehensive manner. It comprises lectures and practical microscopy sessions, the latter making up roughly half the time and consisting of individual study of a unique collection of cases.

Further details and application forms are available from:
Professor B Corrin
Brompton Hospital
London SW3 6NP, UK
Fax: +44 20 7351 8293
E-mail: b.corrin@ic.ac.uk

22–23 September 2005
Breast Diagnostic Histopathology Update
Hammersmith Hospital (Imperial College), London, UK

A 2-day course designed for pathologists at Consultant and Senior Trainee level. The course is a shorter version of the week long course and is also suitable for those who have previously attended that course and wish to participate in discussing new developments in the field. The course will be based on 30, mostly new, cases derived from the arcives of Hammersmith, Charing Cross, Nottingham City and Cambridge Addenbrook's Hospitals and is slanted to practical diagnostic pathology with special emphasis on areas that pose diagnostic difficulties. The participants will be given ample time to study histological preparations, followed by illustrated discussion of the cases. In addition there will be several talks on specific topics, given by breast pathology specialists followed by discussions. The topics will include issues in the interpretation of breast biopsies, examination of breast biopsies after neo-adjuvant chemotherapy, breast immunohistochemistry, dealing with the gross specimen, fibro-epithelial and spindle cell lesions; papillary, lobular, apocrine and metaplastic lesions, proliferative lesions/ carcinoma in situ and sentinel lymph node biopsy. The faculty will include Ian Ellis, Mary Falzon, Andrew Lee, Sarah Pinder and Sami Shousha.

Further details from:
Wolfson Conference Centre,
Hammersmith Hospital,
Du Cane Road,
London W12 ONN, UK
Tel.: (44) 20 8383 3117/3227/3245
Fax: (44) 20 8383 2428
E-mail: wcc@imperial.ac.uk

1–2 December 2005
International Symposium on "Salivary Gland Tumours; Present Concepts of Diagnosis and Management"
Amsterdam, The Netherlands

For further information please contact congress secretariat
Mrs. D. Chavalking
Vrije Universiteit Medical Center (Vumc)
Department of Oral and Maxillofacial Surgery/Oral Pathology
PO Box 7057
1007 MB Amsterdam
The Netherlands
Tel.: +31-20-444-4039
Fax: +31-20-444-4046
E-mail: d.chevalking@vumc.nl
Internet: www.vumc.nl